

P437

Bibliography of Lewis Research Center Technical Publications Announced in 1990

August 1991

(NASA-TM-103753) BIBLIOGRAPHY OF LEWIS
RESEARCH CENTER TECHNICAL PUBLICATIONS
ANNOUNCED IN 1990 (NASA) ~~437~~ CSCL 050

N92-12786

446 P

unclas
G5/82 0053267



NASA Technical Memorandum 103753

Bibliography of Lewis Research Center Technical Publications Announced in 1990

August 1991



National Aeronautics and
Space Administration

Lewis Research Center
Cleveland, Ohio 44135

PREFACE

In 1990, Lewis Research Center's 1396 research authors published 659 technical publications that were announced to and reached the worldwide scientific community. This was our highest number of technical publications in 19 years and 21 more than last year's high production of 638. In addition to this total, 134 contractor-authored research reports were produced at NASA Lewis. Included in this total were more symposium/seminar presentations (311) and more Lewis-hosted conference papers (123) than at any other time.

In 1990, Lewis authors published approximately 59 percent of their research contributions in outside publications and the remainder as NASA research reports. Sixty-six percent of Lewis-authored society presentations and journal articles were addressed to members of the following 10 societies—AIAA, ASME, IEEE, SAE, American Chemical Society, ASEE (American Society of Engineering Education), AIChE, American Nuclear Society, MRS (Material Research Society), and AHS (American Helicopter Society).

Sometimes Lewis scientists and engineers write books or manuals that are of lasting reference value. In 1990 Lewis published five of these reference publications—more than at any other time.

- NASA RP-1240, Liquid Lubrication in Space by Erwin V. Zaretsky
- NASA RP-1228, Fastener Design Manual by Richard T. Barrett
- NASA RP-1235, Exhaust Nozzles for Propulsion Systems With Emphasis on Supersonic Cruise Aircraft by Leonard E. Stitt
- NASA RP-1236, Structural Properties of Laminated Douglas Fir/Epoxy Composite Material by David A. Spera, Jack B. Esgar, Meade Gougeon, and Michael D. Zutech
- NASA RP-1222, Foundations of Measurement and Instrumentation by Isidore Warshawsky

Lewis hosted eight research conferences and workshops in 1990. Three of these resulted in NASA Conference Publications:

- NASA CP-10045 and CP-3078, Computational Fluid Dynamics Symposium on Aeropropulsion, April 24-26
- NASA CP-10051, HITEMP Review 1990: Advanced High Temperature Engine Materials Technology Program, October 30-31
- NASA CP-10059, Vision-21: Space Travel for the Next Millenium, April 3-4

In addition one workshop held in 1989 was published as a NASA Technical Memorandum this year:

- NASA TM-102037, Space Station Freedom: Modular Combustion Facility Assessment Workshop, May 17, 1989

Two of these publications were published at Lewis and made available to the attendees when they registered at the conferences: Computational Fluid Dynamics Symposium on Aeropropulsion and HITEMP Review. Other conferences and workshops hosted or sponsored by Lewis in 1990 included

- 1990 Tri-Services/NASA Cathode Workshop, April 3-5
- Ohio Aerospace Institute Spring Workshop, May 18
- University Design Program Conference, June 12-15
- Preliminary Design Review, July 30—August 3
- 1990 6th Midwest Space Development Conference (MSDC), October 19-21

In 1990, Lewis Research Center received its 59th R&D 100 Award. Since the prestigious award was established by Research and Development magazine in 1962, Lewis has won about 75 percent of all R&D 100 awards given to NASA. This year, the award was shared by Bruce Steinetz of NASA Lewis and Paul Sirocky of Sverdrup Technology, Inc., for their development of a high-temperature, flexible ceramic wafer seal. The seal will keep extremely hot (up to 25 000 °F) gases from leaking from advanced, hypersonic (up to Mach 23) engines. Steinetz and Sirocky also received a patent for their wafer seal. In all, 18 Lewis patent applications were filed in 1990, and 11 patents were issued.

Some of the other patents issued in 1990 were given for composite manufacturing techniques, polymer synthesis, low mass liquid sheet radiators, a process for separating fluid phases in zero gravity, computer codes, ladder polymers, and a graphite fluoride fiber polymer composite.

Lewis researchers also received some awards for their publications. The 1990 Lewis Distinguished Publication Award was presented to Rebecca A. Mackay and Michael V. Nathal for their paper entitled "g1 Coarsening in High Volume Fraction Nickel-Base Alloys." The 1989 Best Paper Award of the American Society of Mechanical Engineers' Aircraft Engine Committee was given this year to Arthur Glassman, Christopher Snyder, and Gerald Knip, Jr., for their paper entitled "Advanced Core Technology Key to Subsonic Propulsion Benefits."

A few of the other awards received by Lewis engineers in 1990 follow. John Adamczyk was named a NASA Senior Aerospace Scientist (one of ten in the entire country); Marvin Goldstein was elected to the National Academy of Engineering; Toni Grobstein was awarded the 1990 Technical Achievement Award by the Cleveland Technical Societies Council; and the Cleveland Section of the Society of Tribologists and Lubrication Engineers (STLE) presented the 1989-90 Distinguished Member of the Year Award to Harold E. Sliney. In addition, six Lewis employees were named Ohio Academy of Science EXEMPLARS (examples to inspire other women to pursue careers in engineering and science): Theresa Babrauckas, Jo Ann Charleston, Diane Swec, Lisa Veitch, Sylvia Yan, Nancy Piltch, and Sheila Bailey.

All of the publications in this collection were announced in the 1990 issues of STAR (Scientific and Technical Aerospace Reports) and IAA (International Aerospace Abstracts). Some 1990 publications will be announced in the 1991 issues of STAR and IAA and will thus appear in the 1991 Lewis Bibliography. However, a few Lewis-authored publications are not included in this compilation because of FEDD (For Early Domestic Dissemination) and ITAR (International Traffic in Arms Regulations) considerations which limit their announcement and distribution.

The arrangement of the material is by NASA subject category, as noted in the Contents. In addition, the various indexes will help locate specific publications by subject, author, corporate source, contract number, and report number.

Richard E. Texler
Chief, Technical Information Services Division

TABLE OF CONTENTS

AERONAUTICS For related information see also *Astronautics*.

01 AERONAUTICS (GENERAL)	1
02 AERODYNAMICS	2
Includes aerodynamics of bodies, combinations, wings, rotors, and control surfaces; and internal flow in ducts and turbomachinery. For related information see also <i>34 Fluid Mechanics and Heat Transfer</i> .	
03 AIR TRANSPORTATION AND SAFETY	15
Includes passenger and cargo air transport operations; and aircraft accidents. For related information see also <i>16 Space Transportation</i> and <i>85 Urban Technology and Transportation</i> .	
04 AIRCRAFT COMMUNICATIONS AND NAVIGATION	N.A.
Includes digital and voice communication with aircraft; air navigation systems (satellite and ground based); and air traffic control. For related information see also <i>17 Space Communications, Spacecraft Communications, Command and Tracking</i> and <i>32 Communications and Radar</i> .	
05 AIRCRAFT DESIGN, TESTING AND PERFORMANCE	17
Includes aircraft simulation technology. For related information see also <i>18 Spacecraft Design, Testing and Performance</i> and <i>39 Structural Mechanics</i> . For land transportation vehicles see <i>85 Urban Technology and Transportation</i> .	
06 AIRCRAFT INSTRUMENTATION	18
Includes cockpit and cabin display devices; and flight instruments. For related information see also <i>19 Spacecraft Instrumentation</i> and <i>35 Instrumentation and Photography</i> .	
07 AIRCRAFT PROPULSION AND POWER	19
Includes prime propulsion systems and systems components, e.g., gas turbine engines and compressors; and onboard auxiliary power plants for aircraft. For related information see also <i>20 Spacecraft Propulsion and Power</i> , <i>28 Propellants and Fuels</i> , and <i>44 Energy Production and Conversion</i> .	
08 AIRCRAFT STABILITY AND CONTROL	36
Includes aircraft handling qualities; piloting; flight controls; and autopilots. For related information see also <i>05 Aircraft Design, Testing and Performance</i> .	
09 RESEARCH AND SUPPORT FACILITIES (AIR)	37
Includes airports, hangars and runways; aircraft repair and overhaul facilities; wind tunnels; shock tubes; and aircraft engine test stands. For related information see also <i>14 Ground Support Systems and Facilities (Space)</i> .	

ASTRONAUTICS For related information see also *Aeronautics*.

12 ASTRONAUTICS (GENERAL)	39
For extraterrestrial exploration see <i>91 Lunar and Planetary Exploration</i> .	
13 ASTRODYNAMICS	40
Includes powered and free-flight trajectories; and orbital and launching dynamics.	
14 GROUND SUPPORT SYSTEMS AND FACILITIES (SPACE)	42
Includes launch complexes, research and production facilities; ground support equipment, e.g., mobile transporters; and simulators. For related information see also <i>09 Research and Support Facilities (Air)</i> .	
15 LAUNCH VEHICLES AND SPACE VEHICLES	44
Includes boosters; operating problems of launch/space vehicle systems; and reusable vehicles. For related information see also <i>20 Spacecraft Propulsion and Power</i> .	
16 SPACE TRANSPORTATION	45
Includes passenger and cargo space transportation, e.g., shuttle operations; and space rescue techniques. For related information see also <i>03 Air Transportation and Safety</i> and <i>18 Spacecraft Design, Testing and Performance</i> . For space suits see <i>54 Man/System Technology and Life Support</i> .	
17 SPACE COMMUNICATIONS, SPACECRAFT COMMUNICATIONS, COMMAND AND TRACKING ...	46
Includes telemetry; space communications networks; astronavigation and guidance; and radio blackout. For related information see also <i>04 Aircraft Communications and Navigation</i> and <i>32 Communications and Radar</i> .	

N.A.—no abstracts were assigned to this category for this issue.

18 SPACECRAFT DESIGN, TESTING AND PERFORMANCE 47
Includes satellites; space platforms; space stations; spacecraft systems and components such as thermal and environmental controls; and attitude controls. For life support systems see *54 Man/System Technology and Life Support*. For related information see also *05 Aircraft Design, Testing and Performance*, *39 Structural Mechanics*, and *16 Space Transportation*.

19 SPACECRAFT INSTRUMENTATION 52
For related information see also *06 Aircraft Instrumentation* and *35 Instrumentation and Photography*.

20 SPACECRAFT PROPULSION AND POWER 53
Includes main propulsion systems and components, e.g., rocket engines; and spacecraft auxiliary power sources. For related information see also *07 Aircraft Propulsion and Power*, *28 Propellants and Fuels*, *44 Energy Production and Conversion*, and *15 Launch Vehicles and Space Vehicles*.

CHEMISTRY AND MATERIALS

23 CHEMISTRY AND MATERIALS (GENERAL) 83

24 COMPOSITE MATERIALS 87
Includes physical, chemical, and mechanical properties of laminates and other composite materials. For ceramic materials see *27 Nonmetallic Materials*.

25 INORGANIC AND PHYSICAL CHEMISTRY 102
Includes chemical analysis, e.g., chromatography; combustion theory; electrochemistry; and photochemistry. For related information see also *77 Thermodynamics and Statistical Physics*.

26 METALLIC MATERIALS 108
Includes physical, chemical, and mechanical properties of metals, e.g., corrosion; and metallurgy.

27 NONMETALLIC MATERIALS 120
Includes physical, chemical, and mechanical properties of plastics, elastomers, lubricants, polymers, textiles, adhesives, and ceramic materials. For composite materials see *24 Composite Materials*.

28 PROPELLANTS AND FUELS 130
Includes rocket propellants, igniters and oxidizers; their storage and handling procedures; and aircraft fuels. For related information see also *07 Aircraft Propulsion and Power*, *20 Spacecraft Propulsion and Power*, and *44 Energy Production and Conversion*.

29 MATERIALS PROCESSING 132
Includes space-based development of products and processes for commercial application. For biological materials see *55 Space Biology*.

ENGINEERING For related information see also *Physics*.

31 ENGINEERING (GENERAL) 136
Includes vacuum technology; control engineering; display engineering; cryogenics; and fire prevention.

32 COMMUNICATIONS AND RADAR 138
Includes radar; land and global communications; communications theory; and optical communications. For related information see also *04 Aircraft Communications and Navigation* and *17 Space Communications, Spacecraft Communications, Command and Tracking*. For search and rescue see *03 Air Transportation and Safety*, and *16 Space Transportation*.

33 ELECTRONICS AND ELECTRICAL ENGINEERING 146
Includes test equipment and maintainability; components, e.g., tunnel diodes and transistors; microminiaturization; and integrated circuitry. For related information see also *60 Computer Operations and Hardware* and *76 Solid-State Physics*.

34 FLUID MECHANICS AND HEAT TRANSFER 156
Includes boundary layers; hydrodynamics; fluidics; mass transfer and ablation cooling. For related information see also *02 Aerodynamics* and *77 Thermodynamics and Statistical Physics*.

35 INSTRUMENTATION AND PHOTOGRAPHY 185
Includes remote sensors; measuring instruments and gauges; detectors; cameras and photographic supplies; and holography. For aerial photography see *43 Earth Resources and Remote Sensing*. For related information see also *06 Aircraft Instrumentation* and *19 Spacecraft Instrumentation*.

36 LASERS AND MASERS 192
Includes parametric amplifiers. For related information see also *76 Solid-State Physics*.

37 MECHANICAL ENGINEERING	192
Includes auxiliary systems (nonpower); machine elements and processes; and mechanical equipment.	
38 QUALITY ASSURANCE AND RELIABILITY	206
Includes product sampling procedures and techniques; and quality control.	
39 STRUCTURAL MECHANICS	208
Includes structural element design and weight analysis; fatigue; and thermal stress. For applications see <i>05 Aircraft Design, Testing and Performance</i> and <i>18 Spacecraft Design, Testing and Performance</i> .	
GEOSCIENCES For related information see also <i>Space Sciences</i> .	
42 GEOSCIENCES (GENERAL)	N.A.
43 EARTH RESOURCES AND REMOTE SENSING	N.A.
Includes remote sensing of earth resources by aircraft and spacecraft; photogrammetry; and aerial photography. For instrumentation see <i>35 Instrumentation and Photography</i> .	
44 ENERGY PRODUCTION AND CONVERSION	224
Includes specific energy conversion systems, e.g., fuel cells; global sources of energy; geophysical conversion; and windpower. For related information see also <i>07 Aircraft Propulsion and Power</i> , <i>20 Spacecraft Propulsion and Power</i> , and <i>28 Propellants and Fuels</i> .	
45 ENVIRONMENT POLLUTION	N.A.
Includes atmospheric, noise, thermal, and water pollution.	
46 GEOPHYSICS	233
Includes aeronomy; upper and lower atmosphere studies; ionospheric and magnetospheric physics; and geomagnetism. For space radiation see <i>93 Space Radiation</i> .	
47 METEOROLOGY AND CLIMATOLOGY	234
Includes weather forecasting and modification.	
48 OCEANOGRAPHY	N.A.
Includes biological, dynamic, and physical oceanography; and marine resources. For related information see also <i>43 Earth Resources and Remote Sensing</i> .	
LIFE SCIENCES	
51 LIFE SCIENCES (GENERAL)	234
52 AEROSPACE MEDICINE	N.A.
Includes physiological factors; biological effects of radiation; and effects of weightlessness on man and animals.	
53 BEHAVIORAL SCIENCES	N.A.
Includes psychological factors; individual and group behavior; crew training and evaluation; and psychiatric research.	
54 MAN/SYSTEM TECHNOLOGY AND LIFE SUPPORT	234
Includes human engineering; biotechnology; and space suits and protective clothing. For related information see also <i>16 Space Transportation</i> .	
55 SPACE BIOLOGY	N.A.
Includes exobiology; planetary biology; and extraterrestrial life.	
MATHEMATICAL AND COMPUTER SCIENCES	
59 MATHEMATICAL AND COMPUTER SCIENCES (GENERAL)	N.A.
60 COMPUTER OPERATIONS AND HARDWARE	235
Includes hardware for computer graphics, firmware, and data processing. For components see <i>33 Electronics and Electrical Engineering</i> .	
61 COMPUTER PROGRAMMING AND SOFTWARE	235
Includes computer programs, routines, algorithms, and specific applications, e.g., CAD/CAM.	
62 COMPUTER SYSTEMS	238
Includes computer networks and special application computer systems.	

63 CYBERNETICS	239
Includes feedback and control theory, artificial intelligence, robotics and expert systems. For related information see also <i>54 Man/System Technology and Life Support</i> .	
64 NUMERICAL ANALYSIS	241
Includes iteration, difference equations, and numerical approximation.	
65 STATISTICS AND PROBABILITY	N.A.
Includes data sampling and smoothing; Monte Carlo method; and stochastic processes.	
66 SYSTEMS ANALYSIS	245
Includes mathematical modeling; network analysis; and operations research.	
67 THEORETICAL MATHEMATICS	N.A.
Includes topology and number theory.	
PHYSICS For related information see also <i>Engineering</i> .	
70 PHYSICS (GENERAL)	246
For precision time and time interval (PTTI) see <i>35 Instrumentation and Photography</i> ; for geophysics, astrophysics or solar physics see <i>46 Geophysics</i> , <i>90 Astrophysics</i> , or <i>92 Solar Physics</i> .	
71 ACOUSTICS	246
Includes sound generation, transmission, and attenuation. For noise pollution see <i>45 Environment Pollution</i> .	
72 ATOMIC AND MOLECULAR PHYSICS	N.A.
Includes atomic structure, electron properties, and molecular spectra.	
73 NUCLEAR AND HIGH-ENERGY PHYSICS	249
Includes elementary and nuclear particles; and reactor theory. For space radiation see <i>93 Space Radiation</i> .	
74 OPTICS	250
Includes light phenomena and optical devices. For lasers see <i>36 Lasers and Masers</i> .	
75 PLASMA PHYSICS	251
Includes magnetohydrodynamics and plasma fusion. For ionospheric plasmas see <i>46 Geophysics</i> . For space plasmas see <i>90 Astrophysics</i> .	
76 SOLID-STATE PHYSICS	253
Includes superconductivity. For related information see also <i>33 Electronics and Electrical Engineering</i> and <i>36 Lasers and Masers</i> .	
77 THERMODYNAMICS AND STATISTICAL PHYSICS	260
Includes quantum mechanics; theoretical physics; and Bose and Fermi statistics. For related information see also <i>25 Inorganic and Physical Chemistry</i> and <i>34 Fluid Mechanics and Heat Transfer</i> .	
SOCIAL SCIENCES	
80 SOCIAL SCIENCES (GENERAL)	261
Includes educational matters.	
81 ADMINISTRATION AND MANAGEMENT	262
Includes management planning and research.	
82 DOCUMENTATION AND INFORMATION SCIENCE	262
Includes information management; information storage and retrieval technology; technical writing; graphic arts; and micrography. For computer documentation see <i>61 Computer Programming and Software</i> .	
83 ECONOMICS AND COST ANALYSIS	N.A.
Includes cost effectiveness studies.	
84 LAW, POLITICAL SCIENCE AND SPACE POLICY	N.A.
Includes NASA appropriation hearings; aviation law; space law and policy; international law; international cooperation; and patent policy.	
85 URBAN TECHNOLOGY AND TRANSPORTATION	263
Includes applications of space technology to urban problems; technology transfer; technology assessment; and surface and mass transportation. For related information see <i>03 Air Transportation and Safety</i> , <i>16 Space Transportation</i> , and <i>44 Energy Production and Conversion</i> .	

SPACE SCIENCES For related information see also *Geosciences*.

88 SPACE SCIENCES (GENERAL)	264
89 ASTRONOMY	N.A.
Includes radio, gamma-ray, and infrared astronomy; and astrometry.	
90 ASTROPHYSICS	264
Includes cosmology; celestial mechanics; space plasmas; and interstellar and interplanetary gases and dust.	
For related information see also <i>75 Plasma Physics</i> .	
91 LUNAR AND PLANETARY EXPLORATION	266
Includes planetology; and manned and unmanned flights. For spacecraft design or space stations see <i>18 Spacecraft Design, Testing and Performance</i> .	
92 SOLAR PHYSICS	N.A.
Includes solar activity, solar flares, solar radiation and sunspots. For related information see <i>93 Space Radiation</i> .	
93 SPACE RADIATION	N.A.
Includes cosmic radiation; and inner and outer earth's radiation belts. For biological effects of radiation see <i>52 Aerospace Medicine</i> . For theory see <i>73 Nuclear and High-Energy Physics</i> .	

GENERAL

Includes aeronautical, astronautical, and space science related histories, biographies, and pertinent reports too broad for categorization; histories or broad overviews of NASA programs.

99 GENERAL	267
SUBJECT INDEX	A-1
PERSONAL AUTHOR INDEX	B-1
CORPORATE SOURCE INDEX	C-1
CONTRACT NUMBER INDEX	D-1
REPORT/ACCESSION NUMBER INDEX	E-1

Bibliography of Lewis Research Center Technical Publications Announced in 1990

01

AERONAUTICS (GENERAL)

N90-13323*# Sverdrup Technology, Inc., Cleveland, OH.
MULTIGRID CALCULATIONS OF 3-D TURBULENT VISCOUS FLOWS Final Report

JEFFREY W. YOKOTA Oct. 1989 18 p Presented at the 1st Canadian Symposium on Aerodynamics, Ottawa, Ontario, 4-5 Dec. 1989; sponsored by Canadian Aeronautics and Space Inst. (Contract NAS3-25266)
(NASA-CR-185154; E-5116; NAS 1.26:185154) Avail: NTIS HC A03/MF A01 CSCL 01/2

Convergence properties of a multigrid algorithm, developed to calculate compressible viscous flows, are analyzed by a vector sequence eigenvalue estimate. The full 3-D Reynolds-averaged Navier-Stokes equations are integrated by an implicit multigrid scheme while a k-epsilon turbulence model is solved, uncoupled from the flow equations. Estimates of the eigenvalue structure for both single and multigrid calculations are compared in an attempt to analyze the process as well as the results of the multigrid technique. The flow through an annular turbine is used to illustrate the scheme's ability to calculate complex 3-D flows. Author

N90-20942*# National Aeronautics and Space Administration.
Lewis Research Center, Cleveland, OH.

LASER-VELOCIMETER-MEASURED FLOW FIELD AROUND AN ADVANCED, SWEEPED, EIGHT-BLADE PROPELLER AT MACH 0.8

HARVEY E. NEUMAN, JOHN A. SERAFINI, DANIEL Y. WHIPPLE, and BRIAN T. HOWARD May 1985 100 p
(NASA-TP-2462; E-2429; NAS 1.60:2462) Avail: Issuing Activity CSCL 01/2

A laser velocimeter has been used to measure velocities in the flow field around an advanced, eight-blade, high-speed propeller in the NASA Lewis 8- by 6-Foot Supersonic Wind Tunnel. The propeller was nominally 62.23 cm (24.5 in.) in diameter and was operated both at windmill and near the design power condition at a free-stream Mach number of 0.8. The detailed three-dimensional velocity data obtained are being made available here to enable researchers to verify emerging advanced propeller design and analysis codes. Data were obtained at two axial positions ahead of the propeller, at two axial positions downstream of the propeller, and at seven radial positions within the bladed passages extending from the inlet of the blades to downstream of the blade exit. A four-beam laser velocimeter system was configured to measure two velocity components simultaneously. Author

N90-20943*# Sverdrup Technology, Inc., Cleveland, OH.
USERS MANUAL FOR THE NASA LEWIS ICE ACCRETION PREDICTION CODE (LEWICE) Final Report

GARY A. RUFF and BRIAN M. BERKOWITZ May 1990 240 p
(Contract NAS3-25266)
(NASA-CR-185129; NAS 1.26:185129) Avail: NTIS HC A11/MF A02 CSCL 01/2

LEWICE is an ice accretion prediction code that applies a

time-stepping procedure to calculate the shape of an ice accretion. The potential flow field is calculated in LEWICE using the Douglas Hess-Smith 2-D panel code (S24Y). This potential flow field is then used to calculate the trajectories of particles and the impingement points on the body. These calculations are performed to determine the distribution of liquid water impinging on the body, which then serves as input to the icing thermodynamic code. The icing thermodynamic model is based on the work of Messinger, but contains several major modifications and improvements. This model is used to calculate the ice growth rate at each point on the surface of the geometry. By specifying an icing time increment, the ice growth rate can be interpreted as an ice thickness which is added to the body, resulting in the generation of new coordinates. This procedure is repeated, beginning with the potential flow calculations, until the desired icing time is reached. The operation of LEWICE is illustrated through the use of five examples. These examples are representative of the types of applications expected for LEWICE. All input and output is discussed, along with many of the diagnostic messages contained in the code. Several error conditions that may occur in the code for certain icing conditions are identified, and a course of action is recommended. LEWICE has been used to calculate a variety of ice shapes, but should still be considered a research code. The code should be exercised further to identify any shortcomings and inadequacies. Any modifications identified as a result of these cases, or of additional experimental results, should be incorporated into the model. Using it as a test bed for improvements to the ice accretion model is one important application of LEWICE. Author

N90-21723*# National Aeronautics and Space Administration.
Lewis Research Center, Cleveland, OH.

THE VIBRO-ACOUSTIC MAPPING OF LOW GRAVITY TRAJECTORIES ON A LEARJET AIRCRAFT

C. M. GRODSINSKY and T. J. SUTLIFF May 1990 16 p
Presented at the 2nd Workshop on Microgravity Experimentation, Ottawa, Ontario, 8-9 May 1990; sponsored by National Research Council of Canada
(NASA-TM-103103; E-5427; NAS 1.15:103103) Avail: NTIS HC A03/MF A01 CSCL 01/2

Terrestrial low gravity research techniques have been employed to gain a more thorough understanding of basic science and technology concepts. One technique frequently used involves flying parabolic trajectories aboard the NASA Lewis Research Center Learjet aircraft. A measurement program was developed to support an isolation system conceptual design. This program primarily was intended to measure time correlated high frequency accelerations (up to 100 Hz) present at various locations throughout the Learjet during a series of trajectories and flights. As suspected, the measurements obtained revealed that the environment aboard such an aircraft can not simply be described in terms of the static level low gravity g vector obtained, but that it also must account for both rigid body and high frequency vibro-acoustic dynamics. Author

N90-21724*# Purdue Univ., West Lafayette, IN.
WINCOF-I CODE FOR PREDICTION OF FAN COMPRESSOR UNIT WITH WATER INGESTION Interim Report
S. N. B. MURTHY and A. MULLICAN Mar. 1990 88 p
(Contract NAG3-481; DTFA03-83-A-00328)

01 AERONAUTICS (GENERAL)

(NASA-CR-185157; NAS 1.26:185157; DOT/FAA/CT-TN89/63; M/NAFA/89-1) Avail: NTIS HC A05/MF A01 CSCL 01/2

The PURDUE-WINCOF code, which provides a numerical method of obtaining the performance of a fan-compressor unit of a jet engine with water ingestion into the inlet, was modified to take into account: (1) the scoop factor, (2) the time required for the setting-in of a quasi-steady distribution of water, and (3) the heat and mass transfer processes over the time calculated under 2. The modified code, named WINCOF-I was utilized to obtain the performance of a fan-compressor unit of a generic jet engine. The results illustrate the manner in which quasi-equilibrium conditions become established in the machine and the redistribution of ingested water in various stages in the form of a film out of the casing wall, droplets across the span, and vapor due to mass transfer.

Author

N90-21725* # National Aeronautics and Space Administration. Lewis Research Center, Cleveland, OH.

PERFORMANCE CHARACTERISTICS OF A ONE-THIRD-SCALE, VECTORABLE VENTRAL NOZZLE FOR SSTOVL AIRCRAFT

BARBARA S. ESKER and JACK G. MCARDLE 1990 12 p Proposed for presentation at the 26th Joint Propulsion Conference, Orlando, FL, 16-18 Jul. 1990; cosponsored by AIAA, ASME, SAE, and ASEE

(NASA-TM-103120; E-5448; NAS 1.15:103120; AIAA-90-2271) Avail: NTIS HC A03/MF A01 CSCL 01/2

Several proposed configurations for supersonic short takeoff, vertical landing aircraft will require one or more ventral nozzles for lift and pitch control. The swivel nozzle is one possible ventral nozzle configuration. A swivel nozzle (approximately one-third scale) was built and tested on a generic model tailpipe. This nozzle was capable of vectoring the flow up to + or - 23 deg from the vertical position. Steady-state performance data were obtained at pressure ratios to 4.5, and pitot-pressure surveys of the nozzle exit plane were made. Two configurations were tested: the swivel nozzle with a square contour of the leading edge of the ventral duct inlet, and the same nozzle with a round leading edge contour. The swivel nozzle showed good performance overall, and the round-leading edge configuration showed an improvement in performance over the square-leading edge configuration. Author

02

AERODYNAMICS

Includes aerodynamics of bodies, combinations, wings, rotors, and control surfaces; and internal flow in ducts and turbomachinery.

A90-11778* # United Technologies Research Center, East Hartford, CT.

CALCULATION OF UNSTEADY EULER FLOWS IN TURBOMACHINERY USING THE LINEARIZED EULER EQUATIONS

KENNETH C. HALL (United Technologies Research Center, East Hartford, CT) and EDWARD F. CRAWLEY (MIT, Cambridge, MA) IN: Unsteady aerodynamics and aeroelasticity of turbomachines and propellers; Proceedings of the Fourth International Symposium, Aachen, Federal Republic of Germany, Sept. 6-10, 1987. Aachen, Federal Republic of Germany, Rheinisch-Westfaelische Technische Hochschule Aachen, 1988, p. 15-38. Research supported by General Electric Co. and General Motors Corp. refs (Contract NSG-3079)

The model used by the present unsteady cascade flow calculation method is based on the linearized unsteady Euler equations and accounts for blade loading and geometry, shock motion, and wake motion. The steady flow that must be determined prior to the unsteady flow is ascertained by means of a Newton iteration procedure. A noteworthy feature of the procedure is the use of shock-fitting to determine steady and unsteady shock

positions; the use of the Euler equations in conjunction with the Rankine-Hugoniot shock-jump conditions is found to directly model the generation of entropy and vorticity at shocks. Results are presented for both channel and cascade flows. O.C.

A90-11779* # Notre Dame Univ., IN.

ANALYSIS OF NONUNIFORM SUBSONIC FLOWS ABOUT A ROW OF MOVING BLADES

H. M. ATASSI (Notre Dame, University, IN) and J. R. SCOTT (NASA, Lewis Research Center, Cleveland, OH) IN: Unsteady aerodynamics and aeroelasticity of turbomachines and propellers; Proceedings of the Fourth International Symposium, Aachen, Federal Republic of Germany, Sept. 6-10, 1987. Aachen, Federal Republic of Germany, Rheinisch-Westfaelische Technische Hochschule Aachen, 1988, p. 39-67. refs (Contract NAG3-732)

The motion of a nonuniform flow about a row of moving blades is modeled as that of a three-dimensional rotational disturbance convected by the mean flow. The aerodynamic theories for such flows are reviewed for both linearly propagating disturbances and disturbances distorted by the mean flow. Linear theories results are examined to assess the effects of the gust variables, the Mach number, and the blade spacing, on the unsteady blade response. For loaded blades, the upstream disturbances are distorted by the blade mean flow. For a potential mean flow, the governing equations can be reduced to a single inhomogeneous nonconstant coefficient convective wave equation. A numerical procedure is developed using an elliptic grid system. The accuracy of the solutions strongly depends on the far-field radiation condition and the optimum determination of the grid system. Solutions are presently obtained for thick symmetric airfoils in three-dimensional gusts. Author

A90-11789* # National Aeronautics and Space Administration. Lewis Research Center, Cleveland, OH.

THE UNSTEADY AERODYNAMICS OF AN OSCILLATING CASCADE IN A COMPRESSIBLE FLOW FIELD

DANIEL H. BUFFUM, DONALD R. BOLDMAN (NASA, Lewis Research Center, Cleveland, OH), and SANFORD FLEETER (Purdue University, West Lafayette, IN) IN: Unsteady aerodynamics and aeroelasticity of turbomachines and propellers; Proceedings of the Fourth International Symposium, Aachen, Federal Republic of Germany, Sept. 6-10, 1987. Aachen, Federal Republic of Germany, Rheinisch-Westfaelische Technische Hochschule Aachen, 1988, p. 293-312. Previously announced in STAR as N88-13346. refs

Fundamental experiments were performed in the NASA Lewis Transonic Oscillating Cascade Facility to investigate and quantify the unsteady aerodynamics of a cascade of biconvex airfoils executing torsion-mode oscillations at realistic reduced frequencies. Flush-mounted, high-response miniature pressure transducers were used to measure the unsteady airfoil surface pressures. The pressures were measured for three interblade phase angles at two inlet Mach numbers, 0.65 and 0.80, and two incidence angles, 0 and 7 deg. The time-variant pressures were analyzed by means of discrete Fourier transform techniques, and these unique data were then compared with predictions from a linearized unsteady cascade model. The experimental results indicate that the interblade phase angle had a major effect on the chordwise distributions of the airfoil surface unsteady pressure, and that reduced frequency, incidence angle, and Mach number had a somewhat less significant effect. Author

A90-11806* # California State Univ., Long Beach.

PROGRESS TOWARDS THE DEVELOPMENT OF AN INVISCID-VISCOUS INTERACTION METHOD FOR UNSTEADY FLOWS IN TURBOMACHINERY CASCADES

T. CEBECI (California State University, Long Beach), M. F. PLATZER, N. G. TENG, A. KRAINER (U.S. Naval Postgraduate School, Monterey, CA), and R. J. SIMONEAU (NASA, Lewis Research Center, Cleveland, OH) IN: Unsteady aerodynamics and aeroelasticity of turbomachines and propellers; Proceedings of the Fourth International Symposium, Aachen, Federal Republic

of Germany, Sept. 6-10, 1987. Aachen, Federal Republic of Germany, Rheinisch-Westfälische Technische Hochschule Aachen, 1988, p. 721-753. refs

The velocity and heat transfer characteristics of blade passage flows subject to onset velocities that vary in space and time are calculated by means of a general method involving the solution of inviscid and boundary-layer equations coupled with the Hilbert integral. The performance of this boundary layer method for flows with prescribed pressure distribution is evaluated in terms of two model problems that give attention to the stagnation region. One model corresponds to an oscillating airfoil with moving stagnation point; the other is a simulation of a blade which is subject to a uniform onset velocity. O.C.

A90-12555*# Pennsylvania State Univ., University Park.
**COMPUTATION OF THREE DIMENSIONAL TURBULENT
 BOUNDARY LAYERS IN INTERNAL FLOWS, INCLUDING
 TURBOMACHINERY ROTOR BLADES**

J. ZHANG and B. LAKSHMINARAYANA (Pennsylvania State University, University Park) IN: International Symposium on Air Breathing Engines, 9th, Athens, Greece, Sept. 3-8, 1989, Proceedings. Volume 1. Washington, DC, American Institute of Aeronautics and Astronautics, 1989, p. 529-538. refs (Contract NSG-3266; NSF INT-87-02083) Copyright

A method is developed for predicting three-dimensional turbulent boundary layers occurring in internal flows, including rotor blades of turbomachinery. These boundary layers are complex, turbulent, and are subject to Coriolis and centrifugal forces. The algebraic Reynolds stress model (ARSM) developed in this paper satisfies the realizability conditions exactly and captures the changes in turbulent structure arising from curvature and rotation. The prediction of pressure driven secondary flow agrees well with the data and all the three turbulent models (k- ϵ , algebraic eddy viscosity, and ARSM) show the same level of agreement. The prediction of boundary layer on rotor blades shows much better agreement with the ARSM. It is essential to employ the higher order models to capture the effects of rotation and curvature and three-dimensional boundary layers in turbomachinery. Author

A90-16753*# National Aeronautics and Space Administration.
 Lewis Research Center, Cleveland, OH.
**PREDICTIONS OF AIRFOIL AERODYNAMIC PERFORMANCE
 DEGRADATION DUE TO ICING**

ROBERT J. SHAW, MARK G. POTAPCZUK, and COLIN S. BIDWELL (NASA, Lewis Research Center, Cleveland, OH) IN: Symposium on Numerical and Physical Aspects of Aerodynamic Flows, 4th, Long Beach, CA, Jan. 16-19, 1989, Proceedings. Long Beach, CA, California State University, 1989, 9 p. Previously announced in STAR as N89-13412. refs

An overview of NASA's ongoing efforts to develop an airfoil icing analysis capability is developed. An indication is given to the approaches being followed to calculate the water droplet trajectories past the airfoil, the buildup of ice on the airfoil, and the resultant changes in aerodynamic performance due to the leading edge ice accretion. Examples are given of current code capabilities/limitations through comparisons of predictions with experimental data gathered in various calibration/validation experiments. A brief discussion of future efforts to extend the analysis to handle three-dimensional components is included. Author

A90-17592* Massachusetts Inst. of Tech., Cambridge.
**A MULTI-DOMAIN SPECTRAL COMPUTATION OF
 THREE-DIMENSIONAL LAMINAR HORSESHOE VORTEX
 FLOW USING INCOMPRESSIBLE NAVIER-STOKES
 EQUATIONS**

C. S. TAN (MIT, Cambridge, MA) Journal of Computational Physics (ISSN 0021-9991), vol. 85, Nov. 1989, p. 130-158. refs (Contract NAG3-660) Copyright

Multidomain spectral methods are presently used to numerically simulate a strut-wall intersection's laminar horseshoe vortex flow

through direct solution of the three-dimensional, incompressible, time-dependent Navier-Stokes equations. Direct expansion in Chebyshev polynomials and spectral element method spatial discretization of flow dependence are used to achieve high-order accuracy, and minimal dispersion errors. Low and moderate Reynolds number results are presented to illustrate the method application. O.C.

A90-17989*# National Aeronautics and Space Administration.
 Lewis Research Center, Cleveland, OH.

**NUMERICAL STUDY OF CHEMICALLY REACTING FLOWS
 USING A LOWER-UPPER SYMMETRIC SUCCESSIVE
 OVERRELAXATION SCHEME**

JIAN SHUN SHUEN (NASA, Lewis Research Center, Cleveland, OH) and SEOKKWAN YOON (NASA, Ames Research Center, Moffett Field, CA) AIAA Journal (ISSN 0001-1452), vol. 27, Dec. 1989, p. 1752-1760. Previously cited in issue 08, p. 1143. Accession no. A88-24825. refs Copyright

A90-18153*# Pennsylvania State Univ., University Park.
**SKIN FRICTION MEASUREMENTS BY LASER
 INTERFEROMETRY IN SWEEP SHOCK/BOUNDARY-LAYER
 INTERACTIONS**

KWANG-SOO KIM and GARY S. SETTLES (Pennsylvania State University, University Park) AIAA Journal (ISSN 0001-1452), vol. 28, Jan. 1990, p. 133-139. Previously cited in issue 07, p. 937. Accession no. A88-22364. refs (Contract AF-AFOSR-86-0082; NAG3-527) Copyright

A90-19978*# Mississippi State Univ., Mississippi State.
**COUNTERROTATING PROP-FAN SIMULATIONS WHICH
 FEATURE A RELATIVE-MOTION MULTIBLOCK GRID
 DECOMPOSITION ENABLING ARBITRARY TIME-STEPS**

J. MARK JANUS and DAVID L. WHITFIELD (Mississippi State University, Mississippi State) AIAA, Aerospace Sciences Meeting, 28th, Reno, NV, Jan. 8-11, 1990. 26 p. refs (Contract NAG3-767; NAG3-869) (AIAA PAPER 90-0687) Copyright

Improvements are presented of a computer algorithm developed for the time-accurate flow analysis of rotating machines. The flow model is a finite volume method utilizing a high-resolution approximate Riemann solver for interface flux definitions. The numerical scheme is a block LU implicit iterative-refinement method which possesses apparent unconditional stability. Multiblock composite gridding is used to orderly partition the field into a specified arrangement of blocks exhibiting varying degrees of similarity. Block-block relative motion is achieved using local grid distortion to reduce grid skewness and accommodate arbitrary time step selection. A general high-order numerical scheme is applied to satisfy the geometric conservation law. An even-blade-count counterrotating unducted fan configuration is chosen for a computational study comparing solutions resulting from altering parameters such as time step size and iteration count. The solutions are compared with measured data. S.A.V.

A90-20010*# Georgia Inst. of Tech., Atlanta.
**NUMERICAL STUDY OF THE EFFECTS OF ICING ON FINITE
 WING AERODYNAMICS**

OH J. KWON and LAKSHMI N. SANKAR (Georgia Institute of Technology, Atlanta) AIAA, Aerospace Sciences Meeting, 28th, Reno, NV, Jan. 8-11, 1990. 10 p. refs (Contract NAG3-768) (AIAA PAPER 90-0757) Copyright

The sectional and total aerodynamics load characteristics of moderate aspect ratio wings with and without simulated glaze leading-edge ice are studied using a three-dimensional, compressible Navier-Stokes solver. The wing has an untwisted, untapered planform shape with NACA 0012 airfoil section. The aspect ratio of the wing is chosen to be 5. Comparisons of computed surface pressures and sectional loads with experimental

02 AERODYNAMICS

data for identical configurations are given. The abrupt decrease in the wing stall angle as a result of the leading edge ice formation is numerically demonstrated. Author

A90-20011*# Nielsen Engineering and Research, Inc., Mountain View, CA.

DEVELOPMENT OF AN UNSTRUCTURED MESH/NAVIER-STOKES METHOD FOR AERODYNAMICS OF AIRCRAFT WITH ICE ACCRETIONS

STEVEN C. CARUSO (Nielsen Engineering and Research, Inc., Mountain View, CA) AIAA, Aerospace Sciences Meeting, 28th, Reno, NV, Jan. 8-11, 1990. 15 p. refs (Contract NAS3-25601)

(AIAA PAPER 90-0758) Copyright

An advanced flowfield prediction method for airfoils with leading edge ice accretions was developed and applied. The method is intended to be eventually used in an aircraft icing analysis. The flowfield is obtained by solving the Euler or Navier-Stokes equations on an unstructured triangular mesh. A new method has been developed to permit efficient mesh generation while providing high grid resolution near complicated airfoil ice accumulations. Unstructured-mesh Euler calculations are presented for clean and iced airfoils; the results are compared to similar structured-mesh calculations to demonstrate the new method's accuracy and efficiency. Author

A90-22153*# Georgia Inst. of Tech., Atlanta.

APPLICATION OF AN EFFICIENT HYBRID SCHEME FOR AEROELASTIC ANALYSIS OF ADVANCED PROPELLERS

R. SRIVASTAVA, N. L. SANKAR (Georgia Institute of Technology, Atlanta), T. S. R. REDDY (Toledo, University, OH), and D. L. HUFF (NASA, Lewis Research Center, Cleveland, OH) AIAA, Aerospace Sciences Meeting, 28th, Reno, NV, Jan. 8-11, 1990. 29 p. Previously announced in STAR as N90-13355. refs (Contract NAG3-730)

(AIAA PAPER 90-0028) Copyright

An efficient 3-D hybrid scheme is applied for solving Euler equations to analyze advanced propellers. The scheme treats the spanwise direction semi-explicitly and the other two directions implicitly, without affecting the accuracy, as compared to a fully implicit scheme. This leads to a reduction in computer time and memory requirement. The calculated power coefficients for two advanced propellers, SR3 and SR7L, and various advanced ratios showed good correlation with experiment. Spanwise distribution of elemental power coefficient and steady pressure coefficient differences also showed good agreement with experiment. A study of the effect of structural flexibility on the performance of the advanced propellers showed that structural deformation due to centrifugal and aero loading should be included for better correlation. Author

A90-22158*# National Aeronautics and Space Administration, Lewis Research Center, Cleveland, OH.

SOME OBSERVATIONS ON TRANSITORY STALL IN CONICAL DIFFUSERS

K. B. M. Q. ZAMAN and M. D. DAHL (NASA, Lewis Research Center, Cleveland, OH) AIAA, Aerospace Sciences Meeting, 28th, Reno, NV, Jan. 8-11, 1990. 11 p. Previously announced in STAR as N90-12561. refs

(AIAA PAPER 90-0048) Copyright

Results from an experimental investigation on the flow through conical diffusers are presented. The mean and fluctuating velocity fields are compared for three diffusers with total diffusion angles of 16, 20 and 24 degrees, in the throat Mach number (M_{sub}) range of 0.05 to 0.95. Each of the diffusers were 14 cm long and had a 5.08 cm inlet diameter, and the flow exited into the ambient. The boundary layer at the throat was thin with the throat diameter (D_{sub}) to momentum thickness (O) ratio being as high as 800 at $M_{sub} = 0.4$. While the 16 deg diffuser flow exited with a top-hat mean velocity profile, increasing losses due to increasing separation resulted in fuller profiles for the 20 and 24 degrees cases. A detailed flow field study was conducted for the 16 deg diffuser. The u^+ -spectrum, measured at the exit plane, exhibited a

peak apparently due to the ensuing jet column instability throughout the M_{sub} range covered. In addition, a much lower frequency spectral peak also occurred in the M_{sub} range of 0.3 to 0.7. Both of the spectral peaks were due to axisymmetric flow fluctuations. A self-sustaining flow oscillation occurred in the M_{sub} range of 0.6 to 0.85, emitting a loud tone, when the jet column instability frequency matched the resonance frequency of the diffuser. Limited data showed that artificial acoustic excitation was effective in reducing the flow fluctuations, with a resultant increase in the pressure recovery, at low M_{sub} . Author

A90-22256*# Nielsen Engineering and Research, Inc., Mountain View, CA.

CHEMICALLY REACTING SUPERSONIC FLOW CALCULATION USING AN ASSUMED PDF MODEL

M. FARSHCHI (Nielsen Engineering and Research, Inc., Mountain View, CA) AIAA, Aerospace Sciences Meeting, 28th, Reno, NV, Jan. 8-11, 1990. 10 p. refs (Contract NAS3-25633)

(AIAA PAPER 90-0731) Copyright

This work is motivated by the need to develop accurate models for chemically reacting compressible turbulent flow fields that are present in a typical supersonic combustion ramjet (SCRAMJET) engine. In this paper the development of a new assumed probability density function (PDF) reaction model for supersonic turbulent diffusion flames and its implementation into an efficient Navier-Stokes solver are discussed. The application of this model to a supersonic hydrogen-air flame will be considered. Author

A90-23650*# National Aeronautics and Space Administration, Lewis Research Center, Cleveland, OH.

EFFECT OF REDUCED AFT DIAMETER AND INCREASED BLADE NUMBER OF HIGH-SPEED COUNTERROTATION PROPELLER PERFORMANCE

E. ROSE GAYLE and ROBERT J. JERACKI (NASA, Lewis Research Center, Cleveland, OH) AIAA, Aerospace Sciences Meeting, 27th, Reno, NV, Jan. 9-12, 1989. 32 p. Previously announced in STAR as N90-13352. refs (AIAA PAPER 89-0438)

Performance data of 0.17-scale model counterrotation pusher propeller configurations were taken in the NASA Lewis 8- by 6-Foot Supersonic Wind Tunnel at Mach numbers of 0.66, 0.71, 0.75, and 0.79. These tests investigated the aerodynamic performance of the unducted fan (UDF) demonstrator propeller engine developed in a joint program by General Electric and NASA. Data were recorded to show the effect on counterrotation propeller cruise efficiency of two takeoff noise-reduction concepts. These two concepts are reduced aft blade diameter and increased forward blade number. The four configurations tested were a baseline (F1/A1 8/8) configuration, a reduced aft diameter (F1/A3 8/8) configuration, an increase forward blade number (F1/A1 9/8) configuration, and a combination of the latter two (F1/A3 9/8) configurations. Data were collected with a complex counterrotation propeller test rig via rotating thrust and torque balances and pressure instrumentation. Data comparisons documented the power differences between the baseline and the reduced aft diameter concepts. Performance comparisons to the baseline configuration showed that reducing the aft blade diameter reduced the net efficiency, and adding a blade to the front rotor increased the net efficiency. The combination of the two concepts showed only slightly lower net efficiency than the baseline configuration. It was also found that the counterrotation demonstrator propeller model (F7/A7 8/8) configuration outperformed the baseline (F1/A1 8/8) configuration. Author

A90-23762*# National Aeronautics and Space Administration, Lewis Research Center, Cleveland, OH.

APPLICATION OF A LOWER-UPPER IMPLICIT SCHEME AND AN INTERACTIVE GRID GENERATION FOR TURBOMACHINERY FLOW FIELD SIMULATIONS

YUNG K. CHOO (NASA, Lewis Research Center, Cleveland, OH), WOO-YUNG SOH (NASA, Lewis Research Center; Sverdrup Technology, Inc., Cleveland, OH), and SEOKKWAN YOON (NASA,

Ames Research Center; MCAT Institute, Moffett Field, CA) ASME, Gas Turbine and Aeroengine Congress and Exposition, Toronto, Canada, June 4-8, 1989. 10 p. refs
(ASME PAPER 89-GT-20)

A finite-volume lower-upper (LU) implicit scheme is used to simulate an inviscid flow in a turbine cascade. This approximate factorization scheme requires only the inversion of sparse lower and upper triangular matrices, which can be done efficiently without extensive storage. As an implicit scheme it allows a large time step to reach the steady state. An interactive grid generation program (TURBO), which is being developed, is used to generate grids. This program uses the control point form of algebraic grid generation which uses a sparse collection of control points from which the shape and position of coordinate curves can be adjusted. A distinct advantage of TURBO compared with other grid generation programs is that it allows the easy change of local mesh structure without affecting the grid outside the domain of dependence. Sample grids are generated by TURBO for a compressor rotor blade and a turbine cascade. The turbine cascade flow is simulated by using the LU implicit scheme on the grid generated by TURBO. Author

A90-23841* National Aeronautics and Space Administration. Lewis Research Center, Cleveland, OH.

SIMULATION OF THREE-DIMENSIONAL VISCOUS FLOW WITHIN A MULTISTAGE TURBINE

JOHN J. ADAMCZYK (NASA, Lewis Research Center, Cleveland, OH), MARK L. CELESTINA, TIM A. BEACH (NASA, Lewis Research Center; Sverdrup Technologies, Inc., Cleveland, OH), and MARK BARNETT (United Technologies Research Center, East Hartford, CT) ASME, Gas Turbine and Aeroengine Congress and Exposition, Toronto, Canada, June 4-8, 1989. 13 p. Previously announced in STAR as N89-14238. refs
(ASME PAPER 89-GT-152)

This work outlines a procedure for simulating the flow field within multistage turbomachinery which includes the effects of unsteadiness, compressibility, and viscosity. The associated modeling equations are the average passage equation system which governs the time-averaged flow field within a typical passage of a blade row embedded within a multistage configuration. The results from a simulation of a low aspect ratio stage and a one-half turbine will be presented and compared with experimental measurements. It will be shown that the secondary flow field generated by the rotor causes the aerodynamic performance of the downstream vane to be significantly different from that of an isolated blade row. Author

A90-25028* National Aeronautics and Space Administration. Lewis Research Center, Cleveland, OH.

UNSTEADY EULER ANALYSIS OF THE FLOWFIELD OF A PROPPAN AT AN ANGLE OF ATTACK

M. NALLASAMY (NASA, Lewis Research Center; Sverdrup Technology, Inc., Cleveland, OH) and J. F. GROENEWEG (NASA, Lewis Research Center, Cleveland, OH) AIAA, Aerospace Sciences Meeting, 28th, Reno, NV, Jan. 8-11, 1990. 18 p. refs
(AIAA PAPER 90-0339) Copyright

The paper examines the effects of angle of attack of a propfan on the blade loading and details of the flowfield by solving the unsteady three-dimensional Euler equations. The configuration considered is the SR7L propeller at cruise condition and the inflow angles considered are 4.6, 1.6 and -0.4 deg. The results indicate that the blade response is nearly sinusoidal at low inflow angles (1.6 and -0.4 deg) and significant deviations from sinusoidal behavior occur at an inflow angle of 4.6 deg due to the presence of strong shocks on both suction and pressure surfaces of the blade. The detailed flow in the blade passages shows that a shock formed on the suction surface during the highly loaded portion of the revolution extends across the passage to the pressure surface. An increase in inflow angle results in an increase in blade loading on the down-going side and a decrease in loading on the up-going side. Author

A90-25041* National Aeronautics and Space Administration. Lewis Research Center, Cleveland, OH.

NUMERICAL SOLUTIONS OF THE LINEARIZED EULER EQUATIONS FOR UNSTEADY VORTICAL FLOWS AROUND LIFTING AIRFOILS

JAMES R. SCOTT (NASA, Lewis Research Center, Cleveland, OH) and HAFIZ M. ATASSI (Notre Dame, University, IN) AIAA, Aerospace Sciences Meeting, 28th, Reno, NV, Jan. 8-11, 1990. 20 p. refs
(AIAA PAPER 90-0694) Copyright

A linearized unsteady aerodynamic analysis is presented for unsteady, subsonic vortical flows around lifting airfoils. The analysis fully accounts for the distortion effects of the nonuniform mean flow on the imposed vortical disturbances. A frequency domain numerical scheme which implements this linearized approach is described, and numerical results are presented for a large variety of flow configurations. The results demonstrate the effects of airfoil thickness, angle of attack, camber, and Mach number on the unsteady lift and moment of airfoils subjected to periodic vortical gusts. The results show that mean flow distortion can have a very strong effect on the airfoil unsteady response, and that the effect depends strongly upon the reduced frequency, Mach number, and gust wave numbers. Author

A90-25042* National Aeronautics and Space Administration. Lewis Research Center, Cleveland, OH.

SWEEP WING ICE ACCRETION MODELING

M. G. POTAPCZUK and C. S. BIDWELL (NASA, Lewis Research Center, Cleveland, OH) AIAA, Aerospace Sciences Meeting, 28th, Reno, NV, Jan. 8-11, 1990. 25 p. refs
(AIAA PAPER 90-0756) Copyright

An effort to develop a three-dimensional ice accretion modeling method is initiated. This first step toward creation of a complete aircraft icing simulation code builds on previously developed methods for calculating three-dimensional flowfields and particle trajectories combined with a two-dimensional ice accretion calculation along coordinate locations corresponding to streamlines. This work is intended as a demonstration of the types of calculations necessary to predict a three-dimensional ice accretion. Results of calculations using the 3D method for a MS-317 swept wing geometry are projected onto a 2D plane normal to the wing leading edge and compared to 2D results for the same geometry. These results indicate that the flowfield over the surface and the particle trajectories differed for the two calculations. This led to lower collection efficiencies, convective heat transfer coefficients, freezing fractions, and ultimately ice accumulation for the 3D calculation. R.E.P.

A90-25043* National Aeronautics and Space Administration. Lewis Research Center, Cleveland, OH.

ENGINE INLET DISTORTION IN A 9.2 PERCENT SCALED VECTORED THRUST STOVL MODEL IN GROUND EFFECT

ALBERT L. JOHNS, GEORGE NEINER (NASA, Lewis Research Center, Cleveland, OH), J. D. FLOOD, K. C. AMUEDO, and T. W. STROCK (McDonnell Aircraft Co., Saint Louis, MO) AIAA, ASME, SAE, and American Society for Engineering Education, Joint Propulsion Conference, 25th, Monterey, CA, July 10-12, 1989. 24 p.
(AIAA PAPER 89-2910) Copyright

Advanced Short Takeoff/Vertical Landing (STOVL) aircraft which can operate from remote locations, damaged runways, and small air capable ships are being pursued for deployment around the turn of the century. To achieve this goal, a cooperative program has been defined for testing in the NASA Lewis 9- by 15-foot Low Speed Wind Tunnel (LSWT) to establish a database for hot gas ingestion, one of the technologies critical to STOVL. This paper presents results showing the engine inlet distortions (both temperature and pressure) in a 9.2 percent scale Vectored Thrust STOVL model in ground effects. Results are shown for the forward nozzle splay angles of 0, -6, and 18 deg. The model support system had 4 deg of freedom, heated high pressure air for nozzle flow, and a suction system exhaust for inlet flow. The headwind (freestream) velocity was varied from 8 to 23 kn. Author

02 AERODYNAMICS

A90-25285*# Ohio State Univ., Columbus.

EFFECTS OF COMPRESSIBILITY ON THE CHARACTERISTICS OF FREE SHEAR LAYERS

M. SAMIMY (Ohio State University, Columbus) and G. S. ELLIOTT AIAA Journal (ISSN 0001-1452), vol. 28, March 1990, p. 439-445. refs

(Contract N00014-87-K-0169; NAG3-764)

Copyright

A high Reynolds number two-dimensional constant pressure compressible shear layer was formed at the trailing edge of an 0.5 mm-thick splitter plate. Convective Mach numbers of 0.51 and 0.64 were investigated using a two-component coincident LDV for the measurements. For the lower convective Mach number case, the nondimensionalized shear-layer and vorticity thickness growth rates were over 20 percent higher and the momentum thickness growth rate was over 30 percent higher than those of the higher convective Mach number case. The results seem to indicate that both small scale and large scale mixing are reduced with increasing convective Mach number.

Author

A90-25290*# Lockheed Aeronautical Systems Co., Marietta, GA.

TOTAL TEMPERATURE EFFECTS ON CENTERLINE MACH NUMBER CHARACTERISTICS OF FREEJETS

J. LEPICOVSKY (Lockheed Aeronautical Systems Co., Marietta, GA) AIAA Journal (ISSN 0001-1452), vol. 28, March 1990, p. 478-482. refs

(Contract NAS3-23708)

Copyright

This paper describes a detailed experimental study of Mach number centerline characteristics of unheated and heated freejets. The jet characteristics were obtained at a range of jet Mach numbers from 0.1 to 0.9 and jet total temperatures up to 900 K. Previously published results showed that the jet total temperature significantly affects the nozzle-exit, boundary-layer characteristics. The results of this study indicate that a strong correlation exists between nozzle-exit, boundary-layer conditions and freejet development. It is clear from this investigation that experimental data on freejet development cannot be meaningfully compared from one facility to another without specific knowledge of nozzle-exit, boundary-layer conditions. It was concluded that direct effect of the jet operating conditions (elevated flow temperature) on freejet development is much less important than the indirect effect due to changed nozzle-exit, boundary-layer characteristics.

Author

A90-26128*# Purdue Univ., West Lafayette, IN.

PROPELLER-WING INTERACTION USING A FREQUENCY DOMAIN PANEL METHOD

MARC H. WILLIAMS (Purdue University, West Lafayette, IN) and JINSOO CHO Journal of Aircraft (ISSN 0021-8669), vol. 27, March 1990, p. 196-203. refs

(Contract NAG3-499)

Copyright

The unsteady aerodynamic coupling between a propeller and a wing is analyzed using linear compressible aerodynamic theory. The periodic loads are decomposed into harmonics, and the harmonic amplitudes are found iteratively. Each stage of the iteration involves the solution of an isolated propeller or wing problem; the interaction is done through the Fourier transform of the induced velocity field. The method was validated by comparing the predicted velocity field about an isolated propeller with detailed laser Doppler velocimeter measurements and by comparison with mean loads measured in a wing-propeller experiment. Comparisons have also been made between the fluctuating loads predicted by the present method and a quasisteady vortex lattice scheme.

Author

A90-26553* National Aeronautics and Space Administration, Lewis Research Center, Cleveland, OH.

INTERACTIVE GRID GENERATION FOR TURBOMACHINERY FLOW FIELD SIMULATIONS

YUNG K. CHOO, CHARLES RENO (NASA, Lewis Research Center,

Cleveland, OH), and PETER R. EISEMAN (NASA, Lewis Research Center, Cleveland, OH; Columbia University, New York) IN: Numerical grid generation in computational fluid mechanics '88; Proceedings of the Second International Conference, Miami Beach, FL, Dec. 5-8, 1988. Swansea, Wales, Pineridge Press, Ltd., 1988, p. 895-904. Previously announced in STAR as N89-11717. refs

Copyright

The control point form of algebraic grid generation presented provides the means that are needed to generate well structured grids of turbomachinery flow simulations. It uses a sparse collection of control points distributed over the flow domain. The shape and position of coordinate curves can be adjusted from these control points while the grid conforms precisely to all boundaries. An interactive program called TURBO, which uses the control point form, is being developed. Basic features of the code are discussed and sample grids are presented. A finite volume LU implicit scheme is used to simulate flow in a turbine cascade on the grid generated by the program.

Author

A90-26967*# Cincinnati Univ., OH.

A FLUX-SPLIT SOLUTION PROCEDURE FOR UNSTEADY INLET FLOWS

H. S. PORDAL, P. K. KHOSLA, and S. G. RUBIN (Cincinnati, University, OH) AIAA, Aerospace Sciences Meeting, 28th, Reno, NV, Jan. 8-11, 1990. 9 p. refs

(Contract NAG3-716; F49620-85-C-0027)

(AIAA PAPER 90-0585) Copyright

The unstart and restart of an axisymmetric inlet is investigated using a flux-split procedure applied to the Euler and Reduced Navier Stokes (RNS) equations. A time consistent direct sparse matrix solver is applied to compute the transient flow field both internal and external to the inlet. Time varying oblique and normal shocks are captured. The code is quite general and is applicable for subsonic, transonic and supersonic free streams. The current analysis is concerned with supersonic flight conditions.

Author

A90-26970*# National Aeronautics and Space Administration, Lewis Research Center, Cleveland, OH.

COMPARISON OF 3-D VISCOUS FLOW COMPUTATIONS OF MACH 5 INLET WITH EXPERIMENTAL DATA

D. R. REDDY (NASA, Lewis Research Center; Sverdrup Technology, Inc., Cleveland, OH), T. J. BENSON, and L. J. WEIR (NASA, Lewis Research Center, Cleveland, OH) AIAA, Aerospace Sciences Meeting, 28th, Reno, NV, Jan. 8-11, 1990. 14 p. refs

(Contract NAS3-25266)

(AIAA PAPER 90-0600) Copyright

The accuracy of the time-marching three-dimensional Navier-Stokes code PARC3D (Cooper et al., 1987) is evaluated using experimental data on a Mach 5 mixed-compression inlet configuration, obtained in the 10 x 10-ft working section of the supersonic wind tunnel at NASA Lewis. The basic principles of the PARC3D computations (in which the inlet and tunnel geometry and the bleed conditions are fully modeled) and the experimental setup are described, and the results are presented in extensive graphs and characterized in detail. PARC3D is shown to give reasonably accurate predictions of the bleed-zone elimination of low-energy vortical flow due to shock/boundary-layer interaction; various possible improvements are briefly considered.

T.K.

A90-27966*# National Aeronautics and Space Administration, Lewis Research Center, Cleveland, OH.

ANALYSIS OF FULLY STALLED COMPRESSOR

WOJCIECH ROSTAFINSKI (NASA, Lewis Research Center, Cleveland, OH) Journal of Propulsion and Power (ISSN 0748-4658), vol. 6, Mar.-Apr. 1990, p. 177-180. Previously cited in issue 17, p. 2470, Accession no. A86-38480. refs

A90-29374*# Toledo Univ., OH.

TIME DOMAIN FLUTTER ANALYSIS OF CASCADES USING A FULL-POTENTIAL SOLVER

MILIND A. BAKHLE, T. S. R. REDDY, and THEO G. KEITH, JR. (Toledo, University, OH) IN: AIAA/ASME/ASCE/AHS/ASC Structures, Structural Dynamics and Materials Conference, 31st,

Long Beach, CA, Apr. 2-4, 1990, Technical Papers. Part 3. Washington, DC, American Institute of Aeronautics and Astronautics, 1990, p. 1489-1496. refs
(Contract NSG-3139)
(AIAA PAPER 90-0984) Copyright

A time domain approach is used to determine the dynamic aeroelastic stability of a cascade of blades. The structural model for each blade is a typical section with two degrees of freedom. The aerodynamic model is the unsteady, two-dimensional, full-potential flow through the cascade of airfoils. The unsteady equations of motion for the structure and the fluid are integrated simultaneously in time starting with the steady flowfield and a small initial disturbance applied to the airfoils. The motion of each blade is analyzed to determine the aeroelastic stability of the cascade. The effect of interblade phase angle is included in the analysis by allowing each blade to have an independent motion and considering a number of blade passages. Calculations are made using an airfoil section and structural parameters that are representative of a propfan. The results are compared with those from a separate frequency domain analysis. Good agreement between the results is observed. With the time domain approach, it is possible to consider nonlinear structural models and nonlinear force-displacement relations. The method allows a realistic simulation of the motion of the fluid and the cascade blades for a better physical understanding and it also has the potential for saving computational time when compared to the frequency domain approach for the flutter analysis of cascades. Author

A90-29392* # Purdue Univ., West Lafayette, IN.

THREE DIMENSIONAL FULL POTENTIAL METHOD FOR THE AEROELASTIC MODELING OF PROPFANS

MARC H. WILLIAMS (Purdue University, West Lafayette, IN) and CHIEH C. KU IN: AIAA/ASME/ASCE/AHS/ASC Structures, Structural Dynamics and Materials Conference, 31st, Long Beach, CA, Apr. 2-4, 1990, Technical Papers. Part 3. Washington, DC, American Institute of Aeronautics and Astronautics, 1990, p. 1727-1735. refs
(Contract NAG3-499)
(AIAA PAPER 90-1120) Copyright

A three-dimensional time dependent full potential aerodynamic analysis of single rotation propellers has been developed. The primary purpose of the code is to provide a capability of doing propfan aeroelastic analysis in the nonlinear transonic regime. A secondary purpose is to provide a validation of the unsteady lifting surface panel method that has been developed. Results will be shown for steady state aerodynamic loading, unsteady aerodynamic response to forced aeroelastic deformations, and free aeroelastic response. Comparisons are made to experimental data and corresponding panel code results. Author

A90-29393* # California Univ., Los Angeles.

AEROELASTIC PROBLEMS IN TURBOMACHINES

ODDVAR O. BENDIKSEN (California, University, Los Angeles) IN: AIAA/ASME/ASCE/AHS/ASC Structures, Structural Dynamics and Materials Conference, 31st, Long Beach, CA, Apr. 2-4, 1990, Technical Papers. Part 3. Washington, DC, American Institute of Aeronautics and Astronautics, 1990, p. 1736-1761. Research supported by NSF. refs
(Contract NAG3-308; NAS3-25574)
(AIAA PAPER 90-1157) Copyright

A review of the field of turbomachinery aeroelasticity is presented. Developments over the past decade are emphasized, and an assessment of possible future directions of research is offered. The paper reviews the areas of unsteady cascade flows, structural modeling, and flutter prediction methods. Representative results for unsteady flow calculations and flutter boundary predictions in subsonic, transonic, and supersonic flows are discussed, including recent calculations based on the methods of computational fluid mechanics. Results from current attempts to correlate experimental data with theoretical predictions are discussed briefly. It is recommended that future research include investigations of novel approaches to flutter calculations that can

take full advantage of parallel processing supercomputers. The feasibility of using mistuning and aeroelastic tailoring as passive flutter suppression techniques should also be pursued. Author

A90-30264* # National Aeronautics and Space Administration. Lewis Research Center, Cleveland, OH.

NUMERICAL SOLUTIONS OF THE LINEARIZED EULER EQUATIONS FOR UNSTEADY VORTICAL FLOWS AROUND LIFTING AIRFOILS

JAMES R. SCOTT (NASA, Lewis Research Center, Cleveland, OH) and HAFIZ M. ATASSI (Notre Dame, University, IN) AIAA, Aerospace Sciences Meeting, 28th, Reno, NV, Jan. 8-11, 1990. 20 p. Previously announced in STAR as N90-17562. refs
Copyright

A linearized unsteady aerodynamic analysis is presented for unsteady, subsonic vortical flows around lifting airfoils. The analysis fully accounts for the distortion effects of the nonuniform mean flow on the imposed vortical disturbances. A frequency domain numerical scheme which implements this linearized approach is described, and numerical results are presented for a large variety of flow configurations. The results demonstrate the effects of airfoil thickness, angle of attack, camber, and Mach number on the unsteady lift and moment of airfoils subjected to periodic vortical gusts. The results show that mean flow distortion can have a very strong effect on the airfoil unsteady response, and that the effect depends strongly upon the reduced frequency, Mach number, and gust wave numbers. Author

A90-31291* # National Central Univ., Chung-Li (Taiwan).

EVALUATION OF THREE TURBULENCE MODELS IN STATIC AIR LOADS AND DYNAMIC STALL PREDICTIONS

JIUNN-CHI WU (National Central University, Chung-Li, Republic of China), DENNIS L. HUFF (NASA, Lewis Research Center, Cleveland, OH), and L. N. SANKAR (Georgia Institute of Technology, Atlanta) Journal of Aircraft (ISSN 0021-8669), vol. 27, April 1990, p. 382-384. Previously cited in issue 09, p. 1284. Accession no. A89-25485. refs
(Contract NAG3-768)
Copyright

A90-36252* # Ohio State Univ., Columbus.

STRUCTURE OF A REATTACHING SUPERSONIC SHEAR LAYER

M. SAMIMY (Ohio State University, Columbus) and B. A. K. ABU-HIJLEH AIAA Journal (ISSN 0001-1452), vol. 28, June 1990, p. 969, 970. Abridged. Previously cited in issue 20, p. 3345. Accession no. A88-48901.
(Contract NAG3-764; N00014-87-K-0168)
Copyright

A90-40686* # United Technologies Corp., Windsor Locks, CT.

INVESTIGATION OF THE NEAR WAKE OF A PROPFAN

D. B. HANSON (United Technologies Corp., Hamilton Standard Div., Windsor Locks, CT) and W. P. PATRICK (United Technologies Research Center, East Hartford, CT) Journal of Aircraft (ISSN 0021-8669), vol. 27, June 1990, p. 536-542. Research supported by United Technologies Corp. Previously cited in issue 13, p. 1940. Accession no. A89-33735. refs
(Contract NAS3-23720)
Copyright

A90-40937* # Purdue Univ., West Lafayette, IN.

COUNTER-ROTATING PROPELLANT ANALYSIS USING A FREQUENCY DOMAIN PANEL METHOD

MARC H. WILLIAMS (Purdue University, West Lafayette, IN) and JINSOO CHO Journal of Propulsion and Power (ISSN 0748-4658), vol. 6, July-Aug. 1990, p. 426-433. refs
(Contract NAG3-499)
Copyright

The unsteady aerodynamic coupling between the front and rear rotors in a counter-rotating propeller system is analyzed using a frequency-domain panel method based on linear compressible aerodynamic theory. The periodic loads are decomposed into

02 AERODYNAMICS

harmonics, and the harmonic amplitudes are found iteratively. Each stage of the interaction involves the solution of an isolated propeller problem, the interaction being done through the Fourier transform of the induced velocity field. The method was validated by comparing mean performance parameters with measured data and by comparing the predicted velocity field with detailed laser Doppler velocimeter measurements. Comparisons have also been made between the fluctuating loads predicted by the present method and a time-domain panel method. Author

A90-42644* Arizona Univ., Tucson.

ON THE INSTABILITIES OF SUPERSONIC MIXING LAYERS - A HIGH-MACH-NUMBER ASYMPTOTIC THEORY

THOMAS F. Balsa (Arizona, University, Tucson) and M. E. GOLDSTEIN (NASA, Lewis Research Center, Cleveland, OH) *Journal of Fluid Mechanics* (ISSN 0022-1120), vol. 216, July 1990, p. 585-611. refs
Copyright

The stability of a family of tanh mixing layers is studied at large Mach numbers using perturbation methods. It is found that the eigenfunction develops a multilayered structure, and the eigenvalue is obtained by solving a simplified version of the Rayleigh equation (with homogeneous boundary conditions) in one of these layers which lies in either of the external streams. This analysis leads to a simple hypersonic similarity law which explains how spatial and temporal phase speeds and growth rates scale with Mach number and temperature ratio. Comparisons are made with numerical results, and it is found that this similarity law provides a good qualitative guide for the behavior of the instability at high Mach numbers. In addition to this asymptotic theory, some fully numerical results are also presented (with no limitation on the Mach number) in order to explain the origin of the hypersonic modes (through mode splitting) and to discuss the role of oblique modes over a very wide range of Mach number and temperature ratio. Author

A90-42709*# Ohio State Univ., Columbus.

PRESSURE-BASED REAL-TIME MEASUREMENTS IN COMPRESSIBLE FREE SHEAR LAYERS

M. SAMIMY (Ohio State University, Columbus), G. S. ELLIOTT, and M. F. REEDER AIAA, SAE, ASME, and ASEE, Joint Propulsion Conference, 26th, Orlando, FL, July 16-18, 1990. 19 p. refs
(Contract N00014-90-J-1730; NAG3-764)
(AIAA PAPER 90-1980) Copyright

A preliminary experimental study has been conducted to gain insight into the temporal and spatial contents of largescale structures in a convective Mach number = 0.51 high Reynolds number planar two-dimensional compressible free shear layer. Power spectra, coherence, and space-time correlations were obtained using single- and two-point pressure measurements. Both developing and fully developed regions of the flow were investigated. The passage frequency of structures were found to be 10-15 kHz in the developing region and 4-8 kHz in the fully developed region. The convective velocity obtained from the space-time correlation in the middle of the shear layer was close to the theoretical value but varied toward the edge of the shear layer. The structures were shown to be surprisingly three-dimensional even in this low compressibility level shear layer. The structures size and spacing were also determined and discussed. Author

A90-42731*# Pennsylvania State Univ., University Park.

COMPUTATION OF TURBINE FLOWFIELDS WITH A NAVIER-STOKES CODE

G. V. HOBSON and B. LAKSHMINARAYANA (Pennsylvania State University, University Park) AIAA, SAE, ASME, and ASEE, Joint Propulsion Conference, 26th, Orlando, FL, July 16-18, 1990. 17 p. refs

(Contract NSG-3266)
(AIAA PAPER 90-2122) Copyright

A new technique has been developed for the solution of the incompressible Navier-Stokes equations. The numerical technique, derived from a pressure substitution method (PSM), overcomes

many of the deficiencies of the pressure correction method. This technique allows for the direct solution of the actual pressure in the form of a Poisson equation which is derived from the pressure weighted substitution of the full momentum equations into the continuity equation. In two-dimensions a turbine flowfield, including heat transfer, has been computed with this method and the prediction of the cascade performance is presented. The extension of the pressure correction method for the solution of three-dimensional flows is also presented for laminar flow in an S-shaped duct and turbulent flow in the end-wall region of a turbine cascade. Author

A90-42734*# Cincinnati Univ., OH.

TRANSIENT BEHAVIOR OF SUPERSONIC FLOW THROUGH INLETS

H. S. PORDAL, P. K. KHOSLA, and S. G. RUBIN (Cincinnati, University, OH) AIAA, SAE, ASME, and ASEE, Joint Propulsion Conference, 26th, Orlando, FL, July 16-18, 1990. 12 p. refs
(Contract NAG3-716; F49620-85-C-0027)
(AIAA PAPER 90-2130) Copyright

A solution technique to compute inlet flow behavior is presented. The phenomena of inlet unstart and restart are investigated using a flux-split procedure applied to the Euler and Reduced Navier Stokes (RNS) equations. A time consistent direct sparse matrix solver in conjunction with a domain decomposition strategy is applied to compute the transient flow behavior both internal and external to the inlet. Time varying shocks and time varying recirculation regions are efficiently analyzed. The code is quite general and is suitable for the computation of flow for a wide variety of geometries and over a wide range of Mach and Reynolds numbers. Author

A90-45873*# General Motors Corp., Indianapolis, IN.

3D EULER ANALYSIS OF DUCTED PROPFAN FLOWFIELDS

EDWARD J. HALL and ROBERT A. DELANEY (General Motors Corp., Allison Gas Turbines Div., Indianapolis, IN) IN: AIAA Applied Aerodynamics Conference, 8th, Portland, OR, Aug. 20-22, 1990, Technical Papers. Part 1. Washington, DC, American Institute of Aeronautics and Astronautics, 1990, p. 306-313. refs
(Contract NAS3-25270)
(AIAA PAPER 90-3034) Copyright

A numerical method is presented for predicting the steady inviscid flow through a ducted propfan based on a time-marching solution of the three-dimensional Euler equations. A four-stage multiple-block Runge-Kutta finite volume numerical technique, utilizing implicit residual smoothing and a blended second and fourth difference dissipation, is applied to predict the transonic flowfield about both single-rotation and counter-rotations ducted rotors. Counter-rotation predictions are based on an average-passage system of equations approach. Calculations are performed for both a single sheared H-type grid system and a multiple-block grid system incorporating a C-type grid about the cowl. Numerical results are compared with experimental data for two cases: a low speed ducted propeller and a 1.15 pressure ratio fan stage. Author

A90-46377* National Aeronautics and Space Administration, Lewis Research Center, Cleveland, OH.

THE LOW FREQUENCY OSCILLATION IN THE FLOW OVER A NACA0012 AIRFOIL WITH AN 'ICED' LEADING EDGE

K. B. M. Q. ZAMAN and M. G. POTAPCZUK (NASA, Lewis Research Center, Cleveland, OH) IN: Low Reynolds number aerodynamics; Proceedings of the Conference, Notre Dame, IN, June 5-7, 1989. Berlin and New York, Springer-Verlag, 1989, p. 271-282. Previously announced in STAR as N89-23417. refs
Copyright

The unusually low frequency oscillation in the wake of an airfoil is explored experimentally as well as computationally for a NACA0012 airfoil with a glaze ice accretion at the leading edge. Experimentally, flow oscillations were observed at low frequencies that correspond to a Strouhal number of about 0.02. This occurred in the angle of attack range of 8 to 9 deg, near the onset of static stall for this airfoil. With a Navier-Stokes computation,

limit-cycle oscillations in the flow and in the aerodynamic forces were also observed at low Strouhal numbers. However, the occurrence of the oscillation is found to depend on the turbulence model in use as well as the Reynolds number. Author

A90-46860*# Allied-Signal Aerospace Co., Phoenix, AZ.
THREE DIMENSIONAL LDV FLOW MEASUREMENTS AND THEORETICAL INVESTIGATION IN A RADIAL INFLOW TURBINE SCROLL

MALAK FOUAD MALAK (Allied-Signal Aerospace Co., Garrett Auxiliary Power Div., Phoenix, AZ), AWATEF HAMED, and WIDEN TABAKOFF (Cincinnati, University, OH) IN: International Congress of Fluid Mechanics, 3rd, Cairo, Egypt, Jan. 2-4, 1990, Proceedings. Volume 1. Mansoura, Egypt, Mansoura University, 1990, p. 427-440. refs
 (Contract NAG3-26)

A two-color LDV system was used in the measurement of three orthogonal velocity components at 758 points located throughout the scroll and the unvaned portion of the nozzle of a radial inflow turbine scroll. The cold flow experimental results are presented for the velocity field at the scroll tongue. In addition, a total pressure loss of 3.5 percent for the scroll is revealed from the velocity measurements combined with the static pressure readings. Moreover, the measurement of the three normal stresses of the turbulence has showed that the flow is anisotropic. Furthermore, the mean velocity components are compared with a numerical solution of the potential flow field using the finite element technique. The theoretical prediction of the exit flow angle variation agrees well with the experimental results. This variation leads to a higher scroll pattern factor which can be avoided by controlling the scroll cross sectional area distribution. Author

A90-46905*# Purdue Univ., Indianapolis, IN.
A BLOCK-BASED ALGORITHM FOR THE SOLUTION OF COMPRESSIBLE FLOWS IN ROTOR-STATOR COMBINATIONS
 H. U. AKAY, A. ECER, and A. BESKOK (Purdue University, Indianapolis, IN) IN: International Congress of Fluid Mechanics, 3rd, Cairo, Egypt, Jan. 2-4, 1990, Proceedings. Volume 4. Mansoura, Egypt, Mansoura University, 1990, p. 1383-1393. refs
 (Contract NAG3-858)

A block-based solution algorithm is developed for the solution of compressible flows in rotor-stator combinations. The method allows concurrent solution of multiple solution blocks in parallel machines. It also allows a time averaged interaction at the stator-rotor interfaces. Numerical results are presented to illustrate the performance of the algorithm. The effect of the interaction between the stator and rotor is evaluated. Author

A90-47213*# National Aeronautics and Space Administration, Lewis Research Center, Cleveland, OH.
ANALYSIS AND DESIGN OF OPTIMIZED TRUNCATED SCARFED NOZZLES SUBJECT TO EXTERNAL FLOW EFFECTS

RICKEY J. SHYNE (NASA, Lewis Research Center, Cleveland, OH) and THEO G. KEITH, JR. (Toledo, University, OH) AIAA, SAE, ASME, and ASEE, Joint Propulsion Conference, 26th, Orlando, FL, July 16-18, 1990. 11 p. Previously announced in STAR as N90-25106. refs
 (AIAA PAPER 90-2222) Copyright

Rao's method for computing optimum thrust nozzles is modified to study the effects of external flow on the performance of a class of exhaust nozzles. Members of this class are termed scarfed nozzles. These are two-dimensional, nonsymmetric nozzles with a flat lower wall. The lower wall (the cowl) is truncated in order to save weight. Results from a parametric investigation are presented to show the effects of the external flowfield on performance. Author

A90-47220*# National Aeronautics and Space Administration, Lewis Research Center, Cleveland, OH.
UNSTEADY BLADE SURFACE PRESSURES ON A LARGE-SCALE ADVANCED PROPELLER - PREDICTION AND DATA

M. NALLASAMY (NASA, Lewis Research Center; Sverdrup Technology, Inc., Brook Park, OH) and J. F. GROENEWEG (NASA, Lewis Research Center, Cleveland, OH) AIAA, SAE, ASME, and ASEE, Joint Propulsion Conference, 26th, Orlando, FL, July 16-18, 1990. 18 p. refs

(AIAA PAPER 90-2402) Copyright

An unsteady three dimensional Euler analysis technique is employed to compute the flowfield of an advanced propeller operating at an angle of attack. The predicted blade pressure waveforms are compared with wind tunnel data at two Mach numbers, 0.5 and 0.2. The inflow angle is three degrees. For an inflow Mach number of 0.5, the predicted pressure response is in fair agreement with data: the predicted phases of the waveforms are in close agreement with data while the magnitudes are underpredicted. At the low Mach number of 0.2 (take-off) the numerical solution shows the formation of a leading edge vortex which is in qualitative agreement with measurements. However, the highly nonlinear pressure response measured on the blade suction surface is not captured in the present inviscid analysis. Author

A90-48954*# National Aeronautics and Space Administration, Lewis Research Center, Cleveland, OH.

EXPERIMENTAL INVESTIGATION OF MULTIELEMENT AIRFOIL ICE ACCRETION AND RESULTING PERFORMANCE DEGRADATION

M. G. POTAPCZUK (NASA, Lewis Research Center, Cleveland, OH) and B. M. BERKOWITZ (Sverdrup Technology, Inc., Brook Park, OH) Journal of Aircraft (ISSN 0021-8669), vol. 27, Aug. 1990, p. 679-691. Previously cited in issue 10, p. 1432, Accession no. A89-28453. refs
 Copyright

A90-50637*# National Aeronautics and Space Administration, Lewis Research Center, Cleveland, OH.

EULER ANALYSIS COMPARISON WITH LDV DATA FOR AN ADVANCED COUNTER-ROTATION PROPFAN AT CRUISE

CHRISTOPHER J. MILLER and GARY G. PODBOY (NASA, Lewis Research Center, Cleveland, OH) AIAA, Applied Aerodynamics Conference, 8th, Portland, OR, Aug. 20-22, 1990. 22 p. Previously announced in STAR as N90-25946. refs
 (AIAA PAPER 90-3033) Copyright

A fine mesh Euler solution of the F4/A4 unducted fan (UDF) model flowfield is compared with laser Doppler velocimeter (LDV) data taken in the NASA Lewis 8- by 6-Foot Supersonic Wind Tunnel. The comparison is made primarily at one axial plane downstream of the front rotor where the LDV particle lag errors are reduced. The agreement between measured and predicted velocities in this axial plane is good. The results show that a dense mesh is needed in the centerbody stagnation region to minimize entropy generation that weakens the aft row passage shock. The predicted radial location of the tip vortex downstream of the front rotor agrees well with the experimental results but the strength is overpredicted. With 40 points per chord line, the integrated performance quantities are nearly converged, but more points are needed to resolve passage shocks and flow field details. Author

A90-51013*# National Aeronautics and Space Administration, Lewis Research Center, Cleveland, OH.

LEAST-SQUARES FINITE ELEMENT METHODS FOR COMPRESSIBLE EULER EQUATIONS

BO-NAN JIANG (NASA, Lewis Research Center, Cleveland, OH) and G. F. CAREY (Texas, University, Austin) International Journal for Numerical Methods in Fluids (ISSN 0271-2091), vol. 10, April 1, 1990, p. 557-568. Research supported by the University of Texas and U.S. Navy. refs
 Copyright

A method based on backward finite differencing in time and a least-squares finite element scheme for first-order systems of partial differential equations in space is applied to the Euler equations for gas dynamics. The scheme minimizes the L-sq-norm of the residual within each time step. The method naturally generates

02 AERODYNAMICS

numerical dissipation proportional to the time step size. An implicit method employing linear elements has been implemented and proves robust. For high-order elements, computed solutions based on the L-sq method may have oscillations for calculations at similar time step sizes. To overcome this difficulty, a scheme which minimizes the weighted H1-norm of the residual is proposed and leads to a successful scheme with high-degree elements. Finally, a conservative least-squares finite element method is also developed. Numerical results for two-dimensional problems are given to demonstrate the shock resolution of the methods and compare different approaches. Author

A90-52618* # National Aeronautics and Space Administration. Lewis Research Center, Cleveland, OH.

AN LDA INVESTIGATION OF THE NORMAL SHOCK WAVE BOUNDARY LAYER INTERACTION

R. M. CHRISS, W. R. HINGST, A. J. STRAZISAR (NASA, Lewis Research Center, Cleveland, OH), and T. G. KEITH (Toledo, University, OH) La Recherche Aerospatiale (English Edition) (ISSN 0379-380X), no. 2, 1990, p. 1-15. refs
Copyright

Nonintrusive measurements have been made of two normal shock wave-boundary layer interactions. Two-dimensional measurements were made throughout the interaction region while three-dimensional measurements were made in the vicinity of the shock wave. The measurements were made in the corner of the test section of a continuous flow supersonic wind tunnel in which a normal shock wave had been stabilized. LDA, surface pressure measurement and flow visualization techniques were employed for two freestream Mach number test cases: 1.6 and 1.3. The former contained separated flow regions and a system of shock waves. The latter was found to be far less complicated. The reported results define the flowfield structure in detail for each case. Author

N90-10004* # Sverdrup Technology, Inc., Cleveland, OH.
A SUPERSONIC THROUGH-FLOW FAN ENGINE AIRFRAME INTEGRATION STUDY Final Report

PAUL J. BARNHART Sep. 1989 11 p Presented at the Aircraft Design, Systems and Operations Conference, Seattle, WA, 31 Jul. - 2 Aug. 1989; cosponsored by AIAA, AHS, and ASEE (Contract NAS3-25266)
(NASA-CR-185140; E-5068; NAS 1.26:185140; AIAA-89-2140)
Avail: NTIS HC A03/MF A01 CSCL 01A

Engine airframe integration effects are investigated for supersonic through-flow fan engines installed on a Mach 3.20 supersonic cruise vehicle. Six different supersonic through-flow fan engine installations covering the effects of engine size, nacelle contour, nacelle placement, and approximate bypass plume effects are presented. The different supersonic through-flow fan installations are compared with a conventional turbine bypass engine configuration on the same basic airframe. The supersonic through-flow fan engine integrations are shown to be comparable to the turbine bypass engine configuration on the basis of installed nacelle wave drag. The supersonic through-flow fan engine airframe integrated vehicles have superior aerodynamic performance on the basis of maximum lift-to-drag ratio than the turbine bypass engine installation over the entire operating Mach number range from 1.10 to 3.20. When approximate bypass plume modeling is included, the supersonic through-flow fan engine configuration shows even larger improvements over the turbine bypass engine configuration. Author

N90-10011* # Lockheed-Georgia Co., Marietta.
ANALYSIS OF RESULTS FROM WIND TUNNEL TESTS OF INLETS FOR AN ADVANCED TURBOPROP NACELLE INSTALLATION Report, 1 Nov. 1982 - 30 Jun. 1985

J. P. HANCOCK, V. LYMAN, and A. P. PENNOCK Jun. 1986 162 p
(Contract NAS3-23710)
(NASA-CR-174937; NAS 1.26:174937; LG85ER0105) Avail: NTIS HC A08/MF A01 CSCL 01A

Inlets for tractor installations of advanced turboprop propulsion

systems were tested in three phases, covering a period from November, 1982 to January, 1984. Nacelle inlet configuration types included single scoop, twin scoop, and annular arrangements. Tests were performed with and without boundary layer diverters and several different diverter heights were tested for the single scoop inlet. This same inlet was also tested at two different axial positions. Test Mach numbers ranged from Mach 0.20 to 0.80. Types of data taken were: (1) internal and external pressures, including inlet throat recoveries; (2) balance forces, including thrust-minus-drag; and (3) propeller blade stresses. Author

N90-10835* # Scientific Research Associates, Inc., Glastonbury, CT.

USER'S MANUAL FOR PEP SIG NASA TIP VORTEX VERSION

TOMMY M. TSAI, FREDERICK J. DEJONG, and RALPH LEVY Aug. 1988 59 p
(Contract NAS3-24881)
(NASA-CR-182178; NAS 1.26:182178; R88-900064-F) Avail: NTIS HC A04/MF A01 CSCL 01/1

The tip vortex flowfield plays a significant role in the performance of advanced aircraft propellers. The flowfield in the tip region is complex, three-dimensional and viscous with large secondary velocities. A computer code was developed to predict the tip vortex flowfield of advanced aircraft propellers. This document is the user's manual. The analysis and a series of test cases are presented in NASA-CR-182179. Author

N90-10836* # Scientific Research Associates, Inc., Glastonbury, CT.

COMPUTATION OF THE TIP VORTEX FLOWFIELD FOR ADVANCED AIRCRAFT PROPELLERS

TOMMY M. TSAI, FREDERICK J. DEJONG, and RALPH LEVY Aug. 1988 62 p
(Contract NAS3-24881)
(NASA-CR-182179; NAS 1.26:182179; R88-900064-F) Avail: NTIS HC A04/MF A01 CSCL 01/1

The tip vortex flowfield plays a significant role in the performance of advanced aircraft propellers. The flowfield in the tip region is complex, three-dimensional and viscous with large secondary velocities. An analysis is presented using an approximate set of equations which contains the physics required by the tip vortex flowfield, but which does not require the resources of the full Navier-Stokes equations. A computer code was developed to predict the tip vortex flowfield of advanced aircraft propellers. A grid generation package was developed to allow specification of a variety of advanced aircraft propeller shapes. Calculations of the tip vortex generation on an SR3 type blade at high Reynolds numbers were made using this code and a parametric study was performed to show the effect of tip thickness on tip vortex intensity. In addition, calculations of the tip vortex generation on a NACA 0012 type blade were made, including the flowfield downstream of the blade trailing edge. Comparison of flowfield calculations with experimental data from an F4 blade was made. A user's manual was also prepared for the computer code (NASA CR-182178). Author

N90-12500* # Georgia Inst. of Tech., Atlanta. School of Aerospace Engineering.

NUMERICAL SIMULATION OF UNSTEADY ROTATIONAL FLOW OVER PROPFAN CONFIGURATIONS Semiannual Status Report, 1 May - 30 Nov. 1989

R. SRIVASTAVA and L. N. SANKAR Nov. 1989 33 p Presented at the AIAA 28th Aerospace Sciences Meeting and Exhibit, Reno, NV, 8-11 Jan. 1990
(Contract NAG3-730)
(NASA-CR-186037; NAS 1.26:186037) Avail: NTIS HC A03/MF A01 CSCL 01/1

The objective is to develop efficient numerical techniques for the study of aeroelastic response of a propfan in an unsteady transonic flow. A three dimensional unsteady Euler solver is being modified to address this problem. Author

N90-12560*# National Aeronautics and Space Administration. Lewis Research Center, Cleveland, OH.

PREDICTION OF UNSTEADY BLADE SURFACE PRESSURES ON AN ADVANCED PROPELLER AT AN ANGLE OF ATTACK
M. NALLASAMY (Sverdrup Technology, Inc., Cleveland, OH.) and J. F. GROENEWEG Nov. 1989 28 p Presented at the 12th Aeroacoustics Conference, San Antonio, TX, 10-12 Apr. 1989; sponsored by AIAA Previously announced in IAA as A89-40473 (Contract NAS3-25266)
(NASA-TM-102374; E-5108; NAS 1.15:102374; AIAA-89-1060)
Avail: NTIS HC A03/MF A01 CSCL 01/1

The numerical solution of the unsteady, three-dimensional, Euler equations is considered in order to obtain the blade surface pressures of an advanced propeller at an angle of attack. The specific configuration considered is the SR7L propeller at cruise conditions with a 4.6 deg inflow angle corresponding to the plus 2 deg nacelle tilt of the Propeller Test Assessment (PTA) flight test condition. The results indicate nearly sinusoidal response of the blade loading, with angle of attack. For the first time, detailed variations of the chordwise loading as a function of azimuthal angle are presented. It is observed that the blade is lightly loaded for part of the revolution and shocks appear from hub to about 80 percent radial station for the highly loaded portion of the revolution.

Author

N90-12561*# National Aeronautics and Space Administration. Lewis Research Center, Cleveland, OH.

SOME OBSERVATIONS ON TRANSITORY STALL IN CONICAL DIFFUSERS
K. B. M. Q. ZAMAN and M. D. DAHL 1989 13 p Presented at the 28th Aerospace Sciences Meeting, Reno, NV, 8-11 Jan. 1990; sponsored by AIAA
(NASA-TM-102387; E-5128; NAS 1.15:102387; AIAA-90-0048)
Avail: NTIS HC A03/MF A01 CSCL 01/1

Results from an experimental investigation on the flow through conical diffusers are presented. The mean and fluctuating velocity fields are compared for three diffusers with total diffusion angles of 16, 20 and 24 degrees, in the throat Mach number ($M_{sub t}$) range of 0.05 to 0.95. Each of the diffusers were 14 cm long and had a 5.08 cm inlet diameter, and the flow exited into the ambient. The boundary layer at the throat was thin with the throat diameter ($D_{sub t}$) to momentum thickness (O) ratio being as high as 800 at $M_{sub t} = 0.4$. While the 16 deg diffuser flow exited with a top-hat mean velocity profile, increasing losses due to increasing separation resulted in fuller profiles for the 20 and 24 degree cases. A detailed flow field study was conducted for the 16 deg. diffuser. The u -spectrum, measured at the exit plane, exhibited a peak apparently due to the ensuing jet column instability throughout the $M_{sub t}$ range covered. In addition, a much lower frequency spectral peak also occurred in the $M_{sub t}$ range of 0.3 to 0.7. Both of the spectral peaks were due to axisymmetric flow fluctuations. A self-sustaining flow oscillation occurred in the $M_{sub t}$ range of 0.6 to 0.85, emitting a loud tone, when the jet column instability frequency matched the resonance frequency of the diffuser. Limited data showed that artificial acoustic excitation was effective in reducing the flow fluctuations, with a resultant increase in the pressure recovery, at low $M_{sub t}$.

Author

N90-13328*# Purdue Univ., West Lafayette, IN. School of Mechanical Engineering.

APPLICATION OF LARGE EDDY INTERACTION MODEL TO A MIXING LAYER Final Report

S. N. B. MURTHY Nov. 1989 50 p
(Contract NAG3-592)
(NASA-CR-185123; NAS 1.26:185123; M/NA/TURB-1) Avail:
NTIS HC A03/MF A01 CSCL 01/1

The large eddy interaction model (LEIM) is a statistical model of turbulence based on the interaction of selected eddies with the mean flow and all of the eddies in a turbulent shear flow. It can be utilized as the starting point for obtaining physical structures in the flow. The possible application of the LEIM to a mixing layer formed between two parallel, incompressible flows with a small

temperature difference is developed by invoking a detailed similarity between the spectra of velocity and temperature.

Author

N90-13352*# National Aeronautics and Space Administration. Lewis Research Center, Cleveland, OH.

EFFECT OF REDUCED AFT DIAMETER AND INCREASED BLADE NUMBER ON HIGH-SPEED COUNTERROTATION PROPELLER PERFORMANCE

GAYLE E. ROSE (Sverdrup Technology, Inc., Cleveland, OH.) and ROBERT J. JERACKI 1989 31 p Presented at the 27th Aerospace Sciences Meeting, Reno, NV, 9-12 Jan. 1989; sponsored by AIAA
(NASA-TM-102077; E-4837; NAS 1.15:102077; AIAA-89-0438)
Avail: NTIS HC A03/MF A01 CSCL 01/1

Performance data of 0.17-scale model counterrotation pusher propeller configurations were taken in the NASA Lewis 8- by 6-Foot Supersonic Wind Tunnel at Mach numbers of 0.66, 0.71, 0.75, and 0.79. These tests investigated the aerodynamic performance of the unducted fan (UDF) demonstrator propeller engine developed in a joint program by General Electric and NASA. Data were recorded to show the effect on counterrotation propeller cruise efficiency of two takeoff noise-reduction concepts. These two concepts are reduced aft blade diameter and increased forward blade number. The four configurations tested were a baseline ($F1/A1$ 8/8) configuration, a reduced aft diameter ($F1/A3$ 8/8) configuration, an increase forward blade number ($F1/A1$ 9/8) configuration, and a combination of the latter two ($F1/A3$ 9/8) configurations. Data were collected with a complex counterrotation propeller test rig via rotating thrust and torque balances and pressure instrumentation. Data comparisons documented the power differences between the baseline and the reduced aft diameter concepts. Performance comparisons to the baseline configuration showed that reducing the aft blade diameter reduced the net efficiency, and adding a blade to the front rotor increased the net efficiency. The combination of the two concepts showed only slightly lower net efficiency than the baseline configuration. It was also found that the counterrotation demonstrator propeller model ($F7/A7$ 8/8) configuration outperformed the baseline ($F1/A1$ 8/8) configuration.

Author

N90-13355*# National Aeronautics and Space Administration. Lewis Research Center, Cleveland, OH.

APPLICATION OF AN EFFICIENT HYBRID SCHEME FOR AEROELASTIC ANALYSIS OF ADVANCED PROPELLERS

R. SRIVASTAVA, N. L. SANKAR, T. S. R. REDDY (Toledo Univ., OH.), and D. L. HUFF 1989 30 p Presented at the 28th Aerospace Sciences Meeting, Reno, NV, 8-11 Jan. 1990; sponsored by AIAA
(NASA-TM-102428; E-5196; NAS 1.15:102428; AIAA-90-0028)
Avail: NTIS HC A03/MF A01 CSCL 01/1

An efficient 3-D hybrid scheme is applied for solving Euler equations to analyze advanced propellers. The scheme treats the spanwise direction semi-explicitly and the other two directions implicitly, without affecting the accuracy, as compared to a fully implicit scheme. This leads to a reduction in computer time and memory requirement. The calculated power coefficients for two advanced propellers, SR3 and SR7L, and various advanced ratios showed good correlation with experiment. Spanwise distribution of elemental power coefficient and steady pressure coefficient differences also showed good agreement with experiment. A study of the effect of structural flexibility on the performance of the advanced propellers showed that structural deformation due to centrifugal and aero loading should be included for better correlation.

Author

N90-14203*# National Aeronautics and Space Administration. Lewis Research Center, Cleveland, OH.

EFFICIENT REAL GAS NAVIER-STOKES COMPUTATIONS OF HIGH SPEED FLOWS USING AN LU SCHEME

WILLIAM J. COIRIER 1990 20 p Presented at the 28th Aerospace Sciences Meeting, Reno, NV, 8-11 Jan. 1990; sponsored by AIAA

02 AERODYNAMICS

(NASA-TM-102429; E-5197; NAS 1.15:102429; AIAA-90-0391)
Avail: NTIS HC A03/MF A01 CSCL 01/1

An efficient method to account for the chemically frozen thermodynamic and transport properties of air in three dimensional Navier-Stokes calculations was demonstrated. This approach uses an explicitly specified equation of state (EOS) so that the fluid pressure, temperature and transport properties are directly related to the flow variables. Since the pressure is explicitly known as a general function of the flow variables no assumptions are made regarding the pressure derivatives in the construction of the flux Jacobians. The method is efficient since no sub-iterations are required to deduce the pressure and temperature from the flux variables and allows different equations of state to be easily supplied to the code. The flexibility of the EOS approach is demonstrated by implementing a high order TVD upwinding scheme based upon flux differencing and Van Leer's flux vector splitting. The EOS approach is demonstrated by computing the hypersonic flow through the corner region of two mutually perpendicular flat plates and through a simplified model of a scramjet module gap-seal configuration. Author

N90-14206* # National Aeronautics and Space Administration. Lewis Research Center, Cleveland, OH.

AN ANALYSIS OF THE VISCOUS FLOW THROUGH A COMPACT RADIAL TURBINE BY THE AVERAGE PASSAGE APPROACH

JAMES D. HEIDMANN and TIMOTHY A. BEACH (Sverdrup Technology, Inc., Cleveland, OH.) 1990 13 p Prepared for presentation at the 35th International Gas Turbine Aeroengine Congress and Exposition, Brussels, Belgium, 11-14 Jun. 1990; sponsored by ASME

(NASA-TM-102471; E-5258; NAS 1.15:102471) Avail: NTIS HC A03/MF A01 CSCL 01/1

A steady, three-dimensional viscous average passage computer code is used to analyze the flow through a compact radial turbine rotor. The code models the flow as spatially periodic from blade passage to blade passage. Results from the code using varying computational models are compared with each other and with experimental data. These results include blade surface velocities and pressures, exit vorticity and entropy contour plots, shroud pressures, and spanwise exit total temperature, total pressure, and swirl distributions. The three computational models used are inviscid, viscous with no blade clearance, and viscous with blade clearance. It is found that modeling viscous effects improves correlation with experimental data, while modeling hub and tip clearances further improves some comparisons. Experimental results such as a local maximum of exit swirl, reduced exit total pressures at the walls, and exit total temperature magnitudes are explained by interpretation of the flow physics and computed secondary flows. Trends in the computed blade loading diagrams are similarly explained. Author

N90-16719* # National Aeronautics and Space Administration. Lewis Research Center, Cleveland, OH.

VISCOUS EFFECTS ON THE INSTABILITY OF AN AXISYMMETRIC JET

K. B. M. Q. ZAMAN and J. M. SEINER (National Aeronautics and Space Administration. Langley Research Center, Hampton, VA.) Feb. 1990 28 p
(NASA-TM-102396; E-4152-1; NAS 1.15:102396) Avail: NTIS HC A03/MF A01 CSCL 01/1

The stability characteristics of a laminar, axisymmetric jet, issuing from fully developed Poiseuille flow, are investigated. The jet preferred frequency, as inferred from surveys of u' -spectra, is found to yield a Strouhal number (St) that depends on the Reynolds number (R); St and R are based on the jet diameter (D) and the average velocity ($U_{sub av}$) at the jet origin. The value of St increases with increasing R in the range 400 less than approximately R less than approximately 4000, attaining an asymptotic value of about 0.45. Flow visualization confirms that the instability is primarily in a helical mode, as predicted by stability analyses. Analyses do predict a similar St versus R variation in

approximately the correct St-range. However, the R-range where this is predicted is lower than that found experimentally. Author

N90-17561* # National Aeronautics and Space Administration. Lewis Research Center, Cleveland, OH.

ENGINE INLET DISTORTION IN A 9.2 PERCENT SCALE VECTORED THRUST STOVL MODEL IN GROUND EFFECT

ALBERT L. JOHNS, GEORGE NEINER, J. D. FLOOD, K. C. AMUEDO, and T. W. STROCK (McDonnell-Douglas Corp., Saint Louis, MO.) 1989 24 p Presented at the 25th Joint Propulsion Conference, Monterey, CA, 10-12 Jul. 1989; cosponsored by AIAA, ASME, SAE, and ASEE

(NASA-TM-102358; E-5072; NAS 1.15:102358; AIAA-89-2910)
Avail: NTIS HC A03/MF A01 CSCL 01/1

Advanced Short Takeoff/Vertical Landing (STOVL) aircraft which can operate from remote locations, damaged runways, and small air capable ships are being pursued for deployment around the turn of the century. To achieve this goal, NASA Lewis Research Center, McDonnell Douglas Aircraft, and DARPA defined a cooperative program for testing in the NASA Lewis 9- by 15-foot low speed wind tunnel (LSWT) to establish a database for hot gas ingestion, one of the technologies critical to STOVL. Results are presented which show the engine inlet distortions (both temperature and pressure) in a 9.2 percent scale vectored thrust STOVL model in ground effects. Results are shown for the forward nozzle splay angles of 0 degrees, -6 degrees, and 18 degrees. The model support system had 4 degrees of freedom, heated high pressure air for nozzle flow, and a suction system exhaust for inlet flow. The headwind (freestream) velocity was varied from 8 to 23 knots. Author

N90-17562* # National Aeronautics and Space Administration. Lewis Research Center, Cleveland, OH.

NUMERICAL SOLUTIONS OF THE LINEARIZED EULER EQUATIONS FOR UNSTEADY VORTICAL FLOWS AROUND LIFTING AIRFOILS

JAMES R. SCOTT and HAFIZ M. ATASSI (Notre Dame Univ., IN.) 1990 21 p Presented at the 28th Aerospace Sciences Meeting, 8-11 Jan. 1990; sponsored by AIAA

(NASA-TM-102466; E-5137; NAS 1.15:102466; AIAA-90-0694)
Avail: NTIS HC A03/MF A01 CSCL 01/1

A linearized unsteady aerodynamic analysis is presented for unsteady, subsonic vortical flows around lifting airfoils. The analysis fully accounts for the distortion effects of the nonuniform mean flow on the imposed vortical disturbances. A frequency domain numerical scheme which implements this linearized approach is described, and numerical results are presented for a large variety of flow configurations. The results demonstrate the effects of airfoil thickness, angle of attack, camber, and Mach number on the unsteady lift and moment of airfoils subjected to periodic vortical gusts. The results show that mean flow distortion can have a very strong effect on the airfoil unsteady response, and that the effect depends strongly upon the reduced frequency, Mach number, and gust wave numbers. Author

N90-18364* McDonnell Aircraft Co., Houston, TX. Engineering Technology Div.

RESEARCH ON A TWO-DIMENSIONAL INLET FOR A SUPERSONIC V/STOL PROPULSION SYSTEM. APPENDIX A Final Report, Sep. 1979 - Jun. 1984

J. L. MARK, M. A. MCGARRY, and P. V. REAGAN Jun. 1984 880 p
(Contract NAS3-22158)

(NASA-CR-174945; NAS 1.26:174945) Avail: NTIS HC A99/MF E06 CSCL 01/1

The inlet system performance requirements associated with supersonic V/STOL aircraft place extreme demands on the inlet designer. The present effort makes maximum use of flow improvement techniques, proven for high subsonic maneuvering flight and adapts them to the critical static and low speed/high angle-of-attack flight regime of the supersonic V/STOL aircraft. A description of the aerodynamic design, model characteristics, data analysis, discussion, and conclusions concerning the most

promising inlet design approaches are contained. The appendix contains the reduced wind tunnel data plots and pressure distribution. Author

N90-19203*# Toledo Univ., OH. Dept. of Chemical Engineering.

HEAT TRANSFER MEASUREMENTS FROM A NACA 0012 AIRFOIL IN FLIGHT AND IN THE NASA LEWIS ICING RESEARCH TUNNEL M.S. Thesis Final Report

PHILIP E. POINSATTE Washington NASA Mar. 1990 194 p

(Contract NAG3-72)

(NASA-CR-4278; E-5228; NAS 1.26:4278) Avail: NTIS HC

A09/MF A01 CSCL 01/1

Local heat transfer coefficients from a smooth and roughened NACA 0012 airfoil were measured using a steady state heat flux method. Heat transfer measurements on the specially constructed 0.533 meter chord airfoil were made both in flight on the NASA Lewis Twin Otter Research Aircraft and in the NASA Lewis Icing Research Tunnel (IRT). Roughness was obtained by the attachment of small, 2 mm diameter, hemispheres of uniform size to the airfoil surface in four distinct patterns. The flight data was taken for the smooth and roughened airfoil at various Reynolds numbers based on chord in the range of 1.24×10^6 to 2.50×10^6 and at various angles of attack up to 4 degrees. During these flight tests the free stream velocity turbulence intensity was found to be very low (less than 0.1 percent). The wind tunnel data was taken in the Reynolds number range of 1.20×10^6 to 4.52×10^6 and at angles of attack from -4 degrees to +8 degrees. The turbulence intensity in the IRT was 0.5 to 0.7 percent with the cloud making spray off. Results for both the flight and tunnel tests are presented as Frossling number based on chord versus position on the airfoil surface for various roughnesses and angle of attack. A table of power law curve fits of Nusselt number as a function of Reynolds number is also provided. The higher level of turbulence in the IRT versus flight had little effect on heat transfer for the lower Reynolds numbers but caused a moderate increase in heat transfer at the higher Reynolds numbers. Turning on the cloud making spray air in the IRT did not alter the heat transfer. Roughness generally increased the heat transfer by locally disturbing the boundary layer flow. Finally, the present data was not only compared with previous airfoil data where applicable, but also with leading edge cylinder and flat plate heat transfer values which are often used to estimate airfoil heat transfer in computer codes. Author

N90-20051*# National Aeronautics and Space Administration. Lewis Research Center, Cleveland, OH.

NUMERICAL SIMULATIONS OF SUPERSONIC FLOW THROUGH OSCILLATING CASCADE SECTIONS

DENNIS L. HUFF and T. S. R. REDDY (Toledo Univ., OH.) 1990 10 p Presented at the 15th Southeastern Conference on Theoretical and Applied Mechanics, Atlanta, GA, 22-23 Mar. 1990; sponsored by Georgia Inst. of Technology (NASA-TM-103100; E-5421; NAS 1.15:103100) Avail: NTIS HC A02/MF A01 CSCL 01/1

A finite difference code was developed for modeling inviscid, unsteady supersonic flow by solution of the compressible Euler equations. The code uses a deforming grid technique to capture the motion of the airfoils and can model oscillating cascades with any arbitrary interblade phase angle. A flat plate cascade is analyzed, and results are compared with results from a small perturbation theory. The results show very good agreement for both the unsteady pressure distributions and the integrated force predictions. The reason for using the numerical Euler code over a small perturbation theory is the ability to model real airfoils that have thickness and camber. Sample predictions are presented for a cascade of loaded airfoils and show appreciable differences in the unsteady surface pressure distributions when compared with the flat plate results. Author

N90-21727*# National Aeronautics and Space Administration. Lewis Research Center, Cleveland, OH.

SWEEP WING ICE ACCRETION MODELING

MARK G. POTAPCZUK and COLIN S. BIDWELL 1990 26 p Presented at the 28th Aerospace Sciences Meeting, Reno, NV, 8-11 Jan. 1990; sponsored by AIAA

(NASA-TM-103114; E-5238; NAS 1.15:103114; AIAA-90-0756)

Avail: NTIS HC A03/MF A01 CSCL 01/1

An effort to develop a three-dimensional modeling method was initiated. This first step towards creation of a complete aircraft icing simulation code builds on previously developed methods for calculating three-dimensional flow fields and particle trajectories combined with a two-dimensional ice accretion calculation along coordinate locations corresponding to streamlines. This work is a demonstration of the types of calculations necessary to predict a three-dimensional ice accretion. Results of calculations using the 3-D method for a MS-317 swept wing geometry are projected onto a 2-D plane normal to the wing leading edge and compared to 2-D results for the same geometry. It is anticipated that many modifications will be made to this approach, however, this effort will lay the groundwork for future modeling efforts. Results indicate that the flow field over the surface and the particle trajectories differed for the two calculations. This led to lower collection efficiencies, convective heat transfer coefficients, freezing fractions, and ultimately ice accumulation for the 3-D calculation. Author

N90-21733*# National Aeronautics and Space Administration. Lewis Research Center, Cleveland, OH.

CONTROL OF FLOW SEPARATION AND MIXING BY AERODYNAMIC EXCITATION

EDWARD J. RICE and JOHN M. ABBOTT 1990 13 p Proposed for presentation at the 17th Congress of the International Council of the Aeronautical Sciences, Stockholm, Sweden, 9-14 Sep. 1990; sponsored by AIAA

(NASA-TM-103131; E-5462; NAS 1.15:103131) Avail: NTIS HC A03/MF A01 CSCL 01/1

The recent research in the control of shear flows using unsteady aerodynamic excitation conducted at the NASA Lewis Research Center is reviewed. The program is of a fundamental nature, concentrating on the physics of the unsteady aerodynamic processes. This field of research is a fairly new development with great promise in the areas of enhanced mixing and flow separation control. Enhanced mixing research includes influence of core turbulence, forced pairing of coherent structures, and saturation of mixing enhancement. Separation flow control studies included are for a two-dimensional diffuser, conical diffusers, and single airfoils. Ultimate applications include aircraft engine inlet flow control at high angle of attack, wide angle diffusers, highly loaded airfoils as in turbomachinery, and ejector/suppressor nozzles for the supersonic transport. An argument involving the Coanda Effect is made that all of the above mentioned application areas really only involve forms of shear layer mixing enhancement. The program also includes the development of practical excitation devices which might be used in aircraft applications. Author

N90-25106*# National Aeronautics and Space Administration. Lewis Research Center, Cleveland, OH.

ANALYSIS AND DESIGN OF OPTIMIZED TRUNCATED SCARFED NOZZLES SUBJECT TO EXTERNAL FLOW EFFECTS

RICKEY J. SHYNE and THEO G. KEITH, JR. (Toledo Univ., OH.) 1990 12 p Presented at the 26th Joint Propulsion Conference, Orlando, FL, 16-18 Jul. 1990; cosponsored by AIAA, SAE, ASME, and ASEE

(NASA-TM-103175; E-5553; NAS 1.15:103175; AIAA-90-2222)

Avail: NTIS HC A03/MF A01 CSCL 01/1

Rao's method for computing optimum thrust nozzles is modified to study the effects of external flow on the performance of a class of exhaust nozzles. Members of this class are termed scarfed nozzles. These are two-dimensional, nonsymmetric nozzles with a flat lower wall. The lower wall (the cowl) is truncated in order to save weight. Results from a parametric investigation are presented

02 AERODYNAMICS

to show the effects of the external flowfield on performance.

Author

N90-25934*# Case Inst. of Tech., Cleveland, OH. Dept. of Mechanical and Aerospace Engineering.

INTERACTIVE CALCULATION PROCEDURES FOR MIXED COMPRESSION INLETS Final Technical Report

ELI RESHOTKO Mar. 1983 7 p

(Contract NAG3-140)

(NASA-CR-186581; NAS 1.26:186581) Avail: NTIS HC A02/MF A01 CSCL 01/1

The proper design of engine nacelle installations for supersonic aircraft depends on a sophisticated understanding of the interactions between the boundary layers and the bounding external flows. The successful operation of mixed external-internal compression inlets depends significantly on the ability to closely control the operation of the internal compression portion of the inlet. This portion of the inlet is one where compression is achieved by multiple reflection of oblique shock waves and weak compression waves in a converging internal flow passage. However weak these shocks and waves may seem gas-dynamically, they are of sufficient strength to separate a laminar boundary layer and generally even strong enough for separation or incipient separation of the turbulent boundary layers. An understanding was developed of the viscous-inviscid interactions and of the shock wave boundary layer interactions and reflections.

Author

N90-25940*# Purdue Univ., West Lafayette, IN.

AN UNSTEADY LIFTING SURFACE METHOD FOR SINGLE ROTATION PROPELLERS Final Report

MARC H. WILLIAMS Washington NASA Jul. 1990 62 p

(Contract NAG3-499)

(NASA-CR-4302; E-5428; NAS 1.26:4302) Avail: NTIS HC A04/MF A01 CSCL 01/1

The mathematical formulation of a lifting surface method for evaluating the steady and unsteady loads induced on single rotation propellers by blade vibration and inflow distortion is described. The scheme is based on 3-D linearized compressible aerodynamics and presumes that all disturbances are simple harmonic in time. This approximation leads to a direct linear integral relation between the normal velocity on the blade (which is determined from the blade geometry and motion) and the distribution of pressure difference across the blade. This linear relation is discretized by breaking the blade up into subareas (panels) on which the pressure difference is treated as approximately constant, and constraining the normal velocity at one (control) point on each panel. The piece-wise constant loads can then be determined by Gaussian elimination. The resulting blade loads can be used in performance, stability and forced response predictions for the rotor. Mathematical and numerical aspects of the method are examined. A selection of results obtained from the method is presented. The appendices include various details of the derivation that were felt to be secondary to the main development in Section 1.

Author

N90-25946*# National Aeronautics and Space Administration. Lewis Research Center, Cleveland, OH.

EULER ANALYSIS COMPARISON WITH LDV DATA FOR AN ADVANCED COUNTER-ROTATION PROPFAN AT CRUISE

CHRISTOPHER J. MILLER and GARY G. PODBOY Aug. 1990 23 p Presented at the 8th Applied Aerodynamics Conference, Portland, OR, 20-22 Aug. 1990; sponsored in part by AIAA

(NASA-TM-103249; E-5676; NAS 1.15:103249; AIAA-90-0438)

Avail: NTIS HC A03/MF A01 CSCL 01/1

A fine mesh Euler solution of the F4/A4 unducted fan (UDF) model flowfield is compared with laser Doppler velocimeter (LDV) data taken in the NASA Lewis 8- by 6-Foot Supersonic Wind Tunnel. The comparison is made primarily at one axial plane downstream of the front rotor where the LDV particle lag errors are reduced. The agreement between measured and predicted velocities in this axial plane is good. The results show that a dense mesh is needed in the centerbody stagnation region to minimize entropy generation that weakens the aft row passage shock. The predicted radial location of the tip vortex downstream

of the front rotor agrees well with the experimental results but the strength is overpredicted. With 40 points per chord line, the integrated performance quantities are nearly converged, but more points are needed to resolve passage shocks and flow field details.

Author

N90-25948*# National Aeronautics and Space Administration. Lewis Research Center, Cleveland, OH.

TWO-DIMENSIONAL EULER AND NAVIER-STOKES TIME ACCURATE SIMULATIONS OF FAN ROTOR FLOWS

A. A. BORETTI (Fiat Research Center, Orbassano, Turin, Italy) Jul. 1990 22 p

(Contract NASA ORDER C-99066-G)

(NASA-TM-102402; E-5155; NAS 1.15:102402; ICOMP-89-29)

Avail: NTIS HC A03/MF A01 CSCL 01/1

Two numerical methods are presented which describe the unsteady flow field in the blade-to-blade plane of an axial fan rotor. These methods solve the compressible, time-dependent, Euler and the compressible, turbulent, time-dependent, Navier-Stokes conservation equations for mass, momentum, and energy. The Navier-Stokes equations are written in Favre-averaged form and are closed with an approximate two-equation turbulence model with low Reynolds number and compressibility effects included. The unsteady aerodynamic component is obtained by superposing inflow or outflow unsteadiness to the steady conditions through time-dependent boundary conditions. The integration in space is performed by using a finite volume scheme, and the integration in time is performed by using k-stage Runge-Kutta schemes, $k = 2, 5$. The numerical integration algorithm allows the reduction of the computational cost of an unsteady simulation involving high frequency disturbances in both CPU time and memory requirements. Less than 200 sec of CPU time are required to advance the Euler equations in a computational grid made up of about 2000 grid during 10,000 time steps on a CRAY Y-MP computer, with a required memory of less than 0.3 megawords.

Author

N90-27655*# United Technologies Research Center, East Hartford, CT.

DEVELOPMENT OF A LINEARIZED UNSTEADY AERODYNAMIC ANALYSIS FOR CASCADE GUST RESPONSE PREDICTIONS Interim Report

JOSEPH M. VERDON and KENNETH C. HALL Washington Jul. 1990 65 p Original contains color illustrations

(Contract NAS3-25425)

(NASA-CR-4308; E-5533; NAS 1.26:4308; R90-957907-2) Avail: NTIS HC A04/MF A01; 12 functional color pages CSCL 01/1

A method for predicting the unsteady aerodynamic response of a cascade of airfoils to entropic, vortical, and acoustic gust excitations is being developed. Here, the unsteady flow is regarded as a small perturbation of a nonuniform isentropic and irrotational steady background flow. A splitting technique is used to decompose the linearized unsteady velocity into rotational and irrotational parts leading to equations for the complex amplitudes of the linearized unsteady entropy, rotational velocity, and velocity potential that are coupled only sequentially. The entropic and rotational velocity fluctuations are described by transport equations for which closed-form solutions in terms of the mean-flow drift and stream functions can be determined. The potential fluctuation is described by an inhomogeneous convected wave equation in which the source term depends on the rotational velocity field, and is determined using finite-difference procedures. The analytical and numerical techniques used to determine the linearized unsteady flow are outlined. Results are presented to indicate the status of the solution procedure and to demonstrate the impact of blade geometry and mean blade loading on the aerodynamic response of cascades to vortical gust excitations. The analysis described herein leads to very efficient predictions of cascade unsteady aerodynamic response phenomena making it useful for turbomachinery aeroelastic and aeroacoustic design applications.

Author

N90-27657*# National Aeronautics and Space Administration. Lewis Research Center, Cleveland, OH.

AERODYNAMICS OF A LINEAR OSCILLATING CASCADE

DANIEL H. BUFFUM and SANFORD FLEETER (Purdue Univ., West Lafayette, IN.) Aug. 1990 265 p
(NASA-TM-103250; E-5677; NAS 1.15:103250) Avail: NTIS HC A12/MF A02 CSCL 01/1

The steady and unsteady aerodynamics of a linear oscillating cascade are investigated using experimental and computational methods. Experiments are performed to quantify the torsion mode oscillating cascade aerodynamics of the NASA Lewis Transonic Oscillating Cascade for subsonic inlet flowfields using two methods: simultaneous oscillation of all the cascaded airfoils at various values of interblade phase angle, and the unsteady aerodynamic influence coefficient technique. Analysis of these data and correlation with classical linearized unsteady aerodynamic analysis predictions indicate that the wind tunnel walls enclosing the cascade have, in some cases, a detrimental effect on the cascade unsteady aerodynamics. An Euler code for oscillating cascade aerodynamics is modified to incorporate improved upstream and downstream boundary conditions and also the unsteady aerodynamic influence coefficient technique. The new boundary conditions are shown to improve the unsteady aerodynamic influence coefficient technique. The new boundary conditions are shown to improve the unsteady aerodynamic predictions of the code, and the computational unsteady aerodynamic influence coefficient technique is shown to be a viable alternative for calculation of oscillating cascade aerodynamics. Author

N90-28504*# Case Western Reserve Univ., Cleveland, OH. Dept. of Mechanical and Aerospace Engineering.

THE ENTRAINMENT RATE FOR A ROW OF TURBULENT JETS M.S. Thesis Final Report

ELIOTT B. GORDON and ISAAC GREBER Sep. 1990 135 p
(Contract NAG3-251)
(NASA-CR-185278; NAS 1.26:185278) Avail: NTIS HC A07/MF A01 CSCL 01/1

Entrainment rates for a row of isothermal circular air jets issuing into a quiescent environment are found by integrating velocity distributions measured by a linearized hot-wire anemometer. Jet spacing to jet diameter ratios of 2.5, 5, 10, and 20 are studied at jet Reynold's numbers ranging from 5110 to 12070. Velocity distributions are determined at regular downstream intervals at axial distances equal to 16.4 to 164 jet diameters from the jet source. The entrainment rates for the four spacing configurations vary monotonically with increasing spacing/diameter between the limiting case of the slot jet entrainment rate (where the jet spacing to diameter ratio is zero) and the circular jet entrainment rate (in which the spacing to diameter ratio is infinity). Author

03

AIR TRANSPORTATION AND SAFETY

Includes passenger and cargo air transport operations; and aircraft accidents.

A90-19735*# Akron Univ., OH.

IMPACT ICE STRESSES IN ROTATING AIRFOILS

R. J. SCAVUZZO, M. L. CHU, and C. J. KELLACKY (Akron, University, OH) AIAA, Aerospace Sciences Meeting, 28th, Reno, NV, Jan. 8-11, 1990. 9 p. refs
(Contract NAG3-479)
(AIAA PAPER 90-0198)

Finite element analysis is used to study the tensile and shear stresses at the interface between impact ice adhering to a rotating airfoil and the metal airfoil surface. A simple rotating beam-ice structure is used to obtain basic understanding of stress distribution in the ice. Calculations show that shear stresses increase linearly with ice thickness and tensile stresses tend to zero for a fully

bonded surface. When shear stresses exceed the ultimate strength, adhesive failure occurs and tensile stresses are developed in the unbonded ice, resulting in tensile failure of the impact ice. A second model is used to study the OH-58 tail rotor with a measured ice profile. Ice shedding predictions are compared to the resulting data using a statistical structural analysis. C.D.

A90-20009*# California State Univ., Long Beach.

FORTIFIED LEWICE WITH VISCOUS EFFECTS

TUNCER CEBECI, H. H. CHEN, and N. ALEMDAROGLU (California State University, Long Beach) AIAA, Aerospace Sciences Meeting, 28th, Reno, NV, Jan. 8-11, 1990. 13 p. refs
(Contract NAG3-935)

(AIAA PAPER 90-0754) Copyright

A method for computing the prediction of ice shapes on airfoils and their effects on the airfoil lift and drag coefficients are described. The previously developed LEWICE code has been modified to avoid problems due to multiple stagnation points. The interactive boundary-layer method developed by Cebeci has been incorporated into LEWICE to improve the accuracy of predicting ice shapes as well as to compute the performance characteristics of iced airfoils. The paper also presents ice shapes calculated without and with viscous effects, the consequences for aerodynamic properties, particularly lift and drag, and evaluation of the time steps used in the ice accretion process. Author

A90-26986*# Texas A&M Univ., College Station.

A STUDY OF ICE SHAPE PREDICTION METHODOLOGIES AND COMPARISON WITH EXPERIMENTAL DATA

K. D. KORKAN and R. K. BRITTON (Texas A & M University, College Station) AIAA, Aerospace Sciences Meeting, 28th, Reno, NV, Jan. 8-11, 1990. 20 p. refs
(Contract NCC3-626)

(AIAA PAPER 90-0753) Copyright

Current analytical ice shape prediction methods are described and evaluated. The analyses of Gray (1958), Wilder (1969), and Bragg (1982) are compared with the prediction of the LEWICE computer analysis. The effects of time stepping and initial surface roughness on analysis predictions are studied utilizing the prediction methods and flight data. Rime, mixed, and glazed ice shapes at the leading edge of an airfoil are analyzed. It is observed that there is no change in ice shape prediction if ice accumulation is less than 0.01, a minimum of 2 time steps is need to incorporate time dependent behavior into the analysis, and the LEWICE analysis provided the most accurate predictions. I.F.

A90-28179* National Aeronautics and Space Administration. Lewis Research Center, Cleveland, OH.

ICING RESEARCH TUNNEL TEST OF A MODEL HELICOPTER ROTOR

THOMAS L. MILLER and THOMAS H. BOND (NASA, Lewis Research Center, Cleveland, OH) IN: AHS, Annual Forum, 45th, Boston, MA, May 22-24, 1989, Proceedings. Alexandria, VA, American Helicopter Society, 1989, p. 367-378. refs
Copyright

An experimental program has been conducted in the NASA Lewis Research Center Icing Research Tunnel (IRT) in which an OH-58 tail rotor assembly was operated in a horizontal plane to simulate the action of a typical main rotor. Ice was accreted on the blades in a variety of rotor and tunnel operating conditions and documentation of the resulting shapes was performed. Rotor torque and vibration are presented as functions of time for several representative test runs, and the effects of various parametric variations on the blade ice shapes are shown. This OH-58 test was the first of its kind in the United States and will encourage additional model rotor icing tunnel testing. Although not a scaled representative of any actual full-scale main rotor system, this rig has produced torque and vibration data which will be useful in assessing the quality of existing rotor icing analyses. Author

03 AIR TRANSPORTATION AND SAFETY

A90-28180* Army Aviation Engineering Flight Activity, Edwards AFB, CA.

INITIAL RESULTS FROM THE JOINT NASA-LEWIS/U.S. ARMY ICING FLIGHT RESEARCH TESTS

DAUMANTS BELTE (U.S. Army, Aviation Engineering Flight Activity, Edwards AFB, CA) and RICHARD J. RANAUDO (NASA, Lewis Research Center, Cleveland, OH) IN: AHS, Annual Forum, 45th, Boston, MA, May 22-24, 1989, Proceedings. Alexandria, VA, American Helicopter Society, 1989, p. 379-392. refs
Copyright

The U.S. Army/NASA joint testing of the various aspects of in-flight and ground-based icing simulation facilities and instrumentation is reviewed. The NASA DN-6 icing research aircraft, the U.S. Army JU-21A aircraft, the portable spray rig, helicopter icing spray system, and icing research tunnel are examined. Natural and artificial icing tests, turbulence measurements, and calibration and icing research tunnel tests are described and test results are reported. C.D.

N90-15062*# National Aeronautics and Space Administration. Lewis Research Center, Cleveland, OH.

NASA'S PROGRAM ON ICING RESEARCH AND TECHNOLOGY

JOHN J. REINMANN, ROBERT J. SHAW, and RICHARD J. RANAUDO /in AGARD, Flight in Adverse Environmental Conditions 31 p Sep. 1989 Previously announced as N89-22569

Copyright Avail: NTIS HC A17/MF A03; Non-NATO Nationals requests available only from AGARD/Scientific Publications Executive CSCL 01/3

NASA's program in aircraft icing research and technology is reviewed. The program relies heavily on computer codes and modern applied physics technology in seeking icing solutions on a finer scale than those offered in earlier programs. Three major goals of this program are to offer new approaches to ice protection, to improve the ability to model the response of an aircraft to an icing encounter, and to provide improved techniques and facilities for ground and flight testing. The following program elements are reviewed: (1) new approaches to ice protection; (2) numerical codes for deicer analysis; (3) measurement and prediction of ice accretion and its effect on aircraft and aircraft components; (4) special wind tunnel test techniques for rotorcraft icing; (5) improvements of icing wind tunnels and research aircraft; (6) ground de-icing fluids used in winter operation; (7) fundamental studies in icing; and (8) droplet sizing instruments for icing clouds. Author

N90-17595*# National Aeronautics and Space Administration. Lewis Research Center, Cleveland, OH.

FIRE SAFETY APPLICATIONS FOR SPACECRAFT

ROBERT FRIEDMAN and SANDRA I. OLSON /in AGARD, Aircraft Fire Safety 15 p Oct. 1989 Previously announced as N89-24413

Copyright Avail: NTIS HC A18/MF A03; Non-NATO Nationals requests available only from AGARD/Scientific Publications Executive CSCL 01/3

Fire safety for spacecraft is reviewed by first describing current practices, many of which are adapted directly from aircraft. Then, current analyses and experimental knowledge in low-gravity combustion, with implications for fire safety are discussed. In orbiting spacecraft, the detection and suppression of flames are strongly affected by the large reduction in buoyant flows under low gravity. Generally, combustion intensity is reduced in low gravity. There are some notable exceptions, however, one example being the strong enhancement of flames by low-velocity ventilation flows in space. Finally, the future requirements in fire safety, particularly the needs of long-duration space stations in fire prevention, detection, extinguishment, and atmospheric control are examined. The goal of spacecraft fire-safety investigations is the establishment of trade-offs that promote maximum safety without hampering the useful human and scientific activities in space. Author

N90-20925*# National Aeronautics and Space Administration. Lewis Research Center, Cleveland, OH.

MODELING OF SURFACE ROUGHNESS EFFECTS ON GLAZE ICE ACCRETION

R. JOHN HANSMAN, JR., KEIKO YAMAGUCHI, BRIAN M. BERKOWITZ (Sverdrup Technology, Inc., Middleburg Heights, OH.), and MARK POTAPCZUK /in NASA, Langley Research Center, Joint University Program for Air Transportation Research, 1988-1989 p 35-42 Mar. 1990

(Contract NAG3-666; NGL-22-009-640; NSF 85-52702)

Avail: NTIS HC A10/MF A02 CSCL 01/3

A series of experimental investigations focused on studying the cause and effect of roughness on accreting glaze ice surfaces were conducted. Detailed microvideo observations were made of glaze ice accretions on 1 to 4 inch diameter cylinders in three icing wind tunnels (the Data Products of New England six inch test facility, the NASA Lewis Icing Research Tunnel, and the B. F. Goodrich Ice Protection Research Facility). Infrared thermal video recordings were made of accreting ice surfaces in the Goodrich facility. Distinct zones of surface water behavior were observed; a smooth wet zone in the stagnation region with a uniform water film; a rough zone where surface tension effects caused coalescence of surface water into stationary beads; a horn zone where roughness elements grow into horn shapes; a runback zone where surface water ran back as rivulets; and a dry zone where rime feathers formed. The location of the transition from the smooth to the rough zone was found to migrate with time towards the stagnation point. The behavior of the transition appeared to be controlled by boundary layer transition and bead formation mechanisms at the interface between the smooth and rough zones. Regions of wet ice growth and enhanced heat transfer were clearly visible in the infrared video recordings of glaze ice surfaces. A simple multi-zone modification to the current glaze ice accretion model was proposed to include spatial variability in surface roughness. Author

N90-20926*# Massachusetts Inst. of Tech., Cambridge. Dept. of Aeronautics and Astronautics.

ULTRASONIC TECHNIQUES FOR AIRCRAFT ICE ACCRETION MEASUREMENT

R. JOHN HANSMAN, JR., MARK S. KIRBY, and FRED LICHTENFELTS (Simmonds Precision Products, Inc., Vergennes, VT.) /in NASA, Langley Research Center, Joint University Program for Air Transportation Research, 1988-1989 p 43-53 Mar. 1990 Sponsored by NSF

(Contract NAG3-666; NGL-22-009-640)

Avail: NTIS HC A10/MF A02 CSCL 01/3

Results of tests to measure ice growth in natural (flight) and artificial (icing wind tunnel) icing conditions are presented. Ice thickness is measured using an ultrasonic pulse-echo technique. Two icing regimes, wet and dry ice growth, are identified and the unique ultrasonic signal characteristics associated with these different types of ice growth are described. Ultrasonic measurements of ice growth on cylinders and airfoils exposed to artificial and natural icing conditions are presented. An accuracy of plus or minus 0.5 mm is achieved for ice thickness measurement using the pulse-echo technique. The performance of two-probe type ice detectors is compared to the surface mounted ultrasonic system. The ultrasonically measured ice accretion rates and ice surface condition (wet or dry) are used to compare the heat transfer characteristics for flight and icing wind tunnel environments. In general the heat transfer coefficient is inferred to be higher in the wind tunnel environment, not likely due to higher freestream turbulence levels. Finally, preliminary results of tests to measure ice growth on airfoil using an array of ultrasonic transducers are described. Ice profiles obtained during flight in natural icing conditions are shown and compared with mechanical and stereo image measurements. Author

N90-20927*# Massachusetts Inst. of Tech., Cambridge.

INVESTIGATION OF SURFACE WATER BEHAVIOR DURING GLAZE ICE ACCRETION

R. JOHN HANSMAN, JR. and STEPHEN R. TURNOCK

05 AIRCRAFT DESIGN, TESTING AND PERFORMANCE

(Southampton Univ., England) In NASA, Langley Research Center, Joint University Program for Air Transportation Research, 1988-1989 p 55-62 Mar. 1990
(Contract NAG3-666; NGL-22-009-640; NSF 85-52702)
Avail: NTIS HC A10/MF A02 CSCL 01/3

A series of experimental investigations that focused on isolating the primary factors that control the behavior of unfrozen surface water during glaze ice accretion were conducted. Detailed microvideo observations were made of glaze ice accretions on 2.54 cm diam cylinders in a closed-loop refrigerated wind tunnel. Distinct zones of surface water behavior were observed; a smooth wet zone in the stagnation region with a uniform water film, a rough zone where surface tension effects caused coalescence of surface water into stationary beads, and a zone where surface water ran back as rivulets. The location of the transition from the smooth to the rough zone was found to migrate towards the stagnation point with time. Comparative tests were conducted to study the effect of the substrate thermal and roughness properties on ice accretion. The importance of surface water behavior was evaluated by the addition of a surface tension reducing agent to the icing tunnel water supply, which significantly altered the accreted glaze ice shape. Measurements were made to determine the contact angle behavior of water droplets on ice. A simple multizone modification to current glaze ice accretion models was proposed to include the observed surface roughness behavior.

Author

N90-20928* Massachusetts Inst. of Tech., Cambridge. Dept. of Aeronautics and Astronautics.

THE INFLUENCE OF ICE ACCRETION PHYSICS ON THE FORECASTING OF AIRCRAFT ICING CONDITIONS

R. JOHN HANSMAN, JR. In NASA, Langley Research Center, Joint University Program for Air Transportation Research, 1988-1989 p 63-67 Mar. 1990 Sponsored by NSF
(Contract NAG3-666; NGL-22-009-640)
Avail: NTIS HC A10/MF A02 CSCL 01/3

The physics which control aircraft ice accretion are reviewed in the context of identifying and forecasting hazardous icing conditions. The severity of aircraft icing is found to be extremely sensitive to temperature, liquid water content and droplet size distribution particularly near the transition between rime and mixed icing. The difficulty in measurement and the variability of these factors with altitude, position and time coupled with variable aircraft sensitivity make forecasting and identifying icing conditions difficult. Automated Pilot Reports (PIREPS) are suggested as one mechanism for improving the data base necessary to forecast icing conditions.

Author

05

AIRCRAFT DESIGN, TESTING AND PERFORMANCE

Includes aircraft simulation technology.

A90-20012* Electroimpact, Inc., Seattle, WA.
THIN FILM EDDY CURRENT IMPULSE DEICER
SAMUEL O. SMITH and PETER B. ZIEVE (Electroimpact, Inc., Seattle, WA) AIAA, Aerospace Sciences Meeting, 28th, Reno, NV, Jan. 8-11, 1990. 7 p. refs
(Contract NAS3-25836; NAS3-25555)
(AIAA PAPER 90-0761) Copyright

Two new styles of electrical impulse deicers has been developed and tested in NASA's Icing Research Tunnel. With the Eddy Current Repulsion Deicing Boot (EDB), a thin and flexible spiral coil is encapsulated between two thicknesses of elastomer. The coil, made by an industrial printed circuit board manufacturer, is bonded to the aluminum aircraft leading edge. A capacitor bank is discharged through the coil. Induced eddy currents repel the coil from the aluminum aircraft structure and shed accumulated ice. A

second configuration, the Eddy Current Repulsion Deicing-Strip (EDS) uses an outer metal erosion strip fastened over the coil. Opposite flowing eddy currents repel the strip and create the impulse deicing force. The outer strip serves as a surface for the collection and shedding of ice and does not require any structural properties. The EDS is suitable for composite aircraft structures. Both systems successfully dispelled over 95 percent of the accumulated ice from airfoils over the range of the FAA icing envelope.

Author

A90-23276* National Aeronautics and Space Administration. Lewis Research Center, Cleveland, OH.

HYPERSONIC AEROSPACE SIZING ANALYSIS FOR THE PRELIMINARY DESIGN OF AEROSPACE VEHICLES

GARY J. HARLOFF and BRIAN M. BERKOWITZ (NASA, Lewis Research Center; Sverdrup Technology, Inc., Cleveland, OH) Journal of Aircraft (ISSN 0021-8669), vol. 27, Feb. 1990, p. 97, 98. Previously announced in STAR as N89-15107. refs
(Contract NAS3-24105)

Copyright

A review of the hypersonic literature indicated that a general weight and sizing analysis was not available for hypersonic orbital, transport, and fighter vehicles. The objective here is to develop such a method for the preliminary design of aerospace vehicles. This report describes the developed methodology and provides examples to illustrate the model, entitled the Hypersonic Aerospace Sizing Analysis (HASA). It can be used to predict the size and weight of hypersonic single-stage and two-stage-to-orbit vehicles and transports, and is also relevant for supersonic transports. HASA is a sizing analysis that determines vehicle length and volume, consistent with body, fuel, structural, and payload weights. The vehicle component weights are obtained from statistical equations for the body, wing, tail, thermal protection system, landing gear, thrust structure, engine, fuel tank, hydraulic system, avionics, electrical system, equipment payload, and propellant. Sample size and weight predictions are given for the Space Shuttle orbiter and other proposed vehicles, including four hypersonic transports, a Mach 6 fighter, a supersonic transport (SST), a single-stage-to-orbit (SSTO) vehicle, a two-stage Space Shuttle with a booster and an orbiter, and two methane-fueled vehicles.

Author

A90-44736* Lockheed Aeronautical Systems Co., Burbank, CA.

INTERIOR NOISE IN THE UNTREATED GULFSTREAM II PROPFAN TEST ASSESSMENT AIRCRAFT

H. L. KUNTZ and R. A. PRYDZ (Lockheed Aeronautical Systems Co., Burbank, CA) Journal of Aircraft (ISSN 0021-8669), vol. 27, July 1990, p. 647-652. Previously cited in issue 13, p. 1943, Accession no. A89-33754. refs
(Contract NAS3-24339)
Copyright

A90-49114* General Dynamics/Fort Worth, TX.
THE IMPLEMENTATION OF STOVL TASK-TAILORED CONTROL MODES IN A FIGHTER COCKPIT

DAVID W. WHATLEY, JOHN C. VIRNIG, and DAVID S. BODDEN (General Dynamics Corp., Fort Worth, TX) AIAA, AHS, and ASEE, Aircraft Design, Systems and Operations Conference, Dayton, OH, Sept. 17-19, 1990. 9 p. refs
(Contract NAS3-25193)
(AIAA PAPER 90-3229) Copyright

The implementation of Short Takeoff/Vertical Landing (STOVL) specific task tailored control modes in a supersonic fighter/attack aircraft cockpit is investigated. A detailed linear model exhibiting STOVL Level 1 handling qualities is implemented in a real time engineering workstation environment with an F-16 cockpit mock-up. Conventional F-16 control inceptors are utilized to achieve effective STOVL operation and reduced pilot workload throughout the transition to hover flight region. Favorable pilot comments indicate the existing F-16 cockpit configuration with a force sidestick is adaptable to STOVL operation.

Author

05 AIRCRAFT DESIGN, TESTING AND PERFORMANCE

N90-10031*# Wichita State Univ., KS. Dept. of Aeronautical Engineering.

ELECTRO-IMPULSE DE-ICING TESTING ANALYSIS AND DESIGN Final Report

G. W. ZUMWALT, R. L. SCHRAG, W. D. BERNHART, and R. A. FRIEDBERG Sep. 1988 352 p

(Contract NAG3-284)

(NASA-CR-4175; E-4279; NAS 1.26:4175) Avail: NTIS HC A16/MF A02 CSCL 01C

Electro-Impulse De-Icing (EIDI) is a method of ice removal by sharp blows delivered by a transient electromagnetic field. Detailed results are given for studies of the electrodynamic phenomena. Structural dynamic tests and computations are described. Also reported are ten sets of tests at NASA's Icing Research Tunnel and flight tests by NASA and Cessna Aircraft Company. Fabrication of system components are described and illustrated. Fatigue and electromagnetic interference tests are reported. Here, the necessary information for the design of an EIDI system for aircraft is provided. Author

N90-20991*# Sverdrup Technology, Inc., Eglin AFB, FL.

AERODYNAMIC OPTIMIZATION BY SIMULTANEOUSLY UPDATING FLOW VARIABLES AND DESIGN PARAMETERS

M. H. RIZK /in AGARD, Computational Methods for Aerodynamic Design (Inverse) and Optimization 18 p Mar. 1990

(Contract NAS3-24855; NAS2-12157)

Copyright Avail: NTIS HC A15/MF A02; Non-NATO Nationals requests available only from AGARD/Scientific Publications Executive CSCL 01/3

The application of conventional optimization schemes to aerodynamic design problems leads to inner-outer iterative procedures that are very costly. An alternative approach is presented based on the idea of updating the flow variable iterative solutions and the design parameter iterative solutions simultaneously. Two schemes based on this idea are applied to problems of correcting wind tunnel wall interference and optimizing advanced propeller designs. The first of these schemes is applicable to a limited class of two-design-parameter problems with an equality constraint. It requires the computation of a single flow solution. The second scheme is suitable for application to general aerodynamic problems. It requires the computation of several flow solutions in parallel. In both schemes, the design parameters are updated as the iterative flow solutions evolve. Computations are performed to test the schemes' efficiency, accuracy, and sensitivity to variations in the computational parameters. Author

N90-23393*# General Electric Co., Cincinnati, OH. Advanced Technology Operations.

EXPERIMENTAL PERFORMANCE AND ACOUSTIC INVESTIGATION OF MODERN, COUNTERROTATING BLADE CONCEPTS Final Report

G. E. HOFF Jan. 1990 659 p

(Contract NAS3-24080)

(NASA-CR-185158; NAS 1.26:185158) Avail: NTIS HC A99/MF A04 CSCL 01/3

The aerodynamic, acoustic, and aeromechanical performance of counterrotating blade concepts were evaluated both theoretically and experimentally. Analytical methods development and design are addressed. Utilizing the analytical methods which evolved during the conduct of this work, aerodynamic and aeroacoustic predictions were developed, which were compared to NASA and GE wind tunnel test results. The detailed mechanical design and fabrication of five different composite shell/titanium spar counterrotating blade set configurations are presented. Design philosophy, analyses methods, and material geometry are addressed, as well as the influence of aerodynamics, aeromechanics, and aeroacoustics on the design procedures. Blade fabrication and quality control procedures are detailed; bench testing procedures and results of blade integrity verification are presented; and instrumentation associated with the bench testing also is identified. Additional hardware to support specialized testing is described, as are operating blade instrumentation and the associated stress limits.

The five counterrotating blade concepts were scaled to a tip diameter of 2 feet, so they could be incorporated into MPS (model propulsion simulators). Aerodynamic and aeroacoustic performance testing was conducted in the NASA Lewis 8 x 6 supersonic and 9 x 15 V/STOL (vertical or short takeoff and landing) wind tunnels and in the GE freejet anechoic test chamber (Cell 41) to generate an experimental data base for these counterrotating blade designs. Test facility and MPS vehicle matrices are provided, and test procedures are presented. Effects on performance of rotor-to-rotor spacing, angle-of-attack, pylon proximity, blade number, reduced-diameter aft blades, and mismatched rotor speeds are addressed. Counterrotating blade and specialized aeromechanical hub stability test results are also furnished. Author

06

AIRCRAFT INSTRUMENTATION

Includes cockpit and cabin display devices; and flight instruments.

N90-13381*# National Aeronautics and Space Administration. Lewis Research Center, Cleveland, OH.

SILICON-ETALON FIBER-OPTIC TEMPERATURE SENSOR

GLENN BEHEIM, KLAUS FRITSCH, JOSEPH M. FLATICO, and MASSOOD TABIB AZAR (Case Western Reserve Univ., Cleveland, OH.) 1989 8 p Presented at the Fiber Optic and Laser Sensors 7 Conference of the OE/Fibers '89 Symposium, Boston, MA, 5-8 Sep. 1989; sponsored by Society of Photo-Optical Instrumentation Engineers

(NASA-TM-102389; E-5130; NAS 1.15:102389) Avail: NTIS HC A02/MF A01 CSCL 01/4

A temperature sensor is described which consists of a silicon etalon that is sputtered directly onto the end of an optical fiber. A two-layer protective cap structure is used to improve the sensor's long-term stability. The sensor's output is wavelength encoded to provide a high degree of immunity from cable and connector effects. This sensor is extremely compact and potentially inexpensive. Author

N90-21006*# Aerometrics, Inc., Sunnyvale, CA.

ADVANCED INSTRUMENTATION FOR AIRCRAFT ICING RESEARCH Final Report

W. BACHALO, J. SMITH, and R. RUDOFF Apr. 1990 103 p (Contract NAS3-25317)

(NASA-CR-185225; NAS 1.26:185225) Avail: NTIS HC A06/MF A01 CSCL 01/4

A compact and rugged probe based on the phase Doppler method was evaluated as a means for characterizing icing clouds using airborne platforms and for advancing aircraft icing research in large scale wind tunnels. The Phase Doppler Particle Analyzer (PDPA) upon which the new probe was based is now widely recognized as an accurate method for the complete characterization of sprays. The prototype fiber optic-based probe was evaluated in simulated aircraft icing clouds and found to have the qualities essential to providing information that will advance aircraft icing research. Measurement comparisons of the size and velocity distributions made with the standard PDPA and the fiber optic probe were in excellent agreement as were the measurements of number density and liquid water content. Preliminary testing in the NASA Lewis Icing Research Tunnel (IRT) produced reasonable results but revealed some problems with vibration and signal quality at high speeds. The cause of these problems were identified and design changes were proposed to eliminate the shortcomings of the probe. Author

AIRCRAFT PROPULSION AND POWER

Includes prime propulsion systems and systems components, e.g., gas turbine engines and compressors; and onboard auxiliary power plants for aircraft.

A90-12502* # National Aeronautics and Space Administration. Lewis Research Center, Cleveland, OH.

ADVANCES IN COMPUTATIONAL DESIGN AND ANALYSIS OF AIRBREATHING PROPULSION SYSTEMS

JOHN M. KLINEBERG (NASA, Lewis Research Center, Cleveland, OH) IN: International Symposium on Air Breathing Engines, 9th, Athens, Greece, Sept. 3-8, 1989, Proceedings. Volume 1. Washington, DC, American Institute of Aeronautics and Astronautics, 1989, p. 3-17. Previously announced in STAR as N89-23465. refs

Copyright

The development of commercial and military aircraft depends, to a large extent, on engine manufacturers being able to achieve significant increases in propulsion capability through improved component aerodynamics, materials, and structures. The recent history of propulsion has been marked by efforts to develop computational techniques that can speed up the propulsion design process and produce superior designs. The availability of powerful supercomputers, such as the NASA Numerical Aerodynamic Simulator, and the potential for even higher performance offered by parallel computer architectures, have opened the door to the use of multi-dimensional simulations to study complex physical phenomena in propulsion systems that have previously defied analysis or experimental observation. An overview of several NASA Lewis research efforts is provided that are contributing toward the long-range goal of a numerical test-cell for the integrated, multidisciplinary design, analysis, and optimization of propulsion systems. Specific examples in Internal Computational Fluid Mechanics, Computational Structural Mechanics, Computational Materials Science, and High Performance Computing are cited and described in terms of current capabilities, technical challenges, and future research directions. Author

A90-12585* # George Washington Univ., Washington, DC.

ROTATING PRIMARY FLOW INDUCTION USING JET-FLAPPED BLADES

STEPHANE J. CORDIER (George Washington University, Washington, DC) IN: International Symposium on Air Breathing Engines, 9th, Athens, Greece, Sept. 3-8, 1989, Proceedings. Volume 2. Washington, DC, American Institute of Aeronautics and Astronautics, 1989, p. 807-814. refs

(Contract DOT-MA91-85-C-50114; NAG3-860)

Copyright

A new concept in ejector design is examined using primary jets exiting from a free spinning bladed rotor. This concept stems from a continuing effort in the development of Rotary-Jet thrust augmentors at George Washington University (GWU). An analysis of a Rotary-Jet rotor with jet-flapped blades is presented, identifying design trends beneficial to its performance. An experimental investigation was conducted to demonstrate the potential of this new concept. Several combinations of blade and shroud geometries were designed, fabricated and tested. The results are presented and discussed. Despite crudeness of fabrication, the maximum thrust augmentations obtained ranged from 1.55 to 2.14. These results demonstrate that this device is superior to all ejector designs tested with similar conventional passive diffusing shrouds. Author

A90-17462* Purdue Univ., West Lafayette, IN.

AEROELASTIC DETUNING FOR STABILITY ENHANCEMENT OF UNSTALLED SUPERSONIC FLUTTER

SANFORD FLEETER (Purdue University, West Lafayette, IN) and DANIEL HOYNIK (NASA, Lewis Research Center, Cleveland,

OH) International Journal of Turbo and Jet-Engines (ISSN 0334-0082), vol. 6, no. 1, 1989, p. 17-26. refs

Copyright

A mathematical model is presented for analyzing the effect of aeroelastic detuning on unstalled supersonic flutter, where the detuning mechanism employed is alternate-blade structural detuning. Two alternative aerodynamic detuning methods are compared: the novel, alternate-chordwise airfoil spacing method, and the alternate circumferential airfoil spacing aerodynamic detuning. A combination of aerodynamic and structural detuning is considered. Relative flutter stability enhancements are assessed for a twelve-blade baseline rotor. O.C.

A90-21225* # National Aeronautics and Space Administration. Lewis Research Center, Cleveland, OH.

PARAMETRIC STUDIES OF ADVANCED TURBOPROPS

D. G. FERTIS (Akron, University, OH), R. A. AIELLO, C. C. CHAMIS (NASA, Lewis Research Center, Cleveland, OH), and J. G. MASER (Structures, Structural Dynamics and Materials Conference, 29th, Williamsburg, VA, Apr. 18-20, 1988, Technical Papers. Part 1, p. 431-440) Journal of Propulsion and Power (ISSN 0748-4658), vol. 6, Jan.-Feb. 1990, p. 58-62. Previously cited in issue 12, p. 1831, Accession no. A88-32223. refs

Copyright

A90-23890* # National Aeronautics and Space Administration. Lewis Research Center, Cleveland, OH.

ADVANCED CORE TECHNOLOGY - KEY TO SUBSONIC PROPULSION BENEFITS

ARTHUR J. GLASSMAN, CHRISTOPHER A. SNYDER, and GERALD KNIP, JR. (NASA, Lewis Research Center, Cleveland, OH) ASME, Gas Turbine and Aeroengine Congress and Exposition, Toronto, Canada, June 4-8, 1989. 8 p. Previously announced in STAR as N89-14237. (ASME PAPER 89-GT-241)

A study was conducted to identify the potential performance benefits and key technology drivers associated with advanced cores for subsonic high bypass turbofan engines. Investigated first were the individual sensitivities of varying compressor efficiency, pressure ratio and bleed (turbine cooling); combustor pressure recovery; and turbine efficiency and inlet temperature on thermal efficiency and core specific power output. Then, engine cycle and mission performance benefits were determined for systems incorporating all potentially achievable technology advancements. The individual thermodynamic sensitivities are shown over a range of turbine temperatures (at cruise) from 2900 to 3500 R and for both constant (current technology) and optimum (maximum thermal efficiency) overall pressure ratios. It is seen that no single parameter alone will provide a large increase in core thermal efficiency, which is the thermodynamic parameter of most concern for transport propulsion. However, when all potentially achievable advancements are considered, there occurs a synergism that produces significant cycle and mission performance benefits. The nature of these benefits are presented along with the technology challenges. Author

A90-23896* # Jordan Univ. of Science and Technology, Irbid.

BLADE MISTUNING COUPLED WITH SHAFT FLEXIBILITY EFFECTS IN ROTOR AEROELASTICITY

NAIM KHADER (Jordan University of Science and Technology, Irbid) and ROBERT G. LOEWY (Rensselaer Polytechnic Institute, Troy, NY) ASME, Gas Turbine and Aeroengine Congress and Exposition, Toronto, Canada, June 4-8, 1989. 8 p. refs

(Contract NAG3-37)

(ASME PAPER 89-GT-330)

The effect of bladed-disk polar dissymmetry, resulting from variations in mass from one blade to another, on aeroelastic stability boundaries for a fan stage is presented. In addition to both in-plane and out-of-plane deformations of the bladed-disk, bending of the supporting shaft in two planes is considered, and the resulting Coriolis forces and gyroscopic moments are included in the analysis. A quasi-steady aerodynamics approach is combined with

07 AIRCRAFT PROPULSION AND POWER

the Lagrangian method to develop the governing equations of motion for the flexible bladed-disk-shaft assembly. Calculations are performed for an actual fan stage. Author

A90-25036*# National Aeronautics and Space Administration. Lewis Research Center, Cleveland, OH.

LOW NO(X) POTENTIAL OF GAS TURBINE ENGINES

ROBERT R. TACINA (NASA, Lewis Research Center, Cleveland, OH) AIAA, Aerospace Sciences Meeting, 28th, Reno, NV, Jan. 8-11, 1990. 19 p. refs

(AIAA PAPER 90-0550) Copyright

Nitrogen oxide levels of low gas turbine engine emissions are correlated in this paper. The predictions of NO(x) emissions are based on a review of the literature of previous low NO(x) combustor programs and analytical chemical kinetic calculations. Concepts included in the literature review consisted of Lean-Premixed-Prevaporized (LPP), Rich Burn/Quick Quench/Lean/Burn (RQL), and Direct Injection. The NO(x) emissions were found to be an exponential function of adiabatic combustion temperature over a wide range of inlet temperatures, pressures and (lean) fuel-air ratios. It is stated that the low NO(x) potential of LPP is offset by the operational disadvantages of its narrow stability limits and its susceptibility to autoignition/ flashback. The RQL and the Direct Injection concepts have the advantage of wider stability limits comparable to conventional combustors. Results were obtained primarily with gaseous fuels and it is noted that the challenge will be to produce the same low levels of NO(x) with liquid fuels. R.E.P.

A90-28571* National Aeronautics and Space Administration. Lewis Research Center, Cleveland, OH.

ADVANCED TECHNOLOGY'S IMPACT ON COMPRESSOR DESIGN AND DEVELOPMENT - A PERSPECTIVE

CALVIN L. BALL (NASA, Lewis Research Center, Cleveland, OH) Cliff Garrett Turbomachinery Award Lectures, 6th, Anaheim, CA, Sept. 25, 1989. 18 p. Previously announced in STAR as N90-10891. refs

(SAE SP-800; SAE PAPER 892213) Copyright

A historical perspective of the impact of advanced technologies on compression system design and development for aircraft gas turbine applications is presented. A bright view of the future is projected in which further advancements in compression system technologies will be made. These advancements will have a significant impact on the ability to meet the ever-more-demanding requirements being imposed on the propulsion system for advanced aircraft. Examples are presented of advanced compression system concepts now being studied. The status and potential impact of transitioning from an empirically derived design system to a computationally oriented system are highlighted. A current NASA Lewis Research Center program to enhance this transitioning is described. Author

A90-32960*# General Motors Corp., Indianapolis, IN.

DESIGN OF AN AIR-COOLED METALLIC HIGH-TEMPERATURE RADIAL TURBINE

PHILIP H. SNYDER (General Motors Corp., Indianapolis, IN) and RICHARD J. ROELKE (NASA, Lewis Research Center, Cleveland, OH) Journal of Propulsion and Power (ISSN 0748-4658), vol. 6, May-June 1990, p. 283-288. Previously cited in issue 18, p. 3006. Accession no. A88-45011. refs

(Contract NAS3-24230; DDAJ02-77-C-0031)

Copyright

A90-37562*# National Aeronautics and Space Administration. Lewis Research Center, Cleveland, OH.

PERFORMANCE CHARACTERISTICS OF A ONE-THIRD-SCALE, VECTORABLE VENTRAL NOZZLE FOR SSTOVL AIRCRAFT

BARBARA S. ESKER and JACK G. MCARDLE (NASA, Lewis Research Center, Cleveland, OH) AIAA, SAE, ASME, and ASEE, Joint Propulsion Conference, 26th, Orlando, FL, July 16-18, 1990. 11 p. Previously announced in STAR as N90-21725.

(AIAA PAPER 90-2271) Copyright

Several proposed configurations for supersonic short takeoff, vertical landing aircraft will require one or more ventral nozzles for lift and pitch control. The swivel nozzle is one possible ventral nozzle configuration. A swivel nozzle (approximately one-third scale) was built and tested on a generic model tailpipe. This nozzle was capable of vectoring the flow up to + or - 23 deg from the vertical position. Steady-state performance data were obtained at pressure ratios to 4.5, and pitot-pressure surveys of the nozzle exit plane were made. Two configurations were tested: the swivel nozzle with a square contour of the leading edge of the ventral duct inlet, and the same nozzle with a round leading edge contour. The swivel nozzle showed good performance overall, and the round-leading-edge configuration showed an improvement in performance over the square-leading-edge configuration. Author

A90-40562*# National Aeronautics and Space Administration. Lewis Research Center, Cleveland, OH.

ON THE USE OF EXTERNAL BURNING TO REDUCE AEROSPACE VEHICLE TRANSONIC DRAG

CHARLES J. TREFNY (NASA, Lewis Research Center, Cleveland, OH) AIAA, SAE, ASME, and ASEE, Joint Propulsion Conference, 26th, Orlando, FL, July 16-18, 1990. 15 p. Previously announced in STAR as N90-21762. refs

(AIAA PAPER 90-1935) Copyright

The external combustion of hydrogen to reduce the transonic drag of aerospace vehicles is currently being investigated. A preliminary analysis based on a constant pressure control volume is discussed. Results indicate that the specific impulse of the external burning process rivals that of a turbojet and depends on the severity of the initial base drag as well as on the Mach flight number and the equivalence ratio. A test program was conducted to investigate hydrogen-air flame stability at the conditions of interest and to demonstrate drag reduction on a simple expansion ramp. Initial test results are presented and compared with the control-volume analysis. The expansion ramp surface pressure coefficient showed little variation with fuel pressure and altitude, in disagreement with the analysis. Flame stability results were encouraging and indicate that stable combustion is possible over an adequate range of conditions. Facility interference and chemical kinetics phenomena that make interpretation of subscale ground test data difficult are discussed. Author

A90-40643*# General Electric Co., Lynn, MA.

CONVERTIBLE ENGINE SYSTEM FOR HIGH SPEED ROTORCRAFT

R. HIRSCHKRON and P. R. HULL (GE Aircraft Engines, Lynn, MA) AIAA, SAE, ASME, and ASEE, Joint Propulsion Conference, 26th, Orlando, FL, July 16-18, 1990. 9 p. refs

(Contract NAS3-25460)

(AIAA PAPER 90-2512) Copyright

The identification of engine technology needed for high speed rotorcraft and to also provide suitable propulsion data for the High Speed Rotor Craft is presented. The several objectives are: (1) to generate technology planning data for NASA, (2) to help understand the propulsion requirements of new aircraft types being considered, and (3) to have a source of consistent engine data for the airframe companies doing the studies. This study is primarily directed at Folding Tilt Rotor types with some consideration given to the X-Wing type. R.E.P.

A90-42168*# National Aeronautics and Space Administration. Lewis Research Center, Cleveland, OH.

A MODELING TECHNIQUE FOR STOVL EJECTOR AND VOLUME DYNAMICS

C. K. DRUMMOND and W. S. BARANKIEWICZ (NASA, Lewis Research Center, Cleveland, OH) AIAA, SAE, ASME, and ASEE, Joint Propulsion Conference, 26th, Orlando, FL, July 16-18, 1990. 13 p. Previously announced in STAR as N90-22566. refs

(AIAA PAPER 90-2417) Copyright

New models for thrust augmenting ejector performance prediction and feeder duct dynamic analysis are presented and applied to a proposed Short Take Off and Vertical Landing (STOVL) aircraft configuration. Central to the analysis is the nontraditional

treatment of the time-dependent volume integrals in the otherwise conventional control-volume approach. In the case of the thrust augmenting ejector, the analysis required a new relationship for transfer of kinetic energy from the primary flow to the secondary flow. Extraction of the required empirical corrections from current steady-state experimental data is discussed; a possible approach for modeling insight through Computational Fluid Dynamics (CFD) is presented. Author

A90-42688*# Sverdrup Technology, Inc., Brook Park, OH.
ANALYSIS OF INTERNAL FLOW IN A VENTRAL NOZZLE FOR STOVL AIRCRAFT

C. FREDERIC SMITH (Sverdrup Technology, Inc., Brook Park, OH) and JACK G. MCARDLE (NASA, Lewis Research Center, Cleveland, OH) AIAA, SAE, ASME, and ASEE, Joint Propulsion Conference, 26th, Orlando, FL, July 16-18, 1990. 20 p. Previously announced in STAR as N90-23404. refs
 (Contract NAS3-25266)
 (AIAA PAPER 90-1899) Copyright

Short takeoff and vertical landing (STOVL) aircraft are planned for possible future development. For these aircraft, the same propulsion system will provide power for lift, hover, and horizontal flight. To accomplish this, many designs include a ventral nozzle to provide part of the vertical thrust required. Understanding and predicting the internal aerodynamic flow caused by a single exhaust duct opening are highly desirable in assessing this concept. A numerical simulation of a ventral nozzle is presented and the results are compared with experimental data. Comparisons include visualizations of the flow along the ventral duct walls and in the tailpipe plane of symmetry. Performance calculations are also compared with measured values. Author

A90-42690*# National Aeronautics and Space Administration.
 Lewis Research Center, Cleveland, OH.

COMPUTATIONAL ANALYSIS OF THE FLOWFIELD OF A TWO-DIMENSIONAL EJECTOR NOZZLE

Y. H. CHOI and W. Y. SOH (NASA, Lewis Research Center, Cleveland, OH; Sverdrup Technology, Inc., Brook Park, OH) AIAA, SAE, ASME, and ASEE, Joint Propulsion Conference, 26th, Orlando, FL, July 16-18, 1990. 16 p. Previously announced in STAR as N90-23406. refs
 (Contract NAS3-25266)
 (AIAA PAPER 90-1901) Copyright

A time-iterative full Navier-Stokes code, PARC, is used to analyze the flowfield of a two-dimensional ejector nozzle system. A parametric study was performed for two controlling parameters, duct to nozzle area ratio and nozzle pressure ratio. Results show that there is an optimum area ratio for the efficient pumping of secondary flow. At high area ratios, a freestream flow passes directly through the mixing duct without giving adequate pumping. At low area ratios, the jet boundary blocks the incoming flow. The nozzle pressure ratio variation shows that the pumping rate increases as the pressure ratio increases, provided there is no interaction between the shroud wall and the shock cell structure. Author

A90-42766*# Illinois Univ., Urbana.
HOT GAS ENVIRONMENT AROUND STOVL AIRCRAFT IN GROUND PROXIMITY. II - NUMERICAL STUDY

D. K. TAFTI and S. P. VANKA (Illinois, University, Urbana) AIAA, SAE, ASME, and ASEE, Joint Propulsion Conference, 26th, Orlando, FL, July 16-18, 1990. 21 p. refs
 (Contract NAG3-1026)
 (AIAA PAPER 90-2270) Copyright

Ingestion of hot exhaust gases by the engines of STOVL aircraft has been an important research problem for several years. The hot gas environment around STOVL aircraft is three-dimensional and turbulent. In this study, the Navier-Stokes equations governing the hot gas ingestion flowfield are solved by an efficient finite-difference calculation procedure. The complete geometry including the head wind and the fuselage is simulated. Four demonstration calculations with variations in the height of the fuselage and the head wind velocity are presented. It is shown

that the calculation procedure efficiently provides a solution to the governing equations and produces realistic descriptions of the flow and temperature fields. Author

A90-42808*# SOL-3 Resources, Inc., Reading, MA.
INTRODUCING THE VRT GAS TURBINE COMBUSTOR

JERRY O. MELCONIAN (SOL-3 Resources, Inc., Reading, MA), ABDU A. MOSTAFA (Textron Lycoming, Stratford, CT), and HUNG LEE NGUYEN (NASA, Lewis Research Center, Cleveland, OH) AIAA, SAE, ASME, and ASEE, Joint Propulsion Conference, 26th, Orlando, FL, July 16-18, 1990. 13 p. Previously announced in STAR as N90-23591. refs
 (AIAA PAPER 90-2452) Copyright

An innovative annular combustor configuration is being developed for aircraft and other gas turbine engines. This design has the potential of permitting higher turbine inlet temperatures by reducing the pattern factor and providing a major reduction in NO(x) emission. The design concept is based on a Variable Residence Time (VRT) technique which allows large fuel particles adequate time to completely burn in the circumferentially mixed primary zone. High durability of the combustor is achieved by dual function use of the incoming air. The feasibility of the concept was demonstrated by water analogue tests and 3-D computer modeling. The computer model predicted a 50 percent reduction in pattern factor when compared to a state of the art conventional combustor. The VRT combustor uses only half the number of fuel nozzles of the conventional configuration. The results of the chemical kinetics model require further investigation, as the NO(x) predictions did not correlate with the available experimental and analytical data base. Author

A90-43218* Jordan Univ. of Science and Technology, Irbid.
SHAFT FLEXIBILITY EFFECTS ON THE FORCED RESPONSE OF A BLADED-DISK ASSEMBLY

N. KHADER (Jordan University of Science and Technology, Irbid) and R. G. LOEWY (Rensselaer Polytechnic Institute, Troy, NY) Journal of Sound and Vibration (ISSN 0022-460X), vol. 139, June 22, 1990, p. 469-485. Research supported by the Jordan University of Science and Technology. refs
 (Contract NAG3-37)
 Copyright

A model analysis approach is used to study the forced response of an actual flexible bladed-disk-shaft system. Both in-plane and out-of-plane flexible deformations of the bladed-disk assembly are considered, in addition to its rigid-body translations and rotations, resulting from the bending of the supporting flexible shaft in two orthogonal planes. The effects of Coriolis forces and structural coupling between flexible and rigid disk motions on the system's response are investigated. Aerodynamic loads acting on the rotating and vibrating bladed-disk assembly are accounted for through a simple quasi-steady representation, to evaluate their influence, combined with shaft flexibility and Coriolis effects. Author

A90-44726*# National Aeronautics and Space Administration.
 Lewis Research Center, Cleveland, OH.

THREE-DIMENSIONAL TURBULENT FLOW CODE CALCULATIONS OF HOT GAS INGESTION

THOMAS J. VANOVERBEKE and JAMES D. HOLDEMAN (NASA, Lewis Research Center, Cleveland, OH) Journal of Aircraft (ISSN 0021-8669), vol. 27, July 1990, p. 577-582. Previously cited in issue 20, p. 3350, Accession no. A88-48752. refs
 Copyright

A90-45414* National Aeronautics and Space Administration.
 Lewis Research Center, Cleveland, OH.

A REAL TIME MICROCOMPUTER IMPLEMENTATION OF SENSOR FAILURE DETECTION FOR TURBOFAN ENGINES

JOHN C. DELAAT and WALTER C. MERRILL (NASA, Lewis Research Center, Cleveland, OH) IEEE Control Systems Magazine (ISSN 0272-1708), vol. 10, June 1990, p. 29-37. Previously announced in STAR as N89-29032. refs
 Copyright

An algorithm was developed that detects, isolates, and

07 AIRCRAFT PROPULSION AND POWER

accommodates sensor failures using analytical redundancy. The performance of this algorithm has been demonstrated on a full-scale F100 turbofan engine. The algorithm was implemented in real-time on a microprocessor-based controls computer which includes parallel processing and high order language programming. Parallel processing was used to achieve the required computational power for the real-time implementation. High order language programming was used in order to reduce the programming and maintenance costs of the algorithm implementation software. The sensor failure algorithm was combined with an existing multivariable control algorithm to give a complete control implementation with sensor analytical redundancy. The real-time microprocessor implementation of the algorithm, which resulted in the successful completion of the algorithm engine demonstration, is described.

Author

A90-46933* National Aeronautics and Space Administration. Lewis Research Center, Cleveland, OH.

THE SELECTION OF CONVERTIBLE ENGINES WITH CURRENT GAS GENERATOR TECHNOLOGY FOR HIGH SPEED ROTORCRAFT

JOSEPH D. EISENBERG (NASA, Lewis Research Center, Cleveland, OH) IN: Vertical Lift Aircraft Design Conference, San Francisco, CA, Jan. 17-19, 1990, Proceedings. Alexandria, VA, American Helicopter Society, 1990, 26 p. refs

NASA-Lewis has sponsored two studies to determine the most promising convertible engine concepts for high speed rotorcraft. These studies projected year 2000 convertible technology limited to present gas generator technology. Propulsion systems for utilization on aircraft needing thrust only during cruise and those aircraft needing both power and thrust at cruise were investigated. Mission calculations for the two contractors involved were based upon the fold tilt rotor concept. Analysis and comparison of the General Electric concepts (geared UDF, clutched fan, and VIGV fan), and the Allison Gas Turbine concepts (clutched fan, VIGV fan, variable pitch fan, single rotation tractor propfan, and counter rotation tractor propfan) are presented.

R.E.P.

A90-47210* General Motors Corp., Indianapolis, IN.

COMPOSITE MATRIX COOLING SCHEME FOR SMALL GAS TURBINE COMBUSTORS

MARC D. PASKIN, PHILLIP T. ROSS, HUKAM C. MONGIA (General Motors Corp., Allison Gas Turbine Div., Indianapolis, IN), and WALDO A. ACOSTA (NASA, Lewis Research Center; U.S. Army, Propulsion Directorate, Cleveland, OH) AIAA, SAE, ASME, and ASEE, Joint Propulsion Conference, 26th, Orlando, FL, July 16-18, 1990. 11 p. refs

(AIAA PAPER 90-2158) Copyright

The design, manufacture, and testing of a compliant metal/ceramic (CMC) wall cooling concept-implementing combustor for small gas turbine engines has been undertaken by a joint U.S. Army/NASA technology development program. CMC in principle promises greater wall cooling effectiveness than conventional designs and materials, thereby facilitating a substantial reduction in combustor cooling air requirements and furnishing greater airflow for the control of burner outlet temperature patterns as well as improving thermodynamic efficiency and reducing pollutant emissions and smoke levels. Rig test results have confirmed the projected benefits of the CMC concept at combustor outlet temperatures of the order of 2460 F, at which approximately 80 percent less cooling air than conventionally required was being employed by the CMC combustor.

O.C.

A90-47218* National Aeronautics and Space Administration. Lewis Research Center, Cleveland, OH.

NASA'S HITEMP PROGRAM FOR UHBR ENGINES

JOSEPH R. STEPHENS (NASA, Lewis Research Center, Cleveland, OH) AIAA, SAE, ASME, and ASEE, Joint Propulsion Conference, 26th, Orlando, FL, July 16-18, 1990. 10 p.

(AIAA PAPER 90-2395) Copyright

NASA's High Temperature Engine Materials Program (HITEMP) is concerned with the laboratory-scale technology development and feasibility demonstration of high-temperature composite

materials, in conjunction with the requisite structural analysis models and test methods for their validation. HITEMP encompasses research on metallic/intermetallic, ceramic, and polymer matrix composites, and is giving attention to high-temperature component composites applicable to future widebody commercial aircraft ultrahigh bypass ratio (UHBR) engines. The UHBR components for which advanced composites are envisioned are fan, compressor, and turbine rotor blades, stator vanes, disks, and shafts, thrust bearings, gearbox bearings and linings, combustor cases and linings, nacelles, and thrust-reversers.

O.C.

A90-47219* National Aeronautics and Space Administration. Lewis Research Center, Cleveland, OH.

COMBUSTOR TECHNOLOGY FOR FUTURE AIRCRAFT

ROBERT R. TACINA (NASA, Lewis Research Center, Cleveland, OH) AIAA, SAE, ASME, and ASEE, Joint Propulsion Conference, 26th, Orlando, FL, July 16-18, 1990. 31 p. refs

(AIAA PAPER 90-2400) Copyright

The continuing improvement of aircraft gas turbine engine operating efficiencies involves increases in overall engine pressure ratio increases that will result in combustor inlet pressure and temperature increases, greater combustion temperature rises, and higher combustor exit temperatures. These conditions entail the development of fuel injectors generating uniform circumferential and radial temperature patterns, as well as combustor liner configurations and materials capable of withstanding increased thermal radiation even as the amount of cooling air is reduced. Low NO(x)-emitting combustor concepts are required which will employ staged combustion. The development status of component technologies answering these requirements are presently evaluated.

O.C.

N90-10036* Detroit Diesel Allison, Indianapolis, IN. Dept. of Engineering.

ADVANCED TURBINE TECHNOLOGY APPLICATIONS

PROJECT (ATTAP) Annual Report, Nov. 1987 - Dec. 1988

1 Jun. 1989 106 p

(Contract DEN3-336; DE-AI01-85CE-50111)

(NASA-CR-185133; NAS 1.26:185133; EDR-14232;

DOE/NASA/O336-1) Avail: NTIS HC A06/MF A01 CSCL 21E

ATTAP activities during the past year were highlighted by an extensive materials assessment, execution of a reference powertrain design, test-bed engine design and development, ceramic component design, materials and component characterization, ceramic component process development and fabrication, component rig design and fabrication, test-bed engine fabrication, and hot gasifier rig and engine testing. Materials assessment activities entailed engine environment evaluation of domestically supplied radial gasifier turbine rotors that were available at the conclusion of the Advanced Gas Turbine (AGT) Technology Development Project as well as an extensive survey of both domestic and foreign ceramic suppliers and Government laboratories performing ceramic materials research applicable to advanced heat engines. A reference powertrain design was executed to reflect the selection of the AGT-5 as the ceramic component test-bed engine for the ATTAP. Test-bed engine development activity focused on upgrading the AGT-5 from a 1038 C (1900 F) metal engine to a durable 1371 C (2500 F) structural ceramic component test-bed engine. Ceramic component design activities included the combustor, gasifier turbine static structure, and gasifier turbine rotor. The materials and component characterization efforts have included the testing and evaluation of several candidate ceramic materials and components being developed for use in the ATTAP. Ceramic component process development and fabrication activities were initiated for the gasifier turbine rotor, gasifier turbine vanes, gasifier turbine scroll, extruded regenerator disks, and thermal insulation. Component rig development activities included combustor, hot gasifier, and regenerator rigs. Test-bed engine fabrication activities consisted of the fabrication of an all-new AGT-5 durability test-bed engine and support of all engine test activities through instrumentation/build/repair. Hot gasifier rig and test-bed engine testing activities were performed.

Author

N90-10037*# General Electric Co., Cincinnati, OH. Aircraft Engines.

PMR GRAPHITE ENGINE DUCT DEVELOPMENT Final Report
C. L. STOTLER and S. A. YOKEL Aug. 1989 190 p LIMITED
REPRODUCIBILITY: More than 20% of this document may be
affected by foldouts
(Contract NAS3-21854)
(NASA-CR-182228; NAS 1.26:182228) Avail: NTIS HC A09/MF
A01 CSCL 21E

The objective was to demonstrate the cost and weight advantages that could be obtained by utilizing the graphite/PMR15 material system to replace titanium in selected turbofan engine applications. The first component to be selected as a basis for evaluation was the outer bypass duct of the General Electric F404 engine. The operating environment of this duct was defined and then an extensive mechanical and physical property test program was conducted using material made by processing techniques which were also established by this program. Based on these properties, design concepts to fabricate a composite version of the duct were established and two complete ducts fabricated. One of these ducts was proof pressure tested and then run successfully on a factory test engine for over 1900 hours. The second duct was static tested to 210 percent design limit load without failure. An improved design was then developed which utilized integral composite end flanges. A complete duct was fabricated and successfully proof pressure tested. The net results of this effort showed that a composite version of the outer duct would be 14 percent lighter and 30 percent less expensive than the titanium duct. The other type of structure chosen for investigation was the F404 fan stator assembly, including the fan stator vanes. It was concluded that it was feasible to utilize composite materials for this type structure but that the requirements imposed by replacing an existing metal design resulted in an inefficient composite design. It was concluded that if composites were to be effectively used in this type structure, the design must be tailored for composite application from the outset. Author

N90-10038*# Pennsylvania State Univ., State College.

THE MEASUREMENT OF BOUNDARY LAYERS ON A COMPRESSOR BLADE IN CASCADE. VOLUME 1: EXPERIMENTAL TECHNIQUE, ANALYSIS AND RESULTS Final Report

WILLIAM C. ZIERKE and STEVEN DEUTSCH Jul. 1989 223 p
(Contract NSG-3264)
(NASA-CR-185118-VOL-1; NAS 1.26:185118-VOL-1) Avail: NTIS
HC A10/MF A02 CSCL 21E

Measurements were made of the boundary layers and wakes about a highly loaded, double-circular-arc compressor blade in cascade. These laser Doppler velocimetry measurements have yielded a very detailed and precise data base with which to test the application of viscous computational codes to turbomachinery. In order to test the computational codes at off-design conditions, the data were acquired at a chord Reynolds number of 500,000 and at three incidence angles. Moreover, these measurements have supplied some physical insight into these very complex flows. Although some natural transition is evident, laminar boundary layers usually detach and subsequently reattach as either fully or intermittently turbulent boundary layers. These transitional separation bubbles play an important role in the development of most of the boundary layers and wakes measured in this cascade and the modeling or computing of these bubbles should prove to be the key aspect in computing the entire cascade flow field. In addition, the nonequilibrium turbulent boundary layers on these highly loaded blades always have some region of separation near the trailing edge of the suction surface. These separated flows, as well as the subsequent near wakes, show no similarity and should prove to be a challenging test for the viscous computational codes. Author

N90-10039*# Pennsylvania State Univ., State College.

THE MEASUREMENT OF BOUNDARY LAYERS ON A COMPRESSOR BLADE IN CASCADE. VOLUME 2: DATA TABLES Final Report

WILLIAM C. ZIERKE and STEVEN DEUTSCH Jul. 1989 209 p
(Contract NSG-3264)
(NASA-CR-185118-VOL-2; NAS 1.26:185118-VOL-2) Avail: NTIS
HC A10/MF A02 CSCL 21E

Measurements were made of the boundary layers and wakes about a highly loaded, double-circular-arc compressor blade in cascade. These laser Doppler velocimetry measurements have yielded a very detailed and precise data base with which to test the application of viscous computational codes to turbomachinery. In order to test the computational codes at off-design conditions, the data have been acquired at a chord Reynolds number of 500,000 and at three incidence angles. Average values and 95 percent confidence bands were tabularized for the velocity, local turbulence intensity, skewness, kurtosis, and percent backflow. Tables also exist for the blade static-pressure distributions and boundary layer velocity profiles reconstructed to account for the normal pressure gradient. Author

N90-10043*# Hamilton Standard, Windsor Locks, CT.

LARGE SCALE PROP-FAN STRUCTURAL DESIGN STUDY.

VOLUME 1: INITIAL CONCEPTS

L. C. BILLMAN, C. J. GRUSKA, R. M. LADDEN, D. K. LEISHMAN,
and J. E. TURNBERG 1988 258 p
(Contract NAS3-22394)
(NASA-CR-174992; NAS 1.26:174992; HSER-11518-VOL-1)
Avail: NTIS HC A12/MF A02 CSCL 21E

In recent years, considerable attention has been directed toward improving aircraft fuel consumption. Studies have shown that the inherent efficiency advantage that turboprop propulsion systems have demonstrated at lower cruise speeds may now be extended to the higher speeds of today's turbofan and turbojet-powered aircraft. To achieve this goal, new propeller designs will require features such as thin, high speed airfoils and aerodynamic sweep, features currently found only in wing designs for high speed aircraft. This is Volume 1 of a 2 volume study to establish structural concepts for such advanced propeller blades, to define their structural properties, to identify any new design, analysis, or fabrication techniques which were required, and to determine the structural tradeoffs involved with several blade shapes selected primarily on the basis of aero/acoustic design considerations. The feasibility of fabricating and testing dynamically scaled models of these blades for aeroelastic testing was also established. The preliminary design of a blade suitable for flight use in a testbed advanced turboprop was conducted and is described in Volume 2. Author

N90-10044*# Hamilton Standard, Windsor Locks, CT.

LARGE SCALE PROP-FAN STRUCTURAL DESIGN STUDY.

VOLUME 2: PRELIMINARY DESIGN OF SR-7

L. C. BILLMAN, C. J. GRUSKA, R. M. LADDEN, D. K. LEISHMAN,
and J. E. TURNBERG 1988 282 p
(Contract NAS3-22394)
(NASA-CR-174993; NAS 1.26:174993; HSER-11518-VOL-2)
Avail: NTIS HC A13/MF A02 CSCL 21E

In recent years, considerable attention has been directed toward improving aircraft fuel consumption. Studies have shown that the inherent efficiency advantage that turboprop propulsion systems have demonstrated at lower cruise speeds may now be extended to the higher speeds of today's turbofan and turbojet-powered aircraft. To achieve this goal, new propeller designs will require features such as thin, high speed airfoils and aerodynamic sweep, features currently found only in wing designs for high speed aircraft. This is Volume 2 of a 2 volume study to establish structural concepts for such advanced propeller blades, to define their structural properties, to identify any new design, analysis, or fabrication techniques which were required, and to determine the structural tradeoffs involved with several blade shapes selected primarily on the basis of aero/acoustic design considerations. The feasibility of fabricating and testing dynamically scaled models of these blades for aeroelastic testing was also established. The preliminary design of a blade suitable for flight use in a testbed advanced turboprop was conducted and is described. Author

07 AIRCRAFT PROPULSION AND POWER

N90-10045*# Hamilton Standard, Windsor Locks, CT.

LARGE-SCALE ADVANCED PROP-FAN (LAP) HIGH SPEED WIND TUNNEL TEST REPORT

WILLIAM A. CAMPBELL, HAROLD S. WAINAUSKI, and PETER J. ARSENEAUX Jul. 1988 199 p
(Contract NAS3-23051)

(NASA-CR-182125; NAS 1.26:182125; HSER-11894) Avail: NTIS HC A09/MF A02 CSCL 21E

High Speed Wind Tunnel testing of the SR-7L Large Scale Advanced Prop-Fan (LAP) is reported. The LAP is a 2.74 meter (9.0 ft) diameter, 8-bladed tractor type rated for 4475 KW (6000 SHP) at 1698 rpm. It was designated and built by Hamilton Standard under contract to the NASA Lewis Research Center. The LAP employs thin swept blades to provide efficient propulsion at flight speeds up to Mach .85. Testing was conducted in the ONERA S1-MA Atmospheric Wind Tunnel in Modane, France. The test objectives were to confirm that the LAP is free from high speed classical flutter, determine the structural and aerodynamic response to angular inflow, measure blade surface pressures (static and dynamic) and evaluate the aerodynamic performance at various blade angles, rotational speeds and Mach numbers. The measured structural and aerodynamic performance of the LAP correlated well with analytical predictions thereby providing confidence in the computer prediction codes used for the design. There were no signs of classical flutter throughout all phases of the test up to and including the 0.84 maximum Mach number achieved. Steady and unsteady blade surface pressures were successfully measured for a wide range of Mach numbers, inflow angles, rotational speeds and blade angles. No barriers were discovered that would prevent proceeding with the PTA (Prop-Fan Test Assessment) Flight Test Program scheduled for early 1987. Author

N90-10046*# Hamilton Standard, Windsor Locks, CT.

LARGE-SCALE ADVANCED PROP-FAN (LAP) TECHNOLOGY ASSESSMENT REPORT

C. L. DEGEORGE Sep. 1988 102 p
(Contract NAS3-23051)

(NASA-CR-182142; NAS 1.26:182142; HSER-11804) Avail: NTIS HC A06/MF A01 CSCL 21E

The technologically significant findings and accomplishments of the Large Scale Advanced Prop-Fan (LAP) program in the areas of aerodynamics, aeroelasticity, acoustics and materials and fabrication are described. The extent to which the program goals related to these disciplines were achieved is discussed, and recommendations for additional research are presented. The LAP program consisted of the design, manufacture and testing of a near full-scale Prop-Fan or advanced turboprop capable of operating efficiently at speeds to Mach .8. An aeroelastically scaled model of the LAP was also designed and fabricated. The goal of the program was to acquire data on Prop-Fan performance that would indicate the technology readiness of Prop-Fans for practical applications in commercial and military aviation. Author

N90-10047*# General Electric Co., Cincinnati, OH. Aircraft Engines Div.

FULL SCALE TECHNOLOGY DEMONSTRATION OF A MODERN COUNTERROTATING UNDUCTED FAN ENGINE CONCEPT: COMPONENT TEST

Dec. 1987 109 p

(Contract NAS3-24210)

(NASA-CR-180868; NAS 1.26:180868) Avail: NTIS HC A06/MF A01 CSCL 21E

The UDF trademark (Unducted Fan) engine is a new aircraft engine concept based on an ungeared, counterrotating, unducted, ultra-high-bypass turbofan configuration. This engine is being developed to provide a high thrust-to-weight ratio powerplant with exceptional fuel efficiency for subsonic aircraft application. This report covers the testing of pertinent components of this engine such as the fan blades, control and actuation system, turbine blades and spools, seals, and mixer frame. Author

N90-10048*# General Electric Co., Cincinnati, OH. Aircraft Engines Div.

FULL SCALE TECHNOLOGY DEMONSTRATION OF A MODERN COUNTERROTATING UNDUCTED FAN ENGINE CONCEPT. DESIGN REPORT

Dec. 1987 368 p

(Contract NAS3-24210)

(NASA-CR-180867; NAS 1.26:180867) Avail: NTIS HC A16/MF A02 CSCL 21E

The Unducted Fan engine (UDF trademark) concept is based on an ungeared, counterrotating, unducted, ultra-high-bypass turbofan configuration. This engine is being developed to provide a high thrust-to-weight ratio power plant with exceptional fuel efficiency for subsonic aircraft application. This report covers the design methodology and details for the major components of this engine. The design intent of the engine is to efficiently produce 25,000 pounds of static thrust while meeting life and stress requirements. The engine is required to operate at Mach numbers of 0.8 or above. Author

N90-10049*# General Electric Co., Cincinnati, OH. Aircraft Engines Div.

FULL SCALE TECHNOLOGY DEMONSTRATION OF A MODERN COUNTERROTATING UNDUCTED FAN ENGINE CONCEPT. ENGINE TEST

Dec. 1987 340 p

(Contract NAS3-24210)

(NASA-CR-180869; NAS 1.26:180869) Avail: NTIS HC A15/MF A02 CSCL 21E

The Unducted Fan (UDF) engine is an innovative aircraft engine concept based on an ungeared, counterrotating, unducted, ultra-high-bypass turbofan configuration. This engine is being developed to provide a high thrust-to-weight ratio power plant with exceptional fuel efficiency for subsonic aircraft application. This report covers the successful ground testing of this engine. A test program exceeding 100-hr duration was completed, in which all the major goals were achieved. The following accomplishments were demonstrated: (1) full thrust (25,000 lb); (2) full counterrotating rotor speeds (1393+ rpm); (3) low specific fuel consumption (less than 0.24 lb/hr/lb); (4) new composite fan design; (5) counterrotation of structures, turbines, and fan blades; (6) control system; (7) actuation system; and (8) reverse thrust. Author

N90-10891*# National Aeronautics and Space Administration, Lewis Research Center, Cleveland, OH.

ADVANCED TECHNOLOGIES IMPACT ON COMPRESSOR DESIGN AND DEVELOPMENT: A PERSPECTIVE

CALVIN L. BALL Sep. 1989 18 p Presented at Aerotech '89, Anaheim, CA, 25-28 Sep. 1989; sponsored by SAE

(NASA-TM-102341; E-5039; NAS 1.15:102341) Avail: NTIS HC A03/MF A01 CSCL 21/5

A historical perspective of the impact of advanced technologies on compression system design and development for aircraft gas turbine applications is presented. A bright view of the future is projected in which further advancements in compression system technologies will be made. These advancements will have a significant impact on the ability to meet the ever-more-demanding requirements being imposed on the propulsion system for advanced aircraft. Examples are presented of advanced compression system concepts now being studied. The status and potential impact of transitioning from an empirically derived design system to a computationally oriented system are highlighted. A current NASA Lewis Research Center program to enhance this transitioning is described. Author

N90-11738*# Lockheed Aeronautical Systems Co., Marietta, GA.

PROPFAN TEST ASSESSMENT (PTA): FLIGHT TEST REPORT

B. H. LITTLE, H. W. BARTEL, N. N. REDDY, G. SWIFT, C. C. WITHERS, and P. C. BROWN (United Technologies Corp., Windsor Locks, CT.) Apr. 1989 276 p

(Contract NAS3-24339)

(NASA-CR-182278; NAS 1.26:182278; LG89ER0026) Avail:
NTIS HC A13/MF A02 CSCL 21/5

The Propfan Test Assessment (PTA) aircraft was flown to obtain glade stress and noise data for a 2.74m (9 ft.) diameter single rotation propfan. Tests were performed at Mach numbers to 0.85 and altitudes to 12,192m (40,000 ft.). The propfan was well-behaved structurally over the entire flight envelope, demonstrating that the blade design technology was completely adequate. Noise data were characterized by strong signals at blade passage frequency and up to 10 harmonics. Cabin noise was not so high as to preclude attainment of comfortable levels with suitable wall treatment. Community noise was not excessive. Author

N90-11739*# Lockheed Aeronautical Systems Co., Marietta, GA.

PROPFAN TEST ASSESSMENT (PTA) Final Report

B. H. LITTLE, D. T. POLAND, H. W. BARTEL, C. C. WITHERS, and P. C. BROWN (United Technologies Corp., Windsor Locks, CT.) Jul. 1989 676 p
(Contract NAS3-24339)
(NASA-CR-185138; NAS 1.26:185138; LG89ER0064) Avail:
NTIS HC A99/MF A04 CSCL 21/5

The objectives of the Propfan Test Assessment (PTA) Program were to validate in flight the structural integrity of large-scale propfan blades and to measure noise characteristics of the propfan in both near and far fields. All program objectives were met or exceeded, on schedule and under budget. A Gulfstream Aerospace Corporation GII aircraft was modified to provide a testbed for the 2.74m (9 ft) diameter Hamilton Standard SR-7 propfan which was driven by a 4475 kw (600 shp) turboshaft engine mounted on the left-hand wing of the aircraft. Flight research tests were performed for 20 combinations of speed and altitude within a flight envelope that extended to Mach numbers of 0.85 and altitudes of 12,192m (40,000 ft). Propfan blade stress, near-field noise on aircraft surfaces, and cabin noise were recorded. Primary variables were propfan power and tip speed, and the nacelle tilt angle. Extensive low altitude far-field noise tests were made to measure flyover and sideline noise and the lateral attenuation of noise. In cooperation with the FAA, tests were also made of flyover noise for the aircraft at 6100m (20,000 ft) and 10,668m (35,000 ft). A final series of tests were flown to evaluate an advanced cabin wall noise treatment that was produced under a separate program by NASA-Langley Research Center. Author

N90-11740*# National Aeronautics and Space Administration, Lewis Research Center, Cleveland, OH.

STOVL PROPULSION SYSTEM VOLUME DYNAMICS APPROXIMATIONS

COLIN K. DRUMMOND 1989 11 p Presented at the 1989 Winter Annual Meeting, San Francisco, CA, 10-15 Dec. 1989, sponsored by ASME
(NASA-TM-102397; E-5147; NAS 1.15:102397) Avail: NTIS HC A03/MF A01 CSCL 21/5

Two approaches to modeling turbofan engine component volume dynamics are explored and compared with a view toward application to real-time simulation of short take-off vertical landing (STOVL) aircraft propulsion systems. The first (and most popular) approach considers only heat and mass balances; the second approach includes a momentum balance and substitutes the heat equation with a complete energy balance. Results for a practical test case are presented and discussed. Author

N90-12617*# Hamilton Standard Div., United Aircraft Corp., Windsor Locks, CT.

LARGE-SCALE ADVANCED PROP-FAN (LAP) STATIC ROTOR TEST REPORT

CHARLES L. DEGEORGE, JAY E. TURNBERG, and HARRY S. WAINAUSKI 1987 156 p
(Contract NAS3-23051)
(NASA-CR-180848; NAS 1.26:180848; HSER-116227) Avail:
NTIS HC A08/MF A01 CSCL 21/5

Discussed is Static Rotor Testing of the SR-7L Large Scale Advanced Prop-Fan (LAP). The LAP is an advanced 9 foot diameter.

8 bladed propeller designed and built by Hamilton Standard under contract to the NASA Lewis Research Center. The Prop-Fan employs thin swept blades to provide efficient propulsion at flight speeds up to Mach .85. Static Testing was conducted on a 10,000 HP whirl rig at Wright Patterson Air Force Base. The test objectives were to investigate the Prop-Fan static aerodynamic and structural dynamic performance, determine the blade steady state stressers and deflections and to measure steady and unsteady pressures on the SR-7L blade surface. The measured performance of the LAP correlated well with analytical predictions at blade pitch angles below 30 deg. A stall buffet phenomenon was observed at blade pitch angles above 30 deg. This phenomenon manifested itself by elevated blade vibratory stress levels and lower than expected thrust produced and power absorbed by the Prop-Fan for a given speed and blade angle. Author

N90-12618*# National Aeronautics and Space Administration, Lewis Research Center, Cleveland, OH.

REAL-TIME SIMULATION OF AN F110/STOVL TURBOFAN ENGINE

COLIN K. DRUMMOND and PETER J. OUZTS Nov. 1989 24 p Presented at the Central/Northeastern ADIUS Conference, Cleveland, OH, 16-17 Oct. 1989; sponsored by Applied Dynamics International
(NASA-TM-102409; E-5162; NAS 1.15:102409) Avail: NTIS HC A03/MF A01 CSCL 21/5

A traditional F110-type turbofan engine model was extended to include a ventral nozzle and two thrust-augmenting ejectors for Short Take-Off Vertical Landing (STOVL) aircraft applications. Development of the real-time F110/STOVL simulation required special attention to the modeling approach to component performance maps, the low pressure turbine exit mixing region, and the tailpipe dynamic approximation. Simulation validation derives by comparing output from the ADSIM simulation with the output for a validated F110/STOVL General Electric Aircraft Engines FORTRAN deck. General Electric substantiated basic engine component characteristics through factory testing and full scale ejector data. Author

N90-13385*# PDA Engineering, Santa Ana, CA.

THE APPLICATION OF CAST SiC/AL TO ROTARY ENGINE COMPONENTS Final Report

H. M. STOLLER, J. R. CARLUCCIO, and J. P. NORMAN 15 Aug. 1986 101 p
(Contract NAS3-24847)
(NASA-CR-179610; NAS 1.26:179610; PDA-86-FR-5333-00-06)
Avail: NTIS HC A06/MF A01 CSCL 21/5

A silicon carbide reinforced aluminum (SiC/Al) material fabricated by Dural Aluminum Composites Corporation was tested for various components of rotary engines. Properties investigated included hardness, high temperature strength, wear resistance, fatigue resistance, thermal conductivity, and expansion. SiC/Al appears to be a viable candidate for cast rotors, and may be applicable to other components, primarily housings. J.P.S.

N90-13387*# National Aeronautics and Space Administration, Lewis Research Center, Cleveland, OH.

APPLICATION OF A TWO-DIMENSIONAL UNSTEADY VISCOUS ANALYSIS CODE TO A SUPERSONIC THROUGHFLOW FAN STAGE

RONALD J. STEINKE Nov. 1989 18 p
(NASA-TM-4141; E-4848; NAS 1.15:4141) Avail: NTIS HC A03/MF A01 CSCL 21/5

The Rai ROTOR1 code for two-dimensional, unsteady viscous flow analysis was applied to a supersonic throughflow fan stage design. The axial Mach number for this fan design increases from 2.0 at the inlet to 2.9 at the outlet. The Rai code uses overlapped O- and H-grids that are appropriately packed. The Rai code was run on a Cray XMP computer; then data postprocessing and graphics were performed to obtain detailed insight into the stage flow. The large rotor wakes uniformly traversed the rotor-stator interface and dispersed as they passed through the stator passage. Only weak blade shock losses were computed, which supports

07 AIRCRAFT PROPULSION AND POWER

the design goals. High viscous effects caused large blade wakes and a low fan efficiency. Rai code flow predictions were essentially steady for the rotor, and they compared well with Chima rotor viscous code predictions based on a C-grid of similar density.

Author

N90-13388*# Pratt and Whitney Aircraft, East Hartford, CT. Commercial Engine Business.

THERMAL BARRIER COATING LIFE PREDICTION MODEL DEVELOPMENT, PHASE 1 Final Report

JEANINE T. DEMASI and MILTON ORTIZ Dec. 1989 338 p (Contract NAS3-23944)

(NASA-CR-182230; NAS 1.26:182230; PWA-5970-40) Avail: NTIS HC A15/MF A02 CSCL 21/5

The objective of this program was to establish a methodology to predict thermal barrier coating (TBC) life on gas turbine engine components. The approach involved experimental life measurement coupled with analytical modeling of relevant degradation modes. Evaluation of experimental and flight service components indicate the predominant failure mode to be thermomechanical spallation of the ceramic coating layer resulting from propagation of a dominant near interface crack. Examination of fractionally exposed specimens indicated that dominant crack formation results from progressive structural damage in the form of subcritical microcrack link-up. Tests conducted to isolate important life drivers have shown MCRAIY oxidation to significantly affect the rate of damage accumulation. Mechanical property testing has shown the plasma deposited ceramic to exhibit a non-linear stress-strain response, creep and fatigue. The fatigue based life prediction model developed accounts for the unusual ceramic behavior and also incorporates an experimentally determined oxide rate model. The model predicts the growth of this oxide scale to influence the intensity of the mechanic driving force, resulting from cyclic strains and stresses caused by thermally induced and externally imposed mechanical loads.

Author

N90-13389*# National Aeronautics and Space Administration. Lewis Research Center, Cleveland, OH.

STOVL AIRCRAFT SIMULATION FOR INTEGRATED FLIGHT AND PROPULSION CONTROL RESEARCH

JAMES R. MIHALOEW and COLIN K. DRUMMOND 1989 23 p Presented at the 10th Applied Dynamics International Users Society Annual Conference, Keystone, CO, 25-28 Jun. 1989 (NASA-TM-102419; E-5185; NAS 1.15:102419) Avail: NTIS HC A03/MF A01 CSCL 21/5

The United States is in the initial stages of committing to a national program to develop a supersonic short takeoff and vertical landing (STOVL) aircraft. The goal of the propulsion community in this effort is to have the enabling propulsion technologies for this type aircraft in place to permit a low risk decision regarding the initiation of a research STOVL supersonic attack/fighter aircraft in the late mid-90's. This technology will effectively integrate, enhance, and extend the supersonic cruise, STOVL and fighter/attack programs to enable U.S. industry to develop a revolutionary supersonic short takeoff and vertical landing fighter/attack aircraft in the post-ATF period. A joint NASA Lewis and NASA Ames research program, with the objective of developing and validating technology for integrated-flight propulsion control design methodologies for short takeoff and vertical landing (STOVL) aircraft, was planned and is underway. This program, the NASA Supersonic STOVL Integrated Flight-Propulsion Controls Program, is a major element of the overall NASA-Lewis Supersonic STOVL Propulsion Technology Program. It uses an integrated approach to develop an integrated program to achieve integrated flight-propulsion control technology. Essential elements of the integrated controls research program are realtime simulations of the integrated aircraft and propulsion systems which will be used in integrated control concept development and evaluations. This paper describes pertinent parts of the research program leading up to the related realtime simulation development and remarks on the simulation structure to accommodate propulsion system hardware drop-in for real system evaluation.

Author

N90-13390*# Southwest Research Inst., San Antonio, TX. **CONSTITUTIVE MODELING FOR ISOTROPIC MATERIALS (HOST) Annual Status Report No. 3**

KWAI S. CHAN, ULRIC S. LINDHOLM, S. R. BODNER, JEFF T. HILL, R. M. WEBER, and T. G. MEYER (Pratt and Whitney Aircraft, East Hartford, CT.) Aug. 1986 129 p

(Contract NAS3-23925; SWRI PROJ. 06-7576)

(NASA-CR-179522; SWRI-7576/45; NAS 1.26:179522) Avail:

NTIS HC A07/MF A01 CSCL 21/5

The results of the third year of work on a program which is part of the NASA Hot Section Technology program (HOST) are presented. The goals of this program are: (1) the development of unified constitutive models for rate dependent isotropic materials; and (2) the demonstration of the use of unified models in structural analyses of hot section components of gas turbine engines. The unified models selected for development and evaluation are those of Bodner-Partom and of Walker. A test procedure was developed for assisting the generation of a data base for the Bodner-Partom model using a relatively small number of specimens. This test procedure involved performing a tensile test at a temperature of interest that involves a succession of strain-rate changes. The results for B1900+Hf indicate that material constants related to hardening and thermal recovery can be obtained on the basis of such a procedure. Strain aging, thermal recovery, and unexpected material variations, however, preluded an accurate determination of the strain-rate sensitivity parameter in this exercise. The effects of casting grain size on the constitutive behavior of B1900+Hf were studied and no particular grain size effect was observed. A systematic procedure was also developed for determining the material constants in the Bodner-Partom model. Both the new test procedure and the method for determining material constants were applied to the alternate material, Mar-M247. Test data including tensile, creep, cyclic and nonproportional biaxial (tension/torsion) loading were collected. Good correlations were obtained between the Bodner-Partom model and experiments. A literature survey was conducted to assess the effects of thermal history on the constitutive behavior of metals. Thermal history effects are expected to be present at temperature regimes where strain aging and change of microstructure are important. Possible modifications to the Bodner-Partom model to account for these effects are outlined. The use of a unified constitutive model for hot section component analyses was demonstrated by applying the Walker model and the MARC finite-element code to a B1900+Hf airfoil problem.

Author

N90-13391*# Southwest Research Inst., San Antonio, TX. **CONSTITUTIVE MODELING FOR ISOTROPIC MATERIALS (HOST) Annual Report No. 1**

ULRIC S. LINDHOLM, KWAI S. CHAN, S. R. BODNER, R. M. WEBER (Pratt and Whitney Aircraft, East Hartford, CT.), K. P. WALKER, and B. N. CASSENTI May 1984 127 p

(Contract NAS3-23925; SWRI PROJ. 06-7576)

(NASA-CR-174718; SWRI-06-7576/13; NAS 1.26:174718) Avail:

NTIS HC A07/MF A01 CSCL 21/5

The results of the first year of work on a program to validate unified constitutive models for isotropic materials utilized in high temperature regions of gas turbine engines and to demonstrate their usefulness in computing stress-strain-time-temperature histories in complex three-dimensional structural components. The unified theories combine all inelastic strain-rate components in a single term avoiding, for example, treating plasticity and creep as separate response phenomena. An extensive review of existing unified theories is given and numerical methods for integrating these stiff time-temperature-dependent constitutive equations are discussed. Two particular models, those developed by Bodner and Partom and by Walker, were selected for more detailed development and evaluation against experimental tensile, creep and cyclic strain tests on specimens of a cast nickel base alloy, B19000+Hf. Initial results comparing computed and test results for tensile and cyclic straining for temperature from ambient to 982 C and strain rates from $10(\exp-7)$ to $10(\exp-3)$ s(exp-1) are given. Some preliminary data correlations are presented also for highly non-proportional biaxial loading which demonstrate an increase in

biaxial cyclic hardening rate over uniaxial or proportional loading conditions. Initial work has begun on the implementation of both constitutive models in the MARC finite element computer code.

Author

N90-13392*# National Aeronautics and Space Administration. Lewis Research Center, Cleveland, OH.

TWO-DIMENSIONAL ANALYSIS OF TWO-PHASE REACTING FLOW IN A FIRING DIRECT-INJECTION DIESEL ENGINE

H. LEE NGUYEN Dec. 1989 21 p
(NASA-TM-102069; E-4826; NAS 1.15:102069) Avail: NTIS HC A03/MF A01 CSCL 21/5

The flow field, spray penetration, and combustion in two-stroke diesel engines are described. Fuel injection begins at 345 degrees after top dead center (ATDC) and n-dodecane is used as the liquid fuel. Arrhenius kinetics is used to calculate the reaction rate term in the quasi-global combustion model. When the temperature, fuel, and oxygen mass fraction are within suitable flammability limits, combustion begins spontaneously. No spark is necessary to ignite a localized high temperature region. Compression is sufficient to increase the gaseous phase temperature to a point where spontaneous chemical reactions occur. Results are described for a swirl angle of 22.5 degrees.

Author

N90-13393*# National Aeronautics and Space Administration. Lewis Research Center, Cleveland, OH.

A PLANAR REACTING SHEAR LAYER SYSTEM FOR THE STUDY OF FLUID DYNAMICS-COMBUSTION INTERACTION

C. J. MAREK, C. T. CHANG, B. GHORASHI, C. C. WEY, C. WEY, and E. J. MULARZ (Army Aviation Research and Development Command, Cleveland, OH.) 1989 21 p Proposed for presentation at the 23rd International Symposium on Combustion, Orleans, France, 22-27 Jul. 1990; sponsored by Orleans Univ. Prepared in cooperation with Army Aviation Research and Development Command, Cleveland, OH
(Contract DA PROJ. 1L1-61102-AH-45)
(NASA-TM-102422; E-5063; NAS 1.15:102422; AVSCOM-TR-89-C-013) Avail: NTIS HC A03/MF A01 CSCL 21/5

A versatile planar reacting shear layer facility is constructed at NASA-Lewis. The research objectives, as well as design, instrumentations and the operational procedures developed for the system are described. The fundamental governing equations and the type of quantitative information that are needed from experiments are described. Additionally, a review of earlier work is presented. Whenever appropriate, comparisons are made with similar systems in other facilities and the main differences are described. Finally, the nonintrusive measurement techniques (PLIF, PMS, LDV, and Schlieren photography) and the type of experiments that are planned are described.

Author

N90-13394*# National Aeronautics and Space Administration. Lewis Research Center, Cleveland, OH.

RECENT PROGRESS IN RESEARCH PERTAINING TO ESTIMATES OF GAS-SIDE HEAT TRANSFER IN AN AIRCRAFT GAS TURBINE

ROBERT W. GRAHAM 1989 9 p Proposed for presentation at the Turbo Expo, Brussels, Belgium, 11-14 Jun. 1990; sponsored by ASME
(NASA-TM-102460; E-5247; NAS 1.15:102460) Avail: NTIS HC A02/MF A01 CSCL 21/5

A decade ago several important fundamental heat transfer phenomena were identified which were considered basic to the ability to predict heat transfer loads in aircraft gas turbines. The progress in addressing these fundamentals over the past ten years is assessed. Much research effort has been devoted to their study in university, industry and government labs and significant progress has been achieved. Advances in computer technology have enabled the modeling of complex 3-D fluid flow in gas turbines so necessary for heat transfer calculations. Advances in instrumentation plus improved data acquisition have brought about more reliable data sets. While much has advanced in the 1980's,

much challenging research remains to be done. Several of these areas are suggested.

Author

N90-14235*# National Aeronautics and Space Administration. Lewis Research Center, Cleveland, OH.

RAMSCRAM: A FLEXIBLE RAMJET/SCRAMJET ENGINE SIMULATION PROGRAM

LEO A. BURKARDT and LEO C. FRANCISCUS 1990 6 p
Prepared for presentation at the 35th International Gas Turbine Aeroengine Congress and Exposition, Brussels, Belgium, 11-14 Jun. 1990; sponsored by ASME
(NASA-TM-102451; E-5236; NAS 1.15:102451) Avail: NTIS HC A02/MF A01 CSCL 21/5

With the resurgence of interest in high supersonic and hypersonic flight there is a need to simulate airbreathing engines which may be used in this flight regime. To meet this requirement the RAMSCRAM code was developed. The code calculates 1-D flow properties at each component interface and the overall performance of the engine. It uses equilibrium thermodynamics which accounts for dissociation and allows for any fuel or combination of fuels. The program can simulate ramjet, scramjet, rocket, and ducted rocket engines.

Author

N90-15923*# National Aeronautics and Space Administration. Lewis Research Center, Cleveland, OH.

ASSESSMENT OF WORM GEARING FOR HELICOPTER TRANSMISSIONS

LEV CHAIKO Jan. 1990 16 p Prepared in cooperation with Army Aviation Systems Command, Cleveland, OH
(Contract DA PROJ. 1L1-61102-AH-45)
(NASA-TM-102441; E-5212; NAS 1.15:102441; AVSCOM-TM-89-C-010) Avail: NTIS HC A03/MF A01 CSCL 13/9

A high-efficiency hydrostatic worm gear drive for helicopter transmissions is assessed. The example given is for a large-cargo helicopter with three 4000-kW engines and transmission reduction ratio of 110. Also contained are: an efficiency calculation, a description of the test stand for evaluating the feasibility of worm gear hydrostatic mesh, a weight calculation, and a comparison with conventional helicopter transmissions of the same power and transmission reduction ratio.

Author

N90-17635*# Sverdrup Technology, Inc., Cleveland, OH.
VISCOUS THREE-DIMENSIONAL ANALYSES FOR NOZZLES FOR HYPERSONIC PROPULSION Final Report

G. J. HARLOFF, D. R. REDDY, and H. T. LAI Jan. 1990 25 p
Proposed for presentation at the AGARD Symposium on Combined Cycle Propulsion for Hypersonic Application, Madrid, Spain, 21-25 May 1990
(Contract NAS3-24105; NAS3-25266)
(NASA-CR-185197; E-5267; NAS 1.26:185197) Avail: NTIS HC A03/MF A01 CSCL 21/5

A Navier-Stokes computer code was validated using a number of two- and three-dimensional configurations for both laminar and turbulent flows. The validation data covers a range of freestream Mach numbers from 3 to 14, includes wall pressures, velocity profiles, and skin friction. Nozzle flow fields computed for a generic scramjet nozzle from Mach 3 to 20, wall pressures, wall skin friction values, heat transfer values, and overall performance are presented. In addition, three-dimensional solutions obtained for two asymmetric, single expansion ramp nozzles at a pressure ratio of 10 consists of the internal expansion region in the converging/diverging sections and the external supersonic exhaust in a quiescent ambient environment. The fundamental characteristics that were captured successfully include expansion fans; Mach wave reflections; mixing layers; and nonsymmetrical, multiple inviscid cell, supersonic exhausts. Comparison with experimental data for wall pressure distributions at the center planes shows good agreement.

Author

N90-17636*# National Aeronautics and Space Administration. Lewis Research Center, Cleveland, OH.

LOW NO(X) POTENTIAL OF GAS TURBINE ENGINES

07 AIRCRAFT PROPULSION AND POWER

ROBERT R. TACINA 1990 20 p Presented at the 28th Aerospace Sciences Meeting, Reno, NV, 8-11 Jan. 1990; sponsored by AIAA (NASA-TM-102452; E-5237; NAS 1.15:102452; AIAA-90-0550) Avail: NTIS HC A03/MF A01 CSCL 21/5

The purpose is to correlate emission levels of gas turbine engines. The predictions of NO(x) emissions are based on a review of the literature of previous low NO(x) combustor programs and analytical chemical kinetic calculations. Concepts included in the literature review consisted of lean-premixed-prevaporized (LPP), rich burn/quick quench/lean burn (RQL), and direct injection. The NO(x) emissions were found to be an exponential function of adiabatic combustion temperature over a wide range of inlet temperatures, pressures and (lean) fuel-air ratios. A simple correlation of NO(x) formation with time was not found. The LPP and direct injection (using gaseous fuels) concepts have the lowest NO(x) emissions of the three concepts. The RQL data has higher values of NO(x) than the LPP concept, probably due to the stoichiometric temperatures and NO(x) production that occur during the quench step. Improvements in the quick quench step could reduce the NO(x) emissions to the LPP levels. The low NO(x) potential of LPP is offset by the operational disadvantages of its narrow stability limits and its susceptibility to autoignition/flashback. The Rich-Burn/Quick-Quench/Lean-Burn (RQL) and the direct injection concepts have the advantage of wider stability limits comparable to conventional combustors. Author

N90-17638*# General Electric Co., Cincinnati, OH. Aircraft Engine Business Group.

ALTITUDE TESTING OF THE 2D V/STOL ADEN

DEMONSTRATOR ON AN F404 ENGINE Final Report

J. T. BLOZY Feb. 1985 110 p

(Contract NAS3-23042)

(NASA-CR-174824; NAS 1.26:174824) Avail: NTIS HC A06/MF A01 CSCL 21/5

The Augmented Deflector Exhaust Nozzle (ADEN) exhaust system was tested in the PSL-3 altitude chamber at the NASA Lewis Research Center in order to evaluate aerodynamic performance, cooling-system effectiveness, and mechanical operation at flight-type conditions. The ADEN, a flight-weight, two-dimensional, thrust-vectoring nozzle, was successfully tested on the F404 engine using a remote engine control system for automatic or manual setting of the throat-area control and available fan air for the nozzle internal cooling system. Throughout the test, the ADEN performed with no adverse effects on the engine or augmentor operation. R.J.F.

N90-18415*# United Technologies Research Center, East Hartford, CT. Computational and Theoretical Fluid Dynamics.

GUST RESPONSE ANALYSIS FOR CASCADES OPERATING IN NONUNIFORM MEAN FLOWS

KENNETH C. HALL and JOSEPH M. VERDON In AGARD, Unsteady Aerodynamic Phenomena in Turbomachines 13 p Feb. 1990

(Contract NAS3-25425)

Copyright Avail: NTIS HC A14/MF A02; Non-NATO Nationals requests available only from AGARD/Scientific Publications Executive CSCL 21/5

The linearized unsteady aerodynamic response of a cascade of airfoils subjected to entropic, vortical, and acoustic gusts is analyzed. Field equations for the first-order unsteady perturbation flow are obtained by linearizing the full time-dependent mass, momentum, and energy conservation equations about a nonlinear, isentropic, and irrotational mean or steady flow. A splitting technique is then used to decompose the unsteady velocity field into irrotational and rotational parts leading to field equations for the unsteady entropy, rotational velocity, and irrotational velocity fluctuations that are coupled only sequentially. The entropic and rotational velocity fluctuations can be described in terms of the mean-flow drift and stream functions which can be computed numerically. The irrotational unsteady velocity is described by an inhomogeneous linearized potential equation which contains a source term that depends on the rotational velocity field. This

equation is solved via a finite difference technique. Results are presented to indicate the status of the numerical solution procedure and to demonstrate the impact of blade geometry and mean blade loading on the aerodynamic response of cascades to vortical gust excitations. The analysis described leads to very efficient predictions of cascade unsteady aerodynamic phenomena making it useful for turbomachinery aeroelastic and aeroacoustic design applications. Author

N90-19234*# National Aeronautics and Space Administration. Lewis Research Center, Cleveland, OH.

INDUCTION MOTOR CONTROL

IRVING G. HANSEN 1990 5 p Prepared for presentation at the National Aerospace and Electronics Conference, Dayton, Ohio, 21-25 May 1990; sponsored in part by the IEEE (NASA-TM-102533; E-5342; NAS 1.15:102533) Avail: NTIS HC A01/MF A01 CSCL 21/5

Electromechanical actuators developed to date have commonly utilized permanent magnet (PM) synchronous motors. More recently switched reluctance (SR) motors have been advocated due to their robust characteristics. Implications of work which utilizes induction motors and advanced control techniques are discussed. When induction motors are operated from an energy source capable of controlling voltages and frequencies independently, drive characteristics are obtained which are superior to either PM or SR motors. By synthesizing the machine frequency from a high frequency carrier (nominally 20 kHz), high efficiencies, low distortion, and rapid torque response are available. At this time multiple horsepower machine drives were demonstrated, and work is on-going to develop a 20 hp average, 40 hp peak class of aerospace actuators. This effort is based upon high frequency power distribution and management techniques developed by NASA for Space Station Freedom. Author

N90-20085*# National Aeronautics and Space Administration. Lewis Research Center, Cleveland, OH.

AEROSPACE INDUCTION MOTOR ACTUATORS DRIVEN FROM A 20-KHZ POWER LINK

IRVING G. HANSEN Jan. 1990 5 p Presented at the 4th International Conference on Power Electronics and Variable Speed Drives, London, England, 17-19 Jul. 1990; sponsored by Institution of Electrical Engineers

(NASA-TM-102482; E-5272; NAS 1.15:102482) Avail: NTIS HC A01/MF A01 CSCL 21/5

Aerospace electromechanical actuators utilizing induction motors are under development in sizes up to 40 kW. While these actuators have immediate application to the Advanced Launch System (ALS) program, several potential applications are currently under study including the Advanced Aircraft Program. Several recent advances developed for the Space Station Freedom have allowed induction motors to be selected as a first choice for such applications. Among these technologies are bi-directional electronics and high frequency power distribution techniques. Each of these technologies are discussed with emphasis on their impact upon induction motor operation. Author

N90-20090*# National Aeronautics and Space Administration. Lewis Research Center, Cleveland, OH.

COMPARISON OF 3-D VISCOUS FLOW COMPUTATIONS OF MACH 5 INLET WITH EXPERIMENTAL DATA

D. R. REDDY (Sverdrup Technology, Inc., Cleveland, OH.), T. J. BENSON, and L. J. WEIR Jan. 1990 15 p Presented at the 28th Aerospace Sciences Meeting, Reno, NV, 8-11 Jan. 1990; sponsored by AIAA Previously announced in IAA as A90-26970 (NASA-TM-102518; E-5322; NAS 1.15:102518) Avail: NTIS HC A03/MF A01 CSCL 21/5

A time marching 3-D full Navier-Stokes code, called PARC3D, is validated for an experimental Mach 5 inlet configuration using the data obtained in the 10 x 10 ft supersonic wind tunnel at the NASA Lewis Research Center. For the first time, a solution is obtained for this configuration with the actual geometry, the tunnel conditions, and all the bleed zones modeled in the computation. Pitot pressure profiles and static pressures at various locations in

the inlet are compared with the corresponding experimental data. The effect of bleed zones, located in different places on the inlet walls, in eliminating the low energy vortical flow generated from the 3-D shock-boundary layer interaction is simulated very well even though some approximations are used in applying the bleed boundary conditions and in the turbulence model. A further detailed study of the effect of individual bleed ports is needed to understand fully the actual mechanism of efficiently eliminating the vortical flow from the inlet. A better turbulence model would help to improve the accuracy even further in predicting the corner flow boundary layer profiles. Author

N90-21025* National Aeronautics and Space Administration. Lewis Research Center, Cleveland, OH.

THE NUMERICAL SIMULATION OF MULTISTAGE TURBOMACHINERY FLOWS

J. J. ADAMCZYK, T. A. BEACH, M. L. CELESTINA, R. A. MULAC, and W. M. TO (Sverdrup Technology, Inc., Cleveland, OH.) In AGARD, Secondary Flows in Turbomachines 13 p Feb. 1990 Copyright Avail: NTIS HC A15/MF A02; Non-NATO Nationals requests available only from AGARD/Scientific Publications Executive CSCL 21/5

The need to account for momentum and energy transport by the unsteady deterministic flow field in modeling the time-averaged flow state within a blade row passage embedded in a multistage compressor is assessed. It was found that, within the endwall regions, large-scale three-dimensional unsteady structures existed which caused significant transport of momentum and energy across the time-averaged stream surface of a stator flow field. These experiments confirmed that the transport process is dominated by turbulent diffusion in the midspan region. A model was then proposed for simulating this transport process, and a limited study was undertaken to assess its validity. Author

N90-21036* National Aeronautics and Space Administration. Lewis Research Center, Cleveland, OH.

PROBABILISTIC MODELING FOR SIMULATION OF AERODYNAMIC UNCERTAINTIES IN PROPULSION SYSTEMS

AWATEF HAMED (Cincinnati Univ., OH.) Dec. 1989 28 p (Contract NASA ORDER C-99066-G) (NASA-TM-102472; ICOMP-89-32; E-5260; NAS 1.15:102472) Avail: NTIS HC A03/MF A01 CSCL 21/5

The numerical simulation of the probabilistic aerothermodynamic response of propulsion system components to randomness in their environment was explored. The reusable rocket engine turbopumps were selected as an example because of the severe cryogenic environment in which they operate. The thermal and combustion instabilities, coupled with the engine thrust requirements from start up to shut down, lead to randomness in the flow variables and uncertainties in the aerodynamic loading. The probabilistic modeling of the turbopumps aerodynamic response was accomplished using the panel method coupled with fast probability integration methods. The aerodynamic response in the form of probabilistic rotor blades and splitter loading were predicted and the results presented for specified flow coefficient and rotor preswirl variance. Possible future applications of the aerothermodynamic probabilistic modeling in engine transient simulation, condition monitoring and engine life prediction are briefly discussed. Author

N90-21037* Sverdrup Technology, Inc., Cleveland, OH. **EXHAUST NOZZLES FOR PROPULSION SYSTEMS WITH EMPHASIS ON SUPERSONIC CRUISE AIRCRAFT**

LEONARD E. STITT May 1990 107 p (Contract NAS3-25266) (NASA-RP-1235; E-4789; NAS 1.61:1235) Avail: NTIS HC A06/MF A01 CSCL 21/5

This compendium summarizes the contributions of the NASA-Lewis and its contractors to supersonic exhaust nozzle research from 1963 to 1985. Two major research and technology efforts sponsored this nozzle research work; the U.S. Supersonic Transport (SST) Program and the follow-on Supersonic Cruise Research (SCR) Program. They account for two generations of nozzle technology: the first from 1963 to 1971, and the second

from 1971 to 1985. First, the equations used to calculate nozzle thrust are introduced. Then the general types of nozzles are presented, followed by a discussion of those types proposed for supersonic aircraft. Next, the first-generation nozzles designed specifically for the Boeing SST and the second-generation nozzles designed under the SCR program are separately reviewed and then compared. A chapter on throttle-dependent afterbody drag is included, since drag has a major effect on the off-design performance of supersonic nozzles. A chapter on the performance of supersonic dash nozzles follows, since these nozzles have similar design problems. Finally, the nozzle test facilities used at NASA-Lewis during this nozzle research effort are identified and discussed. These facilities include static test stands, a transonic wind tunnel, and a flying testbed aircraft. A concluding section points to the future: a third generation of nozzles designed for a new era of high speed civil transports to produce even greater advances in performance, to meet new noise rules, and to ensure the continuity of over two decades of NASA research. Author

N90-21038* National Aeronautics and Space Administration. Lewis Research Center, Cleveland, OH.

SUPERSONIC THROUGH-FLOW FAN ENGINE AND AIRCRAFT MISSION PERFORMANCE

LEO C. FRANCISCUS and JAIME J. MALDONADO (Puerto Rico Univ., Mayaguez.) 1989 15 p Presented at the Aircraft Design, Systems, and Operations Conference, Seattle, WA, 31 Jul. - 2 Aug. 1989; cosponsored by AIAA, AHS, and ASEE (NASA-TM-102304; E-4991; NAS 1.15:102304; AIAA-89-2139) Avail: NTIS HC A03/MF A01 CSCL 21/5

A study was made to evaluate potential improvement to a commercial supersonic transport by powering it with supersonic through-flow fan turbofan engines. A Mach 3.2 mission was considered. The three supersonic fan engines considered were designed to operate at bypass ratios of 0.25, 0.5, and 0.75 at supersonic cruise. For comparison a turbine bypass turbojet was included in the study. The engines were evaluated on the basis of aircraft takeoff gross weight with a payload of 250 passengers for a fixed range of 5000 N.MI. The installed specific fuel consumption of the supersonic fan engines was 7 to 8 percent lower than that of the turbine bypass engine. The aircraft powered by the supersonic fan engines had takeoff gross weights 9 to 13 percent lower than aircraft powered by turbine bypass engines. Author

N90-21761* Pratt and Whitney Aircraft, West Palm Beach, FL. **ASSESSMENT OF HIGH TEMPERATURE SUPERCONDUCTING (HTS) ELECTRIC MOTORS FOR ROTORCRAFT PROPULSION** Final Report

JAY DOERNBACH Apr. 1990 49 p (Contract NAS3-25117) (NASA-CR-185222; NAS 1.26:185222; PW-FR-20668) Avail: NTIS HC A03/MF A01 CSCL 21/5

The successful development of high temperature superconductors (HTS) could have a major impact on future aeronautical propulsion and aeronautical flight vehicle systems. Applications of high temperature superconductors have been envisioned for several classes of aeronautical systems, including subsonic and supersonic transports, hypersonic aircraft, V/STOL aircraft, rotorcraft and solar powered aircraft. The potential of HTS electric motors and generators for providing primary shaft power for rotorcraft propulsion is examined. Three different sized production helicopters were investigated; namely, the Bell Jet Ranger, the Sikorsky Black Hawk and the Sikorsky Super Stallion. These rotorcraft have nominal horsepower ratings of 500, 3600, and 13400 respectively. Preliminary results indicated that an all-electric HTS drive system produces an improvement in rotorcraft Takeoff Gross Weight (TOGW) for those rotorcraft with power ratings above 2000 horsepower. The predicted TOGW improvements are up to 9 percent for the medium-sized Sikorsky Black Hawk and up to 20 percent for the large-sized Sikorsky Super Stallion. The small-sized Bell Jet Ranger, however, experienced a penalty in TOGW with the all-electric HTS drive system. Author

07 AIRCRAFT PROPULSION AND POWER

N90-21762*# National Aeronautics and Space Administration. Lewis Research Center, Cleveland, OH.

ON THE USE OF EXTERNAL BURNING TO REDUCE AEROSPACE VEHICLE TRANSONIC DRAG

CHARLES J. TREFNY 1990 12 p Proposed for presentation at the 26th Joint Propulsion Conference, Orlando, FL, 16-18 Jul. 1990; cosponsored by AIAA, ASME, SAE, and ASEE (NASA-TM-103107; E-5431; NAS 1.15:103107; AIAA-90-1935) Avail: NTIS HC A03/MF A01 CSCL 21/5

The external combustion of hydrogen to reduce the transonic drag of aerospace vehicles is currently being investigated. A preliminary analysis based on a constant pressure control volume is discussed. Results indicate that the specific impulse of the external burning process rivals that of a turbojet and depends on the severity of the initial base drag as well as on the Mach flight number and the equivalence ratio. A test program was conducted to investigate hydrogen-air flame stability at the conditions of interest and to demonstrate drag reduction on a simple expansion ramp. Initial test results are presented and compared with the control-volume analysis. The expansion ramp surface pressure coefficient showed little variation with fuel pressure and altitude, in disagreement with the analysis. Flame stability results were encouraging and indicate that stable combustion is possible over an adequate range of conditions. Facility interference and chemical kinetics phenomena that make interpretation of subscale ground test data difficult are discussed. Author

N90-21763*# Sverdrup Technology, Inc., Brook Park, OH.

PRELIMINARY DESIGN OF A LONG-ENDURANCE MARS AIRCRAFT Final Report

ANTHONY J. COLOZZA Apr. 1990 14 p Proposed for presentation at the 26th Joint Propulsion Conference, Orlando, FL, 16-18 Jul. 1990; sponsored by AIAA, SAE, ASME and ASEE (Contract NAS3-25266) (NASA-CR-185243; E-5475; NAS 1.26:185243; AIAA-90-2000) Avail: NTIS HC A03/MF A01 CSCL 21/5

The preliminary design requirements of a long endurance aircraft capable of flight within the Martian environment was determined. Both radioisotope/heat engine and PV solar array power production systems were considered. Various cases for each power system were analyzed in order to determine the necessary size, weight and power requirements of the aircraft. The analysis method used was an adaptation of the method developed by Youngblood and Talay of NASA-Langley used to design a high altitude earth based aircraft. The analysis is set up to design an aircraft which, for the given conditions, has a minimum wingspan and maximum endurance parameter. The results showed that, for a first approximation, a long endurance aircraft is feasible within the Martian environment. The size and weight of the most efficient solar aircraft were comparable to the radioisotope powered one. Author

N90-22564*# National Aeronautics and Space Administration. Lewis Research Center, Cleveland, OH.

LARGE-SCALE ADVANCED PROPELLER BLADE PRESSURE DISTRIBUTIONS: PREDICTION AND DATA

M. NALLASAMY, O. YAMAMOTO, S. WARSI (Sverdrup Technology, Inc., Cleveland, OH.), and L. J. BOBER 1989 19 p Presented at the 25th Joint Propulsion Conference, Monterey, CA, 10-12 Jul. 1989; cosponsored by AIAA, ASME, SAE, and ASEE Previously announced in IAA as A89-47026 Original contains color illustrations (NASA-TM-102316; E-4914; NAS 1.15:102316; AIAA-89-2696) Avail: NTIS HC A03/MF A01; 5 functional color pages CSCL 21/5

Two Euler analyses techniques, finite difference and finite volume, were employed to predict the blade surface pressure distributions of a large scale advanced propeller. The predicted pressure distributions were compared with wind tunnel data. Both techniques produced blade pressure distributions that are in fairly good agreement with the data over the range of test Mach numbers of 0.2 to 0.78. However, the numerical simulations fail to predict correctly the measured pressure distributions for the low Mach

number, high power case. The data indicate the presence of a leading edge vortex for this case. A discussion of the compressibility effects is also presented. Author

N90-22566*# National Aeronautics and Space Administration. Lewis Research Center, Cleveland, OH.

A MODELING TECHNIQUE FOR STOVL EJECTOR AND VOLUME DYNAMICS

C. K. DRUMMOND and W. S. BARANKIEWICZ 1990 13 p Presented at the 26th Joint Propulsion Conference, Orlando, FL, 16-18 Jul. 1990; cosponsored by AIAA, SAE, ASME, and ASEE (NASA-TM-103167; E-5539; NAS 1.15:103167; AIAA-90-2417) Avail: NTIS HC A03/MF A01 CSCL 21/5

New models for thrust augmenting ejector performance prediction and feeder duct dynamic analysis are presented and applied to a proposed Short Take Off and Vertical Landing (STOVL) aircraft configuration. Central to the analysis is the nontraditional treatment of the time-dependent volume integrals in the otherwise conventional control-volume approach. In the case of the thrust augmenting ejector, the analysis required a new relationship for transfer of kinetic energy from the primary flow to the secondary flow. Extraction of the required empirical corrections from current steady-state experimental data is discussed; a possible approach for modeling insight through Computational Fluid Dynamics (CFD) is presented. Author

N90-22567*# General Motors Corp., Indianapolis, IN. Gas Turbine Div.

INVESTIGATION OF ADVANCED COUNTERROTATION BLADE CONFIGURATION CONCEPTS FOR HIGH SPEED TURBOPROP SYSTEMS, TASK 1: DUCTED PROPFAN ANALYSIS Final Report

EDWARD J. HALL, ROBERT A. DELANEY, and JAMES L. BETTNER Apr. 1990 158 p Original contains color illustrations (Contract NAS3-25270) (NASA-CR-185217; NAS 1.26:185217; EDR-14622) Avail: NTIS HC A08/MF A01; 11 functional color pages CSCL 21/5

The time-dependent three-dimensional Euler equations of gas dynamics were solved numerically to study the steady compressible transonic flow about ducted propfan propulsion systems. Aerodynamic calculations were based on a four-stage Runge-Kutta time-marching finite volume solution technique with added numerical dissipation. An implicit residual smoothing operator was used to aid convergence. Two calculation grids were employed in this study. The first grid utilized an H-type mesh network with a branch cut opening to represent the axisymmetric cowl. The second grid utilized a multiple-block mesh system with a C-type grid about the cowl. The individual blocks were numerically coupled in the Euler solver. Grid systems were generated by a combined algebraic/elliptic algorithm developed specifically for ducted propfans. Numerical calculations were initially performed for unducted propfans to verify the accuracy of the three-dimensional Euler formulation. The Euler analyses were then applied for the calculation of ducted propfan flows, and predicted results were compared with experimental data for two cases. The three-dimensional Euler analyses displayed exceptional accuracy, although certain parameters were observed to be very sensitive to geometric deflections. Both solution schemes were found to be very robust and demonstrated nearly equal efficiency and accuracy, although it was observed that the multi-block C-grid formulation provided somewhat better resolution of the cowl leading edge region. Author

N90-23403*# National Aeronautics and Space Administration. Lewis Research Center, Cleveland, OH.

EXPERIMENTAL EVALUATION OF A TUNED ELECTROMAGNETIC DAMPER FOR VIBRATION CONTROL OF CRYOGENIC TURBOPUMP ROTORS

ELISEO DIRUSSO and GERALD V. BROWN Washington Jun. 1990 17 p (NASA-TP-3005; E-5012; NAS 1.60:3005) Avail: NTIS HC A03/MF A01 CSCL 21/5

Experiments were performed on a passive tuned electromagnetic damper that could be used for damping rotor vibrations in cryogenic turbopumps for rocket engines. The tests were performed in a rig that used liquid nitrogen to produce cryogenic turbopump temperatures. This damper is most effective at cryogenic temperatures and is not a viable damper at room temperature. The unbalanced amplitude response of the rotor shaft was measured for undamped (baseline) and damped conditions at the critical speeds of the rotor (approx. 5900 to 6400 rpm) and the data were compared. The tests were performed for a speed range between 900 and 10 000 rpm. The tests revealed that the damper is very effective for damping single-mode narrow bandwidth amplitude response but is less effective in damping broadband response or multimode amplitude response. Author

N90-23404*# National Aeronautics and Space Administration. Lewis Research Center, Cleveland, OH.

ANALYSIS OF INTERNAL FLOW IN A VENTRAL NOZZLE FOR STOVL AIRCRAFT

C. FREDERIC SMITH (Sverdrup Technology, Inc., Brookpark, OH.) and JACK G. MCARDLE 1990 21 p Presented at the 26th Joint Propulsion Conference, Orlando, FL, 16-18 Jul. 1990; cosponsored by AIAA, SAE, ASME, and ASCE LIMITED REPRODUCIBILITY: More than 20% of this document may be affected by color photographs Original contains color illustrations (Contract NAS3-25266) (NASA-TM-103123; E-5451; NAS 1.15:103123; AIAA-90-1899) Avail: NTIS HC A03/MF A01; 3 functional color pages CSCL 21/5

Short takeoff and vertical landing (STOVL) aircraft are planned for possible future development. For these aircraft, the same propulsion system will provide power for lift, hover, and horizontal flight. To accomplish this, many designs include a ventral nozzle to provide part of the vertical thrust required. Understanding and predicting the internal aerodynamic flow caused by a single exhaust duct opening are highly desirable in assessing this concept. A numerical simulation of a ventral nozzle is presented and the results are compared with experimental data. Comparisons include visualizations of the flow along the ventral duct walls and in the tailpipe plane of symmetry. Performance calculations are also compared with measured values. Author

N90-23405*# Calspan-Buffalo Univ. Research Center, NY.
HEAT TRANSFER AND PRESSURE MEASUREMENTS FOR THE SSME FUEL-SIDE TURBOPUMP

MICHAEL G. DUNN Jul. 1990 29 p
(Contract NAG3-581)
(NASA-CR-184928; NAS 1.26:184928) Avail: NTIS HC A03/MF A01 CSCL 21/5

A measurement program is currently underway at the Calspan-UB Research Center (CUBRC) which utilizes the Rocketdyne two-state fuel-side turbine with the engine geometric configuration reproduced. This is a full two-state turbine for which the vane rows and the blades are the engine hardware currently used on the Space Shuttle turbopump. A status report is provided for the experimental program and a description of the instrumentation and the measurements to be performed. The specific items that will be illustrated and described are as follows: (1) the gas flow path, (2) the heat-flux instrumentation, (3) the surface-pressure instrumentation, (4) the experimental conditions for which data will be obtained, and (5) the specific measurements that will be performed. Author

N90-23406*# Sverdrup Technology, Inc., Brook Park, OH.
COMPUTATIONAL ANALYSIS OF THE FLOWFIELD OF A TWO-DIMENSIONAL EJECTOR NOZZLE Final Report

Y. H. CHOI and W. Y. SOH Jun. 1990 17 p Presented at the 26th Joint Propulsion Conference, Orlando, FL, 16-18 Jul. 1990; cosponsored by AIAA, SAE, and ASME
(Contract NAS3-25266)
(NASA-CR-185255; E-5548; NAS 1.26:185255; AIAA-90-1901) Avail: NTIS HC A03/MF A01 CSCL 21/5

A time-iterative full Navier-Stokes code, PARC, is used to

analyze the flowfield of a two-dimensional ejector nozzle system. A parametric study was performed for two controlling parameters, duct to nozzle area ratio and nozzle pressure ratio. Results show that there is an optimum area ratio for the efficient pumping of secondary flow. At high area ratios, a freestream flow passes directly through the mixing duct without giving adequate pumping. At low area ratios, the jet boundary blocks the incoming flow. The nozzle pressure ratio variation shows that the pumping rate increases as the pressure ratio increases, provided there is no interaction between the shroud wall and the shock cell structure. Author

N90-23407*# National Aeronautics and Space Administration. Lewis Research Center, Cleveland, OH.

NASA LEWIS ICING RESEARCH TUNNEL USER MANUAL

RONALD H. SOEDER and CHARLES R. ANDRACCHIO Jun. 1990 40 p
(NASA-TM-102319; E-5015; NAS 1.15:102319) Avail: NTIS HC A03/MF A01 CSCL 21/5

The Icing Research Tunnel (IRT) at Lewis Research Center is described and information is provided for users who wish to conduct experiments in this facility. The capabilities of the tunnel test section, main drive system, speed control, and spray bars are described. Tunnel performance maps of water droplet size as a function of liquid water content are presented for a range of test section velocities from 43.5 to 217.3 kn (50 to 250 mph) for two types of spray nozzles. Tunnel facility support systems, which include heated air systems, steam and service air systems, altitude exhaust system, and model electrical power are described. Facility instrumentation capabilities regarding temperature and pressure measurements and model attitude simulation are discussed. Photographic documentation and flow visualization techniques are also described. Preliminary and pretest meeting formats and schedules are outlined. Tunnel user responsibility, personnel safety, and cost of tunnel operation are also stated. The Icing Research Tunnel is equipped to support testing of low-speed models. The IRT is a closed-return atmospheric-type tunnel with rectangular cross sections. Author

N90-24273*# National Aeronautics and Space Administration. Lewis Research Center, Cleveland, OH.

EXPERIMENTAL AND ANALYTICAL STUDY OF CLOSE-COUPLED VENTRAL NOZZLES FOR ASTOVL AIRCRAFT

JACK G. MCARDLE and C. FREDERIC SMITH (Sverdrup Technology, Inc., Cleveland, OH.) 1990 16 p Proposed for presentation at the International Powered Lift Conference, London, England, 29-31 Aug. 1990; sponsored by Royal Aeronautical Society
(NASA-TM-103170; E-5499; NAS 1.15:103170) Avail: NTIS HC A03/MF A01 CSCL 21/5

Flow in a generic ventral nozzle system was studied experimentally and analytically with a block version of the PARC3D computational fluid dynamics program (a full Navier-Stokes equation solver) in order to evaluate the program's ability to predict system performance and internal flow patterns. For the experimental work a one-third-size model tailpipe with a single large rectangular ventral nozzle mounted normal to the tailpipe axis was tested with unheated air at steady-state pressure ratios up to 4.0. The end of the tailpipe was closed to simulate a blocked exhaust nozzle. Measurements showed about 5 1/2 percent flow-turning loss, reasonable nozzle performance coefficients, and a significant aftward axial component of thrust due to flow turning loss, reasonable nozzle performance coefficients, and a significant aftward axial component of thrust due to flow turning more than 90 deg. Flow behavior into and through the ventral duct is discussed and illustrated with paint streak flow visualization photographs. For the analytical work the same ventral system configuration was modeled with two computational grids to evaluate the effect of grid density. Both grids gave good results. The finer-grid solution produced more detailed flow patterns and predicted performance parameters, such as thrust and discharge coefficient, within 1 percent of the measured values. PARC3D flow visualization images are shown

07 AIRCRAFT PROPULSION AND POWER

for comparison with the paint streak photographs. Modeling and computational issues encountered in the analytical work are discussed. Author

N90-24274*# General Motors Corp., Indianapolis, IN. Allison Gas Turbine Div.

ADVANCED GEARBOX TECHNOLOGY Final Report, Aug. 1984 - Jan. 1987

N. E. ANDERSON, R. W. CEDOZ, E. E. SALAMA, and D. A. WAGNER Jun. 1987 142 p Presented at the AIAA/SAE/ASME/ASCE 23rd Joint Propulsion Conference, San Diego, CA, Jun. 1987 (Contract NAS3-24341) (NASA-CR-179625; NAS 1.26:179625; EDR-12909) Avail: NTIS HC A07/MF A01 CSCL 21/5

An advanced 13,000 HP, counterrotating (CR) gearbox was designed and successfully tested to provide a technology base for future designs of geared propfan propulsion systems for both commercial and military aircraft. The advanced technology CR gearbox was designed for high efficiency, low weight, long life, and improved maintainability. The differential planetary CR gearbox features double helical gears, double row cylindrical roller bearings integral with planet gears, tapered roller prop support bearings, and a flexible ring gear and diaphragm to provide load sharing. A new Allison propfan back-to-back gearbox test facility was constructed. Extensive rotating and stationary instrumentation was used to measure temperature, strain, vibration, deflection and efficiency under representative flight operating conditions. The tests verified smooth, efficient gearbox operation. The highly-instrumented advanced CR gearbox was successfully tested to design speed and power (13,000 HP), and to a 115 percent overspeed condition. Measured CR gearbox efficiency was 99.3 percent at the design point based on heat loss to the oil. Tests demonstrated low vibration characteristics of double helical gearing, proper gear tooth load sharing, low stress levels, and the high load capacity of the prop tapered roller bearings. Applied external prop loads did not significantly affect gearbox temperature, vibration, or stress levels. Gearbox hardware was in excellent condition after the tests with no indication of distress. Author

N90-25982*# National Aeronautics and Space Administration. Lewis Research Center, Cleveland, OH.

PERFORMANCE OF A SUPERCHARGED DIRECT-INJECTION STRATIFIED-CHARGE ROTARY COMBUSTION ENGINE

TIMOTHY A. BARTRAND (Sverdrup Technology, Inc., Brook Park, OH.) and EDWARD A. WILLIS Apr. 1990 25 p Presented at the Joint Symposium on General Aviation Systems, Ocean City, NJ, 11-12 Apr. 1990; sponsored in part by AIAA and FAA (NASA-TM-103105; E-5430; NAS 1.15:103105) Avail: NTIS HC A03/MF A01 CSCL 21/5

A zero-dimensional thermodynamic performance computer model for direct-injection stratified-charge rotary combustion engines was modified and run for a single rotor supercharged engine. Operating conditions for the computer runs were a single boost pressure and a matrix of speeds, loads and engine materials. A representative engine map is presented showing the predicted range of efficient operation. After discussion of the engine map, a number of engine features are analyzed individually. These features are: heat transfer and the influence insulating materials have on engine performance and exhaust energy; intake manifold pressure oscillations and interactions with the combustion chamber; and performance losses and seal friction. Finally, code running times and convergence data are presented. Author

N90-26009*# National Aeronautics and Space Administration. Lewis Research Center, Cleveland, OH.

HOT GAS INGESTION CHARACTERISTICS AND FLOW VISUALIZATION OF A VECTORED THRUST STOVL CONCEPT

ALBERT L. JOHNS, GEORGE H. NEINER, TIMOTHY J. BENCIC, JOSEPH D. FLOOD, KURT C. AMUEDO, THOMAS W. STROCK, and BEN R. WILLIAMS (McDonnell Aircraft Co., Saint Louis, MO.) 1990 22 p Presented at the International Powered Lift Conference, London, England, 29-31 Aug. 1990; sponsored by

Royal Aeronautical Society (NASA-TM-103212; E-5623; NAS 1.15:103212) Avail: NTIS HC A03/MF A01 CSCL 21/5

A 9.2 percent scale short takeoff and vertical landing (STOVL) hot gas ingestion model was designed and built by McDonnell Douglas Corporation (MCAIR) and tested in the NASA Lewis Research Center 9- by 15-Foot Low Speed Wind Tunnel (LSWT). Hot gas ingestion, the entrainment of heated engine exhaust into the inlet flow field, is a key development issue for advanced short takeoff and vertical landing aircraft. The Phase 1 test program, conducted by NASA Lewis and McDonnell Douglas Corporation, evaluated the hot ingestion phenomena and control techniques and Phase 2 test program which was conducted by NASA Lewis are both reported. The Phase 2 program was conducted at exhaust nozzles temperatures up to 1460 R and utilized a sheet laser system for flow visualization of the model flow field in and out of ground effects. Hot gas ingestion levels were measured for the several forward nozzle splay configurations and with flow control/lift improvement devices which reduced the hot gas ingestion. The model support system had four degrees of freedom, heated high pressure air for nozzle flow, and a suction system exhaust for inlet flow. The headwind (freestream) velocity for Phase 1 was varied from 8 to 90 kn, with primary data taken in the 8 to 23 kn headwind velocity range. Phase 2 headwind velocity varied from 10 to 23 kn. Results of both Phase 1 and 2 are presented. A description of the model, facility, a new model support system, and a sheet laser illumination system are also provided. Results are presented over a range of main landing gear height (model height) above the ground plane at a 10 kn headwind velocity. The results contain the compressor face pressure and temperature distortions, total pressure recovery, compressor face temperature rise, and the environmental effects of the hot gas. The environmental effects include the ground plane temperature and pressure distributions, model airframe heating, and the location of the ground flow separation. Results from the sheet laser flow visualization test are also shown. Author

N90-27722*# National Aeronautics and Space Administration. Lewis Research Center, Cleveland, OH.

COMPUTER CODE FOR PREDICTING COOLANT FLOW AND HEAT TRANSFER IN TURBOMACHINERY

PETER L. MEITNER Washington Sep. 1990 41 p Prepared in cooperation with Army Aviation Systems Command, Cleveland, OH

(Contract DA PROJ. 1L1-61102-AH-45)

(NASA-TP-2985; E-5186; NAS 1.60:2985; AVSCOM-TR-89-C-008) Avail: NTIS HC A03/MF A01 CSCL 21/5

A computer code was developed to analyze any turbomachinery coolant flow path geometry that consist of a single flow passage with a unique inlet and exit. Flow can be bled off for tip-cap impingement cooling, and a flow bypass can be specified in which coolant flow is taken off at one point in the flow channel and reintroduced at a point farther downstream in the same channel. The user may either choose the coolant flow rate or let the program determine the flow rate from specified inlet and exit conditions. The computer code integrates the 1-D momentum and energy equations along a defined flow path and calculates the coolant's flow rate, temperature, pressure, and velocity and the heat transfer coefficients along the passage. The equations account for area change, mass addition or subtraction, pumping, friction, and heat transfer. Author

N90-28552*# Hamilton Standard, Windsor Locks, CT. **MEASUREMENT OF THE STEADY SURFACE PRESSURE DISTRIBUTION ON A SINGLE ROTATION LARGE SCALE ADVANCED PROP-FAN BLADE AT MACH NUMBERS FROM 0.03 TO 0.78 Final Report**

PETER BUSHNELL Jul. 1988 540 p

(Contract NAS3-23051)

(NASA-CR-182124; E-4137; NAS 1.26:182124) Avail: NTIS HC A23/MF A03 CSCL 21/5

The aerodynamic pressure distribution was determined on a rotating Prop-Fan blade at the S1-MA wind tunnel facility operated

by the Office National D'Etudes et de Recherches Aerospatiale (ONERA) in Modane, France. The pressure distributions were measured at thirteen radial stations on a single rotation Large Scale Advanced Prop-Fan (LAP/SR7) blade, for a sequence of operating conditions including inflow Mach numbers ranging from 0.03 to 0.78. Pressure distributions for more than one power coefficient and/or advanced ratio setting were measured for most of the inflow Mach numbers investigated. Due to facility power limitations the Prop-Fan test installation was a two bladed version of the eight design configuration. The power coefficient range investigated was therefore selected to cover typical power loading per blade conditions which occur within the Prop-Fan operating envelope. The experimental results provide an extensive source of information on the aerodynamic behavior of the swept Prop-Fan blade, including details which were elusive to current computational models and do not appear in the two-dimensional airfoil data.

Author

N90-28553*# General Electric Co., Cincinnati, OH. Aircraft Engine Group.

ENERGY EFFICIENT ENGINE HIGH PRESSURE TURBINE COMPONENT TEST PERFORMANCE REPORT

L. P. TIMKO 1984 173 p

(Contract NAS3-20643)

(NASA-CR-168289; NAS 1.26:168289; R82AEB406) Avail: NTIS HC A08/MF A01 CSCL 21/5

The high pressure turbine for the General Electric Energy Efficient Engine is a two stage design of moderate loading. Results of detailed system studies led to selection of this configuration as the most appropriate in meeting the efficiency goals of the component development program. To verify the design features of the high pressure turbine, a full scale warm air turbine test rig with cooling flows simulated was run. Prior to this testing, an annular cascade test was run to select vane unguided turn for the first stage nozzle. Results of this test showed that the base configuration exceeded the lower unguided turning configuration by 0.48 percent in vane kinetic energy efficiency. The air turbine test program, consisting of extensive mapping and cooling flow variation as well as design point evaluation, demonstrated a design point efficiency level of 90.0 percent based on the thermodynamic definition. In terms of General Electric cycle definition, this efficiency was 92.5 percent. Based on this test, it is concluded that efficiency goals for the Flight Propulsion System were met.

Author

N90-28554*# General Electric Co., Cincinnati, OH. Aircraft Engine Business Group.

ENERGY EFFICIENT ENGINE COMBUSTOR TEST HARDWARE DETAILED DESIGN REPORT

D. L. BURRUS, C. A. CHAHROUR, H. L. FOLTZ, P. E. SABLE, S. P. SETO, and J. R. TAYLOR Mar. 1984 474 p

(Contract NAS3-20643)

(NASA-CR-168301; NAS 1.26:168301; R82AEB472) Avail: NTIS HC A20/MF A03 CSCL 21/5

The Energy Efficient Engine (E3) Combustor Development effort was conducted as part of the overall NASA/GE E3 Program. This effort included the selection of an advanced double-annular combustion system design. The primary intent was to evolve a design which meets the stringent emissions and life goals of the E3 as well as all of the usual performance requirements of combustion systems for modern turbofan engines. Numerous detailed design studies were conducted to define the features of the combustion system design. Development test hardware was fabricated, and an extensive testing effort was undertaken to evaluate the combustion system subcomponents in order to verify and refine the design. Technology derived from this development effort will be incorporated into the engine combustion system hardware design. This advanced engine combustion system will then be evaluated in component testing to verify the design intent. What is evolving from this development effort is an advanced combustion system capable of satisfying all of the combustion system design objectives and requirements of the E3. Fuel nozzle, diffuser, starting, and emissions design studies are discussed.

R.J.F.

N90-28555*# General Electric Co., Cincinnati, OH. Aircraft Engine Business Group.

ENERGY EFFICIENT ENGINE (E3) COMBUSTION SYSTEM COMPONENT TECHNOLOGY PERFORMANCE REPORT Draft Report

D. L. BURRUS, C. A. CHAHROUR, H. L. FOLTZ, P. E. SABLE, S. P. SETO, and J. R. TAYLOR Jul. 1984 494 p

(Contract NAS3-20643)

(NASA-CR-168274; NAS 1.26:168274; R82AEB401) Avail: NTIS HC A21/MF A03 CSCL 21/5

The Energy Efficient Engine (E3) combustor effort was conducted as part of the overall NASA/GE E3 Program. This effort included the selection of an advanced double-annular combustion system design. The primary intent of this effort was to evolve a design that meets the stringent emissions and life goals of the E3, as well as all of the usual performance requirements of combustion systems for modern turbofan engines. Numerous detailed design studies were conducted to define the features of the combustion system design. Development test hardware was fabricated, and an extensive testing effort was undertaken to evaluate the combustion system subcomponents in order to verify and refine the design. Technology derived from this effort was incorporated into the engine combustion hardware design. The advanced engine combustion system was then evaluated in component testing to verify the design intent. What evolved from this effort was an advanced combustion system capable of satisfying all of the combustion system design objectives and requirements of the E3.

R.J.F.

N90-28556*# Pratt and Whitney Aircraft, East Hartford, CT. Engineering Div.

ENERGY EFFICIENT ENGINE EXHAUST MIXER MODEL TECHNOLOGY REPORT ADDENDUM; PHASE 3 TEST PROGRAM

M. J. LARKIN and J. R. BLATT Apr. 1984 197 p

(Contract NAS3-20646)

(NASA-CR-174799; NAS 1.26:174799; PWA-5594-271-ADD)

Avail: NTIS HC A09/MF A02 CSCL 21/5

The Phase 3 exhaust mixer test program was conducted to explore the trends established during previous Phases 1 and 2. Combinations of mixer design parameters were tested. Phase 3 testing showed that the best performance achievable within tailpipe length and diameter constraints is 2.55 percent better than an optimized separate flow base line. A reduced penetration design achieved about the same overall performance level at a substantially lower level of excess pressure loss but with a small reduction in mixing. To improve reliability of the data, the hot and cold flow thrust coefficient analysis used in Phases 1 and 2 was augmented by calculating percent mixing from traverse data. Relative change in percent mixing between configurations was determined from thrust and flow coefficient increments. The calculation procedure developed was found to be a useful tool in assessing mixer performance. Detailed flow field data were obtained to facilitate calibration of computer codes.

Author

N90-28557*# General Electric Co., Cincinnati, OH. Aircraft Engine Business Group.

ENERGY EFFICIENT ENGINE ACOUSTIC SUPPORTING TECHNOLOGY REPORT

S. P. LAVIN and P. Y. HO Jun. 1985 371 p

(Contract NAS3-20643)

(NASA-CR-174834; NAS 1.26:174834; R84AEB246) Avail: NTIS HC A16/MF A02 CSCL 21/5

The acoustic development of the Energy Efficient Engine combined testing and analysis using scale model rigs and an integrated Core/Low Spool demonstration engine. The scale model tests show that a cut-on blade/vane ratio fan with a large spacing ($S/C = 2.3$) is as quiet as a cut-off blade/vane ratio with a tighter spacing ($S/C = 1.27$). Scale model mixer tests show that separate flow nozzles are the noisiest, conic nozzles the quietest, with forced mixers in between. Based on projections of ICLS data the Energy Efficient Engine (E3) has FAR 36 margins of 3.7 EPNdB

07 AIRCRAFT PROPULSION AND POWER

at approach, 4.5 EPNdB at full power takeoff, and 7.2 EPNdB at sideline conditions. Author

N90-28558*# General Electric Co., Evendale, OH. Aircraft Engine Business Group.

ENERGY EFFICIENT ENGINE: FLIGHT PROPULSION SYSTEM FINAL DESIGN AND ANALYSIS Report, Nov. 1978 - Aug. 1983 DONALD Y. DAVIS and E. MARSHALL STEARNS Aug. 1985 170 p

(Contract NAS3-20643)

(NASA-CR-168219; NAS 1.26:168219; R83AEB488) Avail: NTIS HC A08/MF A01 CSCL 21/5

The Energy Efficient Engine (E3) is a NASA program to create fuel saving technology for future transport engines. The Flight Propulsion System (FPS) is the engine designed to achieve E3 goals. Achieving these goals required aerodynamic, mechanical and system technologies advanced beyond that of current production engines. These technologies were successfully demonstrated in component rigs, a core engine and a turbofan ground test engine. The design and benefits of the FPS are presented. All goals for efficiency, environmental considerations, and economic payoff were met. The FPS has, at maximum cruise, 10.67 km (35,000 ft), M0.8, standard day, a 16.9 percent lower installed specific fuel consumption than a CF6-50C. It provides an 8.6 percent reduction in direct operating cost for a short haul domestic transport and a 16.2 percent reduction for an international long distance transport. Author

N90-28559*# General Electric Co., Cincinnati, OH. Aircraft Engine Business Group.

ENERGY EFFICIENT ENGINE CORE DESIGN AND PERFORMANCE REPORT Report, Jan. 1978 - Dec. 1982

E. MARSHALL STEARNS et al. Dec. 1982 530 p

(Contract NAS3-20643)

(NASA-CR-168069; NAS 1.26:168069; R82AEB470) Avail: NTIS HC A23/MF A03 CSCL 21/5

The Energy Efficient Engine (E3) is a NASA program to develop fuel saving technology for future large transport aircraft engines. Testing of the General Electric E3 core showed that the core component performance and core system performance necessary to meet the program goals can be achieved. The E3 core design and test results are described. Author

N90-28560*# Pratt and Whitney Aircraft, East Hartford, CT. Engineering Div.

ENERGY EFFICIENT ENGINE PROGRAM ADVANCED TURBOFAN NACELLE DEFINITION STUDY

DAVID C. HOWE and T. A. WYNOSKY May 1985 165 p

(Contract NAS3-20646)

(NASA-CR-174942; NAS 1.26:174942; PWA-5394-315) Avail: NTIS HC A08/MF A01 CSCL 21/5

Advanced, low drag, nacelle configurations were defined for some of the more promising propulsion systems identified in the earlier Benefit/Cost Study, to assess the benefits associated with these advanced technology nacelles and formulate programs for developing these nacelles and low volume thrust reversers/spoilers to a state of technology readiness in the early 1990's. The study results established the design feasibility of advanced technology, slim line nacelles applicable to advanced technology, high bypass ratio turbofan engines. Design feasibility was also established for two low volume thrust reverse/spoiler concepts that meet or exceed the required effectiveness for these engines. These nacelle and thrust reverse/spoiler designs were shown to be applicable in engines with takeoff thrust sizes ranging from 24,000 to 60,000 pounds. The reduced weight, drag, and cost of the advanced technology nacelle installations relative to current technology nacelles offer a mission fuel burn savings ranging from 3.0 to 4.5 percent and direct operating cost plus interest improvements from 1.6 to 2.2 percent. Author

N90-28561*# General Electric Co., Evendale, OH. Aircraft Engine Business Group.

ENERGY EFFICIENT ENGINE INTEGRATED CORE/LOW SPOOL DESIGN AND PERFORMANCE REPORT Topical Report, Jan. 1978 - Aug. 1983

E. MARSHALL STEARNS et al. Feb. 1985 649 p

(Contract NAS3-20643)

(NASA-CR-168211; NAS 1.26:168211; R83AEB503) Avail: NTIS HC A99/MF A04 CSCL 21/5

The Energy Efficient Engine (E3) is a NASA program to create fuel saving technology for future transport aircraft engines. The E3 technology advancements were demonstrated to operate reliably and achieve goal performance in tests of the Integrated Core/Low Spool vehicle. The first build of this undeveloped technology research engine set a record for low fuel consumption. Its design and detailed test results are herein presented. Author

N90-28562*# General Electric Co., Evendale, OH. Aircraft Engine Business Group.

ENERGY EFFICIENT ENGINE: CONTROL SYSTEM COMPONENT PERFORMANCE REPORT

R. S. BEITLER and G. W. BENNETT Oct. 1984 205 p

(Contract NAS3-20643)

(NASA-CR-174651; NAS 1.26:174651; R83AEB623) Avail: NTIS HC A10/MF A02 CSCL 21/5

An Energy Efficient Engine (E3) program was established to develop technology for improving the energy efficiency of future commercial transport aircraft engines. As part of this program, General Electric designed and tested a new engine. The design, fabrication, bench and engine testing of the Full Authority Digital Electronic Control (FADEC) system used for controlling the E3 Demonstrator Engine is described. The system design was based on many of the proven concepts and component designs used on the General Electric family of engines. One significant difference is the use of the FADEC in place of hydromechanical computation currently used. Author

N90-28563*# General Electric Co., Cincinnati, OH. Aircraft Engine Business Group.

NASA/GE ENERGY EFFICIENT ENGINE LOW PRESSURE TURBINE SCALED TEST VEHICLE PERFORMANCE REPORT Topical Report, 1979-1982

M. J. BRIDGEMAN, D. G. CHERRY, and J. PEDERSEN Jul. 1983 259 p

(Contract NAS3-20643)

(NASA-CR-168290; NAS 1.26:168290; R83AEB143) Avail: NTIS HC A12/MF A02 CSCL 21/5

The low pressure turbine for the NASA/General Electric Energy Efficient Engine is a highly loaded five-stage design featuring high outer wall slope, controlled vortex aerodynamics, low stage flow coefficient, and reduced clearances. An assessment of the performance of the LPT has been made based on a series of scaled air-turbine tests divided into two phases: Block 1 and Block 2. The transition duct and the first two stages of the turbine were evaluated during the Block 1 phase from March through August 1979. The full five-stage scale model, representing the final integrated core/low spool (ICLS) design and incorporating redesigns of stages 1 and 2 based on Block 1 data analysis, was tested as Block 2 in June through September 1981. Results from the scaled air-turbine tests, reviewed herein, indicate that the five-stage turbine designed for the ICLS application will attain an efficiency level of 91.5 percent at the Mach 0.8/10.67-km (35,000-ft), max-climb design point. This is relative to program goals of 91.1 percent for the ICLS and 91.7 percent for the flight propulsion system (FPS). Author

N90-28564*# Pratt and Whitney Aircraft, East Hartford, CT. Engineering Div.

ENERGY EFFICIENT ENGINE PROGRAM TECHNOLOGY BENEFIT/COST STUDY. VOLUME 1: EXECUTIVE SUMMARY

D. E. GRAY and WILLIAM B. GARDNER Oct. 1983 19 p

(Contract NAS3-20646)

(NASA-CR-174766-VOL-1; NAS 1.26:174766-VOL-1; PWA-5594-258-VOL-1) Avail: NTIS HC A03/MF A01 CSCL 21/5

Under the NASA sponsored Energy Efficient Engine Program, Pratt and Whitney completed the Benefit/Cost Study to identify turbofan engine technologies required for the years 2000 to 2010, to assess the benefits of those technologies, and to formulate programs for developing the technologies required for that time period. The results verified that there are still many potential benefits to be realized from the advancement of gas turbine technology. The initial effort was to screen and rank preliminary technology concepts that might be amenable to future development. Cycle studies, flowpath definition studies, and mechanical configuration studies were then used to identify and establish the feasibility of the technologies that would be required in the 2000 to 2010 time frame. These efforts showed that a turbofan engine with advancements in aerodynamics, mechanical arrangements, and materials offered significant performance improvements over 1988 technology. The benefits of the technologies were assessed using fuel burn and direct operating cost plus interest (DOC+I). These concepts could yield thrust specific fuel consumption benefits of almost 16 percent, fuel burn benefits of up to 24 percent and DOC+I benefits of up to 14 percent in a long-range airplane relative to Energy Efficient Engine technology levels. Technology development programs were formulated and recommended to realize those benefits. Author

N90-28565* # Pratt and Whitney Aircraft, East Hartford, CT. Engineering Div.

ENERGY EFFICIENT ENGINE PROGRAM TECHNOLOGY BENEFIT/COST STUDY, VOLUME 2

D. E. GRAY and WILLIAM B. GARDNER Oct. 1983 109 p (Contract NAS3-20646)

(NASA-CR-174766-VOL-2; NAS 1.26:174766-VOL-2; PWA-5594-251-VOL-2) Avail: NTIS HC A06/MF A01 CSCL 21/5

The Benefit/Cost Study portion of the NASA-sponsored Energy Efficient Engine Component Development and Integration program was successful in achieving its objectives: identification of air transport propulsion system technology requirements for the years 2000 and 2010, and formulation of programs for developing these technologies. It is projected that the advanced technologies identified, when developed to a state of readiness, will provide future commercial and military turbofan engines with significant savings in fuel consumption and related operating costs. These benefits are significant and far from exhausted. The potential savings translate into billions of dollars in annual savings for the airlines. Analyses indicate that a significant portion of the overall savings is attributed to aerodynamic and structure advancements. Another important consideration in acquiring these benefits is developing a viable reference technology base that will permit engines to operate at substantially higher overall pressure ratios and bypass ratios. Results have pointed the direction for future research and a comprehensive program plan for achieving this was formulated. The next major step is initiating the program effort that will convert the advanced technologies into the expected benefits. Author

N90-28566* # Pratt and Whitney Aircraft, East Hartford, CT. Engineering Div.

ENERGY EFFICIENT ENGINE INTEGRATED CORE/LOW SPOOL TEST HARDWARE DESIGN REPORT

JOHN W. BISSET and DAVID C. HOWE Mar. 1983 223 p (Contract NAS3-20646)

(NASA-CR-168137; NAS 1.26:168137; PWA-5594-231) Avail: NTIS HC A10/MF A02 CSCL 21/5

The Energy Efficient Engine Program is designed to identify and verify the technology required to significantly lower fuel consumption and operating cost for future commercial gas turbine engines. A major task that was completed under this program is the design and analysis of test hardware for the integrated core/low spool, which is a test simulation of the conceptual study engine defined to meet performance, economic and environmental goals.

An evaluation and verification of critical technologies is intended in a full engine operating environment. The design and results of design-related analyses for the integrated core/low spool and its subsystems are described. The design effort included a definition of the engine, major components, internal and external subsystems, test ducting, and test instrumentation. Various analytical representations, in addition to results acquired from supporting component rig and subscale model tests, were used to verify aerodynamic and structural design concepts as well as to predict performance. Author

N90-28567* # Pratt and Whitney Aircraft, East Hartford, CT. Engineering Div.

ENERGY EFFICIENT ENGINE PIN FIN AND CERAMIC COMPOSITE SEGMENTED LINER COMBUSTOR SECTOR RIG TEST REPORT

D. J. DUBIEL, R. P. LOHMANN, S. TANRIKUT, and P. M. MORRIS Sep. 1986 218 p

(Contract NAS3-20646)

(NASA-CR-179534; NAS 1.26:179534; PWA-5594-333; LC-86-23)

Avail: NTIS HC A10/MF A02 CSCL 21/5

Under the NASA-sponsored Energy Efficient Engine program, Pratt and Whitney has successfully completed a comprehensive test program using a 90-degree sector combustor rig that featured an advanced two-stage combustor with a succession of advanced segmented liners. Building on the successful characteristics of the first generation counter-parallel Finwall cooled segmented liner, design features of an improved performance metallic segmented liner were substantiated through representative high pressure and temperature testing in a combustor atmosphere. This second generation liner was substantially lighter and lower in cost than the predecessor configuration. The final test in this series provided an evaluation of ceramic composite liner segments in a representative combustor environment. It was demonstrated that the unique properties of ceramic composites, low density, high fracture toughness, and thermal fatigue resistance can be advantageously exploited in high temperature components. Overall, this Combustor Section Rig Test program has provided a firm basis for the design of advanced combustor liners. Author

N90-28568* # Pratt and Whitney Aircraft, East Hartford, CT. Engineering Div.

ENERGY EFFICIENT ENGINE: COMBUSTOR COMPONENT PERFORMANCE PROGRAM

D. J. DUBIEL Sep. 1986 53 p

(Contract NAS3-20646)

(NASA-CR-179533; NAS 1.26:179533; PWA-5594-329) Avail:

NTIS HC A04/MF A01 CSCL 21/5

The results of the Combustor Component Performance analysis as developed under the Energy Efficient Engine (EEE) program are presented. This study was conducted to demonstrate the aerothermal and environmental goals established for the EEE program and to identify areas where refinements might be made to meet future combustor requirements. In this study, a full annular combustor test rig was used to establish emission levels and combustor performance for comparison with those indicated by the supporting technology program. In addition, a combustor sector test rig was employed to examine differences in emissions and liner temperatures obtained during the full annular performance and supporting technology tests. Author

N90-28569* # Pratt and Whitney Aircraft, East Hartford, CT. Engineering Div.

ENERGY EFFICIENT ENGINE: CONTROL SYSTEM PRELIMINARY DEFINITION REPORT

DAVID C. HOWE Sep. 1986 126 p

(Contract NAS3-20646)

(NASA-CR-179578; NAS 1.26:179578; PWA-5594-331) Avail:

NTIS HC A07/MF A01 CSCL 21/5

The object of the Control Preliminary Definition Program was to define a preliminary control system concept as a part of the Energy Efficient Engine program. The program was limited to a conceptual definition of a full authority digital electronic control

07 AIRCRAFT PROPULSION AND POWER

system. System requirements were determined and a control system was conceptually defined to these requirements. Areas requiring technological development were identified and a plan was established for implementing the identified technological features, including a control technology demonstration. A significant element of this program was a study of the potential benefits of closed-loop active clearance control, along with laboratory tests of candidate clearance sensor elements for a closed loop system.

Author

N90-28570*# Pratt and Whitney Aircraft, East Hartford, CT.
**ENERGY EFFICIENT ENGINE: HIGH-PRESSURE
COMPRESSOR TEST HARDWARE DETAILED DESIGN
REPORT**

DAVID C. HOWE and R. D. MARCHANT Mar. 1988 261 p
(Contract NAS3-20646)
(NASA-CR-180850; NAS 1.26:180850; PWA-5594-287) Avail:
NTIS HC A12/MF A02 CSCL 21/5

The objective of the NASA Energy Efficient Engine program is to identify and verify the technology required to achieve significant reductions in fuel consumption and operating cost for future commercial gas turbine engines. The design and analysis is documented of the high pressure compressor which was tested as part of the Pratt and Whitney effort under the Energy Efficient Engine program. This compressor was designed to produce a 14:1 pressure ratio in ten stages with an adiabatic efficiency of 88.2 percent in the flight propulsion system. The corresponding expected efficiency for the compressor component test rig is 86.5 percent. Other performance goals are a surge margin of 20 percent, a corrected flow rate of 35.2 kg/sec (77.5 lb/sec), and a life of 20,000 missions and 30,000 hours. Low loss, highly loaded airfoils are used to increase efficiency while reducing the parts count. Active clearance control and case trenches in abradable strips over the blade tips are included in the compressor component design to further increase the efficiency potential. The test rig incorporates variable geometry stator vanes in all stages to permit maximum flexibility in developing stage-to-stage matching. This provision precluded active clearance control on the rear case of the test rig. Both the component and rig designs meet or exceed design requirements with the exception of life goals, which will be achievable with planned advances in materials technology.

Author

N90-29394*# TRW Defense and Space Systems Group, Redondo Beach, CA.

**GENERALIZED ADVANCED PROPELLER ANALYSIS SYSTEM
(GAPAS). VOLUME 2: COMPUTER PROGRAM USER MANUAL**
L. GLATT, D. R. CRAWFORD, J. B. KOSMATKA, R. J. SWIGART,
and E. W. WONG Dec. 1986 484 p
(Contract NAS3-22251)
(NASA-CR-185277; NAS 1.26:185277) Avail: NTIS HC A21/MF
A03 CSCL 01/3

The Generalized Advanced Propeller Analysis System (GAPAS) computer code is described. GAPAS was developed to analyze advanced technology multi-bladed propellers which operate on aircraft with speeds up to Mach 0.8 and altitudes up to 40,000 feet. GAPAS includes technology for analyzing aerodynamic, structural, and acoustic performance of propellers. The computer code was developed for the CDC 7600 computer and is currently available for industrial use on the NASA Langley computer. A description of all the analytical models incorporated in GAPAS is included. Sample calculations are also described as well as users requirements for modifying the analysis system. Computer system core requirements and running times are also discussed. Author

08

AIRCRAFT STABILITY AND CONTROL

Includes aircraft handling qualities; piloting; flight controls; and autopilots.

A90-33061*# National Aeronautics and Space Administration.
Lewis Research Center, Cleveland, OH.

**COOPERATIVE SYNTHESIS OF CONTROL AND DISPLAY
AUGMENTATION IN APPROACH AND LANDING**

SANJAY GARG (NASA, Lewis Research Center; Sverdrup Technology, Inc., Cleveland, OH) and DAVID K. SCHMIDT (Purdue University, West Lafayette, IN) Journal of Guidance, Control, and Dynamics (ISSN 0731-5090), vol. 13, May-June 1990, p. 466-475. Research supported by Honeywell, Inc. Previously cited in issue 21, p. 3494, Accession no. A88-50272. refs
(Contract NAG4-1; F33615-86-C-3615)
Copyright

A90-40557*# Arizona State Univ., Tempe.
**ANALYSIS OF AIRFRAME/ENGINE INTERACTIONS - AN
INTEGRATED CONTROL PERSPECTIVE**

DAVID K. SCHMIDT, JOHN D. SCHIERMAN (Arizona State University, Tempe), and SANJAY GARG (NASA, Lewis Research Center; Sverdrup Technology, Inc., Cleveland, OH) AIAA, SAE, ASME, and ASEE, Joint Propulsion Conference, 26th, Orlando, FL, July 16-18, 1990. 12 p. refs
(Contract NAG3-998)
(AIAA PAPER 90-1918) Copyright

Techniques for the analysis of the dynamic interactions between airframe/engine dynamical systems are presented. Critical coupling terms are developed that determine the significance of these interactions with regard to the closed loop stability and performance of the feedback systems. A conceptual model is first used to indicate the potential sources of the coupling, how the coupling manifests itself, and how the magnitudes of these critical coupling terms are used to quantify the effects of the airframe/engine interactions. A case study is also presented involving an unstable airframe with thrust vectoring for attitude control. It is shown for this system with classical, decentralized control laws that there is little airframe/engine interaction, and the stability and performance with those control laws is not affected. Implications of parameter uncertainty in the coupling dynamics is also discussed, and effects of these parameter variations are also demonstrated to be small for this vehicle configuration.

Author

A90-47595*# National Aeronautics and Space Administration.
Lewis Research Center, Cleveland, OH.

**H-INFINITY BASED INTEGRATED FLIGHT/PROPULSION
CONTROL DESIGN FOR A STOVL AIRCRAFT IN TRANSITION
FLIGHT**

SANJAY GARG, DUANE L. MATTERN (NASA, Lewis Research Center; Sverdrup Technology, Inc., Cleveland, OH), MICHELLE BRIGHT, and PETER OUZTS (NASA, Lewis Research Center, Cleveland, OH) IN: AIAA Guidance, Navigation and Control Conference, Portland, OR, Aug. 20-22, 1990, Technical Papers. Part 1. Washington, DC, American Institute of Aeronautics and Astronautics, 1990, p. 183-193. refs
(AIAA PAPER 90-3335) Copyright

This paper presents results from an application of H(infinity) control design methodology to a centralized integrated flight/propulsion control (IFPC) system design for a supersonic STOVL fighter aircraft in transition flight. The overall design methodology consists of a centralized IFPC design with controller partitioning. Design and evaluation vehicle models are summarized, and insight is provided into formulating the H(infinity) control problem such that it reflects the IFPC design objective. The H(infinity) controller is shown to provide decoupled command tracking for the design model. The controller order could be

significantly reduced by modal residualization of the fast controller modes without any deterioration in performance. Author

A90-49110*# Systems Control Technology, Inc., Palo Alto, CA.
FLIGHT CONTROL DESIGN CONSIDERATIONS FOR STOVL POWERED-LIFT FLIGHT
JAMES H. VINCENT and ROB ANEX (Systems Control Technology, Inc., Palo Alto, CA) AIAA, AHS, and ASEE, Aircraft Design, Systems and Operations Conference, Dayton, OH, Sept. 17-19, 1990. 13 p. refs
(Contract NAS3-25193)
(AIAA PAPER 90-3225) Copyright

Short Takeoff Vertical Landing (STOVL) aircraft rely on the propulsion system for the lift and control functions during slow speed flight. The propulsion system provides the entire lifting force and all of the control power for hovering flight at zero airspeed. STOVL designs such as the General Dynamics E-7D ejector configuration incorporate an integrated flight/propulsion control system to manage the aerodynamic and propulsive-lift control effectors and to reduce the pilot's workload for powered-lift flight. Desired flying qualities characteristics are implemented through the utilization of an explicit model following flight control system. With the model following control system, the pilot commands the desired response (e.g., throttle commands vertical velocity in hover, instead of power lever angle). Design considerations for developing a multivariable model-following flight control system are presented in this paper. When the regulator gains are defined in terms of generalized controls, the design problem becomes how to best transform the generalized controls to aerodynamic control surface, thrust and thrust vectoring commands. Author

N90-15112*# National Aeronautics and Space Administration. Lewis Research Center, Cleveland, OH.
ADVANCED DETECTION, ISOLATION, AND ACCOMMODATION OF SENSOR FAILURES IN TURBOFAN ENGINES: REAL-TIME MICROCOMPUTER IMPLEMENTATION
JOHN C. DELAAT and WALTER C. MERRILL Washington Feb. 1990 28 p
(NASA-TP-2925; E-4391; NAS 1.60:2925) Avail: NTIS HC A03/MF A01 CSCL 01/3

The objective of the Advanced Detection, Isolation, and Accommodation Program is to improve the overall demonstrated reliability of digital electronic control systems for turbine engines. For this purpose, an algorithm was developed which detects, isolates, and accommodates sensor failures by using analytical redundancy. The performance of this algorithm was evaluated on a real time engine simulation and was demonstrated on a full scale F100 turbofan engine. The real time implementation of the algorithm is described. The implementation used state-of-the-art microprocessor hardware and software, including parallel processing and high order language programming. Author

N90-26011*# National Aeronautics and Space Administration. Lewis Research Center, Cleveland, OH.
H-INFINITY BASED INTEGRATED FLIGHT-PROPULSION CONTROL DESIGN FOR A STOVL AIRCRAFT IN TRANSITION FLIGHT
SANJAY GARG, DUANE L. MATTERN (Sverdrup Technology, Inc., Brook Park, OH.), MICHELLE M. BRIGHT, and PETER J. OUZTS Aug. 1990 32 p Presented at the Guidance, Navigation and Control Conference, Portland, OR, 20-22 Aug. 1990; sponsored in part by AIAA
(NASA-TM-103198; E-5594; NAS 1.15:103198) Avail: NTIS HC A03/MF A01 CSCL 01/3

Results are presented from an application of H-infinity control design methodology to a centralized integrated flight/propulsion control (IFPC) system design for a supersonic Short Take-Off and Vertical Landing (STOVL) fighter aircraft in transition flight. The overall design methodology consists of a centralized IFPC controller design with controller partitioning. Only the feedback controller design portion of the methodology is addressed. Design and evaluation vehicle models are summarized, and insight is provided into formulating the H-infinity control problem such that it reflects

09 RESEARCH AND SUPPORT FACILITIES (AIR)

the IFPC design objectives. The H-infinity controller is shown to provide decoupled command tracking for the design model. The controller order could be significantly reduced by modal residualization of the fast controller modes without any deterioration in performance. A discussion is presented of the areas in which the controller performance needs to be improved, and ways in which these improvements can be achieved within the framework of an H-infinity based linear control design. Author

09

RESEARCH AND SUPPORT FACILITIES (AIR)

Includes airports, hangars and runways; aircraft repair and overhaul facilities; wind tunnels; shock tubes; and aircraft engine test stands.

A90-22242*# National Aeronautics and Space Administration. Lewis Research Center, Cleveland, OH.

LIQUID WATER CONTENT AND DROPLET SIZE CALIBRATION OF THE NASA LEWIS ICING RESEARCH TUNNEL

ROBERT F. IDE (NASA, Lewis Research Center; U.S. Army, Propulsion Directorate, Cleveland, OH) AIAA, Aerospace Sciences Meeting, 28th, Reno, NV, Jan. 8-11, 1990. 28 p. Previously announced in STAR as N90-13797.
(AIAA PAPER 90-0669) Copyright

The icing research tunnel at the NASA Lewis Research Center underwent a major rehabilitation in 1986 to 1987, necessitating recalibration of the icing cloud. The methods used in the recalibration, including the procedure used to establish a uniform icing cloud and the use of a standard icing blade technique for measurement of liquid water content are described. PMS Forward Scattering Spectrometer and Optical Array probes were used for measurement of droplet size. Examples of droplet size distributions are shown for several median volumetric diameters. Finally, the liquid water content/droplet size operating envelopes of the icing tunnel are shown for a range of airspeeds and are compared to the FAA icing certification criteria. Author

A90-25040*# Boeing Helicopter Co., Philadelphia, PA. **SPRAY NOZZLE INVESTIGATION FOR THE IMPROVED HELICOPTER ICING SPRAY SYSTEM (IHSS)**

ANDREW A. PETERSON (Boeing Helicopters, Philadelphia, PA) and JOHN R. OLDENBURG (NASA, Lewis Research Center, Cleveland, OH) AIAA, Aerospace Sciences Meeting, 28th, Reno, NV, Jan. 8-11, 1990. 9 p. refs
(AIAA PAPER 90-0666) Copyright

A contract has been awarded by the U.S. Army to design, fabricate and test a replacement for the existing Helicopter Icing Spray System. Data are shown for extensive bench and icing tunnel test programs used to select and modify an improved spray nozzle. The IHSS, capable of deployment from any CH-47 helicopter, will include new icing spray nozzles and pneumatic pressure source, and a significantly larger water tank and spray boom. The resulting system will provide a significantly larger icing cloud with droplet characteristics closely matching natural icing conditions. R.E.P.

A90-42791*# National Aeronautics and Space Administration. Lewis Research Center, Cleveland, OH.

A TEST MATRIX SEQUENCER FOR RESEARCH TEST FACILITY AUTOMATION

TIMOTHY P. MCCARTNEY and EDWARD F. EMERY (NASA, Lewis Research Center, Cleveland, OH) AIAA, SAE, ASME, and ASEE, Joint Propulsion Conference, 26th, Orlando, FL, July 16-18, 1990. 8 p. Previously announced in STAR as N90-23416.
(AIAA PAPER 90-2386) Copyright

The hardware and software configuration of a Test Matrix Sequencer, a general purpose test matrix profiler that was

09 RESEARCH AND SUPPORT FACILITIES (AIR)

developed for research test facility automation at the NASA Lewis Research Center, is described. The system provides set points to controllers and contact closures to data systems during the course of a test. The Test Matrix Sequencer consists of a microprocessor controlled system which is operated from a personal computer. The software program, which is the main element of the overall system is interactive and menu driven with pop-up windows and help screens. Analog and digital input/output channels can be controlled from a personal computer using the software program. The Test Matrix Sequencer provides more efficient use of aeronautics test facilities by automating repetitive tasks that were once done manually. Author

N90-15964*# National Aeronautics and Space Administration. Lewis Research Center, Cleveland, OH.

AN ELECTRONIC PRESSURE PROFILE DISPLAY SYSTEM FOR AERONAUTIC TEST FACILITIES

MARK R. WOIKE 1990 13 p Proposed for presentation at the International Instrumentation Symposium, Denver, CO, 6-10 May 1990; sponsored by Instrument Society of America (NASA-TM-102478; E-5265; NAS 1.15:102478) Avail: NTIS HC A03/MF A01 CSCL 14/2

The NASA Lewis Research Center has installed an Electronic Pressure Profile Display system. This system provides for the real-time display of pressure readings on high resolution graphics monitors. The Electronic Pressure Profile Display system will replace manometer banks currently used in aeronautic test facilities. The Electronic Pressure Profile Display system consists of an industrial type Digital Pressure Transmitter (DPT) unit which interfaces with a host computer. The host computer collects the pressure data from the DPT unit, converts it into engineering units, and displays the readings on a high resolution graphics monitor in bar graph format. Software was developed to accomplish the above tasks and also draw facility diagrams as background information on the displays. Data transfer between host computer and DPT unit is done with serial communications. Up to 64 channels are displayed with one second update time. This paper describes the system configuration, its features, and its advantages over existing systems. Author

N90-15965*# National Aeronautics and Space Administration. Lewis Research Center, Cleveland, OH.

A NUMERICAL SIMULATION OF THE FLOW IN THE DIFFUSER OF THE NASA LEWIS ICING RESEARCH TUNNEL

HAROLD E. ADDY, JR. and THEO G. KEITH, JR. (Toledo Univ., OH.) 1990 11 p Presented at the 28th Aerospace Sciences Meeting, Reno, NV, 8-11 Jan. 1990; sponsored by AIAA (NASA-TM-102480; E-5270; NAS 1.15:102480; AIAA-90-0488) Avail: NTIS HC A03/MF A01 CSCL 14/2

The flow in the diffuser section of the Icing Research Tunnel at the NASA Lewis Research Center is numerically investigated. To accomplish this, an existing computer code is utilized. The code, known as PARC3D, is based on the Beam-Warming algorithm applied to the strong conservation law form of the complete Navier-Stokes equations. The first portion of the paper consists of a brief description of the diffuser and its current flow characteristics. A brief discussion of the code work follows. Predicted velocity patterns are then compared with the measured values. Author

N90-19242*# National Aeronautics and Space Administration. Lewis Research Center, Cleveland, OH.

COMPARISON BETWEEN DESIGN AND INSTALLED ACOUSTIC CHARACTERISTICS OF NASA LEWIS 9- BY 15-FOOT LOW-SPEED WIND TUNNEL ACOUSTIC TREATMENT

MILO D. DAHL and RICHARD P. WOODWARD Washington Apr. 1990 28 p Presented at the 115th Meeting of the Acoustical Society of America, Seattle, WA, 16-20 May 1988 (NASA-TP-2996; E-4981; NAS 1.60:2996) Avail: NTIS HC A03/MF A01 CSCL 14/2

The test section of the NASA Lewis 9- by 15-Foot Low-Speed Wind Tunnel was acoustically treated to allow the measurement of sound under simulated free-field conditions. The treatment was

designed for high sound absorption at frequencies above 250 Hz and for withstanding the environmental conditions in the test section. In order to achieve the design requirements, a fibrous, bulk-absorber material was packed into removable panel sections. Each section was divided into two equal-depth layers packed with material to different bulk densities. The lower density was next to the facing of the treatment. The facing consisted of a perforated plate and screening material layered together. Sample tests for normal-incidence acoustic absorption were also conducted in an impedance tube to provide data to aid in the treatment design. Tests with no airflow, involving the measurement of the absorptive properties of the treatment installed in the 9- by 15-foot wind tunnel test section, combined the use of time-delay spectrometry with a previously established free-field measurement method. This new application of time-delay spectrometry enabled these free-field measurements to be made in nonanechoic conditions. The results showed that the installed acoustic treatment had absorption coefficients greater than 0.95 over the frequency range 250 Hz to 4 kHz. The measurements in the wind tunnel were in good agreement with both the analytical prediction and the impedance tube test data. Author

N90-21776*# Pittsburgh Univ., PA. Dept. of Electrical Engineering.

THE INSERTION OF HUMAN DYNAMICS MODELS IN THE FLIGHT CONTROL LOOPS OF V/STOL RESEARCH AIRCRAFT. APPENDIX 2: THE OPTIMAL CONTROL MODEL OF A PILOT IN V/STOL AIRCRAFT CONTROL LOOPS Final Report

MARK E. ZIFF 1989 210 p (Contract NAG3-729) (NASA-CR-186598; NAS 1.26:186598) Avail: NTIS HC A10/MF A02 CSCL 05/8

An overview is presented of research work focussed on the design and insertion of classical models of human pilot dynamics within the flight control loops of V/STOL aircraft. The pilots were designed and configured for use in integrated control system research and design. The models of human behavior that were considered are: McRuer-Krendel (a single variable transfer function model); and Optimal Control Model (a multi-variable approach based on optimal control and stochastic estimation theory). These models attempt to predict human control response characteristics when confronted with compensatory tracking and state regulation tasks. An overview, mathematical description, and discussion of predictive limitations of the pilot models is presented. Design strategies and closed loop insertion configurations are introduced and considered for various flight control scenarios. Models of aircraft dynamics (both transfer function and state space based) are developed and discussed for their use in pilot design and application. Pilot design and insertion are illustrated for various flight control objectives. Results of pilot insertion within the control loops of two V/STOL research aircraft (Sikorski Black Hawk UH-60A, McDonnell Douglas Harrier II AV-8B) are presented and compared against actual pilot flight data. Conclusions are reached on the ability of the pilot models to adequately predict human behavior when confronted with similar control objectives. Author

N90-21777*# Pittsburgh Univ., PA. Dept. of Electrical Engineering.

AN ADAPTIVE HUMAN RESPONSE MECHANISM CONTROLLING THE V/STOL AIRCRAFT. APPENDIX 3: THE ADAPTIVE CONTROL MODEL OF A PILOT IN V/STOL AIRCRAFT CONTROL LOOPS M.S. Thesis. Final Report

SENOLO KUCUK 1988 183 p (Contract NAG3-729) (NASA-CR-186599; NAS 1.26:186599) Avail: NTIS HC A09/MF A01 CSCL 05/8

Importance of the role of human operator in control systems has led to the particular area of manual control theory. Human describing functions were developed to model human behavior for manual control studies to take advantage of the successful and safe human operations. A single variable approach is presented that can be extended for multi-variable tasks where a low order

ASTRONAUTICS (GENERAL)

human response model is used together with its rules, to adapt the model on-line, being capable of responding to the changes in the controlled element dynamics. Basic control theory concepts are used to combine the model, constrained with the physical observations, particularly, for the case of aircraft control. Pilot experience is represented as the initial model parameters. An adaptive root-locus method is presented as the adaptation law of the model where the closed loop bandwidth of the system is to be preserved in a stable manner with the adjustments of the pilot handling qualities which relate the latter to the closed loop bandwidth and damping of the closed loop pilot aircraft combination. A Kalman filter parameter estimator is presented as the controlled element identifier of the adaptive model where any discrepancies of the open loop dynamics from the presented one, are sensed to be compensated. Author

N90-23416* # National Aeronautics and Space Administration. Lewis Research Center, Cleveland, OH.

A TEST MATRIX SEQUENCER FOR RESEARCH TEST FACILITY AUTOMATION

TIMOTHY P. MCCARTNEY and EDWARD F. EMERY Jul. 1990 9 p Presented at the 26th Joint Propulsion Conference, Orlando, FL, 16-18 Jul. 1990; cosponsored by AIAA, SAE, ASME, and ASEE (NASA-TM-103108; E-5432; NAS 1.15:103108; AIAA-90-2386) Avail: NTIS HC A02/MF A01 CSCL 14/2

The hardware and software configuration of a Test Matrix Sequencer, a general purpose test matrix profiler that was developed for research test facility automation at the NASA Lewis Research Center, is described. The system provides set points to controllers and contact closures to data systems during the course of a test. The Test Matrix Sequencer consists of a microprocessor controlled system which is operated from a personal computer. The software program, which is the main element of the overall system is interactive and menu driven with pop-up windows and help screens. Analog and digital input/output channels can be controlled from a personal computer using the software program. The Test Matrix Sequencer provides more efficient use of aeronautics test facilities by automating repetitive tasks that were once done manually. Author

N90-25151* # National Aeronautics and Space Administration. Lewis Research Center, Cleveland, OH.

HIGH-TEMPERATURE TEST FACILITY AT THE NASA LEWIS ENGINE COMPONENTS RESEARCH LABORATORY

RENATO O. COLANTONIO Jun. 1990 22 p Original contains color illustrations (NASA-TM-103143; E-5495; NAS 1.15:103143) Avail: NTIS HC A03/MF A01; 1 functional color page CSCL 14/2

The high temperature test facility (HTTF) at NASA-Lewis Engine Components Research Laboratory (ECRL) is presently used to evaluate the survivability of aerospace materials and the effectiveness of new sensing instrumentation in a realistic afterburner environment. The HTTF has also been used for advanced heat transfer studies on aerospace components. The research rig uses pressurized air which is heated with two combustors to simulate high temperature flow conditions for test specimens. Maximum airflow is 31 pps. The HTTF is pressure rated for up to 150 psig. Combustors are used to regulate test specimen temperatures up to 2500 F. Generic test sections are available to house test plates and advanced instrumentation. Customized test sections can be fabricated for programs requiring specialized features and functions. The high temperature test facility provides government and industry with a facility for testing aerospace components. Its operation and capabilities are described. Author

A90-19988* # Martin Marietta Space Systems, Inc., Denver, CO. **ON-ORBIT LOW GRAVITY CRYOGENIC SCIENTIFIC INVESTIGATIONS USING THE COLD-SAT SATELLITE** W. J. BAILEY (Martin Marietta Space Systems, Denver, CO) AIAA, Aerospace Sciences Meeting, 28th, Reno, NV, Jan. 8-11, 1990. 12 p.

(Contract NAS3-25063)

(AIAA PAPER 90-0718) Copyright

The Cryogenic On-Orbit Liquid Depot Storage, Acquisition and Transfer (COLD-SAT) Satellite is an experimental spacecraft designed to investigate the systems and technologies required for an efficient, effective, and reliable management of cryogenic fluids in reduced-gravity space environment. This paper defines the technology needs and the accompanying experimental three-month baseline mission of the COLD-SAT Satellite; describes the experiment subsystems, major features, and rationale for satisfying primary and secondary experimental requirements, using LH2 as the test fluid; and presents the conceptual design of the COLD-SAT spacecraft subsystems which support the on-orbit experiment. I.S.

A90-23263* # Iowa Univ., Iowa City.

SPACELAB 2 PLASMA DIAGNOSTICS PACKAGE

W. S. KURTH and L. A. FRANK (Iowa, University, Iowa City) Journal of Spacecraft and Rockets (ISSN 0022-4650), vol. 27, Jan.-Feb. 1990, p. 70-75. refs (Contract NAS8-32807; NAG3-449)

Copyright

The Plasma Diagnostics Package is a small, deployable satellite designed to study the interaction of the Space Shuttle Orbiter with the ionospheric environment as well as to be used in joint experiments with the plasma depletion and the vehicle charging and potential investigations during the Spacelab 2 mission. This paper provides a brief description of the small spacecraft, its instrumentation and operation, and the scientific objectives of the investigations. A brief summary of the scientific results obtained thus far is also presented. Author

A90-25655* # Ford Aerospace and Communications Corp., Palo Alto, CA.

SERVICING COMMUNICATION SATELLITES IN GEOSTATIONARY ORBIT

PAUL K. RUSSELL and KENT M. PRICE (Ford Aerospace Corp., Space Systems Div., Palo Alto, CA) IN: AIAA International Communication Satellite Systems Conference and Exhibit, 13th, Los Angeles, CA, Mar. 11-15, 1990, Technical Papers. Part 2. Washington, DC, American Institute of Aeronautics and Astronautics, 1990, p. 456-465.

(Contract NAS3-24253)

(AIAA PAPER 90-0830) Copyright

The economic benefits of a LEO space station are quantified by identifying alternative operating scenarios utilizing the space station's transportation facilities and assembly and repair facilities. Particular consideration is given to the analysis of the impact of on-orbit assembly and servicing on a typical communications satellite is analyzed. The results of this study show that on-orbit servicing can increase the internal rate of return by as much as 30 percent. I.S.

A90-33935* National Aeronautics and Space Administration. Lewis Research Center, Cleveland, OH.

HUMAN EXPLORATION MISSION STUDIES

ROBERT L. CATALDO (NASA, Lewis Research Center, Cleveland, OH) (NASA, Space Electrochemical Research and Technology Conference, 2nd, Cleveland, OH, Apr. 11-13, 1989) Journal of

12 ASTRONAUTICS (GENERAL)

Power Sources (ISSN 0378-7753), vol. 29, Feb. 1990, p. 291-297. Copyright

This paper describes several case studies of human space exploration, considered by the NASA's Office of Exploration in 1988. Special attention is given to the mission scenarios, the critical technology required in these expeditions, and the extraterrestrial power requirements of significant system elements. The cases examined include a manned expedition to Phobos, the inner Martian moon; a human expedition to Mars; the Lunar Observatory; and a lunar outpost to early Mars evolution. I.S.

A90-38105*# National Aeronautics and Space Administration. Lewis Research Center, Cleveland, OH.

ORBIT TO SURFACE BEAMED POWER FOR MARS BASES EXPANSION

RONALD CULL and KARL A. FAYMON (NASA, Lewis Research Center, Cleveland, OH) IN: IECEC-89; Proceedings of the Twenty-fourth Intersociety Energy Conversion Engineering Conference, Washington, DC, Aug. 6-11, 1989. Volume 1. New York, Institute of Electrical and Electronics Engineers, 1989, p. 479-484. refs

A scenario is presented wherein the interplanetary supply vehicles for the expansion of the Mars bases are nuclear powered and electrically propelled. For the initial buildup phase supply vehicles need not return to earth but could be utilized as a one-way transport to a Mars synchronous orbit. Upon arriving at Mars, they would land their cargos with one-way descent vehicles. Base personnel would arrive at Mars in separate, faster vehicles. Once the vehicles are in Mars synchronous orbits, the nuclear power system would no longer be needed for propulsion and could be used as an orbital power station beaming its megawatts of power to locations on the surface of the planet. Placing a number of such power systems at strategically located synchronous orbit positions would permit coverage of the major portion of the Martian surface. I.E.

A90-48819* National Aeronautics and Space Administration. Lewis Research Center, Cleveland, OH.

ADVANCED REFRACTORY METALS AND COMPOSITES FOR EXTRATERRESTRIAL POWER SYSTEMS

R. H. TITRAN and TONI L. GROBSTEIN (NASA, Lewis Research Center, Cleveland, OH) JOM (ISSN 1047-4838), vol. 42, Aug. 1990, p. 8-10. refs Copyright

Concepts for future space power systems include nuclear and focused solar heat sources coupled to static and dynamic power-conversion devices; such systems must be designed for service lives as long as 30 years, despite service temperatures of the order of 1600 K. Materials are a critical technology-development factor in such aspects of these systems as reactor fuel containment, environmental protection, power management, and thermal management. Attention is given to the prospective performance of such refractory metals as Nb, W, and Mo alloys, W fiber-reinforced Nb-matrix composites, and HfC precipitate-strengthened W-Re alloys. O.C.

N90-20457*# National Aeronautics and Space Administration. Lewis Research Center, Cleveland, OH.

HUMAN EXPLORATION MISSION STUDIES

ROBERT L. CATALDO In *its* Space Electrochemical Research and Technology (SERT), 1989 p 9-15 Dec. 1989 Avail: NTIS HC A16/MF A02 CSCL 22/1

The nation's efforts to expand human presence and activity beyond Earth orbit into the solar system was given renewed emphasis in January of 1988 when the Presidential Directive on National Space Policy was signed into effect. The expansion of human presence into the solar system has particular significance, in that it defines long-range goals for NASA's future missions. To embark and achieve such ambitious ventures is a significant undertaking, particularly compared to past space activities. Missions to Mars, the Moon, and Phobos, as well as an observatory based on the dark side of the Moon are discussed. Author

13

ASTRODYNAMICS

Includes powered and free-flight trajectories; and orbital and launching dynamics.

A90-46783* Illinois Univ., Urbana.

OPTIMAL FINITE-THRUST SPACECRAFT TRAJECTORIES USING COLLOCATION AND NONLINEAR PROGRAMMING

PAUL J. ENRIGHT and BRUCE A. CONWAY (Illinois, University, Urbana) IN: Astrodynamics 1989; Proceedings of the AAS/AIAA Astrodynamics Conference, Stowe, VT, Aug. 7-10, 1989. Part 1. San Diego, CA, Univelt, Inc., 1990, p. 479-490. refs (Contract NAG3-805) (AAS PAPER 89-350) Copyright

A new method is described for the determination of optimal spacecraft trajectories in an inverse-square field using finite, fixed thrust. The method employs a recently developed optimization technique which uses a piecewise polynomial representation for the state and controls, and collocation, thus converting the optimal control problem into a nonlinear programming problem, which is solved numerically. This technique has been modified to provide efficient handling of those portions of the trajectory which can be determined analytically, i.e., the coast arcs. Among the problems that have been solved using this method are optimal rendezvous and transfer (including multirevolution cases) and optimal multiburn orbit insertion from hyperbolic approach. Author

A90-46784* Stanford Univ., CA.

MINIMUM FUEL TRAJECTORIES FOR A LOW-THRUST POWER-LIMITED MISSION TO THE MOON AND TO LAGRANGE POINTS L4 AND L5

JOHN V. BREAKWELL (Stanford University, CA) and ODED M. GOLAN IN: Astrodynamics 1989; Proceedings of the AAS/AIAA Astrodynamics Conference, Stowe, VT, Aug. 7-10, 1989. Part 1. San Diego, CA, Univelt, Inc., 1990, p. 491-500. (Contract NAG3-286) (AAS PAPER 89-351) Copyright

Minimum fuel trajectories from a low earth parking orbit to Lagrange points L4 or L5 and to the moon are obtained for a low-thrust limited-power spacecraft, with thrust acceleration levels of the order of 0.001 G. The procedure to find a trajectory to the libration point starts from an analytical description of a slightly elliptical spiral, given by Breakwell and Rauch. The earth moon trajectory is found by matching an earth spiral to a moon spiral on the sphere of influence. Earth oblateness effect is considered. Author

A90-46785* Stanford Univ., CA.

MINIMUM FUEL TRAJECTORY FOR THE AEROSPACE-PLANE

JOHN V. BREAKWELL (Stanford University, CA), ODED GOLAN, and ANNE SAUVAGEOT IN: Astrodynamics 1989; Proceedings of the AAS/AIAA Astrodynamics Conference, Stowe, VT, Aug. 7-10, 1989. Part 1. San Diego, CA, Univelt, Inc., 1990, p. 501-512. refs (Contract NAG3-908) (AAS PAPER 89-352) Copyright

An overall trajectory for a single-stage-to-orbit vehicle with an initial weight of 234 tons is calculated, and four different propulsion models including turbojet, ramjet, scramjet, and rocket are considered. First, the atmospheric flight in the thicker atmosphere is discussed with emphasis on trajectory optimization, optimization problem, aerodynamic problem, propulsion model, and initial conditions. The performance of turbojet and ramjet-scramjet engines is analyzed; and then the flight to orbit is assessed from the optimization point of view. It is shown that roll modulation saves little during the trajectory, and the combined application of airbreathing propulsion and aerodynamic lift is suggested. V.T.

A90-46786* Illinois Univ., Urbana.

OPTIMAL ORBITAL RENDEZVOUS USING HIGH AND LOW THRUST

JOHN E. PRUSSING (Illinois, University, Urbana) and CATHERINE A. LARSON IN: Astrodynamics 1989; Proceedings of the AAS/AIAA Astrodynamics Conference, Stowe, VT, Aug. 7-10, 1989. Part 1. San Diego, CA, Univelt, Inc., 1990, p. 513-532. refs (Contract NAG3-805)

(AAS PAPER 89-354) Copyright

Optimal control theory is used to examine a specific class of spacecraft trajectory problems where high- and low-thrust propulsion systems are utilized. These problems assume a spacecraft is in an established orbit about a planet. It is desired to execute an intercept of a pre-determined position in space in a specified amount of time using an optimal high-thrust program. The spacecraft then returns to the original orbit station using the low-thrust propulsion system in an optimal fashion. A minimum fuel solution is sought using the linearized equations of motion, known as the CW equations, which simplify the necessary computations. Solutions are obtained for problems with a fixed final time. However, for the time-open case, the optimal solution is for the final time to be infinite. With a weighted function of the final time in the performance index, a limited range of optimal single impulse solutions for the time -open case can also be found. Author

A90-53035*# Princeton Univ., NJ.

COMPARISON OF SOLUTION APPROACHES FOR MINIMUM-FUEL, LOW-THRUST, POWER-LIMITED ORBITAL TRANSFERS

KENNETH D. MEASE (Princeton University, NJ), NGUYEN X. VINH (Michigan, University, Ann Arbor), and CHRISTINE M. HAISSIG IN: AIAA/AAS Astrodynamics Conference, Portland, OR, Aug. 20-22, 1990, Technical Papers. Part 2. Washington, DC, American Institute of Aeronautics and Astronautics, 1990, p. 733-741. refs (Contract NAG3-915)

(AIAA PAPER 90-2960) Copyright

An initial assessment of the feasibility of a function space gradient method for computing solutions to minimum-fuel power-limited transfers encompassing a wide range of thrust to weight ratios is conducted. Three transfers between coplanar ellipses are used as test cases. The gradient method performs best at the high end of the thrust to weight ratio range. At the lower end, there is reduced sensitivity of the fuel consumption to the control profiles. The minimum fuel consumption and the trajectory are computed quite accurately but the control profiles are in error. An approximate analytical solution, obtained by Edelbaum using the method of averaging, is discussed. Author

A90-53037*# Illinois Univ., Urbana.

OPTIMAL COOPERATIVE TIME-FIXED IMPULSIVE RENDEZVOUS

KOOROSH MIRFAKHRAIE and BRUCE A. CONWAY (Illinois, University, Urbana) IN: AIAA/AAS Astrodynamics Conference, Portland, OR, Aug. 20-22, 1990, Technical Papers. Part 2. Washington, DC, American Institute of Aeronautics and Astronautics, 1990, p. 757-770. refs (Contract NAG3-805; NAG3-1138)

(AIAA PAPER 90-2962) Copyright

New capabilities have been added to a method that had been developed for determining optimal, i.e., minimum fuel, trajectories for the fixed-time cooperative rendezvous of two spacecraft. The method utilizes the primer vector theory. The new capabilities enable the method to accommodate cases in which there are fuel constraints on the spacecraft and/or enable the addition of a mid-course impulse to one of the vehicle's trajectories. Results are presented for a large number of cases, and the effect of varying parameters, such as vehicle fuel constraints, vehicle initial masses, and time allowed for the rendezvous, is demonstrated. Author

A90-53038*# Illinois Univ., Urbana.

DISCRETE APPROXIMATIONS TO OPTIMAL TRAJECTORIES USING DIRECT TRANSCRIPTION AND NONLINEAR PROGRAMMING

PAUL J. ENRIGHT and BRUCE A. CONWAY (Illinois, University, Urbana) IN: AIAA/AAS Astrodynamics Conference, Portland, OR, Aug. 20-22, 1990, Technical Papers. Part 2. Washington, DC, American Institute of Aeronautics and Astronautics, 1990, p. 771-785. refs (Contract NAG3-805; NAG3-1138)

(AIAA PAPER 90-2963) Copyright

A recently developed method for solving optimal trajectory problems uses a piecewise-polynomial representation of the state and control variables, enforces the equations of motion via a collocation procedure, and thus approximates the original calculus-of-variations problem with a nonlinear-programming problem, which is solved numerically. This paper identifies this method as a direct transcription method and proceeds to investigate the relationship between the original optimal-control problem and the nonlinear-programming problem. The discretized adjoint equation of the collocation method is found to have deficient accuracy, and an alternate scheme which discretizes the equations of motion using an explicit Runge-Kutta parallel-shooting approach is developed. Both methods are applied to finite-thrust spacecraft trajectory problems, including a low-thrust escape spiral, a three-burn rendezvous, and a low-thrust transfer to the moon. Author

A90-53051*# Chung Shan Inst. of Science and Technology, Lung Tan (China).

OPTIMAL IMPULSIVE TIME-FIXED ORBITAL RENDEZVOUS AND INTERCEPTION WITH PATH CONSTRAINTS

D.-R. TAUR (Chung Shan Institute of Science and Technology, Lung-Tan, Republic of China), J. E. PRUSSING (Illinois, University, Urbana), and V. COVERSTONE-CARROLL IN: AIAA/AAS Astrodynamics Conference, Portland, OR, Aug. 20-22, 1990, Technical Papers. Part 2. Washington, DC, American Institute of Aeronautics and Astronautics, 1990, p. 899-906. refs (Contract NAG3-1138)

(AIAA PAPER 90-2972) Copyright

Minimum-fuel, impulsive, time-fixed solutions are obtained for the problem of orbital rendezvous and interception with interior path constraints. Transfers between coplanar circular orbits in an inverse-square gravitational field are considered, subject to a circular path constraint representing a minimum or maximum permissible orbital radius. Primer vector theory is extended to incorporate path constraints. The optimal number of impulses, their times and positions, and the presence of initial or final coasting arcs are determined. The existence of constraint boundary arcs and boundary points is investigated as well as the optimality of a class of singular arc solutions. To illustrate the complexities introduced by path constraints, an analysis is made of optimal rendezvous in field-free space subject to a minimum radius constraint. Author

A90-53054*# Stanford Univ., CA.

MINIMUM FUEL LUNAR TRAJECTORIES FOR A LOW-THRUST POWER-LIMITED SPACECRAFT

JOHN V. BREAKWELL (Stanford University, CA) and ODED M. GOLAN IN: AIAA/AAS Astrodynamics Conference, Portland, OR, Aug. 20-22, 1990, Technical Papers. Part 2. Washington, DC, American Institute of Aeronautics and Astronautics, 1990, p. 926-932. refs (Contract NAG3-286)

(AIAA PAPER 90-2975) Copyright

Minimum-fuel trajectories from a low earth parking orbit to a low moon orbit are obtained for a low-thrust power-limited spacecraft with thrust acceleration levels of the order of 0.001 G. The trajectories are found by matching an earth spiral to a moon spiral at some intermediate distance. Results are given for the planar case and for the three-dimensional case where the moon orbit is polar. Author

14 GROUND SUPPORT SYSTEMS AND FACILITIES (SPACE)

14

GROUND SUPPORT SYSTEMS AND FACILITIES (SPACE)

Includes launch complexes, research and production facilities; ground support equipment, e.g., mobile transporters; and simulators.

A90-13409*# National Aeronautics and Space Administration. Lewis Research Center, Cleveland, OH.

PHOTOVOLTAIC POWER FOR A LUNAR BASE

GEOFFREY A. LANDIS, SHEILA G. BAILEY, HENRY B. CURTIS, DAVID J. BRINKER, and DENNIS J. FLOOD (NASA, Lewis Research Center, Cleveland, OH) IAF, International Astronautical Congress, 40th, Malaga, Spain, Oct. 7-13, 1989. 16 p. refs (IAF PAPER 89-254) Copyright

A lunar base is an attractive option for space exploration plans early in the next century. The primary options for a lunar base power system are solar and nuclear. This paper details the requirements for a photovoltaic powered lunar base. Topics covered are (1) requirements for power during the lunar day and during the night, (2) solar cells, present and future availability, efficiency, specific power, and temperature sensitivity, (3) storage options for the lunar night, (4) arrays and system integration, and (5) the potential for production of photovoltaic arrays and storage capability from locally available materials. Author

A90-16544* National Aeronautics and Space Administration. Lewis Research Center, Cleveland, OH.

ENERGY STORAGE CONSIDERATIONS FOR A ROBOTIC MARS SURFACE SAMPLER

PATRICIA M. O'DONNELL, ROBERT L. CATALDO, and OLGA D. GONZALEZ-SANABRIA (NASA, Lewis Research Center, Cleveland, OH) IN: The case for Mars III: Strategies for exploration - Technical. San Diego, CA, Univelt, Inc., 1989, p. 245-252. (AAS PAPER 87-245) Copyright

A Mars Rover capable of obtaining surface samples will need a power system for motive power and to power scientific instrumentation. Several different power systems are considered in this paper along with a discussion of the location options. The weight and volume advantages of the different systems are described for a particular power profile. The conclusions are that a Mars Rover Sample Return Mission and Extended Mission can be accomplished utilizing photovoltaics and electrochemical storage. Author

A90-16569* National Aeronautics and Space Administration. Lewis Research Center, Cleveland, OH.

MARS MANNED TRANSPORTATION VEHICLE

MARLA E. PEREZ-DAVIS and KARL A. FAYMON (NASA, Lewis Research Center, Cleveland, OH) IN: The case for Mars III: Strategies for exploration - Technical. San Diego, CA, Univelt, Inc., 1989, p. 557-568. Previously announced in STAR as N89-20545. refs (AAS PAPER 87-271) Copyright

A viable power system technology for a surface transportation vehicle to explore the planet Mars is presented. A number of power traction systems were investigated, and it was found that a regenerative hydrogen-oxygen fuel cell appears to be attractive for a manned Mars rover application. Mission requirements were obtained from the Manned Mars Mission Working Group. Power systems weights, power, and reactants requirements were determined as a function of vehicle weights for vehicles weighting from 6,000 to 16,000 lb (2,722 to 7,257 kg), (Earth weight). The vehicle performance requirements were: velocity, 10 km/hr; range, 100 km; slope climbing capability, 30 deg uphill for 50 km; mission duration, 5 days; and crew, 5. Power requirements for the operation of scientific equipment and support system capabilities were also specified and included in this study. The concept developed here would also be applicable to a Lunar based vehicle for Lunar

exploration. The reduced gravity on the Lunar surface, (over that on the Martian surface), would result in an increased range or capability over that of the Mars vehicle since many of the power and energy requirements for the vehicle are gravity dependent.

Author

A90-24791*# National Aeronautics and Space Administration. Lewis Research Center, Cleveland, OH.

LUNAR PRODUCTION OF SOLAR CELLS - A NEAR-TERM PRODUCT FOR A LUNAR INDUSTRIAL FACILITY

GEOFFREY A. LANDIS (NASA, Lewis Research Center, Cleveland, OH) and MARIA ANTONIETTA PERINO (Aeritalia S.p.A., Turin, Italy) IN: Space manufacturing 7 - Space resources to improve life on earth; Proceedings of the Ninth Princeton/AIAA/SSI Conference, Princeton, NJ, May 10-13, 1989. Washington, DC, American Institute of Aeronautics and Astronautics, 1989, p. 144-151. refs Copyright

Because of the much lower escape velocity, there is a great advantage in manufacture of solar cells for use in space on the moon rather than on earth. Silicon is abundant on the moon, and new refining methods allow it to be reduced and purified without extensive reliance on materials unavailable on the moon. Silicon and amorphous silicon solar cells could be manufactured on the moon for use in space. Author

A90-25662*# Harris Corp., Melbourne, FL.

LBR-2 EARTH STATIONS FOR THE ACTS PROGRAM

MICHAEL O'REILLY (Harris Corp., Melbourne, FL), RUSSELL JIRBERG, and ERNIE SPISZ (NASA, Lewis Research Center, Cleveland, OH) IN: AIAA International Communication Satellite Systems Conference and Exhibit, 13th, Los Angeles, CA, Mar. 11-15, 1990, Technical Papers. Part 2. Washington, DC, American Institute of Aeronautics and Astronautics, 1990, p. 514-521. (AIAA PAPER 90-0838) Copyright

Described in this paper is the 'LBR-2' earth station being developed for NASA's Advanced Communications Technology Satellite (ACTS). The LBR-2 is one of two earth station types that operate through the satellite's baseband processor. The LBR-2 is a small VSAT-like earth station that is easily sited on a user's premises, and provides up to 1.792 megabits per second (MBPS) of voice, video, and data communications. Addressed in the paper is the design of the antenna, the rf subsystems, the digital processing equipment, and the user interface equipment. Author

A90-38030*# National Aeronautics and Space Administration. Lewis Research Center, Cleveland, OH.

COMPARISON OF SOLAR PHOTOVOLTAIC AND NUCLEAR REACTOR POWER SYSTEMS FOR A HUMAN-TENDED LUNAR OBSERVATORY

J. M. HICKMAN and H. S. BLOOMFIELD (NASA, Lewis Research Center, Cleveland, OH) IN: IECEC-89; Proceedings of the Twenty-fourth Intersociety Energy Conversion Engineering Conference, Washington, DC, Aug. 6-11, 1989. Volume 1. New York, Institute of Electrical and Electronics Engineers, 1989, p. 1-5. Previously announced in STAR as N89-23397. refs

Photovoltaic and nuclear surface power systems were examined at the 20 to 100 kW power level range for use at a human-tended lunar astronomical observatory, and estimates of the power system masses were made. One system, consisting of an SP-100 thermoelectric nuclear power supply integrated with a lunar lander, is recommended for further study due to its low system mass, potential for modular growth, and applicability to other surface power missions, particularly in the Martian system. Author

A90-38083*# National Aeronautics and Space Administration. Lewis Research Center, Cleveland, OH.

EVALUATION OF POWER CONTROL CONCEPTS USING THE PMAD SYSTEMS TEST BED

R. F. BEACH, G. L. KIMNACH, T. A. JETT, and L. M. TRASH (NASA, Lewis Research Center, Cleveland, OH) IN: IECEC-89; Proceedings of the Twenty-fourth Intersociety Energy Conversion

14 GROUND SUPPORT SYSTEMS AND FACILITIES (SPACE)

Engineering Conference, Washington, DC, Aug. 6-11, 1989. Volume 1. New York, Institute of Electrical and Electronics Engineers, 1989, p. 327-332. refs

The Lewis Research Center's Power Management and Distribution (PMAD) System testbed and its use in the evaluation of control concepts applicable to the NASA Space Station Freedom electric power system (EPS) are described. The facility was constructed to allow testing of control hardware and software in an environment functionally similar to the space station electric power system. Control hardware and software have been developed to allow operation of the testbed power system in a manner similar to a supervisory control and data acquisition (SCADA) system employed by utility power systems for control. The system hardware and software are described. I.E.

A90-38126* National Aeronautics and Space Administration. Lewis Research Center, Cleveland, OH.

DEVELOPMENT AND TESTING OF A 20 KHZ COMPONENT TEST BED

ROBERT M. BUTTON (NASA, Lewis Research Center, Cleveland, OH), ANDREW S. BRUSH (NASA, Lewis Research Center, Cleveland; Sverdrup Technology, Inc., Middleburg Heights, OH), and RICHARD C. SUNDBERG (General Dynamics Corp., Space Systems Div., San Diego, CA) IN: IECEC-89; Proceedings of the Twenty-fourth Intersociety Energy Conversion Engineering Conference, Washington, DC, Aug. 6-11, 1989. Volume 1. New York, Institute of Electrical and Electronics Engineers, 1989, p. 605-610. Previously announced in STAR as N89-25403. refs (Contract NAS3-25266) Copyright

A history of the General Dynamics Space Systems Division 20-kHz breadboard is presented, including its current configuration and its role in the SSF program. Highlights and results are presented of a series of tests conducted on the 20 kHz breadboard. The first test presented is the 20 kHz Breadboard Acceptance test. This test verified the operation of the delivered Breadboard and also characterized the main components of the system. Next, an in-depth efficiency testing effort is presented. The tests attempted to apportion all the power losses in the 20 Hz Breadboard Main Inverter Units. Distortion test data are presented, showing the distortion characteristics of a Mapham inverter. Lastly, current work on the 20 kHz Breadboard is presented including Main Inverter Unit paralleling tests. Conclusions are summarized and references given. Author

A90-38156* National Aeronautics and Space Administration. Lewis Research Center, Cleveland, OH.

PHOTOVOLTAIC POWER SYSTEM OPERATION IN THE MARS ENVIRONMENT

JOSEPH APPELBAUM and DENNIS J. FLOOD (NASA, Lewis Research Center, Cleveland, OH) IN: IECEC-89; Proceedings of the Twenty-fourth Intersociety Energy Conversion Engineering Conference, Washington, DC, Aug. 6-11, 1989. Volume 2. New York, Institute of Electrical and Electronics Engineers, 1989, p. 841-848. Previously announced in STAR as N89-24529. refs

Detailed information on the environmental conditions on Mars are very desirable for the design of photovoltaic systems for establishing outposts on the Martian surface. The variation of solar insolation (global, direct, and diffuse) at the Viking lander's locations is addressed. It can be used, to a first approximation, for other latitudes. The radiation data is based on measured optical depth of the Martian atmosphere derived from images taken of the sun with a special diode on the Viking cameras; and computation based on multiple wavelength and multiple scattering of the solar radiation. The data are used to make estimates of photovoltaic system power, area and mass for a surface power system using regenerative fuel cells for storage and nighttime operation. Author

A90-40587* Sverdrup Technology, Inc., Brook Park, OH.
PRELIMINARY DESIGN OF A LONG-ENDURANCE MARS AIRCRAFT

ANTHONY J. COLOZZA (Sverdrup Technology, Inc., Lewis Research Center Group, Brook Park, OH) AIAA, SAE, ASME,

and ASEE, Joint Propulsion Conference, 26th, Orlando, FL, July 16-18, 1990. 13 p. Previously announced in STAR as N90-21763. refs

(Contract NAS3-25266)

(AIAA PAPER 90-2000) Copyright

The preliminary design requirements of a long endurance aircraft capable of flight within the Martian environment was determined. Both radioisotope/heat engine and PV solar array power production systems were considered. Various cases for each power system were analyzed in order to determine the necessary size, weight and power requirements of the aircraft. The analysis method used was an adaptation of the method developed by Youngblood and Talay of NASA-Langley used to design a high altitude earth based aircraft. The analysis is set up to design an aircraft which, for the given conditions, has a minimum wingspan and maximum endurance parameter. The results showed that, for a first approximation, a long endurance aircraft is feasible within the Martian environment. The size and weight of the most efficient solar aircraft were comparable to the radioisotope powered one. Author

A90-40627* Large Scale Programs Inst., Austin, TX.

A SUPERCONDUCTING QUENCHGUN FOR DELIVERING LUNAR DERIVED OXYGEN TO LUNAR ORBIT

DAVID KORSMEYER, CURT BILBY, and NATHAN NOTTKE (Large Scale Programs Institute, Austin, TX) AIAA, SAE, ASME, and ASEE, Joint Propulsion Conference, 26th, Orlando, FL, July 16-18, 1990. 12 p. refs (Contract NAG3-928)

(AIAA PAPER 90-2369) Copyright

This study defines a superconducting electromagnetic lunar launcher and its necessary support systems. This launcher is to deliver lunar-derived liquid oxygen to lunar orbit. An Electromagnetic Launcher and Systems Sizing Model developed by the Large Scale Programs Institute scales the launcher and supporting systems as a function of liquid oxygen payload and time between launches. The impact an electromagnetic lunar launcher would have to the present NASA Office of Exploration Lunar Evolution Case Study is examined for three lunar oxygen producing scenarios. Author

A90-47225* National Aeronautics and Space Administration. Lewis Research Center, Cleveland, OH.

LOW THRUST ROCKET TEST FACILITY

LYNN A. ARRINGTON (NASA, Lewis Research Center; Sverdrup Technology, Inc., Brook Park, OH) and STEVEN J. SCHNEIDER (NASA, Lewis Research Center, Cleveland, OH) AIAA, SAE, ASME, and ASEE, Joint Propulsion Conference, 26th, Orlando, FL, July 16-18, 1990. 21 p. Previously announced in STAR as N90-25158. refs

(AIAA PAPER 90-2503) Copyright

A low thrust chemical rocket test facility has recently become operational at the NASA-Lewis. The new facility is used to conduct both long duration and performance tests at altitude over a thruster's operating envelope using hydrogen and oxygen gas for propellants. The facility provides experimental support for a broad range of objectives, including fundamental modeling of fluids and combustion phenomena, the evaluation of thruster components, and life testing of full rocket designs. The major mechanical and electrical systems are described along with aspects of the various optical diagnostics available in the test cell. The electrical and mechanical systems are designed for low down time between tests and low staffing requirements for test operations. Initial results are also presented which illustrate the various capabilities of the cell. Author

N90-25158* National Aeronautics and Space Administration. Lewis Research Center, Cleveland, OH.

LOW THRUST ROCKET TEST FACILITY

LYNN A. ARRINGTON (Sverdrup Technology, Inc., Cleveland, OH.) and STEVEN J. SCHNEIDER Jul. 1990 22 p Presented at the 26th Joint Propulsion Conference, Orlando, FL, 16-18 Jul. 1990; sponsored in part by AIAA, SAE, ASME, and ASEE

14 GROUND SUPPORT SYSTEMS AND FACILITIES (SPACE)

(NASA-TM-103206; E-5571; NAS 1.15:103206; AIAA-90-2503)
Avail: NTIS HC A03/MF A01 CSCL 14/2

A low thrust chemical rocket test facility has recently become operational at the NASA-Lewis. The new facility is used to conduct both long duration and performance tests at altitude over a thruster's operating envelope using hydrogen and oxygen gas for propellants. The facility provides experimental support for a broad range of objectives, including fundamental modeling of fluids and combustion phenomena, the evaluation of thruster components, and life testing of full rocket designs. The major mechanical and electrical systems are described along with aspects of the various optical diagnostics available in the test cell. The electrical and mechanical systems are designed for low down time between tests and low staffing requirements for test operations. Initial results are also presented which illustrate the various capabilities of the cell.

Author

N90-26030*# National Aeronautics and Space Administration. Lewis Research Center, Cleveland, OH.

NATIONAL SPACE TEST CENTERS, LEWIS RESEARCH CENTER FACILITIES

RONALD R. ROSKILLY 1990 7 p Proposed for presentation at the Space Programs and Technologies Conference, Huntsville, AL, 25-27 Sep. 1990; sponsored by AIAA (NASA-TM-103187; E-5570; NAS 1.15:103187; AIAA-90-3593)
Avail: NTIS HC A02/MF A01 CSCL 14/2

The Lewis Research Center, NASA, presently has a number of test facilities that constitute a significant national space test resource. It is expected this capability will continue to find wide application in work involving this country's future in space. Testing from basic research to applied technology, to systems development, to ground support will be performed, supporting such activities as Space Station Freedom, the Space Exploration Initiative, Mission to Planet Earth, and many others. The major space test facilities at both Cleveland and Lewis' Plum Brook Station are described. Primary emphasis is on space propulsion facilities; other facilities of importance in space power and microgravity are also included.

Author

15

LAUNCH VEHICLES AND SPACE VEHICLES

Includes boosters; operating problems of launch/space vehicle systems; and reusable vehicles.

A90-18017*# National Aeronautics and Space Administration. Lewis Research Center, Cleveland, OH.

CENTAUR UPPER STAGE

W. GROESBECK (NASA, Lewis Research Center, Cleveland, OH) IN: Orbital debris from upper-stage breakup. Washington, DC, American Institute of Aeronautics and Astronautics, Inc., 1989, p. 211-213.
Copyright

An account is given of the design features of the LOX/LH₂-fueled Centaur upper stage engine and fuel cryotankage, in order to serve as a basis for understanding the Main Engine Cut Off (MECO) system instituted. MECO follows the instant of spacecraft separation from the upper stage. The planetary launch program during 1966-1978 involved 23 Centaur launches and led to no upper stage reentry; LEO missions for HEAO and OAO satellite lofting in 1963-1979 involved nine Centaur launches and led to five reentries. GEO satellite launches in 1969-1986 saw 32 launches and three known reentries.

O.C.

A90-19989*# National Aeronautics and Space Administration. Lewis Research Center, Cleveland, OH.

EVALUATION OF SUPERCRITICAL CRYOGEN STORAGE AND TRANSFER SYSTEMS FOR FUTURE NASA MISSIONS

HUGH ARIF, JOHN C. AYDELOTT, and DAVID J. CHATO (NASA,

Lewis Research Center, Cleveland, OH) AIAA, Aerospace Sciences Meeting, 28th, Reno, NV, Jan. 8-11, 1990. 9 p. Previously announced in STAR as N90-10912. refs

(AIAA PAPER 90-0719) Copyright

Conceptual designs of Space Transportation Vehicles (STV), and their orbital servicing facilities, that utilize supercritical, single phase, cryogenic propellant were established and compared with conventional subcritical, two phases, STV concepts. The analytical study was motivated by the desire to avoid fluid management problems associated with the storage, acquisition and transfer of subcritical liquid oxygen and hydrogen propellants in the low gravity environment of space. Although feasible, the supercritical concepts suffer from STV weight penalties and propellant resupply system power requirements which make the concepts impractical.

Author

A90-23712*# National Aeronautics and Space Administration. Lewis Research Center, Cleveland, OH.

ATOMIC HYDROGEN AS A LAUNCH VEHICLE PROPELLANT

BRYAN A. PALASZEWSKI (NASA, Lewis Research Center, Cleveland, OH) AIAA, Aerospace Sciences Meeting, 28th, Reno, NV, Jan. 8-11, 1990. 11 p. Previously announced in STAR as N90-14284. refs

(AIAA PAPER 90-0715) Copyright

An analysis of several atomic hydrogen launch vehicles was conducted. A discussion of the facilities and the technologies that would be needed for these vehicles is also presented. The Gross Liftoff Weights (GLOW) for two systems were estimated; their specific impulses (I_{sub sp}) were 750 and 1500 lb (sub f)/s/lb(sub m). The atomic hydrogen launch vehicles were also compared to the currently planned Advanced Launch System design concepts. Very significant GLOW reductions of 52 to 58 percent are possible over the Advanced Launch System designs. Applying atomic hydrogen propellants to upper stages was also considered. Very high I_(sub sp) (greater than 750 lb(sub f)/s/lb(sub m)) is needed to enable a mass savings over advanced oxygen/hydrogen propulsion. Associated with the potential benefits of high I_(sub sp) atomic hydrogen are several challenging problems. Very high magnetic fields are required to maintain the atomic hydrogen in a solid kilogauss (3 Tesla). Also the storage temperature of the propellant is 4 K. This very low temperature will require a large refrigeration facility for the launch vehicle. The design considerations for a very high recombination rate for the propellant are also discussed. A recombination rate of 210 cm/s is predicted for atomic hydrogen. This high recombination rate can produce very high acceleration for the launch vehicle. Unique insulation or segmentation to inhibit the propellant may be needed to reduce its recombination rate.

Author

A90-36188*# National Aeronautics and Space Administration. Lewis Research Center, Cleveland, OH.

EFFECT OF ELEVEN YEARS IN EARTH ORBIT ON A MIRROR SURFACE

MICHAEL J. MIRTICH (NASA, Lewis Research Center, Cleveland, OH), HERMAN MARK, and WILLIAM R. KERSLAKE Journal of Spacecraft and Rockets (ISSN 0022-4650), vol. 27, May-June 1990, p. 258-266. Previously cited in issue 05, p. 639, Accession no. A89-17939. refs

Copyright

N90-10912*# National Aeronautics and Space Administration. Lewis Research Center, Cleveland, OH.

EVALUATION OF SUPERCRITICAL CRYOGEN STORAGE AND TRANSFER SYSTEMS FOR FUTURE NASA MISSIONS

HUGH ARIF, JOHN C. AYDELOTT, and DAVID J. CHATO 1989 10 p Prepared for presentation at the 28th Aerospace Sciences Meeting, Reno, NV, 8-11 Jan. 1990; sponsored by AIAA (NASA-TM-102394; E-5144; NAS 1.15:102394; AIAA-90-0719)
Avail: NTIS HC A02/MF A01 CSCL 22/2

Conceptual designs of Space Transportation Vehicles (STV), and their orbital servicing facilities, that utilize supercritical, single phase, cryogenic propellants were established and compared with conventional subcritical, two phase, STV concepts. The analytical

study was motivated by the desire to avoid fluid management problems associated with the storage, acquisition and transfer of subcritical liquid oxygen and hydrogen propellants in the low gravity environment of space. Although feasible, the supercritical concepts suffer from STV weight penalties and propellant resupply system power requirements which make the concepts impractical.

Author

N90-20110* National Aeronautics and Space Administration. Lewis Research Center, Cleveland, OH.

ADVANCED LAUNCH VEHICLE PROPULSION AT THE NASA LEWIS RESEARCH CENTER

BRYAN A. PALASZEWSKI 1990 6 p. Presented at the High Energy Density Materials Contractors' Conference, Long Beach, CA, 26-28 Feb. 1990; sponsored by AFOSR (NASA-TM-103096; E-5417; NAS 1.15:103096) Avail: NTIS HC A02/MF A01 CSDL 22/2

Several programs are investigating the benefits of advanced propellant and propulsion systems for future launch vehicles and upper stages. The two major research areas are the Metallized Propellants Program and the Advanced Concepts Program. Both of these programs have theoretical and experimental studies underway to determine the system-level performance effects of these propellants on future NASA vehicles.

Author

N90-25159* Sverdrup Technology, Inc., Brook Park, OH.
ROCKET ENGINE FAILURE DETECTION USING SYSTEM IDENTIFICATION TECHNIQUES Final Report

CLAUDIA M. MEYER and JUNE F. ZAKRAJSEK Jun. 1990 18 p. Presented at the 26th Joint Propulsion Conference, Orlando, FL, 16-20 Jul. 1990; cosponsored by AIAA, SAE, ASME, and ASEE

(Contract NAS3-25266)
(NASA-CR-185259; E-5585; NAS 1.26:185259; AIAA-90-1993)
Avail: NTIS HC A03/MF A01 CSDL 22/2

The theoretical foundation and application of two univariate failure detection algorithms to Space Shuttle Main Engine (SSME) test firing data is presented. Both algorithms were applied to data collected during steady state operation of the engine. One algorithm, the time series algorithm, is based on time series techniques and involves the computation of autoregressive models. Times series techniques have been previously applied to SSME data. The second algorithm is based on standard signal processing techniques. It consists of tracking the variations in the average signal power with time. The average signal power algorithm is a newly proposed SSME failure detection algorithm. Seven nominal test firings were used to develop failure indication thresholds for each algorithm. These thresholds were tested using four anomalous firings and one additional nominal firing. Both algorithms provided significantly earlier failure indication times than did the current redline limit system. Neither algorithm gave false failure indications for the nominal firing. The strengths and weaknesses of the two algorithms are discussed and compared. The average signal algorithm was found to have several advantages over the time series algorithm.

Author

N90-27732* Sverdrup Technology, Inc., Brook Park, OH.
MULTI-SENSOR ANALYSIS TECHNIQUES FOR SSME SAFETY MONITORING Final Report

WILLIAM A. MAUL, III Jul. 1990 22 p. Presented at the 26th Joint Propulsion Conference, Orlando, FL, 16-18 Jul. 1990; sponsored in part by AIAA, SAE, ASME, and ASEE

(Contract NAS3-25266)
(NASA-CR-185260; E-5591; NAS 1.26:185260; AIAA-90-1990)
Avail: Issuing Activity CSDL 22/2

Two algorithms were developed which utilized multi-sensor analysis techniques to complement the current Space Shuttle Main Engine (SSME) safety monitoring system. The first algorithm analyzed the accumulative error between actual and predicted values of the engine parameter set, while the second algorithm combined these error terms into a response pattern and correlated each pattern with a standard pattern. These algorithms were applied to twelve SSME anomalous test firings and were found to produce

improved failure detection times in eight of those twelve compared to the current engine safety monitoring system. Of the eight detected anomalous test firings, the first algorithm detected all eight, while the second algorithm detected seven of the eight. No false alarms were indicated by either algorithm for twelve nominal test firings. An initial parametric study of these algorithms for optimized parameter selection is presented and algorithm robustness to sensor failure is demonstrated.

Author

16

SPACE TRANSPORTATION

Includes passenger and cargo space transportation, e.g., shuttle operations; and space rescue techniques.

A90-38071* National Aeronautics and Space Administration. Lewis Research Center, Cleveland, OH.

PHOTOVOLTAIC MODULE ON-ORBIT ASSEMBLY FOR SPACE STATION FREEDOM

T. SOURS (NASA, Lewis Research Center, Cleveland, OH), R. LOVELY, and D. CLARK (Rockwell International Corp., Rocketdyne Div., Canoga Park, CA) IN: IECEC-89; Proceedings of the Twenty-fourth Intersociety Energy Conversion Engineering Conference, Washington, DC, Aug. 6-11, 1989. Volume 1. New York, Institute of Electrical and Electronics Engineers, 1989, p. 251-256. Previously announced in STAR as N89-26887. refs

Copyright

One of the elements of the Space Station Freedom power system is the photovoltaic (PV) module. These modules will be assembled on-orbit during the assembly phase of the program. These modules will be assembled either from the Shuttle Orbiter or from the Mobile Servicing Center (MSC). The different types of assembly operations that will be used to assemble PV modules are described.

Author

A90-38078* National Aeronautics and Space Administration. Lewis Research Center, Cleveland, OH.

LAUNCH PACKAGING OPTIONS FOR THE PV POWER MODULE CARGO ELEMENT

MARK A. HOBERECHT (NASA, Lewis Research Center, Cleveland, OH) and SCOTT T. VOGT (Rockwell International Corp., Rocketdyne Div., Canoga Park, CA) IN: IECEC-89; Proceedings of the Twenty-fourth Intersociety Energy Conversion Engineering Conference, Washington, DC, Aug. 6-11, 1989. Volume 1. New York, Institute of Electrical and Electronics Engineers, 1989, p. 295-298. Previously announced in STAR as N89-25275.

Copyright

NASA recently embarked on the Space Station Freedom program, which will utilize the Shuttle Orbiter for transportation to orbit. Each flight is unique in terms of the hardware that is manifested and the method by which it is integrated to form viable cargo elements. Various constraints determine the packaging options for the three PV power module combined assemblies. Several packaging options for the PV power module cargo element are presented. These options are discussed in terms of their impact on the overall flight hardware manifest as determined by the various constraints.

Author

A90-52499* National Aeronautics and Space Administration. Lewis Research Center, Cleveland, OH.

MULTI-SENSOR ANALYSIS TECHNIQUES FOR SSME SAFETY MONITORING

WILLIAM A. MAUL, III (NASA, Lewis Research Center; Sverdrup Technology, Inc., Brook Park, OH) AIAA, SAE, ASME, and ASEE, Joint Propulsion Conference, 26th, Orlando, FL, July 16-18, 1990. 20 p. Previously announced in STAR as N90-27732. refs

(Contract NAS3-25266)

(AIAA PAPER 90-1990) Copyright

Two algorithms were developed which utilized multi-sensor

17 SPACE COMMUNICATIONS, SPACECRAFT COMMUNICATIONS, COMMAND & TRACKING

analysis techniques to complement the current Space Shuttle Main Engine (SSME) safety monitoring system. The first algorithm analyzed the accumulative error between actual and predicted values of the engine parameter set, while the second algorithm combined these error terms into a response pattern and correlated each pattern with a standard pattern. These algorithms were applied to twelve SSME anomalous test firings and were found to produce improved failure detection times in eight of those twelve compared to the current engine safety monitoring system. Of the eight detected anomalous test firings, the first algorithm detected all eight, while the second algorithm detected seven of the eight. No false alarms were indicated by either algorithm for twelve nominal test firings. An initial parametric study of these algorithms for optimized parameter selection is presented and algorithm robustness to sensor failure is demonstrated. Author

17

SPACE COMMUNICATIONS, SPACECRAFT COMMUNICATIONS, COMMAND & TRACKING

Includes telemetry; space communications networks; astronavigation and guidance; and radio blackout.

A90-11822* Drexel Univ., Philadelphia, PA.

HIGH-SPEED ANALOG FIBER OPTIC LINKS FOR SATELLITE COMMUNICATION

A. S. DARYOUSH, P. R. HERCZFELD (Drexel University, Philadelphia, PA), and R. R. KUNATH (NASA, Lewis Research Center, Cleveland, OH) IN: High data rate atmospheric and space communications; Proceedings of the Meeting, Boston, MA, Sept. 8, 9, 1988, Bellingham, WA, Society of Photo-Optical Instrumentation Engineers, 1988, p. 102-107. refs Copyright

Large-aperture phased array antennas operating at millimeter wave frequencies are designed for space-based communications and imaging. Array elements are comprised of active transmit/receive (T/R) modules which are linked to the central processing unit through a high-speed fiberoptic network. This paper demonstrates optical control of active modules for satellite communication at 24 GHz. An approach called T/R level data mixing, which utilizes fiberoptic transmission of a data signal to individual T/R modules to be upconverted by an optically synchronized local oscillator, is demonstrated at 24 GHz. A free-running HEMT oscillator, used as local oscillator at 24 GHz, is synchronized using indirect subharmonic optical injection locking over a locking range of 14 MHz. Results of data link performance over 500-1000 MHz is also reported in terms of gain-bandwidth, linearity and third-order intercept, sensitivity, and dynamic range. Author

A90-25635* Toledo Univ., OH.

A PARALLEL PIPELINED ARCHITECTURE FOR A DIGITAL MULTICARRIER DEMODULATOR

P. J. FERNANDES, L. P. EUGENE, M. M. JAMALI, S. C. KWATRA (Toledo, University, OH), and J. BUDINGER (NASA, Lewis Research Center, Cleveland, OH) IN: AIAA International Communication Satellite Systems Conference and Exhibit, 13th, Los Angeles, CA, Mar. 11-15, 1990, Technical Papers. Part 1. Washington, DC, American Institute of Aeronautics and Astronautics, 1990, p. 285-294. refs (Contract NAG3-799; NAG3-865) (AIAA PAPER 90-0912) Copyright

A parallel pipelined architecture is presented for demultiplexing and demodulating SCPC/FDMA channels in real time. Specific algorithms are selected for each of the operations necessary for multicarrier demodulation. The selection is made based on their suitability for implementation into parallel-pipelined and sharing schemes. The demodulator is programmable and uses a single hardware module which is shared among all the channels for the

recovery of clock, carrier, and data, resulting in large savings of power and hardware. The system is suitable for onboard processing of signals in satellites where power and area requirements are critical. The design is illustrated for the specific case of processing 800 FDMA channels at 64 kb/s each. Author

A90-25639* Ohio State Univ., Columbus.

A HEURISTIC APPROACH TO WORST-CASE CARRIER-TO-INTERFERENCE RATIO MAXIMIZATION IN SATELLITE SYSTEM SYNTHESIS

CHARLES H. REILLY, ERIC K. WALTON, FERNANDO MATA, CLARK A. MOUNT-CAMPBELL, CARL A. OLEN (Ohio State University, Columbus) et al. IN: AIAA International Communication Satellite Systems Conference and Exhibit, 13th, Los Angeles, CA, Mar. 11-15, 1990, Technical Papers. Part 1. Washington, DC, American Institute of Aeronautics and Astronautics, 1990, p. 322-330. refs (Contract NAG3-159) (AIAA PAPER 90-0816)

Consideration is given to the problem of allotting GEO locations to communication satellites so as to maximize the smallest aggregate carrier-to-interference (C/I) ratio calculated at any test point (assumed earth station). The location allotted to each satellite must be within the satellite's service arc, and angular separation constraints are enforced for each pair of satellites to control single-entry EMI. Solutions to this satellite system synthesis problem (SSSP) are found by embedding two heuristic procedures for the satellite location problem (SLP), in a binary search routine to find an estimate of the largest increment to the angular separation values that permits a feasible solution to SLP and SSSP. Numerical results for a 183-satellite, 208-beam example problem are presented. Author

A90-25673* National Aeronautics and Space Administration, Lewis Research Center, Cleveland, OH.

A BURST COMPRESSION AND EXPANSION TECHNIQUE FOR VARIABLE-RATE USERS IN SATELLITE-SWITCHED TDMA NETWORKS

JAMES M. BUDINGER (NASA, Lewis Research Center, Cleveland, OH) IN: AIAA International Communication Satellite Systems Conference and Exhibit, 13th, Los Angeles, CA, Mar. 11-15, 1990, Technical Papers. Part 2. Washington, DC, American Institute of Aeronautics and Astronautics, 1990, p. 623-637. Previously announced in STAR as N90-15983. refs (AIAA PAPER 90-0850) Copyright

A burst compression and expansion technique is described for asynchronously interconnecting variable-data-rate users with cost-efficient ground terminals in a satellite-switched, time-division-multiple-access (SS/TDMA) network. Compression and expansion buffers in each ground terminal convert between lower rate, asynchronous, continuous-user data streams and higher-rate TDMA bursts synchronized with the satellite-switched timing. The technique described uses a first-in, first-out (FIFO) memory approach which enables the use of inexpensive clock sources by both the users and the ground terminals and obviates the need for elaborate user clock synchronization processes. A continuous range of data rates from kilobits per second to that approaching the modulator burst rate (hundreds of megabits per second) can be accommodated. The technique was developed for use in the NASA Lewis Research Center System Integration, Test, and Evaluation (SITE) facility. Some key features of the technique have also been implemented in the ground terminals developed at NASA Lewis for use in on-orbit evaluation of the Advanced Communications Technology Satellite (ACTS) high burst rate (HBR) system. Author

A90-25704* Ford Aerospace and Communications Corp., Palo Alto, CA.

DATA DISTRIBUTION SATELLITE SYSTEM ARCHITECTURE CONCEPT

KENT M. PRICE and RONALD E. JORASCH (Ford Aerospace Corp., Space Systems Div., Palo Alto, CA) IN: AIAA International Communication Satellite Systems Conference and Exhibit, 13th,

Los Angeles, CA, Mar. 11-15, 1990, Technical Papers. Part 2. Washington, DC, American Institute of Aeronautics and Astronautics, 1990, p. 864-877.
(Contract NAS3-24683)
(AIAA PAPER 90-0885) Copyright

This paper describes a future communications satellite system architecture concept called the Data Distribution Satellite (DDS). The DDS is envisioned as a new system to be used as an adjunct to TDRS/TDAS for distributing new NASA science data throughout the U.S. as well as internationally. The DDS would also provide networking capability for interchange of science database files among science users and NASA archive depositories. Experimenters would be able to access and control their experimental packages remotely, relieving astronaut workload. This paper gives a conceptual system design based on year 1995 technology. Features of the design include use of Ku and Ka-bands, use of fixed spot beams, 2 Gb/s throughput, and on-board demodulation and switching. The satellite dry mass is 1,300 kg and end-of-life power is 4 kW. Author

A90-41687* Drexel Univ., Philadelphia, PA.
HIGH-SPEED FIBER-OPTIC LINKS FOR DISTRIBUTION OF SATELLITE TRAFFIC

AFSHIN S. DARYOUSH, REZA SAEDI (Drexel University, Philadelphia, PA), EDWARD ACKERMAN (GE Electronics Laboratory, Syracuse, NY), RICHARD KUNATH, and KURT SHALKHAUSER (NASA, Lewis Research Center, Cleveland, OH) IEEE Transactions on Microwave Theory and Techniques (ISSN 0018-9480), vol. 38, May 1990, p. 510-517. Research supported by General Electric Co. and Du Pont de Nemours and Co. refs Copyright

Low-loss fiberoptic links are designed for distribution of data and the frequency reference in large-aperture phased-array antennas based on the transmit/receive-level data mixing architecture. In particular, design aspects of a fiberoptic link satisfying the distribution requirements of satellite data traffic are presented. The design is addressed in terms of reactively matched optical transmitter and receiver modules. Analog and digital characterization of a 50-m fiberoptic link realized using these modules indicates the applicability of this architecture as the only viable alternative for distribution of data signals inside a satellite at present. It is demonstrated that the design of a reactive matching modules enhances the link performance. A dynamic range of 88 dB/MHz was measured for analog data over a 500-1000-MHz bandwidth. I.E.

N90-15983* National Aeronautics and Space Administration. Lewis Research Center, Cleveland, OH.

A BURST COMPRESSION AND EXPANSION TECHNIQUE FOR VARIABLE-RATE USERS IN SATELLITE-SWITCHED TDMA NETWORKS

JAMES M. BUDINGER Mar. 1990 19 p Prepared for presentation at the 13th International Communication Satellite Systems Conference, Los Angeles, CA, 11-15 Mar. 1990; sponsored in part by AIAA
(NASA-TM-102414; E-5177; NAS 1.15:102414; AIAA-90-0850)
Avail: NTIS HC A03/MF A01 CSCL 17/2

A burst compression and expansion technique is described for asynchronously interconnecting variable-data-rate users with cost-efficient ground terminals in a satellite-switched, time-division-multiple-access (SS/TDMA) network. Compression and expansion buffers in each ground terminal convert between lower rate, asynchronous, continuous-user data streams and higher-rate TDMA bursts synchronized with the satellite-switched timing. The technique described uses a first-in, first-out (FIFO) memory approach which enables the use of inexpensive clock sources by both the users and the ground terminals and obviates the need for elaborate user clock synchronization processes. A continuous range of data rates from kilobits per second to that approaching the modulator burst rate (hundreds of megabits per second) can be accommodated. The technique was developed for use in the NASA Lewis Research Center System Integration, Test, and Evaluation (SITE) facility. Some key features of the

technique have also been implemented in the ground terminals developed at NASA Lewis for use in on-orbit evaluation of the Advanced Communications Technology Satellite (ACTS) high burst rate (HBR) system. Author

N90-27736* National Aeronautics and Space Administration. Lewis Research Center, Cleveland, OH.

A TECHNOLOGY ASSESSMENT OF ALTERNATIVE COMMUNICATIONS SYSTEMS FOR THE SPACE EXPLORATION INITIATIVE

DENISE S. PONCHAK, JOHN E. ZUZK, WAYNE A. WHYTE, JR., RODNEY L. SPENCE, and PHILIP Y. SOHN 1990 25 p Presented at the Space Programs and Technologies Conference, Huntsville, AL, 25-27 Sep. 1990; sponsored by AIAA
(NASA-TM-103243; E-5665; NAS 1.15:103243; AIAA-90-3681)
Avail: NTIS HC A03/MF A01 CSCL 17/2

Telecommunications, Navigation, and Information Management (TNIM) services are vital to accomplish the ambitious goals of the Space Exploration Initiative (SEI). A technology assessment is provided for four alternative lunar and Mars operational TNIM systems based on detailed communications link analyses. The four alternative systems range from a minimum to a fully enhanced capability and use frequencies from S-band, through Ka-band, and up to optical wavelengths. Included are technology development schedules as they relate to present SEI mission architecture time frames. Author

18

SPACECRAFT DESIGN, TESTING AND PERFORMANCE

Includes satellites; space platforms; space stations; spacecraft systems and components such as thermal and environmental controls; and attitude controls.

A90-22252* National Aeronautics and Space Administration. Lewis Research Center, Cleveland, OH.

THE SPACE STATION PHOTOVOLTAIC PANELS PLASMA INTERACTION TEST PROGRAM - TEST PLAN AND RESULTS

HENRY K. NAHRA, MARIAN C. FELDER, BERNARD L. SATER, and JOHN V. STASKUS (NASA, Lewis Research Center, Cleveland, OH) AIAA, Aerospace Sciences Meeting, 28th, Reno, NV, Jan. 8-11, 1990. 11 p. Previously announced in STAR as N90-13581.
(AIAA PAPER 90-0722) Copyright

The plasma Interaction Test performed on two space station solar array panels is addressed. This includes a discussion of the test requirements, test plan, experimental set-up, and test results. It was found that parasitic current collection was insignificant (0.3 percent of the solar array delivered power). The measured arcing threshold ranged from -210 to -457 V with respect to the plasma potential. Furthermore, the dynamic response of the panels showed the panel time constant to range between 1 and 5 microsec, and the panel capacitance to be between .01 and .02 microF. Author

A90-27525* National Aeronautics and Space Administration. Lewis Research Center, Cleveland, OH.

COMPARATIVE THERMAL ANALYSIS OF THE SPACE STATION FREEDOM PHOTOVOLTAIC DEPLOYABLE BOOM STRUCTURE USING TRASYS, NEVADA, AND SINDA PROGRAMS

JOSEPH F. BAUMEISTER (NASA, Lewis Research Center; Analox Corp., Cleveland, OH), DUANE E. BEACH, and SASAN C. ARMAND (NASA, Lewis Research Center, Cleveland, OH) SAE, Intersociety Conference on Environmental Systems, 19th, San Diego, CA, July 24-26, 1989. 9 p. Previously announced in STAR as N89-26177.
(SAE PAPER 891563) Copyright

The proposed Space Station Photovoltaic Deployable Boom was analyzed for operating temperatures. The boom glass/epoxy

18 SPACECRAFT DESIGN, TESTING AND PERFORMANCE

structure design needs protective shielding from environmental degradation. The protective shielding optical properties (solar absorptivity and emissivity) dictate the operating temperatures of the boom components. The Space Station Boom protective shielding must also withstand the effects of the extendible/retractable coiling acting within the mast canister. A thermal analysis method was developed for the Space Station Deployable Boom to predict transient temperatures for a variety of surface properties. The modeling procedures used to evaluate temperatures within the boom structure incorporated the TRASYS, NEVADA, and SINDA thermal analysis programs. Use of these programs led to a comparison between TRASYS and NEVADA analysis methods. Comparing TRASYS and NEVADA results exposed differences in the environmental solar flux predictions.

Author

A90-27527* Grumman Aerospace Corp., Bethpage, NY.
CONCEPTUAL DESIGN OF A LIQUID DROPLET RADIATOR SPACE FLIGHT EXPERIMENT

S. PFEIFFER (Grumman Space Systems Div., Bethpage, NY) and A. WHITE (NASA, Lewis Research Center, Cleveland, OH) SAE, Intersociety Conference on Environmental Systems, 19th, San Diego, CA, July 24-26, 1989. 10 p. refs (SAE PAPER 891565) Copyright

This paper discusses the conceptual design of a shuttle-attached Liquid Droplet Radiator (LDR) experiment. The Liquid Droplet Radiator is an advanced lightweight heat rejection concept that can be used to reject heat from future high-powered space platforms. In the LDR concept, submillimeter-sized droplets are generated, radiate heat as they pass through space and are then collected and recirculated back to the heat source. The LDR experiment is designed to be attached to the shuttle longeron and integrated into the shuttle bay using standard shuttle/experiment interfaces. Overall power, weight, and data requirements of the experiment are detailed. Conceptual design and shuttle integration issues are discussed.

Author

A90-27710* Rockwell International Corp., Canoga Park, CA.
STRUCTURAL CONFIGURATION OPTIONS FOR THE SPACE STATION FREEDOM SOLAR DYNAMIC RADIATOR

ADRIAN TYLIM (Rockwell International Corp., Rocketdyne Div., Canoga Park, CA) (IAF, International Conference on Space Power, Cleveland, OH, June 5-7, 1989) Space Power (ISSN 0883-6272), vol. 8, no. 4, 1989, p. 459-468.

(Contract NAS3-25082)

(IAF PAPER ICOSP89-4-5) Copyright

In order to meet the growing power demands of the Space Station, the electrical power system design includes an option to provide additional power capability in increments of 50 kW of power. Each increment consists of a pair of two solar dynamic power modules (SDPMs), each of which containing a closed Brayton Cycle (CBC) thermodynamic engine. A solar dynamic radiator (SDR) enables the CBC to reject the waste heat to the surrounding space environment. This paper analyzes three alternatives to the baseline configuration of the Space Station Freedom solar dynamic radiator and discusses their merits based on Space Shuttle cargo capabilities, location with respect to the SDPM supporting structure, thermal performance, drag, concentrator shading, mass, and other issues of concern. Results indicating the advantages and disadvantages of each option are presented along with diagrams of the alternative configurations.

I.S.

A90-29281*# Rockwell International Corp., Canoga Park, CA.
SPACE STATION FREEDOM ELECTRIC POWER SYSTEM PHOTOVOLTAIC POWER MODULE INTEGRATED LAUNCH PACKAGE

THEODORE H. NATHANSON, DONALD D. CLEMENS, RAYMOND R. SPATZ (Rockwell International Corp., Rocketdyne Div., Canoga Park, CA), and LUKE A. KIRCH (NASA, Lewis Research Center, Cleveland, OH) IN: AIAA/ASME/ASCE/AHS/ASC Structures, Structural Dynamics and Materials Conference, 31st, Long Beach, CA, Apr. 2-4, 1990, Technical Papers. Part 1. Washington, DC,

American Institute of Aeronautics and Astronautics, 1990, p. 568-571.

(AIAA PAPER 90-1053) Copyright

The launch of the Space Station Freedom solar power module requires a weight efficient structure that will include large components within the limited load capacity of the Space Shuttle cargo bay. The design iterations to meet these requirements have evolved from a proposal concept featuring a separate cradle and integrated equipment assembly (IEA), to a package that interfaces directly with the Shuttle. Size, weight, and cost have been reduced as a result.

Author

A90-34780* Stanford Univ., CA.
THE SHEATH STRUCTURE AROUND A NEGATIVELY CHARGED ROCKET PAYLOAD

T. NEUBERT, B. E. GILCHRIST, P. M. BANKS (Stanford University, CA), M. J. MANDELL (Maxwell Laboratories, Inc., La Jolla, CA), S. SASAKI (Institute for Space and Astronautical Sciences, Tokyo, Japan) et al. Journal of Geophysical Research (ISSN 0148-0227), vol. 95, May 1, 1990, p. 6155-6165. Research sponsored by USAF. refs

(Contract NAGW-1566; NAG5-607; NAS8-35350; NAS3-23881) Copyright

The sheath structure around a rocket payload charged up to 460 V negative relative to the ambient ionospheric plasma is investigated experimentally and by computer simulations. The experimental results come from the Charge 2 sounding rocket experiment in which the payload was split into two separate sections (mother and daughter) connected with a conducting, insulated tether. In one of the experimental modes, the voltage between the payloads was increased linearly from 0 to 460 V in 2.5 s. A floating probe array was mounted on the mother with probes located 25, 50, 75, and 100 cm from the rocket surface. The internal impedance of the array was smaller than the probe/plasma impedance, which influenced the potential measurements. The measurements contain signatures, resulting from the outward expansion of the ion sheath with increasing negative mother potential. This conclusion is substantiated by computer simulations of space charge limited flow.

Author

A90-36191*# Massachusetts Inst. of Tech., Cambridge.
ION DRAG FOR A NEGATIVELY BIASED SOLAR ARRAY IN LOW EARTH ORBIT

DANIEL E. HASTINGS and MENGU CHO (MIT, Cambridge, MA) Journal of Spacecraft and Rockets (ISSN 0022-4650), vol. 27, May-June 1990, p. 279-284. refs

(Contract AF-AFOSR-87-0340; NAG3-695)

Copyright

Highly biased solar arrays in the space environment are found to have a number of significant interactions with the space environment. The enhanced drag suffered by highly biased solar arrays is studied with the particle-in-cell code. The results are compared to recent numerical work. The drag calculations contain the effect of having the conductor surrounded by dielectrics as well as the charging of the dielectric by electrons. The results are used to calculate the attitude change expected on the high-voltage solar array of the Japanese Space Flyer Unit.

Author

A90-38267* National Aeronautics and Space Administration.
Lewis Research Center, Cleveland, OH.

UPDATE OF THE SOLAR CONCENTRATOR ADVANCED DEVELOPMENT PROJECT

ROBERT D. CORRIGAN, TODD T. PETERSON (NASA, Lewis Research Center, Cleveland, OH), and DERIK T. EHRESMAN (Harris Corp., Melbourne, FL) IN: IECEC-89; Proceedings of the Twenty-fourth Intersociety Energy Conversion Engineering Conference, Washington, DC, Aug. 6-11, 1989. Volume 6. New York, Institute of Electrical and Electronics Engineers, 1989, p. 2617-2622.

(Contract NAS3-24670)

Copyright

The Solar Concentrator Advanced Development Project, which has achieved the successful design, fabrication, and testing of a

full-scale prototypical solar dynamic concentrator, is discussed. The design and fabrication process are summarized, and the test results for the reflective facet optical performance and the concentrator structural repeatability are reported. Initial testing of structural repeatability of a seven panel portion of the concentrator was followed by assembly and testing of the full nineteen-panel structure. The testing, which consisted of theodolite and optical measurements over an assembly-disassembly-reassembly cycle, demonstrated that the concentrator maintained the as-built contour and optical characteristics. The facet development effort, which entailed developing a vapor-deposited reflective facet, produced a viable design with demonstrated optical characteristics that are within the project goals. I.E.

A90-38697*# Systems Science and Software, La Jolla, CA.
PLASMA SOURCES FOR SPACECRAFT NEUTRALIZATION

V. A. DAVIS, I. KATZ, and M. J. MANDELL (Systems Science and Software, La Jolla, CA) AIAA, Fluid Dynamics, Plasma Dynamics and Lasers Conference, 21st, Seattle, WA, June 18-20, 1990. 12 p. refs
 (Contract NAS3-23881)
 (AIAA PAPER 90-1556) Copyright

The principles of the operation of plasma sources for the neutralization of the surface of a spacecraft traveling in the presence of hot plasma are discussed with special attention given to the hollow-cathode-based plasma contactors. Techniques are developed that allow the calculation of the potentials and particle densities in the near environment of a hollow cathode plasma contactor in both the test tank and the LEO environment. The techniques and codes were validated by comparison of calculated and measured results. I.S.

A90-41566*# National Aeronautics and Space Administration.
 Lewis Research Center, Cleveland, OH.

**SPACECRAFT ATTITUDE IMPACTS ON COLD-SAT
 NON-VACUUM JACKETED LH2 SUPPLY TANK THERMAL
 PERFORMANCE**

HUGH ARIF (NASA, Lewis Research Center, Cleveland, OH) AIAA and ASME, Joint Thermophysics and Heat Transfer Conference, 5th, Seattle, WA, June 18-20, 1990. 16 p. Previously announced in STAR as N90-22592. refs
 (AIAA PAPER 90-1672) Copyright

The Cryogenic On-Orbit Liquid Depot - Storage, Acquisition and Transfer (COLD-SAT) spacecraft will be launched into low earth orbit to perform fluid management experiments on the behavior of subcritical liquid hydrogen (LH2). For determining the optimum on-orbit attitude for the COLD-SAT satellite, a comparative analytical study was performed to determine the thermal impacts of spacecraft attitude on the performance of the COLD-SAT non-vacuum jacketed LH2 supply tank. Tank thermal performance was quantified by total conductive and radiative heat leakage into the pressure vessel due to the absorbed solar, earth albedo and infra-red on-orbit fluxes, and also by the uniformity of the variation of this leakage on the vessel surface area. Geometric and thermal analysis math models were developed for the spacecraft and the tank as part of this analysis, based on their individual thermal/structural designs. Two quasi-inertial spacecraft attitudes were investigated and their effects on the tank performance compared. The results are one of the criteria by which the spacecraft orientation in orbit was selected for the in-house NASA Lewis Research Center design. Author

N90-10983*# General Dynamics Corp., San Diego, CA. Space Systems Div.

**EVOLUTIONARY SPACE STATION FLUIDS MANAGEMENT
 STRATEGIES Final Report**

Aug. 1989 167 p
 (Contract NAS3-25354)
 (NASA-CR-185137; NAS 1.26:185137; GDSS-CRAD-89-002)
 Avail: NTIS HC A08/MF A01 CSCL 22/2

Results are summarized for an 11-month study to define fluid storage and handling strategies and requirements for various specific mission case studies and their associated design impacts

on the Space Station. There are a variety of fluid users which require a variety of fluids and use rates. Also, the cryogenic propellants required for NASA's STV, Planetary, and Code Z missions are enormous. The storage methods must accommodate fluids ranging from a high pressure gas or supercritical state fluid to a sub-cooled liquid (and superfluid helium). These requirements begin in the year 1994, reach a maximum of nearly 1800 metric tons in the year 2004, and trail off to the year 2018, as currently planned. It is conceivable that the cryogenic propellant needs for the STV and/or Lunar mission models will be met by LTCSF LH2/LO2 tanksets attached to the SS truss structure. Concepts and corresponding transfer and delivery operations have been presented for STV propellant provisioning from the SS. A growth orbit maneuvering vehicle (OMV) and associated servicing capability will be required to move tanksets from delivery launch vehicles to the SS or co-orbiting platforms. Also, appropriate changes to the software used for OMV operation are necessary to allow for the combined operation of the growth OMV. To support fluid management activities at the Space Station for the experimental payloads and propellant provisioning, there must be truss structure space allocated for fluid carriers and propellant tanksets, and substantial beam strengthening may be required. The Station must have two Mobile Remote Manipulator Systems (MRMS) and the growth OMV propellant handling operations for the STV at the SS. Propellant needs for the Planetary Initiatives and Code Z mission models will most likely be provided by co-orbiting propellant platform(s). Space Station impacts for Code Z mission fluid management activities will be minimal. Author

N90-12645*# Wyle Labs., Inc., Huntsville, AL.
**ADVANCED SPACECRAFT FIRE SAFETY: PROPOSED
 PROJECTS AND PROGRAM PLAN Final Report**

WALLACE W. YOUNGBLOOD and M. VEDHA-NAYAGAM Oct. 1989 176 p
 (Contract NAS3-25367)
 (NASA-CR-185147; NAS 1.26:185147; WYLE-60300-1) Avail:
 NTIS HC A09/MF A01 CSCL 22/2

A detailed review identifies spacecraft fire safety issues and the efforts for their resolution, particularly for the threats posed by the increased on-orbit duration, size, and complexity of the Space Station Freedom. Suggestions provided by a survey of Wyle consultants and outside fire safety experts were combined into 30 research and engineering projects. The projects were then prioritized with respect to urgency to meet Freedom design goals, status of enabling technology, cost, and so on, to yield 14 highest priority projects, described in terms of background, work breakdown structure, and schedule. These highest priority projects can be grouped into the thematic areas of fire detection, fire extinguishment, risk assessment, toxicology and human effects, and ground based testing. Recommendations for overall program management stress the need for NASA Headquarters and field center coordination, with information exchange through spacecraft fire safety oversight committees. Author

N90-13581*# National Aeronautics and Space Administration.
 Lewis Research Center, Cleveland, OH.

**THE SPACE STATION PHOTOVOLTAIC PANELS PLASMA
 INTERACTION TEST PROGRAM: TEST PLAN AND RESULTS**

HENRY K. NAHRA, MARIAN C. FELDER, BERNARD L. SATER, and JOHN V. STASKUS 1989 11 p Presented at the 28th Aerospace Sciences Meeting, Reno, NV, 8-11 Jan. 1990; sponsored by AIAA
 (NASA-TM-102474; E-5261; NAS 1.15:102474; AIAA-90-0722)
 Avail: NTIS HC A03/MF A01 CSCL 22/2

The Plasma Interaction Test performed on two space station solar array panels is addressed. This includes a discussion of the test requirements, test plan, experimental set-up, and test results. It was found that parasitic current collection was insignificant (0.3 percent of the solar array delivered power). The measured arcing threshold ranged from -210 to -457 V with respect to the plasma potential. Furthermore, the dynamic response of the panels showed the panel time constant to range between 1 and 5 microsec, and

18 SPACECRAFT DESIGN, TESTING AND PERFORMANCE

the panel capacitance to be between .01 and .02 microF.

Author

N90-14268*# National Aeronautics and Space Administration. Lewis Research Center, Cleveland, OH.

SLUSH HYDROGEN (SLH2) TECHNOLOGY DEVELOPMENT FOR APPLICATION TO THE NATIONAL AEROSPACE PLANE (NASP)

RICHARD L. DEWITT, TERRY L. HARDY, MARGARET V. WHALEN, and G. PAUL RICHTER Jul. 1989 19 p Presented at the Cryogenic Engineering Conference, Los Angeles, CA, 24-28 Jul. 1989; sponsored by the California Univ. at Los Angeles (NASA-TM-102315; E-5001; NAS 1.15:102315) Avail: NTIS HC A03/MF A01 CSCL 22/2

The National Aerospace Plane (NASP) program is giving us the opportunity to reach new unique answers in a number of engineering categories. The answers are considered enhancing technology or enabling technology. Airframe materials and densified propellants are examples of enabling technology. The National Aeronautics and Space Administration's Lewis Research Center has the task of providing the technology data which will be used as the basis to decide if slush hydrogen (SLH2) will be the fuel of choice for the NASP. The objectives of this NASA Lewis program are: (1) to provide, where possible, verified numerical models of fluid production, storage, transfer, and feed systems, and (2) to provide verified design criteria for other engineered aspects of SLH2 systems germane to a NASP. This program is a multiyear multimillion dollar effort. The present pursuit of the above listed objectives is multidimensional, covers a range of problem areas, works these to different levels of depth, and takes advantage of the resources available in private industry, academia, and the U.S. Government. The NASA Lewis overall program plan is summarized. The initial implementation of the plan will be unfolded and the present level of efforts in each of the resource areas will be discussed. Results already in hand will be pointed out. A description of additionally planned near-term experimental and analytical work is described.

Author

N90-14273*# National Aeronautics and Space Administration. Lewis Research Center, Cleveland, OH.

CHARACTERIZATION OF TWO MMIC GAAS SWITCH MATRICES AT MICROWAVE FREQUENCIES

GENE FUJIKAWA 1990 12 p Prepared for presentation at the 13th International Communication Satellite Systems Conference, Los Angeles, CA, 11-15 Mar. 1990; sponsored by AIAA (NASA-TM-102449; E-5234; NAS 1.15:102449) Avail: NTIS HC A03/MF A01 CSCL 22/2

Monolithic GaAs microwave switch matrices for use in satellite switched, time division multiple access communication systems were developed. Two monolithic GaAs MESFET switch matrices were fabricated; one for switching operation at intermediate frequencies, 3.5 to 6.0 GHz, and another for switching at radio frequencies, 17.7 to 20.2 GHz. Key switch parameters were measured for both switch matrices.

Author

N90-15985*# Rockwell International Corp., Canoga Park, CA. Energy Technology Engineering Center.

THE GEVALTIG: AN INERTIAL FUSION POWERED MANNED SPACECRAFT DESIGN FOR OUTER SOLAR SYSTEM MISSIONS Final Report

K. A. MURRAY Oct. 1989 53 p (Contract NASA ORDER C-32002-J) (NASA-CR-185163; NAS 1.26:185163; ETEC-89-7) Avail: NTIS HC A04/MF A01 CSCL 22/2

The Gevaltig is an inertial fusion powered rocket engine capable of manned missions to other planets with round trip mission times as low as 100 days. The Gevaltig design was previously described for a mission to Mars. This effort defines the spacecraft components in terms of mass and presents a mission analysis for a manned trip to Titan, a moon of Saturn. The Gevaltig component masses are provided as a function of fuel pellet ignition frequency. These variable mass components include the fuel tank, radiators, structure

and EM pumps. Fixed mass components include the drivers, coil, coil shield, power processing system, payload, crew shield and laser mirrors. A 6 MW nuclear reactor is included in the design for startup purposes. Various combinations of thrust, mission duration and specific impulse were evaluated to determine a reasonable mission scenario for the Titan mission. The mission analysis yielded several viable mission scenarios, with round trip durations of 370 to 500 days and initial (launch) masses from lunar orbit of 2500 to 20,000 metric tons.

Author

N90-20120*# Arinc Research Corp., Annapolis, MD. **SPACE STATION FREEDOM ELECTRIC POWER SYSTEM AVAILABILITY STUDY Final Report**

SCOTT R. TURNQUIST Feb. 1990 139 p Prepared for Analox Corp., Cleveland, OH (Contract NAS3-24564) (NASA-CR-185181; NAS 1.26:185181; ARINC-4247-01-01-5032) Avail: NTIS HC A07/MF A01 CSCL 22/2

The results are detailed of follow-on availability analyses performed on the Space Station Freedom electric power system (EPS). The scope includes analyses of several EPS design variations, these are: the 4-photovoltaic (PV) module baseline EPS design, a 6-PV module EPS design, and a 3-solar dynamic module EPS design which included a 10 kW PV module. The analyses performed included: determining the discrete power levels that the EPS will operate at upon various component failures and the availability of each of these operating states; ranking EPS components by the relative contribution each component type gives to the power availability of the EPS; determining the availability impacts of including structural and long-life EPS components in the availability models used in the analyses; determining optimum sparing strategies, for storing space EPS components on-orbit, to maintain high average-power-capability with low lift-mass requirements; and analyses to determine the sensitivity of EPS-availability to uncertainties in the component reliability and maintainability data used.

Author

N90-21074*# National Aeronautics and Space Administration. Lewis Research Center, Cleveland, OH.

DETECTION OF POTENTIAL SPACE STATION CONTROL/STRUCTURE INTERACTION WITH CO-ST-IN

KELLY CARNEY, RON GRAHAM, DOUG KYR, and PAUL ANDREW BLELLOCH (SDRC, Inc., San Diego, CA.) In NASA, Langley Research Center, NASA/DOD Controls-Structures Interaction Technology 1989 p 211-228 Aug. 1989 Avail: NTIS HC A23/MF A03 CSCL 22/2

The NASA Lewis Research Center is concerned with the potential of interaction between space station controllers and the solar PV array structures. The models required to handle this problem are very large, and automated methods were developed for the transfer of data between structural dynamic and control system analysis software. These methods emphasize the need to achieve accurate coupled analysis results while using as small a model as possible. Specific tools which help the analyst in this regard include modal order techniques, the use of mode acceleration to calculate internal loads and stresses and the transfer of Craig-Bampton components to reduce problems associated with modal sufficiency. These techniques were applied to a space station model with 366 modes below 1 Hz. Attitude control, and alpha and beta joint control were simulated. The inclusion of alpha and beta joint controllers is important when examining overall space station dynamics. An initial choice of control parameters does indicate a potential for control/structure interaction during reboost. As expected this is exacerbated by increasing the rate gain and decreasing the hysteresis of the reaction control system (RCS) in order to improve rigid body performance.

Author

N90-25172*# TRW Space Technology Labs., Redondo Beach, CA.

CONCEPTUAL DEFINITION OF A HIGH VOLTAGE POWER SUPPLY TEST FACILITY Final Technical Report

JOHN J. BIESS, TEH-MING CHU, and N. JOHN STEVENS Dec.

1989 83 p

(Contract NAS3-25089)

(NASA-CR-185216; NAS 1.26:185216) Avail: NTIS HC A05/MF A01 CSCL 22/2

NASA Lewis Research Center is presently developing a 60 GHz traveling wave tube for satellite cross-link communications. The operating voltage for this new tube is - 20 kV. There is concern about the high voltage insulation system and NASA is planning a space station high voltage experiment that will demonstrate both the 60 GHz communications and high voltage electronics technology. The experiment interfaces, requirements, conceptual design, technology issues and safety issues are determined. A block diagram of the high voltage power supply test facility was generated. It includes the high voltage power supply, the 60 GHz traveling wave tube, the communications package, the antenna package, a high voltage diagnostics package and a command and data processor system. The interfaces with the space station and the attached payload accommodations equipment were determined. A brief description of the different subsystems and a discussion of the technology development needs are presented. Author

N90-25173*# National Aeronautics and Space Administration. Lewis Research Center, Cleveland, OH.

LUNAR ORBITING MICROWAVE BEAM POWER SYSTEM

EDGAR H. FAY (Sverdrup Technology, Inc., Brook Park, OH.) and RONALD C. CULL 1990 9 p Presented at the 25th Intersociety Energy Conversion Engineering Conference, Reno, NV, 12-17 Aug. 1990; cosponsored by AIChE, ANS, SAE, ACS, AIAA, ASME, and IEEE (NASA-TM-103211; E-5620; NAS 1.15:103211) Avail: NTIS HC A02/MF A01 CSCL 22/2

A microwave beam power system using lunar orbiting solar powered satellite(s) and surface rectenna(s) was investigated as a possible energy source for the Moon's surface. The concept has the potential of reduced system mass by placing the power source in orbit. This can greatly reduce and/or eliminate the 14 day energy storage requirement of a lunar surface solar system. Also propellants required to de-orbit to the surface are greatly reduced. To determine the practicality of the concept and the most important factors, a zero-th order feasibility analysis was performed. Three different operational scenarios employing state of the art technology and forecasts for two different sets of advanced technologies were investigated. To reduce the complexity of the problem, satellite(s) were assumed in circular equatorial orbits around the Moon, supplying continuous power to a single equatorial base through a fixed horizontal rectenna on the surface. State of the art technology yielded specific masses greater than 2500 kg/kw, well above projections for surface systems. Using advanced technologies the specific masses are on the order of 100 kg/kw which is within the range of projections for surface nuclear (20 kg/kw) and solar systems (500 kg/kw). Further studies examining optimization of the scenarios, other technologies such as lasers transmitters and nuclear sources, and operational issues such as logistics, maintenance and support are being carried out to support the Space Exploration Initiative (SEI) to the Moon and Mars. Author

N90-25174*# National Aeronautics and Space Administration. Lewis Research Center, Cleveland, OH. Dept. of Engineering Technology.

DYNAMIC ANALYSIS OF SPACE-RELATED LINEAR AND NON-LINEAR STRUCTURES

PAUL A. BOSELA, FRANCIS J. SHAKER, and DEMETER G. FERTIS (Akron Univ., OH.) 1990 9 p Presented at the Southeast Conference of Theoretical and Applied Mechanics, Atlanta, GA, 22 Mar. 1990 (Contract NAG3-1008) (NASA-TM-103490; NAS 1.15:103490) Avail: NTIS HC A02/MF A01 CSCL 22/2

In order to be cost effective, space structures must be extremely light weight, and subsequently, very flexible structures. The power system for Space Station Freedom is such a structure. Each array

consists of a deployable truss mast and a split blanket of photovoltaic solar collectors. The solar arrays are deployed in orbit, and the blanket is stretched into position as the mast is extended. Geometric stiffness due to the preload make this an interesting non-linear problem. The space station will be subjected to various dynamic loads, during shuttle docking, solar tracking, attitude adjustment, etc. Accurate prediction of the natural frequencies and mode shapes of the space station components, including the solar arrays, is critical for determining the structural adequacy of the components, and for designing a dynamic controls system. The process used in developing and verifying the finite element dynamic model of the photo-voltaic arrays is documented. Various problems were identified, such as grounding effects due to geometric stiffness, large displacement effects, and pseudo-stiffness (grounding) due to lack of required rigid body modes. Analysis techniques, such as development of rigorous solutions using continuum mechanics, finite element solution sequence altering, equivalent systems using a curvature basis, Craig-Bampton superelement approach, and modal ordering schemes were utilized. The grounding problems associated with the geometric stiffness are emphasized. Author

N90-26054*# National Aeronautics and Space Administration. Lewis Research Center, Cleveland, OH.

COMPARISON OF CURRENTS PREDICTED BY NASCAP/LEO MODEL SIMULATIONS WITH ELEMENTARY LANGMUIR-TYPE BARE PROBE MODELS FOR AN INSULATED CABLE CONTAINING A SINGLE PINHOLE

JOEL T. GALOFARO Jul. 1990 39 p Original contains color illustrations (NASA-TM-102486; E-5095; NAS 1.15:102486) Avail: NTIS HC A03/MF A01; 9 functional color pages CSCL 22/2

The behavior of a defect in the insulation of a short biased section of cable in a Low Earth Orbit (LEO) space environment was examined. Such studies are of the utmost importance for large space power systems where great quantities of cabling will be deployed. An insulated probe containing a pinhole was placed into a hypothetical high speed LEO plasma. The NASA Charging Analyzer Program (NASCAP/LEO) was used to explore sheath growth about the probe as a function of applied voltage and to predict I-V behavior. A set of independent current calculations using Langmuir's formulations for concentric spheres and coaxial cylinders were also performed. The case of concentric spheres was here extended to include the case of concentric hemispheres. Several simple Langmuir-type models were then constructed to bracket the current collected by the cable. The space-charge sheath radius and impact parameters were used to determine the proper current regime. I-V curves were plotted for the models and comparisons were made with NASCAP/LEO results. Finally, NASCAP/LEO potential contours and surface cell potential plots were examined to explain interesting features in the NASCAP/LEO I-V curve. Author

N90-26055*# National Aeronautics and Space Administration. Lewis Research Center, Cleveland, OH.

BACKGROUND, CURRENT STATUS, AND PROGNOSIS OF THE ONGOING SLUSH HYDROGEN TECHNOLOGY DEVELOPMENT PROGRAM FOR THE NASP

R. L. DEWITT, T. L. HARDY, M. V. WHALEN, G. P. RICHTER, and T. M. TOMSIK 1990 16 p Presented at the 8th World Hydrogen Energy Conference, Honolulu, HI, 22-27 Jul. 1990; sponsored by Hawaii Natural Energy Inst. (NASA-TM-103220; E-5634; NAS 1.15:103220) Avail: NTIS HC A03/MF A01 CSCL 22/2

Among the Hydrogen Projects at the NASA Lewis Research Center (NASA LeRC), is the task of implementing and managing the Slush Hydrogen (SLH2) Technology Program for the United States' National AeroSpace Plane Joint Program Office (NASP JPO). The objectives of this NASA LeRC program are to provide verified numerical models of fluid production, storage, transfer, and feed systems and to provide verified design criteria for other engineered aspects of SLH2 systems germane to a NASP. The pursuit of these objectives is multidimensional, covers a range of

18 SPACECRAFT DESIGN, TESTING AND PERFORMANCE

problem areas, works these to different levels of depth, and takes advantage of the resources available in private industry, academia, and the U.S. Government. A summary of the NASA LeRC overall SLH2 program plan, is presented along with its implementation, the present level of effort in each of the program areas, some of the results already in hand, and the prognosis for the effort in the immediate future. Author

N90-28596*# National Aeronautics and Space Administration. Lewis Research Center, Cleveland, OH.

ATDRS PAYLOAD TECHNOLOGY RESEARCH AND DEVELOPMENT

G. ANZIC, D. J. CONNOLLY, G. FUJIKAWA, M. ANDRO, R. R. KUNATH, and G. R. SHARP 1990 9 p Prepared for presentation at the IEEE Global Telecommunications Conference, San Diego, CA, 2-5 Dec. 1990; sponsored in part by IEEE (NASA-TM-103256; E-5687; NAS 1.15:103256) Avail: NTIS HC A02/MF A01 CSCL 22/2

Four technology development tasks were chosen to reduce (or at least better understand) the technology risks associated with proposed approaches to Advanced Tracking and Data Relay Satellite (ATDRS). The four tasks relate to a Tri-Band Antenna feed system, a Digital Beamforming System for the S Band Multiple Access System (SMA), an SMA Phased Array Antenna, and a Configuration Thermal/Mechanical Analysis task. The objective, approach, and status of each are discussed. Author

19

SPACECRAFT INSTRUMENTATION

A90-36195*# National Aeronautics and Space Administration. Lewis Research Center, Cleveland, OH.

HARDWARE DEVELOPMENT FOR THE SURFACE TENSION DRIVEN CONVECTION EXPERIMENT

A. D. PLINE, T. P. JACOBSON, J. S. WANHAINEN, and D. A. PETRARCA (NASA, Lewis Research Center, Cleveland, OH) Journal of Spacecraft and Rockets (ISSN 0022-4650), vol. 27, May-June 1990, p. 312-317. Previously cited in issue 09, p. 1306, Accession no. A89-25341. refs Copyright

A90-41980*# Sverdrup Technology, Inc., Brook Park, OH.

A CANDIDATE ARCHITECTURE FOR MONITORING AND CONTROL IN CHEMICAL TRANSFER PROPULSION SYSTEMS

MICHAEL BINDER (Sverdrup Technology, Inc., Brook Park, OH) and MARC G. MILLIS (NASA, Lewis Research Center, Cleveland, OH) AIAA, SAE, ASME, and ASEE, Joint Propulsion Conference, 26th, Orlando, FL, July 16-18, 1990. 16 p. Previously announced in STAR as N90-22595. refs (AIAA PAPER 90-1882) Copyright

To support the exploration of space, a reusable space-based rocket engine must be developed. This engine must sustain superior operability and man-rated levels of reliability over several missions with limited maintenance or inspection between flights. To meet these requirements, an expander cycle engine incorporating a highly capable control and health monitoring system is planned. Alternatives for the functional organization and the implementation architecture of the engine's monitoring and control system are discussed. On the basis of this discussion, a decentralized architecture is favored. The trade-offs between several implementation options are outlined and future work is proposed. Author

A90-47229*# National Aeronautics and Space Administration. Lewis Research Center, Cleveland, OH.

INTEGRATED CONTROLS AND HEALTH MONITORING FOR CHEMICAL TRANSFER PROPULSION

MARC G. MILLIS (NASA, Lewis Research Center, Cleveland, OH) and MICHAEL P. BINDER (NASA, Lewis Research Center; Sverdrup Technology, Inc., Brook Park, OH) AIAA, SAE, ASME, and ASEE, Joint Propulsion Conference, 26th, Orlando, FL, July 16-18, 1990. 11 p. Previously announced in STAR as N90-25178. refs

(AIAA PAPER 90-2751) Copyright

NASA is reviewing various propulsion technologies for exploring space. The requirements are examined for one enabling propulsion technology: Integrated Controls and Health Monitoring (ICHM) for Chemical Transfer Propulsion (CTP). Functional requirements for a CTP-ICHM system are proposed from tentative mission scenarios, vehicle configurations, CTP specifications, and technical feasibility. These CTP-ICHM requirements go beyond traditional reliable operation and emergency shutoff control to include: (1) enhanced mission flexibility; (2) continuously variable throttling; (3) tank-head start control; (4) automated prestart and post-shutoff engine check; (5) monitoring of space exposure degradation; and (6) product evolution flexibility. Technology development plans are also discussed. Author

N90-14275*# National Aeronautics and Space Administration. Lewis Research Center, Cleveland, OH.

DESIGN CONSIDERATIONS FOR SPACE FLIGHT HARDWARE

DANIEL GLOVER Jan. 1990 23 p (NASA-TM-102300; E-4979; NAS 1.15:102300) Avail: NTIS HC A03/MF A01 CSCL 22/1

The environmental and design constraints are reviewed along with some insight into the established design and quality assurance practices that apply to low earth orbit (LEO) space flight hardware. It is intended as an introduction for people unfamiliar with space flight considerations. Some basic data and a bibliography are included. Author

N90-22595*# National Aeronautics and Space Administration. Lewis Research Center, Cleveland, OH.

A CANDIDATE ARCHITECTURE FOR MONITORING AND CONTROL IN CHEMICAL TRANSFER PROPULSION SYSTEMS

MICHAEL P. BINDER (Sverdrup Technology, Inc., Cleveland, OH.) and MARC G. MILLIS 1990 17 p Presented at the 26th Joint Propulsion Conference, Orlando, FL, 16-18 Jul. 1990; cosponsored by AIAA, SAE, ASME, and ASEE (NASA-TM-103161; E-5529; NAS 1.15:103161; AIAA-90-1882) Avail: NTIS HC A03/MF A01 CSCL 14/2

To support the exploration of space, a reusable space-based rocket engine must be developed. This engine must sustain superior operability and man-rated levels of reliability over several missions with limited maintenance or inspection between flights. To meet these requirements, an expander cycle engine incorporating a highly capable control and health monitoring system is planned. Alternatives for the functional organization and the implementation architecture of the engine's monitoring and control system are discussed. On the basis of this discussion, a decentralized architecture is favored. The trade-offs between several implementation options are outlined and future work is proposed. Author

N90-25178*# National Aeronautics and Space Administration. Lewis Research Center, Cleveland, OH.

INTEGRATED CONTROLS AND HEALTH MONITORING FOR CHEMICAL TRANSFER PROPULSION

MARC G. MILLIS and MICHAEL P. BINDER (Sverdrup Technology, Inc., Brook Park, OH.) 1990 12 p Presented at the 26th Joint Propulsion Conference, Orlando, FL, 16-18 Jul. 1990; cosponsored by AIAA, SAE, ASME, and ASEE (NASA-TM-103185; E-6657; NAS 1.15:103185; AIAA-90-2751) Avail: NTIS HC A03/MF A01 CSCL 22/2

NASA is reviewing various propulsion technologies for exploring space. The requirements are examined for one enabling propulsion technology: Integrated Controls and Health Monitoring (ICHM) for Chemical Transfer Propulsion (CTP). Functional requirements for a CTP-ICHM system are proposed from tentative mission scenarios, vehicle configurations, CTP specifications, and technical feasibility.

20 SPACECRAFT PROPULSION AND POWER

These CTP-ICHM requirements go beyond traditional reliable operation and emergency shutoff control to include: (1) enhanced mission flexibility; (2) continuously variable throttling; (3) tank-head start control; (4) automated prestart and post-shutoff engine check; (5) monitoring of space exposure degradation; and (6) product evolution flexibility. Technology development plans are also discussed. Author

N90-26063*# Sverdrup Technology, Inc., Brook Park, OH.
A RESISTANCE STRAIN GAGE WITH REPEATABLE AND CANCELLABLE APPARENT STRAIN FOR USE TO 800 C Final Report

J1H-FEN LEI Jul. 1990 10 p Presented at the Spring Conference on Experimental Mechanics, Albuquerque, NM, 4-6 Jun. 1990; sponsored in part by the Society for Experimental Mechanics, Inc. (Contract NAS3-25266)
(NASA-CR-185256; E-5577; NAS 1.26:185256) Avail: NTIS HC A02/MF A01 CSDL 22/2

A temperature compensated static strain gage, which is fabricated from palladium-13w/o chromium (Pd13Cr) alloy and a platinum (Pt) compensator, is being developed and was tested over a temperature range to 800 C at NASA-Lewis. The PdCr compensated strain gage has significantly lower apparent strain to 800 C than other high temperature strain gages. The PdCr compensated gage is protected from oxidation by a flame-sprayed alumina-4w/o zirconia overcoating. Test results to 800 C indicate apparent strain variations of less than 300 micro-epsilon and reproducibility between thermal cycles within 50 micro-epsilon. Apparent strain of the coated PdCr compensated gage can be predicted and cancelled due to its reproducibility and low value. Author

20

SPACECRAFT PROPULSION AND POWER

Includes main propulsion systems and components, e.g., rocket engines; and spacecraft auxiliary power sources.

A90-11992* National Aeronautics and Space Administration.
Lewis Research Center, Cleveland, OH.

THERMAL ENERGY STORAGE FLIGHT EXPERIMENTS

D. NAMKOONG (NASA, Lewis Research Center, Cleveland, OH)
IN: Solar engineering - 1989; Proceedings of the Eleventh Annual ASME Solar Energy Conference, San Diego, CA, Apr. 2-5, 1989. New York, American Society of Mechanical Engineers, 1989, p. 19-24.

Copyright

Consideration is given to the development of an experimental program to study heat transfer, energy storage, fluid movement, and void location under microgravity. Plans for experimental flight packages containing Thermal Energy Storage (TES) material applicable for advanced solar heat receivers are discussed. Candidate materials for TES include fluoride salts, salt eutectics, silicides, and metals. The development of a three-dimensional computer program to describe TES material behavior undergoing melting and freezing under microgravity is also discussed. The TES experiment concept and plans for ground and flight tests are outlined. R.B.

A90-11993* Rockwell International Corp., Canoga Park, CA.
SPACE STATION SOLAR DYNAMIC MODULE MODELLING AND SIMULATION

A. TYLIM (Rockwell International Corp., Rocketdyne Div., Canoga Park, CA) IN: Solar engineering - 1989; Proceedings of the Eleventh Annual ASME Solar Energy Conference, San Diego, CA, Apr. 2-5, 1989. New York, American Society of Mechanical Engineers, 1989, p. 25-30.
(Contract NAS3-25082)

Copyright

Efforts to model and simulate the Solar Dynamic Power Module (SDPM) for the Space Station are discussed. The SDPM configuration is given and the SDPM subsystems are described, including the concentrator assembly, the fine pointing and tracking system, the power generation system, the heat rejection assembly, the electrical equipment, the interface structure and integration hardware, and the beta gimbal assembly. Performance requirements and design considerations are given. The development of models to simulate the SDPM is examined, noting research on models such as the Electric Power System Transient Analysis Model, the Electric Power System on Orbit Performance model, and a spatial flux distribution function. R.B.

A90-13262*# National Aeronautics and Space Administration.
Lewis Research Center, Cleveland, OH.

PERFORMANCE COMPARISONS OF NUCLEAR THERMAL ROCKET AND CHEMICAL PROPULSION SYSTEMS FOR PILOTTED MISSIONS TO PHOBOS/MARS

S. K. BOROWSKI, M. W. MULAC, and O. F. SPURLOCK (NASA, Lewis Research Center, Cleveland, OH) IAF, International Astronautical Congress, 40th, Malaga, Spain, Oct. 7-13, 1989. 13 p. refs

(IAF PAPER 89-027) Copyright

Performance capability of nuclear thermal rocket (NTR) and chemical propulsion systems, operating with and without aerobraking, are compared for a selected set of Mars mission opportunities in the 2000 to 2020 timeframe. Both high- and low-energy mission opportunities are investigated. Results are presented as the required initial mass in low earth orbit (IMLEO) to perform the missions. Missions exclusively using chemical propulsion systems have the greatest initial masses. Significant mass reductions are realized by utilizing either aerobrake or NTR technology or both. As mission energy requirements increase, the benefit of implementing aerobrake or NTR technology increases, resulting in IMLEO mass reductions on the order of 60 to 75 percent when compared with all-propulsive chemical missions. By combining both advanced technologies, still greater mass reductions are possible. Author

A90-13282*# General Dynamics/Astronautics, San Diego, CA.
COLD-SAT - AN ORBITAL CRYOGENIC HYDROGEN TECHNOLOGY EXPERIMENT

J. R. SCHUSTER (General Dynamics Corp., Space Systems Div., San Diego, CA), JOSEPH P. WACHTER (Ford Aerospace Corp., Space Systems Div., Palo Alto, CA), and ALBERT G. POWERS (NASA, Lewis Research Center, Cleveland, OH) IAF, International Astronautical Congress, 40th, Malaga, Spain, Oct. 7-13, 1989. 13 p. Previously announced in STAR as N89-26044.
(Contract NAS3-25062)

(IAF PAPER 89-057) Copyright

The COLD-SAT spacecraft will perform subcritical liquid hydrogen storage and transfer experiments under low-gravity conditions to provide engineering data for future space transportation missions. Consisting of an experiment module mated to a spacecraft bus, COLD-SAT will be placed in an initial 460 km circular orbit by an Atlas I commercial launch vehicle. After deployment, the three-axis-controlled spacecraft bus will provide electric power, experiment control and data management, communications, and attitude control along with propulsive acceleration levels ranging from 10 (-6) to 10 (-4) g. These accelerations are an important aspect of some of the experiments, as it is desired to know the effects that low gravity levels might have on the heat and mass transfer processes involved. The experiment module will contain the three liquid hydrogen tanks, valves, pressurization equipment, and instrumentation. At launch all the hydrogen will be in the largest tank, which has helium-purged MLI and is loaded and topped off by the hydrogen tanking system used for the Centaur upper stage of the Atlas. The two smaller tanks will be utilized in orbit for performing some of the experiments. The experiments are grouped into two classes on the basis of their priority, and include six regarded as enabling technology and nine regarded as enhancing technology. Author

20 SPACECRAFT PROPULSION AND POWER

A90-13295* National Aeronautics and Space Administration. Lewis Research Center, Cleveland, OH.

SPACE STATION FREEDOM POWER MANAGEMENT AND DISTRIBUTION SYSTEM DESIGN

FRED TEREN (NASA, Lewis Research Center, Cleveland, OH) IAF, International Astronautical Congress, 40th, Malaga, Spain, Oct. 7-13, 1989. 9 p. Previously announced in STAR as N89-26045. (IAF PAPER 89-078) Copyright

The design is described of the Space Station Freedom Power Management and Distribution (PMAD) System. In addition, the significant trade studies which were conducted are described, which led to the current PMAD system configuration. Author

A90-13668* National Aeronautics and Space Administration. Lewis Research Center, Cleveland, OH.

OPTICS AND MATERIALS CONSIDERATIONS FOR A LASER-PROPELLED LIGHTSAIL

GEOFFREY A. LANDIS (NASA, Lewis Research Center, Cleveland, OH) IAF, International Astronautical Congress, 40th, Malaga, Spain, Oct. 7-13, 1989. 21 p. refs (IAF PAPER 89-664) Copyright

The principles of a laser-propelled lightsail for an interstellar probe are discussed. The feasibility of a laser-propelled-lightsail round-trip interstellar mission proposed by Forward (1984) is examined, with special attention given to the issues of optics and materials. It is shown that the large lens and a high lens/target distance required by such a mission result in optical difficulties, requiring positioning tolerance for the 1000-km-diam lens of only 3 m, which is unlikely to be achievable. Techniques and sail materials that would reduce this problem are suggested, including the use of LiF and CaF₂ quarter-wave dielectric films and the use of many intermediate lenses spaced between the probe and the source. It is pointed out that, as sail materials, the quarter-wavelength dielectric films have significant advantages over metals. I.S.

A90-14852* Aerospace Corp., El Segundo, CA.

ISSUES AND OPPORTUNITIES IN SPACE PHOTOVOLTAICS

ROBERT W. FRANCIS, W. A. SOMERVILLE (Aerospace Corp., El Segundo, CA), and DENNIS J. FLOOD (NASA, Lewis Research Center, Cleveland, OH) IN: IEEE Photovoltaic Specialists Conference, 20th, Las Vegas, NV, Sept. 26-30, 1988, Conference Record. Volume 1. New York, Institute of Electrical and Electronics Engineers, Inc., 1988, p. 8-20. Previously announced in STAR as N89-15171. refs Copyright

Space power sources are becoming a central focus for determining man's potential and schedule for exploring and utilizing the benefits of space. The ability to search, probe, survey, and communicate throughout the universe will depend on providing adequate power to the instruments to do these jobs. Power requirements for space platforms are increasing and will continue to increase into the 21st century. Photovoltaics have been a dependable power source for space for the last 30 years and have served as the primary source of power on virtually all DOD and NASA satellites. The performance of silicon (Si) solar cells has increased from 10 percent air mass zero (AM0) solar energy conversion efficiency in the early 60's to almost 15 percent on today's spacecraft. Some technologists even think that the potential for solar photovoltaics has reached a plateau. However, present and near-future Air Force and NASA requirements show needs that, if the problems are looked upon as opportunities, can elevate the photovoltaic power source scientist and array structure engineer into the next technological photovoltaic growth curve. Author

A90-14929* National Aeronautics and Space Administration. Lewis Research Center, Cleveland, OH.

ASSESSMENT OF THE EFFECTS OF SPACE DEBRIS AND METEOROID ENVIRONMENT ON THE SPACE STATION SOLAR ARRAY ASSEMBLY

HENRY K. NAHRA (NASA, Lewis Research Center, Cleveland, OH) IN: IEEE Photovoltaic Specialists Conference, 20th, Las Vegas, NV, Sept. 26-30, 1988, Conference Record. Volume 2.

New York, Institute of Electrical and Electronics Engineers, Inc., 1988, p. 868-873. Previously announced in STAR as N88-28959. refs

The methodology used to assess the probability of no impact of space debris and meteoroids on a spacecraft structure is applied to the Space Station solar array assembly. Starting with space debris and meteoroid flux models, the projected surface area of the solar cell string circuit of the solar array panel and the mast longeron, and the design lifetime, the possibility of no impact on the solar mast and solar cell string circuits was determined as a function of particle size. The probability of no impact on the cell string circuits was used to derive the probability of no open circuit panel. The probability of meeting a certain power requirement at the end of the design lifetime was then calculated as a function of impacting particle size. Coupled with a penetration and damage models/correlations which relate the particle size to penetration depth and damage, the results of this analysis can be used to determine the probability of meeting the lower power requirement given a degree of redundancy, and the probability of no impact on the solar array mast. Author

A90-14941* Spectrolab, Inc., Sylmar, CA.

OPTIMIZATION OF SILICON 8 CM X 8 CM WRAPTHROUGH SPACE STATION CELLS FOR 'ON ORBIT' OPERATION

D. R. LILLINGTON, J. R. KUKULKA, A. V. MASON (Spectrolab, Inc., Sylmar, CA), B. L. SATER (NASA, Lewis Research Center, Cleveland, OH), and J. SANCHEZ (Optical Coating Laboratory, Inc., Santa Rosa, CA) IN: IEEE Photovoltaic Specialists Conference, 20th, Las Vegas, NV, Sept. 26-30, 1988, Conference Record. Volume 2. New York, Institute of Electrical and Electronics Engineers, Inc., 1988, p. 934-939. (Contract NAS3-24672) Copyright

The optimization of Space Station cells for on-orbit performance is described. Design trades were performed in which back DAR coating thickness was traded against thermal absorptance and performance under front and back (albedo) illumination. Typical examples of modeled cell performance under different scenarios are given. Experimental illuminated output data under back illumination for specific DAR coating thicknesses are also given. Computer modeling of the solar array using TRASYS and SINDA programs also provide on-orbit thermal data and performance predictions. The overall backside response from albedo illumination was found to make a considerable contribution to the total array performance, particularly during the early stages of space station assembly when the arrays are feathered. I.E.

A90-14954* ENTECH Corp., Dallas-Fort Worth Airport, TX.

AN ADVANCED SPACE PHOTOVOLTAIC CONCENTRATOR ARRAY USING FRESNEL LENSES, GALLIUM ARSENIDE CELLS, AND PRISMATIC CELL COVERS

MARK J. O'NEILL (Entech, Inc., Fort Worth, TX) and MICHAEL F. PISZCZOR (NASA, Lewis Research Center, Cleveland, OH) IN: IEEE Photovoltaic Specialists Conference, 20th, Las Vegas, NV, Sept. 26-30, 1988, Conference Record. Volume 2. New York, Institute of Electrical and Electronics Engineers, Inc., 1988, p. 1007-1012. refs Copyright

The current status of a space concentrator array which uses refractive optics, gallium arsenide cells, and prismatic cell covers to achieve excellent performance at a very low array mass is documented. The prismatically covered cells have established records for space cell performance (24.2 percent efficient at 100 AM0 suns and 25 C) and terrestrial single-junction cell performance (29.3 percent efficient at 200 AM1.5 suns and 25 C). I.E.

A90-16368* National Aeronautics and Space Administration. Lewis Research Center, Cleveland, OH.

SPACE STATION FREEDOM RESISTOJET SYSTEM STUDY

ROBERT R. TACINA (NASA, Lewis Research Center, Cleveland, OH) Journal of Propulsion and Power (ISSN 0748-4658), vol. 5, Nov.-Dec. 1989, p. 694-702. Previously cited in issue 20, p. 3175,

Accession no. A87-45256. refs
Copyright

A90-16369* Michigan State Univ., East Lansing.
**REVIEW OF RESEARCH AND DEVELOPMENT ON THE
MICROWAVE ELECTROTHERMAL THRUSTER**
MARTIN C. HAWLEY, JES ASMUSSEN, JOHN W. FILPUS,
STANLEY WHITEHAIR, CRAIG HOEKSTRA (Michigan State
University, East Lansing) et al. Journal of Propulsion and Power
(ISSN 0748-4658), vol. 5, Nov.-Dec. 1989, p. 703-712. Previously
cited in issue 16, p. 2463, Accession no. A87-38008. refs
(Contract NSG-3299)
Copyright

A90-16374* TRW, Inc., Redondo Beach, CA.
SOLAR DYNAMIC POWER FOR THE SPACE STATION
J. S. ARCHER and E. S. DIAMANT (TRW, Inc., Redondo Beach,
CA) Journal of Propulsion and Power (ISSN 0748-4658), vol. 5,
Nov.-Dec. 1989, p. 744-749. Previously cited in issue 18, p. 2623,
Accession no. A86-39906.
(Contract NAS3-24655)
Copyright

A90-16676* National Aeronautics and Space Administration.
Lewis Research Center, Cleveland, OH.
**NUCLEAR PROPULSION - A VITAL TECHNOLOGY FOR THE
EXPLORATION OF MARS AND THE PLANETS BEYOND**
STANLEY K. BOROWSKI (NASA, Lewis Research Center,
Cleveland, OH) IN: The case for Mars III: Strategies for exploration
- General interest and overview. San Diego, CA, Univelt, Inc.,
1989, p. 451-494. Previously announced in STAR as N89-10944.
refs
(AAS PAPER 87-210) Copyright

The physics and technology issues and performance potential
of various direct thrust fission and fusion propulsion concepts are
examined. Next to chemical propulsion the solid core fission thermal
rocket (SCR) is the only other concept to be experimentally tested
at the power (approx 1.5 to 5.0 GW) and thrust levels (approx
0.33 to 1.11 MN) required for manned Mars missions. With a
specific impulse of approx 850 s, the SCR can perform various
near-earth, cislunar and interplanetary missions with lower mass
and cost requirements than its chemical counterpart. The gas core
fission thermal rocket, with a specific power and impulse of approx
50 kW/kg and 5000 s offers the potential for quick courier trips
to Mars (of about 80 days) or longer duration exploration cargo
missions (lasting about 280 days) with starting masses of about
1000 m tons. Convenient transportation to the outer Solar System
will require the development of magnetic and inertial fusion rockets
(IFRs). Possessing specific powers and impulses of approx 100
kW/kg and 200-300 kilosecs, IFRs will usher in the era of the
true Solar System class spaceship. Even Pluto will be accessible
with roundtrip times of less than 2 years and starting masses of
about 1500 m tons. Author

A90-16688* National Aeronautics and Space Administration.
Lewis Research Center, Cleveland, OH.
**POWER CONSIDERATIONS FOR AN EARLY MANNED MARS
MISSION UTILIZING THE SPACE STATION**
MARTIN E. VALGORA (NASA, Lewis Research Center, Cleveland,
OH) IN: The case for Mars III: Strategies for exploration - General
interest and overview. San Diego, CA, Univelt, Inc., 1989, p.
667-679.
(AAS PAPER 87-223) Copyright

Power requirements and candidate electrical power sources
were examined for the supporting space infrastructure for an early
(2004) manned Mars mission. This two-year mission (60-day stay
time) assumed a single six crew piloted vehicle with a Mars lander
for four of the crew. The transportation vehicle was assumed to
be a hydrogen/oxygen propulsion design with or without large
aerobrakes and assembled and checked out on the LEO Space
Station. The long transit time necessitated artificial gravity of the
crew by rotating the crew compartments. This rotation complicates
power source selection. Candidate power sources were examined

for the Lander, Mars Orbiter, supporting Space Station, co-orbiting
Propellant Storage Depot, and, alternatively, a co-orbiting Propellant
Generation (water electrolysis) Depot. Candidates considered were
photovoltaics with regenerative fuel cells or batteries, solar
dynamics, isotope dynamics, and nuclear power. Author

A90-16689* Jet Propulsion Lab., California Inst. of Tech.,
Pasadena.
**THE SP-100 SPACE REACTOR AS A POWER SOURCE FOR
MARS EXPLORATION MISSIONS**
LON ISENBERG (JPL, Pasadena, CA) and JACK A. HELLER
(NASA, Lewis Research Center, Cleveland, OH) IN: The case
for Mars III: Strategies for exploration - General interest and
overview. San Diego, CA, Univelt, Inc., 1989, p. 681-695. refs
(AAS PAPER 87-224) Copyright

This paper argues that many of the power requirements of
complex, relatively long-duration space missions such as the
exploration of Mars may best be met through the use of power
systems which use nuclear reactors as a thermal energy source.
The development of such a power system, the SP-100, and its
application in Mars mission scenarios is described. The missions
addressed include a freighter mission and a mission involving
exploration of the Martian surface. C.D.

A90-21219* Washington Univ., Saint Louis, MO.
**PREDICTION OF SELF-PRESSURIZATION RATE OF
CRYOGENIC PROPELLANT TANKAGE**
JOHN I. HOCHSTEIN, HYUN-CHUL JI (Washington University,
Saint Louis, MO), and JOHN C. AYDELOTT (NASA, Lewis Research
Center, Cleveland, OH) Journal of Propulsion and Power (ISSN
0748-4658), vol. 6, Jan.-Feb. 1990, p. 11-17. refs
(Contract NAG3-578)
Copyright

The SOLA-ECLIPSE code is being developed to enable
prediction of the behavior of cryogenic propellants in spacecraft
tankage. A brief description of the formulations used for modeling
heat transfer and for determining the thermodynamic state is
presented. Code performance is verified through comparison to
experimental data for the self-pressurization of scale-model liquid
hydrogen tanks. SOLA-ECLIPSE is used to examine the effect of
initial subcooling of the liquid phase on the self-pressurization rate
of an on-orbit full-scale liquid hydrogen tank typical for a
chemical-propulsion orbit transfer vehicle. The computational
predictions show that even small amounts of subcooling will
significantly decrease the self-pressurization rate. Further, if the
cooling is provided by a thermodynamic vent system, it is concluded
that small levels of subcooling will maximize propellant
conservation. Author

A90-21220* National Aeronautics and Space Administration.
Lewis Research Center, Cleveland, OH.
**PERFORMANCE AND ENDURANCE TESTS OF A
LABORATORY MODEL MULTIPROPELLANT RESISTOJET**
W. EARL MORREN, MARGARET V. WHALEN, and JAMES S.
SOVEY (NASA, Lewis Research Center, Cleveland, OH) Journal
of Propulsion and Power (ISSN 0748-4658), vol. 6, Jan.-Feb. 1990,
p. 18-27. refs
Copyright

This paper presents the results of an effort to demonstrate
the technological readiness of a long-life multipropellant resistojet
for Space Station auxiliary propulsion. A laboratory model resistojet
made from grain-stabilized platinum served as a test bed to evaluate
the design characteristics, fabrication methods, and operating
strategies for an engineering model multipropellant resistojet
developed as part of the NASA Space Station propulsion system
Advanced Development Program. The laboratory model thruster
was characterized for performance on a variety of fluids expected
to be available onboard a Space Station, then subjected to a
2000-h, 2400-thermal-cycle endurance test using carbon dioxide
propellant. Maximum thruster temperatures were approximately
1400 C. Significant observations from the laboratory model thruster
performance and endurance tests are discussed as they relate to
the design of the engineering model thruster. Author

20 SPACECRAFT PROPULSION AND POWER

A90-22874* Hughes Research Labs., Malibu, CA.
XENON ION SOURCES FOR SPACE APPLICATIONS

J. R. BEATTIE and J. N. MATOSSIAN (Hughes Research Laboratories, Malibu, CA) Review of Scientific Instruments (ISSN 0034-6748), vol. 61, pt. 2, Jan. 1990, p. 348-353. Research supported by Hughes Aircraft Co. refs
(Contract NAS3-25553)
Copyright

The technology of xenon ion thrusters under development for space-propulsion and plasma-contactor applications is described with particular consideration given to the 1.4-kW Xenon Ion Propulsion Subsystem (XIPS) designed for the upcoming Atmospheric Laboratory for Applications and Science Shuttle-based missions. The 25-cm-diam ion thruster of the XIPS is able to convert input power into thrust-beam power with an efficiency of over 82 percent. The XIPS will be used for satellite stationkeeping and orbit raising and maneuvering and as a plasma contactor. A 1991 flight application is described in which the 25-cm XIPS plasma contactor will be used to stabilize the electrical potential of the Shuttle Orbiter during firings of a 1.5-A electron beam from its payload bay. I.S.

A90-23821*# National Aeronautics and Space Administration, Lewis Research Center, Cleveland, OH.

PROBABILISTIC STRUCTURAL ANALYSIS METHODS OF HOT ENGINE STRUCTURES

C. C. CHAMIS and D. A. HOPKINS (NASA, Lewis Research Center, Cleveland, OH) ASME, Gas Turbine and Aeroengine Congress and Exposition, Toronto, Canada, June 4-8, 1989. 13 p. refs (ASME PAPER 89-GT-122)

Development of probabilistic structural analysis methods for hot engine structures is a major activity at Lewis Research Center. Recent activities have focused on extending the methods to include the combined uncertainties in several factors on structural response. This paper briefly describes recent progress on composite load spectra models, probabilistic finite element structural analysis, and probabilistic strength degradation modeling. Progress is described in terms of fundamental concepts, computer code development, and representative numerical results. C.D.

A90-26837* National Aeronautics and Space Administration, Lewis Research Center, Cleveland, OH.

THE FUEL CELL IN SPACE - YESTERDAY, TODAY AND TOMORROW

MARVIN WARSHAY and PAUL R. PROKOPIUS (NASA, Lewis Research Center, Cleveland, OH) (IBC Technical Services, Ltd., British Gas, PLC, British Petroleum Co., PLC, et al., Grove Anniversary Fuel Cell Symposium, London, England, Sept. 18-21, 1989) Journal of Power Sources (ISSN 0378-7753), vol. 29, Jan. 1990, p. 193-200. Previously announced in STAR as N90-11804.
Copyright

The past, present, and future of space fuel cell power systems is reviewed, starting with the first practical fuel cell by F. T. Bacon which led to the 1.5 kW Apollo alkaline fuel cell. However, the first fuel cell to be used for space power was the Gemini 1.0 kW Acid IEM fuel cell. The successor to the Apollo fuel cell is today's 12 kW Orbiter alkaline fuel cell whose technology is considerably different and considerably better than that of its ancestor, the Bacon cell. And in terms of specific weight there has been a steady improvement from the past to the present, from the close to 200 lb/kW of Apollo to the 20 lb/kW of the orbiter. For NASA future Lunar and Martian surface power requirements the regenerative fuel cell (RFC) energy storage system is enabling technology, with the alkaline and the PEM the leading RFC candidate systems. The U.S. Air Force continues to support fuel cell high power density technology development for its future short duration applications. Author

A90-27960*# GT-Devices, Alexandria, VA.
EXPERIMENTS ON A REPETITIVELY PULSED ELECTROTHERMAL THRUSTER

R. L. BURTON, D. FLEISCHER, S. A. GOLDSTEIN, and D. A. TIDMAN (GT-Devices, Inc., Alexandria, VA) Journal of Propulsion

and Power (ISSN 0748-4658), vol. 6, Mar.-Apr. 1990, p. 139-144. Research supported by GT-Devices, Inc. Previously cited in issue 16, p. 2464, Accession no. A87-38017. refs
(Contract NAS3-24636)
Copyright

A90-27961*# Hughes Research Labs., Malibu, CA.
STATUS OF XENON ION PROPULSION TECHNOLOGY

J. R. BEATTIE, J. N. MATOSSIAN, and R. R. ROBSON (Hughes Research Laboratories, Malibu, CA) Journal of Propulsion and Power (ISSN 0748-4658), vol. 6, Mar.-Apr. 1990, p. 145-150. Previously cited in issue 21, p. 3360, Accession no. A87-48677. refs
(Contract INTELSAT-INTEL-375; NAS3-23860)
Copyright

A90-29328*# Southwest Research Inst., San Antonio, TX.

APPLICATION OF THE PROBABILISTIC APPROXIMATE ANALYSIS METHOD TO A TURBOPUMP BLADE ANALYSIS

B. H. THACKER, R. C. MCCLUNG, and H. R. MILLWATER (Southwest Research Institute, San Antonio, TX) IN: AIAA/ASME/ASCE/AHS/ASC Structures, Structural Dynamics and Materials Conference, 31st, Long Beach, CA, Apr. 2-4, 1990, Technical Papers. Part 2. Washington, DC, American Institute of Aeronautics and Astronautics, 1990, p. 1039-1047. refs
(Contract NAS3-24389)
(AIAA PAPER 90-1098) Copyright

An eigenvalue analysis of a typical space propulsion system turbopump blade is presented using an approximate probabilistic analysis methodology. The methodology was developed originally to investigate the feasibility of computing probabilistic structural response using closed-form approximate models. This paper extends the methodology to structures for which simple closed-form solutions do not exist. The finite element method will be used for this demonstration, but the concepts apply to any numerical method. The results agree with detailed analysis results and indicate the usefulness of using a probabilistic approximate analysis in determining efficient solution strategies. Author

A90-33940* National Aeronautics and Space Administration, Marshall Space Flight Center, Huntsville, AL.

CHARACTERIZATION TESTING OF A 40 AMPERE HOUR BIPOLAR NICKEL-HYDROGEN BATTERY

JEFFREY C. BREWER (NASA, Marshall Space Flight Center, Huntsville, AL), MICHELLE A. MANZO, and RUSSEL P. GEMEINER (NASA, Lewis Research Center, Cleveland, OH) (NASA, Space Electrochemical Research and Technology Conference, 2nd, Cleveland, OH, Apr. 11-13, 1989) Journal of Power Sources (ISSN 0378-7753), vol. 29, Feb. 1990, p. 341-354.
Copyright

Extensive characterization testing has been done on a second 40-ampere hour (A h), 10-cell, bipolar nickel-hydrogen (Ni-H₂) battery, to study the effects of operating parameters such as charge and discharge rates, temperature, and pressure on capacity, A h and watt hour (W h) efficiencies, and end-of-charge and midpoint discharge voltages. Testing to date has produced many interesting results, with the battery performing well throughout the test matrix except during the high-rate (5 C and 10 C) discharges, where poorer than expected results were observed. The exact cause of this poor performance is, as yet, unknown. Small scale 2 in. x 2 in. battery tests are to be used in studying this problem. Low earth orbit cycle life testing at a 40-percent depth of discharge and 10 C is scheduled to follow the characterization testing. Author

A90-33944* National Aeronautics and Space Administration, Lewis Research Center, Cleveland, OH.

HYDROGEN-OXYGEN PROTON-EXCHANGE MEMBRANE FUEL CELLS AND ELECTROLYZERS

R. BALDWIN (NASA, Lewis Research Center, Cleveland, OH), M. PHAM (NASA, Johnson Space Center, Houston, TX), A. LEONIDA, J. MCELROY, and T. NALETTE (United Technologies Corp., Hamilton Standard Div., Windsor Locks, CT) (NASA, Space

Electrochemical Research and Technology Conference, 2nd, Cleveland, OH, Apr. 11-13, 1989) Journal of Power Sources (ISSN 0378-7753), vol. 29, Feb. 1990, p. 399-412.
Copyright

A flight experiment is planned for the validation, in a microgravity environment, of several ground-proven simplification features relating to SPE fuel cells and SPE electrolyzers. With a successful experiment, these features can be incorporated into equipment designs for specific extraterrestrial energy storage applications.

Author

A90-33945* Case Western Reserve Univ., Cleveland, OH.
ELECTROCATALYSIS FOR OXYGEN ELECTRODES IN FUEL CELLS AND WATER ELECTROLYZERS FOR SPACE APPLICATIONS

JAI PRAKASH, DONALD TRYK, and ERNEST YEAGER (Case Western Reserve University, Cleveland, OH) (NASA, Space Electrochemical Research and Technology Conference, 2nd, Cleveland, OH, Apr. 11-13, 1989) Journal of Power Sources (ISSN 0378-7753), vol. 29, Feb. 1990, p. 413-422. Research supported by DOE. refs
(Contract NAG3-964)
Copyright

The lead ruthenate pyrochlore $Pb_2Ru_2O_{6.5}$, in both high- and low-area forms, has been characterized using thermogravimetric analysis, X-ray photoelectron spectroscopy, X-ray diffraction, cyclic voltammetry, and O_2 reduction and generation kinetic-mechanistic studies. Mechanisms are proposed. Compounds in which part of the Ru is substituted with Ir have also been prepared. They exhibit somewhat better performance for O_2 reduction in porous, gas-fed electrodes than the unsubstituted compound. The anodic corrosion resistance of pyrochlore-based porous electrodes was improved by using two different anionically conducting polymer overlayers, which slow down the diffusion of ruthenate and plumbate out of the electrode. The O_2 generation performance was improved with both types of electrodes. With a hydrogel overlayer, the O_2 reduction performance was also improved.

Author

A90-33955* National Aeronautics and Space Administration, Lewis Research Center, Cleveland, OH.

NICKEL-HYDROGEN CAPACITY LOSS ON STORAGE

MICHELLE A. MANZO (NASA, Lewis Research Center, Cleveland, OH) (NASA, Space Electrochemical Research and Technology Conference, 2nd, Cleveland, OH, Apr. 11-13, 1989) Journal of Power Sources (ISSN 0378-7753), vol. 29, Feb. 1990, p. 541-554. refs
Copyright

A controlled experiment evaluating the capacity loss experienced by nickel electrodes stored under various conditions of temperature, hydrogen pressure, and electrolyte concentration was conducted using nickel electrodes from four different manufacturers. It was found that capacity loss varied with regard to hydrogen pressure and storage temperature, as well as with regard to electrode manufacturing processes. Impedance characteristics were monitored and found to be indicative of electrode manufacturing processes and capacity loss. Cell testing to evaluate state-of-charge effects on capacity loss were inconclusive as no loss was sustained by the cells tested in this experiment.

Author

A90-33956* Ford Aerospace and Communications Corp., Palo Alto, CA.

SODIUM-SULFUR BATTERY FLIGHT EXPERIMENT DEFINITION STUDY

REBECCA CHANG (Ford Aerospace Corp., Space Systems Div., Palo Alto, CA) and ROBERT MINCK (Ford Aerospace Corp., Aeronutronic Div., Newport Beach, CA) (NASA, Space Electrochemical Research and Technology Conference, 2nd, Cleveland, OH, Apr. 11-13, 1989) Journal of Power Sources (ISSN 0378-7753), vol. 29, Feb. 1990, p. 555-563. refs
(Contract NAS3-25355)
Copyright

Sodium-sulfur batteries are considered to be one of the most

likely battery systems for space applications. Compared with the Ni-H₂ or Ni-Co battery systems, Na-S batteries offer a mass reduction by a factor of 2 to 4, representing significant launch cost savings or increased payload mass capabilities. The Na-S battery operates at between 300 and 400 C, using liquid sodium and sulfur/polysulfide electrodes and solid ceramic electrolyte; the transport of the electrode materials to the surface of the electrolyte is through wicking/capillary forces. This paper describes five tests identified for the Na-S battery flight experiment definition study, which include the cell characterization test, the reactant distribution test, the current/temperature distribution test, the freeze/thaw test, and the multicell LEO test. A schematic diagram of Na-S cell is included.

I.S.

A90-37854* National Aeronautics and Space Administration, Lewis Research Center, Cleveland, OH.

INDIUM PHOSPHIDE SOLAR CELLS - RECENT DEVELOPMENTS AND ESTIMATED PERFORMANCE IN SPACE

IRVING WEINBERG and DAVID J. BRINKER (NASA, Lewis Research Center, Cleveland, OH) Space Power - Resources, Manufacturing and Development (ISSN 0883-6272), vol. 9, no. 1, 1990, p. 3-14. refs
Copyright

The current status of indium phosphide solar cell research is reviewed. In the NASA research program, efficiencies of 18.8 percent were achieved for standard n/p homojunction InP cells while 17 percent was achieved for ITO/InP cells processed by sputtering n-type indium tin oxide onto p-type indium phosphide. The latter represents a cheaper, simpler processing alternative. Computer modeling calculations indicate that efficiencies of over 21 percent are feasible. Relatively large area cells are produced in Japan with a maximum efficiency of 16.6 percent.

Author

A90-37859* National Aeronautics and Space Administration, Lewis Research Center, Cleveland, OH.

SPACE NUCLEAR REACTOR SHIELDS FOR MANNED AND UNMANNED APPLICATIONS

BARBARA I. MCKISSOCK and HARVEY S. BLOOMFIELD (NASA, Lewis Research Center, Cleveland, OH) Space Power - Resources, Manufacturing and Development (ISSN 0883-6272), vol. 9, no. 1, 1990, p. 57-65. Previously announced in STAR as N89-25272. refs
Copyright

Missions which use nuclear reactor power systems require radiation shielding of payload and/or crew areas to predetermined dose rates. Since shielding can become a significant fraction of the total mass of the system, it is of interest to show the effect of various parameters on shield thickness and mass for manned and unmanned applications. Algorithms were developed to give the thicknesses needed if reactor thermal power, separation distances, and dose rates are given as input. The thickness algorithms were combined with models for four different shield geometries to allow tradeoff studies of shield volume and mass for a variety of manned and unmanned missions. Shield design tradeoffs presented in this study include the effects of: higher allowable dose rates; radiation hardened electronics; shorter crew exposure times; shield geometry; distance of the payload and/or crew from the reactor; and changes in the size of the shielded area. Specific NASA missions that were considered in this study include unmanned outer planetary exploration, manned advanced/evolutionary Space Station, and advanced manned lunar base.

Author

A90-38070* National Aeronautics and Space Administration, Lewis Research Center, Cleveland, OH.

DESIGN OF THE SPACE STATION FREEDOM POWER SYSTEM

RONALD L. THOMAS (NASA, Lewis Research Center, Cleveland, OH) and GEORGE J. HALLINAN (Rockwell International Corp., Rocketdyne Div., Canoga Park, CA) IN: IECEC-89; Proceedings of the Twenty-fourth Intersociety Energy Conversion Engineering Conference, Washington, DC, Aug. 6-11, 1989. Volume 1. New

20 SPACECRAFT PROPULSION AND POWER

York, Institute of Electrical and Electronics Engineers, 1989, p. 245-250.

Copyright

The design of Space Station Freedom's electric power system (EPS) is reviewed, highlighting the key design goals of performance, low cost, reliability and safety. Tradeoff study results that illustrate the competing factors responsible for many of the more important design decisions are discussed. When Freedom's EPS is compared with previous space power designs, two major differences stand out. The first is the size of the EPS, which is larger than any prior system. The second major difference between the EPS and other space power designs is the indefinite expected life of Freedom; 30 years has been used for life-cycle-cost calculations. I.E.

A90-38072* Rockwell International Corp., Canoga Park, CA.
EVOLUTIONARY GROWTH FOR SPACE STATION FREEDOM ELECTRICAL POWER SYSTEM

MATTHEW FISK MARSHALL (Rockwell International Corp., Rocketdyne Div., Canoga Park, CA), KERRY MCLALLIN, and MIKE ZERNIC (NASA, Lewis Research Center, Cleveland, OH) IN: IECEC-89; Proceedings of the Twenty-fourth Intersociety Energy Conversion Engineering Conference, Washington, DC, Aug. 6-11, 1989. Volume 1. New York, Institute of Electrical and Electronics Engineers, 1989, p. 257-262. Previously announced in STAR as N89-28570. refs

Copyright

Over an operational lifetime of at least 30 yr, Space Station Freedom will encounter increased Space Station user requirements and advancing technologies. The Space Station electrical power system is designed with the flexibility to accommodate these emerging technologies and expert systems and is being designed with the necessary software hooks and hardware scars to accommodate increased growth demand. The electrical power system is planned to grow from the initial 75 kW up to 300 kW. The Phase 1 station will utilize photovoltaic arrays to produce the electrical power; however, for growth to 300 kW, solar dynamic power modules will be utilized. Pairs of 25 kW solar dynamic power modules will be added to the station to reach the power growth level. The addition of solar dynamic power in the growth phase places constraints in the initial Space Station systems such as guidance, navigation, and control, external thermal, truss structural stiffness, computational capabilities and storage, which must be planned-in, in order to facilitate the addition of the solar dynamic modules. Author

A90-38073*# National Aeronautics and Space Administration, Lewis Research Center, Cleveland, OH.

SPACE STATION FREEDOM ELECTRICAL POWER SYSTEM HARDWARE COMMONALITY WITH THE UNITED STATES POLAR PLATFORM

LORRA L. RIEKER and FRANCIS M. HARABURDA (NASA, Lewis Research Center, Cleveland, OH) IN: IECEC-89; Proceedings of the Twenty-fourth Intersociety Energy Conversion Engineering Conference, Washington, DC, Aug. 6-11, 1989. Volume 1. New York, Institute of Electrical and Electronics Engineers, 1989, p. 263-270. refs

Information is presented on how the concept of commonality is being implemented with respect to electric power system hardware for the Space Station Freedom and the U.S. Polar Platform. Included is a historical account of the candidate common items which have the potential to serve the same power system functions on both Freedom and the Polar Platform. The Space Station program and objectives are described, focusing on the test and development responsibilities. The program definition and preliminary design phase and the design and development phase are discussed. The goal of this work is to reduce the program cost. I.E.

A90-38074* Arinc Research Corp., Annapolis, MD.
SPACE STATION FREEDOM POWER - A RELIABILITY, AVAILABILITY, AND MAINTAINABILITY ASSESSMENT OF THE PROPOSED SPACE STATION FREEDOM ELECTRIC POWER SYSTEM

S. R. TURNQUIST, M. TWOMBLY (Arinc Research Corp., Annapolis, MD), and D. HOFFMAN (NASA, Lewis Research Center, Cleveland, OH) IN: IECEC-89; Proceedings of the Twenty-fourth Intersociety Energy Conversion Engineering Conference, Washington, DC, Aug. 6-11, 1989. Volume 1. New York, Institute of Electrical and Electronics Engineers, 1989, p. 271-276.

Copyright

A preliminary reliability, availability, and maintainability (RAM) analysis of the proposed Space Station Freedom electric power system (EPS) was performed using the unit reliability, availability, and maintainability (UNIRAM) analysis methodology. Orbital replacement units (ORUs) having the most significant impact on EPS availability measures were identified. Also, the sensitivity of the EPS to variations in ORU RAM data was evaluated for each ORU. Estimates were made of average EPS power output levels and availability of power to the core area of the space station. The results of assessments of the availability of EPS power and power to load distribution points in the space stations are given. Some highlights of continuing studies being performed to understand EPS availability considerations are presented. I.E.

A90-38075* Rockwell International Corp., Canoga Park, CA.
SPACE STATION FREEDOM PHOTOVOLTAIC POWER MODULE DESIGN STATUS

AMADOR P. JIMENEZ (Rockwell International Corp., Rocketdyne Div., Canoga Park, CA) and MARK A. HOBRECHT (NASA, Lewis Research Center, Cleveland, OH) IN: IECEC-89; Proceedings of the Twenty-fourth Intersociety Energy Conversion Engineering Conference, Washington, DC, Aug. 6-11, 1989. Volume 1. New York, Institute of Electrical and Electronics Engineers, 1989, p. 277-281. Previously announced in STAR as N89-25273.

Copyright

Electric power generation for the Space Station Freedom will be provided by four photovoltaic (PV) power modules using silicon solar cells during phase I operation. Each PV power module requires two solar arrays with 32,800 solar cells generating 18.75 kW of dc power for a total of 75 kW. A portion of this power will be stored in nickel-hydrogen batteries for use during eclipse, and the balance will be processed and converted to 20 kHz ac power for distribution to end users through the power management and distribution system. The design incorporates an optimized thermal control system, pointing and tracking provision with the application of gimbals, and the use of orbital replacement units to achieve modularization. The design status of the PV power module, as derived from major trade studies, is discussed at hardware levels ranging from component to system. Details of the design are presented where appropriate. Author

A90-38076* Lockheed Missiles and Space Co., Sunnyvale, CA.
SPACE STATION FREEDOM SOLAR ARRAY DESIGN DEVELOPMENT

CINDY WINSLOW, KEVIN BILGER (Lockheed Missiles and Space Co., Inc., Sunnyvale, CA), and COSMO BARAONA (NASA, Lewis Research Center, Cleveland, OH) IN: IECEC-89; Proceedings of the Twenty-fourth Intersociety Energy Conversion Engineering Conference, Washington, DC, Aug. 6-11, 1989. Volume 1. New York, Institute of Electrical and Electronics Engineers, 1989, p. 283-287.

(Contract NAS3-25082)

Copyright

The Space Station Freedom solar array program is required to provide a 75-kW power module that uses eight solar array (SA) wings over a four-year period in low earth orbit (LEO). Each wing will be capable of providing 23.4 kW at the 4-yr design point. The design of flexible-substrate SAs that must survive exposure to the space environment, including atomic oxygen, for an operating life of fifteen years is discussed. The tradeoff study and development areas being investigated include solar cell module size, solar cell weld pads, panel stiffener frames, materials inherently resistant to atomic oxygen, and weight reduction design alternatives. I.E.

A90-38077* National Aeronautics and Space Administration. Lewis Research Center, Cleveland, OH.

ENERGY STORAGE AND THERMAL CONTROL SYSTEM DESIGN STATUS

STEPHEN N. SIMONS (NASA, Lewis Research Center, Cleveland, OH), BRYAN C. WILLHOITE (Rockwell International Corp., Rocketdyne Div., Canoga Park, CA), and GERT VAN OMMERING (Ford Aerospace Corp., Palo Alto, CA) IN: IECEC-89; Proceedings of the Twenty-fourth Intersociety Energy Conversion Engineering Conference, Washington, DC, Aug. 6-11, 1989. Volume 1. New York, Institute of Electrical and Electronics Engineers, 1989, p. 289-294. Previously announced in STAR as N89-24427.

Copyright

The Space Station Freedom electric power system (EPS) will initially rely on photovoltaics for power generation and Ni/H₂ batteries for electrical energy storage. The current design for the development status of two major subsystems in the PV Power Module is discussed. The energy storage subsystem comprised of high capacity Ni/H₂ batteries and the single-phase thermal control system that rejects the excess heat generated by the batteries and other components associated with power generation and storage is described.

Author

A90-38079* National Aeronautics and Space Administration. Lewis Research Center, Cleveland, OH.

SOLAR DYNAMIC POWER MODULE DESIGN

RICHARD R. SECUNDE, THOMAS L. LABUS (NASA, Lewis Research Center, Cleveland, OH), and RONALD G. LOVELY (Rockwell International Corp., Rocketdyne Div., Canoga Park, CA) IN: IECEC-89; Proceedings of the Twenty-fourth Intersociety Energy Conversion Engineering Conference, Washington, DC, Aug. 6-11, 1989. Volume 1. New York, Institute of Electrical and Electronics Engineers, 1989, p. 299-307. Previously announced in STAR as N89-25269. refs

Copyright

Studies have shown that the use of solar dynamic (SD) power for the growth areas of the Space Station Freedom program will result in life cycle cost savings when compared to power supplied by photovoltaic sources. In the SD power module, a concentrator collects and focuses solar energy into a heat receiver which has integral thermal energy storage. A Power Conversion Unit (PCU) based on the closed Brayton cycle removes thermal energy from the receiver and converts that energy to electrical energy. Since the closed Brayton cycle is a single phase gas cycle, the conversion hardware (heat exchangers, turbine, compressor, etc.) can be designed for operation in low earth orbit, and tested with confidence in test facilities on earth before launch into space. The concentrator subassemblies will be aligned and the receiver/PCU/radiator combination completely assembled and charged with gas and cooling liquid on earth before launch to, and assembly on, orbit.

Author

A90-38080* National Aeronautics and Space Administration. Lewis Research Center, Cleveland, OH.

SPACE STATION FREEDOM POWER MANAGEMENT AND DISTRIBUTION DESIGN STATUS

S. JAVIDI (NASA, Lewis Research Center, Cleveland, OH), E. GHOLDSTON, and P. STROH (Rockwell International Corp., Rocketdyne Div., Canoga Park, CA) IN: IECEC-89; Proceedings of the Twenty-fourth Intersociety Energy Conversion Engineering Conference, Washington, DC, Aug. 6-11, 1989. Volume 1. New York, Institute of Electrical and Electronics Engineers, 1989, p. 309-313.

Copyright

The design status of the power management and distribution electric power system for the Space Station Freedom is presented. The current design is a star architecture, which has been found to be the best approach for meeting the requirement to deliver 120 V dc to the user interface. The architecture minimizes mass and power losses while improving element-to-element isolation and system flexibility. The design is partitioned into three elements: energy collection, storage and conversion, system protection and distribution, and management and control.

I.E.

A90-38081* National Aeronautics and Space Administration. Lewis Research Center, Cleveland, OH.

DEVELOPMENT AND REFINEMENT OF TEST BED SIMULATIONS

N. V. DRAVID, D. R. MILLER (NASA, Lewis Research Center, Cleveland, OH), A. G. PATTERSON (Analex Corp., Fairview Park, OH), and F. J. GOMBOS (Rockwell International Corp., Rocketdyne Div., Canoga Park, CA) IN: IECEC-89; Proceedings of the Twenty-fourth Intersociety Energy Conversion Engineering Conference, Washington, DC, Aug. 6-11, 1989. Volume 1. New York, Institute of Electrical and Electronics Engineers, 1989, p. 315-320. Previously announced in STAR as N89-27702. refs

Copyright

Lewis Research Center of NASA, with support from Rocketdyne, has engaged in a nonreal-time computer simulation effort for the Space Station Freedom Electric Power System (EPS). EASYS, a simulation package, is used as the primary tool for this activity. Early in the design of the EPS, two test beds were set up at Lewis. The Integrated Test Bed (ITB) that combines and upgrades these test beds is in the planning stage. The test beds are designed to functionally represent many of the components of the EPS and their interconnections. The simulation effort is primarily directed towards these test beds. Model verification is performed using test bed data.

Author

A90-38087*# National Aeronautics and Space Administration. Lewis Research Center, Cleveland, OH.

REVIEW OF THE ENVIRONMENTAL EFFECTS ON THE SPACE STATION FREEDOM PHOTOVOLTAIC POWER MODULE

HENRY K. NAHRA (NASA, Lewis Research Center, Cleveland, OH) IN: IECEC-89; Proceedings of the Twenty-fourth Intersociety Energy Conversion Engineering Conference, Washington, DC, Aug. 6-11, 1989. Volume 1. New York, Institute of Electrical and Electronics Engineers, 1989, p. 355-360. Previously announced in STAR as N89-24418. refs

An overview is provided of the environment in the low earth orbit (LEO), the interaction of this environment with the photovoltaic (PV) power system of the Space Station Freedom is reviewed, and the environmental programs are described that are designed to investigate the interaction of the LEO environment with the photovoltaic power system. Such programs will support and impact the design of the subsystems of the PV module in order to survive the design lifetime in the LEO natural and induced environment.

Author

A90-38088* Lockheed Missiles and Space Co., Sunnyvale, CA. **PHOTOVOLTAIC ARRAY ENVIRONMENTAL PROTECTION PROGRAM**

KEVIN M. BILGER, HELEN B. GJERDE (Lockheed Missiles and Space Co., Inc., Sunnyvale, CA), and BERNARD L. SATER (NASA, Lewis Research Center, Cleveland, OH) IN: IECEC-89; Proceedings of the Twenty-fourth Intersociety Energy Conversion Engineering Conference, Washington, DC, Aug. 6-11, 1989. Volume 1. New York, Institute of Electrical and Electronics Engineers, 1989, p. 361-369. refs
(Contract NAS3-25079)
Copyright

During the photovoltaic array environmental protection program, a coating material, application technique, and design approach intended to protect flexible solar array blankets during a nominal fifteen-year operating lifetime were developed. Numerous thin-film coatings for protecting the Kapton polyimide material used in the construction of the Space Station Freedom flexible solar array blanket were evaluated. The critical solar array design features and protection measures are discussed with special emphasis on the effects of solar array fabrication and flexible printed circuit manufacturing processes on coating durability. The results of the mechanical and environmental test evaluation, including oxygen plasma, neutral oxygen beam, and UV/charged-particle combined exposure, are discussed. These results led to the selection of a silicon dioxide thin-film coating to protect the solar array blanket from the low-earth-orbit atomic oxygen environment.

I.E.

20 SPACECRAFT PROPULSION AND POWER

A90-38118* Pennsylvania State Univ., New Kensington.

THE EFFECTS OF NONLINEAR LOADING UPON THE SPACE STATION FREEDOM 20 KHZ POWER SYSTEM

R. THOMAS LESKOVIK (Pennsylvania State University, Monaca) and IRVING G. HANSEN (NASA, Lewis Research Center, Cleveland, OH) IN: IECEC-89; Proceedings of the Twenty-fourth Intersociety Energy Conversion Engineering Conference, Washington, DC, Aug. 6-11, 1989. Volume 1. New York, Institute of Electrical and Electronics Engineers, 1989, p. 555-560. refs Copyright

The Space Station Freedom power distribution system, which consists of dual redundant 20-kHz, 440-V RMS, single-phase power systems, is discussed. The effect of a typical space station nonlinear load on the measurement of RMS current and voltage at various points in the space station power system has been investigated using the Electromagnetic Transients Program (EMTP). The load current distortion at the user interface, its effect on the distribution system, and its relationship to power factor have been studied. Modeling results are compared to test data. The differences under nonlinear loading are evaluated and presented as a measure of distribution voltage distortion and current measurement accuracy. I.E.

A90-38150*# National Aeronautics and Space Administration. Lewis Research Center, Cleveland, OH.

THERMAL ANNEALING OF GAAS CONCENTRATOR SOLAR CELLS

H. B. CURTIS and D. J. BRINKER (NASA, Lewis Research Center, Cleveland, OH) IN: IECEC-89; Proceedings of the Twenty-fourth Intersociety Energy Conversion Engineering Conference, Washington, DC, Aug. 6-11, 1989. Volume 2. New York, Institute of Electrical and Electronics Engineers, 1989, p. 805-810. refs

The thermal annealing of GaAs concentrator cells after electron irradiation is reported. Results are given for cells annealed at 150, 200, and 250 C. Isochronal annealing was done for 20 min intervals up to 350 C. For cells irradiated with electrons of energies between 0.7 and 2.3 MeV, the recovery decreases with increasing electron energy. Isothermal and isochronal annealing produce the same recovery. Cells irradiated to 3×10 to the 15th or 1×10 to the 16th e/sq cm recover to similar unannealed fractions. Significant annealing is seen starting at 150 C, although very long times are required. I.E.

A90-38155* ENTECH Corp., Dallas-Fort Worth Airport, TX.

THE MINI-DOME LENS SPACE CONCENTRATOR ARRAY - RECENT COMPONENT TEST RESULTS AND CURRENT ARRAY DEVELOPMENT STATUS

M. J. O'NEILL, A. J. MCDANAL, J. L. PERRY (Entech, Inc., Dallas, TX), D. J. FLOOD, M. F. PISZCZOR, and C. K. SWARTZ (NASA, Lewis Research Center, Cleveland, OH) IN: IECEC-89; Proceedings of the Twenty-fourth Intersociety Energy Conversion Engineering Conference, Washington, DC, Aug. 6-11, 1989. Volume 2. New York, Institute of Electrical and Electronics Engineers, 1989, p. 835-840. Research supported by SDIO. refs Copyright

The development of a high-performance, lightweight space photovoltaic concentrator array is described. The array is the first space photovoltaic concentrator system to use a refractive optical concentrator in the form of a dome-shaped, point-focus, Fresnel lens. In addition, it is the first such concentrator system to utilize prismatic cell covers to eliminate gridline obscuration losses. By combining these array features with state-of-the-art gallium arsenide cell technology, array areal power values (in watts per square meter) well in excess of present space power system levels are anticipated. In addition, the array has the potential for extremely high specific power values (in watts per kilogram). I.E.

A90-38158* National Aeronautics and Space Administration. Lewis Research Center, Cleveland, OH.

TWO-TIERED DESIGN ANALYSIS OF A RADIATOR FOR A SOLAR DYNAMIC POWERED STIRLING ENGINE

DONALD C. HAINLEY (NASA, Lewis Research Center; Sverdrup Technology, Inc., Cleveland, OH) IN: IECEC-89; Proceedings of

the Twenty-fourth Intersociety Energy Conversion Engineering Conference, Washington, DC, Aug. 6-11, 1989. Volume 2. New York, Institute of Electrical and Electronics Engineers, 1989, p. 855-860. Previously announced in STAR as N89-26031. Copyright

Two separate design approaches for a pumped loop radiator used to transfer heat from the cold end of a solar dynamic powered Stirling engine are described. The first approach uses a standard method to determine radiator requirements to meet specified end of mission conditions. Trade-off studies conducted for the analysis are included. Justification of this concept within the specified parameters of the analysis is provided. The second design approach determines the life performance of the radiator/Stirling system. In this approach, the system performance was altered by reducing the radiator heat transfer area. Performance effects and equilibrium points were determined as radiator segments were removed. This simulates the effect of loss of radiator sections due to micro-meteoroid and space debris penetration. The two designs are compared on the basis of overall system requirements and goals. Author

A90-38159*# National Aeronautics and Space Administration. Lewis Research Center, Cleveland, OH.

A PROGRAM FOR ADVANCING THE TECHNOLOGY OF SPACE CONCENTRATORS

GERALD J. NAUJOKAS (NASA, Lewis Research Center; Sverdrup Technology, Inc., Cleveland, OH) and JOSEPH M. SAVINO (NASA, Lewis Research Center, Cleveland, OH) IN: IECEC-89; Proceedings of the Twenty-fourth Intersociety Energy Conversion Engineering Conference, Washington, DC, Aug. 6-11, 1989. Volume 2. New York, Institute of Electrical and Electronics Engineers, 1989, p. 861-866. Previously announced in STAR as N89-29484.

In 1985, the NASA Lewis Research Center formed a project, the Advanced Solar Dynamics Power Systems Project, for the purpose of advancing the technology of Solar Dynamic Power Systems for space applications beyond 2000. Since then, technology development activities have been initiated for the major components and subsystems such as the concentrator, heat receiver and engine, and radiator. Described here is a program for developing long lived (10 years or more), lighter weight, and more reflective space solar concentrators than is presently possible. The program is progressing along two parallel paths: one is concentrator concept development and the other is the resolution of those critical technology issues that will lead to durable, highly specular, and lightweight reflector elements. Outlined are the specific objectives, long-term goals, approach, planned accomplishments for the future, and the present status of the various program elements. Author

A90-38163*# National Aeronautics and Space Administration. Lewis Research Center, Cleveland, OH.

CONCENTRATION OF OFF-AXIS RADIATION BY SOLAR CONCENTRATORS FOR SPACE POWER

KENT S. JEFFERIES (NASA, Lewis Research Center, Cleveland, OH) IN: IECEC-89; Proceedings of the Twenty-fourth Intersociety Energy Conversion Engineering Conference, Washington, DC, Aug. 6-11, 1989. Volume 2. New York, Institute of Electrical and Electronics Engineers, 1989, p. 887-893. Previously announced in STAR as N89-24438. refs

Four types of off-axis radiation are discussed. These are: (1) small off-axis angles during walk-off, (2) large off-axis angles, (3) an extended off-axis source such as Earth albedo, and (4) miscellaneous off-axis sources including radio frequency sources and local point sources. A code named OFFSET has been developed to represent the solar concentrator being developed for Space Station Freedom. It is a detailed, ray-tracing model which represents 50 ray originating points on the Sun and reflections from 10 points on each of the 456 concentrator facets. Results of this code are generally similar to the PIXEL results although there are small differences due to the more detailed representations of the Sun and concentrator that were used in the OFFSET code. Author

A90-38165* Boeing Aerospace Co., Seattle, WA.

A BRAYTON CYCLE SOLAR DYNAMIC HEAT RECEIVER FOR SPACE

L. M. SEDGWICK, H. L. NORDWALL, K. J. KAUFMANN (Boeing Aerospace and Electronics, Seattle, WA), and S. D. JOHNSON (NASA, Lewis Research Center, Cleveland, OH) IN: IECEC-89; Proceedings of the Twenty-fourth Intersociety Energy Conversion Engineering Conference, Washington, DC, Aug. 6-11, 1989. Volume 2. New York, Institute of Electrical and Electronics Engineers, 1989, p. 905-909. refs

Copyright

The detailed design of a heat receiver developed to meet the requirements of the Space Station Freedom, which will be assembled and operated in low earth orbit beginning in the mid-1990's, is described. The heat receiver supplies thermal energy to a nominal 25-kW closed-Brayton-cycle power conversion unit. The receiver employs an integral thermal energy storage system utilizing the latent heat of a eutectic-salt phase-change mixture to store energy for eclipse operation. The salt is contained within a felt metal matrix which enhances heat transfer and controls the salt void distribution during solidification. I.E.

A90-38168*# National Aeronautics and Space Administration. Lewis Research Center, Cleveland, OH.

NUMERICAL MODEL OF SOLAR DYNAMIC RADIATOR FOR PARAMETRIC ANALYSIS

JENNIFER L. RHATIGAN (NASA, Lewis Research Center, Cleveland, OH) IN: IECEC-89; Proceedings of the Twenty-fourth Intersociety Energy Conversion Engineering Conference, Washington, DC, Aug. 6-11, 1989. Volume 2. New York, Institute of Electrical and Electronics Engineers, 1989, p. 923-930. Previously announced in STAR as N89-22653. refs

Growth power requirements for Space Station Freedom will be met through addition of 25 kW solar dynamic (SD) power modules. Extensive thermal and power cycle modeling capabilities have been developed which are powerful tools in Station design and analysis, but which prove cumbersome and costly for simple component preliminary design studies. In order to aid in refining the SD radiator to the mature design stage, a simple and flexible numerical model was developed. The model simulates heat transfer and fluid flow performance of the radiator and calculates area mass and impact survivability for many combinations of flow tube and panel configurations, fluid and material properties, and environmental and cycle variations. Author

A90-38169* Sanders Associates, Inc., Nashua, NH.

THE CAVITY HEAT PIPE STIRLING RECEIVER FOR SPACE SOLAR DYNAMICS

JAMES B. KESSELI (Sanders Associates, Inc., Nashua, NH) and DOVIE E. LACEY (NASA, Lewis Research Center, Cleveland, OH) IN: IECEC-89; Proceedings of the Twenty-fourth Intersociety Energy Conversion Engineering Conference, Washington, DC, Aug. 6-11, 1989. Volume 2. New York, Institute of Electrical and Electronics Engineers, 1989, p. 931-936.

Copyright

The receiver/storage unit for the low-earth-orbiting Stirling system is discussed. The design, referred to as the cavity heat pipe (CHP), has been optimized for minimum specific mass and volume width. A specific version of this design at the 7-kWe level has been compared to the space station Brayton solar dynamic design. The space station design utilizes a eutectic mixture of LiF and CaF₂. Using the same phase change material, the CHP has been shown to have a specific mass of 40 percent and a volume of 5 percent of that of the space station Brayton at the same power level. Additionally, it complements the free-piston Stirling engine in that it also maintains a relatively flat specific mass down to at least 1 kWe. The technical requirements, tradeoff studies, critical issues, and critical technology experiments are discussed. I.E.

A90-38170* Sundstrand Corp., Rockford, IL.

BRAYTON ADVANCED HEAT RECEIVER DEVELOPMENT PROGRAM

G. R. HEIDENREICH, R. S. DOWNING (Sundstrand Corp., Rockford, IL), and DOVIE E. LACEY (NASA, Lewis Research Center, Cleveland, OH) IN: IECEC-89; Proceedings of the Twenty-fourth Intersociety Energy Conversion Engineering Conference, Washington, DC, Aug. 6-11, 1989. Volume 2. New York, Institute of Electrical and Electronics Engineers, 1989, p. 937-941. refs

Copyright

NASA Lewis Research Center is managing an advanced solar dynamic (ASD) space power program. The objective of the ASD program is to develop small and lightweight solar dynamic systems which show significant improvement in efficiency and specific mass over the baseline design derived from the Space Station Freedom technology. The advanced heat receiver development program is a phased program to design, fabricate and test elements of a 7-kWe heat-receiver/thermal-energy-storage subsystem. Receivers for both Brayton and Stirling heat engines are being developed under separate contracts. Phase I, described here, is the current eighteen month effort to design and perform critical technology experiments on innovative concepts designed to reduce mass without compromising thermal efficiency and reliability. I.E.

A90-38172*# National Aeronautics and Space Administration. Lewis Research Center, Cleveland, OH.

FLIGHT EXPERIMENT OF THERMAL ENERGY STORAGE

DAVID NAMKOONG (NASA, Lewis Research Center, Cleveland, OH) IN: IECEC-89; Proceedings of the Twenty-fourth Intersociety Energy Conversion Engineering Conference, Washington, DC, Aug. 6-11, 1989. Volume 2. New York, Institute of Electrical and Electronics Engineers, 1989, p. 953-957. Previously announced in STAR as N89-24440.

Thermal energy storage (TES) enables a solar dynamic system to deliver constant electric power through periods of sun and shade. Brayton and Stirling power systems under current considerations for missions in the near future require working fluid temperatures in the 1100 to 1300+ K range. TES materials that meet these requirements fall into the fluoride family of salts. Salts shrink as they solidify, a change reaching 30 percent for some salts. Hot spots can develop in the TES container or the container can become distorted if the melting salt cannot expand elsewhere. Analysis of the transient, two-phase phenomenon is being incorporated into a three-dimensional computer code. The objective of the flight program is to verify the predictions of the code, particularly of the void location and its effect on containment temperature. The four experimental packages comprising the program will be the first tests of melting and freezing conducted under microgravity. Author

A90-38196*# National Aeronautics and Space Administration. Lewis Research Center, Cleveland, OH.

CSTI HIGH CAPACITY POWER

JERRY M. WINTER (NASA, Lewis Research Center, Cleveland, OH) IN: IECEC-89; Proceedings of the Twenty-fourth Intersociety Energy Conversion Engineering Conference, Washington, DC, Aug. 6-11, 1989. Volume 2. New York, Institute of Electrical and Electronics Engineers, 1989, p. 1195-1208. Previously announced in STAR as N89-25282. refs

In FY-88, the Advanced Technology Program was incorporated into NASA's Civil Space Technology Initiative (CSTI). The CSTI Program was established to provide the foundation for technology development in automation and robotics, information, propulsion, and power. The CSTI High Capacity Power Program builds on the technology efforts of the SP-100 program, incorporates the previous NASA SP-100 Advanced Technology project, and provides a bridge to NASA Project Pathfinder. The elements of CSTI High Capacity Power development include Conversion Systems, Thermal Management, Power Management, System Diagnostics, and Environmental Interactions. Technology advancement in all areas, including materials, is required to assure the high reliability and 7 to 10 year lifetime demanded for future space nuclear power systems. Author

20 SPACECRAFT PROPULSION AND POWER

A90-38202* Rockwell International Corp., Canoga Park, CA.

SP-100 ADVANCED RADIATOR DESIGNS FOR THERMOELECTRIC AND STIRLING APPLICATIONS

M. P. MORIARTY and W. R. DETERMAN (Rockwell International Corp., Rocketdyne Div., Canoga Park, CA) IN: IECEC-89; Proceedings of the Twenty-fourth Intersociety Energy Conversion Engineering Conference, Washington, DC, Aug. 6-11, 1989. Volume 2. New York, Institute of Electrical and Electronics Engineers, 1989, p. 1245-1250.

(Contract NAS3-25209)

Copyright

Advanced radiator designs employing carbon-carbon liquid metal heat pipe technology, which significantly reduce the mass of the heat rejection subsystem for high temperature space technology systems such as the SP-100 are discussed. This technology is being developed to address the need for lightweight heat transfer components and structures for space applications. Heat pipe and subsystem designs were optimized for thermoelectric- and Stirling-engine-based SP-100 system designs. A multiple, deployed-petal radiator concept was selected for the heat rejection subsystem design as it provided minimum mass. Radiator stowage in the space transportation system cargo bay and deployment schemes were investigated for each of the optimized designs. I.E.

A90-38249* National Aeronautics and Space Administration. Lewis Research Center, Cleveland, OH.

RESULTS FROM BASELINE TESTS OF THE SPRE I AND COMPARISON WITH CODE MODEL PREDICTIONS

JAMES E. CAIRELLI, STEVEN M. GENG (NASA, Lewis Research Center, Cleveland, OH), and ROBERT C. SKUPINSKI (NASA, Lewis Research Center; Sverdrup Technology, Inc., Cleveland, OH) IN: IECEC-89; Proceedings of the Twenty-fourth Intersociety Energy Conversion Engineering Conference, Washington, DC, Aug. 6-11, 1989. Volume 5. New York, Institute of Electrical and Electronics Engineers, 1989, p. 2249-2256. Previously announced in STAR as N89-23527. refs

Copyright

The space power research engine (SPRE), a free-piston Stirling engine with linear alternator, is being tested at NASA-Lewis as a candidate for high capacity space power. Results are presented of baseline engine tests at design and off-design operating conditions. The test results are compared with code model prediction. Author

A90-38266*# National Aeronautics and Space Administration. Lewis Research Center, Cleveland, OH.

PROTOFLIGHT PHOTOVOLTAIC POWER MODULE SYSTEM-LEVEL TESTS IN THE SPACE POWER FACILITY

JUAN C. RIVERA and LUKE A. KIRCH (NASA, Lewis Research Center, Cleveland, OH) IN: IECEC-89; Proceedings of the Twenty-fourth Intersociety Energy Conversion Engineering Conference, Washington, DC, Aug. 6-11, 1989. Volume 6. New York, Institute of Electrical and Electronics Engineers, 1989, p. 2601-2615. Previously announced in STAR as N89-25267. refs

Work Package Four, which includes the NASA-Lewis and Rocketdyne, has selected an approach for the Space Station Freedom Photovoltaic (PV) Power Module flight certification that combines system level qualification and acceptance testing in the thermal vacuum environment: the 'protoflight' vehicle approach. This approach maximizes ground test verification to assure system level performance and to minimize risk of on-orbit failures. The preliminary plans for system level thermal vacuum environmental testing of the protoflight PV Power Module in the NASA-Lewis Space Power Facility (SPF) are addressed. Details of the facility modifications to refurbish SPF, after 13 years of downtime, are briefly discussed. The results of an evaluation of the effectiveness of system level environmental testing in screening out incipient part and workmanship defects and unique failure modes are discussed. Preliminary test objectives, test hardware configurations, test support equipment, and operations, are presented. Author

A90-38280*# National Aeronautics and Space Administration. Lewis Research Center, Cleveland, OH.

THE NASA ADVANCED SOLAR DYNAMICS TECHNOLOGY PROGRAM

MARVIN WARSHAY and THADDEUS S. MROZ (NASA, Lewis Research Center, Cleveland, OH) IN: IECEC-89; Proceedings of the Twenty-fourth Intersociety Energy Conversion Engineering Conference, Washington, DC, Aug. 6-11, 1989. Volume 6. New York, Institute of Electrical and Electronics Engineers, 1989, p. 2711-2715.

The NASA Advanced Solar Dynamics Technology Program, aimed at developing power system technology for versatile, advanced, high-capacity spacecraft and surface power systems, is discussed. The goals of the program are to be achieved by pursuing high-risk but high-payoff technologies, namely, advanced solar concentrators, heat receivers, power conversion dynamic cycles, and radiators. The NASA program is discussed in terms of mission drivers, the technological goals for each of the system's major components, and program status. I.E.

A90-38288* National Aeronautics and Space Administration. Lewis Research Center, Cleveland, OH.

BIPOLAR NICKEL-HYDROGEN BATTERY DEVELOPMENT - A PROGRAM REVIEW

MICHELLE MANZO (NASA, Lewis Research Center, Cleveland, OH), STEPHEN LENHART (Ford Aerospace Corp., Palo Alto, CA), and ARNOLD HALL (Whittaker-Yardney Power Systems, Pawcatuck, CT) IN: IECEC-89; Proceedings of the Twenty-fourth Intersociety Energy Conversion Engineering Conference, Washington, DC, Aug. 6-11, 1989. Volume 6. New York, Institute of Electrical and Electronics Engineers, 1989, p. 2775-2780. refs

Copyright

An overview of spacecraft power system design trends, focusing on higher power bus voltages and improved energy storage systems, is followed by a discussion of bipolar Ni/H₂ battery development efforts. Several 10-cell batteries and one 50-cell battery are described, and performance results are presented. A comparison of individual-pressure-vessel and bipolar Ni/H₂ technologies is used to suggest a new direction for bipolar Ni/H₂ battery development efforts, toward a large number of passively cooled cells in parallel. I.E.

A90-38301*# National Aeronautics and Space Administration. Lewis Research Center, Cleveland, OH.

INITIAL CHARACTERIZATION OF A MODULAR HEAT EXCHANGER WITH AN INTEGRAL HEAT PIPE

JEFFREY G. SCHREIBER (NASA, Lewis Research Center, Cleveland, OH) IN: IECEC-89; Proceedings of the Twenty-fourth Intersociety Energy Conversion Engineering Conference, Washington, DC, Aug. 6-11, 1989. Volume 6. New York, Institute of Electrical and Electronics Engineers, 1989, p. 2891-2895. Previously announced in STAR as N89-25078. refs

As part of the Civil Space Technology Initiative (CSTI) Advanced Technology program, a conceptual design of the Stirling space engine (SSE) was generated to develop the technology base needed to meet the long duration, high capacity power requirements for future NASA space missions. The free-piston Stirling engine (FPSE) was chosen as the growth option in the CSTI program. An existing FPSE was modified as a test bed for a modular heat exchanger evaluation. Evaluation of the individual heat pipes before installation in the engine is described. Author

A90-38307*# National Aeronautics and Space Administration. Lewis Research Center, Cleveland, OH.

ESTIMATED PERFORMANCE AND FUTURE POTENTIAL OF SOLAR DYNAMIC AND PHOTOVOLTAIC POWER SYSTEMS FOR SELECTED LEO AND HEO MISSIONS

DAVID J. BENTS and CHENG Y. LU (NASA, Lewis Research Center, Cleveland, OH) IN: IECEC-89; Proceedings of the Twenty-fourth Intersociety Energy Conversion Engineering Conference, Washington, DC, Aug. 6-11, 1989. Volume 6. New

York, Institute of Electrical and Electronics Engineers, 1989, p. 2949-2959. Previously announced in STAR as N89-25280. refs

Solar photovoltaic and thermal dynamic power systems for application to selected low-earth-orbit (LEO) and high-earth-orbit (HEO) missions are characterized in the regime 7 to 35 kWe. Input parameters to the characterization are varied to correspond to anticipated introduction of improved or new technologies. A comparative assessment is made of the two power system types for emerging technologies in cells and arrays, energy storage, optical surfaces, heat engines, thermal energy storage and thermal management. The assessment is made to common ground rules and assumptions. The four missions (Space Station, sun-synchronous, Van Allen belt, and GEO) are representative of the anticipated range of multikilowatt earth-orbit missions. The results give the expected performance, mass and drag of multikilowatt earth-orbiting solar power systems and show how the overall system figure of merit will improve as new component technologies are incorporated. Author

A90-39111* Virginia Polytechnic Inst. and State Univ., Blacksburg.

HIGH-FREQUENCY AC POWER DISTRIBUTION IN SPACE STATION

FU-SHENG TSAI and FRED C. Y. LEE (Virginia Polytechnic Institute and State University, Blacksburg) IEEE Transactions on Aerospace and Electronic Systems (ISSN 0018-9251), vol. 26, March 1990, p. 239-253. refs
(Contract NAG3-551)
Copyright

A utility-type 20-kHz ac power distribution system for the Space Station, employing resonant power-conversion techniques, is presented. The system converts raw dc voltage from photovoltaic cells or three-phase LF ac voltage from a solar dynamic generator into a regulated 20-kHz ac voltage for distribution among various loads. The results of EASY5 computer simulations of the local and global performance show that the system has fast response and good transient behavior. The ac bus voltage is effectively regulated using the phase-control scheme, which is demonstrated with both line and load variations. The feasibility of paralleling the driver-module outputs is illustrated with the driver modules synchronized and sharing a common feedback loop. An HF sinusoidal ac voltage is generated in the three-phase ac input case, when the driver modules are phased 120 deg away from one another and their outputs are connected in series. I.E.

A90-40545* Cincinnati Univ., OH.

SPACE VEHICLE PROPULSION SYSTEMS - ENVIRONMENTAL SPACE HAZARDS

G. K. BAHR and P. J. DISIMILE (Cincinnati, University, OH) AIAA, SAE, ASME, and ASEE, Joint Propulsion Conference, 26th, Orlando, FL, July 16-18, 1990. 10 p. refs
(Contract NAG3-948)
(AIAA PAPER 90-1881) Copyright

An evaluation of hazards which exist in geo-lunar space and have the potential to negatively affect a long-term mission-oriented spacecraft systems is presented based on published data. The hazards are categorized as pervasive (radiation), incident specific (meteoroids and thermal shock), and chemically corrosive (monatomic oxygen). It appears that the number one priority should be the development of new materials; and the secondary concern should be the development of fabrication techniques for the exterior hull, so that incident specific hazards can be minimized in an active fashion. The pervasive hazard can be dealt with by exploring on-board circuit technology with ancillary monitoring systems. Effects of thermal shock on the exterior nozzle, directional gimbals, and internal combustion chamber geometry seem to need more investigation. N.B.

A90-40583* United Technologies Research Center, East Hartford, CT.
HEALTH MONITORING SYSTEM FOR THE SSME - PROGRAM OVERVIEW
MICHAEL W. HAWMAN (United Technologies Research Center,

East Hartford, CT) AIAA, SAE, ASME, and ASEE, Joint Propulsion Conference, 26th, Orlando, FL, July 16-18, 1990. 11 p. refs
(Contract NAS3-25626)
(AIAA PAPER 90-1987) Copyright

This paper considers the design of a health management system (HMS) program for enhancement of the safety of SSME operations during ground tests and space missions. The fault detection techniques based on time series, nonlinear regression, and clustering algorithms were developed and were demonstrated based on data from SSME ground test failures. The fault detection algorithms of the HMS system exhibited 100 percent detection of faults and an extremely low fault alarm rate, and were robust to sensor loss. A preliminary design of hardware architecture capable of supporting real-time operation of the HMS functions is described. I.S.

A90-40584* United Technologies Research Center, East Hartford, CT.

HEALTH MONITORING SYSTEM FOR THE SSME-FAULT DETECTION ALGORITHMS

S. TULPUL and W. S. GALINAITIS (United Technologies Research Center, East Hartford, CT) AIAA, SAE, ASME, and ASEE, Joint Propulsion Conference, 26th, Orlando, FL, July 16-18, 1990. 11 p. refs
(Contract NAS3-25626)
(AIAA PAPER 90-1988) Copyright

A Health Monitoring System (HMS) Framework for the Space Shuttle Main Engine (SSME) has been developed by United Technologies Corporation (UTC) for the NASA Lewis Research Center. As part of this effort, fault detection algorithms have been developed to detect the SSME faults with sufficient time to shutdown the engine. These algorithms have been designed to provide monitoring coverage during the startup, mainstage and shutdown phases of the SSME operation. The algorithms have the capability to detect multiple SSME faults, and are based on time series, regression and clustering techniques. This paper presents a discussion of candidate algorithms suitable for fault detection followed by a description of the algorithms selected for implementation in the HMS and the results of testing these algorithms with the SSME test stand data. Author

A90-42029* National Aeronautics and Space Administration, Lewis Research Center, Cleveland, OH.

COOLING OF ROCKET THRUST CHAMBERS WITH LIQUID OXYGEN

ELIZABETH S. ARMSTRONG and JULIE A. SCHLUMBERGER (NASA, Lewis Research Center, Cleveland, OH) AIAA, SAE, ASME, and ASEE, Joint Propulsion Conference, 26th, Orlando, FL, July 16-18, 1990. 10 p. Previously announced in STAR as N90-22605. refs
(AIAA PAPER 90-2120) Copyright

Rocket engines using high pressure liquid oxygen (LOX) and kerosene (RP-1) as the propellants have been considered for future launch vehicle propulsion. Generally, in regeneratively cooled engines, the fuel is used to cool the combustion chamber. However, hydrocarbons such as RP-1 are limited in their cooling capability at high temperatures and pressures. Therefore, LOX is being considered as an alternative coolant. However, there has been concern as to the effect on the integrity of the chamber liner if oxygen leaks into the combustion zone through fatigue cracks that may develop between the cooling passages and the hot-gas side wall. To address this concern, an investigation was previously conducted with simulated fatigue cracks upstream of the thrust chamber throat. When these chambers were tested, an unexpected melting in the throat region developed which was not in line with the simulated fatigue cracks. The current experimental program was conducted in order to determine the cause for the failure in the earlier thrust chambers and to further investigate the effects of cracks in the thrust chamber liner upstream of the throat. The thrust chambers were tested at oxygen-to-fuel mixture ratios from 1.5 to 2.86 at a nominal chamber pressure of 8.6 MPa. As a result of the test series, the reason for the failure occurring in the

20 SPACECRAFT PROPULSION AND POWER

earlier work was determined to be injector anomalies. The LOX leaking through the simulated fatigue cracks did not affect the integrity of the chambers. Author

A90-42030*# Aerojet Technical Systems Co., Sacramento, CA. COMBUSTION INTERACTION WITH RADIATION-COOLED CHAMBERS

S. D. ROSENBERG, D. M. JASSOWSKI (Aerojet TechSystems, Sacramento, CA), R. BARLOW, R. LUCHT, K. MCCARTY (Sandia National Laboratories, Livermore, CA) et al. AIAA, SAE, ASME, and ASEE, Joint Propulsion Conference, 26th, Orlando, FL, July 16-18, 1990. 8 p. refs
(Contract NAS3-25646)
(AIAA PAPER 90-2121) Copyright

Over 15 hours of thruster operation at temperatures between 1916 and 2246 C without failure or erosion has been demonstrated using iridium-coated rhenium chamber materials with nitrogen tetroxide/monomethylhydrazine propellants operating over a mixture ratio range of 1.60-2.05. Research is now under way to provide a basic understanding of the mechanisms which make high-temperature operation possible and to extend the capability to a wider range of conditions, including other propellant combinations and chamber materials. Techniques have been demonstrated for studying surface fracture phenomena. These include surface Raman and Auger for study of oxide formation, surface Raman and X-ray diffraction to determine the oxide phase, Auger to study oxide stoichiometry, and sputter Auger to study interdiffusion of alloy species. V.L.

A90-42063*# Rockwell International Corp., Canoga Park, CA. ENHANCED HEAT TRANSFER ROCKET COMBUSTOR TECHNOLOGY COMPONENT HOT-FIRE TEST RESULTS

WILLIAM S. BROWN (Rockwell International Corp., Rocketdyne Div., Canoga Park, CA) AIAA, SAE, ASME, and ASEE, Joint Propulsion Conference, 26th, Orlando, FL, July 16-18, 1990. 8 p.
(Contract NAS3-23773)
(AIAA PAPER 90-2182) Copyright

The evaluation of a method for enhancing combustor hot-gas wall heat extraction by using hot-fire tests of a rocket engine combustor calorimeter with hot-gas wall ribs is presented. The capability for enhanced heat extraction is required to increase available turbine drive energy for high chamber pressure operation, and therefore higher overall expander cycle engine performance. Determination of the rib effectiveness for incorporation into the design of a high-performance combustor for an advanced expander cycle combustor intended for use in an orbital transfer vehicle or advanced space engine, was the objective of these tests. R.E.P.

A90-42536*# Hughes Research Labs., Malibu, CA. HIGH-POWER XENON ION THRUSTERS

J. R. BEATTIE and J. N. MATOSSIAN (Hughes Research Laboratories, Malibu, CA) AIAA, DGLR, and JSASS, International Electric Propulsion Conference, 21st, Orlando, FL, July 18-20, 1990. 9 p. refs
(Contract NAS3-25553)
(AIAA PAPER 90-2540) Copyright

Steady state performance characteristics for a 25-cm diameter laboratory-model xenon ion thruster operating over the power range from 1.8 to 6.8 kW are described. Performance data are also presented for a similar 30-cm diameter thruster operated over the 1.4 to 11.1 kW power range. For each of the two thrusters, thermal characteristics, discharge-chamber performance data, overall thruster performance data, and beam-current density profiles are presented. A high level of performance and stability over a wide range of input power is demonstrated for the two thrusters. It is concluded that there appears to be no technological obstacles in the way of developing flight-design thrusters that operate in the 5- to 10-kW power range for near-term applications to orbit raising. S.A.V.

A90-42559*# Rocket Research Corp., Redmond, WA. QUALIFICATION AND LIFE TESTING OF A FLIGHT DESIGN HYDRAZINE ARCJET SYSTEM

S. C. KNOWLES, S. E. YANO, and R. S. AADLAND (Rocket Research Co., Redmond, WA) AIAA, DGLR, and JSASS, International Electric Propulsion Conference, 21st, Orlando, FL, July 18-20, 1990. 17 p. refs
(Contract NAS3-24631)
(AIAA PAPER 90-2576) Copyright

This paper describes the design and the requirements of a low-power hydrazine arc jet system and presents the results of tests on the system's performance, vibration, and lifetime. The system consists of an arcjet, catalyst bed, power control unit, and interconnecting power cable. Operating at 1.4 kW input power, the system provides a minimum of 450 sec mission average specific impulse, yielding greater than a 100 kg propellant savings over standard monopropellant or bipropellant systems used on communication satellites. I.S.

A90-42570*# Commonwealth Scientific Corp., Alexandria, VA. END-HALL THRUSTERS

H. R. KAUFMAN (Front Range Research, Fort Collins, CO; Commonwealth Scientific Corp., Alexandria, VA), R. S. ROBINSON (Colorado State University, Fort Collins), M. L. DAY (Ford Aerospace Corp., Palo Alto, CA), and T. W. HAAG (NASA, Lewis Research Center, Cleveland, OH) AIAA, DGLR, and JSASS, International Electric Propulsion Conference, 21st, Orlando, FL, July 18-20, 1990. 8 p. Research supported by the Ford Aerospace Corp. refs
(AIAA PAPER 90-2595) Copyright

The end-Hall thruster can provide electric propulsion with fixed masses, specific impulses, and power-to-thrust ratios intermediate of an arcjet and a gridded (electrostatic) ion thruster. With these characteristics, this thruster is a candidate for missions of intermediate difficulty, such as the north-south stationkeeping of geostationary satellites. Author

A90-42587*# Tennessee Univ. Space Inst., Tullahoma. NUMERICAL MODELING OF AN ARCJET THRUSTER

ROBERT P. RHODES and DENNIS KEEFER (Tennessee University, Tullahoma) AIAA, DGLR, and JSASS, International Electric Propulsion Conference, 21st, Orlando, FL, July 18-20, 1990. 9 p. Research supported by SDIO. refs
(Contract NAG3-1159)
(AIAA PAPER 90-2614) Copyright

A numerical model of an arcjet thruster was developed and the results of calculations using this model are compared to the experimental data from a 30 kW arcjet using ammonia as a propellant. The model contains equations for the conservation of mass, radial, axial, and azimuthal momentum, energy, and the radial component of the magnetic field and provides a solution for three components of velocity, temperature, and the axial and radial current as a function of position in an axisymmetric flowfield. The model predicts 12 percent more specific impulse than the experiment when the mass flow and power input are constrained to the experimental values. A major conclusion of this study is that improved procedures for calculating transport properties are necessary if the accuracy of the model is to be improved. Author

A90-42609*# Sverdrup Technology, Inc., Brook Park, OH. PRELIMINARY PLUME CHARACTERISTICS OF AN ARCJET THRUSTER

DAVID H. MANZELLA, ROGER M. MYERS (Sverdrup Technology, Inc., Brook Park, OH), FRANCIS M. CURRAN (NASA, Lewis Research Center, Cleveland, OH), and DIETER M. ZUBE (Stuttgart, Universitaet, Federal Republic of Germany) AIAA, DGLR, and JSASS, International Electric Propulsion Conference, 21st, Orlando, FL, July 18-20, 1990. 15 p. refs
(AIAA PAPER 90-2645)

An experimental program initiated to characterize the near field of an arcjet plume is described. The complete emission spectrum from 3200 to 7200 A at the nozzle exit plane detected the electronically excited species N₂, N₂(+), NH, and H, indicating excitation, dissociation, ionization, and recombination in the nozzle. Axial intensity profiles indicated an exponential decay in excited

state population for H(alpha), H(beta), and NH. The rate of axial decay indicated lower velocities for NH than H in the plume and population of the third excited energy state of hydrogen from the decay of higher energy levels. Rotational temperatures ranged from 750 K for N₂ to 2500 K for NH. Based on these results, the arcjet plume is found to be a highly nonequilibrium plasma. Anode electrical configuration is found to have a large effect on the spectral intensities measured in the plume. C.D.

A90-42625* # Ohio State Univ., Columbus.

DIAGNOSTICS AND PERFORMANCE OF A 1/4-SCALE MPD THRUSTER

T. M. YORK, C. ZAKRZWSKI, and G. SOULAS (Ohio State University, Columbus) AIAA, DGLR, and JSASS, International Electric Propulsion Conference, 21st, Orlando, FL, July 18-20, 1990. 11 p. refs
(Contract NAG3-843)
(AIAA PAPER 90-2665) Copyright

The primary purpose of this study is to evaluate the performance and scaling characteristics of a 1/4-scale magnetoplasmadynamic (MPD) thruster operating with and without applied magnetic nozzle fields. The experiment was carried out with separate pulse forming networks for the thruster and the applied field solenoidal coil. A strong correlation of impact pressure signal with thruster current was noted. Also striking was the larger impact signal when the magnetic nozzle field was applied. Measurements of N(e) and T(e) from Langmuir probes have been made. Compatible interpretation of pressure with N(e), T(e), allow local velocity to be mapped, thus enhancing understanding of the acceleration process. Author

A90-42713* # United Technologies Corp., Windsor Locks, CT. HEALTH MONITORING SYSTEM FOR THE SSME - HARDWARE ARCHITECTURE STUDY

JEFFREY K. KAMENETZ (United Technologies Corp., Hamilton Standard Div., Windsor Locks, CT), MIKE W. HAWMAN, and SHARAYU TULPUL (United Technologies Research Center, East Hartford, CT) AIAA, SAE, ASME, and ASEE, Joint Propulsion Conference, 26th, Orlando, FL, July 16-18, 1990. 12 p. refs
(Contract NAS3-25626)
(AIAA PAPER 90-1989) Copyright

This paper presents a hardware architecture for a health monitoring system (HMS) for the SSME. The architecture study was conducted in conjunction with a NASA sponsored program to develop a framework for SSME HMS for (1) ground test and, potentially (2) flight applications. The requirements for both systems are both stated and analyzed. A multiprocessor distributed VME system is envisioned for the ground-test hardware. By repackaging the boards, the same concept is shown to be usable for the flight system. The paper concludes with an analysis of weight, power, and reliability with respect to variations in functionality. Author

A90-42770* # Cincinnati Univ., OH.

THE SIMULATION OF FLUID DYNAMIC UNCERTAINTIES IN THE SSME TURBOPUMP

AWATEF HAMED (Cincinnati University, OH) AIAA, SAE, ASME, and ASEE, Joint Propulsion Conference, 26th, Orlando, FL, July 16-18, 1990. 10 p. refs
(Contract NASA ORDER C-99066-G)
(AIAA PAPER 90-2294) Copyright

The aerodynamic uncertainties in the reusable rocket engine turbopumps due to randomness in their cryogenic environment are investigated. The probabilistic simulation of the turbopumps' aerodynamic response was accomplished using the panel method coupled with Fast Probability Integration methods. The results are presented for the probabilistic rotor blades and splitter loading and their sensitivity to specified flow coefficient and rotor prewhirl variance. Author

A90-45694* # National Aeronautics and Space Administration. Lewis Research Center, Cleveland, OH.

COMBUSTOR DESIGN AND ANALYSIS USING THE ROCKET COMBUSTOR INTERACTIVE DESIGN (ROCCID)

METHODOLOGY

MARK D. KLEM (NASA, Lewis Research Center, Cleveland, OH), JERRY L. PIEPER, and RICHARD E. WALKER (Aerojet TechSystems, Sacramento, CA) AIAA, SAE, ASME, and ASEE, Joint Propulsion Conference, 26th, Orlando, FL, July 16-18, 1990. 10 p. Previously announced in STAR as N90-24349. refs
(AIAA PAPER 90-2240) Copyright

The ROCKET Combustor Interactive Design (ROCCID) Methodology is a newly developed, interactive computer code for the design and analysis of a liquid propellant rocket combustion chamber. The application of ROCCID to design a liquid rocket combustion chamber is illustrated. Designs for a 50,000 lbf thrust and 1250 psi chamber pressure combustor using liquid oxygen (LOX)/RP-1 propellants are developed and evaluated. Tradeoffs between key design parameters affecting combustor performance and stability are examined. Predicted performance and combustion stability margin for these designs are provided as a function of the combustor operating mixture ratio and chamber pressure. Author

A90-47201* # National Aeronautics and Space Administration. Marshall Space Flight Center, Huntsville, AL.

ENGINE SELECTION FOR THE SPACE EXPLORATION INITIATIVE

LEE W. JONES (NASA, Marshall Space Flight Center, Huntsville, AL) and FRANK D. BERKOPPEC (NASA, Lewis Research Center, Cleveland, OH) AIAA, SAE, ASME, and ASEE, Joint Propulsion Conference, 26th, Orlando, FL, July 16-18, 1990. 15 p.
(AIAA PAPER 90-1880) Copyright

The process used by NASA in the selection of the engine for the Space Exploration Initiative mission is described. The major propulsion requirements of the engine are addressed along with the engine options and key drivers and trades. Special attention is given to the requirements of the propellant feed system and the reaction control system. As a result of the 90-study, four moderate chamber pressure expander-cycle oxygen/hydrogen engines with a thrust level of 20,000 lbf each were selected for the lunar transfer vehicle. The paper also presents results of architecture studies and of advanced engine test bed studies. I.S.

A90-47205* # National Aeronautics and Space Administration. Lewis Research Center, Cleveland, OH.

ROCKET ENGINE FAILURE DETECTION USING SYSTEM IDENTIFICATION TECHNIQUES

CLAUDIA M. MEYER and JUNE F. ZAKRAJSEK (NASA, Lewis Research Center; Sverdrup Technology, Inc., Brook Park, OH) AIAA, SAE, ASME, and ASEE, Joint Propulsion Conference, 26th, Orlando, FL, July 16-18, 1990. 17 p. Previously announced in STAR as N90-25159. refs
(Contract NAS3-25266)
(AIAA PAPER 90-1993) Copyright

The theoretical foundation and application of two univariate failure detection algorithms to Space Shuttle Main Engine (SSME) test firing data is presented. Both algorithms were applied to data collected during steady state operation of the engine. One algorithm, the time series algorithm, is based on time series techniques and involves the computation of autoregressive models. Time series techniques have been previously applied to SSME data. The second algorithm is based on standard signal processing techniques. It consists of tracking the variations in the average signal power with time. The average signal power algorithm is a newly proposed SSME failure detection algorithm. Seven nominal test firings were used to develop failure indication thresholds for each algorithm. These thresholds were tested using four anomalous firings and one additional nominal firing. Both algorithms provided significantly earlier failure indication times than did the current redline limit system. Neither algorithm gave false failure indications for the nominal firing. The strengths and weaknesses of the two

20 SPACECRAFT PROPULSION AND POWER

algorithms are discussed and compared. The average signal algorithm was found to have several advantages over the time series algorithm. Author

A90-47207*# National Aeronautics and Space Administration. Lewis Research Center, Cleveland, OH.

MULTI-REACTOR CONFIGURATIONS FOR MULTI-MEGAWATT SPACECRAFT POWER SUPPLIES

JEFFREY A. GEORGE (NASA, Lewis Research Center, Cleveland, OH) AIAA, SAE, ASME, and ASEE, Joint Propulsion Conference, 26th, Orlando, FL, July 16-18, 1990. 8 p. refs (AIAA PAPER 90-2111) Copyright

Several conceptual designs for a multimegawatt space nuclear power supply system were developed on the basis of hardware and technology from the existing multihundred kilowatt-class SP-100 reactor program. It is shown that net power outputs in the multimegawatt range can be achieved by using a modular multireactor configuration of several SP-100-derived nuclear power supplies. A variety of geometries were examined for their applicability to the multireactor configuration, showing that modular multireactor systems have the advantage of an increased redundancy in the power system, as compared with a single-reactor system, allowing higher reliabilities than those achievable with single-reactor systems. Results are presented on the Mars Cargo Mission analysis, showing that modularity allows the option of redeployment of power systems in Mars and facilitates refurbishment and turnaround of NEP transfer vehicles. I.S.

A90-47208*# National Aeronautics and Space Administration. Lewis Research Center, Cleveland, OH.

ROCKET COMBUSTION CHAMBER LIFE-ENHANCING DESIGN CONCEPTS

R. J. QUENTMEYER (NASA, Lewis Research Center; Sverdrup Technology, Inc., Brook Park, OH) AIAA, SAE, ASME, and ASEE, Joint Propulsion Conference, 26th, Orlando, FL, July 16-18, 1990. 18 p. Previously announced in STAR as N90-25183. refs (AIAA PAPER 90-2116) Copyright

NASA continues to pursue technologies which can lead to an increase in life and reduce the costs of fabrication of the Space Shuttle Main Engine. The joint NASA/Air Force Advanced Launch System Program has set its prime objectives to be high reliability and low cost for their new advanced booster engine. In order to meet these objectives, NASA will utilize the results of several ongoing programs to provide the required technologies. An overview is presented of those programs which address life enhancing design concepts for the combustion chamber. Seven different design concepts, which reduce the thermal strain and/or increase the material strength of the combustion chamber liner wall are discussed. Subscale rocket test results are presented, where available, for life enhancing design concepts. Two techniques for reducing chamber fabrication costs are discussed, as well as issues relating to hydrocarbon fuels/combustion chamber liner materials compatibility. Author

A90-47211*# Aerojet TechSystems Co., Sacramento, CA.

A HIGHLY DURABLE INJECTOR FACEPLATE DESIGN CONCEPT FOR O₂/H₂ PROPELLANTS

H. H. MUEGGENBURG (Aerojet TechSystems, Sacramento, CA) and G. A. REPAS (NASA, Lewis Research Center, Cleveland, OH) AIAA, SAE, ASME, and ASEE, Joint Propulsion Conference, 26th, Orlando, FL, July 16-18, 1990. 5 p. (AIAA PAPER 90-2181) Copyright

Two different O₂/H₂ injector faceplate designs were used in a test bed rocket engine at the NASA Lewis Research Center facility. This test bed was operated in a pulsing mode to evaluate thrust chamber wall materials and coatings. Degradation of the sintered mesh injector face plates resulted in the substitution of a photoetched diffusion-bonded platelet faceplate. This faceplate accumulated over 4200 thermal cycles without damage or degradation. Prior testing for a total of 17,446 cycles required 19 sintered mesh faceplates. This average of 918 cycles per unit showed the diffusion bonded faceplate to have a thermal cycle capability ranging from 150 to 500 percent of that of the sintered

wire unit. The test data also showed that the diffusion-bonded faceplate provided a more uniform flow of gaseous H₂ through its discrete and uniformly spaced propellant orifices resulting in enhanced face cooling (no local hot spots) and increased performance. The injector faceplate designs are described and the results of the injector comparison test data are presented. Author

Author

A90-47215*# National Aeronautics and Space Administration. Lewis Research Center, Cleveland, OH.

AEROELASTIC STABILITY ANALYSIS OF A HIGH-ENERGY TURBINE BLADE

TODD E. SMITH (NASA, Lewis Research Center; Sverdrup Technology, Inc., Brook Park, OH) AIAA, SAE, ASME, and ASEE, Joint Propulsion Conference, 26th, Orlando, FL, July 16-18, 1990. 17 p. refs

(Contract NAS3-25266)

(AIAA PAPER 90-2351) Copyright

The dynamic analysis for the SSME HPOTP first stage turbine blade is presented wherein the rotor aeroelastic stability is assessed. The method employs normal modes analysis to simulate the coupled blade/fluid system. A three-dimensional finite element model of the blade is used in conjunction with a two-dimensional linearized unsteady aerodynamic theory which accounts for steady aerodynamic loading effects. This unsteady aerodynamic model is applied in stacked axisymmetric strips along the airfoil span. The blade dynamic and aerodynamic behaviors are coupled within modal space by expressing the unsteady aerodynamic forces in the frequency domain. A complex eigenvalue problem is solved to determine the stability of the rotor assuming tuned blades. The present analysis indicates that the HPOTP rotor experiences very low aerodynamic damping in the first four vibrational modes. The edgewise mode was found to be dynamically unstable. This mode of the blade became stable when the effect of mechanical damping was considered. Author

A90-47216*# National Aeronautics and Space Administration. Lewis Research Center, Cleveland, OH.

NUMERICAL ANALYSIS OF SECONDARY FLOW IN A TWO-STAGE TURBINE

K. R. KIRTLEY, T. A. BEACH (NASA, Lewis Research Center; Sverdrup Technology, Inc., Cleveland, OH), and J. J. ADAMCZYK (NASA, Lewis Research Center, Cleveland, OH) AIAA, SAE, ASME, and ASEE, Joint Propulsion Conference, 26th, Orlando, FL, July 16-18, 1990. 16 p. refs (AIAA PAPER 90-2356)

The three-dimensional viscous average passage flow in the Pratt and Whitney alternate design Space Shuttle Main Engine fuel turbine has been simulated. The effect of secondary flows generated by upstream blade rows on the performance of downstream blade rows is studied. The numerical results are compared to the design intent to validate improved models in the average passage equations. Analysis of the results centers on the primary spanwise mixing mechanism in this low aspect ratio turbine. A multigrid method has also been incorporated to improve the overall convergence rate of the numerical algorithm. Author

A90-47217*# Boeing Aerospace Co., Seattle, WA.

TANK PRESSURE CONTROL EXPERIMENT - A LOW-G MIXING INVESTIGATION

M. D. BENTZ, J. S. MESEROLE (Boeing Aerospace and Electronics, Seattle, WA), and R. L. KNOLL (NASA, Lewis Research Center, Cleveland, OH) AIAA, SAE, ASME, and ASEE, Joint Propulsion Conference, 26th, Orlando, FL, July 16-18, 1990. 8 p. refs

(AIAA PAPER 90-2376) Copyright

The Tank Pressure Control Experiment (TPCE) was conceived to meet the need for an aspect of cryogenic fluid management technology that is critical to several future national space missions: control of cryogenic storage tank pressures by active mixing. In-space testing is the only means of obtaining the fluid dynamic data necessary to develop and test predictive models of mixing. These models, when validated, will allow future cryogenic systems

to be designed with more efficient and reliable pressure control systems. The objectives of the TPCE project are to characterize the fluid dynamics of jet-induced mixing in low gravity, evaluate the validity of empirical models and correlations, and provide data for use in developing and validating computational fluid dynamic models. This paper discusses prior studies of low-g mixing, the objectives and benefits of TPCE, the design and status of the payload, and preliminary results obtained from low-g aircraft testing. Author

A90-47221*# National Aeronautics and Space Administration. Lewis Research Center, Cleveland, OH.

LUNAR MISSIONS USING ADVANCED CHEMICAL PROPULSION - SYSTEM DESIGN ISSUES

BRYAN PALASZEWSKI (NASA, Lewis Research Center, Cleveland, OH) AIAA, SAE, ASME, and ASEE, Joint Propulsion Conference, 26th, Orlando, FL, July 16-18, 1990. 13 p. refs (AIAA PAPER 90-2431) Copyright

In this paper, the masses in low earth orbit (LEO) were compared for several propulsion systems: nitrogen tetroxide/monomethyl hydrazine, oxygen/methane, oxygen/hydrogen, and metallized O₂/H₂/Al propellants. Also, the payload mass increases enabled with these systems were addressed. In addition, many system design issues involving the engine thrust levels, engine commonality between the transfer vehicle and the excursion vehicle, and the number of launches to place the lunar mission vehicles into LEO are discussed. Analyses of small lunar missions launched from a single STS-C flight are also presented. Author

A90-47224*# National Aeronautics and Space Administration. Lewis Research Center, Cleveland, OH.

CALCULATIONS OF GASEOUS H₂/O₂ THRUSTER

S. C. KIM (NASA, Lewis Research Center; Sverdrup Technology, Inc., Cleveland, OH) and T. J. VANOVERBEKE (NASA, Lewis Research Center, Cleveland, OH) AIAA, SAE, ASME, and ASEE, Joint Propulsion Conference, 26th, Orlando, FL, July 16-18, 1990. 9 p. refs (Contract NAS3-25266) (AIAA PAPER 90-2490)

Calculations were made for the gaseous H₂/O₂ thruster for the Space Station by using the RPLUS code which employs an implicit finite volume, LUSSOR scheme to solve the Navier-Stokes equations and the species equations. The combustion processes of hydrogen and oxygen are modeled by a 9 species and 18 step reaction mechanism and the turbulence is simulated by the Baldwin-Lomax turbulence model for the thruster wall boundary layer and the modified Prandtl's mixing length model for the reacting shear layer. Results are presented for different mixture ratios and fuel film cooling percents and compared with the experimental data. The calculated performance predictions for the thruster agree well with the experimental data and the results demonstrate that the RPLUS code can be used for design and analysis of thrusters and rockets. Author

A90-47226*# National Aeronautics and Space Administration. Lewis Research Center, Cleveland, OH.

ARCJET LOAD CHARACTERISTICS

JOHN A. HAMLEY (NASA, Lewis Research Center, Cleveland, OH) AIAA, SAE, ASME, and ASEE, Joint Propulsion Conference, 26th, Orlando, FL, July 16-18, 1990. 17 p. Previously announced in STAR as N90-25181. refs (AIAA PAPER 90-2579) Copyright

Experiments were conducted to define the interface characteristics and constraints of 1 kW class arcjets run on simulated decomposition products of hydrazine and power processors. The impacts of power supply output current ripple on arcjet performance were assessed by variation of the ripple frequency from 100 Hz to 100 kHz with 10 percent peak-to-peak ripple amplitude at 1.2 kW. Ripple had no significant effects on thrust, specific impulse or efficiency. The impact of output ripple on thruster lifetime was not assessed. The static and dynamic impedances of the arcjet were quantified with two thrusters of

nearly identical configuration. Superposition of an AC component on the DC arc current was used to characterize the dynamic impedance as a function of flow rate and DC current level. A mathematical model was formulated from these data. Both the static and dynamic impedance magnitude were found to be dependent on mass flow rate. The amplitude of the AC component was found to have little effect on the dynamic impedance. Reducing the DC level from 10 to 8 amps led to a large change in the magnitude of the dynamic impedance with no observable phase change. The impedance data compared favorably between the two thrusters. Author

A90-47227*# National Aeronautics and Space Administration. Lewis Research Center, Cleveland, OH.

ADVANCED TUBE-BUNDLE ROCKET THRUST CHAMBER

JOHN M. KAZAROFF (NASA, Lewis Research Center, Cleveland, OH) and ALBERT J. PAVLI (NASA, Lewis Research Center; Sverdrup Technology, Inc., Brook Park, OH) AIAA, SAE, ASME, and ASEE, Joint Propulsion Conference, 26th, Orlando, FL, July 16-18, 1990. 13 p. Previously announced in STAR as N90-25185. (AIAA PAPER 90-2726) Copyright

An advanced rocket thrust chamber for future space application is described along with an improved method of fabrication. Potential benefits of the concept are improved cyclic life, reusability, and performance. Performance improvements are anticipated because of the enhanced heat transfer into the coolant which will enable higher chamber pressure in expander cycle engines. Cyclic life, reusability and reliability improvements are anticipated because of the enhanced structural compliance inherent in the construction. The method of construction involves the forming of the combustion chamber with a tube-bundle of high conductivity copper or copper alloy tubes, and the bonding of these tubes by an electroforming operation. Further, the method of fabrication reduces chamber complexity by incorporating manifolds, jackets, and structural stiffeners while having the potential for thrust chamber cost and weight reduction. Author

A90-50643*# National Aeronautics and Space Administration. Lewis Research Center, Cleveland, OH.

DIGITAL FILTERING OF PLUME EMISSION SPECTRA

GEORGE C. MADZSAR (NASA, Lewis Research Center, Cleveland, OH) AIAA, SAE, ASME, and ASEE, Joint Propulsion Conference, 26th, July 16-18, 1990. 12 p. Previously announced in STAR as N90-26070. refs (AIAA PAPER 90-1994) Copyright

Fourier transformation and digital filtering techniques were used to separate the superpositioned spectral phenomena observed in the exhaust plumes of liquid propellant rocket engines. Space shuttle main engine (SSME) spectral data were used to show that extraction of spectral lines in the spatial frequency domain does not introduce error, and extraction of the background continuum introduces only minimal error. Error introduced during band extraction could not be quantified due to poor spectrometer resolution. Based on the atomic and molecular species found in the SSME plume, it was determined that spectrometer resolution must be 0.03 nm for SSME plume spectral monitoring. Author

A90-52562*# National Aeronautics and Space Administration. Lewis Research Center, Cleveland, OH.

XENON ION PROPULSION FOR ORBIT TRANSFER

V. K. RAWLIN, M. J. PATTERSON, and R. P. GRUBER (NASA, Lewis Research Center, Cleveland, OH) AIAA, DGLR, and JSASS, International Electric Propulsion Conference, 21st, Orlando, FL, July 18-20, 1990. 29 p. refs (AIAA PAPER 90-2527) Copyright

The status of critical ion propulsion system elements is reviewed. Electron bombardment ion thrusters for primary propulsion have evolved to operate on xenon in the 5-10 kW power range. Thruster efficiencies of 0.7 and specific impulse values of 4000 s have been documented. The baseline thruster currently under development by NASA LeRC includes ring-cusp magnetic field plasma containment and dished two-grid ion optics. Based on past experience and demonstrated simplifications, power

20 SPACECRAFT PROPULSION AND POWER

processors for these thrusters should have approximately 500 parts, a mass of 40 kg, and an efficiency near 0.94. Thrust vector control, via individual thruster gimbals, is a mature technology. High pressure, gaseous xenon propellant storage and control schemes, using flight qualified hardware, result in propellant tankage fractions between 0.1 and 0.2. In-space and ground integration testing has demonstrated that ion propulsion systems can be successfully integrated with their host spacecraft. Author

A90-52563*# Jet Propulsion Lab., California Inst. of Tech., Pasadena.

PHOTOVOLTAIC OPTIONS FOR SOLAR ELECTRIC PROPULSION

PAUL M. STELLA (JPL, Pasadena, CA) and DENNIS J. FLOOD (NASA, Lewis Research Center, Cleveland, OH) AIAA, DGLR, and JSASS, International Electric Propulsion Conference, 21st, Orlando, FL, July 18-20, 1990. 9 p. refs (AIAA PAPER 90-2529)

This paper discusses both state-of-the-art and advanced development cell and array technology. Present technology includes rigid, roll-out, and foldout flexible substrate designs, with silicon and GaAs solar cells. The use of concentrator array systems is discussed based on both DOD efforts and NASA work. The benefits of advanced lightweight array technology, for both near term and far term utilization, and of advanced high efficiency thin radiation resistant cells is examined. This includes gallium arsenide/germanium, indium phosphide, and thin film devices such as copper indium diselenide. Author

A90-52564*# National Aeronautics and Space Administration, Lewis Research Center, Cleveland, OH.

5KW XENON ION THRUSTER LIFETEST

MICHAEL J. PATTERSON (NASA, Lewis Research Center, Cleveland, OH) and TIMOTHY R. VERHEY (NASA, Lewis Research Center; Sverdrup Technology, Inc, Cleveland, OH) AIAA, DGLR, and JSASS, International Electric Propulsion Conference, 21st, Orlando, FL, July 18-20, 1990. 52 p. refs (AIAA PAPER 90-2543) Copyright

This paper describes the results of the first lifetest of a high power ring-cusp ion thruster. A 30-cm laboratory model thruster was operated steady-state at a nominal beam power of 5kW on xenon propellant for approximately 900 hours. This test was conducted to identify life-limiting erosion mechanisms and thruster design modifications, and to demonstrate operation using simplified power processing. The results from this test are described including the conclusions derived from extensive post-test analyses of the thruster. Modifications to the thruster and ground support equipment, which have been incorporated to solve problems identified by the lifetest, are also described. Author

A90-52565*# National Aeronautics and Space Administration, Lewis Research Center, Cleveland, OH.

ADVANCED PROPULSION FOR LEO AND GEO PLATFORMS

JAMES S. SOVEY (NASA, Lewis Research Center, Cleveland, OH) and DAVID J. PIDGEON (NASA, Langley Research Center; George Washington University, Hampton, VA) AIAA, DGLR, and JSASS, International Electric Propulsion Conference, 21st, Orlando, FL, July 18-20, 1990. 25 p. Previously announced in STAR as N90-27785. refs (AIAA PAPER 90-2551) Copyright

Mission requirements and mass savings applicable to specific low earth orbit and geostationary earth orbit platforms using three highly developed propulsion systems are described. Advanced hypergolic bipropellant thrusters and hydrazine arcjets can provide about 11 percent additional instrument payload to 14,000 kg LEO platforms. By using electric propulsion on a 8,000 kg class GEO platform, mass savings in excess of 15 percent of the beginning-of-life platform mass are obtained. Effects of large, advanced technology solar arrays and antennas on platform propulsion requirements are also discussed. Author

A90-52566*# Sverdrup Technology, Inc., Brook Park, OH. MULTIMEGAWATT ELECTRIC PROPULSION SYSTEM DESIGN CONSIDERATIONS

J. H. GILLAND, R. M. MYERS (Sverdrup Technology, Inc., Brook Park, OH), and M. J. PATTERSON (NASA, Lewis Research Center, Cleveland, OH) AIAA, DGLR, and JSASS, International Electric Propulsion Conference, 21st, Orlando, FL, July 18-20, 1990. 16 p. refs (AIAA PAPER 90-2552)

Piloted Mars mission requirements of relatively short trip times and low initial mass in earth orbit as identified by the NASA Space Exploration Initiative, indicate the need for multimewatt electric propulsion systems. The design considerations and results for two thruster types, the argon ion and hydrogen magnetoplasmadynamic thrusters, are addressed in terms of configuration, performance, and mass projections. Preliminary estimates of Power Management and Distribution for these systems are given. Some assessment of these systems' performance in a reference Space Exploration Initiative piloted mission are discussed. Research and development requirements of these systems are also described. Author

A90-52568*# National Aeronautics and Space Administration, Lewis Research Center, Cleveland, OH.

LOW POWER ARCJET PERFORMANCE

FRANCIS M. CURRAN and CHARLES J. SARMIENTO (NASA, Lewis Research Center, Cleveland, OH) AIAA, DGLR, and JSASS, International Electric Propulsion Conference, 21st, Orlando, FL, July 18-20, 1990. 14 p. refs (AIAA PAPER 90-2578)

An experimental investigation was performed to evaluate arcjet operation at low power. A standard, 1 kW, constricted arcjet was run using nozzles with three different constrictor diameters. Each nozzle was run over a range of current and mass flow rates to explore stability and performance in the low power regime. A standard pulse-width modulated power processor was modified to accommodate the high operating voltages required under certain conditions. Stable, reliable operation at power levels below 0.5 kW was obtained at efficiencies between 30 and 40 percent. The operating range was found to be somewhat dependent on constrictor geometry at low mass flow rates. Quasi-periodic voltage fluctuations were observed at the low power end of the operating envelope. The nozzle insert geometry was found to have little effect on the performance of the device. The observed performance levels show that specific impulse levels above 350 seconds can be obtained at the 0.5 kW power level. Author

A90-52569*# National Aeronautics and Space Administration, Lewis Research Center, Cleveland, OH.

PERFORMANCE CHARACTERIZATION OF A SEGMENTED ANODE ARCJET THRUSTER

FRANCIS M. CURRAN, ERIC J. PENCIL (NASA, Lewis Research Center, Cleveland, OH), and DAVID H. MANZELLA (NASA, Lewis Research Center; Sverdrup Technology, Inc, Cleveland, OH) AIAA, DGLR, and JSASS, International Electric Propulsion Conference, 21st, Orlando, FL, July 18-20, 1990. 16 p. refs (AIAA PAPER 90-2582)

Results are presented from a continuing experimental program aimed at providing insight into arc energy deposition in the nozzle, the nature of the arc attachment, and its effects on performance characteristics of the device. A modular, 1-2 kW class arcjet thruster incorporating a segmented anode/nozzle was run on a thrust stand to determine performance characteristics under a number of experimental conditions. The nozzle comprised five axial conducting segments isolated from each other by boron nitride spacers. The electrical configuration permitted the current delivered to the arcjet to be collected at any combination of segments. It is concluded that the changes in the electric field in the nozzle that occur as a result of the changes in the current distribution do not significantly affect the momentum transfer or loss mechanisms in the type of nozzle investigated. Performance characteristics show that the segmented anode reasonably simulates the behavior of solid anodes of similar geometry. R.E.P.

A90-52570* # National Aeronautics and Space Administration. Lewis Research Center, Cleveland, OH.

REQUIREMENTS FOR LONG-LIFE OPERATION OF INERT GAS HOLLOW CATHODES - PRELIMINARY RESULTS

TIMOTHY R. VERHEY (NASA, Lewis Research Center; Sverdrup Technology, Inc., Brook Park, OH) and GREGORY S. MACRAE (NASA, Lewis Research Center, Cleveland, OH) AIAA, DGLR, and JSASS, International Electric Propulsion Conference, 21st, Orlando, FL, July 18-20, 1990. 18 p. Previously announced in STAR as N90-27783. refs
(AIAA PAPER 90-2586) Copyright

An experimental investigation was initiated to establish conditioning procedures for reliable hollow cathode operation via the characterization of critical parameters in a representative cathode test facility. From vacuum pumpdown rates, it was found that approximately 1.5 hours were required to achieve pressure levels within 5 percent of the lowest attainable pressure for this facility, depending on the purge conditions. The facility atmosphere was determined by a residual gas analyzer to be composed of primarily air and water vapor. The effects of vacuum pumping and inert gas purging were evaluated. A maximum effective leakage rate of 2.0×10 (exp -3) sccm was observed and its probable causes were examined. An extended test of a 0.64 cm diameter Mo-Re hollow cathode was successfully completed. This test ran for 504 hours at an emission current of 23.0 amperes and a xenon flow rate of 6.1 sccm. Discharge voltage rose continuously from 15 to 21 volts over the course of the test. The temperature of the cathode body during the test was relatively stable at 1160 C. Post-test examination revealed ion-bombardment texturing of the orifice plate to be the only detectable sign of wear on the hollow cathode. Author

A90-52572* # National Aeronautics and Space Administration. Lewis Research Center, Cleveland, OH.

GEOMETRIC EFFECTS IN APPLIED-FIELD MPD THRUSTERS

R. M. MYERS (NASA, Lewis Research Center; Sverdrup Technology, Inc., Brook Park, OH), M. MANTENIEKS, and J. SOVEY (NASA, Lewis Research Center, Cleveland, OH) AIAA, DGLR, and JSASS, International Electric Propulsion Conference, 21st, Orlando, FL, July 18-20, 1990. 19 p. Previously announced in STAR as N90-27782. refs
(AIAA PAPER 90-2669)

Three applied-field magnetoplasma dynamic (MPD) thruster geometries were tested with argon propellant to establish the influence of electrode geometry on thruster performance. The thrust increased approximately linearly with anode radius, while the discharge and electrode fall voltages increased quadratically with anode radius. All these parameters increased linearly with applied-field strength. Thrust efficiency, on the other hand, was not significantly influenced by changes in geometry over the operating range studied, though both thrust and thermal efficiencies increased monotonically with applied field strength. The best performance, 1820 sec I (sub sp) at 20 percent efficiency, was obtained with the largest radius anode at the highest discharge current (1500 amps) and applied field strength (0.4 Tesla). Author

A90-52955* National Aeronautics and Space Administration. Lewis Research Center, Cleveland, OH.

ADVANCED LAUNCH SYSTEM (ALS) ACTUATION AND POWER SYSTEMS IMPACT OPERABILITY AND COST

GALE R. SUNDBERG (NASA, Lewis Research Center, Cleveland, OH) IEEE Aerospace and Electronic Systems Magazine (ISSN 0885-8985), vol. 5, Sept. 1990, p. 20-23. Previously announced in STAR as N90-21271. Copyright

To obtain the Advanced Launch System (ALS) primary goals of reduced costs and improved operability, there must be significant reductions in the launch operations and servicing requirements relative to current vehicle designs and practices. One of the primary methods for achieving these goals is by using vehicle electrical power system and controls for all actuation and avionics requirements. A brief status review of the ALS and its associated

Advanced Development Program is presented to demonstrate maturation of those technologies that will help meet the overall operability and cost goals. The electric power and actuation systems are highlighted as a specific technology ready not only to meet the stringent ALS goals (cryogenic field valves and thrust vector controls with peak power demands to 75 hp), but also those of other launch vehicles, military and civilian aircraft, lunar/Martian vehicles, and a multitude of commercial applications. Author

N90-10147* # Georgia Inst. of Tech., Atlanta.

MILLIMETER-WAVE/INFRARED RECTENNA DEVELOPMENT AT GEORGIA TECH

MARK A. GOUKER /n NASA. Langley Research Center, Second Beamed Space-Power Workshop p 127-137 Jul. 1989
(Contract NAG3-202)

Avail: NTIS HC A19/MF A03 CSCL 10B

The key design issues of the Millimeter Wave/Infrared (MMW/IR) monolithic rectenna have been resolved. The work at Georgia Tech in the last year has focused on increasing the power received by the physically small MMW rectennas in order to increase the rectification efficiency. The solution to this problem is to place a focusing element on the back side of the substrate. The size of the focusing element can be adjusted to help maintain the optimum input power density not only for different power densities called for in various mission scenarios, but also for the nonuniform power density profile of a narrow EM-beam. Author

N90-10158* # National Aeronautics and Space Administration. Lewis Research Center, Cleveland, OH.

POWER FOR THE MOON: IS MICROWAVE POWER BEAMING AN OPTION?

RONALD C. CULL /n NASA. Langley Research Center, Second Beamed Space-Power Workshop p 329-342 Jul. 1989

Avail: NTIS HC A19/MF A03 CSCL 10C

Microwave power beaming options for powering lunar bases are presented in viewgraph form. Information is given on power dependent system masses, a solar source beam power system, a nuclear source beam power system, a three satellite beam power system, antenna configurations, and antenna design. Author

N90-10159* # National Aeronautics and Space Administration. Lewis Research Center, Cleveland, OH.

APPLICABILITY OF THE BEAMED POWER CONCEPT TO LUNAR ROVERS, CONSTRUCTION, MINING, EXPLORERS AND OTHER MOBILE EQUIPMENT

JOSE L. CHRISTIAN, JR. /n NASA. Langley Research Center, Second Beamed Space-Power Workshop p 343-356 Jul. 1989

Avail: NTIS HC A19/MF A03 CSCL 10C

Some of the technical issues dealing with the feasibility of high power (10 Kw to 100 Kw) mobile manned equipment for settlement, exploration and exploitation of Lunar resources are addressed. Short range mining/construction equipment, a moderate range (50 Km) exploration vehicle, and an unlimited range explorer are discussed. Author

N90-10165* # National Aeronautics and Space Administration. Lewis Research Center, Cleveland, OH.

MICROWAVE BEAM POWER

KARL A. FAYMON /n NASA. Langley Research Center, Second Beamed Space-Power Workshop p 397-403 Jul. 1989

Avail: NTIS HC A19/MF A03 CSCL 10B

Information on microwave beam power is given in viewgraph form. Information is given on orbit transfer propulsion applications, costs of delivering 100 kWe of usable power, and costs of delivering a 1 kg payload into orbit. Author

N90-10172* # National Aeronautics and Space Administration. Lewis Research Center, Cleveland, OH.

A ROCKET ENGINE DESIGN EXPERT SYSTEM

KENNETH J. DAVIDIAN Oct. 1989 11 p Presented at the 26th JANNAF Combustion Meeting, Pasadena, CA, 23-27 Oct.

20 SPACECRAFT PROPULSION AND POWER

1989

(NASA-TM-102373; E-5107; NAS 1.15:102373) Avail: NTIS HC A03/MF A01 CSCL 21H

The overall structure and capabilities of an expert system designed to evaluate rocket engine performance are described. The expert system incorporates a JANNAF standard reference computer code to determine rocket engine performance and a state-of-the-art finite element computer code to calculate the interactions between propellant injection, energy release in the combustion chamber, and regenerative cooling heat transfer. Rule-of-thumb heuristics were incorporated for the hydrogen-oxygen coaxial injector design, including a minimum gap size constraint on the total number of injector elements. One-dimensional equilibrium chemistry was employed in the energy release analysis of the combustion chamber and three-dimensional finite-difference analysis of the regenerative cooling channels was used to calculate the pressure drop along the channels and the coolant temperature as it exits the coolant circuit. Inputting values to describe the geometry and state properties of the entire system is done directly from the computer keyboard. Graphical display of all output results from the computer code analyses is facilitated by menu selection of up to five dependent variables per plot.

Author

N90-10174*# National Aeronautics and Space Administration. Lewis Research Center, Cleveland, OH.

A FEASIBILITY ASSESSMENT OF INSTALLATION, OPERATION AND DISPOSAL OPTIONS FOR NUCLEAR REACTOR POWER SYSTEM CONCEPTS FOR A NASA GROWTH SPACE STATION

HARVEY S. BLOOMFIELD and JACK A. HELLER Jun. 1987 37 p

(NASA-TM-89923; E-3622; NAS 1.15:89923) Avail: NTIS HC A03/MF A01 CSCL 21H

A preliminary feasibility assessment of the integration of reactor power system concepts with a projected growth space station architecture was conducted to address a variety of installation, operational disposition, and safety issues. A previous NASA sponsored study, which showed the advantages of space station - attached concepts, served as the basis for this study. A study methodology was defined and implemented to assess compatible combinations of reactor power installation concepts, disposal destinations, and propulsion methods. Three installation concepts that met a set of integration criteria were characterized from a configuration and operational viewpoint, with end-of-life disposal mass identified. Disposal destinations that met current aerospace nuclear safety criteria were identified and characterized from an operational and energy requirements viewpoint, with delta-V energy requirement as a key parameter. Chemical propulsion methods that met current and near-term application criteria were identified and payload mass and delta-V capabilities were characterized. These capabilities were matched against concept disposal mass and destination delta-V requirements to provide the feasibility of each combination.

Author

N90-10175*# General Dynamics Corp., San Diego, CA. Space Systems Div.

BIDIRECTIONAL POWER CONVERTER CONTROL ELECTRONICS Final Report

J. W. MILDICE Nov. 1987 103 p

(Contract NAS3-23878)

(NASA-CR-175070; NAS 1.26:175070) Avail: NTIS HC A06/MF A01 CSCL 21H

The object of this program was to design, build, test, and deliver a set of control electronics suitable for control of bidirectional resonant power processing equipment of the direct output type. The program is described, including the technical background, and results discussed. Even though the initial program tested only the logic outputs, the hardware was subsequently tested with high-power breadboard equipment, and in the testbed of NASA contract NAS3-24399. The completed equipment is now operating as part of the Space Station Power System Test Facility at NASA Lewis Research Center.

Author

N90-11081*# National Aeronautics and Space Administration. Lewis Research Center, Cleveland, OH.

THE EFFECT OF ELECTRODE CONFIGURATION ON ARCJET PERFORMANCE

FRANK M. CURRAN and DAVID H. MANZELLA (Sverdrup Technology, Inc., Cleveland, OH.) 1989 14 p Presented at the 25th Joint Propulsion Conference, Monterey, CA, 10-12 Jul. 1989; cosponsored by AIAA, ASME, SAE, and ASEE Previously announced in IAA as A89-47044

(NASA-TM-102346; E-5054; NAS 1.15:102346) Avail: NTIS HC A03/MF A01 CSCL 21/8

A radiation cooled, segmented anode was tested in a low power (1 kW class) arcjet thruster in order to study the current distribution in the attachment region of the nozzle of the thruster. The nozzle was composed of five segments insulated from one another with boron nitride spacers and matched the critical dimensions of nozzles commonly used in previous testing. The anode was configured so that the current could be collected across any combination of the segments and the potential difference between the cathode and each of the segments was monitored during testing.

Author

N90-11082*# National Aeronautics and Space Administration. Lewis Research Center, Cleveland, OH.

HEAT TRANSFER TO THROAT TUBES IN A SQUARE-CHAMBERED ROCKET ENGINE AT THE NASA LEWIS RESEARCH CENTER

JAMES A. NESBITT and WILLIAM J. BRINDLEY Oct. 1989 33 p

(NASA-TM-102336; E-5045; NAS 1.15:102336) Avail: NTIS HC A03/MF A01 CSCL 21/8

A gaseous H₂/O₂ rocket engine was constructed at the NASA-Lewis to provide a high heat flux source representative of the heat flux to the blades in the high pressure fuel turbopump (HPFTP) during startup of the space shuttle main engines. The high heat flux source was required to evaluate the durability of thermal barrier coatings being investigated for use on these blades. The heat transfer, and specifically, the heat flux to tubes located at the throat of the test rocket engine was evaluated and compared to the heat flux to the blades in the HPFTP during engine startup. Gas temperatures, pressures and heat transfer coefficients in the test rocket engine were measured. Near surface metal temperatures below thin thermal barrier coatings were also measured at various angular orientations around the throat tube to indicate the angular dependence of the heat transfer coefficients. A finite difference model for a throat tube was developed and a thermal analysis was performed using the measured gas temperatures and the derived heat transfer coefficients to predict metal temperatures in the tube. Near surface metal temperatures of an uncoated throat tube were measured at the stagnation point and showed good agreement with temperatures predicted by the thermal model. The maximum heat flux to the throat tube was calculated and compared to that predicted for the leading edge of an HPFTP blade. It is shown that the heat flux to an uncooled throat tube is slightly greater than the heat flux to an HPFTP blade during engine startup.

Author

N90-11804*# National Aeronautics and Space Administration. Lewis Research Center, Cleveland, OH.

THE FUEL CELL IN SPACE: YESTERDAY, TODAY AND TOMORROW

MARVIN WARSHAY and PAUL R. PROKOPIUS Sep. 1989 11 p Presented at the Grove Anniversary (1839-1989) Fuel Cell Symposium, London, England, 18-21 Sep. 1989; sponsored in part by the Royal Institution

(NASA-TM-102366; E-5084; NAS 1.15:102366) Avail: NTIS HC A03/MF A01 CSCL 10/2

The past, present, and future of space fuel cell power systems is reviewed, starting with the first practical fuel cell by F.T. Bacon which led to the 1.5 kW Apollo alkaline fuel cell. However, the first fuel cell to be used for space power was the Gemini 1.0 kW Acid IEM fuel cell. The successor to the Apollo fuel cell is today's 12 kW Orbiter alkaline fuel cell whose technology is considerably

different and considerably better than that of its ancestor, the Bacon cell. And in terms of specific weight there has been a steady improvement from the past to the present, from the close to 200 lb/kW of Apollo to the 20 lb/kW of the orbiter. For NASA future Lunar and Martian surface power requirements the regenerative fuel cell (RFC) energy storage system is enabling technology, with the alkaline and the PEM the leading RFC candidate systems. The U.S. Air Force continues to support fuel cell high power density technology development for its future short duration applications. Author

N90-11805*# Grumman Aerospace Corp., Bethpage, NY. Space Systems.

CONCEPTUAL DESIGN OF LIQUID DROPLET RADIATOR SHUTTLE-ATTACHED EXPERIMENT Final Report

SHLOMO L. PFEIFFER Oct. 1989 60 p

(Contract NAS3-25357)

(NASA-CR-185164; NAS 1.26:185164) Avail: NTIS HC A04/MF A01 CSCL 10/2

The conceptual design of a shuttle-attached liquid droplet radiator (LDR) experiment is discussed. The LDR is an advanced, lightweight heat rejection concept that can be used to reject heat from future high-powered space platforms. In the LDR concept, submillimeter-sized droplets are generated, pass through space, radiate heat before they are collected, and recirculated back to the heat source. The LDR experiment is designed to be attached to the shuttle longeron and integrated into the shuttle bay using standard shuttle/experiment interfaces. Overall power, weight, and data requirements of the experiment are detailed. The conceptual designs of the droplet radiator, droplet collector, and the optical diagnostic system are discussed in detail. Shuttle integration and safety design issues are also discussed. Author

N90-11806*# Grumman Aerospace Corp., Bethpage, NY.

CONCEPTUAL DESIGN OF LIQUID DROPLET RADIATOR SHUTTLE-ATTACHED EXPERIMENT TECHNICAL REQUIREMENTS DOCUMENT

SHLOMO L. PFEIFFER Oct. 1989 31 p

(Contract NAS3-25357)

(NASA-CR-185165; NAS 1.26:185165) Avail: NTIS HC A03/MF A01 CSCL 10/2

The technical requirements of a shuttle-attached Liquid Droplet Radiator (LDR) experiment are discussed. The Liquid Droplet Radiator is an advanced lightweight heat rejection concept that can be used to reject heat from future high powered space platforms. In the LDR concept, submillimeter sized droplets are generated, pass through space, and radiate heat before they are collected and recirculated back to the heat source. The LDR experiment is designed to be attached to the shuttle longeron and integrated into the shuttle bay using standard shuttle/experiment interfaces. Overall power, weight, and data requirements of the experiment are detailed. Shuttle integration and safety design issues are discussed. An overview of the conceptual design of the experiment is presented. Details of the conceptual design are not discussed here, but rather in a separate Final Report. Author

N90-13589*# Rockwell International Corp., Canoga Park, CA. Rocketdyne Div.

LOX/HYDROCARBON COMBUSTION INSTABILITY INVESTIGATION Final Report

R. J. JENSEN, H. C. DODSON, and S. E. CLAFLIN Jul. 1989 177 p

(Contract NAS3-24612)

(NASA-CR-182249; RI/RD-89-179; NAS 1.26:182249) Avail: NTIS HC A09/MF A02 CSCL 21/2

The LOX/Hydrocarbon Combustion Instability Investigation Program was structured to determine if the use of light hydrocarbon combustion fuels with liquid oxygen (LOX) produces combustion performance and stability behavior similar to the LOX/hydrogen propellant combination. In particular methane was investigated to determine if that fuel can be rated for combustion instability using the same techniques as previously used for LOX/hydrogen. These

techniques included fuel temperature ramping and stability bomb tests. The hot fire program probed the combustion behavior of methane from ambient to subambient temperatures. Very interesting results were obtained from this program that have potential importance to future LOX/methane development programs. A very thorough and carefully reasoned documentation of the experimental data obtained is contained. The hot fire test logic and the associated tests are discussed. Subscale performance and stability rating testing was accomplished using 40,000 lb. thrust class hardware. Stability rating tests used both bombs and fuel temperature ramping techniques. The test program was successful in generating data for the evaluation of the methane stability characteristics relative to hydrogen and to anchor stability models. Data correlations, performance analysis, stability analyses, and key stability margin enhancement parameters are discussed. Author

N90-13590*# National Aeronautics and Space Administration. Lewis Research Center, Cleveland, OH.

TANK PRESSURE CONTROL EXPERIMENT ON THE SPACE SHUTTLE

1989 11 p

(NASA-TM-102313; E-5007; NAS 1.15:102313) Avail: NTIS HC A03/MF A01 CSCL 22/2

The tank pressure control experiment is a demonstration of NASA intent to develop new technology for low-gravity management of the cryogenic fluids that will be required for future space systems. The experiment will use freon as the test fluid to measure the effects of jet-induced fluid mixing on storage tank pressure and will produce data on low-gravity mixing processes critical to the design of on-orbit cryogenic storage and resupply systems. Basic data on fluid motion and thermodynamics in low gravity is limited, but such data is critical to the development of space transfer vehicles and spacecraft resupply facilities. An in-space experiment is needed to obtain reliable data on fluid mixing and pressure control because none of the available microgravity test facilities provide a low enough gravity level for a sufficient duration to duplicate in-space flow patterns and thermal processes. Normal gravity tests do not represent the fluid behavior properly; drop-tower tests are limited in length of time available; aircraft low-gravity tests cannot provide the steady near-zero gravity level and long duration needed to study the subtle processes expected in space. Author

N90-13595*# National Aeronautics and Space Administration. Lewis Research Center, Cleveland, OH.

THIN-FILM SENSORS FOR REUSABLE SPACE PROPULSION SYSTEMS

ALOYSIUS F. HEPP and WALTER S. KIM 1989 10 p Presented at the Sensors Expo International, Cleveland, OH, 12-14 Sep. 1989; sponsored by Sensors Magazine

(NASA-TM-102383; E-5122; NAS 1.15:102383) Avail: NTIS HC A02/MF A01 CSCL 21/8

Thin-film thermocouples (TFTCs) were developed for aircraft gas turbine engines and are in use for temperature measurement on turbine blades up to 1800 F. Established aircraft engine gas turbine technology is currently being adapted to turbine engine blade materials and the environment encountered in the Space Shuttle Main Engine (SSME)-severe thermal shock from cryogenic fuel to combustion temperatures. Initial results with coupons of MAR M-246 (+Hf) and PWA 1480 were followed by fabrication of TFTC on SSME turbine blades. Current efforts are focused on preparation for testing in the Turbine Blade Tester at NASA Marshall Space Flight Center. Author

N90-13596*# National Aeronautics and Space Administration. Lewis Research Center, Cleveland, OH.

THE US SPACE STATION AND ITS ELECTRIC POWER SYSTEM

RONALD L. THOMAS 1988 26 p Presented at the 10th South Pacific Electrical International Convention, Brisbane, Australia, 2-5 May 1988; sponsored by the Electrical Development Association of Queensland, Inc.

20 SPACECRAFT PROPULSION AND POWER

(NASA-TM-101974; E-4674; NAS 1.15:101974) Avail: NTIS HC A03/MF A01 CSCL 10/2

The United States has embarked on a major development program to have a space station operating in low earth orbit by the mid-1990s. This endeavor draws on the talents of NASA and most of the aerospace firms in the U.S. Plans are being pursued to include the participation of Canada, Japan, and the European Space Agency in the space station. From the start of the program there was a focus on the utilization of the space station for science, technology, and commercial endeavors. These requirements were utilized in the design of the station and manifest themselves in: pressurized volume; crew time; power availability and level of power; external payload accommodations; microgravity levels; servicing facilities; and the ability to grow and evolve the space station to meet future needs. President Reagan directed NASA to develop a permanently manned space station in his 1984 State of the Union message. Since then the definition phase was completed and the development phase initiated. A major subsystem of the space station is its 75 kW electric power system. The electric power system has characteristics similar to those of terrestrial power systems. Routine maintenance and replacement of failed equipment must be accomplished safely and easily and in a minimum time while providing reliable power to users. Because of the very high value placed on crew time it is essential that the power system operate in an autonomous mode to minimize crew time required. The power system design must also easily accommodate growth as the power demands by users are expected to grow. An overview of the U.S. space station is provided with special emphasis on its electrical power system. Author

N90-14278* Rocket Research Corp., Redmond, WA.
ARCJET THRUSTER RESEARCH AND TECHNOLOGY. PHASE 1: EXECUTIVE SUMMARY
10 Aug. 1987 31 p
(Contract NAS3-24631)
(NASA-CR-182106; NAS 1.26:182106) Avail: NTIS HC A03/MF A01 CSCL 21/8

The principal objective of this two phase program is to conduct the development research required to make the low power arcjet a flight ready technology. Many important results were obtained during Phase 1 to move closer to this objective. Fundamental analyses were performed of the arcjet nozzle, the gas kinetic reaction effects, the thermal environment, and the arc stabilizing vortex. These aided the conceptual understanding of the arcjet and guided design work. A hydrazine (N₂H₄) arcjet was designed that combined a flight qualified catalyst bed with a modular arcjet. Extensive testing was performed which demonstrated the feasibility of using this propellant in an arcjet for the first time. Startup techniques were developed, stability maintained, material compatibility tests conducted, and performance mapping tests performed. Specific impulse values from 400 to 730 seconds were produced with a non-optimized design. These levels are higher than were originally thought possible and proved that extremely high enthalpy values can be obtained with constricted arc technology. Erosion rate data are promising for lifetime extensions to meet flight application requirements. Power control unit (PCU) development was started with the design and fabrication of a laboratory high switching frequency supply. Valuable data were obtained on PCU operation and on the interaction with the dynamic arc. Phase 2 efforts presently underway are resolving key issues for multi-hundred hour lifetimes, are continuing to investigate arcjet/PCU interactions, and will demonstrate duty cycle N₂H₄ arcjet/PCU operation in a simulated flight mode for lifetimes consistent with initial applications. Author

N90-14279*# Toledo Univ., OH. Dept. of Electrical Engineering.
ELECTRICAL PERFORMANCE CHARACTERISTICS OF HIGH POWER CONVERTERS FOR SPACE POWER APPLICATIONS Final Report, 1 Jan. 1988 - 30 Sep. 1989
THOMAS A. STUART and ROGER J. KING Sep. 1989 149 p
(Contract NAG3-708)

(NASA-CR-185947; NAS 1.26:185947) Avail: NTIS HC A07/MF A01 CSCL 10/2

The first goal of this project was to investigate various converters that would be suitable for processing electric power derived from a nuclear reactor. The implementation is indicated of a 20 kHz system that includes a source converter, a ballast converter, and a fixed frequency converter for generating the 20 kHz output. This system can be converted to dc simply by removing the fixed frequency converter. This present study emphasized the design and testing of the source and ballast converters. A push-pull current-fed (PPCF) design was selected for the source converter, and a 2.7 kW version of this was implemented using three 900 watt modules in parallel. The characteristic equation for two converters in parallel was derived, but this analysis did not yield any experimental methods for measuring relative stability. The three source modules were first tested individually and then in parallel as a 2.7 kW system. All tests proved to be satisfactory; the system was stable; efficiency and regulation were acceptable; and the system was fault tolerant. The design of a ballast-load converter, which was operated as a shunt regulator, was investigated. The proposed power circuit is suitable for use with BJTs because proportional base drive is easily implemented. A control circuit which minimizes switching frequency ripple and automatically bypasses a faulty shunt section was developed. A nonlinear state-space-averaged model of the shunt regulator was developed and shown to produce an accurate incremental (small-signal) dynamic model, even though the usual state-space-averaging assumptions were not met. The nonlinear model was also shown to be useful for large-signal dynamic simulation using PSpice. Author

N90-14281*# ENTECH Corp., Dallas-Fort Worth Airport, TX.
CONCEPTUAL DESIGN STUDY OF A 5 KILOWATT SOLAR DYNAMIC BRAYTON POWER SYSTEM USING A DOME FRESNEL LENS SOLAR CONCENTRATOR Final Report
MARK J. ONEILL, A. J. MCDANAL, and DON H. SPEARS Dec. 1989 48 p
(Contract NAS3-24877)
(NASA-CR-185134; NAS 1.26:185134) Avail: NTIS HC A03/MF A01 CSCL 10/2

The primary project objective was to generate a conceptual design for a nominal 5 kW solar dynamic space power system, which uses a unique, patented, transmittance-optimized, dome-shaped, point-focus Fresnel lens as the optical concentrator. Compared to reflective concentrators, the dome lens allows 200 times larger slope errors for the same image displacement. Additionally, the dome lens allows the energy receiver, the power conversion unit (PCU), and the heat rejection radiator to be independently optimized in configuration and orientation, since none of these elements causes any aperture blockage. Based on optical and thermal trade studies, a 6.6 m diameter lens with a focal length of 7.2 m was selected. This lens should provide 87 percent net optical efficiency at 800X geometric concentration ratio. The large lens is comprised of 24 gores, which compactly stow together during launch, and automatically deploy on orbit. The total mass of the microglass lens panels, the graphite/epoxy support structure, and miscellaneous hardware is about 1.2 kg per square meter of aperture. The key problem for the dome lens approach relates to the selection of a space-durable lens material. For the first time, all-glass Fresnel lens samples were successfully made by a sol-gel casting process. Author

N90-14283*# National Aeronautics and Space Administration. Lewis Research Center, Cleveland, OH.
A HEAT RECEIVER DESIGN FOR SOLAR DYNAMIC SPACE POWER SYSTEMS
KARL W. BAKER, MILES O. DUSTIN, and ROGER CRANE (University of South Florida, Tampa.) 1990 7 p Prepared for presentation at the 1990 International Solar Energy Conference, Miami, FL, 1-4 Apr. 1990; sponsored by ASME
(NASA-TM-102473; E-5253; NAS 1.15:102473) Avail: NTIS HC A02/MF A01 CSCL 10/2

An advanced heat pipe receiver designed for a solar dynamic

space power system is described. The power system consists of a solar concentrator, solar heat receiver, Stirling heat engine, linear alternator and waste heat radiator. The solar concentrator focuses the sun's energy into a heat receiver. The engine and alternator convert a portion of this energy to electric power and the remaining heat is rejected by a waste heat radiator. Primary liquid metal heat pipes transport heat energy to the Stirling engine. Thermal energy storage allows this power system to operate during the shade portion of an orbit. Lithium fluoride/calcium fluoride eutectic is the thermal energy storage material. Thermal energy storage canisters are attached to the midsection of each heat pipe. The primary heat pipes pass through a secondary vapor cavity heat pipe near the engine and receiver interface. The secondary vapor cavity heat pipe serves three important functions. First, it smooths out hot spots in the solar cavity and provides even distribution of heat to the engine. Second, the event of a heat pipe failure, the secondary heat pipe cavity can efficiently transfer heat from other operating primary heat pipes to the engine heat exchanger of the defunct heat pipe. Third, the secondary heat pipe vapor cavity reduces temperature drops caused by heat flow into the engine. This unique design provides a high level of reliability and performance. Author

N90-14284*# National Aeronautics and Space Administration. Lewis Research Center, Cleveland, OH.
ATOMIC HYDROGEN AS A LAUNCH VEHICLE PROPELLANT
 BRYAN A. PALASZEWSKI 1990 12 p Presented at the 28th Aerospace Sciences Meeting, Reno, NV, 8-11 Jan. 1990; sponsored by AIAA
 (NASA-TM-102459; E-5246; NAS 1.15:102459; AIAA-90-0715)
 Avail: NTIS HC A03/MF A01 CSCL 21/9

An analysis of several atomic hydrogen launch vehicles was conducted. A discussion of the facilities and the technologies that would be needed for these vehicles is also presented. The Gross Liftoff Weights (GLOW) for two systems were estimated; their specific impulses (I_{sp}) were 750 and 1500 lb(sub f)/s/lb(sub m). The atomic hydrogen launch vehicles were also compared to the currently planned Advanced Launch System design concepts. Very significant GLOW reductions of 52 to 58 percent are possible over the Advanced Launch System designs. Applying atomic hydrogen propellants to upper stages was also considered. Very high I_{sp} (greater than 750 lb(sub f)/s/lb(sub m)) is needed to enable a mass savings over advanced oxygen/hydrogen propulsion. Associated with the potential benefits of high I_{sp} atomic hydrogen are several challenging problems. Very high magnetic fields are required to maintain the atomic hydrogen in a solid hydrogen matrix. The magnetic field strength was estimated to be 30 kilogauss (3 Tesla). Also the storage temperature of the propellant is 4 K. This very low temperature will require a large refrigeration facility for the launch vehicle. The design considerations for a very high recombination rate for the propellant are also discussed. A recombination rate of 210 cm/s is predicted for atomic hydrogen. This high recombination rate can produce very high acceleration for the launch vehicle. Unique insulation or segmentation to inhibit the propellant may be needed to reduce its recombination rate. Author

N90-14285*# National Aeronautics and Space Administration. Lewis Research Center, Cleveland, OH.
ON PROTECTION OF FREEDOM'S SOLAR DYNAMIC RADIATOR FROM THE ORBITAL DEBRIS ENVIRONMENT.
PART 1: PRELIMINARY ANALYSES AND TESTING
 JENNIFER L. RHATIGAN, ERIC L. CHRISTIANSEN, and MICHAEL L. FLEMING (LTV Missiles and Electronics Group, Dallas, TX.) 1990 10 p Prepared for presentation at the International Solar Energy Conference, Miami, FL, 1-4 Apr. 1990; sponsored by ASME
 (NASA-TM-102458; E-5245; NAS 1.15:102458) Avail: NTIS HC A02/MF A01 CSCL 10/2

A great deal of experimentation and analysis was performed to quantify penetration thresholds of components which will experience orbital debris impacts. Penetration was found to depend upon mission specific parameters such as orbital altitude,

inclination, and orientation of the component; and upon component specific parameters such as material, density and the geometry particular to its shielding. Experimental results are highly dependent upon shield configuration and cannot be extrapolated with confidence to alternate shield configurations. Also, current experimental capabilities are limited to velocities which only approach the lower limit of predicted orbital debris velocities. Therefore, prediction of the penetrating particle size for a particular component having a complex geometry remains highly uncertain. An approach is described which was developed to assess on-orbit survivability of the solar dynamic radiator due to micrometeoroid and space debris impacts. Preliminary analyses are presented to quantify the solar dynamic radiator survivability, and include the type of particle and particle population expected to defeat the radiator bumpering (i.e., penetrate a fluid flow tube). Results of preliminary hypervelocity impact testing performed on radiator panel samples (in the 6 to 7 km/sec velocity range) are also presented. Plans for further analyses and testing are discussed. These efforts are expected to lead to a radiator design which will perform to requirements over the expected lifetime. Author

N90-15130*# National Aeronautics and Space Administration. Lewis Research Center, Cleveland, OH.
EXTENDED TEMPERATURE RANGE ROCKET INJECTOR Patent Application
 STEVEN J. SCHNEIDER, inventor (to NASA) 30 Nov. 1989 9 p
 (NASA-CASE-LEW-14846-1; NAS 1.71:LEW-14846-1; US-PATENT-APPL-SN-443523) Avail: NTIS HC A02/MF A01 CSCL 21/8

A rocket injector is provided with multiple sets of manifolds for supplying propellants to injector elements. Sensors transmit the temperatures of the propellants to a suitable controller which is operably connected to valves between these manifolds and propellant storage tanks. When cryogenic propellant temperatures are sensed only a portion of the valves are opened to furnish propellants to some of the manifolds. When lower temperatures are sensed additional valves are opened to furnish propellants to more of the manifolds. NASA

N90-15992*# National Aeronautics and Space Administration. Lewis Research Center, Cleveland, OH.
DESIGN OF A THRUST STAND FOR HIGH POWER ELECTRIC PROPULSION DEVICES
 THOMAS W. HAAG 1989 15 p Presented at the 25th Joint Propulsion Conference, Monterey, CA, 10-14 Jul. 1989; sponsored by AIAA, ASEE, ASME and SAE Previously announced in IAA as A89-47110
 (NASA-TM-102372; E-5104; NAS 1.15:102372; AIAA-89-2829)
 Avail: NTIS HC A03/MF A01 CSCL 21/3

A thrust stand for use with high power electric propulsion devices was designed and tested. The thrust stand was specifically tailored to the needs of a 100 to 250 kW magnetoplasmadynamic (MPD) thruster program currently in progress at the NASA Lewis Research Center. The thrust stand structure was built as an inverted pendulum arrangement, supported at the base by water-cooled electrical power flexures. Thrust stand tares due to thruster discharge current were demonstrated to be negligible. Tares due to an applied field magnet current, after considerable effort, were reduced to less than 3.0 percent of measured thrust. These tares, however, could be determined independently and subtracted from the indicated thrust measurement. A detailed description is given for the thrust stand design and operation with a 100 kW class MPD device. Other thrust stand tares due to vibration and thermal effects are discussed, along with issues of accuracy and repeatability. Author

N90-15996*# Little (Arthur D.), Inc., Cambridge, MA.
CONCEPTUAL DESIGN OF A MOVING BELT RADIATOR SHUTTLE-ATTACHED EXPERIMENTS: TECHNICAL REQUIREMENT DOCUMENT
 JERRY L. AGUILAR Nov. 1989 63 p

20 SPACECRAFT PROPULSION AND POWER

(Contract NAS3-25356)

(NASA-CR-185168; NAS 1.26:185168) Avail: NTIS HC A04/MF A01 CSCL 10/2

The technical requirements for a shuttle-attached Moving Belt Radiator (MBR) experiment are defined. The MBR is an advanced radiator concept in which a rotating belt radiates thermal energy to space. The requirements for integrating the MBR experiment in the shuttle bay are discussed. Requirements for the belt material and working fluid are outlined along with some possible options. The proposed size and relationship to a full scale Moving Belt Radiator are defined. The experiment is defined with the primary goal of dynamic testing and a secondary goal of demonstrating the sealing and heat transfer characteristics. A perturbation system which will simulate a docking maneuver or other type of short term acceleration is proposed for inclusion in the experimental apparatus. A deployment and retraction capability which will aid in evaluating the dynamics of a belt during such a maneuver is also described. The proposed test sequence for the experiment is presented. Details of the conceptual design are not presented herein, but rather in a separate Final Report. Author

N90-17677*# National Aeronautics and Space Administration. Lewis Research Center, Cleveland, OH.

PRELIMINARY EVALUATION OF SPACE STATION TRANSMISSION LINE IN A RING CONFIGURATION

MARY ELLEN ROTH Jan. 1990 7 p

(NASA-TM-102461; E-5248; NAS 1.15:102461) Avail: NTIS HC A02/MF A01 CSCL 10/2

The results of a preliminary evaluation of a space station type transmission line and commercial transmission lines in a ring configuration, are reported. In a ring configuration, each node has two paths for the return current of each wire. The additional path can create an unbalanced condition, where the magnetic fields created by the forward and return currents do not cancel. This evaluation was to quantify the effects of the unbalanced case upon the external fields. The transmission lines evaluated were standard commercial coaxial cables, RG59 and RG213, and a space station designed flat Litz transmission line. Each was evaluated in a balanced and unbalanced mode of operation. Currents and their harmonic content were recorded and compared. As expected, the harmonic content of the different current (I_{Δ}) was substantial for the unbalanced case as compared to the balanced case. For the balanced case, very little difference was noted among the various transmission lines evaluated. The evaluation is discussed, and the test circuit, the measurements, and the resulting data are described. Author

N90-17681*# National Aeronautics and Space Administration. Lewis Research Center, Cleveland, OH.

TOWARD AN ELECTRICAL POWER UTILITY FOR SPACE EXPLORATION

ROBERT W. BERCAW In ESA, European Space Power, Volume 1 p 19-22 Aug. 1989 Previously announced as N89-27704

Copyright Avail: NTIS HC A19/MF A03 CSCL 10/2

Future electrical power requirements for space exploration are discussed. Megawatts of power with enough reliability for multi-year missions and with enough flexibility to adapt to needs unanticipated at design time are some of the criteria which space power systems must be able to meet. The reasons for considering the power management and distribution in the various systems, from a total mission perspective rather than simply extrapolating current spacecraft design practice, are discussed. A utility approach to electric power integrating requirements from a broad selection of current development programs, with studies in which both space and terrestrial technologies are conceptually applied to exploration mission scenarios, is described. ESA

N90-17695*# National Aeronautics and Space Administration. Lewis Research Center, Cleveland, OH.

CHALLENGES FOR FUTURE SPACE POWER SYSTEMS

HENRY W. BRANDHORST, JR. In ESA, European Space Power, Volume 1 p 133-136 Aug. 1989 Previously announced as

N89-25506

Copyright Avail: NTIS HC A19/MF A03 CSCL 10/2

Forecasts of space power needs are presented. The needs fall into three broad categories: survival, self-sufficiency, and industrialization. The cost of delivering payloads to orbital locations and from Low Earth Orbit (LEO) to Mars are determined. Future launch cost reductions are predicted. From these projections the performances necessary for future solar and nuclear space power options are identified. The availability of plentiful cost effective electric power and of low cost access to space are identified as crucial factors in the future extension of human presence in space. ESA

N90-17708*# National Aeronautics and Space Administration. Lewis Research Center, Cleveland, OH.

REGENERATIVE FUEL CELL SYSTEMS FOR PROJECT PATHFINDER

J. R. HUFF, J. HEDSTROM, N. E. VANDERBORGH (Los Alamos National Lab., NM.), and P. PROKOPIUS In ESA, European Space Power, Volume 1 p 217-219 Aug. 1989

Copyright Avail: NTIS HC A19/MF A03 CSCL 10/2

The objectives of a surface power program, an element of the exploration thrust of the Pathfinder project, and plans for meeting them are outlined. Technological assessment and tradeoff studies of fuel cell and electrolyzer technologies suitable for use in a regenerative fuel cell are described. The viability of proton exchange membranes (PEM) in meeting the system requirements is discussed. ESA

N90-17775*# National Aeronautics and Space Administration. Lewis Research Center, Cleveland, OH.

NASA ADVANCED SPACE PHOTOVOLTAIC TECHNOLOGY: STATUS, POTENTIAL AND FUTURE MISSION APPLICATIONS

DENNIS J. FLOOD, MICHAEL PISZCZOR, JR., PAUL M. STELLA, and GARY L. BENNETT In ESA, European Space Power, Volume 2 p 643-646 Aug. 1989 Prepared in cooperation with JPL/CALTECH, Pasadena, CA and NASA, Washington

Copyright Avail: NTIS HC A16/MF A03 CSCL 10/2

The long term goals of the NASA program in space photovoltaic research are presented. The long range goals are to develop technology capable of achieving 300 W/kg for planar arrays and 300 W per sq m for concentrator arrays. InP and GaAs planar and concentrator cell research projects are described. The near term program of developing the Advanced Photovoltaic Solar Array (APSA) intended to produce 130 W/kg using thin (62 micron) silicon cells, is described. Ways in which this program will provide a baseline for development of 300 W/kg arrays are described. ESA

N90-17794*# National Aeronautics and Space Administration. Lewis Research Center, Cleveland, OH.

ON-ORBIT RESULTS OF THE LIPS 3/INP HOMOJUNCTION SOLAR CELL EXPERIMENT

DAVID J. BRINKER In ESA, European Space Power, Volume 2 p 759-764 Aug. 1989 Previously announced as N89-26292

Copyright Avail: NTIS HC A16/MF A03 CSCL 10/2

The flight performance of the NASA indium phosphide homojunction cell module on the LIPS 3 satellite is presented. The experimental objective was to measure the InP cell performance in the natural radiation environment in a circular 1100 km altitude orbit inclined 60 degrees. Flight data for the first year is close to expected values. No degradation in the short-circuit current is seen. Details of cell structure and flight module design are discussed. ESA

N90-18471*# National Aeronautics and Space Administration. Lewis Research Center, Cleveland, OH.

THE PATHFINDER CHEMICAL TRANSFER PROPULSION PROGRAM

NED P. HANNUM, FRANK D. BERKOPEC, and ROBERT L. ZURAWSKI (National Aeronautics and Space Administration, Washington, DC.) In Johns Hopkins Univ., The 1989 JANNAP

Propulsion Meeting, Volume 1 p 191-197 May 1989 Previously announced as N89-24409

Avail: NTIS HC A25/MF A04 CSCL 21/8

Pathfinder is a research and technology initiative by the National Aeronautics and Space Administration (NASA) intended to strengthen the technology base of the United States civil space program in preparation for future space exploration missions. Pathfinder begins in FY-89. One of the four major thrusts is the Chemical Transfer Propulsion program which will provide the propulsion technology for high performance, liquid oxygen/liquid hydrogen expander cycle engines which are expected to be operated and maintained in space. These advanced engines will enhance or enable a variety of future space exploration missions. The goals and objectives, management, technical plan, and technology transfer for the Chemical Transfer Propulsion element of Pathfinder are described. Author

N90-18472*# National Aeronautics and Space Administration. Lewis Research Center, Cleveland, OH.

ADVANCED APS IMPACTS ON VEHICLE PAYLOADS

STEVEN J. SCHNEIDER and BRIAN D. REED In Johns Hopkins Univ., The 1989 JANNAF Propulsion Meeting, Volume 1 p 209-218 May 1989 Previously announced as N89-25254

Avail: NTIS HC A25/MF A04 CSCL 21/8

Advanced auxiliary propulsion system (APS) technology has the potential to both, increase the payload capability of earth-to-orbit (ETO) vehicles by reducing APS propellant mass, and simplify ground operations and logistics by reducing the number of fluids on the vehicle and eliminating toxic, corrosive propellants. The impact of integrated cryogenic APS on vehicle payloads is addressed. In this system, launch propulsion system residuals are scavenged from integral launch propulsion tanks for use in the APS. Sufficient propellant is preloaded into the APS to return to earth with margin and noncomplete scavenging assumed. No propellant conditioning is required by the APS, but ambient heat soak is accommodated. High temperature rocket materials enable the use of the unconditioned hydrogen/oxygen in the APS and are estimated to give APS rockets specific impulse of up to about 444 sec. The payload benefits are quantified and compared with an uprated monomethyl hydrazine/nitrogen tetroxide system in a conservative fashion, by assuming a 25.5 percent weight growth for the hydrogen/oxygen system and a 0 percent weight growth for the uprated system. The combination and scavenging and high performance gives payload impacts which are highly mission specific. A payload benefit of 861 kg (1898 lbm) was estimated for a Space Station Freedom rendezvous mission and 2099 kg (4626 lbm) for a sortie mission, with payload impacts varying with the amount of launch propulsion residual propellants. Missions without liquid propellant scavenging were estimated to have payload penalties, however, operational benefits were still possible.

Author

N90-18474*# National Aeronautics and Space Administration. Lewis Research Center, Cleveland, OH.

ELECTRIC PROPULSION OPTIONS FOR 10 KW CLASS EARTH-SPACE MISSIONS

M. J. PATTERSON and FRANCIS M. CURRAN In Johns Hopkins Univ., The 1989 JANNAF Propulsion Meeting, Volume 1 p 239-265 May 1989 Previously announced as N89-26906

Avail: NTIS HC A25/MF A04 CSCL 21/8

Five and 10 kW ion and arcjet propulsion system options for a near-term space demonstration experiment were evaluated. Analyses were conducted to determine first-order propulsion system performance and system component mass estimates. Overall mission performance of the electric propulsion systems was quantified in terms of the maximum thrusting time, total impulse, and velocity increment capability available when integrated onto a generic spacecraft under fixed mission model assumptions. Maximum available thrusting times for the ion-propelled spacecraft options, launched on a DELTA 2 6920 vehicle, range from approximately 8,600 hours for a 4-engine 10 kW system to more than 29,600 hours for a single-engine 5 kW system. Maximum total impulse values and maximum delta-v's range from 1.2x10

(exp 7) to 2.1x10 (exp 7) N-s, and 3550 to 6200 m/s, respectively. Maximum available thrusting times for the arcjet propelled spacecraft launched on the DELTA 2 6920 vehicle range from approximately 528 hours for the 6-engine 10 kW hydrazine system to 2328 hours for the single-engine 5 kW system. Maximum total impulse values and maximum delta-v's range from 2.2x10 (exp 6) to 3.6x10 (exp 6) N-s, and approximately 662 to 1072 m/s, respectively. Author

N90-18475*# National Aeronautics and Space Administration. Lewis Research Center, Cleveland, OH.

PERFORMANCE OF LARGE AREA XENON ION THRUSTERS FOR ORBIT TRANSFER MISSIONS

VINCENT K. RAWLIN In Johns Hopkins Univ., The 1989 JANNAF Propulsion Meeting, Volume 1 p 267-276 May 1989

Avail: NTIS HC A25/MF A04 CSCL 21/8

Studies have indicated that xenon ion propulsion systems can enable the use of smaller earth-launch vehicles for satellite placement which results in significant cost savings. These analyses have assumed the availability of advanced, high power ion thrusters operating at about 10 kW or higher. A program was initiated to explore the viability of operating 50 cm diameter ion thrusters at this power level. Operation with several discharge chamber and ion extraction grid set combinations was demonstrated and data were obtained at power levels to 16 kW. Fifty cm diameter thrusters using state of the art 30 cm diameter grids or advanced technology 50 cm diameter grids allow discharge power and beam current densities commensurate with long life at power levels up to 10 kW. In addition, 50 cm diameter thrusters are shown to have potential for growth in thrust and power levels beyond 10 kW. Author

N90-18476*# National Aeronautics and Space Administration. Lewis Research Center, Cleveland, OH.

TEST FACILITY AND PRELIMINARY PERFORMANCE OF A 100 KW CLASS MPD THRUSTER

J. S. SOVEY, M. A. MANTENIEKS, THOMAS W. HAAG, P. RAITANO, and J. E. PARKES (Sverdrup Technology, Inc., Cleveland, OH.) In Johns Hopkins Univ., The 1989 JANNAF Propulsion Meeting, Volume 1 p 325-338 May 1989 Previously announced as N89-23520

Avail: NTIS HC A25/MF A04 CSCL 21/8

A 260 kW magnetoplasmadynamic (MPD) thruster test facility was assembled and used to characterize thrusters at power levels up to 130 kW using argon and helium propellants. Sensitivities of discharge characteristics to arc current, mass flow rate, and applied magnetic field were investigated. A thermal efficiency correlation developed by others for low power MPD thrusters defined parametric guidelines to minimize electrode losses in MPD thrusters. Argon and helium results suggest that a parameter defined as the product of arc voltage and the square root of the mass flow rate must exceed 0.7 V/kg(sup 1/2)/sec(sup 1/2) in order to obtain thermal efficiencies in excess of 60 percent.

Author

N90-18477*# National Aeronautics and Space Administration. Lewis Research Center, Cleveland, OH.

ARCJET CATHODE PHENOMENA

FRANCIS M. CURRAN, THOMAS W. HAAG, and JOHN F. RAQUET (Air Force Academy, CO.) In Johns Hopkins Univ., The 1989 JANNAF Propulsion Meeting, Volume 1 p 349-366 May 1989 Previously announced as N89-27121

Avail: NTIS HC A25/MF A04 CSCL 21/8

Cathode tips made from a number of different materials were tested in a modular arcjet thruster in order to examine cathode phenomena. Periodic disassembly and examination, along with the data collected during testing, indicated that all of the tungsten-based materials behaved similarly despite the fact that in one of these samples the percentage of thorium oxide was doubled and another was 25 percent rhenium. The mass loss rate from a 2 percent thoriated rhenium cathode was found to be an order of magnitude greater than that observed using 2 percent thoriated tungsten. Detailed analysis of one of these cathode tips

20 SPACECRAFT PROPULSION AND POWER

showed that the molten crater contained pure tungsten to a depth of about 150 microns. Problems with thermal stress cracking were encountered in the testing of a hafnium carbide tip. Post test analysis showed that the active area of the tip had chemically reacted with the propellant. A 100 hour continuous test was run at about 1 kW. Post test analysis revealed no dendrite formation, such as observed in a 30 kW arcjet lifetest, near the cathode crater. The cathodes from both this test and a previously run 1000 hour cycled test displayed nearly identical arc craters. Data and calculations indicate that the mass losses observed in testing can be explained by evaporation. Author

N90-18478*# National Aeronautics and Space Administration. Lewis Research Center, Cleveland, OH.

ARCJET NOZZLE DESIGN IMPACTS

FRANCIS M. CURRAN, AMY J. SOVIE (Ohio Univ., Athens.), and THOMAS W. HAAG /in Johns Hopkins Univ., The 1989 JANNAF Propulsion Meeting, Volume 1 p 367-380 May 1989 Previously announced as N89-23522

Avail: NTIS HC A25/MF A04 CSCL 21/8

The effect of nozzle configuration on the operating characteristics of a low power dc arcjet thruster was determined. A conical nozzle with a 30 deg converging angle, a 20 deg diverging angle, and an area ratio of 225 served as the baseline case. Variations on the geometry included bell-shaped contours both up and downstream, and a downstream trumpet-shaped contour. The nozzles were operated over a range of specific power near that anticipated for on-orbit operation. Mass flow rate, thrust, current, and voltage were monitored to provide accurate comparisons between nozzles. The upstream contour was found to have minimal effect on arcjet operation. It was determined that the contour of the divergent section of the nozzle, that serves as the anode, was very important in determining the location of arc attachment, and thus had a significant impact on arcjet performance. The conical nozzle was judged to have the optimal current/voltage characteristics and produced the best performance of the nozzles tested. Author

N90-19299*# National Aeronautics and Space Administration. Lewis Research Center, Cleveland, OH.

AEOLIAN REMOVAL OF DUST FROM PHOTOVOLTAIC SURFACES ON MARS

JAMES R. GAIER, MARLA E. PEREZ-DAVIS, and MARK MARABITO (Cleveland State Univ., OH.) Feb. 1990 19 p (NASA-TM-102507; E-5309; NAS 1.15:102507) Avail: NTIS HC A03/MF A01 CSCL 10/1

It is well documented that Mars is totally engulfed in huge dust storms nearly each Martian year. Dust elevated in these global dust storms, or in any of the numerous local dust storms could settle on photovoltaic surfaces and seriously hamper photovoltaic power system performance. Using a recently developed technique to uniformly dust simulated photovoltaic surfaces, samples were subjected to Martian-like winds in an attempt to determine whether natural aeolian processes on Mars would sweep off the settled dust. The effects of wind velocity, angle of attack, height off the Martian surface, and surface coating material were investigated. Principles which can help to guide the design of photovoltaic arrays bound for the Martian surface were uncovered. Most importantly, arrays mounted with an angle of attack approaching 45 deg show the most efficient clearing. Although the angular dependence is not sharp, horizontally mounted arrays required significantly higher wind velocities to clear off the dust. From the perspective of dust-clearing it appears that the arrays may be erected quite near the ground, but previous studies have suggested that saltation effects can be expected to cause such arrays to be covered by sand if they are set up less than about a meter from the ground. Providing that the surface chemistry of Martian dusts is comparable to our test dust, the materials used for protective coating may be optimized for other considerations such as transparency, and chemical or abrasion resistance. The static threshold velocity is low enough that there are regions on Mars which experience winds strong enough to clear off a photovoltaic array if it is properly

oriented. Turbulence fences proved to be an ineffective strategy to keep dust cleared from the photovoltaic surfaces. Author

N90-21108*# Texas A&M Univ., College Station. Dept. of Nuclear Engineering.

A RADIOLOGICAL ASSESSMENT OF NUCLEAR POWER AND PROPULSION OPERATIONS NEAR SPACE STATION

FREEDOM Contract Report, Jan. 1988 - Jan. 1990

WESLEY E. BOLCH, J. KELLY THOMAS, K. LEE PEDDICORD, PAUL NELSON, DAVID T. MARSHALL, and DONNA M. BUSCHE Mar. 1990 115 p (Contract NAG3-944) (NASA-CR-185185; NAS 1.26:185185) Avail: NTIS HC A06/MF A01 CSCL 10/2

Scenarios were identified which involve the use of nuclear power systems in the vicinity of Space Station Freedom (SSF) and their radiological impact on the SSF crew was quantified. Several of the developed scenarios relate to the use of SSF as an evolutionary transportation node for lunar and Mars missions. In particular, radiation doses delivered to SSF crew were calculated for both the launch and subsequent return of a Nuclear Electric Propulsion (NEP) cargo vehicle and a Nuclear Thermal Rocket (NTR) personnel vehicle to low earth orbit. The use of nuclear power on co-orbiting platforms and the storage and handling issues associated with radioisotope power systems were also explored as they relate to SSF. A central philosophy in these analyses was the utilization of a radiation dose budget, defined as the difference between recommended dose limits from all radiation sources and estimated doses received by crew members from natural space radiations. Consequently, for each scenario examined, the dose budget concept was used to identify and quantify constraints on operational parameters such as launch separation distances, returned vehicle parking distances, and reactor shutdown times prior to vehicle approach. The results indicate that realistic scenarios do not exist which would preclude the use of nuclear power sources in the vicinity of SSF. The radiation dose to the SSF crew can be maintained at safe levels solely by implementing proper and reasonable operating procedures. Author

N90-21109*# Ohio State Univ., Columbus. Dept. of Aeronautical and Astronautical Engineering.

THE EFFECTS OF MAGNETIC NOZZLE CONFIGURATIONS ON PLASMA THRUSTERS Semiannual Progress Report, 1 Jul. - 31 Dec. 1989

THOMAS M. YORK Feb. 1990 71 p

(Contract NAG3-843)

(NASA-CR-186465; NAS 1.26:186465; AARL-P-90-1) Avail: NTIS HC A04/MF A01 CSCL 21/3

Plasma thrusters have been operated at power levels from 10 kw to 0.1 MW. When these devices have had magnetic fields applied to them which form a nozzle configuration for the expanding plasma, they have shown marked increases in exhaust velocity which is in direct proportion to the magnitude of the applied field. Further, recent results have shown that electrode erosion may be influenced by applied magnetic fields. This research effort is directed to the experimental and computational study of the effects of applied magnetic field nozzles in the acceleration of plasma flows. Plasma source devices which eliminate the plasma interaction in normal thrusters are studied as most basic. Normal thruster configurations were studied without applied fields and with applied magnetic nozzle fields. Unique computational studies utilize existing codes which accurately include transport processes. Unique diagnostic studies supported the experimental studies to generate new data. Both computation and diagnostics were combined to indicate the physical mechanisms and transport properties that are operative in order to allow scaling and accurate prediction of thruster performance. Author

N90-21110*# National Aeronautics and Space Administration. Lewis Research Center, Cleveland, OH.

THE EFFECT OF LEVELING COATINGS ON THE ATOMIC OXYGEN DURABILITY OF SOLAR CONCENTRATOR SURFACES

KIM K. DEGROH, THERESE M. DEVER, and WILLIAM F. QUINN (Cleveland State Univ., OH.) Apr. 1990 18 p Presented at the 8th International Conference on Thin Films, and the 17th International Conference on Metallurgical Coatings, San Diego, CA, 2-6 Apr. 1990; spon. in part by Intern. Union for Vacuum Sci., Tech., and Appl. and the Amer. Vacuum Society (NASA-TM-102557; E-5375; NAS 1.15:102557) Avail: NTIS HC A03/MF A01 CSCL 10/1

Space power systems for Space Station Freedom will be exposed to the harsh environment of low earth orbit (LEO). Neutral atomic oxygen is the major constituent in LEO and has the potential of severely reducing the efficiency of solar dynamic power systems through degradation of the concentrator surfaces. Several transparent dielectric thin films have been found to provide atomic oxygen protection, but atomic oxygen undercutting at inherent defect sites is still a threat to solar dynamic power system survivability. Leveling coatings smooth microscopically rough surfaces, thus eliminating potential defect sites prone to oxidation attack on concentrator surfaces. The ability of leveling coatings to improve the atomic oxygen durability of concentrator surfaces was investigated. The application of a EPO-TEK 377 epoxy leveling coating on a graphite epoxy substrate resulted in an increase in solar specular reflectance, a decrease in the atomic oxygen defect density by an order of magnitude and a corresponding order of magnitude decrease in the percent loss of specular reflectance during atomic oxygen plasma ashing. Author

N90-21113*# Toledo Univ., OH. Dept. of Electrical Engineering.

A COMPARATIVE STUDY OF ELECTRIC POWER DISTRIBUTION SYSTEMS FOR SPACECRAFT Final Report, 19 Jun. - 31 Dec. 1989

THOMAS A. STUART and ROGER J. KING Jan. 1990 134 p (Contract NAG3-708) (NASA-CR-186531; NAS 1.26:186531) Avail: NTIS HC A07/MF A01 CSCL 22/2

The electric power distribution systems for spacecraft are compared concentrating on two interrelated issues: the choice between dc and high frequency ac, and the converter/inverter topology to be used at the power source. The relative merits of dc and ac distribution are discussed. Specific converter and inverter topologies are identified and analyzed in detail for the purpose of detailed comparison. Finally, specific topologies are recommended for use in dc and ac systems. Author

N90-21114*# National Aeronautics and Space Administration. Lewis Research Center, Cleveland, OH.

RECENT STIRLING ENGINE LOSS-UNDERSTANDING RESULTS

ROY C. TEW, LANNY G. THIEME, and JAMES E. DUDENHOEFER 1990 11 p Prepared for presentation at the 25th Intersociety Energy Conversion Engineering Conference, Reno, NV, 12-17 Aug. 1990; sponsored in part by AIChE, SAE, ACS, AIAA, ASME, and IEEE (NASA-TM-103122; E-5450; NAS 1.15:103122) Avail: NTIS HC A03/MF A01 CSCL 10/2

For several years, NASA and other U.S. government agencies have been funding experimental and analytical efforts to improve the understanding of Stirling thermodynamic losses. NASA's objective is to improve Stirling engine design capability to support the development of new engines for space power. An overview of these efforts was last given at the 1988 IECEC. Recent results of this research are reviewed. Author

N90-21116*# National Aeronautics and Space Administration. Lewis Research Center, Cleveland, OH.

EFFECT OF KOH CONCENTRATION ON LEO CYCLE LIFE OF IPV NICKEL-HYDROGEN FLIGHT BATTERY CELLS

JOHN J. SMITHRICK and STEPHEN W. HALL (Naval Weapons Support Center, Crane, IN.) 1990 8 p Proposed for presentation at the 25th Intersociety Energy Conversion Engineering Conference, Reno, NV, 12-17 Aug. 1990; cosponsored by AIChE, SAE, ACS,

AIAA, ASME, IEEE

(NASA-TM-103127; E-5457; NAS 1.15:103127) Avail: NTIS HC A02/MF A01 CSCL 10/3

A breakthrough in low earth orbit (LEO) cycle life of individual pressure vessel (IPV) nickel hydrogen battery cells was reported. The cycle life of boiler plate cells containing 26 percent potassium hydroxide (KOH) electrolyte was about 40,000 LEO cycles compared to 3500 cycles for cells containing 31 percent KOH. The effect of KOH concentration on cycle life was studied. The cycle regime was a stressful accelerated LEO, which consisted of a 27.5 min charge followed by a 17.5 min charge (2 x normal rate). The depth of discharge (DOD) was 80 percent. The cell temperature was maintained at 23 C. The next step is to validate these results using flight hardware and a real time LEO test. NASA Lewis has a contract with the Naval Weapons Support Center (NWSC), Crane, Indiana, to validate the boiler plate test results. Six 48 A-hr Hughes recirculation design IPV nickel-hydrogen flight battery cells are being evaluated. Three of the cells contain 26 percent KOH (test cells) and three contain 31 percent KOH (control cells). They are undergoing real time LEO cycle life testing. The cycle regime is a 90-min LEO orbit consisting of a 54-min charge followed by a 36-min discharge. The depth-of-discharge is 80 percent. The cell temperature is maintained at 10 C. The cells were cycled for over 8000 cycles in the continuing test. There were no failures for the cells containing 26 percent KOH. There was two failures, however, for the cells containing 31 percent KOH. Author

N90-21795*# National Aeronautics and Space Administration. Lewis Research Center, Cleveland, OH.

FREE-SPACE POWER TRANSMISSION

Washington Nov. 1989 189 p Workshop held in Cleveland, OH, 29-30 Mar. 1988 (NASA-CP-10016; E-4161; NAS 1.55:10016) Avail: NTIS HC A09/MF A02 CSCL 10/2

NASA Lewis Research Center organized a workshop on technology availability for free-space power transmission (beam power). This document contains a collection of viewgraph presentations that describes the effort by academia, industry, and the national laboratories in the area of high-frequency, high-power technology applicable to free-space power transmission systems. The areas covered were rectenna technology, high-frequency, high-power generation (gyrotrons, solar pumped lasers, and free electron lasers), and antenna technology.

N90-21806*# Large Scale Programs Inst., Austin, TX.

A SUPERCONDUCTING QUENCHGUN FOR DELIVERING LUNAR DERIVED OXYGEN TO LUNAR ORBIT Final Report

NATHAN NOTTKE and CURT R. BILBY Apr. 1990 51 p (Contract NAG3-928) (NASA-CR-185161; NAS 1.26:185161; LSPI-901) Avail: NTIS HC A04/MF A01 CSCL 22/4

The development of a parametric model for a superconducting quenchgun for launching lunar derived liquid oxygen to lunar orbit is detailed. An overview is presented of the quenchgun geometry and operating principles, a definition of the required support systems, and the methods used to size the quenchgun launcher and support systems. An analysis assessing the impact of a lunar quenchgun on the OEXP Lunar Evolution Case Study is included. Author

N90-21807*# Large Scale Programs Inst., Austin, TX.

A TRAJECTORY GENERATION AND SYSTEM CHARACTERIZATION MODEL FOR CISLUNAR LOW-THRUST SPACECRAFT. VOLUME 2: TECHNICAL MANUAL

DAVID J. KORSMEYER, ELFEGO PINON, III, BRENDAN M. OCONNOR, and CURT R. BILBY May 1990 61 p (Contract NAG3-928) (NASA-CR-185172; NAS 1.26:185172; LSPI-903) Avail: NTIS HC A04/MF A01 CSCL 21/8

The documentation of the Trajectory Generation and System Characterization Model for the Cislunar Low-Thrust Spacecraft is presented in Technical and User's Manuals. The system

20 SPACECRAFT PROPULSION AND POWER

characteristics and trajectories of low thrust nuclear electric propulsion spacecraft can be generated through the use of multiple system technology models coupled with a high fidelity trajectory generation routine. The Earth to Moon trajectories utilize near Earth orbital plane alignment, midcourse control dependent upon the spacecraft's Jacobian constant, and capture to target orbit utilizing velocity matching algorithms. The trajectory generation is performed in a perturbed two-body equinoctial formulation and the restricted three-body formulation. A single control is determined by the user for the interactive midcourse portion of the trajectory. The full spacecraft system characteristics and trajectory are provided as output.

Author

N90-21808* National Aeronautics and Space Administration. Lewis Research Center, Cleveland, OH.

EFFECT OF LEO CYCLING ON 125 AH ADVANCED DESIGN IPV NICKEL-HYDROGEN BATTERY CELLS

JOHN J. SMITHRICK and STEPHEN W. HALL (Naval Weapons Support Center, Crane, IN.) 1990 8 p Proposed for presentation at the 25th Intersociety Energy Conversion Engineering Conference, Reno, NV, 12-17 Aug. 1990; cosponsored by AIChE, SAE, ACS, AIAA, ASME, and IEEE
(NASA-TM-103128; E-5458; NAS 1.15:103128) Avail: NTIS HC A02/MF A01 CSCL 10/1

An advanced 125 Ah individual pressure vessel (IPV) nickel-hydrogen cell was designed. The primary function of the advanced cell, is to store and deliver energy for long term, low earth-orbit (LEO) spacecraft missions. The new features of this design are: (1) use of 26 percent rather than 31 percent potassium hydroxide (KOH) electrolyte, (2) use of a patented catalyzed wall wick, (3) use of serrated edge separators to facilitate gaseous oxygen and hydrogen flow within the cell, while still maintaining physical contact with the wall wick for electrolyte management, and (4) use of a floating rather than a fixed stack (state-of-the-art) to accommodate nickel electrode expansion. Six 125 Ah flight cells based on this design were fabricated by Eagle-Picher. Three of the cells contain all of the advanced features (test cells) and three are the same as the test cells except they don't have catalyst on the wall wick (control cells). All six cells are in the process of being evaluated in a LEO cycle life test. The cells have accumulated about 4700 LEO cycles (60 percent DOD 10 C). There have been no cell failures, the catalyzed wall wick cells however, are performing better.

Author

N90-21809* United Technologies Research Center, East Hartford, CT.

FRAMEWORK FOR A SPACE SHUTTLE MAIN ENGINE HEALTH MONITORING SYSTEM Final Report

MICHAEL W. HAWMAN, WILLIAM S. GALINAITIS, SHARAYU TULPUL, ANITA K. MATTEDI, and JEFFREY KAMENETZ (United Technologies Corp., Windsor Locks, CT.) May 1990 189 p (Contract NAS3-25626)
(NASA-CR-185224; NAS 1.26:185224; UTRC-R90-997978)
Avail: NTIS HC A09/MF A01 CSCL 21/8

A framework developed for a health management system (HMS) which is directed at improving the safety of operation of the Space Shuttle Main Engine (SSME) is summarized. An emphasis was placed on near term technology through requirements to use existing SSME instrumentation and to demonstrate the HMS during SSME ground tests within five years. The HMS framework was developed through an analysis of SSME failure modes, fault detection algorithms, sensor technologies, and hardware architectures. A key feature of the HMS framework design is that a clear path from the ground test system to a flight HMS was maintained. Fault detection techniques based on time series, nonlinear regression, and clustering algorithms were developed and demonstrated on data from SSME ground test failures. The fault detection algorithms exhibited 100 percent detection of faults, had an extremely low false alarm rate, and were robust to sensor loss. These algorithms were incorporated into a hierarchical decision making strategy for overall assessment of SSME health. A preliminary design for a hardware architecture capable of supporting real time operation of the HMS functions was developed.

Utilizing modular, commercial off-the-shelf components produced a reliable low cost design with the flexibility to incorporate advances in algorithm and sensor technology as they become available.

Author

N90-21812* National Aeronautics and Space Administration. Lewis Research Center, Cleveland, OH.

PHOTOVOLTAIC POWER FOR SPACE STATION FREEDOM

COSMO R. BARAONA 1990 8 p Presented at the 21st Photovoltaic Specialists Conference, Orlando, FL, 21-25 May 1990; sponsored by IEEE
(NASA-TM-102569; E-5391; NAS 1.15:102569) Avail: NTIS HC A02/MF A01 CSCL 10/2

Space Station Freedom is described with special attention given to its electric power system. The photovoltaic arrays, the battery energy storage system, and the power management, and distribution system are also discussed. The current design of Freedom's power system and the system requirements, trade studies, and competing factors which lead to system selections are referenced. This will be the largest power system ever flown in space. This system represents the culmination of many developments that have improved system performance, reduced cost, and improved reliability. Key developments and their evolution into the current space station solar array design are briefly described. The features of the solar cell and the array including the development, design, test, and flight hardware production status are given.

Author

N90-22604* National Aeronautics and Space Administration. Lewis Research Center, Cleveland, OH.

THE INTERNATIONAL SPACE UNIVERSITY

KENNETH J. DAVIDIAN 1990 11 p Presented at the 26th Joint Propulsion Conference, Orlando, FL, 16-18 Jul. 1990; cosponsored by AIAA, SAE, ASME, and ASEE
(NASA-TM-103163; E-5531; NAS 1.15:103163; AIAA-90-2389)
Avail: NTIS HC A03/MF A01 CSCL 22/1

The International Space University (ISU) was founded on the premise that any major space program in the future would require international cooperation as a necessary first step toward its successful completion. ISU is devoted to being a leading center for educating future authorities in the world space industry. ISU's background, goals, current form, and future plans are described. The results and benefits of the type of education and experience gained from ISU include technical reports describing the design projects undertaken by the students, an exposure to the many different disciplines which are a part of a large space project, an awareness of the existing activities from around the world in the space community, and an international professional network which spans all aspects of space activities and covers the globe.

Author

N90-22605* National Aeronautics and Space Administration. Lewis Research Center, Cleveland, OH.

COOLING OF ROCKET THRUST CHAMBERS WITH LIQUID OXYGEN

ELIZABETH S. ARMSTRONG and JULIE A. SCHLUMBERGER 1990 11 p Presented at the 26th Joint Propulsion Conference, Orlando, FL, 16-18 Jul. 1990; cosponsored by AIAA, SAE, ASME, and ASEE
(NASA-TM-103146; E-5498; NAS 1.15:103146; AIAA-90-2120)
Avail: NTIS HC A03/MF A01 CSCL 21/8

Rocket engines using high pressure liquid oxygen (LOX) and kerosene (RP-1) as the propellants have been considered for future launch vehicle propulsion. Generally, in regeneratively cooled engines, the fuel is used to cool the combustion chamber. However, hydrocarbons such as RP-1 are limited in their cooling capability at high temperatures and pressures. Therefore, LOX is being considered as an alternative coolant. However, there has been concern as to the effect on the integrity of the chamber liner if oxygen leaks into the combustion zone through fatigue cracks that may develop between the cooling passages and the hot-gas side wall. To address this concern, an investigation was previously conducted with simulated fatigue cracks upstream of the thrust

chamber throat. When these chambers were tested, an unexpected melting in the throat region developed which was not in line with the simulated fatigue cracks. The current experimental program was conducted in order to determine the cause for the failure in the earlier thrust chambers and to further investigate the effects of cracks in the thrust chamber liner upstream of the throat. The thrust chambers were tested at oxygen-to-fuel mixture ratios from 1.5 to 2.86 at a nominal chamber pressure of 8.6 MPa. As a result of the test series, the reason for the failure occurring in the earlier work was determined to be injector anomalies. The LOX leaking through the simulated fatigue cracks did not affect the integrity of the chambers. Author

N90-22606* National Aeronautics and Space Administration. Lewis Research Center, Cleveland, OH.
PROGRAMMATIC STATUS OF NASA'S CSTI HIGH CAPACITY POWER STIRLING SPACE POWER CONVERTER PROGRAM
 JAMES E. DUDENHOEFER 1990 9 p Proposed for presentation at the 25th Intersociety Energy Conversion Engineering Conference, Reno, NV, 12-17 Aug. 1990; cosponsored by AICHE, SAE, ACS, AIAA, ASME, and IEEE
 (NASA-TM-103142; E-5494; NAS 1.15:103142) Avail: NTIS HC A02/MF A01 CSCL 21/8

An overview is presented of the NASA Lewis Research Center Free-Piston Stirling Space Power Converter Technology Development Program. This work is being conducted under NASA's Civil Space Technology Initiative (CSTI). The goal of the CSTI High Capacity Power element is to develop the technology base needed to meet the long duration, high capacity power requirements for future NASA space initiatives. Efforts are focused upon increasing system thermal and electric energy conversion efficiency at least fivefold over current SP-100 technology, and on achieving systems that are compatible with space nuclear reactors. The status of test activities with the Space Power Research Engine (SPRE) is discussed. Design deficiencies are gradually being corrected and the power converter is now outputting 11.5 kW at a temperature ratio of 2 (design output is 12.5 kW). Detail designs were completed for the 1050 K Component Test Power Converter (CTPC). The success of these and future designs is dependent upon supporting research and technology efforts including heat pipes, gas bearings, superalloy joining technologies and high efficiency alternators. An update of progress in these technologies is provided. Author

N90-23474* Little (Arthur D.), Inc., Cambridge, MA.
CONCEPTUAL DESIGN OF A MOVING BELT RADIATOR (MBR) SHUTTLE-ATTACHED EXPERIMENT Final Report
 JERRY L. AGUILAR Jun. 1990 46 p
 (Contract NAS3-25356)
 (NASA-CR-185169; NAS 1.26:185169) Avail: NTIS HC A03/MF A01 CSCL 21/8

The conceptual design of a shuttle-attached Moving Belt Radiator (MBR) experiment is presented. The MBR is an advanced radiator concept in which a rotating belt is used to radiate thermal energy to space. The experiment is developed with the primary focus being the verification of the dynamic characteristics of a rotating belt with a secondary objective of proving the thermal and sealing aspects in a reduced gravity, vacuum environment. The mechanical design, selection of the belt material and working fluid, a preliminary test plan, and program plan are presented. The strategy used for selecting the basic sizes and materials of the components are discussed. Shuttle and crew member requirements are presented with some options for increasing or decreasing the demands on the STS. An STS carrier and the criteria used in the selection process are presented. The proposed carrier for the Moving Belt Radiator experiment is the Hitchhiker-M. Safety issues are also listed with possible results. This experiment is designed so that a belt can be deployed, run at steady state conditions, run with dynamic perturbations imposed, verify the operation of the interface heat exchanger and seals, and finally be retracted into a stowed position for transport back to earth. Author

N90-24349* National Aeronautics and Space Administration. Lewis Research Center, Cleveland, OH.

COMBUSTOR DESIGN AND ANALYSIS USING THE ROCKET COMBUSTOR INTERACTIVE DESIGN (ROCCID)

METHODOLOGY

MARK D. KLEM, JERRY L. PIEPER, and RICHARD E. WALKER (Aerojet TechSystems Co., Sacramento, CA.) 1990 11 p Presented at the 26th Joint Propulsion Conference, Orlando, FL, 16-18 Jul. 1990; cosponsored by AIAA, SAE, ASME, and ASEE (NASA-TM-103165; E-5537; NAS 1.15:103165; AIAA-90-2240) Avail: NTIS HC A03/MF A01 CSCL 21/8

The Rocket Combustor Interactive Design (ROCCID) Methodology is a newly developed, interactive computer code for the design and analysis of a liquid propellant rocket combustion chamber. The application of ROCCID to design a liquid rocket combustion chamber is illustrated. Designs for a 50,000 lbf thrust and 1250 psi chamber pressure combustor using liquid oxygen (LOX)/RP-1 propellants are developed and evaluated. Tradeoffs between key design parameters affecting combustor performance and stability are examined. Predicted performance and combustion stability margin for these designs are provided as a function of the combustor operating mixture ratio and chamber pressure. Author

N90-25181* National Aeronautics and Space Administration. Lewis Research Center, Cleveland, OH.

ARCJET LOAD CHARACTERISTICS

JOHN A. HAMLEY 1990 18 p Presented at the 21st International Electric Propulsion Conference, Orlando, FL, 18-20 Jul. 1990; cosponsored by AIAA, DGLR, and JSASS (NASA-TM-103190; E-5578; NAS 1.15:103190; AIAA-90-2579) Avail: NTIS HC A03/MF A01 CSCL 21/8

Experiments were conducted to define the interface characteristics and constraints of 1 kW class arcjets run on simulated decomposition products of hydrazine and power processors. The impacts of power supply output current ripple on arcjet performance were assessed by variation of the ripple frequency from 100 Hz to 100 kHz with 10 percent peak-to-peak ripple amplitude at 1.2 kW. Ripple had no significant effects on thrust, specific impulse or efficiency. The impact of output ripple on thruster lifetime was not assessed. The static and dynamic impedances of the arcjet were quantified with two thrusters of nearly identical configuration. Superposition of an AC component on the DC arc current was used to characterize the dynamic impedance as a function of flow rate and DC current level. A mathematical model was formulated from these data. Both the static and dynamic impedance magnitude were found to be dependent on mass flow rate. The amplitude of the AC component was found to have little effect on the dynamic impedance. Reducing the DC level from 10 to 8 amps led to a large change in the magnitude of the dynamic impedance with no observable phase change. The impedance data compared favorably between the two thrusters. Author

N90-25183* Sverdrup Technology, Inc., Brook Park, OH.
ROCKET COMBUSTION CHAMBER LIFE-ENHANCING DESIGN CONCEPTS Final Report

RICHARD J. QUENTMEYER Jul. 1990 19 p Presented at the 26th Joint Propulsion Conference, Orlando, FL, 16-18 Jul. 1990; cosponsored by AIAA, SAE, ASME, and ASEE (Contract NAS3-25266) (NASA-CR-185257; E-5564; NAS 1.26:185257; AIAA-90-2116) Avail: NTIS HC A03/MF A01 CSCL 21/8

NASA continues to pursue technologies which can lead to an increase in life and reduce the costs of fabrication of the Space Shuttle Main Engine. The joint NASA/Air Force Advanced Launch System Program has set its prime objectives to be high reliability and low cost for their new advanced booster engine. In order to meet these objectives, NASA will utilize the results of several ongoing programs to provide the required technologies. An overview is presented of those programs which address life enhancing design concepts for the combustion chamber. Seven different design concepts, which reduce the thermal strain and/or

20 SPACECRAFT PROPULSION AND POWER

increase the material strength of the combustion chamber liner wall are discussed. Subscale rocket test results are presented, where available, for life enhancing design concepts. Two techniques for reducing chamber fabrication costs are discussed, as well as issues relating to hydrocarbon fuels/combustion chamber liner materials compatibility. Author

N90-25184*# National Aeronautics and Space Administration. Lewis Research Center, Cleveland, OH.

AN ANALYSIS OF SPACE POWER SYSTEM MASSES

BARBARA H. KENNY (Sverdrup Technology, Inc., Brook Park, OH.), RONALD C. CULL, and M. DAVID KANKAM 1990 8 p
Proposed for presentation at the 25th Intersociety Energy Conversion Engineering Conference, Reno, NV, 12-17 Aug. 1990; cosponsored by AICHe, ANS, SAE, ACS, AIAA, ASME, and IEEE (NASA-TM-103199; E-5597; NAS 1.15:103199) Avail: NTIS HC A02/MF A01 CSCL 21/8

Various space electrical power system masses are analyzed with particular emphasis on the power management and distribution (PMAD) portion. The electrical power system (EPS) is divided into functional blocks: source, interconnection, storage, transmission, distribution, system control and load. The PMAD subsystem is defined as all the blocks between the source, storage and load, plus the power conditioning equipment required for the source, storage and load. The EPS mass of a wide range of spacecraft is then classified as source, storage or PMAD and tabulated in a database. The intent of the database is to serve as a reference source for PMAD masses of existing and in-design spacecraft. The PMAD masses in the database range from 40 kg/kW to 183 kg/kW across the spacecraft systems studied. Factors influencing the power system mass are identified. These include the total spacecraft power requirements, total amount of load capacity and physical size of the spacecraft. It is found that a new utility class of power systems, represented by Space Station Freedom, is evolving. Author

N90-25185*# National Aeronautics and Space Administration. Lewis Research Center, Cleveland, OH.

ADVANCED TUBE-BUNDLE ROCKET THRUST CHAMBER

JOHN M. KAZAROFF and ALBERT J. PAVLI (Sverdrup Technology, Inc., Brook Park, OH.) 1990 14 p Presented at the 26th Joint Propulsion Conference, Orlando, FL, 16-18 Jul. 1990; cosponsored by AIAA, SAE, ASME, and ASEE (NASA-TM-103139; E-5491; NAS 1.15:103139; AIAA-90-2726) Avail: NTIS HC A03/MF A01 CSCL 21/8

An advanced rocket thrust chamber for future space application is described along with an improved method of fabrication. Potential benefits of the concept are improved cyclic life, reusability, and performance. Performance improvements are anticipated because of the enhanced heat transfer into the coolant which will enable higher chamber pressure in expander cycle engines. Cyclic life, reusability and reliability improvements are anticipated because of the enhanced structural compliance inherent in the construction. The method of construction involves the forming of the combustion chamber with a tube-bundle of high conductivity copper or copper alloy tubes, and the bonding of these tubes by an electroforming operation. Further, the method of fabrication reduces chamber complexity by incorporating manifolds, jackets, and structural stiffeners while having the potential for thrust chamber cost and weight reduction. Author

N90-25186*# National Aeronautics and Space Administration. Lewis Research Center, Cleveland, OH.

A COMPARISON OF ANALYTICAL RESULTS FOR 20 K LOX/HYDROGEN INSTABILITIES

MARK D. KLEM and KEVIN J. BREISACHER Jul. 1990 17 p
Presented at the 26th Joint Propulsion Conference, Orlando, FL, 16-18 Jul. 1990; cosponsored by AIAA, SAE, ASME, and ASEE (NASA-TM-103166; E-5538; NAS 1.15:103166; AIAA-90-2241) Avail: NTIS HC A03/MF A01 CSCL 21/8

Test data from NASA Lewis' Effect of Thrust Per Element on Combustion Stability Characteristics of Hydrogen-Oxygen Rocket Engines test program are used to validate two recently released

stability analysis tools. The first tool is a design methodology called ROCCID (ROCKET Combustor Interactive Design). ROCCID is an interactive design and analysis methodology that uses existing performance and combustion stability analysis codes. The second tool is HICCIP (High frequency Injection Coupled Combustion Instability Program). HICCIP is a recently developed combustion stability analysis model. Using a matrix of models, results from analytic comparisons with 20 K LOX/H₂ experimental data are presented. Author

N90-25187*# Sverdrup Technology, Inc., Cleveland, OH.

AUTONOMOUS POWER EXPERT SYSTEM Final Report

MARK J. RINGER and TODD M. QUINN Jul. 1990 8 p
Presented at the 25th Intersociety Energy Conversion Engineering Conference, Reno, NV, 12-17 Aug. 1990; cosponsored by AICHe, ANS, SAE, ACS, AIAA, ASME, and IEEE (Contract NAS3-25266) (NASA-CR-185263; E-5609; NAS 1.26:185263) Avail: NTIS HC A02/MF A01 CSCL 21/8

The goal of the Autonomous Power System (APS) program is to develop and apply intelligent problem solving and control technologies to the Space Station Freedom Electrical Power Systems (SSF/EPS). The objectives of the program are to establish artificial intelligence/expert system technology paths, to create knowledge based tools with advanced human-operator interfaces, and to integrate and interface knowledge-based and conventional control schemes. This program is being developed at the NASA-Lewis. The APS Brassboard represents a subset of a 20 KHz Space Station Power Management And Distribution (PMAD) testbed. A distributed control scheme is used to manage multiple levels of computers and switchgear. The brassboard is comprised of a set of intelligent switchgear used to effectively switch power from the sources to the loads. The Autonomous Power Expert System (APEX) portion of the APS program integrates a knowledge based fault diagnostic system, a power resource scheduler, and an interface to the APS Brassboard. The system includes knowledge bases for system diagnostics, fault detection and isolation, and recommended actions. The scheduler autonomously assigns start times to the attached loads based on temporal and power constraints. The scheduler is able to work in a near real time environment for both scheduling and dynamic replanning. Author

N90-25521*# National Aeronautics and Space Administration. Lewis Research Center, Cleveland, OH.

AUTONOMOUS POWER EXPERT FAULT DIAGNOSTIC SYSTEM FOR SPACE STATION FREEDOM ELECTRICAL POWER SYSTEM TESTBED

LONG V. TRUONG, JERRY L. WALTERS, MARY ELLEN ROTH, TODD M. QUINN, and WALTER M. KRAWCZONEK (Sverdrup Technology, Inc., Cleveland, OH.) /n NASA, Lyndon B. Johnson Space Center, Third Annual Workshop on Space Operations Automation and Robotics (SOAR 1989) p 181-186 Mar. 1990
Avail: NTIS HC A99/MF A04 CSCL 21/8

The goal of the Autonomous Power System (APS) program is to develop and apply intelligent problem solving and control to the Space Station Freedom Electrical Power System (SSF/EPS) testbed being developed and demonstrated at NASA Lewis Research Center. The objectives of the program are to establish artificial intelligence technology paths, to craft knowledge-based tools with advanced human-operator interfaces for power systems, and to interface and integrate knowledge-based systems with conventional controllers. The Autonomous Power Expert (APEX) portion of the APS program will integrate a knowledge-based fault diagnostic system and a power resource planner-scheduler. Then APEX will interface on-line with the SSF/EPS testbed and its Power Management Controller (PMC). The key tasks include establishing knowledge bases for system diagnostics, fault detection and isolation analysis, on-line information accessing through PMC, enhanced data management, and multiple-level, object-oriented operator displays. The first prototype of the diagnostic expert system for fault detection and isolation has been developed. The knowledge bases and the rule-based model that were developed

for the Power Distribution Control Unit subsystem of the SSF/EPS testbed are described. A corresponding troubleshooting technique is also described. Author

N90-26065*# National Aeronautics and Space Administration. Lewis Research Center, Cleveland, OH.

MARS IN SITU PROPELLANTS: CARBON MONOXIDE AND OXYGEN IGNITION EXPERIMENTS

DIANE L. LINNE, JAMES RONCACE (Sverdrup Technology, Inc., Brook Park, OH.), and MARY F. GROTH Jul. 1990 13 p Presented at the 26th Joint Propulsion Conference, Orlando, FL, 16-18 Jul. 1990; sponsored in part by AIAA, SAE, ASME, and ASEE (NASA-TM-103202; E-5607; NAS 1.15:103202; AIAA-90-1894) Avail: NTIS HC A03/MF A01 CSCL 21/9

Carbon monoxide and oxygen were tested in a standard spark-torch igniter to identify the ignition characteristics of this potential Mars in situ propellant combination. The ignition profiles were determined as functions of mixture ratio, amount of hydrogen added to the carbon monoxide, and oxygen inlet temperature. The experiments indicated that the carbon monoxide and oxygen combination must have small amounts of hydrogen present to initiate reaction. Once the reaction was started, the combustion continued without the presence of hydrogen. A mixture ratio range was identified where ignition occurred, and this range varied with the oxygen inlet temperature. Author

N90-26068*# National Aeronautics and Space Administration. Lewis Research Center, Cleveland, OH.

AEOLIAN REMOVAL OF DUST FROM RADIATOR SURFACES ON MARS

JAMES R. GAIER, MARLA E. PEREZ-DAVIS, SHARON K. RUTLEDGE, and DEBORAH HOTES (Cleveland State Univ., OH.) Aug. 1990 15 p Presented at the AIChE Summer National Meeting, San Diego, CA, 19-22 Aug. 1990 (NASA-TM-103205; E-5547; NAS 1.15:103205) Avail: NTIS HC A03/MF A01 CSCL 10/2

Simulated radiator surfaces made of arc-textured Cu and Nb-1 percent-Zr and ion beam textured graphite and C-C composite were fabricated and their integrated spectral emittance characterized from 300 to 3000 K. A thin layer of aluminum oxide, basalt, or iron (III) oxide dust was then deposited on them, and they were subjected to low pressure winds in the Martian Surface Wind Tunnel. It was found that dust deposited on simulated radiator surfaces may or may not seriously lower their integrated spectral emittance, depending upon the characteristics of the dust. With Al₂O₃ there is no appreciable degradation of emittance on a dusted sample, with basaltic dust there is a 10 to 20 percent degradation, and with Fe₂O₃ a 20 to 40 percent degradation. It was also found that very high winds on dusted highly textured surfaces can result in their abrasion. Degradation in emittance due to abrasion was found to vary with radiator material. Arc-textured Cu and Nb-1 percent Zr was found to be more susceptible to emittance degradation than graphite or C-C composite. The most abrasion occurred at low angles, peaking at the 22.5 deg test samples. Author

N90-26069*# National Aeronautics and Space Administration. Lewis Research Center, Cleveland, OH.

ESTIMATION OF MINORITY CARRIER DIFFUSION LENGTHS IN INP/GAAS SOLAR CELLS

R. K. JAIN and D. J. FLOOD 1990 10 p Presented at the 2nd International Conference on Indium Phosphide and Related Materials, Denver, CO, 23-25 Apr. 1990; sponsored in part by IEEE Lasers and Electro-Optics Society and IEEE Electron Device Society (NASA-TM-103213; E-5624; NAS 1.15:103213) Avail: NTIS HC A02/MF A01 CSCL 10/1

Minority carrier diffusion length is one of the most important parameters affecting the solar cell performance. An attempt is made to estimate the minority carrier diffusion lengths in the emitter and base of InP/GaAs heteroepitaxial solar cells. The PC-1D computer model was used to simulate the experimental cell results

measured at NASA Lewis under AMO (air mass zero) spectrum at 25 C. A 16 nm hole diffusion length in the emitter and a 0.42 micron electron diffusion length in the base gave very good agreement with the I-V curve. The effect of varying minority carrier diffusion lengths on cell short current, open circuit voltage, and efficiency was studied. It is also observed that the front surface recombination velocity has very little influence on the cell performance. The poor output of heteroepitaxial cells is caused primarily by the large number of dislocations generated at the interfaces that propagate through the bulk indium phosphide layers. Cell efficiency as a function of dislocation density was calculated and the effect of improved emitter bulk properties on cell efficiency is presented. It is found that cells with over 16 percent efficiencies should be possible, provided the dislocation density is below 10(exp 6)/sq cm. Author

N90-26070*# National Aeronautics and Space Administration. Lewis Research Center, Cleveland, OH.

DIGITAL FILTERING OF PLUME EMISSION SPECTRA

GEORGE C. MADZSAR Jul. 1990 13 p Presented at the 26th Joint Propulsion Conference, Orlando, FL, 16-18 Jul. 1990; sponsored in part by AIAA, ASME, SAE, and ASEE (NASA-TM-103135; E-5478; NAS 1.15:103135; AIAA-90-1994) Avail: NTIS HC A03/MF A01 CSCL 21/8

Fourier transformation and digital filtering techniques were used to separate the superpositioned spectral phenomena observed in the exhaust plumes of liquid propellant rocket engines. Space shuttle main engine (SSME) spectral data were used to show that extraction of spectral lines in the spatial frequency domain does not introduce error, and extraction of the background continuum introduces only minimal error. Error introduced during band extraction could not be quantified due to poor spectrometer resolution. Based on the atomic and molecular species found in the SSME plume, it was determined that spectrometer resolution must be 0.03 nm for SSME plume spectral monitoring. Author

N90-26071*# National Aeronautics and Space Administration. Lewis Research Center, Cleveland, OH.

PRELIMINARY PLUME CHARACTERISTICS OF AN ARCJET THRUSTER

DAVID H. MANZELLA, FRANCIS M. CURRAN, ROGER M. MYERS, and DIETER M. ZUBE (Stuttgart Univ., Germany, F.R.) 1990 16 p Presented at the 21st International Electric Propulsion Conference, Orlando, FL, 18-20 Jul. 1990; sponsored by AIAA, DGLR, and JSASS (NASA-TM-103241; E-5659; NAS 1.15:103241; AIAA-90-2645) Avail: NTIS HC A03/MF A01 CSCL 21/8

An experimental investigation of a low power arcjet plume was conducted using emission spectroscopy. A laboratory model arcjet incorporating a segmented anode was run on simulated hydrazine at a flow rate of 5 x 10(exp -5) kg/s. The complete visible spectrum measured in the exit plane of the arcjet showed the presence of N₂, N₂(+), NH, and H. Radial intensity profiles for the H alpha, H sub beta, and the NH A(sup 3)Pi yields X(sup 3)Sigma(0,0) transitions at four different axial locations were measured. These line of sight intensity measurements, spaced 0.05 mm apart, were deconvoluted to give the radial intensity distribution using an inverse Abel transformation. The ratio between the intensities from the H sub alpha and H sub beta transitions indicated a non-Boltzmann energy distribution between excited states in the plume. Axial intensity profiles taken on center line indicated the decay rate of excited states in the plume. An electron number density of 2 x 10(exp 13)/cu cm at the exit plane was determined based on Stark broadening of the H sub beta line. Rotational temperatures of 750 K, 1750 K, and 2500 K were determined for N₂, N₂(+), and NH respectively. The results demonstrate that the location of the current attachment on the anode has a measurable effect on the electronically excited species in the plume and that dissociation is the dominant frozen flow loss mechanism in low power arcjets. Author

20 SPACECRAFT PROPULSION AND POWER

N90-26873*# National Aeronautics and Space Administration. Lewis Research Center, Cleveland, OH.

NUCLEAR POWER SYSTEMS FOR LUNAR AND MARS EXPLORATION

R. J. SOVIE and J. M. BOZEK 1990 12 p. Proposed for presentation at the 41st International Astronautical Conference, Dresden, German Democratic Republic, 6-13 Oct. 1990 (NASA-TM-103168; E-5540; NAS 1.15:103168; IAF-90-200) Avail: NTIS HC A03/MF A01 CSCL 18/12

Initial studies of a variety of mission scenarios for the new Space Exploration Initiative, and the technologies necessary to enable or significantly enhance them, have identified the development of advanced space power systems whether solar, chemical or nuclear to be of prime importance. Lightweight, compact, reliable power systems for planetary rovers and a variety of surface vehicles, utility surface power, and power for advanced propulsion systems have been identified as critical needs for these missions. These mission scenarios, the concomitant power system requirements, and power system options considered are discussed. The significant potential benefits of nuclear power are identified for meeting the power needs of the above applications. Author

N90-27782*# National Aeronautics and Space Administration. Lewis Research Center, Cleveland, OH.

GEOMETRIC EFFECTS IN APPLIED-FIELD MPD THRUSTERS

R. M. MYERS (Sverdrup Technology, Inc., Brook Park, OH.), M. MANTENIEKS, and JAMES S. SOVEY 1990 20 p. Presented at the 21st International Electric Propulsion Conference, Orlando, FL, 18-20 Jul. 1990; sponsored by AIAA, DGLR, JSASS (NASA-TM-103259; E-5692; NAS 1.15:103259; AIAA-90-2669) Avail: NTIS HC A01/MF A01 CSCL 21/8

Three applied-field magnetoplasmadynamic (MPD) thruster geometries were tested with argon propellant to establish the influence of electrode geometry on thruster performance. The thrust increased approximately linearly with anode radius, while the discharge and electrode fall voltages increased quadratically with anode radius. All these parameters increased linearly with applied-field strength. Thrust efficiency, on the other hand, was not significantly influenced by changes in geometry over the operating range studied, though both thrust and thermal efficiencies increased monotonically with applied field strength. The best performance, 1820 sec I(sub sp) at 20 percent efficiency, was obtained with the largest radius anode at the highest discharge current (1500 amps) and applied field strength (0.4 Tesla).

Author

N90-27783*# National Aeronautics and Space Administration. Lewis Research Center, Cleveland, OH.

REQUIREMENTS FOR LONG-LIFE OPERATION OF INERT GAS HOLLOW CATHODES: PRELIMINARY REPORT

TIMOTHY R. VERHEY (Sverdrup Technology, Inc., Brook Park, OH.) and GREGORY S. MACRAE Jul. 1990 19 p. Presented at the 21st International Electric Propulsion Conference, Orlando, FL, 18-20 Jul. 1990; cosponsored by the AIAA, DGLR, and JSASS (NASA-TM-103242; E-5662; NAS 1.15:103242; AIAA-90-2586) Avail: NTIS HC A03/MF A01 CSCL 21/8

An experimental investigation was initiated to establish conditioning procedures for reliable hollow cathode operation via the characterization of critical parameters in a representative cathode test facility. From vacuum pumpdown rates, it was found that approximately 1.5 hours were required to achieve pressure levels within 5 percent of the lowest attainable pressure for this facility, depending on the purge conditions. The facility atmosphere was determined by a residual gas analyzer to be composed of primarily air and water vapor. The effects of vacuum pumping and inert gas purging were evaluated. A maximum effective leakage rate of 2.0×10^{-3} sccm was observed and its probable causes were examined. An extended test of a 0.64 cm diameter Mo-Re hollow cathode was successfully completed. This test ran for 504 hours at an emission current of 23.0 amperes and a xenon flow rate of 6.1 sccm. Discharge voltage rose continuously from 15 to 21 volts over the course of the test. The temperature of the

cathode body during the test was relatively stable at 1160 C. Post-test examination revealed ion-bombardment texturing of the orifice plate to be the only detectable sign of wear on the hollow cathode.

Author

N90-27784*# National Aeronautics and Space Administration. Lewis Research Center, Cleveland, OH.

ELECTRICAL CHARACTERIZATION OF A MAPHAM INVERTER USING PULSE TESTING TECHNIQUES

E. D. BAUMANN, I. T. MYERS, and A. N. HAMMOND (Sverdrup Technology, Inc., Brook Park, OH.) 1990 7 p. Presented at the 25th Intersociety Energy Conversion Engineering Conference, Reno, NV, 12-17 Aug. 1990; cosponsored by AIChE, ANS, SAE, ACS, AIAA, ASME, and IEEE (Contract FY1455-89-N-0655) (NASA-TM-103254; E-5683; NAS 1.15:103254) Avail: NTIS HC A02/MF A01 CSCL 21/8

Electric power requirements for aerospace missions have reached megawatt power levels. Within the next few decades, it is anticipated that a manned lunar base, interplanetary travel, and surface exploration of the Martian surface will become reality. Several research and development projects aimed at demonstrating megawatt power level converters for space applications are currently underway at the NASA Lewis Research Center. Innovative testing techniques will be required to evaluate the components and converters, when developed, at their rated power in the absence of costly power sources, loads, and cooling systems. Facilities capable of testing these components and systems at full power are available, but their use may be cost prohibitive. The use of a multiple pulse testing technique is proposed to determine the electrical characteristics of large megawatt level power systems. Characterization of a Mapham inverter is made using the proposed technique and conclusions are drawn concerning its suitability as an experimental tool to evaluate megawatt level power systems.

Author

N90-27785*# National Aeronautics and Space Administration. Lewis Research Center, Cleveland, OH.

ADVANCED PROPULSION FOR LEO AND GEO PLATFORMS

JAMES S. SOVEY and DAVID J. PIDGEON (George Washington Univ., Hampton, VA.) 1990 27 p. Presented at the 21st International Electric Propulsion Conference, Orlando, FL, 18-20 Jul. 1990; cosponsored by AIAA, DGLR, and JSASS (NASA-TM-103228; E-5644; NAS 1.15:103228; AIAA-90-2551) Avail: NTIS HC A03/MF A01 CSCL 21/8

Mission requirements and mass savings applicable to specific low earth orbit and geostationary earth orbit platforms using three highly developed propulsion systems are described. Advanced hypergolic bipropellant thrusters and hydrazine arcjets can provide about 11 percent additional instrument payload to 14,000 kg LEO platforms. By using electric propulsion on a 8,000 kg class GEO platform, mass savings in excess of 15 percent of the beginning-of-life platform mass are obtained. Effects of large, advanced technology solar arrays and antennas on platform propulsion requirements are also discussed.

Author

N90-27786*# National Aeronautics and Space Administration. Lewis Research Center, Cleveland, OH.

ADVANCED ONBOARD PROPULSION BENEFITS AND STATUS

DAVID C. BYERS Mar. 1989 14 p. Presented at the Symposium on Space Commercialization: Role of Developing Countries, Nashville, TN, 5-10 Mar. 1989; sponsored in part by UTISI, UN-OSAD, AIAA, and IAA (NASA-TM-103174; E-5552; NAS 1.15:103174) Avail: NTIS HC A03/MF A01 CSCL 21/8

Future commercial space systems may include geosynchronous-orbit communication satellites; Earth-observing satellites in polar, sun-synchronous orbits; and tended low-earth-orbit platforms. All such space systems require onboard propulsion for a variety of functions, including stationkeeping and drag makeup, apogee motors, and delivery and return. In many cases, the onboard propulsion exerts a major influence on the

overall mission performance, lifetime, and integration. NASA has established a Low Thrust Propulsion Program, which is developing chemical and electric propulsion concepts that offer potential for significant benefits for onboard propulsion for the various classes of commercial spacecraft. The onboard propulsion requirements of future commercial space systems are briefly discussed, followed by a summary of the characteristics and status of relevant elements of the NASA Low Thrust program. Author

N90-28616*# National Aeronautics and Space Administration. Lewis Research Center, Cleveland, OH.

PROBABILISTIC STRUCTURAL ANALYSIS METHODS DEVELOPMENT FOR SSME

C. C. CHAMIS and D. A. HOPKINS In NASA, Marshall Space Flight Center, Advanced Earth-to-Orbit Propulsion Technology 1988, Volume 1 p 54-68 Sep. 1988
 Avail: NTIS HC A99/MF E06 CSCL 21/8

The development of probabilistic structural analysis methods is a major part of the SSME Structural Durability Program and consists of three program elements: composite load spectra, probabilistic finite element structural analysis, and probabilistic structural analysis applications. Recent progress includes: (1) the effects of the uncertainties of several factors on the HPFP blade temperature pressure and torque, (2) the evaluation of the cumulative distribution function of structural response variables based on assumed uncertainties on primitive structural variables, and (3) evaluation of the failure probability. Collectively, the results obtained demonstrate that the structural durability of critical SSME components can be probabilistically evaluated. Author

N90-28657*# National Aeronautics and Space Administration. Lewis Research Center, Cleveland, OH.

LOW POWER ARCJET PERFORMANCE

FRANCIS M. CURRAN and CHARLES J. SARMIENTO Jul. 1990 15 p Presented at the 21st International Electric Propulsion Conference, Orlando, FL, 18-20 July 1990; cosponsored in part by AIAA, DGLR, and JSASS
 (NASA-TM-103280; E-5734; NAS 1.15:103280; AIAA-90-2578)
 Avail: NTIS HC A03/MF A01 CSCL 21/8

An experimental investigation was performed to evaluate arc jet operation at low power. A standard, 1 kW, constricted arc jet was run using nozzles with three different constrictor diameters. Each nozzle was run over a range of current and mass flow rates to explore stability and performance in the low power engine. A standard pulse-width modulated power processor was modified to accommodate the high operating voltages required under certain conditions. Stable, reliable operation at power levels below 0.5 kW was obtained at efficiencies between 30 and 40 percent. The operating range was found to be somewhat dependent on constrictor geometry at low mass flow rates. Quasi-periodic voltage fluctuations were observed at the low power end of the operating envelope. The nozzle insert geometry was found to have little effect on the performance of the device. The observed performance levels show that specific impulse levels above 350 seconds can be obtained at the 0.5 kW power level. Author

N90-28659*# National Aeronautics and Space Administration. Lewis Research Center, Cleveland, OH.

A FAILURE DIAGNOSIS SYSTEM BASED ON A NEURAL NETWORK CLASSIFIER FOR THE SPACE SHUTTLE MAIN ENGINE

AHMET DUYAR (Florida Atlantic Univ., Boca Raton.) and WALTER MERRILL 1990 13 p Proposed for presentation at the 29th Conference on Decision and Control, Honolulu, HI, 5-7 Dec. 1990; sponsored by IEEE
 (NASA-TM-103607; E-5756; NAS 1.15:103607) Avail: NTIS HC A03/MF A01 CSCL 21/8

A conceptual design of a model based failure detection and diagnosis system is developed for the space shuttle main engine. This design relies on the accurate and reliable identification of the parameters of the highly nonlinear and very complex engine. The design approach is presented in some detail and results for

23 CHEMISTRY AND MATERIALS (GENERAL)

a failed valve are presented. These preliminary results verify that the developed parameter identification technique together with a neural network classifier can be used for this purpose. Author

23

CHEMISTRY AND MATERIALS (GENERAL)

A90-14021* National Aeronautics and Space Administration. Lewis Research Center, Cleveland, OH.

UNIVERSAL ASPECTS OF BRITTLE FRACTURE, ADHESION, AND ATOMIC FORCE MICROSCOPY

AMITAVA BANERJEA, JOHN FERRANTE (NASA, Lewis Research Center, Cleveland, OH), and JOHN R. SMITH (GM Research Laboratories, Warren, MI) IN: New materials approaches to tribology: Theory and applications; Proceedings of the Symposium, Boston, MA, Nov. 29-Dec. 2, 1988. Pittsburgh, PA, Materials Research Society, 1989, p. 89-100. refs
 Copyright

This universal relation between binding energy and interatomic separation was originally discovered for adhesion at bimetallic interfaces involving the simple metals Al, Zn, Mg, and Na. It is shown here that the same universal relation extends to adhesion at transition-metal interfaces. Adhesive energies have been computed for the low-index interfaces of Al, Ni, Cu, Ag, Fe, and W, using the equivalent-crystal theory (ECT) and keeping the atoms in each semiinfinite slab fixed rigidly in their equilibrium positions. These adhesive energy curves can be scaled onto each other and onto the universal adhesion curve. The effect of tip shape on the adhesive forces in the atomic-force microscope (AFM) is studied by computing energies and forces using the ECT. While the details of the energy-distance and force-distance curves are sensitive to tip shape, all of these curves can be scaled onto the universal adhesion curve. Author

A90-15049* Akron Univ., OH.

AN EXPERIMENTAL EVALUATION OF THE TENSILE STRENGTH OF IMPACT ICE

X. XIAN, M. L. CHU, R. J. SCAVUZZO, and T. S. SRIVATSAN (Akron, University, OH) Journal of Materials Science Letters (ISSN 0261-8028), vol. 8, Oct. 1989, p. 1205-1208. refs
 (Contract NAG3-479)
 Copyright

The evaluation of the tensile strength of impact built-up ice on structural components has been prompted by such problems as electrical transmission line losses and catastrophic failures in Arctic regions, deicing problems with fixed-wing and rotary-wing aircraft, etc. It is demonstrated that the conventional tensile-testing technique furnishes adequate data on artificially refrigerated ice, and helps establish the influence of extrinsic factors on ice tensile strength. O.C.

A90-17294* National Aeronautics and Space Administration. Lewis Research Center, Cleveland, OH.

TBCs FOR BETTER ENGINE EFFICIENCY

WILLIAM J. BRINDLEY and ROBERT A. MILLER (NASA, Lewis Research Center, Cleveland, OH) Advanced Materials and Processes (ISSN 0882-7958), vol. 136, Aug. 1989, p. 29-33. refs
 Copyright

State-of-the-art thermal barrier coatings (TBCs) developed for aircraft engines can achieve both hot-section component operating temperature reductions and superior oxidation resistance. Such TBCs typically consist of two layers: a metallic, often NiCrAlY 'bond' inner layer in contact with the superalloy structural component, and an outer, insulating ceramic layer. A ceramic frequently used in this role due to its high durability is

23 CHEMISTRY AND MATERIALS (GENERAL)

plasma-sprayed ZrO₂, partially stabilized with 6-8 wt pct Y₂O₃. TBCs can also be useful in nonaircraft gas turbines, which frequently use highly contaminated fuels. O.C.

A90-21930* National Aeronautics and Space Administration. Lewis Research Center, Cleveland, OH.

PROCESSABLE, HIGH TEMPERATURE POLYMERS FROM 1,4,5,8-TETRAHYDRO-1,4;5,8-DIEPOXYANTHRACENE AND BIS-DIENES

MARY ANN B. MEADOR (NASA, Lewis Research Center, Cleveland, OH) *Journal of Polymer Science: Polymer Chemistry Edition* (ISSN 0360-6376), vol. 26, 1988, p. 2907-2916. refs Copyright

1,4,5,8-tetrahydro-1,4;5,8-diepoxyanthracene reacts with various anthracene end-capped polyimide oligomers to form Diels-Alder cycloaddition copolymers. The polymers are soluble in common organic solvents, and have molecular weights of approximately 21,000 to 32,000. These resins exhibit lower weight loss in air than in nitrogen. This is suggested to be due to dehydration (loss of water ranges from 2 to 5 percent) at temperatures of 390 to 400 C to give thermooxidatively stable pentiptycene units along the polymer backbone. Because of their high softening points and good thermooxidative stability, the polymers have potential as processable, matrix resins for high temperature composite applications. Author

A90-22646* Rensselaer Polytechnic Inst. of Connecticut, Inc., East Windsor Hill.

DETERMINATION OF THE MEAN SOLID-LIQUID INTERFACE ENERGY OF PIVALIC ACID

N. B. SINGH and M. E. GLIKSMAN (Rensselaer Polytechnic Institute, Troy, NY) *Journal of Crystal Growth* (ISSN 0022-0248), vol. 98, no. 4, Dec. 1989, p. 573-580. refs (Contract NAS3-25368) Copyright

A high-confidence solid-liquid interfacial energy is determined for an anisotropic material. A coaxial composite having a cylindrical specimen chamber geometry provides a thermal gradient with an axial heating wire. The surface energy is derived from measurements of grain boundary groove shapes. Applying this method to pivalic acid, a surface energy of 2.84 erg/sq cm was determined with a total systematic and random error less than 10 percent. The value of interfacial energy corresponds to 24 percent of the latent heat of fusion per molecule. Author

A90-23830*# United Technologies Corp., East Hartford, CT.

MECHANISMS OF DEGRADATION AND FAILURE IN A PLASMA DEPOSITED THERMAL BARRIER COATING

JEANINE T. DEMASI-MARCIN, KEITH D. SHEFFLER, and SUDHANGSHU BOSE (United Technologies Corp., Pratt and Whitney Group, East Hartford, CT) *ASME, Gas Turbine and Aeroengine Congress and Exposition*, Toronto, Canada, June 4-8, 1989, 8 p. refs (Contract NAS3-23944) (ASME PAPER 89-GT-132)

Failure of a two layer plasma deposited thermal barrier coating is caused by cyclic thermal exposure and occurs by spallation of the outer ceramic layer. Spallation life is quantitatively predictable, based on the severity of cyclic thermal exposure. This paper describes and attempts to explain unusual constitutive behavior observed in the insulative ceramic coating layer, and presents details of the ceramic cracking damage accumulation process which is responsible for spallation failure. Comments also are offered to rationalize the previously documented influence of interfacial oxidation on ceramic damage accumulation and spallation life. Author

A90-31581* National Aeronautics and Space Administration. Lewis Research Center, Cleveland, OH.

EVALUATION OF ATOMIC OXYGEN RESISTANT PROTECTIVE COATINGS FOR FIBERGLASS-EPOXY COMPOSITES IN LEO

SHARON K. RUTLEDGE (NASA, Lewis Research Center, Cleveland, OH), PHILLIP E. PAULSEN (Cleveland State University,

OH), and JOYCE A. BRADY (Sverdrup Technology, Inc., Middleburg Heights, OH) *IN: International SAMPE Symposium and Exhibition*, 34th, Reno, NV, May 8-11, 1989, Proceedings. Book 1. Covina, CA, Society for the Advancement of Material and Process Engineering, 1989, p. 1163-1174. Previously announced in STAR as N89-21100. refs Copyright

Fiberglass-epoxy composite masts are the prime structural members for the Space Station Freedom solar array. At the altitude where Space Station Freedom will operate, atomic oxygen atoms are the most predominant species. Atomic oxygen is highly reactive and has been shown to oxidize organic and some metallic materials. Tests with random and directed atomic oxygen exposure have shown that the epoxy is removed from the composite exposing brittle glass fibers which could be easily removed from the surface where they could contaminate space Station Freedom Systems. Protection or fiber containment systems, inorganic based paints, aluminum braid, and a metal coatings, were evaluated for resistance to atomic oxygen, vacuum ultraviolet radiation, thermal cycling, and mechanical flexing. All appeared to protect well against atomic oxygen and provide fiber containment except for the single aluminum braid covering. UV radiation resistance was acceptable and in general, thermal cycling and flexure had little to no effect on the mass loss rate for most coatings. Author

A90-32833* Pennsylvania State Univ., University Park.

ON THE DRIVING FORCE OF PAH PRODUCTION

MICHAEL FRENKLACH (Pennsylvania State University, University Park) *IN: Symposium (International) on Combustion*, 22nd, Seattle, WA, Aug. 14-19, 1988, Proceedings. Pittsburgh, PA, Combustion Institute, 1989, p. 1075-1082. refs (Contract NAG3-668) Copyright

The kinetic factors affecting the production of polycyclic aromatic hydrocarbons (PAH) in high-temperature pyrolysis and combustion environments are analyzed. A lumped kinetic model representing polymerization-type growth by one irreversible step and two reversible steps is considered. It is shown that at high temperatures, PAH growth is controlled by the superequilibrium of hydrogen atoms; at low temperatures and low H₂ concentrations, the PAH growth rate is proportional to the rate of the H-abstraction of a hydrogen atom from aromatic molecules; while at low temperatures and high H₂ concentrations, it is controlled by the thermodynamics of the H-abstraction and the kinetics of acetylene addition to aromatic radicals. The presence of oxygen mainly affects the small-molecule reactions during the induction period. V.T.

A90-33222*# National Aeronautics and Space Administration. Lewis Research Center, Cleveland, OH.

PHOTOCHEMICAL APPROACHES TO ORDERED POLYMERS

MICHAEL A. MEADOR, MAHMOUD ABDULAZIZ, and MARY ANN B. MEADOR (NASA, Lewis Research Center, Cleveland, OH) *IN: Radiation curing of polymeric materials*. Washington, DC, American Chemical Society, 1990, p. 220-237. refs

The photocyclization of o-benzoyloxyphenyl ketone chromophores provides an efficient, high yield route to the synthesis of 2,3-diphenylbenzofurans. The synthesis and solution of photochemistry of a series of polymers containing this chromophore is described. The photocuring of these polymers is a potential new approach to the synthesis of highly conjugated polymers based upon a p-phenylene bisbenzofuran repeat unit. Author

A90-37458* National Aeronautics and Space Administration. Lewis Research Center, Cleveland, OH.

APPLICATIONS OF SURFACE ANALYSIS AND SURFACE THEORY IN TRIBOLOGY

JOHN FERRANTE (NASA, Lewis Research Center, Cleveland, OH) *SIA - Surface and Interface Analysis* (ISSN 0142-2421), vol. 14, 1989, p. 809-822. Previously announced in STAR as N89-15981. refs Copyright

Tribology, the study of adhesion, friction and wear of materials, is a complex field which requires a knowledge of solid state physics,

surface physics, chemistry, material science, and mechanical engineering. It has been dominated, however, by the more practical need to make equipment work. With the advent of surface analysis and advances in surface and solid-state theory, a new dimension has been added to the analysis of interactions at tribological interfaces. In this paper the applications of tribological studies and their limitations are presented. Examples from research at the NASA Lewis Research Center are given. Emphasis is on fundamental studies involving the effects of monolayer coverage and thick films on friction and wear. A summary of the current status of theoretical calculations of defect energetics is presented. In addition, some new theoretical techniques which enable simplified quantitative calculations of adhesion, fracture, and friction are discussed. Author

A90-39975* National Aeronautics and Space Administration. Lewis Research Center, Cleveland, OH.

MATERIALS PARK, OH

JOSEPH R. STEPHENS (NASA, Lewis Research Center, Cleveland, OH) IN: Metals handbook. Volume 1, 10th Edition: Properties and selection. ASM International, 1989, p. 1009-1022. refs Copyright

An evaluation is made of the supply sources and current availability of elements involved in superalloy compositions, as well as of development trends in the substitution of strategic materials for superalloys, giving attention to the results thus far achieved by NASA's Conservation of Strategic Aerospace Materials program, which formally operated only from 1980 to 1984 but whose various research initiatives have been continued under other NASA programs. Peacetime and wartime economies' need and probable availability analyses are presented for bauxite/aluminum, the Pt-group metals, and the alloying elements Mn, Nb, Ta, Co, Cr, Ni, W, Fe, Cu, Ti, Mo, and Mg. O.C.

A90-42028*# Aerojet Technical Systems Co., Sacramento, CA. **CORROSION PREVENTION IN COPPER COMBUSTION CHAMBER LINERS OF LIQUID OXYGEN/METHANE BOOSTER ENGINES**

S. D. ROSENBERG and M. L. GAGE (Aerojet TechSystems, Sacramento, CA) AIAA, SAE, ASME, and ASEE, Joint Propulsion Conference, 26th, Orlando, FL, July 16-18, 1990. 8 p. refs (Contract NAS3-25070) (AIAA PAPER 90-2119) Copyright

The use of a protective gold coating for preventing the corrosion of copper combustion chamber liners in liquid oxygen/methane booster engines is discussed with reference to experimental results. Gold-plated and unplated copper alloy specimens were tested in a carbothermal test facility providing realistic simulations of booster engine cooling channel conditions, such as temperature, pressure, flow velocity, and heat flux. Metallographic examinations of the unplated specimens showed severe corrosion as a result of the reaction with the sulfur-containing contaminant in the fuel. In contrast, gold-plated specimens showed no corrosion under similar operating conditions. V.L.

A90-43902* Monash Univ., Clayton (Australia). **TENSILE ADHESION TESTING METHODOLOGY FOR THERMALLY SPRAYED COATINGS**

CHRISTOPHER C. BERNDT (Monash University, Clayton, Australia) Journal of Materials Engineering (ISSN 0931-7058), vol. 12, June 1990, p. 151-158. refs (Contract NCC3-27) Copyright

The structure of thermally sprayed coatings consists of lamellae which are oriented parallel to the substrate surface. The lamellae separate and fracture by distinctive mechanisms which are reflected in the failure morphology, and these may be described as adhesive (between the coating and substrate), cohesive (within the coating), or mixed mode. There is a large variability in the failure stress for any nominally identical group of coatings. A lower bound for the fracture toughness of alumina coatings can be calculated as $0.2 \text{ MNm}^{1/2}$. The coating strength values may also be treated as belonging to the statistical distribution of the Weibull function.

The Weibull modulus of the coating strength varied from 1.4 to 3.8. This analysis infers that the flaw size within coatings is highly variable and that the flaws are nonuniformly dispersed. The present work focuses on the question of whether tensile adhesion tests are an appropriate testing method for thermally sprayed materials.

Author

A90-44869* National Aeronautics and Space Administration. Lewis Research Center, Cleveland, OH.

METALLOGRAPHIC TECHNIQUES FOR EVALUATION OF THERMAL BARRIER COATINGS

WILLIAM J. BRINDLEY (NASA, Lewis Research Center, Cleveland, OH) and TODD A. LEONHARDT (Sverdrup Technologies, Inc., Cleveland, OH) Materials Characterization (ISSN 1044-5803), vol. 24, 1990, p. 93-101. refs Copyright

The performance of ceramic thermal barrier coatings is strongly dependent on the amount and shape of the porosity in the coating. Current metallographic techniques do not provide polished surfaces that are adequate for a repeatable interpretation of the coating structures. A technique recently developed at NASA-Lewis for preparation of thermal barrier coating sections combines epoxy impregnation, careful sectioning and polishing, and interference layering to provide previously unobtainable information on processing-induced porosity. In fact, increased contrast and less ambiguous structure developed by the method make automatic quantitative metallography a viable option for characterizing thermal barrier coating structures. Author

A90-49071* Michigan State Univ., East Lansing. **LINEAR ACENE DERIVATIVES - NEW ROUTES TO PENTACENE AND NAPHTHACENE AND THE FIRST SYNTHESIS OF A TRIPTYCENE WITH TWO ANTHRACENE MOIETIES**

JIHMEI LUO and HAROLD HART (Michigan State University, East Lansing) Journal of Organic Chemistry (ISSN 0022-3263), vol. 52, no. 22, 1987, p. 4833-4836. refs (Contract NAG3-670; NSF CHE-83-19578) Copyright

The cycloaddition of o-xylene to arene 1,4-endoxides was used to construct linear arene derivatives. An analogous sequence but with naphthalene 1,4-endoxides gave naphthacenes. Dehydration of the di adducts from 4 and anthracene 1,4:5,8-diendoxides gave a mixture of 5,9,14,18- and 5,8,15,18-tetrahydroheptacenes 3 and 9. The previously unknown triptycene 2 was synthesized from 5,14-dihydropentacene, an intermediate in the new pentacene synthesis, in three steps and 29 percent overall yield. Author

A90-49072* Michigan State Univ., East Lansing. **BISANNELATION WITH A BENZO(1,2-C:4,5-C-PRIME) DIFURAN EQUIVALENT - A NEW ROUTE TO LINEAR ACENE DERIVATIVES**

JIHMEI LUO and HAROLD HART (Michigan State University, East Lansing) Journal of Organic Chemistry (ISSN 0022-3263), vol. 53, no. 6, 1988, p. 1341-1343. refs (Contract NSF CHE-87-12118; NAG3-670) Copyright

It was observed that the base peak in the mass spectra of all the Diels-Alder bis adducts of anthracene diendoxide as well as of its tetrahydro derivative appear at m/e 158, corresponding to the radical cation of benzo(1,2-c:4,5-c-prime) difuran (BDF). This paper describes a synthetic equivalent of BDF and demonstrates its utility for obtaining linear acene derivatives. I.S.

A90-49073* Michigan State Univ., East Lansing. **IPTYCENE SYNTHESIS: A NEW METHOD FOR ATTACHING A 2,3-ANTHRACENE MOIETY TO THE 9,10-POSITIONS OF ANOTHER ANTHRACENE MOIETY - EXCEPTIONAL CONDITIONS FOR A LEWIS ACID CATALYZED DIELS-ALDER REACTION**

YONG-SHING CHEN and HAROLD HART (Michigan State University, East Lansing) (Midwest-America Chinese Science and

23 CHEMISTRY AND MATERIALS (GENERAL)

Technology Conference, Saint Louis, MO, June 4, 1988) Journal of Organic Chemistry (ISSN 0022-3263), vol. 54, no. 11, 1989, p. 2612-2615. refs

(Contract NSF CHE-87-12118; NAG3-670)

Copyright

An efficient three-step method for appending a 2,3-anthracene moiety to the 9,10-positions of an existing anthracene moiety is described. The first step uses excess 1,4-anthraquinone (3 equiv) and aluminum chloride (6 equiv) to obtain the anthracene-quinone cycloadduct (omission of the AlCl_3 resulted in no adduct). The resulting diketone was reduced to the corresponding diol (excess LiAlH_4), which was dehydrated to the arene with phosphorus oxychloride and pyridine. Specific examples include the preparation of heptyptycene 8 from pentiptycene 6 (66 percent overall yield) and a similar conversion of 8 to the noniptycene 13 (75 percent overall yield). The methodology led to a markedly improved synthesis of triptycene 9 and the first synthesis of undecaptycene 14. Author

N90-12658*# National Aeronautics and Space Administration. Lewis Research Center, Cleveland, OH.

TRIBOLOGICAL PROPERTIES OF CERAMIC/TI3AL-NB SLIDING COUPLES FOR USE AS CANDIDATE SEAL MATERIALS TO 700 DEG C

CHRISTOPHER DELLACORTE, BRUCE M. STEINETZ, and PAMELA K. BRINDLEY 1989 21 p Proposed for presentation at the International Conference on Metallurgical Coatings, San Diego, CA, 2-6 Apr. 1990; sponsored by American Vacuum Society (NASA-TM-102401; E-5048; NAS 1.15:102401) Avail: NTIS HC A03/MF A01 CSCL 07/1

Tribological properties of Ti3Al-Nb intermetallic disks sliding against alumina-boria-silicate fabric were ascertained in air at temperatures from 25 to 700 C. These materials are candidates for sliding seal applications for the National AeroSpace Plane. The tests were done using a pin on disk tribometer. Sliding was unidirectional at 0.27 m/sec under a nominal contact stress of 340 kPa. Gold sputter or ion plating deposited films were used to reduce friction and wear. Rhodium and palladium films were used beneath the gold lubricating films to prevent diffusion of the substrate into the gold at high temperature. The friction and wear of the unlubricated specimens was unacceptable. Friction coefficients were generally greater than 1.0. The ion plated gold films, when used with a rhodium diffusion barrier reduced friction by almost a factor of 2. Wear was also substantially reduced. The sputter deposited films were not adherent unless the substrate was sputter cleaned immediately prior to film deposition. Palladium did not function as a diffusion barrier. Author

N90-12659*# National Aeronautics and Space Administration. Lewis Research Center, Cleveland, OH.

TRIBOLOGICAL PROPERTIES OF PM212: A HIGH-TEMPERATURE, SELF-LUBRICATING, POWDER METALLURGY COMPOSITE

CHRISTOPHER DELLACORTE and HAROLD E. SLINNEY 1989 22 p Proposed for presentation at the Annual Meeting of the Society of Tribologists and Lubrication Engineers, Denver, CO, 7-11 May 1990 (NASA-TM-102355; E-5066; NAS 1.15:102355) Avail: NTIS HC A03/MF A01 CSCL 07/1

This paper describes a research program to develop and evaluate a new high temperature, self-lubricating powder metallurgy composite, PM212. PM212 has the same composition as the plasma-sprayed coating, PS212, which contains 70 wt percent metal-bonded chromium carbide, 15 wt percent silver and 15 wt percent barium fluoride/calcium fluoride eutectic. The carbide acts as a wear resistant matrix and the silver and fluorides act as low and high temperature lubricants, respectively. The material is prepared by sequential cold press, cold isostatic pressing and sintering techniques. In this study, hemispherically tipped wear pins of PM212 were prepared and slid against superalloy disks at temperatures from 25 to 850 C in air in a pin-on-disk tribometer. Friction coefficients range from 0.29 to 0.38 and the wear of both

the composite pins and superalloy disks was moderate to low in the $10(\text{exp } -5)$ to $10(\text{exp } -6)$ cubic mm/N-m range. Preliminary tests indicate that the material has a compressive strength of at least 130 MPa over the entire temperature range of 25 to 900 C. This material has promise for use as seal inserts, bushings, small inside diameter parts and other applications where plasma-sprayed coatings are impractical or too costly. Author

N90-13597*# National Aeronautics and Space Administration. Lewis Research Center, Cleveland, OH.

THE MATERIALS DIVISION: A CASE STUDY

SALVATORE J. GRISAFFE and CARL E. LOWELL 1989 13 p Presented at the Quality Improvement Prototype Workshop, Washington, DC, 6 Sep. 1989 (NASA-TM-102380; E-5119; NAS 1.15:102380) Avail: NTIS HC A03/MF A01 CSCL 07/1

The Materials Division at NASA's Lewis Research Center has been engaged in a program to improve the quality of its output. The division, its work, and its customers are described as well as the methodologies developed to assess and improve the quality of the Division's staff and output. Examples of these methodologies are presented and evaluated. An assessment of current progress is also presented along with a summary of future plans. Author

N90-17811*# National Aeronautics and Space Administration. Lewis Research Center, Cleveland, OH.

THE APPLICATION OF A COMPUTER DATA ACQUISITION SYSTEM FOR A NEW HIGH TEMPERATURE TRIBOMETER

CHARLES D. BONHAM (Sverdrup Technology, Inc., Cleveland, OH.) and CHRISTOPHER DELLACORTE 1990 38 p Proposed for presentation at the Annual Meeting for the Society of Tribologists and Lubrication Engineers, Denver, CO, 7-11 May 1990 (NASA-TM-102508; E-5310; NAS 1.15:102508) Avail: NTIS HC A03/MF A01 CSCL 07/1

The two data acquisition computer programs are described which were developed for a high temperature friction and wear test apparatus, a tribometer. The raw data produced by the tribometer and the methods used to sample that data are explained. In addition, the instrumentation and computer hardware and software are presented. Also shown is how computer data acquisition was applied to increase convenience and productivity on a high temperature tribometer. Author

N90-19300* National Aeronautics and Space Administration. Lewis Research Center, Cleveland, OH.

NEW CONDENSATION POLYIMIDES CONTAINING 1,1,1-TRIARYL-2,2,2-TRIFLUOROETHANE STRUCTURES Patent

WILLIAM B. ALSTON, inventor (to NASA) and ROY F. GRATZ, inventor (to NASA) 4 Jul. 1989 18 p Filed 29 Oct. 1986 (NASA-CASE-LEW-14346-1; US-PATENT-4,845,167; US-PATENT-APPL-SN-924470; US-PATENT-CLASS-528-353; US-PATENT-CLASS-528-352; US-PATENT-CLASS-528-229; US-PATENT-CLASS-528-188) Avail: US Patent and Trademark Office CSCL 07/1

The invention relates to a condensation polyimide containing a 1,1,1-triaryl 2,2,2-trifluoroethane structure and other related condensation polyimides. The process for their preparation, which comprises polymerization of a cyclic dianhydride with a diamine is also covered.

Official Gazette of the U.S. Patent and Trademark Office

N90-19301*# National Aeronautics and Space Administration. Lewis Research Center, Cleveland, OH.

FLUORINATED GRAPHITE FIBERS AS A NEW ENGINEERING MATERIAL: PROMISES AND CHALLENGES

CHING-CHEH HUNG and MARTIN LONG (Cleveland State Univ., OH.) 1989 23 p Presented at the 19th Biennial Conference on Carbon, University Park, PA, 25-30 Jun. 1989; sponsored by American Carbon Society (NASA-TM-102511; E-5313; NAS 1.15:102511) Avail: NTIS HC A03/MF A01 CSCL 07/1

Pitch based graphitized carbon fibers with electrical resistivity of 300 micro-Ohm/cm were brominated and partially debrominated to 18 percent bromine at room temperature, and then fluorinated at 300 to 450 C, either continuously or intermittently for several cycles. In addition, on fluorine and titanium fluoride intercalated fiber sample was fluorinated at 270 C from the same fiber source. The mass and conductivity of the brominated-debrominated then fluorinated fibers (with fluorine-to-carbon atom ratio of 0.54 or higher) stabilized at room temperature air in a few days. However, at 200 C, these values decreased rapidly and then more slowly, throughout a 2-week test period. The electrically insulative or semiconductive fibers were found to be compatible with epoxy and have the fluorine-to-carbon atom ratio of 0.65 to 0.68, thermal conductivity of 5 to 24 W/m-K, electrical resistivity of 10(exp 4) to 10(exp 11) Ohm/cm, tensile strength of 70 to 150 ksi, Young's modulus of 20 to 30 msi, and CTE (coefficient of thermal expansion) values of 7 ppm/deg C. Data of these physical property values are preliminary. However, it is concluded that these physical properties can be tailor-made. They depend largely on the fluorine content of the final products and the intercalant in the fibers before fluorination, and, to a smaller extent, on the fluorination temperature histogram. Author

N90-20130*# National Aeronautics and Space Administration. Lewis Research Center, Cleveland, OH.

EXPERIMENTALLY DETERMINED WEAR BEHAVIOR OF AN AL2O3-SIC COMPOSITE FROM 25 TO 1200 C

CHRISTOPHER DELLACORTE, SERENE C. FARMER, and PATRICIA O. BOOK (Cleveland State Univ., OH.) 1990 22 p Presented at the Tribology of Composite Materials, 1-3 May 1990, Oak Ridge, TN; sponsored by ASM International (NASA-TM-102549; E-5361; NAS 1.15:102549) Avail: NTIS HC A03/MF A01 CSCL 07/1

The sliding wear behavior of a self-mated alumina-silicon carbide whisker toughened composite was studied using optical, scanning electron (SEM) and transmission electron (TEM) microscopy. Because of its excellent strength and toughness properties this composite material is under consideration for use in heat engine applications for sliding contacts which operate at elevated temperatures. The composite's wear behavior and especially its wear mechanisms are not well understood. Pin-on-disk specimens were slid in air at 2.7 m/s sliding velocity, under a 26.5-N load, at temperatures 25 to 1200 C. Pin wear increased with increasing temperature. Based upon the microscopic analyses, the wear mechanism seems to be loosening of the reinforcing whiskers due to frictional and bulk heating. This leads to whisker pullout and increased wear. Author

N90-23476*# National Aeronautics and Space Administration. Lewis Research Center, Cleveland, OH.

DEVELOPMENT OF A QUADRUPOLE-BASED SECONDARY-ION MASS SPECTROMETRY (SIMS) SYSTEM AT LEWIS RESEARCH CENTER

CARLOS VARGAS-ABURTO, PAUL R. ARON, and DALE R. LIFF (Kent State Univ., OH.) Jun. 1990 32 p (NASA-TM-102531; E-5341; NAS 1.15:102531) Avail: NTIS HC A03/MF A01 CSCL 07/1

The design, construction, and initial use of an ion microprobe to carry out secondary ion mass spectrometry (SIMS) of solid samples is reported. The system is composed of a differentially pumped custom-made UHV (Ultra High Vacuum) chamber, a quadrupole mass spectrometer and a telefocus A-DIDA ion gun with the capability of producing beams of Cesium, as well as inert and reactive gases. The computer control and acquisition of the data were designed and implemented using a personal computer with plug-in boards, and external circuitry built as required to suit the system needs. The software is being developed by using a FORTH-like language. Initial tests aimed at characterizing the system, as well as preliminary surface and depth-profiling studies are presently underway. Author

N90-26074*# National Aeronautics and Space Administration. Lewis Research Center, Cleveland, OH.

THE CHEMICAL EFFECTS OF THE MARTIAN ENVIRONMENT ON POWER SYSTEM COMPONENT MATERIALS: A THEORETICAL APPROACH

MARLA E. PEREZ-DAVIS and JAMES R. GAIER Aug. 1990 13 p Presented at the AIChE Summer National Meeting, San Diego, CA, 19-22 Aug. 1990 (NASA-TM-103203; E-5608; NAS 1.15:103203) Avail: NTIS HC A03/MF A01 CSCL 07/3

In the foreseeable future, an expedition may be undertaken to explore the planet Mars. Some of the power source options being considered for such a mission are photovoltaics, regenerative fuel cells and nuclear reactors. In addition to electrical power requirements, environmental conditions en route to Mars, in the planetary orbit and on the Martian surface must be simulated and studied in order to anticipate and solve potential problems. Space power systems components such as photovoltaic arrays, radiators, and solar concentrators may be vulnerable to degradation in the Martian environment. Natural characteristics of Mars which may pose a threat to surface power systems include high velocity winds, dust, ultraviolet radiation, large daily variation in temperature, reaction to components of the soil, atmosphere and atmospheric condensates as well as synergistic combinations. Most of the current knowledge of the characteristics of the Martian atmosphere and soil composition was obtained from the Viking 1 and 2 missions in 1976. A theoretical study is presented which was used to assess the effects of the Martian atmospheric conditions on the power systems components. A computer program written at NASA-Lewis for combustion research that uses a free energy minimization technique was used to calculate chemical equilibrium for assigned thermodynamic states of temperature and pressure. The power system component materials selected for this study include: silicon dioxide, silicon, carbon, copper, and titanium. Combinations of environments and materials considered include: (1) Mars atmosphere with power surface material, (2) Mars atmosphere and dust component with power surface material, and (3) Mars atmosphere and hydrogen peroxide or superoxide or superoxide with power system material. The chemical equilibrium calculations were performed at a composition ratio (oxidant to reactant) of 100. The temperature for the silicon dioxide material and silicon, which simulate photovoltaic cells, were 300 and 400 K; for carbon, copper and titanium, which simulate radiator surfaces, 300, 500, and 1000 K. All of the systems were evaluated at pressures of 700, 800, and 900 Pa, which simulate the Martian atmosphere. Author

24

COMPOSITE MATERIALS

Includes physical, chemical, and mechanical properties of laminates and other composite materials.

A90-13237* Alfred Univ., NY.

MEASUREMENT OF INTERFACIAL SHEAR STRENGTH IN SIC-FIBER/Si3N4 COMPOSITES

JAMES W. LAUGHNER (Alfred University, NY) and RHAM T. BHATT (NASA, Lewis Research Center, Cleveland, OH) American Ceramic Society, Communications (ISSN 0002-7820), vol. 72, Oct. 1989, p. 2017-2019. refs

Copyright

An indentation method for measuring shear strength in brittle matrix composites was applied to SiC-fiber/Si3N4-matrix samples. Three methods were used to manufacture the composites: reaction bonding of a Si/SiC preform, hot-pressing, and nitrogen-overpressure sintering. An indentation technique developed by Marshall for thin specimens was used to measure the shear strength of the interface and the interfacial friction stresses. This was done by inverting the sample after the initial

24 COMPOSITE MATERIALS

push through and retesting the pushed fibers. SEM observations showed that the shear strength was determined by the degree of reaction between the fiber and the matrix unless the fiber was pushed out of its (well-bonded) sheath. Author

A90-16938* National Aeronautics and Space Administration. Lewis Research Center, Cleveland, OH.

1200 TO 1400 K SLOW STRAIN RATE COMPRESSIVE PROPERTIES OF NIAL/NI2ALTI-BASE MATERIALS

J. DANIEL WHITTENBERGER (NASA, Lewis Research Center, Cleveland, OH), R. K. VISWANADHAM (Multi-Metals, Louisville, KY), S. K. MANNAN, and K. S. KUMAR (Martin Marietta Laboratories, Baltimore, MD) IN: High-temperature ordered intermetallic alloys III; Proceedings of the Third Symposium, Boston, MA, Nov. 29-Dec. 1, 1988. Pittsburgh, PA, Materials Research Society, 1989, p. 621-626. refs

Copyright

An attempt to apply the Martin Marietta Corporation's XD technology to the fabrication of NiAl-Ni₂AlTi materials with improved creep properties is presented. Composite materials, containing from 0 to 30 vol pct of nominally 1-micron-diameter TiB₂ particles in the intermetallic matrix have been produced by the XD process and compacted by hot pressing. Such composites demonstrated significant strength increases, approaching 3-fold for the 20 vol pct materials, in comparison to the unreinforced aluminide. This behavior was accomplished without deleterious side effects as the grain boundaries and particle-matrix interfaces were intact after compressive deformation to 10 percent or more strain. Typical true compressive stress-strain diagrams for materials tested in air between 1200 and 1400 K at approximate strain rates of 1.7 x 10 to the -6th/sec are presented. C.E.

A90-17295* National Aeronautics and Space Administration. Lewis Research Center, Cleveland, OH.

UP-AND-COMING IMCS

RANDY BOWMAN and RONALD NOEBE (NASA, Lewis Research Center, Cleveland, OH) Advanced Materials and Processes (ISSN 0882-7958), vol. 136, Aug. 1989, p. 35-40.

Copyright

While the good oxidation and environmental resistance, high melting points, and comparatively low densities of such ordered intermetallics as Ti₃Al, NiAl, FeAl, and NbAl₃ render them good candidates for advanced aerospace structures, their poor toughness at low temperatures and low strength at elevated temperatures have prompted the development of fiber-reinforced intermetallic-matrix composites (IMCs) with more balanced characteristics. Fabrication methods for continuous-fiber IMCs under development include the P/M 'powder cloth' method, the foil/fiber method, and thermal spraying. The ultimate success of IMCs depends on fibers truly compatible with the matrix materials. O.C.

A90-17301* National Aeronautics and Space Administration. Lewis Research Center, Cleveland, OH.

CMCS FOR THE LONG RUN

JAMES A. DICARLO (NASA, Lewis Research Center, Cleveland, OH) Advanced Materials and Processes (ISSN 0882-7958), vol. 135, June 1989, p. 41-44.

Copyright

The structural and environmental requirements for ceramic matrix composites (CMCs) are most demanding in aerospace applications involving human transport; this need for extreme reliability has led to intensive investigations of criteria for high CMC integrity. The ideal properties of a fiber-reinforced CMC have been found to depend on the use of high aspect ratio fibers capable of maximum strength retention during fabrication, uniform fiber infiltration by the matrix material, high matrix oxidation resistance in elevated temperature applications, and a fiber/matrix interface that accommodates debonding in the presence of matrix cracks. O.C.

A90-18973* National Aeronautics and Space Administration. Lewis Research Center, Cleveland, OH.

INVESTIGATION OF INTERFACIAL SHEAR STRENGTH IN A SiC FIBRE/Ti-24Al-11Nb COMPOSITE BY A FIBRE PUSH-OUT TECHNIQUE

J. I. ELDRIDGE (NASA, Lewis Research Center, Cleveland; Sverdrup Technology, Inc., Middleburg Heights, OH) and P. K. BRINDLEY (NASA, Lewis Research Center, Cleveland, OH) Journal of Materials Science Letters (ISSN 0261-8028), vol. 8, Dec. 1989, p. 1451-1454. refs

Copyright

A fiber push-out technique applied at several sample thicknesses was used to determine both the debond shear stress and the frictional shear stress at the fiber-matrix interface at room temperature for a unidirectional SiC fiber-reinforced Ti-24Al-11Nb (in at. pct) composite prepared by a powder cloth technique. The push-out technique measures the separate contributions of bond strength and friction to the mechanical shear strength at the fiber-matrix interface. It was found that the fiber-matrix bond shear strength of this material is significantly higher than the fiber-matrix frictional shear stress (119.2 and 47.8 MPa, respectively). I.S.

A90-19149* National Aeronautics and Space Administration. Lewis Research Center, Cleveland, OH.

ANALYSIS OF WHISKER-TOUGHENED CERAMIC COMPONENTS - A DESIGN ENGINEER'S VIEWPOINT

STEPHEN F. DUFFY, JANE M. MANDERSCHIED, and JOSEPH L. PALKO (NASA, Lewis Research Center; Cleveland State University, OH) American Ceramic Society Bulletin (ISSN 0002-7812), vol. 68, Dec. 1989, p. 2078-2083. refs

Copyright

The analysis of components fabricated from whisker-toughened ceramic matrix composites requires a departure from the 'factor-of-safety' design philosophy prevalent in the design of metallic structural component, which are more tolerant of flaws. A public-domain computer algorithm has been developed which, in conjunction with a general-purpose FEM program, can predict the fast-fracture reliability of a structural component under multiaxial loading conditions. The present version of the algorithm, designated 'Toughened Ceramics Analysis and Reliability Evaluation of Structures', accounts for material symmetry imposed by whisker orientation; the processes of crack deflection and crack pinning are also addressed. O.C.

A90-23188* National Aeronautics and Space Administration. Lewis Research Center, Cleveland, OH.

EFFECT OF FIBER SPACING ON INTERFACIAL DAMAGE IN A METAL MATRIX COMPOSITE

REBECCA A. MACKAY (NASA, Lewis Research Center, Cleveland, OH) Scripta Metallurgica et Materialia (ISSN 0956-716X), vol. 24, Jan. 1990, p. 167-172. refs

Copyright

The nature and the location of cracking in a Ti-V-Cr-Al-Sn/SiC composite (Ti-15V-3Cr-3Al-3Sn, in wt pct, reinforced by 33 vol pct of continuous unidirectional SCS-6SiC fibers) before and after unconstrained thermal cycling were investigated. The material was subjected to 10,000 thermal cycles between 300 and 550 C and samples were examined for cracks in the fiber, the matrix, and the fiber-matrix interface, using a back-scattered SEM. The Ti-based metal matrix composite was found to have a substantial amount of interfacial damage in the form of radial cracks, which formed first in the C-rich coating of the SiC fiber and then in the fiber-matrix reaction zone. The cracking was related to the fiber distribution, with consistently more cracking found between the more closely-spaced fibers within a given row, and more radial cracking in the outside fiber rows. I.S.

A90-23835*# Case Western Reserve Univ., Cleveland, OH.

LOCAL-GLOBAL ANALYSIS OF CRACK GROWTH IN CONTINUOUSLY REINFORCED CERAMIC MATRIX COMPOSITES

ROBERTO BALLARINI and SHAMIM AHMED (Case Western Reserve University, Cleveland, OH) ASME, Gas Turbine and

Aeroengine Congress and Exposition, Toronto, Canada, June 4-8, 1989. 12 p. refs
(Contract NAG3-856)
(ASME PAPER 89-GT-138)

This paper describes the development of a mathematical model for predicting the strength and micromechanical failure characteristics of continuously reinforced ceramic matrix composites. The local-global analysis models the vicinity of a propagating crack tip as a local heterogeneous region (LHR) consisting of spring-like representation of the matrix, fibers and interfaces. Parametric studies are conducted to investigate the effects of LHR size, component properties, and interface conditions on the strength and sequence of the failure processes in the unidirectional composite system. Author

A90-23842* Cleveland State Univ., OH.

A REVIEW OF FAILURE MODELS FOR CERAMIC MATRIX COMPOSITE LAMINATES UNDER MONOTONIC LOADS

DAVID E. TRIPP, JOHN H. HEMANN (Cleveland State University, OH), and JOHN P. GYEKENYESI (NASA, Lewis Research Center, Cleveland, OH) ASME, Gas Turbine and Aeroengine Congress and Exposition, Toronto, Canada, June 4-8, 1989. 13 p. Previously announced in STAR as N89-14470. refs
(Contract NCC3-81)
(ASME PAPER 89-GT-153)

Ceramic matrix composites offer significant potential for improving the performance of turbine engines. In order to achieve their potential, however, improvements in design methodology are needed. In the past most components using structural ceramic matrix composites were designed by trial and error since the emphasis of feasibility demonstration minimized the development of mathematical models. To understand the key parameters controlling response and the mechanics of failure, the development of structural failure models is required. A review of short term failure models with potential for ceramic matrix composite laminates under monotonic loads is presented. Phenomenological, semi-empirical, shear-lag, fracture mechanics, damage mechanics, and statistical models for the fast fracture analysis of continuous fiber unidirectional ceramic matrix composites under monotonic loads are surveyed. Author

A90-25238* National Aeronautics and Space Administration. Lewis Research Center, Cleveland, OH.

IDENTIFICATION OF THERMODYNAMICALLY STABLE CERAMIC REINFORCEMENT MATERIALS FOR IRON ALUMINIDE MATRICES

AJAY K. MISRA (NASA, Lewis Research Center; Sverdrup Technology, Inc., Cleveland, OH) Metallurgical Transactions A - Physical Metallurgy and Materials Science (ISSN 0360-2133), vol. 21A, Feb. 1990, p. 441-446. refs
Copyright

Aluminide-base intermetallic matrix composites are currently being considered as potential high-temperature materials. One of the key factors in the selection of a reinforcement material is its chemical stability in the matrix. In this study, chemical interactions between iron aluminides and several potential reinforcement materials, which include carbides, oxides, borides, and nitrides, are analyzed from thermodynamic considerations. Several chemically compatible reinforcement materials are identified for the iron aluminides with Al concentrations ranging from 40 to 50 at. pct. Author

A90-25268* Virginia Polytechnic Inst. and State Univ., Blacksburg.

ROLE OF THE INTERFACIAL THERMAL BARRIER IN THE EFFECTIVE THERMAL DIFFUSIVITY/CONDUCTIVITY OF SIC-FIBER-REINFORCED REACTION-BONDED SILICON NITRIDE

HEMANSHU BHATT, KIMBERLY Y. DONALDSON, D. P. H. HASSELMAN (Virginia Polytechnic Institute and State University, Blacksburg), and R. T. BHATT (NASA, Lewis Research Center, Cleveland, OH) American Ceramic Society, Journal (ISSN

0002-7820), vol. 73, Feb. 1990, p. 312-316. refs
Copyright

Experimental thermal diffusivity data transverse to the fiber direction for composites composed of a reaction bonded silicon nitride matrix reinforced with uniaxially aligned carbon-coated silicon carbide fibers indicate the existence of a significant thermal barrier at the matrix-fiber interface. Calculations of the interfacial thermal conductances indicate that at 300 C and 1-atm N₂, more than 90 percent of the heat conduction across the interface occurs by gaseous conduction. Good agreement is obtained between thermal conductance values for the oxidized composite at 1 atm calculated from the thermal conductivity of the N₂ gas and those inferred from the data for the effective composite thermal conductivity. Author

A90-25609* National Aeronautics and Space Administration. Lewis Research Center, Cleveland, OH.

APPLICATIONS OF HIGH THERMAL CONDUCTIVITY COMPOSITES TO ELECTRONICS AND SPACECRAFT THERMAL DESIGN

G. RICHARD SHARP (NASA, Lewis Research Center, Cleveland, OH) and TIMOTHY A. LOFTIN (DWA Composite Specialties, Inc., Chatsworth, CA) IN: AIAA International Communication Satellite Systems Conference and Exhibit, 13th, Los Angeles, CA, Mar. 11-15, 1990, Technical Papers. Part 1. Washington, DC, American Institute of Aeronautics and Astronautics, 1990, p. 59-64. (AIAA PAPER 90-0783) Copyright

Recently, high thermal conductivity graphite fiber-reinforced metal matrix composites (MMCs) have become available that can save weight over present methods of heat conduction. Another significant advantage is that these materials can be used without the plumbing and testing complexities that accompany the use of liquid heat pipes. A spinoff of this research was the development of other MMCs as electronic device heat sinks. These use particulates rather than fibers and are formulated to match the coefficient of thermal expansion of electronic substrates in order to alleviate thermally induced stresses. The development of both types of these materials as viable weight-saving substitutes for the traditional methods of thermal control for electronics packaging and also for spacecraft thermal control applications are the subjects of this report. Author

A90-26561* Cleveland State Univ., OH.

NONINTERACTIVE MACROSCOPIC RELIABILITY MODEL FOR WHISKER-REINFORCED CERAMIC COMPOSITES

STEPHEN F. DUFFY (Cleveland State University, OH) and STEVEN M. ARNOLD (NASA, Lewis Research Center, Cleveland, OH) Journal of Composite Materials (ISSN 0021-9983), vol. 24, March 1990, p. 293-308. refs
(Contract NCC3-81)
Copyright

Considerable research is underway in the field of material science focusing on incorporating silicon carbide whiskers into silicon nitride and alumina matrices. These composites show the requisite thermal stability and thermal shock resistance necessary for use as components in advanced gas turbines and heat exchangers. This paper presents a macroscopic noninteractive reliability model for whisker-reinforced ceramic composites. The theory is multiaxial and is applicable to composites that can be characterized as transversely isotropic. Enough processing data exists to suggest this idealization encompasses a significantly large class of fabricated components. A qualitative assessment of the model is made by presenting reliability surfaces in several different stress spaces and for different values of model parameters. Author

A90-27065* National Aeronautics and Space Administration. Lewis Research Center, Cleveland, OH.

POLYMER DERIVED NICALON/SI-C-O COMPOSITES - PROCESSING AND MECHANICAL BEHAVIOR

FRANCES I. HURWITZ (NASA, Lewis Research Center, Cleveland, OH), JOHN Z. GYEKENYESI, and PAULA J. CONROY (Cleveland State University, OH) Ceramic Engineering and Science

24 COMPOSITE MATERIALS

Proceedings (ISSN 0196-6219), vol. 10, July-Aug. 1989, p. 750-763. refs

Copyright

Ceramic matrix composites fabricated using Nicalon fiber and several polysilsesquioxane-derived Si-C-O matrices were characterized by optical and SEM and in four-point bending. In the matrix material linear shrinkages of up to 19 percent were observed for the vinylmethyl copolymer pyrolyzed to 1200 C, and up to 13 percent for the phenylmethyl material pyrolyzed to the same temperature, resulting in considerable matrix cracking. Under four-point loading, most composite samples fractured in a brittle manner as the result of strong fiber-matrix bonding. Flexural strengths, moduli, and ultimate strain varied with fiber sizing and processing parameters. Testing and analysis is being applied to promote more fibrous pullout during fracture. Author

A90-27076* Massachusetts Inst. of Tech., Cambridge.
NITRIDING KINETICS OF SI-SiC POWDER MIXTURES AS SIMULATIONS OF REACTION BONDED Si3N4-SiC COMPOSITES

A. LIGHTFOOT, B. W. SHELDON, J. H. FLINT, and J. S. HAGGERTY (MIT, Cambridge, MA) Ceramic Engineering and Science Proceedings (ISSN 0196-6219), vol. 10, Sept.-Oct. 1989, p. 1035-1048. refs
(Contract NAG3-845)

Copyright

The nitriding kinetics of Si and Si plus SiC powder mixtures were studied to simulate the fabrication of RBSN-SiC ceramic matrix composites. Very clean, assynthesized, and solvent-exposed powders were studied; C-rich and Si-rich SiC 0.04-0.05 micron diameter powders were mixed in varying concentrations with SiH4-derived 0.2-0.3 micron diameter Si powder. Complete nitridation is achieved with C-rich SiC powders in 140 min at 1250 C, and in the centers of Si-rich SiC powders in 15 min. The effects on the incubation periods, fast reaction periods, and slow reaction periods that characterize these nitriding processes were studied to explain unusual reverse reaction gradients and other effects of contamination. Author

A90-29228* National Aeronautics and Space Administration. Lewis Research Center, Cleveland, OH.

EVALUATION OF THERMAL AND MECHANICAL LOADING EFFECTS ON THE STRUCTURAL BEHAVIOR OF A SiC/TITANIUM COMPOSITE

J. E. GRADY and B. A. LERCH (NASA, Lewis Research Center, Cleveland, OH) IN: AIAA/ASME/ASCE/AHS/ASC Structures, Structural Dynamics and Materials Conference, 31st, Long Beach, CA, Apr. 2-4, 1990, Technical Papers. Part 1. Washington, DC, American Institute of Aeronautics and Astronautics, 1990, p. 9-15. refs

(AIAA PAPER 90-1026) Copyright

Composite specimens of titanium-15-3 matrix reinforced with continuous SCS-6 silicon carbide fibers were tested under a variety of thermal and mechanical loadings. A combined experimental/finite element approach was used to estimate the effective in situ modulus of the matrix material and to evaluate changes in modulus due to the applied loads. Several fiber orientations were tested. Results indicate that the effect of thermal loads on composite stiffness varies with fiber orientation. Applications of this method to test specimens damaged by uniaxial tension, thermal cycling, and isothermal fatigue loadings are used to illustrate that by monitoring overall structural behavior, changes in stiffness caused by thermomechanical loading can be detected. Author

A90-29704* National Aeronautics and Space Administration. Lewis Research Center, Cleveland, OH.

COMPOSITES BOOST 21ST-CENTURY AIRCRAFT ENGINES

JOSEPH R. STEPHENS (NASA, Lewis Research Center, Cleveland, OH) Advanced Materials and Processes (ISSN 0882-7958), vol. 137, April 1990, p. 35-38.

Copyright

Research and development in light-weight, high-temperature

composite materials for ultrahigh-bypass engines to be used in high-speed civil transport/rotocraft is presented. It is noted that the expected benefits to be attained by this R&D include weight reduction, lowered fuel consumption, and lower direct operating costs. A major effort underway in this area is the Advanced High Temperature Engine Materials Technology Program (HITEMP) of NASA, which focuses on providing revolutionary high-temperature composite materials: to 425 C (800 F) for polymer-matrix composites (PMCs), to 1250 C (2280 F) for metal-matrix/intermetallic-matrix composites (MMCs/IMCs), and to as high as 1650 C (3000 F) for ceramic-matrix composites (CMCs). Analytical modeling is being used to investigate the structural behavior of these advanced materials in six distinct areas: micromechanics, deformation and damage, fatigue, fracture, trade-off studies, and load definition. It is concluded that the development of advanced materials such as high-temperature composites is highly dependent on the availability of high-temperature fibers. The wide range of fiber characteristics needed will require the development of more than one fiber. In general, a candidate fiber should have low density, high strength, high stiffness, a CTE matching the matrix, chemical compatibility with the matrix, environmental stability and appropriate fiber diameter. R.E.P.

A90-29927* National Aeronautics and Space Administration. Lewis Research Center, Cleveland, OH.

LAMINATE BEHAVIOR FOR SiC FIBER-REINFORCED REACTION-BONDED SILICON NITRIDE MATRIX COMPOSITES

RAMAKRISHNA T. BHATT (NASA, Lewis Research Center; U.S. Army, Propulsion Laboratory, Cleveland, OH) and RONALD E. PHILLIPS (BP America, Warrensville, OH) Journal of Composites Technology and Research (ISSN 0885-6804), vol. 12, Spring 1990, p. 13-23. Previously announced in STAR as N89-10952. refs

Copyright
The room temperature mechanical properties of SiC fiber reinforced reaction-bonded silicon nitride matrix composite laminates (SiC/RBSN) have been measured. The laminates contained approx 30 volume fraction of aligned 142-micron diameter SiC fiber in a porous RBSN matrix. Three types of laminate studied were unidirectional: (1) (0) sub 8, (2) (10) sub 8, and (3) (45) sub 8, and (90) sub 8; cross plied laminates (0 sub 2/90 sub 2); and angle plied laminates: (+45 sub 2/-45 sub 2). Each laminate contained eight fiber plies. Results of the unidirectionally reinforced composites tested at various angles to the reinforcement direction indicate large anisotropy in in-plane properties. In addition, strength properties of these composites along the fiber direction were independent of specimen gage length and were unaffected by notches normal to the fiber direction. Splitting parallel to the fiber at the notch tip appears to be the dominant crack blunting mechanism responsible for notch insensitive behavior of these composites. In-plane properties of the composites can be improved by 2-D laminate construction. Mechanical property results for (0 sub 2/90 sub 2) sub s and (+45/-45 sub 2) sub s laminates showed that their matrix failure strains were similar to that for (0) sub 8 laminates, but their primary elastic moduli, matrix cracking strengths, and ultimate composite strengths were lower. The elastic properties of unidirectional, cross-ply, and angle-ply composites can be predicted from modified constitutive equations and laminate theory. Further improvements in laminate properties may be achieved by reducing the matrix porosity and by optimizing the bond strength between the SiC fiber and RBSN matrix. Author

A90-29929* National Aeronautics and Space Administration. Lewis Research Center, Cleveland, OH.

UNIFIED MICROMECHANICS OF DAMPING FOR UNIDIRECTIONAL AND OFF-AXIS FIBER COMPOSITES

DIMITRIS A. SARAVANOS and CHRISTOS C. CHAMIS (NASA, Lewis Research Center, Cleveland, OH) Journal of Composites Technology and Research (ISSN 0885-6804), vol. 12, Spring 1990, p. 31-40. refs

Copyright

An integrated micromechanics methodology for the prediction of damping capacity in fiber-reinforced polymer matrix unidirectional

composites has been developed. Explicit micromechanics equations based on hysteretic damping are presented relating the on-axis damping capacities to the fiber and matrix properties and fiber volume ratio. The damping capacities of unidirectional composites subjected to off-axis loading are synthesized from on-axis damping values. Predicted values correlate satisfactorily with experimental measurements. The hygro-thermal effect on the damping performance of unidirectional composites caused by temperature and moisture variations is also modeled. The damping contributions from interfacial friction between broken fibers and matrix are incorporated. Finally, the temperature rise in continuously vibrating composite plies is estimated. Application examples illustrate the significance of various parameters on the damping performance of unidirectional and off-axis fiber reinforced composites. Author

A90-31555* National Aeronautics and Space Administration. Lewis Research Center, Cleveland, OH.

MEASUREMENTS OF PRINT-THROUGH IN GRAPHITE FIBER EPOXY COMPOSITES

DONALD A. JAWORSKE (NASA, Lewis Research Center, Cleveland, OH), TIMOTHY T. JEUNETTE, and JUDITH M. ANZIC (Cleveland State University, OH) IN: International SAMPE Symposium and Exhibition, 34th, Reno, NV, May 8-11, 1989, Proceedings. Book 1. Covina, CA, Society for the Advancement of Material and Process Engineering, 1989, p. 780-789.

Copyright

High-reflectance accurate-contour mirrors are needed for solar dynamic space power systems. Graphite fiber epoxy composites are attractive candidates for such applications owing to their high modulus, near-zero coefficient of thermal expansion, and low mass. However, mirrors prepared from graphite fiber epoxy composite substrates often exhibit print-through, a distortion of the surface, which causes a loss in solar specular reflectance. Efforts to develop mirror substrates without print-through distortion require a means of quantifying print-through. Methods have been developed to quantify the degree of print-through in graphite fiber epoxy composite specimens using surface profilometry. Author

A90-34169* National Aeronautics and Space Administration. Lewis Research Center, Cleveland, OH.

FIBER REINFORCED SUPERALLOYS

DONALD W. PETRASEK, ROBERT A. SIGNORELLI (NASA, Lewis Research Center, Cleveland, OH), THOMAS CAULFIELD, and JOHN K. TIEN (Columbia University, New York) IN: Superalloys, supercomposites and superceramics. San Diego, CA, Academic Press, Inc., 1989, p. 625-670. Previously announced in STAR as N87-22811. refs

Copyright

Improved performance of heat engines is largely dependent upon maximum cycle temperatures. Tungsten fiber reinforced superalloys (TFRS) are the first of a family of high temperature composites that offer the potential for significantly raising hot component operating temperatures and thus leading to improved heat engine performance. This status review of TFRS research emphasizes the promising property data developed to date, the status of TFRS composite airfoil fabrication technology, and the areas requiring more attention to assure their applicability to hot section components of aircraft gas turbine engines. Author

A90-36746* National Aeronautics and Space Administration. Lewis Research Center, Cleveland, OH.

ISOTHERMAL AND NONISOTHERMAL FATIGUE BEHAVIOR OF A METAL MATRIX COMPOSITE

T. P. GABB, J. GAYDA, and R. A. MACKAY (NASA, Lewis Research Center, Cleveland, OH) Journal of Composite Materials (ISSN 0021-9983), vol. 24, June 1990, p. 667-686. refs

Copyright

The isothermal and nonisothermal fatigue resistance of a metal matrix composite (MMC) consisting of Ti-15V-3Cr-3Al-3Sn (Ti-15-3) matrix reinforced by 33 vol pct continuous SiC fibers was investigated. The fibers were nominally oriented parallel to the specimen axis. Isothermal fatigue tests were performed in air at

300 and 550 C. The MMC had good isothermal fatigue resistance at low cyclic stress, with fatigue cracks initiating from fiber-matrix interfaces and foil laminations. At high cyclic stresses, stress relaxation in the matrix reduced isothermal composite fatigue resistance at 550 C. Nonisothermal fatigue loading substantially degraded composite fatigue resistance. This degradation was produced by a thermomechanical fatigue damage mechanism associated with the fiber-matrix interfaces. Author

A90-36802* National Aeronautics and Space Administration. Lewis Research Center, Cleveland, OH.

CHARACTERIZATION OF INTERFACIAL FAILURE IN SiC REINFORCED Si3N4 MATRIX COMPOSITE MATERIAL BY BOTH FIBER PUSH-OUT TESTING AND AUGER ELECTRON SPECTROSCOPY

J. I. ELDRIDGE (NASA, Lewis Research Center, Cleveland; Sverdrup Technology, Inc., Middleburg Heights, OH) and F. S. HONECY (NASA, Lewis Research Center, Cleveland, OH) Journal of Vacuum Science and Technology A (ISSN 0734-2101), vol. 8, pt. 1, May-June 1990, p. 2101-2106. refs

Copyright

AES depth profiling and a fiber push-out test for interfacial shear-strength determination have been used to ascertain the mechanical/chemical properties of the fiber/matrix interface in SiC-reinforced reaction-bonded Si3N4, with attention to the weak point where interfacial failure occurs. In the cases of both composite fracture and fiber push-outs, the interfacial failure occurred either between the two C-rich coatings that are present on the double-coated SiC fibers, or between the inner C-rich coating and the SiC fiber. Interface failure occurs at points of very abrupt concentration changes. O.C.

A90-37663* National Aeronautics and Space Administration. Lewis Research Center, Cleveland, OH.

MICROSTRUCTURE OF A SiC/Ti-15-3 COMPOSITE

B. A. LERCH, D. R. HULL (NASA, Lewis Research Center, Cleveland, OH), and T. A. LEONHARDT (NASA, Lewis Research Center; Sverdrup Technology, Inc., Cleveland, OH) Composites (ISSN 0010-4361), vol. 21, May 1990, p. 216-224. refs

Copyright

A continuous SiC-fiber-reinforced titanium (Ti-15V-3Cr-3Sn-3Al) composite was metallographically examined. Several methods for examining composite materials were investigated and documented. Polishing techniques for this material are described. An interference layering method was developed to reveal the structure of the fiber, the reaction zone, and various phases within the matrix. Microprobe and TEM analyses were performed on the fiber-matrix interface. Detailed descriptions of the fiber distribution and the microstructure of the fiber and matrix are presented. Author

A90-39627* Aluminum Co. of America, Alcoa Center, PA. **REACTION ZONE MICROSTRUCTURE IN A Ti3Al + Nb/SiC COMPOSITE**

S. F. BAUMANN, S. D. SMITH (Alcoa Technical Center, Alcoa Center, PA), and P. K. BRINDLEY (NASA, Lewis Research Center, Cleveland, OH) Metallurgical Transactions A - Physical Metallurgy and Materials Science (ISSN 0360-2133), vol. 21A, June 1990, p. 1559-1569. refs

Copyright

A composite of Ti-25Al-13Nb (atomic percent) matrix with a continuous SiC fiber (SCS-6) reinforcement was fabricated by hot pressing powder cloths and mats of fiber. The fiber/matrix reaction zone was studied using scanning electron microscopy (SEM) and transmission electron microscopy/analytical electron microscopy (TEM/AEM) techniques. The extent of reaction was determined, phases were identified, and solute partitioning among the phases was determined. It was found that the matrix had reacted only with a portion of the carbon-rich outer layer of the SCS-6 fiber. The reaction zone contained two concentric zones which are distinguished by the presence of different carbide phases. Both zones contained a hexagonal Si-bearing phase, and one of the zones also contained some fine scattered porosity. The results

24 COMPOSITE MATERIALS

are discussed with reference to available phase equilibria data.

Author

A90-44001* National Aeronautics and Space Administration. Lewis Research Center, Cleveland, OH.

THERMODYNAMIC ANALYSIS OF CHEMICAL COMPATIBILITY OF CERAMIC REINFORCEMENT MATERIALS WITH NIOBIUM ALUMINIDES

AJAY K. MISRA (NASA, Lewis Research Center; Sverdrup Technology, Inc., Cleveland, OH) Journal of Materials Research (ISSN 0884-2914), vol. 5, July 1990, p. 1561-1566. Previously announced in STAR as N89-21036. refs
Copyright

Chemical compatibility of several reinforcement materials with three niobium aluminides, Nb₃Al, Nb₂Al, and NbAl₃, were examined from thermodynamic considerations. The reinforcement materials considered in this study include carbides, borides, nitrides, oxides, silicides, and Engel-Brewer compounds. Thermodynamics of the Nb-Al system were reviewed and activities of Nb and Al were derived at desired calculation temperatures. Criteria for chemical compatibility between the reinforcement material and Nb-Al compounds have been defined and several chemically compatible reinforcement materials have been identified.

Author

A90-45271* National Aeronautics and Space Administration. Lewis Research Center, Cleveland, OH.

METAL MATRIX COMPOSITE MICROMECHANICS - IN SITU BEHAVIOR INFLUENCE ON COMPOSITE PROPERTIES

P. L. N. MURTHY, D. A. HOPKINS, and C. C. CHAMIS (NASA, Lewis Research Center, Cleveland, OH) IN: Mechanics of composite materials and structures; Proceedings of the Third Joint ASCE/ASME Mechanics Conference, La Jolla, CA, July 9-12, 1989. New York, American Society of Mechanical Engineers, 1989, p. 41-48.

Copyright

The influence of in situ fiber and matrix properties (such as in situ matrix strength and the interphase degradation) of high-temperature metal matrix composites (HTMMCs) on the unidirectional stress-strain behavior of the composite is examined using results of a numerical investigation of a SiC/Ti-15-3-3-3 unidirectional composite. It is shown that a reduction of the in situ matrix strength substantially decreases the transverse and the longitudinal tensile/compressive strengths, as well as the in-plane shear strength, of the composite. The interphase degradation affects the behavior in transverse tension/compression drastically; both the ultimate strength and strain showed significant reductions. The higher use temperature results in a reduction in the ultimate strength and in the initial tangential modulus for compression and for in-plane shear loading.

I.S.

A90-45621* National Aeronautics and Space Administration. Lewis Research Center, Cleveland, OH.

ELEVATED TEMPERATURE SLOW PLASTIC DEFORMATION OF NIAL-TiB2 PARTICULATE COMPOSITES AT 1200 AND 1300 K

J. DANIEL WHITTENBERGER (NASA, Lewis Research Center, Cleveland, OH), R. K. VISWANADHAM, S. K. MANNAN, and B. SPRISLER (Martin Marietta Laboratories, Baltimore, MD) Journal of Materials Science (ISSN 0022-2461), vol. 25, no. 1A, Jan. 1990, p. 35-44. refs

(Contract N00014-85-C-0639)

Copyright

Elevated temperature compression testing has been conducted in air at 1200 and 1300 K with strain rates varying from about 10 to the -4th to about 10 to the -7th/sec on NiAl-TiB₂ particulate composites. These materials, which consisted of a B2 crystal structure intermetallic Ni-50 at. pct Al matrix and from 0 to 30 vol pct of approximately 1- micron diameter TiB₂ particles, were fabricated by XD synthesis and hot pressed to full density. Flow strength of the composites increased with volume fraction of the strengthening phase with NiAl-30TiB₂ being approximately three times stronger than NiAl. Comparison of the light optical and TEM microstructures of as-received and tested samples revealed that

reactions did not occur between the two phases, and NiAl-TiB₂ interfaces were not cracked during deformation. Additional TEM indicated that the particles stabilize a vastly different microstructure in the NiAl matrix of the composites than that formed in unreinforced NiAl.

Author

A90-46133* National Aeronautics and Space Administration. Lewis Research Center, Cleveland, OH.

SLOW PLASTIC DEFORMATION OF EXTRUDED NIAL-10TiB2 PARTICULATE COMPOSITES AT 1200 AND 1300 K

J. D. WHITTENBERGER (NASA, Lewis Research Center, Cleveland, OH), S. KUMAR, S. K. MANNAN, and R. K. VISWANADHAM (Martin Marietta Laboratories, Baltimore, MD) Journal of Materials Science Letters (ISSN 0261-8028), vol. 9, March 1990, p. 326-328.

Copyright

A dispersion of 1-micron TiB₂ particles in the B2 crystal structure NiAl intermetallic can effectively increase its elevated temperature strength, in association with increasing deformation resistance with TiB₂ volume fraction. Attention is presently given to alternative densification methods, which may increase the initial as-fabricated dislocation density and lead to enhanced elevated-temperature strength. The 'XD' extrusion method was used to produce NiAl with 10 vol pct TiB₂. Although apparent extrusion defects were occasionally found, neither grain-boundary cracking nor particle-matrix separation occurred.

O.C.

A90-46999* Army Propulsion Lab., Cleveland, OH.

THERMAL EFFECTS ON THE MECHANICAL PROPERTIES OF SiC FIBRE REINFORCED REACTION-BONDED SILICON NITRIDE MATRIX COMPOSITES

R. T. BHATT (U.S. Army, Propulsion Directorate, Cleveland, OH) and R. E. PHILLIPS (NASA, Lewis Research Center; Sverdrup Technology, Inc., Cleveland, OH) Journal of Materials Science (ISSN 0022-2461), vol. 25, July 1990, p. 3401-3407. Previously announced in STAR as N89-10134. refs

Copyright

The elevated temperature four-point flexural strength and the room temperature tensile and flexural strength properties after thermal shock were measured for ceramic composites consisting of 30 vol pct uniaxially aligned 142 micron diameter SiC fibers in a reaction bonded Si₃N₄ matrix. The elevated temperature strengths were measured after 15 min of exposure in air at temperatures to 1400 C. Thermal shock treatment was accomplished by heating the composite in air for 15 min at temperatures to 1200 C and then quenching in water at 25 C. The results indicate no significant loss in strength properties either at temperature or after thermal shock when compared with the strength data for composites in the as-fabricated condition.

Author

A90-48115* National Aeronautics and Space Administration. Lewis Research Center, Cleveland, OH.

ISOTHERMAL LIFE PREDICTION OF COMPOSITE LAMINA USING A DAMAGE MECHANICS APPROACH

NADER MOHAMED ABUELFOUTOUH, M. J. VERRILLI, and G. R. HALFORD (NASA, Lewis Research Center, Cleveland, OH) IN: Symposium on High Temperature Composites - Proceedings of the American Society for Composites, Dayton, OH, June 13-15, 1989. Lancaster, PA, Technomic Publishing Co., Inc., 1989, p. 121-130. Previously announced in STAR as N89-24460.

Copyright

A method for predicting isothermal plastic fatigue life of a composite lamina is presented in which both fibers and matrix are isotropic materials. In general, the fatigue resistances of the matrix, fibers, and interfacial material must be known in order to predict composite fatigue life. Composite fatigue life is predicted using only the matrix fatigue resistance due to inelasticity micromechanisms. The effect of the fiber orientation on loading direction is accounted for while predicting composite life. The application is currently limited to isothermal cases where the internal thermal stresses that might arise from thermal strain mismatch between fibers and matrix are negligible. The theory is formulated

to predict the fatigue life of a composite lamina under either load or strain control. It is applied currently to predict the life of tungsten-copper composite lamina at 260 C under tension-tension load control. The calculated life of the lamina is in good agreement with available composite low cycle fatigue data. Author

A90-48636* Martin Marietta Corp., Baltimore, MD.
HIGH-TEMPERATURE SLOW-STRAIN-RATE COMPRESSION STUDIES ON COAL-TiB₂ COMPOSITES

S. K. MANNAN, K. S. KUMAR (Martin Marietta Laboratories, Baltimore, MD), and J. D. WHITTENBERGER (NASA, Lewis Research Center, Cleveland, OH) Metallurgical Transactions A - Physical Metallurgy and Materials Science (ISSN 0360-2133), vol. 21A, Aug. 1990, p. 2179-2188. refs
 (Contract N00014-85-C-0639)
 Copyright

Results are presented of compressive deformation tests performed on particulate-reinforced CoAl-TiB₂ composites in the temperature range 1100-1300 K. Hot-pressed and postdeformation microstructures were characterized by TEM and by optical microscopy. It was found that the addition of TiB₂ particles improves the deformation resistance of the matrix, due to dislocation-particle interactions. I.S.

A90-50068* National Aeronautics and Space Administration.
 Lewis Research Center, Cleveland, OH.

THERMO-OXIDATIVE STABILITY STUDIES OF PMR-15 POLYMER MATRIX COMPOSITES REINFORCED WITH VARIOUS CONTINUOUS FIBERS

KENNETH J. BOWLES (NASA, Lewis Research Center, Cleveland, OH) IN: International SAMPE Symposium and Exhibition, 35th, Anaheim, CA, Apr. 2-5, 1990, Proceedings. Book 1. Covina, CA, Society for the Advancement of Material and Process Engineering, 1990, p. 147-161. refs
 Copyright

An experimental study was conducted to measure the thermooxidative stability of PMR-15 composites reinforced with various fibers and to observe differences in the way they degrade in air. The fibers studied include graphite and the thermally stable Nicalon and Nextel ceramic fibers. Weight-loss rates for the different composites were assessed as a function of mechanical properties, specimen geometry, fiber sizing, and interfacial bond strength. Differences were observed in rates of weight loss, matrix cracking, geometry dependency, and fiber sizing effects. It was shown that Celion 6000 fiber-reinforced composites do not exhibit a straight-line Arrhenius relationship at temperatures above 316 C. Author

A90-50093* National Aeronautics and Space Administration.
 Lewis Research Center, Cleveland, OH.

PARAMETRIC STUDIES TO DETERMINE THE EFFECT OF COMPLIANT LAYERS ON METAL MATRIX COMPOSITE SYSTEMS

J. J. CARUSO, C. C. CHAMIS (NASA, Lewis Research Center, Cleveland, OH), and H. C. BROWN (NASA, Lewis Research Center; Sverdrup Technology, Inc., Cleveland, OH) IN: International SAMPE Symposium and Exhibition, 35th, Anaheim, CA, Apr. 2-5, 1990, Proceedings. Book 1. Covina, CA, Society for the Advancement of Material and Process Engineering, 1990, p. 468-478. Previously announced in STAR as N90-14294. refs
 Copyright

Computational simulation studies are conducted to identify compliant layers to reduce matrix stresses which result from the coefficient of thermal expansion mismatch and the large temperature range over which the current metal matrix composites will be used. The present study includes variations of compliant layers and their properties to determine their influence on unidirectional composite and constituent response. Two simulation methods are used for these studies. The first approach is based on a three-dimensional linear finite element analysis of a 9 fiber unidirectional composite system. The second approach is a micromechanics based nonlinear computer code developed to determine the behavior of metal matrix composite system for

thermal and mechanical loads. The results show that an effective compliant layer for the SCS 6 (SiC)/Ti-24Al-11Nb (Ti3Al + Nb) and SCS 6 (SiC)/Ti-15V-3Cr-3Sn-3Al (Ti-15-3) composite systems should have modulus 15 percent that of the matrix and a coefficient of thermal expansion of the compliant layer roughly equal to that of the composite system without the CL. The matrix stress in the longitudinal and the transverse tangent (loop) direction are tensile for the Ti3Al + Nb and Ti-15-3 composite systems upon cool down from fabrication. The fiber longitudinal stress is compressive from fabrication cool down. Addition of a recommended compliant layer will result in a reduction in the composite modulus. Author

A90-50094* National Aeronautics and Space Administration.
 Lewis Research Center, Cleveland, OH.

INTERFACIAL EFFECTS ON THE BEHAVIOR OF PARTIALLY BONDED METAL MATRIX COMPOSITE PROPERTIES

J. J. CARUSO and C. C. CHAMIS (NASA, Lewis Research Center, Cleveland, OH) IN: International SAMPE Symposium and Exhibition, 35th, Anaheim, CA, Apr. 2-5, 1990, Proceedings. Book 1. Covina, CA, Society for the Advancement of Material and Process Engineering, 1990, p. 479-491. refs
 Copyright

A novel computational method developed at NASA-Lewis in order to predict the behavior of unidirectional composites has been used to explore the effects of partial debonding and fiber fracture on the behavior of room temperature and high temperature metal-matrix composites. Attention is presently given to the influence of disbonding, which occurs with fractured fibers, on the ply properties of metal-matrix composites with orthotropic fibers, in the case of a graphite fiber-reinforced copper-matrix composite. It is shown that, for small amounts of partial bonding on fractured fibers, composite material properties are not significantly affected. O.C.

A90-50095* National Aeronautics and Space Administration.
 Lewis Research Center, Cleveland, OH.

FUNDAMENTAL ASPECTS AND FAILURE MODES IN HIGH-TEMPERATURE COMPOSITES

C. C. CHAMIS and C. A. GINTY (NASA, Lewis Research Center, Cleveland, OH) IN: International SAMPE Symposium and Exhibition, 35th, Anaheim, CA, Apr. 2-5, 1990, Proceedings. Book 1. Covina, CA, Society for the Advancement of Material and Process Engineering, 1990, p. 492-505. refs
 Copyright

Fundamental aspects and attendant failure mechanisms for high-temperature composites are summarized. These include in situ matrix behavior, load transfer, limits on matrix ductility to survive a given number of cyclic loadings, fundamental parameters which govern thermal stresses, vibration stresses and impact resistance, as well as their attendant failure mechanisms and failure sequences. The resulting guidelines are presented in terms of simple equations which are suitable for the preliminary assessment of the merits of a particular high-temperature composite in a specific application. Author

A90-50096* National Aeronautics and Space Administration.
 Lewis Research Center, Cleveland, OH.

OPTIMAL FABRICATION PROCESSES FOR UNIDIRECTIONAL METAL-MATRIX COMPOSITES - A COMPUTATIONAL SIMULATION

D. A. SARAVANOS, P. L. N. MURTHY, and M. MOREL (NASA, Lewis Research Center, Cleveland, OH) IN: International SAMPE Symposium and Exhibition, 35th, Anaheim, CA, Apr. 2-5, 1990, Proceedings. Book 1. Covina, CA, Society for the Advancement of Material and Process Engineering, 1990, p. 506-519. Previously announced in STAR as N90-21143. refs
 Copyright

A method is proposed for optimizing the fabrication process of unidirectional metal matrix composites. The temperature and pressure histories are optimized such that the residual microstresses of the composite at the end of the fabrication process are minimized and the material integrity throughout the process is ensured. The response of the composite during the fabrication is

24 COMPOSITE MATERIALS

simulated based on a nonlinear micromechanics theory. The optimal fabrication problem is formulated and solved with nonlinear programming. Application cases regarding the optimization of the fabrication cool-down phases of unidirectional ultra-high modulus graphite/copper and silicon carbide/titanium composites are presented. Author

A90-50128* Applied Sciences Corp., Yellow Springs, OH.
VAPOR GROWN CARBON FIBER FOR SPACE THERMAL MANAGEMENT SYSTEMS

MAX L. LAKE, J. KYLE HICKOK, KAREN K. BRITO, and LESTER L. BEGG (Applied Sciences, Inc., Yellow Springs, OH) IN: International SAMPE Symposium and Exhibition, 35th, Anaheim, CA, Apr. 2-5, 1990, Proceedings. Book 1. Covina, CA, Society for the Advancement of Material and Process Engineering, 1990, p. 960-969. Research supported by SDIO. refs (Contract NAS3-25470)

Copyright

Research that uses a novel, highly graphitic, vapor grown carbon fiber (VGCF) to fabricate composites for thermal management applications is described. These VGCF/Carbon composites have shown a specific thermal conductivity with values of twenty-to-ten times that of copper in the 500-900 K temperature range needed for waste heat management. It is concluded that development of this high specific thermal conductivity composite for thermal radiator panels will provide the foundation for a reevaluation of space power designs heretofore limited by the mass of waste heat dissipation systems. Further, it is suggested that through optimization of fiber handling and composite processing, thermal conductivities exceeding 1000 W/m-K (at 300 K) are achievable in composites reinforced with VGCF. R.E.P.

A90-50217* Case Western Reserve Univ., Cleveland, OH.
USE OF UNBALANCED LAMINATES AS A SCREENING METHOD FOR MICROCRACKING

DEMETRIOS S. PAPADOPOULOS (Case Western University, Cleveland, OH) and KENNETH J. BOWLES (NASA, Lewis Research Center, Cleveland, OH) IN: International SAMPE Symposium and Exhibition, 35th, Anaheim, CA, Apr. 2-5, 1990, Proceedings. Book 2. Covina, CA, Society for the Advancement of Material and Process Engineering, 1990, p. 2127-2141. Previously announced in STAR as N90-21124. refs

Copyright

State-of-the-art, high temperature polyimide matrix composites, reinforced with continuous graphite fibers are known to be susceptible to intraply cracking when thermally cycled over their useful service temperature range. It is believed that the transply cracking, in part, results from residual stresses caused by differences in coefficients of thermal expansion (CTE) between the polymer matrix and the reinforcement. Thermal cycling tests to investigate this phenomenon involve expensive time and energy consuming programs which are not economically feasible for use as a part of a materials screening process. As an alternative to thermal cycling studies, a study of unbalanced crossply graphite fiber reinforcement composites was conducted to assess the effect of the composite ply layup and surface condition on the residual stresses that remain after the processing of these materials. The residual stresses were assessed by measuring the radii of curvature of the types of laminates that were studied. The temperature at which stress-free conditions existed were determined and a dye penetrant method was used to observe surface damage resulting from excessive residual stress buildup. These results are compared with some published results of thermal cycling tests that were previously conducted on balanced polyimide composites. Author

A90-50496* National Aeronautics and Space Administration, Lewis Research Center, Cleveland, OH.

COMPATIBILITY OF FE-40AL WITH VARIOUS FIBERS

S. L. DRAPER, D. J. GAYDOS, M. V. NATHAL (NASA, Lewis Research Center, Cleveland, OH), and A. K. MISRA (NASA, Lewis Research Center; Sverdrup Technology, Inc., Cleveland, OH) Journal of Materials Research (ISSN 0884-2914), vol. 5, Sept.

1990, p. 1976-1984. refs

Copyright

Chemical reaction can occur at the fiber/matrix interface of intermetallic matrix composites, leading to a degradation of mechanical properties. Fe-40Al matrix composites were fabricated using SiC, B, W, Mo-base, and Al₂O₃ fibers. Composite samples were heat treated up to 1500 K to study the reaction kinetics, and reaction rates were determined from reaction zone thickness measurements. The Al₂O₃ and W fibers were found to be compatible with the Fe-40Al matrix, while the Mo-based fibers reacted moderately and the B and SiC fibers reacted severely. Experimental results are compared to theoretical thermodynamic predictions. Author

A90-51920* Massachusetts Inst. of Tech., Cambridge.
PROPERTIES OF RBSN AND RBSN-SiC COMPOSITES

A. LIGHTFOOT, H. L. KER, J. S. HAGGERTY (MIT, Cambridge, MA), and J. E. RITTER (Massachusetts University, Amherst) Ceramic Engineering and Science Proceedings (ISSN 0196-6219), vol. 11, July-Aug. 1990, p. 842-856. refs (Contract NAG3-845; DAAG03-88-K-0099)

Copyright

Strengths, fracture toughnesses, hardnesses, and dimensional changes have been measured for RBSN and RBSN/SiC composites. Samples were made from mixtures of Si and either Si- or C-rich SiC powders. For pure, 75 pct dense RBSN dispersed with octanol, strengths up to 858 MPa have been achieved. Improved strengths result from a combination of microstructural perfection and increased fracture toughness. The mechanical properties of the composites were approximately equal to those of methanol processed RBSN but not quite equal to those of the octanol-processed RBSN. Results are discussed in terms of observed microstructural features. Author

A90-51924* National Aeronautics and Space Administration, Lewis Research Center, Cleveland, OH.

NICALON/SILICONOCARBIDE CERAMIC COMPOSITES

F. I. HURWITZ (NASA, Lewis Research Center, Cleveland, OH), J. Z. GYKENYESI, P. J. CONROY (Cleveland State University, OH), and A. L. RIVERA (Case Western Reserve University, Cleveland, OH) Ceramic Engineering and Science Proceedings (ISSN 0196-6219), vol. 11, July-Aug. 1990, p. 931-946.

Copyright

A number of polymers of differing molecular structure, viscosity, copolymer composition, and production procedures, screened for production of strong, tough Nicalon/siliconocarbide composites, are discussed. Variables during polymer synthesis include pH, water/methoxy ratio and phenyl/methyl ratio. Final processing temperatures of the composites range from 1200 deg to 1400 deg C. The filler is derived from pyrolysis of the 50 phenyl/50 methyl silsesquioxane copolymer pyrolyzed to 650 deg C, then milled to less than 1-micron powder. Composite samples were fractured to evaluate the influence of matrix composition, final fabrication temperature, and use of filler on the composite mode of failure, modulus, strain capability, and strength. Incorporation of filler was found to increase matrix compressive strength and to influence matrix shrinkage and cracking. B.P.

A90-51927* National Aeronautics and Space Administration, Lewis Research Center, Cleveland, OH.

MATRIX DENSITY EFFECTS ON THE MECHANICAL PROPERTIES OF SiC FIBER-REINFORCED SILICON NITRIDE MATRIX PROPERTIES

RAMAKRISHNA T. BHATT (NASA, Lewis Research Center; U.S. Army, Aviation Research and Technology Activity, Cleveland, OH) and LAMES D. KISER (NASA, Lewis Research Center, Cleveland, OH) Ceramic Engineering and Science Proceedings (ISSN 0196-6219), vol. 11, July-Aug. 1990, p. 974-994. Previously announced in STAR as N90-21826. refs

Copyright

The room temperature mechanical properties were measured for SiC fiber reinforced reaction-bonded silicon nitride composites (SiC/RBSN) of different densities. The composites consisted of

approx. 30 vol percent uniaxially aligned 142 micron diameter SiC fibers (Textron SCS-6) in a reaction-bonded Si₃N₄ matrix. The composite density was varied by changing the consolidation pressure during RBSN processing and by hot isostatically pressing the SiC/RBSN composites. Results indicate that as the consolidation pressure was increased from 27 to 138 MPa, the average pore size of the nitrided composites decreased from 0.04 to 0.02 microns and the composite density increased from 2.07 to 2.45 gm/cc. Nonetheless, these improvements resulted in only small increases in the first matrix cracking stress, primary elastic modulus, and ultimate tensile strength values of the composites. In contrast, HIP consolidation of SiC/RBSN resulted in a fully dense material whose first matrix cracking stress and elastic modulus were approx. 15 and 50 percent higher, respectively, and ultimate tensile strength values were approx. 40 percent lower than those for unHIPed SiC/RBSN composites. The modulus behavior for all specimens can be explained by simple rule-of-mixture theory. Also, the loss in ultimate strength for the HIPed composites appears to be related to a degradation in fiber strength at the HIP temperature. However, the density effect on matrix fracture strength was much less than would be expected based on typical monolithic Si₃N₄ behavior, suggesting that composite theory is indeed operating. Possible practical implications of these observations are discussed. Author

A90-51933* Ohio State Univ., Columbus.
**CRYSTALLIZATION BEHAVIOR AND PROPERTIES OF
 BAO-AL₂O₃-2SiO₂ GLASS MATRICES**

CHARLES H. DRUMMOND, III (Ohio State University, Columbus) and NAROTTAM P. BANSAL (NASA, Lewis Research Center, Cleveland, OH) Ceramic Engineering and Science Proceedings (ISSN 0196-6219), vol. 11, July-Aug. 1990, p. 1072-1086. refs Copyright

Glass of stoichiometric celsian composition, BaO-Al₂O₃-SiO₂, has a density of 3.39 g/cc, a thermal expansion coefficient of 6.6 x 10 to the -6th/C, a glass-transition temperature of 910 C, and a dilatometric softening point of 925 C. On heat treatment, only hexacelsian crystallized out on the surface, but both celsian and hexacelsian were present in the bulk. Effects of cold isostatic pressing (CIP), sintering, and hot-pressing, in the presence and absence of an additive, on the formation of the celsian phase in the glass have been studied. CIP'd samples, after appropriate heat treatments, always crystallized out as celsian, whereas presence of 5-10 wt pct of an additive was necessary for formation of celsian in sintered as well as hot-pressed specimens. Green density increased with CIP'ing pressure but had no effect on sintered density. Hot-pressing resulted in fully dense samples. Author

A90-52783* National Aeronautics and Space Administration.
 Lewis Research Center, Cleveland, OH.

**HIGH-TEMPERATURE TENSILE PROPERTIES OF FIBER
 REINFORCED REACTION BONDED SILICON NITRIDE**

DAVID A. JABLONSKI (Instron Corp., Canton, MA) and RAMAKRISHNA T. BHATT (NASA, Lewis Research Center; U.S. Army, Propulsion Directorate, Cleveland, OH) Journal of Composites Technology and Research (ISSN 0885-6804), vol. 12, Fall 1990, p. 139-146. refs Copyright

Measurements of tensile properties of unidirectional silicon carbide fiber-reinforced reaction-bonded silicon nitride (SiC/RBSN) composite specimens were carried out in air at 25, 1300, and 1500 C, using a new testing technique and a specially designed gripping system that minimizes bending moment and assures that failure always occurred in the gage section. The material was found to display metallike stress-strain behavior at all temperatures tested, and a noncatastrophic failure beyond the matrix fracture. The tensile properties were found to be temperature dependent, with the values of the ultimate tensile strength decreasing with temperature, from 543 MPa at 25 C to 169 at 1500 C. I.S.

N90-10181* National Aeronautics and Space Administration.
 Lewis Research Center, Cleveland, OH.

**COMPOSITE BLADE STRUCTURAL ANALYZER (COBSTRAN)
 THEORETICAL/PROGRAMMER'S MANUAL**

ROBERT A. AIELLO and CHRISTOS C. CHAMIS Aug. 1989
 136 p
 (NASA-TM-101958; E-4986; NAS 1.15:101958) Avail: NTIS HC A07/MF A01 CSCL 11D

This manual describes the organization and flow of data and analysis in the computer code, COBSTRAN (Composite Blade STRUCTural ANalyzer). This code combines composite mechanics and laminate theory with an internal data base of fiber and matrix properties and was developed for the design and analysis of composite turbofan and turboprop blades and composite wind turbine blades. Inputs to the code are constituent fiber and matrix material properties, factors reflecting the fabrication process, composite geometry and blade geometry. COBSTRAN performs the micromechanics and laminate analyses of these fiber composites and generates a NASTRAN finite element model of the blade. This manual describes the equations formulated and solved in the code and the function of each of the seventy-two subroutines. COBSTRAN is written in FORTRAN 77. Author

N90-10184* General Electric Co., Cincinnati, OH. Aircraft Engine Business Group.

**REVOLUTIONARY OPPORTUNITIES FOR MATERIALS AND
 STRUCTURES STUDY**

F. A. SCHWEIGER Feb. 1987 169 p
 (Contract NAS3-24622)
 (NASA-CR-179642; NAS 1.26:179642) Avail: NTIS HC A08/MF A01 CSCL 11D

The revolutionary opportunities for materials and structures study was performed to provide Government and Industry focus for advanced materials technology. Both subsonic and supersonic engine studies and aircraft fuel burn and DOC evaluation are examined. Year 2010 goal materials were used in the advanced engine studies. These goal materials and improved component aero yielded subsonic fuel burn and DOC improvements of 13.4 percent and 5 percent, respectively and supersonic fuel burn and DOC improvements of 21.5 percent and 18 percent, respectively. Conclusions are that the supersonic study engine yielded fuel burn and DOC improvements well beyond the program goals; therefore, it is appropriate that advanced material programs be considered. Author

N90-10185* National Aeronautics and Space Administration.
 Lewis Research Center, Cleveland, OH.

**MECHANICS OF DAMPING FOR FIBER COMPOSITE
 LAMINATES INCLUDING HYGRO-THERMAL EFFECTS**

D. A. SARAVANOS and CHRISTOS C. CHAMIS Apr. 1989
 28 p Presented at the 30th Structures, Structural Dynamics, and Materials Conference, Mobile, AL, 3-5 Apr. 1989; sponsored in part by AIAA, ASME, ASCE, AHS, and ASC Previously announced in IAA as A89-30681
 (NASA-TM-102329; E-5034; NAS 1.15:102329) Avail: NTIS HC A03/MF A01 CSCL 11D

An integrated mechanics theory was developed for the modeling of composite damping from the micromechanics to the laminate level. Simplified, design oriented equations based on hysteretic damping are presented for on-axis plies, off-axis plies, and laminates including the effect of temperature, moisture, and interply hysteretic damping. The temperature rise within vibrating composite laminates resulting from strain energy dissipation is also modeled, and their coupled hygro-thermo-mechanical response is predicted. The method correlates well with reported damping measurements. Application examples illustrate the effect of various ply, laminate, and hygro-thermal parameters on the overall damping performance of composite laminates. Author

N90-10188* National Aeronautics and Space Administration.
 Lewis Research Center, Cleveland, OH.

**MATERIALS FOR ENGINE APPLICATIONS ABOVE 3000 DEG
 F: AN OVERVIEW**

24 COMPOSITE MATERIALS

NANCY J. SHAW, JAMES A. DICARLO, NATHAN S. JACOBSON, STANLEY R. LEVINE, JAMES A. NESBITT, HUBERT B. PROBST, WILLIAM A. SANDERS, and CARL A. STEARNS Oct. 1987 36 p
(NASA-TM-100169; E-3734; NAS 1.15:100169) Avail: NTIS HC A03/MF A01 CSCL 11D

Materials for future generations of aeropropulsion systems will be required to perform at ever-increasing temperatures and have properties superior to the current state of the art. Improved engine efficiency can reduce specific fuel consumption and thus increase range and reduce operating costs. The ultimate payoff gain is expected to come when materials are developed which can perform without cooling at gas temperatures to 2200 C (4000 F). An overview is presented of materials for applications above 1650 C (3000 F), some pertinent physical property data, and the rationale used: (1) to arrive at recommendations of material systems that qualify for further investigation, and (2) to develop a proposed plan of research. From an analysis of available thermochemical data it was included that such materials systems must be composed of oxide ceramics. The required structural integrity will be achieved by developing these materials into fiber-reinforced ceramic composites. Author

N90-11808* National Aeronautics and Space Administration. Lewis Research Center, Cleveland, OH.

AN INTEGRATED METHODOLOGY FOR OPTIMIZING STRUCTURAL COMPOSITE DAMPING

D. A. SARAVANOS and C. C. CHAMIS 1989 25 p Presented at the 1989 Winter Annual Meeting of the ASME, San Francisco, CA, 10-15 Dec. 1989
(NASA-TM-102343; E-5051; NAS 1.15:102343) Avail: NTIS HC A03/MF A01 CSCL 11/4

A method is presented for tailoring plate and shell composite structures for optimal forced damped dynamic response. The damping of specific vibration modes is optimized with respect to dynamic performance criteria including placement of natural frequencies and minimization of resonance amplitudes. The structural composite damping is synthesized from the properties of the constituent materials, laminate parameters, and structural geometry based on a specialty finite element. Application studies include the optimization of laminated composite beams and composite shells with fiber volume ratios and ply angles as design variables. The results illustrate the significance of damping tailoring to the dynamic performance of composite structures, and the effectiveness of the method in optimizing the structural dynamic response. Author

N90-12670* National Aeronautics and Space Administration. Lewis Research Center, Cleveland, OH.

A NEW TEST MACHINE FOR MEASURING FRICTION AND WEAR IN CONTROLLED ATMOSPHERES TO 1200 C

HAROLD E. SLINEY and CHRISTOPHER DELLACORTE 1989 23 p Proposed for presentation at the Annual Meeting of the Society of Tribologists and Lubrication Engineers, Denver, CO, 7-11 May 1990
(NASA-TM-102405; E-5093; NAS 1.15:102405) Avail: NTIS HC A03/MF A01 CSCL 11/4

This paper describes a new high temperature friction and wear test apparatus (tribometer) at NASA Lewis Research Center, Cleveland, Ohio. The tribometer can be used as a pin-on-disk or pin-on-ring configuration and is specially designed to measure the tribological properties of ceramics and high temperature metallic alloys from room temperature to 1200 C. Sliding mode can be selected to be either unidirectional at velocities up to 22 m/sec or oscillating at frequencies up to 4.5 Hz and amplitudes up to + or - 60 deg. The test atmosphere is established by a controlled flow rate of a purge gas. All components within the test chamber are compatible with oxidizing, inert, or reducing gases. Author

N90-14287* National Aeronautics and Space Administration. Lewis Research Center, Cleveland, OH.

OXIDATION EFFECTS ON THE MECHANICAL PROPERTIES OF SiC FIBER-REINFORCED REACTION-BONDED SILICON NITRIDE MATRIX COMPOSITES

RAMAKRISHNA T. BHATT Nov. 1989 38 p Prepared in cooperation with Army Propulsion Lab., Cleveland, OH
(NASA-TM-102360; E-5074; NAS 1.15:102360; AVSCOM-TR-89-C-018; AD-A217852) Avail: NTIS HC A03/MF A01 CSCL 11/4

The room temperature mechanical properties of SiC fiber reinforced reaction bonded silicon nitride composites were measured after 100 hrs exposure at temperatures to 1400 C in nitrogen and oxygen environments. The composites consisted of approx. 30 vol percent uniaxially aligned 142 micron diameter SiC fibers in a reaction bonded Si₃N₄ matrix. The results indicate that composites heat treated in a nitrogen environment at temperatures to 1400 C showed deformation and fracture behavior equivalent to that of the as-fabricated composites. Also, the composites heat treated in an oxidizing environment beyond 400 C yielded significantly lower tensile strength values. Specifically in the temperature range from 600 to 1000 C, composites retained approx. 40 percent of their as-fabricated strength, and those heat treated in the temperatures from 1200 to 1400 C retained 70 percent. Nonetheless, for all oxygen heat treatment conditions, composite specimens displayed strain capability beyond the matrix fracture stress; a typical behavior of a tough composite. Author

N90-14294* National Aeronautics and Space Administration. Lewis Research Center, Cleveland, OH.

PARAMETRIC STUDIES TO DETERMINE THE EFFECT OF COMPLIANT LAYERS ON METAL MATRIX COMPOSITE SYSTEMS

J. J. CARUSO, C. C. CHAMIS, and H. C. BROWN (Sverdrup Technology, Inc., Cleveland, OH.) 1990 13 p Prepared for presentation at the 35th Symposium and Exhibition, Anaheim, CA, 2-5 Apr. 1990; sponsored by Society for the Advancement of Material and Process Engineering
(NASA-TM-102465; E-5252; NAS 1.15:102465) Avail: NTIS HC A03/MF A01 CSCL 11/4

Computational simulation studies are conducted to identify compliant layers to reduce matrix stresses which result from the coefficient of thermal expansion mismatch and the large temperature range over which the current metal matrix composites will be used. The present study includes variations of compliant layers and their properties to determine their influence on unidirectional composite and constituent response. Two simulation methods are used for these studies. The first approach is based on a three-dimensional linear finite element analysis of a 9 fiber unidirectional composite system. The second approach is a micromechanics based nonlinear computer code developed to determine the behavior of metal matrix composite system for thermal and mechanical loads. The results show that an effective compliant layer for the SCS 6 (SiC)/Ti-24Al-11Nb (Ti3Al + Nb) and SCS 6 (SiC)/Ti-15V-3Cr-3Sn-3Al (Ti-15-3) composite systems should have modulus 15 percent that of the matrix and a coefficient of thermal expansion of the compliant layer roughly equal to that of the composite system without the CL. The matrix stress in the longitudinal and the transverse tangent (loop) direction are tensile for the Ti3Al + Nb and Ti-15-3 composite systems upon cool down from fabrication. The fiber longitudinal stress is compressive from fabrication cool down. Addition of a recommended compliant layer will result in a reduction in the composite modulus. Author

N90-15143* National Aeronautics and Space Administration. Lewis Research Center, Cleveland, OH.

EMPIRICAL AND ANALYTICAL DETERMINATION OF THE FRACTURE RESISTANCE OF A TiB₂ PARTICLE/SiC MATRIX COMPOSITE

MICHAEL G. JENKINS, MINORU TAYA, ALBERT S. KOBAYASHI (Washington Univ., Seattle.), and JONATHAN A. SALEM 1989 7 p Presented at the First International SAMPE Symposium and Exhibition on New Materials and Processes for the Future, Chiba,

Japan, 28 Nov. - 1 Dec. 1989
(Contract DE-AC05-84OR-21400)
(NASA-TM-101940; NAS 1.15:101940; DE89-012331;
CONF-891116-1) Avail: NTIS HC A02/MF A01 CSCL 11/4

The addition of TiB₂ particles to an SiC matrix improves machinability and the room temperature fracture resistance of the composite. Empirical tests have revealed, that the fracture resistance of this composite is a function of both loading condition (monotonic or cyclic-type) and temperature (20 to 1400 C) with some dependence on specimen geometry. Both K_{sub} IC and the levels of the flat R-curves decrease with increasing temperature and are dependent on the loading condition. Fractography shows that toughening contributions include particle size effects, micro-cracking at the particle/matrix interface, and crack deflection. Analytical modeling based on the residual stresses within the material due to the thermal mismatch between the particle and matrix materials compares well with the empirical results. DOE

N90-15147*# National Aeronautics and Space Administration. Lewis Research Center, Cleveland, OH.

IMPROVED PROCESS FOR HIP CANNING OF COMPOSITES
Patent Application

JOHN J. JUHAS, inventor (to NASA) 9 Nov. 1989 11 p
Sponsored by NASA
(NASA-CASE-LEW-14990-1-CU; US-PATENT-APPL-SN-433863;
NAS 1.71:LEW-14990-1-CU) Avail: NTIS HC A03/MF A01
CSCL 11/4

A single step is relied on in the canning process for hot isostatic pressing (HIP) metallurgy composites. The composites are made from arc-sprayed and plasma sprayed monotape. The HIP can is of compatible refractory metal and is sealed at high vacuum and temperature. This eliminates outgassing during hot isostatic pressing. NASA

N90-16008*# National Aeronautics and Space Administration. Lewis Research Center, Cleveland, OH.

PROBABILISTIC SIMULATION OF UNCERTAINTIES IN COMPOSITE UNIAXIAL STRENGTHS

C. C. CHAMIS and T. A. STOCK (Cleveland State Univ., OH.)
1990 16 p Presented at the 45th Annual Conference of the Society of Plastics Industry Reinforced Plastics, Washington, DC, 12-16 Feb. 1990
(NASA-TM-102483; E-5269; NAS 1.15:102483) Avail: NTIS HC A03/MF A01 CSCL 11/4

Probabilistic composite micromechanics methods are developed that simulate uncertainties in unidirectional fiber composite strengths. These methods are in the form of computational procedures using composite mechanics with Monte Carlo simulation. The variables for which uncertainties are accounted include constituent strengths and their respective scatter. A graphite/epoxy unidirectional composite (ply) is studied to illustrate the procedure and its effectiveness to formally estimate the probable scatter in the composite uniaxial strengths. The results show that ply longitudinal tensile and compressive, transverse compressive and intralaminar shear strengths are not sensitive to single fiber anomalies (breaks, interfacial disbands, matrix microcracks); however, the ply transverse tensile strength is.

Author

N90-17817*# National Aeronautics and Space Administration. Lewis Research Center, Cleveland, OH.

PREDICTION OF HIGH TEMPERATURE METAL MATRIX COMPOSITE PLY PROPERTIES

J. J. CARUSO and C. C. CHAMIS 1988 19 p Presented at the 29th Structures, Structural Dynamics, and Materials Conference, Williamsburg, VA, 18-20 Apr. 1988; cosponsored by AIAA, ASME, AHS, and ASC
(NASA-TM-102490; E-5280; NAS 1.15:102490) Avail: NTIS HC A03/MF A01 CSCL 11/4

The application of the finite element method (superelement technique) in conjunction with basic concepts from mechanics of materials theory is demonstrated to predict the thermomechanical behavior of high temperature metal matrix composites (HTMMC).

The simulated behavior is used as a basis to establish characteristic properties of a unidirectional composite idealized as an equivalent homogeneous material. The ply properties predicted include: thermal properties (thermal conductivities and thermal expansion coefficients) and mechanical properties (moduli and Poisson's ratio). These properties are compared with those predicted by a simplified, analytical composite micromechanics model. The predictive capabilities of the finite element method and the simplified model are illustrated through the simulation of the thermomechanical behavior of a P100-graphite/copper unidirectional composite at room temperature and near matrix melting temperature. The advantage of the finite element analysis approach is its ability to more precisely represent the composite local geometry and hence capture the subtle effects that are dependent on this. The closed form micromechanics model does a good job at representing the average behavior of the constituents to predict composite behavior. Author

N90-18504*# National Aeronautics and Space Administration. Lewis Research Center, Cleveland, OH.

ANALYSIS OF WHISKER-TOUGHENED CERAMIC COMPONENTS: A DESIGN ENGINEER'S VIEWPOINT

STEPHEN F. DUFFY, JANE M. MANDERSCHIED, and JOSEPH L. PALKO (Cleveland State Univ., OH.) Dec. 1989 10 p Original contains color illustrations
(NASA-TM-102333; E-5042; NAS 1.15:102333) Avail: NTIS HC A02/MF A01; 1 functional color page CSCL 11/4

The use of ceramics components in gas turbines, cutting tools, and heat exchangers has been limited by the relatively low flaw tolerance of monolithic ceramics. The development of whisker toughened ceramic composites offers the potential for considerable improvement in fracture toughness as well as strength. However, the variability of strength is still too high for the application of deterministic design approaches. Several phenomenological reliability theories proposed for this material system are reviewed and the development is reported of a public domain computer algorithm. This algorithm, when coupled with a general purpose finite element program, predicts the fast fracture reliability of a structural component under multiaxial loading conditions. Author

N90-19302*# National Aeronautics and Space Administration. Lewis Research Center, Cleveland, OH.

HEAT TREATMENT STUDY OF THE SiC/Ti-15-3 COMPOSITE SYSTEM Final Report

BRADLEY A. LERCH, TIMOTHY P. GABB, and REBECCA A. MACKAY Washington Jan. 1990 31 p
(NASA-TP-2970; E-4985; NAS 1.60:2970) Avail: NTIS HC A03/MF A01 CSCL 11/4

The oxidation and aging behaviors of a continuous fiber SiC/Ti-15V-3Cr-3Sn-3Al composite (SiC/Ti-15-3) were investigated. The aging characteristic of the composite were compared with those of the unreinforced Ti-15-3 matrix material, which was processed in the same manner as the composite. Various age hardened conditions of both the unreinforced matrix and the composite were evaluated by using optical microscopy, hardness measurements, and room temperature tensile tests (unreinforced matrix only). The Ti-15-3 material formed a thick surface oxide at temperature at or above 550 C when heat treated in air. The in situ composite matrix was softer than the unreinforced matrix for equivalent aging conditions. Both materials hardened to a maximum, then softened during overaging. The temperature at which peak aging occurred was approx. 450 C for both the in situ composite matrix and the unreinforced matrix. The room temperature elastic modulus and ultimate tensile strength of the unreinforced matrix varied as a function of aging treatment and paralleled the hardness behavior. The modulus and tensile strength showed little response to aging up to temperatures of 300 C; however, these properties increased after aging at 550 C. Aging at temperatures above 550 C resulted in a decrease in the modulus and tensile strength. The failure strain was a function of the precipitation state and of the amount of oxidation resulting from the heat treatment. Aging in air at the higher temperatures (greater than 550 C) caused the formation of a thick oxide layer and

24 COMPOSITE MATERIALS

reduced the ductility. Aging in vacuum at these temperatures resulted in significantly higher ductilities. Long term exposures at 700 C caused the formation of a large grain boundary alpha-phase which reduced the ductility, even though the specimens were heat treated in vacuum. Author

N90-19310*# National Aeronautics and Space Administration. Lewis Research Center, Cleveland, OH.

THERMO-OXIDATIVE STABILITY STUDIES OF PMR-15 POLYMER MATRIX COMPOSITES REINFORCED WITH VARIOUS FIBERS

KENNETH J. BOWLES 1990 16 p Presented at the 35th International SAMPE Symposium and Exhibition, Anaheim, CA, 2-5 Apr. 1990

(NASA-TM-102439; E-5208; NAS 1.15:102439) Avail: NTIS HC A03/MF A01 CSCL 11/4

An experimental study was conducted to measure the thermo-oxidative stability of PMR-15 polymer matrix composites reinforced with various fibers and to observe differences in the way they degrade in air. The fibers that were studied included graphite and the thermally stable Nicalon and Nextel ceramic fibers. Weight loss rates for the different composites were assessed as a function of mechanical properties, specimen geometry, fiber sizing, and interfacial bond strength. Differences were observed in rates of weight loss, matrix cracking, geometry dependency, and fiber-sizing effects. It was shown that Celion 6000 fiber-reinforced composites do not exhibit a straight-line Arrhenius relationship at temperatures above 316 C. Author

N90-20138*# National Aeronautics and Space Administration. Lewis Research Center, Cleveland, OH.

COMPOSITE LAMINATE TAILORING WITH PROBABILISTIC CONSTRAINTS AND LOADS

P. B. THANEDAR and C. C. CHAMIS 1990 18 p Presented at the Energy Technology Conference and Exhibition, New Orleans, LA, 14-18 Jan. 1990; sponsored by ASME

(NASA-TM-102515; E-5182; NAS 1.15:102515) Avail: NTIS HC A03/MF A01 CSCL 11/4

A reliability-based structural synthesis procedure was developed to tailor laminates to meet reliability-based (ply) strength requirements and achieve desirable laminate responses. The main thrust is to demonstrate how to integrate the optimization technique in the composite laminate tailoring process to meet reliability design requirements. The question of reliability arises in fiber composite analysis and design because of the inherent scatter that is observed in the constituent (fiber and matrix) material properties during experimentation. Symmetric and asymmetric composite laminates subject to mechanical loadings are considered as application examples. These application examples illustrate the effectiveness and ease with which reliability considerations can be integrated in the design optimization model for composite laminate tailoring. Author

N90-20139*# National Aeronautics and Space Administration. Lewis Research Center, Cleveland, OH.

EVALUATION OF THERMAL AND MECHANICAL LOADING EFFECTS ON THE STRUCTURAL BEHAVIOR OF A SIC/TITANIUM COMPOSITE

JOSEPH E. GRADY and BRADLEY A. LERCH Apr. 1990 15 p Presented at the 31st Structures, Structural Dynamics and Materials Conference, Long Beach, CA, 2-4 Apr. 1990; sponsored in part by AIAA, ASME, ASCE, AHS, and ASC

(NASA-TM-102536; E-5349; NAS 1.15:102536) Avail: NTIS HC A03/MF A01 CSCL 11/4

Composite specimens of titanium-15-3 matrix reinforced with continuous SCS-6 silicon carbide fibers were tested under a variety of thermal and mechanical loadings. A combined experimental/finite element approach was used to estimate the effective in-situ modulus of the matrix material and to evaluate changes in modulus due to the applied loads. Several fiber orientations were tested. Results indicate that the effect of the thermal loads on composite stiffness varies with fiber orientation. Applications of this method to test specimens damaged by uniaxial

tension, thermal cycling, and isothermal fatigue loadings are used to illustrate that by monitoring overall structural behavior, changes in stiffness caused by thermomechanical loading can be detected. Author

N90-20151*# National Aeronautics and Space Administration. Lewis Research Center, Cleveland, OH.

FUNDAMENTAL ASPECTS OF AND FAILURE MODES IN HIGH-TEMPERATURE COMPOSITES

CHRISTOS C. CHAMIS and CAROL A. GINTY 1990 16 p Presented at the 35th International SAMPE Symposium and Exhibition, Anaheim, CA, 2-5 Apr. 1990

(NASA-TM-102558; E-5378; NAS 1.15:102558) Avail: NTIS HC A03/MF A01 CSCL 11/4

Fundamental aspects of and attendant failure mechanisms for high temperature composites are summarized. These include: (1) in-situ matrix behavior; (2) load transfer; (3) limits on matrix ductility to survive a given number of cyclic loadings; (4) fundamental parameters which govern thermal stresses; (5) vibration stresses; and (6) impact resistance. The resulting guidelines are presented in terms of simple equations which are suitable for the preliminary assessment of the merits of a particular high temperature composite in a specific application. Author

N90-21123*# National Aeronautics and Space Administration. Lewis Research Center, Cleveland, OH.

CHARACTERIZATION OF FAILURE PROCESSES IN TUNGSTEN COPPER COMPOSITES UNDER FATIGUE LOADING CONDITIONS

YONG-SUK KIM (National Academy of Sciences - National Research Council, Washington, DC.), MICHAEL J. VERRILLI, and TIMOTHY P. GABB 1989 22 p Presented at the International Symposium for Testing and Failure Analysis (ISTFA '89), Los Angeles, CA, 6-10 Nov. 1989; sponsored by ASM International (NASA-TM-102371; E-5090; NAS 1.15:102371) Avail: NTIS HC A03/MF A01 CSCL 11/4

A fractographic and metallographic investigation was performed on specimens of a tungsten fiber reinforced copper matrix composite (9 vol percent), which had experienced fatigue failures at elevated temperatures. Major failure modes and possible failure mechanisms, with an emphasis placed on characterizing fatigue damage accumulation, were determined. Metallography of specimens fatigued under isothermal cyclic loading suggested that fatigue damage initiates in the matrix. Cracks nucleated within the copper matrix at grain boundaries, and they propagated through cavity coalescence. The growing cracks subsequently interacted with the reinforcing tungsten fibers, producing a localized ductile fiber failure. Examinations of interrupted tests before final failure confirmed the suggested fatigue damage processes. Author

N90-21124*# National Aeronautics and Space Administration. Lewis Research Center, Cleveland, OH.

USE OF UNBALANCED LAMINATES AS A SCREENING METHOD FOR MICROCRACKING

DEMETRIOS S. PAPADOPOULOS (Case Western Reserve Univ., Cleveland, OH.) and KENNETH J. BOWLES 1990 17 p Presented at the 35th International SAMPE Symposium, Anaheim, CA, 2-5 Apr. 1990

(NASA-TM-102517; E-5214; NAS 1.15:102517) Avail: NTIS HC A03/MF A01 CSCL 11/4

State-of-the-art, high temperature polyimide matrix composites, reinforced with continuous graphite fibers are known to be susceptible to intraply cracking when thermally cycled over their useful service temperature range. It is believed that the transply cracking, in part, results from residual stresses caused by differences in coefficients of thermal expansion (CTE) between the polymer matrix and the reinforcement. Thermal cycling tests to investigate this phenomenon involve expensive time and energy consuming programs which are not economically feasible for use as a part of a materials screening process. As an alternative to thermal cycling studies, a study of unbalanced crossply graphite fiber reinforcement composites was conducted to assess the effect of the composite ply layup and surface condition on the residual

stresses that remain after the processing of these materials. The residual stresses were assessed by measuring the radii of curvature of the types of laminates that were studied. The temperature at which stress-free conditions existed were determined and a dye penetrant method was used to observe surface damage resulting from excessive residual stress buildup. These results are compared with some published results of thermal cycling tests that were previously conducted on balanced polyimide composites. Author

N90-21131*# National Aeronautics and Space Administration. Lewis Research Center, Cleveland, OH.

FIBER PUSHOUT TEST: A THREE-DIMENSIONAL FINITE ELEMENT COMPUTATIONAL SIMULATION

SUBODH K. MITAL and CHRISTOS C. CHAMIS Apr. 1990 18 p

(Contract NASA ORDER C-99066-G)

(NASA-TM-102565; ICOMP-90-11; E-5389; NAS 1.15:102565)

Avail: NTIS HC A03/MF A01 CSCL 11/4

A fiber pushthrough process was computationally simulated using three-dimensional finite element method. The interface material is replaced by an anisotropic material with greatly reduced shear modulus in order to simulate the fiber pushthrough process using a linear analysis. Such a procedure is easily implemented and is computationally very effective. It can be used to predict fiber pushthrough load for a composite system at any temperature. The average interface shear strength obtained from pushthrough load can easily be separated into its two components: one that comes from frictional stresses and the other that comes from chemical adhesion between fiber and the matrix and mechanical interlocking that develops due to shrinkage of the composite because of phase change during the processing. Step-by-step procedures are described to perform the computational simulation, to establish bounds on interfacial bond strength and to interpret interfacial bond quality. Author

N90-21132*# National Aeronautics and Space Administration. Lewis Research Center, Cleveland, OH.

MULTI-OBJECTIVE SHAPE AND MATERIAL OPTIMIZATION OF COMPOSITE STRUCTURES INCLUDING DAMPING

D. A. SARAVANOS (Case Western Reserve Univ., Cleveland, OH.) and CHRISTOS C. CHAMIS 1990 19 p Presented at the 31st Structures, Structural Dynamics, and Materials Conference, Long Beach, CA, 2-4 Apr. 1990; cosponsored by AIAA, ASME, ASCE, AHS, and ASC Previously announced in IAA as A90-29262

(NASA-TM-102579; E-5410; NAS 1.15:102579) Avail: NTIS HC A03/MF A01 CSCL 11/4

A multi-objective optimal design methodology is developed for light-weight, low cost composite structures of improved dynamic performance. The design objectives include minimization of resonance amplitudes (or maximization of modal damping), weight, and material cost. The design vector includes micromechanics, laminate, and structural shape parameters. Performance constraints are imposed on static displacements, dynamic amplitudes, and natural frequencies. The effects of damping on the dynamics of composite structures are incorporated. Preliminary applications on a cantilever composite beam illustrated that only the proposed multi-objective optimization, as opposed to single objective functions, simultaneously improved all objectives. The significance of composite damping in the design of advanced composite structures was also demonstrated, indicating the design methods based on undamped dynamics may fail to improve the dynamic performance near resonances. Author

N90-21133*# National Aeronautics and Space Administration. Lewis Research Center, Cleveland, OH.

NICALON/SILICONOXYCARBIDE CERAMIC COMPOSITES

FRANCES I. HURWITZ, JOHN Z. GYKENYESI, PAULA J. CONROY, and ANN L. RIVERA (Case Western Reserve Univ., Cleveland, OH.) 1990 21 p Presented at the 14th Annual Conference on Composites and Advanced Ceramics, Cocoa Beach, FL, 14-17 Jan. 1990; sponsored by American Ceramic Society

(NASA-TM-102563; E-5383; NAS 1.15:102563) Avail: NTIS HC A03/MF A01 CSCL 11/4

A series of silsesquioxane copolymers was synthesized by acid hydrolysis and condensation of trimethoxysilanes of the form $\text{RSi}(\text{OCH}_3)_3$, where R = methyl or phenyl. By varying pH, water/methoxy and methyl/phenyl ratios, the molecular structure, polymer rheology and ceramic composition can be controlled. The polymers form an amorphous siliconoxycarbide on pyrolysis. Composites of Nicalon/siliconoxycarbide were fractured in four-point flexure and in tension to evaluate the influence of matrix composition, final fabrication temperature and use of filler on composite mode of failure, modulus, strain capability and strength. Incorporation of filler was found to increase matrix compressive strength. Employment of processing temperatures of 1375 to 1400 C enhanced strain to failure and reduced the tendency toward brittle fracture. Mixed mode (compression/shear and tension/shear) failures were observed in flexural samples processed to the higher temperatures, giving rise to nonlinear stress-strain curves. Tensile samples pyrolyzed to 1400 C showed linear-elastic behavior and failed by fracture of fiber bundles. Matrix material was found to be adherent to the fiber surface after failure. These results demonstrate the need for tensile testing to establish composite behavior. Author

N90-21137*# National Aeronautics and Space Administration. Lewis Research Center, Cleveland, OH.

STRUCTURAL TAILORING OF SELECT FIBER COMPOSITE STRUCTURES

CHRISTOS C. CHAMIS and ROBERT I. RUBINSTEIN (Sverdrup Technology, Inc., Cleveland, OH.) Feb. 1990 14 p Presented at the 45th Annual Conference on the Society of Plastics Industry Reinforced Plastics/Composites Inst., Washington, DC, 12-16 Feb. 1990

(NASA-TM-102484; E-5273; NAS 1.15:102484) Avail: NTIS HC A03/MF A01 CSCL 11/4

A multidisciplinary design process for aerospace propulsion composite structures was formalized and embedded into computer codes. These computer codes are streamlined to obtain tailored designs for select composite structures. The codes available are briefly described with sample cases to illustrate their applications. The sample cases include aircraft engine blades, propfans (turboprops), flat, and cylindrical panels. Typical results illustrate that the use of these codes enable the designer to obtain designs which meet all the design requirements with maximum benefits in efficiency, noise, weight or thermal distortions. Author

N90-21138*# National Aeronautics and Space Administration. Lewis Research Center, Cleveland, OH.

HIGH TEMPERATURE FATIGUE BEHAVIOR OF TUNGSTEN COPPER COMPOSITES

MICHAEL J. VERRILLI, YONG-SUK KIM, and TIMOTHY P. GABB Oct. 1989 18 p Presented at the Symposium on Fundamental Relationships Between Microstructure and Mechanical Properties of Metal-Matrix Composites, Indianapolis, IN, 1-5 Oct. 1989; sponsored in part by the Metallurgical Society and the American Society for Metals

(NASA-TM-102404; E-5156; NAS 1.15:102404) Avail: NTIS HC A03/MF A01 CSCL 11/4

The high temperature fatigue behavior of a 9 vol percent, tungsten fiber reinforced copper matrix composite was investigated. Load-controlled isothermal fatigue experiments at 260 and 560 C and thermomechanical fatigue (TMF) experiments, both in phase and out of phase between 260 and 560 C, were performed. The stress-strain response displayed considerable inelasticity under all conditions. Also, strain ratcheting was observed during all the fatigue experiments. For the isothermal fatigue and in-phase TMF tests, the ratcheting was always in a tensile direction, continuing until failure. The ratcheting during the out-of-phase TMF test shifted from a tensile direction to a compressive direction. This behavior was thought to be associated with the observed bulging and the extensive cracking of the out-of-phase specimen. For all cases, the fatigue lives were found to be controlled by damage to the copper matrix. Grain boundary cavitation was the dominant damage

24 COMPOSITE MATERIALS

mechanism of the matrix. On a stress basis, TMF loading reduced lives substantially, relative to isothermal cycling. In-phase cycling resulted in the shortest lives, and isothermal fatigue at 260 C, the longest.

Author

N90-21143*# National Aeronautics and Space Administration. Lewis Research Center, Cleveland, OH.

OPTIMAL FABRICATION PROCESSES FOR UNIDIRECTIONAL METAL-MATRIX COMPOSITES: A COMPUTATIONAL SIMULATION

D. A. SARAVANOS, P. L. N. MURTHY, and M. MOREL (Sverdrup Technology, Inc., Cleveland, OH.) 1990 19 p Presented at the 35th International SAMPE Symposium and Exhibition, Anaheim, CA, 2-5 Apr. 1990

(NASA-TM-102559; E-5379; NAS 1.15:102559) Avail: NTIS HC A03/MF A01 CSCL 11/4

A method is proposed for optimizing the fabrication process of unidirectional metal matrix composites. The temperature and pressure histories are optimized such that the residual microstresses of the composite at the end of the fabrication process are minimized and the material integrity throughout the process is ensured. The response of the composite during the fabrication is simulated based on a nonlinear micromechanics theory. The optimal fabrication problem is formulated and solved with non-linear programming. Application cases regarding the optimization of the fabrication cool-down phases of unidirectional ultra-high modulus graphite/copper and silicon carbide/titanium composites are presented.

Author

N90-21821*# National Aeronautics and Space Administration. Lewis Research Center, Cleveland, OH.

COMPUTATIONAL SIMULATION OF STRUCTURAL FRACTURE IN FIBER COMPOSITES

CHRISTOS C. CHAMIS and P. L. N. MURTHY 7 Feb. 1990 20 p Presented at the 8th Conference on Fibrous Composites in Structural Design, Norfolk, VA, 28 Nov. - 1 Dec. 1989; sponsored in part by DOD and FAA

(NASA-TM-102505; E-5307; NAS 1.15:102505) Avail: NTIS HC A03/MF A01 CSCL 11/4

A methodology was developed for the computational simulation of structural fracture in fiber composites. This methodology consists of step-by-step procedures for mixed-mode fracture in generic components and an integrated computer code, Composite Durability Structural Analysis (CODSTRAN). The generic types of composite structural fracture include: (1) single and combined mode fracture in beams; 2) laminate free-edge delamination fracture; and (3) laminate center flaw progressive fracture. Structural fracture is identified by rapid changes in one or all of the following: (1) displacements, (2) frequencies, (3) the buckling loads, or (4) the strain energy release rate. These rapid changes are herein assumed to denote imminent structural fracture. Based on these rapid changes, parameters are identified which can be used as guidelines for structural fracture, inspection intervals and retirement for cause.

Author

N90-21824*# National Aeronautics and Space Administration. Lewis Research Center, Cleveland, OH.

METCAN VERIFICATION STATUS

CHRISTOS C. CHAMIS, J. J. CARUSO, H.-J. LEE, and P. L. N. MURTHY May 1990 16 p

(NASA-TM-103119; E-5443; NAS 1.15:103119) Avail: NTIS HC A03/MF A01 CSCL 11/4

The status of the verification (comparisons of predictions with experimental data) of the METCAN (METal-matrix Composite ANalyzer) code at high temperature is summarized. Verification includes select available room temperature of W/Cu composites for different fiber volume ratios. It also includes high temperature properties for thermal expansion, moduli, strength and stress/strain behavior for SiC/Ti composites. Furthermore it includes limited cases for thermal fatigue strength degradation. The verification results summarized herein indicate that METCAN simulates complex high temperature metal matrix composite behavior with

reasonable accuracy and that it can be used with confidence to identify in-situ nonlinear behavior that influences composite properties.

Author

N90-21825*# National Aeronautics and Space Administration. Lewis Research Center, Cleveland, OH.

PROGRESSION OF DAMAGE AND FRACTURE IN COMPOSITES UNDER DYNAMIC LOADING

LEVON MINNETYAN (Clarkson Univ., Potsdam, NY.), PAPPU L. N. MURTHY, and CHRISTOS C. CHAMIS 1990 17 p Presented at the 31st Structures, Structural Dynamics, and Materials Conference, Long Beach, CA, 2-4 Apr. 1990; cosponsored by AIAA, ASME, ASCE, AHS, and ASCE Previously announced in IAA as A90-29318

(NASA-TM-103118; E-5442; NAS 1.15:103118) Avail: NTIS HC A03/MF A01 CSCL 11/4

A new computational simulation method is presented to evaluate the dynamic aspects of composite structural response and durability that have not been simulated previously. Composite structural behavior under any loading condition, geometry, composite system, laminate configuration, and boundary conditions can now be simulated. Structural degradation, delamination, fracture, and damage propagation are included in the simulation. An angle-ply composite plate structure under normal impact loading is used as an example to demonstrate the versatility of the simulation method.

Author

N90-21826*# National Aeronautics and Space Administration. Lewis Research Center, Cleveland, OH.

MATRIX DENSITY EFFECTS ON THE MECHANICAL PROPERTIES OF SiC/RBSN COMPOSITES

RAMAKRISHNA T. BHATT (Army Aviation Systems Command, Cleveland, OH.) and JAMES D. KISER 1990 17 p Presented at the 14th Annual Conference on Composites and Advanced Ceramics, Cocoa Beach, FL, 14-17 Jan. 1990; sponsored by American Ceramic Society

(NASA-TM-103098; E-5306; NAS 1.15:103098; AVSCOM-TR-90-C-008; AD-A224494) Avail: NTIS HC A03/MF A01 CSCL 11/4

The room temperature mechanical properties were measured for SiC fiber reinforced reaction-bonded silicon nitride composites (SiC/RBSN) of different densities. The composites consisted of approx. 30 vol percent uniaxially aligned 142 micron diameter SiC fibers (Trextron SCS-6) in a reaction-bonded Si₃N₄ matrix. The composite density was varied by changing the consolidation pressure during RBSN processing and by hot isostatically pressing the SiC/RBSN composites. Results indicate that as the consolidation pressure was increased from 27 to 138 MPa, the average pore size of the nitrided composites decreased from 0.04 to 0.02 microns and the composite density increased from 2.07 to 2.45 gm/cc. Nonetheless, these improvements resulted in only small increases in the first matrix cracking stress, primary elastic modulus, and ultimate tensile strength values of the composites. In contrast, HIP consolidation of SiC/RBSN resulted in a fully dense material whose first matrix cracking stress and elastic modulus were approx. 15 and 50 percent higher, respectively, and ultimate tensile strength values were approx. 40 percent lower than those for unHIPed SiC/RBSN composites. The modulus behavior for all specimens can be explained by simple rule-of-mixture theory. Also, the loss in ultimate strength for the HIPed composites appears to be related to a degradation in fiber strength at the HIP temperature. However, the density effect on matrix fracture strength was much less than would be expected based on typical monolithic Si₃N₄ behavior, suggesting that composite theory is indeed operating. Possible practical implications of these observations are discussed.

Author

N90-23477*# National Aeronautics and Space Administration. Lewis Research Center, Cleveland, OH.

STRUCTURAL BEHAVIOR OF COMPOSITES WITH PROGRESSIVE FRACTURE

LEVON MINNETYAN (Clarkson Univ., Potsdam, NY.), CHRISTOS C. CHAMIS, and PAPPU L. N. MURTHY Jan. 1990 19 p

Original contains color illustrations
(NASA-TM-102370; E-5089; NAS 1.15:102370) Avail: NTIS HC A03/MF A01; 10 functional color pages CSCL 11/4

Structural characteristics such as natural frequencies and buckling loads with corresponding mode shapes were investigated during progressive fracture of multilayer, angle-ply polymer matrix composites. A computer program was used to generate the numerical results for overall mechanical response of damaged composites. Variations in structural characteristics as a function of the previously applied loading were studied. Results indicate that most of the overall structural properties were preserved throughout a significant proportion of the ultimate fracture load. For the cases studied, changes in structural behavior began to occur after 70 percent of the ultimate fracture load was applied. However, the individual nature of the structural change was rather varied depending on the laminate configuration, fiber orientation, and the boundary conditions. Author

N90-23493* National Aeronautics and Space Administration. Lewis Research Center, Cleveland, OH.

ONE STEP HIP CANNING OF POWDER METALLURGY COMPOSITES Patent

JOHN J. JUHAS, inventor (to NASA) 27 Feb. 1990 8 p Filed 21 Mar. 1989

(NASA-CASE-LEW-14719-1; US-PATENT-4,904,538; US-PATENT-APPL-SN-326757; US-PATENT-CLASS-428-552; US-PATENT-CLASS-75-228; US-PATENT-CLASS-428-551; US-PATENT-CLASS-419-8; US-PATENT-CLASS-419-24; US-PATENT-CLASS-419-36; US-PATENT-CLASS-419-37) Avail: US Patent and Trademark Office CSCL 11/4

A single step is relied on in the canning process for hot isostatic pressing (HIP) powder metallurgy composites. The binders are totally removed while the HIP can of compatible refractory metal is sealed at high vacuum and temperature. This eliminates outgassing during hot isostatic pressing.

Official Gazette of the U.S. Patent and Trademark Office

N90-24382*# National Aeronautics and Space Administration. Lewis Research Center, Cleveland, OH.

INFLUENCE OF INTERFACIAL SHEAR STRENGTH ON THE MECHANICAL PROPERTIES OF SiC FIBER REINFORCED REACTION-BONDED SILICON NITRIDE MATRIX COMPOSITES
RAMAKRISHNA T. BHATT (Army Aviation Systems Command, Cleveland, OH.) 1990 14 p Presented at the Advanced Metal and Ceramic Material Composites Symposium, Anaheim, CA, 23-27 Feb. 1990; sponsored by the Metallurgical Society (NASA-TM-102462; E-5250; NAS 1.15:102462; AVSCOM-TR-90-C-003; AD-A224968) Avail: NTIS HC A03/MF A01 CSCL 11/4

The influence of fiber/matrix interface microstructure and interfacial shear strength on the mechanical properties of a fiber-reinforced ceramic composite was evaluated. The composite consisted of approximately 30 vol percent uniaxially aligned 142 microns diameter SiC fibers (Textron SCS-6) in a reaction-bonded Si₃N₄ matrix (SiC/RBSN). The interface microstructure was varied by controlling the composite fabrication conditions and by heat treating the composite in an oxidizing environment. Interfacial shear strength was determined by the matrix crack spacing method. The results of microstructural examination indicate that the carbon-rich coating provided with the as-produced SiC fibers was stable in composites fabricated at 1200 C in a nitrogen or in a nitrogen plus 4 percent hydrogen mixture for 40 hr. However this coating degraded in composites fabricated at 1350 C in N₂ + 4 percent H₂ for 40 and 72 hr and also in composites heat treated in an oxidizing environment at 600 C for 100 hr after fabrication at 1200 C in a nitrogen. It was determined that degradation occurred by carbon removal which in turn had a strong influence on interfacial shear strength and other mechanical properties. Specifically, as the carbon coating was removed, the composite interfacial shear strength, primary elastic modulus, first matrix cracking stress, and ultimate tensile strength decreased, but the first matrix cracking strain remained nearly the same. Author

N90-24383*# National Aeronautics and Space Administration. Lewis Research Center, Cleveland, OH.

METAL MATRIX COMPOSITES MICROFRACTURE: COMPUTATIONAL SIMULATION

SUBODH K. MITAL, JOHN J. CARUSO, and CHRISTOS C. CHAMIS 1990 14 p Proposed for presentation at the Symposium on Computational Technology for Flight Vehicles, Washington, DC, 5-7 Nov. 1990; cosponsored by NASA and George Washington Univ.

(Contract NASA ORDER C-99066-G)

(NASA-TM-103153; ICOMP-90-14; E-5514; NAS 1.15:103153)

Avail: NTIS HC A03/MF A01 CSCL 11/4

Fiber/matrix fracture and fiber-matrix interface debonding in a metal matrix composite (MMC) are computationally simulated. These simulations are part of a research activity to develop computational methods for microfracture, microfracture propagation and fracture toughness of the metal matrix composites. The three-dimensional finite element model used in the simulation consists of a group of nine unidirectional fibers in three by three unit cell array of SiC/Ti15 metal matrix composite with a fiber volume ratio of 0.35. This computational procedure is used to predict the fracture process and establish the hierarchy of fracture modes based on strain energy release rate. It is also used to predict stress redistribution to surrounding matrix-fibers due to initial and progressive fracture of fiber/matrix and due to debonding of fiber-matrix interface. Microfracture results for various loading cases such as longitudinal, transverse, shear and bending are presented and discussed. Step-by-step procedures are outlined to evaluate composite microfracture for a given composite system. Author

N90-24384*# National Aeronautics and Space Administration. Lewis Research Center, Cleveland, OH.

SIMPLIFIED DESIGN PROCEDURES FOR FIBER COMPOSITE STRUCTURAL COMPONENTS/JOINTS

P. L. N. MURTHY and CHRISTOS C. CHAMIS 1990 23 p Presented at the Indo-US Workshop on Composite Materials for Aerospace Applications, Bangalore, India, 23-27 Jul. 1990; sponsored by Indian Inst. of Science (NASA-TM-103113; E-5392; NAS 1.15:103113) Avail: NTIS HC A03/MF A01 CSCL 11/4

Simplified step-by-step design procedures are summarized, which are suitable for the preliminary design of composite structural components such as panels (laminates) and composite built-up structures (box beams). Similar procedures are also summarized for the preliminary design of composite bolted and adhesively bonded joints. The summary is presented in terms of sample design cases complemented with typical results. Guidelines are provided which can be used in the design selection process of composite structural components/joints. Also, procedures to account for cyclic loads, hygrothermal effects and lamination residual stresses are included. Author

N90-25193*# National Aeronautics and Space Administration. Lewis Research Center, Cleveland, OH.

A CREEP MODEL FOR METALLIC COMPOSITES BASED ON MATRIX TESTING: APPLICATION TO KANTHAL COMPOSITES

W. K. BINIENDA, D. N. ROBINSON (Akron Univ., OH.), S. M. ARNOLD, and PAUL A. BARTOLOTTA Jun. 1990 19 p (Contract NAG3-379)

(NASA-TM-103172; E-5550; NAS 1.15:103172) Avail: NTIS HC A03/MF A01 CSCL 11/4

An anisotropic creep model is formulated for metallic composites with strong fibers and low to moderate fiber volume percent (less than 40 percent). The idealization admits no creep in the local fiber direction and assumes equal creep strength in longitudinal and transverse shear. Identification of the matrix behavior with that of the isotropic limit of the theory permits characterization of the composite through uniaxial creep tests on the matrix material. Constant and step-wise creep tests are required as a data base. The model provides an upper bound on the transverse creep strength of a composite having strong fibers embedded in a particular matrix material. Comparison of the measured transverse strength with the upper bound gives an assessment of the integrity

24 COMPOSITE MATERIALS

of the composite. Application is made to a Kanthal composite, a model high-temperature composite system. Predictions are made of the creep response of fiber reinforced Kanthal tubes under interior pressure. Author

N90-27874*# National Aeronautics and Space Administration. Lewis Research Center, Cleveland, OH.

AUTOCALVABLE ADDITION POLYIMIDES FOR 371 C COMPOSITE APPLICATIONS

R. D. VANNUCCI, D. C. MALARIK, D. S. PAPADAPPOULOS, and J. F. WATERS 1990 12 p Prepared for presentation at the 22nd International SAMPE Technical Conference, Boston, MA, 6-8 Nov. 1990

(NASA-TM-103233; E-5613; NAS 1.15:103233) Avail: NTIS HC A03/MF A01 CSCL 11/4

Studies were conducted to improve the thermo-oxidative stability (TOS) of PMR type polyimides by the substitution of para-aminostyrene (PAS) for the nadic ester endcap in second generation PMR polyimides (PMR-2). The nadic endcap which provides the PMR polyimides with their relative ease of fabrication, both by limiting the molecular weight of the prepolymer and by undergoing the final addition cure without volatiles, is also the weak link with regard to TOS. A polyimide formulated with PAS endcaps, called V-CAP, utilizes a two step reaction sequence similar to that of the PMR polyimides and can be easily autoclave molded into low void composite materials. Resin studies included two formulations of both PMR-2 and V-CAP, corresponding to $n=9$ and $n=14$ prepolymer stoichiometry. Unidirectional reinforced T40R graphite fiber laminates were fabricated from each of the resins was post-cured in either air at 385 C or nitrogen at 400 C. Composite specimens were aged in air at 371 C and mechanical properties were measured at 371 C before and after exposure.

Author

N90-27875*# National Aeronautics and Space Administration. Lewis Research Center, Cleveland, OH.

IMPROVED TRANSVERSE CRACK DETECTION IN COMPOSITES

J. MICHAEL PEREIRA and EDWARD R. GENERAZIO 1990 11 p Presented at the Society of Plastics Engineers Regional Technical Conference, Los Angeles, CA, 16-18 Oct. 1990

(NASA-TM-103261; E-5650; NAS 1.15:103261) Avail: NTIS HC A03/MF A01 CSCL 11/4

A modified ultrasonic C-scan technique was implemented for improving the detection of a certain type of damage in composite specimens. The type of damage being studied is transverse (through the thickness) cracking of unidirectional off-axis graphite-epoxy specimens. These cracks are difficult to detect using standard through-transmission C-scan techniques. The modification is based on mode conversion to produce transmitted shear waves from incident longitudinal waves. While mode conversion is used extensively with isotropic materials, its use with composites is more limited. This is largely because the computation of wave propagation parameters is significantly more complicated with highly anisotropic materials than with isotropic materials. The appropriate incident angles to produce the desired mode conversion were computed based on the mechanical properties of the composite. Once the angles were computed the technique was simple to implement and resulted in marked improvement in detection of the transverse cracks being studied.

Author

N90-28655*# National Aeronautics and Space Administration. Lewis Research Center, Cleveland, OH.

CERAMIC MATRIX COMPOSITES IN SIMULATED SSME ENVIRONMENTS

THOMAS P. HERBELL and ANDREW J. ECKEL (Sverdrup Technology, Inc., Middleburg Heights, OH.) In NASA, Marshall Space Flight Center, Advanced Earth-to-Orbit Propulsion Technology 1988, Volume 1 p 730-741 Sep. 1988

Avail: NTIS HC A99/MF E06 CSCL 11/4

Future Space Shuttle Main Engine (SSME)-type rocket engines can benefit from the use of fiber-reinforced ceramic matrix composites (FRCMC). Ceramics reinforced with long continuous

fibers exhibit improved tolerance to severe thermomechanical and environmental exposures. An in-house NASA-Lewis program to evaluate the durability of FRCMC in simulated SSME environments is described. Primary tests involve multiple (one second) exposures of FRCMC specimens in a hydrogen/oxygen rocket test rig. This rig generates surface heating rates of 1000 to 2500 C/second. The FRCMC durability evaluation involves measurement of retained strength as a function of thermal shock severity and number of upshock cycles. Preliminary test results for monolithic silicon nitride (Si₃N₄) and silicon carbide (SiC), and one type of silicon based FRCMC, are presented. The test data are examined in terms of simple thermal shock theory.

Author

N90-28670*# National Aeronautics and Space Administration. Lewis Research Center, Cleveland, OH.

THE EFFECTS OF ATOMIC OXYGEN ON THE THERMAL EMITTANCE OF HIGH TEMPERATURE RADIATOR SURFACES

SHARON K. RUTLEDGE, DEBORAH L. HOTES, and PHILLIP E. PAULSEN (Cleveland State Univ., OH.) 1989 25 p Presented at the Spring Meeting of the Materials Research Society, San Diego, CA, 24-29 Apr. 1989

(NASA-TM-103224; E-5640; NAS 1.15:103224) Avail: NTIS HC A03/MF A01 CSCL 11/4

Radiator surfaces on high temperature space power systems such as SP-100 space nuclear power system must maintain a high emittance level in order to reject waste heat effectively. One of the primary materials under consideration for the radiators is carbon-carbon composite. Since carbon is susceptible to attack by atomic oxygen in the low earth orbital environment, it is important to determine the durability of carbon composites in this environment as well as the effect atomic oxygen has on the thermal emittance of the surface if it is to be considered for use as a radiator. Results indicate that the thermal emittance of carbon-carbon composite (as low as 0.42) can be enhanced by exposure to a directed beam of atomic oxygen to levels above 0.85 at 800 K. This emittance enhancement is due to a change in the surface morphology as a result of oxidation. High aspect ratio cones are formed on the surface which allow more efficient trapping of incident radiation. Erosion of the surface due to oxidation is similar to that for carbon, so that at altitudes less than approximately 600 km, thickness loss of the radiator could be significant (as much as 0.1 cm/year). A protective coating or oxidation barrier forming additive may be needed to prevent atomic oxygen attack after the initial high emittance surface is formed. Textured surfaces can be formed in ground based facilities or possibly in space if emittance is not sensitive to the orientation of the atomic oxygen arrival that forms the texture.

Author

25

INORGANIC AND PHYSICAL CHEMISTRY

Includes chemical analysis, e.g., chromatography; combustion theory; electrochemistry; and photochemistry.

A90-16280* Cleveland State Univ., OH.

LIQUID ALKALI METALS - EQUATION OF STATE AND REDUCED-PRESSURE, BULK-MODULUS, SOUND-VELOCITY, AND SPECIFIC-HEAT FUNCTIONS

HERBERT SCHLOSSER (Cleveland State University, OH) and JOHN FERRANTE (NASA, Lewis Research Center, Cleveland, OH) Physical Review B - Condensed Matter, 3rd Series (ISSN 0163-1829), vol. 40, Sept. 15, 1989, p. 6405-6408. Research supported by the Ohio Board of Regents. refs

Copyright

The previous work of Schlosser and Ferrante (1988) on universality in solids is extended to the study of liquid metals. As in the case of solids, to a good approximation, in the absence of phase transitions, plots of the logarithm of the reduced-pressure function H , of the reduced-isothermal-bulk-modulus function b , and

of the reduced-sound-velocity function v are all linear in $1-X$. Finally, it is demonstrated that $\ln(C_p/C/v)$ is also linear in $1-X$, where $X = (V/V_0)/\exp(1/3)$, and $V(0)$ is the volume at zero pressure.

Author

A90-16281* Cleveland State Univ., OH.

PRESSURE DEPENDENCE OF THE MELTING TEMPERATURE OF METALS

HERBERT SCHLOSSER (Cleveland State University, OH), PASCAL VINET (L'Air Liquide, Paris, France), and JOHN FERRANTE (NASA, Lewis Research Center, Cleveland, OH) Physical Review B - Condensed Matter, 3rd Series (ISSN 0163-1829), vol. 40, Sept. 15, 1989, p. 5929-5935. Research supported by the Ohio Board of Regents. refs

Copyright

A new method for the analysis of the experimental data for the pressure dependence of the melting temperature of metals is presented. The method combines Lindemann's law, the Debye model, and a first-order equation of state with the experimental observation that the Grueneisen parameter divided by the volume is constant. It is observed that, based on these assumptions, in the absence of phase transitions, plots of the logarithm of the normalized melting temperature versus the logarithm of the normalized pressure are straight lines. It is found that the normalized-melting-temperature versus normalized-pressure curves accurately satisfy the linear relationship for Al, Ag, Au, Cs, Cu, K, Na, Pt, and Rb. In addition, this technique provides a sensitive tool for detecting phase transitions.

Author

A90-19904* University of South Florida, Tampa.

REDUCED CHEMICAL KINETICS FOR PROPANE COMBUSTION

SHUH-JING YING (South Florida, University, Tampa, FL) and HUNG LEE NGUYEN (NASA, Lewis Research Center, Cleveland, OH) AIAA, Aerospace Sciences Meeting, 28th, Reno, NV, Jan. 8-11, 1990. 10 p. refs

(AIAA PAPER 90-0546) Copyright

It is pointed out that a detailed chemical kinetics mechanism for the combustion of propane consists of 40 chemical species and 118 elementary chemical reactions. An attempt is made to reduce the number of chemical species and elementary chemical reactions so that the computer run times and storage requirements may be greatly reduced in three-dimensional gas turbine combustion flow calculations, while maintaining accurate predictions of the propane combustion and exhaust emissions. By way of a sensitivity analysis, the species of interest and chemical reactions are classified in descending order of importance. Nineteen species are chosen, and their pressure, temperature, and concentration profiles are presented for the reduced mechanisms, which are then compared with those from the full 118 reactions. It is found that 45 reactions involving 27 species have to be kept for comparable agreement. A comparison of the results obtained from the 45 reactions to that of the full 118 shows that the pressure and temperature profiles and concentrations of C_3H_8 , O_2 , N_2 , H_2O , CO , and CO_2 are within 10 percent of maximum change.

S.A.V.

A90-21215* National Aeronautics and Space Administration, Lewis Research Center, Cleveland, OH.

MASS SPECTROMETRIC OBSERVATIONS OF METAL OXYCHLORIDES PRODUCED BY OXIDATION-CHLORINATION REACTIONS

N. S. JACOBSON (NASA, Lewis Research Center, Cleveland, OH), M. J. MCNALLAN (Illinois, University, Chicago), and Y. Y. LEE (Research Institute for Industrial Science and Technology, Pohang, Republic of Korea) Metallurgical Transactions A - Physical Metallurgy and Materials Science (ISSN 0360-2133), vol. 20A, Aug. 1989, p. 1566-1568. refs

(Contract DE-FG02-85ER-45178)

It was recently reported that Cr_2O_3 -forming alloys show less corrosion resistance than Al_2O_3 -forming alloys in Cl_2/O_2 mixtures, which is attributed to the formation of porous Cr_2O_3 scales and stable CrO_2Cl_2 vapor species. This paper reports the results of

direct mass spectrometric observations with a high-pressure sampling mass spectrometer of these metal oxychlorides forming on the surfaces of Hastelloy S and Alloy 600 superalloys. Samples were preoxidized for 2 hrs at 900 C before the exposure to a O_2/Ar gas mixture containing 1 percent Cl_2 . Results of X-ray diffraction showed scales containing Cr_2O_3 and $NiCr_2O_4$ on both alloys. After exposure to Cl_2 , large quantities of CrO_2Cl_2 were demonstrated for both alloys, indicating that this is a route for the breakdown of Cr_2O_3 scales. The Mo present in the Hastelloy S leads to more rapid attack by Cl_2 , resulting in the formation of MoO_2Cl_2 .

I.S.

A90-22238* National Aeronautics and Space Administration, Ames Research Center, Moffett Field, CA.

SMOLDERING COMBUSTION UNDER LOW GRAVITY CONDITIONS

ELIZABETH R. CANTWELL (NASA, Ames Research Center, Moffett Field, CA) and A. C. FERNANDEZ-PELLO (California, University, Berkeley) AIAA, Aerospace Sciences Meeting, 28th, Reno, NV, Jan. 8-11, 1990. 8 p. refs

(Contract NAG3-443)

(AIAA PAPER 90-0648) Copyright

A study is being conducted on the effects of buoyancy in smoldering combustion, and the expected behavior of smolder under low gravity conditions. Initial experiments, on one-dimensional smoldering of polyurethane foam have been conducted, both in ground-based and drop tower facilities, to provide information for the design of space-based experiments. Results from these experiments are presented and discussed in light of our understanding of the various competing physical processes controlling smoldering combustion. These results show that for low forcing flow rates, smolder behaves differently in the absence of gravity than at normal gravity.

Author

A90-23107* Science Applications International Corp., Torrance, CA.

IGNITION AND BEHAVIOR OF LAMINAR GAS-JET DIFFUSION FLAMES IN MICROGRAVITY

M. YOUSEF BAHADORI, RAYMOND B. EDELMAN (Science Applications International Corp., Torrance, CA), DENNIS P. STOCKER, and SANDRA L. OLSON (NASA, Lewis Research Center, Cleveland, OH) AIAA Journal (ISSN 0001-1452), vol. 28, Feb. 1990, p. 236-244. Previously cited in issue 10, p. 1494, Accession no. A88-27722. refs

(Contract NAS3-22822)

A90-24535* Hughes Aircraft Co., Los Angeles, CA.

ELECTROCHEMICAL BEHAVIOR OF HEAVILY CYCLED NICKEL ELECTRODES IN Ni/H_2 CELLS CONTAINING ELECTROLYTES OF VARIOUS KOH CONCENTRATIONS

H. S. LIM and S. A. VERZWYVELT (Hughes Aircraft Co., Los Angeles, CA) Electrochemical Society, Fall Meeting, Hollywood, FL, Oct. 15-20, 1989, Paper. 15 p. refs

(Contract NAS3-22238)

A study has been made of charge and discharge voltage changes with cycling of Ni/H_2 cells containing electrolytes of various KOH concentrations. A study has also been made of electrochemical behavior of the nickel electrodes from the cycled Ni/H_2 cells as a function of overcharge amounts. Discharge voltages depressed gradually with cycling for cells having high KOH concentrations (31 to 36 percent), but the voltages increased for those having low KOH concentrations (21 to 26 percent). To determine if there was a crystallographic change of the active material due to cycling, electrochemical behavior of nickel electrodes was studied in an electrolyte flooded cell containing either 31 or 26 percent KOH electrolyte as a function of the amount of overcharge. The changes in discharge voltage appear to indicate crystal structure changes of active material from gamma-phase to beta-phase in low KOH concentrations, and vice versa in high KOH concentration.

Author

25 INORGANIC AND PHYSICAL CHEMISTRY

A90-25038* # National Aeronautics and Space Administration, Lewis Research Center, Cleveland, OH.

N-DECANE-AIR DROPLET COMBUSTION EXPERIMENTS IN THE NASA-LEWIS 5 SECOND ZERO-GRAVITY FACILITY

JOHN B. HAGGARD, MICHAEL H. BRACE (NASA, Lewis Research Center, Cleveland, OH), FREDERICK L. DRYER, MUN Y. CHOI (Princeton University, NJ), FORMAN A. WILLIAMS (California, University, La Jolla) et al. AIAA, Aerospace Sciences Meeting, 28th, Reno, NV, Jan. 8-11, 1990. 10 p. refs (AIAA PAPER 90-0649) Copyright

The burning of single fuel (n-decane) droplets in a microgravity environment (below 0.00001 of the earth's gravity, achieved in the NASA-Lewis 5-Second Zero-Gravity Facility) was studied, as part of the development of the Droplet Combustion Experiment for eventual operation aboard either the Shuttle middeck or Spacelab. Special attention is given to the combustion equipment used and its operations and performance. Temporal analysis of the local burning rates in these tests showed increasing rates of change in the local burning as droplet combustion progressed. Result point to the need of studying large droplets, with long droplet combustion lifetimes as well as low gas/droplet motion to understand reasons for this unsteadiness. I.S.

A90-25039* # Science Applications International Corp., Torrance, CA.

EFFECTS OF PRESSURE ON MICROGRAVITY HYDROCARBON DIFFUSION FLAMES

M. YOUSEF BAHADORI (Science Applications International Corp., Torrance, CA), DENNIS P. STOCKER (NASA, Lewis Research Center, Cleveland, OH), and RAYMOND B. EDELMAN (Rockwell International Corp., Rocketdyne Div., Canoga Park, CA) AIAA, Aerospace Sciences Meeting, 28th, Reno, NV, Jan. 8-11, 1990. 7 p. refs

(Contract NAS3-22822)
(AIAA PAPER 90-0651)

The effect of pressure on the propane diffusion flames burning in quiescent air under both normal-gravity and microgravity conditions (in the NASA's 2.2-Second Drop Tower at the Lewis Research Center) were studied at pressures of 0.5, 1.0, and 1.5 atm, with three fuel mass-flow rates for each pressure. Compared to normal-gravity flames, the microgravity tests showed enhanced sooting, tip-opening, and soot escape, accompanied with changes in color, size, and luminosity of the flames. At low pressures, less-efficient burning and a broader flame zone was found to exist due to the kinetics effects, while at high pressures, where was more soot and longer soot-burning zones. Results show that there exist a particular intermediate pressure at which both the microgravity and normal-gravity flame heights are minimized. I.S.

A90-28771* California Univ., La Jolla.

THEORY OF INFLUENCE OF A LOW-VOLATILITY, SOLUBLE IMPURITY ON SPHERICALLY-SYMMETRIC COMBUSTION OF FUEL DROPLETS

B. D. SHAW and F. A. WILLIAMS (California, University, La Jolla) International Journal of Heat and Mass Transfer (ISSN 0017-9310), vol. 33, Feb. 1990, p. 301-317. refs

(Contract NAS3-24640)
Copyright

Analyses are given for the evolution of liquid-phase mass fraction profiles and temperature during combustion of fuel droplets composed of binary miscible mixtures of low-volatility and high-volatility constituents, with small initial mass fractions of the low-volatility material, or slow introduction of low-volatility material into the liquid phase by absorption from the gas phase. The gas phase is assumed to remain quasi-steady and the liquid temperature spatially uniform. The ratio of the liquid-phase diffusion coefficient to the initial burning-rate constant is treated as a small parameter. Asymptotic analyses in this parameter are developed, and the conservation equations are integrated numerically in obtaining descriptions of the combustion history. It is shown that at the surface of the droplet a boundary layer arises in which the mass fraction of the low-volatility component increases with time. The

results are used to explain qualitatively some observed conditions of flame contraction and liquid disruption in droplet combustion.

Author

A90-32835* National Aeronautics and Space Administration, Lewis Research Center, Cleveland, OH.

NEAR-LIMIT FLAME SPREAD OVER A THIN SOLID FUEL IN MICROGRAVITY

SANDRA L. OLSON (NASA, Lewis Research Center, Cleveland, OH), PAUL V. FERKUL, and JAMES S. T'EN (Case Western Reserve University, Cleveland, OH) IN: Symposium (International) on Combustion, 22nd, Seattle, WA, Aug. 14-19, 1988, Proceedings. Pittsburgh, PA, Combustion Institute, 1989, p. 1213-1219; Discussion, p. 1220-1222. refs

(Contract NGT-50088)

Copyright

Diffusion flame spread over a thin solid fuel in quiescent and slowly moving atmospheres is studied in microgravity. The flame behavior is observed to depend strongly on the magnitude of the relative velocity between the flame and the atmosphere. In particular, a low velocity quenching limit is found to exist in low oxygen environments. Using both the microgravity results and previously published data at high opposed-flow velocities, the flame spread behavior is examined over a wide velocity range. A flammability map using molar oxygen percentages and characteristic relative velocities as coordinates is constructed. Trends of flame spread rate are determined and mechanisms for flame extinction are discussed.

Author

A90-33723* Research Triangle Inst., Research Triangle Park, NC.

THE IMPEDANCE OF A TUBULAR ELECTRODE - A MODEL FOR A POROUS ELECTRODE

ANDREW S. VINER (Research Triangle Institute, Research Triangle Park, NC) and PETER S. FEDKIW (North Carolina State University, Raleigh) Electrochemical Society, Journal (ISSN 0013-4651), vol. 137, May 1990, p. 1435-1444. refs

(Contract NAG3-649)

Copyright

A cylindrical tube is used as the basis for a two-dimensional mathematical model to calculate the impedance of a flooded porous electrode. The model incorporates charge-transfer, mass-transfer, and ohmic resistances to obtain the axial and radial dependencies of the concentration and potential profiles. A linearized Butler-Volmer kinetic expression for a simple redox reaction $O + e$ yielding R is used, in conjunction with analytical expressions for the surface concentration and overpotential, to compute the open-circuit impedance. The results of the two-dimensional model, which omits double-layer charging, are compared with the results of a more standardly applied one-dimensional model in which radial variations are neglected, with and without double-layer charging. The simpler-to-apply one-dimensional model is found to be satisfactory when mass-transfer and ohmic resistances are small with respect to charge-transfer resistance. The omission of double-layer charging does not introduce error into the two-dimensional model in the frequency range in which capacitive-like effects are caused by mass-transfer limitations.

Author

A90-36268* # Nebraska Univ., Lincoln.

ELLIPSOMETRIC STUDIES OF THE DIFFUSION OF ATOMIC OXYGEN THROUGH SILICON DIOXIDE THIN FILMS

GRANT G. MEYERS, JOHN WOOLLAM (Nebraska, University, Lincoln), DANIEL A. GULINO (NASA, Lewis Research Center, Cleveland, OH), BHOLA N. DE, KAZEM MEMARZADEH, AGUS JULIANTO et al. AIAA Journal (ISSN 0001-1452), vol. 28, June 1990, p. 1065, 1066. Abridged.

(Contract NAG3-95)

Copyright

The application of variable angle spectroscopic ellipsometry to the study of diffusion of atomic oxygen through SiO_2 is presented. Data are found to be well fit to the universal growth parabola,

and the diffusion coefficient is estimated to be 0.00001 sq cm/min. Author

A90-36810* Aerodyne Research, Inc., Billerica, MA.
MODELING OF THE SiC CHEMICAL VAPOR DEPOSITION PROCESS AND COMPARISON WITH EXPERIMENTAL RESULTS

K. D. ANNEN, C. D. STINESPRING (Aerodyne Research, Inc., Billerica, MA), M. A. KUCZMARSKI, and J. A. POWELL (NASA, Lewis Research Center, Cleveland, OH) Journal of Vacuum Science and Technology A (ISSN 0734-2101), vol. 8, pt. II, May-June 1990, p. 2970-2975. refs
 Copyright

A model of the NASA Lewis SiC CVD process is described, and the results presented. A key feature of the model is the direct coupling of gas-phase chemical kinetics with diffusion. A deposition chemistry model using reactive sticking coefficients for each gas-phase species provides the diffusion boundary conditions. SiC deposition rates predicted by the model agree reasonably well with experimentally observed rates. Author

A90-38399*# Physical Sciences, Inc., Andover, MA.
H₂/O₂ THREE-BODY RATES AT HIGH TEMPERATURES
 WILLIAM J. MARINELLI, WILLIAM J. KESSLER, LAWRENCE G. PIPER, and W. TERRY RAWLINS (Physical Sciences, Inc., Andover, MA) AIAA and ASME, Joint Thermophysics and Heat Transfer Conference, 5th, Seattle, WA, June 18-20, 1990. 8 p. refs

(Contract NAS3-25566)

(AIAA PAPER 90-1696) Copyright

The extraction of thrust from air breathing hypersonic propulsion systems is critically dependent on the degree to which chemical equilibrium is reached in the combustion process. In the combustion of H₂/Air mixtures, slow three-body chemical reactions involving H-atoms, O-atoms, and the OH radical play an important role in energy extraction. A first-generation high temperature and pressure flash-photolysis/laser-induced fluorescence reactor was designed and constructed to measure these important three-body rates. The system employs a high power excimer laser to produce these radicals via the photolysis of stable precursors. A novel two-photon laser-induced fluorescence technique is employed to detect H-atoms without optical thickness or O₂ absorption problems. To demonstrate the feasibility of the technique the apparatus in the program is designed to perform preliminary measurements on the H + O₂ + M reaction at temperatures from 300 to 835 K.

R.E.P.

A90-42298* Case Western Reserve Univ., Cleveland, OH.
THE POSSIBILITY OF A REVERSAL OF MATERIAL FLAMMABILITY RANKING FROM NORMAL GRAVITY TO MICROGRAVITY

JAMES S. T'EN (Case Western Reserve University, Cleveland, OH) Combustion and Flame (ISSN 0010-2180), vol. 80, June 1990, p. 355-357. refs

(Contract NAG3-1046)

Copyright

The purpose of the discussion is to show, by a theoretical model, that one of the material flammability indices, the flammability limit, can be reversed in proper circumstances. A stagnation-point diffusion flame adjacent to a spherical solid-fuel surface is considered. It is shown that a reversal of the limiting oxygen indices from normal gravity and microgravity is possible. Although the example is based on a particular theoretical model with a particular flame configuration and specifically for an oxygen limit, the flammability-limit reversal phenomenon is believed to be more general. V.T.

A90-42774*# Sverdrup Technology, Inc., Brook Park, OH.
FUEL-RICH CATALYTIC COMBUSTION - A FUEL PROCESSOR FOR HIGH-SPEED PROPULSION
 THEODORE A. BRABBS (Sverdrup Technology, Inc., Brook Park, OH), R. JAMES ROLLBUHLER, and ERWIN A. LEZBERG (NASA, Lewis Research Center, Cleveland, OH) AIAA, SAE, ASME, and

ASEE, Joint Propulsion Conference, 26th, Orlando, FL, July 16-18, 1990. 10 p. Previously announced in STAR as N90-23518. refs
 (AIAA PAPER 90-2319) Copyright

Fuel-rich catalytic combustion of Jet-A fuel was studied over the equivalence ratio range 4.7 to 7.8, which yielded combustion temperatures of 1250 to 1060 K. The process was soot-free and the gaseous products were similar to those obtained in the iso-octane study. A carbon atom balance across the catalyst bed calculated for the gaseous products accounted for about 70 to 90 percent of the fuel carbon; the balance was condensed as a liquid in the cold trap. It was shown that 52 to 77 percent of the fuel carbon was C₁, C₂, and C₃ molecules. The viability of using fuel-rich catalytic combustion as a technique for preheating a practical fuel to very high temperatures was demonstrated. Preliminary results from the scaled up version of the catalytic combustor produced a high-temperature fuel containing large amounts of hydrogen and carbon monoxide. The balance of the fuel was completely vaporized and in various stages of pyrolysis and oxidation. Visual observations indicate that there was no soot present. Author

A90-43674* Illinois Univ., Urbana.
THE STRUCTURE AND STABILITY OF NONADIABATIC FLAME BALLS

J. BUCKMASTER (Illinois, University, Urbana), G. JOULIN (CNRS, Laboratoire d'Energetique et de Detonique, Poitiers, France), and P. RONNEY (Princeton University, NJ) Combustion and Flame (ISSN 0010-2180), vol. 79, March 1990, p. 381-392. Research supported by USAF and Gas Research Institute. refs

(Contract NSF CBT-86-57228; NAG3-965)

Copyright

Recent experiments in microgravity suggest the possibility of stationary spherical premixed flames (flame balls) in which the only fluxes are diffusional. Stationary solutions of this nature are constructed, starting with simple model equations and using activation energy asymptotics. Sufficiently large volumetric heat losses quench the flame, and for heat losses less than the quenching value there are two possible solutions, a small flame and a large flame. For vanishing heat loss the small solution is identical to one constructed by Zel'dovich, and is known to be unstable, whereas the large solution is characterized by a flame of infinite radius. The linear stability of these stationary solutions is examined, and it is shown that all small flames are unstable to one-dimensional (radial) perturbations. Large flames are unstable to three-dimensional perturbations, but only if they have a radius greater than some critical value. Thus there is a band of large flames, lying between the quenching point and unstable flames, that are stable. Author

A90-44689* National Aeronautics and Space Administration. Lewis Research Center, Cleveland, OH.

HUMIDITY-INDUCED ROOM-TEMPERATURE DECOMPOSITION OF AU CONTACTED INDIUM PHOSPHIDE

NAVID S. FATEMI (NASA, Lewis Research Center, Cleveland, OH; Sverdrup Technology, Inc., Brookpark, OH) and VICTOR G. WEIZER (NASA, Lewis Research Center, Cleveland, OH) Applied Physics Letters (ISSN 0003-6951), vol. 57, July 30, 1990, p. 500-502. refs

(Contract NAS3-25266)

Copyright

It has been found that Au-contacted InP is chemically unstable at room temperature in a humid ambient due to the leaching action of indium nitrate islands that continually remove In from the contact metallization and thus, in effect, from the InP substrate. While similar appearing islands form on Au-contacted GaAs, that system appears to be stable since leaching of the group III element does not take place. Author

A90-50645*# National Aeronautics and Space Administration. Lewis Research Center, Cleveland, OH.
CRITICAL EVALUATION OF JET-A SPRAY COMBUSTION USING PROPANE CHEMICAL KINETICS IN GAS TURBINE COMBUSTION SIMULATED BY KIVA-II

25 INORGANIC AND PHYSICAL CHEMISTRY

H. L. NGUYEN (NASA, Lewis Research Center, Cleveland, OH) and S.-J. YING (South Florida, University, Tampa, FL) AIAA, SAE, ASME, and ASEE, Joint Propulsion Conference, 26th, July 16-18, 1990. 20 p. refs

(Contract NAG3-1112)
(AIAA PAPER 90-2439) Copyright

Numerical solutions of the Jet-A spray combustion were obtained by means of the KIVA-II computer code after Jet-A properties were added to the 12 chemical species the program had initially contained. Three different reaction mechanism models are considered. The first model consists of 131 reactions and 45 species; it is evaluated by comparing calculated ignition delay times with available shock tube data, and it is used in the evaluation of the other two simplified models. The simplified mechanisms consider 45 reactions and 27 species and 5 reactions and 12 species, respectively. In the prediction of pollutants NOx and CO, the full mechanism of 131 reactions is considered to be more reliable. The numerical results indicate that the variation of the maximum flame temperature is within 20 percent as compared with that of the full mechanism of 131 reactions. The chemical compositions of major components such as C3H8, H2O, O2, CO2, and N2 are of the same order of magnitude. However, the concentrations of pollutants are quite different. B.P.

N90-11824* National Aeronautics and Space Administration. Lewis Research Center, Cleveland, OH.

STEAM COOLED RICH-BURN COMBUSTOR LINER Patent

DONALD F. SCHULTZ, inventor (to NASA) 11 Apr. 1989 7 p
Filed 23 Dec. 1982 Supersedes N83-17628 (21 - 8, p 1149)
(NASA-CASE-LEW-13609-1; US-PATENT-4,819,438;
US-PATENT-APPL-SN-452465; US-PATENT-CLASS-60-730;
US-PATENT-CLASS-60-732; US-PATENT-CLASS-165-83;
US-PATENT-CLASS-165-81; US-PATENT-CLASS-165-156;
US-PATENT-CLASS-431-352) Avail: US Patent and Trademark Office CSCL 21/2

Stress on the wall of the primary combustor is minimized. Thus, the steam pressure in the inlet manifold is approximately the same as the combustor discharge pressure at the throat, and annular expansion tubes minimize stresses in the jacket. The second combustor accomplishes lean burning of the gases discharged from primary combustor. The combination of the rich burning of heavy fuels followed by lean burning minimizes the NOx in the exhaust gas discharged from combustor. The novelty of the invention appears to lie in cooling a rich burn combustor with spiral streams of saturated steam flowing between the combustor liner and the jacket at a predetermined pressure; the jacket including stress relief means.

Official Gazette of the U.S. Patent and Trademark Office

N90-12696* National Aeronautics and Space Administration. Lewis Research Center, Cleveland, OH.

CHARACTERIZATION AND CYCLE TESTS OF LIGHTWEIGHT NICKEL ELECTRODES

DORIS L. BRITTON 1989 13 p Presented at the Electrochemical Society Meeting, Hollywood, FL, 16-20 Oct. 1989 (NASA-TM-102399; E-5153; NAS 1.15:102399) Avail: NTIS HC A03/MF A01 CSCL 07/4

Development of a high specific energy nickel electrode is the main goal of the lightweight nickel electrode program at NASA Lewis Research Center. The approach was to improve the nickel electrode by continuing combined in-house and contract efforts to develop a more efficient and lighter weight electrode for the nickel-hydrogen battery. High energy nickel electrodes suffer from having shorter lives than state-of-the-art electrode. However, these lightweight electrodes appear to be favorable for missions requiring moderate cycle lives and depth-of-discharge. Author

N90-14305* Pennsylvania State Univ., University Park. Fuel Science Program.

KINETICS AND MECHANISM OF SOOT FORMATION IN HYDROCARBON COMBUSTION Final Technical Report, 25 Oct. 1985 - 28 Feb. 1989

MICHAEL FRENKLACH 5 Jan. 1990 10 p

(Contract NAG3-668)

(NASA-CR-186162; NAS 1.26:186162) Avail: NTIS HC A02/MF A01 CSCL 21/2

The focus of this work was on kinetic modeling. The specific objectives were: detailed modeling of soot formation in premixed flames, elucidation of the effects of fuel structure on the pathway to soot, and the development of a numerical technique for accurate modeling of soot particle coagulation and surface growth. Those tasks were successfully completed and are briefly summarized.

J.P.S.

N90-19340* North Carolina State Univ., Raleigh. Dept. of Chemical Engineering.

CHARACTERIZATION OF REACTION KINETICS IN A POROUS ELECTRODE Final Report

PETER S. FEDKIW 23 Apr. 1990 128 p

(Contract NAG3-649)

(NASA-CR-186504; NAS 1.26:186504) Avail: NTIS HC A07/MF A01 CSCL 07/4

A continuum-model approach, analogous to porous electrode theory, was applied to a thin-layer cell of rectangular and cylindrical geometry. A reversible redox couple is assumed, and the local reaction current density is related to the potential through the formula of Hubbard and Anson for a uniformly accessible thin-layer cell. The placement of the reference electrode is also accounted for in the analysis. Primary emphasis is placed on the effect of the solution-phase ohmic potential drop on the voltammogram characteristics. Correlation equations for the peak-potential displacement from $E(\text{sup } 0 \text{ prime})$ and the peak current are presented in terms of two dimensionless parameters. Author

N90-21842* National Aeronautics and Space Administration. Lewis Research Center, Cleveland, OH.

DETAILED MECHANISM FOR OXIDATION OF BENZENE

DAVID A. BITTKER May 1990 32 p

(NASA-TM-102443; E-5224; NAS 1.15:102443) Avail: NTIS HC A03/MF A01 CSCL 07/4

A detailed mechanism for the oxidation of benzene is presented and used to compute experimentally obtained concentration profiles and ignition delay times over a wide range of equivalence ratio and temperature. The computed results agree qualitatively with all the experimental trends. Quantitative agreement is obtained with several of the composition profiles and for the temperature dependence of the ignition delay times. There are indications, however, that some important reactions are as yet undiscovered in this mechanism. Recent literature expressions have been used for the rate coefficients of most important reactions, except for some involving phenol. The discrepancy between the phenol pyrolysis rate coefficient used in this work and a recent literature expression remains to be explained. Author

N90-21843* National Aeronautics and Space Administration. Lewis Research Center, Cleveland, OH.

STUDIES ON THE USE OF SUPERCRITICAL AMMONIA FOR CERAMIC NITRIDE SYNTHESIS AND FABRICATION

LINDA CORNELL, Y. C. LIN (Case Western Reserve Univ., Cleveland, OH.), and WARREN H. PHILIPP Apr. 1990 17 p
(NASA-TM-102570; E-4441; NAS 1.15:102570) Avail: NTIS HC A03/MF A01 CSCL 07/4

The extractability of ammonia halides (including ammonium thiocyanate) formed as byproducts from the synthesis of $\text{Si}(\text{NH})_2$ via ammonolysis of the corresponding silicon tetrahalides using supercritical NH_3 as the extraction medium was investigated. It was found that the NH_4SCN byproduct of ammonolysis of $\text{Si}(\text{SCN})_4$ can be almost completely extracted from the insoluble $\text{Si}(\text{NH})_2$ forming a promising system for the synthesis of pure $\text{Si}(\text{NH})_2$, one of the best precursors for Si_3N_4 . In addition it was found that Si_3N_4 , AlN , BN , and $\text{Si}(\text{NH})_2$ are insoluble in SC ammonia. Also discussed are design considerations for a supercritical ammonia extraction unit. Author

N90-21844*# National Aeronautics and Space Administration. Lewis Research Center, Cleveland, OH.

ELECTROCHEMICAL IMPREGNATION AND CYCLE LIFE OF LIGHTWEIGHT NICKEL ELECTRODES FOR NICKEL-HYDROGEN CELLS

DORIS L. BRITTON 1990 6 p Presented at the 34th International Power Sources Conference, Cherry Hill, NJ, 25-28 Jun. 1990; cosponsored by Army and IEEE (NASA-TM-103140; E-5492; NAS 1.15:103140) Avail: NTIS HC A02/MF A01 CSCL 07/4

Development of a high specific energy nickel electrode is the main goal of the lightweight nickel electrode program at NASA-Lewis. The approach was to improve the nickel electrode by continuing combined in-house and contract efforts to develop a more efficient and lighter weight electrode for the nickel-hydrogen cell. Lightweight plaques are used as conductive supports for the nickel hydroxide active material. These plaques are commercial products that are fabricated into nickel electrodes by electrochemically impregnating them with active material. The electrodes are life cycle tested in a low Earth orbit regime at 40 and 80 percent depths-of-discharge. Author

N90-23497* National Aeronautics and Space Administration. Lewis Research Center, Cleveland, OH.

SUBSTITUTED 1,1,1-TRIARYL-2,2,2-TRIFLUOROETHANES AND PROCESSES FOR THEIR SYNTHESIS Patent

WILLIAM B. ALSTON, inventor (to NASA) and ROY F. GRATZ, inventor (to NASA) (Mary Washington Coll., Fredericksburg, VA.) 5 Dec. 1989 12 p Filed 23 Feb. 1988 Division of US-Patent-Appl-SN-924474, filed 29 Oct. 1986 (NASA-CASE-LEW-14345-2; US-PATENT-4,885,116; US-PATENT-APPL-SN-159071; US-PATENT-APPL-SN-924474; US-PATENT-CLASS-562-413; US-PATENT-CLASS-260-395; US-PATENT-CLASS-260-386; US-PATENT-CLASS-549-241; US-PATENT-CLASS-562-415; US-PATENT-CLASS-562-417) Avail: US Patent and Trademark Office CSCL 07/4

Synthetic procedures are disclosed for tetraalkyls, tetraacids, and dianhydrides substituted 1,1,1-triaryl 2,2,2-trifluoroethanes which comprises: (1) 1,1-bis (dialkylaryl) 1-aryl 2,2,2-trifluoroethane, (2) 1,1-bis (dicarboxyaryl) 1-aryl 2,2,2-trifluoroethane, or (3) cyclic dianhydride or diamine of 1,1-bis (dialkylaryl) 1-aryl 2,2,2-trifluoroethanes. The synthesis of (1) is accomplished by the condensation reaction of an aryltrifluoromethyl ketone with a dialkylaryl compound. The synthesis of (2) is accomplished by the oxidation of (1). The synthesis dianhydride of (3) is accomplished by the conversion of (2) to its corresponding cyclic dianhydride. The synthesis of the diamine is accomplished by the similar reaction of an aryltrifluoromethyl ketone with aniline or alkyl substituted or disubstituted anilines. Also, other derivatives of the above are formed by nucleophilic displacement reactions.

Official Gazette of the U.S. Patent and Trademark Office

N90-23518*# National Aeronautics and Space Administration. Lewis Research Center, Cleveland, OH.

FUEL-RICH CATALYTIC COMBUSTION: A FUEL PROCESSOR FOR HIGH-SPEED PROPULSION

THEODORE A. BRABBS (Sverdrup Technology, Inc., Brookpark, OH.), R. JAMES ROLLBUHLER, and ERWIN A. LEZBERG 1990 11 p Presented at the 26th Joint Propulsion Conference, Orlando, FL, 16-18 Jul. 1990; cosponsored by AIAA, SAE, ASME, and ASEE (NASA-TM-103177; E-5555; NAS 1.15:103177; AIAA-90-2319) Avail: NTIS HC A03/MF A01 CSCL 21/2

Fuel-rich catalytic combustion of Jet-A fuel was studied over the equivalence ratio range 4.7 to 7.8, which yielded combustion temperatures of 1250 to 1060 K. The process was soot-free and the gaseous products were similar to those obtained in the iso-octane study. A carbon atom balance across the catalyst bed calculated for the gaseous products accounted for about 70 to 90 percent of the fuel carbon; the balance was condensed as a liquid in the cold trap. It was shown that 52 to 77 percent of the fuel carbon was C1, C2, and C3 molecules. The viability of using fuel-rich catalytic combustion as a technique for preheating a

practical fuel to very high temperatures was demonstrated. Preliminary results from the scaled up version of the catalytic combustor produced a high-temperature fuel containing large amounts of hydrogen and carbon monoxide. The balance of the fuel was completely vaporized and in various stages of pyrolysis and oxidation. Visual observations indicate that there was no soot present. Author

N90-26911*# Pennsylvania State Univ., University Park. Dept. of Mechanical Engineering.

IGNITION AND COMBUSTION CHARACTERISTICS OF METALLIZED PROPELLANTS Semiannual Report, Jan. - Jun. 1990

S. R. TURNS, D. C. MUELLER, and M. J. SCOTT Jul. 1990 41 p

(Contract NAG3-1044) (NASA-CR-186870; NAS 1.26:186870) Avail: NTIS HC A03/MF A01 CSCL 21/2

Shakedown and calibration of the experimental apparatus designed to study secondary atomization and ignition characteristics of aluminum slurry propellants was begun and nears completion. The burner was tested over an array of equivalence ratios and oxygen mass fractions to determine the permissible range of operating conditions. A burner flow control system was designed and fabricated which permits independent control of flame stoichiometry and oxidant O2 concentrations. The Sun slurry formulation was selected as the base for initial testing. Laser beam waists at the focal volume of the single particle sizing system were determined to be 396 microns for the Ar-ion and 81 microns for the He-Ne laser. Size calibrations using pinholes were completed and compared to Mie theory for light scattering from particles. A vibrating orifice droplet generator was used to test the single particle sizing system dynamically by producing a water droplet laden gas flow. The data acquisition and analysis programming was completed and testing is in progress. From initial results, the particle sizing, atomization and ignition detection systems appear to be performing as expected. Author

N90-28627*# National Aeronautics and Space Administration. Lewis Research Center, Cleveland, OH.

CATALYTIC IGNITION OF HYDROGEN/OXYGEN

JAMES M. GREEN (Sverdrup Technology, Inc., Middleburg Heights, OH.) and ROBERT L. ZURAWSKI /in NASA, Marshall Space Flight Center, Advanced Earth-to-Orbit Propulsion Technology 1988, Volume 1 p 231-248 Sep. 1988 Avail: NTIS HC A99/MF E06 CSCL 21/2

An experimental program was conducted to evaluate the catalytic ignition of gaseous hydrogen and oxygen. Shell 405 granular catalyst and a unique monolithic sponge catalyst were tested. Mixture ratio, mass flow rate, propellant inlet temperature, and back pressure were varied parametrically in testing to determine the operational limits of a catalytic igniter. The test results showed that the gaseous hydrogen/oxygen propellant combination can be ignited catalytically using Shell 405 catalyst over a wide range of mixture ratios, mass flow rates, and propellant injection temperatures. These operating conditions must be optimized to ensure reliable ignition for an extended period of time. The results of the experimental program and the established operational limits for a catalytic igniter using both the granular and monolithic catalysts are presented. The capabilities of a facility constructed to conduct the igniter testing and the advantages of a catalytic igniter over other ignition systems for gaseous hydrogen and oxygen are also discussed. Author

N90-28628*# Rockwell International Corp., Canoga Park, CA. Rocketdyne Div.

OXYGEN/METHANE COMBUSTION STABILITY INVESTIGATION

R. J. JENSEN, H. DODSON, and B. TRUEBLOOD /in NASA, Marshall Space Flight Center, Advanced Earth-to-Orbit Propulsion Technology 1988, Volume 1 p 249-269 Sep. 1988 (Contract NAS3-24612)

Avail: NTIS HC A99/MF E06 CSCL 21/2

The LOX/Hydrocarbon Combustion Instability Investigation Program is structured to determine if the use of light hydrocarbon fuels (such as methane) with liquid oxygen (LOX) produces combustion performance and stability behavior similar to the LOX/hydrogen propellant combination. In particular, methane is being investigated to determine if that fuel can be rated for combustion instability using the same techniques as previously used for LOX/hydrogen. These techniques include fuel temperature ramping and stability bomb tests. The hot fire program probed the combustion behavior of methane from ambient to subambient (438 R) temperatures. The 5.66-in. diameter, 82-coaxial element hardware was operated over a mixture ratio range of 2.8 to 3.7 and mainstage durations from 0.1 to 8 sec in tests at a nominal chamber pressure of 2000 psig. Three tests were successfully driven unstable at low fuel temperature during fuel temperature ramping stability rating tests. Three other tests experienced self-induced instabilities at low mixture ratios and ambient fuel temperatures. Relationships between the data, stability analyses, and LOX/hydrogen stability trends are discussed. Author

N90-28629*# National Aeronautics and Space Administration. Lewis Research Center, Cleveland, OH.

COMBUSTION INSTABILITY COUPLING WITH FEED SYSTEM ACOUSTICS

RICHARD J. PRIEM (Priem Consultants, Inc., Cleveland, OH.) and KEVIN J. BREISACHER /in NASA, Marshall Space Flight Center, Advanced Earth-to-Orbit Propulsion Technology 1988, Volume 1 p 270-301 Sep. 1988

Avail: NTIS HC A99/MF E06 CSCL 21/2

High frequency combustion instability has recently been observed by Rocketdyne in a 40K thrust methane/LOX combustion chamber. The oscillations had frequencies as high as 14,000 Hz with pressure amplitudes in the LOX dome of 500 psi at a chamber pressures of 2,000 psi. At this frequency the wave length associated with a period of oscillation is 2.3 inches in LOX and 1.4 inches in methane. These distances are comparable to the lengths of the injector elements which requires that acoustic waves be considered in the feed systems rather than using lumped parameters as is normally considered for feed system coupled oscillations. To expand the capability of existing models, the Feiler and Heidmann feed system coupled instability model was modified to include acoustic oscillations in the feed system. Similarly the vaporization controlled instability model of Heidmann and Wieber was modified to include flow oscillations that would be produced by feed system coupling. The major elements that control oscillations in a rocket combustion chamber are shown and discussed. Author

N90-28696*# National Aeronautics and Space Administration. Lewis Research Center, Cleveland, OH.

SYNTHESIS AND STRUCTURAL CHEMISTRY OF AU(III)-SUBSTITUTED BA₂YCu₃O(7-DELTA)

A. F. HEPP, J. R. GAIER, J. J. POUCH, A. BANERJEA, and P. D. HAMBOURGER (Cleveland State Univ., OH.) Apr. 1988 9 p Presented at the 2nd Annual Conference on Superconductivity and Applications, Buffalo, NY, 18-20 Apr. 1988; sponsored in part by The New York State Institute on Superconductivity and The New York State Energy Research and Development Authority (NASA-TM-103292; E-5752; NAS 1.15:103292) Avail: NTIS HC A02/MF A01 CSCL 07/4

Gold-substituted superconductors, Ba₂Y(Au(x)Cu(1-x))-3O(7-delta) (x = 0-0.1) were synthesized. For x = 0.1, there was no change in the a and b lattice parameters (a = 3.826 Å and b = 3.889 Å) but a 0.06 Å c axis expansion to 11.75 Å was observed. Substituted gold is found to be trivalent by XPS. Replacing Cu(1) in the copper oxide chain with a slight reordering of oxygen is consistent with c axis expansion. The formal charge of the site remains trivalent; remaining Cu in the chains may be reduced resulting in an oxygen stoichiometry is less than or equal to 7. A small effect on T(sub c)(89 K for x = 0.10) is observed upon gold substitution. Author

METALLIC MATERIALS

Includes physical, chemical, and mechanical properties of metals, e.g., corrosion; and metallurgy.

A90-10028* National Aeronautics and Space Administration. Lewis Research Center, Cleveland, OH.

APPARENT ACTIVATION VOLUME FOR CREEP OF COPPER AND ALPHA BRASS AT INTERMEDIATE TEMPERATURES

S. V. RAJ (NASA, Lewis Research Center, Cleveland, OH) Journal of Materials Science (ISSN 0022-2461), vol. 24, Sept. 1989, p. 3196-3204. Research supported by DOE. refs Copyright

Experimental measurements of the apparent activation volume for creep, V-asterisk, of Cu and Cu-30 pct Zn conducted at intermediate temperatures showed two types of strain dependencies. At the lower temperatures and higher stresses, V-asterisk decreased with increasing creep strain, while at higher temperatures and lower stresses, V-asterisk was essentially independent of strain. The low temperature-high stress behavior for Cu and Cu-30 pct Zn was found to be consistent with the dominance of a dislocation intersection mechanism. The high temperature-low stress data for the pure metals suggest that the rate-controlling process involves the nonconservative motion of jogs on screw dislocations. For the latter conditions, an additional contribution from solute drag-limited dislocation glide also appears to be important in governing the creep behavior of the alloy. Author

A90-11534* National Aeronautics and Space Administration. Lewis Research Center, Cleveland, OH.

THE HIGH TEMPERATURE DEFORMATION IN CYCLIC LOADING OF A SINGLE CRYSTAL NICKEL-BASE SUPERALLOY

T. P. GABB (NASA, Lewis Research Center, Cleveland, OH) and G. WELSCH (Case Western Reserve University, Cleveland, OH) Acta Metallurgica (ISSN 0001-6160), vol. 37, Sept. 1989, p. 2507-2516. refs Copyright

The high temperature cyclic stress softening response of the single crystal nickel-base superalloy PWA 1480 was investigated. Specimens oriented near the 001- and 111-lines were tested at 1050 C in low-cycle fatigue and then microstructurally evaluated. The 001- and 111-line specimens had dissimilar flow behavior in monotonic tensile tests, but comparable softening in low-cycle fatigue. This softening was accompanied by rapid generation of dislocation networks at the gamma-gamma-prime interfaces and by a slower time-dependent coarsening of gamma-prime precipitates. Due to the rapid formation of a dislocation substructure at the gamma-gamma-prime interfaces, the cyclic stress softening could be modeled with an existing theory which related cyclic stress to the evolving microstructure and dislocation structure. Author

A90-11651*# National Aeronautics and Space Administration. Lewis Research Center, Cleveland, OH.

MICROSTRUCTURE AND TENSILE PROPERTIES OF Fe-40 AT. PCT AL ALLOYS WITH C, ZR, HF, AND B ADDITIONS

D. J. GAYDOSH, S. L. DRAPER, and M. V. NATHAL (NASA, Lewis Research Center, Cleveland, OH) Metallurgical Transactions A - Physical Metallurgy and Materials Science (ISSN 0360-2133), vol. 20A, Sept. 1989, p. 1701-1714. refs

The influence of small additions of C, Zr, and Hf, alone or in combination with B, on the microstructure and tensile behavior of substoichiometric FeAl was investigated. Tensile properties were determined from 300 to 1100 K on powder which was consolidated by hot extrusion. All materials possessed some ductility at room temperature, although ternary additions generally reduced ductility compared to the binary alloy. Adding B to the C- and Zr-containing

alloys changed the fracture mode from intergranular to transgranular and restored the ductility to approximately 5 percent elongation. Additions of Zr and Hf increased strength up to about 900 K. Fe₆Al₆Zr and Fe₆Al₆Hf precipitates, both with identical body-centered tetragonal structures, were identified as the principal second phase in these alloys. Strength decreased steadily as temperature increased above 700 K, as diffusion-assisted mechanisms became operative. Although all alloys had similar strengths at 1100 K, Hf additions significantly improved high-temperature ductility by suppressing cavitation. Author

A90-11657* Michigan Technological Univ., Houghton.
**THE CORRELATION BETWEEN THE TEMPERATURE
 DEPENDENCE OF THE CRSS AND THE FORMATION OF
 SUPERLATTICE-INTRINSIC STACKING FAULTS IN THE
 NICKEL-BASE SUPERALLOY PWA 1480**

WALTER W. MILLIGAN (Michigan Technological University, Houghton) and STEPHEN D. ANTOLOVICH (Georgia Institute of Technology, Atlanta) Metallurgical Transactions A - Physical Metallurgy and Materials Science (ISSN 0360-2133), vol. 20A, Sept. 1989, p. 1888, 1889. refs
 (Contract NAG3-503)
 Copyright

The PWA 1480 nickel-base superalloy is known to exhibit a unique minimum in the critical resolved shear stress (CRSS) at about 400 C. This paper reports an observation of a deformation mechanism whose temperature dependence correlates exactly with the reduction in the CRSS. It was found that, after monotonic or cyclic deformation of PWA 1480 at 20 C, the deformation substructures typically contain high density of superlattice-intrinsic stacking faults (S-ISFs) within the gamma-prime precipitates. As the temperature of deformation is increased, the density of S-ISFs is reduced, until finally no faults are observed after deformation in the range from 400 to 705 C. The reduction in the fault density corresponds exactly to the reduction in the CRSS, and the temperature at which the fault density is zero corresponds with the minimum in the CRSS. Two possible mechanisms related to the presence of the S-ISFs in the alloy are considered. I.S.

A90-11658* Cleveland State Univ., OH.
**SIDE BRANCH MORPHOLOGY AND COARSENING IN
 DIRECTIONALLY SOLIDIFIED PB-8.4 AT. PCT AU**

S. N. TEWARI (Cleveland State University, OH), DAVID LEE, and V. V. NESARIKAR Metallurgical Transactions A - Physical Metallurgy and Materials Science (ISSN 0360-2133), vol. 20A, Sept. 1989, p. 1889-1893. refs
 (Contract NCC3-95)
 Copyright

The scaling relationships among the morphological features associated with the formation of perturbations (side branches) in the intercellular regions of a directionally solidified Pb-8.4 at. pct Au alloy were investigated. It is shown that the ratio between the initial side-branch spacing near dendrite tips, λ_{bd}^2 , and the dendrite-tip radius, $r(t)$, equals 2 to 2.5. The ratio between the distance from the dendrite tip to the location of the first side branch formation, $\lambda_{bd}(p)$, and the $t(r)$ equals 8 to 10. It was found that the model proposed by Kirkwood (1985) for the secondary dendrite arm coarsening shows a very good quantitative fit to the experimentally observed secondary arm coarsening kinetics during directional solidification. I.S.

A90-11925* Cincinnati Univ., OH.
**TORSIONAL AND BIAxIAL (TENSION-TORSION) FATIGUE
 DAMAGE MECHANISMS IN WASPALOY AT ROOM
 TEMPERATURE**

N. JAYARAMAN and M. M. DITMARS (Cincinnati, University, OH) International Journal of Fatigue (ISSN 0142-1123), vol. 11, Sept. 1989, p. 309-318. refs
 (Contract NSG-3506)
 Copyright

Strain controlled torsional and biaxial (tension-torsion) low cycle fatigue behavior of Waspaloy was studied at room temperature as a function of heat treatment. Biaxial tests were conducted under

proportional and nonproportional cyclic conditions. The deformation behavior under these different cyclic conditions was evaluated by slip trace analysis. For this, a Schmidt-type factor was defined for multiaxial loading conditions, and it was shown that when the slip deformation is predominant, nonproportional cycles are more damaging than proportional or pure axial or torsional cycles. This was attributed to the fact that under nonproportional cyclic conditions, deformation was through multiple slip, as opposed to single slip for other loading conditions, which gave rise to increased hardening. The total life for a given test condition was found to be independent of heat treatment. This was interpreted as being due to the differences in the cycles to initiation and propagation of cracks. Author

A90-13838*# Southwest Research Inst., San Antonio, TX.
**HIGH TEMPERATURE INELASTIC DEFORMATION UNDER
 UNIAXIAL LOADING - THEORY AND EXPERIMENT**

K. S. CHAN, U. S. LINDHOLM (Southwest Research Institute, San Antonio, TX), S. R. BODNER (Technion - Israel Institute of Technology, Haifa), and K. P. WALKER (Engineering Science Software, Inc., Smithfield, RI) ASME, Transactions, Journal of Engineering Materials and Technology (ISSN 0094-4289), vol. 111, Oct. 1989, p. 345-353. refs
 (Contract NAS3-23925)
 Copyright

The elevated-temperature uniaxial inelastic deformation behavior of an Ni-base alloy, B1900 + Hf, is investigated by performing isothermal tensile, creep, cyclic, stress relaxation, and thermomechanical fatigue tests. The range of strain rates examined is from 10 to the -7th to 100 per sec, while the test temperatures range from 25 to 1093 C. This extensive constitutive data base has been used for evaluating the unified constitutive models of Bodner and Partom (1972) and of Walker (1972) which apply for the small-strain regime. Comparison of test results with independent model predictions indicates good agreement over a broad range of loading conditions, demonstrating the applicability of the unified-constitutive-equation approach for describing the strongly nonlinear and temperature-dependent response of metals under a wide range of deformation and thermal histories. Thus the results give confidence that the unified approach is an effective and efficient approach in which complex history-dependent thermoviscoplastic flow can be represented within a single inelastic strain-rate term. Author

A90-14687* National Aeronautics and Space Administration.
 Lewis Research Center, Cleveland, OH.

**PROPERTIES OF OXIDE DISPERSION STRENGTHENED
 ALLOYS**

J. DANIEL WHITTENBERGER (NASA, Lewis Research Center, Cleveland, OH) IN: New materials by mechanical alloying techniques; Proceedings of the Conference, Calw-Hirsau, Federal Republic of Germany, Oct. 3-5, 1988. Oberursel, Federal Republic of Germany, DGM Informationsgesellschaft Verlag, 1989, p. 201-215. refs
 Copyright

A contrast is drawn between the behavior of ODS alloys' matrix compositions and that of more conventional alloys. Mechanical property enhancements associated with ODS alloys are accounted for by both the presence of the dispersoids and, in some cases, the smaller size and number of secondary phases. Data obtained for ODS materials to date indicate the presence of three different threshold stresses, due to dislocation-particle interactions, diffusional creep/grain boundary sliding, and, in the case of the MA 956 ODS alloy, crack nucleation and growth processes. It is critical to establish which threshold stress is in effect, since the latter two stresses can result in failure by cracking. O.C.

A90-15206* National Aeronautics and Space Administration.
 Lewis Research Center, Cleveland, OH.

**ANALYSIS OF GAMMA PRIME SHAPE CHANGES IN A
 SINGLE CRYSTAL NI-BASE SUPERALLOY**

J. GAYDA and R. A. MACKAY (NASA, Lewis Research Center,

Cleveland, OH) Scripta Metallurgica (ISSN 0036-9748), vol. 23, Nov. 1989, p. 1835-1838. refs
Copyright

The microstructural evolution of a commercial single crystal superalloy, NASAIR 100, is analyzed using the existing high-temperature lattice mismatch data and high-temperature moduli obtained from tests on single crystals of gamma and gamma prime. A multiparticle analysis of the microstructural evolution is performed using a novel microstructural lattice simulation technique, MCFET. Under a uniaxial stress, a regular array of gamma prime particles in the simulated microstructure is predicted to coalesce and form a plate morphology, with the broad faces of the plates and stress axis perpendicular in tension but parallel in compression. These results are consistent with changes in gamma prime shape observed in NASAIR 100 following creep testing at 1000 C. V.L.

A90-16741* Engineering Science Software, Inc., Smithfield, RI.
BIAXIAL CONSTITUTIVE MODELLING AND TESTING OF A SINGLE CRYSTAL SUPERALLOY AT ELEVATED TEMPERATURES

K. P. WALKER (Engineering Science Software, Inc., Smithfield, RI) and E. M. JORDAN (Connecticut, University, Storrs) IN: Biaxial and multiaxial fatigue. London, Mechanical Engineering Publications, Ltd., 1989, p. 145-170. refs
(Contract NAG3-512)

Copyright

A viscoplastic constitutive model for single crystal superalloys is developed from crystallographic slip theory. The model is applied to the tension and torsion deformation behavior of the single crystal superalloy PWA 1480 at 871 C (1600 F). Both octahedral and cube slip behavior are needed to model the deformation behavior of single crystal superalloys at elevated temperature. Author

A90-16901* National Aeronautics and Space Administration, Lewis Research Center, Cleveland, OH.

HIGH TEMPERATURE CREEP BEHAVIOR OF SINGLE CRYSTAL GAMMA PRIME AND GAMMA ALLOYS

M. V. NATHAL, J. O. DIAZ, and R. V. MINER (NASA, Lewis Research Center, Cleveland, OH) IN: High-temperature ordered intermetallic alloys III; Proceedings of the Third Symposium, Boston, MA, Nov. 29-Dec. 1, 1988. Pittsburgh, PA, Materials Research Society, 1989, p. 269-274. refs
Copyright

The creep behavior of single crystals of gamma-prime and gamma alloys were investigated and compared to the response of two-phase superalloys tested previously. High temperature deformation in the gamma alloys was characteristic of a climb-controlled mechanism, whereas the gamma-prime based materials exhibited glide-controlled creep behavior. The superalloys were much more creep resistant than their constituent phases, which indicates the importance of the gamma/gamma-prime interface as a barrier for dislocation motion during creep. Author

A90-16930* Pennsylvania State Univ., University Park.
DEFORMATION BEHAVIOR OF NIAL-BASED ALLOYS CONTAINING IRON, COBALT, AND HAFNIUM

D. R. PANK, D. A. KOSS (Pennsylvania State University, University Park), and M. V. NATHAL (NASA, Lewis Research Center, Cleveland, OH) IN: High-temperature ordered intermetallic alloys III; Proceedings of the Third Symposium, Boston, MA, Nov. 29-Dec. 1, 1988. Pittsburgh, PA, Materials Research Society, 1989, p. 561-566. refs
Copyright

The effects of alloying additions on the mechanical properties of the B2 intermetallic NiAl have been investigated in both the melt-spun ribbon and consolidated, bulk form. The study is based on a matrix of NiAl-based alloys with up to 20 at. pct Co and Fe additions and with reduced Al levels in the range of 30-40 at. pct. Characterization of the melt-spun ribbon by optical and scanning electron microscopy indicates a range of microstructures, including single-phase beta, gamma-prime necklace phase surrounding either martensitic or beta grains, and a mixture of equiaxed martensitic and gamma-prime grains. Bend ductility is present in melt-spun

and annealed ribbons exhibiting the gamma-prime necklace structure and in a single-phase beta material containing 20 at. pct Fe. The analysis of compressive flow behavior on consolidated, bulk specimens indicates that the single-phase beta alloys exhibit a continuous decrease in yield stress with increasing temperature and profuse microcracking at grain boundaries. In contrast, multiphase (gamma-prime + either martensite or beta) alloys tend to display a peak in flow stress between 600 and 800 K, with little or no signs of microcracking. In general, heat treatments which convert the martensitic grains to beta + gamma-prime result in improved strength at temperatures above 600 K and better resistance to crack initiation. Author

A90-16940* Dartmouth Coll., Hanover, NH.

IMPROVING THE LOW TEMPERATURE DUCTILITY OF NIAL

SUMIT GUHA, PAUL R. MUNROE, and IAN BAKER (Dartmouth College, Hanover, NH) IN: High-temperature ordered intermetallic alloys III; Proceedings of the Third Symposium, Boston, MA, Nov. 29-Dec. 1, 1988. Pittsburgh, PA, Materials Research Society, 1989, p. 633-638. refs
(Contract NAG3-775)

Copyright

As part of a study aimed at developing a ductile NiAl-based alloy, ingots of Ni-Fe-Al alloys were cast and hot extruded to rods. The purpose of the iron additions was two-fold viz; to produce a change in the slip vector from 001 to 111 line and, in one alloy, to add a L1(2)-structured ductile second phase. Extruded Ni-20Al-30Fe was two-phase, containing a pro-eutectic B2 phase in a fine lamellar structure of B2 + L1(2) phases. Room temperature tensile testing of both single extruded and double extruded alloys resulted in 8-percent and 22-percent plastic elongation and yield stresses of 850 and 760 MPa, respectively. Fracture in both cases occurred by ductile tearing of the eutectic and transgranular cleavage of the proeutectic phase at 1350 MPa. The ductility in double extruded condition is higher than that reported earlier in rapidly solidified wires by Inoue et al. (1984). By comparison, extruded single-phase B2-structured Ni-30Al-20Fe exhibited a fracture strength of 780 MPa, no plasticity, and a mixture of intergranular fracture and transgranular cleavage. This is contrast to earlier work by Inoue et al. where a yield stress of 400 MPa, 5 percent plastic strain, and a mixture of dimple and intergranular fracture was reported. Author

A90-16941* National Aeronautics and Space Administration, Lewis Research Center, Cleveland, OH.

PROCESSING AND MICROSTRUCTURE OF MELT SPUN NIAL ALLOYS

I. E. LOCCI (NASA, Lewis Research Center; Case Western Reserve University, Cleveland, OH), R. D. NOEBE, J. A. MOSER, D. S. LEE, and M. NATHAL (NASA, Lewis Research Center, Cleveland, OH) IN: High-temperature ordered intermetallic alloys III; Proceedings of the Third Symposium, Boston, MA, Nov. 29-Dec. 1, 1988. Pittsburgh, PA, Materials Research Society, 1989, p. 639-646. refs
Copyright

The influence of various melt spinning parameters and the effect of consolidation on the microstructure of melt spun NiAl and NiAl + W alloys have been examined by optical and electron microscopy techniques. It was found that the addition of 0.5 at. pct W to NiAl results in a fine dispersion of W particles after melt spinning which effectively controls grain growth during annealing treatments or consolidation at temperatures between 1523 and 1723 K. Increased wheel speeds are effective at reducing both the ribbon thickness and grain size, such that proper choice of both composition and casting parameters can produce structures with grain sizes as small as 2 microns. Finally, fabrication of continuous fiber-reinforced composites which used pulverized ribbon as the matrix material was demonstrated. Author

A90-19153* National Aeronautics and Space Administration. Lewis Research Center, Cleveland, OH.

OBSERVATIONS ON THE BRITTLE TO DUCTILE TRANSITION TEMPERATURES OF B2 NICKEL ALUMINIDES WITH AND WITHOUT ZIRCONIUM

S. V. RAJ, R. D. NOEBE, and R. BOWMAN (NASA, Lewis Research Center, Cleveland, OH) Scripta Metallurgica (ISSN 0036-9748), vol. 23, Dec. 1989, p. 2049-2054. refs
Copyright

The effect of a zirconium addition (0.05 at. pct) to a stoichiometric NiAl alloy on the brittle-to-ductile transition temperature (BDTT) of this alloy was investigated. Constant velocity tensile tests were conducted to fracture between 300 and 1100 K under initial strain rate 0.00014/sec, and the true stress and true strain values were determined from plots of load vs time after subtracting the elastic strain. The inelastic strain was measured under a traveling microscope. Microstructural characterization of as-extruded and fractured specimens was carried out by SEM and TEM. It was found that, while the addition of 0.05 at. pct Zr strengthened the NiAl alloy, it increased its BDTT; this shift in the BDTT could not be attributed either to variations in grain size or to impurity contents. Little or no room-temperature ductility was observed for either alloy. I.S.

A90-19154* National Aeronautics and Space Administration. Lewis Research Center, Cleveland, OH.

1100 TO 1300 K SLOW PLASTIC COMPRESSION PROPERTIES OF NI-38.5Al COMPOSITES

J. DANIEL WHITTENBERGER (NASA, Lewis Research Center, Cleveland, OH), S. K. MANNAN, and K. S. KUMAR (Martin Marietta Laboratories, Baltimore, MD) Scripta Metallurgica (ISSN 0036-9748), vol. 23, Dec. 1989, p. 2055-2060. refs
Copyright

Compressive properties of Ni-38.5Al (in at. pct) composites containing 4, 7.5, and 15 vol pct Al₂O₃ whiskers or 20 vol pct TiB₂ particles were investigated in samples compacted to full density by vacuum hot pressing at 20.7 MPa and 1725 K, followed by HIP at 207 MPa and 1725 K. Constant-velocity compression tests were conducted in air at 1100, 1200, and 1300 K to 8 percent strain. It was found that the elevated-temperature compressive properties of Ni-38.5Al+Al₂O₃ whisker composites were only marginally better than those of the matrix, and that the composite containing 20 vol pct TiB₂ particles was only slightly stronger than unreinforced Ni-38.5Al. I.S.

A90-19157* National Aeronautics and Space Administration. Lewis Research Center, Cleveland, OH.

COMPRESSIVE STRENGTH OF A B2 MATRIX NIAL-NB INTERMETALLIC AT 1200 AND 1300 K

J. DANIEL WHITTENBERGER, L. J. WESTFALL, and M. V. NATHAL (NASA, Lewis Research Center, Cleveland, OH) Scripta Metallurgica (ISSN 0036-9748), vol. 23, Dec. 1989, p. 2127-2130. refs

Copyright

The effect of a large Nb addition to a NiAl, to a final composition 43.5Ni-45.2Al-0.8Fe-10.5Nb (in at. pct), on the high-temperature compressive strength of NiAl was investigated using cylindrical samples which were compression tested in air at 1200 K and 1300 K under constant-velocity conditions. The compressive strength of the Ni-45Al-10.5Nb was compared to data from all known solid solution-strengthened and/or precipitation-strengthened NiAl-based materials. It was found that, for strain rates higher than 5×10^{-6} th/sec, the Ni-45Al-10.5Nb is stronger than NiAl. However, this advantage disappears at lower strain rates. A comparison of NiAl-based materials indicated that a NiAl+TiB₂ composite containing 20 vol pct 1-micron-diam particles has a strength superiority over all the solid solution and precipitation-hardened aluminides at strain rates below 10^{-6} th/sec. I.S.

A90-20255* Monash Univ., Clayton (Australia).

INSTRUMENTED ADHESION TESTS ON PLASMA SPRAYED THERMAL BARRIER COATINGS

CHRISTOPHER C. BERNDT (Monash University, Clayton, Australia) Journal of Materials Engineering (ISSN 0931-7058), vol. 11, Dec. 1989, p. 275-282. refs
(Contract NCC3-27)

Copyright

The failure mechanisms of plasma-sprayed two-layer coatings consisting of an NiCrAlY or NiCrAlZr bond coat with an yttria-stabilized zirconia overlay are presently examined by tensile adhesion tests. It has been found that adhesive failure within the bond coat exhibits greater failure strain than the cohesive failure of the ceramic overlay, supporting the view of the intermediate coatings being highly compliant. The absolute extension exhibited by failures occurring only through the ceramic coating is greater than that of adhesive failure, since the ceramic coating is much thicker than the bond coat. O.C.

A90-20611* Michigan Technological Univ., Houghton.

ON THE MECHANISM OF CROSS SLIP IN Ni3Al

WALTER W. MILLIGAN (Michigan Technological University, Houghton) and STEPHEN D. ANTOLOVICH (Georgia Institute of Technology, Atlanta) Metallurgical Transactions A - Physical Metallurgy and Materials Science (ISSN 0360-2133), vol. 20A, Dec. 1989, p. 2811-2818. refs
(Contract NAG3-503)

Copyright

The mechanical properties of L1(2) intermetallic alloys have been previously described by models based on the assumption that cube cross slip is the rate-limiting step. In this study, it was demonstrated that the cube cross-slip event must be reversible under a change in loading direction. This observation allows the cross-slip models to remain consistent with cyclic deformation data. Additionally, this observation was used as a critical test of the available cross-slip models. It was demonstrated that the rate-limiting step cannot be a total cross-slip event, in which both a/2 110-line superpartial dislocations cross slip to the cube plane. Conversely, the limited cross-slip event proposed by Paidar et al. (1984), was demonstrated to be consistent with the reversibility constraint. This lends additional experimental support to this model. Author

A90-20612* Arizona Univ., Tucson.

EFFICIENT ESTIMATION OF DIFFUSION DURING DENDRITIC SOLIDIFICATION

K. S. YEUM, D. R. POIRIER (Arizona, University, Tucson), and V. LAXMANAN (GM Research Laboratory, Warren, MI) Metallurgical Transactions A - Physical Metallurgy and Materials Science (ISSN 0360-2133), vol. 20A, Dec. 1989, p. 2847-2856. refs
(Contract NAG3-723; NAG3-417)

Copyright

A very efficient finite difference method has been developed to estimate the solute redistribution during solidification with diffusion in the solid. This method is validated by comparing the computed results with the results of an analytical solution derived by Kobayashi (1988) for the assumptions of a constant diffusion coefficient, a constant equilibrium partition ratio, and a parabolic rate of the advancement of the solid/liquid interface. The flexibility of the method is demonstrated by applying it to the dendritic solidification of a Pb-15 wt pct Sn alloy, for which the equilibrium partition ratio and diffusion coefficient vary substantially during solidification. The fraction eutectic at the end of solidification is also obtained by estimating the fraction solid, in greater resolution, where the concentration of solute in the interdendritic liquid reaches the eutectic composition of the alloy. Author

A90-21009* National Aeronautics and Space Administration. Lewis Research Center, Cleveland, OH.

THE UNUSUAL NEAR-THRESHOLD FCG BEHAVIOR OF A SINGLE CRYSTAL SUPERALLOY AND THE RESOLVED SHEAR STRESS AS THE CRACK DRIVING FORCE

JACK TELESMA and LOUIS J. GHOSN (NASA, Lewis Research Center, Cleveland, OH) Engineering Fracture Mechanics (ISSN 0013-7944), vol. 34, no. 5-6, 1989, p. 1183-1196. refs

Copyright

26 METALLIC MATERIALS

An investigation of the fatigue growth (FCG) behavior of PWA 1480 single crystal nickel base superalloy was conducted. Typical Paris region behavior was observed above a Delta-K of 8 MPa sq rt m. However, below that stress intensity range, the alloy exhibited highly unusual behavior. The behavior consisted of a region where the crack growth rate became essentially independent of the applied stress intensity. The transition in the FCG behavior was related to a change in the observed crack growth mechanisms.

Author

A90-21174* Valpey-Fisher Corp., Hopkinton, MA.
MEASUREMENTS OF DYNAMIC YOUNG'S MODULUS IN SHORT SPECIMENS WITH THE PUCOT

S. N. WICKSTROM (Valpey-Fisher Corp., Hopkinton, MA) and A. WOLFENDEN (Texas A & M University, College Station) Journal of Testing and Evaluation (ISSN 0090-3973), vol. 18, Jan. 1990, p. 81-84.

(Contract NAG3-702)

Copyright

The piezoelectric ultrasonic composite oscillator technique (PUCOT) was used at frequencies in the range 40 to 150 kHz to measure dynamic Young's modulus for short-length single crystals of copper at temperatures in the range 25 to 650 C and for polycrystalline copper at room temperature. Corrections to the modulus for variations in length/diameter resulted in no loss of precision due to wave velocity dispersion.

Author

A90-22656*# Southwest Research Inst., San Antonio, TX.
HIGH TEMPERATURE INELASTIC DEFORMATION OF THE B1900 + HF ALLOY UNDER MULTIAXIAL LOADING - THEORY AND EXPERIMENT

K. S. CHAN, U. S. LINDHOLM, A. NAGY (Southwest Research Institute, San Antonio, TX), and S. R. BODNER (Technion - Israel Institute of Technology, Haifa) ASME, Transactions, Journal of Engineering Materials and Technology (ISSN 0094-4289), vol. 112, Jan. 1990, p. 7-14. refs

(Contract NAS3-23925)

Copyright

The multiaxial deformation behavior of the Ni-based alloy B1900 + Hf has been studied at elevated temperatures in the range of 649-982 C. Combined tension/torsion cyclic tests were performed on thin-wall tubular specimens under both in-phase and out-of-phase strain-controlled loading cycles. Both straining conditions resulted in stress loci of comparable magnitude, exhibiting no difference in cyclic hardening response. A phase angle was observed between the deviatoric stress and the incremental plastic strain vectors during 90-deg out-of-phase strain cycling, and nonproportional stress relaxation occurred under biaxial strain hold. The overall results have been used to assess the flow law, the hardening equations, and the applicability of the J2-based, elastic-viscoplastic model of Bodner-Partom (1979) for multiaxial loading conditions. The overall agreement between theory and experiment is good. Discrepancies are discussed in relation to micromechanical considerations.

Author

A90-22657*# Southwest Research Inst., San Antonio, TX.
INELASTIC DEFORMATION UNDER NONISOTHERMAL LOADING

K. S. CHAN and U. S. LINDHOLM (Southwest Research Institute, San Antonio, TX) ASME, Transactions, Journal of Engineering Materials and Technology (ISSN 0094-4289), vol. 112, Jan. 1990, p. 15-25. refs

(Contract NAS3-23925)

Copyright

The objective of this paper is to evaluate, both experimentally and analytically, the appropriate forms of the hardening evolution equations in unified constitutive models for conditions involving nonisothermal loading. Critical experiments were performed for a cast nickel-base superalloy by using variable temperature tensile, creep, and cyclic tests in the 538-982 C temperature range. These experimental results were compared with both isothermal data and predictions of the Bodner-Partom-Bodner, 1987 elastic-viscoplastic theory to assess the effects of thermal history

on constitutive behavior. The results indicate that the hardening evolution equations based on isothermal data are applicable for nonisothermal loading of these precipitation strengthened alloys. Additional thermal history effect terms in the hardening evolution equations were not required beyond those accounting for the variation of material constants with temperature. Using material constants determined solely from isothermal data, the inelastic deformation behavior of B1900 + Hf subject to thermomechanical loading were adequately predicted by the Bodner-Partom model.

Author

A90-24852* National Aeronautics and Space Administration.
Lewis Research Center, Cleveland, OH.

OXIDATION OF HIGH-TEMPERATURE INTERMETALLICS; PROCEEDINGS OF THE WORKSHOP, CLEVELAND, OH, SEPT. 22, 23, 1988

TONI GROBSTEIN, ED. (NASA, Lewis Research Center, Cleveland, OH) and JOSEPH DOYCHAK, ED. (NASA, Lewis Research Center; Sverdrup Technology, Inc., Cleveland, OH) Workshop sponsored by ASM International, NASA, GE Aircraft Engines, et al. Warrendale, PA, Minerals, Metals, and Materials Society, 1989, 303 p. For individual items see A90-24853 to A90-24869.

Copyright

The present conference on the high-temperature oxidation behavior of aerospace structures-applicable intermetallic compounds discusses the influence of reactive-element additions on the oxidation of Ni3Al base alloys, the effect of Ni3Al oxidation below 850 C on fracture behavior, the oxidation of FeAl + Hf, Zr, and B, the synergistic effect of Al and Si on the oxidation resistance of Fe alloys, and pack cementation coatings of Cr-Al on Fe, Ni, and Co alloys. Also discussed are the formation of alumina on Nb- and Ti-base alloys, the oxidation behavior of titanium aluminide alloys, silicide coatings for refractory metals, the oxidation of chromium disilicide, and the oxidation behavior of nickel beryllides.

O.C.

A90-24855* National Aeronautics and Space Administration.
Lewis Research Center, Cleveland, OH.

THE OXIDATION OF NI-RICH NI-AL INTERMETALLICS

J. DOYCHAK (NASA, Lewis Research Center, Cleveland; Sverdrup Technology, Inc., Middleburg Heights, OH), J. L. SMIALEK, and C. A. BARRETT (NASA, Lewis Research Center, Cleveland, OH) IN: Oxidation of high-temperature intermetallics; Proceedings of the Workshop, Cleveland, OH, Sept. 22, 23, 1988. Warrendale, PA, Minerals, Metals, and Materials Society, 1989, p. 41-55. Previously announced in STAR as N89-15233. refs

Copyright

The oxidation of Ni-Al intermetallic alloys in the beta-NiAl phase field and in the two phase beta-NiAl/gamma'-Ni3Al phase field has been studied between 1000 and 1400 C. The stoichiometric beta-NiAl alloy doped with Zr was superior to other alloy compositions under cyclic and isothermal oxidation. The isothermal growth rates did not increase monotonically as the alloy Al content was decreased. The characteristically ridged alpha-Al2O3 scale morphology, consisting of cells of thin, textured oxide with thick growth ridges at cell boundaries, forms on oxidized beta-NiAl alloys. The correlation of scale features with isothermal growth rates indicates a predominant grain boundary diffusion growth mechanism. The 1200 C cyclic oxidation resistance decreases near the lower end of the beta-NiAl phase field.

Author

A90-24857* National Aeronautics and Space Administration.
Lewis Research Center, Cleveland, OH.

THE EFFECT OF 0.1 ATOMIC PERCENT ZIRCONIUM ON THE CYCLIC OXIDATION BEHAVIOR OF BETA-NIAL FOR 3000 HOURS AT 1200 C

C. A. BARRETT (NASA, Lewis Research Center, Cleveland, OH) IN: Oxidation of high-temperature intermetallics; Proceedings of the Workshop, Cleveland, OH, Sept. 22, 23, 1988. Warrendale, PA, Minerals, Metals, and Materials Society, 1989, p. 67-82. Previously announced in STAR as N89-13566. refs

Copyright

The long time effect of 0.1 at percent Zr (0.2 wt percent Zr)

on the cyclic oxidation behavior of hipped beta-NiAl was studied. Oxidation testing was performed in static air at 1200 C for up to 3000 one-hour exposure cycles. Specific weight change versus time data was modeled with the COSP computer program to analyze cyclic oxidation behavior. The Zr-free stoichiometric alloy oxidized and spalled randomly to bare metal between cycles at a rate high enough to deplete Al to a low enough level that oxidation breakaway took place as nonprotective NiO replaced the alpha-Al₂O₃/NiAl₂O₄ scale as the controlling oxide. The Zr minimized this severe type of spalling maintaining the protective alpha-Al₂O₃ scale even out to 3000 hours for the stoichiometric alloy with no significant Al depletion. A third beta-NiAl alloy containing 0.1 at percent Zr but with 10 percent less Al than the stoichiometric alloy was also tested and showed some depletion of Al, but the protective Al₂O₃/NiAl₂O₄ was still maintained to close to 2700 hours. Author

A90-24858* National Aeronautics and Space Administration. Lewis Research Center, Cleveland, OH.

OXIDATION BEHAVIOR OF FeAl+HF,Zr,B

JAMES L. SMIALEK, JOSEPH DOYCHAK, and DARRELL J. GAYDOSH (NASA, Lewis Research Center, Cleveland, OH) IN: Oxidation of high-temperature intermetallics; Proceedings of the Workshop, Cleveland, OH, Sept. 22, 23, 1988. Warrendale, PA, Minerals, Metals, and Materials Society, 1989, p. 83-95. Previously announced in STAR as N89-14297. refs

Copyright

The oxidation behavior of Fe-40Al-1Hf, Fe-40Al-1Hf-0.4B, and Fe-40Al-0.1Zr-0.4B (at. percent) alloys was characterized after 900, 1000, and 100 C exposures. Isothermal tests revealed parabolic kinetics after a period of transitional theta-alumina scale growth. The parabolic growth rates for the subsequent alpha-alumina scales were about five times higher than those for NiAl+0.1Zr alloys. The isothermally grown scales showed a propensity toward massive scale spallation due to both extensive rumpling from growth stresses and to an inner layer of HfO₂. Cyclic oxidation for 200 1-hr cycles produced little degradation at 900 or 1000 C, but caused significant spallation at 1100 C in the form of small segments of the outer scale. The major difference in the cyclic oxidation of the three FeAl alloys was increased initial spallation for FeAl+Zr,B. Although these FeAl alloys showed many similarities to NiAl alloys, they were generally less oxidation resistant. It is believed that this resulted from nonoptimal levels of dopants and larger thermal expansion mismatch stresses. Author

A90-24861* National Aeronautics and Space Administration. Lewis Research Center, Cleveland, OH.

INFLUENCE OF ALLOYING ELEMENTS ON THE OXIDATION BEHAVIOR OF NbAl₃

M. G. HEBBURN (NASA, Lewis Research Center; Sverdrup Technology, Inc., Cleveland, OH), J. R. STEPHENS, J. L. SMIALEK, C. A. BARRETT, and D. S. FOX (NASA, Lewis Research Center, Cleveland, OH) IN: Oxidation of high-temperature intermetallics; Proceedings of the Workshop, Cleveland, OH, Sept. 22, 23, 1988. Warrendale, PA, Minerals, Metals, and Materials Society, 1989, p. 171-183. Previously announced in STAR as N89-12717. refs

Copyright

NbAl₃ is one candidate material for advanced aeropropulsion systems because of its high melting point, low density, and good oxidation resistance. Although NbAl₃ has the lowest oxidation rate among the binary Nb-Al alloys, it does not form exclusive layers of protective Al₂O₃ scales. Recently Perkin et al., have shown the feasibility of forming alumina scales on Nb-Al alloys at greatly reduced Al contents. However, the objective was to maintain the high Al content, and hence low density, while achieving the capability of growing protective alumina scales. Alloy development followed approaches similar to those used successfully for superalloys and oxidation resistant MCrAl_y coatings. Among the three elements examined (Ti, Si, and Cr) as ternary additions to Nb-Al₃, Cr was the most effective in favoring the selective oxidation of Al. Nb-41Al-8Cr formed exclusive layers of alumina and had a k sub p value of 0.22 mg squared/cm (sup 4)/hr at 1200 C. The addition of 1 wt percent Y to this alloy was also beneficial, resulting

in nearly an order of magnitude decrease in K sub p at 1200 C. Further improvements were achieved by adding about 1 wt percent Si to the quaternary alloy. The k sub p value of 0.012 mg squared/cm (sup 4)/hr for Nb-40Al-8Cr-1Y-1Si at 1200 C was identical to the best NiAl + Zr alloys. These NbAl₃ alloys also exhibited excellent cyclic oxidation resistance for 100 hr at 1200 C, being nearly equivalent to NiAl + Zr. Author

A90-25098* National Aeronautics and Space Administration. Lewis Research Center, Cleveland, OH.

PRELIMINARY INVESTIGATION OF A NIAL COMPOSITE PREPARED BY CRYOMILLING

J. DANIEL WHITTENBERGER (NASA, Lewis Research Center, Cleveland, OH), EDUARD ARZT (Max-Planck-Institut fuer Metallforschung, Stuttgart, Federal Republic of Germany), and MICHAEL J. LUTON (Exxon Research and Engineering Co., Annandale, NJ) Journal of Materials Research (ISSN 0884-2914), vol. 5, Feb. 1990, p. 271-277. refs

Copyright

An attempt has been made to improve the high temperature mechanical strength of the B2 cubic crystal structure intermetallic NiAl by dispersion strengthening. Prealloyed Ni-51 at. pct Al was cryomilled with a Y₂O₃ addition to form an yttria dispersoid within the intermetallic matrix. Following milling, the powder was hot extruded to full density and machined into test coupons. Compression testing between 1200 and 1400 K indicated that the cryogenic process yielded the strongest NiAl based material tested to date. Creep resistance was six times better than NiAl and twice that of a NiAl particulate composite containing 10 vol pct TiB₂. Surprisingly, transmission electron microscopy revealed that the second phase was inhomogeneously distributed. Furthermore, X-ray analysis indicated that the second phase was not Y₂O₃ but rather AlN. Author

A90-25233*# National Aeronautics and Space Administration. Lewis Research Center, Cleveland, OH.

INFLUENCE OF MOLYBDENUM ON THE CREEP PROPERTIES OF NICKEL-BASE SUPERALLOY SINGLE CRYSTALS

R. A. MACKAY, M. V. NATHAL (NASA, Lewis Research Center, Cleveland, OH), and D. D. PEARSON (United Technologies Research Center, East Hartford, CT) Metallurgical Transactions A - Physical Metallurgy and Materials Science (ISSN 0360-2133), vol. 21A, Feb. 1990, p. 381-388. refs

The Mo content of an alloy series based on Ni-6 wt pct Al-6 wt pct Ta was systematically varied from 9.8 to 14.6 wt pct, in order to ascertain the influence of Mo on the creep properties of single crystals. The optimum initial gamma-gamma prime microstructure for raft development and creep strength was established in each alloy before testing. It was found that, as the Mo content increased from 9.8 to 14.0 percent, the magnitude of the lattice mismatch increased; upon reaching 14.6 percent, a degradation of mechanical properties occurred due to the precipitation of a third phase. These results suggest that small refractory metal content and initial gamma-prime variations can profoundly affect mechanical properties. O.C.

A90-28075* National Aeronautics and Space Administration. Lewis Research Center, Cleveland, OH.

DIFFUSIONAL ASPECTS OF THE HIGH-TEMPERATURE OXIDATION OF PROTECTIVE COATINGS

J. A. NESBITT (NASA, Lewis Research Center, Cleveland, OH) IN: Diffusion analysis and applications. Warrendale, PA, Minerals, Metals, and Materials Society, 1989, p. 307-324. refs

Copyright

The role of diffusional transport associated with the high-temperature oxidation of coatings is examined, with special attention given to the low-pressure plasma spraying MCrAl-type overlay coatings and similar Ni-base alloys which form protective Al₂O₃ scales. The use of diffusional analysis to predict the minimum solute concentration necessary to form and grow a solute oxide scale is illustrated. Modeling procedures designed to simulate the diffusional transport in coatings and substrates are presented to

26 METALLIC MATERIALS

show their use in understanding coating degradation, predicting the protective life of a coating, and evaluating various coating parameters to guide coating development. I.S.

A90-28754* # Cincinnati Univ., OH.

A CRYSTALLOGRAPHIC MODEL FOR THE TENSILE AND FATIGUE RESPONSE FOR RENE N4 AT 982 C

M. Y. SHEH and D. C. STOUFFER (Cincinnati, University, OH) ASME, Transactions, Journal of Applied Mechanics (ISSN 0021-8936), vol. 57, March 1990, p. 25-31. refs (Contract NAG3-511)

Copyright

An anisotropic constitutive model based on crystallographic slip theory was formulated for nickel-base single-crystal superalloys. The current equations include both drag stress and back stress state variables to model the local inelastic flow. Specially designed experiments have been conducted to evaluate the existence of back stress in single crystals. The results showed that the back stress effect of reverse inelastic flow on the unloading stress is orientation-dependent, and a back stress state variable in the inelastic flow equation is necessary for predicting inelastic behavior. Model correlations and predictions of experimental data are presented for the single crystal superalloy Rene N4 at 982 C.

Author

A90-30480* Ultramet, Pacoima, CA.

IRIDIUM-COATED RHENIUM THRUSTERS BY CVD

J. T. HARDING (Ultramet, Pacoima, CA), J. M. KAZAROFF (NASA, Lewis Research Center, Cleveland, OH), and M. A. APPEL (JPL, Pasadena, CA) IN: Surface modification technologies II; Proceedings of the Second International Conference, Chicago, IL, Sept. 26-28, 1988. Warrendale, PA, Minerals, Metals and Materials Society, 1989, p. 63-71. Previously announced in STAR as N88-29874. refs

Copyright

Operation of spacecraft thrusters at increased temperature reduces propellant requirements. Inasmuch as propellant comprises the bulk of a satellite's mass, even a small percentage reduction makes possible a significant enhancement of the mission in terms of increased payload. Because of its excellent high temperature strength, rhenium is often the structural material of choice. It can be fabricated into free-standing shapes by chemical vapor deposition (CVD) onto an expendable mandrel. What rhenium lacks is oxidation resistance, but this can be provided by a coating of iridium, also by CVD. This paper describes the process used by Ultramet to fabricate 22-N (5-lbf) and, more recently, 445-N (100-lbf) Ir/Re thrusters; characterizes the CVD-deposited materials; and summarizes the materials effects of firing these thrusters. Optimal propellant mixture ratios can be employed because the materials withstand an oxidizing environment up to the melting temperature of iridium, 2400 C (4350 F).

Author

A90-32266* # Cincinnati Univ., OH.

A CONSTITUTIVE MODEL FOR THE INELASTIC MULTIAXIAL RESPONSE OF RENE 80 AT 871 C AND 982 C

D. C. STOUFFER (Cincinnati, University, OH), V. G. RAMASWAMY, J. H. LAFLEN, R. H. VAN STONE, and R. WILLIAMS (General Electric Co., Aircraft Engine Business Group, Evandale, OH) ASME, Transactions, Journal of Engineering Materials and Technology (ISSN 0094-4289), vol. 112, April 1990, p. 241-246. refs

(Contract NAS3-23927)

Copyright

This paper contains an extension of the uniaxial state variable constitutive model of Ramaswamy et al. (1988) to the case of multiaxial loading. The correlation between uniaxial and multiaxial loading conditions is achieved through the assumptions of material isotropy and conservation of inelastic volume. The multiaxial extension is based only on the material parameters evaluated from uniaxial loading. The research is accompanied by a multiaxial experimental program to evaluate the response of Rene 80 at 871 C and 982 C. Experiments in the program include torsion, proportional axial and torsion, and nonproportional loading. It was

shown experimentally that there is no extra hardening from the multiaxial loading than results from uniaxial loading. Further, it is shown that the multiaxial model is successful in predicting the experimental results using only the parameters determined from the uniaxial experiments. Author

A90-33329* National Aeronautics and Space Administration. Lewis Research Center, Cleveland, OH.

THE ROLE OF INTERFACIAL DISLOCATION NETWORKS IN HIGH TEMPERATURE CREEP OF SUPERALLOYS

T. P. GABB, S. L. DRAPER, D. R. HULL, R. A. MACKAY, and M. V. NATHAL (NASA, Lewis Research Center, Cleveland, OH) Materials Science and Engineering, Part A - Structural Materials: Properties, Microstructure and Processing (ISSN 0921-5093), vol. A118, 1989, p. 59-69. refs

Copyright

The dislocation networks generated during high-temperature creep of several single-crystal nickel-based superalloys are analyzed. The networks continually evolve during creep at relatively low temperatures or eventually reach a more stable configuration at high temperatures. Specifically, the role of these networks in directional coarsening processes are studied, along with their formation kinetics, characteristics, and stability during creep. The results of this study combined with previous findings suggest that the directional coarsening process is strongly influenced by elastic strain energy. The dislocation networks formed during primary creep are found to be stable during all subsequent creep stages. Aspects of these dislocation networks are determined to be a product of both the applied creep stress and coherency strains. V.T.

A90-33340* Case Western Reserve Univ., Cleveland, OH.

PRODUCTION AND PROCESSING OF CU-CR-NB ALLOYS

DAVID L. ELLIS, GARY M. MICHAL (Case Western Reserve University, Cleveland, OH), and NORMAN W. ORTH (NASA, Lewis Research Center, Cleveland, OH) Scripta Metallurgica et Materialia (ISSN 0956-716X), vol. 24, May 1990, p. 885-890. Previously announced in STAR as N90-16053. refs (Contract NGT-50087)

Copyright

A new Cu-based alloy possessing high strength, high conductivity, and good stability at elevated temperatures was recently produced. This paper details the melting of the master alloys, production of rapidly solidified ribbon, and processing of the ribbon to sheet by hot pressing and hot rolling. Author

A90-34152* National Aeronautics and Space Administration. Lewis Research Center, Cleveland, OH.

RESOURCES - SUPPLY AND AVAILABILITY

JOSEPH R. STEPHENS (NASA, Lewis Research Center, Cleveland, OH) IN: Superalloys, supercomposites and superceramics. San Diego, CA, Academic Press, Inc., 1989, p. 9-48. Previously announced in STAR as N87-21077. refs

Copyright

Over the past several decades there have been shortage of strategic materials because of our near total import dependence on such metals as chromium, cobalt, and tantalum. In response to the continued vulnerability of U.S. superalloy producers to disruptions in resource supplies, NASA has undertaken a program to address alternatives to the super-alloys containing significant quantities of the strategic materials such as chromium, cobalt, niobium, and tantalum. The research program called Conservation of Strategic Aerospace Materials (COSAM) focuses on substitution, processing, and alternate materials to achieve its goals. In addition to NASA Lewis Research Center, universities and industry play an important role in the COSAM Program. This paper defines what is meant by strategic materials in the aerospace community, presents a strategic materials index, and reviews the resource supply and availability picture from the U.S. point of view. In addition, research results from the COSAM Program are highlighted and future directions for the use of low strategic material alloys or alternate materials are discussed. Author

A90-34162* Georgia Inst. of Tech., Atlanta.

CYCLIC DEFORMATION, FATIGUE AND FATIGUE CRACK PROPAGATION IN NI-BASE ALLOYS

STEPHEN D. ANTOLOVICH (Georgia Institute of Technology, Atlanta) and BRAD LERCH (NASA, Lewis Research Center, Cleveland, OH) IN: Superalloys, supercomposites and superceramics. San Diego, CA, Academic Press, Inc., 1989, p. 363-411. refs

Copyright

Ni-base superalloys' cumulative glide behavior, damage accumulation, low-cycle fatigue, and crack propagation characteristics are directly dependent on deformation behavior which is in turn a strong function of microstructural characteristics. Microstructural instabilities and environmental interactions become additional factors at elevated temperatures. An account is presently given of microstructural, chemical, and processing techniques that may be used to obtain the properties that appear most critical or desirable in specific applications. O.C.

A90-35071* Pennsylvania State Univ., University Park.

MICROSTRUCTURE AND MECHANICAL PROPERTIES OF MULTIPHASE NIAL-BASED ALLOYS

D. R. PANK, D. A. KOSS (Pennsylvania State University, University Park), and M. V. NATHAL (NASA, Lewis Research Center, Cleveland) Journal of Materials Research (ISSN 0884-2914), vol. 5, May 1990, p. 942-949. refs

(Contract NAG3-827)

Copyright

The effect of the gamma-prime phase on the deformation behavior and fracture resistance of melt-spun ribbons and consolidated bulk specimens of a series of Nial-based alloys with Co and Hf additions has been examined. The morphology, location, and volume fraction of the gamma-prime phase are significant factors in enhancing the fracture resistance of the normally brittle Nial-based alloys. In particular, the results indicate that a continuous-grain-boundary film of gamma-prime can impart limited room-temperature ductility regardless of whether B2 or L10 Nial is present. Guidelines for microstructure control in multiphase Nial-based alloys are also presented. Author

A90-37719* National Aeronautics and Space Administration. Lewis Research Center, Cleveland, OH.

COARSENING IN HIGH VOLUME FRACTION NICKEL-BASE ALLOYS

R. A. MACKAY and M. V. NATHAL (NASA, Lewis Research Center, Cleveland, OH) Acta Metallurgica et Materialia (ISSN 0956-7151), vol. 38, June 1990, p. 993-1005. refs

Copyright

The coarsening behavior of the gamma-prime precipitate has been examined in high volume fraction nickel-base alloys aged at elevated temperatures for times of up to 5000 h. Although the cube rate law was observed during coarsening, none of the presently available coarsening theories showed complete agreement with the experimental particle size distributions (PSDs). These discrepancies were thought to be due to elastic coherency strains which were not considered by the available models. Increasing the Mo content significantly influenced the PSDs and decreased the coarsening rate of the gamma-prime cubes, as a result of increasing the magnitude of the lattice mismatch. After extended aging times, the gamma-prime cubes underwent massive coalescence into plates at a rate which was much faster than the cuboidal coarsening rate. Once the gamma-prime plates were formed, further coarsening was not observed, and this stabilization of the microstructure was attributed to the development of dislocation networks at the gamma-gamma-prime interfaces. Author

A90-39658* National Aeronautics and Space Administration. Lewis Research Center, Cleveland, OH.

INFLUENCE OF TESTING ENVIRONMENT ON THE ROOM TEMPERATURE DUCTILITY OF FEAL ALLOYS

D. J. GAYDOSH and M. V. NATHAL (NASA, Lewis Research

Center, Cleveland, OH) Scripta Metallurgica et Materialia (ISSN 0956-716X), vol. 24, July 1990, p. 1281-1284. refs
Copyright

The effects of testing atmospheres (air, O₂, N₂, and vacuum) on the room-temperature ductility of Fe-40Al, Fe-40Al-0.5B, and Fe-50Al alloys were investigated. The results confirmed the decrease in room-temperature ductility of Fe-rich FeAl alloys by the interaction of the aluminide with water vapor, reported previously by Liu et al. (1989). The highest ductilities were measured in the atmosphere with the lowest moisture levels, i.e., in vacuum. It was found that significant ductility is still restricted to Fe-rich alloys (Fe-40Al), as the Fe-50Al alloy remained brittle under all testing conditions. It was also found that slow cooling after annealing was beneficial, and the effect was additive to the environmental effect. The highest ductility measurements in this study were 9 percent elongation in furnace-cooled Fe-40Al and in Fe-40Al-0.5B, when tested in vacuum. I.S.

A90-39660* National Aeronautics and Space Administration. Lewis Research Center, Cleveland, OH.

CYCLIC OXIDATION OF ALUMINIDE COATINGS ON Ti3Al+NB

JAMES L. SMIALEK, MICHAEL A. GEDWILL, and PAMELA K. BRINDLEY (NASA, Lewis Research Center, Cleveland, OH) Scripta Metallurgica et Materialia (ISSN 0956-716X), vol. 24, July 1990, p. 1291-1296. refs

Copyright

A number of pack aluminide coatings were produced on fiber-reinforced Ti3Al+Nb composites and were compared for their protection effect in cyclic oxidation at 982 C. It was found that pack aluminizing of Ti3Al+Nb can successfully produce an oxidation resistant TiAl₃ coating which forms alpha-Al₂O₃ scales. These coatings offer a substantial improvement over the uncoated matrix material in 982 C cyclic oxidation. Coating cracks were found to contribute to degradation of thick coatings. I.S.

A90-44338* National Aeronautics and Space Administration. Lewis Research Center, Cleveland, OH.

THE EFFECTS OF SURFACE FILMS ON MECHANICAL BEHAVIOR OF B2 ORDERED INTERMETALLIC ALLOYS

R. D. NOEBE, J. T. KIM, J. W. MCVAY, and R. GIBALA (NASA, Lewis Research Center, Cleveland, OH; Michigan, University, Ann Arbor) IN: Strength of metals and alloys (ICSMA 8); Proceedings of the Eighth International Conference, Tampere, Finland, Aug. 22-26, 1988. Volume 1. Oxford, England and Elmsford, NY, Pergamon Press, 1989, p. 415-420. refs

(Contract NSF DMR-85-06705)

Copyright

Surface films deposited on body-centered cubic metals can greatly reduce the yield and flow stresses and increase the ductility at low homologous temperatures. This softening process is associated with the ability of the film-substrate interface to generate large populations of mobile edge dislocations. This phenomenon is extended to B2 ordered intermetallic alloys, which display many deformation characteristics of bcc metals. Single crystal NiAl coated with thermally formed oxide films and polycrystalline FeAl with electrochemically formed Fe-Al-O films display film softening at and below room temperature. The extent of film softening is shown to depend on many factors, including crystal orientation, deformation temperature, operative slip systems, film thickness, film adherence, and film and substrate properties. Author

A90-45304* National Aeronautics and Space Administration. Lewis Research Center, Cleveland, OH.

INVESTIGATION OF WEIBULL STATISTICS IN FRACTURE ANALYSIS OF CAST ALUMINUM

F. A. HOLLAND, JR. and E. V. ZARETSKY (NASA, Lewis Research Center, Cleveland, OH) IN: Failure prevention and reliability - 1989; Proceedings of the Eighth Biennial Conference, Montreal, Canada, Sept. 17-21, 1989. New York, American Society of Mechanical Engineers, 1989, p. 41-51. refs

Copyright

The fracture strengths of two large batches of A357-T6 cast

26 METALLIC MATERIALS

aluminum coupon specimens were compared by using two-parameter Weibull analysis. The minimum number of these specimens necessary to find the fracture strength of the material was determined. The applicability of three-parameter Weibull analysis was also investigated. A design methodology based on the combination of elementary stress analysis and Weibull statistical analysis is advanced and applied to the design of a spherical pressure vessel shell. The results from this design methodology are compared with results from the applicable ASME pressure vessel code. Author

A90-45620* National Aeronautics and Space Administration. Lewis Research Center, Cleveland, OH.

FILTER CLOGGING BY THE EXTRACTED GAMMA PRIME AND ITS MEASUREMENT

F. H. HARF (NASA, Lewis Research Center, Cleveland, OH) *Journal of Materials Science Letters* (ISSN 0261-8028), vol. 9, Jan. 1990, p. 78.

Copyright

The extraction of gamma-prime sample residues from Ni-based superalloys varies greatly in efficiency with the type of heat-treatment that had previously been applied to the alloy; this effect has prompted the present formulation of a standardized procedure for measuring the residues' filter-clogging factor (FCF). The FCF differences between heat treatments can be correlated with the quantity and size distribution of extracted particles; this procedure could accordingly furnish a means of checking the accuracy of heat treatments. O.C.

A90-46677*# National Aeronautics and Space Administration. Lewis Research Center, Cleveland, OH.

REFRACTORY METAL ALLOYS AND COMPOSITES FOR SPACE POWER SYSTEMS

R. STEPHENS, D. W. PETRASEK, and R. H. TITRAN (NASA, Lewis Research Center, Cleveland, OH) *International Journal of Refractory Metals and Hard Materials* (ISSN 0263-4368), vol. 9, June 1990, p. 96-103. refs

Results are presented on recent studies of refractory-metal-alloy and refractory-metal-composite technologies for space power systems, with emphasis on work performed at the Lewis Research Center in support of the Ground Engineering System (GES) for the SP-100 reactor. Special attention is given to the mechanical properties of alloys with compositions Nb-1Zr and Nb-0.1Zr-0.1C (the PWC-11 alloy) and to advanced fiber-reinforced composites. The results to date indicate that, for the GES at a power level of about 100 kWe, the PWC-11 has attractive creep properties that will extend the capabilities of the SP-100 reactor compared to a similar system fabricated from Nb-1Zr. On the other hand, tungsten-reinforced Nb-1Zr composites were found to provide a ten-fold and four-fold creep strength over Nb-1Zr and PWC-11, respectively, at 1400 to 1500 K. I.S.

A90-47091* National Aeronautics and Space Administration. Lewis Research Center, Cleveland, OH.

1300 K COMPRESSIVE PROPERTIES OF SEVERAL DISPERSION STRENGTHENED NIAL MATERIALS

J. DANIEL WHITTENBERGER, D. J. GAYDOSH (NASA, Lewis Research Center, Cleveland, OH), and K. S. KUMAR (Martin Marietta Laboratories, Baltimore, MD) *Journal of Materials Science* (ISSN 0022-2461), vol. 25, June 1990, p. 2771-2776. refs

Copyright

To examine the potential of rapid solidification technology (RST) as a means to fabricate dispersion-strengthened aluminides, cylindrical compression samples were machined from the gauge section of their tensile specimens and tested in air at 1300 K. While microscopy indicates that RST can produce fine dispersions of TiB₂, TiC and HfC in a NiAl matrix, the mechanical property data reveal that only HfC successfully strengthens the intermetallic matrix. The high stress exponents (above 10) and/or independence of strain rate on stress for NiAl-HfC materials suggest elevated temperature mechanical behavior similar to that found in oxide dispersion-strengthened alloys. Furthermore, an apparent example

of departure side pinning has been observed, and as such, it is indicative of a threshold stress for creep. Author

A90-48635* National Aeronautics and Space Administration. Lewis Research Center, Cleveland, OH.

FATIGUE CRACK PROPAGATION BEHAVIOR OF A SINGLE CRYSTALLINE SUPERALLOY

B. A. LERCH (NASA, Lewis Research Center, Cleveland, OH) and STEPHEN D. ANTOLOVICH (Georgia Institute of Technology, Atlanta) *Metallurgical Transactions A - Physical Metallurgy and Materials Science* (ISSN 0360-2133), vol. 21A, Aug. 1990, p. 2169-2177. Research supported by the General Electric Co. refs

Copyright

Crack propagation mechanisms occurring at various temperatures in a single crystalline Ni-base alloy, Rene N4, were investigated. The rates of crack growth at 21, 704, 927, 1038, and 1093 C were measured in specimens with 001-line and 110-line directions parallel to the load axis and the machined notch, respectively, using a pulsed dc potential drop apparatus, and the fracture surfaces at each temperature were examined using SEM. Crack growth rates (CGRs) for specimens tested at or below 927 C were similar, while at two higher temperatures, the CGRs were about an order of magnitude higher than at the lower temperatures. Results of SEM observations showed that surface morphologies depended on temperature. I.S.

A90-51298* Martin Marietta Labs., Baltimore, MD.
COMPRESSION BEHAVIOR OF THE FORGED LL2 COMPOUNDS AL67Ti25Cr8 AND AL66Ti25Mn9

S. A. BROWN, K. S. KUMAR (Martin Marietta Laboratories, Baltimore, MD), and J. D. WHITTENBERGER (NASA, Lewis Research Center, Cleveland, OH) *Scripta Metallurgica et Materialia* (ISSN 0956-716X), vol. 24, Oct. 1990, p. 2001-2006. refs

(Contract NAS3-25787)

Copyright

The paper presents the findings of a compression study as a function of temperature from cryogenic temperatures to 1373 K at a strain rate of about 0.0001/s on forged Al67Ti25Cr8 and Al66Ti25Mn9 compounds. The creep response of these alloys is analyzed at strain rates varying from 2×10^{-5} to the -4 th to 2×10^{-4} s at 1000 K and 1100 K. It is shown that as-cast microstructures for both compounds are dendritic, while both intermetallics forged very well with no edge cracking, with the microstructures appearing fully recrystallized. True comprehensive stress-strain diagrams determined at 1100 K as a function of nominal strain rate reveal a range of behaviors in both materials. V.T.

N90-11854*# National Aeronautics and Space Administration. Lewis Research Center, Cleveland, OH.

CREEP STRENGTH OF NIOBIUM ALLOYS, NB-1%ZR AND PWC-11 Final Report

ROBERT H. TITRAN 1989 10 p Prepared for presentation at the 7th Symposium on Space Nuclear Power Systems, Albuquerque, NM, 7-11 Jan. 1990; sponsored in part by New Mexico Univ.

(Contract DE-AI03-86SF-16310)

(NASA-TM-102390; E-5102; DOE/NASA/16310-13; NAS 1.15:102390) Avail: NTIS HC A02/MF A01 CSCL 11/6

A study is being conducted at NASA Lewis Research Center to determine the feasibility of using a carbide particle strengthened Nb-1 percent Zr base alloy to meet the anticipated temperature and creep resistance requirements of proposed near term space power systems. In order to provide information to aid in the determination of the suitability of the PWC-11 alloy as an alternative to Nb-1 percent Zr in space power systems this study investigated: (1) the long-time high-vacuum creep behavior of the PWC-11 material and the Nb-1 percent Zr alloy, (2) the effect of prior stress-free thermal aging on this creep behavior, (3) the effect of electron beam (EB) welding on this creep behavior, and (4) the stability of creep strengthening carbide particles. Author

N90-13636*# National Aeronautics and Space Administration. Lewis Research Center, Cleveland, OH.

THERMAL BARRIER COATINGS FOR GAS TURBINE AND DIESEL ENGINES

ROBERT A. MILLER, WILLIAM J. BRINDLEY, and M. MURRAY BAILEY 1989 9 p Presented at the 11th Workshop on Ceramic Coatings for Wear and Thermal Applications, Edmonton, Alberta, 16-17 Oct. 1989; sponsored by the Canadian Univ.-Industry-Council on Advanced Ceramics (NASA-TM-102408; E-5160; NAS 1.15:102408) Avail: NTIS HC A02/MF A01 CSCL 11/6

The present state of development of thin thermal barrier coatings for aircraft gas turbine engines and thick thermal barrier coatings for truck diesel engines is assessed. Although current thermal barrier coatings are flying in certain gas turbine engines, additional advances will be needed for future engines. Thick thermal barrier coatings for truck diesel engines have advanced to the point where they are being seriously considered for the next generation of engine. Since coatings for truck engines is a young field of inquiry, continued research and development efforts will be required to help bring this technology to commercialization.

Author

N90-14335*# National Aeronautics and Space Administration. Lewis Research Center, Cleveland, OH.

CALIBRATION APPROACH TO ELECTRON PROBE MICROANALYSIS: A STUDY WITH PWA-1480, A NICKEL BASE SUPERALLOY

F. M. TEREPA, M. VIJAYAKUMAR, and S. N. TEWARI (Cleveland State Univ., OH.) Dec. 1989 18 p (Contract NAG8-091) (NASA-TM-102393; E-5138; NAS 1.15:102393) Avail: NTIS HC A03/MF A01 CSCL 11/6

The utility of an indirect calibration approach in electron probe microanalysis is explored. The methodology developed is based on establishing a functional relationship between the uncorrected k-ratios and the corresponding concentrations obtained using one of the ZAF correction schemes, for all the desired elements in the concentration range of interest. In cases where a very large number of analyses are desired, such a technique significantly reduces the total time required for the microprobe analysis without any significant loss of precision in the data. A typical application of the method in the concentration mapping of the transverse cross-section of a dendrite in directionally solidified PWA-1480, a nickel-based superalloy, is described.

Author

N90-15211*# National Aeronautics and Space Administration. Lewis Research Center, Cleveland, OH.

SECONDARY ELECTRON EMISSION CHARACTERISTICS OF MOLYBDENUM-MASKED, ION-TEXTURED OFHC COPPER

ARTHUR N. CURREN, KENNETH A. JENSEN, and ROBERT F. ROMAN Jan. 1990 15 p (NASA-TP-2967; E-5009; NAS 1.60:2967) Avail: NTIS HC A03/MF A01 CSCL 11/6

A method for producing a uniform, highly textured surface on oxygen-free, high conductivity (OFHC) copper by ion bombardment using sputtered molybdenum as a texture-inducing masking film was developed and used to provide samples for study. The purpose was to develop a basically OFHC copper surface having very low secondary electron emission characteristics. Surfaces having low secondary electron emission are a requirement for the electrodes of very high efficiency multistage depressed collectors (MDC's). Such MDC's are used in microwave amplifier traveling wave tubes for space communications and other applications. OFHC copper is the material most commonly used for MDC electrodes because it has high thermal conductivity, it is easy to machine, and its fabrication and brazing procedures are well established. However, its untreated surface displays relatively very high levels of secondary electron emissions. Textured OFHC copper samples were tested for true secondary electron emission and relative reflected primary electron yield at primary electron beam energy levels from 200 to 2000 eV and at direct (0 deg) to oblique (60 deg) beam impingement angles. The test results for three of the

samples, each of which was processed in a slightly different way, are compared with each other and with test results for a machined OFHC copper sample. Although the textured samples are not represented here as having been processed optimally, their measured secondary electron emission characteristics are significantly lower than those of the untreated OFHC copper sample over the range of conditions studied. Importantly, the relative reflected primary electron yield of one of the textured samples is conspicuously lower than that of the others. Clearly, with further development, the molybdenum-masked ion-textured OFHC copper surface will be a promising material for high-efficiency MDC electrodes.

Author

N90-16053*# National Aeronautics and Space Administration. Lewis Research Center, Cleveland, OH.

PRODUCTION AND PROCESSING OF CU-CR-NB ALLOYS

DAVID L. ELLIS, GARY M. MICHAL (Case Western Reserve Univ., Cleveland, OH.), and NORMAN W. ORTH Jan. 1990 14 p (NASA-TM-102495; E-5286; NAS 1.15:102495) Avail: NTIS HC A03/MF A01 CSCL 11/6

A new Cu-based alloy possessing high strength, high conductivity, and good stability at elevated temperatures was recently produced. This paper details the melting of the master alloys, production of rapidly solidified ribbon, and processing of the ribbon to sheet by hot pressing and hot rolling.

Author

N90-16911*# National Aeronautics and Space Administration. Lewis Research Center, Cleveland, OH.

THERMAL MODELLING OF VARIOUS THERMAL BARRIER COATINGS IN A HIGH HEAT FLUX ROCKET ENGINE

JAMES A. NESBITT Dec. 1989 31 p (NASA-TM-102418; E-5184; NAS 1.15:102418) Avail: NTIS HC A03/MF A01 CSCL 11/6

Traditional Air Plasma Sprayed (APS) ZrO₂-Y₂O₃ Thermal Barrier Coatings (TBC's) and Low Pressure Plasma Sprayed (LPPS) ZrO₂-Y₂O₃/Ni-Cr-Al-Y cermet coatings were tested in a H₂/O₂ rocket engine. The traditional ZrO₂-Y₂O₃ (TBC's) showed considerable metal temperature reductions during testing in the hydrogen-rich environment. A thermal model was developed to predict the thermal response of the tubes with the various coatings. Good agreement was observed between predicted temperatures and measured temperatures at the inner wall of the tube and in the metal near the coating/metal interface. The thermal model was also used to examine the effect of the differences in the reported values of the thermal conductivity of plasma sprayed ZrO₂-Y₂O₃ ceramic coatings, the effect of 100 micron (0.004 in.) thick metallic bond coat, the effect of tangential heat transfer around the tube, and the effect or radiation from the surface of the ceramic coating. It was shown that for the short duration testing in the rocket engine, the most important of these considerations was the effect of the uncertainty in the thermal conductivity of temperatures (greater than 100 C) predicted in the tube. The thermal model was also used to predict the thermal response of the coated rod in order to quantify the difference in the metal temperatures between the two substrate geometries and to explain the previously-observed increased life of coatings on rods over that on tubes. A thermal model was also developed to predict heat transfer to the leading edge of High Pressure Fuel Turbopump (HPFTP) blades during start-up of the space shuttle main engines. The ability of various TBC's to reduce metal temperatures during the two thermal excursions occurring on start-up was predicted. Temperature reductions of 150 to 470 C were predicted for 165 micron (0.0065 in.) coatings for the greater of the two thermal excursions.

Author

N90-17868*# Pratt and Whitney Aircraft, East Hartford, CT. Engineering Div.

MATE (MATERIALS FOR ADVANCED TURBINE ENGINES) PROGRAM, PROJECT 3. VOLUME 2: DESIGN, FABRICATION AND EVALUATION OF AN OXIDE DISPERSION STRENGTHENED SHEET ALLOY COMBUSTOR LINER Final Report

S. BOSE and K. D. SHEFFLER Feb. 1988 9 p

26 METALLIC MATERIALS

(Contract NAS3-20072)
(NASA-CR-180892; NAS 1.26:180892; PWA-5574-223-VOL-2)
Avail: NTIS HC A02/MF A01 CSCL 11/6

The suitability of wrought oxide dispersion strengthened (ODS) superalloy sheet for gas turbine engine combustor applications was evaluated. Two yttria (Y₂O₃) dispersion strengthened alloys were evaluated; Incoloy MA956 and Haynes Development Alloy (HDA) 8077 (NiCrAl base). Preliminary tests showed both alloys to be potentially viable combustor materials, with neither alloy exhibiting a significant advantage over the other. MA956 was selected as the final alloy based on manufacturing reproducibility for evaluation as a burner liner. A hybrid PW2037 inner burner liner containing MA956 and Hastelloy X components and using a louvered configuration was designed and constructed. The louvered configuration was chosen because of field experience and compatibility with the bill of material PW2037 design. The simulated flight cycle for the ground based engine tests consisted of 4.5 min idle, 1.5 min takeoff and intermediate conditions in a PW2037 engine with average uncorrected combustor exit temperature of 1527 C. Post test evaluation consisting of visual observations and fluorescent penetrant inspections was conducted after 500 cycles of testing. No loss of integrity in the burner liner was shown.

Author

N90-18559*# United Technologies Research Center, East Hartford, CT.

IDENTIFICATION OF A CAST IRON ALLOY CONTAINING NONSTRATEGIC ELEMENTS Final Report

C. V. COOPER, D. L. ANTON, F. D. LEMKEY, H. NOWOTNY, R. S. BAILEY, L. H. FAVROW, J. G. SMEGGIL, and D. B. SNOW
Jun. 1989 79 p

(Contract DEN3-282; DE-AI01-77CS-51040)
(NASA-CR-185174; DOE/NASA/0282-1; NAS 1.26:185174;
R89-917447-32) Avail: NTIS HC A05/MF A01 CSCL 11/6

A program was performed to address the mechanical and environmental needs of Stirling engine heater head and regenerator housing components, while reducing the dependence on strategic materials. An alloy was developed which contained no strategic elemental additions per se. The base is iron with additions of manganese, molybdenum, carbon, silicon, niobium, and ferro-chromium. Such an alloy should be producible on a large scale at very low cost. The resulting alloy, designated as NASAUT 4G-Al, contained 15 Mn, 15 Cr, 2 Mo, 1.5 C, 1.0 Si, 1.0 Nb (in weight percent) with a balance of Fe. This alloy was optimized for chemistry, based upon tensile strength, creep-rupture strength, fracture behavior, and fatigue resistance up to 800 C. Alloys were also tested for environmental compatibility. The microstructure and mechanic properties (including hardness) were assessed in the as-cast condition and following several heat treatments, including one designed to simulate a required braze cycle. The alloy was fabricated and characterized in the form of both equiaxed and columnar-grained castings. The columnar grains were produced by directional solidification, and the properties were characterized in both the longitudinal and transverse orientations. The NASAUT 4G-Al alloy was found to be good in cyclic-oxidation resistance and excellent in both hydrogen and hot-corrosion resistance, especially in comparison to the baseline XF-818 alloy. The mechanical properties of yield strength, stress-rupture life, high-cycle-fatigue resistance, and low-cycle-fatigue resistance were good to excellent in comparison to the current alloy for this application, HS-31 (X-40), with precise results depending in a complex manner on grain orientation and temperature. If required, the ductility could be improved by lowering the carbon content.

Author

N90-20181*# National Aeronautics and Space Administration. Lewis Research Center, Cleveland, OH.

MECHANICAL PROPERTIES OF PURE NICKEL ALLOYS AFTER LONG TERM EXPOSURES TO LIOH AND VACUUM AT 775 K

J. DANIEL WHITTENBERGER and E. J. VESELY, JR. (IIT Research Inst., Chicago, IL.) Jan. 1990 23 p

(NASA-TM-102403; E-5142; NAS 1.15:102403) Avail: NTIS HC A03/MF A01 CSCL 11/6

The solid to liquid phase transformation of LiOH at 744.3 K is considered to be an ideal candidate thermal energy storage (TES) mechanism for a Rankine heat engine based solar dynamic system operating at approximately 682 K. While pure nickel is thought to be a suitable containment material for LiOH, long term containment is of concern because molten hydroxides are usually corrosive. Two commercially pure nickel alloys, Ni-200 and Ni-201, were exposed to molten LiOH, its vapor, and vacuum at 775 K for periods ranging from 50 to 5000 h, and simple mechanical property measurements (77 to 900 K tensile and 750 K creep rupture) of exposed alloys were undertaken. The mechanical property test procedures are described and tabular lists of the test data are presented.

Author

N90-21165*# Aerojet Technical Systems Co., Sacramento, CA. HYDROCARBON-FUEL/COMBUSTION-CHAMBER-LINER MATERIALS COMPATIBILITY Interim Final Report, 7 Nov. 1986 - 31 Oct. 1989

MARK L. GAGE Apr. 1990 249 p

(Contract NAS3-25070)
(NASA-CR-185203; NAS 1.26:185203; KBQ-FR-1; RPT/D0406-54;
AD-A227392) Avail: NTIS HC A11/MF A02 CSCL 11/6

Results of material compatibility experiments using hydrocarbon fuels in contact with copper-based combustion chamber liner materials are presented. Mil-Spec RP-1, n-dodecane, propane, and methane fuels were tested in contact with OFHC, NASA-Z, and ZrCu coppers. Two distinct test methods were employed. Static tests, in which copper coupons were exposed to fuel for long durations at constant temperature and pressure, provided compatibility data in a precisely controlled environment. Dynamic tests, using the Aerojet Carbothermal Test Facility, provided fuel and copper compatibility data under realistic booster engine service conditions. Tests were conducted using very pure grades of each fuel and fuels to which a contaminant, e.g., ethylene or methyl mercaptan, was added to define the role played by fuel impurities. Conclusions are reached as to degradation mechanisms and effects, methods for the elimination of these mechanisms, selection of copper alloy combustion chamber liners, and hydrocarbon fuel purchase specifications.

Author

N90-21849*# Carnegie-Mellon Univ., Pittsburgh, PA. THE EFFECT OF HYDROGEN AND MICROSTRUCTURE ON THE DEFORMATION AND FRACTURE BEHAVIOR OF A SINGLE CRYSTAL NICKEL-BASE SUPERALLOY Final Report Ph.D. Thesis

WILLIAM S. WALSTON Apr. 1990 254 p

(Contract NAG3-463)
(NASA-CR-185219; NAS 1.26:185219) Avail: NTIS HC A12/MF A02 CSCL 11/6

A study was conducted on the effects of internal hydrogen and microstructure on the deformation and fracture of a single crystal nickel-base superalloy. In particular, room temperature plane strain fracture toughness and tensile tests were performed on hydrogen-free and hydrogen charged samples of PWA 1480. The role of microstructure was incorporated by varying the levels of porosity and eutectic gamma/gamma prime through hot isostatic pressing and heat treatment. The room temperature behavior of PWA 1480 was unusual because precipitate shearing was not the primary deformation mechanism at all strains. At strains over 1 percent, dislocations were trapped in the gamma matrix and an attempt was made to relate this behavior to compositional differences between PWA 1480 and other superalloys. Another unique feature of the tensile behavior was cleavage of the eutectic gamma/gamma prime, which is believed to initiate the failure process. Fracture occurred on (111) planes and is likely a result of shear localization along these planes. Elimination of the eutectic gamma/gamma prime greatly improved the tensile ductility, but porosity had no effect on tensile properties. Large quantities of hydrogen (1.74 at. percent) were gas-phase charged into the material, but surprisingly this was not a function of the amount of porosity or eutectic gamma/gamma prime present. Desorption

experiments suggest that the vast majority of hydrogen is at reversible lattice trapping sites. This large, uniform concentration of hydrogen dramatically reduced the tensile strain to failure, but only slightly affected the reduction in area. Available hydrogen embrittlement models were examined in light of these results and it was found that the hydrogen enhanced localized plasticity model can explain much of the tensile behavior. K(IC) fracture toughness tests were conducted, but it was necessary to also perform J(IC) tests to provide valid data. Author

N90-22646* # National Aeronautics and Space Administration. Lewis Research Center, Cleveland, OH.

FATIGUE CRACK GROWTH IN A UNIDIRECTIONAL SCS-6/TI-15-3 COMPOSITE

PETER KANTZOS, JACK TELESMA, and LOUIS GHOSH (Sverdrup Technology, Inc., Cleveland, OH.) 1989 36 p Presented at the 3rd Symposium on Composite Materials: Fatigue and Fracture, Orlando, FL, 6-9 Nov. 1989; sponsored by American Society for Testing Materials (NASA-TM-103095; E-5413; NAS 1.15:103095) Avail: NTIS HC A03/MF A01 CSCL 11/6

An investigation was conducted to characterize and model the fatigue crack growth (FCG) behavior of a SCS-6/Ti-15-3 metal matrix composite. Part of the study was conducted using a fatigue loading stage mounted inside a scanning electron microscope (SEM). This unique facility allowed high magnification viewing of the composite fatigue processes and measurement of the near crack tip displacements. The unidirectional composite was tested in the (0)8 (i.e., longitudinal) and (90)8 (i.e., transverse) orientations. For comparison purposes unreinforced matrix material produced by the identical process as the reinforced material was also tested. The results of the study reveal that the fatigue crack growth behavior of the composite is a function of specimen geometry, fiber orientation and the interaction of local stress fields with the highly anisotropic composite. In the case of (0)8 oriented single edge notch (SEN) specimens and (90)8 oriented compact tension (CT) specimens, the crack growth was normal to the loading direction. However, for the (0)8 CT specimens the crack grew mostly parallel to the loading and the fiber direction. The unusual fatigue behavior of the (0)8 CT specimens was attributed to the specimen geometry and the associated high tensile bending stresses perpendicular to the fiber direction. These stresses resulted in preferential cracking in the weak interface region perpendicular to the fiber direction. The interface region, and in particular the carbon coating surrounding the fiber proved to be the composites weakest link. In the (0)8 SEN the crack growth was confined to the matrix leaving behind unbroken fibers which bridged the cracked surfaces. As the crack grew longer, more fibers bridged the crack resulting in a progressive decrease in the crack growth rates and eventual crack arrest. The actual near crack tip displacement measurements were used in a proposed formulation for a bridging-corrected effective crack driving force, $\Delta K(\text{sub eff})$. This parameter was able to account for most of the experienced bridging and correlated the (0)8 SEN fatigue crack growth data reasonably well. Author

N90-23536* # National Aeronautics and Space Administration. Lewis Research Center, Cleveland, OH.

ASSESSMENT OF FUNDAMENTAL MATERIALS NEEDS FOR THICK THERMAL BARRIER COATINGS (TTBC'S) FOR TRUCK DIESEL ENGINES Final Report

ROBERT A. MILLER May 1990 56 p (Contract DE-AI05-87OR-21749) (NASA-TM-103130; E-5460; DOE/NASA/21749-1; NAS 1.15:103130) Avail: NTIS HC A04/MF A01 CSCL 11/6

The present state of development of thick thermal barrier coatings for truck diesel engines is assessed and areas where improved fundamental understanding is needed to properly pursue development are identified. Emphasis is given to the coating systems and design approaches that are being developed for the next generation of truck diesel engines under DOE/NASA support. It is noted that, while considerable progress has been made, the current level of understanding of coating system behavior is

inadequate and this lack of fundamental understanding may impede current and future development. Several areas where improved understanding would be especially valuable are identified and recommendations for research into those areas are offered. Author

N90-25211* # National Aeronautics and Space Administration. Lewis Research Center, Cleveland, OH.

THE OXIDATION AND CORROSION OF ODS ALLOYS

CARL E. LOWELL and CHARLES A. BARRETT Jun. 1990 25 p Submitted for publication (NASA-TM-102555; E-4030; NAS 1.15:102555) Avail: NTIS HC A03/MF A01 CSCL 11/6

The oxidation and hot corrosion of high temperature oxide dispersion strengthened (ODS) alloys are reviewed. The environmental resistance of such alloys are classified by oxide growth rate, oxide volatility, oxide spalling, and hot corrosion limitations. Also discussed are environmentally resistant coatings for ODS materials. It is concluded that ODS NiCrAl and FeCrAl alloys are highly oxidation and corrosion resistant and can probably be used uncoated. Author

N90-28642* # National Aeronautics and Space Administration. Lewis Research Center, Cleveland, OH.

HIGH TEMPERATURE FATIGUE BEHAVIOR OF HAYNES 188

GARY R. HALFORD, JAMES F. SALTSMAN, and SREERAMESH KALLURI (Sverdrup Technology, Inc., Cleveland, OH.) In NASA, Marshall Space Flight Center, Advanced Earth-to-Orbit Propulsion Technology 1988, Volume 1 p 497-509 Sep. 1988 Avail: NTIS HC A99/MF E06 CSCL 11/6

The high temperature, creep-fatigue behavior of Haynes 188 was investigated as an element in a broader thermomechanical fatigue life prediction model development program at the NASA-Lewis. The models are still in the development stage, but the data that were generated possess intrinsic value on their own. Results generated to date is reported. Data were generated to characterize isothermal low cycle fatigue resistance at temperatures of 316, 704, and 927 C with cyclic failure lives ranging from 10 to more than 20,000. These results follow trends that would be predicted from a knowledge of tensile properties, i.e., as the tensile ductility varies with temperature, so varies the cyclic inelastic straining capacity. Likewise, as the tensile strength decreases, so does the high cyclic fatigue resistance. A few two-minute hold-time cycles at peak compressive strain were included in tests at 760 C. These results were obtained in support of a redesign effort for the Orbital Maneuverable System engine. No detrimental effects on cyclic life were noted despite the added exposure time for creep and oxidation. Finally, a series of simulated thermal fatigue tests, referred to as bithermal fatigue tests, were conducted using 316 C as the minimum and 760 C as the maximum temperature. Only out-of-phase bithermal tests were conducted to date. These test results are intended for use as input to a more general thermomechanical fatigue life prediction model based on the concepts of the total strain version of Strainrange Partitioning. Author

N90-28643* # Pratt and Whitney Aircraft, East Hartford, CT.

CONSTITUTIVE AND LIFE MODELING OF SINGLE CRYSTAL BLADE ALLOYS FOR ROOT ATTACHMENT ANALYSIS

T. G. MEYER, G. J. MCCARTHY, L. H. FAVROW, D. L. ANTON, and JOE BAK (United Technologies Research Center, East Hartford, CT.) In NASA, Marshall Space Flight Center, Advanced Earth-to-Orbit Propulsion Technology 1988, Volume 1 p 510-518 Sep. 1988 (Contract NAS3-23939)

Avail: NTIS HC A99/MF E06 CSCL 11/6

Work to develop fatigue life prediction and constitutive models for uncoated attachment regions of single crystal gas turbine blades is described. At temperatures relevant to attachment regions, deformation is dominated by slip on crystallographic planes. However, fatigue crack initiation and early crack growth are not always observed to be crystallographic. The influence of natural occurring microporosity will be investigated by testing both hot

26 METALLIC MATERIALS

isostatically pressed and conventionally cast PWA 1480 single crystal specimens. Several different specimen configurations and orientations relative to the natural crystal axes are being tested to investigate the influence of notch acuity and the material's anisotropy. Global and slip system stresses in the notched regions were determined from three dimensional stress analyses and will be used to develop fatigue life prediction models consistent with the observed lives and crack characteristics. Author

N90-28644* National Aeronautics and Space Administration. Lewis Research Center, Cleveland, OH.

THE FATIGUE DAMAGE BEHAVIOR OF A SINGLE CRYSTAL SUPERALLOY

MICHAEL A. MCGAW /in NASA, Marshall Space Flight Center, Advanced Earth-to-Orbit Propulsion Technology 1988, Volume 1 p 519-562 Sep. 1988

Avail: NTIS HC A99/MF E06 CSCL 11/6

The uniaxial fatigue behavior of a single crystal superalloy, PWA 1480, is described. Both monotonic tensile and constant amplitude fatigue tests were conducted at room temperature, in an effort to assess the applicability of polycrystalline-based fatigue life prediction methods to a single crystal superalloy. The observed constant amplitude behavior correlated best using a stress-based life criterion. Nearly all specimens failed at surface or slightly subsurface microporosity; this is thought to be responsible for the unusually large amount of scatter in the test results. An additional term is developed in the stress-life equation for the purpose of accounting for the effect of microporosity on fatigue life. The form chosen is a function of the effective area of the failure-producing microporosity projected on a plane perpendicular to the loading axis, as well as the applied stress. This additional term correlated the data to within factors of two on life. Although speculative, extrapolation of the microporosity relation to zero micropore area indicates that approximately an order of magnitude improvement in fatigue life should result. Author

27

NONMETALLIC MATERIALS

Includes physical, chemical, and mechanical properties of plastics, elastomers, lubricants, polymers, textiles, adhesives, and ceramic materials.

A90-13230* Ohio State Univ., Columbus.

MICROSTRUCTURAL CHANGES IN BETA-SILICON NITRIDE GRAINS UPON CRYSTALLIZING THE GRAIN-BOUNDARY GLASS

WILLIAM E. LEE and GREGORY E. HILMAS (Ohio State University, Columbus) American Ceramic Society, Journal (ISSN 0002-7820), vol. 72, Oct. 1989, p. 1931-1937. refs

(Contract NAG3-824)

Copyright

Crystallizing the grain-boundary glass of a liquid-phase-sintered Si₃N₄ ceramic for 2 h or less at 1500 C led to formation of delta-Y₂Si₂O₇. After 5 h at 1500 C, the delta-Y₂Si₂O₇ had transformed to beta-Y₂Si₂O₇ with a concurrent dramatic increase in dislocation density within beta-Si₃N₄ grains. Reasons for the increased dislocation density are discussed. Annealing for 20 h at 1500 C reduced dislocation densities to the levels found in as-sintered material. Author

A90-15375* National Aeronautics and Space Administration. Lewis Research Center, Cleveland, OH.

DENSIFICATION AND COARSENING DURING SOLID STATE SINTERING OF CERAMICS: A REVIEW OF THE MODELS. II - GRAIN GROWTH

NANCY J. SHAW (NASA, Lewis Research Center, Cleveland, OH) Powder Metallurgy International (ISSN 0048-5012), vol. 21,

Oct. 1989, p. 31-33. refs

Copyright

Two processes occur simultaneously during the sintering of a ceramic powder compact: densification and coarsening (or grain growth). Both processes have as their driving force the reduction of the excess free surface energy of the powder particles. Several different mechanisms of atom transport, operating concurrently or consecutively, may be responsible for the two processes. Algebraic, geometric and topological models have been proposed and refined in attempts to determine the mechanism, or mechanisms, responsible for densification under defined processing conditions. These efforts have met with varying degrees of success. Recently, it has become apparent that more attention must be paid to the coarsening processes during sintering. The models for both densification and coarsening during solid state sintering are reviewed with particular emphasis on their applicability to engineering ceramics. Author

A90-16278* National Aeronautics and Space Administration. Lewis Research Center, Cleveland, OH.

TRIBOLOGICAL REACTIONS OF PERFLUOROALKYL POLYETHER OILS WITH STAINLESS STEEL UNDER ULTRAHIGH VACUUM CONDITIONS AT ROOM TEMPERATURE

SHIGEYUKI MORI and WILFREDO MORALES (NASA, Lewis Research Center, Cleveland, OH) Wear (ISSN 0043-1648), vol. 132, 1989, p. 111-121. refs

Copyright

The reaction between three types of commercial perfluoroalkyl polyether (PFPE) oils and stainless steel 440C was investigated experimentally during sliding under ultrahigh vacuum conditions at room temperature. It is found that the tribological reaction of PFPE is mainly affected by the activity of the mechanically formed fresh surfaces of metals rather than the heat generated at the sliding contacts. The fluorides formed on the wear track act as a boundary layer, reducing the friction coefficient. V.L.

A90-16279* National Aeronautics and Space Administration. Lewis Research Center, Cleveland, OH.

EFFECT OF HEAT-TREATMENT TEMPERATURE OF VAPOR-GROWN GRAPHITE FIBERS. I - PROPERTIES OF THEIR BROMINE INTERCALATION COMPOUNDS

JAMES R. GAIER (NASA, Lewis Research Center, Cleveland, OH), PAUL D. HAMBOURGER, and MELISSA E. SLABE (Cleveland State University, OH) Synthetic Metals (ISSN 0379-6779), vol. 31, 1989, p. 229-240. refs

(Contract NCC3-19)

Copyright

Vapor-grown graphite fibers were heat treated at 2000, 2200, 2400, 2600, 2800, and 3000 C, brominated at room temperature for two days, and then characterized by X-ray diffraction analysis, differential scanning calorimetry, and resistivity measurements. Fibers greater than 13 microns in diameter had low resistivities (50 microhms or less) irrespective of the heat treatment temperature. An analysis of the results obtained suggests that resistivities below 6 microhms cannot be achieved through a further reduction in defect level unless the amount of bromine is increased. V.L.

A90-18217* Nebraska Univ., Lincoln.

ELLIPSOMETRIC STUDY OF AL₂O₃/AG/SI AND SiO₂/AG/QUARTZ ASHED IN AN OXYGEN PLASMA

BHOLA N. DE and JOHN A. WOOLLAM (Nebraska, University, Lincoln) Journal of Applied Physics (ISSN 0021-8979), vol. 66, Dec. 1, 1989, p. 5602-5607. refs

(Contract NAG3-95)

Copyright

The growth of silver oxide (proposed as a potentially useful protective coating for space environment) on a silver mirror coated with an Al₂O₃ or a SiO₂ protective layer was investigated using the monolayer-sensitive variable angle of incidence spectroscopic ellipsometry technique. The samples were exposed to a pure oxygen plasma in a plasma asher, and the silver oxide growth

was monitored as a function of the exposure time. It was found that atomic oxygen in the asher penetrated through the SiO_2 or Al_2O_3 coatings to convert the silver underneath to silver oxide, and that the quantity of the silver oxide formed was proportional to the ashing time. The band gap of silver oxide was determined to be 1.3 eV. A schematic diagram of the variable angle of incidence spectroscopic ellipsometer is included. I.S.

A90-18879* University of Southern California, Los Angeles.
THE HIGH TEMPERATURE CREEP DEFORMATION OF
 $\text{Si}_3\text{N}_4\text{-6Y}_2\text{O}_3\text{-2Al}_2\text{O}_3$

J. A. TODD and ZHI-YUE XU (Southern California, University, Los Angeles, CA) Journal of Materials Science (ISSN 0022-2461), vol. 24, Dec. 1989, p. 4443-4452. Previously announced in STAR as N88-28981. refs

(Contract NAG3-685; DE-AC05-76OR-00033)

Copyright

The creep properties of silicon nitride containing 6 wt percent yttria and 2 wt percent alumina have been determined in the temperature range 1573 to 1673 K. The stress exponent, n , in the equation $\epsilon \propto \sigma^n$ varies as σ sup n , was determined to be 2.00 ± 0.15 and the true activation energy was found to be 692 ± 25 kJ/mol. Transmission electron microscopy studies showed that deformation occurred in the grain boundary glassy phase accompanied by microcrack formation and cavitation. The steady state creep results are consistent with a diffusion controlled creep mechanism involving nitrogen diffusion through the grain boundary glassy phase. Author

A90-21175* National Aeronautics and Space Administration.
 Lewis Research Center, Cleveland, OH.

CRYSTALLIZATION KINETICS OF $\text{BaO-Al}_2\text{O}_3\text{-SiO}_2$ GLASSES
 NAROTTAM P. BANSAL and MARK J. HYATT (NASA, Lewis Research Center, Cleveland, OH) Journal of Materials Research (ISSN 0884-2914), vol. 4, Sep.-Oct. 1989, p. 1257-1265. Previously announced in STAR as N89-20252. refs

Copyright

Barium aluminosilicate glasses are being investigated as matrix materials in high-temperature ceramic composites for structural applications. Kinetics of crystallization of two refractory glass compositions in the barium aluminosilicate system were studied by differential thermal analysis (DTA), X-ray diffraction (XRD), and scanning electron microscopy (SEM). From variable heating rate DTA, the crystallization activation energies for glass compositions (wt percent) $10\text{BaO-38Al}_2\text{O}_3\text{-51SiO}_2\text{-1MoO}_3$ (glass A) and $39\text{BaO-25Al}_2\text{O}_3\text{-35SiO}_2\text{-1MoO}_3$ (glass B) were determined to be 553 and 558 kJ/mol, respectively. On thermal treatment, the crystalline phases in glasses A and B were identified as mullite ($3\text{Al}_2\text{O}_3\text{-2SiO}_2$) and hexacelsian ($\text{BaO-Al}_2\text{O}_3\text{-2SiO}_2$), respectively. Hexacelsian is a high-temperature polymorph which is metastable below 1590 C. It undergoes structural transformation into the orthorhombic form at approximately 300 C accompanied by a large volume change which is undesirable for structural applications. A process needs to be developed where stable monoclinic celsian, rather than hexacelsian, precipitates out as the crystal phase in glass B. Author

A90-21214* National Aeronautics and Space Administration.
 Lewis Research Center, Cleveland, OH.

CORROSION OF CORDIERITE CERAMICS BY SODIUM SULPHATE AT 1000 C

ROBERT BIANCO and NATHAN JACOBSON (NASA, Lewis Research Center, Cleveland, OH) Journal of Materials Science (ISSN 0022-2461), vol. 24, Aug. 1989, p. 2903-2910. refs

Copyright

The corrosion of a sintered cordierite ($2\text{MgO-2Al}_2\text{O}_3\text{-5SiO}_2$) ceramic by sodium sulphate (Na_2SO_4) was investigated at 1000 C. Laboratory tests with thin films of $\text{Na}_2\text{SO}_4/\text{O}_2$ and $\text{Na}_2\text{SO}_4/1$ percent $\text{SO}_2\text{-O}_2$ were performed. In the $\text{Na}_2\text{SO}_4/\text{O}_2$ case, the cordierite reacted to form NaAlSiO_4 . After several hours of corrosion, the Na_2SO_4 appeared to induce surface cracks in the cordierite. In the $\text{Na}_2\text{SO}_4/1$ percent $\text{SO}_2\text{-O}_2$ case, other dissolution reactions occurred. The material was also tested in a burner rig

with No. 2 Diesel fuel and 2 ppm sodium. The corrosion process was similar to that observed in the $\text{Na}_2\text{SO}_4/\text{O}_2$ furnace tests, with more severe attack occurring. Author

A90-25267* National Aeronautics and Space Administration.
 Lewis Research Center, Cleveland, OH.

BURNER RIG HOT CORROSION OF SILICON CARBIDE AND SILICON NITRIDE

DENNIS S. FOX and JAMES L. SMIALEK (NASA, Lewis Research Center, Cleveland, OH) American Ceramic Society, Journal (ISSN 0002-7820), vol. 73, Feb. 1990, p. 303-311. Research sponsored by DOE. refs

Copyright

A number of commercially available SiC and Si_3N_4 materials were exposed to 1000 C for 40 h in a high-velocity, pressurized burner rig as a simulation of an aircraft turbine environment. Na impurities (2 ppm) added to the burner flame resulted in molten Na_2SO_4 deposition, attack of the SiC and Si_3N_4 , and formation of substantial $\text{Na}_2\text{O} + x(\text{SiO}_2)$ corrosion product. Room-temperature strength of the materials decreased as a result of the formation of corrosion pits in SiC and grain-boundary dissolution and pitting in Si_3N_4 . Author

A90-25273* National Aeronautics and Space Administration.
 Lewis Research Center, Cleveland, OH.

INTERGRANULAR FRACTURE OF LITHIUM FLUORIDE-22 PERCENT CALCIUM FLUORIDE HYPEREUTECTIC SALT AT 800 K

SUBRAMANIAM V. RAJ and J. DANIEL WHITTENBERGER (NASA, Lewis Research Center, Cleveland, OH) American Ceramic Society, Journal (ISSN 0002-7820), vol. 73, Feb. 1990, p. 403-408. refs

(Contract NCC3-72)

Copyright

Substantial strain-hardening was noted during the initial stages of deformation in constant-velocity compression tests conducted on as-cast samples of the LiF-22 mol pct CaF_2 hypereutectic salt at 800 K. The deformed specimens exhibited extensive grain-boundary cracking and cavitation, suggesting that such cracking, in conjunction with interfacial sliding, is important for cavity nucleation at grain boundaries and at the LiF- CaF_2 interfaces. Cavity growth and interlinkage occur through the preferential failure of the weaker LiF phase. O.C.

A90-27107* Ohio State Univ., Columbus.

CRYSTALLIZATION OF A BARIUM-ALUMINOSILICATE GLASS
 C. H. DRUMMOND, III, W. E. LEE (Ohio State University, Columbus), N. P. BANSAL, and M. J. HYATT (NASA, Lewis Research Center, Cleveland, OH) Ceramic Engineering and Science Proceedings (ISSN 0196-6219), vol. 10, Sept.-Oct. 1989, p. 1485-1502. refs

Copyright

The crystallization of a celsian glass composition was investigated as a possible high-temperature ceramic matrix material. Heat treatments invariably resulted in crystallization of the hexacelsian phase unless a flux, such as lithia, was added or a nucleating agent used (e.g., celsian seeds). TEM analysis revealed complex microstructures. Glasses with Mo additions contained hexacelsian, mullite, and an Mo-rich glass. Li_2O additions stabilized celsian but mullite and Mo-rich glass were still present. Author

A90-27691* National Aeronautics and Space Administration.
 Lewis Research Center, Cleveland, OH.

SLURRY-PRESSING CONSOLIDATION OF SILICON NITRIDE

WILLIAM A. SANDERS, JAMES D. KISER, and MARC R. FREEDMAN (NASA, Lewis Research Center, Cleveland, OH) American Ceramic Society Bulletin (ISSN 0002-7812), vol. 68, Oct. 1989, p. 1836-1841. Previously announced in STAR as N89-12746. refs

Copyright

A baseline slurry-pressing method for a silicon nitride material is developed. The Si_3N_4 composition contained 5.8 wt percent SiO_2 and 6.4 wt percent Y_2O_3 . Slurry-pressing variables included

27 NONMETALLIC MATERIALS

volume percent solids, application of ultrasonic energy, and pH. Twenty vol percent slurry-pressed material was approximately 11 percent stronger than both 30 vol percent slurry-pressed and dry-pressed materials. The Student's t-test showed the difference to be significant at the 99 percent confidence level. Twenty volume percent (300 h) slurry-pressed test bars exhibited strengths as high as 980 MPa. Large, columnar beta-Si₃N₄ grains caused failure in the highest strength specimens. The improved strength correlated with better structural uniformity as determined by radiography, optical microscopy, and image analysis. Author

A90-33317* National Aeronautics and Space Administration. Lewis Research Center, Cleveland, OH.

TWO-LAYER THERMAL BARRIER COATING. I - EFFECTS OF COMPOSITION AND TEMPERATURE ON OXIDATION BEHAVIOR AND FAILURE

STEPHAN STECURA (NASA, Lewis Research Center, Cleveland, OH) Thin Solid Films (ISSN 0040-6090), vol. 182, 1989, p. 121-139. refs
Copyright

The effects of 21 bond and 2 ceramic coating compositions on the specific mass gain, internal crack location at failure, and life of a two-layer thermal barrier coating (TBC) were studied by cyclic testing in a furnace. MAR-M 200 + Hf alloy specimens were completely coated with bond and thermal barrier (ceramic) coatings. Both coatings were applied by air plasma spray deposition. Cyclic test data were obtained at 1110, 1160, and 1220 deg C. The data show that the specific mass gain and the TBC life are significantly affected by the composition of the bond coating and the temperature and only slightly affected by the composition of the ceramic coating. Author

A90-33332* National Aeronautics and Space Administration. Lewis Research Center, Cleveland, OH.

THE EFFECT OF LENGTH AND DIAMETER ON THE RESISTIVITY OF BROMINE INTERCALATED GRAPHITE FIBERS

JAMES R. GAIER (NASA, Lewis Research Center, Cleveland, OH) Synthetic Metals (ISSN 0379-6779), vol. 34, 1989, p. 745-750. refs
Copyright

The resistivity of bromine intercalated graphite fibers has been shown to vary with both the diameter and the length of the fibers. This is due to bromine depletion from the fiber surface. Model calculations assuming a 1.0 micron bromine depletion zone for P-100, and 3.0 microns for vapor-grown graphite fibers fit the respective diameter dependence of their resistivities quite well. Length dependence data imply a bromine depletion zone along the length of P-100 fibers which is also a few microns, but that of vapor grown fibers appears to be as large as 300 microns. Despite these values, microfilaments, which are much smaller than the expected depletion zones, do form residual bromine intercalation compounds with resistivities about one-half of their pristine value. Author

A90-34569* National Aeronautics and Space Administration. Lewis Research Center, Cleveland, OH.

DIAMONDLIKE CARBON PROTECTIVE COATINGS FOR OPTICAL WINDOWS

DIANE M. SWEC and MICHAEL J. MIRTICH (NASA, Lewis Research Center, Cleveland, OH) IN: Window and dome technologies and materials; Proceedings of the Meeting, Orlando, FL, Mar. 27-29, 1989. Bellingham, WA, Society of Photo-Optical Instrumentation Engineers, 1989, p. 162-173. Previously announced in STAR as N89-27506. refs
Copyright

Diamondlake carbon (DLC) films were deposited on infrared transmitting optical windows and were evaluated as protective coatings for these windows exposed to particle and rain erosion. The DLC films were deposited on zinc selenide (ZnSe) and zinc sulfide (ZnS) by three different ion beam methods: (1) sputter deposition from a carbon target using an 8-cm argon ion source; (2) direct deposition by a 30-cm hollow cathode ion source with

hydrocarbon gas in argon; and (3) dual beam direct deposition by the 30-cm hollow cathode ion source and an 8-cm argon ion source. In an attempt to improve the adherence of the DLC films on ZnSe and ZnS, ion beam cleaning, ion implantation with helium and neon ions, or sputter deposition of a thin, ion beam intermediate coating was employed prior to deposition of the DLC film. The protection that the DLC films afforded the windows from particle and rain erosion was evaluated, along with the hydrogen content, adherence, intrinsic stress, and infrared transmittance of the films. Because of the elevated stress levels in the ion beam sputtered DLC films and in those ion beam deposited with butane, films thicker than 0.1 micron and with good adherence on ZnS and ZnSe could not be generated. An intermediate coating of germanium successfully allowed the DLC films to remain adherent to the optical windows and caused only negligible reduction in the specular transmittance of the ZnS and ZnSe at 10 microns. Author

A90-35473* National Aeronautics and Space Administration. Lewis Research Center, Cleveland, OH.

HIGH-STRENGTH SILICON CARBIDES BY HOT ISOSTATIC PRESSING

SUNIL DUTTA (NASA, Lewis Research Center, Cleveland, OH) IN: Ceramic materials and components for engines; Proceedings of the Third International Symposium, Las Vegas, NV, Nov. 27-30, 1988. Westerville, OH, American Ceramic Society, Inc., 1989, p. 683-695. Previously announced in STAR as N89-13666. refs
Copyright

Silicon carbide has strong potential for heat engine hardware and other high-temperature applications because of its low density, good strength, high oxidation resistance, and good high-temperature creep resistance. Hot isostatic pressing (HIP) was used for producing alpha and beta silicon carbide (SiC) bodies with near-theoretical density, ultrafine grain size, and high strength at processing temperatures of 1900 to 2000 C. The HIPed materials exhibited ultrafine grain size. Furthermore, no phase transformation from beta to alpha was observed in HIPed beta-SiC. Both materials exhibited very high average flexural strength. It was also shown that alpha-SiC bodies without any sintering aids, when HIPed to high final density, can exhibit very high strength. Fracture toughness K (sub C) values were determined to be 3.6 to 4.0 MPa m (sup 1/2) for HIPed alpha-SiC and 3.7 to 4.1 MPa m (sup 1/2) for HIPed beta-SiC. In the HIPed specimens strength-controlling flaws were typically surface related. In spite of improvements in material properties such as strength and fracture toughness by elimination of the larger strength-limiting flaws and by grain size refinement, HIPing has no effect on the Weibull modulus. Author

A90-35509* Norton Co., Northboro, MA.

DEVELOPMENT OF Si₃N₄ FOR GAS TURBINE APPLICATIONS

ANTONI P. TAGLIAVARE (Norton Co., Northboro, MA) IN: Ceramic materials and components for engines; Proceedings of the Third International Symposium, Las Vegas, NV, Nov. 27-30, 1988. Westerville, OH, American Ceramic Society, Inc., 1989, p. 1376-1383. Research supported by DOE. refs
(Contract DEN3-335)
Copyright

Activities associated with materials research are often concerned with composition and intrinsic properties as opposed to formability. To overcome this problem, Taguchi-designed experiments were utilized to develop process parameters for a formable Si₃N₄ powder. Using these experiments, the transfer of a research-based material (prepared by isostatic pressing) to a component formable material (prepared by casting) was accomplished while preserving properties required for gas-turbine applications. Author

A90-40714* National Aeronautics and Space Administration. Lewis Research Center, Cleveland, OH.

DECOMPOSITION OF PERFLUOROALKYLPOLYETHERS (PFPE) IN ULTRA-HIGH VACUUM UNDER SLIDING CONDITIONS

SHIGEYUKI MORI and WILFREDO MORALES (NASA, Lewis

Research Center, Cleveland, OH) (STLE, Annual Meeting, 44th, Atlanta, GA, May 1-4, 1989) STLE Tribology Transactions (ISSN 0569-8197), vol. 33, July 1990, p. 325-332. Previously announced in STAR as N89-26091. refs
Copyright

Reactions of perfluoroalkylpolyethers (PFPE: Fomblin, Demnum and Krytox) were studied during the sliding contact of stainless steel specimens under ultrahigh vacuum conditions. All three fluids reacted with the steel specimens during sliding. Fomblin, which has acetal linkages, decomposed under the sliding conditions generating gaseous products, (COF₂ and fluorinated carbons) which were detected by a quadrupole mass spectrometer. Gaseous products were not detected for the Demnum and Krytox fluids. The amount of gaseous products from Fomblin increased with increasing sliding speed. At the end of the sliding experiments, the wear scar and deposits on the specimens were examined by small spot size XPS. The oxide layer on the specimen surface was removed during sliding, and metal fluorides were formed on the worn surface. The surface of the wear scar and deposits were covered with adsorbed PFPE. Based on these results, it was concluded that the decomposition reaction on Fomblin was initiated by contacting the fluid with a fresh metal surface which was formed during sliding. Author

A90-43119* State Univ. of New York, Buffalo.

A BRIEF SURVEY OF RADIATION EFFECTS ON POLYMER DIELECTRICS

JAVOID R. LAGHARI (New York, State University, Buffalo) and AHMAD N. HAMMOUD (NASA, Lewis Research Center; Sverdrup Technology, Inc., Cleveland, OH) IEEE Transactions on Nuclear Science (ISSN 0018-9499), vol. 37, pt. 2, April 1990, p. 1076-1083. refs

Copyright

Future space power needs are extrapolated to be at least three to four orders of magnitude more than is currently available. This long-term reliable power will be required on missions such as the Space Station, Pathfinder, Space Plane, and high-powered satellites, and for defense. Electrical insulation and dielectrics are the key electrical materials needed to support these power systems, where a single-point system failure could prove catastrophic or even fatal for the whole mission. Therefore, the impact of radiation, an environmental stress, on the properties and performance of insulation and dielectrics must be understood. The influence of radiation on polymer dielectrics, the insulating materials most commonly used for power transmission and storage, is reviewed. The effects of the type of radiation, dose, rate, and total exposure on the key electrical, mechanical, and physical properties of polymer dielectrics are described and explained. I.E.

A90-43580* Utah Univ., Salt Lake City.

EQUIVALENCE OF PHYSICALLY BASED STATISTICAL FRACTURE THEORIES FOR RELIABILITY ANALYSIS OF CERAMICS IN MULTIAXIAL LOADING

LUEN-YUAN CHAO and DINESH K. SHETTY (Utah, University, Salt Lake City) American Ceramic Society, Journal (ISSN 0002-7820), vol. 73, July 1990, p. 1917-1921. refs
(Contract NAG3-789)

Copyright

The present comparison of the Batdorf (1974) flaw density and orientation distribution approach with Evans' (1978) elemental strength approach, with a view to identities in fracture criteria and distribution functions, notes that despite their fundamental differences in multiaxial loading fracture probabilities, the two approaches yield identical predictions. Lamon's (1988) assertion to the contrary, in light of different theoretical predictions by the two methods for the case of alumina disks loaded in flexure, is demonstrated to be in error. O.C.

A90-44376* National Aeronautics and Space Administration. Lewis Research Center, Cleveland, OH.

THE MECHANICAL PROPERTIES OF FLUORIDE SALTS AT ELEVATED TEMPERATURES

S. V. RAJ and J. D. WHITTENBERGER (NASA, Lewis Research

Center, Cleveland, OH) IN: Strength of metals and alloys (ICSMA 8); Proceedings of the Eighth International Conference, Tampere, Finland, Aug. 22-26, 1988. Volume 2. Oxford, England and Elmsford, NY, Pergamon Press, 1989, p. 1007-1012. Copyright

The deformation behavior of CaF₂ and LiF single crystals compressed in the 111 and the 100 line directions, respectively, are compared with the mechanical properties of polycrystalline LiF-22 (mol pct) CaF₂ eutectic mixture in the temperature range 300 to 1275 K for strain rates varying between 7 x 10 to the -7th and 0.2/s. The true stress-strain curves for the single crystals were found to exhibit three stages in an intermediate range of temperatures and strain rates, whereas those for the eutectic showed negative work-hardening rates after a maximum stress. The true stress-strain rate data for CaF₂ and LiF-22 CaF₂ could be represented by a power-law relation with the strain rate sensitivities lying between 0.05 and 0.2 for both materials. A similar relation was found to be unsatisfactory in the case of LiF.

Author

A90-44864* National Aeronautics and Space Administration. Lewis Research Center, Cleveland, OH.

PLASMA-DEPOSITED AMORPHOUS HYDROGENATED CARBON FILMS AND THEIR TRIBOLOGICAL PROPERTIES

K. MIYOSHI, J. J. POUCH, and S. A. ALTEROVITZ (NASA, Lewis Research Center, Cleveland, OH) Materials Science Forum (ISSN 0255-5476), vol. 52-53, 1989, p. 645-656. Previously announced in STAR as N90-11880. refs

Copyright

Recent work on the properties of diamondlike carbon films and their dependence on preparation conditions are reviewed. The results of the study indicate that plasma deposition enables one to deposit a variety of amorphous hydrogenated carbon (a-C:H) films exhibiting more diamondlike behavior to more graphitic behavior. The plasma-deposited a-C:H can be effectively used as hard, wear-resistant, and protective lubricating films on ceramic materials such as Si(sub 3)N(sub 4) under a variety of environmental conditions such as moist air, dry nitrogen, and vacuum. Author

A90-45830* National Aeronautics and Space Administration. Lewis Research Center, Cleveland, OH.

REACTIONS OF SiC WITH H₂/H₂O/AR MIXTURES AT 1300 C

NATHAN S. JACOBSON, ANDREW J. ECKEL, AJAY K. MISRA, and DONALD L. HUMPHREY (NASA, Lewis Research Center, Cleveland, OH) American Ceramic Society, Journal (ISSN 0002-7820), vol. 73, Aug. 1990, p. 2330-2332. refs

Copyright

Thermochemical modeling anticipates the existence of three reaction regions for the case of a sintered alpha-SiC with 5 percent H₂/H₂O/Ar at 1300 C, depending on the initial water vapor or, equivalently, oxygen, content of the gas stream. While a high oxygen content leads to SiC-protecting SiO₂ surface film formation and limits consumption of the SiC through passive oxidation, intermediate oxygen contents lead to SiO and CO formation and rapid SiC consumption. In this intermediate region, reaction rates appear to be controlled by H₂O gas-phase transport to the sample; reacted microstructures exhibit extensive grain-boundary attack in this region. Very low oxygen content is predicted to selectively remove carbon, with free silicon formation. O.C.

A90-47093* National Aeronautics and Space Administration. Lewis Research Center, Cleveland, OH.

PHASE TRANSFORMATIONS IN XEROGELS OF MULLITE COMPOSITION

MARK J. HYATT and NAROTTAM P. BANSAL (NASA, Lewis Research Center, Cleveland, OH) Journal of Materials Science (ISSN 0022-2461), vol. 25, June 1990, p. 2815-2821. Previously announced in STAR as N89-11038. refs

Copyright

Monophasic and diphasic xerogels have been prepared as precursors for mullite (3Al₂O₃-2SiO₂). Monophasic xerogel was synthesized from tetraethyl orthosilicate and aluminum nitrate

27 NONMETALLIC MATERIALS

nanohydrate and the diphasic xerogel from colloidal suspension of silica and boehmite. The chemical and structural evolutions, as a function of thermal treatment, in these two types of sol-gel derived mullite precursor powders have been characterized by DTA, TGA, X-ray diffraction, SEM and infrared spectroscopy. Monophasic xerogel transforms to an Al-Si spinel from an amorphous structure at approximately 980 C. The spinel then changes into mullite on further heating. Diphasic xerogel forms mullite at approximately 1360 C. The components of the diphasic powder react independently up to the point of mullite formation. The transformation in the monophasic powder occurs rapidly and yields strongly crystalline mullite with no other phases present. The diphasic powder, however, transforms rather slowly and contains remnants of the starting materials (α -Al₂O₃, cristobalite) even after heating at high temperatures for long times (1600 C, 6 hr). The diphasic powder could be sintered to high density but not the monophasic powder in spite of its molecular level homogeneity.

Author

A90-48550* National Aeronautics and Space Administration. Lewis Research Center, Cleveland, OH.

X-RAY PHOTOELECTRON SPECTROSCOPY PEAK ASSIGNMENT FOR PERFLUOROPOLYETHER OILS

SHIGEYUKI MORI and WILFREDO MORALES (NASA, Lewis Research Center, Cleveland, OH) *Journal of Vacuum Science and Technology A* (ISSN 0734-2101), vol. 8, July-Aug. 1990, p. 3354-3356. refs

Copyright

Perfluoroalkylpolyether (PFPE) oils are increasingly being used as vacuum pump oils and as lubricants for magnetic recording media and instrumentation for satellites. In this paper, the relative binding energies of three PFPE oils are determined. When sample oils are continuously irradiated during X-ray spectroscopy (XPS) measurements, the relative peak intensity of the spectra is altered significantly, indicating that gaseous products form from the oils during XPS measurements. Thus, attention should be paid to chemical changes when XPE is used to characterize fluorinated carbons such as PFPE oils.

C.D.

A90-49054* National Aeronautics and Space Administration. Lewis Research Center, Cleveland, OH.

FUNDAMENTAL TRIBOLOGICAL PROPERTIES OF ION-BEAM-DEPOSITED BORON NITRIDE FILMS

K. MIYOSHI (NASA, Lewis Research Center, Cleveland, OH) *Materials Science Forum* (ISSN 0255-5476), vol. 54-55, 1990, p. 375-397. Previously announced in STAR as N90-11881. refs

Copyright

The adhesion, friction, and micromechanical properties of ion-beam-deposited boron nitride (BN) films are reviewed. The BN films are examined in contact with BN metals and other harder materials. For simplicity of discussion, the tribological properties of concern in the processes are separated into two parts. First, the pull-off force (adhesion) and the shear force required to break the interfacial junctions between contacting surfaces are discussed. The effects of surface films, hardness of metals, and temperature on tribological response with respect to adhesion and friction are considered. The second part deals with the abrasion of the BN films. Elastic, plastic, and fracture behavior of the BN films in solid-state contact are discussed. The scratch technique of determining the critical load needed to fracture interfacial adhesive bonds of BN films deposited on substrates is also addressed.

Author

A90-49061* National Aeronautics and Space Administration. Lewis Research Center, Cleveland, OH.

DENSITY OF INTERCALATED GRAPHITE FIBERS

JAMES R. GAIER (NASA, Lewis Research Center, Cleveland, OH) and MELISSA E. SLABE (Cleveland State University, OH) *Carbon* (ISSN 0008-6223), vol. 28, no. 5, 1990, p. 669-674. Previously announced in STAR as N90-14362. refs

Copyright

The density of Amoco P-55, P-75, P-100, and P-120 pitch-based graphite fibers and their intercalation compounds with bromine,

iodine monochloride, and copper (II) chloride have been measured using a density gradient column. The distribution of densities within a fiber type is found to be a sensitive indicator of the quality of the intercalation reaction. In all cases the density was found to increase, indicating that the mass added to the graphite is dominant over fiber expansion. Density increases are small (less than 10 percent) giving credence to a model of the intercalated graphite fibers which have regions which are intercalated and regions which are not.

Author

A90-49086* National Aeronautics and Space Administration. Lewis Research Center, Cleveland, OH.

DEFORMATION OF AS-CAST LiF-22 MOL PCT CaF₂ HYPEREUTECTIC SALT BETWEEN 500 AND 1015 K

S. V. RAJ and J. D. WHITTENBERGER (NASA, Lewis Research Center, Cleveland, OH) *Materials Science and Engineering, Part A - Structural Materials: Properties, Microstructure and Processing* (ISSN 0921-5093), vol. 124, 1990, p. 113-123. refs (Contract NCC3-72)

Copyright

Results are presented on compression tests conducted on as-cast LiF-22 mol pct CaF₂ hypereutectic specimens at nominal strain rates between 1.8×10^{-3} to the -6th/sec and 0.25/sec over the temperature range 500-1015 K. In all instances, the stress-strain curves showed broad maxima, with negative strain-hardening rates after the peak stress σ_{max} . It was found that, at low temperatures and high stresses, the CaF₂ lamellae are rigid while the LiF matrix exhibits extensive transgranular cavitation, while at high temperatures and low stresses the CaF₂ lamellae break down and spheroidize while the LiF matrix does not cavitate. It was concluded that the mechanical properties of the as-cast hypereutectic LiF-22 mol pct CaF₂ are governed by the rate of deformation of the CaF₂ phase. It is suggested that, for thermal energy storage applications, a spheroidal microstructure is more desirable than a lamellar structure.

I.S.

N90-10262*# National Aeronautics and Space Administration. Lewis Research Center, Cleveland, OH.

FRICTION AND WEAR OF OXIDE-CERAMIC SLIDING AGAINST IN-718 NICKEL BASE ALLOY AT 25 TO 800 C IN ATMOSPHERIC AIR

HAROLD E. SLINEY and DANIEL L. DEADMORE Aug. 1989 27 p (NASA-TM-102291; E-4963; NAS 1.15:102291) Avail: NTIS HC A03/MF A01 CSCL 11C

The friction and wear of oxide-ceramics sliding against the nickel base alloy IN-718 at 25 to 800 C were measured. The oxide materials tested were mullite (3Al₂O₃·2SiO₂); lithium aluminum silicate (LiAlSi₂O₆); polycrystalline monolithic alpha alumina (α -Al₂O₃); single crystal α -Al₂O₃ (sapphire); zirconia (ZrO₂); and silicon carbide (SiC) whisker-reinforced Al₂O₃ composites. At 25 C the mullite and zirconia had the lowest friction and the polycrystalline monolithic alumina had the lowest wear. At 800 C the Al₂O₃-8 vol/percent SiC whisker composite had the lowest friction and the Al₂O₃-25 vol/percent SiC composite had the lowest wear. The friction of the Al₂O₃-SiC whisker composites increased with increased whisker content while the wear decreased. In general, the wear-resistance of the ceramics improve with their hardness.

Author

N90-10293*# Ford Motor Co., Dearborn, MI. Scientific Lab. **IMPROVED SILICON CARBIDE FOR ADVANCED HEAT ENGINES** Final Annual Report No. 2, 15 Feb. 1986 - 14 Feb. 1987

THOMAS J. WHALEN Oct. 1987 80 p (Contract NAS3-24384)

(NASA-CR-180831; NAS 1.26:180831) Avail: NTIS HC A05/MF A01 CSCL 11C

This is the second annual technical report entitled, Improved Silicon Carbide for Advanced Heat Engines, and includes work performed during the period February 16, 1986 to February 15, 1987. The program is conducted for NASA under contract NAS3-24384. The objective is the development of high strength,

high reliability silicon carbide parts with complex shapes suitable for use in advanced heat engines. The fabrication methods used are to be adaptable for mass production of such parts on an economically sound basis. Injection molding is the forming method selected. This objective is to be accomplished in a two-phase program: (1) to achieve a 20 percent improvement in strength and a 100 percent increase in Weibull modulus of the baseline material; and (2) to produce a complex shaped part, a gas turbine rotor, for example, with the improved mechanical properties attained in the first phase. Eight tasks are included in the first phase covering the characterization of the properties of a baseline material, the improvement of those properties and the fabrication of complex shaped parts. Activities during the first contract year concentrated on two of these areas: fabrication and characterization of the baseline material (Task 1) and improvement of material and processes (Task 7). Activities during the second contract year included an MOR bar matrix study to improve mechanical properties (Task 2), materials and process improvements (Task 7), and a Ford-funded task to mold a turbocharger rotor with an improved material (Task 8). Author

N90-10294*# Materials and Electrochemical Research Corp., Tucson, AZ.

ZIRCONIA TOUGHENED SiC WHISKER REINFORCED ALUMINA COMPOSITES SMALL BUSINESS INNOVATION RESEARCH Final Report, Dec. 1985 - Oct. 1986

R. O. LOUTFY, K. L. STUFFLE, J. C. WITHERS, and C. T. LEE
Oct. 1987 48 p
(Contract NAS3-24872)
(NASA-CR-179629; NAS 1.26:179629) Avail: NTIS HC A03/MF A01 CSCL 11C

The objective of this phase 1 project was to develop a ceramic composite with superior fracture toughness and high strength, based on combining two toughness inducing materials: zirconia for transformation toughening and SiC whiskers for reinforcement, in a controlled microstructure alumina matrix. The controlled matrix microstructure is obtained by controlling the nucleation frequency of the alumina gel with seeds (submicron alpha-alumina). The results demonstrate the technical feasibility of producing superior binary composites (Al₂O₃-ZrO₂) and tertiary composites (Al₂O₃-ZrO₂-SiC). Thirty-two composites were prepared, consolidated, and fracture toughness tested. Statistical analysis of the results showed that: (1) the SiC type is the key statistically significant factor for increased toughness; (2) sol-gel processing with a-alumina seed had a statistically significant effect on increasing toughness of the binary and tertiary composites compared to the corresponding mixed powder processing; and (3) ZrO₂ content within the range investigated had a minor effect. Binary composites with an average critical fracture toughness of 6.6 MPa^{1/2} were obtained. Tertiary composites with critical fracture toughness in the range of 9.3 to 10.1 MPa^{1/2} were obtained. Results indicate that these composites are superior to zirconia toughened alumina and SiC whisker reinforced alumina ceramic composites produced by conventional techniques with similar composition from published data. Author

N90-11144*# National Aeronautics and Space Administration, Lewis Research Center, Cleveland, OH.

HYDROGEN-SILICON CARBIDE INTERACTIONS

ANDREW J. ECKEL, NATHAN S. JACOBSON, AJAY K. MISRA, and DONALD L. HUMPHREY Sep. 1989 12 p Presented at the 4th International Conference on Hydrogen Effects on Material Behavior, Moran, WY, 12-16 Sep. 1989; sponsored in part by The Metallurgical Society Prepared in cooperation with Sverdrup Technology, Inc., Cleveland, OH
(NASA-TM-102382; E-5120; NAS 1.15:102382) Avail: NTIS HC A03/MF A01 CSCL 11/3

A study of the thermochemistry and kinetics of hydrogen environmental attack of silicon carbide was conducted for temperatures in the range from 1100 C to 1400 C. Thermodynamic maps based on the parameters of pressure and oxygen/moisture content were constructed. With increasing moisture levels, four distinct regions of attack were identified. Each region is defined

by the thermodynamically stable solid phases. The theoretically stable solid phases of Region 1 are silicon carbide and silicon. Experimental evidence is provided to support this thermodynamic prediction. Silicon carbide is the single stable solid phase in Region 2. Active attack of the silicon carbide in this region occurs by the formation of gases of SiO, CO, CH₄, SiH₄, and SiH. Analysis of the kinetics of reaction for Region 2 at 1300 C show the attack of the silicon carbide to be controlled by gas phase diffusion of H₂O to the sample. Silicon carbide and silica are the stable phases common to Regions 3 and 4. These two regions are characterized by the passive oxidation of silicon carbide and formation of a protective silica layer. Author

N90-11880*# National Aeronautics and Space Administration, Lewis Research Center, Cleveland, OH.

PLASMA-DEPOSITED AMORPHOUS HYDROGENATED CARBON FILMS AND THEIR TRIBOLOGICAL PROPERTIES

KAZUHISA MIYOSHI, JOHN J. POUCH, and SAMUEL A. ALTEROVITZ Oct. 1989 13 p Submitted for publication
(NASA-TM-102379; E-5118; NAS 1.15:102379) Avail: NTIS HC A03/MF A01 CSCL 11/3

Recent work on the properties of diamondlike carbon films and their dependence on preparation conditions are reviewed. The results of the study indicate that plasma deposition enables one to deposit a variety of amorphous hydrogenated carbon (a-C:H) films exhibiting more diamondlike behavior to more graphitic behavior. The plasma-deposited a-C:H can be effectively used as hard, wear-resistant, and protective lubricating films on ceramic materials such as Si(sub 3)N(sub 4) under a variety of environmental conditions such as moist air, dry nitrogen, and vacuum. Author

N90-11881*# National Aeronautics and Space Administration, Lewis Research Center, Cleveland, OH.

FUNDAMENTAL TRIBOLOGICAL PROPERTIES OF ION-BEAM-DEPOSITED BORON NITRIDE FILMS

KAZUHISA MIYOSHI Oct. 1989 25 p Submitted for publication
(NASA-TM-102088; E-4850; NAS 1.15:102088) Avail: NTIS HC A03/MF A01 CSCL 11/3

The adhesion, friction, and micromechanical properties of ion-beam-deposited boron nitride (BN) films are reviewed. The BN films are examined in contact with BN metals and other harder materials. For simplicity of discussion, the tribological properties of concern in the processes are separated into two parts. First, the pull-off force (adhesion) and the shear force required to break the interfacial junctions between contacting surfaces are discussed. The effects of surface films, hardness of metals, and temperature on tribological response with respect to adhesion and friction are considered. The second part deals with the abrasion of the BN films. Elastic, plastic, and fracture behavior of the BN films in solid-state contact are discussed. The scratch technique of determining the critical load needed to fracture interfacial adhesive bonds of BN films deposited on substrates is also addressed. Author

N90-11882*# Southwest Research Inst., San Antonio, TX.
SLIDING SEAL MATERIALS FOR LOW HEAT REJECTION ENGINES

KEVIN BEATY, JAMES LANKFORD, and SHANNON VINYARD Jul. 1989 134 p Prepared in cooperation with Department of Energy, Washington, DC
(Contract DEN3-352; DE-AI01-86CE-50162)
(NASA-CR-182262; NAS 1.26:182262; DOE/NASA/0352-3; SWRI-06-7963) Avail: NTIS HC A07/MF A01 CSCL 11/1

Sliding friction coefficients and wear rates of promising piston seal materials were measured under temperature, environmental, velocity, and loading conditions that are representative of the low heat rejection (LHR) diesel engine environment. These materials included carbides, oxides, and nitrides. In addition, silicon nitride and partially stabilized zirconia disks (cylinder liners) were ion-implanted with Ti, Ni, Co, and Cr, and subsequently run against carbide pins (piston rings), with the objective of producing

27 NONMETALLIC MATERIALS

reduced friction via solid lubrication at elevated temperature. Friction and wear measurements were obtained using pin-on-disk laboratory experiments and a unique engine friction test rig. Unmodified ceramic sliding couples were characterized at all temperatures by friction coefficients of 0.24 and above during the pin-on-disk tests. The coefficient at 800 C in an oxidizing environment was reduced to below 0.1, for certain material combination, by the ion-implantation of TiNi or Co. This beneficial effect was found to derive from the lubricious Ti, Ni, and Co oxides. Similar results were demonstrated on the engine friction test rig at lower temperatures. The structural integrity and feasibility of engine application with the most promising material combination were demonstrated during a 30-hour single-cylinder, direct-injection diesel engine test.

Author

N90-13666*# National Aeronautics and Space Administration. Lewis Research Center, Cleveland, OH.

THERMODYNAMIC PROPERTIES OF SOME METAL OXIDE-ZIRCONIA SYSTEMS

NATHAN S. JACOBSON Dec. 1989 63 p
(NASA-TM-102351; E-5060; NAS 1.15:102351) Avail: NTIS HC A04/MF A01 CSCL 11/3

Metal oxide-zirconia systems are a potential class of materials for use as structural materials at temperatures above 1900 K. These materials must have no destructive phase changes and low vapor pressures. Both alkaline earth oxide (MgO, CaO, SrO, and BaO)-zirconia and some rare earth oxide (Y₂O₃, Sc₂O₃, La₂O₃, CeO₂, Sm₂O₃, Gd₂O₃, Yb₂O₃, Dy₂O₃, Ho₂O₃, and Er₂O₃)-zirconia system are examined. For each system, the phase diagram is discussed and the vapor pressure for each vapor species is calculated via a free energy minimization procedure. The available thermodynamic literature on each system is also surveyed. Some of the systems look promising for high temperature structural materials.

Author

N90-14362*# National Aeronautics and Space Administration. Lewis Research Center, Cleveland, OH.

DENSITY OF INTERCALATED GRAPHITE FIBERS

JAMES R. GAIER and MELISSA E. SLABE (Cleveland State Univ., OH.) Dec. 1989 15 p
(NASA-TM-102411; E-5167; NAS 1.15:102411) Avail: NTIS HC A03/MF A01 CSCL 11/3

The density of Amoco P-55, P-75, P-100, and P-120 pitch-based graphite fibers and their intercalation compounds with bromine, iodine monochloride, and copper (II) chloride have been measured using a density gradient column. The distribution of densities within a fiber type is found to be a sensitive indicator of the quality of the intercalation reaction. In all cases the density was found to increase, indicating that the mass added to the graphite is dominant over fiber expansion. Density increases are small (less than 10 percent) giving credence to a model of the intercalated graphite fibers which have regions which are intercalated and regions which are not.

Author

N90-14363*# National Aeronautics and Space Administration. Lewis Research Center, Cleveland, OH.

THE 3F CONDENSATION POLYIMIDES: REVIEW AND UPDATE

WILLIAM B. ALSTON and ROY F. GRATZ (Mary Washington Coll., Fredricksburg, VA.) 1989 6 p Presented at the 1st Pacific Polymer Conference, Maui, HI, 12-15 Dec. 1989; sponsored by Pacific Polymer Federation, Inc. Prepared in cooperation with Army Aviation Systems Command, Cleveland, OH
(NASA-TM-102353; E-5062; NAS 1.15:102353; AVSCOM-TR-89-C-017; AD-A217851) Avail: NTIS HC A02/MF A01 CSCL 11/3

Nine new condensation polyimides containing the phenyltrifluoroethylidene (3F) linkage were synthesized by the amic-acid route. Several other polyimides, including some with hexafluoroisopropylidene (6F) linkage, were also prepared as controls. Amic-acid solutions were characterized by determining their inherent viscosities prior to thermal conversion into polyimide films. Glass transition temperatures (T_{sub g}), thermogravimetric analysis (TGA), and isothermal weight loss data (at 316, 371, and

371 C under 0.5 MPa air pressure) were obtained for the films. The films were pulverized into molding powders which, in turn, were thermally processed under pressure into neat resin disks. The disks were also characterized by T_{sub g}'s and 316 and 371 C isothermal weight losses. The film study identified two new polyimides with T_{sub g}'s greater than 371 C and two new polyimides with low rates of weight loss. The resin disks exhibited the same overall trends in T_{sub g} and weight loss as the respective films, however the weight loss per unit surface area was always greater, presumably due to molecular degradation induced during preparation of the molding powders. The overall results indicate that polyimides containing the 3F linkage have T_{sub g}'s and thermo-oxidative stability comparable to polyimides containing the 6F group. Alternate technology was also shown by the synthesis of two new polyalkyl substituted 3F diamines and five more new 3F polymers. Their potential as photoresists was demonstrated by T_{sub g} advancement after ultraviolet exposure. Last, four U.S. patents on 3F monomers and polymers were issued and up to eight more are pending.

Author

N90-14368*# National Aeronautics and Space Administration. Lewis Research Center, Cleveland, OH.

STRENGTH AND TOUGHNESS OF MONOLITHIC AND COMPOSITE SILICON NITRIDES

JONATHAN A. SALEM Jan. 1990 20 p
(Contract DE-AI05-87OR-21749)
(NASA-TM-102423; E-5188; NAS 1.15:102423) Avail: NTIS HC A03/MF A01 CSCL 11/3

The strength and toughness of two composite and two monolithic silicon nitrides were measured from 25 to 1400 C. The monolithic and composite materials were made from similar starting powders. Both of the composite materials contained 30 vol percent silicon carbide whiskers. All measurements were made by four point flexure in surrounding air and humidity. The composite and monolithic materials exhibited similar fast fracture properties as a function of temperature.

Author

N90-15262*# National Aeronautics and Space Administration. Lewis Research Center, Cleveland, OH.

BROMINATED GRAPHITIZED CARBON FIBERS Patent Application

CHING-CHEN HUNG, inventor (to NASA) 30 Nov. 1989 13 p
(NASA-CASE-LEW-14698-2; NAS 1.71:LEW-14698-2; US-PATENT-APPL-SN-443289) Avail: NTIS HC A03/MF A01 CSCL 11/3

Low cost, high break elongation graphitized carbon fibers having low degree of graphitization are inert to bromine at room or higher temperatures, but are brominated at -7 to 20 C, and then debrominated at ambient. Repetition of this bromination-debromination process can bring the bromine content to 18 percent. Electrical conductivity of the brominated fibers is three times of the before-bromination value.

NASA

N90-16072*# Sverdrup Technology, Inc., Cleveland, OH. THERMODYNAMIC ANALYSIS OF CHEMICAL STABILITY OF CERAMIC MATERIALS IN HYDROGEN-CONTAINING ATMOSPHERES AT HIGH TEMPERATURES Final Report

AJAY K. MISRA Jan. 1990 26 p
(Contract NAS3-25266; NRA-88-ARC-1(BJY))
(NASA-CR-4271; E-4954; NAS 1.26:4271) Avail: NTIS HC A03/MF A01 CSCL 11/3

The chemical stability of several ceramic materials in hydrogen-containing environments was analyzed with thermodynamic considerations in mind. Equilibrium calculations were made as a function of temperature, moisture content, and total system pressure. The following ceramic materials were considered in this study: SiC, Si₃N₄, SiO₂, Al₂O₃, mullite, ZrO₂, Y₂O₃, CaO, MgO, BeO, TiB₂, TiC, HfC, and ZrC. On the basis of purely thermodynamic arguments, upper temperature limits are suggested for each material for long-term use in H₂-containing atmospheres.

Author

N90-16944*# National Aeronautics and Space Administration. Lewis Research Center, Cleveland, OH.

THE EXPERIMENTAL EVALUATION AND APPLICATION OF HIGH-TEMPERATURE SOLID LUBRICANTS Ph.D. Thesis -

Case Western Reserve Univ., 1989 Final Report

CHRISTOPHER DELLACORTE Jan. 1990 57 p

(Contract DE-AI01-85CE-50162)

(NASA-TM-102476; E-5263; DOE/NASA/50162-3; NAS

1.15:102476) Avail: NTIS HC A04/MF A01 CSCL 11/3

A research program is described which develops an understanding of high-temperature solid lubrication and experimental techniques through the development of a composite lubricant coating system. The knowledge gained through this research was then applied to a specific engineering challenge, the tribology of a sliding seal for hypersonic flight vehicles. The solid lubricant coating is a chromium carbide based composite combined with silver, which acts as a low temperature lubricant, and barium fluoride/calcium fluoride eutectic, which acts as a high-temperature lubricant. This composite coating provides good wear resistance and low friction for sliding contacts from room temperature to over 900 C in reducing or oxidative environments. The specific research on this coating included a composition screening using a foil gas bearing test rig and the use of thin silver films to reduce initial wear using a pin-on-disk test rig. The chemical stability of the materials used was also addressed. This research indicated that soft metallic films and materials which become soft at elevated temperatures are potentially good lubricants. The general results from the experiments with the model solid lubricant coating were then applied to a sliding seal design concept. This seal design requires that a braided ceramic fabric slide against a variety of metal counterface materials at temperatures from 25 to 850 C in an oxidative environment. A pin-on-disk tribometer was used to evaluate the tribological properties of these materials and to develop lubrication techniques. The results indicate that these seal materials must be lubricated to prevent wear and reduce friction. Thin films of silver, gold and calcium fluoride provided lubrication to the sliding materials.

Author

N90-17101*# National Aeronautics and Space Administration. Lewis Research Center, Cleveland, OH.

POLYMER SOLUTION PHASE SEPARATION: MICROGRAVITY SIMULATION

LAWRENCE C. CERNY (Utica Coll., NY.) and JAMES K. SUTTER *In its* NASA Laser Light Scattering Advanced Technology Development Workshop, 1988 p 229-234 Aug. 1989

Avail: NTIS HC A14/MF A02 CSCL 11/3

In many multicomponent systems, a transition from a single phase of uniform composition to a multiphase state with separated regions of different composition can be induced by changes in temperature and shear. The density difference between the phase and thermal and/or shear gradients within the system results in buoyancy driven convection. These differences affect kinetics of the phase separation if the system has a sufficiently low viscosity. This investigation presents more preliminary developments of a theoretical model in order to describe effects of the buoyancy driven convection in phase separation kinetics. Polymer solutions were employed as model systems because of the ease with which density differences can be systematically varied and because of the importance of phase separation in the processing and properties of polymeric materials. The results indicate that the kinetics of the phase separation can be performed viscometrically using laser light scattering as a principle means of following the process quantitatively. Isopycnic polymer solutions were used to determine the viscosity and density difference limits for polymer phase separation.

Author

N90-17875*# National Aeronautics and Space Administration. Lewis Research Center, Cleveland, OH.

DETERMINATION OF THE THERMAL STABILITY OF PERFLUOROALKYLETERS

LARRY S. HELMICK and WILLIAM R. JONES, JR. Feb. 1990 21 p Proposed for presentation at the Japan International

Tribology Conference, Nagaya, Japan, 29 Oct. - 1 Nov. 1990; sponsored by Japan Society of Tribologists

(NASA-TM-102493; E-5211; NAS 1.15:102493) Avail: NTIS HC

A03/MF A01 CSCL 11/2

The thermal decomposition temperatures of several commercial and custom synthesized perfluoroalkylether fluids were determined with a computerized tensimeter. In general, the decomposition temperatures of the commercial fluids were all similar and significantly higher than those for custom synthesized fluids. Correlation of the decomposition temperatures with the molecular structures of the primary components of the commercial fluids revealed that the stability of the fluids is not affected by intrinsic factors such as carbon chain length, branching, or cumulated difluoroformal groups. Instead, correlation with extrinsic factors revealed that the stability may be limited by the presence of small quantities of thermally unstable material and/or chlorine-containing material arising from the use of chlorine-containing solvents during synthesis. Finally, correlation of decomposition temperatures with molecular weights for Demnum and Krytox fluids supports a chain cleavage reaction mechanism for Demnum fluids and an unzipping reaction mechanism for Krytox fluids.

Author

N90-19373*# National Aeronautics and Space Administration. Lewis Research Center, Cleveland, OH.

HOT FILAMENT TECHNIQUE FOR MEASURING THE THERMAL CONDUCTIVITY OF MOLTEN LITHIUM FLUORIDE

DONALD A. JAWORSKE and WILLIAM D. PERRY (Auburn Univ., AL.) 1990 13 p Proposed for presentation at the AIChE Summer National Meeting Session on Space Power Systems Technology, San Diego, CA, 19-22 Aug. 1990; sponsored by American Institute of Chemical Engineers

(NASA-TM-102506; E-5308; NAS 1.15:102506) Avail: NTIS HC

A03/MF A01 CSCL 11/3

Molten salts, such as lithium fluoride, are attractive candidates for thermal energy storage in solar dynamic space power systems because of their high latent heat of fusion. However, these same salts have poor thermal conductivities which inhibit the transfer of heat into the solid phase and out of the liquid phase. One concept for improving the thermal conductivity of the thermal energy storage system is to add a conductive filler material to the molten salt. High thermal conductivity pitch-based graphite fibers are being considered for this application. Although there is some information available on the thermal conductivity of lithium fluoride solid, there is very little information on lithium fluoride liquid, and no information on molten salt graphite fiber composites. This paper describes a hot filament technique for determining the thermal conductivity of molten salts. The hot filament technique was used to find the thermal conductivity of molten lithium fluoride at 930 C, and the thermal conductivity values ranged from 1.2 to 1.6 W/mK. These values are comparable to the slightly larger value of 5.0 W/mK for lithium fluoride solid. In addition, two molten salt graphite fiber composites were characterized with the hot filament technique and these results are also presented.

Author

N90-19374*# Ohio State Univ., Columbus. Dept. of Materials Science and Engineering.

CRYSTALLIZATION BEHAVIOR AND PROPERTIES OF BAO-AL2O3-2SiO2 GLASS MATRICES Final Report

CHARLES H. DRUMMOND, III and NAROTTAM P. BANSAL (Case Western Reserve Univ., Cleveland, OH.) Feb. 1990 23 p Presented at the 14th Annual Conference on Composite and Advanced Ceramics, Cocoa Beach, FL, 14-17 Jan. 1990; sponsored by American Ceramic Society

(Contract NCC3-133)

(NASA-CR-185209; E-5314; NAS 1.26:185209) Avail: NTIS HC

A03/MF A01 CSCL 11/3

Glass of stoichiometric celsian composition, BaO-Al₂O₃-2SiO₂, is a potential glass-ceramic matrix for high-temperature composites. The glass has a density of 3.39 g/cu cm, thermal expansion coefficient of 6.6 x 10⁻⁶/deg C glass transition temperature of 910 C, and dilatometric softening point of 925 C. On heat treatment, only hexacelsian crystallized out on the surface, but both celsian and hexacelsian were present in the bulk. Effects of

27 NONMETALLIC MATERIALS

cold isostatic pressing (CIP), sintering, and hot pressing, in the presence and absence of an additive, on the formation of the celsian phase in the glass were studied. CIP'ed samples, after appropriate heat treatments, always crystallized out as celsian whereas the presence of 5 to 10 weight percent of an additive was necessary for formation of celsian in sintered as well as hot pressed specimens. Green density increased with CIP'ing pressure but had no effect on sintered density. Hot pressing resulted in fully dense samples. Author

N90-21181*# National Aeronautics and Space Administration. Lewis Research Center, Cleveland, OH.

FEASIBILITY OF INTERCALATED GRAPHITE RAILGUN ARMATURES

JAMES R. GAIER, CLARENCE E. GOODEN, DOREEN YASHAN, and STEVEN NAUD (Naval Coastal Systems Center, Panama City, FL.) Apr. 1990 7 p Presented at the 5th Symposium on Electromagnetic Launch Technology, Fort Walton Beach, FL, 2-5 Apr. 1990; sponsored by IEEE (NASA-TM-102546; E-5332; NAS 1.15:102546) Avail: NTIS HC A03/MF A01 CSCL 11/3

Graphite intercalation compounds may provide an excellent material for the fabrication of electro-magnetic railgun armatures. As a pulse of power is fed into the armature the intercalate could be excited into the plasma state around the edges of the armature, while the bulk of the current would be carried through the graphite block. Such an armature would have the desirable characteristics of both diffuse plasma armatures and bulk conduction armatures. In addition, the highly anisotropic nature of these materials could enable the electrical and thermal conductivity to be tailored to meet the specific requirements of electromagnetic railgun armatures. Preliminary investigations were performed in an attempt to determine the feasibility of using graphite intercalation compounds as railgun armatures. Issues of fabrication, resistivity, stability, and electrical current spreading are addressed for the case of highly oriented pyrolytic graphite. Author

N90-21182*# National Aeronautics and Space Administration. Lewis Research Center, Cleveland, OH.

STUDIES OF MECHANO-CHEMICAL INTERACTIONS IN THE TRIBOLOGICAL BEHAVIOR OF MATERIALS

KAZUHISA MIYOSHI 1990 22 p Presented at the 8th International Conference on Thin Films, San Diego, CA, 2-6 Apr. 1990; sponsored by the American Vacuum Society (NASA-TM-102545; E-5301; NAS 1.15:102545) Avail: NTIS HC A03/MF A01 CSCL 11/3

Mechano-chemical interaction studies can contribute to the understanding of wear and friction of materials. Specific examples of experimental results relative to the subject are discussed. There are two parts: one describes the synergistic effect of corrosion and wear of iron sliding on sapphire in sulfuric acid, and the other describes the effect of surface films on the wear and friction of plasma-deposited diamondlike carbon (amorphous hydrogenated carbon) films in sliding contact with silicon nitride. The concentration of acid (pH) is an important factor in controlling the iron loss caused by wear-corrosion processes in sulfuric acid. The mechanical action can cause chemical reactions to proceed much faster than they would otherwise. The diamondlike carbon (DLC) films are shown to behave tribologically much like bulk diamond. In a dry nitrogen environment, a mechano-chemical reaction produces a substance which greatly decreases the coefficient of friction. In a moist air environment, mechano-chemical interactions drastically reduce the wear life of DLC films and water vapor greatly increases friction. Author

N90-21192*# National Aeronautics and Space Administration. Lewis Research Center, Cleveland, OH.

RESISTIVITY OF PRISTINE AND INTERCALATED GRAPHITE FIBER EPOXY COMPOSITES

JAMES R. GAIER, PAUL D. HAMBOURGER (Cleveland State Univ., OH.), and MELISSA E. SLABE 1989 18 p Presented at the 19th Biennial Conference on Carbon, University Park, PA, 25-30 Jun. 1989; sponsored by American Carbon Society

(Contract NCC3-19)

(NASA-TM-102576; E-5406; NAS 1.15:102576) Avail: NTIS HC A03/MF A01 CSCL 11/3

Laminar composites were fabricated from pristine and bromine intercalated Amoco P-55, P-75, and P-100 graphite fibers and Hysol-Grafil EAG101-1 film epoxy. The thickness and r.f. eddy current resistivity of several samples were measured at grid points and averaged point by point to obtain final values. Although the values obtained this way have high precision (less than 3 percent deviation), the resistivity values appear to be 20 to 90 percent higher than resistivities measured on high aspect ratio samples using multi-point techniques, and by those predicted by theory. The temperature dependence of the resistivity indicates that the fibers are neither damaged nor deintercalated by the composite fabrication process. The resistivity of the composites is a function of sample thickness (i.e., resin content). Composite resistivity is dominated by fiber resistivity, so lowering the resistivity of the fibers, either through increased graphitization or intercalation, results in a lower composite resistivity. A modification of the simple rule of mixtures model appears to predict the conductivity of high aspect ratio samples measured along a fiber direction, but a directional dependence appears which is not predicted by the theory. The resistivity of these materials is clearly more complex than that of homogeneous materials. Author

N90-21858*# National Aeronautics and Space Administration. Lewis Research Center, Cleveland, OH.

POLYSILOXANES DERIVED FROM THE CONTROLLED HYDROLYSIS OF TETRAETHOXYLANE AS PRECURSORS TO SILICA FOR USE IN CERAMIC PROCESSING

WARREN H. PHILIPP Jan. 1990 21 p (NASA-TM-102489; E-4527; NAS 1.15:102489) Avail: NTIS HC A03/MF A01 CSCL 11/3

Synthesis, properties, and potential applications in ceramic processing for two polysiloxane silica precursors derived from the controlled hydrolysis of tetraethoxysilane (TEOS) are presented. The higher molecular weight TEOS-A is a thick adhesive liquid of viscosity 8000 to 12,000 c.p. having a SiO₂ char yield of about 55 percent. The lower molecular weight TEOS-B is a more fluid liquid of viscosity 150 to 200 c.p. having a SiO₂ char yield of about 52 percent. The acid catalyzed hydrolysis of TEOS to hydrated silica gel goes through a series of polysiloxane intermediates. The rate of this transition increases with the quantity of water added to the TEOS; thus, for ease of polymer isolation, the amount of water added must be carefully determined so as to produce the desired polymer in a reasonable time. The water to TEOS mole ratio falls in the narrow range of 1.05 for TEOS-A and 0.99 for TEOS-B. Further polymerization or gelation is prevented by storing at -5 C in a freezer. Both polysiloxanes thermoset to a glassy solid at 115 C. The liquid polymers are organic in nature in that they are miscible with toluene and ethanol, slightly soluble in heptane, but immiscible with water. For both polymers, results on viscosity versus time are given at several temperatures and water additions. Based on these results, some examples of practical utilization of the precursors for ceramic fabrication are given. B.H.A.

N90-21862*# National Aeronautics and Space Administration. Lewis Research Center, Cleveland, OH.

SELF-LUBRICATING POLYMER COMPOSITES AND POLYMER TRANSFER FILM LUBRICATION FOR SPACE APPLICATIONS

ROBERT L. FUSARO Feb. 1990 49 p (NASA-TM-102492; E-5284; NAS 1.15:102492) Avail: NTIS HC A03/MF A01 CSCL 11/3

The use of self-lubricating polymers and polymer composites in space is somewhat limited today. In general, they are only used when other methods are inadequate. There is potential, however, for these materials to make a significant impact on future space missions if properly utilized. Some of the different polymers and fillers used to make self-lubricating composites are surveyed. The mechanisms of composite lubrication and wear, the theory behind transfer film lubricating mechanisms, and some factors which affect polymer composite wear and transfer are examined.

In addition, some of the current space tribology application areas for self-lubricating polymer composites and polymer transfer are mentioned. Author

N90-23543* National Aeronautics and Space Administration. Lewis Research Center, Cleveland, OH.

CONTROLLED CRACK GROWTH SPECIMEN FOR BRITTLE SYSTEMS

ANTHONY M. CALOMINO and DAVID N. BREWER (Army Aviation Systems Command, Cleveland, OH.) May 1990 10 p (Contract DA PROJ. 1L1-61102-AH-45) (NASA-TM-103126; E-5454; NAS 1.15:103126; AVSCOM-TR-90-C-009; AD-A227150) Avail: NTIS HC A02/MF A01 CSCL 11/6

A pure Mode I fracture specimen and test procedure has been developed which provides extended, stable, through-thickness crack growth in ceramics and other brittle, nonmetallic materials. Fixed displacement loading, applied at the crack mouth, promotes stable crack extension by reducing the stored elastic strain energy. Extremely fine control of applied displacements is achieved by utilizing the Poisson's expansion of a compressively loaded cylindrical pin. Stable cracks were successfully grown in soda-lime glass and monolithic Al₂O₃ for lengths in excess of 20 mm without uncontrollable catastrophic failure. Author

N90-26132* National Aeronautics and Space Administration. Lewis Research Center, Cleveland, OH.

DETERMINATION OF THE STRESS DISTRIBUTIONS IN A CERAMIC: TENSILE SPECIMEN USING NUMERICAL TECHNIQUES

M. G. JENKINS, M. K. FERBER, V. J. TENNERY (Oak Ridge National Lab., TN.), and J. A. SALEM 1990 8 p Presented at the ASME International Conference on Computers in Engineering, Boston, MA, 5-9 Aug. 1990 (Contract DE-AC05-84OR-21400) (NASA-TM-101914; NAS 1.15:101914; DE90-010499; CONF-900837-2) Avail: NTIS HC A02/MF A01 CSCL 11/3

Finite element analyses (FEA) were used to determine the stress distributions in a ceramic, tensile specimen with two types of button-head gripping systems. The FEA revealed stress raisers at both the button-head and the transition from the gage section to the shank. However, the stress field within the bulk of the gage section is uniform and uniaxial. The stress ratio, $k(\text{sub } t)$, between the button-head and gage section stresses varied from 0.35 to 0.72 for the tapered collet or the straight collet systems, respectively. Previous empirical tests confirm these results whereby, the tapered collet system, compared to the straight collet system, sustained over twice the average load before failure at the button-head. DOE

N90-26142* Cleveland State Univ., OH. Dept. of Civil Engineering.

EXTENSION OF A NONINTERACTIVE RELIABILITY MODEL FOR CERAMIC MATRIX COMPOSITES Final Report

STEPHEN F. DUFFY, ROBERT C. WETHERHOLD, and LALIT K. JAIN (State Univ. of New York, Buffalo.) Aug. 1990 10 p (Contract NCC3-89; NAG3-862) (NASA-CR-185267; E-5621; NAS 1.26:185267) Avail: NTIS HC A02/MF A01 CSCL 11/3

Developments in the processing of high temperature ceramic composites demand innovative and progressive design protocols that adequately predict the thermal and mechanical behavior of these materials. The focus here is the extension of a reliability model for orthotropic ceramic composites. The approach chosen to describe failures leads to a noninteractive formulation of reliability that is phenomenological. This particular criterion, which was constructed using tensorial invariant theory, allows six potential failure modes to emerge. Author

N90-28651* National Aeronautics and Space Administration. Lewis Research Center, Cleveland, OH.

DURABILITY OF THERMAL BARRIER COATINGS IN A HIGH HEAT FLUX ENVIRONMENT

WILLIAM J. BRINDLEY and JAMES A. NESBITT In NASA, Marshall Space Flight Center, Advanced Earth-to-Orbit Propulsion Technology 1988, Volume 1 p 661-674 Sep. 1988 Avail: NTIS HC A99/MF E06 CSCL 11/3

Thermal shock is a significant factor in the limited service life of Space Shuttle Main Engine (SSME) high pressure, fuel turbopump (HPFTP) turbine blades. Addition of advanced thermal barrier coatings (TBCs) to the blades could serve to dampen the thermal shock, thereby increasing the life of the blades. However, testing and use of TBCs to date is performed primarily under moderate heat flux conditions which are typical of aircraft turbines. Only limited testing was conducted that addresses high heat flux and severe thermal shock conditions. Therefore, it is not clear if TBCs can survive severe thermal shocks or provide adequate thermal shock protection to the HPFTP turbine blades. The purpose is to experimentally evaluate the potential durability and protective capability of a variety of advanced TBCs in a cyclic thermal shock environment. A secondary goal is to identify significant parameters affecting TBC life during high heat flux testing. Parameters investigated include top coat thickness, bond coat thickness, substrate type, and substrate geometry. Author

N90-28652* National Aeronautics and Space Administration. Lewis Research Center, Cleveland, OH.

THERMAL ANALYSIS OF THERMAL BARRIER COATINGS IN A HIGH HEAT FLUX ENVIRONMENT

JAMES A. NESBITT and WILLIAM J. BRINDLEY In NASA, Marshall Space Flight Center, Advanced Earth-to-Orbit Propulsion Technology 1988, Volume 1 p 675-691 Sep. 1988 Avail: NTIS HC A99/MF E06 CSCL 11/3

Gas temperatures and pressures were measured around the second test position in the H₂/O₂ rocket engine at NASA-Lewis. Measured gas temperatures generally varied from 1210 to 1390 C. Measured pressures were in good agreement with other studies for throat tubes in a square chamber rocket engine. Heat transfer coefficients were measured at 90 and 180 degrees from the stagnation point and resulted in values of 27.5 and 8.5 kW/sq m C, respectively. A thermal model was developed to predict temperatures in bare and coated tubes and rods. Agreement between measured and predicted temperatures below the surface of a bare Mar-M 246 tube was very good for most of the heat up and cool down period. Predicted temperatures were significantly below measured temperatures for the coated tubes. A thermal model to simulate heat transfer to the leading edge of an HPFTP blade was developed and showed that TBCs can significantly dampen the thermal transient which occurs in the HPFTP during the startup of the SSME. Author

N90-28735* Ford Motor Co., Dearborn, MI.

IMPROVED SILICON CARBIDE FOR ADVANCED HEAT ENGINES Annual Report No. 3

THOMAS J. WHALEN Aug. 1988 69 p (Contract NAS3-24384) (NASA-CR-182186; NAS 1.26:182186) Avail: NTIS HC A04/MF A01 CSCL 11/3

This is the third annual technical report for the program entitled, Improved Silicon Carbide for Advanced Heat Engines, for the period February 16, 1987 to February 15, 1988. The objective of the original program was the development of high strength, high reliability silicon carbide parts with complex shapes suitable for use in advanced heat engines. Injection molding is the forming method selected for the program because it is capable of forming complex parts adaptable for mass production on an economically sound basis. The goals of the revised program are to reach a Weibull characteristic strength of 550 MPa (80 ksi) and a Weibull modulus of 16 for bars tested in 4-point loading. Two tasks are discussed: Task 1 which involves materials and process improvements, and Task 2 which is a MOR bar matrix to improve strength and reliability. Many statistically designed experiments were completed under task 1 which improved the composition of the batches, the mixing of the powders, the sinter and anneal cycles. The best results were obtained by an attritor mixing process which yielded strengths in excess of 550 MPa (80 ksi) and an

27 NONMETALLIC MATERIALS

individual Weibull modulus of 16.8 for a 9-sample group. Strengths measured at 1200 and 1400 C were equal to the room temperature strength. Annealing of machined test bars significantly improved the strength. Molding yields were measured and flaw distributions were observed to follow a Poisson process. The second iteration of the Task 2 matrix experiment is described. Author

N90-28740* # National Aeronautics and Space Administration. Lewis Research Center, Cleveland, OH.

HIGH-TEMPERATURE DEFORMATION AND MICROSTRUCTURAL ANALYSIS FOR Si3N4-SC2O3

DEOCK-SOO CHEONG and WILLIAM A. SANDERS Apr. 1990 25 p Presented at the 92nd Annual Meeting of the American Ceramic Society, Dallas, TX, 23-27 Apr. 1990 (NASA-TM-103239; E-5593; NAS 1.15:103239) Avail: NTIS HC A03/MF A01 CSCL 11/3

It was indicated that Si3N4 doped with Sc2O3 may exhibit high temperature mechanical properties superior to Si3N4 systems with various other oxide sintered additives. High temperature deformation of samples was studied by characterizing the microstructures before and after deformation. It was found that elements of the additive, such as Sc and O, exist in small amounts at very thin grain boundary layers and most of them stay in secondary phases at triple and multiple grain boundary junctions. These secondary phases are devitrified as crystalline Sc2Si2O7. Deformation of the samples was dominated by cavitation processes rather than movements of dislocations. Thus the excellent deformation resistance of the samples at high temperature can be attributed to the very small thickness of the grain boundary layers and the crystalline secondary phase. Author

28

PROPELLANTS AND FUELS

Includes rocket propellants, igniters, and oxidizers; their storage and handling procedures; and aircraft fuels.

A90-47204* # National Aeronautics and Space Administration. Lewis Research Center, Cleveland, OH.

HIGH ENERGY-DENSITY LIQUID ROCKET FUEL PERFORMANCE

DOUGLAS C. RAPP (NASA, Lewis Research Center; Sverdrup Technology, Inc., Cleveland, OH) AIAA, SAE, ASME, and ASEE, Joint Propulsion Conference, 26th, Orlando, FL, July 16-18, 1990. 13 p. refs

(Contract NAS3-25266)

(AIAA PAPER 90-1968)

A fuel performance database of liquid hydrocarbons and aluminum-hydrocarbon fuels was compiled using engine parameters from the Space Transportation Engine Program as a baseline. Propellant performance parameters are introduced. General hydrocarbon fuel performance trends are discussed with respect to hydrogen-to-carbon ratio and heat of formation. Aluminum-hydrocarbon fuel performance is discussed with respect to aluminum metal loading. Hydrocarbon and aluminum-hydrocarbon fuel performance is presented with respect to fuel density, specific impulse and propellant density specific impulse. Author

A90-47214* # National Aeronautics and Space Administration. Lewis Research Center, Cleveland, OH.

A COMPARISON OF ANALYTICAL RESULTS FOR 20 K LOX/HYDROGEN INSTABILITIES

MARK D. KLEM and KEVIN J. BREISACHER (NASA, Lewis Research Center, Cleveland, OH) AIAA, SAE, ASME, and ASEE, Joint Propulsion Conference, 26th, Orlando, FL, July 16-18, 1990. 16 p. Previously announced in STAR as N90-25186. refs

(AIAA PAPER 90-2241) Copyright

Test data from NASA Lewis' Effect of Thrust Per Element on

Combustion Stability Characteristics of Hydrogen-Oxygen Rocket Engines test program are used to validate two recently released stability analysis tools. The first tool is a design methodology called ROCCID (ROCKET Combustor Interactive Design). ROCCID is an interactive design and analysis methodology that uses existing performance and combustion stability analysis codes. The second tool is HICCIP (High frequency Injection Coupled Combustion Instability Program). HICCIP is a recently developed combustion stability analysis model. Using a matrix of models, results from analytic comparisons with 20 K LOX/H2 experimental data are presented. Author

A90-50642* # National Aeronautics and Space Administration. Lewis Research Center, Cleveland, OH.

MARS IN SITU PROPELLANTS - CARBON MONOXIDE AND OXYGEN IGNITION EXPERIMENTS

DIANE L. LINNE, MARY F. GROTH (NASA, Lewis Research Center, Cleveland, OH), and JAMES RONCACE (Sverdrup Technology, Inc., Brook Park, OH) AIAA, SAE, ASME, and ASEE, Joint Propulsion Conference, 26th, July 16-18, 1990. 12 p. Previously announced in STAR as N90-26065. refs

(AIAA PAPER 90-1894) Copyright

Carbon monoxide and oxygen were tested in a standard spark-torch igniter to identify the ignition characteristics of this potential Mars in situ propellant combination. The ignition profiles were determined as functions of mixture ratio, amount of hydrogen added to the carbon monoxide, and oxygen inlet temperature. The experiments indicated that the carbon monoxide and oxygen combination must have small amounts of hydrogen present to initiate reaction. Once the reaction was started, the combustion continued without the presence of hydrogen. A mixture ratio range was identified where ignition occurred, and this range varied with the oxygen inlet temperature. Author

N90-13675* # National Aeronautics and Space Administration. Lewis Research Center, Cleveland, OH.

BUOYANCY EFFECTS ON THE VAPOR CONDENSATION RATE ON A HORIZONTAL LIQUID SURFACE

MOHAMMAD M. HASAN and CHIN-SHUN LIN (Analex Corp., Cleveland, OH.) 1989 14 p Presented at the 28th Aerospace Sciences Meeting, Reno, NV, 8-11 Jan. 1990; sponsored by AIAA (NASA-TM-102437; E-5206; NAS 1.15:102437; AIAA-90-0353) Avail: NTIS HC A03/MF A01 CSCL 21/9

The results are presented of a numerical study of the effects of buoyancy on the direct condensation of saturated or nearly saturated vapor on a horizontal liquid surface in a cylindrical tank. The liquid motion beneath the liquid-vapor interface is induced by an axisymmetric laminar jet of subcooled liquid. Analysis and numerical results show that the dominant parameter which determines the influence of buoyancy on the condensation rate is the Richardson number. However, the effect of buoyancy on the condensation rate cannot be quantified in terms of the Richardson number alone. The critical value of the Richardson number below which the condensation rate is not significantly reduced depends on the Reynolds number as well as the Prandtl number. Author

N90-17890* # National Aeronautics and Space Administration. Lewis Research Center, Cleveland, OH.

FLUSH: A TOOL FOR THE DESIGN OF SLUSH HYDROGEN FLOW SYSTEMS

TERRY L. HARDY Feb. 1990 71 p (NASA-TM-102467; E-5255; NAS 1.15:102467) Avail: NTIS HC A04/MF A01 CSCL 21/9

As part of the National Aerospace Plane Project an analytical model was developed to perform calculations for in-line transfer of solid-liquid mixtures of hydrogen. This code, called FLUSH, calculates pressure drop and solid fraction loss for the flow of slush hydrogen through pipe systems. The model solves the steady-state, one-dimensional equation of energy to obtain slush loss estimates. A description of the code is provided as well as a guide for users of the program. Preliminary results are also presented showing the anticipated degradation of slush hydrogen solid content for various piping systems. Author

N90-19386*# Battelle Columbus Labs., OH. Metals and Ceramics Information Center.

THE MEASUREMENT, MODELING, AND PREDICTION OF TRACTION FOR ROCKET PROPELLANT 1 Final Report

J. L. TEVAARWERK Oct. 1989 72 p
(Contract NASA ORDER C-30012-M; DLA900-83-C-1744)
(NASA-CR-185186; NAS 1.26:185186; G8558-8701) Avail: NTIS HC A04/MF A01 CSCL 21/9

Traction tests were performed on RP-1, a common kerosene based rocket propellant. Traction data on this fluid are required for purposes of turbopump bearing design, using codes such as SHABERTH. To obtain the traction data, an existing twin disc machine was used, operating under the side slip mode and using elliptical contacts. The range of test variables were: contact peak Hertz stress from 1.0 to 2.0 GPa, disc surface speed from 10 to 50 m/s, fluid inlet temperature from 30 to 70 C, and with a contact aspect ratio of 1.7. The resulting traction curves were reduced to fundamental fluid property parameters using the Johnson and Tevaarwerk traction model. Theoretical traction predictions were performed by back substitution of the fundamental properties into the traction model. Comparison of the predicted with the measured curves gives a high degree of confidence in the correctness of the traction model. For purposes of input to the NASA SHABERTH program, the traction model was next used to predict the expected traction of RP-1 under line contact conditions. Author

N90-21869*# National Aeronautics and Space Administration. Lewis Research Center, Cleveland, OH.

HIGH SPEED COMMERCIAL TRANSPORT FUELS CONSIDERATIONS AND RESEARCH NEEDS

C. M. LEE and R. W. NIEDZWIECKI 1989 10 p Presented at the Symposium on the Structure of Future Jet Fuels 2, Miami Beach, FL, 10-15 Sep. 1989; sponsored by American Chemical Society
(NASA-TM-102535; E-5345; NAS 1.15:102535) Avail: NTIS HC A02/MF A01 CSCL 21/4

NASA is currently evaluating the potential of incorporating High Speed Civil Transport (HSCT) aircraft in the commercial fleet in the beginning of the 21st century. NASA sponsored HSCT enabling studies currently underway with airframers and engine manufacturers, are addressing a broad range of technical, environmental, economic, and related issues. Supersonic cruise speeds for these aircraft were originally focused in the Mach 2 to 5 range. At these flight speeds, both jet fuels and liquid methane were considered potential fuel candidates. For the year 2000 to 2010, cruise Mach numbers of 2 to 3+ are projected for aircraft fuel with thermally stable liquid jet fuels. For 2015 and beyond, liquid methane fueled aircraft cruising at Mach numbers of 4+ may be viable candidates. Operation at supersonic speeds will be much more severe than those encountered at subsonic flight. One of the most critical problems is the potential deterioration of the fuel due to the high temperature environment. HSCT fuels will not only be required to provide the energy necessary for flight, but will also be subject to aerodynamic heating and, will be required to serve as the primary heat sink for cooling the engine and airframe. To define fuel problems for high speed flight, a fuels workshop was conducted at NASA Lewis Research Center. The purpose of the workshop was to gather experts on aviation fuels, airframe fuel systems, airport infrastructure, and combustion systems to discuss high speed fuel alternatives, fuel supply scenarios, increased thermal stability approaches and measurements, safety considerations, and to provide directional guidance for future R and D efforts. Subsequent follow-up studies defined airport infrastructure impacts of high speed fuel candidates. The results of these activities are summarized. In addition, an initial case study using modified in-house refinery simulation model Gordian code (1) is briefly discussed. This code can be used to simulate different types of refineries, emphasizing jet fuel production and relative cost factors. Author

N90-23574*# Rockwell International Corp., Canoga Park, CA. Rocketdyne Div.

HEALTH MANAGEMENT SYSTEM FOR ROCKET ENGINES

Final Report

EDWARD NEMETH Jun. 1990 247 p
(Contract NAS3-25625)
(NASA-CR-185223; NAS 1.26:185223) Avail: NTIS HC A11/MF A02 CSCL 21/9

The functional framework of a failure detection algorithm for the Space Shuttle Main Engine (SSME) is developed. The basic algorithm is based only on existing SSME measurements. Supplemental measurements, expected to enhance failure detection effectiveness, are identified. To support the algorithm development, a figure of merit is defined to estimate the likelihood of SSME criticality 1 failure modes and the failure modes are ranked in order of likelihood of occurrence. Nine classes of failure detection strategies are evaluated and promising features are extracted as the basis for the failure detection algorithm. The failure detection algorithm provides early warning capabilities for a wide variety of SSME failure modes. Preliminary algorithm evaluation, using data from three SSME failures representing three different failure types, demonstrated indications of imminent catastrophic failure well in advance of redline cutoff in all three cases. Author

N90-26160*# National Aeronautics and Space Administration. Lewis Research Center, Cleveland, OH.

PREDICTION OF THE ULLAGE GAS THERMAL STRATIFICATION IN A NASP VEHICLE PROPELLANT TANK EXPERIMENTAL SIMULATION USING FLOW-3D

TERRY L. HARDY and THOMAS M. TOMSIK Jul. 1990 27 p
(NASA-TM-103217; E-5629; NAS 1.15:103217) Avail: NTIS HC A03/MF A01 CSCL 07/4

As part of the National Aero-Space Plane (NASP) project, the multi-dimensional effects of gravitational force, initial tank pressure, initial ullage temperature, and heat transfer rate on the 2-D temperature profiles were studied. FLOW-3D, a commercial finite difference fluid flow model, was used for the evaluation. These effects were examined on the basis of previous liquid hydrogen experimental data with gaseous hydrogen pressurant. FLOW-3D results were compared against an existing 1-D model. In addition, the effects of mesh size and convergence criteria on the analytical results were investigated. Suggestions for future modifications and uses of FLOW-3D for modeling of a NASP tank are also presented. Author

N90-28742*# Sverdrup Technology, Inc., Brook Park, OH.

HIGH ENERGY-DENSITY LIQUID ROCKET FUEL

PERFORMANCE Final Report

DOUGLAS C. RAPP Jul. 1990 14 p Presented at the 26th Joint Propulsion Conference, Orlando, FL, 16-18 Jul. 1990; cosponsored by AIAA, SAE, ASME, and ASEE
(Contract NAS3-25266)
(NASA-CR-185279; E-5667; NAS 1.26:185279; AIAA-90-1968)
Avail: NTIS HC A03/MF A01 CSCL 21/9

A fuel performance database of liquid hydrocarbons and aluminum-hydrocarbon fuels was compiled using engine parametrics from the Space Transportation Engine Program as a baseline. Propellant performance parameters are introduced. General hydrocarbon fuel performance trends are discussed with respect to hydrogen-to-carbon ratio and heat of formation. Aluminum-hydrocarbon fuel performance is discussed with respect to aluminum metal loading. Hydrocarbon and aluminum-hydrocarbon fuel performance is presented with respect to fuel density, specific impulse, and propellant density specific impulse. Author

MATERIALS PROCESSING

Includes space-based development of products and processes for commercial applications.

A90-17825*# National Aeronautics and Space Administration. Lewis Research Center, Cleveland, OH.

EFFECTS OF CRUCIBLE WETTING DURING SOLIDIFICATION OF IMMISCIBLE PB-ZN ALLOYS

HENRY C. DE GROH, III and HUBERT B. PROBST (NASA, Lewis Research Center, Cleveland, OH) *Journal of Spacecraft and Rockets* (ISSN 0022-4650), vol. 26, Dec. 1989, p. 476-479. Previously cited in issue 09, p. 1327, Accession no. A89-25261. refs

Copyright

A90-18292* Arizona Univ., Tucson.

FINITE ELEMENT SIMULATIONS OF THERMOSOLUTAL CONVECTION IN VERTICAL SOLIDIFICATION OF BINARY ALLOYS

J. C. HEINRICH and S. FELICELLI (Arizona, University, Tucson) IN: *Finite element analysis in fluids; Proceedings of the Seventh International Conference on Finite Element Methods in Flow Problems*, Huntsville, AL, Apr. 3-7, 1989. Huntsville, AL, University of Alabama in Huntsville Press, 1989, p. 596-603. refs (Contract NAG3-723)

Copyright

Dendritic vertical solidification of a binary alloy is modeled using the finite element method to assess the effect of thermosolutal convection in macrosegregation. The mathematical model assumes steady-state solidification with a planar, undeformable surface defined by the dendrite tips and the eutectic isotherm. The dendritic region is assumed to advance at a constant solidification velocity v . The stability of the modeled system has been investigated and nonlinear calculations performed that show finger-like convection when the system is unstable. Results for lead-tin alloys show that when the system is unstable, convection is only significant in the uppermost part of the mush and is entirely driven by convection in the bulk fluid.

Author

A90-19999*# National Aeronautics and Space Administration. Lewis Research Center, Cleveland, OH.

NONINTRUSIVE INERTIAL VIBRATION ISOLATION TECHNOLOGY FOR MICROGRAVITY SPACE EXPERIMENTS

CARLOS M. GRODSINSKY and GERALD V. BROWN (NASA, Lewis Research Center, Cleveland, OH) *AIAA, Aerospace Sciences Meeting*, 28th, Reno, NV, Jan. 8-11, 1990. 9 p. Previously announced in STAR as N90-11901. refs (AIAA PAPER 90-0741) Copyright

The dynamic acceleration environment observed on Space Shuttle flights to date and predicted for the Space Station has complicated the analysis of prior microgravity experiments and prompted concern for the viability of proposed space experiments requiring long-term, microgravity environments. Isolation systems capable of providing significant improvements to this environment exist, but at present have not been demonstrated in flight configurations. A summary of the theoretical evaluation for two one degree-of-freedom (DOF) active magnetic isolators and their predicted response to both direct and base excitations is presented. These isolators can be used independently or in concert to isolate acceleration-sensitive microgravity space experiments, dependent on the isolation capability required for specific experimenter needs.

Author

A90-20000*# GTE Labs., Inc., Waltham, MA.

FREE FLOAT ACCELERATION MEASUREMENTS ABOARD NASA'S KC-135 MICROGRAVITY RESEARCH AIRCRAFT

A. H. BELLOW, D. H. MATTHIESEN, and G. A. DUCHENE (GTE Laboratories, Inc., Waltham, MA) *AIAA, Aerospace Sciences Meeting*, 28th, Reno, NV, Jan. 8-11, 1990. 5 p. Research supported

by USAF. refs

(Contract NAS3-24644)

(AIAA PAPER 90-0742) Copyright

A three-axis accelerometer subsystem, developed as part of a get-away-special Ga-As crystal growth system for the Space Shuttle, is described. Each axis of this subsystem contains a quartz flexure accelerometer capable of dc measurements, custom-designed measurement circuitry, a programmable microcomputer for measurement control and data reduction, and memory for recording data. The subsystem was flown as a free float experiment aboard the NASA KC-135 microgravity research aircraft, yielding measurements of accelerations during free float at a resolution of 10 micro-g.

I.S.

A90-20525*# Westinghouse Research and Development Center, Pittsburgh, PA.

EVALUATION OF TRANSPORT CONDITIONS DURING PHYSICAL VAPOR TRANSPORT GROWTH OF OPTO-ELECTRONIC CRYSTALS

N. B. SINGH, R. MAZELSKY (Westinghouse Research and Development Center, Pittsburgh, PA), and M. E. GLICKSMAN (Rensselaer Polytechnic Institute, Troy, NY) *Journal of Thermophysics and Heat Transfer* (ISSN 0887-8722), vol. 4, Jan. 1990, p. 126-128. Previously cited in issue 09, p. 1326, Accession no. A89-25197. refs

(Contract NAS3-25274)

Copyright

A90-22878* Colorado Univ., Boulder.

MODELING OF COLLISION AND COALESCENCE OF DROPLETS DURING MICROGRAVITY PROCESSING OF ZN-BI IMMISCIBLE ALLOYS

R. H. DAVIS (Colorado, University, Boulder) and J. R. ROGERS *Metallurgical Transactions A - Physical Metallurgy and Materials Science* (ISSN 0360-2133), vol. 21A, Jan. 1990, p. 59-68. refs (Contract NAGW-951; NAG3-993; NGT-50367)

Copyright

A population balance model is presented for the coarsening of the dispersed phase of liquid-liquid two-phase mixtures in microgravity due to gravity sedimentation and Marangoni migration, which lead to the collision and coalescence of droplets. The model is used to predict the evolution of the size distribution of the dispersed phase in a liquid-phase miscibility gap system, Zn-Bi, which has been used in a number of experimental microgravity processing studies in which significant phase segregation has been observed. The analysis shows that increasing the temperature gradient, gravity level, volume fraction of the dispersed phase, initial average drop radius, initial standard deviation of droplet radii, or the temperature coefficient of the interfacial tension leads to an increase in the rate of droplet growth due to collision and coalescence. Comparison of the distribution evolutions for unimodal and bimodal initial distributions shows that the latter yield significantly more rapid droplet growth. Finally, it is shown that droplet growth can be dramatically reduced with antiparallel orientation of the gravity vector and the temperature gradient, provided that the relative magnitude of these two vectors is properly chosen.

Author

A90-23713*# National Aeronautics and Space Administration. Lewis Research Center, Cleveland, OH.

PRIMARY ARM SPACING IN DIRECTIONALLY SOLIDIFIED PB-10 WT PCT SN ALLOYS

M. A. CHOPRA (NASA, Lewis Research Center; Cleveland State University, OH) and S. N. TEWARI (Cleveland State University, OH) *AIAA, Aerospace Sciences Meeting*, 28th, Reno, NV, Jan. 8-11, 1990. 18 p. Previously announced in STAR as N90-14398. refs

(Contract NCC3-95)

(AIAA PAPER 90-0740) Copyright

The dependence of primary arm spacings on growth speed was investigated for cellular and dendritic arrays in Pb-10 wt percent Sn samples directionally solidified under a constant positive thermal gradient in the melt. The gradient of constitutional supercooling

was varied from almost zero (near the break-down of the planar liquid-solid interface at small growth speeds, cellular morphology) to near unity (large growth speeds, dendritic morphology). The spatial arrangements of cells and dendrites, as given by their coordination number, are not very different from each other. It appears that primary arm spacing maxima and the cell to dendrite transition are strongly influenced by the magnitude of the solute partition coefficient. The planar to cellular bifurcation is supercritical in Pb-Sn which has a high partition coefficient, as compared to the subcritical behavior reported in Al-Cu and succinonitrile-acetone, both of which have low partition coefficients. The primary arm spacing model due to Hunt agrees with the experimentally observed trend for the whole growth regime. There is a good quantitative agreement at higher gradients of supercooling. However, the model overpredicts the primary arm spacings at low gradients of constitutional supercooling. Author

A90-25031*# National Aeronautics and Space Administration. Lewis Research Center, Cleveland, OH.

COUPLED EFFECTS OF CONDUCTION IN THE CRYSTAL AND THERMO-SOLUTAL CONVECTION IN A RECTANGULAR INCLINED ENCLOSURE

CHRISTOPHE MENNETRIER and WALTER M. B. DUVAL (NASA, Lewis Research Center, Cleveland, OH) AIAA, Aerospace Sciences Meeting, 28th, Reno, NV, Jan. 8-11, 1990. 9 p. Research sponsored by the Universities Space Research Association. refs (AIAA PAPER 90-0408) Copyright

To date modeling of crystal growth of optoelectronic materials using Physical Vapor Transport has been limited to the study of the fluid phase. To achieve it, the equations of coupled heat, mass and momentum transfer in the gas have to be solved. The first objective of this study is to examine the effect of heat conduction in the crystal on the fluid flow in the neighborhood of the interface. Heat transfer boundary conditions on both interfaces were modified to take into account the additional heat flux between gas and solid. It is proved that heat conduction does not affect the fluid flow. In the presence of gravity, density gradients in the fluid phase generate convection responsible for the problem of a nonplanar growth of the interface. The second objective is to study systematically under one-g the different possible flows in order to solve this problem. Depending on the parameters, a diffusive mode and three convective modes (thermal, solutal and thermo-solutal) are observed. The competition between thermal and solutal convections leads to a mathematical condition which can be used to achieve a planar growth. It is proven that, under the physical conditions chosen, this mathematical condition cannot be thermodynamically satisfied. Author

A90-25032*# National Aeronautics and Space Administration. Lewis Research Center, Cleveland, OH.

CONVECTION PHENOMENA IN LOW-GRAVITY PROCESSING - THE GTE GAAS SPACE EXPERIMENT

W. A. ARNOLD, D. A. JACOMIN, R. L. GAUG, and A. CHAIT (NASA, Lewis Research Center, Cleveland, OH) AIAA, Aerospace Sciences Meeting, 28th, Reno, NV, Jan. 8-11, 1990. 8 p. refs (AIAA PAPER 90-0409) Copyright

A numerical model for the proposed GTE GaAs space experiment is presented. The model includes the actual ampule design and the experimentally obtained furnace thermal profiles. Results are presented based on both the traditional steady-state models and on fully time dependent simulations. It is demonstrated that the commonly presumed axisymmetric flows in numerical studies are physically accurate only when the local gravitational acceleration vector is parallel to the ampule's axis. Other gravitational orientations result in nontrivial three-dimensional flows which must be resolved using full three-dimensional models. Implications of the resulting flow and thermal fields on the growing crystal at conditions available during space processing are also discussed. Author

A90-48720* Arizona State Univ., Tempe.

ENERGY STABILITY OF THERMOCAPILLARY CONVECTION IN A MODEL OF THE FLOAT-ZONE CRYSTAL-GROWTH PROCESS

Y. SHEN, G. P. NEITZEL, D. F. JANKOWSKI, and H. D. MITTELMANN (Arizona State University, Tempe) Journal of Fluid Mechanics (ISSN 0022-1120), vol. 217, Aug. 1990, p. 639-660. refs

(Contract NAG3-568; NSF MSM-83-51490; AF-AFOSR-84-0315) Copyright

Energy stability theory has been applied to a basic state of thermocapillary convection occurring in a cylindrical half-zone of finite length to determine conditions under which the flow will be stable. Because of the finite length of the zone, the basic state must be determined numerically. Instead of obtaining stability criteria by solving the related Euler-Lagrange equations, the variational problem is attacked directly by discretization of the integrals in the energy identity using finite differences. Results of the analysis are values of the Marangoni number below which axisymmetric disturbances to the basic state will decay, for various values of the other parameters governing the problem. Author

A90-49060* National Aeronautics and Space Administration. Lewis Research Center, Cleveland, OH.

EFFECT OF GAS AND SURFACE RADIATION ON CRYSTAL GROWTH FROM THE VAPOR PHASE

MOHAMMAD KASSEMI and WALTER M. B. DUVAL (NASA, Lewis Research Center, Cleveland, OH) PQH/PhysicoChemical Hydrodynamics (ISSN 0191-9059), vol. 11, no. 5-6, 1989, p. 737-751. Research supported by the U.S. National Research Council. refs

Copyright

Growth of single crystals from vapor in closed ampoules is governed by an intricate interplay between the mass, momentum and heat transfer processes. The objective of this study is to examine and isolate the effects of radiative heat transfer on vapor transport in enclosed ampoules using a two-dimensional mathematical model. The formulation consists of a set of coupled nonlinear partial differential equations for conservation of mass, momentum, energy and species, and the integrodifferential equations which represent radiative exchange. Attention is focused on the vertical enclosure in the stable convective configuration. It is shown that for this case, even when relatively small temperature differences exist between the source and the crystal, because of the convection caused by radiative transfer, significant non-uniformity is introduced in the growth flux. The different and sometimes opposing roles of gas and surface radiation are discussed and the importance of the thermal boundary conditions imposed by the furnace is examined. Finally, it is shown that in this configuration, the low gravity environment provided by orbiting spacecraft can be effectively exploited to produce better crystals. Author

N90-11196*# National Aeronautics and Space Administration. Lewis Research Center, Cleveland, OH.

DROPLET COMBUSTION EXPERIMENT DROP TOWER TESTS USING MODELS OF THE SPACE FLIGHT APPARATUS

J. B. HAGGARD, M. H. BRACE, J. L. KROPP, and F. L. DRYER (Princeton Univ., NJ.) 1989 13 p Presented at the 27th Aerospace Sciences Meeting, Reno, NV, 9-12 Jan. 1989; sponsored by AIAA Previously announced in IAA A89-28418 (NASA-TM-101472; E-4586; NAS 1.15:101472; AIAA-89-0501) Avail: NTIS HC A03/MF A01 CSCI 22/1

The Droplet Combustion Experiment (DCE) is an experiment that is being developed to ultimately operate in the shuttle environment (middeck or Spacelab). The current experiment implementation is for use in the 2.2 or 5 sec drop towers at NASA Lewis Research Center. Initial results were reported in the 1986 symposium of this meeting. Since then significant progress was made in drop tower instrumentation. The 2.2 sec drop tower apparatus, a conceptual level model, was improved to give more reproducible performance as well as operate over a wider range of test conditions. Some very low velocity deployments of ignited

29 MATERIALS PROCESSING

droplets were observed. An engineering model was built at TRW. This model will be used in the 5 sec drop tower operation to obtain science data. In addition, it was built using the flight design except for changes to accommodate the drop tower requirements. The mechanical and electrical assemblies have the same level of complexity as they will have in flight. The model was tested for functional operation and then delivered to NASA Lewis. The model was then integrated into the 5 sec drop tower. The model is currently undergoing initial operational tests prior to starting the science tests. Author

N90-13679*# National Aeronautics and Space Administration. Lewis Research Center, Cleveland, OH.

FACILITIES FOR MICROGRAVITY COMBUSTION RESEARCH
KURT R. SACKSTEDER 1988 20 p Presented at the 39th Annual Astronautical Congress of the International Astronautical Federation, Bangalore, India, 8-15 Oct. 1988
(NASA-TM-102014; E-4726; NAS 1.15:102014; IAF-88-355)
Avail: NTIS HC A03/MF A01 CSCL 21/2

Combustion science and applications have benefited in unforeseen ways from experimental research performed in the low-gravity environment. The capability to control for the first time the influence of gravitational buoyancy has provided some insight into soot formation in droplet combustion, the nature of flammability limits in premixed gases, and the relationship between normal-gravity and low-gravity material flammability that may influence how materials are best selected for routine use in habitable spacecraft. The opportunity to learn about these complex phenomena is derived from the control of the ambient body-force field and, perhaps as importantly, the simplified boundary conditions that can be established in well designed low-gravity combustion experiments. A description of the test facilities and typical experimental apparatus are provided; and conceptual plans for a Space Station Freedom capability, the Modular Combustion Facility, are described. Author

N90-13680*# National Aeronautics and Space Administration. Lewis Research Center, Cleveland, OH.

AN INVESTIGATION OF FLAME SPREAD OVER SHALLOW LIQUID POOLS IN MICROGRAVITY AND NONAIR ENVIRONMENTS

HOWARD D. ROSS and RAYMOND G. SOTOS 1989 19 p
Proposed for presentation at the 23rd International Symposium on Combustion, Orleans, France, 22-27 Jul. 1990; sponsored by Orleans Univ.
(NASA-TM-102425; E-5190; NAS 1.15:102425) Avail: NTIS HC A03/MF A01 CSCL 21/2

Experiments of interest to combustion fundamentals and spacecraft fire safety investigated flame spread of alcohol fuels over shallow, 15 cm diameter pools in a 5.2 sec free-fall, microgravity facility. Results showed that, independent of O₂ concentration, alcohol fuel, and diluent types, microgravity flame spread rates were nearly identical to those corresponding normal-gravity flames for conditions where the normal gravity flames spread uniformly. This similarity indicated buoyancy-related convection in either phase does not affect flame spread, at least for the physical scale of the experiments. However, microgravity extinction coincided with the onset conditions for pulsating spread in normal gravity, implicating gas phase, buoyant flow as a requirement for pulsating spread. When the atmospheric nitrogen was replaced with argon, the conditions for the onset of normal-gravity pulsating flame spread and microgravity flame extinction were changed, in agreement with the expected lowering of the flash point through the thermal properties of the diluent. Helium-diluted flames, however, showed unexpected results with a shift to apparently higher flash-point temperatures and high normal gravity pulsation amplitudes. Author

N90-14398*# Cleveland State Univ., OH. Dept. of Chemical Engineering.

PRIMARY ARM SPACING IN DIRECTIONALLY SOLIDIFIED PB-10 WT PERCENT SN ALLOYS Final Report

M. A. CHOPRA and S. N. TEWARI Jan. 1990 19 p Presented

at the 28th Aerospace Sciences Meeting, Reno, NV, 8-11 Jan. 1990; sponsored by AIAA
(Contract NCC3-95)
(NASA-CR-185190; E-5141; NAS 1.26:185190; AIAA-90-0740)
Avail: NTIS HC A03/MF A01 CSCL 11/6

The dependence of primary arm spacings on growth speed was investigated for cellular and dendritic arrays in Pb-10 wt percent Sn samples directionally solidified under a constant positive thermal gradient in the melt. The gradient of constitutional supercooling was varied from almost zero (near the break-down of the planar liquid-solid interface at small growth speeds, cellular morphology) to near unity (large growth speeds, dendritic morphology). The spatial arrangements of cells and dendrites, as given by their coordination number, are not very different from each other. It appears that primary arm spacing maxima and the cell to dendrite transition are strongly influenced by the magnitude of the solute partition coefficient. The planar to cellular bifurcation is supercritical in Pb-Sn which has a high partition coefficient, as compared to the subcritical behavior reported in Al-Cu and succinonitrile-acetone, both of which have low partition coefficients. The primary arm spacing model due to Hunt agrees with the experimentally observed trend for the whole growth regime. There is a good quantitative agreement at higher gradients of supercooling. However, the model overpredicts the primary arm spacings at low gradients of constitutional supercooling. Author

N90-16087*# National Aeronautics and Space Administration. Lewis Research Center, Cleveland, OH.

CONCEPTUAL DESIGN FOR THE SPACE STATION FREEDOM MODULAR COMBUSTION FACILITY

17 May 1989 63 p Presented at the MCF Assessment Workshop, Cleveland, OH, 17-18 May 1989; sponsored by NASA, Washington
(NASA-TM-102037; E-4786; NAS 1.15:102037) Avail: NTIS HC A04/MF A01 CSCL 22/1

A definition study and conceptual design for a combustion science facility that will be located in the Space Station Freedom's baseline U.S. Laboratory module is being performed. This modular, user-friendly facility, called the Modular Combustion Facility, will be available for use by industry, academic, and government research communities in the mid-1990's. The Facility will support research experiments dealing with the study of combustion and its byproducts. Because of the lack of gravity-induced convection, research into the mechanisms of combustion in the absence of gravity will help to provide a better understanding of the fundamentals of the combustion process. The background, current status, and future activities of the effort are covered. Author

N90-16966*# National Aeronautics and Space Administration. Lewis Research Center, Cleveland, OH.

A COMPARISON OF EUROPEAN AND AMERICAN MICROGRAVITY COMBUSTION EXPERIMENTAL TECHNIQUES

KURT SACKSTEDER In ESA, Combustion Experiments during KC-135 Parabolic Flight p 65-69 Aug. 1989 Original contains color illustrations
Copyright Avail: NTIS HC A04/MF A01; ESA Publications Div., ESTEC, Noordwijk, Netherlands, 30 Dutch guilders

The European and the NASA microgravity combustion programs are complementary in many aspects. Differences appear in the technical approaches and cooperative efforts are beneficial. Droplet combustion gaseous fuel studies and the study of solid-fuel combustion are areas of common interest. It is recognized that the progress that can be made in low gravity combustion investigations, depends on advanced diagnostic tools, developed for normal gravity laboratories. The benefits of combustion experiments in reduced gravity, the ground-based low gravity facilities and the NASA microgravity combustion program are also considered. ESA

N90-17897*# National Aeronautics and Space Administration. Lewis Research Center, Cleveland, OH.

MICROGRAVITY NONCONTACT TEMPERATURE REQUIREMENTS AT NASA LEWIS RESEARCH CENTER

G. SANTORO *In* JPL, Proceedings of the Second Noncontact Temperature Measurement Workshop p 19-32 1 Jun. 1989
 Avail: NTIS HC A16/MF A03 CSCL 22/1

NASA Lewis Research Center is currently supporting 66 microgravity science and applications projects. The 66 projects are separated into 23 flight projects and 43 ground-based projects. The part of the NASA Lewis program dealing with flight experiments is divided into six areas: Combustion Science, Materials Science, Fluid Physics, Instrumentation/Equipment, Advanced Technology Development, and Space Station Multi-User Facility studies. The part of the NASA Lewis program dealing with ground-based experiments is coincidentally also divided into six areas: Electronic Materials, Combustion Science, Fluid Dynamics and Transport Phenomena, Metals and Alloys, Glasses and Ceramics, and Physics and Chemistry Experiments. Several purposes exist for ground-based experimenting. Preliminary information is necessary before a decision can be made for flight status, the short low gravity durations available in ground facilities are adequate for a particular study, or extensive ground-based research must be conducted to define and support the microgravity science endeavors contemplated for space. Not all of the 66 microgravity science and application projects at NASA Lewis have temperature requirements, but most do. Since space allocation does not permit a review of all the pertinent projects, a decision was made to restrict the coverage to the science flight projects, flight projects minus the advanced technology development, and multiuser facility efforts. Very little is lost by this decision as the types of temperature requirements for science flight projects can be considered representative of those for the ground-based projects. The noncontact temperature needs at NASA Lewis, as represented by the science flight projects are discussed by describing briefly the experiments themselves, by displaying an illustration of each experimental setup, and by specifying their temperature requisites. Author

N90-17900* # National Aeronautics and Space Administration. Lewis Research Center, Cleveland, OH.

NON-CONTACT TEMPERATURE MEASUREMENTS IN SUPPORT OF MICROGRAVITY COMBUSTION EXPERIMENTS

PAUL S. GREENBERG *In* JPL, Proceedings of the Second Noncontact Temperature Measurement Workshop p 50-59 1 Jun. 1989

Avail: NTIS HC A16/MF A03 CSCL 22/1

Recent conceptual advances in the understanding of combustion science fundamentals in the context of microgravity processes and phenomenology have resulted in an increased demand for diagnostic systems of greater sophistication. Owing primarily to the severe operational constraints that accompany the space flight environment, measurement systems to date remain fairly primitive in nature. Qualitative pictures provided by photographic recording media comprise the majority of the existing data, the remainder consisting of the output of conventional transducers, such as thermocouples, hot wires, and pressure transducers. The absence of the rather strong influence of buoyant convection renders microgravity combustion phenomena more fragile than their 1-G counterparts. The emphasis was placed on nonperturbing optical diagnostics. Other factors such as limited supplies of expendable reactants, and periods of microgravity time of sufficient duration, coupled with more fundamental questions regarding inherent length and time scales and reproducibility have favored multipoint or multidimensional techniques. While the development of optical diagnostics for application to combustion science is an extremely active area at present, the peculiarities of space flight hardware severely restrict the feasibility of implementing the majority of techniques which are being utilized in terrestrial applications. The additional requirements for system reliability and operational simplicity have tended to promote somewhat less commonly emphasized techniques such as refractive index mapping and molecular Rayleigh scattering, which are briefly discussed. Author

N90-20237* # Case Western Reserve Univ., Cleveland, OH. Dept. of Material Science and Engineering.

INSTANTANEOUSLY GENERATED FOAM AND ITS APPLICABILITY TO REDUCED GRAVITY Final Report

ALI ILHAN, DONG-SANG KIM, and PAVEL HRMA Feb. 1990 58 p

(Contract NAG3-740)

(NASA-CR-185208; E-5282; NAS 1.26:185208) Avail: NTIS HC A04/MF A01 CSCL 22/1

The objective of this study is two-fold: (1) understanding the generation and collapse of foam in molten glass, and (2) determining the role of gravity in transient foam dynamics. Both theoretical considerations and experiments show that gravity affects evolution of transient foams. Provided that Marangoni forces are absent, the lack of bubble motion under microgravity will prevent formation of surface foam and, as a result, only bulk foam will be generated. Also, the absence of gravity drainage will affect the foam collapse rate and mode when a surface foam has been produced prior to its exposure to microgravity. The progress follows three steps: (1) selection of appropriate materials and development of experimental techniques; (2) experimental study of transient foams on earth and developing a theoretical model; and (3) experimental study of transient foams under microgravity during free fall in a drop tower. The main results are presented of the first phase of the research which involves most of the ground based work needed to accomplish the first two steps. The suggestions for the final stage is also included. Earth bound experiments have shown that it is possible to produce transient foams suitable for drop tower experiments and to record their behavior by a video or still camera in a simple experimental set-up. Transient cellular foams were produced and studied in soda lime glass with sulfate at 1400 to 1500 C. The study of foams in model systems under convenient ambient temperature conditions helped to gather a significant amount of information in a short time. The relationship between foam behavior and structure was analyzed and the relationship between foam structure and the system properties is currently under development. Author

N90-20253* # National Aeronautics and Space Administration. Lewis Research Center, Cleveland, OH.

DESIGN AND TEST OF A COMPACT OPTICS SYSTEM FOR THE POOL BOILING EXPERIMENT

JERRI S. LING and JAMES R. LAUBENTHAL Mar. 1990 17 p (NASA-TM-102530; E-5339; NAS 1.15:102530) Avail: NTIS HC A03/MF A01 CSCL 22/1

The experiment described seeks to improve the understanding of the fundamental mechanisms that constitute nucleate pool boiling. The vehicle for accomplishing this is an investigation, including tests to be conducted in microgravity and coupled with appropriate analyses, of the heat transfer and vapor bubble dynamics associated with nucleation, bubble growth/collapse and subsequent motion, considering the interrelations between buoyancy, momentum and surface tension which will govern the motion of the vapor and surrounding liquid, as a function of the heating rate at the heat transfer surface and the temperature level and distribution in the bulk liquid. The experiment is designed to be contained within the confines of a Get-Away-Special Canister (GAS Can) installed in the bay of the space shuttle. When the shuttle reaches orbit, the experiment will be turned on and testing will proceed automatically. In the proposed Pool Boiling Experiment a pool of liquid, initially at a precisely defined pressure and temperature, will be subjected to a step imposed heat flux from a semitransparent thin-film heater forming part of one wall of the container such that boiling is initiated and maintained for a defined period of time at a constant pressure level. Transient measurements of the heater surface and fluid temperatures near the surface will be made, noting especially the conditions at the onset of boiling, along with motion photography of the boiling process in two simultaneous views, from beneath the heating surface and from the side. The conduct of the experiment and the data acquisition will be completely automated and self-contained. For the initial flight, a total of nine tests are proposed, with three levels of heat flux and three levels of subcooling. The design process used in

29 MATERIALS PROCESSING

the development and check-out of the compact photographic/optics system for the Pool Boiling Experiment is documented.

Author

N90-21871*# National Aeronautics and Space Administration. Lewis Research Center, Cleveland, OH.

PROBABILISTIC ANALYSIS OF BLADED TURBINE DISKS AND THE EFFECT OF MISTUNING

A. R. SHAH, V. K. NAGPAL (Sverdrup Technology, Inc., Cleveland, OH.), and CHRISTOS C. CHAMIS 1990 11 p Presented at the 31st Structures, Structural Dynamics and Materials Conference, Long Beach, CA, 2-4 Apr. 1990; sponsored by AIAA, ASME, ASCE, AHS and ASC Previously announced in IAA as A90-29327 (NASA-TM-102564; E-5388; NAS 1.15:102564) Avail: NTIS HC A03/MF A01 CSCL 22/1

Probabilistic assessment of the maximum blade response on a mistuned rotor disk is performed using the computer code NESSUS. The uncertainties in natural frequency, excitation frequency, amplitude of excitation and damping are included to obtain the cumulative distribution function (CDF) of blade responses. Advanced mean value first order analysis is used to compute CDF. The sensitivities of different random variables are identified. Effect of the number of blades on a rotor on mistuning is evaluated. It is shown that the uncertainties associated with the forcing function parameters have significant effect on the response distribution of the bladed rotor.

Author

N90-25238*# Arizona Univ., Tucson. Coll. of Engineering and Mines.

THE ROLE OF GRAVITY ON MACROSEGREGATION IN ALLOYS Final Report, 30 Apr. 1986 - 29 Apr. 1989

D. R. POIRIER, C. F. CHEN, and J. C. HEINRICH 10 May 1990 65 p

(Contract NAG3-723)

(NASA-CR-186530; NAS 1.26:186530) Avail: NTIS HC A04/MF A01 CSCL 22/1

During dendritic solidification liquid flow is induced both by buoyancy forces and solidification shrinkage. There is strong evidence that the major reason for the liquid flow is the former, i.e., thermosolutal convection. In the microgravity environment, it is thought that the thermosolutal convection will be greatly diminished so that convection will be confined mainly to the flow of interdendritic liquid required to satisfy the solidification shrinkage. An attempt is made to provide improved models of dendritic solidification with emphasis on convection and macrosegregation. Macrosegregation is an extremely important subject to the commercial casting community. The simulation of thermosolutal convection in directionally solidified (DS) alloys is described. A linear stability analysis was used to predict marginal stability curves for a system that comprises a mushy zone underlying an all-liquid zone. The supercritical thermosolutal convection in directionally solidified dendritic alloys was also modeled. The model assumes a nonconvective initial state with planar and horizontal isotherms and isoconcentration that move upward at a constant solidification velocity. Results are presented for systems involving lead-tin alloys and show significant differences with results of plane-front solidification.

Author

N90-26163*# National Aeronautics and Space Administration. Lewis Research Center, Cleveland, OH.

NEW FINDINGS AND INSTRUMENTATION FROM THE NASA LEWIS MICROGRAVITY FACILITIES

HOWARD D. ROSS and PAUL S. GREENBERG May 1990 8 p Presented at the 2nd Workshop on Microgravity Experimentation, Ottawa, Ontario, 8-9 May 1990

(NASA-TM-103189; E-5575; NAS 1.15:103189) Avail: NTIS HC A02/MF A01 CSCL 22/1

The study of fundamental combustion and fluid physics in a microgravity environment is a relatively new scientific endeavor. The microgravity environment enables a new range of experiments to be performed since: buoyancy-induced flows are nearly eliminated; normally obscured forces and flows may be isolated; gravitational settling or sedimentation is nearly eliminated; and

larger time or length scales in experiments become permissible. Unexpected phenomena have been observed, with surprising frequency, in microgravity experiments, raising questions about the degree of accuracy and completeness of the classical understanding. An overview is provided of some new phenomena found through ground-based, microgravity research, the instrumentation used in this research, and plans for new instrumentation.

Author

31

ENGINEERING (GENERAL)

Includes vacuum technology; control engineering; display engineering; cryogenics; and fire prevention.

A90-46246* National Aeronautics and Space Administration. Lewis Research Center, Cleveland, OH.

LOW FREQUENCY VIBRATION ISOLATION TECHNOLOGY FOR MICROGRAVITY SPACE EXPERIMENTS

C. M. GRODSINSKY and G. V. BROWN (NASA, Lewis Research Center, Cleveland, OH) IN: Machinery dynamics - Applications and vibration control problems; Proceedings of the Twelfth Biennial ASME Conference on Mechanical Vibration and Noise, Montreal, Canada, Sept. 17-21, 1989. New York, American Society of Mechanical Engineers, 1989, p. 295-302. Previously announced in STAR as N89-20324. refs

Copyright

The dynamic acceleration environment observed on Space Shuttle flights to date and predicted for the Space Station has complicated the analysis of prior microgravity experiments and prompted concern for the viability of proposed space experiments requiring long-term, low-g environments. Isolation systems capable of providing significant improvements in this environment exist, but have not been demonstrated in flight configurations. This paper presents a summary of the theoretical evaluation for two one degree-of-freedom (DOF) active magnetic isolators and their predicted response to both direct and base excitations, that can be used to isolate acceleration sensitive microgravity space experiments.

Author

A90-50641*# National Aeronautics and Space Administration. Lewis Research Center, Cleveland, OH.

INITIAL EXPERIMENTATION ON THE NONVENTED FILL OF A 0.14 CU M (5 CU FT) DEWAR WITH NITROGEN AND HYDROGEN

DAVID J. CHATO, MATTHEW E. MORAN, and TED W. NYLAND (NASA, Lewis Research Center, Cleveland, OH) AIAA and ASME, Joint Thermophysics and Heat Transfer Conference, 5th, Seattle, WA, June 18-20, 1990. 19 p. Previously announced in STAR as N90-26278.

(AIAA PAPER 90-1681) Copyright

A series of nonvented fills were performed on a 0.14 cu m (5 cu ft) stainless steel dewar. Fills were conducted with a 120 deg cone angle spray nozzle over a range of inflow and initial wall temperatures with both liquid nitrogen and liquid hydrogen. Fill levels in excess of 85 percent liquid were achieved for four out of four nitrogen and two out of five hydrogen tests. Previously developed analytical models were compared to the test results and shown to have general trend agreement.

Author

N90-10309*# National Aeronautics and Space Administration. Lewis Research Center, Cleveland, OH.

TOTAL HEMISPHERICAL EMITTANCE MEASURED AT HIGH TEMPERATURES BY THE CALORIMETRIC METHOD

FRANK DIFILIPPO, MICHAEL J. MIRTICH, BRUCE A. BANKS, CURTIS STIDHAM, and MICHAEL KUSSMAUL (Cleveland State Univ., OH.) 1989 19 p Presented at the 16th International Conference on Metallurgical Coatings, San Diego, CA, 17-21 Apr.

1989; sponsored by the American Vacuum Society (NASA-TM-102322; E-4704; NAS 1.15:102322) Avail: NTIS HC A03/MF A01 CSCL 13B

A calorimetric vacuum emissometer (CVE) capable of measuring total hemispherical emittance of surfaces at elevated temperatures was designed, built, and tested. Several materials with a wide range of emittances were measured in the CVE between 773 to 923 K. These results were compared to values calculated from spectral emittance curves measured in a room temperature Hohlraum reflectometer and in an open-air elevated temperature emissometer. The results differed by as much as 0.2 for some materials but were in closer agreement for the more highly-emitting, diffuse-reflecting samples. The differences were attributed to temperature, atmospheric, and directional effects, and errors in the Hohlraum and emissometer measurements (plus or minus 5 percent). The probable error of the CVE measurements was typically less than 1 percent. Author

N90-11901*# National Aeronautics and Space Administration. Lewis Research Center, Cleveland, OH.

NONINTRUSIVE INERTIAL VIBRATION ISOLATION TECHNOLOGY FOR MICROGRAVITY SPACE EXPERIMENTS

CARLOS M. GRODSINSKY and GERALD V. BROWN 1989 10 p Proposed for presentation at the 28th Aerospace Sciences Meeting, Reno, NV, 8-11 Jan. 1990; sponsored by AIAA (NASA-TM-102386; E-5127; NAS 1.15:102386; AIAA-90-0741) Avail: NTIS HC A02/MF A01 CSCL 22/1

The dynamic acceleration environment observed on Space Shuttle flights to date and predicted for the Space Station has complicated the analysis of prior microgravity experiments and prompted concern for the viability of proposed space experiments requiring long-term, microgravity environments. Isolation systems capable of providing significant improvements to this environment exist, but at present have not been demonstrated in flight configurations. A summary of the theoretical evaluation for two one degree-of-freedom (DOF) active magnetic isolators and their predicted response to both direct and base excitations is presented. These isolators can be used independently or in concert to isolate acceleration-sensitive microgravity space experiments, dependent on the isolation capability required for specific experimenter needs. Author

N90-11902*# National Aeronautics and Space Administration. Lewis Research Center, Cleveland, OH.

ADVANCES AND DIRECTIONS OF ION NITRIDING/CARBURIZING

TALIVALDIS SPALVINS Sep. 1989 6 p Presented at the 2nd International Ion Nitriding/Carburizing Conference, Cincinnati, OH, 18-20 Sep. 1989; sponsored in part by ASM (NASA-TM-102398; E-5148; NAS 1.15:102398) Avail: NTIS HC A02/MF A01 CSCL 13/2

Ion nitriding and carburizing are plasma activated thermodynamic processes for the production of case hardened surface layers not only for ferrous materials, but also for an increasing number of nonferrous metals. When the treatment variables are properly controlled, the use of nitrogenous or carbonaceous glow discharge medium offers great flexibility in tailoring surface/near-surface properties independently of the bulk properties. The ion nitriding process has reached a high level of maturity and has gained wide industrial acceptance, while the more recently introduced ion carburizing process is rapidly gaining industrial acceptance. The current status of plasma mass transfer mechanisms into the surface regarding the formation of compound and diffusion layers in ion nitriding and carbon build-up ion carburizing is reviewed. In addition, the recent developments in design and construction of advanced equipment for obtaining optimized and controlled case/core properties is summarized. Also, new developments and trends such as duplex plasma treatments and alternatives to dc diode nitriding are highlighted. Author

N90-17929*# National Aeronautics and Space Administration. Lewis Research Center, Cleveland, OH.

A NEW APPROACH TO ACTIVE VIBRATION ISOLATION FOR MICROGRAVITY SPACE EXPERIMENTS

ALOK SINHA, CHIKUAN K. KAO (Pennsylvania State Univ., University Park.), and CARLOS M. GRODSINSKY Feb. 1990 11 p

(Contract NAG3-949)

(NASA-TM-102470; E-5257; NAS 1.15:102470) Avail: NTIS HC A03/MF A01 CSCL 13/9

A new method was developed to design an active vibration isolation system for microgravity space experiments. This method yields the required controller transfer functions for a specified transmissibility ratio. Hence, it is a straightforward task to guarantee that the desired vibration isolation performance is achieved at each frequency. The theory for such a controller design was presented by considering a single degree of freedom system. In addition, the magnitude of the input required by the new method has been found to be less than that used by a standard phase lead/lag compensator. Author

N90-21210*# National Aeronautics and Space Administration. Lewis Research Center, Cleveland, OH.

INFLUENCE OF THE DEPOSITION CONDITIONS ON RADIOFREQUENCY MAGNETRON SPUTTERED MOS₂ FILMS

PIERRE A. STEINMANN and TALIVALDIS SPALVINS Apr. 1990 11 p

(NASA-TP-2994; E-5181; NAS 1.60:2994) Avail: NTIS HC

A03/MF A01 CSCL 13/2

By varying the radiofrequency (RF) power, the Ar pressure, and the potential on the substrates, MoS₂(x) films of various stoichiometry, density, adhesion, and morphology were produced. An increase of RF power increased the deposition rate and density of the MoS₂ films as well as improved adhesion. However, the stoichiometry remained constant. An increase of Ar pressure increased the deposition rate but decreased the density, whereas both stoichiometry and adhesion were maximized at around 20 mtorr Ar pressure. Furthermore, a transition from compact film growth to columnar film growth was observed when the pressure was varied from 5 to 15 mtorr. Substoichiometric films were grown when a negative (bias) voltage was applied to the substrates. Author

N90-22703*# National Aeronautics and Space Administration. Lewis Research Center, Cleveland, OH.

ELEMENTS OF ACTIVE VIBRATION CONTROL FOR ROTATING MACHINERY

HEINZ ULBRICH May 1990 50 p

(NASA-TM-102368; E-5036; NAS 1.15:102368) Avail: NTIS HC

A03/MF A01 CSCL 13/2

The success or failure of active vibration control is determined by the availability of suitable actuators, modeling of the entire system including all active elements, positioning of the actuators and sensors, and implementation of problem-adapted control concepts. All of these topics are outlined and their special problems are discussed in detail. Special attention is given to efficient modeling of systems, especially for considering the active elements. Finally, design methods for and the application of active vibration control on rotating machinery are demonstrated by several real applications. Author

N90-23591*# National Aeronautics and Space Administration. Lewis Research Center, Cleveland, OH.

INTRODUCING THE VRT GAS TURBINE COMBUSTOR

JERRY O. MELCONIAN, ABDU A. MOSTAFA (Textron Lycoming, Stratford, CT.), and HUNG LEE NGUYEN 1990 14 p Presented at the 26th Joint Propulsion Conference, Orlando, FL, 16-18 Jul. 1990; cosponsored by AIAA, SAE, ASME, and ASEE

(NASA-TM-103176; E-5554; NAS 1.15:103176; AIAA-90-2452)

Avail: NTIS HC A03/MF A01 CSCL 21/5

An innovative annular combustor configuration is being developed for aircraft and other gas turbine engines. This design has the potential of permitting higher turbine inlet temperatures

31 ENGINEERING (GENERAL)

by reducing the pattern factor and providing a major reduction in NO(x) emission. The design concept is based on a Variable Residence Time (VRT) technique which allows large fuel particles adequate time to completely burn in the circumferentially mixed primary zone. High durability of the combustor is achieved by dual function use of the incoming air. The feasibility of the concept was demonstrated by water analogue tests and 3-D computer modeling. The computer model predicted a 50 percent reduction in pattern factor when compared to a state of the art conventional combustor. The VRT combustor uses only half the number of fuel nozzles of the conventional configuration. The results of the chemical kinetics model require further investigation, as the NO(x) predictions did not correlate with the available experimental and analytical data base. Author

N90-26170* National Aeronautics and Space Administration. Lewis Research Center, Cleveland, OH.

CRITICAL EVALUATION OF JET-A SPRAY COMBUSTION USING PROPANE CHEMICAL KINETICS IN GAS TURBINE COMBUSTION SIMULATED BY KIVA-2

H. L. NGUYEN and S.-J. YING (University of South Florida, Tampa.) Jul. 1990 21 p Presented at the 26th Joint Propulsion Conference, Orlando, FL, 16-18 Jul. 1990; sponsored in part by AIAA, SAE, ASME, and ASCE (NASA-TM-103173; E-5551; NAS 1.15:103173) Avail: NTIS HC A03/MF A01 CSCL 21/2

Jet-A spray combustion has been evaluated in gas turbine combustion with the use of propane chemical kinetics as the first approximation for the chemical reactions. Here, the numerical solutions are obtained by using the KIVA-2 computer code. The KIVA-2 code is the most developed of the available multidimensional combustion computer programs for application of the in-cylinder combustion dynamics of internal combustion engines. The released version of KIVA-2 assumes that 12 chemical species are present; the code uses an Arrhenius kinetic-controlled combustion model governed by a four-step global chemical reaction and six equilibrium reactions. Researchers efforts involve the addition of Jet-A thermophysical properties and the implementation of detailed reaction mechanisms for propane oxidation. Three different detailed reaction mechanism models are considered. The first model consists of 131 reactions and 45 species. This is considered as the full mechanism which is developed through the study of chemical kinetics of propane combustion in an enclosed chamber. The full mechanism is evaluated by comparing calculated ignition delay times with available shock tube data. However, these detailed reactions occupy too much computer memory and CPU time for the computation. Therefore, it only serves as a benchmark case by which to evaluate other simplified models. Two possible simplified models were tested in the existing computer code KIVA-2 for the same conditions as used with the full mechanism. One model is obtained through a sensitivity analysis using LSENS, the general kinetics and sensitivity analysis program code of D. A. Bittker and K. Radhakrishnan. This model consists of 45 chemical reactions and 27 species. The other model is based on the work published by C. K. Westbrook and F. L. Dryer. Author

N90-26171* Cincinnati Univ., OH.

COMPUTER SIMULATION OF GEAR TOOTH MANUFACTURING PROCESSES Final Report

DIMITRI MAVRIPLIS and RONALD L. HUSTON Feb. 1990 53 p Sponsored in part by AVSCOM, Cleveland, OH. (Contract NSG-3188; DA PROJ. 1L1-62209-A-47-A) (NASA-CR-185200; NAS 1.26:185200; AVSCOM-TM-90-C-003; AD-A227148) Avail: NTIS HC A04/MF A01 CSCL 13/9

The use of computer graphics to simulate gear tooth manufacturing procedures is discussed. An analytical basis for the simulation is established for spur gears. The simulation itself, however, is developed not only for spur gears, but for straight bevel gears as well. The applications of the developed procedure extend from the development of finite element models of heretofore intractable geometrical forms, to exploring the fabrication of nonstandard tooth forms. Author

N90-26172* National Aeronautics and Space Administration. Lewis Research Center, Cleveland, OH.

ANALYSIS OF A MARS-STATIONARY ORBITING MICROWAVE POWER TRANSMISSION SYSTEM

KENWYN J. LONG Jul. 1990 22 p (NASA-TM-101344; E-4367; NAS 1.15:101344) Avail: NTIS HC A03/MF A01 CSCL 20/14

To determine the feasibility of providing efficient RF power transmission from a Mars-stationary orbit to the surface of the planet, an assessment was made focussing on RF propagation in the 2.45- to 300-GHz range. The proposed orbiting system configuration provides for power generation by either photovoltaic array or nuclear reactor, the conversion of the dc output to RF, and subsequent propagation of RF energy from the orbiting array to the Martian surface. On the planet, a rectenna array will convert RF to dc power to be distributed for planetary power needs. Total efficiency of the energy conversion chain from dc to RF in orbit through RF to dc on the planetary surface was derived for several representative frequencies in the range of study. Tradeoffs between component efficiency and transmitting antenna requirements were considered for each of these frequencies. Rectenna element power density thresholds and desired received power levels were used to determine receiving antenna criteria. Recommendations are presented for research into developing technologies which may afford enhanced viability of the proposed microwave power transmission system. Author

N90-28754* National Aeronautics and Space Administration. Lewis Research Center, Cleveland, OH.

DEVELOPMENT AND APPROACH TO LOW-FREQUENCY MICROGRAVITY ISOLATION SYSTEMS

CARLOS M. GRODSINSKY Washington Aug. 1990 24 p (NASA-TP-2984; E-5287; NAS 1.60:2984) Avail: NTIS HC A03/MF A01 CSCL 22/1

The low-gravity environment provided by space flight has afforded the science community a unique arena for the study of fundamental and technological sciences. However, the dynamic environment observed on space shuttle flights and predicted for Space Station Freedom has complicated the analysis of prior microgravity experiments and prompted concern for the viability of proposed space experiments requiring long-term, low-gravity environments. Thus, isolation systems capable of providing significant improvements to this random environment are being developed. The design constraints imposed by acceleration-sensitive, microgravity experiment payloads in the unique environment of space and a theoretical background for active isolation are discussed. A design is presented for a six-degree-of-freedom, active, inertial isolation system based on the baseline relative and inertial isolation techniques described. Author

32

COMMUNICATIONS AND RADAR

Includes radar; land and global communications; communications theory; and optical communications.

A90-13935* Drexel Univ., Philadelphia, PA.

DESIGN FOR STEERING ACCURACY IN ANTENNA ARRAYS USING SHARED OPTICAL PHASE SHIFTERS

MOSHE KAM, PETER R. HERCZFELD (Drexel University, Philadelphia, PA), and JEFFREY WILCOX (System Planning Corp., Arlington, VA) IEEE Transactions on Antennas and Propagation (ISSN 0018-926X), vol. 37, Sept. 1989, p. 1102-1108. refs (Contract NAG3-763; NSF IRI-88-10168) Copyright

Uniform linear phased arrays where many radiating elements share a relatively small number of phase shifters are investigated. Such architectures arise in arrays which derive the time delays in

the signal paths from a small group of independent phase shifters. In particular, a true time-delay device which has been suggested recently for optically controlled arrays is used as the basic phase shifter. Different architectures, viz. alternative procedures of deriving the necessary time delay for each antenna in the face of phase-shifter inaccuracies, are examined. The variance of the steered beam's direction is used as the performance criterion. The direction-optimal architecture is obtained by means of quadratic programming, and is shown not to be unique. The nonuniqueness of the optimal architecture is exploited to improve other characteristics of the array's beam shape, and the optimal solution is shown to compare favorably with a suboptimal interleaved solution which is easier to implement. I.E.

A90-13936* Ohio State Univ., Columbus.

EFFECTS OF DESIRED SIGNAL ON THE PERFORMANCE OF A SIDELobe CANCELLER

INDER J. GUPTA and JAMES WARD (Ohio State University, Columbus) IEEE Transactions on Antennas and Propagation (ISSN 0018-926X), vol. 37, Sept. 1989, p. 1109-1115. refs (Contract NAG3-536) Copyright

The performance of a sidelobe canceller is studied in a communication system where the desired signal is continually present and its amplitude in the auxiliary antennas may be large (above thermal noise). In such a system, to avoid the cancellation of the desired signal, one can use a reference signal and adjust the auxiliary antenna weights to minimize the error between the reference signal and the sidelobe canceller output or one can use a steering vector. It is shown that in spite of the reference signal or a steering vector, the presence of the desired signal in the auxiliary antennas degrades the interference suppression provided by a sidelobe canceller. The amount of degradation depends on the number of degrees of freedom, the strength of the various signals, and the angular resolution of the auxiliary antenna array. Signal scenarios involving a single interfering signal as well as those involving multiple interfering signals are considered. I.E.

A90-16566* National Aeronautics and Space Administration. Lewis Research Center, Cleveland, OH.

AN EVOLUTIONARY COMMUNICATIONS SCENARIO FOR MARS EXPLORATION

STEVEN M. STEVENSON (NASA, Lewis Research Center, Cleveland, OH) IN: The case for Mars III: Strategies for exploration - Technical. San Diego, CA, Univelt, Inc., 1989, p. 527-538. Previously announced in STAR as N88-13515. refs (AAS PAPER 87-268) Copyright

As Mars exploration grows in complexity with time, the corresponding communication needs will grow in variety and complexity also. From initial Earth/Mars links, further needs will arise for complete surface connectivity for the provision of navigation, position location, and voice, data, and video communications services among multiple Mars bases and remote exploration sites. This paper addresses the likely required communication functions over the first few decades of Martian exploration and postulates systems for providing these services. Required technologies are identified and development requirements indicated. Author

A90-23261* # Toledo Univ., OH.

ENCODING Y,I,Q COMPONENT ESTIMATES OF AN NTSC COMPOSITE SIGNAL

DAVID A. BORDER (Digital Automation Associates, Bowling Green, OH) and S. C. KWATRA (Toledo, University, OH) Journal of Spacecraft and Rockets (ISSN 0022-4650), vol. 27, Jan.-Feb. 1990, p. 61-63. refs (Contract NAG3-42) Copyright

Several new techniques for reducing the entropy of a Y,I,Q component digital transmission are presented. A discussion of each technique is presented along with objective and subjective analysis. For a set of four test pictures, the average Y,I,Q entropy/pixel

was reduced by nearly 80 percent. An initial component system entropy of 11.08 bits/pixel was reduced to 2.33 bits/pixel. Although exact numeric results are dependent on the separation technique used, the methods presented may be applied to systems using other component separation methods. Author

A90-25617* # Ford Aerospace and Communications Corp., Palo Alto, CA.

ROLE OF COMMUNICATIONS SATELLITES IN THE FIBER ERA

KENT M. PRICE, RONALD E. JORASCH (Ford Aerospace Corp., Space Systems Div., Palo Alto, CA), and WALTER L. MORGAN (Communications Center, Clarksburg, MD) IN: AIAA International Communication Satellite Systems Conference and Exhibit, 13th, Los Angeles, CA, Mar. 11-15, 1990, Technical Papers. Part 1. Washington, DC, American Institute of Aeronautics and Astronautics, 1990, p. 126-134. (Contract NAS3-24683) (AIAA PAPER 90-0792) Copyright

System descriptions of satellite and fiber optic networks are developed for the benchmark years 1983 and 1986, and forecasts are made for the years 1990 and 1995. Based on this information, the impact of fiber optics on satellite communications in the years 1995 and 2000 is assessed. Ten services are identified which are likely to be supplied at least in part by satellite in the 1995-2000 time frame. Estimates are made of the probability of existence and the number of transponders used by these future satellite services. Author

A90-25620* # National Aeronautics and Space Administration. Lewis Research Center, Cleveland, OH.

SATELLITE RANGE DELAY SIMULATOR FOR A MATRIX-SWITCHED TIME DIVISION MULTIPLE-ACCESS NETWORK SIMULATION SYSTEM

LAWRENCE A. NAGY (NASA, Lewis Research Center, Cleveland, OH) IN: AIAA International Communication Satellite Systems Conference and Exhibit, 13th, Los Angeles, CA, Mar. 11-15, 1990, Technical Papers. Part 1. Washington, DC, American Institute of Aeronautics and Astronautics, 1990, p. 154-164. Previously announced in STAR as N90-12813. (AIAA PAPER 90-0795) Copyright

The Systems Integration, Test, and Evaluation (SITE) facility at NASA Lewis Research Center is presently configured as a satellite-switched time division multiple access (SS-TDMA) network simulator. The purpose of SITE is to demonstrate and evaluate advanced communication satellite technologies, presently embodied by POC components developed under NASA contracts in addition to other hardware, such as ground terminals, designed and built in-house at NASA Lewis. Each ground terminal in a satellite communications system will experience a different aspect of the satellite's motion due mainly to daily tidal effects and station keeping, hence a different duration and rate of variation in the range delay. As a result of this and other effects such as local oscillator instability, each ground terminal must constantly adjust its transmit burst timing so that data bursts from separate ground terminals arrive at the satellite in their assigned time slots, preventing overlap and keeping the system in synchronism. On the receiving end, ground terminals must synchronize their local clocks using reference transmissions received through the satellite link. A feature of the SITE facility is its capability to simulate the varying propagation delays and associated Doppler frequency shifts that the ground terminals in the network have to cope with. Delay is achieved by means of two NASA Lewis designed and built range delay simulator (RDS) systems, each independently controlled locally with front panel switches or remotely by an experiment control and monitor (EC/M) computer. Author

A90-25627* # National Aeronautics and Space Administration. Lewis Research Center, Cleveland, OH.

A NEW FABRICATION METHOD FOR PRECISION ANTENNA REFLECTORS FOR SPACE FLIGHT AND GROUND TEST

G. RICHARD SHARP, JOYCE S. WANHAINEN (NASA, Lewis Research Center, Cleveland, OH), and DEAN A. KETELSEN

32 COMMUNICATIONS AND RADAR

(Arizona, University, Tucson) IN: AIAA International Communication Satellite Systems Conference and Exhibit, 13th, Los Angeles, CA, Mar. 11-15, 1990, Technical Papers. Part 1. Washington, DC, American Institute of Aeronautics and Astronautics, 1990, p. 217-228. refs
(AIAA PAPER 90-0803) Copyright

The use of higher frequencies on communications satellites has led to the requirement for increasingly precise antenna reflectors for use in space. Typical industry fabrication methods for space antenna reflectors employ successive molding techniques for reflector face sheets and a final fit-up to a master mold in order to achieve the required accuracies. However, new missions at much higher frequencies will require greater accuracies than may be achievable using these present methods. A new approach for the fabrication of ground-test antenna reflectors is to machine the reflective surface into a stainless steel and fiberglass composite structure. A 2.7-m diameter ground-test antenna reflector fabricated using this method has an accuracy of better than 0.013 mm (0.0005 in.) rms. A similar design concept for a solid surface reflector for use on spacecraft would involve fabrication in a similar manner but using space-qualified materials. This report describes the design, analysis, and fabrication of the 2.7-m-diameter precision antenna reflector for antenna ground test and the extension of this technology to precision space antenna reflectors. Author

A90-25634*# National Aeronautics and Space Administration, Lewis Research Center, Cleveland, OH.
**PERFORMANCE MEASUREMENTS FOR A
LABORATORY-SIMULATED 30/20 GHZ COMMUNICATION
SATELLITE TRANSPONDER**

ROBERT J. KERCZEWSKI (NASA, Lewis Research Center, Cleveland, OH) IN: AIAA International Communication Satellite Systems Conference and Exhibit, 13th, Los Angeles, CA, Mar. 11-15, 1990, Technical Papers. Part 1. Washington, DC, American Institute of Aeronautics and Astronautics, 1990, p. 277-284. refs
(AIAA PAPER 90-0808) Copyright

NASA has developed a digital satellite communications system simulator and test bed facility, known as the SITE (System Integration, Test and Evaluation) Project. The purpose of the facility is to evaluate satellite system components, develop and verify system concepts, and perform satellite system experiments. A recently completed set of experiments measured the performance of the 30/20 GHz satellite transponder portion of the system in terms of RF parameters and high rate digital data transmission. The results of these tests indicate the quality of data transmission which can be obtained under various transponder operating conditions, as well as the relative effects of degraded RF performance on the bit-error rate (BER) of transmitted data.

Author

A90-25658*# Communications Satellite Corp., Clarksburg, MD.
**A USERS PERSPECTIVE OF THE ACTS HOPPING BEAM
TDMA SYSTEM**

S. JOSEPH CAMPANELLA, B. A. PONTANO, and D. M. CHITRE (COMSAT Laboratories, Clarksburg, MD) IN: AIAA International Communication Satellite Systems Conference and Exhibit, 13th, Los Angeles, CA, Mar. 11-15, 1990, Technical Papers. Part 2. Washington, DC, American Institute of Aeronautics and Astronautics, 1990, p. 484-489.
(Contract NAS3-25084)

(AIAA PAPER 90-0833) Copyright

NASA's ACTS offers a number of satellite communications technology innovations that go far beyond any of the concepts that are currently in operational use today. One of the most interesting is its use of multiple hopping beams, onboard circuit switching and Time Division Multiple Access (TDMA) transmission to create a telephone switching center in geostationary orbit. This paper describes the ACTS hopping beam TDMA system in simple terms that will equip potential users of ACTS LBR earth terminals with a useful understanding of the concept. Author

A90-25663*# National Aeronautics and Space Administration, Washington, DC.

**ADVANCED COMMUNICATIONS TECHNOLOGY SATELLITE
(ACTS)**

DEAN A. OLMSTEAD (NASA, Washington, DC) and RONALD J. SCHERTLER (NASA, Lewis Research Center, Cleveland, OH) IN: AIAA International Communication Satellite Systems Conference and Exhibit, 13th, Los Angeles, CA, Mar. 11-15, 1990, Technical Papers. Part 2. Washington, DC, American Institute of Aeronautics and Astronautics, 1990, p. 522-528.

(AIAA PAPER 90-0839) Copyright

The benefits that will be offered by the NASA-sponsored communication spacecraft ACTS which is scheduled for launch in 1992 are described together with examples of demonstrations on proposed data, video, and voice applications supported by the advanced ACTS technologies. Compared to existing satellite service, the ACTS will provide lower cost, better service, greater convenience, and improved service reliability of telecommunications to customers around the world. In addition, the pioneering ACTS technology will provide many capabilities qualitatively different from those of current satellite systems, such as on-demand assignment, frequency reuse, and the flexible targeting of spot beams directly to the very-small-aperture terminals at customer premises. I.S.

A90-25681*# General Electric Co., Princeton, NJ.
SPACECRAFT DESIGNS FOR VSAT NETWORKS

ALAN L. STERN (General Electric Co., Astro-Space Div., Princeton, NJ) and DAVID L. WRIGHT (NASA, Lewis Research Center, Cleveland, OH) IN: AIAA International Communication Satellite Systems Conference and Exhibit, 13th, Los Angeles, CA, Mar. 11-15, 1990, Technical Papers. Part 2. Washington, DC, American Institute of Aeronautics and Astronautics, 1990, p. 689-693.
(AIAA PAPER 90-0895) Copyright

Results are presented from a study to determine the commercial applications of the technology developed for ACTS. Two systems are discussed: point-to-point transmission of T1 (1.544 Mb/s) data channels using Very Small Aperture Terminals, and point-to-point transmission of single channel per carrier data from extremely small ground terminals. Satellite communications systems designed for each of these applications are described. R.B.

A90-25697*# National Aeronautics and Space Administration, Lewis Research Center, Cleveland, OH.

**EFFECTS OF AMPLITUDE DISTORTIONS AND IF
EQUALIZATION ON SATELLITE COMMUNICATION SYSTEM
BIT-ERROR RATE PERFORMANCE**

ROBERT J. KERCZEWSKI, GENE FUJIKAWA (NASA, Lewis Research Center, Cleveland, OH), JAMES S. SVOBODA (NASA, Lewis Research Center; Sverdrup Technology, Inc., Cleveland, OH), and PAUL J. LIZANICH (NASA, Lewis Research Center; Analox Corp., Cleveland, OH) IN: AIAA International Communication Satellite Systems Conference and Exhibit, 13th, Los Angeles, CA, Mar. 11-15, 1990, Technical Papers. Part 2. Washington, DC, American Institute of Aeronautics and Astronautics, 1990, p. 807-817. refs

(Contract NAS3-25266; NAS3-24564)

(AIAA PAPER 90-0878) Copyright

Satellite communications links are subject to distortions which result in an amplitude versus frequency response which deviates from the ideal flat response. Such distortions result from propagation effects such as multipath fading and scintillation and from transponder and ground terminal hardware imperfections. Laboratory experiments performed at NASA Lewis measured the bit-error-rate (BER) degradation resulting from several types of amplitude response distortions. Additional tests measured the amount of BER improvement obtained by flattening the amplitude response of a distorted laboratory-simulated satellite channel. This paper presents the results of these experiments. Author

A90-34914* National Aeronautics and Space Administration. Lewis Research Center, Cleveland, OH.

A UNIFIED STATISTICAL RAIN-ATTENUATION MODEL FOR COMMUNICATION LINK FADE PREDICTIONS AND OPTIMAL STOCHASTIC FADE CONTROL DESIGN USING A LOCATION-DEPENDENT RAIN-STATISTIC DATABASE

ROBERT M. MANNING (NASA, Lewis Research Center, Cleveland, OH) International Journal of Satellite Communications (ISSN 0737-2884), vol. 8, Jan.-Feb. 1990, p. 11-30. refs
Copyright

A static and dynamic rain-attenuation model is presented which describes the statistics of attenuation on an arbitrarily specified satellite link for any location for which there are long-term rainfall statistics. The model may be used in the design of the optimal stochastic control algorithms to mitigate the effects of attenuation and maintain link reliability. A rain-statistics data base is compiled, which makes it possible to apply the model to any location in the continental U.S. with a resolution of 0.5 degrees in latitude and longitude. The model predictions are compared with experimental observations, showing good agreement. I.E.

A90-36717* Massachusetts Inst. of Tech., Lexington.
CONVERGENCE OF THE SMI AND THE DIAGONALLY LOADED SMI ALGORITHMS WITH WEAK INTERFERENCE

MATTHEW W. GANZ, SANFORD L. WILSON (MIT, Lexington, MA), and RANDOLPH L. MOSES (Ohio State University, Columbus) IEEE Transactions on Antennas and Propagation (ISSN 0018-926X), vol. 38, March 1990, p. 394-399. Research supported by the U.S. Navy. refs
(Contract F19628-85-C-0002; NAG3-536)
(AD-A22639; ESD-TR-90-048) Copyright

Approximations for the power levels at the output of an adaptive array that uses the diagonally loaded sample-matrix inversion (SMI) algorithm are derived. Diagonal loading is a technique where the diagonal of the covariance matrix is augmented with a positive or negative constant prior to inversion. This paper examines how the signal-to-interference-plus-noise ratio (SINR) and signal-to-interference ratio (SIR) at the array output vary with the number of samples taken when the input signals are CW. It is shown that positive loading produces more rapid convergence with a reduction in output SIR. Negative loading provides an improved SIR level, but positive loading produces more rapid convergence. Negative loading provides an improved SIR level, but the output power levels are erratic and slow to converge. Simulation results which verify the theoretical procedure are given. I.E.

A90-37312* National Aeronautics and Space Administration. Lewis Research Center, Cleveland, OH.

EXPERIMENTAL STUDY OF THE CROSS-POLARIZATION CHARACTERISTICS OF RECTANGULAR MICROSTRIP ANTENNAS

R. Q. LEE (NASA, Lewis Research Center, Cleveland, OH), T. HUYNH (Akron, University, OH), and K. F. LEE (Toledo, University, OH) Microwave and Optical Technology Letters (ISSN 0895-2477), vol. 2, July 1989, p. 247-249.
Copyright

The cross polarization characteristics of rectangular patch antennas are studied experimentally. Data are presented showing the dependence of the copolarization to cross-polarization ratio on the aspect ratio in both the E and H planes. Three substrate thicknesses are included and the variation with resonant frequency is examined. Author

A90-39056* Naval Postgraduate School, Monterey, CA.
A PERFORMANCE ANALYSIS OF DS-CDMA AND SCPC VSAT NETWORKS

DAVID P. HAYES (Analytic Sciences Corp., Reston, VA) and TRI T. HA (U.S. Naval Postgraduate School, Monterey, CA) IEEE Transactions on Aerospace and Electronic Systems (ISSN 0018-9251), vol. 26, Jan. 1990, p. 12-21. Research supported by the Virginia Polytechnic Institute and State University and U.S. Navy. refs

(Contract NAS3-24887)

Copyright

Spread-spectrum and single-channel-per-carrier (SCPC) transmission techniques work well in very small aperture terminal (VSAT) networks for multiple-access purposes while allowing the earth station antennas to remain small. Direct-sequence code-division multiple-access (DS-CDMA) is the simplest spread-spectrum technique to use in a VSAT network since a frequency synthesizer is not required for each terminal. An examination is made of the DS-CDMA and SCPC Ku-band VSAT satellite systems for low-density (64-kb/s or less) communications. A method for improving the standard link analysis of DS-CDMA satellite-switched networks by including certain losses is developed. The performance of 50-channel full mesh and star network architectures is analyzed. The selection of operating conditions producing optimum performance is demonstrated. I.E.

A90-41586* Toledo Univ., OH.

MICROSTRIP SUBARRAY WITH COPLANAR AND STACKED PARASITIC ELEMENTS

K. F. LEE, T. TALTY (Toledo, University, OH), and R. Q. LEE (NASA, Lewis Research Center, Cleveland, OH) Electronics Letters (ISSN 0013-5194), vol. 26, May 10, 1990, p. 668, 669.
refs

Copyright

A parasitic subarray configuration combining the coplanar and stacked geometries is proposed and studied. It is numerically shown that a two-layer cross offers a gain enhancement of several decibels compared with either the coplanar cross or the two-layer electromagnetically coupled antenna. Preliminary experimental results appear to be in agreement with this estimate. C.D.

A90-45398* Illinois Univ., Urbana.

REFLECTOR SPILLOVER LOSS OF AN OPEN-ENDED RECTANGULAR AND CIRCULAR WAVEGUIDE FEED

SHUNG WU LEE and MARTIN L. ZIMMERMAN (Illinois, University, Urbana) IEEE Transactions on Antennas and Propagation (ISSN 0018-926X), vol. 38, June 1990, p. 940-942. refs
(Contract NAG3-419)

Copyright

An important and frequently used parameter in the design of a feed for a reflector antenna is the spillover loss. A set of spillover curves is presented for several common feeds, namely circular waveguides with TE₁₁ or TE₂₁ excitations, rectangular guides for the monopulse application, etc. The difference between two common methods of normalizing the feed input power is also discussed. I.E.

A90-48440* Harris Corp., Melbourne, FL.

A FORWARD ERROR CORRECTION TECHNIQUE USING A HIGH-SPEED, HIGH-RATE SINGLE CHIP CODEC

R. W. BOYD, W. F. HARTMAN (Harris Corp., Melbourne, FL), and ROBERT E. JONES (NASA, Lewis Research Center, Cleveland, OH) IN: MILCOM '89 - IEEE Military Communications Conference, Boston, MA, Oct. 15-18, 1989, Conference Record. Volume 1. New York, Institute of Electrical and Electronics Engineers, Inc., 1989, p. 166-170.

(Contract NAS3-25087)

Copyright

The authors describe an error-correction coding approach that allows operation in either burst or continuous modes at data rates of multiple hundreds of megabits per second. Bandspreading is low since the code rate is 7/8 or greater, which is consistent with high-rate link operation. The encoder, along with a hard-decision decoder, fits on a single application-specific integrated circuit (ASIC) chip. Soft-decision decoding is possible utilizing applique hardware in conjunction with the hard-decision decoder. Expected coding gain is a function of the application and is approximately 2.5 dB for hard-decision decoding at 10⁻⁵ bit-error rate with phase-shift-keying modulation and additive Gaussian white noise interference. The principal use envisioned for this technique is to achieve a modest amount of coding gain on high-data-rate, bandwidth-constrained channels. Data rates of up to 300 Mb/s

32 COMMUNICATIONS AND RADAR

can be accommodated by the codec chip. The major objective is burst-mode communications, where code words are composed of 32 n data bits followed by 32 overhead bits. I.E.

A90-51165* National Aeronautics and Space Administration. Lewis Research Center, Cleveland, OH.

ADVANCED COMMUNICATIONS TECHNOLOGY SATELLITE (ACTS) AND POTENTIAL SYSTEM APPLICATIONS

DAVID L. WRIGHT, JOSEPH R. BALOMBIN, and PHILIP Y. SOHN (NASA, Lewis Research Center, Cleveland, OH) IEEE, Proceedings (ISSN 0018-9219), vol. 78, July 1990, p. 1165-1175. Copyright

A description of the advanced communications technology satellite (ACTS) system is given with special emphasis on the communication characteristics. Potential satellite communications scenarios, including future operational ACTS-like satellite systems, are discussed. The description of the ACTS system updates previously published ACTS system references. Detailed information on items such as experimental ground stations is presented. The potential services can be generically described as voice, video, and data services. The implementation of these services on future operational ACTS-like systems can lead to unique quality, flexibility, and capacity characteristics at lower service costs. The specific service applications that could be supported range from low to high data rates and include both domestic and international applications. I.E.

A90-51167* National Aeronautics and Space Administration. Lewis Research Center, Cleveland, OH.

THE ROLE OF TECHNOLOGY IN INFLUENCING FUTURE CIVIL COMMUNICATIONS SATELLITES

JAMES W. BAGWELL (NASA, Lewis Research Center, Cleveland, OH) and CHRISTOPH E. MAHLE (COMSAT Laboratories, Clarksburg, MD) IEEE, Proceedings (ISSN 0018-9219), vol. 78, July 1990, p. 1190-1205. refs Copyright

Technology, both as an enabler and as a driver of new and improved communication satellites, is discussed. A brief look at the beginnings and evolution of satellite communications is given to reveal the continuing influence of technology over the past 25 years. An assessment of the current state of the art which serves as a benchmark representing how far technology has come and as a basis for comparison for future possibilities is presented. A short tutorial on communications satellite basics is presented, followed by an assessment of technologies used for satellite antennas and signal amplification and routing. A discussion of future service requirements follows, and emerging technologies are identified along with possible improved communications capabilities that can result from them. The outlook for the role of technology for future communication satellites is summarized. I.E.

A90-51306* National Aeronautics and Space Administration. Lewis Research Center, Cleveland, OH.

DIGITAL CODEC FOR REAL-TIME PROCESSING OF BROADCAST QUALITY VIDEO SIGNALS AT 1.8 BITS/PIXEL

MARY JO SHALKHAUSER and WAYNE A. WHYTE, JR. (NASA, Lewis Research Center, Cleveland, OH) IN: GLOBECOM '89 - IEEE Global Telecommunications Conference and Exhibition, Dallas, TX, Nov. 27-30, 1989, Conference Record. Volume 1. New York, Institute of Electrical and Electronics Engineers, Inc., 1989, p. 242-249. Copyright

The authors present the hardware implementation of a digital television bandwidth compression algorithm which processes standard NTSC (National Television Systems Committee) composite color television signals and produces broadcast-quality video in real time at an average of 1.8 b/pixel. The sampling rate used with this algorithm results in 768 samples over the active portion of each video line by 512 active video lines per video frame. The algorithm is based on differential pulse code modulation (DPCM), but additionally utilizes a nonadaptive predictor, nonuniform quantizer, and multilevel Huffman coder to reduce the

data rate substantially below that achievable with straight DPCM. The nonadaptive predictor and multilevel Huffman coder combine to set this technique apart from prior-art DPCM encoding algorithms. The authors describe the data compression algorithm and the hardware implementation of the codec and provide performance results. I.E.

N90-10155*# National Aeronautics and Space Administration. Lewis Research Center, Cleveland, OH.

OVERVIEW OF MICROWAVE CONCEPTS

KARL A. FAYMON /n NASA. Langley Research Center, Second Beamed Space-Power Workshop p 287-290 Jul. 1989 Avail: NTIS HC A19/MF A03 CSCL 20N

An overview of microwave beamed power concepts is given in outline form. Concepts such as power transmission to operational satellites, spacecraft propulsion, lunar/planetary outpost power and planetary rover propulsion are listed in chart form and characterized in columns titled power level, benefits, and comments. Author

N90-11210*# Hughes Aircraft Co., El Segundo, CA. Space and Communications Group.

ANTENNA BEAMFORMING USING OPTICAL PROCESSING

L. P. ANDERSON, JR., F. BOLDISSAR, and D. C. D. CHANG Jun. 1987 66 p Previously announced in IAA as A89-15844 (Contract NAS3-24889) (NASA-CR-180844; NAS 1.26:180844) Avail: NTIS HC A04/MF A01 CSCL 20/14

This work concerns itself with the analytical investigation into the feasibility of optical processor based beamforming for microwave array antennas. The primary focus is on systems utilizing the 20 and 30 GHz communications band and a transmit configuration exclusively to serve this band. A mathematical model is developed for computation of candidate design configurations. The model is capable of determination of the necessary design parameters required for both spatial aspects of the microwave footprint (beam) formation as well as transmitted signal quality. Computed example beams transmitted from geosynchronous orbit are presented to demonstrate network capabilities. A comprehensive device/component survey is also conducted in parallel to determine the feasibility of breadboarding a transmit processor. Recommendations are made for the configuration of such a processor and the components which would comprise such a network. Author

N90-11211*# Ohio State Univ., Columbus. ElectroScience Lab. **AN EXPERIMENTAL SMI ADAPTIVE ANTENNA ARRAY FOR WEAK INTERFERING SIGNALS**

R. L. DILSAVOR and I. J. GUPTA Oct. 1989 89 p (Contract NAS3-536) (NASA-CR-185976; NAS 1.26:185976; ESL-TR-716111-7) Avail: NTIS HC A05/MF A01 CSCL 17/2

A modified sample matrix inversion (SMI) algorithm designed to increase the suppression of weak interference is implemented on an existing experimental array system. The algorithm itself is fully described as are a number of issues concerning its implementation and evaluation, such as sample scaling, snapshot formation, weight normalization, power calculation, and system calibration. Several experiments show that the steady state performance (i.e., many snapshots are used to calculate the array weights) of the experimental system compares favorably with its theoretical performance. It is demonstrated that standard SMI does not yield adequate suppression of weak interference. Modified SMI is then used to experimentally increase this suppression by as much as 13dB. Author

N90-11915*# National Aeronautics and Space Administration. Lewis Research Center, Cleveland, OH.

SATELLITE-MATRIX-SWITCHED, TIME-DIVISION-MULTIPLE-ACCESS NETWORK SIMULATOR

WILLIAM D. IVANCIC, MONTY ANDRO, LAWRENCE A. NAGY, JAMES M. BUDINGER, and MARY JO SHALKHAUSER Washington Oct. 1989 21 p Proposed for presentation at the 13th AIAA International Communication Satellite System

Conference, 11-15 Mar. 1990
(NASA-TP-2944; E-4813; NAS 1.60:2944) Avail: NTIS HC
A03/MF A01 CSCL 17/2

A versatile experimental Ka-band network simulator has been implemented at the NASA Lewis Research Center to demonstrate and evaluate a satellite-matrix-switched, time-division-multiple-access (SMS-TDMA) network and to evaluate future digital ground terminals and radiofrequency (RF) components. The simulator was implemented by using proof-of-concept RF components developed under NASA contracts and digital ground terminal and link simulation hardware developed at Lewis. This simulator provides many unique capabilities such as satellite range delay and variation simulation and rain fade simulation. All network parameters (e.g., signal-to-noise ratio, satellite range variation rate, burst density, and rain fade) are controlled and monitored by a central computer. The simulator is presently configured as a three-ground-terminal SMS-TDMA network. Author

N90-12784*# Ohio State Univ., Columbus. ElectroScience Lab.
**ADAPTIVE ANTENNA ARRAYS FOR SATELLITE
COMMUNICATION Final Report**

INDER J. GUPTA Sep. 1989 139 p
(Contract NAG3-536)

(NASA-CR-185989; REPT-716111-09; NAS 1.26:185989) Avail:
NTIS HC A07/MF A01 CSCL 20/14

The feasibility of using adaptive antenna arrays to provide interference protection in satellite communications was studied. The feedback loops as well as the sample matrix inversion (SMI) algorithm for weight control were studied. Appropriate modifications in the two were made to achieve the required interference suppression. An experimental system was built to test the modified feedback loops and the modified SMI algorithm. The performance of the experimental system was evaluated using bench generated signals and signals received from TVRO geosynchronous satellites. A summary of results is given. Some suggestions for future work are also presented. Author

N90-12813*# National Aeronautics and Space Administration.
Lewis Research Center, Cleveland, OH.

**SATELLITE RANGE DELAY SIMULATOR FOR A
MATRIX-SWITCHED TIME DIVISION MULTIPLE-ACCESS
NETWORK SIMULATOR**

LAWRENCE A. NAGY 1989 14 p Proposed for presentation
at the 13th International Communications Satellite Systems
Conference, Los Angeles, CA, 11-15 Mar. 1990; sponsored by
AIAA

(NASA-TM-102407; E-5159; NAS 1.15:102407) Avail: NTIS HC
A03/MF A01 CSCL 17/2

The Systems Integration, Test, and Evaluation (SITE) facility at NASA Lewis Research Center is presently configured as a satellite-switched time division multiple access (SS-TDMA) network simulator. The purpose of SITE is to demonstrate and evaluate advanced communication satellite technologies, presently embodied by POC components developed under NASA contracts in addition to other hardware, such as ground terminals, designed and built in-house at NASA Lewis. Each ground terminal in a satellite communications system will experience a different aspect of the satellite's motion due mainly to daily tidal effects and station keeping, hence a different duration and rate of variation in the range delay. As a result of this and other effects such as local oscillator instability, each ground terminal must constantly adjust its transmit burst timing so that data bursts from separate ground terminals arrive at the satellite in their assigned time slots, preventing overlap and keeping the system in synchronism. On the receiving end, ground terminals must synchronize their local clocks using reference transmissions received through the satellite link. A feature of the SITE facility is its capability to simulate the varying propagation delays and associated Doppler frequency shifts that the ground terminals in the network have to cope with. Delay is achieved by means of two NASA Lewis designed and built range delay simulator (RDS) systems, each independently

controlled locally with front panel switches or remotely by an experiment control and monitor (EC/M) computer. Author

N90-14452*# Analox Corp., Cleveland, OH.

**DATA COMPRESSION TECHNIQUES APPLIED TO HIGH
RESOLUTION HIGH FRAME RATE VIDEO TECHNOLOGY Final
Report**

WILLIAM G. HARTZ, ROBERT E. ALEXOVICH, and MARC S.
NEUSTADTER Washington NASA Dec. 1989 139 p

(Contract NAS3-24564)

(NASA-CR-4263; E-5126; NAS 1.26:4263) Avail: NTIS HC
A07/MF A01 CSCL 17/2

An investigation is presented of video data compression applied to microgravity space experiments using High Resolution High Frame Rate Video Technology (HHVT). An extensive survey of methods of video data compression, described in the open literature, was conducted. The survey examines compression methods employing digital computing. The results of the survey are presented. They include a description of each method and assessment of image degradation and video data parameters. An assessment is made of present and near term future technology for implementation of video data compression in high speed imaging system. Results of the assessment are discussed and summarized. The results of a study of a baseline HHVT video system, and approaches for implementation of video data compression, are presented. Case studies of three microgravity experiments are presented and specific compression techniques and implementations are recommended. Author

N90-16103*# Ohio State Univ., Columbus. ElectroScience Lab.
**HIGH-FREQUENCY ASYMPTOTIC METHODS FOR ANALYZING
THE EM SCATTERING BY OPEN-ENDED WAVEGUIDE
CAVITIES**

R. J. BURKHOLDER and P. H. PATHAK Sep. 1989 271 p
(Contract NAG3-476)

(NASA-CR-186244; NAS 1.26:186244; ESL-TR-719630-3) Avail:
NTIS HC A12/MF A02 CSCL 20/14

Four high-frequency methods are described for analyzing the electromagnetic (EM) scattering by electrically large open-ended cavities. They are: (1) a hybrid combination of waveguide modal analysis and high-frequency asymptotics, (2) geometrical optics (GO) ray shooting, (3) Gaussian beam (GB) shooting, and (4) the generalized ray expansion (GRE) method. The hybrid modal method gives very accurate results but is limited to cavities which are made up of sections of uniform waveguides for which the modal fields are known. The GO ray shooting method can be applied to much more arbitrary cavity geometries and can handle absorber treated interior walls, but it generally only predicts the major trends of the RCS pattern and not the details. Also, a very large number of rays need to be tracked for each new incidence angle. Like the GO ray shooting method, the GB shooting method can handle more arbitrary cavities, but it is much more efficient and generally more accurate than the GO method because it includes the fields diffracted by the rim at the open end which enter the cavity. However, due to beam divergence effects the GB method is limited to cavities which are not very long compared to their width. The GRE method overcomes the length-to-width limitation of the GB method by replacing the GB's with GO ray tubes which are launched in the same manner as the GB's to include the interior rim diffracted field. This method gives good accuracy and is generally more efficient than the GO method, but a large number of ray tubes needs to be tracked. Author

N90-17977*# National Aeronautics and Space Administration.
Lewis Research Center, Cleveland, OH.

**PERFORMANCE MEASUREMENTS FOR A
LABORATORY-SIMULATED 30/20 GHZ COMMUNICATION
SATELLITE TRANSPONDER**

ROBERT J. KERCZEWSKI and GENE FUJIKAWA 1990 10 p
Presented at the 13th International Communication Satellite
Systems Conference, Los Angeles, CA, 11-15 Mar. 1990;
sponsored by AIAA

32 COMMUNICATIONS AND RADAR

(NASA-TM-102424; E-5189; NAS 1.15:102424; AIAA-90-0808)
Avail: NTIS HC A02/MF A01 CSCL 17/2

NASA has developed a digital satellite communications system simulator and test bed facility, known as the Systems Integration, Test and Evaluation (SITE) Project. The purpose of the facility is to evaluate satellite system components, develop and verify system concepts, and perform satellite system experiments. A recently completed set of experiments measured the performance of the 30/20 GHz satellite transponder portion of the system in terms of RF parameters and high rate digital data transmission. The results of these tests indicate the quality of data transmission which can be obtained under various transponder conditions, as well as the relative effects of degraded RF performance on the bit-error rate (BER) of transmitted data. Author

N90-19264*# National Aeronautics and Space Administration. Lewis Research Center, Cleveland, OH.

A COMPARISON OF REFLECTOR ANTENNA DESIGNS FOR WIDE-ANGLE SCANNING

M. ZIMMERMAN, S. W. LEE, B. HOUSHMAND, Y. RAHMATSAMII (Jet Propulsion Lab., California Inst. of Tech., Pasadena.), and R. J. ACOSTA /in NASA, Langley Research Center, Earth Science Geostationary Platform Technology p 217-240 Jul. 1989 Previously announced as N89-21138

Avail: NTIS HC A17/MF A03 CSCL 20/14

Conventional reflector antennas are typically designed for up to + or - 20 beamwidths scan. An attempt was made to stretch this scan range to some + or - 300 beamwidths. Six single and dual reflector antennas were compared. It is found that a symmetrical parabolic reflector with $f/D = 2$ and a single circular waveguide feed has the minimum scan loss (only 0.6 dB at Theta sub 0 = 8 deg, or a 114 beamwidths scan). The scan is achieved by tilting the parabolic reflector by an angle equal to the half-scan angle. The f/D may be shortened if a cluster 7 to 19 elements instead of one element is used for the feed. The cluster excitation is adjusted for each new beam scan direction to compensate for the imperfect field distribution over the reflector aperture. The antenna can be folded into a Cassegrain configuration except that, due to spillover and blockage considerations, the amount of folding achievable is small. Author

N90-19266*# National Aeronautics and Space Administration. Lewis Research Center, Cleveland, OH.

CONJUGATE FIELD APPROACHES FOR ACTIVE ARRAY COMPENSATION

R. J. ACOSTA /in NASA, Langley Research Center, Earth Science Geostationary Platform Technology p 265-271 Jul. 1989

Avail: NTIS HC A17/MF A03 CSCL 20/14

Two approaches for calculating the compensating feed array complex excitations are namely, the indirect conjugate field matching (ICFM) and the direct conjugate field matching (DCFM) approach. In the ICFM approach the compensating feed array excitations are determined by considering the transmitting mode and the reciprocity principle. The DCFM, in contrast calculates the array excitations by integrating directly the induced surface currents on the reflector under a receiving mode. DCFM allows the reflector to be illuminated by an incident plane wave with a tapered amplitude. The level of taper can effectively control the sidelobe level of the compensated antenna pattern. Both approaches are examined briefly. Author

N90-19267*# National Aeronautics and Space Administration. Lewis Research Center, Cleveland, OH.

REFLECTOR SURFACE DISTORTION ANALYSIS TECHNIQUES (THERMAL DISTORTION ANALYSIS OF ANTENNAS IN SPACE)

R. SHARP, M. LIAO, J. GIRIUNAS, J. HEIGHWAY, A. LAGIN, and R. STEINBACH /in NASA, Langley Research Center, Earth Science Geostationary Platform Technology p 273293 Jul. 1989

Avail: NTIS HC A17/MF A03 CSCL 20/14

A group of large computer programs are used to predict the farfield antenna pattern of reflector antennas in the thermal environment of space. Thermal Radiation Analysis Systems

(TRASYS) is a thermal radiation analyzer that interfaces with Systems Improved Numerical Differencing Analyzer (SINDA), a finite difference thermal analysis program. The programs linked together for this analysis can now be used to predict antenna performance in the constantly changing space environment. They can be used for very complex spacecraft and antenna geometries. Performance degradation caused by methods of antenna reflector construction and materials selection are also taken into consideration. However, the principal advantage of using this program linkage is to account for distortions caused by the thermal environment of space and the hygroscopic effects of the dry-out of graphite/epoxy materials after the antenna is placed into orbit. The results of this type of analysis could ultimately be used to predict antenna reflector shape versus orbital position. A phased array antenna distortion compensation system could then use this data to make RF phase front corrections. That is, the phase front could be adjusted to account for the distortions in the antenna feed and reflector geometry for a particular orbital position. Author

N90-19454*# National Aeronautics and Space Administration. Lewis Research Center, Cleveland, OH.

EFFECTS OF AMPLITUDE DISTORTIONS AND IF EQUALIZATION ON SATELLITE COMMUNICATION SYSTEM BIT-ERROR RATE PERFORMANCE

ROBERT J. KERCZEWSKI, GENE FUJIKAWA, JAMES S. SVOBODA, and PAUL J. LIZANICH (Analex Corp., Cleveland, OH.) 1990 13 p Presented at the 13th International Communication Satellite Systems Conference, Los Angeles, CA, 11-15 Mar. 1990; sponsored by AIAA

(Contract NAS3-25266; NAS3-24564)

(NASA-TM-102415; E-5180; NAS 1.15:102415; AIAA-90-0878)

Avail: NTIS HC A03/MF A01 CSCL 17/2

Satellite communications links are subject to distortions which result in an amplitude versus frequency response which deviates from the ideal flat response. Such distortions result from propagation effects such as multipath fading and scintillation and from transponder and ground terminal hardware imperfections. Bit-error rate (BER) degradation resulting from several types of amplitude response distortions were measured. Additional tests measured the amount of BER improvement obtained by flattening the amplitude response of a distorted laboratory simulated satellite channel. The results of these experiments are presented. Author

N90-19466*# Ohio State Univ., Columbus. ElectroScience Lab. **ELECTROMAGNETIC PROPERTIES OF MATERIAL COATED SURFACES Annual Report**

L. BEARD, J. BERRIE, R. BURKHOLDER, A. DOMINEK, E. WALTON, and N. WANG Oct. 1989 48 p

(Contract NAG3-913)

(NASA-CR-186466; NAS 1.26:186466; OSU-TR-720964-5) Avail: NTIS HC A03/MF A01 CSCL 20/14

The electromagnetic properties of material coated conducting surfaces were investigated. The coating geometries consist of uniform layers over a planar surface, irregularly shaped formations near edges and randomly positioned, electrically small, irregularly shaped formations over a surface. Techniques to measure the scattered field and constitutive parameters from these geometries were studied. The significance of the scattered field from these geometries warrants further study. Author

N90-20264*# National Aeronautics and Space Administration. Lewis Research Center, Cleveland, OH.

NUMERICAL ARC SEGMENTATION ALGORITHM FOR A RADIO CONFERENCE-NASARC (VERSION 4.0) TECHNICAL MANUAL

WAYNE A. WHYTE, JR., ANN O. HEYWARD, DENISE S. PONCHAK, RODNEY L. SPENCE, and JOHN E. ZUZEK 6 Oct. 1988 156 p

(NASA-TM-101453; E-4736; NAS 1.15:101453) Avail: NTIS HC A08/MF A01 CSCL 17/2

The information contained in the NASARC (Version 4.0) Technical Manual and NASARC (Version 4.0) User's Manual relates to the Numerical Arc Segmentation Algorithm for a Radio

Conference (NASARC) software development through November 1, 1988. The Technical Manual describes the NASARC concept and the algorithms used to implement the concept. The User's Manual provides information on computer system considerations, installation instructions, description of input files, and program operation instructions. Significant revisions were incorporated in the Version 4.0 software over prior versions. These revisions have further enhanced the modeling capabilities of the NASARC procedure and provide improved arrangements of predetermined arcs within the geostationary orbits. Array dimensions within the software were structured to fit within the currently available 12 megabyte memory capacity of the International Frequency Registration Board (IFRB) computer facility. A piecewise approach to predetermined arc generation in NASARC (Version 4.0) allows worldwide planning problem scenarios to be accommodated within computer run time and memory constraints with enhanced likelihood and ease of solution. Author

N90-20270*# Communications Satellite Corp., Clarksburg, MD.
ADVANCED MODULATION TECHNOLOGY DEVELOPMENT FOR EARTH STATION DEMODULATOR APPLICATIONS. CODED MODULATION SYSTEM DEVELOPMENT Final Report
 SUSAN P. MILLER, J. MARK KAPPES, DAVID H. LAYER, and PETER N. JOHNSON Apr. 1990 95 p
 (Contract NAS3-24680)
 (NASA-CR-185149; NAS 1.26:185149; CTD-90/022) Avail: NTIS HC A05/MF A01 CSCL 17/2

A jointly optimized coded modulation system is described which was designed, built, and tested by COMSAT Laboratories for NASA LeRC which provides a bandwidth efficiency of 2 bits/s/Hz at an information rate of 160 Mbit/s. A high speed rate 8/9 encoder with a Viterbi decoder and an Octal PSK modem are used to achieve this. The BER performance is approximately 1 dB from the theoretically calculated value for this system at a BER of 5×10^{-7} under nominal conditions. The system operates in burst mode for downlink applications and tests have demonstrated very little degradation in performance with frequency and level offset. Unique word miss rate measurements were conducted which demonstrate reliable acquisition at low values of E_b/N_0 . Codec self tests have verified the performance of this subsystem in a stand alone mode. The codec is capable of operation at a 200 Mbit/s information rate as demonstrated using a codec test set which introduces noise digitally. The measured performance is within 0.2 dB of the computer simulated predictions. A gate array implementation of the most time critical element of the high speed Viterbi decoder was completed. This gate array add-compare-select chip significantly reduces the power consumption and improves the manufacturability of the decoder. This chip has general application in the implementation of high speed Viterbi decoders. Author

N90-20271*# Ohio State Univ., Columbus. ElectroScience Lab.
EFFECTS OF ADDITIONAL INTERFERING SIGNALS ON ADAPTIVE ARRAY PERFORMANCE
 RANDOLPH L. MOSES Sep. 1989 29 p
 (Contract NAG3-536)
 (NASA-CR-186508; NAS 1.26:186508; OSU-TR-716111-8) Avail: NTIS HC A03/MF A01 CSCL 20/14

The effects of additional interference signals on the performance of a fully adaptive array are considered. The case where the number of interference signals exceeds the number of array degrees of freedom is addressed. It is shown how performance is affected as a function of the number of array elements, the number of interference signals, and the directivity of the array antennas. By using directive auxiliary elements, the performance of the array can be as good as the performance when the additional interference signals are not present. Author

N90-21250*# National Aeronautics and Space Administration. Lewis Research Center, Cleveland, OH.
NUMERICAL ARC SEGMENTATION ALGORITHM FOR A RADIO CONFERENCE (NASARC), VERSION 4.0: USER'S MANUAL
 WAYNE A. WHYTE, JR., ANN O. HEYWARD, DENISE S.

PONCHAK, RODNEY L. SPENCE, and JOHN E. ZUZK 6 Oct. 1988 112 p
 (NASA-TM-101454; E-4987; NAS 1.15:101454) Avail: NTIS HC A06/MF A01 CSCL 17/2

The information in the NASARC (Version 4.0) Technical Manual (NASA-TM-101453) and NASARC (Version 4.0) User's Manual (NASA-TM-101454) relates to the state of Numerical Arc Segmentation Algorithm for a Radio Conference (NASARC) software development through November 1, 1988. The Technical Manual describes the NASARC concept and the algorithms used to implement the concept. The User's Manual provides information on computer system considerations, installation instructions, description of input files, and program operation instructions. Significant revisions were incorporated in the Version 4.0 software over prior versions. These revisions have further enhanced the modeling capabilities of the NASARC procedure and provide improved arrangements of predetermined arcs within the geostationary orbit. Array dimensions within the software were structured to fit within the currently available 12-megabyte memory capacity of the International Frequency Registration Board (IFRB) computer facility. A piecewise approach to predetermined arc generation in NASARC (Version 4.0) allows worldwide planning problem scenarios to be accommodated within computer run time and memory constraints with enhanced likelihood and ease of solution. Author

N90-21261*# National Aeronautics and Space Administration. Lewis Research Center, Cleveland, OH.
BIT-ERROR-RATE TESTING OF FIBER OPTIC DATA LINKS FOR MMIC-BASED PHASED ARRAY ANTENNAS
 K. A. SHALKHAUSER, R. R. KUNATH, and A. S. DARYOUSH (Drexel Univ., Philadelphia, PA.) Jan. 1990 10 p Presented at the Optoelectronics and Laser Applications in Science and Engineering Conference, Los Angeles, CA, 14-19 Jan. 1990; sponsored in part by the Society of Photo-Optical Instrumentation Engineers
 (NASA-TM-102523; E-5330; NAS 1.15:102523) Avail: NTIS HC A02/MF A01 CSCL 17/2

The measured bit-error-rate (BER) performance of a fiber optic data link to be used in satellite communications systems is presented and discussed. In the testing, the link was measured for its ability to carry high burst rate, serial-minimum shift keyed (SMSK) digital data similar to those used in actual space communications systems. The fiber optic data link, as part of a dual-segment injection-locked RF fiber optic link system, offers a means to distribute these signals to the many radiating elements of a phased array antenna. Test procedures, experimental arrangements, and test results are presented. Author

N90-21263*# National Aeronautics and Space Administration. Lewis Research Center, Cleveland, OH.
A NEW RECTANGULAR WAVEGUIDE TO COPLANAR WAVEGUIDE TRANSITION
 GEORGE E. PONCHAK and RAINEE N. SIMONS 1990 4 p Presented at the 1990 IEEE MTT-S International Microwave Symposium, Dallas, TX, 8-10 May 1990
 (Contract NAG3-816)
 (NASA-TM-102477; E-5264; NAS 1.15:102477) Avail: NTIS HC A01/MF A01 CSCL 20/14

A new rectangular waveguide to coplanar waveguide (CPW) transition is described. The transition uses a ridge in one of the broad walls of the waveguide and a nonradiating slot in the opposite wall to split and rotate the electromagnetic fields of the rectangular waveguide TE₁₀ mode into the CPW fields. Author

N90-24514*# Virginia Univ., Charlottesville. Computer Networks Lab.
AIRNET: A REAL-TIME COMMUNICATIONS NETWORK FOR AIRCRAFT Final Report
 ALFRED C. WEAVER, BRENDAN G. CAIN, M. ALEXANDER COLVIN, and ROBERT SIMONCIC Jun. 1990 47 p
 (Contract NAG3-630)

32 COMMUNICATIONS AND RADAR

(NASA-CR-186140; NAS 1.26:186140; UVA/528238/CS90/101)
Avail: NTIS HC A03/MF A01 CSCL 17/2

A real-time local area network was developed for use on aircraft and space vehicles. It uses token ring technology to provide high throughput, low latency, and high reliability. The system was implemented on PCs and PC/ATs operating on PCbus, and on Intel 8086/186/286/386s operating on Multibus. A standard IEEE 802.2 logical link control interface was provided to (optional) upper layer software; this permits the controls designer to utilize standard communications protocols (e.g., ISO, TCP/IP) if time permits, or to utilize a very fast link level protocol directly if speed is critical. Both unacknowledged datagram and reliable virtual circuit services are supported. A station operating an 8 MHz Intel 286 as a host can generate a sustained load of 1.8 megabits per second per station, and a 100-byte message can be delivered from the transmitter's user memory to the receiver's user memory, including all operating system and network overhead, in under 4 milliseconds.

Author

N90-24528*# Honeywell, Inc., Bloomington, MN. Sensors and Signal Processing Lab.

THE 30-GHZ MONOLITHIC RECEIVE MODULE Interim Report, 1 Nov. 1985 - 31 Oct. 1987

P. BAUHAHN, J. GEDDES, V. SOKOLOV, and T. CONTOLATIS
Apr. 1988 150 p

(Contract NAS3-23356)

(NASA-CR-180849; NAS 1.26:180849) Avail: NTIS HC A07/MF A01 CSCL 17/2

The fourth year progress is described on a program to develop a 27.5 to 30 GHz GaAs monolithic receive module for spaceborne-communication antenna feed array applications, and to deliver submodules for experimental evaluation. Program goals include an overall receive module noise figure of 5 dB, a 30 dB RF to IF gain with six levels of intermediate gain control, a five bit phase shifter, and a maximum power consumption of 250 mW. Submicron gate length single and dual gate FETs are described and applied in the development of monolithic gain control amplifiers and low noise amplifiers. A two-stage monolithic gain control amplifier based on ion implanted dual gate MESFETs was designed and fabricated. The gain control amplifier has a gain of 12 dB at 29 GHz with a gain control range of over 13 dB. A two-stage monolithic low noise amplifier based on ion implanted MESFETs which provides 7 dB gain with 6.2 dB noise figure at 29 GHz was also developed. An interconnected receive module containing LNA, gain control, and phase shifter submodules was built using the LNA and gain control ICs as well as a monolithic phase shifter developed previously under this program. The design, fabrication, and evaluation of this interconnected receiver is presented. Progress in the development of an RF/IF submodule containing a unique ion implanted diode mixer diode and a broadband balanced mixer monolithic IC with on-chip IF amplifier and the initial design of circuits for the RF portion of a two submodule receiver are also discussed.

Author

N90-26234*# New York Univ., New York. Dept. of Applied Science.

FIGURE OF MERIT STUDIES OF BEAM POWER CONCEPTS FOR ADVANCED SPACE EXPLORATION

GABRIEL MILLER and MURALI N. KADIRAMANGALAM 1990
52 p

(Contract NAG3-1048)

(NASA-CR-186720; NAS 1.26:186720) Avail: NTIS HC A04/MF A01 CSCL 20/14

Surface to surface, millimeter wavelength beam power systems for power transmission on the lunar base were investigated. Qualitative/quantitative analyses and technology assessment of 35, 110 and 140 GHz beam power systems were conducted. System characteristics including mass, stowage volume, cost and efficiency as a function of range and power level were calculated. A simple figure of merit analysis indicates that the 35 GHz system would be the preferred choice for lunar base applications, followed closely by the 110 GHz system. System parameters of a 35 GHz

beam power system appropriate for power transmission on a recent lunar base concept studied by NASA-Johnson and the necessary deployment sequence are suggested.

Author

N90-28768*# National Aeronautics and Space Administration. Lewis Research Center, Cleveland, OH.

RAIN-FADE SIMULATION AND POWER AUGMENTATION FOR SATELLITE COMMUNICATION SYSTEMS

KURT A. SHALKHAUSER, LAWRENCE A. NAGY, and JAMES S. SVOBODA (Sverdrup Technology, Inc., Brook Park, OH.) Sep. 1990 11 p

(Contract NAS3-25266)

(NASA-TM-103134; E-5476; NAS 1.15:103134) Avail: NTIS HC A03/MF A01 CSCL 17/2

The design and implementation of an automated rain-fade simulation and power augmentation system is presented. The system experimentally simulates and measures the effects of radiofrequency power fade on a 20 GHz communication link using a multimode travelling wave tube amplifier for loss compensation. Precision, computer-controlled attenuators are used in the fade simulation. Test plans for analog and digital testing are discussed.

Author

33

ELECTRONICS AND ELECTRICAL ENGINEERING

Includes test equipment and maintainability; components, e.g., tunnel diodes and transistors; microminiaturization; and integrated circuitry.

A90-11774* Case Western Reserve Univ., Cleveland, OH.

HIGH FREQUENCY GAALAS MODULATOR AND PHOTODETECTOR FOR PHASED ARRAY ANTENNA APPLICATIONS

P. C. CLASPY, C. M. CHOREY, S. M. HILL (Case Western Reserve University, Cleveland, OH), and K. B. BHASIN (NASA, Lewis Research Center, Cleveland, OH) IN: High frequency analog communications; Proceedings of the Meeting, Boston, MA, Sept. 6, 7, 1988. Bellingham, WA, Society of Photo-Optical Instrumentation Engineers, 1989, p. 151-156. Previously announced in STAR as N88-30048. refs

(Contract NCC3-99)

Copyright

A waveguide Mach-Zehnder electro-optic modulator and an interdigitated photoconductive detector designed to operate at 820 nm, fabricated on different GaAlAs/GaAs heterostructure materials, are being investigated for use in optical interconnects in phased array antenna systems. Measured optical attenuation effects in the modulator are discussed and the observed modulation performance up to 1 GHz is presented. Measurements of detector frequency response are described and results presented.

Author

A90-20861* Texas Instruments, Inc., Dallas.

ALGAAS/INGAAS HETEROSTRUCTURES WITH DOPED CHANNELS FOR DISCRETE DEVICES AND MONOLITHIC AMPLIFIERS

PAUL SAUNIER and HUA QUEN TSERNG (Texas Instruments Central Research Laboratories, Dallas) IEEE Transactions on Electron Devices (ISSN 0018-9383), vol. 36, Oct. 1989, p. 2231-2235. refs

(Contract NAS3-24239)

Copyright

AlGaAs/InGaAs/GaAs-type heterostructure with one or two doped channels have been used to fabricate both discrete devices and monolithic amplifiers for millimeter-wave operation. Maximum current densities of 1 A/mm and maximum transconductances of 530 mS/mm were obtained. 0.25 x 50 micron discrete devices delivered a power density of 1 W/mm with 2.9-dB gain and 25 percent efficiency at 60 GHz. A 100-micron monolithic one-stage

amplifier demonstrated 93 mW (0.93-W/mm power density) at 31.5 GHz with 4.2-dB gain and 29 percent efficiency. A record 34 percent efficiency was achieved with a 53.7-mW output power and 4.8-dB gain. I.E.

A90-25671* # National Aeronautics and Space Administration. Lewis Research Center, Cleveland, OH.

SATELLITE-MATRIX-SWITCHED, TIME-DIVISION-MULTIPLE-ACCESS NETWORK SIMULATOR
WILLIAM D. IVANCIC, MONTY ANDRO, LAWRENCE A. NAGY, JAMES M. BUDINGER, and MARY JO SHALKHAUSER (NASA, Lewis Research Center, Cleveland, OH) IN: AIAA International Communication Satellite Systems Conference and Exhibit, 13th, Los Angeles, CA, Mar. 11-15, 1990, Technical Papers. Part 2. Washington, DC, American Institute of Aeronautics and Astronautics, 1990, p. 595-612. Previously announced in STAR as N90-11915. refs

(AIAA PAPER 90-0848) Copyright

A versatile experimental Ka-band network simulator has been implemented at the NASA Lewis Research Center to demonstrate and evaluate a satellite-matrix-switched, time-division-multiple-access (SMS-TDMA) network and to evaluate future digital ground terminals and radiofrequency (RF) components. The simulator was implemented by using proof-of-concept RF components developed under NASA contracts and digital ground terminal and link simulation hardware developed at Lewis. This simulator provides many unique capabilities such as satellite range delay and variation simulation and rain fade simulation. All network parameters (e.g., signal-to-noise ratio, satellite range variation rate, burst density, and rain fade) are controlled and monitored by a central computer. The simulator is presently configured as a three-ground-terminal SMS-TDMA network. Author

A90-25686* # National Aeronautics and Space Administration. Lewis Research Center, Cleveland, OH.

CHARACTERIZATION OF TWO MMIC GAAS SWITCH MATRICES AT MICROWAVE FREQUENCIES

GENE FUJIKAWA (NASA, Lewis Research Center, Cleveland, OH) IN: AIAA International Communication Satellite Systems Conference and Exhibit, 13th, Los Angeles, CA, Mar. 11-15, 1990, Technical Papers. Part 2. Washington, DC, American Institute of Aeronautics and Astronautics, 1990, p. 731-740. Previously announced in STAR as N90-14273. refs

(Contract NAS3-24252; NAS3-24895)

(AIAA PAPER 90-0866) Copyright

Monolithic GaAs microwave switch matrices for use in satellite switched, time division multiple access communication systems were developed. Two monolithic GaAs MESFET switch matrices were fabricated; one for switching operation at intermediate frequencies, 3.5 to 6.0 GHz, and another for switching at radio frequencies, 17.7 to 20.2 GHz. Key switch parameters were measured for both switch matrices. Author

A90-25691* # Hughes Aircraft Co., Torrance, CA.

K-BAND TWT USING NEW DIAMOND ROD TECHNOLOGY

S. L. ALDANA and R. N. TAMASHIRO (Hughes Aircraft Co., Electron Dynamics Div., Torrance, CA) IN: AIAA International Communication Satellite Systems Conference and Exhibit, 13th, Los Angeles, CA, Mar. 11-15, 1990, Technical Papers. Part 2. Washington, DC, American Institute of Aeronautics and Astronautics, 1990, p. 766-770.

(Contract NAS3-24897)

(AIAA PAPER 90-0870) Copyright

A 75-W CW helix TWT for satellite communications systems is being developed to operate at 20 GHz with an efficiency goal of 60 percent. A nonbraided nonbonded diamond rod fabrication technique is used to develop the helix-type TWT. Techniques to enhance TWT efficiency are described, including the incorporation of a velocity tapered helix and a multistage graphite collector. Results from testing a breadboard TWT show a CW output power greater than 100 W and a 54.6 overall efficiency. R.B.

A90-33644* National Aeronautics and Space Administration. Lewis Research Center, Cleveland, OH.

KA-BAND PROPAGATION CHARACTERISTICS OF MICROSTRIP LINES ON GAAS SUBSTRATES AT CRYOGENIC TEMPERATURES

R. R. ROMANOFISKY, J. C. MARTINEZ, B. J. VIERGUTZ, and K. B. BHASIN (NASA, Lewis Research Center, Cleveland, OH) Microwave and Optical Technology Letters (ISSN 0895-2477), vol. 3, April 1990, p. 117-119.

Copyright

Effective permittivity and loss characteristics of gold microstrip lines on GaAs substrates were obtained by characterizing GaAs linear resonators at cryogenic temperatures (300 to 20 K) from 30-40 GHz. A slight decrease in effective permittivity and a significant reduction in loss were observed with lower temperatures. Author

A90-33726* North Carolina State Univ., Raleigh.

DEEP-LEVEL DOMINATED ELECTRICAL CHARACTERISTICS OF AU CONTACTS ON BETA-SiC

K. DAS, H. S. KONG, J. B. PETIT, J. W. BUMGARNER, R. F. DAVIS (North Carolina State University, Raleigh), and L. G. MATUS (NASA, Lewis Research Center, Cleveland, OH) Electrochemical Society, Journal (ISSN 0013-4651), vol. 137, May 1990, p. 1598-1603. refs

(Contract NAG3-782; N00014-85-K-0182-P005)

Copyright

Electrical characteristics of Au contacts on beta-SiC films, grown epitaxially on both nominal and off-axis (100) silicon substrates, are reported. An analysis of the logarithmic I-V plots of the Au/beta-SiC diodes revealed information pertaining to the deep states present in the materials. It was found that while the beta-SiC films grown on nominally (100) oriented substrates show the presence of two deep levels located between 0.26 and 0.38 eV below the conduction bandedge, the beta-SiC films deposited on off-axis substrates have only one deep level, located about 0.49 eV below the conduction bandedge for the 2-deg off (100) substrates and 0.57 eV for the 4-deg off (100) substrates. The presence of the shallower deep states in the beta-SiC films grown on nominal (100) substrates is attributed to the electrical activity of antiphase domain boundaries. I.S.

A90-36913* General Electric Co., Erie, PA.

A 2.5 KW CASCADED SCHWARZ CONVERTER FOR 20 KHZ POWER DISTRIBUTION

RUSSELL E. SHETLER (General Electric Co., Erie, PA) and THOMAS A. STUART (Toledo, University, OH) IN: PESC '89 - Annual IEEE Power Electronics Specialists Conference, 20th, Milwaukee, WI, June 26-29, 1989, Record. Volume 2. New York, Institute of Electrical and Electronics Engineers, Inc., 1989, p. 987-993. Research supported by USAF. refs

(Contract NAG3-708)

Copyright

Because it avoids the high currents in a parallel loaded capacitor, the cascaded Schwarz converter should offer better component utilization than converters with sinusoidal output voltages. The circuit is relatively easy to protect, and it provides a predictable trapezoidal voltage waveform that should be satisfactory for 20-kHz distribution systems. Analysis of the system is enhanced by plotting curves of normalized variables vs. gamma(1), where gamma(1) is proportional to the variable frequency of the first stage. Light-load operation is greatly improved by the addition of a power recycling rectifier bridge that is back biased at medium to heavy loads. Operation has been verified on a 2.5-kW circuit that uses input and output voltages in the same range as those anticipated for certain future spacecraft power systems. I.E.

A90-37301* Case Western Reserve Univ., Cleveland, OH.

MICROWAVE RESPONSE OF A HEMT PHOTOCONDUCTIVE DETECTOR

P. C. CLASPY (Case Western Reserve University, Cleveland, OH) and K. B. BHASIN (NASA, Lewis Research Center, Cleveland,

33 ELECTRONICS AND ELECTRICAL ENGINEERING

OH) Microwave and Optical Technology Letters (ISSN 0895-2477), vol. 2, Jan. 1989, p. 1-3. refs
Copyright

Interdigitated photoconductive detectors with 5-micron geometry have been fabricated on HEMT material and their optical response characteristics at 820 nm have been examined at dc and in the frequency range of 2-8 GHz. These have been compared with characteristics of similar 1-micron devices on MESFET material. The shapes of the frequency responses were found to differ, but the useful bandwidth of both types of devices was found to be similar. Author

A90-37864* Case Western Reserve Univ., Cleveland, OH.
COMPLEX PERMITTIVITY OF LANTHANUM ALUMINATE IN THE 20 TO 300 K TEMPERATURE RANGE FROM 26.5 TO 40.0 GHZ

F. A. MIRANDA, W. L. GORDON (Case Western Reserve University, Cleveland, OH), K. B. BHASIN, B. T. EBIHARA, V. O. HEINEN (NASA, Lewis Research Center, Cleveland, OH), and C. M. CHOREY (NASA, Lewis Research Center; Sverdrup Technology, Inc., Cleveland, OH) Microwave and Optical Technology Letters (ISSN 0895-2477), vol. 3, Jan. 1990, p. 11-13. refs
Copyright

Dielectric constants of microwave substrates are required in the design of superconducting microwave circuits at various temperatures. In this paper, the results are reported of a study of the complex permittivity of the newly developed lanthanum aluminate (LaAlO_3) substrate, in the 20 to 300 K temperature range at frequencies from 26.5 to 40.0 GHz. The value of the complex permittivity was obtained by measuring the sample scattering parameters using a microwave waveguide technique. It is observed that, while the dielectric constant did not change appreciably with frequency, its value decreased by approximately 14 percent from room temperature to 20 K. Author

A90-38084* Sverdrup Technology, Inc., Middleburg Heights, OH.

FREQUENCY DOMAIN MODEL FOR ANALYSIS OF PARALLELED, SERIES-OUTPUT-CONNECTED MAPHAM INVERTERS

ANDREW S. BRUSH (Sverdrup Technology, Inc., Middleburg Heights, OH), RICHARD C. SUNDBERG (General Dynamics Corp., San Diego, CA), and ROBERT M. BUTTON (NASA, Lewis Research Center, Cleveland, OH) IN: IECEC-89; Proceedings of the Twenty-fourth Intersociety Energy Conversion Engineering Conference, Washington, DC, Aug. 6-11, 1989. Volume 1. New York, Institute of Electrical and Electronics Engineers, 1989, p. 333-338. Previously announced in STAR as N89-26149. refs
(Contract NAS3-25266)
Copyright

The Mapham resonant inverter is characterized as a two-port network driven by a selected periodic voltage. The two-port model is then used to model a pair of Mapham inverters connected in series and employing phasor voltage regulation. It is shown that the model is useful for predicting power output in paralleled inverter units, and for predicting harmonic current output of inverter pairs, using standard power flow techniques. Some sample results are compared to data obtained from testing hardware inverters. Author

A90-38119*# National Aeronautics and Space Administration. Lewis Research Center, Cleveland, OH.

VARIABLE SPEED INDUCTION MOTOR OPERATION FROM A 20-KHZ POWER BUS

IRVING G. HANSEN (NASA, Lewis Research Center, Cleveland, OH) IN: IECEC-89; Proceedings of the Twenty-fourth Intersociety Energy Conversion Engineering Conference, Washington, DC, Aug. 6-11, 1989. Volume 1. New York, Institute of Electrical and Electronics Engineers, 1989, p. 561-565. Previously announced in STAR as N89-25271. refs

Induction motors are recognized for their simple rugged construction to date, however, their application to variable speed or servo drives has been hampered by limitations on their control.

Induction motor drives tend to be complex and to display troublesome low speed characteristics due in part to nonsinusoidal driving voltages. A technique was developed which involves direct synthesis of sinusoidal driving voltages from a high frequency power bus and independent control of frequency and voltages. Separation of frequency and voltage allows independent control of rotor and stator flux, full four-quadrant operation, and instantaneous torque control. Recent test results, current status of the technology, and proposed aerospace applications will be discussed. Author

A90-38124* National Aeronautics and Space Administration. Lewis Research Center, Cleveland, OH.

20 KHZ MAIN INVERTER UNIT

S. HUSSEY (NASA, Lewis Research Center, Cleveland, OH) IN: IECEC-89; Proceedings of the Twenty-fourth Intersociety Energy Conversion Engineering Conference, Washington, DC, Aug. 6-11, 1989. Volume 1. New York, Institute of Electrical and Electronics Engineers, 1989, p. 591-595.
(Contract NAS3-24653)
Copyright

A proof-of-concept main inverter unit has demonstrated the operation of a pulse-width-modulated parallel resonant power stage topology as a 20-kHz ac power source driver, showing simple output regulation, parallel operation, power sharing and short-circuit operation. The use of a two-stage dc input filter controls the electromagnetic compatibility (EMC) characteristics of the dc power bus, and the use of an ac harmonic trap controls the EMC characteristics of the 20-kHz ac power bus. I.E. 9@

A90-38125* General Dynamics Corp., San Diego, CA.
DISTORTION AND REGULATION CHARACTERIZATION OF A MAPHAM INVERTER

RICHARD C. SUNDBERG (General Dynamics Corp., Space Systems Div., San Diego, CA), ANDREW S. BRUSH (NASA, Lewis Research Center; Sverdrup Technology, Inc., Cleveland, OH), ROBERT M. BUTTON (NASA, Lewis Research Center, Cleveland, OH), and ALEXANDER G. PATTERSON (NASA, Lewis Research Center; Analox Corp., Cleveland, OH) IN: IECEC-89; Proceedings of the Twenty-fourth Intersociety Energy Conversion Engineering Conference, Washington, DC, Aug. 6-11, 1989. Volume 1. New York, Institute of Electrical and Electronics Engineers, 1989, p. 597-604. Previously announced in STAR as N89-26148. refs
Copyright

Output-voltage total harmonic distortion (THD) of a 20-kHz, 6-kVA Mapham resonant inverter is characterized as a function of its switching-to-resonant frequency ratio, $f(s)/f(r)$, using the EASY5 Engineering Analysis System. EASY5 circuit simulation results are compared with hardware test results to verify the accuracy of the simulations. The effects of load on the THD versus $f(s)/f(r)$ is investigated for resistive, leading, and lagging power factor load impedances. The effect of the series output capacitor on the Mapham inverter output-voltage distortion and inherent load regulation is characterized under loads of various power factors and magnitudes. An optimum series capacitor value which improves the inherent load regulation to better than 3 percent is identified. The optimum series capacitor value is different from the value predicted from a modeled frequency domain analysis. An explanation is proposed which takes into account the conduction overlap in the inductor pairs during steady-state inverter operation, which decreases the effective inductance of a Mapham inverter. A fault protection and current limit method is discussed which allows the Mapham inverter to operate into a short circuit, even when the inverter resonant circuit becomes overdamped. Author

A90-38128* Wisconsin Univ., Madison.

PERFORMANCE TESTING OF A HIGH FREQUENCY LINK CONVERTER FOR SPACE STATION POWER DISTRIBUTION SYSTEM

S. K. SUL, I. ALAN, and T. A. LIPO (Wisconsin, University, Madison) IN: IECEC-89; Proceedings of the Twenty-fourth Intersociety Energy Conversion Engineering Conference, Washington, DC, Aug. 6-11, 1989. Volume 1. New York, Institute

of Electrical and Electronics Engineers, 1989, p. 617-623. refs
(Contract NAG3-786)
Copyright

The testing of a brassboard version of a 20-kHz high-frequency ac voltage link prototype converter dynamics for Space Station application is presented. The converter is based on a three-phase six-pulse bridge concept. The testing includes details of the operation of the converter when it is driving an induction machine source/load. By adapting a field orientation controller (FOC) to the converter, four-quadrant operation of the induction machine from the converter has been achieved. Circuit modifications carried out to improve the performance of the converter are described. The performance of two 400-Hz induction machines powered by the converter with simple V/f regulation mode is reported. The testing and performance results for the converter utilizing the FOC, which provides the capability for rapid torque changes, speed reversal, and four-quadrant operation, are reported. I.E.

A90-38134* National Aeronautics and Space Administration. Lewis Research Center, Cleveland, OH.

POWER TRANSMISSION CABLE DEVELOPMENT FOR THE SPACE STATION FREEDOM ELECTRICAL POWER SYSTEM

GREGORY V. SCHMITZ (NASA, Lewis Research Center, Cleveland, OH) and JOHN J. BIESS (TRW Space and Technology Group, Redondo Beach, CA) IN: IECEC-89; Proceedings of the Twenty-fourth Intersociety Energy Conversion Engineering Conference, Washington, DC, Aug. 6-11, 1989. Volume 1. New York, Institute of Electrical and Electronics Engineers, 1989, p. 657-661.

Copyright

Power transmission cable is presently being evaluated under a NASA Lewis Research Center advanced development contract for application in the Space Station Freedom (SSF) electrical power system (EPS). Evaluation testing has been performed by TRW and NASA Lewis Research Center. The results of this development contract are presented. The primary cable design goals are to provide (1) a low characteristic inductance to minimize line voltage drop at 20 kHz, (2) electromagnetic compatibility control of the 20-kHz ac power current, (3) a physical configuration that minimizes ac resistance and (4) release of trapped air for corona-free operation. I.E.

A90-38144* National Aeronautics and Space Administration. Lewis Research Center, Cleveland, OH.

MAGNIFICATION OF STARTING TORQUES OF DC MOTORS BY MAXIMUM POWER POINT TRACKERS IN PHOTOVOLTAIC SYSTEMS

J. APPELBAUM (NASA, Lewis Research Center, Cleveland, OH) and S. SINGER (Colorado, University, Colorado Springs) IN: IECEC-89; Proceedings of the Twenty-fourth Intersociety Energy Conversion Engineering Conference, Washington, DC, Aug. 6-11, 1989. Volume 2. New York, Institute of Electrical and Electronics Engineers, 1989, p. 749-754. refs

Copyright

A calculation of the starting torque ratio of permanent magnet, series, and shunt-excited dc motors powered by solar cell arrays is presented for two cases, i.e., with and without a maximum-power-point tracker (MPPT). Defining motor torque magnification by the ratio of the motor torque with an MPPT to the motor torque without an MPPT, a magnification of 3 for the permanent magnet motor and a magnification of 7 for both the series and shunt motors are obtained. The study also shows that all motor types are less sensitive to solar insolation variation in systems including MPPTs as compared to systems without MPPTs. I.E.

A90-38275* National Aeronautics and Space Administration. Lewis Research Center, Cleveland, OH.

20 KHZ, 25 KVA NODE POWER TRANSFORMER

S. HUSSEY (NASA, Lewis Research Center, Cleveland, OH) IN: IECEC-89; Proceedings of the Twenty-fourth Intersociety Energy Conversion Engineering Conference, Washington, DC, Aug. 6-11, 1989. Volume 6. New York, Institute of Electrical and Electronics

Engineers, 1989, p. 2667-2671.
(Contract NAS3-24667)

Copyright

The electrical and mechanical design information and the electrical and thermal testing performed on the 440-208-V rms, 20-kHz, 25-kVa prototype node transformer are summarized. The calculated efficiency of the node transformer is 99.3 percent based on core loss and copper loss test data, and its maximum calculated load regulation is 0.7 percent. The node transformer has a weight of 19.7 lb and has a power density of 0.8 lb/kW. The hot-spot temperature rise is estimated to be 33 C above the cold plate mounting base. This proof-of-concept transformer design is a viable candidate for the space station Freedom application. I.E.

A90-39761* Oberlin Coll., OH.

SIMPLE EVAPORATION CONTROLLER FOR THIN-FILM DEPOSITION FROM A RESISTIVELY HEATED BOAT

JOHN H. SCOFIELD, LOU BAJUK, and WILLIAM MOHLER (Oberlin College, OH) Review of Scientific Instruments (ISSN 0034-6748), vol. 61, July 1990, p. 1994-1996.

(Contract NAG3-885)

Copyright

A simple, inexpensive circuit is described for switching the current through a resistively heated evaporation boat during thin-film deposition. The circuit uses a silicon-controlled rectifier (SCR) to switch the 0-15-A current in the primary of a 2-kV A step-down transformer that supplies the 0-200-A current to an evaporation boat. The circuit is controlled by a 0-10 V-dc signal similar to that furnished by an Inficon XTC deposition-rate controller. This circuit may be assembled from a handful of parts for a cost of about \$400, nearly one-tenth the cost of similar commercial units. Minimum construction is required, since the circuit is built around an off-the-shelf, self-contained SCR unit. Author

A90-41238* National Aeronautics and Space Administration. Lewis Research Center, Cleveland, OH.

OPTICAL DETECTORS FOR GAAS MMIC INTEGRATION - TECHNOLOGY ASSESSMENT

P. C. CLASPY and K. B. BHASIN (NASA, Lewis Research Center, Cleveland, OH) IN: Optical technology for microwave applications IV; Proceedings of the Meeting, Orlando, FL, Mar. 28, 29, 1989. Bellingham, WA, Society of Photo-Optical Instrumentation Engineers, 1989, p. 53-60. Previously announced in STAR as N89-22020. refs

Copyright

Fiber optic links are being considered to transmit digital and analog signals in phased array antenna feed networks in space communications systems. The radiating elements in these arrays will be GaAs monolithic microwave integrated circuits (MMIC's) in numbers ranging from a few hundred to several thousand. If such optical interconnects are to be practical it appears essential that the associated components, including detectors, be monolithically integrated on the same chip as the microwave circuitry. The general issue of monolithic integration of microwave and optoelectronic components is addressed from the point of view of fabrication technology and compatibility. Particular attention is given to the fabrication technology of various types of GaAs optical detectors that are designed to operate at a wavelength of 830 nm. Author

A90-41605* National Aeronautics and Space Administration. Lewis Research Center, Cleveland, OH.

COAX-TO-CHANNELISED COPLANAR WAVEGUIDE IN-PHASE N-WAY, RADIAL POWER DIVIDER

R. N. SIMONS and G. E. PONCHAK (NASA, Lewis Research Center, Cleveland, OH) Electronics Letters (ISSN 0013-5194), vol. 26, May 24, 1990, p. 754-756. refs

Copyright

A novel nonplanar, wideband power divider which makes use of a coax-to-CCPW transition is demonstrated. The transition utilizes a coaxial transformer whose outer conductor is slotted along the length for RF power division and also for exciting the CCPWs in equal amplitude and phase at the radial junction. The measured (8-16 GHz) excess insertion loss at the output ports is 0.5 dB for

33 ELECTRONICS AND ELECTRICAL ENGINEERING

a four-way divider. The amplitude and phase balance are within 0.5 dB and 5 deg, respectively. The power divider should find applications in the feed network of phased arrays. Author

A90-41700* National Aeronautics and Space Administration. Lewis Research Center, Cleveland, OH.

CONTROL OF A GAAS MONOLITHIC KA-BAND PHASE SHIFTER USING A HIGH-SPEED OPTICAL INTERCONNECT

K. B. BHASIN, R. R. ROMANOVSKY (NASA, Lewis Research Center, Cleveland, OH), P. C. CLASPY, M. A. RICHARD (Case Western Reserve University, Cleveland, OH), M. BENDETT (Honeywell Sensors and Signal Processing Laboratory, Bloomington, MN) et al. IEEE Transactions on Microwave Theory and Techniques (ISSN 0018-9480), vol. 38, May 1990, p. 686-688. refs

Copyright

The use of a high-speed optical interconnect in the control of a Ka-band GaAs monolithic phase shifter is described. A 16-b serial control signal was used to modulate the output of a laser transmitter, and the transmitted optical signal was detected and demultiplexed into 16 parallel electrical outputs using a high-speed hybrid GaAs optoelectronic integrated circuit. Four of the parallel output lines were interfaced to the 4-b phase shifter, and high-speed, optically controlled switching of the phase shifter was observed at clock frequencies to 30 MHz using an interferometric technique. I.E.

A90-42400* National Aeronautics and Space Administration. Lewis Research Center, Cleveland, OH.

REFLECTING BOUNDARY CONDITIONS FOR GRADED P-N JUNCTIONS

S. E. SCHACHAM (NASA, Lewis Research Center, Cleveland, OH) Journal of Applied Physics (ISSN 0021-8979), vol. 68, July 15, 1990, p. 865-867. refs

Copyright

In a graded junction, the formalism for handling reflecting boundary conditions must be modified. Since a significant drift term is present, zero recombination velocity at the surface does not imply a zero excess carrier gradient but rather zero overall flux. A model for analyzing p-n junctions fabricated by implantation or diffusion is presented, assuming the dominant recombination mechanism in the graded region is Auger. The model enables optimization of diode design. By proper selection of parameters, mainly by reducing surface concentration or by increasing the steepness of the dopant profile, it is possible to drastically reduce the saturation current generated by the graded region. Author

A90-47108*# Massachusetts Inst. of Tech., Cambridge. THEORY OF PLASMA CONTACTORS IN GROUND-BASED EXPERIMENTS AND LOW EARTH ORBIT

M. J. GERVER, D. E. HASTINGS, and M. R. OBERHARDT (MIT, Cambridge, MA) Journal of Spacecraft and Rockets (ISSN 0022-4650), vol. 27, July-Aug. 1990, p. 391-402. refs (Contract NAG3-681)

Copyright

An examination of several models of electron collection by plasma contactors leads to a definition of the range of validity and applicability for each model. It is noted that most present ground-based experiments are of limited relevance to space applications of plasma contactors, since they operate in a regime where the magnetic field and effective collisions are at most only marginally important. An exception is the experiment of Stenzel and Urrutia (1986), which examined a plasma whose electron Larmor radius was small by comparison to the scale of the potential, and in which the anomalous transport of electrons across the magnetic field was important. The enhanced electron current was not continuous in time, but occurred in periodic bursts as the instabilities periodically emerged, saturated, and decayed. O.C.

A90-48492* Texas Instruments, Inc., Dallas. DOPED-CHANNEL HETEROJUNCTION STRUCTURES FOR MILLIMETER-WAVE DISCRETE DEVICES AND MMICS

P. SAUNIER, Y. C. KAO, A. M. KHATIBZADEH, H. Q. TSERNG,

and K. BRADSHAW (Texas Instruments Central Research Laboratories, Dallas) IN: MILCOM '89 - IEEE Military Communications Conference, Boston, MA, Oct. 15-18, 1989, Conference Record. Volume 3. New York, Institute of Electrical and Electronics Engineers, Inc., 1989, p. 730-734. refs (Contract NAS3-24239)

Copyright

AlGaAs/InGaAs/GaAs-type heterostructures with one or two channels have been used to fabricate both discrete devices and monolithic amplifiers for millimeter-wave operation. The authors report that 0.25-micron x 50-micron discrete devices delivered a power density of 1 W/mm with 2.9-dB gain and 25 percent efficiency at 60 GHz. A 100-micron monolithic single-stage amplifier demonstrated a record 40 percent efficiency at 32 GHz, and a two-stage monolithic amplifier achieved a record 31.3 percent efficiency with 72-mW power and 13-dB gain at 32 GHz. I.E.

A90-51168* National Aeronautics and Space Administration. Lewis Research Center, Cleveland, OH.

ON-BOARD SWITCHING AND PROCESSING

JOSEPH L. HARROLD, JAMES M. BUDINGER, and GRADY H. STEVENS (NASA, Lewis Research Center, Cleveland, OH) IEEE, Proceedings (ISSN 0018-9219), vol. 78, July 1990, p. 1206-1213. refs

Copyright

Findings from NASA's space electronics division's (SED's) advanced systems studies related to future communications satellite services that will require onboard switching and processing technology are reviewed. SED's digital signal switching and processing technology program is reviewed. This program responds to specific systems technology development needs for enabling commercial development of future satellite services. The technologies include: modulators, demodulators, and forward error-correction hardware for space- and ground-based applications; onboard information switching and processing, onboard network control, and health monitoring; and cost-efficient ground terminals. The in-house systems integration, test, and evaluation (SITE) project, which includes a laboratory testbed for evaluating technology in a simulated systems environment, is reviewed. I.E.

N90-10166*# National Aeronautics and Space Administration. Lewis Research Center, Cleveland, OH.

CENTRAL ELECTRICAL UTILITY POWER FOR A SATELLITE RING CITY IN LOW EARTH ORBIT SPACE

IRA T. MYERS, KARL A. FAYMON, and A. D. PATTON (Texas A&M Univ., College Station.) IN: NASA. Langley Research Center, Second Beamed Space-Power Workshop p 409-418 Jul. 1989 Avail: NTIS HC A19/MF A03 CSCL 10C

Information is given in viewgraph form on central electrical power for a satellite ring city, defined as a group of large free flyers of 10 to 20 units with perhaps 100 people in each unit, and organized in a circle so that power can be fed from a central location. The free flyers would be located at 300 to 700 miles in altitude, and spaced about a kilometer apart. Potential activities of a ring city are listed as well as the electrical power needs. Information is given on costs and individual and centralized solar arrays and nuclear reactor systems. Author

N90-11943*# National Aeronautics and Space Administration. Lewis Research Center, Cleveland, OH.

CHANNELIZED COPLANAR WAVEGUIDE PIN-DIODE SWITCHES

G. E. PONCHAK and R. N. SIMONS (Case Western Reserve Univ., Cleveland, OH.) Nov. 1989 10 p Presented at the European Microwave Conference, London, England, 8 Sep. 1989; sponsored in part by IEEE, IEE, URSI, and EUREL (NASA-TM-102289; E-4959; NAS 1.15:102289) Avail: NTIS HC A02/MF A01 CSCL 09/1

Three different types of p-i-n diode, reflective CPW switches are presented. The first two switches are the series and the shunt mounted diode switches. Each has achieved greater than 15 dB of isolation over a broad bandwidth. The third switch is a narrow

band, high isolation switched filter which has achieved 19 dB of isolation. Equivalent circuits and measured performance for each switch is presented. Author

N90-14467*# Wisconsin Univ., Madison. Dept. of Electrical and Computer Engineering.

HIGH POWER DENSITY DC/DC CONVERTER: SELECTION OF CONVERTER TOPOLOGY Interim Report, Jul. 1987 - Jun. 1988

DEEPAKRAJ M. DIVAN 3 Jan. 1990 92 p

(Contract NAG3-804)

(NASA-CR-186129; NAS 1.26:186129) Avail: NTIS HC A05/MF A01 CSCL 09/3

The work involved in the identification and selection of a suitable converter topology is described. Three new dc/dc converter topologies are proposed: Phase-Shifted Single Active Bridge DC/DC Converter; Single Phase Dual Active Bridges DC/DC Converter; and Three Phase Dual Active Bridges DC/DC Converter (Topology C). The salient features of these topologies are: (1) All are minimal in structure, i.e., each consists of an input and output bridge, input and output filter and a transformer, all components essential for a high power dc/dc conversion process; (2) All devices of both the bridges can operate under near zero-voltage conditions, making possible a reduction of device switching losses and hence, an increase in switching frequency; (3) All circuits operate at a constant frequency, thus simplifying the task of the magnetic and filter elements; (4) Since, the leakage inductance of the transformer is used as the main current transfer element, problems associated with the diode reverse recovery are eliminated. Also, this mode of operation allows easy paralleling of multiple modules for extending the power capacity of the system; (5) All circuits are least sensitive to parasitic impedances, in fact the parasitics are efficiently utilized; and (6) The soft switching transitions, result in low electromagnetic interference. A detailed analysis of each topology was carried out. Based on the analysis, the various device and component ratings for each topology operating at an optimum point, and under the given specifications, are tabulated and discussed. Author

N90-17009*# National Aeronautics and Space Administration. Lewis Research Center, Cleveland, OH.

UNIVERSAL NONDESTRUCTIVE MM-WAVE INTEGRATED CIRCUIT TEST FIXTURE Patent Application

ROBERT R. ROMANOFISKY, inventor (to NASA) and KURT A. SHALKHAUSER, inventor (to NASA) 10 Aug. 1989 17 p (NASA-CASE-LEW-14746-1; US-PATENT-APPL-SN-392239; NAS 1.71:LEW-14746-1) Avail: NTIS HC A03/MF A01 CSCL 09/1

Monolithic microwave integrated circuit (MMIC) test includes a bias module having spring-loaded contacts which electrically engage member. RF frequency is applied to and passed from the chip carrier by chamfered edges of ridges in the waveguide passages of housings which are removably attached to the base member. Thru, Delay, and Short calibration standards having dimensions identical to those of the chip carrier assure accuracy and reliability of the test. The MMIC chip fits in an opening in the chip carrier with the boundaries of the MMIC lying on movable reference planes thereby establishing accuracy and flexibility. NASA

N90-17987*# Cincinnati Univ., OH. Dept. of Electrical and Computer Engineering.

ELECTRON-BEAM INDUCED DAMAGE IN THIN INSULATING FILMS ON COMPOUND SEMICONDUCTORS M.S. Thesis, 1988

DRAGAN M. PANTIC Nov. 1989 121 p

(Contract NCC3-75)

(NASA-CR-185177; NAS 1.26:185177) Avail: NTIS HC A06/MF A01 CSCL 09/1

Phosphorus rich plasma enhanced chemical vapor deposition (PECVD) of silicon nitride and silicon dioxide films on n-type indium phosphide (InP) substrates were exposed to electron-beam irradiation in the 5 to 40 keV range for the purpose of characterizing the damage induced in the dielectric. The electron-beam exposure was on the range of $10(\exp -7)$ to $10(\exp -3)$ C/sq cm. The damage to the devices was characterized by capacitance-voltage

(C-V) measurements of the metal insulator semiconductor (MIS) capacitors. These results were compared to results obtained for radiation damage of thermal silicon dioxide on silicon (Si) MOS capacitors with similar exposures. The radiation induced damage in the PECVD silicon nitride films on InP was successfully annealed out in an hydrogen/nitrogen (H₂/N₂) ambient at 400 C for 15 min. The PECVD silicon dioxide films on InP had the least radiation damage, while the thermal silicon dioxide films on Si had the most radiation damage. Author

N90-18634*# National Aeronautics and Space Administration. Lewis Research Center, Cleveland, OH.

PERFORMANCE AND MODELING OF SUPERCONDUCTING RING RESONATORS AT MILLIMETER-WAVE FREQUENCIES

K. B. BHASIN, C. M. CHOREY, J. D. WARNER, R. R. ROMANOFISKY, V. O. HEINEN, K. S. KONG, H. Y. LEE, and T. ITOH (Texas Univ., Austin.) 1990 9 p Prepared for presentation at the 1990 IEEE MIT-S International Microwave Symposium, Dallas, TX, 8-10 May 1990

(NASA-TM-102526; E-5334; NAS 1.15:102526) Avail: NTIS HC A02/MF A01 CSCL 09/1

Microstrip ring resonators operating at 35 GHz were fabricated from laser ablated YBCO thin films deposited on lanthanum aluminate substrates. They were measured over a range of temperatures and their performance compared to identical resonators made of evaporated gold. Below 60 Kelvin the superconducting strip performed better than the gold, reaching an unloaded Q approximately 1.5 times that of gold at 25 K. A shift in the resonant frequency follows the form predicted by the London equations. The Phenomenological Loss Equivalence Method is applied to the ring resonator and the theoretically calculated Q values are compared to the experimental results. Author

N90-19484*# National Aeronautics and Space Administration. Lewis Research Center, Cleveland, OH.

HIGH POWER, HIGH FREQUENCY COMPONENT TEST FACILITY

MARY ELLEN ROTH and WALTER KRAWCZONEK (Sverdrup Technology, Inc., Cleveland, OH.) Feb. 1990 12 p

(NASA-TM-102500; E-5297; NAS 1.15:102500) Avail: NTIS HC A03/MF A01 CSCL 09/1

The NASA Lewis Research Center has available a high frequency, high power laboratory facility for testing various components of aerospace and/or terrestrial power systems. This facility is described here. All of its capabilities and potential applications are detailed. Author

N90-20286*# National Aeronautics and Space Administration. Lewis Research Center, Cleveland, OH.

EXPERIMENTAL INVESTIGATIONS ON CHANNELIZED COPLANAR WAVEGUIDE

RAINEE N. SIMONS, GEORGE E. PONCHAK, KONSTANTINAS S. MARTZAKLIS (Akron Univ., OH.), and ROBERT R. ROMANOFISKY Apr. 1990 17 p

(Contract NAG3-816)

(NASA-TM-102494; E-5285; NAS 1.15:102494) Avail: NTIS HC A03/MF A01 CSCL 09/1

A new variant of coplanar waveguide (CPW) which was termed channelized coplanar waveguide (CCPW) is presented. Measured propagation characteristics for CCPW such as epsilon(eff) and unloaded Q as a function of geometrical parameters and frequency are presented. The measured and modeled epsilon(eff) are also compared. Equivalent circuit model element values are presented for a CCPW open circuit and a CCPW right angle bend. A CCPW matched T-junction, matched 1:3 junction, and a novel coax-to-CCPW in-phase, N-way, radial power divider are also demonstrated. Author

N90-20301*# National Aeronautics and Space Administration. Lewis Research Center, Cleveland, OH.

POWER CONDITIONING TECHNIQUES

E. D. BAUMANN 1989 7 p Presented at the Neutral Particle Beam Technology Symposium, Monterey, CA, 18-21 Jul. 1989;

33 ELECTRONICS AND ELECTRICAL ENGINEERING

sponsored by Strategic Defense Initiative Organization

(Contract MIPR-FY1455-89-N0655)

(NASA-TM-102577; E-5408; NAS 1.15:102577) Avail: NTIS HC A02/MF A01 CSCL 09/3

The technological developments required to reduce the electrical power system component weights from the state-of-the-art 2.0 kg/kW to the range of 0.1 to 0.2 kg/kW are discussed. Power level requirements and their trends in aerospace applications are identified and presented. The projected weight and launch costs for a 1MW power converter built using state-of-the-art technology are established to illustrate the need for reliable, ultralightweight advanced power components. The key factors affecting converter weight are given and some of the tradeoffs between component ratings and circuit topology are identified. The weight and launch costs for a 1MW converter using 0.1 kg/kW technology are presented. Finally, the objectives and goals of the Multi-Megawatt Program at the NASA Lewis Research Center, which is funded by the SDIO through the Air Force, are given.

Author

N90-21271*# National Aeronautics and Space Administration. Lewis Research Center, Cleveland, OH.

ADVANCED LAUNCH SYSTEM (ALS): ELECTRICAL ACTUATION AND POWER SYSTEMS IMPROVE OPERABILITY AND COST PICTURE

GALE R. SUNDBERG 1990 8 p Proposed for presentation at the National Aerospace and Electronics Conference, Dayton, OH, 21-25 May 1990; sponsored by IEEE (NASA-TM-102547; E-5358; NAS 1.15:102547) Avail: NTIS HC A02/MF A01 CSCL 09/3

To obtain the Advanced Launch System (ALS) primary goals of reduced costs and improved operability, there must be significant reductions in the launch operations and servicing requirements relative to current vehicle designs and practices. One of the primary methods for achieving these goals is by using vehicle electrical power system and controls for all actuation and avionics requirements. A brief status review of the ALS and its associated Advanced Development Program is presented to demonstrate maturation of those technologies that will help meet the overall operability and cost goals. The electric power and actuation systems are highlighted as a specific technology ready not only to meet the stringent ALS goals (cryogenic field valves and thrust vector controls with peak power demands to 75 hp), but also those of other launch vehicles, military and civilian aircraft, lunar/Martian vehicles, and a multitude of commercial applications.

Author

N90-21272*# National Aeronautics and Space Administration. Lewis Research Center, Cleveland, OH.

ELECTROMECHANICAL ACTUATION FOR THRUST VECTOR CONTROL APPLICATIONS

MARY ELLEN ROTH 1990 5 p Proposed for presentation at the National Aerospace and Electronics Conference (NAECON), Dayton, OH, 21-25 May 1990; sponsored by IEEE (Contract NAS3-25799) (NASA-TM-102548; E-5359; NAS 1.15:102548) Avail: NTIS HC A01/MF A01 CSCL 09/1

At present, actuation systems for the Thrust Vector Control (TVC) for launch vehicles are hydraulic systems. The Advanced Launch System (ALS), a joint initiative between NASA and the Air Force, is a launch vehicle that is designed to be cost effective, highly reliable and operationally efficient with a goal of reducing the cost per pound to orbit. As part of this initiative, an electromechanical actuation system is being developed as an attractive alternative to the hydraulic systems used today. NASA-Lewis is developing and demonstrating an Induction Motor Controller Actuation System with a 40 hp peak rating. The controller will integrate 20 kHz resonant link Power Management and Distribution (PMAD) technology and Pulse Population Modulation (PPM) techniques to implement Field Oriented Vector Control (FOVC) of a new advanced induction motor. Through PPM, multiphase variable frequency, variable voltage waveforms can be synthesized from the 20 kHz source. FOVC shows that varying

both the voltage and frequency and their ratio (V/F), permits independent control of both torque and speed while operating at maximum efficiency at any point on the torque-speed curve. The driver and the FOVC will be microprocessor controlled. For increased system reliability, a Built-in Test (BITE) capability will be included. This involves introducing testability into the design of a system such that testing is calibrated and exercised during the design, manufacturing, maintenance and prelaunch activities. An actuator will be integrated with the motor controller for performance testing of the EMA TVC system. The design and fabrication of the motor controller is being done by General Dynamics Space Systems Division. The University of Wisconsin-Madison will assist in the design of the advanced induction motor and in the implementation of the FOVC theory. A 75 hp electronically controlled dynamometer will be used to test the motor controller in all four quadrants of operation using flight type control algorithms. Integrated testing of the controller and actuator will be conducted at a facility yet to be named. The EMA system described above is discussed in detail.

Author

N90-21273*# National Aeronautics and Space Administration. Lewis Research Center, Cleveland, OH.

COPLANAR WAVEGUIDE FED PHASED ARRAY ANTENNA

RAINEE N. SIMONS, GEORGE E. PONCHAK, R. Q. LEE, and N. S. FERNANDEZ (Puerto Rico Univ., Rio Piedras.) 1990 6 p Proposed for presentation at the 1990 IEEE AP-S International Symposium and URSI Radio Science Meeting, Dallas, TX, 7-1 May 1990

(NASA-TM-102522; E-5327; NAS 1.15:102522) Avail: NTIS HC A02/MF A01 CSCL 09/1

A K-band four element linear phased array was designed and tested. Coplanar waveguide (CPW) is used for the microwave distribution system. A CPW to twin strip transition is used to interface with the printed dipole antennas. MMIC phased shifters are used for phase control.

Author

N90-21274*# National Aeronautics and Space Administration. Lewis Research Center, Cleveland, OH.

RECENT RESULTS FROM ADVANCED RESEARCH ON SPACE SOLAR CELLS AT NASA

DENNIS J. FLOOD 1990 9 p Presented at the International Solar Energy Conference, Miami, FL, 1-4 Apr. 1990; sponsored by ASME

(NASA-TM-102485; E-5251; NAS 1.15:102485) Avail: NTIS HC A02/MF A01 CSCL 10/1

The NASA program in space photovoltaic research and development encompasses a wide range of emerging options for future space power systems, and includes both cell and array technology development. The long range goals are to develop technology capable of achieving 300 W/kg for planar arrays, and 300 W/sq m for concentrator arrays. InP and GaAs planar and concentrator cell technologies are under investigation for their potential high efficiency and good radiation resistance. The Advanced Photovoltaic Solar Array (APSA) program is a near term effort aimed at demonstrating 130 W/kg beginning of life specific power using thin (62 pm) silicon cells. It is intended to be technology transparent to future high efficiency cells and provides the baseline for development of the 300 W/kg array.

Author

N90-21275*# National Aeronautics and Space Administration. Lewis Research Center, Cleveland, OH.

OPTICAL CONTROL OF AN 8-ELEMENT KA-BAND PHASED ARRAY USING A HIGH-SPEED OPTOELECTRONIC INTERCONNECT

M. A. RICHARD, P. C. CLASPY, K. B. BHASIN, and M. BENDETT (Honeywell, Inc., Bloomington, MN.) 1990 6 p Proposed for presentation at the 1990 AP-S International Symposium, Dallas, TX, 7-11 May 1990; sponsored by IEEE

(NASA-TM-102550; E-5365; NAS 1.15:102550) Avail: NTIS HC A02/MF A01 CSCL 09/3

Optical distribution of control signals in electronically steered phased array antennas is being considered. A demonstration experiment is described in which a high speed hybrid GaAs

optoelectronic integrated circuit (OEIC) was used to control an eight element phased array antenna. The OEIC, which accepts a serial optical control signal as input and converts it to 16 demultiplexed parallel outputs, was used to control the monolithic GaAs phase shifters of a Ka-band patch panel array antenna. Antenna pattern switching speeds of 2.25 microsec, limited by interface circuitry, were observed. Author

N90-21277*# National Aeronautics and Space Administration. Lewis Research Center, Cleveland, OH.

INTENSITY TO FREQUENCY CONVERSION TECHNIQUE IN INTENSITY MODULATED FIBER OPTIC SENSING SYSTEMS

G. ADAMOVSKY and T. W. CARR (Case Western Reserve Univ., Cleveland, OH.) Mar. 1990 7 p
(NASA-TM-102562; E-5376; NAS 1.15:102562) Avail: NTIS HC A02/MF A01 CSCL 09/3

A novel sensing technique based on intensity-to-frequency conversion is explained and demonstrated. Experimental data are presented and a comparison with a theoretical model is made. Author

N90-21278*# National Aeronautics and Space Administration. Lewis Research Center, Cleveland, OH.

COPLANAR WAVEGUIDE DISCONTINUITIES FOR P-I-N DIODE SWITCHES AND FILTER APPLICATIONS

N. I. DIB, P. B. KATEHI, GEORGE E. PONCHAK, and RAINEE N. SIMONS (Case Western Reserve Univ., Cleveland, OH.) 1990 10 p Presented at the 1990 IEEE MTT-S International Microwave Symposium, Dallas, TX, 8-10 May 1990
(Contract NSF ECS-86-57951)
(NASA-TM-102534; E-5343; NAS 1.15:102534) Avail: NTIS HC A02/MF A01 CSCL 09/3

A full wave space domain integral equation (SDIE) analysis of coplanar waveguide (CPW) two port discontinuities is presented. An experimental setup to measure the S-parameters of such discontinuities is described. Experimental and theoretical results for CPW realizations of pass-band and stop-band filters are presented. The S-parameters of such structures are plotted in the frequency range 5 to 25 GHz. Author

N90-21282*# Analox Corp., Cleveland, OH. APERTURE TAPER DETERMINATION FOR THE HALF-SCALE ACCURATE ANTENNA REFLECTOR Final Report

KEVIN M. LAMBERT Apr. 1990 22 p
(Contract NAS3-24564)
(NASA-CR-185215; E-5373; NAS 1.26:185215) Avail: NTIS HC A03/MF A01 CSCL 09/3

A simulation is described of a proposed microwave reflectance measurement in which the half scale reflector is used in a compact range type of application. The simulation is used to determine an acceptable aperture taper for the reflector which will allow for accurate measurements. Information on the taper is used in the design of a feed for the reflector. Author

N90-21283*# National Aeronautics and Space Administration. Lewis Research Center, Cleveland, OH.

CIVIL AIR TRANSPORT: A FRESH LOOK AT POWER-BY-WIRE AND FLY-BY-LIGHT

GALE R. SUNDBERG May 1990 6 p Presented at the National Aerospace and Electronics Conference, Dayton, OH, 21-25 May 1990; sponsored by IEEE
(NASA-TM-102574; E-5402; NAS 1.15:102574) Avail: NTIS HC A02/MF A01 CSCL 09/3

Power-by-wire (PBW) is a key element under subsonic transport flight systems technology with potential savings of over 10 percent in gross take-off-weight and in fuel consumption compared to today's transport aircraft. The PBW technology substitutes electrical actuation in place of centralized hydraulics, uses internal starter-motor/generators and eliminates the need for variable engine bleed air to supply cabin comfort. The application of advanced fiber optics to the electrical power system controls, to built-in-test (BITE) equipment, and to fly-by-light (FBL) flight controls provides additional benefits in lightning and high energy radio

frequency (HERF) immunity over existing mechanical or even fly-by-wire controls. The program plan is reviewed and a snapshot is given of the key technologies and their benefits to all future aircraft, both civil and military. Author

N90-21287*# National Aeronautics and Space Administration. Lewis Research Center, Cleveland, OH.

PEELED FILM GAAS SOLAR CELLS FOR SPACE POWER

D. M. WILT, F. L. DEANGELO, R. D. THOMAS, S. G. BAILEY, G. A. LANDIS, D. J. BRINKER, and N. S. FATEMI (Sverdrup Technology, Inc., Cleveland, OH.) May 1990 8 p
(NASA-TM-103125; E-5453; NAS 1.15:103125) Avail: NTIS HC A02/MF A01 CSCL 10/1

Gallium arsenide (GaAs) peeled film solar cells were fabricated, by Organo-Metallic Vapor Phase Epitaxy (OMVPE), incorporating an aluminum arsenide (AlAs) parting layer between the device structure and the GaAs substrate. This layer was selectively removed by etching in dilute hydrofluoric (HF) acid to release the epitaxial film. Test devices exhibit high series resistance due to insufficient back contact area. A new design is presented which uses a coverglass superstrate for structural support and incorporates a coplanar back contact design. Devices based on this design should have a specific power approaching 700 W/Kg. Author

N90-21952*# Cleveland State Univ., OH. Dept. of Electrical Engineering.

ANALYTICAL AND EXPERIMENTAL STUDY OF HIGH PHASE ORDER INDUCTION MOTORS Final Technical Report

EUGENE A. KLINGSHIRN Aug. 1989 120 p
(Contract NAG3-108)
(NASA-CR-186580; NAS 1.26:186580) Avail: NTIS HC A06/MF A01 CSCL 09/1

Induction motors having more than three phases were investigated to determine their suitability for electric vehicle applications. The objective was to have a motor with a current rating lower than that of a three-phase motor. The name chosen for these is high phase order (HPO) motors. Motors having six phases and nine phases were given the most attention. It was found that HPO motors are quite suitable for electric vehicles, and for many other applications as well. They have characteristics which are as good as or better than three-phase motors for practically all applications where polyphase induction motors are appropriate. Some of the analysis methods are presented, and several of the equivalent circuits which facilitate the determination of harmonic currents and losses, or currents with unbalanced sources, are included. The sometimes large stator currents due to harmonics in the source voltages are pointed out. Filters which can limit these currents were developed. An analysis and description of these filters is included. Experimental results which confirm and illustrate much of the theory are also included. These include locked rotor test results and full-load performance with an open phase. Also shown are oscillograms which display the reduction in harmonic currents when a filter is used with the experimental motor supplied by a non-sinusoidal source. Author

N90-22724*# National Aeronautics and Space Administration. Lewis Research Center, Cleveland, OH.

MINIATURE TRAVELING WAVE TUBE AND METHOD OF MAKING Patent

HENRY G. KOSMAHL 26 Dec. 1989 8 p Filed 8 Dec. 1987
Supersedes N88-23936 (26 - 17, p 2335)
(Contract NAS3-24565)
(NASA-CASE-LEW-14520-1; US-PATENT-APPL-SN-130058; US-PATENT-CLASS-315-3.5; US-PATENT-CLASS-315-3; US-PATENT-CLASS-331-82; INT-PATENT-CLASS-H01J-25/34; US-Patent-4,890,036) Avail: US Patent and Trademark Office CSCL 09/1

A miniature traveling wave tube is provided which will have most of the advantages of solid state circuitry but with higher efficiency and without being highly sensitive to temperature and various types of electromagnetic radiation and subatomic particles as are solid state devices. The traveling wave tube is about 2.5

33 ELECTRONICS AND ELECTRICAL ENGINEERING

cm in length and includes a slow wave circuit (SWS) comprised of apertured fins with a top cover which is insulated from the fins by strips or rungs of electrically insulating, dielectric material. An extremely small SWS is constructed by employing various grooving and etching methods, and by providing insulating strips or rungs by various deposition and masking techniques.

Official Gazette of the U.S. Patent and Trademark Office

N90-22731*# National Aeronautics and Space Administration. Lewis Research Center, Cleveland, OH.

FIELD ORIENTED CONTROL OF INDUCTION MOTORS

LINDA M. BURROWS, DON S. ZINGER (Akron Univ., OH.), and MARY ELLEN ROTH 1990 8 p Proposed for presentation at the 25th Intersociety Energy Conversion Engineering Conference, Reno, NV, 12-17 Aug. 1990; cosponsored by AICHE, SAE, ACS, AIAA, ASME, and IEEE

(NASA-TM-103154; E-5516; NAS 1.15:103154) Avail: NTIS HC A02/MF A01 CSCL 09/3

Induction motors have always been known for their simple rugged construction, but until lately were not suitable for variable speed or servo drives due to the inherent complexity of the controls. With the advent of field oriented control (FOC), however, the induction motor has become an attractive option for these types of drive systems. An FOC system which utilizes the pulse population modulation method to synthesize the motor drive frequencies is examined. This system allows for a variable voltage to frequency ratio and enables the user to have independent control of both the speed and torque of an induction motor. A second generation of the control boards were developed and tested with the next point of focus being the minimization of the size and complexity of these controls. Many options were considered with the best approach being the use of a digital signal processor (DSP) due to its inherent ability to quickly evaluate control algorithms. The present test results of the system and the status of the optimization process using a DSP are discussed. Author

N90-22732*# National Aeronautics and Space Administration. Lewis Research Center, Cleveland, OH.

PHOTORESPONSE OF YBA2CU3O(7-DELTA) GRANULAR AND EPITAXIAL SUPERCONDUCTING THIN FILMS

G. J. VALCO, P. CLASPY (Case Western Reserve Univ., Cleveland, OH.), J. D. WARNER, N. VARALJAY, and K. B. BHASIN 1990 12 p Presented at the Technical Symposium on Optical Engineering and Photonics in Aerospace Sensing, Orlando, FL, 16-20 Apr. 1990; sponsored by Society of Photo-Optical Instrumentation Engineers (Contract NCC3-105)

(NASA-TM-103144; E-5496; NAS 1.15:103144) Avail: NTIS HC A03/MF A01 CSCL 20/2

The response is reported of thin films of YBa₂Cu₃O(7-delta) with either a very grainy or a smooth epitaxial morphology to visible radiation. SrTiO₃ substrates were employed for both types of films. The grainy films were formed by sequential multi-layer electron beam evaporation while the epitaxial films were formed by laser ablation. Both films were patterned into H shaped detectors via a negative photolithographic process employing a Br/ethanol etchant. The bridge region of the H was 50 microns wide. The patterned films formed by laser ablation and sequential evaporation had critical temperatures of 74 K and 72 K respectively. The bridge was current biased and illuminated with chopped He-Ne laser radiation and the voltage developed in response to the illumination was measured. A signal was detected only above the critical temperature and the peak of the response coincided with the resistive transition for both types of films although the correspondence was less exact for the grainy film. The details of the responses and their analysis are presented. Author

N90-23662*# National Aeronautics and Space Administration. Lewis Research Center, Cleveland, OH.

NEW DIRECTIONS IN INP SOLAR CELL RESEARCH

I. WEINBERG, C. K. SWARTZ, and D. J. BRINKER 1990 7 p Proposed for presentation at the 25th Intersociety Energy Conversion Engineering Conference, Reno, NV, 12-17 Aug. 1990;

cosponsored by AICHE, SAE, ACS, AIAA, ASME, and IEEE (NASA-TM-103160; E-5528; NAS 1.15:103160) Avail: NTIS HC A02/MF A01 CSCL 10/1

Recent research efforts representing new directions in InP solar cell research are reviewed. These include heteroepitaxial growth on silicon and gallium arsenide substrates, V-grooved cells, large area high efficiency cells, and surface passivation. Improvements in heteroepitaxial cell efficiency are described together with processing of 19.1 percent, 4 sq cm cells. Recommendations are made for improvements in processing leading to increased efficiencies. Author

N90-23663*# National Aeronautics and Space Administration. Lewis Research Center, Cleveland, OH.

HIGH FREQUENCY, HIGH TEMPERATURE SPECIFIC CORE LOSS AND DYNAMIC B-H HYSTERESIS LOOP CHARACTERISTICS OF SOFT MAGNETIC ALLOYS

W. R. WIESERMAN, G. E. SCHWARZE, and J. M. NIEDRA (Sverdrup Technology, Inc., Brookpark, OH.) 1990 8 p Proposed for presentation at the 25th Intersociety Energy Conversion Engineering Conference, Reno, NV, 12-17 Aug. 1990; cosponsored by AICHE, SAE, ACS, AIAA, ASME, and IEEE (NASA-TM-103164; E-5536; NAS 1.15:103164) Avail: NTIS HC A02/MF A01 CSCL 09/3

Limited experimental data exists for the specific core loss and dynamic B-H loops for soft magnetic materials for the combined conditions of high frequency and high temperature. This experimental study investigates the specific core loss and dynamic B-H loop characteristics of Supermalloy and Metglas 2605SC over the frequency range of 1 to 50 kHz and temperature range of 23 to 300 C under sinusoidal voltage excitation. The experimental setup used to conduct the investigation is described. The effects of the maximum magnetic flux density, frequency, and temperature on the specific core loss and on the size and shape of the B-H loops are examined. Author

N90-23664*# Johns Hopkins Univ., Baltimore, MD. Center for Nondestructive Evaluation.

ACOUSTO-ULTRASONIC NONDESTRUCTIVE EVALUATION OF MATERIALS USING LASER BEAM GENERATION AND DETECTION M.S. Thesis

ROBERT D. HUBER and ROBERT E. GREEN, JR. 1990 97 p (Contract NAG3-728) (NASA-CR-186694; NAS 1.26:186694) Avail: NTIS HC A05/MF A01 CSCL 09/3

The acousto-ultrasonic method has proven to be a most interesting technique for nondestructive evaluation of the mechanical properties of a variety of materials. Use of the technique or a modification thereof, has led to correlation of the associated stress wave factor with mechanical properties of both metals and composite materials. The method is applied to the nondestructive evaluation of selected fiber reinforced structural composites. For the first time, conventional piezoelectric transducers were replaced with laser beam ultrasonic generators and detectors. This modification permitted true non-contact acousto-ultrasonic measurements to be made, which yielded new information about the basic mechanisms involved as well as proved the feasibility of making such non-contact measurements on terrestrial and space structures and heat engine components. A state-of-the-art laser based acousto-ultrasonic system, incorporating a compact pulsed laser and a fiber-optic heterodyne interferometer, was delivered to the NASA Lewis Research Center. Author

N90-25273*# National Aeronautics and Space Administration. Lewis Research Center, Cleveland, OH.

SEQUENTIALLY EVAPORATED THIN FILM YBA2CU3O(7-X) SUPERCONDUCTING MICROWAVE RING RESONATOR

NORMAN J. ROHRER, HING Y. TO, GEORGE J. VALCO, KUL B. BHASIN, CHRIS CHOREY (Sverdrup Technology, Inc., Brook Park, OH.), and JOSEPH D. WARNER 1990 12 p Presented at the Conference on the Science and Technology of Thin Film Superconductors, Denver, CO, 30 Apr. - 4 May 1990; sponsored by DOE

(Contract NCC3-105)
(NASA-TM-103180; E-5557; NAS 1.15:103180; UPI307-51-00)
Avail: NTIS HC A03/MF A01 CSCL 09/1

There is great interest in the application of thin film high temperature superconductors in high frequency electronic circuits. A ring resonator provides a good test vehicle for assessing the microwave losses in the superconductor and for comparing films made by different techniques. Ring resonators made of $\text{YBa}_2\text{Cu}_3\text{O}_{7-x}$ have been investigated on LaAlO_3 substrates. The superconducting thin films were deposited by sequential electron beam evaporation of Cu, Y, and BaF_2 with a post anneal. Patterning of the superconducting film was done using negative photolithography. A ring resonator was also fabricated from a thin gold film as a control. Both resonators had a gold ground plane on the backside of the substrate. The ring resonators' reflection coefficients were measured as a function of frequency from 33 to 37 GHz at temperatures ranging from 20 K to 68 K. The resonator exhibited two resonances which were at 34.5 and 35.7 GHz at 68 K. The resonant frequencies increased with decreasing temperature. The magnitude of the reflection coefficients was in the calculation of the unloaded Q-values. The performance of the evaporated and gold resonator are compared with the performance of a laser ablated $\text{YBa}_2\text{Cu}_3\text{O}_{7-x}$ resonator. The causes of the double resonance are discussed. Author

N90-25278*# National Aeronautics and Space Administration. Lewis Research Center, Cleveland, OH.

NEUTRON AND GAMMA IRRADIATION EFFECTS ON POWER SEMICONDUCTOR SWITCHES

G. E. SCHWARZE and A. J. FRASCA (Wittenberg Univ., Springfield, OH.) Aug. 1990 8 p Prepared for presentation at the 25th Intersociety Energy Conversion Engineering Conference, Reno, NV, 12-17 Aug. 1990; cosponsored by AICHE, ANS, SAE, ACS, AIAA, ASME, and IEEE

(NASA-TM-103200; E-5598; NAS 1.15:103200) Avail: NTIS HC A02/MF A01 CSCL 09/1

The performance characteristics of high power semiconductor switches subjected to high levels of neutron fluence and gamma dose must be known by the designer of the power conditioning, control and transmission subsystem of space nuclear power systems. Location and the allowable shielding mass budget will determine the level of radiation tolerance required by the switches to meet performance and reliability requirements. Neutron and gamma ray interactions with semiconductor materials and how these interactions affect the electrical and switching characteristics of solid state power switches is discussed. The experimental measurement system and radiation facilities are described. Experimental data showing the effects of neutron and gamma irradiation on the performance characteristics are given for power-type NPN Bipolar Junction Transistors (BJTs), and Metal-Oxide-Semiconductor Field Effect Transistors (MOSFETs). BJTs show a rapid decrease in gain, blocking voltage, and storage time for neutron irradiation, and MOSFETs show a rapid decrease in the gate threshold voltage for gamma irradiation. Author

N90-26250*# National Aeronautics and Space Administration. Lewis Research Center, Cleveland, OH.

DESIGN OF AN OPTICALLY CONTROLLED KA-BAND GAAS MMIC PHASED-ARRAY ANTENNA

RICHARD R. KUNATH, PAUL C. CLASPY, MARK A. RICHARD (Case Western Reserve Univ., Cleveland, OH.), and KUL B. BHASIN 1990 9 p Presented at the Optoelectronics and Laser Applications in Science and Engineering, Los Angeles, CA, 14-19 Jan. 1990; sponsored by Society of Photo-Optical Instrumentation Engineers

(NASA-TM-103147; E-5500; NAS 1.15:103147) Avail: NTIS HC A02/MF A01 CSCL 09/1

Phased array antennas long were investigated to support the agile, multibeam radiating apertures with rapid reconfigurability needs of radar and communications. With the development of the Monolithic Microwave Integrated Circuit (MMIC), phased array antennas having the stated characteristics are becoming realizable. However, at K-band frequencies (20 to 40 GHz) and higher, the

problem of controlling the MMICs using conventional techniques either severely limits the array size or becomes insurmountable due to the close spacing of the radiating elements necessary to achieve the desired antenna performance. Investigations were made that indicate using fiber optics as a transmission line for control information for the MMICs provides a potential solution. By adding an optical interface circuit to pre-existing MMIC designs, it is possible to take advantage of the small size, lightweight, mechanical flexibility and RFI/EMI resistant characteristics of fiber optics to distribute MMIC control signals. The architecture, circuit development, testing and integration of optically controlled K-band MMIC phased array antennas are described. Author

N90-27844*# National Aeronautics and Space Administration. Lewis Research Center, Cleveland, OH.

MICROWAVE CONDUCTIVITY OF LASER ABLATED YBACUO SUPERCONDUCTING FILMS AND ITS RELATION TO MICROSTRIP TRANSMISSION LINE

K. B. BHASIN, J. D. WARNER, C. M. CHOREY, B. T. EBIHARA, R. R. ROMANOFISKY, V. O. HEINEN, F. A. MIRANDA, and W. L. GORDON (Case Western Reserve Univ., Cleveland, OH.) In NASA, Goddard Space Flight Center, AMSAHS 1990: Advances in Materials Science and Applications of High Temperature Superconductors p 78-81 Apr. 1990

Avail: NTIS HC A07/MF A02 CSCL 09/3

The discovery of high temperature superconductor oxides has raised the possibility of a new class of millimeter and microwave devices operating at temperatures considerably higher than liquid helium temperatures. Therefore, materials properties such as conductivity, current density, and sheet resistance as a function of temperature and frequency, possible anisotropies, moisture absorption, thermal expansion, and others, have to be well characterized and understood. The millimeter wave response was studied of laser ablated $\text{YBa}_2\text{Cu}_3\text{O}_{7-x}/\text{LaAlO}_3$ thin films as a function of temperature and frequency. In particular, the evaluation of their microwave conductivity was emphasized, since knowledge of this parameter provides a basis for the derivation of other relevant properties of these superconducting oxides, and for using them in the fabrication of actual passive circuits. The microwave conductivity for these films was measured at frequencies from 26.5 to 40.0 GHz, in the temperature range from 20 to 300 K. The values of the conductivity are obtained from the millimeter wave power transmitted through the films, using a two fluid model. Author

N90-27965*# National Aeronautics and Space Administration. Lewis Research Center, Cleveland, OH.

SPENT-BEAM REFOCUSING ANALYSIS AND MULTISTAGE DEPRESSED COLLECTOR DESIGN FOR A 75-W, 59- TO 64-GHZ COUPLED-CAVITY TRAVELING-WAVE TUBE

JEFFREY D. WILSON, PETER RAMINS, and DALE A. FORCE Aug. 1990 22 p

(NASA-TP-3039; E-5455; NAS 1.60:3039) Avail: NTIS HC A03/MF A01 CSCL 09/1

A computational design technique for coupled-cavity tubes (TWTs) equipped with spent-beam refocusers (SBRs) and multistage depressed collectors (MDCs) is described. A large-signal multidimensional computer program was used to analyze the TWT-SBR performance and to generate the spent-beam models used for MDC design. The results of a design involving a 75-W, 59 to 64 GHz TWT are presented. The SBR and MDC designs are shown, and the computed TWT, SBR, and MDC performances are described. Collector efficiencies in excess of 94 percent led to projected overall TWT efficiencies in the 40-percent range. Author

N90-27966*# National Aeronautics and Space Administration. Lewis Research Center, Cleveland, OH.

ANALYSIS OF MICROSTRIP LINES WITH ALTERNATIVE IMPLEMENTATION OF CONDUCTORS AND SUPERCONDUCTORS

K.-S. KONG, H.-Y. LEE, T. ITOH, C. M. CHOREY (Sverdrup Technology, Inc., Brook Park, OH.), and K. B. BHASIN Sep.

33 ELECTRONICS AND ELECTRICAL ENGINEERING

1990 7 p Prepared for presentation at the Asia-Pacific Microwave Conference, Tokyo, Japan, 18-21 Sep. 1990; sponsored in part by the Inst. of Electronics, Information and Commercialization Engineers

(NASA-TM-103182; E-5562; NAS 1.15:103182) Avail: NTIS HC A02/MF A01 CSCL 09/1

An analysis of microstrip line structures in which either the strip or the ground plane or both are made of a high T_c superconductor is presented. The effect of implementation of a superconductor to the strip and the ground plane is explained with the calculation of a conductor loss of the structure by the Phenomenological Loss Equivalence Method (PEM). The theoretical values are compared with the experimental results from a ring resonator which is made of a gold ground plane and a high T_c superconductor, $YBa_2Cu_3O_{7-x}$, strip. Author

N90-28786* National Aeronautics and Space Administration. Lewis Research Center, Cleveland, OH.

HIGH TEMPERATURE SUPERCONDUCTING THIN FILM MICROWAVE CIRCUITS: FABRICATION, CHARACTERIZATION, AND APPLICATIONS

K. B. BHASIN, J. D. WARNER, R. R. ROMANOFSKY, V. O. HEINEN, and C. M. CHOREY (Sverdrup Technology, Inc., Brook Park, OH.) 1990 14 p Presented at the Technical Symposium on Optical Engineering and Photonics in Aerospace Sensing, Orlando, FL, 16-20 Apr. 1990; sponsored by Society of Photo-Optical Instrumentation Engineers

(NASA-TM-103235; E-5515; NAS 1.15:103235) Avail: NTIS HC A03/MF A01 CSCL 09/1

Epitaxial $YBa_2Cu_3O_7$ films were grown on several microwave substrates. Surface resistance and penetration depth measurements were performed to determine the quality of these films. Here the properties of these films on key microwave substrates are described. The fabrication and characterization of a microwave ring resonator circuit to determine transmission line losses are presented. Lower losses than those observed in gold resonator circuits were observed at temperatures lower than critical transition temperature. Based on these results, potential applications of microwave superconducting circuits such as filters, resonators, oscillators, phase shifters, and antenna elements in space communication systems are identified. Author

34

FLUID MECHANICS AND HEAT TRANSFER

Includes boundary layers; hydrodynamics; fluidics; mass transfer; and ablation cooling.

A90-11559* National Aeronautics and Space Administration. Lewis Research Center, Cleveland, OH.

TWO-COMPONENT PHASE-AVERAGED TURBULENCE STATISTICS DOWNSTREAM OF A ROTATING SPOKED-WHEEL WAKE GENERATOR

J. E. O'BRIEN (NASA, Lewis Research Center, Cleveland, OH) and S. P. CAPP (Pittsburgh, University, Johnstown, PA) ASME, Transactions, Journal of Turbomachinery (ISSN 0889-504X), vol. 111, Oct. 1989, p. 475-482. refs Copyright

Flow-field measurements of unsteady turbulent flow downstream of a rotating spoked-wheel wake generator were performed in a short-duration light-piston tunnel, and the instantaneous-velocity data were phase averaged based on a signal synchronized with the bar-passing frequency. Mean axial velocities were found to agree well with those obtained from measurements behind a stationary cylinder and to be independent of both Reynolds and bar-passing Strouhal numbers. Reynolds stresses were found to be consistent with related cylinder-wake measurements, but were significantly higher than corresponding measurements obtained in large-scale research turbomachines. Phase-averaged triple velocity

correlations were calculated from the digital velocity records, revealing the sign and the magnitude of skewness in the velocity probability density distributions for the two components. I.S.

A90-11598* National Aeronautics and Space Administration. Lewis Research Center, Cleveland, OH.

TIME-DEPENDENT VISCOUS INCOMPRESSIBLE NAVIER-STOKES EQUATIONS - THE FINITE DIFFERENCE GALERKIN FORMULATION AND STREAMFUNCTION ALGORITHMS

JOHN W. GOODRICH (NASA, Lewis Research Center, Cleveland, OH) and W. Y. SOH (NASA, Lewis Research Center; Sverdrup Technology, Inc., Cleveland, OH) Journal of Computational Physics (ISSN 0021-9991), vol. 84, Sept. 1989, p. 207-241. refs Copyright

Numerical techniques are developed to solve the Navier-Stokes equations for unsteady incompressible flow. The extension of the finite-difference Galerkin (FDG) method of Stephens et al. (1984) to the continuous-time case in two or three space dimensions is explained, and the numerical implementation of the method is discussed with particular attention to the staggered-MAC-grid primitive-variable discretization, the application of discrete mass balance to avoid problems inherent in FDG schemes, the direct interpretation of the FDG expansion variables as a discrete streamfunction, and a mass-balance approach to two-dimensional problems with throughflow or obstacles. Numerical results are presented graphically for the evolution of asymptotic steady flow in a driven cavity at Reynolds number 400, 1000, or 3200; good agreement with published experimental data is demonstrated, with accurate predictions of secondary-vortex formation from wall bubble recirculations at Reynolds number 1000. T.K.

A90-12606* National Aeronautics and Space Administration. Lewis Research Center, Cleveland, OH.

ADVANCED COMPUTATIONAL TECHNIQUES FOR HYPERSONIC PROPULSION

LOUIS A. POVINELLI (NASA, Lewis Research Center, Cleveland, OH) IN: International Symposium on Air Breathing Engines, 9th, Athens, Greece, Sept. 3-8, 1989, Proceedings. Volume 2. Washington, DC, American Institute of Aeronautics and Astronautics, 1989, p. 993-1008. Previously announced in STAR as N89-23809. refs

Computational Fluid Dynamics (CFD) has played a major role in the resurgence of hypersonic flight, on the premise that numerical methods will allow performance of simulations at conditions for which no ground test capability exists. Validation of CFD methods is being established using the experimental data base available, which is below Mach 8. It is important, however, to realize the limitations involved in the extrapolation process as well as the deficiencies that exist in numerical methods at the present time. Current features of CFD codes are examined for application to propulsion system components. The shortcomings in simulation and modeling are identified and discussed. Author

A90-12636* Boyce Engineering International, Inc., Houston, TX.

NEAR WALL FLOW PARAMETERS IN THE BLADE END-WALL CORNER REGION

R. K. BHARGAVA (Boyce Engineering International, Inc., Houston, TX) and R. RAJ (City College, New York) IN: International Symposium on Air Breathing Engines, 9th, Athens, Greece, Sept. 3-8, 1989, Proceedings. Volume 2. Washington, DC, American Institute of Aeronautics and Astronautics, 1989, p. 1269-1281. refs

(Contract NAG3-122) Copyright

The effects of secondary end-wall corner flows on near wall flow parameters in turbomachinery are studied. Important near wall flow parameters such as the wall shear stress vector, the mean wall pressure, the wall pressure fluctuations, and the correlation of the wall pressure fluctuation with the velocity fluctuation in three-dimensional turbulent flows are first experimentally investigated. The blade end-wall corner region is

simulated by mounting airfoil section of symmetric blades on both sides of the flat plate with semicircular leading edge. Observed changes in the maximum values of the wall shear stress and its location from the corner line could be associated with the stretching and attenuation of the horseshoe vortex. The values of wall pressure fluctuation intensity in the blade end-wall corner region are found to be influenced by the changes of the strength of the horseshoe vortex. The correlation of the wall pressure fluctuation with the velocity fluctuation indicated higher values of correlation coefficient in the inner region as compared to the outer region of the shear layer. The values of wall pressure-velocity correlation coefficient in the blade end-wall corner region also decrease in the streamwise direction while increasing in the presence of favorable and adverse pressure gradients. C.E.

A90-12836*# Flow Research, Inc., Kent, WA.
**PROGRESS IN DIRECT NUMERICAL SIMULATIONS OF
 TURBULENT REACTING FLOWS**

W.-H. JOU (Flow Research Co., Kent, WA) and JAMES J. RILEY (Washington University, Seattle) AIAA Journal (ISSN 0001-1452), vol. 27, Nov. 1989, p. 1543-1556. Research supported by Johns Hopkins University. Previously cited in issue 19, p. 3012, Accession no. A87-44930. refs
 (Contract NAS3-23351; NAS3-24229; F49620-85-C-0067; N00014-84-C-0359; N00014-87-K-0174)
 Copyright

A90-13091* Texas A&M Univ., College Station.
**AUGMENTED HEAT TRANSFER IN RECTANGULAR
 CHANNELS OF NARROW ASPECT RATIOS WITH RIB
 TURBULATORS**

J. C. HAN, S. OU, J. S. PARK, and C. K. LEI (Texas A & M University, College Station) International Journal of Heat and Mass Transfer (ISSN 0017-9310), vol. 32, Sept. 1989, p. 1619-1630. refs
 (Contract NAG3-311; NAS3-24227)
 Copyright

The effects of the rib angle-of-attack on the distributions of the local heat transfer coefficient and on the friction factors in short rectangular channels of narrow aspect ratios with a pair of opposite rib-roughened walls are determined for Reynolds numbers from 10,000 to 60,000. The channel width-to-height ratios are 2/4 and 1/4; the corresponding rib angles-of-attack are 90, 60, 45, and 30 deg, respectively. The results indicate that the narrow-aspect-ratio channels give better heat transfer performance than the wide-aspect-ratio channels for a constant pumping power. Semiempirical friction and heat transfer correlations are obtained. The results can be used in the design of turbine cooling channels of narrow aspect ratios. Author

A90-13092* Minnesota Univ., Minneapolis.
**THE MODELLING OF HEAT, MASS AND SOLUTE
 TRANSPORT IN SOLIDIFICATION SYSTEMS**

V. R. VOLLER, A. D. BRENT (Minnesota, University, Minneapolis), and C. PRAKASH (GE Research and Development Center, Schenectady, NY) International Journal of Heat and Mass Transfer (ISSN 0017-9310), vol. 32, Sept. 1989, p. 1719-1731. Research supported by the University of Minnesota and AT&T Information Systems, Inc. refs
 (Contract NAS3-25331)
 Copyright

The aim of this paper is to explore the range of possible one-phase models of binary alloy solidification. Starting from a general two-phase description, based on the two-fluid model, three limiting cases are identified which result in one-phase models of binary systems. Each of these models can be readily implemented in standard single phase flow numerical codes. Differences between predictions from these models are examined. In particular, the effects of the models on the predicted macro-segregation patterns are evaluated. Author

A90-13093* Kentucky Univ., Lexington.
**INVERSE HEAT TRANSFER ANALYSIS OF BRIDGMAN
 CRYSTAL GROWTH**

K. TAGHAVI (Kentucky University, Lexington,) and W. M. B. DUVAL (NASA, Lewis Research Center, Cleveland, OH) International Journal of Heat and Mass Transfer (ISSN 0017-9310), vol. 32, Sept. 1989, p. 1741-1750. refs
 Copyright

The effects of asymmetry in furnace temperature profile and pulling velocity on the crystal interface shape are demonstrated while neglecting the latent heat of solidification. It is seen that the furnace temperature profile may be varied in order to influence the shape of the melt-crystal interface. An exact thermal analysis is then performed on the Bridgman technique by including the latent heat of solidification as a source term. The exact temperature field required for yielding a flat melt-crystal interface is obtained. The earlier observation regarding the influence of furnace temperature profile on the interface shape is confirmed and a criterion for achieving a flat interface is obtained. Various furnace temperature profiles are selected and their corresponding melt-crystal interface results are presented. Author

A90-13095* National Aeronautics and Space Administration.
 Lewis Research Center, Cleveland, OH.

**SOME ASPECTS OF TRANSIENT COOLING OF A RADIATING
 RECTANGULAR MEDIUM**

ROBERT SIEGEL (NASA, Lewis Research Center, Cleveland, OH) International Journal of Heat and Mass Transfer (ISSN 0017-9310), vol. 32, Oct. 1989, p. 1955-1966. refs
 Copyright

The emission from a gray radiating medium is analyzed for transient cooling in surroundings at a low temperature. The medium is rectangular with no variations in the direction normal to the cross section. The integral equation for the transient temperature distribution is solved numerically using a two-dimensional Gaussian integration subroutine. The emissive ability for a rectangle at uniform temperature is compared with that for transient cooling where the temperature distribution of the region has reached a fully developed shape, as shown by a separation of variables solution. The two solutions provide the upper and lower bounds for the emittance of a rectangle during transient cooling. The emittances for various aspect ratios are presented as a function of the mean length of the rectangle and are compared with results for a plane layer and a cylinder. Author

A90-13511*# National Aeronautics and Space Administration.
 Lewis Research Center, Cleveland, OH.

NUMERICAL MODELING OF ENCLOSURE CONVECTION

J. C. DUH (NASA, Lewis Research Center; Sverdrup Technology, Inc., Cleveland, OH) IAF, International Astronautical Congress, 40th, Malaga, Spain, Oct. 7-13, 1989. 9 p. refs
 (IAF PAPER 89-403)

A numerical study on the steady and unsteady natural convection in two-dimensional rectangular enclosures has been performed by a time-accurate ADI finite difference scheme. The study covered a range of Rayleigh numbers between 1000 and 10 to the 7th, aspect ratios between 0.2 and 10.0, and tilt angles between -90 (heating from bottom) and +90 deg (heating from top). Various Prandtl numbers have been studied, but only the results of water ($Pr = 7.0$) are reported here due to space limitations. The physics revealed, however, includes the convection phenomena and the Rayleigh-Benard stability, as well as the combined mechanism of these two. The onset of secondary cells is determined by using a velocity map, which is simpler and cleaner, instead of a streamline plot. The critical Ra number for the occurrence of these secondary cells is shown to be lower than can be detected by experimental studies. On the Rayleigh-Benard stability part, a second transition from stable single-cell convection to periodic multicellular convection is disclosed. Author

34 FLUID MECHANICS AND HEAT TRANSFER

A90-13907* Brown Univ., Providence, RI.

CONTRIBUTIONS TO THE UNDERSTANDING OF LARGE-SCALE COHERENT STRUCTURES IN DEVELOPING FREE TURBULENT SHEAR FLOWS

J. T. C. LIU (Brown University, Providence, RI) IN: Advances in applied mechanics. Volume 26. San Diego, CA, Academic Press, Inc., 1988, p. 183-309. Research supported by DARPA and U.S.-China Cooperative Research Program. refs

(Contract NSF MSM-83-20307; NSF INT-85-14196; NAG1-379; NAG3-673; NATO-343/85)

Copyright

The physical problem of large-scale coherent structures in real, developing free turbulent shear flows are discussed from the point of view of a broader interpretation of the nonlinear aspects of hydrodynamic stability. Variations on the Amsden and Harlow problem are considered, and the role of linear theory in nonlinear problems is addressed. Spatially developing two-dimensional coherent structures and three-dimensional nonlinear effects in large-scale coherent mode interactions are considered. C.D.

A90-14086* Yale Univ., New Haven, CT.

SIDE-WALL GAS 'CREEP' AND 'THERMAL STRESS CONVECTION' IN MICROGRAVITY EXPERIMENTS ON FILM GROWTH BY VAPOR TRANSPORT

DANIEL E. ROSNER (Yale University, New Haven, CT) Physics of Fluids A (ISSN 0899-8213), vol. 1, Nov. 1989, p. 1761-1763. refs

(Contract NAG3-898)

Copyright

While 'no-slip' boundary conditions and the Navier-Stokes equations of continuum fluid mechanics have served the vapor transport community well until now, it is pointed out that transport conditions within highly nonisothermal ampoules are such that the nonisothermal side walls 'drive' the dominant convective flow, and the familiar Stokes-Fourier-Fick laws governing the molecular fluxes of momentum, energy, and (species) mass in the 'continuum' field equations will often prove to be inadequate, even at Knudsen numbers as small as 0.001. The implications of these interesting gas kinetic phenomena under microgravity conditions, and even under 'earth-bound' experimental conditions, are outlined here, along with a tractable approach to their systematic treatment.

Author

A90-15389* National Aeronautics and Space Administration, Lewis Research Center, Cleveland, OH.

A CIRCULAR COMBUSTOR CONFIGURATION WITH MULTIPLE INJECTION PORTS FOR MIXING ENHANCEMENT

B. GHORASHI, K. CHUN, P. KANG, and R. NEIDZWECKI (NASA, Lewis Research Center, Cleveland, OH) IN: Heat Transfer and Fluid Mechanics Institute, 31st, Sacramento, CA, June 1, 2, 1989, Proceedings. Sacramento, CA, California State University, 1989, p. 39-57. refs

Copyright

A circular combustor design by Ghorashi (1988) which resembles a continuously-stirred tank reactor with multiple injection ports is presented with a view to the enhanced control of mixing, NO(x) reduction, and combustion efficiency maximization. Attention is given to the prototype apparatus for this type of circular combustor, which takes the form of a transparent cold-flow reactor for flow visualization studies under 'chemically frozen' conditions.

O.C.

A90-15729* State Univ. of New York at Buffalo, Amherst.

MODEL-FREE SIMULATIONS OF TURBULENT REACTIVE FLOWS

PEYMAN GIVI (New York, State University, Amherst) Progress in Energy and Combustion Science (ISSN 0360-1285), vol. 15, no. 1, 1989, p. 1-107. Research supported by the State University of New York and AChS. refs

(Contract NAG3-1011; NSF CPE-80-14661; F49620-85-C-0067; F33615-87-C-2790)

Copyright

The current computational methods for solving transport

equations of turbulent reacting single-phase flows are critically reviewed, with primary attention given to those methods that lead to model-free simulations. In particular, consideration is given to direct numerical simulations using spectral (Galerkin) and pseudospectral (collocation) methods, spectral element methods, and Lagrangian methods. The discussion also covers large eddy simulations and turbulence modeling. V.L.

A90-15942* National Aeronautics and Space Administration, Lewis Research Center, Cleveland, OH.

NONLINEAR EVOLUTION OF OBLIQUE WAVES ON COMPRESSIBLE SHEAR LAYERS

M. E. GOLDSTEIN (NASA, Lewis Research Center, Cleveland, OH) and S. J. LEIB (NASA, Lewis Research Center; Sverdrup Technology, Inc., Cleveland, OH) Journal of Fluid Mechanics (ISSN 0022-1120), vol. 207, Oct. 1989, p. 73-96. refs

Copyright

The effects of critical-layer nonlinearity on spatially growing oblique instability waves on compressible shear layers between two parallel streams are considered. The analysis shows that mean temperature nonuniformities cause nonlinearity to occur at much smaller amplitudes than it does when the flow is isothermal. The nonlinear instability wave growth rate effects are described by an integrodifferential equation which bears some resemblance to the Landau equation, in that it involves a cubic-type nonlinearity. The numerical solutions to this equation are worked out and discussed in some detail. Inviscid solutions always end in a singularity at a finite downstream distance, but viscosity can eliminate this singularity for certain parameter ranges. Author

A90-15943* National Aeronautics and Space Administration, Lewis Research Center, Cleveland, OH.

NONLINEAR EVOLUTION OF INTERACTING OBLIQUE WAVES ON TWO-DIMENSIONAL SHEAR LAYERS

M. E. GOLDSTEIN and S.-W. CHOI (NASA, Lewis Research Center, Cleveland, OH) Journal of Fluid Mechanics (ISSN 0022-1120), vol. 207, Oct. 1989, p. 97-120. Previously announced in STAR as N89-24575. refs

Copyright

The effects of critical layer nonlinearity are considered on spatially growing oblique instability waves on nominally two-dimensional shear layers between parallel streams. The analysis shows that three-dimensional effects cause nonlinearity to occur at much smaller amplitudes than it does in two-dimensional flows. The nonlinear instability wave amplitude is determined by an integro-differential equation with cubic type nonlinearity. The numerical solutions to this equation are worked out and discussed in some detail. The numerical solutions always end in a singularity at a finite downstream distance. Author

A90-15947* Arizona Univ., Tucson.

EXPERIMENTAL INVESTIGATION OF CONVECTIVE STABILITY IN A SUPERPOSED FLUID AND POROUS LAYER WHEN HEATED FROM BELOW

FALIN CHEN and C. F. CHEN (Arizona, University, Tucson) Journal of Fluid Mechanics (ISSN 0022-1120), vol. 207, Oct. 1989, p. 311-321. refs

(Contract NAG3-723; NSF MSM-87-02732)

Copyright

Experiments have been carried out in a horizontal superposed fluid and porous layer contained in a test box 24 cm x 12 cm x 4 cm high. The porous layer consisted of 3 mm diameter glass beads, and the fluids used were water, 60 and 90 percent glycerin-water solutions, and 100 percent glycerin. The depth ratio d , which is the ratio of the thickness of the fluid layer to that of the porous layer, varied from 0 to 1.0. Fluids of increasingly higher viscosity were used for cases with larger d in order to keep the temperature difference across the tank within reasonable limits. The size of the convection cells was inferred from temperature measurements made with embedded thermocouples and from temperature distributions at the top of the layer by use of liquid crystal film. The experimental results showed: (1) a precipitous decrease in the critical Rayleigh number as the depth of the fluid

layer was increased from zero, and (2) an eightfold decrease in the critical wavelength between $d = 0.1$ and 0.2 . Both of these results were predicted by the linear stability theory reported earlier (Chen and Chen, 1988). Author

A90-17578* Cornell Univ., Ithaca, NY.

SHEAR STABILIZATION OF THE CAPILLARY BREAKUP OF A CYLINDRICAL INTERFACE

MATHEW J. RUSSO and PAUL H. STEEN (Cornell University, Ithaca, NY) *Physics of Fluids A* (ISSN 0899-8213), vol. 1, Dec. 1989, p. 1926-1937. Research supported by the U.S. Army. refs (Contract NAG3-801) (AD-A219268) Copyright

A cylindrical interface containing a viscous liquid set into axial motion is subject to a capillary and to a surface-wave instability. Clues from previous studies suggest that, even though both mechanisms separately are destabilizing, under certain circumstances their mutual interaction can lead to a stable interface; shear can stabilize capillary breakup. Here, an axial flow through an annular cross section bounded on the inside by a rigid rod and on the outside by a deformable interface is considered. The competition between the two mechanisms is studied through the temporal growth of infinitesimal axisymmetric and nonaxisymmetric disturbances. This examination of temporal stability shows that, indeed, for geometries corresponding to thin annular layers both instabilities can be completely suppressed (disturbances of all wavelengths decay). Author

A90-18071* Houston Univ., TX.

ELLIPTIC JETS. I - CHARACTERISTICS OF UNEXCITED AND EXCITED JETS

FAZLE HUSSAIN and HYDER S. HUSAIN (Houston, University, TX) *Journal of Fluid Mechanics* (ISSN 0022-1120), vol. 208, Nov. 1989, p. 257-320. refs (Contract NAG3-639; DE-FG05-88ER-13839) Copyright

Experimental studies of incompressible elliptic jets of different aspect ratios and initial conditions are summarized along with the effects of excitations at selected frequencies and amplitudes. The experimental facilities and procedures are described and jet spread and decay are discussed. The instability of elliptic shear layers, the behavior of the jet column under controlled excitation, and the time-average measures of unexcited jets are addressed. C.D.

A90-18246* National Aeronautics and Space Administration. Lewis Research Center, Cleveland, OH.

LEAST-SQUARES FINITE ELEMENT METHOD FOR FLUID DYNAMICS

BO-NAN JIANG (NASA, Lewis Research Center; Cleveland State University, OH) and LOUIS A. POVINELLI (NASA, Lewis Research Center, Cleveland, OH) IN: Finite element analysis in fluids; Proceedings of the Seventh International Conference on Finite Element Methods in Flow Problems, Huntsville, AL, Apr. 3-7, 1989. Huntsville, AL, University of Alabama in Huntsville Press, 1989, p. 105-110. Previously announced in STAR as N89-30008. refs Copyright

An overview is given of new developments of the least squares finite element method (LSFEM) in fluid dynamics. Special emphasis is placed on the universality of LSFEM; the symmetry and positiveness of the algebraic systems obtained from LSFEM; the accommodation of LSFEM to equal order interpolations for incompressible viscous flows; and the natural numerical dissipation of LSFEM for convective transport problems and high speed compressible flows. The performance of LSFEM is illustrated by numerical examples. Author

A90-18288* Colorado Univ., Boulder.

TREATMENT OF COUPLED FLUID-STRUCTURE INTERACTION PROBLEMS BY A MIXED VARIATIONAL PRINCIPLE

CARLOS A. FELIPPA (Colorado, University, Boulder) and ROGER OHAYON (ONERA, Chatillon-sous-Bagneux, France) IN: Finite

element analysis in fluids; Proceedings of the Seventh International Conference on Finite Element Methods in Flow Problems, Huntsville, AL, Apr. 3-7, 1989. Huntsville, AL, University of Alabama in Huntsville Press, 1989, p. 555-563. refs (Contract NAG3-934) Copyright

A general three-field variational principle is obtained for the motion of an acoustic fluid enclosed in a rigid or flexible container by the method of canonical decomposition applied to a modified form of the wave equation in the displacement potential. The general principle is specialized to a mixed two-field principle that contains the fluid displacement potential and pressure as independent fields. Semidiscrete finite-element equations of motion based on this principle are displayed. Author

A90-18505*# Maine Univ., Orono.

ASYMMETRICAL BOUNDARY LAYER SEPARATION AT THE BASE OF A TWO CYLINDER GEOMETRY

M. T. BOYLE (Maine, University, Orono) and L. S. LANGSTON (Connecticut, University, Storrs) *ASME, Transactions, Journal of Fluids Engineering* (ISSN 0098-2202), vol. 111, Dec. 1989, p. 443-448. refs (Contract NSG-3238) Copyright

This paper reports on the experimental description of the three-dimensional horseshoe vortex system occurring at the base of two cylinder mounted side by side on an endwall. The spacing between the two cylinders is adjusted to generate a family of viscous flows. Flow visualization performed in a water tunnel provides a qualitative understanding of the flow over a range of flow variables. A detailed wind tunnel experiment provides a quantitative description of the flow at a single test condition. At $Re(D) = 2.5 \times 10^5$ to the 5th the measurements show an asymmetrical primary vortex with a wide flat cross section. A small counterrotating vortex is found between the primary vortex and the cylinder leading edge. Author

A90-19633*# National Aeronautics and Space Administration. Lewis Research Center, Cleveland, OH.

A NONOSCILLATORY, CHARACTERISTICALLY CONVECTED, FINITE VOLUME SCHEME FOR MULTIDIMENSIONAL CONVECTION PROBLEMS

JEFFREY W. YOKOTA (NASA, Lewis Research Center; Sverdrup Technology, Inc., Cleveland, OH) and HUNG T. HUYNH (NASA, Lewis Research Center, Cleveland, OH) *AIAA, Aerospace Sciences Meeting, 28th, Reno, NV, Jan. 8-11, 1990*. 16 p. Previously announced in STAR as N90-11497. refs (AIAA PAPER 90-0015) Copyright

A new, nonoscillatory upwind scheme is developed for the multidimensional convection equation. The scheme consists of an upwind, nonoscillatory interpolation of data to the surfaces of an intermediate finite volume; a characteristic convection of surface data to a midpoint time level; and a conservative time integration based on the midpoint rule. This procedure results in a convection scheme capable of resolving discontinuities neither aligned with, nor convected along, grid lines. Author

A90-19635*# National Aeronautics and Space Administration. Lewis Research Center, Cleveland, OH.

RECIPROCAL INTERACTIONS OF HAIRPIN-SHAPED VORTICES AND A BOUNDARY LAYER

N.-S. LIU (NASA, Lewis Research Center, Cleveland, OH; Scientific Research Associates, Inc., Glastonbury, CT), S. J. SHAMROTH, and H. MCDONALD (Scientific Research Associates, Inc., Glastonbury, CT) *AIAA, Aerospace Sciences Meeting, 28th, Reno, NV, Jan. 8-11, 1990*. 11 p. refs (Contract F49620-86-C-0028) (AIAA PAPER 90-0017) Copyright

The present effort simulates the flow dynamics resulting from hairpin-shaped vortices in a boundary layer through the solution of the time-dependent, three-dimensional, compressible Navier-Stokes equations. Two simulations have been carried out. In the first case, the initial condition contains only one imposed

34 FLUID MECHANICS AND HEAT TRANSFER

hairpin-shaped vortex. In the second case, there are two incipient vortices separated by a short distance in the streamwise direction. The results add to the detailed understanding of the dynamic role of hairpin vortices in the entrainment, production and continual replenishment of turbulent structure, as well as the process of the interaction, intertwining and eventual conglomeration of vortices in boundary layers. Author

A90-19649*# National Aeronautics and Space Administration. Lewis Research Center, Cleveland, OH.

CALCULATION OF REATTACHING SHEAR LAYERS IN DIVERGENT CHANNEL WITH A MULTIPLE-TIME-SCALE TURBULENCE MODEL

S.-W. KIM (NASA, Lewis Research Center, Cleveland, OH) AIAA, Aerospace Sciences Meeting, 28th, Reno, NV, Jan. 8-11, 1990. 10 p. Previously announced in STAR as N89-28749. refs (AIAA PAPER 90-0047)

Numerical calculations of turbulent reattaching shear layers in a divergent channel are presented. The turbulence is described by a multiple-time-scale turbulence model. The turbulent flow equations are solved by a control-volume based finite difference method. The computational results are compared with those obtained using k-epsilon turbulence models and algebraic Reynolds stress turbulence models. It is shown that the multiple-time-scale turbulence model yields significantly improved computational results than the other turbulence models in the region where the turbulence is in a strongly inequilibrium state. Author

A90-19693*# Arizona Univ., Tucson.

SALT-FINGER CONVECTION UNDER REDUCED GRAVITY

C. F. CHEN (Arizona, University, Tucson) AIAA, Aerospace Sciences Meeting, 28th, Reno, NV, Jan. 8-11, 1990. 12 p. refs (Contract NSF MSM-87-02732; NAG3-723) (AIAA PAPER 90-0122) Copyright

Salt-finger convection in a double-diffusive system is a motion driven by the release of gravitational potential due to differential diffusion rates. Because of the fact that the destabilizing effect of the concentration gradient is amplified by the Lewis number (the ratio of thermal diffusivity to solute diffusivity) salt-finger convection can be generated at very much reduced gravity levels. This effect may be of importance in the directional solidification of binary alloys carried out in space. The transport of solute and heat by salt-finger convection at microgravity conditions is considered; instability arising from surface tension gradients, the Marangoni instability, is discussed, and the possible consequences of combined salt-finger and Marangoni instability are considered. Author

A90-19749*# Pennsylvania State Univ., University Park.

FULLY ELLIPTIC INCOMPRESSIBLE FLOW CALCULATIONS ON REGULAR GRID BY A NEW PRESSURE SUBSTITUTION METHOD

G. V. HOBSON and B. LAKSHMINARAYANA (Pennsylvania State University, University Park) AIAA, Aerospace Sciences Meeting, 28th, Reno, NV, Jan. 8-11, 1990. 19 p. refs (Contract NSG-3266) (AIAA PAPER 90-0239) Copyright

A new method is presented for the solution of incompressible flow in generalized coordinates. This method is based on the substitution of the pressure weighted form of the momentum equations into the continuity equation. The algorithm is rigorously derived and a Fourier analysis is used to assess its suitability to act as an error smoother. Linear stability analysis results indicate that the performance of the new pressure substitution method (PSM) and the pressure correction method (PCM) is about the same at low Reynolds numbers, with no significant pressure gradient. At high Reynolds numbers the PSM shows much faster convergence. Likewise prediction of various flows indicate that the PSM has better accuracy for high Reynolds number flows with significant pressure gradients. Since most practical aerodynamic flows have significant pressure gradients, the PSM seems to be attractive for such flows. Solutions for both laminar

and turbulent flow are compared with the experimental data. A two-equation low Reynolds number turbulence model is used to resolve the turbulent flowfield. Author

A90-19752*# National Aeronautics and Space Administration. Lewis Research Center, Cleveland, OH.

CALCULATION OF TURBULENCE-DRIVEN SECONDARY MOTION IN DUCTS WITH ARBITRARY CROSS-SECTION

A. O. DEMUREN (NASA, Lewis Research Center, Cleveland, OH) AIAA, Aerospace Sciences Meeting, 28th, Reno, NV, Jan. 8-11, 1990. 10 p. Previously announced in STAR as N89-27115. refs (AIAA PAPER 90-0245) Copyright

Calculation methods for turbulent duct flows are generalized for ducts with arbitrary cross-sections. The irregular physical geometry is transformed into a regular one in computational space, and the flow equations are solved with a finite-volume numerical procedure. The turbulent stresses are calculated with an algebraic stress model derived by simplifying model transport equations for the individual Reynolds stresses. Two variants of such a model are considered. These procedures enable the prediction of both the turbulence-driven secondary flow and the anisotropy of the Reynolds stresses, in contrast to some of the earlier calculation methods. Model predictions are compared to experimental data for developed flow in triangular duct, trapezoidal duct and a rod-bundle geometry. The correct trends are predicted, and the quantitative agreement is mostly fair. The simpler variant of the algebraic stress model procured better agreement with the measured data. Author

A90-19788*# Lehigh Univ., Bethlehem, PA.

COMPUTATION OF THREE-DIMENSIONAL TURBULENT BOUNDARY LAYERS WITH HEAT TRANSFER IN A PLANE OF SYMMETRY USING EMBEDDED WALL-LAYER FUNCTIONS

A. T. DEGANI and J. D. A. WALKER (Lehigh University, Bethlehem, PA) AIAA, Aerospace Sciences Meeting, 28th, Reno, NV, Jan. 8-11, 1990. 17 p. refs (Contract NAG3-771) (AIAA PAPER 90-0307) Copyright

In the calculation of turbulent boundary layers, a large number of mesh points are required to adequately resolve the intense variation in the velocity and enthalpy in the near-wall region. A substantial reduction in computational effort may be realized by representing the velocity and enthalpy profiles in the wall layer by analytical embedded functions. The effectively inviscid flow in the outer part of the boundary layer may then be resolved by employing a relatively coarser mesh. To obtain complete profiles, the outer numerical solution is matched asymptotically to the inner wall-layer analytical solution. To date, this approach has been restricted to two-dimensional flows; in the present study, a method which may be utilized for turbulent boundary layers with heat transfer in a plane of symmetry is developed as a first step in the application of the embedded-function method to full three-dimensional flows. The present method uses only about half as many mesh points as that required in a conventional procedure, which calculates the flow all the way to the wall, but there is no degradation in accuracy of the computed results. Author

A90-19804*# National Aeronautics and Space Administration. Lewis Research Center, Cleveland, OH.

CONVERGENCE ACCELERATION FOR VECTOR SEQUENCES AND APPLICATIONS TO COMPUTATIONAL FLUID DYNAMICS

AVRAM SIDI (NASA, Lewis Research Center, Cleveland, OH) and MARK L. CELESTINA (NASA, Lewis Research Center; Sverdrup Technology, Inc., Cleveland, OH) AIAA, Aerospace Sciences Meeting, 28th, Reno, NV, Jan. 8-11, 1990. 11 p. Previously announced in STAR as N88-30377. refs (AIAA PAPER 90-0338) Copyright

Some recent developments in acceleration of convergence methods for vector sequences are reviewed. The methods considered are the minimal polynomial extrapolation, the reduced rank extrapolation, and the modified minimal polynomial extrapolation. The vector sequences to be accelerated are those that are obtained from the iterative solution of linear or nonlinear

systems of equations. The convergence and stability properties of these methods as well as different ways of numerical implementation are discussed in detail. Based on the convergence and stability results, strategies that are useful in practical applications are suggested. Two applications to computational fluid mechanics involving the three dimensional Euler equations for ducted and external flows are considered. The numerical results demonstrate the usefulness of the methods in accelerating the convergence of the time marching techniques in the solution of steady state problems. Author

A90-19878*# Temple Univ., Philadelphia, PA.
ON THE MATHEMATICAL MODELING OF THE REYNOLDS STRESS'S EQUATIONS

AVI LIN (Temple University, Philadelphia, PA) AIAA, Aerospace Sciences Meeting, 28th, Reno, NV, Jan. 8-11, 1990. 10 p. refs (Contract NAG3-1002) (AIAA PAPER 90-0498) Copyright

By considering the Reynolds stress equations as a possible descriptor of complex turbulent fields, pressure-velocity interaction and turbulence dissipation are studied as two of the main physical contributions to Reynolds stress balancing in turbulent flow fields. It is proven that the pressure interaction term contains turbulence generation elements. However, the usual 'return to isotropy' element appears more weakly than in the standard models. In addition, convection-like elements are discovered mathematically, but there is no mathematical evidence that the pressure fluctuations contribute to the turbulent transport mechanism. Calculations of some simple one-dimensional fields indicate that this extra convection, rather than the turbulent transport, is needed mathematically. Similarly, an expression for the turbulence dissipation is developed. The end result is a dynamic equation for the dissipation tensor which is based on the tensorial length scales. S.A.V.

A90-19976*# General Motors Corp., Indianapolis, IN.
CALCULATION OF TURBULENT THREE-DIMENSIONAL JET-INDUCED FLOW IN A RECTANGULAR ENCLOSURE

M. NIKJOOY, K. C. KARKI, and H. C. MONGIA (General Motors Corp., Allison Gas Turbine Div., Indianapolis, IN) AIAA, Aerospace Sciences Meeting, 28th, Reno, NV, Jan. 8-11, 1990. 11 p. refs (Contract NAS3-24350) (AIAA PAPER 90-0684) Copyright

The application of a flux-spline scheme to three-dimensional fluid flow is reported. A comparison is made of the performance of this scheme with that of the Power-law differencing scheme. The numerical results are compared with experimental data. For the problem considered in this study, the flux-spline scheme is more accurate than the Power-law. For a prescribed accuracy, the flux-spline scheme requires a far fewer number of grid points. Thus, it has the potential of providing a numerical error-free solution, especially for three-dimensional flows, without requiring an excessively fine grid. Author

A90-19984*# Ohio State Univ., Columbus.
COMPRESSIBILITY EFFECTS IN FREE SHEAR LAYERS

M. SAMIMY (Ohio State University, Columbus) and G. S. ELLIOTT AIAA, Aerospace Sciences Meeting, 28th, Reno, NV, Jan. 8-11, 1990. 10 p. refs (Contract N00014-87-K-0169; NAG3-764) (AIAA PAPER 90-0705) Copyright

High-Reynolds-number compressible free shear layers were studied experimentally to explore the effects of compressibility on the turbulence field. A reduction in both the level and the lateral extent of turbulence fluctuations with increasing convective Mach number (Mc) (reported earlier for Mc of 0.51 and 0.64) is much higher at Mc of 0.86. The higher-order moments of turbulence fluctuations such as skewness and flatness show that the intermittency due to the excursion of large-scale structures into the free streams at the edge of shear layers was significantly reduced (both in the level and the extent) due to increased Mc. Author

A90-20511*# California State Univ., Long Beach.
UNSTEADY HEAT TRANSFER ON TURBINE BLADES

TUNCER CEBECI (California State University, Long Beach), ROBERT J. SIMONEAU (NASA, Lewis Research Center, Cleveland, OH), and MAX F. PLATZER (U.S. Naval Postgraduate School, Monterey, CA) Journal of Thermophysics and Heat Transfer (ISSN 0887-8722), vol. 4, Jan. 1990, p. 47-52. refs

This paper describes a method for calculating heat transfer on turbine blades subjected to passing wakes. It is based on the numerical solution of the boundary-layer equations for laminar, transitional, and turbulent flows with a novel procedure to account for the movement of the stagnation point. Results are presented for a model flow and show that the procedure is numerically sound and produces results that can give good agreement with measurements provided that the turbulence model is adequate. Author

A90-20519*# National Aeronautics and Space Administration.
 Lewis Research Center, Cleveland, OH.

TWO-DIMENSIONAL CONVECTION AND RADIATION WITH SCATTERING FROM A POISEUILLE FLOW

M. KASSEMI (NASA, Lewis Research Center, Cleveland; Akron, University, OH) and B. T. F. CHUNG (Akron, University, OH) Journal of Thermophysics and Heat Transfer (ISSN 0887-8722), vol. 4, Jan. 1990, p. 98-105. refs Copyright

Two-dimensional combined convection and radiation heat transfer from a gray scattering fluid in a reflecting channel is considered. The model, represented by a set of simultaneous nonlinear integro-partial differential equations, is solved numerically. The effects of aspect ratio, conduction-radiation parameter, scattering albedo, and wall emissivity, are systematically investigated. It is found that these parameters have a significant influence on the temperature field and alter the radiative and convective fluxes at the hot and cold walls. In particular, when radiation effects are considerable, the heat-transfer characteristics of the fluid at the hot and cold walls are very different. Author

A90-20520*# National Aeronautics and Space Administration.
 Lewis Research Center, Cleveland, OH.

EMITTANCE BOUNDS FOR TRANSIENT RADIATIVE COOLING OF A SCATTERING RECTANGULAR REGION

ROBERT SIEGEL (NASA, Lewis Research Center, Cleveland, OH) Journal of Thermophysics and Heat Transfer (ISSN 0887-8722), vol. 4, Jan. 1990, p. 106-114. refs Copyright

Transient cooling was analyzed for a two-dimensional gray rectangular region that emits, absorbs, and isotropically scatters radiation. The region, initially at uniform temperature, is placed in surroundings at a much lower temperature. The cooling analysis yields two simultaneous equations for the transient temperature and scattering source function distributions. The region starts to cool with the medium at uniform temperature. For this condition, the local emittance around the perimeter was obtained by a numerical solution of the radiative equations, and the rate of heat loss from the entire medium was evaluated. As cooling continues, the emissive ability decreases because of the lower temperatures in the outer regions of the rectangle. Based on some previous work, a lower limit for the transient overall emittance was found by obtaining a similarity solution. For some ranges of optical thickness and scattering albedo, the lower limit is only a small amount below the initial emittance. For these conditions, the initial emittance can be used to compute the entire transient resulting in a considerable simplification. Author

A90-21422*# Ohio State Univ., Columbus.
A NUMERICAL STUDY OF THE INTERACTION BETWEEN UNSTEADY FREE-STREAM DISTURBANCES AND LOCALIZED VARIATIONS IN SURFACE GEOMETRY

R. J. BODONYI, M. TADJFAR (Ohio State University, Columbus), W. J. C. WELCH, and P. W. DUCK (Manchester, Victoria University, England) Journal of Fluid Mechanics (ISSN 0022-1120), vol.

34 FLUID MECHANICS AND HEAT TRANSFER

209, Dec. 1989, p. 285-308. refs
(Contract NAG3-743; SERC-GR/E/25702)
Copyright

A numerical study of the generation of Tollmien-Schlichting (T-S) waves due to the interaction between a small free-stream disturbance and a small localized variation of the surface geometry has been carried out using both finite-difference and spectral methods. The nonlinear steady flow is of the viscous-inviscid interactive type while the unsteady disturbed flow is assumed to be governed by the Navier-Stokes equations linearized about this flow. Numerical solutions illustrate the growth or decay of the T-S waves generated by the interaction between the free-stream disturbance and the surface distortion, depending on the value of the scaled Strouhal number. An important result of this receptivity problem is the numerical determination of the amplitude of the T-S waves. Author

A90-21424* Notre Dame Univ., IN.
UNSTEADY DISTURBANCES OF STREAMING MOTIONS AROUND BODIES

H. M. ATASSI and J. GRZEDZINSKI (Notre Dame, University, IN) Journal of Fluid Mechanics (ISSN 0022-1120), vol. 209, Dec. 1989, p. 385-403. refs
(Contract F49620-88-C-0022; NAG3-732)
Copyright

The present investigation of flows around bodies with a stagnation point notes that the vortical part of such flows becomes singular along the entire body surface and its wake; as a result, the potential part of the flow will also be singular along the entire surface. A modified splitting of the velocity field is proposed which encompasses: (1) a vortical part having zero streamwise and normal components along the body surface; (2) an entropy-dependent part; and (3) a regular part similar to the potential part which satisfies a linear inhomogeneous wave equation with a modified source term. O.C.

A90-21937* National Aeronautics and Space Administration, Lewis Research Center, Cleveland, OH.
CALCULATION OF SHOCKED ONE-DIMENSIONAL FLOWS ON ABRUPTLY CHANGING GRIDS BY MATHEMATICAL PROGRAMMING

JOHN E. LAVERY (NASA, Lewis Research Center, Cleveland, OH) Journal of Computational Physics (ISSN 0021-9991), vol. 86, Jan. 1990, p. 1-17. refs
Copyright

Cell-centered finite differences on cells of an arbitrarily spaced grid are presently used to discretize the steady-state inviscid and nearly inviscid Burgers' equations for steady-state shocked flow in a quasi-one-dimensional nozzle. The overdetermined system of nonlinear algebraic equations thus obtained is solved by a procedure which minimizes a weighted sum of the residuals' absolute values. Numerical solutions for both viscous and inviscid problems are accurate and nonoscillatory, on grids whose abrupt mesh lengths refinements are as great as a factor of 10,000. O.C.

A90-22180* National Aeronautics and Space Administration, Lewis Research Center, Cleveland, OH.

CONVECTIVE HEAT TRANSFER MEASUREMENTS FROM A NACA 0012 AIRFOIL IN FLIGHT AND IN THE NASA LEWIS ICING RESEARCH TUNNEL

PHILIP E. POINSATTE, G. JAMES VAN FOSSEN (NASA, Lewis Research Center, Cleveland, OH), and KENNETH J. DEWITT (Toledo, University, OH) AIAA, Aerospace Sciences Meeting, 28th, Reno, NV, Jan. 8-11, 1990. 19 p. Previously announced in STAR as N90-13750. refs
(AIAA PAPER 90-0199) Copyright

Local heat transfer coefficients were measured on a smooth and roughened NACA 0012 airfoil. Heat transfer measurements on the 0.533 m chord airfoil were made both in flight on the NASA Lewis Twin Otter Icing Research Aircraft and in the NASA Icing Research Tunnel (IRT). Roughness was obtained by the attachment of uniform 2 mm diameter hemispheres to the airfoil

surface in 4 distinct patterns. Flight data were taken for the smooth and roughened airfoil at various Reynolds numbers based on chord in the range 1.24 to 2.50 x 10 (exp 6) and at various angles of attack up to 4 deg. During these flight tests, the free stream velocity turbulence intensity was found to be very low (less than 0.1 percent). Wind tunnel data were acquired in the Reynolds number range 1.20 to 4.25 x 10 (exp 6) and at angles of attack from -4 to 8 deg. The turbulence intensity in the IRT was 0.5 to 0.7 percent with the cloud generating sprays off. A direct comparison was made between the results obtained in flight and in the IRT. The higher level of turbulence in the IRT vs. flight had little effect on the heat transfer for the lower Reynolds numbers but caused a moderate increase in heat transfer at the high Reynolds numbers. Roughness generally increased the heat transfer. Author

A90-22181* Massachusetts Inst. of Tech., Cambridge.
HEAT TRANSFER ON ACCRETING ICE SURFACES

KEIKO YAMAGUCHI and R. JOHN HANSMAN, JR. (MIT, Cambridge, MA) AIAA, Aerospace Sciences Meeting, 28th, Reno, NV, Jan. 8-11, 1990. 10 p. Research supported by FAA. refs
(Contract NAG3-666; NGL-22-009-640)
(AIAA PAPER 90-0200) Copyright

Based on previous observations of glaze ice accretion, a 'Multi-Zone' model with distinct zones of different surface roughness is demonstrated. The use of surface roughness in the LEWICE ice accretion prediction code is examined. It was found that roughness is used in two ways: to determine the laminar to turbulent transition location and to calculate the turbulent heat transfer coefficient. A two zone version of the Multi-Zone model is implemented in the LEWICE code, and compared with experimental heat transfer coefficient and ice accretion results. The analysis of the boundary layer transition, surface roughness, and viscous flow field effects significantly increased the accuracy in predicting heat transfer coefficients. The Multi-Zone model was found to greatly improve the ice accretion prediction for the cases compared. Author

A90-22200* National Aeronautics and Space Administration, Lewis Research Center, Cleveland, OH.

AN INTERACTIVE GRID GENERATION PROCEDURE FOR AXIAL AND RADIAL FLOW TURBOMACHINERY

T. A. BEACH (NASA, Lewis Research Center; Sverdrup Technology, Inc., Cleveland, OH) AIAA, Aerospace Sciences Meeting, 28th, Reno, NV, Jan. 8-11, 1990. 12 p. Previously announced in STAR as N90-13968. refs
(Contract NAS3-25266)
(AIAA PAPER 90-0344) Copyright

A combination algebraic/elliptic technique is presented for the generation of three dimensional grids about turbo-machinery blade rows for both axial and radial flow machinery. The technique is built around use of an advanced engineering workstation to construct several two dimensional grids interactively on predetermined blade-to-blade surfaces. A three dimensional grid is generated by interpolating these surface grids onto an axisymmetric grid. On each blade-to-blade surface, a grid is created using algebraic techniques near the blade to control orthogonality within the boundary layer region and elliptic techniques in the mid-passage to achieve smoothness. The interactive definition of bezier curves as internal boundaries is the key to simple construction. This procedure lends itself well to zonal grid construction, an important example being the tip clearance region. Calculations done to date include a space shuttle main engine turbopump blade, a radial inflow turbine blade, and the first stator of the United Technologies Research Center large scale rotating rig. A finite Navier-Stokes solver was used in each case. Author

A90-22201* National Aeronautics and Space Administration, Lewis Research Center, Cleveland, OH.

BUOYANCY EFFECTS ON THE VAPOR CONDENSATION RATE ON A HORIZONTAL LIQUID SURFACE

MOHAMMAD M. HASAN (NASA, Lewis Research Center, Cleveland, OH) and CHIN-SHUN LIN (NASA, Lewis Research

Center; Analex Corp., Cleveland, OH) AIAA, Aerospace Sciences Meeting, 28th, Reno, NV, Jan. 8-11, 1990. 14 p. Previously announced in STAR as N90-13675. refs
(AIAA PAPER 90-0353) Copyright

The results are presented of a numerical study of the effects of buoyancy on the direct condensation of saturated or nearly saturated vapor on a horizontal liquid surface in a cylindrical tank. The liquid motion beneath the liquid-vapor interface is induced by an axisymmetric laminar jet of subcooled liquid. Analysis and numerical results show that the dominant parameter which determines the influence of buoyancy on the condensation rate is the Richardson number. However, the effect of buoyancy on the condensation rate cannot be quantified in terms of the Richardson number alone. The critical value of the Richardson number below which the condensation rate is not significantly reduced depends on the Reynolds number as well as the Prandtl number. Author

A90-22202*# National Aeronautics and Space Administration. Lewis Research Center, Cleveland, OH.
VAPOR CONDENSATION ON LIQUID SURFACE DUE TO LAMINAR JET-INDUCED MIXING - THE EFFECTS OF SYSTEM PARAMETERS

CHIN-SHUN LIN (NASA, Lewis Research Center; Analex Corp., Cleveland, OH) and MOHAMMAD M. HASAN (NASA, Lewis Research Center, Cleveland, OH) AIAA, Aerospace Sciences Meeting, 28th, Reno, NV, Jan. 8-11, 1990. 21 p. Previously announced in STAR as N90-13751. refs
(AIAA PAPER 90-0354) Copyright

The effects of system parameters on the interface condensation rate in a laminar jet induced mixing tank are numerically studied. The physical system consists of a partially filled cylindrical tank with a slightly subcooled jet discharged from the center of the tank bottom toward the liquid-vapor interface which is at a saturation temperature corresponding to the constant tank pressure. Liquid is also withdrawn from the outer part of the tank bottom to maintain the constant liquid level. The jet velocity is selected to be low enough such that the free surface is approximately flat. The effect of vapor superheat is assumed to be negligible. Therefore, the interface condensation rate can be determined from the resulting temperature field in the liquid region alone. The nondimensional form of the steady state conservation equations are solved by a finite difference method for various system parameters including liquid height to tank diameter ratio, tank to jet diameter ratio, liquid inflow to outflow area ratio, and a heat leak parameter which characterizes the uniform wall heat flux. Detailed analyses based on the numerical solutions are performed and simplified equations are suggested for the prediction of condensation rate. Author

A90-22237*# National Aeronautics and Space Administration. Lewis Research Center, Cleveland, OH.

ANALYSIS OF ROTARY ENGINE COMBUSTION PROCESSES BASED ON UNSTEADY, THREE-DIMENSIONAL COMPUTATIONS

M. S. RAJU (NASA, Lewis Research Center; Sverdrup Technology, Inc., Cleveland, OH) and E. A. WILLIS (NASA, Lewis Research Center, Cleveland, OH) AIAA, Aerospace Sciences Meeting, 28th, Reno, NV, Jan. 8-11, 1990. 37 p. Previously announced in STAR as N90-13749. refs
(Contract NAS3-26266)
(AIAA PAPER 90-0643) Copyright

A new computer code was developed for predicting the turbulent and chemically reacting flows with sprays occurring inside of a stratified charge rotary engine. The solution procedure is based on an Eulerian Lagrangian approach where the unsteady, three-dimensional Navier-Stokes equations for a perfect gas mixture with variable properties are solved in generalized, Eulerian coordinates on a moving grid by making use of an implicit finite volume, Steger-Warming flux vector splitting scheme, and the liquid phase equations are solved in Lagrangian coordinates. Both the details of the numerical algorithm and the finite difference predictions of the combustor flow field during the opening of exhaust and/or intake, and also during fuel vaporization and combustion, are presented. Author

A90-22239*# California Univ., Irvine.

EFFECTS OF G-JITTER ON A THERMAL, BUOYANT FLOW

F. TSAU, S. ELGHOBASHI, and W. A. SIRIGNANO (California, University, Irvine) AIAA, Aerospace Sciences Meeting, 28th, Reno, NV, Jan. 8-11, 1990. 26 p. refs
(Contract NAG3-627)

(AIAA PAPER 90-0653) Copyright

The effects of g-jitter on a buoyant flow in a cylindrical enclosure is examined via a finite-difference method. The enclosure is heated nonuniformly from above and a periodic gravitational acceleration is imposed on the flow inside to simulate gravity jittering. It is found that the flow field responding to the imposed gravitational acceleration also exhibits periodic behavior and that the heat transfer rate to the fluid is increased compared to the case without g-jitter. The modulations on the three gravity components all contribute to the increase in heat transfer rate but in ways different in nature. The flow field, sometimes, cannot remain quasi-steady with the imposed gravity changes and hot, isolated packets of fluid are created away from the heat source. It is also found that reducing the total gravity level is more efficient than eliminating the gravity jittering itself in averting the effects of g-jitter after a system has been disturbed. Author

A90-22651*# California Univ., Irvine.

INFLUENCE OF THE CONTINUOUS AND DISPERSED PHASES ON THE SYMMETRY OF A GAS TURBINE AIR-BLAST ATOMIZER

V. G. MCDONELL and G. S. SAMUELSEN (California, University, Irvine) ASME, Transactions, Journal of Engineering for Gas Turbines and Power (ISSN 0022-0825), vol. 112, Jan. 1990, p. 44-51. Research supported by General Motors Corp. refs
(Contract NAS3-24350)

(ASME PAPER 89-GT-303) Copyright

Current trends in liquid-fueled practical combustion systems are leaving less tolerance for fuel injection deficiencies such as poor spray field symmetry. The present paper evaluates the symmetry of the flowfield produced by a practical airblast atomizer. Specifically, the influence of both the continuous phase and dispersed phase on the spray field symmetry is assessed. In the present case, asymmetry in volume flux is associated principally with disparities in the injection of the dispersed phase, which is manifested by a maldistribution of larger drops. Asymmetries observed in the continuous phase without the dispersed phase are reduced in magnitude by the presence of the dispersed phase, but still contribute to asymmetry in radial spread of the dispersed phase. Author

A90-23111*# National Aeronautics and Space Administration. Lewis Research Center, Cleveland, OH.

TIME-ACCURATE SIMULATIONS OF A SHEAR LAYER FORCED AT A SINGLE FREQUENCY

R. W. CLAUS (NASA, Lewis Research Center, Cleveland, OH), P. G. HUANG (Michigan Technological University, Houghton), and J. M. MACINNES (Princeton University, NJ) AIAA Journal (ISSN 0001-1452), vol. 28, Feb. 1990, p. 267-275. Previously cited in issue 10, p. 1526, Accession no. A88-27716. refs

A90-23112*# North Carolina State Univ., Raleigh.

INVESTIGATION OF TURBULENT TRANSPORT IN AN AXISYMMETRIC SUDDEN EXPANSION

RICHARD D. GOULD (North Carolina State University, Raleigh), WARREN H. STEVENSON, and H. DOYLE THOMPSON (Purdue University, West Lafayette, IN) AIAA Journal (ISSN 0001-1452), vol. 28, Feb. 1990, p. 276-283. refs
(Contract NAG3-502)

Copyright

Simultaneous two-component laser velocimeter measurements were made in the incompressible turbulent flowfield following an axisymmetric sudden expansion. Mean velocities, Reynolds stresses, and triple products were measured and are presented at axial positions ranging from $x/H = 0.2-14$. A balance of the turbulent kinetic energy in the flow was performed. The production, convection, and diffusion of turbulent kinetic energy were computed

directly from the experimental data using central differencing. A specially designed correction lens was employed to correct for optical aberrations introduced by the circular tube. This lens system allowed the accurate simultaneous measurement of axial and radial velocities in the test section. The experimental measurements were compared to predictions generated by a code that employed the k-epsilon turbulence model. Agreement was good for mean axial velocities, turbulent kinetic energy, and turbulent shear stresses. However, the modeled turbulent normal stresses were in poor agreement with the measured values. The modeled diffusion of turbulent kinetic energy was underpredicted in the region between the shear layer and the centerline of the flow giving lower values of turbulent kinetic energy downstream of the potential core than measured.

Author

A90-23212* National Aeronautics and Space Administration. Lewis Research Center, Cleveland, OH.

NUMERICAL ANALYSIS OF NATURAL CONVECTION IN LIQUID DROPLETS BY PHASE CHANGE

J. C. DUH (NASA, Lewis Research Center; Sverdrup Technology, Inc., Cleveland OH) and WEN-JEI YANG (Michigan, University, Ann Arbor) Numerical Heat Transfer, Part A: Applications (ISSN 1040-7782), vol. 16, no. 2, Sept. 1989, p. 129-154. refs Copyright

A numerical analysis is performed on thermocapillary buoyancy convection induced by phase change in a liquid droplet. A finite-difference code is developed using an alternating-direction implicit (ADI) scheme. The intercoupling relation between thermocapillary force, buoyancy force, fluid property, heat transfer, and phase change, along with their effects on the induced flow patterns, are disclosed. The flow is classified into three types: thermocapillary, buoyancy, and combined convection. Among the three mechanisms, the combined convection simulates the experimental observations quite well, and the basic mechanism of the observed convection inside evaporating sessile drops is thus identified. It is disclosed that evaporation initiates unstable convection, while condensation always brings about a stable density distribution which eventually damps out all fluid disturbances. Another numerical model is presented to study the effect of boundary recession due to evaporation, and the 'peeling-off' effect (the removal of the surface layer of fluid by evaporation) is shown to be relevant.

Author

A90-23213* National Aeronautics and Space Administration. Lewis Research Center, Cleveland, OH.

NUMERICAL SIMULATION OF THERMOCAPILLARY BUBBLE MIGRATION UNDER MICROGRAVITY FOR LARGE REYNOLDS AND MARANGONI NUMBERS

R. BALASUBRAMANIAM and JOHN E. LAVERY (NASA, Lewis Research Center, Cleveland, OH) Numerical Heat Transfer, Part A: Applications (ISSN 1040-7782), vol. 16, no. 2, Sept. 1989, p. 175-187. refs Copyright

A numerical procedure in which the Navier-Stokes equations are discretized using tightly coupled discretizations of pressure derivatives and continuity equations is used here to extend the range of known terminal velocities of gaseous bubbles in liquids well beyond that in previous investigations. Computations performed for Reynolds numbers up to 2000 and Marangoni numbers up to 1000 show only a modest variation of the scaled bubble velocity between 0.16 and 0.5. The bubble velocity is influenced more by the Marangoni number than by the Reynolds number.

C.D.

A90-23702*# National Aeronautics and Space Administration. Lewis Research Center, Cleveland, OH.

THERMAL/STRUCTURAL ANALYSES OF SEVERAL HYDROGEN-COOLED LEADING-EDGE CONCEPTS FOR HYPERSONIC FLIGHT VEHICLES

HERBERT J. GLADDEN, MATTHEW E. MELIS, THEODORE T. MOCKLER, and MIKE TONG (NASA, Lewis Research Center, Cleveland, OH) AIAA, Aerospace Sciences Meeting, 28th, Reno,

NV, Jan. 8-11, 1990. 15 p. Previously announced in STAR as N90-14511. refs

(AIAA PAPER 90-0053) Copyright

The aerodynamic heating at high flight Mach numbers, when shock interference heating is included, can be extremely high and can exceed the capability of most conventional metallic and potential ceramic materials available. Numerical analyses of the heat transfer and thermal stresses are performed on three actively cooled leading-edge geometries (models) made of three different materials to address the issue of survivability in a hostile environment. These analyses show a mixture of results from one configuration to the next. Results for each configuration are presented and discussed. Combinations of enhanced internal film coefficients and high material thermal conductivity of copper and tungsten are predicted to maintain the maximum wall temperature for each concept within acceptable operating limits. The exception is the TD nickel material which is predicted to melt for most cases. The wide range of internal impingement film coefficients (based on correlations) for these conditions can lead to a significant uncertainty in expected leading-edge wall temperatures. The equivalent plastic strain, inherent in each configuration which results from the high thermal gradients, indicates a need for further cyclic analysis to determine component life.

Author

A90-23706*# National Aeronautics and Space Administration. Lewis Research Center, Cleveland, OH.

EFFICIENT REAL GAS NAVIER-STOKES COMPUTATIONS OF HIGH SPEED FLOWS USING AN LU SCHEME

WILLIAM J. COIRIER (NASA, Lewis Research Center, Cleveland, OH) AIAA, Aerospace Sciences Meeting, 28th, Reno, NV, Jan. 8-11, 1990. 19 p. Previously announced in STAR as N90-14203. refs

(AIAA PAPER 90-0391) Copyright

An efficient method to account for the chemically frozen thermodynamic and transport properties of air in three dimensional Navier-Stokes calculations was demonstrated. This approach uses an explicitly specified equation of state (EOS) so that the fluid pressure, temperature and transport properties are directly related to the flow variables. Since the pressure is explicitly known as a general function of the flow variables no assumptions are made regarding the pressure derivatives in the construction of the flux Jacobians. The method is efficient since no sub-iterations are required to deduce the pressure and temperature from the flux variables and allows different equations of state to be easily supplied to the code. The flexibility of the EOS approach is demonstrated by implementing a high order TVD upwinding scheme based upon flux differencing and Van Leer's flux vector splitting. The EOS approach is demonstrated by computing the hypersonic flow through the corner region of two mutually perpendicular flat plates and through a simplified model of a scramjet module gap-seal configuration.

Author

A90-23711*# National Aeronautics and Space Administration. Lewis Research Center, Cleveland, OH.

COMPARISON OF TWO DROPLET SIZING SYSTEMS IN AN ICING WIND TUNNEL

JOHN R. OLDENBURG (NASA, Lewis Research Center, Cleveland, OH) and ROBERT F. IDE (NASA, Lewis Research Center; U.S. Army, Aviation Research and Technology Activity, Cleveland, OH) AIAA, Aerospace Sciences Meeting, 28th, Reno, NV, Jan. 8-11, 1990. 18 p. Previously announced in STAR as N90-14617. refs (AIAA PAPER 90-0668) Copyright

A comparison between the Phase Doppler Analyzer and the combined measurements from the Particle Measuring Systems Forward Scattering Spectrometer Probe and the Optical Array Probe was conducted in an icing wind tunnel using NASA Icing Research Tunnel spray nozzles to produce the icing cloud. Clouds with a range of volume median diameters from 10 to greater than 50 microns were used for the instrument comparisons. A comparison of the volume median diameter from the Phase Doppler Particle Analyzer and only the Forward Scattering Spectrometer Probe indicated agreement up to 18 microns. A combined volume median diameter was calculated from the droplet distribution of

the Optical Array Probe and the Forward Scattering Spectrometer Probe. A comparison of the combined volume median diameters and the Phase Doppler Particle Analyzer volume median diameters showed agreement up to 30 microns with the agreement deteriorating rapidly above 30 microns. Droplet distributions from the Phase Doppler Particle Analyzer, the Forward Scattering Spectrometer Probe, and Optical Array Probe are presented.

Author

A90-23792*# General Motors Corp., Indianapolis, IN.
AN EXPERIMENTAL STUDY OF TURBINE VANE HEAT TRANSFER WITH LEADING EDGE AND DOWNSTREAM FILM COOLING

V. NIRMALAN and L. D. HYLTON (General Motors Corp., Allison Gas Turbine Div., Indianapolis, IN) ASME, Gas Turbine and Aeroengine Congress and Exposition, Toronto, Canada, June 4-8, 1989. 11 p. refs
 (Contract NAS3-24619)
 (ASME PAPER 89-GT-69)

This paper presents the effects of downstream film cooling, with and without leading edge showerhead film cooling, on turbine-vane external heat transfer. Steady-state experimental measurements were made in a three-vane linear two-dimensional cascade. The principal independent parameters were maintained over ranges consistent with actual engine conditions. The test matrix was structured to provide an assessment of the independent influence of parameters of interest, namely, exit Mach number, exit Reynolds number, coolant-to-gas temperature ratio, and coolant-to-gas pressure ratio. The data obtained indicate that considerable cooling benefits can be achieved by utilizing downstream film cooling. The downstream film cooling process was shown to be a complex interaction of two competing mechanisms. The thermal dilution effect, associated with the injection of relatively cold fluid, results in a decrease in the heat transfer to the airfoil. Conversely, the turbulence augmentation, produced by the injection process, results in increased heat transfer to the airfoil.

Author

A90-23793*# Pennsylvania State Univ., University Park.
THE MEASUREMENT OF BOUNDARY LAYERS ON A COMPRESSOR BLADE IN CASCADE. IV - FLOW FIELDS FOR INCIDENCE ANGLES OF -1.5 AND -8.5 DEGREES

W. C. ZIERKE and S. DEUTSCH (Pennsylvania State University, University Park) ASME, Gas Turbine and Aeroengine Congress and Exposition, Toronto, Canada, June 4-8, 1989. 16 p. refs
 (Contract NSG-3264)
 (ASME PAPER 89-GT-72)

Measurements, made with laser Doppler velocimetry, about a double-circular-arc compressor blade in a cascade are presented for -1.5 and -8.5 degree incidence angles and a chord Reynolds number near 500,000. Comparisons between the results of the current study and those of an earlier work at a 5.0 degree incidence are made. It is found that, in spite of the relative sophistication of the measurement techniques, transition on the pressure surface at the -1.5 degree incidence is dominated by a separation 'bubble' too small to be detected by the laser Doppler velocimeter. The development of the boundary layers at -1.5 and 5.0 degrees are found to be similar. In contrast to the flow at these two incidence angles, the leading edge separation 'bubble' is on the pressure surface for the -8.5 degree incidence.

Author

A90-23815*# National Aeronautics and Space Administration, Lewis Research Center, Cleveland, OH.
HEAT FLUX MEASUREMENTS

CURT H. LIEBERT and DONALD H. WEIKLE (NASA, Lewis Research Center, Cleveland, OH) ASME, Gas Turbine and Aeroengine Congress and Exposition, Toronto, Canada, June 4-8, 1989. 9 p. refs
 (ASME PAPER 89-GT-107)

This paper discusses a new automated, computer-controlled heat flux measurement facility. Continuous transient and steady-state surface heat flux values varying from about 0.3 to 6 MW/sq m over a temperature range of 100 to 1200 K can be

obtained in the facility. An application of this facility is the development of heat flux gages for continuous fast transient surface heat flux measurement on turbine blades operating in Space Shuttle main engine turbopumps. The facility is also useful for durability testing at fast temperature transients.

Author

A90-23832*# Calspan-Buffalo Univ. Research Center, NY.

PHASE AND TIME-RESOLVED MEASUREMENTS OF UNSTEADY HEAT TRANSFER AND PRESSURE IN A FULL-STAGE ROTATING TURBINE

M. G. DUNN (Calspan-UB Research Center, Buffalo, NY) ASME, Gas Turbine and Aeroengine Congress and Exposition, Toronto, Canada, June 4-8, 1989. 9 p. Research supported by USAF. refs
 (Contract NAG3-581)
 (ASME PAPER 89-GT-135)

This paper presents detailed phase-resolved heat-flux data obtained on rotor blades and a comparison of simultaneously obtained time-resolved heat-flux and static pressure data obtained on the stationary shroud of a Garrett TFE 731-2 HP full-stage rotating turbine. A shock tube is used to generate a short-duration source of heated and pressurized air and platinum thin-film gages are used to obtain heat-flux measurements. Blade results are presented at several selected blade locations. Shroud surface pressure and heat-flux time histories are presented for comparable locations relative to the blade position.

Author

A90-23880*# National Aeronautics and Space Administration, Lewis Research Center, Cleveland, OH.

EXPERIMENTAL DETERMINATION OF STATOR ENDWALL HEAT TRANSFER

ROBERT J. BOYLE and LOUIS M. RUSSELL (NASA, Lewis Research Center, Cleveland, OH) ASME, Gas Turbine and Aeroengine Congress and Exposition, Toronto, Canada, June 4-8, 1989. 15 p. Previously announced in STAR as N89-15366. refs
 (ASME PAPER 89-GT-219)

Local Stanton numbers were experimentally determined for the endwall surface of a turbine vane passage. A six vane linear cascade having vanes with an axial chord of 13.81 cm was used. Results were obtained for Reynolds numbers based on inlet velocity and axial chord between 75,000 and 495,000. The test section was connected to a low pressure exhaust system. Ambient air was drawn into the test section, inlet velocity was controlled up to a maximum of 59.4 m/sec. The effect of the inlet boundary layer thickness on the endwall heat transfer was determined for a range of test section flow rates. The liquid crystal measurement technique was used to measure heat transfer. Endwall heat transfer was determined by applying electrical power to a foil heater attached to the cascade endwall. The temperature at which the liquid crystal exhibited a specific color was known from a calibration test. Lines showing this specific color were isotherms, and because of uniform heat generation they were also lines of nearly constant heat transfer. Endwall static pressures were measured, along with surveys of total pressure and flow angles at the inlet and exit of the cascade.

Author

A90-24837*# Texas A&M Univ., College Station.
PRESSURE DROP AND MASS TRANSFER IN TWO-PASS RIBBED CHANNELS

P. R. CHANDRA and J. C. HAN (Texas A & M University, College Station) Journal of Thermophysics and Heat Transfer (ISSN 0887-8722), vol. 3, July 1989, p. 315-320. refs
 (Contract NAS3-24227)
 Copyright

The combined effects of the sharp 180-deg turn and of the rib configuration on the pressure drop and mass transfer characteristics in a two-pass square channel with a pair of opposite rib-roughened walls (to simulate turbine airfoil cooling passages) were determined for a Reynolds number range of 10,000-60,000. Heat transfer enhancements were compared for the first pass and for the two-pass channel with the sharp 180-deg turn. Correlations for the fully-developed friction factors and loss coefficients were obtained.

Author

34 FLUID MECHANICS AND HEAT TRANSFER

A90-24840*# National Aeronautics and Space Administration. Lewis Research Center, Cleveland, OH.

SOLIDIFICATION BY RADIATIVE COOLING OF A CYLINDRICAL REGION FILLED WITH DROPS

ROBERT SIEGEL (NASA, Lewis Research Center, Cleveland, OH) Journal of Thermophysics and Heat Transfer (ISSN 0887-8722), vol. 3, July 1989, p. 340-344. refs
Copyright

Transient cooling by radiation is analyzed for a cylindrical region filled with axially flowing streams of drops that are becoming solidified. This is of interest for the dissipation of waste heat from orbiting power system in space. The drops absorb, emit, and scatter radiation, and the surroundings are at a lower uniform temperature. The radiative properties are assumed gray, and the scattering is isotropic. The radiating region is a two-phase mixture that remains at the melting temperature of the drops. Its temperature uniformity maintains a high emissive power as energy is lost. This is an advantage over a sensible heat radiator in which the temperature decreases, thereby reducing the emissive power. The results provide the axial length that remains two-phase and the fraction of energy dissipated within this length in which the emissive power has not decreased because of sensible cooling. It is also shown how the radial distribution of the axial velocity of the drops can be modified to increase this energy fraction. Author

A90-25026*# National Aeronautics and Space Administration. Lewis Research Center, Cleveland, OH.

A NEW MIXING LENGTH MODEL FOR SUPERSONIC SHEAR LAYERS

S. C. KIM (NASA, Lewis Research Center; Sverdrup Technology, Inc., Cleveland, OH) AIAA, Aerospace Sciences Meeting, 28th, Reno, NV, Jan. 8-11, 1990. 7 p. refs
(Contract NAS3-25266)
(AIAA PAPER 90-0018) Copyright

A new mixing length model is presented for supersonic shear flows. In this model, the characteristic scale of the mixing region is not constant across the shear layer at each axial position but is determined locally by the lateral distance between the two points where flow moves sonic relative to the local point. Supersonic free shear layers at various Mach numbers were calculated by solving the compressible boundary layer equations with the new model. The results demonstrate the decrease of spreading rate with increasing Mach number and agree well with experimental data. Author

A90-25029*# National Aeronautics and Space Administration. Lewis Research Center, Cleveland, OH.

MULTIWAVE NONLINEAR INTERACTIONS IN THE AXISYMMETRIC MODE

REDA R. MANKBADI (NASA, Lewis Research Center, Cleveland, OH) AIAA, Aerospace Sciences Meeting, 28th, Reno, NV, Jan. 8-11, 1990. 9 p. refs
(AIAA PAPER 90-0365) Copyright

Nonlinear wave-wave interactions in turbulent jets were investigated based on the integrated energy of each scale of motion in a cross section of the jet. The analysis indicates that two frequency components in the axisymmetric mode can interact with other background frequencies in the axisymmetric mode, thereby amplifying an enormous number of other frequencies. The present computations produce several features consistent with experimental observations such as dependency of the interactions on the initial phase differences; enhancement of the momentum thickness under multi-frequency forcing; and an increase in background turbulence under forcing. Author

A90-25030*# National Aeronautics and Space Administration. Lewis Research Center, Cleveland, OH.

THE OSHER SCHEME FOR REAL GASES

AMBADY SURESH (NASA, Lewis Research Center; Sverdrup Technology, Inc., Cleveland, OH) and MENG-SING LIOU (NASA, Lewis Research Center, Cleveland, OH) AIAA, Aerospace Sciences Meeting, 28th, Reno, NV, Jan. 8-11, 1990. 12 p. refs

(Contract NAS3-25266)

(AIAA PAPER 90-0397) Copyright

An extension of Osher's approximate Riemann solver to include gases with an arbitrary equation of state is presented. By a judicious choice of thermodynamic variables, the Riemann invariants are reduced to quadratures which are then approximated numerically. The extension is rigorous and does not involve any further assumptions or approximations over the ideal gas case. Numerical results are presented to demonstrate the feasibility and accuracy of the proposed method. Author

A90-25033*# National Aeronautics and Space Administration. Lewis Research Center, Cleveland, OH.

GROUND-BASED EXPERIMENTS ON THERMAL AND THERMOSOLUTAL CONVECTION IN INCLINED LOW-ASPECT-RATIO ENCLOSURES

L. W. WANG (Yuan-Tze Memorial College of Engineering, Republic of China), A. T. CHAI, and N. RASHIDNIA (NASA, Lewis Research Center, Cleveland, OH) AIAA, Aerospace Sciences Meeting, 28th, Reno, NV, Jan. 8-11, 1990. 8 p. refs
(AIAA PAPER 90-0413) Copyright

Thermal and thermosolutal convection driven by buoyancy forces are investigated experimentally in inclined low-aspect-ratio enclosures. Thermal and thermosolutal convection are important in crystal growth processes. The transport process in the fluid phase during the growth of a crystal has a profound influence on the structure and quality of the solid phase. The present work is concerned with natural convection in a shallow rectangular enclosure with imposed inclined temperature and/or concentration gradients. Various complex flow patterns are observed with different experimental conditions. A flow instability under certain conditions is reported. The flow instability is found to depend not only on the thermal and solutal Grashof numbers, the aspect ratios, but also the inclined angles. Author

A90-25034*# National Aeronautics and Space Administration. Lewis Research Center, Cleveland, OH.

A NUMERICAL SIMULATION OF THE FLOW IN THE DIFFUSER OF THE NASA LEWIS ICING RESEARCH TUNNEL

HAROLD E. ADDY, JR. (NASA, Lewis Research Center, Cleveland, OH) and THEO G. KEITH, JR. (Toledo, University, OH) AIAA, Aerospace Sciences Meeting, 28th, Reno, NV, Jan. 8-11, 1990. 10 p. Previously announced in STAR as N90-15965.
(AIAA PAPER 90-0488) Copyright

The flow in the diffuser section of the Icing Research Tunnel at the NASA Lewis Research Center is numerically investigated. To accomplish this, an existing computer code is utilized. The code, known as PARC3D, is based on the Beam-Warming algorithm applied to the strong conservation law form of the complete Navier-Stokes equations. The first portion of the paper consists of a brief description of the diffuser and its current flow characteristics. A brief discussion of the code work follows. Predicted velocity patterns are then compared with the measured values. Author

A90-25035*# National Aeronautics and Space Administration. Lewis Research Center, Cleveland, OH.

PHASE DEVELOPMENT AND ITS ROLE ON SUBHARMONIC CONTROL

REDA R. MANKBADI, GANESH RAMAN, and EDWARD J. RICE (NASA, Lewis Research Center, Cleveland, OH) AIAA, Aerospace Sciences Meeting, 28th, Reno, NV, Jan. 8-11, 1990. 12 p. refs
(AIAA PAPER 90-0503) Copyright

The conditions for resonance interaction between two instability waves in an axisymmetric jet were investigated. Considerations of the energy equation of the wave resulting from the interaction indicate that the phase angle between the wave-induced stresses and the wave-induced strains plays a crucial role in the resonance interaction. This fact is demonstrated experimentally by exciting a jet at fundamental and subharmonic frequencies. The phase angle between the waves' stresses and strains was varied by varying the initial phase-difference between the two excitation waves. The subharmonic resonance was found to be highly dependent on this angle. Favorable agreement was found between the phase

angles predicted by a nonlinear theory and the measured ones. The theory is used to explain the subharmonic's resonance in terms of the phase-angles. Author

A90-25451* National Aeronautics and Space Administration. Lewis Research Center, Cleveland, OH.

SPLITTING OF INVISCID FLUXES FOR REAL GASES

MENG-SING LIOU (NASA, Lewis Research Center, Cleveland, OH), BRAM VAN LEER (NASA, Lewis Research Center, Cleveland, OH; Michigan, University, Ann Arbor), and JIAN-SHUN SHUEN (NASA, Lewis Research Center; Sverdrup Technology, Inc., Cleveland, OH) Journal of Computational Physics (ISSN 0021-9991), vol. 87, March 1990, p. 1-24. Previously announced in STAR as N88-21717. refs Copyright

Flux-vector and flux-difference splittings for the inviscid terms of the compressible flow equations are derived under the assumption of a general equation of state for a real gas in equilibrium. No necessary assumptions, approximations for auxiliary quantities are introduced. The formulas derived include several particular cases known for ideal gases and readily apply to curvilinear coordinates. Applications of the formulas in a TVD algorithm to one-dimensional shock-tube and nozzle problems show their quality and robustness. Author

A90-25594* National Aeronautics and Space Administration. Lewis Research Center, Cleveland, OH.

PARALLEL FLOWS WITH SORET EFFECT IN TILTED CYLINDERS

DAVID JACQMIN (NASA, Lewis Research Center, Cleveland, OH) Journal of Fluid Mechanics (ISSN 0022-1120), vol. 211, Feb. 1990, p. 355-372. refs Copyright

Henry and Roux (1986, 1987, 1988) have conducted extensive numerical studies on the interaction of Soret separation with convection in cylindrical geometry. Many of their solutions exhibit parallel flow away from end walls. Their parallel flow results can be matched by closed-form solutions. Solutions are nonunique in some parameter regions. Disappearance of one branch of solutions correlates with a sudden transition of Henry and Roux's results from a separated to a well-mixed flow. Author

A90-26334* Manhattan Coll., New York.

RADIATIVE CONFIGURATION FACTORS FROM CYLINDERS TO COAXIAL AXISYMMETRIC BODIES

C. SALTIEL and M. H. N. NARAGHI (Manhattan College, Riverdale, NY) International Journal of Heat and Mass Transfer (ISSN 0017-9310), vol. 33, Jan. 1990, p. 215-218. refs (Contract NAG3-892) Copyright

Exact solutions are obtained for the radiative configuration factor between differential elements of arbitrary orientation and cylinders. A general method is then proposed for calculating the view factor from a cylinder to a coaxial axisymmetric body using only a single numerical integration. The method is illustrated for axisymmetric bodies with function generators described by a power law equation. The method may be useful in calculating radiative heat transfer between cylindrical bodies and high-density exhaust gases and between annular radiative fins and their bases. V.L.

A90-26369* Maryland Univ., College Park.

CRITICAL SPEEDING UP IN PURE FLUIDS

HACENE BOUKARI, J. N. SHAUMEYER, MATTHEW E. BRIGGS, and ROBERT W. GAMMON (Maryland, University, College Park) Physical Review A - Statistical Physics, Plasmas, Fluids, and Related Interdisciplinary Topics, 3rd Series (ISSN 0556-2791), vol. 41, Feb. 15, 1990, p. 2260-2263. refs (Contract NAS3-25370) Copyright

The extreme compressibility of a pure fluid near its critical point significantly affects its bulk dynamic response to temperature changes through adiabatic processes. Equations that describe the dynamics in the absence of gravity are developed, and the

magnitude of the effect is illustrated with numerical solutions in one dimension. The results are remarkable: 5 mm of critical xenon, quenched from 20 to 10 mK above its critical temperature, cools by over 99 percent in less than 5 s. Moreover, adiabatic cooling is faster when the fluid is closer to the critical point. Author

A90-26506* Sverdrup Technology, Inc., Middleburg Heights, OH.

THREE-DIMENSIONAL ADAPTIVE GRID GENERATION FOR BODY-FITTED COORDINATE SYSTEM

S. C. CHEN (Sverdrup Technology, Inc., Middleburg Heights, OH) IN: Numerical grid generation in computational fluid mechanics '88; Proceedings of the Second International Conference, Miami Beach, FL, Dec. 5-8, 1988. Swansea, Wales, Pineridge Press, Ltd., 1988, p. 309-318. Previously announced in STAR as N88-27520.

(Contract NAS3-24105)

Copyright

This report describes a numerical method for generating 3-D grids for general configurations. The basic method involves the solution of a set of quasi-linear elliptic partial differential equations via pointwise relaxation with a local relaxation factor. It allows specification of the grid spacing off the boundary surfaces and the grid orthogonality at the boundary surfaces. It includes adaptive mechanisms to improve smoothness, orthogonality, and flow resolution in the grid interior. Author

A90-26940*# National Aeronautics and Space Administration. Lewis Research Center, Cleveland, OH.

COMPARATIVE STUDY OF COMPUTATIONAL EFFICIENCY OF TWO LU SCHEMES FOR NON-EQUILIBRIUM REACTING FLOWS

Y.-L. PETER TSAI and K.-C. HSIEH (NASA, Lewis Research Center; Sverdrup Technology, Inc., Cleveland, OH) AIAA, Aerospace Sciences Meeting, 28th, Reno, NV, Jan. 8-11, 1990. 15 p. refs (AIAA PAPER 90-0396) Copyright

The systems of equations governing chemically nonequilibrium flows are solved numerically by two lower-upper(LU) algorithms, namely, LU-SSOR (Yoon and Jameson, 1987) and LU-SW (Steger and Warming, 1981). The methods of flux-Jacobian splitting differentiate the two LU algorithms. The LU-SSOR gives a simpler implicit operator with less temporal damping, while the LU-SW converges faster but requires more computation for each iteration. Relative efficiencies and mutual merits of these two LU algorithms are compared. The results show that LU-SW with upwind-differenced right-hand-side gives the best convergence. Author

A90-26952*# National Aeronautics and Space Administration. Lewis Research Center, Cleveland, OH.

MULTIGRID CALCULATIONS OF A JET IN CROSSFLOW

R. W. CLAUS (NASA, Lewis Research Center, Cleveland, OH) and S. P. VANKA (Illinois, University, Urbana) AIAA, Aerospace Sciences Meeting, 28th, Reno, NV, Jan. 8-11, 1990. 8 p. refs (AIAA PAPER 90-0444) Copyright

A series of numerical calculations are made of a jet in crossflow using progressive mesh refinement up to 2.4 million grid points. A solution algorithm that combined the features of a point-coupled solution of the momentum and continuity equations with multigrid acceleration demonstrated efficient convergence of the governing equations. In comparisons with experimental data, some features of the jet flow field were found to be predicted reasonably well, but the results still remain affected by numerical diffusion. Author

A90-27983*# General Motors Corp., Indianapolis, IN.

THREE-DIMENSIONAL FLUID FLOW CALCULATIONS USING A FLUX-SPLINE METHOD

K. C. KARKI, H. C. MONGIA (General Motors Corp., Indianapolis, IN), and S. V. PATANKAR (Minnesota, University, Minneapolis) AIAA Journal (ISSN 0001-1452), vol. 28, April 1990, p. 631-634. Previously cited in issue 09, p. 1352, Accession no. A89-25543.

34 FLUID MECHANICS AND HEAT TRANSFER

refs

(Contract NAS3-24350)

Copyright

A90-28143* Massachusetts Inst. of Tech., Cambridge.

ON SUBLAYER STREAKS

M. T. LANDAHL (MIT, Cambridge, MA) Journal of Fluid Mechanics (ISSN 0022-1120), vol. 212, March 1990, p. 593-614. Research supported by Flygtekniska Forsöksanstalten of Sweden. refs (Contract NCC3-177)

Copyright

Turbulent sublayer streaks are studied with the aid of a simplified theoretical model. In this the nonlinear activity is assumed to be intermittent and to act locally in space during a very short initial time so as to set up the initial conditions for the subsequent linear and inviscid evolution of the resulting three-dimensional flow disturbance. The mean shear flow is taken as a parallel one and a correction for the long-term effects of viscosity is applied. A model for the initial nonlinear phase is chosen to represent the local Reynolds stresses that would be produced by a patch of local inflectional instability. The streamwise dimension of the resulting eddy is found to grow linearly with time in accordance with the algebraic instability mechanism (Landahl 1980). The associated Reynolds shear stress is expressible in a simple manner in terms of the liftup of the fluid elements and is suggestive of an algebraic-type Reynolds stress model similar to, but not identical to, that of Prandtl's (1925) mixing-length theory. Author

A90-32171* National Aeronautics and Space Administration. Lewis Research Center, Cleveland, OH.

SIMULATING TRANSITIONAL FLOW AND HEAT TRANSFER OVER THE FLAT PLATE AND CIRCULAR CYLINDER USING A K-EPSILON TURBULENCE MODEL

T. J. SULLIVAN (NASA, Lewis Research Center; Sverdrup Technology, Inc., Sharonville, OH) and M. IBRAHIM (Cleveland State University, OH) IN: Heat transfer in gas turbine engines; Proceedings of the Symposium, ASME Winter Annual Meeting, San Francisco, CA, Dec. 10-15, 1989. New York, American Society of Mechanical Engineers, 1989, p. 43-50. refs

Copyright

A boundary layer computer code, called TEXTAN, has been used to simulate external, transitional, fluid flow and heat transfer over the flat plate and circular cylinder. Turbulence modeling was accomplished by using a low-Reynolds number K-epsilon turbulence model. The study was made for free-stream turbulence intensities less than 15 percent. The comparison of the flat plate heat transfer predictions to experimental data showed good agreement, for the location of transition as well as in the heat transfer coefficient. The typical discrepancy in predicting the heat transfer coefficient was less than 5 percent of the measured value. Author

A90-32225* California Univ., Davis.

THE PDF APPROACH TO TURBULENT FLOW

W. KOLLMANN (California, University, Davis) Theoretical and Computational Fluid Dynamics (ISSN 0935-4964), vol. 1, no. 5, 1990, p. 249-285. Research supported by CAICYT. refs (Contract NAG3-667; NAG3-836)

Copyright

This paper provides a detailed discussion of the theory and application of probability density function (pdf) methods, which provide a complete statistical description of turbulent flow fields at a single point or a finite number of points. The basic laws governing the flow of Newtonian fluids are set up in the Eulerian and the Lagrangian frame, and the exact and linear equations for the characteristic functionals in those frames are discussed. Pdf equations in both frames are derived as Fourier transforms of the equations of the characteristic functions. Possible formulations for the nonclosed terms in the pdf equation are discussed, their properties are assessed, and closure modes for the molecular-transport and the fluctuating pressure-gradient terms are reviewed. The application of pdf methods to turbulent combustion

flows, supersonic flows, and the interaction of turbulence with shock waves is discussed. C.D.

A90-32293* Akron Univ., OH.

A LASER BASED COMPUTER AIDED NON-INTRUSIVE TECHNIQUE FOR FULL FIELD FLOW CHARACTERIZATION IN MACROSCOPIC CURVED CHANNELS

M. J. BRAUN, V. A. CANACCI (Akron, University, OH), L. RUSSELL, and R. C. HENDRICKS (NASA, Lewis Research Center, Cleveland, OH) IN: Flow visualization - 1989; Proceedings of the Symposium, ASME Winter Annual Meeting, San Francisco, CA, Dec. 10-15, 1989. New York, American Society of Mechanical Engineers, 1989, p. 15-22. refs

(Contract NCC3-93)

Copyright

This paper presents the application of a laser based, computer aided image processing technique for the nonintrusive evaluation of field velocities and accelerations in a 180 deg curved channel geometry, characteristic of inlet passages of the cowls of airbreathing aircraft engines. The method based on the illumination of the test section with a laser generated planar sheet of light, allows microscopic or macroscopic surveillance of fluid flow across or along large cross sections for relatively long (greater than 1 sec) periods of time. The method is Lagrangian in concept and permits identification and tracking of the same particle, thus facilitating construction of more comprehensive trajectories and the calculation of velocities and accelerations. Author

A90-32456*# National Aeronautics and Space Administration. Lewis Research Center, Cleveland, OH.

NUMERICAL ANALYSIS OF THREE-DIMENSIONAL VISCOUS INTERNAL FLOWS

RODRICK V. CHIMA (NASA, Lewis Research Center, Cleveland, OH) and JEFFREY W. YOKOTA (Sverdrup Technology, Inc., Cleveland, OH) AIAA Journal (ISSN 0001-1452), vol. 28, May 1990, p. 798-806. Previously cited in issue 20, p. 3386, Accession no. A88-48779. refs

Copyright

A90-32841* Kentucky Univ., Lexington.

OPPOSED-FLOW FLAME SPREAD AND EXTINCTION IN MIXED-CONVECTION BOUNDARY LAYERS

R. A. ALTENKIRCH and M. WEDHA-NAYAGAM (Kentucky, University, Lexington) IN: Symposium (International) on Combustion, 22nd, Seattle, WA, Aug. 14-19, 1988, Proceedings. Pittsburgh, PA, Combustion Institute, 1989, p. 1495-1500. refs (Contract NSG-3114; NAS3-23901)

Copyright

Experimental data for flame spread down thin fuel samples in an opposing, mixed-convection, boundary-layer flow are analyzed to determine the gas-phase velocity that characterizes how the flame reacts as it spreads toward the leading edge of the fuel sample into a thinning boundary layer. In the forced-flow limit where the cube of the Reynolds number divided by the Grashof number, $Re \exp 3/Gr$, is large, $L(q)/L(e)$, where $L(q)$ is a theoretical flame standoff distance at extinction and $L(e)$ is the measured distance from the leading edge of the sample where extinction occurs, is found to be proportional to $Re \exp n$ with $n = -0.874$ and Re based on $L(e)$. The value of n is established by the character of the flow field near the leading edge of the flame. The Re dependence is used, along with a correction for the mixed-convection situation where $Re \exp 3/Gr$ is not large, to construct a Damkohler number with which the measured spread rates correlate for all values of $Re \exp 3/Gr$. Author

A90-33516* National Aeronautics and Space Administration. Lewis Research Center, Cleveland, OH.

THE VIBRATING RIBBON PROBLEM REVISITED

DAVID E. ASHPIS (NASA, Lewis Research Center, Cleveland, OH) and ELI RESHOTKO (Case Western Reserve University, Cleveland, OH) Journal of Fluid Mechanics (ISSN 0022-1120), vol. 213, April 1990, p. 531-547. Research supported by USAF. refs

Copyright

A revised formal solution of the vibrating ribbon problem of hydrodynamic stability is presented. The initial formulation of Gaster (1965) is modified by application of the Briggs method and a careful treatment of the complex double Fourier transform inversions. Expressions are obtained in a natural way for the discrete spectrum as well as for the four branches of the continuous spectra. These correspond to discrete and branch-cut singularities in the complex wavenumber plane. The solutions from the continuous spectra decay both upstream and downstream of the ribbon, with the decay in the upstream direction being much more rapid than that in the downstream direction. Comments and clarification of related prior work are made. Author

A90-35183*# Case Western Reserve Univ., Cleveland, OH.
SOME CHARACTERISTICS OF BYPASS TRANSITION IN A HEATED BOUNDARY LAYER

K. H. SOHN, E. RESHOTKO (Case Western Reserve University, Cleveland, OH), and J. E. O'BRIEN (NASA, Lewis Research Center, Cleveland, OH) IN: Symposium on Turbulent Shear Flows, 7th, Stanford, CA, Aug. 21-23, 1989, Proceedings. Volume 1. University Park, PA, Pennsylvania State University, 1989, p. 2.4.1-2.4.6. Previously announced in STAR as N89-24577. refs

Experimental measurements of both mean and conditionally sampled characteristics of laminar, transitional and low Reynolds number turbulent boundary layers on a heated flat plate are presented. Measurements were obtained in air over a range of freestream turbulence intensities from 0.3 percent to 6 percent with a freestream velocity of 30.5 m/s and zero pressure gradient. Conditional sampling performed in the transitional boundary layers indicate the existence of a near-wall drop in intermittency, especially pronounced at low intermittencies. Nonturbulent intervals were observed to possess large levels of low-frequency unsteadiness, and turbulent intervals had peak intensities as much as 50 percent higher than were measured at fully turbulent stations. Heat transfer results were consistent with results of previous researches and Reynolds analogy factors were found to be well predicted by laminar and turbulent correlations which accounted for unheated starting length. A small dependence of the turbulent Reynolds analogy factors on freestream turbulence level was observed. Laminar boundary layer spectra indicated selective amplification of unstable frequencies. These instabilities appear to play a dominant role in the transition process only for the lowest freestream turbulence level studied, however. Author

A90-35219*# Michigan State Univ., East Lansing.
THE EFFECTS OF FORCING ON A SINGLE STREAM SHEAR LAYER AND ITS PARENT BOUNDARY LAYER

R. C. HAW and J. F. FOSS (Michigan State University, East Lansing) IN: Symposium on Turbulent Shear Flows, 7th, Stanford, CA, Aug. 21-23, 1989, Proceedings. Volume 1. University Park, PA, Pennsylvania State University, 1989, p. 11.1.1-11.1.6. refs (Contract NAG3-671)

The detailed response of a large single-stream shear layer to a sinusoidal forcing at $x = 0$ is quantitatively defined. Phase-averaged data are used to characterize the increased disturbance convection velocity and a width measure of the disturbance field. These findings are consistent with and complement those of Fiedler and Mensing (1985). C.D.

A90-35222*# Princeton Univ., NJ.
TIME-DEPENDENT CALCULATION OF A FORCED MIXING LAYER USING A K-EPSILON TURBULENCE MODEL

J. M. MACINNES (Princeton University, NJ), R. W. CLAUS (NASA, Lewis Research Center, Cleveland, OH), and P. G. HUANG (Stanford University, CA) IN: Symposium on Turbulent Shear Flows, 7th, Stanford, CA, Aug. 21-23, 1989, Proceedings. Volume 1. University Park, PA, Pennsylvania State University, 1989, p. 11.4.1-11.4.6. refs

A two-dimensional-dependent calculation of a forced turbulent mixing layer is reported. The approach employs a k-epsilon turbulence model to represent the effects of motions which are three dimensional or out of phase with the forcing cycle. Calculations that correspond to conditions of the measurements

of Weisbrot (1984) and Weisbrot and Wygnanski (1988) indicate that the main features of the mixing layer development are captured by the computation. The effect of grid refinement on the computed result indicates the importance of adequate resolution of the near field in correctly reproducing the flow evolution. The inlet boundary condition, similarly, is shown to play a decisive role in determining subsequent development. Author

A90-35247*# Stanford Univ., CA.
EFFECTS OF VERY HIGH TURBULENCE ON HEAT TRANSFER
 PAUL K. MACIEJEWSKI and ROBERT J. MOFFAT (Stanford University, CA) IN: Symposium on Turbulent Shear Flows, 7th, Stanford, CA, Aug. 21-23, 1989, Proceedings. Volume 2. University Park, PA, Pennsylvania State University, 1989, p. 20.3.1-20.3.5. refs

(Contract NAG3-522)

The effects of very high free stream turbulence on heat transfer were investigated experimentally by placing a flat plate, constant temperature heat transfer surface in a large diameter turbulent-free jet. The heat transfer rates measured were two to four times greater than those that would be predicted by accepted correlations for turbulent boundary layers. Thus, rather than establish a particular high turbulence flow field and then measure its effect on heat transfer, search for a flow field with very aggressive heat transfer characteristics and description of the aspects of the free stream turbulence associated with high levels of heat transfer is examined. R.E.P.

A90-37124*# Evansville Univ., IN.
KINETIC THEORY MODEL FOR THE FLOW OF A SIMPLE GAS FROM A TWO-DIMENSIONAL NOZZLE

B. R. RILEY (Evansville, University, IN) and K. W. SCHELLER IN: Rarefied gas dynamics: Space-related studies; International Symposium, 16th, Pasadena, CA, July 10-16, 1988, Technical Papers. Washington, DC, American Institute of Aeronautics and Astronautics, Inc., 1989, p. 352-362. refs (Contract NAG3-746)

Copyright

A system of nonlinear integral equations equivalent to the Krook kinetic equation for the steady state is the mathematical basis used to develop a computer code to model the flowfields for low-thrust two-dimensional nozzles. The method of characteristics was used to solve numerically by an iteration process the approximated Boltzmann equation for the number density, temperature, and velocity profiles of a simple gas as it exhausts into a vacuum. Results predict backscatter and show the effect of the inside wall boundary layer on the flowfields external to the nozzle. Author

A90-37328* National Aeronautics and Space Administration.
 Lewis Research Center, Cleveland, OH.

NEAR-WALL TURBULENCE MODEL AND ITS APPLICATION TO FULLY DEVELOPED TURBULENT CHANNEL AND PIPE FLOWS

S.-W. KIM (NASA, Lewis Research Center, Cleveland, OH) Numerical Heat Transfer, Part B: Fundamentals (ISSN 1040-7790), vol. 17, Jan. 1990, p. 101-122. refs

Copyright

A near-wall turbulence model and its incorporation into a multiple-timescale turbulence model are presented. The near-wall turbulence model is obtained from a k-equation turbulence model and a near-wall analysis. In the method, the equations for the conservation of mass, momentum, and turbulent kinetic energy are integrated up to the wall, and the energy transfer and the dissipation rates inside the near-wall layer are obtained from algebraic equations. Fully developed turbulent channel and pipe flows are solved using a finite element method. The computational results compare favorably with experimental data. It is also shown that the turbulence model can resolve the overshoot phenomena of the turbulent kinetic energy and the dissipation rate in the region very close to the wall. Author

34 FLUID MECHANICS AND HEAT TRANSFER

A90-38036* Science Applications International Corp., Albuquerque, NM.

SPRITE - A COMPUTER CODE FOR THE OPTIMIZATION OF SPACE BASED HEAT PIPE RADIATOR SYSTEMS

JOHN J. BUKSA and KENNETH A. WILLIAMS (Science Applications International Corp., Albuquerque, NM) IN: IECEC-89; Proceedings of the Twenty-fourth Intersociety Energy Conversion Engineering Conference, Washington, DC, Aug. 6-11, 1989. Volume 1. New York, Institute of Electrical and Electronics Engineers, 1989, p. 39-44.

(Contract NAS3-25210)

Copyright

An integrated analytical tool has been developed for use in designing optimized space-based heat pipe radiator systems. This code, SPRITE-1, incorporates the thermal, structural, and reliability aspects of the radiator into a single framework from which a physically consistent design can be obtained. A parametric study of the integral heat pipe panel radiator was performed using SPRITE-1, and a preliminary minimum mass design was obtained. The radiator design is summarized, and the mass minimization method and results are presented. I.E.

A90-38037*# National Aeronautics and Space Administration. Lewis Research Center, Cleveland, OH.

SCALING RESULTS FOR THE LIQUID SHEET RADIATOR

DONALD L. CHUBB and FREDERICK D. CALFO (NASA, Lewis Research Center, Cleveland, OH) IN: IECEC-89; Proceedings of the Twenty-fourth Intersociety Energy Conversion Engineering Conference, Washington, DC, Aug. 6-11, 1989. Volume 1. New York, Institute of Electrical and Electronics Engineers, 1989, p. 45-50. Previously announced in STAR as N89-25277. refs

Surface tension forces at the edges of a thin liquid (approx 100 micrometers) sheet flow result in a triangularly shaped sheet. Such a geometry is ideal for an external flow radiator. The experimental investigation of such sheet flows was extended to large sheets (width = 23.5 cm, length = 3.5 m). Experimental L/W results are greater than the calculated results. However, more experimental results are necessary for a complete comparison. The calculated emissivity of a sheet of Dow-Corning 705 silicone oil, which is low temperature (300-400 K) candidate for a liquid sheet radiator (LSR), is greater than 0.8 for sheet thicknesses greater than 100 micrometers. Author

A90-38042* Space Power, Inc., San Jose, CA.

ADVANCED RADIATOR CONCEPTS

L. L. BEGG and E. H. ENGDAHL (Space Power, Inc., San Jose, CA) IN: IECEC-89; Proceedings of the Twenty-fourth Intersociety Energy Conversion Engineering Conference, Washington, DC, Aug. 6-11, 1989. Volume 1. New York, Institute of Electrical and Electronics Engineers, 1989, p. 75-80.

(Contract NAS3-25208)

Copyright

Two radiator systems to reject heat from future space nuclear power systems were conceptually designed. One design would dissipate 1.7 MWt of heat at 600 K, and the other would reject 2.4 MWt at 875 K. The low-temperature radiator utilized a pumped loop system constructed of titanium, and achieved a specific mass of 5.8 kg/sq m, including pumps and structure. The high-temperature radiator system utilized potassium heat pipes constructed of SiC-reinforced titanium, and achieved a specific mass of 5.5 kg/sq m. Both radiators took advantage of light, high-thermal-conductivity carbon/graphite composite fins to distribute and radiate the rejected heat. I.E.

A90-38290* Cleveland State Univ., OH.

TWO-DIMENSIONAL NUMERICAL SIMULATION OF A STIRLING ENGINE HEAT EXCHANGER

MOUNIR IBRAHIM (Cleveland State University, OH), ROY C. TEW, and JAMES E. DUDENHOEFER (NASA, Lewis Research Center, Cleveland, OH) IN: IECEC-89; Proceedings of the Twenty-fourth Intersociety Energy Conversion Engineering Conference, Washington, DC, Aug. 6-11, 1989. Volume 6. New York, Institute

of Electrical and Electronics Engineers, 1989, p. 2795-2802. refs

Copyright

The first phase of an effort to develop multidimensional models of Stirling engine components is described. The ultimate goal is to model an entire engine working space. Parallel plate and tubular heat exchanger models are described, with emphasis on the central part of the channel (i.e., ignoring hydrodynamic and thermal end effects). The model assumes laminar, incompressible flow with constant thermophysical properties. In addition, a constant axial temperature gradient is imposed. The governing equations describing the model have been solved using the Crank-Nicolson finite-difference scheme. Model predictions are compared with analytical solutions for oscillating/reversing flow and heat transfer in order to check numerical accuracy. Excellent agreement is obtained for flow both in circular tubes and between parallel plates. The computational heat transfer results are in good agreement with the analytical heat transfer results for parallel plates. I.E.

A90-38396*# National Aeronautics and Space Administration. Ames Research Center, Moffett Field, CA.

EFFICIENT MONTE CARLO SIMULATION OF RAREFIED FLOW IN A SMALL NOZZLE

IAIN D. BOYD (NASA, Ames Research Center, Moffett Field; Elore Institute, Palo Alto, CA), PAUL F. PENKO, and LYNNETTE M. CARNEY (NASA, Lewis Research Center, Cleveland, OH) AIAA and ASME, Joint Thermophysics and Heat Transfer Conference, 5th, Seattle, WA, June 18-20, 1990. 11 p. refs

(Contract NCC2-582)

(AIAA PAPER 90-1693)

The flow of carbon dioxide through a small conical nozzle is computed using two different numerical approaches. The first of these is the direct simulation Monte Carlo method in which the physical phenomena are modeled at the molecular level. The second technique solves the Navier-Stokes equations of fluid flow. The purpose of the paper is to compare the solutions generated by these two methods for the conditions prevailing in a small, low density nozzle. The comparison between the two sets of solutions reveals only small differences. However, the flow properties in the thick viscous layer close to the nozzle at the exit plane show important deviations which have implications for the subsequent determination of the plume backflow. Author

A90-38397*# Toledo Univ., OH.

NUMERICAL SIMULATION OF RAREFIED GAS FLOW THROUGH A SLIT

THEO G. KEITH, JR., DUEN-REN JENG, KENNETH J. DE WITT (Toledo, University, OH), and CHAN-HONG CHUNG AIAA and ASME, Joint Thermophysics and Heat Transfer Conference, 5th, Seattle, WA, June 18-20, 1990. 12 p. refs

(Contract NAG3-577)

(AIAA PAPER 90-1694) Copyright

Two different approaches, the finite-difference method coupled with the discrete-ordinate method (FDDO), and the direct-simulation Monte Carlo (DSMC) method, are used in the analysis of the flow of a rarefied gas from one reservoir to another through a two-dimensional slit. The cases considered are for hard vacuum downstream pressure, finite pressure ratios, and isobaric pressure with thermal diffusion, which are not well established in spite of the simplicity of the flow field. In the FDDO analysis, by employing the discrete-ordinate method, the Boltzmann equation simplified by a model collision integral is transformed to a set of partial differential equations which are continuous in physical space but are point functions in molecular velocity space. The set of partial differential equations are solved by means of a finite-difference approximation. In the DSMC analysis, three kinds of collision sampling techniques, the time counter (TC) method, the null collision (NC) method, and the no time counter (NTC) method, are used. Author

A90-38614*# Princeton Univ., NJ.

A STUDY OF THE UNSTEADINESS OF CROSSING SHOCK WAVE TURBULENT BOUNDARY LAYER INTERACTIONS

K. PODDAR and S. M. BOGDONOFF (Princeton University, NJ) AIAA, Fluid Dynamics, Plasma Dynamics and Lasers Conference, 21st, Seattle, WA, June 18-20, 1990. 14 p. refs (Contract AF-AFOSR-89-0033; NAG3-926) (AIAA PAPER 90-1456) Copyright

The unsteadiness of crossing shock wave turbulent boundary layer interactions at a nominal Mach number of 3 was examined by measuring wall pressure fluctuations using multiple, high frequency response, pressure transducers. The unsteadiness in the initial part of the interaction for all the interactions is similar to that of single fin interaction as studied by Tran and Bogdonoff (1987). However, for stronger interactions, flow downstream of the inviscid shock crossing position has a significant unsteady characteristic. In this unsteady region of the interaction, mean surface pressure rises significantly over the value obtained from the inviscid shock approximation. The energy spectrum of the fluctuating pressure signal shows a significant increase in the energy level at the higher frequencies. Author

A90-38651*# Tennessee Univ., Tullahoma. INFLUENCE OF BULK TURBULENCE AND ENTRANCE BOUNDARY LAYER THICKNESS ON THE CURVED DUCT FLOW FIELD

AHMAD A. SHOHADAEI, ROGER A. CRAWFORD, and ALI HEDAYATPOUR (Tennessee, University, Tullahoma) AIAA, Fluid Dynamics, Plasma Dynamics and Lasers Conference, 21st, Seattle, WA, June 18-20, 1990. 7 p. Previously announced in STAR as N89-12896. (Contract NAG3-617) (AIAA PAPER 90-1502) Copyright

The objective of this investigation was the experimental evaluation of bulk turbulence and boundary thickness influence on the secondary flow development in a square, 90 deg turning duct. A three dimensional laser velocimetry system was utilized to measure the mean and fluctuating components of velocity in the large curved duct facility. The three dimensional development of the viscous shear layers in the curved duct has a strong influence on the complete flow field. Since ducted three dimensional flows are found in many engineering applications, including gas turbine engines, and contain high turbulence levels and high wall heat transfer rates, they present a difficult challenge to computational fluid mechanics codes. Turbulence modeling remains one of constraints to CFD advance due to inadequate physical understanding and experimental definition of turbulent shear flows. The results of this investigation expand the curved duct data base to higher turbulence levels and thicker entrance boundary layers. The experimental results provide a challenging benchmark data base for computational fluid dynamics code development and validation. The variation of inlet bulk turbulence intensity provides additional information to aid in turbulence model evaluation. Author

A90-38654*# National Aeronautics and Space Administration. Lewis Research Center, Cleveland, OH. EXPERIMENTAL INVESTIGATION OF TURBULENT FLOW THROUGH A CIRCULAR-TO-RECTANGULAR TRANSITION DUCT

D. O. DAVIS (NASA, Lewis Research Center, Cleveland, OH; Washington, University, Seattle) and F. B. GESSNER (Washington, University, Seattle) AIAA, Fluid Dynamics, Plasma Dynamics and Lasers Conference, 21st, Seattle, WA, June 18-20, 1990. 13 p. refs (Contract NAG3-376) (AIAA PAPER 90-1505) Copyright

An incompressible, turbulent, swirl-free flow through a circular-to-rectangular transition duct was studied experimentally. The cross-sectional geometry all along the duct was defined using the equation of a superellipse. The three mean velocity components and the six Reynolds stress components were measured at two axial stations downstream from the transition. It is shown that a secondary flow vortex pair which develops along the duct sidewalls significantly distorts the mean and turbulence fields. At the duct exit, the flow is not in local equilibrium, but recovers to local

equilibrium conditions in the rectangular extension duct. Analysis demonstrates that conventional wall functions are not applicable at all streamwise locations in the duct. N.B.

A90-38685*# Aerospace Corp., El Segundo, CA. EXPERIMENTAL INVESTIGATION OF FLOW ABOUT A STRUT-ENDWALL CONFIGURATION

P. S. CHANG (Aerospace Corp., El Segundo, CA) and F. B. GESSNER (Washington, University, Seattle) AIAA, Fluid Dynamics, Plasma Dynamics and Lasers Conference, 21st, Seattle, WA, June 18-20, 1990. 13 p. refs (Contract NAG3-376) (AIAA PAPER 90-1541) Copyright

An experimental study was conducted to investigate incompressible flow about a strut-endwall configuration positioned within a constant area duct. The endwall boundary layer was tripped, but natural transition occurred on the strut surface. The results indicate that spanwise varying transition on this surface leads to the formation of a secondary vortex which coexists with the horseshoe vortex generated by endwall flow separation upstream of the strut leading edge. Both vortices are similar in strength downstream of the strut trailing edge, and both distort the primary flow and local turbulence structure in the wake-endwall region. The level of distortion is demonstrated by means of axial mean velocity contours, turbulence kinetic energy contours, and Reynolds shear stress contours measured in the cross plane at two streamwise locations. Analysis of the results shows that conventional eddy viscosity and k-epsilon transport equation models are not wholly adequate for predicting this flow situation. Author

A90-38799* General Motors Corp., Indianapolis, IN. AN EXPERIMENTAL AND NUMERICAL STUDY OF PARTICLE-LADEN COAXIAL JET FLOWS

A. A. MOSTAFA, H. C. MONGIA (General Motors Corp., Allison Gas Turbine Div., Indianapolis, IN), V. G. MCDONELL, and G. S. SAMUELSEN (California, University, Irvine) International Journal of Heat and Fluid Flow (ISSN 0142-727X), vol. 11, June 1990, p. 90-97. refs (Contract NAS3-24350) Copyright

A detailed experimental and numerical study of the developing region of coaxial jet flows with and without glass beads is performed. A two-component phase/Doppler interferometer is used to measure mean and fluctuating velocity components for each phase and particle-number density. The numerical calculation is based on a stochastic Lagrangian treatment for the particles and a recently proposed two-equation turbulence model for two-phase flows. Results show that the particle-number density profile becomes narrower than the corresponding profile for round jet flow and that the particles attain a uniform velocity across the jet radius. The particles attenuate the level of gas turbulence and increase their anisotropy level. The numerical calculations yield reasonable and encouraging agreement with the measurements. Author

A90-38978* Cornell Univ., Ithaca, NY. THE COUPLING OF MARANGONI AND CAPILLARY INSTABILITIES IN AN ANNULAR THREAD OF LIQUID

HENK A. DIJKSTRA (Cornell University, Ithaca, NY) Journal of Colloid and Interface Science (ISSN 0021-9797), vol. 136, April 1990, p. 151-159. Research supported by the U.S. Army. refs (Contract NAG3-801) Copyright

It is shown that the coupling of the Marangoni and capillary instabilities in an annular thread of liquid heated along its axis can give rise to traveling waves. It is also shown that the coupling of both instabilities is not able to stabilize capillary breakup. However, the capillary breakup can be stabilized by a temperature-dependent surface tension, with $Ma(0)$ less than 0. N.B.

34 FLUID MECHANICS AND HEAT TRANSFER

A90-39625* National Aeronautics and Space Administration. Lewis Research Center, Cleveland, OH.

A TECHNIQUE FOR MEASUREMENT OF INSTANTANEOUS HEAT TRANSFER IN STEADY-FLOW AMBIENT-TEMPERATURE FACILITIES

JAMES E. O'BRIEN (NASA, Lewis Research Center, Cleveland, OH) Experimental Thermal and Fluid Science (ISSN 0894-1777), vol. 3, July 1990, p. 416-430. refs
Copyright

An experimental technique is described for obtaining time-resolved heat flux measurements with high-frequency response (up to 100 kHz) in a steady-flow ambient-temperature facility. The heat transfer test object is preheated and suddenly injected into an established steady flow. Thin-film gages deposited on the test surface detect the unsteady substrate surface temperature. Analog circuitry designed for use in short-duration facilities and based on one-dimensional semiinfinite heat conduction is used to perform the temperature/heat flux transformation. A detailed description of substrate properties, instrumentation, experimental procedure, and data reduction is given, along with representative results obtained in the stagnation region of a circular cylinder subjected to a wake-dominated unsteady flow. An in-depth discussion of related work is also provided. Author

A90-40930*# California Univ., Irvine.

SYMMETRY ASSESSMENT OF AN AIR-BLAST ATOMIZER SPRAY

V. G. MCDONNELL, C. D. CAMERON, and G. S. SAMUELSEN (California, University, Irvine) Journal of Propulsion and Power (ISSN 0748-4658), vol. 6, July-Aug. 1990, p. 375-381. refs
(Contract NAS3-24350; F08635-86-C-0309)
Copyright

This study represents an evaluation of the extent to which conventional and recently introduced modern diagnostics can assess the symmetry of sprays formed by three atomizers of identical design. The conventional diagnostics include sheet-lit photography, patterning, and laser diffraction. The modern diagnostic is laser interferometry (phase Doppler). Symmetry is assessed in ambient conditions for four atomizer orientations, and comparisons are made between the diagnostic techniques. The results demonstrate that conventional and modern diagnostics are consistent in the assessment of symmetry, patterning and phase Doppler are most effective in establishing symmetry of mass flux, and phase Doppler, although more tedious to employ, provides the additional information necessary to establish the sources of detected asymmetries in terms of nonuniformities in droplet velocities, size distributions, volume flux, and concentration. Author

A90-41163*# National Aeronautics and Space Administration. Lewis Research Center, Cleveland, OH.

CFD PROPELS NASP PROPULSION PROGRESS

LOUIS A. POVINELLI (NASA, Lewis Research Center, Cleveland, OH), DOUGLAS L. DWOYER (NASA, Langley Research Center, Hampton, VA), and MICHAEL J. GREEN (NASA, Ames Research Center, Moffett Field, CA) Aerospace America (ISSN 0740-722X), vol. 28, July 1990, p. 26, 27, 86.
Copyright

The most complex aerothermodynamics encountered in the National Aerospace Plane (NASP) propulsion system are associated with the fuel-mixing and combustion-reaction flows of its combustor section; adequate CFD tools must be developed to model shock-wave systems, turbulent hydrogen/air mixing, flow separation, and combustion. Improvements to existing CFD codes have involved extension from two dimensions to three, as well as the addition of finite-rate hydrogen-air chemistry. A novel CFD code for the treatment of reacting flows throughout the NASP, designated GASP, uses the most advanced upwind-differencing technology. O.C.

A90-42426*# National Aeronautics and Space Administration. Lewis Research Center, Cleveland, OH.

MULTIGRID CALCULATIONS OF 3-D TURBULENT VISCOUS FLOWS

JEFFREY W. YOKOTA (NASA, Lewis Research Center; Sverdrup Technology, Inc., Cleveland, OH) IN: Canadian Symposium on Aerodynamics, 1st, Ottawa, Canada, Dec. 4, 5, 1989, Proceedings. Ottawa, Canada, Canadian Aeronautics and Space Institute, 1989, p. 29-1 to 29-16. Previously announced in STAR as N90-13323. refs

Convergence properties of a multigrid algorithm, developed to calculate compressible viscous flows, are analyzed by a vector sequence eigenvalue estimate. The full 3-D Reynolds-averaged Navier-Stokes equations are integrated by an implicit multigrid scheme while a k-epsilon turbulence model is solved, uncoupled from the flow equations. Estimates of the eigenvalue structure for both single and multigrid calculations are compared in an attempt to analyze the process as well as the results of the multigrid technique. The flow through an annular turbine is used to illustrate the scheme's ability to calculate complex 3-D flows. Author

A90-44011* National Aeronautics and Space Administration. Lewis Research Center, Cleveland, OH.

NONLINEAR REYNOLDS STRESS MODELS AND THE RENORMALIZATION GROUP

ROBERT RUBINSTEIN and J. MICHAEL BARTON (NASA, Lewis Research Center; Sverdrup Technology, Inc., Cleveland, OH) Physics of Fluids A (ISSN 0899-8213), vol. 2, Aug. 1990, p. 1472-1476. refs
(Contract NAS3-25266)
Copyright

The renormalization group is applied to derive a nonlinear algebraic Reynolds stress model of anisotropic turbulence in which the Reynolds stresses are quadratic functions of the mean velocity gradients. The model results from a perturbation expansion that is truncated systematically at second order with subsequent terms contributing no further information. The resulting turbulence model applied to both low and high Reynolds number flows without requiring wall functions or ad hoc modifications of the equations. All constants are derived from the renormalization group procedure; no adjustable constants arise. The model permits inequality of the Reynolds normal stresses, a necessary condition for calculating turbulence-driven secondary flows in noncircular ducts. Author

A90-44462* Maryland Univ., College Park.

COMPARISON BETWEEN PRESSURE GRADIENT METHOD AND MAC METHOD ON HIGH RE CALCULATION

C.-H. TAN (Maryland, University, College Park) and J. C. DUH (NASA, Lewis Research Center; Sverdrup Technology, Inc., Cleveland, OH) IN: International Symposium on Numerical Methods in Engineering, 5th, Lausanne, Switzerland, Sept. 11-15, 1989, Proceedings. Volume 2. Southampton, England and New York/Berlin, Computational Mechanics Publications/Springer-Verlag, 1989, p. 465-471. refs
Copyright

A cavity flow driven by shear and buoyancy forces is used as a test problem in the application of a nonstaggered pressure gradient (PG) method in solving the two-dimensional incompressible Navier-Stokes equations. Twelve finite differencing schemes are used to solve the cavity flow problem. The schemes consist of various combinations of grid arrangements, upwinding treatments, and conservativeness of convection terms. An artificial source term is introduced, and the solutions are compared with those obtained by the conventional marker-and-cell (MAC) method. The comparisons favor the PG method. Numerical results obtained by the twelve schemes are compared with exact solutions in order to assess the stability and accuracy of each scheme. S.A.V.

A90-44541* National Aeronautics and Space Administration. Lewis Research Center, Cleveland, OH.

SURFACE REORIENTATION AND SETTLING IN CYLINDERS UPON STEP REDUCTION IN GRAVITY

MARK M. WEISLOGEL and H. D. ROSS (NASA, Lewis Research

Center, Cleveland, OH) Microgravity Science and Technology (ISSN 0938-0108), vol. 3, May 1990, p. 24-32. refs
Copyright

A large literature exists concerning the equilibrium configurations of free liquid/gas surfaces in reduced gravity environments. Such conditions generally yield surfaces of constant curvature contracting the container wall at a particular angle. The time required to reach and stabilize about this configuration is less studied for the case of sudden changes in gravity level; e.g., from normal- to low-gravity, as can occur in many drop tower experiments. The particular interest here was to determine the total reorientation time for such surfaces in cylinders, as a function primarily of contact angle and kinematic viscosity, in order to aid in the development of drop tower experiment design. A large parametric range of tests were performed and, based on an accompanying scale analysis, the complete data set was correlated. The results of other investigations are included for comparison. Author

A90-45317* National Aeronautics and Space Administration. Lewis Research Center, Cleveland, OH.

NUMERICAL STUDIES OF CONVECTIVE HEAT TRANSFER IN AN INCLINED SEMI-ANNULAR ENCLOSURE

L.-W. WANG, A.-T. CHAI (NASA, Lewis Research Center, Cleveland, OH), C.-N. YUNG (Toledo, University, OH), and N. RASHIDNIA (NASA, Lewis Research Center; Sverdrup Technology, Inc., Cleveland, OH) IN: Numerical heat transfer with personal computers and supercomputing; Proceedings of the ASME National Heat Transfer Conference, Philadelphia, PA, Aug. 6-9, 1989. New York, American Society of Mechanical Engineers, 1989, p. 73-77. Previously announced in STAR as N89-28666. refs
Copyright

Natural convection heat transfer in a two-dimensional differentially heated semiannular enclosure is studied. The enclosure is isothermally heated and cooled at the inner and outer walls, respectively. A commercial software based on the SIMPLER algorithm was used to simulate the velocity and temperature profiles. Various parameters that affect the momentum and heat transfer processes were examined. These parameters include the Rayleigh number, Prandtl number, radius ratio, and the angle of inclination. A flow regime extending from conduction-dominated to convection-dominated flow was examined. The computed results of heat transfer are presented as a function of flow parameter and geometric factors. It is found that the heat transfer rate attains a minimum when the enclosure is tilted about + 50 deg with respect to the gravitational direction. Author

A90-46885*# National Aeronautics and Space Administration. Lewis Research Center, Cleveland, OH.

EVOLUTION AND INTERACTION OF TWO- AND THREE-DIMENSIONAL INSTABILITY WAVES

R. R. MANKBADI (NASA, Lewis Research Center, Cleveland, OH) IN: International Congress of Fluid Mechanics, 3rd, Cairo, Egypt, Jan. 2-4, 1990, Proceedings. Volume 3. Mansoura, Egypt, Mansoura University, 1990, p. 853-866. refs

The present work is concerned with the nonlinear interactions of high-amplitude two- and three-dimensional instability waves in jets. A jet is excited by multifrequency axisymmetric and helical modes. Formulations are presented here for the nonlinear development of both the amplitudes and phases of the instability waves. The development of these waves are also coupled with the development of the mean flow and the background turbulence. In formulating this model it is assumed that each flow component can be characterized by conservation equations supplemented by closure models. Author

A90-46895*# National Aeronautics and Space Administration. Lewis Research Center, Cleveland, OH.

GAS-PHASE FLOWRATE EFFECT ON DISINTEGRATING CRYOGENIC LIQUID-JETS

ROBERT D. INGEBE (NASA, Lewis Research Center, Cleveland, OH) IN: International Congress of Fluid Mechanics, 3rd, Cairo, Egypt, Jan. 2-4, 1990, Proceedings. Volume 3. Mansoura, Egypt,

Mansoura University, 1990, p. 1105-1110. Previously announced in STAR as N90-11277. refs

Two phase liquid and gaseous nitrogen flow in a pneumatic two fluid atomizer was investigated. Characteristic dropsize for cryogenic sprays were measured with a scattered light scanning instrument developed at NASA-Lewis. Tests were conducted primarily in the aerodynamic stripping regime of liquid jet atomization. At a sampling distance of $\bar{x} = 1.3$ cm, the Sauter mean, $D_{(sub\ 32)}$, and volume median, $D_{(sub\ v.5)}$, drop diameters were measured and correlated with nitrogen gas flowrate, $W_{(sub\ n)}$, to give the following expressions: $D_{sub\ 32}$ to the $-1 = 210W_{(sub\ n)}$ to the -1.33 and $D_{(sub\ v.5)}$ to the $-1 = 150 W_{(sub\ n)}$ to the -1.33 , where reciprocal diameters and gas flowrate are in cm (-1) and g/sec, respectively. The exponent 1.33 for nitrogen gas flowrate, $W_{(sub\ n)}$, is the same as that predicted by atomization theory for liquid-jet breakup in high velocity gasflow. When the spray was sampled at axial distances of $\bar{x} = 2.5$ and 4.5 cm downstream of the atomizer, the exponent decreased to 1.2 and 0.9, respectively. This was attributed to the loss of small droplets due to their rapid vaporization. Author

A90-46902*# Virginia Polytechnic Inst. and State Univ., Blacksburg.

THE GROWTH AND DEVELOPMENT OF A TURBULENT JUNCTION VORTEX SYSTEM

F. J. PIERCE (Virginia Polytechnic Institute and State University, Blacksburg) and J. SHIN (NASA, Lewis Research Center, Cleveland, OH) IN: International Congress of Fluid Mechanics, 3rd, Cairo, Egypt, Jan. 2-4, 1990, Proceedings. Volume 4. Mansoura, Egypt, Mansoura University, 1990, p. 1311-1324. refs

The growth and development of a vortex system in an incompressible three-dimensional flow generated by a streamlined cylinder mounted with its axis normal to a flat surface was investigated using data from surface flow visualizations, surface pressure measurements, and mean flow measurements. The results from velocity measurements revealed the presence of a single large dominant vortex and a small vortex in the junction between the cylinder and the flat surface. This second vortex is tentatively identified as being connected with a corner separation occurring just downstream of the body at its thickest cross section. It is shown that, as the principal horseshoe vortex develops downstream, the strength of the vortex decreases, while its length scale increases. I.S.

A90-47203*# Florida Univ., Gainesville.

EFFECT OF VANE TWIST ON THE PERFORMANCE OF DOME SWIRLERS FOR GAS TURBINE AIRBLAST ATOMIZERS

GERALD J. MICKLOW, ANJU S. DOGRA (Florida, University, Gainesville), and H. LEE NGUYEN (NASA, Lewis Research Center, Cleveland, OH) AIAA, SAE, ASME, and ASCE, Joint Propulsion Conference, 26th, Orlando, FL, July 16-18, 1990. 14 p. Previously announced in STAR as N90-25289. refs
(AIAA PAPER 90-1955) Copyright

For advanced gas turbine engines, two combustor systems, the lean premixed/prevaporized (LPP) and the rich burn/quick quench/lean burn (RQL) offer great potential for reducing NO(x) emissions. An important consideration for either concept is the development of an advanced fuel injection system that will provide a stable, efficient, and very uniform combustion system over a wide operating range. High-shear airblast fuel injectors for gas turbine combustors have exhibited superior atomization and mixing compared with pressure-atomizing fuel injectors. This improved mixing has lowered NO(x) emissions and the pattern factor, and has enabled combustors to alternate fuels while maintaining a stable, efficient combustion system. The performance of high-shear airblast fuel injectors is highly dependent on the design of the dome swirl vanes. The type of swirl vanes most widely used in gas turbine combustors are usually flat for ease of manufacture, but vanes with curvature will, in general, give superior aerodynamic performance. The design and performance of high-turning, low-loss curved dome swirl vanes with twist along the span are investigated. The twist induces a secondary vortex flow pattern which will improve the atomization of the fuel, thereby producing a more

34 FLUID MECHANICS AND HEAT TRANSFER

uniform fuel-air distribution. This uniform distribution will increase combustion efficiency while lowering NO(x) emissions. A systematic swirl vane design system is presented based on one-, two-, and three-dimensional flowfield calculations, with variations in vane-turning angle, rate of turning, vane solidity, and vane twist as design parameters. Author

A90-47206* National Aeronautics and Space Administration. Lewis Research Center, Cleveland, OH.

THREE-DIMENSIONAL COMPRESSIBLE JET-IN-CROSSFLOW CALCULATIONS USING IMPROVED VISCOSITY MODELS AND ADAPTED GRID

JOHN K. LYTLE (NASA, Lewis Research Center, Cleveland, OH), GARY J. HARLOFF, and ANDREW T. HSU (NASA, Lewis Research Center; Sverdrup Technology, Inc., Brook Park, OH) AIAA, SAE, ASME, and ASEE, Joint Propulsion Conference, 26th, Orlando, FL, July 16-18, 1990. 11 p. refs

(Contract NAS3-25266)

(AIAA PAPER 90-2100) Copyright

Previous calculations of jet-in-crossflow problems have been sensitive to the turbulence and artificial viscosity models and to the grid. Consequently, the eddy viscosity model in the PARC3D code was modified to consider the turbulent jet by switching from the Baldwin-Lomax (1978) model to an axisymmetric jet model. A modified artificial viscosity model has been utilized and evaluated in this study as well. The new model includes cell size scaling and a directional dependence in the coefficients. Computational results from PARC3D demonstrate the effects of the viscosity models on the pressure distribution fore and aft of the jet and the ability of the adaptive grid scheme to adjust to the three-dimensional gradients around the jet. Author

A90-48404* National Aeronautics and Space Administration. Lewis Research Center, Cleveland, OH.

MATHEMATICAL MODELING AND ANALYSIS OF HEAT PIPE START-UP FROM THE FROZEN STATE

J. H. JANG (NASA, Lewis Research Center, Cleveland, OH), A. FAGHRI (Wright State University, Dayton, OH), W. S. CHANG, and E. T. MAHEFKEY (USAF, Wright Research and Development Center, Wright-Patterson AFB, OH) ASME, Transactions, Journal of Heat Transfer (ISSN 0022-1481), vol. 112, Aug. 1990, p. 586-594. Previously announced in STAR as N89-28747. refs

(Contract F33615-88-C-2820)

Copyright

The start-up process of a frozen heat pipe is described and a complete mathematical model for the start-up of the frozen heat pipe is developed based on the existing experimental data, which is simplified and solved numerically. The two-dimensional transient model for the wall and wick is coupled with the one-dimensional transient model for the vapor flow when vaporization and condensation occur at the interface. A parametric study is performed to examine the effect of the boundary specification at the surface of the outer wall on the successful start-up from the frozen state. For successful start-up, the boundary specification at the outer wall surface must melt the working substance in the condenser before dry-out takes place in the evaporator. Author

A90-48548* National Aeronautics and Space Administration. Lewis Research Center, Cleveland, OH.

HOPF BIFURCATION IN THE DRIVEN CAVITY

JOHN W. GOODRICH (NASA, Lewis Research Center, Cleveland, OH), KARL GUSTAFSON (Colorado, University, Boulder), and KADOSA HALASI (Kansas State University, Manhattan) Journal of Computational Physics (ISSN 0021-9991), vol. 90, Sept. 1990, p. 219-261. refs

Copyright

The algorithm employed in the present incompressible two-dimensional calculations of an impulsively-started lid-driven cavity has its basis in the time-dependent stream-function equation. While a Crank-Nicholson differencing scheme is used for the diffusion terms, the Adams-Bashforth scheme is used for the convection terms. The periodic asymptotic solutions obtained for

Reynolds numbers of 5000 and 10,000 are found to be precisely periodic; it is demonstrated that they have reached asymptotic states. The indicators of that achievement are discussed. O.C.

A90-49789* National Aeronautics and Space Administration. Lewis Research Center, Cleveland, OH.

DIAGONALLY INVERTED LOWER-UPPER FACTORED IMPLICIT MULTIGRID SCHEME FOR THE THREE-DIMENSIONAL NAVIER-STOKES EQUATIONS

JEFFREY W. YOKOTA (NASA, Lewis Research Center; Sverdrup Technology, Inc., Cleveland, OH) AIAA Journal (ISSN 0001-1452), vol. 28, Sept. 1990, p. 1642-1649. Previously cited in issue 09, p. 1349, Accession no. A89-25382. refs

Copyright

A90-50511* Massachusetts Inst. of Tech., Cambridge.

RATE CORRELATION FOR CONDENSATION OF PURE VAPOR ON TURBULENT, SUBCOOLED LIQUID

J. STEVEN BROWN, BOO CHEONG KHOO, and AIN A. SONIN (MIT, Cambridge, MA) International Journal of Heat and Mass Transfer (ISSN 0017-9310), vol. 33, Sept. 1990, p. 2001-2018. refs

(Contract NAG3-731)

Copyright

An empirical correlation is presented for the condensation of pure vapor on a subcooled, turbulent liquid with a shear-free interface. The correlation expresses the dependence of the condensation rate on fluid properties, on the liquid-side turbulence (which is imposed from below), and on the effects of buoyancy in the interfacial thermal layer. The correlation is derived from experiments with steam and water, but under conditions which simulate typical cryogenic fluids. Author

A90-51019* Cincinnati Univ., OH.

GLOBAL PRESSURE RELAXATION FOR LAMINAR TWO-DIMENSIONAL INTERNAL FLOW

D. ROSENBAUM and S. G. RUBIN (Cincinnati, University, OH) International Journal for Numerical Methods in Fluids (ISSN 0271-2091), vol. 10, May 1990, p. 827-848. refs

(Contract NAG3-397)

Copyright

This study extends the reduced Navier-Stokes (RNS) global pressure relaxation procedure developed by Rubin and co-workers for external flow to internal flow applications. The streamwise pressure gradient is split into a backward-differenced or initial value component, as in boundary layer marching, and a forward-differenced or boundary value component that represents the elliptic downstream effects. The streamwise convection terms are upwind-differenced and all other streamwise derivatives are backward-differenced. A standard boundary layer marching technique imbedded in a conventional line relaxation technique is obtained. For compressible flow the pressure iteration determines the interior flow interaction as well as the inlet mass flux that is consistent with the outflow pressure boundary condition. Results have been computed for incompressible flow in both rectangular and curved channels, and for subsonic compressible flow in the simulation of an aerofoil in a wind tunnel. Converged solutions were obtained over a range of Reynolds numbers generating small to moderately large separation bubbles. Author

A90-52275* National Aeronautics and Space Administration. Lewis Research Center, Cleveland, OH.

INVISCID FLUX-SPLITTING ALGORITHMS FOR REAL GASES WITH NON-EQUILIBRIUM CHEMISTRY

JIAN-SHUN SHUEN (NASA, Lewis Research Center; Sverdrup Technology, Inc., Cleveland, OH), MENG-SING LIOU (NASA, Lewis Research Center, Cleveland, OH), and BRAM VAN LEER (NASA, Lewis Research Center; Institute for Computational Mechanics in Propulsion, Cleveland, OH; Michigan, University, Ann Arbor) Journal of Computational Physics (ISSN 0021-9991), vol. 90, Oct. 1990, p. 371-395. refs

Copyright

Formulations of inviscid flux splitting algorithms for chemical

nonequilibrium gases are presented. A chemical system for air dissociation and recombination is described. Numerical results for one-dimensional shock tube and nozzle flows of air in chemical nonequilibrium are examined. C.D.

A90-52500*# National Aeronautics and Space Administration. Lewis Research Center, Cleveland, OH.

NUMERICAL INVESTIGATION OF THE THERMAL STRATIFICATION IN CRYOGENIC TANKS SUBJECTED TO WALL HEAT FLUX

CHIN-SHUN LIN (NASA, Lewis Research Center; Analox Corp., Fairview Park, OH) and MOHAMMED M. HASAN (NASA, Lewis Research Center, Cleveland, OH) AIAA, SAE, ASME, and ASEE, Joint Propulsion Conference, 26th, Orlando, FL, July 16-18, 1990. 19 p. Previously announced in STAR as N90-27984. refs (AIAA PAPER 90-2375) Copyright

The flow pattern and thermal stratification of a cryogenic cylindrical tank are numerically studied. The tank sidewall is subjected to either a uniform heat-flux or two discrete levels of uniform heat-flux at the upper and lower halves of the tank wall. The tank bottom is kept at a constant temperature controlled by the heat exchanger of a thermodynamic vent system. The tank pressure is also assumed constant resulting in a constant saturation temperature at the interface which is higher than the tank bottom temperature. The effects of vapor motion and vapor superheat on the mass and heat transfer processes at the interface are assumed negligible such that the calculations of liquid region can be decoupled from the vapor region. Dimensionless steady-state conservation equations are solved by a finite-difference method. The effects of modified Rayleigh number, Prandtl number, tank aspect ratio, wall heat-flux parameter, and wall heat-flux distribution on the liquid velocity and temperature fields are investigated. Also, their effects on the rate of heat transfer through the interface and the tank bottom are examined. Author

N90-11245*# National Aeronautics and Space Administration. Lewis Research Center, Cleveland, OH.

LASER ANEMOMETER MEASUREMENTS IN A TRANSONIC AXIAL-FLOW FAN ROTOR

ANTHONY J. STRAZISAR, JERRY R. WOOD, MICHAEL D. HATHAWAY, and KENNETH L. SUDER Washington Nov. 1989 216 p (NASA-TP-2879; E-4480; NAS 1.60:2879) Avail: NTIS HC A10/MF A02 CSCL 20/4

Laser anemometer surveys were made of the 3-D flow field in NASA rotor 67, a low aspect ratio transonic axial-flow fan rotor. The test rotor has a tip relative Mach number of 1.38. The flowfield was surveyed at design speed at near peak efficiency and near stall operating conditions. Data is presented in the form of relative Mach number and relative flow angle distributions on surfaces of revolution at nine spanwise locations evenly spaced from hub to tip. At each spanwise location, data was acquired upstream, within, and downstream of the rotor. Aerodynamic performance measurements and detailed rotor blade and annulus geometry are also presented so that the experimental results can be used as a test case for 3-D turbomachinery flow analysis codes. Author

N90-11250*# National Aeronautics and Space Administration. Lewis Research Center, Cleveland, OH.

WALL-LAYER ERUPTIONS IN TURBULENT FLOWS

J. D. A. WALKER (Lehigh Univ., Bethlehem, PA.) Sep. 1989 13 p (Contract NASA ORDER C-99066-G) (NASA-TM-102362; E-5078; ICOMP-89-26; NAS 1.15:102362) Avail: NTIS HC A03/MF A01 CSCL 20/4

The near-wall region of a turbulent flow is investigated in the limit of large Reynolds numbers. When low-speed streaks are present, the governing equations are shown to be of the boundary-layer type. Physical processes leading to local breakdown and a strong interaction with the outer region are considered. It is argued that convected vortices, predominantly of the hairpin type, will provoke eruptions and regenerative interactions with the outer region. Author

N90-11256*# Elrod (Harold G.), Old Saybrook, CT. EFFICIENT NUMERICAL METHOD FOR COMPUTATION OF THERMOHYDRODYNAMICS OF LAMINAR LUBRICATING FILMS Final Report

HAROLD G. ELROD Aug. 1989 25 p (Contract NASA ORDER C-22406-M; DA PROJ. 1L1-61102-AH-45) (NASA-CR-185136; NAS 1.26:185136; AVSCOM-TR-89-C-015) Avail: NTIS HC A03/MF A01 CSCL 20/4

The purpose of this paper is to describe an accurate, yet economical, method for computing temperature effects in laminar lubricating films in two dimensions. The procedure presented here is a sequel to one presented in Leeds in 1986 that was carried out for the one-dimensional case. Because of the marked dependence of lubricant viscosity on temperature, the effect of viscosity variation both across and along a lubricating film can dwarf other deviations from ideal constant-property lubrication. In practice, a thermohydrodynamics program will involve simultaneous solution of the film lubrication problem, together with heat conduction in a solid, complex structure. The extent of computation required makes economy in numerical processing of utmost importance. In pursuit of such economy, we here use techniques similar to those for Gaussian quadrature. We show that, for many purposes, the use of just two properly positioned temperatures (Lobatto points) characterizes well the transverse temperature distribution. Author

N90-11969*# National Aeronautics and Space Administration. Lewis Research Center, Cleveland, OH.

HOPF BIFURCATION IN THE DRIVEN CAVITY

JOHN W. GOODRICH, KARL GUSTAFSON, and KADOSA HALASI (Kansas State Univ., Manhattan.) Oct. 1989 52 p Submitted for publication (Contract NASA ORDER C-99066-G) (NASA-TM-102334; E-4957-1; ICOMP-89-21; NAS 1.15:102334) Avail: NTIS HC A04/MF A01 CSCL 20/4

Incompressible two dimensional calculations are reported for the impulsively started lid driven cavity with aspect ratio two. The algorithm is based on the time dependent streamfunction equation, with a Crank-Nicolson differencing scheme for the diffusion terms, and with an Adams-Bashforth scheme for the convection terms. A multigrid method is used to solve the linear implicit equations at each time step. Periodic asymptotic solutions have been found for $Re = 10000$ and for $Re = 5000$. The $Re = 5000$ results are validated by grid refinement calculations. The solutions are shown to be precisely periodic, and care is taken to demonstrate that asymptotic states were reached. A discussion is included about the indicators that are used to show that an asymptotic state was reached, and to show that the asymptotic state is indeed periodic. Author

N90-12882*# California Univ., Berkeley. Dept. of Mechanical Engineering.

INVESTIGATION OF TURBULENT FLOW IN HIGHLY CURVED DUCTS WITH APPLICATION TO TURBOMACHINERY COMPONENTS Final Report

J. A. C. HUMPHREY and M. P. ARNAL 1987 166 p (Contract NAG3-624; NAG3-735) (NASA-CR-186060; NAS 1.26:186060) Avail: NTIS HC A08/MF A01 CSCL 20/4

Numerical predictions were performed using a semi-elliptic calculation procedure for the case of turbulent flow in passage through a 90 deg bend of square cross section. Two versions of the isotropic turbulent viscosity two equation k-epsilon model were used. The first, the wall function model (WFM), employs the logarithmic law-of-the-wall relation and the notion of equilibrium flow to set all the necessary boundary conditions at the first grid point adjacent to a solid wall. The second model, the Van Driest model (VDM), employs Prandtl's original mixing length formulation, in conjunction with Van Driest's semi-empirical relation for the mixing length, to calculate the turbulent viscosity in the near wall regions of the flow. In this case, boundary conditions for k and epsilon, required to calculate these quantities in the core of the

34 FLUID MECHANICS AND HEAT TRANSFER

flow, are obtained by matching the mixing length and Reynolds number model formulations in an overlapping region of the flow near the walls. In both cases the results obtained show an improvement over earlier calculations using an elliptic numerical procedure. This is attributed to the finer grids possible in the present work. Of the two models, the VDM formulation shows better overall conformity with the mean flow measurements. Neither model reproduces well the details of the stress distribution as a result of the implied isotropic turbulent viscosity. Author

N90-13719*# National Aeronautics and Space Administration. Lewis Research Center, Cleveland, OH.

EFFECT OF SPATIAL RESOLUTION ON APPARENT SENSITIVITY TO INITIAL CONDITIONS OF A DECAYING FLOW AS IT BECOMES TURBULENT

ROBERT G. DEISSLER and FRANK B. MOLLS Nov. 1989 8 p Submitted for publication (NASA-TM-102377; E-5115; NAS 1.15:102377) Avail: NTIS HC A02/MF A01 CSCL 20/4

Grids with 32(exp 3), 64(exp 3), and 128(exp 3) points are used in numerical solutions for a decaying flow. The sensitivity of initially neighboring solutions to small changes in initial conditions increases as the spatial resolution improves. A fourth-order finite-difference method is used for the solutions with 32(exp 3) and 64(exp 3) grid points, and a pseudospectral method is used for 128(exp 3) grid points. The latter solutions appear to be rather well-resolved, in spite of the formation of steep velocity gradients in the flow. Author

N90-13748*# Sverdrup Technology, Inc., Cleveland, OH.

AN IMPROVED ALGORITHM FOR THE MODELING OF VAPOR FLOW IN HEAT PIPES Final Report

LEONARD K. TOWER and DONALD C. HAINLEY Dec. 1989 12 p Proposed for presentation at the 7th International Heat Pipe Conference, Minsk, USSR, 21-25 May 1990; sponsored by Luikov Heat and Mass Transfer Inst. (Contract NAS3-25266) (NASA-CR-185179; E-5195; NAS 1.26:185179) Avail: NTIS HC A03/MF A01 CSCL 20/4

A heat pipe vapor flow algorithm suitable for use in codes on microcomputers is presented. The incompressible heat pipe vapor flow studies of Busse are extended to incorporate compressibility effects. The Busse velocity profile factor is treated as a function of temperature and pressure. The assumption of a uniform saturated vapor temperature determined by the local pressure at each cross section of the pipe is not made. Instead, a mean vapor temperature, defined by an energy integral, is determined in the course of the solution in addition to the pressure, saturation temperature at the wall, and the Busse velocity profile factor. For alkali metal working fluids, local species equilibrium is assumed. Temperature and pressure profiles are presented for several cases involving sodium heat pipes. An example for a heat pipe with an adiabatic section and two evaporators in sequence illustrates the ability to handle axially varying heat input. A sonic limit plot for a short evaporator falls between curves for the Busse and Levy inviscid sonic limits. Author

N90-13749*# National Aeronautics and Space Administration. Lewis Research Center, Cleveland, OH.

ANALYSIS OF ROTARY ENGINE COMBUSTION PROCESSES BASED ON UNSTEADY, THREE-DIMENSIONAL COMPUTATIONS

M. S. RAJU (Sverdrup Technology, Inc., Cleveland, OH.) and E. A. WILLIS 1989 37 p Presented at the 28th Aerospace Sciences Meeting, Reno, NV, 8-11 Jan. 1990; sponsored by AIAA (NASA-TM-102469; E-5249; NAS 1.15:102469; AIAA-90-0643) Avail: NTIS HC A03/MF A01 CSCL 20/4

A new computer code was developed for predicting the turbulent, and chemically reacting flows with sprays occurring inside of a stratified charge rotary engine. The solution procedure is based on an Eulerian Lagrangian approach where the unsteady, 3-D Navier-Stokes equations for a perfect gas mixture with variable properties are solved in generalized, Eulerian coordinates on a

moving grid by making use of an implicit finite volume, Steger-Warming flux vector splitting scheme, and the liquid phase equations are solved in Lagrangian coordinates. Both the details of the numerical algorithm and the finite difference predictions of the combustor flow field during the opening of exhaust and/or intake, and also during fuel vaporization and combustion, are presented. Author

N90-13750*# National Aeronautics and Space Administration. Lewis Research Center, Cleveland, OH.

CONVECTIVE HEAT TRANSFER MEASUREMENTS FROM A NACA 0012 AIRFOIL IN FLIGHT AND IN THE NASA LEWIS ICING RESEARCH TUNNEL

PHILIP E. POINSATTE, G. JAMES VANFOSSSEN, and KENNETH J. DEWITT (Toledo Univ., OH.) 1989 20 p Presented at the 28th Aerospace Sciences Meeting, Reno, NV, 8-11 Jan. 1990; sponsored by AIAA (NASA-TM-102448; E-5232; NAS 1.15:102448) Avail: NTIS HC A03/MF A01 CSCL 20/4

Local heat transfer coefficients were measured on a smooth and roughened NACA 0012 airfoil. Heat transfer measurements on the 0.533 m chord airfoil were made both in flight on the NASA Lewis Twin Otter Icing Research Aircraft and in the NASA Lewis Icing Research Tunnel (IRT). Roughness was obtained by the attachment of uniform 2 mm diameter hemispheres to the airfoil surface in 4 distinct patterns. Flight data were taken for the smooth and roughened airfoil at various Reynolds numbers based on chord in the range 1.24 to 2.50 x 10⁶ (exp 6) and at various angles of attack up to 4 deg. During these flight tests, the free stream velocity turbulence intensity was found to be very low (less than 0.1 percent). Wind tunnel data were acquired in the Reynolds number range 1.20 to 4.25 x 10⁶ (exp 6) and at angles of attack from -4 to 8 deg. The turbulence intensity in the IRT was 0.5 to 0.7 percent with the cloud generating sprays off. A direct comparison was made between the results obtained in flight and in the IRT. The higher level of turbulence in the IRT vs. flight had little effect on the heat transfer for the lower Reynolds numbers but caused a moderate increase in heat transfer at the high Reynolds numbers. Roughness generally increased the heat transfer. Author

N90-13751*# National Aeronautics and Space Administration. Lewis Research Center, Cleveland, OH.

VAPOR CONDENSATION ON LIQUID SURFACE DUE TO LAMINAR JET-INDUCED MIXING: THE EFFECTS OF SYSTEM PARAMETERS

CHIN-SHUN LIN (Analex Corp., Cleveland, OH.) and MOHAMMAD M. HASAN 1989 21 p Presented at the 28th Aerospace Sciences Meeting, Reno, NV, 8-11 Jan. 1990; sponsored by AIAA (NASA-TM-102433; E-5201; NAS 1.15:102433; AIAA-90-0354) Avail: NTIS HC A03/MF A01 CSCL 20/4

The effects of system parameters on the interface condensation rate in a laminar jet induced mixing tank are numerically studied. The physical system consists of a partially filled cylindrical tank with a slightly subcooled jet discharged from the center of the tank bottom toward the liquid-vapor interface which is at a saturation temperature corresponding to the constant tank pressure. Liquid is also withdrawn from the outer part of the tank bottom to maintain the constant liquid level. The jet velocity is selected to be low enough such that the free surface is approximately flat. The effect of vapor superheat is assumed to be negligible. Therefore, the interface condensation rate can be determined from the resulting temperature field in the liquid region alone. The nondimensional form of the steady state conservation equations are solved by a finite difference method for various system parameters including liquid height to tank diameter ratio, tank to jet diameter ratio, liquid inflow to outflow area ratio, and a heat leak parameter which characterizes the uniform wall heat flux. Detailed analyses based on the numerical solutions are performed and simplified equations are suggested for the prediction of condensation rate. Author

N90-14494* # United Technologies Research Center, East Hartford, CT.

LASER VELOCIMETER AND TOTAL PRESSURE MEASUREMENTS IN CIRCULAR-TO-RECTANGULAR TRANSITION DUCTS Final Report

WILLIAM P. PATRICK and DUANE C. MCCORMICK Jun. 1988 121 p

(Contract NAS3-24616)

(NASA-CR-182286; NAS 1.26:182286; UTRC-87-41) Avail: NTIS HC A06/MF A01 CSCL 20/4

A comprehensive set of total pressure and three-component laser velocimetry (LV) data were obtained within two circular-to-rectangular transition ducts at low subsonic speeds. This set of reference data was acquired for use in identifying secondary flow mechanisms and for assessing the accuracy of computational procedures for calculating such flows. Data were obtained at the inlet and exit planes of an aspect ratio three duct having a length-to-diameter ratio of one (AR310) and an aspect ratio six duct having a length-to-diameter ratio of three (AR630). Each duct was unseparated throughout its transition section. It is therefore concluded that secondary flows can play an important part in the fluid dynamics of transition ducts and needs to be addressed in computational analysis. The strength of the secondary flows depends on both the aspect ratio and relative axial duct length.

Author

N90-14511* # National Aeronautics and Space Administration. Lewis Research Center, Cleveland, OH.

THERMAL/STRUCTURAL ANALYSES OF SEVERAL HYDROGEN-COOLED LEADING-EDGE CONCEPTS FOR HYPERSONIC FLIGHT VEHICLES

HERBERT J. GLADDEN, MATTHEW E. MELIS, THEODORE T. MOCKLER, and MIKE TONG (Sverdrup Technology, Inc., Cleveland, OH.) 1990 16 p Presented at the 28th Aerospace Sciences Meeting, Reno, NV, 8-11 Jan. 1990; sponsored by AIAA Original contains color illustrations

(NASA-TM-102391; E-4788; NAS 1.15:102391; AIAA-90-0053)

Avail: NTIS HC A03/MF A01 CSCL 20/4

The aerodynamic heating at high flight Mach numbers, when shock interference heating is included, can be extremely high and can exceed the capability of most conventional metallic and potential ceramic materials available. Numerical analyses of the heat transfer and thermal stresses are performed on three actively cooled leading-edge geometries (models) made of three different materials to address the issue of survivability in a hostile environment. These analyses show a mixture of results from one configuration to the next. Results for each configuration are presented and discussed. Combinations of enhanced internal film coefficients and high material thermal conductivity of copper and tungsten are predicted to maintain the maximum wall temperature for each concept within acceptable operating limits. The exception is the TD nickel material which is predicted to melt for most cases. The wide range of internal impingement film coefficients (based on correlations) for these conditions can lead to a significant uncertainty in expected leading-edge wall temperatures. The equivalent plastic strain, inherent in each configuration which results from the high thermal gradients, indicates a need for further cyclic analysis to determine component life.

Author

N90-14512* # Sverdrup Technology, Inc., Cleveland, OH.

THERMOCAPILLARY MIGRATION OF LIQUID DROPLETS IN A TEMPERATURE GRADIENT IN A DENSITY MATCHED SYSTEM Final Report

N. RASHIDNIA and R. BALASUBRAMANIAM (Case Western Reserve Univ., Cleveland, OH.) Dec. 1989 28 p (Contract NAS3-25266; NCC3-140)

(NASA-CR-185178; E-5192; NAS 1.26:185178) Avail: NTIS HC A03/MF A01 CSCL 20/4

An experimental investigation of thermocapillary flow in droplets of a vegetable oil (partially hydrogenated soybean oil) immersed in silicone oil was conducted in a test cell with a heated top wall and a cooled bottom wall. The liquids are nearly immiscible and have equal densities at a temperature below the room temperature,

thus providing a simulation of low-gravity conditions by reducing the buoyancy forces. The interfacial tension between the two oils was measured in the temperature range 20 to 50 C using a capillary tube and $(d\sigma)/(dT)$ was determined to be negative. Droplets ranging in sizes from 3 mm to 1 cm diameter were injected into the silicone oil. The vertical temperature profile in the bulk liquid (silicone oil) produces temperature variations along the interface which induce variations in the interfacial tension. The flow inside the droplet driven by the resulting interfacial shear stresses was observed using a laser light-sheet flow visualization technique. The flow direction is consistent with the sign of $(d\sigma)/(dT)$. The observed maximum surface velocities are compared to the theoretical predictions of Young et al. (1959).

Author

N90-14517* # National Aeronautics and Space Administration. Lewis Research Center, Cleveland, OH.

SPATIAL EVOLUTION OF NONLINEAR ACOUSTIC MODE INSTABILITIES ON HYPERSONIC BOUNDARY LAYERS

M. E. GOLDSTEIN and D. W. WUNDROW (State Univ. of New York, Buffalo.) Dec. 1989 30 p

(Contract NAS3-25266; NGT-50085; NASA ORDER C-99066-G) (NASA-TM-102431; E-5075-1; ICOMP-89-30; NAS 1.15:102431)

Avail: NTIS HC A03/MF A01 CSCL 20/4

The effects are considered of strong critical layer nonlinearity on the spatial evolution of an initially linear acoustic mode instability wave on a hypersonic flat plate boundary layer. The analysis shows that nonlinearity, which is initially confined to a thin critical layer, first becomes important when the amplitude of the pressure fluctuations become $O(1/M \exp 4 \ln M \exp 2)$, where M is the free stream Mach number. The flow outside the critical layer is still determined by linear dynamics and therefore takes the form of a linear instability wave, but with its amplitude completely determined by the flow within the critical layer. The latter flow is determined by a coupled set of nonlinear equations, which were solved numerically.

Author

N90-15363* # Georgia Inst. of Tech., Atlanta. School of Mechanical Engineering.

FEASIBILITY ANALYSIS OF RECIPROCATING MAGNETIC HEAT PUMPS Final Report

A. V. LARSON, J. G. HARTLEY, SAM V. SHELTON, and M. M. SMITH Dec. 1989 59 p

(Contract NAG3-600)

(NASA-CR-186205; NAS 1.26:186205) Avail: NTIS HC A04/MF A01 CSCL 20/4

A reciprocating gadolinium core in a regeneration fluid column in the warm bore of a superconducting solenoidal magnet is considered for magnetic refrigeration in 3.517 MW (1000 ton) applications. A procedure is presented to minimize the amount of superconducting cable needed in the magnet design. Estimated system capital costs for an ideal magnetic refrigerator of this type become comparable to conventional chillers as the frequency of reciprocation approaches 10 Hertz. A 1-D finite difference analysis of a regenerator cycling at 0.027 Hertz is presented which exhibits some of the features seen in the experiments of G. V. Brown.

Author

N90-15364* # Calspan-Buffalo Univ. Research Center, NY. **DEVELOPMENT OF AN INTEGRATED BEM APPROACH FOR HOT FLUID STRUCTURE INTERACTION Annual Report, Nov. 1988 - Nov. 1989**

G. F. DARGUSH and P. K. BANERJEE (State Univ. of New York, Buffalo.) 1989 119 p

(Contract NAG3-712)

(NASA-CR-186214; NAS 1.26:186214) Avail: NTIS HC A06/MF A01 CSCL 20/4

The progress made toward the development of a boundary element formulation for the study of hot fluid-structure interaction in Earth-to-Orbit engine hot section components is reported. The convective viscous integral formulation was derived and implemented in the general purpose computer program GP-BEST. The new convective kernel functions, in turn, necessitated the development of refined integration techniques. As a result, however,

34 FLUID MECHANICS AND HEAT TRANSFER

since the physics of the problem is embedded in these kernels, boundary element solutions can now be obtained at very high Reynolds number. Flow around obstacles can be solved approximately with an efficient linearized boundary-only analysis or, more exactly, by including all of the nonlinearities present in the neighborhood of the obstacle. The other major accomplishment was the development of a comprehensive fluid-structure interaction capability within GP-BEST. This new facility is implemented in a completely general manner, so that quite arbitrary geometry, material properties and boundary conditions may be specified. Thus, a single analysis code (GP-BEST) can be used to run structures-only problems, fluids-only problems, or the combined fluid-structure problem. In all three cases, steady or transient conditions can be selected, with or without thermal effects. Nonlinear analyses can be solved via direct iteration or by employing a modified Newton-Raphson approach. M.G.

N90-17076* # National Aeronautics and Space Administration. Lewis Research Center, Cleveland, OH.

ON THE NUMERICAL SOLUTION OF THE DYNAMICALLY LOADED HYDRODYNAMIC LUBRICATION OF THE POINT CONTACT PROBLEM

SANG G. LIM, DAVID E. BREWE, and JOSEPH M. PRAHL (Case Western Reserve Univ., Cleveland, OH.) Feb. 1990 30 p Proposed for presentation at the Annual Meeting of the Society of Tribologists and Lubrication Engineers, Denver, CO, 7-11 May 1990 Prepared in cooperation with Army Aviation Research and Development Command, Cleveland, OH (Contract DA PROJ. 1L1-61102-AH-45) (NASA-TM-102427; E-5193; NAS 1.15:102427; AVSCOM-TR-89-C-021; AD-A219299) Avail: NTIS HC A03/MF A01 CSCL 20/4

The transient analysis of hydrodynamic lubrication of a point-contact is presented. A body-fitted coordinate system is introduced to transform the physical domain to a rectangular computational domain, enabling the use of the Newton-Raphson method for determining pressures and locating the cavitation boundary, where the Reynolds boundary condition is specified. In order to obtain the transient solution, an explicit Euler method is used to effect a time march. The transient dynamic load is a sinusoidal function of time with frequency, fractional loading, and mean load as parameters. Results include the variation of the minimum film thickness and phase-lag with time as functions of excitation frequency. The results are compared with the analytic solution to the transient step bearing problem with the same dynamic loading function. The similarities of the results suggest an approximate model of the point contact minimum film thickness solution. Author

N90-18005* # National Aeronautics and Space Administration. Lewis Research Center, Cleveland, OH.

RESPONSE OF A CHEMICALLY REACTING LAYER TO STREAMWISE VORTICITY

RUSSELL W. CLAUS Dec. 1989 12 p Previously announced in IAA as A89-40400 (NASA-TM-102288; E-4956; NAS 1.15:102288) Avail: NTIS HC A03/MF A01 CSCL 20/4

A series of Direct Numerical Simulations of a temporally evolving shear layer subject to both harmonic (2D) and streamwise (3D) forcing were performed. The interaction and coupling of these various 2D and 3D modes is shown to significantly alter the development of the flow. The scale of the 3D modes is quite important to the coupling process with greatly enhanced mixing and product formation resulting from 3D modes that are rapidly amplified by the spanwise vorticity. In general, the longer wavelength 3D modes are found to be highly efficient at increasing the momentum transport while the shorter wavelengths increase mass transport. Author

N90-18665* # National Aeronautics and Space Administration. Lewis Research Center, Cleveland, OH.

INVESTIGATION OF METHODS TO PRODUCE A UNIFORM CLOUD OF FUEL PARTICLES IN A FLAME TUBE

CLIFFORD E. SIEGERT, FREDERIC G. PLA, ROBERT RUBINSTEIN (Sverdrup Technology, Inc., Cleveland, OH.), THOMAS F. NIEZGODA, ROBERT J. BURNS, and JEROME A. JOHNSON Feb. 1990 25 p (NASA-TM-102376; E-5110; NAS 1.15:102376) Avail: NTIS HC A03/MF A01 CSCL 20/4

The combustion of a uniform, quiescent cloud of 30-micron fuel particles in a flame tube was proposed as a space-based, low-gravity experiment. The subject is the normal- and low-gravity testing of several methods to produce such a cloud, including telescoping propeller fans, air pumps, axial and quadrature acoustical speakers, and combinations of these devices. When operated in steady state, none of the methods produced an acceptably uniform cloud (+ or - 5 percent of the mean concentration), and voids in the cloud were clearly visible. In some cases, severe particle agglomeration was observed; however, these clusters could be broken apart by a short acoustic burst from an axially in-line speaker. Analyses and experiments reported elsewhere suggest that transient, acoustic mixing methods can enhance cloud uniformity while minimizing particle agglomeration. Author

N90-18667* # National Aeronautics and Space Administration. Lewis Research Center, Cleveland, OH.

A SIMPLE ALGEBRAIC GRID ADAPTATION SCHEME WITH APPLICATIONS TO TWO- AND THREE-DIMENSIONAL FLOW PROBLEMS

ANDREW T. HSU (Sverdrup Technology, Inc., Cleveland, OH.) and JOHN K. LYTLE 1989 10 p Presented at the 9th Computational Fluid Dynamics Conference, Buffalo, NY, 14-16 Jun. 1989; sponsored by AIAA Previously announced in IAA as A89-41827 (Contract NAS3-25266) (NASA-TM-102446; E-5229; NAS 1.15:102446) Avail: NTIS HC A02/MF A01 CSCL 20/4

An algebraic adaptive grid scheme based on the concept of arc equidistribution is presented. The scheme locally adjusts the grid density based on gradients of selected flow variables from either finite difference or finite volume calculations. A user-prescribed grid stretching can be specified such that control of the grid spacing can be maintained in areas of known flowfield behavior. For example, the grid can be clustered near a wall for boundary layer resolution and made coarse near the outer boundary of an external flow. A grid smoothing technique is incorporated into the adaptive grid routine, which is found to be more robust and efficient than the weight function filtering technique employed by other researchers. Since the present algebraic scheme requires no iteration or solution of differential equations, the computer time needed for grid adaptation is trivial, making the scheme useful for three-dimensional flow problems. Applications to two- and three-dimensional flow problems show that a considerable improvement in flowfield resolution can be achieved by using the proposed adaptive grid scheme. Although the scheme was developed with steady flow in mind, it is a good candidate for unsteady flow computations because of its efficiency. Author

N90-20326* # National Aeronautics and Space Administration. Lewis Research Center, Cleveland, OH.

AMPLITUDE-DEPENDENT NEUTRAL MODES IN COMPRESSIBLE BOUNDARY LAYER FLOWS

J. S. B. GAJJAR Mar. 1990 19 p (Contract NASA ORDER C-99066-G) (NASA-TM-102524; ICOMP-90-06; E-5331; NAS 1.15:102524) Avail: NTIS HC A03/MF A01 CSCL 20/4

The ideas of Benney and Bergeron (1969) and Davies (1970) on nonlinear critical layers are extended, and some new nonlinear neutral modes are computed for compressible boundary layer flow. A special case of the work is when the generalized inflexion point criterion holds. Neutral modes are found for a range of phase-speeds, dependent on the Mach number, and the properties of these are discussed. As in the linear case when the flow is relatively supersonic, multiple neutral modes exist. The behavior of the neutral amplitude in some limiting cases is also considered,

and it is found that the results are significantly different from that in incompressible flow when the flow is locally supersonic.

Author

N90-20337*# National Aeronautics and Space Administration. Lewis Research Center, Cleveland, OH.

UNSTEADY THREE-DIMENSIONAL MARGINAL SEPARATION, INCLUDING BREAKDOWN

PETER W. DUCK (Manchester Univ., England) Feb. 1990 31 p

(Contract NASA ORDER C-99066-G)

(NASA-TM-102525; ICOMP-90-07; E-5333; NAS 1.15:102525)

Avail: NTIS HC A03/MF A01 CSCL 20/4

A situation involving a three-dimensional marginal separation is considered, where a (steady) boundary layer flow is on the verge of separating at a point (located along a line of symmetry/centerline). At this point, a triple-deck is included, thereby permitting a small amount of interaction to occur. Unsteadiness is included within this interaction region through some external means. It is shown that the problem reduces to the solution of a nonlinear, unsteady, partial-integro system, which is solved numerically by means of time-marching together with a pseudo-spectral method spatially. A number of solutions to this system are presented which strongly suggest a breakdown of this system may occur, at a finite spatial position, at a finite time. The structure and details of this breakdown are then described.

Author

N90-20338*# National Aeronautics and Space Administration. Lewis Research Center, Cleveland, OH.

MASS TRANSFER FROM A SPHERE IN AN OSCILLATING FLOW WITH ZERO MEAN VELOCITY

COLIN K. DRUMMOND and FREDERIC A. LYMAN (Syracuse Univ., Utica, NY.) Apr. 1990 21 p

(NASA-TM-102566; E-5202; NAS 1.15:102566) Avail: NTIS HC

A03/MF A01 CSCL 20/4

A pseudospectral numerical method is used for the solution of the Navier-Stokes and mass transport equations for a sphere in a sinusoidally oscillating flow with zero mean velocity. The flow is assumed laminar and axisymmetric about the sphere's polar axis. Oscillating flow results were obtained for Reynolds numbers (based on the free-stream oscillatory flow amplitude) between 1 and 150, and Strouhal numbers between 1 and 1000. Sherwood numbers were computed and their dependency on the flow frequency and amplitude discussed. An assessment of the validity of the quasi-steady assumption for mass transfer is based on these results.

Author

N90-21291*# National Aeronautics and Space Administration. Lewis Research Center, Cleveland, OH.

A COST-EFFECTIVE STRATEGY FOR NONOSCILLATORY CONVECTION WITHOUT CLIPPING

B. P. LEONARD and H. S. NIKNAFS (Norton Co., Stow, OH.) Mar. 1990 24 p

(Contract NASA ORDER C-99066-G)

(NASA-TM-102538; ICOMP-90-09; E-5336; NAS 1.15:102538)

Avail: NTIS HC A03/MF A01 CSCL 20/4

Clipping of narrow extrema and distortion of smooth profiles is a well known problem associated with so-called high resolution nonoscillatory convection schemes. A strategy is presented for accurately simulating highly convective flows containing discontinuities such as density fronts or shock waves, without distorting smooth profiles or clipping narrow local extrema. The convection algorithm is based on non-artificially diffusive third-order upwinding in smooth regions, with automatic adaptive stencil expansion to (in principle, arbitrarily) higher order upwinding locally, in regions of rapidly changing gradients. This is highly cost effective because the wider stencil is used only where needed-in isolated narrow regions. A recently developed universal limiter assures sharp monotonic resolution of discontinuities without introducing artificial diffusion or numerical compression. An adaptive discriminator is constructed to distinguish between spurious overshoots and physical peaks; this automatically relaxes the limiter near local

turning points, thereby avoiding loss of resolution in narrow extrema. Examples are given for one-dimensional pure convection of scalar profiles at constant velocity.

Author

N90-21295*# National Aeronautics and Space Administration. Lewis Research Center, Cleveland, OH.

LIQUID TRANSFER CRYOGENIC TEST FACILITY: INITIAL HYDROGEN AND NITROGEN NO-VENT FILL DATA

MATTHEW E. MORAN, TED W. NYLAND, and S. STEPHEN PAPELL (Analex Corp., Cleveland, OH.) Mar. 1990 28 p

(NASA-TM-102572; E-5396; NAS 1.15:102572) Avail: NTIS HC

A03/MF A01 CSCL 20/4

The Liquid Transfer Cryogenic Test Facility is a versatile testbed for ground-based cryogenic fluid storage, handling, and transfer experimentation. The test rig contains two well instrumented tanks, and a third interchangeable tank, designed to accommodate liquid nitrogen or liquid hydrogen testing. The internal tank volumes are approx. 18, 5, and 1.2 cu. ft. Tank pressures can be varied from 2 to 30 psia. Preliminary no vent fill tests with nitrogen and hydrogen were successfully completed with the test rig. Initial results indicate that no vent fills of nitrogen above 90 percent full are achievable using this test configuration, in a 1-g environment, and with inlet liquid temperatures as high as 143 R, and an average tank wall temperature of nearly 300 R. This inlet temperature corresponds to a saturation pressure of 19 psia for nitrogen. Hydrogen proved considerably more difficult to transfer between tanks without venting. The highest temperature conditions resulting in a fill level greater than 90 percent were with an inlet liquid temperature of 34 R, and an estimated tank wall temperature of slightly more than 100 R. Saturation pressure for hydrogen at this inlet temperature is 10 psia. All preliminary no vent fill tests were performed with a top mounted full cone nozzle for liquid injection. The nozzle produces a 120 degree conical droplet spray at a differential pressure of 10 psi. Pressure in the receiving tank was held to less than 30 psia for all tests.

Author

N90-21296*# National Aeronautics and Space Administration. Lewis Research Center, Cleveland, OH.

THERMAL RADIATION CHARACTERISTICS OF NONISOTHERMAL CYLINDRICAL ENCLOSURES USING A NUMERICAL RAY TRACING TECHNIQUE

JOSEPH F. BAUMEISTER 1990 9 p Proposed for presentation at the 5th Thermophysics and Heat Transfer Conference, Seattle, WA, 18-20 Jun. 1990; cosponsored by AIAA and ASME

(NASA-TM-102527; E-5335; NAS 1.15:102527) Avail: NTIS HC

A02/MF A01 CSCL 20/4

Analysis of energy emitted from simple or complex cavity designs can lead to intricate solutions due to nonuniform radiosity and irradiation within a cavity. A numerical ray tracing technique was applied to simulate radiation propagating within and from various cavity designs. To obtain the energy balance relationships between isothermal and nonisothermal cavity surfaces and space, the computer code NEVADA was utilized for its statistical technique applied to numerical ray tracing. The analysis method was validated by comparing results with known theoretical and limiting solutions, and the electrical resistance network method. In general, for nonisothermal cavities the performance (apparent emissivity) is a function of cylinder length-to-diameter ratio, surface emissivity, and cylinder surface temperatures. The extent of nonisothermal conditions in a cylindrical cavity significantly affects the overall cavity performance. Results are presented over a wide range of parametric variables for use as a possible design reference.

Author

N90-21300*# National Aeronautics and Space Administration. Lewis Research Center, Cleveland, OH.

NAVIER-STOKES ANALYSIS OF TURBINE BLADE HEAT TRANSFER

R. J. BOYLE 1990 21 p Prepared for presentation at the 35th International Gas Turbine and Aeroengine Congress and Exposition, Brussels, Belgium, 11-14 Jun. 1990; sponsored in part by ASME

34 FLUID MECHANICS AND HEAT TRANSFER

(NASA-TM-102496; E-5219; NAS 1.15:102496) Avail: NTIS HC A03/MF A01 CSCL 20/4

Comparisons with experimental heat transfer and surface pressures were made for seven turbine vane and blade geometries using a quasi-three-dimensional thin-layer Navier-Stokes analysis. Comparisons are made for cases with both separated and unseparated flow over a range of Reynolds numbers and freestream turbulence intensities. The analysis used a modified Baldwin-Lomax turbulent eddy viscosity mode. Modifications were made to account for the effects of: (1) freestream turbulence on both transition and leading edge heat transfer; (2) strong favorable pressure gradients on relaminarization; and (3) variable turbulent Prandtl number heat transfer. In addition, the effect of heat transfer on the near wall model of Deissler is compared with the Van Driest model.

Author

N90-21301*# Michigan State Univ., East Lansing. Dept. of Mechanical Engineering.

THE EFFECTS OF FORCING ON A SINGLE STREAM SHEAR LAYER AND ITS PARENT BOUNDARY LAYER

RICHARD C. HAW and JOHN F. FOSS 1990 194 p
(Contract NAG3-671)

(NASA-CR-186529; NAS 1.26:186529; MSU-ENGR-90-006; TSF1-R-014) Avail: NTIS HC A09/MF A01 CSCL 20/4

Forcing and its effect on fluid flows has become an accepted tool in the study and control of flow systems. It has been used both as a diagnostic tool, to explore the development and interaction of coherent structures, and as a method of controlling the behavior of the flow. A number of forcing methods have been used in order to provide a perturbation to the flow; among these are the use of an oscillating trailing edge, acoustically driven slots, external acoustic forcing, and mechanical piston methods. The effect of a planar mechanical piston forcing on a single stream shear layer is presented; it can be noted that this is one of the lesser studied free shear layers. The single stream shear layer can be characterized by its primary flow velocity scale and the thickness of the separating boundary layer. The velocity scale is constant over the length of the flow field; theta (x) can be used as a width scale to characterize the unforced shear layer. In the case of the forced shear layer the velocity field is a function of phase time and definition of a width measure becomes somewhat problematic.

Author

N90-21303*# National Aeronautics and Space Administration. Lewis Research Center, Cleveland, OH.

PROTEUS TWO-DIMENSIONAL NAVIER-STOKES COMPUTER CODE, VERSION 1.0. VOLUME 1: ANALYSIS DESCRIPTION

CHARLES E. TOWNE, JOHN R. SCHWAB, THOMAS J. BENSON, and AMBADY SURESH (Sverdrup Technology, Inc., Cleveland, OH.) Mar. 1990 71 p

(NASA-TM-102551; E-5366; NAS 1.15:102551) Avail: NTIS HC A04/MF A01 CSCL 20/4

A new computer code was developed to solve the two-dimensional or axisymmetric, Reynolds averaged, unsteady compressible Navier-Stokes equations in strong conservation law form. The thin-layer or Euler equations may also be solved. Turbulence is modeled using an algebraic eddy viscosity model. The objective was to develop a code for aerospace applications that is easy to use and easy to modify. Code readability, modularity, and documentation were emphasized. The equations are written in nonorthogonal body-fitted coordinates, and solved by marching in time using a fully-coupled alternating direction-implicit procedure with generalized first- or second-order time differencing. All terms are linearized using second-order Taylor series. The boundary conditions are treated implicitly, and may be steady, unsteady, or spatially periodic. Simple Cartesian or polar grids may be generated internally by the program. More complex geometries require an externally generated computational coordinate system. The documentation is divided into three volumes. Volume 1 is the Analysis Description, and describes in detail the governing equations, the turbulence model, the linearization of the equations and boundary conditions, the time and space differencing formulas,

the ADI solution procedure, and the artificial viscosity models.

Author

N90-21306*# National Aeronautics and Space Administration. Lewis Research Center, Cleveland, OH.

PROTEUS TWO-DIMENSIONAL NAVIER-STOKES COMPUTER CODE, VERSION 1.0. VOLUME 2: USER'S GUIDE

CHARLES E. TOWNE, JOHN R. SCHWAB, THOMAS J. BENSON, and AMBADY SURESH (Sverdrup Technology, Inc., Cleveland, OH.) Mar. 1990 110 p

(NASA-TM-102552; E-5367; NAS 1.15:102552) Avail: NTIS HC A06/MF A01 CSCL 20/4

A new computer code was developed to solve the two-dimensional or axisymmetric, Reynolds averaged, unsteady compressible Navier-Stokes equations in strong conservation law form. The thin-layer or Euler equations may also be solved. Turbulence is modeled using an algebraic eddy viscosity model. The objective was to develop a code for aerospace applications that is easy to use and easy to modify. Code readability, modularity, and documentation were emphasized. The equations are written in nonorthogonal body-fitted coordinates, and solved by marching in time using a fully-coupled alternating direction-implicit procedure with generalized first- or second-order time differencing. All terms are linearized using second-order Taylor series. The boundary conditions are treated implicitly, and may be steady, unsteady, or spatially periodic. Simple Cartesian or polar grids may be generated internally by the program. More complex geometries require an externally generated computational coordinate system. The documentation is divided into three volumes. Volume 2 is the User's Guide, and describes the program's general features, the input and output, the procedure for setting up initial conditions, the computer resource requirements, the diagnostic messages that may be generated, the job control language used to run the program, and several test cases.

Author

N90-21307*# National Aeronautics and Space Administration. Lewis Research Center, Cleveland, OH.

PROTEUS TWO-DIMENSIONAL NAVIER-STOKES COMPUTER CODE, VERSION 1.0. VOLUME 3: PROGRAMMER'S REFERENCE

CHARLES E. TOWNE, JOHN R. SCHWAB, THOMAS J. BENSON, and AMBADY SURESH (Sverdrup Technology, Inc., Cleveland, OH.) Mar. 1990 249 p

(NASA-TM-102553; E-5368; NAS 1.15:102553) Avail: NTIS HC A11/MF A02 CSCL 20/4

A new computer code was developed to solve the 2-D or axisymmetric, Reynolds-averaged, unsteady compressible Navier-Stokes equations in strong conservation law form. The thin-layer or Euler equations may also be solved. Turbulence is modeled using an algebraic eddy viscosity model. The objective was to develop a code for aerospace applications that is easy to use and easy to modify. Code readability, modularity, and documentation were emphasized. The equations are written in nonorthogonal body-fitted coordinates, and solved by marching in time using a fully-coupled alternating-direction-implicit procedure with generalized first- or second-order time differencing. All terms are linearized using second-order Taylor series. The boundary conditions are treated implicitly, and may be steady, unsteady, or spatially periodic. Simple Cartesian or polar grids may be generated internally by the program. More complex geometries require an externally generated computational coordinate system. The documentation is divided into three volumes. Volume 3 is the Programmer's Reference, and describes the program structure, the FORTRAN variables stored in common blocks, and the details of each subprogram.

Author

N90-21962*# National Aeronautics and Space Administration. Lewis Research Center, Cleveland, OH. Inst. for Computational Mechanics in Propulsion.

NUMERICAL INVESTIGATION OF SEPARATED TRANSONIC TURBULENT FLOWS WITH A MULTIPLE-TIME-SCALE TURBULENCE MODEL

S.-W. KIM Jan. 1990 40 p

(Contract NASA ORDER C-99066-G)
(NASA-TM-102499; ICOMP-90-04; E-5295; NAS 1.15:102499)
Avail: NTIS HC A03/MF A01 CSCL 20/4

A numerical investigation of transonic turbulent flows separated by curvature and shock wave - boundary layer interaction is presented. The free stream Mach numbers considered are 0.4, 0.5, 0.6, 0.7, 0.8, 0.825, 0.85, 0.875, 0.90, and 0.925. In the numerical method, the conservation of mass equation is replaced by a pressure correction equation for compressible flows and thus incremental pressure is solved for instead of density. The turbulence is described by a multiple-time-scale turbulence model supplemented with a near-wall turbulence model. The present numerical results show that there exists a reversed flow region at all free stream Mach numbers considered whereas various k-epsilon turbulence models fail to predict such a reversed flow region at low free stream Mach numbers. The numerical results also show that the size of the reversed flow region grows extensively due to the shock wave - turbulent boundary layer interaction as the free stream Mach number is increased. These numerical results show that the turbulence model can resolve the turbulence field subjected to extra strains caused by the curvature and the shock wave - turbulent boundary layer interaction and that the numerical method yields a significantly accurate solution for the complex compressible turbulent flow. Author

N90-21974*# National Aeronautics and Space Administration. Lewis Research Center, Cleveland, OH.

ANALYSIS OF THERMAL ENERGY STORAGE MATERIAL WITH CHANGE-OF-PHASE VOLUMETRIC EFFECTS

THOMAS W. KERSLAKE and MOUNIR B. IBRAHIM (Cleveland State Univ., OH.) Feb. 1990 34 p Presented at the 1990 International Solar Energy Conference, Miami, FL, 1-4 Apr. 1990; sponsored by ASME

(NASA-TM-102457; E-5244; NAS 1.15:102457) Avail: NTIS HC A03/MF A01 CSCL 20/4

NASA's Space Station Freedom proposed hybrid power system includes photovoltaic arrays with nickel hydrogen batteries for energy storage and solar dynamic collectors driving Brayton heat engines with change-of-phase Thermal Energy Storage (TES) devices. A TES device is comprised of multiple metallic, annular canisters which contain a eutectic composition LiF-CaF₂ Phase Change Material (PCM) that melts at 1040 K. A moderately sophisticated LiF-CaF₂ PCM computer model is being developed in three stages considering 1-D, 2-D, and 3-D canister geometries, respectively. The 1-D model results indicate that the void has a marked effect on the phase change process due to PCM displacement and dynamic void heat transfer resistance. Equally influential are the effects of different boundary conditions and liquid PCM natural convection. For the second stage, successful numerical techniques used in the 1-D phase change model are extended to a 2-D (r,z) PCM containment canister model. A prototypical PCM containment canister is analyzed and the results are discussed. Author

N90-22000*# Kansas Univ. Center for Research, Inc., Lawrence. Flight Research Lab.

MODERN DEVELOPMENTS IN SHEAR FLOW CONTROL WITH SWIRL Final Report

SAEED FAROKHI and R. TAGHAVI May 1990 48 p (Contract NCC3-56)

(NASA-CR-186586; NAS 1.26:186586; KU-FRL-724-4) Avail: NTIS HC A03/MF A01 CSCL 20/4

Passive and active control of swirling turbulent jets is experimentally investigated. Initial swirl distribution is shown to dominate the free jet evolution in the passive mode. Vortex breakdown, a manifestation of high intensity swirl, was achieved at below critical swirl number ($S = 0.48$) by reducing the vortex core diameter. The response of a swirling turbulent jet to single frequency, plane wave acoustic excitation was shown to depend strongly on the swirl number, excitation Strouhal number, amplitude of the excitation wave, and core turbulence in a low speed cold jet. A 10 percent reduction of the mean centerline velocity at $x/D = 9.0$ (and a corresponding increase in the shear layer momentum

thickness) was achieved by large amplitude internal plane wave acoustic excitation. Helical instability waves of negative azimuthal wave numbers exhibit larger amplification rates than the plane waves in swirling free jets, according to hydrodynamic stability theory. Consequently, an active swirling shear layer control is proposed to include the generation of helical instability waves of arbitrary helicity and the promotion of modal interaction, through multifrequency forcing. Author

N90-22011*# National Aeronautics and Space Administration. Lewis Research Center, Cleveland, OH.

COMPUTATIONAL MODELING AND VALIDATION FOR HYPERSONIC INLETS

LOUIS A. POVINELLI 1990 11 p Presented at the 75th Symposium on Hypersonic Combined Cycle Propulsion, Madrid, Spain, 28 May - 1 Jun. 1990; sponsored by Propulsion and Energetics Panel of AGARD

(NASA-TM-103111; E-5435; NAS 1.15:103111) Avail: NTIS HC A03/MF A01 CSCL 20/4

Hypersonic inlet research activity at NASA is reviewed. The basis is the experimental tests performed with three inlets: the NASA Lewis Research Center Mach 5, the McDonnell Douglas Mach 12, and the NASA Langley Mach 18. Both three-dimensional parabolized Navier-Stokes and Navier-Stokes codes were used to compute the flow within the three inlets. Modeling assumptions in the codes involve the turbulence model, the nature of the boundary layer, shock wave boundary layer interaction, and the flow spilled to the outside of the inlet. Use of the codes in conjunction with the experimental data are helping to develop a clearer understanding of the inlet flow physics and to focus on the modeling improvements required in order to arrive at validated codes. Author

N90-22016*# National Aeronautics and Space Administration. Lewis Research Center, Cleveland, OH.

AN UNSTEADY TIME ASYMPTOTIC FLOW IN THE SQUARE DRIVEN CAVITY

JOHN W. GOODRICH 1990 12 p Presented at the IMACS 1st International Conference on Computational Physics, Boulder, CO, 11-15 Jun. 1990; cosponsored by International Association of Mathematics and Computers in Simulation and Colorado Univ.

(NASA-TM-103141; E-5493; NAS 1.15:103141) Avail: NTIS HC A03/MF A01 CSCL 20/4

Summary details of an aperiodic time asymptotic numerical solution for the square drive cavity at $Re = 10000$ are presented. The data presented is for 6100 less than t less than or equal to 7100, and is representative of the data that characterizes the aperiodic asymptotic state. Author

N90-22017*# Arizona Univ., Tucson. Dept. of Aerospace and Mechanical Engineering.

INSTABILITIES AND SUBHARMONIC RESONANCES OF SUBSONIC HEATED ROUND JETS, VOLUME 2 Ph.D. Thesis Final Report

LIAN LAI NG 1990 186 p

(Contract NAS1-18599; NAG3-485)

(NASA-CR-186058; NAS 1.26:186058) Avail: NTIS HC A09/MF A01 CSCL 20/4

When a jet is perturbed by a periodic excitation of suitable frequency, a large-scale coherent structure develops and grows in amplitude as it propagates downstream. The structure eventually rolls up into vortices at some downstream location. The wavy flow associated with the roll-up of a coherent structure is approximated by a parallel mean flow and a small, spatially periodic, axisymmetric wave whose phase velocity and mode shape are given by classical (primary) stability theory. The periodic wave acts as a parametric excitation in the differential equations governing the secondary instability of a subharmonic disturbance. The (resonant) conditions for which the periodic flow can strongly destabilize a subharmonic disturbance are derived. When the resonant conditions are met, the periodic wave plays a catalytic role to enhance the growth rate of the subharmonic. The stability characteristics of the subharmonic disturbance, as a function of

34 FLUID MECHANICS AND HEAT TRANSFER

jet Mach number, jet heating, mode number and the amplitude of the periodic wave, are studied via a secondary instability analysis using two independent but complementary methods: (1) method of multiple scales, and (2) normal mode analysis. It is found that the growth rates of the subharmonic waves with azimuthal numbers $\beta = 0$ and $\beta = 1$ are enhanced strongly, but comparably, when the amplitude of the periodic wave is increased. Furthermore, compressibility at subsonic Mach numbers has a moderate stabilizing influence on the subharmonic instability modes. Heating suppresses moderately the subharmonic growth rate of an axisymmetric mode, and it reduces more significantly the corresponding growth rate for the first spinning mode. Calculations also indicate that while the presence of a finite-amplitude periodic wave enhances the growth rates of subharmonic instability modes, it minimally distorts the mode shapes of the subharmonic waves.

Author

N90-22761* # National Aeronautics and Space Administration. Lewis Research Center, Cleveland, OH.

ACQUISITION AND CORRELATION OF CRYOGENIC NITROGEN MASS FLOW DATA THROUGH A MULTIPLE ORIFICE JOULE-THOMSON DEVICE

S. STEPHEN PAPELL (Analex Corp., Cleveland, OH.), NASEEM H. SAIYED, and TED W. NYLAND May 1990 23 p (NASA-TM-103121; E-5449; NAS 1.15:103121) Avail: NTIS HC A03/MF A01 CSCL 20/4

Liquid nitrogen mass flow rate, pressure drop, and temperature drop data were obtained for a series of multiple orifice Joule-Thomson devices, known as Visco Jets, over a wide range of flow resistance. The test rig used to acquire the data was designed to minimize heat transfer so that fluid expansion through the Visco Jets would be isenthalpic. The data include a range of fluid inlet pressures from 30 to 60 psia, fluid inlet temperatures from 118 to 164 R, outlet pressures from 2.8 to 55.8 psia, outlet temperatures from 117 to 162 R and flow rate from 0.04 to 4.0 lbm/hr of nitrogen. A flow rate equation supplied by the manufacturer was found to accurately predict single-phase (noncavitating) liquid nitrogen flow through the Visco Jets. For cavitating flow, the manufacturer's equation was found to be inaccurate. Greatly improved results were achieved with a modified version of the single-phase equation. The modification consists of a multiplication factor to the manufacturer's equation equal to one minus the downstream quality on an isenthalpic expansion of the fluid across the Visco Jet. For a range of flow resistances represented by Visco Jet Lohm ratings between 17,600 and 80,000, 100 percent of the single-phase data and 85 percent of the two-phase data fall within ± 10 percent of predicted values.

Author

N90-23674* # Arizona Univ., Tucson. Dept. of Aerospace and Mechanical Engineering.

NONLINEAR INTERACTIONS IN MIXING LAYERS AND COMPRESSIBLE HEATED ROUND JETS Ph.D. Thesis Final Report

YOUSSEF MOHD JARRAH 1989 171 p (Contract NAG3-485) (NASA-CR-186303; NAS 1.26:186303) Avail: NTIS HC A08/MF A01 CSCL 20/4

The nonlinear interactions between a fundamental instability mode and both its harmonics and the changing mean flow are studied using the weakly nonlinear stability theory of Stuart and Watson, and numerical solutions of coupled nonlinear partial differential equations. The first part focuses on incompressible cold (or isothermal; constant temperature throughout) mixing layers, and for these, the first and second Landau constants are calculated as functions of wavenumber and Reynolds number. It is found that the dominant contribution to the Landau constants arises from the mean flow changes and not from the higher harmonics. In order to establish the range of validity of the weakly nonlinear theory, the weakly nonlinear and numerical solutions are compared and the limitation of each is discussed. At small amplitudes and at low-to-moderate Reynolds numbers, the two results compare well in describing the saturation of the fundamental, the distortion

of the mean flow, and the initial stages of vorticity roll-up. At larger amplitudes, the interaction between the fundamental, second harmonic, and the mean flow is strongly nonlinear and the numerical solution predicts flow oscillations, whereas the weakly nonlinear theory yields saturation. In the second part, the weakly nonlinear theory is extended to heated (or nonisothermal; mean temperature distribution) subsonic round jets where quadratic and cubic nonlinear interactions are present, and the Landau constants also depend on jet temperature ratio, Mach number and azimuthal mode number. Under exponential growth and nonlinear saturation, it is found that heating and compressibility suppress the growth of instability waves, that the first azimuthal mode is the dominant instability mode, and that the weakly nonlinear solution describes the early stages of the roll-up of an axisymmetric shear layer. The receptivity of a typical jet flow to pulse type input disturbance is also studied by solving the initial value problem and then examining the behavior of the long-time solution.

Author

N90-25289* # National Aeronautics and Space Administration. Lewis Research Center, Cleveland, OH.

EFFECT OF VANE TWIST ON THE PERFORMANCE OF DOME SWIRLERS FOR GAS TURBINE AIRBLAST ATOMIZERS

GERALD J. MICKLOW, ANJU S. DOGRA (Florida Univ., Gainesville.), and H. LEE NGUYEN Jun. 1990 15 p Presented at the 26th Joint Propulsion Conference, Orlando, FL, 16-18 Jul. 1990; sponsored in part by AIAA, SAE, ASME, and ASEE Original contains color illustrations (NASA-TM-103195; E-5589; NAS 1.15:103195; AIAA-90-1955) Avail: NTIS HC A03/MF A01; 1 functional color page CSCL 20/4

For advanced gas turbine engines, two combustor systems, the lean premixed/prevaporized (LPP) and the rich burn/quick quench/lean burn (RQL) offer great potential for reducing NO(x) emissions. An important consideration for either concept is the development of an advanced fuel injection system that will provide a stable, efficient, and very uniform combustion system over a wide operating range. High-shear airblast fuel injectors for gas turbine combustors have exhibited superior atomization and mixing compared with pressure-atomizing fuel injectors. This improved mixing has lowered NO(x) emissions and the pattern factor, and has enabled combustors to alternate fuels while maintaining a stable, efficient combustion system. The performance of high-shear airblast fuel injectors is highly dependent on the design of the dome swirl vanes. The type of swirl vanes most widely used in gas turbine combustors are usually flat for ease of manufacture, but vanes with curvature will, in general, give superior aerodynamic performance. The design and performance of high-turning, low-loss curved dome swirl vanes with twist along the span are investigated. The twist induces a secondary vortex flow pattern which will improve the atomization of the fuel, thereby producing a more uniform fuel-air distribution. This uniform distribution will increase combustion efficiency while lowering NO(x) emissions. A systematic swirl vane design system is presented based on one-, two-, and three-dimensional flowfield calculations, with variations in vane-turning angle, rate of turning, vane solidity, and vane twist as design parameters.

Author

N90-26269* # Texas Univ., Austin. Dept. of Mechanical Engineering.

AN INVESTIGATION INTO THE NUMERICAL PREDICTION OF BOUNDARY LAYER TRANSITION USING THE K.Y. CHIEN TURBULENCE MODEL Final Report

CRAIG A. STEPHENS and MICHAEL E. CRAWFORD Jun. 1990 192 p (Contract NAG3-864) (NASA-CR-185252; NAS 1.26:185252; REPT-89-3) Avail: NTIS HC A09/MF A01 CSCL 20/4

Assessments were made of the simulation capabilities of transition models developed at the University of Minnesota, as applied to the Launder-Sharma and Lam-Bremhorst two-equation turbulence models, and at The University of Texas at Austin, as applied to the K. Y. Chien two-equation turbulence model. A major shortcoming in the use of the basic K. Y. Chien turbulence model

for low-Reynolds number flows was identified. The problem with the Chien model involved premature start of natural transition and a damped response as the simulation moved to fully turbulent flow at the end of transition. This is in contrast to the other two-equation turbulence models at comparable freestream turbulence conditions. The damping of the transition response of the Chien turbulence model leads to an inaccurate estimate of the start and end of transition for freestream turbulence levels greater than 1.0 percent and to difficulty in calculating proper model constants for the transition model. Author

N90-26272*# Sverdrup Technology, Inc., Brook Park, OH.
TRANSIENT CHARACTERISTICS OF A GROOVED WATER HEAT PIPE WITH VARIABLE HEAT LOAD Final Report
 JONG HOON JANG Jul. 1990 8 p Proposed for presentation at the 1990 Winter Annual Meeting of ASME, Dallas, TX, 25-30 Nov. 1990
 (Contract NAS3-24105; NAS3-25266)
 (NASA-CR-185280; E-5668; NAS 1.26:185280) Avail: NTIS HC A02/MF A01 CSCL 20/4

The transient characteristics of a grooved water heat pipe were studied by using variable heat load. First, the effects of the property variations of the working fluid with temperature were investigated by operating the water heat pipe at several different temperatures. The experimental results show that, even for the same heat input profile and heat pipe configuration, the heat pipe transports more heat at higher temperature within the tested temperature range. Adequate liquid return to the evaporator due to decreasing viscosity of the working fluid permits continuous vaporization of water without dry-out. Second, rewetting of the evaporator was studied after the evaporator had experienced dry-out. To rewet the evaporator, the elevation of the condenser end was the most effective way. Without elevating the condenser end, rewetting is not straight-forward even with power turned off unless the heat pipe is kept at isothermal condition for sufficiently long time. Author

N90-26273*# National Aeronautics and Space Administration. Lewis Research Center, Cleveland, OH.
LOW-GRAVITY FLUID PHYSICS: A PROGRAM OVERVIEW
 Aug. 1990 39 p
 (NASA-TM-103215; E-5626; NAS 1.15:103215) Avail: NTIS HC A03/MF A01 CSCL 20/4

An overview is presented of the microgravity fluid physics program at Lewis Research Center. One of the main reasons for conducting low gravity research in fluid physics is to study phenomena such as surface tension, interfacial contact angles, and diffusion independent of such gravitationally induced effects as buoyant convection. Fluid physics is at the heart of many space-based technologies including power systems, thermal control systems, and life support systems. Fundamental understanding of fluid physics is a key ingredient to successful space systems design. In addition to describing ground-based and space-based low-gravity facilities, selected experiments are presented which highlight Lewis work in fluid physics. These experiments can be categorized into five theme areas which summarize the work being conducted at Lewis for OSSA: (1) isothermal/iso-solutal capillary phenomena; (2) capillary phenomena with thermal/solutal gradients; (3) thermal-solutal convection; (4) first- and second-order phase transitions in a static fluid; and (5) multiphase flow. Author

N90-26275*# National Aeronautics and Space Administration. Lewis Research Center, Cleveland, OH.
COMPUTATIONAL EXPERIENCE WITH A THREE-DIMENSIONAL ROTARY ENGINE COMBUSTION MODEL
 M. S. RAJU (Sverdrup Technology, Inc., Brook Park, OH.) and E. A. WILLIS Apr. 1990 24 p Presented at the Joint Symposium on General Aviation Systems, Ocean City, NJ, 11-12 Apr. 1990; sponsored in part by AIAA and FAA
 (Contract NAS3-25266)
 (NASA-TM-103104; E-5249; NAS 1.15:103104) Avail: NTIS HC A03/MF A01 CSCL 20/4

A new computer code was developed to analyze the chemically

reactive flow and spray combustion processes occurring inside a stratified-charge rotary engine. Mathematical and numerical details of the new code were recently described by the present authors. The results are presented of limited, initial computational trials as a first step in a long-term assessment/validation process. The engine configuration studied was chosen to approximate existing rotary engine flow visualization and hot firing test rigs. Typical results include: (1) pressure and temperature histories, (2) torque generated by the nonuniform pressure distribution within the chamber, (3) energy release rates, and (4) various flow-related phenomena. These are discussed and compared with other predictions reported in the literature. The adequacy or need for improvement in the spray/combustion models and the need for incorporating an appropriate turbulence model are also discussed. Author

N90-26276*# National Aeronautics and Space Administration. Lewis Research Center, Cleveland, OH.
GALERKIN FINITE DIFFERENCE LAPLACIAN OPERATORS ON ISOLATED UNSTRUCTURED TRIANGULAR MESHES BY LINEAR COMBINATIONS
 KENNETH J. BAUMEISTER 1990 10 p Proposed for presentation at the 1990 Winter Annual Meeting of the ASME, Dallas, TX, 25-30 Nov. 1990
 (NASA-TM-103209; E-5617; NAS 1.15:103209) Avail: NTIS HC A02/MF A01 CSCL 20/4

The Galerkin weighted residual technique using linear triangular weight functions is employed to develop finite difference formulae in Cartesian coordinates for the Laplacian operator on isolated unstructured triangular grids. The weighted residual coefficients associated with the weak formulation of the Laplacian operator along with linear combinations of the residual equations are used to develop the algorithm. The algorithm was tested for a wide variety of unstructured meshes and found to give satisfactory results. Author

N90-26278*# National Aeronautics and Space Administration. Lewis Research Center, Cleveland, OH.
INITIAL EXPERIMENTATION ON THE NONVENTED FILL OF A 0.14M3 (5 FT. 3) DEWAR WITH NITROGEN AND HYDROGEN
 DAVID J. CHATO, MATTHEW E. MORAN, and TED W. NYLAND Jun. 1990 20 p Presented at the 5th Joint Thermophysics and Heat Transfer Conference, Seattle, WA, 18-20 Jun. 1990; sponsored in part by AIAA and ASME
 (NASA-TM-103155; E-5517; NAS 1.15:103155; AIAA-90-1681) Avail: NTIS HC A03/MF A01 CSCL 20/4

A series of nonvented fills were performed on a 0.14 cu m (5 cu ft) stainless steel dewar. Fills were conducted with a 120 deg cone angle spray nozzle over a range of inflow and initial wall temperatures with both liquid nitrogen and liquid hydrogen. Fill levels in excess of 85 percent liquid were achieved for four out of four nitrogen and two out of five hydrogen tests. Previously developed analytical models were compared to the test results and shown to have general trend agreement. Author

N90-26279*# National Aeronautics and Space Administration. Lewis Research Center, Cleveland, OH.
TWO-DIMENSIONAL MODEL OF A SPACE STATION FREEDOM THERMAL ENERGY STORAGE CANISTER
 THOMAS W. KERSLAKE and MOUNIR B. IBRAHIM (Cleveland State Univ., OH.) Aug. 1990 11 p Presented at the 25th Intersociety Energy Conversion Engineering Conference, Reno, NV, 12-17 Aug. 1990; sponsored in part by AICHe, SAE, ACS, AIAA, ASME, and IEEE
 (NASA-TM-103124; E-5474; NAS 1.15:103124) Avail: NTIS HC A03/MF A01 CSCL 20/4

The Solar Dynamic Power Module being developed for Space Station Freedom uses a eutectic mixture of LiF-CaF₂ phase change salt contained in toroidal canisters for thermal energy storage. Results are presented from heat transfer analyses of the phase change salt containment canister. A 2-D, axisymmetric finite difference computer program which models the canister walls, salt, void, and heat engine working fluid coolant was developed.

34 FLUID MECHANICS AND HEAT TRANSFER

Analyses included effects of conduction in canister walls and solid salt, conduction and free convection in liquid salt, conduction and radiation across salt vapor filled void regions and forced convection in the heat engine working fluid. Void shape, location, growth or shrinkage (due to density difference between the solid and liquid salt phases) were prescribed based on engineering judgement. The salt phase change process was modeled using the enthalpy method. Discussion of results focuses on the role of free-convection in the liquid salt on canister heat transfer performance. This role is shown to be important for interpreting the relationship between ground based canister performance (in 1-g) and expected on-orbit performance (in micro-g). Attention is also focused on the influence of void heat transfer on canister wall temperature distributions. The large thermal resistance of void regions is shown to accentuate canister hot spots and temperature gradients. Author

N90-26282* National Aeronautics and Space Administration, Lewis Research Center, Cleveland, OH.

CALCULATION OF 3D TURBULENT JETS IN CROSSFLOW WITH A MULTIGRID METHOD AND A SECOND-MOMENT CLOSURE MODEL

A. O. DEMUREN 1990 18 p Proposed for presentation at the International Symposium on Engineering Turbulence Modelling and Measurements, Dubrovnik, Yugoslavia, 24-28 Sep. 1990; sponsored by Assembly of World Conferences on Experimental Heat Transfer, Fluid Mechanics, and Thermodynamics (Contract NASA ORDER C-99066-G) (NASA-TM-103159; ICOMP-90-15; E-5527; NAS 1.15:103159) Avail: NTIS HC A03/MF A01 CSCL 20/4

A multigrid method is presented for calculating turbulent jets in crossflow. Fairly rapid convergence is obtained with the k-epsilon turbulence model, but computations with a full Reynolds stress turbulence model (RSM) are not yet very efficient. Grid dependency tests show that there are slight differences between results obtained on the two finest grid levels. Computations using the RSM are significantly different from those with k-epsilon model and compare better to experimental data. Some work is still required to improve the efficiency of the computations with the RSM. Author

N90-27982* National Aeronautics and Space Administration, Lewis Research Center, Cleveland, OH.

IMPLICIT SOLUTION OF THREE-DIMENSIONAL INTERNAL TURBULENT FLOWS

V. MICHELASSI (Florence Univ., Italy), M.-S. LIOU, and L. A. POVINELLI Jul. 1990 45 p (Contract NASA-ORDER C-99066-G) (NASA-TM-103099; ICOMP-90-13; E-5420; NAS 1.15:103099) Avail: NTIS HC A03/MF A01 CSCL 20/4

The scalar form of the approximate factorization method was used to develop a new code for the solution of three-dimensional internal laminar and turbulent compressible flows. The Navier-Stokes equations in their Reynolds-averaged form are iterated in time until a steady solution is reached. Evidence is given to the implicit and explicit artificial damping schemes that proved to be particularly efficient in speeding up convergence and enhancing the algorithm robustness. A conservative treatment of these terms at domain boundaries is proposed in order to avoid undesired mass and/or momentum artificial fluxes. Turbulence effects are accounted for by the zero-equation Baldwin-Lomax turbulence model and the q-omega two-equation model. For the first, an investigation on the model behavior in case of multiple boundaries is performed. The flow in a developing S-duct is then solved in the laminar regime at Reynolds number (Re) 790 and in the turbulent regime at Re=40,000 using the Baldwin-Lomax model. The Stanitz elbow is then solved using an inviscid version of the same code at M(sub inlet)=0.4. Grid dependence and convergence rate are investigated showing that for this solver the implicit damping scheme may play a critical role for convergence characteristics. The same flow at Re=2.5x10(exp 6) is solved with the Baldwin-Lomax and the q-omega models. Both approaches showed satisfactory agreement with experiments, although the q-omega model is slightly more accurate. Author

N90-27983* National Aeronautics and Space Administration, Lewis Research Center, Cleveland, OH.

AN IMPROVED K-EPSILON MODEL FOR NEAR-WALL TURBULENCE AND COMPARISON WITH DIRECT NUMERICAL SIMULATION

T. H. SHIH Aug. 1990 22 p Sponsored in part by Stanford Univ., CA

(Contract NASA ORDER C-99066-G)

(NASA-TM-103221; ICOMP-90-16; E-5635; NAS 1.15:103221)

Avail: NTIS HC A03/MF A01 CSCL 20/4

An improved k-epsilon model for low Reynolds number turbulence near a wall is presented. The near-wall asymptotic behavior of the eddy viscosity and the pressure transport term in the turbulent kinetic energy equation is analyzed. Based on this analysis, a modified eddy viscosity model, having correct near-wall behavior, is suggested, and a model for the pressure transport term in the k-equation is proposed. In addition, a modeled dissipation rate equation is reformulated. Fully developed channel flows were used for model testing. The calculations using various k-epsilon models are compared with direct numerical simulations. The results show that the present k-epsilon model performs well in predicting the behavior of near-wall turbulence. Significant improvement over previous k-epsilon models is obtained. Author

N90-27984* National Aeronautics and Space Administration, Lewis Research Center, Cleveland, OH.

NUMERICAL INVESTIGATION OF THE THERMAL STRATIFICATION IN CRYOGENIC TANKS SUBJECTED TO WALL HEAT FLUX

CHIN-SHUN LIN (Analex Corp., Fairview Park, OH.) and MOHAMMAD H. HASAN 1990 20 p Presented at the 26th Joint Propulsion Conference, Orlando, FL, 16-18 Jul. 1990; cosponsored by AIAA, SAE, ASME, and ASEE (NASA-TM-103194; E-5545; NAS 1.15:103194; AIAA-90-2375) Avail: NTIS HC A03/MF A01 CSCL 20/4

The flow pattern and thermal stratification of a cryogenic cylindrical tank are numerically studied. The tank sidewall is subjected to either a uniform heat-flux or two discrete levels of uniform heat-flux at the upper and lower halves of the tank wall. The tank bottom is kept at a constant temperature controlled by the heat exchanger of a thermodynamic vent system. The tank pressure is also assumed constant resulting in a constant saturation temperature at the interface which is higher than the tank bottom temperature. The effects of vapor motion and vapor superheat on the mass and heat transfer processes at the interface are assumed negligible such that the calculations of liquid region can be decoupled from the vapor region. Dimensionless steady-state conservation equations are solved by a finite-difference method. The effects of modified Rayleigh number, Prandtl number, tank aspect ratio, wall heat-flux parameter, and wall heat-flux distribution on the liquid velocity and temperature fields are investigated. Also, their effects on the rate of heat transfer through the interface and the tank bottom are examined. Author

N90-27985* National Aeronautics and Space Administration, Lewis Research Center, Cleveland, OH.

NUMERICAL SOLUTION FOR THE VELOCITY-DERIVATIVE SKEWNESS OF A LOW-REYNOLDS-NUMBER DECAYING NAVIER-STOKES FLOW

ROBERT G. DEISSLER Jun. 1990 10 p

(NASA-TM-103186; E-5568; NAS 1.15:103186) Avail: NTIS HC A02/MF A01 CSCL 20/4

The variation of the velocity-derivative skewness of a Navier-Stokes flow as the Reynolds number goes toward zero is calculated numerically. The value of the skewness, which has been somewhat controversial, is shown to become small at low Reynolds numbers. Author

N90-28009* National Aeronautics and Space Administration, Lewis Research Center, Cleveland, OH.

MODELING OF NEAR-WALL TURBULENCE

T. H. SHIH and N. N. MANSOUR (National Aeronautics and Space Administration, Ames Research Center, Moffett Field, CA.) 1990

INSTRUMENTATION AND PHOTOGRAPHY

Includes remote sensors; measuring instruments and gages; detectors; cameras and photographic supplies; and holography.

16 p Presented at the International Symposium on Engineering Turbulence Modeling and Measurements, Dubrovnik, Yugoslavia, 24-28 Sep. 1990
(Contract NASA ORDER C-99066-G)
(NASA-TM-103222; ICOMP-90-0017; E-5636; NAS 1.15:103222)
Avail: NTIS HC A03/MF A01 CSCL 20/4

An improved k-epsilon model and a second order closure model is presented for low Reynolds number turbulence near a wall. For the k-epsilon model, a modified form of the eddy viscosity having correct asymptotic near wall behavior is suggested, and a model for the pressure diffusion term in the turbulent kinetic energy equation is proposed. For the second order closure model, the existing models are modified for the Reynolds stress equations to have proper near wall behavior. A dissipation rate equation for the turbulent kinetic energy is also reformulated. The proposed models satisfy realizability and will not produce unphysical behavior. Fully developed channel flows are used for model testing. The calculations are compared with direct numerical simulations. It is shown that the present models, both the k-epsilon model and the second order closure model, perform well in predicting the behavior of the near wall turbulence. Significant improvements over previous models are obtained. Author

N90-28792* National Aeronautics and Space Administration. Lewis Research Center, Cleveland, OH.

EVALUATION OF A HYBRID KINETICS/MIXING-CONTROLLED COMBUSTION MODEL FOR TURBULENT PREMIXED AND DIFFUSION COMBUSTION USING KIVA-2

H. LEE NGUYEN and MING-JYH WEY (MBR Combustion Research, Inc., Princeton, NJ.) 1990 22 p Presented at the 26th Joint Propulsion Conference, Orlando, FL, 16-18 Jul. 1990; cosponsored by AIAA, SAE, ASME, and ASEE
(NASA-TM-103196; E-5590; NAS 1.15:103196; AIAA-90-2450)
Avail: NTIS HC A03/MF A01 CSCL 20/4

Two dimensional calculations were made of spark ignited premixed-charge combustion and direct injection stratified-charge combustion in gasoline fueled piston engines. Results are obtained using kinetic-controlled combustion submodel governed by a four-step global chemical reaction or a hybrid laminar kinetics/mixing-controlled combustion submodel that accounts for laminar kinetics and turbulent mixing effects. The numerical solutions are obtained by using KIVA-2 computer code which uses a kinetic-controlled combustion submodel governed by a four-step global chemical reaction (i.e., it assumes that the mixing time is smaller than the chemistry). A hybrid laminar/mixing-controlled combustion submodel was implemented into KIVA-2. In this model, chemical species approach their thermodynamics equilibrium with a rate that is a combination of the turbulent-mixing time and the chemical-kinetics time. The combination is formed in such a way that the longer of the two times has more influence on the conversion rate and the energy release. An additional element of the model is that the laminar-flame kinetics strongly influence the early flame development following ignition. Author

N90-29610* Program Development Corp., White Plains, NY.
THE FUNDAMENTALS OF ADAPTIVE GRID MOVEMENT
PETER R. EISEMAN (Columbia Univ., New York, NY.) In VKI, Numerical Grid Generation 85 p 1990
(Contract NAG3-715; AF-AFOSR-0307-86)
Avail: NTIS HC A21/MF A03

Basic grid point movement schemes are studied. The schemes are referred to as adaptive grids. Weight functions and equidistribution in one dimension are treated. The specification of coefficients in the linear weight, attraction to a given grid or a curve, and evolutionary forces are considered. Curve by curve and finite volume methods are described. The temporal coupling of partial differential equations solvers and grid generators was discussed. ESA

A90-10472* National Aeronautics and Space Administration. Lewis Research Center, Cleveland, OH.

FIBER OPTIC SENSING SYSTEMS USING HIGH FREQUENCY RESONANT SENSING HEADS WITH INTENSITY SENSORS

GRIGORY ADAMOVSKY (NASA, Lewis Research Center, Cleveland, OH) and DUNCAN J. MAITLAND, IV (Cleveland State University, OH) IN: High bandwidth analog applications of photonics II; Proceedings of the Meeting, Boston, MA, Sept. 8, 9, 1988. Bellingham, WA, Society of Photo-Optical Instrumentation Engineers, 1989, p. 29-34. Previously announced in STAR as N88-28293. refs
(Contract NCC3-58)
Copyright

Optical fibers have an inherent capability of transmitting high bandwidth analog and digital signals. To apply this property of fiber optics to remote sensing, special sensing heads as well as signal processing electronics have to be developed. In systems employing intensity modulating sensors, there is also a need for a referencing technique to compensate for changes in the transmission of the connecting fibers and light source intensity. Fiber optic sensing systems incorporated in sensing heads of a special configuration are discussed. Different modes of operation as well as resonant conditions are explained. Theoretical and experimental analyses are also given. Author

A90-11702* National Aeronautics and Space Administration. Lewis Research Center, Cleveland, OH.

FIBER OPTICS FOR ADVANCED AIRCRAFT

ROBERT J. BAUMBICK (NASA, Lewis Research Center, Cleveland, OH) IN: Fiber optic and laser sensors VI; Proceedings of the Meeting, Boston, MA, Sept. 6, 7, 1988. Bellingham, WA, Society of Photo-Optical Instrumentation Engineers, 1989, p. 5-11. Previously announced in STAR as N88-26328.
Copyright

The increased use of composites makes the digital control more susceptible to electromagnetic effects. In order to provide the protection to the digital control additional shielding will be required as well as protective circuitry for the electronics. This results in increased weight and reduced reliability. The advantages that fiber optic technology provides for advanced aircraft applications is recognized. The use of optical signals to carry information between the aircraft and the control module provides immunity from contamination by electromagnetic sources as well as other important benefits such as reduced weight and volume resulting from the elimination of the shielding and the replacement of metal conductors with low weight glass fibers. In 1975 NASA began work to develop passive optical sensors for use with fiber optics in aircraft control systems. The problem now is to choose the best optical sensor concepts and evaluate them for use. In 1985 NASA and DOD entered into a joint program, Fiber Optic Control System Integration (FOCSI), to look at optical technology specifically for use in advanced aircraft systems. The results of this program are discussed. The conclusion of the study indicated that the use of fiber optic technology in advanced aircraft systems is feasible and desirable. The study pointed to a lack of available sensors from vendors capable of operating in the adverse environments of advanced aircraft. Author

A90-11706* National Aeronautics and Space Administration. Lewis Research Center, Cleveland, OH.

MODULATED-SPLITTING-RATIO FIBER-OPTIC TEMPERATURE SENSOR

GLENN BEHEIM (NASA, Lewis Research Center, Cleveland, OH), DONALD J. ANTHAN, JOHN R. RYS (Cleveland State University,

35 INSTRUMENTATION AND PHOTOGRAPHY

OH), KLAUS FRITSCH (John Carroll University, Cleveland, OH), and WALTER R. RUPPE (Case Western Reserve University, Cleveland, OH) IN: Fiber optic and laser sensors VI; Proceedings of the Meeting, Boston, MA, Sept. 6, 7, 1988. Bellingham, WA, Society of Photo-Optical Instrumentation Engineers, 1989, p. 82-88. refs

Copyright

A fiber-optic temperature sensor is described that uses a small silicon beamsplitter whose splitting ratio varies as a function of temperature. A four-beam technique is used to measure the sensor's temperature-indicating splitting ratio. This referencing method provides a measurement that is largely independent of the transmission properties of the sensor's optical fiber link. A significant advantage of this sensor, relative to other fiber-optic sensors, is its high stability, which permits the fiber-optic components to be readily substituted, thereby simplifying the sensor's installation and maintenance. Author

A90-22483* National Aeronautics and Space Administration. Lewis Research Center, Cleveland, OH.

A HIGH-SPEED GAAS MESFET OPTICAL CONTROLLER

P. C. CLASPY, K. B. BHASIN (NASA, Lewis Research Center, Cleveland, OH), M. RICHARD (Case Western Reserve University, Cleveland, OH), M. BENDETT, G. GUSTAFSON (Honeywell Sensors and Signal Processing Laboratory, Bloomington, MN) et al. IEEE Photonics Technology Letters (ISSN 1041-1135), vol. 1, Nov. 1989, p. 389-391. refs

Copyright

Optical interconnects are being considered for control signal distribution in phased array antennas. A packaged hybrid GaAs optical controller with a 1:16 demultiplexed output that is suitable for this application is described. The controller, which was fabricated using enhancement/depletion mode MESFET technology, operates at demultiplexer-limited input data rates up to 305 Mb/s and requires less than 200 microW optical input power. I.E.

A90-26978*# Aerometrics, Inc., Sunnyvale, CA. DEVELOPMENT OF A PHASE DOPPLER BASED PROBE FOR ICING CLOUD DROPLET CHARACTERIZATION

R. C. RUOFF, J. N. SMITH, and W. D. BACHALO (Aerometrics, Inc., Sunnyvale Technology Center, CA) AIAA, Aerospace Sciences Meeting, 28th, Reno, NV, Jan. 8-11, 1990. 13 p. refs (Contract NAS3-25653)

(AIAA PAPER 90-0667) Copyright

The development and evaluation of a compact optical fiber probe (OFP) for airborne and wind tunnel icing cloud characterizations is described. This probe was based upon the proven phase Doppler technique for measuring the size and velocity of spherical drops. Direct comparisons of the size distributions from the standard PDPA with the OFP were used to confirm the reliability of the probe. After some improvements in the fiber coupling efficiency, the number density and liquid water content data agreed to within 15 percent. Author

A90-32853* California Univ., Irvine.

APPLICATION OF TWO-COMPONENT PHASE DOPPLER INTERFEROMETRY TO THE MEASUREMENT OF PARTICLE SIZE, MASS FLUX, AND VELOCITIES IN TWO-PHASE FLOWS

V. G. MCDONELL and G. S. SAMUELSEN (California, University, Irvine) IN: Symposium (International) on Combustion, 22nd, Seattle, WA, Aug. 14-19, 1988, Proceedings. Pittsburgh, PA, Combustion Institute, 1989, p. 1961-1969; Discussion, p. 1969-1971. Research supported by Parker Hannifin Corp. refs (Contract F08635-86-C-0309; NAS3-23450)

Copyright

Two-component phase Doppler interferometry is described, along with its application for the spatially-resolved measurements of particle size, velocity, and mass flux as well as continuous phase velocity. This technique measures single particle events at a point in the flow; droplet size is deduced from the spatial phase shift of the Doppler signal. Particle size influence and discrimination of continuous and discrete phases are among issues covered.

Applications are presented for four cases: an example of the discrimination of two sizes of glass beads in a jet flow; a demonstration of the discrimination of phases in a spray field; an assessment of atomizer symmetry with respect to fuel distribution; and a characterization of a droplet field in a reacting spray. It is noted that the above technique is especially powerful in delineating droplet interactions in the swirling, complex flows typical of realistic systems. V.T.

A90-40560*# McDonnell-Douglas Research Labs., Saint Louis, MO.

EXPERIMENTAL INVESTIGATION OF TERMINAL SHOCK SENSORS IN MIXED-COMPRESSION INLETS

MIKLOS SAJBEN, JOHN F. DONOVAN, and MARTIN J. MORRIS (McDonnell Douglas Research Laboratories, Saint Louis, MO) AIAA, SAE, ASME, and ASCE, Joint Propulsion Conference, 26th, Orlando, FL, July 16-18, 1990. 11 p. refs (Contract NAS3-25446)

(AIAA PAPER 90-1931) Copyright

This paper describes experimental investigations of devices designed for the nonintrusive detection of terminal shock location in mixed-compression inlets at high supersonic flight speeds. Systems based on sensing wall pressures by an array of wall-mounted transducers were selected for detailed study. Pressure signals were processed by three different methods: (1) interpretation of instantaneous pressure distributions, (2) detection of the turbulent intensity amplification occurring at the shock, and (3) determination of the upstream limit to which a search-tone, introduced at the downstream end of the channel, can propagate. The first two of these methods were tested in real time. The third method appeared feasible for weak shocks only; at high shock strengths, propagation upstream of the source could not be detected. Author

A90-41120* Illinois Inst. of Tech., Chicago.

A ROTATING HOT-WIRE TECHNIQUE FOR SPATIAL SAMPLING OF DISTURBED AND MANIPULATED DUCT FLOWS

C. E. WARK, H. M. NAGIB (Illinois Institute of Technology, Chicago), and M. J. JENNINGS (Ricardo-ITI, Westmont, IL) Experiments in Fluids (ISSN 0723-4864), vol. 9, no. 4, June 1990, p. 191-196. refs

(Contract NSG-3220; NAG3-565)

Copyright

A duct flow spatial sampling technique, in which an X-wire probe is rotated about the center of a cylindrical test section at a radius equal to one-half that of the test section in order to furnish nearly instantaneous multipoint measurements of the streamwise and azimuthal components, is presently evaluated in view of the control of flow disturbances downstream of various open inlet contractions. The effectiveness of a particular contraction in controlling ingested flow disturbances was ascertained by artificially introducing disturbances upstream of the contractions; control effectiveness if found to be strongly dependent on inlet contraction, with consequences for the reduction of passing-blade frequency noise during gas turbine engine ground testing. O.C.

A90-42373*# National Aeronautics and Space Administration. Lewis Research Center, Cleveland, OH.

HOLOGRAPHIC INTERFEROMETRY WITH AN INJECTION SEEDED ND:YAG LASER AND TWO REFERENCE BEAMS

ARTHUR J. DECKER (NASA, Lewis Research Center, Cleveland, OH) Applied Optics (ISSN 0003-6935), vol. 29, June 20, 1990, p. 2696-2700. Previously announced in STAR as N89-24591. refs

Copyright

The performance of twin injection seeded Nd:YAG lasers is compared with the performance of an argon-ion laser for recording dual-reference-beam holograms in AGFA 8E56 emulsion. Optical heterodyning is used to measure interference, and the results are expressed in terms of heterodyning signal level and intensity signal-to-noise. The Nd:YAG laser system is to be used for optical

inspections of structures for cracks, defects, gas leaks, and structural changes. Author

A90-42755*# Cleveland State Univ., OH.
DEVELOPING A SELF-DIAGNOSTIC SYSTEM FOR PIEZOELECTRIC SENSORS

PATRICK M. FLANAGAN and WILLIAM J. ATHERTON (Cleveland State University, OH) AIAA, SAE, ASME, and ASEE, Joint Propulsion Conference, 26th, Orlando, FL, July 16-18, 1990. 6 p. (Contract NAG3-1151)
 (AIAA PAPER 90-2230) Copyright

Measurement techniques for developing a self-diagnostic system for piezoelectric sensors are presented. The self-diagnostic system uses two types of measurement techniques based on passive and active evaluation of the piezoelectric element. Both hard and soft failures can be detected by this system. Hard failures such as loss of sensor signal and change in sensor output resistance are determined by monitoring the sensor's output resistance, voltage or current. These are passive measurements of the sensor's output condition. Soft failures include changes in sensor calibration and mounting conditions. Soft failures are detected by measuring structural/electrical impedance of the piezoelectric sensor. Active measurement techniques are used to calculate changes in piezoelectric element properties related to soft failures. This paper describes the general operating principles of a self-diagnostic system and discusses the design of an active/passive measurement technique required for this system to function. Experimental results using two types of piezoelectric accelerometers are presented. Author

A90-44485* Connecticut Univ., Storrs.
X-RAY BEAM METHOD FOR DISPLACEMENT MEASUREMENT IN HOSTILE ENVIRONMENTS

ERIC H. JORDAN, D. M. PEASE, H. CANISTRARO, and DALE BREW (Connecticut, University, Storrs) IN: Hostile environments and high temperature measurements; Proceedings of the Conference, Kansas City, MO, Nov. 6-8, 1989. Bethel, CT, Society for Experimental Mechanics, Inc., 1989, p. 27-30. (Contract NAG3-1004)
 Copyright

A new method of extensometry using an X-ray beam was devised, and the results of current testing reveal it to be highly feasible. This technique has been shown to provide a non-contacting system that is immune to problems associated with density variations in gaseous environments, that plague currently available optical methods. This advantage is a result of the non-refracting penetrating nature of X-rays. The method is based on X-ray-induced X-ray fluorescence of targets, which subsequently serve as fiducial markers. Some target materials have melting points over 1600 degrees C which will facilitate measurement at extremely high temperatures. A highly focused intense X-ray beam, which is produced using a Johansen 'bent crystal', is then scanned across the target, which responds by fluorescing X-rays when stimulated by the incident beam. This secondary radiation is monitored using a detector. By carefully measuring beam orientation, change in target edge position can be determined. Many variations on this basic theme are now possible such as two targets demarcating a gage length, or a beam shadowing method using opaque targets. Author

A90-47212*# Aerojet TechSystems Co., Sacramento, CA.
FABRY-PEROT INTERFEROMETER DEVELOPMENT FOR ROCKET ENGINE PLUME SPECTROSCOPY

R. L. BICKFORD (Aerojet TechSystems, Sacramento, CA) and G. MADZSAR (NASA, Lewis Research Center, Cleveland, OH) AIAA, SAE, ASME, and ASEE, Joint Propulsion Conference, 26th, Orlando, FL, July 16-18, 1990. 8 p. (AIAA PAPER 90-2234) Copyright

This paper describes a new rugged high-resolution Fabry-Perot interferometer (FPI) designed for rocket engine plume spectroscopy, which is capable of detecting spectral signatures of eroding engine components during rocket engine tests and/or flight operations. The FPI system will make it possible to predict and to

respond to the incipient rocket engine failures and to indicate the presence of rocket components degradation. The design diagram of the FPI spectrometer is presented. I.S.

A90-48750*# National Aeronautics and Space Administration. Lewis Research Center, Cleveland, OH.

NEW SPACE DOMAIN PROCESSING TECHNIQUE FOR PULSED LASER VELOCIMETRY

MARK P. WERNET (NASA, Lewis Research Center, Cleveland, OH) and ROBERT V. EDWARDS (Case Western Reserve University, Cleveland, OH) Applied Optics (ISSN 0003-6935), vol. 29, Aug. 10, 1990, p. 3399-3417. refs
 Copyright

A new and fast data processing technique for pulsed-laser-velocimetry data is described. A simplified cross correlation algorithm was developed which uses the time history information of the recorded particle images. It is shown that, the use of the particle time history information (which can be obtained using an electronic camera to record the particle exposures) facilitates high speed processing and unambiguous velocity vector information. It was found that a complex convection vortex flow can be recorded and completely processed in less than 2 min on a personal computer, producing a two-dimensional map of the flow field containing over 300 velocity vectors. I.S.

N90-10415*# National Aeronautics and Space Administration. Lewis Research Center, Cleveland, OH.

ADJUSTABLE DEPTH GAGE Patent Application

ROGER C. FORSGREN, inventor (to NASA) 7 Jul. 1989 10 p (NASA-CASE-LEW-14880-1; NAS 1.71:LEW-14880-1; US-PATENT-APPL-SN-376738) Avail: NTIS HC A02/MF A01 CSCL 14B

A quick adjust depth gage includes a handle-clamp assembly wherein the clamp includes an opening in which a cylindrical shaft with suitable depth measurement markings thereon is reviewed. Turning the handle on the clamp enables the gage to be set to the desired depth. NASA

N90-11277*# National Aeronautics and Space Administration. Lewis Research Center, Cleveland, OH.

GAS-PHASE FLOWRATE EFFECT ON DISINTEGRATING CRYOGENIC LIQUID-JETS

ROBERT D. INGEBRO 1989 8 p Prepared for presentation at the 3rd International Congress on Fluid Mechanics, Cairo, Egypt, 2-4 Jan. 1990
 (NASA-TM-102357; E-5071; NAS 1.15:102357) Avail: NTIS HC A02/MF A01 CSCL 14/2

Two phase liquid and gaseous nitrogen flow in a pneumatic two fluid atomizer was investigated. Characteristic droplet size for cryogenic sprays were measured with a scattered light scanning instrument developed at NASA-Lewis. Tests were conducted primarily in the aerodynamic stripping regime of liquid jet atomization. At a sampling distance of bar-x=1.3 cm, the Sauter mean, D(sub 32), and volume median, D(sub v.5), drop diameters were measured and correlated with nitrogen gas flowrate, W(sub n), to give the following expressions: D sub 32 to the -1=210W(sub n) to the -1.33 and D(sub v.5) to the -1=150 W(sub n) to the -1.33, where reciprocal diameters and gas flowrate are in cm (-1) and g/sec, respectively. The exponent 1.33 for nitrogen gas flowrate, W(sub n), is the same as that predicted by atomization theory for liquid-jet breakup in high velocity gasflow. When the spray was sampled at axial distances of bar-x=2.5 and 4.5 cm downstream of the atomizer, the exponent decreased to 1.2 and 0.9, respectively. This was attributed to the loss of small droplets due to their rapid vaporization. Author

N90-11999*# Sverdrup Technology, Inc., Cleveland, OH.
DROPLET SIZING INSTRUMENTATION USED FOR ICING RESEARCH: OPERATION, CALIBRATION, AND ACCURACY Final Report

EDWARD A. HOVENAC Aug. 1989 53 p Sponsored by FAA, Atlantic City International Airport, NJ
 (Contract NAS3-25266)

35 INSTRUMENTATION AND PHOTOGRAPHY

(NASA-CR-182293; E-4538; NAS 1.26:182293; DOT/FAA/CD-89/13) Avail: NTIS HC A04/MF A01 CSCL 14/2

The accuracy of the Forward Scattering Spectrometer Probe (FSSP) is determined using laboratory tests, wind tunnel comparisons, and computer simulations. Operation in an icing environment is discussed and a new calibration device for the FSSP (the rotating pinhole) is demonstrated to be a valuable tool. Operation of the Optical Array Probe is also presented along with a calibration device (the rotating reticle) which is suitable for performing detailed analysis of that instrument. Author

N90-13761*# Sverdrup Technology, Inc., Cleveland, OH.
DEVELOPMENT AND CHARACTERIZATION OF PDCR TEMPERATURE-COMPENSATED WIRE RESISTANCE STRAIN GAGE Final Report

JIH-FEN LEI Oct. 1989 9 p Presented at the Sensors Expo International, Cleveland, OH, 12-14 Sep. 1989; sponsored by Sensors Magazine (Contract NAS3-25266)

(NASA-CR-185153; E-5112; NAS 1.26:185153) Avail: NTIS HC A02/MF A01 CSCL 14/2

A temperature-compensated resistance static strain gage with potential to be used to 600 C was recently developed. Gages were fabricated from specially developed palladium-13 w/o chromium (Pd-13Cr) wire and platinum (Pt) compensator. When bonded to high temperature Hastelloy X, the apparent strain from room temperature to 600 C was within 400 microstrain for gages with no preheat treatment and within 3500 microstrain for gages with 16 hours prestabilization at 640 C. The apparent strain versus temperature relationship of stabilized PdCr gages were repeatable with the reproducibility within 100 microstrain during three thermal cycles to 600 C and an 11 hours soak at 600 C. The gage fabrication, construction and installation is described. Also, the coating system used for this compensated resistance strain gage is explained. The electrical properties of the strain sensing element and main characteristics of the compensated gage including apparent strain, drift and reproducibility are discussed. Author

N90-14534*# Northwestern Univ., Evanston, IL. Dept. of Materials Science and Engineering.

ELECTRICAL PROPERTIES OF MATERIALS FOR HIGH TEMPERATURE STRAIN GAGE APPLICATIONS Final Report

JOHN O. BRITAIN 28 Feb. 1989 26 p

(Contract NAG3-501)

(NASA-CR-186192; NAS 1.26:186192) Avail: NTIS HC A03/MF A01 CSCL 14/2

A study was done on the electrical resistance of materials that are potentially useful as resistance strain gages at high temperatures under static strain conditions. Initially a number of binary alloys were investigated. Later, third elements were added to these alloys, all of which were prepared by arc melting. Several transition metals were selected for experimentation, most prepared as thin films. Difficulties with electrical contacts thwarted efforts to extend measurements to the targeted 1000 C, but results obtained did suggest ways of improving the electrical resistance characteristics of certain materials. J.P.S.

N90-16212*# National Aeronautics and Space Administration. Lewis Research Center, Cleveland, OH.

DATA COMPRESSION FOR THE MICROGRAVITY EXPERIMENTS

KHALID SAYOOD, WAYNE A. WHYTE, JR., KAREN S. ANDERSON, MARY JO SHALKHAUSER, and ANNE M. SUMMERS (Nebraska Univ., Lincoln.) In NASA, Langley Research Center, Visual Information Processing for Television and Telerobotics p 93-107 Nov. 1989 Sponsored in part by NASA, Goddard Space Flight Center

(Contract NAG3-806; NAG5-916)

Avail: NTIS HC A12/MF A02 CSCL 14/2

Researchers present the environment and conditions under which data compression is to be performed for the microgravity experiment. Also presented are some coding techniques that would

be useful for coding in this environment. It should be emphasized that researchers are currently at the beginning of this program and the toolkit mentioned is far from complete. Author

N90-17085*# National Aeronautics and Space Administration. Lewis Research Center, Cleveland, OH.

NASA LASER LIGHT SCATTERING ADVANCED TECHNOLOGY DEVELOPMENT WORKSHOP, 1988

WILLIAM V. MEYER, ed. (Case Western Reserve Univ., Cleveland, OH.) Aug. 1989 306 p Workshop held in Cleveland, OH, 7-8 Sep. 1988

(NASA-CP-10033; E-4915; NAS 1.55:10033) Avail: NTIS HC A14/MF A02 CSCL 14/2

The major objective of the workshop was to explore the capabilities of existing and prospective laser light scattering hardware and to assess user requirements and needs for a laser light scattering instrument in a reduced gravity environment. The workshop addressed experimental needs and stressed hardware development.

N90-17922*# National Aeronautics and Space Administration. Lewis Research Center, Cleveland, OH.

DEVELOPMENT OF AN INFRARED IMAGING SYSTEM FOR THE SURFACE TENSION DRIVEN CONVECTION EXPERIMENT

ALEXANDER D. PLINE In JPL, Proceedings of the Second Noncontact Temperature Measurement Workshop p 284-293 1 Jun. 1989 Previously announced as N89-17211

Avail: NTIS HC A16/MF A03 CSCL 14/2

An infrared imaging system is used to quantify the imposed surface temperature distribution along a liquid/gas free surface in support of the Surface Tension Driven Convection Experiment, a planned Space Transportation System flight experiment. For ground-based work a commercially available instrument was used to determine the feasibility of using this type of imaging system for this experiment. The ground-based work was used as a baseline for compiling specifications for a flight qualified imager to be designed, fabricated, tested and qualified for flight. The requirements and the specifications for the flight model are given along with the reasons for departures from the ground-based equipment. The flight qualification requirements discussed are a representative sample of the necessary procedures which must be followed to flight qualify diagnostic equipment for use aboard the STS. The potential problems and concerns associated with operating an imaging system on orbit are also discussed. Author

N90-18025*# National Aeronautics and Space Administration. Lewis Research Center, Cleveland, OH.

LASER DIFFRACTION PARTICLE SIZING: INSTRUMENT PROBE VOLUME RELOCATION AND ELONGATION

ROBERT C. ANDERSON, DONALD R. BUCHELE, EDWARD A. HOVENAC, and JAMES A. LOCK (Cleveland State Univ., OH.) 1990 12 p Presented at the 2nd International Congress on Optical Particle Sizing, Tempe, AZ, 5-8 Mar. 1990; sponsored by Arizona State Univ.

(NASA-TM-102512; E-5315; NAS 1.15:102512) Avail: NTIS HC A03/MF A01 CSCL 14/2

The effective probe volume of laser diffraction particle sizing instruments depends on many instrument parameters. In particular the probe volume axial boundaries and its location along laser beam are essentially defined by the onset of a vignetting effect where light scattered at large angles from small particles misses the transform lens. This vignetting effect results in a probe volume that must be inconveniently close to the lens in order to detect smaller diameter particles (less than 100 micrometers). With the addition of an appropriately designed Keplerian telescope, the probe volume may be relocated and elongated. The theory of operation of this supplemental optical system is described. Design considerations for these supplemental optical systems are described, including recommendations for lens specifications, assembly and use. An image transfer system is described which has been designed for use on a Malvern 2600HSD instrument. Experimental validation of this image transfer system is described. Author

N90-20352*# National Aeronautics and Space Administration. Lewis Research Center, Cleveland, OH.

SPACELAB QUALIFIED INFRARED IMAGER FOR MICROGRAVITY SCIENCE EXPERIMENTS

ALEXANDER D. PLINE and ROBERT L. BUTCHER 1990 11 p Presented at the Technical Symposium on Optical Engineering and Photonics in Aerospace Sensing, Orlando, FL, 16-20 Apr. 1990; sponsored by Society of Photo-Optical Instrumentation Engineers (NASA-TM-102503; E-5304; NAS 1.15:102503) Avail: NTIS HC A03/MF A01 CSCL 14/2

The Lewis Research Center is developing, under contract, a Spacelab (manned module in the Space Shuttle payload bay) qualified infrared imager for noncontact surface temperature measurement in the Surface Tension Driven Convection Experiment, a microgravity fluid physics experiment. A versatile design philosophy was used in order to provide other experiments with essentially an off the shelf Shuttle qualified instrument, eliminating the duplication of the rigorous development and flight qualification processes. An Inframetrics Model 600 Scanning Infrared Radiometer is being modified to satisfy both experimental and flight requirements, while maintaining the basic performance parameters of the commercial instrument. The modifications include an efficient, low power closed cycle cryogenic cooler to cool the detector, a ruggedized scanner mechanism, 8 bit A/D conversion, Mil-STD components (where possible), size and weight optimization, and the addition of a microprocessor to perform automatic gain control. Features such as detector spectral response, the addition of spectral filters, and target temperature ranges could easily be changed to make this instrument useful as both a qualitative and quantitative diagnostic tool for Spacelab microgravity experiments, in combustion and fluid physics. Author

N90-20353*# National Aeronautics and Space Administration. Lewis Research Center, Cleveland, OH.

DESIGN AND CALIBRATION OF A VACUUM COMPATIBLE SCANNING TUNNELING MICROSCOPE

PHILLIP B. ABEL Mar. 1990 13 p (NASA-TM-102514; E-5317; NAS 1.15:102514) Avail: NTIS HC A03/MF A01 CSCL 14/2

A vacuum compatible scanning tunneling microscope was designed and built, capable of imaging solid surfaces with atomic resolution. The single piezoelectric tube design is compact, and makes use of sample mounting stubs standard to a commercially available surface analysis system. Image collection and display is computer controlled, allowing storage of images for further analysis. Calibration results from atomic scale images are presented. Author

N90-20358*# National Aeronautics and Space Administration. Lewis Research Center, Cleveland, OH.

TiCl₄ AS A SOURCE OF TiO₂ PARTICLES FOR LASER ANEMOMETRY MEASUREMENTS IN HOT GAS

DONALD H. WEIKLE, RICHARD G. SEASHOLTZ, and LAWRENCE G. OBERLE Apr. 1990 6 p (NASA-TM-102581; E-5412; NAS 1.15:102581) Avail: NTIS HC A02/MF A01 CSCL 14/2

A method of reacting TiCl₄ with water saturated gaseous nitrogen (GN₂) at the entrance into a high temperature gas flow is described. The TiO₂ particles formed are then entrained in the gas flow and used as seed particles for making laser anemometry (LA) measurements of the flow velocity distribution in the hot gas. Scanning electron microscope photographs of the TiO₂ particles are shown. Data rate of the LA processor was measured to determine the amount of TiO₂ formed. The TiCl₄ and mixing gas flow diagram is shown. This work was performed in an open jet burner. Author

N90-21351*# National Aeronautics and Space Administration. Lewis Research Center, Cleveland, OH.

FOUNDATIONS OF MEASUREMENT AND INSTRUMENTATION

ISIDORE WARSHAWSKY Apr. 1990 232 p

(NASA-RP-1222; E-3786; NAS 1.61:1222) Avail: NTIS HC A11/MF A02 CSCL 14/2

The user of instrumentation has provided an understanding of the factors that influence instrument performance, selection, and application, and of the methods of interpreting and presenting the results of measurements. Such understanding is prerequisite to the successful attainment of the best compromise among reliability, accuracy, speed, cost, and importance of the measurement operation in achieving the ultimate goal of a project. Some subjects covered are dimensions; units; sources of measurement error; methods of describing and estimating accuracy; deduction and presentation of results through empirical equations, including the method of least squares; experimental and analytical methods of determining the static and dynamic behavior of instrumentation systems, including the use of analogs. Author

N90-21360*# National Aeronautics and Space Administration. Lewis Research Center, Cleveland, OH.

A FIBER OPTIC SENSOR FOR NONCONTACT MEASUREMENT OF SHAFT SPEED, TORQUE, AND POWER

GEORGE C. MADZSAR 1990 11 p Presented at the 36th International Instrumentation Symposium, Denver, CO, 6-10 May 1990; sponsored by Instrument Society of America (NASA-TM-102481; E-5271; NAS 1.15:102481) Avail: NTIS HC A03/MF A01 CSCL 14/2

A fiber optic sensor which enables noncontact measurement of the speed, torque and power of a rotating shaft was fabricated and tested. The sensor provides a direct measurement of shaft rotational speed and shaft angular twist, from which torque and power can be determined. Angles of twist between 0.005 and 10 degrees were measured. Sensor resolution is limited by the sampling rate of the analog to digital converter, while accuracy is dependent on the spot size of the focused beam on the shaft. Increasing the sampling rate improves measurement resolution, and decreasing the focused spot size increases accuracy. Digital processing allows for enhancement of an electronically or optically degraded signal. Author

N90-21361*# National Aeronautics and Space Administration. Lewis Research Center, Cleveland, OH.

ATTACHMENT OF LEAD WIRES TO THIN FILM THERMOCOUPLES MOUNTED ON HIGH TEMPERATURE MATERIALS USING THE PARALLEL GAP WELDING PROCESS

RAYMOND HOLANDA, WALTER S. KIM, ERIC PENCIL, MARY GROTH (Cincinnati Univ., OH.), and GERALD A. DANZEY 1990 19 p Presented at the 177th Meeting of the Electrochemical Society, Montreal, Quebec, 6-11 May 1990 (NASA-TM-102442; E-5218; NAS 1.15:102442) Avail: NTIS HC A03/MF A01 CSCL 14/2

Parallel gap resistance welding was used to attach lead wires to sputtered thin film sensors. Ranges of optimum welding parameters to produce an acceptable weld were determined. The thin film sensors were Pt13Rh/Pt thermocouples; they were mounted on substrates of MCrAlY-coated superalloys, aluminum oxide, silicon carbide and silicon nitride. The entire sensor system is designed to be used on aircraft engine parts. These sensor systems, including the thin-film-to-lead-wire connectors, were tested to 1000 C. Author

N90-22021*# National Aeronautics and Space Administration. Lewis Research Center, Cleveland, OH.

SCATTERED-LIGHT SCANNER MEASUREMENTS OF CRYOGENIC LIQUID-JET BREAKUP

ROBERT D. INGEBO and DONALD R. BUCHELE 1990 14 p Presented at the 2nd International Congress Optical Particle Sizing, Tempe, AZ, 5-9 Mar. 1990; sponsored by Arizona State Univ. (NASA-TM-102432; E-5200; NAS 1.15:102432) Avail: NTIS HC A03/MF A01 CSCL 14/2

The effect of highly turbulent Mach 1 gas flow and high thermal gradients on drop size measurements was investigated with a scattered light scanner. The instrument, developed at NASA-Lewis, was used to measure characteristic drop diameters or cryogenic liquid sprays. By correcting for gas turbulence and thermal gradient

35 INSTRUMENTATION AND PHOTOGRAPHY

affects, it was possible to obtain good reproducible data with the scattered light scanner. Tests were conducted primarily in the aerodynamic-stripping regime of liquid atomization and it was found that the loss of small droplets due to vaporization and dispersion had a marked effect on drop size measurements. The nitrogen gas flow rate exponent of 1.33 is the same as that predicted by atomization theory for liquid jet breakup in high velocity gas flow. However, when the sprays were sampled farther downstream of the atomizer, at axial distances of 2.5 and 4.5 cm, the exponent for $W_{sub n}$ decreased 1.2 and 0.9, respectively. This was attributed to the loss of small droplets due to vaporization when values of downstream axial distances exceeded 1.3 cm. Author

N90-22022* Purdue Univ., West Lafayette, IN. School of Mechanical Engineering.

SATURATED FLUORESCENCE MEASUREMENTS OF THE HYDROXYL RADICAL IN LAMINAR HIGH-PRESSURE FLAMES **Final Report**

CAMPBELL D. CARTER, GALEN B. KING, and NORMAND M. LAURENDEAU Feb. 1990 222 p
(Contract NAG3-351)
(NASA-CR-185218; NAS 1.26:185218) Avail: NTIS HC A10/MF A02 CSCL 14/2

The efficacy of laser saturated fluorescence (LSF) for OH concentration measurements in high pressure flames was studied theoretically and experimentally. Using a numerical model describing the interaction of hydroxyl with nonuniform laser excitation, the effect of pressure on the validity of the balanced cross-rate model was studied along with the sensitivity of the depopulation of the laser-coupled levels to the ratio of rate coefficients describing: (1) electronic quenching to (sup 2) Sigma (+) (v double prime greater than 0), and (2) vibrational relaxation from v double prime greater than 0 to v double prime = 0. At sufficiently high pressures and near-saturated conditions, the total population of the laser-coupled levels reaches an asymptotic value, which is insensitive to the degree of saturation. When the ratio of electronic quenching to vibrational relaxation is small and the rate of coefficients for rotational transfer in the ground and excited electronic states are nearly the same, the balanced cross-rate model remains a good approximation for all pressures. When the above ratio is large, depopulation of the laser-coupled levels becomes significant at high pressures, and thus the balanced cross-rate model no longer holds. Under these conditions, however, knowledge of the depletion of the laser-coupled levels can be used to correct the model. A combustion facility for operation up to 20 atm was developed to allow LSF measurements of OH in high pressure flames. Using this facility, partial saturation in laminar high pressure (less than or equal to 12.3 atm) C₂H₆/O₂/N₂ flames was achieved. To evaluate the limits of the balanced cross-rate model, absorption and calibrated LSF measurements at 3.1 and 6.1 atm were compared. The fluorescence voltages were calibrated with absorption measurements in an atmospheric flame and corrected for their finite sensitivity to quenching with: (1) estimated quenching rate coefficients, and (2) an in situ measurement from a technique employing two fluorescence detection geometries. Author

N90-22024* National Aeronautics and Space Administration. Lewis Research Center, Cleveland, OH.

ZERO-G PHASE DETECTOR AND SEPARATOR Patent

STEVEN J. SCHNEIDER, inventor (to NASA) 27 Mar. 1990 7 p Filed 21 Mar. 1989
(NASA-CASE-LEW-14844-1; US-PATENT-4,911,738;
US-PATENT-APPL-SN-326766; US-PATENT-CLASS-55-160;
US-PATENT-CLASS-55-203; US-PATENT-CLASS-55-204;
US-PATENT-CLASS-210-512.1; US-PATENT-CLASS-210-97)
Avail: US Patent and Trademark Office CSCL 14/2

The gaseous phase is detected and then separated from a liquid phase in a fluid. This is accomplished by centrifuging the liquid phase while the gaseous phase migrates to the axis. When the expected phase is detected at a predetermined port, a signal is generated to open the liquid or gas valve at the respective

outlet ports and to modulate these valves in such a manner as to withdraw fluid at the same volume rate at which it is admitted.

Official Gazette of the U.S. Patent and Trademark Office

N90-22773* National Aeronautics and Space Administration. Lewis Research Center, Cleveland, OH.

A FIBER-OPTIC CURRENT SENSOR FOR AEROSPACE APPLICATIONS

RICHARD L. PATTERSON, A. H. ROSE, D. TANG, and G. W. DAY (National Inst. of Standards and Technology, Boulder, CO.) 1990 7 p Proposed for presentation at the 25th Intersociety Energy Conversion Engineering Conference, Reno, NV, 12-17 Aug. 1990; cosponsored by AIChE, SAE, ACS, AIAA, ASME, and IEEE (NASA-TM-103152; E-5513; NAS 1.15:103152) Avail: NTIS HC A02/MF A01 CSCL 14/2

A robust, accurate, broad-band, alternating current sensor using fiber optics is being developed for space applications at power frequencies as high as 20 kHz. It can also be used in low and high voltage 60 Hz terrestrial power systems and in 400 Hz aircraft systems. It is intrinsically electromagnetic interference (EMI) immune and has the added benefit of excellent isolation. The sensor uses the Faraday effect in optical fiber and standard polarimetric measurements to sense electrical current. The primary component of the sensor is a specially treated coil of single-mode optical fiber, through which the current carrying conductor passes. Improved precision is accomplished by temperature compensation by means of signals from a novel fiber-optic temperature sensor embedded in the sensing head. The technology contained in the sensor is examined and the results of precision tests conducted at various temperatures within the wide operating range are given. The results of early EMI tests are also given. Author

N90-23712* National Aeronautics and Space Administration. Lewis Research Center, Cleveland, OH.

FATIGUE TESTING APPARATUS Patent

ROBERT J. BUZZARD, inventor (to NASA) 17 Apr. 1990 8 p Filed 21 Aug. 1989 Supersedes N89-28806 (27 - 23, p 3296)
(NASA-CASE-LEW-14124-1; US-PATENT-4,916,954;
US-PATENT-APPL-SN-396263; US-PATENT-CLASS-73-799;
US-PATENT-CLASS-73-845; INT-PATENT-CLASS-G01N-3/32)
Avail: US Patent and Trademark Office CSCL 14/2

An apparatus is provided for obtaining a single crack in fatigue loading which emanates from a predetermined starting notch in a test specimen. This crack propagates in a direction in line with that of the applied Mode 2 load. The loading may be performed either monotonically or in a cyclic fatigue.

Official Gazette of the U.S. Patent and Trademark Office

N90-23714* National Aeronautics and Space Administration. Lewis Research Center, Cleveland, OH.

MULTIWAVELENGTH PYROMETRY TO CORRECT FOR REFLECTED RADIATION

DANIEL L. P. NG Jun. 1990 13 p
(NASA-TM-102578; E-5409; NAS 1.15:102578) Avail: NTIS HC A03/MF A01 CSCL 14/2

Computer curve fitting is used in multiwavelength pyrometry to measure the temperature of a surface in the presence of reflected radiation by decomposing its radiation spectrum. Computer-simulated spectra (at a surface temperature of 1000 K; in the wavelength region 0.3 to 20 microns; with a reflected radiation-source temperature of 700 to 2500 K; and reflector emissivity from 0.1 to 0.9) were generated and decomposed. This method of pyrometry determined the surface temperatures under these conditions to within 5 percent. The practicability of the method was further demonstrated by the successful analysis of a related problem--decomposition of the real spectrum of an infrared source containing two emitters to determine their temperatures. Author

N90-25323* National Aeronautics and Space Administration. Lewis Research Center, Cleveland, OH.

OPTICAL TECHNIQUES FOR DETERMINATION OF NORMAL SHOCK POSITION IN SUPERSONIC FLOWS FOR AEROSPACE APPLICATIONS

GRIGORY ADAMOVSKY and JOHN G. EUSTACE (John Carroll Univ., Cleveland, OH.) 1990 9 p Presented at the 3d Conference on Optical Testing and Metrology, San Diego, CA, 8-13 Jul. 1990; sponsored by the Society of Photo-Optical Instrumentation Engineers (NASA-TM-103201; E-5599; NAS 1.15:103201) Avail: NTIS HC A02/MF A01 CSCL 14/2

Techniques for the quantitative determination of shock position in supersonic flows using direct and indirect methods is presented. A description of an experimental setup is also presented, different configurations of shock position sensing systems are explained, and some experimental results are given. All of the methods discussed are analyzed to determine the ease of technology transfer from the laboratory to in-flight operation. Author

N90-25324*# Sverdrup Technology, Inc., Brook Park, OH.
FEASIBILITY STUDY FOR THE ADVANCED ONE-DIMENSIONAL HIGH TEMPERATURE OPTICAL STRAIN MEASUREMENT SYSTEM, PHASE 3 Final Report
CHRISTIAN T. LANT Jun. 1990 21 p
(Contract NAS3-25266)
(NASA-CR-185254; E-5546; NAS 1.26:185254) Avail: NTIS HC A03/MF A01 CSCL 14/2

The Instrumentation and Control Technology Division is developing optical strain measurement systems for applications using high temperature wire and fiber specimens. This feasibility study has determined that stable optical signals can be obtained from specimens at temperatures beyond 2,400 C. A system using an area array sensor is proposed to alleviate off-axis decorrelation arising from rigid body motions. A digital signal processor (DSP) is recommended to perform speckle correlations at a rate near the data acquisition rate. Design parameters are discussed, and fundamental limits on the speckle shift strain measurement technique are defined. Author

N90-26299*# National Aeronautics and Space Administration. Lewis Research Center, Cleveland, OH.
OPTICAL CHARACTERIZATION OF CLOUDS OF FINE LIQUID-NITROGEN PARTICLES
ROBERT D. INGEBRO 1990 7 p Presented at the 21st Annual Meeting of the Fine Particle Society, San Diego, CA, 21-25 Aug. 1990
(NASA-TM-103208; E-5616; NAS 1.15:103208) Avail: NTIS HC A02/MF A01 CSCL 14/2

Characteristic drop size, $D_{sub 32}$, of clouds of fine liquid nitrogen particles was measured with a scattered light scanning instrument developed at NASA-Lewis. Calibration of the instrument was accomplished with suspensions of monosized polystyrene spheres and the scattered light scanner was then used to investigate the mechanism of liquid nitrogen jet disintegration in high velocity gas flow. The Sauter mean diameter, $D_{sub 32}$, was found to vary inversely with nitrogen gas mass-flux raised to the 1.33 power. Values of $D_{sub 32}$ varied from 5 to 25 microns and the mass-flux exponent 1.33 agrees well with theory for liquid jet breakup in high velocity gas flow. Loss of fine particles due to the high vaporization rate of liquid nitrogen was avoided by sampling the spray 1.3 cm downstream of the nozzle orifice. The presence of high velocity and thermal gradients in the gas phase also made sampling of the particles quite difficult. As a result, it was necessary to correct the measurements for background noise produced by both highly turbulent gas flow and thermally induced density gradients in the gas phase. Author

N90-28031*# National Aeronautics and Space Administration. Lewis Research Center, Cleveland, OH.
PROGRESS IN HIGH TEMPERATURE SPECKLE-SHIFT STRAIN MEASUREMENT SYSTEM
CHRISTIAN T. LANT (Sverdrup Technology, Inc., Brook Park, OH.) and JOHN P. BARRANGER 1990 9 p Prepared for presentation at the International Conference on Hologram Interferometry and Speckle Metrology, Baltimore, MD, 5-8 Nov. 1990; sponsored in part by the Society of Experimental Mechanics

(NASA-TM-103255; E-5684; NAS 1.15:103255) Avail: NTIS HC A02/MF A01 CSCL 14/2

A fast, easy to use speckle tracking system is under development for the speckle-shift strain measurement technique. Preliminary correlation tests on wire specimens show strong correlations of well-developed speckle patterns. Stable cross-correlations were obtained from a tungsten filament at 2480 C. An analysis of the optical system determines the minimum required sampling frequency of the speckle pattern to be 2.55 pixels per speckle. Author

N90-28033*# National Aeronautics and Space Administration. Lewis Research Center, Cleveland, OH.

FIBER-OPTIC PROJECTED-FRINGE DIGITAL INTERFEROMETRY
CAROLYN R. MERCER and GLENN BEHEIM 1990 9 p Proposed for presentation at the 1990 Fall Conference on Hologram Interferometry and Speckle Metrology, Baltimore, MD, 4-7 Nov. 1990; sponsored by Society for Experimental Mechanics (NASA-TM-103252; E-5681; NAS 1.15:103252) Avail: NTIS HC A02/MF A01 CSCL 14/2

A phase-stepped projected-fringe interferometer was developed which uses a closed-loop fiber-optic phase-control system to make very accurate surface profile measurements. The closed-loop phase-control system greatly reduces phase-stepping error, which is frequently the dominant source of error in digital interferometers. Two beams emitted from a fiber-optic coupler are combined to form an interference fringe pattern on a diffusely reflecting object. Reflections off of the fibers' output faces are used to create a phase-indicating signal for the closed-loop optical phase controller. The controller steps the phase difference between the two beams by $\pi/2$ radians in order to determine the object's surface profile using a solid-state camera and a computer. The system combines the ease of alignment and automated data reduction of phase-stepping projected-fringe interferometry with the greatly improved phase-stepping accuracy of our closed-loop phase-controller. The system is demonstrated by measuring the profile of a plate containing several convex surfaces whose heights range from 15 to 25 micron high. Author

N90-28827*# National Aeronautics and Space Administration. Lewis Research Center, Cleveland, OH.
FREQUENCY RESPONSE OF A THERMOCOUPLE WIRE: EFFECTS OF AXIAL CONDUCTION Progress Report, Apr. - Sep. 1990
L. J. FORNEY (Georgia Inst. of Tech., Atlanta.) and G. C. FRALICK Sep. 1990 40 p
(Contract NCC3-135)
(NASA-CR-180454; NAS 1.26:180454; E19-666-1) Avail: NTIS HC A03/MF A01 CSCL 14/2

Theoretical expressions are derived for the steady-state frequency response of a thermocouple wire. In particular, the effects of axial heat conduction are demonstrated for both a uniform thermocouple wire and a nonuniform wire with unequal material properties and wire diameters across the junction. For the case of a uniform wire, the amplitude ratio and phase angle compare favorably with the series solution of Scadron and Warshawsky (1952) except near the ends of the wire. For the case of a non-uniform wire, the amplitude ratio at low frequency omega yields 0 agrees with the results of Scadron and Warshawsky for a steady-state temperature distribution. Moreover, the frequency response for a non-uniform wire in the limit of infinite length l yields infinity is shown to reduce to a simple expression that is analogous to the classic first order solution for a thermocouple wire with uniform properties. Author

N90-29622*# Rockwell International Corp., Canoga Park, CA. Rocketdyne Div.
INTEGRATED CONTROLS AND HEALTH MONITORING FIBEROPTIC SHAFT MONITOR Final Report
P. COLEMAN, H. DAREJEH, and J. J. COLLINS Nov. 1989 28 p Original contains color illustrations

36 LASERS AND MASERS

(Contract NAS3-23773)

(NASA-CR-185210; NAS 1.26:185210; RI/RD-90-177) Avail: NTIS HC A03/MF A01; 2 functional color pages CSCL 14/2

Recent work was performed on development optical technology to provide real time monitoring of shaft speed, shaft axial displacement, and shaft orbit of the OTVE hydrostatic bearing tester. Results show shaft axial displacement can be optically measured (at the same time as shaft orbital motion and speed) to within 0.3 mills by two fiber optic deflectometers. The final results of this condition monitoring development effort are presented. Author

36

LASERS AND MASERS

Includes parametric amplifiers.

A90-11593* State Univ. of New York, Stony Brook.
FIBER OPTIC DETECTOR PROBES FOR LASER LIGHT SCATTERING

HARBANS S. DHADWAL, CHI WU, and BENJAMIN CHU (New York, State University, Stony Brook) Applied Optics (ISSN 0003-6935), vol. 28, Oct. 1, 1989, p. 4199-4205. refs (Contract NAG3-963; NSF DMR-86-17820)

Copyright

An experimental investigation of the role of fiber optic detector probes in laser light scattering is presented. A quantitative comparison between different detector configurations is accomplished by measuring the time taken for one million photocounts to be accumulated in the extrapolated zeroth delay channel of the net unnormalized intensity time correlation function. A considerable reduction in the accumulation time is achieved by relaxing a rather stringent requirement for the spatial coherence of the optical field. Author

N90-22784*# National Aeronautics and Space Administration. Lewis Research Center, Cleveland, OH.

TWO-DIMENSIONAL SURFACE STRAIN MEASUREMENT BASED ON A VARIATION OF YAMAGUCHI'S LASER-SPECKLE STRAIN GAUGE

JOHN P. BARRANGER 1990 12 p Presented at the Conference on Optical Testing and Metrology 3, San Diego, CA, 8-13 Jul. 1990; sponsored by Society of Photo-Optical Instrumentation Engineers (NASA-TM-103162; E-5530; NAS 1.15:103162) Avail: NTIS HC A03/MF A01 CSCL 20/5

A novel optical method of measuring 2-D surface strain is proposed. Two linear strains along orthogonal axes and the shear strain between those axes is determined by a variation of Yamaguchi's laser-speckle strain gage technique. It offers the advantages of shorter data acquisition times, less stringent alignment requirements, and reduced decorrelation effects when compared to a previously implemented optical strain rosette technique. The method automatically cancels the translational and rotational components of rigid body motion while simplifying the optical system and improving the speed of response. Author

N90-28833*# National Aeronautics and Space Administration. Lewis Research Center, Cleveland, OH.

DESIGN OF A CO2 LASER POWER CONTROL SYSTEM FOR A SPACELAB MICROGRAVITY EXPERIMENT

CARL J. WENZLER and DENNIS J. EICHENBERG Aug. 1990 42 p (NASA-TM-103112; E-5436; NAS 1.15:103112) Avail: NTIS HC A03/MF A01 CSCL 20/5

The surface tension driven convection experiment (STDCE) is a Space Transportation System flight experiment manifested to fly aboard the USML-1 Spacelab mission. A CO2 laser is used to heat a spot on the surface of silicone oil contained inside a test

chamber. Several CO2 laser control systems were evaluated and the selected system will be interfaced with the balance of the experimental hardware to constitute a working engineering model. Descriptions and a discussion of these various design approaches are presented. Author

37

MECHANICAL ENGINEERING

Includes auxiliary systems (nonpower); machine elements and processes; and mechanical equipment.

A90-13750* Akron Univ., OH.
EXPERIMENTAL AND ANALYTICAL EVALUATION OF DYNAMIC LOAD VIBRATION OF A 2240-KW (3000-HP) ROTORCRAFT TRANSMISSION

FRED K. CHOY (Akron, University, OH), DENNIS P. TOWNSEND, and FRED B. OSWALD (NASA, Lewis Research Center, Cleveland, OH) Franklin Institute, Journal (ISSN 0016-0032), vol. 326, no. 5, 1989, p. 721-735. Previously announced in STAR as N87-20556. refs

Copyright

A dynamic analysis of a 2240-kW (3000-hp) helicopter planetary system is presented. Results from both analytical and experimental studies show good correlation in gear-tooth loads. A parametric study indicates that the mesh damping ratio has a significant effect on maximum gear tooth load, stress, and vibration. Correlation with experimental results indicates that the Sun-planet mesh damping ratio can significantly differ from the planet ring mesh damping ratio. A numerical fast Fourier transform (FFT) procedure was applied to examine the mesh load components in the frequency domain and the magnitudes of multiple tooth pass frequencies excited by nonsynchronous meshing of the planets. Effects of tooth-spacing errors and tooth-profile modifications with tip relief are examined. A general discussion of results and correlation with the experimental study are also presented. Author

A90-14020* National Aeronautics and Space Administration. Lewis Research Center, Cleveland, OH.

FUNDAMENTALS OF TRIBOLOGY AT THE ATOMIC LEVEL

JOHN FERRANTE and STEPHEN V. PEPPER (NASA, Lewis Research Center, Cleveland, OH) IN: New materials approaches to tribology: Theory and applications; Proceedings of the Symposium, Boston, MA, Nov. 29-Dec. 2, 1988. Pittsburgh, PA, Materials Research Society, 1989, p. 37-50. refs

Tribology, the science and engineering of solid surfaces in moving contact, is a field that encompasses many disciplines: solid state physics, chemistry, materials science, and mechanical engineering. In spite of the practical importance and maturity of the field, the fundamental understanding of basic phenomena has only recently been attacked. An attempt to define some of these problems and indicate some profitable directions for future research is presented. There are three broad classifications: (1) fluid properties (compression, rheology, additives and particulates); (2) material properties of the solids (deformation, defect formation and energy loss mechanisms); and (3) interfacial properties (adhesion, friction chemical reactions, and boundary films). Research in the categories has traditionally been approached by considering macroscopic material properties. Recent activity has shown that some issues can be approached at the atomic level: the atoms in the materials can be manipulated both experimentally and theoretically, and can produce results related to macroscopic phenomena. Author

A90-17018* Ohio State Univ., Columbus.

MODAL ANALYSIS OF GEAR HOUSING AND MOUNTS

TEIK C. LIM, RAJENDRA SINGH (Ohio State University, Columbus), and JAMES J. ZAKRAJSEK (NASA, Lewis Research Center,

Cleveland, OH) IN: International Modal Analysis Conference, 7th, Las Vegas, NV, Jan. 30-Feb. 2, 1989, Proceedings. Volume 2. Bethel, CT, Society for Experimental Mechanics, Inc., 1989, p. 1072-1078. Previously announced in STAR as N89-21244. refs
Copyright

Dynamic finite element analysis of a real gear housing is presented. The analysis was conducted for the housing without the rotating components (gears, shafts, and bearings). Both rigid and flexible mounting conditions for the gear housing are considered in this analysis. The flexible support simulates the realistic mounting condition on a rotorcraft, and the rigid one is analyzed for comparison purposes. The effect of gear housing stiffeners is also evaluated. The results indicate that the first six natural modes of the flexibly mounted gear housing in the 0 to 200 Hz range correspond to the translational and rotational rigid body vibration modes of the housing. Above this range, the housing plate elastic modes begin to occur. In the case of the rigid mount, only the housing plate elastic modes are observed which are verified by modal analysis experiments. Parametric studies show that the housing plate stiffeners and rigid mounts tend to increase most of the natural frequencies, the lower ones being affected the most. Author

A90-18355* Virginia Polytechnic Inst. and State Univ., Blacksburg.

IMPACT DAMAGE DEVELOPMENT IN DAMAGED COMPOSITE MATERIALS

J. C. DUKE, JR. and M. T. KIERNAN (Virginia Polytechnic Institute and State University, Blacksburg) IN: Japan-U.S. Conference on Composite Materials, 4th, Washington, DC, June 27-29, 1988, Proceedings. Lancaster, PA, Technomic Publishing Co., Inc., 1989, p. 63-71.

(Contract NAG3-172)

Copyright

A procedure for predicting the nature of impact damage development based on the measured acousto-ultrasonic (AU) response of fiber reinforced crossply laminates with or without damage is described. Results of AU evaluation as well as penetrant enhanced radiographs of damaged laminates are presented. Author

A90-21107*# Cincinnati Univ., OH.

COMPARISON OF BOUNDARY ELEMENT AND FINITE ELEMENT METHODS IN SPUR GEAR ROOT STRESS ANALYSIS

H. SUN, D. MAVRIPLIS, R. L. HUSTON (Cincinnati, University, OH), and F. B. OSWALD (NASA, Lewis Research Center, Cleveland, OH) IN: 1989 International Power Transmission and Gearing Conference, 5th, Chicago, IL, Apr. 25-28, 1989, Proceedings. Volume 1. New York, American Society of Mechanical Engineers, 1989, p. 163-166. refs

(Contract NSG-3188)

Copyright

The boundary element method (BEM) is used to compute fillet stress concentration in spur gear teeth. The results are shown to compare favorably with analogous results obtained using the finite element method (FEM). A partially supported thin rim gear is studied. The loading is applied at the pitch point. A three-dimensional analysis is conducted using both the BEM and FEM (NASTRAN). The results are also compared with those of a two-dimensional finite element model. An advantage of the BEM over the FEM is that fewer elements are needed with the BEM. Indeed, in the current study the BEM used 92 elements and 270 nodes whereas the FEM used 320 elements and 2037 nodes. Moreover, since the BEM is especially useful in problems with high stress gradients it is potentially a very useful tool for fillet stress analyses. Author

A90-21112*# Akron Univ., OH.

TOOTH CONTACT SHIFT IN LOADED SPIRAL BEVEL GEARS

M. SAVAGE, P. C. ALTIDIS (Akron, University, OH), D. G. LEWICKI (NASA, Lewis Research Center; U.S. Army, Propulsion Directorate, Cleveland, OH), J. J. COY (NASA, Lewis Research Center,

Cleveland, OH), and F. L. LITVIN (Illinois, University, Chicago) IN: 1989 International Power Transmission and Gearing Conference, 5th, Chicago, IL, Apr. 25-28, 1989, Proceedings. Volume 1. New York, American Society of Mechanical Engineers, 1989, p. 203-212. Previously announced in STAR as N89-14453. refs

(Contract NAG3-55)

Copyright

An analytical method is presented to predict the shifts of the contact ellipses of spiral bevel gear teeth under load. The contact ellipse shift is the motion of the tooth contact position from the ideal pitch point to its location under load. The shifts are due to the elastic motions of the gear and pinion supporting shafts and bearings. The calculations include the elastic deflections of the gear shafts and the deflections of the four shaft bearings. The method assumes that the surface curvature of each tooth is constant near the unloaded pitch point. Results from these calculations will help designers reduce transmission weight without seriously reducing transmission performance. Author

A90-21113*# National Aeronautics and Space Administration. Lewis Research Center, Cleveland, OH.

EFFICIENCY TESTING OF A HELICOPTER TRANSMISSION PLANETARY REDUCTION STAGE

R. F. HANDSCHUH (U.S. Army, Propulsion Directorate, Cleveland, OH) and D. A. ROHN (NASA, Lewis Research Center, Cleveland, OH) IN: 1989 International Power Transmission and Gearing Conference, 5th, Chicago, IL, Apr. 25-28, 1989, Proceedings. Volume 1. New York, American Society of Mechanical Engineers, 1989, p. 243-257. Previously announced in STAR as N88-15224. refs

Copyright

A parametric study of the efficiency of a 310-kW (420-hp) helicopter transmission planetary test section (four planets) was performed. The purpose was to determine the planetary contribution to the overall transmission power loss. Test parameters varied were oil flow rate, oil inlet temperature, lubricant type, shaft speed, and applied torque. The measured efficiency over all the test variables ranged from 99.44 to 99.75 percent. These experimental results were compared with other experimental and computational results. Author

A90-21115*# National Aeronautics and Space Administration. Lewis Research Center, Cleveland, OH.

EFFECT OF ADVANCED COMPONENT TECHNOLOGY ON HELICOPTER TRANSMISSIONS

D. G. LEWICKI (NASA, Lewis Research Center; U.S. Army, Propulsion Directorate, Cleveland, OH) and D. P. TOWNSEND (NASA, Lewis Research Center, Cleveland, OH) IN: 1989 International Power Transmission and Gearing Conference, 5th, Chicago, IL, Apr. 25-28, 1989, Proceedings. Volume 1. New York, American Society of Mechanical Engineers, 1989, p. 267-279. Previously announced in STAR as N89-13794. refs

Copyright

Experimental tests were performed on the NASA/Bell Helicopter Textron (BHT) 500 hp advanced technology transmission (ATT) at the NASA Lewis Research Center. The ATT was a retrofit of the OH-58C helicopter 236 kW (317 hp) main rotor transmission, upgraded to 373 kW (500 hp), with a design goal of retaining long life with a minimum increase in cost, weight, and size. Vibration, strain, efficiency, deflection, and temperature experiments were performed and the results were compared to previous experiments on the OH-58A, OH-58C, and UH-60A transmissions. The high-contact-ratio gears and the cantilevered-mounted, flexible ring gear of the ATT reduced vibration compared to that of the OH-58C. The ATT flexible ring gear improved planetary load sharing compared to that of the rigid ring gear of the UH-60A transmission. The ATT mechanical efficiency was lower than that of the OH-58A transmission, probably due to the high-contact-ratio planetary gears. Author

37 MECHANICAL ENGINEERING

A90-21118*# California State Univ., Long Beach.
THE ROLE OF THERMAL AND LUBRICANT BOUNDARY LAYERS IN THE TRANSIENT THERMAL ANALYSIS OF SPUR GEARS

L. E. EL-BAYOUMY, L. S. AKIN (California State University, Long Beach), D. P. TOWNSEND (NASA, Lewis Research Center, Cleveland, OH), and F. C. CHOY (Akron, University, OH) IN: 1989 International Power Transmission and Gearing Conference, 5th, Chicago, IL, Apr. 25-28, 1989, Proceedings. Volume 1. New York, American Society of Mechanical Engineers, 1989, p. 313-325. Previously announced in STAR as N89-14452. refs
Copyright

An improved convection heat-transfer model has been developed for the prediction of the transient tooth surface temperature of spur gears. The dissipative quality of the lubricating fluid is shown to be limited to the capacity extent of the thermal boundary layer. This phenomenon can be of significance in the determination of the thermal limit of gears accelerating to the point where gear scoring occurs. Steady-state temperature prediction is improved considerably through the use of a variable integration time step that substantially reduces computer time. Computer-generated plots of temperature contours enable the user to animate the propagation of the thermal wave as the gears come into and out of contact, thus contributing to better understanding of this complex problem. This model has a much better capability at predicting gear-tooth temperatures than previous models. Author

A90-21119*# Mechanical Engineering Lab., Tsukuba (Japan).
EFFECTS OF LUBRICATION ON THE PERFORMANCE OF HIGH SPEED SPUR GEARS

H. MIZUTANI, Y. ISIKAWA (Mechanical Engineering Laboratory, Tsukuba, Japan), and D. P. TOWNSEND (NASA, Lewis Research Center, Cleveland, OH) IN: 1989 International Power Transmission and Gearing Conference, 5th, Chicago, IL, Apr. 25-28, 1989, Proceedings. Volume 1. New York, American Society of Mechanical Engineers, 1989, p. 327-334. Previously announced in STAR as N89-22919. refs
Copyright

An experimental analysis was conducted to determine power loss and gear noise of high speed spur gears with long addendum under various conditions of load, speed, and oil jet pressure for into mesh lubrication. Power losses were calculated from temperature measurements of lubricating oil, gears, gear box, and oil flow rate. Furthermore, power loss was divided into windage loss, friction loss and churning loss. The results show that windage loss and churning loss were the main components of gear power loss of high gear speed. In addition, lubricating conditions had some influences on gear noise especially under low oil temperature or high viscosity. Author

A90-21121*# Aerojet Electrosystems Co., Azusa, CA.
WEAR CONSIDERATION IN GEAR DESIGN FOR SPACE APPLICATIONS

L. S. AKIN (Aerojet ElectroSystems Co., Azusa, CA) and D. P. TOWNSEND (NASA, Lewis Research Center, Cleveland, OH) IN: 1989 International Power Transmission and Gearing Conference, 5th, Chicago, IL, Apr. 25-28, 1989, Proceedings. Volume 1. New York, American Society of Mechanical Engineers, 1989, p. 361-365. Previously announced in STAR as N89-15414. refs
Copyright

A procedure is described that was developed for evaluating the wear in a set of gears in mesh under high load and low rotational speed. The method can be used for any low-speed gear application, with nearly negligible oil film thickness, and is especially useful in space stepping mechanism applications where determination of pointing error due to wear is important, such as in long life sensor antenna drives. A method is developed for total wear depth at the ends of the line of action using a very simple formula with the slide to roll ratio $V_{\text{sub s}}/V_{\text{sub r}}$. A method is also developed that uses the wear results to calculate the transmission error also known as pointing error of a gear mesh. Author

A90-21122*# California State Univ., Long Beach.
LUBRICANT JET FLOW PHENOMENA IN SPUR AND HELICAL GEARS WITH MODIFIED ADDENDUMS - FOR RADIALLY DIRECTED INDIVIDUAL JETS

L. S. AKIN (California State University, Long Beach) and D. P. TOWNSEND (NASA, Lewis Research Center, Cleveland, OH) IN: 1989 International Power Transmission and Gearing Conference, 5th, Chicago, IL, Apr. 25-28, 1989, Proceedings. Volume 1. New York, American Society of Mechanical Engineers, 1989, p. 367-374. Previously announced in STAR as N89-15415. refs
Copyright

This paper develops the mathematical relations for the Virtual Kinetic Model as an improvement over the vectorial model developed earlier. The model solution described provides the most energy efficient means of cooling gears, i.e., it requires the least pressure or pumping power to distribute the coolant onto the tooth surface. Further, this nozzle orientation allows impingement to the root of the tooth if needed and provides the most cooling control when compared to into-mesh and out-of-mesh cooling. Author

A90-21123*# Ohio State Univ., Columbus.
DYNAMIC ANALYSIS OF GEARED ROTORS BY FINITE ELEMENTS

A. KAHRAMAN, H. N. OZGUVEN, D. R. HOUSER (Ohio State University, Columbus), and J. ZAKRAJSEK (NASA, Lewis Research Center, Cleveland, OH) IN: 1989 International Power Transmission and Gearing Conference, 5th, Chicago, IL, Apr. 25-28, 1989, Proceedings. Volume 1. New York, American Society of Mechanical Engineers, 1989, p. 375-382. refs
(Contract NAG3-773)
Copyright

The finite element model of a geared rotor system on flexible bearings has been developed. The model includes the rotary inertia of shaft elements, the axial loading on shafts, flexibility and damping of bearings, material damping of shafts and the stiffness and the damping of gear mesh. The coupling between the torsional and transverse vibrations of gears were considered in the model. A constant mesh stiffness was assumed. The analysis procedure can be used for forced vibration analysis of geared rotors by calculating the critical speeds and determining the response of any point on the shaft to mass unbalances, geometric eccentricities of gears and displacement transmission error excitation at the mesh point. The dynamic mesh forces due to these excitations can also be calculated. The model has been applied to several systems for the demonstration of its accuracy and for studying the effect of bearing compliances on system dynamics. Author

A90-21124*# Akron Univ., OH.
VIBRATION SIGNATURE ANALYSIS OF MULTISTAGE GEAR TRANSMISSION

F. K. CHOY, Y. K. TU, M. SAVAGE (Akron, University, OH), and D. P. TOWNSEND (NASA, Lewis Research Center, Cleveland, OH) IN: 1989 International Power Transmission and Gearing Conference, 5th, Chicago, IL, Apr. 25-28, 1989, Proceedings. Volume 1. New York, American Society of Mechanical Engineers, 1989, p. 383-390. Previously announced in STAR as N89-18685. refs
Copyright

An analysis is presented for multistage multimesh gear transmission systems. The analysis predicts the overall system dynamics and the transmissibility to the gear box or the enclosed structure. The modal synthesis approach of the analysis treats the uncoupled lateral/torsional model characteristics of each stage or component independently. The vibration signature analysis evaluates the global dynamics coupling in the system. The method synthesizes the interaction of each modal component or stage with the nonlinear gear mesh dynamics and the modal support geometry characteristics. The analysis simulates transient and steady state vibration events to determine the resulting torque variations, speeds, changes, rotor imbalances, and support gear box motion excitations. A vibration signature analysis examines the overall dynamic characteristics of the system, and the individual

model component responses. The gear box vibration analysis also examines the spectral characteristics of the support system.

Author

A90-21126*# Memphis State Univ., TN.

DYNAMIC LOADING OF SPUR GEARS WITH LINEAR OR PARABOLIC TOOTH PROFILE MODIFICATIONS

H. H. LIN (Memphis State University, TN), F. B. OSWALD, and D. P. TOWNSEND (NASA, Lewis Research Center, Cleveland, OH) IN: 1989 International Power Transmission and Gearing Conference, 5th, Chicago, IL, Apr. 25-28, 1989, Proceedings. Volume 1. New York, American Society of Mechanical Engineers, 1989, p. 409-419. Previously announced in STAR as N89-15413. refs

Copyright

A computer simulation was conducted to investigate the effects of both linear and parabolic tooth profile modification on the dynamic response of low-contact-ratio spur gears. The effect of the total amount of modification and the length of the modification zone were studied at various loads and speeds to find the optimal profile modification for minimal dynamic loading. Design charts consisting of normalized maximum dynamic load curves were generated for gear systems operated at various loads and with different tooth profile modification. An optimum profile modification can be determined from these design charts to minimize the dynamic loads of spur gear systems.

Author

A90-21128*# Memphis State Univ., TN.

PROFILE MODIFICATION TO MINIMIZE SPUR GEAR DYNAMIC LOADING

H. H. LIN (Memphis State University, TN), D. P. TOWNSEND, and F. B. OSWALD (NASA, Lewis Research Center, Cleveland, OH) IN: 1989 International Power Transmission and Gearing Conference, 5th, Chicago, IL, Apr. 25-28, 1989, Proceedings. Volume 1. New York, American Society of Mechanical Engineers, 1989, p. 455-465. Previously announced in STAR as N87-28918. refs

Copyright

An analytical computer simulation program for dynamic modeling of low-contact-ratio spur gear systems is presented. The procedure computes the static transmission error of the gears operating under load and uses a fast Fourier transform to generate the frequency spectrum of the static transmission error at various tooth profile modifications. The dynamic loading response of an unmodified (perfect involute) gear pair was compared with that of gears with various profile modifications. Correlations were found between various profile modifications and the resulting dynamic loads. An effective error, obtained from frequency domain analysis of the static transmission error of the gears, gave a very good indication of the optimum profile modification to reduce gear dynamic loading. Design curves generated by dynamic simulation at various profile modifications are given for gear systems operated at various loads. Optimum profile modifications can be determined from these design curves for improved gear design.

Author

A90-21131*# Cincinnati Univ., OH.

COMPUTER AIDED DESIGN OF SPUR GEAR TEETH

R. L. HUSTON, D. MAVRIPLIS (Cincinnati, University, OH), and F. B. OSWALD (NASA, Lewis Research Center, Cleveland, OH) IN: 1989 International Power Transmission and Gearing Conference, 5th, Chicago, IL, Apr. 25-28, 1989, Proceedings. Volume 2. New York, American Society of Mechanical Engineers, 1989, p. 539-545.

(Contract NSG-3188)

Copyright

Procedures for computer-modeling of spur gear tooth fabrication are given. It is shown that the standard involute tooth form results from a cutter with an involute shape rolling onto a gear blank. Specifically, the envelope of an involute is an involute. Examples are given and applications are discussed.

Author

A90-21132*# Illinois Univ., Chicago.

TOPOLOGY OF MODIFIED HELICAL GEARS

F. L. LITVIN, J. ZHANG (Illinois, University, Chicago), R. F. HANDSCHUH, and J. J. COY (NASA, Lewis Research Center; U. S. Army, Propulsion Directorate, Cleveland, OH) IN: 1989 International Power Transmission and Gearing Conference, 5th, Chicago, IL, Apr. 25-28, 1989, Proceedings. Volume 2. New York, American Society of Mechanical Engineers, 1989, p. 547-554. Previously announced in STAR as N89-28015. refs

Copyright

The topology of several types of modified surfaces of helical gears is proposed. The modified surfaces allow absorption of a linear or almost linear function of transmission errors. These errors are caused by gear misalignment and an improvement of the contact of gear tooth surfaces. Principles and corresponding programs for computer aided simulation of meshing and contact of gears have been developed. The results of this investigation are illustrated with numerical examples.

Author

A90-21136*# IBM Watson Research Center, Yorktown Heights, NY.

COMPUTER AIDED DESIGN OF BEVEL GEAR TOOTH SURFACES

S. H. CHANG (IBM Thomas J. Watson Research Center, Yorktown Heights, NY), R. L. HUSTON (Cincinnati, University, OH), and J. J. COY (NASA, Lewis Research Center, Cleveland, OH) IN: 1989 International Power Transmission and Gearing Conference, 5th, Chicago, IL, Apr. 25-28, 1989, Proceedings. Volume 2. New York, American Society of Mechanical Engineers, 1989, p. 585-591. Previously announced in STAR as N89-17248. refs

(Contract NSG-3188)

Copyright

This paper presents a computer-aided design procedure for generating bevel gears. The development is based on examining a perfectly plastic, cone-shaped gear blank rolling over a cutting tooth on a plane crown rack. The resulting impression on the plastic gear blank is the envelope of the cutting tooth. This impression and envelope thus form a conjugate tooth surface. Equations are presented for the locus of points on the tooth surface. The same procedures are then extended to simulate the generation of a spiral bevel gear. The corresponding governing equations are presented.

Author

A90-23814*# Allied-Signal Aerospace Co., Phoenix, AZ.

ATTAP/AGT101 CERAMICS TECHNOLOGY UPDATE

G. L. BOYD and D. M. KREINER (Allied-Signal Aerospace Co., Garrett Auxiliary Power Div., Phoenix, AZ) ASME, Gas Turbine and Aeroengine Congress and Exposition, Toronto, Canada, June 4-8, 1989. 6 p.

(Contract DEN3-335)

(ASME PAPER 89-GT-105)

The feasibility of applying ceramics to the gas turbine was demonstrated during the AGT101 Program, when over 250 hours were accumulated on ceramic components in engine tests at temperatures up to 1204C (2200F). The follow-on program, designated the Advanced Turbine Technology Applications Project (ATTAP), began in late August 1987 to further develop ceramic technology. This program addresses ceramic component fabrication technology, design methods development and the supporting data base, and verification of ceramic component durability in an operating engine environment. These technologies must be demonstrated so that a commercialization development decision can be made at the end of ATTAP.

Author

A90-23838*# National Aeronautics and Space Administration. Lewis Research Center, Cleveland, OH.

SOME COMPOSITE BEARING AND SEAL MATERIALS FOR GAS TURBINE APPLICATIONS - A REVIEW

HAROLD E. SLINEY (NASA, Lewis Research Center, Cleveland, OH) ASME, Gas Turbine and Aeroengine Congress and Exposition, Toronto, Canada, June 4-8, 1989. 8 p. Previously announced in STAR as N89-14338. refs

(ASME PAPER 89-GT-144)

A review is made of the selection and tribological testing of materials for high-temperature bearings and seals. The goal is to

achieve good tribological properties over a wide range of temperatures because bearings and seals must be functional from low temperature start-up conditions on up to the maximum temperatures encountered during engine operation. Plasma sprayed composite coatings with favorable tribological properties from 25 to 900 C are discussed. The performance of these coatings in simple tribological bench tests is described. Examples are also given of their performance in high-speed sliding contact seals and as Stirling cylinder liner materials, and as backup lubricants for compliant foil gas bearings. Author

A90-26899* National Aeronautics and Space Administration. Lewis Research Center, Cleveland, OH.

PRELIMINARY STUDY ON PRESSURE BRAZING AND DIFFUSION WELDING OF Nb-1Zr TO INCONEL 718

T. J. MOORE (NASA, Lewis Research Center, Cleveland, OH) Welding Journal, Research Supplement (ISSN 0043-2296), vol. 69, March 1990, p. 98-s to 102-s. refs Copyright

Future space power systems may include Nb-1Zr/Inconel 718 dissimilar metal joints for operation at 1000 K for 60,000 h. The serviceability of pressure-brazed and diffusion-welded joints was investigated. Ni-based metallic glass foil filler metals were used for brazing. Ni and Fe foils were used as diffusion welding inter-layers. Joint soundness was determined by metallographic examination in the as-brazed and as-welded condition, after aging at 1000 K, and after thermal cycling. Brazed joints thermally cycled in the as-brazed condition and diffusion-welded joints were unsatisfactory because of cracking problems. Brazed joints may meet the service requirements if the joints are aged at 1000 K prior to thermal cycling. Author

A90-27091* Detroit Diesel Allison, MI. CERAMIC VALVE DEVELOPMENT FOR HEAVY-DUTY LOW HEAT REJECTION DIESEL ENGINES

K. E. WEBER and C. J. MICU (Detroit Diesel Corp., MI) Ceramic Engineering and Science Proceedings (ISSN 0196-6219), vol. 10, Sept.-Oct. 1989, p. 1254-1268. Research supported by DOE. (Contract DEN3-329) Copyright

Monolithic ceramic valves can be successfully operated in a heavy-duty diesel engine, even under extreme low heat rejection operating conditions. This paper describes the development of a silicon nitride valve from the initial design stage to actual engine testing. Supplier involvement, finite element analysis, and preliminary proof of concept demonstration testing played a significant role in this project's success. Author

A90-27095* Detroit Diesel Allison, MI. CERAMIC PORT SHIELDS CAST IN AN IRON ENGINE HEAD NABIL S. HAKIM and MARK A. GROENEWEG (Detroit Diesel Corp., MI) Ceramic Engineering and Science Proceedings (ISSN 0196-6219), vol. 10, Sept.-Oct. 1989, p. 1304-1314. Research supported by DOE. (Contract DEN3-329) Copyright

Silicon nitride exhaust and intake port shields have been successfully cast into a gray iron cylinder head of a heavy duty diesel single cylinder research engine. Careful design considerations, finite element, and probability of survival analyses indicated viability of the design. Foundry experience, NDE, and failure investigations are reported. Author

A90-29327*# National Aeronautics and Space Administration. Lewis Research Center, Cleveland, OH.

PROBABILISTIC ANALYSIS OF BLADED TURBINE DISKS AND THE EFFECT OF MISTUNING

ASHWIN SHAH, V. K. NAGPAL (Sverdrup Technology, Inc., Brookpark, OH), and C. C. CHAMIS (NASA, Lewis Research Center, Cleveland, OH) IN: AIAA/ASME/ASCE/AHS/ASC Structures, Structural Dynamics and Materials Conference, 31st, Long Beach, CA, Apr. 2-4, 1990, Technical Papers. Part 2. Washington, DC,

American Institute of Aeronautics and Astronautics, 1990, p. 1033-1038. refs (AIAA PAPER 90-1097) Copyright

Probabilistic assessment of the maximum blade response on a mistuned rotor disk is performed using the computer code NESSUS. The uncertainties in natural frequency, excitation frequency, amplitude of excitation and damping have been included to obtain the cumulative distribution function (CDF) of blade responses. Advanced mean value first order analysis is used to compute CDF. The sensitivities of different random variables are identified. Effect of the number of blades on a rotor on mistuning is evaluated. It is shown that the uncertainties associated with the forcing function parameters have significant effect on the response distribution of the bladed rotor. Author

A90-33225* National Aeronautics and Space Administration. Lewis Research Center, Cleveland, OH.

SOLID STATE PROCESSING FOR HIGH TEMPERATURE ALLOYS AND COMPOSITES

J. DANIEL WHITTENBERGER (NASA, Lewis Research Center, Cleveland, OH) IN: Solid state powder processing. Warrendale, PA, Minerals, Metals and Materials Society, 1990, p. 137-155. refs Copyright

A variety of solid state powder processing methods have been examined for their potential to produce high temperature materials. These techniques included solid state diffusion, mechanical alloying, reaction milling, and exothermic reactions. While both mechanical alloying and exothermic reactions are capable of producing high temperature composites in addition to yielding solid solution and precipitation hardened alloys, reaction milling can only be used to make composite materials. Although at present this method has only been applied to make carbide strengthened Al, recent work indicates that reaction milling is capable of yielding high strength NiAl-AlN composites. Author

A90-33555*# Virginia Polytechnic Inst. and State Univ., Blacksburg.

AN ANNULAR GAS SEAL ANALYSIS USING EMPIRICAL ENTRANCE AND EXIT REGION FRICTION FACTORS

D. A. ELROD (Virginia Polytechnic Institute and State University, Blacksburg), D. W. CHILDS, and C. C. NELSON (Texas A & M University, College Station) (STLE and ASME, Joint Tribology Conference, Fort Lauderdale, FL, Oct. 16-19, 1989) ASME, Transactions, Journal of Tribology (ISSN 0742-4787), vol. 112, April 1990, p. 196-204. refs (Contract NAG3-181)

(ASME PAPER 89-TRIB-46) Copyright

Wall shear stress results from stationary-rotor flow tests of five annular gas seals are used to develop entrance and exit region friction factor models. The friction factor models are used in a bulk-flow seal analysis which predicts leakage and rotor-dynamic coefficients. The predictions of the analysis are compared to experimental results and to the predictions of Nelson's analysis (1985). The comparisons are for smooth-rotor seals with smooth and honeycomb-stators. The present analysis predicts the destabilizing cross-coupled stiffness of a seal better than Nelson's analysis. Both analyses predict direct damping well and direct stiffness poorly. Author

A90-38248* Sverdrup Technology, Inc., Middleburg Heights, OH.

ON THE DYNAMIC RESPONSE OF PRESSURE TRANSMISSION LINES IN THE RESEARCH OF HELIUM-CHARGED FREE PISTON STIRLING ENGINES

ERIC L. MILLER (Sverdrup Technology, Inc., Middleburg Heights, OH) and JAMES E. DUDENHOEFER (NASA, Lewis Research Center, Cleveland, OH) IN: IECEC-89; Proceedings of the Twenty-fourth Intersociety Energy Conversion Engineering Conference, Washington, DC, Aug. 6-11, 1989. Volume 5. New York, Institute of Electrical and Electronics Engineers, 1989, p. 2243-2248.

Copyright

The signal distortion inherent to pressure transmission lines in free-piston Stirling engine research is discussed. Based on results from classical analysis, guidelines are formulated to describe the dynamic response properties of a volume-terminated transmission tube for applications involving the helium-charged free-piston Stirling engines. The underdamped flow regime is described, the primary resonance frequency is derived, and the pressure phase and amplitude distortion are discussed. The scope and limitation of the dynamic response analysis are considered. I.E.

A90-40713* Carnegie-Mellon Univ., Pittsburgh, PA.
A SIMPLIFIED MODEL FOR TWO PHASE FACE SEAL DESIGN
 S. Y. LAU, W. F. HUGHES (Carnegie-Mellon University, Pittsburgh, PA), P. BASU (EG&G Sealol, Cranston, RI), and P. A. BEATTY (Vermont University, Burlington) (STLE, Annual Meeting, 44th, Atlanta, GA, May 1-4, 1989) STLE Tribology Transactions (ISSN 0569-8197), vol. 33, July 1990, p. 315-324. refs
 (Contract NAG3-166) Copyright

A simplified quasi-isothermal low-leakage laminar model for analyzing the stiffness and the stability characteristics of two-phase face seals with real fluids is developed. Sample calculations with this model for low-leakage operations are compared with calculations for high-leakage operations, performed using the adiabatic turbulent model of Beatty and Hughes (1987). It was found that the seal characteristics predicted using the two extreme models tend to overlap with each other, indicating that the simplified laminar model may be a useful tool for seal design. The effect of coning was investigated using the simplified model. The results show that, for the same balance, a coned seal has a higher leakage rate than a parallel face seal. I.S.

A90-42000* Mechanical Technology, Inc., Latham, NY.
ANALYSIS AND DESIGN OF HELIUM-BUFFERED FACE SEALS FOR THE SSME HIGH-PRESSURE OXYGEN TURBOPUMP
 WILBUR SHAPIRO (Mechanical Technology, Inc., Latham, NY) AIAA, SAE, ASME, and ASEE, Joint Propulsion Conference, 26th, Orlando, FL, July 16-18, 1990. 9 p. refs
 (Contract NAS3-24645) (AIAA PAPER 90-2049) Copyright

One form of a gas-buffered seal consists of two opposed fluid-film face seals, each mating against a single collar. The buffer fluid is introduced at the OD and flows through the radial clearances of each seal to opposite and separate environments at the IDs. This arrangement was investigated for the helium buffer seals applied to the oxidizer pump of the Space Shuttle Main Engine (SSME). A variety of face configurations were considered, and the self-energized-hydrostatic and spiral-groove geometries were selected for detailed evaluation. Fluid-film performance, dynamic response, and thermoelastic distortions were determined. Because of very high temperature gradients, distortions of the turbine-side seal ring were excessive. Otherwise, performance was excellent in all respects. Author

A90-42049* National Aeronautics and Space Administration. Lewis Research Center, Cleveland, OH.
SURFACE PITTING FATIGUE LIFE OF NONINVOLUTE, LOW-CONTACT-RATIO GEARS
 DENNIS P. TOWNSEND (NASA, Lewis Research Center, Cleveland, OH) AIAA, SAE, ASME, and ASEE, Joint Propulsion Conference, 26th, Orlando, FL, July 16-18, 1990. 8 p. Previously announced in STAR as N90-22790. refs
 (AIAA PAPER 90-2153) Copyright

Spur gear endurance tests were conducted to investigate the surface pitting fatigue life of noninvolute gears with low numbers of teeth and low contact ratios for use in advanced applications. The results were compared with those for a standard involute design with a low number of teeth. The gear pitch diameter was 8.89 cm (3.50 in.) with 12 teeth on both gear designs. Test conditions were an oil inlet temperature of 320 K (116 F), an oil outlet temperature of 350 K (170 F), a maximum Hertz stress of 1.49 GPa (216 ksi), and a speed of 10,000 rpm. The following results were obtained: the noninvolute gear had a surface pitting

fatigue life approximately 1.6 times that of the standard involute gear of a similar design; and the surface pitting fatigue life of the 3.43-pitch AISI 8620 noninvolute gear was approximately equal to the surface pitting fatigue life of an 8-pitch, 28-tooth AISI 9310 gear at the same load but at a considerably higher maximum Hertz stress. Author

A90-42165* Allied-Signal Aerospace Co., Phoenix, AZ.
DEVELOPMENT OF IMPACT DESIGN METHODS FOR CERAMIC GAS TURBINE COMPONENTS
 J. SONG, J. CUCCIO, and H. KINGTON (Allied-Signal Aerospace Co., Garrett Auxiliary Power Div., Phoenix, AZ) AIAA, SAE, ASME, and ASEE, Joint Propulsion Conference, 26th, Orlando, FL, July 16-18, 1990. 8 p. Research supported by DOE. refs
 (Contract DEN3-335) (AIAA PAPER 90-2413) Copyright

Impact damage prediction methods are being developed to aid in the design of ceramic gas turbine engine components with improved impact resistance. Two impact damage modes were characterized: local, near the impact site, and structural, usually fast fracture away from the impact site. Local damage to Si₃N₄ impacted by Si₃N₄ spherical projectiles consists of ring and/or radial cracks around the impact point. In a mechanistic model being developed, impact damage is characterized as microcrack nucleation and propagation. The extent of damage is measured as volume fraction of microcracks. Model capability is demonstrated by simulating late impact tests. Structural failure is caused by tensile stress during impact exceeding material strength. The EPIC3 code was successfully used to predict blade structural failures in different size particle impacts on radial and axial blades. Author

A90-46074* National Aeronautics and Space Administration. Lewis Research Center, Cleveland, OH.
OPTIMUM STRUCTURAL DESIGN OF ROBOTIC MANIPULATORS WITH FIBER REINFORCED COMPOSITE MATERIALS
 D. A. SARAVANOS (NASA, Lewis Research Center, Cleveland, OH) and J. S. LAMANCUSA (Pennsylvania State University, University Park) Computers and Structures (ISSN 0045-7949), vol. 36, no. 1, 1990, p. 119-132. refs
 (Contract N00024-85-C-6041) Copyright

High-speed robotic arms with advanced structural characteristics can be fabricated from optimally tailored fiber reinforced composites. An integrated design methodology is presented for the optimal structural synthesis of composite robotic manipulators. Optimum configurations of ply angles and ply thicknesses are predicted for maximum structural end-effector stiffness and maximum end-effector load carrying capacity, without altering the geometric dimensions of the links. Multiple posture finite element-based static performance criteria are implemented. A new finite element has been developed for the modeling of tubular composite links. Unique features are the inclusion of shear effects and coupling between stretching and flexure. Numerical solutions are obtained via an efficient optimization algorithm. Applications to an existing SCARA-class manipulator illustrate the effectiveness of the method and demonstrate the dramatic influence of the multi-postural design criteria on the optimal design. For a filament wound structure using a high strength carbon fiber in a thermoplastic matrix, the resultant optimum ply configurations have increased the specific stiffness and specific load capacity by factors of 1.5 and 16, respectively, in comparison to identically sized aluminum links. Author

A90-46222* National Aeronautics and Space Administration. Lewis Research Center, Cleveland, OH.
ACTIVE VIBRATION CONTROL FOR FLEXIBLE ROTOR BY OPTIMAL DIRECT-OUTPUT FEEDBACK CONTROL
 K. NONAMI, E. DIRUSSO, and D. P. FLEMING (NASA, Lewis Research Center, Cleveland, OH) IN: Rotating machinery dynamics; Proceedings of the Twelfth Annual ASME Conference on Mechanical Vibration and Noise, Montreal, Canada, Sept. 17-21,

37 MECHANICAL ENGINEERING

1989. New York, American Society of Mechanical Engineers, 1989, p. 327-333. Previously announced in STAR as N89-22605. refs Copyright

Experimental research tests were performed to actively control the rotor vibrations of a flexible rotor mounted on flexible bearing supports. The active control method used in the tests is called optimal direct-output feedback control. This method uses four electrodynamic actuators to apply control forces directly to the bearing housings in order to achieve effective vibration control of the rotor. The force actuators are controlled by an analog controller that accepts rotor displacement as input. The controller is programmed with experimentally determined feedback coefficients; the output is a control signal to the force actuators. The tests showed that this active control method reduced the rotor resonance peaks due to unbalance from approximately 250 microns down to approximately 25 microns (essentially runout level). The tests were conducted over a speed range from 0 to 10,000 rpm; the rotor system had nine critical speeds within this speed range. The method was effective in significantly reducing the rotor vibration for all of the vibration modes and critical speeds. Author

A90-46224* Arizona State Univ., Tempe.

AN ACTIVE OPTIMAL CONTROL STRATEGY OF ROTOR VIBRATIONS USING EXTERNAL FORCES

W. ZHU, I. CASTELAZO, and H. D. NELSON (Arizona State University, Tempe) IN: Rotating machinery dynamics; Proceedings of the Twelfth Biennial ASME Conference on Mechanical Vibration and Noise, Montreal, Canada, Sept. 17-21, 1989. New York, American Society of Mechanical Engineers, 1989, p. 351-359. refs

(Contract NAG3-580)

Copyright

An active control strategy for lateral rotor vibrations using external forces is proposed. An extended state observer is used to reconstruct the full states and the unbalance distribution. An optimal controller which accommodates persistent unbalance excitation is derived with feedback of estimated states and unbalances. Numerical simulations were conducted for two separate four degree of freedom rotor systems. These simulations indicated that the proposed strategy can achieve almost complete vibration cancellation. This was shown to be true even when the number of external control forces was less than the system order so long as coordinate coupling was present. Both steady state and transient response at a constant speed are presented. Author

A90-46226* Texas A&M Univ., College Station.

TEST AND THEORY FOR PIEZOELECTRIC ACTUATOR-ACTIVE VIBRATION CONTROL OF ROTATING MACHINERY

A. B. PALAZZOLO, R. R. LIN, R. M. ALEXANDER (Texas A & M University, College Station), A. F. KASCAK (NASA, Lewis Research Center; U.S. Army, Cleveland, OH), and J. MONTAGUE (Sverdrup Technology, Inc., Middleburg Heights, OH) IN: Rotating machinery dynamics; Proceedings of the Twelfth Biennial ASME Conference on Mechanical Vibration and Noise, Montreal, Canada, Sept. 17-21, 1989. New York, American Society of Mechanical Engineers, 1989, p. 367-374. Research supported by Texas A & M Turbomachinery Research Consortium. refs

(Contract NAG3-763)

Copyright

The application of piezoelectric actuators for active vibration control (AVC) of rotating machinery is examined. Theory is derived and the resulting predictions are shown to agree closely with results of tests performed on an air turbine driven-overhung rotor. The test results show significant reduction in unbalance, transient and sub-synchronous responses. Results from a 30-hour endurance test support the AVC system reliability. Various aspects of the electro-mechanical stability of the control system are also discussed and illustrated. Finally, application of the AVC system to an actual jet engine is discussed. Author

A90-46228* Southwest Research Inst., San Antonio, TX.

SPRAY AUTOMATED BALANCING OF ROTORS - HOW PROCESS PARAMETERS INFLUENCE PERFORMANCE

A. J. SMALLEY, R. M. BALDWIN (Southwest Research Institute, San Antonio, TX), D. P. FLEMING (NASA, Lewis Research Center, Cleveland, OH), and J. S. YUHAS (U.S. Army, Propulsion Directorate, Cleveland, OH) IN: Rotating machinery dynamics; Proceedings of the Twelfth Biennial ASME Conference on Mechanical Vibration and Noise, Montreal, Canada, Sept. 17-21, 1989. New York, American Society of Mechanical Engineers, 1989, p. 381-387. refs

Copyright

This paper addresses the application of spray-automated balancing of rotors, and the influence that various operating parameters will have on balancing performance. Spray-automated balancing uses the fuel-air repetitive explosion process to imbed short, discrete bursts of high velocity, high temperature powder into a rotating part at an angle selected to reduce unbalance of the part. The shortness of the burst, the delay in firing of the gun, the speed of the disk and the variability in speed all influence the accuracy and effectiveness of the automated balancing process. The paper evaluates this influence by developing an analytical framework and supplementing the analysis with empirical data obtained while firing the gun at a rotating disk. Encouraging results are obtained, and it is shown that the process should perform satisfactorily over a wide range of operating parameters. Further experimental results demonstrate the ability of the method to reduce vibration levels induced by mass unbalance in a rotating disk. Author

A90-46232* National Aeronautics and Space Administration. Lewis Research Center, Cleveland, OH.

ACTUATOR DESIGN FOR ROTOR CONTROL

H. ULBRICH and J. ALTHAUS (NASA, Lewis Research Center, Cleveland, OH; Muenchen, Technische Universitaet, Munich, Federal Republic of Germany) IN: Machinery dynamics - Applications and vibration control problems; Proceedings of the Twelfth Biennial ASME Conference on Mechanical Vibration and Noise, Montreal, Canada, Sept. 17-21, 1989. New York, American Society of Mechanical Engineers, 1989, p. 17-22. refs

Copyright

Active control of dynamical behavior of rotor systems involves the following modeling of the rotor system including active elements as a control process, positioning of actuators and sensors, implementation of problem-adapted control concepts. The key to attaining the desired influence on the dynamic behavior of rotor systems lies in the presence of suitable actuators. Some types of actuators (magnetic, electrohydraulic and piezoelectric) will be discussed and their respective drawbacks indicated. Their design will be outlined and functional correlations will be presented. Theoretical and experimental results demonstrate that an improvement of the system dynamics by the use of control forces is always possible. Author

A90-47209*# Case Western Reserve Univ., Cleveland, OH.

NUMERICAL MODELING OF FLOWS IN SIMULATED BRUSH SEAL CONFIGURATIONS

R. L. MULLEN (Case Western Reserve University, Cleveland, OH), M. J. BRAUN (Akron, University, OH), and R. C. HENDRICKS (NASA, Lewis Research Center, Cleveland, OH) AIAA, SAE, ASME, and ASSE, Joint Propulsion Conference, 26th, Orlando, FL, July 16-18, 1990. 5 p. refs

(AIAA PAPER 90-2141) Copyright

The two-dimensional flow field in a linear brush seal configuration is modeled and the flow field determined numerically using an FEM model consisting of a matrix of 6 x 6 uniformly spaced circular bristles with a uniform flow field upstream of the simulated brush element. Results from the numerical model are compared to earlier work for a circular seal of similar configuration. Temporal disturbance of the upstream flow field is studied to elucidate system dynamics; however, only the local velocity field is investigated. The effect of tangential flow at the upstream

boundary is also studied. Tangential flow produces changes in the pressure applied to the bristle but has little effect on the axial flow rates. Author

A90-47222* # Akron Univ., OH.

FLOW VISUALIZATION AND MOTION ANALYSIS FOR A SERIES OF FOUR SEQUENTIAL BRUSH SEALS

M. J. BRAUN, V. A. CANACCI (Akron, University, OH), and R. C. HENDRICKS (NASA, Lewis Research Center, Cleveland, OH) AIAA, SAE, ASME, and ASEE, Joint Propulsion Conference, 26th, Orlando, FL, July 16-18, 1990. 10 p.

(Contract NAG3-969)

(AIAA PAPER 90-2482) Copyright

Applying the Full Flow Field Tracking (FFFT) method, the flow patterns and the accompanying fluid velocities inside a series of brushes were nonintrusively determined and graphically reconstructed. The visualized flow field revealed regions that are characteristically river-jetting, vortical, and crossflow, and exist upstream, downstream, or within the seal. These flows are especially engendered by variations in fiber void that are spatial and temporal and affect changes in seal leakage and stability. The deformation of the upper half of each of the four sequential brushes as a function of upstream pressure and mass flow was determined. The axial pressure variation across the set of four brushes and the mass flow as a function of the pressure drops are also presented. Author

A90-47223* # National Aeronautics and Space Administration. Lewis Research Center, Cleveland, OH.

DEVELOPMENT OF A COMPACT, LIGHT WEIGHT MAGNETIC BEARING

CRAWFORD MEEKS (Advanced Controls Technology, Inc., Northridge, CA), ELISEO DIRUSSO, and GERALD V. BROWN (NASA, Lewis Research Center, Cleveland, OH) AIAA, SAE, ASME, and ASEE, Joint Propulsion Conference, 26th, Orlando, FL, July 16-18, 1990. 9 p. refs

(Contract NAS3-25572)

(AIAA PAPER 90-2483) Copyright

A compact, lightweight radial-load bearing has been devised with permanent magnet bias and actively controlled radial loading. The novel design uses permanent magnets to generate a coaxial magnetic field that energizes two radial air gaps. Two electromechanical stators modulate the airgap field in order to impart stability and control. Attention is given to the implementation of this design in an application involving operation at ambient and cryogenic temperatures at loads of up to 500 lbs. Stiffnesses of up to 17,500 N/mm have been obtained. O.C.

A90-47228* # Texas A&M Univ., College Station.

VIBRATION DAMPERS FOR CRYOGENIC TURBOMACHINERY

ALAN B. PALAZZOLO, EMMANUEL OLAN, AZMAN SYED IBRAHIM (Texas A & M University, College Station), and ALBERT F. KASCAK (NASA, Lewis Research Center, Cleveland, OH) AIAA, SAE, ASME, and ASEE, Joint Propulsion Conference, 26th, Orlando, FL, July 16-18, 1990. 10 p. refs

(AIAA PAPER 90-2740) Copyright

This paper describes the development of effective and reliable minimum-weight and minimum-envelope vibration dampers for cryogenic turbines. To meet this objective, a high speed test rig was designed and fabricated, which is currently used to test a curved beam type damper. The operation, capacity, structural characteristics, measurement system, and safety features of the cryogenic damper test rig are discussed. I.S.

A90-50644* # National Aeronautics and Space Administration. Lewis Research Center, Cleveland, OH.

EFFICIENCY STUDY COMPARING TWO HELICOPTER PLANETARY REDUCTION STAGES

TIMOTHY L. KRANTZ and ROBERT F. HANDSCHUH (NASA, Lewis Research Center; U.S. Army, Propulsion Directorate, Cleveland, OH) AIAA, SAE, ASME, and ASEE, Joint Propulsion Conference, 26th, July 16-18, 1990. 10 p. Previously announced

in STAR as N90-26334. refs
(AIAA PAPER 90-2156)

A study was conducted to compare the efficiency of two helicopter transmission planetary reduction stages. Experimental measurements and analytical predictions were made. The analysis predicted and experiments verified that one planetary stage was a more efficient design due to the type of planet bearing used in the stage. The effects of torque, speed, lubricant type, and lubricant temperature on planetary efficiency are discussed. Author

N90-10437* # Hamilton Standard, Windsor Locks, CT.

TWO STAGE GEAR TOOTH DYNAMICS PROGRAM Final Report

LINDA S. BOYD Aug. 1989 49 p

(Contract NAS3-25281)

(NASA-CR-185110; NAS 1.26:185110; AVSCOM-TM-89-C-003; HSER-12648; AD-A216002) Avail: NTIS HC A03/MF A01 CSDL 13/9

The epicyclic gear dynamics program was expanded to add the option of evaluating the tooth pair dynamics for two epicyclic gear stages with peripheral components. This was a practical extension to the program as multiple gear stages are often used for speed reduction, space, weight, and/or auxiliary units. The option was developed for either stage to be a basic planetary, star, single external-external mesh, or single external-internal mesh. The two stage system allows for modeling of the peripherals with an input mass and shaft, an output mass and shaft, and a connecting shaft. Execution of the initial test case indicated an instability in the solution with the tooth pair loads growing to excessive magnitudes. A procedure to trace the instability is recommended as well as a method of reducing the program's computation time by reducing the number of boundary condition iterations. Author

N90-12033* # Illinois Univ., Chicago. Dept. of Mechanical Engineering.

GENERATION AND TOOTH CONTACT ANALYSIS OF SPIRAL BEVEL GEARS WITH PREDESIGNED PARABOLIC FUNCTIONS OF TRANSMISSION ERRORS Final Report

FAYDOR L. LITVIN and HONG-TAO LEE Washington NASA Nov. 1989 215 p

(Contract NAG3-783; DA PROJ. 1L1-62209-A-47-A)

(NASA-CR-4259; E-4977; AVSCOM-TR-89-C-014; NAS 1.26:4259; AD-A217853) Avail: NTIS HC A10/MF A02 CSDL 13/9

A new approach for determination of machine-tool settings for spiral bevel gears is proposed. The proposed settings provide a predesigned parabolic function of transmission errors and the desired location and orientation of the bearing contact. The predesigned parabolic function of transmission errors is able to absorb piece-wise linear functions of transmission errors that are caused by the gear misalignment and reduce gear noise. The gears are face-milled by head cutters with conical surfaces or surfaces of revolution. A computer program for simulation of meshing, bearing contact and determination of transmission errors for misaligned gear has been developed. Author

N90-12936* # Ohio State Univ., Columbus. Dept. of Mechanical Engineering.

VIBRATION TRANSMISSION THROUGH ROLLING ELEMENT BEARINGS IN GEARED ROTOR SYSTEM, PART 1 Ph.D.

Thesis Final Report

RAJENDRA SINGH and TEIK CHIN LIM Dec. 1989 146 p

(Contract NAG3-773)

(NASA-CR-186093; NAS 1.26:186093) Avail: NTIS HC A07/MF A01 CSDL 13/9

A mathematical model is proposed to examine the vibration transmission through rolling element bearings in geared rotor systems. Current bearing models, based on either ideal boundary conditions for the shaft or purely translational stiffness element description, cannot explain how the vibratory motion may be transmitted from the rotating shaft to the casing. This study clarifies this issue qualitatively and quantitatively by developing a comprehensive bearing stiffness matrix of dimension 6 model for

37 MECHANICAL ENGINEERING

the precision rolling element bearings from basic principles. The proposed bearing formulation is extended to analyze the overall geared rotor system dynamics including casing and mounts. The bearing stiffness matrix is included in discrete system models using lumped parameter and/or dynamic finite element techniques. Eigensolution and forced harmonic response due to rotating mass unbalance or kinematic transmission error excitation for a number of examples are computed.

Author

N90-13785* National Aeronautics and Space Administration. Lewis Research Center, Cleveland, OH.

AN INVESTIGATION OF GEAR MESH FAILURE PREDICTION TECHNIQUES M.S. Thesis - Cleveland State Univ.

JAMES J. ZAKRAJSEK Nov. 1989 100 p Prepared in cooperation with Army Aviation Systems Command, Cleveland, OH

(Contract DA PROJ. 1L1-62209-A4-7A)

(NASA-TM-102340; E-5049; NAS 1.15:102340;

AVSCOM-TM-89-C-005; AD-A217844) Avail: NTIS HC A05/MF A01 CSCL 13/9

A study was performed in which several gear failure prediction methods were investigated and applied to experimental data from a gear fatigue test apparatus. The primary objective was to provide a baseline understanding of the prediction methods and to evaluate their diagnostic capabilities. The methods investigated use the signal average in both the time and frequency domain to detect gear failure. Data from eleven gear fatigue tests were recorded at periodic time intervals as the gears were run from initiation to failure. Four major failure modes, consisting of heavy wear, tooth breakage, single pits, and distributed pitting were observed among the failed gears. Results show that the prediction methods were able to detect only those gear failures which involved heavy wear or distributed pitting. None of the methods could predict fatigue cracks, which resulted in tooth breakage, or single pits. It is suspected that the fatigue cracks were not detected because of limitations in data acquisition rather than in methodology. Additionally, the frequency response between the gear shaft and the transducer was found to significantly affect the vibration signal. The specific frequencies affected were filtered out of the signal average prior to application of the methods.

Author

N90-13786* National Aeronautics and Space Administration. Lewis Research Center, Cleveland, OH.

ELASTICITY EFFECTS ON CAVITATION IN A SQUEEZE FILM DAMPER UNDERGOING NONCENTERED CIRCULAR WHIRL

DAVID E. BREWE (Army Aviation Research and Development Command, Cleveland, OH.) 1988 20 p Presented at the Nordic Symposium on Tribology, Trondheim, Norway, 26-29 Jun. 1988; sponsored by Wear Magazine

(Contract DA PROJ. 1L1-61102-AH-45)

(NASA-TM-102392; E-4224; NAS 1.15:102392;

AVSCOM-TM-89-C-012; AD-A217846) Avail: NTIS HC A03/MF A01 CSCL 13/9

Elasticity of the liner and its effects on cavitation were numerically determined for a squeeze film damper subjected to dynamic loading. The loading was manifested as a prescribed motion of the rotor undergoing noncentered circular whirl. The boundary conditions were implemented using Elrod's algorithm which conserves lineal mass flux through the moving cavitation bubble as well as the oil film region of the damper. Computational movies were used to analyze the rapidly changing pressures and vapor bubble dynamics throughout the dynamic cycle for various flexibilities in the damper liner. The effects of liner elasticity on cavitation were only noticeable for the intermediate and high values of viscosity used in this study.

Author

N90-13794* Teledyne Brown Engineering, Huntsville, AL. **USER NEEDS, BENEFITS, AND INTEGRATION OF ROBOTIC SYSTEMS IN A SPACE STATION LABORATORY Final Report, Oct. 1987 - Oct. 1989**

W. R. DODD, M. B. BADGLEY, and C. R. KONKEL Oct. 1989 78 p

(Contract NAS3-25278)

(NASA-CR-185150; NAS 1.26:185150; TBE-SSD-P601-89-191)

Avail: NTIS HC A05/MF A01 CSCL 13/9

The methodology, results and conclusions of all tasks of the User Needs, Benefits, and Integration Study (UNBIS) of Robotic Systems in a Space Station Laboratory are summarized. Study goals included the determination of user requirements for robotics within the Space Station, United States Laboratory. In Task 1, three experiments were selected to determine user needs and to allow detailed investigation of microgravity requirements. In Task 2, a NASTRAN analysis of Space Station response to robotic disturbances, and acceleration measurement of a standard industrial robot (Intellex Model 660) resulted in selection of two ranges of microgravity manipulation: Level 1 (10-3 to 10-5 G at greater than 1 Hz) and Level 2 (less than equal 10-6 G at 0.1 Hz). This task included an evaluation of microstepping methods for controlling stepper motors and concluded that an industrial robot actuator can perform milli-G motion without modification. Relative merits of end-effectors and manipulators were studied in Task 3 in order to determine their ability to perform a range of tasks related to the three microgravity experiments. An Effectivity Rating was established for evaluating these robotic system capabilities. Preliminary interface requirements for an orbital flight demonstration were determined in Task 4. Task 5 assessed the impact of robotics.

Author

N90-13797* National Aeronautics and Space Administration. Lewis Research Center, Cleveland, OH.

LIQUID WATER CONTENT AND DROPLET SIZE CALIBRATION OF THE NASA LEWIS ICING RESEARCH TUNNEL

ROBERT F. IDE (Army Aviation Research and Development Command, Cleveland, OH.) 1989 28 p Presented at the 28th Aerospace Sciences Meeting, Reno, NV, 8-11 Jan. 1990; sponsored by AIAA Prepared in cooperation with Army Aviation Research and Development Command, Cleveland, OH

(Contract DA PROJ. 1L1-62209-A47-A)

(NASA-TM-102447; E-5231; NAS 1.15:102447;

AVSCOM-TM-89-C-014; AIAA-90-0669) Avail: NTIS HC A03/MF A01 CSCL 14/2

The icing research tunnel at the NASA Lewis Research Center underwent a major rehabilitation in 1986 to 1987, necessitating recalibration of the icing cloud. The methods used in the recalibration, including the procedure used to establish a uniform icing cloud and the use of a standard icing blade technique for measurement of liquid water content are described. PMS Forward Scattering Spectrometer and Optical Array probes were used for measurement of droplet size. Examples of droplet size distributions are shown for several median volumetric diameters. Finally, the liquid water content/droplet size operating envelopes of the icing tunnel are shown for a range of airspeeds and are compared to the FAA icing certification criteria.

Author

N90-14617* National Aeronautics and Space Administration. Lewis Research Center, Cleveland, OH.

COMPARISON OF TWO DROPLET SIZING SYSTEMS IN AN ICING WIND TUNNEL

J. R. OLDENBURG and R. F. IDE (Army Aviation Systems Command, Cleveland, OH.) 1990 19 p Presented at the 28th Aerospace Sciences Meeting, Reno, NV, 8-11 Jan. 1990; sponsored by AIAA

(Contract DA PROJ. 1L1-62209-A4-7A)

(NASA-TM-102456; E-5240; NAS 1.15:102456;

AVSCOM-TM-89-C-015; AIAA-90-0668) Avail: NTIS HC A03/MF A01 CSCL 13/2

A comparison between the Phase Doppler Analyzer and the combined measurements from the Particle Measuring Systems Forward Scattering Spectrometer Probe and the Optical Array Probe was conducted in an icing wind tunnel using NASA Icing Research Tunnel spray nozzles to produce the icing cloud. Clouds with a range of volume median diameters from 10 to greater than 50 microns were used for the instrument comparisons. A comparison of the volume median diameter from the Phase Doppler

Particle Analyzer and only the Forward Scattering Spectrometer Probe indicated agreement up to 18 microns. A combined volume median diameter was calculated from the droplet distribution of the Optical Array Probe and the Forward Scattering Spectrometer Probe. A comparison of the combined volume median diameters and the Phase Doppler Particle Analyzer volume median diameters showed agreement up to 30 microns with the agreement deteriorating rapidly above 30 microns. Droplet distributions from the Phase Doppler Particle Analyzer, the Forward Scattering Spectrometer Probe, and Optical Array Probe are presented.

Author

N90-15434*# Cincinnati Univ., OH. Dept. of Mechanical and Industrial Engineering.

MESH REFINEMENT IN FINITE ELEMENT ANALYSIS BY MINIMIZATION OF THE STIFFNESS MATRIX TRACE Final Report

MADAN G. KITTUR and RONALD L. HUSTON Nov. 1989 108 p Prepared in cooperation with Army Aviation Systems Command, Cleveland, OH
(Contract NSG-3188; DA PROJ. 1L1-62209-A-47-A)
(NASA-CR-185170; USAAVSCOM-TR-89-C-019; NAS 1.26:185170; AD-A219303) Avail: NTIS HC A06/MF A01 CSCL 13/9

Most finite element packages provide means to generate meshes automatically. However, the user is usually confronted with the problem of not knowing whether the mesh generated is appropriate for the problem at hand. Since the accuracy of the finite element results is mesh dependent, mesh selection forms a very important step in the analysis. Indeed, in accurate analyses, meshes need to be refined or rezoned until the solution converges to a value so that the error is below a predetermined tolerance. A-posteriori methods use error indicators, developed by using the theory of interpolation and approximation theory, for mesh refinements. Some use other criterions, such as strain energy density variation and stress contours for example, to obtain near optimal meshes. Although these methods are adaptive, they are expensive. Alternatively, a priori methods, until now available, use geometrical parameters, for example, element aspect ratio. Therefore, they are not adaptive by nature. An adaptive a-priori method is developed. The criterion is that the minimization of the trace of the stiffness matrix with respect to the nodal coordinates, leads to a minimization of the potential energy, and as a consequence provide a good starting mesh. In a few examples the method is shown to provide the optimal mesh. The method is also shown to be relatively simple and amenable to development of computer algorithms. When the procedure is used in conjunction with a-posteriori methods of grid refinement, it is shown that fewer refinement iterations and fewer degrees of freedom are required for convergence as opposed to when the procedure is not used. The mesh obtained is shown to have uniform distribution of stiffness among the nodes and elements which, as a consequence, leads to uniform error distribution. Thus the mesh obtained meets the optimality criterion of uniform error distribution.

Author

N90-15444*# National Aeronautics and Space Administration. Lewis Research Center, Cleveland, OH.

HIGH TEMPERATURE, FLEXIBLE, THERMAL BARRIER SEAL Patent Application

PAUL J. SIROCKY and BRUCE M. STEINETZ 27 Nov. 1989 13 p
(NASA-CASE-LEW-14672-1; NAS 1.71:LEW-14672-1; US-PATENT-APPL-SN-441672) Avail: NTIS HC A03/MF A01 CSCL 11/1

This device seals the sliding interfaces between structural panels that are roughly perpendicular to each other or whose edges are butted against one another. The nonuniformity of the gap between the panels requires significant flexibility along the seal length. The seal is mounted in a rectangular groove in a moveable structural panel. A plurality of particles or balls is densely packed in an outer sheathing. The balls are laterally preloaded to maintain sealing contact with the adjacent wall using a pressurized linear bellows. Distortions in the adjacent panel are accommodated

by rearrangement of the particles within the outer sheathing. Leakage through the seal is minimized by densely compacting the internal particles and by maintaining positive preload along the back side of the seal. The braid architecture of the outer sheathing is selected to minimize leakage through the seal and to resist mechanical abrasion.

NASA

N90-15445*# National Aeronautics and Space Administration. Lewis Research Center, Cleveland, OH.

FULLY ARTICULATED FOUR-POINT-BEND LOADING FIXTURE Patent Application

ANTHONY M. CALOMINO, inventor (to NASA) 28 Dec. 1989 11 p
(NASA-CASE-LEW-14776-1; US-PATENT-APPL-SN-458274; NAS 1.71:LEW-14776-1) Avail: NTIS HC A03/MF A01 CSCL 13/9

A fully articulated four-point bend loading fixture for Modulus of Rupture (MOR) and fracture toughness specimens utilizes an upper loading plate in combination with a lower loading plate. The lower plate has a pair of spring loaded ball bearings which seat in V-shaped grooves located in the upper plate. The ball bearings are carried in the arms of the lower plate. A load is applied to the specimen through steel rollers, one large roller and one smaller roller each located on both the upper and lower plates. The large rollers have needle roller bearings which enable a single loading roller to rotate relative to the plate to which it is attached.

NASA

N90-15447*# Carnegie-Mellon Univ., Pittsburgh, PA. The Robotics Inst.

BASE REACTION OPTIMIZATION OF REDUNDANT MANIPULATORS FOR SPACE APPLICATIONS

C. L. CHUNG, S. DE SA, and C. W. DESILVA (British Columbia Univ., Vancouver.) 1988 32 p
(Contract NAG3-811)

(NASA-CR-186274; NAS 1.26:186274; CMU-RI-TR-88-17)

Copyright Avail: NTIS HC A03/MF A01 CSCL 13/9

One of the problems associated with redundant manipulators which were proposed for space applications is that the reactions transmitted to the base of the manipulator as a result of the motion of the manipulator will cause undesirable effects on the dynamic behavior of the supporting space structure. It is therefore necessary to minimize the magnitudes of the forces and moments transmitted to the base. It is shown that kinematic redundancy can be used to solve the dynamic problem of minimizing the magnitude of the base reactions. The methodology described is applied to a four degree-of-freedom spatial manipulator with one redundant degree-of-freedom.

Author

N90-16286*# National Aeronautics and Space Administration. Lewis Research Center, Cleveland, OH.

DYNAMIC ANALYSIS OF GEARED ROTORS BY FINITE ELEMENTS

AHMET KAHRAMAN, H. NEVZAT OZGUVEN, DONALD R. HOUSER (Ohio State Univ., Columbus.), and JAMES J. ZAKRAJSEK Jan. 1990 22 p Prepared in cooperation with Army Aviation Systems Command, Cleveland, OH
(Contract NAG3-773; DA PROJ. 1L1-62209-A4-7A)
(NASA-TM-102349; E-5058; NAS 1.15:102349; AVSCOM-TM-89-C-006) Avail: NTIS HC A03/MF A01 CSCL 13/9

A finite-element model of a geared rotor system on flexible bearings was developed. The model includes the rotary inertia of shaft elements, the axial loading on shafts, flexibility and damping of bearings, material damping of shafts and the stiffness and the damping of gear mesh. The coupling between the torsional and transverse vibrations of gears were considered in the model. A constant mesh stiffness was assumed. The analysis procedure can be used for forced vibration analysis of geared rotors by calculating the critical speeds and determining the response of any point on the shaft to mass unbalances, geometric eccentricities of gears and displacement transmission error excitation at the mesh point. The dynamic mesh forces due to these excitations can also be calculated. The model has been applied to several

37 MECHANICAL ENGINEERING

systems for the demonstration of its accuracy and for studying the effect of bearing compliances on system dynamics. Author

N90-17147*# National Aeronautics and Space Administration. Lewis Research Center, Cleveland, OH.

COMPARISON OF DROP SIZE DISTRIBUTIONS FROM TWO DROPLET SIZING SYSTEMS

JOHN R. OLDENBURG and ROBERT F. IDE (Army Aviation Research and Development Command, Cleveland, OH.) 1990 18 p Presented at the 2nd International Congress on Optical Particle Sizing, Phoenix, AZ, 5-9 Mar. 1990; sponsored by Arizona State Univ. and NSF Prepared in cooperation with Army Aviation Research and Development Command, Cleveland, OH (Contract DA PROJ. 1L1-62209-AH-47A) (NASA-TM-102520; E-5324; NAS 1.15:102520; AVSCOM-TM-90-C-001; AD-A221523) Avail: NTIS HC A03/MF A01 CSCL 13/9

A comparison between the Phase Doppler Particle Analyzer and the combined measurements from Particle Measuring Systems' Forward Scattering Spectrometer Probe and the Optical Array Probe was conducted in an icing wind tunnel using NASA Icing Research Tunnel spray nozzles to produce the supercooled water droplet cloud. Clouds having a range of volume median diameters from 10 to greater than 50 microns were used for the instrument comparisons. A volume median diameter was calculated from combining the droplet distributions of the Optical Array Probe and the Forward Scattering Spectrometer Probe. A comparison of the combined volume median diameters and the Phase Doppler Particle Analyzer volume median diameters showed agreement from 10 microns up to 30 microns. Typical drop size distributions from the Phase Doppler Particle Analyzer, the Forward Scattering Spectrometer Probe, and Optical Array Probe are presented for several median volume diameters. A comparison of the distributions illustrates regions of the distributions where there is good agreement and other regions where there are discrepancies between the Phase Doppler Particle Analyzer and the Particle Measuring Systems' droplet size instruments. Author

N90-18041*# National Aeronautics and Space Administration. Lewis Research Center, Cleveland, OH.

GEAR NOISE, VIBRATION, AND DIAGNOSTIC STUDIES AT NASA LEWIS RESEARCH CENTER

JAMES J. ZAKRAJSEK, FRED B. OSWALD, DENNIS P. TOWNSEND, and JOHN J. COY 1990 10 p Prepared for presentation at the 1st International Conference on Gear Box Noise and Vibration, Cambridge, England, 10-11 Apr. 1990; sponsored by the Institution of Mechanical Engineers (Contract DA PROJ. 1L1-62209-A4-7A) (NASA-TM-102435; E-5204; NAS 1.15:102435; AVSCOM-TR-89-C-020) Avail: NTIS HC A02/MF A01 CSCL 13/9

The NASA Lewis Research Center and the U.S. Army Aviation Systems Command are involved in a joint research program to advance the technology of rotorcraft transmissions. This program consists of analytical as well as experimental efforts to achieve the overall goals of reducing weight, noise, and vibration, while increasing life and reliability. Recent analytical activities are highlighted in the areas of gear noise, vibration, and diagnostics performed in-house and through NASA and U.S. Army sponsored grants and contracts. These activities include studies of gear tooth profiles to reduce transmission error and vibration as well as gear housing and rotordynamic modeling to reduce structural vibration transmission and noise radiation, and basic research into current gear failure diagnostic methodologies. Results of these activities are presented along with an overview of near term research plans in the gear noise, vibration, and diagnostics area. Author

N90-18740*# National Aeronautics and Space Administration. Lewis Research Center, Cleveland, OH.

FASTENER DESIGN MANUAL

RICHARD T. BARRETT Mar. 1990 99 p (NASA-RP-1228; E-4911; NAS 1.61:1228) Avail: NTIS HC A05/MF A01 CSCL 13/11

This manual was written for design engineers to enable them to choose appropriate fasteners for their designs. Subject matter includes fastener material selection, platings, lubricants, corrosion, locking methods, washers, inserts, thread types and classes, fatigue loading, and fastener torque. A section on design criteria covers the derivation of torque formulas, loads on a fastener group, combining simultaneous shear and tension loads, pullout load for tapped holes, grip length, head styles, and fastener strengths. The second half of this manual presents general guidelines and selection criteria for rivets and lockbolts. Author

N90-19593*# Illinois Univ., Chicago. Dept. of Mechanical Engineering.

THEORY OF GEARING

FAYDOR L. LITVIN 1989 479 p Prepared in cooperation with Army Aviation Systems Command, Cleveland, OH (Contract NAG3-783; NAG3-655; DA PROJ. 1L1-62209-AH-76) (NASA-RP-1212; E-2641; NAS 1.61:1212; AVSCOM-TR-88-C-035; L-89-600204) Avail: NTIS HC A21/MF A03; Also Avail: SOD HC \$40.00 as 033-000-01068-1 CSCL 13/9

Basic mathematical problems on the theory of gearing are covered in this book, such as the necessary and sufficient conditions of envelope existence, relations between principal curvatures and directions for surfaces of mating gears. Also included are singularities of surfaces accompanied by undercutting the process of generation, the phenomena of envelope of lines of contact, and the principles for generation of conjugate surfaces. Special attention is given to the algorithms for computer aided simulation of meshing and tooth contact. This edition was complemented with the results of research recently performed by the author and his doctoral students. The book contains sample problems and also problems for the reader to solve. K.C.D.

N90-20391*# National Aeronautics and Space Administration. Lewis Research Center, Cleveland, OH.

BEARING AND GEAR STEELS FOR AEROSPACE APPLICATIONS

ERWIN V. ZARETSKY Mar. 1990 30 p Submitted for publication (NASA-TM-102529; E-5300; NAS 1.15:102529) Avail: NTIS HC A03/MF A01 CSCL 13/9

Research in metallurgy and processing for bearing and gear steels has resulted in improvements in rolling-element bearing and gear life for aerospace application by a factor of approximately 200 over that obtained in the early 1940's. The selection and specification of a bearing or gear steel is dependent on the integration of multiple metallurgical and physical variables. For most aerospace bearings, through-hardened VIM-VAR AISI M-50 steel is the material of preference. For gears, the preferential material is case-carburized VAR AISI 9310. However, the VAR processing for this material is being replaced by VIM-VAR processing. Since case-carburized VIM-VAR M-50NiL incorporates the desirable qualities of both the AISI M-50 and AISI 9310 materials, optimal life and reliability can be achieved in both bearings and gears with a single steel. Hence, this material offers the promise of a common steel for both bearings and gears for future aerospace applications. Author

N90-20392*# National Aeronautics and Space Administration. Lewis Research Center, Cleveland, OH.

AN APPLICATIONAL PROCESS FOR DYNAMIC BALANCING OF TURBOMACHINERY SHAFTING

VINCENT G. VERHOFF Mar. 1990 36 p (NASA-TM-102537; E-4768; NAS 1.15:102537) Avail: NTIS HC A03/MF A01 CSCL 13/9

The NASA Lewis Research Center has developed and implemented a time-efficient methodology for dynamically balancing turbomachinery shafting. This methodology minimizes costly facility downtime by using a balancing arbor (mandrel) that simulates the turbomachinery (rig) shafting. The need for precision dynamic balancing of turbomachinery shafting and for a dynamic balancing methodology is discussed in detail. Additionally, the inherent problems (and their causes and effects) associated with unbalanced

turbomachinery shafting as a function of increasing shaft rotational speeds are discussed. Included are the design criteria concerning rotor weight differentials for rotors made of different materials that have similar parameters and shafting. The balancing methodology for applications where rotor replaceability is a requirement is also covered. This report is intended for use as a reference when designing, fabricating, and troubleshooting turbomachinery shafting. Author

N90-20393*# National Aeronautics and Space Administration. Lewis Research Center, Cleveland, OH.

ELECTRON BEAM INDUCED DAMAGE IN PECVD Si₃N₄ AND SiO₂ FILMS ON INP

DRAGAN M. PANTIC, VIK J. KAPOOR, PAUL G. YOUNG (Cincinnati Univ., OH.), WALLACE D. WILLIAMS, and JOHN E. DICKMAN Mar. 1990 17 p Presented at the Dielectric Films on Compound Semiconductors Symposium, Honolulu, HI, 18-23 Oct. 1987; sponsored by The Electrochemical Society (NASA-TM-102544; E-5356; NAS 1.15:102544) Avail: NTIS HC A03/MF A01 CSCL 13/9

Phosphorus rich plasma enhanced chemical vapor deposition (PECVD) of silicon nitride and silicon dioxide films on n-type indium phosphide (InP) substrates were exposed to electron beam irradiation in the 5 to 40 keV range for the purpose of characterizing the damage induced in the dielectric. The electron beam exposure was on the range of 10(exp -7) to 10(exp -3) C/sq cm. The damage to the devices was characterized by capacitance-voltage (C-V) measurements of the metal insulator semiconductor (MIS) capacitors. These results were compared to results obtained for radiation damage of thermal silicon dioxide on silicon (Si) MOS capacitors with similar exposures. The radiation induced damage in the PECVD silicon nitride films on InP was successfully annealed out in an hydrogen/nitrogen (H₂/N₂) ambient at 400 C for 15 min. The PECVD silicon dioxide films on InP had the least radiation damage, while the thermal silicon dioxide films on Si had the most radiation damage. Author

N90-21387*# Ohio State Univ., Columbus. Dept. of Mechanical Engineering.

A REVIEW OF GEAR HOUSING DYNAMICS AND ACOUSTICS LITERATURE Interim Report

TEIK CHIN LIM and RAJENDRA SINGH Oct. 1989 85 p (Contract NAG3-773; DA PROJ. 1L1-62209-A47-A) (NASA-CR-185148; NAS 1.26:185148; AVSCOM-TM-89-C-009) Avail: NTIS HC A05/MF A01 CSCL 13/9

A review of the available literature on gear housing vibration and noise radiation is presented. Analytical and experimental methodologies used for bearing dynamics, housing vibration and noise, mounts and suspensions, and the overall gear and housing system are discussed. Typical design guidelines, as outlined by various investigators, are also included. Results of this review indicate that although many attempts were made to characterize the dynamics of gearbox system components, no comprehensive set of design criteria currently exist. Moreover, the literature contains conflicting reports concerning relevant design guidelines. Author

N90-21394*# National Aeronautics and Space Administration. Lewis Research Center, Cleveland, OH.

TRANSMISSION RESEARCH ACTIVITIES AT NASA LEWIS RESEARCH CENTER

D. G. LEWICKI 1990 31 p Presented at the Helicopter Transmission Design and Maintenance Workshop, Quebec City, Quebec, 21-25 May 1990; sponsored by Canadian Department of National Defense Prepared in cooperation with Army Aviation Systems Command, Cleveland, OH (Contract DA PROJ. 1L1-2211-A-47-A) (NASA-TM-103132; E-5469; NAS 1.15:103132; AVSCOM-TM-90-C-006; AD-A224967) Avail: NTIS HC A03/MF A01 CSCL 13/9

A joint research program, to advance the technology of rotorcraft transmissions, consists of analytical and experimental efforts to achieve the overall goals of reducing transmission weight

and noise, while increasing life and reliability. Recent activities in the areas of transmission and related component research are highlighted. Current areas include specific technologies in support of military rotary wing aviation, gearing technology, transmission noise reduction studies, a recent interest in gearbox diagnostics, and advanced transmission system studies. Results of recent activities are presented along with near term research plans. Author

N90-22041*# National Aeronautics and Space Administration. Lewis Research Center, Cleveland, OH.

BEARING ELASTOHYDRODYNAMIC LUBRICATION: A COMPLEX CALCULATION MADE SIMPLE

ERWIN V. ZARETSKY Apr. 1990 11 p (NASA-TM-102575; E-5360; NAS 1.15:102575) Avail: NTIS HC A03/MF A01 CSCL 11/8

The lubricant elastohydrodynamic (EHD) film thickness formula is reduced to a simplified form whereby only the rolling-element bearing inside and outside diameters and speed (in revolutions per minute) and the lubricant type and viscosity (in centipoise) at temperature are required for its use. Additionally, a graph is provided for the first time that is based upon experimental data giving an EHD film reduction factor as a function of contact lubricant flow number. This reduction factor accounts for lubricant starvation within the Hertzian contact. A graph relating the ratio of minimum film thickness to composite surface roughness and a lubrication-life correction factor is also provided. The life correction factor is used to determine resultant bearing life. Author

N90-22054*# National Aeronautics and Space Administration. Lewis Research Center, Cleveland, OH.

COMPUTERIZED INSPECTION OF GEAR TOOTH SURFACES

FAYDOR L. LITVIN, ZHANG YI, JONATHAN KIEFFER, ROBERT F. HANDSCHUH (Army Research and Technology Labs., Cleveland, OH.), and JOHN J. COY 1989 18 p Presented at the SIAM Conference on Geometric Design, Tempe, AZ, 6-10 Nov. 1989 (Contract DA PROJ. 1L1-62209-AH-47-A) (NASA-TM-102395; E-5113; NAS 1.15:102395; AVSCOM-TR-89-C-011) Avail: NTIS HC A03/MF A01 CSCL 13/9

An approach is proposed that uses coordinate measurements of the real surface of spiral bevel gears to determine the actual machine tool setting applied during the gear manufacturing process. The deviations of the real surface from the theoretical one are also determined. Adjustments are then applied by machine tool corrections to minimize these surface deviations. This is accomplished by representing the real surface analytically in the same Gaussian coordinates as the theoretical surface. Author

N90-22790*# National Aeronautics and Space Administration. Lewis Research Center, Cleveland, OH.

SURFACE PITTING FATIGUE LIFE OF NONINVOLUTE, LOW-CONTACT-RATIO GEARS

DENNIS P. TOWNSEND 1990 9 p Presented at the 26th Joint Propulsion Conference, Orlando, FL, 16-18 Jul. 1990; cosponsored by AIAA, SAE, ASME, and ASCE (Contract DA PROJ. 1L1-62209-A4-7A) (NASA-TM-103116; E-5440; NAS 1.15:103116; AVSCOM-TM-90-C-008; AIAA-90-2153) Avail: NTIS HC A02/MF A01 CSCL 13/9

Spur gear endurance tests were conducted to investigate the surface pitting fatigue life of noninvolute gears with low numbers of teeth and low contact ratios for use in advanced applications. The results were compared with those for a standard involute design with a low number of teeth. The gear pitch diameter was 8.89 cm (3.50 in.) with 12 teeth on both gear designs. Test conditions were an oil inlet temperature of 320 K (116 F), an oil outlet temperature of 350 K (170 F), a maximum Hertz stress of 1.49 GPa (216 ksi), and a speed of 10 000 rpm. The following results were obtained: the noninvolute gear had a surface pitting fatigue life approximately 1.6 times that of the standard involute gear of a similar design; and the surface pitting fatigue life of the

37 MECHANICAL ENGINEERING

3.43-pitch AISI 8620 noninvolute gear was approximately equal to the surface pitting fatigue life of an 8-pitch, 28-tooth AISI 9310 gear at the same load but at a considerably higher maximum Hertz stress.

Author

N90-22796*# National Aeronautics and Space Administration. Lewis Research Center, Cleveland, OH.

INFLUENCE OF LINEAR PROFILE MODIFICATION AND LOADING CONDITIONS ON THE DYNAMIC TOOTH LOAD AND STRESS OF HIGH CONTACT RATIO GEARS

CHINWAI LEE, HSIANG HSI LIN (Memphis State Univ., TN.), FRED B. OSWALD, and DENNIS P. TOWNSEND 1990 13 p Prepared for presentation at the ASME Mechanism Conference, Chicago, IL, 16-19 Sep. 1990 Prepared in cooperation with Army Aviation Systems Command, Cleveland, OH (NASA-TM-103136; E-5384; NAS 1.15:103136; AVSCOM-TM-90-C-004; AD-A224492) Avail: NTIS HC A03/MF A01 CSCL 13/9

A computer simulation for the dynamic response of high-contact-ratio spur gear transmissions is presented. High contact ratio gears have the potential to produce lower dynamic tooth loads and minimum root stress but they can be sensitive to tooth profile errors. The analysis presented examines various profile modifications under realistic loading conditions. The effect of these modifications on the dynamic load (force) between mating gear teeth and the dynamic root stress is presented. Since the contact stress is dependent on the dynamic load, minimizing dynamic loads will also minimize contact stresses. It is shown that the combination of profile modification and the applied load (torque) carried by a gear system has a significant influence on gear dynamics. The ideal modification at one value of applied load will not be the best solution for a different load. High-contact-ratio gears were found to require less modification than standard low-contact-ratio gears. High-contact-ratio gears are more adversely affected by excess modification than by under modification. In addition, the optimal profile modification required to minimize the dynamic load (hence the contact stress) on a gear tooth differs from the optimal modification required to minimize the dynamic root (bending) stress. Computer simulation can help find the design tradeoffs to determine the best profile modification to satisfy the conflicting constraints of minimizing both the load and root stress in gears which must operate over a range of applied loads.

Author

N90-23732*# Ohio State Univ., Columbus. Dept. of Mechanical Engineering.

NON-LINEAR DYNAMIC ANALYSIS OF GEARED SYSTEMS, PART 2 Final Report

RAJENDRA SINGH, DONALD R. HOUSER, and AHMET KAHRAMAN Feb. 1990 263 p (Contract NAG3-773)

(NASA-CR-180495; NAS 1.26:180495) Avail: NTIS HC A12/MF A02 CSCL 13/9

A good understanding of the steady state dynamic behavior of a geared system is required in order to design reliable and quiet transmissions. This study focuses on a system containing a spur gear pair with backlash and periodically time-varying mesh stiffness, and rolling element bearings with clearance type non-linearities. A dynamic finite element model of the linear time-invariant (LTI) system is developed. Effects of several system parameters, such as torsional and transverse flexibilities of the shafts and prime mover/load inertias, on free and forced vibration characteristics are investigated. Several reduced order LTI models are developed and validated by comparing their eigen solution with the finite element model results. Several key system parameters such as mean load and damping ratio are identified and their effects on the non-linear frequency response are evaluated quantitatively. Other fundamental issues such as the dynamic coupling between non-linear modes, dynamic interactions between component non-linearities and time-varying mesh stiffness, and the existence of subharmonic and chaotic solutions including routes to chaos have also been examined in depth.

Author

N90-23751* National Aeronautics and Space Administration. Lewis Research Center, Cleveland, OH.

HIGH TEMPERATURE FLEXIBLE SEAL Patent

BRUCE M. STEINETZ, inventor (to NASA) and PAUL J. SIROCKY, inventor (to NASA) 17 Apr. 1990 9 p Filed 30 Dec. 1988 Supersedes N89-28830 (27 - 23, p 3301)

(NASA-CASE-LEW-14695-1; US-PATENT-4,917,302;

US-PATENT-APPL-SN-292146; US-PATENT-CLASS-239-265.11;

US-PATENT-CLASS-277-34; US-PATENT-CLASS-277-158;

INT-PATENT-CLASS-B64D-33/04;

INT-PATENT-CLASS-F16J-15/46) Avail: US Patent and

Trademark Office CSCL 11/1

This device is concerned with sealing the sliding interfaces between structural panels that are roughly perpendicular to each other or whose edges are butted against one another. The gap which the seal element must seal is not uniform along the seal length requiring significant seal flexibility. The seal is mounted in a rectangular groove in a moveable structural panel. The seal comprises a plurality of rectangular shaped wafers stacked next to one another and preloaded in the axial direction to minimize leakage between wafers. The wafers are laterally preloaded to maintain sealing contact along the wafer faces which engage the adjacent wall of a sidewall using one of several approaches, such as the pressurized linear bellows. The seal accommodates distortions in the adjacent panel by relative sliding between adjacent wafers. Leakage between wafers is further minimized with good wafer surface finishes. Leakage between the seal nose and the adjacent structural panel is minimized when sealing against a distorted sidewall with relatively thin wafers and suitable seal preload apparatus. Leakage behind the seal is minimized with good groove tolerances and good sealing contact between the preload system and the back of the peripheral edge of the wafers. Official Gazette of the U.S. Patent and Trademark Office

N90-26320*# Rockwell International Corp., Canoga Park, CA. Rocketdyne Div.

REUSABLE ROCKET ENGINE TURBOPUMP HEALTH MONITORING SYSTEM, PART 3 Final Report

JOHN G. PERRY 14 Mar. 1989 42 p

(Contract NAS3-25279)

(NASA-CR-182294; NAS 1.26:182294; RI/RD89-171-PT-3) Avail: NTIS HC A03/MF A01 CSCL 13/9

Degradation mechanisms and sensor identification/selection resulted in a list of degradation modes and a list of sensors that are utilized in the diagnosis of these degradation modes. The sensor list is divided into primary and secondary indicators of the corresponding degradation modes. The signal conditioning requirements are discussed, describing the methods of producing the Space Shuttle Main Engine (SSME) post-hot-fire test data to be utilized by the Health Monitoring System. Development of the diagnostic logic and algorithms is also presented. The knowledge engineering approach, as utilized, includes the knowledge acquisition effort, characterization of the expert's problem solving strategy, conceptually defining the form of the applicable knowledge base, and rule base, and identifying an appropriate inferencing mechanism for the problem domain. The resulting logic flow graphs detail the diagnosis/prognosis procedure as followed by the experts. The nature and content of required support data and databases is also presented. The distinction between deep and shallow types of knowledge is identified. Computer coding of the Health Monitoring System is shown to follow the logical inferencing of the logic flow graphs/algorithms.

Author

N90-26338*# National Aeronautics and Space Administration. Lewis Research Center, Cleveland, OH.

A HIGH-SPEED PHOTOGRAPHY STUDY OF CAVITATION IN A DYNAMICALLY LOADED JOURNAL BEARING

D. C. SUN (State Univ. of New York, Binghamton.) and D. E. BREWE 1990 27 p Presented at the Joint Tribology Conference, Toronto, Ontario, 7-10 Oct. 1990; sponsored by ASME and STLE (Contract DA PROJ. 1L1-61102-AH-45)

(NASA-TM-103178; E-5547; NAS 1.15:103178;

AVSCOM-TR-90-C-013; AD-A225679) Avail: NTIS HC A03/MF A01 CSCL 13/9

The earlier study made by Jacobson and Hamrock on the cavitation of liquid lubricant films in a dynamically loaded journal bearing was repeated with a quartz sleeve, which was more rigid than the Polymethylmethacrylate (PMMA) sleeve used previously. Various improvements of the test rig were made concomitantly so that the experimental errors could be better controlled and assessed. The updated speed photography experiment and its results are described. Author

N90-28060*# National Aeronautics and Space Administration. Lewis Research Center, Cleveland, OH.

DYNAMICS OF MULTISTAGE GEAR TRANSMISSION WITH EFFECTS OF GEARBOX VIBRATIONS

F. K. CHOY, Y. K. TU (Akron Univ., OH.), J. J. ZAKRAJSEK, and DENNIS P. TOWNSEND Jun. 1990 25 p Presented at the CSME Mechanical Engineering Forum, Toronto, Ontario, 3-9 Jun. 1990; sponsored in part by Canadian Society of Mechanical Engineers

(Contract DA PROJ. 1L1-62209-A-47-A)

(NASA-TM-103109; E-5433; NAS 1.15:103109;

AVSCOM-TR-90-C-022; AD-A227151) Avail: NTIS HC A03/MF A01 CSCL 13/9

A comprehensive approach is presented in analyzing the dynamic behavior of multistage gear transmission systems with the effects of gearbox induced vibrations and mass imbalances of the rotor. The modal method, with undamped frequencies and planar mode shapes, is used to reduce the degrees of freedom of the gear system for time-transient dynamic analysis. Both the lateral and torsional vibration modes of each rotor-bearing-gear stage as well as the interstage vibrational characteristics are coupled together through localized gear mesh tooth interactions. In addition, gearbox vibrations are also coupled to the rotor-bearing-gear system dynamics through bearing support forces between the rotor and the gearbox. Transient and steady state dynamics of lateral and torsional vibrations of the geared system are examined in both time and frequency domains to develop interpretations of the overall modal dynamic characteristics under various operating conditions. A typical three-stage geared system is used as an example. Effects of mass imbalance and gearbox vibrations on the system dynamic behavior are presented in terms of modal excitation functions for both lateral and torsional vibrations. Operational characteristics and conclusions are drawn from the results presented. Author

N90-28062*# National Aeronautics and Space Administration. Lewis Research Center, Cleveland, OH.

REACTION-COMPENSATION TECHNOLOGY FOR MICROGRAVITY LABORATORY ROBOTS

DOUGLAS A. ROHN, CHARLES LAWRENCE, and JEFFREY H. MILLER (Sverdrup Technology, Inc., Brook Park, OH.) 1990 5 p Proposed for presentation at the i-SAIRAS 1990 International Symposium on Artificial Intelligence, Robotics and Automation in Space, Kobe, Japan, 18-20 Nov. 1990

(NASA-TM-103271; E-5713; NAS 1.15:103271) Avail: NTIS HC A01/MF A01 CSCL 13/9

Robots operating in the microgravity environment of an orbiting laboratory should be capable of manipulating payloads such that the motion of the robot does not disturb adjacent experiments. The current results of a NASA Lewis Research Center technology program to develop smooth, reaction-compensated manipulation based on both mechanism technology and trajectory planning strategies are present. Experimental validation of methods to reduce robot base reactions through the use of redundant degrees of freedom is discussed. Merits of smooth operation roller-driven robot joints for microgravity manipulators are also reviewed. Author

N90-28063*# National Aeronautics and Space Administration. Lewis Research Center, Cleveland, OH.

LIQUID LUBRICATION IN SPACE

ERWIN V. ZARETSKY Jul. 1990 26 p (NASA-RP-1240; E-5094; NAS 1.61:1240) Avail: NTIS HC A03/MF A01 CSCL 13/9

The requirement for long-term, reliable operation of aerospace mechanisms has, with a few exceptions, pushed the state of the art in tribology. Space mission life requirements in the early 1960s were generally 6 months to a year. The proposed U.S. space station schedule to be launched in the 1990s must be continuously usable for 10 to 20 years. Liquid lubrication systems are generally used for mission life requirements longer than a year. Although most spacecraft or satellites have reached their required lifetimes without a lubrication-related failure, the application of liquid lubricants in the space environment presents unique challenges. The state of the art of liquid lubrication in space as well as the problems and their solutions are reviewed. Author

N90-28065*# National Aeronautics and Space Administration. Lewis Research Center, Cleveland, OH.

COMPUTER-AIDED DESIGN OF HIGH-CONTACT-RATIO GEARS FOR MINIMUM DYNAMIC LOAD AND STRESS

HSIANG HSI LIN, CHINWAI LEE (Memphis State Univ., TN.), FRED B. OSWALD, and DENNIS P. TOWNSEND 1990 12 p Proposed for presentation at the Design Productivity International Conference, Honolulu, HI, 6-8 Feb. 1991; sponsored by ASME (Contract NAG3-961; DA PROJ. 1L1-62211-A-47-A)

(NASA-TM-103275; E-5686; NAS 1.15:103275;

AVSCOM-TR-90-C-016; AD-A227149) Avail: NTIS HC A03/MF A01 CSCL 13/9

A computer aided design procedure is presented for minimizing dynamic effects on high contact ratio gears by modification of the tooth profile. Both linear and parabolic tooth profile modifications of high contact ratio gears under various loading conditions are examined and compared. The effects of the total amount of modification and the length of the modification zone were systematically studied at various loads and speeds to find the optimum profile design for minimizing the dynamic load and the tooth bending stress. Parabolic profile modification is preferred over linear profile modification for high contact ratio gears because of its lower sensitivity to manufacturing errors. For parabolic modification, a greater amount of modification at the tooth tip and a longer modification zone are required. Design charts are presented for high contact ratio gears with various profile modifications operating under a range of loads. A procedure is illustrated for using the charts to find the optimum profile design. Author

N90-28066*# National Aeronautics and Space Administration. Lewis Research Center, Cleveland, OH.

MODIFICATION OF THE SHABERTH BEARING CODE TO INCORPORATE RP-1 AND A DISCUSSION OF THE TRACTION MODEL

CLAUDIA M. WOODS Sep. 1990 30 p (NASA-TP-3017; E-5407; NAS 1.60:3017) Avail: NTIS HC A03/MF A01 CSCL 13/9

Recently developed traction data for Rocket Propellant 1 (RP-1), a hydrocarbon fuel of the kerosene family, was used to develop the parameters needed by the bearing code SHABERTH in order to include RP-1 as a lubricant choice. The procedure for inputting data for a new lubricant choice is reviewed, and the theoretical fluid traction model is discussed. Comparisons are made between experimental traction data and those predicted by SHABERTH for RP-1. All data needed to modify SHABERTH for use with RP-1 as a lubricant are specified. Author

N90-28622*# National Aeronautics and Space Administration. Lewis Research Center, Cleveland, OH.

BEARING OPTIMIZATION FOR SSME HPOTP APPLICATION

ELIZABETH S. ARMSTRONG and HAROLD H. COE In NASA, Marshall Space Flight Center, Advanced Earth-to-Orbit Propulsion Technology 1988, Volume 1 p 159-174 Sep. 1988

Avail: NTIS HC A99/MF E06 CSCL 13/9

The space shuttle main engine (SSME) high-pressure oxygen turbopumps (HPOTP) have not experienced the service life required

38 QUALITY ASSURANCE AND RELIABILITY

of them. To improve the life of the existing turbopump bearings, modifications to the bearings that could be retrofitted into the present bearing cavity are being investigated. Several bearing parameters were optimized using the computer program SHABERTH, which performs a thermomechanical simulation of a load support system. The computer analysis showed that improved bearing performance is feasible if low friction coefficients can be attained. Bearing geometries were optimized considering heat generation, equilibrium temperatures, and relative life. Two sets of curvatures were selected from the optimization: an inner-raceway curvature of 0.54, an outer-raceway curvature of 0.52, and an inner-raceway curvature of 0.55, an outer-raceway curvature of 0.53. A contact angle of 16 deg was also selected. Thermal gradients through the bearings were found to be lower with liquid lubrication than with solid film lubrication. As the coolant flowrate through the bearing increased, the ball temperature decreased but at a continuously decreasing rate. The optimum flowrate was approximately 4 kg/s. The analytical modeling used to determine these feasible modifications to improve bearing performance is described.

Author

38

QUALITY ASSURANCE AND RELIABILITY

Includes product sampling procedures and techniques; and quality control.

A90-30706* # National Aeronautics and Space Administration. Lewis Research Center, Cleveland, OH.

THREE APPROACHES TO RELIABILITY ANALYSIS

DANIEL L. PALUMBO (NASA, Langley Research Center, Hampton, VA) IN: NAECON 89; Proceedings of the IEEE National Aerospace and Electronics Conference, Dayton, OH, May 22-26, 1989. Volume 1. New York, Institute of Electrical and Electronics Engineers, Inc., 1989, p. 308-315. refs

It is noted that current reliability analysis tools differ not only in their solution techniques, but also in their approach to model abstraction. The analyst must be satisfied with the constraints that are intrinsic to any combination of solution technique and model abstraction. To get a better idea of the nature of these constraints, three reliability analysis tools (HARP, ASSIST/SURE, and CAME) were used to model portions of the Integrated Airframe/Propulsion Control System architecture. When presented with the example problem, all three tools failed to produce correct results. In all cases, either the tool or the model had to be modified. It is suggested that most of the difficulty is rooted in the large model size and long computational times which are characteristic of Markov model solutions.

I.E.

A90-35508* Allied-Signal Aerospace Co., Phoenix, AZ.

THE ROLE OF NDE IN CERAMIC TURBINE ENGINE COMPONENT DEVELOPMENT

JANET MINTER (Allied-Signal Aerospace Co., Garrett Auxiliary Power Div., Phoenix, AZ) IN: Ceramic materials and components for engines; Proceedings of the Third International Symposium, Las Vegas, NV, Nov. 27-30, 1988. Westerville, OH, American Ceramic Society, Inc., 1989, p. 1289-1298. Research supported by DOE. refs
(Contract DEN3-335)
Copyright

A systematic approach to the use of nondestructive evaluation (NDE) throughout the ceramic engine component development cycle is necessary to achieve the high reliability required for turbine engine applications. Specifically, NDE techniques must be developed and applied to component design, development, fabrication, and test to ensure adequate materials characterization. This approach has the potential of reducing ceramic component cost by optimizing the initial design and eliminating unacceptable components early in the fabrication cycle. Although research NDE

techniques have been developed that have the potential to solve the problems of ceramic component inspection, systematic application of these NDE techniques for inspection and process control has not yet occurred. The application of NDE techniques for both material characterization and flaw detection is discussed as well as an approach for applying NDE throughout the fabrication process to achieve highly reliable ceramic components. Author

A90-43731* National Aeronautics and Space Administration. Lewis Research Center, Cleveland, OH.

A MODIFIED VAPEPS METHOD FOR PREDICTING VIBROACOUSTIC RESPONSE OF UNREINFORCED MASS LOADED HONEYCOMB PANELS

MARK E. MCNELIS (NASA, Lewis Research Center, Cleveland, OH) IN: Institute of Environmental Sciences, Annual Technical Meeting, 35th, Anaheim, CA, May 1-5, 1989, Proceedings. Mount Prospect, IL, Institute of Environmental Sciences, 1989, p. 64-71. Previously announced in STAR as N89-16905. refs
Copyright

VAPEPS (vibroAcoustic Payload Environment Prediction System) is a computer program used to predict the vibroacoustic response of a structure. An alternate VAPEPS modeling technique, the Modified NASA Lewis Method, is an improvement for modeling unreinforced mass loaded honeycomb panels. The Modified NASA Lewis Method prediction is compared to the standard ASMS VAPEPS prediction, and the acoustic test data for three spacecraft panels. An analytical method of computing variance is presented and used to compute 95 percent confidence levels. These levels are compared to the standard VAPEPS confidence levels and to the envelope of the test data. As a result of using the new methodology suggested in the paper, both the mean prediction and the 95 percent confidence level prediction agree well with the test data in both spectral shape and magnitude. Therefore, the Modified NASA Lewis Method prediction methodology may be used to define more realistic random vibration test levels.

Author

N90-12034* # National Aeronautics and Space Administration. Lewis Research Center, Cleveland, OH.

MODEL 0A WIND TURBINE GENERATOR FMEA Final Report

WILLIAM E. KLEIN (National Aeronautics and Space Administration. Plum Brook Reactor Facility, Sandusky, OH.) and VINCENT R. LALLI Oct. 1989 8 p Proposed for presentation at the 1990 Annual Reliability and Maintainability Symposium, Los Angeles, CA, 23-25 Jan. 1990; cosponsored by ASME, ASQC, IIE, IEEE, SOLE, IES, AIAA, SSS, and SRE
(Contract DE-AB29-79ET-20370)
(NASA-TM-102378; E-5117; NAS 1.15:102378;
DOE/NASA/20370-23) Avail: NTIS HC A02/MF A01 CSCL 10/1

The results of Failure Modes and Effects Analysis (FMEA) conducted for the Wind Turbine Generators are presented. The FMEA was performed for the functional modes of each system, subsystem, or component. The single-point failures were eliminated for most of the systems. The blade system was the only exception. The qualitative probability of a blade separating was estimated at level D-remote. Many changes were made to the hardware as a result of this analysis. The most significant change was the addition of the safety system. Operational experience and need to improve machine availability have resulted in subsequent changes to the various systems which are also reflected in this FMEA. Author

N90-17167* # National Aeronautics and Space Administration. Lewis Research Center, Cleveland, OH.

SUBTLE POROSITY VARIATION IN THE YBA2CU3O(7-X) HIGH-TEMPERATURE SUPERCONDUCTOR REVEALED BY ULTRASONIC IMAGING

D. J. ROTH, E. R. GENERAZIO, D. B. STANG (Sverdrup Technology, Inc., Cleveland, OH.), and A. F. HEPP Jan. 1990 11 p
(NASA-TM-102130; E-4917; NAS 1.15:102130) Avail: NTIS HC A03/MF A01 CSCL 14/4

The characterization of global porosity variation within a

nominally 93-percent-dense specimen of $\text{YBa}_2\text{Cu}_3\text{O}(7-x)$ high-temperature superconductor is reported. With a computer-controlled scanning system, precision ultrasonic velocity measurements were obtained at 100 micron increments over an 8- by 8-mm area of the $\text{YBa}_2\text{Cu}_3\text{O}(7-x)$ specimen. The measurements were used to form a color map of velocity variation across the scanned region of the specimen. Subtle velocity variation on the order of 1 percent was observed. The specimen was shown by experimental methods to be single-phase, untextured, and free of nonuniform residual microstresses. From this knowledge and an established velocity-density relationship, a likely conclusion is that the observed velocity variations are solely due to porosity variations of similar magnitude. Locating these subtle porosity variations is critical since they can result in an order of magnitude variation in $J(\text{sub } c)$ for dense YBCO specimens. Thus, mapping the global porosity distribution within $\text{YBa}_2\text{Cu}_3\text{O}(7-x)$ may reveal regions that have poorer superconducting properties. Ultrasonic velocity results are translated into useful microstructural information for the material scientist. Author

N90-21399*# National Aeronautics and Space Administration. Lewis Research Center, Cleveland, OH.

AEROPROPULSION FACILITIES CONFIGURATION CONTROL: PROCEDURES MANUAL

JAMES J. LAVELLE Mar. 1990 24 p
(NASA-TM-102541; E-5351; NAS 1.15:102541) Avail: NTIS HC A03/MF A01 CSCL 14/4

Lewis Research Center senior management directed that the aeropropulsion facilities be put under configuration control. A Configuration Management (CM) program was established by the Facilities Management Branch of the Aeropropulsion Facilities and Experiments Division. Under the CM program, a support service contractor was engaged to staff and implement the program. The Aeronautics Directorate has over 30 facilities at Lewis of various sizes and complexities. Under the program, a Facility Baseline List (FBL) was established for each facility, listing which systems and their documents were to be placed under configuration control. A Change Control System (CCS) was established requiring that any proposed changes to FBL systems or their documents were to be processed as per the CCS. Limited access control of the FBL master drawings was implemented and an audit system established to ensure all facility changes are properly processed. This procedures manual sets forth the policy and responsibilities to ensure all key documents constituting a facilities configuration are kept current, modified as needed, and verified to reflect any proposed change. This is the essence of the CM program. Author

N90-21401*# National Aeronautics and Space Administration. Lewis Research Center, Cleveland, OH.

ULTRASONIC AND RADIOGRAPHIC EVALUATION OF ADVANCED AEROSPACE MATERIALS: CERAMIC COMPOSITES

EDWARD R. GENERAZIO 1990 12 p Presented at Physics Dept. Seminars, University Heights, OH, 11 Apr. 1990; sponsored by John Carroll Univ.
(NASA-TM-102540; E-5403; NAS 1.15:102540) Avail: NTIS HC A03/MF A01 CSCL 14/4

Two conventional nondestructive evaluation techniques were used to evaluate advanced ceramic composite materials. It was shown that neither ultrasonic C-scan nor radiographic imaging can individually provide sufficient data for an accurate nondestructive evaluation. Both ultrasonic C-scan and conventional radiographic imaging are required for preliminary evaluation of these complex systems. The material variations that were identified by these two techniques are porosity, delaminations, bond quality between laminae, fiber alignment, fiber registration, fiber parallelism, and processing density flaws. The degree of bonding between fiber and matrix cannot be determined by either of these methods. An alternative ultrasonic technique, angular power spectrum scanning (APSS) is recommended for quantification of this interfacial bond. Author

N90-21402*# National Aeronautics and Space Administration. Lewis Research Center, Cleveland, OH.

REVIEW AND STATISTICAL ANALYSIS OF THE ULTRASONIC VELOCITY METHOD FOR ESTIMATING THE POROSITY FRACTION IN POLYCRYSTALLINE MATERIALS

D. J. ROTH, S. M. SWICKARD, D. B. STANG, and M. R. DEGUIRE (Case Western Reserve Univ., Cleveland, OH.) 7 1990 47 p Revised
(NASA-TM-102501-REV; E-5298; NAS 1.15:102501-REV) Avail: NTIS HC A03/MF A01 CSCL 14/4

A review and statistical analysis of the ultrasonic velocity method for estimating the porosity fraction in polycrystalline materials is presented. Initially, a semi-empirical model is developed showing the origin of the linear relationship between ultrasonic velocity and porosity fraction. Then, from a compilation of data produced by many researchers, scatter plots of velocity versus percent porosity data are shown for Al_2O_3 , MgO , porcelain-based ceramics, PZT, SiC , Si_3N_4 , steel, tungsten, UO_2 , $(\text{U}_0.30\text{Pu}_0.70)\text{C}$, and $\text{YBa}_2\text{Cu}_3\text{O}(7-x)$. Linear regression analysis produced predicted slope, intercept, correlation coefficient, level of significance, and confidence interval statistics for the data. Velocity values predicted from regression analysis for fully-dense materials are in good agreement with those calculated from elastic properties. Author

N90-22801*# National Aeronautics and Space Administration. Lewis Research Center, Cleveland, OH.

RECENT ADVANCES IN NONDESTRUCTIVE EVALUATION MADE POSSIBLE BY NOVEL USES OF VIDEO SYSTEMS

EDWARD R. GENERAZIO and DON J. ROTH 1990 20 p
Presented at the MiCon 90: Advances in Video Technology: Materials Science Applications, San Francisco, CA, 23-25 May 1990; sponsored by American Society for Testing and Materials Original contains color illustrations
(NASA-TM-102491; E-5283; NAS 1.15:102491) Avail: NTIS HC A03/MF A01; 4 functional color pages CSCL 14/4

Complex materials are being developed for use in future advanced aerospace systems. High temperature materials have been targeted as a major area of materials development. The development of composites consisting of ceramic matrix and ceramic fibers or whiskers is currently being aggressively pursued internationally. These new advanced materials are difficult and costly to produce; however, their low density and high operating temperature range are needed for the next generation of advanced aerospace systems. These materials represent a challenge to the nondestructive evaluation community. Video imaging techniques not only enhance the nondestructive evaluation, but they are also required for proper evaluation of these advanced materials. Specific research examples are given, highlighting the impact that video systems have had on the nondestructive evaluation of ceramics. An image processing technique for computerized determination of grain and pore size distribution functions from microstructural images is discussed. The uses of video and computer systems for displaying, evaluating, and interpreting ultrasonic image data are presented. Author

N90-23754*# National Aeronautics and Space Administration. Lewis Research Center, Cleveland, OH.

THEORY AND EXPERIMENTAL TECHNIQUE FOR NONDESTRUCTIVE EVALUATION OF CERAMIC COMPOSITES

EDWARD R. GENERAZIO 1990 18 p Presented at the March Meeting of the American Society for Nondestructive Testing, Columbus, OH, 15 Mar. 1990
(NASA-TM-102561; E-5381; NAS 1.15:102561) Avail: NTIS HC A03/MF A01 CSCL 14/5

The important ultrasonic scattering mechanisms for SiC and Si_3N_4 ceramic composites were identified by examining the interaction of ultrasound with individual fibers, pores, and grains. The dominant scattering mechanisms were identified as asymmetric refractive scattering due to porosity gradients in the matrix material, and symmetric diffractive scattering at the fiber-to-matrix interface and at individual pores. The effect of the ultrasonic reflection coefficient and surface roughness in the ultrasonic evaluation was highlighted. A new nonintrusive ultrasonic evaluation technique,

38 QUALITY ASSURANCE AND RELIABILITY

angular power spectrum scanning (APSS), was presented that is sensitive to microstructural variations in composites. Preliminary results indicate that APSS will yield information on the composite microstructure that is not available by any other nondestructive technique. Author

N90-28097* # Massachusetts Inst. of Tech., Cambridge. Dept. of Mechanical Engineering.

INPUT-OUTPUT CHARACTERIZATION OF FIBER REINFORCED COMPOSITES BY P WAVES Final Report

JOHN D. RENNEISEN and JAMES H. WILLIAMS, JR. Sep. 1990 89 p

(Contract NAG3-1105)

(NASA-CR-185287; NAS 1.26:185287) Avail: NTIS HC A05/MF A01 CSCL 14/4

Input-output characterization of fiber composites is studied theoretically by tracing P waves in the media. A new path motion to aid in the tracing of P and the reflection generated SV wave paths in the continuum plate is developed. A theoretical output voltage from the receiving transducer is calculated for a tone burst. The study enhances the quantitative and qualitative understanding of the nondestructive evaluation of fiber composites which can be modeled as transversely isotropic media. Author

N90-28858* # Massachusetts Inst. of Tech., Cambridge. Dept. of Mechanical Engineering.

ULTRASONIC VERIFICATION OF FIVE WAVE FRONTS IN UNIDIRECTIONAL GRAPHITE EPOXY COMPOSITE Final Report

HAN-SONG SENG and JAMES H. WILLIAMS, JR. Sep. 1990 55 p

(Contract NAG3-1105)

(NASA-CR-185288; NAS 1.26:185288) Avail: NTIS HC A04/MF A01 CSCL 14/4

The existence of five different waves fronts in a unidirectional graphite fiber reinforced epoxy composite with energy flux propagation at the angle of 60 deg with respect to the fiber direction is verified by measuring their corresponding group and phase velocities of longitudinal and shear waves using the through transmission technique. The experimental and theoretical values of phase velocities show excellent agreement for all three modes of wave propagation. It is also verified that the maximum output voltage amplitude is obtained when the line joining the centers of the transmitting and receiving transducers is parallel to the energy propagation direction defined by the deviation angle. Author

39

STRUCTURAL MECHANICS

Includes structural element design and weight analysis; fatigue; and thermal stress.

A90-15704* National Aeronautics and Space Administration. Lewis Research Center, Cleveland, OH.

FINITE ELEMENT IMPLEMENTATION OF ROBINSON'S UNIFIED VISCOPLASTIC MODEL AND ITS APPLICATION TO SOME UNIAXIAL AND MULTIAXIAL PROBLEMS

V. K. ARYA and A. KAUFMAN (NASA, Lewis Research Center, Cleveland, OH) Engineering Computations (ISSN 0264-4401), vol. 6, Sept. 1989, p. 237-247. Previously announced in STAR as N87-23010. refs

Copyright

A description of the finite element implementation of Robinson's unified viscoplastic model into the General Purpose Finite Element Program (MARC) is presented. To demonstrate its application, the implementation is applied to some uniaxial and multiaxial problems. A comparison of the results for the multiaxial problem of a thick internally pressurized cylinder, obtained using the finite element

implementation and an analytical solution, is also presented. The excellent agreement obtained confirms the correct finite element implementation of Robinson's model. Author

A90-16371* # Rensselaer Polytechnic Inst., Troy, NY.

SHAFT FLEXIBILITY EFFECTS ON AEROELASTIC STABILITY OF A ROTATING BLADED DISK

NAIM KHADER (Jordan University of Science and Technology, Irbid) and ROBERT LOEWY (Rensselaer Polytechnic Institute, Troy, NY) Journal of Propulsion and Power (ISSN 0748-4658), vol. 5, Nov.-Dec. 1989, p. 718-726. Research supported by Jordan University of Science and Technology. refs

(Contract NAG3-37)

Copyright

A comprehensive study of Coriolis forces and shaft flexibility effects on the structural dynamics and aeroelastic stability of a rotating bladed-disk assembly attached to a cantilever, massless, flexible shaft is presented. Analyses were performed for an actual bladed-disk assembly, used as the first stage in the fan of the 'E3' engine. In the structural model, both in-plane and out-of-plane elastic deformation of the bladed-disk assembly were considered relative to their hub, in addition to rigid disk translations and rotations introduced by shaft flexibility. Besides structural coupling between blades (through the flexible disk), additional coupling is introduced through quasisteady aerodynamic loads. Rotational effects are accounted for throughout the work, and some mode shapes for the whole structure are presented at a selected rpm. Author

A90-16723* National Aeronautics and Space Administration. Lewis Research Center, Cleveland, OH.

ASSUMED STRAIN DISTRIBUTIONS FOR A FINITE STRIP PLATE BENDING ELEMENT USING MINDLIN-REISSNER PLATE THEORY

ABHISAK CHULYA (NASA, Lewis Research Center, Cleveland, OH) and ROBERT L. MULLEN (Case Western Reserve University, Cleveland, OH) Computers and Structures (ISSN 0045-7949), vol. 33, no. 2, 1989, p. 513-521. refs

Copyright

A linear finite strip plate element based on Mindlin-Reissner plate theory is developed. The analysis is suitable for both thin and thick plates. In the formulation, new transverse shear strains are introduced and assumed constant in each two-node linear strip. The element stiffness matrix is explicitly formulated for efficient computation and computer implementation. Numerical results showing the efficiency and predictive capability of the element for the analysis of plates are presented for different support and loading conditions and a wide range of thicknesses. No sign of shear locking is observed with the newly developed element. Author

A90-16959* National Aeronautics and Space Administration. Lewis Research Center, Cleveland, OH.

CHARACTERIZATION OF DAMPED STRUCTURAL CONNECTIONS FOR MULTI-COMPONENT SYSTEMS

CHARLES LAWRENCE (NASA, Lewis Research Center, Cleveland, OH) and ARTHUR A. HUCKELBRIDGE (Case Western Reserve University, Cleveland, OH) IN: International Modal Analysis Conference, 7th, Las Vegas, NV, Jan. 30-Feb. 2, 1989, Proceedings. Volume 1. Bethel, CT, Society for Experimental Mechanics, Inc., 1989, p. 71-78. Previously announced in STAR as N88-18974. refs

Copyright

The inability to model connections adequately has historically limited the ability to predict overall system dynamic response. Connections between structural components are often mechanically complex and difficult to accurately model analytically. Improved analytical models for connections are needed to improve system dynamic predictions. This study explores combining Component Mode Synthesis methods for coupling structural components with Parameter Identification procedures for improving the analytical modeling of the connections. Improvements in the connection stiffness and damping properties are computed in terms of physical

parameters so the physical characteristics of the connections can be better understood, in addition to providing improved input for the system model. Author

A90-17001* SDRC, Inc., San Diego, CA.

MODAL SELECTION IN STRUCTURAL DYNAMICS

PAUL A. BLELLOCH (SDRC, Inc., San Diego, CA) and KELLY S. CARNEY (NASA, Lewis Research Center, Cleveland, OH) IN: International Modal Analysis Conference, 7th, Las Vegas, NV, Jan. 30-Feb. 2, 1989, Proceedings. Volume 2. Bethel, CT, Society for Experimental Mechanics, Inc., 1989, p. 742-749. refs
Copyright

An overview of two modal selection procedures for lightly damped structural dynamic models is presented. Both procedures order the modes in terms of their contribution to the input/output dynamics of the model. A complex model of the Phase I Space Station is used to illustrate the application of these procedures to a realistic structure. Author

A90-19109* Cincinnati Univ., OH.

IMPROVEMENT OF FINITE ELEMENT MESHES - HEAT TRANSFER IN AN INFINITE CYLINDER

MADAN G. KITTUR, RONALD L. HUSTON (Cincinnati University, OH), and FRED B. OSWALD (NASA, Lewis Research Center, Cleveland, OH) Computers and Structures (ISSN 0045-7949), vol. 33, no. 5, 1989, p. 1215-1221. Previously announced in STAR as N89-14450. refs
(Contract NSG-3188)
Copyright

An extension of a structural finite element mesh improvement technique to heat conduction analysis is presented. The mesh improvement concept was originally presented by Prager in studying tapered, axially loaded bars. It was further shown that an improved mesh can be obtained by minimizing the trace of the stiffness matrix. These procedures are extended and applied to the analysis of heat conduction in an infinitely long hollow circular cylinder. Author

A90-19132* National Aeronautics and Space Administration. Lewis Research Center, Cleveland, OH.

ANALYTICAL AND FINITE ELEMENT SOLUTIONS OF SOME PROBLEMS USING A VISCOPLASTIC MODEL

V. K. ARYA (NASA, Lewis Research Center, Cleveland, OH) Computers and Structures (ISSN 0045-7949), vol. 33, no. 4, 1989, p. 957-967. refs
Copyright

The feasibility of using a viscoplastic model developed by Robinson to perform a nonlinear structural analysis was investigated. The paper presents analytical solutions for three classical problems: (1) a pressurized thick-walled cylinder, (2) a thin rotating disk, and (3) a pressurized thick-walled sphere. The analytical expressions derived for the stress and the strain rates for these components are general in nature as they consider both the mechanical and thermal loadings to be time-dependent. A computer program VISTAN (Viscoplastic STructural ANalyzer) was developed to obtain the stress and strain distributions. The finite element solutions for these problems are also presented. The numerical results pertaining to isothermal loading conditions are provided. The results obtained demonstrate the feasibility of using the viscoplastic model developed by Robinson to perform nonlinear structural analyses. Author

A90-20061* National Aeronautics and Space Administration. Lewis Research Center, Cleveland, OH.

RELATIONSHIP BETWEEN FATIGUE LIFE IN THE CREEP-FATIGUE REGION AND STRESS-STRAIN RESPONSE

A. BERKOVITS (NASA, Lewis Research Center, Cleveland, OH) and S. NADIV IN: International Congress on Experimental Mechanics, 6th, Portland, OR, June 6-10, 1988, Proceedings. Volume 2. Bethel, CT, Society for Experimental Mechanics, Inc., 1988, p. 787-794. Previously announced in STAR as N88-18040. refs
Copyright

On the basis of mechanical tests and metallographic studies, strainrange partitioned lives were predicted by introducing stress-strain materials parameters into the Universal Slopes Equation. This was the result of correlating fatigue damage mechanisms and deformation mechanisms operating at elevated temperatures on the basis of observed mechanical and microstructural behavior. Correlation between high temperature fatigue and stress strain properties for nickel base superalloys and stainless steel substantiated the method. Parameters which must be evaluated for PP- and CC- life are the maximum stress achievable under entirely plastic and creep conditions respectively and corresponding inelastic strains, and the two more pairs of stress strain parameters must be ascertained. Author

A90-23013* Aerostructures, Inc., Arlington, VA.

FINITE ELEMENT MESH REFINEMENT CRITERIA FOR STRESS ANALYSIS

MADAN G. KITTUR (Aerostructures, Inc., Arlington, VA) and RONALD L. HUSTON (Cincinnati University, OH) Computers and Structures (ISSN 0045-7949), vol. 34, no. 2, 1990, p. 251-255. refs
(Contract NSG-3188)
Copyright

This paper discusses procedures for finite-element mesh selection and refinement. The objective is to improve accuracy. The procedures are based on (1) the minimization of the stiffness matrix trace (optimizing node location); (2) the use of h-version refinement (rezoning, element size reduction, and increasing the number of elements); and (3) the use of p-version refinement (increasing the order of polynomial approximation of the elements). A step-by-step procedure of mesh selection, improvement, and refinement is presented. The criteria for 'goodness' of a mesh are based on strain energy, displacement, and stress values at selected critical points of a structure. An analysis of an aircraft lug problem is presented as an example. Author

A90-23827*# Cleveland State Univ., OH.

NONINTERACTIVE MACROSCOPIC RELIABILITY MODEL FOR CERAMIC MATRIX COMPOSITES WITH ORTHOTROPIC MATERIAL SYMMETRY

STEPHEN F. DUFFY (Cleveland State University, OH) and JANE M. MANDERSCHIED (NASA, Lewis Research Center, Cleveland, OH) ASME, Gas Turbine and Aeroengine Congress and Exposition, Toronto, Canada, June 4-8, 1989. 7 p. Previously announced in STAR as N89-15437. refs
(Contract NCC3-81)
(ASME PAPER 89-GT-129)

A macroscopic noninteractive reliability model for ceramic matrix composites is presented. The model is multiaxial and applicable to composites that can be characterized as orthotropic. Tensorial invariant theory is used to create an integrity basis with invariants that correspond to physical mechanisms related to fracture. This integrity basis is then used to construct a failure function per unit volume (or area) of material. It is assumed that the overall strength of the composite is governed by weakest link theory. This leads to a Weibull type model similar in nature to the principle of independent action (PIA) model for isotropic monolithic ceramics. An experimental program to obtain model parameters is briefly discussed. In addition, qualitative features of the model are illustrated by presenting reliability surfaces for various model parameters. Author

A90-23828*# General Electric Co., Cincinnati, OH.

APPLICATION OF HOST TECHNOLOGY TO THE SSME HPFTP BLADE

R. L. MCKNIGHT, T. S. COOK, G. S. BECHTEL, and H. T. HUANG (General Electric Co., Cincinnati, OH) ASME, Gas Turbine and Aeroengine Congress and Exposition, Toronto, Canada, June 4-8, 1989. 12 p. refs
(Contract NAS3-24861)
(ASME PAPER 89-GT-130)

The development of turbine blade analysis tools as they moved from research contracts under the NASA HOST (Hot Section

39 STRUCTURAL MECHANICS

Technology) program to a PC-based system for preliminary design and to use in evaluating the SSME HPFTP (Space Shuttle Main Engine High Pressure Fuel Turbo Pump) blade is discussed. The heat transfer and structural analysis of the blade, the development of a data base for constitutive modeling of the blade materials, including coatings, and the use of advanced nonlinear finite element methods are addressed. C.D.

A90-24384* Colorado Univ., Boulder.

A VARIATIONAL JUSTIFICATION OF THE ASSUMED NATURAL STRAIN FORMULATION OF FINITE ELEMENTS. I - VARIATIONAL PRINCIPLES. II - THE C(0) FOUR-NODE PLATE ELEMENT

CARMELO MILITELLO and CARLOS A. FELIPPA (Colorado, University, Boulder) Computers and Structures (ISSN 0045-7949), vol. 34, no. 3, 1990, p. 431-444. refs

(Contract NAG3-934)

Copyright

The assumed natural strain formulation of finite elements is interpreted from a variational standpoint. The approach is based on hybrid extensions of the Reissner-type functional which uses the strains and displacements as independent fields. Consideration is restricted to linear elasticity. The four-node C(0) plate-bending quadrilateral is used as a specific example to illustrate the application of the present interpretation. A key finding is that any change in the strain-displacement interpolation from the variationally consistent interpolation must be associated in some way to the addition of incompatible displacement modes. C.D.

A90-26787* SDRC, Inc., San Diego, CA.

SELECTION OF COMPONENT MODES

PAUL A. BLELLOCH (SDRC, Inc., Engineering Services Div., San Diego, CA) and KELLY S. CARNEY (NASA, Lewis Research Center, Cleveland, OH) IN: AIAA Dynamics Specialists Conference, Long Beach, CA, Apr. 5, 6, 1990, Technical Papers. Washington, DC, American Institute of Aeronautics and Astronautics, 1990, p. 105-112. refs

(AIAA PAPER 90-1201) Copyright

Structural dynamic models of complex spacecraft are often assembled from a number of component models. In this paper, three methods for reducing the order of these component models are presented by selecting 'important' fixed interface component modes. These methods are applied to two component structures of the Space Station Freedom: a photovoltaic (PV) array and a solar dynamic collector. The reduced order models of these components retain a small fraction of the number of modes in the original models while accurately representing a set of outputs chosen by the user. Author

A90-28755* Tulane Univ., New Orleans, LA.

CRACK-PATH EFFECT ON MATERIAL TOUGHNESS

ASHER A. RUBINSTEIN (Tulane University, New Orleans, LA) ASME, Transactions, Journal of Applied Mechanics (ISSN 0021-8936), vol. 57, March 1990, p. 97-103. refs

(Contract NAG3-815)

(ASME PAPER 89-WA/APM-43) Copyright

The main features of a toughening mechanism associated with a curvilinear crack path are examined using a model consisting of a macrocrack in a brittle solid with a curvilinear segment at the crack tip. A numerical procedure for finite and semiinfinite cracks is formulated and evaluated using an example which has an exact solution (a finite crack in the form of a circular arc in a uniform stress field). It is shown that, for a relatively small amplitude of crack path oscillations, the toughening ratio can be taken equal to the ratio of the corresponding crack path lengths. V.L.

A90-29215* Syracuse Univ., NY.

THE EQUIVALENCE BETWEEN DISLOCATION PILE-UPS AND CRACKS

H. W. LIU (Syracuse University, NY) and Q. GAO (Southwest Jiaotong University, Sichuan, People's Republic of China) Theoretical and Applied Fracture Mechanics (ISSN 0167-8442),

vol. 12, Feb. 1990, p. 195-204. refs

(Contract NAG3-837)

Copyright

Cracks and dislocation pile-ups are equivalent to each other. In this paper, the physical equivalence between cracks and pile-ups is delineated, and the relationships between crack-extension force, force on the leading dislocation, stress-intensity factor, and dislocation density are reviewed and summarized. These relations make it possible to extend quantitatively the recent advances in the concepts and practices of fracture mechanics to the studies of microfractures and microplastic deformations. Author

A90-29260* Florida Univ., Gainesville.

NEUROBIOLOGICAL COMPUTATIONAL MODELS IN STRUCTURAL ANALYSIS AND DESIGN

P. HAJELA (Florida, University, Gainesville) and L. BERKE (NASA, Lewis Research Center, Cleveland, OH) IN: AIAA/ASME/ASCE/AHS/ASC Structures, Structural Dynamics and Materials Conference, 31st, Long Beach, CA, Apr. 2-4, 1990, Technical Papers. Part 1. Washington, DC, American Institute of Aeronautics and Astronautics, 1990, p. 345-355. refs

(Contract NAG3-1086)

(AIAA PAPER 90-1133) Copyright

The present paper examines the role of neural computing strategies in structural analysis and design. A principal focus of the work resides in the use of neural networks to represent the force-displacement relationship in static structural analysis. Such models provide computationally efficient capabilities for reanalysis, and appear to be well suited for application in numerical optimum design. The paper presents an overview of the neural computing approach, with special emphasis on supervised learning techniques adopted in the present work. Special features of such learning strategies which have a direct bearing on numerical accuracy and efficiency, are examined in the context of representative structural optimization problems. Author

A90-29262* National Aeronautics and Space Administration. Lewis Research Center, Cleveland, OH.

MULTI-OBJECTIVE SHAPE AND MATERIAL OPTIMIZATION OF COMPOSITE STRUCTURES INCLUDING DAMPING

D. A. SARAVANOS and C. C. CHAMIS (NASA, Lewis Research Center, Cleveland, OH) IN: AIAA/ASME/ASCE/AHS/ASC Structures, Structural Dynamics and Materials Conference, 31st, Long Beach, CA, Apr. 2-4, 1990, Technical Papers. Part 1. Washington, DC, American Institute of Aeronautics and Astronautics, 1990, p. 371-377. refs

(AIAA PAPER 90-1135) Copyright

A multi-objective optimal design methodology is developed for light-weight, low-cost composite structures of improved dynamic performance. The design objectives include minimization of resonance amplitudes (or maximization of modal damping), weight, and material cost. The design vector includes micromechanics, laminate, and structural shape parameters. Performance constraints are imposed on static displacements, dynamic amplitudes, and natural frequencies. The effects of damping on the dynamics of composite structures are incorporated. Preliminary applications on a cantilever composite beam illustrated that only the proposed multi-objective optimization, as opposed to single objective functions, simultaneously improved all objectives. The significance of composite damping in the design of advanced composite structures was also demonstrated, indicating that design methods based on undamped dynamics may fail to improve the dynamic performance near resonances. Author

A90-29318* Clarkson Univ., Potsdam, NY.

PROGRESSION OF DAMAGE AND FRACTURE IN COMPOSITES UNDER DYNAMIC LOADING

LEVON MINNETYAN (Clarkson University, Potsdam, NY), PAPPU L. N. MURTHY, and CHRISTOS CHAMIS (NASA, Lewis Research Center, Cleveland, OH) IN: AIAA/ASME/ASCE/AHS/ASC Structures, Structural Dynamics and Materials Conference, 31st, Long Beach, CA, Apr. 2-4, 1990, Technical Papers. Part 2.

Washington, DC, American Institute of Aeronautics and Astronautics, 1990, p. 941-949. refs
(AIAA PAPER 90-0916) Copyright

A new computational simulation method is presented to evaluate the dynamic aspects of composite structural response and durability that could not be simulated previously. Composite structural behavior under any loading, geometry, composite system, laminate configuration, and boundary conditions can now be simulated. Structural degradation, delamination, fracture, and damage propagation are included in the simulation. An angle-ply composite plate structure under normal impact loading is used as an example to demonstrate the versatility of the simulation method. Author

A90-29324*# Worcester Polytechnic Inst., MA.
**LOCAL AND GLOBAL ACCURACY ESTIMATES FOR
BOUNDARY ELEMENT ANALYSIS**

JOSEPH J. RENCIS (Worcester Polytechnic Institute, MA), DALE A. HOPKINS, and CHRIS C. CHAMIS (NASA, Lewis Research Center, Cleveland, OH) IN: AIAA/ASME/ASCE/AHS/ASC Structures, Structural Dynamics and Materials Conference, 31st, Long Beach, CA, Apr. 2-4, 1990, Technical Papers. Part 2. Washington, DC, American Institute of Aeronautics and Astronautics, 1990, p. 1002-1009. refs
(AIAA PAPER 90-0930) Copyright

An a posteriori error estimation strategy for the boundary element solution of two-dimensional heat conduction problem is presented. The error estimate formulation is based on the boundary element equations and employs a least squares fit of the solutions obtained from these equations. A local error estimate is evaluated for the unknown quantity in each element. The global error estimates are found from local (element) quantities. The range and accuracy of the proposed strategy is very good as demonstrated by problems containing smooth and non-smooth solutions. Author

A90-29329*# Southwest Research Inst., San Antonio, TX.
**PROBABILISTIC ANALYSIS OF A MATERIALLY NONLINEAR
STRUCTURE**

H. R. MILLWATER, Y.-T. WU, and A. F. FOSSUM (Southwest Research Institute, San Antonio, TX) IN: AIAA/ASME/ASCE/AHS/ASC Structures, Structural Dynamics and Materials Conference, 31st, Long Beach, CA, Apr. 2-4, 1990, Technical Papers. Part 2. Washington, DC, American Institute of Aeronautics and Astronautics, 1990, p. 1048-1053. refs
(Contract NAS3-24389)
(AIAA PAPER 90-1099) Copyright

A probabilistic finite element program is used to perform probabilistic analysis of a materially nonlinear structure. The program used in this study is NESSUS (Numerical Evaluation of Stochastic Structure Under Stress), under development at Southwest Research Institute. The cumulative distribution function (CDF) of the radial stress of a thick-walled cylinder under internal pressure is computed and compared with the analytical solution. In addition, sensitivity factors showing the relative importance of the input random variables are calculated. Significant plasticity is present in this problem and has a pronounced effect on the probabilistic results. The random input variables are the material yield stress and internal pressure with Weibull and normal distributions, respectively. The results verify the ability of NESSUS to compute the CDF and sensitivity factors of a materially nonlinear structure. In addition, the ability of the Advanced Mean Value (AMV) procedure to assess the probabilistic behavior of structures which exhibit a highly nonlinear response is shown. Thus, the AMV procedure can be applied with confidence to other structures which exhibit nonlinear behavior. Author

A90-29332*# National Aeronautics and Space Administration.
Lewis Research Center, Cleveland, OH.
**A METHODOLOGY FOR EVALUATING THE RELIABILITY AND
RISK OF STRUCTURES UNDER COMPLEX SERVICE
ENVIRONMENTS**
MICHAEL C. SHIAO (NASA, Lewis Research Center; Sverdrup

Technology, Inc., Cleveland, OH) and CHRISTOS C. CHAMIS (NASA, Lewis Research Center, Cleveland, OH) IN: AIAA/ASME/ASCE/AHS/ASC Structures, Structural Dynamics and Materials Conference, 31st, Long Beach, CA, Apr. 2-4, 1990, Technical Papers. Part 2. Washington, DC, American Institute of Aeronautics and Astronautics, 1990, p. 1070-1080. refs
(AIAA PAPER 90-1102) Copyright

The theoretical basis and numerical implementation of NESSUS (Numerical Evaluation of Stochastic Structures Under Stress; Cruse et al., 1988), a computer code for probabilistic structural analyses of aerospace components, are described, with an emphasis on the use of NESSUS for reliability and risk assessment. Topics addressed include the structure of NESSUS, the material-properties model, computational procedures, probabilistic models of fatigue-crack initiation, risk/cost evaluation, fatigue-fracture analyses, and fatigue-crack propagation. Numerical results from typical applications are presented in extensive graphs and briefly characterized; the usefulness of NESSUS predictions for establishing inspection and retirement schedules and for component certification is indicated. T.K.

A90-29380*# National Aeronautics and Space Administration.
Lewis Research Center, Cleveland, OH.
**CONCURRENT PROCESSING ADAPTATION OF
AEROELASTIC ANALYSIS OF PROPPANS**

DURBHA V. MURTHY (NASA, Lewis Research Center, Cleveland; Toledo, University, OH) and DAVID C. JANETZKE (NASA, Lewis Research Center, Cleveland, OH) IN: AIAA/ASME/ASCE/AHS/ASC Structures, Structural Dynamics and Materials Conference, 31st, Long Beach, CA, Apr. 2-4, 1990, Technical Papers. Part 3. Washington, DC, American Institute of Aeronautics and Astronautics, 1990, p. 1551-1559. refs
(AIAA PAPER 90-1036) Copyright

This paper reports on a study involving the adaptation of an advanced aeroelastic analysis program to run concurrently on a shared memory multiple processor computer. The program uses a three-dimensional compressible unsteady aerodynamic model and blade normal modes to calculate aeroelastic stability and response of propfan blades. The identification of the computational parallelism within the sequential code and the scheduling of the concurrent subtasks to minimize processor idle time are discussed. Processor idle time in the calculation of the unsteady aerodynamic coefficients was reduced by the simple strategy of appropriately ordering the computations. Speedup and efficiency results are presented for the calculation of the matched flutter point of an experimental propfan model. The results show that efficiencies above 70 percent can be obtained using the present implementation with 7 processors. The parallel computational strategy described here is also applicable to other aeroelastic analysis procedures based on parallel methods. Author

A90-30250* National Aeronautics and Space Administration.
Lewis Research Center, Cleveland, OH.
**TAILORING OF COMPOSITE LINKS FOR OPTIMAL DAMPED
ELASTO-DYNAMIC PERFORMANCE**
D. A. SARAVANOS and C. C. CHAMIS (NASA, Lewis Research Center, Cleveland, OH) IN: Advances in design automation. New York, American Society of Mechanical Engineers, 1989, p. 151-159. Previously announced in STAR as N89-26912. refs
Copyright

A method is developed for the optimal design of composite links based on dynamic performance criteria directly related to structural modal damping and dynamic stiffness. An integrated mechanics theory correlates structural composite damping to the parameters of basic composite material systems, laminate parameters, link shape, and modal deformations. The inclusion of modal properties allows the selective minimization of vibrations associated with specific modes. Ply angles and fiber volumes are tailored to obtain optimal combinations of damping and stiffness. Applications to simple composite links indicate wide margins for trade-offs and illustrate the importance of various design variables to the optimal design. Author

39 STRUCTURAL MECHANICS

A90-32264* # State Univ. of New York, Buffalo.

DEVELOPMENT OF AN INTEGRATED BEM FOR HOT FLUID-STRUCTURE INTERACTION

G. F. DARGUSH and P. K. BANERJEE (New York, State University, Buffalo) ASME, Transactions, Journal of Engineering for Gas Turbines and Power (ISSN 0022-0825), vol. 112, April 1990, p. 243-250. refs

(Contract NAG3-712)

(ASME PAPER 89-GT-128) Copyright

A boundary element approach is developed for problems of hot fluid-structure interaction. The structure is idealized as a thermoelastic solid, and a time-domain, boundary-only integral formulation is described. Meanwhile, several approaches are discussed for the hot fluid. Integrals equations are developed for both compressible and incompressible thermoviscous flow. Due to the presence of nonlinear convective terms in the governing differential equations, domain discretization is generally required. However, with the introduction of reference velocities, volume modeling often can be confined to regions near obstacles and walls. All formulations are implemented for two-dimensional problems in GPO-BEST, a general purpose boundary element computer program. An overview of this numerical implementation is provided, along with several illustrative examples. The present fluid formulations are appropriate in the low to medium Reynolds number ranges; however, some enhancements required for higher speed simulations are noted.

Author

A90-34851* Colorado Univ., Boulder.

MIXED VARIATIONAL FORMULATION OF FINITE ELEMENT ANALYSIS OF ACOUSTOELASTIC/SLOSH FLUID-STRUCTURE INTERACTION

C. A. FELIPPA (Colorado, University, Boulder) and R. OHAYON (ONERA, Chatillon, France) Journal of Fluids and Structures (ISSN 0889-9746), vol. 4, Jan. 1990, p. 35-57. refs

(Contract NAG3-934)

Copyright

A general three-field variational principle is obtained for the motion of an acoustic fluid enclosed in a rigid or flexible container by the method of canonical decomposition applied to a modified form of the wave equation in the displacement potential. The general principle is specialized to a mixed two-field principle that contains the fluid displacement potential and pressure as independent fields. This principle contains a free parameter α . Semidiscrete finite-element equations of motion based on this principle are displayed and applied to the transient response and free-vibrations of the coupled fluid-structure problem. It is shown that a particular setting of α yields a rich set of formulations that can be customized to fit physical and computational requirements. The variational principle is then extended to handle slosh motions in a uniform gravity field, and used to derived semidiscrete equations of motion that account for such effects.

Author

A90-35429* Case Western Reserve Univ., Cleveland, OH.

BOUNDARY FLEXIBILITY METHOD OF COMPONENT MODE SYNTHESIS USING STATIC RITZ VECTORS

A. A. ABDALLAH and A. A. HUCKELBRIDGE (Case Western Reserve University, Cleveland, OH) Computers and Structures (ISSN 0045-7949), vol. 35, no. 1, 1990, p. 51-61. refs

(Contract NAG3-707)

Copyright

A method of dynamic substructuring is presented which provides for the incorporation of a set of static Ritz vectors, referred to as boundary flexibility vectors, as a replacement and/or supplement to conventional eigenvectors in component mode synthesis. The suggested boundary flexibility Ritz vectors are generated by an extension of Wilson's load-dependent Ritz vector algorithm for transient dynamic analysis. The extended algorithm is not load-dependent, is applicable to both fixed-and free-interface components, and results in a general component mode synthesis model appropriate for any type of dynamic analysis.

Author

A90-35462* National Aeronautics and Space Administration. Lewis Research Center, Cleveland, OH.

CALCULATION OF WEIBULL STRENGTH PARAMETERS AND BATDORF FLOW-DENSITY CONSTANTS FOR VOLUME- AND SURFACE-FLAW-INDUCED FRACTURE IN CERAMICS

S. PAI SHANTARAM (NASA, Lewis Research Center; W. L. Tanksley and Associates, Inc., Cleveland, OH) and JOHN P. GYEKENYESI (NASA, Lewis Research Center, Cleveland, OH) IN: Ceramic materials and components for engines; Proceedings of the Third International Symposium, Las Vegas, NV, Nov. 27-30, 1988. Westerville, OH, American Ceramic Society, Inc., 1989, p. 565-585. Previously announced in STAR as N89-12930. refs

Copyright

The calculation of shape and scale parameters of the two-parameter Weibull distribution is described using the least-squares analysis and maximum likelihood methods for volume- and surface-flaw-induced fracture in ceramics with complete and censored samples. Detailed procedures are given for evaluating 90 percent confidence intervals for maximum likelihood estimates of shape and scale parameters, the unbiased estimates of the shape parameters, and the Weibull mean values and corresponding standard deviations. Furthermore, the necessary steps are described for detecting outliers and for calculating the Kolmogorov-Smirnov and the Anderson-Darling goodness-of-fit statistics and 90 percent confidence bands about the Weibull distribution. It also shows how to calculate the Batdorf flaw-density constants by using the Weibull distribution statistical parameters. The techniques described were verified with several example problems, from the open literature, and were coded in the Structural Ceramics Analysis and Reliability Evaluation (SCARE) design program.

Author

A90-41223* # Akron Univ., OH.

EFFECTS OF STATE RECOVERY ON CREEP BUCKLING UNDER VARIABLE LOADING

D. N. ROBINSON (Akron, University, OH) and S. M. ARNOLD (NASA, Lewis Research Center, Cleveland, OH) ASME, Transactions, Journal of Applied Mechanics (ISSN 0021-8936), vol. 57, June 1990, p. 313-320. Previously announced in STAR as N88-21527. refs

(Contract NAG3-379)

Copyright

Structural alloys embody internal mechanisms that allow recovery of state with varying stress and elevated temperature, i.e., they can return to a softer state following periods of hardening. Such material behavior is known to strongly influence structural response under some important thermomechanical loadings, for example, that involving thermal ratchetting. The influence of dynamic and thermal recovery on the creep buckling of a column under variable loading is investigated. The column is taken as the idealized (Shanley) sandwich column. The constitutive model, unlike the commonly employed Norton creep model, incorporates a representation of both dynamic and thermal (state) recovery. The material parameters of the constitutive model are chosen to characterize Narloy Z, a representative copper alloy used in thrust nozzle liners of reusable rocket engines. Variable loading histories include rapid cyclic unloading/reloading sequences and intermittent reductions of load for extended periods of time; these are superimposed on a constant load. The calculated results show that state recovery significantly affects creep buckling under variable loading.

Author

A90-41278* Illinois Univ., Chicago.

A PROBABILISTIC APPROACH TO CRACK INSTABILITY

A. CHUDNOVSKY and B. KUNIN (Illinois, University, Chicago) IN: Advances in fracture research; Proceedings of the Seventh International Conference on Fracture (ICF7), Houston, TX, Mar. 20-24, 1989. Volume 1. Oxford, England and Elmsford, NY, Pergamon Press, 1989, p. 23-25. Research supported by the U.S. Navy. refs

(Contract NAG3-754)

Copyright

A probabilistic model of brittle fracture is examined with

reference to two-dimensional problems. The model is illustrated by using experimental data obtained for 25 macroscopically identical specimens made of short-fiber-reinforced composites. It is shown that the model proposed here provides a predictive formalism for the probability distributions of critical crack depth, critical loads, and crack arrest depths. It also provides similarity criteria for small-scale testing. V.L.

A90-41372* Illinois Univ., Chicago.

ENERGY ANALYSIS OF CRACK-DAMAGE INTERACTION

A. CHUDNOVSKY and SHAOFU WU (Illinois, University, Chicago) IN: Advances in fracture research; Proceedings of the Seventh International Conference on Fracture (ICF7), Houston, TX, Mar. 20-24, 1989. Volume 3. Oxford, England and Elmsford, NY, Pergamon Press, 1989, p. 2153-2160. refs
(Contract NAG3-754; AF-AFOSR-88-003)
Copyright

The energy release rates associated with a main crack propagating into a surrounding damage zone, and a damage zone translation relative to the main crack, as well as an energy of interaction between the two are analyzed. The displacement and stress fields for the crack-damage interaction problem are reconstructed employing a semi-empirical stress analysis and experimental evaluation of the average craze density in the crazed zone. Author

A90-43883* University of Southwest Jiaotong, Sichuan (China).

CHARACTERIZATION OF THE TIP FIELD OF A DISCRETE DISLOCATION PILEUP FOR THE DEVELOPMENT OF PHYSICALLY BASED MICROMECHANICS

Q. GAO (Southwest Jiaotong University, Chengdu, People's Republic of China) and H. W. LIU (Syracuse University, NY) Metallurgical Transactions A - Physical Metallurgy and Materials Science (ISSN 0360-2133), vol. 21A, July 1990, p. 2087-2089. refs
(Contract NAG3-837)
Copyright

It is shown, on the basis of calculations by Eshelby et al. (1951), Armstrong et al. (1966), and Chou and Li (1969), that a single parameter, such as the force on the leading dislocation (F), the crack extension force, or the stress intensity factor, is capable of characterizing uniquely the entire tip field of a discrete dislocation pileup, including the positions of mobile dislocations behind the locked leading dislocation at the tip. Conversely, the position of the i -th mobile dislocation $X(i)$ is related to the value of F and is capable of characterizing the entire stress, strain, and displacement fields at the tip of a discrete dislocation pileup. If the interactions between dislocations are linear elastic, the measured positions of the mobile dislocations can be used to determine the value of F , which can then be used as a quantitative measure of the strength of a dislocation barrier resisting the propagation of a microslip or the nucleation of a microfracture. I.S.

A90-45770* State Univ. of New York, Buffalo.

ADVANCED APPLICATIONS OF BEM TO INELASTIC ANALYSIS OF SOLIDS

P. K. BANERJEE and D. P. HENRY, JR. (New York, State University, Buffalo) IN: Industrial applications of boundary element methods. London and New York, Elsevier Applied Science, 1989, p. 39-75. Research supported by United Technologies Corp. refs
(Contract NAS3-23697)
Copyright

Newly evolved boundary element solution algorithms are utilized for solving a range of elastoplastic and thermoplastic problems. The first algorithm is the typical iterative procedure in which the unknown boundary solution and the initial stress (or strain) rates are found together in an incremental iterative fashion. The second one is a variable stiffness type approach in which the incremental boundary solution is obtained in a direct (noniterative) manner. The third procedure differs from the two prior algorithms in that volume integration is not needed to incorporate the nonlinear effects in the analysis. Instead, initial stress rates are introduced

in the boundary element system by way of particular integrals. The methodology is used in a general purpose, multiregion system that employs quadratic isoparametric shape functions to model the geometry and field variables of the body and can admit up to 15 substructured areas of different material properties. R.E.P.

A90-45771* State Univ. of New York, Buffalo.

ADVANCED DEVELOPMENT OF BEM FOR ELASTIC AND INELASTIC DYNAMIC ANALYSIS OF SOLIDS

P. K. BANERJEE, S. AHMAD, and H. C. WANG (New York, State University, Buffalo) IN: Industrial applications of boundary element methods. London and New York, Elsevier Applied Science, 1989, p. 77-117. Research supported by United Technologies Corp. refs
(Contract NAS3-23697)
Copyright

Direct Boundary Element formulations and their numerical implementation for periodic and transient elastic as well as inelastic transient dynamic analyses of two-dimensional, axisymmetric and three-dimensional solids are presented. The inelastic formulation is based on an initial stress approach and is the first of its kind in the field of Boundary Element Methods. This formulation employs the Navier-Cauchy equation of motion, Graffi's dynamic reciprocal theorem, Stokes' fundamental solution, and the divergence theorem, together with kinematical and constitutive equations to obtain the pertinent integral equations of the problem in the time domain within the context of the small displacement theory of elastoplasticity. The dynamic (periodic, transient as well as nonlinear transient) formulations have been applied to a range of problems. The numerical formulations presented here are included in the BEST3D and GPBEST systems. Author

A90-46068* Colorado Univ., Boulder.

VARIATIONAL FORMULATION OF HIGH-PERFORMANCE FINITE ELEMENTS - PARAMETRIZED VARIATIONAL PRINCIPLES

C. A. FELIPPA and C. MILITELLO (Colorado, University, Boulder) Computers and Structures (ISSN 0045-7949), vol. 36, no. 1, 1990, p. 1-11. refs
(Contract NAG3-934)
Copyright

High-performance (HP) elements are simple finite elements constructed to deliver engineering accuracy with coarse arbitrary grids. This paper is part of a series on the variational basis of HP elements, with emphasis on those constructed with the free formulation (FF) and assumed natural strain (ANS) methods. The present paper studies parametrized variational principles that provide a foundation for the FF and ANS methods, as well as for a combination of both methods. Author

A90-46172* National Aeronautics and Space Administration. Lewis Research Center, Cleveland, OH.

CHARACTERIZATION OF STRUCTURAL CONNECTIONS USING FREE AND FORCED RESPONSE TEST DATA

C. LAWRENCE (NASA, Lewis Research Center, Cleveland, OH) and A. A. HUCKELBRIDGE (Case Western Reserve University, Cleveland, OH) IN: Structural vibration and acoustics; Proceedings of the Twelfth Biennial ASME Conference on Mechanical Vibration and Noise, Montreal, Canada, Sept. 17-21, 1989. New York, American Society of Mechanical Engineers, 1989, p. 45-52. Previously announced in STAR as N89-21266. refs
Copyright

The accurate prediction of system dynamic response often has been limited by deficiencies in existing capabilities to characterize connections adequately. Connections between structural components often are complex mechanically, and difficult to accurately model analytically. Improved analytical models for connections are needed to improve system dynamic predictions. A procedure for identifying physical connection properties from free and forced response test data is developed, then verified utilizing a system having both a linear and nonlinear connection. Connection properties are computed in terms of physical parameters so that the physical characteristics of the connections

39 STRUCTURAL MECHANICS

can better be understood, in addition to providing improved input for the system model. The identification procedure is applicable to multi-degree of freedom systems, and does not require that the test data be measured directly at the connection locations.

Author

A90-46288* Colorado Univ., Boulder.

DEVELOPMENTS IN VARIATIONAL METHODS FOR HIGH PERFORMANCE PLATE AND SHELL ELEMENTS

C. A. FELIPPA and C. MITTELLO (Colorado, University, Boulder)
IN: Analytical and computational models of shells; Proceedings of the Symposium, ASME Winter Annual Meeting, San Francisco, CA, Dec. 10-15, 1989. New York, American Society of Mechanical Engineers, 1989, p. 191-215. refs
(Contract NAG3-934)

Copyright

This paper is part of a series on the variational foundations of high-performance elements, with emphasis on plate and shell elements constructed with the free formulation (FF) and assumed natural strain (ANS) methods. Attention is given to parametrized variational principles that provide a common foundation for the FF and ANS methods, as well as a combination of both. From this unified formulation, a variant of the ANS formulation called the 'assumed natural deviatoric strain' (ANDES) formulation, emerges as an important case. The first ANDES element, a high-performance 9-dof triangular Kirchhoff plate bending element, is briefly described to illustrate the use of the new formulation.

Author

A90-47567* National Aeronautics and Space Administration. Lewis Research Center, Cleveland, OH.

ANALYSIS OF IMPACT RESPONSE IN COMPOSITE PLATES

A. P. CHRISTOFOROU (NASA, Lewis Research Center, Cleveland, OH; Utah, University, Salt Lake City) and S. R. SWANSON (Utah, University, Salt Lake City) International Journal of Solids and Structures (ISSN 0020-7683), vol. 27, no. 2, 1991, p. 161-170. refs

Copyright

The problem of impact is of considerable interest in laminated composite materials. Although important contributions have been made in the understanding the impact problem through numerical solutions, an analytical solution has not been available for the problem of impact of laminated plates. The present work gives an analytical solution to this problem, based on the usual Fourier series expansion for simply-supported plates, combined with Laplace transform techniques for the impact problem solution.

Author

A90-49269* Illinois Univ., Chicago.

EFFECT OF CRACK-MICROCRACKS INTERACTION ON ENERGY RELEASE RATES

A. CHUDNOVSKY and SHAOFU WU (Illinois, University, Chicago) International Journal of Fracture (ISSN 0376-9429), vol. 44, July 1, 1990, p. 43-56. refs

(Contract NAG3-754; AF-AFOSR-88-003)

Copyright

The energy release rates associated with the main crack advancing into its surrounding damage zone, and the damage zone translation relative to the main crack, as well as the energy of interaction between the crack and the damage zone are analyzed. The displacement and stress fields for this crack-damage interaction problem are reconstructed by employing a semi-empirical stress analysis which involves experimental evaluation of the average microcrack density in the damage zone.

Author

A90-49792*# Southwest Research Inst., San Antonio, TX.

ADVANCED PROBABILISTIC STRUCTURAL ANALYSIS METHOD FOR IMPLICIT PERFORMANCE FUNCTIONS

Y.-T. WU, H. R. MILLWATER, and T. A. CRUSE (Southwest Research Institute, San Antonio, TX) AIAA Journal (ISSN 0001-1452), vol. 28, Sept. 1990, p. 1663-1669. Previously cited in

issue 12, p. 1859, Accession no. A89-30846. refs
(Contract NAS3-24389)
Copyright

A90-49869* Colorado Univ., Boulder.

ELECTROMAGNETIC FINITE ELEMENTS BASED ON A FOUR-POTENTIAL VARIATIONAL PRINCIPLE

JAMES SCHULER and CARLOS A. FELIPPA (Colorado, University, Boulder) Finite Elements in Analysis and Design (ISSN 0168-874X), vol. 6, June 1990, p. 321-339. refs
(Contract NAG3-934)

Copyright

Electromagnetic finite elements based on a variational principle that uses the electromagnetic four-potential as primary variable are derived. This choice is used to construct elements suitable for downstream coupling with mechanical and thermal finite elements for the analysis of electromagnetic/mechanical systems that involve superconductors. The main advantages of the four-potential as a basis for finite element formulation are: (1) the number of degrees of freedom per node remains modest as the problem dimensionality increases, (2) jump discontinuities on interfaces are naturally accommodated, and (3) statics as well as dynamics may be treated without any a priori approximations. The new elements are tested on an axisymmetric problem under steady-state forcing conditions. The results are in excellent agreement with analytical solutions.

Author

A90-50562* General Electric Co., Cincinnati, OH.

SIMULATION OF CRACK GROWTH AND CRACK CLOSURE UNDER LARGE CYCLIC PLASTICITY

K. S. KIM, R. H. VAN STONE, J. H. LAFLIN (GE Aircraft Engines, Cincinnati, OH), and T. W. ORANGE (NASA, Lewis Research Center, Cleveland, OH) IN: Fracture mechanics; Proceedings of the Twenty-first ASTM National Symposium, Annapolis, MD, June 28-30, 1988. Philadelphia, PA, American Society for Testing and Materials, 1990, p. 421-447. Research supported by GE Aircraft Engines. refs

(Contract NAS3-23940)

Copyright

The propagation of a crack during cyclic loading with large plasticity was simulated using a finite element method. The numerical procedure included the determination of crack closing and opening by examining the contact condition of the crack surfaces in the plasticity iteration. The method was applied to the growth of cracks in Alloy 718 single edge notch specimens at 538 C subject to strain cycling under both nominally elastic and elastoplastic conditions. The results show, among other things, that the crack closure and opening stresses become more compressive as the loading becomes more plastic, and that, under a given control condition, the closure and opening stresses become less compressive as the crack propagates.

Author

A90-50566* National Aeronautics and Space Administration. Lewis Research Center, Cleveland, OH.

METHOD AND MODELS FOR R-CURVE INSTABILITY CALCULATIONS

THOMAS W. ORANGE (NASA, Lewis Research Center, Cleveland, OH) IN: Fracture mechanics; Proceedings of the Twenty-first ASTM National Symposium, Annapolis, MD, June 28-30, 1988. Philadelphia, PA, American Society for Testing and Materials, 1990, p. 545-559. Previously announced in STAR as N88-23278. refs

Copyright

This paper presents a simple method for performing elastic R-curve instability calculations. For a single material-structure combination, the calculations can be done on some pocket calculators. On microcomputers and larger, it permits the development of a comprehensive program having libraries of driving force equations for different configurations and R-curve model equations for different materials. The paper also presents several model equations for fitting to experimental R-curve data, both linear elastic and elastoplastic. The models are fit to data from the literature to demonstrate their viability.

Author

A90-51480* State Univ. of New York, Buffalo.
**INELASTIC TRANSIENT DYNAMIC ANALYSIS OF
 THREE-DIMENSIONAL PROBLEMS BY BEM**
 S. AHMAD and P. K. BANERJEE (New York, State University,
 Buffalo) International Journal for Numerical Methods in
 Engineering (ISSN 0029-5981), vol. 29, Feb. 1990, p. 371-390.
 refs
 (Contract NAS3-23697)
 Copyright

A general direct boundary element formulation and its numerical
 implementation for solving transient dynamic problems of
 three-dimensional isotropic homogeneous or piecewise homo-
 geneous solids involving material nonlinearities are presented.
 The algorithm produces accurate results for static nonlinear
 problems by using large time steps. When a large value of yield
 stress is selected, the incremental inelastic transient algorithm
 produces results identical to those obtained by elastodynamic
 analysis. C.D.

A90-52007* United Technologies Corp., East Hartford, CT.
**FREE-VIBRATION ANALYSIS OF THREE-DIMENSIONAL
 SOLIDS BY BEM**

R. B. WILSON, N. M. MILLER (United Technologies Corp., Pratt
 and Whitney Group, East Hartford, CT), and P. K. BANERJEE
 (New York, State University, Buffalo) International Journal for
 Numerical Methods in Engineering (ISSN 0029-5981), vol. 30, June
 1990, p. 1737-1757. refs
 (Contract NAS3-23697)
 Copyright

This paper discusses the calculation of natural frequencies and
 mode shapes of three-dimensional solids, using the boundary
 element method. The method developed is based on the use of
 particular integrals of the elastic equilibrium equations, and employs
 only real arithmetic. It represents an extension to three dimensions
 of work previously carried out for two-dimensional problems by
 Ahmad and Banerjee (1986) and Nardini and Brebbia (1982). The
 method has been incorporated, for multiregion analysis, in the
 BEST3D (Boundary Element Solution Technology, Three-
 Dimensional) computer program. Results of the boundary
 element calculations are compared with analytical, finite element,
 and experimental results. Author

A90-52571* National Aeronautics and Space Administration.
 Lewis Research Center, Cleveland, OH.

**STATUS OF STRUCTURAL ANALYSIS OF 30 CM DIAMETER
 ION OPTICS**

GREGORY S. MACRAE and GARY T. HERING (NASA, Lewis
 Research Center, Cleveland, OH) AIAA, DGLR, and JSASS,
 International Electric Propulsion Conference, 21st, Orlando, FL,
 July 18-20, 1990. 15 p. refs
 (AIAA PAPER 90-2649) Copyright

Three structural finite element programs are compared with
 theory, experimental data, and each other to evaluate their
 usefulness for modeling the thermomechanical deflection of ion
 engine electrodes. Two programs, NASTRAN and MARC, used a
 Cray XMP and the third, Algor, used an IBM compatible personal
 computer. The shape of the applied temperature gradient greatly
 affects off-axis displacement, implying that an accurate temperature
 distribution is required to analyze new designs. The use of bulk
 material constants to model the perforated electrodes was
 investigated. The stress and displacement predictions are shown
 to be sensitive to the temperature gradient and the Young's
 modulus, and insensitive to number of nodes, above some minimum
 value, and the Poisson ratio used. The models are shown to be
 useful tools for evaluating designs. Experimental measurement of
 temperatures and displacements was identified as the most critical
 area for further work. Author

N90-10450* MARC Analysis Research Corp., Palo Alto, CA.
 Finite Element Factory.
**THE MHOST FINITE ELEMENT PROGRAM: 3-D INELASTIC
 ANALYSIS METHODS FOR HOT SECTION COMPONENTS.
 VOLUME 2: USER'S MANUAL Final Report**

SHOHEI NAKAZAWA Jul. 1989 136 p
 (Contract NAS3-23697)
 (NASA-CR-182235-VOL-2; NAS 1.26:182235-VOL-2;
 FEF/PD/1101/89-VOL-2) Avail: NTIS HC A07/MF A01 CSCL
 20/11

The user options available for running the MHOST finite element
 analysis package is described. MHOST is a solid and structural
 analysis program based on the mixed finite element technology,
 and is specifically designed for 3-D inelastic analysis. A family of
 2- and 3-D continuum elements along with beam and shell structural
 elements can be utilized, many options are available in the
 constitutive equation library, the solution algorithms and the analysis
 capabilities. The outline of solution algorithms is discussed along
 with the data input and output, analysis options including the user
 subroutines and the definition of the finite elements implemented
 in the program package. Author

N90-10451* MARC Analysis Research Corp., Palo Alto, CA.
 Finite Element Factory.

**THE MHOST FINITE ELEMENT PROGRAM: 3-D INELASTIC
 ANALYSIS METHODS FOR HOT SECTION COMPONENTS.
 VOLUME 3: SYSTEMS' MANUAL Final Report**

SHOHEI NAKAZAWA Jul. 1989 216 p
 (Contract NAS3-23697)
 (NASA-CR-182236; NAS 1.26:182236; FEF/PD/1102/89-VOL-3)
 Avail: NTIS HC A10/MF A02 CSCL 20/11

The internal structure is discussed of the MHOST finite element
 program designed for 3-D inelastic analysis of gas turbine hot
 section components. The computer code is the first implementation
 of the mixed iterative solution strategy for improved efficiency and
 accuracy over the conventional finite element method. The control
 structure of the program is covered along with the data storage
 scheme and the memory allocation procedure and the file handling
 facilities including the read and/or write sequences. Author

N90-10455* Tulane Univ., New Orleans, LA.

MECHANICS OF THE CRACK PATH FORMATION Final Report

ASHER A. RUBINSTEIN Sep. 1989 21 p
 (Contract NAG3-815)
 (NASA-CR-185143; NAS 1.26:185143; E-5070) Avail: NTIS HC
 A03/MF A01 CSCL 20/11

A detailed analysis of experimentally obtained curvilinear crack
 path trajectories formed in a heterogeneous stress field is
 presented. Experimental crack path trajectories were used as data
 for numerical simulations, recreating the actual stress field
 governing the development of the crack path. Thus, the current
 theories of crack curving and kinking could be examined by
 comparing them with the actual stress field parameters as they
 develop along the experimentally observed crack path. The
 experimental curvilinear crack path trajectories were formed in the
 tensile specimens with a hole positioned in the vicinity of a potential
 crack path. The numerical simulation, based on the solution of
 equivalent boundary value problems with the possible perturbations
 of the crack path, is presented here. Author

N90-11332* Case Western Reserve Univ., Cleveland, OH. Dept.
 of Civil Engineering.

**THREE-DIMENSIONAL ANALYSIS OF SURFACE
 CRACK-HERTZIAN STRESS FIELD INTERACTION Final
 Report**

R. BALLARINI and Y. HSU Washington NASA Oct. 1989
 165 p
 (Contract NAG3-396)
 (NASA-CR-4254; E-5013; NAS 1.26:4254) Avail: NTIS HC
 A08/MF A01 CSCL 20/11

The results are presented of a stress intensity factor analysis
 of semicircular surface cracks in the inner raceway of an engine
 bearing. The loading consists of a moving spherical Hertzian
 contact load and an axial stress due to rotation and shrink fit. A
 3-D linear elastic Boundary Element Method code was developed
 to perform the stress analysis. The element library includes linear
 and quadratic isoparametric surface elements. Singular quarter
 point elements were employed to capture the square root

39 STRUCTURAL MECHANICS

displacement variation and the inverse square root stress singularity along the crack front. The program also possesses the capability to separate the whole domain into two subregions. This procedure enables one to solve nonsymmetric fracture mechanics problems without having to separate the crack surfaces a priori. A wide range of configuration parameters was investigated. The ratio of crack depth to bearing thickness was varied from one-sixtieth to one-fifth for several different locations of the Hertzian load. The stress intensity factors for several crack inclinations were also investigated. The results demonstrate the efficiency and accuracy of the Boundary Element Method. Moreover, the results can provide the basis for crack growth calculations and fatigue life prediction.

Author

N90-12041*# National Aeronautics and Space Administration. Lewis Research Center, Cleveland, OH.

EFFECTS OF MISTUNING AND MATRIX STRUCTURE ON THE TOPOLOGY OF FREQUENCY RESPONSE CURVES

DARE AFOLABI Oct. 1989 48 p

(Contract NASA ORDER C-99066-G)

(NASA-TM-102290; ICOMP-89-17; E-4960; NAS 1.15:102290)

Avail: NTIS HC A03/MF A01 CSCL 20/11

The stability of a frequency response curve under mild perturbations of the system's matrix is investigated. Using recent developments in the theory of singularities of differentiable maps, it is shown that the stability of a response curve depends on the structure of the system's matrix. In particular, the frequency response curves of a cyclic system are shown to be unstable. Consequently, slight parameter variations engendered by mistuning will induce a significant difference in the topology of the forced response curves, if the mistuning transformation crosses the bifurcation set.

Author

N90-12950*# National Aeronautics and Space Administration. Lewis Research Center, Cleveland, OH.

A THERMOELASTIC TRANSVERSELY ISOTROPIC THICK WALLED CYLINDER/DISK APPLICATION: AN ANALYTICAL SOLUTION AND STUDY

S. M. ARNOLD Oct. 1989 46 p

(NASA-TM-102320; E-5016; NAS 1.15:102320) Avail: NTIS HC

A03/MF A01 CSCL 20/11

A continuum theory is utilized to represent the thermoelastic behavior of a thick walled composite cylinder that can be idealized as transversely isotropic. A multiaxial statement of the constitutive theory employed is presented, as well as the out of the plane of isotropy, plane stress, and plane strain reductions. The derived analytical solution presented is valid for a cylindrical tube or thin disk with a concentric hole, subjected to internal and/or external pressure and a general radial temperature distribution. A specific problem examined is that of a thick walled cylinder subjected to an internal and external pressure loading and a linear radial temperature distribution. The results are expressed in non-dimensional form and the effects on the response behavior are examined for various material properties, fiber orientation and types of loadings.

Author

N90-13819*# National Aeronautics and Space Administration. Lewis Research Center, Cleveland, OH.

MEAN STRESS AND THE EXHAUSTION OF FATIGUE-DAMAGE RESISTANCE

AVRAHAM BERKOVITS Nov. 1989 18 p

(NASA-TM-101311; E-4307; NAS 1.15:101311) Avail: NTIS HC

A03/MF A01 CSCL 20/11

Mean-stress effects on fatigue life are critical in isothermal and thermomechanically loaded materials and composites. Unfortunately, existing mean-stress life-prediction methods do not incorporate physical fatigue damage mechanisms. An objective is to examine the relation between mean-stress induced damage (as measured by acoustic emission) and existing life-prediction methods. Acoustic emission instrumentation has indicated that, as with static yielding, fatigue damage results from dislocation buildup and motion until dislocation saturation is reached, after which void formation and coalescence predominate. Correlation of damage

processes with similar mechanisms under monotonic loading led to a reinterpretation of Goodman diagrams for 40 alloys and a modification of Morrow's formulation for life prediction under mean stresses. Further testing, using acoustic emission to monitor dislocation dynamics, can generate data for developing a more general model for fatigue under mean stress.

Author

N90-14640*# National Aeronautics and Space Administration. Lewis Research Center, Cleveland, OH.

VISCOPLASTICITY: A THERMODYNAMIC FORMULATION

A. D. FREED and J. L. CHABOCHE (Office National d'Etudes et de Recherches Aerospatiales, Paris, France) Nov. 1989 21 p

Submitted for publication

(NASA-TM-102388; E-5129; NAS 1.15:102388) Avail: NTIS HC

A03/MF A01 CSCL 20/11

A thermodynamic foundation using the concept of internal state variables is given for a general theory of viscoplasticity, as it applies to initially isotropic materials. Three fundamental internal state variables are admitted. They are: a tensor valued back stress for kinematic effects, and the scalar valued drag and yield strengths for isotropic effects. All three are considered to phenomenologically evolve according to competitive processes between strain hardening, strain induced dynamic recovery, and time induced static recovery. Within this phenomenological framework, a thermodynamically admissible set of evolution equations is put forth. This theory allows each of the three fundamental internal variables to be composed as a sum of independently evolving constituents.

Author

N90-14641*# National Aeronautics and Space Administration. Lewis Research Center, Cleveland, OH.

THERMAL FATIGUE DURABILITY FOR ADVANCED PROPULSION MATERIALS

GARY R. HALFORD Oct. 1989 13 p Presented at the Australian Aeronautical Conference, Melbourne, Australia, 9-11 Oct. 1989; sponsored in part by The Inst. of Engineers, Australia; The Royal Aeronautical Society; and The Aeronautical Research Lab. (NASA-TM-102348; E-5057; NAS 1.15:102348) Avail: NTIS HC

A03/MF A01 CSCL 20/11

A review is presented of thermal and thermomechanical fatigue (TMF) crack initiation life prediction and cyclic constitutive modeling efforts sponsored recently by the NASA Lewis Research Center in support of advanced aeronautical propulsion research. A brief description is provided of the more significant material durability models that were created to describe TMF fatigue resistance of both isotropic and anisotropic superalloys, with and without oxidation resistant coatings. The two most significant crack initiation models are the cyclic damage accumulation model and the total strain version of strainrange partitioning. Unified viscoplastic cyclic constitutive models are also described. A troika of industry, university, and government research organizations contributed to the generation of these analytic models. Based upon current capabilities and established requirements, an attempt is made to project which TMF research activities most likely will impact future generation propulsion systems.

Author

N90-14642*# National Aeronautics and Space Administration. Lewis Research Center, Cleveland, OH.

A NONLINEAR HIGH TEMPERATURE FRACTURE MECHANICS BASIS FOR STRAINRANGE PARTITIONING

TAKAYUKI KITAMURA (Kyoto Univ., Japan) and GARY R. HALFORD Oct. 1989 17 p

(NASA-TM-4133; E-4733; NAS 1.15:4133) Avail: NTIS HC

A03/MF A01 CSCL 20/11

A direct link was established between Strainrange Partitioning (SRP) and high temperature fracture mechanics by deriving the general SRP inelastic strain range versus cyclic life relationships from high temperature, nonlinear, fracture mechanics considerations. The derived SRP life relationships are in reasonable agreement based on the experience of the SRP behavior of many high temperature alloys. In addition, fracture mechanics has served as a basis for derivation of the Ductility-Normalized SRP life equations, as well as for examination of SRP relations that are

applicable to thermal fatigue life prediction. Areas of additional links between nonlinear fracture mechanics and SRP were identified for future exploration. These include effects of multiaxiality as well as low strain, nominally elastic, long life creep fatigue interaction.

Author

N90-14652*# Ohio Univ., Athens. Dept. of Civil Engineering.
**PARALLEL EIGENANALYSIS OF FINITE ELEMENT MODELS
 IN A COMPLETELY CONNECTED ARCHITECTURE Final
 Report**

F. A. AKL and M. R. MOREL Nov. 1989 112 p
 (Contract NAG3-762)
 (NASA-CR-185166; NAS 1.26:185166) Avail: NTIS HC A06/MF
 A01 CSCL 20/11

A parallel algorithm is presented for the solution of the generalized eigenproblem in linear elastic finite element analysis, $(K)(\phi) = (M)(\phi)(\omega)$, where (K) and (M) are of order N , and (ω) is order of q . The concurrent solution of the eigenproblem is based on the multifrontal/modified subspace method and is achieved in a completely connected parallel architecture in which each processor is allowed to communicate with all other processors. The algorithm was successfully implemented on a tightly coupled multiple-instruction multiple-data parallel processing machine, Cray X-MP. A finite element model is divided into m domains each of which is assumed to process n elements. Each domain is then assigned to a processor or to a logical processor (task) if the number of domains exceeds the number of physical processors. The macrotasking library routines are used in mapping each domain to a user task. Computational speed-up and efficiency are used to determine the effectiveness of the algorithm. The effect of the number of domains, the number of degrees-of-freedom located along the global fronts and the dimension of the subspace on the performance of the algorithm are investigated. A parallel finite element dynamic analysis program, p-feda, is documented and the performance of its subroutines in parallel environment is analyzed.

Author

N90-14655*# National Aeronautics and Space Administration.
 Lewis Research Center, Cleveland, OH.

**A NEW UNIFORMLY VALID ASYMPTOTIC INTEGRATION
 ALGORITHM FOR ELASTO-PLASTIC-CREEP AND UNIFIED
 VISCOPLASTIC THEORIES INCLUDING CONTINUUM DAMAGE**

A. CHULYA and K. P. WALKER (Engineering Science Software, Inc., Smithfield, RI.) Dec. 1989 72 p
 (Contract NASA ORDER C-99066-G)
 (NASA-TM-102344; E-5052; ICOMP-89-22; NAS 1.15:102344)
 Avail: NTIS HC A04/MF A01 CSCL 20/11

A new scheme to integrate a system of stiff differential equations for both the elasto-plastic creep and the unified viscoplastic theories is presented. The method has high stability, allows large time increments, and is implicit and iterative. It is suitable for use with continuum damage theories. The scheme was incorporated into MARC, a commercial finite element code through a user subroutine called HYPELA. Results from numerical problems under complex loading histories are presented for both small and large scale analysis. To demonstrate the scheme's accuracy and efficiency, comparisons to a self-adaptive forward Euler method are made.

Author

N90-14656*# National Aeronautics and Space Administration.
 Lewis Research Center, Cleveland, OH.

**CONCURRENT PROCESSING ADAPTATION OF
 AEROPLASTIC ANALYSIS OF PROPFANS**

DAVID C. JANETZKE and DURBHA V. MURTHY (Toledo Univ., OH.) Jan. 1990 24 p Prepared for presentation at the 31st Structures, Structural Dynamics, and Materials Conference, Long Beach, CA, 2-4 Apr. 1990; cosponsored by AIAA, ASME, ASCE, AHS, and ASC
 (Contract NAG3-742)
 (NASA-TM-102455; E-5105; NAS 1.15:102455) Avail: NTIS HC
 A03/MF A01 CSCL 20/11

Discussed here is a study involving the adaptation of an advanced aeroelastic analysis program to run concurrently on a

shared memory multiple processor computer. The program uses a three-dimensional compressible unsteady aerodynamic model and blade normal modes to calculate aeroelastic stability and response of propfan blades. The identification of the computational parallelism within the sequential code and the scheduling of the concurrent subtasks to minimize processor idle time are discussed. Processor idle time in the calculation of the unsteady aerodynamic coefficients was reduced by the simple strategy of appropriately ordering the computations. Speedup and efficiency results are presented for the calculation of the matched flutter point of an experimental propfan model. The results show that efficiencies above 70 percent can be obtained using the present implementation with 7 processors. The parallel computational strategy described here is also applicable to other aeroelastic analysis procedures based on panel methods.

Author

N90-17173*# National Aeronautics and Space Administration.
 Lewis Research Center, Cleveland, OH.

**EIGENSOLUTION OF FINITE ELEMENT PROBLEMS IN A
 COMPLETELY CONNECTED PARALLEL ARCHITECTURE**

FRED A. AKL and MICHAEL R. MOREL (Ohio Univ., Athens.) 1989 12 p Presented at the 30th Structures, Structural Dynamics, and Materials Conference, Mobile, AL, 3-5 Apr. 1989; cosponsored by AIAA, ASME, ASCE, AHS, and ACS
 (Contract NASA ORDER C-99066-G)
 (NASA-TM-102450; E-5235; ICOMP-89-31; NAS 1.15:102450;
 AIAA-89-1395) Avail: NTIS HC A03/MF A01 CSCL 20/11

A parallel algorithm for the solution of the generalized eigenproblem in linear elastic finite element analysis, $(K)(\phi) = (M)(\phi)(\omega)$, where (K) and (M) are of order N , and (ω) is of order q is presented. The parallel algorithm is based on a completely connected parallel architecture in which each processor is allowed to communicate with all other processors. The algorithm has been successfully implemented on a tightly coupled multiple-instruction-multiple-data (MIMD) parallel processing computer, Cray X-MP. A finite element model is divided into m domains each of which is assumed to process n elements. Each domain is then assigned to a processor, or to a logical processor (task) if the number of domains exceeds the number of physical processors. The macro-tasking library routines are used in mapping each domain to a user task. Computational speed-up and efficiency are used to determine the effectiveness of the algorithm. The effect of the number of domains, the number of degrees-of-freedom located along the global fronts and the dimension of the subspace on the performance of the algorithm are investigated. For a 64-element rectangular plate, speed-ups of 1.86, 3.13, 3.18 and 3.61 are achieved on two, four, six and eight processors, respectively.

Author

N90-17180*# National Aeronautics and Space Administration.
 Lewis Research Center, Cleveland, OH.

**COMPATIBILITY CONDITIONS OF STRUCTURAL MECHANICS
 FOR FINITE ELEMENT ANALYSIS**

SURYA N. PATNAIK, LASZLO BERKE, and RICHARD H. GALLAGHER (Clarkson Univ., Potsdam, NY.) Jan. 1990 35 p
 (NASA-TM-102413; E-4966; NAS 1.15:102413) Avail: NTIS HC
 A03/MF A01 CSCL 20/11

The equilibrium equations and the compatibility conditions are fundamental to the analyses of structures. However, anyone who undertakes even a cursory generic study of the compatibility conditions can discover, with little effort, that historically this facet of structural mechanics had not been adequately researched by the profession. Now the compatibility conditions (CC's) have been researched and are understood to a great extent. For finite element discretizations, the CC's are banded and can be divided into three distinct categories: (1) the interface CC's; (2) the cluster or field CC's; and (3) the external CC's. The generation of CC's requires the separating of a local region, then writing the deformation displacement relation (ddr) for the region, and finally, the eliminating of the displacements from the ddr. The procedure to generate all three types of CC's is presented and illustrated through examples of finite element models. The uniqueness of the CC's thus generated is shown.

Author

39 STRUCTURAL MECHANICS

N90-18064*# National Aeronautics and Space Administration. Lewis Research Center, Cleveland, OH.

STEADY-STATE AND TRANSIENT ZENER PARAMETERS IN VISCOPLASTICITY: DRAG STRENGTH VERSUS YIELD STRENGTH

A. D. FREED and K. P. WALKER (Engineering Science Software, Inc., Smithfield, RI.) 1990 12 p Proposed for presentation at the 11th US National Congress of Applied Mechanics, Tucson, AZ, 21-25 May 1990
(NASA-TM-102487; E-5278; NAS 1.15:102487) Avail: NTIS HC A03/MF A01 CSCL 20/11

A hypothesis is put forth which enables the viscoplastician to formulate a theory of viscoplasticity that reduces, in closed form, to the classical theory of creep. This hypothesis is applied to a variety of drag and yield strength models. Because of two theoretical restrictions that are a consequence of this hypothesis, three different yield strength models and one drag strength model are shown to be theoretically admissible. One of these yield strength models is selected as being the most appropriate representation for isotropic hardening. Author

N90-18071*# Pittsburgh Univ., PA. Dept. of Mechanical Engineering.

TRANSIENT FINITE ELEMENT COMPUTATIONS ON THE TRANSPUTER SYSTEM Final Report

PATRICK J. SMOLINSKI Feb. 1990 37 p
(Contract NAG3-829)
(NASA-CR-185199; NAS 1.26:185199) Avail: NTIS HC A03/MF A01 CSCL 20/11

The aim was to study the solution of transient finite element problems on the Transputer system of parallel processors. The central difference time integration rule was used so that no equation solving was necessary. Also investigated was subcycling time integration which uses different time steps in different subdomains of the finite element mesh. A one-dimensional bar problem was analyzed using the parallel time integration algorithm. This involves subdividing the bar into subproblems which are assigned to different processors. Results show that the significant speed-up can be obtained through parallel processing. Also subcycling can give an additional speed-up in certain classes of problems. A two-dimensional problem was also examined to evaluate the effect of the communication to computation ratio on solution time. Author

N90-18081*# National Aeronautics and Space Administration. Lewis Research Center, Cleveland, OH.

INTEGRATED FORCE METHOD VERSUS DISPLACEMENT METHOD FOR FINITE ELEMENT ANALYSIS

SURYA N. PATNAIK, LASZLO BERKE, and RICHARD H. GALLAGHER (Clarkson Univ., Potsdam, NY.) Washington Feb. 1990 33 p
(NASA-TP-2937; E-4604; NAS 1.60:2937) Avail: NTIS HC A03/MF A01 CSCL 20/11

A novel formulation termed the integrated force method (IFM) has been developed in recent years for analyzing structures. In this method all the internal forces are taken as independent variables, and the system equilibrium equations (EE's) are integrated with the global compatibility conditions (CC's) to form the governing set of equations. In IFM the CC's are obtained from the strain formulation of St. Venant, and no choices of redundant load systems have to be made, in contrast to the standard force method (SFM). This property of IFM allows the generation of the governing equation to be automated straightforwardly, as it is in the popular stiffness method (SM). In this report IFM and SM are compared relative to the structure of their respective equations, their conditioning, required solution methods, overall computational requirements, and convergence properties as these factors influence the accuracy of the results. Overall, this new version of the force method produces more accurate results than the stiffness method for comparable computational cost. Author

N90-18470*# National Aeronautics and Space Administration. Lewis Research Center, Cleveland, OH.

PROBABILITY OF FAILURE AND RISK ASSESSMENT OF PROPULSION STRUCTURAL COMPONENTS

MICHAEL C. SHIAO (Sverdrup Technology, Inc., Cleveland, OH.) and CHRISTOS C. CHAMIS In Johns Hopkins Univ., The 1989 JANNAF Propulsion Meeting, Volume 1 p 135-162 May 1989
Avail: NTIS HC A25/MF A04 CSCL 20/11

Due to increasing need to account for the uncertainties in material properties, loading conditions, or geometries, a methodology was developed to determine structural reliability and the assess the risk associated with it. The methodology consists of a probabilistic structural analysis by a probabilistic finite element computer code Nonlinear Evaluation of Stochastic Structures Under Stress (NESSUS) and a generic probabilistic material properties model. The methodology is versatile and is equally applicable to high and cryogenic temperature structures. Results obtained demonstrate that the whole issue of structural reliability and risk can be formally evaluated using the methodology developed which is inclusive of uncertainties in material properties, structural parameters and loading conditions. The methodology is described in some detail with illustrative examples. Author

N90-18745*# National Aeronautics and Space Administration. Lewis Research Center, Cleveland, OH.

A GLOBAL APPROACH FOR THE IDENTIFICATION OF STRUCTURAL CONNECTION PROPERTIES

CHARLES LAWRENCE and ARTHUR A. HUCKELBRIDGE (Case Western Reserve Univ., Cleveland, OH.) Feb. 1990 16 p
(NASA-TM-102502; E-5303; NAS 1.15:102502) Avail: NTIS HC A03/MF A01 CSCL 20/11

A general procedure is developed for identifying properties of structural joints. The procedure, which uses experimental response data, is considered general because it is applicable to any size or type of structural system. The present procedure, which identifies characteristics such as damping and stiffness, accommodates both linear and nonlinear joint properties and may process test data measured at arbitrary stations on the structural system. The method identifies joint characteristics by performing a global fit between predicted and measured data. It overcomes limitations of previous methods in that it can better deal with parameter-dependent constraints (e.g., gaps). The method is demonstrated with a simplified model of a bladed disk assembly having friction damping and mistuning. Author

N90-19617*# National Aeronautics and Space Administration. Lewis Research Center, Cleveland, OH.

A TRANSIENT PLASTICITY STUDY AND LOW CYCLE FATIGUE ANALYSIS OF THE SPACE STATION FREEDOM PHOTOVOLTAIC SOLAR ARRAY BLANKET

SASAN C. ARMAND, MEI-HWA LIAO, and RONALD W. MORRIS (Sverdrup Technology, Inc., Cleveland, OH.) 1990 16 p
Presented at the 1990 MSC World Users Conference, Los Angeles, CA, 26-30 Mar. 1990; sponsored by Macneal-Schwendler Corporation
(NASA-TM-102516; E-5321; NAS 1.15:102516) Avail: NTIS HC A03/MF A01 CSCL 20/11

The Space Station Freedom photovoltaic solar array blanket assembly is comprised of several layers of materials having dissimilar elastic, thermal, and mechanical properties. The operating temperature of the solar array, which ranges from -75 to +60 C, along with the material incompatibility of the blanket assembly components combine to cause an elastic-plastic stress in the weld points of the assembly. The weld points are secondary structures in nature, merely serving as electrical junctions for gathering the current. The thermal mechanical loading of the blanket assembly operating in low earth orbit continually changes throughout each 90 min orbit, which raises the possibility of fatigue induced failure. A series of structural analyses were performed in an attempt to predict the fatigue life of the solar cell in the Space Station Freedom photovoltaic array blanket. A nonlinear elastic-plastic MSC/NASTRAN analysis followed by a fatigue calculation indicated a fatigue life of 92,000 to 160,000 cycles for the solar cell weld

tabs. Additional analyses predict a permanent buckling phenomenon in the copper interconnect after the first loading cycle. This should reduce or eliminate the pulling of the copper interconnect on the joint where it is welded to the silicon solar cell. It is concluded that the actual fatigue life of the solar array blanket assembly should be significantly higher than the calculated 92,000 cycles, and thus the program requirement of 87,500 cycles (orbits) will be met. Another important conclusion that can be drawn from the overall analysis is that, the strain results obtained from the MSC/NASTRAN nonlinear module are accurate to use for low-cycle fatigue analysis, since both thermal cycle testing of solar cells and analysis have shown higher fatigue life than the minimum program requirement of 87,500 cycles. Author

N90-19629*# National Aeronautics and Space Administration. Lewis Research Center, Cleveland, OH.
DEMONSTRATION OF CAPABILITIES OF HIGH TEMPERATURE COMPOSITES ANALYZER CODE HITCAN
 SURENDRA N. SINGHAL, JOSEPH J. LACKNEY (Sverdrup Technology, Inc., Cleveland, OH.), CHRISTOS C. CHAMIS, and PAPPU L. N. MURTHY Mar. 1990 56 p
 (NASA-TM-102560; E-5380; NAS 1.15:102560) Avail: NTIS HC A04/MF A01 CSCL 20/11

The capabilities a high temperature composites analyzer code, HITCAN which predicts global structural and local stress-strain response of multilayered metal matrix composite structures, are demonstrated. The response can be determined both at the constituent (fiber, matrix, and interphase) and the structure level and includes the fabrication process effects. The thermo-mechanical properties of the constituents are considered to be nonlinearly dependent on several parameters including temperature, stress, and stress rate. The computational procedure employs an incremental iterative nonlinear approach utilizing a multifactor-interactive constituent material behavior model. Various features of the code are demonstrated through example problems for typical structures. Author

N90-20428*# National Aeronautics and Space Administration. Lewis Research Center, Cleveland, OH.
COMPUTER SIMULATION OF THE MATHEMATICAL MODELING INVOLVED IN CONSTITUTIVE EQUATION DEVELOPMENT: VIA SYMBOLIC COMPUTATIONS
 S. M. ARNOLD, H. Q. TAN, and X. DONG (Akron Univ., OH.) 1989 13 p Presented at the 7th International Conference on Mathematical and Computer Modeling, Chicago, IL, 2-5 Aug. 1989; cosponsored by IAMCM and IMACS
 (NASA-TM-102532; E-5276; NAS 1.15:102532) Avail: NTIS HC A03/MF A01 CSCL 20/11

Development of new material models for describing the high temperature constitutive behavior of real materials represents an important area of research in engineering disciplines. Derivation of mathematical expressions (constitutive equations) which describe this high temperature material behavior can be quite time consuming, involved and error prone; thus intelligent application of symbolic systems to facilitate this tedious process can be of significant benefit. A computerized procedure (SDICE) capable of efficiently deriving potential based constitutive models, in analytical form is presented. This package, running under MACSYMA, has the following features: partial differentiation, tensor computations, automatic grouping and labeling of common factors, expression substitution and simplification, back substitution of invariant and tensorial relations and a relational data base. Also limited aspects of invariant theory were incorporated into SDICE due to the utilization of potentials as a starting point and the desire for these potentials to be frame invariant (objective). Finally not only calculation of flow and/or evolutionary laws were accomplished but also the determination of history independent nonphysical coefficients in terms of physically measurable parameters, e.g., Young's modulus, was achieved. The uniqueness of SDICE resides in its ability to manipulate expressions in a general yet predefined order and simplify expressions so as to limit expression growth. Results are displayed when applicable utilizing index notation. Author

N90-20431*# National Aeronautics and Space Administration. Lewis Research Center, Cleveland, OH.
MODEL DEVELOPMENT IN VISCOPLASTIC RATCHETTING
 ALAN D. FREED and KEVIN P. WALKER (Engineering Science Software, Inc., Smithfield, RI.) Apr. 1990 32 p
 (NASA-TM-102509; E-5311; NAS 1.15:102509) Avail: NTIS HC A03/MF A01 CSCL 20/11

Space Station Freedom's solar dynamic power modules, like all power plants, contain components that are subjected to conditions which favor thermally driven ratchetting. Existing viscoplastic models tend to overpredict ratchetting behavior, because their back stress (the kinematic variable) seems to stick more than it should during unloading. For this reason, a study was undertaken to compare a variety of possible modifications to the evolution equation for back stress. All models considered herein have a hardening vs. dynamic-recovery format. To remove the stickiness of the back stress, a linear dependence on stress rate is introduced into the evolution equation for back stress in a variety of ways. Several favorable models were screened out of the field of candidates by qualitatively determining their relative ability to fit experimentally observed behavior through six numerical experiments. A final selection must be made by quantitatively correlating the proposed models with experimental data, and then seeing which candidate does the best job of predicting observed ratchetting behavior. This is a subject of future work. Author

N90-20432*# National Aeronautics and Space Administration. Lewis Research Center, Cleveland, OH.
COMPUTATIONAL SIMULATION OF DAMPING IN COMPOSITE STRUCTURES
 D. A. SARAVANOS and C. C. CHAMIS Jul. 1989 26 p Presented at the 2nd National Congress in Mechanics, Athens, Greece, 29 Jun. - 1 Jul. 1989
 (NASA-TM-102567; E-5143; NAS 1.15:102567) Avail: NTIS HC A03/MF A01 CSCL 20/11

A computational methodology is developed for the prediction of passive damping in composite structures. The method involves multiple levels of damping modeling by integrating micromechanics, laminate, and structural damping theories. The effects of temperature and moisture on structural damping are included. The simulation of damping in the structural level is accomplished with finite-element discretization. Applications are performed on graphite/epoxy composite beams, plates, and shells to illustrate the methodology. Additional parametric studies demonstrate the variation of structural modal damping with respect to ply angles, fiber volume ratio, and temperature. Author

N90-20438*# National Aeronautics and Space Administration. Lewis Research Center, Cleveland, OH.
COMGEN: A COMPUTER PROGRAM FOR GENERATING FINITE ELEMENT MODELS OF COMPOSITE MATERIALS AT THE MICRO LEVEL
 MATTHEW E. MELIS Apr. 1990 24 p
 (NASA-TM-102556; E-5372; NAS 1.15:102556) Avail: NTIS HC A03/MF A01 CSCL 20/11

COMGEN (Composite Model Generator) is an interactive FORTRAN program which can be used to create a wide variety of finite element models of continuous fiber composite materials at the micro level. It quickly generates batch or session files to be submitted to the finite element pre- and postprocessor PATRAN based on a few simple user inputs such as fiber diameter and percent fiber volume fraction of the composite to be analyzed. In addition, various mesh densities, boundary conditions, and loads can be assigned easily to the models within COMGEN. PATRAN uses a session file to generate finite element models and their associated loads which can then be translated to virtually any finite element analysis code such as NASTRAN or MARC. Author

N90-21420*# Sverdrup Technology, Inc., Cleveland, OH.
THERMOMECHANICAL DEFORMATION TESTING AND MODELING IN THE PRESENCE OF METALLURGICAL INSTABILITIES M.S. Thesis - Akron Univ. Final Report

39 STRUCTURAL MECHANICS

MICHAEL G. CASTELLI Jan. 1990 172 p
(Contract NAS3-25266)
(NASA-CR-185188; E-5243; NAS 1.26:185188) Avail: NTIS HC A08/MF A01 CSCL 20/11

A number of viscoplastic constitutive models were developed to describe deformation behavior under complex combinations of thermal and mechanical loading. Questions remain, however, regarding the validity of procedures used to characterize these models for specific structural alloys. One area of concern is that the majority of experimental data available for this purpose are determined under isothermal conditions. This experimental study is aimed at determining whether viscoplastic constitutive theories characterized using an isothermal data base can adequately model material response under the complex thermomechanical loading conditions typical of power generation service. The approach adopted was to conduct a series of carefully controlled thermomechanical experiments on a nickel-based superalloy, Hastelloy Alloy X. Previous investigations had shown that this material experiences metallurgical instabilities leading to complex hardening behavior, termed dynamic strain aging. Investigating this phenomenon under full thermomechanical conditions leads to a number of challenging experimental difficulties which up to the present work were unresolved. To correct this situation, a number of advances were made in thermomechanical testing techniques. Advanced methods for dynamic temperature gradient control, phasing control and thermal strain compensation were developed and incorporated into real time test control software. These advances allowed the thermomechanical data to be analyzed with minimal experimental uncertainty. The thermomechanical results were evaluated on both a phenomenological and microstructural basis. Phenomenological results revealed that the thermomechanical hardening trends were not bounded by those displayed under isothermal conditions. For the case of Hastelloy Alloy X (and similar dynamic strain aging materials), this strongly suggests that some form of thermomechanical testing is necessary when characterizing a thermoviscoplastic deformation model. Transmission electron microscopy was used to study the microstructural physics, and analyze the unique phenomenological behavior.

Author

N90-22117*# National Aeronautics and Space Administration. Lewis Research Center, Cleveland, OH.

FATIGUE CRACK GROWTH IN UNIDIRECTIONAL METAL MATRIX COMPOSITE

LOUIS J. GHOSN (Sverdrup Technology, Inc., Cleveland, OH.), JACK TELESMA, and PETER KANTZOS 1990 9 p Proposed for presentation at the International Fatigue Series, Honolulu, HI, 15-20 Jul. 1990

(NASA-TM-103102; E-5426; NAS 1.15:103102) Avail: NTIS HC A02/MF A01 CSCL 20/11

The weight function method was used to determine the effective stress intensity factor and the crack opening profile for a fatigue tested composite which exhibited fiber bridging. The bridging mechanism was modeled using two approaches; the crack closure approach and the shear lag approach. The numerically determined stress intensity factor values from both methods were compared and correlated with the experimentally obtained crack growth rates for SiC/Ti-15-3 (0)(sub 8) oriented composites. The near crack tip opening profile was also determined for both methods and compared with the experimentally obtained measurements.

Author

N90-22808*# National Aeronautics and Space Administration. Lewis Research Center, Cleveland, OH.

FINITE ELEMENT ELASTIC-PLASTIC-CREEP AND CYCLIC LIFE ANALYSIS OF A COWL LIP

VINOD K. ARYA (Toledo Univ., OH.), MATTHEW E. MELIS, and GARY R. HALFORD Apr. 1990 10 p Submitted for publication Original contains color illustrations
(NASA-TM-102342; E-5050; NAS 1.15:102342) Avail: NTIS HC A02/MF A01; 3 functional color pages CSCL 20/11

Results are presented of elastic, elastic-plastic, and elastic-plastic-creep analyses of a test-rig component of an actively

cooled cowl lip. A cowl lip is part of the leading edge of an engine inlet of proposed hypersonic aircraft and is subject to severe thermal loadings and gradients during flight. Values of stresses calculated by elastic analysis are well above the yield strength of the cowl lip material. Such values are highly unrealistic, and thus elastic stress analyses are inappropriate. The inelastic (elastic-plastic and elastic-plastic-creep) analyses produce more reasonable and acceptable stress and strain distributions in the component. Finally, using the results from these analyses, predictions are made for the cyclic crack initiation life of a cowl lip. A comparison of predicted cyclic lives shows the cyclic life prediction from the elastic-plastic-creep analysis to be the lowest and, hence, most realistic.

Author

N90-22813*# Case Western Reserve Univ., Cleveland, OH. Dept. of Civil Engineering.

DYNAMIC SUBSTRUCTURING BY THE BOUNDARY FLEXIBILITY VECTOR METHOD OF COMPONENT MODE SYNTHESIS Ph.D. Thesis

AYMAN AHMED ABDALLAH 12 Jan. 1990 139 p
(Contract NAG3-707)

(NASA-CR-182445; NAS 1.26:182445) Avail: NTIS HC A07/MF A01 CSCL 20/11

Component mode synthesis (CMS) is a method of dynamic analysis, for structures having a large number of degrees of freedom (DOF). These structures often required lengthy computer CPU time and large computer memory resources, if solved directly by the finite-element method (FEM). In CMS, the structure is divided into independent components in which the DOF are defined by a set of generalized coordinates defined by displacement shapes. The number of the generalized coordinates are much less than the original number of physical DOF, in the component. The displacement shapes are used to transform the component property matrices and any applied external loads, to a reduced system of coordinates. Reduced system property matrices are assembled, and any type of dynamic analysis is carried out in the reduced coordinate system. Any obtained results are back transformed to the original component coordinate systems. In all conventional methods of CMS, the mode shapes used for components are dynamic mode shapes, supplemented by static deflected shapes. Historically, all the dynamic mode shapes used in conventional CMS are the natural modes (eigenvectors) of components. A new method of CMS, namely the boundary flexibility vector method of CMS, is presented. The method provides for the incorporation of a set of static Ritz vectors, referred to as boundary flexibility vectors, as a replacement and/or supplement to conventional eigenvectors, as displacement shapes for components. The generation of these vectors does not require the solution of a costly eigenvalue problem, as in the case of natural modes in conventional CMS, and hence a substantial saving in CPU time can be achieved. The boundary flexibility vectors are generated from flexibility (or stiffness) properties of components. The formulation presented is for both free and fixed-interface components, and for both the free and forced vibration problems. Free and forced vibration numerical examples are presented to verify the accuracy of the method and the saving in CPU time. Compared to conventional methods of CMS, the results indicate that by using the new method, more accurate results can be obtained with a substantial saving in CPU time.

Author

N90-22822*# National Aeronautics and Space Administration. Lewis Research Center, Cleveland, OH.

HIGH TEMPERATURE FATIGUE BEHAVIOR OF A SiC/Ti-24Al-11Nb COMPOSITE

P. A. BARTOLOTTA and P. K. BRINDLEY 1990 15 p Presented at the 10th Symposium on Composite Materials: Testing and Design, San Francisco, CA, 24-25 Apr. 1990; sponsored by American Society for Testing Materials
(NASA-TM-103157; E-5524; NAS 1.15:103157) Avail: NTIS HC A03/MF A01 CSCL 20/11

A series of tension-tension strain- and load-controlled tests were conducted on unidirectional SiC/Ti-24Al-11Nb (at percent) composites at 425 and 815 C. Several regimes of damage were

identified using Talrega's concept of fatigue life diagrams. Issues of test technique, test control mode, and definition of failure were also addressed. Author

N90-22823*# National Aeronautics and Space Administration. Lewis Research Center, Cleveland, OH.

PROBABILISTIC STRUCTURAL ANALYSIS OF AEROSPACE COMPONENTS USING NESSUS

MICHAEL C. SHIAO, VINOD K. NAGPAL (Sverdrup Technology, Inc., Cleveland, OH.), and CHRISTOS C. CHAMIS 1988 10 p Presented at the 29th Structures, Structural Dynamics, and Materials Conference, Williamsburg, VA, 18-20 Apr. 1988; cosponsored by AIAA, ASME, ASCE, AHS, and ACS Previously announced in IAA as A88-32310 Original contains color illustrations

(NASA-TM-102324; E-5020; NAS 1.15:102324) Avail: NTIS HC A02/MF A01; 5 functional color pages CSCL 20/11

Probabilistic structural analysis of a Space Shuttle main engine turbopump blade is conducted using the computer code NESSUS (numerical evaluation of stochastic structures under stress). The goal of the analysis is to derive probabilistic characteristics of blade response given probabilistic descriptions of uncertainties in blade geometry, material properties, and temperature and pressure distributions. Probability densities are derived for critical blade responses. Risk assessment and failure life analysis is conducted assuming different failure models. Author

N90-23757*# Toledo Univ., OH. Dept. of Mechanical Engineering.

APPLICATION OF FINITE-ELEMENT-BASED SOLUTION TECHNOLOGIES FOR VISCOPLASTIC STRUCTURAL ANALYSES Final Report

V. K. ARYA Mar. 1990 14 p Original contains color illustrations

(Contract NCC3-120)

(NASA-CR-185196; E-5187; NAS 1.26:185196) Avail: NTIS HC A03/MF A01; 1 functional color page CSCL 20/11

Finite-element solution technology developed for use in conjunction with advanced viscoplastic models is described. The development of such solution technology is necessary for performing stress/life analyses of engineering structural problems where the complex geometries and loadings make the conventional analytical solutions difficult. The versatility of the solution technology is demonstrated by applying it to viscoplastic models possessing different mathematical structures and encompassing isotropic and anisotropic material. The computational results qualitatively replicate deformation behavior observed in experiments on prototypical structural components. Author

N90-23769*# Toledo Univ., OH.
FINITE ELEMENT ANALYSIS OF STRUCTURAL COMPONENTS USING VISCOPLASTIC MODELS WITH APPLICATION TO A COWL LIP PROBLEM Final Report

V. K. ARYA Jun. 1990 19 p Original contains color illustrations

(Contract NCC3-120)

(NASA-CR-185189; E-4920; NAS 1.26:185189) Avail: NTIS HC A03/MF A01; 4 functional color pages CSCL 20/11

The viability of advanced viscoplastic models for nonlinear finite element analyses of structural components is investigated. Several uniaxial and a multiaxial problem are analyzed using the finite element implementation of Freed's viscoplastic model. Good agreement between the experimental and calculated uniaxial results validates the finite element implementation and gives confidence to apply it to more complex multiaxial problems. A comparison of results for a sample structural component (the cowl lip of a hypersonic engine inlet) with the earlier elastic, elastic-plastic, and elastic-plastic-creep analyses available in the literature shows that the elastic-viscoplastic analyses yield more reasonable stress and strain distributions. Finally, the versatility of the finite-element-based solution technology presented herein is demonstrated by applying it to another viscoplastic model. Author

N90-23770*# National Aeronautics and Space Administration. Lewis Research Center, Cleveland, OH.

A VISCOPLASTIC MODEL WITH APPLICATION TO LiF-22 PERCENT CaF₂ HYPEREUTECTIC SALT

A. D. FREED and K. P. WALKER (Engineering Science Software, Inc., Smithfield, RI.) 1990 13 p Proposed for presentation at the 3rd International Conference on Constitutive Laws for Engineering Materials: Theory and Applications and Workshop on Innovative Use of Materials in Industrial and Infrastructure Design and Manufacturing, Tucson, AZ, 7-12 Jan. 1991; sponsored by Arizona Univ.

(NASA-TM-103181; E-5559; NAS 1.15:103181) Avail: NTIS HC A03/MF A01 CSCL 20/11

A viscoplastic model for class M (metal-like behavior) materials is presented. One novel feature is its use of internal variables to change the stress exponent of creep (where n is approximately = 5) to that of natural creep (where $n = 3$), in accordance with experimental observations. Another feature is the introduction of a coupling in the evolution equations of the kinematic and isotropic internal variables, making thermal recovery of the kinematic variable implicit. These features enable the viscoplastic model to reduce to that of steady-state creep in closed form. In addition, the hardening parameters associated with the two internal state variables (one scalar-valued, the other tensor-valued) are considered to be functions of state, instead of being taken as constant-valued. This feature enables each internal variable to represent a much wider spectrum of internal states for the material. The model is applied to a LiF-22 percent CaF₂ hypereutectic salt, which is being considered as a thermal energy storage material for space-based solar dynamic power systems. Author

N90-23773*# National Aeronautics and Space Administration. Lewis Research Center, Cleveland, OH.

STRESS VERSUS TEMPERATURE DEPENDENT ACTIVATION ENERGIES IN CREEP

A. D. FREED, S. V. RAJ, and K. P. WALKER (Engineering Science Software, Inc., Smithfield, RI.) 1990 12 p Proposed for presentation at the 3rd International Conference on Constitutive Laws for Engineering Materials: Theory and Applications and Workshop on Innovative Use of Materials in Industrial and Infrastructure Design and Manufacturing, Tucson, AZ, 7 Jan. 1991; sponsored by Arizona Univ.

(NASA-TM-103192; E-5580; NAS 1.15:103192) Avail: NTIS HC A03/MF A01 CSCL 20/11

The activation energy for creep at low stresses and elevated temperatures is lattice diffusion, where the rate controlling mechanism for deformation is dislocation climb. At higher stresses and intermediate temperatures, the rate controlling mechanism changes from that of dislocation climb to one of obstacle-controlled dislocation glide. Along with this change, there occurs a change in the activation energy. It is shown that a temperature-dependent Gibbs free energy does a good job of correlating steady-state creep data, while a stress-dependent Gibbs free energy does a less desirable job of correlating the same data. Applications are made to copper and a LiF-22 mol. percent CaF₂ hypereutectic salt. Author

N90-24647*# National Aeronautics and Space Administration. Lewis Research Center, Cleveland, OH.

LOW VELOCITY IMPACT ANALYSIS WITH NASTRAN

DANIEL A. TROWBRIDGE (Analex Corp., Fairview Park, OH.), JOSEPH E. GRADY, and ROBERT A. AIELLO In COSMIC, 18th NASTRAN (R) Users' Colloquium p 115-134 Apr. 1990 Sponsored in part by Naval Weapons Center, China Lake, CA Avail: NTIS HC A09/MF A01; also available from COSMIC, Athens, GA 30602 CSCL 20/11

A nonlinear elastic force-displacement relationship is used to calculate the transient impact force and local deformation at the point of contact between impactor and target. The nonlinear analysis and transfer function capabilities of NASTRAN are used to define a finite element model that behaves globally linearly elastic, and locally nonlinear elastic to model the local contact behavior. Results are presented for two different structures: a

39 STRUCTURAL MECHANICS

uniform cylindrical rod impacted longitudinally; and an orthotropic plate impacted transversely. Calculated impact force and transient structural response of the targets are shown to compare well with results measured in experimental tests. Author

N90-24653* # Georgia Inst. of Tech., Atlanta. School of Aerospace Engineering.

ANALYSIS OF SHELL-TYPE STRUCTURES SUBJECTED TO TIME-DEPENDENT MECHANICAL AND THERMAL LOADING

Final Technical Report, 15 Apr. 1984 - 10 Mar. 1990

GEORGE J. SIMITSES Mar. 1990 91 p

(Contract NAG3-534)

(NASA-CR-185077; NAS 1.26:185077) Avail: NTIS HC A05/MF A01 CSCL 20/11

The development of a general mathematical model and solution methodologies for analyzing structural response of thin, metallic shell-like structures under dynamic and/or static thermomechanical loads is examined. In the mathematical model, geometric as well as material-type of nonlinearities are considered. Traditional as well as novel approaches are reported and detailed applications are presented in the appendices. The emphasis for the mathematical model, the related solution schemes, and the applications, is on thermal viscoelastic and viscoplastic phenomena, which can predict creep and ratchetting. Author

N90-25367* # National Aeronautics and Space Administration. Lewis Research Center, Cleveland, OH.

THERMOMECHANICAL TESTING TECHNIQUES FOR HIGH-TEMPERATURE COMPOSITES: TMF BEHAVIOR OF SiC(SCS-6)/Ti-15-3

MICHAEL G. CASTELLI (Sverdrup Technology, Inc., Brook Park, OH.), J. RODNEY ELLIS, and PAUL A. BARTOLOTTA 1990 20 p Presented at the 10th Symposium on Composite Materials: Testing and Design, San Francisco, CA, 24-25 Aug. 1990; sponsored by American Society for Testing and Materials (NASA-TM-103171; E-5543; NAS 1.15:103171) Avail: NTIS HC A03/MF A01 CSCL 20/11

Thermomechanical testing techniques recently developed for monolithic structural alloys were successfully extended to continuous fiber reinforced composite materials in plate form. The success of this adaptation was verified on a model metal matrix composite (MMC) material, namely SiC(SCS-6)/Ti-15V-3Cr-3Al-3Sn. Effects of heating system type and specimen preparation are also addressed. Cyclic lives determined under full thermo-mechanical conditions were shown to be significantly reduced from those obtained under comparable isothermal and in-phase bi-thermal conditions. Fractography and metallography from specimens subjected to isothermal, out-of-phase and in-phase conditions reveal distinct differences in damage-failure modes. Isothermal metallography revealed extensive matrix cracking associated with fiber damage throughout the entire cross-section of the specimen. Out-of-phase metallography revealed extensive matrix damage associated with minimal (if any) fiber cracking. However, the damage was located exclusively at surface and near-surface locations. In-phase conditions produced extensive fiber cracking throughout the entire cross-section, associated with minimal (if any) matrix damage. Author

N90-26355* # General Electric Co., Cincinnati, OH. Aircraft Engine Business Group.

ELEVATED TEMPERATURE CRACK GROWTH Final Report

K. S. KIM, R. H. VANSTONE, S. N. MALIK, and J. H. LAFLIN Nov. 1988 293 p

(Contract NAS3-23940)

(NASA-CR-182247; NAS 1.26:182247; R89AEB-325) Avail: NTIS HC A13/MF A02 CSCL 20/11

A study was performed to examine the applicability of path-independent (P-I) integrals to crack growth problems in hot section components of gas turbine aircraft engines. Alloy 718 was used and the experimental parameters included combined temperature and strain cycling, thermal gradients, elastic-plastic strain levels, and mean strains. A literature review was conducted

of proposed P-I integrals, and those capable of analyzing hot section component problems were selected and programmed into the postprocessor of a finite element code. Detailed elastic-plastic finite element analyses were conducted to simulate crack growth and crack closure of the test specimen, and to evaluate the P-I integrals. It was shown that the selected P-I integrals are very effective for predicting crack growth for isothermal conditions. Author

N90-26359* # National Aeronautics and Space Administration. Lewis Research Center, Cleveland, OH.

DESIGN OF CERAMIC COMPONENTS WITH THE NASA/CARES COMPUTER PROGRAM

NOEL N. NEMETH, JANE M. MANDERSCHIED, and JOHN P. GYEKENYESI Apr. 1990 14 p Submitted for publication Original contains color illustrations

(NASA-TM-102369; E-5038; NAS 1.15:102369) Avail: NTIS HC A03/MF A01; 2 functional color pages CSCL 20/11

The ceramics analysis and reliability evaluation of structures (CARES) computer program is described. The primary function of the code is to calculate the fast-fracture reliability or failure probability of macroscopically isotropic ceramic components. These components may be subjected to complex thermo-mechanical loadings, such as those found in heat engine applications. CARES uses results from MSC/NASTRAN or ANSYS finite-element analysis programs to evaluate how inherent surface and/or volume type flaws component reliability. CARES utilizes the Batdorf model and the two-parameter Weibull cumulative distribution function to describe the effects of multiaxial stress states on material strength. The principle of independent action (PIA) and the Weibull normal stress averaging models are also included. Weibull material strength parameters, the Batdorf crack density coefficient, and other related statistical quantities are estimated from four-point bend bar or uniform uniaxial tensile specimen fracture strength data. Parameter estimation can be performed for a single or multiple failure modes by using a least-squares analysis or a maximum likelihood method. Kolmogorov-Smirnov and Anderson-Darling goodness-to-fit-tests, 90 percent confidence intervals on the Weibull parameters, and Kanofsky-Srinivasan 90 percent confidence band values are also provided. Examples are provided to illustrate the various features of CARES. Author

N90-26364* # National Aeronautics and Space Administration. Lewis Research Center, Cleveland, OH.

APPLICATION OF SYMBOLIC COMPUTATIONS TO THE CONSTITUTIVE MODELING OF STRUCTURAL MATERIALS

STEVEN M. ARNOLD, H. Q. TAN, and X. DONG (Akron Univ., OH.) 1990 17 p Proposed for presentation at the 1990 Winter Annual Meeting of ASME, Dallas, TX, 25-30 Nov. 1990 (Contract NAG3-872)

(NASA-TM-103225; E-5641; NAS 1.15:103225) Avail: NTIS HC A03/MF A01 CSCL 20/11

In applications involving elevated temperatures, the derivation of mathematical expressions (constitutive equations) describing the material behavior can be quite time consuming, involved and error-prone. Therefore intelligent application of symbolic systems to facilitate this tedious process can be of significant benefit. Presented here is a problem oriented, self contained symbolic expert system, named SDICE, which is capable of efficiently deriving potential based constitutive models in analytical form. This package, running under DOE MACSYMA, has the following features: (1) potential differentiation (chain rule), (2) tensor computations (utilizing index notation) including both algebraic and calculus; (3) efficient solution of sparse systems of equations; (4) automatic expression substitution and simplification; (5) back substitution of invariant and tensorial relations; (6) the ability to form the Jacobian and Hessian matrix; and (7) a relational data base. Limited aspects of invariant theory were also incorporated into SDICE due to the utilization of potentials as a starting point and the desire for these potentials to be frame invariant (objective). The uniqueness of SDICE resides in its ability to manipulate expressions in a general yet pre-defined order and simplify

expressions so as to limit expression growth. Results are displayed, when applicable, utilizing index notation. SDICE was designed to aid and complement the human constitutive model developer. A number of examples are utilized to illustrate the various features contained within SDICE. It is expected that this symbolic package can and will provide a significant incentive to the development of new constitutive theories. Author

N90-26372*# State Univ. of New York, Buffalo. Dept. of Mechanical and Aerospace Engineering.
RELIABILITY ANALYSIS OF CONTINUOUS FIBER COMPOSITE LAMINATES Final Report
 DAVID J. THOMAS and ROBERT C. WETHERHOLD Jul. 1990 31 p
 (Contract NAG3-862)
 (NASA-CR-185265; NAS 1.26:185265) Avail: NTIS HC A03/MF A01 CSCL 20/11

A composite lamina may be viewed as a homogeneous solid whose directional strengths are random variables. Calculation of the lamina reliability under a multi-axial stress state can be approached by either assuming that the strengths act separately (modal or independent action), or that they interact through a quadratic interaction criterion. The independent action reliability may be calculated in closed form, while interactive criteria require simulations; there is currently insufficient data to make a final determination of preference between them. Using independent action for illustration purposes, the lamina reliability may be plotted in either stress space or in a non-dimensional representation. For the typical laminated plate structure, the individual lamina reliabilities may be combined in order to produce formal upper and lower bounds of reliability for the laminate, similar in nature to the bounds on properties produced from variational elastic methods. These bounds are illustrated for a (0/plus or minus 15)_{sub s} Graphite/Epoxy (GR/EP) laminate. And addition, simple physically plausible phenomenological rules are proposed for redistribution of load after a lamina has failed. These rules are illustrated by application to (0/plus or minus 15)_{sub s} and (90/plus or minus 45/0)_{sub s} GR/EP laminates and results are compared with respect to the proposed bounds. Author

N90-26373*# National Aeronautics and Space Administration. Lewis Research Center, Cleveland, OH.
STRUCTURAL DYNAMICS BRANCH RESEARCH AND ACCOMPLISHMENTS Report, FY 1989
 Jul. 1990 51 p
 (NASA-TM-102488; E-5279; NAS 1.15:102488) Avail: NTIS HC A04/MF A01 CSCL 20/11

Summaries are presented of fiscal year 1989 research highlights from the Structural Dynamics Branch at NASA Lewis Research Center. Highlights from the branch's major work areas include aeroelasticity, vibration control, dynamic systems, and computation structural methods. A listing of the fiscal year 1989 branch publications is given. Author

N90-28099*# National Aeronautics and Space Administration. Lewis Research Center, Cleveland, OH.
CERAMICS ANALYSIS AND RELIABILITY EVALUATION OF STRUCTURES (CARES). USERS AND PROGRAMMERS MANUAL
 NOEL N. NEMETH (Aerospace Design and Fabrication, Inc., Brook Park, OH.), JANE M. MANDERSCHIED, and JOHN P. GYEKENYESI Washington Aug. 1990 232 p
 (NASA-TP-2916; E-4722-1; NAS 1.60:2916) Avail: NTIS HC A11/MF A02 CSCL 11/3

This manual describes how to use the Ceramics Analysis and Reliability Evaluation of Structures (CARES) computer program. The primary function of the code is to calculate the fast fracture reliability or failure probability of macroscopically isotropic ceramic components. These components may be subjected to complex thermomechanical loadings, such as those found in heat engine applications. The program uses results from MSC/NASTRAN or ANSYS finite element analysis programs to evaluate component reliability due to inherent surface and/or volume type flaws. CARES

utilizes the Batdorf model and the two-parameter Weibull cumulative distribution function to describe the effect of multiaxial stress states on material strength. The principle of independent action (PIA) and the Weibull normal stress averaging models are also included. Weibull material strength parameters, the Batdorf crack density coefficient, and other related statistical quantities are estimated from four-point bend bar or uniform uniaxial tensile specimen fracture strength data. Parameter estimation can be performed for single or multiple failure modes by using the least-square analysis or the maximum likelihood method. Kolmogorov-Smirnov and Anderson-Darling goodness-of-fit tests, ninety percent confidence intervals on the Weibull parameters, and Kanofsky-Srinivasan ninety percent confidence band values are also provided. The probabilistic fast-fracture theories used in CARES, along with the input and output for CARES, are described. Example problems to demonstrate various feature of the program are also included. This manual describes the MSC/NASTRAN version of the CARES program. Author

N90-28110*# Akron Univ., OH.
CREEP AND CREEP RUPTURE OF STRONGLY REINFORCED METALLIC COMPOSITES Final Report
 D. N. ROBINSON, W. K. BINIENDA, and M. MITI-KAVUMA Aug. 1990 23 p
 (Contract NAG3-379)
 (NASA-CR-185286; NAS 1.26:185286) Avail: NTIS HC A03/MF A01 CSCL 20/11

A creep and creep damage theory is presented for metallic composites with strong fibers. Application is to reinforced structures in which the fiber orientation may vary throughout but a distinct fiber direction can be identified locally (local transverse isotropy). The creep deformation model follows earlier work and is based on a flow potential function that depends on invariants reflecting stress and the material symmetry. As the focus is on the interaction of creep and damage, primary creep is ignored. The creep rupture model is an extension of continuum damage mechanics and includes an isochronous damage function that depends on invariants specifying the local maximum transverse tension and the maximum longitudinal shear stress. It is posited that at high temperature and low stress, appropriate to engineering practice, these stress components damage the fiber/matrix interface through diffusion controlled void growth, eventually causing creep rupture. Experiments are outlined for characterizing a composite through creep rupture tests under transverse tension and longitudinal shear. Application is made to a thin-walled pressure vessel with reinforcing fibers at an arbitrary helical angle. The results illustrate the usefulness of the model as a means of achieving optimal designs of composite structures where creep and creep rupture are life limiting. Author

N90-28111*# National Aeronautics and Space Administration. Lewis Research Center, Cleveland, OH.
COLLISION FORCES FOR COMPLIANT PROJECTILES
 JOSEPH E. GRADY Washington Aug. 1990 12 p
 (NASA-TM-4203; E-5215; NAS 1.15:4203) Avail: NTIS HC A03/MF A01 CSCL 20/11

Force histories resulting from the impact of compliant projectiles were determined experimentally. A long instrumented rod was used as the target, and the impact force was calculated directly from the measured strain response. Results from a series of tests on several different sized impactors were used to define four dimensionless parameters that determine, for a specified impactor velocity and size, the amplitude, duration, shape, and impulse of the impact force history. Author

N90-28112*# National Aeronautics and Space Administration. Lewis Research Center, Cleveland, OH.
RELIABILITY ANALYSIS OF A STRUCTURAL CERAMIC COMBUSTION CHAMBER
 JONATHAN A. SALEM, JANE M. MANDERSCHIED, MARC R. FREEDMAN, and JOHN P. GYEKENYESI Aug. 1990 23 p
 Proposed for presentation at the 36th International Gas Turbine and Aeroengine Congress and Exposition, Orlando, FL, 3-6 Jun.

39 STRUCTURAL MECHANICS

1991; sponsored by ASME

(NASA-TM-103264; E-5699; NAS 1.15:103264) Avail: NTIS HC A03/MF A01 CSCL 20/11

The Weibull modulus, fracture toughness and thermal properties of a silicon nitride material used to make a gas turbine combustor were experimentally measured. The location and nature of failure origins resulting from bend tests were determined with fractographic analysis. The measured Weibull parameters were used along with thermal and stress analysis to determine failure probabilities of the combustor with the CARES design code. The effect of data censoring, FEM mesh refinement, and fracture criterion were considered in the analysis.

Author

N90-28113* # Tulane Univ., New Orleans, LA.

MICROMECHANICAL MODEL OF CRACK GROWTH IN FIBER REINFORCED CERAMICS Final Report

ASHER A. RUBINSTEIN and KANG XU Washington Sep. 1990 32 p

(Contract NAG3-967)

(NASA-CR-4321; E-5670; NAS 1.26:4321) Avail: NTIS HC A03/MF A01 CSCL 20/11

A model based on the micromechanical mechanism of crack growth resistance in fiber reinforced ceramics is presented. The formulation of the model is based on a small scale geometry of a macrocrack with a bridging zone, the process zone, which governs the resistance mechanism. The effect of high toughness of the fibers in retardation of the crack advance, and the significance of the fiber pullout mechanism on the crack growth resistance, are reflected in this model. The model allows one to address issues such as influence of fiber spacing, fiber flexibility, and fiber matrix friction. Two approaches were used. One represents the fracture initiation and concentrated on the development of the first microcracks between fibers. An exact closed form solution was obtained for this case. The second case deals with the development of an array of microcracks between fibers forming the bridging zone. An implicit exact solution is formed for this case. In both cases, a discrete fiber distribution is incorporated into the solution.

Author

N90-28641* # Georgia Inst. of Tech., Atlanta. School of Materials Engineering.

MICROMECHANICS OF CYCLIC DEFORMATION IN SSME TURBOPUMP BLADE MATERIALS

WALTER W. MILLIGAN and STEPHEN D. ANTOLOVICH *In* NASA, Marshall Space Flight Center, Advanced Earth-to-Orbit Propulsion Technology 1988, Volume 1 p 487-496 Sep. 1988 (Contract NAG3-503)

Avail: NTIS HC A99/MF E06 CSCL 20/11

Current and candidate Space Shuttle Main Engine (SSME) turbopump blade materials are anisotropic, both in their elastic and plastic response. The major objective is to characterize the plastic deformation behavior of a typical single crystal nickel-base superalloy, PWA 1480, and to use this information to help guide the development of anisotropic constitutive models.

Author

N90-28649* # National Aeronautics and Space Administration. Lewis Research Center, Cleveland, OH.

STRUCTURAL RESPONSE OF SSME TURBINE BLADE AIRFOILS

V. K. ARYA, A. ABDUL-AZIZ (Sverdrup Technology, Inc., Cleveland, OH.), and R. L. THOMPSON *In* NASA, Marshall Space Flight Center, Advanced Earth-to-Orbit Propulsion Technology 1988, Volume 1 p 634-652 Sep. 1988

Avail: NTIS HC A99/MF E06 CSCL 20/11

Reusable space propulsion hot gas-path components are required to operate under severe thermal and mechanical loading conditions. These operating conditions produce elevated temperature and thermal transients which results in significant thermally induced inelastic strains, particularly, in the turbopump turbine blades. An inelastic analysis for this component may therefore be necessary. Anisotropic alloys such as MAR M-247 or PWA-1480 are being considered to meet the safety and durability requirements of this component. An anisotropic inelastic structural

analysis for an SSME fuel turbopump turbine blade was performed. The thermal loads used resulted from a transient heat transfer analysis of a turbine blade. A comparison of preliminary results from the elastic and inelastic analyses is presented.

Author

N90-28878* # Case Western Reserve Univ., Cleveland, OH. Dept. of Civil Engineering.

GREEN'S FUNCTIONS FOR DISLOCATIONS IN BONDED STRIPS AND RELATED CRACK PROBLEMS Final Report

R. BALLARINI and H. A. LUO Sep. 1990 47 p

(Contract NAG3-856)

(NASA-CR-185291; NAS 1.26:185291) Avail: NTIS HC A03/MF A01 CSCL 20/11

Green's functions are derived for the plane elastostatics problem of a dislocation in a bimaterial strip. Using these fundamental solutions as kernels, various problems involving cracks in a bimaterial strip are analyzed using singular integral equations. For each problem considered, stress intensity factors are calculated for several combinations of the parameters which describe loading, geometry and material mismatch.

Author

N90-28880* # Cincinnati Univ., OH. Dept. of Materials Science and Engineering.

MICROSTRUCTURE: PROPERTY CORRELATION Final Technical Report

N. JAYARAMAN 1 Oct. 1990 54 p

(Contract NAG3-506)

(NASA-CR-180406; NAS 1.26:180406) Avail: NTIS HC A04/MF A01 CSCL 20/11

Strain controlled torsional and biaxial (tension-torsion) low cycle fatigue behavior of Waspaloy was studied at room temperature as a function of heat treatment. Biaxial tests were conducted under proportional (when the axial and torsional strain cycles are in-phase) and non-proportional (when the axial and torsional strain cycles are 90 deg out-of-phase) cyclic conditions. The deformation behavior under these different cyclic conditions were evaluated by slip trace analysis. For this, a Schmidt-type factor was defined for multiaxial loading conditions and it was shown that when the slip deformation is predominant, non-proportional cycles are more damaging than proportional or pure axial or torsional cycles. This was attributed to the fact that under non-proportional cyclic conditions, deformation was through multiple slip as opposed single slip for other loading conditions, which gave rise to increased hardening. The total life for a given test condition was found to be independent of heat treatment. This was interpreted as being due to the differences in the cycles to initiation and propagation of cracks.

Author

44

ENERGY PRODUCTION AND CONVERSION

Includes specific energy conversion systems, e.g., fuel cells; global sources of energy; geophysical conversion; and windpower.

A90-14858* Spire Corp., Bedford, MA.

HIGH EFFICIENCY GAAS/GE MONOLITHIC TANDEM SOLAR CELLS

S. P. TOBIN, S. M. VERNON, C. BAJGAR, V. E. HAVEN, L. M. GEOFFROY, M. M. SANFACON (Spire Corp., Bedford, MA), D. R. LILLINGTON (Spectrolab, Inc., Sylmar, CA), R. E. HART, JR. (NASA, Lewis Research Center, Cleveland, OH) et al. *IN: IEEE Photovoltaic Specialists Conference, 20th, Las Vegas, NV, Sept. 26-30, 1988, Conference Record. Volume 1. New York, Institute of Electrical and Electronics Engineers, Inc., 1988, p. 405-410, refs*

Copyright

Two-terminal monolithic tandem cells consisting of a GaAs solar cell grown epitaxially on a Ge solar cell substrate are very attractive for space applications. Tandem cells of GaAs grown by

metal-organic chemical vapor deposition on thin Ge were investigated to address both higher efficiency and reduced weight. Two materials growth issues associated with this heteroepitaxial system, autodoping of the GaAs layers by Ge and diffusion of Ga and As into the Ge substrate, were addressed. The latter appears to result in information of an unintentional p-n junction in the Ge. Early simulator measurements gave efficiencies as high as 21.7 percent for 4 cm² GaAs/Ge cells, but recent high-altitude testing has given efficiencies of 18 percent. Sources of errors in simulator measurements of two-terminal tandem cells are discussed. A limiting efficiency of about 36 percent for the tandem cell at AMO was calculated. Ways to improve the performance of present cells, primarily by increasing the I_{sc} and V_{oc} of the Ge cell, are proposed. I.E.

A90-14869* Midwest Research Inst., Golden, CO.
AN EMPIRICAL INVESTIGATION OF THE INP SHALLOW-HOMOJUNCTION SOLAR CELL

M. W. WANLASS, T. A. GESSERT, K. A. EMERY, and T. J. COUTTS (SERI, Golden, CO) IN: IEEE Photovoltaic Specialists Conference, 20th, Las Vegas, NV, Sept. 26-30, 1988, Conference Record. Volume 1. New York, Institute of Electrical and Electronics Engineers, Inc., 1988, p. 491-496. refs
 (Contract DE-AC02-83CH-10093; NASA ORDER C-30005-K)
 Copyright

An experimental study of the performance of epitaxially grown InP shallow-homojunction solar cells as a function of the thickness and carrier concentration in the base and emitter layers is presented. Identification of improvements to cell design leading to higher performance is emphasized. As a result, using a near-optimum set of design parameters, cells with conversion efficiencies of 20.3 percent (global) and 17.6 percent (AMO) have been achieved. For such cells, it is shown that the internal response of the base layer is essentially perfect, whereas the emitter-layer properties can be improved substantially and warrant further investigation. Discrepancies between the results of the present study and those of earlier modeling efforts are discussed. I.E.

A90-14887* National Aeronautics and Space Administration.
 Lewis Research Center, Cleveland, OH.

A V-GROOVED GAAS SOLAR CELL

S. G. BAILEY, N. FATEMI, G. A. LANDIS, D. M. WILT, R. D. THOMAS, and A. ARRISON (NASA, Lewis Research Center, Cleveland, OH) IN: IEEE Photovoltaic Specialists Conference, 20th, Las Vegas, NV, Sept. 26-30, 1988, Conference Record. Volume 1. New York, Institute of Electrical and Electronics Engineers, Inc., 1988, p. 625-628. Previously announced in STAR as N89-22177. refs

Copyright

V-grooved GaAs solar cells promise the benefits of improved optical coupling, higher short-circuit current, and increased tolerance to particle radiation compared to planar cells. A GaAs homojunction cell was fabricated by etching a V-groove pattern into an n-epilayer (2.1 x 10 to the 17th power per cu cm) grown by metalorganic chemical vapor deposition (MOCVD) on an n+ substrate (2.8 x 10 to the 18th power per cu cm) and then depositing an MOCVD p epilayer (4.2 x 10 to the 18th power per cu cm). Reflectivity measurements on cells with and without an antireflective coating confirm the expected decrease in reflectance of the microgrooved cell compared to the planar structure. The short-circuit current of the V-grooved solar cell was 13 percent higher than that of the planar control. Author

A90-14888* National Aeronautics and Space Administration.
 Lewis Research Center, Cleveland, OH.

CONTACT FORMATION IN GALLIUM ARSENIDE SOLAR CELLS

VICTOR G. WEIZER (NASA, Lewis Research Center, Cleveland, OH) and NAVID S. FATEMI (Sverdrup Technology, Inc., Middleburg Heights, OH) IN: IEEE Photovoltaic Specialists Conference, 20th, Las Vegas, NV, Sept. 26-30, 1988, Conference Record. Volume 1. New York, Institute of Electrical and Electronics Engineers, Inc.,

1988, p. 629-634. refs

Copyright

Gold and gold-based alloys, commonly used as solar cell contact materials, are known to react readily with gallium arsenide. Experiments were performed to identify the mechanisms involved in these GaAs-metal interactions. It is shown that the reaction of GaAs with gold takes place via a dissociative diffusion process. It is shown further that the GaAs-metal reaction rate is controlled to a very great extent by the condition of the free surface of the contact metal, an interesting example of which is the previously unexplained increase in the reaction rate that has been observed for samples annealed in a vacuum environment as compared to those annealed in a gaseous ambient. A number of other hard-to-explain observations, such as the low-temperature formation of voids in the gold lattice and crystallite growth on the gold surface, are explained by invoking this mechanism. I.E.

A90-14893* Midwest Research Inst., Golden, CO.

HYBRID SOLAR CELLS BASED ON DC MAGNETRON SPUTTERED FILMS OF N-ITO ON APMOVPE GROWN P-INP

T. J. COUTTS, X. LI, M. W. WANLASS, K. A. EMERY, and T. A. GESSERT (SERI, Golden, CO) IN: IEEE Photovoltaic Specialists Conference, 20th, Las Vegas, NV, Sept. 26-30, 1988, Conference Record. Volume 1. New York, Institute of Electrical and Electronics Engineers, Inc., 1988, p. 660-665. refs
 (Contract DE-AC02-83CH-10093; NASA ORDER C-30005-K)
 Copyright

Hybrid indium-tin-oxide (ITO)/InP solar cells are discussed. The cells are constructed by dc magnetron sputter deposition of ITO onto high-quality InP films grown by atmospheric pressure metal-organic vapor-phase epitaxy (APMOVPE). A record efficiency of 18.9 percent, measured under standard Solar Energy Research Institute reporting conditions, has been obtained. The p-InP surface is shown to be type converted, principally by the ITO, but with the extent of conversion being modified by the nature of the sputtering gas. The deposition process, in itself, is not responsible for the type conversion. Dark currents have been suppressed by more than three orders of magnitude by the addition of hydrogen to the sputtering gas during deposition of a thin (5 nm) interface layer. Without this layer, and using only the more usual argon/oxygen mixture, the devices had poorer efficiencies and were unstable. A discussion of associated quantum efficiencies and capacitance/voltage measurements is also presented from which it is concluded that further improvements in efficiency will result from better control over the type-conversion process. I.E.

A90-14898* Cleveland State Univ., OH.

PREDICTED PERFORMANCE OF NEAR-OPTIMALLY DESIGNED INDIUM PHOSPHIDE SPACE SOLAR CELLS AT HIGH INTENSITIES AND TEMPERATURES

CHANDRA GORADIA, WILLIAM THESLING, MANJU GHALLA GORADIA (Cleveland State University, OH), IRVING WEINBERG, and CLIFFORD K. SWARTZ (NASA, Lewis Research Center, Cleveland, OH) IN: IEEE Photovoltaic Specialists Conference, 20th, Las Vegas, NV, Sept. 26-30, 1988, Conference Record. Volume 1. New York, Institute of Electrical and Electronics Engineers, Inc., 1988, p. 695-701. refs
 Copyright

The authors calculated the expected performance dependence of near-optimally designed shallow homojunction n+pp+ InP solar cells on incident intensities up to 200 AMO and temperatures up to 100 deg C (373 K). Both circular and rectangular cells were considered, the former for use in a Cassegrainian concentrator array at 100 AMO, 80-100 deg C and the latter for use in a Slats concentrator array at 20 AMO, 80-100 deg C. With efficiencies near 22 percent at 80 deg C, both the circular and rectangular InP shallow homojunction solar cells compare very favorably to GaAs cells of the same design and may be preferable to the GaAs cells for space applications because of the superior radiation tolerance of the InP cells. I.E.

44 ENERGY PRODUCTION AND CONVERSION

A90-14899* Midwest Research Inst., Golden, CO.

MODELING AND SIMULATION OF INP HOMOJUNCTION SOLAR CELLS

A. H. YAHIA, M. W. WANLASS, and T. J. COUTTS (SERI, Golden, CO) IN: IEEE Photovoltaic Specialists Conference, 20th, Las Vegas, NV, Sept. 26-30, 1988, Conference Record. Volume 1. New York, Institute of Electrical and Electronics Engineers, Inc., 1988, p. 702-707. refs

(Contract DE-AC02-83CH-10093; NASA ORDER C-30005-K)

Copyright

Modeling and simulation of single-crystal InP homojunction solar cells has been performed using the PC-1D code. Cell design and performance have been optimized using the best available estimates of the various materials parameters. A comparison has been made of the predictions of the PC-1D model to those of other models. The optimum performance is predicted to give an efficiency approaching 21 percent at AM0. It is shown that in order to describe the performance of actual cells it is necessary to use larger values of the intrinsic carrier concentration and the surface recombination velocity (SRV) than have been reported in the literature. However, even with a near-maximum value of SRV (e.g., 10 to the 7th cm/s) it is necessary to reduce the minority carrier diffusion length in the emitter to only 0.01 micron in order to account for the relatively low quantum efficiency in the blue part of the spectrum. This indicates that improvement in the emitter bulk properties could be much more important than the SRV. Other loss mechanisms are also discussed; in particular, it is shown that recombination in the base, for good quality material, is relatively insignificant. I.E.

A90-14900* National Aeronautics and Space Administration. Lewis Research Center, Cleveland, OH.

THIN, LIGHT-TRAPPING SILICON SOLAR CELLS FOR SPACE
GEOFFREY A. LANDIS (NASA, Lewis Research Center, Cleveland, OH) IN: IEEE Photovoltaic Specialists Conference, 20th, Las Vegas, NV, Sept. 26-30, 1988, Conference Record. Volume 1. New York, Institute of Electrical and Electronics Engineers, Inc., 1988, p. 708-712. Research supported by DOE. refs
Copyright

Ultrathin silicon solar cells with high efficiency and radiation tolerance can be made by incorporating light-trapping and heterojunction surface passivation. Calculations show that a 2-micron-thick light-trapping cell remains over 18 percent efficient after the equivalent of 20 years in geosynchronous orbit. Including a 50-micron coverglass, the thin cells had, after irradiation, a specific power over ten times higher than that of the baseline design. I.E.

A90-14910* National Aeronautics and Space Administration. Lewis Research Center, Cleveland, OH.

HIGH ALTITUDE CURRENT-VOLTAGE MEASUREMENT OF GAAS/GE SOLAR CELLS

RUSSELL E. HART, JR., DAVID J. BRINKER (NASA, Lewis Research Center, Cleveland, OH), and KEITH A. EMERY (SERI, Golden, CO) IN: IEEE Photovoltaic Specialists Conference, 20th, Las Vegas, NV, Sept. 26-30, 1988, Conference Record. Volume 1. New York, Institute of Electrical and Electronics Engineers, Inc., 1988, p. 764, 765.

Copyright

Measurements of high-voltage (Voc of 1.2 V) gallium arsenide on germanium tandem junction solar cells at air mass 0.22 showed that the insolation in the red portion of the solar spectrum is insufficient to obtain high fill factor. On the basis of measurements in the LeRC X-25L solar simulator, these cells were believed to be as efficient as 21.68 percent AM0. Solar simulator spectrum errors in the red end allowed the fill factor to be as high as 78.7 percent. When a similar cell's current-voltage characteristic was measured at high altitude in the NASA Lear Jet Facility, a loss of 15 percentage points in fill factor was observed. This decrease was caused by insufficient current in the germanium bottom cell of the tandem stack. I.E.

A90-14921* National Aeronautics and Space Administration. Lewis Research Center, Cleveland, OH.

INP HOMOJUNCTION SOLAR CELL PERFORMANCE ON THE LIPS III FLIGHT EXPERIMENT

DAVID J. BRINKER, RUSSELL E. HART, JR., IRVING WEINBERG (NASA, Lewis Research Center, Cleveland, OH), and BRIAN S. SMITH (Spectrolab, Inc., Sylmar, CA) IN: IEEE Photovoltaic Specialists Conference, 20th, Las Vegas, NV, Sept. 26-30, 1988, Conference Record. Volume 2. New York, Institute of Electrical and Electronics Engineers, Inc., 1988, p. 819-823. Previously announced in STAR as N89-12123. refs

Copyright

Performance data for the NASA Lewis Research Center indium phosphide n+p homojunction solar cell module on the LIPS 3 flight experiment is presented. The objective of the experiment is to measure the performance of InP cells in the natural radiation environment of the 1100 km altitude, 60+ deg inclination orbit. Analysis of flight data indicates that the performance of the four cells throughout the first year is near expected values. No degradation in short-circuit current was seen, as was expected from radiation tolerance studies of similar cells. Details of the cell structure and flight module design are discussed. The results of the temperature dependency and radiation tolerance studies necessary for normalization and analysis of the data are included.

Author

A90-14930* National Aeronautics and Space Administration. Lewis Research Center, Cleveland, OH.

LUNAR PRODUCTION OF SPACE PHOTOVOLTAIC ARRAYS

GEOFFREY A. LANDIS (NASA, Lewis Research Center, Cleveland, OH) IN: IEEE Photovoltaic Specialists Conference, 20th, Las Vegas, NV, Sept. 26-30, 1988, Conference Record. Volume 2. New York, Institute of Electrical and Electronics Engineers, Inc., 1988, p. 874-879. refs

Copyright

The advantages of manufacturing solar cells for use in space on the moon rather than on Earth are discussed. It is shown how solar cells manufactured on the moon could significantly reduce the cost of transportation of power systems to space destinations, including the moon, Mars, earth orbit, and transfer orbits. Silicon is abundant on the moon, and refining processes are demonstrated which do not depend on extensive use of reactants imported from Earth. Because of the lower requirements for refined silicon, the amorphous silicon process is preferred, despite lower efficiencies. Calculations show that the specific power of amorphous silicon cells can be adequate for most uses. I.E.

A90-14933* National Aeronautics and Space Administration. Lewis Research Center, Cleveland, OH.

RADIATION RESISTANCE AND COMPARATIVE PERFORMANCE OF ITO/INP AND N/P INP HOMOJUNCTION SOLAR CELLS

I. WEINBERG, C. K. SWARTZ, R. E. HART, JR. (NASA, Lewis Research Center, Cleveland, OH), and T. J. COUTTS (SERI, Golden, CO) IN: IEEE Photovoltaic Specialists Conference, 20th, Las Vegas, NV, Sept. 26-30, 1988, Conference Record. Volume 2. New York, Institute of Electrical and Electronics Engineers, Inc., 1988, p. 893-897. Previously announced in STAR as N89-12819. refs

Copyright

The radiation resistance of ITO/InP cells processed by dc magnetron sputtering is compared to that of standard n/p InP and GaAs homojunction cells. After 20 MeV proton irradiations, it is found that the radiation resistance of the present ITO/InP cell is comparable to that of the n/p homojunction InP cell and that both InP cell types have radiation resistances significantly greater than GaAs. The relatively lower radiation resistance, observed at higher fluence, for the InP cell with the deepest junction depth, is attributed to losses in the cells emitter region. Diode parameters obtained from $I_{sub} sc - V_{sub} oc$ plots, data from surface Raman spectroscopy, and determinations of surface conductivity type are used to investigate the configuration of the ITO/InP cells. It is

concluded that these latter cells are n/p homojunctions, the n-region consisting of a disordered layer at the oxide semiconductor. Author

A90-14952* Wayne State Univ., Detroit, MI. **RADIATION RESISTANCE STUDIES OF AMORPHOUS SILICON FILMS**

J. SCOTT PAYSON and JAMES R. WOODYARD (Wayne State University, Detroit, MI) IN: IEEE Photovoltaic Specialists Conference, 20th, Las Vegas, NV, Sept. 26-30, 1988, Conference Record. Volume 2. New York, Institute of Electrical and Electronics Engineers, Inc., 1988, p. 990-995. Research supported by Wayne State University. refs
(Contract NAG3-833)
Copyright

A study of hydrogenated amorphous silicon thin films irradiated with 2.00 MeV helium ions using fluences ranging from 1×10^{11} to 1×10^{15} /sq cm is presented. The films were characterized using photothermal deflection spectroscopy, transmission and reflection spectroscopy, and photoconductivity and annealing measurements. Large changes were observed in the subband-gap optical absorption for energies between 0.9 and 1.7 eV. The steady-state photoconductivity showed decreases of almost five orders of magnitude for a fluence of 1×10^{15} /sq cm, but the slope of the intensity dependence of the photoconductivity remained almost constant for all fluences. Substantial annealing occurs even at room temperature, and for temperatures greater than 448 K the damage is completely annealed. The data are analyzed to describe the defects and the density of states function. I.E.

A90-14956* National Aeronautics and Space Administration. Lewis Research Center, Cleveland, OH.

PERFORMANCE OF GAAS CONCENTRATOR CELLS UNDER ELECTRON IRRADIATIONS FROM 0.4 TO 2.3 MEV

HENRY B. CURTIS and RUSSELL E. HART, JR. (NASA, Lewis Research Center, Cleveland, OH) IN: IEEE Photovoltaic Specialists Conference, 20th, Las Vegas, NV, Sept. 26-30, 1988, Conference Record. Volume 2. New York, Institute of Electrical and Electronics Engineers, Inc., 1988, p. 1020-1023.

Gallium arsenide concentrator cells were irradiated with electrons with energies varying from 0.4 to 2.3 MeV, and their electrical performance was measured. The cells are 5 x 5 mm square with a 4-mm diameter illuminated area. At each of four different electron energy levels (0.4, 0.7, 1.0, and 2.3 MeV), three n/p and two p/n cells were irradiated. I-V performance measurements were made prior to irradiation and at several intermediate fluence levels. The final fluence level was 3×10 to the 15th e/sq cm. It is concluded that the power degradation is independent of the temperature at which it is measured. I.E.

A90-27709* National Aeronautics and Space Administration. Lewis Research Center, Cleveland, OH.

CRYOGENIC REACTANT STORAGE FOR LUNAR BASE REGENERATIVE FUEL CELLS

LISA L. KOHOUT (NASA, Lewis Research Center, Cleveland, OH) (IAF, International Conference on Space Power, Cleveland, OH, June 5-7, 1989) Space Power (ISSN 0883-6272), vol. 8, no. 4, 1989, p. 443-457. Previously announced in STAR as N89-21419. refs
(IAF PAPER ICOSP89-3-8) Copyright

There are major advantages to be gained by integrating a cryogenic reactant storage system with a hydrogen-oxygen regenerative fuel cell (RFC) to provide on-site electrical power during the lunar night. Although applicable to any power system using hydrogen-oxygen RFC's for energy storage, cryogenic reactant storage offers a significant benefit whenever the sun/shade cycle and energy storage period approach hundreds of hours. For solar power installations on the moon, cryogenic reactant storage reduces overall specific mass and meteoroid vulnerability of the system. In addition, it offers synergistic benefits to on-site users, such as availability of primary fuel cell reactants for surface rover vehicles and cryogenic propellants for OTV's. The integration involves processing and storing the RFC reactant

streams as cryogenic liquids rather than pressurized gases, so that reactant containment (tankage per unit mass of reactants) can be greatly reduced. Hydrogen-oxygen alkaline RFC's, GaAs photovoltaic (PV) arrays and space cryogenic processing/refrigeration technologies are assumed to be available for the conceptual system design. Advantages are demonstrated by comparing the characteristics of two power system concepts: a conventional lunar surface PV/RFC power system using pressurized gas storage in SOA filament wound pressure vessels and, that same system with gas liquefaction and storage replacing the pressurized storage. Comparisons are made at 20 and 250 kWe. Although cryogenic storage adds a processing plant (drying and liquefaction) to the system plus 30 percent more solar array to provide processing power, the approximate order of magnitude reduction in tankage mass, confirmed by this analysis, results in a reduction in overall total system mass of approximately 50 percent. Author

A90-28359* National Aeronautics and Space Administration. Lewis Research Center, Cleveland, OH.

WIDE-BANDGAP EPITAXIAL HETEROJUNCTION WINDOWS FOR SILICON SOLAR CELLS

GEOFFREY A. LANDIS (NASA, Lewis Research Center, Cleveland, OH), JOSEPH J. LOFERSKI, ROLAND BEAULIEU (Brown University, Providence), PATRICIA A. SEKULA-MOISE, STANLEY M. VERNON (Spire Corp., Bedford, MA) et al. IEEE Transactions on Electron Devices (ISSN 0018-9383), vol. 37, Feb. 1990, p. 372-381. refs
(Contract DE-AC02-84ER-80186; NAS3-24641)
Copyright

It is shown that the efficiency of a solar cell can be improved if minority carriers are confined by use of a wide-bandgap heterojunction window. For silicon (lattice constant $a = 5.43$ Å), nearly lattice-matched wide-bandgap materials are ZnS ($a = 5.41$ Å) and GaP ($a = 5.45$ Å). Isotype n-n heterojunctions of both ZnS/Si and GaP/Si were grown on silicon n-p homojunction solar cells. Successful deposition processes used were metalorganic chemical vapor deposition (MO-CVD) for GaP and ZnS, and vacuum evaporation of ZnS. Planar (100) and (111) and texture-etched - (111)-faceted - surfaces were used. A decrease in minority-carrier surface recombination compared to a bare surface was seen from increased short-wavelength spectral response, increased open-circuit voltage, and reduced dark saturation current, with no degradation of the minority carrier diffusion length. I.E.

A90-33932* National Aeronautics and Space Administration. Lewis Research Center, Cleveland, OH.

SPACE ELECTROCHEMICAL RESEARCH AND TECHNOLOGY CONFERENCE, 2ND, CLEVELAND, OH, APR. 11-13, 1989, PROCEEDINGS

PATRICIA M. O'DONNELL, ED. (NASA, Lewis Research Center, Cleveland, OH) Conference sponsored by NASA. Journal of Power Sources (ISSN 0378-7753), vol. 29, Feb. 1990, 329 p. For individual items see A90-33933 to A90-33958.

Copyright

Attention is given to topics of advanced concepts, hydrogen-oxygen fuel cells and electrolyzers, nickel electrodes, and advanced rechargeable batteries. Papers are presented on human exploration mission studies, advanced rechargeable sodium batteries with novel cathodes, advanced double-layer capacitors, recent advances in solid-polymer electrolyte fuel cell technology with low platinum loading electrodes, electrocatalysts for oxygen electrodes in fuel cells and water electrolyzers for space applications, and the corrosion testing of candidates for the alkaline fuel cell cathode. Other papers are on a structural comparison of nickel electrodes and precursor phases, the application of electrochemical impedance spectroscopy for characterizing the degradation of Ni(OH)₂/NiOOH electrodes, advances in lightweight nickel electrode technology, multimission nickel-hydrogen battery cell for the 1990s, a sodium-sulfur battery flight experiment definition study, and advances in ambient-temperature secondary lithium cells. I.S.

44 ENERGY PRODUCTION AND CONVERSION

A90-33946* Giner, Inc., Waltham, MA.

OXYGEN ELECTRODES FOR RECHARGEABLE ALKALINE FUEL CELLS. II

L. SWETTE and N. KACKLEY (Giner, Inc., Waltham, MA) (NASA, Space Electrochemical Research and Technology Conference, 2nd, Cleveland, OH, Apr. 11-13, 1989) Journal of Power Sources (ISSN 0378-7753), vol. 29, Feb. 1990, p. 423-436. refs (Contract NAS3-24635)
Copyright

The primary objective of this program is the investigation and development of electrocatalysts and supports for the positive electrode of moderate temperature, single-unit, rechargeable alkaline fuel cells. Approximately six support materials and five catalyst materials have been identified to date for further development.
Author

A90-33948* National Aeronautics and Space Administration, Lewis Research Center, Cleveland, OH.

CORROSION TESTING OF CANDIDATES FOR THE ALKALINE FUEL CELL CATHODE

JOSEPH SINGER and WILLIAM L. FIELDER (NASA, Lewis Research Center, Cleveland, OH) (NASA, Space Electrochemical Research and Technology Conference, 2nd, Cleveland, OH, Apr. 11-13, 1989) Journal of Power Sources (ISSN 0378-7753), vol. 29, Feb. 1990, p. 443-450. refs (Contract NAS3-25199)
Copyright

Current/voltage data have been obtained for specially made corrosion electrodes of some oxides and of gold materials for the purpose of developing a screening test of catalysts and supports for use at the cathode of the alkaline fuel cell. The data consist of measurements of current at fixed potentials and cyclic voltammograms. These data will have to be correlated with longtime performance data in order to evaluate fully this approach to corrosion screening.
Author

A90-33949* Michigan Technological Univ., Houghton.

STRUCTURAL COMPARISON OF NICKEL ELECTRODES AND PRECURSOR PHASES

BAHNE C. CORNILSEN, XIAOYIN SHAN, and PATRICIA L. LOYSELLE (Michigan Technological University, Houghton) (NASA, Space Electrochemical Research and Technology Conference, 2nd, Cleveland, OH, Apr. 11-13, 1989) Journal of Power Sources (ISSN 0378-7753), vol. 29, Feb. 1990, p. 453-466. refs (Contract NAG3-519)
Copyright

In this paper the previous Raman spectroscopic results are summarized and important structural differences in the various phases of active mass and active mass precursors are discussed. Raman spectra provide unique signatures for these phases, and allow one to distinguish each phase, even when the compound is amorphous to X-rays (i.e., does not scatter X-rays because of a lack of order and/or small particle size). The structural changes incurred during formation, charge and discharge, cobalt addition, and aging will be discussed. The oxidation states and dopant contents are explained in terms of the nonstoichiometric structures.
Author

A90-33950* National Aeronautics and Space Administration, Lewis Research Center, Cleveland, OH.

IMPEDANCE STUDIES OF NICKEL/CADMIUM AND NICKEL-HYDROGEN CELLS USING THE CELL CASE AS A REFERENCE ELECTRODE

MARGARET A. REID (NASA, Lewis Research Center, Cleveland, OH) (NASA, Space Electrochemical Research and Technology Conference, 2nd, Cleveland, OH, Apr. 11-13, 1989) Journal of Power Sources (ISSN 0378-7753), vol. 29, Feb. 1990, p. 467-476. refs
Copyright

Impedance measurements have been made on several Ni/Cd and Ni/H₂ flight-weight cells using the case as a reference electrode. For these measurements, the voltage of the case with respect to the anode or cathode is unimportant provided that it

remains stable during the measurement of the impedance. In the cells measured so far, the voltage of the cell cases with respect to the individual electrodes differ from cell to cell, even at the same overall cell voltage, but they remain stable with time. The measurements can thus be used to separate the cell impedance into the contributions of each electrode, allowing improved diagnosis of cell problems.
Author

A90-33952* Hughes Aircraft Co., Torrance, CA.

KOH CONCENTRATION EFFECT ON THE CYCLE LIFE OF NICKEL-HYDROGEN CELLS. IV - RESULTS OF FAILURE ANALYSIS

H. S. LIM and S. A. VERZWYVELT (Hughes Aircraft Co., Torrance, CA) (NASA, Space Electrochemical Research and Technology Conference, 2nd, Cleveland, OH, Apr. 11-13, 1989) Journal of Power Sources (ISSN 0378-7753), vol. 29, Feb. 1990, p. 503-519. refs (Contract NAS3-22238)
Copyright

Potassium hydroxide concentration effects on the cycle life of a Ni/H₂ cell have been studied by carrying out a cycle life test on ten Ni/H₂ boiler plate cells which contain electrolytes of various KOH concentrations. Failure analyses of these cells were carried out after completion of the life test, which accumulated up to 40,000 cycles at an 80-percent depth of discharge over a period of 3.7 years. These failure analyses included studies on changes of electrical characteristics of test cells, and component analyses after disassembly of the cell. The component analyses included visual inspections, dimensional changes, capacity measurements of nickel electrodes, scanning electron microscopy, surface area measurements, and chemical analyses. Results have indicated that failure mode and change in the nickel electrode varied as the concentration was varied, especially when the concentration was changed from 31 percent or higher to 26 percent or lower.
Author

A90-38110* National Aeronautics and Space Administration, Lewis Research Center, Cleveland, OH.

MATHEMATICAL OPTIMIZATION OF PHOTOVOLTAIC CONVERTERS FOR DIODE LASERS

GILBERT H. WALKER (NASA, Langley Research Center, Hampton, VA) and JOHN H. HEINBOCKEL (Old Dominion University, Norfolk, VA) IN: IECEC-89; Proceedings of the Twenty-fourth Intersociety Energy Conversion Engineering Conference, Washington, DC, Aug. 6-11, 1989. Volume 1. New York, Institute of Electrical and Electronics Engineers, 1989, p. 507-511. refs
Copyright

The mathematical optimization of vertical-junction photovoltaic converters for use with diode laser arrays supplying powers up to 1 MW is discussed. Photovoltaic parameters were optimized using a mathematical model. The optimized converters have 500 single junctions connected in series. The efficiency varies from 41 percent for a 0.73-micron diode laser to 46 percent for a 0.83-micron diode laser. The optimum width of the single-junction converter is small, 3.0 microns, in order for the p-n junction to be within a diffusion length of the light-generated carriers. Another critical parameter is the series resistance; the optimum value of 0.001 ohms should be achievable. Another critical parameter is the donor carrier concentration, for which an optimum value of 5 x 10 to the 15th carriers/cu cm has been chosen.
I.E.

A90-38217* National Aeronautics and Space Administration, Lewis Research Center, Cleveland, OH.

NASA AEROSPACE BATTERY SYSTEMS PROGRAM UPDATE

MICHELLE A. MANZO (NASA, Lewis Research Center, Cleveland, OH) and NORMAN R. SCHULZE (NASA, Washington, DC) IN: IECEC-89; Proceedings of the Twenty-fourth Intersociety Energy Conversion Engineering Conference, Washington, DC, Aug. 6-11, 1989. Volume 3. New York, Institute of Electrical and Electronics Engineers, 1989, p. 1401-1404.

An overview of a battery systems program designed to enhance the safety, reliability, and performance of NASA's aerospace primary and secondary batteries as well as battery power systems

is presented. The status of research in all three areas is reviewed. The approach to achieving the program objectives involves increasing the fundamental understanding of primary and secondary cells; providing for improved nickel-cadmium manufacturing process control; providing for the establishment of a NASA standard nickel-hydrogen cell design; establishing specifications, design and operational guidelines for both primary and secondary cells and batteries; providing training relating to the above areas; and opening and maintaining communication lines within NASA and the aerospace battery community. I.E.

A90-38254* # National Aeronautics and Space Administration. Lewis Research Center, Cleveland, OH.

COMPARISON OF CONCEPTUAL DESIGNS FOR 25 KWE ADVANCED STIRLING CONVERSION SYSTEMS FOR DISH ELECTRIC APPLICATIONS

RICHARD K. SHALTENS and JEFFREY G. SCHREIBER (NASA, Lewis Research Center, Cleveland, OH) IN: IECEC-89; Proceedings of the Twenty-fourth Intersociety Energy Conversion Engineering Conference, Washington, DC, Aug. 6-11, 1989. Volume 5. New York, Institute of Electrical and Electronics Engineers, 1989, p. 2305-2315. Previously announced in STAR as N89-26781. refs

The Advanced Stirling Conversion System (ASCS) Project is managed by NASA Lewis Research Center through a cooperative interagency agreement with DOE. Conceptual designs for the ASCS's were completed under parallel contracts in 1987 by Mechanical Technology Inc. (MTI) of Latham, NY, and Stirling Technology Company (STC) of Richland, WA. Each design features a free-piston Stirling engine, a liquid metal heat pipe receiver, and a means to provide about 25 kW of electric power to a utility grid while meeting DOE's long term performance and cost goals. An independent assessment showed that both designs are manufacturable and have the potential to easily meet DOE's long term cost goals. Author

N90-13886* # Arizona State Univ., Tempe.

THE PHOTOVOLTAIC PROPERTIES OF AN AL IN AS/INP HETEROJUNCTIONS GROWN BY LPE METHOD Final Technical Report

EDWARD Y. WANG 27 Oct. 1989 18 p

(Contract NAG3-383)

(NASA-CR-185996; NAS 1.26:185996) Avail: NTIS HC A03/MF A01 CSCL 10/1

Work is presented on heterojunction solar cells which were studied under the NASA/Arizona State University intern program. The heterojunction solar cells were fabricated by the liquid phase epitaxy method. The basic conversion efficiency was measured at 5 percent. It was determined that a thicker epilayer is needed, and that the density of recombination center should be reduced to give a smaller saturation current and hence a larger open-circuit voltage. J.P.S.

N90-14678* # National Aeronautics and Space Administration. Lewis Research Center, Cleveland, OH.

TECHNOLOGY DEVELOPMENT PROGRAM FOR AN ADVANCED MICROSHEET GLASS CONCENTRATOR

SCOTT W. RICHTER (Sverdrup Technology, Inc., Cleveland, OH.) and DOVIE E. LACY 1990 8 p Prepared for presentation at the 1990 International Solar Energy Conference, Miami, FL, 1-4 Apr. 1990; sponsored in part by ASME

(NASA-TM-102406; E-5158; NAS 1.15:102406) Avail: NTIS HC A02/MF A01 CSCL 10/1

Solar Dynamic Space Power Systems are candidate electrical power generating systems for future NASA missions. One of the key components in a solar dynamic power system is the concentrator which collects the sun's energy and focuses it into a receiver. In 1985, the NASA Lewis Research Center initiated the Advanced Solar Dynamic Concentrator Program with funding from NASA's Office of Aeronautics and Space Technology (OAST). The objectives of the Advanced Concentrator Program is to develop the technology that will lead to lightweight, highly reflective, accurate, scaleable, and long lived (7 to 10 years) space solar

dynamic concentrators. The Advanced Concentrator Program encompasses new and innovative concepts, fabrication techniques, materials selection, and simulated space environmental testing. The Advanced Microsheet Glass Concentrator Program, a reflector concept, that is currently being investigated both in-house and under contract is discussed. Author

N90-15506* # Oak Ridge National Lab., TN.

SELECTION OF PHASE-CHANGE AND CONTAINMENT MATERIALS FOR THERMAL ENERGY STORAGE

D. F. WILSON, J. H. DEVAN, and M. HOWELL 1989 14 p Presented at the ASME Winter Annual Meeting, San Francisco, CA, 10-15 Dec. 1989

(Contract NASA ORDER C-3003-J; DE-AC05-84OR-21400)

(NASA-CR-186228; NAS 1.26:186228; DE89-014778;

CONF-891208-6) Avail: NTIS HC A03/MF A01 CSCL 10/1

The high thermal conductivity and generally low volume change on melting of germanium and alloys based on silicon make them attractive for storage of thermal energy in space power systems. However, this application obviously depends on identification of suitable container materials that are compatible with these metals at the temperature of interest (greater than 1223 K). An approach to solving the containment problem, involving both chemical and physical compatibility, preparation of NiSi/NiSi₂, and initial results for containment of germanium and NiSi/NiSi₂ are presented. DOE

N90-17754* # National Aeronautics and Space Administration. Lewis Research Center, Cleveland, OH.

GAAS SOLAR CELLS WITH V-GROOVED EMITTERS

S. G. BAILEY, N. FATEMI, D. M. WILT, G. A. LANDIS, and R. D. THOMAS /n ESA, European Space Power, Volume 2 p 515-518 Aug. 1989

Copyright Avail: NTIS HC A16/MF A03 CSCL 10/2

A GaAs solar cell with a V-grooved front surface is described. It shows improved optical coupling and higher short-circuit current compared to planar cells. The GaAs homojunction cells, manufactured by OrganoMetallic Chemical Vapor Deposition (OMCVD), are described. The V-grooves were formed by anisotropic etching. Reflectivity measurements show significantly lower reflectance for the microgrooved cell compared to the planar structure. The short circuit current of the V-grooved solar cell is consistently higher than that of the planar controls. ESA

N90-17758* # National Aeronautics and Space Administration. Lewis Research Center, Cleveland, OH.

INDIUM PHOSPHIDE SOLAR CELL RESEARCH IN THE UNITED STATES: COMPARISON WITH NON-PHOTOVOLTAIC SOURCES

I. WEINBERG, C. K. SWARTZ, and R. E. HART, JR. /n ESA, European Space Power, Volume 2 p 537-542 Aug. 1989 Previously announced as N89-27868

Copyright Avail: NTIS HC A16/MF A03 CSCL 10/1

Highlights of the InP solar cell research program are presented. Homojunction cells with efficiencies approaching 19 percent are demonstrated, while 17 percent is achieved for ITO/InP cells. The superior radiation resistance of the two latter cell configurations over both Si and GaAs cells has been shown. InP cells aboard the LIPS3 satellite show no degradation after more than a year in orbit. Computed array specific powers are used to compare the performance of an InP solar cell array to solar dynamic and nuclear systems. ESA

N90-18097* # National Aeronautics and Space Administration. Lewis Research Center, Cleveland, OH.

CHANGES IN IMPEDANCE OF NI ELECTRODES UPON STANDING AND CYCLING

MARGARET A. REID 1989 16 p Presented at the 1989 Fall Meeting of the Electrochemical Society, Hollywood, FL, 15-20 Oct. 1989

(NASA-TM-102438; E-5207; NAS 1.15:102438) Avail: NTIS HC A03/MF A01 CSCL 10/1

Impedances of Ni electrodes vary with many factors including

44 ENERGY PRODUCTION AND CONVERSION

voltage, cycling, and manufacturer. However, results from Ni/H₂ cells being tested for Space Station Freedom show that consistent results are obtained within a group of cells from the same manufacturer if the cells are cycled and stored in the same manner. Impedance changes with storage and cycling are being investigated. Impedances are low in the fully charged state but rise abruptly by several orders of magnitude at a voltage corresponding to a very low state-of-charge. After standing for several months, this increase occurred at a higher voltage, consistent with an increase in structural order during storage which hinders diffusion of protons and reduces high rate capacity. Early measurements on the effects of cycling on Ni/H₂ cells being tested for Space Station Freedom show differences between cells from different manufacturers. Author

N90-18808*# International Fuel Cells Corp., South Windsor, CT. **INTEGRATED REGENERATIVE FUEL CELL EXPERIMENTAL EVALUATION Final Report, 11 Jan. 1988 - 30 Jun. 1989** RONALD E. MARTIN 1990 65 p (Contract NAS3-22234) (NASA-CR-185183; NAS 1.26:185183; FCR-10555A) Avail: NTIS HC A04/MF A01 CSCL 10/2

An experimental test program was conducted to investigate the performance characteristics of an integrated regenerative fuel cell (IRFC) concept. The IRFC consists of a separate fuel cell unit and electrolysis cell unit in the same structure, with internal storage of fuel cell product water and external storage of electrolysis cell produced hydrogen and oxygen. The fuel cell unit incorporates an enhanced Orbiter-type cell capable of improved performance at reduced weight. The electrolysis cell features a NiCo₂O₄ catalyst oxygen evolution electrode with a porous Teflon cover to retard electrolyte loss. Six complete IRFC assemblies were assembled and performance tested at an operating temperature of 200 F (93.3 C) and reactant pressures up to 170 psia (117.2 n/cu cm) on IRFC No. 4. Anomalous pressure charge/discharge characteristics were encountered during performance evaluation. A reversible fuel cell incorporating a proprietary bi-functional oxygen electrode operated satisfactorily at 200 F (93.3 C) at reactant pressures up to 50 psia (41.4 n/cu cm) as a regenerative fuel cell for one cycle, before developing an electrical short in the fuel cell mode. Electrolysis cell 300-hour endurance tests demonstrated the electrolyte retention capability of the electrode Teflon cover and the performance stability of the bi-functional oxygen electrode at high potential. Author

N90-20454*# National Aeronautics and Space Administration. Lewis Research Center, Cleveland, OH. **SPACE ELECTROCHEMICAL RESEARCH AND TECHNOLOGY (SERT), 1989** RICHARD S. BALDWIN, ed. Washington Dec. 1989 351 p Conference held in Cleveland, OH, 11-13 Apr. 1989 (NASA-CP-3056; E-4708; NAS 1.55:3056) Avail: NTIS HC A16/MF A02 CSCL 10/1

The proceedings of NASA's second Space Electrochemical Research and Technology Conference are presented. The objectives of the conference were to examine current technologies, research efforts, and advanced ideas, and to identify technical barriers which affect the advancement of electrochemical energy storage systems for space applications. The conference provided a forum for the exchange of ideas and opinions of those actively involved in the field, with the intention of coalescing views and findings into conclusions on progress in the field, prospects for future advances, areas overlooked, and the directions of future efforts. Related overviews were presented in the areas of NASA advanced mission models. Papers were presented and workshops conducted in four technical areas: advanced concepts, hydrogen-oxygen fuel cells and electrolyzers, the nickel electrode, and advanced rechargeable batteries.

N90-20463*# National Aeronautics and Space Administration. Lewis Research Center, Cleveland, OH. **CHARACTERIZATION TESTING OF A 40 AHR BIPOLAR NICKEL-HYDROGEN BATTERY**

JEFFREY C. BREWER (National Aeronautics and Space Administration. Marshall Space Flight Center, Huntsville, AL.), MICHELLE A. MANZO, and RUSSEL P. GEMEINER *In its Space Electrochemical Research and Technology (SERT)*, 1989 p 69-82 Dec. 1989

Avail: NTIS HC A16/MF A02 CSCL 10/3

Extensive characterization testing has been done on a second 40 amp-hour (Ahr), 10-cell bipolar nickel-hydrogen (Ni-H₂) battery to study the effects of such operating parameters as charge and discharge rates, temperature, and pressure, on capacity, Ahr and watt-hour (Whr) efficiencies, end-of-charge (EOC) and mid-point discharge voltages. Testing to date has produced many interesting results, with the battery performing well throughout all of the test matrix except during the high-rate (5C and 10C) discharges, where poorer than expected results were observed. The exact cause of this poor performance is, as yet, unknown. Small scale 2 x 2 inch battery tests are to be used in studying this problem. Low earth orbit (LEO) cycle life testing at a 40 percent depth of discharge (DOD) and 10 C is scheduled to follow the characterization testing. Author

N90-20467*# National Aeronautics and Space Administration. Lewis Research Center, Cleveland, OH.

HYDROGEN-OXYGEN PROTON-EXCHANGE MEMBRANE FUEL CELLS AND ELECTROLYZERS

R. BALDWIN, M. PHAM, A. LEONIDA, J. MCELROY, and T. NALETTE (Hamilton Standard, Windsor Locks, CT.) *In its Space Electrochemical Research and Technology (SERT)*, 1989 p 127-136 Dec. 1989

Avail: NTIS HC A16/MF A02 CSCL 10/3

Hydrogen-oxygen solid polymer electrolyte (SPE) fuel cells and SPE electrolyzers (products of Hamilton Standard) both use a Proton-Exchange Membrane (PEM) as the sole electrolyte. These solid electrolyte devices have been under continuous development for over 30 years. This experience has resulted in a demonstrated ten-year SPE cell life capability under load conditions. Ultimate life of PEM fuel cells and electrolyzers is primarily related to the chemical stability of the membrane. For perfluorocarbon proton exchange membranes an accurate measure of the membrane stability is the fluoride loss rate. Millions of cell hours have contributed to establishing a relationship between fluoride loss rates and average expected ultimate cell life. This relationship is shown. Several features have been introduced into SPE fuel cells and SPE electrolyzers such that applications requiring greater than or equal to 100,000 hours of life can be considered. Equally important as the ultimate life is the voltage stability of hydrogen-oxygen fuel cells and electrolyzers. Here again the features of SPE fuel cells and SPE electrolyzers have shown a cell voltage stability in the order of 1 microvolt per hour. That level of stability has been demonstrated for tens of thousands of hours in SPE fuel cells at up to 500 amps per square foot (ASF) current density. Author

N90-20468*# Case Western Reserve Univ., Cleveland, OH. Dept. of Chemistry.

ELECTROCATALYSIS FOR OXYGEN ELECTRODES IN FUEL CELLS AND WATER ELECTROLYZERS FOR SPACE APPLICATIONS

JAI PRAKASH, DONALD TRYK, and ERNEST YEAGER *In NASA, Lewis Research Center, Space Electrochemical Research and Technology (SERT)*, 1989 p 137-147 Dec. 1989 Previously announced at N89-22997

(Contract NAG3-964)

Avail: NTIS HC A16/MF A02 CSCL 10/3

In most instances separate electrocatalysts are needed to promote the reduction of O₂ in the fuel cell mode and to generate O₂ in the energy storage-water electrolysis mode in aqueous electrochemical systems operating at low and moderate temperatures (T greater than or equal to 200 C). Interesting exceptions are the lead and bismuth ruthenate pyrochlores in alkaline electrolytes. These catalysts on high area carbon supports have high catalytic activity for both O₂ reduction and generation. Rotating ring-disk electrode measurements provide evidence that

the O₂ reduction proceeds by a parallel four-electron pathway. The ruthenates can also be used as self-supported catalysts to avoid the problems associated with carbon oxidation, but the electrode performance so far achieved in the research at Case Western Reserve University (CWRU) is considerably less. At the potentials involved in the anodic mode the ruthenate pyrochlores have substantial equilibrium solubility in concentrated alkaline electrolyte. This results in the loss of catalyst into the bulk solution and a decline in catalytic activity. Furthermore, the hydrogen generation counter electrode may become contaminated with reduction products from the pyrochlores (lead, ruthenium).

Author

N90-20469* # Giner, Inc., Waltham, MA.

OXYGEN ELECTRODES FOR RECHARGEABLE ALKALINE FUEL CELLS-II

L. SWETTE and N. KACKLEY *In* NASA, Lewis Research Center, Space Electrochemical Research and Technology (SERT), 1989 p 149-163 Dec. 1989
(Contract NAS3-24635)
Avail: NTIS HC A16/MF A02 CSCL 10/3

The primary objective of this program is the investigation and development of electrocatalysts and supports for the positive electrode of moderate temperature single-unit rechargeable alkaline fuel cells. Approximately six support materials and five catalyst materials have been identified to date for further development.

Author

N90-20471* # National Aeronautics and Space Administration. Lewis Research Center, Cleveland, OH.

CORROSION TESTING OF CANDIDATES FOR THE ALKALINE FUEL CELL CATHODE

JOSEPH SINGER and WILLIAM L. FIELDER *In* its Space Electrochemical Research and Technology (SERT), 1989 p 171-180 Dec. 1989
(Contract NAS3-25199)
Avail: NTIS HC A16/MF A02 CSCL 10/3

Current/voltage data was obtained for specially made corrosion electrodes of some oxides and of gold materials for the purpose of developing a screening test of catalysts and supports for use at the cathode of the alkaline fuel cell. The data consists of measurements of current at fixed potentials and cyclic voltammograms. These data will have to be correlated with longtime performance data in order to fully evaluate this approach to corrosion screening. Corrosion test screening of candidates for the oxygen reduction electrode of the alkaline fuel cell was applied to two substances, the pyrochlore Pb₂Ru₂O_{6.5} and the spinel NiCo₂O₄. The substrate gold screen and a sample of the IFC Orbiter Pt-Au performance electrode were included as blanks. The pyrochlore data indicate relative stability, although nothing yet can be said about long term stability. The spinel was plainly unstable. For this type of testing to be validated, comparisons will have to be made with long term performance tests.

Author

N90-20472* # Michigan Technological Univ., Houghton.

STRUCTURAL COMPARISON OF NICKEL ELECTRODES AND PRECURSOR PHASES

BAHNE C. CORNILSEN, XIAOYIN SHAN, and PATRICIA LOYSELLE *In* NASA, Lewis Research Center, Space Electrochemical Research and Technology (SERT), 1989 p 181-196 Dec. 1989
(Contract NAG3-519)
Avail: NTIS HC A16/MF A02 CSCL 10/3

Researchers summarize previous Raman spectroscopic results and discuss important structural differences in the various phases of active mass and active mass precursors. Raman spectra provide unique signatures for these phases, and allow one to distinguish each phase, even when the compound is amorphous to x rays (i.e., does not scatter x rays because of a lack of order and/or small particle size). The structural changes incurred during formation, charge and discharge, cobalt addition, and aging are discussed. The oxidation states and dopant contents are explained in terms of the nonstoichiometric structures.

Author

N90-20473* # National Aeronautics and Space Administration. Lewis Research Center, Cleveland, OH.

IMPEDANCE STUDIES OF NI/CD AND NI/H₂ CELLS USING THE CELL CASE AS A REFERENCE ELECTRODE

MARGARET A. REID *In* its Space Electrochemical Research and Technology (SERT), 1989 p 197-209 Dec. 1989
Avail: NTIS HC A16/MF A02 CSCL 10/3

Impedance measurements have been made on several Ni/Cd and Ni/H₂ flightweight cells using the case as a reference electrode. For these measurements the voltage of the case with respect to the anode or cathode is unimportant provided that it remains stable during the measurement of the impedance. In the cells measured so far, the voltages of the cell cases with respect to the individual electrodes differ from cell to cell even at the same overall cell voltage, but they remain stable with time. The measurements can thus be used to separate the cell impedance into the contributions of each electrode, allowing improved diagnosis of cell problems.

Author

N90-20478* # National Aeronautics and Space Administration. Lewis Research Center, Cleveland, OH.

NICKEL-HYDROGEN CAPACITY LOSS ON STORAGE

MICHELLE A. MANZO *In* its Space Electrochemical Research and Technology (SERT), 1989 p 279-295 Dec. 1989
Avail: NTIS HC A16/MF A02 CSCL 10/3

A controlled experiment evaluating the capacity loss experienced by nickel electrodes stored under various conditions of temperature, hydrogen pressure, and electrolyte concentration was conducted using nickel electrodes from four different manufacturers. It was found that capacity loss varied with respect to hydrogen pressure, and storage temperature as well as with respect to electrode manufacturing processes. Impedance characteristics were monitored and found to be indicative of electrode manufacturing processes and capacity loss. Cell testing to evaluate state-of-charge effects on capacity loss were inconclusive as no loss was sustained by the cells tested in this experiment.

Author

N90-20479* # Ford Aerospace and Communications Corp., Palo Alto, CA. Space Systems Div.

SODIUM-SULFUR BATTERY FLIGHT EXPERIMENT DEFINITION STUDY

REBECCA CHANG and ROBERT MINCK (Ford Aerospace Corp., Newport Beach, CA.) *In* NASA, Lewis Research Center, Space Electrochemical Research and Technology (SERT), 1989 p 297-306 Dec. 1989
(Contract NAS3-25355)
Avail: NTIS HC A16/MF A02 CSCL 10/3

NaS batteries have been identified as the most likely successor to space Ni-H₂ or Ni-Cd batteries, primarily due to a mass reduction by a factor 2 to 3 over Ni-H₂ and by a factor of 4 over Ni-Cd. This yields major launch cost reductions or payload mass improvements. NaS batteries support NASA OAST's proposed Civil Space Technology Initiative goal of a factor of two improvement in spacecraft 2000 initiative. Since Ni-H₂ and Ni-Cd batteries have been space flight proven, it is essential to have the flight experiment to establish a national space technology base to demonstrate the operation of the NaS battery for space applications.

Author

N90-21469* # National Aeronautics and Space Administration. Lewis Research Center, Cleveland, OH.

O₂ REDUCTION AT THE IFC ORBITER FUEL CELL O₂ ELECTRODE

WILLIAM L. FIELDER and JOSEPH SINGER Apr. 1990 15 p (NASA-TM-102580; E-5411; NAS 1.15:102580) Avail: NTIS HC A03/MF A01 CSCL 10/2

O₂ reduction Tafel data were obtained for the IFC Orbiter fuel cell O₂ electrode (Au-10 percent Pt catalyst) at temperatures between 24 and 81 C. BET measurements gave an electrode surface area of about 2040 sq cm per sq cm of geometric area. The Tafel data could be fitted to three straight line regions. For current densities less than 0.001 A/sq cm, the slope was essentially independent of temperature with a value of about 0.032 V/decade.

44 ENERGY PRODUCTION AND CONVERSION

Above 0.001 A/sq cm, the two regions, designated in the present study as the 0.04 and 0.12 V/decade regions, were temperature dependent. The apparent energies of activation for these two regions were about 9.3 and 6.5 kcal/mol, respectively. Tafel data (1 atmosphere O₂) were extrapolated to 120 C for predicting changes in overpotential with increasing temperature. A mechanism is presented for O₂ reduction.

Author

N90-22834*# Harris Corp., Melbourne, FL. Government Aerospace Systems Div.

SOLAR CONCENTRATOR ADVANCED DEVELOPMENT PROGRAM Final Report

DON KNASEL and DERIK EHRESMAN Oct. 1989 333 p
Original contains color illustrations
(Contract NAS3-24670)
(NASA-CR-185173; NAS 1.26:185173) Avail: NTIS HC A15/MF A02; 1 functional color page CSCL 10/1

The Solar Concentrator Advanced Development Project has successfully designed, fabricated, and tested a full scale prototypical solar dynamic concentrator for space station applications. A Truss Hexagonal Panel reflector was selected as a viable solar concentrator concept to be used for space station applications. This concentrator utilizes a modular design approach and is flexible in attainable flux profiles and assembly techniques. The detailed design of the concentrator, which included structural, thermal and optical analysis, identified the feasibility of the design and specific technologies that were required to fabricate it. The needed surface accuracy of the reflectors surface was found to be very tight, within 5 mrad RMS slope error, and results in very close tolerances for fabrication. To meet the design requirements, a modular structure composed of hexagonal panels was used. The panels, made up of graphite epoxy box beams provided the strength, stiffness and dimensional stability needed. All initial project requirements were met or exceeded by hardware demonstration. Initial testing of structural repeatability of a seven panel portion of the concentrator was followed by assembly and testing of the full nineteen panel structure. The testing, which consisted of theodolite and optical measurements over an assembly-disassembly-reassembly cycle, demonstrated that the concentrator maintained the as-built contour and optical characteristics. The facet development effort within the project, which included developing the vapor deposited reflective facet, produced a viable design with demonstrated optical characteristics that are within the project goals.

Author

N90-22835*# Case Western Reserve Univ., Cleveland, OH. Center for Electrochemical Sciences.

CATALYSTS FOR ULTRAHIGH CURRENT DENSITY OXYGEN CATHODES FOR SPACE FUEL CELL APPLICATIONS Final Report, 1 Feb. 1989 - 31 Jan. 1990

D. TRYK, E. YEAGER, M. SHINGLER, W. ALDRED, and C. WANG 11 Jun. 1990 30 p
(Contract NAG3-694)
(NASA-CR-180650; NAS 1.26:180650) Avail: NTIS HC A03/MF A01 CSCL 10/1

The objective of this research was to identify promising electrocatalyst/support systems for the oxygen cathode in alkaline fuel cells operating at relatively high temperatures, O₂ pressures and current densities. A number of materials were prepared, including Pb-Ru and Pb-Ir pyrochlores, RuO₂ and Pt-doped RuO₂, and lithiated NiO. Several of these were prepared using techniques that had not been previously used to prepare them. Particularly interesting is the use of the alkaline solution technique to prepare the Pt-doped Pb-Ru pyrochlore in high area form. Well-crystallized Pb(2)Ru(2)O(7-y) was used to fabricate high performance O₂ cathodes with relatively good stability in room temperature KOH. This material was also found to be stable over a useful potential range at approximately 140 C in concentrated KOH. Other pyrochlores were found to be either unstable (amorphous samples) or the fabrication of the gas-fed electrodes could not be fully optimized during this project period. Future work may be directed at this problem. High area platinum supported on conductive metal oxide supports produced mixed results: small improvements in O₂

reduction performance for Pb(2)Ru(2)O(7-y) but a large improvement for Li-doped NiO at room temperature. Nearly reversible behavior was observed for the O₂/OH couple for Li-doped NiO at approximately 200 C.

Author

N90-22843*# National Aeronautics and Space Administration. Lewis Research Center, Cleveland, OH.

LATERAL SPREADING OF AU CONTACTS ON INP

NAVID S. FATEMI (Sverdrup Technology, Inc., Cleveland, OH.) and VICTOR G. WEIZER 1990 10 p Presented at the 1990 Spring Meeting of the Materials Research Society, San Francisco, CA, 16-21 Apr. 1990
(Contract NAS3-25266)
(NASA-TM-103133; E-5472; NAS 1.15:103133) Avail: NTIS HC A02/MF A01 CSCL 10/1

The contact spreading phenomenon observed when small area Au contacts on InP are annealed at temperatures above about 400 C was investigated. It was found that the rapid lateral expansion of the contact metallization which consumes large quantities of InP during growth is closely related to the third stage in the series of solid state reactions that occur between InP and Au, i.e., to the Au₃In-to-Au₉In₄ transition. Detailed descriptions are presented of both the spreading process and the Au₃In-to-Au₉In₄ transition along with arguments that the two processes are manifestations of the same basic phenomenon.

Author

N90-22847*# National Aeronautics and Space Administration. Lewis Research Center, Cleveland, OH.

NUCLEAR TECHNOLOGY AND THE SPACE EXPLORATION MISSIONS

HENRY W. BRANDHORST and RONALD J. SOVIE 1990 11 p Proposed for presentation at the 25th Intersociety Energy Conversion Engineering Conference, Reno, NV, 12-17 Aug. 1990; cosponsored by AIChE, SAE, ACS, AIAA, ASME, and IEEE
(NASA-TM-103156; E-5518; NAS 1.15:103156) Avail: NTIS HC A03/MF A01 CSCL 10/2

The strategy for a major exploration initiative leading to permanent human presence beyond earth orbit is still being developed; however enough is known to begin defining the role of nuclear technologies. Three broad areas are discussed: low power (less than 10 kWe) rover/vehicle power systems; integrated, evolutionary base power systems (25 to 100 kW) and nuclear energy for electric propulsion (2 to 100 MWe); and direct thermal propulsion (1000s MW). A phased, evolutionary approach is described for both the moon and Mars, and the benefits of nuclear technologies relative to solar and their integration are described.

Author

N90-25418*# Colby Coll., Waterville, ME. Dept. of Physics and Astronomy.

LEO HIGH VOLTAGE SOLAR ARRAY ARCING RESPONSE MODEL, CONTINUATION 5 Interim Report

ROGER N. METZ Apr. 1989 89 p
(Contract NAG3-576)
(NASA-CR-186505; NAS 1.26:186505) Avail: NTIS HC A05/MF A01 CSCL 10/1

The modeling of the Debye Approximation electron sheaths in the edge and strip geometries was completed. Electrostatic potentials in these sheaths were compared to NASCAP/LEO solutions for similar geometries. Velocity fields, charge densities and particle fluxes to the biased surfaces were calculated for all cases. The major conclusion to be drawn from the comparisons of our Debye Approximation calculations with NASCAP-LEO output is that, where comparable biased structures can be defined and sufficient resolution obtained, these results are in general agreement. Numerical models for the Child-Langmuir, high-voltage electron sheaths in the edge and strip geometries were constructed. Electrostatic potentials were calculated for several cases in each of both geometries. Velocity fields and particle fluxes were calculated. The self-consistent solution process was carried through one cycle and output electrostatic potentials compared to NASCAP-type input potentials.

Author

N90-25419*# National Aeronautics and Space Administration. Lewis Research Center, Cleveland, OH.

ENERGY STORAGE FOR A LUNAR BASE BY THE REVERSIBLE CHEMICAL REACTION: $\text{CaO} + \text{H}_2\text{O}$ REVERSIBLE REACTION $\text{Ca}(\text{OH})_2$

MARLA E. PEREZ-DAVIS and FRANK DIFILIPPO (Case Western Reserve Univ., Cleveland, OH.) Jun. 1990 7 p (NASA-TM-103145; E-5497; NAS 1.15:103145) Avail: NTIS HC A02/MF A01 CSCL 10/3

A thermochemical solar energy storage concept involving the reversible reaction $\text{CaO} + \text{H}_2\text{O}$ yields $\text{Ca}(\text{OH})_2$ is proposed as a power system element for a lunar base. The operation and components of such a system are described. The $\text{CaO}/\text{H}_2\text{O}$ system is capable of generating electric power during both the day and night. The specific energy (energy to mass ratio) of the system was estimated to be 155 W-hr/kg. Mass of the required amount of CaO is neglected since it is obtained from lunar soil. Potential technical problems, such as reactor design and lunar soil processing, are reviewed. Author

N90-25420*# National Aeronautics and Space Administration. Lewis Research Center, Cleveland, OH.

AN ANALYSIS OF THE CONTACT SINTERING PROCESS IN III-V SOLAR CELLS

VICTOR G. WEIZER and NAVID S. FATEMI (Sverdrup Technology, Inc., Brook Park, OH.) 1990 8 p Presented at the 21st Photovoltaics Specialists Conference, Kissimmee, FL, 21-25 May 1990; sponsored by IEEE (Contract NAS3-25266) (NASA-TM-103179; E-5556; NAS 1.15:103179) Avail: NTIS HC A02/MF A01 CSCL 10/1

The possibility of eliminating the gross mechanical changes that take place during sintering while retaining the processes that reduce contact resistivity is investigated. Before considering the electrical aspects, however, it is necessary to understand the relevant metallurgy. As the sintering process proceeds in the InP-Au system, dramatic color changes occur that enable a precise measurement of the kinetics of each step. A detailed insight into the processes that control each stage in the InP-Au interaction has resulted. It is shown that contact sintering in the InP-Au system consists of three consecutive stages, each of which is controlled by a separate mechanism. Author

N90-25558*# National Aeronautics and Space Administration. Lewis Research Center, Cleveland, OH.

SOLAR ARRAY ARCING IN PLASMAS

DALE C. FERGUSON In NASA, Lyndon B. Johnson Space Center, Third Annual Workshop on Space Operations Automation and Robotics (SOAR 1989) p 509-513 Mar. 1990 Avail: NTIS HC A99/MF A04 CSCL 10/1

Solar cells in space plasma conditions are known to arc into the plasma when the interconnects are at a negative potential of a few hundred volts, relative to plasma potential. For cells with silver-coated interconnects, a threshold voltage for arcing exists at about -230 V, as found in both ground and LEO experiments. The arc rate beyond the threshold voltage depends nearly linearly on plasma density, but has a strong power-law dependence on voltage, such that for small increments in operating voltage there is a large increment in arc rate. The arcs generate broadband radio interference and visible light. In ground tests, interconnects have been damaged by arcs in cells having insufficient isolation from a source of high current. Models for the arcs are highly dependent on the choice of interconnect conductor material exposed to the plasma and possibly on the geometry and choice of adjacent insulator material. Finally, new technology solar cells use copper for the cell interconnects, a material which may have a lower arcing threshold voltage than silver. It is expected, from ground tests of simulated solar cells, that any junction of conductor and insulator exposed to space plasma conditions will arc into the plasma at a few hundred volts negative potential, relative to the local plasma. Author

N90-26396*# National Aeronautics and Space Administration. Lewis Research Center, Cleveland, OH.

MODELING AND OPTIMIZATION OF A REGENERATIVE FUEL CELL SYSTEM USING THE ASPEN PROCESS SIMULATOR

THOMAS M. MALONEY (Sverdrup Technology, Inc., Brook Park, OH.) and HAROLD F. LEIBECKI 1990 7 p Presented at the 25th Intersociety Energy Conversion Engineering Conference, Reno, NV, 12-17 Aug. 1990; cosponsored by AIChE, ANS, SAE, ACS, AIAA, ASME, and IEEE (NASA-TM-103210; E-5618; NAS 1.15:103210) Avail: NTIS HC A02/MF A01 CSCL 10/3

The Hydrogen-Oxygen Regenerative Fuel Cell System was identified as a key component for energy storage in support of future lunar missions. Since the $\text{H}_2\text{-O}_2$ regenerative electrochemical conversion technology has not yet been tested in space applications, it is necessary to implement predictive techniques to develop initial feasible system designs. The ASPEN simulation software furnishes a constructive medium for analyzing and for optimizing such systems. A rudimentary regenerative fuel cell system design was examined using the ASPEN simulator and this modular approach allows for easy addition of supplementary ancillary components and easy integration with life support systems. The modules included in the preliminary analyses may serve as the fundamental structure for more complicated energy storage systems. Author

N90-26397*# National Aeronautics and Space Administration. Lewis Research Center, Cleveland, OH.

NASA AEROSPACE FLIGHT BATTERY SYSTEMS PROGRAM

MICHELLE A. MANZO and PATRICIA M. O'DONNELL 1990 7 p Presented at the 25th Intersociety Energy Conversion Engineering Conference, Reno, NV, 12-17 Aug. 1990; cosponsored by AIChE, ANS, SAE, ACS, AIAA, ASME, and IEEE (NASA-TM-103237; E-5656; NAS 1.15:103237) Avail: NTIS HC A02/MF A01 CSCL 10/3

The major objective of the NASA Aerospace Flight Battery Systems Program is to provide NASA with the policy and posture to increase and ensure the safety, performance and reliability of batteries for space power systems. The program plan has been modified in the past year to reflect changes in the agency's approach to battery related problems that are affecting flight programs. Primary attention in the Battery Program is being devoted to the development of an advanced nickel-cadmium cell design and the qualification of vendors to produce cells for flight programs. As part of a unified Battery Program, the development of a nickel-hydrogen standard and primary cell issues are also being pursued to provide high performance NASA Standards and space qualified state-of-the-art primary cells. The resolution of issues is being addressed with the full participation of the aerospace battery community. Author

46

GEOPHYSICS

Includes aeronomy; upper and lower atmosphere studies; ionospheric and magnetospheric physics; and geomagnetism.

A90-43609* Utah State Univ., Logan.

A TWO-DIMENSIONAL MODEL OF PLASMA EXPANSION IN THE IONOSPHERE

T.-Z. MA and R. W. SCHUNK (Utah State University, Logan) Planetary and Space Science (ISSN 0032-0633), vol. 38, June 1990, p. 723-741. refs (Contract NAG3-792; NAGW-77; F49620-86-C-0109) Copyright

A systematic parameter study is conducted of the motion of artificial plasma clouds across the geomagnetic field at ionospheric altitudes. The study is based on a two-dimensional numerical model. Taken into consideration are the effects solar cycle variations on

46 GEOPHYSICS

the cloud evolution, as well as the effects of seasonal and geomagnetic activity conditions, and variations in the ionospheric release conditions. The effects of magnetospheric electric fields and thermospheric winds are also considered. The plasma cloud model and related assumptions are discussed, and numerical results are presented. S.A.V.

N90-12984*# National Aeronautics and Space Administration. Lewis Research Center, Cleveland, OH.

THE GEM-T2 GRAVITATIONAL MODEL

J. G. MARSH, F. J. LERCH, B. H. PUTNEY, T. L. FELSENTERGER, B. V. SANCHEZ, S. M. KLOSKO, G. B. PATEL, J. W. ROBBINS, R. G. WILLIAMSON, T. E. ENGELIS (ST Systems Corp., Lanham, MD.) et al. Oct. 1989 91 p Prepared in cooperation with Maryland Univ., College Park (NASA-TM-100746; REPT-89B00244; NAS 1.15:100746) Avail: NTIS HC A05/MF A01 CSCL 08/5

The GEM-T2 is the latest in a series of Goddard Earth Models of the terrestrial field. It was designed to bring modeling capabilities one step closer towards ultimately determining the TOPEX/Poseidon satellite's radial position to an accuracy of 10-cm RMS (root mean square). It also improves models of the long wavelength geoid to support many oceanographic and geophysical applications. The GEM-T2 extends the spherical harmonic field to include more than 600 coefficients above degree 36 (which was the limit for its predecessor, GEM-T1). Like GEM-T1, it was produced entirely from satellite tracking data, but it now uses nearly twice as many satellites (31 vs. 17), contains four times the number of observations (2.4 million), has twice the number of data arcs (1132), and utilizes precise laser tracking from 11 satellites. The estimation technique for the solution has been augmented to include an optimum data weighting procedure with automatic error calibration for the gravitational parameters. Results for the GEM-T2 error calibration indicate significant improvement over previous satellite-only models. The error of commission in determining the geoid has been reduced from 155 cm in GEM-T1 to 105 cm for GEM-T2 for the 36 x 36 portion of the field, and 141 cm for the entire model. The orbital accuracies achieved using GEM-T2 are likewise improved. Also, the projected radial error on the TOPEX satellite orbit indicates 9.4 cm RMS for GEM-T2, compared to 24.1 cm for GEM-T1. Author

47

METEOROLOGY AND CLIMATOLOGY

Includes weather forecasting and modification.

A90-38363* Colorado Univ., Boulder.

THE EFFECTS OF VAN DER WAALS ATTRACTIONS ON CLOUD DROPLET GROWTH BY COALESCENCE

JAN R. ROGERS and ROBERT H. DAVIS (Colorado, University, Boulder) Journal of the Atmospheric Sciences (ISSN 0022-4928), vol. 47, May 1, 1990, p. 1075-1080. refs (Contract NAGW-951; NAG3-993) Copyright

The inclusion of van der Waals attractions in the interaction between cloud droplets has been recently shown to significantly increase the collision efficiencies of the smaller droplets. In the current work, these larger values for the collision efficiencies are used in a population dynamics model of the droplet size distribution evolution with time, in hopes of at least partially resolving the long-standing paradox in cloud microphysics that predicted rates of the onset of precipitation are generally much lower than those which are observed. Evolutions of several initial cloud droplet spectra have been tracked in time. Size evolutions are compared as predicted from the use of collision efficiencies computed using two different models to allow for droplet-droplet contact: one which considers slip flow effects only, and one which considers the combined effects of van der Waals forces and slip flow. The rate

at which the droplet mass density function shifts to larger droplet sizes is increased by typically 20-25 percent, when collision efficiencies which include van der Waals forces are used.

Author

51

LIFE SCIENCES (GENERAL)

A90-28084* Mount Sinai School of Medicine, New York, NY. **A GEOMETRIC ANALYSIS OF SEMICIRCULAR CANALS AND INDUCED ACTIVITY IN THEIR PERIPHERAL AFFERENTS IN THE RHESUS MONKEY**

H. REISINE (Mount Sinai School of Medicine, New York; Zuerich, Universitaet, Zurich, Switzerland), J. I. SIMPSON (New York University, NY), and V. HENN (Zuerich, Universitaet, Zurich, Switzerland) New York Academy of Sciences, Annals (ISSN 0077-8923), vol. 545, Dec. 26, 1988, p. 10-20. Research supported by the EMDO Foundation and Eidgenoessische Technische Hochschule Zuerich. refs (Contract SNSF-3,718,80; NAG3-336; NIH-NS-13742) Copyright

Experiments were carried out to determine anatomically the planes of the semicircular canals of two juvenile rhesus monkeys, using plastic casts of the semicircular canals, and the anatomical measurements were related to the directional coding of neural signals transmitted by primary afferents innervating the same semicircular canals. In the experiments, animals were prepared for monitoring the eye position by the implantation of silver-silver chloride electrodes into the bony orbit. Following the recording of semicircular canal afferent activity, the animals were sacrificed; plastic casting resin was injected into the bony canals; and, when the temporal bone was demineralized and removed, the coordinates of points spaced along the circumference of the canal casts were measured. A comparison of the sensitivity vectors determined in these experiments and the anatomical measures showed that the average difference between a sensitivity vector and its respective normal vector was 6.3 deg. I.S.

54

MAN/SYSTEM TECHNOLOGY AND LIFE SUPPORT

Includes human engineering; biotechnology; and space suits and protective clothing.

N90-25499*# Carnegie-Mellon Univ., Pittsburgh, PA. Robotics Inst.

A GLOBAL APPROACH FOR USING KINEMATIC REDUNDANCY TO MINIMIZE BASE REACTIONS OF MANIPULATORS

C. L. CHUNG and S. DESA Mar. 1989 32 p (Contract NAG3-811) (NASA-CR-186825; NAS 1.26:186825; CMU-RI-TR-89-9) Copyright Avail: NTIS HC A03/MF A01 CSCL 05/8

An important consideration in the use of manipulators in microgravity environments is the minimization of the base reactions, i.e. the magnitude of the force and the moment exerted by the manipulator on its base as it performs its tasks. One approach which was proposed and implemented is to use the redundant degree of freedom in a kinematically redundant manipulator to plan manipulator trajectories to minimize base reactions. A global approach was developed for minimizing the magnitude of the base reactions for kinematically redundant manipulators which integrates

the Partitioned Jacobian method of redundancy resolution, a 4-3-4 joint-trajectory representation and the minimization of a cost function which is the time-integral of the magnitude of the base reactions. The global approach was also compared with a local approach developed earlier for the case of point-to-point motion of a three degree-of-freedom planar manipulator with one redundant degree-of-freedom. The results show that the global approach is more effective in reducing and smoothing the base force while the local approach is superior in reducing the base moment.

Author

60

COMPUTER OPERATIONS AND HARDWARE

Includes hardware for computer graphics, firmware, and data processing.

N90-14783*# Sverdrup Technology, Inc., Cleveland, OH.
USER'S GUIDE TO PMESH: A GRID-GENERATION PROGRAM FOR SINGLE-ROTATION AND COUNTERROTATION ADVANCED TURBOPROPS Final Report
 SAIF A. WARSJ Dec. 1989 25 p
 (Contract NAS3-24105)
 (NASA-CR-185156; E-5152; NAS 1.26:185156) Avail: NTIS HC A03/MF A01 CSCL 09/2

A detailed operating manual is presented for a grid generating program that produces 3-D meshes for advanced turboprops. The code uses both algebraic and elliptic partial differential equation methods to generate single rotation and counterrotation, H or C type meshes for the z - r planes and H type for the z - theta planes. The code allows easy specification of geometrical constraints (such as blade angle, location of bounding surfaces, etc.), mesh control parameters (point distribution near blades and nacelle, number of grid points desired, etc.), and it has good runtime diagnostics. An overview is provided of the mesh generation procedure, sample input dataset with detailed explanation of all input, and example meshes.

Author

N90-25579*# Toledo Univ., OH. Dept. of Computer Science and Engineering.
MULTIPROCESSOR ARCHITECTURE: SYNTHESIS AND EVALUATION
 HILDA M. STANDLEY 1990 5 p
 (Contract NAG3-699)
 (NASA-CR-186618; NAS 1.26:186618) Avail: NTIS HC A01/MF A01 CSCL 09/2

Multiprocessor computed architecture evaluation for structural computations is the focus of the research effort described. Results obtained are expected to lead to more efficient use of existing architectures and to suggest designs for new, application specific, architectures. The brief descriptions given outline a number of related efforts directed toward this purpose. The difficulty is analyzing an existing architecture or in designing a new computer architecture lies in the fact that the performance of a particular architecture, within the context of a given application, is determined by a number of factors. These include, but are not limited to, the efficiency of the computation algorithm, the programming language and support environment, the quality of the program written in the programming language, the multiplicity of the processing elements, the characteristics of the individual processing elements, the interconnection network connecting processors and non-local memories, and the shared memory organization covering the spectrum from no shared memory (all local memory) to one global access memory. These performance determiners may be loosely classified as being software or hardware related. This distinction is not clear or even appropriate in many cases. The effect of the choice of algorithm is ignored by assuming that the algorithm is specified as given. Effort directed toward the removal of the effect of the programming language and program resulted in the design

61 COMPUTER PROGRAMMING AND SOFTWARE

of a high-level parallel programming language. Two characteristics of the fundamental structure of the architecture (memory organization and interconnection network) are examined. Author

N90-26512*# Toledo Univ., OH. Dept. of Computer Science.
COMPUTER ARCHITECTURE EVALUATION FOR STRUCTURAL DYNAMICS COMPUTATIONS: PROJECT SUMMARY Final Technical Report, 10 Feb. 1986 - 7 Aug. 1989
 HILDA M. STANDLEY 1989 10 p
 (Contract NAG3-699)
 (NASA-CR-186137; NAS 1.26:186137) Avail: NTIS HC A02/MF A01 CSCL 09/2

The intent of the proposed effort is the examination of the impact of the elements of parallel architectures on the performance realized in a parallel computation. To this end, three major projects are developed: a language for the expression of high level parallelism, a statistical technique for the synthesis of multicomputer interconnection networks based upon performance prediction, and a queueing model for the analysis of shared memory hierarchies.

Author

61

COMPUTER PROGRAMMING AND SOFTWARE

Includes computer programs, routines, and algorithms, and specific applications, e.g., CAD/CAM.

A90-19147* Tanksley (W. L.) and Associates, Inc., Cleveland, OH.
DESIGNING CERAMIC COMPONENTS WITH THE CARES COMPUTER PROGRAM
 NOEL N. NEMETH (W. L. Tanksley and Associates, Inc., Cleveland, OH), JANE M. MANDERSCHIED, and JOHN P. GYKENYESI (NASA, Lewis Research Center, Cleveland, OH) American Ceramic Society Bulletin (ISSN 0002-7812), vol. 68, Dec. 1989, p. 2064-2072. refs
 Copyright

NASA-Lewis has developed a public-domain computer program, designated 'Ceramic Analysis and Reliability Evaluation of Structures' (CARES) for calculating the fast-fracture reliability of macroscopically isotropic ceramic components subjected to the complex thermomechanical loadings typical of heat engines. The design methodology employed by CARES encompasses linear elastic fracture mechanics theory, extreme value statistics, and material microstructures; component integrity is conceived as a function of the entire field solution of the stresses, rather than being based solely on the most highly stressed point.

O.C.

A90-20188* Pittsburgh Univ., PA.
PARALLEL MULTI-TIME STEP INTEGRATION ON A TRANSPUTER SYSTEM
 P. SMOLINSKI (Pittsburgh, University, PA) Computers and Structures (ISSN 0045-7949), vol. 33, no. 6, 1989, p. 1529-1535. refs
 (Contract NAG3-829)
 Copyright

An algorithm which allows different nodes of the finite element mesh to be integrated with different time steps is presented for second order finite element systems. The implementation of this algorithm on a system of transputer processors is discussed and a numerical example is used to evaluate the efficiency of the algorithm.

Author

A90-22257*# National Aeronautics and Space Administration. Lewis Research Center, Cleveland, OH.
FLIGHT SOFTWARE DEVELOPMENT FOR THE ISOTHERMAL DENDRITIC GROWTH EXPERIMENT
 LAURIE H. LEVINSON, EDWARD A. WINSA (NASA, Lewis Research Center, Cleveland, OH), and M. E. GLICKSMAN

61 COMPUTER PROGRAMMING AND SOFTWARE

(Rensselaer Polytechnic Institute, Troy, NY) AIAA, Aerospace Sciences Meeting, 28th, Reno, NV, Jan. 8-11, 1990. 10 p. Previously announced in STAR as N90-13988. refs
(AIAA PAPER 90-0744) Copyright

The Isothermal Dendritic Growth Experiment (IDGE) is a microgravity materials science experiment scheduled to fly in the cargo bay of the shuttle on the United States Microgravity Payload (USMP) carrier. The experiment will be operated by real-time control software which will not only monitor and control onboard experiment hardware, but will also communicate, via downlink data and unlink commands, with the Payload Operations Control Center (POCC) at NASA George C. Marshall Space Flight Center (MSFC). The software development approach being used to implement this system began with software functional requirements specification. This was accomplished using the Yourdon/DeMarco methodology as supplemented by the Ward/Mellor real-time extensions. The requirements specification in combination with software prototyping was then used to generate a detailed design consisting of structure charts, module prologues, and Program Design Language (PDL) specifications. This detailed design will next be used to code the software, followed finally by testing against the functional requirements. The result will be a modular real-time control software system with traceability through every phase of the development process.

Author

A90-26082* Akron Univ., OH.
MULTI-LEVEL HIERARCHICAL POLY TREE COMPUTER ARCHITECTURES

JOE PADOVAN and DOUG GUTE (Akron, University, OH) Computers and Structures (ISSN 0045-7949), vol. 34, no. 5, 1990, p. 685-713. refs
(Contract NAG3-664) Copyright

Based on the concept of hierarchical substructuring, this paper develops an optimal multi-level Hierarchical Poly Tree (HPT) parallel computer architecture scheme which is applicable to the solution of finite element and difference simulations. Emphasis is given to minimizing computational effort, in-core/out-of-core memory requirements, and the data transfer between processors. In addition, a simplified communications network that reduces the number of I/O channels between processors is presented. HPT configurations that yield optimal superlinearities are also demonstrated. Moreover, to generalize the scope of applicability, special attention is given to developing: (1) multi-level reduction trees which provide an orderly/optimal procedure by which model densification/simplification can be achieved, as well as (2) methodologies enabling processor grading that yields architectures with varying types of multi-level granularity.

Author

A90-29268* National Aeronautics and Space Administration. Lewis Research Center, Cleveland, OH.

ROBUSTNESS, GENERALITY AND EFFICIENCY OF OPTIMIZATION ALGORITHMS IN PRACTICAL APPLICATIONS
P. B. THANEDAR (NASA, Lewis Research Center, Cleveland, OH), J. S. ARORA, G. Y. LI, and T. C. LIN (Iowa, University, Iowa City) IN: AIAA/ASME/ASCE/AHS/ASC Structures, Structural Dynamics and Materials Conference, 31st, Long Beach, CA, Apr. 2-4, 1990, Technical Papers, Part 1. Washington, DC, American Institute of Aeronautics and Astronautics, 1990, p. 425-435. refs
(AIAA PAPER 90-1177) Copyright

The theoretical foundations of two approaches, sequential quadratic programming (SQP) and optimality criteria (OC), are analyzed and compared, with emphasis on the critical importance of parameters such as accuracy, generality, robustness, efficiency, and ease of use in large scale structural optimization. A simplified fighter wing and active control of space structures are considered with other example problems. When applied to general system identification problems, the OC methods are shown to lose simplicity and demonstrate lack of generality, accuracy and robustness. It is concluded that the SQP method with a potential constraint strategy is a better choice as compared to the currently prevalent mathematical programming and OC approaches. N.B.

A90-29333* Southwest Research Inst., San Antonio, TX.
COMPUTATIONAL METHODS FOR PROBABILITY OF INSTABILITY CALCULATIONS

Y.-T. WU and O. H. BURNSIDE (Southwest Research Institute, San Antonio, TX) IN: AIAA/ASME/ASCE/AHS/ASC Structures, Structural Dynamics and Materials Conference, 31st, Long Beach, CA, Apr. 2-4, 1990, Technical Papers, Part 2. Washington, DC, American Institute of Aeronautics and Astronautics, 1990, p. 1081-1091. refs
(Contract NAS3-24389)
(AIAA PAPER 90-1139) Copyright

This paper summarizes the development of the methods and a computer program to compute the probability of instability of a dynamic system than can be represented by a system of second-order ordinary linear differential equations. Two instability criteria based upon the roots of the characteristics equation or Routh-Hurwitz test functions are investigated. Computational methods based on system reliability analysis methods and importance sampling concepts are proposed to perform efficient probabilistic analysis. Numerical examples are provided to demonstrate the methods.

Author

A90-38082* National Aeronautics and Space Administration. Lewis Research Center, Cleveland, OH.
DEVELOPMENT OF ADA LANGUAGE CONTROL SOFTWARE FOR THE NASA POWER MANAGEMENT AND DISTRIBUTION TEST BED

TED WRIGHT, MICHAEL MACKIN (NASA, Lewis Research Center, Cleveland, OH), and DAVE GANTOSE (Sverdrup Technology, Inc., Middleburg Heights, OH) IN: IECEC-89; Proceedings of the Twenty-fourth Intersociety Energy Conversion Engineering Conference, Washington, DC, Aug. 6-11, 1989. Volume 1. New York, Institute of Electrical and Electronics Engineers, 1989, p. 321-326.
Copyright

The Ada language software developed to control the NASA Lewis Research Center's Power Management and Distribution testbed is described. The testbed is a reduced-scale prototype of the electric power system to be used on space station Freedom. It is designed to develop and test hardware and software for a 20-kHz power distribution system. The distributed, multiprocessor, testbed control system has an easy-to-use operator interface with an understandable English-text format. A simple interface for algorithm writers that uses the same commands as the operator interface is provided, encouraging interactive exploration of the system.

I.E.

A90-38089* Maxwell Labs., Inc., La Jolla, CA.
THE ENVIRONMENT-POWER SYSTEM ANALYSIS TOOL DEVELOPMENT PROGRAM

GARY A. JONGEWARD, ROBERT A. KUHARSKI, ERIC M. KENNEDY, KATHERINE G. WILCOX (Maxwell Laboratories, Inc., La Jolla, CA), N. JOHN STEVENS, RAND M. PUTNAM (TRW, Inc., Redondo Beach, CA), and JAMES C. ROCHE (NASA, Lewis Research Center, Cleveland, OH) IN: IECEC-89; Proceedings of the Twenty-fourth Intersociety Energy Conversion Engineering Conference, Washington, DC, Aug. 6-11, 1989. Volume 1. New York, Institute of Electrical and Electronics Engineers, 1989, p. 371-374.
(Contract NAS3-25347) Copyright

The Environment Power System Analysis Tool (EPSAT) is being developed to provide engineers with the ability to assess the effects of a broad range of environmental interactions on space power systems. A unique user-interface-data-dictionary code architecture oversees a collection of existing and future environmental modeling codes (e.g., neutral density) and physical interaction models (e.g., sheath ionization). The user-interface presents the engineer with tables, graphs, and plots which, under supervision of the data dictionary, are automatically updated in response to parameter change. EPSAT thus provides the engineer with a comprehensive and responsive environmental assessment tool and the scientist

with a framework into which new environmental or physical models can be easily incorporated. I.E.

A90-47188* National Aeronautics and Space Administration. Langley Research Center, Hampton, VA.

GRID GENERATION FOR THE SOLUTION OF PARTIAL DIFFERENTIAL EQUATIONS

PETER R. EISEMAN (Columbia University, New York) and GORDON ERLEBACHER (NASA, Langley Research Center, Hampton, VA) IN: State-of-the-art surveys on computational mechanics. New York, American Society of Mechanical Engineers, 1989, p. 367-440. Previously announced in STAR as N87-30076. refs

(Contract NAG3-715; AF-AFOSR-86-0307)

Copyright

A general survey of grid generators is presented with a concern for understanding why grids are necessary, how they are applied, and how they are generated. After an examination of the need for meshes, the overall applications setting is established with a categorization of the various connectivity patterns. This is split between structured grids and unstructured meshes. Altogether, the categorization establishes the foundation upon which grid generation techniques are developed. The two primary categories are algebraic techniques and partial differential equation techniques. These are each split into basic parts, and accordingly are individually examined in some detail. In the process, the interrelations between the various parts are accented. From the established background in the primary techniques, consideration is shifted to the topic of interactive grid generation and then to adaptive meshes. The setting for adaptivity is established with a suitable means to monitor severe solution behavior. Adaptive grids are considered first and are followed by adaptive triangular meshes. Then the consideration shifts to the temporal coupling between grid generators and PDE-solvers. To conclude, a reflection upon the discussion, herein, is given. Author

N90-13968*# Sverdrup Technology, Inc., Cleveland, OH. **AN INTERACTIVE GRID GENERATION PROCEDURE FOR AXIAL AND RADIAL FLOW TURBOMACHINERY Final Report** TIMOTHY A. BEACH Nov. 1989 13 p Presented at the 28th Aerospace Sciences Meeting, Reno, NV, 8-11 Jan. 1990; sponsored by AIAA

(Contract NAS3-25266)

(NASA-CR-185167; E-5151; NAS 1.26:185167; AIAA-90-0344)

Avail: NTIS HC A03/MF A01 CSCL 09/2

A combination algebraic/elliptic technique is presented for the generation of three dimensional grids about turbo-machinery blade rows for both axial and radial flow machinery. The technique is built around use of an advanced engineering workstation to construct several two dimensional grids interactively on predetermined blade-to-blade surfaces. A three dimensional grid is generated by interpolating these surface grids onto an axisymmetric grid. On each blade-to-blade surface, a grid is created using algebraic techniques near the blade to control orthogonality within the boundary layer region and elliptic techniques in the mid-passage to achieve smoothness. The interactive definition of bezier curves as internal boundaries is the key to simple construction. This procedure lends itself well to zonal grid construction, an important example being the tip clearance region. Calculations done to date include a space shuttle main engine turbopump blade, a radial inflow turbine blade, and the first stator of the United Technologies Research Center large scale rotating rig. A finite Navier-Stokes solver was used in each case. Author

N90-15622*# National Aeronautics and Space Administration. Lewis Research Center, Cleveland, OH.

CRYOTRAN USER'S MANUAL, VERSION 1.0

GLENN R. COWGILL, DAVID J. CHATO, and EHAB SAAD (Analex Corp., Cleveland, OH.) Dec. 1989 326 p (NASA-TM-102468; E-5256; NAS 1.15:102468) Avail: NTIS HC A15/MF A02 CSCL 09/2

The development of cryogenic fluid management systems for space operation is a major portion of the efforts of the Cryogenic

Fluids Technology Office (CFTO) at the NASA Lewis Research Center. Analytical models are a necessary part of experimental programs which are used to verify the results of experiments and are also used as a predictor for parametric studies. The CryoTran computer program is a bridge to obtain analytical results. The object of CryoTran is to coordinate these separate analyses into an integrated framework with a user-friendly interface and a common cryogenic property database. CryoTran is an integrated software system designed to help solve a diverse set of problems involving cryogenic fluid storage and transfer in both ground and low-g environments. Author

N90-20708*# National Aeronautics and Space Administration. Lewis Research Center, Cleveland, OH.

GRID2D/3D: A COMPUTER PROGRAM FOR GENERATING GRID SYSTEMS IN COMPLEX-SHAPED TWO- AND THREE-DIMENSIONAL SPATIAL DOMAINS. PART 2: USER'S MANUAL AND PROGRAM LISTING

R. T. BAILEY, T. I.-P. SHIH (Carnegie-Mellon Univ., Pittsburgh, PA.), H. L. NGUYEN, and R. J. ROELKE Apr. 1990 73 p

(Contract NAG3-828)

(NASA-TM-102454; E-5242; NAS 1.15:102454) Avail: NTIS HC A04/MF A01 CSCL 09/2

An efficient computer program, called GRID2D/3D, was developed to generate single and composite grid systems within geometrically complex two- and three-dimensional (2- and 3-D) spatial domains that can deform with time. GRID2D/3D generates single grid systems by using algebraic grid generation methods based on transfinite interpolation in which the distribution of grid points within the spatial domain is controlled by stretching functions. All single grid systems generated by GRID2D/3D can have grid lines that are continuous and differentiable everywhere up to the second-order. Also, grid lines can intersect boundaries of the spatial domain orthogonally. GRID2D/3D generates composite grid systems by patching together two or more single grid systems. The patching can be discontinuous or continuous. For continuous composite grid systems, the grid lines are continuous and differentiable everywhere up to the second-order except at interfaces where different single grid systems meet. At interfaces where different single grid systems meet, the grid lines are only differentiable up to the first-order. For 2-D spatial domains, the boundary curves are described by using either cubic or tension spline interpolation. For 3-D spatial domains, the boundary surfaces are described by using either linear Coon's interpolation, bi-hyperbolic spline interpolation, or a new technique referred to as 3-D bi-directional Hermite interpolation. Since grid systems generated by algebraic methods can have grid lines that overlap one another, GRID2D/3D contains a graphics package for evaluating the grid systems generated. With the graphics package, the user can generate grid systems in an interactive manner with the grid generation part of GRID2D/3D. GRID2D/3D is written in FORTRAN 77 and can be run on any IBM PC, XT, or AT compatible computer. In order to use GRID2D/3D on workstations or mainframe computers, some minor modifications must be made in the graphics part of the program; no modifications are needed in the grid generation part of the program. The theory and method used in GRID2D/3D is described. Author

N90-21552*# Sverdrup Technology, Inc., Cleveland, OH. **HYPERCLUSTER PARALLEL PROCESSING LIBRARY USER'S MANUAL Final Report**

ANGELA QUEALY Apr. 1990 75 p

(Contract NAS3-25266)

(NASA-CR-185231; NAS 1.26:185231) Avail: NTIS HC A04/MF A01 CSCL 09/2

This User's Manual describes the Hypercluster Parallel Processing Library, composed of FORTRAN-callable subroutines which enable a FORTRAN programmer to manipulate and transfer information throughout the Hypercluster at NASA Lewis Research Center. Each subroutine and its parameters are described in detail. A simple heat flow application using Laplace's equation is included to demonstrate the use of some of the library's subroutines. The

61 COMPUTER PROGRAMMING AND SOFTWARE

manual can be used initially as an introduction to the parallel features provided by the library. Thereafter it can be used as a reference when programming an application. Author

N90-22262*# National Aeronautics and Space Administration. Lewis Research Center, Cleveland, OH.

GRID2D/3D: A COMPUTER PROGRAM FOR GENERATING GRID SYSTEMS IN COMPLEX-SHAPED TWO- AND THREE-DIMENSIONAL SPATIAL DOMAINS. PART 1: THEORY AND METHOD

T. I.-P. SHIH, R. T. BAILEY (Florida Univ., Gainesville.), H. L. NGUYEN, and R. J. ROELKE Mar. 1990 103 p
(Contract NAG3-929; NAG3-997)
(NASA-TM-102453; E-5241; NAS 1.15:102453) Avail: NTIS HC A06/MF A01 CSCL 09/2

An efficient computer program, called GRID2D/3D was developed to generate single and composite grid systems within geometrically complex two- and three-dimensional (2- and 3-D) spatial domains that can deform with time. GRID2D/3D generates single grid systems by using algebraic grid generation methods based on transfinite interpolation in which the distribution of grid points within the spatial domain is controlled by stretching functions. All single grid systems generated by GRID2D/3D can have grid lines that are continuous and differentiable everywhere up to the second-order. Also, grid lines can intersect boundaries of the spatial domain orthogonally. GRID2D/3D generates composite grid systems by patching together two or more single grid systems. The patching can be discontinuous or continuous. For continuous composite grid systems, the grid lines are continuous and differentiable everywhere up to the second-order except at interfaces where different single grid systems meet. At interfaces where different single grid systems meet, the grid lines are only differentiable up to the first-order. For 2-D spatial domains, the boundary curves are described by using either cubic or tension spline interpolation. For 3-D spatial domains, the boundary surfaces are described by using either linear Coon's interpolation, bi-hyperbolic spline interpolation, or a new technique referred to as 3-D bi-directional Hermite interpolation. Since grid systems generated by algebraic methods can have grid lines that overlap one another, GRID2D/3D contains a graphics package for evaluating the grid systems generated. With the graphics package, the user can generate grid systems in an interactive manner with the grid generation part of GRID2D/3D. GRID2D/3D is written in FORTRAN 77 and can be run on any IBM PC, XT, or AT compatible computer. In order to use GRID2D/3D on workstations or mainframe computers, some minor modifications must be made in the graphics part of the program; no modifications are needed in the grid generation part of the program. This technical memorandum describes the theory and method used in GRID2D/3D. Author

62

COMPUTER SYSTEMS

Includes computer networks and special application computer systems.

A90-37482* Toledo Univ., OH.

A GENERAL MODEL FOR MEMORY INTERFERENCE IN A MULTIPROCESSOR SYSTEM WITH MEMORY HIERARCHY

BADIE A. TAHA and HILDA M. STANDLEY (Toledo, University, OH) IN: 1989 International Conference on Parallel Processing, University Park, PA, Aug. 8-12, 1989, Proceedings. Volume 1. University Park, PA, Pennsylvania State University Press, 1989, p. I-225 to I-232. refs
(Contract NAG3-699)
Copyright

The problem of memory interference in a multiprocessor system with a hierarchy of shared buses and memories is addressed.

The behavior of the processors is represented by a sequence of memory requests with each followed by a determined amount of processing time. A statistical queuing network model for determining the extent of memory interference in multiprocessor systems with clusters of memory hierarchies is presented. The performance of the system is measured by the expected number of busy memory clusters. The results of the analytic model are compared with simulation results, and the correlation between them is found to be very high. I.E.

N90-13988*# National Aeronautics and Space Administration. Lewis Research Center, Cleveland, OH.

FLIGHT SOFTWARE DEVELOPMENT FOR THE ISOTHERMAL DENDRITIC GROWTH EXPERIMENT

LAURIE H. LEVINSON, EDWARD A. WINSKA, and MARTIN E. GLICKSMAN (Rensselaer Polytechnic Inst., Troy, NY.) 1989 11 p Proposed for presentation at the 28th Aerospace Sciences Meeting, Reno, NV, 8-11 Jan. 1990; sponsored by AIAA (NASA-TM-102412; E-5170; NAS 1.15:102412; AIAA-90-0744) Avail: NTIS HC A03/MF A01 CSCL 09/2

The Isothermal Dendritic Growth Experiment (IDGE) is a microgravity materials science experiment scheduled to fly in the cargo bay of the shuttle on the United States Microgravity Payload (USMP) carrier. The experiment will be operated by real-time control software which will not only monitor and control onboard experiment hardware, but will also communicate, via downlink data and uplink commands, with the Payload Operations Control Center (POCC) at NASA George C. Marshall Space Flight Center (MSFC). The software development approach being used to implement this system began with software functional requirements specification. This was accomplished using the Yourdon/DeMarco methodology as supplemented by the Ward/Mellor real-time extensions. The requirements specification in combination with software prototyping was then used to generate a detailed design consisting of structure charts, module prologues, and Program Design Language (PDL) specifications. This detailed design will next be used to code the software, followed finally by testing against the functional requirements. The result will be a modular real-time control software system with traceability through every phase of the development process. Author

N90-25604*# Toledo Univ., OH. Dept. of Computer Science and Engineering.

MODELING AND SYNTHESIS OF MULTICOMPUTER INTERCONNECTION NETWORKS

HILDA M. STANDLEY and D. STEVE AUXTER 1990 10 p
(Contract NAG3-699)
(NASA-CR-186619; NAS 1.26:186619) Avail: NTIS HC A02/MF A01 CSCL 09/2

The type of interconnection network employed has a profound effect on the performance of a multicomputer and multiprocessor design. Adequate models are needed to aid in the design and development of interconnection networks. A novel modeling approach using statistical and optimization techniques is described. This method represents an attempt to compare diverse interconnection network designs in a way that allows not only the best of existing designs to be identified but to suggest other, perhaps hybrid, networks that may offer better performance. Stepwise linear regression is used to develop a polynomial surface representation of performance in a $(k+1)$ space with a total of k quantitative and qualitative independent variables describing graph-theoretic characteristics such as size, average degree, diameter, radius, girth, node-connectivity, edge-connectivity, minimum dominating set size, and maximum number of prime node and edge cutsets. Dependent variables used to measure performance are average message delay and the ratio of message completion rate to network connection cost. Response Surface Methodology (RSM) optimizes a response variable from a polynomial function of several independent variables. Steepest ascent path may also be used to approach optimum points. Author

CYBERNETICS

Includes feedback and control theory, artificial intelligence, robotics and expert systems.

A90-47697* # Arizona State Univ., Tempe.

EXTENDED IMPLICIT MODEL FOLLOWING AS APPLIED TO INTEGRATED FLIGHT AND PROPULSION CONTROL

DAVID K. SCHMIDT and JOHN D. SCHIERMAN (Arizona State University, Tempe) IN: AIAA Guidance, Navigation and Control Conference, Portland, OR, Aug. 20-22, 1990, Technical Papers. Part 2. Washington, DC, American Institute of Aeronautics and Astronautics, 1990, p. 1159-1169. refs

(Contract NAG3-998)

(AIAA PAPER 90-3444) Copyright

An extended model-following control-synthesis method, including loop-transfer recovery, is presented and applied to synthesize control laws for integrated flight and propulsion control (IFPC). The vehicle considered is representative of an unstable modern fighter aircraft; with a two-dimensional thrust-vectoring and thrust-reversing nozzle. The linearized design model includes both airframe and engine dynamics. A model-following formulation of the LQR problem is extended to handle this hybrid problem. Compensators are then obtained to realize an output-feedback control law, by using a loop-transfer-recovery procedure. The airframe and engine responses are decoupled, and perfect airframe response following is obtained. The loop transfers also reveal good stability robustness and reasonable loop cross-over frequencies that would not lead to excessive actuation requirements. Author

A90-49899* Mississippi State Univ., Mississippi State.

AN OBSERVER-BASED COMPENSATOR FOR DISTRIBUTED DELAYS

ROGELIO LUCK (Mississippi State University, Drawer) and ASOK RAY (Pennsylvania State University, University Park) Automatica (ISSN 0005-1098), vol. 26, Sept. 1990, p. 903-908. refs

(Contract NAG3-823)

Copyright

This paper presents an algorithm for compensating delays that are distributed between the sensor(s), controller and actuator(s) within a control loop. This observer-based algorithm is specially suited to compensation of network-induced delays in integrated communication and control systems. The robustness of the algorithm relative to plant model uncertainties has been examined. Author

A90-51266* # Pennsylvania State Univ., University Park.

INTEGRATED COMMUNICATION AND CONTROL SYSTEMS. III - NONIDENTICAL SENSOR AND CONTROLLER SAMPLING

LUEN-WOEI LIOU and A. RAY (Pennsylvania State University, University Park) ASME, Transactions, Journal of Dynamic Systems, Measurement, and Control (ISSN 0022-0434), vol. 112, Sept. 1990, p. 357-364. refs

(Contract NAG3-823; NSF DMC-87-07648)

Copyright

Networking in Integrated Communication and Control Systems (ICCS) introduces randomly varying delays which degrade the system dynamic performance and are a source of potential instability. In Part I of this sequence of papers, a discrete-time, finite-dimensional model of the delayed control system for analysis and design of ICCS was developed where the sensor and controller have identical sampling rates. In Part II, two alternate approaches for ICCS design, namely, identical and nonidentical sampling rates for sensor and controller were proposed. This Part III presents extended modeling of ICCS for nonidentical sensor and controller sampling rates. This model is also suitable for analyzing tracking problems, i.e., control systems with time-dependent reference inputs. Author

A90-51267* # Technion - Israel Inst. of Tech., Haifa.

PERFORMANCE ANALYSIS OF INTEGRATED COMMUNICATION AND CONTROL SYSTEM NETWORKS

Y. HALEVI (Technion - Israel Institute of Technology, Haifa) and A. RAY (Pennsylvania State University, University Park) ASME, Transactions, Journal of Dynamic Systems, Measurement, and Control (ISSN 0022-0434), vol. 112, Sept. 1990, p. 365-371. refs

(Contract NAG3-823; NSF DMC-87-07648)

Copyright

This paper presents statistical analysis of delays in Integrated Communication and Control System (ICCS) networks that are based on asynchronous time-division multiplexing. The models are obtained in closed form for analyzing control systems with randomly varying delays. The results of this research are applicable to ICCS design for complex dynamical processes like advanced aircraft and spacecraft, autonomous manufacturing plants, and chemical and processing plants. Author

A90-52881* Akron Univ., OH.

THE DETERMINATION OF THIRD ORDER LINEAR MODELS FROM A SEVENTH ORDER NONLINEAR JET ENGINE MODEL

RICK J. LALONDE, TOM T. HARTLEY, and J. ALEX DE ABREU-GARCIA (Akron, University, OH) IN: IEEE International Conference on Systems Engineering, Dayton, OH, Aug. 24-26, 1989, Proceedings. New York, Institute of Electrical and Electronics Engineers, Inc., 1989, p. 467-470. refs

(Contract NAG3-778)

Copyright

Results are presented that demonstrate how good reduced-order models can be obtained directly by recursive parameter identification using input/output (I/O) data of high-order nonlinear systems. Three different methods of obtaining a third-order linear model from a seventh-order nonlinear turbojet engine model are compared. The first method is to obtain a linear model from the original model and then reduce the linear model by standard reduction techniques such as residualization and balancing. The second method is to identify directly a third-order linear model by recursive least-squares parameter estimation using I/O data of the original model. The third method is to obtain a reduced-order model from the original model and then linearize the reduced model. Frequency responses are used as the performance measure to evaluate the reduced models. The reduced-order models along with their Bode plots are presented for comparison purposes. I.E.

N90-21564* # National Aeronautics and Space Administration. Lewis Research Center, Cleveland, OH.

A REAL TIME NEURAL NET ESTIMATOR OF FATIGUE LIFE

T. TROUDET (Sverdrup Technology, Inc., Cleveland, OH.) and W. MERRILL 1990 11 p Presented at the International Joint Conference on Neural Networks, San Diego, CA, 17-21 Jun. 1990; cosponsored by IEEE and INNS

(NASA-TM-103117; E-5217; NAS 1.15:103117) Avail: NTIS HC A03/MF A01 CSCL 09/2

A neural net architecture is proposed to estimate, in real-time, the fatigue life of mechanical components, as part of the Intelligent Control System for Reusable Rocket Engines. Arbitrary component loading values were used as input to train a two hidden-layer feedforward neural net to estimate component fatigue damage. The ability of the net to learn, based on a local strain approach, the mapping between load sequence and fatigue damage has been demonstrated for a uniaxial specimen. Because of its demonstrated performance, the neural computation may be extended to complex cases where the loads are biaxial or triaxial, and the geometry of the component is complex (e.g., turbopump blades). The generality of the approach is such that load/damage mappings can be directly extracted from experimental data without requiring any knowledge of the stress/strain profile of the component. In addition, the parallel network architecture allows real-time life calculations even for high frequency vibrations. Owing to its distributed nature, the neural implementation will be robust and reliable, enabling its use in hostile environments such as rocket

63 CYBERNETICS

engines. This neural net estimator of fatigue life is seen as the enabling technology to achieve component life prognosis, and therefore would be an important part of life extending control for reusable rocket engines. Author

N90-22306*# National Aeronautics and Space Administration. Lewis Research Center, Cleveland, OH.

AUTONOMOUS POWER EXPERT SYSTEM

JERRY L. WALTERS, EDWARD J. PETRIK, MARY ELLEN ROTH, LONG VAN TRUONG, TODD QUINN, and WALTER M. KRAWCZONEK (Sverdrup Technology, Inc., Cleveland, OH.) In NASA, Goddard Space Flight Center, The 1990 Goddard Conference on Space Applications of Artificial Intelligence p 147-156 May 1990

Avail: NTIS HC A15/MF A02 CSCL 09/2

The Autonomous Power Expert (APEX) system was designed to monitor and diagnose fault conditions that occur within the Space Station Freedom Electrical Power System (SSF/EPS) Testbed. APEX is designed to interface with SSF/EPS testbed power management controllers to provide enhanced autonomous operation and control capability. The APEX architecture consists of three components: (1) a rule-based expert system, (2) a testbed data acquisition interface, and (3) a power scheduler interface. Fault detection, fault isolation, justification of probable causes, recommended actions, and incipient fault analysis are the main functions of the expert system component. The data acquisition component requests and receives pertinent parametric values from the EPS testbed and asserts the values into a knowledge base. Power load profile information is obtained from a remote scheduler through the power scheduler interface component. The current APEX design and development work is discussed. Operation and use of APEX by way of the user interface screens is also covered. Author

N90-22323*# National Aeronautics and Space Administration. Lewis Research Center, Cleveland, OH.

ELECTRIC POWER SCHEDULING: A DISTRIBUTED PROBLEM-SOLVING APPROACH

PAMELA A. MELLOR, JAMES L. DOLCE, and JOSEPH C. KRUPP (Decision-Science Applications, Inc., Arlington, VA.) 1990 8 p Proposed for presentation at the 25th Intersociety Energy Conversion Engineering Conference, Reno, NV, 12-17 Aug. 1990; cosponsored by AICHE, SAE, ACS, AIAA, ASME, and IEEE (NASA-TM-103149; E-5503; NAS 1.15:103149) Avail: NTIS HC A02/MF A01 CSCL 09/2

Space Station Freedom's power system, along with the spacecraft's other subsystems, needs to carefully conserve its resources and yet strive to maximize overall Station productivity. Due to Freedom's distributed design, each subsystem must work cooperatively within the Station community. There is a need for a scheduling tool which will preserve this distributed structure, allow each subsystem the latitude to satisfy its own constraints, and preserve individual value systems while maintaining Station-wide integrity. The value-driven free-market economic model is such a tool. Author

N90-22324*# National Aeronautics and Space Administration. Lewis Research Center, Cleveland, OH.

AUTOMATING SECURITY MONITORING AND ANALYSIS FOR SPACE STATION FREEDOM'S ELECTRIC POWER SYSTEM

JAMES L. DOLCE, DEJAN J. SOBAJIC, and YOH-HAN PAO (Case Western Reserve Univ., Cleveland, OH.) 1990 10 p Proposed for presentation at the 25th Intersociety Energy Conversion Engineering Conference, Reno, NV, 12-17 Aug. 1990; cosponsored by AICHE, SAE, ACS, AIAA, ASME, and IEEE (NASA-TM-103148; E-5502; NAS 1.15:103148) Avail: NTIS HC A02/MF A01 CSCL 09/2

Operating a large, space power system requires classifying the system's status and analyzing its security. Conventional algorithms are used by terrestrial electric utilities to provide such information to their dispatchers, but their application aboard Space Station Freedom will consume too much processing time. A new approach for monitoring and analysis using adaptive pattern techniques is

presented. This approach yields an on-line security monitoring and analysis algorithm that is accurate and fast; and thus, it can free the Space Station Freedom's power control computers for other tasks. Author

N90-22325*# National Aeronautics and Space Administration. Lewis Research Center, Cleveland, OH.

AN EXPERT SYSTEM FOR SIMULATING ELECTRIC LOADS ABOARD SPACE STATION FREEDOM

GEORGE KUKICH (Analytical Engineering Corp., North Olmsted, OH.) and JAMES L. DOLCE 1990 7 p Proposed for presentation at the 25th Intersociety Energy Conversion Engineering Conference, Reno, NV, 12-17 Aug. 1990; cosponsored by AICHE, SAE, ACS, AIAA, ASME, and IEEE (NASA-TM-103150; E-5504; NAS 1.15:103150) Avail: NTIS HC A02/MF A01 CSCL 09/2

Space Station Freedom will provide an infrastructure for space experimentation. This environment will feature regulated access to any resources required by an experiment. Automated systems are being developed to manage the electric power so that researchers can have the flexibility to modify their experiment plan for contingencies or for new opportunities. To define these flexible power management characteristics for Space Station Freedom, a simulation is required that captures the dynamic nature of space experimentation; namely, an investigator is allowed to restructure his experiment and to modify its execution. This changes the energy demands for the investigator's range of options. An expert system competent in the domain of cryogenic fluid management experimentation was developed. It will be used to help design and test automated power scheduling software for Freedom's electric power system. The expert system allows experiment planning and experiment simulation. The former evaluates experimental alternatives and offers advice on the details of the experiment's design. The latter provides a real-time simulation of the experiment replete with appropriate resource consumption. Author

N90-23125*# National Aeronautics and Space Administration. Lewis Research Center, Cleveland, OH.

AUTOMATED ELECTRIC POWER MANAGEMENT AND CONTROL FOR SPACE STATION FREEDOM

JAMES L. DOLCE, PAMELA A. MELLOR, and JAMES A. KISH 1990 8 p Proposed for presentation at the 25th Intersociety Energy Conversion Engineering Conference, Reno, NV, 12-17 Aug. 1990; cosponsored by AICHE, SAE, ACS, AIAA, ASME, and IEEE (NASA-TM-103151; E-5505; NAS 1.15:103151) Avail: NTIS HC A02/MF A01 CSCL 09/2

A comprehensive automation design is being developed for Space Station Freedom's electric power system. It strives to increase station productivity by applying expert systems and conventional algorithms to automate power system operation. An integrated approach to the power system command and control problem is defined and used to direct technology development in: diagnosis, security monitoring and analysis, battery management, and cooperative problem-solving for resource allocation. The prototype automated power system is developed using simulations and test-beds. Author

N90-23991*# National Aeronautics and Space Administration. Lewis Research Center, Cleveland, OH.

AN EXPERT SYSTEM TO PERFORM ON-LINE CONTROLLER TUNING

JONATHAN S. LITT 1990 15 p Presented at the 1990 American Control Conference, San Diego, CA, 23-25 May 1990; sponsored by American Automatic Control Council (Contract DA PROJ. 1L1-62211-A4-7A) (NASA-TM-103101; E-5422; NAS 1.15:103101; AVSCOM-TR-90-C-007; AD-A224969) Avail: NTIS HC A03/MF A01 CSCL 09/2

An expert system which tunes a Proportional-Integral-Derivative (PID) controller on-line for a single-input-single-output multiple-lag process with dead time is described. The expert system examines features of the previous transient responses and their

corresponding sets of controller parameters. It determines a new set of controller gains to obtain a more desirable time response. This technique can be used to determine and implement a different set of PID gains for each operating regime and, once in steady state, the system can be used to find optimal parameters for load disturbance rejection. The expert system can be applied to any system of the specified form (aerospace, industrial, etc.) and can be expanded to include additional process models. Author

N90-25607*# National Aeronautics and Space Administration. Lewis Research Center, Cleveland, OH.

NEUROMORPHIC LEARNING OF CONTINUOUS-VALUED MAPPINGS FROM NOISE-CORRUPTED DATA. APPLICATION TO REAL-TIME ADAPTIVE CONTROL

TERRY TROUDET (Sverdrup Technology, Inc., Cleveland, OH.) and WALTER C. MERRILL Washington May 1990 25 p (NASA-TM-4176; E-4967; NAS 1.15:4176) Avail: NTIS HC A03/MF A01 CSDL 09/2

The ability of feed-forward neural network architectures to learn continuous valued mappings in the presence of noise was demonstrated in relation to parameter identification and real-time adaptive control applications. An error function was introduced to help optimize parameter values such as number of training iterations, observation time, sampling rate, and scaling of the control signal. The learning performance depended essentially on the degree of embodiment of the control law in the training data set and on the degree of uniformity of the probability distribution function of the data that are presented to the net during sequence. When a control law was corrupted by noise, the fluctuations of the training data biased the probability distribution function of the training data sequence. Only if the noise contamination is minimized and the degree of embodiment of the control law is maximized, can a neural net develop a good representation of the mapping and be used as a neurocontroller. A multilayer net was trained with back-error-propagation to control a cart-pole system for linear and nonlinear control laws in the presence of data processing noise and measurement noise. The neurocontroller exhibited noise-filtering properties and was found to operate more smoothly than the teacher in the presence of measurement noise. Author

N90-26581*# Cellulose Conversion Enterprises, Berkeley, CA. Robotics/Electronic Photography.

BEAM RIDER FOR AN ARTICULATED ROBOT MANIPULATOR (ARM) ACCURATE POSITIONING OF LONG FLEXIBLE MANIPULATORS Final Report

M. J. MALACHOWSKI Apr. 1990 180 p (Contract NAS3-25917) (NASA-CR-185151; NAS 1.26:185151) Avail: NTIS HC A09/MF A01 CSDL 09/2

Laser beam positioning and beam rider modules were incorporated into the long hollow flexible segment of an articulated robot manipulator (ARM). Using a single laser beam, the system determined the position of the distal ARM endtip, with millimetric precision, in six degrees of freedom, at distances of up to 10 meters. Preliminary designs, using space rated technology for the critical systems, of a two segmented physical ARM, with a single and a dual degree of freedom articulation, were developed, prototyped, and tested. To control the positioning of the physical ARM, an indirect adaptive controller, which used the mismatch between the position of the laser beam under static and dynamic conditions, was devised. To predict the behavior of the system and test the concept, a computer simulation model was constructed. A hierarchical artificially intelligent real time ADA operating system program structure was created. The software was designed for implementation on a dedicated VME bus based Intel 80386 administered parallel processing multi-tasking computer system. Author

N90-29121*# National Aeronautics and Space Administration. Lewis Research Center, Cleveland, OH.

AN EXPERT SYSTEM TO PERFORM ON-LINE CONTROLLER RESTRUCTURING FOR ABRUPT MODEL CHANGES

JONATHAN S. LITT 1990 12 p Prepared for presentation at

the Rotary Wing Propulsion Specialists' Meeting, Williamsburg, VA, 13-15 Nov. 1990; sponsored in part by the Hampton Roads Chapter of the Southeast Region of the American Helicopter Society Prepared in cooperation with Army Aviation Systems Command, Cleveland, OH

(Contract DA PROJ. 1L1-61102-AH-45)

(NASA-TM-103609; E-5761; NAS 1.15:103609;

AVSCOM-TR-90-C-018) Avail: NTIS HC A03/MF A01 CSDL 09/2

Work in progress on an expert system used to reconfigure and tune airframe/engine control systems on-line in real time in response to battle damage or structural failures is presented. The closed loop system is monitored constantly for changes in structure and performance, the detection of which prompts the expert system to choose and apply a particular control restructuring algorithm based on the type and severity of the damage. Each algorithm is designed to handle specific types of failures and each is applicable only in certain situations. The expert system uses information about the system model to identify the failure and to select the technique best suited to compensate for it. A depth-first search is used to find a solution. Once a new controller is designed and implemented it must be tuned to recover the original closed-loop handling qualities and responsiveness from the degraded system. Ideally, the pilot should not be able to tell the difference between the original and redesigned systems. The key is that the system must have inherent redundancy so that degraded or missing capabilities can be restored by creative use of alternate functionalities. With enough redundancy in the control system, minor battle damage affecting individual control surfaces or actuators, compressor efficiency, etc., can be compensated for such that the closed-loop performance is not noticeably altered. The work is applied to a Black Hawk/T700 system. Author

64

NUMERICAL ANALYSIS

Includes iteration, difference equations, and numerical approximation.

A90-21918* National Aeronautics and Space Administration. Lewis Research Center, Cleveland, OH.

SOLUTION OF STEADY-STATE ONE-DIMENSIONAL CONSERVATION LAWS BY MATHEMATICAL PROGRAMMING

J. E. LAVERY (NASA, Lewis Research Center, Cleveland, OH; U.S. Navy, Office of Naval Research, Arlington, VA) SIAM Journal on Numerical Analysis (ISSN 0036-1429), vol. 26, Oct. 1989, p. 1081-1089. refs

Copyright

Solution techniques for a class of steady-state scalar conservation laws are developed analytically. Discretization by finite-volume formulas is employed to obtain an overdetermined system of algebraic equations, which are then perturbed nonsingularly (with perturbation coefficient = epsilon) and solved using the l(1) mathematical-programming algorithm of Seneta and Steiger (1984); this approach limits the matrix bandwidth to two, so that an explicit solution can be found efficiently. It is shown that, for small values of epsilon, the l(1) solutions exhibit sharp correctly located shocks and are nonoscillatory O(epsilon) approximations of the physically relevant solutions. T.K.

A90-21940* National Aeronautics and Space Administration. Lewis Research Center, Cleveland, OH.

A CRITICAL ANALYSIS OF THE MODIFIED EQUATION TECHNIQUE OF WARMING AND HYETT

SIN-CHUNG CHANG (NASA, Lewis Research Center, Cleveland, OH) Journal of Computational Physics (ISSN 0021-9991), vol. 86, Jan. 1990, p. 107-126. refs

Copyright

The modified equation technique of Warming and Hyett (1974),

64 NUMERICAL ANALYSIS

which evaluates the behavior of a difference scheme by means of the coefficients of a certain modified equation, established a link between such coefficients and the multiplication factor obtained from the von Neumann analysis. It follows from this pioneering work that modified equations should be derived from the difference scheme, rather than from the original differential equation; a rigorous investigation is presently made of this link without resort to their original interpretation. Only partial validity is establishable for the case of multilevel schemes. O.C.

A90-23110* # Cornell Univ., Ithaca, NY.

DIAGONAL INVERSION OF LOWER-UPPER IMPLICIT SCHEMES

JEFFREY W. YOKOTA (Sverdrup Technology, Inc., Cleveland, OH), DAVID A. CAUGHEY (Cornell University, Ithaca, NY), and RODRICK V. CHIMA (NASA, Lewis Research Center, Cleveland, OH) AIAA Journal (ISSN 0001-1452), vol. 28, Feb. 1990, p. 263-266. Previously cited in issue 20, p. 3440, Accession no. A88-48791. refs

Copyright

A90-26499* Southern Methodist Univ., Dallas, TX.

A 'TRANSIENT' AUTOMATED MAPPING PROCEDURE FOR COMPLEX GEOMETRIES

PETER E. RAAD (Southern Methodist University, Dallas, TX) and JAMES W. WHITE (Santa Clara, University, CA) IN: Numerical grid generation in computational fluid mechanics '88; Proceedings of the Second International Conference, Miami Beach, FL, Dec. 5-8, 1988. Swansea, Wales, Pineridge Press, Ltd., 1988, p. 237-245.

(Contract NAG3-18)

Copyright

A numerical procedure is presented which is applicable to the general curvilinear mappings of complex geometries and is unrestricted by slow convergence or strong dependence on the initial conditions of physical space. The scheme, employing a time-dependent factored-implicit scheme, is shown to be general and robust. In the illustrative applications presented, complex, closed geometries are routinely mapped even when they begin with unreasonable initial conditions created through the analytical and computer graphics inputs. Due to the natural damping introduced into the governing equations, fast convergence is achieved and high stability is observed. O.C.

A90-26535* National Aeronautics and Space Administration. Lewis Research Center, Cleveland, OH.

DISCRETIZATION FORMULAS FOR UNSTRUCTURED GRIDS

KENNETH J. BAUMEISTER (NASA, Lewis Research Center, Cleveland, OH) IN: Numerical grid generation in computational fluid mechanics '88; Proceedings of the Second International Conference, Miami Beach, FL, Dec. 5-8, 1988. Swansea, Wales, Pineridge Press, Ltd., 1988, p. 665-674. Previously announced in STAR as N89-10242.

Copyright

The Galerkin weighted residual technique using linear triangular weight functions is employed to develop finite difference formula in cartesian coordinates for the Laplacian operator, first derivative operators and the function for unstructured triangular grids. The weighted residual coefficients associated with the weak formulation of the Laplacian operator are shown to agree with the Taylor series approach on a global average. In addition, a simple algorithm is presented to determine the Voronoi (finite difference) area of an unstructured grid. Author

A90-34549* Alberta Univ., Edmonton.

ABSORBING BOUNDARY CONDITIONS FOR SECOND-ORDER HYPERBOLIC EQUATIONS

HONG JIANG (Alberta, University, Edmonton, Canada) and YAU SHU WONG (NASA, Lewis Research Center, Cleveland, OH; Alberta, University, Edmonton, Canada) Journal of Computational Physics (ISSN 0021-9991), vol. 88, May 1990, p. 205-231. Research supported by the National Aeronautical Establishment of Canada.

Previously announced in STAR as N89-22397. refs
Copyright

A uniform approach to construct absorbing artificial boundary conditions for second-order linear hyperbolic equations is proposed. The nonlocal boundary condition is given by a pseudodifferential operator that annihilates travelling waves. It is obtained through the dispersion relation of the differential equation by requiring that the initial-boundary value problem admits the wave solutions travelling in one direction only. Local approximation of this global boundary condition yields an nth-order differential operator. It is shown that the best approximations must be in the canonical forms which can be factorized into first-order operators. These boundary conditions are perfectly absorbing for wave packets propagating at certain group velocities. A hierarchy of absorbing boundary conditions is derived for transonic small perturbation equations of unsteady flows. These examples illustrate that the absorbing boundary conditions are easy to derive, and the effectiveness is demonstrated by the numerical experiments.

Author

N90-10635* # National Aeronautics and Space Administration. Lewis Research Center, Cleveland, OH.

QUOTIENT-DIFFERENCE TYPE GENERALIZATIONS OF THE POWER METHOD AND THEIR ANALYSIS

AVRAM SIDI and WILLIAM F. FORD Sep. 1989 18 p Prepared in cooperation with Technion-Israel Inst. of Tech., Haifa (Contract NASA ORDER C-99066-G) (NASA-TM-102361; ICOMP-89-25; E-5077; NAS 1.15:102361) Avail: NTIS HC A03/MF A01 CSCL 12/1

The recursion relations that were proposed by W. F. Ford and A. Sidi (Appl. Numer. Math., 4 (1988), pp. 477-489) for implementing vector extrapolation methods are used for devising generalizations of the power method for linear operators. These generalizations are shown to produce approximations to largest eigenvalues of a linear operator under certain conditions. They are similar in form to the quotient-difference algorithm and share similar convergence properties with the latter. These convergence properties also resemble those obtained for the basic LR and QR algorithms. Finally, it is shown that the convergence rate produced by one of these generalizations is twice as fast for normal operators as it is for nonnormal operators.

Author

N90-11497* # National Aeronautics and Space Administration. Lewis Research Center, Cleveland, OH.

A NONOSCILLATORY, CHARACTERISTICALLY CONVECTED, FINITE VOLUME SCHEME FOR MULTIDIMENSIONAL CONVECTION PROBLEMS

JEFFREY W. YOKOTA and HUNG T. HUYNH 1989 20 p Prepared for presentation at the 28th Aerospace Sciences Meeting, Reno, NV, 8-11 Jan. 1990; sponsored in part by AIAA Prepared in cooperation with Sverdrup Technology, Inc., Cleveland, OH (NASA-TM-102354; E-5069; NAS 1.15:102354) Avail: NTIS HC A03/MF A01 CSCL 12/1

A new, nonoscillatory upwind scheme is developed for the multidimensional convection equation. The scheme consists of an upwind, nonoscillatory interpolation of data to the surfaces of an intermediate finite volume; a characteristic convection of surface data to a midpoint time level; and a conservative time integration based on the midpoint rule. This procedure results in a convection scheme capable of resolving discontinuities neither aligned with, nor convected along, grid lines.

Author

N90-12231* # National Aeronautics and Space Administration. Lewis Research Center, Cleveland, OH.

A LEAST-SQUARES FINITE ELEMENT METHOD FOR INCOMPRESSIBLE NAVIER-STOKES PROBLEMS

BO-NAN JIANG Oct. 1989 22 p (Contract NASA ORDER C-99066-G) (NASA-TM-102385; E-5124; ICOMP-89-28; NAS 1.15:102385) Avail: NTIS HC A03/MF A01 CSCL 12/1

A least-squares finite element method, based on the velocity-pressure-vorticity formulation, is developed for solving steady incompressible Navier-Stokes problems. This method leads

to a minimization problem rather than to a saddle-point problem by the classic mixed method, and can thus accommodate equal-order interpolations. This method has no parameter to tune. The associated algebraic system is symmetric, and positive definite. Numerical results for the cavity flow at Reynolds number up to 10,000 and the backward-facing step flow at Reynolds number up to 900 are presented. Author

N90-14002* # National Aeronautics and Space Administration. Lewis Research Center, Cleveland, OH.

APPLICATION OF MULTI-GRID METHODS FOR SOLVING THE NAVIER-STOKES EQUATIONS

A. O. DEMUREN Oct. 1989 23 p Reprint from the Proceedings of the Inst. of Mechanical Engineers, Part C, 1989, by permission of the Council of the Inst. Previously announced in IAA as A89-53172 Prepared in cooperation with Lagos Univ., Nigeria (Contract NASA ORDER C-99066-G) (NASA-TM-102359; ICOMP-89-24; E-4655; NAS 1.15:102359) Avail: NTIS HC A03/MF A01 CSCL 12/1

The application of a class of multi-grid methods to the solution of the Navier-Stokes equations for two-dimensional laminar flow problems is discussed. The methods consist of combining the full approximation scheme-full multi-grid technique (FAS-FMG) with point-, line-, or plane-relaxation routines for solving the Navier-Stokes equations in primitive variables. The performance of the multi-grid methods is compared to that of several single-grid methods. The results show that much faster convergence can be procured through the use of the multi-grid approach than through the various suggestions for improving single-grid methods. The importance of the choice of relaxation scheme for the multi-grid method is illustrated. Author

N90-14844* # National Aeronautics and Space Administration. Lewis Research Center, Cleveland, OH.

ON THE APPLICATION OF SUBCELL RESOLUTION TO CONSERVATION LAWS WITH STIFF SOURCE TERMS

SHIH-HUNG CHANG (Cleveland State Univ., OH.) Nov. 1989 14 p (Contract NASA ORDER C-99066-G) (NASA-TM-102384; E-5123; ICOMP-89-27; NAS 1.15:102384) Avail: NTIS HC A03/MF A01 CSCL 12/1

LeVeque and Yee recently investigated a one-dimensional scalar conservation law with stiff source terms modeling the reacting flow problems and discovered that for the very stiff case most of the current finite difference methods developed for non-reacting flows would produce wrong solutions when there is a propagating discontinuity. A numerical scheme, essentially nonoscillatory/subcell resolution - characteristic direction (ENO/SRCD), is proposed for solving conservation laws with stiff source terms. This scheme is a modification of Harten's ENO scheme with subcell resolution, ENO/SR. The locations of the discontinuities and the characteristic directions are essential in the design. Strang's time-splitting method is used and time evolutions are done by advancing along the characteristics. Numerical experiment using this scheme shows excellent results on the model problem of LeVeque and Yee. Comparisons of the results of ENO, ENO/SR, and ENO/SRCD are also presented. Author

N90-18198* # National Aeronautics and Space Administration. Lewis Research Center, Cleveland, OH.

CONDITIONS AT THE DOWNSTREAM BOUNDARY FOR SIMULATIONS OF VISCOUS INCOMPRESSIBLE FLOW

THOMAS HAGSTROM (State Univ. of New York, Stony Brook.) Feb. 1990 26 p (Contract NASA ORDER C-99066-G) (NASA-TM-102510; ICOMP-90-05; E-5312; NAS 1.15:102510) Avail: NTIS HC A03/MF A01 CSCL 12/1

The proper specification of boundary conditions at artificial boundaries for the simulation of time-dependent fluid flows has long been a matter of controversy. A general theory of asymptotic boundary conditions for dissipative waves is applied to the design of simple, accurate conditions at downstream boundary for

incompressible flows. For Reynolds numbers far enough below the critical value for linear stability, a scaling is introduced which greatly simplifies the construction of the asymptotic conditions. Numerical experiments with the nonlinear dynamics of vortical disturbances to plane Poiseuille flow are presented which illustrate the accuracy of our approach. The consequences of directly applying the scalings to the equations are also considered. Author

N90-18927* # National Aeronautics and Space Administration. Lewis Research Center, Cleveland, OH. Inst. for Computational Mechanics in Propulsion.

ASYMPTOTIC BOUNDARY CONDITIONS FOR DISSIPATIVE WAVES: GENERAL THEORY

THOMAS HAGSTROM (State Univ. of New York, Stony Brook.) Jan. 1990 21 p (Contract NASA ORDER C-99066-G; NSF DMS-89-05314) (NASA-TM-102497; ICOMP-90-02; E-5291; NAS 1.15:102497) Avail: NTIS HC A03/MF A01 CSCL 12/1

An outstanding issue in the computational analysis of time dependent problems is the imposition of appropriate radiation boundary conditions at artificial boundaries. Accurate conditions are developed which are based on the asymptotic analysis of wave propagation over long ranges. Employing the method of steepest descents, dominant wave groups are identified and simple approximations to the dispersion relation are considered in order to derive local boundary operators. The existence of a small number of dominant wave groups may be expected for systems with dissipation. Estimates of the error as a function of domain size are derived under general hypotheses, leading to convergence results. Some practical aspects of the numerical construction of the asymptotic boundary operators are also discussed. Author

N90-19783* # National Aeronautics and Space Administration. Lewis Research Center, Cleveland, OH. Inst. for Computational Mechanics in Propulsion.

PARALLEL ALGORITHMS FOR BOUNDARY VALUE PROBLEMS

AVI LIN (Temple Univ., Philadelphia, PA.) Jan. 1990 21 p (Contract NASA ORDER C-99066-G) (NASA-TM-102498; ICOMP-90-03; E-5292; NAS 1.15:102498) Avail: NTIS HC A03/MF A01 CSCL 12/1

A general approach to solve boundary value problems numerically in a parallel environment is discussed. The basic algorithm consists of two steps: the local step where all the P available processors work in parallel, and the global step where one processor solves a tridiagonal linear system of the order P. The main advantages of this approach are two fold. First, this suggested approach is very flexible, especially in the local step and thus the algorithm can be used with any number of processors and with any of the SIMD or MIMD machines. Secondly, the communication complexity is very small and thus can be used as easily with shared memory machines. Several examples for using this strategy are discussed. Author

N90-20769* # National Aeronautics and Space Administration. Lewis Research Center, Cleveland, OH.

INSTITUTE FOR COMPUTATIONAL MECHANICS IN PROPULSION (ICOMP) FOURTH ANNUAL REVIEW, 1989

Mar. 1990 59 p (Contract NASA ORDER C-99066-G) (NASA-TM-102519; ICOMP-90-01; E-5323; NAS 1.15:102519) Avail: NTIS HC A04/MF A01 CSCL 12/1

The Institute for Computational Mechanics in Propulsion (ICOMP) is operated jointly by Case Western Reserve University and the NASA Lewis Research Center. The purpose of ICOMP is to develop techniques to improve problem solving capabilities in all aspects of computational mechanics related to propulsion. The activities at ICOMP during 1989 are described. Author

64 NUMERICAL ANALYSIS

N90-21567*# National Aeronautics and Space Administration.
Lewis Research Center, Cleveland, OH.

HIGH ACCURACY SOLUTIONS OF INCOMPRESSIBLE NAVIER-STOKES EQUATIONS

MURLI M. GUPTA Mar. 1990 27 p

(Contract NASA ORDER C-99066-G)

(NASA-TM-102539; ICOMP-90-10; E-5350; NAS 1.15:102539)

Avail: NTIS HC A03/MF A01 CSCL 12/1

In recent years, high accuracy finite difference approximations were developed for partial differential equations of elliptic type, with particular emphasis on the convection-diffusion equation. These approximations are of compact type, have a local truncation error of fourth order, and allow the use of standard iterative schemes to solve the resulting systems of algebraic equations. These high accuracy approximations are extended to the solution of Navier-Stokes equations. Solutions are obtained for the model problem of driven cavity and are compared with solutions obtained using other approximations and those obtained by other authors. It is discovered that the high order approximations do indeed produce high accuracy solutions and have a potential for use in solving important problems of viscous fluid flows. Author

N90-21570*# National Aeronautics and Space Administration.
Lewis Research Center, Cleveland, OH.

ULTRA-SHARP NONOSCILLATORY CONVECTION SCHEMES FOR HIGH-SPEED STEADY MULTIDIMENSIONAL FLOW

B. P. LEONARD and SIMIN MOKHTARI (Akron Univ., OH.) Apr. 1990 50 p

(Contract NASA ORDER C-99066-G)

(NASA-TM-102568; ICOMP-90-12; E-5320; NAS 1.15:102568)

Avail: NTIS HC A03/MF A01 CSCL 12/1

For convection-dominated flows, classical second-order methods are notoriously oscillatory and often unstable. For this reason, many computational fluid dynamicists have adopted various forms of (inherently stable) first-order upwinding over the past few decades. Although it is now well known that first-order convection schemes suffer from serious inaccuracies attributable to artificial viscosity or numerical diffusion under high convection conditions, these methods continue to enjoy widespread popularity for numerical heat transfer calculations, apparently due to a perceived lack of viable high accuracy alternatives. But alternatives are available. For example, nonoscillatory methods used in gasdynamics, including currently popular TVD schemes, can be easily adapted to multidimensional incompressible flow and convective transport. This, in itself, would be a major advance for numerical convective heat transfer, for example. But, as is shown, second-order TVD schemes form only a small, overly restrictive, subclass of a much more universal, and extremely simple, nonoscillatory flux-limiting strategy which can be applied to convection schemes of arbitrarily high order accuracy, while requiring only a simple tridiagonal ADI line-solver, as used in the majority of general purpose iterative codes for incompressible flow and numerical heat transfer. The new universal limiter and associated solution procedures form the so-called ULTRA-SHARP alternative for high resolution nonoscillatory multidimensional steady state high speed convective modelling. Author

N90-26614*# National Aeronautics and Space Administration.
Lewis Research Center, Cleveland, OH.

PARALLEL/DISTRIBUTED DIRECT METHOD FOR SOLVING LINEAR SYSTEMS

AVI LIN (Temple Univ., Philadelphia, PA.) Jul. 1990 18 p

(Contract NASA ORDER C-99066-G)

(NASA-TM-103229; ICOMP-90-18; E-5645; NAS 1.15:103229)

Avail: NTIS HC A03/MF A01 CSCL 12/1

A new family of parallel schemes for directly solving linear systems is presented and analyzed. It is shown that these schemes exhibit a near optimal performance and enjoy several important features: (1) For large enough linear systems, the design of the appropriate parallelized algorithm is insensitive to the number of processors as its performance grows monotonically with them; (2) It is especially good for large matrices, with dimensions large relative to the number of processors in the system; (3) It can be

used in both distributed parallel computing environments and tightly coupled parallel computing systems; and (4) This set of algorithms can be mapped onto any parallel architecture without any major programming difficulties or algorithmical changes. Author

N90-26615*# National Aeronautics and Space Administration.
Lewis Research Center, Cleveland, OH.

ASYMPTOTIC ANALYSIS OF DISSIPATIVE WAVES WITH APPLICATIONS TO THEIR NUMERICAL SIMULATION

THOMAS HAGSTROM (State Univ. of New York, Stony Brook.)

Aug. 1990 15 p

(Contract NASA ORDER C-99066-G; NSF DMS-89-05314)

(NASA-TM-103231; ICOMP-90-19; E-5647; NAS 1.15:103231)

Avail: NTIS HC A03/MF A01 CSCL 12/1

Various problems involving the interplay of asymptotics and numerics in the analysis of wave propagation in dissipative systems are studied. A general approach to the asymptotic analysis of linear, dissipative waves is developed. It was applied to the derivation of asymptotic boundary conditions for numerical solutions on unbounded domains. Applications include the Navier-Stokes equations. Multidimensional traveling wave solutions to reaction-diffusion equations are also considered. A preliminary numerical investigation of a thermo-diffusive model of flame propagation in a channel with heat loss at the walls is presented. Author

N90-26616*# National Aeronautics and Space Administration.
Lewis Research Center, Cleveland, OH.

EFFICIENT IMPLEMENTATION OF MINIMAL POLYNOMIAL AND REDUCED RANK EXTRAPOLATION METHODS

AVRAM SIDI (Israel Inst. of Tech., Haifa.) Aug. 1990 43 p

(Contract NASA ORDER C-99066-G)

(NASA-TM-103240; ICOMP-90-20; E-5658; NAS 1.15:103240)

Avail: NTIS HC A03/MF A01 CSCL 12/1

The minimal polynomial extrapolation (MPE) and reduced rank extrapolation (RRE) are two effective techniques that have been used in accelerating the convergence of vector sequences, such as those that are obtained from iterative solution of linear and nonlinear systems of equation. Their definitions involve some linear least squares problems, and this causes difficulties in their numerical implementation. Timewise efficient and numerically stable implementations for MPE and RRE are developed. A computer program written in FORTRAN 77 is also appended and applied to some model problems. Author

N90-29124*# National Aeronautics and Space Administration.
Lewis Research Center, Cleveland, OH.

CONSISTENCY AND CONVERGENCE FOR NUMERICAL RADIATION CONDITIONS

THOMAS HAGSTROM Aug. 1990 12 p Prepared in cooperation with State Univ. of New York, Stony Brook

(Contract NASA ORDER C-99066-G; NSF DMS-89-05314)

(NASA-TM-103262; ICOMP-90-21; E-5695; NAS 1.15:103262)

Avail: NTIS HC A03/MF A01 CSCL 12/1

The problem of imposing radiation conditions at artificial boundaries for the numerical simulation of wave propagation is considered. Emphasis is on the behavior and analysis of the error which results from the restriction of the domain. The theory of error estimation is briefly outlined for boundary conditions. Use is made of the asymptotic analysis of propagating wave groups to derive and analyze boundary operators. For dissipative problems this leads to local, accurate conditions, but falls short in the hyperbolic case. A numerical experiment on the solution of the wave equation with cylindrical symmetry is described. A unified presentation of a number of conditions which have been proposed in the literature is given and the time dependence of the error which results from their use is displayed. The results are in qualitative agreement with theoretical considerations. It was found, however, that for this model problem it is particularly difficult to force the error to decay rapidly in time. Author

SYSTEMS ANALYSIS

Includes mathematical modeling; network analysis; and operations research.

A90-10373* National Aeronautics and Space Administration. Lewis Research Center, Cleveland, OH.

SPACE STATION POWER SYSTEM AUTONOMY DEMONSTRATION

JAMES A. KISH, JAMES L. DOLCE (NASA, Lewis Research Center, Cleveland, OH), and DAVID J. WEEKS (NASA, Marshall Space Flight Center, Huntsville, AL) IN: Space Station automation IV; Proceedings of the Meeting, Cambridge, MA, Nov. 7-9, 1988. Bellingham, WA, Society of Photo-Optical Instrumentation Engineers, 1988, p. 218-225. refs

Copyright

The Systems Autonomy Demonstration Program (SADP) represents NASA's major effort to demonstrate, through a series of complex ground experiments, the application and benefits of applying advanced automation technologies to the Space Station project. Lewis Research Center (LeRC) and Marshall Space Flight Center (MSFC) will first jointly develop an autonomous power system using existing Space Station testbed facilities at each center. The subsequent 1990 power-thermal demonstration will then involve the cooperative operation of the LeRC/MSFC power system with the Johnson Space Center (JSC's) thermal control and DMS/OMS testbed facilities. The testbeds and expert systems at each of the NASA centers will be interconnected via communication links. The appropriate knowledge-based technology will be developed for each testbed and applied to problems requiring intersystem cooperation. Primary emphasis will be focused on failure detection and classification, system reconfiguration, planning and scheduling of electrical power resources, and integration of knowledge-based and conventional control system software into the design and operation of Space Station testbeds.

C.E.

A90-25638*# National Aeronautics and Space Administration. Lewis Research Center, Cleveland, OH.

APPLICATION OF HEURISTIC SATELLITE PLAN SYNTHESIS ALGORITHMS TO REQUIREMENTS OF THE WARC-88 ALLOTMENT PLAN

ANN O. HEYWARD (NASA, Lewis Research Center, Cleveland, OH), CHARLES H. REILLY, ERIC K. WALTON, FERNANDO MATA, and CARL OLEN (Ohio State University, Columbus) IN: AIAA International Communication Satellite Systems Conference and Exhibit, 13th, Los Angeles, CA, Mar. 11-15, 1990, Technical Papers. Part 1. Washington, DC, American Institute of Aeronautics and Astronautics, 1990, p. 311-321. Previously announced in STAR as N90-14856. refs

(Contract NAG3-159)

(AIAA PAPER 90-0815) Copyright

Creation of an Allotment Plan for the Fixed Satellite Service at the 1988 Space World Administrative Radio Conference (WARC) represented a complex satellite plan synthesis problem, involving a large number of planned and existing systems. Solutions to this problem at WARC-88 required the use of both automated and manual procedures to develop an acceptable set of system positions. Development of an Allotment Plan may also be attempted through solution of an optimization problem, known as the Satellite Location Problem (SLP). Three automated heuristic procedures, developed specifically to solve SLP, are presented. The heuristics are then applied to two specific WARC-88 scenarios. Solutions resulting from the fully automated heuristics are then compared with solutions obtained at WARC-88 through a combination of both automated and manual planning efforts.

Author

A90-26975*# Maxwell Labs., Inc., La Jolla, CA.

EPSAT - A WORKBENCH FOR DESIGNING HIGH-POWER SYSTEMS FOR THE SPACE ENVIRONMENT

R. A. KUHARSKI, G. A. JONGEWARD, K. G. WILCOX, E. M. KENNEDY (Maxwell Laboratories, Inc., La Jolla, CA), N. J. STEVENS, R. M. PUTNAM (TRW, Inc., Space and Technology Group, Redondo Beach, CA), and J. C. ROCHE (NASA, Lewis Research Center, Cleveland, OH) AIAA, Aerospace Sciences Meeting, 28th, Reno, NV, Jan. 8-11, 1990. 5 p.

(AIAA PAPER 90-0637) Copyright

The Environment Power System Analysis Tool (EPSAT) is being developed to provide space power system design engineers with an analysis tool for determining the performance of power systems in both naturally occurring and self-induced environments. This paper presents the results of the project after two years of a three-year development program. The relevance of the project result for SDI are pointed out, and models of the interaction of the environment and power systems are discussed.

C.D.

N90-10674*# National Aeronautics and Space Administration. Lewis Research Center, Cleveland, OH.

APPLICATION OF A HYBRID GENERATION/UTILITY ASSESSMENT HEURISTIC TO A CLASS OF SCHEDULING PROBLEMS

ANN O. HEYWARD 1989 13 p Prepared for presentation at the International Conference on Systems, Man, and Cybernetics, Cambridge, MA, 14-17 Nov. 1989; sponsored by IEEE (NASA-TM-102367; E-5086; NAS 1.15:102367) Avail: NTIS HC A03/MF A01 CSCL 12/2

A two-stage heuristic solution approach for a class of multiobjective, n-job, 1-machine scheduling problems is described. Minimization of job-to-job interference for n jobs is sought. The first stage generates alternative schedule sequences by interchanging pairs of schedule elements. The set of alternative sequences can represent nodes of a decision tree; each node is reached via decision to interchange job elements. The second stage selects the parent node for the next generation of alternative sequences through automated paired comparison of objective performance for all current nodes. An application of the heuristic approach to communications satellite systems planning is presented.

Author

N90-14060*# National Aeronautics and Space Administration. Lewis Research Center, Cleveland, OH.

MODELING OF POWER ELECTRONIC SYSTEMS WITH EMTP

KWA-SUR TAM (Virginia Polytechnic Inst. and State Univ., Blacksburg) and NARAYAN V. DRAVID Dec. 1989 10 p (NASA-TM-102375; E-5109; NAS 1.15:102375) Avail: NTIS HC A02/MF A01 CSCL 12/2

In view of the potential impact of power electronics on power systems, there is need for a computer modeling/analysis tool to perform simulation studies on power systems with power electronic components as well as to educate engineering students about such systems. The modeling of the major power electronic components of the NASA Space Station Freedom Electric Power System is described along with ElectroMagnetic Transients Program (EMTP) and it is demonstrated that EMTP can serve as a very useful tool for teaching, design, analysis, and research in the area of power systems with power electronic components. EMTP modeling of power electronic circuits is described and simulation results are presented.

Author

N90-14856*# National Aeronautics and Space Administration. Lewis Research Center, Cleveland, OH.

APPLICATION OF HEURISTIC SATELLITE PLAN SYNTHESIS ALGORITHMS TO REQUIREMENTS OF THE WARC-88 ALLOTMENT PLAN

ANN O. HEYWARD, CHARLES H. REILLY, ERIC K. WALTON, FERNANDO MATA, and CARL OLEN (Ohio State Univ., Columbus) 1990 13 p Prepared for presentation at the 13th International Communications Satellite Systems Conference, Los Angeles, CA, 11-15 Mar. 1990; sponsored by AIAA

(Contract NAG3-159)
(NASA-TM-102479; E-5266; NAS 1.15:102479; AIAA-90-0815)
Avail: NTIS HC A03/MF A01 CSCL 12/2

Creation of an Allotment Plan for the Fixed Satellite Service at the 1988 Space World Administrative Radio Conference (WARC) represented a complex satellite plan synthesis problem, involving a large number of planned and existing systems. Solutions to this problem at WARC-88 required the use of both automated and manual procedures to develop an acceptable set of system positions. Development of an Allotment Plan may also be attempted through solution of an optimization problem, known as the Satellite Location Problem (SLP). Three automated heuristic procedures, developed specifically to solve SLP, are presented. The heuristics are then applied to two specific WARC-88 scenarios. Solutions resulting from the fully automated heuristics are then compared with solutions obtained at WARC-88 through a combination of both automated and manual planning efforts. Author

N90-28393*# National Aeronautics and Space Administration. Lewis Research Center, Cleveland, OH.

A SOLAR POWER SYSTEM FOR AN EARLY MARS EXPEDITION

BARBARA I. MCKISSOCK, LISA L. KOHOUT, and PAUL C. SCHMITZ (Sverdrup Technology, Inc., Brook Park, OH.) 1990 12 p Presented at the American Institute of Chemical Engineers Summer National Meeting, San Diego, CA, 19-22 Aug. 1990 (NASA-TM-103219; E-5632; NAS 1.15:103219) Avail: NTIS HC A03/MF A01 CSCL 12/2

As NASA looks at missions that will expand human presence in the solar system, the power requirements for such missions need to be defined, developed and analyzed. One mission under consideration consists of a 40 day manned Mars surface expedition to perform science experiments. The mission time was centered around an aerocentric longitude (Ls) of 90 deg to lessen the probability of an occurrence of a local or planetary dust storm. The mission site was arbitrarily located at the Martian equator. The power requirements were assumed to be 40 kWe for life support and experiment power during the Martian day and 20 kWe for life support during the Martian night. A solar energy system consisting of roll-out amorphous silicon arrays and a hydrogen-oxygen regenerative fuel cell energy storage system was chosen for the study. The power available from a roll-out array, when plotted against time, approaches a cosine-like curve and depends on both array area and the amount of solar irradiance impinging on its horizontal surface. The array is sized to provide at least 20 KWe when the sun is 12.5 deg above the horizon and ramp up to 140 kWe peak power at Martian noon. In this configuration, the array is capable of supplying 40 KWe continuously to the user for the majority of the Martian day while supplying the excess energy to the electrolyzer portion of the energy storage system. A roll-out, pumped loop radiator system is used to dissipate the waste heat produced by the fuel cell. The power management and distribution system inverts the power from the individual solar array sub-modules and the fuel cell stacks and connects them to a 440 VAC single phase 20 kHz main bus. The total power system is comprised of 80 individual solar array modules with an integral bus and three energy storage modules consisting of fuel cell and electrolyzer stacks, reactant storage tanks, and a roll-out radiator. Power system mass, stowed volume, and deployed area were determined. Day/night power splits of 40/10 kWe, 40/30 kWe, and 40/40 kWe were also considered to determine the impact of a range of nighttime power requirements on the baseline system. Author

PHYSICS (GENERAL)

N90-12282*# National Aeronautics and Space Administration. Lewis Research Center, Cleveland, OH.

PARAMETRIC STUDY OF POWER ABSORPTION FROM ELECTROMAGNETIC WAVES BY SMALL FERRITE SPHERES

GERALD W. ENGLERT Nov. 1989 22 p
(NASA-TP-2949; E-4601; NAS 1.60:2949) Avail: NTIS HC A03/MF A01 CSCL 20/3

Algebraic expressions in terms of elementary mathematical functions are derived for power absorption and dissipation by eddy currents and magnetic hysteresis in ferrite spheres. Skin depth is determined by using a variable inner radius in descriptive integral equations. Numerical results are presented for sphere diameters less than one wavelength. A generalized power absorption parameter for both eddy currents and hysteresis is expressed in terms of the independent parameters involving wave frequency, sphere radius, resistivity, and complex permeability. In general, the hysteresis phenomenon has a greater sensitivity to these independent parameters than do eddy currents over the ranges of independent parameters studied herein. Working curves are presented for obtaining power losses from input to the independent parameters. Author

ACOUSTICS

Includes sound generation, transmission, and attenuation.

A90-14342* Texas A&M Univ., College Station.

PERFORMANCE AND ACOUSTIC PREDICTION OF COUNTERROTATING PROPELLER CONFIGURATIONS

B. W. DENNER and K. D. KORKAN (Texas A & M University, College Station) SAE, General Aviation Aircraft Meeting and Exposition, Wichita, KS, Apr. 11-13, 1989. 17 p. refs
(Contract NAG3-354)

(SAE PAPER 891035) Copyright

The Davidson (1981) numerical method is used to predict the performance of a counterrotating propeller configuration over a range of different front and back disk rotation speeds with constant-speed propellers; this has yielded such overall performance parameters as integrated thrust, torque, and power, as well as the radial variation of blade torque and thrust. Since the unsteady component of the noise from a counterrotating propeller configuration is minimal in the plane of the propeller disk, this approach is restricted to noise-level predictions for observer locations in this region. O.C.

A90-19725*# Texas A&M Univ., College Station.

APPLICATION OF THE COMPUTATIONAL AEROACOUSTICS METHOD TO AN ADVANCED COUNTERROTATING PROPPAN CONFIGURATION

JINHAN KIM (Texas A & M University, College Station) AIAA, Aerospace Sciences Meeting, 28th, Reno, NV, Jan. 8-11, 1990. 12 p. refs

(Contract NAG3-354)

(AIAA PAPER 90-0183) Copyright

The acoustical near field of a counterrotating propeller configuration of unducted fan (UDF) type is presently predicted by means of a numerical methodology employing the transonic flow field generated by the three-dimensional numerical flow solver designated SSTAGE. This numerical approach simulates the time-averaged, three-dimensional inviscid flow field of the UDF by

means of a four-stage Runge-Kutta integration scheme which marches the equations forward in time toward an asymptotic limit. The near field pressure time history is obtained directly from the flow field solution; by converting these histories with a Fourier series representation, specific data on the acoustic signal frequency spectra can be obtained. O.C.

A90-32505* National Aeronautics and Space Administration. Lewis Research Center, Cleveland, OH.

NOISE OF A SIMULATED INSTALLED MODEL COUNTERROTATION PROPELLER AT ANGLE-OF-ATTACK AND TAKEOFF/APPROACH CONDITIONS

RICHARD P. WOODWARD (NASA, Lewis Research Center, Cleveland, OH) AIAA, Aerospace Sciences Meeting, 28th, Reno, NV, Jan. 8-11, 1990. 24 p. refs
(AIAA PAPER 90-0283) Copyright

Acoustic results for two model counterrotation propellers are presented. The propellers were tested over a range of rotational speeds and propeller axis angles of attack in both the baseline configuration and the installed configuration consisting of a simulated upstream nacelle support pylon and fuselage section. Acoustic data were taken with a polar microphone probe attached to the downstream propeller housing, capable of surveying directivities at several azimuthal locations. The forward and aft rotor power coefficients and fundamental rotor-alone tone levels are found to be directly controlled by propeller axis angle of attack. The second-order rotor-alone tones are strongly influenced by the upstream pylon wake at 80 percent speed; however, rotor-alone mechanisms control the tone level at 90 percent speed, while rotor-rotor interaction tones are essentially unaffected by the presence of the simulated installation. V.T.

A90-33313* National Aeronautics and Space Administration. Lewis Research Center, Cleveland, OH.

EFFECTS OF FIBER MOTION ON THE ACOUSTIC BEHAVIOR OF AN ANISOTROPIC, FLEXIBLE FIBROUS MATERIAL

MILO D. DAHL, EDWARD J. RICE, and DONALD E. GROESBECK (NASA, Lewis Research Center, Cleveland, OH) Acoustical Society of America, Journal (ISSN 0001-4966), vol. 87, Jan. 1990, p. 54-66. Previously announced in STAR as N87-25826. refs
Copyright

The acoustic behavior of a flexible fibrous material was studied experimentally. The material consisted of cylindrically shaped fibers arranged in a batting with the fibers primarily aligned parallel to the face of the batting. This type of material was considered anisotropic, with the acoustic propagation constant depending on whether the direction of sound propagation was parallel or normal to the fiber arrangement. Normal incidence sound absorption measurements were taken for both fiber orientations over the frequency range 140 to 1500 Hz and with bulk densities ranging from 4.6 to 67 kg/cu m. When the sound propagated in a direction normal to the fiber alignment, the measured sound absorption showed the occurrence of a strong resonance, which increased absorption above that attributed to viscous and thermal effects. When the sound propagated in a direction parallel to the fiber alignment, indications of strong resonances in the data were not present. The resonance in the data for fibers normal to the direction of sound propagation is attributed to fiber motion. An analytical model was developed for the acoustic behavior of the material displaying the same fiber motion characteristics shown in the measurements. Author

A90-35903* Florida State Univ., Gainesville.

THEORETICAL MODEL OF DISCRETE TONE GENERATION BY IMPINGING JETS

CHRISTOPHER K. W. TAM (Florida State University, Tallahassee) and K. K. AHUJA (Lockheed Aeronautical Systems Co., Marietta, GA) Journal of Fluid Mechanics (ISSN 0022-1120), vol. 214, May 1990, p. 67-87. refs
(Contract NAS3-23798)
Copyright

A new feedback mechanism is proposed for discrete tone generation by impinging jets. It is suggested that the feedback is

achieved by upstream-propagating waves associated with the lowest-order intrinsic neutral wave modes of the jet flow. These wave modes have well-defined radial and azimuthal pressure and velocity distributions, which are determined by the mean flow of the jets in the case of the Kelvin-Helmholtz instability waves. The model proposed here allows the prediction of the average Strouhal number of impingement tones as a function of the jet Mach number. V.L.

A90-47202* Pratt and Whitney Aircraft Group, East Hartford, CT.

MIXER-EJECTOR NOZZLE FOR JET NOISE SUPPRESSION

W. K. LORD, C. W. JONES, A. M. STERN (United Technologies Corp., Pratt and Whitney Group, East Hartford, CT), V. L. HEAD, and E. A. KREJSA (NASA, Lewis Research Center, Cleveland, OH) AIAA, SAE, ASME, and ASCE, Joint Propulsion Conference, 26th, Orlando, FL, July 16-18, 1990. 20 p. refs
(AIAA PAPER 90-1909) Copyright

An aero/acoustic model test of a mixer-ejector nozzle was conducted at the 9 x 15 foot low-speed acoustic wind tunnel at NASA Lewis Research Center. The objective of the test was to get a preliminary assessment of ejector pumping and noise reduction potential of this device for possible application in the exhaust system of an advanced supersonic civil transport. The results of the test showed that goal levels of pumping were achieved. Exit pressure/temperature traverse data showed that there was good mixing between the primary and secondary streams. Acoustics data were dominated by shock noise; jet mixing noise levels were low because of a facility limit on primary temperature. The mixer-ejector did significantly reduce shock noise relative to the baseline conic nozzle. Because the relative magnitudes of jet mixing noise and shock noise were not in the correct proportion to properly model engine noise, an Effective Perceived Noise Level (EPNL) assessment was precluded. Author

N90-10683* Hamilton Standard, Windsor Locks, CT.

ACOUSTIC TEST AND ANALYSIS OF A COUNTERROTATING PROP-FAN MODEL Final Report

BERNARD MAGLIOZZI, PAUL BROWN, and DAVID PARZYCH Oct. 1987 156 p
(Contract NAS3-24222)
(NASA-CR-179590; NAS 1.26:179590) Avail: NTIS HC A08/MF A01 CSCL 20/1

Results of acoustic tests of a 62.2 cm (24.5 in) diameter model counterrotating Prop-Fan are presented. The model was tested as a tractor and a pusher downstream of a pylon, both at 0 degrees and at 4 degrees angle-of-attack. The effects on noise of spacing between rotors and between the pylons and the rotors were also measured. Effects of rotor spacing were found to cause small changes in noise over the range of spacings tested. The presence of the pylon resulted in a 2 to 3 EPNdB increase in noise. Angle-of-attack effects showed an increase of 3 to 4 EPNdB for the tractor and only about 1 EPNdB for the pusher configuration. Speed was found to be the strongest parameter in minimizing noise. However, the decrease in noise with tip speeds below 200 m/sec (650 ft/sec) became significantly smaller than at higher tip speeds. Comparison of noise spectra between single rotation and counterrotating Prop-Fans showed that the counterrotating Prop-Fan has significantly higher levels of higher frequency noise which radiates in the forward direction. Correlations between measurement and prediction are discussed. Predictions are made of far-field noise during takeoff and near-field noise during cruise. Author

N90-11549* General Electric Co., Cincinnati, OH. Advanced Engineering Technologies Dept.

AN INVESTIGATION OF COUNTERROTATING TIP VORTEX INTERACTION

R. K. MAJJIGI, K. UENISHI, and P. R. GLIEBE Oct. 1989 124 p
(Contract NAS3-24080)
(NASA-CR-185135; NAS 1.26:185135) Avail: NTIS HC A06/MF A01 CSCL 20/1

71 ACOUSTICS

A tip vortex interaction model originally developed for compressors has been extended and adapted for use with counterrotating open rotors. Comparison of available acoustic data with predictions (made with and without the tip vortex model included) illustrate the importance of this interaction effect. This report documents the analytical modeling, a limited experimental verification, and certain key parametric studies pertaining to the tip vortex as a noise source mechanism for the unsteady loading noise of counterrotating propellers. Author

N90-17413* # National Aeronautics and Space Administration. Lewis Research Center, Cleveland, OH.

PREDICTED AND MEASURED BOUNDARY LAYER REFRACTION FOR ADVANCED TURBOPROP PROPELLER NOISE

JAMES H. DITTMAR and EUGENE A. KREJSA Jan. 1990 20 p
(NASA-TM-102365; E-5081; NAS 1.15:102365) Avail: NTIS HC A03/MF A01 CSCL 20/1

Currently, boundary layer refraction presents a limitation to the measurement of forward arc propeller noise measured on an acoustic plate in the NASA Lewis 8- by 6-Foot Supersonic Wind Tunnel. The use of a validated boundary layer refraction model to adjust the data could remove this limitation. An existing boundary layer refraction model is used to predict the refraction for cases where boundary layer refraction was measured. In general, the model exhibits the same qualitative behavior as the measured refraction. However, the prediction method does not show quantitative agreement with the data. In general, it overpredicts the amount of refraction for the far forward angles at axial Mach number of 0.85 and 0.80 and underpredicts the refraction at axial Mach numbers of 0.75 and 0.70. A more complete propeller source description is suggested as a way to improve the prediction method. Author

N90-18228* # Texas A&M Univ., College Station. Dept. of Aerospace Engineering.

AN APPROXIMATE MODEL FOR THE PERFORMANCE AND ACOUSTIC PREDICTIONS OF COUNTERROTATING PROPELLER CONFIGURATIONS M.S. Thesis

BRETT WILLIAM DENNER Dec. 1989 182 p
(Contract NAG3-354)
(NASA-CR-180667; E-126:180667) Avail: NTIS HC A09/MF A01 CSCL 20/1

An approximate method was developed to analyze and predict the acoustics of a counterrotating propeller configuration. The method employs the analytical techniques of Lock and Theodorsen as described by Davidson to predict the steady performance of a counterrotating configuration. Then, a modification of the method of Lesieur is used to predict the unsteady forces on the blades. Finally, the steady and unsteady loads are used in the numerical method of Succi to predict the unsteady acoustics of the propeller. The numerical results are compared with experimental acoustic measurements of a counterrotating propeller configuration by Gazzaniga operating under several combinations of advance ratio, blade pitch, and number of blades. In addition, a constant-speed commuter-class propeller configuration was designed with the Davidson method and the acoustics analyzed at three advance ratios. Noise levels and frequency spectra were calculated at a number of locations around the configuration. The directivity patterns of the harmonics in both the horizontal and vertical planes were examined, with the conclusion that the noise levels of the even harmonics are relatively independent of direction whereas the noise levels of the odd harmonics are extremely dependent on azimuthal direction in the horizontal plane. The equations of Succi are examined to explain this behavior. Author

N90-18229* # National Aeronautics and Space Administration. Lewis Research Center, Cleveland, OH.

UNSTEADY EULER ANALYSIS OF THE FLOW FIELD OF A PROPFAN AT AN ANGLE OF ATTACK

M. NALLASAMY (Sverdrup Technology, Inc., Cleveland, OH.) and J. F. GROENEWEG 1990 19 p Presented at the 28th

Aerospace Sciences Meeting, Reno, NV, 8-11 Jan. 1990; sponsored by AIAA

(NASA-TM-102426; E-5191; NAS 1.15:102426; AIAA-90-0339)

Avail: NTIS HC A03/MF A01 CSCL 20/1

The effects of angle of attack of a propfan on the blade loading and details of the flow field by solving the unsteady three-dimensional Euler equations are examined. The configuration considered is the SR7L propeller at cruise condition and the inflow angles considered are 4.6 degrees, 1.6 degrees and -0.4 degrees. The results indicate that the blade response is nearly sinusoidal at low inflow angles (1.6 degrees and -0.4 degrees) and significant deviations from sinusoidal behavior occur at an inflow angle of 4.6 degrees due to the presence of strong shocks on both suction and pressure surfaces of the blade. The detailed flow in the blade passages shows that a shock formed on the suction surface during the highly loaded portion of the revolution extends across the passage to the pressure surface. An increase in inflow angle results in an increase in blade loading on the down-going side and a decrease in loading on the up-going side. Author

N90-20794* # National Aeronautics and Space Administration. Lewis Research Center, Cleveland, OH.

NOISE OF A SIMULATED INSTALLED MODEL COUNTERROTATION PROPELLER AT ANGLE-OF-ATTACK AND TAKEOFF/APPROACH CONDITIONS

RICHARD P. WOODWARD 1990 25 p Presented at the 28th Aerospace Sciences Meeting, Reno, NV, 8-11 Jan. 1990; sponsored by AIAA

(NASA-TM-102440; E-5210; NAS 1.15:102440; AIAA-90-0283)

Avail: NTIS HC A03/MF A01 CSCL 20/1

Two modern high-speed advanced counterrotation propellers, F7/A7 and F7/A3 were tested in the NASA Lewis Research Center's 9- by 15-Foot Anechoic Wind Tunnel at simulated takeoff/approach conditions of 0.2 Mach. Both rotors were of similar diameter on the F7/A7 propeller, while the aft diameter of the F7/A3 propeller was 85 percent of the forward propeller to reduce tip vortex-aft rotor interaction. The two propellers were designed for similar performance. The propellers were tested in both the baseline configuration and installed configuration consisting of a simulated upstream nacelle support pylon and fuselage section. Acoustic measurements were made with a polar microphone probe which recorded sideline directivities at various azimuthal locations. Aerodynamic measurements were also made to establish propeller operating conditions. The propellers were run at initial blade setting angles adjusted to achieve equal forward/aft torque ratios at angle of attack with the pylon and fuselage simulation in place. Data are presented for propeller operation at 80 and 90 percent of design speed (the forward rotor design tip speed was 238 m/sec (780 ft/sec). Both propellers were tested at the maximum rotor-rotor spacing of 14.99 cm (5.90 in.) based on the pitch change axis separation. Author

N90-21600* # Sverdrup Technology, Inc., Cleveland, OH.

MICROGRAVITY ACOUSTIC MIXING FOR PARTICLE CLOUD COMBUSTORS Final Report

FREDERIC PLA and ROBERT I. RUBINSTEIN Mar. 1990 153 p

(Contract NAS3-25266)

(NASA-CR-185159; E-5347; NAS 1.26:185159) Avail: NTIS HC A08/MF A01 CSCL 20/1

Experimental and theoretical investigations of acoustic mixing procedures designed to uniformly distribute fuel particles in a combustion tube for application in the proposed Particle Cloud Combustion Experiment (PCCE) are described. Two acoustic mixing methods are investigated: mixing in a cylindrical tube using high frequency spinning modes generated by suitably phased, or quadrature speakers, and acoustic premixing in a sphere. Quadrature mixing leads to rapid circumferential circulation of the powder around the tube. Good mixing is observed in the circulating regions. However, because axial inhomogeneities are necessarily present in the acoustic field, this circulation does not extend throughout the tube. Simultaneous operation of the quadrature-speaker set and the axial-speaker was observed to

produce considerably enhanced mixing compared to operation of the quadrature-speaker set alone. Mixing experiments using both types of speakers were free of the longitudinal powder drift observed using axial-speakers alone. Vigorous powder mixing was obtained in the sphere for many normal modes; however, in no case was the powder observed to fill the sphere entirely. Theoretical analysis indicated that mixing under steady conditions cannot fill more than a hemisphere except under very unusual conditions. Premixing in a hemisphere may be satisfactory; otherwise, complete mixing in microgravity might be possible by operating the speaker in short bursts. A general conclusion is that acoustic transients are more likely to produce good mixing than steady state conditions. The reason is that in steady conditions, flow structures like nodal planes are possible and often even unavoidable. These tend to separate the mixing region into cells across which powder cannot be transferred. In contrast, transients not only are free of such structures, they also have the characteristics, desirable for mixing, of randomness and disorder. This conclusion is corroborated by mixing experiments using axial waves. Author

N90-21602*# General Electric Co., Schenectady, NY.
THE RADIATION OF SOUND FROM A PROPELLER AT ANGLE OF ATTACK Final Report

RAMANI MANI Washington, DC NASA Jan. 1990 53 p
 (Contract NAS3-23721)
 (NASA-CR-4264; E-5139; NAS 1.26:4264) Avail: NTIS HC A04/MF A01 CSCL 20/1

The mechanism by which the noise generated at the blade passing frequency by a propeller is altered when the propeller axis is at an angle of attack to the freestream is examined. The measured noise field is distinctly non axially symmetric under such conditions with far field sound pressure levels both diminished and increased relative to the axially symmetric values produced with the propeller at zero angle of attack. Attempts have been made to explain this non axially symmetric sound field based on the unsteady (once per rev) loading experienced by the propeller blades when the propeller axis is at non zero angle of attack. A calculation based on this notion appears to greatly underestimate the measured azimuthal asymmetry of noise for high tip speed, highly loaded propellers. A new mechanism is proposed; namely, that at angle of attack, there is a non axially symmetric modulation of the radiative efficiency of the steady loading and thickness noise which is the primary cause of the non axially symmetric sound field at angle of attack for high tip speed, heavily loaded propellers with a large number of blades. A calculation of this effect to first order in the crossflow Mach number (component of freestream Mach number normal to the propeller axis) is carried out and shows much better agreement with measured noise data on the angle of attack effect. Author

N90-26633*# General Electric Co., Cincinnati, OH. Advanced Technology Operations.
HIGH SPEED TURBOPROP AEROACOUSTIC STUDY (COUNTERROTATION). VOLUME 1: MODEL DEVELOPMENT Final Report
 C. E. WHITFIELD, R. MANI, and P. R. GLIEBE Jul. 1990 121 p
 (Contract NAS3-23721)
 (NASA-CR-185241; NAS 1.26:185241) Avail: NTIS HC A06/MF A01 CSCL 20/1

The isolated counterrotating high speed turboprop noise prediction program was compared with model data taken in the GE Aircraft Engines Cell 41 anechoic facility, the Boeing Transonic Wind Tunnel, and in NASA-Lewis' 8x6 and 9x15 wind tunnels. The predictions show good agreement with measured data under both low and high speed simulated flight conditions. The installation effect model developed for single rotation, high speed turboprops was extended to include counterrotation. The additional effect of mounting a pylon upstream of the forward rotor was included in the flow field modeling. A nontraditional mechanism concerning the acoustic radiation from a propeller at angle of attack was investigated. Predictions made using this approach show results that are in much closer agreement with measurement over a range

of operating conditions than those obtained via traditional fluctuating force methods. The isolated rotors and installation effects models were combined into a single prediction program, results of which were compared with data taken during the flight test of the B727/UDF engine demonstrator aircraft. Satisfactory comparisons between prediction and measured data for the demonstrator airplane, together with the identification of a nontraditional radiation mechanism for propellers at angle of attack are achieved. Author

N90-26635*# National Aeronautics and Space Administration. Lewis Research Center, Cleveland, OH.

AEROACOUSTICS OF ADVANCED PROPELLERS

JOHN F. GROENEWEG 1990 21 p Presented at the 17th Congress of the International Council of Aeronautical Sciences, Stockholm, Sweden, 9-14 Sep. 1990; sponsored by AIAA (NASA-TM-103137; E-5446; NAS 1.15:103137) Avail: NTIS HC A03/MF A01 CSCL 20/1

The aeroacoustics of advanced, high speed propellers (propfans) are reviewed from the perspective of NASA research conducted in support of the Advanced Turboprop Program. Aerodynamic and acoustic components of prediction methods for near and far field noise are summarized for both single and counterrotation propellers in uninstalled and configurations. Experimental results from tests at both takeoff/approach and cruise conditions are reviewed with emphasis on: (1) single and counterrotation model tests in the NASA Lewis 9 by 15 (low speed) and 8 by 6 (high speed) wind tunnels, and (2) full scale flight tests of a 9 ft (2.74 m) diameter single rotation wing mounted tractor and a 11.7 ft (3.57 m) diameter counterrotation aft mounted pusher propeller. Comparisons of model data projected to flight with full scale flight data show good agreement validating the scale model wind tunnel approach. Likewise, comparisons of measured and predicted noise level show excellent agreement for both single and counterrotation propellers. Progress in describing angle of attack and installation effects is also summarized. Finally, the aeroacoustic issues associated with ducted propellers (very high bypass fans) are discussed. Author

73

NUCLEAR AND HIGH-ENERGY PHYSICS

Includes elementary and nuclear particles; and reactor theory.

A90-19303*# Case Western Reserve Univ., Cleveland, OH.
PHASE TRANSITIONS IN FERMIONIC SYSTEMS WITH MANY-BODY INTERACTION

G. BOZZOLO (Case Western Reserve University, Cleveland, OH), A. PLASTINO (La Plata, Universidad Nacional, Argentina), and J. FERRANTE (NASA, Lewis Research Center, Cleveland, OH) Zeitschrift fuer Physik A - Atomic Nuclei (ISSN 0930-1151), vol. 333, 1989, p. 119-123. refs
 (Contract NCC3-71)
 Copyright

A linearized version of the Hartree-Fock method is used as a probe to investigate phase transitions in fermionic systems with many-body interactions. An application to a new exactly solvable model which includes two- and three-body forces is shown. Author

N90-16496*# National Aeronautics and Space Administration. Lewis Research Center, Cleveland, OH.

SCALING STUDY FOR SP-100 REACTOR TECHNOLOGY

A. C. MARSHALL (Sandia National Labs., Albuquerque, NM.) and B. MCKISSOCK 1989 8 p Presented at the 7th Symposium on Space Nuclear Power Systems, Albuquerque, NM, 7-11 Jan. 1990
 (Contract DE-AC04-76DP-00789)

73 NUCLEAR AND HIGH-ENERGY PHYSICS

(NASA-TM-897140; NAS 1.15:897140; DE89-014967; SAND-89-1635C; CONF-900109-4) Avail: NTIS HC A02/MF A01 CSDL 18/9

Several ways were explored of extending SP-100 reactor technology to higher power levels. One approach was to use the reference SP-100 pin design and increase the fuel pin length and the number of fuel pins as needed to provide higher capability. The impact on scaling of a modified and advanced SP-100 reactor technology was also explored. Finally, the effect of using alternative power conversion subsystems, with SP-100 reactor technology was investigated. One of the principal concerns for any space based system is mass; consequently, this study focused on estimating reactor, shield, and total system mass. The RSMAS code (Marshall 1986) was used to estimate reactor and shield mass. Simple algorithms developed at NASA-Lewis were used to estimate the balance of system mass. Power ranges from 100 kWe to 10 MWe were explored assuming both one year and seven years of operation. Thermoelectric, Stirling, Rankine, and Brayton power conversion systems were investigated. The impact on safety, reliability, and other system attributes, caused by extending the technology to higher power levels, was also investigated. DOE

N90-17424* National Aeronautics and Space Administration. Lewis Research Center, Cleveland, OH.

RESULTS OF AN ATTEMPT TO MEASURE INCREASED RATES OF THE REACTION D-2 + D-2 YIELDS HE-3 + N IN A NONELECTROCHEMICAL COLD FUSION EXPERIMENT

GUSTAVE C. FRALICK, ARTHUR J. DECKER, and JAMES W. BLUE Dec. 1989 24 p
(NASA-TM-102430; E-5198; NAS 1.15:102430) Avail: NTIS HC A03/MF A01 CSDL 20/8

An experiment was performed to look for evidence of deuterium fusion in palladium. The experiment, which involved introducing deuterium into the palladium filter of a hydrogen purifier, was designed to detect neutrons produced in the reaction $D-2 + D-2$ yields $He-3 + n$ as well as heat production. The neutron counts for deuterium did not differ significantly from background or from the counts for a hydrogen control. Heat production was detected when deuterium, but not hydrogen, was pumped from the purifier.

Author

74

OPTICS

Includes light phenomena and optical devices.

A90-11310* National Aeronautics and Space Administration. Lewis Research Center, Cleveland, OH.

ACTIVE PHASE COMPENSATION SYSTEM FOR FIBER OPTIC HOLOGRAPHY

CAROLYN R. MERCER and GLENN BEHEIM (NASA, Lewis Research Center, Cleveland, OH) IN: Current developments in optical engineering III; Proceedings of the Meeting, San Diego, CA, Aug. 15, 16, 18, 1988. Bellingham, WA, Society of Photo-Optical Instrumentation Engineers, 1989, p. 104-108. Previously announced in STAR as N88-26641.

Copyright

Fiber optic delivery systems promise to extend the application of holography to severe environments by simplifying test configurations and permitting the laser to be remotely placed in a more benign location. However, the introduction of optical fiber leads to phase stability problems. Environmental effects cause the pathlengths of the fibers to change randomly, preventing the formation of stationary interference patterns which are required for holography. An active phase control system has been designed and used with an all-fiber optical system to stabilize the phase difference between light emitted from two fibers, and to step the phase difference by 90 deg without applying any constraints on the placement of the fibers. The accuracy of the phase steps is

shown to be better than 0.02 deg., and a stable phase difference can be maintained for 30 min. This system can be applied to both conventional and electro-optic holography, as well as to any system where the maintenance of an accurate phase difference between two coherent beams is required.

Author

A90-20151* Illinois Univ., Urbana.

ON PHYSICAL OPTICS FOR CALCULATING SCATTERING FROM COATED BODIES

J. BALDAUF, S. W. LEE (Illinois, University, Urbana), H. LING (Texas, University, Austin), and R. CHOU (Ohio State University, Columbus) Journal of Electromagnetic Waves and Applications (ISSN 0920-5071), vol. 3, no. 8, 1989, p. 725-746. Research supported by MIT and University of Illinois. refs
(Contract NAG3-475)

Copyright

The familiar physical optics (PO) approximation is no longer valid when the perfectly conducting scatterer is coated with dielectric material. This paper reviews several possible PO formulations. By comparing the PO formulation with the moment method solution based on the impedance boundary condition for the case of the coated cone-sphere, a PO formulation using both electric and magnetic currents consistently gives the best numerical results. Comparisons of the exact moment method with the PO formulations using the impedance boundary condition and the PO formulation using the Fresnel reflection coefficient for the case of scattering from the cone-ellipsoid demonstrate that the Fresnel reflection coefficient gives the best numerical results in general.

Author

A90-41247* Drexel Univ., Philadelphia, PA.

HIGH-SPEED DIGITAL FIBER OPTIC LINKS FOR SATELLITE TRAFFIC

A. S. DARYOUSH, E. ACKERMAN, R. SAEDI, R. R. KUNATH (Drexel University, Philadelphia, PA), and K. SHALKHAUSER (NASA, Lewis Research Center, Cleveland, OH) IN: Optical technology for microwave applications IV; Proceedings of the Meeting, Orlando, FL, Mar. 28, 29, 1989. Bellingham, WA, Society of Photo-Optical Instrumentation Engineers, 1989, p. 142-150. refs

Copyright

Large aperture phased array antennas operating at millimeter wave frequencies are designed for space-based communications and imaging platforms. Array elements are comprised of active T/R modules which are linked to the central processing unit through high-speed fiber-optic networks. The system architecture satisfying system requirements at millimeter wave frequency is T/R level data mixing where data and frequency reference signals are distributed independently before mixing at the T/R modules. This paper demonstrates design procedures of a low loss high-speed fiber-optic link used for transmission of data signals over 600-900 MHz bandwidth inside satellite. The fiber-optic link is characterized for transmission of analog and digital data. A dynamic range of 79 dB/MHz was measured for analog data over the bandwidth. On the other hand, for burst SMSK satellite traffic at 220 Mbps rates, BER of 2×10^{-7} was measured for $E(b)/N(o)$ of 14.3 dB.

Author

A90-42754* Rockwell International Corp., Canoga Park, CA.

DETERMINATION OF THE DURABILITY OF THE FIBEROPTICS IN ROCKET ENGINE ENVIRONMENTS

R. DELCHER, D. DINNSEN, S. BARKHOUDARIAN, and I. CANNON (Rockwell International Corp., Rocketdyne Div., Canoga Park, CA) AIAA, SAE, ASME, and ASEE, Joint Propulsion Conference, 26th, Orlando, FL, July 16-18, 1990. 4 p.
(Contract NAS3-25346)

(AIAA PAPER 90-2229) Copyright

The results of a testing program in which selected optical fibers were exposed to extreme environments representative of those experienced on rocket engines are discussed. Included in the experiment are cold-bend testing, a moisture embrittlement test, a thermal cycling test, temperature extremes testing, vibration testing,

and shock testing. Two of the fibers selected, the titanium-carbide-coated and the aluminum-jacketed silica samples succeeded in passing all the tests without a failure. V.T.

A90-45947* National Aeronautics and Space Administration. Lewis Research Center, Cleveland, OH.

INTERFACE PROPERTIES OF VARIOUS PASSIVATIONS OF HGCDE

S. E. SCHACHAM (NASA, Lewis Research Center, Cleveland, OH; Technion - Israel Institute of Technology, Haifa) and E. FINKMAN (Technion - Israel Institute of Technology, Haifa) Optical Engineering (ISSN 0091-3286), vol. 29, July 1990, p. 795-799. refs

Copyright

The effects of different surface treatments of the p-type Hg(x-1)Cd(x)Te (x about 0.2) alloy, including anodic-sulfide, anodic-oxide, and ZnS coatings, on the surface charge density and surface mobility were investigated. Measurements of surface recombination velocities in samples passivated by either a ZnS coating on a freshly etched surface or by anodic native sulfide combined with deposited ZnS showed essentially the same temperature dependence down to 50 K. For the same original material, both the surface state density and the activation energy were found to be similar. It is suggested that, for both passivations, the surface is controlled by traps that can be related to lattice defects, such as vacancies. I.S.

N90-15733*# National Aeronautics and Space Administration. Lewis Research Center, Cleveland, OH.

FIBER OPTIC SENSING SYSTEM Patent Application

GRIGORY ADAMOVSKY, inventor (to NASA) 7 Sep. 1989 14 p

(NASA-CASE-LEW-14795-1; NAS 1.71:LEW-14795-1; US-PATENT-APPL-SN-404291) Avail: NTIS HC A03/MF A01 CSCL 20/6

A fiber optic interferometer utilizes a low coherence light emitting diode (LED) laser as a light source which is filtered and driven at two RF frequencies, high and low, that are specific to the initial length of the resonator chamber. A displacement of a reflecting mirror changes the length traveled by the nonreferencing signal. The low frequency light undergoes destructive interference which reduces the average intensity of the wave while the high frequency light undergoes constructive interference which increases the average intensity of the wave. The ratio of these two intensity measurements is proportional to the displacement incurred.

NASA

N90-17087*# Maryland Univ., College Park. Inst. for Physical Science and Technology.

CRITICAL FLUID LIGHT SCATTERING

ROBERT W. GAMMON /n NASA, Lewis Research Center, NASA Laser Light Scattering Advanced Technology Development Workshop, 1988 p 25-44 Aug. 1989 Previously announced in IAA as A88-33009 (Contract NAG3-727)

Avail: NTIS HC A14/MF A02 CSCL 20/1

Thermal fluctuations give rise to a host of thermodynamic anomalies near critical points. The background for these phenomena is presented, and an experimental design on STS flight experiment called Zeno is described. The objective is to measure the decay rates of critical density fluctuations in a simple fluid (xenon) very near its liquid-vapor critical point using laser light scattering and photon correlation spectroscopy. Such experiments have been limited on Earth by the presence of gravity, which causes large density gradients in the sample. Fluctuation decay rates in xenon will be measured at least 100 times closer to the critical point than is possible on Earth. This will require taking data as close as 145 micro K to the critical temperature, after locating it to + or - 10 micro K. The minimum mission time of 100 hours will allow a complete range of temperature points to be covered, limited by the thermal response of the sample. An essential part of the apparatus is the thermostat. Its design principles and key features are given together with some observed

performance characteristics of a prototype: + or - 20 micro K stability for 18 hours, and one minute programmed step response for steps less than 10 mK. Author

75

PLASMA PHYSICS

Includes magnetohydrodynamics and plasma fusion.

A90-10725* Systems Science and Software, La Jolla, CA. **A VAN DER WAALS-LIKE THEORY OF PLASMA DOUBLE LAYERS**

IRA KATZ and V. A. DAVIS (Systems Science and Software, La Jolla, CA) Physics of Fluids B (ISSN 0899-8221), vol. 1, Oct. 1989, p. 2121-2125. refs (Contract NAS3-23881) Copyright

A theory describing plasma double layers in terms of multiple roots of the charge density expression is presented. The theory presented uses the fact that equilibrium plasmas shield small potential perturbations linearly; for high potentials, the shielding decreases. The approach is analogous to Van der Waals' theory of simple fluids in which inclusion of approximate expressions for both excluded volume and long range attractive forces sufficiently describes the first-order liquid-gas phase transition. K.K.

A90-22254*# Systems Science and Software, La Jolla, CA. **HIGH-VOLTAGE PLASMA INTERACTIONS CALCULATIONS USING NASCAP/LEO**

M. J. MANDELL and I. KATZ (Systems Science and Software, La Jolla, CA) AIAA, Aerospace Sciences Meeting, 28th, Reno, NV, Jan. 8-11, 1990. 16 p. refs (Contract NAS3-23881) (AIAA PAPER 90-0725) Copyright

This paper reviews four previous simulations (two laboratory and two space-flight) of interactions of a high-voltage spacecraft with a plasma under low-earth orbit conditions, performed using a three-dimensional computer code NASCAP/LEO. Results show that NASCAP/LEO can perform meaningful simulations of high-voltage plasma interactions taking into account three-dimensional effects of geometry, spacecraft motion, and magnetic field. Two new calculations are presented: (1) for current collection by 1-mm pinholes in wires (showing that a pinhole in a wire can collect far more current than a similar pinhole in a flat plate); and (2) current collection by Charge-2 mother vehicle launched in December 1985. It is shown that the Charge-2 calculations predicted successfully ion collection at negative bias, the floating potential of a probe outside or inside the sheath under negative bias conditions, and magnetically limited electron collection under electron beam operation at high altitude. I.S.

A90-22255*# Systems Science and Software, La Jolla, CA. **PLASMA CONTACTOR MODELING WITH NASCAP/LEO - EXTENDING LABORATORY RESULTS TO SPACE SYSTEMS**

V. A. DAVIS, I. KATZ, and M. J. MANDELL (Systems Science and Software, La Jolla, CA) AIAA, Aerospace Sciences Meeting, 28th, Reno, NV, Jan. 8-11, 1990. 6 p. refs (Contract NAS3-23881) (AIAA PAPER 90-0726) Copyright

In the laboratory, hollow cathode-based plasma contactors have been observed to both emit and collect ampere-level electron currents with low impedance. The laboratory behavior of hollow cathode-based plasma contactors and the limited space experience with hollow cathodes suggest that, for many applications, a hollow cathode-based plasma contactor is the ideal device to provide electrical connection with the space plasma. In order to confidently extend the laboratory experience to the low-earth-orbit environment, a series of plasma contactor computer models has been developed. Calculations show that a hollow cathode plasma contactor that

75 PLASMA PHYSICS

collects 0.5 A in the laboratory will only collect 2.4 mA in space. The simplest way to boost the collected current is to increase the gas flow. A mole of gas is enough to collect ampere level currents for 5-1/2 hours. Author

A90-24933* Maxwell Labs., Inc., San Diego, CA.
COMPUTER MODELING OF CURRENT COLLECTION BY THE CHARGE-2 MOTHER PAYLOAD

M. J. MANDELL, J. R. LILLEY, JR., I. KATZ (Maxwell Laboratories, Inc., S-Cubed Div., San Diego, CA), T. NEUBERT (Stanford University, CA), and NEIL B. MYERS (Utah State University, Logan) Geophysical Research Letters (ISSN 0094-8276), vol. 17, Feb. 1990, p. 135-138. refs
(Contract NAS3-23881; F19628-86-C-0056)
Copyright

The three-dimensional computer codes NASCAP/LEO and POLAR have been used to calculate current collection by the mother payload of the CHARGE-2 rocket under conditions of positive and negative potential up to several hundred volts. For negative bias (ion collection), the calculations lie about 25 percent above the data, indicating that the ions were less dense, colder, or heavier than the input parameters. For positive bias (electron collection), NASCAP/LEO and POLAR calculations show similar agreement with the measurements at the highest altitudes. This agreement indicates that the current is classically magnetically limited, even during electron beam emission. However, the calculated values fall well below the data at lower altitudes. It is suggested that beam-plasma-neutral interactions are responsible for the high values of collected current at altitudes below 240 km. Author

A90-26665* National Aeronautics and Space Administration. Lewis Research Center, Cleveland, OH.

NATURE OF CONVECTION-STABILIZED DC ARCS IN DUAL-FLOW NOZZLE GEOMETRY. I - THE COLD FLOW FIELD AND DC ARC CHARACTERISTICS. II - OPTICAL DIAGNOSTICS AND THEORY

ILTER SERBETCI (NASA, Lewis Research Center, Cleveland, OH) and H. T. NAGAMATSU (Rensselaer Polytechnic Institute, Troy, NY) IEEE Transactions on Plasma Science (ISSN 0093-3813), vol. 18, Feb. 1990, p. 91-114. Research supported by the Electric Power Research Institute. refs
Copyright

Steady-state low-current air arcs in a dual-flow nozzle system are studied experimentally. The cold flow field with no arc is investigated using a 12.7-mm diameter dual-flow nozzle in a steady-flow facility. Mach number and mass flux distributions are determined for various nozzle-pressure ratios and nozzle-gap spacing. It is found that the shock waves in the converging-diverging nozzles result in a decrease in overall resistance by about 15 percent. Also, Schlieren and differential interferometry techniques are used to visualize the density gradients within the arc plasma and thermal mantle. Both optical techniques reveal a laminar arc structure for a reservoir pressure of 1 atm at various current levels. Experimentally determined axial static pressure and cold-flow mass flux rate distributions and a channel-flow model with constant arc temperature are used to solve the energy integral for the arc radius as a function of axial distance. The arc electric field strength, voltage, resistance, and power are determined with Ohm's law and the total heat transfer is related to arc power. R.B.

A90-42602* Military Academy, West Point, NY.
DIAGNOSTIC EVALUATIONS OF MICROWAVE GENERATED HELIUM AND NITROGEN PLASMA MIXTURES

SCOTT S. HARABURDA (U.S. Military Academy, West Point, NY), MARTIN C. HAWLEY (Michigan State University, East Lansing), and DUANE W. DINKEL AIAA, DGLR, and JSASS, International Electric Propulsion Conference, 21st, Orlando, FL, July 18-20, 1990. 11 p. refs
(Contract NSG-3299)
(AIAA PAPER 90-2634)

The goal of this work is to continue the development to fundamentally understand the plasma processes as applied to

spacecraft propulsion. The diagnostic experiments used are calorimetric, dimensional, and spectroscopic measurements using the TM 011 and TM 012 modes in the resonance cavity. These experimental techniques are highly important in furthering the understanding of plasma phenomena and of designing rocket thrusters. Several experimental results are included using nitrogen and helium gas mixtures. Author

N90-10718*# National Aeronautics and Space Administration. Lewis Research Center, Cleveland, OH.

PLASMA GUN WITH COAXIAL POWDER FEED AND ADJUSTABLE CATHODE Patent Application

ISIDOR ZAPLATYNSKY, inventor (to NASA) 7 Jul. 1989 12 p (NASA-CASE-LEW-14901-1; NAS 1.71:LEW-14901-1; US-PATENT-APPL-SN-376488) Avail: NTIS HC A03/MF A01 CSCL 20/9

An improved plasma gun coaxially injects particles of ceramic materials having high melting temperatures into the central portion of a plasma jet. This results in a more uniform and higher temperature and velocity distribution of the sprayed particles. The position of the cathode is adjustable to facilitate optimization of the performance of the gun wherein grains of the ceramic material are melted at lower power input levels. NASA

N90-22389*# Colorado State Univ., Fort Collins. Dept. of Mechanical Engineering.

PLASMA CONTACTOR RESEARCH, 1989 Annual Report, 1 Jan. 1989 - 1 Jan. 1990

JOHN D. WILLIAMS Feb. 1990 67 p
(Contract NAG3-776)

(NASA-CR-185212; NAS 1.26:185212) Avail: NTIS HC A04/MF A01 CSCL 20/9

The characteristics of double layers observed by researchers investigating magnetospheric phenomena are contrasted to those observed in plasma contacting experiments. Experiments in the electron collection mode of the plasma contacting process were performed and the results confirm a simple model of this process for current levels ranging to 3 A. Experimental results were also obtained in a study of the process of electron emission from a hollow cathode plasma contactor. High energy ions are observed coming from the cathode in addition to the electrons and a phenomenological model that suggests a mechanism by which this could occur is presented. Experimental results showing the effects of the design parameters of the ambient plasma simulator on the plasma potential, electron temperature, electron density and plasma noise levels induced in plasma contacting experiments are presented. A preferred simulator design is selected on the basis of these results. Author

N90-25545*# National Aeronautics and Space Administration. Lewis Research Center, Cleveland, OH.

PLASMA INTERACTIONS AND EFFECTS FOR LARGE SYSTEMS

DAVID B. SNYDER /in NASA, Lyndon B. Johnson Space Center, Third Annual Workshop on Space Operations Automation and Robotics (SOAR 1989) p 393-404 Mar. 1990
Avail: NTIS HC A99/MF A04 CSCL 20/9

Information on plasma-spacecraft interactions and the effects on spacecraft systems and materials is given in viewgraph form. Information is given on plasma characteristics, ionospheric charge density, spacecraft floating potential, floating potentials of self-biased solar arrays, and geosynchronous earth orbit issues. Author

SOLID-STATE PHYSICS

Includes superconductivity.

A90-11491* National Aeronautics and Space Administration. Lewis Research Center, Cleveland, OH.

GLASS-DERIVED SUPERCONDUCTING CERAMICS WITH ZERO RESISTANCE AT 107 K IN THE $\text{Bi(1.5)Pb(0.5)Sr}_2\text{Ca}_2\text{Cu}_3\text{O}(x)$ SYSTEM

NAROTTAM P. BANSAL and D. E. FARRELL (NASA, Lewis Research Center, Cleveland, OH) Applied Physics Letters (ISSN 0003-6951), vol. 55, Oct. 9, 1989, p. 1572-1574. refs
Copyright

A melt of composition $\text{Bi(1.5)Pb(0.5)Sr}_2\text{Ca}_2\text{Cu}_3\text{O}(x)$ was fast quenched to form a glass. This was subsequently air annealed and the influence of annealing time and temperature on the formation of various crystalline phases was investigated. X-ray powder diffraction indicate that none of the resulting samples were single phase. However, for an annealing temperature of 840 C, the volume fraction of the high T_c phase (isostructural with $\text{Bi}_2\text{Sr}_2\text{Ca}_2\text{Cu}_3\text{O}_{10}$) increased with annealing time. A specimen annealed at this temperature for 243 h followed by slow cooling showed a sharp transition and $T_c (R = 0) = 107.2 \text{ K}$. Author

A90-12808* Michigan Univ., Ann Arbor.

MOLECULAR BEAM EPITAXIAL GROWTH OF HIGH-QUALITY InSb ON InP AND GaAs SUBSTRATES

J. E. OH, P. K. BHATTACHARYA, Y. C. CHEN, and S. TSUKAMOTO (Michigan, University, Ann Arbor) Journal of Applied Physics (ISSN 0021-8979), vol. 66, Oct. 15, 1989, p. 3618-3621. Previously announced in STAR as N89-26739. refs
(Contract NSF ECS-88-00659; NAG3-988)
Copyright

Epitaxial layers of InSb were grown on InP and GaAs substrates by molecular beam epitaxy. The dependence of the epilayer quality on flux ratio, $J_{\text{sub Sb4}}/J_{\text{sub In}}$, was studied. Deviation from an optimum value of $J_{\text{sub Sb4}}/J_{\text{sub In}}$ (approx. 2) during growth led to deterioration in the surface morphology and the electrical and crystalline qualities of the films. Room temperature electron mobilities as high as 70,000 and 53,000 sq cm/V-s were measured in InSb layers grown on InP and GaAs substrates, respectively. Unlike the previous results, the conductivity in these films is n-type even at $T = 13 \text{ K}$, and no degradation of the electron mobility due to the high density of dislocations was observed. The measured electron mobilities (and carrier concentrations) at 77 K in InSb layers grown on InP and GaAs substrates are 110,000 sq cm/V-s ($3 \times 10^{15} \text{ cm}^{-3}$) and 55,000 sq cm/V-s ($4.95 \times 10^{15} \text{ cm}^{-3}$), respectively, suggesting their application to electronic devices at cryogenic temperatures. Author

A90-15136* National Aeronautics and Space Administration. Lewis Research Center, Cleveland, OH.

EFFECT OF CRYSTAL ORIENTATION ON ANISOTROPIC ETCHING AND MOCVD GROWTH OF GROOVES ON GaAs

SHEILA G. BAILEY, GEOFFREY A. LANDIS, and DAVID M. WILT (NASA, Lewis Research Center, Cleveland, OH) Electrochemical Society, Journal (ISSN 0013-4651), vol. 136, Nov. 1989, p. 3444-3449. refs
Copyright

Grooves can be formed on GaAs by wet-chemical anisotropic etching of surfaces masked by photoresist stripes. The effect of crystal orientation on the shape of the grooves etched and on subsequent epitaxial growth by MOCVD is presented. The polar lattice increases the complexity of the etching and growth processes. The slow-etch planes defined by anisotropic etching are not always the same as the growth facets produced during MOCVD deposition, especially for deposition on higher order planes. Author

A90-17399* Arizona Univ., Tucson.

SOLUTE REDISTRIBUTION IN DENDRITIC SOLIDIFICATION WITH DIFFUSION IN THE SOLID

S. GANESAN and D. R. POIRIER (Arizona, University, Tucson) Journal of Crystal Growth (ISSN 0022-0248), vol. 97, no. 3-4, Oct. 1989, p. 851-859. Research supported by the Aluminum Company of America. refs
(Contract NAG3-723)
Copyright

An investigation of solute redistribution during dendritic solidification with diffusion in the solid has been performed using numerical techniques. The extent of diffusion is characterized by the instantaneous and average diffusion parameters. These parameters are functions of the diffusion Fourier number, the partition ratio and the fraction solid. Numerical results are presented as an approximate model, which is used to predict the average diffusion parameter and calculate the composition of the interdendritic liquid during solidification. Author

A90-19284* Rensselaer Polytechnic Inst., Troy, NY.

EFFECTS OF CRYSTAL-MELT INTERFACIAL ENERGY ANISOTROPY ON DENDRITIC MORPHOLOGY AND GROWTH KINETICS

M. E. GLICKSMAN (Rensselaer Polytechnic Institute, Troy, NY) and N. B. SINGH (Westinghouse Research and Development Center, Pittsburgh, PA) Journal of Crystal Growth (ISSN 0022-0248), vol. 98, no. 3, Nov. 1989, p. 277-284. refs
(Contract NAS3-25368)
Copyright

Morphological and kinetic studies of succinonitrile, a BCC crystal with a low (0.5 percent) anisotropy and pivalic acid, and FCC crystal with relatively large (5 percent) anisotropy in solid-liquid interfacial energy, show clearly that anisotropy in the solid-liquid interfacial energy does not affect the tip radius-velocity relationship, but has a profound influence on the tip region and the rate of amplification of branching waves. Anisotropy of the solid-liquid interfacial energy may be one of the key factors by which the microstructural characteristics of cast structures reflect individual material behavior, especially crystal symmetry. Author

A90-19285* Westinghouse Research and Development Center, Pittsburgh, PA.

FREE DENDRITIC GROWTH IN VISCOUS MELTS - CYCLOHEXANOL

N. B. SINGH (Westinghouse Research and Development Center, Pittsburgh, PA) and M. E. GLICKSMAN (Rensselaer Polytechnic Institute, Troy, NY) Journal of Crystal Growth (ISSN 0022-0248), vol. 98, no. 3, Nov. 1989, p. 534-540. refs
(Contract NAG3-333)
Copyright

Experiments were carried out to measure the growth speed, V , and dendritic tip radius, R , of highly purified cyclohexanol. The data show that VR -squared = constant over the entire experimentally observed supercooling range, ΔT is between 0.1 and 1 K. The stability parameter estimated from this result indicates that $\sigma(\text{asterisk}) = 0.027$, a value in good agreement with the values of $\sigma(\text{asterisk})$ found for the cubic plastic crystals succinonitrile pivalic acid. Cyclohexanol differs from other carefully measured plastic crystals in that the viscosity of its melt at the melting point is about 20 times higher, so gravity-induced convection remains weak even at small supercoolings. Author

A90-19300* National Aeronautics and Space Administration. Lewis Research Center, Cleveland, OH.

SYNTHESIS AND CHARACTERIZATION OF HIGH- T_c SUPERCONDUCTORS IN THE TL-Ca-Ba-Cu-O SYSTEM

NAROTTAM P. BANSAL (NASA, Lewis Research Center, Cleveland, OH) and D. E. FARRELL (Case Western Reserve University, Cleveland, OH) International Journal of Modern Physics B (ISSN 0217-9792), vol. 3, May 1989, p. 733-741. refs
Copyright

Both $\text{Ti}_2\text{Ca}_2\text{Ba}_2\text{Cu}_3\text{O}_{10}$ and $\text{TiCa}_3\text{BaCu}_3\text{O}_{8.5}$ are investigated for superconductivity as a function of the sintering temperature.

time, atmosphere, and quench rate in an effort to synthesize the high- T_c superconducting phase in the thallium system. The samples are characterized by electrical resistivity measurements, X-ray diffraction, and scanning electron microscopy. Samples of starting composition $Tl_2Ca_2Ba_2Cu_3O_{10}$ fired in air at 860-900 C and rapidly quenched show a T_c of 96-107 K. In contrast, specimens of starting composition $TlCa_3BaCu_3O_{8.5}$ when baked at 900 C and slowly cooled in oxygen superconduct at 116 K and above and consist of $Tl_2Ca_2Ba_2Cu_3O_{(10+x)}$ as the dominant phase. The results also show that, in contrast to the case of $YBa_2Cu_3O_{(7-x)}$, doping with a small concentration of fluorine sharpens the resistive transition and produces a large T_c increase in thallium-based superconductors. S.A.V.

A90-19793* GTE Labs., Inc., Waltham, MA.

INTERFACE DEMARCATION IN GAAS BY CURRENT PULSING

D. H. MATTHIESSEN, J. A. KAFALAS, G. A. DUCHENE, and A. H. BELLOWS (GTE Laboratories, Inc., Waltham, MA) AIAA, Aerospace Sciences Meeting, 28th, Reno, NV, Jan. 8-11, 1990. 7 p. Research supported by USAF. refs (Contract NAS3-24644) (AIAA PAPER 90-0319) Copyright

GTE Laboratories is currently conducting a program to investigate the effect of convection in the melt on the properties of bulk grown gallium arsenide (GaAs). In addition to extensive ground based experimentation, a Get Away Special growth system has been developed to grow two GaAs crystals aboard the Space Shuttle, each with a one inch diameter. In order to perform a complete segregation analysis of the crystals grown in space, it is necessary to measure the interface shape and growth rate as well as the spatial distribution of the selenium dopant. The techniques for interface demarcation in selenium doped GaAs by current pulsing have been developed at GTE Laboratories and successful interface demarcation has been achieved for current pulses ranging from 20 to 90 amps, in both single crystal and polycrystalline regions. Author

A90-21348* Notre Dame Univ., IN.

HIGH FREQUENCY CAPACITANCE-VOLTAGE CHARACTERISTICS OF THERMALLY GROWN SiO_2 FILMS ON BETA-SiC

S. M. TANG, W. B. BERRY (Notre Dame, University, IN), R. KWOR (Colorado, University, Colorado Springs), M. V. ZELLER, and L. G. MATUS (NASA, Lewis Research Center, Cleveland, OH) Electrochemical Society, Journal (ISSN 0013-4651), vol. 137, Jan. 1990, p. 221-225. refs (Contract NAG3-428) Copyright

Silicon dioxide films grown under dry and wet oxidation environment on beta-SiC films have been studied. The beta-SiC films had been heteroepitaxially grown on both on-axis and 2-deg off-axis (001) Si substrates. Capacitance-voltage and conductance-voltage characteristics of metal-oxide-semiconductor structures were measured in a frequency range of 10 kHz to 1 MHz. From these measurements, the interface trap density and the effective fixed oxide charge density were observed to be generally lower for off-axis samples. Author

A90-21920* National Aeronautics and Space Administration. Lewis Research Center, Cleveland, OH.

ON THE STABILITY OF THE CREEP SUBSTRUCTURE IN NaCl SINGLE CRYSTALS

S. V. RAJ, J. D. WHITTENBERGER (NASA, Lewis Research Center, Cleveland, OH), and G. M. PHARR (Rice University, Houston, TX) (International Conference on Low-Energy Dislocation Structures, 2nd, Charlottesville, VA, Aug. 13-17, 1989) Materials Science and Engineering, Part A: Structural Materials: Properties, Microstructure and Processing (ISSN 0921-5093), vol. A113, 1989, p. 161-175. Research supported by IBM Corp. refs Copyright

Microstructural observations were conducted on NaCl single crystals after creep. The microstructure after a stress increase followed by a stress decrease consisted primarily of cells; no

significant number of subgrains were observed although they were present in the microstructures produced during uninterrupted tests. Prestraining in the exponential creep regime produced an uniform distribution of dislocations and a few subboundaries which transformed to equiaxed subgrains when tested in the power law creep region. This substructure was similar to that observed in an as-received specimen deformed to an equivalent strain. Prior creep in the power law creep region produced equiaxed subgrains whose boundaries were found to be mechanically stable when the specimen was retested in the exponential creep region. The role of subboundary migration in the formation of new subgrains is discussed. Author

A90-21926* National Aeronautics and Space Administration. Lewis Research Center, Cleveland, OH.

SYNTHESIS AND CHARACTERIZATION OF HIGH-T(C) SCREEN-PRINTED Y-Ba-Cu-O FILMS ON ALUMINA

NAROTTAM P. BANSAL, RAINEE N. SIMONS (NASA, Lewis Research Center, Cleveland, OH), and D. E. FARRELL (Case Western Reserve University, Cleveland, OH) IN: Ceramic superconductors II - Research update, 1988; Proceedings of the Second Annual Ceramic Superconductor Symposium, Cincinnati, OH, May 3-5, 1988. Columbus, OH, American Ceramic Society, Inc., 1988, p. 474-482. Previously announced in STAR as N88-22805. refs Copyright

Thick films of $YBa_2Cu_3O_{(sub\ 7-x)}$ have been deposited on highly polished alumina substrates by the screen printing technique. To optimize the post-printing heat treatment, the films were baked at various temperatures for different lengths of time and oxygen-annealed at a lower temperature. The resulting films were characterized by electrical resistivity measurements, X-ray diffraction, and optical and scanning electron microscopy. Properties of the films were found to be highly sensitive to the post-printing thermal treatment. Films baked for 15 min at 1000 C in oxygen were hard, adherent, near single phase, and superconducting with $T_{(sub\ c)}$ (onset) approx 96 K, $T_{(sub\ c)}$ (zero) approx 66 K and $\Delta T_{sub\ c}$ (10 to 90 percent) approx 10 K. Author

A90-24448* California Univ., La Jolla.

THIN FILMS OF THE $Bi_2Sr_2Ca_2Cu_3O_{(x)}$ SUPERCONDUCTOR

YU MEI, H. L. LUO, and ROGER HU (California, University, La Jolla) Applied Physics Letters (ISSN 0003-6951), vol. 56, Feb. 5, 1990, p. 581-583. Research supported by the California MICRO Program and Hughes Aircraft Co. refs (Contract NAG3-1015) Copyright

Using RF sputtering technique, thin films of near single phase $Bi_2Sr_2Ca_2Cu_3O_{(x)}$ were successfully prepared on $SrTiO_3(100)$, $MgO(100)$, and $LaAlO_3(012)$ substrates. Zero resistance of these films occurred in the range of 90-105 K. Author

A90-25084* National Aeronautics and Space Administration. Lewis Research Center, Cleveland, OH.

THE KINETICS OF THE Au-INP INTERACTION

NAVID S. FATEMI (NASA, Lewis Research Center; Sverdrup Technology, Inc., Cleveland, OH) and VICTOR G. WEIZER (NASA, Lewis Research Center, Cleveland, OH) Journal of Applied Physics (ISSN 0021-8979), vol. 67, Feb. 15, 1990, p. 1934-1939. refs (Contract NAS3-25266) Copyright

An analysis of the reaction of Au and Au-In alloys with InP has permitted the identification of the mechanisms occurring during the first two stages of the Au-InP interaction. The first stage of the interaction, during which the Au is converted to a saturated Au (In) solution, is controlled by the vacancy-generation rate at the free surface of the metallization. The activation energy for this process is the activation energy for Au self-diffusion. Evidence is presented for the existence of large localized variations in this value due to surface related effects. At the completion of stage I stage II becomes active and continues until the metallization is converted to Au_3In . This process, proceeding via an interstitial

interchange mechanism, is many orders of magnitude slower than stage I. The rate-limiting step, with an activation energy of 2.8 eV, is shown to be the diffusion of In from the InP-metal interface. The P atoms that are released when In enters the metallization during stage I leave the system without reacting, whereas in stage II they form a compound (Au₂P₃) at the InP-metal interface. The presence of the Au₂P₃ severely retards the stage II interaction rate. Author

A90-29596* National Aeronautics and Space Administration. Lewis Research Center, Cleveland, OH.

GROWTH OF IMPROVED QUALITY 3C-SiC FILMS ON 6H-SiC SUBSTRATES

J. A. POWELL, L. G. MATUS (NASA, Lewis Research Center, Cleveland, OH), W. J. CHOYKE, J. L. BRADSHAW (Pittsburgh, University, PA), D. J. LARKIN et al. Applied Physics Letters (ISSN 0003-6951), vol. 56, April 2, 1990, p. 1353-1355. refs Copyright

Previously reported chemical vapor deposition of 3C-SiC on 6H-SiC has resulted in films with a high density of double positioning boundaries (DPBs). It is found that growth on as-grown faces of 6H-SiC crystals can yield films that are largely free of DPBs. The (111) 3C-SiC films, up to 12 microns thick, were evaluated by optical and electron microscopy and low-temperature photoluminescence (LTPL). The LTPL spectra of the films were similar to those of high quality Lely-grown 3C-SiC. Author

A90-29739* National Aeronautics and Space Administration. Lewis Research Center, Cleveland, OH.

EXPERIMENTAL EVIDENCE OF A DIMENSIONAL CROSSOVER IN Y1Ba2Cu3O(7-DELTA)

D. E. FARRELL (NASA, Lewis Research Center, Cleveland, OH), J. P. RICE, D. M. GINSBERG (Illinois, University, Urbana), and J. Z. LIU (Argonne National Laboratory, IL) Physical Review Letters (ISSN 0031-9007), vol. 64, March 26, 1990, p. 1573-1576. refs (Contract NAG3-814; NSF DMR-87-14555; W-31-109-ENG-38) Copyright

High-resolution torque-magnetometry data have been obtained on an untwinned single crystal of Y1Ba2Cu3O(7-delta) in the temperature range 63-88 K ($T_c = 90.5$ K). At $T = 80$ K and above, the data are fitted extremely well with the accepted three-dimensional phenomenological theory, but below this temperature an anomalous torque develops when the magnetic field lies close to the Cu-O planes. The qualitative and quantitative features of these results provide strong evidence that breakdown of the three-dimensional description below 80 K is associated with a crossover to two-dimensional superconducting behavior. Author

A90-29952* National Aeronautics and Space Administration. Lewis Research Center, Cleveland, OH.

GROWTH OF HIGH QUALITY 6H-SiC EPITAXIAL FILMS ON VICINAL (0001) 6H-SiC WAFERS

J. A. POWELL, D. J. LARKIN, L. G. MATUS (NASA, Lewis Research Center, Cleveland, OH), W. J. CHOYKE, J. L. BRADSHAW (Pittsburgh, University, PA) et al. Applied Physics Letters (ISSN 0003-6951), vol. 56, April 9, 1990, p. 1442-1444. refs Copyright

Previously reported growth of SiC films on SiC by chemical vapor deposition (CVD) used alpha-SiC crystal substrates. The CVD growth and evaluation of high quality 6H-SiC films on 6H-SiC wafers cut from large boules grown by the modified-sublimation process is reported. The single-crystal 6H-SiC films were grown on wafers oriented 3 to 4 deg off the (0001) plane toward the 11-20 direction. The films, up to 12 microns thick, had surfaces that were smooth and featureless. The high quality of the films was demonstrated by optical and electron microscopy, and low-temperature photoluminescence. Author

A90-33224* National Aeronautics and Space Administration. Lewis Research Center, Cleveland, OH.

PROPERTIES OF PB(1-X)BI(X)/BA2YCU3O(X) COMPOSITES - REACTION OF BA2YCU3O(X) WITH PB AND BI

A. F. HEPP, S. L. OLSON, J. R. GAIER (NASA, Lewis Research Center, Cleveland, OH), and P. D. HAMBOURGER (Cleveland State University, OH) IN: Physical chemistry of powder metals - Production and processing. Warrendale, PA, Minerals, Metals and Materials Society, 1989, p. 509-517. refs (Contract NAG3-873; NCC3-19) Copyright

This paper describes experiments conducted with a purpose of fabricating superconducting composites from Pb, Bi, and Ba₂YCu₃O(x), together the results of SEM examinations and energy dispersive spectroscopy performed on products. Results showed a limited utility of Pb and Pb(1-x)Bi(x) as matrices for ceramic superconductors. It was found that cold pressing followed by sintering at 200 C resulted in a composite which excluded flux below 90 K but did not show zero electrical resistance until the metal superconducting transition. Processing at 400 or 950 C resulted in oxygen depleted perovskite and/or metal oxides; these materials displayed greatly degraded superconducting properties. Finally, processing at 800 C resulted in high T_c only for composites containing more than 90 wt pct ceramic. I.S.

A90-33330* National Aeronautics and Space Administration. Lewis Research Center, Cleveland, OH.

CREEP SUBSTRUCTURE FORMATION IN SODIUM CHLORIDE SINGLE CRYSTALS IN THE POWER LAW AND EXPONENTIAL CREEP REGIMES

S. V. RAJ (NASA, Lewis Research Center, Cleveland, OH) and G. M. PHARR (Rice University, Houston, TX) Materials Science and Engineering, Part A - Structural Materials: Properties, Microstructure and Processing (ISSN 0921-5093), vol. A122, 1989, p. 233-242. Research supported by the IBM Corp. refs (Contract NCC3-72) Copyright

Creep tests conducted on NaCl single crystals in the temperature range from 373 to 1023 K show that true steady state creep is obtained only above 873 K when the ratio of the applied stress to the shear modulus is less than or equal to 0.0001. Under other stress and temperature conditions, corresponding to both power law and exponential creep, the creep rate decreases monotonically with increasing strain. The transition from power law to exponential creep is shown to be associated with increases in the dislocation density, the cell boundary width, and the aspect ratio of the subgrains along the primary slip planes. The relation between dislocation structure and creep behavior is also assessed. V.T.

A90-34011* Cincinnati Univ., OH.

ANTIFERROMAGNETISM IN CO-57-DOPED LA2CUO(4-Y) STUDIED BY MOESSBAUER SPECTROSCOPY

S. JHA, C. MITROS, AMER LAHAMER, SHERIF YEHIA (Cincinnati, University, OH), GLENN M. JULIAN (Miami University, Oxford, OH) et al. Hyperfine Interactions (ISSN 0304-3843), vol. 50, 1989, p. 607-612. Research supported by Miami University. refs (Contract NAG3-847) Copyright

Moessbauer effect studies of Co-57-doped La₂CuO(4-y) were performed at temperatures between 4.2 K and room temperature. These confirm the antiferromagnetic ordering of these compounds below room temperature. Temperature dependence of the quadrupole splitting shows that the hyperfine field is at an angle with the c-axis. Author

A90-34012* Cincinnati Univ., OH.

HYPERFINE MAGNETIC FIELD ON CD-111 IN HEUSLER ALLOYS CO2MNZ (Z = SI, GA, GE, SN)

S. JHA, C. MITROS, AMER LAHAMER, SHERIF YEHIA (Cincinnati, University, OH), GLENN M. JULIAN (Miami University, Oxford, OH) et al. Hyperfine Interactions (ISSN 0304-3843), vol. 51, 1989, p. 987-992. Research supported by Miami University. refs (Contract NAG3-847) Copyright

The time differential perturbed angular correlation method has been used to measure, as a function of temperature, the hyperfine

magnetic field at Cd sites in the Heusler alloys Co_2MnZ ($Z = \text{Si, Ga, Ge, Sn}$). The hyperfine fields, normalized to the total magnetic moment per formula unit, show an approximately linear trend toward more positive values with increasing lattice parameter. Author

A90-34020* Cincinnati Univ., OH.

FE-57 AND SN-119 MOESSBAUER STUDY OF $\text{La}_2\text{CuO}_{4-y}$, $\text{YBa}_2\text{Cu}_3\text{O}_{7-y}$ AND $\text{SMBa}_2\text{Cu}_3\text{O}_{7-y}$

S. JHA, C. MITROS, S. YEHIA, AMER LAHAMER (Cincinnati, University, OH), GLENN M. JULIAN (Miami University, Oxford, OH) et al. *Physica C - Superconductivity* (ISSN 0921-4534), vol. 153-155, 1988, p. 1555, 1556. refs
(Contract NAG3-847)

Copyright

Mossbauer studies reveal antiferromagnetic order in doped $\text{La}_2\text{CuO}_{4-y}$: at 77 K, $H = 476$ kOe at Fe-57 and H is less than 10 kOe at Sn-119. Split-source and conventional absorber experiments on $\text{RbBa}_2\text{Cu}_3\text{O}_{7-y}$ ($R = \text{Y, Sm}$) are consistent with occupation of 3 sites by Fe-57, the relative population depending on sample preparation and Fe concentration. Author

A90-35153* Case Western Reserve Univ., Cleveland, OH.

SUPERCONDUCTING GLASS-CERAMICS IN THE BI-SR-CA-CU-O SYSTEM

MARK R. DE GUIRE, CHEOL J. KIM (Case Western Reserve University, Cleveland, OH), and NAROTTAM P. BAUSAL (NASA, Lewis Research Center; Case Western Reserve University, Cleveland, OH) *American Ceramic Society, Journal* (ISSN 0002-7820), vol. 73, May 1990, p. 1165-1171. refs

Copyright

Differential thermal analysis, XRD, SEM, and resistivity measurements, have been used to study the recrystallization during various heat treatments of a $\text{Bi}_{1.5}\text{SrCaCu}_2\text{O}_z$ glass obtained by rapid quenching from the melt. Heating at 450 C formed the $\text{Bi}_{2-x}\text{Sr}_{2-x}\text{CuO}_z$ solid solution designated 'R'. Between 765 and 845 C, R reacts slowly with the glass to form the 80 K superconductor $\text{Bi}_2(\text{Sr,Ca})_3\text{Cu}_2\text{O}_z$, together with CuO . Heating for 7 days at the higher temperature, followed by slow cooling, raised the temperature of zero resistance to 77 K. O.C.

A90-36232 Michigan Univ., Ann Arbor.

TRANSPORT PROPERTIES OF $\text{InAs}(\text{x})\text{Sb}(1-\text{x})$ ($\text{x} = 0-0.55$) ON INP GROWN BY MOLECULAR-BEAM EPITAXY

S. TSUKAMOTO, P. BHATTACHARYA, Y. C. CHEN, and J. H. KIM (Michigan, University, Ann Arbor) *Journal of Applied Physics* (ISSN 0021-8979), vol. 67, June 1, 1990, p. 6819-6822. refs
(Contract NAG3-988; NSF ECS-88-00659)

Copyright

Molecular-beam epitaxy has been successfully used to grow $\text{InAs}(\text{x})\text{Sb}(1-\text{x})$ on InP substrates with good electrical characteristics. The samples are all n type with electron concentrations varying in the range $(3-9) \times 10$ to the 15th/cu cm. The mobilities are high (70,000 and 110,000 sq cm/V s at 300 and 77 K, respectively) in InSb and the alloys. More importantly, the mobilities remain high at the low temperatures in the alloys also, without any type conversion. The mobility data have been analyzed taking into account the appropriate scattering mechanisms. The alloy scattering potential in $\text{InAs}_{0.24}\text{Sb}_{0.76}$ is estimated to be 0.3 V. Author

A90-36799* Midwest Research Inst., Golden, CO.

INVESTIGATION OF BURIED HOMOJUNCTIONS IN P-INP FORMED DURING SPUTTER DEPOSITION OF BOTH INDIUM TIN OXIDE AND INDIUM OXIDE

T. A. GESSERT, X. LI, M. W. WANLASS, A. J. NELSON, and T. J. COUTTS (SERI, Golden, CO) *Journal of Vacuum Science and Technology A* (ISSN 0734-2101), vol. 8, pt. 1, May-June 1990, p. 1912-1916. refs
(Contract DE-AC02-83CH-10093; NASA ORDER C-3000-K)

Copyright

While dc magnetron sputter deposition of indium tin oxide leads to the formation of a buried homojunction in single crystal p-type InP, the mechanism of type conversion of the InP surface is not

apparent. In view of the recent achievement of nearly 17-percent global efficiencies for cells fabricated solely by sputter deposition of In_2O_3 , it is presently surmised that tin may not be an essential element in type conversion. A variety of electrical and optical techniques are presently used to evaluate the changes at both indium tin oxide/InP and indium oxide/InP interfaces. Such mechanisms as the passivation of acceptors by hydrogen, and sputter damage, are found to occur simultaneously. O.C.

A90-38140* National Aeronautics and Space Administration, Lewis Research Center, Cleveland, OH.

EFFECT OF GA AND P DOPANTS ON THE THERMOELECTRIC PROPERTIES OF N-TYPE SiGe

S. L. DRAPER (NASA, Lewis Research Center, Cleveland, OH), J. W. VANDERSANDE, C. WOOD (JPL, Pasadena, CA), R. MASTERS, and V. RAAG (Thermo Electron Technologies Corp., Waltham, MA) IN: *IECEC-89; Proceedings of the Twenty-fourth Intersociety Energy Conversion Engineering Conference*, Washington, DC, Aug. 6-11, 1989. Volume 2. New York, Institute of Electrical and Electronics Engineers, 1989, p. 711-714. refs

Copyright

The purpose of this study was to hot-press improved n-type $\text{Si}_{80}\text{Ge}_{20}/\text{GaP}$ samples directly (without any heat treatment) and to confirm that a Ga/P ratio less than one increases the solubility of P and, hence, improves the power factor and Z. One of the three samples ($\text{Ga/P} = 0.43$) had an improvement in Z of about 20 percent between 400 and 1000 C over that for standard SiGe. This demonstrates that improved samples can be pressed directly and that a Ga/P ratio less than one is necessary. The other two samples ($\text{Ga/P} = 0.33$ and 0.50) had Z's equal to or less than that of standard SiGe but had a lower hot-pressing temperature than the improved sample. I.E.

A90-43568* National Aeronautics and Space Administration, Lewis Research Center, Cleveland, OH.

SUPERCONDUCTING $\text{Bi}_{1.5}\text{Pb}_{0.5}\text{Sr}_2\text{Ca}_2\text{Cu}_3\text{O}(\text{x})$ CERAMICS BY RAPID MELT QUENCHING AND GLASS CRYSTALLIZATION

NAROTTAM P. BANSAL (NASA, Lewis Research Center, Cleveland, OH) *Journal of Applied Physics* (ISSN 0021-8979), vol. 68, Aug. 1, 1990, p. 1143-1150. refs

Copyright

The preparation of superconducting $\text{Bi}_{1.5}\text{Pb}_{0.5}\text{Sr}_2\text{Ca}_2\text{Cu}_3\text{O}(\text{x})$ in the glassy state is described, and the results of a study of its crystallization kinetics are presented. The annealing parameters for transforming the glass into a superconductor containing a large fraction of the high- T_c phase were determined. It was found that prolonged annealing (longer than 10 days) in air at 840 C, followed by slow cooling, results in the T_c of 107.2 K and a sharp transition of 2 K. I.S.

A90-44022* Northwestern Univ., Evanston, IL.

MEASUREMENT OF THE INTRINSIC BOND STRENGTH OF BRITTLE THIN FILMS ON FLEXIBLE SUBSTRATES

Q. GUO, L. M. KEER (Northwestern University, Evanston, IL), H. OSAKI (Sony Magnetic Products, Inc., Tagajo, Japan), and D. R. WHEELER (NASA, Lewis Research Center, Cleveland, OH) *Journal of Applied Physics* (ISSN 0021-8979), vol. 68, Aug. 15, 1990, p. 1649-1654. Research supported by USAF. refs

Copyright

The brittle cracking and subsequent debonding of nickel films deposited on polymer substrates subjected to uniaxial strain is investigated. Stress analyses for a film/substrate system are performed. Based on the analysis, the interfacial bond strength between brittle thin films and flexible substrates can be evaluated in terms of the tensile strength of the coating and the length of the largest segment that first debonds. Experiments were performed on Ni films with different thicknesses evaporated on polyethylene terephthalate substrates and the intrinsic bond strength was evaluated. The interfacial bond strengths were shown to be relatively independent of the film thickness for the range studied. Author

A90-45193* Nebraska Univ., Lincoln.

STUDY OF INDIUM TIN OXIDE FILMS EXPOSED TO ATOMIC OXYGEN

PAUL G. SNYDER, BHOLA N. DE, JOHN A. WOOLLAM (Nebraska, University, Lincoln), T. J. COUTTS, and X. LI (Solar Energy Research Institute, Golden, CO) IN: Space optical materials and space qualification of optics; Proceedings of the Meeting, Orlando, FL, Mar. 30, 31, 1989. Bellingham, WA, Society of Photo-Optical Instrumentation Engineers, 1989, p. 133-135. refs

(Contract NAG3-95)

Copyright

A qualitative simulation of the effects of atomic oxygen has been conducted on indium tin oxide (ITO) films prepared by dc sputtering onto room-temperature substrates, by exposing them to an RF-excited oxygen plasma and characterizing the resulting changes in optical, electrical, and structural properties as functions of exposure time with ellipsometry, spectrophotometry, resistivity, and X-ray measurements. While the films thus exposed exhibit reduced resistivity and optical transmission; both of these effects, as well as partial crystallization of the films, may be due to sample heating by the plasma. Film resistivity is found to stabilize after a period of exposure. O.C.

A90-45948* National Aeronautics and Space Administration. Lewis Research Center, Cleveland, OH.

CONTRIBUTION OF THE GRADED REGION OF A HGCDTE DIODE TO ITS SATURATION CURRENT

S. E. SCHACHAM (NASA, Lewis Research Center, Cleveland, OH; Technion - Israel Institute of Technology, Haifa) and E. FINKMAN (Technion - Israel Institute of Technology, Haifa) Optical Engineering (ISSN 0091-3286), vol. 29, July 1990, p. 800-803. refs

Copyright

Experimental results show that the contribution of the graded region to the current of $Hg(1-x)Cd(x)Te$ diodes is not negligible, as compared to that of the p type bulk. The theoretical analysis reveals the influence of the electric field present outside the depletion region on the current generated by the graded region. The analysis shows the importance of the lifetime profile in the graded region, which is a function of the specific recombination mechanism and its dependence on the local dopant concentration. The effect of parameters such as substrate concentration, surface concentration, and junction depth on this current is discussed.

Author

A90-48661* National Aeronautics and Space Administration. Lewis Research Center, Cleveland, OH.

CONTACT SPREADING AND THE AU₃IN-TO-AU₉IN₄ TRANSITION IN THE AU-INP SYSTEM

VICTOR G. WEIZER (NASA, Lewis Research Center, Cleveland, OH) and NAVID S. FATEMI (NASA, Lewis Research Center; Sverdrup Technology, Inc., Cleveland, OH) Journal of Applied Physics (ISSN 0021-8979), vol. 68, Sept. 1, 1990, p. 2275-2284. refs

(Contract NAS3-25266)

Copyright

An investigation is made of the third stage in the series of solid-state reactions that occur between InP and its most commonly used contact material, Au. This reaction, which results in the transformation of the contacting metallization from the pink-colored Au₃In to the silver-colored Au₉In₄, is shown to be controlled by an In-Au exchange or knockout mechanism operating at the interface between the two phases. Contact spreading, a rapid lateral expansion of the contact metallization that can consume large quantities of InP during growth, is shown to be another manifestation of this final stage in the InP-Au reaction. A detailed description of the mechanisms, including an investigation of the kinetics of the processes involved, is presented. Author

A90-48694* Case Western Reserve Univ., Cleveland, OH.

MILLIMETER-WAVE SURFACE RESISTANCE OF LASER-ABLATED YBa₂Cu₃O₇(δ) SUPERCONDUCTING FILMS

F. A. MIRANDA, W. L. GORDON (Case Western Reserve University, Cleveland, OH), K. B. BHASIN, and J. D. WARNER (NASA, Lewis Research Center, Cleveland, OH) Applied Physics Letters (ISSN 0003-6951), vol. 57, Sept. 3, 1990, p. 1058-1060. refs

Copyright

The millimeter-wave surface resistance of YBa₂Cu₃O₇(δ) superconducting films was measured in a gold-plated copper host cavity at 58.6 GHz between 25 and 300 K. High-quality laser-ablated films of 1.2-micron thickness were deposited on SrTiO₃ and LaGaO₃ substrates. Their transition temperatures were 90.0 and 88.9 K, with a surface resistance at 70 K of 82 and 116 milliohms, respectively. These values are better than the values for the gold-plated cavity at the same temperature and frequency.

Author

N90-10737*# National Aeronautics and Space Administration. Lewis Research Center, Cleveland, OH.

STUDY OF DEPOSITION OF YBa₂Cu₃O_{7-x} ON CUBIC ZIRCONIA

JOSEPH D. WARNER, JOSEPH E. MEOLA, and KIMBERLY A. JENKINS (Ohio Univ., Athens.) 1989 7 p Presented at the 3rd Annual Conference on Superconductivity and Applications, Buffalo, NY, 19-21 Sep. 1989; sponsored by New York State Inst. on Superconductivity

(NASA-TM-102350; E-5059; NAS 1.15:102350) Avail: NTIS HC A02/MF A01 CSCL 20/12

Films of YBa₂Cu₃O_{7-x} were grown on (100) cubic zirconia with 8 percent yttria by laser ablation from sintered targets of YBa₂Cu₃O_{7-x}. The temperature of the zirconia substrate during growth was varied between 700 and 780 C. The atmosphere during growth was 170 mtorr of O₂. The films were subsequently slowly cooled in-situ in 1 atm of O₂. The best films were c-axis aligned and had a transition temperature of 87.7 K. The superconducting transition temperature and the X-ray diffraction analysis is reported as a function of the substrate temperature and of the angle between the laser beam and the target's normal.

Author

N90-10738*# National Aeronautics and Space Administration. Lewis Research Center, Cleveland, OH.

OPTICAL DISPERSION RELATIONS FOR DIAMONDLIKE CARBON FILMS

SAMUEL A. ALTEROVITZ, ROBERT M. SIEG, NEIL S. SHOEMAKER (Case Western Reserve Univ., Cleveland, OH.), and JOHN J. POUCH 1989 9 p Presented at the 1989 Spring Meeting of the Materials Research Society, San Diego, CA, 24-29 Apr. 1989

(NASA-TM-102356; E-4769; NAS 1.15:102356) Avail: NTIS HC A02/MF A01 CSCL 20/12

Ellipsometric measurements on plasma deposited diamondlike amorphous carbon (a-C:H) films were taken in the visible, (E=1.75 to 3.5 eV). The films were deposited on Si and their properties were varied using high temperature (up to 750 C) anneals. The real (n) and imaginary (k) parts of the complex index of refraction N were obtained simultaneously. Following the theory of Forouhi and Bloomer, a least squares fit was used to find the dispersion relations n(E) and k(E). Reasonably good fits were obtained, showing that the theory can be used for a-C:H films. Moreover, the value of the energy gap (E_g) obtained in this way was compared to the E_g value using conventional Tauc plots and reasonably good agreement was obtained.

Author

N90-11603*# Ohio State Univ., Columbus. ElectroScience Lab. **CONSTITUTIVE PARAMETER MEASUREMENTS OF LOSSY MATERIALS**

A. DOMINEK and A. PARK Sep. 1989 45 p

(Contract NAG3-1000)

(NASA-CR-183398; NAS 1.26:183398; ESL-721837-1) Avail: NTIS HC A03/MF A01 CSCL 20/12

The electrical constitutive parameters of lossy materials are considered. A discussion of the NRL arch for lossy coatings is presented involving analytical analyses of the reflected field using the geometrical theory of diffraction (GTD) and physical optics (PO). The actual values for these parameters can be obtained

through a traditional transmission technique which is examined from an error analysis standpoint. Alternate sample geometries are suggested for this technique to reduce sample tolerance requirements for accurate parameter determination. The performance for one alternate geometry is given. Author

N90-11606*# Case Western Reserve Univ., Cleveland, OH.
SUPERCONDUCTING CERAMICS IN THE $\text{Bi}_{1.5}\text{SrCaCu}_2\text{O}_x$ SUB X SYSTEM BY MELT QUENCHING TECHNIQUE Final Report

NAROTTAM P. BANSAL and MARK R. DEGUIRE Oct. 1989
 20 p Presented at the 91st Annual Meeting of the American Ceramic Society, Indianapolis, IN, 23-27 Apr. 1989
 (Contract NCC3-133)
 (NASA-CR-185139; E-5064; NAS 1.26:185139) Avail: NTIS HC A03/MF A01 CSCL 20/12

Bi sub 1.5 SrCaCu sub 2 O sub x has been prepared in the glassy state by rapid quenching of the melt. The kinetics of crystallization of various phases in the glass have been evaluated by a variable heating rate differential scanning calorimetry method. The formation various phases on thermal treatments of the glass has been investigated by powder X-ray diffraction and electrical resistivity measurements. Heating at 450 C formed Bi sub 2 Sr sub 2 CuO sub 6, which disappeared on further heating at 765 C, where Bi sub 2 Sr sub 2 CaCu sub 2 O sub 8 formed. Prolonged heating at 845 C resulted in the formation of a small amount of a phase with T sub c onset of approx. 108 K, believed to be Bi sub 2 Sr sub 2 Ca sub 2 Cu sub 3 O sub 10. This specimen showed zero resistivity at 54 K. The glass ceramic approach could offer several advantages in the fabrication of the high-T sub c superconductors in desired practical shapes such as continuous fibers, wires, tapes, etc. Author

N90-12348*# National Aeronautics and Space Administration. Lewis Research Center, Cleveland, OH.
FORTAN PROGRAM FOR X RAY PHOTOELECTRON SPECTROSCOPY DATA REFORMATTING
 PHILLIP B. ABEL Nov. 1989 10 p
 (NASA-TP-2957; E-4867; NAS 1.60:2957) Avail: NTIS HC A02/MF A01 CSCL 20/12

A FORTAN program has been written for use on an IBM PC/XT or AT or compatible microcomputer (personal computer, PC) that converts a column of ASCII-format numbers into a binary-format file suitable for interactive analysis on a Digital Equipment Corporation (DEC) computer running the VGS-5000 Enhanced Data Processing (EDP) software package. The incompatible floating-point number representations of the two computers were compared, and a subroutine was created to correctly store floating-point numbers on the IBM PC, which can be directly read by the DEC computer. Any file transfer protocol having provision for binary data can be used to transmit the resulting file from the PC to the DEC machine. The data file header required by the EDP programs for an x ray photoelectron spectrum is also written to the file. The user is prompted for the relevant experimental parameters, which are then properly coded into the format used internally by all of the VGS-5000 series EDP packages. Author

N90-14108*# Case Western Reserve Univ., Cleveland, OH.
PREPARATION OF 110K (Bi , Pb)- Sr - Ca - Cu - O SUPERCONDUCTOR FROM GLASS PRECURSOR Final Report
 NAROTTAM P. BANSAL Oct. 1989 14 p Presented at the 1st International Ceramic Science and Technology Congress, Anaheim, CA, 31 Oct. - 3 Nov. 1989; sponsored by the American Ceramic Society
 (Contract NCC3-133)
 (NASA-CR-185162; E-5131; NAS 1.26:185162) Avail: NTIS HC A03/MF A01 CSCL 20/12

The $\text{Bi}_{1.5}\text{Pb}_{0.5}\text{Sr}_2\text{Ca}_2\text{Cu}_3\text{O}(x)$ glass, prepared by rapid quenching of the melt, showed $T(\text{sub } g)$ of 383 C, crystallization temperature of approx. 446 C, melting temperature of approx. 855 C, and bulk density of 5.69 g/cu. cm. in air. The as-quenched glass was oxygen deficient. On heating in O_2 , it showed a slow,

irreversible, and continuous weight gain starting at approx. 530 C. The influence of annealing conditions on the formation of various phases was investigated by XRD and electrical resistivity measurements. The 110K-T(sub c) phase did not form below 840 C. The amount of this phase increased with the sintering time at 840 C. A sample annealed at 840 C for 243 h in air and furnace cooled showed the highest $T(\text{sub } c)(R=0)$ of 107.2K and transition width $\Delta T(\text{sub } c)(10 \text{ to } 90 \text{ percent})$ of approx. 2 K. Author

N90-17454*# National Aeronautics and Space Administration. Lewis Research Center, Cleveland, OH.

METHOD OF FORMING LOW COST, FORMABLE HIGH T(SUBC) SUPERCONDUCTING WIRE Patent Application

JAMES L. SMIALEK, inventor (to NASA) 28 Dec. 1989 9 p
 Sponsored by NASA
 (NASA-CASE-LEW-14676-2; US-PATENT-APPL-SN-458467; NAS 1.71:LEW-14676-2) Avail: NTIS HC A02/MF A01 CSCL 20/12

A ceramic superconductivity part, such as a wire, is produced through the partial oxidation of a specially formulated copper alloy in a core. The alloys contains low level of quantities of rare earth and alkaline earth dopant elements. Upon oxidation at high temperatures, and superconducting oxide phases are formed as a thin film. NASA

N90-17465*# Case Western Reserve Univ., Cleveland, OH. Dept. of Materials Science and Engineering.
SUPERCONDUCTING $\text{Bi}_{1.5}\text{Pb}_{0.5}\text{Sr}_2\text{Ca}_2\text{Cu}_3\text{O}(x)$ CERAMICS BY RAPID MELT QUENCHING AND GLASS CRYSTALLIZATION Final Report

NAROTTAM P. BANSAL Dec. 1989 29 p Submitted for publication
 (Contract NCC3-133)
 (NASA-CR-185184; E-5216; NAS 1.26:185184) Avail: NTIS HC A03/MF A01 CSCL 20/12

A glass of nominal $\text{Bi}_{1.5}\text{Pb}_{0.5}\text{Sr}_2\text{Ca}_2\text{Cu}_3\text{O}(x)$ composition, prepared by rapid quenching of the melt, showed a glass transition temperature of 383 C, crystallization temperature of 446 C, melting temperature of 855 C, and bulk density of 5.69 g/cu cm in air. The activation energy for crystallization of the glass was estimated to be 292kJ/mol from non-isothermal DSC. On heating in oxygen, the glass showed a slow and continuous weight gain starting at approximately 530 C which reached a plateau at approximately 820 C. The weight gained during heating was retained on cooling to ambient conditions indicating an irreversible oxidation step. The influence of annealing conditions on the formation of various phases in the glass has been investigated. The $\text{Bi}_2(\text{Sr}_2)\text{Ca}(\text{O})\text{Cu}(\text{O})_6$ phase crystallized out first followed by formation of other phases at higher temperatures. The high-T(sub c) phase, isostructural with $\text{Bi}_2(\text{Sr}_2)\text{Ca}(\text{O})\text{Cu}(\text{O})_{10}$ was not detected below 840 C, but its fraction increased with the annealing time at 840 C. A sample annealed at 840 C for 243h in air and furnace cooled showed the highest $T(\text{sub } c)(R=0)$ of 107.2K and a narrow transition width, $\Delta T(\text{sub } c)(10 \text{ to } 90 \text{ percent})$, of approximately 2 K. The high T(sub c) phase does not seem to crystallize out directly from the glass but is rather produced at high temperature by reaction between the phases formed at lower temperatures. The kinetics of 110K phase formation was sluggish. It appears that the presence of lead helps in the formation and/or stabilization of the 110 K phase. Author

N90-19873*# North Carolina State Univ., Raleigh. College of Engineering.
SILICON CARBIDE SEMICONDUCTOR DEVICE FABRICATION AND CHARACTERIZATION Final Report, 10 Feb. 1987 - 9 Feb. 1990

R. F. DAVIS and K. DAS 8 Feb. 1990 35 p
 (Contract NAG3-782; N00014-85-K-0182)
 (NASA-CR-186354; NAS 1.26:186354) Avail: NTIS HC A03/MF A01 CSCL 20/12

A number of basic building blocks i.e., rectifying and ohmic contacts, implanted junctions, MOS capacitors, pnnp diodes and devices, such as, MESFETs on both alpha and beta SiC films were fabricated and characterized. Gold forms a rectifying contact

on beta SiC. Since Au contacts degrade at high temperatures, these are not considered to be suitable for high temperature device applications. However, it was possible to utilize Au contact diodes for electrically characterizing SiC films. Preliminary work indicates that sputtered Pt or Pt/Si contacts on beta SiC films are somewhat superior to Au contacts. Sputtered Pt layers on alpha SiC films form excellent rectifying contacts, whereas Ni layers following anneal at approximately 1050 C provide an ohmic contact. It has demonstrated that ion implantation of Al in substrates held at 550 C can be successfully employed for the fabrication of rectifying junction diodes. Feasibility of fabricating pnpn diodes and platinum gated MESFETs on alpha SiC films was also demonstrated.

Author

N90-20886*# National Aeronautics and Space Administration. Lewis Research Center, Cleveland, OH.

MILLIMETER WAVE SURFACE RESISTANCE OF RBA2CU3O(7-DELTA) (R=Y,EU,DY,SM,ER) SUPERCONDUCTORS

F. A. MIRANDA, W. L. GORDON, T. G. ECK (Case Western Reserve Univ., Cleveland, OH.), K. B. BHASIN, J. D. WARNER, and K. A. JENKINS 1990 9 p Presented at the March Meeting of the American Physical Society, Anaheim, CA, 12-16 Mar. 1990

(NASA-TM-102571; E-5395; NAS 1.15:102571) Avail: NTIS HC A02/MF A01 CSCL 20/12

The measurements are reported of the millimeter wave surface resistance $R_{\text{sub s}}$ at 58.6 GHz of bulk samples of $\text{RBA}_2\text{Cu}_3\text{O}(7-\delta)$ ($R = \text{Y, Eu, Dy, Sm, Er}$) and of $\text{YBa}_2\text{Cu}_3\text{O}(7-\delta)$ superconducting films, in the temperature range from 20 to 300 K. The bulk samples were prepared by cold pressing the powders of $\text{RBA}_2\text{Cu}_3\text{O}(7-\delta)$ into one in. disks. The powders were prepared by several sinterings in one atmosphere of oxygen at 925 C, with grindings between sinterings, to obtain the superconducting phase. The thin films were deposited on SrTiO_3 and LaGaO_3 substrates by pulsed laser ablation. Each sample was measured by replacing the end wall of a gold-plated Te sub 013 circular mode copper cavity with the sample and determining the cavity quality factor. From the difference in the Q-factor of the cavity, with and without the sample, the $R_{\text{sub s}}$ of the sample was determined.

Author

N90-22421*# National Aeronautics and Space Administration. Lewis Research Center, Cleveland, OH.

GROWTH AND PATTERNING OF LASER ABLATED SUPERCONDUCTING YBA2CU3O7 FILMS ON LAAO3 SUBSTRATES

J. D. WARNER, K. B. BHASIN, N. C. VARALJAY, D. Y. BOHMAN, and C. M. CHOREY (Sverdrup Technology, Inc., Cleveland, OH.) 1989 8 p Presented at the 36th National Symposium and Topical Conference, Boston, MA, 23-27 Oct. 1989; sponsored by American Vacuum Society

(NASA-TM-102436; E-5205; NAS 1.15:102436) Avail: NTIS HC A02/MF A01 CSCL 20/12

A high quality superconducting film on a substrate with a low dielectric constant is desired for passive microwave circuit applications. In addition, it is essential that the patterning process does not effect the superconducting properties of the thin films to achieve the highest circuit operating temperatures. $\text{YBa}_2\text{Cu}_3\text{O}_7$ superconducting films were grown on lanthanum aluminate substrates using laser ablation with resulting maximum transition temperature ($T_{\text{sub c}}$) of 90 K. The films were grown on a LaAlO_3 which was at 775 C and in 170 mtorr of oxygen and slowly cooled to room temperature in 1 atm of oxygen. These films were then processed using photolithography and a negative photoresist with an etch solution of bromine and ethanol. Results are presented on the effect of the processing on $T_{\text{sub c}}$ of the film and the microwave properties of the patterned films.

Author

N90-24952*# National Aeronautics and Space Administration. Lewis Research Center, Cleveland, OH.

HIGH-TEMPERATURE SUPERCONDUCTORS FOR SPACE POWER TRANSMISSION LINES

JOHN R. HULL (Argonne National Lab., IL.) and IRA T. MYERS Aug. 1989 24 p Presented at the ASME Winter Annual Meeting Conference, San Francisco, CA, 10-15 Dec. 1989

(Contract W-31-109-ENG-38)

(NASA-TM-103459; NAS 1.15:103459; DE90-009725;

CONF-891208-32) Avail: NTIS HC A03/MF A01 CSCL 20/12

Analysis of high temperature superconductors (HTS) for space power transmission lines shows that they have the potential to provide low weight alternatives to conventional power distribution systems, especially for line lengths greater than 100 m. The use of directional radiators, combined with the natural vacuum of space, offers the possibility of reducing or eliminating the heat flux from the environment that dominates loss in terrestrial systems. This leads to scaling laws that favor flat conductor geometries. From a total launch weight viewpoint, HTS transmission lines appear superior, even with presently attainable values of current density.

DOE

N90-24964*# Sandia National Labs., Albuquerque, NM.

RAPID THERMAL PROCESSING OF HIGH TEMPERATURE SUPERCONDUCTING FIBER

J. W. HALLORAN, M. J. NEAL, D. S. GINLEY, E. L. VENTURINI, J. F. KWAK, R. J. BAUGHMAN, M. A. MITCHELL, B. MOROSIN, S. N. BASU, and T. E. MITCHELL (Los Alamos National Lab., NM.) 1990 7 p Presented at the Spring Meeting of the Materials Research Society, San Francisco, CA, 16-21 Apr. 1990

Sponsored in part by High Temperature Superconductor Pilot Center

(Contract NAS3-25876; N00014-88-C-0512;

DE-AC04-76DP-00789; W-7405-ENG-36)

(NASA-CR-186803; NAS 1.26:186803; DE90-011236;

SAND-90-1229C; CONF-900466-44) Avail: NTIS HC A02/MF

A01 CSCL 20/12

We report on the rapid thermal processing (RTP) of Y-123 fibers with and without presintering to form the orthorhombic phase. We show that fibers which were originally semiconducting and tetragonal before rapid thermal processing form normal twinned orthorhombic material after processing for 2 to 4 seconds at greater than 1000 C with a 3 min. cool down in oxygen. They subsequently show (T_c) to 90 K and magnetization indicative of substantial diamagnetic shielding. We present the effects of varying the RTP parameters on the morphology, phase, and superconducting properties of a number of tetragonal and orthorhombic Y-123 fibers.

DOE

N90-26664*# Akron Univ., OH. Dept. of Mechanical Engineering.

TEMPERATURE AND MELT SOLID INTERFACE CONTROL DURING CRYSTAL GROWTH Final Technical Report, 1 May - 14 Nov. 1989

CELAL BATUR Jul. 1990 47 p

(Contract NCC3-109)

(NASA-CR-186731; NAS 1.26:186731) Avail: NTIS HC A03/MF A01 CSCL 20/12

Findings on the adaptive control of a transparent Bridgman crystal growth furnace are summarized. The task of the process controller is to establish a user specified axial temperature profile by controlling the temperatures in eight heating zones. The furnace controller is built around a computer. Adaptive PID (Proportional Integral Derivative) and Pole Placement control algorithms are applied. The need for adaptive controller stems from the fact that the zone dynamics changes with respect to time. The controller was tested extensively on the Lead Bromide crystal growth. Several different temperature profiles and ampoule's translational rates are tried. The feasibility of solid liquid interface quantification by image processing was determined. The interface is observed by a color video camera and the image data file is processed to determine if the interface is flat, convex or concave.

Author

N90-26682*# National Aeronautics and Space Administration. Lewis Research Center, Cleveland, OH.

ELLIPSOMETRIC STUDY OF YBA2CU3O(7-X) LASER ABLATED AND CO-EVAPORATED FILMS

S. A. ALTEROVITZ, R. E. SIEG, J. D. WARNER, M. A. STAN (Kent State Univ., OH.), and S. VITTA 1990 8 p Presented at the International Conference on Electronic Materials 1990, Newark, NJ, 17-19 Sep. 1990; sponsored by Materials Research Society (NASA-TM-103223; E-5637; NAS 1.15:103223) Avail: NTIS HC A02/MF A01 CSCL 20/12

High temperature superconducting films of YBa₂Cu₃O(7-x) (YBCO) were grown on SrTiO₃, LaAlO₃, and YSZ substrates using two techniques: excimer laser ablation with in situ annealing and co-evaporation of Y, Cu, and BaF₂ with ex-situ annealing. Film thicknesses were typically 5000 Å, with predominant c-axis alignment perpendicular to the substrate. Critical temperatures up to T_c(R=0)=90 K were achieved by both techniques. Ellipsometric measurements were taken in the range 1.6 to 4.3 eV using a variable angle spectroscopic ellipsometer. The complex dielectric function of the laser ablated films was reproducible from run to run, and was found to be within 10 percent of that previously reported for (001) oriented single crystals. A dielectric overlayer was observed in these films, with an index of refraction of approximately 1.55 and nearly zero absorption. For the laser ablated films the optical properties were essentially independent of substrate material. The magnitude of the dielectric function obtained for the co-evaporated films was much lower than the value reported for single crystals, and was sample dependent. Author

N90-26683* National Aeronautics and Space Administration. Lewis Research Center, Cleveland, OH.

DIELECTRIC FUNCTION OF INGAAS IN THE VISIBLE

S. A. ALTEROVITZ, R. E. SIEG, H. D. YAO, P. G. SNYDER, J. A. WOOLLAM, J. PAMULAPATI, P. K. BHATTACHARYA, and P. A. SEKULA-MOISE (Spire Corp., Bedford, MA.) 1990 8 p Presented at the 2nd International Conference on Electronic Materials, Newark, NJ, 17-19 Sep. 1990; sponsored by Materials Research Society (Contract NAG3-988; NAS3-25867) (NASA-TM-103246; E-5672; NAS 1.15:103246) Avail: NTIS HC A02/MF A01 CSCL 20/12

Measurements are reported of the dielectric function of thermodynamically stable In_xGa(1-x)As in the composition range 0.3 equal to or less than X = to or less than 0.7. The optically thick samples of InGaAs were made by molecular beam epitaxy (MBE) in the range 0.4 = to or less than X = to or less than 0.7 and by metal-organic chemical vapor deposition (MOCVD) for X = 0.3. The MBE made samples, usually 1 micron thick, were grown on semi-insulating InP and included a strain release structure. The MOCVD sample was grown on GaAs and was 2 microns thick. The dielectric functions were measured by variable angle spectroscopic ellipsometry in the range 1.55 to 4.4 eV. The data was analyzed assuming an optically thick InGaAs material with an oxide layer on top. The thickness of this layer was estimated by comparing the results for the InP lattice matched material, i.e., X = 0.53, with results published in the literature. The top oxide layer mathematically for X = 0.3 and X = 0.53 was removed to get the dielectric function of the bare InGaAs. In addition, the dielectric function of GaAs in vacuum, after a protective arsenic layer was removed. The dielectric functions for X = 0, 0.3, and 0.53 together with the X = 1 result from the literature to evaluate an algorithm for calculating the dielectric function of InGaAs for an arbitrary value of X(0 = to or less than X = to or less than 1) were used. Results of the dielectric function calculated using the algorithm were compared with experimental data. Author

N90-27808* National Aeronautics and Space Administration. Lewis Research Center, Cleveland, OH.

LASER ABLATED HIGH T(SUB C) SUPERCONDUCTING THIN YBA2CU3O(7-X) FILMS ON SUBSTRATES SUITABLE FOR MICROWAVE APPLICATIONS Abstract Only

J. D. WARNER, J. E. MEOLA, K. A. JENKINS, and K. B. BHASIN /In NASA, Goddard Space Flight Center, AMSAHS 1990: Advances in Materials Science and Applications of High Temperature Superconductors p 26 Apr. 1990 Avail: NTIS HC A07/MF A02 CSCL 20/12

The development of high temperature superconducting YBa₂Cu₃O(7-x) thin films on substrates suitable for microwave applications is of great interest for evaluating their applications for space radar, communication, and sensor systems. Thin films of YBa₂Cu₃O(7-x) were formed on SrTiO₃, ZrO₂, MgO, and LaAlO₃ substrates by laser ablation. The wavelength used was 248 nm from a KrF excimer laser. During deposition the films were heated to 600 C in a flowing oxygen environment, and required no post annealing. The low substrate temperature during deposition with no post annealing gave films which were smooth, which had their c-axis aligned to the substrates, and which had grains ranging from 0.2 to 0.5 microns in size. The films being c-axis aligned gave excellent surface resistance at 35 GHz which was lower than that of copper at 77 K. At present, LaAlO₃ substrates with a dielectric constant of 22, appears suitable as a substrate for microwave and electronic applications. The films were characterized by resistance-temperature measurements, scanning electron microscopy, and x ray diffraction. The highest critical transition temperatures (T sub c) are above 89 K for films on SrTiO₃ and LaAlO₃, above 88 K for ZrO₂, and above 86 K for MgO. The critical current density (J sub c) of the films on SrTiO₃ is above 2 x 10(exp 6) amperes/sq cm at 77 K. The T(sub c) and J(sub c) are reported as a function of laser power, composition of the substrate, and temperature of the substrate during deposition. Author

N90-29219* National Aeronautics and Space Administration. Lewis Research Center, Cleveland, OH.

XANES AND EXAFS STUDY OF AU-SUBSTITUTED YBA2CU3O(7-DELTA)

MARK W. RUCKMAN (Brookhaven National Lab., Upton, NY.) and ALOYSIUS F. HEPP Sep. 1990 11 p Presented at the 4th Annual Conference on Superconductivity and Applications, Buffalo, NY, 18-20 Sep. 1990; sponsored by The New York State Institute on Superconductivity (NASA-TM-103291; E-5751; NAS 1.15:103291) Avail: NTIS HC A03/MF A01 CSCL 20/12

The near-edge structure (XANES) of the Au L₃ and Cu K edges of YBa₂Au(0.3)Cu(2.7)O(7-delta) was studied. X ray diffraction suggests that Au goes on the Cu(1) site and XANES shows that this has little effect on the oxidation state of the remaining copper. The gold L₃ edge develops a white line feature whose position lies between that of trivalent gold oxide (Au₂O₃) and monovalent potassium gold cyanide (KAu(CN)₂) and whose intensity relative to the edge step is smaller than in the two reference compounds. The L₃ EXAFS for Au in the superconductor resembles that of Au₂O₃. However, differences in the envelope of the Fourier filtered component for the first shell suggest that the local structure of the Au in the superconductor is not equivalent to Au₂O₃. Author

77

THERMODYNAMICS AND STATISTICAL PHYSICS

Includes quantum mechanics; theoretical physics; and Bose and Fermi statistics.

A90-21904* National Aeronautics and Space Administration. Lewis Research Center, Cleveland, OH.

RADIATIVE TRANSFER THEORY FOR INHOMOGENEOUS MEDIA WITH RANDOM EXTINCTION AND SCATTERING COEFFICIENTS

ROBERT M. MANNING (NASA, Lewis Research Center, Cleveland, OH) Journal of Mathematical Physics (ISSN 0022-2488), vol. 30, Oct. 1989, p. 2432-2440. refs Copyright

The small-angle scattering approximation of the scalar radiative transfer equation (RTE) is examined for the case where the extinction and scattering coefficients have a component that is a

deterministic function of position along the propagation path and a component that is a random function of position transverse to the propagation direction. It is found that the resulting stochastic RTE can be reduced to a system of two stochastic integrodifferential equations for the average and fluctuating components of the radiant intensity. Two transfer equations are obtained describing the average radiant intensity and the spatial correlation function of the intensity fluctuations. The average intensity equation is then solved and applied to a simple propagation scenario. An approximate solution is also derived for the equation giving the correlation function. The developed equations can be applied to problems involving short wavelength electromagnetic wave propagation through media possessing the variable characteristics of turbulence and turbidity, such as plasmas, the atmosphere, and the ocean. S.A.V.

A90-27612* Cleveland State Univ., OH.

AN ACCURATE ANALYTIC APPROXIMATION TO THE NON-LINEAR CHANGE IN VOLUME OF SOLIDS WITH APPLIED PRESSURE

HERBERT SCHLOSSER (Cleveland State University, OH) and JOHN FERRANTE (NASA, Lewis Research Center, Cleveland, OH) *Journal of Physics: Condensed Matter* (ISSN 0953-8984), vol. 1, 1989, p. 2727-2730. Research supported by the Ohio Board of Regents. refs
Copyright

An accurate analytic expression for the nonlinear change of the volume of a solid as a function of applied pressure is of great interest in high-pressure experimentation. It is found that a two-parameter analytic expression, fits the experimental volume-change data to within a few percent over the entire experimentally attainable pressure range. Results are presented for 24 different materials including metals, ceramic semiconductors, polymers, and ionic and rare-gas solids. Author

A90-31670*# Sverdrup Technology, Inc., Cleveland, OH.
EQUILIBRIUM STATISTICAL THERMODYNAMICS OF A MANY-PARTICLE SYSTEM COUPLED TO AN EXTERNAL SCALAR FIELD

R. E. SALVINO (Sverdrup Technology, Inc., Cleveland, OH) *Physical Review A - Statistical Physics, Plasmas, Fluids, and Related Interdisciplinary Topics, 3rd Series* (ISSN 0556-2791), vol. 41, April 15, 1990, p. 4236-4250. refs
(Contract NAS3-25266)

The equilibrium thermodynamics of a many-particle assembly in the presence of an external scalar field is examined. Two types of scalar coupling are considered: an external field coupled to the particle density and an external scalar field coupled to the energy density. It is shown that the broken translational and rotational invariance of the system due to the external field is reflected in the macroscopic physics by loss of the usual extensivity property of the system and by means of anisotropy in the response of the system to changes in the system lengths or to the system shape. In addition, the assumptions used in local equilibrium analyses are shown to be incorrect in principle. Nonlocal effects due to the external field must be included in the determination of the equation of state. Simple model calculations for a system in an external gravitational field and an externally imposed temperature field are presented as illustrations. Author

A90-31675* Ohio State Univ., Columbus.

SURFACE ENTROPY OF LIQUIDS VIA A DIRECT MONTE CARLO APPROACH - APPLICATION TO LIQUID SI

Z. Q. WANG and D. STROUD (Ohio State University, Columbus) *Physical Review A - Statistical Physics, Plasmas, Fluids, and Related Interdisciplinary Topics, 3rd Series* (ISSN 0556-2791), vol. 41, April 15, 1990, p. 4582-4584. refs
(Contract NAG3-999)
Copyright

Two methods are presented for a direct Monte Carlo evaluation of the surface entropy $S(s)$ of a liquid interacting by specified, volume-independent potentials. The first method is based on an application of the approach of Ferrenberg and Swendsen (1988,

1989) to Monte Carlo simulations at two different temperatures; it gives much more reliable results for $S(s)$ in liquid Si than previous calculations based on numerical differentiation. The second method expresses the surface entropy directly as a canonical average at fixed temperature. Author

A90-43941* National Inst. of Standards and Technology, Gaithersburg, MD.

CRITICAL EXPONENT FOR THE VISCOSITY OF CARBON DIOXIDE AND XENON

R. F. BERG and M. R. MOLDOVER (NIST, Thermophysics Div., Gaithersburg, MD) *Journal of Chemical Physics* (ISSN 0021-9606), vol. 93, Aug. 1, 1990, p. 1926-1938. refs
(Contract NASA ORDER C-86129-D)
Copyright

The viscosities of carbon dioxide and xenon have been measured near their critical points and the critical exponent γ characterizing the asymptotic divergence has been determined. Both fluids yielded exponents in the range $\gamma = 0.041 \pm$ or -0.001 and thus also fell in the range $\gamma = 0.042 \pm$ or -0.002 from an earlier study of four binary liquids. This agreement between experiments is the first evidence that pure fluids and binary liquids are in the same dynamic universality class. A recent theoretical value for γ is 0.032. The 30 percent discrepancy is much greater than the combined errors from experiment and theory. The torsion oscillator viscometer operated at low frequency and low shear rate to avoid systematic errors caused by critical slowing down. Far from $T(c)$ the analysis accounted for the crossover from critical to noncritical temperature dependence, where the latter was obtained from previously published correlations. Corrections for gravitational stratification were included close to $T(c)$. Author

80

SOCIAL SCIENCES (GENERAL)

Includes educational matters.

A90-42152*# National Aeronautics and Space Administration, Lewis Research Center, Cleveland, OH.

THE INTERNATIONAL SPACE UNIVERSITY

KENNETH J. DAVIDIAN (NASA, Lewis Research Center, Cleveland, OH) AIAA, SAE, ASME, and ASEE, Joint Propulsion Conference, 26th, Orlando, FL, July 16-18, 1990. 10 p. Previously announced in STAR as N90-22604. refs
(AIAA PAPER 90-2389) Copyright

The International Space University (ISU) was founded on the premise that any major space program in the future would require international cooperation as a necessary first step toward its successful completion. ISU is devoted to being a leading center for educating future authorities in the world space industry. ISU's background, goals, current form, and future plans are described. The results and benefits of the type of education and experience gained from ISU include technical reports describing the design projects undertaken by the students, an exposure to the many different disciplines which are a part of a large space project, an awareness of the existing activities from around the world in the space community, and an international professional network which spans all aspects of space activities and covers the globe. Author

81 ADMINISTRATION AND MANAGEMENT

N90-26693*# National Aeronautics and Space Administration. Lewis Research Center, Cleveland, OH.

LAUNCHING A DREAM: A TEACHERS GUIDE TO A SIMULATED SPACE SHUTTLE MISSION

1989 105 p

(NASA-TM-89715; NAS 1.15:89715) Avail: NTIS HC A06/MF A01 CSCL 05/9

Two simulated shuttle missions cosponsored by the NASA Lewis Research Center and Cleveland, Ohio, area schools are highlighted in this manual for teachers. A simulated space shuttle mission is an opportunity for students of all ages to plan, train for, and conduct a shuttle mission. Some students are selected to be astronauts, flight planners, and flight controllers. Other students build and test the experiments that the astronauts will conduct. Some set up mission control, while others design the mission patch. Students also serve as security officers or carry out public relations activities. For the simulated shuttle mission, school buses or recreation vehicles are converted to represent shuttle orbiters. All aspects of a shuttle mission are included. During preflight activities the shuttle is prepared, and experiments and a flight plan are made ready for launch day. The flight itself includes lifting off, conducting experiments on orbit, and rendezvousing with the crew from the sister school. After landing back at the home school, the student astronauts are debriefed and hold press conferences. The astronauts celebrate their successful missions with their fellow students at school and with the community at an evening postflight recognition program. To date, approximately 6,000 students have been involved in simulated shuttle missions with the Lewis Research Center. A list of participating schools, along with the names of their space shuttles, is included. Educations outcomes and other positive effects for the students are described. J.P.S.

81

ADMINISTRATION AND MANAGEMENT

Includes management planning and research.

N90-20901*# National Aeronautics and Space Administration. Lewis Research Center, Cleveland, OH.

MIDDLE MANAGEMENT OF RESEARCH

ROBERT W. GRAHAM Jan. 1990 14 p Submitted for publication

(NASA-TM-102417; E-5183; NAS 1.15:102417) Avail: NTIS HC A03/MF A01 CSCL 05/1

The role of the middle manager in a research organization is discussed. The middle manager serves as a liaison between upper management and researchers to assure that individual research projects manifest the goals of the organization. The author draws on his long experience in this role to describe management practices that have proven successful. A general discussion is presented of the makeup of a research environment, derived from a study of a division involved in aerospace research and development (R and D). The study emphasized the importance of planning and management style in producing an attractive environment. Management practices are described, which include goal setting, planning, staffing, reviewing and evaluating, and rewarding. The importance of selecting and defining an appropriate research area is discussed. It is emphasized that in relating to the staff the middle manager must cultivate the human side of supervision, develop the art of delegating responsibility, judiciously select facilities, and provide recognition and meaningful rewards to develop a productive research staff. The development of the staff is probably the most important and challenging role of the manager. Author

82

DOCUMENTATION AND INFORMATION SCIENCE

Includes information management; information storage and retrieval technology; technical writing; graphic arts; and micrography.

N90-12388* National Aeronautics and Space Administration. Lewis Research Center, Cleveland, OH.

CRISS-CROSS DIRECTORY OF NASA N NUMBERS AND DOD AD NUMBERS. VOLUME 2, PART 1: AD TO N, 1979-1986. N TO AD, 1962-1986

GEORGE MANDEL, ed. Feb. 1988 449 p Prepared in cooperation with Special Libraries Association, Chicago, IL (NASA-TM-101814; NAS 1.15:101814) Avail: MS 60-1, NASA Lewis Research Center, 21000 Brookpark Road, Cleveland, OH 44135 HC \$55.00. Make checks available to Aerospace Div., SLA CSCL 05/2

This directory presents a tabular listing of DOD AD report numbers and corresponding NASA N numbers for the periods 1979-1986 (AD to N) and 1962-1986 (N to AD). In addition, tables are provided that map the various NASA Research Report series to N numbers. Those series include Conference Papers (CP), Contractor Reports (CR), Educational Publications (EP), Reference Publications (RP), Special Publications (SP), Technical Papers (TP), Technical Translations (TT), and Technical Memorandums (TM). Part 1 of the directory includes the AD to N listing, Research Report tables, and a portion of the N to AD listing. Author

N90-12389* National Aeronautics and Space Administration. Lewis Research Center, Cleveland, OH.

CRISS-CROSS DIRECTORY OF NASA N NUMBERS AND DOD AD NUMBERS. VOLUME 2, PART 2: AD TO N, 1979-1986. N TO AD, 1962-1986

GEORGE MANDEL Feb. 1988 451 p Prepared in cooperation with Special Libraries Association, Chicago, IL (NASA-TM-101815; NAS 1.15:101815) Avail: MS 60-1, NASA Lewis Research Center, 21000 Brookpark Road, Cleveland, OH 44135 HC \$55.00. Make checks available to Aerospace Div., SLA CSCL 05/2

This directory presents a tabular listing of DOD AD report numbers and corresponding NASA N numbers for the periods 1979-1986 (AD to N) and 1962-1986 (N to AD). In addition, tables mapping the various NASA Research Report series to N numbers are provided. Part 2 of the directory continues the N to AD listing. Author

N90-15846*# National Aeronautics and Space Administration. Lewis Research Center, Cleveland, OH.

BIBLIOGRAPHY OF LEWIS RESEARCH CENTER TECHNICAL PUBLICATIONS ANNOUNCED IN 1988

Jul. 1989 371 p

(NASA-TM-102034; E-4780; NAS 1.15:102034) Avail: NTIS HC A16/MF A02 CSCL 05/2

This bibliography contains abstracts of the technical reports that resulted from the scientific and engineering work performed and managed by the Lewis Research Center in 1988. Subject, author, and corporate source indexes are also included. All the publications were announced in the 1988 issues of STAR (Scientific and Technical Aerospace Reports) and/or IAA (International Aerospace Abstracts). Included are research reports, journal articles, conference presentations, patents and patent applications, and theses. Author

URBAN TECHNOLOGY AND TRANSPORTATION

Includes applications of space technology to urban problems; technology transfer; technology assessment; and surface and mass transportation.

N90-11654*# Mechanical Technology, Inc., Latham, NY. Stirling Engine Systems Div.

AUTOMOTIVE STIRLING ENGINE DEVELOPMENT PROGRAM Semiannual Technical Progress Report, 1 Jul. - 31 Dec. 1986
R. FARRELL, C. HINDES, R. BATTISTA, M. CONNELLY, M. CRONIN, R. HOWARTH, A. DONAHUE, E. SLATE, R. STOTTS, R. LACY et al. Feb. 1988 59 p
(Contract DEN3-32; DE-A101-85CE-50112)
(NASA-CR-180839; DOE/NASA/0032-30; NAS 1.26:180839; MTI-87ASE555SA11) Avail: NTIS HC A04/MF A01 CSCL 13/9

The study of high power kinematic Stirling engines for transportation use, testing of Mod I and Mod II Stirling engines, and component development activities are summarized. Mod II development testing was performed to complete the development of the basic engine and begin characterization of performance. Mod I engines were used for Mod II component development and to obtain independent party (U.S. Air Force) evaluation of Stirling engine vehicle performance. Author

N90-14153*# Allied-Signal Aerospace Co., Phoenix, AZ. Garrett Auxiliary Power Div.

ADVANCED TURBINE TECHNOLOGY APPLICATIONS PROJECT (ATTAP) Annual Report, 1988

Apr. 1989 249 p
(Contract DEN3-335)
(NASA-CR-185109; DOE/NASA/0335-1; NAS 1.26:185109; GARRETT-31-8071(1)) Avail: NTIS HC A11/MF A02 CSCL 10/2

Work to develop and demonstrate the technology of structural ceramics for automotive engines and similar applications is described. Long-range technology is being sought to produce gas turbine engines for automobiles with reduced fuel consumption and reduced environmental impact. The Advanced Turbine Technology Application Project (ATTAP) test bed engine is designed such that, when installed in a 3,000 pound inertia weight automobile, it will provide low emissions, 42 miles per gallon fuel economy on diesel fuel, multifuel capability, costs competitive with current spark ignition engines, and noise and safety characteristics that meet Federal standards. Author

N90-18326*# Martini Engineering, Richland, WA.
DEVELOPMENT OF FREE-PISTON STIRLING ENGINE PERFORMANCE AND OPTIMIZATION CODES BASED ON MARTINI SIMULATION TECHNIQUE

WILLIAM R. MARTINI Sep. 1989 269 p
(Contract NAS3-22256)
(NASA-CR-182210; NAS 1.26:182210) Avail: NTIS HC A12/MF A02 CSCL 10/2

A FORTRAN computer code is described that could be used to design and optimize a free-displacer, free-piston Stirling engine similar to the RE-1000 engine made by Sunpower. The code contains options for specifying displacer and power piston motion or for allowing these motions to be calculated by a force balance. The engine load may be a dashpot, inertial compressor, hydraulic pump or linear alternator. Cycle analysis may be done by isothermal analysis or adiabatic analysis. Adiabatic analysis may be done using the Martini moving gas node analysis or the Rios second-order Runge-Kutta analysis. Flow loss and heat loss equations are included. Graphical display of engine motions and pressures and temperatures are included. Programming for optimizing up to 15 independent dimensions is included. Sample performance results are shown for both specified and unconstrained piston motions; these results are shown as

generated by each of the two Martini analyses. Two sample optimization searches are shown using specified piston motion isothermal analysis. One is for three adjustable input and one is for four. Also, two optimization searches for calculated piston motion are presented for three and for four adjustable inputs. The effect of leakage is evaluated. Suggestions for further work are given. Author

N90-26728*# Garrett Turbine Engine Co., Phoenix, AZ.

ADVANCED TURBINE TECHNOLOGY APPLICATIONS PROJECT (ATTAP) Annual Report, 1989

Feb. 1990 215 p
(Contract DEN3-335)
(NASA-CR-185240; DOE/NASA/0335-2; NAS 1.26:185240; GARRETT-31-8071(2)) Avail: NTIS HC A10/MF A02 CSCL 21/5

This report is the second in a series of Annual Technical Summary Reports for the Advanced Turbine Technology Applications Project (ATTAP). Plans and progress are covered for ceramics development for commercial automotive applications over the period January 1 through December 31, 1989. Project effort conducted under this contract is part of the DOE Gas Turbine Highway Vehicle System program. This program is directed to provide the U.S. automotive industry the high-risk, long-range technology necessary to produce gas turbine engines for automobiles with reduced fuel consumption, reduced environmental impact, and a decreased reliance on scarce materials and resources. The program is oriented toward developing the high-risk technology of ceramic structural component design and fabrication, such that industry can carry this technology forward to production in the 1990s. The ATTAP test bed engine, carried over from the previous AGT101 project, is being used for verification testing of the durability of next generation ceramic components, and their suitability for service at Reference Powertrain Design conditions. The technical effort conducted by GAPD and the ATTAP subcontractors over the second year of the project is reported. Topics covered include ceramic processing definition and refinement, design improvements to the ATTAP test bed engine and test rigs and the methodology development of ceramic impact and fracture mechanisms. Appendices include reports by ATTAP subcontractors in the development of silicon nitride and silicon carbide families of materials and processes. Author

N90-26729*# National Aeronautics and Space Administration. Lewis Research Center, Cleveland, OH.

PRELIMINARY DESIGNS FOR 25 KWE ADVANCED STIRLING CONVERSION SYSTEMS FOR DISH ELECTRIC APPLICATIONS Final Report

RICHARD K. SHALTENS and JEFFREY G. SCHREIBER 1990 19 p Presented at the 25th Intersociety Conversion Engineering Conference, Reno, NV, 12-17 Aug. 1990; sponsored by AICHE, ANS, SAE, ACS, AIAA, ASME, and IEEE Prepared for DOE, Washington, DC

(Contract DE-AT04-85AL-33408)
(NASA-TM-103188; DOE/NASA/33408-4; E-5573; NAS 1.15:103188) Avail: NTIS HC A03/MF A01 CSCL 10/1

Under the Department of Energy's (DOE) Solar Thermal Technology Program, Sandia National Laboratories is evaluating heat engines for terrestrial Solar Distributed Heat Receivers. The Stirling engine has been identified by Sandia as one of the most promising engines for terrestrial applications. The Stirling engine also has the potential to meet DOE's performance and cost goals. The NASA Lewis Research Center is conducting Stirling engine technology development activities directed toward a dynamic power source for space applications. Space power systems requirements include high reliability, very long life, low vibration and high efficiency. The free-piston Stirling engine has the potential for future high power space conversion systems, either nuclear or solar powered. Although both applications appear to be quite different, their requirements complement each other. Preliminary designs feature a free-piston Stirling engine, a liquid metal heat transport system, and a means to provide nominally 25 kW electric power to a utility grid while meeting DOE's performance and long term

85 URBAN TECHNOLOGY AND TRANSPORTATION

cost goals. The Cummins design incorporates a linear alternator to provide the electrical output, while the STC design generates electrical power indirectly through a hydraulic pump/motor coupled to an induction generator. Both designs for the ASCS's will use technology which can reasonably be expected to be available in the early 1990's

Author

N90-29260* Medical Technology, Inc., Syracuse, NY. Engine Systems Div.

**AUTOMOTIVE STIRLING ENGINE DEVELOPMENT PROGRAM
Semiannual Technical Progress Report No. 12, 1 Jan. - 30 Jun. 1987**

ROGER A. FARRELL, A. RICHEY, and J. MUNDY Feb. 1988
73 p

(Contract DEN3-32; DE-AI01-85CE-50112)

(NASA-CR-180840; NAS 1.26:180840; MTI-87ASE575SA12;
DOE/NASA/0032-31) Avail: NTIS HC A04/MF A01 CSCI
10/1

A study of high-power kinematic Stirling engines for transportation use, testing of Mod I and Mod II Stirling engines, and component development activities is reviewed. Mod II development testing included performance, emissions, and noise as well as the impact of varying regenerator porosity, working gas, and heater head geometry. Mod I engines were used for Mod II component development and to obtain independent party (U.S. Air Force) evaluation of Stirling engine vehicle performance.

Author

88

SPACE SCIENCES (GENERAL)

N90-22464* National Aeronautics and Space Administration. Lewis Research Center, Cleveland, OH.

EXTRATERRESTRIAL LIFE IN THE UNIVERSE

ROBERT W. GRAHAM Feb. 1990 10 p Presented at the Lewis Special Summer Lecture Series, Cleveland, OH, 18 Jul. 1989

(NASA-TM-102363; E-5080; NAS 1.15:102363) Avail: NTIS HC A02/MF A01 CSCI 06/3

The possibility that life exists elsewhere in the universe, even in our own planetary system, has intrigued scientists, philosophers, and theologians for centuries. The spaceflight programs of NASA have provided much new information about our planetary neighbors and have put to rest some speculations about the existence of life on those planets or their satellites. However, there are still undetermined questions about the possibility of some form of life existing in the far distant past in our planetary system. Beyond our planetary system, the astronomical quest for scientific clues about life continues, largely via the radio telescope. Thus far there is no conclusive evidence. Here, some of the recent findings about our planetary neighbors are reviewed and the question about life elsewhere in the universe is addressed.

Author

90

ASTROPHYSICS

Includes cosmology; celestial mechanics; space plasmas; and interstellar and interplanetary gases and dust.

A90-12669* National Aeronautics and Space Administration. Lewis Research Center, Cleveland, OH.

IS THE SUB-MILLISECOND PULSAR STRANGE?

JOSHUA A. FRIEMAN and ANGELA V. OLINTO (NASA/Fermilab

Astrophysics Center, Batavia, IL) Nature (ISSN 0028-0836), vol. 341, Oct. 19, 1989, p. 633-635. Research supported by DOE. refs

Copyright

The possibility that the submillisecond pulsar from supernova 1987A is composed of strange matter is theoretically discussed. It is shown that for a range of hadron parameters, the maximum rotation rate of secularly stable strange stars may exceed that of the half-millisecond pulsar and the nonrotating maximum mass is greater than 1.52 solar mass. The low-mass companion(s) to SN1987A, inferred from the periodic modulations of the optical signal, can be accounted for by stable strange-matter lump(s) ejected from the young strange star.

C.D.

A90-17643* Lawrence Livermore National Lab., CA.
THE SHOCKING DEVELOPMENT OF LITHIUM (AND BORON) IN SUPERNOVAE

DAVID S. P. DEARBORN (Lawrence Livermore National Laboratory, Livermore, CA), DAVID N. SCHRAMM (NASA/Fermilab Astrophysics Center, Batavia; Chicago, University, IL), GARY STEIGMAN (Ohio State University, Columbus), and JAMES TRURAN (Illinois, University, Urbana) Astrophysical Journal, Part 1 (ISSN 0004-637X), vol. 347, Dec. 1, 1989, p. 455-460. Research supported by DOE and Fermi National Accelerator Laboratory. Previously announced in STAR as N89-22545. refs

(Contract NAGW-1321; NSF AST-85-15447)

Copyright

It is shown that significant amounts of Li-7 and B-11 are produced in Type 2 supernovae. The synthesis of these rare elements occurs as the supernova shock traverses the base of the hydrogen envelope burning He-3 to masses 7 and 11 via alpha capture. The yields in this process are sufficient to account for the difference in lithium abundance observed between Pop 2 and Pop 1 stars. Since lithium (and boron) would, in this manner, be created in the same stars that produce the bulk of the heavy elements, the lithium abundance even in old Pop 1 stars would be high (as observed). The B-11 production may remedy the long-standing problem of the traditional spallation scenario to account for the observed isotopic ratio of boron. Observational consequences of this mechanism are discussed, including the evolution of lithium and boron isotope ratios in the Galaxy and the possible use of the boron yields to constrain the number of blue progenitor Type 2 supernovae.

Author

A90-24671* California Univ., Berkeley.
UNITARITY LIMITS ON THE MASS AND RADIUS OF DARK-MATTER PARTICLES

KIM GRIEST (California, University, Berkeley) and MARC KAMIONKOWSKI (NASA/Fermilab Astrophysics Center, Batavia; Chicago, University, IL) Physical Review Letters (ISSN 0031-9007), vol. 64, Feb. 5, 1990, p. 615-618. Research supported by DOE. Previously announced in STAR as N90-14164. refs

(Contract NAGW-1340; NSF AST-88-09616)

Copyright

Using partial wave unitarity and the observed density of the Universe, it is shown that a stable elementary particle which was once in thermal equilibrium cannot have a mass greater than 340 TeV. An extended object which was once in thermal equilibrium cannot have a radius less than $7.5 \times 10(\exp -7)$ fm. A lower limit to the relic abundance of such particles is also found.

Author

A90-25889* National Aeronautics and Space Administration. Lewis Research Center, Cleveland, OH.

COSMIC-STRING-INDUCED HOT DARK MATTER PERTURBATIONS

ANTHONY VAN DALEN (NASA/Fermilab Astrophysics Center, Batavia; Chicago, University, IL) Astrophysical Journal, Part 1 (ISSN 0004-637X), vol. 351, March 10, 1990, p. 356-363. Research supported by DOE. refs

(Contract NSF AST-85-15447)

Copyright

This paper investigates the evolution of initially relativistic matter, radiation, and baryons around cosmic string seed perturbations. A

detailed analysis of the linear evolution of spherical perturbations in a universe is carried out, and this formalism is used to study the evolution of perturbations around a sphere of uniform density and fixed radius, approximating a loop of cosmic string. It was found that, on scales less than a few megaparsec, the results agree with the nonrelativistic calculation of previous authors. On greater scales, there is a deviation approaching a factor of 2-3 in the perturbation mass. It is shown that a scenario with cosmic strings, hot dark matter, and a Hubble constant greater than 75 km/sec per Mpc can generally produce structure on the observed mass scales and at the appropriate time: $1 + z = \text{about } 4$ for galaxies and $1 + z = \text{about } 1.5$ for Abell clusters. I.S.

A90-30909* National Aeronautics and Space Administration. Lewis Research Center, Cleveland, OH.

NEUTRON STARS AND WHITE DWARFS IN GALACTIC HALOS?

DONGSU RYU (NASA/Fermilab Astrophysics Center, Batavia, IL), KEITH A. OLIVE (Minnesota, University, Minneapolis), and JOSEPH SILK (California, University, Berkeley) *Astrophysical Journal*, Part 1 (ISSN 0004-637X), vol. 353, April 10, 1990, p. 81-89. Research supported by NSF. Previously announced in STAR as N89-26783. refs

(Contract NAGW-1340; DE-AC02-83ER-40105)

Copyright

The possibility that galactic halos are composed of stellar remnants such as neutron stars and white dwarfs is discussed. On the basis of a simple model for the evolution of galactic halos, researchers follow the history of halo matter, luminosity, and metal and helium abundances. They assume conventional yields for helium and the heavier elements. By comparing with the observational constraints, which may be considered as fairly conservative, it is found that, for an exponentially decreasing star formation rate (SFR) with e-folding time τ , only values between $6 \times 10(8)$ less than similar to τ less than similar to $2 \times 10(9)$ years are allowed together with a very limited range of masses for the initial mass function (IMF). Star formation is allowed for 2 solar mass less than similar to m less than similar to 8 solar mass if $\tau = 2 \times 10(9)$ years, and for 4 solar mass less than similar to m less than similar to 6 solar mass if $\tau = 10(9)$ years. For $\tau = 6 \times 10(8)$ years, the lower and upper mass limits merge to similar to 5 solar mass. Researchers conclude that, even though the possibility of neutron stars as halo matter may be ruled out, that of white dwarfs may still be a viable hypothesis, though with very stringent constraints on allowed parameters, that merits further consideration. Author

A90-31407* Drexel Univ., Philadelphia, PA.

BIG BANG NUCLEOSYNTHESIS AND THE QUARK-HADRON TRANSITION

HANNU KURKI-SUONIO (Drexel University, Philadelphia, PA), RICHARD A. MATZNER (Texas, University, Austin), KEITH A. OLIVE (Minnesota, University, Minneapolis), and DAVID N. SCHRAMM (NASA/Fermilab Astrophysics Center, Batavia; Chicago, University, IL) *Astrophysical Journal*, Part 1 (ISSN 0004-637X), vol. 353, April 20, 1990, p. 406-410. Previously announced in STAR as N90-14168. refs

(Contract DE-AC02-83ER-40105; NSF PHY-88-06567)

Copyright

An examination and brief review is made of the effects of quark-hadron transition induced fluctuations on Big Bang nucleosynthesis. It is shown that cosmologically critical densities in baryons are difficult to reconcile with observation, but the traditional baryon density constraints from homogeneous calculations might be loosened by as much as 50 percent, to 0.3 of critical density, and the limit on the number of neutrino flavors remains about $N(\text{sub } \nu)$ is less than or approximately 4. To achieve baryon densities of greater than or approximately 0.3 of critical density would require initial density contrasts R is much greater the $10(\text{exp } e)$, whereas the simplest models for the transition seem to restrict R to less than of approximately $10(\text{exp } 2)$. Author

A90-34505* National Aeronautics and Space Administration. Lewis Research Center, Cleveland, OH.

A MODEL FOR THE DISTRIBUTION OF THE INTERGALACTIC MEDIUM

DONGSU RYU (NASA/Fermilab Astrophysics Center, Batavia, IL; Texas, University, Austin), ETHAN T. VISHNIAC (Texas, University, Austin), and WEI-HWAN CHIANG (Texas, University, Austin; IBM Corp., Kingston, NY) *Astrophysical Journal*, Part 1 (ISSN 0004-637X), vol. 354, May 10, 1990, p. 389-399. Research supported by TARP and DOE. refs

(Contract NSF AST-84-51736)

Copyright

The evolution and distribution of the intergalactic medium (IGM) in a universe dominated by cold dark matter with $\Omega(0) = 1$ and $h = 0.5$ are investigated. Galaxies form and eject energy into the IGM from z about 20 up to the present, and the distribution of the IGM is dominated by large connected structures. The power spectrum and two-point correlation function of the IGM show a suppressed growth due to the energy injected from galaxies and the mass subtraction to form galaxies. The high-temperature regions of the IGM correspond to the low-density regions and the low-temperature regions correspond to the high-density regions. The temperature of the IGM increases from $z = 1$ to $z = 0$, while the pressure decreases. The present temperature distribution shows a peak at about 10 million K. The mass fraction of the IGM with temperature below 100,000 K is negligible, indicating almost all the hydrogen is ionized. C.D.

A90-35291* National Aeronautics and Space Administration. Lewis Research Center, Cleveland, OH.

PHASE TRANSITIONS AS THE ORIGIN OF LARGE SCALE STRUCTURE IN THE UNIVERSE

NEIL TUROK (NASA/Fermilab Astrophysics Center, Batavia, IL) IN: Particle physics and astrophysics - Current viewpoints. Berlin and New York, Springer-Verlag, 1989, p. 267-309. Research supported by DOE. refs

Copyright

A review of the formation of large scale structure through gravitational growth of primordial perturbations is given. This is followed by a discussion of how symmetry breaking phase transitions in the early universe might have produced the required perturbations, in particular through the formation and evolution of a network of cosmic strings. Author

A90-40088* Carnegie-Mellon Univ., Pittsburgh, PA.

GRAVITATIONAL COUPLINGS OF THE INFLATON IN EXTENDED INFLATION

RICHARD HOLMAN, YUN WANG (Carnegie-Mellon University, Pittsburgh, PA), and EDWARD W. KOLB (NASA/Fermilab Astrophysics Center, Batavia; Chicago, University, IL) *Physical Review Letters* (ISSN 0031-9007), vol. 65, July 2, 1990, p. 17-20. Previously announced in STAR as N90-22504. refs

(Contract DE-AC02-76ER-03066; NAGW-1340)

Copyright

A new extended inflationary scenario evading the difficulties of the original model is discussed. The model can thermalize the energy in the bubble walls by the necessary epoch, and establish a Robertson-Walker frame in the bubble clusters. The essential new ingredient in the model is the observation that the coupling of the inflaton to the Jordan-Brans-Dicke field is expected to be different from that of visible matter. Author

A90-40093* Waseda Univ., Tokyo (Japan).

SOFT INFLATION

ANDREW L. BERKIN (Waseda University, Tokyo, Japan), KEI-ICHI MAEDA (Waseda University, Tokyo, Japan; NASA/Fermilab Astrophysics Center, Batavia, IL), and JUN-ICHI YOKOYAMA (Tokyo, University, Japan; NASA/Fermilab Astrophysics Center, Batavia, IL) *Physical Review Letters* (ISSN 0031-9007), vol. 65, July 9, 1990, p. 141-144. Previously announced in STAR as N90-22506. refs

(Contract NAGW-1340)

Copyright

90 ASTROPHYSICS

The cosmology resulting from two coupled scalar fields was studied, one which is either a new inflation or chaotic type inflation, and the other which has an exponentially decaying potential. Such a potential may appear in the conformally transformed frame of generalized Einstein theories like the Jordan-Brans-Dicke theory. The constraints necessary for successful inflation are examined. Conventional GUT models such as SU(5) were found to be compatible with new inflation, while restrictions on the self-coupling constant are significantly loosened for chaotic inflation. Author

A90-44095* National Aeronautics and Space Administration. Lewis Research Center, Cleveland, OH.

DARK MATTER CANDIDATES

MICHAEL S. TURNER (NASA/Fermilab Astrophysics Center, Batavia; Chicago, University, IL) IN: Astronomy, cosmology and fundamental physics; Proceedings of the Third ESO-CERN Symposium, Bologna, Italy, May 16-20, 1988. Dordrecht, Netherlands and Boston, MA, Kluwer Academic Publishers, 1989, p. 279-286; Discussion, p. 286. refs
(Contract DE-AC02-80ER-10587)
Copyright

The types of particles which may provide the nonluminous mass required by big-bang cosmological models are listed and briefly characterized. The observational evidence for the existence of dark matter (outweighing the luminous component by at least a factor of 10) is reviewed; the theoretical arguments favoring mainly nonbaryonic dark matter are summarized; and particular attention is given to weakly interacting massive particles (WIMPs) remaining as relics from the early universe. The WIMPs are classified as thermal relics (heavy stable neutrinos and lighter neutralinos), asymmetric relics (including baryons), nonthermal relics (superheavy magnetic monopoles, axions, and soliton stars), and truly exotic relics (relativistic debris or vacuum energy). Explanations for the current apparent baryon/exotica ratio of about 0.1 in different theoretical scenarios are considered, and the problems of experimental and/or observational dark-matter detection are examined. T.K.

A90-45560* National Aeronautics and Space Administration. Lewis Research Center, Cleveland, OH.

A MODEL FOR THE DISTRIBUTION OF DARK MATTER, GALAXIES, AND THE INTERGALACTIC MEDIUM IN A COLD DARK MATTER-DOMINATED UNIVERSE

DONGSU RYU (NASA/Fermilab Astrophysics Center, Batavia, IL), ETHAN T. VISHNIAC, and WEI-HWAN CHIANG (Texas, University, Austin) (NASA, NSF, Texas Academy of Science, et al., Texas Symposium on Relativistic Astrophysics, 14th, Dallas, TX, Dec. 11-16, 1988) New York Academy of Sciences, Annals (ISSN 0077-8923), vol. 571, 1989, p. 228-238. refs
Copyright

The spatial distribution of the cold-dark-matter (CDM) and baryonic components of CDM-dominated cosmological models are characterized, summarizing the results of recent theoretical investigations. The evolution and distribution of matter in an Einstein-de Sitter universe on length scales small enough so that the Newtonian approximation is valid is followed chronologically, assuming (1) that the galaxies, CDM, and the intergalactic medium (IGM) are coupled by gravity, (2) that galaxies form by taking mass and momentum from the IGM, and (3) that the IGM responds to the energy input from the galaxies. The results of the numerical computations are presented in extensive graphs and discussed in detail. T.K.

N90-22488* National Aeronautics and Space Administration. Lewis Research Center, Cleveland, OH.

SPACE STATION FREEDOM SOLAR ARRAY PANELS PLASMA INTERACTION TEST FACILITY

DONALD F. MARTIN and KENNETH D. MELLOTT 1989 14 p
Presented at the Spacecraft Charging Technology Conference, Monterey, CA, 31 Oct. - 3 Nov. 1989; sponsored by Naval Postgraduate School
(NASA-TM-102475; E-5262; NAS 1.15:102475) Avail: NTIS HC A03/MF A01 CSCL 03/2

The Space Station Freedom Power System will make extensive use of photovoltaic (PV) power generation. The phase 1 power system consists of two PV power modules each capable of delivering 37.5 KW of conditioned power to the user. Each PV module consists of two solar arrays. Each solar array is made up of two solar blankets. Each solar blanket contains 82 PV panels. The PV power modules provide a 160 V nominal operating voltage. Previous research has shown that there are electrical interactions between a plasma environment and a photovoltaic power source. The interactions take two forms: parasitic current loss (occurs when the current produced by the PV panel leaves at a high potential point and travels through the plasma to a lower potential point, effectively shorting that portion of the PV panel); and arcing (occurs when the PV panel electrically discharges into the plasma). The PV solar array panel plasma interaction test was conceived to evaluate the effects of these interactions on the Space Station Freedom type PV panels as well as to conduct further research. The test article consists of two active solar array panels in series. Each panel consists of two hundred 8 cm x 8 cm silicon solar cells. The test requirements dictated specifications in the following areas: plasma environment/plasma sheath; outgassing; thermal requirements; solar simulation; and data collection requirements. B.H.A.

91

LUNAR AND PLANETARY EXPLORATION

Includes planetology; and manned and unmanned flights.

A90-24814* National Aeronautics and Space Administration. Lewis Research Center, Cleveland, OH.

SOLAR POWER FOR THE LUNAR NIGHT

GEOFFREY A. LANDIS (NASA, Lewis Research Center, Cleveland, OH) IN: Space manufacturing 7 - Space resources to improve life on earth; Proceedings of the Ninth Princeton/AIAA/SSI Conference, Princeton, NJ, May 10-13, 1989. Washington, DC, American Institute of Aeronautics and Astronautics, 1989, p. 290-296. Previously announced in STAR as N89-26799. refs
Copyright

Providing power over the 354 hour lunar night provides a considerable challenge to solar power concepts for a moonbase. Concepts are reviewed for providing night power for a solar powered moonbase. The categories of solutions considered are electrical storage, physical storage, transmitted power, and innovative concepts. Electrical storage is the most well-developed option. Less developed electrical storage options are capacitors and superconducting inductors. Physical storage options include storage of potential energy and storage of energy in flywheels. Thermal storage has potentially high energy/weight, but problems of conduction and radiation losses during the night need to be addressed. Transmitted power considers use of microwave or laser beams to transmit power either from orbit or directly from the earth. Finally, innovative concepts proposed include reflecting light from orbital mirrors, locating the moonbase at a lunar pole, converting reflected earthlight, or moving the moonbase to follow the sun. Author

A90-35441* National Aeronautics and Space Administration. Lewis Research Center, Cleveland, OH.

DEGRADATION OF THE LUNAR VACUUM BY A MOON BASE

GEOFFREY LANDIS (NASA, Lewis Research Center, Cleveland, OH) Acta Astronautica (ISSN 0094-5765), vol. 21, March 1990, p. 183-187. refs
Copyright

Several industrial processes requiring high and ultra-high vacuum similar to the lunar vacuum are outlined. The effects of a 20-person lunar base and a 250-person industrial facility on this vacuum are discussed. It is shown that exhaust from transport spacecraft and leakage from the habitat will be comparable to

the daytime gas pressure for the 20-person base, and will degrade the vacuum to the range of 2×10 to the -9 th torr for the use of 250-person facility. This will result in replacing the mostly nonreactive gases hydrogen, helium, and neon with more reactive gases containing carbon and oxygen. This vacuum is still good enough to perform many important vacuum processes such as plasma-deposition of amorphous silicon for solar cells, but processes such as molecular beam epitaxy or locating an intersecting beam accelerator on the moon will require additional vacuum pumping. V.T.

N90-15030*# National Aeronautics and Space Administration. Lewis Research Center, Cleveland, OH.

SP-100 POWER SYSTEM CONCEPTUAL DESIGN FOR LUNAR BASE APPLICATIONS

LEE S. MASON, HARVEY S. BLOOMFIELD, and DONALD C. HAINLEY (Sverdrup Technology, Inc., Cleveland, OH.) 1989 22 p Presented at the 6th Symposium on Space Nuclear Power Systems, Albuquerque, NM, 8-12 Jan. 1989; sponsored by Inst. for Space Nuclear Power Studies (NASA-TM-102090; E-5083; NAS 1.15:102090) Avail: NTIS HC A03/MF A01 CSCL 03/2

A conceptual design is presented for a nuclear power system utilizing an SP-100 reactor and multiple Stirling cycle engines for operation on the lunar surface. Based on the results of this study, it was concluded that this power plant could be a viable option for an evolutionary lunar base. The design concept consists of a 2500 kWt (kilowatt thermal) SP-100 reactor coupled to eight free-piston Stirling engines. Two of the engines are held in reserve to provide conversion system redundancy. The remaining engines operate at 91.7 percent of their rated capacity of 150 kWe. The design power level for this system is 825 kWe. Each engine has a pumped heat-rejection loop connected to a heat pipe radiator. Power system performance, sizing, layout configurations, shielding options, and transmission line characteristics are described. System components and integration options are compared for safety, high performance, low mass, and ease of assembly. The power plant was integrated with a proposed human lunar base concept to ensure mission compatibility. This study should be considered a preliminary investigation; further studies are planned to investigate the effect of different technologies on this baseline design.

Author

99

GENERAL

N90-23339*# National Aeronautics and Space Administration. Lewis Research Center, Cleveland, OH.

ROMANS TO MARS

D. J. BENTS 1990 22 p Presented at the 28th Goddard Memorial Symposium, Washington, DC, 14-16 Mar. 1990; sponsored by the American Astronautical Society (NASA-TM-103094; E-5416; NAS 1.15:103094) Avail: NTIS HC A03/MF A01 CSCL 05/4

The key role played by technology advancement with respect to the anticipated era of discovery and exploration (in space) is illustrated: how bold new initiatives may or may not be enabled. A truly enabling technology not only renders the proposed missions technically feasible, but also makes them viable economically; that is, low enough in cost (relative to the economy supporting them) that urgent national need is not required for justification, low enough in cost that high risk can be programmatically tolerated. A fictional parallel is drawn to the Roman Empire of the second century A.D., shown to have possessed by that time the necessary knowledge, motivation, means, and technical capability of mounting, through the use of innovative mission planning, an initiative similar to Columbus' voyage. They failed to do so because they lacked

the advanced technology necessary to make it an acceptable proposition economically. Speculation, based on the historical perspective, is made on the outcome of contemporary plans for future exploration showing how they will be subjected to the same historical forces, within limits imposed by the state of technology development, that shaped the timing of that previous era of discovery and exploration. Author

N90-24220*# National Aeronautics and Space Administration. Lewis Research Center, Cleveland, OH.

TECHNICAL ACCOMPLISHMENTS OF THE NASA LEWIS RESEARCH CENTER, 1989 Annual Report, 1989

1990 252 p Original contains color illustrations (NASA-TM-102296; NAS 1.15:102296) Avail: NTIS HC A12/MF A02; 13 functional color pages CSCL 05/1

Topics addressed include: high-temperature composite materials; structural mechanics; fatigue life prediction for composite materials; internal computational fluid mechanics; instrumentation and controls; electronics; stirling engines; aeropropulsion and space propulsion programs, including a study of slush hydrogen; space power for use in the space station, in the Mars rover, and other applications; thermal management; plasma and radiation; cryogenic fluid management in space; microgravity physics; combustion in reduced gravity; test facilities and resources. J.P.S.

N90-26789*# National Aeronautics and Space Administration. Lewis Research Center, Cleveland, OH.

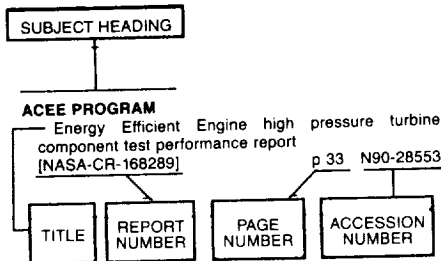
THE LESSONS OF VARSOVIAN'S RECONNAISSANCE

D. J. BENTS Jun. 1990 27 p Presented at the Case for Mars 4, Boulder, CO, 4-8 Jun. 1990; sponsored in part by JPL, NASA Ames Research Center, NASA Johnson Space Center, NASA Marshall Space Flight Center, American Astronautical Society, LANL, and Planetary Society (NASA-TM-103207; E-5615; NAS 1.15:103207) Avail: NTIS HC A03/MF A01 CSCL 05/4

The role played by advanced technology is illustrated with respect to the anticipated era of discovery and exploration (in space): how bold new exploration initiatives may or may not be enabled. Enabling technology makes the mission feasible. To be truly enabling, however, the technology must not only render the proposed mission technically feasible, but also make it viable economically; that is, low enough in cost (relative to the economy supporting it) that urgent national need is not required for justification, low enough that risks can be programmatically tolerated. An allegorical parallel is drawn to the Roman Empire of the second century AD, shown to have possessed by that time the necessary knowledge, motivation, means, and technical capability of mounting, through the use of innovative mission planning, an initiative similar to Columbus' voyage. They failed to do so; not because they lacked the vision, but because their technology was not advanced enough to make it an acceptable proposition economically. Speculation, based on the historical perspective, is made on the outcome of contemporary plans for future exploration showing how they will be subjected to the same historical forces, within limits imposed by the state of technology development, that shaped the timing of that previous era of discovery and exploration. Author

SUBJECT INDEX

Typical Subject Index Listing



The subject heading is a key to the subject content of the document. Titles, report numbers, and accession numbers of pertinent documents are provided under each subject heading. When the title is insufficiently descriptive of document content, a title extension is added, separated from the title by three hyphens. The report number helps to indicate the type of document cited (e.g., NASA report, NASA translation, NASA contractor report). The accession number is the number by which the document abstracts are arranged in this journal and by which the document is sold or requested. The titles, with title extensions if present, are arranged under each subject heading in ascending accession number order. The subject headings have been selected from the latest revision of the *NASA Thesaurus* (NASA SP-7064).

A

ABLATION

Growth and patterning of laser ablated superconducting YBa₂Cu₃O₇ films on LaAlO₃ substrates
[NASA-TM-102436] p 259 N90-22421

Ellipsometric study of YBa₂Cu₃O₇(x) laser ablated and co-evaporated films
[NASA-TM-103223] p 259 N90-26682

Laser ablated high T_c(sub c) superconducting thin YBa₂Cu₃O₇(x) films on substrates suitable for microwave applications p 260 N90-27808

ABRASION

Aeolian removal of dust from radiator surfaces on Mars
[NASA-TM-103205] p 81 N90-26068

ABSORPTION SPECTROSCOPY

Saturated fluorescence measurements of the hydroxyl radical in laminar high-pressure flames
[NASA-CR-185218] p 190 N90-22022

ABSORPTIVITY

A V-grooved GaAs solar cell p 225 A90-14887
XANES and EXAFS study of Au-substituted YBa₂Cu₃O₇(delta)
[NASA-TM-103291] p 260 N90-29219

ACCELERATED LIFE TESTS

Qualification and life testing of a flight design hydrazine arcjet system
[AIAA PAPER 90-2576] p 64 A90-42559

5kW xenon ion thruster lifetest
[AIAA PAPER 90-2543] p 68 A90-52564

ACCELERATION (PHYSICS)

The vibro-acoustic mapping of low gravity trajectories on a Learjet aircraft
[NASA-TM-103103] p 1 N90-21723
Collision forces for compliant projectiles
[NASA-TM-4203] p 223 N90-28111

ACCUMULATORS

Spent-beam refocusing analysis and multistage depressed collector design for a 75-W, 59- to 64-GHz coupled-cavity traveling-wave tube
[NASA-TP-3039] p 155 N90-27965

ACCURACY

Foundations of measurement and instrumentation
[NASA-RP-1222] p 189 N90-21351

ACEE PROGRAM

Energy Efficient Engine high pressure turbine component test performance report
[NASA-CR-168289] p 33 N90-28553

Energy Efficient Engine combustor test hardware detailed design report
[NASA-CR-168301] p 33 N90-28554

Energy Efficient Engine acoustic supporting technology report
[NASA-CR-174834] p 33 N90-28557

Energy Efficient Engine: Flight propulsion system final design and analysis
[NASA-CR-168219] p 34 N90-28558

Energy Efficient Engine core design and performance report
[NASA-CR-168069] p 34 N90-28559

Energy Efficient Engine integrated core/low spool design and performance report
[NASA-CR-168211] p 34 N90-28561

Energy Efficient Engine: Control system component performance report
[NASA-CR-174651] p 34 N90-28562

NASA/GE Energy Efficient Engine low pressure turbine scaled test vehicle performance report
[NASA-CR-168290] p 34 N90-28563

Energy efficient engine program technology benefit/cost study. Volume 1: Executive summary
[NASA-CR-174766-VOL-1] p 34 N90-28564

Energy efficient engine program technology benefit/cost study. Volume 2
[NASA-CR-174766-VOL-2] p 35 N90-28565

Energy efficient engine pin fin and ceramic composite segmented liner combustor sector rig test report
[NASA-CR-179534] p 35 N90-28567

Energy Efficient Engine: Combustor component performance program
[NASA-CR-179533] p 35 N90-28568

Energy Efficient Engine: High-pressure compressor test hardware detailed design report
[NASA-CR-180850] p 36 N90-28570

ACOUSTIC ATTENUATION

Comparison between design and installed acoustic characteristics of NASA Lewis 9- by 15-foot low-speed wind tunnel acoustic treatment
[NASA-TP-2996] p 38 N90-19242

ACOUSTIC COUPLING

Combustion instability coupling with feed system acoustics
[NASA-TP-2996] p 108 N90-28629

ACOUSTIC FREQUENCIES

The radiation of sound from a propeller at angle of attack
[NASA-CR-4264] p 249 N90-21602

ACOUSTIC INSTABILITY

Spatial evolution of nonlinear acoustic mode instabilities on hypersonic boundary layers
[NASA-TM-102431] p 177 N90-14517

ACOUSTIC MEASUREMENT

Effects of fiber motion on the acoustic behavior of an anisotropic, flexible fibrous material p 247 A90-33313
Acoustic test and analysis of a counterrotating prop-fan model
[NASA-CR-179590] p 247 N90-10683

Comparison between design and installed acoustic characteristics of NASA Lewis 9- by 15-foot low-speed wind tunnel acoustic treatment
[NASA-TP-2996] p 38 N90-19242

ACOUSTIC PROPAGATION

Mixed variational formulation of finite element analysis of acoustoelastic/slosh fluid-structure interaction
[NASA-TP-2996] p 212 A90-34851

ACOUSTIC STREAMING

Microgravity acoustic mixing for particle cloud combustors
[NASA-CR-185159] p 248 N90-21600

ACOUSTICS

A modified VAPEPS method for predicting vibroacoustic response of unreinforced mass loaded honeycomb panels p 206 A90-43731

An approximate model for the performance and acoustic predictions of counterrotating propeller configurations
[NASA-CR-180667] p 248 N90-18228

The vibro-acoustic mapping of low gravity trajectories on a Learjet aircraft
[NASA-TM-103103] p 1 N90-21723

Acousto-ultrasonic nondestructive evaluation of materials using laser beam generation and detection
[NASA-CR-186694] p 154 N90-23664

Energy Efficient Engine acoustic supporting technology report
[NASA-CR-174834] p 33 N90-28557

ACOUSTO-OPTICS

Evaluation of transport conditions during physical vapor transport growth of opto-electronic crystals
[NASA-TP-2996] p 132 A90-20525

ACTIVATION ENERGY

Stress versus temperature dependent activation energies in creep
[NASA-TM-103192] p 221 N90-23773

ACTIVE CONTROL

Active phase compensation system for fiber optic holography p 250 A90-11310
Active vibration control for flexible rotor by optimal direct-output feedback control p 197 A90-46222

Test and theory for piezoelectric actuator-active vibration control of rotating machinery p 198 A90-46226
Actuator design for rotor control p 198 A90-46232

Development of a compact, light weight magnetic bearing
[AIAA PAPER 90-2483] p 199 A90-47223

Modern developments in shear flow control with swirl
[NASA-CR-186586] p 181 N90-22000

Elements of active vibration control for rotating machinery
[NASA-TM-102368] p 137 N90-22703

Autonomous power expert system
[NASA-CR-185263] p 80 N90-25187

ACTS

LBR-2 earth stations for the ACTS program
[AIAA PAPER 90-0838] p 42 A90-25662

Advanced Communications Technology Satellite (ACTS)
[AIAA PAPER 90-0839] p 140 A90-25663

Advanced Communications Technology Satellite (ACTS) and potential system applications p 142 A90-51165

ACTUATORS

Variable speed induction motor operation from a 20-kHz power bus p 148 A90-38119
Test and theory for piezoelectric actuator-active vibration control of rotating machinery p 198 A90-46226

Actuator design for rotor control p 198 A90-46232
Advanced Launch System (ALS) actuation and power systems impact operability and cost p 69 A90-52955

Aerospace induction motor actuators driven from a 20-kHz power link
[NASA-TM-102482] p 28 N90-20085

Advanced Launch System (ALS): Electrical actuation and power systems improve operability and cost picture
[NASA-TM-102547] p 152 N90-21271

Electromechanical actuation for thrust vector control applications
[NASA-TM-102548] p 152 N90-21272

Civil air transport: A fresh look at power-by-wire and fly-by-light
[NASA-TM-102574] p 153 N90-21283

Elements of active vibration control for rotating machinery
[NASA-TM-102368] p 137 N90-22703

Field oriented control of induction motors
[NASA-TM-103154] p 154 N90-22731

ADA (PROGRAMMING LANGUAGE)

Development of Ada language control software for the NASA power management and distribution test bed
[NASA-TM-4203] p 236 A90-38082

ADAPTIVE CONTROL

- Convergence of the SMI and the diagonally loaded SMI algorithms with weak interference
[AD-A22639] p 141 A90-36717
- Low frequency vibration isolation technology for microgravity space experiments p 136 A90-46246
- A new approach to active vibration isolation for microgravity space experiments
[NASA-TM-102470] p 137 N90-17929
- An adaptive human response mechanism controlling the V/STOL aircraft. Appendix 3: The adaptive control model of a pilot in V/STOL aircraft control loops
[NASA-CR-186599] p 38 N90-21777
- Neuromorphic learning of continuous-valued mappings from noise-corrupted data. Application to real-time adaptive control
[NASA-TM-4176] p 241 N90-25607
- Beam rider for an Articulated Robot Manipulator (ARM) accurate positioning of long flexible manipulators
[NASA-CR-185151] p 241 N90-26581
- Temperature and melt solid interface control during crystal growth
[NASA-CR-186731] p 259 N90-26664
- An expert system to perform on-line controller restructuring for abrupt model changes
[NASA-TM-103609] p 241 N90-29121
- ADAPTIVE FILTERS**
- A simple algebraic grid adaptation scheme with applications to two- and three-dimensional flow problems
[NASA-TM-102446] p 178 N90-18667
- ADDITION RESINS**
- Autoclavable addition polyimides for 371 C composite applications
[NASA-TM-103233] p 102 N90-27874
- ADDITIVES**
- Crystallization behavior and properties of BaO-Al₂O₃-2SiO₂ glass matrices
[NASA-CR-185209] p 127 N90-19374
- ADHESION**
- Applications of surface analysis and surface theory in tribology p 84 A90-37458
- Fundamental tribological properties of ion-beam-deposited boron nitride films p 124 A90-49054
- Fundamental tribological properties of ion-beam-deposited boron nitride films
[NASA-TM-102088] p 125 N90-11881
- ADHESION TESTS**
- Instrumented adhesion tests on plasma sprayed thermal barrier coatings p 111 A90-20255
- Tensile adhesion testing methodology for thermally sprayed coatings p 85 A90-43902
- ADHESIVE BONDING**
- Universal aspects of brittle fracture, adhesion, and atomic force microscopy p 83 A90-14021
- Simplified design procedures for fiber composite structural components/joints
[NASA-TM-103113] p 101 N90-24384
- ADIABATIC CONDITIONS**
- Critical speeding up in pure fluids p 167 A90-26369
- ADVANCED LAUNCH SYSTEM (STS)**
- Advanced Launch System (ALS) actuation and power systems impact operability and cost p 69 A90-52955
- Aerospace induction motor actuators driven from a 20-kHz power link
[NASA-TM-102482] p 28 N90-20085
- Advanced Launch System (ALS): Electrical actuation and power systems improve operability and cost picture
[NASA-TM-102547] p 152 N90-21271
- Electromechanical actuation for thrust vector control applications
[NASA-TM-102548] p 152 N90-21272
- AEROACOUSTICS**
- Application of the computational aeroacoustics method to an advanced counterrotating propfan configuration
[AIAA PAPER 90-0183] p 246 A90-19725
- Investigation of the near wake of a propfan p 7 A90-40686
- Mixer-ejector nozzle for jet noise suppression
[AIAA PAPER 90-1909] p 247 A90-47202
- Large-scale Advanced Prop-fan (LAP) technology assessment report
[NASA-CR-182142] p 24 N90-10046
- An investigation of counterrotating tip vortex interaction
[NASA-CR-185135] p 247 N90-11549
- Predicted and measured boundary layer refraction for advanced turboprop propeller noise
[NASA-TM-102365] p 248 N90-17413
- Experimental performance and acoustic investigation of modern, counterrotating blade concepts
[NASA-CR-185158] p 18 N90-23393
- Aeroacoustics of advanced propellers
[NASA-TM-103137] p 249 N90-26635

- Development of a linearized unsteady aerodynamic analysis for cascade gust response predictions
[NASA-CR-4308] p 14 N90-27655
- Generalized Advanced Propeller Analysis System (GAPAS). Volume 2: Computer program user manual
[NASA-CR-185277] p 36 N90-29394

AERODYNAMIC CHARACTERISTICS

- Numerical study of the effects of icing on finite wing aerodynamics
[AIAA PAPER 90-0757] p 3 A90-20010
- Effects of compressibility on the characteristics of free shear layers p 6 A90-25285
- Large-scale Advanced Prop-fan (LAP) static rotor test report
[NASA-CR-180848] p 25 N90-12617
- Concurrent processing adaptation of aeroplastic analysis of propfans
[NASA-TM-102455] p 217 N90-14656
- Experimental performance and acoustic investigation of modern, counterrotating blade concepts
[NASA-CR-185158] p 18 N90-23393
- Development of a linearized unsteady aerodynamic analysis for cascade gust response predictions
[NASA-CR-4308] p 14 N90-27655
- Generalized Advanced Propeller Analysis System (GAPAS). Volume 2: Computer program user manual
[NASA-CR-185277] p 36 N90-29394

AERODYNAMIC COEFFICIENTS

- Fortified LEWICE with viscous effects --- Lewis Ice Accretion Prediction Code
[AIAA PAPER 90-0754] p 15 A90-20009

AERODYNAMIC CONFIGURATIONS

- An approximate model for the performance and acoustic predictions of counterrotating propeller configurations
[NASA-CR-180667] p 248 N90-18228
- Energy Efficient Engine high pressure turbine component test performance report
[NASA-CR-168289] p 33 N90-28553
- Energy Efficient Engine program advanced turbopfan nacelle definition study
[NASA-CR-174942] p 34 N90-28560

AERODYNAMIC DRAG

- On the use of external burning to reduce aerospace vehicle transonic drag
[AIAA PAPER 90-1935] p 20 A90-40562
- Exhaust nozzles for propulsion systems with emphasis on supersonic cruise aircraft
[NASA-RP-1235] p 29 N90-21037
- On the use of external burning to reduce aerospace vehicle transonic drag
[NASA-TM-103107] p 30 N90-21762

AERODYNAMIC FORCES

- Counter-rotating propellant analysis using a frequency domain panel method p 7 A90-40937
- Shaft flexibility effects on the forced response of a bladed-disk assembly p 21 A90-43218

AERODYNAMIC HEAT TRANSFER

- Heat transfer measurements from a NACA 0012 airfoil in flight and in the NASA Lewis icing research tunnel
[NASA-CR-4278] p 13 N90-19203

AERODYNAMIC HEATING

- Thermal/structural analyses of several hydrogen-cooled leading-edge concepts for hypersonic flight vehicles
[AIAA PAPER 90-0053] p 164 A90-23702
- Thermal/structural analyses of several hydrogen-cooled leading-edge concepts for hypersonic flight vehicles
[NASA-TM-102391] p 177 N90-14511

AERODYNAMIC LOADS

- Unsteady Euler analysis of the flowfield of a propfan at an angle of attack
[AIAA PAPER 90-0339] p 5 A90-25028
- Evaluation of three turbulence models in static air loads and dynamic stall predictions p 7 A90-31291
- The radiation of sound from a propeller at angle of attack
[NASA-CR-4264] p 249 N90-21602
- NASA/GE Energy Efficient Engine low pressure turbine scaled test vehicle performance report
[NASA-CR-168290] p 34 N90-28563

AERODYNAMIC STABILITY

- Aeroelastic detuning for stability enhancement of unstalled supersonic flutter p 19 A90-17462
- Aeroelastic stability analysis of a high-energy turbine blade --- for SSME High Pressure Oxidizer TurboPump first stage
[AIAA PAPER 90-2351] p 66 A90-47215

AERODYNAMIC STALLING

- Some observations on transitory stall in conical diffusers
[AIAA PAPER 90-0048] p 4 A90-22158
- Analysis of fully stalled compressor p 6 A90-27966
- Some observations on transitory stall in conical diffusers
[NASA-TM-102387] p 11 N90-12561

AERODYNAMICS

- The unsteady aerodynamics of an oscillating cascade in a compressible flow field p 2 A90-11789
- An unsteady lifting surface method for single rotation propellers
[NASA-CR-4302] p 14 N90-25940
- Aerodynamics of a linear oscillating cascade
[NASA-TM-103250] p 15 N90-27657

AEROELASTICITY

- Shaft flexibility effects on aeroelastic stability of a rotating bladed disk p 208 A90-16371
- Aeroelastic detuning for stability enhancement of unstalled supersonic flutter p 19 A90-17462
- Application of an efficient hybrid scheme for aeroelastic analysis of advanced propellers
[AIAA PAPER 90-0028] p 4 A90-22153
- Blade mistuning coupled with shaft flexibility effects in rotor aeroelasticity
[ASME PAPER 89-GT-330] p 19 A90-23896
- Time domain flutter analysis of cascades using a full-potential solver
[AIAA PAPER 90-0984] p 6 A90-29374
- Concurrent processing adaptation of aeroelastic analysis of propfans
[AIAA PAPER 90-1036] p 211 A90-29380
- Three dimensional full potential method for the aeroelastic modeling of propfans
[AIAA PAPER 90-1120] p 7 A90-29392
- Aeroelastic problems in turbomachines
[AIAA PAPER 90-1157] p 7 A90-29393
- Shaft flexibility effects on the forced response of a bladed-disk assembly p 21 A90-43218
- Aeroelastic stability analysis of a high-energy turbine blade --- for SSME High Pressure Oxidizer TurboPump first stage
[AIAA PAPER 90-2351] p 66 A90-47215
- Large-scale Advanced Prop-fan (LAP) technology assessment report
[NASA-CR-182142] p 24 N90-10046
- Numerical simulation of unsteady rotational flow over propfan configurations
[NASA-CR-186037] p 10 N90-12500
- Application of an efficient hybrid scheme for aeroelastic analysis of advanced propellers
[NASA-TM-102428] p 11 N90-13355
- Concurrent processing adaptation of aeroplastic analysis of propfans
[NASA-TM-102455] p 217 N90-14656
- Structural dynamics branch research and accomplishments
[NASA-TM-102488] p 223 N90-26373

AERONAUTICAL ENGINEERING

- Bibliography of Lewis Research Center technical publications announced in 1988
[NASA-TM-102034] p 262 N90-15846

AEROSPACE ENGINEERING

- Bibliography of Lewis Research Center technical publications announced in 1988
[NASA-TM-102034] p 262 N90-15846
- Power conditioning techniques
[NASA-TM-102577] p 151 N90-20301
- Bearing and gear steels for aerospace applications
[NASA-TM-102529] p 202 N90-20391
- Optical techniques for determination of normal shock position in supersonic flows for aerospace applications
[NASA-TM-103201] p 190 N90-25323

AEROSPACE ENVIRONMENTS

- On-orbit low gravity cryogenic scientific investigations using the COLD-SAT Satellite
[AIAA PAPER 90-0718] p 39 A90-19988
- Wear consideration in gear design for space applications p 194 A90-21121
- EPSAT - A workbench for designing high-power systems for the space environment
[AIAA PAPER 90-0637] p 245 A90-26975
- Space Station Freedom solar array design development p 58 A90-38076
- Space vehicle propulsion systems - Environmental space hazards
[AIAA PAPER 90-1881] p 63 A90-40545
- Reflector surface distortion analysis techniques (thermal distortion analysis of antennas in space) p 144 N90-19267
- Comparison of currents predicted by NASCAP/LEO model simulations with elementary Langmuir-type bare probe models for an insulated cable containing a single pinhole
[NASA-TM-102486] p 51 N90-26054
- AEROSPACE INDUSTRY**
- Resources - Supply and availability --- of superalloys for United States aerospace industry p 114 A90-34152
- AEROSPACE PLANES**
- Minimum fuel trajectory for the aerospace-plane
[AAS PAPER 89-352] p 40 A90-46785

- Slush Hydrogen (SLH2) technology development for application to the National Aerospace Plane (NASP) [NASA-TM-102315] p 50 N90-14268
- Background, current status, and prognosis of the ongoing slush hydrogen technology development program for the NASP [NASA-TM-103220] p 51 N90-26055
- Prediction of the ullage gas thermal stratification in a NASP vehicle propellant tank experimental simulation using FLOW-3D [NASA-TM-103217] p 131 N90-26160
- AEROSPACE SAFETY**
- Multi-sensor analysis techniques for SSME safety monitoring [AIAA PAPER 90-1990] p 45 A90-52499
- Fire safety applications for spacecraft p 16 N90-17595
- Multi-sensor analysis techniques for SSME safety monitoring [NASA-CR-185260] p 45 N90-27732
- AEROSPACE SYSTEMS**
- NASA aerospace battery systems program update p 228 A90-38217
- Low-gravity fluid physics: A program overview [NASA-TM-103215] p 183 N90-26273
- NASA aerospace flight battery systems program [NASA-TM-103237] p 233 N90-26397
- Preliminary designs for 25 kW advanced Stirling conversion systems for dish electric applications [NASA-TM-103188] p 263 N90-26729
- Advanced onboard propulsion benefits and status [NASA-TM-103174] p 82 N90-27786
- AEROSPACE TECHNOLOGY TRANSFER**
- Application of HOST technology to the SSME HPFTP blade [ASME PAPER 89-GT-130] p 209 A90-23828
- Enhanced heat transfer rocket combustor technology component hot-fire test results [AIAA PAPER 90-2182] p 64 A90-42063
- AEROSPACE VEHICLES**
- On the use of external burning to reduce aerospace vehicle transonic drag [AIAA PAPER 90-1935] p 20 A90-40562
- Fire safety applications for spacecraft p 16 N90-17595
- On the use of external burning to reduce aerospace vehicle transonic drag [NASA-TM-103107] p 30 N90-21762
- AEROTHERMOCHEMISTRY**
- Comparative study of computational efficiency of two LU schemes for non-equilibrium reacting flows [AIAA PAPER 90-0396] p 167 A90-26940
- AEROTHERMODYNAMICS**
- CFD propels NASP propulsion progress p 172 A90-41163
- Heat transfer measurements from a NACA 0012 airfoil in flight and in the NASA Lewis icing research tunnel [NASA-CR-4278] p 13 N90-19203
- Probabilistic modeling for simulation of aerodynamic uncertainties in propulsion systems p 29 N90-21036
- [NASA-TM-102472] p 29 N90-21036
- Navier-Stokes analysis of turbine blade heat transfer [NASA-TM-102496] p 179 N90-21300
- AFFERENT NERVOUS SYSTEMS**
- A geometric analysis of semicircular canals and induced activity in their peripheral afferents in the rhesus monkey p 234 A90-28084
- AFTERBURNING**
- High-temperature test facility at the NASA Lewis engine components research laboratory [NASA-TM-103143] p 39 N90-25151
- AGING (METALLURGY)**
- Heat treatment study of the SiC/Ti-15-3 composite system [NASA-TP-2970] p 97 N90-19302
- AIR**
- WINCOF-I code for prediction of fan compressor unit with water ingestion [NASA-CR-185157] p 1 N90-21724
- AIR COOLING**
- Design of an air-cooled metallic high-temperature radial turbine p 20 A90-32960
- AIR JETS**
- The entrainment rate for a row of turbulent jets [NASA-CR-185278] p 15 N90-28504
- AIRCRAFT COMMUNICATION**
- AIRNET: A real-time communications network for aircraft [NASA-CR-186140] p 145 N90-24514
- AIRCRAFT COMPARTMENTS**
- Interior noise in the untreated Gulfstream II Propfan Test Assessment aircraft p 17 A90-44736
- AIRCRAFT CONFIGURATIONS**
- A modeling technique for STOVL ejector and volume dynamics [AIAA PAPER 90-2417] p 20 A90-42168
- A modeling technique for STOVL ejector and volume dynamics [NASA-TM-103167] p 30 N90-22566
- AIRCRAFT CONSTRUCTION MATERIALS**
- Composite Blade Structural Analyzer (COBSTRAN) theoretical/programmer's manual [NASA-TM-101958] p 95 N90-10181
- Materials for engine applications above 3000 deg F: An overview [NASA-TM-100169] p 95 N90-10188
- Ultrasonic and radiographic evaluation of advanced aerospace materials: Ceramic composites [NASA-TM-102540] p 207 N90-21401
- AIRCRAFT CONTROL**
- Cooperative synthesis of control and display augmentation in approach and landing p 36 A90-33061
- H-infinity based integrated flight/propulsion control design for a STOVL aircraft in transition flight [AIAA PAPER 90-3335] p 36 A90-47595
- The implementation of STOVL task-tailored control modes in a fighter cockpit [AIAA PAPER 90-3229] p 17 A90-49114
- The insertion of human dynamics models in the flight control loops of V/STOL research aircraft. Appendix 2: The optimal control model of a pilot in V/STOL aircraft control loops [NASA-CR-186598] p 38 N90-21776
- An adaptive human response mechanism controlling the V/STOL aircraft. Appendix 3: The adaptive control model of a pilot in V/STOL aircraft control loops [NASA-CR-186599] p 38 N90-21777
- An expert system to perform on-line controller restructuring for abrupt model changes [NASA-TM-103609] p 241 N90-29121
- AIRCRAFT DESIGN**
- Research on a two-dimensional inlet for a supersonic V/STOL propulsion system. Appendix A [NASA-CR-174945] p 12 N90-18364
- Energy efficient engine program technology benefit/cost study, volume 2 [NASA-CR-174766-VOL-2] p 35 N90-28565
- AIRCRAFT ENGINES**
- Augmented heat transfer in rectangular channels of narrow aspect ratios with rib turbulators p 157 A90-13091
- TBCs for better engine efficiency --- thermal barrier coatings p 83 A90-17294
- Parametric studies of advanced turboprops p 19 A90-21225
- Effect of reduced aft diameter and increased blade number of high-speed counterrotation propeller performance [AIAA PAPER 89-0438] p 4 A90-23650
- Burner rig hot corrosion of silicon carbide and silicon nitride p 121 A90-25267
- Advanced technology's impact on compressor design and development - A perspective [SAE SP-800] p 20 A90-28571
- Composites boost 21st-century aircraft engines p 90 A90-29704
- Fiber reinforced superalloys p 91 A90-34169
- Convertible engine system for high speed rotorcraft [AIAA PAPER 90-2512] p 20 A90-40643
- Transient behavior of supersonic flow through inlets [AIAA PAPER 90-2130] p 8 A90-42734
- NASA's HITEMP program for UHBR engines [AIAA PAPER 90-2395] p 22 A90-47218
- Combustor technology for future aircraft [AIAA PAPER 90-2400] p 22 A90-47219
- A supersonic through-flow fan engine airframe integration study [NASA-CR-185140] p 10 N90-10004
- Full scale technology demonstration of a modern counterrotating unducted fan engine concept: Component test [NASA-CR-180868] p 24 N90-10047
- Full scale technology demonstration of a modern counterrotating unducted fan engine concept: Design report [NASA-CR-180867] p 24 N90-10048
- Full scale technology demonstration of a modern counterrotating unducted fan engine concept: Engine test [NASA-CR-180869] p 24 N90-10049
- Advanced technologies impact on compressor design and development: A perspective [NASA-TM-102341] p 24 N90-10891
- Effect of reduced aft diameter and increased blade number on high-speed counterrotation propeller performance [NASA-TM-102077] p 11 N90-13352
- Structural tailoring of select fiber composite structures [NASA-TM-102484] p 99 N90-21137
- Attachment of lead wires to thin film thermocouples mounted on high temperature materials using the parallel gap welding process [NASA-TM-102442] p 189 N90-21361
- Aeropropulsion facilities configuration control: Procedures manual [NASA-TM-102541] p 207 N90-21399
- Control of flow separation and mixing by aerodynamic excitation [NASA-TM-103131] p 13 N90-21733
- Elevated temperature crack growth [NASA-CR-182247] p 222 N90-26355
- Energy efficient engine program technology benefit/cost study. Volume 1: Executive summary [NASA-CR-174766-VOL-1] p 34 N90-28564
- Energy efficient engine program technology benefit/cost study, volume 2 [NASA-CR-174766-VOL-2] p 35 N90-28565
- Energy Efficient Engine: Control system preliminary definition report [NASA-CR-179578] p 35 N90-28569
- AIRCRAFT EQUIPMENT**
- Electro-impulse de-icing testing analysis and design [NASA-CR-4175] p 18 N90-10031
- AIRCRAFT HAZARDS**
- NASA's program on icing research and technology p 16 N90-15062
- Modeling of surface roughness effects on glaze ice accretion p 16 N90-20925
- Ultrasonic techniques for aircraft ice accretion measurement p 16 N90-20926
- Investigation of surface water behavior during glaze ice accretion p 16 N90-20927
- The influence of ice accretion physics on the forecasting of aircraft icing conditions p 17 N90-20928
- Advanced instrumentation for aircraft icing research [NASA-CR-185225] p 18 N90-21006
- AIRCRAFT NOISE**
- Noise of a simulated installed model counterrotation propeller at angle-of-attack and takeoff/approach conditions [AIAA PAPER 90-0283] p 247 A90-32505
- Interior noise in the untreated Gulfstream II Propfan Test Assessment aircraft p 17 A90-44736
- Propfan Test Assessment (PTA): Flight test report [NASA-CR-182278] p 24 N90-11738
- Comparison between design and installed acoustic characteristics of NASA Lewis 9- by 15-foot low-speed wind tunnel acoustic treatment [NASA-TP-2996] p 38 N90-19242
- Noise of a simulated installed model counterrotation propeller at angle-of-attack and takeoff/approach conditions [NASA-TM-102440] p 248 N90-20794
- High speed turboprop aeroacoustic study (counterrotation). Volume 1: Model development [NASA-CR-185241] p 249 N90-26633
- AIRCRAFT PERFORMANCE**
- Supersonic through-flow fan engine and aircraft mission performance [NASA-TM-102304] p 29 N90-21038
- AIRCRAFT POWER SUPPLIES**
- Preliminary design of a long-endurance Mars aircraft [AIAA PAPER 90-2000] p 43 A90-40587
- Civil air transport: A fresh look at power-by-wire and fly-by-light [NASA-TM-102574] p 153 N90-21283
- Preliminary design of a long-endurance Mars aircraft [NASA-CR-185243] p 30 N90-21763
- AIRCRAFT SAFETY**
- Electro-impulse de-icing testing analysis and design [NASA-CR-4175] p 18 N90-10031
- AIRCRAFT STRUCTURES**
- Development of a phase Doppler based probe for icing cloud droplet characterization [AIAA PAPER 90-0667] p 186 A90-26978
- AIRCRAFT WAKES**
- The low frequency oscillation in the flow over a NACA0012 airfoil with an 'iced' leading edge p 8 A90-46377
- AIRFOIL OSCILLATIONS**
- The low frequency oscillation in the flow over a NACA0012 airfoil with an 'iced' leading edge p 8 A90-46377
- AIRFOIL PROFILES**
- Fortified LEWICE with viscous effects --- Lewis Ice Accretion Prediction Code [AIAA PAPER 90-0754] p 15 A90-20009
- Numerical solutions of the linearized Euler equations for unsteady vortical flows around lifting airfoils [AIAA PAPER 90-0694] p 5 A90-25041
- The low frequency oscillation in the flow over a NACA0012 airfoil with an 'iced' leading edge p 8 A90-46377

AIRFOILS

- Predictions of airfoil aerodynamic performance degradation due to icing p 3 A90-16753
- Development of an unstructured mesh/Navier-Stokes method for aerodynamics of aircraft with ice accretions [AIAA PAPER 90-0758] p 4 A90-20011
- Convective heat transfer measurements from a NACA 0012 airfoil in flight and in the NASA Lewis Icing Research Tunnel
- [AIAA PAPER 90-0199] p 162 A90-22180
- Fiber reinforced superalloys p 91 A90-34169
- Experimental investigation of multi-element airfoil ice accretion and resulting performance degradation p 9 A90-48954
- Convective heat transfer measurements from a NACA 0012 airfoil in flight and in the NASA Lewis Icing Research Tunnel
- [NASA-TM-102448] p 176 N90-13750
- Numerical solutions of the linearized Euler equations for unsteady vortical flows around lifting airfoils
- [NASA-TM-102466] p 12 N90-17562
- Heat transfer measurements from a NACA 0012 airfoil in flight and in the NASA Lewis icing research tunnel
- [NASA-CR-4278] p 13 N90-19203
- Numerical simulations of supersonic flow through oscillating cascade sections
- [NASA-TM-103100] p 13 N90-20051
- Ultrasonic techniques for aircraft ice accretion measurement p 16 N90-20926
- Control of flow separation and mixing by aerodynamic excitation
- [NASA-TM-103131] p 13 N90-21733
- Development of a linearized unsteady aerodynamic analysis for cascade gust response predictions
- [NASA-CR-4308] p 14 N90-27655
- Aerodynamics of a linear oscillating cascade
- [NASA-TM-103250] p 15 N90-27657
- AIRFRAMES**
- Three approaches to reliability analysis p 206 A90-30706
- A supersonic through-flow fan engine airframe integration study
- [NASA-CR-185140] p 10 N90-10004
- ALCOHOLS**
- Free dendritic growth in viscous melts - Cyclohexanol p 253 A90-19285
- An investigation of flame spread over shallow liquid pools in microgravity and nonair environments
- [NASA-TM-102425] p 134 N90-13680
- ALGEBRA**
- A simple algebraic grid adaptation scheme with applications to two- and three-dimensional flow problems
- [NASA-TM-102446] p 178 N90-18667
- High accuracy solutions of incompressible Navier-Stokes equations
- [NASA-TM-102539] p 244 N90-21567
- Application of symbolic computations to the constitutive modeling of structural materials
- [NASA-TM-103225] p 222 N90-26364
- ALGORITHMS**
- Analysis of rotary engine combustion processes based on unsteady, three-dimensional computations
- [AIAA PAPER 90-0643] p 163 A90-22237
- Application of heuristic satellite plan synthesis algorithms to requirements of the WARC-88 allotment plan
- [AIAA PAPER 90-0815] p 245 A90-25638
- Space nuclear reactor shields for manned and unmanned applications p 57 A90-37859
- An observer-based compensator for distributed delays p 239 A90-49899
- Multi-sensor analysis techniques for SSME safety monitoring
- [AIAA PAPER 90-1990] p 45 A90-52499
- Quotient-difference type generalizations of the power method and their analysis p 242 N90-10635
- [NASA-TM-102361]
- An experimental SMI adaptive antenna array for weak interfering signals
- [NASA-CR-185976] p 142 N90-11211
- An improved algorithm for the modeling of vapor flow in heat pipes
- [NASA-CR-185179] p 176 N90-13748
- Analysis of rotary engine combustion processes based on unsteady, three-dimensional computations
- [NASA-TM-102469] p 176 N90-13749
- Data compression techniques applied to high resolution high frame rate video technology
- [NASA-CR-4263] p 143 N90-14452
- A new uniformly valid asymptotic integration algorithm for elasto-plastic-creep and unified viscoplastic theories including continuum damage
- [NASA-TM-102344] p 217 N90-14655

- Application of heuristic satellite plan synthesis algorithms to requirements of the WARC-88 allotment plan
- [NASA-TM-102479] p 245 N90-14856
- Advanced detection, isolation, and accommodation of sensor failures in turbofan engines: Real-time microcomputer implementation
- [NASA-TP-2925] p 37 N90-15112
- Mesh refinement in finite element analysis by minimization of the stiffness matrix trace
- [NASA-CR-185170] p 201 N90-15434
- A numerical simulation of the flow in the diffuser of the NASA Lewis icing research tunnel
- [NASA-TM-102480] p 38 N90-15965
- Scaling study for SP-100 reactor technology
- [NASA-TM-897140] p 249 N90-16496
- Eigensolution of finite element problems in a completely connected parallel architecture
- [NASA-TM-102450] p 217 N90-17173
- Analysis of whisker-toughened ceramic components: A design engineer's viewpoint
- [NASA-TM-102333] p 97 N90-18504
- Parallel algorithms for boundary value problems
- [NASA-TM-102498] p 243 N90-19783
- Numerical Arc Segmentation Algorithm for a Radio Conference-NASARC (version 4.0) technical manual
- [NASA-TM-101453] p 144 N90-20264
- Effects of additional interfering signals on adaptive array performance
- [NASA-CR-186508] p 145 N90-20271
- Numerical Arc Segmentation Algorithm for a Radio Conference (NASARC), version 4.0: User's manual
- [NASA-TM-101454] p 145 N90-21250
- Electromechanical actuation for thrust vector control applications
- [NASA-TM-102548] p 152 N90-21272
- A cost-effective strategy for nonoscillatory convection without clipping
- [NASA-TM-102538] p 179 N90-21291
- A trajectory generation and system characterization model for cislunar low-thrust spacecraft. Volume 2: Technical manual
- [NASA-CR-185172] p 77 N90-21807
- Framework for a space shuttle main engine health monitoring system
- [NASA-CR-185224] p 78 N90-21809
- Automating security monitoring and analysis for Space Station Freedom's electric power system
- [NASA-TM-103148] p 240 N90-22324
- Parallel/distributed direct method for solving linear systems
- [NASA-TM-103229] p 244 N90-26614
- Multi-sensor analysis techniques for SSME safety monitoring
- [NASA-CR-185260] p 45 N90-27732
- ALIGNMENT**
- Topology of modified helical gears p 195 A90-21132
- ALKALI METALS**
- Liquid alkali metals - Equation of state and reduced-pressure, bulk-modulus, sound-velocity, and specific-heat functions p 102 A90-16280
- ALKALINE BATTERIES**
- Oxygen electrodes for rechargeable alkaline fuel cells-II p 231 N90-20469
- ALKALINE EARTH OXIDES**
- Oxygen electrodes for rechargeable alkaline fuel cells. II p 228 A90-33946
- Corrosion testing of candidates for the alkaline fuel cell cathode p 228 A90-33948
- ALKYL COMPOUNDS**
- Decomposition of perfluoroalkylpolyethers (PFPE) in ultra-high vacuum under sliding conditions p 122 A90-40714
- Determination of the thermal stability of perfluoroalkylethers
- [NASA-TM-102493] p 127 N90-17875
- ALLOYING**
- Microstructure and tensile properties of Fe-40 at. pct Al alloys with C, Zr, Hf, and B additions p 108 A90-11651
- Influence of alloying elements on the oxidation behavior of NbAl₃ p 113 A90-24861
- Solid state processing for high temperature alloys and composites p 196 A90-33225
- ALLOYS**
- High temperature creep behavior of single crystal gamma prime and gamma alloys p 110 A90-16901
- Electrical properties of materials for high temperature strain gage applications
- [NASA-CR-186192] p 188 N90-14534
- The oxidation and corrosion of ODS alloys
- [NASA-TM-102555] p 119 N90-25211
- Creep and creep rupture of strongly reinforced metallic composites
- [NASA-CR-185286] p 223 N90-28110

ALTERNATING CURRENT

- A comparative study of electric power distribution systems for spacecraft
- [NASA-CR-186531] p 77 N90-21113
- ALTERNATING DIRECTION IMPLICIT METHODS**
- Numerical modeling of enclosure convection
- [IAF PAPER 89-403] p 157 A90-13511
- Numerical analysis of natural convection in liquid droplets by phase change p 164 A90-23212
- ALTITUDE TESTS**
- Altitude testing of the 2D V-STOL ADEN demonstrator on an F404 engine
- [NASA-CR-174824] p 28 N90-17638
- ALUMINATES**
- Growth and patterning of laser ablated superconducting YBa₂Cu₃O₇ films on LaAlO₃ substrates
- [NASA-TM-102436] p 259 N90-22421
- ALUMINIDES**
- Deformation behavior of NiAl-based alloys containing iron, cobalt, and hafnium p 110 A90-16930
- Improving the low temperature ductility of NiAl p 110 A90-16940
- Observations on the brittle to ductile transition temperatures of B2 nickel aluminides with and without zirconium p 111 A90-19153
- 1100 to 1300 K slow plastic compression properties of Ni-38.5Al composites p 111 A90-19154
- The effect of 0.1 atomic percent zirconium on the cyclic oxidation behavior of beta-NiAl for 3000 hours at 1200 C p 112 A90-24857
- Identification of thermodynamically stable ceramic reinforcement materials for iron aluminide matrices p 89 A90-25238
- Influence of testing environment on the room temperature ductility of FeAl alloys p 115 A90-39658
- Cyclic oxidation of aluminide coatings on Ti3Al + Nb p 115 A90-39660
- Thermodynamic analysis of chemical compatibility of ceramic reinforcement materials with niobium aluminides p 92 A90-44001
- Compatibility of Fe-40Al with various fibers p 94 A90-50496
- ALUMINUM**
- High frequency GaAlAs modulator and photodetector for phased array antenna applications p 146 A90-11774
- The oxidation of Ni-rich Ni-Al intermetallics p 112 A90-24855
- Oxidation behavior of FeAl + Hf, Zr, B p 113 A90-24858
- Tribological properties of ceramic/Ti3Al-Nb sliding couples for use as candidate seal materials to 700 deg C
- [NASA-TM-102401] p 86 N90-12658
- ALUMINUM ALLOYS**
- Microstructure and tensile properties of Fe-40 at. pct Al alloys with C, Zr, Hf, and B additions p 108 A90-11651
- Analysis of gamma prime shape changes in a single crystal Ni-base superalloy p 109 A90-15206
- Deformation behavior of NiAl-based alloys containing iron, cobalt, and hafnium p 110 A90-16930
- 1200 to 1400 K slow strain rate compressive properties of NiAl/Ni₂AlTi-base materials p 88 A90-16938
- Processing and microstructure of melt spun NiAl alloys p 110 A90-16941
- Compressive strength of a B2 matrix NiAl-Nb intermetallic at 1200 and 1300 K p 111 A90-19157
- On the mechanism of cross slip in Ni3Al p 111 A90-20611
- Influence of alloying elements on the oxidation behavior of NbAl₃ p 113 A90-24861
- Preliminary investigation of a NiAl composite prepared by cryomilling p 113 A90-25098
- Microstructure and mechanical properties of multiphase NiAl-based alloys p 115 A90-35071
- Thermodynamic analysis of chemical compatibility of ceramic reinforcement materials with niobium aluminides p 92 A90-44001
- Investigation of Weibull statistics in fracture analysis of cast aluminum p 115 A90-45304
- Elevated temperature slow plastic deformation of NiAl-TiB₂ particulate composites at 1200 and 1300 K p 92 A90-45621
- High-temperature slow-strain-rate compression studies on CoAl-TiB₂ composites p 93 A90-48636
- Compression behavior of the forged L12 compounds Al₆Ti₂Cr₈ and Al₆Ti₂Mn₉ p 116 A90-51298
- ALUMINUM ARSENIDES**
- Peeled film GaAs solar cells for space power
- [NASA-TM-103125] p 153 N90-21287
- ALUMINUM CARBIDES**
- The application of cast SiC/Al to rotary engine components
- [NASA-CR-179610] p 255 N90-13385

SUBJECT INDEX

ALUMINUM GALLIUM ARSENIDES

- AlGaAs/InGaAs heterostructures with doped channels for discrete devices and monolithic amplifiers p 146 A90-20861
- Mathematical optimization of photovoltaic converters for diode lasers --- for spacecraft power supplies p 228 A90-38110
- Doped-channel heterojunction structures for millimeter-wave discrete devices and MMICs p 150 A90-48492

ALUMINUM OXIDES

- Ellipsometric study of Al₂O₃/Ag/Si and SiO₂/Ag/quartz ashed in an oxygen plasma --- protective coatings to prevent degradation of materials in low earth orbits p 120 A90-18217
- The high temperature creep deformation of Si₃N₄-6Y₂O₃-2Al₂O₃ p 121 A90-18879
- Synthesis and characterization of high-T(c) screen-printed Y-Ba-Cu-O films on alumina p 254 A90-21926
- Crystallization behavior and properties of BaO-Al₂O₃-2SiO₂ glass matrices p 95 A90-51933
- Zirconia toughened SiC whisker reinforced alumina composites small business innovation research [NASA-CR-179629] p 125 N90-10294
- Experimentally determined wear behavior of an Al₂O₃-SiC composite from 25 to 1200 C [NASA-TM-102549] p 87 N90-20130

ALUMINUM SILICATES

- Crystallization of a barium-aluminosilicate glass p 121 A90-27107
- Phase transformations in xerogels of mullite composition p 123 A90-47093

AMBIENT TEMPERATURE

- Determination of the durability of the fiber optics in rocket engine environments [AIAA PAPER 90-2229] p 250 A90-42754

AMMETERS

- A fiber-optic current sensor for aerospace applications [NASA-TM-103152] p 190 N90-22773

AMMONIA

- Numerical modeling of an arcjet thruster [AIAA PAPER 90-2614] p 64 A90-42587

AMMONIUM COMPOUNDS

- Studies on the use of supercritical ammonia for ceramic nitride synthesis and fabrication [NASA-TM-102570] p 106 N90-21843

AMMONOLYSIS

- Studies on the use of supercritical ammonia for ceramic nitride synthesis and fabrication [NASA-TM-102570] p 106 N90-21843

AMORPHOUS MATERIALS

- Optical dispersion relations for diamondlike carbon films [NASA-TM-102356] p 257 N90-10738

AMORPHOUS SILICON

- Radiation resistance studies of amorphous silicon films p 227 A90-14952

AMPLIFIER DESIGN

- The 30-GHz monolithic receive module [NASA-CR-180849] p 146 N90-24528

AMPLITUDE MODULATION

- Effects of amplitude distortions and IF equalization on satellite communication system bit-error rate performance [AIAA PAPER 90-0878] p 140 A90-25697

AMPLITUDES

- Effects of amplitude distortions and IF equalization on satellite communication system bit-error rate performance [NASA-TM-102415] p 144 N90-19454

ANALOGS

- Introducing the VRT gas turbine combustor [AIAA PAPER 90-2452] p 21 A90-42808
- Introducing the VRT gas turbine combustor [NASA-TM-103176] p 137 N90-23591

ANALYSIS (MATHEMATICS)

- A thermoelastic transversely isotropic thick walled cylinder/disk application. An analytical solution and study [NASA-TM-102320] p 216 N90-12950
- Institute for Computational Mechanics in Propulsion (ICOMP) fourth annual review, 1989 [NASA-TM-102519] p 243 N90-20769

ANELASTICITY

- High temperature inelastic deformation under uniaxial loading - Theory and experiment p 109 A90-13838
- A constitutive model for the inelastic multiaxial response of Rene 80 at 871 C and 982 C p 114 A90-32266

ANEMOMETERS

- A rotating hot-wire technique for spatial sampling of disturbed and manipulated duct flows p 186 A90-41120

ANGLE OF ATTACK

- Unsteady Euler analysis of the flowfield of a propfan at an angle of attack [AIAA PAPER 90-0339] p 5 A90-25028
- Prediction of unsteady blade surface pressures on an advanced propeller at an angle of attack [NASA-TM-102374] p 11 N90-12560
- Unsteady Euler analysis of the flow field of a propfan at an angle of attack [NASA-TM-102426] p 248 N90-18229

ANHYDRIDES

- Substituted 1,1,1-triaryl-2,2,2-trifluoroethanes and processes for their synthesis [NASA-CASE-LEW-14345-2] p 107 N90-23497

ANISOTROPIC MEDIA

- Nonlinear Reynolds stress models and the renormalization group p 172 A90-44011

ANISOTROPY

- Effect of crystal orientation on anisotropic etching and MOCVD growth of grooves on GaAs p 253 A90-15136

- Effects of fiber motion on the acoustic behavior of an anisotropic, flexible fibrous material p 247 A90-33313

ANNEALING

- Glass-derived superconducting ceramics with zero resistance at 107 K in the Bi(1.5)Pb(0.5)Sr₂Ca₂Cu₃O(x) system p 253 A90-11491
- Thermal annealing of GaAs concentrator solar cells --- during electron irradiation p 60 A90-38150
- Silicon carbide semiconductor device fabrication and characterization [NASA-CR-186354] p 258 N90-19873
- Lateral spreading of Au contacts on InP [NASA-TM-103133] p 232 N90-22843
- Ellipsometric study of YBa₂Cu₃O(7-x) laser ablated and co-evaporated films [NASA-TM-103223] p 259 N90-26682

ANNIHILATION REACTIONS

- Unitarity limits on the mass and radius of dark-matter particles p 264 A90-24671

ANNULAR FLOW

- Calculation of turbulent three-dimensional jet-induced flow in a rectangular enclosure [AIAA PAPER 90-0684] p 161 A90-19976
- Numerical studies of convective heat transfer in an inclined semi-annular enclosure p 173 A90-45317

ANODES

- Performance characterization of a segmented anode arcjet thruster [AIAA PAPER 90-2582] p 68 A90-52569
- Geometric effects in applied-field MPD thrusters [AIAA PAPER 90-2669] p 69 A90-52572
- Impedance studies of Ni/Cd and Ni/H₂ cells using the cell case as a reference electrode p 231 N90-20473
- Geometric effects in applied-field MPD thrusters [NASA-TM-103259] p 82 N90-27782

ANTENNA ARRAYS

- High frequency GaAlAs modulator and photodetector for phased array antenna applications p 146 A90-11774

- Design for steering accuracy in antenna arrays using shared optical phase shifters p 138 A90-13935
- A high-speed GaAs MESFET optical controller p 186 A90-22483

- Convergence of the SMI and the diagonally loaded SMI algorithms with weak interference [AD-A222639] p 141 A90-36717

- Microstrip subarray with coplanar and stacked parasitic elements p 141 A90-41586

- High-speed fiber-optic links for distribution of satellite traffic p 47 A90-41687

- Antenna beamforming using optical processing [NASA-CR-180844] p 142 N90-11210

- An experimental SMI adaptive antenna array for weak interfering signals [NASA-CR-185976] p 142 N90-11211

- Adaptive antenna arrays for satellite communication [NASA-CR-185989] p 143 N90-12784

- Effects of additional interfering signals on adaptive array performance [NASA-CR-186508] p 145 N90-20271

- Coplanar waveguide fed phased array antenna [NASA-TM-102522] p 152 N90-21273

- Optical control of an 8-element Ka-band phased array using a high-speed optoelectronic interconnect [NASA-TM-102550] p 152 N90-21275

- Design of an optically controlled Ka-band GaAs MMIC phased-array antenna [NASA-TM-103147] p 155 N90-26250

ANTENNA DESIGN

- A new fabrication method for precision antenna reflectors for space flight and ground test [AIAA PAPER 90-0803] p 139 A90-25627

- Microstrip subarray with coplanar and stacked parasitic elements p 141 A90-41586

ARC JET ENGINES

- A comparison of reflector antenna designs for wide-angle scanning p 144 N90-19264
- Conjugate field approaches for active array compensation p 144 N90-19266
- Reflector surface distortion analysis techniques (thermal distortion analysis of antennas in space) p 144 N90-19267

- Aperture taper determination for the half-scale accurate antenna reflector [NASA-CR-185215] p 153 N90-21282

- ATDRS payload technology research and development [NASA-TM-103256] p 52 N90-28596

ANTENNA FEEDS

- Microstrip subarray with coplanar and stacked parasitic elements p 141 A90-41586

- Reflector spillover loss of an open-ended rectangular and circular waveguide feed p 141 A90-45398

- A comparison of reflector antenna designs for wide-angle scanning p 144 N90-19264

- The 30-GHz monolithic receive module [NASA-CR-180849] p 146 N90-24528

- ATDRS payload technology research and development [NASA-TM-103256] p 52 N90-28596

ANTENNA RADIATION PATTERNS

- Effects of desired signal on the performance of a sidelobe canceller p 139 A90-13936

- Experimental study of the cross-polarization characteristics of rectangular microstrip antennas p 141 A90-37312

- Conjugate field approaches for active array compensation p 144 N90-19266

ANTENNAS

- An experimental SMI adaptive antenna array for weak interfering signals [NASA-CR-185976] p 142 N90-11211

ANTHRACENE

- Processable, high temperature polymers from 1,4,5,8-tetrahydro-1,4,5,8-diepoxyanthracene and bis-dienes p 84 A90-21930

- Linear acene derivatives - New routes to pentacene and naphthalene and the first synthesis of a triptycene with two anthracene moieties p 85 A90-49071

- Iptycene synthesis: A new method for attaching a 2,3-anthracene moiety to the 9,10-positions of another anthracene moiety - Exceptional conditions for a Lewis acid catalyzed Diels-Alder reaction p 85 A90-49073

ANTIFERROMAGNETISM

- Antiferromagnetism in Co-57-doped La₂CuO₄(y) studied by Moessbauer spectroscopy p 255 A90-34011

APERTURES

- Aperture taper determination for the half-scale accurate antenna reflector [NASA-CR-185215] p 153 N90-21282

APPLICATION SPECIFIC INTEGRATED CIRCUITS

- A forward error correction technique using a high-speed, high-rate single chip codec p 141 A90-48440

APPLICATIONS PROGRAMS (COMPUTERS)

- Finite element implementation of Robinson's unified viscoplastic model and its application to some uniaxial and multiaxial problems p 208 A90-15704

- Flight experiment of thermal energy storage --- for spacecraft power systems p 61 A90-38172

- User's manual for PEPSIG NASA tip vortex version [NASA-CR-182178] p 10 N90-10835

APPROACH INDICATORS

- Cooperative synthesis of control and display augmentation in approach and landing p 36 A90-33061

APPROXIMATION

- Absorbing boundary conditions for second-order hyperbolic equations p 242 A90-34549

- An approximate model for the performance and acoustic predictions of counterrotating propeller configurations [NASA-CR-180667] p 248 N90-18228

- Implicit solution of three-dimensional internal turbulent flows [NASA-TM-103099] p 184 N90-27982

ARC JET ENGINES

- Qualification and life testing of a flight design hydrazine arcjet system [AIAA PAPER 90-2576] p 64 A90-42559

- End-hall thrusters [AIAA PAPER 90-2595] p 64 A90-42570

- Numerical modeling of an arcjet thruster [AIAA PAPER 90-2614] p 64 A90-42587

- Preliminary plume characteristics of an arcjet thruster [AIAA PAPER 90-2645] p 64 A90-42609

- Arcjet load characteristics [AIAA PAPER 90-2579] p 67 A90-47226

- Advanced propulsion for LEO and GEO platforms [AIAA PAPER 90-2551] p 68 A90-52565

- Low power arcjet performance [AIAA PAPER 90-2578] p 68 A90-52568

- Performance characterization of a segmented anode arcjet thruster
[AIAA PAPER 90-2582] p 68 A90-52569
The effect of electrode configuration on arcjet performance p 70 N90-11081
[NASA-TM-102346] p 70 N90-11081
Arcjet thruster research and technology. Phase 1: Executive summary p 72 N90-14278
[NASA-CR-182106] p 72 N90-14278
Electric propulsion options for 10 kW class earth-space missions p 75 N90-18474
Test facility and preliminary performance of a 100 kW class MPD thruster p 75 N90-18476
Arcjet cathode phenomena p 75 N90-18477
Arcjet nozzle design impacts p 76 N90-18478
Arcjet load characteristics p 79 N90-25181
[NASA-TM-103190] p 79 N90-25181
Preliminary plume characteristics of an arcjet thruster [NASA-TM-103241] p 81 N90-26071
Advanced propulsion for LEO and GEO platforms [NASA-TM-103228] p 82 N90-27785
Low power arcjet performance [NASA-TM-103280] p 83 N90-28657
- ARC SPRAYING**
Improved process for HIP canning of composites [NASA-CASE-LEW-14990-1-CU] p 97 N90-15147
- ARCHITECTURE (COMPUTERS)**
Multi-level Hierarchical Poly Tree computer architectures p 236 A90-26082
A general model for memory interference in a multiprocessor system with memory hierarchy p 238 A90-37482
A candidate architecture for monitoring and control in chemical transfer propulsion systems [AIAA PAPER 90-1882] p 52 A90-41980
Health monitoring system for the SSME - Hardware architecture study [AIAA PAPER 90-1989] p 65 A90-42713
Parallel eigenanalysis of finite element models in a completely connected architecture [NASA-CR-185166] p 217 N90-14652
Eigensolution of finite element problems in a completely connected parallel architecture [NASA-TM-102450] p 217 N90-17173
Autonomous power expert system p 240 N90-22306
A candidate architecture for monitoring and control in chemical transfer propulsion systems [NASA-TM-103161] p 52 N90-22595
AIRNET: A real-time communications network for aircraft [NASA-CR-186140] p 145 N90-24514
Multiprocessor architecture: Synthesis and evaluation [NASA-CR-186618] p 235 N90-25579
Modeling and synthesis of multicomputer interconnection networks [NASA-CR-186619] p 238 N90-25604
Neuromorphic learning of continuous-valued mappings from noise-corrupted data. Application to real-time adaptive control [NASA-TM-4176] p 241 N90-25607
Computer architecture evaluation for structural dynamics computations: Project summary [NASA-CR-186137] p 235 N90-26512
- ARGON**
Reactions of SiC with H₂/H₂O/Ar mixtures at 1300 C p 123 A90-45830
- ARMATURES**
Feasibility of intercalated graphite railgun armatures [NASA-TM-102546] p 128 N90-21181
- AROMATIC COMPOUNDS**
On the driving force of PAH production p 84 A90-32833
Bisannulation with a benzo(1,2-c:4,5-c'-prime) difuran equivalent - A new route to linear acene derivatives p 85 A90-49072
- ARTIFICIAL CLOUDS**
A two-dimensional model of plasma expansion in the ionosphere p 233 A90-43609
- ARTIFICIAL INTELLIGENCE**
User needs, benefits, and integration of robotic systems in a space station laboratory [NASA-CR-185150] p 200 N90-13794
Autonomous power expert fault diagnostic system for Space Station Freedom electrical power system testbed p 80 N90-25521
- ASSESSMENTS**
Probability of failure and risk assessment of propulsion structural components p 218 N90-18470
- ASTRODYNAMICS**
Comparison of solution approaches for minimum-fuel, low-thrust, power-limited orbital transfers [AIAA PAPER 90-2960] p 41 A90-53035
- ASTRONOMICAL MODELS**
The shocking development of lithium (and boron) in supernovae p 264 A90-17643
Big bang nucleosynthesis and the quark-hadron transition p 265 A90-31407
A model for the distribution of the intergalactic medium p 265 A90-34505
Dark matter candidates p 266 A90-44095
A model for the distribution of dark matter, galaxies, and the intergalactic medium in a cold dark matter-dominated universe p 266 A90-45560
- ASTRONOMICAL OBSERVATORIES**
Comparison of solar photovoltaic and nuclear reactor power systems for a human-tended lunar observatory p 42 A90-38030
- ASTROPHYSICS**
The shocking development of lithium (and boron) in supernovae p 264 A90-17643
- ASYMPTOTIC METHODS**
On the instabilities of supersonic mixing layers - A high-Mach-number asymptotic theory p 8 A90-42644
Hopf bifurcation in the driven cavity [NASA-TM-102334] p 175 N90-11969
A new uniformly valid asymptotic integration algorithm for elasto-plastic-creep and unified viscoplastic theories including continuum damage [NASA-TM-102344] p 217 N90-14655
High-frequency asymptotic methods for analyzing the EM scattering by open-ended waveguide cavities [NASA-CR-186244] p 143 N90-16103
Conditions at the downstream boundary for simulations of viscous incompressible flow [NASA-TM-102510] p 243 N90-18198
Asymptotic boundary conditions for dissipative waves: General theory [NASA-TM-102497] p 243 N90-18927
An unsteady time asymptotic flow in the square driven cavity [NASA-TM-103141] p 181 N90-22016
- ASYMPTOTIC PROPERTIES**
Critical exponent for the viscosity of carbon dioxide and xenon p 261 A90-43941
- ASYMPTOTIC SERIES**
Asymptotic analysis of dissipative waves with applications to their numerical simulation [NASA-TM-103231] p 244 N90-26615
Consistency and convergence for numerical radiation conditions [NASA-TM-103262] p 244 N90-29124
- ATMOSPHERIC ATTENUATION**
A unified statistical rain-attenuation model for communication link fade predictions and optimal stochastic fade control design using a location-dependent rain-statistic database p 141 A90-34914
- ATMOSPHERIC CHEMISTRY**
Digital filtering of plume emission spectra [AIAA PAPER 90-1994] p 67 A90-50643
Digital filtering of plume emission spectra [NASA-TM-103135] p 81 N90-26070
- ATMOSPHERIC MOISTURE**
Humidity-induced room-temperature decomposition of Au contacted indium phosphide p 105 A90-44689
Rain-fade simulation and power augmentation for satellite communication systems [NASA-TM-103134] p 146 N90-28768
- ATMOSPHERIC RADIATION**
A radiological assessment of nuclear power and propulsion operations near Space Station Freedom [NASA-CR-185185] p 76 N90-21108
- ATOMIC INTERACTIONS**
Fundamentals of tribology at the atomic level p 192 A90-14020
- ATOMIZERS**
Influence of the continuous and dispersed phases on the symmetry of a gas turbine air-blast atomizer [ASME PAPER 89-GT-303] p 163 A90-22651
Symmetry assessment of an air-blast atomizer spray p 172 A90-40930
Effect of vane twist on the performance of dome swirlers for gas turbine airblast atomizers [AIAA PAPER 90-1955] p 173 A90-47203
Effect of vane twist on the performance of dome swirlers for gas turbine airblast atomizers [NASA-TM-103195] p 182 N90-25289
- ATOMIZING**
Effect of vane twist on the performance of dome swirlers for gas turbine airblast atomizers [AIAA PAPER 90-1955] p 173 A90-47203
Effect of vane twist on the performance of dome swirlers for gas turbine airblast atomizers [NASA-TM-103195] p 182 N90-25289
Ignition and combustion characteristics of metalized propellants [NASA-CR-186870] p 107 N90-26911
- ATTITUDE (INCLINATION)**
NASA Lewis icing research tunnel user manual [NASA-TM-102319] p 31 N90-23407
- AUGER SPECTROSCOPY**
Characterization of interfacial failure in SiC reinforced Si₃N₄ matrix composite material by both fiber push-out testing and Auger electron spectroscopy p 91 A90-36802
- AUTOCCLAVING**
Autoclavable addition polyimides for 371 C composite applications [NASA-TM-102333] p 102 N90-27874
- AUTOMATED PILOT ADVISORY SYSTEM**
The influence of ice accretion physics on the forecasting of aircraft icing conditions p 17 N90-20928
- AUTOMATIC CONTROL**
Flight software development for the isothermal dendritic growth experiment [AIAA PAPER 90-0744] p 235 A90-22257
Flight software development for the isothermal dendritic growth experiment [NASA-TM-102412] p 238 N90-13988
Automated electric power management and control for Space Station Freedom [NASA-TM-103151] p 240 N90-23125
- AUTOMOBILE ENGINES**
ATTAP/AGT101 ceramics technology update [ASME PAPER 89-GT-105] p 195 A90-23814
Advanced Turbine Technology Applications Project (ATTAP) [NASA-CR-185133] p 22 N90-10036
Automotive Stirling engine development program [NASA-CR-180839] p 263 N90-11654
- AUTOMOBILES**
Automotive Stirling engine development program [NASA-CR-180840] p 264 N90-29260
- AUTONOMY**
Space Station power system autonomy demonstration p 245 A90-10373
Autonomous power expert system p 240 N90-22306
Autonomous power expert system [NASA-CR-185263] p 80 N90-25187
- AUTOREGRESSIVE PROCESSES**
Health monitoring system for the SSME - Program overview [AIAA PAPER 90-1987] p 63 A90-40583
- AUXILIARY POWER SOURCES**
Advanced Turbine Technology Applications Project (ATTAP) [NASA-CR-185240] p 263 N90-26728
- AUXILIARY PROPULSION**
Advanced APS impacts on vehicle payloads p 75 N90-18472
Low power arcjet performance [NASA-TM-103280] p 83 N90-28657
- AVAILABILITY**
Space Station Freedom power - A reliability, availability, and maintainability assessment of the proposed Space Station Freedom electric power system p 58 A90-38074
- AVIONICS**
Fiber optics for advanced aircraft p 185 A90-11702
Advanced Launch System (ALS) actuation and power systems impact operability and cost p 69 A90-52955
Advanced Launch System (ALS): Electrical actuation and power systems improve operability and cost picture [NASA-TM-102547] p 152 N90-21271
- AXIAL FLOW**
An interactive grid generation procedure for axial and radial flow turbomachinery [AIAA PAPER 90-0344] p 162 A90-22200
Solidification by radiative cooling of a cylindrical region filled with drops p 166 A90-24840
Laser anemometer measurements in a transonic axial-flow fan rotor [NASA-TP-2879] p 175 N90-11245
An interactive grid generation procedure for axial and radial flow turbomachinery [NASA-CR-185167] p 237 N90-13968
- AXIAL LOADS**
High temperature inelastic deformation of the B1900 + Hf alloy under multiaxial loading - Theory and experiment p 112 A90-22656
A constitutive model for the inelastic multiaxial response of Rene 80 at 871 C and 982 C p 114 A90-32266
Equivalence of physically based statistical fracture theories for reliability analysis of ceramics in multiaxial loading p 123 A90-43580
- AXIAL STRAIN**
Finite element analysis of structural components using viscoplastic models with application to a cowl lip problem [NASA-CR-185189] p 221 N90-23769
Microstructure: Property correlation --- multiaxial fatigue damage evolution in waspaloy [NASA-CR-180406] p 224 N90-28880

AXISYMMETRIC BODIES

Radiative configuration factors from cylinders to coaxial axisymmetric bodies p 167 A90-26334

AXISYMMETRIC FLOW

Investigation of turbulent transport in an axisymmetric sudden expansion p 163 A90-23112
Multiwave nonlinear interactions in the axisymmetric mode [AIAA PAPER 90-0365] p 166 A90-25029
Three-dimensional compressible jet-in-crossflow calculations using improved viscosity models and adapted grid [AIAA PAPER 90-2100] p 174 A90-47206
Viscous effects on the instability of an axisymmetric jet [NASA-TM-102396] p 12 N90-16719
The radiation of sound from a propeller at angle of attack [NASA-CR-4264] p 249 N90-21602

B

BALANCING

Spray automated balancing of rotors - How process parameters influence performance p 198 A90-46228
An applicational process for dynamic balancing of turbomachinery shafting [NASA-TM-102537] p 202 N90-20392

BALL BEARINGS

Fully articulated four-point-bend loading fixture [NASA-CASE-LEW-14776-1] p 201 N90-15445
Bearing optimization for SSME HPOTP application p 205 N90-28622

BALLISTIC TRAJECTORIES

The vibro-acoustic mapping of low gravity trajectories on a Learjet aircraft [NASA-TM-103103] p 1 N90-21723

BANDPASS FILTERS

Coplanar waveguide discontinuities for P-I-N diode switches and filter applications [NASA-TM-102534] p 153 N90-21278

BANDSTOP FILTERS

Coplanar waveguide discontinuities for P-I-N diode switches and filter applications [NASA-TM-102534] p 153 N90-21278

BARIUM

Synthesis and characterization of high-T(c) screen-printed Y-Ba-Cu-O films on alumina p 254 A90-21926

BARIUM COMPOUNDS

Crystallization of a barium-aluminosilicate glass p 121 A90-27107

BARIUM OXIDES

Growth and patterning of laser ablated superconducting YBa₂Cu₃O₇ films on LaAlO₃ substrates [NASA-TM-102436] p 259 N90-22421
Photoresponse of YBa₂Cu₃O₇(δ) granular and epitaxial superconducting thin films [NASA-TM-103144] p 154 N90-22732
Sequentially evaporated thin film YBa₂Cu₃O₇(δ -x) superconducting microwave ring resonator [NASA-TM-103180] p 154 N90-25273
Ellipsometric study of YBa₂Cu₃O₇(δ -x) laser ablated and co-evaporated films [NASA-TM-103223] p 259 N90-26682
Laser ablated high T(sub c) superconducting thin YBa₂Cu₃O₇(δ -x) films on substrates suitable for microwave applications p 260 N90-27808
Synthesis and structural chemistry of Au(III)-substituted Ba₂YCu₃O₇(δ -x) [NASA-TM-103292] p 108 N90-28696

BARRIER LAYERS

High temperature, flexible, thermal barrier seal [NASA-CASE-LEW-14672-1] p 201 N90-15444
Thermal analysis of thermal barrier coatings in a high heat flux environment p 129 N90-28652

BEAM NEUTRALIZATION

Plasma sources for spacecraft neutralization [AIAA PAPER 90-1556] p 49 A90-38697

BEAM SWITCHING

A users perspective of the ACTS hopping beam TDMA system [AIAA PAPER 90-0833] p 140 A90-25658
Antenna beamforming using optical processing [NASA-CR-180844] p 142 N90-11210

BEAMS (RADIATION)

Applicability of the beamed power concept to lunar rovers, construction, mining, explorers and other mobile equipment p 69 N90-10159

BEAMS (SUPPORTS)

Boundary flexibility method of component mode synthesis using static Ritz vectors p 212 A90-35429
Dynamic analysis of space-related linear and non-linear structures [NASA-TM-103490] p 51 N90-25174

BEARINGS

Tooth contact shift in loaded spiral bevel gears p 193 A90-21112
Some composite bearing and seal materials for gas turbine applications - A review [ASME PAPER 89-GT-144] p 195 A90-23838
Three-dimensional analysis of surface crack-Hertzian stress field interaction [NASA-CR-4254] p 215 N90-11332
Vibration transmission through rolling element bearings in geared rotor system, part 1 [NASA-CR-186093] p 199 N90-12936
Bearing and gear steels for aerospace applications [NASA-TM-102529] p 202 N90-20391
Bearing elastohydrodynamic lubrication: A complex calculation made simple [NASA-TM-102575] p 203 N90-22041

BEND TESTS

Strength and toughness of monolithic and composite silicon nitrides [NASA-TM-102423] p 126 N90-14368

BENDING

Green's functions for dislocations in bonded strips and related crack problems [NASA-CR-185291] p 224 N90-28878

BENDING MOMENTS

Assumed strain distributions for a finite strip plate bending element using Mindlin-Reissner plate theory p 208 A90-16723

BENZENE

Detailed mechanism for oxidation of benzene [NASA-TM-102443] p 106 N90-21842

BIBLIOGRAPHIES

Bibliography of Lewis Research Center technical publications announced in 1988 [NASA-TM-102034] p 262 N90-15846

BIG BANG COSMOLOGY

Big bang nucleosynthesis and the quark-hadron transition p 265 A90-31407
Phase transitions as the origin of large scale structure in the universe p 265 A90-35291

BINARY ALLOYS

The modelling of heat, mass and solute transport in solidification systems p 157 A90-13092
Finite element simulations of thermosolutal convection in vertical solidification of binary alloys p 132 A90-18292

Electrical properties of materials for high temperature strain gage applications [NASA-CR-186192] p 188 N90-14534

BINARY DATA

FORTTRAN program for x ray photoelectron spectroscopy data reformatting [NASA-TP-2957] p 258 N90-12348

BINARY FLUIDS

Solidification by radiative cooling of a cylindrical region filled with drops p 166 A90-24840

BINARY SYSTEMS (MATERIALS)

Properties of oxide dispersion strengthened alloys p 109 A90-14687

BIPOLAR TRANSISTORS

Neutron and gamma irradiation effects on power semiconductor switches [NASA-TM-103200] p 155 N90-25278

BIPOLARITY

Bipolar nickel-hydrogen battery development - A program review p 62 A90-38288
Characterization testing of a 40 AHR bipolar nickel-hydrogen battery p 230 N90-20463

BISMUTH ALLOYS

Modeling of collision and coalescence of droplets during microgravity processing of Zn-Bi immiscible alloys p 132 A90-22878

BISMUTH OXIDES

Glass-derived superconducting ceramics with zero resistance at 107 K in the Bi(1.5)Pb(0.5)Sr₂Ca₂Cu₃O(x) system p 253 A90-11491
Superconducting glass-ceramics in the Bi-Sr-Ca-Cu-O system p 256 A90-35153
Superconducting Bi(1.5)Pb(0.5)Sr₂Ca₂Cu₃O(x) ceramics by rapid melt quenching and glass crystallization p 256 A90-43568

BIT ERROR RATE

Spacecraft designs for VSAT networks [AIAA PAPER 90-0895] p 140 A90-25681
Effects of amplitude distortions and IF equalization on satellite communication system bit-error rate performance [AIAA PAPER 90-0878] p 140 A90-25697
Effects of amplitude distortions and IF equalization on satellite communication system bit-error rate performance [NASA-TM-102415] p 144 N90-19454
Bit-error-rate testing of fiber optic data links for MMIC-based phased array antennas [NASA-TM-102523] p 145 N90-21261

BLADE TIPS

User's manual for PEP SIG NASA tip vortex version [NASA-CR-182178] p 10 N90-10835
Computation of the tip vortex flowfield for advanced aircraft propellers [NASA-CR-182179] p 10 N90-10836

BLADE-VORTEX INTERACTION

Noise of a simulated installed model counterrotation propeller at angle-of-attack and takeoff/approach conditions [AIAA PAPER 90-0283] p 247 A90-32505
User's manual for PEP SIG NASA tip vortex version [NASA-CR-182178] p 10 N90-10835
Computation of the tip vortex flowfield for advanced aircraft propellers [NASA-CR-182179] p 10 N90-10836
An investigation of counterrotating tip vortex interaction [NASA-CR-185135] p 247 N90-11549

BODY CENTERED CUBIC LATTICES

High frequency capacitance-voltage characteristics of thermally grown SiO₂ films on beta-SiC p 254 A90-21348
Deep-level dominated electrical characteristics of Au contacts on beta-SiC p 147 A90-33726
The effects of surface films on mechanical behavior of B2 ordered intermetallic alloys p 115 A90-44338

BOILING

Design and test of a compact optics system for the pool boiling experiment [NASA-TM-102530] p 135 N90-20253

BOLTED JOINTS

Simplified design procedures for fiber composite structural components/joints [NASA-TM-103113] p 101 N90-24384

BONDING

Measurement of the intrinsic bond strength of brittle thin films on flexible substrates p 256 A90-44022

BOOMS (EQUIPMENT)

Comparative thermal analysis of the Space Station Freedom photovoltaic deployable boom structure using TRASYS, NEVADA, and SINDA programs [SAE PAPER 891563] p 47 A90-27525

BOOSTER ROCKET ENGINES

Corrosion prevention in copper combustion chamber liners of liquid oxygen/methane booster engines [AIAA PAPER 90-2119] p 85 A90-42028
Hydrocarbon-fuel/combustion-chamber-liner materials compatibility [NASA-CR-185203] p 118 N90-21165

BORON

The shocking development of lithium (and boron) in supernovae p 264 A90-17643
Oxidation behavior of FeAl + Hf,Zr,B p 113 A90-24858

BORON NITRIDES

Fundamental tribological properties of ion-beam-deposited boron nitride films p 124 A90-49054
Fundamental tribological properties of ion-beam-deposited boron nitride films [NASA-TM-102088] p 125 N90-11881

BOUNDARY CONDITIONS

Absorbing boundary conditions for second-order hyperbolic equations p 242 A90-34549
Reflecting boundary conditions for graded p-n junctions p 150 A90-42400
Asymptotic boundary conditions for dissipative waves: General theory [NASA-TM-102497] p 243 N90-18927
Consistency and convergence for numerical radiation conditions [NASA-TM-103262] p 244 N90-29124

BOUNDARY ELEMENT METHOD

Comparison of boundary element and finite element methods in spur gear root stress analysis p 193 A90-21107
Local and global accuracy estimates for boundary element analysis [AIAA PAPER 90-0930] p 211 A90-29324
Development of an integrated BEM for hot fluid-structure interaction [ASME PAPER 89-GT-128] p 212 A90-32264
Advanced applications of BEM to inelastic analysis of solids p 213 A90-45770
Advanced development of BEM for elastic and inelastic dynamic analysis of solids p 213 A90-45771
Inelastic transient dynamic analysis of three-dimensional problems by BEM p 215 A90-51480
Free-vibration analysis of three-dimensional solids by BEM p 215 A90-52007
Three-dimensional analysis of surface crack-Hertzian stress field interaction [NASA-CR-4254] p 215 N90-11332

BOUNDARY LAYER EQUATIONS

- Development of an integrated BEM approach for hot fluid structure interaction
[NASA-CR-186214] p 177 N90-15364
- BOUNDARY LAYER EQUATIONS**
Unsteady heat transfer on turbine blades p 161 A90-20511
- BOUNDARY LAYER FLOW**
Reciprocal interactions of hairpin-shaped vortices and a boundary layer p 159 A90-19635
[AIAA PAPER 90-0017]
The measurement of boundary layers on a compressor blade in cascade. IV - Flow fields for incidence angles of -1.5 and -8.5 degrees p 165 A90-23793
[ASME PAPER 89-GT-72]
Opposed-flow flame spread and extinction in mixed-convection boundary layers p 168 A90-32841
Influence of bulk turbulence and entrance boundary layer thickness on the curved duct flow field p 171 A90-38651
[AIAA PAPER 90-1502]
Spatial evolution of nonlinear acoustic mode instabilities on hypersonic boundary layers p 177 N90-14517
[NASA-TM-102431]
The effects of forcing on a single stream shear layer and its parent boundary layer p 180 N90-21301
[NASA-CR-186529]
- BOUNDARY LAYER SEPARATION**
Asymmetrical boundary layer separation at the base of a two cylinder geometry p 159 A90-18505
Some observations on transitory stall in conical diffusers p 4 A90-22158
[AIAA PAPER 90-0048]
The effects of forcing on a single stream shear layer and its parent boundary layer p 169 A90-35219
Some observations on transitory stall in conical diffusers p 11 N90-12561
[NASA-TM-102387]
Unsteady three-dimensional marginal separation, including breakdown p 179 N90-20337
[NASA-TM-102525]
Control of flow separation and mixing by aerodynamic excitation p 13 N90-21733
[NASA-TM-103131]
- BOUNDARY LAYER STABILITY**
Wall-layer eruptions in turbulent flows p 175 N90-11250
[NASA-TM-102362]
Spatial evolution of nonlinear acoustic mode instabilities on hypersonic boundary layers p 177 N90-14517
[NASA-TM-102431]
- BOUNDARY LAYER TRANSITION**
Heat transfer on accreting ice surfaces p 162 A90-22181
[AIAA PAPER 90-0200]
Some characteristics of bypass transition in a heated boundary layer p 169 A90-35183
Experimental investigation of flow about a strut-endwall configuration p 171 A90-38685
[AIAA PAPER 90-1541]
The measurement of boundary layers on a compressor blade in cascade. Volume 1. Experimental technique, analysis and results p 23 N90-10038
[NASA-CR-185118-VOL-1]
The measurement of boundary layers on a compressor blade in cascade. Volume 2. Data tables p 23 N90-10039
[NASA-CR-185118-VOL-2]
An investigation into the numerical prediction of boundary layer transition using the K.Y. Chien turbulence model p 182 N90-26269
[NASA-CR-185252]
- BOUNDARY LAYERS**
Predicted and measured boundary layer refraction for advanced turboprop propeller noise p 248 N90-17413
[NASA-TM-102365]
- BOUNDARY LUBRICATION**
Liquid lubrication in space p 205 N90-28063
[NASA-RP-1240]
- BOUNDARY VALUE PROBLEMS**
Absorbing boundary conditions for second-order hyperbolic equations p 242 A90-34549
Mechanics of the crack path formation p 215 N90-10455
[NASA-CR-185143]
Conditions at the downstream boundary for simulations of viscous incompressible flow p 243 N90-18198
[NASA-TM-102510]
Asymptotic boundary conditions for dissipative waves: General theory p 243 N90-18927
[NASA-TM-102497]
Parallel algorithms for boundary value problems p 243 N90-19783
[NASA-TM-102498]
Amplitude-dependent neutral modes in compressible boundary layer flows p 178 N90-20326
[NASA-TM-102524]
The fundamentals of adaptive grid movement p 185 N90-29610
- BOX BEAMS**
Solar Concentrator Advanced Development Program [NASA-CR-185173] p 232 N90-22834

BOXES (CONTAINERS)

- Advanced gearbox technology [NASA-CR-179625] p 32 N90-24274

BRANCHING (MATHEMATICS)

- Hopf bifurcation in the driven cavity p 174 A90-48548

BRAYTON CYCLE

- Solar dynamic power module design p 59 A90-38079
A Brayton cycle solar dynamic heat receiver for space p 61 A90-38165
Brayton advanced heat receiver development program p 61 A90-38170
The NASA Advanced Solar Dynamics Technology Program p 62 A90-38280
Conceptual design study of a 5 kilowatt solar dynamic Brayton power system using a dome Fresnel lens solar concentrator p 72 N90-14281
[NASA-CR-185134]
Analysis of thermal energy storage material with change-of-phase volumetric effects p 181 N90-21974
[NASA-TM-102457]

BRAZING

- Preliminary study on pressure brazing and diffusion welding of Nb-1Zr to Inconel 718 p 196 A90-26899

BREADBOARD MODELS

- Development and testing of a 20 kHz component test bed --- for space station power supplies p 43 A90-38126

BRIDGMAN METHOD

- Inverse heat transfer analysis of Bridgman crystal growth p 157 A90-13093
Temperature and melt solid interface control during crystal growth p 259 N90-26664
[NASA-CR-186731]

BRITTLE MATERIALS

- Universal aspects of brittle fracture, adhesion, and atomic force microscopy p 83 A90-14021
Measurement of the intrinsic bond strength of brittle thin films on flexible substrates p 256 A90-44022
Controlled crack growth specimen for brittle systems [NASA-TM-103126] p 129 N90-23543
Green's functions for dislocations in bonded strips and related crack problems p 224 N90-28878
[NASA-CR-185291]

BRITTLENESS

- Observations on the brittle to ductile transition temperatures of B2 nickel aluminides with and without zirconium p 111 A90-19153
Controlled crack growth specimen for brittle systems [NASA-TM-103126] p 129 N90-23543

BROMINATION

- Effect of heat-treatment temperature of vapor-grown graphite fibers. I - Properties of their bromine intercalation compounds p 120 A90-16279
Brominated graphitized carbon fibers [NASA-CASE-LEW-14698-2] p 126 N90-15262

BROMINE

- The effect of length and diameter on the resistivity of bromine intercalated graphite fibers p 122 A90-33332
Brominated graphitized carbon fibers [NASA-CASE-LEW-14698-2] p 126 N90-15262

BRUSHES (ELECTRICAL CONTACTS)

- Numerical modeling of flows in simulated brush seal configurations p 198 A90-47209
[AIAA PAPER 90-2141]
Flow visualization and motion analysis for a series of four sequential brush seals p 199 A90-47222
[AIAA PAPER 90-2482]

BUBBLES

- Numerical simulation of thermocapillary bubble migration under microgravity for large Reynolds and Marangoni numbers p 164 A90-23213
Gravitational couplings of the inflaton in extended inflation p 265 A90-40088
Soft inflation --- in cosmology p 265 A90-40093

BUCKLING

- Effect of crack-microcracks interaction on energy release rates p 214 A90-49269
Structural behavior of composites with progressive fracture [NASA-TM-102370] p 100 N90-23477

BUOYANCY

- Salt-finger convection under reduced gravity [AIAA PAPER 90-0122] p 160 A90-19693
Buoyancy effects on the vapor condensation rate on a horizontal liquid surface p 162 A90-22201
[AIAA PAPER 90-0353]
Buoyancy effects on the vapor condensation rate on a horizontal liquid surface p 130 N90-13675
[NASA-TM-102437]
Facilities for microgravity combustion research p 134 N90-13679
[NASA-TM-102014]
Polymer solution phase separation: Microgravity simulation p 127 N90-17101

SUBJECT INDEX

- Non-contact temperature measurements in support of microgravity combustion experiments p 135 N90-17900

- The role of gravity on macrosegregation in alloys [NASA-CR-186530] p 136 N90-25238

BURGER EQUATION

- Solution of steady-state one-dimensional conservation laws by mathematical programming p 241 A90-21918
Calculation of shocked one-dimensional flows on abruptly changing grids by mathematical programming p 162 A90-21937

BURNERS

- Burner rig hot corrosion of silicon carbide and silicon nitride p 121 A90-25267

BURSTS

- Spray automated balancing of rotors - How process parameters influence performance p 198 A90-46228

BYPASS RATIO

- Some characteristics of bypass transition in a heated boundary layer p 169 A90-35183
NASA's HITEMP program for UHBR engines [AIAA PAPER 90-2395] p 22 A90-47218

C

CADMIUM

- Impedance studies of Ni/Cd and Ni/H₂ cells using the cell case as a reference electrode p 231 N90-20473

CADMIUM ALLOYS

- Hyperfine magnetic field on Cd-111 in Heusler alloys Co₂MnZ (Z = Si, Ga, Ge, Sn) p 255 A90-34012

CALCIUM

- Energy storage for a lunar base by the reversible chemical reaction: CaO + H₂O reversible reaction Ca(OH)₂ [NASA-TM-103145] p 233 N90-25419

CALCIUM FLUORIDES

- Intergranular fracture of lithium fluoride-22 percent calcium fluoride hypereutectic salt at 800 K p 121 A90-25273
The mechanical properties of fluoride salts at elevated temperatures --- candidate thermal energy storage materials for solar dynamic systems p 123 A90-44376
Deformation of as-cast LiF-22 mol pct CaF₂ hypereutectic salt between 500 and 1015 K p 124 A90-49086

- A viscoplastic model with application to LiF-22 percent CaF₂ hypereutectic salt [NASA-TM-103181] p 221 N90-23770

CALCULUS

- Application of symbolic computations to the constitutive modeling of structural materials [NASA-TM-103225] p 222 N90-26364

CALIBRATING

- Liquid water content and droplet size calibration of the NASA Lewis Icing Research Tunnel [AIAA PAPER 90-0669] p 37 A90-22242
Developing a self-diagnostic system for piezoelectric sensors p 187 A90-42755
[AIAA PAPER 90-2230]

- Droplet sizing instrumentation used for icing research: Operation, calibration, and accuracy p 187 N90-11999
[NASA-CR-182293]

- Liquid water content and droplet size calibration of the NASA Lewis Icing Research Tunnel [NASA-TM-102447] p 200 N90-13797
Calibration approach to electron probe microanalysis: A study with PWA-1480, a nickel base superalloy [NASA-TM-102393] p 117 N90-14335

- Design and calibration of a vacuum compatible scanning tunneling microscope [NASA-TM-102514] p 189 N90-20353

- Optical characterization of clouds of fine liquid-nitrogen particles [NASA-TM-103208] p 191 N90-26299

CANNING

- One step HIP canning of powder metallurgy composites [NASA-CASE-LEW-14719-1] p 101 N90-23493

CANS

- Improved process for HIP canning of composites [NASA-CASE-LEW-14990-1-CU] p 97 N90-15147
Two-dimensional model of a Space Station Freedom thermal energy storage canister [NASA-TM-103124] p 183 N90-26279

CAPACITANCE

- Nickel-hydrogen capacity loss on storage p 57 A90-33955

CAPACITANCE-VOLTAGE CHARACTERISTICS

- High frequency capacitance-voltage characteristics of thermally grown SiO₂ films on beta-SiC p 254 A90-21348
Deep-level dominated electrical characteristics of Au contacts on beta-SiC p 147 A90-33726

SUBJECT INDEX

- Electron beam induced damage in PECVD Si₃N₄ and SiO₂ films on InP [NASA-TM-102544] p 203 N90-20393
- CAPILLARIES**
Energy stability of thermocapillary convection in a model of the float-zone crystal-growth process p 133 A90-48720
- CAPILLARY FLOW**
Shear stabilization of the capillary breakup of a cylindrical interface [AD-A219268] p 159 A90-17578
Numerical simulation of thermocapillary bubble migration under microgravity for large Reynolds and Marangoni numbers p 164 A90-23213
Hardware development for the surface tension driven convection experiment p 52 A90-36195
The coupling of Marangoni and capillary instabilities in an annular thread of liquid p 171 A90-38978
- CARBIDES**
Creep strength of niobium alloys, Nb-1%Zr and PWC-11 [NASA-TM-102390] p 116 N90-11854
- CARBON**
Diamondlike carbon protective coatings for optical windows p 122 A90-34569
Fuel-rich catalytic combustion - A fuel processor for high-speed propulsion [AIAA PAPER 90-2319] p 105 A90-42774
Plasma-deposited amorphous hydrogenated carbon films and their tribological properties p 123 A90-44864
Optical dispersion relations for diamondlike carbon films [NASA-TM-102356] p 257 N90-10738
Plasma-deposited amorphous hydrogenated carbon films and their tribological properties [NASA-TM-102379] p 125 N90-11880
Fuel-rich catalytic combustion: A fuel processor for high-speed propulsion [NASA-TM-103177] p 107 N90-23518
- CARBON COMPOUNDS**
Polymer derived Nicalon/Si-C-O composites - Processing and mechanical behavior p 89 A90-27065
- CARBON DIOXIDE**
Efficient Monte Carlo simulation of rarefied flow in a small nozzle [AIAA PAPER 90-1693] p 170 A90-38396
Critical exponent for the viscosity of carbon dioxide and xenon p 261 A90-43941
- CARBON DIOXIDE LASERS**
Design of a CO₂ laser power control system for a Spacelab microgravity experiment [NASA-TM-103112] p 192 N90-28833
- CARBON FIBER REINFORCED PLASTICS**
Applications of high thermal conductivity composites to electronics and spacecraft thermal design [AIAA PAPER 90-0783] p 89 A90-25609
Ultrasonic verification of five wave fronts in unidirectional graphite epoxy composite [NASA-CR-185288] p 208 N90-28858
- CARBON FIBERS**
Effect of heat-treatment temperature of vapor-grown graphite fibers. I - Properties of their bromine intercalation compounds p 120 A90-16279
The effect of length and diameter on the resistivity of bromine intercalated graphite fibers p 122 A90-33332
Vapor grown carbon fiber for space thermal management systems p 94 A90-50128
Brominated graphitized carbon fibers [NASA-CASE-LEW-14698-2] p 126 N90-15262
Fluorinated graphite fibers as a new engineering material: Promises and challenges [NASA-TM-102511] p 86 N90-19301
- CARBON MONOXIDE**
Mars in situ propellants - Carbon monoxide and oxygen ignition experiments [AIAA PAPER 90-1894] p 130 A90-50642
Mars in situ propellants: Carbon monoxide and oxygen ignition experiments [NASA-TM-103202] p 81 N90-26065
- CARBON STEELS**
Bearing and gear steels for aerospace applications [NASA-TM-102529] p 202 N90-20391
- CARBON-CARBON COMPOSITES**
The effects of atomic oxygen on the thermal emittance of high temperature radiator surfaces [NASA-TM-103224] p 102 N90-28670
- CARBURIZING**
Advances and directions of ion nitriding/carburizing [NASA-TM-102398] p 137 N90-11902
- CARRIER DENSITY (SOLID STATE)**
An empirical investigation of the InP shallow-homojunction solar cell p 225 A90-14869
Reflecting boundary conditions for graded p-n junctions p 150 A90-42400

- CARRIER FREQUENCIES**
Numerical Arc Segmentation Algorithm for a Radio Conference-NASARC (version 4.0) technical manual [NASA-TM-101453] p 144 N90-20264
- CARRIER TO NOISE RATIOS**
A heuristic approach to worst-case carrier-to-interference ratio maximization in satellite system synthesis [AIAA PAPER 90-0816] p 46 A90-25639
- CARTESIAN COORDINATES**
Galerkin finite difference Laplacian operators on isolated unstructured triangular meshes by linear combinations [NASA-TM-103209] p 183 N90-26276
- CASCADE CONTROL**
A 2.5 kW cascaded Schwarz converter for 20 kHz power distribution p 147 A90-36913
- CASCADE FLOW**
Calculation of unsteady Euler flows in turbomachinery using the linearized Euler equations p 2 A90-11778
Analysis of nonuniform subsonic flows about a row of moving blades p 2 A90-11779
The unsteady aerodynamics of an oscillating cascade in a compressible flow field p 2 A90-11789
Progress towards the development of an inviscid-viscous interaction method for unsteady flows in turbomachinery cascades p 2 A90-11806
Computation of three dimensional turbulent boundary layers in internal flows, including turbomachinery rotor blades p 3 A90-12555
The measurement of boundary layers on a compressor blade in cascade. IV - Flow fields for incidence angles of -1.5 and -8.5 degrees [ASME PAPER 89-GT-72] p 165 A90-23793
Time domain flutter analysis of cascades using a full-potential solver [AIAA PAPER 90-0984] p 6 A90-29374
Aeroelastic problems in turbomachines [AIAA PAPER 90-1157] p 7 A90-29393
Numerical analysis of three-dimensional viscous internal flows p 168 A90-32456
Computation of turbine flowfields with a Navier-Stokes code [AIAA PAPER 90-2122] p 8 A90-42731
The measurement of boundary layers on a compressor blade in cascade. Volume 1: Experimental technique, analysis and results [NASA-CR-185118-VOL-1] p 23 N90-10038
The measurement of boundary layers on a compressor blade in cascade. Volume 2: Data tables [NASA-CR-185118-VOL-2] p 23 N90-10039
Gust response analysis for cascades operating in nonuniform mean flows p 28 N90-18415
Aerodynamics of a linear oscillating cascade [NASA-TM-103250] p 15 N90-27657
- CASSEGRAIN OPTICS**
A comparison of reflector antenna designs for wide-angle scanning p 144 N90-19264
- CAST ALLOYS**
Constitutive modeling for isotropic materials (HOST) [NASA-CR-179522] p 26 N90-13390
Constitutive modeling for isotropic materials (HOST) [NASA-CR-174718] p 26 N90-13391
Identification of a cast iron alloy containing nonstrategic elements [NASA-CR-185174] p 118 N90-18559
- CASTING**
The role of gravity on macrosegregation in alloys [NASA-CR-186530] p 136 N90-25238
- CATALOGS (PUBLICATIONS)**
Criss-cross directory of NASA N numbers and DOD AD numbers. Volume 2, part 1: AD to N, 1979-1986. N to AD, 1962-1986 [NASA-TM-101814] p 262 N90-12388
Criss-cross directory of NASA N numbers and DOD AD numbers. Volume 2, part 2: AD to N, 1979-1986. N to AD, 1962-1986 [NASA-TM-101815] p 262 N90-12389
- CATALYSTS**
Catalytic ignition of hydrogen/oxygen p 107 N90-28627
- CATHODES**
Plasma gun with coaxial powder feed and adjustable cathode [NASA-CASE-LEW-14901-1] p 252 N90-10718
Arcjet cathode phenomena p 75 N90-18477
Corrosion testing of candidates for the alkaline fuel cell cathode p 231 N90-20471
Impedance studies of Ni/Cd and Ni/H₂ cells using the cell case as a reference electrode p 231 N90-20473
- CAVITATION FLOW**
Elasticity effects on cavitation in a squeeze film damper undergoing noncentered circular whirl [NASA-TM-102392] p 200 N90-13786
A high-speed photography study of cavitation in a dynamically loaded journal bearing [NASA-TM-103178] p 204 N90-26338

CERAMIC MATRIX COMPOSITES

- CAVITIES**
Hopf bifurcation in the driven cavity p 174 A90-48548
High-frequency asymptotic methods for analyzing the EM scattering by open-ended waveguide cavities [NASA-CR-186244] p 143 N90-16103
Thermal radiation characteristics of nonisothermal cylindrical enclosures using a numerical ray tracing technique [NASA-TM-102527] p 179 N90-21296
An unsteady time asymptotic flow in the square driven cavity [NASA-TM-103141] p 181 N90-22016
- CELL CATHODES**
Corrosion testing of candidates for the alkaline fuel cell cathode p 228 A90-33948
Corrosion testing of candidates for the alkaline fuel cell cathode p 231 N90-20471
Catalysts for ultrahigh current density oxygen cathodes for space fuel cell applications [NASA-CR-180650] p 232 N90-22835
- CENTAUR LAUNCH VEHICLE**
Centaur upper stage p 44 A90-18017
- CENTRAL PROCESSING UNITS**
Concurrent processing adaptation of aeroplasic analysis of proplans [NASA-TM-102455] p 217 N90-14656
Transient finite element computations on the transputer system [NASA-CR-185199] p 218 N90-18071
Parallel algorithms for boundary value problems [NASA-TM-102498] p 243 N90-19783
- CENTRIFUGAL FORCE**
Computation of three dimensional turbulent boundary layers in internal flows, including turbomachinery rotor blades p 3 A90-12555
- CERAMIC COATINGS**
Mechanisms of degradation and failure in a plasma deposited thermal barrier coating [ASME PAPER 89-GT-132] p 84 A90-23830
Two-layer thermal barrier coating. I - Effects of composition and temperature on oxidation behavior and failure p 122 A90-33317
Deep-level dominated electrical characteristics of Au contacts on beta-SiC p 147 A90-33726
Metallographic techniques for evaluation of thermal barrier coatings p 85 A90-44869
- CERAMIC FIBERS**
Characterization of interfacial failure in SiC reinforced Si₃N₄ matrix composite material by both fiber push-out testing and Auger electron spectroscopy p 91 A90-36802
Microstructure of a SiC/Ti-15-3 composite p 91 A90-37663
Fatigue crack growth in a unidirectional SCS-6/Ti-15-3 composite [NASA-TM-103095] p 119 N90-22646
High temperature fatigue behavior of a SiC/Ti-24Al-11Nb composite [NASA-TM-103157] p 220 N90-22822
- CERAMIC MATRIX COMPOSITES**
Microstructural changes in beta-silicon nitride grains upon crystallizing the grain-boundary glass p 120 A90-13230
Measurement of interfacial shear strength in SiC-fiber/Si₃N₄ composites p 87 A90-13237
Up-and-coming IMCs --- Intermetallic-Matrix Composites p 88 A90-17295
CMCs for the long run --- ceramic-matrix composites p 88 A90-17301
Analysis of whisker-toughened ceramic components - A design engineer's viewpoint p 88 A90-19149
Noninteractive macroscopic reliability model for ceramic matrix composites with orthotropic material symmetry [ASME PAPER 89-GT-129] p 209 A90-23827
Local-global analysis of crack growth in continuously reinforced ceramic matrix composites [ASME PAPER 89-GT-138] p 88 A90-23835
A review of failure models for ceramic matrix composite laminates under monotonic loads p 89 A90-23842
Role of the interfacial thermal barrier in the effective thermal diffusivity/conductivity of SiC-fiber-reinforced reaction-bonded silicon nitride p 89 A90-25268
Noninteractive macroscopic reliability model for whisker-reinforced ceramic composites p 89 A90-26561
Polymer derived Nicalon/Si-C-O composites - Processing and mechanical behavior p 89 A90-27065
Nitriding kinetics of Si-SiC powder mixtures as simulations of reaction bonded Si₃N₄-SiC composites p 90 A90-27076
Crystallization of a barium-aluminosilicate glass p 121 A90-27107

- Laminate behavior for SiC fiber-reinforced reaction-bonded silicon nitride matrix composites p 90 A90-29927
- Characterization of interfacial failure in SiC reinforced Si3N4 matrix composite material by both fiber push-out testing and Auger electron spectroscopy p 91 A90-36802
- Thermal effects on the mechanical properties of SiC fibre reinforced reaction-bonded silicon nitride matrix composites p 92 A90-46999
- Properties of RBSN and RBSN-SiC composites --- Reaction Bonded Silicon Nitride p 94 A90-51920
- Nicalon/siliconoxycarbide ceramic composites p 94 A90-51924
- Crystallization behavior and properties of BaO-Al2O3-2SiO2 glass matrices p 95 A90-51933
- Zirconia toughened SiC whisker reinforced alumina composites small business innovation research [NASA-CR-179629] p 125 N90-10294
- Plasma gun with coaxial powder feed and adjustable cathode [NASA-CASE-LEW-14901-1] p 252 N90-10718
- Superconducting ceramics in the Bi1.5SrCaCu2O sub x system by melt quenching technique [NASA-CR-185139] p 258 N90-11606
- Sliding seal materials for low heat rejection engines [NASA-CR-182262] p 125 N90-11882
- Tribological properties of ceramic/Ti3Al-Nb sliding couples for use as candidate seal materials to 700 deg C [NASA-TM-102401] p 86 N90-12658
- Thermal barrier coatings for gas turbine and diesel engines [NASA-TM-102408] p 117 N90-13636
- Preparation of 110K (Bi,Pb)-Sr-Ca-Cu-O superconductor from glass precursor [NASA-CR-185162] p 258 N90-14108
- Advanced Turbine Technology Applications Project (ATTAP) [NASA-CR-185109] p 263 N90-14153
- Thermal/structural analyses of several hydrogen-cooled leading-edge concepts for hypersonic flight vehicles [NASA-TM-102391] p 177 N90-14511
- Thermodynamic analysis of chemical stability of ceramic materials in hydrogen-containing atmospheres at high temperatures [NASA-CR-4271] p 126 N90-16072
- Superconducting Bi1.5Pb0.5Sr2Ca2Cu3O(x) ceramics by rapid melt quenching and glass crystallization [NASA-CR-185184] p 258 N90-17465
- Analysis of whisker-toughened ceramic components: A design engineer's viewpoint [NASA-TM-102333] p 97 N90-18504
- Nicalon/siliconoxycarbide ceramic composites [NASA-TM-102563] p 99 N90-21133
- Ultrasonic and radiographic evaluation of advanced aerospace materials: Ceramic composites [NASA-TM-102540] p 207 N90-21401
- Studies on the use of supercritical ammonia for ceramic nitride synthesis and fabrication [NASA-TM-102570] p 106 N90-21843
- Polysiloxanes derived from the controlled hydrolysis of tetraethoxysilane as precursors to silica for use in ceramic processing [NASA-TM-102489] p 128 N90-21858
- Recent advances in nondestructive evaluation made possible by novel uses of video systems [NASA-TM-102491] p 207 N90-22801
- Controlled crack growth specimen for brittle systems [NASA-TM-103126] p 129 N90-23543
- Determination of the stress distributions in a ceramic: Tensile specimen using numerical techniques [NASA-TM-101914] p 129 N90-26132
- Extension of a noninteractive reliability model for ceramic matrix composites [NASA-CR-185267] p 129 N90-26142
- Design of ceramic components with the NASA/CARES computer program [NASA-TM-102369] p 222 N90-26359
- Advanced Turbine Technology Applications Project (ATTAP) [NASA-CR-185240] p 263 N90-26728
- Ceramics Analysis and Reliability Evaluation of Structures (CARES) Users and programmers manual [NASA-TP-2916] p 223 N90-28099
- Micromechanical model of crack growth in fiber reinforced ceramics [NASA-CR-4321] p 224 N90-28113
- Energy efficient engine pin fin and ceramic composite segmented liner combustor sector rig test report [NASA-CR-179534] p 35 N90-28567
- Improved silicon carbide for advanced heat engines [NASA-CR-182186] p 129 N90-28735
- CERMETS**
- Investigation of interfacial shear strength in a SiC fibre/Ti-24Al-11Nb composite by a fibre push-out technique p 88 A90-18973
- Properties of Pb(1-x)Bi(x)/Ba2YCu3O(x) composites - Reaction of Ba2YCu3O(x) with Pb and Bi p 255 A90-33224
- Composite matrix cooling scheme for small gas turbine combustors [AIAA PAPER 90-2158] p 22 A90-47210
- CHANNEL FLOW**
- Calculation of reattaching shear layers in divergent channel with a multiple-time-scale turbulence model [AIAA PAPER 90-0047] p 160 A90-19649
- Pressure drop and mass transfer in two-pass ribbed channels p 165 A90-24837
- A laser based computer aided non-intrusive technique for full field flow characterization in macroscopic curved channels p 168 A90-32293
- Near-wall turbulence model and its application to fully developed turbulent channel and pipe flows p 169 A90-37328
- Numerical simulation of rarefied gas flow through a slit [AIAA PAPER 90-1694] p 170 A90-38397
- Investigation of turbulent flow in highly curved ducts with application to turbomachinery components [NASA-CR-186060] p 175 N90-12882
- Experimental investigations on channelized coplanar waveguide [NASA-TM-102494] p 151 N90-20286
- An improved k-epsilon model for near-wall turbulence and comparison with direct numerical simulation [NASA-TM-103221] p 184 N90-27983
- CHARACTERIZATION**
- Synthesis and characterization of high-T(c) screen-printed Y-Ba-Cu-O films on alumina p 254 A90-21926
- Characterization and cycle tests of lightweight nickel electrodes [NASA-TM-102399] p 106 N90-12696
- Universal nondestructive MM-wave integrated circuit test fixture [NASA-CASE-LEW-14746-1] p 151 N90-17009
- High temperature superconducting thin film microwave circuits: Fabrication, characterization, and applications [NASA-TM-103235] p 156 N90-28786
- CHARGE COUPLED DEVICES**
- Optical techniques for determination of normal shock position in supersonic flows for aerospace applications [NASA-TM-103201] p 190 N90-25323
- CHARGE DISTRIBUTION**
- A Van der Waals-like theory of plasma double layers p 251 A90-10725
- CHARGE EFFICIENCY**
- Characterization testing of a 40 ampere hour bipolar nickel-hydrogen battery p 56 A90-33940
- CHEMICAL ANALYSIS**
- Thermodynamic analysis of chemical stability of ceramic materials in hydrogen-containing atmospheres at high temperatures [NASA-CR-4271] p 126 N90-16072
- CHEMICAL COMPOSITION**
- Two-layer thermal barrier coating I - Effects of composition and temperature on oxidation behavior and failure p 122 A90-33317
- Phase transformations in xerogels of mullite composition p 123 A90-47093
- Deformation of as-cast LiF-22 mol pct CaF2 hypereutectic salt between 500 and 1015 K p 124 A90-49086
- Identification of a cast iron alloy containing nonstrategic elements [NASA-CR-185174] p 118 N90-18559
- CHEMICAL EFFECTS**
- The chemical effects of the Martian environment on power system component materials: A theoretical approach [NASA-TM-103203] p 87 N90-26074
- CHEMICAL EQUILIBRIUM**
- H2/O2 three-body rates at high temperatures [AIAA PAPER 90-1696] p 105 A90-38399
- Inviscid flux-splitting algorithms for real gases with non-equilibrium chemistry p 174 A90-52275
- CHEMICAL PROPULSION**
- Performance comparisons of nuclear thermal rocket and chemical propulsion systems for piloted missions to Phobos/Mars [IAF PAPER 89-027] p 53 A90-13262
- A candidate architecture for monitoring and control in chemical transfer propulsion systems [AIAA PAPER 90-1882] p 52 A90-41980
- Lunar missions using advanced chemical propulsion - System design issues [AIAA PAPER 90-2431] p 67 A90-47221
- Low thrust rocket test facility [AIAA PAPER 90-2503] p 43 A90-47225
- Integrated controls and health monitoring for chemical transfer propulsion [AIAA PAPER 90-2751] p 52 A90-47229
- A candidate architecture for monitoring and control in chemical transfer propulsion systems [NASA-TM-103161] p 52 N90-22595
- Low thrust rocket test facility [NASA-TM-103206] p 43 N90-25158
- Integrated controls and health monitoring for chemical transfer propulsion [NASA-TM-103185] p 52 N90-25178
- CHEMICAL REACTIONS**
- Numerical study of chemically reacting flows using a lower-upper symmetric successive overrelaxation scheme p 3 A90-17989
- Humidity-induced room-temperature decomposition of Au contacted indium phosphide p 105 A90-44689

SUBJECT INDEX

- Bisannulation with a benzo(1,2-c:4,5-c'-prime) difuran equivalent - A new route to linear acene derivatives
[NASA-TM-102288] p 85 A90-49072
- Response of a chemically reacting layer to streamwise vorticity
[NASA-TM-102288] p 178 N90-18005
- TiCl₄ as a source of TiO₂ particles for laser anemometry measurements in hot gas
[NASA-TM-102581] p 189 N90-20358
- Critical evaluation of Jet-A spray combustion using propane chemical kinetics in gas turbine combustion simulated by KIVA-2
[NASA-TM-103173] p 138 N90-26170
- CHEMICAL REACTORS**
Energy storage for a lunar base by the reversible chemical reaction: CaO + H₂O reversible reaction Ca(OH)₂
[NASA-TM-103145] p 233 N90-25419
- CHILD-LANGMUIR LAW**
LEO high voltage solar array arcing response model, continuation 5
[NASA-CR-186505] p 232 N90-25418
- CHLORIDES**
Mass spectrometric observations of metal oxychlorides produced by oxidation-chlorination reactions
p 103 A90-21215
- CHLORINATION**
Mass spectrometric observations of metal oxychlorides produced by oxidation-chlorination reactions
p 103 A90-21215
- CHROMIUM ALLOYS**
Production and processing of Cu-Cr-Nb alloys
p 114 A90-33340
- Production and processing of Cu-Cr-Nb alloys
[NASA-TM-102495] p 117 N90-16053
- A resistance strain gage with repeatable and cancellable apparent strain for use to 800 C
[NASA-CR-185256] p 53 N90-26063
- CIRCULAR CYLINDERS**
Shear stabilization of the capillary breakup of a cylindrical interface
[AD-A219268] p 159 A90-17578
- Asymmetrical boundary layer separation at the base of a two cylinder geometry
p 159 A90-18505
- Simulating transitional flow and heat transfer over the flat plate and circular cylinder using a K-epsilon turbulence model
p 168 A90-32171
- CIRCULAR ORBITS**
Optimal impulsive time-fixed orbital rendezvous and interception with path constraints
[AIAA PAPER 90-2972] p 41 A90-53051
- Lunar orbiting microwave beam power system
[NASA-TM-103211] p 51 N90-25173
- CIRCULAR WAVEGUIDES**
Reflector spillover loss of an open-ended rectangular and circular waveguide feed
p 141 A90-45398
- CISLUNAR SPACE**
A trajectory generation and system characterization model for cislunar low-thrust spacecraft. Volume 2: Technical manual
[NASA-CR-185172] p 77 N90-21807
- CIVIL AVIATION**
Civil air transport: A fresh look at power-by-wire and fly-by-light
[NASA-TM-102574] p 153 N90-21283
- CLASSIFIERS**
A failure diagnosis system based on a neural network classifier for the space shuttle main engine
[NASA-TM-103607] p 83 N90-28659
- CLEARANCES**
Assessment of worm gearing for helicopter transmissions
[NASA-TM-102441] p 27 N90-15923
- NASA/GE Energy Efficient Engine low pressure turbine scaled test vehicle performance report
[NASA-CR-168290] p 34 N90-28563
- CLOSURE LAW**
Calculation of 3D turbulent jets in crossflow with a multigrid method and a second-moment closure model
[NASA-TM-103159] p 184 N90-26282
- Modeling of near-wall turbulence
[NASA-TM-103222] p 184 N90-28009
- CLOUDS**
Optical characterization of clouds of fine liquid-nitrogen particles
[NASA-TM-103208] p 191 N90-26299
- CLOUDS (METEOROLOGY)**
The effects of van der Waals attractions on cloud droplet growth by coalescence
p 234 A90-38363
- COALESCING**
Modeling of collision and coalescence of droplets during microgravity processing of Zn-Bi immiscible alloys
p 132 A90-22878
- Investigation of surface water behavior during glaze ice accretion
p 16 N90-20927
- COANDA EFFECT**
Control of flow separation and mixing by aerodynamic excitation
[NASA-TM-103131] p 13 N90-21733
- COATING**
Electromagnetic properties of material coated surfaces
[NASA-CR-186466] p 144 N90-19466
- COATINGS**
On physical optics for calculating scattering from coated bodies
p 250 A90-20151
- Indium-coated rhenium thrusters by CVD
p 114 A90-30480
- Constitutive parameter measurements of lossy materials
[NASA-CR-183398] p 257 N90-11603
- Electromagnetic properties of material coated surfaces
[NASA-CR-186466] p 144 N90-19466
- A resistance strain gage with repeatable and cancellable apparent strain for use to 800 C
[NASA-CR-185256] p 53 N90-26063
- COAXIAL CABLES**
Coax-to-channelised coplanar waveguide in-phase N-way, radial power divider
p 149 A90-41605
- COAXIAL FLOW**
An experimental and numerical study of particle-laden coaxial jet flows
p 171 A90-38799
- COBALT ALLOYS**
High-temperature slow-strain-rate compression studies on CoAl-TiB₂ composites
p 93 A90-48636
- COCKPITS**
The implementation of STOVU task-tailored control modes in a fighter cockpit
[AIAA PAPER 90-3229] p 17 A90-49114
- CODE DIVISION MULTIPLE ACCESS**
A performance analysis of DS-SS and SCPC VSAT networks
p 141 A90-39056
- CODERS**
Advanced modulation technology development for earth station demodulator applications. Coded modulation system development
[NASA-CR-185149] p 145 N90-20270
- CODING**
Data compression for the microgravity experiments
p 188 N90-16212
- COEFFICIENT OF FRICTION**
Studies of mechano-chemical interactions in the tribological behavior of materials
[NASA-TM-102545] p 128 N90-21182
- COLD FLOW TESTS**
Nature of convection-stabilized dc arcs in dual-flow nozzle geometry. I - The cold flow field and dc arc characteristics. II - Optical diagnostics and theory
p 252 A90-26665
- COLD PRESSING**
Crystallization behavior and properties of BaO-Al₂O₃-2SiO₂ glass matrices
[NASA-CR-185209] p 127 N90-19374
- Millimeter wave surface resistance of RbBa₂Cu₃O₇(δ) superconductors (R = Y, Eu, Dy, Sm, Er)
[NASA-TM-102571] p 259 N90-20886
- COLLIMATION**
Antenna beamforming using optical processing
[NASA-CR-180844] p 142 N90-11210
- COLLISIONLESS PLASMAS**
A Van der Waals-like theory of plasma double layers
p 251 A90-10725
- COLLISIONS**
Collision forces for compliant projectiles
[NASA-TM-4203] p 223 N90-28111
- COLOR**
An analysis of the contact sintering process in III-V solar cells
[NASA-TM-103179] p 233 N90-25420
- COMBUSTIBLE FLOW**
Progress in direct numerical simulations of turbulent reacting flows
p 157 A90-12836
- Model-free simulations of turbulent reactive flows
p 158 A90-15729
- Numerical study of chemically reacting flows using a lower-upper symmetric successive overrelaxation scheme
p 3 A90-17989
- Reduced chemical kinetics for propane combustion
[AIAA PAPER 90-0546] p 103 A90-19904
- Chemically reacting supersonic flow calculation using an assumed PDF model
[AIAA PAPER 90-0731] p 4 A90-22256
- Comparative study of computational efficiency of two LU schemes for non-equilibrium reacting flows
[AIAA PAPER 90-0396] p 167 A90-25940
- A planar reacting shear layer system for the study of fluid dynamics-combustion interaction
[NASA-TM-102422] p 27 N90-13393
- Development of an integrated BEM approach for hot fluid structure interaction
[NASA-CR-186214] p 177 N90-15364
- Response of a chemically reacting layer to streamwise vorticity
[NASA-TM-102288] p 178 N90-18005
- COMBUSTION**
On the use of external burning to reduce aerospace vehicle transonic drag
[AIAA PAPER 90-1935] p 20 A90-40562
- A comparison of European and American microgravity combustion experimental techniques
p 134 N90-16966
- Non-contact temperature measurements in support of microgravity combustion experiments
p 135 N90-17900
- On the use of external burning to reduce aerospace vehicle transonic drag
[NASA-TM-103107] p 30 N90-21762
- Saturated fluorescence measurements of the hydroxyl radical in laminar high-pressure flames
[NASA-CR-185218] p 190 N90-22022
- Critical evaluation of Jet-A spray combustion using propane chemical kinetics in gas turbine combustion simulated by KIVA-2
[NASA-TM-103173] p 138 N90-26170
- Ignition and combustion characteristics of metallized propellants
[NASA-CR-186870] p 107 N90-26911
- Energy Efficient Engine combustor test hardware detailed design report
[NASA-CR-168301] p 33 N90-28554
- COMBUSTION CHAMBERS**
A circular combustor configuration with multiple injection ports for mixing enhancement
p 158 A90-15389
- Corrosion prevention in copper combustion chamber liners of liquid oxygen/methane booster engines
[AIAA PAPER 90-2119] p 85 A90-42028
- Cooling of rocket thrust chambers with liquid oxygen
[AIAA PAPER 90-2120] p 63 A90-42029
- Enhanced heat transfer rocket combustor technology component hot-fire test results
[AIAA PAPER 90-2182] p 64 A90-42063
- Introducing the VRT gas turbine combustor
[AIAA PAPER 90-2452] p 21 A90-42808
- Effect of vane twist on the performance of dome swirlers for gas turbine airblast atomizers
[AIAA PAPER 90-1955] p 173 A90-47203
- Rocket combustion chamber life-enhancing design concepts
[AIAA PAPER 90-2116] p 66 A90-47208
- Composite matrix cooling scheme for small gas turbine combustors
[AIAA PAPER 90-2158] p 22 A90-47210
- Steam cooled rich-burn combustor liner
[NASA-CASE-LEW-13609-1] p 106 N90-11824
- Conceptual design for the space station Freedom modular combustion facility
[NASA-TM-102037] p 134 N90-16087
- MATE (Materials for Advanced Turbine Engines) Program, Project 3. Volume 2: Design, fabrication and evaluation of an oxide dispersion strengthened sheet alloy combustor liner
[NASA-CR-180892] p 117 N90-17868
- Hydrocarbon-fuel/combustion-chamber-liner materials compatibility
[NASA-CR-185203] p 118 N90-21165
- Microgravity acoustic mixing for particle cloud combustors
[NASA-CR-185159] p 248 N90-21600
- Cooling of rocket thrust chambers with liquid oxygen
[NASA-TM-103146] p 78 N90-22605
- Introducing the VRT gas turbine combustor
[NASA-TM-103176] p 137 N90-23591
- Rocket combustion chamber life-enhancing design concepts
[NASA-CR-185257] p 79 N90-25183
- Effect of vane twist on the performance of dome swirlers for gas turbine airblast atomizers
[NASA-TM-103195] p 182 N90-25289
- Reliability analysis of a structural ceramic combustion chamber
[NASA-TM-103264] p 223 N90-28112
- Energy Efficient Engine combustor test hardware detailed design report
[NASA-CR-168301] p 33 N90-28554
- Energy Efficient Engine (E3) combustion system component technology performance report
[NASA-CR-168274] p 33 N90-28555
- Energy efficient engine pin fin and ceramic composite segmented liner combustor sector rig test report
[NASA-CR-179534] p 35 N90-28567
- COMBUSTION CHEMISTRY**
On the driving force of PAH production
p 84 A90-32833

COMBUSTION EFFICIENCY

- Combustion interaction with radiation-cooled chambers
[AIAA PAPER 90-2121] p 64 A90-42030
Critical evaluation of Jet-A spray combustion using propane chemical kinetics in gas turbine combustion simulated by KIVA-II
[AIAA PAPER 90-2439] p 105 A90-50645
Critical evaluation of Jet-A spray combustion using propane chemical kinetics in gas turbine combustion simulated by KIVA-2
[NASA-TM-103173] p 138 N90-26170

COMBUSTION EFFICIENCY

- Effect of vane twist on the performance of dome swirlers for gas turbine airblast atomizers
[AIAA PAPER 90-1955] p 173 A90-47203
Effect of vane twist on the performance of dome swirlers for gas turbine airblast atomizers
[NASA-TM-103195] p 182 N90-25289
Energy Efficient Engine combustor test hardware detailed design report
[NASA-CR-168301] p 33 N90-28554
Energy Efficient Engine (E3) combustion system component technology performance report
[NASA-CR-168274] p 33 N90-28555
Energy efficient engine program technology benefit/cost study. Volume 1: Executive summary
[NASA-CR-174766-VOL-1] p 34 N90-28564
Energy efficient engine program technology benefit/cost study, volume 2
[NASA-CR-174766-VOL-2] p 35 N90-28565
Energy Efficient Engine: Combustor component performance program
[NASA-CR-179533] p 35 N90-28568

COMBUSTION PHYSICS

- Smoldering combustion under low gravity conditions
[AIAA PAPER 90-0648] p 103 A90-22238
Theory of influence of a low-volatility, soluble impurity on spherically-symmetric combustion of fuel droplets
p 104 A90-28771
Application of two-component phase Doppler interferometry to the measurement of particle size, mass flux, and velocities in two-phase flows
p 186 A90-32853
Mars in situ propellants - Carbon monoxide and oxygen ignition experiments
[AIAA PAPER 90-1894] p 130 A90-50642
Droplet combustion experiment drop tower tests using models of the space flight apparatus
[NASA-TM-101472] p 133 N90-11196
Facilities for microgravity combustion research
[NASA-TM-102014] p 134 N90-13679
Microgravity noncontact temperature requirements at NASA Lewis Research Center
p 134 N90-17897
Non-contact temperature measurements in support of microgravity combustion experiments
p 135 N90-17900
Spacelab qualified infrared imager for microgravity science experiments
[NASA-TM-102503] p 189 N90-20352
Mars in situ propellants: Carbon monoxide and oxygen ignition experiments
[NASA-TM-103202] p 81 N90-26065
New findings and instrumentation from the NASA Lewis microgravity facilities
[NASA-TM-103189] p 136 N90-26163
Critical evaluation of Jet-A spray combustion using propane chemical kinetics in gas turbine combustion simulated by KIVA-2
[NASA-TM-103173] p 138 N90-26170
Computational experience with a three-dimensional rotary engine combustion model
[NASA-TM-103104] p 183 N90-26275

COMBUSTION STABILITY

- The structure and stability of nonadiabatic flame balls
p 105 A90-43674
Combustor design and analysis using the ROCKET Combustor Interactive Design (ROCCID) Methodology
[AIAA PAPER 90-2240] p 65 A90-45694
A comparison of analytical results for 20 K LOX/hydrogen instabilities
[AIAA PAPER 90-2241] p 130 A90-47214
LOX/hydrocarbon combustion instability investigation
[NASA-CR-182249] p 71 N90-13589
Combustor design and analysis using the Rocket Combustor Interactive Design (ROCCID) methodology
[NASA-TM-103165] p 79 N90-24349
A comparison of analytical results for 20 K LOX/hydrogen instabilities
[NASA-TM-103166] p 80 N90-25186
Oxygen/methane combustion stability investigation
p 107 N90-28628
Combustion instability coupling with feed system acoustics
p 108 N90-28629

COMBUSTION TEMPERATURE

- H₂/O₂ three-body rates at high temperatures
[AIAA PAPER 90-1696] p 105 A90-38399

- Combustor technology for future aircraft
[AIAA PAPER 90-2400] p 22 A90-47219
COMMERCIAL AIRCRAFT
NASA's HITEMP program for UHBR engines
[AIAA PAPER 90-2395] p 22 A90-47218

COMMERCIAL SPACECRAFT

- The role of technology in influencing future civil communications satellites
p 142 A90-51167
Advanced onboard propulsion benefits and status
[NASA-TM-103174] p 82 N90-27786

COMMUNICATION EQUIPMENT

- AIRNET: A real-time communications network for aircraft
[NASA-CR-186140] p 145 N90-24514

COMMUNICATION NETWORKS

- An evolutionary communications scenario for Mars exploration
[AAS PAPER 87-268] p 139 A90-16566
Advanced Communications Technology Satellite (ACTS)
[AIAA PAPER 90-0839] p 140 A90-25663
Satellite-matrix-switched, time-division-multiple-access network simulator
[AIAA PAPER 90-0848] p 147 A90-25671
A performance analysis of DS-CDMA and SCPC VSAT networks
p 141 A90-39056
Performance analysis of Integrated Communication and Control System networks
p 239 A90-51267
Satellite-matrix-switched, time-division-multiple-access network simulator
[NASA-TP-2944] p 142 N90-11915

COMMUNICATION SATELLITES

- Role of communications satellites in the fiber era
[AIAA PAPER 90-0792] p 139 A90-25617
A new fabrication method for precision antenna reflectors for space flight and ground test
[AIAA PAPER 90-0803] p 139 A90-25627
Performance measurements for a laboratory-simulated 30/20 GHz communication satellite transponder
[AIAA PAPER 90-0808] p 140 A90-25634
Servicing communication satellites in geostationary orbit
[AIAA PAPER 90-0830] p 39 A90-25655
A users perspective of the ACTS hopping beam TDMA system
[AIAA PAPER 90-0833] p 140 A90-25658
Satellite-matrix-switched, time-division-multiple-access network simulator
[AIAA PAPER 90-0848] p 147 A90-25671
Spacecraft designs for VSAT networks
[AIAA PAPER 90-0895] p 140 A90-25681
Data distribution satellite system architecture concept
[AIAA PAPER 90-0885] p 46 A90-25704
Satellite-matrix-switched, time-division-multiple-access network simulator
[NASA-TP-2944] p 142 N90-11915
Performance measurements for a laboratory-simulated 30/20 GHz communication satellite transponder
[NASA-TM-102424] p 143 N90-17977
Advanced onboard propulsion benefits and status
[NASA-TM-103174] p 82 N90-27786

COMPARISON

- A comparison of European and American microgravity combustion experimental techniques
p 134 N90-16966

COMPATIBILITY

- Compatibility conditions of structural mechanics for finite element analysis
[NASA-TM-102413] p 217 N90-17180

COMPONENT RELIABILITY

- CSTI high capacity power --- Civil Space Technology Initiative
p 61 A90-38196
Integrated controls and health monitoring for chemical transfer propulsion
[AIAA PAPER 90-2751] p 52 A90-47229
Advanced Turbine Technology Applications Project (ATTAP)
[NASA-CR-185109] p 263 N90-14153
Space Station Freedom electric power system availability study
[NASA-CR-185181] p 50 N90-20120
Integrated controls and health monitoring for chemical transfer propulsion
[NASA-TM-103185] p 52 N90-25178
Design of ceramic components with the NASA/CARES computer program
[NASA-TM-102369] p 222 N90-26359
Ceramic matrix composites in simulated SSME environments
p 102 N90-28655

COMPOSITE MATERIALS

- Some composite bearing and seal materials for gas turbine applications - A review
[ASME PAPER 89-GT-144] p 195 A90-23838
Composites boost 21st-century aircraft engines
p 90 A90-29704

SUBJECT INDEX

- Solid state processing for high temperature alloys and composites
p 196 A90-33225
Thermodynamic analysis of chemical compatibility of ceramic reinforcement materials with niobium aluminides
p 92 A90-44001
Elevated temperature slow plastic deformation of NiAl-TiB₂ particulate composites at 1200 and 1300 K
p 92 A90-45621
Composite matrix cooling scheme for small gas turbine combustors
[AIAA PAPER 90-2158] p 22 A90-47210
Advanced refractory metals and composites for extraterrestrial power systems
p 40 A90-48819
Composite Blade Structural Analyzer (COBSTAN) theoretical/programmer's manual
[NASA-TM-101958] p 95 N90-10181
The application of cast SiC/Al to rotary engine components
[NASA-CR-179610] p 25 N90-13385
The Materials Division: A case study
[NASA-TM-102380] p 86 N90-13597
Empirical and analytical determination of the fracture resistance of a TiB₂ particle/SiC matrix composite
[NASA-TM-101940] p 96 N90-15143
Green's functions for dislocations in bonded strips and related crack problems
[NASA-CR-185291] p 224 N90-28878
COMPOSITE STRUCTURES
Multi-objective shape and material optimization of composite structures including damping
[AIAA PAPER 90-1135] p 210 A90-29262
Progression of damage and fracture in composites under dynamic loading
[AIAA PAPER 90-0916] p 210 A90-29318
NASA's HITEMP program for UHBR engines
[AIAA PAPER 90-2395] p 22 A90-47218
Effect of crack-microcracks interaction on energy release rates
p 214 A90-49269
PMR graphite engine duct development
[NASA-CR-182228] p 23 N90-10037
An integrated methodology for optimizing structural composite damping
[NASA-TM-102343] p 96 N90-11808
A thermoelastic transversely isotropic thick walled cylinder/disk application: An analytical solution and study
[NASA-TM-102320] p 216 N90-12950
Strength and toughness of monolithic and composite silicon nitrides
[NASA-TM-102423] p 126 N90-14368
Improved process for HIP canning of composites
[NASA-CASE-LEW-14990-1-CU] p 97 N90-15147
Demonstration of capabilities of high temperature composites analysis code HITCAN
[NASA-TM-102560] p 219 N90-19629
Computational simulation of damping in composite structures
[NASA-TM-102567] p 219 N90-20432
Multi-objective shape and material optimization of composite structures including damping
[NASA-TM-102579] p 99 N90-21132
Structural tailoring of select fiber composite structures
[NASA-TM-102484] p 99 N90-21137
Simplified design procedures for fiber composite structural components/joints
[NASA-TM-103113] p 101 N90-24384
Creep and creep rupture of strongly reinforced metallic composites
[NASA-CR-185286] p 223 N90-28110
Energy efficient engine pin fin and ceramic composite segmented liner combustor sector rig test report
[NASA-CR-179534] p 35 N90-28567
COMPRESSIBILITY EFFECTS
Effects of compressibility on the characteristics of free shear layers
p 6 A90-25285
COMPRESSIBLE BOUNDARY LAYER
Amplitude-dependent neutral modes in compressible boundary layer flows
[NASA-TM-102524] p 178 N90-20326
COMPRESSIBLE FLOW
The unsteady aerodynamics of an oscillating cascade in a compressible flow field
p 2 A90-11789
Nonlinear evolution of oblique waves on compressible shear layers
p 158 A90-15942
Compressibility effects in free shear layers
[AIAA PAPER 90-0705] p 161 A90-19984
Chemically reacting supersonic flow calculation using an assumed PDF model
[AIAA PAPER 90-0731] p 4 A90-22256
Effects of compressibility on the characteristics of free shear layers
p 6 A90-25285
Splitting of inviscid fluxes for real gases
p 167 A90-25451
Pressure-based real-time measurements in compressible free shear layers
[AIAA PAPER 90-1980] p 8 A90-42709

SUBJECT INDEX

- A block-based algorithm for the solution of compressible flows in rotor-stator combinations p 9 A90-46905
- Three-dimensional compressible jet-in-crossflow calculations using improved viscosity models and adapted grid [AIAA PAPER 90-2100] p 174 A90-47206
- Diagonally inverted lower-upper factored implicit multigrid scheme for the three-dimensional Navier-Stokes equations p 174 A90-49789
- Least-squares finite element methods for compressible Euler equations p 9 A90-51013
- PROTEUS two-dimensional Navier-Stokes computer code, version 1.0. Volume 1: Analysis description [NASA-TM-102551] p 180 N90-21303
- PROTEUS two-dimensional Navier-Stokes computer code, version 1.0. Volume 2: User's guide [NASA-TM-102552] p 180 N90-21306
- Numerical investigation of separated transonic turbulent flows with a multiple-time-scale turbulence model [NASA-TM-102499] p 180 N90-21962
- Investigation of advanced counterrotation blade configuration concepts for high speed turboprop systems, task 1: Ducted propfan analysis [NASA-CR-185217] p 30 N90-22567
- Implicit solution of three-dimensional internal turbulent flows [NASA-TM-103099] p 184 N90-27982
- COMPRESSIBLE FLUIDS**
- Treatment of coupled fluid-structure interaction problems by a mixed variational principle p 159 A90-18288
- COMPRESSION LOADS**
- Tooth contact shift in loaded spiral bevel gears p 193 A90-21112
- The mechanical properties of fluoride salts at elevated temperatures --- candidate thermal energy storage materials for solar dynamic systems p 123 A90-44376
- Slow plastic deformation of extruded NiAl-TiB₂ particulate composites at 1200 and 1300 K p 92 A90-46133
- COMPRESSION TESTS**
- 1200 to 1400 K slow strain rate compressive properties of NiAl/Ni₂AlTi-base materials p 88 A90-16938
- High-temperature slow-strain-rate compression studies on CoAl-TiB₂ composites p 93 A90-48636
- Deformation of as-cast LiF-22 mol pct CaF₂ hyperutectic salt between 500 and 1015 K p 124 A90-49086
- Compression behavior of the forged Li₂ compounds Al₆7Ti₂Cr₈ and Al₆6Ti₂5Mn₉ p 116 A90-51298
- COMPRESSIVE STRENGTH**
- 1100 to 1300 K slow plastic compression properties of Ni-38.5Al composites p 111 A90-19154
- Compressive strength of a B2 matrix NiAl-Nb intermetallic at 1200 and 1300 K p 111 A90-19157
- 1300 K compressive properties of several dispersion strengthened NiAl materials p 116 A90-47091
- COMPRESSOR BLADES**
- The measurement of boundary layers on a compressor blade in cascade. IV - Flow fields for incidence angles of -1.5 and -8.5 degrees [ASME PAPER 89-GT-72] p 165 A90-23793
- The measurement of boundary layers on a compressor blade in cascade. Volume 1: Experimental technique, analysis and results [NASA-CR-185118-VOL-1] p 23 N90-10038
- The measurement of boundary layers on a compressor blade in cascade. Volume 2: Data tables [NASA-CR-185118-VOL-2] p 23 N90-10039
- COMPRESSOR EFFICIENCY**
- Advanced core technology - Key to subsonic propulsion benefits [ASME PAPER 89-GT-241] p 19 A90-23890
- Energy Efficient Engine acoustic supporting technology report [NASA-CR-174834] p 33 N90-28557
- COMPRESSOR ROTORS**
- Analysis of fully stalled compressor p 6 A90-27966
- Advanced technology's impact on compressor design and development - A perspective [SAE SP-800] p 20 A90-28571
- Advanced technologies impact on compressor design and development: A perspective [NASA-TM-102341] p 24 N90-10891
- COMPRESSORS**
- WINCOF-I code for prediction of fan compressor unit with water ingestion [NASA-CR-185157] p 1 N90-21724
- COMPUTATION**
- Bearing elastohydrodynamic lubrication: A complex calculation made simple [NASA-TM-102575] p 203 N90-22041
- COMPUTATIONAL FLUID DYNAMICS**
- Advances in computational design and analysis of airbreathing propulsion systems p 19 A90-12502

- Computation of three dimensional turbulent boundary layers in internal flows, including turbomachinery rotor blades p 3 A90-12555
- Advanced computational techniques for hypersonic propulsion p 156 A90-12606
- Numerical modeling of enclosure convection [IAF PAPER 89-403] p 157 A90-13511
- Contributions to the understanding of large-scale coherent structures in developing free turbulent shear flows p 158 A90-13907
- Model-free simulations of turbulent reactive flows p 158 A90-15729
- Nonlinear evolution of interacting oblique waves on two-dimensional shear layers p 158 A90-15943
- A multi-domain spectral computation of three-dimensional laminar horseshoe vortex flow using incompressible Navier-Stokes equations p 3 A90-17592
- Numerical study of chemically reacting flows using a lower-upper symmetric successive overrelaxation scheme p 3 A90-17989
- Least-squares finite element method for fluid dynamics p 159 A90-18246
- Treatment of coupled fluid-structure interaction problems by a mixed variational principle p 159 A90-18288
- Fully elliptic incompressible flow calculations on regular grid by a new pressure substitution method [AIAA PAPER 90-0239] p 160 A90-19749
- Calculation of turbulence-driven secondary motion in ducts with arbitrary cross-section [AIAA PAPER 90-0245] p 160 A90-19752
- Convergence acceleration for vector sequences and applications to computational fluid dynamics [AIAA PAPER 90-0338] p 160 A90-19804
- On the mathematical modeling of the Reynolds stress's equations [AIAA PAPER 90-0498] p 161 A90-19878
- Reduced chemical kinetics for propane combustion [AIAA PAPER 90-0546] p 103 A90-19904
- Counterrotating prop-fan simulations which feature a relative-motion multiblock grid decomposition enabling arbitrary time-steps [AIAA PAPER 90-0687] p 3 A90-19978
- Development of an unstructured mesh/Navier-Stokes method for aerodynamics of aircraft with ice accretions [AIAA PAPER 90-0758] p 4 A90-20011
- A numerical study of the interaction between unsteady free-stream disturbances and localized variations in surface geometry p 161 A90-21422
- Chemically reacting supersonic flow calculation using an assumed PDF model [AIAA PAPER 90-0731] p 4 A90-22256
- Time-accurate simulations of a shear layer forced at a single frequency p 163 A90-23111
- Investigation of turbulent transport in an axisymmetric sudden expansion p 163 A90-23112
- Efficient real gas Navier-Stokes computations of high speed flows using an LU scheme [AIAA PAPER 90-0391] p 164 A90-23706
- The Osher scheme for real gases [AIAA PAPER 90-0397] p 166 A90-25030
- A numerical simulation of the flow in the diffuser of the NASA Lewis Icing Research Tunnel [AIAA PAPER 90-0488] p 166 A90-25034
- Phase development and its role on subharmonic control [AIAA PAPER 90-0503] p 166 A90-25035
- Numerical solutions of the linearized Euler equations for unsteady vortical flows around lifting airfoils [AIAA PAPER 90-0694] p 5 A90-25041
- Parallel flows with Soret effect in tilted cylinders p 167 A90-25594
- A 'transient' automated mapping procedure for complex geometries p 242 A90-26499
- Comparative study of computational efficiency of two LU schemes for non-equilibrium reacting flows [AIAA PAPER 90-0396] p 167 A90-26940
- Multigrid calculations of a jet in crossflow [AIAA PAPER 90-0444] p 167 A90-26952
- A flux-split solution procedure for unsteady inlet flows [AIAA PAPER 90-0585] p 6 A90-26967
- Comparison of 3-D viscous flow computations of Mach 5 inlet with experimental data [AIAA PAPER 90-0600] p 6 A90-26970
- Numerical solutions of the linearized Euler equations for unsteady vortical flows around lifting airfoils p 7 A90-30264
- Development of an integrated BEM for hot fluid-structure interaction [ASME PAPER 89-GT-128] p 212 A90-32264
- Numerical simulation of rarefied gas flow through a slit [AIAA PAPER 90-1694] p 170 A90-38397
- CFD propels NASP propulsion progress p 172 A90-41163

COMPUTATIONAL FLUID DYNAMICS

- A modeling technique for STOVL ejector and volume dynamics [AIAA PAPER 90-2417] p 20 A90-42168
- Numerical modeling of an arcjet thruster [AIAA PAPER 90-2614] p 64 A90-42587
- Computational analysis of the flowfield of a two-dimensional ejector nozzle [AIAA PAPER 90-1901] p 21 A90-42690
- Computation of turbine flowfields with a Navier-Stokes code [AIAA PAPER 90-2122] p 8 A90-42731
- The simulation of fluid dynamic uncertainties in the SSME turbopump [AIAA PAPER 90-2294] p 65 A90-42770
- Comparison between pressure gradient method and MAC method on high Re calculation p 172 A90-44462
- A block-based algorithm for the solution of compressible flows in rotor-stator combinations p 9 A90-46905
- Numerical analysis of secondary flow in a two-stage turbine [AIAA PAPER 90-2356] p 66 A90-47216
- Calculations of gaseous H₂/O₂ thruster [AIAA PAPER 90-2490] p 67 A90-47224
- Hopf bifurcation in the driven cavity p 174 A90-48548
- Diagonally inverted lower-upper factored implicit multigrid scheme for the three-dimensional Navier-Stokes equations p 174 A90-49789
- Least-squares finite element methods for compressible Euler equations p 9 A90-51013
- Global pressure relaxation for laminar two-dimensional internal flow p 174 A90-51019
- The measurement of boundary layers on a compressor blade in cascade. Volume 1: Experimental technique, analysis and results [NASA-CR-185118-VOL-1] p 23 N90-10038
- The measurement of boundary layers on a compressor blade in cascade. Volume 2: Data tables [NASA-CR-185118-VOL-2] p 23 N90-10039
- Computation of the tip vortex flowfield for advanced aircraft propellers [NASA-CR-182179] p 10 N90-10836
- Hopf bifurcation in the driven cavity [NASA-TM-102334] p 175 N90-11969
- Recent progress in research pertaining to estimates of gas-side heat transfer in an aircraft gas turbine [NASA-TM-102460] p 27 N90-13394
- Efficient real gas Navier-Stokes computations of high speed flows using an LU scheme [NASA-TM-102429] p 11 N90-14203
- An analysis of the viscous flow through a compact radial turbine by the average passage approach [NASA-TM-102471] p 12 N90-14206
- A numerical simulation of the flow in the diffuser of the NASA Lewis icing research tunnel [NASA-TM-102480] p 38 N90-15965
- Numerical solutions of the linearized Euler equations for unsteady vortical flows around lifting airfoils [NASA-TM-102466] p 12 N90-17562
- Viscous three-dimensional analyses for nozzles for hypersonic propulsion [NASA-CR-185197] p 27 N90-17635
- Conditions at the downstream boundary for simulations of viscous incompressible flow [NASA-TM-102510] p 243 N90-18198
- Gust response analysis for cascades operating in nonuniform mean flows p 28 N90-18415
- Numerical simulations of supersonic flow through oscillating cascade sections [NASA-TM-103100] p 13 N90-20051
- Comparison of 3-D viscous flow computations of Mach 5 inlet with experimental data [NASA-TM-102518] p 28 N90-20090
- Mass transfer from a sphere in an oscillating flow with zero mean velocity [NASA-TM-102566] p 179 N90-20338
- GRID2D/3D: A computer program for generating grid systems in complex-shaped two- and three-dimensional spatial domains. Part 2: User's manual and program listing [NASA-TM-102454] p 237 N90-20708
- A cost-effective strategy for nonoscillatory convection without clipping [NASA-TM-102538] p 179 N90-21291
- PROTEUS two-dimensional Navier-Stokes computer code, version 1.0. Volume 1: Analysis description [NASA-TM-102551] p 180 N90-21303
- PROTEUS two-dimensional Navier-Stokes computer code, version 1.0. Volume 2: User's guide [NASA-TM-102552] p 180 N90-21306
- PROTEUS two-dimensional Navier-Stokes computer code, version 1.0. Volume 3: Programmer's reference [NASA-TM-102553] p 180 N90-21307
- Swept wing ice accretion modeling [NASA-TM-103114] p 13 N90-21727

Computational modeling and validation for hypersonic inlets
[NASA-TM-103111] p 181 N90-22011

GRID2D/3D: A computer program for generating grid systems in complex-shaped two- and three-dimensional spatial domains. Part 1: Theory and method
[NASA-TM-102453] p 238 N90-22262

A modeling technique for STOVJ ejector and volume dynamics
[NASA-TM-103167] p 30 N90-22566

Investigation of advanced counterrotation blade configuration concepts for high speed turboprop systems, task 1: Ducted propfan analysis
[NASA-CR-185217] p 30 N90-22567

Computational analysis of the flowfield of a two-dimensional ejector nozzle
[NASA-CR-185255] p 31 N90-23406

Nonlinear interactions in mixing layers and compressible heated round jets
[NASA-CR-186303] p 182 N90-23674

Experimental and analytical study of close-coupled ventral nozzles for ASTOVJ aircraft
[NASA-TM-103170] p 31 N90-24273

Computational experience with a three-dimensional rotary engine combustion model
[NASA-TM-103104] p 183 N90-26275

Aerodynamics of a linear oscillating cascade
[NASA-TM-103250] p 15 N90-27657

Measurement of the steady surface pressure distribution on a single rotation large scale advanced prop-fan blade at Mach numbers from 0.03 to 0.78
[NASA-CR-182124] p 32 N90-28552

COMPUTATIONAL GEOMETRY
A 'transient' automated mapping procedure for complex geometries p 242 A90-26499

COMPUTATIONAL GRIDS
Fully elliptic incompressible flow calculations on regular grid by a new pressure substitution method
[AIAA PAPER 90-0239] p 160 A90-19749

Computation of three-dimensional turbulent boundary layers with heat transfer in a plane of symmetry using embedded wall-layer functions
[AIAA PAPER 90-0307] p 160 A90-19788

Development of an unstructured mesh/Navier-Stokes method for aerodynamics of aircraft with ice accretions
[AIAA PAPER 90-0758] p 4 A90-20011

Parallel multi-time step integration on a transputer system p 235 A90-20188

Calculation of shocked one-dimensional flows on abruptly changing grids by mathematical programming p 162 A90-21937

A critical analysis of the modified equation technique of Warming and Hyett p 241 A90-21940

Finite element mesh refinement criteria for stress analysis p 209 A90-23013

Diagonal inversion of lower-upper implicit schemes p 242 A90-23110

Discretization formulas for unstructured grids p 242 A90-26535

Interactive grid generation for turbomachinery flow field simulations p 6 A90-26553

Multigrid calculations of a jet in crossflow
[AIAA PAPER 90-0444] p 167 A90-26952

Three-dimensional fluid flow calculations using a flux-spline method p 167 A90-27983

Multigrid calculations of 3-D turbulent viscous flows p 172 A90-42426

Grid generation for the solution of partial differential equations p 237 A90-47188

Euler analysis comparison with LDV data for an advanced counter-rotation propfan at cruise
[AIAA PAPER 90-3033] p 9 A90-50637

Multigrid calculations of 3-D turbulent viscous flows
[NASA-CR-185154] p 1 N90-13323

Effect of spatial resolution on apparent sensitivity to initial conditions of a decaying flow as it becomes turbulent
[NASA-TM-102377] p 176 N90-13719

Application of multi-grid methods for solving the Navier-Stokes equations
[NASA-TM-102359] p 243 N90-14002

Mesh refinement in finite element analysis by minimization of the stiffness matrix trace
[NASA-CR-185170] p 201 N90-15434

A simple algebraic grid adaptation scheme with applications to two- and three-dimensional flow problems
[NASA-TM-102446] p 178 N90-18667

GRID2D/3D: A computer program for generating grid systems in complex-shaped two- and three-dimensional spatial domains. Part 2: User's manual and program listing
[NASA-TM-102454] p 237 N90-20708

Resistivity of pristine and intercalated graphite fiber epoxy composites
[NASA-TM-102576] p 128 N90-21192

GRID2D/3D: A computer program for generating grid systems in complex-shaped two- and three-dimensional spatial domains. Part 1: Theory and method
[NASA-TM-102453] p 238 N90-22262

Euler analysis comparison with LDV data for an advanced counter-rotation propfan at cruise
[NASA-TM-103249] p 14 N90-25946

Galerkin finite difference Laplacian operators on isolated unstructured triangular meshes by linear combinations
[NASA-TM-103209] p 183 N90-26276

Calculation of 3D turbulent jets in crossflow with a multigrid method and a second-moment closure model
[NASA-TM-103159] p 184 N90-26282

The fundamentals of adaptive grid movement p 185 N90-29610

COMPUTER AIDED DESIGN
Advances in computational design and analysis of airbreathing propulsion systems p 19 A90-12502

Designing ceramic components with the CARES computer program p 235 A90-19147

Analysis of whisker-toughened ceramic components - A design engineer's viewpoint p 88 A90-19149

Computer aided design of spur gear teeth p 195 A90-21131

Computer aided design of bevel gear tooth surfaces p 195 A90-21136

Multi-level Hierarchical Poly Tree computer architectures p 236 A90-26082

EPSAT - A workbench for designing high-power systems for the space environment p 245 A90-26975

[AIAA PAPER 90-0637] p 245 A90-26975

Neurobiological computational models in structural analysis and design p 210 A90-29260

[AIAA PAPER 90-1133] p 210 A90-29260

Tailoring of composite links for optimal damped elasto-dynamic performance p 211 A90-30250

SPRITE - A computer code for the optimization of space based heat pipe radiator systems p 170 A90-38036

Combustor design and analysis using the ROCKET Combustor Interactive Design (ROCCID) Methodology
[AIAA PAPER 90-2240] p 65 A90-45694

Combustor design and analysis using the Rocket Combustor Interactive Design (ROCCID) methodology
[NASA-TM-103165] p 79 N90-24349

Extension of a noninteractive reliability model for ceramic matrix composites p 129 N90-26142

[NASA-CR-185267] p 129 N90-26142

Modeling and optimization of a regenerative fuel cell system using the ASPEN process simulator
[NASA-TM-103210] p 233 N90-26396

Spent-beam refocusing analysis and multistage depressed collector design for a 75-W, 59- to 64-GHz coupled-cavity traveling-wave tube
[NASA-TP-3039] p 155 N90-27965

Computer-aided design of high-contact-ratio gears for minimum dynamic load and stress
[NASA-TM-103275] p 205 N90-28065

COMPUTER AIDED MANUFACTURING
Computer aided design of spur gear teeth p 195 A90-21131

Multi-level Hierarchical Poly Tree computer architectures p 236 A90-26082

Computerized inspection of gear tooth surfaces
[NASA-TM-102395] p 203 N90-22054

COMPUTER GRAPHICS
Advances in computational design and analysis of airbreathing propulsion systems p 19 A90-12502

Interactive grid generation for turbomachinery flow field simulations p 6 A90-26553

Computer simulation of gear tooth manufacturing processes
[NASA-CR-185200] p 138 N90-26171

COMPUTER NETWORKS
Modeling and synthesis of multicomputer interconnection networks
[NASA-CR-186619] p 238 N90-25604

Computer architecture evaluation for structural dynamics computations: Project summary
[NASA-CR-186137] p 235 N90-26512

COMPUTER PROGRAMMING
Grid generation for the solution of partial differential equations p 237 A90-47188

Numerical Arc Segmentation Algorithm for a Radio Conference-NASARC (version 4.0) technical manual
[NASA-TM-101453] p 144 N90-20264

Numerical Arc Segmentation Algorithm for a Radio Conference (NASARC), version 4.0: User's manual
[NASA-TM-101454] p 145 N90-21250

COMPUTER PROGRAMS
Predictions of airflow aerodynamic performance degradation due to icing p 3 A90-16753

Designing ceramic components with the CARES computer program p 235 A90-19147

Fortified LEWICE with viscous effects --- Lewis Ice Accretion Prediction Code
[AIAA PAPER 90-0754] p 15 A90-20009

Analysis of rotary engine combustion processes based on unsteady, three-dimensional computations
[AIAA PAPER 90-0643] p 163 A90-22237

Comparative thermal analysis of the Space Station Freedom photovoltaic deployable boom structure using TRASYS, NEVADA, and SINDA programs
[SAE PAPER 891563] p 47 A90-27525

Computational methods for probability of instability calculations
[AIAA PAPER 90-1139] p 236 A90-29333

Evaluation of three turbulence models in static air loads and dynamic stall predictions p 7 A90-31291

Influence of bulk turbulence and entrance boundary layer thickness on the curved duct flow field
[AIAA PAPER 90-1502] p 171 A90-38651

Computational analysis of the flowfield of a two-dimensional ejector nozzle p 21 A90-42690

[AIAA PAPER 90-1901] p 21 A90-42690

A test matrix sequencer for research test facility automation
[AIAA PAPER 90-2386] p 37 A90-42791

Numerical studies of convective heat transfer in an inclined semi-annular enclosure p 173 A90-45317

Combustor design and analysis using the ROCKET Combustor Interactive Design (ROCCID) Methodology
[AIAA PAPER 90-2240] p 65 A90-45694

A comparison of analytical results for 20 K LOX/hydrogen instabilities p 130 A90-47214

[AIAA PAPER 90-2241] p 130 A90-47214

Two stage gear tooth dynamics program p 199 N90-10437

[NASA-CR-185110] p 199 N90-10437

The MHOST finite element program: 3-D inelastic analysis methods for hot section components. Volume 2: User's manual p 215 N90-10450

[NASA-CR-182235-VOL-2] p 215 N90-10450

The MHOST finite element program: 3-D inelastic analysis methods for hot section components. Volume 3: Systems' manual p 215 N90-10451

[NASA-CR-182236] p 215 N90-10451

Generation and tooth contact analysis of spiral bevel gears with predesigned parabolic functions of transmission errors p 199 N90-12033

[NASA-CR-4259] p 199 N90-12033

FORTAN program for x ray photoelectron spectroscopy data reformatting p 258 N90-12348

[NASA-TP-2957] p 258 N90-12348

Application of a two-dimensional unsteady viscous analysis code to a supersonic throughflow fan stage
[NASA-TM-4141] p 25 N90-13387

[NASA-TM-4141] p 25 N90-13387

An improved algorithm for the modeling of vapor flow in heat pipes p 176 N90-13748

[NASA-CR-185179] p 176 N90-13748

Analysis of rotary engine combustion processes based on unsteady, three-dimensional computations p 176 N90-13749

[NASA-TM-102469] p 176 N90-13749

An analysis of the viscous flow through a compact radial turbine by the average passage approach
[NASA-TM-102471] p 12 N90-14206

[NASA-TM-102471] p 12 N90-14206

RAMSCRAM: A flexible ramjet/scramjet engine simulation program p 27 N90-14235

[NASA-TM-102451] p 27 N90-14235

User's guide to PMESH: A grid-generation program for single-rotation and counterrotation advanced turboprops
[NASA-CR-185156] p 235 N90-14783

[NASA-CR-185156] p 235 N90-14783

CryoTran user's manual, version 1.0 p 237 N90-15622

[NASA-TM-102468] p 237 N90-15622

A numerical simulation of the flow in the diffuser of the NASA Lewis icing research tunnel p 38 N90-15965

[NASA-TM-102480] p 38 N90-15965

Viscous three-dimensional analyses for nozzles for hypersonic propulsion p 27 N90-17635

[NASA-CR-185197] p 27 N90-17635

The application of a computer data acquisition system for a new high temperature tribometer p 86 N90-17811

[NASA-TM-102508] p 86 N90-17811

FLUSH: A tool for the design of slush hydrogen flow systems p 130 N90-17890

[NASA-TM-102467] p 130 N90-17890

Development of free-piston Stirling engine performance and optimization codes based on Martini simulation technique p 263 N90-18326

[NASA-CR-182210] p 263 N90-18326

Heat transfer measurements from a NACA 0012 airfoil in flight and in the NASA Lewis icing research tunnel
[NASA-CR-4278] p 13 N90-19203

Conjugate field approaches for active array compensation p 144 N90-19266

[NASA-TM-102454] p 144 N90-19266

Reflector surface distortion analysis techniques (thermal distortion analysis of antennas in space) p 144 N90-19267

[NASA-TM-102454] p 144 N90-19267

The measurement, modeling, and prediction of traction for rocket propellant 1 p 131 N90-19386

[NASA-CR-185186] p 131 N90-19386

Demonstration of capabilities of high temperature composites analyzer code HITCAN p 219 N90-19629

[NASA-TM-102560] p 219 N90-19629

Comparison of 3-D viscous flow computations of Mach 5 inlet with experimental data p 28 N90-20090 [NASA-TM-102518]

Composite laminate tailoring with probabilistic constraints and loads p 98 N90-20138 [NASA-TM-102515]

Computer simulation of the mathematical modeling involved in constitutive equation development: Via symbolic computations p 219 N90-20428 [NASA-TM-102532]

COMGEN: A computer program for generating finite element models of composite materials at the micro level p 219 N90-20438 [NASA-TM-102556]

GRID2D/3D: A computer program for generating grid systems in complex-shaped two- and three-dimensional spatial domains. Part 2: User's manual and program listing p 237 N90-20708 [NASA-TM-102454]

Detection of potential space station control/structure interaction with CO-ST-IN p 50 N90-21074

Structural tailoring of select fiber composite structures [NASA-TM-102484] p 99 N90-21137

Thermal radiation characteristics of nonisothermal cylindrical enclosures using a numerical ray tracing technique p 179 N90-21296 [NASA-TM-102527]

PROTEUS two-dimensional Navier-Stokes computer code, version 1.0. Volume 1: Analysis description p 180 N90-21303 [NASA-TM-102551]

PROTEUS two-dimensional Navier-Stokes computer code, version 1.0. Volume 2: User's guide p 180 N90-21306 [NASA-TM-102552]

PROTEUS two-dimensional Navier-Stokes computer code, version 1.0. Volume 3: Programmer's reference p 180 N90-21307 [NASA-TM-102553]

Aeropropulsion facilities configuration control: Procedures manual p 207 N90-21399 [NASA-TM-102541]

Hypercluster parallel processing library user's manual p 237 N90-21552 [NASA-CR-185231]

WINCOF-I code for prediction of fan compressor unit with water ingestion p 1 N90-21724 [NASA-CR-185157]

Computational simulation of structural fracture in fiber composites p 100 N90-21821 [NASA-TM-102505]

METCAN verification status p 100 N90-21824 [NASA-TM-103119]

Probabilistic analysis of bladed turbine disks and the effect of mistuning p 136 N90-21871 [NASA-TM-102564]

GRID2D/3D: A computer program for generating grid systems in complex-shaped two- and three-dimensional spatial domains. Part 1: Theory and method p 238 N90-22262 [NASA-TM-102453]

Computational analysis of the flowfield of a two-dimensional ejector nozzle p 31 N90-23406 [NASA-CR-185255]

A test matrix sequencer for research test facility automation p 39 N90-23416 [NASA-TM-103108]

Health management system for rocket engines p 131 N90-23574 [NASA-CR-185223]

Combustor design and analysis using the Rocket Combustor Interactive Design (ROCCID) methodology p 79 N90-24349 [NASA-TM-103165]

A comparison of analytical results for 20 K LOX/hydrogen instabilities p 80 N90-25186 [NASA-TM-103166]

Prediction of the ullage gas thermal stratification in a NASP vehicle propellant tank experimental simulation using FLOW-3D p 131 N90-26160 [NASA-TM-103217]

Critical evaluation of Jet-A spray combustion using propane chemical kinetics in gas turbine combustion simulated by KIVA-2 p 138 N90-26170 [NASA-TM-103173]

Design of ceramic components with the NASA/CARES computer program p 222 N90-26359 [NASA-TM-102369]

Efficient implementation of minimal polynomial and reduced rank extrapolation methods p 244 N90-26616 [NASA-TM-103240]

Computer code for predicting coolant flow and heat transfer in turbomachinery p 32 N90-27722 [NASA-TP-2985]

Modification of the SHABERTH bearing code to incorporate RP-1 and a discussion of the traction model p 205 N90-28066 [NASA-TP-3017]

Ceramics Analysis and Reliability Evaluation of Structures (CARES). Users and programmers manual p 223 N90-28399 [NASA-TP-2916]

Bearing optimization for SSME HPOTP application p 205 N90-28622

Generalized Advanced Propeller Analysis System (GAPAS). Volume 2: Computer program user manual [NASA-CR-185277] p 36 N90-29394

COMPUTER SYSTEMS PERFORMANCE

A general model for memory interference in a multiprocessor system with memory hierarchy p 238 A90-37482

COMPUTER SYSTEMS PROGRAMS

Robustness, generality and efficiency of optimization algorithms in practical applications p 236 A90-29268 [AIAA PAPER 90-1177]

COMPUTER TECHNIQUES

A laser based computer aided non-intrusive technique for full field flow characterization in macroscopic curved channels p 168 A90-32293

Boundary flexibility method of component mode synthesis using static Ritz vectors p 212 A90-35429

Status of structural analysis of 30 cm diameter ion optics p 215 A90-52571 [AIAA PAPER 90-2649]

Recent progress in research pertaining to estimates of gas-side heat transfer in an aircraft gas turbine p 27 N90-13394 [NASA-TM-102460]

Institute for Computational Mechanics in Propulsion (ICOMP) fourth annual review, 1989 p 243 N90-20769 [NASA-TM-102519]

COMPUTERIZED SIMULATION

Advances in computational design and analysis of airbreathing propulsion systems p 19 A90-12502

Advanced computational techniques for hypersonic propulsion p 156 A90-12606

Progress in direct numerical simulations of turbulent reacting flows p 157 A90-12836

Modeling and simulation of InP homojunction solar cells p 226 A90-14899

Optimization of silicon 8 cm x 8 cm wrapthrough Space Station cells for 'on orbit' operation p 54 A90-14941

Model-free simulations of turbulent reactive flows p 158 A90-15729

Predictions of airfoil aerodynamic performance degradation due to icing p 3 A90-16753

Computer aided design of spur gear teeth p 195 A90-21131

Prediction of self-pressurization rate of cryogenic propellant tankage p 55 A90-21219

High-voltage plasma interactions calculations using NASCAP/LEO p 251 A90-22254 [AIAA PAPER 90-0725]

Plasma contactor modeling with NASCAP/LEO - Extending laboratory results to space systems p 251 A90-22255 [AIAA PAPER 90-0726]

Application of a lower-upper implicit scheme and an interactive grid generation for turbomachinery flow field simulations p 4 A90-23762 [ASME PAPER 89-GT-20]

Computer modeling of current collection by the CHARGE-2 mother payload p 252 A90-24933

Interactive grid generation for turbomachinery flow field simulations p 6 A90-26553

Simulating transitional flow and heat transfer over the flat plate and circular cylinder using a K-epsilon turbulence model p 168 A90-32171

Development and refinement of test bed simulations --- for space station power supplies p 59 A90-38081

Evaluation of power control concepts using the PMAD systems test bed --- Power Management and Distribution p 42 A90-38083

Efficient Monte Carlo simulation of rarefied flow in a small nozzle p 170 A90-38396 [AIAA PAPER 90-1693]

High-frequency ac power distribution in Space Station p 63 A90-39111

Introducing the VRT gas turbine combustor p 21 A90-42808 [AIAA PAPER 90-2452]

Numerical modeling of flows in simulated brush seal configurations p 198 A90-47209 [AIAA PAPER 90-2141]

Critical evaluation of Jet-A spray combustion using propane chemical kinetics in gas turbine combustion simulated by KIVA-II p 105 A90-50645 [AIAA PAPER 90-2439]

STOVL propulsion system volume dynamics approximations p 25 N90-11740 [NASA-TM-102397]

Generation and tooth contact analysis of spiral bevel gears with predesigned parabolic functions of transmission errors p 199 N90-12033 [NASA-CR-4259]

Real-time simulation of an F110/STOVL turbofan engine p 25 N90-12618 [NASA-TM-102409]

STOVL aircraft simulation for integrated flight and propulsion control research p 26 N90-13389 [NASA-TM-102419]

Modeling of power electronic systems with EMTF p 245 N90-14060 [NASA-TM-102375]

RAMSCRAM: A flexible ramjet/scramjet engine simulation program p 27 N90-14235 [NASA-TM-102451]

CryoTran user's manual, version 1.0 p 237 N90-15622 [NASA-TM-102468]

Probabilistic simulation of uncertainties in composite uniaxial strengths p 97 N90-16008 [NASA-TM-102483]

Conditions at the downstream boundary for simulations of viscous incompressible flow p 243 N90-18198 [NASA-TM-102510]

Development of free-piston Stirling engine performance and optimization codes based on Martini simulation technique p 263 N90-18326 [NASA-CR-182210]

Advanced modulation technology development for earth station demodulator applications. Coded modulation system development p 145 N90-20270 [NASA-CR-185149]

Computer simulation of the mathematical modeling involved in constitutive equation development: Via symbolic computations p 219 N90-20428 [NASA-TM-102532]

The numerical simulation of multistage turbomachinery flows p 29 N90-21025

Detection of potential space station control/structure interaction with CO-ST-IN p 50 N90-21074

Fiber pushout test: A three-dimensional finite element computational simulation p 99 N90-21131 [NASA-TM-102565]

Swept wing ice accretion modeling p 13 N90-21727 [NASA-TM-103114]

Computational simulation of structural fracture in fiber composites p 100 N90-21821 [NASA-TM-102505]

Progression of damage and fracture in composites under dynamic loading p 100 N90-21825 [NASA-TM-103118]

An expert system for simulating electric loads aboard Space Station Freedom p 240 N90-22325 [NASA-TM-103150]

Influence of linear profile modification and loading conditions on the dynamic tooth load and stress of high contact ratio gears p 204 N90-22796 [NASA-TM-103136]

Probabilistic structural analysis of aerospace components using NESSUS p 221 N90-22823 [NASA-TM-102324]

Introducing the VRT gas turbine combustor p 137 N90-23591 [NASA-TM-103176]

Multiwavelength pyrometry to correct for reflected radiation p 190 N90-23714 [NASA-TM-102578]

Metal matrix composites microfracture: Computational simulation p 101 N90-24383 [NASA-TM-103153]

Two-dimensional Euler and Navier-Stokes Time accurate simulations of fan rotor flows p 14 N90-25948 [NASA-TM-102402]

Performance of a supercharged direct-injection stratified-charge rotary combustion engine p 32 N90-25982 [NASA-TM-103105]

Computer simulation of gear tooth manufacturing processes p 138 N90-26171 [NASA-CR-185200]

Modeling and optimization of a regenerative fuel cell system using the ASPEN process simulator p 233 N90-26396 [NASA-TM-103210]

Beam rider for an Articulated Robot Manipulator (ARM) accurate positioning of long flexible manipulators p 241 N90-26581 [NASA-CR-185151]

An improved k-epsilon model for near-wall turbulence and comparison with direct numerical simulation p 184 N90-27983 [NASA-TM-103221]

CONCENTRATION (COMPOSITION)

Low NO(x) potential of gas turbine engines p 27 N90-17636 [NASA-TM-102452]

CONCENTRATORS

A program for advancing the technology of space concentrators p 60 A90-38159

Update of the Solar Concentrator Advanced Development Project p 48 A90-38267

CONCURRENT PROCESSING

Concurrent processing adaptation of aeroelastic analysis of proflaps p 211 A90-29380 [AIAA PAPER 90-1036]

Concurrent processing adaptation of aeroelastic analysis of proflaps p 217 N90-14656 [NASA-TM-102455]

CONDENSATION

Rate correlation for condensation of pure vapor on turbulent, subcooled liquid p 174 A90-50511

CONDENSING

Buoyancy effects on the vapor condensation rate on a horizontal liquid surface p 162 A90-22201 [AIAA PAPER 90-0353]

CONDUCTIVE HEAT TRANSFER

SUBJECT INDEX

- Vapor condensation on liquid surface due to laminar jet-induced mixing - The effects of system parameters [AIAA PAPER 90-0354] p 163 A90-22202
- Buoyancy effects on the vapor condensation rate on a horizontal liquid surface [NASA-TM-102437] p 130 N90-13675
- Vapor condensation on liquid surface due to laminar jet-induced mixing: The effects of system parameters [NASA-TM-102433] p 176 N90-13751
- ### CONDUCTIVE HEAT TRANSFER
- Local and global accuracy estimates for boundary element analysis [AIAA PAPER 90-0930] p 211 A90-29324
- Frequency response of a thermocouple wire: Effects of axial conduction [NASA-CR-180454] p 191 N90-28827
- ### CONDUCTORS
- Solar array arcing in plasmas p 233 N90-25558
- Analysis of microstrip lines with alternative implementation of conductors and superconductors [NASA-TM-103182] p 155 N90-27966
- ### CONFERENCES
- Oxidation of high-temperature intermetallics; Proceedings of the Workshop, Cleveland, OH, Sept. 22, 23, 1988 p 112 A90-24852
- Space Electrochemical Research and Technology Conference, 2nd, Cleveland, OH, Apr. 11-13, 1989, Proceedings p 227 A90-33932
- Space Electrochemical Research and Technology (SERT), 1989 [NASA-CP-3056] p 230 N90-20454
- Free-Space Power Transmission [NASA-CP-10016] p 77 N90-21795
- ### CONFIGURATION MANAGEMENT
- Aeropropulsion facilities configuration control: Procedures manual [NASA-TM-102541] p 207 N90-21399
- ### CONICAL FLOW
- Some observations on transitory stall in conical diffusers [AIAA PAPER 90-0048] p 4 A90-22158
- Some observations on transitory stall in conical diffusers [NASA-TM-102387] p 11 N90-12561
- ### CONICAL NOZZLES
- Efficient Monte Carlo simulation of rarefied flow in a small nozzle [AIAA PAPER 90-1693] p 170 A90-38396
- Arjet nozzle design impacts p 76 N90-18478
- ### CONJUGATES
- Conjugate field approaches for active array compensation p 144 N90-19266
- ### CONNECTORS
- Characterization of structural connections using free and forced response test data p 213 A90-46172
- ### CONSERVATION LAWS
- Solution of steady-state one-dimensional conservation laws by mathematical programming p 241 A90-21918
- On the application of subcell resolution to conservation laws with stiff source terms [NASA-TM-102384] p 243 N90-14844
- ### CONSISTENCY
- Consistency and convergence for numerical radiation conditions [NASA-TM-103262] p 244 N90-29124
- ### CONSOLIDATION
- Slurry-pressing consolidation of silicon nitride p 121 A90-27691
- ### CONSTITUTIVE EQUATIONS
- Biaxial constitutive modelling and testing of a single crystal superalloy at elevated temperatures p 110 A90-16741
- Constitutive modeling for isotropic materials (HOST) [NASA-CR-179522] p 26 N90-13390
- Constitutive modeling for isotropic materials (HOST) [NASA-CR-174718] p 26 N90-13391
- Computer simulation of the mathematical modeling involved in constitutive equation development: Via symbolic computations [NASA-TM-102532] p 219 N90-20428
- Application of symbolic computations to the constitutive modeling of structural materials [NASA-TM-103225] p 222 N90-26364
- ### CONSTRICTORS
- Low power arcjet performance [AIAA PAPER 90-2578] p 68 A90-52568
- Low power arcjet performance [NASA-TM-103280] p 83 N90-28657
- ### CONTACT LOADS
- Fundamentals of tribology at the atomic level p 192 A90-14020
- Tooth contact shift in loaded spiral bevel gears p 193 A90-21112
- Surface pitting fatigue life of noninvolute, low-contact-ratio gears [AIAA PAPER 90-2153] p 197 A90-42049
- Influence of linear profile modification and loading conditions on the dynamic tooth load and stress of high contact ratio gears [NASA-TM-103136] p 204 N90-22796
- Computer-aided design of high-contact-ratio gears for minimum dynamic load and stress [NASA-TM-103275] p 205 N90-28065
- ### CONTACT RESISTANCE
- An analysis of the contact sintering process in III-V solar cells [NASA-TM-103179] p 233 N90-25420
- ### CONTAINMENT
- Selection of phase-change and containment materials for thermal energy storage [NASA-CR-186228] p 229 N90-15506
- ### CONTINUUM MECHANICS
- Mechanics of damping for fiber composite laminates including hygro-thermal effects [NASA-TM-102329] p 95 N90-10185
- A new uniformly valid asymptotic integration algorithm for elasto-plastic-creep and unified viscoplastic theories including continuum damage [NASA-TM-102344] p 217 N90-14655
- ### CONTINUUM MODELING
- Characterization of reaction kinetics in a porous electrode [NASA-CR-186504] p 106 N90-19340
- ### CONTRAROTATING PROPELLERS
- Performance and acoustic prediction of counterrotating propeller configurations [SAE PAPER 891035] p 246 A90-14342
- Noise of a simulated installed model counterrotation propeller at angle-of-attack and takeoff/approach conditions [AIAA PAPER 90-0283] p 247 A90-32505
- Counter-rotating propellant analysis using a frequency domain panel method p 7 A90-40937
- User's guide to PMESH: A grid-generation program for single-rotation and counterrotation advanced turboprops [NASA-CR-185156] p 235 N90-14783
- An approximate model for the performance and acoustic predictions of counterrotating propeller configurations [NASA-CR-180667] p 248 N90-18228
- Investigation of advanced counterrotation blade configuration concepts for high speed turboprop systems, task 1: Ducted propfan analysis [NASA-CR-185217] p 30 N90-22567
- Experimental performance and acoustic investigation of modern, counterrotating blade concepts [NASA-CR-185158] p 18 N90-23393
- ### CONTROL EQUIPMENT
- Autonomous power expert fault diagnostic system for Space Station Freedom electrical power system testbed p 80 N90-25521
- ### CONTROL SYSTEMS DESIGN
- Fiber optics for advanced aircraft p 185 A90-11702
- Advances in computational design and analysis of airbreathing propulsion systems p 19 A90-12502
- A high-speed GaAs MESFET optical controller p 186 A90-22483
- Space Station Freedom power management and distribution design status p 59 A90-38080
- Analysis of airframe/engine interactions - An integrated control perspective [AIAA PAPER 90-1918] p 36 A90-40557
- A candidate architecture for monitoring and control in chemical transfer propulsion systems [AIAA PAPER 90-1882] p 52 A90-41980
- Tank Pressure Control Experiment - A low-g mixing investigation [AIAA PAPER 90-2376] p 66 A90-47217
- H-infinity based integrated flight/propulsion control design for a STOLV aircraft in transition flight [AIAA PAPER 90-3335] p 36 A90-47595
- Extended implicit model following as applied to integrated flight and propulsion control [AIAA PAPER 90-3444] p 239 A90-47697
- Flight control design considerations for STOLV powered-lift flight [AIAA PAPER 90-3225] p 37 A90-49110
- An observer-based compensator for distributed delays p 239 A90-49899
- Integrated Communication and Control Systems. III - Nonidentical sensor and controller sampling p 239 A90-51266
- Performance analysis of Integrated Communication and Control System networks p 239 A90-51267
- Bidirectional power converter control electronics [NASA-CR-175070] p 70 N90-10175
- Induction motor control [NASA-TM-102533] p 28 N90-19234
- Detection of potential space station control/structure interaction with CO-ST-IN p 50 N90-21074
- A candidate architecture for monitoring and control in chemical transfer propulsion systems [NASA-TM-103161] p 52 N90-22595
- Elements of active vibration control for rotating machinery [NASA-TM-102368] p 137 N90-22703
- Dynamic analysis of space-related linear and non-linear structures [NASA-TM-103490] p 51 N90-25174
- Hot gas ingestion characteristics and flow visualization of a vectored thrust STOLV concept [NASA-TM-103212] p 32 N90-26009
- H-infinity based integrated flight-propulsion control design for a STOLV aircraft in transition flight [NASA-TM-103198] p 37 N90-26011
- Energy Efficient Engine: Control system preliminary definition report [NASA-CR-179578] p 35 N90-28569
- Design of a CO2 laser power control system for a Spacelab microgravity experiment [NASA-TM-103112] p 192 N90-28833
- An expert system to perform on-line controller restructuring for abrupt model changes [NASA-TM-103609] p 241 N90-29121
- ### CONTROL THEORY
- Neuromorphic learning of continuous-valued mappings from noise-corrupted data: Application to real-time adaptive control [NASA-TM-1476] p 241 N90-25607
- ### CONTROLLABILITY
- Elements of active vibration control for rotating machinery [NASA-TM-102368] p 137 N90-22703
- ### CONTROLLERS
- Simple evaporation controller for thin-film deposition from a resistively heated boat p 149 A90-39761
- Electromechanical actuation for thrust vector control applications [NASA-TM-102548] p 152 N90-21272
- Field oriented control of induction motors [NASA-TM-103154] p 154 N90-22731
- An expert system to perform on-line controller tuning [NASA-TM-103101] p 240 N90-23991
- H-infinity based integrated flight-propulsion control design for a STOLV aircraft in transition flight [NASA-TM-103198] p 37 N90-26011
- Temperature and melt solid interface control during crystal growth [NASA-CR-186731] p 259 N90-26664
- Fiber-optic projected-fringe digital interferometry [NASA-TM-103252] p 191 N90-28033
- ### CONVECTION
- Side-wall gas 'creep' and 'thermal stress convection' in microgravity experiments on film growth by vapor transport p 158 A90-14086
- Salt-finger convection under reduced gravity [AIAA PAPER 90-0122] p 160 A90-19693
- Non-contact temperature measurements in support of microgravity combustion experiments p 135 N90-17900
- Development of an infrared imaging system for the surface tension driven convection experiment p 188 N90-17922
- Spacelab qualified infrared imager for microgravity science experiments [NASA-TM-102503] p 189 N90-20352
- A cost-effective strategy for nonoscillatory convection without clipping [NASA-TM-102538] p 179 N90-21291
- ### CONVECTION CURRENTS
- Polymer solution phase separation: Microgravity simulation p 127 N90-17101
- ### CONVECTIVE FLOW
- Numerical modeling of enclosure convection [IAF PAPER 89-403] p 157 A90-13511
- Experimental investigation of convective stability in a superposed fluid and porous layer when heated from below p 158 A90-15947
- A nonoscillatory, characteristically convected, finite volume scheme for multidimensional convection problems [AIAA PAPER 90-0015] p 159 A90-19633
- Compressibility effects in free shear layers [AIAA PAPER 90-0705] p 161 A90-19984
- Opposed-flow flame spread and extinction in mixed-convection boundary layers p 168 A90-32841
- A nonoscillatory, characteristically convected, finite volume scheme for multidimensional convection problems [NASA-TM-102354] p 242 N90-11497
- A cost-effective strategy for nonoscillatory convection without clipping [NASA-TM-102538] p 179 N90-21291
- ### CONVECTIVE HEAT TRANSFER
- Interface demarcation in GaAs by current pulsing [AIAA PAPER 90-0319] p 254 A90-19793
- Two-dimensional convection and radiation with scattering from a Poiseuille flow p 161 A90-20519

- Convective heat transfer measurements from a NACA 0012 airfoil in flight and in the NASA Lewis Icing Research Tunnel
[AIAA PAPER 90-0199] p 162 A90-22180
- Coupled effects of conduction in the crystal and thermo-solutal convection in a rectangular inclined enclosure
[AIAA PAPER 90-0408] p 133 A90-25031
- Numerical studies of convective heat transfer in an inclined semi-annular enclosure
p 173 A90-45317
- Convective heat transfer measurements from a NACA 0012 airfoil in flight and in the NASA Lewis Icing Research Tunnel
[NASA-TM-102448] p 176 N90-13750
- ULTRA-SHARP nonoscillatory convection schemes for high-speed steady multidimensional flow
[NASA-TM-102568] p 244 N90-21570
- CONVERGENCE**
- Convergence acceleration for vector sequences and applications to computational fluid dynamics
[AIAA PAPER 90-0338] p 160 A90-19804
- Consistency and convergence for numerical radiation conditions
[NASA-TM-103262] p 244 N90-29124
- CONVERTIBLE FAN-SHAFT ENGINES**
- Convertible engine system for high speed rotorcraft
[AIAA PAPER 90-2512] p 20 A90-40643
- The selection of convertible engines with current gas generator technology for high speed rotorcraft
p 22 A90-46933
- COOLING**
- Lubricant jet flow phenomena in spur and helical gears with modified addendums - For radially directed individual jets
p 194 A90-21122
- Thermal/structural analyses of several hydrogen-cooled leading-edge concepts for hypersonic flight vehicles
[AIAA PAPER 90-0053] p 164 A90-23702
- Cooling of rocket thrust chambers with liquid oxygen
[AIAA PAPER 90-2120] p 63 A90-42029
- Steam cooled rich-burn combustor liner
[NASA-CASE-LEW-13609-1] p 106 N90-11824
- Thermal/structural analyses of several hydrogen-cooled leading-edge concepts for hypersonic flight vehicles
[NASA-TM-102391] p 177 N90-14511
- Cooling of rocket thrust chambers with liquid oxygen
[NASA-TM-103146] p 78 N90-22605
- COOLING SYSTEMS**
- Scaling results for the liquid sheet radiator
p 170 A90-38037
- Numerical model of solar dynamic radiator for parametric analysis
p 61 A90-38168
- Combustion interaction with radiation-cooled chambers
[AIAA PAPER 90-2121] p 64 A90-42030
- Composite matrix cooling scheme for small gas turbine combustors
[AIAA PAPER 90-2158] p 22 A90-47210
- COORDINATES**
- Three-dimensional adaptive grid generation for body-fitted coordinate system
p 167 A90-26506
- COPOLYMERS**
- Nicalon/siliconoxycarbide ceramic composites
[NASA-TM-102563] p 99 N90-21133
- COPPER**
- Measurements of dynamic Young's modulus in short specimens with the PUCOT - Piezoelectric Ultrasonic Composite Oscillator Technique
p 112 A90-21174
- Corrosion prevention in copper combustion chamber liners of liquid oxygen/methane booster engines
[AIAA PAPER 90-2119] p 85 A90-42028
- Secondary electron emission characteristics of molybdenum-masked, ion-textured OFHC copper
[NASA-TP-2967] p 117 N90-15211
- Hydrocarbon-fuel/combustion-chamber-liner materials compatibility
[NASA-CR-185203] p 118 N90-21165
- COPPER ALLOYS**
- Apparent activation volume for creep of copper and alpha brass at intermediate temperatures
p 108 A90-10028
- Production and processing of Cu-Cr-Nb alloys
p 114 A90-33340
- Production and processing of Cu-Cr-Nb alloys
[NASA-TM-102495] p 117 N90-16053
- Method of forming low cost, formable High T(sub c) superconducting wire
[NASA-CASE-LEW-14676-2] p 258 N90-17454
- High temperature fatigue behavior of tungsten copper composites
[NASA-TM-102404] p 99 N90-21138
- COPPER OXIDES**
- Synthesis and characterization of high-Tc superconductors in the Ti-Ca-Ba-Cu-O system
p 253 A90-19300
- Synthesis and characterization of high-T(c) screen-printed Y-Ba-Cu-O films on alumina
p 254 A90-21926
- Thin films of the Bi2Sr2Ca2Cu3O(x) superconductor
p 254 A90-24448
- Experimental evidence of a dimensional crossover in Y1Ba2Cu3O(7-delta)
p 255 A90-29739
- Antiferromagnetism in Co-57-doped La2CuO(4-y) studied by Moessbauer spectroscopy
p 255 A90-34011
- Fe-57 and Sn-119 Moessbauer study of La2CuO(4-y), YBa2Cu3O(7-y) and SmBa2Cu3O(7-y)
p 256 A90-34020
- Study of deposition of YBa2Cu3O7-x on cubic zirconia
[NASA-TM-102350] p 257 N90-10737
- Growth and patterning of laser ablated superconducting YBa2Cu3O7 films on LaAlO3 substrates
[NASA-TM-102436] p 259 N90-22421
- Photoresponse of YBa2Cu3O(7-delta) granular and epitaxial superconducting thin films
[NASA-TM-103144] p 154 N90-22732
- Sequentially evaporated thin film YBa2Cu3O(7-x) superconducting microwave ring resonator
[NASA-TM-103180] p 154 N90-25273
- Ellipsometric study of YBa2Cu3O(7-x) laser ablated and co-evaporated films
[NASA-TM-103223] p 259 N90-26682
- Laser ablated high T(sub c) superconducting thin YBa2Cu3O(7-x) films on substrates suitable for microwave applications
p 260 N90-27808
- Microwave conductivity of laser ablated YBaCuO superconducting films and its relation to microstrip transmission line
p 155 N90-27844
- Synthesis and structural chemistry of Au(III)-substituted Ba2YCu3O(7-delta)
[NASA-TM-103292] p 108 N90-28696
- CORDIERITE**
- Corrosion of cordierite ceramics by sodium sulphate at 1000 C
p 121 A90-21214
- CORE FLOW**
- Energy Efficient Engine core design and performance report
[NASA-CR-168069] p 34 N90-28559
- COROLIS EFFECT**
- Shaft flexibility effects on aeroelastic stability of a rotating bladed disk
p 208 A90-16371
- CORNER FLOW**
- Near wall flow parameters in the blade end-wall corner region
p 156 A90-12636
- CORRECTION**
- Computerized inspection of gear tooth surfaces
[NASA-TM-102395] p 203 N90-22054
- CORRELATION COEFFICIENTS**
- Review and statistical analysis of the ultrasonic velocity method for estimating the porosity fraction in polycrystalline materials
[NASA-TM-102501-REV] p 207 N90-21402
- CORROSION**
- Fastener design manual
[NASA-RP-1228] p 202 N90-18740
- Corrosion testing of candidates for the alkaline fuel cell cathode
p 231 N90-20471
- The oxidation and corrosion of ODS alloys
[NASA-TM-102555] p 119 N90-25211
- CORROSION PREVENTION**
- Corrosion prevention in copper combustion chamber liners of liquid oxygen/methane booster engines
[AIAA PAPER 90-2119] p 85 A90-42028
- CORROSION RESISTANCE**
- Analysis of whisker-toughened ceramic components - A design engineer's viewpoint
p 88 A90-19149
- CORROSION TESTS**
- Corrosion testing of candidates for the alkaline fuel cell cathode
p 228 A90-33948
- Corrosion testing of candidates for the alkaline fuel cell cathode
p 231 N90-20471
- COSMOLOGY**
- The shocking development of lithium (and boron) in supernovae
p 264 A90-17643
- A model for the distribution of the intergalactic medium
p 265 A90-34505
- Gravitational couplings of the inflation in extended inflation
p 265 A90-40088
- Soft inflation --- in cosmology
p 265 A90-40093
- COST ANALYSIS**
- Challenges for future space power systems
p 74 N90-17695
- COST EFFECTIVENESS**
- A cost-effective strategy for nonoscillatory convection without clipping
[NASA-TM-102538] p 179 N90-21291
- Energy efficient engine program technology benefit/cost study, Volume 1: Executive summary
[NASA-CR-174766-VOL-1] p 34 N90-28564
- Energy Efficient Engine: High-pressure compressor test hardware detailed design report
[NASA-CR-180850] p 36 N90-28570
- COST REDUCTION**
- Rocket combustion chamber life-enhancing design concepts
[AIAA PAPER 90-2116] p 66 A90-47208
- Rocket combustion chamber life-enhancing design concepts
[NASA-CR-185257] p 79 N90-25183
- Energy efficient engine program technology benefit/cost study, volume 2
[NASA-CR-174766-VOL-2] p 35 N90-28565
- COSTS**
- Preliminary designs for 25 kWe advanced Stirling conversion systems for dish electric applications
[NASA-TM-103188] p 263 N90-26729
- COUNTER ROTATION**
- Application of the computational aeroacoustics method to an advanced counterrotating propfan configuration
[AIAA PAPER 90-0183] p 246 A90-19725
- Counterrotating prop-fan simulations which feature a relative-motion multiblock grid decomposition enabling arbitrary time-steps
[AIAA PAPER 90-0687] p 3 A90-19978
- Effect of reduced aft diameter and increased blade number of high-speed counterrotation propeller performance
[AIAA PAPER 89-0438] p 4 A90-23650
- Euler analysis comparison with LDV data for an advanced counter-rotation propfan at cruise
[AIAA PAPER 90-3033] p 9 A90-50637
- Full scale technology demonstration of a modern counterrotating unducted fan engine concept: Component test
[NASA-CR-180868] p 24 N90-10047
- Full scale technology demonstration of a modern counterrotating unducted fan engine concept: Design report
[NASA-CR-180867] p 24 N90-10048
- Full scale technology demonstration of a modern counterrotating unducted fan engine concept: Engine test
[NASA-CR-180869] p 24 N90-10049
- Acoustic test and analysis of a counterrotating prop-fan model
[NASA-CR-179590] p 247 N90-10683
- An investigation of counterrotating tip vortex interaction
[NASA-CR-185135] p 247 N90-11549
- Effect of reduced aft diameter and increased blade number on high-speed counterrotation propeller performance
[NASA-TM-102077] p 11 N90-13352
- Noise of a simulated installed model counterrotation propeller at angle-of-attack and takeoff/approach conditions
[NASA-TM-102440] p 248 N90-20794
- Advanced gearbox technology
[NASA-CR-179625] p 32 N90-24274
- Euler analysis comparison with LDV data for an advanced counter-rotation propfan at cruise
[NASA-TM-103249] p 14 N90-25946
- High speed turboprop aeroacoustic study (counterrotation). Volume 1: Model development
[NASA-CR-185241] p 249 N90-26633
- COUNTER-ROTATING WHEELS**
- Theory of gearing
[NASA-RP-1212] p 202 N90-19593
- COWLINGS**
- Finite element analysis of structural components using viscoplastic models with application to a cowl lip problem
[NASA-CR-185189] p 221 N90-23769
- CRACK ARREST**
- Fatigue crack growth in a unidirectional SCS-6/Ti-15-3 composite
[NASA-TM-103095] p 119 N90-22646
- CRACK CLOSURE**
- Simulation of crack growth and crack closure under large cyclic plasticity
p 214 A90-50562
- Elevated temperature crack growth
[NASA-CR-182247] p 222 N90-26355
- CRACK INITIATION**
- Isothermal and nonisothermal fatigue behavior of a metal matrix composite
p 91 A90-36746
- Thermal fatigue durability for advanced propulsion materials
[NASA-TM-102348] p 216 N90-14641
- CRACK PROPAGATION**
- The unusual near-threshold FCG behavior of a single crystal superalloy and the resolved shear stress as the crack driving force
p 111 A90-21009
- Effect of fiber spacing on interfacial damage in a metal matrix composite
p 88 A90-23188

Local-global analysis of crack growth in continuously reinforced ceramic matrix composites
[ASME PAPER 89-GT-138] p 88 A90-23835

Cyclic deformation, fatigue and fatigue crack propagation in Ni-base alloys p 115 A90-34162

A probabilistic approach to crack instability p 212 A90-41278

Energy analysis of crack-damage interaction p 213 A90-41372

Fatigue crack propagation behavior of a single crystalline superalloy p 116 A90-48635

Simulation of crack growth and crack closure under large cyclic plasticity p 214 A90-50562

Mechanics of the crack path formation
[NASA-CR-185143] p 215 A90-10455

A nonlinear high temperature fracture mechanics basis for strainrange partitioning p 216 A90-14642

Fatigue crack growth in unidirectional metal matrix composite p 220 A90-22117

Fatigue crack growth in a unidirectional SCS-6/Ti-15-3 composite p 119 A90-22646

Controlled crack growth specimen for brittle systems
[NASA-TM-103126] p 129 A90-23543

Fatigue testing apparatus
[NASA-CASE-LEW-14124-1] p 190 A90-23712

Elevated temperature crack growth
[NASA-CR-182247] p 222 A90-26355

Improved transverse crack detection in composites
[NASA-TM-103261] p 102 A90-27875

Micromechanical model of crack growth in fiber reinforced ceramics p 224 A90-28113

Green's functions for dislocations in bonded strips and related crack problems
[NASA-CR-185291] p 224 A90-28878

CRACK TIPS

Local-global analysis of crack growth in continuously reinforced ceramic matrix composites
[ASME PAPER 89-GT-138] p 88 A90-23835

Characterization of the tip field of a discrete dislocation pileup for the development of physically based micromechanics p 213 A90-43883

CRACKING (FRACTURING)

Mechanisms of degradation and failure in a plasma deposited thermal barrier coating
[ASME PAPER 89-GT-132] p 84 A90-23830

Crack-path effect on material toughness
[ASME PAPER 89-WA/APM-43] p 210 A90-28755

The equivalence between dislocation pile-ups and cracks p 210 A90-29215

Cooling of rocket thrust chambers with liquid oxygen
[AIAA PAPER 90-2120] p 63 A90-42029

Cooling of rocket thrust chambers with liquid oxygen
[NASA-TM-103146] p 78 A90-22605

CRACKS

Mechanics of the crack path formation
[NASA-CR-185143] p 215 A90-10455

Arcjet cathode phenomena p 75 A90-18477

Influence of interfacial shear strength on the mechanical properties of SiC fiber reinforced reaction-bonded silicon nitride matrix composites
[NASA-TM-102462] p 101 A90-24382

CREEP ANALYSIS

On the stability of the creep substructure in NaCl single crystals p 254 A90-21920

CREEP BUCKLING

Effects of state recovery on creep buckling under variable loading p 212 A90-41223

CREEP PROPERTIES

Apparent activation volume for creep of copper and alpha brass at intermediate temperatures p 108 A90-10028

Finite element implementation of Robinson's unified viscoplastic model and its application to some uniaxial and multiaxial problems p 208 A90-15704

The high temperature creep deformation of Si3N4-6Y2O3-2Al2O3 p 121 A90-18879

Relationship between fatigue life in the creep-fatigue region and stress-strain response p 209 A90-20061

Influence of molybdenum on the creep properties of nickel-base superalloy single crystals p 113 A90-25233

The role of interfacial dislocation networks in high temperature creep of superalloys p 114 A90-33329

A nonlinear high temperature fracture mechanics basis for strainrange partitioning
[NASA-TM-4133] p 216 A90-14642

Steady-state and transient Zener parameters in viscoplasticity: Drag strength versus yield strength
[NASA-TM-102487] p 218 A90-18064

A viscoplastic model with application to LiF-22 percent CaF2 hypereutectic salt
[NASA-TM-103181] p 221 A90-23770

Stress versus temperature dependent activation energies in creep
[NASA-TM-103192] p 221 A90-23773

A creep model for metallic composites based on matrix testing: Application to Kanthal composites
[NASA-TM-103172] p 101 A90-25193

Creep and creep rupture of strongly reinforced metallic composites
[NASA-CR-185286] p 223 A90-28110

CREEP RUPTURE STRENGTH

Refractory metal alloys and composites for space power systems p 116 A90-46677

Identification of a cast iron alloy containing nonstrategic elements
[NASA-CR-185174] p 118 A90-18559

Mechanical properties of pure nickel alloys after long term exposures to LiOH and vacuum at 775 K
[NASA-TM-102403] p 118 A90-20181

CREEP STRENGTH

High temperature creep behavior of single crystal gamma prime and gamma alloys p 110 A90-16901

Creep strength of niobium alloys, Nb-1%Zr and PWC-11 p 116 A90-11854

A creep model for metallic composites based on matrix testing: Application to Kanthal composites
[NASA-TM-103172] p 101 A90-25193

CREEP TESTS

Inelastic deformation under nonisothermal loading p 112 A90-22657

Creep substructure formation in sodium chloride single crystals in the power law and exponential creep regimes p 255 A90-33330

A creep model for metallic composites based on matrix testing: Application to Kanthal composites
[NASA-TM-103172] p 101 A90-25193

CREW WORKSTATIONS

Space nuclear reactor shields for manned and unmanned applications p 57 A90-37859

CRITERIA

Amplitude-dependent neutral modes in compressible boundary layer flows
[NASA-TM-102524] p 178 A90-20326

CRITICAL POINT

Critical speeding up in pure fluids p 167 A90-26369

Critical exponent for the viscosity of carbon dioxide and xenon p 261 A90-43941

Critical fluid light scattering p 251 A90-17087

CRITICAL TEMPERATURE

Critical speeding up in pure fluids p 167 A90-26369

Critical fluid light scattering p 251 A90-17087

CROSS CORRELATION

Progress in high temperature speckle-shift strain measurement system
[NASA-TM-103255] p 191 A90-28031

CROSS COUPLING

Analysis of airframe/engine interactions - An integrated control perspective
[AIAA PAPER 90-1918] p 36 A90-40557

CROSS FLOW

Multigrid calculations of a jet in crossflow
[AIAA PAPER 90-0444] p 167 A90-26952

Three-dimensional compressible jet-in-crossflow calculations using improved viscosity models and adapted grid
[AIAA PAPER 90-2100] p 174 A90-47206

Flow visualization and motion analysis for a series of four sequential brush seals
[AIAA PAPER 90-2482] p 199 A90-47222

Calculation of 3D turbulent jets in crossflow with a multigrid method and a second-moment closure model
[NASA-TM-103159] p 184 A90-26282

CROSS POLARIZATION

Experimental study of the cross-polarization characteristics of rectangular microstrip antennas p 141 A90-37312

CROSSLINKING

Conceptual definition of a high voltage power supply test facility
[NASA-CR-185216] p 50 A90-25172

CRUCIBLES

Effects of crucible wetting during solidification of immiscible Pb-Zn alloys p 132 A90-17825

CRYOGENIC EQUIPMENT

Development of a compact, light weight magnetic bearing
[AIAA PAPER 90-2483] p 199 A90-47223

Vibration dampers for cryogenic turbomachinery
[AIAA PAPER 90-2740] p 199 A90-47228

Initial experimentation on the nonvented fill of a 0.14 cu m (5 cu ft) dewar with nitrogen and hydrogen
[AIAA PAPER 90-1681] p 136 A90-50641

Initial experimentation on the nonvented fill of a 0.14m3 (5 ft. 3) dewar with nitrogen and hydrogen
[NASA-TM-103155] p 183 A90-26278

CRYOGENIC FLUID STORAGE

COLD-SAT - An orbital cryogenic hydrogen technology experiment
[IAF PAPER 89-057] p 53 A90-13282

Evaluation of supercritical cryogen storage and transfer systems for future NASA missions
[AIAA PAPER 90-0719] p 44 A90-19989

Spacecraft attitude impacts on COLD-SAT non-vacuum jacketed LH2 supply tank thermal performance
[AIAA PAPER 90-1672] p 49 A90-41566

Tank Pressure Control Experiment - A low-g mixing investigation p 66 A90-47217

Numerical investigation of the thermal stratification in cryogenic tanks subjected to wall heat flux
[AIAA PAPER 90-2375] p 175 A90-52500

Evaluation of supercritical cryogen storage and transfer systems for future NASA missions
[NASA-TM-102394] p 44 A90-10912

Evolutionary space station fluids management strategies
[NASA-CR-185137] p 49 A90-10983

Liquid Transfer Cryogenic Test Facility: Initial hydrogen and nitrogen no-vent fill data
[NASA-TM-102572] p 179 A90-21295

Acquisition and correlation of cryogenic nitrogen mass flow data through a multiple orifice Joule-Thomson device
[NASA-TM-103121] p 182 A90-22761

Numerical investigation of the thermal stratification in cryogenic tanks subjected to wall heat flux
[NASA-TM-103194] p 184 A90-27984

CRYOGENIC FLUIDS

On-orbit low gravity cryogenic scientific investigations using the COLD-SAT Satellite p 39 A90-19988

Gas-phase flowrate effect on disintegrating cryogenic liquid-jets p 173 A90-46895

Evolutionary space station fluids management strategies
[NASA-CR-185137] p 49 A90-10983

Gas-phase flowrate effect on disintegrating cryogenic liquid-jets p 187 A90-11277

Tank pressure control experiment on the space shuttle
[NASA-TM-102313] p 71 A90-13590

CryoTran user's manual, version 1.0
[NASA-TM-102468] p 237 A90-15622

Scattered-light scanner measurements of cryogenic liquid-jet breakup
[NASA-TM-102432] p 189 A90-22021

CRYOGENIC ROCKET PROPELLANTS

Evaluation of supercritical cryogen storage and transfer systems for future NASA missions
[AIAA PAPER 90-0719] p 44 A90-19989

Prediction of self-pressurization rate of cryogenic propellant tankage p 55 A90-21219

Evaluation of supercritical cryogen storage and transfer systems for future NASA missions
[NASA-TM-102394] p 44 A90-10912

Evolutionary space station fluids management strategies
[NASA-CR-185137] p 49 A90-10983

Advanced APS impacts on vehicle payloads p 75 A90-18472

Technical accomplishments of the NASA Lewis Research Center, 1989
[NASA-TM-102296] p 267 A90-24220

CRYOGENIC STORAGE

On-orbit low gravity cryogenic scientific investigations using the COLD-SAT Satellite p 39 A90-19988

Prediction of self-pressurization rate of cryogenic propellant tankage p 55 A90-21219

CRYOGENIC TEMPERATURE

Ka-band propagation characteristics of microstrip lines on GaAs substrates at cryogenic temperatures p 147 A90-33644

Experimental evaluation of a tuned electromagnetic damper for vibration control of cryogenic turbopump rotors
[NASA-TP-3005] p 30 A90-23403

CRYOGENICS

Preliminary investigation of a NiAl composite prepared by cryomilling p 113 A90-25098

Cryogenic reactant storage for lunar base regenerative fuel cells
[IAF PAPER ICOSP89-3-8] p 227 A90-27709

Advanced Launch System (ALS) actuation and power systems impact operability and cost p 69 A90-52955

Advanced Launch System (ALS): Electrical actuation and power systems improve operability and cost picture
[NASA-TM-102547] p 152 A90-21271

Liquid Transfer Cryogenic Test Facility: Initial hydrogen and nitrogen no-vent fill data
[NASA-TM-102572] p 179 N90-21295

CRYSTAL DEFECTS

The correlation between the temperature dependence of the CRSS and the formation of superlattice-intrinsic stacking faults in the nickel-base superalloy PWA 1480
--- critical resolved shear stress p 109 A90-11657

CRYSTAL DISLOCATIONS

Molecular beam epitaxial growth of high-quality InSb on InP and GaAs substrates p 253 A90-12808
High temperature creep behavior of single crystal gamma prime and gamma alloys p 110 A90-16901
The role of interfacial dislocation networks in high temperature creep of superalloys p 114 A90-33329
Characterization of the tip field of a discrete dislocation pileup for the development of physically based micromechanics p 213 A90-43883

CRYSTAL GROWTH

A V-grooved GaAs solar cell p 225 A90-14887
Effect of crystal orientation on anisotropic etching and MOCVD growth of grooves on GaAs p 253 A90-15136
Evaluation of transport conditions during physical vapor transport growth of opto-electronic crystals p 132 A90-20525
High frequency capacitance-voltage characteristics of thermally grown SiO₂ films on beta-SiC p 254 A90-21348

Flight software development for the isothermal dendritic growth experiment p 235 A90-22257
[AIAA PAPER 90-0744]
Primary arm spacing in directionally solidified Pb-10 wt pct Sn alloys p 132 A90-23713
[AIAA PAPER 90-0740]
Coupled effects of conduction in the crystal and thermo-solutal convection in a rectangular inclined enclosure p 133 A90-25031
[AIAA PAPER 90-0408]
Ground-based experiments on thermal and thermosolutal convection in inclined low-aspect-ratio enclosures p 166 A90-25033
[AIAA PAPER 90-0413]
Growth of improved quality 3C-SiC films on 6H-SiC substrates p 255 A90-29596

The effect of length and diameter on the resistivity of bromine intercalated graphite fibers p 122 A90-33332
Energy stability of thermocapillary convection in a model of the float-zone crystal-growth process p 133 A90-48720
Effect of gas and surface radiation on crystal growth from the vapor phase p 133 A90-49060
Flight software development for the isothermal dendritic growth experiment p 238 N90-13988
[NASA-TM-102412]
Primary arm spacing in directionally solidified Pb-10 wt percent Sn alloys p 134 N90-14398
[NASA-CR-185190]
Temperature and melt solid interface control during crystal growth p 259 N90-26664
[NASA-CR-186731]

CRYSTAL STRUCTURE
Free dendritic growth in viscous melts - Cyclohexanol p 253 A90-19285
Creep substructure formation in sodium chloride single crystals in the power law and exponential creep regimes p 255 A90-33330

CRYSTALLIZATION

Micromicrostructural changes in beta-silicon nitride grains upon crystallizing the grain-boundary glass p 120 A90-13230
Crystallization kinetics of BaO-Al₂O₃-SiO₂ glasses p 121 A90-21175
Superconducting Bi(1.5)Pb(0.5)Sr₂Ca₂Cu₃O(x) ceramics by rapid melt quenching and glass crystallization p 256 A90-43568
Superconducting Bi_{1.5}Pb_{0.5}Sr₂Ca₂Cu₃O(x) ceramics by rapid melt quenching and glass crystallization [NASA-CR-185184] p 258 N90-17465
Crystallization behavior and properties of BaO-Al₂O₃-2SiO₂ glass matrices p 127 N90-19374
[NASA-CR-185209]

CRYSTALLOGRAPHY

A crystallographic model for the tensile and fatigue response for Rene N4 at 982 C p 114 A90-28754

CUMULATIVE DAMAGE

Progression of damage and fracture in composites under dynamic loading p 210 A90-29318
[AIAA PAPER 90-0916]

CURING

Photochemical approaches to ordered polymers p 84 A90-33222

CURRENT DENSITY

A V-grooved GaAs solar cell p 225 A90-14887
Contribution of the graded region of a HgCdTe diode to its saturation current p 257 A90-45948

Catalysts for ultrahigh current density oxygen cathodes for space fuel cell applications p 232 N90-22835
[NASA-CR-180650]
Microwave conductivity of laser ablated YBaCuO superconducting films and its relation to microstrip transmission line p 155 N90-27844

CURRENT REGULATORS

Distortion and regulation characterization of a Mapham inverter p 148 A90-38125

CURVATURE

Theory of gearing p 202 N90-19593
[NASA-RP-1212]

CURVED BEAMS

Vibration dampers for cryogenic turbomachinery p 199 A90-47228
[AIAA PAPER 90-2740]

CURVES

Method and models for R-curve instability calculations p 214 A90-50566

Theory of gearing p 202 N90-19593
[NASA-RP-1212]

CYCLES

Changes in impedance of Ni electrodes upon standing and cycling p 229 N90-18097
[NASA-TM-102438]

CYCLIC COMPOUNDS

On the driving force of PAH production p 84 A90-32833

CYCLIC HYDROCARBONS

Linear acene derivatives - New routes to pentacene and naphthalene and the first synthesis of a triptycene with two anthracene moieties p 85 A90-49071
Iptycene synthesis: A new method for attaching a 2,3-anthracene moiety to the 9,10-positions of another anthracene moiety - Exceptional conditions for a Lewis acid catalyzed Diels-Alder reaction p 85 A90-49073

CYCLIC LOADS

The high temperature deformation in cyclic loading of a single crystal nickel-base superalloy p 108 A90-11534
A constitutive model for the inelastic multiaxial response of Rene 80 at 871 C and 982 C p 114 A90-32266
Cyclic deformation, fatigue and fatigue crack propagation in Ni-base alloys p 115 A90-34162
Simulation of crack growth and crack closure under large cyclic plasticity p 214 A90-50562
Characterization of failure processes in tungsten copper composites under fatigue loading conditions p 98 N90-21123
[NASA-TM-102371]

CYCLOHEXANE

Free dendritic growth in viscous melts - Cyclohexanol p 253 A90-19285

CYCLOTRON RESONANCE DEVICES

Free-Space Power Transmission p 77 N90-21795
[NASA-CP-10016]

CYLINDRICAL BODIES

Improvement of finite element meshes - Heat transfer in an infinite cylinder p 209 A90-19109
Radiative configuration factors from cylinders to coaxial axisymmetric bodies p 167 A90-26334
Controlled crack growth specimen for brittle systems p 129 N90-23543
[NASA-TM-103126]
Low velocity impact analysis with NASTRAN p 221 N90-24647

CYLINDRICAL SHELLS

The impedance of a tubular electrode - A model for a porous electrode p 104 A90-33723
Effect of crack-microcracks interaction on energy release rates p 214 A90-49269
A thermoelastic transversely isotropic thick walled cylinder/disk application: An analytical solution and study p 216 N90-12950
[NASA-TM-102320]

CYLINDRICAL TANKS

Effects of g-jitter on a thermal, buoyant flow p 163 A90-22239
[AIAA PAPER 90-0653]
Numerical investigation of the thermal stratification in cryogenic tanks subjected to wall heat flux p 175 A90-52500
[AIAA PAPER 90-2375]
Numerical investigation of the thermal stratification in cryogenic tanks subjected to wall heat flux p 184 N90-27984
[NASA-TM-103194]

D**DAMAGE**

Relationship between fatigue life in the creep-fatigue region and stress-strain response p 209 A90-20061
Use of unbalanced laminates as a screening method for microcracking p 94 A90-50217
A new uniformly valid asymptotic integration algorithm for elasto-plastic-creep and unified viscoplastic theories including continuum damage p 217 N90-14655
[NASA-TM-102344]

Use of unbalanced laminates as a screening method for microcracking p 98 N90-21124
[NASA-TM-102517]

Progression of damage and fracture in composites under dynamic loading p 100 N90-21825
[NASA-TM-103118]
Creep and creep rupture of strongly reinforced metallic composites p 223 N90-28110
[NASA-CR-185286]

DAMAGE ASSESSMENT

Torsional and biaxial (tension-torsion) fatigue damage mechanisms in Waspaloy at room temperature p 109 A90-11925

Progression of damage and fracture in composites under dynamic loading p 210 A90-29318
[AIAA PAPER 90-0916]

Energy analysis of crack-damage interaction p 213 A90-41372

Mean stress and the exhaustion of fatigue-damage resistance p 216 N90-13819
[NASA-TM-101311]

The fatigue damage behavior of a single crystal superalloy p 120 N90-28644

DAMPERS (VALVES)

Elasticity effects on cavitation in a squeeze film damper undergoing noncentered circular whirl p 200 N90-13786
[NASA-TM-102392]

DAMPING

Characterization of damped structural connections for multi-component systems p 208 A90-16959
Mechanics of damping for fiber composite laminates including hygro-thermal effects p 95 N90-10185
[NASA-TM-102329]
An integrated methodology for optimizing structural composite damping p 96 N90-11808
[NASA-TM-102343]

DARK MATTER

Unitarity limits on the mass and radius of dark-matter particles p 264 A90-24671

Cosmic-string-induced hot dark matter perturbations p 264 A90-25889

A model for the distribution of the intergalactic medium p 265 A90-34505

Dark matter candidates p 266 A90-44095

A model for the distribution of dark matter, galaxies, and the intergalactic medium in a cold dark matter-dominated universe p 266 A90-45560

DATA ACQUISITION

The application of a computer data acquisition system for a new high temperature tribometer p 86 N90-17811
[NASA-TM-102508]

DATA BASES

The influence of ice accretion physics on the forecasting of aircraft icing conditions p 17 N90-20928
Reusable rocket engine turbopump health monitoring system, part 3 p 204 N90-26320
[NASA-CR-182294]
Application of symbolic computations to the constitutive modeling of structural materials p 222 N90-26364
[NASA-TM-103225]
High energy-density liquid rocket fuel performance p 131 N90-28742
[NASA-CR-185279]

DATA COMPRESSION

Digital codec for real-time processing of broadcast quality video signals at 1.8 bits/pixel p 142 A90-51306

Data compression techniques applied to high resolution high frame rate video technology p 143 N90-14452
[NASA-CR-4263]

Data compression for the microgravity experiments p 188 N90-16212

DATA LINKS

High-speed analog fiber optic links for satellite communication p 46 A90-11822
Data distribution satellite system architecture concept p 46 A90-25704
[AIAA PAPER 90-0885]
A forward error correction technique using a high-speed, high-rate single chip codec p 141 A90-48440
Bit-error-rate testing of fiber optic data links for MMIC-based phased array antennas p 145 N90-21261
[NASA-TM-102523]

DATA PROCESSING

A global approach for the identification of structural connection properties p 218 N90-18745
[NASA-TM-102502]

Multiprocessor architecture: Synthesis and evaluation p 235 N90-25579
[NASA-CR-186618]

Neuromorphic learning of continuous-valued mappings from noise-corrupted data. Application to real-time adaptive control p 241 N90-25607
[NASA-TM-4176]

DATA REDUCTION

New space domain processing technique for pulsed laser velocimetry p 187 A90-48750

DATA SAMPLING

DATA SAMPLING

Integrated Communication and Control Systems. III -
Nonidentical sensor and controller sampling
p 239 A90-51266

DATA STORAGE

The MHOST finite element program: 3-D inelastic
analysis methods for hot section components. Volume 3:
Systems' manual
[NASA-CR-182236] p 215 N90-10451

DATA SYSTEMS

A test matrix sequencer for research test facility
automation
[AIAA PAPER 90-2386] p 37 A90-42791
A test matrix sequencer for research test facility
automation
[NASA-TM-103108] p 39 N90-23416

DATA TRANSFER (COMPUTERS)

A forward error correction technique using a high-speed,
high-rate single chip codec p 141 A90-48440

DECISION MAKING

The lessons of Varsovian's reconnaissance
[NASA-TM-103207] p 267 N90-26789

DECISION THEORY

Application of a hybrid generation/utility assessment
heuristic to a class of scheduling problems
[NASA-TM-102367] p 245 N90-10674

DECOMPOSITION

Arcjet load characteristics
[AIAA PAPER 90-2579] p 67 A90-47226
Arcjet load characteristics
[NASA-TM-103190] p 79 N90-25181

DEFECTS

Calculation of Weibull strength parameters and Batdorf
flow-density constants for volume- and
surface-flaw-induced fracture in ceramics
p 212 A90-35462
Arcjet cathode phenomena p 75 N90-18477
Comparison of currents predicted by NASCAP/LEO
model simulations with elementary Langmuir-type bare
probe models for an insulated cable containing a single
pinhole
[NASA-TM-102486] p 51 N90-26054

DEFENSE PROGRAM

EPSAT - A workbench for designing high-power systems
for the space environment
[AIAA PAPER 90-0637] p 245 A90-26975

DEFLECTION

Tooth contact shift in loaded spiral bevel gears
p 193 A90-21112

DEFORMATION

The high temperature deformation in cyclic loading of
a single crystal nickel-base superalloy
p 108 A90-11534
Deformation behavior of NiAl-based alloys containing
iron, cobalt, and hafnium p 110 A90-16930
The high temperature creep deformation of
Si3N4-6Y2O3-2Al2O3 p 121 A90-18879
Cyclic deformation, fatigue and fatigue crack
propagation in Ni-base alloys p 115 A90-34162
Deformation of as-cast LiF-22 mol pct CaF2
hyper-eutectic salt between 500 and 1015 K
p 124 A90-49086
Thermomechanical deformation testing and modeling in
the presence of metallurgical instabilities
[NASA-CR-185188] p 219 N90-21420
The effect of hydrogen and microstructure on the
deformation and fracture behavior of a single crystal
nickel-base superalloy
[NASA-CR-185219] p 118 N90-21849
Low velocity impact analysis with NASTRAN
p 221 N90-24647
High-temperature deformation and microstructural
analysis for Si3N4-Sc2O3
[NASA-TM-103239] p 130 N90-28740

DEGRADATION

Predictions of airfoil aerodynamic performance
degradation due to icing p 3 A90-16753
Experimental investigation of multielement airfoil ice
accretion and resulting performance degradation
p 9 A90-48954
Advanced modulation technology development for earth
station demodulator applications. Coded modulation
system development
[NASA-CR-185149] p 145 N90-20270
Aeolian removal of dust from radiator surfaces on
Mars
[NASA-TM-103205] p 81 N90-26068
The chemical effects of the Martian environment on
power system component materials: A theoretical
approach
[NASA-TM-103203] p 87 N90-26074
Reusable rocket engine turbopump health monitoring
system, part 3
[NASA-CR-182294] p 204 N90-26320

DEGREES OF FREEDOM

Dynamic substructuring by the boundary flexibility vector
method of component mode synthesis
[NASA-CR-182445] p 220 N90-22813
Reaction-compensation technology for microgravity
laboratory robots
[NASA-TM-103271] p 205 N90-28062

DEICERS

Thin film eddy current impulse deicer
[AIAA PAPER 90-0761] p 17 A90-20012

DEICING

Impact ice stresses in rotating airfoils
[AIAA PAPER 90-0198] p 15 A90-19735
Electro-impulse de-icing testing analysis and design
[NASA-CR-4175] p 18 N90-10031
NASA's program on icing research and technology
p 16 N90-15062
Modeling of surface roughness effects on glaze ice
accretion p 16 N90-20925

DELAMINATING

Interfacial effects on the behavior of partially bonded
metal matrix composite properties p 93 A90-50094
Green's functions for dislocations in bonded strips and
related crack problems
[NASA-CR-185291] p 224 N90-28878

DELAY LINES

Satellite range delay simulator for a matrix-switched time
division multiple-access network simulation system
[AIAA PAPER 90-0795] p 139 A90-25620
Satellite range delay simulator for a matrix-switched time
division multiple-access network simulator
[NASA-TM-102407] p 143 N90-12813

DEMODULATORS

A parallel pipelined architecture for a digital multicarrier
demodulator
[AIAA PAPER 90-0812] p 46 A90-25635
Advanced modulation technology development for earth
station demodulator applications. Coded modulation
system development
[NASA-CR-185149] p 145 N90-20270

DENDRITIC CRYSTALS

Solute redistribution in dendritic solidification with
diffusion in the solid p 253 A90-17399
Finite element simulations of thermosolutal convection
in vertical solidification of binary alloys
p 132 A90-18292
Effects of crystal-melt interfacial energy anisotropy on
dendritic morphology and growth kinetics
p 253 A90-19284
Free dendritic growth in viscous melts - Cyclohexanol
p 253 A90-19285
Efficient estimation of diffusion during dendritic
solidification p 111 A90-20612
Flight software development for the isothermal dendritic
growth experiment
[AIAA PAPER 90-0744] p 235 A90-22257
Primary arm spacing in directionally solidified Pb-10 wt
pct Sn alloys
[AIAA PAPER 90-0740] p 132 A90-23713
Flight software development for the isothermal dendritic
growth experiment
[NASA-TM-102412] p 238 N90-13988
Primary arm spacing in directionally solidified Pb-10 wt
percent Sn alloys
[NASA-CR-185190] p 134 N90-14398

DENSIFICATION

Densification and coarsening during solid state sintering
of ceramics: A review of the models. II - Grain growth
p 120 A90-15375

DENSITY (MASS/VOLUME)

Density of intercalated graphite fibers
p 124 A90-49061
Density of intercalated graphite fibers
[NASA-TM-102411] p 126 N90-14362

DEPOSITION

Diamondlike carbon protective coatings for optical
windows p 122 A90-34569
Plasma-deposited amorphous hydrogenated carbon
films and their tribological properties
p 123 A90-44864
Fundamental tribological properties of
ion-beam-deposited boron nitride films
p 124 A90-49054
Plasma-deposited amorphous hydrogenated carbon
films and their tribological properties
[NASA-TM-102379] p 125 N90-11880
Fundamental tribological properties of
ion-beam-deposited boron nitride films
[NASA-TM-102088] p 125 N90-11881
Influence of the deposition conditions on radiofrequency
magnetron sputtered MoS2 films
[NASA-TP-2994] p 137 N90-21210

DEPTH MEASUREMENT

Adjustable depth gage
[NASA-CASE-LEW-14880-1] p 187 N90-10415

DESIGN ANALYSIS

Advances in computational design and analysis of
airbreathing propulsion systems p 19 A90-12502
Wear consideration in gear design for space
applications p 194 A90-21121
Computer aided design of bevel gear tooth surfaces
p 195 A90-21136
Advanced radiator concepts --- for nuclear powered
spacecraft p 170 A90-38042
Design of the Space Station Freedom power system
p 57 A90-38070
Space Station Freedom solar array design
development p 58 A90-38076
Review of the environmental effects on the Space
Station Freedom photovoltaic power module
p 59 A90-38087
Combustor design and analysis using the Rocket
Combustor Interactive Design (ROCCID) Methodology
[AIAA PAPER 90-2240] p 65 A90-45694
Large scale prop-fan structural design study. Volume
1: Initial concepts
[NASA-CR-174992] p 23 N90-10043
Large scale prop-fan structural design study. Volume
2: Preliminary design of SR-7
[NASA-CR-174993] p 23 N90-10044
Full scale technology demonstration of a modern
counterrotating unducted fan engine concept. Design
report
[NASA-CR-180867] p 24 N90-10048
An integrated methodology for optimizing structural
composite damping
[NASA-TM-102343] p 96 N90-11808
Numerical solutions of the linearized Euler equations
for unsteady vortical flows around lifting airfoils
[NASA-TM-102466] p 12 N90-17562
Research on a two-dimensional inlet for a supersonic
V/STOL propulsion system. Appendix A
[NASA-CR-174945] p 12 N90-18364
Fastener design manual
[NASA-RP-1228] p 202 N90-18740
Composite laminate tailoring with probabilistic
constraints and loads
[NASA-TM-102515] p 98 N90-20138
Design and test of a compact optics system for the
pool boiling experiment
[NASA-TM-102530] p 135 N90-20253
An applicational process for dynamic balancing of
turbomachinery shafting
[NASA-TM-102537] p 202 N90-20392
Aerodynamic optimization by simultaneously updating
flow variables and design parameters
p 18 N90-20991
Combustor design and analysis using the Rocket
Combustor Interactive Design (ROCCID) methodology
[NASA-TM-103165] p 79 N90-24349
Simplified design procedures for fiber composite
structural components/joints
[NASA-TM-103113] p 101 N90-24384
Feasibility study for the advanced one-dimensional high
temperature optical strain measurement system, phase 3
[NASA-CR-185254] p 191 N90-25324
Modeling and synthesis of multicomputer
interconnection networks
[NASA-CR-186619] p 238 N90-25604
Background, current status, and prognosis of the
ongoing slush hydrogen technology development program
for the NASP
[NASA-TM-103220] p 51 N90-26055
Spent-beam refocusing analysis and multistage
depressed collector design for a 75-W, 59- to 64-GHz
coupled-cavity traveling-wave tube
[NASA-TP-3039] p 155 N90-27965
Energy Efficient Engine integrated core/low spool test
hardware design report
[NASA-CR-168137] p 35 N90-28566
Energy Efficient Engine: High-pressure compressor test
hardware detailed design report
[NASA-CR-180850] p 36 N90-28570

DESTABILIZATION

Instabilities and subharmonic resonances of subsonic
heated round jets, volume 2
[NASA-CR-186058] p 181 N90-22017

DESTRUCTIVE TESTS

Investigation of Weibull statistics in fracture analysis of
cast aluminum p 115 A90-45304

DETECTION

Rocket engine failure detection using system
identification techniques
[AIAA PAPER 90-1993] p 65 A90-47205
Rocket engine failure detection using system
identification techniques
[NASA-CR-185259] p 45 N90-25159
Autonomous power expert fault diagnostic system for
Space Station Freedom electrical power system testbed
p 80 N90-25521

SUBJECT INDEX

SUBJECT INDEX

DEUTERIUM

Results of an attempt to measure increased rates of the reaction $D-2 + D-2$ yields $He-3 + n$ in a nonelectrochemical cold fusion experiment
[NASA-TM-102430] p 250 N90-17424

DIAGNOSIS

Gear noise, vibration, and diagnostic studies at NASA Lewis Research Center
[NASA-TM-102435] p 202 N90-18041
Autonomous power expert fault diagnostic system for Space Station Freedom electrical power system testbed
[NASA-TM-102552] p 80 N90-25521

DIAMETERS

Effect of reduced aft diameter and increased blade number of high-speed counterrotation propeller performance
[AIAA PAPER 89-0438] p 4 A90-23650
Effect of reduced aft diameter and increased blade number on high-speed counterrotation propeller performance
[NASA-TM-102077] p 11 N90-13352

DIAMONDS

K-band TWT using new diamond rod technology
[AIAA PAPER 90-0870] p 147 A90-25691
Studies of mechano-chemical interactions in the tribological behavior of materials
[NASA-TM-102545] p 128 N90-21182

DIELECTRIC PROPERTIES

Ellipsometric study of YBa₂Cu₃O_{7-x} laser ablated and co-evaporated films
[NASA-TM-103223] p 259 N90-26682
Dielectric function of InGaAs in the visible
[NASA-TM-103246] p 260 N90-26683

DIELECTRICS

A brief survey of radiation effects on polymer dielectrics
[NASA-TM-103119] p 123 A90-43119
Electron-beam induced damage in thin insulating films on compound semiconductors
[NASA-CR-185177] p 151 N90-17987
Electromagnetic properties of material coated surfaces
[NASA-CR-186466] p 144 N90-19466

DIELS-ALDER REACTIONS

Processable, high temperature polymers from 1,4,5,8-tetrahydro-1,4,5,8-diepoxyanthracene and bis-dienes
[AIAA PAPER 89-0438] p 84 A90-21930
Bisannulation with a benzo(1,2-c:4,5-c'-prime) difuran equivalent - A new route to linear acene derivatives
[AIAA PAPER 89-0438] p 85 A90-49072
Iptycene synthesis: A new method for attaching a 2,3-anthracene moiety to the 9,10-positions of another anthracene moiety - Exceptional conditions for a Lewis acid catalyzed Diels-Alder reaction
[AIAA PAPER 89-0438] p 85 A90-49073

DIESEL ENGINES

Ceramic valve development for heavy-duty low heat rejection diesel engines
[NASA-TM-102709] p 196 A90-27091
Ceramic port shields cast in an iron engine head
[NASA-TM-102709] p 196 A90-27095
Sliding seal materials for low heat rejection engines
[NASA-CR-182262] p 125 N90-11882
Two-dimensional analysis of two-phase reacting flow in a firing direct-injection diesel engine
[NASA-TM-102069] p 27 N90-13392
Assessment of fundamental materials needs for Thick Thermal Barrier Coatings (TTBC's) for truck diesel engines
[NASA-TM-103130] p 119 N90-23536

DIFFERENTIAL EQUATIONS

Numerical solutions of the linearized Euler equations for unsteady vortical flows around lifting airfoils
[NASA-TM-102466] p 7 A90-30264
Numerical solutions of the linearized Euler equations for unsteady vortical flows around lifting airfoils
[NASA-TM-102466] p 12 N90-17562
PROTEUS two-dimensional Navier-Stokes computer code, version 1.0. Volume 3: Programmer's reference
[NASA-TM-102553] p 180 N90-21307
Instabilities and subharmonic resonances of subsonic heated round jets, volume 2
[NASA-CR-186058] p 181 N90-22017

DIFFERENTIAL PRESSURE

Liquid Transfer Cryogenic Test Facility: Initial hydrogen and nitrogen no-vent fill data
[NASA-TM-102572] p 179 N90-21295

DIFFERENTIAL PULSE CODE MODULATION

Digital codec for real-time processing of broadcast quality video signals at 1.8 bits/pixel
[NASA-TM-102512] p 142 A90-51306

DIFFRACTION

Laser diffraction particle sizing: Instrument probe volume relocation and elongation
[NASA-TM-102512] p 188 N90-18025

DIFFUSERS

A numerical simulation of the flow in the diffuser of the NASA Lewis Icing Research Tunnel
[AIAA PAPER 90-0488] p 166 A90-25034

DIFFUSION

Salt-finger convection under reduced gravity
[AIAA PAPER 90-0122] p 160 A90-19693
Some observations on transitory stall in conical diffusers
[AIAA PAPER 90-0048] p 4 A90-22158
Some observations on transitory stall in conical diffusers
[NASA-TM-102387] p 11 N90-12561

DIFFUSION COEFFICIENT

Efficient estimation of diffusion during dendritic solidification
[AIAA PAPER 90-0651] p 111 A90-20612
Theory of influence of a low-volatility, soluble impurity on spherically-symmetric combustion of fuel droplets
[AIAA PAPER 90-0651] p 104 A90-28771

DIFFUSION ELECTRODES

Electrocatalysis for oxygen electrodes in fuel cells and water electrolyzers for space applications
[AIAA PAPER 90-0651] p 230 N90-20468

DIFFUSION FLAMES

Ignition and behavior of laminar gas-jet diffusion flames in microgravity
[AIAA PAPER 90-0651] p 103 A90-23107
Effects of pressure on microgravity hydrocarbon diffusion flames
[AIAA PAPER 90-0651] p 104 A90-25039
Near-limit flame spread over a thin solid fuel in microgravity
[AIAA PAPER 90-0651] p 104 A90-32835

DIFFUSION LENGTH

Estimation of minority carrier diffusion lengths in InP/GaAs solar cells
[AIAA PAPER 90-0651] p 81 N90-26069

DIFFUSION WELDING

Preliminary study on pressure brazing and diffusion welding of Nb-12Zr to Inconel 718
[AIAA PAPER 90-0651] p 196 A90-26899

DIGITAL COMPUTERS

Data compression techniques applied to high resolution high frame rate video technology
[NASA-CR-4263] p 143 N90-14452

DIGITAL DATA

Bit-error-rate testing of fiber optic data links for MMIC-based phased array antennas
[NASA-TM-102523] p 145 N90-21261

DIGITAL ELECTRONICS

A real time microcomputer implementation of sensor failure detection for turbofan engines
[AIAA PAPER 90-1994] p 21 A90-45414
Advanced detection, isolation, and accommodation of sensor failures in turbofan engines: Real-time microcomputer implementation
[NASA-TP-2925] p 37 N90-15112
Energy Efficient Engine: Control system preliminary definition report
[NASA-CR-179578] p 35 N90-28569

DIGITAL FILTERS

Digital filtering of plume emission spectra
[AIAA PAPER 90-1994] p 67 A90-50643
Digital filtering of plume emission spectra
[NASA-TM-103135] p 81 N90-26070

DIGITAL SIMULATION

Response of a chemically reacting layer to streamwise vorticity
[NASA-TM-102288] p 178 N90-18005

DIGITAL SPACECRAFT TELEVISION

High-speed digital fiber optic links for satellite traffic
[NASA-TM-103135] p 250 A90-41247

DIGITAL SYSTEMS

A parallel pipelined architecture for a digital multicarrier demodulator
[AIAA PAPER 90-0812] p 46 A90-25635
Feasibility study for the advanced one-dimensional high temperature optical strain measurement system, phase 3
[NASA-CR-185254] p 191 N90-25324
ATDRS payload technology research and development
[NASA-TM-103256] p 52 N90-28596

DIGITAL TECHNIQUES

Encoding Y,I,Q component estimates of an NTSC composite signal
[NASA-TM-103256] p 139 A90-23261
On-board switching and processing
[NASA-TM-103256] p 150 A90-51168
Digital codec for real-time processing of broadcast quality video signals at 1.8 bits/pixel
[NASA-TM-102512] p 142 A90-51306

Data compression techniques applied to high resolution high frame rate video technology
[NASA-CR-4263] p 143 N90-14452

DIMENSIONAL ANALYSIS

Fiber pushout test: A three-dimensional finite element computational simulation
[NASA-TM-102565] p 99 N90-21131

DIMENSIONAL STABILITY

Solar Concentrator Advanced Development Program
[NASA-CR-185173] p 232 N90-22834

DIODES

Coplanar waveguide discontinuities for P-I-N diode switches and filter applications
[NASA-TM-102534] p 153 N90-21278

DISTRIBUTED PARAMETER SYSTEMS

DIPOLE ANTENNAS

Millimeter-wave/infrared rectenna development at Georgia Tech
[NASA-CR-186531] p 69 N90-10147

DIRECT CURRENT

Magnification of starting torques of dc motors by maximum power point trackers in photovoltaic systems
[NASA-CR-186531] p 149 A90-38144

A comparative study of electric power distribution systems for spacecraft
[NASA-CR-186531] p 77 N90-21113

DIRECT POWER GENERATORS

Electrical performance characteristics of high power converters for space power applications
[NASA-CR-185947] p 72 N90-14279

DIRECTIONAL SOLIDIFICATION (CRYSTALS)

Side branch morphology and coarsening in directionally solidified Pb-8.4 at. pct Au
[AIAA PAPER 90-0740] p 109 A90-11658
Solute redistribution in dendritic solidification with diffusion in the solid
[AIAA PAPER 90-0409] p 253 A90-17399
Finite element simulations of thermosolutal convection in vertical solidification of binary alloys
[AIAA PAPER 90-0740] p 132 A90-18292

Primary arm spacing in directionally solidified Pb-10 wt pct Sn alloys
[AIAA PAPER 90-0740] p 132 A90-23713

Convection phenomena in low-gravity processing - The GTE GaAs space experiment
[AIAA PAPER 90-0409] p 133 A90-25032

Primary arm spacing in directionally solidified Pb-10 wt percent Sn alloys
[NASA-CR-185190] p 134 N90-14398

DIRECTORIES

Cross-cross directory of NASA N numbers and DOD AD numbers. Volume 2, part 1: AD to N, 1979-1986. N to AD, 1962-1986
[NASA-TM-101814] p 262 N90-12388
Cross-cross directory of NASA N numbers and DOD AD numbers. Volume 2, part 2: AD to N, 1979-1986. N to AD, 1962-1986
[NASA-TM-101815] p 262 N90-12389

DISCRETE FUNCTIONS

Discretization formulas for unstructured grids
[NASA-TM-101815] p 242 A90-26535

DISKS (SHAPES)

A thermoelastic transversely isotropic thick walled cylinder/disk application: An analytical solution and study
[NASA-TM-102320] p 216 N90-12950

DISLOCATIONS (MATERIALS)

The equivalence between dislocation pile-ups and cracks
[NASA-TM-102320] p 210 A90-29215

DISPERSION

MATE (Materials for Advanced Turbine Engines) Program, Project 3. Volume 2: Design, fabrication and evaluation of an oxide dispersion strengthened sheet alloy combustor liner
[NASA-CR-180892] p 117 N90-17868

DISPLACEMENT

Two stage gear tooth dynamics program
[NASA-CR-185110] p 199 N90-10437
Integrated force method versus displacement method for finite element analysis
[NASA-TP-2937] p 218 N90-18081

DISPLACEMENT MEASUREMENT

X-ray beam method for displacement measurement in hostile environments
[NASA-TM-102478] p 187 A90-44485

DISPLAY DEVICES

Cooperative synthesis of control and display augmentation in approach and landing
[NASA-TM-102478] p 36 A90-33061

An electronic pressure profile display system for aeronautic test facilities
[NASA-TM-102478] p 38 N90-15964

DISSIPATION

Asymptotic boundary conditions for dissipative waves: General theory
[NASA-TM-102497] p 243 N90-18927
Asymptotic analysis of dissipative waves with applications to their numerical simulation
[NASA-TM-103231] p 244 N90-26615

DISTANCE MEASURING EQUIPMENT

Adjustable depth gage
[NASA-CASE-LEW-14880-1] p 187 N90-10415

DISTORTION

Distortion and regulation characterization of a Mapham inverter
[NASA-TM-102358] p 148 A90-38125
Engine inlet distortion in a 9.2 percent scale vectored thrust STOV model in ground effect
[NASA-TM-102358] p 12 N90-17561
Nonlinear interactions in mixing layers and compressible heated round jets
[NASA-CR-186303] p 182 N90-23674

DISTRIBUTED PARAMETER SYSTEMS

An observer-based compensator for distributed delays
[NASA-TM-102358] p 239 A90-49899

- Autonomous power expert system
[NASA-CR-185263] p 80 N90-25187
- DISTRIBUTED PROCESSING**
Parallel/distributed direct method for solving linear systems
[NASA-TM-103229] p 244 N90-26614
- DISTRIBUTION FUNCTIONS**
Neuromorphic learning of continuous-valued mappings from noise-corrupted data. Application to real-time adaptive control
[NASA-TM-4176] p 241 N90-25607
- DIVERTERS**
Analysis of results from wind tunnel tests of inlets for an advanced turboprop nacelle installation
[NASA-CR-174937] p 10 N90-10011
- DOCUMENTATION**
Criss-cross directory of NASA N numbers and DOD AD numbers. Volume 2, part 1: AD to N, 1979-1986. N to AD, 1962-1986
[NASA-TM-101814] p 262 N90-12388
Criss-cross directory of NASA N numbers and DOD AD numbers. Volume 2, part 2: AD to N, 1979-1986. N to AD, 1962-1986
[NASA-TM-101815] p 262 N90-12389
- DOPED CRYSTALS**
AlGaAs/InGaAs heterostructures with doped channels for discrete devices and monolithic amplifiers
p 146 A90-20861
Antiferromagnetism in Co-57-doped La₂CuO₄(y) studied by Moessbauer spectroscopy
p 255 A90-34011
Fe-57 and Sn-119 Moessbauer study of La₂CuO₄(y), YBa₂Cu₃O(7-y) and SmBa₂Cu₃O(7-y)
p 256 A90-34020
Effect of Ga and P dopants on the thermoelectric properties of n-type SiGe
p 256 A90-38140
Reflecting boundary conditions for graded p-n junctions
p 150 A90-42400
Doped-channel heterojunction structures for millimeter-wave discrete devices and MMICs
p 150 A90-48492
High-temperature deformation and microstructural analysis for Si₃N₄-Sc₂O₃
[NASA-TM-103239] p 130 N90-28740
XANES and EXAFS study of Au-substituted YBa₂Cu₃O(7-delta)
[NASA-TM-103291] p 260 N90-29219
- DOPPLER RADAR**
Advanced instrumentation for aircraft icing research
[NASA-CR-185225] p 18 N90-21006
- DOWNLINKING**
Advanced modulation technology development for earth station demodulator applications. Coded modulation system development
[NASA-CR-185149] p 145 N90-20270
- DRAW COEFFICIENTS**
Ion drag for a negatively biased solar array in low earth orbit
p 48 A90-36191
- DRAG REDUCTION**
On the use of external burning to reduce aerospace vehicle transonic drag
[AIAA PAPER 90-1935] p 20 A90-40562
On the use of external burning to reduce aerospace vehicle transonic drag
[NASA-TM-103107] p 30 N90-21762
- DRILLING**
Adjustable depth gage
[NASA-CASE-LEW-14880-1] p 187 N90-10415
- DROP SIZE**
Liquid water content and droplet size calibration of the NASA Lewis Icing Research Tunnel
[AIAA PAPER 90-0669] p 37 A90-22242
Comparison of two droplet sizing systems in an icing wind tunnel
[AIAA PAPER 90-0668] p 164 A90-23711
Development of a phase Doppler based probe for icing cloud droplet characterization
[AIAA PAPER 90-0667] p 186 A90-26978
The effects of van der Waals attractions on cloud droplet growth by coalescence
p 234 A90-38363
Liquid water content and droplet size calibration of the NASA Lewis Icing Research Tunnel
[NASA-TM-102447] p 200 N90-13797
Comparison of two droplet sizing systems in an icing wind tunnel
[NASA-TM-102456] p 200 N90-14617
Comparison of drop size distributions from two droplet sizing systems
[NASA-TM-102520] p 202 N90-17147
Scattered-light scanner measurements of cryogenic liquid-jet breakup
[NASA-TM-102432] p 189 N90-22021
NASA Lewis icing research tunnel user manual
[NASA-TM-102319] p 31 N90-23407
- Optical characterization of clouds of fine liquid-nitrogen particles
[NASA-TM-103208] p 191 N90-26299
- DROP TESTS**
Conceptual design of a Liquid Droplet Radiator space flight experiment
[SAE PAPER 891565] p 48 A90-27527
- DROP TOWERS**
Droplet combustion experiment drop tower tests using models of the space flight apparatus
[NASA-TM-101472] p 133 N90-11196
- DROPS (LIQUIDS)**
Numerical analysis of natural convection in liquid droplets by phase change
p 164 A90-23212
Solidification by radiative cooling of a cylindrical region filled with drops
p 166 A90-24840
Conceptual design of a Liquid Droplet Radiator space flight experiment
[SAE PAPER 891565] p 48 A90-27527
The effects of van der Waals attractions on cloud droplet growth by coalescence
p 234 A90-38363
Conceptual design of liquid droplet radiator shuttle-attached experiment
[NASA-CR-185164] p 71 N90-11805
Conceptual design of liquid droplet radiator shuttle-attached experiment technical requirements document
[NASA-CR-185165] p 71 N90-11806
Droplet sizing instrumentation used for icing research: Operation, calibration, and accuracy
[NASA-CR-182293] p 187 N90-11999
Facilities for microgravity combustion research
[NASA-TM-102014] p 134 N90-13679
Thermocapillary migration of liquid droplets in a temperature gradient in a density matched system
[NASA-CR-185178] p 177 N90-14512
Comparison of drop size distributions from two droplet sizing systems
[NASA-TM-102520] p 202 N90-17147
- DUCT GEOMETRY**
Experimental investigation of turbulent flow through a circular-to-rectangular transition duct
[AIAA PAPER 90-1505] p 171 A90-38654
- DUCTED FAN ENGINES**
3D Euler analysis of ducted propfan flowfields
[AIAA PAPER 90-3034] p 8 A90-45873
- DUCTED FLOW**
Experimental investigation of turbulent flow through a circular-to-rectangular transition duct
[AIAA PAPER 90-1505] p 171 A90-38654
Experimental investigation of flow about a strut-endwall configuration
[AIAA PAPER 90-1541] p 171 A90-38685
A rotating hot-wire technique for spatial sampling of disturbed and manipulated duct flows
p 186 A90-41120
Analysis of internal flow in a ventral nozzle for STOVL aircraft
[AIAA PAPER 90-1899] p 21 A90-42688
Nonlinear Reynolds stress models and the renormalization group
p 172 A90-44011
Investigation of turbulent flow in highly curved ducts with application to turbomachinery components
[NASA-CR-186060] p 175 N90-12882
Analysis of internal flow in a ventral nozzle for STOVL aircraft
[NASA-TM-103123] p 31 N90-23404
- DUCTILITY**
Improving the low temperature ductility of NiAl
p 110 A90-16940
Observations on the brittle to ductile transition temperatures of B2 nickel aluminides with and without zirconium
p 111 A90-19153
Influence of testing environment on the room temperature ductility of FeAl alloys
p 115 A90-39658
Cyclic oxidation of aluminide coatings on TiAl+Ni
p 115 A90-39660
- DUCTS**
Calculation of turbulence-driven secondary motion in ducts with arbitrary cross-section
[AIAA PAPER 90-0245] p 160 A90-19752
PMR graphite engine duct development
[NASA-CR-182228] p 23 N90-10037
Laser velocimeter and total pressure measurements in circular-to-rectangular transition ducts
[NASA-CR-182286] p 177 N90-14494
Experimental and analytical study of close-coupled ventral nozzles for ASTOVL aircraft
[NASA-TM-103170] p 31 N90-24273
- DURABILITY**
Introducing the VRT gas turbine combustor
[AIAA PAPER 90-2452] p 21 A90-42808
The effect of leveling coatings on the atomic oxygen durability of solar concentrator surfaces
[NASA-TM-102557] p 76 N90-21110
- Computational simulation of structural fracture in fiber composites
[NASA-TM-102505] p 100 N90-21821
Progression of damage and fracture in composites under dynamic loading
[NASA-TM-103118] p 100 N90-21825
Introducing the VRT gas turbine combustor
[NASA-TM-103176] p 137 N90-23591
Advanced Turbine Technology Applications Project (ATTAP)
[NASA-CR-185240] p 263 N90-26728
The effects of atomic oxygen on the thermal emittance of high temperature radiator surfaces
[NASA-TM-103224] p 102 N90-28670
- DUST**
Aeolian removal of dust from photovoltaic surfaces on Mars
[NASA-TM-102507] p 76 N90-19299
Aeolian removal of dust from radiator surfaces on Mars
[NASA-TM-103205] p 81 N90-26068
- DUST STORMS**
Aeolian removal of dust from photovoltaic surfaces on Mars
[NASA-TM-102507] p 76 N90-19299
- DYNAMIC CHARACTERISTICS**
Base reaction optimization of redundant manipulators for space applications
[NASA-CR-186274] p 201 N90-15447
An application process for dynamic balancing of turbomachinery shafting
[NASA-TM-102537] p 202 N90-20392
High frequency, high temperature specific core loss and dynamic B-H hysteresis loop characteristics of soft magnetic alloys
[NASA-TM-103164] p 154 N90-23663
Non-linear dynamic analysis of geared systems, part 2
[NASA-CR-180495] p 204 N90-23732
Dynamics of multistage gear transmission with effects of gearbox vibrations
[NASA-TM-103109] p 205 N90-28060
- DYNAMIC CONTROL**
Dynamic analysis of space-related linear and non-linear structures
[NASA-TM-103490] p 51 N90-25174
- DYNAMIC LOADS**
Experimental and analytical evaluation of dynamic load vibration of a 2240-kW (3000-hp) rotorcraft transmission
p 192 A90-13750
Dynamic loading of spur gears with linear or parabolic tooth profile modifications
p 195 A90-21126
Profile modification to minimize spur gear dynamic loading
p 195 A90-21128
Progression of damage and fracture in composites under dynamic loading
[AIAA PAPER 90-0916] p 210 A90-29318
Two stage gear tooth dynamics program
[NASA-CR-185110] p 199 N90-10437
Elasticity effects on cavitation in a squeeze film damper undergoing noncentered circular whirl
[NASA-TM-102392] p 200 N90-13786
Progression of damage and fracture in composites under dynamic loading
[NASA-TM-103118] p 100 N90-21825
Influence of linear profile modification and loading conditions on the dynamic tooth load and stress of high contact ratio gears
[NASA-TM-103136] p 204 N90-22796
Analysis of shell-type structures subjected to time-dependent mechanical and thermal loading
[NASA-CR-185077] p 222 N90-24653
- DYNAMIC MODELS**
Numerical modeling of flows in simulated brush seal configurations
[AIAA PAPER 90-2141] p 198 A90-47209
A global approach for the identification of structural connection properties
[NASA-TM-102502] p 218 N90-18745
Non-linear dynamic analysis of geared systems, part 2
[NASA-CR-180495] p 204 N90-23732
- DYNAMIC MODULUS OF ELASTICITY**
Measurements of dynamic Young's modulus in short specimens with the PUCOT --- Piezoelectric Ultrasonic Composite Oscillator Technique
p 112 A90-21174
- DYNAMIC RESPONSE**
Tailoring of composite links for optimal damped elasto-dynamic performance
p 211 A90-30250
Influence of linear profile modification and loading conditions on the dynamic tooth load and stress of high contact ratio gears
[NASA-TM-103136] p 204 N90-22796
Dynamic substructuring by the boundary flexibility vector method of component mode synthesis
[NASA-CR-182445] p 220 N90-22813

SUBJECT INDEX

- Structural dynamics branch research and accomplishments
[NASA-TM-102488] p 223 N90-26373
- Development of a linearized unsteady aerodynamic analysis for cascade gust response predictions
[NASA-CR-4308] p 14 N90-27655
- DYNAMIC STABILITY**
Computational methods for probability of instability calculations
[AIAA PAPER 90-1139] p 236 A90-29333
- DYNAMIC STRUCTURAL ANALYSIS**
Characterization of damped structural connections for multi-component systems p 208 A90-16959
Modal selection in structural dynamics
p 209 A90-17001
Dynamic analysis of geared rotors by finite elements
p 194 A90-21123
- Selection of component modes
[AIAA PAPER 90-1201] p 210 A90-26787
Application of the probabilistic approximate analysis method to a turbopump blade analysis --- for Space Shuttle Main Engine
[AIAA PAPER 90-1098] p 56 A90-29328
Probabilistic analysis of a materially nonlinear structure
[AIAA PAPER 90-1099] p 211 A90-29329
A methodology for evaluating the reliability and risk of structures under complex service environments
[AIAA PAPER 90-1102] p 211 A90-29332
Boundary flexibility method of component mode synthesis using static Ritz vectors p 212 A90-35429
Advanced development of BEM for elastic and inelastic dynamic analysis of solids p 213 A90-45771
Characterization of structural connections using free and forced response test data p 213 A90-46172
Analysis of impact response in composite plates
p 214 A90-47567
Effect of crack-microcracks interaction on energy release rates p 214 A90-49269
Inelastic transient dynamic analysis of three-dimensional problems by BEM p 215 A90-51480
Status of structural analysis of 30 cm diameter ion optics
[AIAA PAPER 90-2649] p 215 A90-52571
Effects of mistuning and matrix structure on the topology of frequency response curves
[NASA-TM-102290] p 216 N90-12041
Dynamic analysis of geared rotors by finite elements
[NASA-TM-102349] p 201 N90-16286
A global approach for the identification of structural connection properties
[NASA-TM-102502] p 218 N90-18745
Computational simulation of damping in composite structures
[NASA-TM-102567] p 219 N90-20432
Progression of damage and fracture in composites under dynamic loading
[NASA-TM-103118] p 100 N90-21825
Dynamic substructuring by the boundary flexibility vector method of component mode synthesis
[NASA-CR-182445] p 220 N90-22813
Structural dynamics branch research and accomplishments
[NASA-TM-102488] p 223 N90-26373
- DYNAMIC TESTS**
Full scale technology demonstration of a modern counterrotating unducted fan engine concept: Component test
[NASA-CR-180868] p 24 N90-10047
Conceptual design of a moving belt radiator shuttle-attached experiments: Technical requirement Document
[NASA-CR-185168] p 73 N90-15996
- DYNAMICAL SYSTEMS**
A critical analysis of the modified equation technique of Warming and Hyett p 241 A90-21940
Computational methods for probability of instability calculations
[AIAA PAPER 90-1139] p 236 A90-29333
Actuator design for rotor control p 198 A90-46232

E

- EARTH IONOSPHERE**
Spacelab 2 Plasma Diagnostics Package
p 39 A90-23263
A two-dimensional model of plasma expansion in the ionosphere p 233 A90-43609
- EARTH ORBITAL ENVIRONMENTS**
Optimization of silicon 8 cm x 8 cm wrapthrough Space Station cells for 'on orbit' operation p 54 A90-14941
Power considerations for an early manned Mars mission utilizing the Space Station
[AAS PAPER 87-223] p 55 A90-16688

- High-voltage plasma interactions calculations using NASCAP/LEO p 251 A90-22254
[AIAA PAPER 90-0725] p 42 A90-24791
Lunar production of solar cells - A near-term product for a lunar industrial facility p 48 A90-36191
Ion drag for a negatively biased solar array in low earth orbit p 104 A90-36268
Ellipsometric studies of the diffusion of atomic oxygen through silicon dioxide thin films p 58 A90-38076
Space Station Freedom solar array design development p 59 A90-38087
Review of the environmental effects on the Space Station Freedom photovoltaic power module p 59 A90-38087
Photovoltaic array environmental protection program --- in Space Station Freedom p 59 A90-38088
Space vehicle propulsion systems - Environmental space hazards
[AIAA PAPER 90-1881] p 63 A90-40545
- EARTH ORBITS**
Theory of plasma contactors in ground-based experiments and low earth orbit p 150 A90-47108
Design considerations for space flight hardware
[NASA-TM-102300] p 52 N90-14275
- EARTH-MOON SYSTEM**
Minimum fuel lunar trajectories for a low-thrust power-limited spacecraft
[AIAA PAPER 90-2975] p 41 A90-53054
- EARTH-MOON TRAJECTORIES**
Minimum fuel trajectories for a low-thrust power-limited mission to the moon and to Lagrange points L4 and L5
[AAS PAPER 89-351] p 40 A90-46784
- ECCENTRIC ORBITS**
Estimated performance and future potential of solar dynamic and photovoltaic power systems for selected LEO and HEO missions p 62 A90-38307
- EDDY CURRENTS**
Thin film eddy current impulse deicer
[AIAA PAPER 90-0761] p 17 A90-20012
Parametric study of power absorption from electromagnetic waves by small ferrite spheres
[NASA-TP-2949] p 246 N90-12282
- EDDY VISCOSITY**
Nonlinear Reynolds stress models and the renormalization group p 172 A90-44011
Three-dimensional compressible jet-in-crossflow calculations using improved viscosity models and adapted grid
[AIAA PAPER 90-2100] p 174 A90-47206
Application of large eddy interaction model to a mixing layer
[NASA-CR-185123] p 11 N90-13328
PROTEUS two-dimensional Navier-Stokes computer code, version 1.0. Volume 2: User's guide
[NASA-TM-102552] p 180 N90-21306
PROTEUS two-dimensional Navier-Stokes computer code, version 1.0. Volume 3: Programmer's reference
[NASA-TM-102553] p 180 N90-21307
An improved k-epsilon model for near-wall turbulence and comparison with direct numerical simulation
[NASA-TM-103221] p 184 N90-27983
Modeling of near-wall turbulence
[NASA-TM-103222] p 184 N90-28009
- EDGE DISLOCATIONS**
Biaxial constitutive modelling and testing of a single crystal superalloy at elevated temperatures p 110 A90-16741
On the mechanism of cross slip in Ni3Al p 111 A90-20611
- EDUCATION**
The International Space University
[AIAA PAPER 90-2389] p 261 A90-42152
The International Space University
[NASA-TM-103163] p 78 N90-22604
- EFFICIENCY**
On-orbit results of the LIPS 3/InP homojunction solar cell experiment p 74 N90-17794
- EIGENVALUES**
Quotient-difference type generalizations of the power method and their analysis
[NASA-TM-102361] p 242 N90-10635
Parallel eigenanalysis of finite element models in a completely connected architecture
[NASA-CR-185166] p 217 N90-14652
- EIGENVECTORS**
The pdf approach to turbulent flow p 168 A90-32225
Parallel eigenanalysis of finite element models in a completely connected architecture
[NASA-CR-185166] p 217 N90-14652
- EJECTORS**
Rotating primary flow induction using jet-flapped blades p 19 A90-12585
Computational analysis of the flowfield of a two-dimensional ejector nozzle
[AIAA PAPER 90-1901] p 21 A90-42690

ELECTRIC ENERGY STORAGE

- Computational analysis of the flowfield of a two-dimensional ejector nozzle
[NASA-CR-185255] p 31 N90-23406
- ELASTIC ANISOTROPY**
Improved transverse crack detection in composites
[NASA-TM-103261] p 102 N90-27875
- ELASTIC BODIES**
Mixed variational formulation of finite element analysis of acoustoelastic/slosh fluid-structure interaction p 212 A90-34851
- ELASTIC DEFORMATION**
Advanced development of BEM for elastic and inelastic dynamic analysis of solids p 213 A90-45771
A review of gear housing dynamics and acoustics literature
[NASA-CR-185148] p 203 N90-21387
Collision forces for compliant projectiles
[NASA-TM-4203] p 223 N90-28111
- ELASTIC PROPERTIES**
A transient plasticity study and low cycle fatigue analysis of the Space Station Freedom photovoltaic solar array blanket
[NASA-TM-102516] p 218 N90-19617
Review and statistical analysis of the ultrasonic velocity method for estimating the porosity fraction in polycrystalline materials
[NASA-TM-102501-REV] p 207 N90-21402
- ELASTIC WAVES**
Unsteady blade surface pressures on a large-scale advanced propeller - Prediction and data
[AIAA PAPER 90-2402] p 9 A90-47220
- ELASTODYNAMICS**
Tailoring of composite links for optimal damped elasto-dynamic performance p 211 A90-30250
- ELASTOHYDRODYNAMICS**
Bearing elastohydrodynamic lubrication: A complex calculation made simple
[NASA-TM-102575] p 203 N90-22041
- ELASTOPLASTICITY**
Advanced applications of BEM to inelastic analysis of solids p 213 A90-45770
Advanced development of BEM for elastic and inelastic dynamic analysis of solids p 213 A90-45771
The MHOST finite element program: 3-D inelastic analysis methods for hot section components. Volume 2: User's manual
[NASA-CR-182235-VOL-2] p 215 N90-10450
The MHOST finite element program: 3-D inelastic analysis methods for hot section components. Volume 3: Systems' manual
[NASA-CR-182236] p 215 N90-10451
A new uniformly valid asymptotic integration algorithm for elasto-plastic-creep and unified viscoplastic theories including continuum damage
[NASA-TM-102344] p 217 N90-14655
- ELASTOSTATICS**
Green's functions for dislocations in bonded strips and related crack problems
[NASA-CR-185291] p 224 N90-28878
- ELECTRIC ARCS**
Nature of convection-stabilized dc arcs in dual-flow nozzle geometry. I - The cold flow field and dc arc characteristics. II - Optical diagnostics and theory p 252 A90-26665
- ELECTRIC BATTERIES**
Space Electrochemical Research and Technology Conference, 2nd, Cleveland, OH, Apr. 11-13, 1989, Proceedings p 227 A90-33932
Space Electrochemical Research and Technology (SERT), 1989
[NASA-CP-3056] p 230 N90-20454
- ELECTRIC BRIDGES**
High power density dc/dc converter: Selection of converter topology
[NASA-CR-186129] p 151 N90-14467
- ELECTRIC CONTACTS**
Contact formation in gallium arsenide solar cells p 225 A90-14888
Deep-level dominated electrical characteristics of Au contacts on beta-SiC p 147 A90-33726
Contact spreading and the Au3In-to-Au9In4 transition in the Au-In system p 257 A90-48661
On the numerical solution of the dynamically loaded hydrodynamic lubrication of the point contact problem
[NASA-TM-102427] p 178 N90-17076
Lateral spreading of Au contacts on InP
[NASA-TM-103133] p 232 N90-22843
- ELECTRIC CURRENT**
Preliminary evaluation of space station transmission line in a ring configuration p 74 N90-17677
[NASA-TM-102461] p 190 N90-22773
A fiber-optic current sensor for aerospace applications
[NASA-TM-103152] p 190 N90-22773
- ELECTRIC ENERGY STORAGE**
Nickel-hydrogen capacity loss on storage p 57 A90-33955

- Space Electrochemical Research and Technology (SERT), 1989
[NASA-CP-3056] p 230 N90-20454
- ELECTRIC EQUIPMENT TESTS**
20 kHz, 25 kVA node power transformer p 149 A90-38275
- ELECTRIC GENERATORS**
Comparison of solar photovoltaic and nuclear reactor power systems for a human-tended lunar observatory p 42 A90-38030
Assessment of High Temperature Superconducting (HTS) electric motors for rotorcraft propulsion [NASA-CR-185222] p 29 N90-21761
- ELECTRIC MOTOR VEHICLES**
Analytical and experimental study of high phase order induction motors [NASA-CR-186580] p 153 N90-21952
- ELECTRIC MOTORS**
Magnification of starting torques of dc motors by maximum power point trackers in photovoltaic systems p 149 A90-38144
Assessment of High Temperature Superconducting (HTS) electric motors for rotorcraft propulsion [NASA-CR-185222] p 29 N90-21761
- ELECTRIC POTENTIAL**
Changes in impedance of Ni electrodes upon standing and cycling [NASA-TM-102438] p 229 N90-18097
Hydrogen-oxygen proton-exchange membrane fuel cells and electrolyzers p 230 N90-20467
Conceptual definition of a high voltage power supply test facility [NASA-CR-185216] p 50 N90-25172
Comparison of currents predicted by NASCAP/LEO model simulations with elementary Langmuir-type bare probe models for an insulated cable containing a single pinhole [NASA-TM-102486] p 51 N90-26054
- ELECTRIC POWER**
Space Station Freedom electrical power system hardware commonality with the United States Polar Platform p 58 A90-38073
Space Station Freedom power management and distribution design status p 59 A90-38080
- ELECTRIC POWER SUPPLIES**
Space Station power system autonomy demonstration p 245 A90-10373
Photovoltaic module on-orbit assembly for Space Station Freedom p 45 A90-38071
Development and refinement of test bed simulations --- for space station power supplies p 59 A90-38081
Power transmission cable development for the Space Station Freedom electrical power system p 149 A90-38134
Advanced Launch System (ALS) actuation and power systems impact operability and cost p 69 A90-52955
The US space station and its electric power system [NASA-TM-101974] p 71 N90-13596
Space Station Freedom electric power system availability study [NASA-CR-185181] p 50 N90-20120
Power conditioning techniques [NASA-TM-102577] p 151 N90-20301
Advanced Launch System (ALS): Electrical actuation and power systems improve operability and cost picture [NASA-TM-102547] p 152 N90-21271
Nuclear technology and the space exploration missions [NASA-TM-103156] p 232 N90-22847
- ELECTRIC POWER TRANSMISSION**
A comparative study of electric power distribution systems for spacecraft [NASA-CR-186531] p 77 N90-21113
An expert system for simulating electric loads aboard Space Station Freedom [NASA-TM-103150] p 240 N90-22325
- ELECTRIC PROPULSION**
Experiments on a repetitively pulsed electrothermal thruster p 56 A90-27960
End-hall thrusters [AIAA PAPER 90-2595] p 64 A90-42570
Advanced propulsion for LEO and GEO platforms [AIAA PAPER 90-2551] p 68 A90-52565
Multimegawatt electric propulsion system design considerations [AIAA PAPER 90-2552] p 68 A90-52566
Design of a thrust stand for high power electric propulsion devices [NASA-TM-102372] p 73 N90-15992
Electric propulsion options for 10 kW class earth-space missions p 75 N90-18474
Advanced propulsion for LEO and GEO platforms [NASA-TM-103228] p 82 N90-27785
Advanced onboard propulsion benefits and status [NASA-TM-103174] p 82 N90-27786
- Low power arcjet performance [NASA-TM-103280] p 83 N90-28657
- ELECTRIC PULSES**
Interface demarcation in GaAs by current pulsing [AIAA PAPER 90-0319] p 254 A90-19793
- ELECTRIC ROCKET ENGINES**
Geometric effects in applied-field MPD thrusters [AIAA PAPER 90-2669] p 69 A90-52572
Arcjet nozzle design impacts p 76 N90-18478
Geometric effects in applied-field MPD thrusters [NASA-TM-103259] p 82 N90-27782
- ELECTRICAL FAULTS**
Autonomous power expert fault diagnostic system for Space Station Freedom electrical power system testbed p 80 N90-25521
- ELECTRICAL IMPEDANCE**
The impedance of a tubular electrode - A model for a porous electrode p 104 A90-33723
Impedance studies of nickel/cadmium and nickel/hydrogen cells using the cell case as a reference electrode p 228 A90-33950
- ELECTRICAL MEASUREMENT**
High altitude current-voltage measurement of GaAs/Ge solar cells p 226 A90-14910
A fiber-optic current sensor for aerospace applications [NASA-TM-103152] p 190 N90-22773
Electrical characterization of a Mapham inverter using pulse testing techniques [NASA-TM-103254] p 82 N90-27784
- ELECTRICAL PROPERTIES**
A brief survey of radiation effects on polymer dielectrics p 123 A90-43119
Electrical properties of materials for high temperature strain gage applications [NASA-CR-186192] p 188 N90-14534
- ELECTRICAL RESISTANCE**
Glass-derived superconducting ceramics with zero resistance at 107 K in the Bi(1.5)Pb(0.5)Sr2Ca2Cu3O(x) system p 253 A90-11491
- ELECTRICAL RESISTIVITY**
Properties of Pb(1-x)Bi(x)/Ba2YCu3O(x) composites - Reaction of Ba2YCu3O(x) with Pb and Bi p 255 A90-33224
The effect of length and diameter on the resistivity of bromine intercalated graphite fibers p 122 A90-33332
Resistivity of pristine and intercalated graphite fiber epoxy composites [NASA-TM-102576] p 128 N90-21192
High-temperature superconductors for space power transmission lines [NASA-TM-103459] p 259 N90-24952
An analysis of the contact sintering process in III-V solar cells [NASA-TM-103179] p 233 N90-25420
- ELECTRO-OPTICS**
Coupled effects of conduction in the crystal and thermo-solutal convection in a rectangular inclined enclosure [AIAA PAPER 90-0408] p 133 A90-25031
- ELECTROCATALYSTS**
Electrocatalysis for oxygen electrodes in fuel cells and water electrolyzers for space applications p 57 A90-33945
Oxygen electrodes for rechargeable alkaline fuel cells. II p 228 A90-33946
Space Electrochemical Research and Technology (SERT), 1989 [NASA-CP-3056] p 230 N90-20454
Electrocatalysis for oxygen electrodes in fuel cells and water electrolyzers for space applications p 230 N90-20468
Catalysts for ultrahigh current density oxygen cathodes for space fuel cell applications [NASA-CR-180650] p 232 N90-22835
- ELECTROCHEMICAL CELLS**
Electrochemical behavior of heavily cycled nickel electrodes in Ni/H2 cells containing electrolytes of various KOH concentrations p 103 A90-24535
Space Electrochemical Research and Technology Conference, 2nd, Cleveland, OH, Apr. 11-13, 1989, Proceedings p 227 A90-33932
- ELECTROCHEMISTRY**
Space Electrochemical Research and Technology (SERT), 1989 [NASA-CP-3056] p 230 N90-20454
Electrochemical impregnation and cycle life of lightweight nickel electrodes for nickel-hydrogen cells [NASA-TM-103140] p 107 N90-21844
- ELECTRODE MATERIALS**
Electrochemical behavior of heavily cycled nickel electrodes in Ni/H2 cells containing electrolytes of various KOH concentrations p 103 A90-24535
The impedance of a tubular electrode - A model for a porous electrode p 104 A90-33723
- Electrocatalysis for oxygen electrodes in fuel cells and water electrolyzers for space applications p 57 A90-33945
Structural comparison of nickel electrodes and precursor phases p 228 A90-33949
Impedance studies of nickel/cadmium and nickel/hydrogen cells using the cell case as a reference electrode p 228 A90-33950
Space Electrochemical Research and Technology (SERT), 1989 [NASA-CP-3056] p 230 N90-20454
Catalysts for ultrahigh current density oxygen cathodes for space fuel cell applications [NASA-CR-180650] p 232 N90-22835
- ELECTRODES**
Characterization and cycle tests of lightweight nickel electrodes [NASA-TM-102399] p 106 N90-12696
Changes in impedance of Ni electrodes upon standing and cycling [NASA-TM-102438] p 229 N90-18097
Characterization of reaction kinetics in a porous electrode [NASA-CR-186504] p 106 N90-19340
Oxygen electrodes for rechargeable alkaline fuel cells-II p 231 N90-20469
Corrosion testing of candidates for the alkaline fuel cell cathode p 231 N90-20471
Structural comparison of nickel electrodes and precursor phases p 231 N90-20472
Impedance studies of Ni/Cd and Ni/H2 cells using the cell case as a reference electrode p 231 N90-20473
Nickel-hydrogen capacity loss on storage p 231 N90-20478
O2 reduction at the IFC orbiter fuel cell O2 electrode [NASA-TM-102580] p 231 N90-21469
Effect of LEO cycling on 125 Ah advanced design IPV nickel-hydrogen battery cells [NASA-TM-103128] p 78 N90-21808
Electrochemical impregnation and cycle life of lightweight nickel electrodes for nickel-hydrogen cells [NASA-TM-103140] p 107 N90-21844
- ELECTROLYSIS**
Integrated regenerative fuel cell experimental evaluation [NASA-CR-185183] p 230 N90-18808
Electrocatalysis for oxygen electrodes in fuel cells and water electrolyzers for space applications p 230 N90-20468
- ELECTROLYTES**
Integrated regenerative fuel cell experimental evaluation [NASA-CR-185183] p 230 N90-18808
Nickel-hydrogen capacity loss on storage p 231 N90-20478
Effect of KOH concentration on LEO cycle life of IPV nickel-hydrogen flight battery cells [NASA-TM-103127] p 77 N90-21116
Effect of LEO cycling on 125 Ah advanced design IPV nickel-hydrogen battery cells [NASA-TM-103128] p 78 N90-21808
- ELECTROLYTIC CELLS**
Impedance studies of Ni/Cd and Ni/H2 cells using the cell case as a reference electrode p 231 N90-20473
- ELECTROMAGNETIC COMPATIBILITY**
Power transmission cable development for the Space Station Freedom electrical power system p 149 A90-38134
- ELECTROMAGNETIC FIELDS**
Electromagnetic finite elements based on a four-potential variational principle p 214 A90-49869
Electro-impulse de-icing testing analysis and design [NASA-CR-4175] p 18 N90-10031
A new rectangular waveguide to coplanar waveguide transition [NASA-TM-102477] p 145 N90-21263
- ELECTROMAGNETIC INTERFERENCE**
A heuristic approach to worst-case carrier-to-interference ratio maximization in satellite system synthesis [AIAA PAPER 90-0816] p 46 A90-25639
Convergence of the SMI and the diagonally loaded SMI algorithms with weak interference [AD-A222639] p 141 A90-36717
Effects of additional interfering signals on adaptive array performance [NASA-CR-186508] p 145 N90-20271
- ELECTROMAGNETIC PROPERTIES**
Electromagnetic properties of material coated surfaces [NASA-CR-186466] p 144 N90-19466
- ELECTROMAGNETIC PROPULSION**
A superconducting quenchgun for delivering lunar derived oxygen to lunar orbit [AIAA PAPER 90-2369] p 43 A90-40627

- A superconducting quenchgun for delivering lunar derived oxygen to lunar orbit
[NASA-CR-185161] p 77 N90-21806
- ELECTROMAGNETIC PULSES**
Modeling of power electronic systems with EMT
[NASA-TM-102375] p 245 N90-14060
- ELECTROMAGNETIC RADIATION**
Parametric study of power absorption from electromagnetic waves by small ferrite spheres
[NASA-TP-2949] p 246 N90-12282
- ELECTROMAGNETIC SCATTERING**
High-frequency asymptotic methods for analyzing the EM scattering by open-ended waveguide cavities
[NASA-CR-186244] p 143 N90-16103
- ELECTROMAGNETISM**
Experimental evaluation of a tuned electromagnetic damper for vibration control of cryogenic turbopump rotors
[NASA-TP-3005] p 30 N90-23403
- ELECTROMECHANICAL DEVICES**
Induction motor control
[NASA-TM-102533] p 28 N90-19234
- ELECTROMECHANICS**
Aerospace induction motor actuators driven from a 20-kHz power link
[NASA-TM-102482] p 28 N90-20085
- ELECTRON BEAM WELDING**
Refractory metal alloys and composites for space power systems
p 116 A90-46677
- ELECTRON BEAMS**
Electron beam induced damage in PECVD Si₃N₄ and SiO₂ films on InP
[NASA-TM-102544] p 203 N90-20393
- ELECTRON BOMBARDMENT**
Secondary electron emission characteristics of molybdenum-masked, ion-textured OFHC copper
[NASA-TP-2967] p 117 N90-15211
- ELECTRON CAPTURE**
Theory of plasma contactors in ground-based experiments and low earth orbit
p 150 A90-47108
- ELECTRON DENSITY (CONCENTRATION)**
Plasma contactor research, 1989
[NASA-CR-185212] p 252 N90-22389
- ELECTRON DIFFUSION**
Estimation of minority carrier diffusion lengths in InP/GaAs solar cells
[NASA-TM-103213] p 81 N90-26069
- ELECTRON EMISSION**
Plasma contactor research, 1989
[NASA-CR-185212] p 252 N90-22389
- ELECTRON IRRADIATION**
Performance of GaAs concentrator cells under electron irradiations from 0.4 to 2.3 MeV
p 227 A90-14956
Thermal annealing of GaAs concentrator solar cells during electron irradiation
p 60 A90-38150
- ELECTRON OPTICS**
Status of structural analysis of 30 cm diameter ion optics
[AIAA PAPER 90-2649] p 215 A90-52571
- ELECTRON PROBES**
Calibration approach to electron probe microanalysis: A study with PWA-1480, a nickel base superalloy
[NASA-TM-102393] p 117 N90-14335
- ELECTRON RADIATION**
A brief survey of radiation effects on polymer dielectrics
p 123 A90-43119
- ELECTRON SPECTROSCOPY**
FORTRAN program for x ray photoelectron spectroscopy data reformatting
[NASA-TP-2957] p 258 N90-12348
- ELECTRON TUNNELING**
Design and calibration of a vacuum compatible scanning tunneling microscope
[NASA-TM-102514] p 189 N90-20353
- ELECTRONIC CONTROL**
A real time microcomputer implementation of sensor failure detection for turbofan engines
p 21 A90-45414
Advanced detection, isolation, and accommodation of sensor failures in turbofan engines: Real-time microcomputer implementation
[NASA-TP-2925] p 37 N90-15112
- ELECTRONIC EQUIPMENT**
Modeling of power electronic systems with EMT
[NASA-TM-102375] p 245 N90-14060
An electronic pressure profile display system for aeronautic test facilities
[NASA-TM-102478] p 38 N90-15964
- ELECTRONIC FILTERS**
20 kHz main inverter unit for space station power supplies
p 148 A90-38124
- ELECTROSTATICS**
LEO high voltage solar array arcing response model, continuation 5
[NASA-CR-186505] p 232 N90-25418
- ELECTROTHERMAL ENGINES**
Review of research and development on the microwave electrothermal thruster
p 55 A90-16369
Experiments on a repetitively pulsed electrothermal thruster
p 56 A90-27960
- ELLIPSOIDMETERS**
Ellipsometric study of Al₂O₃/Ag/Si and SiO₂/Ag/quartz ashed in an oxygen plasma --- protective coatings to prevent degradation of materials in low earth orbits
p 120 A90-18217
Ellipsometric study of YBa₂Cu₃O(7-x) laser ablated and co-evaporated films
[NASA-TM-103223] p 259 N90-26682
- ELLIPSOIDMETRY**
Ellipsometric studies of the diffusion of atomic oxygen through silicon dioxide thin films
p 104 A90-36268
- ELLIPTIC DIFFERENTIAL EQUATIONS**
A 'transient' automated mapping procedure for complex geometries
p 242 A90-26499
- ELONGATION**
Brominated graphitized carbon fibers
[NASA-CASE-LEW-14698-2] p 126 N90-15262
- EMBEDDING**
Structural tailoring of select fiber composite structures
[NASA-TM-102484] p 99 N90-21137
- EMBRITTLMENT**
Determination of the durability of the fiber optics in rocket engine environments
[AIAA PAPER 90-2229] p 250 A90-42754
- EMISSION SPECTRA**
Preliminary plume characteristics of an arcjet thruster
[AIAA PAPER 90-2645] p 64 A90-42609
Digital filtering of plume emission spectra
[AIAA PAPER 90-1994] p 67 A90-50643
Digital filtering of plume emission spectra
[NASA-TM-103135] p 81 N90-26070
- EMISSIVITY**
Total hemispherical emittance measured at high temperatures by the calorimetric method
[NASA-TM-102322] p 136 N90-10309
Multiwavelength pyrometry to correct for reflected radiation
[NASA-TM-102578] p 190 N90-23714
- EMITTANCE**
Emittance bounds for transient radiative cooling of a scattering rectangular region
p 161 A90-20520
Total hemispherical emittance measured at high temperatures by the calorimetric method
[NASA-TM-102322] p 136 N90-10309
Thermal radiation characteristics of nonisothermal cylindrical enclosures using a numerical ray tracing technique
[NASA-TM-102527] p 179 N90-21296
The effects of atomic oxygen on the thermal emittance of high temperature radiator surfaces
[NASA-TM-103224] p 102 N90-28670
- EMULSIONS**
Holographic interferometry with an injection seeded Nd:YAG laser and two reference beams
p 186 A90-42373
- ENCAPSULATING**
Selection of phase-change and containment materials for thermal energy storage
[NASA-CR-186228] p 229 N90-15506
- END EFFECTORS**
Optimum structural design of robotic manipulators with fiber reinforced composite materials
p 197 A90-46074
- END PLATES**
Experimental determination of stator endwall heat transfer
[ASME PAPER 89-GT-219] p 165 A90-23880
- ENERGY CONSERVATION**
Energy Efficient Engine: Flight propulsion system final design and analysis
[NASA-CR-168219] p 34 N90-28558
Energy Efficient Engine core design and performance report
[NASA-CR-168069] p 34 N90-28559
Energy Efficient Engine integrated core/low spool design and performance report
[NASA-CR-168211] p 34 N90-28561
Energy efficient engine program technology benefit/cost study, Volume 1: Executive summary
[NASA-CR-174766-VOL-1] p 34 N90-28564
Energy Efficient Engine: Control system preliminary definition report
[NASA-CR-179578] p 35 N90-28569
- ENERGY CONVERSION**
Comparison of solar photovoltaic and nuclear reactor power systems for a human-tended lunar observatory
p 42 A90-38030
Space Station Freedom power management and distribution design status
p 59 A90-38080
Bidirectional power converter control electronics
[NASA-CR-175070] p 70 N90-10175
- Analysis of a Mars-stationary orbiting microwave power transmission system
[NASA-TM-101344] p 138 N90-26172
- ENERGY CONVERSION EFFICIENCY**
High efficiency GaAs/Ge monolithic tandem solar cells
p 224 A90-14858
Predicted performance of near-optimally designed indium phosphide space solar cells at high intensities and temperatures
p 225 A90-14898
Thin, light-trapping silicon solar cells for space
p 226 A90-14900
Wide-bandgap epitaxial heterojunction windows for silicon solar cells
p 227 A90-28359
Indium phosphide solar cells - Recent developments and estimated performance in space
p 57 A90-37854
Energy storage and thermal control system design status for space station power supplies
p 59 A90-38077
Effect of Ga and P dopants on the thermoelectric properties of n-type SiGe
p 256 A90-38140
The mini-dome lens space concentrator array - Recent component test results and current array development status
p 60 A90-38155
The photovoltaic properties of an Al In As/InP heterojunctions grown by LPE method
[NASA-CR-185996] p 229 N90-13886
GaAs solar cells with V-grooved emitters
p 229 N90-17754
Indium phosphide solar cell research in the United States: Comparison with non-photovoltaic sources
p 229 N90-17758
Energy Efficient Engine high pressure turbine component test performance report
[NASA-CR-168289] p 33 N90-28553
Energy Efficient Engine acoustic supporting technology report
[NASA-CR-174834] p 33 N90-28557
Energy Efficient Engine: Flight propulsion system final design and analysis
[NASA-CR-168219] p 34 N90-28558
Energy Efficient Engine program advanced turbofan nacelle definition study
[NASA-CR-174942] p 34 N90-28560
- ENERGY DISSIPATION**
Rain-fade simulation and power augmentation for satellite communication systems
[NASA-TM-103134] p 146 N90-28768
- ENERGY GAPS (SOLID STATE)**
Wide-bandgap epitaxial heterojunction windows for silicon solar cells
p 227 A90-28359
Optical dispersion relations for diamondlike carbon films
[NASA-TM-102356] p 257 N90-10738
- ENERGY STORAGE**
Energy storage considerations for a robotic Mars surface sampler
[AAS PAPER 87-245] p 42 A90-16544
Solar power for the lunar night
p 266 A90-24814
Cryogenic reactant storage for lunar base regenerative fuel cells
[IAF PAPER ICOSP89-3-8] p 227 A90-27709
Space Station Freedom electrical power system hardware commonality with the United States Polar Platform
p 58 A90-38073
Space Station Freedom power management and distribution design status
p 59 A90-38080
Performance testing of a high frequency link converter for Space Station power distribution system
p 148 A90-38128
Photovoltaic power system operation in the Mars environment
p 43 A90-38156
Brayton advanced heat receiver development program
p 61 A90-38170
A heat receiver design for solar dynamic space power systems
[NASA-TM-102473] p 72 N90-14283
Selection of phase-change and containment materials for thermal energy storage
[NASA-CR-186228] p 229 N90-15506
Analysis of thermal energy storage material with change-of-phase volumetric effects
[NASA-TM-102457] p 181 N90-21974
Lunar orbiting microwave beam power system
[NASA-TM-103211] p 51 N90-25173
Energy storage for a lunar base by the reversible chemical reaction: CaO + H₂O reversible reaction
Ca(OH)₂
[NASA-TM-103145] p 233 N90-25419
A solar power system for an early Mars expedition
[NASA-TM-103219] p 246 N90-28393
- ENERGY TECHNOLOGY**
Update of the Solar Concentrator Advanced Development Project
p 48 A90-38267
The NASA Advanced Solar Dynamics Technology Program
p 62 A90-38280

ENERGY TRANSFER

The numerical simulation of multistage turbomachinery flows p 29 N90-21025

ENGINE AIRFRAME INTEGRATION

Analysis of airframe/engine interactions - An integrated control perspective
[AIAA PAPER 90-1918] p 36 A90-40557
Extended implicit model following as applied to integrated flight and propulsion control
[AIAA PAPER 90-3444] p 239 A90-47697
A supersonic through-flow fan engine airframe integration study
[NASA-CR-185140] p 10 N90-10004

ENGINE CONTROL

H-infinity based integrated flight/propulsion control design for a STOVL aircraft in transition flight
[AIAA PAPER 90-3335] p 36 A90-47595
Full scale technology demonstration of a modern counterrotating unducted fan engine concept. Engine test
[NASA-CR-180869] p 24 N90-10049

ENGINE COOLANTS

Cooling of rocket thrust chambers with liquid oxygen
[AIAA PAPER 90-2120] p 63 A90-42029
Cooling of rocket thrust chambers with liquid oxygen
[NASA-TM-103146] p 78 N90-22605
Computer code for predicting coolant flow and heat transfer in turbomachinery
[NASA-TP-2985] p 32 N90-27722

ENGINE DESIGN

TBCs for better engine efficiency --- thermal barrier coatings p 83 A90-17294
A review of failure models for ceramic matrix composite laminates under monotonic loads
[ASME PAPER 89-GT-153] p 89 A90-23842
Advanced technology's impact on compressor design and development - A perspective
[SAE SP-800] p 20 A90-28571
Design of an air-cooled metallic high-temperature radial turbine p 20 A90-32960
Two-tiered design analysis of a radiator for a solar dynamic powered Stirling engine p 60 A90-38158
Results from baseline tests of the SPRE I and comparison with code model predictions p 62 A90-38249

Comparison of conceptual designs for 25 kW advanced Stirling conversion systems for dish electric applications p 229 A90-38254

Convertible engine system for high speed rotorcraft
[AIAA PAPER 90-2512] p 20 A90-40643
Development of impact design methods for ceramic gas turbine components
[AIAA PAPER 90-2413] p 197 A90-42165

Qualification and life testing of a flight design hydrazine arcjet system
[AIAA PAPER 90-2576] p 64 A90-42559

Rocket combustion chamber life-enhancing design concepts
[AIAA PAPER 90-2116] p 66 A90-47208
Integrated controls and health monitoring for chemical transfer propulsion
[AIAA PAPER 90-2751] p 52 A90-47229

A supersonic through-flow fan engine airframe integration study
[NASA-CR-185140] p 10 N90-10004

Advanced Turbine Technology Applications Project (ATTAP)
[NASA-CR-185133] p 22 N90-10036

Large-scale Advanced Prop-fan (LAP) technology assessment report
[NASA-CR-182142] p 24 N90-10046

Full scale technology demonstration of a modern counterrotating unducted fan engine concept. Design report
[NASA-CR-180867] p 24 N90-10048
Revolutionary opportunities for materials and structures study
[NASA-CR-179642] p 95 N90-10184

Advanced technologies impact on compressor design and development. A perspective
[NASA-TM-102341] p 24 N90-10891

Automotive Stirling engine development program
[NASA-CR-180839] p 263 N90-11654

Advanced Turbine Technology Applications Project (ATTAP)
[NASA-CR-185109] p 263 N90-14153

SP-100 power system conceptual design for lunar base applications
[NASA-TM-102090] p 267 N90-15030

Supersonic through-flow fan engine and aircraft mission performance
[NASA-TM-102304] p 29 N90-21038
Recent Stirling engine loss-understanding results
[NASA-TM-103122] p 77 N90-21114

Assessment of fundamental materials needs for Thick Thermal Barrier Coatings (TBC's) for truck diesel engines
[NASA-TM-103130] p 119 N90-23536

Integrated controls and health monitoring for chemical transfer propulsion
[NASA-TM-103185] p 52 N90-25178
Rocket combustion chamber life-enhancing design concepts
[NASA-CR-185257] p 79 N90-25183

Preliminary designs for 25 kW advanced Stirling conversion systems for dish electric applications
[NASA-TM-103188] p 263 N90-26729
Energy Efficient Engine combustor test hardware detailed design report
[NASA-CR-168301] p 33 N90-28554

Energy Efficient Engine (E3) combustion system component technology performance report
[NASA-CR-168274] p 33 N90-28555
Energy Efficient Engine exhaust mixer model technology report addendum; phase 3 test program
[NASA-CR-174799] p 33 N90-28556

Energy Efficient Engine: Flight propulsion system final design and analysis
[NASA-CR-168219] p 34 N90-28558
Energy Efficient Engine core design and performance report
[NASA-CR-168069] p 34 N90-28559

Energy Efficient Engine program advanced turbofan nacelle definition study
[NASA-CR-174942] p 34 N90-28560
Energy Efficient Engine: Control system component performance report
[NASA-CR-174651] p 34 N90-28562

NASA/GE Energy Efficient Engine low pressure turbine scaled test vehicle performance report
[NASA-CR-168290] p 34 N90-28563
Energy Efficient Engine integrated core/low spool test hardware design report
[NASA-CR-168137] p 35 N90-28566

A failure diagnosis system based on a neural network classifier for the space shuttle main engine
[NASA-TM-103607] p 83 N90-28659
Automotive Stirling engine development program
[NASA-CR-180840] p 264 N90-29260

ENGINE FAILURE

Health monitoring system for the SSME - Program overview
[AIAA PAPER 90-1987] p 63 A90-40583
Health Monitoring System for the SSME-fault detection algorithms
[AIAA PAPER 90-1988] p 63 A90-40584

Rocket engine failure detection using system identification techniques
[AIAA PAPER 90-1993] p 65 A90-47205
Multi-sensor analysis techniques for SSME safety monitoring
[AIAA PAPER 90-1990] p 45 A90-52499

Framework for a space shuttle main engine health monitoring system
[NASA-CR-185224] p 78 N90-21809
Rocket engine failure detection using system identification techniques
[NASA-CR-185259] p 45 N90-25159

Multi-sensor analysis techniques for SSME safety monitoring
[NASA-CR-185260] p 45 N90-27732

ENGINE INLETS

Engine inlet distortion in a 9.2 percent scaled vectored thrust STOVL model in ground effect
[AIAA PAPER 89-2910] p 5 A90-25043
Influence of bulk turbulence and entrance boundary layer thickness on the curved duct flow field
[AIAA PAPER 90-1502] p 171 A90-38651

Combustor technology for future aircraft
[AIAA PAPER 90-2400] p 22 A90-47219
Engine inlet distortion in a 9.2 percent scale vectored thrust STOVL model in ground effect
[NASA-TM-102358] p 12 N90-17561

Control of flow separation and mixing by aerodynamic excitation
[NASA-TM-103131] p 13 N90-21733
Finite element elastic-plastic-creep and cyclic life analysis of a cowl lip
[NASA-TM-102342] p 220 N90-22808

Finite element analysis of structural components using viscoplastic models with application to a cowl lip problem
[NASA-CR-185189] p 221 N90-23769

ENGINE MONITORING INSTRUMENTS

Health monitoring system for the SSME - Program overview
[AIAA PAPER 90-1987] p 63 A90-40583
Health Monitoring System for the SSME-fault detection algorithms
[AIAA PAPER 90-1988] p 63 A90-40584

Health monitoring system for the SSME - Hardware architecture study
[AIAA PAPER 90-1989] p 65 A90-42713

Multi-sensor analysis techniques for SSME safety monitoring
[AIAA PAPER 90-1990] p 45 A90-52499
Framework for a space shuttle main engine health monitoring system
[NASA-CR-185224] p 78 N90-21809

Reusable rocket engine turbopump health monitoring system, part 3
[NASA-CR-182294] p 204 N90-26320
Multi-sensor analysis techniques for SSME safety monitoring
[NASA-CR-185260] p 45 N90-27732

ENGINE PARTS
ATTAP/AGT101 ceramics technology update
[ASME PAPER 89-GT-105] p 195 A90-23814

A review of failure models for ceramic matrix composite laminates under monotonic loads
[ASME PAPER 89-GT-153] p 89 A90-23842
Noninteractive macroscopic reliability model for whisker-reinforced ceramic composites p 89 A90-26561

Ceramic valve development for heavy-duty low heat rejection diesel engines p 196 A90-27091
Ceramic port shields cast in an iron engine head p 196 A90-27095

The role of NDE in ceramic turbine engine component development p 206 A90-35508
Development of Si3N4 for gas turbine applications p 122 A90-35509

Two-dimensional numerical simulation of a Stirling engine heat exchanger p 170 A90-38290
Development of impact design methods for ceramic gas turbine components
[AIAA PAPER 90-2413] p 197 A90-42165

Full scale technology demonstration of a modern counterrotating unducted fan engine concept: Component test
[NASA-CR-180868] p 24 N90-10047
Materials for engine applications above 3000 deg F: An overview p 95 N90-10188

Improved silicon carbide for advanced heat engines
[NASA-CR-180831] p 124 N90-10293
Automotive Stirling engine development program
[NASA-CR-180839] p 263 N90-11654

Real-time simulation of an F110/STOVL turbofan engine
[NASA-TM-102409] p 25 N90-12618
Constitutive modeling for isotropic materials (HOST)
[NASA-CR-179522] p 26 N90-13390

Constitutive modeling for isotropic materials (HOST)
[NASA-CR-174718] p 26 N90-13391
Development of an integrated BEM approach for hot fluid structure interaction
[NASA-CR-186214] p 177 N90-15364

Probability of failure and risk assessment of propulsion structural components p 218 N90-18470
Attachment of lead wires to thin film thermocouples mounted on high temperature materials using the parallel gap welding process
[NASA-TM-102442] p 189 N90-21361

High-temperature test facility at the NASA Lewis engine components research laboratory
[NASA-TM-103143] p 39 N90-25151
Energy Efficient Engine: Control system component performance report
[NASA-CR-174651] p 34 N90-28562

Improved silicon carbide for advanced heat engines
[NASA-CR-182186] p 129 N90-28735

ENGINE TESTING LABORATORIES
Test facility and preliminary performance of a 100 kW class MPD thruster p 75 N90-18476

ENGINE TESTS
Efficiency testing of a helicopter transmission planetary reduction stage p 193 A90-21113
ATTAP/AGT101 ceramics technology update
[ASME PAPER 89-GT-105] p 195 A90-23814

Ceramic valve development for heavy-duty low heat rejection diesel engines p 196 A90-27091
On the dynamic response of pressure transmission lines in the research of helium-charged free piston Stirling engines p 196 A90-38248

Results from baseline tests of the SPRE I and comparison with code model predictions p 62 A90-38249
Initial characterization of a modular heat exchanger with an integral heat pipe --- for Stirling space engine p 62 A90-38301

Enhanced heat transfer rocket combustor technology component hot-fire test results
[AIAA PAPER 90-2182] p 64 A90-42063

- Diagnostics and performance of a 1/4-scale MPD thruster
[AIAA PAPER 90-2665] p 65 A90-42625
- Health monitoring system for the SSME - Hardware architecture study
[AIAA PAPER 90-1989] p 65 A90-42713
- A real time microcomputer implementation of sensor failure detection for turbofan engines p 21 A90-45414
- 5kW xenon ion thruster lifetest
[AIAA PAPER 90-2543] p 68 A90-52564
- Full scale technology demonstration of a modern counterrotating unducted fan engine concept: Component test
[NASA-CR-180868] p 24 N90-10047
- Full scale technology demonstration of a modern counterrotating unducted fan engine concept: Engine test
[NASA-CR-180869] p 24 N90-10049
- The effect of electrode configuration on arcjet performance
[NASA-TM-102346] p 70 N90-11081
- Automotive Stirling engine development program
[NASA-CR-180839] p 263 N90-11654
- Advanced Turbine Technology Applications Project (ATTAP)
[NASA-CR-185109] p 263 N90-14153
- Advanced detection, isolation, and accommodation of sensor failures in turbofan engines: Real-time microcomputer implementation
[NASA-TP-2925] p 37 N90-15112
- Test facility and preliminary performance of a 100 kW class MPD thruster p 75 N90-18476
- Advanced Turbine Technology Applications Project (ATTAP)
[NASA-CR-185240] p 263 N90-26728
- Energy Efficient Engine: Control system component performance report
[NASA-CR-174651] p 34 N90-28562
- Energy Efficient Engine integrated core/low spool test hardware design report
[NASA-CR-168137] p 35 N90-28566
- Energy Efficient Engine: Combustor component performance program
[NASA-CR-179533] p 35 N90-28568
- ENTRAINMENT**
The entrainment rate for a row of turbulent jets
[NASA-CR-185278] p 15 N90-28504
- ENVIRONMENT SIMULATION**
Ceramic matrix composites in simulated SSME environments p 102 N90-28655
- ENVIRONMENTAL TESTS**
Photovoltaic array environmental protection program --- in Space Station Freedom p 59 A90-38088
- The Environment-Power System Analysis Tool development program --- for spacecraft power supplies p 236 A90-38089
- Influence of testing environment on the room temperature ductility of FeAl alloys p 115 A90-39658
- Determination of the durability of the fiber optics in rocket engine environments
[AIAA PAPER 90-2229] p 250 A90-42754
- The chemical effects of the Martian environment on power system component materials: A theoretical approach
[NASA-TM-103203] p 87 N90-26074
- EPITAXY**
Growth of high quality 6H-SiC epitaxial films on vicinal (0001) 6H-SiC wafers p 255 A90-29952
- New directions in InP solar cell research
[NASA-TM-103160] p 154 N90-23662
- EPOXY MATRIX COMPOSITES**
Evaluation of atomic oxygen resistant protective coatings for fiberglass-epoxy composites in LEO
[NASA-TM-102576] p 84 A90-31581
- Resistivity of pristine and intercalated graphite fiber epoxy composites
[NASA-TM-102576] p 128 N90-21192
- EQUATIONS OF MOTION**
A nonoscillatory, characteristically convected, finite volume scheme for multidimensional convection problems
[AIAA PAPER 90-0015] p 159 A90-19633
- A nonoscillatory, characteristically convected, finite volume scheme for multidimensional convection problems
[NASA-TM-102354] p 242 N90-11497
- EQUATIONS OF STATE**
Liquid alkali metals - Equation of state and reduced-pressure, bulk-modulus, sound-velocity, and specific-heat functions p 102 A90-16280
- Pressure dependence of the melting temperature of metals p 103 A90-16281
- EQUILIBRIUM EQUATIONS**
Compatibility conditions of structural mechanics for finite element analysis
[NASA-TM-102413] p 217 N90-17180
- Integrated force method versus displacement method for finite element analysis
[NASA-TP-2937] p 218 N90-18081
- EQUIVALENT CIRCUITS**
Analytical and experimental study of high phase order induction motors
[NASA-CR-186580] p 153 N90-21952
- EROSION**
Diamondlike carbon protective coatings for optical windows p 122 A90-34569
- ERROR ANALYSIS**
Profile modification to minimize spur gear dynamic loading p 195 A90-21128
- Performance measurements for a laboratory-simulated 30/20 GHz communication satellite transponder
[AIAA PAPER 90-0808] p 140 A90-25634
- Local and global accuracy estimates for boundary element analysis
[AIAA PAPER 90-0930] p 211 A90-29324
- Foundations of measurement and instrumentation
[NASA-RP-1222] p 189 N90-21351
- Consistency and convergence for numerical radiation conditions
[NASA-TM-103262] p 244 N90-29124
- ERROR CORRECTING CODES**
A forward error correction technique using a high-speed, high-rate single chip codec p 141 A90-48440
- ERROR FUNCTIONS**
Asymptotic boundary conditions for dissipative waves: General theory
[NASA-TM-102497] p 243 N90-18927
- ETCHING**
A V-grooved GaAs solar cell p 225 A90-14887
- Effect of crystal orientation on anisotropic etching and MOCVD growth of grooves on GaAs p 253 A90-15136
- ETHANE**
Substituted 1,1,1-triaryl-2,2,2-trifluoroethanes and processes for their synthesis
[NASA-CASE-LEW-14345-2] p 107 N90-23497
- ETHERS**
Determination of the thermal stability of perfluoroalkylethers
[NASA-TM-102493] p 127 N90-17875
- EULER EQUATIONS OF MOTION**
Calculation of unsteady Euler flows in turbomachinery using the linearized Euler equations p 2 A90-11778
- Application of an efficient hybrid scheme for aeroelastic analysis of advanced propellers
[AIAA PAPER 90-0028] p 4 A90-22153
- Diagonal inversion of lower-upper implicit schemes
[NASA-TM-102428] p 242 A90-23110
- Unsteady Euler analysis of the flowfield of a propfan at an angle of attack
[AIAA PAPER 90-0339] p 5 A90-25028
- Numerical solutions of the linearized Euler equations for unsteady vortical flows around lifting airfoils
[AIAA PAPER 90-0694] p 5 A90-25041
- 3D Euler analysis of ducted propfan flowfields
[AIAA PAPER 90-3034] p 8 A90-45873
- Least-squares finite element methods for compressible Euler equations p 9 A90-51013
- Numerical simulation of unsteady rotational flow over propfan configurations
[NASA-CR-186037] p 10 N90-12500
- Application of an efficient hybrid scheme for aeroelastic analysis of advanced propellers
[NASA-TM-102428] p 11 N90-13355
- On the numerical solution of the dynamically loaded hydrodynamic lubrication of the point contact problem
[NASA-TM-102427] p 178 N90-17076
- Unsteady Euler analysis of the flow field of a propfan at an angle of attack
[NASA-TM-102426] p 248 N90-18229
- Numerical simulations of supersonic flow through oscillating cascade sections
[NASA-TM-103100] p 13 N90-20051
- PROTEUS two-dimensional Navier-Stokes computer code, version 1.0. Volume 1: Analysis description
[NASA-TM-102551] p 180 N90-21303
- PROTEUS two-dimensional Navier-Stokes computer code, version 1.0. Volume 2: User's guide
[NASA-TM-102552] p 180 N90-21306
- Investigation of advanced counterrotation blade configuration concepts for high speed turboprop systems, task 1: Ducted propfan analysis
[NASA-CR-185217] p 30 N90-22567
- EUROPEAN SPACE PROGRAMS**
A comparison of European and American microgravity combustion experimental techniques p 134 N90-16966
- EUTECTIC COMPOSITES**
Tribological properties of PM212: A high-temperature, self-lubricating, powder metallurgy composite
[NASA-TM-102355] p 86 N90-12659
- EUTECTICS**
Intergranular fracture of lithium fluoride-22 percent calcium fluoride hypereutectic salt at 800 K p 121 A90-25273
- The experimental evaluation and application of high-temperature solid lubricants
[NASA-TM-102476] p 127 N90-16944
- Two-dimensional model of a Space Station Freedom thermal energy storage canister
[NASA-TM-103124] p 183 N90-26279
- EVALUATION**
Experimental and analytical evaluation of dynamic load vibration of a 2240-kW (3000-hp) rotorcraft transmission p 192 A90-13750
- EVAPORATION**
Simple evaporation controller for thin-film deposition from a resistively heated boat p 149 A90-39761
- Sequentially evaporated thin film YBa₂Cu₃O_{7-x} superconducting microwave ring resonator
[NASA-TM-103180] p 154 N90-25273
- Ellipsometric study of YBa₂Cu₃O_{7-x} laser ablated and co-evaporated films
[NASA-TM-103223] p 259 N90-26682
- EXCIMER LASERS**
Laser ablated high T_c superconducting thin YBa₂Cu₃O_{7-x} films on substrates suitable for microwave applications p 260 N90-27808
- EXHAUST CLOUDS**
Preliminary plume characteristics of an arcjet thruster
[AIAA PAPER 90-2645] p 64 A90-42609
- EXHAUST EMISSION**
Low NO_x potential of gas turbine engines
[AIAA PAPER 90-0550] p 20 A90-25036
- Energy Efficient Engine exhaust mixer model technology report addendum: phase 3 test program
[NASA-CR-174799] p 33 N90-28556
- EXHAUST FLOW SIMULATION**
Analysis of internal flow in a ventral nozzle for STOVL aircraft
[AIAA PAPER 90-1899] p 21 A90-42688
- Analysis of internal flow in a ventral nozzle for STOVL aircraft
[NASA-TM-103123] p 31 N90-23404
- EXHAUST GASES**
Hot gas environment around STOVL aircraft in ground proximity. II - Numerical study
[AIAA PAPER 90-2270] p 21 A90-42766
- Digital filtering of plume emission spectra
[AIAA PAPER 90-1994] p 67 A90-50643
- Digital filtering of plume emission spectra
[NASA-TM-103135] p 81 N90-26070
- EXHAUST NOZZLES**
Performance characteristics of a one-third-scale, vectorable ventral nozzle for SSTOVL aircraft
[AIAA PAPER 90-2271] p 20 A90-37562
- Analysis and design of optimized truncated scarfed nozzles subject to external flow effects
[AIAA PAPER 90-2222] p 9 A90-47213
- Altitude testing of the 2D V-STOL ADEN demonstrator on an F404 engine
[NASA-CR-174824] p 28 N90-17638
- Exhaust nozzles for propulsion systems with emphasis on supersonic cruise aircraft
[NASA-RP-1235] p 29 N90-21037
- Performance characteristics of a one-third-scale, vectorable ventral nozzle for SSTOVL aircraft
[NASA-TM-103120] p 2 N90-21725
- Experimental and analytical study of close-coupled ventral nozzles for ASTOVL aircraft
[NASA-TM-103170] p 31 N90-24273
- Analysis and design of optimized truncated scarfed nozzles subject to external flow effects
[NASA-TM-103175] p 13 N90-25106
- Hot gas ingestion characteristics and flow visualization of a vectored thrust STOVL concept
[NASA-TM-103212] p 32 N90-26009
- EXHAUST VELOCITY**
The effects of magnetic nozzle configurations on plasma thrusters
[NASA-CR-186465] p 76 N90-21109
- EXPERIMENT DESIGN**
Hardware development for the surface tension driven convection experiment p 52 A90-36195
- Conceptual design of liquid droplet radiator shuttle-attached experiment
[NASA-CR-185164] p 71 N90-11805
- Conceptual design of liquid droplet radiator shuttle-attached experiment technical requirements document
[NASA-CR-185165] p 71 N90-11806
- Design considerations for space flight hardware
[NASA-TM-102300] p 52 N90-14275
- Conceptual design of a moving belt radiator shuttle-attached experiments: Technical requirement Document
[NASA-CR-185168] p 73 N90-15996

EXPERIMENTATION

SUBJECT INDEX

- Conceptual design of a Moving Belt Radiator (MBR) shuttle-attached experiment
[NASA-CR-185169] p 79 N90-23474
- Launching a dream: A teachers guide to a simulated space shuttle mission
[NASA-TM-89715] p 261 N90-26693
- ### EXPERIMENTATION
- Microgravity noncontact temperature requirements at NASA Lewis Research Center p 134 N90-17897
- ### EXPERT SYSTEMS
- Evolutionary growth for Space Station Freedom electrical power system p 58 A90-38072
- A rocket engine design expert system
[NASA-TM-102373] p 69 N90-10172
- Computer simulation of the mathematical modeling involved in constitutive equation development: Via symbolic computations
[NASA-TM-102532] p 219 N90-20428
- Autonomous power expert system p 240 N90-22306
- An expert system for simulating electric loads aboard Space Station Freedom
[NASA-TM-103150] p 240 N90-22325
- Automated electric power management and control for Space Station Freedom
[NASA-TM-103151] p 240 N90-23125
- An expert system to perform on-line controller tuning
[NASA-TM-103101] p 240 N90-23991
- Autonomous power expert system
[NASA-CR-185263] p 80 N90-25187
- Autonomous power expert fault diagnostic system for Space Station Freedom electrical power system testbed p 80 N90-25521
- Reusable rocket engine turbopump health monitoring system, part 3
[NASA-CR-182294] p 204 N90-26320
- Application of symbolic computations to the constitutive modeling of structural materials
[NASA-TM-103225] p 222 N90-26364
- An expert system to perform on-line controller restructuring for abrupt model changes
[NASA-TM-103609] p 241 N90-29121
- ### EXPONENTIAL FUNCTIONS
- Creep substructure formation in sodium chloride single crystals in the power law and exponential creep regimes p 255 A90-33330
- ### EXPOSURE
- Integrated controls and health monitoring for chemical transfer propulsion
[AIAA PAPER 90-2751] p 52 A90-47229
- Integrated controls and health monitoring for chemical transfer propulsion
[NASA-TM-103185] p 52 N90-25178
- ### EXTINCTION
- Opposed-flow flame spread and extinction in mixed-convection boundary layers p 168 A90-32841
- An investigation of flame spread over shallow liquid pools in microgravity and nonair environments
[NASA-TM-102425] p 134 N90-13680
- ### EXTRACTION
- Studies on the use of supercritical ammonia for ceramic nitride synthesis and fabrication
[NASA-TM-102570] p 106 N90-21843
- ### EXTRAPOLATION
- Convergence acceleration for vector sequences and applications to computational fluid dynamics
[AIAA PAPER 90-0338] p 160 A90-19804
- Efficient implementation of minimal polynomial and reduced rank extrapolation methods
[NASA-TM-103240] p 244 N90-26616
- ### EXTRATERRESTRIAL LIFE
- Extraterrestrial life in the universe
[NASA-TM-102363] p 264 N90-22464
- ### EXTRATERRESTRIAL RESOURCES
- Human exploration mission studies p 39 A90-33935
- ### EXTREMELY HIGH FREQUENCIES
- K-band TWT using new diamond rod technology
[AIAA PAPER 90-0870] p 147 A90-25691
- Ka-band propagation characteristics of microstrip lines on GaAs substrates at cryogenic temperatures p 147 A90-33644
- ### EYE MOVEMENTS
- A geometric analysis of semicircular canals and induced activity in their peripheral afferents in the rhesus monkey p 234 A90-28084
- ## F
- ### FABRICATION
- A V-grooved GaAs solar cell p 225 A90-14887
- A new fabrication method for precision antenna reflectors for space flight and ground test
[AIAA PAPER 90-0803] p 139 A90-25627
- K-band TWT using new diamond rod technology
[AIAA PAPER 90-0870] p 147 A90-25691
- Optical detectors for GaAs MMIC integration - Technology assessment p 149 A90-41238
- PMR graphite engine duct development
[NASA-CR-182228] p 23 N90-10037
- Development and characterization of PdCr temperature-compensated wire resistance strain gage
[NASA-CR-185153] p 188 N90-13761
- Technology development program for an advanced microsheet glass concentrator
[NASA-TM-102406] p 229 N90-14678
- Performance and modeling of superconducting ring resonators at millimeter-wave frequencies
[NASA-TM-102526] p 151 N90-18634
- Silicon carbide semiconductor device fabrication and characterization
[NASA-CR-186354] p 258 N90-19873
- An applicational process for dynamic balancing of turbomachinery shafting
[NASA-TM-102537] p 202 N90-20392
- Studies on the use of supercritical ammonia for ceramic nitride synthesis and fabrication
[NASA-TM-102570] p 106 N90-21843
- Miniature traveling wave tube and method of making
[NASA-CASE-LEW-14520-1] p 153 N90-22724
- Solar Concentrator Advanced Development Program
[NASA-CR-185173] p 232 N90-22834
- The 30-GHz monolithic receive module
[NASA-CR-180849] p 146 N90-24528
- Rapid thermal processing of high temperature superconducting fiber
[NASA-CR-186803] p 259 N90-24964
- High-temperature test facility at the NASA Lewis engine components research laboratory
[NASA-TM-103143] p 39 N90-25151
- A resistance strain gage with repeatable and cancellable apparent strain for use to 800 C
[NASA-CR-185256] p 53 N90-26063
- Advanced Turbine Technology Applications Project (ATTAP)
[NASA-CR-185240] p 263 N90-26728
- High temperature superconducting thin film microwave circuits: Fabrication, characterization, and applications
[NASA-TM-103235] p 156 N90-28786
- ### FABRICS
- The experimental evaluation and application of high-temperature solid lubricants
[NASA-TM-102476] p 127 N90-16944
- ### FABRY-PEROT INTERFEROMETERS
- Fabry-Perot interferometer development for rocket engine plume spectroscopy
[AIAA PAPER 90-2234] p 187 A90-47212
- Optical techniques for determination of normal shock position in supersonic flows for aerospace applications
[NASA-TM-103201] p 190 N90-25323
- ### FACE CENTERED CUBIC LATTICES
- Analysis of gamma prime shape changes in a single crystal Ni-base superalloy p 109 A90-15206
- Effects of crystal-melt interfacial energy anisotropy on dendritic morphology and growth kinetics p 253 A90-19284
- Coarsening in high volume fraction nickel-base alloys p 115 A90-37719
- ### FACTORIZATION
- Implicit solution of three-dimensional internal turbulent flows
[NASA-TM-103099] p 184 N90-27982
- ### FAILURE ANALYSIS
- Two-layer thermal barrier coating. I - Effects of composition and temperature on oxidation behavior and failure p 122 A90-33317
- KOH concentration effect on the cycle life of nickel-hydrogen cells. IV - Results of failure analysis p 228 A90-33952
- Characterization of interfacial failure in SiC reinforced Si3N4 matrix composite material by both fiber push-out testing and Auger electron spectroscopy p 91 A90-36802
- Investigation of Weibull statistics in fracture analysis of cast aluminum p 115 A90-45304
- A real time microcomputer implementation of sensor failure detection for turbofan engines p 21 A90-45414
- Fundamental aspects and failure modes in high-temperature composites p 93 A90-50095
- Model OA wind turbine generator FMEA
[NASA-TM-102378] p 206 N90-12034
- Thermal barrier coating life prediction model development, phase 1
[NASA-CR-182230] p 26 N90-13388
- An investigation of gear mesh failure prediction techniques
[NASA-TM-102340] p 200 N90-13785
- Probability of failure and risk assessment of propulsion structural components p 218 N90-18470
- Space Station Freedom electric power system availability study
[NASA-CR-185181] p 50 N90-20120
- Fundamental aspects of and failure modes in high-temperature composites p 98 N90-20151
- Effect of KOH concentration on LEO cycle life of IPV nickel-hydrogen flight battery cells
[NASA-TM-103127] p 77 N90-21116
- Characterization of failure processes in tungsten copper composites under fatigue loading conditions
[NASA-TM-102371] p 98 N90-21123
- Health management system for rocket engines
[NASA-CR-185223] p 131 N90-23574
- Metal matrix composites microfracture: Computational simulation p 101 N90-24383
- Design of ceramic components with the NASA/CARES computer program
[NASA-TM-102369] p 222 N90-26359
- ### FAILURE MODES
- Instrumented adhesion tests on plasma sprayed thermal barrier coatings p 111 A90-20255
- Local-global analysis of crack growth in continuously reinforced ceramic matrix composites
[ASME PAPER 89-GT-138] p 88 A90-23835
- A review of failure models for ceramic matrix composite laminates under monotonic loads
[ASME PAPER 89-GT-153] p 89 A90-23842
- Three approaches to reliability analysis p 206 A90-30706
- Tensile adhesion testing methodology for thermally sprayed coatings p 85 A90-43902
- Fundamental aspects and failure modes in high-temperature composites p 93 A90-50095
- Model OA wind turbine generator FMEA
[NASA-TM-102378] p 206 N90-12034
- An investigation of gear mesh failure prediction techniques
[NASA-TM-102340] p 200 N90-13785
- Fundamental aspects of and failure modes in high-temperature composites p 98 N90-20151
- Framework for a space shuttle main engine health monitoring system
[NASA-CR-185224] p 78 N90-21809
- Probabilistic structural analysis of aerospace components using NESSUS
[NASA-TM-102324] p 221 N90-22823
- Health management system for rocket engines
[NASA-CR-185223] p 131 N90-23574
- Fatigue testing apparatus
[NASA-CASE-LEW-14124-1] p 190 N90-23712
- Extension of a noninteractive reliability model for ceramic matrix composites p 129 N90-26142
- Ceramics Analysis and Reliability Evaluation of Structures (CARES): Users and programmers manual
[NASA-TP-2916] p 223 N90-28099
- ### FAN BLADES
- Blade mistuning coupled with shaft flexibility effects in rotor aeroelasticity
[ASME PAPER 89-GT-330] p 19 A90-23896
- Laser anemometer measurements in a transonic axial-flow fan rotor
[NASA-TP-2879] p 175 N90-11245
- ### FANS
- WINCOF-I code for prediction of fan compressor unit with water ingestion
[NASA-CR-185157] p 1 N90-21724
- ### FASTENERS
- Fastener design manual
[NASA-RP-1228] p 202 N90-18740
- ### FATIGUE (MATERIALS)
- A methodology for evaluating the reliability and risk of structures under complex service environments
[AIAA PAPER 90-1102] p 211 A90-29332
- Cooling of rocket thrust chambers with liquid oxygen
[AIAA PAPER 90-2120] p 63 A90-42029
- An investigation of gear mesh failure prediction techniques
[NASA-TM-102340] p 200 N90-13785
- Identification of a cast iron alloy containing nonstrategic elements
[NASA-CR-185174] p 118 N90-18559
- Characterization of failure processes in tungsten copper composites under fatigue loading conditions
[NASA-TM-102371] p 98 N90-21123
- A real time neural net estimator of fatigue life
[NASA-TM-103117] p 239 N90-21564
- Fatigue crack growth in unidirectional metal matrix composite p 220 N90-22117
- Cooling of rocket thrust chambers with liquid oxygen
[NASA-TM-103146] p 78 N90-22605
- Fatigue crack growth in a unidirectional SCS-6/Ti-15-3 composite
[NASA-TM-103095] p 119 N90-22646

SUBJECT INDEX

- Energy efficient engine pin fin and ceramic composite segmented liner combustor sector rig test report [NASA-CR-179534] p 35 N90-28567
- FATIGUE LIFE**
- Torsional and biaxial (tension-torsion) fatigue damage mechanisms in Waspaloy at room temperature p 109 A90-11925
- Relationship between fatigue life in the creep-fatigue region and stress-strain response p 209 A90-20061
- Surface pitting fatigue life of noninvolute, low-contact-ratio gears [NASA PAPER 90-2153] p 197 A90-42049
- Shaft flexibility effects on the forced response of a bladed-disk assembly p 21 A90-43218
- Isothermal life prediction of composite lamina using a damage mechanics approach p 92 A90-48115
- Thermal fatigue durability for advanced propulsion materials [NASA-TM-102348] p 216 N90-14641
- A transient plasticity study and low cycle fatigue analysis of the Space Station Freedom photovoltaic solar array blanket [NASA-TM-102516] p 218 N90-19617
- A real time neural net estimator of fatigue life [NASA-TM-103117] p 239 N90-21564
- Surface pitting fatigue life of noninvolute, low-contact-ratio gears [NASA-TM-103116] p 203 N90-22790
- High temperature fatigue behavior of a SiC/Ti-24Al-11Nb composite [NASA-TM-103157] p 220 N90-22822
- Constitutive and life modeling of single crystal blade alloys for root attachment analysis p 119 N90-28643
- The fatigue damage behavior of a single crystal superalloy p 120 N90-28644
- FATIGUE TESTS**
- Measurements of dynamic Young's modulus in short specimens with the PUCOT --- Piezoelectric Ultrasonic Composite Oscillator Technique p 112 A90-21174
- Isothermal and nonisothermal fatigue behavior of a metal matrix composite p 91 A90-36746
- An investigation of gear mesh failure prediction techniques [NASA-TM-102340] p 200 N90-13785
- Fatigue testing apparatus [NASA-CASE-LEW-14124-1] p 190 N90-23712
- Microstructure: Property correlation --- multiaxial fatigue damage evolution in waspaloy [NASA-CR-180406] p 224 N90-28880
- FAULT TOLERANCE**
- Autonomous power expert system p 240 N90-22306
- FEASIBILITY ANALYSIS**
- A feasibility assessment of installation, operation and disposal options for nuclear reactor power system concepts for a NASA growth space station [NASA-TM-89923] p 70 N90-10174
- Lunar orbiting microwave beam power system [NASA-TM-103211] p 51 N90-25173
- Feasibility study for the advanced one-dimensional high temperature optical strain measurement system, phase 3 [NASA-CR-185254] p 191 N90-25324
- FEED SYSTEMS**
- Combustion instability coupling with feed system acoustics p 108 N90-28629
- FEEDBACK CONTROL**
- Analysis of airframe/engine interactions - An integrated control perspective [AIAA PAPER 90-1918] p 36 A90-40557
- Active vibration control for flexible rotor by optimal direct-output feedback control p 197 A90-46222
- Advanced detection, isolation, and accommodation of sensor failures in turbofan engines: Real-time microcomputer implementation [NASA-TP-2925] p 37 N90-15112
- Fiber-optic projected-fringe digital interferometry [NASA-TM-103252] p 191 N90-28033
- An expert system to perform on-line controller restructuring for abrupt model changes [NASA-TM-103609] p 241 N90-29121
- FEEDERS**
- Plasma gun with coaxial powder feed and adjustable cathode [NASA-CASE-LEW-14901-1] p 252 N90-10718
- FERMIONS**
- Phase transitions in fermionic systems with many-body interaction p 249 A90-19303
- FERRITES**
- Parametric study of power absorption from electromagnetic waves by small ferrite spheres [NASA-TP-2949] p 246 N90-12282
- FIBER COMPOSITES**
- Up-and-coming IMCs --- Intermetallic-Matrix Composites p 88 A90-17295
- CMCs for the long run --- ceramic-matrix composites p 88 A90-17301
- Impact damage development in damaged composite materials p 193 A90-18355
- Investigation of interfacial shear strength in a SiC fibre/Ti-24Al-11Nb composite by a fibre push-out technique p 88 A90-18973
- Local-global analysis of crack growth in continuously reinforced ceramic matrix composites [ASME PAPER 89-GT-138] p 88 A90-23835
- Polymer derived Nicalon/Si-C-O composites - Processing and mechanical behavior p 89 A90-27065
- Evaluation of thermal and mechanical loading effects on the structural behavior of a SiC/titanium composite [AIAA PAPER 90-1026] p 90 A90-29228
- Multi-objective shape and material optimization of composite structures including damping [AIAA PAPER 90-1135] p 210 A90-29262
- Composites boost 21st-century aircraft engines p 90 A90-29704
- Laminate behavior for SiC fiber-reinforced reaction-bonded silicon nitride matrix composites p 90 A90-29927
- Unified micromechanics of damping for unidirectional and off-axis fiber composites p 90 A90-29929
- Tailoring of composite links for optimal damped elasto-dynamic performance p 211 A90-30250
- Measurements of print-through in graphite fiber epoxy composites p 91 A90-31555
- Effects of fiber motion on the acoustic behavior of an anisotropic, flexible fibrous material p 247 A90-33313
- Fiber reinforced superalloys p 91 A90-34169
- Reaction zone microstructure in a Ti3Al + Nb/SiC composite p 91 A90-39627
- Metal matrix composite micromechanics - In situ behavior influence on composite properties p 92 A90-45271
- Optimum structural design of robotic manipulators with fiber reinforced composite materials p 197 A90-46074
- Isothermal life prediction of composite lamina using a damage mechanics approach p 92 A90-48115
- Thermo-oxidative stability studies of PMR-15 polymer matrix composites reinforced with various continuous fibers p 93 A90-50068
- Parametric studies to determine the effect of compliant layers on metal matrix composite systems p 93 A90-50093
- Interfacial effects on the behavior of partially bonded metal matrix composite properties p 93 A90-50094
- Fundamental aspects and failure modes in high-temperature composites p 93 A90-50095
- Use of unbalanced laminates as a screening method for microcracking p 94 A90-50217
- Compatibility of Fe-40Al with various fibers p 94 A90-50496
- Matrix density effects on the mechanical properties of SiC fiber-reinforced silicon nitride matrix properties p 94 A90-51927
- High-temperature tensile properties of fiber reinforced reaction bonded silicon nitride p 95 A90-52783
- Mechanics of damping for fiber composite laminates including hygro-thermal effects [NASA-TM-102329] p 95 N90-10185
- Zirconia toughened SiC whisker reinforced alumina composites small business innovation research [NASA-CR-179629] p 125 N90-10294
- An integrated methodology for optimizing structural composite damping [NASA-TM-102343] p 96 N90-11808
- Oxidation effects on the mechanical properties of SiC fiber-reinforced reaction-bonded silicon nitride matrix composites [NASA-TM-102360] p 96 N90-14287
- Parametric studies to determine the effect of compliant layers on metal matrix composite systems [NASA-TM-102465] p 96 N90-14294
- Probabilistic simulation of uncertainties in composite uniaxial strengths [NASA-TM-102483] p 97 N90-16008
- Heat treatment study of the SiC/Ti-15-3 composite system [NASA-TP-2970] p 97 N90-19302
- Thermo-oxidative stability studies of PMR-15 polymer matrix composites reinforced with various fibers [NASA-TM-102439] p 98 N90-19310
- Composite laminate tailoring with probabilistic constraints and loads p 98 N90-20138
- COMGEN: A computer program for generating finite element models of composite materials at the micro level [NASA-TM-102556] p 219 N90-20438
- Characterization of failure processes in tungsten copper composites under fatigue loading conditions [NASA-TM-102371] p 98 N90-21123
- Use of unbalanced laminates as a screening method for microcracking [NASA-TM-102517] p 98 N90-21124
- Multi-objective shape and material optimization of composite structures including damping [NASA-TM-102579] p 99 N90-21132
- Structural tailoring of select fiber composite structures [NASA-TM-102484] p 99 N90-21137
- High temperature fatigue behavior of tungsten copper composites [NASA-TM-102404] p 99 N90-21138
- Computational simulation of structural fracture in fiber composites [NASA-TM-102505] p 100 N90-21821
- METCAN verification status [NASA-TM-103119] p 100 N90-21824
- Matrix density effects on the mechanical properties of SiC/RBSN composites [NASA-TM-103098] p 100 N90-21826
- Fatigue crack growth in a unidirectional SCS-6/Ti-15-3 composite [NASA-TM-103095] p 119 N90-22646
- High temperature fatigue behavior of a SiC/Ti-24Al-11Nb composite [NASA-TM-103157] p 220 N90-22822
- Acousto-ultrasonic nondestructive evaluation of materials using laser beam generation and detection [NASA-CR-186694] p 154 N90-23664
- Influence of interfacial shear strength on the mechanical properties of SiC fiber reinforced reaction-bonded silicon nitride matrix composites [NASA-TM-102462] p 101 N90-24382
- Simplified design procedures for fiber composite structural components/joints [NASA-TM-103113] p 101 N90-24384
- A creep model for metallic composites based on matrix testing: Application to Kanthal composites [NASA-TM-103172] p 101 N90-25193
- Thermomechanical testing techniques for high-temperature composites: TMF behavior of SiC(SCS-6)/Ti-15-3 [NASA-TM-103171] p 222 N90-25367
- Reliability analysis of continuous fiber composite laminates [NASA-CR-185265] p 223 N90-26372
- Input-output characterization of fiber reinforced composites by P waves [NASA-CR-185287] p 208 N90-28097
- Micromechanical model of crack growth in fiber reinforced ceramics [NASA-CR-4321] p 224 N90-28113
- FIBER OPTICS**
- Fiber optic sensing systems using high frequency resonant sensing heads with intensity sensors p 185 A90-10472
- Active phase compensation system for fiber optic holography p 250 A90-11310
- Fiber optic detector probes for laser light scattering p 192 A90-11593
- Fiber optics for advanced aircraft p 185 A90-11702
- Modulated-splitting-ratio fiber-optic temperature sensor p 185 A90-11706
- High-speed analog fiber optic links for satellite communication p 46 A90-11822
- Role of communications satellites in the fiber era [AIAA PAPER 90-0792] p 139 A90-25617
- Development of a phase Doppler based probe for icing cloud droplet characterization [AIAA PAPER 90-0667] p 186 A90-26978
- Optical detectors for GaAs MMIC integration - Technology assessment p 149 A90-41238
- High-speed digital fiber optic links for satellite traffic p 250 A90-41247
- High-speed fiber-optic links for distribution of satellite traffic p 47 A90-41687
- Silicon-etalon fiber-optic temperature sensor [NASA-TM-102389] p 18 N90-13381
- Fiber optic sensing system [NASA-CASE-LEW-14795-1] p 251 N90-15733
- NASA Laser Light Scattering Advanced Technology Development Workshop, 1988 [NASA-CP-10033] p 188 N90-17085
- Advanced instrumentation for aircraft icing research [NASA-CR-185225] p 18 N90-21006
- Bit-error-rate testing of fiber optic data links for MMIC-based phased array antennas [NASA-TM-102523] p 145 N90-21261
- Intensity to frequency conversion technique in intensity modulated fiber optic sensing systems [NASA-TM-102562] p 153 N90-21277
- Civil air transport: A fresh look at power-by-wire and fly-by-light [NASA-TM-102574] p 153 N90-21283
- A fiber optic sensor for noncontact measurement of shaft speed, torque, and power [NASA-TM-102481] p 189 N90-21360
- A fiber-optic current sensor for aerospace applications [NASA-TM-103152] p 190 N90-22773

- Design of an optically controlled Ka-band GaAs MMIC phased-array antenna
[NASA-TM-103147] p 155 N90-26250
- Fiber-optic projected-fringe digital interferometry
[NASA-TM-103252] p 191 N90-28033
- FIBER ORIENTATION**
- Unified micromechanics of damping for unidirectional and off-axis fiber composites p 90 A90-29929
- Effects of fiber motion on the acoustic behavior of an anisotropic, flexible fibrous material p 247 A90-33313
- Resistivity of pristine and intercalated graphite fiber epoxy composites
[NASA-TM-102576] p 128 N90-21192
- Fatigue crack growth in unidirectional metal matrix composite
[NASA-TM-103102] p 220 N90-22117
- Structural behavior of composites with progressive fracture
[NASA-TM-102370] p 100 N90-23477
- Creep and creep rupture of strongly reinforced metallic composites
[NASA-CR-185286] p 223 N90-28110
- FIBER STRENGTH**
- Matrix density effects on the mechanical properties of SiC fiber-reinforced silicon nitride matrix properties
p 94 A90-51927
- Matrix density effects on the mechanical properties of SiC/RBSN composites
[NASA-TM-103098] p 100 N90-21826
- FIBERS**
- Thermal effects on the mechanical properties of SiC fibre reinforced reaction-bonded silicon nitride matrix composites p 92 A90-46999
- Density of intercalated graphite fibers
p 124 A90-49061
- Density of intercalated graphite fibers
[NASA-TM-102411] p 126 N90-14362
- Fiber pushout test: A three-dimensional finite element computational simulation
[NASA-TM-102565] p 99 N90-21131
- Rapid thermal processing of high temperature superconducting fiber
[NASA-CR-186803] p 259 N90-24964
- FIELD EFFECT TRANSISTORS**
- A high-speed GaAs MESFET optical controller
p 186 A90-22483
- Silicon carbide semiconductor device fabrication and characterization
[NASA-CR-186354] p 258 N90-19873
- The 30-GHz monolithic receive module
[NASA-CR-180849] p 146 N90-24528
- Neutron and gamma irradiation effects on power semiconductor switches
[NASA-TM-103200] p 155 N90-25278
- FIGHTER AIRCRAFT**
- The implementation of STOVL task-tailored control modes in a fighter cockpit
[AIAA PAPER 90-3229] p 17 A90-49114
- FILM COOLING**
- An experimental study of turbine vane heat transfer with leading edge and downstream film cooling
[ASME PAPER 89-GT-69] p 165 A90-23792
- Scaling results for the liquid sheet radiator
p 170 A90-38037
- FILM THICKNESS**
- On the numerical solution of the dynamically loaded hydrodynamic lubrication of the point contact problem
[NASA-TM-102427] p 178 N90-17076
- Ellipsometric study of YBa₂Cu₃O_{7-x} laser ablated and co-evaporated films
[NASA-TM-103223] p 259 N90-26682
- FINITE STRUCTURE**
- XANES and EXAFS study of Au-substituted YBa₂Cu₃O_{7-delta}
[NASA-TM-103291] p 260 N90-29219
- FINITE DIFFERENCE THEORY**
- Efficient estimation of diffusion during dendritic solidification p 111 A90-20612
- A critical analysis of the modified equation technique of Warming and Hyett p 241 A90-21940
- A 'transient' automated mapping procedure for complex geometries p 242 A90-26499
- Numerical simulation of rarefied gas flow through a slit
[AIAA PAPER 90-1694] p 170 A90-38397
- On the application of subcell resolution to conservation laws with stiff source terms
[NASA-TM-102384] p 243 N90-14844
- PROTEUS two-dimensional Navier-Stokes computer code, version 1.0. Volume 3: Programmer's reference
[NASA-TM-102553] p 180 N90-21307
- High accuracy solutions of incompressible Navier-Stokes equations
[NASA-TM-102539] p 244 N90-21567
- Large-scale advanced propeller blade pressure distributions: Prediction and data
[NASA-TM-102316] p 30 N90-22564
- Galerkin finite difference Laplacian operators on isolated unstructured triangular meshes by linear combinations
[NASA-TM-103209] p 183 N90-26276
- Two-dimensional model of a Space Station Freedom thermal energy storage canister
[NASA-TM-103124] p 183 N90-26279
- FINITE ELEMENT METHOD**
- Finite element implementation of Robinson's unified viscoplastic model and its application to some uniaxial and multiaxial problems p 208 A90-15704
- Assumed strain distributions for a finite strip plate bending element using Mindlin-Reissner plate theory
p 208 A90-16723
- Modal analysis of gear housing and mounts
p 192 A90-17018
- Least-squares finite element method for fluid dynamics p 159 A90-18246
- Finite element simulations of thermosolutal convection in vertical solidification of binary alloys
p 132 A90-18292
- Improvement of finite element meshes - Heat transfer in an infinite cylinder p 209 A90-19109
- Analytical and finite element solutions of some problems using a viscoplastic model p 209 A90-19132
- Impact ice stresses in rotating airfoils
[AIAA PAPER 90-0198] p 15 A90-19735
- Parallel multi-time step integration on a transputer system p 235 A90-20188
- Comparison of boundary element and finite element methods in spur gear root stress analysis
p 193 A90-21107
- Dynamic analysis of geared rotors by finite elements
p 194 A90-21123
- Finite element mesh refinement criteria for stress analysis p 209 A90-23013
- A variational justification of the assumed natural strain formulation of finite elements. I - Variational principles. II - The C(0) four-node plate element p 210 A90-24384
- Probabilistic analysis of a materially nonlinear structure
[AIAA PAPER 90-1099] p 211 A90-29329
- Mixed variational formulation of finite element analysis of acoustoelastic/slosh fluid-structure interaction
p 212 A90-34851
- Variational formulation of high-performance finite elements - Parametrized variational principles
p 213 A90-46068
- Developments in variational methods for high performance plate and shell elements
p 214 A90-46288
- Numerical modeling of flows in simulated brush seal configurations
[AIAA PAPER 90-2141] p 198 A90-47209
- Electromagnetic finite elements based on a four-potential variational principle p 214 A90-49869
- Least-squares finite element methods for compressible Euler equations p 9 A90-51013
- The MHOST finite element program: 3-D inelastic analysis methods for hot section components. Volume 2: User's manual
[NASA-CR-182235-VOL-2] p 215 N90-10450
- The MHOST finite element program: 3-D inelastic analysis methods for hot section components. Volume 3: Systems' manual
[NASA-CR-182236] p 215 N90-10451
- A least-squares finite element method for incompressible Navier-Stokes problems
[NASA-TM-102385] p 242 N90-12231
- Constitutive modeling for isotropic materials (HOST)
[NASA-CR-174718] p 26 N90-13391
- Parallel eigenanalysis of finite element models in a completely connected architecture
[NASA-CR-185166] p 217 N90-14652
- Mesh refinement in finite element analysis by minimization of the stiffness matrix trace
[NASA-CR-185170] p 201 N90-15434
- Dynamic analysis of geared rotors by finite elements
[NASA-TM-102349] p 201 N90-16286
- Eigensolution of finite element problems in a completely connected parallel architecture
[NASA-TM-102450] p 217 N90-17173
- Compatibility conditions of structural mechanics for finite element analysis
[NASA-TM-102413] p 217 N90-17180
- Prediction of high temperature metal matrix composite properties
[NASA-TM-102490] p 97 N90-17817
- Transient finite element computations on the transputer system
[NASA-CR-185199] p 218 N90-18071
- Integrated force method versus displacement method for finite element analysis
[NASA-TP-2937] p 218 N90-18081
- COMGEN: A computer program for generating finite element models of composite materials at the micro level
[NASA-TM-102556] p 219 N90-20438
- Fiber pushout test: A three-dimensional finite element computational simulation
[NASA-TM-102565] p 99 N90-21131
- Computational simulation of structural fracture in fiber composites
[NASA-TM-102505] p 100 N90-21821
- Finite element elastic-plastic-creep and cyclic life analysis of a cowl lip
[NASA-TM-102342] p 220 N90-22808
- Non-linear dynamic analysis of geared systems, part 2
[NASA-CR-180495] p 204 N90-23732
- Application of finite-element-based solution technologies for viscoplastic structural analyses
[NASA-CR-185196] p 221 N90-23757
- Finite element analysis of structural components using viscoplastic models with application to a cowl lip problem
[NASA-CR-185189] p 221 N90-23769
- Metal matrix composites microfracture: Computational simulation
[NASA-TM-103153] p 101 N90-24383
- Low velocity impact analysis with NASTRAN
p 221 N90-24647
- Determination of the stress distributions in a ceramic: Tensile specimen using numerical techniques
[NASA-TM-101914] p 129 N90-26132
- Computer simulation of gear tooth manufacturing processes
[NASA-CR-185200] p 138 N90-26171
- Design of ceramic components with the NASA/CARES computer program
[NASA-TM-102369] p 222 N90-26359
- Probabilistic structural analysis methods development for SSME p 83 N90-28616
- FINITE VOLUME METHOD**
- A nonoscillatory, characteristically convected, finite volume scheme for multidimensional convection problems
[AIAA PAPER 90-0015] p 159 A90-19633
- Calculation of turbulence-driven secondary motion in ducts with arbitrary cross-section
[AIAA PAPER 90-0245] p 160 A90-19752
- Application of a lower-upper implicit scheme and an interactive grid generation for turbomachinery flow field simulations
[ASME PAPER 89-GT-20] p 4 A90-23762
- Calculations of gaseous H₂/O₂ thruster
[AIAA PAPER 90-2490] p 67 A90-47224
- A nonoscillatory, characteristically convected, finite volume scheme for multidimensional convection problems
[NASA-TM-102354] p 242 N90-11497
- Large-scale advanced propeller blade pressure distributions: Prediction and data
[NASA-TM-102316] p 30 N90-22564
- The fundamentals of adaptive grid movement
p 185 N90-29610
- FIRE EXTINGUISHERS**
- Advanced spacecraft fire safety: Proposed projects and program plan
[NASA-CR-185147] p 49 N90-12645
- Fire safety applications for spacecraft
p 16 N90-17595
- FIRE PREVENTION**
- Advanced spacecraft fire safety: Proposed projects and program plan
[NASA-CR-185147] p 49 N90-12645
- Fire safety applications for spacecraft
p 16 N90-17595
- FIRES**
- Fire safety applications for spacecraft
p 16 N90-17595
- FITNESS**
- Three-dimensional adaptive grid generation for body-fitted coordinate system p 167 A90-26506
- FLAME PROPAGATION**
- Ignition and behavior of laminar gas-jet diffusion flames in microgravity p 103 A90-23107
- Near-limit flame spread over a thin solid fuel in microgravity p 104 A90-32835
- Opposed-flow flame spread and extinction in mixed-convection boundary layers p 168 A90-32841
- An investigation of flame spread over shallow liquid pools in microgravity and nonair environments
[NASA-TM-102425] p 134 N90-13680
- Asymptotic analysis of dissipative waves with applications to their numerical simulation
[NASA-TM-103231] p 244 N90-26615
- FLAME SPECTROSCOPY**
- Fabry-Perot interferometer development for rocket engine plume spectroscopy
[AIAA PAPER 90-2234] p 187 A90-47212

FLAME STABILITY

- On the use of external burning to reduce aerospace vehicle transonic drag
 - [AIAA PAPER 90-1935] p 20 A90-40562
- The structure and stability of nonadiabatic flame balls
 - p 105 A90-43674
- On the use of external burning to reduce aerospace vehicle transonic drag
 - [NASA-TM-103107] p 30 N90-21762

FLAMES

- Investigation of methods to produce a uniform cloud of fuel particles in a flame tube
 - [NASA-TM-102376] p 178 N90-18665
- Saturated fluorescence measurements of the hydroxyl radical in laminar high-pressure flames
 - [NASA-CR-185218] p 190 N90-22022
- Asymptotic analysis of dissipative waves with applications to their numerical simulation
 - [NASA-TM-103231] p 244 N90-26615
- Ignition and combustion characteristics of metallized propellants
 - [NASA-CR-186870] p 107 N90-26911

FLAMMABILITY

- The possibility of a reversal of material flammability ranking from normal gravity to microgravity
 - p 105 A90-42298
- Advanced spacecraft fire safety: Proposed projects and program plan
 - [NASA-CR-185147] p 49 N90-12645

FLAT PLATES

- Near wall flow parameters in the blade end-wall corner region
 - p 156 A90-12636
- Simulating transitional flow and heat transfer over the flat plate and circular cylinder using a K-epsilon turbulence model
 - p 168 A90-32171
- Some characteristics of bypass transition in a heated boundary layer
 - p 169 A90-35183
- Effects of very high turbulence on heat transfer
 - p 169 A90-35247
- Numerical simulations of supersonic flow through oscillating cascade sections
 - [NASA-TM-103100] p 13 N90-20051

FLEXIBILITY

- Tooth contact shift in loaded spiral bevel gears
 - p 193 A90-21112
- Blade mistuning coupled with shaft flexibility effects in rotor aeroelasticity
 - [ASME PAPER 89-GT-330] p 19 A90-23896
- Effects of fiber motion on the acoustic behavior of an anisotropic, flexible fibrous material
 - p 247 A90-33313
- Numerical simulation of unsteady rotational flow over propfan configurations
 - [NASA-CR-186037] p 10 N90-12500
- High temperature flexible seal
 - [NASA-CASE-LEW-14695-1] p 204 N90-23751

FLEXIBLE BODIES

- Shaft flexibility effects on the forced response of a bladed-disk assembly
 - p 21 A90-43218

FLIGHT CHARACTERISTICS

- H-infinity based integrated flight-propulsion control design for a STOVL aircraft in transition flight
 - [NASA-TM-103198] p 37 N90-26011

FLIGHT CONTROL

- H-infinity based integrated flight/propulsion control design for a STOVL aircraft in transition flight
 - [AIAA PAPER 90-3335] p 36 A90-47595
- Extended implicit model following as applied to integrated flight and propulsion control
 - [AIAA PAPER 90-3444] p 239 A90-47697
- Flight control design considerations for STOVL powered-lift flight
 - [AIAA PAPER 90-3225] p 37 A90-49110
- STOVL aircraft simulation for integrated flight and propulsion control research
 - [NASA-TM-102419] p 26 N90-13389
- Civil air transport: A fresh look at power-by-wire and fly-by-light
 - [NASA-TM-102574] p 153 N90-21283
- The insertion of human dynamics models in the flight control loops of V/STOL research aircraft. Appendix 2: The optimal control model of a pilot in V/STOL aircraft control loops
 - [NASA-CR-186598] p 38 N90-21776

FLIGHT SIMULATION

- Launching a dream: A teachers guide to a simulated space shuttle mission
 - [NASA-TM-89715] p 261 N90-26693

FLIGHT TESTS

- Thermal energy storage flight experiments
 - p 53 A90-11992
- InP homojunction solar cell performance on the LIPS III flight experiment
 - p 226 A90-14921
- Initial results from the joint NASA-Lewis/U.S. Army icing flight research tests
 - p 16 A90-28180
- Advanced Communications Technology Satellite (ACTS) and potential system applications
 - p 142 A90-51165

- Electro-impulse de-icing testing analysis and design
 - [NASA-CR-4175] p 18 N90-10031
 - Propan Test Assessment (PTA): Flight test report
 - [NASA-CR-182278] p 24 N90-11738
 - Propan Test Assessment (PTA)
 - [NASA-CR-185138] p 25 N90-11739
 - NASA's program on icing research and technology
 - p 16 N90-15062
 - Heat transfer measurements from a NACA 0012 airfoil in flight and in the NASA Lewis icing research tunnel
 - [NASA-CR-4278] p 13 N90-19203
 - Aeroacoustics of advanced propellers
 - [NASA-TM-103137] p 249 N90-26635
- FLOAT ZONES**
- Energy stability of thermocapillary convection in a model of the float-zone crystal-growth process
 - p 133 A90-48720

FLOW CHARACTERISTICS

- Structure of a reattaching supersonic shear layer
 - p 7 A90-36252
- The simulation of fluid dynamic uncertainties in the SSME turbopump
 - [AIAA PAPER 90-2294] p 65 A90-42770
- Wall-layer eruptions in turbulent flows
 - [NASA-TM-102362] p 175 N90-11250
- A numerical simulation of the flow in the diffuser of the NASA Lewis icing research tunnel
 - [NASA-TM-102480] p 38 N90-15965
- Aerodynamic optimization by simultaneously updating flow variables and design parameters
 - p 18 N90-20991

FLOW DEFLECTION

- Experimental and analytical study of close-coupled ventral nozzles for ASTOVL aircraft
 - [NASA-TM-103170] p 31 N90-24273

FLOW DISTRIBUTION

- The unsteady aerodynamics of an oscillating cascade in a compressible flow field
 - p 2 A90-11789
- Numerical study of chemically reacting flows using a lower-upper symmetric successive overrelaxation scheme
 - p 3 A90-17989
- Least-squares finite element method for fluid dynamics
 - p 159 A90-18246
- A nonoscillatory, characteristically convected, finite volume scheme for multidimensional convection problems
 - [AIAA PAPER 90-0015] p 159 A90-19633
- Application of an efficient hybrid scheme for aeroelastic analysis of advanced propellers
 - [AIAA PAPER 90-0028] p 4 A90-22153
- Convective heat transfer measurements from a NACA 0012 airfoil in flight and in the NASA Lewis Icing Research Tunnel
 - [AIAA PAPER 90-0199] p 162 A90-22180
- An interactive grid generation procedure for axial and radial flow turbomachinery
 - [AIAA PAPER 90-0344] p 162 A90-22200
- Application of a lower-upper implicit scheme and an interactive grid generation for turbomachinery flow field simulations
 - [ASME PAPER 89-GT-20] p 4 A90-23762
- Unsteady Euler analysis of the flowfield of a propfan at an angle of attack
 - [AIAA PAPER 90-0339] p 5 A90-25028
- Ground-based experiments on thermal and thermosolutal convection in inclined low-aspect-ratio enclosures
 - [AIAA PAPER 90-0413] p 166 A90-25033
- Interactive grid generation for turbomachinery flow field simulations
 - p 6 A90-26553
- Nature of convection-stabilized dc arcs in dual-flow nozzle geometry. I - The cold flow field and dc arc characteristics. II - Optical diagnostics and theory
 - p 252 A90-26665
- On sublayer streaks
 - p 168 A90-28143
- A laser based computer aided non-intrusive technique for full field flow characterization in macroscopic curved channels
 - p 168 A90-32293
- The effects of forcing on a single stream shear layer and its parent boundary layer
 - p 169 A90-35219
- Time-dependent calculation of a forced mixing layer using a k-epsilon turbulence model
 - p 169 A90-35222
- Influence of bulk turbulence and entrance boundary layer thickness on the curved duct flow field
 - [AIAA PAPER 90-1502] p 171 A90-38651
- Symmetry assessment of an air-blast atomizer spray
 - p 172 A90-40930
- A rotating hot-wire technique for spatial sampling of disturbed and manipulated duct flows
 - p 186 A90-41120
- Computational analysis of the flowfield of a two-dimensional ejector nozzle
 - [AIAA PAPER 90-1901] p 21 A90-42690
- Three-dimensional turbulent flow code calculations of hot gas ingestion
 - p 21 A90-44726

- The low frequency oscillation in the flow over a NACA0012 airfoil with an 'iced' leading edge
 - p 8 A90-46377
- Analysis and design of optimized truncated scarfed nozzles subject to external flow effects
 - [AIAA PAPER 90-2222] p 9 A90-47213
- Euler analysis comparison with LDV data for an advanced counter-rotation propfan at cruise
 - [AIAA PAPER 90-3033] p 9 A90-50637
- Numerical investigation of the thermal stratification in cryogenic tanks subjected to wall heat flux
 - [AIAA PAPER 90-2375] p 175 A90-52500
- User's manual for PEP SIG NASA tip vortex version
 - [NASA-CR-186178] p 10 N90-10835
- Computation of the tip vortex flowfield for advanced aircraft propellers
 - [NASA-CR-182179] p 10 N90-10836
- A nonoscillatory, characteristically convected, finite volume scheme for multidimensional convection problems
 - [NASA-TM-102354] p 242 N90-11497
- Investigation of turbulent flow in highly curved ducts with application to turbomachinery components
 - [NASA-CR-186060] p 175 N90-12882
- Application of an efficient hybrid scheme for aeroelastic analysis of advanced propellers
 - [NASA-TM-102426] p 11 N90-13355
- A planar reacting shear layer system for the study of fluid dynamics-combustion interaction
 - [NASA-TM-102422] p 27 N90-13393
- Convective heat transfer measurements from a NACA 0012 airfoil in flight and in the NASA Lewis Icing Research Tunnel
 - [NASA-TM-102448] p 176 N90-13750
- An interactive grid generation procedure for axial and radial flow turbomachinery
 - [NASA-CR-185167] p 237 N90-13968
- An analysis of the viscous flow through a compact radial turbine by the average passage approach
 - [NASA-TM-102471] p 12 N90-14206
- Spatial evolution of nonlinear acoustic mode instabilities on hypersonic boundary layers
 - [NASA-TM-102431] p 177 N90-14517
- Viscous three-dimensional analyses for nozzles for hypersonic propulsion
 - [NASA-CR-185197] p 27 N90-17635
- FLUSH: A tool for the design of slush hydrogen flow systems
 - [NASA-TM-102467] p 130 N90-17890
- Unsteady Euler analysis of the flow field of a propfan at an angle of attack
 - [NASA-TM-102426] p 248 N90-18229
- Laser-velocimeter-measured flow field around an advanced, swept, eight-blade propeller at Mach 0.8
 - [NASA-TP-2462] p 1 N90-20942
- Users manual for the NASA Lewis Ice Accretion Prediction Code (LEWICE)
 - [NASA-CR-185129] p 1 N90-20943
- The effects of forcing on a single stream shear layer and its parent boundary layer
 - [NASA-CR-186529] p 180 N90-21301
- Investigation of advanced counterrotation blade configuration concepts for high speed turboprop systems, task 1: Ducted propfan analysis
 - [NASA-CR-185217] p 30 N90-22567
- Computational analysis of the flowfield of a two-dimensional ejector nozzle
 - [NASA-CR-185255] p 31 N90-23406
- Experimental and analytical study of close-coupled ventral nozzles for ASTOVL aircraft
 - [NASA-TM-103170] p 31 N90-24273
- Analysis and design of optimized truncated scarfed nozzles subject to external flow effects
 - [NASA-TM-103175] p 13 N90-25106
- Euler analysis comparison with LDV data for an advanced counter-rotation propfan at cruise
 - [NASA-TM-103249] p 14 N90-25946
- Two-dimensional Euler and Navier-Stokes Time accurate simulations of fan rotor flows
 - [NASA-TM-102402] p 14 N90-25948
- Hot gas ingestion characteristics and flow visualization of a vectored thrust STOVL concept
 - [NASA-TM-103212] p 32 N90-26009
- High speed turboprop aerodynamic study (counterrotation). Volume 1: Model development
 - [NASA-CR-185241] p 249 N90-26633
- Aerodynamics of a linear oscillating cascade
 - [NASA-TM-103250] p 15 N90-27657
- Computer code for predicting coolant flow and heat transfer in turbomachinery
 - [NASA-TP-2985] p 32 N90-27722
- Numerical investigation of the thermal stratification in cryogenic tanks subjected to wall heat flux
 - [NASA-TM-103194] p 184 N90-27984

FLOW EQUATIONS

Investigation of advanced counterrotation blade configuration concepts for high speed turboprop systems, task 1: Ducted propfan analysis
[NASA-CR-185217] p 30 N90-22567

FLOW GEOMETRY

Augmented heat transfer in rectangular channels of narrow aspect ratios with rib turbulators p 157 A90-13091
A circular combustor configuration with multiple injection ports for mixing enhancement p 158 A90-15389
Elliptic jets. I - Characteristics of unexcited and excited jets p 159 A90-18071
Calculation of turbulent three-dimensional jet-induced flow in a rectangular enclosure
[AIAA PAPER 90-0684] p 161 A90-19976
Nature of convection-stabilized dc arcs in dual-flow nozzle geometry. I - The cold flow field and dc arc characteristics II - Optical diagnostics and theory p 252 A90-26665

FLOW MEASUREMENT

The measurement of boundary layers on a compressor blade in cascade. IV - Flow fields for incidence angles of -1.5 and -8.5 degrees
[ASME PAPER 89-GT-72] p 165 A90-23793
Three dimensional LDV flow measurements and theoretical investigation in a radial inflow turbine scroll p 9 A90-46860

FLOW RESISTANCE

Acquisition and correlation of cryogenic nitrogen mass flow data through a multiple orifice Joule-Thomson device
[NASA-TM-103121] p 182 N90-22761

FLOW STABILITY

Nonlinear evolution of oblique waves on compressible shear layers p 158 A90-15942
Experimental investigation of convective stability in a superposed fluid and porous layer when heated from below p 158 A90-15947
The vibrating ribbon problem revisited --- in hydrodynamic stability p 168 A90-33516
Scaling results for the liquid sheet radiator p 170 A90-38037
On the instabilities of supersonic mixing layers - A high-Mach-number asymptotic theory p 8 A90-42644
Evolution and interaction of two- and three-dimensional instability waves p 173 A90-46885
Viscous effects on the instability of an axisymmetric jet
[NASA-TM-102396] p 12 N90-16719
Amplitude-dependent neutral modes in compressible boundary layer flows
[NASA-TM-102524] p 178 N90-20326
Modern developments in shear flow control with swirl
[NASA-CR-186586] p 181 N90-22000
Nonlinear interactions in mixing layers and compressible heated round jets
[NASA-CR-186303] p 182 N90-23674
Near-limit flame spread over a thin solid fuel in microgravity p 104 A90-32835
Scaling results for the liquid sheet radiator p 170 A90-38037
Experimental investigation of turbulent flow through a circular-to-rectangular transition duct
[AIAA PAPER 90-1505] p 171 A90-38654
A rotating hot-wire technique for spatial sampling of disturbed and manipulated duct flows p 186 A90-41120
Gas-phase flowrate effect on disintegrating cryogenic liquid-jets p 173 A90-46895
Arcjet load characteristics
[AIAA PAPER 90-2579] p 67 A90-47226
Laser anemometer measurements in a transonic axial-flow fan rotor p 175 N90-11245
Gas-phase flowrate effect on disintegrating cryogenic liquid-jets
[NASA-TM-102357] p 187 N90-11277
The effects of forcing on a single stream shear layer and its parent boundary layer
[NASA-CR-186529] p 180 N90-21301
Arcjet load characteristics
[NASA-TM-103190] p 79 N90-25181

FLOW VISUALIZATION

Asymmetrical boundary layer separation at the base of a two cylinder geometry p 159 A90-18505
Flow visualization and motion analysis for a series of four sequential brush seals
[AIAA PAPER 90-2482] p 199 A90-47222
Viscous effects on the instability of an axisymmetric jet
[NASA-TM-102396] p 12 N90-16719
Hot gas ingestion characteristics and flow visualization of a vectored thrust STOVL concept
[NASA-TM-103212] p 32 N90-26009

FLUID DYNAMICS

Reciprocal interactions of hairpin-shaped vortices and a boundary layer
[AIAA PAPER 90-0017] p 159 A90-19635
Evaluation of three turbulence models in static air loads and dynamic stall predictions p 7 A90-31291
A least-squares finite element method for incompressible Navier-Stokes problems
[NASA-TM-102385] p 242 N90-12231
Application of multi-grid methods for solving the Navier-Stokes equations
[NASA-TM-102359] p 243 N90-14002
Laser velocimeter and total pressure measurements in circular-to-rectangular transition ducts
[NASA-CR-182286] p 177 N90-14494
On the application of subcell resolution to conservation laws with stiff source terms
[NASA-TM-102384] p 243 N90-14844
Microgravity noncontact temperature requirements at NASA Lewis Research Center p 134 N90-17897
Spacelab qualified infrared imager for microgravity science experiments
[NASA-TM-102503] p 189 N90-20352
High accuracy solutions of incompressible Navier-Stokes equations
[NASA-TM-102539] p 244 N90-21567
WINCOF-I code for prediction of fan compressor unit with water ingestion
[NASA-CR-185157] p 1 N90-21724
New findings and instrumentation from the NASA Lewis microgravity facilities p 136 N90-26163
Low-gravity fluid physics: A program overview
[NASA-TM-103215] p 183 N90-26273
Implicit solution of three-dimensional internal turbulent flows
[NASA-TM-103099] p 184 N90-27982
An improved k-epsilon model for near-wall turbulence and comparison with direct numerical simulation
[NASA-TM-103221] p 184 N90-27983
Numerical solution for the velocity-derivative skewness of a low-Reynolds-number decaying Navier-Stokes flow
[NASA-TM-103186] p 184 N90-27985

FLUID FILLED SHELLS

Treatment of coupled fluid-structure interaction problems by a mixed variational principle p 159 A90-18288
Mixed variational formulation of finite element analysis of acoustoelastic/slosh fluid-structure interaction p 212 A90-34851

FLUID FILMS

A high-speed photography study of cavitation in a dynamically loaded journal bearing
[NASA-TM-103178] p 204 N90-26338

FLUID FLOW

On the application of subcell resolution to conservation laws with stiff source terms p 243 N90-14844
Prediction of the ullage gas thermal stratification in a NASP vehicle propellant tank experimental simulation using FLOW-3D
[NASA-TM-103217] p 131 N90-26160
Computational experience with a three-dimensional rotary engine combustion model
[NASA-TM-103104] p 183 N90-26275

FLUID JETS

Elliptic jets. I - Characteristics of unexcited and excited jets p 159 A90-18071
Evolution and interaction of two- and three-dimensional instability waves p 173 A90-46885

FLUID MANAGEMENT

On-orbit low gravity cryogenic scientific investigations using the COLD-SAT Satellite
[AIAA PAPER 90-0718] p 39 A90-19988
Evaluation of supercritical cryogen storage and transfer systems for future NASA missions
[AIAA PAPER 90-0719] p 44 A90-19989
Spacecraft attitude impacts on COLD-SAT non-vacuum jacketed LH2 supply tank thermal performance
[AIAA PAPER 90-1672] p 49 A90-41566
Evaluation of supercritical cryogen storage and transfer systems for future NASA missions
[NASA-TM-102394] p 44 N90-10912
Evolutionary space station fluids management strategies
[NASA-CR-185137] p 49 N90-10983
CryoTran user's manual, version 1.0
[NASA-TM-102468] p 237 N90-15622
Acquisition and correlation of cryogenic nitrogen mass flow data through a multiple orifice Joule-Thomson device
[NASA-TM-103121] p 182 N90-22761
Tank pressure control experiment on the space shuttle
[NASA-TM-102313] p 71 N90-13590

Technical accomplishments of the NASA Lewis Research Center, 1989
[NASA-TM-102296] p 267 N90-24220
Optical techniques for determination of normal shock position in supersonic flows for aerospace applications
[NASA-TM-103201] p 190 N90-25323

FLUID-SOLID INTERACTIONS

Treatment of coupled fluid-structure interaction problems by a mixed variational principle p 159 A90-18288
A numerical study of the interaction between unsteady free-stream disturbances and localized variations in surface geometry p 161 A90-21422
Unsteady disturbances of streaming motions around bodies p 162 A90-21424
Development of an integrated BEM for hot fluid-structure interaction
[ASME PAPER 89-GT-128] p 212 A90-32264
Mixed variational formulation of finite element analysis of acoustoelastic/slosh fluid-structure interaction p 212 A90-34851

FLUORIDES

Flight experiment of thermal energy storage --- for spacecraft power systems p 61 A90-38172

FLUORINATION

Fluorinated graphite fibers as a new engineering material: Promises and challenges
[NASA-TM-102511] p 86 N90-19301

FLUORO COMPOUNDS

Substituted 1,1,1-triaryl-2,2,2-trifluoroethanes and processes for their synthesis
[NASA-CASE-LEW-14345-2] p 107 N90-23497

FLUOROHYDROCARBONS

New Condensation polyimides containing 1,1,1-triaryl-2,2,2-trifluoroethane structures
[NASA-CASE-LEW-14346-1] p 86 N90-19300

FLUOROPOLYMERS

The 3F condensation polyimides: Review and update
[NASA-TM-102353] p 126 N90-14363
New Condensation polyimides containing 1,1,1-triaryl-2,2,2-trifluoroethane structures
[NASA-CASE-LEW-14346-1] p 86 N90-19300

FLUTTER ANALYSIS

Time domain flutter analysis of cascades using a full-potential solver
[AIAA PAPER 90-0984] p 6 A90-29374
Aeroelastic problems in turbomachines
[AIAA PAPER 90-1157] p 7 A90-29393

FLUX DENSITY

High frequency, high temperature specific core loss and dynamic B-H hysteresis loop characteristics of soft magnetic alloys
[NASA-TM-103164] p 154 N90-23663
Ultrasonic verification of five wave fronts in undirectional graphite epoxy composite
[NASA-CR-185288] p 208 N90-28858

FLUX VECTOR SPLITTING

Splitting of inviscid fluxes for real gases p 167 A90-25451
A flux-split solution procedure for unsteady inlet flows
[AIAA PAPER 90-0585] p 6 A90-26967
Transient behavior of supersonic flow through inlets
[AIAA PAPER 90-2130] p 8 A90-42734
Inviscid flux-splitting algorithms for real gases with non-equilibrium chemistry p 174 A90-52275

FLYWHEELS

Solar power for the lunar night p 266 A90-24814

FOAMING

Instantaneously generated foam and its applicability to reduced gravity
[NASA-CR-185208] p 135 N90-20237

FOAMS

Instantaneously generated foam and its applicability to reduced gravity
[NASA-CR-185208] p 135 N90-20237

FOCUSING

Millimeter-wave/infrared rectenna development at Georgia Tech p 69 N90-10147

FORCED CONVECTION

A technique for measurement of instantaneous heat transfer in steady-flow ambient-temperature facilities p 172 A90-39625

FORCED VIBRATION

The vibrating ribbon problem revisited --- in hydrodynamic stability p 168 A90-33516
Dynamic analysis of geared rotors by finite elements
[NASA-TM-102349] p 201 N90-16286
Gust response analysis for cascades operating in nonuniform mean flows p 28 N90-18415

FORMAT

FORTTRAN program for x ray photoelectron spectroscopy data reformatting
[NASA-TP-2957] p 258 N90-12348

FORTRAN

FORTRAN program for x ray photoelectron spectroscopy data reformatting
[NASA-TP-2957] p 258 N90-12348

FORWARD SCATTERING

Droplet sizing instrumentation used for icing research: Operation, calibration, and accuracy
[NASA-CR-182293] p 187 N90-11999

FRACTOGRAPHY

Refractory metal alloys and composites for space power systems p 116 A90-46677

FRACTURE MECHANICS

Universal aspects of brittle fracture, adhesion, and atomic force microscopy p 83 A90-14021
Improving the low temperature ductility of NIAI p 110 A90-16940

Burner rig hot corrosion of silicon carbide and silicon nitride p 121 A90-25267
Intergranular fracture of lithium fluoride-22 percent calcium fluoride hypereutectic salt at 800 K p 121 A90-25273

The equivalence between dislocation pile-ups and cracks p 210 A90-29215
Progression of damage and fracture in composites under dynamic loading p 210 A90-29318

Calculation of Weibull strength parameters and Batdorf flow-density constants for volume- and surface-flaw-induced fracture in ceramics p 212 A90-35462

Equivalence of physically based statistical fracture theories for reliability analysis of ceramics in multiaxial loading p 123 A90-43580

Fatigue crack propagation behavior of a single crystalline superalloy p 116 A90-48635
Fundamental tribological properties of ion-beam-deposited boron nitride films p 124 A90-49054

Use of unbalanced laminates as a screening method for microcracking p 94 A90-50217
High-temperature tensile properties of fiber reinforced reaction bonded silicon nitride p 95 A90-52783

Mechanics of the crack path formation [NASA-CR-185143] p 215 N90-10455
Fundamental tribological properties of ion-beam-deposited boron nitride films p 125 N90-11881

A nonlinear high temperature fracture mechanics basis for strainrange partitioning [NASA-TM-4133] p 216 N90-14642
Identification of a cast iron alloy containing nonstrategic elements [NASA-CR-185174] p 118 N90-18559

Use of unbalanced laminates as a screening method for microcracking [NASA-TM-102517] p 98 N90-21124
Computational simulation of structural fracture in fiber composites [NASA-TM-102505] p 100 N90-21821

The effect of hydrogen and microstructure on the deformation and fracture behavior of a single crystal nickel-base superalloy [NASA-CR-185219] p 118 N90-21849
Controlled crack growth specimen for brittle systems [NASA-TM-103126] p 129 N90-23543

FRACTURE STRENGTH

Analysis of whisker-toughened ceramic components - A design engineer's viewpoint p 88 A90-19149
Crack-path effect on material toughness [ASME PAPER 89-WA/APM-43] p 210 A90-28755

Microstructure and mechanical properties of multiphase NIAI-based alloys p 115 A90-35071
High-strength silicon carbides by hot isostatic pressing p 122 A90-35473

Tensile adhesion testing methodology for thermally sprayed coatings p 85 A90-43902
Investigation of Weibull statistics in fracture analysis of cast aluminum p 115 A90-45304

Strength and toughness of monolithic and composite silicon nitrides [NASA-TM-102423] p 126 N90-14368
Empirical and analytical determination of the fracture resistance of a TiB₂ particle/SiC matrix composite [NASA-TM-101940] p 96 N90-15143

Fully articulated four-point-bend loading fixture [NASA-CASE-LEW-14776-1] p 201 N90-15445
Analysis of whisker-toughened ceramic components: A design engineer's viewpoint p 97 N90-18504

Micromechanical model of crack growth in fiber reinforced ceramics [NASA-CR-4321] p 224 N90-28113

FRACTURES (MATERIALS)

Metal matrix composites microfracture: Computational simulation [NASA-TM-103153] p 101 N90-24383

FRACTURING

Computational simulation of structural fracture in fiber composites [NASA-TM-102505] p 100 N90-21821
Progression of damage and fracture in composites under dynamic loading [NASA-TM-103118] p 100 N90-21825

Structural behavior of composites with progressive fracture [NASA-TM-102370] p 100 N90-23477

FREE CONVECTION

Numerical modeling of enclosure convection [IAF PAPER 89-403] p 157 A90-13511
Finite element simulations of thermosolutal convection in vertical solidification of binary alloys p 132 A90-18292

Free float acceleration measurements aboard NASA's KC-135 Microgravity Research Aircraft [AIAA PAPER 90-0742] p 132 A90-20000
Effects of g-jitter on a thermal, buoyant flow [AIAA PAPER 90-0653] p 163 A90-22239

Numerical analysis of natural convection in liquid droplets by phase change p 164 A90-23212
Ground-based experiments on thermal and thermosolutal convection in inclined low-aspect-ratio enclosures [AIAA PAPER 90-0413] p 166 A90-25033

Hardware development for the surface tension driven convection experiment p 52 A90-36195

FREE ELECTRON LASERS

Free-Space Power Transmission [NASA-CP-10016] p 77 N90-21795

FREE FLOW

Contributions to the understanding of large-scale coherent structures in developing free turbulent shear flows p 158 A90-13907
Compressibility effects in free shear layers [AIAA PAPER 90-0705] p 161 A90-19984

A numerical study of the interaction between unsteady free-stream disturbances and localized variations in surface geometry p 161 A90-21422
The effects of forcing on a single stream shear layer and its parent boundary layer p 169 A90-35219

Effects of very high turbulence on heat transfer p 169 A90-35247
Pressure-based real-time measurements in compressible free shear layers [AIAA PAPER 90-1980] p 8 A90-42709

FREE JETS

Vapor condensation on liquid surface due to laminar jet-induced mixing - The effects of system parameters [AIAA PAPER 90-0354] p 163 A90-22202
Total temperature effects on centerline Mach number characteristics of freejets p 6 A90-25290

Vapor condensation on liquid surface due to laminar jet-induced mixing: The effects of system parameters [NASA-TM-102433] p 176 N90-13751
The entrainment rate for a row of turbulent jets [NASA-CR-185278] p 15 N90-28504

FREE RADICALS

Atomic hydrogen as a launch vehicle propellant [AIAA PAPER 90-0715] p 44 A90-23712
Atomic hydrogen as a launch vehicle propellant [NASA-TM-102459] p 73 N90-14284

FREE VIBRATION

Free-vibration analysis of three-dimensional solids by BEM p 215 A90-52007

FREE-PISTON ENGINES

On the dynamic response of pressure transmission lines in the research of helium-charged free piston Stirling engines p 196 A90-38248
Results from baseline tests of the SPRE I and comparison with code model predictions p 62 A90-38249

Comparison of conceptual designs for 25 kW advanced Stirling conversion systems for dish electric applications p 229 A90-38254

FREEZING

Flight experiment of thermal energy storage ... for spacecraft power systems p 61 A90-38172

FREQUENCIES

High frequency GaAlAs modulator and photodetector for phased array antenna applications p 146 A90-11774

FREQUENCY ASSIGNMENT

Application of heuristic satellite plan synthesis algorithms to requirements of the WARC-88 allotment plan [AIAA PAPER 90-0815] p 245 A90-25638

Application of heuristic satellite plan synthesis algorithms to requirements of the WARC-88 allotment plan [NASA-TM-102479] p 245 N90-14856

Numerical Arc Segmentation Algorithm for a Radio Conference-NASARC (version 4.0) technical manual [NASA-TM-101453] p 144 N90-20264

FREQUENCY CONTROL

Variable speed induction motor operation from a 20-kHz power bus p 148 A90-38119

FREQUENCY CONVERTERS

Intensity to frequency conversion technique in intensity modulated fiber optic sensing systems [NASA-TM-102562] p 153 N90-21277

FREQUENCY DISTRIBUTION

Induction motor control [NASA-TM-102533] p 28 N90-19234

FREQUENCY DIVISION MULTIPLE ACCESS

A parallel pipelined architecture for a digital multicarrier demodulator [AIAA PAPER 90-0812] p 46 A90-25635

FREQUENCY HOPPING

A users perspective of the ACTS hopping beam TDMA system [AIAA PAPER 90-0833] p 140 A90-25658

FREQUENCY RESPONSE

Effects of amplitude distortions and IF equalization on satellite communication system bit-error rate performance [AIAA PAPER 90-0878] p 140 A90-25697

Microwave response of a HEMT photoconductive detector p 147 A90-37301
Effects of mistuning and matrix structure on the topology of frequency response curves [NASA-TM-102290] p 216 N90-12041

FRESNEL LENSES

The mini-dome lens space concentrator array - Recent component test results and current array development status p 60 A90-38155

Conceptual design study of a 5 kilowatt solar dynamic Brayton power system using a dome Fresnel lens solar concentrator [NASA-CR-185134] p 72 N90-14281

FRICTION

Effects of lubrication on the performance of high speed spur gears p 194 A90-21119
Applications of surface analysis and surface theory in tribology p 84 A90-37458

Friction and wear of oxide-ceramic sliding against IN-718 nickel base alloy at 25 to 800 C in atmospheric air [NASA-TM-102291] p 124 N90-10262

A new test machine for measuring friction and wear in controlled atmospheres to 1200 C [NASA-TM-102405] p 96 N90-12670

The experimental evaluation and application of high-temperature solid lubricants [NASA-TM-102476] p 127 N90-16944

FRICTION FACTOR

An annular gas seal analysis using empirical entrance and exit region friction factors [ASME PAPER 89-TRIB-46] p 196 A90-33555

Experimentally determined wear behavior of an Al₂O₃-SiC composite from 25 to 1200 C [NASA-TM-102549] p 87 N90-20130
Fiber pushout test: A three-dimensional finite element computational simulation [NASA-TM-102565] p 99 N90-21131

FRICTION REDUCTION

Fundamentals of tribology at the atomic level p 192 A90-14020

FUEL CELLS

Electrocatalysis for oxygen electrodes in fuel cells and water electrolyzers for space applications p 57 A90-33945

Oxygen electrodes for rechargeable alkaline fuel cells. II p 228 A90-33946
Corrosion testing of candidates for the alkaline fuel cell cathode p 228 A90-33948

Hydrogen-oxygen proton-exchange membrane fuel cells and electrolyzers p 230 N90-20467
Electrocatalysis for oxygen electrodes in fuel cells and water electrolyzers for space applications p 230 N90-20468

Oxygen electrodes for rechargeable alkaline fuel cells. II p 231 N90-20469
Corrosion testing of candidates for the alkaline fuel cell cathode p 231 N90-20471

O₂ reduction at the IFC orbiter fuel cell O₂ electrode [NASA-TM-102580] p 231 N90-21469
Catalysts for ultrahigh current density oxygen cathodes for space fuel cell applications [NASA-CR-180650] p 232 N90-22835

FUEL COMBUSTION

Analysis of rotary engine combustion processes based on unsteady, three-dimensional computations [AIAA PAPER 90-0643] p 163 A90-22237

Theory of influence of a low-volatility, soluble impurity on spherically-symmetric combustion of fuel droplets p 104 A90-28771
Opposed-flow flame spread and extinction in mixed-convection boundary layers p 168 A90-32841

- Fuel-rich catalytic combustion - A fuel processor for high-speed propulsion
[AIAA PAPER 90-2319] p 105 A90-42774
- Revolutionary opportunities for materials and structures study
[NASA-CR-179642] p 95 N90-10184
- Two-dimensional analysis of two-phase reacting flow in a firing direct-injection diesel engine
[NASA-TM-102069] p 27 N90-13392
- Investigation of flame spread over shallow liquid pools in microgravity and nonair environments
[NASA-TM-102425] p 134 N90-13680
- Analysis of rotary engine combustion processes based on unsteady, three-dimensional computations
[NASA-TM-102469] p 176 N90-13749
- Investigation of methods to produce a uniform cloud of fuel particles in a flame tube
[NASA-TM-102376] p 178 N90-18665
- Detailed mechanism for oxidation of benzene
[NASA-TM-102443] p 106 N90-21842
- High speed commercial transport fuels considerations and research needs
[NASA-TM-102535] p 131 N90-21869
- Fuel-rich catalytic combustion: A fuel processor for high-speed propulsion
[NASA-TM-103177] p 107 N90-23518
- Performance of a supercharged direct-injection stratified-charge rotary combustion engine
[NASA-TM-103105] p 32 N90-25982
- Evaluation of a hybrid kinetics/mixing-controlled combustion model for turbulent premixed and diffusion combustion using KIVA-2
[NASA-TM-103196] p 185 N90-28792
- FUEL CONSUMPTION**
- A circular combustor configuration with multiple injection ports for mixing enhancement p 158 A90-15389
- Minimum fuel trajectories for a low-thrust power-limited mission to the moon and to Lagrange points L4 and L5
[AAS PAPER 89-351] p 40 A90-46784
- Minimum fuel trajectory for the aerospace-plane
[AAS PAPER 89-352] p 40 A90-46785
- Comparison of solution approaches for minimum-fuel, low-thrust, power-limited orbital transfers
[AIAA PAPER 90-2960] p 41 A90-53035
- Optimal cooperative time-fixed impulsive rendezvous
[AIAA PAPER 90-2962] p 41 A90-53037
- Civil air transport: A fresh look at power-by-wire and fly-by-light
[NASA-TM-102574] p 153 N90-21283
- Advanced Turbine Technology Applications Project (ATTAP)
[NASA-CR-185240] p 263 N90-26728
- Energy Efficient Engine acoustic supporting technology report
[NASA-CR-174834] p 33 N90-28557
- Energy Efficient Engine core design and performance report
[NASA-CR-168069] p 34 N90-28559
- Energy Efficient Engine program advanced turbofan nacelle definition study
[NASA-CR-174942] p 34 N90-28560
- Energy Efficient Engine integrated core/low spool design and performance report
[NASA-CR-168211] p 34 N90-28561
- Energy efficient engine program technology benefit/cost study, volume 2
[NASA-CR-174766-VOL-2] p 35 N90-28565
- Energy Efficient Engine: Combustor component performance program
[NASA-CR-179533] p 35 N90-28568
- Energy Efficient Engine: Control system preliminary definition report
[NASA-CR-179578] p 35 N90-28569
- Energy Efficient Engine: High-pressure compressor test hardware detailed design report
[NASA-CR-180850] p 36 N90-28570
- FUEL INJECTION**
- A circular combustor configuration with multiple injection ports for mixing enhancement p 158 A90-15389
- Analysis of rotary engine combustion processes based on unsteady, three-dimensional computations
[AIAA PAPER 90-0643] p 163 A90-22237
- Influence of the continuous and dispersed phases on the symmetry of a gas turbine air-blast atomizer
[ASME PAPER 89-GT-303] p 163 A90-22651
- Effect of vane twist on the performance of dome swirlers for gas turbine airblast atomizers
[AIAA PAPER 90-1955] p 173 A90-47203
- A comparison of analytical results for 20 K LOX/hydrogen instabilities
[AIAA PAPER 90-2241] p 130 A90-47214
- Two-dimensional analysis of two-phase reacting flow in a firing direct-injection diesel engine
[NASA-TM-102069] p 27 N90-13392
- LOX/hydrocarbon combustion instability investigation
[NASA-CR-182249] p 71 N90-13589

- Analysis of rotary engine combustion processes based on unsteady, three-dimensional computations
[NASA-TM-102469] p 176 N90-13749
- Extended temperature range rocket injector
[NASA-CASE-LEW-14846-1] p 73 N90-15130
- A comparison of analytical results for 20 K LOX/hydrogen instabilities
[NASA-TM-103166] p 80 N90-25186
- Effect of vane twist on the performance of dome swirlers for gas turbine airblast atomizers
[NASA-TM-103195] p 182 N90-25289
- Evaluation of a hybrid kinetics/mixing-controlled combustion model for turbulent premixed and diffusion combustion using KIVA-2
[NASA-TM-103196] p 185 N90-28792
- FUEL SPRAYS**
- Influence of the continuous and dispersed phases on the symmetry of a gas turbine air-blast atomizer
[ASME PAPER 89-GT-303] p 163 A90-22651
- N-decane-air droplet combustion experiments in the NASA-Lewis 5 Second Zero-Gravity Facility
[AIAA PAPER 90-0649] p 104 A90-25038
- Introducing the VRT gas turbine combustor
[AIAA PAPER 90-2452] p 21 A90-42808
- Critical evaluation of Jet-A spray combustion using propane chemical kinetics in gas turbine combustion simulated by KIVA-II
[AIAA PAPER 90-2439] p 105 A90-50645
- Microgravity acoustic mixing for particle cloud combustors
[NASA-CR-185159] p 248 N90-21600
- Introducing the VRT gas turbine combustor
[NASA-TM-103176] p 137 N90-23591
- FUEL-AIR RATIO**
- N-decane-air droplet combustion experiments in the NASA-Lewis 5 Second Zero-Gravity Facility
[AIAA PAPER 90-0649] p 104 A90-25038
- A planar reacting shear layer system for the study of fluid dynamics-combustion interaction
[NASA-TM-102422] p 27 N90-13393
- FUNCTIONAL DESIGN SPECIFICATIONS**
- Integrated controls and health monitoring for chemical transfer propulsion
[AIAA PAPER 90-2751] p 52 A90-47229
- Integrated controls and health monitoring for chemical transfer propulsion
[NASA-TM-103185] p 52 N90-25178
- FURANS**
- Bisannulation with a benzo(1,2-c:4,5-c'-prime) difuran equivalent - A new route to linear acene derivatives
p 85 A90-49072

- FURNACES**
- Temperature and melt solid interface control during crystal growth
[NASA-CR-186731] p 259 N90-26664
- G**
- GALACTIC CLUSTERS**
- Cosmic-string-induced hot dark matter perturbations
p 264 A90-25889
- GALACTIC MASS**
- A model for the distribution of dark matter, galaxies, and the intergalactic medium in a cold dark matter-dominated universe
p 266 A90-45560
- GALACTIC STRUCTURE**
- A model for the distribution of dark matter, galaxies, and the intergalactic medium in a cold dark matter-dominated universe
p 266 A90-45560
- GALAXIES**
- Neutron stars and white dwarfs in galactic halos?
p 265 A90-30909
- GALERKIN METHOD**
- Time-dependent viscous incompressible Navier-Stokes equations - The finite difference Galerkin formulation and streamfunction algorithms
p 156 A90-11598
- Discretization formulas for unstructured grids
p 242 A90-26535
- Galerkin finite difference Laplacian operators on isolated unstructured triangular meshes by linear combinations
[NASA-TM-103209] p 183 N90-26276
- GALLIUM ARSENIDE LASERS**
- Mathematical optimization of photovoltaic converters for diode lasers --- for spacecraft power supplies
p 228 A90-38110
- GALLIUM ARSENIDES**
- High frequency GaAlAs modulator and photodetector for phased array antenna applications
p 146 A90-11774
- Molecular beam epitaxial growth of high-quality InSb on InP and GaAs substrates
p 253 A90-12808
- High efficiency GaAs/Ge monolithic tandem solar cells
p 224 A90-14858
- A V-grooved GaAs solar cell
p 225 A90-14887

- Contact formation in gallium arsenide solar cells
p 225 A90-14888
- High altitude current-voltage measurement of GaAs/Ge solar cells
p 226 A90-14910
- An advanced space photovoltaic concentrator array using Fresnel lenses, gallium arsenide cells, and prismatic cell covers
p 54 A90-14954
- Performance of GaAs concentrator cells under electron irradiations from 0.4 to 2.3 MeV
p 227 A90-14956
- Effect of crystal orientation on anisotropic etching and MOCVD growth of grooves on GaAs
p 253 A90-15136
- Interface demarcation in GaAs by current pulsing
[AIAA PAPER 90-0319] p 254 A90-19793
- Free float acceleration measurements aboard NASA's KC-135 Microgravity Research Aircraft
[AIAA PAPER 90-0742] p 132 A90-20000
- A high-speed GaAs MESFET optical controller
p 186 A90-22483
- Convection phenomena in low-gravity processing - The GTE GaAs space experiment
[AIAA PAPER 90-0409] p 133 A90-25032
- Characterization of two MMIC GaAs switch matrices at microwave frequencies
[AIAA PAPER 90-0866] p 147 A90-25686
- Ka-band propagation characteristics of microstrip lines on GaAs substrates at cryogenic temperatures
p 147 A90-33644
- Microwave response of a HEMT photoconductive detector
p 147 A90-37301
- Thermal annealing of GaAs concentrator solar cells --- during electron irradiation
p 60 A90-38150
- The mini-dome lens space concentrator array - Recent component test results and current array development status
p 60 A90-38155
- Optical detectors for GaAs MMIC integration - Technology assessment
p 149 A90-41238
- Control of a GaAs monolithic Ka-band phase shifter using a high-speed optical interconnect
p 150 A90-41700
- Characterization of two MMIC GaAs switch matrices at microwave frequencies
[NASA-TM-102449] p 50 N90-14273
- Peeled film GaAs solar cells for space power
[NASA-TM-103125] p 153 N90-21287
- The 30-GHz monolithic receive module
[NASA-CR-180849] p 146 N90-24528
- Dielectric function of InGaAs in the visible
[NASA-TM-103246] p 260 N90-26683
- GALLIUM PHOSPHIDES**
- Effect of Ga and P dopants on the thermoelectric properties of n-type SiGe
p 256 A90-38140
- GAMMA RAYS**
- Neutron and gamma irradiation effects on power semiconductor switches
[NASA-TM-103200] p 155 N90-25278
- GAS ANALYSIS**
- Requirements for long-life operation of inert gas hollow cathodes - Preliminary results
[AIAA PAPER 90-2586] p 69 A90-52570
- Requirements for long-life operation of inert gas hollow cathodes: Preliminary report
[NASA-TM-103242] p 82 N90-27783
- GAS DETECTORS**
- Requirements for long-life operation of inert gas hollow cathodes - Preliminary results
[AIAA PAPER 90-2586] p 69 A90-52570
- Requirements for long-life operation of inert gas hollow cathodes: Preliminary report
[NASA-TM-103242] p 82 N90-27783
- GAS DYNAMICS**
- Least-squares finite element methods for compressible Euler equations
p 9 A90-51013
- GAS EVOLUTION**
- Integrated regenerative fuel cell experimental evaluation
[NASA-CR-185183] p 230 N90-18808
- GAS FLOW**
- Kinetic theory model for the flow of a simple gas from a two-dimensional nozzle
p 169 A90-37124
- Gas-phase flowrate effect on disintegrating cryogenic liquid-jets
p 173 A90-46895
- Gas-phase flowrate effect on disintegrating cryogenic liquid-jets
[NASA-TM-102357] p 187 N90-11277
- Recent progress in research pertaining to estimates of gas-side heat transfer in an aircraft gas turbine
[NASA-TM-102460] p 27 N90-13394
- TiCl4 as a source of TiO2 particles for laser anemometry measurements in hot gas
[NASA-TM-102581] p 189 N90-20358
- Scattered-light scanner measurements of cryogenic liquid-jet breakup
[NASA-TM-102432] p 189 N90-22021

SUBJECT INDEX

- Optical characterization of clouds of fine liquid-nitrogen particles
[NASA-TM-103208] p 191 N90-26299
- GAS IONIZATION**
High-power xenon ion thrusters
[AIAA PAPER 90-2540] p 64 A90-42536
- GAS JETS**
Gas-phase flowrate effect on disintegrating cryogenic liquid-jets
p 173 A90-46895
Gas-phase flowrate effect on disintegrating cryogenic liquid-jets
[NASA-TM-102357] p 187 N90-11277
Instabilities and subharmonic resonances of subsonic heated round jets, volume 2
[NASA-CR-186058] p 181 N90-22017
Nonlinear interactions in mixing layers and compressible heated round jets
[NASA-CR-186303] p 182 N90-23674
- GAS MIXTURES**
FLUSH: A tool for the design of slush hydrogen flow systems
[NASA-TM-102467] p 130 N90-17890
- GAS PRESSURE**
An annular gas seal analysis using empirical entrance and exit region friction factors
[ASME PAPER 89-TRIB-46] p 196 A90-33555
- GAS TURBINE ENGINES**
Augmented heat transfer in rectangular channels of narrow aspect ratios with rib turbulators
p 157 A90-13091
A circular combustor configuration with multiple injection ports for mixing enhancement
p 158 A90-15389
Reduced chemical kinetics for propane combustion
[AIAA PAPER 90-0546] p 103 A90-19904
Influence of the continuous and dispersed phases on the symmetry of a gas turbine air-blast atomizer
[ASME PAPER 89-GT-303] p 163 A90-22651
An experimental study of turbine vane heat transfer with leading edge and downstream film cooling
[ASME PAPER 89-GT-69] p 165 A90-23792
Low NO(x) potential of gas turbine engines
[AIAA PAPER 90-0550] p 20 A90-25036
Advanced technology's impact on compressor design and development - A perspective
[SAE SP-800] p 20 A90-28571
Design of an air-cooled metallic high-temperature radial turbine
p 20 A90-32960
Fiber reinforced superalloys
p 91 A90-34169
Development of impact design methods for ceramic gas turbine components
p 197 A90-42165
Introducing the VRT gas turbine combustor
[AIAA PAPER 90-2452] p 21 A90-42808
The selection of convertible engines with current gas generator technology for high speed rotorcraft
p 22 A90-46933
Effect of vane twist on the performance of dome swirlers for gas turbine airblast atomizers
[AIAA PAPER 90-1955] p 173 A90-47203
Composite matrix cooling scheme for small gas turbine combustors
[AIAA PAPER 90-2158] p 22 A90-47210
Combustor technology for future aircraft
[AIAA PAPER 90-2400] p 22 A90-47219
Critical evaluation of Jet-A spray combustion using propane chemical kinetics in gas turbine combustion simulated by KIVA-II
[AIAA PAPER 90-2439] p 105 A90-50645
Advanced Turbine Technology Applications Project (ATTAP)
[NASA-CR-185133] p 22 N90-10036
The MHOST finite element program: 3-D inelastic analysis methods for hot section components. Volume 3: Systems' manual
[NASA-CR-182236] p 215 N90-10451
Advanced technologies impact on compressor design and development: A perspective
[NASA-TM-102341] p 24 N90-10891
Constitutive modeling for isotropic materials (HOST)
[NASA-CR-179522] p 26 N90-13390
Constitutive modeling for isotropic materials (HOST)
[NASA-CR-174718] p 26 N90-13391
Recent progress in research pertaining to estimates of gas-side heat transfer in an aircraft gas turbine
[NASA-TM-102460] p 27 N90-13394
Low NO(x) potential of gas turbine engines
[NASA-TM-102452] p 27 N90-17636
Introducing the VRT gas turbine combustor
[NASA-TM-103176] p 137 N90-23591
Effect of vane twist on the performance of dome swirlers for gas turbine airblast atomizers
[NASA-TM-103195] p 182 N90-25289
Elevated temperature crack growth
[NASA-CR-182247] p 222 N90-26355

- Advanced Turbine Technology Applications Project (ATTAP)
[NASA-CR-185240] p 263 N90-26728
Energy Efficient Engine exhaust mixer model technology report addendum, phase 3 test program
[NASA-CR-174799] p 33 N90-28556
Energy Efficient Engine integrated core/low spool design and performance report
[NASA-CR-168211] p 34 N90-28561
Energy Efficient Engine integrated core/low spool test hardware design report
[NASA-CR-168137] p 35 N90-28566
Energy Efficient Engine: High-pressure compressor test hardware detailed design report
[NASA-CR-180850] p 36 N90-28570
- GAS TURBINES**
Some composite bearing and seal materials for gas turbine applications - A review
[ASME PAPER 89-GT-144] p 195 A90-23838
Development of Si3N4 for gas turbine applications
p 122 A90-35509
Three dimensional LDV flow measurements and theoretical investigation in a radial inflow turbine scroll
p 9 A90-46860
Effect of vane twist on the performance of dome swirlers for gas turbine airblast atomizers
[AIAA PAPER 90-1955] p 173 A90-47203
Improved silicon carbide for advanced heat engines
[NASA-CR-180831] p 124 N90-10293
Advanced gearbox technology
[NASA-CR-179625] p 32 N90-24274
Effect of vane twist on the performance of dome swirlers for gas turbine airblast atomizers
[NASA-TM-103195] p 182 N90-25289
Critical evaluation of Jet-A spray combustion using propane chemical kinetics in gas turbine combustion simulated by KIVA-2
[NASA-TM-103173] p 138 N90-26170
Reliability analysis of a structural ceramic combustion chamber
[NASA-TM-103264] p 223 N90-28112
Structural response of SSME turbine blade airfoils
p 224 N90-28649
- GAS VALVES**
Zero-G phase detector and separator
[NASA-CASE-LEW-14844-1] p 190 N90-22024
- GAS-LIQUID INTERACTIONS**
Rate correlation for condensation of pure vapor on turbulent, subcooled liquid
p 174 A90-50511
- GASEOUS DIFFUSION**
Ellipsometric studies of the diffusion of atomic oxygen through silicon dioxide thin films
p 104 A90-36268
- GASEOUS ROCKET PROPELLANTS**
Calculations of gaseous H2/O2 thruster
[AIAA PAPER 90-2490] p 67 A90-47224
Catalytic ignition of hydrogen/oxygen
p 107 N90-28627
- GEAR TEETH**
Comparison of boundary element and finite element methods in spur gear root stress analysis
p 193 A90-21107
Tooth contact shift in loaded spiral bevel gears
p 193 A90-21112
The role of thermal and lubricant boundary layers in the transient thermal analysis of spur gears
p 194 A90-21118
Effects of lubrication on the performance of high speed spur gears
p 194 A90-21119
Lubricant jet flow phenomena in spur and helical gears with modified addendums - For radially directed individual jets
p 194 A90-21122
Computer aided design of spur gear teeth
p 195 A90-21131
Topology of modified helical gears
p 195 A90-21132
Computer aided design of bevel gear tooth surfaces
p 195 A90-21136
Surface pitting fatigue life of noninvolute, low-contact-ratio gears
[AIAA PAPER 90-2153] p 197 A90-42049
Two stage gear tooth dynamics program
[NASA-CR-185110] p 199 N90-10437
Generation and tooth contact analysis of spiral bevel gears with predesigned parabolic functions of transmission errors
p 199 N90-12033
Gear noise, vibration, and diagnostic studies at NASA Lewis Research Center
[NASA-TM-102435] p 202 N90-18041
Theory of gearing
[NASA-RP-1212] p 202 N90-19593
A review of gear housing dynamics and acoustics literature
[NASA-CR-185148] p 203 N90-21387
Transmission research activities at NASA Lewis Research Center
[NASA-TM-103132] p 203 N90-21394
Surface pitting fatigue life of noninvolute, low-contact-ratio gears
[NASA-TM-103116] p 203 N90-22790
Advanced gearbox technology
[NASA-CR-179625] p 32 N90-24274
Computer simulation of gear tooth manufacturing processes
[NASA-CR-185200] p 138 N90-26171
Dynamics of multistage gear transmission with effects of gearbox vibrations
[NASA-TM-103109] p 205 N90-28060
- GEOMAGNETISM**
Computer modeling of current collection by the CHARGE-2 mother payload
p 252 A90-24933
- GEOMETRICAL OPTICS**
High-frequency asymptotic methods for analyzing the EM scattering by open-ended waveguide cavities
[NASA-CR-186244] p 143 N90-16103
- GEOMETRICAL THEORY OF DIFFRACTION**
Constitutive parameter measurements of lossy materials
[NASA-CR-183398] p 257 N90-11603
- GEOMETRY**
Probability of failure and risk assessment of propulsion structural components
p 218 N90-18470
- GEOPOTENTIAL**
The GEM-T2 gravitational model
[NASA-TM-100746] p 234 N90-12984
- GEOSYNCHRONOUS ORBITS**
Lunar production of solar cells - A near-term product for a lunar industrial facility
p 42 A90-24791

GEOSYNCHRONOUS ORBITS

- Surface pitting fatigue life of noninvolute, low-contact-ratio gears
[NASA-TM-103116] p 203 N90-22790
Influence of linear profile modification and loading conditions on the dynamic tooth load and stress of high contact ratio gears
[NASA-TM-103136] p 204 N90-22796
Non-linear dynamic analysis of geared systems, part 2
[NASA-CR-180495] p 204 N90-23732
Computer simulation of gear tooth manufacturing processes
[NASA-CR-185200] p 138 N90-26171
Dynamics of multistage gear transmission with effects of gearbox vibrations
[NASA-TM-103109] p 205 N90-28060
Computer-aided design of high-contact-ratio gears for minimum dynamic load and stress
[NASA-TM-103275] p 205 N90-28065
- GEARS**
Modal analysis of gear housing and mounts
p 192 A90-17018
Efficiency testing of a helicopter transmission planetary reduction stage
p 193 A90-21113
Wear consideration in gear design for space applications
p 194 A90-21121
Dynamic analysis of geared rotors by finite elements
p 194 A90-21123
Vibration signature analysis of multistage gear transmission
p 194 A90-21124
Dynamic loading of spur gears with linear or parabolic tooth profile modifications
p 195 A90-21126
Profile modification to minimize spur gear dynamic loading
p 195 A90-21128
Topology of modified helical gears
p 195 A90-21132
Computer aided design of bevel gear tooth surfaces
p 195 A90-21136
Generation and tooth contact analysis of spiral bevel gears with predesigned parabolic functions of transmission errors
[NASA-CR-4259] p 199 N90-12033
Vibration transmission through rolling element bearings in geared rotor system, part 1
[NASA-CR-186093] p 199 N90-12936
An investigation of gear mesh failure prediction techniques
[NASA-TM-102340] p 200 N90-13785
Assessment of worm gearing for helicopter transmissions
[NASA-TM-102441] p 27 N90-15923
Dynamic analysis of geared rotors by finite elements
[NASA-TM-102349] p 201 N90-16286
Gear noise, vibration, and diagnostic studies at NASA Lewis Research Center
[NASA-TM-102435] p 202 N90-18041
Theory of gearing
[NASA-RP-1212] p 202 N90-19593
Bearing and gear steels for aerospace applications
[NASA-TM-102529] p 202 N90-20391
A review of gear housing dynamics and acoustics literature
[NASA-CR-185148] p 203 N90-21387
Transmission research activities at NASA Lewis Research Center
[NASA-TM-103132] p 203 N90-21394
Surface pitting fatigue life of noninvolute, low-contact-ratio gears
[NASA-TM-103116] p 203 N90-22790
Advanced gearbox technology
[NASA-CR-179625] p 32 N90-24274
Computer simulation of gear tooth manufacturing processes
[NASA-CR-185200] p 138 N90-26171
Dynamics of multistage gear transmission with effects of gearbox vibrations
[NASA-TM-103109] p 205 N90-28060
- GEOMAGNETISM**
Computer modeling of current collection by the CHARGE-2 mother payload
p 252 A90-24933
- GEOMETRICAL OPTICS**
High-frequency asymptotic methods for analyzing the EM scattering by open-ended waveguide cavities
[NASA-CR-186244] p 143 N90-16103
- GEOMETRICAL THEORY OF DIFFRACTION**
Constitutive parameter measurements of lossy materials
[NASA-CR-183398] p 257 N90-11603
- GEOMETRY**
Probability of failure and risk assessment of propulsion structural components
p 218 N90-18470
- GEOPOTENTIAL**
The GEM-T2 gravitational model
[NASA-TM-100746] p 234 N90-12984
- GEOSYNCHRONOUS ORBITS**
Lunar production of solar cells - A near-term product for a lunar industrial facility
p 42 A90-24791

- Advanced propulsion for LEO and GEO platforms
[AIAA PAPER 90-2551] p 68 A90-52565
Numerical Arc Segmentation Algorithm for a Radio
Conference (NASARC), version 4.0: User's manual
[NASA-TM-101454] p 145 N90-21250
Plasma interactions and effects for large systems
p 252 N90-25545
Advanced propulsion for LEO and GEO platforms
[NASA-TM-103228] p 82 N90-27785
- GERMANIUM**
High efficiency GaAs/Ge monolithic tandem solar
cells p 224 A90-14858
- GERMANIUM ALLOYS**
Effect of Ga and P dopants on the thermoelectric
properties of n-type SiGe p 256 A90-38140
- GET AWAY SPECIALS (STS)**
Flight experiment of thermal energy storage --- for
spacecraft power systems p 61 A90-38172
Design and test of a compact optics system for the
pool boiling experiment
[NASA-TM-102530] p 135 N90-20253
- GIBBS FREE ENERGY**
Stress versus temperature dependent activation
energies in creep
[NASA-TM-103192] p 221 N90-23773
- GLASS**
Glass-derived superconducting ceramics with zero
resistance at 107 K in the Bi(1.5)Pb(0.5)Sr₂Ca₂Cu₃O(x)
system p 253 A90-11491
Microstructural changes in beta-silicon nitride grains
upon crystallizing the grain-boundary glass
p 120 A90-13230
Crystallization kinetics of BaO-Al₂O₃-SiO₂ glasses
p 121 A90-21175
Superconducting glass-ceramics in the Bi-Sr-Ca-Cu-O
system p 256 A90-35153
Crystallization behavior and properties of
BaO-Al₂O₃-2SiO₂ glass matrices p 95 A90-51933
Preparation of 110K (Bi, Pb)-Sr-Ca-Cu-O superconductor
from glass precursor p 258 N90-14108
Superconducting Bi_{1.5}Pb_{0.5}Sr₂Ca₂Cu₃O(x) ceramics
by rapid melt quenching and glass crystallization
[NASA-CR-185184] p 258 N90-17465
Crystallization behavior and properties of
BaO-Al₂O₃-2SiO₂ glass matrices p 127 N90-19374
Instantaneously generated foam and its applicability to
reduced gravity p 135 N90-20237
- GLASS COATINGS**
Superconducting ceramics in the Bi_{1.5}SrCaCu₂O sub
x system by melt quenching technique
[NASA-CR-185139] p 258 N90-11606
- GLASS FIBER REINFORCED PLASTICS**
Evaluation of atomic oxygen resistant protective
coatings for fiberglass-epoxy composites in LEO
p 84 A90-31581
- GLASS TRANSITION TEMPERATURE**
The 3F condensation polyimides: Review and update
[NASA-TM-102353] p 126 N90-14363
- GLOW DISCHARGES**
Advances and directions of ion nitriding/carburizing
[NASA-TM-102398] p 137 N90-11902
- GLYCEROLS**
Experimental investigation of convective stability in a
superposed fluid and porous layer when heated from
below p 158 A90-15947
- GOLD**
The kinetics of the Au-InP interaction p 254 A90-25084
Deep-level dominated electrical characteristics of Au
contacts on beta-SiC p 147 A90-33726
Humidity-induced room-temperature decomposition of
Au contacted indium phosphide p 105 A90-44689
Lateral spreading of Au contacts on InP p 232 N90-22843
[NASA-TM-103133] p 232 N90-22843
An analysis of the contact sintering process in III-V solar
cells [NASA-TM-103179] p 233 N90-25420
Synthesis and structural chemistry of Au(III)-substituted
Ba₂Cu₃O(7-delta) p 108 N90-28696
[NASA-TM-103292] p 108 N90-28696
XANES and EXAFS study of Au-substituted
YBa₂Cu₃O(7-delta) p 260 N90-29219
[NASA-TM-103291] p 260 N90-29219
- GOLD ALLOYS**
Side branch morphology and coarsening in directionally
solidified Pb-8.4 at. pct Au p 109 A90-11658
Contact spreading and the Au₃In-to-Au₅In₄ transition
in the Au-InP system p 257 A90-48661
- GRADIENTS**
Profile modification to minimize spur gear dynamic
loading p 195 A90-21128
- GRAIN BOUNDARIES**
Microstructural changes in beta-silicon nitride grains
upon crystallizing the grain-boundary glass p 120 A90-13230
Characterization of failure processes in tungsten copper
composites under fatigue loading conditions
[NASA-TM-102371] p 98 N90-21123
High-temperature deformation and microstructural
analysis for Si₃N₄-SiC₂O₃ p 130 N90-28740
[NASA-TM-103239] p 130 N90-28740
- GRAIN SIZE**
Side branch morphology and coarsening in directionally
solidified Pb-8.4 at. pct Au p 109 A90-11658
- GRAND TOURS**
The Gervallig: An inertial fusion powered manned
spacecraft design for outer solar system missions
[NASA-CR-185163] p 50 N90-15985
- GRAPHITE**
Density of intercalated graphite fibers p 124 A90-49061
PMR graphite engine duct development
[NASA-CR-182228] p 23 N90-10037
Density of intercalated graphite fibers
[NASA-TM-102411] p 126 N90-14362
Fluorinated graphite fibers as a new engineering
material: Promises and challenges
[NASA-TM-102511] p 86 N90-19301
Resistivity of pristine and intercalated graphite fiber
epoxy composites [NASA-TM-102576] p 128 N90-21192
- GRAPHITE-EPOXY COMPOSITES**
Impact damage development in damaged composite
materials p 193 A90-18355
Measurements of print-through in graphite fiber epoxy
composites p 91 A90-31555
Vapor grown carbon fiber for space thermal
management systems p 94 A90-50128
Probabilistic simulation of uncertainties in composite
uniaxial strengths p 97 N90-16008
[NASA-TM-102483] p 97 N90-16008
Reliability analysis of continuous fiber composite
laminates [NASA-CR-185265] p 223 N90-26372
Improved transverse crack detection in composites
[NASA-TM-103261] p 102 N90-27875
Ultrasonic verification of five wave fronts in unidirectional
graphite epoxy composite [NASA-CR-185288] p 208 N90-28858
- GRAPHITIZATION**
Brominated graphitized carbon fibers
[NASA-CASE-LEW-14698-2] p 126 N90-15262
Fluorinated graphite fibers as a new engineering
material: Promises and challenges
[NASA-TM-102511] p 86 N90-19301
- GRAVIMETRY**
The GEM-T2 gravitational model
[NASA-TM-100746] p 234 N90-12984
- GRAVITATIONAL EFFECTS**
Salt-finger convection under reduced gravity
[AIAA PAPER 90-0122] p 160 A90-19693
Effects of g-jitter on a thermal, buoyant flow
[AIAA PAPER 90-0653] p 163 A90-22239
The possibility of a reversal of material flammability
ranking from normal gravity to microgravity p 105 A90-42298
Facilities for microgravity combustion research
[NASA-TM-102014] p 134 N90-13679
Data compression for the microgravity experiments
p 188 N90-16212
Non-contact temperature measurements in support of
microgravity combustion experiments p 135 N90-17900
A new approach to active vibration isolation for
microgravity space experiments
[NASA-TM-102470] p 137 N90-17929
Instantaneously generated foam and its applicability to
reduced gravity [NASA-CR-185208] p 135 N90-20237
Spacelab qualified infrared imager for microgravity
science experiments [NASA-TM-102503] p 189 N90-20352
The role of gravity on macrosegregation in alloys
[NASA-CR-186530] p 136 N90-25238
New findings and instrumentation from the NASA Lewis
microgravity facilities [NASA-TM-103189] p 136 N90-26163
Development and approach to low-frequency
microgravity isolation systems [NASA-TP-2984] p 138 N90-28754
- GRAVITATIONAL FIELDS**
Shear stabilization of the capillary breakup of a cylindrical
interface [AD-A219268] p 159 A90-15758
Gravitational couplings of the inflation in extended
inflation p 265 A90-40088
- Optimal impulsive time-fixed orbital rendezvous and
interception with path constraints [AIAA PAPER 90-2972] p 41 A90-53051
The GEM-T2 gravitational model
[NASA-TM-100746] p 234 N90-12984
- GREEN'S FUNCTIONS**
Green's functions for dislocations in bonded strips and
related crack problems [NASA-CR-185291] p 224 N90-28878
- GRID GENERATION (MATHEMATICS)**
Improvement of finite element meshes - Heat transfer
in an infinite cylinder p 209 A90-19109
Fully elliptic incompressible flow calculations on regular
grid by a new pressure substitution method
[AIAA PAPER 90-0239] p 160 A90-19749
An interactive grid generation procedure for axial and
radial flow turbomachinery [AIAA PAPER 90-0344] p 162 A90-22200
Finite element mesh refinement criteria for stress
analysis p 209 A90-23013
Application of a lower-upper implicit scheme and an
interactive grid generation for turbomachinery flow field
simulations [ASME PAPER 89-GT-20] p 4 A90-23762
A 'transient' automated mapping procedure for complex
geometries p 242 A90-26499
Three-dimensional adaptive grid generation for
body-fitted coordinate system p 167 A90-26506
Interactive grid generation for turbomachinery flow field
simulations p 6 A90-26553
Computation of turbine flowfields with a Navier-Stokes
code [AIAA PAPER 90-2122] p 8 A90-42731
Grid generation for the solution of partial differential
equations p 237 A90-47188
An interactive grid generation procedure for axial and
radial flow turbomachinery [NASA-CR-185167] p 237 N90-13968
User's guide to PMESH: A grid-generation program for
single-rotation and counterrotation advanced turboprops
[NASA-CR-185156] p 235 N90-14783
Mesh refinement in finite element analysis by
minimization of the stiffness matrix trace
[NASA-CR-185170] p 201 N90-15434
A simple algebraic grid adaptation scheme with
applications to two- and three-dimensional flow
problems [NASA-TM-102446] p 178 N90-18667
GRID2D/3D: A computer program for generating grid
systems in complex-shaped two- and three-dimensional
spatial domains. Part 2: User's manual and program
listing [NASA-TM-102454] p 237 N90-20708
GRID2D/3D: A computer program for generating grid
systems in complex-shaped two- and three-dimensional
spatial domains. Part 1: Theory and method
[NASA-TM-102453] p 238 N90-22262
The fundamentals of adaptive grid movement
p 185 N90-29610
- GROOVES**
A V-grooved GaAs solar cell p 225 A90-14887
- GROOVING**
GaAs solar cells with V-grooved emitters
p 229 N90-17754
- GROUND EFFECT (AERODYNAMICS)**
Engine inlet distortion in a 9.2 percent scaled vectored
thrust STOVL model in ground effect [AIAA PAPER 89-2910] p 5 A90-25043
Hot gas environment around STOVL aircraft in ground
proximity. II - Numerical study [AIAA PAPER 90-2270] p 21 A90-42766
Three-dimensional turbulent flow code calculations of
hot gas ingestion p 21 A90-44726
Engine inlet distortion in a 9.2 percent scale vectored
thrust STOVL model in ground effect [NASA-TM-102358] p 12 N90-17561
- GROUND STATIONS**
LBR-2 earth stations for the ACTS program
[AIAA PAPER 90-0838] p 42 A90-25662
On-board switching and processing p 150 A90-51168
- GROUND TESTS**
Initial results from the joint NASA-Lewis/U.S. Army icing
flight research tests p 16 A90-28180
Theory of plasma contactors in ground-based
experiments and low earth orbit p 150 A90-47108
Full scale technology demonstration of a modern
counterrotating ducted fan engine concept. Engine
test [NASA-CR-180869] p 24 N90-10049
NASA's program on icing research and technology
p 16 N90-15062
- GROUND WIND**
Aeolian removal of dust from radiator surfaces on
Mars [NASA-TM-103205] p 81 N90-26068

SUBJECT INDEX

GUIDE VANES

Two-component phase-averaged turbulence statistics downstream of a rotating spoke-wheel wake generator p 156 A90-11559

GUN LAUNCHERS

A superconducting quenchgun for delivering lunar derived oxygen to lunar orbit p 77 N90-21806 [NASA-CR-185161]

GUST LOADS

Gust response analysis for cascades operating in nonuniform mean flows p 28 N90-18415

GUSTS

Development of a linearized unsteady aerodynamic analysis for cascade gust response predictions [NASA-CR-4308] p 14 N90-27655

H

HADRONS

Big bang nucleosynthesis and the quark-hadron transition p 265 A90-31407

HAFNIUM

Oxidation behavior of FeAl + Hf,Zr,B p 113 A90-24858

HALIDES

Studies on the use of supercritical ammonia for ceramic nitride synthesis and fabrication [NASA-TM-102570] p 106 N90-21843

HALL EFFECT

End-hall thrusters [AIAA PAPER 90-2595] p 64 A90-42570

HALOS

Neutron stars and white dwarfs in galactic halos? p 265 A90-30909

HARMONIC CONTROL

Phase development and its role on subharmonic control [AIAA PAPER 90-0503] p 166 A90-25035

HARMONICS

Distortion and regulation characterization of a Mapham inverter p 148 A90-38125

Nonlinear interactions in mixing layers and compressible heated round jets [NASA-CR-186303] p 182 N90-23674

HARTREE APPROXIMATION

Phase transitions in fermionic systems with many-body interaction p 249 A90-19303

HEAD MOVEMENT

A geometric analysis of semicircular canals and induced activity in their peripheral afferents in the rhesus monkey p 234 A90-28084

HEAD-UP DISPLAYS

Cooperative synthesis of control and display augmentation in approach and landing p 36 A90-33061

HEAT EXCHANGERS

Two-dimensional numerical simulation of a Stirling engine heat exchanger p 170 A90-38290

Numerical investigation of the thermal stratification in cryogenic tanks subjected to wall heat flux [AIAA PAPER 90-2375] p 175 A90-52500

Two-dimensional model of a Space Station Freedom thermal energy storage canister [NASA-TM-103124] p 183 N90-26279

Numerical investigation of the thermal stratification in cryogenic tanks subjected to wall heat flux [NASA-TM-103194] p 184 N90-27984

HEAT FLUX

Heat flux measurements [ASME PAPER 89-GT-107] p 165 A90-23815

Phase and time-resolved measurements of unsteady heat transfer and pressure in a full-stage rotating turbine [ASME PAPER 89-GT-135] p 165 A90-23832

A technique for measurement of instantaneous heat transfer in steady-flow ambient-temperature facilities p 172 A90-39625

Mathematical modeling and analysis of heat pipe start-up from the frozen state p 174 A90-48404

Numerical investigation of the thermal stratification in cryogenic tanks subjected to wall heat flux [AIAA PAPER 90-2375] p 175 A90-52500

Heat transfer to throat tubes in a square-chambered rocket engine at the NASA Lewis Research Center [NASA-TM-102336] p 70 N90-11082

Thermal modelling of various thermal barrier coatings in a high heat flux rocket engine [NASA-TM-102418] p 117 N90-16911

Numerical investigation of the thermal stratification in cryogenic tanks subjected to wall heat flux [NASA-TM-103194] p 184 N90-27984

HEAT MEASUREMENT

Heat flux measurements [ASME PAPER 89-GT-107] p 165 A90-23815

Phase and time-resolved measurements of unsteady heat transfer and pressure in a full-stage rotating turbine [ASME PAPER 89-GT-135] p 165 A90-23832

A technique for measurement of instantaneous heat transfer in steady-flow ambient-temperature facilities p 172 A90-39625

HEAT PIPES

The cavity heat pipe Stirling receiver for space solar dynamics p 61 A90-38169

Comparison of conceptual designs for 25 kW advanced Stirling conversion systems for dish electric applications p 229 A90-38254

Initial characterization of a modular heat exchanger with an integral heat pipe --- for Stirling space engine p 62 A90-38301

Mathematical modeling and analysis of heat pipe start-up from the frozen state p 174 A90-48404

An improved algorithm for the modeling of vapor flow in heat pipes p 176 N90-13748 [NASA-CR-185179]

A heat receiver design for solar dynamic space power systems [NASA-TM-102473] p 72 N90-14283

Transient characteristics of a grooved water heat pipe with variable heat load [NASA-CR-185280] p 183 N90-26272

HEAT PUMPS

Feasibility analysis of reciprocating magnetic heat pumps [NASA-CR-186205] p 177 N90-15363

HEAT RADIATORS

Conceptual design of a Liquid Droplet Radiator space flight experiment [SAE PAPER 891565] p 48 A90-27527

Scaling results for the liquid sheet radiator p 170 A90-38037

Two-tiered design analysis of a radiator for a solar dynamic powered Stirling engine p 60 A90-38158

SP-100 advanced radiator designs for thermoelectric and Stirling applications p 62 A90-38202

Aeolian removal of dust from radiator surfaces on Mars [NASA-TM-103205] p 81 N90-26068

The effects of atomic oxygen on the thermal emittance of high temperature radiator surfaces [NASA-TM-103224] p 102 N90-28670

HEAT RESISTANT ALLOYS

The high temperature deformation in cyclic loading of a single crystal nickel-base superalloy p 108 A90-11534

The correlation between the temperature dependence of the CRSS and the formation of superlattice-intrinsic stacking faults in the nickel-base superalloy PWA 1480 --- critical resolved shear stress p 109 A90-11657

High temperature inelastic deformation under uniaxial loading - Theory and experiment p 109 A90-13838

Properties of oxide dispersion strengthened alloys p 109 A90-14687

Analysis of gamma prime shape changes in a single crystal Ni-base superalloy p 109 A90-15206

Biaxial constitutive modelling and testing of a single crystal superalloy at elevated temperatures p 110 A90-16741

The unusual near-threshold FCG behavior of a single crystal superalloy and the resolved shear stress as the crack driving force p 111 A90-21009

Mass spectrometric observations of metal oxychlorides produced by oxidation-chlorination reactions p 103 A90-21215

High temperature inelastic deformation of the B1900 + Hf alloy under multiaxial loading - Theory and experiment p 112 A90-22656

Influence of molybdenum on the creep properties of nickel-base superalloy single crystals p 113 A90-25233

A crystallographic model for the tensile and fatigue response for Rene N4 at 982 C p 114 A90-28754

A constitutive model for the inelastic multiaxial response of Rene 80 at 871 C and 982 C p 114 A90-32266

The role of interfacial dislocation networks in high temperature creep of superalloys p 114 A90-33329

Resources - Supply and availability --- of superalloys for United States aerospace industry p 114 A90-34152

Cyclic deformation, fatigue and fatigue crack propagation in Ni-base alloys p 115 A90-34162

Fiber reinforced superalloys p 91 A90-34169

Coarsening in high volume fraction nickel-base alloys p 115 A90-37719

Materials Park, OH p 85 A90-39975

Filter clogging by the extracted gamma prime and its measurement p 116 A90-45620

1300 K compressive properties of several dispersion strengthened NiAl materials p 116 A90-47091

Fatigue crack propagation behavior of a single crystalline superalloy p 116 A90-48635

Constitutive modeling for isotropic materials (HOST) [NASA-CR-179522] p 26 N90-13390

Constitutive modeling for isotropic materials (HOST) [NASA-CR-174718] p 26 N90-13391

Calibration approach to electron probe microanalysis: A study with PWA-1480, a nickel base superalloy [NASA-TM-102393] p 117 N90-14335

Thermal fatigue durability for advanced propulsion materials [NASA-TM-102348] p 216 N90-14641

Attachment of lead wires to thin film thermocouples mounted on high temperature materials using the parallel gap welding process [NASA-TM-102442] p 189 N90-21361

Micromechanics of cyclic deformation in SSME turbopump blade materials p 224 N90-28641

High temperature fatigue behavior of Haynes 188 p 119 N90-28642

Constitutive and life modeling of single crystal blade alloys for root attachment analysis p 119 N90-28643

The fatigue damage behavior of a single crystal superalloy p 120 N90-28644

HEAT STORAGE

Thermal energy storage flight experiments p 53 A90-11992

Flight experiment of thermal energy storage --- for spacecraft power systems p 61 A90-38172

A heat receiver design for solar dynamic space power systems [NASA-TM-102473] p 72 N90-14283

Selection of phase-change and containment materials for thermal energy storage [NASA-CR-186228] p 229 N90-15506

Mechanical properties of pure nickel alloys after long term exposures to LiOH and vacuum at 775 K [NASA-TM-102403] p 118 N90-20181

Analysis of thermal energy storage material with change-of-phase volumetric effects [NASA-TM-102457] p 181 N90-21974

Two-dimensional model of a Space Station Freedom thermal energy storage canister [NASA-TM-103124] p 183 N90-26279

HEAT TRANSFER

Augmented heat transfer in rectangular channels of narrow aspect ratios with rib turbulators p 157 A90-13091

The modelling of heat, mass and solute transport in solidification systems p 157 A90-13092

Inverse heat transfer analysis of Bridgman crystal growth p 157 A90-13093

Improvement of finite element meshes - Heat transfer in an infinite cylinder p 209 A90-19109

Computation of three-dimensional turbulent boundary layers with heat transfer in a plane of symmetry using embedded wall-layer functions [AIAA PAPER 90-0307] p 160 A90-19788

Unsteady heat transfer on turbine blades p 161 A90-20511

Effects of g-jitter on a thermal, buoyant flow [AIAA PAPER 90-0653] p 163 A90-22239

An experimental study of turbine vane heat transfer with leading edge and downstream film cooling [ASME PAPER 89-GT-69] p 165 A90-23792

Phase and time-resolved measurements of unsteady heat transfer and pressure in a full-stage rotating turbine [ASME PAPER 89-GT-135] p 165 A90-23832

Experimental determination of stator endwall heat transfer [ASME PAPER 89-GT-219] p 165 A90-23880

Pressure drop and mass transfer in two-pass ribbed channels p 165 A90-24837

Simulating transitional flow and heat transfer over the flat plate and circular cylinder using a K-epsilon turbulence model p 168 A90-32171

Some characteristics of bypass transition in a heated boundary layer p 169 A90-35183

A technique for measurement of instantaneous heat transfer in steady-flow ambient-temperature facilities p 172 A90-39625

Enhanced heat transfer rocket combustor technology component hot-fire test results [AIAA PAPER 90-2182] p 64 A90-42063

Rate correlation for condensation of pure vapor on turbulent, subcooled liquid p 174 A90-50511

Numerical investigation of the thermal stratification in cryogenic tanks subjected to wall heat flux [AIAA PAPER 90-2375] p 175 A90-52500

Heat transfer to throat tubes in a square-chambered rocket engine at the NASA Lewis Research Center [NASA-TM-102336] p 70 N90-11082

Recent progress in research pertaining to estimates of gas-side heat transfer in an aircraft gas turbine [NASA-TM-102460] p 27 N90-13394

HEAT TRANSFER COEFFICIENTS

SUBJECT INDEX

- Conceptual design of a moving belt radiator shuttle-attached experiments: Technical requirement Document
[NASA-CR-185168] p 73 N90-15996
- Thermal modelling of various thermal barrier coatings in a high heat flux rocket engine
[NASA-TM-102418] p 117 N90-16911
- Viscous three-dimensional analyses for nozzles for hypersonic propulsion
[NASA-CR-185197] p 27 N90-17635
- Design and test of a compact optics system for the pool boiling experiment
[NASA-TM-102530] p 135 N90-20253
- Ultrasonic techniques for aircraft ice accretion measurement
p 16 N90-20926
- Users manual for the NASA Lewis Ice Accretion Prediction Code (LEWICE)
[NASA-CR-185129] p 1 N90-20943
- Navier-Stokes analysis of turbine blade heat transfer
[NASA-TM-102496] p 179 N90-21300
- ULTRA-SHARP nonoscillatory convection schemes for high-speed steady multidimensional flow
[NASA-TM-102568] p 244 N90-21570
- WINCOF-I code for prediction of fan compressor unit with water ingestion
[NASA-CR-185157] p 1 N90-21724
- Heat transfer and pressure measurements for the SSME fuel-side turbopump
[NASA-CR-184928] p 31 N90-23405
- Performance of a supercharged direct-injection stratified-charge rotary combustion engine
[NASA-TM-103105] p 32 N90-25982
- Prediction of the ullage gas thermal stratification in a NASP vehicle propellant tank experimental simulation using FLOW-3D
[NASA-TM-103217] p 131 N90-26160
- Transient characteristics of a grooved water heat pipe with variable heat load
[NASA-CR-185280] p 183 N90-26272
- Two-dimensional model of a Space Station Freedom thermal energy storage canister
[NASA-TM-103124] p 183 N90-26279
- Preliminary designs for 25 kW advanced Stirling conversion systems for dish electric applications
[NASA-TM-103186] p 263 N90-26729
- Computer code for predicting coolant flow and heat transfer in turbomachinery
[NASA-TP-2985] p 32 N90-27722
- Numerical investigation of the thermal stratification in cryogenic tanks subjected to wall heat flux
[NASA-TM-103194] p 184 N90-27984
- ### HEAT TRANSFER COEFFICIENTS
- Convective heat transfer measurements from a NACA 0012 airfoil in flight and in the NASA Lewis Icing Research Tunnel
[AIAA PAPER 90-0199] p 162 A90-22180
- Heat transfer on accreting ice surfaces
[AIAA PAPER 90-0200] p 162 A90-22181
- Effects of very high turbulence on heat transfer
p 169 A90-35247
- Convective heat transfer measurements from a NACA 0012 airfoil in flight and in the NASA Lewis Icing Research Tunnel
[NASA-TM-102448] p 176 N90-13750
- Ultrasonic techniques for aircraft ice accretion measurement
p 16 N90-20926
- ### HEAT TREATMENT
- Effect of heat-treatment temperature of vapor-grown graphite fibers. I - Properties of their bromine intercalation compounds
p 120 A90-16279
- Filter clogging by the extracted gamma prime and its measurement
p 116 A90-45620
- Crystallization behavior and properties of BaO-Al₂O₃-2SiO₂ glass matrices
[NASA-CR-185209] p 127 N90-19374
- ### HEATING
- Thermomechanical testing techniques for high-temperature composites: TMF behavior of SiC(SCS-6)/Ti-15-3
[NASA-TM-103171] p 222 N90-25367
- ### HELICOPTER ENGINES
- Efficiency testing of a helicopter transmission planetary reduction stage
p 193 A90-21113
- ### HELICOPTER PROPELLER DRIVE
- Efficiency study comparing two helicopter planetary reduction stages
[AIAA PAPER 90-2156] p 199 A90-50644
- ### HELICOPTER TAIL ROTORS
- Icing Research Tunnel test of a model helicopter rotor
p 15 A90-28179
- ### HELICOPTERS
- Effect of advanced component technology on helicopter transmissions
p 193 A90-21115
- Assessment of worm gearing for helicopter transmissions
[NASA-TM-102441] p 27 N90-15923
- ### HELIUM IONS
- Radiation resistance studies of amorphous silicon films
p 227 A90-14952
- ### HELIUM ISOTOPES
- Results of an attempt to measure increased rates of the reaction D-2 + D-2 yields He-3 + n in a nonelectrochemical cold fusion experiment
[NASA-TM-102430] p 250 N90-17424
- ### HELIUM PLASMA
- Diagnostic evaluations of microwave generated helium and nitrogen plasma mixtures
[AIAA PAPER 90-2634] p 252 A90-42602
- ### HELIUM-NEON LASERS
- Fiber optic detector probes for laser light scattering
p 192 A90-11593
- ### HESSIAN MATRICES
- Application of symbolic computations to the constitutive modeling of structural materials
[NASA-TM-103225] p 222 N90-26364
- ### HETEROJUNCTION DEVICES
- AlGaAs/InGaAs heterostructures with doped channels for discrete devices and monolithic amplifiers
p 146 A90-20861
- Wide-bandgap epitaxial heterojunction windows for silicon solar cells
p 227 A90-28359
- Doped-channel heterojunction structures for millimeter-wave discrete devices and MMICs
p 150 A90-48492
- The photovoltaic properties of an Al In As/InP heterojunctions grown by LPE method
[NASA-CR-185996] p 229 N90-13886
- ### HETEROJUNCTIONS
- Thin, light-trapping silicon solar cells for space
p 226 A90-14900
- ### HEURISTIC METHODS
- A heuristic approach to worst-case carrier-to-interference ratio maximization in satellite system synthesis
[AIAA PAPER 90-0816] p 46 A90-25639
- Application of a hybrid generation/utility assessment heuristic to a class of scheduling problems
[NASA-TM-102367] p 245 N90-10674
- ### HIGH ALTITUDE
- High altitude current-voltage measurement of GaAs/Ge solar cells
p 226 A90-14910
- ### HIGH ELECTRON MOBILITY TRANSISTORS
- Microwave response of a HEMT photoconductive detector
p 147 A90-37301
- ### HIGH ENERGY PROPELLANTS
- High energy-density liquid rocket fuel performance
[NASA-CR-185279] p 131 N90-28742
- ### HIGH FREQUENCIES
- High frequency GaAlAs modulator and photodetector for phased array antenna applications
p 146 A90-11774
- High power, high frequency component test facility
[NASA-TM-102500] p 151 N90-19484
- High frequency, high temperature specific core loss and dynamic B-H hysteresis loop characteristics of soft magnetic alloys
[NASA-TM-103164] p 154 N90-23663
- ### HIGH REYNOLDS NUMBER
- Compressibility effects in free shear layers
[AIAA PAPER 90-0705] p 161 A90-19984
- Numerical simulation of thermocapillary bubble migration under microgravity for large Reynolds and Marangoni numbers
p 164 A90-23213
- Effects of compressibility on the characteristics of free shear layers
p 6 A90-25285
- Comparison between pressure gradient method and MAC method on high Re calculation
p 172 A90-44462
- ### HIGH SPEED
- Efficient real gas Navier-Stokes computations of high speed flows using an LU scheme
[AIAA PAPER 90-0391] p 164 A90-23706
- Fuel-rich catalytic combustion - A fuel processor for high-speed propulsion
[AIAA PAPER 90-2319] p 105 A90-42774
- Large-scale Advanced Prop-fan (LAP) high speed wind tunnel test report
[NASA-CR-182125] p 24 N90-10045
- Efficient real gas Navier-Stokes computations of high speed flows using an LU scheme
[NASA-TM-102429] p 11 N90-14203
- Fuel-rich catalytic combustion: A fuel processor for high-speed propulsion
[NASA-TM-103177] p 107 N90-23518
- ### HIGH SPEED PHOTOGRAPHY
- A high-speed photography study of cavitation in a dynamically loaded journal bearing
[NASA-TM-103178] p 204 N90-26338
- ### HIGH STRENGTH ALLOYS
- Properties of oxide dispersion strengthened alloys
p 109 A90-14687
- Materials Park, OH
p 85 A90-39975
- ### MATE (Materials for Advanced Turbine Engines) Program, Project 3. Volume 2: Design, fabrication and evaluation of an oxide dispersion strengthened sheet alloy combustor liner [NASA-CR-180892] p 117 N90-17868 HIGH TEMPERATURE The high temperature creep deformation of Si₃N₄-6Y₂O₃-2Al₂O₃ p 121 A90-18879 Total temperature effects on centerline Mach number characteristics of freejets p 6 A90-25290 Effects of state recovery on creep buckling under variable loading p 212 A90-41223 Spray automated balancing of rotors - How process parameters influence performance p 198 A90-46228 Materials for engine applications above 3000 deg F: An overview [NASA-TM-100169] p 95 N90-10188 Electrical properties of materials for high temperature strain gage applications [NASA-CR-186192] p 188 N90-14534 High temperature, flexible, thermal barrier seal [NASA-CASE-LEW-14672-1] p 201 N90-15444 The application of a computer data acquisition system for a new high temperature tribometer [NASA-TM-102508] p 86 N90-17811 Prediction of high temperature metal matrix composite ply properties [NASA-TM-102490] p 97 N90-17817 Demonstration of capabilities of high temperature composites analyzer code HITCAN [NASA-TM-102560] p 219 N90-19629 Fundamental aspects of and failure modes in high-temperature composites [NASA-TM-102558] p 98 N90-20151 High temperature fatigue behavior of tungsten copper composites [NASA-TM-102404] p 99 N90-21138 High frequency, high temperature specific core loss and dynamic B-H hysteresis loop characteristics of soft magnetic alloys [NASA-TM-103164] p 154 N90-23663 High temperature flexible seal [NASA-CASE-LEW-14695-1] p 204 N90-23751 Rapid thermal processing of high temperature superconducting fiber [NASA-CR-186803] p 259 N90-24964 Feasibility study for the advanced one-dimensional high temperature optical strain measurement system, phase 3 [NASA-CR-185254] p 191 N90-25324 Thermomechanical testing techniques for high-temperature composites: TMF behavior of SiC(SCS-6)/Ti-15-3 [NASA-TM-103171] p 222 N90-25367 Extension of a noninteractive reliability model for ceramic matrix composites [NASA-CR-185267] p 129 N90-26142 Elevated temperature crack growth [NASA-CR-182247] p 222 N90-26355 Application of symbolic computations to the constitutive modeling of structural materials [NASA-TM-103225] p 222 N90-26364 Progress in high temperature speckle-shift strain measurement system [NASA-TM-103255] p 191 N90-28031 The effects of atomic oxygen on the thermal emittance of high temperature radiator surfaces [NASA-TM-103224] p 102 N90-28670 Improved silicon carbide for advanced heat engines [NASA-CR-182186] p 129 N90-28735 High-temperature deformation and microstructural analysis for Si₃N₄-Sc₂O₃ [NASA-TM-103239] p 130 N90-28740 High temperature superconducting thin film microwave circuits: Fabrication, characterization, and applications [NASA-TM-103235] p 156 N90-28786 HIGH TEMPERATURE ENVIRONMENTS Designing ceramic components with the CARES computer program p 235 A90-19147 X-ray beam method for displacement measurement in hostile environments p 187 A90-44485 HIGH TEMPERATURE GASES Design of an air-cooled metallic high-temperature radial turbine p 20 A90-32960 Hot gas environment around STOVLC aircraft in ground proximity. II - Numerical study [AIAA PAPER 90-2270] p 21 A90-42766 Three-dimensional turbulent flow code calculations of hot gas ingestion p 21 A90-44726 TiCl₄ as a source of TiO₂ particles for laser anemometry measurements in hot gas [NASA-TM-102581] p 189 N90-20358 Hot gas ingestion characteristics and flow visualization of a vectored thrust STOVLC concept [NASA-TM-103212] p 32 N90-26009

SUBJECT INDEX

HIGH TEMPERATURE LUBRICANTS

The experimental evaluation and application of high-temperature solid lubricants
[NASA-TM-102476] p 127 N90-16944

HIGH TEMPERATURE PLASMAS

Plasma sources for spacecraft neutralization
[AIAA PAPER 90-1556] p 49 A90-38697

HIGH TEMPERATURE RESEARCH

The Materials Division: A case study
[NASA-TM-102380] p 86 N90-13597

HIGH TEMPERATURE SUPERCONDUCTORS

Glass-derived superconducting ceramics with zero resistance at 107 K in the Bi(1.5)Pb(0.5)Sr₂Ca₂Cu₃O(x) system
p 253 A90-11491

Synthesis and characterization of high-Tc superconductors in the Ti-Ca-Ba-Cu-O system
p 253 A90-19300

Thin films of the Bi₂Sr₂Ca₂Cu₃O(x) superconductor
p 254 A90-24448

Experimental evidence of a dimensional crossover in YBa₂Cu₃O(7-delta)
p 255 A90-29739

Properties of Pb(1-x)Bi(x)/Ba₂YCu₃O(x) composites - Reaction of Ba₂YCu₃O(x) with Pb and Bi
p 255 A90-33224

Fe-57 and Sn-119 Moessbauer study of La₂CuO(4-y), YBa₂Cu₃O(7-y) and SmBa₂Cu₃O(7-y)
p 256 A90-34020

Superconducting glass-ceramics in the Bi-Sr-Ca-Cu-O system
p 256 A90-35153

Complex permittivity of lanthanum aluminate in the 20 to 300 K temperature range from 26.5 to 40.0 GHz
p 148 A90-37864

Superconducting Bi(1.5)Pb(0.5)Sr₂Ca₂Cu₃O(x) ceramics by rapid melt quenching and glass crystallization
p 256 A90-43568

Millimeter-wave surface resistance of laser-ablated YBa₂Cu₃O(7-delta) superconducting films
p 257 A90-48694

Study of deposition of YBa₂Cu₃O(7-x) on cubic zirconia
[NASA-TM-102350] p 257 N90-10737

Preparation of 110K (Bi,Pb)-Sr-Ca-Cu-O superconductor from glass precursor
p 258 N90-14108

Subtle porosity variation in the YBa₂Cu₃O(7-x) high-temperature superconductor revealed by ultrasonic imaging
[NASA-TM-102130] p 206 N90-17167

Assessment of High Temperature Superconducting (HTS) electric motors for rotorcraft propulsion
[NASA-CR-185222] p 29 N90-21761

High-temperature superconductors for space power transmission lines
[NASA-TM-103459] p 259 N90-24952

Sequentially evaporated thin film YBa₂Cu₃O(7-x) superconducting microwave ring resonator
[NASA-TM-103180] p 154 N90-25273

Laser ablated high T(sub c) superconducting thin YBa₂Cu₃O(7-x) films on substrates suitable for microwave applications
p 260 N90-27808

Microwave conductivity of laser ablated YBaCuO superconducting films and its relation to microstrip transmission line
p 155 N90-27844

Analysis of microstrip lines with alternative implementation of conductors and superconductors
[NASA-TM-103182] p 155 N90-27966

Synthesis and structural chemistry of Au(III)-substituted Ba₂YCu₃O(7-delta)
[NASA-TM-103292] p 108 N90-28696

XANES and EXAFS study of Au-substituted YBa₂Cu₃O(7-delta)
[NASA-TM-103291] p 260 N90-29219

HIGH TEMPERATURE TESTS

The high temperature deformation in cyclic loading of a single crystal nickel-base superalloy
p 108 A90-11534

High temperature inelastic deformation under uniaxial loading - Theory and experiment
p 109 A90-13838

High temperature creep behavior of single crystal gamma prime and gamma alloys
p 110 A90-16901

CMCs for the long run --- ceramic-matrix composites
p 88 A90-17301

Corrosion of cordierite ceramics by sodium sulphate at 1000 C
p 121 A90-21214

High temperature inelastic deformation of the B1900 + Hf alloy under multiaxial loading - Theory and experiment
p 112 A90-22656

Inelastic deformation under nonisothermal loading
p 112 A90-22657

ATTAP/AGT101 ceramics technology update
[ASME PAPER 89-GT-105] p 195 A90-23814

Oxidation of high-temperature intermetallics; Proceedings of the Workshop, Cleveland, OH, Sept. 22, 23, 1988
p 112 A90-24852

Noninteractive macroscopic reliability model for whisker-reinforced ceramic composites
p 89 A90-26561

The role of interfacial dislocation networks in high temperature creep of superalloys
p 114 A90-33329

Cyclic oxidation of aluminide coatings on Ti3Al+ Nb
p 115 A90-39660

The mechanical properties of fluoride salts at elevated temperatures --- candidate thermal energy storage materials for solar dynamic systems
p 123 A90-44376

Refractory metal alloys and composites for space power systems
p 116 A90-46677

1300 K compressive properties of several dispersion strengthened NiAl materials
p 116 A90-47091

Deformation of as-cast LiF-22 mol pct CaF₂ hyperutectic salt between 500 and 1015 K
p 124 A90-49086

Total hemispherical emittance measured at high temperatures by the calorimetric method
[NASA-TM-102322] p 136 N90-10309

A new test machine for measuring friction and wear in controlled atmospheres to 1200 C
[NASA-TM-102405] p 96 N90-12670

Mechanical properties of pure nickel alloys after long term exposures to LiOH and vacuum at 775 K
[NASA-TM-102403] p 118 N90-20181

High-temperature test facility at the NASA Lewis engine components research laboratory
[NASA-TM-103143] p 39 N90-25151

HIGH THRUST

Optimal orbital rendezvous using high and low thrust
[AAS PAPER 89-354] p 41 A90-46786

HIGH VACUUM

Development of a quadrupole-based Secondary-Ion Mass Spectrometry (SIMS) system at Lewis Research Center
[NASA-TM-102531] p 87 N90-23476

HIGH VOLTAGES

High-voltage plasma interactions calculations using NASCAP/LEO
[AIAA PAPER 90-0725] p 251 A90-22254

Conceptual definition of a high voltage power supply test facility
[NASA-CR-185216] p 50 N90-25172

LEO high voltage solar array arcing response model, continuation 5
[NASA-CR-186505] p 232 N90-25418

HISTORIES

The fuel cell in space - Yesterday, today and tomorrow
p 56 A90-26837

The fuel cell in space: Yesterday, today and tomorrow
[NASA-TM-102366] p 70 N90-11804

The lessons of Varsovian's reconnaissance
[NASA-TM-103207] p 267 N90-26789

HOHLRAUMS

Total hemispherical emittance measured at high temperatures by the calorimetric method
[NASA-TM-102322] p 136 N90-10309

HOLLOW CATHODES

Plasma contactor modeling with NASCAP/LEO - Extending laboratory results to space systems
[AIAA PAPER 90-0726] p 251 A90-22255

Requirements for long-life operation of inert gas hollow cathodes - Preliminary results
[AIAA PAPER 90-2586] p 69 A90-52570

Plasma contactor research, 1989
[NASA-CR-185212] p 252 N90-22389

Requirements for long-life operation of inert gas hollow cathodes: Preliminary report
[NASA-TM-103242] p 82 N90-27783

HOLOGRAPHIC INTERFEROMETRY

Holographic interferometry with an injection seeded Nd:YAG laser and two reference beams
p 186 A90-42373

HOLOGRAPHY

Active phase compensation system for fiber optic holography
p 250 A90-11310

HOMOJUNCTIONS

An empirical investigation of the InP shallow-homojunction solar cell
p 225 A90-14869

Predicted performance of near-optimally designed indium phosphide space solar cells at high intensities and temperatures
p 225 A90-14898

Modeling and simulation of InP homojunction solar cells
p 226 A90-14899

InP homojunction solar cell performance on the LIPS III flight experiment
p 226 A90-14921

Investigation of buried homojunctions in p-InP formed during sputter deposition of both indium tin oxide and indium oxide
p 256 A90-36799

On-orbit results of the LIPS 3/InP homojunction solar cell experiment
p 74 N90-17794

HONEYCOMB STRUCTURES

A modified VAPEPS method for predicting vibroacoustic response of unreinforced mass loaded honeycomb panels
p 206 A90-43731

HYDROCARBON COMBUSTION

HORSESHOE VORTICES

A multi-domain spectral computation of three-dimensional laminar horseshoe vortex flow using incompressible Navier-Stokes equations
p 3 A90-17592

Reciprocal interactions of hairpin-shaped vortices and a boundary layer
[AIAA PAPER 90-0017] p 159 A90-19635

HOT CORROSION

Corrosion of cordierite ceramics by sodium sulphate at 1000 C
p 121 A90-21214

Oxidation of high-temperature intermetallics; Proceedings of the Workshop, Cleveland, OH, Sept. 22, 23, 1988
p 112 A90-24852

Burner rig hot corrosion of silicon carbide and silicon nitride
p 121 A90-25267

Diffusional aspects of the high-temperature oxidation of protective coatings
p 113 A90-28075

The oxidation and corrosion of ODS alloys
[NASA-TM-102555] p 119 N90-25211

HOT ISOSTATIC PRESSING

High-strength silicon carbides by hot isostatic pressing
p 122 A90-35473

Improved process for HIP canning of composites
[NASA-CASE-LEW-14990-1-CU] p 97 N90-15147

One step HIP canning of powder metallurgy composites
[NASA-CASE-LEW-14719-1] p 101 N90-23493

HOT PRESSING

Production and processing of Cu-Cr-Nb alloys
p 114 A90-33340

Production and processing of Cu-Cr-Nb alloys
[NASA-TM-102495] p 117 N90-16053

Crystallization behavior and properties of BaO-Al₂O₃-2SiO₂ glass matrices
[NASA-CR-185209] p 127 N90-19374

HOT-WIRE FLOWMETERS

Enhanced heat transfer rocket combustor technology component hot-fire test results
[AIAA PAPER 90-2182] p 64 A90-42063

HOUSINGS

The application of cast SiC/Al to rotary engine components
[NASA-CR-179610] p 25 N90-13385

Gear noise, vibration, and diagnostic studies at NASA Lewis Research Center
[NASA-TM-102435] p 202 N90-18041

A review of gear housing dynamics and acoustics literature
[NASA-CR-185148] p 203 N90-21387

HUMAN BEHAVIOR

The insertion of human dynamics models in the flight control loops of V/STOL research aircraft. Appendix 2: The optimal control model of a pilot in V/STOL aircraft control loops
[NASA-CR-186598] p 38 N90-21776

HUMAN FACTORS ENGINEERING

The insertion of human dynamics models in the flight control loops of V/STOL research aircraft. Appendix 2: The optimal control model of a pilot in V/STOL aircraft control loops
[NASA-CR-186598] p 38 N90-21776

HUMAN REACTIONS

An adaptive human response mechanism controlling the V/STOL aircraft. Appendix 3: The adaptive control model of a pilot in V/STOL aircraft control loops
[NASA-CR-186598] p 38 N90-21777

HYDRAULIC TEST TUNNELS

Liquid water content and droplet size calibration of the NASA Lewis Icing Research Tunnel
[AIAA PAPER 90-0669] p 37 A90-22242

Liquid water content and droplet size calibration of the NASA Lewis Icing Research Tunnel
[NASA-TM-102447] p 200 N90-13797

HYDRAZINE ENGINES

Qualification and life testing of a flight design hydrazine arcjet system
[AIAA PAPER 90-2576] p 64 A90-42559

HYDRAZINES

Arcjet load characteristics
[AIAA PAPER 90-2579] p 67 A90-47226

Advanced propulsion for LEO and GEO platforms
[AIAA PAPER 90-2551] p 68 A90-52565

Arcjet thruster research and technology. Phase 1: Executive summary
[NASA-CR-182106] p 72 N90-14278

Arcjet load characteristics
[NASA-TM-103190] p 79 N90-25181

Advanced propulsion for LEO and GEO platforms
[NASA-TM-103228] p 82 N90-27785

HYDROCARBON COMBUSTION

Reduced chemical kinetics for propane combustion
[AIAA PAPER 90-0546] p 103 A90-18904

N-decane-air droplet combustion experiments in the NASA-Lewis 5 Second Zero-Gravity Facility
[AIAA PAPER 90-0649] p 104 A90-25038

- Effects of pressure on microgravity hydrocarbon diffusion flames
[AIAA PAPER 90-0651] p 104 A90-25039
- Kinetics and mechanism of soot formation in hydrocarbon combustion
[NASA-CR-186162] p 106 N90-14305
- HYDROCARBON FUELS**
On the driving force of PAH production p 84 A90-32833
- High energy-density liquid rocket fuel performance
[AIAA PAPER 90-1968] p 130 A90-47204
- Hydrocarbon-fuel/combustion-chamber-liner materials compatibility
[NASA-CR-185203] p 118 N90-21165
- High energy-density liquid rocket fuel performance
[NASA-CR-185279] p 131 N90-28742
- HYDRODYNAMICS**
On the numerical solution of the dynamically loaded hydrodynamic lubrication of the point contact problem
[NASA-TM-102427] p 178 N90-17076
- HYDROGEN**
On the use of external burning to reduce aerospace vehicle transonic drag
[AIAA PAPER 90-1935] p 20 A90-40562
- Reactions of SiC with H₂/H₂O/Ar mixtures at 1300 C
p 123 A90-45830
- Mars in situ propellants - Carbon monoxide and oxygen ignition experiments
[AIAA PAPER 90-1894] p 130 A90-50642
- Hydrogen-silicon carbide interactions
[NASA-TM-102382] p 125 N90-11144
- FLUSH: A tool for the design of slush hydrogen flow systems
[NASA-TM-102467] p 130 N90-17890
- Impedance studies of Ni/Cd and Ni/H₂ cells using the cell case as a reference electrode p 231 N90-20473
- On the use of external burning to reduce aerospace vehicle transonic drag
[NASA-TM-103107] p 30 N90-21762
- The effect of hydrogen and microstructure on the deformation and fracture behavior of a single crystal nickel-base superalloy
[NASA-CR-185219] p 118 N90-21849
- Mars in situ propellants: Carbon monoxide and oxygen ignition experiments
[NASA-TM-103202] p 81 N90-26065
- Catalytic ignition of hydrogen/oxygen p 107 N90-28627
- HYDROGEN ATOMS**
Atomic hydrogen as a launch vehicle propellant
[AIAA PAPER 90-0715] p 44 A90-23712
- Atomic hydrogen as a launch vehicle propellant
[NASA-TM-102459] p 73 N90-14284
- HYDROGEN FUELS**
H₂/O₂ three-body rates at high temperatures
[AIAA PAPER 90-1696] p 105 A90-38399
- Slush Hydrogen (SLH₂) technology development for application to the National Aerospace Plane (NASP)
[NASA-TM-102315] p 50 N90-14268
- HYDROGEN OXYGEN ENGINES**
Power considerations for an early manned Mars mission utilizing the Space Station
[AAS PAPER 87-223] p 55 A90-16688
- Centaur upper stage p 44 A90-18017
- A highly durable injector faceplate design concept for O₂/H₂ propellants
[AIAA PAPER 90-2181] p 66 A90-47211
- A comparison of analytical results for 20 K LOX/hydrogen instabilities
[AIAA PAPER 90-2241] p 130 A90-47214
- Calculations of gaseous H₂/O₂ thruster
[AIAA PAPER 90-2490] p 67 A90-47224
- A rocket engine design expert system
[NASA-TM-102373] p 69 N90-10172
- Heat transfer to throat tubes in a square-chambered rocket engine at the NASA Lewis Research Center
[NASA-TM-102336] p 70 N90-11082
- The Pathfinder chemical transfer propulsion program p 74 N90-18471
- Advanced APS impacts on vehicle payloads p 75 N90-18472
- A comparison of analytical results for 20 K LOX/hydrogen instabilities
[NASA-TM-103166] p 80 N90-25186
- HYDROGEN OXYGEN FUEL CELLS**
Mars manned transportation vehicle
[AAS PAPER 87-271] p 42 A90-16569
- Cryogenic reactant storage for lunar base regenerative fuel cells
[IAF PAPER ICOSP89-3-8] p 227 A90-27709
- Hydrogen-oxygen proton-exchange membrane fuel cells and electrolyzers p 56 A90-33944
- Integrated regenerative fuel cell experimental evaluation
[NASA-CR-185183] p 230 N90-18808
- Space Electrochemical Research and Technology (SERT), 1989
[NASA-CP-3056] p 230 N90-20454
- Hydrogen-oxygen proton-exchange membrane fuel cells and electrolyzers p 230 N90-20467
- A solar power system for an early Mars expedition
[NASA-TM-103219] p 246 N90-28393
- HYDROLYSIS**
Polysiloxanes derived from the controlled hydrolysis of tetraethoxysilane as precursors to silica for use in ceramic processing
[NASA-TM-102489] p 128 N90-21858
- HYDROSTATICS**
Assessment of worm gearing for helicopter transmissions
[NASA-TM-102441] p 27 N90-15923
- Integrated controls and health monitoring fiberoptic shaft monitor
[NASA-CR-185210] p 191 N90-29622
- HYDROXYL RADICALS**
Saturated fluorescence measurements of the hydroxyl radical in laminar high-pressure flames
[NASA-CR-185218] p 190 N90-22022
- HYGRAL PROPERTIES**
Mechanics of damping for fiber composite laminates including hygro-thermal effects
[NASA-TM-102329] p 95 N90-10185
- HYPERBOLIC DIFFERENTIAL EQUATIONS**
Absorbing boundary conditions for second-order hyperbolic equations p 242 A90-34549
- HYPERSONIC COMBUSTION**
Advanced computational techniques for hypersonic propulsion p 156 A90-12606
- H₂/O₂ three-body rates at high temperatures
[AIAA PAPER 90-1696] p 105 A90-38399
- HYPERSONIC FLIGHT**
Advanced computational techniques for hypersonic propulsion p 156 A90-12606
- Thermal/structural analyses of several hydrogen-cooled leading-edge concepts for hypersonic flight vehicles
[AIAA PAPER 90-0053] p 164 A90-23702
- Thermal/structural analyses of several hydrogen-cooled leading-edge concepts for hypersonic flight vehicles
[NASA-TM-102391] p 177 N90-14511
- Viscous three-dimensional analyses for nozzles for hypersonic propulsion
[NASA-CR-185197] p 27 N90-17635
- HYPERSONIC FLOW**
Efficient real gas Navier-Stokes computations of high speed flows using an LU scheme
[AIAA PAPER 90-0391] p 164 A90-23706
- Efficient real gas Navier-Stokes computations of high speed flows using an LU scheme
[NASA-TM-102429] p 11 N90-14203
- Spatial evolution of nonlinear acoustic mode instabilities on hypersonic boundary layers
[NASA-TM-102431] p 177 N90-14517
- HYPERSONIC INLETS**
Computational modeling and validation for hypersonic inlets
[NASA-TM-103111] p 181 N90-22011
- Finite element analysis of structural components using viscoplastic models with application to a cowl lip problem
[NASA-CR-185189] p 221 N90-23769
- HYPERSONIC VEHICLES**
Hypersonic aerospace sizing analysis for the preliminary design of aerospace vehicles p 17 A90-23276
- Thermal/structural analyses of several hydrogen-cooled leading-edge concepts for hypersonic flight vehicles
[AIAA PAPER 90-0053] p 164 A90-23702
- Thermal/structural analyses of several hydrogen-cooled leading-edge concepts for hypersonic flight vehicles
[NASA-TM-102391] p 177 N90-14511
- HYPERVELOCITY IMPACT**
Effect of eleven years in earth orbit on a mirror surface p 44 A90-36188
- On protection of Freedom's solar dynamic radiator from the orbital debris environment. Part 1: Preliminary analyses and testing
[NASA-TM-102458] p 73 N90-14285
- HYSTERESIS**
Parametric study of power absorption from electromagnetic waves by small ferrite spheres
[NASA-TP-2949] p 246 N90-12282
- High frequency, high temperature specific core loss and dynamic B-H hysteresis loop characteristics of soft magnetic alloys
[NASA-TM-103164] p 154 N90-23663
- ICE**
Modeling of surface roughness effects on glaze ice accretion p 16 N90-20925
- Ultrasonic techniques for aircraft ice accretion measurement p 16 N90-20926
- Investigation of surface water behavior during glaze ice accretion p 16 N90-20927
- The influence of ice accretion physics on the forecasting of aircraft icing conditions p 17 N90-20928
- ICE CLOUDS**
Development of a phase Doppler based probe for icing cloud droplet characterization
[AIAA PAPER 90-0667] p 186 A90-26978
- Initial results from the joint NASA-Lewis/U.S. Army icing flight research tests p 16 A90-28180
- ICE FORMATION**
Predictions of airfoil aerodynamic performance degradation due to icing p 3 A90-16753
- Fortified LEWICE with viscous effects --- Lewis Ice Accretion Prediction Code
[AIAA PAPER 90-0754] p 15 A90-20009
- Numerical study of the effects of icing on finite wing aerodynamics p 3 A90-20010
- Development of an unstructured mesh/Navier-Stokes method for aerodynamics of aircraft with ice accretions
[AIAA PAPER 90-0758] p 4 A90-20011
- Convective heat transfer measurements from a NACA 0012 airfoil in flight and in the NASA Lewis Icing Research Tunnel
[AIAA PAPER 90-0199] p 162 A90-22180
- Heat transfer on accreting ice surfaces
[AIAA PAPER 90-0200] p 162 A90-22181
- Liquid water content and droplet size calibration of the NASA Lewis Icing Research Tunnel
[AIAA PAPER 90-0669] p 37 A90-22242
- Comparison of two droplet sizing systems in an icing wind tunnel
[AIAA PAPER 90-0668] p 164 A90-23711
- A numerical simulation of the flow in the diffuser of the NASA Lewis Icing Research Tunnel
[AIAA PAPER 90-0488] p 166 A90-25034
- Spray nozzle investigation for the Improved Helicopter Icing Spray System (IHSS)
[AIAA PAPER 90-0666] p 37 A90-25040
- Swept wing ice accretion modeling
[AIAA PAPER 90-0756] p 5 A90-25042
- Development of a phase Doppler based probe for icing cloud droplet characterization
[AIAA PAPER 90-0667] p 186 A90-26978
- A study of ice shape prediction methodologies and comparison with experimental data
[AIAA PAPER 90-0753] p 15 A90-26986
- Icing Research Tunnel test of a model helicopter rotor p 15 A90-28179
- Initial results from the joint NASA-Lewis/U.S. Army icing flight research tests p 16 A90-28180
- The low frequency oscillation in the flow over a NACA0012 airfoil with an 'iced' leading edge p 8 A90-46377
- Experimental investigation of multielement airfoil ice accretion and resulting performance degradation p 9 A90-48954
- Convective heat transfer measurements from a NACA 0012 airfoil in flight and in the NASA Lewis Icing Research Tunnel
[NASA-TM-102448] p 176 N90-13750
- Liquid water content and droplet size calibration of the NASA Lewis Icing Research Tunnel
[NASA-TM-102447] p 200 N90-13797
- Comparison of two droplet sizing systems in an icing wind tunnel
[NASA-TM-102456] p 200 N90-14617
- NASA's program on icing research and technology p 16 N90-15062
- A numerical simulation of the flow in the diffuser of the NASA Lewis icing research tunnel
[NASA-TM-102480] p 38 N90-15965
- Comparison of drop size distributions from two droplet sizing systems p 202 N90-17147
- Heat transfer measurements from a NACA 0012 airfoil in flight and in the NASA Lewis icing research tunnel
[NASA-CR-4278] p 13 N90-19203
- Modeling of surface roughness effects on glaze ice accretion p 16 N90-20925
- Ultrasonic techniques for aircraft ice accretion measurement p 16 N90-20926
- Investigation of surface water behavior during glaze ice accretion p 16 N90-20927
- The influence of ice accretion physics on the forecasting of aircraft icing conditions p 17 N90-20928
- Users manual for the NASA Lewis Ice Accretion Prediction Code (LEWICE)
[NASA-CR-185129] p 1 N90-20943
- Advanced instrumentation for aircraft icing research
[NASA-CR-185225] p 18 N90-21006
- Swept wing ice accretion modeling
[NASA-TM-103114] p 13 N90-21727

SUBJECT INDEX

NASA Lewis icing research tunnel user manual
[NASA-TM-102319] p 31 N90-23407

ICE PREVENTION
An experimental evaluation of the tensile strength of impact ice p 83 A90-15049
Impact ice stresses in rotating airfoils
[AIAA PAPER 90-0198] p 15 A90-19735
NASA's program on icing research and technology p 16 N90-15062
Modeling of surface roughness effects on glaze ice accretion p 16 N90-20925

ICE REPORTING
Impact ice stresses in rotating airfoils
[AIAA PAPER 90-0198] p 15 A90-19735

IGNITION
Mars in situ propellants - Carbon monoxide and oxygen ignition experiments p 130 A90-50642
[AIAA PAPER 90-1894] p 130 A90-50642
The Gevaltig: An inertial fusion powered manned spacecraft design for outer solar system missions p 50 N90-15985
[NASA-CR-185163] p 50 N90-15985
Detailed mechanism for oxidation of benzene [NASA-TM-102443] p 106 N90-21842
Mars in situ propellants: Carbon monoxide and oxygen ignition experiments p 81 N90-26065
[NASA-TM-103202] p 81 N90-26065
Critical evaluation of Jet-A spray combustion using propane chemical kinetics in gas turbine combustion simulated by KIVA-2 p 138 N90-26170
[NASA-TM-103173] p 138 N90-26170
Ignition and combustion characteristics of metallized propellants p 107 N90-26911
[NASA-CR-186870] p 107 N90-26911

IGNITION LIMITS
Ignition and behavior of laminar gas-jet diffusion flames in microgravity p 103 A90-23107

IGNITION SYSTEMS
Ignition and combustion characteristics of metallized propellants p 107 N90-26911
[NASA-CR-186870] p 107 N90-26911
Catalytic ignition of hydrogen/oxygen p 107 N90-28627

IMAGE PROCESSING
A laser based computer aided non-intrusive technique for full field flow characterization in macroscopic curved channels p 168 A90-32293

IMAGING TECHNIQUES
Data compression techniques applied to high resolution high frame rate video technology p 143 N90-14452
[NASA-CR-4263] p 143 N90-14452
Data compression for the microgravity experiments p 188 N90-16212
Subtle porosity variation in the $YBa_2Cu_3O_{7-x}$ high-temperature superconductor revealed by ultrasonic imaging p 206 N90-17167
[NASA-TM-102130] p 206 N90-17167
Development of an infrared imaging system for the surface tension driven convection experiment p 188 N90-17922
Design and calibration of a vacuum compatible scanning tunneling microscope p 189 N90-20353
[NASA-TM-102514] p 189 N90-20353
Ultrasonic and radiographic evaluation of advanced aerospace materials: Ceramic composites p 207 N90-21401
[NASA-TM-102540] p 207 N90-21401
Recent advances in nondestructive evaluation made possible by novel uses of video systems p 207 N90-22801
[NASA-TM-102491] p 207 N90-22801

IMPACT DAMAGE
Assessment of the effects of space debris and meteoroids environment on the Space Station solar array assembly p 54 A90-14929
Impact damage development in damaged composite materials p 193 A90-18355
Progression of damage and fracture in composites under dynamic loading p 210 A90-29318
[AIAA PAPER 90-0916] p 210 A90-29318
Development of impact design methods for ceramic gas turbine components p 197 A90-42165
[AIAA PAPER 90-2413] p 197 A90-42165

IMPACT LOADS
Analysis of impact response in composite plates p 214 A90-47567
Collision forces for compliant projectiles p 223 N90-28111
[NASA-TM-4203] p 223 N90-28111

IMPACT RESISTANCE
Development of impact design methods for ceramic gas turbine components p 197 A90-42165
[AIAA PAPER 90-2413] p 197 A90-42165

IMPACT TESTS
On protection of Freedom's solar dynamic radiator from the orbital debris environment. Part 1: Preliminary analyses and testing p 73 N90-14285
[NASA-TM-102458] p 73 N90-14285
Collision forces for compliant projectiles p 223 N90-28111
[NASA-TM-4203] p 223 N90-28111

IMPACTORS

Low velocity impact analysis with NASTRAN p 221 N90-24647
Collision forces for compliant projectiles p 223 N90-28111
[NASA-TM-4203] p 223 N90-28111

IMPEDANCE

Distortion and regulation characterization of a Mapham inverter p 148 A90-38125
Changes in impedance of Ni electrodes upon standing and cycling p 229 N90-18097
[NASA-TM-102438] p 229 N90-18097
Impedance studies of Ni/Cd and Ni/H₂ cells using the cell case as a reference electrode p 231 N90-20473
Nickel-hydrogen capacity loss on storage p 231 N90-20478

IMPEDANCE MEASUREMENT

Impedance studies of Ni/Cd and Ni/H₂ cells using the cell case as a reference electrode p 231 N90-20473

IMPROVEMENT

Improved silicon carbide for advanced heat engines p 129 N90-28735
[NASA-CR-182186] p 129 N90-28735

IMPURITIES

Theory of influence of a low-volatility, soluble impurity on spherically-symmetric combustion of fuel droplets p 104 A90-28771

IN-FLIGHT MONITORING

On-orbit results of the LIPS 3/InP homojunction solar cell experiment p 74 N90-17794

INCIDENT RADIATION

Concentration of off-axis radiation by solar concentrators for space power p 60 A90-38163

INCOMPRESSIBLE FLOW

Time-dependent viscous incompressible Navier-Stokes equations - The finite difference Galerkin formulation and streamfunction algorithms p 156 A90-11598
A multi-domain spectral computation of three-dimensional laminar horseshoe vortex flow using incompressible Navier-Stokes equations p 3 A90-17592
Elliptic jets. I - Characteristics of unexcited and excited jets p 159 A90-18071
Least-squares finite element method for fluid dynamics p 159 A90-18246
Fully elliptic incompressible flow calculations on regular grid by a new pressure substitution method p 160 A90-19749
[AIAA PAPER 90-0239] p 160 A90-19749
Experimental investigation of flow about a strut-endwall configuration p 171 A90-38685
[AIAA PAPER 90-1541] p 171 A90-38685
Computation of turbine flowfields with a Navier-Stokes code p 8 A90-42731
[AIAA PAPER 90-2122] p 8 A90-42731
Comparison between pressure gradient method and MAC method on high Re calculation p 172 A90-44462
Hopf bifurcation in the driven cavity p 174 A90-48548
A least-squares finite element method for incompressible Navier-Stokes problems p 242 N90-12231
[NASA-TM-102385] p 242 N90-12231
Conditions at the downstream boundary for simulations of viscous incompressible flow p 243 N90-18198
[NASA-TM-102510] p 243 N90-18198
High accuracy solutions of incompressible Navier-Stokes equations p 244 N90-21567
[NASA-TM-102539] p 244 N90-21567
ULTRA-SHARP nonoscillatory convection schemes for high-speed steady multidimensional flow p 244 N90-21570
[NASA-TM-102568] p 244 N90-21570
An unsteady time asymptotic flow in the square driven cavity p 181 N90-22016
[NASA-TM-103141] p 181 N90-22016
Numerical solution for the velocity-derivative skewness of a low-Reynolds-number decaying Navier-Stokes flow p 184 N90-27985
[NASA-TM-103186] p 184 N90-27985

INCONEL (TRADEMARK)
Preliminary study on pressure brazing and diffusion welding of Nb-1Zr to Inconel 718 p 196 A90-26899

INDEXES (DOCUMENTATION)
Criss-cross directory of NASA N numbers and DOD AD numbers. Volume 2, part 1: AD to N, 1979-1986. N to AD, 1962-1986 p 262 N90-12388
[NASA-TM-101814] p 262 N90-12388
Criss-cross directory of NASA N numbers and DOD AD numbers. Volume 2, part 2: AD to N, 1979-1986. N to AD, 1962-1986 p 262 N90-12389
[NASA-TM-101815] p 262 N90-12389
Bibliography of Lewis Research Center technical publications announced in 1988 p 262 N90-15846
[NASA-TM-102034] p 262 N90-15846

INDIUM ANTIMONIDES

Molecular beam epitaxial growth of high-quality InSb on InP and GaAs substrates p 253 A90-12808
Transport properties of InAs(x)Sb(1-x) (x = 0-0.55) on InP grown by molecular-beam epitaxy p 256 A90-36232

INDIUM ARSENIDES

AlGaAs/InGaAs heterostructures with doped channels for discrete devices and monolithic amplifiers p 146 A90-20861
Transport properties of InAs(x)Sb(1-x) (x = 0-0.55) on InP grown by molecular-beam epitaxy p 256 A90-36232

INDIUM COMPOUNDS

Study of indium tin oxide films exposed to atomic oxygen p 257 A90-45193
Dielectric function of InGaAs in the visible p 260 N90-26683
[NASA-TM-103246] p 260 N90-26683

INDIUM PHOSPHIDES

Molecular beam epitaxial growth of high-quality InSb on InP and GaAs substrates p 253 A90-12808
An empirical investigation of the InP shallow-homojunction solar cell p 225 A90-14869
Hybrid solar cells based on dc magnetron sputtered films of n-ITO on APMOVPE grown p-InP p 225 A90-14893
Predicted performance of near-optimally designed indium phosphide space solar cells at high intensities and temperatures p 225 A90-14898
Modeling and simulation of InP homojunction solar cells p 226 A90-14899
InP homojunction solar cell performance on the LIPS III flight experiment p 226 A90-14921
Radiation resistance and comparative performance of ITO/InP and n/p InP homojunction solar cells p 226 A90-14933
The kinetics of the Au-InP interaction p 254 A90-25084

Investigation of buried homojunctions in p-InP formed during sputter deposition of both indium tin oxide and indium oxide p 256 A90-36799
Indium phosphide solar cells - Recent developments and estimated performance in space p 57 A90-37854
Humidity-induced room-temperature decomposition of Au contacted indium phosphide p 105 A90-44689
Contact spreading and the Au3In-to-Au9In4 transition in the Au-InP system p 257 A90-48661
Indium phosphide solar cell research in the United States: Comparison with non-photovoltaic sources p 229 N90-17758
On-orbit results of the LIPS 3/InP homojunction solar cell experiment p 74 N90-17794
Electron beam induced damage in PECVD Si₃N₄ and SiO₂ films on InP p 203 N90-20393
[NASA-TM-102544] p 203 N90-20393
Lateral spreading of Au contacts on InP p 232 N90-22843
[NASA-TM-103133] p 232 N90-22843
New directions in InP solar cell research p 154 N90-23662
[NASA-TM-103160] p 154 N90-23662
An analysis of the contact sintering process in III-V solar cells p 233 N90-25420
[NASA-TM-103179] p 233 N90-25420

INDUCTION MOTORS

Variable speed induction motor operation from a 20-kHz power bus p 148 A90-38119
Induction motor control p 28 N90-19234
[NASA-TM-102533] p 28 N90-19234
Aerospace induction motor actuators driven from a 20-kHz power link p 28 N90-20085
[NASA-TM-102482] p 28 N90-20085
Electromechanical actuation for thrust vector control applications p 152 N90-21272
[NASA-TM-102548] p 152 N90-21272
Analytical and experimental study of high phase order induction motors p 153 N90-21952
[NASA-CR-186580] p 153 N90-21952
Field oriented control of induction motors p 154 N90-22731
[NASA-TM-103154] p 154 N90-22731

INERTIAL CONFINEMENT FUSION

The Gevaltig: An inertial fusion powered manned spacecraft design for outer solar system missions p 50 N90-15985
[NASA-CR-185163] p 50 N90-15985

INFLATABLE STRUCTURES

Free-Space Power Transmission p 77 N90-21795
[NASA-CR-10016] p 77 N90-21795

INFLATING

Gravitational couplings of the inflator in extended inflation p 265 A90-40088

INFORMATION MANAGEMENT

A technology assessment of alternative communications systems for the space exploration initiative p 47 N90-27736
[NASA-TM-103243] p 47 N90-27736

INFRARED IMAGERY

Development of an infrared imaging system for the surface tension driven convection experiment p 188 N90-17922

INFRARED RADIATION

Millimeter-wave/infrared rectenna development at Georgia Tech p 69 N90-10147

INGESTION (ENGINES)

Engine inlet distortion in a 9.2 percent scaled vectored thrust STOVL model in ground effect p 5 A90-25043
[AIAA PAPER 89-2910] p 5 A90-25043

- Hot gas environment around STOL aircraft in ground proximity. II - Numerical study
[AIAA PAPER 90-2270] p 21 A90-42766
- INJECTION**
Low NO(x) potential of gas turbine engines
[NASA-TM-102452] p 27 N90-17636
- INJECTION MOLDING**
Improved silicon carbide for advanced heat engines
[NASA-CR-180831] p 124 N90-10293
Improved silicon carbide for advanced heat engines
[NASA-CR-182186] p 129 N90-28735
- INJECTORS**
A highly durable injector faceplate design concept for O2/H2 propellants
[AIAA PAPER 90-2181] p 66 A90-47211
A rocket engine design expert system
[NASA-TM-102373] p 69 N90-10172
Extended temperature range rocket injector
[NASA-CASE-LEW-14846-1] p 73 N90-15130
- INLET FLOW**
Advanced computational techniques for hypersonic propulsion
p 156 A90-12606
A flux-split solution procedure for unsteady inlet flows
[AIAA PAPER 90-0585] p 6 A90-26967
Comparison of 3-D viscous flow computations of Mach 5 inlet with experimental data
[AIAA PAPER 90-0600] p 6 A90-26970
Influence of bulk turbulence and entrance boundary layer thickness on the curved duct flow field
[AIAA PAPER 90-1502] p 171 A90-38651
Transient behavior of supersonic flow through inlets
[AIAA PAPER 90-2130] p 8 A90-42734
Three dimensional LDV flow measurements and theoretical investigation in a radial inflow turbine scroll
p 9 A90-46880
Research on a two-dimensional inlet for a supersonic V/STOL propulsion system. Appendix A
[NASA-CR-174945] p 12 N90-18364
Control of flow separation and mixing by aerodynamic excitation
[NASA-TM-103131] p 13 N90-21733
Computational modeling and validation for hypersonic inlets
[NASA-TM-103111] p 181 N90-22011
Aerodynamics of a linear oscillating cascade
[NASA-TM-103250] p 15 N90-27657
- INLET PRESSURE**
Experimental investigation of terminal shock sensors in mixed-compression inlets
[AIAA PAPER 90-1931] p 186 A90-40560
- INPUT/OUTPUT ROUTINES**
A test matrix sequencer for research test facility automation
[AIAA PAPER 90-2386] p 37 A90-42791
A test matrix sequencer for research test facility automation
[NASA-TM-103108] p 39 N90-23416
- INSPECTION**
Computerized inspection of gear tooth surfaces
[NASA-TM-102395] p 203 N90-22054
- INSTRUMENT ERRORS**
Developing a self-diagnostic system for piezoelectric sensors
[AIAA PAPER 90-2230] p 187 A90-42755
- INSULATION**
Comparison of currents predicted by NASCAP/LEO model simulations with elementary Langmuir-type bare probe models for an insulated cable containing a single pinhole
[NASA-TM-102486] p 51 N90-26054
- INSULATORS**
Solar array arcing in plasmas
p 233 N90-25558
- INTAKE SYSTEMS**
Analysis of results from wind tunnel tests of inlets for an advanced turboprop nacelle installation
[NASA-CR-174937] p 10 N90-10011
- INTEGRALS**
Elevated temperature crack growth
[NASA-CR-182247] p 222 N90-26355
- INTEGRATED CIRCUITS**
Characterization of two MMIC GaAs switch matrices at microwave frequencies
[AIAA PAPER 90-0866] p 147 A90-25686
Optical detectors for GaAs MMIC integration - Technology assessment
p 149 A90-41238
Doped-channel heterojunction structures for millimeter-wave discrete devices and MMICs
p 150 A90-48492
Characterization of two MMIC GaAs switch matrices at microwave frequencies
[NASA-TM-102449] p 50 N90-14273
Universal nondestructive MM-wave integrated circuit test fixture
[NASA-CASE-LEW-14746-1] p 151 N90-17009
Coplanar waveguide fed phased array antenna
[NASA-TM-102522] p 152 N90-21273
- Optical control of an 8-element Ka-band phased array using a high-speed optoelectronic interconnect
[NASA-TM-102550] p 152 N90-21275
Design of an optically controlled Ka-band GaAs MMIC phased-array antenna
[NASA-TM-103147] p 155 N90-26250
- INTEGRATED OPTICS**
Optical detectors for GaAs MMIC integration - Technology assessment
p 149 A90-41238
High-speed digital fiber optic links for satellite traffic
p 250 A90-41247
- INTERACTIONAL AERODYNAMICS**
Fortified LEWICE with viscous effects --- Lewis Ice Accretion Prediction Code
[AIAA PAPER 90-0754] p 15 A90-20009
A numerical study of the interaction between unsteady free-stream disturbances and localized variations in surface geometry
p 161 A90-21422
Multiscale nonlinear interactions in the axisymmetric mode
[AIAA PAPER 90-0365] p 166 A90-25029
A block-based algorithm for the solution of compressible flows in rotor-stator combinations
p 9 A90-46905
An LDA investigation of the normal shock wave boundary layer interaction
p 10 A90-52618
- INTERACTIONS**
Detection of potential space station control/structure interaction with CO-ST-IN
p 50 N90-21074
- INTERATOMIC FORCES**
Universal aspects of brittle fracture, adhesion, and atomic force microscopy
p 83 A90-14021
- INTERCALATION**
Effect of heat-treatment temperature of vapor-grown graphite fibers. I - Properties of their bromine intercalation compounds
p 120 A90-16279
Density of intercalated graphite fibers
p 124 A90-49061
Density of intercalated graphite fibers
[NASA-TM-102411] p 126 N90-14362
Feasibility of intercalated graphite railgun armatures
[NASA-TM-102546] p 128 N90-21181
Resistivity of pristine and intercalated graphite fiber epoxy composites
[NASA-TM-102576] p 128 N90-21192
- INTERDIGITAL TRANSDUCERS**
Microwave response of a HEMT photoconductive detector
p 147 A90-37301
- INTERFACE STABILITY**
Effect of fiber spacing on interfacial damage in a metal matrix composite
p 88 A90-23188
- INTERFACES**
High temperature, flexible, thermal barrier seal
[NASA-CASE-LEW-14672-1] p 201 N90-15444
- INTERFACIAL ENERGY**
Shear stabilization of the capillary breakup of a cylindrical interface
[AD-A219268] p 159 A90-17578
Effects of crystal-melt interfacial energy anisotropy on dendritic morphology and growth kinetics
p 253 A90-19284
- INTERFACIAL TENSION**
Investigation of interfacial shear strength in a SiC fiber/Ti-24Al-11Nb composite by a fibre push-out technique
p 88 A90-18973
Surface entropy of liquids via a direct Monte Carlo approach - Application to liquid Si
p 261 A90-31675
Hardware development for the surface tension driven convection experiment
p 52 A90-36195
Thermocapillary migration of liquid droplets in a temperature gradient in a density matched system
[NASA-CR-185178] p 177 N90-14512
Development of an infrared imaging system for the surface tension driven convection experiment
p 188 N90-17922
Spacelab qualified infrared imager for microgravity science experiments
[NASA-TM-102503] p 189 N90-20352
Design of a CO2 laser power control system for a Spacelab microgravity experiment
[NASA-TM-103112] p 192 N90-28833
- INTERFERENCE**
A general model for memory interference in a multiprocessor system with memory hierarchy
p 238 A90-37482
- INTERFEROMETERS**
Fiber optic sensing system
[NASA-CASE-LEW-14795-1] p 251 N90-15733
Fiber-optic projected-fringe digital interferometry
[NASA-TM-103252] p 191 N90-28033
- INTERFEROMETRY**
Application of two-component phase Doppler interferometry to the measurement of particle size, mass flux, and velocities in two-phase flows
p 186 A90-32853
Fiber-optic projected-fringe digital interferometry
[NASA-TM-103252] p 191 N90-28033
- INTERGALACTIC MEDIA**
A model for the distribution of the intergalactic medium
p 265 A90-34505
A model for the distribution of dark matter, galaxies, and the intergalactic medium in a cold dark matter-dominated universe
p 266 A90-45560
- INTERGRANULAR CORROSION**
Intergranular fracture of lithium fluoride-22 percent calcium fluoride hypereutectic salt at 800 K
p 121 A90-25273
- INTERMETALLICS**
Deformation behavior of NiAl-based alloys containing iron, cobalt, and hafnium
p 110 A90-16930
Up-and-coming IMCs --- Intermetallic-Matrix Composites
p 88 A90-17295
Compressive strength of a B2 matrix NiAl-Nb intermetallic at 1200 and 1300 K
p 111 A90-19157
Effect of fiber spacing on interfacial damage in a metal matrix composite
p 88 A90-23188
Oxidation of high-temperature intermetallics; Proceedings of the Workshop, Cleveland, OH, Sept. 22, 23, 1988
p 112 A90-24852
The oxidation of Ni-rich Ni-Al intermetallics
p 112 A90-24855
The effects of surface films on mechanical behavior of B2 ordered intermetallic alloys
p 115 A90-44338
Filter clogging by the extracted gamma prime and its measurement
p 116 A90-45620
1300 K compressive properties of several dispersion strengthened NiAl materials
p 116 A90-47091
Compatibility of Fe-40Al with various fibers
p 94 A90-50496
Compression behavior of the forged Li2 compounds Al67Ti25Cr8 and Al66Ti25Mn9
p 116 A90-51298
Selection of phase-change and containment materials for thermal energy storage
[NASA-CR-186228] p 229 N90-15506
High temperature fatigue behavior of a SiC/Ti-24Al-11Nb composite
[NASA-TM-103157] p 220 N90-22822
- INTERNAL COMBUSTION ENGINES**
Critical evaluation of Jet-A spray combustion using propane chemical kinetics in gas turbine combustion simulated by KIVA-2
[NASA-TM-103173] p 138 N90-26170
- INTERNATIONAL COOPERATION**
The International Space University
[AIAA PAPER 90-2389] p 261 A90-42152
A comparison of European and American microgravity combustion experimental techniques
p 134 N90-16966
The International Space University
[NASA-TM-103163] p 78 N90-22604
- INTERPLANETARY FLIGHT**
Nuclear propulsion - A vital technology for the exploration of Mars and the planets beyond
[AAS PAPER 87-210] p 55 A90-16676
Engine selection for the Space Exploration Initiative
[AIAA PAPER 90-1880] p 65 A90-47201
- INTERPLANETARY SPACECRAFT**
Orbit to surface beamed power for Mars bases expansion
p 40 A90-38105
- INVERTED CONVERTERS (DC TO AC)**
20 kHz main inverter unit --- for space station power supplies
p 148 A90-38124
- INVERTERS**
Frequency domain model for analysis of paralleled, series-output-connected Mapham inverters
p 148 A90-38084
Distortion and regulation characterization of a Mapham inverter
p 148 A90-38125
Electrical characterization of a Mapham inverter using pulse testing techniques
[NASA-TM-103254] p 82 N90-27784
- INVISCID FLOW**
Progress towards the development of an inviscid-viscous interaction method for unsteady flows in turbomachinery cascades
p 2 A90-11806
Application of a lower-upper implicit scheme and an interactive grid generation for turbomachinery flow field simulations
[ASME PAPER 89-GT-20] p 4 A90-23762
Splitting of inviscid fluxes for real gases
p 167 A90-25451
Inviscid flux-splitting algorithms for real gases with non-equilibrium chemistry
p 174 A90-52275
- ION BEAMS**
Fundamental tribological properties of ion-beam-deposited boron nitride films
p 124 A90-49054
Fundamental tribological properties of ion-beam-deposited boron nitride films
[NASA-TM-102088] p 125 N90-11881
Advances and directions of ion nitriding/carburizing
[NASA-TM-102398] p 137 N90-11902

ION DENSITY (CONCENTRATION)

- Ion drag for a negatively biased solar array in low earth orbit p 48 A90-36191

ION ENGINES

- Status of xenon ion propulsion technology p 56 A90-27961
- High-power xenon ion thrusters [AIAA PAPER 90-2540] p 64 A90-42536
- End-hall thrusters [AIAA PAPER 90-2595] p 64 A90-42570
- Xenon ion propulsion for orbit transfer [AIAA PAPER 90-2527] p 67 A90-52562
- Status of structural analysis of 30 cm diameter ion optics [AIAA PAPER 90-2649] p 215 A90-52571

ION EXCHANGE MEMBRANE ELECTROLYTES

- Hydrogen-oxygen proton-exchange membrane fuel cells and electrolyzers p 56 A90-33944
- Regenerative fuel cell systems for project Pathfinder p 74 A90-17708
- Electrocatalysis for oxygen electrodes in fuel cells and water electrolyzers for space applications p 230 A90-20468

ION IMPLANTATION

- Silicon carbide semiconductor device fabrication and characterization [NASA-CR-186354] p 258 A90-19873

ION IRRADIATION

- Radiation resistance studies of amorphous silicon films p 227 A90-14952

ION PROBES

- Development of a quadrupole-based Secondary-Ion Mass Spectrometry (SIMS) system at Lewis Research Center [NASA-TM-102531] p 87 A90-23476

ION PROPULSION

- Xenon ion sources for space applications p 56 A90-22874
- Status of xenon ion propulsion technology p 56 A90-27961
- High-power xenon ion thrusters [AIAA PAPER 90-2540] p 64 A90-42536
- Xenon ion propulsion for orbit transfer [AIAA PAPER 90-2527] p 67 A90-52562
- Performance of large area xenon ion thrusters for orbit transfer missions p 75 A90-18475

ION SHEATHS

- The sheath structure around a negatively charged rocket payload p 48 A90-34780

ION SOURCES

- Xenon ion sources for space applications p 56 A90-22874

IONIC CRYSTALS

- The mechanical properties of fluoride salts at elevated temperatures --- candidate thermal energy storage materials for solar dynamic systems p 123 A90-44376

IRIDIUM

- Iridium-coated rhenium thrusters by CVD p 114 A90-30480

IRON

- Studies of mechano-chemical interactions in the tribological behavior of materials [NASA-TM-102545] p 128 A90-21182

IRON ALLOYS

- Microstructure and tensile properties of Fe-40 at. pct Al alloys with C, Zr, Hf, and B additions p 108 A90-11651
- Oxidation behavior of FeAl + Hf, Zr, B p 113 A90-24858
- The effects of surface films on mechanical behavior of B2 ordered intermetallic alloys p 115 A90-44338
- Compatibility of Fe-40Al with various fibers p 94 A90-50496
- Identification of a cast iron alloy containing nonstrategic elements [NASA-CR-185174] p 118 A90-18559

IRON COMPOUNDS

- Identification of thermodynamically stable ceramic reinforcement materials for iron aluminide matrices p 89 A90-25238

- Influence of testing environment on the room temperature ductility of FeAl alloys p 115 A90-39658

IRON OXIDES

- Fe-57 and Sn-119 Moessbauer study of La₂CuO₄(-y), YBa₂Cu₃O₇(-y) and SmBa₂Cu₃O₇(-y) p 256 A90-34020

IRRADIATION

- Electron-beam induced damage in thin insulating films on compound semiconductors [NASA-CR-185177] p 151 A90-17987
- Electron beam induced damage in PECVD Si₃N₄ and SiO₂ films on InP [NASA-TM-102544] p 203 A90-20393
- Neutron and gamma irradiation effects on power semiconductor switches [NASA-TM-103200] p 155 A90-25278

ISOTROPIC MEDIA

- Viscoplasticity: A thermodynamic formulation [NASA-TM-102388] p 216 A90-14640
- Input-output characterization of fiber reinforced composites by P waves [NASA-CR-185287] p 208 A90-28097

ISOTROPY

- A thermoelastic transversely isotropic thick walled cylinder/disk application: An analytical solution and study [NASA-TM-102320] p 216 A90-12950
- A viscoplastic model with application to LiF-22 percent CaF₂ hypereutectic salt [NASA-TM-103181] p 221 A90-23770
- A creep model for metallic composites based on matrix testing: Application to Kanthal composites [NASA-TM-103172] p 101 A90-25193

ITERATION

- High accuracy solutions of incompressible Navier-Stokes equations [NASA-TM-102539] p 244 A90-21567
- Neuromorphic learning of continuous-valued mappings from noise-corrupted data. Application to real-time adaptive control [NASA-TM-4176] p 241 A90-25607

ITERATIVE SOLUTION

- Convergence acceleration for vector sequences and applications to computational fluid dynamics [AIAA PAPER 90-0338] p 160 A90-19804
- The MHOST finite element program: 3-D inelastic analysis methods for hot section components. Volume 3: Systems' manual [NASA-CR-182236] p 215 A90-10451
- Efficient implementation of minimal polynomial and reduced rank extrapolation methods [NASA-TM-103240] p 244 A90-26616

ITO (SEMICONDUCTORS)

- Hybrid solar cells based on dc magnetron sputtered films of n-ITO on APMOPE grown p-InP p 225 A90-14893
- Indium phosphide solar cell research in the United States: Comparison with non-photovoltaic sources p 229 A90-17758

J**J INTEGRAL**

- Method and models for R-curve instability calculations p 214 A90-50566

JET AIRCRAFT NOISE

- Mixer-ejector nozzle for jet noise suppression [AIAA PAPER 90-1909] p 247 A90-47202

JET ENGINES

- Test and theory for piezoelectric actuator-active vibration control of rotating machinery p 198 A90-46226
- The determination of third order linear models from a seventh order nonlinear jet engine model p 239 A90-52881

- WINCOF-I code for prediction of fan compressor unit with water ingestion [NASA-CR-185157] p 1 A90-21724

JET FLAPS

- Rotating primary flow induction using jet-flapped blades p 19 A90-12585

JET FLOW

- Elliptic jets. I - Characteristics of unexcited and excited jets p 159 A90-18071
- Calculation of turbulent three-dimensional jet-induced flow in a rectangular enclosure [AIAA PAPER 90-0684] p 161 A90-19976
- Lubricant jet flow phenomena in spur and helical gears with modified addendums - For radially directed individual jets p 194 A90-21122

- Phase development and its role on subharmonic control [AIAA PAPER 90-0503] p 166 A90-25035

- An experimental and numerical study of particle-laden coaxial jet flows p 171 A90-38799

- Three-dimensional compressible jet-in-crossflow calculations using improved viscosity models and adapted grid [AIAA PAPER 90-2100] p 174 A90-47206

- Flow visualization and motion analysis for a series of four sequential brush seals [AIAA PAPER 90-2482] p 199 A90-47222

- Viscous effects on the instability of an axisymmetric jet [NASA-TM-102396] p 12 A90-16719

JET IMPINGEMENT

- Theoretical model of discrete tone generation by impinging jets p 247 A90-35903

JET MIXING FLOW

- Buoyancy effects on the vapor condensation rate on a horizontal liquid surface [AIAA PAPER 90-0353] p 162 A90-22201

- Vapor condensation on liquid surface due to laminar jet-induced mixing - The effects of system parameters [AIAA PAPER 90-0354] p 163 A90-22202

- Total temperature effects on centerline Mach number characteristics of freejets p 6 A90-25290

- Buoyancy effects on the vapor condensation rate on a horizontal liquid surface [NASA-TM-102437] p 130 A90-13675

- Vapor condensation on liquid surface due to laminar jet-induced mixing: The effects of system parameters [NASA-TM-102433] p 176 A90-13751

JET NOZZLES

- The effect of electrode configuration on arcjet performance [NASA-TM-102346] p 70 A90-11081

JET PROPULSION

- Advanced core technology - Key to subsonic propulsion benefits [ASME PAPER 89-GT-241] p 19 A90-23890
- STOVL aircraft simulation for integrated flight and propulsion control research [NASA-TM-102419] p 26 A90-13389

JOINTS (JUNCTIONS)

- Characterization of damped structural connections for multi-component systems p 208 A90-16959
- A global approach for the identification of structural connection properties [NASA-TM-102502] p 218 A90-18745
- Thermo-oxidative stability studies of PMR-15 polymer matrix composites reinforced with various fibers [NASA-TM-102439] p 98 A90-19310
- Fiber pushout test: A three-dimensional finite element computational simulation [NASA-TM-102565] p 99 A90-21131

JOULE-THOMSON EFFECT

- Acquisition and correlation of cryogenic nitrogen mass flow data through a multiple orifice Joule-Thomson device [NASA-TM-103121] p 182 A90-22761

JOURNAL BEARINGS

- A high-speed photography study of cavitation in a dynamically loaded journal bearing [NASA-TM-103178] p 204 A90-26338

JUNCTION DIODES

- Contribution of the graded region of a HgCdTe diode to its saturation current p 257 A90-45948

JUNCTION TRANSISTORS

- Neutron and gamma irradiation effects on power semiconductor switches [NASA-TM-103200] p 155 A90-25278

K**K-EPSILON TURBULENCE MODEL**

- Simulating transitional flow and heat transfer over the flat plate and circular cylinder using a K-epsilon turbulence model p 168 A90-32171
- Near-wall turbulence model and its application to fully developed turbulent channel and pipe flows p 169 A90-37328

- Multigrid calculations of 3-D turbulent viscous flows p 172 A90-42426

- Diagonally inverted lower-upper factored implicit multigrid scheme for the three-dimensional Navier-Stokes equations p 174 A90-49789

- Investigation of turbulent flow in highly curved ducts with application to turbomachinery components [NASA-CR-186060] p 175 A90-12882

- Multigrid calculations of 3-D turbulent viscous flows [NASA-CR-185154] p 1 A90-13323

- Calculation of 3D turbulent jets in crossflow with a multigrid method and a second-moment closure model [NASA-TM-103159] p 184 A90-26282

- Modeling of near-wall turbulence [NASA-TM-103222] p 184 A90-28009

KALMAN FILTERS

- An adaptive human response mechanism controlling the V/STOL aircraft. Appendix 3: The adaptive control model of a pilot in V/STOL aircraft control loops [NASA-CR-186599] p 38 A90-21777

KEROSENE

- The measurement, modeling, and prediction of traction for rocket propellant 1 [NASA-CR-185186] p 131 A90-19386

KINEMATICS

- Theory of gearing [NASA-RP-1212] p 202 A90-19593
- Model development in viscoplastic ratchetting [NASA-TM-102509] p 219 A90-20431

- A viscoplastic model with application to LiF-22 percent CaF₂ hypereutectic salt [NASA-TM-103181] p 221 A90-23770

- A global approach for using kinematic redundancy to minimize base reactions of manipulators [NASA-CR-186825] p 234 A90-25499

KINETIC ENERGY

An improved k-epsilon model for near-wall turbulence and comparison with direct numerical simulation
[NASA-TM-103221] p 184 N90-27983

KINETIC EQUATIONS

Kinetics and mechanism of soot formation in hydrocarbon combustion
[NASA-CR-186162] p 106 N90-14305

KINETIC THEORY

Kinetic theory model for the flow of a simple gas from a two-dimensional nozzle
p 169 A90-37124

KNOWLEDGE BASES (ARTIFICIAL INTELLIGENCE)

Space Station power system autonomy demonstration
p 245 A90-10373

Autonomous power expert fault diagnostic system for Space Station Freedom electrical power system testbed
p 80 N90-25521

L**LABYRINTH SEALS**

An annular gas seal analysis using empirical entrance and exit region friction factors
[ASME PAPER 89-TRIB-46] p 196 A90-33555

LAGRANGIAN EQUILIBRIUM POINTS

Minimum fuel lunar trajectories for a low-thrust power-limited spacecraft
[AIAA PAPER 90-2975] p 41 A90-53054

LAMELLA (METALLURGY)

Tensile adhesion testing methodology for thermally sprayed coatings
p 85 A90-43902

LAMINAR BOUNDARY LAYER

Some characteristics of bypass transition in a heated boundary layer
p 169 A90-35183

Interactive calculation procedures for mixed compression inlets
[NASA-CR-186581] p 14 N90-25934

LAMINAR FLOW

A multi-domain spectral computation of three-dimensional laminar horseshoe vortex flow using incompressible Navier-Stokes equations
p 3 A90-17592

Two-dimensional convection and radiation with scattering from a Poiseuille flow
p 161 A90-20519

Ignition and behavior of laminar gas-jet diffusion flames in microgravity
p 103 A90-23107

Two-dimensional numerical simulation of a Stirling engine heat exchanger
p 170 A90-38290

A simplified model for two phase face seal design
p 187 A90-40713

Global pressure relaxation for laminar two-dimensional internal flow
p 174 A90-51019

Application of multi-grid methods for solving the Navier-Stokes equations
p 243 N90-14002

Viscous effects on the instability of an axisymmetric jet
[NASA-TM-102396] p 12 N90-16719

Saturated fluorescence measurements of the hydroxyl radical in laminar high-pressure flames
[NASA-CR-185218] p 190 N90-22022

LAMINAR MIXING

Buoyancy effects on the vapor condensation rate on a horizontal liquid surface
[AIAA PAPER 90-0353] p 162 A90-22201

Vapor condensation on liquid surface due to laminar jet-induced mixing - The effects of system parameters
[AIAA PAPER 90-0354] p 163 A90-22202

Buoyancy effects on the vapor condensation rate on a horizontal liquid surface
[NASA-TM-102437] p 130 N90-13675

Vapor condensation on liquid surface due to laminar jet-induced mixing: The effects of system parameters
[NASA-TM-102433] p 176 N90-13751

LAMINATES

Impact damage development in damaged composite materials
p 193 A90-18355

Laminate behavior for SiC fiber-reinforced reaction-bonded silicon nitride matrix composites
p 90 A90-29927

Tailoring of composite links for optimal damped elasto-dynamic performance
p 211 A90-30250

Analysis of impact response in composite plates
p 214 A90-47567

Use of unbalanced laminates as a screening method for microcracking
p 94 A90-50217

Mechanics of damping for fiber composite laminates including hygro-thermal effects
[NASA-TM-102329] p 95 N90-10185

Use of unbalanced laminates as a screening method for microcracking
[NASA-TM-102517] p 98 N90-21124

Computational simulation of structural fracture in fiber composites
[NASA-TM-102505] p 100 N90-21821

Reliability analysis of continuous fiber composite laminates
[NASA-CR-185265] p 223 N90-26372

LANDING INSTRUMENTS

Cooperative synthesis of control and display augmentation in approach and landing
p 36 A90-33061

LANTHANUM

Growth and patterning of laser ablated superconducting YBaCu3O7 films on LaAlO3 substrates
[NASA-TM-102436] p 259 N90-22421

LANTHANUM OXIDES

Antiferromagnetism in Co-57-doped La2CuO4-y studied by Moessbauer spectroscopy
p 255 A90-34011

Complex permittivity of lanthanum aluminate in the 20 to 300 K temperature range from 26.5 to 40.0 GHz
p 148 A90-37864

LAPLACE TRANSFORMATION

Galerkin finite difference Laplacian operators on isolated unstructured triangular meshes by linear combinations
[NASA-TM-103209] p 183 N90-26276

LARGE SPACE STRUCTURES

Selection of component modes
[AIAA PAPER 90-1201] p 210 A90-26787

Dynamic analysis of space-related linear and non-linear structures
[NASA-TM-103490] p 51 N90-25174

LASER ANEMOMETERS

Laser anemometer measurements in a transonic axial-flow fan rotor
[NASA-TP-2879] p 175 N90-11245

TiCl4 as a source of TiO2 particles for laser anemometry measurements in hot gas
[NASA-TM-102581] p 189 N90-20358

LASER APPLICATIONS

A laser based computer aided non-intrusive technique for full field flow characterization in macroscopic curved channels
p 168 A90-32293

Ellipsometric study of YBaCu3O7-x laser ablated and co-evaporated films
[NASA-TM-103223] p 259 N90-26682

Microwave conductivity of laser ablated YBaCuO superconducting films and its relation to microstrip transmission line
p 155 N90-27844

LASER BEAMS

Fiber optic detector probes for laser light scattering
p 192 A90-11593

Study of deposition of YBaCu3O7-x on cubic zirconia
[NASA-TM-102350] p 257 N90-10737

NASA Laser Light Scattering Advanced Technology Development Workshop, 1988
[NASA-CP-10033] p 188 N90-17085

Critical fluid light scattering
p 251 N90-17087

Polymer solution phase separation: Microgravity simulation
p 127 N90-17101

Laser diffraction particle sizing: Instrument probe volume relocation and elongation
[NASA-TM-102512] p 188 N90-18025

Acousto-ultrasonic nondestructive evaluation of materials using laser beam generation and detection
[NASA-CR-186694] p 154 N90-23664

Beam rider for an Articulated Robot Manipulator (ARM) accurate positioning of long flexible manipulators
[NASA-CR-185151] p 241 N90-26581

LASER DOPPLER VELOCIMETERS

Development of a phase Doppler based probe for icing cloud droplet characterization
[AIAA PAPER 90-0667] p 186 A90-26978

Application of two-component phase Doppler interferometry to the measurement of particle size, mass flux, and velocities in two-phase flows
p 186 A90-32853

Three dimensional LDV flow measurements and theoretical investigation in a radial inflow turbine scroll
p 9 A90-46860

Euler analysis comparison with LDV data for an advanced counter-rotation propfan at cruise
[AIAA PAPER 90-3033] p 9 A90-50637

An LDA investigation of the normal shock wave boundary layer interaction
p 10 A90-52618

Laser velocimeter and total pressure measurements in circular-to-rectangular transition ducts
[NASA-CR-182286] p 177 N90-14494

Laser-velocimeter-measured flow field around an advanced, swept, eight-blade propeller at Mach 0.8
[NASA-TP-2462] p 1 N90-20942

Euler analysis comparison with LDV data for an advanced counter-rotation propfan at cruise
[NASA-TM-103249] p 14 N90-25946

LASER HEATING

Hardware development for the surface tension driven convection experiment
p 52 A90-36195

LASER INDUCED FLUORESCENCE

Saturated fluorescence measurements of the hydroxyl radical in laminar high-pressure flames
[NASA-CR-185218] p 190 N90-22022

LASER INTERFEROMETRY

Skin friction measurements by laser interferometry in swept shock/boundary-layer interactions
p 3 A90-18153

LASER OUTPUTS

Fiber optic sensing system
[NASA-CASE-LEW-14795-1] p 251 N90-15733

Design of a CO2 laser power control system for a Spacelab microgravity experiment
[NASA-TM-103112] p 192 N90-28833

LASER PROPULSION

Optics and materials considerations for a laser-propelled lightsail
[IAF PAPER 89-664] p 54 A90-13668

LASERS

Laser diffraction particle sizing: Instrument probe volume relocation and elongation
[NASA-TM-102512] p 188 N90-18025

Performance and modeling of superconducting ring resonators at millimeter-wave frequencies
[NASA-TM-102526] p 151 N90-18634

Growth and patterning of laser ablated superconducting YBaCu3O7 films on LaAlO3 substrates
[NASA-TM-102436] p 259 N90-22421

Lunar orbiting microwave beam power system
[NASA-TM-103211] p 51 N90-25173

LATERAL OSCILLATION

An active optimal control strategy of rotor vibrations using external forces
p 198 A90-46224

LATTICE PARAMETERS

Synthesis and structural chemistry of Au(III)-substituted Ba2YCu3O(7-delta)
[NASA-TM-103292] p 108 N90-28696

LAUNCH VEHICLE CONFIGURATIONS

A superconducting quenchgun for delivering lunar derived oxygen to lunar orbit
[AIAA PAPER 90-2369] p 43 A90-40627

LAUNCH VEHICLES

Atomic hydrogen as a launch vehicle propellant
[AIAA PAPER 90-0715] p 44 A90-23712

Advanced Launch System (ALS) actuation and power systems impact operability and cost
p 69 A90-52955

Atomic hydrogen as a launch vehicle propellant
[NASA-TM-102459] p 73 N90-14284

Advanced launch vehicle propulsion at the NASA Lewis Research Center
[NASA-TM-103096] p 45 N90-20110

Advanced Launch System (ALS): Electrical actuation and power systems improve operability and cost picture
[NASA-TM-102547] p 152 N90-21271

LEACHING

Humidity-induced room-temperature decomposition of Au contacted indium phosphide
p 105 A90-44689

LEAD (METAL)

Effects of crucible wetting during solidification of immiscible Pb-Zn alloys
p 132 A90-17825

LEAD ALLOYS

Side branch morphology and coarsening in directionally solidified Pb-8.4 at. pct Au
p 109 A90-11658

Efficient estimation of diffusion during dendritic solidification
p 111 A90-20612

Primary arm spacing in directionally solidified Pb-10 wt pct Sn alloys
[AIAA PAPER 90-0740] p 132 A90-23713

Primary arm spacing in directionally solidified Pb-10 wt percent Sn alloys
[NASA-CR-185190] p 134 N90-14398

LEAD COMPOUNDS

Catalysts for ultrahigh current density oxygen cathodes for space fuel cell applications
[NASA-CR-180650] p 232 N90-22835

LEADING EDGES

Development of an unstructured mesh/Navier-Stokes method for aerodynamics of aircraft with ice accretions
[AIAA PAPER 90-0758] p 4 A90-20011

Thermal/structural analyses of several hydrogen-cooled leading-edge concepts for hypersonic flight vehicles
[AIAA PAPER 90-0053] p 164 A90-23702

An experimental study of turbine vane heat transfer with leading edge and downstream film cooling
[ASME PAPER 89-GT-69] p 165 A90-23792

The low frequency oscillation in the flow over a NACA0012 airfoil with an 'iced' leading edge
p 8 A90-46377

Thermal/structural analyses of several hydrogen-cooled leading-edge concepts for hypersonic flight vehicles
[NASA-TM-102391] p 177 N90-14511

Large-scale advanced propeller blade pressure distributions: Prediction and data
[NASA-TM-102316] p 30 N90-22564

SUBJECT INDEX

- Finite element elastic-plastic-creep and cyclic life analysis of a cowl lip
[NASA-TM-102342] p 220 N90-22808
- LEAKAGE**
A simplified model for two phase face seal design
p 197 A90-40713
Requirements for long-life operation of inert gas hollow cathodes - Preliminary results
[AIAA PAPER 90-2586] p 69 A90-52570
High temperature flexible seal
[NASA-CASE-LEW-14695-1] p 204 N90-23751
Requirements for long-life operation of inert gas hollow cathodes: Preliminary report
[NASA-TM-103242] p 82 N90-27783
- LEAST SQUARES METHOD**
Least-squares finite element method for fluid dynamics
p 159 A90-18246
Least-squares finite element methods for compressible Euler equations
p 9 A90-51013
A least-squares finite element method for incompressible Navier-Stokes problems
[NASA-TM-102385] p 242 N90-12231
- LENS DESIGN**
Optics and materials considerations for a laser-propelled lightsail
[IAF PAPER 89-664] p 54 A90-13668
Conceptual design study of a 5 kilowatt solar dynamic Brayton power system using a dome Fresnel lens solar concentrator
[NASA-CR-185134] p 72 N90-14281
- LENSES**
Laser diffraction particle sizing: Instrument probe volume relocation and elongation
[NASA-TM-102512] p 188 N90-18025
- LEVELING**
The effect of leveling coatings on the atomic oxygen durability of solar concentrator surfaces
[NASA-TM-102557] p 76 N90-21110
- LIBRARIES**
Hypercluster parallel processing library user's manual
[NASA-CR-185231] p 237 N90-21552
- LIFE (DURABILITY)**
Review of the environmental effects on the Space Station Freedom photovoltaic power module
p 59 A90-38087
Advanced tube-bundle rocket thrust chamber
[AIAA PAPER 90-2726] p 67 A90-47227
Requirements for long-life operation of inert gas hollow cathodes - Preliminary results
[AIAA PAPER 90-2586] p 69 A90-52570
Mean stress and the exhaustion of fatigue-damage resistance
p 216 N90-13819
Advanced Turbine Technology Applications Project (ATTAP)
[NASA-CR-185109] p 263 N90-14153
Bearing and gear steels for aerospace applications
[NASA-TM-102529] p 202 N90-20391
Characterization testing of a 40 AHR bipolar nickel-hydrogen battery
p 230 N90-20463
Effect of KOH concentration on LEO cycle life of IPV nickel-hydrogen flight battery cells
[NASA-TM-103127] p 77 N90-21116
Electrochemical impregnation and cycle life of lightweight nickel electrodes for nickel-hydrogen cells
[NASA-TM-103140] p 107 N90-21844
Finite element elastic-plastic-creep and cyclic life analysis of a cowl lip
[NASA-TM-102342] p 220 N90-22808
Advanced tube-bundle rocket thrust chamber
[NASA-TM-103139] p 80 N90-25185
Requirements for long-life operation of inert gas hollow cathodes: Preliminary report
[NASA-TM-103242] p 82 N90-27783
Structural response of SSME turbine blade airfoils
p 224 N90-28649
Thermal analysis of thermal barrier coatings in a high heat flux environment
p 129 N90-28652
Ceramic matrix composites in simulated SSME environments
p 102 N90-28655
- LIFE SUPPORT SYSTEMS**
A solar power system for an early Mars expedition
[NASA-TM-103219] p 246 N90-28393
- LIFT**
Numerical solutions of the linearized Euler equations for unsteady vortical flows around lifting airfoils
[AIAA PAPER 90-0694] p 5 A90-25041
- LIFTING BODIES**
Numerical solutions of the linearized Euler equations for unsteady vortical flows around lifting airfoils
p 7 A90-30264
- LIGHT EMITTING DIODES**
Fiber optic sensing system
[NASA-CASE-LEW-14795-1] p 251 N90-15733

LIGHT MODULATION

- Control of a GaAs monolithic Ka-band phase shifter using a high-speed optical interconnect
p 150 A90-41700

LIGHT SCATTERING

- Fiber optic detector probes for laser light scattering
p 192 A90-11593
Droplet sizing instrumentation used for icing research: Operation, calibration, and accuracy
[NASA-CR-182293] p 187 N90-11999
NASA Laser Light Scattering Advanced Technology Development Workshop, 1988
[NASA-CP-10033] p 188 N90-17085
Critical fluid light scattering
p 251 N90-17087
Polymer solution phase separation: Microgravity simulation
p 127 N90-17101
Optical characterization of clouds of fine liquid-nitrogen particles
[NASA-TM-103208] p 191 N90-26299

LIGHT SOURCES

- Fiber optic sensing systems using high frequency resonant sensing heads with intensity sensors
p 185 A90-10472

LINEAR EQUATIONS

- Efficient implementation of minimal polynomial and reduced rank extrapolation methods
[NASA-TM-103240] p 244 N90-26616

LINEAR QUADRATIC REGULATOR

- Extended implicit model following as applied to integrated flight and propulsion control
[AIAA PAPER 90-3444] p 239 A90-47697

LINEAR SYSTEMS

- The determination of third order linear models from a seventh order nonlinear jet engine model
p 239 A90-52881
Parallel algorithms for boundary value problems
[NASA-TM-102498] p 243 N90-19783
Parallel/distributed direct method for solving linear systems
[NASA-TM-103229] p 244 N90-26614

LINEARITY

- Dynamic loading of spur gears with linear or parabolic tooth profile modifications
p 195 A90-21126

LININGS

- Steam cooled rich-burn combustor liner
[NASA-CASE-LEW-13609-1] p 106 N90-11824
Elasticity effects on cavitation in a squeeze film damper undergoing noncentered circular whirl
[NASA-TM-102392] p 200 N90-13786
MATE (Materials for Advanced Turbine Engines) Program, Project 3. Volume 2: Design, fabrication and evaluation of an oxide dispersion strengthened sheet alloy combustor liner
[NASA-CR-180892] p 117 N90-17868
Hydrocarbon-fuel/combustion-chamber-liner materials compatibility
[NASA-CR-185203] p 118 N90-21165
Energy efficient engine pin fin and ceramic composite segmented liner combustor sector rig test report
[NASA-CR-179534] p 35 N90-28567

LINKAGES

- Tailoring of composite links for optimal damped elasto-dynamic performance
p 211 A90-30250

LIQUEFIED GASES

- High speed commercial transport fuels considerations and research needs
[NASA-TM-102535] p 131 N90-21869

LIQUID ATOMIZATION

- Scattered-light scanner measurements of cryogenic liquid-jet breakup
[NASA-TM-102432] p 189 N90-22021

LIQUID COOLING

- Rate correlation for condensation of pure vapor on turbulent, subcooled liquid
p 174 A90-50511

LIQUID FLOW

- Scaling results for the liquid sheet radiator
p 170 A90-38037
The role of gravity on macrosegregation in alloys
[NASA-CR-186530] p 136 N90-25238

LIQUID FUELS

- Theory of influence of a low-volatility, soluble impurity on spherically-symmetric combustion of fuel droplets
p 104 A90-28771

- High energy-density liquid rocket fuel performance
[AIAA PAPER 90-1968] p 130 A90-47204

LIQUID HYDROGEN

- COLD-SAT - An orbital cryogenic hydrogen technology experiment
[IAF PAPER 89-057] p 53 A90-13282
Spacecraft attitude impacts on COLD-SAT non-vacuum jacketed LH2 supply tank thermal performance
[AIAA PAPER 90-1672] p 49 A90-41566
Initial experimentation on the nonvented fill of a 0.14 cu m (5 cu ft) dewar with nitrogen and hydrogen
[AIAA PAPER 90-1681] p 136 A90-50641

LIQUID-SOLID INTERFACES

- Initial experimentation on the nonvented fill of a 0.14m3 (5 ft. 3) dewar with nitrogen and hydrogen
[NASA-TM-103155] p 183 N90-26278

LIQUID INJECTION

- Liquid Transfer Cryogenic Test Facility: Initial hydrogen and nitrogen non-vent fill data
[NASA-TM-102572] p 179 N90-21295

LIQUID METALS

- Liquid alkali metals - Equation of state and reduced-pressure, bulk-modulus, sound-velocity, and specific-heat functions
p 102 A90-16280
Mathematical modeling and analysis of heat pipe start-up from the frozen state
p 174 A90-48404

LIQUID NITROGEN

- Initial experimentation on the nonvented fill of a 0.14 cu m (5 cu ft) dewar with nitrogen and hydrogen
[AIAA PAPER 90-1681] p 136 A90-50641
Acquisition and correlation of cryogenic nitrogen mass flow data through a multiple orifice Joule-Thomson device
[NASA-TM-103121] p 182 N90-22761
Initial experimentation on the nonvented fill of a 0.14m3 (5 ft. 3) dewar with nitrogen and hydrogen
[NASA-TM-103155] p 183 N90-26278
Optical characterization of clouds of fine liquid-nitrogen particles
[NASA-TM-103208] p 191 N90-26299

LIQUID OXYGEN

- A superconducting quenchgun for delivering lunar derived oxygen to lunar orbit
[AIAA PAPER 90-2369] p 43 A90-40627
Corrosion prevention in copper combustion chamber liners of liquid oxygen/methane booster engines
[AIAA PAPER 90-2119] p 85 A90-42028
Cooling of rocket thrust chambers with liquid oxygen
[AIAA PAPER 90-2120] p 63 A90-42029
A superconducting quenchgun for delivering lunar derived oxygen to lunar orbit
[NASA-CR-185161] p 77 N90-21806
Cooling of rocket thrust chambers with liquid oxygen
[NASA-TM-103146] p 78 N90-22605
Oxygen/methane combustion stability investigation
p 107 N90-28628

LIQUID PHASE EPITAXY

- The photovoltaic properties of an Al In As/InP heterojunctions grown by LPE method
[NASA-CR-185996] p 229 N90-13886

LIQUID PHASES

- Two-dimensional model of a Space Station Freedom thermal energy storage canister
[NASA-TM-103124] p 183 N90-26279

LIQUID PROPELLANT ROCKET ENGINES

- Health Monitoring System for the SSME-fault detection algorithms
[AIAA PAPER 90-1988] p 63 A90-40584
Cooling of rocket thrust chambers with liquid oxygen
[AIAA PAPER 90-2120] p 63 A90-42029
A rocket engine design expert system
[NASA-TM-102373] p 69 N90-10172
Cooling of rocket thrust chambers with liquid oxygen
[NASA-TM-103146] p 78 N90-22605

LIQUID ROCKET PROPELLANTS

- High energy-density liquid rocket fuel performance
[AIAA PAPER 90-1968] p 130 A90-47204
Advanced propulsion for LEO and GEO platforms
[AIAA PAPER 90-2551] p 68 A90-52565
Extended temperature range rocket injector
[NASA-CASE-LEW-14846-1] p 73 N90-15130
Advanced propulsion for LEO and GEO platforms
[NASA-TM-103228] p 82 N90-27785
High energy-density liquid rocket fuel performance
[NASA-CR-185279] p 131 N90-28742

LIQUID SLOSHING

- Effects of g-jitter on a thermal, buoyant flow
[AIAA PAPER 90-0653] p 163 A90-22239

LIQUID SURFACES

- Surface entropy of liquids via a direct Monte Carlo approach - Application to liquid Si
p 261 A90-31675
Surface reorientation and settling in cylinders upon step reduction in gravity
p 172 A90-44541

LIQUID-SOLID INTERFACES

- Side branch morphology and coarsening in directionally solidified Pb-8.4 at. pct Au
p 109 A90-11658
Inverse heat transfer analysis of Bridgman crystal growth
p 157 A90-13093
Effects of crucible wetting during solidification of immiscible Pb-Zn alloys
p 132 A90-17825
Effects of crystal-melt interfacial energy anisotropy on dendritic morphology and growth kinetics
p 253 A90-19284
Free dendritic growth in viscous melts - Cyclohexanol
p 253 A90-19285
Interface demarcation in GaAs by current pulsing
[AIAA PAPER 90-0319] p 254 A90-19793
Determination of the mean solid-liquid interface energy of pivalic acid
p 84 A90-22646

LIQUID-VAPOR EQUILIBRIUM

- Critical speeding up in pure fluids p 167 A90-26369
Surface reorientation and settling in cylinders upon step reduction in gravity p 172 A90-44541

LIQUID-VAPOR INTERFACES

- Buoyancy effects on the vapor condensation rate on a horizontal liquid surface
[AIAA PAPER 90-0353] p 162 A90-22201
Vapor condensation on liquid surface due to laminar jet-induced mixing - The effects of system parameters [AIAA PAPER 90-0354] p 163 A90-22202
The coupling of Marangoni and capillary instabilities in an annular thread of liquid p 171 A90-38978
Surface reorientation and settling in cylinders upon step reduction in gravity p 172 A90-44541
Buoyancy effects on the vapor condensation rate on a horizontal liquid surface [NASA-TM-102437] p 130 N90-13675
Vapor condensation on liquid surface due to laminar jet-induced mixing: The effects of system parameters [NASA-TM-102433] p 176 N90-13751

LITHIUM

- The shocking development of lithium (and boron) in supernovae p 264 A90-17643

LITHIUM FLUORIDES

- Intergranular fracture of lithium fluoride-22 percent calcium fluoride hypereutectic salt at 800 K p 121 A90-25273
The mechanical properties of fluoride salts at elevated temperatures --- candidate thermal energy storage materials for solar dynamic systems p 123 A90-44376
Deformation of as-cast LiF-22 mol pct CaF₂ hypereutectic salt between 500 and 1015 K p 124 A90-49086
Hot filament technique for measuring the thermal conductivity of molten lithium fluoride [NASA-TM-102506] p 127 N90-19373
A viscoplastic model with application to LiF-22 percent CaF₂ hypereutectic salt [NASA-TM-103181] p 221 N90-23770

LITHIUM HYDROXIDES

- Mechanical properties of pure nickel alloys after long term exposures to LiOH and vacuum at 775 K [NASA-TM-102403] p 118 N90-20181

LOAD DISTRIBUTION (FORCES)

- High temperature inelastic deformation under uniaxial loading - Theory and experiment p 109 A90-13838
Computer-aided design of high-contact-ratio gears for minimum dynamic load and stress [NASA-TM-103275] p 205 N90-28065

LOAD TESTING MACHINES

- Fully articulated four-point-bend loading fixture [NASA-CASE-LEW-14776-1] p 201 N90-15445

LOAD TESTS

- Composites boost 21st-century aircraft engines p 90 A90-29704

LOADING RATE

- On the mechanism of cross slip in Ni₃Al p 111 A90-20611

LOADS (FORCES)

- Distortion and regulation characterization of a Mapham inverter p 148 A90-38125
Effects of state recovery on creep buckling under variable loading p 212 A90-41223
A modified VAPEPS method for predicting vibroacoustic response of unreinforced mass loaded honeycomb panels p 206 A90-43731
Arcjet load characteristics [AIAA PAPER 90-2579] p 67 A90-47226
Integrated force method versus displacement method for finite element analysis [NASA-TP-2937] p 218 N90-18081
Fastener design manual [NASA-RP-1228] p 202 N90-18740
Experimentally determined wear behavior of an Al₂O₃-SiC composite from 25 to 1200 C [NASA-TM-102549] p 87 N90-20130
Composite laminate tailoring with probabilistic constraints and loads [NASA-TM-102515] p 98 N90-20138
COMGEN: A computer program for generating finite element models of composite materials at the micro level [NASA-TM-102556] p 219 N90-20438
An expert system for simulating electric loads aboard Space Station Freedom [NASA-TM-103150] p 240 N90-22325
Fatigue testing apparatus [NASA-CASE-LEW-14124-1] p 190 N90-23712
Arcjet load characteristics [NASA-TM-103190] p 79 N90-25181
An analysis of space power system masses [NASA-TM-103199] p 80 N90-25184
An unsteady lifting surface method for single rotation propellers [NASA-CR-4302] p 14 N90-25940

- Energy Efficient Engine high pressure turbine component test performance report [NASA-CR-168289] p 33 N90-28553
Probabilistic structural analysis methods development for SSME p 83 N90-28616

LOCAL AREA NETWORKS

- AIRNET: A real-time communications network for aircraft [NASA-CR-186140] p 145 N90-24514

LONG DURATION SPACE FLIGHT

- The International Space University [AIAA PAPER 90-2389] p 261 A90-42152
The International Space University [NASA-TM-103163] p 78 N90-22604

LOSSES

- FLUSH: A tool for the design of slush hydrogen flow systems [NASA-TM-102467] p 130 N90-17890
Nickel-hydrogen capacity loss on storage p 231 N90-20478
High frequency, high temperature specific core loss and dynamic B-H hysteresis loop characteristics of soft magnetic alloys [NASA-TM-103164] p 154 N90-23663

LOSSY MEDIA

- Constitutive parameter measurements of lossy materials [NASA-CR-183398] p 257 N90-11603

LOW ALTITUDE

- Theory of plasma contactors in ground-based experiments and low earth orbit p 150 A90-47108

LOW ASPECT RATIO

- Augmented heat transfer in rectangular channels of narrow aspect ratios with rib turbulators p 157 A90-13091
Ground-based experiments on thermal and thermosolutal convection in inclined low-aspect-ratio enclosures [AIAA PAPER 90-0413] p 166 A90-25033

LOW FREQUENCIES

- The low frequency oscillation in the flow over a NACA0012 airfoil with an 'iced' leading edge p 8 A90-46377

LOW PRESSURE

- NASA/GE Energy Efficient Engine low pressure turbine scaled test vehicle performance report [NASA-CR-168290] p 34 N90-28563

LOW REYNOLDS NUMBER

- The growth and development of a turbulent junction vortex system p 173 A90-46902
Numerical solution for the velocity-derivative skewness of a low-Reynolds-number decaying Navier-Stokes flow [NASA-TM-103186] p 184 N90-27985

LOW SPEED

- Low velocity impact analysis with NASTRAN p 221 N90-24647

LOW SPEED WIND TUNNELS

- Engine inlet distortion in a 9.2 percent scaled vectored thrust STOVL model in ground effect [AIAA PAPER 89-2910] p 5 A90-25043
Comparison between design and installed acoustic characteristics of NASA Lewis 9- by 15-foot low-speed wind tunnel acoustic treatment [NASA-TP-2996] p 38 N90-19242

LOW THRUST

- Optimal orbital rendezvous using high and low thrust [AAS PAPER 89-354] p 41 A90-46786
Low thrust rocket test facility [AIAA PAPER 90-2503] p 43 A90-47225
A trajectory generation and system characterization model for cislunar low-thrust spacecraft. Volume 2: Technical manual [NASA-CR-185172] p 77 N90-21807
Low thrust rocket test facility [NASA-TM-103206] p 43 N90-25158

LOW THRUST PROPULSION

- Minimum fuel trajectories for a low-thrust power-limited mission to the moon and to Lagrange points L4 and L5 [AAS PAPER 89-351] p 40 A90-46784
Comparison of solution approaches for minimum-fuel, low-thrust, power-limited orbital transfers [AIAA PAPER 90-2960] p 41 A90-53035
Minimum fuel lunar trajectories for a low-thrust power-limited spacecraft [AIAA PAPER 90-2975] p 41 A90-53054
Advanced onboard propulsion benefits and status [NASA-TM-103174] p 82 N90-27786

LUBRICANTS

- The role of thermal and lubricant boundary layers in the transient thermal analysis of spur gears p 194 A90-21118
Plasma-deposited amorphous hydrogenated carbon films and their tribological properties p 123 A90-44864

- Plasma-deposited amorphous hydrogenated carbon films and their tribological properties [NASA-TM-102379] p 125 N90-11880

- Influence of the deposition conditions on radiofrequency magnetron sputtered MoS₂ films [NASA-TP-2994] p 137 N90-21210

- Self-lubricating polymer composites and polymer transfer film lubrication for space applications [NASA-TM-102492] p 128 N90-21862

- Bearing elastohydrodynamic lubrication: A complex calculation made simple [NASA-TM-102575] p 203 N90-22041

- A high-speed photography study of cavitation in a dynamically loaded journal bearing [NASA-TM-103178] p 204 N90-26338

LUBRICATING OILS

- Tribological reactions of perfluoroalkyl polyether oils with stainless steel under ultrahigh vacuum conditions at room temperature p 120 A90-16278
Effects of lubrication on the performance of high speed spur gears p 194 A90-21119
X-ray photoelectron spectroscopy peak assignment for perfluoropolyether oils p 124 A90-48550
Liquid lubrication in space [NASA-RP-1240] p 205 N90-28063

LUBRICATION

- Lubricant jet flow phenomena in spur and helical gears with modified addendums - For radially directed individual jets p 194 A90-21122
Efficient numerical method for computation of thermohydrodynamics of laminar lubricating films [NASA-CR-185136] p 175 N90-11256
Tribological properties of ceramic/Ti₃Al-Nb sliding couples for use as candidate seal materials to 700 deg C [NASA-TM-102401] p 86 N90-12658

- On the numerical solution of the dynamically loaded hydrodynamic lubrication of the point contact problem [NASA-TM-102427] p 178 N90-17076

- Bearing elastohydrodynamic lubrication: A complex calculation made simple [NASA-TM-102575] p 203 N90-22041
Liquid lubrication in space [NASA-RP-1240] p 205 N90-28063

LUBRICATION SYSTEMS

- Liquid lubrication in space [NASA-RP-1240] p 205 N90-28063

LUMINOUS INTENSITY

- Fiber optic sensing systems using high frequency resonant sensing heads with intensity sensors p 185 A90-10472

LUNAR BASES

- Photovoltaic power for a lunar base [IAF PAPER 89-254] p 42 A90-13409
Lunar production of space photovoltaic arrays p 226 A90-14930
Solar power for the lunar night p 266 A90-24814
Degradation of the lunar vacuum by a moon base p 266 A90-35441

- Comparison of solar photovoltaic and nuclear reactor power systems for a human-tended lunar observatory p 42 A90-38030

- Power for the moon: Is microwave power beaming an option? p 69 N90-10158

- SP-100 power system conceptual design for lunar base applications [NASA-TM-102090] p 267 N90-15030

- Energy storage for a lunar base by the reversible chemical reaction: CaO + H₂O reversible reaction Ca(OH)₂ [NASA-TM-103145] p 233 N90-25419

- Figure of merit studies of beam power concepts for advanced space exploration [NASA-CR-186720] p 146 N90-26234

LUNAR CRUST

- Lunar production of solar cells - A near-term product for a lunar industrial facility p 42 A90-24791

LUNAR EXPLORATION

- Applicability of the beamed power concept to lunar rovers, construction, mining, explorers and other mobile equipment p 69 N90-10159

LUNAR LAUNCH

- A superconducting quenchgun for delivering lunar derived oxygen to lunar orbit [AIAA PAPER 90-2369] p 43 A90-40627

LUNAR OBSERVATORIES

- Comparison of solar photovoltaic and nuclear reactor power systems for a human-tended lunar observatory p 42 A90-38030

- Human exploration mission studies p 40 N90-20457

LUNAR ORBITS

- Space vehicle propulsion systems - Environmental space hazards [AIAA PAPER 90-1881] p 63 A90-40545

SUBJECT INDEX

- Minimum fuel lunar trajectories for a low-thrust power-limited spacecraft [AIAA PAPER 90-2975] p 41 A90-53054
- A superconducting quenchgun for delivering lunar derived oxygen to lunar orbit [NASA-CR-185161] p 77 N90-21806
- LUNAR ROCKS**
- Lunar production of space photovoltaic arrays p 226 A90-14930
- LUNAR ROVING VEHICLES**
- Applicability of the beamed power concept to lunar rovers, construction, mining, explorers and other mobile equipment p 69 N90-10159
- LUNAR SOIL**
- Lunar production of solar cells - A near-term product for a lunar industrial facility p 42 A90-24791
- Energy storage for a lunar base by the reversible chemical reaction: $\text{CaO} + \text{H}_2\text{O}$ reversible reaction Ca(OH)_2 [NASA-TM-103145] p 233 N90-25419
- LUNAR SPACECRAFT**
- Lunar missions using advanced chemical propulsion - System design issues [AIAA PAPER 90-2431] p 67 A90-47221

M

- MACH NUMBER**
- Total temperature effects on centerline Mach number characteristics of freejets p 6 A90-25290
- Comparison of 3-D viscous flow computations of Mach 5 inlet with experimental data [AIAA PAPER 90-0600] p 6 A90-26970
- On the instabilities of supersonic mixing layers - A high-Mach-number asymptotic theory p 8 A90-42644
- Instabilities and subharmonic resonances of subsonic heated round jets, volume 2 [NASA-CR-186058] p 181 N90-22017
- MACHINE TOOLS**
- Computerized inspection of gear tooth surfaces [NASA-TM-102395] p 203 N90-22054
- MACHINERY**
- Elements of active vibration control for rotating machinery [NASA-TM-102368] p 137 N90-22703
- MAGNETIC BEARINGS**
- Development of a compact, light weight magnetic bearing [AIAA PAPER 90-2483] p 199 A90-47223
- MAGNETIC COOLING**
- Feasibility analysis of reciprocating magnetic heat pumps [NASA-CR-186205] p 177 N90-15363
- MAGNETIC EFFECTS**
- The effects of magnetic nozzle configurations on plasma thrusters [NASA-CR-186465] p 76 N90-21109
- MAGNETIC FIELD CONFIGURATIONS**
- Experimental evidence of a dimensional crossover in $\text{YBa}_2\text{Cu}_3\text{O}_{7-\delta}$ p 255 A90-29739
- MAGNETIC FIELDS**
- Hyperfine magnetic field on Cd-111 in Heusler alloys Co_2MnZ ($\text{Z} = \text{Si, Ga, Ge, Sn}$) p 255 A90-34012
- Preliminary evaluation of space station transmission line in a ring configuration [NASA-TM-102461] p 74 N90-17677
- The effects of magnetic nozzle configurations on plasma thrusters [NASA-CR-186465] p 76 N90-21109
- MAGNETIC FLUX**
- High frequency, high temperature specific core loss and dynamic B-H hysteresis loop characteristics of soft magnetic alloys [NASA-TM-103164] p 154 N90-23663
- MAGNETIC MEASUREMENT**
- Experimental evidence of a dimensional crossover in $\text{YBa}_2\text{Cu}_3\text{O}_{7-\delta}$ p 255 A90-29739
- High frequency, high temperature specific core loss and dynamic B-H hysteresis loop characteristics of soft magnetic alloys [NASA-TM-103164] p 154 N90-23663
- MAGNETIZATION**
- Hyperfine magnetic field on Cd-111 in Heusler alloys Co_2MnZ ($\text{Z} = \text{Si, Ga, Ge, Sn}$) p 255 A90-34012
- MAGNETOHYDRODYNAMIC FLOW**
- The effects of magnetic nozzle configurations on plasma thrusters [NASA-CR-186465] p 76 N90-21109
- MAGNETOPLASMA DYNAMICS**
- Diagnostics and performance of a 1/4-scale MPD thruster [AIAA PAPER 90-2665] p 65 A90-42625
- Multimegawatt electric propulsion system design considerations [AIAA PAPER 90-2552] p 68 A90-52566
- Geometric effects in applied-field MPD thrusters [AIAA PAPER 90-2669] p 69 A90-52572
- Design of a thrust stand for high power electric propulsion devices [NASA-TM-102372] p 73 N90-15992
- Test facility and preliminary performance of a 100 kW class MPD thruster p 75 N90-18476
- Geometric effects in applied-field MPD thrusters [NASA-TM-103259] p 82 N90-27782
- MAGNETOSPHERIC ELECTRON DENSITY**
- Computer modeling of current collection by the CHARGE-2 mother payload p 252 A90-24933
- MAGNETOSPHERIC ION DENSITY**
- Computer modeling of current collection by the CHARGE-2 mother payload p 252 A90-24933
- MAGNETRON SPUTTERING**
- Hybrid solar cells based on dc magnetron sputtered films of n-ITO on APMOPE grown p-InP p 225 A90-14893
- Investigation of buried homojunctions in p-InP formed during sputter deposition of both indium tin oxide and indium oxide p 256 A90-36799
- Influence of the deposition conditions on radiofrequency magnetron sputtered MoS_2 films [NASA-TP-2994] p 137 N90-21210
- MAINTAINABILITY**
- Space Station Freedom power - A reliability, availability, and maintainability assessment of the proposed Space Station Freedom electric power system p 58 A90-38074
- Space Station Freedom electric power system availability study [NASA-CR-185181] p 50 N90-20120
- MAINTENANCE**
- The US space station and its electric power system [NASA-TM-101974] p 71 N90-13596
- Autonomous power expert fault diagnostic system for Space Station Freedom electrical power system testbed p 80 N90-25521
- MAN ENVIRONMENT INTERACTIONS**
- Degradation of the lunar vacuum by a moon base p 266 A90-35441
- MAN MACHINE SYSTEMS**
- An adaptive human response mechanism controlling the V/STOL aircraft. Appendix 3: The adaptive control model of a pilot in V/STOL aircraft control loops [NASA-CR-186599] p 38 N90-21777
- MAN-COMPUTER INTERFACE**
- The Environment-Power System Analysis Tool development program --- for spacecraft power supplies p 236 A90-38089
- MANAGEMENT ANALYSIS**
- Middle management of research [NASA-TM-102417] p 262 N90-20901
- MANAGEMENT PLANNING**
- Toward an electrical power utility for space exploration p 74 N90-17681
- The Pathfinder chemical transfer propulsion program p 74 N90-18471
- MANAGEMENT SYSTEMS**
- Detection of potential space station control/structure interaction with CO-ST-IN p 50 N90-21074
- Automated electric power management and control for Space Station Freedom [NASA-TM-103151] p 240 N90-23125
- Health management system for rocket engines [NASA-CR-185223] p 131 N90-23574
- MANGANESE ALLOYS**
- Hyperfine magnetic field on Cd-111 in Heusler alloys Co_2MnZ ($\text{Z} = \text{Si, Ga, Ge, Sn}$) p 255 A90-34012
- MANIFOLDS**
- Extended temperature range rocket injector [NASA-CASE-LEW-14846-1] p 73 N90-15130
- MANIPULATORS**
- Optimum structural design of robotic manipulators with fiber reinforced composite materials p 197 A90-46074
- Base reaction optimization of redundant manipulators for space applications [NASA-CR-186274] p 201 N90-15447
- A global approach for using kinematic redundancy to minimize base reactions of manipulators [NASA-CR-186825] p 234 N90-25499
- Beam rider for an Articulated Robot Manipulator (ARM) accurate positioning of long flexible manipulators [NASA-CR-185151] p 241 N90-26581
- Reaction-compensation technology for microgravity laboratory robots [NASA-TM-103271] p 205 N90-28062
- MANNED MARS MISSIONS**
- Performance comparisons of nuclear thermal rocket and chemical propulsion systems for piloted missions to Phobos/Mars [IAF PAPER 89-027] p 53 A90-13262
- Power considerations for an early manned Mars mission utilizing the Space Station [AAS PAPER 87-223] p 55 A90-16688

MASS DISTRIBUTION

- The SP-100 space reactor as a power source for Mars exploration missions [AAS PAPER 87-224] p 55 A90-16689
- Human exploration mission studies p 39 A90-33935
- A solar power system for an early Mars expedition [NASA-TM-103219] p 246 N90-28393
- MANNED SPACE FLIGHT**
- Engine selection for the Space Exploration Initiative [AIAA PAPER 90-1880] p 65 A90-47201
- The Gevaltig: An inertial fusion powered manned spacecraft design for outer solar system missions [NASA-CR-185163] p 50 N90-15985
- MANUALS**
- Fastener design manual [NASA-RP-1228] p 202 N90-18740
- Launching a dream: A teachers guide to a simulated space shuttle mission [NASA-TM-89715] p 261 N90-26693
- MANUFACTURING**
- Computer aided design of bevel gear tooth surfaces p 195 A90-21136
- Computer simulation of gear tooth manufacturing processes [NASA-CR-185200] p 138 N90-26171
- MANY BODY PROBLEM**
- Phase transitions in fermionic systems with many-body interaction p 249 A90-19303
- MARANGONI CONVECTION**
- Numerical simulation of thermocapillary bubble migration under microgravity for large Reynolds and Marangoni numbers p 164 A90-23213
- The coupling of Marangoni and capillary instabilities in an annular thread of liquid p 171 A90-38978
- Energy stability of thermocapillary convection in a model of the float-zone crystal-growth process p 133 A90-48720
- MARKOV PROCESSES**
- Three approaches to reliability analysis p 206 A90-30706
- MARS (PLANET)**
- An evolutionary communications scenario for Mars exploration [AAS PAPER 87-268] p 139 A90-16566
- MARS ATMOSPHERE**
- Photovoltaic power system operation in the Mars environment p 43 A90-38156
- Preliminary design of a long-endurance Mars aircraft [AIAA PAPER 90-2000] p 43 A90-40587
- Mars in situ propellants - Carbon monoxide and oxygen ignition experiments [AIAA PAPER 90-1894] p 130 A90-50642
- Preliminary design of a long-endurance Mars aircraft [NASA-CR-185243] p 30 N90-21763
- Mars in situ propellants: Carbon monoxide and oxygen ignition experiments [NASA-TM-103202] p 81 N90-26065
- The chemical effects of the Martian environment on power system component materials: A theoretical approach [NASA-TM-103203] p 87 N90-26074
- MARS ENVIRONMENT**
- Aeolian removal of dust from photovoltaic surfaces on Mars [NASA-TM-102507] p 76 N90-19299
- MARS SAMPLE RETURN MISSIONS**
- Energy storage considerations for a robotic Mars surface sampler [AAS PAPER 87-245] p 42 A90-16544
- MARS SURFACE**
- An evolutionary communications scenario for Mars exploration [AAS PAPER 87-268] p 139 A90-16566
- Mars manned transportation vehicle [AAS PAPER 87-271] p 42 A90-16569
- Nuclear propulsion - A vital technology for the exploration of Mars and the planets beyond [AAS PAPER 87-210] p 55 A90-16676
- Orbit to surface beamed power for Mars bases expansion p 40 A90-38105
- Aeolian removal of dust from photovoltaic surfaces on Mars [NASA-TM-102507] p 76 N90-19299
- Aeolian removal of dust from radiator surfaces on Mars [NASA-TM-103205] p 81 N90-26068
- The chemical effects of the Martian environment on power system component materials: A theoretical approach [NASA-TM-103203] p 87 N90-26074
- Analysis of a Mars-stationary orbiting microwave power transmission system [NASA-TM-101344] p 138 N90-26172
- MASS DISTRIBUTION**
- A modified VAPEPS method for predicting vibroacoustic response of unreinforced mass loaded honeycomb panels p 206 A90-43731

MASS FLOW

Application of two-component phase Doppler interferometry to the measurement of particle size, mass flux, and velocities in two-phase flows p 186 A90-32853

MASS FLOW RATE

Low power arcjet performance [AIAA PAPER 90-2578] p 68 A90-52568
Acquisition and correlation of cryogenic nitrogen mass flow data through a multiple orifice Joule-Thomson device [NASA-TM-103121] p 182 N90-22761
The entrainment rate for a row of turbulent jets [NASA-CR-185278] p 15 N90-28504

MASS SPECTROMETERS

Development of a quadrupole-based Secondary-Ion Mass Spectrometry (SIMS) system at Lewis Research Center [NASA-TM-102531] p 87 N90-23476

MASS SPECTROSCOPY

Mass spectrometric observations of metal oxychlorides produced by oxidation-chlorination reactions p 103 A90-21215
Development of a quadrupole-based Secondary-Ion Mass Spectrometry (SIMS) system at Lewis Research Center [NASA-TM-102531] p 87 N90-23476

MASS TO LIGHT RATIOS

Dark matter candidates p 266 A90-44095

MASS TRANSFER

The modelling of heat, mass and solute transport in solidification systems p 157 A90-13092
Pressure drop and mass transfer in two-pass ribbed channels p 165 A90-24837
Mass transfer from a sphere in an oscillating flow with zero mean velocity [NASA-TM-102566] p 179 N90-20338
WINCOF-I code for prediction of fan compressor unit with water ingestion [NASA-CR-185157] p 1 N90-21724

MATCHING

Conjugate field approaches for active array compensation p 144 N90-19266

MATERIALS HANDLING

Technical accomplishments of the NASA Lewis Research Center, 1989 [NASA-TM-102296] p 267 N90-24220

MATERIALS TESTS

Noninteractive macroscopic reliability model for ceramic matrix composites with orthotropic material symmetry [ASME PAPER 89-GT-129] p 209 A90-23827
Crack-path effect on material toughness [ASME PAPER 89-WA/APM-43] p 210 A90-28755

MATHEMATICAL MODELS

Aeroelastic detuning for stability enhancement of unstalled supersonic flutter p 19 A90-17462
Vibration signature analysis of multistage gear transmission p 194 A90-21124
Efficient real gas Navier-Stokes computations of high speed flows using an LU scheme [AIAA PAPER 90-0391] p 164 A90-23706
The impedance of a tubular electrode - A model for a porous electrode p 104 A90-33723
Theoretical model of discrete tone generation by impinging jets p 247 A90-35903
Mathematical optimization of photovoltaic converters for diode lasers --- for spacecraft power supplies p 228 A90-38110
Numerical model of solar dynamic radiator for parametric analysis p 61 A90-38168
Gravitational couplings of the inflator in extended inflation p 265 A90-40088
Soft inflation --- in cosmology p 265 A90-40093
A modeling technique for STOVL ejector and volume dynamics [AIAA PAPER 90-2417] p 20 A90-42168
Numerical modeling of an arcjet thruster [AIAA PAPER 90-2614] p 64 A90-42587
Characterization of structural connections using free and forced response test data p 213 A90-46172
Mathematical modeling and analysis of heat pipe start-up from the frozen state p 174 A90-48404
Method and models for R-curve instability calculations p 214 A90-50566
The measurement of boundary layers on a compressor blade in cascade. Volume 1: Experimental technique, analysis and results [NASA-CR-185118-VOL-1] p 23 N90-10038
The MHOST finite element program: 3-D inelastic analysis methods for hot section components. Volume 2: User's manual [NASA-CR-182235-VOL-2] p 215 N90-10450
An integrated methodology for optimizing structural composite damping [NASA-TM-102343] p 96 N90-11808

Thermal barrier coating life prediction model development, phase 1 [NASA-CR-182230] p 26 N90-13388
Constitutive modeling for isotropic materials (HOST) [NASA-CR-179522] p 26 N90-13390
Constitutive modeling for isotropic materials (HOST) [NASA-CR-174718] p 26 N90-13391
An improved algorithm for the modeling of vapor flow in heat pipes [NASA-CR-185179] p 176 N90-13748
Modeling of power electronic systems with EMTP [NASA-TM-102375] p 245 N90-14060
Efficient real gas Navier-Stokes computations of high speed flows using an LU scheme [NASA-TM-102429] p 11 N90-14203
Slush Hydrogen (SLH2) technology development for application to the National Aerospace Plane (NASP) [NASA-TM-102315] p 50 N90-14268
Kinetics and mechanism of soot formation in hydrocarbon combustion [NASA-CR-186162] p 106 N90-14305
Thermal fatigue durability for advanced propulsion materials [NASA-TM-102348] p 216 N90-14641
Development of an integrated BEM approach for hot fluid structure interaction [NASA-CR-186214] p 177 N90-15364
CryoTran user's manual, version 1.0 [NASA-TM-102468] p 237 N90-15622
Eigenanalysis of finite element problems in a completely connected parallel architecture [NASA-TM-102450] p 217 N90-17173
Prediction of high temperature metal matrix composite ply properties [NASA-TM-102490] p 97 N90-17817
FLUSH: A tool for the design of slush hydrogen flow systems [NASA-TM-102467] p 130 N90-17890
Steady-state and transient Zener parameters in viscoplasticity: Drag strength versus yield strength [NASA-TM-102487] p 218 N90-18064
An approximate model for the performance and acoustic predictions of counterrotating propeller configurations [NASA-CR-180667] p 248 N90-18228
The measurement, modeling, and prediction of traction for rocket propellant 1 [NASA-CR-185186] p 131 N90-19386
Amplitude-dependent neutral modes in compressible boundary layer flows [NASA-TM-102524] p 178 N90-20326
Computer simulation of the mathematical modeling involved in constitutive equation development: Via symbolic computations [NASA-TM-102532] p 219 N90-20428
Model development in viscoplastic ratchetting [NASA-TM-102509] p 219 N90-20431
Computational simulation of damping in composite structures [NASA-TM-102567] p 219 N90-20432
COMGEN: A computer program for generating finite element models of composite materials at the micro level [NASA-TM-102556] p 219 N90-20438
The numerical simulation of multistage turbomachinery flows p 29 N90-21025
Intensity to frequency conversion technique in intensity modulated fiber optic sensing systems [NASA-TM-102562] p 153 N90-21277
PROTEUS two-dimensional Navier-Stokes computer code, version 1.0. Volume 1: Analysis description [NASA-TM-102551] p 180 N90-21303
PROTEUS two-dimensional Navier-Stokes computer code, version 1.0. Volume 2: User's guide [NASA-TM-102552] p 180 N90-21306
PROTEUS two-dimensional Navier-Stokes computer code, version 1.0. Volume 3: Programmer's reference [NASA-TM-102553] p 180 N90-21307
Thermomechanical deformation testing and modeling in the presence of metallurgical instabilities [NASA-CR-185188] p 219 N90-21420
The insertion of human dynamics models in the flight control loops of V/STOL research aircraft. Appendix 2: The optimal control model of a pilot in V/STOL aircraft control loops [NASA-CR-186598] p 38 N90-21776
Computerized inspection of gear tooth surfaces [NASA-TM-102395] p 203 N90-22054
A modeling technique for STOVL ejector and volume dynamics [NASA-TM-103167] p 30 N90-22566
Non-linear dynamic analysis of geared systems, part 2 [NASA-CR-180495] p 204 N90-23732
A viscoplastic model with application to LiF-22 percent CaF₂ hypereutectic salt [NASA-TM-103181] p 221 N90-23770

Metal matrix composites microfracture: Computational simulation [NASA-TM-103153] p 101 N90-24383
Analysis of shell-type structures subjected to time-dependent mechanical and thermal loading [NASA-CR-185077] p 222 N90-24653
LEO high voltage solar array arcing response model, continuation 5 [NASA-CR-186505] p 232 N90-25418
Performance of a supercharged direct-injection stratified-charge rotary combustion engine [NASA-TM-103105] p 32 N90-25982
Background, current status, and prognosis of the ongoing slush hydrogen technology development program for the NASP [NASA-TM-103220] p 51 N90-26055
Extension of a noninteractive reliability model for ceramic matrix composites [NASA-CR-185267] p 129 N90-26142
An investigation into the numerical prediction of boundary layer transition using the K.Y. Chien turbulence model [NASA-CR-185252] p 182 N90-26269
Application of symbolic computations to the constitutive modeling of structural materials [NASA-TM-103225] p 222 N90-26364
Dielectric function of InGaAs in the visible [NASA-TM-103246] p 260 N90-26683
Modification of the SHABERTH bearing code to incorporate RP-1 and a discussion of the traction model [NASA-TP-3017] p 205 N90-28066
Micromechanical model of crack growth in fiber reinforced ceramics [NASA-CR-4321] p 224 N90-28113
Micromechanics of cyclic deformation in SSME turbopump blade materials p 224 N90-28641
High temperature fatigue behavior of Haynes 188 p 119 N90-28642
Structural response of SSME turbine blade airfoils p 224 N90-28649
Thermal analysis of thermal barrier coatings in a high heat flux environment p 129 N90-28652
Evaluation of a hybrid kinetics/mixing-controlled combustion model for turbulent premixed and diffusion combustion using KIVA-2 [NASA-TM-103196] p 185 N90-28792
Green's functions for dislocations in bonded strips and related crack problems [NASA-CR-185291] p 224 N90-28878

MATHEMATICAL PROGRAMMING
Solution of steady-state one-dimensional conservation laws by mathematical programming p 241 A90-21918
Calculation of shocked one-dimensional flows on abruptly changing grids by mathematical programming p 162 A90-21937
Robustness, generality and efficiency of optimization algorithms in practical applications [AIAA PAPER 90-1177] p 236 A90-29268

MATRICES (CIRCUITS)
Characterization of two MMIC GaAs switch matrices at microwave frequencies [AIAA PAPER 90-0866] p 147 A90-25686
Characterization of two MMIC GaAs switch matrices at microwave frequencies [NASA-TM-102449] p 50 N90-14273

MATRICES (MATHEMATICS)
Parallel eigenanalysis of finite element models in a completely connected architecture [NASA-CR-185166] p 217 N90-14652
METCAN verification status [NASA-TM-103119] p 100 N90-21824

MATRIX MATERIALS
1200 to 1400 K slow strain rate compressive properties of NiAl/Ni₂AlTi-base materials p 88 A90-16938
Up-and-coming IMCs --- Intermetallic-Matrix Composites p 88 A90-17295
Compressive strength of a B2 matrix NiAl-Nb intermetallic at 1200 and 1300 K p 111 A90-19157
Crystallization kinetics of BaO-Al₂O₃-SiO₂ glasses p 121 A90-21175
Composites boost 21st-century aircraft engines p 90 A90-29704
Tailoring of composite links for optimal damped elasto-dynamic performance p 211 A90-30250
Matrix density effects on the mechanical properties of SiC fiber-reinforced silicon nitride matrix properties p 94 A90-51927
Crystallization behavior and properties of BaO-Al₂O₃-2SiO₂ glass matrices p 95 A90-51933
Composite laminate tailoring with probabilistic constraints and loads [NASA-TM-102515] p 98 N90-20138
Matrix density effects on the mechanical properties of SiC/RBSN composites [NASA-TM-103098] p 100 N90-21826

SUBJECT INDEX

Theory and experimental technique for nondestructive evaluation of ceramic composites p 207 N90-23754 [NASA-TM-102561]

A creep model for metallic composites based on matrix testing: Application to Kanthal composites [NASA-TM-103172] p 101 N90-25193

MATRIX METHODS

Influence of interfacial shear strength on the mechanical properties of SiC fiber reinforced reaction-bonded silicon nitride matrix composites [NASA-TM-102462] p 101 N90-24382

MEASUREMENT

Foundations of measurement and instrumentation [NASA-RP-1222] p 189 N90-21351

MEASURING INSTRUMENTS

Universal nondestructive MM-wave integrated circuit test fixture [NASA-CASE-LEW-14746-1] p 151 N90-17009

Foundations of measurement and instrumentation [NASA-RP-1222] p 189 N90-21351

MECHANICAL DRIVES

Modal analysis of gear housing and mounts p 192 A90-17018

Assessment of worm gearing for helicopter transmissions [NASA-TM-102441] p 27 N90-15923

MECHANICAL ENGINEERING

Conceptual design of a Moving Belt Radiator (MBR) shuttle-attached experiment [NASA-CR-185169] p 79 N90-23474

MECHANICAL PROPERTIES

CMCs for the long run --- ceramic-matrix composites p 88 A90-17301

Designing ceramic components with the CARES computer program p 235 A90-19147

On the mechanism of cross slip in Ni₃Al p 111 A90-20611

Crystallization kinetics of BaO-Al₂O₃-SiO₂ glasses p 121 A90-21175

Preliminary investigation of a NiAl composite prepared by cryomilling p 113 A90-25098

Resources - Supply and availability --- of superalloys for United States aerospace industry p 114 A90-34152

Coarsening in high volume fraction nickel-base alloys p 115 A90-37719

A brief survey of radiation effects on polymer dielectrics p 123 A90-43119

Equivalence of physically based statistical fracture theories for reliability analysis of ceramics in multiaxial loading p 123 A90-43580

The effects of surface films on mechanical behavior of B2 ordered intermetallic alloys p 115 A90-44338

The mechanical properties of fluoride salts at elevated temperatures --- candidate thermal energy storage materials for solar dynamic systems p 123 A90-44376

Metal matrix composite micromechanics - In situ behavior influence on composite properties p 92 A90-45271

Thermal effects on the mechanical properties of SiC fibre reinforced reaction-bonded silicon nitride matrix composites p 92 A90-46999

Thermo-oxidative stability studies of PMR-15 polymer matrix composites reinforced with various continuous fibers p 93 A90-50068

Properties of RBSN and RBSN-SiC composites --- Reaction Bonded Silicon Nitride p 94 A90-51920

The application of cast SiC/Al to rotary engine components [NASA-CR-179610] p 25 N90-13385

Prediction of high temperature metal matrix composite ply properties [NASA-TM-102490] p 97 N90-17817

Identification of a cast iron alloy containing nonstrategic elements [NASA-CR-185174] p 118 N90-18559

Thermo-oxidative stability studies of PMR-15 polymer matrix composites reinforced with various fibers [NASA-TM-102439] p 98 N90-19310

A transient plasticity study and low cycle fatigue analysis of the Space Station Freedom photovoltaic solar array blanket [NASA-TM-102516] p 218 N90-19617

Structural behavior of composites with progressive fracture [NASA-TM-102370] p 100 N90-23477

Acousto-ultrasonic nondestructive evaluation of materials using laser beam generation and detection [NASA-CR-186694] p 154 N90-23664

Influence of interfacial shear strength on the mechanical properties of SiC fiber reinforced reaction-bonded silicon nitride matrix composites [NASA-TM-102462] p 101 N90-24382

Extension of a noninteractive reliability model for ceramic matrix composites [NASA-CR-185267] p 129 N90-26142

Design of ceramic components with the NASA/CARES computer program [NASA-TM-102369] p 222 N90-26359

MELT SPINNING

Processing and microstructure of melt spun NiAl alloys p 110 A90-16941

Microstructure and mechanical properties of multiphase NiAl-based alloys p 115 A90-35071

MELTING

Production and processing of Cu-Cr-Nb alloys p 114 A90-33340

Flight experiment of thermal energy storage --- for spacecraft power systems p 61 A90-38172

Production and processing of Cu-Cr-Nb alloys [NASA-TM-102495] p 117 N90-16053

Superconducting Bi_{1.5}Pb_{0.5}Sr₂Ca₂Cu₃O(x) ceramics by rapid melt quenching and glass crystallization [NASA-CR-185184] p 258 N90-17465

MELTING POINTS

Pressure dependence of the melting temperature of metals p 103 A90-16281

MELTS (CRYSTAL GROWTH)

Inverse heat transfer analysis of Bridgman crystal growth p 157 A90-13093

Effects of crystal-melt interfacial energy anisotropy on dendritic morphology and growth kinetics p 253 A90-19284

Free dendritic growth in viscous melts - Cyclohexanol p 253 A90-19285

Interface demarcation in GaAs by current pulsing [AIAA PAPER 90-0319] p 254 A90-19793

Free float acceleration measurements aboard NASA's KC-135 Microgravity Research Aircraft [AIAA PAPER 90-0742] p 132 A90-20000

Crystallization of a barium-aluminosilicate glass p 121 A90-27107

Superconducting Bi_{1.5}Pb_{0.5}Sr₂Ca₂Cu₃O(x) ceramics by rapid melt quenching and glass crystallization [NASA-CR-185184] p 258 N90-17465

MEMBRANES

Hydrogen-oxygen proton-exchange membrane fuel cells and electrolyzers p 230 N90-20467

MEMORY (COMPUTERS)

A general model for memory interference in a multiprocessor system with memory hierarchy p 238 A90-37482

The MHOST finite element program: 3-D inelastic analysis methods for hot section components. Volume 3: Systems' manual [NASA-CR-182236] p 215 N90-10451

Concurrent processing adaptation of aeroplastic analysis of propfans p 217 N90-14656

Numerical Arc Segmentation Algorithm for a Radio Conference (NASARC), version 4.0: User's manual [NASA-TM-101454] p 145 N90-21250

Multiprocessor architecture: Synthesis and evaluation [NASA-CR-186618] p 235 N90-25579

Computer architecture evaluation for structural dynamics computations: Project summary [NASA-CR-186137] p 235 N90-26512

MERCURY CADMIUM TELLURIDES

Interface properties of various passivations of HgCdTe p 251 A90-45947

Contribution of the graded region of a HgCdTe diode to its saturation current p 257 A90-45948

MERCURY COMPOUNDS

Evaluation of transport conditions during physical vapor transport growth of opto-electronic crystals p 132 A90-20525

Coupled effects of conduction in the crystal and thermo-solutal convection in a rectangular inclined enclosure [AIAA PAPER 90-0408] p 133 A90-25031

MESH

Improvement of finite element meshes - Heat transfer in an infinite cylinder p 209 A90-19109

MESSAGE PROCESSING

AIRNET: A real-time communications network for aircraft [NASA-CR-186140] p 145 N90-24514

METAL BONDING

Lateral spreading of Au contacts on InP [NASA-TM-103133] p 232 N90-22843

METAL COATINGS

Cyclic oxidation of aluminide coatings on Ti₃Al + Nb p 115 A90-39660

METAL FATIGUE

The unusual near-threshold FCG behavior of a single crystal superalloy and the resolved shear stress as the crack driving force p 111 A90-21009

A crystallographic model for the tensile and fatigue response for Rene N4 at 982 C p 114 A90-28754

Fatigue crack propagation behavior of a single crystalline superalloy p 116 A90-48635

METAL MATRIX COMPOSITES

Mean stress and the exhaustion of fatigue-damage resistance [NASA-TM-101311] p 216 N90-13819

A nonlinear high temperature fracture mechanics basis for strainrange partitioning [NASA-TM-4133] p 216 N90-14642

High temperature fatigue behavior of Haynes 188 p 119 N90-28642

Constitutive and life modeling of single crystal blade alloys for root attachment analysis p 119 N90-28643

The fatigue damage behavior of a single crystal superalloy p 120 N90-28644

Microstructure: Property correlation --- multiaxial fatigue damage evolution in waspaloy [NASA-CR-180406] p 224 N90-28880

METAL FIBERS

Characterization of failure processes in tungsten copper composites under fatigue loading conditions [NASA-TM-102371] p 98 N90-21123

High temperature fatigue behavior of tungsten copper composites [NASA-TM-102404] p 99 N90-21138

METAL FILMS

Measurement of the intrinsic bond strength of brittle thin films on flexible substrates p 256 A90-44022

The effects of surface films on mechanical behavior of B2 ordered intermetallic alloys p 115 A90-44338

Sequentially evaporated thin film YBa₂Cu₃O(7-x) superconducting microwave ring resonator [NASA-TM-103180] p 154 N90-25273

METAL HALIDES

Evaluation of transport conditions during physical vapor transport growth of opto-electronic crystals p 132 A90-20525

METAL MATRIX COMPOSITES

Up-and-coming IMCs --- Intermetallic-Matrix Composites p 88 A90-17295

Investigation of interfacial shear strength in a SiC fibre/Ti-24Al-11Nb composite by a fibre push-out technique p 88 A90-18973

1100 to 1300 K slow plastic compression properties of Ni-38.5Al composites p 111 A90-19154

Effect of fiber spacing on interfacial damage in a metal matrix composite p 88 A90-23188

Identification of thermodynamically stable ceramic reinforcement materials for iron aluminide matrices p 89 A90-25238

Applications of high thermal conductivity composites to electronics and spacecraft thermal design [AIAA PAPER 90-0783] p 89 A90-25609

Evaluation of thermal and mechanical loading effects on the structural behavior of a SiC/titanium composite [AIAA PAPER 90-1026] p 90 A90-29228

Properties of Pb(1-x)Bi(x)/Ba₂Cu₃O(x) composites - Reaction of Ba₂Cu₃O(x) with Pb and Bi p 255 A90-33224

Isothermal and nonisothermal fatigue behavior of a metal matrix composite p 91 A90-36746

Microstructure of a SiC/Ti-15-3 composite p 91 A90-37663

Metal matrix composite micromechanics - In situ behavior influence on composite properties p 92 A90-45271

Slow plastic deformation of extruded NiAl-10TiB₂ particulate composites at 1200 and 1300 K p 92 A90-46133

Isothermal life prediction of composite lamina using a damage mechanics approach p 92 A90-48115

High-temperature slow-strain-rate compression studies on CoAl-TiB₂ composites p 93 A90-48636

Parametric studies to determine the effect of compliant layers on metal matrix composite systems p 93 A90-50093

Interfacial effects on the behavior of partially bonded metal matrix composite properties p 93 A90-50094

Fundamental aspects and failure modes in high-temperature composites p 93 A90-50095

Optimal fabrication processes for unidirectional metal-matrix composites - A computational simulation p 93 A90-50096

Compatibility of Fe-40Al with various fibers p 94 A90-50496

Parametric studies to determine the effect of compliant layers on metal matrix composite systems [NASA-TM-102465] p 96 N90-14294

Prediction of high temperature metal matrix composite ply properties [NASA-TM-102490] p 97 N90-17817

Demonstration of capabilities of high temperature composites analyzer code HITCAN [NASA-TM-102560] p 219 N90-19629

Evaluation of thermal and mechanical loading effects on the structural behavior of a SiC/titanium composite [NASA-TM-102536] p 98 N90-20139

- Fundamental aspects of and failure modes in high-temperature composites
[NASA-TM-102558] p 98 N90-20151
- High temperature fatigue behavior of tungsten copper composites
[NASA-TM-102404] p 99 N90-21138
- Optimal fabrication processes for unidirectional metal-matrix composites: A computational simulation
[NASA-TM-102559] p 100 N90-21143
- METCAN verification status
[NASA-TM-103119] p 100 N90-21824
- Fatigue crack growth in unidirectional metal matrix composite
[NASA-TM-103102] p 220 N90-22117
- Fatigue crack growth in a unidirectional SCS-6/Ti-15-3 composite
[NASA-TM-103095] p 119 N90-22646
- High temperature fatigue behavior of a SiC/Ti-24Al-11Nb composite
[NASA-TM-103157] p 220 N90-22822
- Metal matrix composites microfracture: Computational simulation
[NASA-TM-103153] p 101 N90-24383
- Thermomechanical testing techniques for high-temperature composites: TMF behavior of SiC(SCS-6)/Ti-15-3
[NASA-TM-103171] p 222 N90-25367
- METAL OXIDE SEMICONDUCTORS**
- Neutron and gamma irradiation effects on power semiconductor switches
[NASA-TM-103200] p 155 N90-25278
- METAL OXIDES**
- Properties of oxide dispersion strengthened alloys
p 109 A90-14687
- Mass spectrometric observations of metal oxychlorides produced by oxidation-chlorination reactions
p 103 A90-21215
- Thermodynamic properties of some metal oxide-zirconia systems
[NASA-TM-102351] p 126 N90-13666
- METAL POWDER**
- Tribological properties of PM212: A high-temperature, self-lubricating, powder metallurgy composite
[NASA-TM-102355] p 86 N90-12659
- METAL PROPELLANTS**
- Ignition and combustion characteristics of metallized propellants
[NASA-CR-186870] p 107 N90-26911
- METAL SURFACES**
- Contact formation in gallium arsenide solar cells
p 225 A90-14888
- METAL-METAL BONDING**
- Universal aspects of brittle fracture, adhesion, and atomic force microscopy
p 83 A90-14021
- METALLIC GLASSES**
- Preliminary study on pressure brazing and diffusion welding of Nb-12r to Inconel 718
p 196 A90-26899
- Crystallization of a barium-aluminosilicate glass
p 121 A90-27107
- METALLIZING**
- The kinetics of the Au-InP interaction
p 254 A90-25084
- METALLOGRAPHY**
- Metallographic techniques for evaluation of thermal barrier coatings
p 85 A90-44869
- METALS**
- Pressure dependence of the melting temperature of metals
p 103 A90-16281
- Acousto-ultrasonic nondestructive evaluation of materials using laser beam generation and detection
[NASA-CR-186694] p 154 N90-23664
- METEORITIC DAMAGE**
- Effect of eleven years in earth orbit on a mirror surface
p 44 A90-36188
- METEOROID HAZARDS**
- Assessment of the effects of space debris and meteoroids environment on the Space Station solar array assembly
p 54 A90-14929
- Space vehicle propulsion systems - Environmental space hazards
[AIAA PAPER 90-1881] p 63 A90-40545
- METEOROID PROTECTION**
- On protection of Freedom's solar dynamic radiator from the orbital debris environment. Part 1: Preliminary analyses and testing
[NASA-TM-102458] p 73 N90-14285
- METHANE**
- High speed commercial transport fuels considerations and research needs
[NASA-TM-102535] p 131 N90-21869
- Oxygen/methane combustion stability investigation
p 107 N90-28628
- METHODOLOGY**
- A review of failure models for ceramic matrix composite laminates under monotonic loads
[ASME PAPER 89-GT-153] p 89 A90-23842

MICROANALYSIS

- Calibration approach to electron probe microanalysis: A study with PWA-1480, a nickel base superalloy
[NASA-TM-102393] p 117 N90-14335

MICROCOMPUTERS

- A real time microcomputer implementation of sensor failure detection for turbofan engines
p 21 A90-45414

MICROCRACKS

- Use of unbalanced laminates as a screening method for microcracking
p 94 A90-50217
- Use of unbalanced laminates as a screening method for microcracking
[NASA-TM-102517] p 98 N90-21124
- Metal matrix composites microfracture: Computational simulation
[NASA-TM-103153] p 101 N90-24383

MICROGRAVITY APPLICATIONS

- Side-wall gas 'creep' and 'thermal stress convection' in microgravity experiments on film growth by vapor transport
p 158 A90-14086
- Modeling of collision and coalescence of droplets during microgravity processing of Zn-Bi immiscible alloys
p 132 A90-22878
- The NASA Advanced Solar Dynamics Technology Program
p 62 A90-38280
- Facilities for microgravity combustion research
[NASA-TM-102014] p 134 N90-13679
- Microgravity noncontact temperature requirements at NASA Lewis Research Center
p 134 N90-17897

MICROMECHANICS

- High temperature inelastic deformation of the B1900 + Hf alloy under multiaxial loading - Theory and experiment
p 112 A90-22656
- Local-global analysis of crack growth in continuously reinforced ceramic matrix composites
[ASME PAPER 89-GT-138] p 88 A90-23835
- Unified micromechanics of damping for unidirectional and off-axis fiber composites
p 90 A90-29929
- Tailoring of composite links for optimal damped elasto-dynamic performance
p 211 A90-30250
- Characterization of the tip field of a discrete dislocation pileup for the development of physically based micromechanics
p 213 A90-43883
- Metal matrix composite micromechanics - In situ behavior influence on composite properties
p 92 A90-45271

- Parametric studies to determine the effect of compliant layers on metal matrix composite systems
p 93 A90-50093

- Interfacial effects on the behavior of partially bonded metal matrix composite properties
p 93 A90-50094
- Optimal fabrication processes for unidirectional metal-matrix composites - A computational simulation
p 93 A90-50096

- Parametric studies to determine the effect of compliant layers on metal matrix composite systems
[NASA-TM-102465] p 96 N90-14294

- Probabilistic simulation of uncertainties in composite uniaxial strengths
[NASA-TM-102483] p 97 N90-16008

- Prediction of high temperature metal matrix composite ply properties
[NASA-TM-102490] p 97 N90-17817

- Composite laminate tailoring with probabilistic constraints and loads
[NASA-TM-102515] p 98 N90-20138
- Computational simulation of damping in composite structures
[NASA-TM-102567] p 219 N90-20432

- Multi-objective shape and material optimization of composite structures including damping
[NASA-TM-102579] p 99 N90-21132

- Optimal fabrication processes for unidirectional metal-matrix composites: A computational simulation
[NASA-TM-102559] p 100 N90-21143

- Micromechanical model of crack growth in fiber reinforced ceramics
[NASA-CR-4321] p 224 N90-28113

MICROMETEORITIC

- Assessment of the effects of space debris and meteoroids environment on the Space Station solar array assembly
p 54 A90-14929

- Effect of eleven years in earth orbit on a mirror surface
p 44 A90-36188

- On protection of Freedom's solar dynamic radiator from the orbital debris environment. Part 1: Preliminary analyses and testing
[NASA-TM-102458] p 73 N90-14285

MICROSTRIP ANTENNAS

- Experimental study of the cross-polarization characteristics of rectangular microstrip antennas
p 141 A90-37312

- Microstrip subarray with coplanar and stacked parasitic elements
p 141 A90-41586

- Millimeter-wave/infrared rectenna development at Georgia Tech
p 69 N90-10147

MICROSTRIP TRANSMISSION LINES

- Ka-band propagation characteristics of microstrip lines on GaAs substrates at cryogenic temperatures
p 147 A90-33644

- Microwave conductivity of laser ablated YBaCuO superconducting films and its relation to microstrip transmission line
p 155 N90-27844

- Analysis of microstrip lines with alternative implementation of conductors and superconductors
[NASA-TM-103182] p 155 N90-27966

MICROSTRUCTURE

- Microstructure and tensile properties of Fe-40 at. pct Al alloys with C, Zr, Hf, and B additions
p 108 A90-11851

- Microstructural changes in beta-silicon nitride grains upon crystallizing the grain-boundary glass
p 120 A90-13230

- Analysis of gamma prime shape changes in a single crystal Ni-base superalloy
p 109 A90-15206

- Processing and microstructure of melt spun NiAl alloys
p 110 A90-16941

- Relationship between fatigue life in the creep-fatigue region and stress-strain response
p 209 A90-20061

- On the stability of the creep substructure in NaCl single crystals
p 254 A90-21920

- Primary arm spacing in directionally solidified Pb-10 wt pct Sn alloys
[AIAA PAPER 90-0740] p 132 A90-23713

- Microstructure and mechanical properties of multiphase NiAl-based alloys
p 115 A90-35071

- High-strength silicon carbides by hot isostatic pressing
p 122 A90-35473

- Microstructure of a SiC/Ti-15-3 composite
p 91 A90-37663

- Reaction zone microstructure in a Ti3Al + Nb/SiC composite
p 91 A90-39627

- Primary arm spacing in directionally solidified Pb-10 wt percent Sn alloys
[NASA-CR-185190] p 134 N90-14398

- Subtle porosity variation in the YBa2Cu3O(7-x) high-temperature superconductor revealed by ultrasonic imaging
[NASA-TM-102130] p 206 N90-17167

- Characterization of failure processes in tungsten copper composites under fatigue loading conditions
[NASA-TM-102371] p 98 N90-21123

- Thermomechanical deformation testing and modeling in the presence of metallurgical instabilities
[NASA-CR-185188] p 219 N90-21420

- The effect of hydrogen and microstructure on the deformation and fracture behavior of a single crystal nickel-base superalloy
[NASA-CR-185219] p 118 N90-21849

- Recent advances in nondestructive evaluation made possible by novel uses of video systems
[NASA-TM-102491] p 207 N90-22801

- Influence of interfacial shear strength on the mechanical properties of SiC fiber reinforced reaction-bonded silicon nitride matrix composites
[NASA-TM-102462] p 101 N90-24382

- High-temperature deformation and microstructural analysis for Si3N4-Sc2O3
[NASA-TM-103239] p 130 N90-28740

- XANES and EXAFS study of Au-substituted YBa2Cu3O(7-delta)
[NASA-TM-103291] p 260 N90-29219

MICROWAVE AMPLIFIERS

- AlGaAs/InGaAs heterostructures with doped channels for discrete devices and monolithic amplifiers
p 146 A90-20861

- K-band TWT using new diamond rod technology
[AIAA PAPER 90-0870] p 147 A90-25691

- Doped-channel heterojunction structures for millimeter-wave discrete devices and MMICs
p 150 A90-48492

MICROWAVE ANTENNAS

- Power for the moon: Is microwave power beaming an option?
p 69 N90-10158

- Antenna beamforming using optical processing
[NASA-CR-180844] p 142 N90-11210

- Optical control of an 8-element Ka-band phased array using a high-speed optoelectronic interconnect
[NASA-TM-102550] p 152 N90-21275

- Design of an optically controlled Ka-band GaAs MMIC phased-array antenna
[NASA-TM-103147] p 155 N90-26250

MICROWAVE ATTENUATION

- Millimeter-wave surface resistance of laser-ablated YBa2Cu3O(7-delta) superconducting films
p 257 A90-48694

MICROWAVE CIRCUITS

- Microwave response of a HEMT photoconductive detector
p 147 A90-37301

- Optical detectors for GaAs MMIC integration - Technology assessment
p 149 A90-41238

SUBJECT INDEX

- Universal nondestructive MM-wave integrated circuit test fixture
[NASA-CASE-LEW-14746-1] p 151 N90-17009
- Coplanar waveguide fed phased array antenna
[NASA-TM-102522] p 152 N90-21273
- High temperature superconducting thin film microwave circuits: Fabrication, characterization, and applications
[NASA-TM-103235] p 156 N90-28786
- MICROWAVE OSCILLATORS**
- Sequentially evaporated thin film YBa₂Cu₃O_{7-x} superconducting microwave ring resonator
[NASA-TM-103180] p 154 N90-25273
- High temperature superconducting thin film microwave circuits: Fabrication, characterization, and applications
[NASA-TM-103235] p 156 N90-28786
- MICROWAVE POWER BEAMING**
- Overview of microwave concepts p 142 N90-10155
- Power for the moon: Is microwave power beaming an option? p 69 N90-10158
- Microwave beam power p 69 N90-10165
- Lunar orbiting microwave beam power system
[NASA-TM-103211] p 51 N90-25173
- Analysis of a Mars-stationary orbiting microwave power transmission system
[NASA-TM-101344] p 138 N90-26172
- MICROWAVE SCATTERING**
- Complex permittivity of lanthanum aluminate in the 20 to 300 K temperature range from 26.5 to 40.0 GHz p 148 A90-37864
- MICROWAVE SWITCHING**
- Characterization of two MMIC GaAs switch matrices at microwave frequencies
[AIAA PAPER 90-0866] p 147 A90-25686
- Channelized coplanar waveguide pin-diode switches
[NASA-TM-102289] p 150 N90-11943
- Characterization of two MMIC GaAs switch matrices at microwave frequencies
[NASA-TM-102449] p 50 N90-14273
- MICROWAVE TRANSMISSION**
- Power for the moon: Is microwave power beaming an option? p 69 N90-10158
- Channelized coplanar waveguide pin-diode switches
[NASA-TM-102289] p 150 N90-11943
- MICROWAVES**
- Review of research and development on the microwave electrothermal thruster p 55 A90-16369
- Overview of microwave concepts p 142 N90-10155
- Power for the moon: Is microwave power beaming an option? p 69 N90-10158
- Microwave beam power p 69 N90-10165
- Microwave conductivity of laser ablated YBaCuO superconducting films and its relation to microstrip transmission line p 155 N90-27844
- MIDCOURSE TRAJECTORIES**
- A trajectory generation and system characterization model for cislunar low-thrust spacecraft. Volume 2: Technical manual
[NASA-CR-185172] p 77 N90-21807
- MILITARY HELICOPTERS**
- Spray nozzle investigation for the Improved Helicopter Icing Spray System (IHIS) p 37 A90-25040
- Initial results from the joint NASA-Lewis/U.S. Army icing flight research tests p 16 A90-28180
- MILLIMETER WAVES**
- AlGaAs/InGaAs heterostructures with doped channels for discrete devices and monolithic amplifiers p 146 A90-20861
- Doped-channel heterojunction structures for millimeter-wave discrete devices and MMICs p 150 A90-48492
- Millimeter-wave/infrared rectenna development at Georgia Tech p 69 N90-10147
- Performance and modeling of superconducting ring resonators at millimeter-wave frequencies
[NASA-TM-102526] p 151 N90-18634
- Millimeter wave surface resistance of RBa₂Cu₃O_{7-delta} (R=Y, Eu, Dy, Sm, Er) superconductors p 259 N90-20886
- Figure of merit studies of beam power concepts for advanced space exploration
[NASA-CR-186720] p 146 N90-26234
- MILLING**
- PMR graphite engine duct development
[NASA-CR-182228] p 23 N90-10037
- MIMD (COMPUTERS)**
- Parallel multi-time step integration on a transputer system p 235 A90-20188
- Eigensolution of finite element problems in a completely connected parallel architecture
[NASA-TM-102450] p 217 N90-17173
- MINIATURIZATION**
- Miniature traveling wave tube and method of making
[NASA-CASE-LEW-14520-1] p 153 N90-22724

MINORITY CARRIERS

- Wide-bandgap epitaxial heterojunction windows for silicon solar cells p 227 A90-28359
- Reflecting boundary conditions for graded p-n junctions p 150 A90-42400
- Estimation of minority carrier diffusion lengths in InP/GaAs solar cells
[NASA-TM-103213] p 81 N90-26069

MIRRORS

- Effect of eleven years in earth orbit on a mirror surface p 44 A90-36188

MISALIGNMENT

- Topology of modified helical gears p 195 A90-21132

MISSION PLANNING

- The SP-100 space reactor as a power source for Mars exploration missions
[AAS PAPER 87-224] p 55 A90-16689
- Toward an electrical power utility for space exploration p 74 N90-17681
- Launching a dream: A teachers guide to a simulated space shuttle mission
[NASA-TM-89715] p 261 N90-26693
- The lessons of Varsovian's reconnaissance
[NASA-TM-103207] p 267 N90-26789

MIXED OXIDES

- Glass-derived superconducting ceramics with zero resistance at 107 K in the Bi(1.5)Pb(0.5)Sr₂Ca₂Cu₃O_x system p 253 A90-11491
- Synthesis and characterization of high-Tc superconductors in the Ti-Ca-Ba-Cu-O system p 253 A90-19300
- Experimental evidence of a dimensional crossover in Y1Ba₂Cu₃O_{7-delta} p 255 A90-29739
- Properties of Pb(1-x)Bi(x)/Ba₂YCu₃O_x composites - Reaction of Ba₂YCu₃O_x with Pb and Bi p 255 A90-33224
- Fe-57 and Sn-119 Moessbauer study of La₂CuO_{4-y}, YBa₂Cu₃O_{7-y} and SmBa₂Cu₃O_{7-y} p 256 A90-34020
- Superconducting glass-ceramics in the Bi-Sr-Ca-Cu-O system p 256 A90-35153
- Complex permittivity of lanthanum aluminate in the 20 to 300 K temperature range from 26.5 to 40.0 GHz p 148 A90-37864
- Superconducting Bi(1.5)Pb(0.5)Sr₂Ca₂Cu₃O_x ceramics by rapid melt quenching and glass system crystallization p 256 A90-43568
- Millimeter-wave surface resistance of laser-ablated YBa₂Cu₃O_{7-delta} superconducting films p 257 A90-48694
- Crystallization behavior and properties of BaO-Al₂O₃-2SiO₂ glass matrices p 95 A90-51933

MIXERS

- Energy Efficient Engine exhaust mixer model technology report addendum: phase 3 test program
[NASA-CR-174799] p 33 N90-28556

MIXING

- Effect of vane twist on the performance of dome swirlers for gas turbine airblast atomizers
[AIAA PAPER 90-1955] p 173 A90-47203
- Tank Pressure Control Experiment - A low-g mixing investigation
[AIAA PAPER 90-2376] p 66 A90-47217
- Investigation of methods to produce a uniform cloud of fuel particles in a flame tube
[NASA-TM-102376] p 178 N90-18665
- Microgravity acoustic mixing for particle cloud combustors
[NASA-CR-185159] p 248 N90-21600
- Control of flow separation and mixing by aerodynamic excitation
[NASA-TM-103131] p 13 N90-21733
- Effect of vane twist on the performance of dome swirlers for gas turbine airblast atomizers
[NASA-TM-103195] p 182 N90-25289

MIXING LAYERS (FLUIDS)

- Nonlinear evolution of oblique waves on compressible shear layers p 158 A90-15942
- Experimental investigation of convective stability in a superposed fluid and porous layer when heated from below p 158 A90-15947
- Time-dependent calculation of a forced mixing layer using a k-epsilon turbulence model p 169 A90-35222
- On the instabilities of supersonic mixing layers - A high-Mach-number asymptotic theory p 8 A90-42644
- Application of large eddy interaction model to a mixing layer
[NASA-CR-185123] p 11 N90-13328
- A planar reacting shear layer system for the study of fluid dynamics-combustion interaction
[NASA-TM-102422] p 27 N90-13393
- Nonlinear interactions in mixing layers and compressible heated round jets
[NASA-CR-186303] p 182 N90-23674

MOLECULAR BEAM EPITAXY

MIXING LENGTH FLOW THEORY

- A circular combustor configuration with multiple injection ports for mixing enhancement p 158 A90-15389
- A new mixing length model for supersonic shear layers
[AIAA PAPER 90-0018] p 166 A90-25026

MIXTURES

- WINCOF-I code for prediction of fan compressor unit with water ingestion
[NASA-CR-185157] p 1 N90-21724

MODAL RESPONSE

- Modal selection in structural dynamics p 209 A90-17001
- Probabilistic analysis of bladed turbine disks and the effect of mistuning
[AIAA PAPER 90-1097] p 196 A90-29327
- Tailoring of composite links for optimal damped elasto-dynamic performance p 211 A90-30250
- Aeroelastic stability analysis of a high-energy turbine blade --- for SSME High Pressure Oxidizer TurboPump first stage
[AIAA PAPER 90-2351] p 66 A90-47215
- Structural behavior of composites with progressive fracture
[NASA-TM-102370] p 100 N90-23477

MODELS

- Characterization of damped structural connections for multi-component systems p 208 A90-16959
- Noninteractive macroscopic reliability model for ceramic matrix composites with orthotropic material symmetry
[ASME PAPER 89-GT-129] p 209 A90-23827
- Frequency domain model for analysis of paralleled, series-output-connected Mapham inverters p 148 A90-38084
- Reactions of SiC with H₂/H₂O/Ar mixtures at 1300 C p 123 A90-45830
- Acoustic test and analysis of a counterrotating prop-fan model
[NASA-CR-179590] p 247 N90-10683
- The GEM-T2 gravitational model
[NASA-TM-100746] p 234 N90-12984
- H-infinity based integrated flight-propulsion control design for a STOVL aircraft in transition flight
[NASA-TM-103198] p 37 N90-26011

MODULATION

- Advanced modulation technology development for earth station demodulator applications. Coded modulation system development
[NASA-CR-185149] p 145 N90-20270

MODULATORS

- High frequency GaAlAs modulator and photodetector for phased array antenna applications p 146 A90-11774

MODULES

- Space Station Freedom resistojet system study p 54 A90-16368
- Photovoltaic module on-orbit assembly for Space Station Freedom p 45 A90-38071
- Conceptual design for the space station Freedom modular combustion facility
[NASA-TM-102037] p 134 N90-16087

MODULUS OF ELASTICITY

- Parametric studies to determine the effect of compliant layers on metal matrix composite systems p 93 A90-50093
- Matrix density effects on the mechanical properties of SiC fiber-reinforced silicon nitride matrix properties p 94 A90-51927
- Parametric studies to determine the effect of compliant layers on metal matrix composite systems
[NASA-TM-102465] p 96 N90-14294
- Fluorinated graphite fibers as a new engineering material: Promises and challenges
[NASA-TM-102511] p 86 N90-19301
- Matrix density effects on the mechanical properties of SiC/RBSN composites
[NASA-TM-103098] p 100 N90-21826

MOISTURE CONTENT

- Liquid water content and droplet size calibration of the NASA Lewis Icing Research Tunnel
[AIAA PAPER 90-0669] p 37 A90-22242
- Liquid water content and droplet size calibration of the NASA Lewis Icing Research Tunnel
[NASA-TM-102447] p 200 N90-13797
- Thermodynamic analysis of chemical stability of ceramic materials in hydrogen-containing atmospheres at high temperatures
[NASA-CR-4271] p 126 N90-16072
- NASA Lewis icing research tunnel user manual
[NASA-TM-102319] p 31 N90-23407

MOLECULAR BEAM EPITAXY

- Molecular beam epitaxial growth of high-quality InSb on InP and GaAs substrates p 253 A90-12808
- Transport properties of InAs_xSb_{1-x} (x = 0-0.55) on InP grown by molecular-beam epitaxy p 256 A90-36232

- Dielectric function of InGaAs in the visible
[NASA-TM-103246] p 260 N90-26683
- MOLECULAR GASES**
Digital filtering of plume emission spectra
[AIAA PAPER 90-1994] p 67 A90-50643
Digital filtering of plume emission spectra
[NASA-TM-103135] p 81 N90-26070
- MOLECULAR STRUCTURE**
Structural comparison of nickel electrodes and precursor phases p 228 A90-33949
Determination of the thermal stability of perfluoroalkylethers
[NASA-TM-102493] p 127 N90-17875
Nicalon/siliconoxycarbide ceramic composites
[NASA-TM-102563] p 99 N90-21133
- MOLECULAR WEIGHT**
Processable, high temperature polymers from 1,4,5,8-tetrahydro-1,4,5,8-diepoxyanthracene and bis-dienes p 84 A90-21930
- MOLTEN SALTS**
Hot filament technique for measuring the thermal conductivity of molten lithium fluoride
[NASA-TM-102506] p 127 N90-19373
Mechanical properties of pure nickel alloys after long term exposures to LiOH and vacuum at 775 K
[NASA-TM-102403] p 118 N90-20181
- MOLYBDENUM**
Influence of molybdenum on the creep properties of nickel-base superalloy single crystals p 113 A90-25233
Secondary electron emission characteristics of molybdenum-masked, ion-textured OFHC copper
[NASA-TP-2967] p 117 N90-15211
- MOMENTUM TRANSFER**
Numerical studies of convective heat transfer in an inclined semi-annular enclosure p 173 A90-45317
The numerical simulation of multistage turbomachinery flows p 29 N90-21025
- MONITORS**
Automating security monitoring and analysis for Space Station Freedom's electric power system
[NASA-TM-103148] p 240 N90-22324
Integrated controls and health monitoring fiberoptic shaft monitor
[NASA-CR-185210] p 191 N90-29622
- MONOMERS**
New Condensation polyimides containing 1,1,1-triaryl-2,2,2-trifluoroethane structures
[NASA-CASE-LEW-14346-1] p 86 N90-19300
- MONTI CARLO METHOD**
Surface entropy of liquids via a direct Monte Carlo approach - Application to liquid Si p 261 A90-31675
Efficient Monte Carlo simulation of rarefied flow in a small nozzle
[AIAA PAPER 90-1693] p 170 A90-38396
Numerical simulation of rarefied gas flow through a slit
[AIAA PAPER 90-1694] p 170 A90-38397
Probabilistic simulation of uncertainties in composite uniaxial strengths
[NASA-TM-102483] p 97 N90-16008
- MOON**
Lunar orbiting microwave beam power system
[NASA-TM-103211] p 51 N90-25173
- MORPHOLOGY**
Crystallization kinetics of BaO-Al₂O₃-SiO₂ glasses p 121 A90-21175
Influence of the deposition conditions on radiofrequency magnetron sputtered MoS₂ films
[NASA-TP-2994] p 137 N90-21210
Photoreponse of YBa₂Cu₃O₇(δ) granular and epitaxial superconducting thin films
[NASA-TM-103144] p 154 N90-22732
- MOSSBAUER EFFECT**
Antiferromagnetism in Co-57-doped La₂CuO₄(-y) studied by Moessbauer spectroscopy p 255 A90-34011
Fe-57 and Sn-119 Moessbauer study of La₂CuO₄(-y), YBa₂Cu₃O₇(-y) and SmBa₂Cu₃O₇(-y) p 256 A90-34020
- MOUNTING**
Constitutive and life modeling of single crystal blade alloys for root attachment analysis p 119 N90-28643
- MULLITES**
Phase transformations in xerogels of mullite composition p 123 A90-47093
- MULTIGRID METHODS**
Multigrid calculations of a jet in crossflow
[AIAA PAPER 90-0444] p 167 A90-26952
Diagonally inverted lower-upper factored implicit multigrid scheme for the three-dimensional Navier-Stokes equations p 174 A90-49789
- MULTIPATH TRANSMISSION**
Effects of amplitude distortions and IF equalization on satellite communication system bit-error rate performance
[NASA-TM-102415] p 144 N90-19454

MULTIPHASE FLOW

- Gas-phase flowrate effect on disintegrating cryogenic liquid-jets p 173 A90-46895
Gas-phase flowrate effect on disintegrating cryogenic liquid-jets
[NASA-TM-102357] p 187 N90-11277
Scattered-light scanner measurements of cryogenic liquid-jet breakup
[NASA-TM-102432] p 189 N90-22021
Low-gravity fluid physics: A program overview
[NASA-TM-103215] p 183 N90-26273

MULTIPLE ACCESS

- ATDRS payload technology research and development
[NASA-TM-103256] p 52 N90-28596

MULTIPROCESSING (COMPUTERS)

- A general model for memory interference in a multiprocessor system with memory hierarchy p 238 A90-37482
Multiprocessor architecture: Synthesis and evaluation
[NASA-CR-186618] p 235 N90-25579
Modeling and synthesis of multicomputer interconnection networks
[NASA-CR-186619] p 238 N90-25604
Computer architecture evaluation for structural dynamics computations: Project summary
[NASA-CR-186137] p 235 N90-26512

MULTISENSOR APPLICATIONS

- Multi-sensor analysis techniques for SSME safety monitoring
[AIAA PAPER 90-1990] p 45 A90-52499
Multi-sensor analysis techniques for SSME safety monitoring
[NASA-CR-185260] p 45 N90-27732

N**N-TYPE SEMICONDUCTORS**

- Transport properties of InAs(x)Sb(1-x) (x = 0-0.55) on InP grown by molecular-beam epitaxy p 256 A90-36232

NACELLES

- Analysis of results from wind tunnel tests of inlets for an advanced turboprop nacelle installation
[NASA-CR-174937] p 10 N90-10011
Interactive calculation procedures for mixed compression inlets
[NASA-CR-186581] p 14 N90-25934
Energy Efficient Engine program advanced turbofan nacelle definition study
[NASA-CR-174942] p 34 N90-28560

NASA PROGRAMS

- A numerical simulation of the flow in the diffuser of the NASA Lewis Icing Research Tunnel
[AIAA PAPER 90-0488] p 166 A90-25034
Comparison of conceptual designs for 25 kWe advanced Stirling conversion systems for dish electric applications p 229 A90-38254
Bibliography of Lewis Research Center technical publications announced in 1988
[NASA-TM-102034] p 262 N90-15846
A comparison of European and American microgravity combustion experimental techniques p 134 N90-16966
A solar power system for an early Mars expedition
[NASA-TM-103219] p 246 N90-28393

NASA SPACE PROGRAMS

- Resources - Supply and availability --- of superalloys for United States aerospace industry p 114 A90-34152
NASA aerospace battery systems program update p 228 A90-38217
Advanced Communications Technology Satellite (ACTS) and potential system applications p 142 A90-51165
The role of technology in influencing future civil communications satellites p 142 A90-51167
The Pathfinder chemical transfer propulsion program p 74 N90-18471

NASTRAN

- Application of an efficient hybrid scheme for aeroelastic analysis of advanced propellers
[AIAA PAPER 90-0028] p 4 A90-22153
Composite Blade Structural Analyzer (COBSTRAN) theoretical/programmer's manual
[NASA-TM-101958] p 95 N90-10181
Application of an efficient hybrid scheme for aeroelastic analysis of advanced propellers
[NASA-TM-102428] p 11 N90-13355
COMGEN: A computer program for generating finite element models of composite materials at the micro level
[NASA-TM-102556] p 219 N90-20438
Low velocity impact analysis with NASTRAN p 221 N90-24647

- Design of ceramic components with the NASA/CARES computer program
[NASA-TM-102369] p 222 N90-26359
Ceramics Analysis and Reliability Evaluation of Structures (CARES). Users and programmers manual
[NASA-TP-2916] p 223 N90-28099

NATIONAL AEROSPACE PLANE PROGRAM

- CFD propels NASP propulsion progress p 172 A90-41163
Slush Hydrogen (SLH2) technology development for application to the National Aerospace Plane (NASP)
[NASA-TM-102315] p 50 N90-14268
Background, current status, and prognosis of the ongoing slush hydrogen technology development program for the NASP
[NASA-TM-103220] p 51 N90-26055
Prediction of the ullage gas thermal stratification in a NASP vehicle propellant tank experimental simulation using FLOW-3D
[NASA-TM-103217] p 131 N90-26160

NAVIER-STOKES EQUATION

- Time-dependent viscous incompressible Navier-Stokes equations - The finite difference Galerkin formulation and streamfunction algorithms p 156 A90-11598
A multi-domain spectral computation of three-dimensional laminar horseshoe vortex flow using incompressible Navier-Stokes equations p 3 A90-17592
Reciprocal interactions of hairpin-shaped vortices and a boundary layer
[AIAA PAPER 90-0017] p 159 A90-19635
Development of an unstructured mesh/Navier-Stokes method for aerodynamics of aircraft with ice accretions
[AIAA PAPER 90-0758] p 4 A90-20011
Analysis of rotary engine combustion processes based on unsteady, three-dimensional computations
[AIAA PAPER 90-0643] p 163 A90-22237
Time-accurate simulations of a shear layer forced at a single frequency p 163 A90-23111
Efficient real gas Navier-Stokes computations of high speed flows using an LU scheme
[AIAA PAPER 90-0391] p 164 A90-23706
Evaluation of three turbulence models in static air loads and dynamic stall predictions p 7 A90-31291
Numerical analysis of three-dimensional viscous internal flows p 168 A90-32456
Multigrid calculations of 3-D turbulent viscous flows p 172 A90-42426
Computational analysis of the flowfield of a two-dimensional ejector nozzle
[AIAA PAPER 90-1901] p 21 A90-42690
Computation of turbine flowfields with a Navier-Stokes code
[AIAA PAPER 90-2122] p 8 A90-42731
Comparison between pressure gradient method and MAC method on high Re calculation p 172 A90-44462
Calculations of gaseous H₂/O₂ thruster
[AIAA PAPER 90-2490] p 67 A90-47224
Hopf bifurcation in the driven cavity p 174 A90-48548
Diagonally inverted lower-upper factored implicit multigrid scheme for the three-dimensional Navier-Stokes equations p 174 A90-49789
Hopf bifurcation in the driven cavity
[NASA-TM-102334] p 175 N90-11969
A least-squares finite element method for incompressible Navier-Stokes problems
[NASA-TM-102385] p 242 N90-12231
Multigrid calculations of 3-D turbulent viscous flows
[NASA-CR-185154] p 1 N90-13323
Analysis of rotary engine combustion processes based on unsteady, three-dimensional computations
[NASA-TM-102469] p 176 N90-13749
Application of multi-grid methods for solving the Navier-Stokes equations
[NASA-TM-102359] p 243 N90-14002
Efficient real gas Navier-Stokes computations of high speed flows using an LU scheme
[NASA-TM-102429] p 11 N90-14203
Viscous three-dimensional analyses for nozzles for hypersonic propulsion
[NASA-CR-185197] p 27 N90-17635
Conditions at the downstream boundary for simulations of viscous incompressible flow
[NASA-TM-102510] p 243 N90-18198
Comparison of 3-D viscous flow computations of Mach 5 inlet with experimental data
[NASA-TM-102518] p 28 N90-20090
Mass transfer from a sphere in an oscillating flow with zero mean velocity
[NASA-TM-102566] p 179 N90-20338
Navier-Stokes analysis of turbine blade heat transfer
[NASA-TM-102496] p 179 N90-21300

SUBJECT INDEX

- PROTEUS two-dimensional Navier-Stokes computer code, version 1.0. Volume 1: Analysis description [NASA-TM-102551] p 180 N90-21303
- PROTEUS two-dimensional Navier-Stokes computer code, version 1.0. Volume 2: User's guide [NASA-TM-102552] p 180 N90-21306
- PROTEUS two-dimensional Navier-Stokes computer code, version 1.0. Volume 3: Programmer's reference [NASA-TM-102553] p 180 N90-21307
- High accuracy solutions of incompressible Navier-Stokes equations [NASA-TM-102539] p 244 N90-21567
- Computational modeling and validation for hypersonic inlets [NASA-TM-103111] p 181 N90-22011
- An unsteady time asymptotic flow in the square driven cavity [NASA-TM-103141] p 181 N90-22016
- Computational analysis of the flowfield of a two-dimensional ejector nozzle [NASA-CR-185255] p 31 N90-23406
- Experimental and analytical study of close-coupled ventral nozzles for ASTOVL aircraft [NASA-TM-103170] p 31 N90-24273
- Two-dimensional Euler and Navier-Stokes Time accurate simulations of fan rotor flows [NASA-TM-102402] p 14 N90-25948
- Implicit solution of three-dimensional internal turbulent flows [NASA-TM-103099] p 184 N90-27982
- Numerical solution for the velocity-derivative skewness of a low-Reynolds-number decaying Navier-Stokes flow [NASA-TM-103186] p 184 N90-27985
- NAVIGATION**
- A technology assessment of alternative communications systems for the space exploration initiative [NASA-TM-103243] p 47 N90-27736
- NEAR WAKES**
- Investigation of the near wake of a propfan p 7 A90-40686
- NEODYMIUM LASERS**
- Holographic interferometry with an injection seeded Nd:YAG laser and two reference beams p 186 A90-42373
- NETWORK CONTROL**
- Satellite range delay simulator for a matrix-switched time division multiple-access network simulation system [AIAA PAPER 90-0795] p 139 A90-25620
- Satellite range delay simulator for a matrix-switched time division multiple-access network simulator [NASA-TM-102407] p 143 N90-12813
- Modeling and synthesis of multicomputer interconnection networks [NASA-CR-186619] p 238 N90-25604
- NEURAL NETS**
- Neurobiological computational models in structural analysis and design [AIAA PAPER 90-1133] p 210 A90-29260
- A real time neural net estimator of fatigue life [NASA-TM-103117] p 239 N90-21564
- Neuromorphic learning of continuous-valued mappings from noise-corrupted data. Application to real-time adaptive control [NASA-TM-4176] p 241 N90-25607
- A failure diagnosis system based on a neural network classifier for the space shuttle main engine [NASA-TM-103607] p 83 N90-28659
- NEUTRINOS**
- Unitarity limits on the mass and radius of dark-matter particles p 264 A90-24671
- NEUTRON IRRADIATION**
- Neutron and gamma irradiation effects on power semiconductor switches [NASA-TM-103200] p 155 N90-25278
- NEUTRON STARS**
- Neutron stars and white dwarfs in galactic halos? p 265 A90-30909
- NEUTRONS**
- Results of an attempt to measure increased rates of the reaction $D-2 + D-2$ yields $He-3 + n$ in a nonelectrochemical cold fusion experiment [NASA-TM-102430] p 250 N90-17424
- NEWTONIAN FLUIDS**
- The pdf approach to turbulent flow p 168 A90-32225
- NICKEL**
- Structural comparison of nickel electrodes and precursor phases p 228 A90-33949
- Measurement of the intrinsic bond strength of brittle thin films on flexible substrates p 256 A90-44022
- Structural comparison of nickel electrodes and precursor phases p 231 N90-20472
- Impedance studies of Ni/Cd and Ni/H₂ cells using the cell case as a reference electrode p 231 N90-20473

NICKEL ALLOYS

- The high temperature deformation in cyclic loading of a single crystal nickel-base superalloy p 108 A90-11534
- The correlation between the temperature dependence of the CRSS and the formation of superlattice-intrinsic stacking faults in the nickel-base superalloy PWA 1480 --- critical resolved shear stress p 109 A90-11657
- Properties of oxide dispersion strengthened alloys p 109 A90-14687
- Analysis of gamma prime shape changes in a single crystal Ni-base superalloy p 109 A90-15206
- High temperature creep behavior of single crystal gamma prime and gamma alloys p 110 A90-16901
- Deformation behavior of NiAl-based alloys containing iron, cobalt, and hafnium p 110 A90-16930
- 1200 to 1400 K slow strain rate compressive properties of NiAl/Ni₂AlTi-base materials p 88 A90-16938
- Improving the low temperature ductility of NiAl p 110 A90-16940
- Processing and microstructure of melt spun NiAl alloys p 110 A90-16941
- Compressive strength of a B2 matrix NiAl-Nb intermetallic at 1200 and 1300 K p 111 A90-19157
- On the mechanism of cross slip in NiAl p 111 A90-20611
- The unusual near-threshold FCG behavior of a single crystal superalloy and the resolved shear stress as the crack driving force p 111 A90-21009
- High temperature inelastic deformation of the B1900 + Hf alloy under multiaxial loading - Theory and experiment p 112 A90-22656
- Inelastic deformation under nonisothermal loading p 112 A90-22657
- The oxidation of Ni-rich Ni-Al intermetallics p 112 A90-24855
- The effect of 0.1 atomic percent zirconium on the cyclic oxidation behavior of beta-NiAl for 3000 hours at 1200 C p 112 A90-24857
- Preliminary investigation of a NiAl composite prepared by cryomilling p 113 A90-25098
- Influence of molybdenum on the creep properties of nickel-base superalloy single crystals p 113 A90-25233
- A crystallographic model for the tensile and fatigue response for Rene N4 at 982 C p 114 A90-28754
- Solid state processing for high temperature alloys and composites p 196 A90-33225
- The role of interfacial dislocation networks in high temperature creep of superalloys p 114 A90-33329
- Cyclic deformation, fatigue and fatigue crack propagation in Ni-base alloys p 115 A90-34162
- Microstructure and mechanical properties of multiphase NiAl-based alloys p 115 A90-35071
- Coarsening in high volume fraction nickel-base alloys p 115 A90-37719
- The effects of surface films on mechanical behavior of B2 ordered intermetallic alloys p 115 A90-44338
- Filter clogging by the extracted gamma prime and its measurement p 116 A90-45620
- Elevated temperature slow plastic deformation of NiAl-TiB₂ particulate composites at 1200 and 1300 K p 92 A90-45621
- 1300 K compressive properties of several dispersion strengthened NiAl materials p 116 A90-47091
- Friction and wear of oxide-ceramic sliding against IN-718 nickel base alloy at 25 to 800 C in atmospheric air [NASA-TM-102291] p 124 N90-10262
- Constitutive modeling for isotropic materials (HOST) [NASA-CR-179522] p 26 N90-13390
- Constitutive modeling for isotropic materials (HOST) [NASA-CR-174718] p 26 N90-13391
- Mechanical properties of pure nickel alloys after long term exposures to LiOH and vacuum at 775 K [NASA-TM-102403] p 118 N90-20181
- The effect of hydrogen and microstructure on the deformation and fracture behavior of a single crystal nickel-base superalloy [NASA-CR-185219] p 118 N90-21849
- NICKEL CADMIUM BATTERIES**
- Impedance studies of nickel/cadmium and nickel/hydrogen cells using the cell case as a reference electrode p 228 A90-33950
- Changes in impedance of Ni electrodes upon standing and cycling p 229 N90-18097
- NASA aerospace flight battery systems program [NASA-TM-103237] p 233 N90-26397
- NICKEL COMPOUNDS**
- Improving the low temperature ductility of NiAl p 110 A90-16940
- Observations on the brittle to ductile transition temperatures of B2 nickel aluminides with and without zirconium p 111 A90-19153
- 1100 to 1300 K slow plastic compression properties of Ni-38.5Al composites p 111 A90-19154

- Slow plastic deformation of extruded NiAl-10TiB₂ particulate composites at 1200 and 1300 K p 92 A90-46133

NICKEL HYDROGEN BATTERIES

- Electrochemical behavior of heavily cycled nickel electrodes in Ni/H₂ cells containing electrolytes of various KOH concentrations p 103 A90-24535
- Characterization testing of a 40 ampere hour bipolar nickel-hydrogen battery p 56 A90-33940
- Impedance studies of nickel/cadmium and nickel/hydrogen cells using the cell case as a reference electrode p 228 A90-33950
- KOH concentration effect on the cycle life of nickel-hydrogen cells. IV - Results of failure analysis p 228 A90-33952
- Nickel-hydrogen capacity loss on storage p 57 A90-33955
- Energy storage and thermal control system design status --- for space station power supplies p 59 A90-38077
- Bipolar nickel-hydrogen battery development - A program review p 62 A90-38288
- Characterization and cycle tests of lightweight nickel electrodes [NASA-TM-102399] p 106 N90-12696
- Changes in impedance of Ni electrodes upon standing and cycling [NASA-TM-102438] p 229 N90-18097
- Space Electrochemical Research and Technology (SERT), 1989 p 230 N90-20454
- Characterization testing of a 40 AHR bipolar nickel-hydrogen battery p 230 N90-20463
- Nickel-hydrogen capacity loss on storage p 231 N90-20478
- Effect of KOH concentration on LEO cycle life of IPV nickel-hydrogen flight battery cells [NASA-TM-103127] p 77 N90-21116
- Effect of LEO cycling on 125 Ah advanced design IPV nickel-hydrogen battery cells [NASA-TM-103128] p 78 N90-21808
- Photovoltaic power for Space Station Freedom [NASA-TM-102569] p 78 N90-21812
- Electrochemical impregnation and cycle life of lightweight nickel electrodes for nickel-hydrogen cells [NASA-TM-103140] p 107 N90-21844
- Analysis of thermal energy storage material with change-of-phase volumetric effects [NASA-TM-102457] p 181 N90-21974
- NASA aerospace flight battery systems program [NASA-TM-103237] p 233 N90-26397
- NIGHT**
- Energy storage for a lunar base by the reversible chemical reaction: $CaO + H_2O$ reversible reaction $Ca(OH)_2$ [NASA-TM-103145] p 233 N90-25419
- NIObIUM ALLOYS**
- Compressive strength of a B2 matrix NiAl-Nb intermetallic at 1200 and 1300 K p 111 A90-19157
- Influence of alloying elements on the oxidation behavior of NbAl₃ p 113 A90-24861
- Preliminary study on pressure brazing and diffusion welding of Nb-12Zr to Inconel 718 p 196 A90-26899
- Production and processing of Cu-Cr-Nb alloys p 114 A90-33340
- Thermodynamic analysis of chemical compatibility of ceramic reinforcement materials with niobium aluminides p 92 A90-44001
- Creep strength of niobium alloys, Nb-1%Zr and PWC-11 [NASA-TM-102390] p 116 N90-11854
- Production and processing of Cu-Cr-Nb alloys [NASA-TM-102495] p 117 N90-16053
- NITRIDES**
- Studies on the use of supercritical ammonia for ceramic nitride synthesis and fabrication [NASA-TM-102570] p 106 N90-21843
- NITRIDING**
- Nitriding kinetics of Si-SiC powder mixtures as simulations of reaction bonded Si₃N₄-SiC composites p 90 A90-27076
- Advances and directions of ion nitriding/carburizing [NASA-TM-102398] p 137 N90-11902
- NITROGEN OXIDES**
- Low NO(x) potential of gas turbine engines [AIAA PAPER 90-0550] p 20 A90-25036
- Low NO(x) potential of gas turbine engines [NASA-TM-102452] p 27 N90-17636
- NITROGEN PLASMA**
- Diagnostic evaluations of microwave generated helium and nitrogen plasma mixtures [AIAA PAPER 90-2634] p 252 A90-42602
- NOISE INTENSITY**
- Effects of lubrication on the performance of high speed spur gears p 194 A90-21119
- Aeroacoustics of advanced propellers [NASA-TM-103137] p 249 N90-26635

NOISE MEASUREMENT

NOISE MEASUREMENT

Interior noise in the untreated Gulfstream II Propfan Test Assessment aircraft p 17 A90-44736
Neuromorphic learning of continuous-valued mappings from noise-corrupted data. Application to real-time adaptive control [NASA-TM-4176] p 241 N90-25607

NOISE PREDICTION

High speed turboprop aeroacoustic study (counterrotation). Volume 1: Model development [NASA-CR-185241] p 249 N90-26633

NOISE PREDICTION (AIRCRAFT)

Performance and acoustic prediction of counterrotating propeller configurations [SAE PAPER 891035] p 246 A90-14342
Noise of a simulated installed model counterrotation propeller at angle-of-attack and takeoff/approach conditions [AIAA PAPER 90-0283] p 247 A90-32505
Aeroacoustics of advanced propellers [NASA-TM-103137] p 249 N90-26635

NOISE REDUCTION

Effect of advanced component technology on helicopter transmissions p 193 A90-21115
Mixer-ejector nozzle for jet noise suppression [AIAA PAPER 90-1909] p 247 A90-47202
Adaptive antenna arrays for satellite communication [NASA-CR-185989] p 143 N90-12784
A review of gear housing dynamics and acoustics literature [NASA-CR-185148] p 203 N90-21387
Transmission research activities at NASA Lewis Research Center [NASA-TM-103132] p 203 N90-21394

NONDESTRUCTIVE TESTS

The role of NDE in ceramic turbine engine component development p 206 A90-35506
Low thrust rocket test facility [AIAA PAPER 90-2503] p 43 A90-47225
Subtle porosity variation in the YBaCu3O(7-x) high-temperature superconductor revealed by ultrasonic imaging [NASA-TM-102130] p 206 N90-17167
Ultrasonic and radiographic evaluation of advanced aerospace materials: Ceramic composites [NASA-TM-102540] p 207 N90-21401
Two-dimensional surface strain measurement based on a variation of Yamaguchi's laser-speckle strain gauge [NASA-TM-103162] p 192 N90-22784
Recent advances in nondestructive evaluation made possible by novel uses of video systems [NASA-TM-102491] p 207 N90-22801
Acousto-ultrasonic nondestructive evaluation of materials using laser beam generation and detection [NASA-CR-186694] p 154 N90-23664
Theory and experimental technique for nondestructive evaluation of ceramic composites [NASA-TM-102561] p 207 N90-23754
Low thrust rocket test facility [NASA-TM-103206] p 43 N90-25158
Input-output characterization of fiber reinforced composites by P waves [NASA-CR-185287] p 208 N90-28097
Ultrasonic verification of five wave fronts in unidirectional graphite epoxy composite [NASA-CR-185288] p 208 N90-28858

NONEQUILIBRIUM CONDITIONS

Inviscid flux-splitting algorithms for real gases with non-equilibrium chemistry p 174 A90-52275

NONEQUILIBRIUM FLOW

Comparative study of computational efficiency of two LU schemes for non-equilibrium reacting flows [AIAA PAPER 90-0396] p 167 A90-26940

NONISOTHERMAL PROCESSES

Inelastic deformation under nonisothermal loading p 112 A90-22657

NONLINEAR EQUATIONS

Convergence acceleration for vector sequences and applications to computational fluid dynamics [AIAA PAPER 90-0338] p 160 A90-19804
Multiwave nonlinear interactions in the axisymmetric mode [AIAA PAPER 90-0365] p 166 A90-25029
Efficient implementation of minimal polynomial and reduced rank extrapolation methods [NASA-TM-103240] p 244 N90-26616

NONLINEAR EVOLUTION EQUATIONS

Nonlinear evolution of interacting oblique waves on two-dimensional shear layers p 158 A90-15943

NONLINEAR PROGRAMMING

Optimal finite-thrust spacecraft trajectories using collocation and nonlinear programming [AAS PAPER 89-350] p 40 A90-46783
Discrete approximations to optimal trajectories using direct transcription and nonlinear programming [AIAA PAPER 90-2963] p 41 A90-53038

NONLINEAR SYSTEMS

Probabilistic analysis of a materially nonlinear structure [AIAA PAPER 90-1099] p 211 A90-29329
The determination of third order linear models from a seventh order nonlinear jet engine model p 239 A90-52881

NONLINEARITY

Nonlinear evolution of interacting oblique waves on two-dimensional shear layers p 158 A90-15943
Amplitude-dependent neutral modes in compressible boundary layer flows [NASA-TM-102524] p 178 N90-20326
Nonlinear interactions in mixing layers and compressible heated round jets [NASA-CR-186303] p 182 N90-23674
Non-linear dynamic analysis of geared systems, part 2 [NASA-CR-180495] p 204 N90-23732
Dynamic analysis of space-related linear and non-linear structures [NASA-TM-103490] p 51 N90-25174

NONUNIFORM FLOW

Analysis of nonuniform subsonic flows about a row of moving blades p 2 A90-11779

NORMAL DENSITY FUNCTIONS

Efficient numerical method for computation of thermohydrodynamics of laminar lubricating films [NASA-CR-185136] p 175 N90-11256

NORMAL SHOCK WAVES

Experimental investigation of terminal shock sensors in mixed-compression inlets [AIAA PAPER 90-1931] p 186 A90-40560
An LDA investigation of the normal shock wave boundary layer interaction p 10 A90-52618

NOZZLE DESIGN

Advanced computational techniques for hypersonic propulsion p 156 A90-12606
Mixer-ejector nozzle for jet noise suppression [AIAA PAPER 90-1909] p 247 A90-47202
Analysis and design of optimized truncated scarfed nozzles subject to external flow effects [AIAA PAPER 90-2222] p 9 A90-47213
Performance characterization of a segmented anode arcjet thruster [AIAA PAPER 90-2582] p 68 A90-52569
Arcjet nozzle design impacts p 76 N90-18478
Analysis and design of optimized truncated scarfed nozzles subject to external flow effects [NASA-TM-103175] p 13 N90-25106

NOZZLE EFFICIENCY

Experimental and analytical study of close-coupled ventral nozzles for ASTOVL aircraft [NASA-TM-103170] p 31 N90-24273

NOZZLE FLOW

Advanced computational techniques for hypersonic propulsion p 156 A90-12606
Nature of convection-stabilized dc arcs in dual-flow nozzle geometry. I - The cold flow field and dc arc characteristics. II - Optical diagnostics and theory p 252 A90-26665

Kinetic theory model for the flow of a simple gas from a two-dimensional nozzle p 169 A90-37124
Efficient Monte Carlo simulation of rarefied flow in a small nozzle [AIAA PAPER 90-1693] p 170 A90-38396

Analysis of internal flow in a ventral nozzle for STOVL aircraft [AIAA PAPER 90-1899] p 21 A90-42688

Computational analysis of the flowfield of a two-dimensional ejector nozzle [AIAA PAPER 90-1901] p 21 A90-42690

Engine inlet distortion in a 9.2 percent scale vectored thrust STOVL model in ground effect [NASA-TM-102358] p 12 N90-17561

Viscous three-dimensional analyses for nozzles for hypersonic propulsion [NASA-CR-185197] p 27 N90-17635

Analysis of internal flow in a ventral nozzle for STOVL aircraft [NASA-TM-103123] p 31 N90-23404

Computational analysis of the flowfield of a two-dimensional ejector nozzle [NASA-CR-185255] p 31 N90-23406

Hot gas ingestion characteristics and flow visualization of a vectored thrust STOVL concept [NASA-TM-103212] p 32 N90-26009

NOZZLE GEOMETRY

Elliptic jets. I - Characteristics of unexcited and excited jets p 159 A90-18071
Analysis and design of optimized truncated scarfed nozzles subject to external flow effects [AIAA PAPER 90-2222] p 9 A90-47213
Analysis and design of optimized truncated scarfed nozzles subject to external flow effects [NASA-TM-103175] p 13 N90-25106

SUBJECT INDEX

Low power arcjet performance [NASA-TM-103280] p 83 N90-28657

NOZZLE INSERTS

Low power arcjet performance [AIAA PAPER 90-2578] p 68 A90-52568

NUCLEAR ASTROPHYSICS

Is the sub-millisecond pulsar strange? p 264 A90-12669
Dark matter candidates p 266 A90-44095

NUCLEAR ELECTRIC POWER GENERATION

Challenges for future space power systems p 74 N90-17695
Nuclear technology and the space exploration missions [NASA-TM-103156] p 232 N90-22847

NUCLEAR ELECTRIC PROPULSION

A radiological assessment of nuclear power and propulsion operations near Space Station Freedom [NASA-CR-185185] p 76 N90-21108
A trajectory generation and system characterization model for cis-lunar low-thrust spacecraft. Volume 2: Technical manual [NASA-CR-185172] p 77 N90-21807

NUCLEAR ENGINE FOR ROCKET VEHICLES

Nuclear propulsion - A vital technology for the exploration of Mars and the planets beyond [AAS PAPER 87-210] p 55 A90-16676

NUCLEAR FUEL ELEMENTS

Scaling study for SP-100 reactor technology [NASA-TM-897140] p 249 N90-16496

NUCLEAR FUSION

Big bang nucleosynthesis and the quark-hadron transition p 265 A90-31407
Results of an attempt to measure increased rates of the reaction D-2 + D-2 yields He-3 + n in a nonelectrochemical cold fusion experiment [NASA-TM-102430] p 250 N90-17424

NUCLEAR MAGNETIC RESONANCE

Photochemical approaches to ordered polymers p 84 A90-33222

NUCLEAR POWER REACTORS

Space nuclear reactor shields for manned and unmanned applications p 57 A90-37859
CSTI high capacity power --- Civil Space Technology Initiative p 61 A90-38196
SP-100 advanced radiator designs for thermoelectric and Stirling applications p 62 A90-38202

NUCLEAR PROPULSION

Performance comparisons of nuclear thermal rocket and chemical propulsion systems for piloted missions to Phobos/Mars [IAF PAPER 89-027] p 53 A90-13262

Nuclear propulsion - A vital technology for the exploration of Mars and the planets beyond [AAS PAPER 87-210] p 55 A90-16676

Nuclear technology and the space exploration missions [NASA-TM-103156] p 232 N90-22847

Nuclear power systems for lunar and Mars exploration [NASA-TM-103168] p 82 N90-26873

NUCLEAR REACTORS

Central electrical utility power for a satellite ring city in low earth orbit space p 150 N90-10166
The Gevaltig: An inertial fusion powered manned spacecraft design for outer solar system missions [NASA-CR-185163] p 50 N90-15985

The chemical effects of the Martian environment on power system component materials: A theoretical approach [NASA-TM-103203] p 87 N90-26074

Analysis of a Mars-stationary orbiting microwave power transmission system [NASA-TM-103144] p 138 N90-26172

NUMERICAL ANALYSIS

Analysis of internal flow in a ventral nozzle for STOVL aircraft [AIAA PAPER 90-1899] p 21 A90-42688

Grid generation for the solution of partial differential equations p 237 A90-47188

Analysis of internal flow in a ventral nozzle for STOVL aircraft [NASA-TM-103123] p 31 N90-23404

Structural behavior of composites with progressive fracture [NASA-TM-102370] p 100 N90-23477

Asymptotic analysis of dissipative waves with applications to their numerical simulation [NASA-TM-103231] p 244 N90-26615

NUMERICAL CONTROL

Development of Ada language control software for the NASA power management and distribution test bed p 236 A90-38082

Evaluation of power control concepts using the PMAD systems test bed --- Power Management and Distribution p 42 A90-38083

A test matrix sequencer for research test facility automation
[AIAA PAPER 90-2386] p 37 A90-42791

Subtle porosity variation in the YBa₂Cu₃O_{7-x} high-temperature superconductor revealed by ultrasonic imaging
[NASA-TM-102130] p 206 N90-17167

Computerized inspection of gear tooth surfaces
[NASA-TM-102395] p 203 N90-22054

A test matrix sequencer for research test facility automation
[NASA-TM-103108] p 39 N90-23416

Development of a quadrupole-based Secondary-Ion Mass Spectrometry (SIMS) system at Lewis Research Center
[NASA-TM-102531] p 87 N90-23476

NUMERICAL FLOW VISUALIZATION

Progress in direct numerical simulations of turbulent reacting flows
[IAF PAPER 89-403] p 157 A90-12836

Numerical modeling of enclosure convection
[IAF PAPER 89-403] p 157 A90-13511

A laser based computer aided non-intrusive technique for full field flow characterization in macroscopic curved channels
[NASA-TM-102531] p 168 A90-32293

NUMERICAL STABILITY

A nonoscillatory, characteristically convected, finite volume scheme for multidimensional convection problems
[AIAA PAPER 90-0015] p 159 A90-19633

A critical analysis of the modified equation technique of Warming and Hyett
[AIAA PAPER 90-0015] p 241 A90-21940

A nonoscillatory, characteristically convected, finite volume scheme for multidimensional convection problems
[NASA-TM-102354] p 242 N90-11497

O

O RING SEALS

High temperature, flexible, thermal barrier seal
[NASA-CASE-LEW-14672-1] p 201 N90-15444

OBLIQUE SHOCK WAVES

Nonlinear evolution of interacting oblique waves on two-dimensional shear layers
[NASA-CR-186581] p 158 A90-15943

Interactive calculation procedures for mixed compression inlets
[NASA-CR-186581] p 14 N90-25934

OBSERVABILITY (SYSTEMS)

An observer-based compensator for distributed delays
[NASA-TM-102368] p 239 A90-49899

Elements of active vibration control for rotating machinery
[NASA-TM-102368] p 137 N90-22703

OILS

Thermocapillary migration of liquid droplets in a temperature gradient in a density matched system
[NASA-CR-185178] p 177 N90-14512

ON-LINE SYSTEMS

Automating security monitoring and analysis for Space Station Freedom's electric power system
[NASA-TM-103148] p 240 N90-22324

An expert system to perform on-line controller tuning
[NASA-TM-103101] p 240 N90-23991

Autonomous power expert fault diagnostic system for Space Station Freedom electrical power system testbed
[NASA-TM-103101] p 80 N90-25521

An expert system to perform on-line controller restructuring for abrupt model changes
[NASA-TM-103609] p 241 N90-29121

ONBOARD DATA PROCESSING

A users perspective of the ACTS hopping beam TDMA system
[AIAA PAPER 90-0833] p 140 A90-25658

Spacecraft designs for VSAT networks
[AIAA PAPER 90-0895] p 140 A90-25681

On-board switching and processing
[AIAA PAPER 90-0895] p 150 A90-51168

ONBOARD EQUIPMENT

Advanced Communications Technology Satellite (ACTS)
[AIAA PAPER 90-0839] p 140 A90-25663

ONE DIMENSIONAL FLOW

Calculation of shocked one-dimensional flows on abruptly changing grids by mathematical programming
[NASA-TM-103609] p 162 A90-21937

OPEN CIRCUIT VOLTAGE

Predicted performance of near-optimally designed indium phosphide space solar cells at high intensities and temperatures
[NASA-TM-103609] p 225 A90-14898

OPERATING COSTS

Revolutionary opportunities for materials and structures study
[NASA-CR-179642] p 95 N90-10184

Energy Efficient Engine program advanced turbofan nacelle definition study
[NASA-CR-174942] p 34 N90-28560

Energy Efficient Engine: High-pressure compressor test hardware detailed design report
[NASA-CR-180850] p 36 N90-28570

OPERATIONS RESEARCH

Launching a dream: A teachers guide to a simulated space shuttle mission
[NASA-TM-89715] p 261 N90-26693

OPERATORS (MATHEMATICS)

Galerkin finite difference Laplacian operators on isolated unstructured triangular meshes by linear combinations
[NASA-TM-103209] p 183 N90-26276

OPTICAL COMMUNICATION

Fiber optics for advanced aircraft
[NASA-TM-103209] p 185 A90-11702

High-speed analog fiber optic links for satellite communication
[NASA-TM-103209] p 46 A90-11822

Control of a GaAs monolithic Ka-band phase shifter using a high-speed optical interconnect
[NASA-TM-103209] p 150 A90-41700

Optical control of an 8-element Ka-band phased array using a high-speed optoelectronic interconnect
[NASA-TM-102550] p 152 N90-21275

OPTICAL COMPUTERS

Antenna beamforming using optical processing
[NASA-CR-180844] p 142 N90-11210

OPTICAL COUPLING

High-speed fiber-optic links for distribution of satellite traffic
[NASA-TM-103209] p 47 A90-41687

Control of a GaAs monolithic Ka-band phase shifter using a high-speed optical interconnect
[NASA-TM-103209] p 150 A90-41700

OPTICAL DATA PROCESSING

New space domain processing technique for pulsed laser velocimetry
[NASA-TM-103209] p 187 A90-48750

OPTICAL EQUIPMENT

A high-speed GaAs MESFET optical controller
[NASA-TM-103209] p 186 A90-22483

Diamondlike carbon protective coatings for optical windows
[NASA-TM-103209] p 122 A90-34569

Comparison of drop size distributions from two droplet sizing systems
[NASA-TM-102520] p 202 N90-17147

Design and test of a compact optics system for the pool boiling experiment
[NASA-TM-102530] p 135 N90-20253

OPTICAL FIBERS

Fiber optic sensing systems using high frequency resonant sensing heads with intensity sensors
[NASA-TM-103209] p 185 A90-10472

Determination of the durability of the fiber optics in rocket engine environments
[AIAA PAPER 90-2229] p 250 A90-42754

OPTICAL HETERODYNING

Holographic interferometry with an injection seeded Nd:YAG laser and two reference beams
[NASA-TM-103209] p 186 A90-42373

OPTICAL MATERIALS

Optics and materials considerations for a laser-propelled lightsail
[IAF PAPER 89-664] p 54 A90-13668

OPTICAL MEASUREMENT

Feasibility study for the advanced one-dimensional high temperature optical strain measurement system, phase 3
[NASA-CR-185254] p 191 N90-25324

OPTICAL MEASURING INSTRUMENTS

Fiber optic detector probes for laser light scattering
[NASA-TM-103209] p 192 A90-11593

Fiber optics for advanced aircraft
[NASA-TM-103209] p 185 A90-11702

Modulated-splitting-ratio fiber-optic temperature sensor
[NASA-TM-103209] p 185 A90-11706

OPTICAL PROPERTIES

Solar Concentrator Advanced Development Program
[NASA-CR-185173] p 232 N90-22834

Ellipsometric study of YBa₂Cu₃O_{7-x} laser ablated and co-evaporated films
[NASA-TM-103223] p 259 N90-26682

OPTICAL REFLECTION

On physical optics for calculating scattering from coated bodies
[NASA-TM-103209] p 250 A90-20151

OPTICAL RESONATORS

Sequentially evaporated thin film YBa₂Cu₃O_{7-x} superconducting microwave ring resonator
[NASA-TM-103180] p 154 N90-25273

OPTICAL THICKNESS

Photovoltaic power system operation in the Mars environment
[NASA-TM-103209] p 43 A90-38156

OPTIMAL CONTROL

Active vibration control for flexible rotor by optimal direct-output feedback control
[NASA-TM-103209] p 197 A90-46222

An active optimal control strategy of rotor vibrations using external forces
[NASA-TM-103209] p 198 A90-46224

Discrete approximations to optimal trajectories using direct transcription and nonlinear programming
[AIAA PAPER 90-2963] p 41 A90-53038

Minimum fuel lunar trajectories for a low-thrust power-limited spacecraft
[AIAA PAPER 90-2975] p 41 A90-53054

The insertion of human dynamics models in the flight control loops of V/STOL research aircraft. Appendix 2: The optimal control model of a pilot in V/STOL aircraft control loops
[NASA-CR-186598] p 38 N90-21776

OPTIMIZATION

Application of heuristic satellite plan synthesis algorithms to requirements of the WARC-88 allotment plan
[AIAA PAPER 90-0815] p 245 A90-25638

Multi-objective shape and material optimization of composite structures including damping
[AIAA PAPER 90-1135] p 210 A90-29262

Robustness, generality and efficiency of optimization algorithms in practical applications
[AIAA PAPER 90-1177] p 236 A90-29268

Tailoring of composite links for optimal damped elasto-dynamic performance
[AIAA PAPER 90-1177] p 211 A90-30250

SPRITE - A computer code for the optimization of space based heat pipe radiator systems
[AIAA PAPER 90-1177] p 170 A90-38036

Optimal fabrication processes for unidirectional metal-matrix composites - A computational simulation
[AIAA PAPER 90-1177] p 93 A90-50096

An integrated methodology for optimizing structural composite damping
[NASA-TM-102343] p 96 N90-11808

Application of heuristic satellite plan synthesis algorithms to requirements of the WARC-88 allotment plan
[NASA-TM-102479] p 245 N90-14856

Base reaction optimization of redundant manipulators for space applications
[NASA-CR-186274] p 201 N90-15447

Development of free-piston Stirling engine performance and optimization codes based on Martini simulation technique
[NASA-CR-182210] p 263 N90-18326

Composite laminate tailoring with probabilistic constraints and loads
[NASA-TM-102515] p 98 N90-20138

Aerodynamic optimization by simultaneously updating flow variables and design parameters
[NASA-TM-102515] p 18 N90-20991

Multi-objective shape and material optimization of composite structures including damping
[NASA-TM-102579] p 99 N90-21132

Optimal fabrication processes for unidirectional metal-matrix composites: A computational simulation
[NASA-TM-102559] p 100 N90-21143

Modeling and optimization of a regenerative fuel cell system using the ASPEN process simulator
[NASA-TM-103210] p 233 N90-26396

Bearing optimization for SSME HPOTP application
[NASA-TM-103210] p 205 N90-28622

OPTOELECTRONIC DEVICES

Optical detectors for GaAs MMIC integration - Technology assessment
[NASA-TM-103152] p 149 A90-41238

Control of a GaAs monolithic Ka-band phase shifter using a high-speed optical interconnect
[NASA-TM-103209] p 150 A90-41700

A fiber-optic current sensor for aerospace applications
[NASA-TM-103152] p 190 N90-22773

ORBIT CALCULATION

The GEM-T2 gravitational model
[NASA-TM-100746] p 234 N90-12984

ORBIT SPECTRUM UTILIZATION

Application of heuristic satellite plan synthesis algorithms to requirements of the WARC-88 allotment plan
[AIAA PAPER 90-0815] p 245 A90-25638

Application of heuristic satellite plan synthesis algorithms to requirements of the WARC-88 allotment plan
[NASA-TM-102479] p 245 N90-14856

ORBIT TRANSFER VEHICLES

Launch packaging options for the PV power module cargo element --- for space station power supplies
[NASA-TM-103209] p 45 A90-38078

Microwave beam power
[NASA-TM-103209] p 69 N90-10165

ORBITAL ASSEMBLY

Photovoltaic module on-orbit assembly for Space Station Freedom
[NASA-TM-103209] p 45 A90-38071

ORBITAL MANEUVERS

Space Station Freedom resistojet system study
[NASA-TM-103209] p 54 A90-16368

Performance of large area xenon ion thrusters for orbit transfer missions
[NASA-TM-103209] p 75 N90-18475

ORBITAL RENDEZVOUS

Optimal orbital rendezvous using high and low thrust
[AAS PAPER 89-354] p 41 A90-46786

Optimal cooperative time-fixed impulsive rendezvous
[AIAA PAPER 90-2962] p 41 A90-53037

- Optimal impulsive time-fixed orbital rendezvous and interception with path constraints
[AIAA PAPER 90-2972] p 41 A90-53051
- ORBITAL SERVICING**
Servicing communication satellites in geostationary orbit
[AIAA PAPER 90-0830] p 39 A90-25655
- ORBITAL SPACE TESTS**
On-orbit results of the LIPS 3/InP homojunction solar cell experiment p 74 N90-17794
- ORGANIC COMPOUNDS**
Effects of crystal-melt interfacial energy anisotropy on dendritic morphology and growth kinetics p 253 A90-19284
- ORGANOMETALLIC COMPOUNDS**
Effect of crystal orientation on anisotropic etching and MOCVD growth of grooves on GaAs p 253 A90-15136
- ORTHOTROPIC PLATES**
Low velocity impact analysis with NASTRAN p 221 N90-24647
- ORTHOTROPISM**
Noninteractive macroscopic reliability model for ceramic matrix composites with orthotropic material symmetry [ASME PAPER 89-GT-129] p 209 A90-23827
- OSCILLATING FLOW**
The unsteady aerodynamics of an oscillating cascade in a compressible flow field p 2 A90-11789
Effects of g-jitter on a thermal, buoyant flow
[AIAA PAPER 90-0653] p 163 A90-22239
Mass transfer from a sphere in an oscillating flow with zero mean velocity
[NASA-TM-102566] p 179 N90-20338
ULTRA-SHARP nonoscillatory convection schemes for high-speed steady multidimensional flow
[NASA-TM-102568] p 244 N90-21570
- OSCILLATION DAMPERS**
Low frequency vibration isolation technology for microgravity space experiments p 136 A90-46246
- OSCILLATIONS**
Numerical simulations of supersonic flow through oscillating cascade sections
[NASA-TM-103100] p 13 N90-20051
- OUTGASSING**
Improved process for HIP canning of composites
[NASA-CASE-LEW-14990-1-CU] p 97 N90-15147
- OXIDATION**
Mass spectrometric observations of metal oxychlorides produced by oxidation-chlorination reactions p 103 A90-21215
The oxidation of Ni-rich Ni-Al intermetallics p 112 A90-24855
The effect of 0.1 atomic percent zirconium on the cyclic oxidation behavior of beta-NiAl for 3000 hours at 1200 C p 112 A90-24857
Fuel-rich catalytic combustion - A fuel processor for high-speed propulsion
[AIAA PAPER 90-2319] p 105 A90-42774
Thermo-oxidative stability studies of PMR-15 polymer matrix composites reinforced with various continuous fibers p 93 A90-50068
Hydrogen-silicon carbide interactions
[NASA-TM-102382] p 125 N90-11144
Heat treatment study of the SiC/Ti-15-3 composite system
[NASA-TP-2970] p 97 N90-19302
Structural comparison of nickel electrodes and precursor phases p 231 N90-20472
Detailed mechanism for oxidation of benzene
[NASA-TM-102443] p 106 N90-21842
Fuel-rich catalytic combustion: A fuel processor for high-speed propulsion
[NASA-TM-103177] p 107 N90-23518
A resistance strain gage with repeatable and cancellable apparent strain for use to 800 C
[NASA-CR-185256] p 53 N90-26063
- OXIDATION RESISTANCE**
Oxidation of high-temperature intermetallics; Proceedings of the Workshop, Cleveland, OH, Sept. 22, 23, 1988 p 112 A90-24852
Oxidation behavior of FeAl + Hf,Zr,B p 113 A90-24858
Influence of alloying elements on the oxidation behavior of NbAl₃ p 113 A90-24861
Evaluation of atomic oxygen resistant protective coatings for fiberglass-epoxy composites in LEO p 84 A90-31581
Two-layer thermal barrier coating. I - Effects of composition and temperature on oxidation behavior and failure p 122 A90-33317
Cyclic oxidation of aluminide coatings on Ti3Al + Nb p 115 A90-39660
Oxidation effects on the mechanical properties of SiC fiber-reinforced reaction-bonded silicon nitride matrix composites
[NASA-TM-102360] p 96 N90-14287

- The oxidation and corrosion of ODS alloys
[NASA-TM-102555] p 119 N90-25211
- OXIDE FILMS**
Study of indium tin oxide films exposed to atomic oxygen p 257 A90-45193
- OXIDES**
Polymer derived Nicalon/Si-C-O composites - Processing and mechanical behavior p 89 A90-27065
Materials for engine applications above 3000 deg F: An overview p 95 N90-10188
Preparation of 110K (Bi, Pb)-Sr-Ca-Cu-O superconductor from glass precursor
[NASA-CR-185162] p 258 N90-14108
The oxidation and corrosion of ODS alloys
[NASA-TM-102555] p 119 N90-25211
- OXIDIZERS**
Ignition and combustion characteristics of metallized propellants
[NASA-CR-186870] p 107 N90-26911
- OXYGEN**
Mars in situ propellants - Carbon monoxide and oxygen ignition experiments
[AIAA PAPER 90-1894] p 130 A90-50642
Oxygen electrodes for rechargeable alkaline fuel cells-II p 231 N90-20469
O₂ reduction at the IFC orbiter fuel cell O₂ electrode
[NASA-TM-102580] p 231 N90-21469
Mars in situ propellants: Carbon monoxide and oxygen ignition experiments
[NASA-TM-103202] p 81 N90-26065
Catalytic ignition of hydrogen/oxygen p 107 N90-28627
- OXYGEN ATOMS**
Evaluation of atomic oxygen resistant protective coatings for fiberglass-epoxy composites in LEO p 84 A90-31581
Ellipsometric studies of the diffusion of atomic oxygen through silicon dioxide thin films p 104 A90-36268
The effect of leveling coatings on the atomic oxygen durability of solar concentrator surfaces
[NASA-TM-102557] p 76 N90-21110
The effects of atomic oxygen on the thermal emittance of high temperature radiator surfaces
[NASA-TM-103224] p 102 N90-28670
- OXYGEN PLASMA**
Ellipsometric study of Al₂O₃/Ag/Si and SiO₂/Ag/quartz ashed in an oxygen plasma --- protective coatings to prevent degradation of materials in low earth orbits p 120 A90-18217
Study of indium tin oxide films exposed to atomic oxygen p 257 A90-45193
- OXYGEN-HYDROCARBON ROCKET ENGINES**
Cooling of rocket thrust chambers with liquid oxygen
[AIAA PAPER 90-2120] p 63 A90-40209
LOX/hydrocarbon combustion instability investigation
[NASA-CR-182249] p 71 N90-13589
Cooling of rocket thrust chambers with liquid oxygen
[NASA-TM-103146] p 78 N90-22605

P

- P WAVES**
Input-output characterization of fiber reinforced composites by P waves
[NASA-CR-185287] p 208 N90-28097
- P-I-N JUNCTIONS**
Channelized coplanar waveguide pin-diode switches
[NASA-TM-102289] p 150 N90-11943
Coplanar waveguide discontinuities for P-I-N diode switches and filter applications
[NASA-TM-102534] p 153 N90-21278
- P-N JUNCTIONS**
Reflecting boundary conditions for graded p-n junctions p 150 A90-42400
- P-TYPE SEMICONDUCTORS**
Investigation of buried homojunctions in p-InP formed during sputter deposition of both indium tin oxide and indium oxide p 256 A90-36799
Interface properties of various passivations of HgCdTe p 251 A90-45947
- PANEL METHOD (FLUID DYNAMICS)**
Propeller-wing interaction using a frequency domain panel method p 6 A90-26128
Counter-rotating propellant analysis using a frequency domain panel method p 7 A90-40937
The simulation of fluid dynamic uncertainties in the SSME turbopump
[AIAA PAPER 90-2294] p 65 A90-42770
Users manual for the NASA Lewis Ice Accretion Prediction Code (LEWICE)
[NASA-CR-185129] p 1 N90-20943
Probabilistic modeling for simulation of aerodynamic uncertainties in propulsion systems
[NASA-TM-102472] p 29 N90-21036
- An unsteady lifting surface method for single rotation propellers
[NASA-CR-4302] p 14 N90-25940
- PANELS**
The Space Station photovoltaic panels plasma interaction test program - Test plan and results
[AIAA PAPER 90-0722] p 47 A90-22252
A modified VAPEPS method for predicting vibroacoustic response of unreinforced mass loaded honeycomb panels p 206 A90-43731
The Space Station Photovoltaic Panels Plasma Interaction Test Program: Test plan and results
[NASA-TM-102474] p 49 N90-13581
High temperature, flexible, thermal barrier seal
[NASA-CASE-LEW-14672-1] p 201 N90-15444
Comparison between design and installed acoustic characteristics of NASA Lewis 9- by 15-foot low-speed wind tunnel acoustic treatment
[NASA-TP-2996] p 38 N90-19242
High temperature flexible seal
[NASA-CASE-LEW-14695-1] p 204 N90-23751
- PARABOLAS**
Dynamic loading of spur gears with linear or parabolic tooth profile modifications p 195 A90-21126
- PARABOLIC REFLECTORS**
Concentration of off-axis radiation by solar concentrators for space power p 60 A90-38163
Comparison of conceptual designs for 25 kWe advanced Stirling conversion systems for dish electric applications p 229 A90-38254
- PARABOLOID MIRRORS**
Measurements of print-through in graphite fiber epoxy composites p 91 A90-31555
- PARALLEL COMPUTERS**
Parallel multi-time step integration on a transputer system p 235 A90-20188
- PARALLEL FLOW**
Nonlinear evolution of oblique waves on compressible shear layers p 158 A90-15942
Parallel flows with Soret effect in tilted cylinders p 167 A90-25594
Instabilities and subharmonic resonances of subsonic heated round jets, volume 2
[NASA-CR-186058] p 181 N90-22017
- PARALLEL PROCESSING (COMPUTERS)**
Advances in computational design and analysis of airbreathing propulsion systems p 19 A90-12502
Multi-level Hierarchical Poly Tree computer architectures p 236 A90-26082
A block-based algorithm for the solution of compressible flows in rotor-stator combinations p 9 A90-46905
Parallel eigenanalysis of finite element models in a completely connected architecture
[NASA-CR-185166] p 217 N90-14652
Eigensolution of finite element problems in a completely connected parallel architecture
[NASA-TM-102450] p 217 N90-17173
Transient finite element computations on the transputer system
[NASA-CR-185199] p 218 N90-18071
Parallel algorithms for boundary value problems
[NASA-TM-102498] p 243 N90-19783
Hypercluster parallel processing library user's manual
[NASA-CR-185231] p 237 N90-21552
Parallel/distributed direct method for solving linear systems
[NASA-TM-103229] p 244 N90-26614
- PARALLEL PROGRAMMING**
A parallel pipelined architecture for a digital multicarrier demodulator
[AIAA PAPER 90-0812] p 46 A90-25635
Hypercluster parallel processing library user's manual
[NASA-CR-185231] p 237 N90-21552
Multiprocessor architecture: Synthesis and evaluation
[NASA-CR-186618] p 235 N90-25579
- PARAMETER IDENTIFICATION**
Characterization of structural connections using free and forced response test data p 213 A90-46172
The determination of third order linear models from a seventh order nonlinear jet engine model p 239 A90-52881
A global approach for the identification of structural connection properties
[NASA-TM-102502] p 218 N90-18745
Autonomous power expert system p 240 N90-22306
Neuromorphic learning of continuous-valued mappings from noise-corrupted data. Application to real-time adaptive control
[NASA-TM-4176] p 241 N90-25607
A failure diagnosis system based on a neural network classifier for the space shuttle main engine
[NASA-TM-103607] p 83 N90-28659

SUBJECT INDEX

PARAMETERIZATION

Constitutive parameter measurements of lossy materials p 237 A90-47188
[NASA-CR-183398] p 257 N90-11603

PARTIAL DIFFERENTIAL EQUATIONS

Grid generation for the solution of partial differential equations p 237 A90-47188
User's guide to PMESH: A grid-generation program for single-rotation and counterrotation advanced turboprops [NASA-CR-185156] p 235 N90-14783
High accuracy solutions of incompressible Navier-Stokes equations [NASA-TM-102539] p 244 N90-21567
Nonlinear interactions in mixing layers and compressible heated round jets [NASA-CR-186303] p 182 N90-23674

PARTICLE DENSITY (CONCENTRATION)

Equilibrium statistical thermodynamics of a many-particle system coupled to an external scalar field p 261 A90-31670

PARTICLE DIFFUSION

Solute redistribution in dendritic solidification with diffusion in the solid p 253 A90-17399
The kinetics of the Au-InP interaction p 254 A90-25084

PARTICLE INTERACTIONS

The kinetics of the Au-InP interaction p 254 A90-25084
Big bang nucleosynthesis and the quark-hadron transition p 265 A90-31407
Phase transitions as the origin of large scale structure in the universe p 265 A90-35291

PARTICLE LADEN JETS

An experimental and numerical study of particle-laden coaxial jet flows p 171 A90-38799

PARTICLE MASS

Unity limits on the mass and radius of dark-matter particles p 264 A90-24671

PARTICLE SIZE DISTRIBUTION

Modeling of collision and coalescence of droplets during microgravity processing of Zn-Bi immiscible alloys p 132 A90-22878
Comparison of two droplet sizing systems in an icing wind tunnel [AIAA PAPER 90-0668] p 164 A90-23711
Application of two-component phase Doppler interferometry to the measurement of particle size, mass flux, and velocities in two-phase flows p 186 A90-32853
Droplet sizing instrumentation used for icing research: Operation, calibration, and accuracy [NASA-CR-182293] p 187 N90-11999
Comparison of two droplet sizing systems in an icing wind tunnel [NASA-TM-102456] p 200 N90-14617

PARTICLE THEORY

Equilibrium statistical thermodynamics of a many-particle system coupled to an external scalar field p 261 A90-31670

PARTICLE TRAJECTORIES

Swept wing ice accretion modeling [NASA-TM-103114] p 13 N90-21727

PARTICULATES

Elevated temperature slow plastic deformation of NiAl-TiB2 particulate composites at 1200 and 1300 K p 92 A90-45621

PASSIVITY

Interface properties of various passivations of HgCdTe p 251 A90-45947
New directions in InP solar cell research [NASA-TM-103160] p 154 N90-23662

PATHFINDER NUCLEAR REACTOR

Regenerative fuel cell systems for project pathfinder p 74 N90-17708

PAYLOAD CONTROL

Space nuclear reactor shields for manned and unmanned applications p 57 A90-37859

PAYLOAD DELIVERY (STS)

Advanced APS impacts on vehicle payloads p 75 N90-18472

PAYLOADS

Computer modeling of current collection by the CHARGE-2 mother payload p 252 A90-24933
Microwave beam power p 69 N90-10165
Reaction-compensation technology for microgravity laboratory robots [NASA-TM-103271] p 205 N90-28062
ATDRS payload technology research and development [NASA-TM-103256] p 52 N90-28596
Development and approach to low-frequency microgravity isolation systems [NASA-TP-2984] p 138 N90-28754

PERFLUORO COMPOUNDS

Tribological reactions of perfluoroalkyl polyether oils with stainless steel under ultrahigh vacuum conditions at room temperature p 120 A90-16278
Decomposition of perfluoroalkylpolyethers (PFPE) in ultra-high vacuum under sliding conditions p 122 A90-40714
Determination of the thermal stability of perfluoroalkylethers [NASA-TM-102493] p 127 N90-17875

PERFLUOROALKANE

X-ray photoelectron spectroscopy peak assignment for perfluoropolyether oils p 124 A90-48550

PERFORATED PLATES

Comparison between design and installed acoustic characteristics of NASA Lewis 9- by 15-foot low-speed wind tunnel acoustic treatment [NASA-TP-2996] p 38 N90-19242

PERFORMANCE PREDICTION

Predictions of airfoil aerodynamic performance degradation due to icing p 3 A90-16753
A study of ice shape prediction methodologies and comparison with experimental data [AIAA PAPER 90-0753] p 15 A90-26986
Indium phosphide solar cells - Recent developments and estimated performance in space p 57 A90-37854
Frequency domain model for analysis of paralleled, series-output-connected Mapham inverters p 148 A90-38084

Estimated performance and future potential of solar dynamic and photovoltaic power systems for selected LEO and HEO missions p 62 A90-38307
A performance analysis of DS-CDMA and SCPC VSAT networks p 141 A90-39056
A modeling technique for STOVL ejector and volume dynamics [AIAA PAPER 90-2417] p 20 A90-42168

Isothermal life prediction of composite lamina using a damage mechanics approach p 92 A90-48115
Performance analysis of Integrated Communication and Control System networks p 239 A90-51267
Large-scale Advanced Prop-fan (LAP) high speed wind tunnel test report [NASA-CR-182125] p 24 N90-10045

Numerical simulation of unsteady rotational flow over propan configurations [NASA-CR-186037] p 10 N90-12500
An investigation of gear mesh failure prediction techniques [NASA-TM-102340] p 200 N90-13785

An approximate model for the performance and acoustic predictions of counterrotating propeller configurations [NASA-CR-180667] p 248 N90-18228
Model development in viscoplastic ratchetting [NASA-TM-102509] p 219 N90-20431
A modeling technique for STOVL ejector and volume dynamics [NASA-TM-103167] p 30 N90-22566

Performance of a supercharged direct-injection stratified-charge rotary combustion engine [NASA-TM-103105] p 32 N90-25982
Modeling and optimization of a regenerative fuel cell system using the ASPEN process simulator [NASA-TM-103210] p 233 N90-26396

PERFORMANCE TESTS

Radiation resistance and comparative performance of ITO/InP and n/p InP homojunction solar cells p 226 A90-14933
Effect of advanced component technology on helicopter transmissions p 193 A90-21115
Development and testing of a 20 kHz component test bed --- for space station power supplies p 43 A90-38126

Performance testing of a high frequency link converter for Space Station power distribution system p 148 A90-38128
Protoflight photovoltaic power module system-level tests in the Space Power Facility p 62 A90-38266

Diagnostics and performance of a 1/4-scale MPD thruster [AIAA PAPER 90-2665] p 65 A90-42625
Experimental investigation of multielement airfoil ice accretion and resulting performance degradation p 9 A90-48954
Low power arcjet performance [AIAA PAPER 90-2578] p 68 A90-52568
LOX/hydrocarbon combustion instability investigation [NASA-CR-182249] p 71 N90-13589

Arcjet thruster research and technology. Phase 1: Executive summary [NASA-CR-182106] p 72 N90-14278
Altitude testing of the 2D V/STOL ADEN demonstrator on an F404 engine [NASA-CR-174824] p 28 N90-17638

PHASE TRANSFORMATIONS

Research on a two-dimensional inlet for a supersonic V/STOL propulsion system. Appendix A [NASA-CR-174945] p 12 N90-18364

Integrated regenerative fuel cell experimental evaluation [NASA-CR-185183] p 230 N90-18808

A comparison of reflector antenna designs for wide-angle scanning p 144 N90-19264
High power, high frequency component test facility [NASA-TM-102500] p 151 N90-19484

Characterization testing of a 40 AHR bipolar nickel-hydrogen battery p 230 N90-20463
Sodium-sulfur battery flight experiment definition study p 231 N90-20479

Effect of KOH concentration on LEO cycle life of IPV nickel-hydrogen flight battery cells [NASA-TM-103127] p 77 N90-21116

Advanced Turbine Technology Applications Project (ATTAP) [NASA-CR-185240] p 263 N90-26728

Energy Efficient Engine exhaust mixer model technology report addendum; phase 3 test program [NASA-CR-174799] p 33 N90-28556
Energy efficient engine pin fin and ceramic composite segmented liner combustor sector rig test report [NASA-CR-179534] p 35 N90-28567

Integrated controls and health monitoring fiberoptic shaft monitor [NASA-CR-185210] p 191 N90-29622

PERMANENT MAGNETS

Magnification of starting torques of dc motors by maximum power point trackers in photovoltaic systems p 149 A90-38144

PERMITTIVITY

Induction motor control [NASA-TM-102533] p 28 N90-19234

PERMITTIVITY

Ka-band propagation characteristics of microstrip lines on GaAs substrates at cryogenic temperatures p 147 A90-33644
Complex permittivity of lanthanum aluminate in the 20 to 300 K temperature range from 26.5 to 40.0 GHz p 148 A90-37864

PEROVSKITES

Antiferromagnetism in Co-57-doped La2CuO4(4-y) studied by Moessbauer spectroscopy p 255 A90-34011

PERSONNEL MANAGEMENT

Middle management of research [NASA-TM-102417] p 262 N90-20901

PERTURBATION THEORY

Numerical simulations of supersonic flow through oscillating cascade sections [NASA-TM-103100] p 13 N90-20051
The effects of forcing on a single stream shear layer and its parent boundary layer [NASA-CR-186529] p 180 N90-21301

PHASE CHANGE MATERIALS

Selection of phase-change and containment materials for thermal energy storage [NASA-CR-186228] p 229 N90-15506
Analysis of thermal energy storage material with change-of-phase volumetric effects [NASA-TM-102457] p 181 N90-21974

PHASE CONTROL

Active phase compensation system for fiber optic holography p 250 A90-11310
Phase development and its role on subharmonic control [AIAA PAPER 90-0503] p 166 A90-25035
Fiber-optic projected-fringe digital interferometry [NASA-TM-103252] p 191 N90-28033

PHASE DETECTORS

Advanced instrumentation for aircraft icing research [NASA-CR-185225] p 18 N90-21006
Zero-G phase detector and separator [NASA-CASE-LEW-14844-1] p 190 N90-22024

PHASE SEPARATION (MATERIALS)

Polymer solution phase separation: Microgravity simulation p 127 N90-17101

PHASE SHIFT CIRCUITS

Design for steering accuracy in antenna arrays using shared optical phase shifters p 138 A90-13935
Control of a GaAs monolithic Ka-band phase shifter using a high-speed optical interconnect p 150 A90-41700

PHASE SHIFT KEYING

A forward error correction technique using a high-speed, high-rate single chip codec p 141 A90-48440
Advanced modulation technology development for earth station demodulator applications. Coded modulation system development [NASA-CR-185149] p 145 N90-20270

PHASE TRANSFORMATIONS

Numerical analysis of natural convection in liquid droplets by phase change p 164 A90-23212

- Big bang nucleosynthesis and the quark-hadron transition p 265 A90-31407
- Phase transitions as the origin of large scale structure in the universe p 265 A90-35291
- High-strength silicon carbides by hot isostatic pressing p 122 A90-35473
- Phase transformations in xerogels of mullite composition p 123 A90-47093
- Low-gravity fluid physics: A program overview [NASA-TM-103215] p 183 A90-26273
- PHASE VELOCITY**
- Instabilities and subharmonic resonances of subsonic heated round jets, volume 2 [NASA-CR-186058] p 181 A90-22017
- PHASED ARRAYS**
- High frequency GaAs modulator and photodetector for phased array antenna applications p 146 A90-11774
- Design for steering accuracy in antenna arrays using shared optical phase shifters p 138 A90-13935
- A high-speed GaAs MESFET optical controller p 186 A90-22483
- Convergence of the SMI and the diagonally loaded SMI algorithms with weak interference [AD-A22639] p 141 A90-36717
- High-speed fiber-optic links for distribution of satellite traffic p 47 A90-41687
- Antenna beamforming using optical processing [NASA-CR-180844] p 142 A90-11210
- Bit-error-rate testing of fiber optic data links for MMIC-based phased array antennas [NASA-TM-102523] p 145 A90-21261
- Coplanar waveguide fed phased array antenna [NASA-TM-102522] p 152 A90-21273
- Optical control of an 8-element Ka-band phased array using a high-speed optoelectronic interconnect [NASA-TM-102550] p 152 A90-21275
- Design of an optically controlled Ka-band GaAs MMIC phased-array antenna [NASA-TM-103147] p 155 A90-26250
- ATDRS payload technology research and development [NASA-TM-103256] p 52 A90-28596
- PHENOMENOLOGY**
- Performance and modeling of superconducting ring resonators at millimeter-wave frequencies [NASA-TM-102526] p 151 A90-18634
- PHOBOS**
- Performance comparisons of nuclear thermal rocket and chemical propulsion systems for piloted missions to Phobos/Mars [IAF PAPER 89-027] p 53 A90-13262
- PHOSPHORUS**
- Electron beam induced damage in PECVD Si₃N₄ and SiO₂ films on InP [NASA-TM-102544] p 203 A90-20393
- PHOTOCHEMICAL REACTIONS**
- Photochemical approaches to ordered polymers p 84 A90-33222
- PHOTOCONDUCTIVITY**
- Radiation resistance studies of amorphous silicon films p 227 A90-14952
- PHOTOCONDUCTORS**
- Microwave response of a HEMT photoconductive detector p 147 A90-37301
- PHOTODIODES**
- Contribution of the graded region of a HgCdTe diode to its saturation current p 257 A90-45948
- NASA Laser Light Scattering Advanced Technology Development Workshop, 1988 [NASA-CP-10033] p 188 A90-17085
- Optical techniques for determination of normal shock position in supersonic flows for aerospace applications [NASA-TM-103201] p 190 A90-25323
- PHOTOLITHOGRAPHY**
- Photoreponse of YBa₂Cu₃O₇(δ) granular and epitaxial superconducting thin films [NASA-TM-103144] p 154 A90-22732
- PHOTOMETERS**
- High frequency GaAs modulator and photodetector for phased array antenna applications p 146 A90-11774
- Microwave response of a HEMT photoconductive detector p 147 A90-37301
- PHOTOVOLTAIC CELLS**
- Issues and opportunities in space photovoltaics p 54 A90-14852
- Lunar production of space photovoltaic arrays p 226 A90-14930
- An advanced space photovoltaic concentrator array using Fresnel lenses, gallium arsenide cells, and prismatic cell covers p 54 A90-14954
- Solar power for the lunar night p 266 A90-24814
- Selection of component modes [AIAA PAPER 90-1201] p 210 A90-26787
- Comparative thermal analysis of the Space Station Freedom photovoltaic deployable boom structure using TRASYS, NEVADA, and SINDA programs [SAE PAPER 891563] p 47 A90-27525
- Space Station Freedom electric power system photovoltaic power module integrated launch package [AIAA PAPER 90-1053] p 48 A90-29281
- Evolutionary growth for Space Station Freedom electrical power system p 58 A90-38072
- The mini-dome lens space concentrator array - Recent component test results and current array development status p 60 A90-38155
- Protoflight photovoltaic power module system-level tests in the Space Power Facility p 62 A90-38266
- Photovoltaic options for solar electric propulsion [AIAA PAPER 90-2529] p 68 A90-52563
- Aeolian removal of dust from photovoltaic surfaces on Mars [NASA-TM-102507] p 76 A90-19299
- A transient plasticity study and low cycle fatigue analysis of the Space Station Freedom photovoltaic solar array blanket [NASA-TM-102516] p 218 A90-19617
- Analysis of thermal energy storage material with change-of-phase volumetric effects [NASA-TM-102457] p 181 A90-21974
- PHOTOVOLTAIC CONVERSION**
- Photovoltaic power for a lunar base [IAF PAPER 89-254] p 42 A90-13409
- Space Station Freedom electrical power system hardware commonality with the United States Polar Platform p 58 A90-38073
- Space Station Freedom photovoltaic power module design status p 58 A90-38075
- Launch packaging options for the PV power module cargo element --- for space station power supplies p 45 A90-38078
- Mathematical optimization of photovoltaic converters for diode lasers --- for spacecraft power supplies p 228 A90-38110
- Magnification of starting torques of dc motors by maximum power point trackers in photovoltaic systems p 149 A90-38144
- Estimated performance and future potential of solar dynamic and photovoltaic power systems for selected LEO and HEO missions p 62 A90-38307
- NASA advanced space photovoltaic technology: Status, potential and future mission applications p 74 A90-17775
- Recent results from advanced research on space solar cells at NASA [NASA-TM-102485] p 152 A90-21274
- Space Station Freedom solar array panels plasma interaction test facility [NASA-TM-102475] p 266 A90-22488
- The chemical effects of the Martian environment on power system component materials: A theoretical approach [NASA-TM-103203] p 87 A90-26074
- PHOTOVOLTAIC EFFECT**
- Photovoltaic module on-orbit assembly for Space Station Freedom p 45 A90-38071
- PHYSICAL OPTICS**
- On physical optics for calculating scattering from coated bodies p 250 A90-20151
- Constitutive parameter measurements of lossy materials [NASA-CR-183398] p 257 A90-11603
- PIEZOELECTRIC GAGES**
- Developing a self-diagnostic system for piezoelectric sensors [AIAA PAPER 90-2230] p 187 A90-42755
- PIEZOELECTRIC TRANSDUCERS**
- Test and theory for piezoelectric actuator-active vibration control of rotating machinery p 198 A90-46226
- PINHOLES**
- Comparison of currents predicted by NASCAP/LEO model simulations with elementary Langmuir-type bare probe models for an insulated cable containing a single pinhole [NASA-TM-102486] p 51 A90-26054
- PINS**
- Controlled crack growth specimen for brittle systems [NASA-TM-103126] p 129 A90-23543
- PIPE FLOW**
- Near-wall turbulence model and its application to fully developed turbulent channel and pipe flows p 169 A90-37328
- Mathematical modeling and analysis of heat pipe start-up from the frozen state p 174 A90-48404
- An improved algorithm for the modeling of vapor flow in heat pipes [NASA-CR-185179] p 176 A90-13748
- PIPELINING (COMPUTERS)**
- A parallel pipelined architecture for a digital multicarrier demodulator [AIAA PAPER 90-0812] p 46 A90-25635
- PIPES (TUBES)**
- FLUSH: A tool for the design of slush hydrogen flow systems [NASA-TM-102467] p 130 A90-17890
- PISTON ENGINES**
- Ceramic port shields cast in an iron engine head p 196 A90-27095
- Development of free-piston Stirling engine performance and optimization codes based on Martini simulation technique [NASA-CR-182210] p 263 A90-18326
- PISTONS**
- Sliding seal materials for low heat rejection engines [NASA-CR-182262] p 125 A90-11882
- PITTING**
- Surface pitting fatigue life of noninvolute, low-contact-ratio gears [AIAA PAPER 90-2153] p 197 A90-42049
- Surface pitting fatigue life of noninvolute, low-contact-ratio gears [NASA-TM-103116] p 203 A90-22790
- PLANAR STRUCTURES**
- Experimental investigations on channelized coplanar waveguide [NASA-TM-102494] p 151 A90-20286
- A new rectangular waveguide to coplanar waveguide transition [NASA-TM-102477] p 145 A90-21263
- Coplanar waveguide fed phased array antenna [NASA-TM-102522] p 152 A90-21273
- Coplanar waveguide discontinuities for P-I-N diode switches and filter applications [NASA-TM-102534] p 153 A90-21278
- PLANETARY BASES**
- Figure of merit studies of beam power concepts for advanced space exploration [NASA-CR-186720] p 146 A90-26234
- PLANETARY GEOLOGY**
- Aeolian removal of dust from photovoltaic surfaces on Mars [NASA-TM-102507] p 76 A90-19299
- PLANETARY ORBITS**
- Orbit to surface beamed power for Mars bases expansion p 40 A90-38105
- PLANETARY SURFACES**
- Analysis of a Mars-stationary orbiting microwave power transmission system [NASA-TM-101344] p 138 A90-26172
- PLANETS**
- Extraterrestrial life in the universe [NASA-TM-102363] p 264 A90-22464
- PLASMA CLOUDS**
- A two-dimensional model of plasma expansion in the ionosphere p 233 A90-43609
- Theory of plasma contactors in ground-based experiments and low earth orbit p 150 A90-47108
- PLASMA CONDUCTIVITY**
- Theory of plasma contactors in ground-based experiments and low earth orbit p 150 A90-47108
- PLASMA CURRENTS**
- The Space Station photovoltaic panels plasma interaction test program - Test plan and results [AIAA PAPER 90-0722] p 47 A90-22252
- The Space Station Photovoltaic Panels Plasma Interaction Test Program: Test plan and results [NASA-TM-102474] p 49 A90-13581
- PLASMA DIAGNOSTICS**
- Review of research and development on the microwave electrothermal thruster p 55 A90-16369
- Spacelab 2 Plasma Diagnostics Package p 39 A90-23263
- Diagnostic evaluations of microwave generated helium and nitrogen plasma mixtures [AIAA PAPER 90-2634] p 252 A90-42602
- PLASMA ELECTRODES**
- Plasma contactor modeling with NASCAP/LEO - Extending laboratory results to space systems [AIAA PAPER 90-0726] p 251 A90-22255
- PLASMA ENGINES**
- Review of research and development on the microwave electrothermal thruster p 55 A90-16369
- Diagnostics and performance of a 1/4-scale MPD thruster [AIAA PAPER 90-2665] p 65 A90-42625
- The effects of magnetic nozzle configurations on plasma thrusters [NASA-CR-186465] p 76 A90-21109
- PLASMA GUNS**
- Plasma gun with coaxial powder feed and adjustable cathode [NASA-CASE-LEW-14901-1] p 252 A90-10718

SUBJECT INDEX

PLASMA INTERACTIONS

- The Space Station photovoltaic panels plasma interaction test program - Test plan and results [AIAA PAPER 90-0722] p 47 A90-22252
- High-voltage plasma interactions calculations using NASCAP/LEO [AIAA PAPER 90-0725] p 251 A90-22254
- The Space Station Photovoltaic Panels Plasma Interaction Test Program: Test plan and results [NASA-TM-102474] p 49 N90-13581
- Space Station Freedom solar array panels plasma interaction test facility [NASA-TM-102475] p 266 N90-22488

PLASMA LAYERS

- A Van der Waals-like theory of plasma double layers p 251 A90-10725

PLASMA PHYSICS

- Plasma contactor research, 1989 [NASA-CR-185212] p 252 N90-22389

PLASMA POTENTIALS

- Plasma contactor research, 1989 [NASA-CR-185212] p 252 N90-22389
- Solar array arcing in plasmas p 233 N90-25558

PLASMA PROPULSION

- Diagnostic evaluations of microwave generated helium and nitrogen plasma mixtures [AIAA PAPER 90-2634] p 252 A90-42602
- Geometric effects in applied-field MPD thrusters [AIAA PAPER 90-2669] p 69 A90-52572
- Test facility and preliminary performance of a 100 kW class MPD thruster p 75 N90-18476
- Geometric effects in applied-field MPD thrusters [NASA-TM-103259] p 82 N90-27782

PLASMA SHEATHS

- Comparison of currents predicted by NASCAP/LEO model simulations with elementary Langmuir-type bare probe models for an insulated cable containing a single pinhole [NASA-TM-102486] p 51 N90-26054

PLASMA SPRAYING

- Instrumented adhesion tests on plasma sprayed thermal barrier coatings p 111 A90-20255
- Mechanisms of degradation and failure in a plasma deposited thermal barrier coating [ASME PAPER 89-GT-132] p 84 A90-23830
- Metallographic techniques for evaluation of thermal barrier coatings p 85 A90-44869
- Plasma gun with coaxial powder feed and adjustable cathode [NASA-CASE-LEW-14901-1] p 252 N90-10718
- Improved process for HIP canning of composites [NASA-CASE-LEW-14990-1-CU] p 97 N90-15147

PLASMA-PARTICLE INTERACTIONS

- Plasma sources for spacecraft neutralization [AIAA PAPER 90-1556] p 49 A90-38697

PLASMAS (PHYSICS)

- Plasma-deposited amorphous hydrogenated carbon films and their tribological properties p 123 A90-44864
- Plasma-deposited amorphous hydrogenated carbon films and their tribological properties [NASA-TM-102379] p 125 N90-11880
- Advances and directions of ion nitriding/carburizing [NASA-TM-102398] p 137 N90-11902
- Electron-beam induced damage in thin insulating films on compound semiconductors p 151 N90-17987
- Electron beam induced damage in PECVD Si₃N₄ and SiO₂ films on InP [NASA-TM-102544] p 203 N90-20393
- Plasma contactor research, 1989 [NASA-CR-185212] p 252 N90-22389
- Technical accomplishments of the NASA Lewis Research Center, 1989 [NASA-TM-102296] p 267 N90-24220

PLASTIC DEFORMATION

- High temperature inelastic deformation under uniaxial loading - Theory and experiment p 109 A90-13838
- High temperature inelastic deformation of the B1900 + Hf alloy under multiaxial loading - Theory and experiment p 112 A90-22656
- Inelastic deformation under nonisothermal loading p 112 A90-22657
- Elevated temperature slow plastic deformation of NiAl-TiB₂ particulate composites at 1200 and 1300 K p 92 A90-45621
- Advanced applications of BEM to inelastic analysis of solids p 213 A90-45770
- Advanced development of BEM for elastic and inelastic dynamic analysis of solids p 213 A90-45771
- Slow plastic deformation of extruded NiAl-10TiB₂ particulate composites at 1200 and 1300 K p 92 A90-46133
- Simulation of crack growth and crack closure under large cyclic plasticity p 214 A90-50562

- Micromechanics of cyclic deformation in SSME turbopump blade materials p 224 N90-28841
- Microstructure: Property correlation --- multiaxial fatigue damage evolution in wasp alloy [NASA-CR-180406] p 224 N90-28880

PLASTIC PROPERTIES

- 1100 to 1300 K slow plastic compression properties of Ni-38.5Al composites p 111 A90-19154
- Isothermal life prediction of composite lamina using a damage mechanics approach p 92 A90-48115
- A transient plasticity study and low cycle fatigue analysis of the Space Station Freedom photovoltaic solar array blanket [NASA-TM-102516] p 218 N90-19617

PLATE THEORY

- Assumed strain distributions for a finite strip plate bending element using Mindlin-Reissner plate theory p 208 A90-16723
- A variational justification of the assumed natural strain formulation of finite elements. I - Variational principles. II - The C(0) four-node plate element p 210 A90-24384

PLATES

- Fully articulated four-point-bend loading fixture [NASA-CASE-LEW-14776-1] p 201 N90-15445

PLATES (STRUCTURAL MEMBERS)

- Developments in variational methods for high performance plate and shell elements p 214 A90-46288

- Analysis of impact response in composite plates p 214 A90-47567

- Progression of damage and fracture in composites under dynamic loading [NASA-TM-103118] p 100 N90-21825

- Reliability analysis of continuous fiber composite laminates [NASA-CR-185265] p 223 N90-26372

PLATINUM

- A resistance strain gage with repeatable and cancellable apparent strain for use to 800 C [NASA-CR-185256] p 53 N90-26063

PLUMES

- Preliminary plume characteristics of an arcjet thruster [AIAA PAPER 90-2645] p 64 A90-42609
- Fabry-Perot interferometer development for rocket engine plume spectroscopy [AIAA PAPER 90-2234] p 187 A90-47212
- Digital filtering of plume emission spectra [AIAA PAPER 90-1994] p 67 A90-50643
- Digital filtering of plume emission spectra [NASA-TM-103135] p 81 N90-26070
- Preliminary plume characteristics of an arcjet thruster [NASA-TM-103241] p 81 N90-26071

PLY ORIENTATION

- Impact damage development in damaged composite materials p 193 A90-18355

POINT TO POINT COMMUNICATION

- Spacecraft designs for VSAT networks [AIAA PAPER 90-0895] p 140 A90-25681

POLYCRYSTALS

- Review and statistical analysis of the ultrasonic velocity method for estimating the porosity fraction in polycrystalline materials [NASA-TM-102501-REV] p 207 N90-21402

POLYETHER RESINS

- Decomposition of perfluoroalkylpolyethers (PFPE) in ultra-high vacuum under sliding conditions p 122 A90-40714

POLYIMIDE RESINS

- Thermo-oxidative stability studies of PMR-15 polymer matrix composites reinforced with various continuous fibers p 93 A90-50068

- Autoclavable addition polyimides for 371 C composite applications [NASA-TM-103233] p 102 N90-27874

POLYIMIDES

- The 3F condensation polyimides: Review and update [NASA-TM-102353] p 126 N90-14363

- New Condensation polyimides containing 1,1,1-triaryl-2,2,2-trifluoroethane structures [NASA-CASE-LEW-14346-1] p 86 N90-19300

POLYMER CHEMISTRY

- Processable, high temperature polymers from 1,4,5,8-tetrahydro-1,4,5,8-diepoxyanthracene and bis-dienes p 84 A90-21930

- Photochemical approaches to ordered polymers p 84 A90-33222

- The 3F condensation polyimides: Review and update [NASA-TM-102353] p 126 N90-14363

- New Condensation polyimides containing 1,1,1-triaryl-2,2,2-trifluoroethane structures [NASA-CASE-LEW-14346-1] p 86 N90-19300

- Polysiloxanes derived from the controlled hydrolysis of tetraethoxysilane as precursors to silica for use in ceramic processing [NASA-TM-102489] p 128 N90-21858

POTASSIUM HYDROXIDES

POLYMER MATRIX COMPOSITES

- Unified micromechanics of damping for unidirectional and off-axis fiber composites p 90 A90-29929
- Tailoring of composite links for optimal damped elasto-dynamic performance p 211 A90-30250
- Thermo-oxidative stability studies of PMR-15 polymer matrix composites reinforced with various continuous fibers p 93 A90-50068
- Use of unbalanced laminates as a screening method for microcracking p 94 A90-50217
- Thermo-oxidative stability studies of PMR-15 polymer matrix composites reinforced with various fibers [NASA-TM-102439] p 98 N90-19310
- Use of unbalanced laminates as a screening method for microcracking [NASA-TM-102517] p 98 N90-21124
- Self-lubricating polymer composites and polymer transfer film lubrication for space applications [NASA-TM-102492] p 128 N90-21862
- Structural behavior of composites with progressive fracture [NASA-TM-102370] p 100 N90-23477

POLYMERIC FILMS

- The 3F condensation polyimides: Review and update [NASA-TM-102353] p 126 N90-14363

POLYMERIZATION

- The 3F condensation polyimides: Review and update [NASA-TM-102353] p 126 N90-14363

- New Condensation polyimides containing 1,1,1-triaryl-2,2,2-trifluoroethane structures [NASA-CASE-LEW-14346-1] p 86 N90-19300

- Polysiloxanes derived from the controlled hydrolysis of tetraethoxysilane as precursors to silica for use in ceramic processing [NASA-TM-102489] p 128 N90-21858

POLYMERS

- A brief survey of radiation effects on polymer dielectrics p 123 A90-43119

POLYNOMIALS

- Efficient implementation of minimal polynomial and reduced rank extrapolation methods [NASA-TM-103240] p 244 N90-26616

POLYQUINOXALINES

- Polymer derived Nicalon/Si-C-O composites - Processing and mechanical behavior p 89 A90-27065

POLYURETHANE FOAM

- Smoldering combustion under low gravity conditions [AIAA PAPER 90-0648] p 103 A90-22238

POROSITY

- Subtle porosity variation in the YBa₂Cu₃O(7-x) high-temperature superconductor revealed by ultrasonic imaging [NASA-TM-102130] p 206 N90-17167

- Characterization of reaction kinetics in a porous electrode [NASA-CR-186504] p 106 N90-19340

- Review and statistical analysis of the ultrasonic velocity method for estimating the porosity fraction in polycrystalline materials [NASA-TM-102501-REV] p 207 N90-21402

- The fatigue damage behavior of a single crystal superalloy p 120 N90-28644

POROUS MATERIALS

- Experimental investigation of convective stability in a superposed fluid and porous layer when heated from below p 158 A90-15947

- The impedance of a tubular electrode - A model for a porous electrode p 104 A90-33723

- Metallographic techniques for evaluation of thermal barrier coatings p 85 A90-44869

POSITION (LOCATION)

- Optical techniques for determination of normal shock position in supersonic flows for aerospace applications [NASA-TM-103201] p 190 N90-25323

POSITION SENSING

- Optical techniques for determination of normal shock position in supersonic flows for aerospace applications [NASA-TM-103201] p 190 N90-25323

POSITIONING

- Beam rider for an Articulated Robot Manipulator (ARM) accurate positioning of long flexible manipulators [NASA-CR-185151] p 241 N90-26581

POTASSIUM HYDROXIDES

- Electrochemical behavior of heavily cycled nickel electrodes in Ni/H₂ cells containing electrolytes of various KOH concentrations p 103 A90-24535

- KOH concentration effect on the cycle life of nickel-hydrogen cells. IV - Results of failure analysis p 228 A90-33952

- Effect of KOH concentration on LEO cycle life of IPV nickel-hydrogen flight battery cells [NASA-TM-103127] p 77 N90-21116

- Effect of LEO cycling on 125 Ah advanced design IPV nickel-hydrogen battery cells p 78 N90-21808

POTENTIAL FLOW

POTENTIAL FLOW

- Time domain flutter analysis of cascades using a full-potential solver
[AIAA PAPER 90-0984] p 6 A90-29374
- Three dimensional full potential method for the aeroleastic modeling of propfans
[AIAA PAPER 90-1120] p 7 A90-29392
- Users manual for the NASA Lewis Ice Accretion Prediction Code (LEWICE)
[NASA-CR-185129] p 1 N90-20943

POTENTIAL THEORY

- Electromagnetic finite elements based on a four-potential variational principle p 214 A90-49869

POWDER (PARTICLES)

- Millimeter wave surface resistance of $R\text{Ba}_2\text{Cu}_3\text{O}(7-\delta)$ (R = Y, Eu, Dy, Sm, Er) superconductors
[NASA-TM-102571] p 259 N90-20886

POWDER METALLURGY

- Solid state processing for high temperature alloys and composites p 196 A90-33225
- Tribological properties of PM212: A high-temperature, self-lubricating, powder metallurgy composite
[NASA-TM-102355] p 86 N90-12659
- One step HIP canning of powder metallurgy composites
[NASA-CASE-LEW-14719-1] p 101 N90-23493

POWDERED ALUMINUM

- High energy-density liquid rocket fuel performance
[NASA-CR-185279] p 131 N90-28742

POWER BEAMING

- Orbit to surface beamed power for Mars bases expansion p 40 A90-38105
- Applicability of the beamed power concept to lunar rovers, construction, mining, explorers and other mobile equipment p 69 N90-10159
- Central electrical utility power for a satellite ring city in low earth orbit space p 150 N90-10166
- Figure of merit studies of beam power concepts for advanced space exploration
[NASA-CR-186720] p 146 N90-26234

POWER CONDITIONING

- Photovoltaic power for a lunar base
[IAF PAPER 89-254] p 42 A90-13409
- A 2.5 kW cascaded Schwarz converter for 20 kHz power distribution p 147 A90-36913
- Space Station Freedom electrical power system hardware commonality with the United States Polar Platform p 58 A90-38073
- Space Station Freedom power - A reliability, availability, and maintainability assessment of the proposed Space Station Freedom electric power system p 58 A90-38074

- Space Station Freedom power management and distribution design status p 59 A90-38080
- Development of Ada language control software for the NASA power management and distribution test bed p 236 A90-38082

- Evaluation of power control concepts using the PMAD systems test bed --- Power Management and Distribution p 42 A90-38083

- The effects of nonlinear loading upon the Space Station Freedom 20 kHz power system p 60 A90-38118
- Performance testing of a high frequency link converter for Space Station power distribution system p 148 A90-38128

- Power transmission cable development for the Space Station Freedom electrical power system p 149 A90-38134

- 20 kHz, 25 kVA node power transformer p 149 A90-38275

- High-frequency ac power distribution in Space Station p 63 A90-39111

- The US space station and its electric power system
[NASA-TM-101974] p 71 N90-13596

- Power conditioning techniques
[NASA-TM-102577] p 151 N90-20301

- Electric power scheduling: A distributed problem-solving approach
[NASA-TM-103149] p 240 N90-22323

- Conceptual definition of a high voltage power supply test facility
[NASA-CR-185216] p 50 N90-25172

- An analysis of space power system masses
[NASA-TM-103199] p 80 N90-25184

POWER CONVERTERS

- A 2.5 kW cascaded Schwarz converter for 20 kHz power distribution p 147 A90-36913

- 20 kHz main inverter unit --- for space station power supplies p 148 A90-38124

- Numerical model of solar dynamic radiator for parametric analysis p 61 A90-38168

- High-frequency ac power distribution in Space Station p 63 A90-39111

- Programmatic status of NASA's CSTI high capacity power Stirling space power converter program
[NASA-TM-103142] p 79 N90-22606

- Electrical characterization of a Mapham inverter using pulse testing techniques
[NASA-TM-103254] p 82 N90-27784

POWER EFFICIENCY

- Efficiency testing of a helicopter transmission planetary reduction stage p 193 A90-21113

- Effects of lubrication on the performance of high speed spur gears p 194 A90-21119

- Estimated performance and future potential of solar dynamic and photovoltaic power systems for selected LEO and HEO missions p 62 A90-38307

- The effect of electrode configuration on arcjet performance
[NASA-TM-102346] p 70 N90-11081

- Energy Efficient Engine exhaust mixer model technology report addendum; phase 3 test program
[NASA-CR-174799] p 33 N90-28556

POWER FACTOR CONTROLLERS

- The effects of nonlinear loading upon the Space Station Freedom 20 kHz power system p 60 A90-38118

POWER LINES

- Power transmission cable development for the Space Station Freedom electrical power system p 149 A90-38134

POWER MODULES (STS)

- Prototyped photovoltaic power module system-level tests in the Space Power Facility p 62 A90-38266

POWER SPECTRA

- Theory and experimental technique for nondestructive evaluation of ceramic composites
[NASA-TM-102561] p 207 N90-23754

POWER TRANSMISSION

- Solar power for the lunar night p 266 A90-24814
- Power transmission cable development for the Space Station Freedom electrical power system p 149 A90-38134

- Coax-to-channelised coplanar waveguide in-phase N-way, radial power divider p 149 A90-41605
- Free-Space Power Transmission
[NASA-CP-10018] p 77 N90-21795

PRECIPITATION HARDENING

- Properties of oxide dispersion strengthened alloys p 109 A90-14687

- Preliminary investigation of a NiAl composite prepared by cryomilling p 113 A90-25098

- Solid state processing for high temperature alloys and composites p 196 A90-33225

- Coarsening in high volume fraction nickel-base alloys p 115 A90-37719

- 1300 K compressive properties of several dispersion strengthened NiAl materials p 116 A90-47091

- Thermomechanical deformation testing and modeling in the presence of metallurgical instabilities
[NASA-CR-185188] p 219 N90-21420

PRECIPITATION PARTICLE MEASUREMENT

- Comparison of two droplet sizing systems in an icing wind tunnel
[AIAA PAPER 90-0668] p 164 A90-23711

- Comparison of two droplet sizing systems in an icing wind tunnel
[NASA-TM-102456] p 200 N90-14617

PRECISION

- Foundations of measurement and instrumentation
[NASA-RP-1222] p 189 N90-21351

PREDICTION ANALYSIS TECHNIQUES

- Performance and acoustic prediction of counterrotating propeller configurations
[SAE PAPER 891035] p 246 A90-14342

- Vibration signature analysis of multistage gear transmission p 194 A90-21124

- Unsteady blade surface pressures on a large-scale advanced propeller - Prediction and data
[AIAA PAPER 90-2402] p 9 A90-47220

- Efficiency study comparing two helicopter planetary reduction stages
[AIAA PAPER 90-2156] p 199 A90-50644

- Status of structural analysis of 30 cm diameter ion optics
[AIAA PAPER 90-2649] p 215 A90-52571

- Mean stress and the exhaustion of fatigue-damage resistance
[NASA-TM-101311] p 216 N90-13819

- Predicted and measured boundary layer refraction for advanced turboprop propeller noise
[NASA-TM-102365] p 248 N90-17413

- Modeling and optimization of a regenerative fuel cell system using the ASPEN process simulator
[NASA-TM-103210] p 233 N90-26396

- Aeroacoustics of advanced propellers
[NASA-TM-103137] p 249 N90-26635

- High temperature fatigue behavior of Haynes 188 p 119 N90-28642

- Constitutive and life modeling of single crystal blade alloys for root attachment analysis p 119 N90-28643
- The fatigue damage behavior of a single crystal superalloy p 120 N90-28644
- Thermal analysis of thermal barrier coatings in a high heat flux environment p 129 N90-28652

PREDICTIONS

- A modified VAPEPS method for predicting vibroacoustic response of unreinforced mass loaded honeycomb panels p 206 A90-43731

- Thermal barrier coating life prediction model development, phase 1
[NASA-CR-182230] p 26 N90-13388

- An investigation into the numerical prediction of boundary layer transition using the K.Y. Chien turbulence model
[NASA-CR-185252] p 182 N90-26269

- Elevated temperature crack growth
[NASA-CR-182247] p 222 N90-26355

- Development of a linearized unsteady aerodynamic analysis for cascade gust response predictions
[NASA-CR-4308] p 14 N90-27655

PREMIXED FLAMES

- The structure and stability of nonadiabatic flame balls p 105 A90-43674

- Kinetics and mechanism of soot formation in hydrocarbon combustion
[NASA-CR-186162] p 106 N90-14305

PREMIXING

- Low NO(x) potential of gas turbine engines
[NASA-TM-102452] p 27 N90-17636

PREPOLYMERS

- Autoclavable addition polyimides for 371 C composite applications
[NASA-TM-103233] p 102 N90-27874

PRESSING

- Slurry-pressing consolidation of silicon nitride p 121 A90-27691

PRESSURE DEPENDENCE

- Pressure dependence of the melting temperature of metals p 103 A90-16281

PRESSURE DISTRIBUTION

- Global pressure relaxation for laminar two-dimensional internal flow p 174 A90-51019

- Prediction of unsteady blade surface pressures on an advanced propeller at an angle of attack
[NASA-TM-102374] p 11 N90-12560

- An electronic pressure profile display system for aeronautic test facilities
[NASA-TM-102478] p 38 N90-15964

- Large-scale advanced propeller blade pressure distributions: Prediction and data
[NASA-TM-102316] p 30 N90-22564

- Measurement of the steady surface pressure distribution on a single rotation large scale advanced prop-fan blade at Mach numbers from 0.03 to 0.78
[NASA-CR-182124] p 32 N90-28552

PRESSURE DROP

- Pressure drop and mass transfer in two-pass ribbed channels p 165 A90-24837

PRESSURE EFFECTS

- COLD-SAT - An orbital cryogenic hydrogen technology experiment
[IAF PAPER 89-057] p 53 A90-13282

- Effects of pressure on microgravity hydrocarbon diffusion flames
[AIAA PAPER 90-0651] p 104 A90-25039

- An accurate analytic approximation to the non-linear change in volume of solids with applied pressure p 261 A90-27612

- Thermodynamic analysis of chemical stability of ceramic materials in hydrogen-containing atmospheres at high temperatures
[NASA-CR-4271] p 126 N90-16072

PRESSURE GRADIENTS

- Fully elliptic incompressible flow calculations on regular grid by a new pressure substitution method
[AIAA PAPER 90-0239] p 160 A90-19749

- Comparison between pressure gradient method and MAC method on high Re calculation p 172 A90-44462

PRESSURE MEASUREMENT

- On the dynamic response of pressure transmission lines in the research of helium-charged free piston Stirling engines p 196 A90-38248

- Pressure-based real-time measurements in compressible free shear layers
[AIAA PAPER 90-1980] p 8 A90-42709

- Tank Pressure Control Experiment - A low-g mixing investigation
[AIAA PAPER 90-2376] p 66 A90-47217

- Laser velocimeter and total pressure measurements in circular-to-rectangular transition ducts
[NASA-CR-182286] p 177 N90-14494

SUBJECT INDEX

- Heat transfer and pressure measurements for the SSME fuel-side turbopump [NASA-CR-184928] p 31 N90-23405
- PRESSURE OSCILLATIONS**
A study of the unsteadiness of crossing shock wave turbulent boundary layer interactions [AIAA PAPER 90-1456] p 170 A90-38614
Unsteady blade surface pressures on a large-scale advanced propeller - Prediction and data [AIAA PAPER 90-2402] p 9 A90-47220
- PRESSURE RECOVERY**
Some observations on transitory stall in conical diffusers [AIAA PAPER 90-0048] p 4 A90-22158
Some observations on transitory stall in conical diffusers [NASA-TM-102387] p 11 N90-12561
- PRESSURE REGULATORS**
Tank pressure control experiment on the space shuttle [NASA-TM-102313] p 71 N90-13590
- PRESSURE SENSORS**
Experimental investigation of terminal shock sensors in mixed-compression inlets [AIAA PAPER 90-1931] p 186 A90-40560
- PRESSURE VESSELS**
Probabilistic analysis of a materially nonlinear structure [AIAA PAPER 90-1099] p 211 A90-29329
Effect of LEO cycling on 125 Ah advanced design IPV nickel-hydrogen battery cells [NASA-TM-103128] p 78 N90-21808
Creep and creep rupture of strongly reinforced metallic composites [NASA-CR-185286] p 223 N90-28110
- PRESSURIZING**
Prediction of self-pressurization rate of cryogenic propellant tankage p 55 A90-21219
- PRIMARY BATTERIES**
NASA aerospace flight battery systems program [NASA-TM-103237] p 233 N90-26397
- PRINTING**
Synthesis and characterization of high-T(c) screen-printed Y-Ba-Cu-O films on alumina p 254 A90-21926
- PROBABILITY DENSITY FUNCTIONS**
Chemically reacting supersonic flow calculation using an assumed PDF model [AIAA PAPER 90-0731] p 4 A90-22256
The pdf approach to turbulent flow p 168 A90-32225
- PROBABILITY THEORY**
Probabilistic structural analysis methods of hot engine structures [ASME PAPER 89-GT-122] p 56 A90-23821
Probabilistic analysis of bladed turbine disks and the effect of mistuning [AIAA PAPER 90-1097] p 196 A90-29327
Application of the probabilistic approximate analysis method to a turbopump blade analysis --- for Space Shuttle Main Engine [AIAA PAPER 90-1098] p 56 A90-29328
Probabilistic analysis of a materially nonlinear structure [AIAA PAPER 90-1099] p 211 A90-29329
A methodology for evaluating the reliability and risk of structures under complex service environments [AIAA PAPER 90-1102] p 211 A90-29332
Computational methods for probability of instability calculations [AIAA PAPER 90-1139] p 236 A90-29333
A probabilistic approach to crack instability p 212 A90-41278
Advanced probabilistic structural analysis method for implicit performance functions p 214 A90-49792
Probability of failure and risk assessment of propulsion structural components p 218 N90-18470
Probabilistic modeling for simulation of aerodynamic uncertainties in propulsion systems [NASA-TM-102472] p 29 N90-21036
Probabilistic structural analysis of aerospace components using NESSUS [NASA-TM-102324] p 221 N90-22823
Neuromorphic learning of continuous-valued mappings from noise-corrupted data. Application to real-time adaptive control [NASA-TM-4176] p 241 N90-25607
Design of ceramic components with the NASA/CARES computer program [NASA-TM-102369] p 222 N90-26359
Ceramics Analysis and Reliability Evaluation of Structures (CARES). Users and programmers manual [NASA-TP-2916] p 223 N90-28099
A solar power system for an early Mars expedition [NASA-TM-103219] p 246 N90-28393

- Probabilistic structural analysis methods development for SSME p 83 N90-28616
- PROBLEM SOLVING**
Application of a hybrid generation/utility assessment heuristic to a class of scheduling problems [NASA-TM-102367] p 245 N90-10674
Application of multi-grid methods for solving the Navier-Stokes equations [NASA-TM-102359] p 243 N90-14002
Institute for Computational Mechanics in Propulsion (ICOMP) fourth annual review, 1989 [NASA-TM-102519] p 243 N90-20769
High accuracy solutions of incompressible Navier-Stokes equations [NASA-TM-102539] p 244 N90-21567
Automated electric power management and control for Space Station Freedom [NASA-TM-103151] p 240 N90-23125
Autonomous power expert system [NASA-CR-185263] p 80 N90-25187
Reusable rocket engine turbopump health monitoring system, part 3 [NASA-CR-182294] p 204 N90-26320
Efficient implementation of minimal polynomial and reduced rank extrapolation methods [NASA-TM-103240] p 244 N90-26616
- PRODUCT DEVELOPMENT**
The role of NDE in ceramic turbine engine component development p 206 A90-35508
Development of Si3N4 for gas turbine applications p 122 A90-35509
- PRODUCTIVITY**
The Materials Division: A case study [NASA-TM-102380] p 86 N90-13597
The application of a computer data acquisition system for a new high temperature tribometer [NASA-TM-102508] p 86 N90-17811
- PROFILES**
Dynamic loading of spur gears with linear or parabolic tooth profile modifications p 195 A90-21126
- PROGRAM VERIFICATION (COMPUTERS)**
METCAN verification status [NASA-TM-103119] p 100 N90-21824
- PROJECT PLANNING**
A program for advancing the technology of space concentrators p 60 A90-38159
Middle management of research [NASA-TM-102417] p 262 N90-20901
Conceptual design of a Moving Belt Radiator (MBR) shuttle-attached experiment [NASA-CR-185169] p 79 N90-23474
Background, current status, and prognosis of the ongoing slush hydrogen technology development program for the NASP [NASA-TM-103220] p 51 N90-26055
- PROJECTILES**
Collision forces for compliant projectiles [NASA-TM-4203] p 223 N90-28111
- PROP-FAN TECHNOLOGY**
Application of the computational aeroacoustics method to an advanced counterrotating propfan configuration [AIAA PAPER 90-0183] p 246 A90-19725
Counterrotating prop-fan simulations which feature a relative-motion multiblock grid decomposition enabling arbitrary time-steps [AIAA PAPER 90-0687] p 3 A90-19978
Unsteady Euler analysis of the flowfield of a propfan at an angle of attack [AIAA PAPER 90-0339] p 5 A90-25028
Concurrent processing adaptation of aeroelastic analysis of propfans [AIAA PAPER 90-1036] p 211 A90-29380
Three dimensional full potential method for the aeroelastic modeling of propfans [AIAA PAPER 90-1120] p 7 A90-29392
Investigation of the near wake of a propfan p 7 A90-40686
Interior noise in the untreated Gulfstream II Propfan Test Assessment aircraft p 17 A90-44736
3D Euler analysis of ducted propfan flowfields [AIAA PAPER 90-3034] p 8 A90-45873
The selection of convertible engines with current gas generator technology for high speed rotorcraft p 22 A90-46933
Euler analysis comparison with LDV data for an advanced counter-rotation propfan at cruise [AIAA PAPER 90-3033] p 9 A90-50637
Large scale prop-fan structural design study. Volume 1: Initial concepts [NASA-CR-174992] p 23 N90-10043
Large scale prop-fan structural design study. Volume 2: Preliminary design of SR-7 [NASA-CR-174993] p 23 N90-10044
Large-scale Advanced Prop-fan (LAP) high speed wind tunnel test report [NASA-CR-182125] p 24 N90-10045

PROPELLANT STORAGE

- Large-scale Advanced Prop-fan (LAP) technology assessment report [NASA-CR-182142] p 24 N90-10046
Full scale technology demonstration of a modern counterrotating unducted fan engine concept: Component test [NASA-CR-180868] p 24 N90-10047
Full scale technology demonstration of a modern counterrotating unducted fan engine concept: Design report [NASA-CR-180867] p 24 N90-10048
Full scale technology demonstration of a modern counterrotating unducted fan engine concept: Engine test [NASA-CR-180869] p 24 N90-10049
Acoustic test and analysis of a counterrotating prop-fan model [NASA-CR-179590] p 247 N90-10683
Propfan Test Assessment (PTA): Flight test report [NASA-CR-182278] p 24 N90-11738
Propfan Test Assessment (PTA) [NASA-CR-185138] p 25 N90-11739
Numerical simulation of unsteady rotational flow over propfan configurations [NASA-CR-186037] p 10 N90-12500
Large-scale Advanced Prop-fan (LAP) static rotor test report [NASA-CR-180848] p 25 N90-12617
Unsteady Euler analysis of the flow field of a propfan at an angle of attack [NASA-TM-102426] p 248 N90-18229
Structural tailoring of select fiber composite structures [NASA-TM-102484] p 99 N90-21137
Investigation of advanced counterrotation blade configuration concepts for high speed turboprop systems, task 1: Ducted propfan analysis [NASA-CR-185217] p 30 N90-22567
Experimental performance and acoustic investigation of modern, counterrotating blade concepts [NASA-CR-185158] p 18 N90-23393
Advanced gearbox technology [NASA-CR-179625] p 32 N90-24274
Euler analysis comparison with LDV data for an advanced counter-rotation propfan at cruise [NASA-TM-103249] p 14 N90-25946
Aeroacoustics of advanced propellers [NASA-TM-103137] p 249 N90-26635
Measurement of the steady surface pressure distribution on a single rotation large scale advanced prop-fan blade at Mach numbers from 0.03 to 0.78 [NASA-CR-182124] p 32 N90-28552
- PROPANE**
Reduced chemical kinetics for propane combustion [AIAA PAPER 90-0546] p 103 A90-19904
Critical evaluation of Jet-A spray combustion using propane chemical kinetics in gas turbine combustion simulated by KIVA-2 [NASA-TM-103173] p 138 N90-26170
- PROPELLANT ADDITIVES**
Ignition and combustion characteristics of metallized propellants [NASA-CR-186870] p 107 N90-26911
High energy-density liquid rocket fuel performance [NASA-CR-185279] p 131 N90-28742
- PROPELLANT COMBUSTION**
Combustor design and analysis using the ROCKET Combustor Interactive Design (ROCCID) Methodology [AIAA PAPER 90-2240] p 65 A90-45694
Mars in situ propellants - Carbon monoxide and oxygen ignition experiments [AIAA PAPER 90-1894] p 130 A90-50642
Combustor design and analysis using the Rocket Combustor Interactive Design (ROCCID) methodology [NASA-TM-103165] p 79 N90-24349
Mars in situ propellants: Carbon monoxide and oxygen ignition experiments [NASA-TM-103202] p 81 N90-26065
Energy Efficient Engine (E3) combustion system component technology performance report [NASA-CR-168274] p 33 N90-28555
Oxygen/methane combustion stability investigation p 107 N90-28628
Combustion instability coupling with feed system acoustics p 108 N90-28629
High energy-density liquid rocket fuel performance [NASA-CR-185279] p 131 N90-28742
- PROPELLANT STORAGE**
Power considerations for an early manned Mars mission utilizing the Space Station [AAS PAPER 87-223] p 55 A90-16688
Evaluation of supercritical cryogen storage and transfer systems for future NASA missions [AIAA PAPER 90-0719] p 44 A90-19989
Atomic hydrogen as a launch vehicle propellant [AIAA PAPER 90-0715] p 44 A90-23712

PROPELLANT TANKS

- Evaluation of supercritical cryogen storage and transfer systems for future NASA missions
[NASA-TM-102394] p 44 N90-10912
- Evolutionary space station fluids management strategies
[NASA-CR-185137] p 49 N90-10983
- Atomic hydrogen as a launch vehicle propellant
[NASA-TM-102459] p 73 N90-14284

PROPELLANT TANKS

- Centaur upper stage
[NASA-TM-102313] p 44 A90-18017
- Tank Pressure Control Experiment - A low-g mixing investigation
[AIAA PAPER 90-2376] p 66 A90-47217
- Tank pressure control experiment on the space shuttle
[NASA-TM-102313] p 71 N90-13590
- Prediction of the ullage gas thermal stratification in a NASP vehicle propellant tank experimental simulation using FLOW-3D
[NASA-TM-103217] p 131 N90-26160

PROPELLANT TESTS

- The measurement, modeling, and prediction of traction for rocket propellant 1
[NASA-CR-185186] p 131 N90-19386

PROPELLANT TRANSFER

- COLD-SAT - An orbital cryogenic hydrogen technology experiment
[IAF PAPER 89-057] p 53 A90-13282
- Evaluation of supercritical cryogen storage and transfer systems for future NASA missions
[AIAA PAPER 90-0719] p 44 A90-19989
- Initial experimentation on the nonvented fill of a 0.14 cu m (5 cu ft) dewar with nitrogen and hydrogen
[AIAA PAPER 90-1681] p 136 A90-50641
- Evaluation of supercritical cryogen storage and transfer systems for future NASA missions
[NASA-TM-102394] p 44 N90-10912
- Initial experimentation on the nonvented fill of a 0.14m3 (5 ft. 3) dewar with nitrogen and hydrogen
[NASA-TM-103155] p 183 N90-26278

PROPELLANTS

- Mars in situ propellants - Carbon monoxide and oxygen ignition experiments
[AIAA PAPER 90-1894] p 130 A90-50642
- Mars in situ propellants: Carbon monoxide and oxygen ignition experiments
[NASA-TM-103202] p 81 N90-26065

PROPELLER BLADES

- Analysis of nonuniform subsonic flows about a row of moving blades
[NASA-TM-103155] p 2 A90-11779
- Parametric studies of advanced turboprops
[NASA-TM-103155] p 19 A90-21225

- Application of an efficient hybrid scheme for aeroelastic analysis of advanced propellers
[AIAA PAPER 90-0028] p 4 A90-22153
- Effect of reduced aft diameter and increased blade number of high-speed counterrotation propeller performance
[AIAA PAPER 89-0438] p 4 A90-23650

- Unsteady blade surface pressures on a large-scale advanced propeller - Prediction and data
[AIAA PAPER 90-2402] p 9 A90-47220
- User's manual for PEP SIG NASA tip vortex version
[NASA-CR-182178] p 10 N90-10835

- Computation of the tip vortex flowfield for advanced aircraft propellers
[NASA-CR-182179] p 10 N90-10836
- Prediction of unsteady blade surface pressures on an advanced propeller at an angle of attack
[NASA-TM-102374] p 11 N90-12560

- Large-scale Advanced Prop-fan (LAP) static rotor test report
[NASA-CR-180848] p 25 N90-12617
- Effect of reduced aft diameter and increased blade number on high-speed counterrotation propeller performance
[NASA-TM-102077] p 11 N90-13352

- Application of an efficient hybrid scheme for aeroelastic analysis of advanced propellers
[NASA-TM-102428] p 11 N90-13355
- Large-scale advanced propeller blade pressure distributions: Prediction and data
[NASA-TM-102316] p 30 N90-22564

PROPELLER EFFICIENCY

- Application of an efficient hybrid scheme for aeroelastic analysis of advanced propellers
[AIAA PAPER 90-0028] p 4 A90-22153
- Application of an efficient hybrid scheme for aeroelastic analysis of advanced propellers
[NASA-TM-102428] p 11 N90-13355

- Experimental performance and acoustic investigation of modern, counterrotating blade concepts
[NASA-CR-185158] p 18 N90-23393

PROPELLER FANS

- Euler analysis comparison with LDV data for an advanced counter-rotation propfan at cruise
[AIAA PAPER 90-3033] p 9 A90-50637
- Concurrent processing adaptation of aeroplastic analysis of propfans
[NASA-TM-102455] p 217 N90-14656
- Unsteady Euler analysis of the flow field of a propfan at an angle of attack
[NASA-TM-102426] p 248 N90-18229
- Investigation of advanced counterrotation blade configuration concepts for high speed turboprop systems, task 1: Ducted propfan analysis
[NASA-CR-185217] p 30 N90-22567
- Euler analysis comparison with LDV data for an advanced counter-rotation propfan at cruise
[NASA-TM-103249] p 14 N90-25946
- Aeroacoustics of advanced propellers
[NASA-TM-103137] p 249 N90-26635

PROPELLER NOISE

- Performance and acoustic prediction of counterrotating propeller configurations
[SAE PAPER 891035] p 246 A90-14342
- An investigation of counterrotating tip vortex interaction
[NASA-CR-185135] p 247 N90-11549
- Predicted and measured boundary layer refraction for advanced turboprop propeller noise
[NASA-TM-102365] p 248 N90-17413
- The radiation of sound from a propeller at angle of attack
[NASA-CR-4264] p 249 N90-21602

PROPELLERS

- Propeller-wing interaction using a frequency domain panel method
[NASA-TM-103137] p 6 A90-26128
- Large scale prop-fan structural design study. Volume 2: Preliminary design of SR-7
[NASA-CR-174993] p 23 N90-10044
- Noise of a simulated installed model counterrotation propeller at angle-of-attack and takeoff/approach conditions
[NASA-TM-102440] p 248 N90-20794
- Laser-velocimeter-measured flow field around an advanced, swept, eight-blade propeller at Mach 0.8
[NASA-TP-2462] p 1 N90-20942
- Aerodynamic optimization by simultaneously updating flow variables and design parameters
[NASA-TM-102991] p 18 N90-20991
- An unsteady lifting surface method for single rotation propellers
[NASA-CR-4302] p 14 N90-25940
- Aeroacoustics of advanced propellers
[NASA-TM-103137] p 249 N90-26635
- Generalized Advanced Propeller Analysis System (GAPAS). Volume 2: Computer program user manual
[NASA-CR-185277] p 36 N90-29394

PROPULSION

- Advanced computational techniques for hypersonic propulsion
[NASA-TM-102606] p 156 A90-12606
- Fuel-rich catalytic combustion - A fuel processor for high-speed propulsion
[AIAA PAPER 90-2319] p 105 A90-42774
- Fuel-rich catalytic combustion: A fuel processor for high-speed propulsion
[NASA-TM-103177] p 107 N90-23518
- Technical accomplishments of the NASA Lewis Research Center, 1989
[NASA-TM-102296] p 267 N90-24220
- H-infinity based integrated flight-propulsion control design for a STOVL aircraft in transition flight
[NASA-TM-103198] p 37 N90-26011

PROPULSION SYSTEM CONFIGURATIONS

- Advances in computational design and analysis of airbreathing propulsion systems
[NASA-TM-102606] p 156 A90-12606
- Prediction of self-pressurization rate of cryogenic propellant tankage
[NASA-TM-102129] p 55 A90-21219
- CFD propels NASP propulsion progress
[NASA-TM-102606] p 172 A90-41163
- A candidate architecture for monitoring and control in chemical transfer propulsion systems
[AIAA PAPER 90-1882] p 52 A90-41980
- Analysis of internal flow in a ventral nozzle for STOVL aircraft
[AIAA PAPER 90-1899] p 21 A90-42688
- Engine selection for the Space Exploration Initiative
[AIAA PAPER 90-1880] p 65 A90-47201
- Multi-reactor configurations for multi-megawatt spacecraft power supplies
[AIAA PAPER 90-2111] p 66 A90-47207
- Advanced propulsion for LEO and GEO platforms
[AIAA PAPER 90-2551] p 68 A90-52565
- Performance characterization of a segmented anode arcjet thruster
[AIAA PAPER 90-2582] p 68 A90-52569

Materials for engine applications above 3000 deg F: An overview

- [NASA-TM-100169] p 95 N90-10188
- STOVL propulsion system volume dynamics approximations
[NASA-TM-102397] p 25 N90-11740
- Large-scale Advanced Prop-fan (LAP) static rotor test report
[NASA-CR-180848] p 25 N90-12617
- Electric propulsion options for 10 kW class earth-space missions
[NASA-TM-102397] p 75 N90-18474
- Performance of large area xenon ion thrusters for orbit transfer missions
[NASA-TM-102397] p 75 N90-18475
- Advanced launch vehicle propulsion at the NASA Lewis Research Center
[NASA-TM-103096] p 45 N90-20110
- Probabilistic modeling for simulation of aerodynamic uncertainties in propulsion systems
[NASA-TM-102472] p 29 N90-21036
- Exhaust nozzles for propulsion systems with emphasis on supersonic cruise aircraft
[NASA-RP-1235] p 29 N90-21037
- A candidate architecture for monitoring and control in chemical transfer propulsion systems
[NASA-TM-103161] p 52 N90-22595
- Analysis of internal flow in a ventral nozzle for STOVL aircraft
[NASA-TM-103123] p 31 N90-23404
- Advanced gearbox technology
[NASA-CR-179625] p 32 N90-24274
- Nuclear power systems for lunar and Mars exploration
[NASA-TM-103168] p 82 N90-26873
- Advanced propulsion for LEO and GEO platforms
[NASA-TM-103228] p 82 N90-27785

PROPULSION SYSTEM PERFORMANCE

- Performance and endurance tests of a laboratory model multipropellant resistojet
[NASA-TM-103161] p 55 A90-21220
- Status of xenon ion propulsion technology
[NASA-TM-103161] p 56 A90-27961
- Three approaches to reliability analysis
[NASA-TM-103161] p 206 A90-30706
- Preliminary design of a long-endurance Mars aircraft
[AIAA PAPER 90-2000] p 43 A90-40587
- CFD propels NASP propulsion progress
[NASA-TM-102606] p 172 A90-41163

- A candidate architecture for monitoring and control in chemical transfer propulsion systems
[AIAA PAPER 90-1882] p 52 A90-41980
- Lunar missions using advanced chemical propulsion - System design issues
[AIAA PAPER 90-2431] p 67 A90-47221

- Extended implicit model following as applied to integrated flight and propulsion control
[AIAA PAPER 90-3444] p 239 A90-47697
- Advanced propulsion for LEO and GEO platforms
[AIAA PAPER 90-2551] p 68 A90-52565
- A rocket engine design expert system
[NASA-TM-102373] p 69 N90-10172

- Advanced APS impacts on vehicle payloads
[NASA-TM-102373] p 75 N90-18472
- Electric propulsion options for 10 kW class earth-space missions
[NASA-TM-102373] p 75 N90-18474

- Performance of large area xenon ion thrusters for orbit transfer missions
[NASA-TM-102373] p 75 N90-18475
- Test facility and preliminary performance of a 100 kW class MPD thruster
[NASA-TM-102373] p 75 N90-18476

- Advanced launch vehicle propulsion at the NASA Lewis Research Center
[NASA-TM-103096] p 45 N90-20110
- Probabilistic modeling for simulation of aerodynamic uncertainties in propulsion systems
[NASA-TM-102472] p 29 N90-21036

- Exhaust nozzles for propulsion systems with emphasis on supersonic cruise aircraft
[NASA-RP-1235] p 29 N90-21037
- Assessment of High Temperature Superconducting (HTS) electric motors for rotorcraft propulsion
[NASA-CR-185222] p 29 N90-21761

- Preliminary design of a long-endurance Mars aircraft
[NASA-CR-185243] p 30 N90-21763
- A candidate architecture for monitoring and control in chemical transfer propulsion systems
[NASA-TM-103161] p 52 N90-22595

- Advanced propulsion for LEO and GEO platforms
[NASA-TM-103228] p 82 N90-27785
- Low power arcjet performance
[NASA-TM-103280] p 83 N90-28657

PROPULSIVE EFFICIENCY

- Parametric studies of advanced turboprops
[NASA-TM-103161] p 19 A90-21225
- Advanced core technology - Key to subsonic propulsion benefits
[ASME PAPER 89-GT-241] p 19 A90-23890
- Advanced APS impacts on vehicle payloads
[NASA-TM-102373] p 75 N90-18472

SUBJECT INDEX

- Energy Efficient Engine (E3) combustion system component technology performance report
[NASA-CR-168274] p 33 N90-28555
- Energy Efficient Engine core design and performance report
[NASA-CR-168069] p 34 N90-28559
- Energy Efficient Engine integrated core/low spool test hardware design report
[NASA-CR-168137] p 35 N90-28586
- Energy Efficient Engine: High-pressure compressor test hardware detailed design report
[NASA-CR-180850] p 36 N90-28570
- PROTECTIVE COATINGS**
- TBCs for better engine efficiency --- thermal barrier coatings
p 83 A90-17294
- Ellipsometric study of Al₂O₃/Ag/Si and SiO₂/Ag/quartz ashed in an oxygen plasma --- protective coatings to prevent degradation of materials in low earth orbits
p 120 A90-18217
- Diffusional aspects of the high-temperature oxidation of protective coatings
p 113 A90-28075
- Evaluation of atomic oxygen resistant protective coatings for fiberglass-epoxy composites in LEO
p 84 A90-31581
- Diamondlike carbon protective coatings for optical windows
p 122 A90-34569
- Microstructure of a SiC/Ti-15-3 composite
p 91 A90-37663
- Photovoltaic array environmental protection program --- in Space Station Freedom
p 59 A90-38088
- Aeolian removal of dust from photovoltaic surfaces on Mars
[NASA-TM-102507] p 76 N90-19299
- The effect of leveling coatings on the atomic oxygen durability of solar concentrator surfaces
[NASA-TM-102557] p 76 N90-21110
- PROTOCOL (COMPUTERS)**
- Extension of a noninteractive reliability model for ceramic matrix composites
[NASA-CR-185267] p 129 N90-26142
- PROTONS**
- Hydrogen-oxygen proton-exchange membrane fuel cells and electrolyzers
p 56 A90-33944
- PROVING**
- Comparison of 3-D viscous flow computations of Mach 5 inlet with experimental data
[NASA-TM-102518] p 28 N90-20090
- PULSARS**
- Is the sub-millisecond pulsar strange?
p 264 A90-12669
- PULSE COMMUNICATION**
- Performance measurements for a laboratory-simulated 30/20 GHz communication satellite transponder
[AIAA PAPER 90-0808] p 140 A90-25634
- Effects of amplitude distortions and IF equalization on satellite communication system bit-error rate performance
[AIAA PAPER 90-0878] p 140 A90-25697
- Performance measurements for a laboratory-simulated 30/20 GHz communication satellite transponder
[NASA-TM-102424] p 143 N90-17977
- PULSE DURATION**
- Intensity to frequency conversion technique in intensity modulated fiber optic sensing systems
[NASA-TM-102562] p 153 N90-21277
- PULSE DURATION MODULATION**
- 20 kHz main inverter unit --- for space station power supplies
p 148 A90-38124
- PULSED JET ENGINES**
- Experiments on a repetitively pulsed electrothermal thruster
p 56 A90-27960
- PULSED LASERS**
- New space domain processing technique for pulsed laser velocimetry
p 187 A90-48750
- PUMP SEALS**
- Analysis and design of helium-buffered face seals for the SSME high-pressure oxygen turbopump
[AIAA PAPER 90-2049] p 197 A90-42000
- PURIFICATION**
- Results of an attempt to measure increased rates of the reaction D-2 + D-2 yields He-3 + n in a nonelectrochemical cold fusion experiment
[NASA-TM-102430] p 250 N90-17424
- PYROLYSIS**
- Fuel-rich catalytic combustion - A fuel processor for high-speed propulsion
[AIAA PAPER 90-2319] p 105 A90-42774
- Fuel-rich catalytic combustion: A fuel processor for high-speed propulsion
[NASA-TM-103177] p 107 N90-23518
- PYROLYTIC GRAPHITE**
- Feasibility of intercalated graphite railgun armatures
[NASA-TM-102546] p 128 N90-21181

PYROMETERS

- Multiwavelength pyrometry to correct for reflected radiation
[NASA-TM-102578] p 190 N90-23714

Q

QUADRUPOLES

- Development of a quadrupole-based Secondary-Ion Mass Spectrometry (SIMS) system at Lewis Research Center
[NASA-TM-102531] p 87 N90-23476

QUALIFICATIONS

- Spacelab qualified infrared imager for microgravity science experiments
[NASA-TM-102503] p 189 N90-20352

QUALITY CONTROL

- Molecular beam epitaxial growth of high-quality InSb on InP and GaAs substrates
p 253 A90-12808
- The Materials Division: A case study
[NASA-TM-102380] p 86 N90-13597

QUANTUM EFFICIENCY

- Hybrid solar cells based on dc magnetron sputtered films of n-ITO on APMOPE grown p-InP
p 225 A90-14893

QUANTUM STATISTICS

- Phase transitions in fermionic systems with many-body interaction
p 249 A90-19303

QUARKS

- Big bang nucleosynthesis and the quark-hadron transition
p 265 A90-31407

QUATERNARY ALLOYS

- Influence of alloying elements on the oxidation behavior of NbAl₃
p 113 A90-24861

QUEUEING THEORY

- Computer architecture evaluation for structural dynamics computations: Project summary
[NASA-CR-186137] p 235 N90-26512

R

RADAR ANTENNAS

- Effects of desired signal on the performance of a sidelobe canceller
p 139 A90-13936

RADAR CROSS SECTIONS

- Electromagnetic properties of material coated surfaces
[NASA-CR-186466] p 144 N90-19466

RADAR SCATTERING

- Electromagnetic properties of material coated surfaces
[NASA-CR-186466] p 144 N90-19466

RADIAL FLOW

- An interactive grid generation procedure for axial and radial flow turbomachinery
[AIAA PAPER 90-0344] p 162 A90-22200
- Design of an air-cooled metallic high-temperature radial turbine
p 20 A90-32960
- Three dimensional LDV flow measurements and theoretical investigation in a radial inflow turbine scroll
p 9 A90-46860

- An interactive grid generation procedure for axial and radial flow turbomachinery
[NASA-CR-185167] p 237 N90-13968

RADIANT COOLING

- Some aspects of transient cooling of a radiating rectangular medium
p 157 A90-13095
- Emission bounds for transient radiative cooling of a scattering rectangular region
p 161 A90-20520
- Solidification by radiative cooling of a cylindrical region filled with drops
p 166 A90-24840
- Combustion interaction with radiation-cooled chambers
[AIAA PAPER 90-2121] p 64 A90-42030

RADIATION ABSORPTION

- Radiative transfer theory for inhomogeneous media with random extinction and scattering coefficients
p 260 A90-21904
- Parametric study of power absorption from electromagnetic waves by small ferrite spheres
[NASA-TP-2949] p 246 N90-12282

RADIATION DAMAGE

- Electron-beam induced damage in thin insulating films on compound semiconductors
[NASA-CR-185177] p 151 N90-17987
- Electron beam induced damage in PECVD Si₃N₄ and SiO₂ films on InP
[NASA-TM-102544] p 203 N90-20393

RADIATION DISTRIBUTION

- Radiative transfer theory for inhomogeneous media with random extinction and scattering coefficients
p 260 A90-21904

RADIO FREQUENCY INTERFERENCE

RADIATION DOSAGE

- A radiological assessment of nuclear power and propulsion operations near Space Station Freedom
[NASA-CR-185185] p 76 N90-21108
- Neutron and gamma irradiation effects on power semiconductor switches
[NASA-TM-103200] p 155 N90-25278

RADIATION EFFECTS

- Radiation resistance and comparative performance of ITO/InP and n/p InP homojunction solar cells
p 226 A90-14933
- Evaluation of atomic oxygen resistant protective coatings for fiberglass-epoxy composites in LEO
p 84 A90-31581
- Photovoltaic power system operation in the Mars environment
p 43 A90-38156
- A brief survey of radiation effects on polymer dielectrics
p 123 A90-43119

RADIATION HAZARDS

- Space vehicle propulsion systems - Environmental space hazards
[AIAA PAPER 90-1881] p 63 A90-40545

RADIATION SHIELDING

- Space nuclear reactor shields for manned and unmanned applications
p 57 A90-37859
- Scaling study for SP-100 reactor technology
[NASA-TM-897140] p 249 N90-16496
- Neutron and gamma irradiation effects on power semiconductor switches
[NASA-TM-103200] p 155 N90-25278

RADIATION SOURCES

- Multiwavelength pyrometry to correct for reflected radiation
[NASA-TM-102578] p 190 N90-23714

RADIATION TOLERANCE

- Thin, light-trapping silicon solar cells for space
p 226 A90-14900
- Radiation resistance studies of amorphous silicon films
p 227 A90-14952
- Indium phosphide solar cell research in the United States: Comparison with non-photovoltaic sources
p 229 N90-17758

- Neutron and gamma irradiation effects on power semiconductor switches
[NASA-TM-103200] p 155 N90-25278

RADIATIVE HEAT TRANSFER

- Some aspects of transient cooling of a radiating rectangular medium
p 157 A90-13095
- Two-dimensional convection and radiation with scattering from a Poiseuille flow
p 161 A90-20519
- Emission bounds for transient radiative cooling of a scattering rectangular region
p 161 A90-20520
- Solidification by radiative cooling of a cylindrical region filled with drops
p 166 A90-24840
- Radiative configuration factors from cylinders to coaxial axisymmetric bodies
p 167 A90-26334
- Effect of gas and surface radiation on crystal growth from the vapor phase
p 133 A90-49060

RADIATIVE TRANSFER

- Radiative transfer theory for inhomogeneous media with random extinction and scattering coefficients
p 260 A90-21904

RADIO ATTENUATION

- Rain-fade simulation and power augmentation for satellite communication systems
[NASA-TM-103134] p 146 N90-28768

RADIO COMMUNICATION

- Conceptual definition of a high voltage power supply test facility
[NASA-CR-185216] p 50 N90-25172
- Rain-fade simulation and power augmentation for satellite communication systems
[NASA-TM-103134] p 146 N90-28768

RADIO FREQUENCIES

- Thin films of the Bi₂Se₂Ca₂Cu₃O(x) superconductor
p 254 A90-24448

- Fiber optic sensing system
[NASA-CASE-LEW-14795-1] p 251 N90-15733

- Influence of the deposition conditions on radiofrequency magnetron sputtered MoS₂ films
[NASA-TP-2994] p 137 N90-21210

- The 30-GHz monolithic receive module
[NASA-CR-180849] p 146 N90-24528

- Analysis of a Mars-stationary orbiting microwave power transmission system
[NASA-TM-101344] p 138 N90-26172

RADIO FREQUENCY HEATING

- Review of research and development on the microwave electrothermal thruster
p 55 A90-16369

RADIO FREQUENCY INTERFERENCE

- An experimental SMI adaptive antenna array for weak interfering signals
[NASA-CR-185976] p 142 N90-11211
- Adaptive antenna arrays for satellite communication
[NASA-CR-185989] p 143 N90-12784
- Solar array arcing in plasmas
p 233 N90-25558

RADIOISOTOPE BATTERIES

- Preliminary design of a long-endurance Mars aircraft [AIAA PAPER 90-2000] p 43 A90-40587
- Preliminary design of a long-endurance Mars aircraft [NASA-CR-185243] p 30 N90-21763

RADIOLOGY

- A radiological assessment of nuclear power and propulsion operations near Space Station Freedom [NASA-CR-185185] p 76 N90-21108

RAILGUN ACCELERATORS

- Feasibility of intercalated graphite railgun armatures [NASA-TM-102546] p 128 N90-21181

RAIN

- A unified statistical rain-attenuation model for communication link fade predictions and optimal stochastic fade control design using a location-dependent rain-statistic database p 141 A90-34914
- The effects of van der Waals attractions on cloud droplet growth by coalescence p 234 A90-38363

RAMAN SPECTRA

- Structural comparison of nickel electrodes and precursor phases p 231 N90-20472

RANDOM VARIABLES

- Effects of state recovery on creep buckling under variable loading p 212 A90-41223

RANDOM VIBRATION

- Probabilistic analysis of bladed turbine disks and the effect of mistuning p 196 A90-29327
- Probabilistic analysis of bladed turbine disks and the effect of mistuning [NASA-TM-102564] p 136 N90-21871

RAPID QUENCHING (METALLURGY)

- Production and processing of Cu-Cr-Nb alloys p 114 A90-33340
- Superconducting Bi(1.5)Pb(0.5)Sr₂Ca₂Cu₃O(x) ceramics by rapid melt quenching and glass crystallization p 256 A90-43568
- 1300 K compressive properties of several dispersion strengthened NiAl materials p 116 A90-47091
- Production and processing of Cu-Cr-Nb alloys [NASA-TM-102495] p 117 N90-16053
- Superconducting Bi_{1.5}Pb_{0.5}Sr₂Ca₂Cu₃O(x) ceramics by rapid melt quenching and glass crystallization [NASA-CR-185184] p 258 N90-17465

RARE EARTH COMPOUNDS

- Thermodynamic properties of some metal oxide-zirconia systems [NASA-TM-102351] p 126 N90-13666

RARE GASES

- Requirements for long-life operation of inert gas hollow cathodes - Preliminary results [AIAA PAPER 90-2586] p 69 A90-52570
- Requirements for long-life operation of inert gas hollow cathodes: Preliminary report [NASA-TM-103242] p 82 N90-27783

RAREFIED GAS DYNAMICS

- Efficient Monte Carlo simulation of rarefied flow in a small nozzle [AIAA PAPER 90-1693] p 170 A90-38396
- Numerical simulation of rarefied gas flow through a slit [AIAA PAPER 90-1694] p 170 A90-38397

RAY TRACING

- Thermal radiation characteristics of nonisothermal cylindrical enclosures using a numerical ray tracing technique [NASA-TM-102527] p 179 N90-21296

REACTION BONDING

- Measurement of interfacial shear strength in SiC-fiber/Si₃N₄ composites p 87 A90-13237
- Role of the interfacial thermal barrier in the effective thermal diffusivity/conductivity of SiC-fiber-reinforced reaction-bonded silicon nitride p 89 A90-25268
- Nitriding kinetics of Si-SiC powder mixtures as simulations of reaction bonded Si₃N₄-SiC composites p 90 A90-27076
- Laminate behavior for SiC fiber-reinforced reaction-bonded silicon nitride matrix composites p 90 A90-29927
- Thermal effects on the mechanical properties of SiC fibre reinforced reaction-bonded silicon nitride matrix composites p 92 A90-46999
- Properties of RBSN and RBSN-SiC composites --- Reaction Bonded Silicon Nitride p 94 A90-51920
- High-temperature tensile properties of fiber reinforced reaction bonded silicon nitride p 95 A90-52783
- Oxidation effects on the mechanical properties of SiC fiber-reinforced reaction-bonded silicon nitride matrix composites [NASA-TM-102360] p 96 N90-14287

REACTION KINETICS

- Reduced chemical kinetics for propane combustion [AIAA PAPER 90-0546] p 103 A90-19904
- Crystallization kinetics of BaO-Al₂O₃-SiO₂ glasses p 121 A90-21175
- Effects of pressure on microgravity hydrocarbon diffusion flames [AIAA PAPER 90-0651] p 104 A90-25039
- The kinetics of the Au-InP interaction p 254 A90-25084
- Nitriding kinetics of Si-SiC powder mixtures as simulations of reaction bonded Si₃N₄-SiC composites p 90 A90-27076
- On the driving force of PAH production p 84 A90-32833
- Modeling of the SiC chemical vapor deposition process and comparison with experimental results p 105 A90-36810
- H₂/O₂ three-body rates at high temperatures [AIAA PAPER 90-1696] p 105 A90-38399
- On the use of external burning to reduce aerospace vehicle transonic drag [AIAA PAPER 90-1935] p 20 A90-40562
- Low thrust rocket test facility [AIAA PAPER 90-2503] p 43 A90-47225
- Critical evaluation of Jet-A spray combustion using propane chemical kinetics in gas turbine combustion simulated by KIVA-II [AIAA PAPER 90-2439] p 105 A90-50645
- Hydrogen-silicon carbide interactions [NASA-TM-102382] p 125 N90-11144
- Results of an attempt to measure increased rates of the reaction D-2 + D-2 yields He-3 + n in a nonelectrochemical cold fusion experiment [NASA-TM-102430] p 250 N90-17424
- Superconducting Bi_{1.5}Pb_{0.5}Sr₂Ca₂Cu₃O(x) ceramics by rapid melt quenching and glass crystallization [NASA-CR-185184] p 258 N90-17465
- Low NO(x) potential of gas turbine engines [NASA-TM-102452] p 27 N90-17636
- Characterization of reaction kinetics in a porous electrode [NASA-CR-186504] p 106 N90-19340
- On the use of external burning to reduce aerospace vehicle transonic drag [NASA-TM-103107] p 30 N90-21762
- Detailed mechanism for oxidation of benzene [NASA-TM-102443] p 106 N90-21842
- Low thrust rocket test facility [NASA-TM-103206] p 43 N90-25158
- An analysis of the contact sintering process in III-V solar cells [NASA-TM-103179] p 233 N90-25420
- Critical evaluation of Jet-A spray combustion using propane chemical kinetics in gas turbine combustion simulated by KIVA-2 [NASA-TM-103173] p 138 N90-26170
- Evaluation of a hybrid kinetics/mixing-controlled combustion model for turbulent premixed and diffusion combustion using KIVA-2 [NASA-TM-103196] p 185 N90-28792

REACTIVITY

- Hydrocarbon-fuel/combustion-chamber-liner materials compatibility [NASA-CR-185203] p 118 N90-21165

REACTOR DESIGN

- Energy storage for a lunar base by the reversible chemical reaction: CaO + H₂O reversible reaction Ca(OH)₂ [NASA-TM-103145] p 233 N90-25419

REACTOR TECHNOLOGY

- Scaling study for SP-100 reactor technology [NASA-TM-897140] p 249 N90-16496

REAL GASES

- Efficient real gas Navier-Stokes computations of high speed flows using an LU scheme [AIAA PAPER 90-0391] p 164 A90-23706
- The Osher scheme for real gases [AIAA PAPER 90-0397] p 166 A90-25030
- Splitting of inviscid fluxes for real gases p 167 A90-25451
- Inviscid flux-splitting algorithms for real gases with non-equilibrium chemistry p 174 A90-52275
- Efficient real gas Navier-Stokes computations of high speed flows using an LU scheme [NASA-TM-102429] p 11 N90-14203

REAL TIME OPERATION

- Flight software development for the isothermal dendritic growth experiment [AIAA PAPER 90-0744] p 235 A90-22257
- A real time microcomputer implementation of sensor failure detection for turbofan engines p 21 A90-45414
- Digital codec for real-time processing of broadcast quality video signals at 1.8 bits/pixel p 142 A90-51306
- Real-time simulation of an F110/STOVL turbofan engine [NASA-TM-102409] p 25 N90-12618
- Flight software development for the isothermal dendritic growth experiment [NASA-TM-102412] p 238 N90-13988

- An electronic pressure profile display system for aeronautic test facilities [NASA-TM-102478] p 38 N90-15964
- Effect of KOH concentration on LEO cycle life of IPV nickel-hydrogen flight battery cells [NASA-TM-103127] p 77 N90-21116
- A real time neural net estimator of fatigue life [NASA-TM-103117] p 239 N90-21564
- AIRNET: A real-time communications network for aircraft [NASA-CR-186140] p 145 N90-24514
- Autonomous power expert system [NASA-CR-185263] p 80 N90-25187
- Neuromorphic learning of continuous-valued mappings from noise-corrupted data. Application to real-time adaptive control [NASA-TM-4176] p 241 N90-25607
- An expert system to perform on-line controller restructuring for abrupt model changes [NASA-TM-103609] p 241 N90-29121
- Integrated controls and health monitoring fiberoptic shaft monitor [NASA-CR-185210] p 191 N90-29622

REATTACHED FLOW

- Calculation of reattaching shear layers in divergent channel with a multiple-time-scale turbulence model [AIAA PAPER 90-0047] p 160 A90-19649
- Structure of a reattaching supersonic shear layer p 7 A90-36252

RECEIVERS

- A heat receiver design for solar dynamic space power systems [NASA-TM-102473] p 72 N90-14283
- The 30-GHz monolithic receive module [NASA-CR-180849] p 146 N90-24528

RECIPROCATION

- Feasibility analysis of reciprocating magnetic heat pumps [NASA-CR-186205] p 177 N90-15363

RECIRCULATIVE FLUID FLOW

- Three-dimensional fluid flow calculations using a flux-spline method p 167 A90-27983

RECTANGULAR WAVEGUIDES

- Experimental study of the cross-polarization characteristics of rectangular microstrip antennas p 141 A90-37312
- Reflector spillover loss of an open-ended rectangular and circular waveguide feed p 141 A90-45398
- A new rectangular waveguide to coplanar waveguide transition [NASA-TM-102477] p 145 N90-21263

RECTENNAS

- Millimeter-wave/infrared rectenna development at Georgia Tech p 69 N90-10147
- Lunar orbiting microwave beam power system [NASA-TM-103211] p 51 N90-25173
- Analysis of a Mars-stationary orbiting microwave power transmission system [NASA-TM-101344] p 138 N90-26172

RECTIFICATION

- Millimeter-wave/infrared rectenna development at Georgia Tech p 69 N90-10147

RECURSIVE FUNCTIONS

- Quotient-difference type generalizations of the power method and their analysis [NASA-TM-102361] p 242 N90-10635

REDUCED GRAVITY

- Side-wall gas 'creep' and 'thermal stress convection' in microgravity experiments on film growth by vapor transport p 158 A90-14086
- Effects of crucible wetting during solidification of immiscible Pb-Zn alloys p 132 A90-17825
- Salt-finger convection under reduced gravity [AIAA PAPER 90-0122] p 160 A90-19693
- On-orbit low gravity cryogenic scientific investigations using the COLD-SAT Satellite [AIAA PAPER 90-0718] p 39 A90-19988
- Nonintrusive inertial vibration isolation technology for microgravity space experiments [AIAA PAPER 90-0741] p 132 A90-19999
- Free float acceleration measurements aboard NASA's KC-135 Microgravity Research Aircraft [AIAA PAPER 90-0742] p 132 A90-20000
- Smoldering combustion under low gravity conditions [AIAA PAPER 90-0648] p 103 A90-22238
- Flight software development for the isothermal dendritic growth experiment [AIAA PAPER 90-0744] p 235 A90-22257
- Ignition and behavior of laminar gas-jet diffusion flames in microgravity p 103 A90-23107
- Numerical simulation of thermocapillary bubble migration under microgravity for large Reynolds and Marangoni numbers p 164 A90-23213
- Convection phenomena in low-gravity processing - The GTE GaAs space experiment [AIAA PAPER 90-0409] p 133 A90-25032

Effects of pressure on microgravity hydrocarbon diffusion flames
[AIAA PAPER 90-0651] p 104 A90-25039

Near-limit flame spread over a thin solid fuel in microgravity p 104 A90-32835

The coupling of Marangoni and capillary instabilities in an annular thread of liquid p 171 A90-38978

The possibility of a reversal of material flammability ranking from normal gravity to microgravity p 105 A90-42298

The structure and stability of nonadiabatic flame balls p 105 A90-43674

Surface reorientation and settling in cylinders upon step reduction in gravity p 172 A90-44541

Low frequency vibration isolation technology for microgravity space experiments p 136 A90-46246

Tank Pressure Control Experiment - A low-g mixing investigation p 66 A90-47217
[AIAA PAPER 90-2376]

Nonintrusive inertial vibration isolation technology for microgravity space experiments p 137 N90-11901
[NASA-TM-102386]

An investigation of flame spread over shallow liquid pools in microgravity and nonair environments p 134 N90-13680
[NASA-TM-102425]

User needs, benefits, and integration of robotic systems in a space station laboratory p 200 N90-13794
[NASA-CR-185150]

Flight software development for the isothermal dendritic growth experiment p 238 N90-13988
[NASA-TM-102412]

Thermocapillary migration of liquid droplets in a temperature gradient in a density matched system p 177 N90-14512
[NASA-CR-185178]

Data compression for the microgravity experiments p 188 N90-16212

A comparison of European and American microgravity combustion experimental techniques p 134 N90-16966

NASA Laser Light Scattering Advanced Technology Development Workshop, 1988 p 188 N90-17085
[NASA-CP-10033]

Polymer solution phase separation: Microgravity simulation p 127 N90-17101

Fire safety applications for spacecraft p 16 N90-17595

Microgravity noncontact temperature requirements at NASA Lewis Research Center p 134 N90-17897

Non-contact temperature measurements in support of microgravity combustion experiments p 135 N90-17900

A new approach to active vibration isolation for microgravity space experiments p 137 N90-17929
[NASA-TM-102470]

Investigation of methods to produce a uniform cloud of fuel particles in a flame tube p 178 N90-18665
[NASA-TM-102376]

Instantaneously generated foam and its applicability to reduced gravity p 135 N90-20237
[NASA-CR-185208]

Design and test of a compact optics system for the pool boiling experiment p 135 N90-20253
[NASA-TM-102530]

Microgravity acoustic mixing for particle cloud combustors p 248 N90-21600
[NASA-CR-185159]

The vibro-acoustic mapping of low gravity trajectories on a Learjet aircraft p 1 N90-21723
[NASA-TM-103103]

Technical accomplishments of the NASA Lewis Research Center, 1989 p 267 N90-24220
[NASA-TM-102296]

A global approach for using kinematic redundancy to minimize base reactions of manipulators p 234 N90-25499
[NASA-CR-186825]

New findings and instrumentation from the NASA Lewis microgravity facilities p 136 N90-26163
[NASA-TM-103189]

Low-gravity fluid physics: A program overview p 183 N90-26273
[NASA-TM-103215]

Reaction-compensation technology for microgravity laboratory robots p 205 N90-28062
[NASA-TM-103271]

Development and approach to low-frequency microgravity isolation systems p 138 N90-28754
[NASA-TP-2984]

Design of a CO₂ laser power control system for a Spacelab microgravity experiment p 192 N90-28833
[NASA-TM-103112]

REDUCED ORDER FILTERS

The determination of third order linear models from a seventh order nonlinear jet engine model p 239 A90-52881

REDUCTION (CHEMISTRY)

Electrocatalysis for oxygen electrodes in fuel cells and water electrolyzers for space applications p 57 A90-33945

O₂ reduction at the IFC orbiter fuel cell O₂ electrode p 231 N90-21469
[NASA-TM-102580]

REDUNDANCY

Base reaction optimization of redundant manipulators for space applications p 201 N90-15447
[NASA-CR-186274]

A global approach for using kinematic redundancy to minimize base reactions of manipulators p 234 N90-25499
[NASA-CR-186825]

REFLECTANCE

A V-grooved GaAs solar cell p 225 A90-14887

Effect of eleven years in earth orbit on a mirror surface p 44 A90-36188

REFLECTED WAVES

Concentration of off-axis radiation by solar concentrators for space power p 60 A90-38163

Multiwavelength pyrometry to correct for reflected radiation p 190 N90-23714
[NASA-TM-102578]

REFLECTOR ANTENNAS

A new fabrication method for precision antenna reflectors for space flight and ground test p 139 A90-25627
[AIAA PAPER 90-0803]

Reflector spillover loss of an open-ended rectangular and circular waveguide feed p 141 A90-45398

A comparison of reflector antenna designs for wide-angle scanning p 144 N90-19264

Reflector surface distortion analysis techniques (thermal distortion analysis of antennas in space) p 144 N90-19267

Aperture taper determination for the half-scale accurate antenna reflector p 153 N90-21282
[NASA-CR-185215]

REFLECTORS

Reflector surface distortion analysis techniques (thermal distortion analysis of antennas in space) p 144 N90-19267

Solar Concentrator Advanced Development Program p 232 N90-22834
[NASA-CR-185173]

REFRACTION

Predicted and measured boundary layer refraction for advanced turboprop propeller noise p 248 N90-17413
[NASA-TM-102365]

REFRACTIVITY

Optical techniques for determination of normal shock position in supersonic flows for aerospace applications p 190 N90-25323
[NASA-TM-103201]

REFRACTORY COATINGS

TBCs for better engine efficiency --- thermal barrier coatings p 83 A90-17294

Superconducting ceramics in the Bi_{1.5}SrCaCu₂O sub x system by melt quenching technique p 258 N90-11606
[NASA-CR-185139]

REFRACTORY MATERIALS

Isothermal life prediction of composite lamina using a damage mechanics approach p 92 A90-48115

Fundamental aspects and failure modes in high-temperature composites p 93 A90-50095

Tribological properties of ceramic/Ti3Al-Nb sliding couples for use as candidate seal materials to 700 deg C p 86 N90-12658
[NASA-TM-102401]

Tribological properties of PM212: A high-temperature, self-lubricating, powder metallurgy composite p 86 N90-12659
[NASA-TM-102355]

Thermodynamic properties of some metal oxide-zirconia systems p 126 N90-13666
[NASA-TM-102351]

Attachment of lead wires to thin film thermocouples mounted on high temperature materials using the parallel gap welding process p 189 N90-21361
[NASA-TM-102442]

Recent advances in nondestructive evaluation made possible by novel uses of video systems p 207 N90-22801
[NASA-TM-102491]

Theory and experimental technique for nondestructive evaluation of ceramic composites p 207 N90-23754
[NASA-TM-102561]

Technical accomplishments of the NASA Lewis Research Center, 1989 p 267 N90-24220
[NASA-TM-102296]

REFRACTORY METAL ALLOYS

Oxidation of high-temperature intermetallics; Proceedings of the Workshop, Cleveland, OH, Sept. 22, 23, 1988 p 112 A90-24852

Advanced refractory metals and composites for extraterrestrial power systems p 40 A90-48819

REFRACTORY METALS

Refractory metal alloys and composites for space power systems p 116 A90-46677

Advanced refractory metals and composites for extraterrestrial power systems p 40 A90-48819

One step HIP canning of powder metallurgy composites p 101 N90-23493
[NASA-CASE-LEW-14719-1]

REGENERATIVE COOLING

Feasibility analysis of reciprocating magnetic heat pumps p 177 N90-15363
[NASA-CR-186205]

REGENERATIVE FUEL CELLS

The fuel cell in space - Yesterday, today and tomorrow p 56 A90-26837

Cryogenic reactant storage for lunar base regenerative fuel cells p 227 A90-27709
[IAF PAPER ICOSP89-3-8]

The fuel cell in space: Yesterday, today and tomorrow p 70 N90-11804
[NASA-TM-102366]

Regenerative fuel cell systems for project Pathfinder p 74 N90-17708

Integrated regenerative fuel cell experimental evaluation p 230 N90-18808
[NASA-CR-185183]

The chemical effects of the Martian environment on power system component materials: A theoretical approach p 87 N90-26074
[NASA-TM-103203]

Modeling and optimization of a regenerative fuel cell system using the ASPEN process simulator p 233 N90-26396
[NASA-TM-103210]

A solar power system for an early Mars expedition p 246 N90-28393
[NASA-TM-103219]

REGRESSION ANALYSIS

Review and statistical analysis of the ultrasonic velocity method for estimating the porosity fraction in polycrystalline materials p 207 N90-21402
[NASA-TM-102501-REV]

REINFORCING FIBERS

Effect of fiber spacing on interfacial damage in a metal matrix composite p 88 A90-23188

Creep and creep rupture of strongly reinforced metallic composites p 223 N90-28110
[NASA-CR-185286]

Ceramic matrix composites in simulated SSME environments p 102 N90-28655

REINFORCING MATERIALS

The application of cast SiC/Al to rotary engine components p 25 N90-13385
[NASA-CR-179610]

REISSNER THEORY

Assumed strain distributions for a finite strip plate bending element using Mindlin-Reissner plate theory p 208 A90-16723

RELAXATION METHOD (MATHEMATICS)

Global pressure relaxation for laminar two-dimensional internal flow p 174 A90-51019

RELIABILITY

Performance and endurance tests of a laboratory model multipropellant resistojet p 55 A90-21220

Design of the Space Station Freedom power system p 57 A90-38070

Preliminary designs for 25 kWe advanced Stirling conversion systems for dish electric applications p 263 N90-26729
[NASA-TM-103188]

RELIABILITY ANALYSIS

A methodology for evaluating the reliability and risk of structures under complex service environments p 211 A90-29332
[AIAA PAPER 90-1102]

Computational methods for probability of instability calculations p 236 A90-29333
[AIAA PAPER 90-1139]

Three approaches to reliability analysis p 206 A90-30706

Equivalence of physically based statistical fracture theories for reliability analysis of ceramics in multiaxial loading p 123 A90-43580

Advanced probabilistic structural analysis method for implicit performance functions p 214 A90-49792

Extension of a noninteractive reliability model for ceramic matrix composites p 129 N90-26142
[NASA-CR-185267]

Reliability analysis of continuous fiber composite laminates p 223 N90-26372
[NASA-CR-185265]

Ceramics Analysis and Reliability Evaluation of Structures (CARES). Users and programmers manual p 223 N90-28099
[NASA-TP-2916]

Reliability analysis of a structural ceramic combustion chamber p 223 N90-28112
[NASA-TM-103264]

RELIABILITY ENGINEERING

Space Station Freedom power - A reliability, availability, and maintainability assessment of the proposed Space Station Freedom electric power system p 58 A90-38074

Rocket combustion chamber life-enhancing design concepts p 66 A90-47208
[AIAA PAPER 90-2116]

- Rocket combustion chamber life-enhancing design concepts
[NASA-CR-185257] p 79 N90-25183
- RELIC RADIATION**
Phase transitions as the origin of large scale structure in the universe p 265 A90-35291
- REMOTE MANIPULATOR SYSTEM**
Photovoltaic module on-orbit assembly for Space Station Freedom p 45 A90-38071
- REMOTE SENSING**
Fiber optic sensing systems using high frequency resonant sensing heads with intensity sensors p 185 A90-10472
- REMOTELY PILOTED VEHICLES**
Preliminary design of a long-endurance Mars aircraft [AIAA PAPER 90-2000] p 43 A90-40587
Preliminary design of a long-endurance Mars aircraft [NASA-CR-185243] p 30 N90-21763
- RENDEZVOUS TRAJECTORIES**
Optimal cooperative time-fixed impulsive rendezvous [AIAA PAPER 90-2962] p 41 A90-53037
Optimal impulsive time-fixed orbital rendezvous and interception with path constraints [AIAA PAPER 90-2972] p 41 A90-53051
- REQUIREMENTS**
Conceptual design of liquid droplet radiator shuttle-attached experiment technical requirements document [NASA-CR-185165] p 71 N90-11806
- RESEARCH AIRCRAFT**
Free float acceleration measurements aboard NASA's KC-135 Microgravity Research Aircraft [AIAA PAPER 90-0742] p 132 A90-20000
STOVL aircraft simulation for integrated flight and propulsion control research [NASA-TM-102419] p 26 N90-13389
- RESEARCH AND DEVELOPMENT**
Review of research and development on the microwave electrothermal thruster p 55 A90-16369
Indium phosphide solar cells - Recent developments and estimated performance in space p 57 A90-37854
Update of the Solar Concentrator Advanced Development Project p 48 A90-38267
Middle management of research [NASA-TM-102417] p 262 N90-20901
- RESEARCH FACILITIES**
A burst compression and expansion technique for variable-rate users in satellite-switched TDMA networks [AIAA PAPER 90-0850] p 46 A90-25673
A test matrix sequencer for research test facility automation [AIAA PAPER 90-2386] p 37 A90-42791
A burst compression and expansion technique for variable-rate users in satellite-switched TDMA networks [NASA-TM-102414] p 47 N90-15983
Conceptual design for the space station Freedom modular combustion facility [NASA-TM-102037] p 134 N90-16087
High power, high frequency component test facility [NASA-TM-102500] p 151 N90-19484
Aeropropulsion facilities configuration control: Procedures manual [NASA-TM-102541] p 207 N90-21399
NASA Lewis icing research tunnel user manual [NASA-TM-102319] p 31 N90-23407
A test matrix sequencer for research test facility automation [NASA-TM-103108] p 39 N90-23416
Technical accomplishments of the NASA Lewis Research Center, 1989 [NASA-TM-102296] p 267 N90-24220
New findings and instrumentation from the NASA Lewis microgravity facilities [NASA-TM-103189] p 136 N90-26163
Structural dynamics branch research and accomplishments [NASA-TM-102488] p 223 N90-26373
- RESEARCH MANAGEMENT**
The Pathfinder chemical transfer propulsion program p 74 N90-18471
Middle management of research [NASA-TM-102417] p 262 N90-20901
- RESIDUAL STRESS**
Optimal fabrication processes for unidirectional metal-matrix composites - A computational simulation p 93 A90-50096
Use of unbalanced laminates as a screening method for microcracking p 94 A90-50217
Use of unbalanced laminates as a screening method for microcracking [NASA-TM-102517] p 98 N90-21124
Fiber pushout test: A three-dimensional finite element computational simulation [NASA-TM-102565] p 99 N90-21131
- Optimal fabrication processes for unidirectional metal-matrix composites: A computational simulation [NASA-TM-102559] p 100 N90-21143
- RESISTANCE HEATING**
Simple evaporation controller for thin-film deposition from a resistively heated boat p 149 A90-39761
- RESISTOJET ENGINES**
Space Station Freedom resistojets system study p 54 A90-16368
Performance and endurance tests of a laboratory model multipropellant resistojets p 55 A90-21220
- RESONANT FREQUENCIES**
Distortion and regulation characterization of a Mapham inverter p 148 A90-38125
Performance and modeling of superconducting ring resonators at millimeter-wave frequencies [NASA-TM-102526] p 151 N90-18634
Probabilistic analysis of bladed turbine disks and the effect of mistuning [NASA-TM-102564] p 136 N90-21871
Structural behavior of composites with progressive fracture [NASA-TM-102370] p 100 N90-23477
Dynamic analysis of space-related linear and non-linear structures [NASA-TM-103490] p 51 N90-25174
- RESONATORS**
Performance and modeling of superconducting ring resonators at millimeter-wave frequencies [NASA-TM-102526] p 151 N90-18634
- RESOURCE ALLOCATION**
Automated electric power management and control for Space Station Freedom [NASA-TM-103151] p 240 N90-23125
- RESPONSE BIAS**
Ion drag for a negatively biased solar array in low earth orbit p 48 A90-36191
- REUSABLE ROCKET ENGINES**
Health Monitoring System for the SSME-fault detection algorithms [AIAA PAPER 90-1988] p 63 A90-40584
The Pathfinder chemical transfer propulsion program p 74 N90-18471
Probabilistic modeling for simulation of aerodynamic uncertainties in propulsion systems [NASA-TM-102472] p 29 N90-21036
A real time neural net estimator of fatigue life [NASA-TM-103117] p 239 N90-21564
- REVISIONS**
Dynamic loading of spur gears with linear or parabolic tooth profile modifications p 195 A90-21126
- REYNOLDS EQUATION**
On the mathematical modeling of the Reynolds stress's equations [AIAA PAPER 90-0498] p 161 A90-19878
- REYNOLDS NUMBER**
Opposed-flow flame spread and extinction in mixed-convection boundary layers p 168 A90-32841
Navier-Stokes analysis of turbine blade heat transfer [NASA-TM-102496] p 179 N90-21300
- REYNOLDS STRESS**
Calculation of turbulence-driven secondary motion in ducts with arbitrary cross-section [AIAA PAPER 90-0245] p 160 A90-19752
On the mathematical modeling of the Reynolds stress's equations [AIAA PAPER 90-0498] p 161 A90-19878
Experimental investigation of turbulent flow through a circular-to-rectangular transition duct [AIAA PAPER 90-1505] p 171 A90-38654
Nonlinear Reynolds stress models and the renormalization group p 172 A90-44011
Wall-layer eruptions in turbulent flows [NASA-TM-102362] p 175 N90-11250
- RHENIUM**
Iridium-coated rhenium thrusters by CVD p 114 A90-30480
- RHEOLOGY**
Nicalon/siliconoxycarbide ceramic composites [NASA-TM-102563] p 99 N90-21133
- RIBBONS**
The vibrating ribbon problem revisited ... in hydrodynamic stability p 168 A90-33516
Microstructure and mechanical properties of multiphase NiAl-based alloys p 115 A90-35071
- RIGID STRUCTURES**
Detection of potential space station control/structure interaction with CO-ST-IN p 50 N90-21074
- RISK**
Probability of failure and risk assessment of propulsion structural components p 218 N90-18470
- RIT ENGINES**
5kW xenon ion thruster lifetest [AIAA PAPER 90-2543] p 68 A90-52564
- Multimegawatt electric propulsion system design considerations [AIAA PAPER 90-2552] p 68 A90-52566
- RITZ AVERAGING METHOD**
Boundary flexibility method of component mode synthesis using static Ritz vectors p 212 A90-35429
- RIVETS**
Fastener design manual [NASA-RP-1228] p 202 N90-18740
- ROBOT ARMS**
Beam rider for an Articulated Robot Manipulator (ARM) accurate positioning of long flexible manipulators [NASA-CR-185151] p 241 N90-26581
Reaction-compensation technology for microgravity laboratory robots [NASA-TM-103271] p 205 N90-28062
- ROBOT DYNAMICS**
Reaction-compensation technology for microgravity laboratory robots [NASA-TM-103271] p 205 N90-28062
- ROBOTICS**
Energy storage considerations for a robotic Mars surface sampler [AAS PAPER 87-245] p 42 A90-16544
Optimum structural design of robotic manipulators with fiber reinforced composite materials p 197 A90-46074
User needs, benefits, and integration of robotic systems in a space station laboratory [NASA-CR-185150] p 200 N90-13794
- ROBOTS**
Reaction-compensation technology for microgravity laboratory robots [NASA-TM-103271] p 205 N90-28062
- ROBUSTNESS (MATHEMATICS)**
Robustness, generality and efficiency of optimization algorithms in practical applications [AIAA PAPER 90-1177] p 236 A90-29268
Extended implicit model following as applied to integrated flight and propulsion control [AIAA PAPER 90-3444] p 239 A90-47697
An observer-based compensator for distributed delays p 239 A90-49899
- ROCKET ENGINE DESIGN**
Performance and endurance tests of a laboratory model multipropellant resistojets p 55 A90-21220
Probabilistic structural analysis methods of hot engine structures [ASME PAPER 89-GT-122] p 56 A90-23821
5kW xenon ion thruster lifetest [AIAA PAPER 90-2543] p 68 A90-52564
A rocket engine design expert system [NASA-TM-102373] p 69 N90-10172
The Pathfinder chemical transfer propulsion program p 74 N90-18471
Low power arcjet performance [NASA-TM-103280] p 83 N90-28657
- ROCKET ENGINES**
Iridium-coated rhenium thrusters by CVD p 114 A90-30480
Enhanced heat transfer rocket combustor technology component hot-fire test results [AIAA PAPER 90-2182] p 64 A90-42063
Determination of the durability of the fiberoptics in rocket engine environments [AIAA PAPER 90-2229] p 250 A90-42754
Rocket engine failure detection using system identification techniques [AIAA PAPER 90-1993] p 65 A90-47205
A highly durable injector faceplate design concept for O₂/H₂ propellants [AIAA PAPER 90-2181] p 66 A90-47211
Fabry-Perot interferometer development for rocket engine plume spectroscopy [AIAA PAPER 90-2234] p 187 A90-47212
A comparison of analytical results for 20 K LOX/hydrogen instabilities [AIAA PAPER 90-2241] p 130 A90-47214
Extended temperature range rocket injector [NASA-CASE-LEW-14846-1] p 73 N90-15130
Development of an integrated BEM approach for hot fluid structure interaction [NASA-CR-186214] p 177 N90-15364
Thermal modelling of various thermal barrier coatings in a high heat flux rocket engine [NASA-TM-102418] p 117 N90-16911
Experimental evaluation of a tuned electromagnetic damper for vibration control of cryogenic turbopump rotors [NASA-TP-3005] p 30 N90-23403
Rocket engine failure detection using system identification techniques [NASA-CR-185259] p 45 N90-25159
A comparison of analytical results for 20 K LOX/hydrogen instabilities [NASA-TM-103166] p 80 N90-25186

SUBJECT INDEX

ROCKET LININGS

- Corrosion prevention in copper combustion chamber liners of liquid oxygen/methane booster engines
[AIAA PAPER 90-2119] p 85 A90-42028
Cooling of rocket thrust chambers with liquid oxygen
[AIAA PAPER 90-2120] p 63 A90-42029
Cooling of rocket thrust chambers with liquid oxygen
[NASA-TM-103146] p 78 N90-22605

ROCKET PROPELLANTS

- Performance and endurance tests of a laboratory model multipropellant resistojet p 55 A90-21220
Atomic hydrogen as a launch vehicle propellant
[AIAA PAPER 90-0715] p 44 A90-23712
Combustion interaction with radiation-cooled chambers
[AIAA PAPER 90-2121] p 64 A90-42030
Numerical modeling of an arcjet thruster
[AIAA PAPER 90-2614] p 64 A90-42587
Atomic hydrogen as a launch vehicle propellant
[NASA-TM-102459] p 73 N90-14284
The measurement, modeling, and prediction of traction for rocket propellant 1
[NASA-CR-185186] p 131 N90-19386

ROCKET SOUNDING

- Computer modeling of current collection by the CHARGE-2 mother payload p 252 A90-24933
The sheath structure around a negatively charged rocket payload p 48 A90-34780

ROCKET TEST FACILITIES

- Low thrust rocket test facility
[AIAA PAPER 90-2503] p 43 A90-47225
Low thrust rocket test facility
[NASA-TM-103206] p 43 N90-25158

ROCKET THRUST

- Advanced tube-bundle rocket thrust chamber
[AIAA PAPER 90-2726] p 67 A90-47227
Advanced tube-bundle rocket thrust chamber
[NASA-TM-103139] p 80 N90-25185

RODS

- Low velocity impact analysis with NASTRAN p 221 N90-24647

ROLLER BEARINGS

- Non-linear dynamic analysis of geared systems, part 2
[NASA-CR-180495] p 204 N90-23732
Modification of the SHABERTH bearing code to incorporate RP-1 and a discussion of the traction model
[NASA-TP-3017] p 205 N90-28066

ROLLERS

- Fully articulated four-point-bend loading fixture
[NASA-CASE-LEW-14776-1] p 201 N90-15445

ROLLING

- Production and processing of Cu-Cr-Nb alloys p 114 A90-33340
Production and processing of Cu-Cr-Nb alloys
[NASA-TM-102495] p 117 N90-16053

ROOM TEMPERATURE

- Torsional and biaxial (tension-torsion) fatigue damage mechanisms in Waspaloy at room temperature p 109 A90-11925
Influence of testing environment on the room temperature ductility of FeAl alloys p 115 A90-39658

ROTARY ENGINES

- Analysis of rotary engine combustion processes based on unsteady, three-dimensional computations
[AIAA PAPER 90-0643] p 163 A90-22237
The application of cast SiC/Al to rotary engine components
[NASA-CR-179610] p 25 N90-13385
Analysis of rotary engine combustion processes based on unsteady, three-dimensional computations
[NASA-TM-102469] p 176 N90-13749
Performance of a supercharged direct-injection stratified-charge rotary combustion engine
[NASA-TM-103105] p 32 N90-25982
Computational experience with a three-dimensional rotary engine combustion model
[NASA-TM-103104] p 183 N90-26275

ROTARY STABILITY

- Shaft flexibility effects on aeroelastic stability of a rotating bladed disk p 208 A90-16371

ROTARY WING AIRCRAFT

- Experimental and analytical evaluation of dynamic load vibration of a 2240-kW (3000-hp) rotorcraft transmission p 192 A90-13750
NASA's program on icing research and technology p 16 N90-15062
Transmission research activities at NASA Lewis Research Center
[NASA-TM-103132] p 203 N90-21394

- Assessment of High Temperature Superconducting (HTS) electric motors for rotorcraft propulsion
[NASA-CR-185222] p 29 N90-21761

ROTARY WINGS

- Impact ice stresses in rotating airfoils
[AIAA PAPER 90-0198] p 15 A90-19735

- Icing Research Tunnel test of a model helicopter rotor p 15 A90-28179

ROTATING BODIES

- Phase and time-resolved measurements of unsteady heat transfer and pressure in a full-stage rotating turbine
[ASME PAPER 89-GT-135] p 165 A90-23832

ROTATING DISKS

- Performance and acoustic prediction of counterrotating propeller configurations p 246 A90-14342
[SAE PAPER 891035]
Shaft flexibility effects on aeroelastic stability of a rotating bladed disk p 208 A90-16371
Analytical and finite element solutions of some problems using a viscoplastic model p 209 A90-19132
Blade mistuning coupled with shaft flexibility effects in rotor aeroelasticity p 19 A90-23896
[ASME PAPER 89-GT-330]
Spray automated balancing of rotors - How process parameters influence performance p 198 A90-46228

ROTATING FLUIDS

- Rotating primary flow induction using jet-flapped blades p 19 A90-12585

ROTATING SHAFTS

- Vibration transmission through rolling element bearings in geared rotor system, part 1 p 199 N90-12936
[NASA-CR-186093]
A fiber optic sensor for noncontact measurement of shaft speed, torque, and power p 189 N90-21360
[NASA-TM-102481]

ROTATION

- Conceptual design of a Moving Belt Radiator (MBR) shuttle-attached experiment p 79 N90-23474
[NASA-CR-185169]
An unsteady lifting surface method for single rotation propellers p 14 N90-25940
[NASA-CR-4302]

ROTOR AERODYNAMICS

- Counter-rotating propellant analysis using a frequency domain panel method p 7 A90-40937
A block-based algorithm for the solution of compressible flows in rotor-stator combinations p 9 A90-46905
An investigation of counterrotating tip vortex interaction p 247 N90-11549
[NASA-CR-185135]
Prediction of unsteady blade surface pressures on an advanced propeller at an angle of attack p 11 N90-12560
[NASA-TM-102374]
Experimental performance and acoustic investigation of modern, counterrotating blade concepts p 18 N90-23393
[NASA-CR-185158]

ROTOR BLADES

- Time domain flutter analysis of cascades using a full-potential solver p 6 A90-29374
[AIAA PAPER 90-0984]
Shaft flexibility effects on the forced response of a bladed-disk assembly p 21 A90-43218
Application of a two-dimensional unsteady viscous analysis code to a supersonic throughflow fan stage p 25 N90-13387
[NASA-TM-4141]

ROTOR BLADES (TURBOMACHINERY)

- Progress towards the development of an inviscid-viscous interaction method for unsteady flows in turbomachinery cascades p 2 A90-11806
Computation of three dimensional turbulent boundary layers in internal flows, including turbomachinery rotor blades p 3 A90-12555
Aeroelastic problems in turbomachines
[AIAA PAPER 90-1157] p 7 A90-29393
Laser anemometer measurements in a transonic axial-flow fan rotor p 175 N90-11245
[NASA-TP-2879]
Numerical simulation of unsteady rotational flow over propfan configurations p 10 N90-12500
[NASA-CR-186037]
An analysis of the viscous flow through a compact radial turbine by the average passage approach p 12 N90-14206
[NASA-TM-102471]
Gust response analysis for cascades operating in nonuniform mean flows p 28 N90-18415
Measurement of the steady surface pressure distribution on a single rotation large scale advanced prop-fan blade at Mach numbers from 0.03 to 0.78 p 32 N90-28552
[NASA-CR-182124]

ROTOR BODY INTERACTIONS

- Propeller-wing interaction using a frequency domain panel method p 6 A90-26128

ROTOR DYNAMICS

- Dynamic analysis of geared rotors by finite elements p 194 A90-21123
Probabilistic analysis of bladed turbine disks and the effect of mistuning
[AIAA PAPER 90-1097] p 196 A90-29327
Actuator design for rotor control p 198 A90-46232
Gear noise, vibration, and diagnostic studies at NASA Lewis Research Center
[NASA-TM-102435] p 202 N90-18041

SAFETY FACTORS

- Probabilistic analysis of bladed turbine disks and the effect of mistuning p 136 N90-21871
[NASA-TM-102564]
Elements of active vibration control for rotating machinery p 137 N90-22703
[NASA-TM-102368]
Experimental performance and acoustic investigation of modern, counterrotating blade concepts p 18 N90-23393
[NASA-CR-185158]

ROTOR SPEED

- An active optimal control strategy of rotor vibrations using external forces p 198 A90-46224
Experimental evaluation of a tuned electromagnetic damper for vibration control of cryogenic turbopump rotors p 30 N90-23403
[NASA-TP-3005]

ROTORCRAFT AIRCRAFT

- Convertible engine system for high speed rotorcraft
[AIAA PAPER 90-2512] p 20 A90-40643

ROTORS

- Active vibration control for flexible rotor by optimal direct-output feedback control p 197 A90-46222
Spray automated balancing of rotors - How process parameters influence performance p 198 A90-46228
Improved silicon carbide for advanced heat engines
[NASA-CR-180831] p 124 N90-10293
Large-scale Advanced Prop-fan (LAP) static rotor test report p 25 N90-12617
[NASA-CR-180848]
Vibration transmission through rolling element bearings in geared rotor system, part 1 p 199 N90-12936
[NASA-CR-186093]
The application of cast SiC/Al to rotary engine components p 25 N90-13385
[NASA-CR-179610]
Elasticity effects on cavitation in a squeeze film damper undergoing noncentered circular whirl p 200 N90-13786
[NASA-TM-102392]
Dynamic analysis of geared rotors by finite elements
[NASA-TM-102349] p 201 N90-16286
Noise of a simulated installed model counterrotation propeller at angle-of-attack and takeoff/approach conditions p 248 N90-20794
[NASA-TM-102440]
Experimental evaluation of a tuned electromagnetic damper for vibration control of cryogenic turbopump rotors p 30 N90-23403
[NASA-TP-3005]
An unsteady lifting surface method for single rotation propellers p 14 N90-25940
[NASA-CR-4302]
Two-dimensional Euler and Navier-Stokes Time accurate simulations of fan rotor flows p 14 N90-25948
[NASA-TM-102402]
Dynamics of multistage gear transmission with effects of gearbox vibrations p 205 N90-28060
[NASA-TM-103109]

ROVING VEHICLES

- Energy storage considerations for a robotic Mars surface sampler p 42 A90-16544
[AAS PAPER 87-245]
Mars manned transportation vehicle p 42 A90-16569
[AAS PAPER 87-271]
Nuclear power systems for lunar and Mars exploration
[NASA-TM-103168] p 82 N90-26873

RP-1 ROCKET PROPELLANTS

- Modification of the SHABERTH bearing code to incorporate RP-1 and a discussion of the traction model
[NASA-TP-3017] p 205 N90-28066

RUNGE-KUTTA METHOD

- Two-dimensional Euler and Navier-Stokes Time accurate simulations of fan rotor flows p 14 N90-25948
[NASA-TM-102402]

RUPTURING

- Fully articulated four-point-bend loading fixture
[NASA-CASE-LEW-14776-1] p 201 N90-15445

RUTHENIUM COMPOUNDS

- Electrocatalysis for oxygen electrodes in fuel cells and water electrolyzers for space applications p 57 A90-33945
Catalysts for ultrahigh current density oxygen cathodes for space fuel cell applications p 232 N90-22835
[NASA-CR-180650]

S

S WAVES

- Improved transverse crack detection in composites
[NASA-TM-103261] p 102 N90-27875

SAFETY FACTORS

- Advanced spacecraft fire safety: Proposed projects and program plan p 49 N90-12645
[NASA-CR-185147]
Health management system for rocket engines p 131 N90-23574
[NASA-CR-185223]

SAFETY MANAGEMENT

- The US space station and its electric power system
[NASA-TM-101974] p 71 N90-13596
Fire safety applications for spacecraft p 16 N90-17595

SAMPLING

- Optical characterization of clouds of fine liquid-nitrogen particles
[NASA-TM-103208] p 191 N90-26299

SANDWICH STRUCTURES

- Effect of crack-microcracks interaction on energy release rates p 214 A90-49269

SATELLITE ANTENNAS

- A new fabrication method for precision antenna reflectors for space flight and ground test
[AIAA PAPER 90-0803] p 139 A90-25627

SATELLITE COMMUNICATION

- Role of communications satellites in the fiber era
[AIAA PAPER 90-0792] p 139 A90-25617
Satellite range delay simulator for a matrix-switched time division multiple-access network simulation system
[AIAA PAPER 90-0795] p 139 A90-25620
A parallel pipelined architecture for a digital multicarrier demodulator
[AIAA PAPER 90-0812] p 46 A90-25635
A heuristic approach to worst-case carrier-to-interference ratio maximization in satellite system synthesis
[AIAA PAPER 90-0816] p 46 A90-25639
K-band TWT using new diamond rod technology
[AIAA PAPER 90-0870] p 147 A90-25691
Effects of amplitude distortions and IF equalization on satellite communication system bit-error rate performance
[AIAA PAPER 90-0878] p 140 A90-25697
A unified statistical rain-attenuation model for communication link fade predictions and optimal stochastic fade control design using a location-dependent rain-statistic database p 141 A90-34914
High-speed digital fiber optic links for satellite traffic p 250 A90-41247
High-speed fiber-optic links for distribution of satellite traffic p 47 A90-41687
Advanced Communications Technology Satellite (ACTS) and potential system applications p 142 A90-51165
The role of technology in influencing future civil communications satellites p 142 A90-51167
On-board switching and processing p 150 A90-51168
Adaptive antenna arrays for satellite communication [NASA-CR-185989] p 143 N90-12784
Satellite range delay simulator for a matrix-switched time division multiple-access network simulator [NASA-TM-102407] p 143 N90-12813
Performance measurements for a laboratory-simulated 30/20 GHz communication satellite transponder [NASA-TM-102424] p 143 N90-17977
Conceptual definition of a high voltage power supply test facility [NASA-CR-185216] p 50 N90-25172
Rain-fade simulation and power augmentation for satellite communication systems [NASA-TM-103134] p 146 N90-28768

SATELLITE DESIGN

- Spacecraft designs for VSAT networks
[AIAA PAPER 90-0895] p 140 A90-25681
Data distribution satellite system architecture concept [AIAA PAPER 90-0885] p 46 A90-25704

SATELLITE GROUND SUPPORT

- LBR-2 earth stations for the ACTS program
[AIAA PAPER 90-0838] p 42 A90-25662

SATELLITE LIFETIME

- Arcjet nozzle design impacts p 76 N90-18478

SATELLITE NETWORKS

- Satellite range delay simulator for a matrix-switched time division multiple-access network simulation system [AIAA PAPER 90-0795] p 139 A90-25620
Data distribution satellite system architecture concept [AIAA PAPER 90-0885] p 46 A90-25704
A performance analysis of DS-CDMA and SCPC VSAT networks p 141 A90-39056
Satellite range delay simulator for a matrix-switched time division multiple-access network simulator [NASA-TM-102407] p 143 N90-12813

SATELLITE ORBITS

- Application of heuristic satellite plan synthesis algorithms to requirements of the WARC-88 allotment plan
[AIAA PAPER 90-0815] p 245 A90-25638
The GEM-T2 gravitational model [NASA-TM-100746] p 234 N90-12984
Application of heuristic satellite plan synthesis algorithms to requirements of the WARC-88 allotment plan [NASA-TM-102479] p 245 N90-14856

SATELLITE ORIENTATION

- Spacecraft attitude impacts on COLD-SAT non-vacuum jacketed LH2 supply tank thermal performance
[AIAA PAPER 90-1672] p 49 A90-41566

SATELLITE POWER TRANSMISSION

- Overview of microwave concepts p 142 N90-10155
Power for the moon: Is microwave power beaming an option? p 69 N90-10158

SATELLITE SOLAR POWER STATIONS

- Lunar production of space photovoltaic arrays p 226 A90-14930

SATELLITE TEMPERATURE

- Spacecraft attitude impacts on COLD-SAT non-vacuum jacketed LH2 supply tank thermal performance
[AIAA PAPER 90-1672] p 49 A90-41566

SATELLITE TRACKING

- Application of heuristic satellite plan synthesis algorithms to requirements of the WARC-88 allotment plan
[AIAA PAPER 90-0815] p 245 A90-25638
The GEM-T2 gravitational model [NASA-TM-100746] p 234 N90-12984
Application of heuristic satellite plan synthesis algorithms to requirements of the WARC-88 allotment plan [NASA-TM-102479] p 245 N90-14856

SATELLITE TRANSMISSION

- Performance measurements for a laboratory-simulated 30/20 GHz communication satellite transponder [NASA-TM-102424] p 143 N90-17977
Effects of amplitude distortions and IF equalization on satellite communication system bit-error rate performance [NASA-TM-102415] p 144 N90-19454
Numerical Arc Segmentation Algorithm for a Radio Conference-NASARC (version 4.0) technical manual [NASA-TM-101453] p 144 N90-20264
Rain-fade simulation and power augmentation for satellite communication systems [NASA-TM-103134] p 146 N90-28768

SCALARS

- Equilibrium statistical thermodynamics of a many-particle system coupled to an external scalar field p 261 A90-31670
Soft inflation --- in cosmology p 265 A90-40093
On the application of subcell resolution to conservation laws with stiff source terms [NASA-TM-102384] p 243 N90-14844

SCALE (CORROSION)

- Diffusional aspects of the high-temperature oxidation of protective coatings p 113 A90-28075

SCALE EFFECT

- Scaling study for SP-100 reactor technology [NASA-TM-897140] p 249 N90-16496

SCALE MODELS

- Diagnostics and performance of a 1/4-scale MPD thruster [AIAA PAPER 90-2665] p 65 A90-42625
Engine inlet distortion in a 9.2 percent scale vectored thrust STOVL model in ground effect [NASA-TM-102358] p 12 N90-17561

SCALING

- Scaling results for the liquid sheet radiator p 170 A90-38037

SCANNERS

- Optical characterization of clouds of fine liquid-nitrogen particles [NASA-TM-103208] p 191 N90-26299

SCANNING TUNNELING MICROSCOPY

- Design and calibration of a vacuum compatible scanning tunneling microscope [NASA-TM-102514] p 189 N90-20353

SCATTERING

- On physical optics for calculating scattering from coated bodies p 250 A90-20151
High-frequency asymptotic methods for analyzing the EM scattering by open-ended waveguide cavities [NASA-CR-186244] p 143 N90-16103
Theory and experimental technique for nondestructive evaluation of ceramic composites [NASA-TM-102561] p 207 N90-23754

SCATTERING COEFFICIENTS

- Radiative transfer theory for inhomogeneous media with random extinction and scattering coefficients p 260 A90-21904

SCATTERING FUNCTIONS

- Two-dimensional convection and radiation with scattering from a Poiseuille flow p 161 A90-20519
Emittance bounds for transient radiative cooling of a scattering rectangular region p 161 A90-20520

SCHEDULES

- A technology assessment of alternative communications systems for the space exploration initiative [NASA-TM-103243] p 47 N90-27736

SCHEDULING

- Application of a hybrid generation/utility assessment heuristic to a class of scheduling problems [NASA-TM-102367] p 245 N90-10674
Electric power scheduling: A distributed problem-solving approach

- [NASA-TM-103149] p 240 N90-22323
An expert system for simulating electric loads aboard Space Station Freedom [NASA-TM-103150] p 240 N90-22325

SCHOOLS

- Launching a dream: A teachers guide to a simulated space shuttle mission [NASA-TM-89715] p 261 N90-26693

SCIENTIFIC SATELLITES

- Spacecraft attitude impacts on COLD-SAT non-vacuum jacketed LH2 supply tank thermal performance [AIAA PAPER 90-1672] p 49 A90-41566

SEALING

- High temperature, flexible, thermal barrier seal [NASA-CASE-LEW-14672-1] p 201 N90-15444
High temperature flexible seal [NASA-CASE-LEW-14695-1] p 204 N90-23751

SEALS (STOPPERS)

- Some composite bearing and seal materials for gas turbine applications - A review [ASME PAPER 89-GT-144] p 195 A90-23838
A simplified model for two phase face seal design p 197 A90-40713

- Flow visualization and motion analysis for a series of four sequential brush seals [AIAA PAPER 90-2482] p 199 A90-47222

- Sliding seal materials for low heat rejection engines [NASA-CR-182262] p 125 N90-11882

- High temperature flexible seal [NASA-CASE-LEW-14695-1] p 204 N90-23751

SECONDARY EMISSION

- Secondary electron emission characteristics of molybdenum-masked, ion-textured OFHC copper [NASA-TP-2967] p 117 N90-15211

SECONDARY FLOW

- Influence of bulk turbulence and entrance boundary layer thickness on the curved duct flow field [AIAA PAPER 90-1502] p 171 A90-38651
Nonlinear Reynolds stress models and the renormalization group p 172 A90-44011
Numerical analysis of secondary flow in a two-stage turbine [AIAA PAPER 90-2356] p 66 A90-47216

SECURITY

- Automating security monitoring and analysis for Space Station Freedom's electric power system [NASA-TM-103148] p 240 N90-22324

SEGMENTS

- Numerical Arc Segmentation Algorithm for a Radio Conference-NASARC (version 4.0) technical manual [NASA-TM-101453] p 144 N90-20264

SELF LUBRICATING MATERIALS

- Tribological properties of PM212: A high-temperature, self-lubricating, powder metallurgy composite [NASA-TM-102355] p 86 N90-12659

SELF LUBRICATION

- Self-lubricating polymer composites and polymer transfer film lubrication for space applications [NASA-TM-102492] p 128 N90-21862

SELF TESTS

- Advanced modulation technology development for earth station demodulator applications. Coded modulation system development [NASA-CR-185149] p 145 N90-20270

SEMICIRCULAR CANALS

- A geometric analysis of semicircular canals and induced activity in their peripheral afferents in the rhesus monkey p 234 A90-28084

SEMICONDUCTING FILMS

- Growth of improved quality 3C-SiC films on 6H-SiC substrates p 255 A90-29596

SEMICONDUCTOR DEVICES

- Silicon carbide semiconductor device fabrication and characterization [NASA-CR-186354] p 258 N90-19873
Lateral spreading of Au contacts on InP [NASA-TM-103133] p 232 N90-22843

SEMICONDUCTOR DIODES

- Mathematical optimization of photovoltaic converters for diode lasers --- for spacecraft power supplies p 228 A90-38110

- Channelized coplanar waveguide pin-diode switches [NASA-TM-102289] p 150 N90-11943

SEMICONDUCTOR JUNCTIONS

- Contribution of the graded region of a HgCdTe diode to its saturation current p 257 A90-45848

SEMICONDUCTOR LASERS

- Fiber optic sensing system [NASA-CASE-LEW-14795-1] p 251 N90-15733

SUBJECT INDEX

SEMICONDUCTORS (MATERIALS)

High frequency capacitance-voltage characteristics of thermally grown SiO₂ films on beta-SiC p 254 A90-21348

Electrical properties of materials for high temperature strain gage applications [NASA-CR-186192] p 188 N90-14534

Electron-beam induced damage in thin insulating films on compound semiconductors [NASA-CR-185177] p 151 N90-17987

Neutron and gamma irradiation effects on power semiconductor switches [NASA-TM-103200] p 155 N90-25278

An analysis of the contact sintering process in III-V solar cells [NASA-TM-103179] p 233 N90-25420

SENSITIVITY

Effect of spatial resolution on apparent sensitivity to initial conditions of a decaying flow as it becomes turbulent [NASA-TM-102377] p 176 N90-13719

SENSORIMOTOR PERFORMANCE

A geometric analysis of semicircular canals and induced activity in their peripheral afferents in the rhesus monkey p 234 A90-28084

SEPARATED FLOW

Unsteady disturbances of streaming motions around bodies p 162 A90-21424

Evaluation of three turbulence models in static air loads and dynamic stall predictions p 7 A90-31291

Experimental investigation of flow about a strut-endwall configuration [AIAA PAPER 90-1541] p 171 A90-38685

Unsteady three-dimensional marginal separation, including breakdown [NASA-TM-102525] p 179 N90-20337

Navier-Stokes analysis of turbine blade heat transfer [NASA-TM-102496] p 179 N90-21300

Control of flow separation and mixing by aerodynamic excitation [NASA-TM-103131] p 13 N90-21733

Numerical investigation of separated transonic turbulent flows with a multiple-time-scale turbulence model [NASA-TM-102499] p 180 N90-21962

SEPARATORS

Zero-G phase detector and separator [NASA-CASE-LEW-14844-1] p 190 N90-22024

SEQUENCING

Application of a hybrid generation/utility assessment heuristic to a class of scheduling problems [NASA-TM-102367] p 245 N90-10674

SERVICE LIFE

KOH concentration effect on the cycle life of nickel-hydrogen cells. IV - Results of failure analysis p 228 A90-33952

Space Station Freedom solar array design development p 58 A90-38076

Rocket combustion chamber life-enhancing design concepts [AIAA PAPER 90-2116] p 66 A90-47208

Thermal barrier coating life prediction model development, phase 1 [NASA-CR-182230] p 26 N90-13388

A nonlinear high temperature fracture mechanics basis for strainrange partitioning [NASA-TM-4133] p 216 N90-14642

Changes in impedance of Ni electrodes upon standing and cycling [NASA-TM-102438] p 229 N90-18097

Rocket combustion chamber life-enhancing design concepts [NASA-CR-185257] p 79 N90-25183

Liquid lubrication in space [NASA-RP-1240] p 205 N90-28063

Energy Efficient Engine (E3) combustion system component technology performance report [NASA-CR-168274] p 33 N90-28555

Probabilistic structural analysis methods development for SSME p 83 N90-28616

Bearing optimization for SSME HPOTP application p 205 N90-28622

Durability of thermal barrier coatings in a high heat flux environment p 129 N90-28651

SHADOWGRAPH PHOTOGRAPHY

Optical techniques for determination of normal shock position in supersonic flows for aerospace applications [NASA-TM-103201] p 190 N90-25323

SHAFTS (MACHINE ELEMENTS)

Shaft flexibility effects on aeroelastic stability of a rotating bladed disk p 208 A90-16371

Modal analysis of gear housing and mounts p 192 A90-17018

Blade mistuning coupled with shaft flexibility effects in rotor aeroelasticity [ASME PAPER 89-GT-330] p 19 A90-23896

An applicational process for dynamic balancing of turbomachinery shafting [NASA-TM-102537] p 202 N90-20392

Assessment of High Temperature Superconducting (HTS) electric motors for rotorcraft propulsion [NASA-CR-185222] p 29 N90-21761

Experimental evaluation of a tuned electromagnetic damper for vibration control of cryogenic turbopump rotors [NASA-TP-3005] p 30 N90-23403

Non-linear dynamic analysis of geared systems, part 2 [NASA-CR-180495] p 204 N90-23732

Integrated controls and health monitoring fiberoptic shaft monitor [NASA-CR-185210] p 191 N90-29622

SHEAR FLOW

Contributions to the understanding of large-scale coherent structures in developing free turbulent shear flows p 158 A90-13907

Shear stabilization of the capillary breakup of a cylindrical interface [AD-A219268] p 159 A90-17578

The effects of forcing on a single stream shear layer and its parent boundary layer p 169 A90-35219

Structure of a reattaching supersonic shear layer p 7 A90-36252

A planar reacting shear layer system for the study of fluid dynamics-combustion interaction [NASA-TM-102422] p 27 N90-13393

Control of flow separation and mixing by aerodynamic excitation [NASA-TM-103131] p 13 N90-21733

Modern developments in shear flow control with swirl [NASA-CR-186586] p 181 N90-22000

SHEAR LAYERS

Nonlinear evolution of oblique waves on compressible shear layers p 158 A90-15942

Nonlinear evolution of interacting oblique waves on two-dimensional shear layers p 158 A90-15943

Calculation of reattaching shear layers in divergent channel with a multiple-time-scale turbulence model [AIAA PAPER 90-0047] p 160 A90-19649

Compressibility effects in free shear layers [AIAA PAPER 90-0705] p 161 A90-19984

Time-accurate simulations of a shear layer forced at a single frequency p 163 A90-23111

A new mixing length model for supersonic shear layers [AIAA PAPER 90-0018] p 166 A90-25026

Effects of compressibility on the characteristics of free shear layers p 6 A90-25285

The effects of forcing on a single stream shear layer and its parent boundary layer p 169 A90-35219

Pressure-based real-time measurements in compressible free shear layers [AIAA PAPER 90-1980] p 8 A90-42709

A planar reacting shear layer system for the study of fluid dynamics-combustion interaction [NASA-TM-102422] p 27 N90-13393

Response of a chemically reacting layer to streamwise vorticity [NASA-TM-102288] p 178 N90-18005

The effects of forcing on a single stream shear layer and its parent boundary layer p 180 N90-21301

[NASA-CR-186529] p 180 N90-21301

Control of flow separation and mixing by aerodynamic excitation [NASA-TM-103131] p 13 N90-21733

SHEAR STRAIN

A variational justification of the assumed natural strain formulation of finite elements. I - Variational principles. II - The C(0) four-node plate element p 210 A90-24384

The equivalence between dislocation pile-ups and cracks p 210 A90-29215

Two-dimensional surface strain measurement based on a variation of Yamaguchi's laser-speckle strain gauge [NASA-TM-103162] p 192 N90-22784

SHEAR STRENGTH

Measurement of interfacial shear strength in SiC-fiber/Si₃N₄ composites p 87 A90-13237

Investigation of interfacial shear strength in a SiC fiber/Ti-24Al-11Nb composite by a fibre push-out technique p 88 A90-18973

Fiber pushout test: A three-dimensional finite element computational simulation [NASA-TM-102565] p 99 N90-21131

Influence of interfacial shear strength on the mechanical properties of SiC fiber reinforced reaction-bonded silicon nitride matrix composites [NASA-TM-102462] p 101 N90-24382

SHEAR STRESS

The correlation between the temperature dependence of the CRSS and the formation of superlattice-intrinsic stacking faults in the nickel-base superalloy PWA 1480 --- critical resolved shear stress p 109 A90-11657

SHORT TAKEOFF AIRCRAFT

Near wall flow parameters in the blade end-wall corner region p 156 A90-12636

Computation of three-dimensional turbulent boundary layers with heat transfer in a plane of symmetry using embedded wall-layer functions [AIAA PAPER 90-0307] p 160 A90-19788

The unusual near-threshold FCG behavior of a single crystal superalloy and the resolved shear stress as the crack driving force p 111 A90-21009

A constitutive model for the inelastic multiaxial response of Rene 80 at 871 C and 982 C p 114 A90-32266

An annular gas seal analysis using empirical entrance and exit region friction factors [ASME PAPER 89-TRIB-46] p 196 A90-33555

Creep and creep rupture of strongly reinforced metallic composites [NASA-CR-185286] p 223 N90-28110

SHELLS (STRUCTURAL FORMS)

Developments in variational methods for high performance plate and shell elements p 214 A90-46288

SHIELDING

On protection of Freedom's solar dynamic radiator from the orbital debris environment. Part 1: Preliminary analyses and testing [NASA-TM-102458] p 73 N90-14285

SHOCK FRONTS

Optical techniques for determination of normal shock position in supersonic flows for aerospace applications [NASA-TM-103201] p 190 N90-25323

SHOCK HEATING

Thermal/structural analyses of several hydrogen-cooled leading-edge concepts for hypersonic flight vehicles [AIAA PAPER 90-0053] p 164 A90-23702

Thermal/structural analyses of several hydrogen-cooled leading-edge concepts for hypersonic flight vehicles [NASA-TM-102391] p 177 N90-14511

SHOCK WAVE INTERACTION

Skin friction measurements by laser interferometry in swept shock/boundary-layer interactions p 3 A90-18153

A study of the unsteadiness of crossing shock wave turbulent boundary layer interactions [AIAA PAPER 90-1456] p 170 A90-38614

An LDA investigation of the normal shock wave boundary layer interaction p 10 A90-52618

Numerical investigation of separated transonic turbulent flows with a multiple-time-scale turbulence model [NASA-TM-102499] p 180 N90-21962

Computational modeling and validation for hypersonic inlets [NASA-TM-103111] p 181 N90-22011

Interactive calculation procedures for mixed compression inlets [NASA-CR-186581] p 14 N90-25934

SHOCK WAVES

The shocking development of lithium (and boron) in supernovae p 264 A90-17643

Calculation of shocked one-dimensional flows on abruptly changing grids by mathematical programming p 162 A90-21937

Nature of convection-stabilized dc arcs in dual-flow nozzle geometry. I - The cold flow field and dc arc characteristics. II - Optical diagnostics and theory p 252 A90-26665

Optical techniques for determination of normal shock position in supersonic flows for aerospace applications [NASA-TM-103201] p 190 N90-25323

SHORT CIRCUIT CURRENTS

A V-grooved GaAs solar cell p 225 A90-14887

High altitude current-voltage measurement of GaAs/Ge solar cells p 226 A90-14910

Performance of GaAs concentrator cells under electron irradiations from 0.4 to 2.3 MeV p 227 A90-14956

SHORT TAKEOFF AIRCRAFT

Engine inlet distortion in a 9.2 percent scaled vectored thrust STOVL model in ground effect [AIAA PAPER 89-2910] p 5 A90-25043

Cooperative synthesis of control and display augmentation in approach and landing p 36 A90-33061

Performance characteristics of a one-third-scale, vectorable ventral nozzle for SSTOVL aircraft [AIAA PAPER 90-2271] p 20 A90-37562

Hot gas environment around STOVL aircraft in ground proximity. II - Numerical study [AIAA PAPER 90-2270] p 21 A90-42766

Three-dimensional turbulent flow code calculations of hot gas ingestion p 21 A90-44726

Flight control design considerations for STOVL powered-lift flight [AIAA PAPER 90-3225] p 37 A90-49110

The implementation of STOVL task-tailored control modes in a fighter cockpit [AIAA PAPER 90-3229] p 17 A90-49114

- STOVL propulsion system volume dynamics approximations p 25 N90-11740
[NASA-TM-102397]
Real-time simulation of an F110/STOVL turbofan engine p 25 N90-12618
[NASA-TM-102409]
STOVL aircraft simulation for integrated flight and propulsion control research p 26 N90-13389
[NASA-TM-102419]
Performance characteristics of a one-third-scale, vectorable ventral nozzle for SSTOVL aircraft p 2 N90-21725
[NASA-TM-103120]
- SHROUDED TURBINES**
Advanced Turbine Technology Applications Project (ATTAP) p 22 N90-10036
[NASA-CR-185133]
- SIDELobe REDUCTION**
Effects of desired signal on the performance of a sidelobe canceller p 139 A90-13936
- SIDELOBES**
Effects of additional interfering signals on adaptive array performance p 145 N90-20271
[NASA-CR-186508]
- SIGNAL ANALYZERS**
Feasibility study for the advanced one-dimensional high temperature optical strain measurement system, phase 3 p 191 N90-25324
[NASA-CR-185254]
- SIGNAL DISTORTION**
Effects of amplitude distortions and IF equalization on satellite communication system bit-error rate performance p 140 A90-25697
[AIAA PAPER 90-0878]
Effects of amplitude distortions and IF equalization on satellite communication system bit-error rate performance p 144 N90-19454
[NASA-TM-102415]
- SIGNAL FADING**
A unified statistical rain-attenuation model for communication link fade predictions and optimal stochastic fade control design using a location-dependent rain-statistic database p 141 A90-34914
Effects of amplitude distortions and IF equalization on satellite communication system bit-error rate performance p 144 N90-19454
[NASA-TM-102415]
- SIGNAL PROCESSING**
Encoding Y,I,Q component estimates of an NTSC composite signal p 139 A90-23261
Rocket engine failure detection using system identification techniques p 65 A90-47205
[AIAA PAPER 90-1993]
An experimental SMI adaptive antenna array for weak interfering signals p 142 N90-11211
[NASA-CR-185976]
Intensity to frequency conversion technique in intensity modulated fiber optic sensing systems p 153 N90-21277
[NASA-TM-102562]
Zero-G phase detector and separator p 190 N90-22024
[NASA-CASE-LEW-14844-1]
Field oriented control of induction motors p 154 N90-22731
[NASA-TM-103154]
Rocket engine failure detection using system identification techniques p 45 N90-25159
[NASA-CR-185259]
Feasibility study for the advanced one-dimensional high temperature optical strain measurement system, phase 3 p 191 N90-25324
[NASA-CR-185254]
- SIGNAL TO NOISE RATIOS**
Convergence of the SMI and the diagonally loaded SMI algorithms with weak interference p 141 A90-36717
[AD-A222639]
Adaptive antenna arrays for satellite communication p 143 N90-12784
[NASA-CR-185989]
- SIGNAL TRANSMISSION**
Effects of desired signal on the performance of a sidelobe canceller p 139 A90-13936
- SIGNATURE ANALYSIS**
Vibration signature analysis of multistage gear transmission p 194 A90-21124
- SILICON**
Surface entropy of liquids via a direct Monte Carlo approach - Application to liquid Si p 261 A90-31675
Silicon-etalon fiber-optic temperature sensor p 18 N90-13381
[NASA-TM-102389]
- SILICON ALLOYS**
Effect of Ga and P dopants on the thermoelectric properties of n-type SiGe p 256 A90-38140
- SILICON CARBIDES**
Measurement of interfacial shear strength in SiC-fiber/Si₃N₄ composites p 87 A90-13237
Investigation of interfacial shear strength in a SiC fiber/Ti-24Al-11Nb composite by a fibre push-out technique p 88 A90-18973
High frequency capacitance-voltage characteristics of thermally grown SiO₂ films on beta-SiC p 254 A90-21348
- Burner rig hot corrosion of silicon carbide and silicon nitride p 121 A90-25267
Role of the interfacial thermal barrier in the effective thermal diffusivity/conductivity of SiC-fiber-reinforced reaction-bonded silicon nitride p 89 A90-25268
Nitriding kinetics of Si-SiC powder mixtures as simulations of reaction bonded Si₃N₄-SiC composites p 90 A90-27076
Evaluation of thermal and mechanical loading effects on the structural behavior of a SiC/titanium composite [AIAA PAPER 90-1026] p 90 A90-29228
Growth of improved quality 3C-SiC films on 6H-SiC substrates p 255 A90-29596
Growth of high quality 6H-SiC epitaxial films on vicinal (0001) 6H-SiC wafers p 255 A90-29952
Deep-level dominated electrical characteristics of Au contacts on beta-SiC p 147 A90-33726
High-strength silicon carbides by hot isostatic pressing p 122 A90-35473
Isothermal and nonisothermal fatigue behavior of a metal matrix composite p 91 A90-36746
Modeling of the SiC chemical vapor deposition process and comparison with experimental results p 105 A90-36810
Microstructure of a SiC/Ti-15-3 composite p 91 A90-37663
Reaction zone microstructure in a Ti₃Al + Nb/SiC composite p 91 A90-39627
Reactions of SiC with H₂/H₂O/Ar mixtures at 1300 C p 123 A90-45830
Thermal effects on the mechanical properties of SiC fiber reinforced reaction-bonded silicon nitride matrix composites p 92 A90-46999
Nicalon/siliconoxycarbide ceramic composites p 94 A90-51924
Improved silicon carbide for advanced heat engines [NASA-CR-180831] p 124 N90-10293
Zirconia toughened SiC whisker reinforced alumina composites small business innovation research [NASA-CR-179629] p 125 N90-10294
Hydrogen-silicon carbide interactions p 125 N90-11144
[NASA-TM-102382]
Oxidation effects on the mechanical properties of SiC fiber-reinforced reaction-bonded silicon nitride matrix composites p 96 N90-14287
[NASA-TM-102360]
Empirical and analytical determination of the fracture resistance of a TiB₂ particle/SiC matrix composite [NASA-TM-101940] p 96 N90-15143
Heat treatment study of the SiC/Ti-15-3 composite system p 97 N90-19302
[NASA-TP-2970]
Silicon carbide semiconductor device fabrication and characterization p 258 N90-19873
[NASA-CR-186354]
Evaluation of thermal and mechanical loading effects on the structural behavior of a SiC/titanium composite [NASA-TM-102536] p 98 N90-20139
High temperature fatigue behavior of a SiC/Ti-24Al-11Nb composite p 220 N90-22822
[NASA-TM-103157]
Theory and experimental technique for nondestructive evaluation of ceramic composites p 207 N90-23754
[NASA-TM-102561]
Influence of interfacial shear strength on the mechanical properties of SiC fiber reinforced reaction-bonded silicon nitride matrix composites p 101 N90-24382
[NASA-TM-102462]
Thermomechanical testing techniques for high-temperature composites: TMF behavior of SiC(SCS-6)/Ti-15-3 p 222 N90-25367
[NASA-TM-103171]
Improved silicon carbide for advanced heat engines [NASA-CR-182186] p 129 N90-28735
- SILICON COMPOUNDS**
Polymer derived Nicalon/Si-C-O composites - Processing and mechanical behavior p 89 A90-27065
- SILICON DIOXIDE**
Ellipsometric study of Al₂O₃/Ag/Si and SiO₂/Ag/quartz ashed in an oxygen plasma --- protective coatings to prevent degradation of materials in low earth orbits p 120 A90-18217
Ellipsometric studies of the diffusion of atomic oxygen through silicon dioxide thin films p 104 A90-36268
Electron-beam induced damage in thin insulating films on compound semiconductors p 151 N90-17987
[NASA-CR-185177]
Polysiloxanes derived from the controlled hydrolysis of tetraethoxysilane as precursors to silica for use in ceramic processing p 128 N90-21858
[NASA-TM-102489]
- SILICON NITRIDES**
Microstructural changes in beta-silicon nitride grains upon crystallizing the grain-boundary glass p 120 A90-13230
- Measurement of interfacial shear strength in SiC-fiber/Si₃N₄ composites p 87 A90-13237
The high temperature creep deformation of Si₃N₄-6Y₂O₃-2Al₂O₃ p 121 A90-18879
Burner rig hot corrosion of silicon carbide and silicon nitride p 121 A90-25267
Role of the interfacial thermal barrier in the effective thermal diffusivity/conductivity of SiC-fiber-reinforced reaction-bonded silicon nitride p 89 A90-25268
Nitriding kinetics of Si-SiC powder mixtures as simulations of reaction bonded Si₃N₄-SiC composites p 90 A90-27076
Ceramic port shields cast in an iron engine head p 196 A90-27095
Slurry-pressing consolidation of silicon nitride p 121 A90-27691
Laminate behavior for SiC fiber-reinforced reaction-bonded silicon nitride matrix composites p 90 A90-29927
Development of Si₃N₄ for gas turbine applications p 122 A90-35509
Properties of RBSN and RBSN-SiC composites --- Reaction Bonded Silicon Nitride p 94 A90-51920
Matrix density effects on the mechanical properties of SiC fiber-reinforced silicon nitride matrix properties p 94 A90-51927
High-temperature tensile properties of fiber reinforced reaction bonded silicon nitride p 95 A90-52783
Oxidation effects on the mechanical properties of SiC fiber-reinforced reaction-bonded silicon nitride matrix composites p 96 N90-14287
[NASA-TM-102360]
Strength and toughness of monolithic and composite silicon nitrides p 126 N90-14368
[NASA-TM-102423]
Electron-beam induced damage in thin insulating films on compound semiconductors p 151 N90-17987
[NASA-CR-185177]
Matrix density effects on the mechanical properties of SiC/RBSN composites p 100 N90-21826
[NASA-TM-103098]
Theory and experimental technique for nondestructive evaluation of ceramic composites p 207 N90-23754
[NASA-TM-102561]
Influence of interfacial shear strength on the mechanical properties of SiC fiber reinforced reaction-bonded silicon nitride matrix composites p 101 N90-24382
[NASA-TM-102462]
Reliability analysis of a structural ceramic combustion chamber p 223 N90-28112
[NASA-TM-103264]
- SILICON OXIDES**
High frequency capacitance-voltage characteristics of thermally grown SiO₂ films on beta-SiC p 254 A90-21348
Experimentally determined wear behavior of an Al₂O₃-SiC composite from 25 to 1200 C p 87 N90-20130
[NASA-TM-102549]
- SILICON RADIATION DETECTORS**
Modulated-splitting-ratio fiber-optic temperature sensor p 185 A90-11706
- SILOXANES**
Nicalon/siliconoxycarbide ceramic composites p 94 A90-51924
Polysiloxanes derived from the controlled hydrolysis of tetraethoxysilane as precursors to silica for use in ceramic processing p 128 N90-21858
[NASA-TM-102489]
- SILVER OXIDES**
Ellipsometric study of Al₂O₃/Ag/Si and SiO₂/Ag/quartz ashed in an oxygen plasma --- protective coatings to prevent degradation of materials in low earth orbits p 120 A90-18217
- SIMPLIFICATION**
Two-dimensional surface strain measurement based on a variation of Yamaguchi's laser-speckle strain gauge [NASA-TM-103162] p 192 N90-22784
- SIMULATION**
Simulation of three-dimensional viscous flow within a multistage turbine p 5 A90-23841
[ASME PAPER 89-GT-152]
Thermocapillary migration of liquid droplets in a temperature gradient in a density matched system p 177 N90-14512
[NASA-CR-185178]
Technology development program for an advanced microsheet glass concentrator p 229 N90-14678
[NASA-TM-102406]
Computational simulation of damping in composite structures p 219 N90-20432
[NASA-TM-102567]
Aperture taper determination for the half-scale accurate antenna reflector p 153 N90-21822
[NASA-CR-185215]
The role of gravity on macrosegregation in alloys p 136 N90-25238
[NASA-CR-186530]

- Comparison of currents predicted by NASCAP/LEO model simulations with elementary Langmuir-type bare probe models for an insulated cable containing a single pinhole
[NASA-TM-102486] p 51 N90-26054
- SIMULATORS**
Satellite range delay simulator for a matrix-switched time division multiple-access network simulation system
[AIAA PAPER 90-0795] p 139 A90-25620
Satellite-matrix-switched, time-division-multiple-access network simulator
[AIAA PAPER 90-0848] p 147 A90-25671
Satellite-matrix-switched, time-division-multiple-access network simulator
[NASA-TP-2944] p 142 N90-11915
Satellite range delay simulator for a matrix-switched time division multiple-access network simulator
[NASA-TM-102407] p 143 N90-12813
Performance measurements for a laboratory-simulated 30/20 GHz communication satellite transponder
[NASA-TM-102424] p 143 N90-17977
Plasma contactor research, 1989
[NASA-CR-185212] p 252 N90-22389
- SINGLE CHANNEL PER CARRIER TRANSMISSION**
A parallel pipelined architecture for a digital multicarrier demodulator
[AIAA PAPER 90-0812] p 46 A90-25635
A performance analysis of DS-CDMA and SCPC VSAT networks
p 141 A90-39056
- SINGLE CRYSTALS**
An empirical investigation of the InP shallow-homojunction solar cell
p 225 A90-14869
Modeling and simulation of InP homojunction solar cells
p 226 A90-14899
Analysis of gamma prime shape changes in a single crystal Ni-base superalloy
p 109 A90-15206
Biaxial constitutive modelling and testing of a single crystal superalloy at elevated temperatures
p 110 A90-16741
High temperature creep behavior of single crystal gamma prime and gamma alloys
p 110 A90-16901
The unusual near-threshold FCG behavior of a single crystal superalloy and the resolved shear stress as the crack driving force
p 111 A90-21009
On the stability of the creep substructure in NaCl single crystals
p 254 A90-21920
Influence of molybdenum on the creep properties of nickel-base superalloy single crystals
p 113 A90-25233
Experimental evidence of a dimensional crossover in $YBa_2Cu_3O_{7-\delta}$
p 255 A90-29739
Growth of high quality 6H-SiC epitaxial films on vicinal (0001) 6H-SiC wafers
p 255 A90-29952
Creep substructure formation in sodium chloride single crystals in the power law and exponential creep regimes
p 255 A90-33330
The mechanical properties of fluoride salts at elevated temperatures --- candidate thermal energy storage materials for solar dynamic systems
p 123 A90-44376
Fatigue crack propagation behavior of a single crystalline superalloy
p 116 A90-48635
The effect of hydrogen and microstructure on the deformation and fracture behavior of a single crystal nickel-base superalloy
p 118 N90-21849
The fatigue damage behavior of a single crystal superalloy
p 120 N90-28644
- SINTERING**
Densification and coarsening during solid state sintering of ceramics: A review of the models. II - Grain growth
p 120 A90-15375
Synthesis and characterization of high-Tc superconductors in the Ti-Ca-Ba-Cu-O system
p 253 A90-19300
Reactions of SiC with $H_2/H_2O/Ar$ mixtures at 1300 C
p 123 A90-45830
Crystallization behavior and properties of $BaO-Al_2O_3-2SiO_2$ glass matrices
[NASA-CR-185209] p 127 N90-19374
Rapid thermal processing of high temperature superconducting fiber
[NASA-CR-186803] p 259 N90-24964
An analysis of the contact sintering process in III-V solar cells
[NASA-TM-103179] p 233 N90-25420
- SISO (CONTROL SYSTEMS)**
An expert system to perform on-line controller tuning
[NASA-TM-103101] p 240 N90-23991
- SIZE (DIMENSIONS)**
The effect of length and diameter on the resistivity of bromine intercalated graphite fibers
p 122 A90-33332
- SIZE DETERMINATION**
Droplet sizing instrumentation used for icing research: Operation, calibration, and accuracy
[NASA-CR-182293] p 187 N90-11999
- SIZE DISTRIBUTION**
Comparison of drop size distributions from two droplet sizing systems
[NASA-TM-102520] p 202 N90-17147
- SIZING**
Hypersonic aerospace sizing analysis for the preliminary design of aerospace vehicles
p 17 A90-23276
- SKENEWS**
Numerical solution for the velocity-derivative skewness of a low-Reynolds-number decaying Navier-Stokes flow
[NASA-TM-103186] p 184 N90-27985
- SKIN FRICTION**
Skin friction measurements by laser interferometry in swept shock/boundary-layer interactions
p 3 A90-18153
Viscous three-dimensional analyses for nozzles for hypersonic propulsion
[NASA-CR-185197] p 27 N90-17635
- SLIDING**
Friction and wear of oxide-ceramic sliding against IN-718 nickel base alloy at 25 to 800 C in atmospheric air
[NASA-TM-102291] p 124 N90-10262
The experimental evaluation and application of high-temperature solid lubricants
[NASA-TM-102476] p 127 N90-16944
- SLIDING FRICTION**
Decomposition of perfluoroalkylpolyethers (PFPE) in ultra-high vacuum under sliding conditions
p 122 A90-40714
Tribological properties of ceramic/Ti3Al-Nb sliding couples for use as candidate seal materials to 700 deg C
[NASA-TM-102401] p 86 N90-12658
- SLITS**
Numerical simulation of rarefied gas flow through a slit
[AIAA PAPER 90-1694] p 170 A90-38397
- SLURRIES**
Slurry-pressing consolidation of silicon nitride
p 121 A90-27691
- SLURRY PROPELLANTS**
Ignition and combustion characteristics of metallized propellants
[NASA-CR-186870] p 107 N90-26911
- SLUSH**
Slush Hydrogen (SLH2) technology development for application to the National Aerospace Plane (NASP)
[NASA-TM-102315] p 50 N90-14268
FLUSH: A tool for the design of slush hydrogen flow systems
[NASA-TM-102467] p 130 N90-17890
- SLUSH HYDROGEN**
Background, current status, and prognosis of the ongoing slush hydrogen technology development program for the NASP
[NASA-TM-103220] p 51 N90-26055
- SMALL PERTURBATION FLOW**
Absorbing boundary conditions for second-order hyperbolic equations
p 242 A90-34549
- SMOKE DETECTORS**
Fire safety applications for spacecraft
p 16 N90-17595
- SMOOTHING**
A global approach for using kinematic redundancy to minimize base reactions of manipulators
[NASA-CR-186825] p 234 N90-25499
- SODIUM CHLORIDES**
On the stability of the creep substructure in NaCl single crystals
p 254 A90-21920
Creep substructure formation in sodium chloride single crystals in the power law and exponential creep regimes
p 255 A90-33330
- SODIUM SULFATES**
Corrosion of cordierite ceramics by sodium sulphate at 1000 C
p 121 A90-21214
- SODIUM SULFUR BATTERIES**
Sodium-sulfur battery flight experiment definition study
p 57 A90-33956
Sodium-sulfur battery flight experiment definition study
p 231 N90-20479
- SOFTWARE ENGINEERING**
Counterrotating prop-fan simulations which feature a relative-motion multiblock grid decomposition enabling arbitrary time-steps
[AIAA PAPER 90-0687] p 3 A90-19978
Flight software development for the isothermal dendritic growth experiment
p 235 A90-22257
Grid generation for the solution of partial differential equations
p 237 A90-47188
Flight software development for the isothermal dendritic growth experiment
[NASA-TM-102412] p 238 N90-13988
Numerical Arc Segmentation Algorithm for a Radio Conference (NASARC), version 4.0: User's manual
[NASA-TM-101454] p 145 N90-21250
- SOFTWARE TOOLS**
Development of Ada language control software for the NASA power management and distribution test bed
p 236 A90-38082
Evaluation of power control concepts using the PMAD systems test bed --- Power Management and Distribution
p 42 A90-38083
- SOLAR ARRAYS**
Assessment of the effects of space debris and meteoroids environment on the Space Station solar array assembly
p 54 A90-14929
Lunar production of space photovoltaic arrays
p 226 A90-14930
Optimization of silicon 8 cm x 8 cm wrapthrough Space Station cells for 'on orbit' operation
p 54 A90-14941
An advanced space photovoltaic concentrator array using Fresnel lenses, gallium arsenide cells, and prismatic cell covers
p 54 A90-14954
The Space Station photovoltaic panels plasma interaction test program - Test plan and results
[AIAA PAPER 90-0722] p 47 A90-22252
Selection of component modes
[AIAA PAPER 90-1201] p 210 A90-26787
Ion drag for a negatively biased solar array in low earth orbit
p 48 A90-36191
Photovoltaic module on-orbit assembly for Space Station Freedom
p 45 A90-38071
Space Station Freedom photovoltaic power module design status
p 58 A90-38075
Space Station Freedom solar array design development
p 58 A90-38076
Launch packaging options for the PV power module cargo element --- for space station power supplies
p 45 A90-38078
Photovoltaic array environmental protection program --- in Space Station Freedom
p 59 A90-38088
20 kHz main inverter unit --- for space station power supplies
p 148 A90-38124
The mini-dome lens space concentrator array - Recent component test results and current array development status
p 60 A90-38155
Preliminary design of a long-endurance Mars aircraft
[AIAA PAPER 90-2000] p 43 A90-40587
Photovoltaic options for solar electric propulsion
[AIAA PAPER 90-2529] p 68 A90-52563
Applicability of the beamed power concept to lunar rovers, construction, mining, explorers and other mobile equipment
p 69 N90-10159
Central electrical utility power for a satellite ring city in low earth orbit space
p 150 N90-10166
The Space Station Photovoltaic Panels Plasma Interaction Test Program: Test plan and results
[NASA-TM-102474] p 49 N90-13581
NASA advanced space photovoltaic technology: Status, potential and future mission applications
p 74 N90-17775
A transient plasticity study and low cycle fatigue analysis of the Space Station Freedom photovoltaic solar array blanket
[NASA-TM-102516] p 218 N90-19617
Recent results from advanced research on space solar cells at NASA
[NASA-TM-102485] p 152 N90-21274
Preliminary design of a long-endurance Mars aircraft
[NASA-CR-185243] p 30 N90-21763
Photovoltaic power for Space Station Freedom
[NASA-TM-102569] p 78 N90-21812
Analysis of thermal energy storage material with change-of-phase volumetric effects
[NASA-TM-102457] p 181 N90-21974
Space Station Freedom solar array panels plasma interaction test facility
[NASA-TM-102475] p 266 N90-22488
Dynamic analysis of space-related linear and non-linear structures
[NASA-TM-103490] p 51 N90-25174
LEO high voltage solar array arcing response model, continuation 5
[NASA-CR-186505] p 232 N90-25418
Solar array arcing in plasmas
p 233 N90-25558
The chemical effects of the Martian environment on power system component materials: A theoretical approach
[NASA-TM-103203] p 87 N90-26074
Analysis of a Mars-stationary orbiting microwave power transmission system
[NASA-TM-101344] p 138 N90-26172
A solar power system for an early Mars expedition
[NASA-TM-103219] p 246 N90-28393
- SOLAR CELLS**
Issues and opportunities in space photovoltaics
p 54 A90-14852
High efficiency GaAs/Ge monolithic tandem solar cells
p 224 A90-14858
An empirical investigation of the InP shallow-homojunction solar cell
p 225 A90-14869

- A V-grooved GaAs solar cell p 225 A90-14887
 Contact formation in gallium arsenide solar cells p 225 A90-14888
 Hybrid solar cells based on dc magnetron sputtered films of n-ITO on APMOPE grown p-InP p 225 A90-14893
 Predicted performance of near-optimally designed indium phosphide space solar cells at high intensities and temperatures p 225 A90-14898
 Modeling and simulation of InP homojunction solar cells p 226 A90-14899
 Thin, light-trapping silicon solar cells for space p 226 A90-14900
 InP homojunction solar cell performance on the LIPS III flight experiment p 226 A90-14921
 Lunar production of space photovoltaic arrays p 226 A90-14930
 Radiation resistance and comparative performance of ITO/InP and n/p InP homojunction solar cells p 226 A90-14933
 Optimization of silicon 8 cm x 8 cm wrapthrough Space Station cells for 'on orbit' operation p 54 A90-14941
 An advanced space photovoltaic concentrator array using Fresnel lenses, gallium arsenide cells, and prismatic cell covers p 54 A90-14954
 Lunar production of solar cells - A near-term product for a lunar industrial facility p 54 A90-24791
 Solar power for the lunar night p 266 A90-24814
 Wide-bandgap epitaxial heterojunction windows for silicon solar cells p 227 A90-28359
 Indium phosphide solar cells - Recent developments and estimated performance in space p 57 A90-37854
 Comparison of solar photovoltaic and nuclear reactor power systems for a human-tended lunar observatory p 42 A90-38030
 Energy storage and thermal control system design status --- for space station power supplies p 59 A90-38077
 Magnification of starting torques of dc motors by maximum power point trackers in photovoltaic systems p 149 A90-38144
 Thermal annealing of GaAs concentrator solar cells --- during electron irradiation p 60 A90-38150
 Photovoltaic power system operation in the Mars environment p 43 A90-38156
 Estimated performance and future potential of solar dynamic and photovoltaic power systems for selected LEO and HEO missions p 62 A90-38307
 Photovoltaic options for solar electric propulsion [AIAA PAPER 90-2529] p 68 A90-52563
 The photovoltaic properties of an Al In As/InP heterojunctions grown by LPE method [NASA-CR-185996] p 229 N90-13886
 GaAs solar cells with V-grooved emitters p 229 N90-17754
 Indium phosphide solar cell research in the United States: Comparison with non-photovoltaic sources p 229 N90-17758
 NASA advanced space photovoltaic technology: Status, potential and future mission applications p 74 N90-17775
 On-orbit results of the LIPS 3/InP homojunction solar cell experiment p 74 N90-17794
 Recent results from advanced research on space solar cells at NASA [NASA-TM-102485] p 152 N90-21274
 Peeled film GaAs solar cells for space power [NASA-TM-103125] p 153 N90-21287
 Automating security monitoring and analysis for Space Station Freedom's electric power system [NASA-TM-103148] p 240 N90-22324
 Space Station Freedom solar array panels plasma interaction test facility [NASA-TM-102475] p 266 N90-22488
 New directions in InP solar cell research [NASA-TM-103160] p 154 N90-23662
 Solar array arcing in plasmas p 233 N90-25558
 Estimation of minority carrier diffusion lengths in InP/GaAs solar cells [NASA-TM-103213] p 81 N90-26069
- SOLAR COLLECTORS**
 An advanced space photovoltaic concentrator array using Fresnel lenses, gallium arsenide cells, and prismatic cell covers p 54 A90-14954
 Performance of GaAs concentrator cells under electron irradiations from 0.4 to 2.3 MeV p 227 A90-14956
 Selection of component modes [AIAA PAPER 90-1201] p 210 A90-26787
 Effect of eleven years in earth orbit on a mirror surface p 44 A90-36188
 Solar dynamic power module design p 59 A90-38079
 A program for advancing the technology of space concentrators p 60 A90-38159
 A Brayton cycle solar dynamic heat receiver for space p 61 A90-38165
 The cavity heat pipe Stirling receiver for space solar dynamics p 61 A90-38169
- Brayton advanced heat receiver development program p 61 A90-38170
 Update of the Solar Concentrator Advanced Development Project p 48 A90-38267
 Conceptual design study of a 5 kilowatt solar dynamic Brayton power system using a dome Fresnel lens solar concentrator [NASA-CR-185134] p 72 N90-14281
 Technology development program for an advanced microsheet glass concentrator [NASA-TM-102406] p 229 N90-14678
 The effect of leveling coatings on the atomic oxygen durability of solar concentrator surfaces [NASA-TM-102557] p 76 N90-21110
 Recent results from advanced research on space solar cells at NASA [NASA-TM-102485] p 152 N90-21274
 Solar Concentrator Advanced Development Program [NASA-CR-185173] p 232 N90-22834
 Dynamic analysis of space-related linear and non-linear structures [NASA-TM-103490] p 51 N90-25174
 Preliminary designs for 25 kW advanced Stirling conversion systems for dish electric applications [NASA-TM-103188] p 263 N90-26729
- SOLAR DYNAMIC POWER SYSTEMS**
 Thermal energy storage flight experiments p 53 A90-11992
 Space Station Solar Dynamic Module modelling and simulation p 53 A90-11993
 Solar dynamic power for the Space Station p 55 A90-16374
 Structural configuration options for the Space Station Freedom solar dynamic radiator [IAF PAPER ICOSP89-4-5] p 48 A90-27710
 Measurements of print-through in graphite fiber epoxy composites p 91 A90-31555
 Solar dynamic power module design p 59 A90-38079
 A program for advancing the technology of space concentrators p 60 A90-38159
 Concentration of off-axis radiation by solar concentrators for space power p 60 A90-38163
 A Brayton cycle solar dynamic heat receiver for space p 61 A90-38165
 Numerical model of solar dynamic radiator for parametric analysis p 61 A90-38168
 The cavity heat pipe Stirling receiver for space solar dynamics p 61 A90-38169
 Brayton advanced heat receiver development program p 61 A90-38170
 Flight experiment of thermal energy storage --- for spacecraft power systems p 61 A90-38172
 The NASA Advanced Solar Dynamics Technology Program p 62 A90-38280
 Estimated performance and future potential of solar dynamic and photovoltaic power systems for selected LEO and HEO missions p 62 A90-38307
 Conceptual design study of a 5 kilowatt solar dynamic Brayton power system using a dome Fresnel lens solar concentrator [NASA-CR-185134] p 72 N90-14281
 A heat receiver design for solar dynamic space power systems [NASA-TM-102473] p 72 N90-14283
 On protection of Freedom's solar dynamic radiator from the orbital debris environment. Part 1: Preliminary analyses and testing [NASA-TM-102458] p 73 N90-14285
 Technology development program for an advanced microsheet glass concentrator [NASA-TM-102406] p 229 N90-14678
 Hot filament technique for measuring the thermal conductivity of molten lithium fluoride [NASA-TM-102506] p 127 N90-19373
 Mechanical properties of pure nickel alloys after long term exposures to LiOH and vacuum at 775 K [NASA-TM-102403] p 118 N90-20181
 Model development in viscoplastic ratchetting [NASA-TM-102509] p 219 N90-20431
 Photovoltaic power for Space Station Freedom [NASA-TM-102568] p 78 N90-21812
- SOLAR ELECTRIC PROPULSION**
 Photovoltaic options for solar electric propulsion [AIAA PAPER 90-2529] p 68 A90-52563
- SOLAR ENERGY**
 Energy storage for a lunar base by the reversible chemical reaction: $\text{CaO} + \text{H}_2\text{O}$ reversible reaction Ca(OH)_2 [NASA-TM-103145] p 233 N90-25419
 A solar power system for an early Mars expedition [NASA-TM-103219] p 246 N90-28393
- SOLAR ENERGY CONVERSION**
 Space Station Freedom electric power system photovoltaic power module integrated launch package [AIAA PAPER 90-1053] p 48 A90-29281
- Solar dynamic power module design p 59 A90-38079
 A program for advancing the technology of space concentrators p 60 A90-38159
 Comparison of conceptual designs for 25 kW advanced Stirling conversion systems for dish electric applications p 229 A90-38254
 Electric power scheduling: A distributed problem-solving approach [NASA-TM-103149] p 240 N90-22323
- SOLAR GENERATORS**
 Solar dynamic power for the Space Station p 55 A90-16374
 Challenges for future space power systems p 74 N90-17695
 Automating security monitoring and analysis for Space Station Freedom's electric power system [NASA-TM-103148] p 240 N90-22324
 An analysis of space power system masses [NASA-TM-103199] p 80 N90-25184
- SOLAR POWER SATELLITES**
 Solar dynamic power for the Space Station p 55 A90-16374
 Applicability of the beamed power concept to lunar rovers, construction, mining, explorers and other mobile equipment p 69 N90-10159
 Lunar orbiting microwave beam power system [NASA-TM-103211] p 51 N90-25173
- SOLAR RADIATION**
 Photovoltaic power system operation in the Mars environment p 43 A90-38156
- SOLAR SYSTEM**
 Human exploration mission studies p 40 N90-20457
- SOLAR-PUMPED LASERS**
 Free-Space Power Transmission [NASA-CP-10016] p 77 N90-21795
- SOLID ELECTRODES**
 Oxygen electrodes for rechargeable alkaline fuel cells. II. Structural comparison of nickel electrodes and precursor phases p 228 A90-33946
 The effect of electrode configuration on arcjet performance [NASA-TM-102346] p 70 N90-11081
- SOLID ELECTROLYTES**
 Hydrogen-oxygen proton-exchange membrane fuel cells and electrolyzers p 230 N90-20467
- SOLID LUBRICANTS**
 The experimental evaluation and application of high-temperature solid lubricants [NASA-TM-102476] p 127 N90-16944
- SOLID MECHANICS**
 An accurate analytic approximation to the non-linear change in volume of solids with applied pressure p 261 A90-27612
 Free-vibration analysis of three-dimensional solids by BEM p 215 A90-52007
- SOLID PROPELLANT COMBUSTION**
 Near-limit flame spread over a thin solid fuel in microgravity p 104 A90-32835
- SOLID SOLUTIONS**
 Solid state processing for high temperature alloys and composites p 196 A90-33225
- SOLID STATE**
 Densification and coarsening during solid state sintering of ceramics: A review of the models. II - Grain growth p 120 A90-15375
 Contact spreading and the Au3In-to-Au9In4 transition in the Au-InP system p 257 A90-48661
- SOLID STATE PHYSICS**
 Superconducting ceramics in the Bi1.5SrCaCu2O sub x system by melt quenching technique [NASA-CR-185139] p 258 N90-11606
- SOLID SURFACES**
 Fundamentals of tribology at the atomic level p 192 A90-14020
 A numerical study of the interaction between unsteady free-stream disturbances and localized variations in surface geometry p 161 A90-21422
- SOLID-SOLID INTERFACES**
 Measurement of interfacial shear strength in SiC-fiber/Si3N4 composites p 87 A90-13237
 Characterization of interfacial failure in SiC reinforced Si3N4 matrix composite material by both fiber push-out testing and Auger electron spectroscopy p 91 A90-36802
 Humidity-induced room-temperature decomposition of Au contacted indium phosphide p 105 A90-44689
 Interface properties of various passivations of HgCdTe p 251 A90-45947
 Contact spreading and the Au3In-to-Au9In4 transition in the Au-InP system p 257 A90-48661
 Interfacial effects on the behavior of partially bonded metal matrix composite properties p 93 A90-50094
 Compatibility of Fe-40Al with various fibers p 94 A90-50496

SUBJECT INDEX

SOLIDIFICATION

- The modelling of heat, mass and solute transport in solidification systems p 157 A90-13092
- Effects of crucible wetting during solidification of immiscible Pb-Zn alloys p 132 A90-17825
- Efficient estimation of diffusion during dendritic solidification p 111 A90-20612
- The role of gravity on macrosegregation in alloys [NASA-CR-186530] p 136 N90-25238

SOLUTES

- Solute redistribution in dendritic solidification with diffusion in the solid p 253 A90-17399

SOOT

- Kinetics and mechanism of soot formation in hydrocarbon combustion [NASA-CR-186162] p 106 N90-14305

SORET COEFFICIENT

- Parallel flows with Soret effect in tilted cylinders p 167 A90-25594

SOUND FIELDS

- Microgravity acoustic mixing for particle cloud combustors [NASA-CR-185159] p 248 N90-21600
- The radiation of sound from a propeller at angle of attack [NASA-CR-4264] p 249 N90-21602

SOUND GENERATORS

- Theoretical model of discrete tone generation by impinging jets p 247 A90-35903
- Acousto-ultrasonic nondestructive evaluation of materials using laser beam generation and detection [NASA-CR-186894] p 154 N90-23664

SOUND PRESSURE

- The radiation of sound from a propeller at angle of attack [NASA-CR-4264] p 249 N90-21602

SOUND WAVES

- Theoretical model of discrete tone generation by impinging jets p 247 A90-35903
- Gear noise, vibration, and diagnostic studies at NASA Lewis Research Center [NASA-TM-102435] p 202 N90-18041
- Combustion instability coupling with feed system acoustics p 108 N90-28629

SPACE COMMUNICATION

- An evolutionary communications scenario for Mars exploration [AAS PAPER 87-268] p 139 A90-16566

SPACE DEBRIS

- Assessment of the effects of space debris and meteoroids environment on the Space Station solar array assembly p 54 A90-14929
- On protection of Freedom's solar dynamic radiator from the orbital debris environment. Part 1: Preliminary analyses and testing [NASA-TM-102458] p 73 N90-14285

SPACE ENVIRONMENT SIMULATION

- Plasma contactor modeling with NASCAP/LEO - Extending laboratory results to space systems [AIAA PAPER 90-0726] p 251 A90-22255
- Droplet combustion experiment drop tower tests using models of the space flight apparatus [NASA-TM-101472] p 133 N90-11196

SPACE EXPLORATION

- Issues and opportunities in space photovoltaics p 54 A90-14852
- An evolutionary communications scenario for Mars exploration [AAS PAPER 87-268] p 139 A90-16566
- The SP-100 space reactor as a power source for Mars exploration missions [AAS PAPER 87-224] p 55 A90-16689
- Human exploration mission studies p 39 A90-33935
- Engine selection for the Space Exploration Initiative [AIAA PAPER 90-1880] p 65 A90-47201
- Human exploration mission studies p 40 N90-20457
- Romans to Mars [NASA-TM-103094] p 267 N90-23339
- The lessons of Varsovia's reconnaissance [NASA-TM-103207] p 267 N90-26789
- Nuclear power systems for lunar and Mars exploration [NASA-TM-103168] p 82 N90-26873
- A technology assessment of alternative communications systems for the space exploration initiative [NASA-TM-103243] p 47 N90-27736

SPACE FLIGHT

- Conceptual design of a Liquid Droplet Radiator space flight experiment [SAE PAPER 891565] p 48 A90-27527
- Design considerations for space flight hardware [NASA-TM-102300] p 52 N90-14275
- Extraterrestrial life in the universe [NASA-TM-102363] p 264 N90-22464

SPACE LABORATORIES

- User needs, benefits, and integration of robotic systems in a space station laboratory [NASA-CR-185150] p 200 N90-13794

SPACE MANUFACTURING

- Lunar production of solar cells - A near-term product for a lunar industrial facility p 42 A90-24791
- Degradation of the lunar vacuum by a moon base p 266 A90-35441

SPACE MISSIONS

- Space nuclear reactor shields for manned and unmanned applications p 57 A90-37859
- Nuclear technology and the space exploration missions [NASA-TM-103156] p 232 N90-22847
- Romans to Mars [NASA-TM-103094] p 267 N90-23339
- Liquid lubrication in space [NASA-RP-1240] p 205 N90-28063

SPACE PLASMAS

- Plasma contactor modeling with NASCAP/LEO - Extending laboratory results to space systems [AIAA PAPER 90-0726] p 251 A90-22255
- Spacelab 2 Plasma Diagnostics Package p 39 A90-23263
- The sheath structure around a negatively charged rocket payload p 48 A90-34780
- Plasma contactor research, 1989 [NASA-CR-185212] p 252 N90-22389
- Space Station Freedom solar array panels plasma interaction test facility [NASA-TM-102475] p 266 N90-22488
- Plasma interactions and effects for large systems p 232 N90-25545
- Solar array arcing in plasmas p 233 N90-25558

SPACE PLATFORMS

- Advanced propulsion for LEO and GEO platforms [AIAA PAPER 90-2551] p 68 A90-52565
- Advanced propulsion for LEO and GEO platforms [NASA-TM-103228] p 82 N90-27785

SPACE POWER REACTORS

- Photovoltaic power for a lunar base [IAF PAPER 89-254] p 42 A90-13409
- The SP-100 space reactor as a power source for Mars exploration missions [AAS PAPER 87-224] p 55 A90-16689
- EPSAT - A workbook for designing high-power systems for the space environment [AIAA PAPER 90-0637] p 245 A90-26975
- Comparison of solar photovoltaic and nuclear reactor power systems for a human-tended lunar observatory p 42 A90-38030
- Advanced radiator concepts --- for nuclear powered spacecraft p 170 A90-38042
- SP-100 advanced radiator designs for thermoelectric and Stirling applications p 62 A90-38202
- Multi-reactor configurations for multi-megawatt spacecraft power supplies [AIAA PAPER 90-2111] p 66 A90-47207
- A feasibility assessment of installation, operation and disposal options for nuclear reactor power system concepts for a NASA growth space station [NASA-TM-89923] p 70 N90-10174
- Creep strength of niobium alloys, Nb-1%Zr and PWC-11 [NASA-TM-102390] p 116 N90-11854
- Electrical performance characteristics of high power converters for space power applications [NASA-CR-185947] p 72 N90-14279
- Scaling study for SP-100 reactor technology [NASA-TM-897140] p 249 N90-16496
- Nuclear technology and the space exploration missions [NASA-TM-103156] p 232 N90-22847
- High-temperature superconductors for space power transmission lines [NASA-TM-103459] p 259 N90-24952
- The effects of atomic oxygen on the thermal emittance of high temperature radiator surfaces [NASA-TM-103224] p 102 N90-28670

SPACE POWER UNIT REACTORS

- CSTI high capacity power --- Civil Space Technology Initiative p 61 A90-38196
- SP-100 power system conceptual design for lunar base applications [NASA-TM-102090] p 267 N90-15030

SPACE PROBES

- Optics and materials considerations for a laser-propelled lightsail [IAF PAPER 89-664] p 54 A90-13668

SPACE PROCESSING

- Effects of crucible wetting during solidification of immiscible Pb-Zn alloys p 132 A90-17825
- Free float acceleration measurements aboard NASA's KC-135 Microgravity Research Aircraft [AIAA PAPER 90-0742] p 132 A90-20000

SPACE SHUTTLE MISSIONS

Modeling of collision and coalescence of droplets during microgravity processing of Zn-Bi immiscible alloys p 132 A90-22878

Coupled effects of conduction in the crystal and thermo-solutal convection in a rectangular inclined enclosure [AIAA PAPER 90-0408] p 133 A90-25031

Convection phenomena in low-gravity processing - The GTE GaAs space experiment [AIAA PAPER 90-0409] p 133 A90-25032

SPACE PROGRAMS

- The International Space University [AIAA PAPER 90-2389] p 261 A90-42152
- The International Space University [NASA-TM-103163] p 78 N90-22604
- Technical accomplishments of the NASA Lewis Research Center, 1989 [NASA-TM-102296] p 267 N90-24220

SPACE RENDEZVOUS

- Optimal cooperative time-fixed impulsive rendezvous [AIAA PAPER 90-2962] p 41 A90-53037

SPACE SHUTTLE MAIN ENGINE

- Heat flux measurements [ASME PAPER 89-GT-107] p 165 A90-23815
- Probabilistic structural analysis methods of hot engine structures [ASME PAPER 89-GT-122] p 56 A90-23821
- Application of HOST technology to the SSME HPFTP blade [ASME PAPER 89-GT-130] p 209 A90-23828
- Application of the probabilistic approximate analysis method to a turbopump blade analysis --- for Space Shuttle Main Engine [AIAA PAPER 90-1098] p 56 A90-29328
- Health monitoring system for the SSME - Program overview [AIAA PAPER 90-1987] p 63 A90-40583
- Health Monitoring System for the SSME-fault detection algorithms [AIAA PAPER 90-1988] p 63 A90-40584
- Analysis and design of helium-buffered face seals for the SSME high-pressure oxygen turbopump [AIAA PAPER 90-2049] p 197 A90-42000
- Health monitoring system for the SSME - Hardware architecture study [AIAA PAPER 90-1989] p 65 A90-42713
- The simulation of fluid dynamic uncertainties in the SSME turbopump [AIAA PAPER 90-2294] p 65 A90-42770
- Rocket combustion chamber life-enhancing design concepts [AIAA PAPER 90-2116] p 66 A90-47208
- Numerical analysis of secondary flow in a two-stage turbine [AIAA PAPER 90-2356] p 66 A90-47216
- Digital filtering of plume emission spectra [AIAA PAPER 90-1994] p 67 A90-50643
- Multi-sensor analysis techniques for SSME safety monitoring [AIAA PAPER 90-1990] p 45 A90-52499
- Framework for a space shuttle main engine health monitoring system [NASA-CR-185224] p 78 N90-21809
- Heat transfer and pressure measurements for the SSME fuel-side turbopump [NASA-CR-184928] p 31 N90-23405
- Health management system for rocket engines [NASA-CR-185223] p 131 N90-23574
- Rocket combustion chamber life-enhancing design concepts [NASA-CR-185257] p 79 N90-25183
- Digital filtering of plume emission spectra [NASA-TM-103135] p 81 N90-26070
- Reusable rocket engine turbopump health monitoring system, part 3 [NASA-CR-182294] p 204 N90-26320
- Multi-sensor analysis techniques for SSME safety monitoring [NASA-CR-185260] p 45 N90-27732
- Probabilistic structural analysis methods development for SSME p 83 N90-28616
- Bearing optimization for SSME HPOTP application p 205 N90-28622
- Structural response of SSME turbine blade airfoils p 224 N90-28649
- A failure diagnosis system based on a neural network classifier for the space shuttle main engine [NASA-TM-103607] p 83 N90-28659

SPACE SHUTTLE MISSIONS

- Launching a dream: A teachers guide to a simulated space shuttle mission [NASA-TM-89715] p 261 N90-26693

SPACE SHUTTLE ORBITERS

Conceptual design of a moving belt radiator shuttle-attached experiments: Technical requirement Document
[NASA-CR-185168] p 73 N90-15996

SPACE SHUTTLE PAYLOADS

Flight software development for the isothermal dendritic growth experiment
[AIAA PAPER 90-0744] p 235 A90-22257
Conceptual design of liquid droplet radiator shuttle-attached experiment
[NASA-CR-185164] p 71 N90-11805
Flight software development for the isothermal dendritic growth experiment
[NASA-TM-102412] p 238 N90-13988
Development of an infrared imaging system for the surface tension driven convection experiment
p 188 N90-17922
Spacelab qualified infrared imager for microgravity science experiments
[NASA-TM-102503] p 189 N90-20352

SPACE SHUTTLES

Nonintrusive inertial vibration isolation technology for microgravity space experiments
[AIAA PAPER 90-0741] p 132 A90-19999
Low frequency vibration isolation technology for microgravity space experiments
p 136 A90-46246
Nonintrusive inertial vibration isolation technology for microgravity space experiments
[NASA-TM-102386] p 137 N90-11901
Tank pressure control experiment on the space shuttle
[NASA-TM-102313] p 71 N90-13590
Development and approach to low-frequency microgravity isolation systems
[NASA-TP-2984] p 138 N90-28754

SPACE STATION PAYLOADS

Conceptual design of a Liquid Droplet Radiator space flight experiment
[SAE PAPER 891565] p 48 A90-27527
Facilities for microgravity combustion research
[NASA-TM-102014] p 134 N90-13679

SPACE STATION POLAR PLATFORMS

Space Station Freedom solar array panels plasma interaction test facility
[NASA-TM-102475] p 266 N90-22488

SPACE STATION POWER SUPPLIES

Space Station power system autonomy demonstration
p 245 A90-10373
Space Station Solar Dynamic Module modelling and simulation
p 53 A90-11993
Space Station Freedom power management and distribution system design
[IAF PAPER 89-078] p 54 A90-13295
Solar dynamic power for the Space Station
p 55 A90-16374
Power considerations for an early manned Mars mission utilizing the Space Station
[AAS PAPER 87-223] p 55 A90-16688
The Space Station photovoltaic panels plasma interaction test program - Test plan and results
[AIAA PAPER 90-0722] p 47 A90-22252
Structural configuration options for the Space Station Freedom solar dynamic radiator
[IAF PAPER ICOSP89-4-5] p 48 A90-27710
Space Station Freedom electric power system photovoltaic power module integrated launch package
[AIAA PAPER 90-1053] p 48 A90-29281
Design of the Space Station Freedom power system
p 57 A90-38070

Evolutionary growth for Space Station Freedom electrical power system
p 58 A90-38072

Space Station Freedom electrical power system hardware commonality with the United States Polar Platform
p 58 A90-38073

Space Station Freedom power - A reliability, availability, and maintainability assessment of the proposed Space Station Freedom electric power system
p 58 A90-38074

Space Station Freedom photovoltaic power module design status
p 58 A90-38075

Space Station Freedom solar array design development
p 58 A90-38076

Energy storage and thermal control system design status --- for space station power supplies
p 59 A90-38077

Solar dynamic power module design
p 59 A90-38079

Space Station Freedom power management and distribution design status
p 59 A90-38080

Development and refinement of test bed simulations --- for space station power supplies
p 59 A90-38081
Development of Ada language control software for the NASA power management and distribution test bed
p 236 A90-38082

Evaluation of power control concepts using the PMAD systems test bed --- Power Management and Distribution
p 42 A90-38083

Photovoltaic array environmental protection program --- in Space Station Freedom
p 59 A90-38088

The effects of nonlinear loading upon the Space Station Freedom 20 kHz power system
p 60 A90-38118

20 kHz main inverter unit --- for space station power supplies
p 148 A90-38124

Performance testing of a high frequency link converter for Space Station power distribution system
p 148 A90-38128

Power transmission cable development for the Space Station Freedom electrical power system
p 149 A90-38134

Concentration of off-axis radiation by solar concentrators for space power
p 60 A90-38163

A Brayton cycle solar dynamic heat receiver for space
p 61 A90-38165

Numerical model of solar dynamic radiator for parametric analysis
p 61 A90-38168

The cavity heat pipe Stirling receiver for space solar dynamics
p 61 A90-38169

Brayton advanced heat receiver development program
p 61 A90-38170

20 kHz, 25 kVA node power transformer
p 149 A90-38275

High-frequency ac power distribution in Space Station
p 63 A90-39111

Advanced refractory metals and composites for extraterrestrial power systems
p 40 A90-48819

A feasibility assessment of installation, operation and disposal options for nuclear reactor power system concepts for a NASA growth space station
[NASA-TM-89923] p 70 N90-10174

Bidirectional power converter control electronics
[NASA-CR-175070] p 70 N90-10175

The Space Station Photovoltaic Panels Plasma Interaction Test Program: Test plan and results
[NASA-TM-102474] p 49 N90-13581

The US space station and its electric power system
[NASA-TM-101974] p 71 N90-13596

Modeling of power electronic systems with EMTF
[NASA-TM-102375] p 245 N90-14060

Space Station Freedom electric power system availability study
[NASA-CR-185181] p 50 N90-20120

Model development in viscoplastic ratcheting
[NASA-TM-102509] p 219 N90-20431

Photovoltaic power for Space Station Freedom
[NASA-TM-102569] p 78 N90-21812

Electric power scheduling: A distributed problem-solving approach
[NASA-TM-103149] p 240 N90-22323

Space Station Freedom solar array panels plasma interaction test facility
[NASA-TM-102475] p 266 N90-22488

Automated electric power management and control for Space Station Freedom
[NASA-TM-103151] p 240 N90-23125

SPACE STATION PROPULSION

Space Station Freedom resistojet system study
p 54 A90-16368

Calculations of gaseous H₂/O₂ thruster
[AIAA PAPER 90-2490] p 67 A90-47224

SPACE STATION STRUCTURES

Space Station Freedom photovoltaic power module design status
p 58 A90-38075

Solar dynamic power module design
p 59 A90-38079

Assessment of the effects of space debris and meteoroids environment on the Space Station solar array assembly
p 54 A90-14929

Optimization of silicon 8 cm x 8 cm wrapthrough Space Station cells for 'on orbit' operation
p 54 A90-14941

Modal selection in structural dynamics
p 209 A90-17001

Comparative thermal analysis of the Space Station Freedom photovoltaic deployable boom structure using TRASYS, NEVADA, and SINDA programs
[SAE PAPER 891563] p 47 A90-27525

Photovoltaic module on-orbit assembly for Space Station Freedom
p 45 A90-38071

Evolutionary space station fluids management strategies
[NASA-CR-185137] p 49 N90-10983

Advanced spacecraft fire safety: Proposed projects and program plan
[NASA-CR-185147] p 49 N90-12645

User needs, benefits, and integration of robotic systems in a space station laboratory
[NASA-CR-185150] p 200 N90-13794

Conceptual design for the space station Freedom modular combustion facility
[NASA-TM-102037] p 134 N90-16087

Preliminary evaluation of space station transmission line in a ring configuration
[NASA-TM-102461] p 74 N90-17677

A transient plasticity study and low cycle fatigue analysis of the Space Station Freedom photovoltaic solar array blanket
[NASA-TM-102516] p 218 N90-19617

Aerospace induction motor actuators driven from a 20-kHz power link
[NASA-TM-102482] p 28 N90-20085

Space Station Freedom electric power system availability study
[NASA-TM-185181] p 50 N90-20120

Detection of potential space station control/structure interaction with CO-ST-IN
p 50 N90-21074

Photovoltaic power for Space Station Freedom
[NASA-TM-102569] p 78 N90-21812

Automating security monitoring and analysis for Space Station Freedom's electric power system
[NASA-TM-103148] p 240 N90-22324

An expert system for simulating electric loads aboard Space Station Freedom
[NASA-TM-103150] p 240 N90-22325

Conceptual definition of a high voltage power supply test facility
[NASA-CR-185216] p 50 N90-25172

Dynamic analysis of space-related linear and non-linear structures
[NASA-TM-103490] p 51 N90-25174

An analysis of space power system masses
[NASA-TM-103199] p 80 N90-25184

Autonomous power expert system
[NASA-CR-185263] p 80 N90-25187

Autonomous power expert fault diagnostic system for Space Station Freedom electrical power system testbed
p 80 N90-25521

Plasma interactions and effects for large systems
p 252 N90-25545

National space test centers, Lewis research center facilities
[NASA-TM-103187] p 44 N90-26030

Two-dimensional model of a Space Station Freedom thermal energy storage canister
[NASA-TM-103124] p 183 N90-26279

Development and approach to low-frequency microgravity isolation systems
[NASA-TP-2984] p 138 N90-28754

SPACE STORAGE

Evolutionary space station fluids management strategies
[NASA-CR-185137] p 49 N90-10983

A superconducting quenchgun for delivering lunar derived oxygen to lunar orbit
[AIAA PAPER 90-2369] p 43 A90-40627

SPACE TRANSPORTATION SYSTEM
Launch packaging options for the PV power module cargo element --- for space station power supplies
p 45 A90-38078

Conceptual design of a Moving Belt Radiator (MBR) shuttle-attached experiment
[NASA-CR-185169] p 79 N90-23474

SPACEBORNE EXPERIMENTS
COLD-SAT - An orbital cryogenic hydrogen technology experiment
[IAF PAPER 89-057] p 53 A90-13282

Nonintrusive inertial vibration isolation technology for microgravity space experiments
[AIAA PAPER 90-0741] p 132 A90-19999

Hydrogen-oxygen proton-exchange membrane fuel cells and electrolyzers
p 56 A90-33944

Sodium-sulfur battery flight experiment definition study
p 57 A90-33956

Hardware development for the surface tension driven convection experiment
p 52 A90-36195

Flight experiment of thermal energy storage --- for spacecraft power systems
p 61 A90-38172

Spacecraft attitude impacts on COLD-SAT non-vacuum jacketed LH₂ supply tank thermal performance
[AIAA PAPER 90-1672] p 49 A90-41566

Droplet combustion experiment drop tower tests using models of the space flight apparatus
[NASA-TM-101472] p 133 N90-11196

SUBJECT INDEX

- Nonintrusive inertial vibration isolation technology for microgravity space experiments
[NASA-TM-102386] p 137 N90-11901
- Design considerations for space flight hardware
[NASA-TM-102300] p 52 N90-14275
- Critical fluid light scattering p 251 N90-17087
- Development of an infrared imaging system for the surface tension driven convection experiment
p 188 N90-17922
- A new approach to active vibration isolation for microgravity space experiments
[NASA-TM-102470] p 137 N90-17929
- Investigation of methods to produce a uniform cloud of fuel particles in a flame tube
[NASA-TM-102376] p 178 N90-18665
- An expert system for simulating electric loads aboard Space Station Freedom
[NASA-TM-103150] p 240 N90-22325
- Development and approach to low-frequency microgravity isolation systems
[NASA-TP-2984] p 138 N90-28754
- Design of a CO₂ laser power control system for a Spacelab microgravity experiment
[NASA-TM-103112] p 192 N90-28833
- ### SPACECRAFT CHARGING
- High-voltage plasma interactions calculations using NASCAP/LEO
[AIAA PAPER 90-0725] p 251 A90-22254
- The sheath structure around a negatively charged rocket payload
p 48 A90-34780
- Plasma sources for spacecraft neutralization
[AIAA PAPER 90-1556] p 49 A90-38697
- Plasma interactions and effects for large systems
p 252 N90-25545
- Comparison of currents predicted by NASCAP/LEO model simulations with elementary Langmuir-type bare probe models for an insulated cable containing a single pinhole
[NASA-TM-102486] p 51 N90-26054
- ### SPACECRAFT COMMUNICATION
- High-speed analog fiber optic links for satellite communication
p 46 A90-11822
- Effects of amplitude distortions and IF equalization on satellite communication system bit-error rate performance
[NASA-TM-102415] p 144 N90-19454
- ### SPACECRAFT COMPONENTS
- Materials for engine applications above 3000 deg F: An overview
[NASA-TM-100169] p 95 N90-10188
- Plasma interactions and effects for large systems
p 252 N90-25545
- ### SPACECRAFT CONSTRUCTION MATERIALS
- Up-and-coming IMCs --- Intermetallic-Matrix Composites
p 88 A90-17295
- The possibility of a reversal of material flammability ranking from normal gravity to microgravity
p 105 A90-42298
- Advanced refractory metals and composites for extraterrestrial power systems
p 40 A90-48819
- Ultrasonic and radiographic evaluation of advanced aerospace materials: Ceramic composites
[NASA-TM-102540] p 207 N90-21401
- Plasma interactions and effects for large systems
p 252 N90-25545
- ### SPACECRAFT DESIGN
- Space Station Freedom power management and distribution system design
[IAF PAPER 89-078] p 54 A90-13295
- The SP-100 space reactor as a power source for Mars exploration missions
[AAS PAPER 87-224] p 55 A90-16689
- On-orbit low gravity cryogenic scientific investigations using the COLD-SAT Satellite
[AIAA PAPER 90-0718] p 39 A90-19988
- Hypersonic aerospace sizing analysis for the preliminary design of aerospace vehicles
p 17 A90-23276
- Spacecraft designs for VSAT networks
[AIAA PAPER 90-0895] p 140 A90-25681
- Evolutionary growth for Space Station Freedom electrical power system
p 58 A90-38072
- Solar dynamic power module design
p 59 A90-38079
- Numerical model of solar dynamic radiator for parametric analysis
p 61 A90-38168
- Design considerations for space flight hardware
[NASA-TM-102300] p 52 N90-14275
- The Gevaltig: An inertial fusion powered manned spacecraft design for outer solar system missions
[NASA-CR-185163] p 50 N90-15985
- Structural dynamics branch research and accomplishments
[NASA-TM-102488] p 223 N90-26373

SPACECRAFT ELECTRONIC EQUIPMENT

- Applications of high thermal conductivity composites to electronics and spacecraft thermal design
[AIAA PAPER 90-0783] p 89 A90-25609
- ### SPACECRAFT INSTRUMENTS
- Microgravity noncontact temperature requirements at NASA Lewis Research Center
p 134 N90-17897
- ### SPACECRAFT LAUNCHING
- Advanced Launch System (ALS) actuation and power systems impact operability and cost
p 69 A90-52955
- Advanced Launch System (ALS): Electrical actuation and power systems improve operability and cost picture
[NASA-TM-102547] p 152 N90-21271
- ### SPACECRAFT LUBRICATION
- Modification of the SHABERTH bearing code to incorporate RP-1 and a discussion of the traction model
[NASA-TP-3017] p 205 N90-28066
- ### SPACECRAFT POWER SUPPLIES
- Thermal energy storage flight experiments
p 53 A90-11992
- Issues and opportunities in space photovoltaics
p 54 A90-14852
- Thin, light-trapping silicon solar cells for space
p 226 A90-14900
- InP homojunction solar cell performance on the LIPS III flight experiment
p 226 A90-14921
- An advanced space photovoltaic concentrator array using Fresnel lenses, gallium arsenide cells, and prismatic cell covers
p 54 A90-14954
- Performance of GaAs concentrator cells under electron irradiations from 0.4 to 2.3 MeV
p 227 A90-14956
- The SP-100 space reactor as a power source for Mars exploration missions
[AIAA PAPER 87-224] p 55 A90-16689
- The fuel cell in space - Yesterday, today and tomorrow
p 56 A90-26837
- Space Electrochemical Research and Technology Conference, 2nd, Cleveland, OH, Apr. 11-13, 1989, Proceedings
p 227 A90-33932
- Characterization testing of a 40 ampere hour bipolar nickel-hydrogen battery
p 56 A90-33940
- Hydrogen-oxygen proton-exchange membrane fuel cells and electrolyzers
p 56 A90-33944
- Electrocatalysis for oxygen electrodes in fuel cells and water electrolyzers for space applications
p 57 A90-33945
- Nickel-hydrogen capacity loss on storage
p 57 A90-33955
- Sodium-sulfur battery flight experiment definition study
p 57 A90-33956
- A 2.5 kW cascaded Schwarz converter for 20 kHz power distribution
p 147 A90-36913
- Indium phosphide solar cells - Recent developments and estimated performance in space
p 57 A90-37854
- Launch packaging options for the PV power module cargo element --- for space station power supplies
p 45 A90-38078
- Frequency domain model for analysis of paralleled, series-output-connected Mapham inverters
p 148 A90-38084
- The Environment-Power System Analysis Tool development program --- for spacecraft power supplies
p 236 A90-38089
- Orbit to surface beamed power for Mars bases expansion
p 40 A90-38105
- Mathematical optimization of photovoltaic converters for diode lasers --- for spacecraft power supplies
p 228 A90-38110
- Development and testing of a 20 kHz component test bed --- for space station power supplies
p 43 A90-38126
- Thermal annealing of GaAs concentrator solar cells --- during electron irradiation
p 60 A90-38150
- A program for advancing the technology of space concentrators
p 60 A90-38159
- Results from baseline tests of the SPRE I and comparison with code model predictions
p 62 A90-38249
- Comparison of conceptual designs for 25 kW advanced Stirling conversion systems for dish electric applications
p 229 A90-38254
- The NASA Advanced Solar Dynamics Technology Program
p 62 A90-38280
- Bipolar nickel-hydrogen battery development - A program review
p 62 A90-38288
- Refractory metal alloys and composites for space power systems
p 116 A90-46677
- Multi-reactor configurations for multi-megawatt spacecraft power supplies
[AIAA PAPER 90-2111] p 66 A90-47207
- Advanced refractory metals and composites for extraterrestrial power systems
p 40 A90-48819
- Overview of microwave concepts
p 142 N90-10155
- Central electrical utility power for a satellite ring city in low earth orbit space
p 150 N90-10166

SPACECRAFT PROPULSION

- The fuel cell in space: Yesterday, today and tomorrow
[NASA-TM-102366] p 70 N90-11804
- Electrical performance characteristics of high power converters for space power applications
[NASA-CR-185947] p 72 N90-14279
- A heat receiver design for solar dynamic space power systems
[NASA-TM-102473] p 72 N90-14283
- Conceptual design of a moving belt radiator shuttle-attached experiments: Technical requirement Document
[NASA-CR-185168] p 73 N90-15996
- Toward an electrical power utility for space exploration
p 74 N90-17681
- Challenges for future space power systems
p 74 N90-17695
- Hot filament technique for measuring the thermal conductivity of molten lithium fluoride
[NASA-TM-102506] p 127 N90-19373
- High power, high frequency component test facility
[NASA-TM-102500] p 151 N90-19484
- Space Electrochemical Research and Technology (SERT), 1989
p 230 N90-20454
- Sodium-sulfur battery flight experiment definition study
p 231 N90-20479
- A comparative study of electric power distribution systems for spacecraft
[NASA-CR-186531] p 77 N90-21113
- Recent Stirling engine loss-understanding results
[NASA-TM-103122] p 77 N90-21114
- Recent results from advanced research on space solar cells at NASA
[NASA-TM-102485] p 152 N90-21274
- Peeled film GaAs solar cells for space power
[NASA-TM-103125] p 153 N90-21287
- Effect of LEO cycling on 125 Ah advanced design IPV nickel-hydrogen battery cells
[NASA-TM-103128] p 78 N90-21808
- Automating security monitoring and analysis for Space Station Freedom's electric power system
[NASA-TM-103148] p 240 N90-22324
- Programmatic status of NASA's CSTI high capacity power Stirling space power converter program
[NASA-TM-103142] p 79 N90-22606
- Technical accomplishments of the NASA Lewis Research Center, 1989
[NASA-TM-102296] p 267 N90-24220
- Conceptual definition of a high voltage power supply test facility
[NASA-CR-185216] p 50 N90-25172
- An analysis of space power system masses
[NASA-TM-103199] p 80 N90-25184
- Autonomous power expert fault diagnostic system for Space Station Freedom electrical power system testbed
p 80 N90-25521
- The chemical effects of the Martian environment on power system component materials: A theoretical approach
[NASA-TM-103203] p 87 N90-26074
- NASA aerospace flight battery systems program
[NASA-TM-103237] p 233 N90-26397
- Nuclear power systems for lunar and Mars exploration
[NASA-TM-103168] p 82 N90-26873
- Electrical characterization of a Mapham inverter using pulse testing techniques
[NASA-TM-103254] p 82 N90-27784
- ### SPACECRAFT PROPULSION
- Xenon ion sources for space applications
p 56 A90-22874
- Experiments on a repetitively pulsed electrothermal thruster
p 56 A90-27960
- Space vehicle propulsion systems - Environmental space hazards
[AIAA PAPER 90-1881] p 63 A90-40545
- End-hall thrusters
[AIAA PAPER 90-2595] p 64 A90-42570
- Diagnostic evaluations of microwave generated helium and nitrogen plasma mixtures
[AIAA PAPER 90-2634] p 252 A90-42602
- Minimum fuel lunar trajectories for a low-thrust power-limited spacecraft
[AIAA PAPER 90-2975] p 41 A90-53054
- Overview of microwave concepts
p 142 N90-10155
- Microwave beam power
p 69 N90-10165
- The effect of electrode configuration on arcjet performance
[NASA-TM-102346] p 70 N90-11081
- Thin-film sensors for reusable space propulsion systems
[NASA-TM-102383] p 71 N90-13595
- Design of a thrust stand for high power electric propulsion devices
[NASA-TM-102372] p 73 N90-15992
- The Pathfinder chemical transfer propulsion program
p 74 N90-18471

- Advanced APS impacts on vehicle payloads
p 75 N90-18472
- Electric propulsion options for 10 kW class earth-space missions
p 75 N90-18474
- Test facility and preliminary performance of a 100 kW class MPD thruster
p 75 N90-18476
- Advanced launch vehicle propulsion at the NASA Lewis Research Center
[NASA-TM-103096] p 45 N90-20110
- A radiological assessment of nuclear power and propulsion operations near Space Station Freedom
[NASA-CR-185185] p 76 N90-21108
- National space test centers, Lewis research center facilities
[NASA-TM-103187] p 44 N90-26030
- Low power arcjet performance
[NASA-TM-103280] p 83 N90-28657
- SPACECRAFT RADIATORS**
- Conceptual design of a Liquid Droplet Radiator space flight experiment
[SAE PAPER 891565] p 48 A90-27527
- Structural configuration options for the Space Station Freedom solar dynamic radiator
[IAF PAPER ICOSP89-4-5] p 48 A90-27710
- SPRITE - A computer code for the optimization of space based heat pipe radiator systems
p 170 A90-38036
- Scaling results for the liquid sheet radiator
p 170 A90-38037
- Advanced radiator concepts --- for nuclear powered spacecraft
p 170 A90-38042
- Two-tiered design analysis of a radiator for a solar dynamic powered Stirling engine
p 60 A90-38158
- Numerical model of solar dynamic radiator for parametric analysis
p 61 A90-38168
- Total hemispherical emittance measured at high temperatures by the calorimetric method
[NASA-TM-102322] p 136 N90-10309
- Conceptual design of liquid droplet radiator shuttle-attached experiment
[NASA-CR-185164] p 71 N90-11805
- Conceptual design of liquid droplet radiator shuttle-attached experiment technical requirements document
[NASA-CR-185165] p 71 N90-11806
- An improved algorithm for the modeling of vapor flow in heat pipes
[NASA-CR-185179] p 176 N90-13748
- On protection of Freedom's solar dynamic radiator from the orbital debris environment. Part 1: Preliminary analyses and testing
[NASA-TM-102458] p 73 N90-14285
- Conceptual design of a moving belt radiator shuttle-attached experiments: Technical requirement Document
[NASA-CR-185168] p 73 N90-15996
- Conceptual design of a Moving Belt Radiator (MBR) shuttle-attached experiment
[NASA-CR-185169] p 79 N90-23474
- SPACECRAFT STRUCTURES**
- Base reaction optimization of redundant manipulators for space applications
[NASA-CR-186274] p 201 N90-15447
- Dynamic analysis of space-related linear and non-linear structures
[NASA-TM-103490] p 51 N90-25174
- SPACECRAFT TRAJECTORIES**
- Discrete approximations to optimal trajectories using direct transcription and nonlinear programming
[AIAA PAPER 90-2963] p 41 A90-53038
- Optimal impulsive time-fixed orbital rendezvous and interception with path constraints
[AIAA PAPER 90-2972] p 41 A90-53051
- SPACECREWS**
- A radiological assessment of nuclear power and propulsion operations near Space Station Freedom
[NASA-CR-185185] p 76 N90-21108
- SPACELAB**
- Spacelab qualified infrared imager for microgravity science experiments
[NASA-TM-102503] p 189 N90-20352
- SPACELAB PAYLOADS**
- Spacelab 2 Plasma Diagnostics Package
p 39 A90-23263
- SPACING**
- Primary arm spacing in directionally solidified Pb-10 wt pct Sn alloys
[AIAA PAPER 90-0740] p 132 A90-23713
- Primary arm spacing in directionally solidified Pb-10 wt percent Sn alloys
[NASA-CR-185190] p 134 N90-14398
- SPALLATION**
- Mechanisms of degradation and failure in a plasma deposited thermal barrier coating
[ASME PAPER 89-GT-132] p 84 A90-23830
- SPALLING**
- The effect of 0.1 atomic percent zirconium on the cyclic oxidation behavior of beta-NiAl for 3000 hours at 1200 C
p 112 A90-24857
- Thermal barrier coating life prediction model development, phase 1
[NASA-CR-182230] p 26 N90-13388
- SPARK IGNITION**
- Evaluation of a hybrid kinetics/mixing-controlled combustion model for turbulent premixed and diffusion combustion using KIVA-2
[NASA-TM-103196] p 185 N90-28792
- SPATIAL DISTRIBUTION**
- Spatial evolution of nonlinear acoustic mode instabilities on hypersonic boundary layers
[NASA-TM-102431] p 177 N90-14517
- SPATIAL RESOLUTION**
- Effect of spatial resolution on apparent sensitivity to initial conditions of a decaying flow as it becomes turbulent
[NASA-TM-102377] p 176 N90-13719
- SPECIFIC IMPULSE**
- Qualification and life testing of a flight design hydrazine arcjet system
[AIAA PAPER 90-2576] p 64 A90-42559
- High energy-density liquid rocket fuel performance
[AIAA PAPER 90-1968] p 130 A90-47204
- SPECIMEN GEOMETRY**
- Investigation of Weibull statistics in fracture analysis of cast aluminum
p 115 A90-45304
- Thermo-oxidative stability studies of PMR-15 polymer matrix composites reinforced with various fibers
[NASA-TM-102439] p 98 N90-19310
- SPECKLE PATTERNS**
- Two-dimensional surface strain measurement based on a variation of Yamaguchi's laser-speckle strain gauge
[NASA-TM-103162] p 192 N90-22784
- Progress in high temperature speckle-shift strain measurement system
[NASA-TM-103255] p 191 N90-28031
- SPECTRAL METHODS**
- A multi-domain spectral computation of three-dimensional laminar horseshoe vortex flow using incompressible Navier-Stokes equations
p 3 A90-17592
- Unsteady three-dimensional marginal separation, including breakdown
[NASA-TM-102525] p 179 N90-20337
- SPECTROMETERS**
- Droplet sizing instrumentation used for icing research: Operation, calibration, and accuracy
[NASA-CR-182293] p 187 N90-11999
- SPECTROSCOPY**
- NASA Laser Light Scattering Advanced Technology Development Workshop, 1988
[NASA-CP-10033] p 188 N90-17085
- Structural comparison of nickel electrodes and precursor phases
p 231 N90-20472
- Preliminary plume characteristics of an arcjet thruster
[NASA-TM-103241] p 81 N90-26071
- SPECULAR REFLECTION**
- The effect of leveling coatings on the atomic oxygen durability of solar concentrator surfaces
[NASA-TM-102557] p 76 N90-21110
- SPHERES**
- Parametric study of power absorption from electromagnetic waves by small ferrite spheres
[NASA-TP-2949] p 246 N90-12282
- Mass transfer from a sphere in an oscillating flow with zero mean velocity
[NASA-TM-102566] p 179 N90-20338
- SPINEL**
- Corrosion testing of candidates for the alkaline fuel cell cathode
p 231 N90-20471
- SPLINE FUNCTIONS**
- Three-dimensional fluid flow calculations using a flux-spline method
p 167 A90-27983
- GRID2D/3D: A computer program for generating grid systems in complex-shaped two- and three-dimensional spatial domains. Part 1: Theory and method
[NASA-TM-102453] p 238 N90-22262
- SPRAY NOZZLES**
- Spray nozzle investigation for the Improved Helicopter Icing Spray System (IHSS)
[AIAA PAPER 90-0666] p 37 A90-25040
- SPRAYED COATINGS**
- TBCs for better engine efficiency --- thermal barrier coatings
p 83 A90-17294
- Instrumented adhesion tests on plasma sprayed thermal barrier coatings
p 111 A90-20255
- Tensile adhesion testing methodology for thermally sprayed coatings
p 85 A90-43902
- Thermal modelling of various thermal barrier coatings in a high heat flux rocket engine
[NASA-TM-102418] p 117 N90-16911
- SPRAYERS**
- Symmetry assessment of an air-blast atomizer spray
p 172 A90-40930
- Critical evaluation of Jet-A spray combustion using propane chemical kinetics in gas turbine combustion simulated by KIVA-2
[NASA-TM-103173] p 138 N90-26170
- SPREAD SPECTRUM TRANSMISSION**
- A performance analysis of DS-CDMA and SCPC VSAT networks
p 141 A90-39056
- SPUTTERING**
- Silicon carbide semiconductor device fabrication and characterization
[NASA-CR-186354] p 258 N90-19873
- SQUEEZE FILMS**
- Elasticity effects on cavitation in a squeeze film damper undergoing noncentered circular whirl
[NASA-TM-102392] p 200 N90-13786
- STABILITY**
- Method and models for R-curve instability calculations
p 214 A90-50566
- Low NO(x) potential of gas turbine engines
[NASA-TM-102452] p 27 N90-17636
- Thermo-oxidative stability studies of PMR-15 polymer matrix composites reinforced with various fibers
[NASA-TM-102439] p 98 N90-19310
- Instabilities and subharmonic resonances of subsonic heated round jets, volume 2
[NASA-CR-186058] p 181 N90-22017
- Controlled crack growth specimen for brittle systems
[NASA-TM-103126] p 129 N90-23543
- STABILITY TESTS**
- The role of gravity on macrosegregation in alloys
[NASA-CR-186530] p 136 N90-25238
- STAGNATION POINT**
- Unsteady disturbances of streaming motions around bodies
p 162 A90-21424
- STAINLESS STEELS**
- Tribological reactions of perfluoroalkyl polyether oils with stainless steel under ultrahigh vacuum conditions at room temperature
p 120 A90-16278
- Decomposition of perfluoroalkylpolyethers (PFPE) in ultra-high vacuum under sliding conditions
p 122 A90-40714
- STARTING**
- Mathematical modeling and analysis of heat pipe start-up from the frozen state
p 174 A90-48404
- STATE ESTIMATION**
- Viscoplasticity: A thermodynamic formulation
[NASA-TM-102388] p 216 N90-14640
- STATIC LOADS**
- A variational justification of the assumed natural strain formulation of finite elements. I - Variational principles. II - The C(0) four-node plate element
p 210 A90-24384
- Analysis of shell-type structures subjected to time-dependent mechanical and thermal loading
[NASA-CR-185077] p 222 N90-24653
- STATIC PRESSURE**
- The measurement of boundary layers on a compressor blade in cascade. Volume 2: Data tables
[NASA-CR-185118-VOL-2] p 23 N90-10039
- STATIC TESTS**
- Large-scale Advanced Prop-fan (LAP) static rotor test report
[NASA-CR-180848] p 25 N90-12617
- STATIONARY ORBITS**
- Servicing communication satellites in geostationary orbit
[AIAA PAPER 90-0830] p 39 A90-25655
- STATIONKEEPING**
- Xenon ion sources for space applications
p 56 A90-22874
- End-hall thrusters
[AIAA PAPER 90-2595] p 64 A90-42570
- STATISTICAL ANALYSIS**
- Equilibrium statistical thermodynamics of a many-particle system coupled to an external scalar field
p 261 A90-31670
- Performance analysis of Integrated Communication and Control System networks
p 239 A90-51267
- Vibration transmission through rolling element bearings in geared rotor system, part 1
[NASA-CR-186093] p 199 N90-12936
- Review and statistical analysis of the ultrasonic velocity method for estimating the porosity fraction in polycrystalline materials
[NASA-TM-102501-REV] p 207 N90-21402
- Modeling and synthesis of multicomputer interconnection networks
[NASA-CR-186619] p 238 N90-25604
- Computer architecture evaluation for structural dynamics computations: Project summary
[NASA-CR-186137] p 235 N90-26512

SUBJECT INDEX

STATISTICAL DISTRIBUTIONS

Equivalence of physically based statistical fracture theories for reliability analysis of ceramics in multiaxial loading p 123 A90-43580

STATORS

Experimental determination of stator endwall heat transfer [ASME PAPER 89-GT-219] p 165 A90-23880
A block-based algorithm for the solution of compressible flows in rotor-stator combinations p 9 A90-46905
The numerical simulation of multistage turbomachinery flows p 29 N90-21025
Analytical and experimental study of high phase order induction motors [NASA-CR-186580] p 153 N90-21952

STEADY FLOW

Three dimensional full potential method for the aeroelastic modeling of propfans [AIAA PAPER 90-1120] p 7 A90-29392
A technique for measurement of instantaneous heat transfer in steady-flow ambient-temperature facilities p 172 A90-39625
Unsteady three-dimensional marginal separation, including breakdown [NASA-TM-102525] p 179 N90-20337
ULTRA-SHARP nonoscillatory convection schemes for high-speed steady multidimensional flow [NASA-TM-102568] p 244 N90-21570

STEADY STATE

Steady-state and transient Zener parameters in viscoplasticity: Drag strength versus yield strength [NASA-TM-102487] p 218 N90-18064
Investigation of methods to produce a uniform cloud of fuel particles in a flame tube p 178 N90-18665 [NASA-TM-102376]

STEADY STATE CREEP

Creep substructure formation in sodium chloride single crystals in the power law and exponential creep regimes p 255 A90-33330

STEAM

Steam cooled rich-burn combustor liner [NASA-CASE-LEW-13609-1] p 106 N90-11824

STEERABLE ANTENNAS

Design for steering accuracy in antenna arrays using shared optical phase shifters p 138 A90-13935
Effects of additional interfering signals on adaptive array performance [NASA-CR-186508] p 145 N90-20271

STELLAR EVOLUTION

Neutron stars and white dwarfs in galactic halos? p 265 A90-30909
Soft inflation --- in cosmology p 265 A90-40093

STELLAR MODELS

Is the sub-millisecond pulsar strange? p 264 A90-12669

STELLAR ROTATION

Is the sub-millisecond pulsar strange? p 264 A90-12669

STIFFNESS

Tailoring of composite links for optimal damped elastodynamic performance p 211 A90-30250
Integrated force method versus displacement method for finite element analysis [NASA-TP-2937] p 218 N90-18081
A global approach for the identification of structural connection properties [NASA-TM-102502] p 218 N90-18745

STIFFNESS MATRIX

Mesh refinement in finite element analysis by minimization of the stiffness matrix trace [NASA-CR-185170] p 201 N90-15434

STIRLING CYCLE

The cavity heat pipe Stirling receiver for space solar dynamics p 61 A90-38169
SP-100 advanced radiator designs for thermoelectric and Stirling applications p 62 A90-38202
Comparison of conceptual designs for 25 kWe advanced Stirling conversion systems for dish electric applications p 229 A90-38254
The NASA Advanced Solar Dynamics Technology Program p 62 A90-38280
Initial characterization of a modular heat exchanger with an integral heat pipe --- for Stirling space engine p 62 A90-38301
SP-100 power system conceptual design for lunar base applications [NASA-TM-102090] p 267 N90-15030
Recent Stirling engine loss-understanding results [NASA-TM-103122] p 77 N90-21114
Preliminary designs for 25 kWe advanced Stirling conversion systems for dish electric applications [NASA-TM-103188] p 263 N90-26729

STIRLING ENGINES

Two-tiered design analysis of a radiator for a solar dynamic powered Stirling engine p 60 A90-38158

CSTI high capacity power --- Civil Space Technology Initiative p 61 A90-38196
On the dynamic response of pressure transmission lines in the research of helium-charged free piston Stirling engines p 196 A90-38248
Results from baseline tests of the SPRE I and comparison with code model predictions p 62 A90-38249

Comparison of conceptual designs for 25 kWe advanced Stirling conversion systems for dish electric applications p 229 A90-38254

Two-dimensional numerical simulation of a Stirling engine heat exchanger p 170 A90-38290
Initial characterization of a modular heat exchanger with an integral heat pipe --- for Stirling space engine p 62 A90-38301

Automotive Stirling engine development program [NASA-CR-180839] p 263 N90-11654
SP-100 power system conceptual design for lunar base applications [NASA-TM-102090] p 267 N90-15030

Development of free-piston Stirling engine performance and optimization codes based on Martini simulation technique [NASA-CR-182210] p 263 N90-18326

Identification of a cast iron alloy containing nonstrategic elements [NASA-CR-185174] p 118 N90-18559

Recent Stirling engine loss-understanding results [NASA-TM-103122] p 77 N90-21114

Programmatic status of NASA's CSTI high capacity power Stirling space power converter program [NASA-TM-103142] p 79 N90-22606

Preliminary designs for 25 kWe advanced Stirling conversion systems for dish electric applications [NASA-TM-103188] p 263 N90-26729

Automotive Stirling engine development program [NASA-CR-180840] p 264 N90-29260

STOCHASTIC PROCESSES

Radiative transfer theory for inhomogeneous media with random extinction and scattering coefficients p 260 A90-21904

A unified statistical rain-attenuation model for communication link fade predictions and optimal stochastic fade control design using a location-dependent rain-statistic database p 141 A90-34914

STOICHIOMETRY

Influence of the deposition conditions on radiofrequency magnetron sputtered MoS₂ films [NASA-TP-2994] p 137 N90-21210

Ignition and combustion characteristics of metallized propellants [NASA-CR-186870] p 107 N90-26911

Synthesis and structural chemistry of Au(III)-substituted Ba₂YCu₃O₇(δ) [NASA-TM-103292] p 108 N90-28696

STORAGE BATTERIES

Cryogenic reactant storage for lunar base regenerative fuel cells [IAF PAPER ICOSP89-3-8] p 227 A90-27709

Photovoltaic power for Space Station Freedom [NASA-TM-102569] p 78 N90-21812

STORAGE STABILITY

Nickel-hydrogen capacity loss on storage p 57 A90-33955

Nickel-hydrogen capacity loss on storage p 231 N90-20478

STORAGE TANKS

Spacecraft attitude impacts on COLD-SAT non-vacuum jacketed LH₂ supply tank thermal performance [AIAA PAPER 90-1672] p 49 A90-41566

Numerical investigation of the thermal stratification in cryogenic tanks subjected to wall heat flux [AIAA PAPER 90-2375] p 175 A90-52500

Numerical investigation of the thermal stratification in cryogenic tanks subjected to wall heat flux [NASA-TM-103194] p 184 N90-27984

STRAIN DISTRIBUTION

Assumed strain distributions for a finite strip plate bending element using Mindlin-Reissner plate theory p 208 A90-16723

Finite element elastic-plastic-creep and cyclic life analysis of a cowl lip [NASA-TM-102342] p 220 N90-22808

Finite element analysis of structural components using viscoplastic models with application to a cowl lip problem [NASA-CR-185189] p 221 N90-23769

STRAIN ENERGY RELEASE RATE

Energy analysis of crack-damage interaction p 213 A90-41372

STRAIN GAGES

Development and characterization of PdCr temperature-compensated wire resistance strain gage [NASA-CR-185153] p 188 N90-13761

Electrical properties of materials for high temperature strain gage applications [NASA-CR-186192] p 188 N90-14534

Two-dimensional surface strain measurement based on a variation of Yamaguchi's laser-speckle strain gage [NASA-TM-103162] p 192 N90-22784

A resistance strain gage with repeatable and cancellable apparent strain for use to 800 C [NASA-CR-185256] p 53 N90-26063

STRAIN HARDENING

Viscoplasticity: A thermodynamic formulation [NASA-TM-102388] p 216 N90-14640

Steady-state and transient Zener parameters in viscoplasticity: Drag strength versus yield strength [NASA-TM-102487] p 218 N90-18064

A viscoplastic model with application to LiF-22 percent CaF₂ hypereutectic salt [NASA-TM-103181] p 221 N90-23770

STRAIN MEASUREMENT

Two-dimensional surface strain measurement based on a variation of Yamaguchi's laser-speckle strain gage [NASA-TM-103162] p 192 N90-22784

Feasibility study for the advanced one-dimensional high temperature optical strain measurement system, phase 3 [NASA-CR-185254] p 191 N90-25324

Progress in high temperature speckle-shift strain measurement system [NASA-TM-103255] p 191 N90-28031

STRAIN RATE

1200 to 1400 K slow strain rate compressive properties of NiAl/Ni₂AlTi-base materials p 88 A90-16938

Advanced applications of BEM to inelastic analysis of solids p 213 A90-45770

High-temperature slow-strain-rate compression studies on CoAl-TiB₂ composites p 93 A90-48636

Compression behavior of the forged Li₂ compounds Al₆Ti₂SiCr₈ and Al₆Ti₂SiMn₉ p 116 A90-51298

STRATEGIC MATERIALS

Resources - Supply and availability --- of superalloys for United States aerospace industry p 114 A90-34152

Materials Park, OH p 85 A90-39975
Identification of a cast iron alloy containing nonstrategic elements [NASA-CR-185174] p 118 N90-18559

STRATIFICATION

Numerical investigation of the thermal stratification in cryogenic tanks subjected to wall heat flux [AIAA PAPER 90-2375] p 175 A90-52500

Numerical investigation of the thermal stratification in cryogenic tanks subjected to wall heat flux [NASA-TM-103194] p 184 N90-27984

STREAM FUNCTIONS (FLUIDS)

Time-dependent viscous incompressible Navier-Stokes equations - The finite difference Galerkin formulation and streamfunction algorithms p 156 A90-11598

STRESS ANALYSIS

Model analysis of gear housing and mounts p 192 A90-17018

Comparison of boundary element and finite element methods in spur gear root stress analysis p 193 A90-21107

Finite element mesh refinement criteria for stress analysis p 209 A90-23013

Energy analysis of crack-damage interaction p 213 A90-41372

Parametric studies to determine the effect of compliant layers on metal matrix composite systems p 93 A90-50093

Analysis of results from wind tunnel tests of inlets for an advanced turboprop nacelle installation [NASA-CR-174937] p 10 N90-10011

Mean stress and the exhaustion of fatigue-damage resistance [NASA-TM-101311] p 216 N90-13819

Parametric studies to determine the effect of compliant layers on metal matrix composite systems [NASA-TM-102465] p 96 N90-14294

Model development in viscoplastic ratchetting [NASA-TM-102509] p 219 N90-20431

Determination of the stress distributions in a ceramic: Tensile specimen using numerical techniques [NASA-TM-101914] p 129 N90-26132

Calculation of 3D turbulent jets in crossflow with a multigrid method and a second-moment closure model [NASA-TM-103159] p 184 N90-26282

Design of ceramic components with the NASA/CARES computer program [NASA-TM-102369] p 222 N90-26359

Constitutive and life modeling of single crystal blade alloys for root attachment analysis p 119 N90-28643

STRESS DISTRIBUTION

Three-dimensional analysis of surface crack-Hertzian stress field interaction [NASA-CR-4254] p 215 N90-11332

- Finite element elastic-plastic-creep and cyclic life analysis of a cowl lip
[NASA-TM-102342] p 220 N90-22808
- Finite element analysis of structural components using viscoplastic models with application to a cowl lip problem
[NASA-CR-185189] p 221 N90-23769
- Determination of the stress distributions in a ceramic: Tensile specimen using numerical techniques
[NASA-TM-101914] p 129 N90-26132
- Computer-aided design of high-contact-ratio gears for minimum dynamic load and stress
[NASA-TM-103275] p 205 N90-28065
- STRESS INTENSITY FACTORS**
- The unusual near-threshold FCG behavior of a single crystal superalloy and the resolved shear stress as the crack driving force
p 111 A90-21009
- Three-dimensional analysis of surface crack-Hertzian stress field interaction
[NASA-CR-4254] p 215 N90-11332
- Fatigue crack growth in unidirectional metal matrix composite
[NASA-TM-103102] p 220 N90-22117
- STRESS RELAXATION**
- Effects of state recovery on creep buckling under variable loading
p 212 A90-41223
- STRESS RELIEVING**
- Steam cooled rich-burn combustor liner
[NASA-CASE-LEW-13609-1] p 106 N90-11824
- STRESS WAVES**
- Acousto-ultrasonic nondestructive evaluation of materials using laser beam generation and detection
[NASA-CR-186694] p 154 N90-23664
- STRESS-STRAIN DIAGRAMS**
- Slow plastic deformation of extruded NiAl-10TiB2 particulate composites at 1200 and 1300 K
p 92 A90-46133
- Compression behavior of the forged Li2 compounds Al6Ti25Cr6 and Al6Ti25Mn9
p 116 A90-51298
- STRESS-STRAIN RELATIONSHIPS**
- Analytical and finite element solutions of some problems using a viscoplastic model
p 209 A90-19132
- Relationship between fatigue life in the creep-fatigue region and stress-strain response
p 209 A90-20061
- Advanced applications of BEM to inelastic analysis of solids
p 213 A90-45770
- Status of structural analysis of 30 cm diameter ion optics
[AIAA PAPER 90-2649] p 215 A90-52571
- Demonstration of capabilities of high temperature composites analyzer code HITCAN
[NASA-TM-102560] p 219 N90-19629
- Nicalon/siliconoxycarbide ceramic composites
[NASA-TM-102563] p 99 N90-21133
- Finite element analysis of structural components using viscoplastic models with application to a cowl lip problem
[NASA-CR-185189] p 221 N90-23769
- A viscoplastic model with application to LiF-22 percent CaF2 hypereutectic salt
[NASA-TM-103181] p 221 N90-23770
- STRESSES**
- Two stage gear tooth dynamics program
[NASA-CR-185110] p 199 N90-10437
- Influence of linear profile modification and loading conditions on the dynamic tooth load and stress of high contact ratio gears
[NASA-TM-103136] p 204 N90-22796
- Stress versus temperature dependent activation energies in creep
[NASA-TM-103192] p 221 N90-23773
- Determination of the stress distributions in a ceramic: Tensile specimen using numerical techniques
[NASA-TM-101914] p 129 N90-26132
- STRING THEORY**
- Cosmic-string-induced hot dark matter perturbations
p 264 A90-25889
- Phase transitions as the origin of large scale structure in the universe
p 265 A90-35291
- Gravitational couplings of the inflaton in extended inflation
p 265 A90-40088
- STRIP TRANSMISSION LINES**
- Experimental investigations on channelized coplanar waveguide
[NASA-TM-102494] p 151 N90-20286
- STRUCTURAL ANALYSIS**
- Finite element implementation of Robinson's unified viscoplastic model and its application to some uniaxial and multiaxial problems
p 208 A90-15704
- Analytical and finite element solutions of some problems using a viscoplastic model
p 209 A90-19132
- Probabilistic structural analysis methods of hot engine structures
[ASME PAPER 89-GT-122] p 56 A90-23821
- Application of HOST technology to the SSME HPFTP blade
[ASME PAPER 89-GT-130] p 209 A90-23828
- Crack-path effect on material toughness
[ASME PAPER 89-WA/APM-43] p 210 A90-28755
- Evaluation of thermal and mechanical loading effects on the structural behavior of a SiC/titanium composite
[AIAA PAPER 90-1026] p 90 A90-29228
- Neurobiological computational models in structural analysis and design
[AIAA PAPER 90-1133] p 210 A90-29260
- Variational formulation of high-performance finite elements - Parametrized variational principles
p 213 A90-46068
- Developments in variational methods for high performance plate and shell elements
p 214 A90-46288
- Advanced probabilistic structural analysis method for implicit performance functions
p 214 A90-49792
- Composite Blade Structural Analyzer (COBSTRAN) theoretical/programmer's manual
[NASA-TM-101958] p 95 N90-10181
- The MHOST finite element program: 3-D inelastic analysis methods for hot section components. Volume 2: User's manual
[NASA-CR-182235-VOL-2] p 215 N90-10450
- Constitutive modeling for isotropic materials (HOST)
[NASA-CR-179522] p 26 N90-13390
- Constitutive modeling for isotropic materials (HOST)
[NASA-CR-174718] p 26 N90-13391
- Compatibility conditions of structural mechanics for finite element analysis
[NASA-TM-102413] p 217 N90-17180
- Integrated force method versus displacement method for finite element analysis
[NASA-TP-2937] p 218 N90-18081
- Probability of failure and risk assessment of propulsion structural components
p 218 N90-18470
- A transient plasticity study and low cycle fatigue analysis of the Space Station Freedom photovoltaic solar array blanket
[NASA-TM-102516] p 218 N90-19617
- Computational simulation of structural fracture in fiber composites
[NASA-TM-102505] p 100 N90-21821
- Probabilistic structural analysis of aerospace components using NESSUS
[NASA-TM-102324] p 221 N90-22823
- Solar Concentrator Advanced Development Program
[NASA-CR-185173] p 232 N90-22834
- Structural behavior of composites with progressive fracture
[NASA-TM-102370] p 100 N90-23477
- Application of finite-element-based solution technologies for viscoplastic structural analyses
[NASA-CR-185196] p 221 N90-23757
- Finite element analysis of structural components using viscoplastic models with application to a cowl lip problem
[NASA-CR-185189] p 221 N90-23769
- Analysis of shell-type structures subjected to time-dependent mechanical and thermal loading
[NASA-CR-185077] p 222 N90-24653
- Multiprocessor architecture: Synthesis and evaluation
[NASA-CR-186618] p 235 N90-25579
- Design of ceramic components with the NASA/CARES computer program
[NASA-TM-102369] p 222 N90-26359
- Ceramics Analysis and Reliability Evaluation of Structures (CARES). Users and programmers manual
[NASA-TP-2916] p 223 N90-28099
- Probabilistic structural analysis methods development for SSME
p 83 N90-28616
- Structural response of SSME turbine blade airfoils
p 224 N90-28649
- Generalized Advanced Propeller Analysis System (GAPAS). Volume 2: Computer program user manual
[NASA-CR-185277] p 36 N90-29394
- STRUCTURAL DESIGN**
- The fuel cell in space - Yesterday, today and tomorrow
p 56 A90-26837
- Neurobiological computational models in structural analysis and design
[AIAA PAPER 90-1133] p 210 A90-29260
- Multi-objective shape and material optimization of composite structures including damping
[AIAA PAPER 90-1135] p 210 A90-29262
- Robustness, generality and efficiency of optimization algorithms in practical applications
[AIAA PAPER 90-1177] p 236 A90-29268
- Space Station Freedom photovoltaic power module design status
p 58 A90-38075
- Two-tiered design analysis of a radiator for a solar dynamic powered Stirling engine
p 60 A90-38158
- SP-100 advanced radiator designs for thermoelectric and Stirling applications
p 62 A90-38202
- Optimum structural design of robotic manipulators with fiber reinforced composite materials
p 197 A90-46074
- Large scale prop-fan structural design study. Volume 1: Initial concepts
[NASA-CR-174992] p 23 N90-10043
- Large scale prop-fan structural design study. Volume 2: Preliminary design of SR-7
[NASA-CR-174993] p 23 N90-10044
- The fuel cell in space: Yesterday, today and tomorrow
[NASA-TM-102366] p 70 N90-11804
- Technology development program for an advanced microsheet glass concentrator
[NASA-TM-102406] p 229 N90-14678
- Design of a thrust stand for high power electric propulsion devices
[NASA-TM-102372] p 73 N90-15992
- Conceptual design for the space station Freedom modular combustion facility
[NASA-TM-102037] p 134 N90-16087
- Probability of failure and risk assessment of propulsion structural components
p 218 N90-18470
- Aerodynamic optimization by simultaneously updating flow variables and design parameters
p 18 N90-20991
- Detection of potential space station control/structure interaction with CO-ST-IN
p 50 N90-21074
- Multi-objective shape and material optimization of composite structures including damping
[NASA-TM-102579] p 99 N90-21132
- Structural tailoring of select fiber composite structures
[NASA-TM-102484] p 99 N90-21137
- Application of finite-element-based solution technologies for viscoplastic structural analyses
[NASA-CR-185196] p 221 N90-23757
- Simplified design procedures for fiber composite structural components/joints
[NASA-TM-103113] p 101 N90-24384
- Dynamic analysis of space-related linear and non-linear structures
[NASA-TM-103490] p 51 N90-25174
- Advanced Turbine Technology Applications Project (ATTAP)
[NASA-CR-185240] p 263 N90-26728
- Measurement of the steady surface pressure distribution on a single rotation large scale advanced prop-fan blade at Mach numbers from 0.03 to 0.78
[NASA-CR-182124] p 32 N90-28552
- STRUCTURAL DESIGN CRITERIA**
- Analysis of fully stalled compressor
p 6 A90-27966
- Analysis of results from wind tunnel tests of inlets for an advanced turboprop nacelle installation
[NASA-CR-174937] p 10 N90-10011
- STRUCTURAL FAILURE**
- Composite Blade Structural Analyzer (COBSTRAN) theoretical/programmer's manual
[NASA-TM-101958] p 95 N90-10181
- Reliability analysis of a structural ceramic combustion chamber
[NASA-TM-103264] p 223 N90-28112
- STRUCTURAL MEMBERS**
- An experimental evaluation of the tensile strength of impact ice
p 83 A90-15049
- Characterization of damped structural connections for multi-component systems
p 208 A90-16959
- STRUCTURAL RELIABILITY**
- Noninteractive macroscopic reliability model for ceramic matrix composites with orthotropic material symmetry
[ASME PAPER 89-GT-129] p 209 A90-23827
- A methodology for evaluating the reliability and risk of structures under complex service environments
[AIAA PAPER 90-1102] p 211 A90-29332
- Advanced probabilistic structural analysis method for implicit performance functions
p 214 A90-49792
- Analysis of whisker-toughened ceramic components: A design engineer's viewpoint
[NASA-TM-102333] p 97 N90-18504
- STRUCTURAL STABILITY**
- Computational methods for probability of instability calculations
[AIAA PAPER 90-1139] p 236 A90-29333
- Integrated force method versus displacement method for finite element analysis
[NASA-TP-2937] p 218 N90-18081
- STRUCTURAL VIBRATION**
- Modal selection in structural dynamics
p 209 A90-17001
- Icing Research Tunnel test of a model helicopter rotor
p 15 A90-28179
- Boundary flexibility method of component mode synthesis using static Ritz vectors
p 212 A90-35429
- Free-vibration analysis of three-dimensional solids by BEM
p 215 A90-52007
- Vibration transmission through rolling element bearings in geared rotor system, part 1
[NASA-CR-186093] p 199 N90-12936

- Computational simulation of damping in composite structures
[NASA-TM-102567] p 219 N90-20432
- Dynamic substructuring by the boundary flexibility vector method of component mode synthesis
[NASA-CR-182445] p 220 N90-22813
- STRUCTURAL WEIGHT**
- Scaling study for SP-100 reactor technology
[NASA-TM-897140] p 249 N90-16496
- Electrochemical impregnation and cycle life of lightweight nickel electrodes for nickel-hydrogen cells
[NASA-TM-103140] p 107 N90-21844
- STRUTS**
- Experimental investigation of flow about a strut-endwall configuration
[AIAA PAPER 90-1541] p 171 A90-38685
- STUDENTS**
- The International Space University
[AIAA PAPER 90-2389] p 261 A90-42152
- The International Space University
[NASA-TM-103163] p 78 N90-22604
- SUBROUTINES**
- Hypercluster parallel processing library user's manual
[NASA-CR-185231] p 237 N90-21552
- SUBSONIC FLOW**
- Analysis of nonuniform subsonic flows about a row of moving blades p 2 A90-11779
- Total temperature effects on centerline Mach number characteristics of freejets p 6 A90-25290
- Instabilities and subharmonic resonances of subsonic heated round jets, volume 2
[NASA-CR-186058] p 181 N90-22017
- SUBSONIC SPEED**
- Advanced core technology - Key to subsonic propulsion benefits
[ASME PAPER 89-GT-241] p 19 A90-23890
- SUBSTRATES**
- Synthesis and characterization of high-T(c) screen-printed Y-Ba-Cu-O films on alumina p 254 A90-21926
- On sublayer streaks p 168 A90-28143
- Measurement of the intrinsic bond strength of brittle thin films on flexible substrates p 256 A90-44022
- Growth and patterning of laser ablated superconducting YBa₂Cu₃O₇ films on LaAlO₃ substrates
[NASA-TM-102436] p 259 N90-22421
- New directions in InP solar cell research
[NASA-TM-103160] p 154 N90-23662
- Laser ablated high T(sub c) superconducting thin YBa₂Cu₃O₇(-x) films on substrates suitable for microwave applications p 260 N90-27808
- SUBSTRUCTURES**
- Boundary flexibility method of component mode synthesis using static Ritz vectors p 212 A90-35429
- SUPERCONDUCTING FILMS**
- Thin films of the Bi₂Sr₂Ca₂Cu₃O(x) superconductor p 254 A90-24448
- Complex permittivity of lanthanum aluminate in the 20 to 300 K temperature range from 26.5 to 40.0 GHz p 148 A90-37864
- Millimeter-wave surface resistance of laser-ablated YBa₂Cu₃O₇(-delta) superconducting films p 257 A90-48694
- Study of deposition of YBa₂Cu₃O₇-x on cubic zirconia
[NASA-TM-102350] p 257 N90-10737
- Millimeter wave surface resistance of RBa₂Cu₃O₇(-delta) superconductors (R=Y, Eu, Dy, Sm, Er)
[NASA-TM-102571] p 259 N90-20886
- Growth and patterning of laser ablated superconducting YBa₂Cu₃O₇ films on LaAlO₃ substrates
[NASA-TM-102436] p 259 N90-22421
- Photoresponse of YBa₂Cu₃O₇(-delta) granular and epitaxial superconducting thin films p 154 N90-22732
- Sequentially evaporated thin film YBa₂Cu₃O₇(-x) superconducting microwave ring resonator
[NASA-TM-103180] p 154 N90-25273
- Ellipsometric study of YBa₂Cu₃O₇(-x) laser ablated and co-evaporated films p 259 N90-26682
- Laser ablated high T(sub c) superconducting thin YBa₂Cu₃O₇(-x) films on substrates suitable for microwave applications p 260 N90-27808
- Microwave conductivity of laser ablated YBaCuO superconducting films and its relation to microstrip transmission line p 155 N90-27844
- SUPERCONDUCTING MAGNETS**
- Feasibility analysis of reciprocating magnetic heat pumps
[NASA-CR-186205] p 177 N90-15363
- SUPERCONDUCTIVITY**
- Synthesis and characterization of high-Tc superconductors in the Ti-Ca-Ba-Cu-O system p 253 A90-19300
- Synthesis and characterization of high-T(c) screen-printed Y-Ba-Cu-O films on alumina p 254 A90-21926
- Properties of Pb(1-x)Bi(x)/Ba₂YCu₃O(x) composites - Reaction of Ba₂YCu₃O(x) with Pb and Bi p 255 A90-33224
- A superconducting quenchgun for delivering lunar derived oxygen to lunar orbit p 43 A90-40627
- Superconducting ceramics in the Bi_{1.5}SrCaCu₂O sub x system by melt quenching technique
[NASA-CR-185139] p 258 N90-11606
- Superconducting Bi_{1.5}Pb_{0.5}Sr₂Ca₂Cu₃O(x) ceramics by rapid melt quenching and glass crystallization
[NASA-CR-185184] p 258 N90-17465
- Performance and modeling of superconducting ring resonators at millimeter-wave frequencies
[NASA-TM-102526] p 151 N90-18634
- Millimeter wave surface resistance of RBa₂Cu₃O₇(-delta) superconductors (R=Y, Eu, Dy, Sm, Er)
[NASA-TM-102571] p 259 N90-20886
- A superconducting quenchgun for delivering lunar derived oxygen to lunar orbit p 77 N90-21806
- Growth and patterning of laser ablated superconducting YBa₂Cu₃O₇ films on LaAlO₃ substrates
[NASA-TM-102436] p 259 N90-22421
- Photoresponse of YBa₂Cu₃O₇(-delta) granular and epitaxial superconducting thin films p 154 N90-22732
- Rapid thermal processing of high temperature superconducting fiber
[NASA-CR-186803] p 259 N90-24964
- Sequentially evaporated thin film YBa₂Cu₃O₇(-x) superconducting microwave ring resonator
[NASA-TM-103180] p 154 N90-25273
- High temperature superconducting thin film microwave circuits: Fabrication, characterization, and applications
[NASA-TM-103235] p 156 N90-28786
- SUPERCONDUCTORS**
- Electromagnetic finite elements based on a four-potential variational principle p 214 A90-49869
- Method of forming low cost, formable High T(sub c) superconducting wire
[NASA-CASE-LEW-14676-2] p 258 N90-17454
- Millimeter wave surface resistance of RBa₂Cu₃O₇(-delta) superconductors (R=Y, Eu, Dy, Sm, Er)
[NASA-TM-102571] p 259 N90-20886
- Sequentially evaporated thin film YBa₂Cu₃O₇(-x) superconducting microwave ring resonator
[NASA-TM-103180] p 154 N90-25273
- High temperature superconducting thin film microwave circuits: Fabrication, characterization, and applications
[NASA-TM-103235] p 156 N90-28786
- SUPERCritical FLUIDS**
- Evaluation of supercritical cryogen storage and transfer systems for future NASA missions
[AIAA PAPER 90-0719] p 44 A90-19989
- Evaluation of supercritical cryogen storage and transfer systems for future NASA missions
[NASA-TM-102394] p 44 N90-10912
- SUPERHIGH FREQUENCIES**
- Performance measurements for a laboratory-simulated 30/20 GHz communication satellite transponder
[AIAA PAPER 90-0808] p 140 A90-25634
- SUPERLATTICES**
- The correlation between the temperature dependence of the CRSS and the formation of superlattice-intrinsic stacking faults in the nickel-base superalloy PWA 1480 --- critical resolved shear stress p 109 A90-11657
- SUPERNOVA 1987A**
- Is the sub-millisecond pulsar strange? p 264 A90-12669
- SUPERNOVAE**
- The shocking development of lithium (and boron) in supernovae p 264 A90-17643
- SUPERSONIC AIRCRAFT**
- A supersonic through-flow fan engine airframe integration study
[NASA-CR-185140] p 10 N90-10004
- Interactive calculation procedures for mixed compression inlets
[NASA-CR-186581] p 14 N90-25934
- SUPERSONIC BOUNDARY LAYERS**
- A study of the unsteadiness of crossing shock wave turbulent boundary layer interactions
[AIAA PAPER 90-1456] p 170 A90-38614
- SUPERSONIC COMBUSTION**
- Chemically reacting supersonic flow calculation using an assumed PDF model p 4 A90-22256
- SUPERSONIC COMBUSTION RAMJET ENGINES**
- RAMSCRAM: A flexible ramjet/scramjet engine simulation program
[NASA-TM-102451] p 27 N90-14235
- SUPERSONIC CRUISE AIRCRAFT RESEARCH**
- A supersonic through-flow fan engine airframe integration study
[NASA-CR-185140] p 10 N90-10004
- SUPERSONIC FLIGHT**
- RAMSCRAM: A flexible ramjet/scramjet engine simulation program
[NASA-TM-102451] p 27 N90-14235
- SUPERSONIC FLOW**
- Numerical study of chemically reacting flows using a lower-upper symmetric successive overrelaxation scheme p 3 A90-17989
- A new mixing length model for supersonic shear layers
[AIAA PAPER 90-0018] p 166 A90-25026
- Structure of a reattaching supersonic shear layer p 7 A90-36252
- On the instabilities of supersonic mixing layers - A high-Mach-number asymptotic theory p 8 A90-42644
- Application of a two-dimensional unsteady viscous analysis code to a supersonic throughflow fan stage
[NASA-TM-4141] p 25 N90-13387
- Numerical simulations of supersonic flow through oscillating cascade sections
[NASA-TM-103100] p 13 N90-20051
- Exhaust nozzles for propulsion systems with emphasis on supersonic cruise aircraft
[NASA-RP-1235] p 29 N90-21037
- Optical techniques for determination of normal shock position in supersonic flows for aerospace applications
[NASA-TM-103201] p 190 N90-25323
- SUPERSONIC FLUTTER**
- Aeroelastic detuning for stability enhancement of unstalled supersonic flutter p 19 A90-17462
- SUPERSONIC INLETS**
- Experimental investigation of terminal shock sensors in mixed-compression inlets
[AIAA PAPER 90-1931] p 186 A90-40560
- Transient behavior of supersonic flow through inlets
[AIAA PAPER 90-2130] p 8 A90-42734
- Comparison of 3-D viscous flow computations of Mach 5 inlet with experimental data
[NASA-TM-102518] p 28 N90-20090
- SUPERSONIC NOZZLES**
- Exhaust nozzles for propulsion systems with emphasis on supersonic cruise aircraft
[NASA-RP-1235] p 29 N90-21037
- SUPERSONIC SPEED**
- High speed commercial transport fuels considerations and research needs
[NASA-TM-102535] p 131 N90-21869
- SUPERSONIC TRANSPORTS**
- Hypersonic aerospace sizing analysis for the preliminary design of aerospace vehicles p 17 A90-23276
- Revolutionary opportunities for materials and structures study
[NASA-CR-179642] p 95 N90-10184
- Supersonic through-flow fan engine and aircraft mission performance
[NASA-TM-102304] p 29 N90-21038
- SUPERSONIC TURBINES**
- Revolutionary opportunities for materials and structures study
[NASA-CR-179642] p 95 N90-10184
- Supersonic through-flow fan engine and aircraft mission performance
[NASA-TM-102304] p 29 N90-21038
- SUPERSONIC WIND TUNNELS**
- Euler analysis comparison with LDV data for an advanced counter-rotation propfan at cruise
[AIAA PAPER 90-3033] p 9 A90-50637
- An LDA investigation of the normal shock wave boundary layer interaction p 10 A90-52618
- Comparison of 3-D viscous flow computations of Mach 5 inlet with experimental data
[NASA-TM-102518] p 28 N90-20090
- Euler analysis comparison with LDV data for an advanced counter-rotation propfan at cruise
[NASA-TM-103249] p 14 N90-25946
- SUPPORT SYSTEMS**
- NASA Lewis icing research tunnel user manual
[NASA-TM-102319] p 31 N90-23407
- SUPPORTS**
- A global approach for using kinematic redundancy to minimize base reactions of manipulators
[NASA-CR-186825] p 234 N90-25499
- SURFACE CRACKS**
- Energy analysis of crack-damage interaction p 213 A90-41372
- Three-dimensional analysis of surface crack-Hertzian stress field interaction
[NASA-CR-4254] p 215 N90-11332

- SURFACE DIFFUSION**
Diffusional aspects of the high-temperature oxidation of protective coatings p 113 A90-28075
- SURFACE DISTORTION**
Reflector surface distortion analysis techniques (thermal distortion analysis of antennas in space) p 144 N90-19267
- SURFACE GEOMETRY**
A numerical study of the interaction between unsteady free-stream disturbances and localized variations in surface geometry p 161 A90-21422
Surface reorientation and settling in cylinders upon step reduction in gravity p 172 A90-44541
- SURFACE PROPERTIES**
Applications of surface analysis and surface theory in tribology p 84 A90-37458
Metallographic techniques for evaluation of thermal barrier coatings p 85 A90-44869
Arcjet cathode phenomena p 75 N90-18477
Design and calibration of a vacuum compatible scanning tunneling microscope p 189 N90-20353
Computerized inspection of gear tooth surfaces [NASA-TM-102395] p 203 N90-22054
- SURFACE REACTIONS**
Tribological reactions of perfluoroalkyl polyether oils with stainless steel under ultrahigh vacuum conditions at room temperature p 120 A90-16278
Aeolian removal of dust from photovoltaic surfaces on Mars [NASA-TM-102507] p 76 N90-19299
- SURFACE ROUGHNESS**
Convective heat transfer measurements from a NACA 0012 airfoil in flight and in the NASA Lewis icing Research Tunnel [AIAA PAPER 90-0199] p 162 A90-22180
Heat transfer on accreting ice surfaces [AIAA PAPER 90-0200] p 162 A90-22181
A study of ice shape prediction methodologies and comparison with experimental data [AIAA PAPER 90-0753] p 15 A90-26986
Convective heat transfer measurements from a NACA 0012 airfoil in flight and in the NASA Lewis icing Research Tunnel [NASA-TM-102448] p 176 N90-13750
Heat transfer measurements from a NACA 0012 airfoil in flight and in the NASA Lewis icing research tunnel [NASA-CR-4278] p 13 N90-19203
Investigation of surface water behavior during glaze ice accretion p 16 N90-20927
Bearing elastohydrodynamic lubrication: A complex calculation made simple [NASA-TM-102575] p 203 N90-22041
- SURFACE ROUGHNESS EFFECTS**
Pressure drop and mass transfer in two-pass ribbed channels p 165 A90-24837
An annular gas seal analysis using empirical entrance and exit region friction factors [ASME PAPER 89-TRIB-46] p 196 A90-33555
Modeling of surface roughness effects on glaze ice accretion p 16 N90-20925
- SURFACE TEMPERATURE**
Development of an infrared imaging system for the surface tension driven convection experiment p 188 N90-17922
Design and test of a compact optics system for the pool boiling experiment [NASA-TM-102530] p 135 N90-20253
Thermal radiation characteristics of nonisothermal cylindrical enclosures using a numerical ray tracing technique [NASA-TM-102527] p 179 N90-21296
Multiwavelength pyrometry to correct for reflected radiation [NASA-TM-102578] p 190 N90-23714
- SURFACE WATER**
Investigation of surface water behavior during glaze ice accretion p 16 N90-20927
- SURFACE WAVES**
Shear stabilization of the capillary breakup of a cylindrical interface [AD-A219268] p 159 A90-17578
- SURFACES**
Theory of gearing [NASA-RP-1212] p 202 N90-19593
- SURVEYS**
Laser anemometer measurements in a transonic axial-flow fan rotor [NASA-TP-2879] p 175 N90-11245
- SWEEP EFFECT**
Parametric studies of advanced turboprops p 19 A90-21225
- SWEPT WINGS**
Swept wing ice accretion modeling [AIAA PAPER 90-0756] p 5 A90-25042
- Swept wing ice accretion modeling [NASA-TM-103114] p 13 N90-21727
- SWIRLING**
Modern developments in shear flow control with swirl [NASA-CR-186586] p 181 N90-22000
- SWITCHES**
Neutron and gamma irradiation effects on power semiconductor switches [NASA-TM-103200] p 155 N90-25278
- SWITCHING**
Induction motor control [NASA-TM-102533] p 28 N90-19234
- SWITCHING CIRCUITS**
Characterization of two MMIC GaAs switch matrices at microwave frequencies [AIAA PAPER 90-0866] p 147 A90-25686
Performance testing of a high frequency link converter for Space Station power distribution system p 148 A90-38128
On-board switching and processing p 150 A90-51168
Characterization of two MMIC GaAs switch matrices at microwave frequencies [NASA-TM-102449] p 50 N90-14273
High power density dc/dc converter: Selection of converter topology [NASA-CR-186129] p 151 N90-14467
- SWIVELS**
Performance characteristics of a one-third-scale, vectorable ventral nozzle for SSTOVL aircraft [AIAA PAPER 90-2271] p 20 A90-37562
Performance characteristics of a one-third-scale, vectorable ventral nozzle for SSTOVL aircraft [NASA-TM-103120] p 2 N90-21725
- SYMMETRY**
Symmetry assessment of an air-blast atomizer spray p 172 A90-40930
- SYNCHRONISM**
A burst compression and expansion technique for variable-rate users in satellite-switched TDMA networks [AIAA PAPER 90-0850] p 46 A90-25673
A burst compression and expansion technique for variable-rate users in satellite-switched TDMA networks [NASA-TM-102414] p 47 N90-15983
- SYNCHRONOUS MOTORS**
Induction motor control [NASA-TM-102533] p 28 N90-19234
- SYNCHRONOUS SATELLITES**
Servicing communication satellites in geostationary orbit [AIAA PAPER 90-0830] p 39 A90-25655
Status of xenon ion propulsion technology p 56 A90-27961
- SYNTHESIS (CHEMISTRY)**
Synthesis and characterization of high-T(c) screen-printed Y-Ba-Cu-O films on alumina p 254 A90-21926
Linear acene derivatives - New routes to pentacene and naphthalene and the first synthesis of a triptycene with two anthracene moieties p 85 A90-49071
Bisannulation with a benzo(1,2-c:4,5-c'-prime) difuran equivalent - A new route to linear acene derivatives p 85 A90-49072
Iptycene synthesis: A new method for attaching a 2,3-anthracene moiety to the 9,10-positions of another anthracene moiety - Exceptional conditions for a Lewis acid catalyzed Diels-Alder reaction p 85 A90-49073
New Condensation polyimides containing 1,1,1-triaryl-2,2,2-trifluoroethane structures [NASA-CASE-LEW-14346-1] p 86 N90-19300
Polysiloxanes derived from the controlled hydrolysis of tetraethoxysilane as precursors to silica for use in ceramic processing [NASA-TM-102489] p 128 N90-21858
Substituted 1,1,1-triaryl-2,2,2-trifluoroethanes and processes for their synthesis [NASA-CASE-LEW-14345-2] p 107 N90-23497
Synthesis and structural chemistry of Au(III)-substituted Ba₂YCu₃O(7- δ) [NASA-TM-103292] p 108 N90-28696
- SYSTEM EFFECTIVENESS**
Characterization and cycle tests of lightweight nickel electrodes [NASA-TM-102399] p 106 N90-12696
- SYSTEM FAILURES**
Developing a self-diagnostic system for piezoelectric sensors [AIAA PAPER 90-2230] p 187 A90-42755
- SYSTEM IDENTIFICATION**
Rocket engine failure detection using system identification techniques [AIAA PAPER 90-1993] p 65 A90-47205
Rocket engine failure detection using system identification techniques [NASA-CR-185259] p 45 N90-25159
- SYSTEMS ANALYSIS**
Detection of potential space station control/structure interaction with CO-ST-IN p 50 N90-21074
Electric power scheduling: A distributed problem-solving approach [NASA-TM-103149] p 240 N90-22323
- SYSTEMS ENGINEERING**
Predicted performance of near-optimally designed indium phosphide space solar cells at high intensities and temperatures p 225 A90-14898
Thin film eddy current impulse deicer [AIAA PAPER 90-0761] p 17 A90-20012
Encoding Y,I,Q component estimates of an NTSC composite signal p 139 A90-23261
Cryogenic reactant storage for lunar base regenerative fuel cells [IAF PAPER ICOSP89-3-8] p 227 A90-27709
Lunar missions using advanced chemical propulsion - System design issues [AIAA PAPER 90-2431] p 67 A90-47221
An electronic pressure profile display system for aeronautic test facilities [NASA-TM-102478] p 38 N90-15964
Progression of damage and fracture in composites under dynamic loading [NASA-TM-103118] p 100 N90-21825
Assessment of fundamental materials needs for Thick Thermal Barrier Coatings (TTBC's) for truck diesel engines [NASA-TM-103130] p 119 N90-23536
National space test centers, Lewis research center facilities [NASA-TM-103187] p 44 N90-26030
Low-gravity fluid physics: A program overview [NASA-TM-103215] p 183 N90-26273
- SYSTEMS INTEGRATION**
A burst compression and expansion technique for variable-rate users in satellite-switched TDMA networks [AIAA PAPER 90-0850] p 46 A90-25673
H-infinity based integrated flight/propulsion control design for a STOVL aircraft in transition flight [AIAA PAPER 90-3335] p 36 A90-47595
Integrated Communication and Control Systems. III - Nonidentical sensor and controller sampling p 239 A90-51266
Performance analysis of Integrated Communication and Control System networks p 239 A90-51267
STOVL aircraft simulation for integrated flight and propulsion control research [NASA-TM-102419] p 26 N90-13389
User needs, benefits, and integration of robotic systems in a space station laboratory [NASA-CR-185150] p 200 N90-13794
A burst compression and expansion technique for variable-rate users in satellite-switched TDMA networks [NASA-TM-102414] p 47 N90-15983
Performance measurements for a laboratory-simulated 30/20 GHz communication satellite transponder [NASA-TM-102424] p 143 N90-17977
Integrated regenerative fuel cell experimental evaluation [NASA-CR-185183] p 230 N90-18808
- SYSTEMS MANAGEMENT**
Space Station Freedom power management and distribution system design [IAF PAPER 89-078] p 54 A90-13295
- SYSTEMS SIMULATION**
Space Station Solar Dynamic Module modelling and simulation p 53 A90-11993
Noise of a simulated installed model counterrotation propeller at angle-of-attack and takeoff/approach conditions [AIAA PAPER 90-0283] p 247 A90-32505
Probabilistic modeling for simulation of aerodynamic uncertainties in propulsion systems [NASA-TM-102472] p 29 N90-21036
- SYSTEMS STABILITY**
Analysis of airframe/engine interactions - An integrated control perspective [AIAA PAPER 90-1918] p 36 A90-40557
- SYSTOLIC ARRAYS**
Multi-level Hierarchical Poly Tree computer architectures p 236 A90-26082

T

TAPERING

- Aperture taper determination for the half-scale accurate antenna reflector [NASA-CR-185215] p 153 N90-21282

TARGETS

- Low velocity impact analysis with NASTRAN p 221 N90-24647

SUBJECT INDEX

TAYLOR SERIES

PROTEUS two-dimensional Navier-Stokes computer code, version 1.0. Volume 3: Programmer's reference [NASA-TM-102553] p 180 N90-21307

TDR SATELLITES

ATDRS payload technology research and development [NASA-TM-103256] p 52 N90-28596

TECHNOLOGICAL FORECASTING

Composites boost 21st-century aircraft engines p 90 A90-29704
Toward an electrical power utility for space exploration p 74 N90-17681
Challenges for future space power systems p 74 N90-17695
NASA advanced space photovoltaic technology: Status, potential and future mission applications p 74 N90-17775

TECHNOLOGY ASSESSMENT

Issues and opportunities in space photovoltaics p 54 A90-14852
Xenon ion sources for space applications p 56 A90-22874
ATTAP/AGT101 ceramics technology update [ASME PAPER 89-GT-105] p 195 A90-23814
Integrated controls and health monitoring for chemical transfer propulsion p 52 A90-47229
Large scale prop-fan structural design study. Volume 1: Initial concepts [NASA-CR-174992] p 23 N90-10043
Large scale prop-fan structural design study. Volume 2: Preliminary design of SR-7 [NASA-CR-174993] p 23 N90-10044
Regenerative fuel cell systems for project Pathfinder p 74 N90-17708

Romans to Mars [NASA-TM-103094] p 267 N90-23339
Integrated controls and health monitoring for chemical transfer propulsion [NASA-TM-103185] p 52 N90-25178
Figure of merit studies of beam power concepts for advanced space exploration [NASA-CR-186720] p 146 N90-26234
The lessons of Varsovia's reconnaissance [NASA-TM-103207] p 267 N90-26789
A technology assessment of alternative communications systems for the space exploration initiative [NASA-TM-103243] p 47 N90-27736
Energy efficient engine program technology benefit/cost study. Volume 1: Executive summary [NASA-CR-174766-VOL-1] p 34 N90-28564

TECHNOLOGY TRANSFER

EPSAT - A workbench for designing high-power systems for the space environment [AIAA PAPER 90-0637] p 245 A90-26975

TECHNOLOGY UTILIZATION

The role of technology in influencing future civil communications satellites p 142 A90-51167
Base reaction optimization of redundant manipulators for space applications [NASA-CR-186274] p 201 N90-15447
Advanced Turbine Technology Applications Project (ATTAP) [NASA-CR-185240] p 263 N90-26728
Preliminary designs for 25 kWe advanced Stirling conversion systems for dish electric applications [NASA-TM-103188] p 263 N90-26729

TELECOMMUNICATION

A burst compression and expansion technique for variable-rate users in satellite-switched TDMA networks [AIAA PAPER 90-0850] p 46 A90-25673
Integrated Communication and Control Systems. III - Nonidentical sensor and controller sampling p 239 A90-51266

A burst compression and expansion technique for variable-rate users in satellite-switched TDMA networks [NASA-TM-102414] p 47 N90-15983
A technology assessment of alternative communications systems for the space exploration initiative [NASA-TM-103243] p 47 N90-27736

TELESCOPES

Laser diffraction particle sizing: Instrument probe volume relocation and elongation [NASA-TM-102512] p 188 N90-18025

TELEVISION TRANSMISSION

Encoding Y,I,Q component estimates of an NTSC composite signal p 139 A90-23261

TEMPERATURE CONTROL

Applications of high thermal conductivity composites to electronics and spacecraft thermal design [AIAA PAPER 90-0783] p 89 A90-25609

TEMPERATURE DEPENDENCE

Apparent activation volume for creep of copper and alpha brass at intermediate temperatures p 108 A90-10028

O2 reduction at the IFC orbiter fuel cell O2 electrode [NASA-TM-102580] p 231 N90-21469
Detailed mechanism for oxidation of benzene [NASA-TM-102443] p 106 N90-21842
Stress versus temperature dependent activation energies in creep [NASA-TM-103192] p 221 N90-23773

TEMPERATURE DISTRIBUTION

Numerical investigation of the thermal stratification in cryogenic tanks subjected to wall heat flux [AIAA PAPER 90-2375] p 175 A90-52500
Development of an infrared imaging system for the surface tension driven convection experiment p 188 N90-17922
Design and test of a compact optics system for the pool boiling experiment [NASA-TM-102530] p 135 N90-20253
Numerical investigation of the thermal stratification in cryogenic tanks subjected to wall heat flux [NASA-TM-103194] p 184 N90-27984
Frequency response of a thermocouple wire: Effects of axial conduction [NASA-CR-180454] p 191 N90-28827

TEMPERATURE EFFECTS

Total temperature effects on centerline Mach number characteristics of freejets p 6 A90-25290
Thermal effects on the mechanical properties of SiC fibre reinforced reaction-bonded silicon nitride matrix composites p 92 A90-46999
Optimal fabrication processes for unidirectional metal-matrix composites - A computational simulation p 93 A90-50096
Efficient numerical method for computation of thermohydrodynamics of laminar lubricating films [NASA-CR-185136] p 175 N90-11256
Superconducting ceramics in the Bi1.5SrCaCu2O sub x system by melt quenching technique [NASA-CR-185139] p 258 N90-11606
Thermal barrier coatings for gas turbine and diesel engines [NASA-TM-102408] p 117 N90-13636
Strength and toughness of monolithic and composite silicon nitrides p 126 N90-14368
Thermodynamic analysis of chemical stability of ceramic materials in hydrogen-containing atmospheres at high temperatures [NASA-CR-42711] p 126 N90-16072
Thermal modelling of various thermal barrier coatings in a high heat flux rocket engine [NASA-TM-102418] p 117 N90-16911
Evaluation of thermal and mechanical loading effects on the structural behavior of a SiC/titanium composite [NASA-TM-102536] p 98 N90-20139
Fundamental aspects of and failure modes in high-temperature composites [NASA-TM-102558] p 98 N90-20151
Optimal fabrication processes for unidirectional metal-matrix composites: A computational simulation [NASA-TM-102559] p 100 N90-21143
METCAN verification status [NASA-TM-103119] p 100 N90-21824
High-temperature superconductors for space power transmission lines [NASA-TM-103459] p 259 N90-24952
Extension of a noninteractive reliability model for ceramic matrix composites [NASA-CR-185267] p 129 N90-26142
High temperature fatigue behavior of Haynes 188 p 119 N90-28642
Durability of thermal barrier coatings in a high heat flux environment p 129 N90-28651
High-temperature deformation and microstructural analysis for Si3N4-Sc2O3 [NASA-TM-103239] p 130 N90-28740
Frequency response of a thermocouple wire: Effects of axial conduction [NASA-CR-180454] p 191 N90-28827

TEMPERATURE GRADIENTS

Thermocapillary migration of liquid droplets in a temperature gradient in a density matched system [NASA-CR-185178] p 177 N90-14512
Thermomechanical deformation testing and modeling in the presence of metallurgical instabilities [NASA-CR-185188] p 219 N90-21420
Scattered-light scanner measurements of cryogenic liquid-jet breakup [NASA-TM-102432] p 189 N90-22021

TEMPERATURE MEASUREMENT

Non-contact temperature measurements in support of microgravity combustion experiments p 135 N90-17900
Spacelab qualified infrared imager for microgravity science experiments [NASA-TM-102503] p 189 N90-20352

Multiwavelength pyrometry to correct for reflected radiation [NASA-TM-102578] p 190 N90-23714
Feasibility study for the advanced one-dimensional high temperature optical strain measurement system, phase 3 [NASA-CR-185254] p 191 N90-25324

TEMPERATURE MEASURING INSTRUMENTS

Modulated-splitting-ratio fiber-optic temperature sensor p 185 A90-11706
Silicon-etalon fiber-optic temperature sensor [NASA-TM-102389] p 18 N90-13381

TENSILE PROPERTIES

Microstructure and tensile properties of Fe-40 at. pct Al alloys with C, Zr, Hf, and B additions p 108 A90-11651
An experimental evaluation of the tensile strength of impact ice p 83 A90-15049
A crystallographic model for the tensile and fatigue response for Rene N4 at 982 C p 114 A90-28754
High-temperature tensile properties of fiber reinforced reaction bonded silicon nitride p 95 A90-52783

TENSILE STRENGTH

An experimental evaluation of the tensile strength of impact ice p 83 A90-15049
Matrix density effects on the mechanical properties of SiC fiber-reinforced silicon nitride matrix properties p 94 A90-51927
Fluorinated graphite fibers as a new engineering material: Promises and challenges [NASA-TM-102511] p 86 N90-19301
Heat treatment study of the SiC/Ti-15-3 composite system [NASA-TP-2970] p 97 N90-19302
Mechanical properties of pure nickel alloys after long term exposures to LiOH and vacuum at 775 K [NASA-TM-102403] p 118 N90-20181
Matrix density effects on the mechanical properties of SiC/RBSN composites [NASA-TM-103098] p 100 N90-21826

TENSILE STRESS

Torsional and biaxial (tension-torsion) fatigue damage mechanisms in Waspaloy at room temperature p 109 A90-11925
Microstructure: Property correlation --- multiaxial fatigue damage evolution in waspaloy [NASA-CR-180406] p 224 N90-28880

TENSILE TESTS

Instrumented adhesion tests on plasma sprayed thermal barrier coatings p 111 A90-20255
Inelastic deformation under nonisothermal loading p 112 A90-22657
Tensile adhesion testing methodology for thermally sprayed coatings p 85 A90-43902
Mechanics of the crack path formation [NASA-CR-185143] p 215 N90-10455
Constitutive modeling for isotropic materials (HOST) [NASA-CR-179522] p 26 N90-13390

TENSORS

Application of symbolic computations to the constitutive modeling of structural materials [NASA-TM-103225] p 222 N90-26364

TEST EQUIPMENT

Development of Ada language control software for the NASA power management and distribution test bed p 236 A90-38082
Evaluation of power control concepts using the PMAD systems test bed --- Power Management and Distribution p 42 A90-38083

TEST FACILITIES

Protoflight photovoltaic power module system-level tests in the Space Power Facility p 62 A90-38266
A test matrix sequencer for research test facility automation [AIAA PAPER 90-2386] p 37 A90-42791
Requirements for long-life operation of inert gas hollow cathodes - Preliminary results [AIAA PAPER 90-2586] p 69 A90-52570
Liquid Transfer Cryogenic Test Facility: Initial hydrogen and nitrogen no-vent fill data [NASA-TM-102572] p 179 N90-21295
A test matrix sequencer for research test facility automation [NASA-TM-103108] p 39 N90-23416
High-temperature test facility at the NASA Lewis engine components research laboratory [NASA-TM-103143] p 39 N90-25151
Conceptual definition of a high voltage power supply test facility [NASA-CR-185216] p 50 N90-25172
National space test centers, Lewis research center facilities [NASA-TM-103187] p 44 N90-26030
Requirements for long-life operation of inert gas hollow cathodes: Preliminary report [NASA-TM-103242] p 82 N90-27783

TEST FIRING

- Rocket engine failure detection using system identification techniques
[AIAA PAPER 90-1993] p 65 A90-47205
- Performance characterization of a segmented anode arcjet thruster
[AIAA PAPER 90-2582] p 68 A90-52569
- Rocket engine failure detection using system identification techniques
[NASA-CR-185259] p 45 N90-25159
- Ceramic matrix composites in simulated SSME environments p 102 N90-28655

TEST STANDS

- Design of a thrust stand for high power electric propulsion devices
[NASA-TM-102372] p 73 N90-15992
- Energy Efficient Engine acoustic supporting technology report
[NASA-CR-174834] p 33 N90-28557

THALLIUM COMPOUNDS

- Synthesis and characterization of high-Tc superconductors in the Ti-Ca-Ba-Cu-O system
p 253 A90-19300

THERMAL ANALYSIS

- The role of thermal and lubricant boundary layers in the transient thermal analysis of spur gears
p 194 A90-21118
- Probabilistic structural analysis methods of hot engine structures
[ASME PAPER 89-GT-122] p 56 A90-23821
- Comparative thermal analysis of the Space Station Freedom photovoltaic deployable boom structure using TRASYS, NEVADA, and SINDA programs
[SAE PAPER 891563] p 47 A90-27525
- Spacecraft attitude impacts on COLD-SAT non-vacuum jacketed LH2 supply tank thermal performance
[AIAA PAPER 90-1672] p 49 A90-41566
- Reflector surface distortion analysis techniques (thermal distortion analysis of antennas in space)
p 144 A90-19267
- Solar Concentrator Advanced Development Program
[NASA-CR-185173] p 232 N90-22834
- Thermal analysis of thermal barrier coatings in a high heat flux environment p 129 N90-28652

THERMAL BOUNDARY LAYER

- The role of thermal and lubricant boundary layers in the transient thermal analysis of spur gears
p 194 A90-21118

THERMAL CONDUCTIVITY

- Thermal/structural analyses of several hydrogen-cooled leading-edge concepts for hypersonic flight vehicles
[AIAA PAPER 90-0053] p 164 A90-23702
- Role of the interfacial thermal barrier in the effective thermal diffusivity/conductivity of SiC-fiber-reinforced reaction-bonded silicon nitride p 89 A90-25268
- Applications of high thermal conductivity composites to electronics and spacecraft thermal design
[AIAA PAPER 90-0783] p 89 A90-25609
- Vapor grown carbon fiber for space thermal management systems p 94 A90-50128
- Thermal/structural analyses of several hydrogen-cooled leading-edge concepts for hypersonic flight vehicles
[NASA-TM-102391] p 177 N90-14511
- Selection of phase-change and containment materials for thermal energy storage
[NASA-CR-186228] p 229 N90-15506
- Thermal modelling of various thermal barrier coatings in a high heat flux rocket engine
[NASA-TM-102418] p 117 N90-16911
- Hot filament technique for measuring the thermal conductivity of molten lithium fluoride
[NASA-TM-102506] p 127 N90-19373
- Frequency response of a thermocouple wire: Effects of axial conduction
[NASA-CR-180454] p 191 N90-28827
- THERMAL CONTROL COATINGS**
- Instrumented adhesion tests on plasma sprayed thermal barrier coatings p 111 A90-20255
- Mechanisms of degradation and failure in a plasma deposited thermal barrier coating
[ASME PAPER 89-GT-132] p 84 A90-23830
- Two-layer thermal barrier coating. I - Effects of composition and temperature on oxidation behavior and failure p 122 A90-33317
- Energy storage and thermal control system design status --- for space station power supplies p 59 A90-38077
- Metallographic techniques for evaluation of thermal barrier coatings p 85 A90-44869
- Heat transfer to throat tubes in a square-chambered rocket engine at the NASA Lewis Research Center
[NASA-TM-102336] p 70 N90-11082
- Thermal barrier coating life prediction model development, phase 1
[NASA-CR-182230] p 26 N90-13388

- Thermal barrier coatings for gas turbine and diesel engines
[NASA-TM-102408] p 117 N90-13636
- Thermal modelling of various thermal barrier coatings in a high heat flux rocket engine
[NASA-TM-102418] p 117 N90-16911
- Assessment of fundamental materials needs for Thick Thermal Barrier Coatings (TTBC's) for truck diesel engines
[NASA-TM-103130] p 119 N90-23536
- Durability of thermal barrier coatings in a high heat flux environment p 129 N90-28651
- Thermal analysis of thermal barrier coatings in a high heat flux environment p 129 N90-28652

THERMAL CYCLING TESTS

- High temperature inelastic deformation under uniaxial loading - Theory and experiment p 109 A90-13838
- Effect of fiber spacing on interfacial damage in a metal matrix composite p 88 A90-23188
- Determination of the durability of the fiber optics in rocket engine environments
[AIAA PAPER 90-2229] p 250 A90-42754
- Use of unbalanced laminates as a screening method for microcracking p 94 A90-50217
- Use of unbalanced laminates as a screening method for microcracking
[NASA-TM-102517] p 98 N90-21124

THERMAL DECOMPOSITION

- Determination of the thermal stability of perfluoroalkylethers
[NASA-TM-102493] p 127 N90-17875

THERMAL DEGRADATION

- Arcjet cathode phenomena p 75 N90-18477

THERMAL DIFFUSION

- Ground-based experiments on thermal and thermosolutal convection in inclined low-aspect-ratio enclosures
[AIAA PAPER 90-0413] p 166 A90-25033

THERMAL DIFFUSIVITY

- Role of the interfacial thermal barrier in the effective thermal diffusivity/conductivity of SiC-fiber-reinforced reaction-bonded silicon nitride p 89 A90-25268

THERMAL ENERGY

- Thermal energy storage flight experiments
p 53 A90-11992
- Brayton advanced heat receiver development program
p 61 A90-38170
- Flight experiment of thermal energy storage --- for spacecraft power systems p 61 A90-38172
- A heat receiver design for solar dynamic space power systems
[NASA-TM-102473] p 72 N90-14283
- Selection of phase-change and containment materials for thermal energy storage
[NASA-CR-186228] p 229 N90-15506
- Conceptual design of a Moving Belt Radiator (MBR) shuttle-attached experiment
[NASA-CR-185169] p 79 N90-23474
- THERMAL ENVIRONMENTS**
- Arcjet thruster research and technology. Phase 1: Executive summary
[NASA-CR-182106] p 72 N90-14278

THERMAL EXPANSION

- Composites boost 21st-century aircraft engines
p 90 A90-29704
- Isothermal and nonisothermal fatigue behavior of a metal matrix composite p 91 A90-36746
- Use of unbalanced laminates as a screening method for microcracking p 94 A90-50217
- Fluorinated graphite fibers as a new engineering material: Promises and challenges
[NASA-TM-102511] p 86 N90-19301
- Crystallization behavior and properties of BaO-Al₂O₃-2SiO₂ glass matrices
[NASA-CR-185209] p 127 N90-19374
- Use of unbalanced laminates as a screening method for microcracking
[NASA-TM-102517] p 98 N90-21124

THERMAL FATIGUE

- Cyclic deformation, fatigue and fatigue crack propagation in Ni-base alloys p 115 A90-34162
- Thermal fatigue durability for advanced propulsion materials
[NASA-TM-102348] p 216 N90-14641
- High temperature fatigue behavior of tungsten copper composites
[NASA-TM-102404] p 99 N90-21138
- High temperature fatigue behavior of a SiC/Ti-24Al-11Nb composite
[NASA-TM-103157] p 220 N90-22822
- High temperature fatigue behavior of Haynes 188 p 119 N90-28642
- Structural response of SSME turbine blade airfoils p 224 N90-28649

THERMAL PROTECTION

- TBCs for better engine efficiency --- thermal barrier coatings p 83 A90-17294
- Comparative thermal analysis of the Space Station Freedom photovoltaic deployable boom structure using TRASYS, NEVADA, and SINDA programs
[SAE PAPER 891563] p 47 A90-27525

THERMAL RADIATION

- Thermal radiation characteristics of nonisothermal cylindrical enclosures using a numerical ray tracing technique
[NASA-TM-102527] p 179 N90-21296

THERMAL RESISTANCE

- Creep strength of niobium alloys, Nb-1%Zr and PWC-11 p 116 N90-11854
- Finite element analysis of structural components using viscoplastic models with application to a cowl lip problem
[NASA-CR-185189] p 221 N90-23769

THERMAL SHOCK

- Noninteractive macroscopic reliability model for whisker-reinforced ceramic composites p 89 A90-26561
- Durability of thermal barrier coatings in a high heat flux environment p 129 N90-28651
- Ceramic matrix composites in simulated SSME environments p 102 N90-28655

THERMAL STABILITY

- Microstructure and tensile properties of Fe-40 at. pct Al alloys with C, Zr, Hf, and B additions p 108 A90-11651
- Processable, high temperature polymers from 1,4,5,8-tetrahydro-1,4,5,8-diepoxyanthracene and bis-dienes p 84 A90-21930
- Preliminary investigation of a NiAl composite prepared by cryomilling p 113 A90-25098
- Noninteractive macroscopic reliability model for whisker-reinforced ceramic composites p 89 A90-26561
- Thermo-oxidative stability studies of PMR-15 polymer matrix composites reinforced with various continuous fibers p 93 A90-50068
- Mechanics of damping for fiber composite laminates including hygro-thermal effects
[NASA-TM-102329] p 95 N90-10185
- The 3F condensation polyimides: Review and update
[NASA-TM-102533] p 126 N90-14363
- Determination of the thermal stability of perfluoroalkylethers
[NASA-TM-102493] p 127 N90-17875
- Thermo-oxidative stability studies of PMR-15 polymer matrix composites reinforced with various fibers
[NASA-TM-102439] p 98 N90-19310
- High speed commercial transport fuels considerations and research needs
[NASA-TM-102535] p 131 N90-21869

THERMAL STRESSES

- Side-wall gas 'creep' and 'thermal stress convection' in microgravity experiments on film growth by vapor transport p 158 A90-14086
- Thermal/structural analyses of several hydrogen-cooled leading-edge concepts for hypersonic flight vehicles
[AIAA PAPER 90-0053] p 164 A90-23702
- Development of an integrated BEM for hot fluid-structure interaction
[ASME PAPER 89-GT-128] p 212 A90-32264
- Isothermal life prediction of composite lamina using a damage mechanics approach p 92 A90-48115
- Optimal fabrication processes for unidirectional metal-matrix composites - A computational simulation p 93 A90-50096
- Thermal/structural analyses of several hydrogen-cooled leading-edge concepts for hypersonic flight vehicles
[NASA-TM-102391] p 177 N90-14511
- Fiber pushout test: A three-dimensional finite element computational simulation
[NASA-TM-102565] p 99 N90-21131
- Optimal fabrication processes for unidirectional metal-matrix composites: A computational simulation
[NASA-TM-102559] p 100 N90-21143
- THERMAL VACUUM TESTS**
- Protoflight photovoltaic power module system-level tests in the Space Power Facility p 82 A90-38266
- Space Station Freedom solar array panels plasma interaction test facility
[NASA-TM-102475] p 266 N90-22488
- THERMOCHEMISTRY**
- Determination of the mean solid-liquid interface energy of pivalic acid p 84 A90-22646
- Reactions of SiC with H₂/H₂O/Ar mixtures at 1300 C p 123 A90-45830
- Hydrogen-silicon carbide interactions
[NASA-TM-102382] p 125 N90-11144

SUBJECT INDEX

- Energy storage for a lunar base by the reversible chemical reaction: $\text{CaO} + \text{H}_2\text{O}$ reversible reaction $\text{Ca}(\text{OH})_2$ [NASA-TM-103145] p 233 N90-25419
- THERMOCOUPLES**
Thin-film sensors for reusable space propulsion systems [NASA-TM-102383] p 71 N90-13595
Attachment of lead wires to thin film thermocouples mounted on high temperature materials using the parallel gap welding process [NASA-TM-102442] p 189 N90-21361
Frequency response of a thermocouple wire: Effects of axial conduction [NASA-CR-180454] p 191 N90-28827
- THERMODYNAMIC CYCLES**
Flight experiment of thermal energy storage --- for spacecraft power systems p 61 A90-38172
- THERMODYNAMIC EQUILIBRIUM**
Unitarity limits on the mass and radius of dark-matter particles p 264 A90-24671
Equilibrium statistical thermodynamics of a many-particle system coupled to an external scalar field p 261 A90-31670
- RAMSCRAM: A flexible ramjet/scramjet engine simulation program** [NASA-TM-102451] p 27 N90-14235
Critical fluid light scattering p 251 N90-17087
- THERMODYNAMIC PROPERTIES**
Liquid alkali metals - Equation of state and reduced-pressure, bulk-modulus, sound-velocity, and specific-heat functions p 102 A90-16280
Efficient real gas Navier-Stokes computations of high speed flows using an LU scheme [AIAA PAPER 90-0391] p 164 A90-23706
Advanced core technology - Key to subsonic propulsion benefits [ASME PAPER 89-GT-241] p 19 A90-23890
Identification of thermodynamically stable ceramic reinforcement materials for iron aluminide matrices p 89 A90-25238
Thermodynamic analysis of chemical compatibility of ceramic reinforcement materials with niobium aluminides p 92 A90-44001
Efficient numerical method for computation of the thermohydrodynamics of laminar lubricating films [NASA-CR-185136] p 175 N90-11256
The application of cast SiC/Al to rotary engine components [NASA-CR-179610] p 25 N90-13385
Thin-film sensors for reusable space propulsion systems [NASA-TM-102383] p 71 N90-13595
Thermodynamic properties of some metal oxide-zirconia systems [NASA-TM-102351] p 126 N90-13666
Efficient real gas Navier-Stokes computations of high speed flows using an LU scheme [NASA-TM-102429] p 11 N90-14203
Prediction of high temperature metal matrix composite ply properties [NASA-TM-102490] p 97 N90-17817
A transient plasticity study and low cycle fatigue analysis of the Space Station Freedom photovoltaic solar array blanket [NASA-TM-102516] p 218 N90-19617
Investigation of surface water behavior during glaze ice accretion p 16 N90-20927
- THERMODYNAMICS**
Numerical investigation of the thermal stratification in cryogenic tanks subjected to wall heat flux [AIAA PAPER 90-2375] p 175 A90-52500
Viscoplasticity: A thermodynamic formulation [NASA-TM-102388] p 216 N90-14640
Thermal fatigue durability for advanced propulsion materials [NASA-TM-102348] p 216 N90-14641
Thermodynamic analysis of chemical stability of ceramic materials in hydrogen-containing atmospheres at high temperatures [NASA-CR-4271] p 126 N90-16072
Demonstration of capabilities of high temperature composites analyzer code HITCAN [NASA-TM-102560] p 219 N90-19629
Evaluation of thermal and mechanical loading effects on the structural behavior of a SiC/titanium composite [NASA-TM-102536] p 98 N90-20139
High temperature fatigue behavior of tungsten copper composites [NASA-TM-102404] p 99 N90-21138
Thermomechanical testing techniques for high-temperature composites: TMF behavior of SiC(SCS-6)/Ti-15-3 [NASA-TM-103171] p 222 N90-25367

- Performance of a supercharged direct-injection stratified-charge rotary combustion engine [NASA-TM-103105] p 32 N90-25982
Numerical investigation of the thermal stratification in cryogenic tanks subjected to wall heat flux [NASA-TM-103194] p 184 N90-27984
- THERMOELASTICITY**
Development of an integrated BEM for hot fluid-structure interaction [ASME PAPER 89-GT-128] p 212 A90-32264
A thermoelastic transversely isotropic thick walled cylinder/disk application: An analytical solution and study [NASA-TM-102320] p 216 N90-12950
- THERMOELECTRIC MATERIALS**
Effect of Ga and P dopants on the thermoelectric properties of n-type SiGe p 256 A90-38140
- THERMOELECTRIC POWER GENERATION**
Comparison of solar photovoltaic and nuclear reactor power systems for a human-tended lunar observatory p 42 A90-38030
SP-100 advanced radiator designs for thermoelectric and Stirling applications p 62 A90-38202
- THERMOELECTRICITY**
CSTI high capacity power --- Civil Space Technology Initiative p 61 A90-38196
- THERMONUCLEAR POWER GENERATION**
Comparison of solar photovoltaic and nuclear reactor power systems for a human-tended lunar observatory p 42 A90-38030
- THERMOPHYSICAL PROPERTIES**
Energy stability of thermocapillary convection in a model of the float-zone crystal-growth process p 133 A90-48720
Critical evaluation of Jet-A spray combustion using propane chemical kinetics in gas turbine combustion simulated by KIVA-2 [NASA-TM-103173] p 138 N90-26170
- THERMOPLASTICITY**
Advanced applications of BEM to inelastic analysis of solids p 213 A90-45770
- THICK FILMS**
Synthesis and characterization of high-T(c) screen-printed Y-Ba-Cu-O films on alumina p 254 A90-21926
- THICK WALLS**
Analytical and finite element solutions of some problems using a viscoplastic model p 209 A90-19132
A thermoelastic transversely isotropic thick walled cylinder/disk application: An analytical solution and study [NASA-TM-102320] p 216 N90-12950
- THICKNESS**
Ultrasonic techniques for aircraft ice accretion measurement p 16 N90-20926
Assessment of fundamental materials needs for Thick Thermal Barrier Coatings (TTBC's) for truck diesel engines [NASA-TM-103130] p 119 N90-23536
- THIN FILMS**
Side-wall gas 'creep' and 'thermal stress convection' in microgravity experiments on film growth by vapor transport p 158 A90-14086
Radiation resistance studies of amorphous silicon films p 227 A90-14952
Thin film eddy current impulse deicer [AIAA PAPER 90-0761] p 17 A90-20012
Thin films of the $\text{Bi}_2\text{Sr}_2\text{Ca}_2\text{Cu}_3\text{O}_x$ superconductor p 254 A90-24448
Growth of high quality 6H-SiC epitaxial films on vicinal (0001) 6H-SiC wafers p 255 A90-29952
Diamondlike carbon protective coatings for optical windows p 122 A90-34569
Ellipsometric studies of the diffusion of atomic oxygen through silicon dioxide thin films p 104 A90-36268
Simple evaporation controller for thin-film deposition from a resistively heated boat p 149 A90-39761
Measurement of the intrinsic bond strength of brittle thin films on flexible substrates p 256 A90-44022
Plasma-deposited amorphous hydrogenated carbon films and their tribological properties p 123 A90-44864
Photovoltaic options for solar electric propulsion [AIAA PAPER 90-2529] p 68 A90-52563
Optical dispersion relations for diamondlike carbon films [NASA-TM-102356] p 257 N90-10738
Efficient numerical method for computation of thermohydrodynamics of laminar lubricating films [NASA-CR-185136] p 175 N90-11256
Plasma-deposited amorphous hydrogenated carbon films and their tribological properties [NASA-TM-102379] p 125 N90-11880
Thin-film sensors for reusable space propulsion systems [NASA-TM-102383] p 71 N90-13595

THREE DIMENSIONAL FLOW

- Electron-beam induced damage in thin insulating films on compound semiconductors [NASA-CR-185177] p 151 N90-17987
Millimeter wave surface resistance of $\text{RbBa}_2\text{Cu}_3\text{O}(7-\delta)$ (R = Y, Eu, Dy, Sm, Er) superconductors [NASA-TM-102571] p 259 N90-20886
The effect of leveling coatings on the atomic oxygen durability of solar concentrator surfaces [NASA-TM-102557] p 76 N90-21110
Influence of the deposition conditions on radiofrequency magnetron sputtered MoS_2 films [NASA-TP-2994] p 137 N90-21210
Peeled film GaAs solar cells for space power [NASA-TM-103125] p 153 N90-21287
Attachment of lead wires to thin film thermocouples mounted on high temperature materials using the parallel gap welding process [NASA-TM-102442] p 189 N90-21361
Growth and patterning of laser ablated superconducting YBa $_2$ Cu $_3$ O $_7$ films on LaAlO_3 substrates [NASA-TM-102436] p 259 N90-22421
Photoresponse of YBa $_2$ Cu $_3$ O $_7(7-\delta)$ granular and epitaxial superconducting thin films p 154 N90-22732
Sequentially evaporated thin film YBa $_2$ Cu $_3$ O $_7(x)$ superconducting microwave ring resonator [NASA-TM-103180] p 154 N90-25273
Laser ablated high T(sub c) superconducting thin YBa $_2$ Cu $_3$ O $_7(7-x)$ films on substrates suitable for microwave applications p 260 N90-27808
High temperature superconducting thin film microwave circuits: Fabrication, characterization, and applications [NASA-TM-102325] p 156 N90-28786
- THIN PLATES**
Assumed strain distributions for a finite strip plate bending element using Mindlin-Reissner plate theory p 208 A90-16723
- THREADS**
Fastener design manual [NASA-RP-1228] p 202 N90-18740
- THREE DIMENSIONAL BODIES**
Advanced development of BEM for elastic and inelastic dynamic analysis of solids p 213 A90-45771
Free-vibration analysis of three-dimensional solids by BEM p 215 A90-52007
- THREE DIMENSIONAL BOUNDARY LAYER**
Computation of three dimensional turbulent boundary layers in internal flows, including turbomachinery rotor blades p 3 A90-12555
Computation of three-dimensional turbulent boundary layers with heat transfer in a plane of symmetry using embedded wall-layer functions [AIAA PAPER 90-0307] p 160 A90-19788
- THREE DIMENSIONAL FLOW**
Analysis of nonuniform subsonic flows about a row of moving blades p 2 A90-11779
Near wall flow parameters in the blade end-wall corner region p 156 A90-12636
A multi-domain spectral computation of three-dimensional laminar horseshoe vortex flow using incompressible Navier-Stokes equations p 3 A90-17592
Asymmetrical boundary layer separation at the base of a two cylinder geometry p 159 A90-18505
Reciprocal interactions of hairpin-shaped vortices and a boundary layer [AIAA PAPER 90-0017] p 159 A90-19635
Application of the computational aeroacoustics method to an advanced counterrotating propfan configuration [AIAA PAPER 90-0183] p 246 A90-19725
Calculation of turbulent three-dimensional jet-induced flow in a rectangular enclosure [AIAA PAPER 90-0684] p 161 A90-19976
Effects of g-jitter on a thermal, buoyant flow [AIAA PAPER 90-0653] p 163 A90-22239
Diagonal inversion of lower-upper implicit schemes p 242 A90-23110
Simulation of three-dimensional viscous flow within a multistage turbine [ASME PAPER 89-GT-152] p 5 A90-23841
Convection phenomena in low-gravity processing - The GTE GaAs space experiment [AIAA PAPER 90-0409] p 133 A90-25032
Comparison of 3-D viscous flow computations of Mach 5 inlet with experimental data [AIAA PAPER 90-0600] p 6 A90-26970
Three-dimensional fluid flow calculations using a flux-spline method p 167 A90-27983
Numerical analysis of three-dimensional viscous internal flows p 168 A90-32456
Multigrid calculations of 3-D turbulent viscous flows p 172 A90-42426
3D Euler analysis of ducted propfan flowfields [AIAA PAPER 90-3034] p 8 A90-45873

- Three dimensional LDV flow measurements and theoretical investigation in a radial inflow turbine scroll p 9 A90-46860
- Evolution and interaction of two- and three-dimensional instability waves p 173 A90-46885
- The growth and development of a turbulent junction vortex system p 173 A90-46902
- Three-dimensional compressible jet-in-crossflow calculations using improved viscosity models and adapted grid [AIAA PAPER 90-2100] p 174 A90-47206
- Diagonally inverted lower-upper factored implicit multigrid scheme for the three-dimensional Navier-Stokes equations p 174 A90-49789
- Multigrid calculations of 3-D turbulent viscous flows [NASA-CR-185154] p 1 N90-13323
- Recent progress in research pertaining to estimates of gas-side heat transfer in an aircraft gas turbine [NASA-TM-102460] p 27 N90-13394
- A simple algebraic grid adaptation scheme with applications to two- and three-dimensional flow problems [NASA-TM-102446] p 178 N90-18667
- Swept wing ice accretion modeling [NASA-TM-103114] p 13 N90-21727
- Investigation of advanced counterrotation blade configuration concepts for high speed turboprop systems, task 1: Ducted propfan analysis [NASA-CR-185217] p 30 N90-22567
- Implicit solution of three-dimensional internal turbulent flows [NASA-TM-103099] p 184 N90-27982
- ### THREE DIMENSIONAL MODELS
- Numerical study of the effects of icing on finite wing aerodynamics [AIAA PAPER 90-0757] p 3 A90-20010
- Convection phenomena in low-gravity processing - The GTE GaAs space experiment [AIAA PAPER 90-0409] p 133 A90-25032
- Swept wing ice accretion modeling [AIAA PAPER 90-0756] p 5 A90-25042
- Three-dimensional adaptive grid generation for body-fitted coordinate system p 167 A90-26506
- Three dimensional full potential method for the aeroelastic modeling of propfans [AIAA PAPER 90-1120] p 7 A90-29392
- Introducing the VRT gas turbine combustor [AIAA PAPER 90-2452] p 21 A90-42808
- Inelastic transient dynamic analysis of three-dimensional problems by BEM p 215 A90-51480
- An analysis of the viscous flow through a compact radial turbine by the average passage approach [NASA-TM-102471] p 12 N90-14206
- Response of a chemically reacting layer to streamwise vorticity [NASA-TM-102288] p 178 N90-18005
- Unsteady three-dimensional marginal separation, including breakdown [NASA-TM-102525] p 179 N90-20337
- Swept wing ice accretion modeling [NASA-TM-103114] p 13 N90-21727
- Introducing the VRT gas turbine combustor [NASA-TM-103176] p 137 N90-23591
- Metal matrix composites microfracture: Computational simulation [NASA-TM-103153] p 101 N90-24383
- Computational experience with a three-dimensional rotary engine combustion model [NASA-TM-103104] p 183 N90-26275
- ### THROATS
- Heat transfer to throat tubes in a square-chambered rocket engine at the NASA Lewis Research Center [NASA-TM-102336] p 70 N90-11082
- ### THRUST
- Iridium-coated rhenium thrusters by CVD p 114 A90-30480
- H2/O2 three-body rates at high temperatures [AIAA PAPER 90-1696] p 105 A90-38399
- A modeling technique for STOVL ejector and volume dynamics [AIAA PAPER 90-2417] p 20 A90-42168
- Low thrust rocket test facility [AIAA PAPER 90-2503] p 43 A90-47225
- Geometric effects in applied-field MPD thrusters [AIAA PAPER 90-2669] p 69 A90-52572
- Design of a thrust stand for high power electric propulsion devices [NASA-TM-102372] p 73 N90-15992
- Engine inlet distortion in a 9.2 percent scale vectored thrust STOVL model in ground effect [NASA-TM-102358] p 12 N90-17561
- A modeling technique for STOVL ejector and volume dynamics [NASA-TM-103167] p 30 N90-22566
- Low thrust rocket test facility [NASA-TM-103206] p 43 N90-25158
- Geometric effects in applied-field MPD thrusters [NASA-TM-103259] p 82 N90-27782
- ### THRUST CHAMBERS
- Cooling of rocket thrust chambers with liquid oxygen [AIAA PAPER 90-2120] p 63 A90-42029
- High-power xenon ion thrusters [AIAA PAPER 90-2540] p 64 A90-42536
- Preliminary plume characteristics of an arcjet thruster [AIAA PAPER 90-2645] p 64 A90-42609
- Diagnostics and performance of a 1/4-scale MPD thruster [AIAA PAPER 90-2665] p 65 A90-42625
- Combustor design and analysis using the ROCKET Combustor Interactive Design (ROCCID) Methodology [AIAA PAPER 90-2240] p 65 A90-45694
- A highly durable injector faceplate design concept for O2/H2 propellants [AIAA PAPER 90-2181] p 66 A90-47211
- Calculations of gaseous H2/O2 thruster [AIAA PAPER 90-2490] p 67 A90-47224
- Advanced tube-bundle rocket thrust chamber [AIAA PAPER 90-2726] p 67 A90-47227
- A rocket engine design expert system [NASA-TM-102373] p 69 N90-10172
- Cooling of rocket thrust chambers with liquid oxygen [NASA-TM-103146] p 78 N90-22605
- Combustor design and analysis using the Rocket Combustor Interactive Design (ROCCID) methodology [NASA-TM-103165] p 79 N90-24349
- Advanced tube-bundle rocket thrust chamber [NASA-TM-103139] p 80 N90-25185
- ### THRUST MEASUREMENT
- Arcjet nozzle design impacts p 76 N90-18478
- ### THRUST PROGRAMMING
- Optimal finite-thrust spacecraft trajectories using collocation and nonlinear programming [AAS PAPER 89-350] p 40 A90-46783
- ### THRUST VECTOR CONTROL
- Space Station Freedom resistojet system study p 54 A90-16368
- Engine inlet distortion in a 9.2 percent scaled vectored thrust STOVL model in ground effect [AIAA PAPER 89-2910] p 5 A90-25043
- Flight control design considerations for STOVL powered-lift flight [AIAA PAPER 90-3225] p 37 A90-49110
- Electromechanical actuation for thrust vector control applications [NASA-TM-102548] p 152 N90-21272
- ### TILT ROTOR AIRCRAFT
- The selection of convertible engines with current gas generator technology for high speed rotorcraft p 22 A90-46933
- ### TILTING ROTORS
- The selection of convertible engines with current gas generator technology for high speed rotorcraft p 22 A90-46933
- ### TIME DEPENDENCE
- Time-dependent viscous incompressible Navier-Stokes equations - The finite difference Galerkin formulation and streamfunction algorithms p 156 A90-11598
- Analysis of shell-type structures subjected to time-dependent mechanical and thermal loading [NASA-CR-185077] p 222 N90-24653
- ### TIME DIVISION MULTIPLE ACCESS
- Satellite range delay simulator for a matrix-switched time division multiple-access network simulation system [AIAA PAPER 90-0795] p 139 A90-25620
- A users perspective of the ACTS hopping beam TDMA system [AIAA PAPER 90-0833] p 140 A90-25658
- Satellite-matrix-switched, time-division-multiple-access network simulator [AIAA PAPER 90-0848] p 147 A90-25671
- A burst compression and expansion technique for variable-rate users in satellite-switched TDMA networks [AIAA PAPER 90-0850] p 46 A90-25673
- Characterization of two MMIC GaAs switch matrices at microwave frequencies [AIAA PAPER 90-0866] p 147 A90-25686
- Advanced Communications Technology Satellite (ACTS) and potential system applications p 142 A90-51165
- Satellite-matrix-switched, time-division-multiple-access network simulator [NASA-TP-2944] p 142 N90-11915
- Satellite range delay simulator for a matrix-switched time division multiple-access network simulator [NASA-TM-102407] p 143 N90-12813
- Characterization of two MMIC GaAs switch matrices at microwave frequencies [NASA-TM-102449] p 50 N90-14273
- A burst compression and expansion technique for variable-rate users in satellite-switched TDMA networks [NASA-TM-102414] p 47 N90-15983
- ### TIME DIVISION MULTIPLEXING
- Performance analysis of Integrated Communication and Control System networks p 239 A90-51267
- ### TIME LAG
- An observer-based compensator for distributed delays p 239 A90-49899
- ### TIME OPTIMAL CONTROL
- Optimal impulsive time-fixed orbital rendezvous and interception with path constraints [AIAA PAPER 90-2972] p 41 A90-53051
- ### TIME SERIES ANALYSIS
- Health monitoring system for the SSME - Program overview [AIAA PAPER 90-1987] p 63 A90-40583
- Rocket engine failure detection using system identification techniques [AIAA PAPER 90-1993] p 65 A90-47205
- Rocket engine failure detection using system identification techniques [NASA-CR-185259] p 45 N90-25159
- ### TIN ALLOYS
- Efficient estimation of diffusion during dendritic solidification p 111 A90-20612
- Primary arm spacing in directionally solidified Pb-10 wt pct Sn alloys [AIAA PAPER 90-0740] p 132 A90-23713
- Primary arm spacing in directionally solidified Pb-10 wt percent Sn alloys [NASA-CR-185190] p 134 N90-14398
- ### TIN OXIDES
- Fe-57 and Sn-119 Moessbauer study of La2CuO(4-y), YBa2Cu3O(7-y) and SmBa2Cu3O(7-y) p 256 A90-34020
- Investigation of buried homojunctions in p-InP formed during sputter deposition of both indium tin oxide and indium oxide p 256 A90-36799
- ### TITANATES
- Heat treatment study of the SiC/Ti-15-3 composite system [NASA-TP-2970] p 97 N90-19302
- ### TITANIUM ALLOYS
- Investigation of interfacial shear strength in a SiC fibre/Ti-24Al-11Nb composite by a fibre push-out technique p 88 A90-18973
- Evaluation of thermal and mechanical loading effects on the structural behavior of a SiC/titanium composite [AIAA PAPER 90-1026] p 90 A90-29228
- Isothermal and nonisothermal fatigue behavior of a metal matrix composite p 91 A90-36746
- Microstructure of a SiC/Ti-15-3 composite p 91 A90-37663
- Reaction zone microstructure in a Ti3Al + Nb/SiC composite p 91 A90-39627
- Cyclic oxidation of aluminide coatings on Ti3Al + Nb p 115 A90-39660
- Tribological properties of ceramic/Ti3Al-Nb sliding couples for use as candidate seal materials to 700 deg C [NASA-TM-102401] p 86 N90-12658
- ### TITANIUM BORIDES
- 1200 to 1400 K slow strain rate compressive properties of NiAl/Ni2AlTi-base materials p 88 A90-18938
- Elevated temperature slow plastic deformation of NiAl-TiB2 particulate composites at 1200 and 1300 K p 92 A90-45621
- High-temperature slow-strain-rate compression studies on CoAl-TiB2 composites p 93 A90-48636
- Empirical and analytical determination of the fracture resistance of a TiB2 particle/SiC matrix composite [NASA-TM-101940] p 96 N90-15143
- ### TITANIUM CHLORIDES
- TiCl4 as a source of TiO2 particles for laser anemometry measurements in hot gas [NASA-TM-102581] p 189 N90-20358
- ### TITANIUM COMPOUNDS
- Slow plastic deformation of extruded NiAl-10TiB2 particulate composites at 1200 and 1300 K p 92 A90-46133
- ### TITANIUM OXIDES
- TiCl4 as a source of TiO2 particles for laser anemometry measurements in hot gas [NASA-TM-102581] p 189 N90-20358
- ### TOLERANCES (MECHANICS)
- Solar Concentrator Advanced Development Program [NASA-CR-185173] p 232 N90-22834
- ### TOOLS
- Adjustable depth gage [NASA-CASE-LEW-14880-1] p 187 N90-10415
- ### TOPOGRAPHY
- Design and calibration of a vacuum compatible scanning tunneling microscope [NASA-TM-102514] p 189 N90-20353
- ### TOPOLOGY
- Topology of modified helical gears p 195 A90-21132

SUBJECT INDEX

TORQUE

- Variable speed induction motor operation from a 20-kHz power bus p 148 A90-38119
- A fiber optic sensor for noncontact measurement of shaft speed, torque, and power [NASA-TM-102481] p 189 N90-21360

TORQUE MOTORS

- Magnification of starting torques of dc motors by maximum power point trackers in photovoltaic systems p 149 A90-38144

TORQUEMETERS

- A fiber optic sensor for noncontact measurement of shaft speed, torque, and power [NASA-TM-102481] p 189 N90-21360

TORSION

- Effect of crack-microcracks interaction on energy release rates p 214 A90-49269

TORSIONAL STRESS

- Torsional and biaxial (tension-torsion) fatigue damage mechanisms in Waspaloy at room temperature p 109 A90-11925
- A constitutive model for the inelastic multiaxial response of Rene 80 at 871 C and 982 C p 114 A90-32266
- Microstructure: Property correlation --- multiaxial fatigue damage evolution in waspaloy [NASA-CR-180406] p 224 N90-28880

TORSIONAL VIBRATION

- Dynamics of multistage gear transmission with effects of gearbox vibrations [NASA-TM-103109] p 205 N90-28060

TRACTION

- The measurement, modeling, and prediction of traction for rocket propellant 1 [NASA-CR-185186] p 131 N90-19386

TRAJECTORY CONTROL

- Reaction-compensation technology for microgravity laboratory robots [NASA-TM-103271] p 205 N90-28062

TRAJECTORY OPTIMIZATION

- Optimal finite-thrust spacecraft trajectories using collocation and nonlinear programming [AAS PAPER 89-350] p 40 A90-46783
- Minimum fuel trajectories for a low-thrust power-limited mission to the moon and to Lagrange points L4 and L5 [AAS PAPER 89-351] p 40 A90-46784
- Minimum fuel trajectory for the aerospace-plane [AAS PAPER 89-352] p 40 A90-46785
- Optimal orbital rendezvous using high and low thrust [AAS PAPER 89-354] p 41 A90-46786
- Optimal cooperative time-fixed impulsive rendezvous [AIAA PAPER 90-2962] p 41 A90-53037
- Discrete approximations to optimal trajectories using direct transcription and nonlinear programming [AIAA PAPER 90-2963] p 41 A90-53038

TRANSFER ORBITS

- Xenon ion propulsion for orbit transfer [AAS PAPER 90-2527] p 67 A90-52562
- Comparison of solution approaches for minimum-fuel, low-thrust, power-limited orbital transfers [AIAA PAPER 90-2960] p 41 A90-53035

TRANSFORMERS

- 20 kHz, 25 kVA node power transformer p 149 A90-38275
- High power density dc/dc converter: Selection of converter topology [NASA-CR-186129] p 151 N90-14467

TRANSIENT HEATING

- Some aspects of transient cooling of a radiating rectangular medium p 157 A90-13095
- Emission bounds for transient radiative cooling of a scattering rectangular region p 161 A90-20520
- The role of thermal and lubricant boundary layers in the transient thermal analysis of spur gears p 194 A90-21118

TRANSIENT RESPONSE

- Characterization of structural connections using free and forced response test data p 213 A90-46172
- Inelastic transient dynamic analysis of three-dimensional problems by BEM p 215 A90-51480
- An expert system to perform on-line controller tuning [NASA-TM-103101] p 240 N90-23991
- Low velocity impact analysis with NASTRAN p 221 N90-24647

TRANSITION FLIGHT

- H-infinity based integrated flight/propulsion control design for a STOVL aircraft in transition flight [AIAA PAPER 90-3335] p 36 A90-47595
- H-infinity based integrated flight/propulsion control design for a STOVL aircraft in transition flight [NASA-TM-103198] p 37 N90-26011

TRANSITION FLOW

- Simulating transitional flow and heat transfer over the flat plate and circular cylinder using a K-epsilon turbulence model p 168 A90-32171

TRANSITION METALS

- Electrical properties of materials for high temperature strain gage applications [NASA-CR-186192] p 188 N90-14534

TRANSITION TEMPERATURE

- Observations on the brittle to ductile transition temperatures of B2 nickel aluminides with and without zirconium p 111 A90-19153

TRANSMISSION

- Profile modification to minimize spur gear dynamic loading p 195 A90-21128
- Conjugate field approaches for active array compensation p 144 A90-19266

TRANSMISSION CIRCUITS

- Modeling of power electronic systems with EMT [NASA-TM-102375] p 245 N90-14060

TRANSMISSION LINES

- Preliminary evaluation of space station transmission line in a ring configuration [NASA-TM-102461] p 74 N90-17677
- High-temperature superconductors for space power transmission lines [NASA-TM-103459] p 259 N90-24952

TRANSMISSION LOSS

- Ka-band propagation characteristics of microstrip lines on GaAs substrates at cryogenic temperatures p 147 A90-33644

TRANSMISSIONS (MACHINE ELEMENTS)

- Experimental and analytical evaluation of dynamic load vibration of a 2240-kW (3000-hp) rotorcraft transmission p 192 A90-13750
- Efficiency testing of a helicopter transmission planetary reduction stage p 193 A90-21113
- Effect of advanced component technology on helicopter transmissions p 193 A90-21115
- Vibration signature analysis of multistage gear transmission p 194 A90-21124
- Topology of modified helical gears p 195 A90-21132
- Efficiency study comparing two helicopter planetary reduction stages [AIAA PAPER 90-2156] p 199 A90-50644
- Assessment of worm gearing for helicopter transmissions [NASA-TM-102441] p 27 N90-15923
- Transmission research activities at NASA Lewis Research Center p 203 N90-21394
- [NASA-TM-103132] p 203 N90-21394
- Influence of linear profile modification and loading conditions on the dynamic tooth load and stress of high contact ratio gears p 204 N90-22796
- Non-linear dynamic analysis of geared systems, part 2 [NASA-CR-180495] p 204 N90-23732
- Dynamics of multistage gear transmission with effects of gearbox vibrations [NASA-TM-103109] p 205 N90-28060

TRANSMITTERS

- Lunar orbiting microwave beam power system [NASA-TM-103211] p 51 N90-25173

TRANSONIC FLOW

- Application of the computational aeroacoustics method to an advanced counterrotating propfan configuration [AIAA PAPER 90-0183] p 246 A90-19725
- Absorbing boundary conditions for second-order hyperbolic equations p 242 A90-34549
- Laser anemometer measurements in a transonic axial-flow fan rotor [NASA-TP-2879] p 175 N90-11245
- Numerical investigation of separated transonic turbulent flows with a multiple-time-scale turbulence model [NASA-TM-102499] p 180 N90-21962
- Investigation of advanced counterrotation blade configuration concepts for high speed turboprop systems, task 1: Ducted propfan analysis [NASA-CR-185217] p 30 N90-22567

TRANSPONDERS

- Performance measurements for a laboratory-simulated 30/20 GHz communication satellite transponder [AIAA PAPER 90-0808] p 140 A90-25634
- Performance measurements for a laboratory-simulated 30/20 GHz communication satellite transponder [NASA-TM-102424] p 143 N90-17977

TRANSPORT AIRCRAFT

- Civil air transport: A fresh look at power-by-wire and fly-by-light [NASA-TM-102574] p 153 N90-21283
- High speed commercial transport fuels considerations and research needs [NASA-TM-102535] p 131 N90-21869
- Energy Efficient Engine: Flight propulsion system final design and analysis [NASA-CR-168219] p 34 N90-28558

TRANSPORT PROPERTIES

- Investigation of turbulent transport in an axisymmetric sudden expansion p 163 A90-23112

TRIMETHYL COMPOUNDS

TRANSPORT THEORY

- Model-free simulations of turbulent reactive flows p 158 A90-15729
- Efficient real gas Navier-Stokes computations of high speed flows using an LU scheme [AIAA PAPER 90-0391] p 164 A90-23706
- Transport properties of InAs(x)Sb(1-x) (x = 0-0.55) on InP grown by molecular-beam epitaxy p 256 A90-36232
- Efficient real gas Navier-Stokes computations of high speed flows using an LU scheme [NASA-TM-102429] p 11 N90-14203
- The numerical simulation of multistage turbomachinery flows p 29 N90-21025

TRANSPUTERS

- Parallel multi-time step integration on a transputer system p 235 A90-20188
- Transient finite element computations on the transputer system [NASA-CR-185199] p 218 N90-18071

TRANVERSE OSCILLATION

- Dynamic analysis of geared rotors by finite elements [NASA-TM-102349] p 201 N90-16286

TRAVELING WAVE TUBES

- K-band TWT using new diamond rod technology [AIAA PAPER 90-0870] p 147 A90-25691
- Secondary electron emission characteristics of molybdenum-masked, ion-textured OFHC copper [NASA-TP-2967] p 117 N90-15211
- Miniature traveling wave tube and method of making [NASA-CASE-LEW-14520-1] p 153 N90-22724
- Conceptual definition of a high voltage power supply test facility [NASA-CR-185216] p 50 N90-25172
- Spent-beam refocusing analysis and multistage depressed collector design for a 75-W, 59- to 64-GHz coupled-cavity traveling-wave tube [NASA-TP-3039] p 155 N90-27965
- Rain-fade simulation and power augmentation for satellite communication systems [NASA-TM-103134] p 146 N90-28768

TREES (MATHEMATICS)

- Multi-level Hierarchical Poly Tree computer architectures p 236 A90-26082

TRENDS

- Power conditioning techniques [NASA-TM-102577] p 151 N90-20301

TRIBOLOGY

- Fundamentals of tribology at the atomic level p 192 A90-14020
- Tribological reactions of perfluoroalkyl polyether oils with stainless steel under ultrahigh vacuum conditions at room temperature p 120 A90-16278
- Applications of surface analysis and surface theory in tribology p 84 A90-37458
- Plasma-deposited amorphous hydrogenated carbon films and their tribological properties p 123 A90-44864
- Fundamental tribological properties of ion-beam-deposited boron nitride films p 124 A90-49054
- Plasma-deposited amorphous hydrogenated carbon films and their tribological properties [NASA-TM-102379] p 125 N90-11880
- Fundamental tribological properties of ion-beam-deposited boron nitride films [NASA-TM-102088] p 125 N90-11881
- Tribological properties of ceramic/TiAl-Nb sliding couples for use as candidate seal materials to 700 deg C [NASA-TM-102401] p 86 N90-12658
- Tribological properties of PM212: A high-temperature, self-lubricating, powder metallurgy composite [NASA-TM-102355] p 86 N90-12659
- A new test machine for measuring friction and wear in controlled atmospheres to 1200 C [NASA-TM-102405] p 96 N90-12670
- The experimental evaluation and application of high-temperature solid lubricants [NASA-TM-102476] p 127 N90-16944
- The application of a computer data acquisition system for a new high temperature tribometer [NASA-TM-102508] p 86 N90-17811
- Experimentally determined wear behavior of an Al2O3-SiC composite from 25 to 1200 C [NASA-TM-102549] p 87 N90-20130
- Studies of mechano-chemical interactions in the tribological behavior of materials [NASA-TM-102545] p 128 N90-21182
- Self-lubricating polymer composites and polymer transfer film lubrication for space applications [NASA-TM-102492] p 128 N90-21862

TRIMETHYL COMPOUNDS

- Determination of the mean solid-liquid interface energy of pivalic acid p 84 A90-22646

TRUSSES

TRUSSES

Solar Concentrator Advanced Development Program
[NASA-CR-185173] p 232 N90-22834
Dynamic analysis of space-related linear and non-linear
structures
[NASA-TM-103490] p 51 N90-25174

TUBE HEAT EXCHANGERS

Initial characterization of a modular heat exchanger with
an integral heat pipe --- for Stirling space engine
p 62 A90-38301

TUBES

The impedance of a tubular electrode - A model for a
porous electrode p 104 A90-33723

TUNGSTEN

Fiber reinforced superalloys p 91 A90-34169

TUNGSTEN ALLOYS

High temperature fatigue behavior of tungsten copper
composites
[NASA-TM-102404] p 99 N90-21138

TUNING

Effects of mistuning and matrix structure on the topology
of frequency response curves
[NASA-TM-102290] p 216 N90-12041

TURBINE BLADES

Shaft flexibility effects on aeroelastic stability of a rotating
bladed disk p 208 A90-16371
Unsteady heat transfer on turbine blades
p 161 A90-20511

Heat flux measurements

[ASME PAPER 89-GT-107] p 165 A90-23815
Phase and time-resolved measurements of unsteady
heat transfer and pressure in a full-stage rotating turbine
[ASME PAPER 89-GT-135] p 165 A90-23832

Probabilistic analysis of bladed turbine disks and the
effect of mistuning
[AIAA PAPER 90-1097] p 196 A90-29327

Aeroelastic stability analysis of a high-energy turbine
blade --- for SSME High Pressure Oxidizer TurboPump
first stage
[AIAA PAPER 90-2351] p 66 A90-47215

Large scale prop-fan structural design study. Volume
1: Initial concepts
[NASA-CR-174992] p 23 N90-10043

Large scale prop-fan structural design study. Volume
2: Preliminary design of SR-7
[NASA-CR-174993] p 23 N90-10044

Heat transfer to throat tubes in a square-chambered
rocket engine at the NASA Lewis Research Center
[NASA-TM-102336] p 70 N90-11082

Model 0A wind turbine generator FMEA
[NASA-TM-102378] p 206 N90-12034

Effects of mistuning and matrix structure on the topology
of frequency response curves
[NASA-TM-102290] p 216 N90-12041

Navier-Stokes analysis of turbine blade heat transfer
[NASA-TM-102496] p 179 N90-21300

Probabilistic analysis of bladed turbine disks and the
effect of mistuning
[NASA-TM-102564] p 136 N90-21871

Probabilistic structural analysis of aerospace
components using NESSUS
[NASA-TM-102324] p 221 N90-22823

Heat transfer and pressure measurements for the SSME
fuel-side turbopump
[NASA-CR-184928] p 31 N90-23405

Micromechanics of cyclic deformation in SSME
turbopump blade materials p 224 N90-28641

Constitutive and life modeling of single crystal blade
alloys for root attachment analysis p 119 N90-28643

Structural response of SSME turbine blade airfoils
p 224 N90-28649

Durability of thermal barrier coatings in a high heat flux
environment p 129 N90-28651

Thermal analysis of thermal barrier coatings in a high
heat flux environment p 129 N90-28652

TURBINE ENGINES

A review of failure models for ceramic matrix composite
laminates under monotonic loads
[ASME PAPER 89-GT-153] p 89 A90-23842

Effect of vane twist on the performance of dome swirlers
for gas turbine airblast atomizers
[AIAA PAPER 90-1955] p 173 A90-47203

Vibration dampers for cryogenic turbomachinery
[AIAA PAPER 90-2740] p 199 A90-47228

Advanced Turbine Technology Applications Project
(ATTAP)
[NASA-CR-185109] p 263 N90-14153

Effect of vane twist on the performance of dome swirlers
for gas turbine airblast atomizers
[NASA-TM-103195] p 182 N90-25289

Energy Efficient Engine: Flight propulsion system final
design and analysis
[NASA-CR-168219] p 34 N90-28558

Energy Efficient Engine core design and performance
report
[NASA-CR-168069] p 34 N90-28559

NASA/GE Energy Efficient Engine low pressure turbine
scaled test vehicle performance report
[NASA-CR-168290] p 34 N90-28563

TURBINE PUMPS

Heat flux measurements
[ASME PAPER 89-GT-107] p 165 A90-23815

Application of HOST technology to the SSME HPFTP
blade
[ASME PAPER 89-GT-130] p 209 A90-23828

Application of the probabilistic approximate analysis
method to a turbopump blade analysis --- for Space Shuttle
Main Engine
[AIAA PAPER 90-1098] p 56 A90-29328

The simulation of fluid dynamic uncertainties in the SSME
turbopump
[AIAA PAPER 90-2294] p 65 A90-42770

Aeroelastic stability analysis of a high-energy turbine
blade --- for SSME High Pressure Oxidizer TurboPump
first stage
[AIAA PAPER 90-2351] p 66 A90-47215

Probabilistic modeling for simulation of aerodynamic
uncertainties in propulsion systems
[NASA-TM-102472] p 29 N90-21036

Experimental evaluation of a tuned electromagnetic
damper for vibration control of cryogenic turbopump
rotors
[NASA-TP-3005] p 30 N90-23403

Heat transfer and pressure measurements for the SSME
fuel-side turbopump
[NASA-CR-184928] p 31 N90-23405

Reusable rocket engine turbopump health monitoring
system, part 3
[NASA-CR-182294] p 204 N90-26320

Bearing optimization for SSME HPOTP application
p 205 N90-28622

Micromechanics of cyclic deformation in SSME
turbopump blade materials p 224 N90-28641

TURBINE WHEELS

Advanced technology's impact on compressor design
and development - A perspective
[SAE SP-800] p 20 A90-28571

Probabilistic analysis of bladed turbine disks and the
effect of mistuning
[AIAA PAPER 90-1097] p 196 A90-29327

Advanced technologies impact on compressor design
and development: A perspective
[NASA-TM-102341] p 24 N90-10891

Probabilistic analysis of bladed turbine disks and the
effect of mistuning
[NASA-TM-102564] p 136 N90-21871

TURBINES

An analysis of the viscous flow through a compact radial
turbine by the average passage approach
[NASA-TM-102471] p 12 N90-14206

Heat transfer and pressure measurements for the SSME
fuel-side turbopump
[NASA-CR-184928] p 31 N90-23405

TURBOCOMPRESSORS

Simulation of three-dimensional viscous flow within a
multistage turbine
[ASME PAPER 89-GT-152] p 5 A90-23841

Analysis and design of helium-buffered face seals for
the SSME high-pressure oxygen turbopump
[AIAA PAPER 90-2049] p 197 A90-42000

Improved silicon carbide for advanced heat engines
[NASA-CR-180831] p 124 N90-10293

TURBOFAN AIRCRAFT

Energy efficient engine program technology benefit/cost
study. Volume 1: Executive summary
[NASA-CR-174766-VOL-1] p 34 N90-28564

Energy efficient engine program technology benefit/cost
study, volume 2
[NASA-CR-174766-VOL-2] p 35 N90-28565

TURBOFAN ENGINES

Advanced core technology - Key to subsonic propulsion
benefits
[ASME PAPER 89-GT-241] p 19 A90-23890

Advanced technology's impact on compressor design
and development - A perspective
[SAE SP-800] p 20 A90-28571

A real time microcomputer implementation of sensor
failure detection for turbofan engines p 21 A90-45414

PMR graphite engine duct development
[NASA-CR-182228] p 23 N90-10037

Full scale technology demonstration of a modern
counterrotating unducted fan engine concept: Component
test
[NASA-CR-180868] p 24 N90-10047

Full scale technology demonstration of a modern
counterrotating unducted fan engine concept. Design
report
[NASA-CR-180867] p 24 N90-10048

Full scale technology demonstration of a modern
counterrotating unducted fan engine concept. Engine
test
[NASA-CR-180869] p 24 N90-10049

Advanced technologies impact on compressor design
and development: A perspective
[NASA-TM-102341] p 24 N90-10891

STOVL propulsion system volume dynamics
approximations
[NASA-TM-102397] p 25 N90-11740

Real-time simulation of an F110/STOVL turbofan
engine
[NASA-TM-102409] p 25 N90-12618

Advanced detection, isolation, and accommodation of
sensor failures in turbofan engines: Real-time
microcomputer implementation
[NASA-TP-2925] p 37 N90-15112

Altitude testing of the 2D V-STOL ADEN demonstrator
on an F404 engine
[NASA-CR-174824] p 28 N90-17638

Supersonic through-flow fan engine and aircraft mission
performance
[NASA-TM-102304] p 29 N90-21038

Energy Efficient Engine combustor test hardware
detailed design report
[NASA-CR-168301] p 33 N90-28554

Energy Efficient Engine (E3) combustion system
component technology performance report
[NASA-CR-168274] p 33 N90-28555

Energy Efficient Engine acoustic supporting technology
report
[NASA-CR-174834] p 33 N90-28557

Energy Efficient Engine program advanced turbofan
nacelle definition study
[NASA-CR-174942] p 34 N90-28560

Energy Efficient Engine: Control system component
performance report
[NASA-CR-174651] p 34 N90-28562

Energy efficient engine program technology benefit/cost
study. Volume 1: Executive summary
[NASA-CR-174766-VOL-1] p 34 N90-28564

Energy efficient engine program technology benefit/cost
study, volume 2
[NASA-CR-174766-VOL-2] p 35 N90-28565

TURBOJET ENGINE CONTROL

A real time microcomputer implementation of sensor
failure detection for turbofan engines p 21 A90-45414

TURBOJET ENGINES

On the use of external burning to reduce aerospace
vehicle transonic drag
[AIAA PAPER 90-1935] p 20 A90-40562

On the use of external burning to reduce aerospace
vehicle transonic drag
[NASA-TM-103107] p 30 N90-21762

TURBOMACHINE BLADES

Numerical analysis of three-dimensional viscous internal
flows p 168 A90-32456

Composite Blade Structural Analyzer (COBSTRAN)
theoretical/programmer's manual
[NASA-TM-101958] p 95 N90-10181

TURBOMACHINERY

Calculation of unsteady Euler flows in turbomachinery
using the linearized Euler equations p 2 A90-11778

Aeroelastic detuning for stability enhancement of
uninstalled supersonic flutter p 19 A90-17462

An interactive grid generation procedure for axial and
radial flow turbomachinery
[AIAA PAPER 90-0344] p 162 A90-22200

Application of a lower-upper implicit scheme and an
interactive grid generation for turbomachinery flow field
simulations
[ASME PAPER 89-GT-20] p 4 A90-23762

Simulation of three-dimensional viscous flow within a
multistage turbine
[ASME PAPER 89-GT-152] p 5 A90-23841

Experimental determination of stator endwall heat
transfer
[ASME PAPER 89-GT-219] p 165 A90-23880

Interactive grid generation for turbomachinery flow field
simulations p 6 A90-26553

An annular gas seal analysis using empirical entrance
and exit region friction factors
[ASME PAPER 89-TRIB-46] p 196 A90-33555

Test and theory for piezoelectric actuator-active vibration
control of rotating machinery p 198 A90-46226

Application of a two-dimensional unsteady viscous
analysis code to a supersonic throughflow fan stage
[NASA-TM-4141] p 25 N90-13387

An interactive grid generation procedure for axial and
radial flow turbomachinery
[NASA-CR-185167] p 237 N90-13968

An applicational process for dynamic balancing of
turbomachinery shafting
[NASA-TM-102537] p 202 N90-20392

GRID2D/3D: A computer program for generating grid
systems in complex-shaped two- and three-dimensional
spatial domains. Part 2: User's manual and program
listing
[NASA-TM-102454] p 237 N90-20708

SUBJECT INDEX

- The numerical simulation of multistage turbomachinery flows p 29 N90-21025
- Computer code for predicting coolant flow and heat transfer in turbomachinery [NASA-TP-2985] p 32 N90-27722
- ### TURBOPROP AIRCRAFT
- Noise of a simulated installed model counterrotation propeller at angle-of-attack and takeoff/approach conditions [NASA-TM-102440] p 248 N90-20794
- High speed turboprop aeroacoustic study (counterrotation). Volume 1: Model development [NASA-CR-185241] p 249 N90-26633
- ### TURBOPROP ENGINES
- Parametric studies of advanced turboprops p 19 A90-21225
- Investigation of the near wake of a propfan p 7 A90-40686
- Large-scale Advanced Prop-fan (LAP) high speed wind tunnel test report [NASA-CR-182125] p 24 N90-10045
- Full scale technology demonstration of a modern counterrotating unducted fan engine concept. Design report [NASA-CR-180867] p 24 N90-10048
- Propfan Test Assessment (PTA) [NASA-CR-185138] p 25 N90-11739
- User's guide to PMESH: A grid-generation program for single-rotation and counterrotation advanced turboprops [NASA-CR-185156] p 235 N90-14783
- Advanced gearbox technology [NASA-CR-179625] p 32 N90-24274
- ### TURBULENCE
- Application of large eddy interaction model to a mixing layer [NASA-CR-185123] p 11 N90-13328
- Two-dimensional analysis of two-phase reacting flow in a firing direct-injection diesel engine [NASA-TM-102069] p 27 N90-13392
- Effect of spatial resolution on apparent sensitivity to initial conditions of a decaying flow as it becomes turbulent [NASA-TM-102377] p 176 N90-13719
- Scattered-light scanner measurements of cryogenic liquid-jet breakup [NASA-TM-102432] p 189 N90-22021
- An improved k-epsilon model for near-wall turbulence and comparison with direct numerical simulation [NASA-TM-103221] p 184 N90-27983
- ### TURBULENCE EFFECTS
- Effects of very high turbulence on heat transfer p 169 A90-35247
- Control of flow separation and mixing by aerodynamic excitation [NASA-TM-103131] p 13 N90-21733
- ### TURBULENCE MODELS
- Calculation of reattaching shear layers in divergent channel with a multiple-time-scale turbulence model [AIAA PAPER 90-0047] p 160 A90-19649
- Calculation of turbulence-driven secondary motion in ducts with arbitrary cross-section [AIAA PAPER 90-0245] p 160 A90-19752
- On the mathematical modeling of the Reynolds stress's equations [AIAA PAPER 90-0498] p 161 A90-19878
- Evaluation of three turbulence models in static air loads and dynamic stall predictions p 7 A90-31291
- Time-dependent calculation of a forced mixing layer using a k-epsilon turbulence model p 169 A90-35222
- An experimental and numerical study of particle-laden coaxial jet flows p 171 A90-38799
- Application of large eddy interaction model to a mixing layer [NASA-CR-185123] p 11 N90-13328
- Comparison of 3-D viscous flow computations of Mach 5 inlet with experimental data [NASA-TM-102518] p 28 N90-20090
- PROTEUS two-dimensional Navier-Stokes computer code, version 1.0. Volume 1: Analysis description [NASA-TM-102551] p 180 N90-21303
- Numerical investigation of separated transonic turbulent flows with a multiple-time-scale turbulence model [NASA-TM-102499] p 180 N90-21962
- Computational modeling and validation for hypersonic inlets [NASA-TM-103111] p 181 N90-22011
- An investigation into the numerical prediction of boundary layer transition using the K.Y. Chien turbulence model [NASA-CR-185252] p 182 N90-26269
- Implicit solution of three-dimensional internal turbulent flows [NASA-TM-103099] p 184 N90-27982

TURBULENT BOUNDARY LAYER

- Computation of three dimensional turbulent boundary layers in internal flows, including turbomachinery rotor blades p 3 A90-12555
- Skin friction measurements by laser interferometry in swept shock/boundary-layer interactions p 3 A90-18153
- Reciprocal interactions of hairpin-shaped vortices and a boundary layer [AIAA PAPER 90-0017] p 159 A90-19635
- Computation of three-dimensional turbulent boundary layers with heat transfer in a plane of symmetry using embedded wall-layer functions [AIAA PAPER 90-0307] p 160 A90-19788
- On sublayer streaks p 168 A90-28143
- Some characteristics of bypass transition in a heated boundary layer p 169 A90-35183
- Structure of a reattaching supersonic shear layer p 7 A90-36252
- A study of the unsteadiness of crossing shock wave turbulent boundary layer interactions [AIAA PAPER 90-1456] p 170 A90-38614
- The growth and development of a turbulent junction vortex system p 173 A90-46902
- An LDA investigation of the normal shock wave boundary layer interaction p 10 A90-52618
- The measurement of boundary layers on a compressor blade in cascade. Volume 1: Experimental technique, analysis and results [NASA-CR-185118-VOL-1] p 23 N90-10038
- Wall-layer eruptions in turbulent flows [NASA-TM-102362] p 175 N90-11250
- Numerical investigation of separated transonic turbulent flows with a multiple-time-scale turbulence model [NASA-TM-102499] p 180 N90-21962
- Interactive calculation procedures for mixed compression inlets [NASA-CR-186581] p 14 N90-25934
- ### TURBULENT DIFFUSION
- Application of large eddy interaction model to a mixing layer [NASA-CR-185123] p 11 N90-13328
- The numerical simulation of multistage turbomachinery flows p 29 N90-21025
- ### TURBULENT FLOW
- Two-component phase-averaged turbulence statistics downstream of a rotating spoked-wheel wake generator p 156 A90-11559
- Near wall flow parameters in the blade end-wall corner region p 156 A90-12636
- Progress in direct numerical simulations of turbulent reacting flows p 157 A90-12836
- Contributions to the understanding of large-scale coherent structures in developing free turbulent shear flows p 158 A90-13907
- Model-free simulations of turbulent reactive flows p 158 A90-15729
- Calculation of reattaching shear layers in divergent channel with a multiple-time-scale turbulence model [AIAA PAPER 90-0047] p 160 A90-19649
- Calculation of turbulence-driven secondary motion in ducts with arbitrary cross-section [AIAA PAPER 90-0245] p 160 A90-19752
- On the mathematical modeling of the Reynolds stress's equations [AIAA PAPER 90-0498] p 161 A90-19878
- Compressibility effects in free shear layers [AIAA PAPER 90-0705] p 161 A90-19984
- Chemically reacting supersonic flow calculation using an assumed PDF model [AIAA PAPER 90-0731] p 4 A90-22256
- Time-accurate simulations of a shear layer forced at a single frequency p 163 A90-23111
- Investigation of turbulent transport in an axisymmetric sudden expansion p 163 A90-23112
- On sublayer streaks p 168 A90-28143
- Evaluation of three turbulence models in static air loads and dynamic stall predictions p 7 A90-31291
- The pdf approach to turbulent flow p 168 A90-32225
- Time-dependent calculation of a forced mixing layer using a k-epsilon turbulence model p 169 A90-35222
- Effects of very high turbulence on heat transfer p 169 A90-35247
- Near-wall turbulence model and its application to fully developed turbulent channel and pipe flows p 169 A90-37328
- Two-dimensional numerical simulation of a Stirling engine heat exchanger p 170 A90-38290
- Experimental investigation of turbulent flow through a circular-to-rectangular transition duct [AIAA PAPER 90-1505] p 171 A90-38654
- A simplified model for two phase face seal design p 197 A90-40713
- Multigrid calculations of 3-D turbulent viscous flows p 172 A90-42426

TWO DIMENSIONAL FLOW

- Computation of turbine flowfields with a Navier-Stokes code [AIAA PAPER 90-2122] p 8 A90-42731
- Nonlinear Reynolds stress models and the renormalization group p 172 A90-44011
- Three-dimensional turbulent flow code calculations of hot gas ingestion p 21 A90-44726
- The growth and development of a turbulent junction vortex system p 173 A90-46902
- Rate correlation for condensation of pure vapor on turbulent, subcooled liquid p 174 A90-50511
- Wall-layer eruptions in turbulent flows [NASA-TM-102362] p 175 N90-11250
- Investigation of turbulent flow in highly curved ducts with application to turbomachinery components [NASA-CR-186060] p 175 N90-12882
- Multigrid calculations of 3-D turbulent viscous flows [NASA-CR-185154] p 1 N90-13323
- Application of large eddy interaction model to a mixing layer [NASA-CR-185123] p 11 N90-13328
- A planar reacting shear layer system for the study of fluid dynamics-combustion interaction [NASA-TM-102422] p 27 N90-13393
- Effect of spatial resolution on apparent sensitivity to initial conditions of a decaying flow as it becomes turbulent [NASA-TM-102377] p 176 N90-13719
- Numerical investigation of separated transonic turbulent flows with a multiple-time-scale turbulence model [NASA-TM-102499] p 180 N90-21962
- An investigation into the numerical prediction of boundary layer transition using the K.Y. Chien turbulence model [NASA-CR-185252] p 182 N90-26269
- Implicit solution of three-dimensional internal turbulent flows [NASA-TM-103099] p 184 N90-27982
- Numerical solution for the velocity-derivative skewness of a low-Reynolds-number decaying Navier-Stokes flow [NASA-TM-103186] p 184 N90-27985
- Modeling of near-wall turbulence [NASA-TM-103222] p 184 N90-28009
- ### TURBULENT HEAT TRANSFER
- Heat transfer on accreting ice surfaces [AIAA PAPER 90-0200] p 162 A90-22181
- ### TURBULENT JETS
- Calculation of turbulent three-dimensional jet-induced flow in a rectangular enclosure [AIAA PAPER 90-0684] p 161 A90-19976
- Multiscale nonlinear interactions in the axisymmetric mode [AIAA PAPER 90-0365] p 166 A90-25029
- Multigrid calculations of a jet in crossflow [AIAA PAPER 90-0444] p 167 A90-26952
- Modern developments in shear flow control with swirl [NASA-CR-186586] p 181 N90-22000
- Calculation of 3D turbulent jets in crossflow with a multigrid method and a second-moment closure model [NASA-TM-103159] p 184 N90-26282
- The entrainment rate for a row of turbulent jets [NASA-CR-185278] p 15 N90-28504
- ### TURBULENT WAKES
- Two-component phase-averaged turbulence statistics downstream of a rotating spoked-wheel wake generator p 156 A90-11559
- ### TVD SCHEMES
- ULTRA-SHARP nonoscillatory convection schemes for high-speed steady multidimensional flow [NASA-TM-102568] p 244 N90-21570
- ### TWISTING
- Parametric studies of advanced turboprops p 19 A90-21225
- ### TWO DIMENSIONAL BOUNDARY LAYER
- Wall-layer eruptions in turbulent flows [NASA-TM-102362] p 175 N90-11250
- ### TWO DIMENSIONAL FLOW
- Numerical modeling of enclosure convection [IAF PAPER 89-403] p 157 A90-13511
- Nonlinear evolution of interacting oblique waves on two-dimensional shear layers p 158 A90-15943
- Two-dimensional convection and radiation with scattering from a Poiseuille flow p 161 A90-20519
- Time-dependent calculation of a forced mixing layer using a k-epsilon turbulence model p 169 A90-35222
- Kinetic theory model for the flow of a simple gas from a two-dimensional nozzle p 169 A90-37124
- Pressure-based real-time measurements in compressible free shear layers [AIAA PAPER 90-1980] p 8 A90-42709
- Comparison between pressure gradient method and MAC method on high Re calculation p 172 A90-44462
- Evolution and interaction of two- and three-dimensional instability waves p 173 A90-46885

- Numerical modeling of flows in simulated brush seal configurations
[AIAA PAPER 90-2141] p 198 A90-47209
Hopf bifurcation in the driven cavity p 174 A90-48548
Global pressure relaxation for laminar two-dimensional internal flow p 174 A90-51019
A simple algebraic grid adaptation scheme with applications to two- and three-dimensional flow problems
[NASA-TM-102446] p 178 N90-18667
PROTEUS two-dimensional Navier-Stokes computer code, version 1.0. Volume 1: Analysis description
[NASA-TM-102551] p 180 N90-21303
- TWO DIMENSIONAL MODELS**
Some aspects of transient cooling of a radiating rectangular medium p 157 A90-13095
Two-dimensional numerical simulation of a Stirling engine heat exchanger p 170 A90-38290
A two-dimensional model of plasma expansion in the ionosphere p 233 A90-43609
Two-dimensional analysis of two-phase reacting flow in a firing direct-injection diesel engine
[NASA-TM-102069] p 27 N90-13392
- TWO PHASE FLOW**
Application of two-component phase Doppler interferometry to the measurement of particle size, mass flux, and velocities in two-phase flows p 186 A90-32853
Two-dimensional analysis of two-phase reacting flow in a firing direct-injection diesel engine
[NASA-TM-102069] p 27 N90-13392
- TWO STAGE TURBINES**
Numerical analysis of secondary flow in a two-stage turbine
[AIAA PAPER 90-2356] p 66 A90-47216
Heat transfer and pressure measurements for the SSME fuel-side turbopump
[NASA-CR-184928] p 31 N90-23405
Energy Efficient Engine high pressure turbine component test performance report
[NASA-CR-168289] p 33 N90-28553
- U**
- ULLAGE**
Prediction of the ullage gas thermal stratification in a NASP vehicle propellant tank experimental simulation using FLOW-3D
[NASA-TM-103217] p 131 N90-26160
- ULTRASONIC FLAW DETECTION**
Impact damage development in damaged composite materials p 193 A90-18355
Improved transverse crack detection in composites
[NASA-TM-103261] p 102 N90-27875
- ULTRASONIC RADIATION**
Ultrasonic verification of five wave fronts in unidirectional graphite epoxy composite
[NASA-CR-185288] p 208 N90-28858
- ULTRASONIC TESTS**
Measurements of dynamic Young's modulus in short specimens with the PUCOT --- Piezoelectric Ultrasonic Composite Oscillator Technique p 112 A90-21174
Recent advances in nondestructive evaluation made possible by novel uses of video systems
[NASA-TM-102491] p 207 N90-22801
Input-output characterization of fiber reinforced composites by P waves
[NASA-CR-185287] p 208 N90-28097
- ULTRASONIC WAVE TRANSDUCERS**
Ultrasonic techniques for aircraft ice accretion measurement p 16 N90-20926
- ULTRASONICS**
Subtle porosity variation in the YBa₂Cu₃O_{7-x} high-temperature superconductor revealed by ultrasonic imaging
[NASA-TM-102130] p 206 N90-17167
Acousto-ultrasonic nondestructive evaluation of materials using laser beam generation and detection
[NASA-CR-186694] p 154 N90-23664
Theory and experimental technique for nondestructive evaluation of ceramic composites
[NASA-TM-102561] p 207 N90-23754
- UNIVERSE**
Unitarity limits on the mass and radius of dark-matter particles p 264 A90-24671
Phase transitions as the origin of large scale structure in the universe p 265 A90-35291
Extraterrestrial life in the universe
[NASA-TM-102363] p 264 N90-22464
- UNSTEADY AERODYNAMICS**
The unsteady aerodynamics of an oscillating cascade in a compressible flow field p 2 A90-11789

- Progress towards the development of an inviscid-viscous interaction method for unsteady flows in turbomachinery cascades p 2 A90-11806
Aeroelastic detuning for stability enhancement of unstalled supersonic flutter p 19 A90-17462
Numerical solutions of the linearized Euler equations for unsteady vortical flows around lifting airfoils
[AIAA PAPER 90-0694] p 5 A90-25041
Propeller-wing interaction using a frequency domain panel method p 6 A90-26128
Time domain flutter analysis of cascades using a full-potential solver
[AIAA PAPER 90-0984] p 6 A90-29374
Concurrent processing adaptation of aeroelastic analysis of propfans
[AIAA PAPER 90-1036] p 211 A90-29380
Three dimensional full potential method for the aeroelastic modeling of propfans
[AIAA PAPER 90-1120] p 7 A90-29392
Numerical solutions of the linearized Euler equations for unsteady vortical flows around lifting airfoils p 7 A90-30264
Counter-rotating propellant analysis using a frequency domain panel method p 7 A90-40937
Aeroelastic stability analysis of a high-energy turbine blade --- for SSME High Pressure Oxidizer TurboPump first stage
[AIAA PAPER 90-2351] p 66 A90-47215
Unsteady blade surface pressures on a large-scale advanced propeller - Prediction and data
[AIAA PAPER 90-2402] p 9 A90-47220
An investigation of counterrotating tip vortex interaction
[NASA-CR-185135] p 247 N90-11549
Prediction of unsteady blade surface pressures on an advanced propeller at an angle of attack
[NASA-TM-102374] p 11 N90-12560
Concurrent processing adaptation of aerodynamic analysis of propfans
[NASA-TM-102455] p 217 N90-14656
Numerical solutions of the linearized Euler equations for unsteady vortical flows around lifting airfoils
[NASA-TM-102466] p 12 N90-17562
Gust response analysis for cascades operating in nonuniform mean flows p 28 N90-18415
Control of flow separation and mixing by aerodynamic excitation
[NASA-TM-103131] p 13 N90-21733
Two-dimensional Euler and Navier-Stokes Time accurate simulations of fan rotor flows
[NASA-TM-102402] p 14 N90-25948
Development of a linearized unsteady aerodynamic analysis for cascade gust response predictions
[NASA-CR-4308] p 14 N90-27655
Aerodynamics of a linear oscillating cascade
[NASA-TM-103250] p 15 N90-27657
- UNSTEADY FLOW**
Calculation of unsteady Euler flows in turbomachinery using the linearized Euler equations p 2 A90-11778
The unsteady aerodynamics of an oscillating cascade in a compressible flow field p 2 A90-11789
Model-free simulations of turbulent reactive flows p 158 A90-15729
Unsteady heat transfer on turbine blades p 161 A90-20511
A numerical study of the interaction between unsteady free-stream disturbances and localized variations in surface geometry p 161 A90-21422
Unsteady disturbances of streaming motions around bodies p 162 A90-21424
Diagonal inversion of lower-upper implicit schemes p 242 A90-23110
Unsteady Euler analysis of the flowfield of a propfan at an angle of attack
[AIAA PAPER 90-0339] p 5 A90-25028
A flux-split solution procedure for unsteady inlet flows
[AIAA PAPER 90-0585] p 6 A90-26967
Aeroelastic problems in turbomachines
[AIAA PAPER 90-1157] p 7 A90-29393
Numerical solutions of the linearized Euler equations for unsteady vortical flows around lifting airfoils p 7 A90-30264
Absorbing boundary conditions for second-order hyperbolic equations p 242 A90-34549
A study of the unsteadiness of crossing shock wave turbulent boundary layer interactions
[AIAA PAPER 90-1456] p 170 A90-38614
A technique for measurement of instantaneous heat transfer in steady-flow ambient-temperature facilities p 172 A90-39625
Transient behavior of supersonic flow through inlets
[AIAA PAPER 90-2130] p 8 A90-42734
Numerical simulation of unsteady rotational flow over propfan configurations
[NASA-CR-186037] p 10 N90-12500

- Application of a two-dimensional unsteady viscous analysis code to a supersonic throughflow fan stage
[NASA-TM-4141] p 25 N90-13387
Numerical solutions of the linearized Euler equations for unsteady vortical flows around lifting airfoils
[NASA-TM-102466] p 12 N90-17562
Conditions at the downstream boundary for simulations of viscous incompressible flow
[NASA-TM-102510] p 243 N90-18198
Unsteady Euler analysis of the flow field of a propfan at an angle of attack
[NASA-TM-102426] p 248 N90-18229
Mass transfer from a sphere in an oscillating flow with zero mean velocity
[NASA-TM-102566] p 179 N90-20338
PROTEUS two-dimensional Navier-Stokes computer code, version 1.0. Volume 1: Analysis description
[NASA-TM-102551] p 180 N90-21303
An unsteady time asymptotic flow in the square driven cavity
[NASA-TM-103141] p 181 N90-22016
An unsteady lifting surface method for single rotation propellers
[NASA-CR-4302] p 14 N90-25940
Two-dimensional Euler and Navier-Stokes Time accurate simulations of fan rotor flows
[NASA-TM-102402] p 14 N90-25948
- USER MANUALS (COMPUTER PROGRAMS)**
Composite Blade Structural Analyzer (COBSTRAN) theoretical/programmer's manual
[NASA-TM-101958] p 95 N90-10181
The MHOST finite element program: 3-D inelastic analysis methods for hot section components. Volume 2: User's manual
[NASA-CR-182235-VOL-2] p 215 N90-10450
User's manual for PEP SIG NASA tip vortex version
[NASA-CR-182178] p 10 N90-10835
User's guide to PMESH: A grid-generation program for single-rotation and counterrotation advanced turboprops
[NASA-CR-185156] p 235 N90-14783
CryoTran user's manual, version 1.0
[NASA-TM-102468] p 237 N90-15622
Numerical Arc Segmentation Algorithm for a Radio Conference-NASARC (version 4.0) technical manual
[NASA-TM-101453] p 144 N90-20264
GRID2D/3D: A computer program for generating grid systems in complex-shaped two- and three-dimensional spatial domains. Part 2: User's manual and program listing
[NASA-TM-102454] p 237 N90-20708
Users manual for the NASA Lewis Ice Accretion Prediction Code (LEWICE)
[NASA-CR-185129] p 1 N90-20943
Numerical Arc Segmentation Algorithm for a Radio Conference (NASARC), version 4.0: User's manual
[NASA-TM-101454] p 145 N90-21250
PROTEUS two-dimensional Navier-Stokes computer code, version 1.0. Volume 2: User's guide
[NASA-TM-102552] p 180 N90-21306
Hypercluster parallel processing library user's manual
[NASA-CR-185231] p 237 N90-21552
NASA Lewis icing research tunnel user manual
[NASA-TM-102319] p 31 N90-23407
Generalized Advanced Propeller Analysis System (GAPAS). Volume 2: Computer program user manual
[NASA-CR-185277] p 36 N90-29394
- USER REQUIREMENTS**
Mars manned transportation vehicle
[AAS PAPER 87-271] p 42 A90-16569
Integrated controls and health monitoring for chemical transfer propulsion
[AIAA PAPER 90-2751] p 52 A90-47229
User needs, benefits, and integration of robotic systems in a space station laboratory
[NASA-CR-185150] p 200 N90-13794
Integrated controls and health monitoring for chemical transfer propulsion
[NASA-TM-103185] p 52 N90-25178
- V**
- V GROOVES**
GaAs solar cells with V-grooved emitters p 229 N90-17754
- V/STOL AIRCRAFT**
A modeling technique for STOVL ejector and volume dynamics
[AIAA PAPER 90-2417] p 20 A90-42168
Analysis of internal flow in a ventral nozzle for STOVL aircraft
[AIAA PAPER 90-1899] p 21 A90-42688
Three-dimensional turbulent flow code calculations of hot gas ingestion p 21 A90-44726

- H-infinity based integrated flight/propulsion control design for a STOVL aircraft in transition flight
[AIAA PAPER 90-3335] p 36 A90-47595
- The implementation of STOVL task-tailored control modes in a fighter cockpit
[AIAA PAPER 90-3229] p 17 A90-49114
- Engine inlet distortion in a 9.2 percent scale vectored thrust STOVL model in ground effect
[NASA-TM-102358] p 12 N90-17561
- Research on a two-dimensional inlet for a supersonic V/STOL propulsion system. Appendix A
[NASA-CR-174945] p 12 N90-18364
- The insertion of human dynamics models in the flight control loops of V/STOL research aircraft. Appendix 2: The optimal control model of a pilot in V/STOL aircraft control loops
[NASA-CR-186598] p 38 N90-21776
- An adaptive human response mechanism controlling the V/STOL aircraft. Appendix 3: The adaptive control model of a pilot in V/STOL aircraft control loops
[NASA-CR-186599] p 38 N90-21777
- A modeling technique for STOVL ejector and volume dynamics
[NASA-TM-103167] p 30 N90-22566
- Analysis of internal flow in a ventral nozzle for STOVL aircraft
[NASA-TM-103123] p 31 N90-23404
- Experimental and analytical study of close-coupled ventral nozzles for ASTOVL aircraft
[NASA-TM-103170] p 31 N90-24273
- Hot gas ingestion characteristics and flow visualization of a vectored thrust STOVL concept
[NASA-TM-103212] p 32 N90-26009
- H-infinity based integrated flight-propulsion control design for a STOVL aircraft in transition flight
[NASA-TM-103198] p 37 N90-26011
- VACUUM**
- Degradation of the lunar vacuum by a moon base
p 266 A90-35441
- Requirements for long-life operation of inert gas hollow cathodes - Preliminary results
[AIAA PAPER 90-2586] p 69 A90-52570
- Design and calibration of a vacuum compatible scanning tunneling microscope
[NASA-TM-102514] p 189 N90-20353
- Requirements for long-life operation of inert gas hollow cathodes: Preliminary report
[NASA-TM-103242] p 82 N90-27783
- VACUUM CHAMBERS**
- Development of a quadrupole-based Secondary-Ion Mass Spectrometry (SIMS) system at Lewis Research Center
[NASA-TM-102531] p 87 N90-23476
- VACUUM EFFECTS**
- Decomposition of perfluoroalkylpolyethers (PFPE) in ultra-high vacuum under sliding conditions
p 122 A90-40714
- Requirements for long-life operation of inert gas hollow cathodes - Preliminary results
[AIAA PAPER 90-2586] p 69 A90-52570
- Requirements for long-life operation of inert gas hollow cathodes: Preliminary report
[NASA-TM-103242] p 82 N90-27783
- VACUUM MELTING**
- Bearing and gear steels for aerospace applications
[NASA-TM-102529] p 202 N90-20391
- VACUUM TESTS**
- Tribological reactions of perfluoroalkyl polyether oils with stainless steel under ultrahigh vacuum conditions at room temperature
p 120 A90-16278
- VALVES**
- Ceramic valve development for heavy-duty low heat rejection diesel engines
p 196 A90-27091
- VAN DER WAAL FORCES**
- A Van der Waals-like theory of plasma double layers
p 251 A90-10725
- The effects of van der Waals attractions on cloud droplet growth by coalescence
p 234 A90-38363
- VANADIUM ALLOYS**
- Processing and microstructure of melt spun NiAl alloys
p 110 A90-16941
- VANES**
- An experimental study of turbine vane heat transfer with leading edge and downstream film cooling
[ASME PAPER 89-GT-69] p 165 A90-23792
- Experimental determination of stator endwall heat transfer
[ASME PAPER 89-GT-219] p 165 A90-23880
- Effect of vane twist on the performance of dome swirlers for gas turbine airblast atomizers
[AIAA PAPER 90-1955] p 173 A90-47203
- Navier-Stokes analysis of turbine blade heat transfer
[NASA-TM-102496] p 179 N90-21300
- Heat transfer and pressure measurements for the SSME fuel-side turbopump
[NASA-CR-184928] p 31 N90-23405
- Effect of vane twist on the performance of dome swirlers for gas turbine airblast atomizers
[NASA-TM-103195] p 182 N90-25289
- VAPOR DEPOSITION**
- Side-wall gas 'creep' and 'thermal stress convection' in microgravity experiments on film growth by vapor transport
p 158 A90-14086
- High efficiency GaAs/Ge monolithic tandem solar cells
p 224 A90-14858
- A V-grooved GaAs solar cell
p 225 A90-14887
- Effect of crystal orientation on anisotropic etching and MOCVD growth of grooves on GaAs
p 253 A90-15136
- Effect of heat-treatment temperature of vapor-grown graphite fibers. I - Properties of their bromine intercalation compounds
p 120 A90-16279
- Evaluation of transport conditions during physical vapor transport growth of opto-electronic crystals
p 132 A90-20525
- Wide-bandgap epitaxial heterojunction windows for silicon solar cells
p 227 A90-28359
- Growth of improved quality 3C-SiC films on 6H-SiC substrates
p 255 A90-29596
- Growth of high quality 6H-SiC epitaxial films on vicinal (0001) 6H-SiC wafers
p 255 A90-29952
- Iridium-coated rhenium thrusters by CVD
p 114 A90-30480
- Modeling of the SiC chemical vapor deposition process and comparison with experimental results
p 105 A90-36810
- Simple evaporation controller for thin-film deposition from a resistively heated boat
p 149 A90-39761
- Vapor grown carbon fiber for space thermal management systems
p 94 A90-50128
- Electron beam induced damage in PECVD Si₃N₄ and SiO₂ films on InP
p 203 N90-20393
- Dielectric function of InGaAs in the visible
[NASA-TM-103246] p 260 N90-26683
- VAPOR PHASE EPITAXY**
- An empirical investigation of the InP shallow-homojunction solar cell
p 225 A90-14869
- Hybrid solar cells based on dc magnetron sputtered films of n-ITO on APMOPE grown p-InP
p 225 A90-14893
- Effect of gas and surface radiation on crystal growth from the vapor phase
p 133 A90-49060
- Peeled film GaAs solar cells for space power
[NASA-TM-103125] p 153 N90-21287
- VAPOR PHASES**
- Buoyancy effects on the vapor condensation rate on a horizontal liquid surface
[AIAA PAPER 90-0353] p 162 A90-22201
- Vapor condensation on liquid surface due to laminar jet-induced mixing - The effects of system parameters
[AIAA PAPER 90-0354] p 163 A90-22202
- Rate correlation for condensation of pure vapor on turbulent, subcooled liquid
p 174 A90-50511
- Buoyancy effects on the vapor condensation rate on a horizontal liquid surface
[NASA-TM-102437] p 130 N90-13675
- Vapor condensation on liquid surface due to laminar jet-induced mixing: The effects of system parameters
[NASA-TM-102433] p 176 N90-13751
- VAPORIZING**
- Fuel-rich catalytic combustion - A fuel processor for high-speed propulsion
[AIAA PAPER 90-2319] p 105 A90-42774
- Fuel-rich catalytic combustion: A fuel processor for high-speed propulsion
[NASA-TM-103177] p 107 N90-23518
- VARIABLE PITCH PROPELLERS**
- An approximate model for the performance and acoustic predictions of counterrotating propeller configurations
[NASA-CR-180667] p 248 N90-18228
- VARIATIONAL PRINCIPLES**
- Treatment of coupled fluid-structure interaction problems by a mixed variational principle
p 159 A90-18288
- A variational justification of the assumed natural strain formulation of finite elements. I - Variational principles. II - The C(0) four-node plate element
p 210 A90-24384
- Mixed variational formulation of finite element analysis of acoustoelastic/slosh fluid-structure interaction
p 212 A90-34851
- Variational formulation of high-performance finite elements - Parametrized variational principles
p 213 A90-46068
- Developments in variational methods for high performance plate and shell elements
p 214 A90-46288
- Electromagnetic finite elements based on a four-potential variational principle
p 214 A90-49869
- VECTORS (MATHEMATICS)**
- Quotient-difference type generalizations of the power method and their analysis
[NASA-TM-102361] p 242 N90-10635
- VELOCITY DISTRIBUTION**
- New space domain processing technique for pulsed laser velocimetry
p 187 A90-48750
- Laser anemometer measurements in a transonic axial-flow fan rotor
[NASA-TP-2879] p 175 N90-11245
- Viscous three-dimensional analyses for nozzles for hypersonic propulsion
[NASA-CR-185197] p 27 N90-17635
- Gust response analysis for cascades operating in nonuniform mean flows
p 28 N90-18415
- TiCl₄ as a source of TiO₂ particles for laser anemometry measurements in hot gas
[NASA-TM-102581] p 189 N90-20358
- VELOCITY MEASUREMENT**
- A fiber optic sensor for noncontact measurement of shaft speed, torque, and power
[NASA-TM-102481] p 189 N90-21360
- VENTILATION**
- Fire safety applications for spacecraft
p 16 N90-17595
- VENTING**
- Liquid Transfer Cryogenic Test Facility: Initial hydrogen and nitrogen non-vent fill data
[NASA-TM-102572] p 179 N90-21295
- VERTICAL LANDING**
- Performance characteristics of a one-third-scale, vectorable ventral nozzle for SSTOVL aircraft
[AIAA PAPER 90-2271] p 20 A90-37562
- Hot gas environment around STOVL aircraft in ground proximity. II - Numerical study
[AIAA PAPER 90-2270] p 21 A90-42766
- Flight control design considerations for STOVL powered-lift flight
[AIAA PAPER 90-3225] p 37 A90-49110
- The implementation of STOVL task-tailored control modes in a fighter cockpit
[AIAA PAPER 90-3229] p 17 A90-49114
- STOVL propulsion system volume dynamics approximations
[NASA-TM-102397] p 25 N90-11740
- Performance characteristics of a one-third-scale, vectorable ventral nozzle for SSTOVL aircraft
[NASA-TM-103120] p 2 N90-21725
- VIBRATION**
- Vibration signature analysis of multistage gear transmission
p 194 A90-21124
- Effects of mistuning and matrix structure on the topology of frequency response curves
[NASA-TM-102290] p 216 N90-12041
- Gear noise, vibration, and diagnostic studies at NASA Lewis Research Center
[NASA-TM-102435] p 202 N90-18041
- Evaluation of thermal and mechanical loading effects on the structural behavior of a SiC/titanium composite
[NASA-TM-102536] p 98 N90-20139
- An unsteady lifting surface method for single rotation propellers
[NASA-CR-4302] p 14 N90-25940
- Dynamics of multistage gear transmission with effects of gearbox vibrations
[NASA-TM-103109] p 205 N90-28060
- VIBRATION DAMPING**
- Modal selection in structural dynamics
p 209 A90-17001
- Multi-objective shape and material optimization of composite structures including damping
[AIAA PAPER 90-1135] p 210 A90-29262
- Aeroelastic problems in turbomachines
[AIAA PAPER 90-1157] p 7 A90-29393
- Unified micromechanics of damping for unidirectional and off-axis fiber composites
p 90 A90-29929
- Tailoring of composite links for optimal damped elasto-dynamic performance
p 211 A90-30250
- Active vibration control for flexible rotor by optimal direct-output feedback control
p 197 A90-46222
- A new approach to active vibration isolation for microgravity space experiments
[NASA-TM-102470] p 137 N90-17929
- Computational simulation of damping in composite structures
[NASA-TM-102567] p 219 N90-20432
- Multi-objective shape and material optimization of composite structures including damping
[NASA-TM-102579] p 99 N90-21132
- A review of gear housing dynamics and acoustics literature
[NASA-CR-185148] p 203 N90-21387
- The vibro-acoustic mapping of low gravity trajectories on a Learjet aircraft
[NASA-TM-103103] p 1 N90-21723
- Elements of active vibration control for rotating machinery
[NASA-TM-102368] p 137 N90-22703

- Experimental evaluation of a tuned electromagnetic damper for vibration control of cryogenic turbopump rotors
[NASA-TP-3005] p 30 N90-23403
- Structural dynamics branch research and accomplishments
[NASA-TM-102488] p 223 N90-26373
- Reaction-compensation technology for microgravity laboratory robots
[NASA-TM-103271] p 205 N90-28062
- VIBRATION ISOLATORS**
- Nonintrusive inertial vibration isolation technology for microgravity space experiments
[AIAA PAPER 90-0741] p 132 A90-19999
- Low frequency vibration isolation technology for microgravity space experiments
[NASA-TM-102488] p 136 A90-46246
- Vibration dampers for cryogenic turbomachinery
[AIAA PAPER 90-2740] p 199 A90-47228
- Nonintrusive inertial vibration isolation technology for microgravity space experiments
[NASA-TM-102386] p 137 N90-11901
- A new approach to active vibration isolation for microgravity space experiments
[NASA-TM-102470] p 137 N90-17929
- Development and approach to low-frequency microgravity isolation systems
[NASA-TP-2984] p 138 N90-28754
- VIBRATION MEASUREMENT**
- Experimental and analytical evaluation of dynamic load vibration of a 2240-kW (3000-hp) rotorcraft transmission
[NASA-TP-2984] p 192 A90-13750
- VIBRATION MODE**
- Instabilities and subharmonic resonances of subsonic heated round jets, volume 2
[NASA-CR-186058] p 181 N90-22017
- Dynamic analysis of space-related linear and non-linear structures
[NASA-TM-103490] p 51 N90-25174
- Dynamics of multistage gear transmission with effects of gearbox vibrations
[NASA-TM-103109] p 205 N90-28060
- VIBRATION TESTS**
- Measurements of dynamic Young's modulus in short specimens with the PUCOT --- Piezoelectric Ultrasonic Composite Oscillator Technique
[AIAA PAPER 90-1026] p 112 A90-21174
- Evaluation of thermal and mechanical loading effects on the structural behavior of a SiC/titanium composite
[AIAA PAPER 90-1026] p 90 A90-29228
- A modified VAPEPS method for predicting vibroacoustic response of unreinforced mass loaded honeycomb panels
[NASA-TM-103203] p 206 A90-43731
- VIBRATORY LOADS**
- An active optimal control strategy of rotor vibrations using external forces
[NASA-TM-103203] p 198 A90-46224
- VIDEO DATA**
- Data compression techniques applied to high resolution high frame rate video technology
[NASA-CR-4263] p 143 N90-14452
- VIDEO SIGNALS**
- Digital codec for real-time processing of broadcast quality video signals at 1.8 bits/pixel
[NASA-TM-103109] p 142 A90-51306
- VIEW EFFECTS**
- Radiative configuration factors from cylinders to coaxial axisymmetric bodies
[NASA-TM-102334] p 167 A90-26334
- VIKING MARS PROGRAM**
- The chemical effects of the Martian environment on power system component materials: A theoretical approach
[NASA-TM-103203] p 87 N90-26074
- VISCOPLASTICITY**
- Finite element implementation of Robinson's unified viscoplastic model and its application to some uniaxial and multiaxial problems
[NASA-TM-102388] p 208 A90-15704
- Analytical and finite element solutions of some problems using a viscoplastic model
[NASA-TM-102388] p 209 A90-19132
- Effects of state recovery on creep buckling under variable loading
[NASA-TM-102388] p 212 A90-41223
- Viscoplasticity: A thermodynamic formulation
[NASA-TM-102388] p 216 N90-14640
- A new uniformly valid asymptotic integration algorithm for elasto-plastic-creep and unified viscoplastic theories including continuum damage
[NASA-TM-102344] p 217 N90-14655
- Steady-state and transient Zener parameters in viscoplasticity: Drag strength versus yield strength
[NASA-TM-102487] p 218 N90-18064
- Model development in viscoplastic ratchetting
[NASA-TM-102509] p 219 N90-20431
- Thermomechanical deformation testing and modeling in the presence of metallurgical instabilities
[NASA-CR-185188] p 219 N90-21420
- Application of finite-element-based solution technologies for viscoplastic structural analyses
[NASA-CR-185196] p 221 N90-23757
- Finite element analysis of structural components using viscoplastic models with application to a cowl lip problem
[NASA-CR-185189] p 221 N90-23769
- A viscoplastic model with application to LiF-22 percent CaF2 hypereutectic salt
[NASA-TM-103181] p 221 N90-23770
- VISCOSITY**
- Critical exponent for the viscosity of carbon dioxide and xenon
[NASA-TM-103181] p 261 A90-43941
- VISCOUS FLOW**
- Time-dependent viscous incompressible Navier-Stokes equations - The finite difference Galerkin formulation and streamfunction algorithms
[NASA-TM-103181] p 156 A90-11598
- Progress towards the development of an inviscid-viscous interaction method for unsteady flows in turbomachinery cascades
[NASA-TM-103181] p 2 A90-11806
- Least-squares finite element method for fluid dynamics
[NASA-TM-103181] p 159 A90-18246
- Asymmetrical boundary layer separation at the base of a two cylinder geometry
[NASA-TM-103181] p 159 A90-18505
- Fortified LEWICE with viscous effects --- Lewis Ice Accretion Prediction Code
[AIAA PAPER 90-0754] p 15 A90-20009
- Simulation of three-dimensional viscous flow within a multistage turbine
[ASME PAPER 89-GT-152] p 5 A90-23841
- Comparison of 3-D viscous flow computations of Mach 5 inlet with experimental data
[AIAA PAPER 90-0600] p 6 A90-26970
- Numerical analysis of three-dimensional viscous internal flows
[NASA-TM-103181] p 168 A90-32456
- Multigrid calculations of 3-D turbulent viscous flows
[NASA-TM-103181] p 172 A90-42426
- Diagonally inverted lower-upper factored implicit multigrid scheme for the three-dimensional Navier-Stokes equations
[NASA-TM-103181] p 174 A90-49789
- Hopf bifurcation in the driven cavity
[NASA-TM-102334] p 175 N90-11969
- A least-squares finite element method for incompressible Navier-Stokes problems
[NASA-TM-102385] p 242 N90-12231
- Multigrid calculations of 3-D turbulent viscous flows
[NASA-CR-185154] p 1 N90-13323
- Application of a two-dimensional unsteady viscous analysis code to a supersonic throughflow fan stage
[NASA-TM-4141] p 25 N90-13387
- An analysis of the viscous flow through a compact radial turbine by the average passage approach
[NASA-TM-102471] p 12 N90-14206
- Development of an integrated BEM approach for hot fluid structure interaction
[NASA-CR-186214] p 177 N90-15364
- Viscous effects on the instability of an axisymmetric jet
[NASA-TM-102396] p 12 N90-16719
- Viscous three-dimensional analyses for nozzles for hypersonic propulsion
[NASA-CR-185197] p 27 N90-17635
- Conditions at the downstream boundary for simulations of viscous incompressible flow
[NASA-TM-102510] p 243 N90-18198
- Comparison of 3-D viscous flow computations of Mach 5 inlet with experimental data
[NASA-TM-102518] p 28 N90-20090
- PROTEUS two-dimensional Navier-Stokes computer code, version 1.0. Volume 2: User's guide
[NASA-TM-102552] p 180 N90-21306
- VISCOUS FLUIDS**
- Experimental investigation of convective stability in a superposed fluid and porous layer when heated from below
[NASA-TM-102396] p 158 A90-15947
- VISUAL OBSERVATION**
- Fuel-rich catalytic combustion - A fuel processor for high-speed propulsion
[AIAA PAPER 90-2319] p 105 A90-42774
- Fuel-rich catalytic combustion: A fuel processor for high-speed propulsion
[NASA-TM-103177] p 107 N90-23518
- VITERBI DECODERS**
- Advanced modulation technology development for earth station demodulator applications. Coded modulation system development
[NASA-CR-185149] p 145 N90-20270
- VOICE COMMUNICATION**
- Advanced Communications Technology Satellite (ACTS) and potential system applications
[NASA-TM-102552] p 142 A90-51165
- On-board switching and processing
[NASA-TM-102552] p 150 A90-51168
- VOIDS**
- Arjet cathode phenomena
[NASA-TM-102376] p 75 N90-18477
- Investigation of methods to produce a uniform cloud of fuel particles in a flame tube
[NASA-TM-102376] p 178 N90-18665
- VOLT-AMPERE CHARACTERISTICS**
- High efficiency GaAs/Ge monolithic tandem solar cells
[NASA-TM-102488] p 224 A90-14858
- High altitude current-voltage measurement of GaAs/Ge solar cells
[NASA-TM-102488] p 226 A90-14910
- Performance of GaAs concentrator cells under electron irradiations from 0.4 to 2.3 MeV
[NASA-TM-102488] p 227 A90-14956
- Deep-level dominated electrical characteristics of Au contacts on beta-SiC
[NASA-TM-102488] p 147 A90-33726
- VOLTAGE CONVERTERS (AC TO AC)**
- Performance testing of a high frequency link converter for Space Station power distribution system
[NASA-TM-102488] p 148 A90-38128
- VOLTAGE CONVERTERS (DC TO DC)**
- High power density dc/dc converter: Selection of converter topology
[NASA-CR-186129] p 151 N90-14467
- VOLTAGE REGULATORS**
- Distortion and regulation characterization of a Mapham inverter
[NASA-TM-102488] p 148 A90-38125
- Electrical performance characteristics of high power converters for space power applications
[NASA-CR-185947] p 72 N90-14279
- VOLUME**
- An accurate analytic approximation to the non-linear change in volume of solids with applied pressure
[NASA-TM-102488] p 261 A90-27612
- VOLUMETRIC STRAIN**
- Coarsening in high volume fraction nickel-base alloys
[NASA-TM-102488] p 115 A90-37719
- VORTEX BREAKDOWN**
- Modern developments in shear flow control with swirl
[NASA-CR-186586] p 181 N90-22000
- VORTEX GENERATORS**
- Unsteady disturbances of streaming motions around bodies
[NASA-TM-102488] p 162 A90-21424
- VORTICES**
- Asymmetrical boundary layer separation at the base of a two cylinder geometry
[NASA-TM-102488] p 159 A90-18505
- Numerical solutions of the linearized Euler equations for unsteady vortical flows around lifting airfoils
[NASA-TM-102488] p 7 A90-30264
- Experimental investigation of flow about a strut-endwall configuration
[AIAA PAPER 90-1541] p 171 A90-38685
- The growth and development of a turbulent junction vortex system
[NASA-TM-102488] p 173 A90-46902
- Flow visualization and motion analysis for a series of four sequential brush seals
[AIAA PAPER 90-2482] p 199 A90-47222
- Euler analysis comparison with LDV data for an advanced counter-rotation propfan at cruise
[AIAA PAPER 90-3033] p 9 A90-50637
- Computation of the tip vortex flowfield for advanced aircraft propellers
[NASA-CR-182179] p 10 N90-10836
- An investigation of counterrotating tip vortex interaction
[NASA-CR-185135] p 247 N90-11549
- Hopf bifurcation in the driven cavity
[NASA-TM-102334] p 175 N90-11969
- Numerical solutions of the linearized Euler equations for unsteady vortical flows around lifting airfoils
[NASA-TM-102466] p 12 N90-17562
- Gust response analysis for cascades operating in nonuniform mean flows
[NASA-TM-102466] p 28 N90-18415
- Instabilities and subharmonic resonances of subsonic heated round jets, volume 2
[NASA-CR-186058] p 181 N90-22017
- Large-scale advanced propeller blade pressure distributions: Prediction and data
[NASA-TM-102316] p 30 N90-22564
- Euler analysis comparison with LDV data for an advanced counter-rotation propfan at cruise
[NASA-TM-103249] p 14 N90-25946
- VORTICITY**
- Time-accurate simulations of a shear layer forced at a single frequency
[NASA-TM-102288] p 163 A90-23111
- Numerical solutions of the linearized Euler equations for unsteady vortical flows around lifting airfoils
[AIAA PAPER 90-0694] p 5 A90-25041
- Response of a chemically reacting layer to streamwise vorticity
[NASA-TM-102288] p 178 N90-18005
- VSAT (NETWORK)**
- LBR-2 earth stations for the ACTS program
[AIAA PAPER 90-0838] p 42 A90-25662
- Spacecraft designs for VSAT networks
[AIAA PAPER 90-0895] p 140 A90-25681
- A performance analysis of DS-CDMA and SCPC VSAT networks
[NASA-TM-102488] p 141 A90-39056

W

WALL FLOW

- Near wall flow parameters in the blade end-wall corner region p 156 A90-12636
On sublayer streaks p 168 A90-28143
Near-wall turbulence model and its application to fully developed turbulent channel and pipe flows p 169 A90-37328

Numerical investigation of the thermal stratification in cryogenic tanks subjected to wall heat flux [AIAA PAPER 90-2375] p 175 A90-52500

Investigation of turbulent flow in highly curved ducts with application to turbomachinery components [NASA-CR-186060] p 175 N90-12882

Aerodynamic optimization by simultaneously updating flow variables and design parameters p 18 N90-20991

Numerical investigation of the thermal stratification in cryogenic tanks subjected to wall heat flux [NASA-TM-103194] p 184 A90-27984

Modeling of near-wall turbulence [NASA-TM-103222] p 184 A90-28009

WALL PRESSURE

A study of the unsteadiness of crossing shock wave turbulent boundary layer interactions [AIAA PAPER 90-1456] p 170 A90-38614

Experimental investigation of terminal shock sensors in mixed-compression inlets [AIAA PAPER 90-1931] p 186 A90-40560

WALLS

Asymptotic analysis of dissipative waves with applications to their numerical simulation [NASA-TM-103231] p 244 A90-26615

An improved k-epsilon model for near-wall turbulence and comparison with direct numerical simulation [NASA-TM-103221] p 184 A90-27983

WASPALOY

Torsional and biaxial (tension-torsion) fatigue damage mechanisms in Waspaloy at room temperature p 109 A90-11925

Microstructure: Property correlation --- multiaxial fatigue damage evolution in waspaloy [NASA-CR-180406] p 224 A90-28880

WASTE ENERGY UTILIZATION

Conceptual design of liquid droplet radiator shuttle-attached experiment [NASA-CR-185164] p 71 N90-11805

Conceptual design of liquid droplet radiator shuttle-attached experiment technical requirements document [NASA-CR-185165] p 71 N90-11806

WATER

Reactions of SiC with H₂/H₂O/Ar mixtures at 1300 C p 123 A90-45830

WINCOF-I code for prediction of fan compressor unit with water ingestion [NASA-CR-185157] p 1 N90-21724

Transient characteristics of a grooved water heat pipe with variable heat load [NASA-CR-185280] p 183 A90-26272

WATER HEATING

Experimental investigation of convective stability in a superposed fluid and porous layer when heated from below p 158 A90-15947

WAVE DISPERSION

Optical dispersion relations for diamondlike carbon films [NASA-TM-102356] p 257 N90-10738

Asymptotic boundary conditions for dissipative waves: General theory [NASA-TM-102497] p 243 N90-18927

WAVE EQUATIONS

Asymptotic analysis of dissipative waves with applications to their numerical simulation [NASA-TM-103231] p 244 A90-26615

Consistency and convergence for numerical radiation conditions [NASA-TM-103262] p 244 A90-29124

WAVE EXCITATION

Modern developments in shear flow control with swirl [NASA-CR-186586] p 181 A90-22000

WAVE FRONTS

Ultrasonic verification of five wave fronts in unidirectional graphite epoxy composite [NASA-CR-185288] p 208 N90-28858

WAVE INTERACTION

Multiwave nonlinear interactions in the axisymmetric mode [AIAA PAPER 90-0365] p 166 A90-25029

Phase development and its role on subharmonic control [AIAA PAPER 90-0503] p 166 A90-25035

Evolution and interaction of two- and three-dimensional instability waves p 173 A90-46885

WAVE PROPAGATION

Nonlinear evolution of oblique waves on compressible shear layers p 158 A90-15942

Absorbing boundary conditions for second-order hyperbolic equations p 242 A90-34549

Asymptotic boundary conditions for dissipative waves: General theory [NASA-TM-102497] p 243 N90-18927

Asymptotic analysis of dissipative waves with applications to their numerical simulation [NASA-TM-103231] p 244 A90-26615

Input-output characterization of fiber reinforced composites by P waves [NASA-CR-185287] p 208 N90-28097

Ultrasonic verification of five wave fronts in unidirectional graphite epoxy composite [NASA-CR-185288] p 208 N90-28858

Consistency and convergence for numerical radiation conditions [NASA-TM-103262] p 244 A90-29124

WAVE REFLECTION

Measurements of print-through in graphite fiber epoxy composites p 91 A90-31555

Improved transverse crack detection in composites [NASA-TM-103261] p 102 N90-27875

WAVE RESISTANCE

Millimeter wave surface resistance of RBa₂Cu₃O₇(δ) superconductors (R = Y, Eu, Dy, Sm, Er) [NASA-TM-102571] p 259 N90-20886

WAVEGUIDE ANTENNAS

Coplanar waveguide fed phased array antenna [NASA-TM-102522] p 152 N90-21273

WAVEGUIDES

Coax-to-channelised coplanar waveguide in-phase N-way, radial power divider p 149 A90-41605

Constitutive parameter measurements of lossy materials [NASA-CR-183398] p 257 N90-11603

Channelized coplanar waveguide pin-diode switches [NASA-TM-102289] p 150 N90-11943

High-frequency asymptotic methods for analyzing the EM scattering by open-ended waveguide cavities [NASA-CR-186244] p 143 N90-16103

Universal nondestructive MM-wave integrated circuit test fixture [NASA-CASE-LEW-14746-1] p 151 N90-17009

Experimental investigations on channelized coplanar waveguide [NASA-TM-102494] p 151 N90-20286

Coplanar waveguide discontinuities for P-I-N diode switches and filter applications [NASA-TM-102534] p 153 N90-21278

WEAR

Wear consideration in gear design for space applications p 194 A90-21121

Applications of surface analysis and surface theory in tribology p 84 A90-37458

Requirements for long-life operation of inert gas hollow cathodes - Preliminary results [AIAA PAPER 90-2586] p 69 A90-52570

Friction and wear of oxide-ceramic sliding against IN-718 nickel base alloy at 25 to 800 C in atmospheric air [NASA-TM-102291] p 124 N90-10262

Sliding seal materials for low heat rejection engines [NASA-CR-182262] p 125 N90-11882

Experimentally determined wear behavior of an Al₂O₃-SiC composite from 25 to 1200 C [NASA-TM-102549] p 87 N90-20130

Studies of mechano-chemical interactions in the tribological behavior of materials [NASA-TM-102545] p 128 N90-21182

Self-lubricating polymer composites and polymer transfer film lubrication for space applications [NASA-TM-102492] p 128 N90-21862

Requirements for long-life operation of inert gas hollow cathodes: Preliminary report [NASA-TM-103242] p 82 N90-27783

WEAR RESISTANCE

Friction and wear of oxide-ceramic sliding against IN-718 nickel base alloy at 25 to 800 C in atmospheric air [NASA-TM-102291] p 124 N90-10262

Tribological properties of ceramic/Ti₃Al-Nb sliding couples for use as candidate seal materials to 700 deg C [NASA-TM-102401] p 86 N90-12658

The experimental evaluation and application of high-temperature solid lubricants [NASA-TM-102476] p 127 N90-16944

WEAR TESTS

Effects of lubrication on the performance of high speed spur gears p 194 A90-21119

Some composite bearing and seal materials for gas turbine applications - A review [ASME PAPER 89-GT-144] p 195 A90-23838

Tribological properties of PM212: A high-temperature, self-lubricating, powder metallurgy composite [NASA-TM-102355] p 86 N90-12659

A new test machine for measuring friction and wear in controlled atmospheres to 1200 C [NASA-TM-102405] p 96 N90-12670

WEATHER FORECASTING

The influence of ice accretion physics on the forecasting of aircraft icing conditions p 17 N90-20928

WEIBULL DENSITY FUNCTIONS

Calculation of Weibull strength parameters and Batdorf flow-density constants for volume- and surface-flaw-induced fracture in ceramics p 212 A90-35462

Investigation of Weibull statistics in fracture analysis of cast aluminum p 115 A90-45304

Reliability analysis of a structural ceramic combustion chamber [NASA-TM-103264] p 223 N90-28112

WEIGHT REDUCTION

Effect of advanced component technology on helicopter transmissions p 183 A90-21115

Applications of high thermal conductivity composites to electronics and spacecraft thermal design [AIAA PAPER 90-0783] p 89 A90-25609

Multi-objective shape and material optimization of composite structures including damping [AIAA PAPER 90-1135] p 210 A90-29262

A program for advancing the technology of space concentrators p 60 A90-38159

Advanced tube-bundle rocket thrust chamber [AIAA PAPER 90-2726] p 67 A90-47227

Characterization and cycle tests of lightweight nickel electrodes [NASA-TM-102399] p 106 N90-12696

Multi-objective shape and material optimization of composite structures including damping [NASA-TM-102579] p 99 N90-21132

Transmission research activities at NASA Lewis Research Center [NASA-TM-103132] p 203 N90-21394

Advanced tube-bundle rocket thrust chamber [NASA-TM-103139] p 80 N90-25185

WEIGHTING FUNCTIONS

Discretization formulas for unstructured grids p 242 A90-26535

Fatigue crack growth in unidirectional metal matrix composite [NASA-TM-103102] p 220 N90-22117

WEIGHTLESSNESS

N-decane-air droplet combustion experiments in the NASA-Lewis 5 Second Zero-Gravity Facility [AIAA PAPER 90-0649] p 104 A90-25038

Zero-G phase detector and separator [NASA-CASE-LEW-14844-1] p 190 N90-22024

WEIGHTLESSNESS SIMULATION

The vibro-acoustic mapping of low gravity trajectories on a Learjet aircraft [NASA-TM-103103] p 1 N90-21723

WELDED JOINTS

Preliminary study on pressure brazing and diffusion welding of Nb-1Zr to Inconel 718 p 196 A90-26899

WELDING

Attachment of lead wires to thin film thermocouples mounted on high temperature materials using the parallel gap welding process [NASA-TM-102442] p 189 N90-21361

WETTABILITY

Effects of crucible wetting during solidification of immiscible Pb-Zn alloys p 132 A90-17825

WHISKER COMPOSITES

Analysis of whisker-toughened ceramic components - A design engineer's viewpoint p 88 A90-19149

Noninteractive macroscopic reliability model for whisker-reinforced ceramic composites p 89 A90-26561

Friction and wear of oxide-ceramic sliding against IN-718 nickel base alloy at 25 to 800 C in atmospheric air [NASA-TM-102291] p 124 N90-10262

Zirconia toughened SiC whisker reinforced alumina composites small business innovation research [NASA-CR-179629] p 125 N90-10294

Analysis of whisker-toughened ceramic components: A design engineer's viewpoint [NASA-TM-102333] p 97 N90-18504

Experimentally determined wear behavior of an Al₂O₃-SiC composite from 25 to 1200 C [NASA-TM-102549] p 87 N90-20130

WHITE DWARF STARS

Neutron stars and white dwarfs in galactic halos? p 265 A90-30909

WICKS

Mathematical modeling and analysis of heat pipe start-up from the frozen state p 174 A90-48404

WIND (METEOROLOGY)

WIND (METEOROLOGY)

Aeolian removal of dust from radiator surfaces on Mars
[NASA-TM-103205] p 81 N90-26068

WIND EFFECTS

Aeolian removal of dust from photovoltaic surfaces on Mars
[NASA-TM-102507] p 76 N90-19299

WIND TUNNEL TESTS

Thin film eddy current impulse deicer
[AIAA PAPER 90-0761] p 17 A90-20012

Icing Research Tunnel test of a model helicopter rotor
p 15 A90-28179

Initial results from the joint NASA-Lewis/U.S. Army icing flight research tests
p 16 A90-28180

Noise of a simulated installed model counterrotation propeller at angle-of-attack and takeoff/approach conditions
[AIAA PAPER 90-0283] p 247 A90-32505

Structure of a reattaching supersonic shear layer
p 7 A90-36252

Experimental investigation of turbulent flow through a circular-to-rectangular transition duct
[AIAA PAPER 90-1505] p 171 A90-38654

Investigation of the near wake of a propfan
p 7 A90-40686

Mixer-ejector nozzle for jet noise suppression
[AIAA PAPER 90-1909] p 247 A90-47202

Experimental investigation of multielement airfoil ice accretion and resulting performance degradation
p 9 A90-48954

Analysis of results from wind tunnel tests of inlets for an advanced turboprop nacelle installation
[NASA-CR-174937] p 10 N90-10011

Large-scale Advanced Prop-fan (LAP) high speed wind tunnel test report
[NASA-CR-182125] p 24 N90-10045

NASA's program on icing research and technology
p 16 N90-15062

Heat transfer measurements from a NACA 0012 airfoil in flight and in the NASA Lewis icing research tunnel
[NASA-CR-4278] p 13 N90-19203

Noise of a simulated installed model counterrotation propeller at angle-of-attack and takeoff/approach conditions
[NASA-TM-102440] p 248 N90-20794

Laser-velocimeter-measured flow field around an advanced, swept, eight-blade propeller at Mach 0.8
[NASA-TP-2462] p 1 N90-20942

Advanced instrumentation for aircraft icing research
[NASA-CR-185225] p 18 N90-21006

Experimental performance and acoustic investigation of modern, counterrotating blade concepts
[NASA-CR-185158] p 18 N90-23393

WIND TUNNEL WALLS

Aerodynamics of a linear oscillating cascade
[NASA-TM-103250] p 15 N90-27657

WIND TUNNELS

Comparison of two droplet sizing systems in an icing wind tunnel
[AIAA PAPER 90-0668] p 164 A90-23711

Comparison of two droplet sizing systems in an icing wind tunnel
[NASA-TM-102458] p 200 N90-14617

Comparison of drop size distributions from two droplet sizing systems
[NASA-TM-102520] p 202 N90-17147

Modeling of surface roughness effects on glaze ice accretion
p 16 N90-20925

WIND TURBINES

Model OA wind turbine generator FMEA
[NASA-TM-102378] p 206 N90-12034

WINDOWS (APERTURES)

Diamondlike carbon protective coatings for optical windows
p 122 A90-34569

WING PROFILES

Numerical study of the effects of icing on finite wing aerodynamics
[AIAA PAPER 90-0757] p 3 A90-20010

WINGS

Propeller-wing interaction using a frequency domain panel method
p 6 A90-26128

WIRE

Development and characterization of PdCr temperature-compensated wire resistance strain gage
[NASA-CR-185153] p 188 N90-13761

Method of forming low cost, formable High T(sub c) superconducting wire
[NASA-CASE-LEW-14676-2] p 258 N90-17454

Attachment of lead wires to thin film thermocouples mounted on high temperature materials using the parallel gap welding process
[NASA-TM-102442] p 189 N90-21361

Progress in high temperature speckle-shift strain measurement system
[NASA-TM-103255] p 191 N90-28031

Frequency response of a thermocouple wire: Effects of axial conduction
[NASA-CR-180454] p 191 N90-28827

WORKING FLUIDS

Flight experiment of thermal energy storage --- for spacecraft power systems
p 61 A90-38172

Mathematical modeling and analysis of heat pipe start-up from the frozen state
p 174 A90-48404

Transient characteristics of a grooved water heat pipe with variable heat load
[NASA-CR-185280] p 183 N90-26272

Two-dimensional model of a Space Station Freedom thermal energy storage canister
[NASA-TM-103124] p 183 N90-26279

WROUGHT ALLOYS

MATE (Materials for Advanced Turbine Engines) Program, Project 3. Volume 2: Design, fabrication and evaluation of an oxide dispersion strengthened sheet alloy combustor liner
[NASA-CR-180892] p 117 N90-17868

X

X RAY FLUORESCENCE

X-ray beam method for displacement measurement in hostile environments
p 187 A90-44485

X RAY SPECTROSCOPY

X-ray photoelectron spectroscopy peak assignment for perfluoropolyether oils
p 124 A90-48550

FORTTRAN program for x ray photoelectron spectroscopy data reformatting
[NASA-TP-2957] p 258 N90-12348

XENON

Xenon ion sources for space applications
p 56 A90-22874

Critical speeding up in pure fluids
p 167 A90-26369

Status of xenon ion propulsion technology
p 56 A90-27961

High-power xenon ion thrusters
[AIAA PAPER 90-2540] p 64 A90-42536

Critical exponent for the viscosity of carbon dioxide and xenon
p 261 A90-43941

Xenon ion propulsion for orbit transfer
[AIAA PAPER 90-2527] p 67 A90-52562

5kW xenon ion thruster lifetest
[AIAA PAPER 90-2543] p 68 A90-52564

Critical fluid light scattering
p 251 N90-17087

Performance of large area xenon ion thrusters for orbit transfer missions
p 75 N90-18475

Y

YAG LASERS

Holographic interferometry with an injection seeded Nd:YAG laser and two reference beams
p 186 A90-42373

YTTERBIUM COMPOUNDS

Photoresponse of YBa₂Cu₃O(7-delta) granular and epitaxial superconducting thin films
[NASA-TM-103144] p 154 N90-22732

Ellipsometric study of YBa₂Cu₃O(7-x) laser ablated and co-evaporated films
[NASA-TM-103223] p 259 N90-26682

YTTRIUM

The high temperature creep deformation of Si₃N₄-6Y₂O₃-2Al₂O₃
p 121 A90-18879

Synthesis and characterization of high-T(c) screen-printed Y-Ba-Cu-O films on alumina
p 254 A90-21926

YTTRIUM COMPOUNDS

Thermal barrier coatings for gas turbine and diesel engines
[NASA-TM-102408] p 117 N90-13636

YTTRIUM OXIDES

MATE (Materials for Advanced Turbine Engines) Program, Project 3. Volume 2: Design, fabrication and evaluation of an oxide dispersion strengthened sheet alloy combustor liner
[NASA-CR-180892] p 117 N90-17868

Growth and patterning of laser ablated superconducting YBa₂Cu₃O₇ films on LaAlO₃ substrates
[NASA-TM-102436] p 259 N90-22421

Sequentially evaporated thin film YBa₂Cu₃O(7-x) superconducting microwave ring resonator
[NASA-TM-103180] p 154 N90-25273

Laser ablated high T(sub c) superconducting thin YBa₂Cu₃O(7-x) films on substrates suitable for microwave applications
p 260 N90-27808

SUBJECT INDEX

Z

ZENER EFFECT

Steady-state and transient Zener parameters in viscoplasticity: Drag strength versus yield strength
[NASA-TM-102487] p 218 N90-18064

ZERO ANGLE OF ATTACK

The radiation of sound from a propeller at angle of attack
[NASA-CR-4264] p 249 N90-21602

ZINC

Effects of crucible wetting during solidification of immiscible Pb-Zn alloys
p 132 A90-17825

ZINC ALLOYS

Modeling of collision and coalescence of droplets during microgravity processing of Zn-Bi immiscible alloys
p 132 A90-22878

ZINC SELENIDES

Diamondlike carbon protective coatings for optical windows
p 122 A90-34569

ZINC SULFIDES

Diamondlike carbon protective coatings for optical windows
p 122 A90-34569

ZIRCONIUM

Observations on the brittle to ductile transition temperatures of B2 nickel aluminides with and without zirconium
p 111 A90-19153

The effect of 0.1 atomic percent zirconium on the cyclic oxidation behavior of beta-NiAl for 3000 hours at 1200 C
p 112 A90-24857

Oxidation behavior of FeAl + Hf, Zr, B
p 113 A90-24858

ZIRCONIUM COMPOUNDS

Thermal barrier coatings for gas turbine and diesel engines
[NASA-TM-102408] p 117 N90-13636

ZIRCONIUM OXIDES

Two-layer thermal barrier coating. I - Effects of composition and temperature on oxidation behavior and failure
p 122 A90-33317

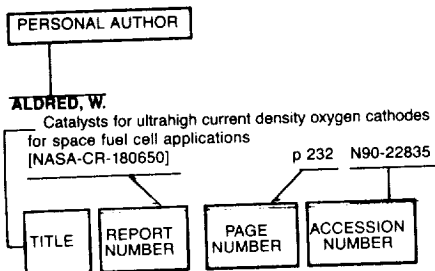
Zirconia toughened SiC whisker reinforced alumina composites small business innovation research
[NASA-CR-179629] p 125 N90-10294

Study of deposition of YBa₂Cu₃O_{7-x} on cubic zirconia
[NASA-TM-102350] p 257 N90-10737

Thermodynamic properties of some metal oxide-zirconia systems
[NASA-TM-102351] p 126 N90-13666

PERSONAL AUTHOR INDEX

Typical Personal Author Index Listing



Listings in this index are arranged alphabetically by personal author. The accession number denotes the number by which the citation is identified.

A

- AADLAND, R. S.**
Qualification and life testing of a flight design hydrazine arcjet system
[AIAA PAPER 90-2576] p 64 A90-42559
- ABBOTT, JOHN M.**
Control of flow separation and mixing by aerodynamic excitation
[NASA-TM-103131] p 13 N90-21733
- ABDALLAH, A. A.**
Boundary flexibility method of component mode synthesis using static Ritz vectors p 212 A90-35429
- ABDALLAH, AYMAN AHMED**
Dynamic substructuring by the boundary flexibility vector method of component mode synthesis
[NASA-CR-182445] p 220 N90-22813
- ABDUL-AZIZ, A.**
Structural response of SSME turbine blade airfoils p 224 N90-28649
- ABDULAZIZ, MAHMOUD**
Photochemical approaches to ordered polymers p 84 A90-33222
- ABEL, PHILLIP B.**
FORTRAN program for x ray photoelectron spectroscopy data reformatting
[NASA-TP-2957] p 258 N90-12348
- Design and calibration of a vacuum compatible scanning tunneling microscope
[NASA-TM-102514] p 189 N90-20353
- ABU-HULEH, B. A. K.**
Structure of a reattaching supersonic shear layer p 7 A90-36252
- ABUELFOUTOUH, NADER MOHAMED**
Isothermal life prediction of composite lamina using a damage mechanics approach p 92 A90-48115
- ACKERMAN, E.**
High-speed digital fiber optic links for satellite traffic p 250 A90-41247
- ACKERMAN, EDWARD**
High-speed fiber-optic links for distribution of satellite traffic p 47 A90-41687
- ACOSTA, R. J.**
A comparison of reflector antenna designs for wide-angle scanning p 144 N90-19264

- Conjugate field approaches for active array compensation p 144 N90-19266
- ACOSTA, WALDO A.**
Composite matrix cooling scheme for small gas turbine combustors
[AIAA PAPER 90-2158] p 22 A90-47210
- ADAMCZYK, J. J.**
Numerical analysis of secondary flow in a two-stage turbine
[AIAA PAPER 90-2356] p 66 A90-47216
- The numerical simulation of multistage turbomachinery flows p 29 N90-21025
- ADAMCZYK, JOHN J.**
Simulation of three-dimensional viscous flow within a multistage turbine
[ASME PAPER 89-GT-152] p 5 A90-23841
- ADAMOVSKY, G.**
Intensity to frequency conversion technique in intensity modulated fiber optic sensing systems
[NASA-TM-102562] p 153 N90-21277
- ADAMOVSKY, GRIGORY**
Fiber optic sensing systems using high frequency resonant sensing heads with intensity sensors p 185 A90-10472
- Fiber optic sensing system
[NASA-CASE-LEW-14795-1] p 251 N90-15733
- Optical techniques for determination of normal shock position in supersonic flows for aerospace applications
[NASA-TM-103201] p 190 N90-25323
- ADDY, HAROLD E., JR.**
A numerical simulation of the flow in the diffuser of the NASA Lewis Icing Research Tunnel
[AIAA PAPER 90-0488] p 166 A90-25034
- A numerical simulation of the flow in the diffuser of the NASA Lewis icing research tunnel
[NASA-TM-102480] p 38 N90-15965
- AFOLABI, DARE**
Effects of mistuning and matrix structure on the topology of frequency response curves
[NASA-TM-102290] p 216 N90-12041
- AGUILAR, JERRY L.**
Conceptual design of a moving belt radiator shuttle-attached experiments: Technical requirement Document
[NASA-CR-185168] p 73 N90-15996
- Conceptual design of a Moving Belt Radiator (MBR) shuttle-attached experiment
[NASA-CR-185169] p 79 N90-23474
- AHMAD, S.**
Advanced development of BEM for elastic and inelastic dynamic analysis of solids p 213 A90-45771
- Inelastic transient dynamic analysis of three-dimensional problems by BEM p 215 A90-51480
- AHMED, SHAMIM**
Local-global analysis of crack growth in continuously reinforced ceramic matrix composites
[ASME PAPER 89-GT-138] p 88 A90-23835
- AHUJA, K. K.**
Theoretical model of discrete tone generation by impinging jets p 247 A90-35903
- AIELLO, R. A.**
Parametric studies of advanced turboprops p 19 A90-21225
- AIELLO, ROBERT A.**
Composite Blade Structural Analyzer (COBSTRAN) theoretical/programmer's manual p 95 N90-10181
- Low velocity impact analysis with NASTRAN p 221 N90-24647
- AKAY, H. U.**
A block-based algorithm for the solution of compressible flows in rotor-stator combinations p 9 A90-46905
- AKIN, L. S.**
The role of thermal and lubricant boundary layers in the transient thermal analysis of spur gears p 194 A90-21118
- Wear consideration in gear design for space applications p 194 A90-21121
- Lubricant jet flow phenomena in spur and helical gears with modified addendums - For radially directed individual jets p 194 A90-21122
- AKL, F. A.**
Parallel eigenanalysis of finite element models in a completely connected architecture
[NASA-CR-185166] p 217 N90-14652
- AKL, FRED A.**
Eigensolution of finite element problems in a completely connected parallel architecture
[NASA-TM-102450] p 217 N90-17173
- ALAN, I.**
Performance testing of a high frequency link converter for Space Station power distribution system p 148 A90-38128
- ALDANA, S. L.**
K-band TWT using new diamond rod technology
[AIAA PAPER 90-0870] p 147 A90-25691
- ALDRED, W.**
Catalysts for ultrahigh current density oxygen cathodes for space fuel cell applications
[NASA-CR-180650] p 232 N90-22835
- ALEMDAROGLU, N.**
Fortified LEWICE with viscous effects
[AIAA PAPER 90-0754] p 15 A90-20009
- ALEXANDER, R. M.**
Test and theory for piezoelectric actuator-active vibration control of rotating machinery p 198 A90-46226
- ALEXOVICH, ROBERT E.**
Data compression techniques applied to high resolution high frame rate video technology
[NASA-CR-4263] p 143 N90-14452
- ALSTON, WILLIAM B.**
The 3F condensation polyimides: Review and update
[NASA-TM-102353] p 126 N90-14363
- New Condensation polyimides containing 1,1,1-triaryl-2,2,2-trifluoroethane structures
[NASA-CASE-LEW-14346-1] p 86 N90-19300
- Substituted 1,1,1-triaryl-2,2,2-trifluoroethanes and processes for their synthesis
[NASA-CASE-LEW-14345-2] p 107 N90-23497
- ALTENKIRCH, R. A.**
Opposed-flow flame spread and extinction in mixed-convection boundary layers p 168 A90-32841
- ALTEROVITZ, S. A.**
Plasma-deposited amorphous hydrogenated carbon films and their tribological properties p 123 A90-44864
- Ellipsometric study of YBa₂Cu₃O_{7-x} laser ablated and co-evaporated films
[NASA-TM-103223] p 259 N90-26682
- Dielectric function of InGaAs in the visible
[NASA-TM-103246] p 260 N90-26683
- ALTEROVITZ, SAMUEL A.**
Optical dispersion relations for diamondlike carbon films
[NASA-TM-102356] p 257 N90-10738
- Plasma-deposited amorphous hydrogenated carbon films and their tribological properties
[NASA-TM-102379] p 125 N90-11880
- ALTHAUS, J.**
Actuator design for rotor control p 198 A90-46232
- ALTIDIS, P. C.**
Tooth contact shift in loaded spiral bevel gears p 193 A90-21112
- AMUEDO, K. C.**
Engine inlet distortion in a 9.2 percent scaled vectored thrust STOVL model in ground effect
[AIAA PAPER 89-2910] p 5 A90-25043
- Engine inlet distortion in a 9.2 percent scale vectored thrust STOVL model in ground effect
[NASA-TM-102358] p 12 N90-17561
- AMUEDO, KURT C.**
Hot gas ingestion characteristics and flow visualization of a vectored thrust STOVL concept
[NASA-TM-103212] p 32 N90-26009
- ANDERSON, KAREN S.**
Data compression for the microgravity experiments p 188 N90-16212
- ANDERSON, L. P., JR.**
Antenna beamforming using optical processing
[NASA-CR-180844] p 142 N90-11210
- ANDERSON, N. E.**
Advanced gearbox technology
[NASA-CR-179625] p 32 N90-24274

ANDERSON, ROBERT C.

PERSONAL AUTHOR INDEX

- ANDERSON, ROBERT C.**
Laser diffraction particle sizing: Instrument probe volume relocation and elongation
[NASA-TM-102512] p 188 N90-18025
- ANDRACCHIO, CHARLES R.**
NASA Lewis icing research tunnel user manual
[NASA-TM-102319] p 31 N90-23407
- ANDRO, M.**
ATDRS payload technology research and development
[NASA-TM-103256] p 52 N90-28596
- ANDRO, MONTY**
Satellite-matrix-switched, time-division-multiple-access network simulator
[AIAA PAPER 90-0848] p 147 A90-25671
Satellite-matrix-switched, time-division-multiple-access network simulator
[NASA-TP-2944] p 142 N90-11915
- ANEX, ROB**
Flight control design considerations for STOVL powered-lift flight
[AIAA PAPER 90-3225] p 37 A90-49110
- ANNEN, K. D.**
Modeling of the SiC chemical vapor deposition process and comparison with experimental results
p 105 A90-36810
- ANTHAN, DONALD J.**
Modulated-splitting-ratio fiber-optic temperature sensor
p 185 A90-11706
- ANTOLOVICH, STEPHEN D.**
The correlation between the temperature dependence of the CRSS and the formation of superlattice-intrinsic stacking faults in the nickel-base superalloy PWA 1480
p 109 A90-11657
On the mechanism of cross slip in Ni3Al
p 111 A90-20811
Cyclic deformation, fatigue and fatigue crack propagation in Ni-base alloys
p 115 A90-34162
Fatigue crack propagation behavior of a single crystalline superalloy
p 116 A90-48635
Micromechanics of cyclic deformation in SSME turbopump blade materials
p 224 N90-28641
- ANTON, D. L.**
Identification of a cast iron alloy containing nonstrategic elements
[NASA-CR-185174] p 118 N90-18559
Constitutive and life modeling of single crystal blade alloys for root attachment analysis
p 119 N90-28643
- ANZIC, G.**
ATDRS payload technology research and development
[NASA-TM-103256] p 52 N90-28596
- ANZIC, JUDITH M.**
Measurements of print-through in graphite fiber epoxy composites
p 91 A90-31555
- APPEL, M. A.**
Iridium-coated rhenium thrusters by CVD
p 114 A90-30480
- APPELBAUM, J.**
Magnification of starting torques of dc motors by maximum power point trackers in photovoltaic systems
p 149 A90-38144
- APPELBAUM, JOSEPH**
Photovoltaic power system operation in the Mars environment
p 43 A90-38156
- ARCHER, J. S.**
Solar dynamic power for the Space Station
p 55 A90-16374
- ARIF, HUGH**
Evaluation of supercritical cryogen storage and transfer systems for future NASA missions
[AIAA PAPER 90-0719] p 44 A90-19989
Spacecraft attitude impacts on COLD-SAT non-vacuum jacketed LH2 supply tank thermal performance
[AIAA PAPER 90-1672] p 49 A90-41566
Evaluation of supercritical cryogen storage and transfer systems for future NASA missions
[NASA-TM-102394] p 44 N90-10912
- ARMANDO, SASAN C.**
Comparative thermal analysis of the Space Station Freedom photovoltaic deployable boom structure using TRASYS, NEVADA, and SINDA programs
[SAE PAPER 891563] p 47 A90-27525
A transient plasticity study and low cycle fatigue analysis of the Space Station Freedom photovoltaic solar array blanket
[NASA-TM-102516] p 218 N90-19617
- ARMSTRONG, ELIZABETH S.**
Cooling of rocket thrust chambers with liquid oxygen
[AIAA PAPER 90-2120] p 63 A90-42029
Cooling of rocket thrust chambers with liquid oxygen
[NASA-TM-103146] p 78 N90-22605
Bearing optimization for SSME HPOTP application
p 205 N90-28622
- ARNAL, M. P.**
Investigation of turbulent flow in highly curved ducts with application to turbomachinery components
[NASA-CR-186060] p 175 N90-12882
- ARNOLD, S. M.**
Effects of state recovery on creep buckling under variable loading
p 212 A90-41223
A thermoelastic transversely isotropic thick walled cylinder/disk application: An analytical solution and study
[NASA-TM-102320] p 216 N90-12950
Computer simulation of the mathematical modeling involved in constitutive equation development: Via symbolic computations
[NASA-TM-102532] p 219 N90-20428
A creep model for metallic composites based on matrix testing: Application to Kanthal composites
[NASA-TM-103172] p 101 N90-25193
- ARNOLD, STEVEN M.**
Noninteractive macroscopic reliability model for whisker-reinforced ceramic composites
p 89 A90-26561
Application of symbolic computations to the constitutive modeling of structural materials
[NASA-TM-103225] p 222 N90-26364
- ARNOLD, W. A.**
Convection phenomena in low-gravity processing - The GTE GaAs space experiment
[AIAA PAPER 90-0409] p 133 A90-25032
- ARON, PAUL R.**
Development of a quadrupole-based Secondary-Ion Mass Spectrometry (SIMS) system at Lewis Research Center
[NASA-TM-102531] p 87 N90-23476
- ARORA, J. S.**
Robustness, generality and efficiency of optimization algorithms in practical applications
[AIAA PAPER 90-1177] p 236 A90-29268
- ARRINGTON, LYNN A.**
Low thrust rocket test facility
[AIAA PAPER 90-2503] p 43 A90-47225
Low thrust rocket test facility
[NASA-TM-103206] p 43 N90-25158
- ARRISON, A.**
A V-grooved GaAs solar cell
p 225 A90-14887
- ARSENEAUX, PETER J.**
Large-scale Advanced Prop-fan (LAP) high speed wind tunnel test report
[NASA-CR-182125] p 24 N90-10045
- ARYA, V. K.**
Finite element implementation of Robinson's unified viscoplastic model and its application to some uniaxial and multiaxial problems
p 208 A90-15704
Analytical and finite element solutions of some problems using a viscoplastic model
p 209 A90-19132
Application of finite-element-based solution technologies for viscoplastic structural analyses
[NASA-CR-185196] p 221 N90-23757
Finite element analysis of structural components using viscoplastic models with application to a cowl lip problem
[NASA-CR-185189] p 221 N90-23769
Structural response of SSME turbine blade airfoils
p 224 N90-28649
- ARYA, VINOD K.**
Finite element elastic-plastic-creep and cyclic life analysis of a cowl lip
[NASA-TM-102342] p 220 N90-22808
- ARZT, EDUARD**
Preliminary investigation of a NiAl composite prepared by cryomilling
p 113 A90-25098
- ASHPIS, DAVID E.**
The vibrating ribbon problem revisited
p 168 A90-33516
- ASMUSSEN, JES**
Review of research and development on the microwave electrothermal thruster
p 55 A90-16369
- ATASSI, H. M.**
Analysis of nonuniform subsonic flows about a row of moving blades
p 2 A90-11779
Unsteady disturbances of streaming motions around bodies
p 162 A90-21424
- ATASSI, HAFIZ M.**
Numerical solutions of the linearized Euler equations for unsteady vortical flows around lifting airfoils
[AIAA PAPER 90-0694] p 5 A90-25041
Numerical solutions of the linearized Euler equations for unsteady vortical flows around lifting airfoils
p 7 A90-30264
Numerical solutions of the linearized Euler equations for unsteady vortical flows around lifting airfoils
[NASA-TM-102466] p 12 N90-17562
- ATHERTON, WILLIAM J.**
Developing a self-diagnostic system for piezoelectric sensors
[AIAA PAPER 90-2230] p 187 A90-42755
- AUXTER, D. STEVE**
Modeling and synthesis of multicomputer interconnection networks
[NASA-CR-186619] p 238 N90-25604
- AYDELOTT, JOHN C.**
Evaluation of supercritical cryogen storage and transfer systems for future NASA missions
[AIAA PAPER 90-0719] p 44 A90-19989
Prediction of self-pressurization rate of cryogenic propellant tankage
p 55 A90-21219
Evaluation of supercritical cryogen storage and transfer systems for future NASA missions
[NASA-TM-102394] p 44 N90-10912
- AZAR, MASSOOD TABIB**
Silicon-etalon fiber-optic temperature sensor
[NASA-TM-102389] p 18 N90-13381

B

- BACHALO, W.**
Advanced instrumentation for aircraft icing research
[NASA-CR-185225] p 18 N90-21006
- BACHALO, W. D.**
Development of a phase Doppler based probe for icing cloud droplet characterization
[AIAA PAPER 90-0667] p 186 A90-26978
- BADGLEY, M. B.**
User needs, benefits, and integration of robotic systems in a space station laboratory
[NASA-CR-185150] p 200 N90-13794
- BAGWELL, JAMES W.**
The role of technology in influencing future civil communications satellites
p 142 A90-51187
- BAHADORI, M. YOUSEF**
Ignition and behavior of laminar gas-jet diffusion flames in microgravity
p 103 A90-23107
Effects of pressure on microgravity hydrocarbon diffusion flames
[AIAA PAPER 90-0651] p 104 A90-25039
- BAHR, G. K.**
Space vehicle propulsion systems - Environmental space hazards
[AIAA PAPER 90-1881] p 63 A90-40545
- BAILEY, M. MURRAY**
Thermal barrier coatings for gas turbine and diesel engines
[NASA-TM-102408] p 117 N90-13636
- BAILEY, R. S.**
Identification of a cast iron alloy containing nonstrategic elements
[NASA-CR-185174] p 118 N90-18559
- BAILEY, R. T.**
GRID2D/3D: A computer program for generating grid systems in complex-shaped two- and three-dimensional spatial domains. Part 2: User's manual and program listing
[NASA-TM-102454] p 237 N90-20708
GRID2D/3D: A computer program for generating grid systems in complex-shaped two- and three-dimensional spatial domains. Part 1: Theory and method
[NASA-TM-102453] p 238 N90-22262
- BAILEY, S. G.**
A V-grooved GaAs solar cell
p 225 A90-14887
GaAs solar cells with V-grooved emitters
p 229 N90-17754
Peeled film GaAs solar cells for space power
[NASA-TM-103125] p 153 N90-21287
- BAILEY, SHEILA G.**
Photovoltaic power for a lunar base
[IAF PAPER 89-254] p 42 A90-13409
Effect of crystal orientation on anisotropic etching and MOCVD growth of grooves on GaAs
p 253 A90-15136
- BAILEY, W. J.**
On-orbit low gravity cryogenic scientific investigations using the COLD-SAT Satellite
[AIAA PAPER 90-0718] p 39 A90-19988
- BAJGAR, C.**
High efficiency GaAs/Ge monolithic tandem solar cells
p 224 A90-14858
- BAJUK, LOU**
Simple evaporation controller for thin-film deposition from a resistively heated boat
p 149 A90-39761
- BAK, JOE**
Constitutive and life modeling of single crystal blade alloys for root attachment analysis
p 119 N90-28643
- BAKER, IAN**
Improving the low temperature ductility of NiAl
p 110 A90-16940
- BAKER, KARL W.**
A heat receiver design for solar dynamic space power systems
[NASA-TM-102473] p 72 N90-14283

- BAKHLE, MILIND A.**
Time domain flutter analysis of cascades using a full-potential solver
[AIAA PAPER 90-0984] p 6 A90-29374
- BALASUBRAMANIAM, R.**
Numerical simulation of thermocapillary bubble migration under microgravity for large Reynolds and Marangoni numbers p 164 A90-23213
Thermocapillary migration of liquid droplets in a temperature gradient in a density matched system
[NASA-CR-185178] p 177 N90-14512
- BALDAUF, J.**
On physical optics for calculating scattering from coated bodies p 250 A90-20151
- BALDWIN, R.**
Hydrogen-oxygen proton-exchange membrane fuel cells and electrolyzers p 56 A90-33944
Hydrogen-oxygen proton-exchange membrane fuel cells and electrolyzers p 230 N90-20467
- BALDWIN, R. M.**
Spray automated balancing of rotors - How process parameters influence performance p 198 A90-46228
- BALDWIN, RICHARD S.**
Space Electrochemical Research and Technology (SERT), 1989
[NASA-CP-3056] p 230 N90-20454
- BALL, CALVIN L.**
Advanced technology's impact on compressor design and development - A perspective
[SAE SP-800] p 20 A90-28571
Advanced technologies impact on compressor design and development: A perspective
[NASA-TM-102341] p 24 N90-10891
- BALLARINI, R.**
Three-dimensional analysis of surface crack-Hertzian stress field interaction
[NASA-CR-4254] p 215 N90-11332
Green's functions for dislocations in bonded strips and related crack problems
[NASA-CR-185291] p 224 N90-28878
- BALLARINI, ROBERTO**
Local-global analysis of crack growth in continuously reinforced ceramic matrix composites
[ASME PAPER 89-GT-138] p 88 A90-23835
- BALOMBIN, JOSEPH R.**
Advanced Communications Technology Satellite (ACTS) and potential system applications p 142 A90-51165
- BALSA, THOMAS F.**
On the instabilities of supersonic mixing layers - A high-Mach-number asymptotic theory p 8 A90-42644
- BANERJEA, A.**
Synthesis and structural chemistry of Au(III)-substituted Ba₂YCu₃O₇(δ)
[NASA-TM-103292] p 108 N90-28696
- BANERJEA, AMITAVA**
Universal aspects of brittle fracture, adhesion, and atomic force microscopy p 83 A90-14021
- BANERJEE, P. K.**
Development of an integrated BEM for hot fluid-structure interaction
[ASME PAPER 89-GT-128] p 212 A90-32264
Advanced applications of BEM to inelastic analysis of solids p 213 A90-45770
Advanced development of BEM for elastic and inelastic dynamic analysis of solids p 213 A90-45771
Inelastic transient dynamic analysis of three-dimensional problems by BEM p 215 A90-51480
Free-vibration analysis of three-dimensional solids by BEM p 215 A90-52007
Development of an integrated BEM approach for hot fluid structure interaction
[NASA-CR-186214] p 177 N90-15364
- BANKS, BRUCE A.**
Total hemispherical emittance measured at high temperatures by the calorimetric method
[NASA-TM-102322] p 136 N90-10309
- BANKS, P. M.**
The sheath structure around a negatively charged rocket payload p 48 A90-34780
- BANSAL, N. P.**
Crystallization of a barium-aluminosilicate glass p 121 A90-27107
- BANSAL, NAROTTAM P.**
Glass-derived superconducting ceramics with zero resistance at 107 K in the Bi(1.5)Pb(0.5)Sr₂Ca₂Cu₃O(x) system p 253 A90-11491
Synthesis and characterization of high-T_c superconductors in the Ti-Ca-Ba-Cu-O system p 253 A90-19300
Crystallization kinetics of BaO-Al₂O₃-SiO₂ glasses p 121 A90-21175
Synthesis and characterization of high-T(c) screen-printed Y-Ba-Cu-O films on alumina p 254 A90-21926
- Superconducting Bi(1.5)Pb(0.5)Sr₂Ca₂Cu₃O(x) ceramics by rapid melt quenching and glass crystallization p 256 A90-43568
Phase transformations in xerogels of mullite composition p 123 A90-47093
Crystallization behavior and properties of BaO-Al₂O₃-2SiO₂ glass matrices p 95 A90-51933
Superconducting ceramics in the Bi_{1.5}Sr₂CaCu₂O sub x system by melt quenching technique
[NASA-CR-185139] p 258 N90-11606
Preparation of 110K (Bi, Pb)-Sr-Ca-Cu-O superconductor from glass precursor p 258 N90-14108
[NASA-CR-185162] p 258 N90-14108
Superconducting Bi_{1.5}Pb_{0.5}Sr₂Ca₂Cu₃O(x) ceramics by rapid melt quenching and glass crystallization
[NASA-CR-185184] p 258 N90-17465
Crystallization behavior and properties of BaO-Al₂O₃-2SiO₂ glass matrices
[NASA-CR-185209] p 127 N90-19374
- BARANKIEWICZ, W. S.**
A modeling technique for STOVJ ejector and volume dynamics
[AIAA PAPER 90-2417] p 20 A90-42168
A modeling technique for STOVJ ejector and volume dynamics
[NASA-TM-103167] p 30 N90-22566
- BARAONA, COSMO**
Space Station Freedom solar array design development p 58 A90-38076
- BARAONA, COSMO R.**
Photovoltaic power for Space Station Freedom
[NASA-TM-102569] p 78 N90-21812
- BARKHOUDARIAN, S.**
Determination of the durability of the fiber optics in rocket engine environments
[AIAA PAPER 90-2229] p 250 A90-42754
- BARLOW, R.**
Combustion interaction with radiation-cooled chambers
[AIAA PAPER 90-2121] p 64 A90-42030
- BARNETT, MARK**
Simulation of three-dimensional viscous flow within a multistage turbine
[ASME PAPER 89-GT-152] p 5 A90-23841
- BARNHART, PAUL J.**
A supersonic through-flow fan engine airframe integration study
[NASA-CR-185140] p 10 N90-10004
- BARRANGER, JOHN P.**
Two-dimensional surface strain measurement based on a variation of Yamaguchi's laser-speckle strain gauge
[NASA-TM-103162] p 192 N90-22784
Progress in high temperature speckle-shift strain measurement system
[NASA-TM-103255] p 191 N90-28031
- BARRETT, C. A.**
The oxidation of Ni-rich Ni-Al intermetallics p 112 A90-24855
The effect of 0.1 atomic percent zirconium on the cyclic oxidation behavior of beta-NiAl for 3000 hours at 1200 C p 112 A90-24857
Influence of alloying elements on the oxidation behavior of NbAl₃ p 113 A90-24861
- BARRETT, CHARLES A.**
The oxidation and corrosion of ODS alloys
[NASA-TM-102555] p 119 N90-25211
- BARRETT, RICHARD T.**
Fastener design manual p 202 N90-18740
[NASA-RP-1228]
- BARTEL, H. W.**
Propfan Test Assessment (PTA): Flight test report
[NASA-CR-182278] p 24 N90-11738
Propfan Test Assessment (PTA)
[NASA-CR-185138] p 25 N90-11739
- BARTOLOTTA, P. A.**
High temperature fatigue behavior of a SiC/Ti-24Al-11Nb composite
[NASA-TM-103157] p 220 N90-22822
- BARTOLOTTA, PAUL A.**
A creep model for metallic composites based on matrix testing: Application to Kanthal composites
[NASA-TM-103172] p 101 N90-25193
Thermomechanical testing techniques for high-temperature composites: TMF behavior of SiC(SCS-6)/Ti-15-3
[NASA-TM-103171] p 222 N90-25367
- BARTON, J. MICHAEL**
Nonlinear Reynolds stress models and the renormalization group p 172 A90-44011
- BARTRAND, TIMOTHY A.**
Performance of a supercharged direct-injection stratified-charge rotary combustion engine
[NASA-TM-103105] p 32 N90-25982
- BASU, P.**
A simplified model for two phase face seal design p 197 A90-40713
- BASU, S. N.**
Rapid thermal processing of high temperature superconducting fiber
[NASA-CR-186803] p 259 N90-24964
- BATTISTA, R.**
Automotive Stirling engine development program
[NASA-CR-180839] p 263 N90-11654
- BATUR, CELAL**
Temperature and melt solid interface control during crystal growth
[NASA-CR-186731] p 259 N90-26664
- BAUGHMAN, R. J.**
Rapid thermal processing of high temperature superconducting fiber
[NASA-CR-186803] p 259 N90-24964
- BAUHAHN, P.**
The 30-GHz monolithic receive module
[NASA-CR-180849] p 146 N90-24528
- BAUMANN, E. D.**
Power conditioning techniques
[NASA-TM-102577] p 151 N90-20301
Electrical characterization of a Mapham inverter using pulse testing techniques
[NASA-TM-103254] p 82 N90-27784
- BAUMANN, S. F.**
Reaction zone microstructure in a Ti₃Al + Nb/SiC composite p 91 A90-39627
- BAUMBICK, ROBERT J.**
Fiber optics for advanced aircraft p 185 A90-11702
- BAUMEISTER, JOSEPH F.**
Comparative thermal analysis of the Space Station Freedom photovoltaic deployable boom structure using TRASYS, NEVADA, and SINDA programs
[SAE PAPER 891563] p 47 A90-27525
Thermal radiation characteristics of nonisothermal cylindrical enclosures using a numerical ray tracing technique
[NASA-TM-102527] p 179 N90-21296
- BAUMEISTER, KENNETH J.**
Discretization formulas for unstructured grids p 242 A90-26535
Galerkin finite difference Laplacian operators on isolated unstructured triangular meshes by linear combinations
[NASA-TM-103209] p 183 N90-26276
- BAUSAL, NAROTTAM P.**
Superconducting glass-ceramics in the Bi-Sr-Ca-Cu-O system p 256 A90-35153
- BEACH, DUANE E.**
Comparative thermal analysis of the Space Station Freedom photovoltaic deployable boom structure using TRASYS, NEVADA, and SINDA programs
[SAE PAPER 891563] p 47 A90-27525
- BEACH, R. F.**
Evaluation of power control concepts using the PMAD systems test bed p 42 A90-38083
- BEACH, T. A.**
An interactive grid generation procedure for axial and radial flow turbomachinery
[AIAA PAPER 90-0344] p 162 A90-22200
Numerical analysis of secondary flow in a two-stage turbine
[AIAA PAPER 90-2356] p 66 A90-47216
The numerical simulation of multistage turbomachinery flows p 29 N90-21025
- BEACH, TIM A.**
Simulation of three-dimensional viscous flow within a multistage turbine
[ASME PAPER 89-GT-152] p 5 A90-23841
- BEACH, TIMOTHY A.**
An interactive grid generation procedure for axial and radial flow turbomachinery
[NASA-CR-185167] p 237 N90-13968
An analysis of the viscous flow through a compact radial turbine by the average passage approach
[NASA-TM-102471] p 12 N90-14206
- BEARD, L.**
Electromagnetic properties of material coated surfaces
[NASA-CR-186466] p 144 N90-19466
- BEATTIE, J. R.**
Xenon ion sources for space applications p 56 A90-22874
Status of xenon ion propulsion technology p 56 A90-27961
High-power xenon ion thrusters
[AIAA PAPER 90-2540] p 64 A90-42536
- BEATTY, P. A.**
A simplified model for two phase face seal design p 197 A90-40713
- BEATY, KEVIN**
Sliding seal materials for low heat rejection engines
[NASA-CR-182262] p 125 N90-11882
- BEAULIEU, ROLAND**
Wide-bandgap epitaxial heterojunction windows for silicon solar cells p 227 A90-28359

- BECHTEL, G. S.**
Application of HOST technology to the SSME HPFPT blade
[ASME PAPER 89-GT-130] p 209 A90-23828
- BEGG, L. L.**
Advanced radiator concepts p 170 A90-38042
- BEGG, LESTER L.**
Vapor grown carbon fiber for space thermal management systems p 94 A90-50128
- BEHEIM, GLENN**
Active phase compensation system for fiber optic holography p 250 A90-11310
Modulated-splitting-ratio fiber-optic temperature sensor p 185 A90-11706
Silicon-etalon fiber-optic temperature sensor [NASA-TM-102389] p 18 A90-13381
Fiber-optic projected-fringe digital interferometry [NASA-TM-102352] p 191 A90-28033
- BEITLER, R. S.**
Energy Efficient Engine: Control system component performance report [NASA-CR-174651] p 34 A90-28562
- BELLOWS, A. H.**
Interface demarcation in GaAs by current pulsing [AIAA PAPER 90-0319] p 254 A90-19793
Free float acceleration measurements aboard NASA's KC-135 Microgravity Research Aircraft [AIAA PAPER 90-0742] p 132 A90-20000
- BELTE, DAUMANTS**
Initial results from the joint NASA-Lewis/U.S. Army icing flight research tests p 16 A90-28180
- BENCIC, TIMOTHY J.**
Hot gas ingestion characteristics and flow visualization of a vectored thrust STOVL concept [NASA-TM-103212] p 32 A90-26009
- BENDETT, M.**
A high-speed GaAs MESFET optical controller p 186 A90-22483
Control of a GaAs monolithic Ka-band phase shifter using a high-speed optical interconnect p 150 A90-41700
Optical control of an 8-element Ka-band phased array using a high-speed optoelectronic interconnect [NASA-TM-102550] p 152 A90-21275
- BENDIKSEN, ODDVAR O.**
Aeroelastic problems in turbomachines [AIAA PAPER 90-1157] p 7 A90-29393
- BENNETT, G. W.**
Energy Efficient Engine: Control system component performance report [NASA-CR-174651] p 34 A90-28562
- BENNETT, GARY L.**
NASA advanced space photovoltaic technology: Status, potential and future mission applications p 74 A90-17775
- BENSON, T. J.**
Comparison of 3-D viscous flow computations of Mach 5 inlet with experimental data [AIAA PAPER 90-0600] p 6 A90-26970
Comparison of 3-D viscous flow computations of Mach 5 inlet with experimental data [NASA-TM-102518] p 28 A90-20090
- BENSON, THOMAS J.**
PROTEUS two-dimensional Navier-Stokes computer code, version 1.0. Volume 1: Analysis description [NASA-TM-102551] p 180 A90-21303
PROTEUS two-dimensional Navier-Stokes computer code, version 1.0. Volume 2: User's guide [NASA-TM-102552] p 180 A90-21306
PROTEUS two-dimensional Navier-Stokes computer code, version 1.0. Volume 3: Programmer's reference [NASA-TM-102553] p 180 A90-21307
- BENTS, D. J.**
Romans to Mars [NASA-TM-103094] p 267 A90-23339
The lessons of Varsovian's reconnaissance [NASA-TM-103207] p 267 A90-26789
- BENTS, DAVID J.**
Estimated performance and future potential of solar dynamic and photovoltaic power systems for selected LEO and HEO missions p 62 A90-38307
- BENTZ, M. D.**
Tank Pressure Control Experiment - A low-g mixing investigation [AIAA PAPER 90-2376] p 66 A90-47217
- BERCAW, ROBERT W.**
Toward an electrical power utility for space exploration p 74 A90-17681
- BERG, R. F.**
Critical exponent for the viscosity of carbon dioxide and xenon p 261 A90-43941
- BERKE, L.**
Neurobiological computational models in structural analysis and design [AIAA PAPER 90-1133] p 210 A90-29260
- BERKE, LASZLO**
Compatibility conditions of structural mechanics for finite element analysis [NASA-TM-102413] p 217 A90-17180
Integrated force method versus displacement method for finite element analysis [NASA-TP-2937] p 218 A90-18081
- BERKIN, ANDREW L.**
Soft inflation p 265 A90-40093
- BERKOPEC, FRANK D.**
Engine selection for the Space Exploration Initiative [AIAA PAPER 90-1880] p 65 A90-47201
The Pathfinder chemical transfer propulsion program p 74 A90-18471
- BERKOVITS, A.**
Relationship between fatigue life in the creep-fatigue region and stress-strain response p 209 A90-20061
- BERKOVITS, AVRAHAM**
Mean stress and the exhaustion of fatigue-damage resistance [NASA-TM-101311] p 216 A90-13819
- BERKOWITZ, B. M.**
Experimental investigation of multielement airfoil ice accretion and resulting performance degradation p 9 A90-48954
- BERKOWITZ, BRIAN M.**
Hypersonic aerospace sizing analysis for the preliminary design of aerospace vehicles p 17 A90-23276
Modeling of surface roughness effects on glaze ice accretion p 16 A90-20925
Users manual for the NASA Lewis Ice Accretion Prediction Code (LEWICE) [NASA-CR-185129] p 1 A90-20943
- BERNDT, CHRISTOPHER C.**
Instrumented adhesion tests on plasma sprayed thermal barrier coatings p 111 A90-20255
Tensile adhesion testing methodology for thermally sprayed coatings p 85 A90-43902
- BERNHART, W. D.**
Electro-impulse de-icing testing analysis and design [NASA-CR-4175] p 18 A90-10031
- BERRIE, J.**
Electromagnetic properties of material coated surfaces [NASA-CR-186466] p 144 A90-19466
- BERRY, W. B.**
High frequency capacitance-voltage characteristics of thermally grown SiO₂ films on beta-SiC p 254 A90-21348
- BESKOK, A.**
A block-based algorithm for the solution of compressible flows in rotor-stator combinations p 9 A90-46905
- BETTNER, JAMES L.**
Investigation of advanced counterrotation blade configuration concepts for high speed turboprop systems, task 1: Ducted propfan analysis [NASA-CR-185217] p 30 A90-22567
- BHARGAVA, R. K.**
Near wall flow parameters in the blade end-wall corner region p 156 A90-12636
- BHASIN, K. B.**
High frequency GaAs modulator and photodetector for phased array antenna applications p 146 A90-11774
A high-speed GaAs MESFET optical controller p 186 A90-22483
Ka-band propagation characteristics of microstrip lines on GaAs substrates at cryogenic temperatures p 147 A90-33644
Microwave response of a HEMT photoconductive detector p 147 A90-37301
Complex permittivity of lanthanum aluminate in the 20 to 300 K temperature range from 26.5 to 40.0 GHz p 148 A90-37864
Optical detectors for GaAs MMIC integration - Technology assessment p 149 A90-41238
Control of a GaAs monolithic Ka-band phase shifter using a high-speed optical interconnect p 150 A90-41700
Millimeter-wave surface resistance of laser-ablated YBa₂Cu₃O₇(δ) superconducting films p 257 A90-48694
Performance and modeling of superconducting ring resonators at millimeter-wave frequencies [NASA-TM-102526] p 151 A90-18634
Millimeter wave surface resistance of RbBa₂Cu₃O₇(δ) superconductors (R = Y, Eu, Dy, Sm, Er) [NASA-TM-102571] p 259 A90-20886
Optical control of an 8-element Ka-band phased array using a high-speed optoelectronic interconnect [NASA-TM-102550] p 152 A90-21275
Growth and patterning of laser ablated superconducting YBa₂Cu₃O₇ films on LaAlO₃ substrates [NASA-TM-102436] p 259 A90-22421
- Photoresponse of YBa₂Cu₃O₇(δ) granular and epitaxial superconducting thin films [NASA-TM-103144] p 154 A90-22732
Laser ablated high T(sub c) superconducting thin YBa₂Cu₃O₇(δ) films on substrates suitable for microwave applications p 260 A90-27808
Microwave conductivity of laser ablated YBaCuO superconducting films and its relation to microstrip transmission line p 155 A90-27844
Analysis of microstrip lines with alternative implementation of conductors and superconductors [NASA-TM-103182] p 155 A90-27966
High temperature superconducting thin film microwave circuits: Fabrication, characterization, and applications [NASA-TM-103235] p 156 A90-28786
- BHASIN, KUL B.**
Sequentially evaporated thin film YBa₂Cu₃O₇(δ) superconducting microwave ring resonator [NASA-TM-103180] p 154 A90-25273
Design of an optically controlled Ka-band GaAs MMIC phased-array antenna [NASA-TM-103147] p 155 A90-26250
- BHATT, HEMANSHU**
Role of the interfacial thermal barrier in the effective thermal diffusivity/conductivity of SiC-fiber-reinforced reaction-bonded silicon nitride p 89 A90-25268
- BHATT, R. T.**
Role of the interfacial thermal barrier in the effective thermal diffusivity/conductivity of SiC-fiber-reinforced reaction-bonded silicon nitride p 89 A90-25268
Thermal effects on the mechanical properties of SiC fibre reinforced reaction-bonded silicon nitride matrix composites p 92 A90-46999
- BHATT, RAMAKRISHNA T.**
Laminate behavior for SiC fiber-reinforced reaction-bonded silicon nitride matrix composites p 90 A90-29927
Matrix density effects on the mechanical properties of SiC fiber-reinforced silicon nitride matrix properties p 94 A90-51927
High-temperature tensile properties of fiber reinforced reaction bonded silicon nitride p 95 A90-52783
Oxidation effects on the mechanical properties of SiC fiber-reinforced reaction-bonded silicon nitride matrix composites p 96 A90-14287
Matrix density effects on the mechanical properties of SiC/RBSN composites [NASA-TM-103098] p 100 A90-21826
Influence of interfacial shear strength on the mechanical properties of SiC fiber reinforced reaction-bonded silicon nitride matrix composites [NASA-TM-102462] p 101 A90-24382
- BHATT, RHAM T.**
Measurement of interfacial shear strength in SiC-fiber/Si₃N₄ composites p 87 A90-13237
- BHATTACHARYA, P.**
Transport properties of InAs(x)Sb(1-x) (x = 0-0.55) on InP grown by molecular-beam epitaxy p 256 A90-36232
- BHATTACHARYA, P. K.**
Molecular beam epitaxial growth of high-quality InSb on InP and GaAs substrates p 253 A90-12808
Dielectric function of InGaAs in the visible [NASA-TM-103246] p 260 A90-26683
- BIANCO, ROBERT**
Corrosion of cordierite ceramics by sodium sulphate at 1000 C p 121 A90-21214
- BICKFORD, R. L.**
Fabry-Perot interferometer development for rocket engine plume spectroscopy [AIAA PAPER 90-2234] p 187 A90-47212
- BIDWELL, C. S.**
Swept wing ice accretion modeling [AIAA PAPER 90-0756] p 5 A90-25042
- BIDWELL, COLIN S.**
Predictions of airfoil aerodynamic performance degradation due to icing p 3 A90-16753
Swept wing ice accretion modeling [NASA-TM-103114] p 13 A90-21727
- BIESS, JOHN J.**
Power transmission cable development for the Space Station Freedom electrical power system p 149 A90-38134
Conceptual definition of a high voltage power supply test facility [NASA-CR-185216] p 50 A90-25172
- BILBY, CURT**
A superconducting quenchgun for delivering lunar derived oxygen to lunar orbit [AIAA PAPER 90-2369] p 43 A90-40627
- BILBY, CURT R.**
A superconducting quenchgun for delivering lunar derived oxygen to lunar orbit [NASA-CR-185161] p 77 A90-21806

PERSONAL AUTHOR INDEX

- A trajectory generation and system characterization model for cislunar low-thrust spacecraft. Volume 2: Technical manual
[NASA-CR-185172] p 77 N90-21807
- BILGER, KEVIN**
Space Station Freedom solar array design development p 58 A90-38076
- BILGER, KEVIN M.**
Photovoltaic array environmental protection program p 59 A90-38088
- BILLMAN, L. C.**
Large scale prop-fan structural design study. Volume 1: Initial concepts p 23 N90-10043
[NASA-CR-174992]
Large scale prop-fan structural design study. Volume 2: Preliminary design of SR-7 p 23 N90-10044
[NASA-CR-174993]
- BINDER, MICHAEL**
A candidate architecture for monitoring and control in chemical transfer propulsion systems p 52 A90-41980
[AIAA PAPER 90-1882]
- BINDER, MICHAEL P.**
Integrated controls and health monitoring for chemical transfer propulsion p 52 A90-47229
[AIAA PAPER 90-2751]
A candidate architecture for monitoring and control in chemical transfer propulsion systems p 52 N90-22595
[NASA-TM-103161]
Integrated controls and health monitoring for chemical transfer propulsion p 52 N90-25178
[NASA-TM-103185]
- BINIENDA, W. K.**
A creep model for metallic composites based on matrix testing: Application to Kanthal composites p 101 N90-25193
[NASA-TM-103172]
Creep and creep rupture of strongly reinforced metallic composites p 223 N90-28110
[NASA-CR-185286]
- BISSET, JOHN W.**
Energy Efficient Engine integrated core/low spool test hardware design report p 35 N90-28566
[NASA-CR-168137]
- BITTKER, DAVID A.**
Detailed mechanism for oxidation of benzene p 106 N90-21842
[NASA-TM-102443]
- BLATT, J. R.**
Energy Efficient Engine exhaust mixer model technology report addendum: phase 3 test program p 33 N90-28556
[NASA-CR-174799]
- BLELLOCH, PAUL A.**
Modal selection in structural dynamics p 209 A90-17001
Selection of component modes p 210 A90-26787
[AIAA PAPER 90-1201]
- BLELLOCH, PAUL ANDREW**
Detection of potential space station control/structure interaction with CO-ST-IN p 50 N90-21074
- BLOOMFIELD, H. S.**
Comparison of solar photovoltaic and nuclear reactor power systems for a human-tended lunar observatory p 42 A90-38030
- BLOOMFIELD, HARVEY S.**
Space nuclear reactor shields for manned and unmanned applications p 57 A90-37859
A feasibility assessment of installation, operation and disposal options for nuclear reactor power system concepts for a NASA growth space station p 70 N90-10174
[NASA-TM-89923]
SP-100 power system conceptual design for lunar base applications p 267 N90-15030
[NASA-TM-102090]
- BLOZY, J. T.**
Altitude testing of the 2D V-STOL ADEN demonstrator on an F404 engine p 28 N90-17638
[NASA-CR-174824]
- BLUE, JAMES W.**
Results of an attempt to measure increased rates of the reaction $D-2 + D-2$ yields $He-3 + n$ in a nonelectrochemical cold fusion experiment p 250 N90-17424
[NASA-TM-102430]
- BOBER, L. J.**
Large-scale advanced propeller blade pressure distributions: Prediction and data p 30 N90-22564
[NASA-TM-102316]
- BODDEN, DAVID S.**
The implementation of STOVL task-tailored control modes in a fighter cockpit p 17 A90-49114
[AIAA PAPER 90-3229]
- BODNER, S. R.**
High temperature inelastic deformation under uniaxial loading - Theory and experiment p 109 A90-13838
High temperature inelastic deformation of the B1900 + Hf alloy under multiaxial loading - Theory and experiment p 112 A90-22656
Constitutive modeling for isotropic materials (HOST) p 26 N90-13390
[NASA-CR-179522]
- Constitutive modeling for isotropic materials (HOST) p 26 N90-13391
[NASA-CR-174718]
- BODONYI, R. J.**
A numerical study of the interaction between unsteady free-stream disturbances and localized variations in surface geometry p 161 A90-21422
- BOGDONOFF, S. M.**
A study of the unsteadiness of crossing shock wave turbulent boundary layer interactions p 170 A90-38614
[AIAA PAPER 90-1456]
- BOHMAN, D. Y.**
Growth and patterning of laser ablated superconducting YBa₂Cu₃O₇ films on LaAlO₃ substrates p 259 N90-22421
[NASA-TM-102436]
- BOLCH, WESLEY E.**
A radiological assessment of nuclear power and propulsion operations near Space Station Freedom p 76 N90-21108
[NASA-CR-185185]
- BOLDISSAR, F.**
Antenna beamforming using optical processing p 142 N90-11210
[NASA-CR-180844]
- BOLDMAN, DONALD R.**
The unsteady aerodynamics of an oscillating cascade in a compressible flow field p 2 A90-11789
- BOND, THOMAS H.**
Icing Research Tunnel test of a model helicopter rotor p 15 A90-28179
- BONHAM, CHARLES D.**
The application of a computer data acquisition system for a new high temperature tribometer p 86 N90-17811
[NASA-TM-102508]
- BOOK, PATRICIA O.**
Experimentally determined wear behavior of an Al₂O₃-SiC composite from 25 to 1200 C p 87 N90-20130
[NASA-TM-102549]
- BORDER, DAVID A.**
Encoding Y,I,Q component estimates of an NTSC composite signal p 139 A90-23261
- BORETTI, A. A.**
Two-dimensional Euler and Navier-Stokes Time accurate simulations of fan rotor flows p 14 N90-25948
[NASA-TM-102402]
- BOROWSKI, S. K.**
Performance comparisons of nuclear thermal rocket and chemical propulsion systems for piloted missions to Phobos/Mars p 53 A90-13262
[IAF PAPER 89-027]
- BOROWSKI, STANLEY K.**
Nuclear propulsion - A vital technology for the exploration of Mars and the planets beyond p 55 A90-16676
[AAS PAPER 87-210]
- BOSE, S.**
MATE (Materials for Advanced Turbine Engines) Program, Project 3. Volume 2: Design, fabrication and evaluation of an oxide dispersion strengthened sheet alloy combustor liner p 117 N90-17868
[NASA-CR-180892]
- BOSE, SUDHANGSHU**
Mechanisms of degradation and failure in a plasma deposited thermal barrier coating p 84 A90-23830
[ASME PAPER 89-GT-132]
- BOSELA, PAUL A.**
Dynamic analysis of space-related linear and non-linear structures p 51 N90-25174
[NASA-TM-103490]
- BOUKARI, HACENE**
Critical speeding up in pure fluids p 167 A90-26369
- BOWLES, KENNETH J.**
Thermo-oxidative stability studies of PMR-15 polymer matrix composites reinforced with various continuous fibers p 93 A90-50068
Use of unbalanced laminates as a screening method for microcracking p 94 A90-50217
Thermo-oxidative stability studies of PMR-15 polymer matrix composites reinforced with various fibers p 98 N90-19310
[NASA-TM-102439]
Use of unbalanced laminates as a screening method for microcracking p 98 N90-21124
[NASA-TM-102517]
- BOWMAN, R.**
Observations on the brittle to ductile transition temperatures of B2 nickel aluminides with and without zirconium p 111 A90-19153
- BOWMAN, RANDY**
Up-and-coming IMCs p 88 A90-17295
- BOYD, G. L.**
ATTAP/AGT101 ceramics technology update p 195 A90-23814
[ASME PAPER 89-GT-105]
- BOYD, IAIN D.**
Efficient Monte Carlo simulation of rarefied flow in a small nozzle p 170 A90-38396
[AIAA PAPER 90-1693]
- BOYD, LINDA S.**
Two stage gear tooth dynamics program p 199 N90-10437
[NASA-CR-185110]
- BOYD, R. W.**
A forward error correction technique using a high-speed, high-rate single chip codec p 141 A90-48440
- BOYLE, M. T.**
Asymmetrical boundary layer separation at the base of a two cylinder geometry p 159 A90-18505
- BOYLE, R. J.**
Navier-Stokes analysis of turbine blade heat transfer p 179 N90-21300
[NASA-TM-102496]
- BOYLE, ROBERT J.**
Experimental determination of stator endwall heat transfer p 165 A90-23880
[ASME PAPER 89-GT-219]
- BOZEK, J. M.**
Nuclear power systems for lunar and Mars exploration p 82 N90-26873
[NASA-TM-103168]
- BOZZOLO, G.**
Phase transitions in fermionic systems with many-body interaction p 249 A90-19303
- BRABBS, THEODORE A.**
Fuel-rich catalytic combustion - A fuel processor for high-speed propulsion p 105 A90-42774
[AIAA PAPER 90-2319]
Fuel-rich catalytic combustion: A fuel processor for high-speed propulsion p 107 N90-23518
[NASA-TM-103177]
- BRACE, M. H.**
Droplet combustion experiment drop tower tests using models of the space flight apparatus p 133 N90-11196
[NASA-TM-101472]
- BRACE, MICHAEL H.**
N-decane-air droplet combustion experiments in the NASA-Lewis 5 Second Zero-Gravity Facility p 104 A90-25038
[AIAA PAPER 90-0649]
- BRADSHAW, J. L.**
Growth of improved quality 3C-SiC films on 6H-SiC substrates p 255 A90-29596
Growth of high quality 6H-SiC epitaxial films on vicinal (0001) 6H-SiC wafers p 255 A90-29952
- BRADSHAW, K.**
Doped-channel heterojunction structures for millimeter-wave discrete devices and MMICs p 150 A90-48492
- BRADY, JOYCE A.**
Evaluation of atomic oxygen resistant protective coatings for fiberglass-epoxy composites in LEO p 84 A90-31581
- BRANDHORST, HENRY W.**
Nuclear technology and the space exploration missions p 232 N90-22847
[NASA-TM-103156]
- BRANDHORST, HENRY W., JR.**
Challenges for future space power systems p 74 N90-17695
- BRAUN, M. J.**
A laser based computer aided non-intrusive technique for full field flow characterization in macroscopic curved channels p 168 A90-32293
Numerical modeling of flows in simulated brush seal configurations p 198 A90-47209
[AIAA PAPER 90-2141]
Flow visualization and motion analysis for a series of four sequential brush seals p 199 A90-47222
[AIAA PAPER 90-2482]
- BREAKWELL, JOHN V.**
Minimum fuel trajectories for a low-thrust power-limited mission to the moon and to Lagrange points L4 and L5 p 40 A90-46784
[AAS PAPER 89-351]
Minimum fuel trajectory for the aerospace-plane p 40 A90-46785
[AAS PAPER 89-352]
Minimum fuel lunar trajectories for a low-thrust power-limited spacecraft p 41 A90-53054
[AIAA PAPER 90-2975]
- BREISACHER, KEVIN J.**
A comparison of analytical results for 20 K LOX/hydrogen instabilities p 130 A90-47214
[AIAA PAPER 90-2241]
A comparison of analytical results for 20 K LOX/hydrogen instabilities p 80 N90-25186
[NASA-TM-103166]
Combustion instability coupling with feed system acoustics p 108 N90-28629
- BRENT, A. D.**
The modelling of heat, mass and solute transport in solidification systems p 157 A90-13092
- BREW, DALE**
X-ray beam method for displacement measurement in hostile environments p 187 A90-44485
- BREWE, D. E.**
A high-speed photography study of cavitation in a dynamically loaded journal bearing p 204 N90-26338
[NASA-TM-103178]
- BREWE, DAVID E.**
Elasticity effects on cavitation in a squeeze film damper undergoing noncentered circular whirl p 200 N90-13786
[NASA-TM-102392]

- On the numerical solution of the dynamically loaded hydrodynamic lubrication of the point contact problem [NASA-TM-102427] p 178 N90-17076
- BREWER, DAVID N.**
Controlled crack growth specimen for brittle systems [NASA-TM-103126] p 129 N90-23543
- BREWER, JEFFREY C.**
Characterization testing of a 40 ampere hour bipolar nickel-hydrogen battery p 56 A90-33940
Characterization testing of a 40 AHR bipolar nickel-hydrogen battery p 230 N90-20463
- BRIDGEMAN, M. J.**
NASA/GE Energy Efficient Engine low pressure turbine scaled test vehicle performance report [NASA-CR-168290] p 34 N90-28563
- BRIGGS, MATTHEW E.**
Critical speeding up in pure fluids p 167 A90-26369
- BRIGHT, MICHELLE**
H-infinity based integrated flight/propulsion control design for a STOVL aircraft in transition flight [AIAA PAPER 90-3335] p 36 A90-47595
- BRIGHT, MICHELLE M.**
H-infinity based integrated flight-propulsion control design for a STOVL aircraft in transition flight [NASA-TM-103198] p 37 N90-26011
- BRINDLEY, P. K.**
Investigation of interfacial shear strength in a SiC fibre/Ti-24Al-11Nb composite by a fibre push-out technique p 88 A90-18973
Reaction zone microstructure in a Ti3Al + Nb/SiC composite p 91 A90-39627
High temperature fatigue behavior of a SiC/Ti-24Al-11Nb composite [NASA-TM-103157] p 220 N90-22822
- BRINDLEY, PAMELA K.**
Cyclic oxidation of aluminate coatings on Ti3Al + Nb p 115 A90-39660
Tribological properties of ceramic/Ti3Al-Nb sliding couples for use as candidate seal materials to 700 deg C [NASA-TM-102401] p 86 N90-12658
- BRINDLEY, WILLIAM J.**
TBCs for better engine efficiency p 83 A90-17294
Metallographic techniques for evaluation of thermal barrier coatings p 85 A90-44869
Heat transfer to throat tubes in a square-chambered rocket engine at the NASA Lewis Research Center [NASA-TM-102336] p 70 N90-11082
Thermal barrier coatings for gas turbine and diesel engines [NASA-TM-102408] p 117 N90-13636
Durability of thermal barrier coatings in a high heat flux environment p 129 N90-28651
Thermal analysis of thermal barrier coatings in a high heat flux environment p 129 N90-28652
- BRINKER, D. J.**
Thermal annealing of GaAs concentrator solar cells p 60 A90-38150
Peeled film GaAs solar cells for space power [NASA-TM-103125] p 153 N90-21287
New directions in InP solar cell research [NASA-TM-103160] p 154 N90-23662
- BRINKER, DAVID J.**
Photovoltaic power for a lunar base [IAF PAPER 89-254] p 42 A90-13409
High altitude current-voltage measurement of GaAs/Ge solar cells p 226 A90-14910
InP homojunction solar cell performance on the LIPS III flight experiment p 226 A90-14921
Indium phosphide solar cells - Recent developments and estimated performance in space p 57 A90-37854
On-orbit results of the LIPS 3/InP homojunction solar cell experiment p 74 N90-17794
- BRITO, KARREN K.**
Vapor grown carbon fiber for space thermal management systems p 94 A90-50128
- BRITTAIN, JOHN O.**
Electrical properties of materials for high temperature strain gage applications [NASA-CR-186192] p 188 N90-14534
- BRITTON, DORIS L.**
Characterization and cycle tests of lightweight nickel electrodes [NASA-TM-102399] p 106 N90-12696
Electrochemical impregnation and cycle life of lightweight nickel electrodes for nickel-hydrogen cells [NASA-TM-103140] p 107 N90-21844
- BRITTON, R. K.**
A study of ice shape prediction methodologies and comparison with experimental data [AIAA PAPER 90-0753] p 15 A90-26986
- BROWN, G. V.**
Low frequency vibration isolation technology for microgravity space experiments p 136 A90-46246
- BROWN, GERALD V.**
Nonintrusive inertial vibration isolation technology for microgravity space experiments [AIAA PAPER 90-0741] p 132 A90-19999
Development of a compact, light weight magnetic bearing [AIAA PAPER 90-2483] p 199 A90-47223
Nonintrusive inertial vibration isolation technology for microgravity space experiments [NASA-TM-102386] p 137 N90-11901
Experimental evaluation of a tuned electromagnetic damper for vibration control of cryogenic turbopump rotors [NASA-TP-3005] p 30 N90-23403
- BROWN, H. C.**
Parametric studies to determine the effect of compliant layers on metal matrix composite systems p 93 A90-50093
Parametric studies to determine the effect of compliant layers on metal matrix composite systems [NASA-TM-102465] p 96 N90-14294
- BROWN, J. STEVEN**
Rate correlation for condensation of pure vapor on turbulent, subcooled liquid p 174 A90-50511
- BROWN, P. C.**
Propfan Test Assessment (PTA): Flight test report [NASA-CR-182278] p 24 N90-11738
Propfan Test Assessment (PTA) [NASA-CR-185138] p 25 N90-11739
- BROWN, PAUL**
Acoustic test and analysis of a counterrotating prop-fan model [NASA-CR-179590] p 247 N90-10683
- BROWN, S. A.**
Compression behavior of the forged Li2 compounds Al6Ti12Cr8 and Al6Ti12Mn9 p 116 A90-51298
- BROWN, WILLIAM S.**
Enhanced heat transfer rocket combustor technology component hot-fire test results [AIAA PAPER 90-2182] p 64 A90-42063
- BRUSH, ANDREW S.**
Frequency domain model for analysis of paralleled, series-output-connected Mapham inverters p 148 A90-38084
Distortion and regulation characterization of a Mapham inverter p 148 A90-38125
Development and testing of a 20 kHz component test bed p 43 A90-38126
- BUCHLE, DONALD R.**
Laser diffraction particle sizing: Instrument probe volume relocation and elongation [NASA-TM-102512] p 188 N90-18025
Scattered-light scanner measurements of cryogenic liquid-jet breakup [NASA-TM-102432] p 189 N90-22021
- BUCKMASTER, J.**
The structure and stability of nonadiabatic flame balls p 105 A90-43674
- BUDINGER, J.**
A parallel pipelined architecture for a digital multicarrier demodulator [AIAA PAPER 90-0812] p 46 A90-25635
- BUDINGER, JAMES M.**
Satellite-matrix-switched, time-division-multiple-access network simulator [AIAA PAPER 90-0848] p 147 A90-25671
A burst compression and expansion technique for variable-rate users in satellite-switched TDMA networks [NASA-PAPER 90-0850] p 46 A90-25673
On-board switching and processing p 150 A90-51168
Satellite-matrix-switched, time-division-multiple-access network simulator [NASA-TP-2944] p 142 N90-11915
A burst compression and expansion technique for variable-rate users in satellite-switched TDMA networks [NASA-TM-102414] p 47 N90-15983
- BUFFUM, DANIEL H.**
The unsteady aerodynamics of an oscillating cascade in a compressible flow field p 2 A90-11789
Aerodynamics of a linear oscillating cascade [NASA-TM-103250] p 15 N90-27657
- BUKSA, JOHN J.**
SPRITE - A computer code for the optimization of space based heat pipe radiator systems p 170 A90-38036
- BUMGARDNER, J. W.**
Deep-level dominated electrical characteristics of Au contacts on beta-SiC p 147 A90-33726
- BURKARDT, LEO A.**
RAMSCRAM: A flexible ramjet/scramjet engine simulation program [NASA-TM-102451] p 27 N90-14235
- BURKHOLDER, R.**
Electromagnetic properties of material coated surfaces [NASA-CR-186466] p 144 N90-19466
- BURKHOLDER, R. J.**
High-frequency asymptotic methods for analyzing the EM scattering by open-ended waveguide cavities [NASA-CR-186244] p 143 N90-16103
- BURNS, ROBERT J.**
Investigation of methods to produce a uniform cloud of fuel particles in a flame tube [NASA-TM-102376] p 178 N90-18665
- BURNSIDE, O. H.**
Computational methods for probability of instability calculations [AIAA PAPER 90-1139] p 236 A90-29333
- BURROWS, LINDA M.**
Field oriented control of induction motors [NASA-TM-103154] p 154 N90-22731
- BURRUS, D. L.**
Energy Efficient Engine combustor test hardware detailed design report [NASA-CR-168301] p 33 N90-28554
Energy Efficient Engine (E3) combustion system component technology performance report [NASA-CR-168274] p 33 N90-28555
- BURTON, R. L.**
Experiments on a repetitively pulsed electrothermal thruster p 56 A90-27960
- BUSCHE, DONNA M.**
A radiological assessment of nuclear power and propulsion operations near Space Station Freedom [NASA-CR-185185] p 76 N90-21108
- BUSHNELL, PETER**
Measurement of the steady surface pressure distribution on a single rotation large scale advanced prop-fan blade at Mach numbers from 0.03 to 0.78 [NASA-CR-182124] p 32 N90-28552
- BUTCHER, ROBERT L.**
Spacelab qualified infrared imager for microgravity science experiments [NASA-TM-102503] p 189 N90-20352
- BUTTON, ROBERT M.**
Frequency domain model for analysis of paralleled, series-output-connected Mapham inverters p 148 A90-38084
Distortion and regulation characterization of a Mapham inverter p 148 A90-38125
Development and testing of a 20 kHz component test bed p 43 A90-38126
- BUZZARD, ROBERT J.**
Fatigue testing apparatus [NASA-CASE-LEW-14124-1] p 190 N90-23712
- BYERS, DAVID C.**
Advanced onboard propulsion benefits and status [NASA-TM-103174] p 82 N90-27786

C

- CAIN, BRENDAN G.**
AIRNET: A real-time communications network for aircraft [NASA-CR-186140] p 145 N90-24514
- CAIRELLI, JAMES E.**
Results from baseline tests of the SPRE I and comparison with code model predictions p 62 A90-38249
- CALFO, FREDERICK D.**
Scaling results for the liquid sheet radiator p 170 A90-38037
- CALOMINO, ANTHONY M.**
Fully articulated four-point-bend loading fixture [NASA-CASE-LEW-14776-1] p 201 N90-15445
Controlled crack growth specimen for brittle systems [NASA-TM-103126] p 129 N90-23543
- CAMERON, C. D.**
Symmetry assessment of an air-blast atomizer spray p 172 A90-40930
- CAMPANELLA, S. JOSEPH**
A users perspective of the ACTS hopping beam TDMA system [AIAA PAPER 90-0833] p 140 A90-25658
- CAMPBELL, WILLIAM A.**
Large-scale Advanced Prop-fan (LAP) high speed wind tunnel test report [NASA-CR-182125] p 24 N90-10045
- CANACCI, V. A.**
A laser based computer aided non-intrusive technique for full field flow characterization in macroscopic curved channels p 168 A90-32293
Flow visualization and motion analysis for a series of four sequential brush seals [AIAA PAPER 90-2482] p 199 A90-47222
- CANISTRARO, H.**
X-ray beam method for displacement measurement in hostile environments p 187 A90-44485

- CANNON, I.**
Determination of the durability of the fiber optics in rocket engine environments
[AIAA PAPER 90-2229] p 250 A90-42754
- CANTWELL, ELIZABETH R.**
Smoldering combustion under low gravity conditions
[AIAA PAPER 90-0648] p 103 A90-22238
- CAPP, S. P.**
Two-component phase-averaged turbulence statistics downstream of a rotating spoked-wheel wake generator
p 156 A90-11559
- CAREY, G. F.**
Least-squares finite element methods for compressible Euler equations
p 9 A90-51013
- CARLUCCIO, J. R.**
The application of cast SiC/Al to rotary engine components
[NASA-CR-179610] p 25 N90-13385
- CARNEY, KELLY**
Detection of potential space station control/structure interaction with CO-ST-IN
p 50 N90-21074
- CARNEY, KELLY S.**
Modal selection in structural dynamics
p 209 A90-17001
Selection of component modes
[AIAA PAPER 90-1201] p 210 A90-26787
- CARNEY, LYNNETTE M.**
Efficient Monte Carlo simulation of rarefied flow in a small nozzle
[AIAA PAPER 90-1693] p 170 A90-38396
- CARR, T. W.**
Intensity to frequency conversion technique in intensity modulated fiber optic sensing systems
[NASA-TM-102562] p 153 N90-21277
- CARTER, CAMPBELL D.**
Saturated fluorescence measurements of the hydroxyl radical in laminar high-pressure flames
[NASA-CR-185218] p 190 N90-22022
- CARUSO, J. J.**
Parametric studies to determine the effect of compliant layers on metal matrix composite systems
p 93 A90-50093
Interfacial effects on the behavior of partially bonded metal matrix composite properties
p 93 A90-50094
Parametric studies to determine the effect of compliant layers on metal matrix composite systems
[NASA-TM-102465] p 96 N90-14294
Prediction of high temperature metal matrix composite ply properties
[NASA-TM-102490] p 97 N90-17817
METCAN verification status
[NASA-TM-103119] p 100 N90-21824
- CARUSO, JOHN J.**
Metal matrix composites microfracture: Computational simulation
[NASA-TM-103153] p 101 N90-24383
- CARUSO, STEVEN C.**
Development of an unstructured mesh/Navier-Stokes method for aerodynamics of aircraft with ice accretions
[AIAA PAPER 90-0758] p 4 A90-20011
- CASSENTI, B. N.**
Constitutive modeling for isotropic materials (HOST)
[NASA-CR-174718] p 26 N90-13391
- CASTELAZO, I.**
An active optimal control strategy of rotor vibrations using external forces
p 198 A90-46224
- CASTELLI, MICHAEL G.**
Thermomechanical deformation testing and modeling in the presence of metallurgical instabilities
[NASA-CR-185188] p 219 N90-21420
Thermomechanical testing techniques for high-temperature composites: TMF behavior of SiC(SCS-6)/Ti-15-3
[NASA-TM-103171] p 222 N90-25367
- CATALDO, ROBERT L.**
Energy storage considerations for a robotic Mars surface sampler
[AAS PAPER 87-245] p 42 A90-16544
Human exploration mission studies
p 39 A90-33935
Human exploration mission studies
p 40 N90-20457
- CAUGHEY, DAVID A.**
Diagonal inversion of lower-upper implicit schemes
p 242 A90-23110
- CAULFIELD, THOMAS**
Fiber reinforced superalloys
p 91 A90-34169
- CEBECI, T.**
Progress towards the development of an inviscid-viscous interaction method for unsteady flows in turbomachinery cascades
p 2 A90-11806
- CEBECI, TUNCER**
Fortified LEWICE with viscous effects
[AIAA PAPER 90-0754] p 15 A90-20009
Unsteady heat transfer on turbine blades
p 161 A90-20511
- CEDOZ, R. W.**
Advanced gearbox technology
[NASA-CR-179625] p 32 N90-24274
- CELESTINA, M. L.**
The numerical simulation of multistage turbomachinery flows
p 29 N90-21025
- CELESTINA, MARK L.**
Convergence acceleration for vector sequences and applications to computational fluid dynamics
[AIAA PAPER 90-0338] p 160 A90-19804
Simulation of three-dimensional viscous flow within a multistage turbine
[ASME PAPER 89-GT-152] p 5 A90-23841
- CERNY, LAWRENCE C.**
Polymer solution phase separation: Microgravity simulation
p 127 N90-17101
- CHABOCHE, J. L.**
Viscoplasticity: A thermodynamic formulation
[NASA-TM-102388] p 216 N90-14640
- CHAHROUR, C. A.**
Energy Efficient Engine combustor test hardware detailed design report
[NASA-CR-168301] p 33 N90-28554
Energy Efficient Engine (E3) combustion system component technology performance report
[NASA-CR-168274] p 33 N90-28555
- CHAI, A. T.**
Ground-based experiments on thermal and thermosolutal convection in inclined low-aspect-ratio enclosures
[AIAA PAPER 90-0413] p 166 A90-25033
- CHAI, A.-T.**
Numerical studies of convective heat transfer in an inclined semi-annular enclosure
p 173 A90-45317
- CHAIKO, LEV**
Assessment of worm gearing for helicopter transmissions
[NASA-TM-102441] p 27 N90-15923
- CHAIT, A.**
Convection phenomena in low-gravity processing - The GTE GaAs space experiment
[AIAA PAPER 90-0409] p 133 A90-25032
- CHAMIS, C. C.**
Parametric studies of advanced turboprops
p 19 A90-21225
Probabilistic structural analysis methods of hot engine structures
[ASME PAPER 89-GT-122] p 56 A90-23821
Multi-objective shape and material optimization of composite structures including damping
[AIAA PAPER 90-1135] p 210 A90-29262
Probabilistic analysis of bladed turbine disks and the effect of mistuning
[AIAA PAPER 90-1097] p 196 A90-29327
Tailoring of composite links for optimal damped elasto-dynamic performance
p 211 A90-30250
Metal matrix composite micromechanics - In situ behavior influence on composite properties
p 92 A90-45271
Parametric studies to determine the effect of compliant layers on metal matrix composite systems
p 93 A90-50093
Interfacial effects on the behavior of partially bonded metal matrix composite properties
p 93 A90-50094
Fundamental aspects and failure modes in high-temperature composites
p 93 A90-50095
An integrated methodology for optimizing structural composite damping
[NASA-TM-102343] p 96 N90-11808
Parametric studies to determine the effect of compliant layers on metal matrix composite systems
[NASA-TM-102465] p 96 N90-14294
Probabilistic simulation of uncertainties in composite uniaxial strengths
[NASA-TM-102483] p 97 N90-16008
Prediction of high temperature metal matrix composite ply properties
[NASA-TM-102490] p 97 N90-17817
Composite laminate tailoring with probabilistic constraints and loads
[NASA-TM-102515] p 98 N90-20138
Computational simulation of damping in composite structures
[NASA-TM-102567] p 219 N90-20432
Probabilistic structural analysis methods development for SSME
p 83 N90-28616
- CHAMIS, CHRIS C.**
Local and global accuracy estimates for boundary element analysis
[AIAA PAPER 90-0930] p 211 A90-29324
- CHAMIS, CHRISTOS**
Progression of damage and fracture in composites under dynamic loading
[AIAA PAPER 90-0916] p 210 A90-29318
- CHAMIS, CHRISTOS C.**
A methodology for evaluating the reliability and risk of structures under complex service environments
[AIAA PAPER 90-1102] p 211 A90-29332
Unified micromechanics of damping for unidirectional and off-axis fiber composites
p 90 A90-29929
Composite Blade Structural Analyzer (COBSTRAN) theoretical/programmer's manual
[NASA-TM-101958] p 95 N90-10181
Mechanics of damping for fiber composite laminates including hygro-thermal effects
[NASA-TM-102329] p 95 N90-10185
Probability of failure and risk assessment of propulsion structural components
p 218 N90-18470
Demonstration of capabilities of high temperature composites analyzer code HITCAN
[NASA-TM-102560] p 219 N90-19629
Fundamental aspects of and failure modes in high-temperature composites
[NASA-TM-102558] p 98 N90-20151
Fiber pushout test: A three-dimensional finite element computational simulation
[NASA-TM-102565] p 99 N90-21131
Multi-objective shape and material optimization of composite structures including damping
[NASA-TM-102579] p 99 N90-21132
Structural tailoring of select fiber composite structures
[NASA-TM-102484] p 99 N90-21137
Computational simulation of structural fracture in fiber composites
[NASA-TM-102505] p 100 N90-21821
METCAN verification status
[NASA-TM-103119] p 100 N90-21824
Progression of damage and fracture in composites under dynamic loading
[NASA-TM-103118] p 100 N90-21825
Probabilistic analysis of bladed turbine disks and the effect of mistuning
[NASA-TM-102564] p 136 N90-21871
Probabilistic structural analysis of aerospace components using NESSUS
[NASA-TM-102324] p 221 N90-22823
Structural behavior of composites with progressive fracture
[NASA-TM-102370] p 100 N90-23477
Metal matrix composites microfracture: Computational simulation
[NASA-TM-103153] p 101 N90-24383
Simplified design procedures for fiber composite structural components/joints
[NASA-TM-103113] p 101 N90-24384
- CHAN, K. S.**
High temperature inelastic deformation under uniaxial loading - Theory and experiment
p 109 A90-13838
High temperature inelastic deformation of the B1900 + Hf alloy under multiaxial loading - Theory and experiment
p 112 A90-22656
Inelastic deformation under nonisothermal loading
p 112 A90-22657
- CHAN, KWAI S.**
Constitutive modeling for isotropic materials (HOST)
[NASA-CR-179522] p 26 N90-13390
Constitutive modeling for isotropic materials (HOST)
[NASA-CR-174718] p 26 N90-13391
- CHANDRA, P. R.**
Pressure drop and mass transfer in two-pass ribbed channels
p 165 A90-24837
- CHANG, C. T.**
A planar reacting shear layer system for the study of fluid dynamics-combustion interaction
[NASA-TM-102422] p 27 N90-13393
- CHANG, D. C. D.**
Antenna beamforming using optical processing
[NASA-CR-180844] p 142 N90-11210
- CHANG, P. S.**
Experimental investigation of flow about a strut-endwall configuration
[AIAA PAPER 90-1541] p 171 A90-38685
- CHANG, REBECCA**
Sodium-sulfur battery flight experiment definition study
p 57 A90-33956
Sodium-sulfur battery flight experiment definition study
p 231 N90-20479
- CHANG, S. H.**
Computer aided design of bevel gear tooth surfaces
p 195 A90-21136
- CHANG, SHIH-HUNG**
On the application of subcell resolution to conservation laws with stiff source terms
[NASA-TM-102384] p 243 N90-14844
- CHANG, SIN-CHUNG**
A critical analysis of the modified equation technique of Warming and Hyett
p 241 A90-21940
- CHANG, W. S.**
Mathematical modeling and analysis of heat pipe start-up from the frozen state
p 174 A90-48404

- CHAO, LUEN-YUAN**
Equivalence of physically based statistical fracture theories for reliability analysis of ceramics in multiaxial loading p 123 A90-43580
- CHATO, DAVID J.**
Evaluation of supercritical cryogen storage and transfer systems for future NASA missions [AIAA PAPER 90-0719] p 44 A90-19989
Initial experimentation on the nonvented fill of a 0.14 cu m (5 cu ft) dewar with nitrogen and hydrogen [AIAA PAPER 90-1681] p 136 A90-50641
Evaluation of supercritical cryogen storage and transfer systems for future NASA missions [NASA-TM-102394] p 44 N90-10912
CryoTran user's manual, version 1.0 [NASA-TM-102468] p 237 N90-15622
Initial experimentation on the nonvented fill of a 0.14m³ (5 ft. 3) dewar with nitrogen and hydrogen [NASA-TM-103155] p 183 N90-26278
- CHEN, C. F.**
Experimental investigation of convective stability in a superposed fluid and porous layer when heated from below p 158 A90-15947
Salt-finger convection under reduced gravity [AIAA PAPER 90-0122] p 160 A90-19693
The role of gravity on macrosegregation in alloys [NASA-CR-186530] p 136 N90-25238
- CHEN, FALIN**
Experimental investigation of convective stability in a superposed fluid and porous layer when heated from below p 158 A90-15947
- CHEN, H. H.**
Fortified LEWICE with viscous effects [AIAA PAPER 90-0754] p 15 A90-20009
- CHEN, S. C.**
Three-dimensional adaptive grid generation for body-fitted coordinate system p 167 A90-26506
- CHEN, Y. C.**
Molecular beam epitaxial growth of high-quality InSb on InP and GaAs substrates p 253 A90-12808
Transport properties of InAs(x)Sb(1-x) (x = 0-0.55) on InP grown by molecular-beam epitaxy p 256 A90-36232
- CHEN, YONG-SHING**
Iptycene synthesis: A new method for attaching a 2,3-anthracene moiety to the 9,10-positions of another anthracene moiety - Exceptional conditions for a Lewis acid catalyzed Diels-Alder reaction p 85 A90-49073
- CHEONG, DEOCK-SOO**
High-temperature deformation and microstructural analysis for Si3N4-Sc2O3 [NASA-TM-103239] p 130 N90-28740
- CHERRY, D. G.**
NASA/GE Energy Efficient Engine low pressure turbine scaled test vehicle performance report [NASA-CR-188290] p 34 N90-28563
- CHIANG, WEI-HWAN**
A model for the distribution of the intergalactic medium p 265 A90-34505
A model for the distribution of dark matter, galaxies, and the intergalactic medium in a cold dark matter-dominated universe p 266 A90-45560
- CHILDS, D. W.**
An annular gas seal analysis using empirical entrance and exit region friction factors [ASME PAPER 89-TRIB-46] p 196 A90-33555
- CHIMA, RODRICK V.**
Diagonal inversion of lower-upper implicit schemes p 242 A90-23110
Numerical analysis of three-dimensional viscous internal flows p 168 A90-32456
- CHITRE, D. M.**
A users perspective of the ACTS hopping beam TDMA system [AIAA PAPER 90-0833] p 140 A90-25658
- CHO, JINSOO**
Propeller-wing interaction using a frequency domain panel method p 6 A90-26128
Counter-rotating propellant analysis using a frequency domain panel method p 7 A90-40937
- CHO, MENGU**
Ion drag for a negatively biased solar array in low earth orbit p 48 A90-36191
- CHOI, MUN Y.**
N-decane-air droplet combustion experiments in the NASA-Lewis 5 Second Zero-Gravity Facility [AIAA PAPER 90-0649] p 104 A90-25038
- CHOI, S.-W.**
Nonlinear evolution of interacting oblique waves on two-dimensional shear layers p 158 A90-15943
- CHOI, Y. H.**
Computational analysis of the flowfield of a two-dimensional ejector nozzle [AIAA PAPER 90-1901] p 21 A90-42690
- Computational analysis of the flowfield of a two-dimensional ejector nozzle p 31 N90-23406
- CHOO, YUNG K.**
Application of a lower-upper implicit scheme and an interactive grid generation for turbomachinery flow field simulations [ASME PAPER 89-GT-20] p 4 A90-23762
Interactive grid generation for turbomachinery flow field simulations p 6 A90-26553
- CHOPRA, M. A.**
Primary arm spacing in directionally solidified Pb-10 wt pct Sn alloys [AIAA PAPER 90-0740] p 132 A90-23713
Primary arm spacing in directionally solidified Pb-10 wt percent Sn alloys [NASA-CR-185190] p 134 N90-14398
- CHOEY, C. M.**
High frequency GaAlAs modulator and photodetector for phased array antenna applications p 146 A90-11774
Complex permittivity of lanthanum aluminate in the 20 to 300 K temperature range from 26.5 to 40.0 GHz p 148 A90-37864
Performance and modeling of superconducting ring resonators at millimeter-wave frequencies [NASA-TM-102526] p 151 N90-18634
Growth and patterning of laser ablated superconducting YBa2Cu3O7 films on LaAlO3 substrates [NASA-TM-102436] p 259 N90-22421
Microwave conductivity of laser ablated YBaCuO superconducting films and its relation to microstrip transmission line p 155 N90-27844
Analysis of microstrip lines with alternative implementation of conductors and superconductors [NASA-TM-103182] p 155 N90-27966
High temperature superconducting thin film microwave circuits: Fabrication, characterization, and applications [NASA-TM-103235] p 156 N90-28786
- CHOEY, CHRIS**
Sequentially evaporated thin film YBa2Cu3O(7-x) superconducting microwave ring resonator [NASA-TM-103180] p 154 N90-25273
- CHOU, R.**
On physical optics for calculating scattering from coated bodies p 250 A90-20151
- CHOY, F. C.**
The role of thermal and lubricant boundary layers in the transient thermal analysis of spur gears p 194 A90-21118
- CHOY, F. K.**
Vibration signature analysis of multistage gear transmission p 194 A90-21124
Dynamics of multistage gear transmission with effects of gearbox vibrations [NASA-TM-103109] p 205 N90-28060
- CHOY, FRED K.**
Experimental and analytical evaluation of dynamic load vibration of a 2240-kW (3000-hp) rotorcraft transmission p 192 A90-13750
- CHOYKE, W. J.**
Growth of improved quality 3C-SiC films on 6H-SiC substrates p 255 A90-29596
Growth of high quality 6H-SiC epitaxial films on vicinal (0001) 6H-SiC wafers p 255 A90-29952
- CHRISS, R. M.**
An LDA investigation of the normal shock wave boundary layer interaction p 10 A90-52618
- CHRISTIAN, JOSE L., JR.**
Applicability of the beamed power concept to lunar rovers, construction, mining, explorers and other mobile equipment p 69 N90-10159
- CHRISTIANSEN, ERIC L.**
On protection of Freedom's solar dynamic radiator from the orbital debris environment. Part 1: Preliminary analyses and testing [NASA-TM-102458] p 73 N90-14265
- CHRISTOFOROU, A. P.**
Analysis of impact response in composite plates p 214 A90-47567
- CHU, BENJAMIN**
Fiber optic detector probes for laser light scattering p 192 A90-11593
- CHU, M. L.**
An experimental evaluation of the tensile strength of impact ice p 83 A90-15049
Impact ice stresses in rotating airfoils [AIAA PAPER 90-0198] p 15 A90-19735
- CHU, TEH-MING**
Conceptual definition of a high voltage power supply test facility [NASA-CR-185216] p 50 N90-25172
- CHUBB, DONALD L.**
Scaling results for the liquid sheet radiator p 170 A90-38037
- CHUDNOVSKY, A.**
A probabilistic approach to crack instability p 212 A90-41278
Energy analysis of crack-damage interaction p 213 A90-41372
Effect of crack-microcracks interaction on energy release rates p 214 A90-49269
- CHULYA, A.**
A new uniformly valid asymptotic integration algorithm for elasto-plastic-creep and unified viscoplastic theories including continuum damage [NASA-TM-102344] p 217 N90-14655
- CHULYA, ABHISAK**
Assumed strain distributions for a finite strip plate bending element using Mindlin-Reissner plate theory p 208 A90-16723
- CHUN, K.**
A circular combustor configuration with multiple injection ports for mixing enhancement p 158 A90-15389
- CHUNG, B. T. F.**
Two-dimensional convection and radiation with scattering from a Poiseuille flow p 161 A90-20519
- CHUNG, C. L.**
Base reaction optimization of redundant manipulators for space applications [NASA-CR-186274] p 201 N90-15447
A global approach for using kinematic redundancy to minimize base reactions of manipulators [NASA-CR-186825] p 234 N90-25499
- CHUNG, CHAN-HONG**
Numerical simulation of rarefied gas flow through a slit [AIAA PAPER 90-1694] p 170 A90-38397
- CLAFLIN, S. E.**
LOX/hydrocarbon combustion instability investigation [NASA-CR-182249] p 71 N90-13589
- CLARK, D.**
Photovoltaic module on-orbit assembly for Space Station Freedom p 45 A90-38071
- CLASPY, P.**
Photoreponse of YBa2Cu3O(7-delta) granular and epitaxial superconducting thin films [NASA-TM-103144] p 154 N90-22732
- CLASPY, P. C.**
High frequency GaAlAs modulator and photodetector for phased array antenna applications p 146 A90-11774
A high-speed GaAs MESFET optical controller p 186 A90-22483
Microwave response of a HEMT photoconductive detector p 147 A90-37301
Optical detectors for GaAs MMIC integration - Technology assessment p 149 A90-41238
Control of a GaAs monolithic Ka-band phase shifter using a high-speed optical interconnect p 150 A90-41700
Optical control of an 8-element Ka-band phased array using a high-speed optoelectronic interconnect [NASA-TM-102550] p 152 N90-21275
- CLASPY, PAUL C.**
Design of an optically controlled Ka-band GaAs MMIC phased-array antenna [NASA-TM-103147] p 155 N90-26250
- CLAUS, R. W.**
Time-accurate simulations of a shear layer forced at a single frequency p 163 A90-23111
Multigrid calculations of a jet in crossflow [AIAA PAPER 90-0444] p 167 A90-26952
Time-dependent calculation of a forced mixing layer using a k-epsilon turbulence model p 169 A90-35222
- CLAUS, RUSSELL W.**
Response of a chemically reacting layer to streamwise vorticity [NASA-TM-102288] p 178 N90-18005
- CLEMENS, DONALD D.**
Space Station Freedom electric power system photovoltaic power module integrated launch package [AIAA PAPER 90-1053] p 48 A90-29281
- COE, HAROLD H.**
Bearing optimization for SSME HPOTP application p 205 N90-28622
- COIRIER, WILLIAM J.**
Efficient real gas Navier-Stokes computations of high speed flows using an LU scheme [AIAA PAPER 90-0391] p 164 A90-23706
Efficient real gas Navier-Stokes computations of high speed flows using an LU scheme [NASA-TM-102429] p 11 N90-14203
- COLANTONIO, RENATO O.**
High-temperature test facility at the NASA Lewis engine components research laboratory [NASA-TM-103143] p 39 N90-25151
- COLEMAN, P.**
Integrated controls and health monitoring fiberoptic shaft monitor [NASA-CR-185210] p 191 N90-29622

- COLLINS, J. J.**
Integrated controls and health monitoring fiberoptic shaft monitor
[NASA-CR-185210] p 191 N90-29622
- COLOZZA, ANTHONY J.**
Preliminary design of a long-endurance Mars aircraft
[AIAA PAPER 90-2000] p 43 A90-40587
Preliminary design of a long-endurance Mars aircraft
[NASA-CR-185243] p 30 N90-21763
- COLVIN, M. ALEXANDER**
AIRNET: A real-time communications network for aircraft
[NASA-CR-186140] p 145 N90-24514
- CONNELLY, M.**
Automotive Stirling engine development program
[NASA-CR-180839] p 263 N90-11654
- CONNOLLY, D. J.**
ATDRS payload technology research and development
[NASA-TM-103256] p 52 N90-28596
- CONROY, P. J.**
Nicalon/siliconoxycarbide ceramic composites
p 94 A90-51924
- CONROY, PAULA J.**
Polymer derived Nicalon/Si-C-O composites - Processing and mechanical behavior p 89 A90-27065
Nicalon/siliconoxycarbide ceramic composites
[NASA-TM-102563] p 99 N90-21133
- CONTOLATIS, T.**
The 30-GHz monolithic receive module
[NASA-CR-180849] p 146 N90-24528
- CONWAY, BRUCE A.**
Optimal finite-thrust spacecraft trajectories using collocation and nonlinear programming
[AAS PAPER 89-350] p 40 A90-46783
Optimal cooperative time-fixed impulsive rendezvous
[AIAA PAPER 90-2962] p 41 A90-53037
Discrete approximations to optimal trajectories using direct transcription and nonlinear programming
[AIAA PAPER 90-2963] p 41 A90-53038
- COOK, T. S.**
Application of HOST technology to the SSME HPFTP blade
[ASME PAPER 89-GT-130] p 209 A90-23828
- COOPER, C. V.**
Identification of a cast iron alloy containing nonstrategic elements
[NASA-CR-185174] p 118 N90-18559
- CORDIER, STEPHANE J.**
Rotating primary flow induction using jet-flapped blades
p 19 A90-12585
- CORNELL, LINDA**
Studies on the use of supercritical ammonia for ceramic nitride synthesis and fabrication
[NASA-TM-102570] p 106 N90-21843
- CORNILSEN, BAHNE C.**
Structural comparison of nickel electrodes and precursor phases p 228 A90-33949
Structural comparison of nickel electrodes and precursor phases p 231 N90-20472
- CORRIGAN, ROBERT D.**
Update of the Solar Concentrator Advanced Development Project p 48 A90-38267
- COUTTS, T. J.**
An empirical investigation of the InP shallow-homojunction solar cell p 225 A90-14869
Hybrid solar cells based on dc magnetron sputtered films of n-ITO on APMOVPE grown p-InP p 225 A90-14893
Modeling and simulation of InP homojunction solar cells p 226 A90-14899
Radiation resistance and comparative performance of ITO/InP and n/p InP homojunction solar cells p 226 A90-14933
Investigation of buried homojunctions in p-InP formed during sputter deposition of both indium tin oxide and indium oxide p 256 A90-36799
Study of indium tin oxide films exposed to atomic oxygen p 257 A90-45193
- COVERSTONE-CARROLL, V.**
Optimal impulsive time-fixed orbital rendezvous and interception with path constraints
[AIAA PAPER 90-2972] p 41 A90-53051
- COWGILL, GLENN R.**
CryoTran user's manual, version 1.0
[NASA-TM-102468] p 237 N90-15622
- COY, J. J.**
Tooth contact shift in loaded spiral bevel gears p 193 A90-21112
Topology of modified helical gears p 195 A90-21132
Computer aided design of bevel gear tooth surfaces p 195 A90-21136
- COY, JOHN J.**
Gear noise, vibration, and diagnostic studies at NASA Lewis Research Center
[NASA-TM-102435] p 202 N90-18041
- Computerized inspection of gear tooth surfaces
[NASA-TM-102395] p 203 N90-22054
- CRANE, ROGER**
A heat receiver design for solar dynamic space power systems
[NASA-TM-102473] p 72 N90-14283
- CRAWFORD, D. R.**
Generalized Advanced Propeller Analysis System (GAPAS). Volume 2: Computer program user manual
[NASA-CR-185277] p 36 N90-29394
- CRAWFORD, MICHAEL E.**
An investigation into the numerical prediction of boundary layer transition using the K.Y. Chien turbulence model
[NASA-CR-185252] p 182 N90-26269
- CRAWFORD, ROGER A.**
Influence of bulk turbulence and entrance boundary layer thickness on the curved duct flow field
[AIAA PAPER 90-1502] p 171 A90-38651
- CRAWLEY, EDWARD F.**
Calculation of unsteady Euler flows in turbomachinery using the linearized Euler equations p 2 A90-11778
- CRONIN, M.**
Automotive Stirling engine development program
[NASA-CR-180839] p 263 N90-11654
- CRUSE, T. A.**
Advanced probabilistic structural analysis method for implicit performance functions p 214 A90-49792
- CUCCIO, J.**
Development of impact design methods for ceramic gas turbine components
[AIAA PAPER 90-2413] p 197 A90-42165
- CULL, RONALD**
Orbit to surface beamed power for Mars bases expansion p 40 A90-38105
- CULL, RONALD C.**
Power for the moon: Is microwave power beaming an option? p 69 N90-10158
Lunar orbiting microwave beam power system
[NASA-TM-103211] p 51 N90-25173
An analysis of space power system masses
[NASA-TM-103199] p 80 N90-25184
- CURRAN, FRANCIS M.**
Preliminary plume characteristics of an arcjet thruster
[AIAA PAPER 90-2645] p 64 A90-42609
Low power arcjet performance
[AIAA PAPER 90-2578] p 68 A90-52568
Performance characterization of a segmented anode arcjet thruster
[AIAA PAPER 90-2582] p 68 A90-52569
Electric propulsion options for 10 kW class earth-space missions p 75 N90-18474
Arcjet cathode phenomena p 75 N90-18477
Arcjet nozzle design impacts p 76 N90-18478
Preliminary plume characteristics of an arcjet thruster
[NASA-TM-103241] p 81 N90-26071
Low power arcjet performance
[NASA-TM-103280] p 83 N90-28657
- CURRAN, FRANK M.**
The effect of electrode configuration on arcjet performance
[NASA-TM-102346] p 70 N90-11081
- CURREN, ARTHUR N.**
Secondary electron emission characteristics of molybdenum-masked, ion-textured OFHC copper
[NASA-TP-2967] p 117 N90-15211
- CURTIS, H. B.**
Thermal annealing of GaAs concentrator solar cells p 60 A90-38150
- CURTIS, HENRY B.**
Photovoltaic power for a lunar base
[IAF PAPER 89-254] p 42 A90-13409
Performance of GaAs concentrator cells under electron irradiations from 0.4 to 2.3 MeV p 227 A90-14956
- D**
- DAHL, M. D.**
Some observations on transitory stall in conical diffusers
[AIAA PAPER 90-0048] p 4 A90-22158
Some observations on transitory stall in conical diffusers
[NASA-TM-102387] p 11 N90-12561
- DAHL, MILO D.**
Effects of fiber motion on the acoustic behavior of an anisotropic, flexible fibrous material p 247 A90-33313
Comparison between design and installed acoustic characteristics of NASA Lewis 9- by 15-foot low-speed wind tunnel acoustic treatment
[NASA-TP-2996] p 38 N90-19242
- DANZEY, GERALD A.**
Attachment of lead wires to thin film thermocouples mounted on high temperature materials using the parallel gap welding process
[NASA-TM-102442] p 189 N90-21361
- DAREJEH, H.**
Integrated controls and health monitoring fiberoptic shaft monitor
[NASA-CR-185210] p 191 N90-29622
- DARGUSH, G. F.**
Development of an integrated BEM for hot fluid-structure interaction
[ASME PAPER 89-GT-128] p 212 A90-32264
Development of an integrated BEM approach for hot fluid structure interaction
[NASA-CR-186214] p 177 N90-15364
- DARYOUSH, A. S.**
High-speed analog fiber optic links for satellite communication p 46 A90-11822
High-speed digital fiber optic links for satellite traffic p 250 A90-41247
Bit-error-rate testing of fiber optic data links for MMIC-based phased array antennas
[NASA-TM-102523] p 145 N90-21261
- DARYOUSH, AFSHIN S.**
High-speed fiber-optic links for distribution of satellite traffic p 47 A90-41687
- DAS, K.**
Deep-level dominated electrical characteristics of Au contacts on beta-SiC p 147 A90-33726
Silicon carbide semiconductor device fabrication and characterization
[NASA-CR-186354] p 258 N90-19873
- DAVIDIAN, KENNETH J.**
The International Space University
[AIAA PAPER 90-2389] p 261 A90-42152
A rocket engine design expert system
[NASA-TM-102373] p 69 N90-10172
The International Space University
[NASA-TM-103163] p 78 N90-22604
- DAVIS, D. O.**
Experimental investigation of turbulent flow through a circular-to-rectangular transition duct
[AIAA PAPER 90-1505] p 171 A90-38654
- DAVIS, DONALD Y.**
Energy Efficient Engine: Flight propulsion system final design and analysis
[NASA-CR-186219] p 34 N90-28558
- DAVIS, R. F.**
Deep-level dominated electrical characteristics of Au contacts on beta-SiC p 147 A90-33726
Silicon carbide semiconductor device fabrication and characterization
[NASA-CR-186354] p 258 N90-19873
- DAVIS, R. H.**
Modeling of collision and coalescence of droplets during microgravity processing of Zn-Bi immiscible alloys p 132 A90-22878
- DAVIS, ROBERT H.**
The effects of van der Waals attractions on cloud droplet growth by coalescence p 234 A90-38383
- DAVIS, V. A.**
A Van der Waals-like theory of plasma double layers p 251 A90-10725
Plasma contactor modeling with NASCAP/LEO - Extending laboratory results to space systems
[AIAA PAPER 90-0726] p 251 A90-22255
Plasma sources for spacecraft neutralization
[AIAA PAPER 90-1556] p 49 A90-38697
- DAY, G. W.**
A fiber-optic current sensor for aerospace applications
[NASA-TM-103152] p 190 N90-22773
- DAY, M. L.**
End-hall thrusters
[AIAA PAPER 90-2595] p 64 A90-42570
- DE ABREU-GARCIA, J. ALEX**
The determination of third order linear models from a seventh order nonlinear jet engine model p 239 A90-52881
- DE GROH, HENRY C., III**
Effects of crucible wetting during solidification of immiscible Pb-Zn alloys p 132 A90-17825
- DE GUIRE, MARK R.**
Superconducting glass-ceramics in the Bi-Sr-Ca-Cu-O system p 256 A90-35153
- DE WITT, KENNETH J.**
Numerical simulation of rarefied gas flow through a slit
[AIAA PAPER 90-1694] p 170 A90-38397
- DE, BHOLA N.**
Ellipsometric study of Al₂O₃/Ag/Si and SiO₂/Ag/quartz ashed in an oxygen plasma p 120 A90-18217
Ellipsometric studies of the diffusion of atomic oxygen through silicon dioxide thin films p 104 A90-36268
Study of indium tin oxide films exposed to atomic oxygen p 257 A90-45193

- DEADMORE, DANIEL L.**
Friction and wear of oxide-ceramic sliding against IN-718 nickel base alloy at 25 to 800 C in atmospheric air [NASA-TM-102291] p 124 N90-10262
- DEANGELO, F. L.**
Peeled film GaAs solar cells for space power [NASA-TM-103125] p 153 N90-21287
- DEARBORN, DAVID S. P.**
The shocking development of lithium (and boron) in supernovae p 264 A90-17643
- DECKER, ARTHUR J.**
Holographic interferometry with an injection seeded Nd:YAG laser and two reference beams p 186 A90-42373
Results of an attempt to measure increased rates of the reaction D-2 + D-2 yields He-3 + n in a nonelectrochemical cold fusion experiment [NASA-TM-102430] p 250 N90-17424
- DEGANI, A. T.**
Computation of three-dimensional turbulent boundary layers with heat transfer in a plane of symmetry using embedded wall-layer functions [AIAA PAPER 90-0307] p 160 A90-19788
- DEGEORGE, C. L.**
Large-scale Advanced Prop-fan (LAP) technology assessment report [NASA-CR-182142] p 24 N90-10046
- DEGEORGE, CHARLES L.**
Large-scale Advanced Prop-fan (LAP) static rotor test report [NASA-CR-180848] p 25 N90-12617
- DEGROH, KIM K.**
The effect of leveling coatings on the atomic oxygen durability of solar concentrator surfaces [NASA-TM-102557] p 76 N90-21110
- DEQUIRE, M. R.**
Review and statistical analysis of the ultrasonic velocity method for estimating the porosity fraction in polycrystalline materials [NASA-TM-102501-REV] p 207 N90-21402
- DEQUIRE, MARK R.**
Superconducting ceramics in the Bi_{1.5}SrCaCu₂O sub x system by melt quenching technique [NASA-CR-185139] p 258 N90-11606
- DEISSLER, ROBERT G.**
Effect of spatial resolution on apparent sensitivity to initial conditions of a decaying flow as it becomes turbulent [NASA-TM-102377] p 176 N90-13719
Numerical solution for the velocity-derivative skewness of a low-Reynolds-number decaying Navier-Stokes flow [NASA-TM-103186] p 184 N90-27985
- DEJONG, FREDERICK J.**
User's manual for PEPIS NASA tip vortex version [NASA-CR-182178] p 10 N90-10835
Computation of the tip vortex flowfield for advanced aircraft propellers [NASA-CR-182179] p 10 N90-10836
- DELAAT, JOHN C.**
A real time microcomputer implementation of sensor failure detection for turbofan engines p 21 A90-45414
Advanced detection, isolation, and accommodation of sensor failures in turbofan engines: Real-time microcomputer implementation [NASA-TP-2925] p 37 N90-15112
- DELANEY, ROBERT A.**
3D Euler analysis of ducted propan flowfields [AIAA PAPER 90-3034] p 8 A90-45873
Investigation of advanced counterrotation blade configuration concepts for high speed turboprop systems, task 1: Ducted propan analysis [NASA-CR-185217] p 30 N90-22567
- DELCHER, R.**
Determination of the durability of the fiberoptics in rocket engine environments [AIAA PAPER 90-2229] p 250 A90-42754
- DELLACORTE, CHRISTOPHER**
Tribological properties of ceramic/TiAl₃-Nb sliding couples for use as candidate seal materials to 700 deg C [NASA-TM-102401] p 86 N90-12658
Tribological properties of PM212: A high-temperature, self-lubricating, powder metallurgy composite [NASA-TM-102355] p 86 N90-12659
A new test machine for measuring friction and wear in controlled atmospheres to 1200 C [NASA-TM-102405] p 96 N90-12670
The experimental evaluation and application of high-temperature solid lubricants [NASA-TM-102476] p 127 N90-16944
The application of a computer data acquisition system for a new high temperature tribometer [NASA-TM-102508] p 86 N90-17811
Experimentally determined wear behavior of an Al₂O₃-SiC composite from 25 to 1200 C [NASA-TM-102549] p 87 N90-20130
- DEMASI-MARCIN, JEANINE T.**
Mechanisms of degradation and failure in a plasma deposited thermal barrier coating [ASME PAPER 89-GT-132] p 84 A90-23830
- DEMASI, JEANINE T.**
Thermal barrier coating life prediction model development, phase 1 [NASA-CR-182230] p 26 N90-13388
- DEMUREN, A. O.**
Calculation of turbulence-driven secondary motion in ducts with arbitrary cross-section [AIAA PAPER 90-0245] p 160 A90-19752
Application of multi-grid methods for solving the Navier-Stokes equations [NASA-TM-102359] p 243 N90-14002
Calculation of 3D turbulent jets in crossflow with a multigrid method and a second-moment closure model [NASA-TM-103159] p 184 N90-26282
- DENNER, B. W.**
Performance and acoustic prediction of counterrotating propeller configurations [SAE PAPER 891035] p 246 A90-14342
- DENNER, BRETT WILLIAM**
An approximate model for the performance and acoustic predictions of counterrotating propeller configurations [NASA-CR-180667] p 248 N90-18228
- DESA, S.**
Base reaction optimization of redundant manipulators for space applications [NASA-CR-186274] p 201 N90-15447
A global approach for using kinematic redundancy to minimize base reactions of manipulators [NASA-CR-186825] p 234 N90-25499
- DESILVA, C. W.**
Base reaction optimization of redundant manipulators for space applications [NASA-CR-186274] p 201 N90-15447
- DETERMAN, W. R.**
SP-100 advanced radiator designs for thermoelectric and Stirling applications p 62 A90-38202
- DEUTSCH, S.**
The measurement of boundary layers on a compressor blade in cascade. IV - Flow fields for incidence angles of -1.5 and -8.5 degrees [ASME PAPER 89-GT-72] p 165 A90-23793
- DEUTSCH, STEVEN**
The measurement of boundary layers on a compressor blade in cascade. Volume 1: Experimental technique, analysis and results [NASA-CR-185118-VOL-1] p 23 N90-10038
The measurement of boundary layers on a compressor blade in cascade. Volume 2: Data tables [NASA-CR-185118-VOL-2] p 23 N90-10039
- DEVAN, J. H.**
Selection of phase-change and containment materials for thermal energy storage [NASA-CR-186228] p 229 N90-15506
- DEVER, THERESA M.**
The effect of leveling coatings on the atomic oxygen durability of solar concentrator surfaces [NASA-TM-102557] p 76 N90-21110
- DEWITT, KENNETH J.**
Convective heat transfer measurements from a NACA 0012 airfoil in flight and in the NASA Lewis Icing Research Tunnel [AIAA PAPER 90-0199] p 162 A90-22180
Convective heat transfer measurements from a NACA 0012 airfoil in flight and in the NASA Lewis Icing Research Tunnel [NASA-TM-102448] p 176 N90-13750
- DEWITT, R. L.**
Background, current status, and prognosis of the ongoing slush hydrogen technology development program for the NASP [NASA-TM-103220] p 51 N90-26055
- DEWITT, RICHARD L.**
Slush Hydrogen (SLH2) technology development for application to the National Aerospace Plane (NASP) [NASA-TM-102315] p 50 N90-14268
- DHADWAL, HARBANS S.**
Fiber optic detector probes for laser light scattering p 192 A90-11593
- DIAMANT, E. S.**
Solar dynamic power for the Space Station p 55 A90-16374
- DIAZ, J. O.**
High temperature creep behavior of single crystal gamma prime and gamma alloys p 110 A90-16901
- DIB, N. I.**
Coplanar waveguide discontinuities for P-I-N diode switches and filter applications [NASA-TM-102534] p 153 N90-21278
- DICARLO, JAMES A.**
CMCs for the long run p 88 A90-17301
- Materials for engine applications above 3000 deg F: An overview [NASA-TM-100169] p 95 N90-10188
- DICKMAN, JOHN E.**
Electron beam induced damage in PECVD Si₃N₄ and SiO₂ films on InP [NASA-TM-102544] p 203 N90-20393
- DIFILIPPO, FRANK**
Energy storage for a lunar base by the reversible chemical reaction: CaO + H₂O reversible reaction Ca(OH)₂ [NASA-TM-103145] p 233 N90-25419
- DIFILIPPO, FRANK**
Total hemispherical emittance measured at high temperatures by the calorimetric method [NASA-TM-102322] p 136 N90-10309
- DIJKSTRA, HENK A.**
The coupling of Marangoni and capillary instabilities in an annular thread of liquid p 171 A90-38978
- DILSAVOR, R. L.**
An experimental SMI adaptive antenna array for weak interfering signals [NASA-CR-185976] p 142 N90-11211
- DINKEL, DUANE W.**
Diagnostic evaluations of microwave generated helium and nitrogen plasma mixtures [AIAA PAPER 90-2634] p 252 A90-42602
- DINNSEN, D.**
Determination of the durability of the fiberoptics in rocket engine environments [AIAA PAPER 90-2229] p 250 A90-42754
- DIRUSSO, E.**
Active vibration control for flexible rotor by optimal direct-output feedback control p 197 A90-46222
- DIRUSSO, ELISEO**
Development of a compact, light weight magnetic bearing [AIAA PAPER 90-2483] p 199 A90-47223
Experimental evaluation of a tuned electromagnetic damper for vibration control of cryogenic turbopump rotors [NASA-TP-3005] p 30 N90-23403
- DISIMILE, P. J.**
Space vehicle propulsion systems - Environmental space hazards [AIAA PAPER 90-1881] p 63 A90-40545
- DITMARS, M. M.**
Torsional and biaxial (tension-torsion) fatigue damage mechanisms in Waspaloy at room temperature p 109 A90-11925
- DITTMAR, JAMES H.**
Predicted and measured boundary layer refraction for advanced turboprop propeller noise [NASA-TM-102365] p 248 N90-17413
- DIVAN, DEEPAKRAJ M.**
High power density dc/dc converter: Selection of converter topology [NASA-CR-186129] p 151 N90-14467
- DODD, W. R.**
User needs, benefits, and integration of robotic systems in a space station laboratory [NASA-CR-185150] p 200 N90-13794
- DODSON, H.**
Oxygen/methane combustion stability investigation p 107 N90-28628
- DODSON, H. C.**
LOX/hydrocarbon combustion instability investigation [NASA-CR-182249] p 71 N90-13589
- DOERNBACH, JAY**
Assessment of High Temperature Superconducting (HTS) electric motors for rotorcraft propulsion [NASA-CR-185222] p 29 N90-21761
- DOGRA, ANJU S.**
Effect of vane twist on the performance of dome swirlers for gas turbine airblast atomizers [AIAA PAPER 90-1955] p 173 A90-47203
Effect of vane twist on the performance of dome swirlers for gas turbine airblast atomizers [NASA-TM-103195] p 182 N90-25289
- DOLCE, JAMES L.**
Space Station power system autonomy demonstration p 245 A90-10373
Electric power scheduling: A distributed problem-solving approach [NASA-TM-103149] p 240 N90-22323
Automating security monitoring and analysis for Space Station Freedom's electric power system [NASA-TM-103148] p 240 N90-22324
An expert system for simulating electric loads aboard Space Station Freedom [NASA-TM-103150] p 240 N90-22325
Automated electric power management and control for Space Station Freedom [NASA-TM-103151] p 240 N90-23125

- DOMINEK, A.**
Constitutive parameter measurements of lossy materials p 257 N90-11603
[NASA-CR-183398]
Electromagnetic properties of material coated surfaces p 144 N90-19466
[NASA-CR-186466]
- DONAHUE, A.**
Automotive Stirling engine development program p 263 N90-11654
[NASA-CR-180839]
- DONALDSON, KIMBERLY Y.**
Role of the interfacial thermal barrier in the effective thermal diffusivity/conductivity of SiC-fiber-reinforced reaction-bonded silicon nitride p 89 A90-25268
- DONG, X.**
Computer simulation of the mathematical modeling involved in constitutive equation development: Via symbolic computations p 219 N90-20428
[NASA-TM-102532]
Application of symbolic computations to the constitutive modeling of structural materials p 222 N90-26364
[NASA-TM-103225]
- DONOVAN, JOHN F.**
Experimental investigation of terminal shock sensors in mixed-compression inlets p 186 A90-40560
[AIAA PAPER 90-1931]
- DOWNING, R. S.**
Brayton advanced heat receiver development program p 61 A90-38170
- DOYCHAK, J.**
The oxidation of Ni-rich Ni-Al intermetallics p 112 A90-24855
- DOYCHAK, JOSEPH**
Oxidation of high-temperature intermetallics; Proceedings of the Workshop, Cleveland, OH, Sept. 22, 23, 1988 p 112 A90-24852
Oxidation behavior of FeAl + Hf, Zr, B p 113 A90-24858
- DRAPER, S. L.**
Microstructure and tensile properties of Fe-40 at. pct Al alloys with C, Zr, Hf, and B additions p 108 A90-11651
The role of interfacial dislocation networks in high temperature creep of superalloys p 114 A90-33329
Effect of Ga and P dopants on the thermoelectric properties of n-type SiGe p 256 A90-38140
Compatibility of Fe-40Al with various fibers p 94 A90-50496
- DRAVID, N. V.**
Development and refinement of test bed simulations p 59 A90-38081
- DRAVID, NARAYAN V.**
Modeling of power electronic systems with EMTF [NASA-TM-102375] p 245 N90-14060
- DRUMMOND, C. H., III**
Crystallization of a barium-aluminosilicate glass p 121 A90-27107
- DRUMMOND, C. K.**
A modeling technique for STOVL ejector and volume dynamics p 20 A90-42168
[AIAA PAPER 90-2417]
A modeling technique for STOVL ejector and volume dynamics p 30 N90-22566
[NASA-TM-103167]
- DRUMMOND, CHARLES H., III**
Crystallization behavior and properties of BaO-Al₂O₃-2SiO₂ glass matrices p 95 A90-51933
Crystallization behavior and properties of BaO-Al₂O₃-2SiO₂ glass matrices p 127 N90-19374
[NASA-CR-185209]
- DRUMMOND, COLIN K.**
STOVL propulsion system volume dynamics approximations p 25 N90-11740
[NASA-TM-102397]
Real-time simulation of an F110/STOVL turbofan engine p 25 N90-12618
[NASA-TM-102409]
STOVL aircraft simulation for integrated flight and propulsion control research p 26 N90-13389
[NASA-TM-102419]
Mass transfer from a sphere in an oscillating flow with zero mean velocity p 179 N90-20338
[NASA-TM-102566]
- DRYER, F. L.**
Droplet combustion experiment drop tower tests using models of the space flight apparatus p 133 N90-11196
[NASA-TM-101472]
- DRYER, FREDERICK L.**
N-decane-air droplet combustion experiments in the NASA-Lewis 5 Second Zero-Gravity Facility p 104 A90-25038
[AIAA PAPER 90-0649]
- DUBIEL, D. J.**
Energy efficient engine pin fin and ceramic composite segmented liner combustor sector rig test report p 35 N90-28567
[NASA-CR-179534]
- Energy Efficient Engine: Combustor component performance program p 35 N90-28568
[NASA-CR-179533]
- DUCHENE, G. A.**
Interface demarcation in GaAs by current pulsing p 254 A90-19793
[AIAA PAPER 90-0319]
Free float acceleration measurements aboard NASA's KC-135 Microgravity Research Aircraft p 132 A90-20000
[AIAA PAPER 90-0742]
- DUCK, P. W.**
A numerical study of the interaction between unsteady free-stream disturbances and localized variations in surface geometry p 161 A90-21422
- DUCK, PETER W.**
Unsteady three-dimensional marginal separation, including breakdown p 179 N90-20337
[NASA-TM-102525]
- DUDEHOEFER, JAMES E.**
On the dynamic response of pressure transmission lines in the research of helium-charged free piston Stirling engines p 196 A90-38248
Two-dimensional numerical simulation of a Stirling engine heat exchanger p 170 A90-38290
Recent Stirling engine loss-understanding results p 77 N90-21114
[NASA-TM-103122]
Programmatic status of NASA's CSTI high capacity power Stirling space power converter program p 79 N90-22606
[NASA-TM-103142]
- DUFFY, STEPHEN F.**
Analysis of whisker-toughened ceramic components - A design engineer's viewpoint p 88 A90-19149
Noninteractive macroscopic reliability model for ceramic matrix composites with orthotropic material symmetry p 209 A90-23827
[ASME PAPER 89-GT-129]
Noninteractive macroscopic reliability model for whisker-reinforced ceramic composites p 89 A90-26561
Analysis of whisker-toughened ceramic components: A design engineer's viewpoint p 97 N90-18504
[NASA-TM-102333]
Extension of a noninteractive reliability model for ceramic matrix composites p 129 N90-26142
[NASA-CR-185267]
- DUH, J. C.**
Numerical modeling of enclosure convection p 157 A90-13511
[IAF PAPER 89-403]
Numerical analysis of natural convection in liquid droplets by phase change p 164 A90-23212
Comparison between pressure gradient method and MAC method on high Re calculation p 172 A90-44462
- DUKE, J. C., JR.**
Impact damage development in damaged composite materials p 193 A90-18355
- DUNN, M. G.**
Phase and time-resolved measurements of unsteady heat transfer and pressure in a full-stage rotating turbine p 165 A90-23832
[ASME PAPER 89-GT-135]
- DUNN, MICHAEL G.**
Heat transfer and pressure measurements for the SSME fuel-side turbopump p 31 N90-23405
[NASA-CR-184928]
- DUSTIN, MILES O.**
A heat receiver design for solar dynamic space power systems p 72 N90-14283
[NASA-TM-102473]
- DUTTA, SUNIL**
High-strength silicon carbides by hot isostatic pressing p 122 A90-35473
- DUVAL, W. M. B.**
Inverse heat transfer analysis of Bridgman crystal growth p 157 A90-13093
- DUVAL, WALTER M. B.**
Coupled effects of conduction in the crystal and thermo-solutal convection in a rectangular inclined enclosure p 133 A90-25031
[AIAA PAPER 90-0408]
Effect of gas and surface radiation on crystal growth from the vapor phase p 133 A90-49060
- DUYAR, AHMET**
A failure diagnosis system based on a neural network classifier for the space shuttle main engine p 83 N90-28659
[NASA-TM-103607]
- DWOYER, DOUGLAS L.**
CFD propels NASP propulsion progress p 172 A90-41163
- Microwave conductivity of laser ablated YBaCuO superconducting films and its relation to microstrip transmission line p 155 N90-27844
- ECER, A.**
A block-based algorithm for the solution of compressible flows in rotor-stator combinations p 9 A90-46905
- ECK, T. G.**
Millimeter wave surface resistance of RBa₂Cu₃O(7-delta) superconductors (R = Y, Eu, Dy, Sm, Er) p 259 N90-20886
[NASA-TM-102571]
- ECKEL, ANDREW J.**
Reactions of SiC with H₂/H₂O/Ar mixtures at 1300 C p 123 A90-45830
Hydrogen-silicon carbide interactions p 125 N90-11144
[NASA-TM-102382]
Ceramic matrix composites in simulated SSME environments p 102 N90-28655
- EDELMAN, RAYMOND B.**
Ignition and behavior of laminar gas-jet diffusion flames in microgravity p 103 A90-23107
Effects of pressure on microgravity hydrocarbon diffusion flames p 104 A90-25039
[AIAA PAPER 90-0651]
- EDWARDS, ROBERT V.**
New space domain processing technique for pulsed laser velocimetry p 187 A90-48750
- EHRESMAN, DERIK**
Solar Concentrator Advanced Development Program p 232 N90-22834
[NASA-CR-185173]
- EHRESMAN, DERIK T.**
Update of the Solar Concentrator Advanced Development Project p 48 A90-38267
- EICHENBERG, DENNIS J.**
Design of a CO₂ laser power control system for a Spacelab microgravity experiment p 192 N90-28833
[NASA-TM-103112]
- EISEMAN, PETER R.**
Interactive grid generation for turbomachinery flow field simulations p 6 A90-26553
Grid generation for the solution of partial differential equations p 237 A90-47188
The fundamentals of adaptive grid movement p 185 N90-29610
- EISENBERG, JOSEPH D.**
The selection of convertible engines with current gas generator technology for high speed rotorcraft p 22 A90-46933
- EL-BAYOUMY, L. E.**
The role of thermal and lubricant boundary layers in the transient thermal analysis of spur gears p 194 A90-21118
- ELDRIDGE, J. I.**
Investigation of interfacial shear strength in a SiC fibre/Ti-24Al-11Nb composite by a fibre push-out technique p 88 A90-18973
Characterization of interfacial failure in SiC reinforced Si₃N₄ matrix composite material by both fiber push-out testing and Auger electron spectroscopy p 91 A90-36802
- ELGHOBASHI, S.**
Effects of g-jitter on a thermal, buoyant flow p 163 A90-22239
[AIAA PAPER 90-0653]
- ELLIOTT, G. S.**
Compressibility effects in free shear layers p 161 A90-19984
[AIAA PAPER 90-0705]
Effects of compressibility on the characteristics of free shear layers p 6 A90-25285
Pressure-based real-time measurements in compressible free shear layers p 8 A90-42709
[AIAA PAPER 90-1980]
- ELLIS, DAVID L.**
Production and processing of Cu-Cr-Nb alloys p 114 A90-33340
Production and processing of Cu-Cr-Nb alloys p 117 N90-16053
[NASA-TM-102495]
- ELLIS, J. RODNEY**
Thermomechanical testing techniques for high-temperature composites: TMF behavior of SiC(SCS-6)/Ti-15-3 p 222 N90-25367
[NASA-TM-103171]
- ELROD, D. A.**
An annular gas seal analysis using empirical entrance and exit region friction factors p 196 A90-33555
[ASME PAPER 89-TRIB-46]
- ELROD, HAROLD G.**
Efficient numerical method for computation of thermohydrodynamics of laminar lubricating films p 175 N90-11256
[NASA-CR-185136]
- EMERY, EDWARD F.**
A test matrix sequencer for research test facility automation p 37 A90-42791
[AIAA PAPER 90-2386]
A test matrix sequencer for research test facility automation p 39 N90-23416
[NASA-TM-103108]

- EMERY, K. A.**
An empirical investigation of the InP shallow-homojunction solar cell p 225 A90-14869
Hybrid solar cells based on dc magnetron sputtered films of n-ITO on APMOVPE grown p-InP p 225 A90-14893
- EMERY, KEITH A.**
High altitude current-voltage measurement of GaAs/Ge solar cells p 226 A90-14910
- ENGDAHL, E. H.**
Advanced radiator concepts p 170 A90-38042
- ENGELIS, T. E.**
The GEM-T2 gravitational model [NASA-TM-100746] p 234 N90-12984
- ENGLERT, GERALD W.**
Parametric study of power absorption from electromagnetic waves by small ferrite spheres [NASA-TP-2949] p 246 N90-12282
- ENRIGHT, PAUL J.**
Optimal finite-thrust spacecraft trajectories using collocation and nonlinear programming [AAS PAPER 89-350] p 40 A90-46783
Discrete approximations to optimal trajectories using direct transcription and nonlinear programming [AIAA PAPER 90-2963] p 41 A90-53038
- ERLEBACHER, GORDON**
Grid generation for the solution of partial differential equations p 237 A90-47188
- ESKER, BARBARA S.**
Performance characteristics of a one-third-scale, vectorable ventral nozzle for SSTOVL aircraft [AIAA PAPER 90-2271] p 20 A90-37562
Performance characteristics of a one-third-scale, vectorable ventral nozzle for SSTOVL aircraft [NASA-TM-103120] p 2 N90-21725
- EUGENE, L. P.**
A parallel pipelined architecture for a digital multicarrier demodulator [AIAA PAPER 90-0812] p 46 A90-25635
- EUSTACE, JOHN G.**
Optical techniques for determination of normal shock position in supersonic flows for aerospace applications [NASA-TM-103201] p 190 N90-25323
- F**
- FAGHRI, A.**
Mathematical modeling and analysis of heat pipe start-up from the frozen state p 174 A90-48404
- FARMER, SERENE C.**
Experimentally determined wear behavior of an Al₂O₃-SiC composite from 25 to 1200 C [NASA-TM-102549] p 87 N90-20130
- FAROKHI, SAEED**
Modern developments in shear flow control with swirl [NASA-CR-186586] p 181 N90-22000
- FARRELL, D. E.**
Glass-derived superconducting ceramics with zero resistance at 107 K in the Bi(1.5)Pb(0.5)Sr₂Ca₂Cu₃O(x) system p 253 A90-11491
Synthesis and characterization of high-T_c superconductors in the Ti-Ca-Ba-Cu-O system p 253 A90-19300
Synthesis and characterization of high-T(c) screen-printed Y-Ba-Cu-O films on alumina p 254 A90-21926
Experimental evidence of a dimensional crossover in Y1Ba2Cu3O7(δ) p 255 A90-29739
- FARRELL, R.**
Automotive Stirling engine development program [NASA-CR-180839] p 263 N90-11654
- FARRELL, ROGER A.**
Automotive Stirling engine development program [NASA-CR-180840] p 264 N90-29260
- FARSHCHI, M.**
Chemically reacting supersonic flow calculation using an assumed PDF model [AIAA PAPER 90-0731] p 4 A90-22256
- FATEMI, N.**
A V-grooved GaAs solar cell p 225 A90-14887
GaAs solar cells with V-grooved emitters p 229 N90-17754
- FATEMI, N. S.**
Peeled film GaAs solar cells for space power [NASA-TM-103125] p 153 N90-21287
- FATEMI, NAVID S.**
Contact formation in gallium arsenide solar cells p 225 A90-14888
The kinetics of the Au-InP interaction p 254 A90-25084
Humidity-induced room-temperature decomposition of Au contacted indium phosphide p 105 A90-44689
Contact spreading and the Au₃In₃-to-Au₃In₄ transition in the Au-InP system p 257 A90-48661
Lateral spreading of Au contacts on InP [NASA-TM-103133] p 232 N90-22843
- An analysis of the contact sintering process in III-V solar cells [NASA-TM-103179] p 233 N90-25420
- FAVROW, L. H.**
Identification of a cast iron alloy containing nonstrategic elements [NASA-CR-185174] p 118 N90-18559
Constitutive and life modeling of single crystal blade alloys for root attachment analysis p 119 N90-28643
- FAY, EDGAR H.**
Lunar orbiting microwave beam power system [NASA-TM-103211] p 51 N90-25173
- FAYMON, KARL A.**
Mars manned transportation vehicle [AAS PAPER 87-271] p 42 A90-16569
Orbit to surface beamed power for Mars bases expansion p 40 A90-38105
Overview of microwave concepts p 142 N90-10155
Microwave beam power p 69 N90-10165
Central electrical utility power for a satellite ring city in low earth orbit space p 150 N90-10166
- FEDKIW, PETER S.**
The impedance of a tubular electrode - A model for a porous electrode p 104 A90-33723
Characterization of reaction kinetics in a porous electrode [NASA-CR-186504] p 106 N90-19340
- FELDER, MARIAN C.**
The Space Station photovoltaic panels plasma interaction test program - Test plan and results [AIAA PAPER 90-0722] p 47 A90-22252
The Space Station Photovoltaic Panels Plasma Interaction Test Program: Test plan and results [NASA-TM-102474] p 49 N90-13581
- FELICELLI, S.**
Finite element simulations of thermosolutal convection in vertical solidification of binary alloys p 132 A90-18292
- FELIPPA, C. A.**
Mixed variational formulation of finite element analysis of acoustoelastic/slosh fluid-structure interaction p 212 A90-34851
Variational formulation of high-performance finite elements - Parametrized variational principles p 213 A90-46068
Developments in variational methods for high performance plate and shell elements p 214 A90-46288
- FELIPPA, CARLOS A.**
Treatment of coupled fluid-structure interaction problems by a mixed variational principle p 159 A90-18288
A variational justification of the assumed natural strain formulation of finite elements. I - Variational principles. II - The C(0) four-node plate element p 210 A90-24384
Electromagnetic finite elements based on a four-potential variational principle p 214 A90-49869
- FELSENTREGER, T. L.**
The GEM-T2 gravitational model [NASA-TM-100746] p 234 N90-12984
- FERBER, M. K.**
Determination of the stress distributions in a ceramic: Tensile specimen using numerical techniques [NASA-TM-101914] p 129 N90-26132
- FERGUSON, DALE C.**
Solar array arcing in plasmas p 233 N90-25558
- FERKUL, PAUL V.**
Near-limit flame spread over a thin solid fuel in microgravity p 104 A90-32835
- FERNANDES, P. J.**
A parallel pipelined architecture for a digital multicarrier demodulator [AIAA PAPER 90-0812] p 46 A90-25635
- FERNANDEZ-PELLO, A. C.**
Smoldering combustion under low gravity conditions [AIAA PAPER 90-0648] p 103 A90-22238
- FERNANDEZ, N. S.**
Coplanar waveguide fed phased array antenna [NASA-TM-102522] p 152 N90-21273
- FERRANTE, J.**
Phase transitions in fermionic systems with many-body interaction p 249 A90-19303
- FERRANTE, JOHN**
Fundamentals of tribology at the atomic level p 192 A90-14020
Universal aspects of brittle fracture, adhesion, and atomic force microscopy p 83 A90-14021
Liquid alkali metals - Equation of state and reduced-pressure, bulk-modulus, sound-velocity, and specific-heat functions p 102 A90-16280
Pressure dependence of the melting temperature of metals p 103 A90-16281
An accurate analytic approximation to the non-linear change in volume of solids with applied pressure p 261 A90-27612
- Applications of surface analysis and surface theory in tribology p 84 A90-37458
- FERTIS, D. G.**
Parametric studies of advanced turboprops p 19 A90-21225
- FERTIS, DEMETER G.**
Dynamic analysis of space-related linear and non-linear structures [NASA-TM-103490] p 51 N90-25174
- FIELDER, WILLIAM L.**
Corrosion testing of candidates for the alkaline fuel cell cathode p 228 A90-33948
Corrosion testing of candidates for the alkaline fuel cell cathode p 231 N90-20471
O₂ reduction at the IFC orbiter fuel cell O₂ electrode [NASA-TM-102580] p 231 N90-21469
- FILPUS, JOHN W.**
Review of research and development on the microwave electrothermal thruster p 55 A90-46369
- FINKMAN, E.**
Interface properties of various passivations of HgCdTe p 251 A90-45947
Contribution of the graded region of a HgCdTe diode to its saturation current p 257 A90-45948
- FLANAGAN, PATRICK M.**
Developing a self-diagnostic system for piezoelectric sensors [AIAA PAPER 90-2230] p 187 A90-42755
- FLATICO, JOSEPH M.**
Silicon-etalon fiber-optic temperature sensor [NASA-TM-102389] p 18 N90-13381
- FLEETER, SANFORD**
The unsteady aerodynamics of an oscillating cascade in a compressible flow field p 2 A90-11789
Aeroelastic detuning for stability enhancement of unstalled supersonic flutter p 19 A90-17462
Aerodynamics of a linear oscillating cascade [NASA-TM-103250] p 15 N90-27657
- FLEISCHER, D.**
Experiments on a repetitively pulsed electrothermal thruster p 56 A90-27960
- FLEMING, D. P.**
Active vibration control for flexible rotor by optimal direct-output feedback control p 197 A90-46222
Spray automated balancing of rotors - How process parameters influence performance p 198 A90-46228
- FLEMING, MICHAEL L.**
On protection of Freedom's solar dynamic radiator from the orbital debris environment. Part 1: Preliminary analyses and testing [NASA-TM-102458] p 73 N90-14285
- FLINT, J. H.**
Nitriding kinetics of Si-SiC powder mixtures as simulations of reaction bonded Si₃N₄-SiC composites p 90 A90-27076
- FLOOD, D. J.**
The mini-dome lens space concentrator array - Recent component test results and current array development status p 60 A90-38155
Estimation of minority carrier diffusion lengths in InP/GaAs solar cells [NASA-TM-103213] p 81 N90-26069
- FLOOD, DENNIS J.**
Photovoltaic power for a lunar base [IAF PAPER 89-254] p 42 A90-13409
Issues and opportunities in space photovoltaics p 54 A90-14852
Photovoltaic power system operation in the Mars environment p 43 A90-38156
Photovoltaic options for solar electric propulsion [AIAA PAPER 90-2529] p 68 A90-52563
NASA advanced space photovoltaic technology: Status, potential and future mission applications p 74 N90-17775
Recent results from advanced research on space solar cells at NASA [NASA-TM-102485] p 152 N90-21274
- FLOOD, J. D.**
Engine inlet distortion in a 9.2 percent scaled vectored thrust STOVL model in ground effect [AIAA PAPER 89-2910] p 5 A90-25043
Engine inlet distortion in a 9.2 percent scale vectored thrust STOVL model in ground effect [NASA-TM-102358] p 12 N90-17561
- FLOOD, JOSEPH D.**
Hot gas ingestion characteristics and flow visualization of a vectored thrust STOVL concept [NASA-TM-103212] p 32 N90-26009
- FOLTZ, H. L.**
Energy Efficient Engine combustor test hardware detailed design report [NASA-CR-168301] p 33 N90-28554
Energy Efficient Engine (E3) combustion system component technology performance report [NASA-CR-168274] p 33 N90-28555

- FORCE, DALE A.**
Spent-beam refocusing analysis and multistage depressed collector design for a 75-W, 59- to 64-GHz coupled-cavity traveling-wave tube
[NASA-TP-3039] p 155 N90-27965
- FORD, WILLIAM F.**
Quotient-difference type generalizations of the power method and their analysis
[NASA-TM-102361] p 242 N90-10635
- FORNEY, L. J.**
Frequency response of a thermocouple wire: Effects of axial conduction
[NASA-CR-180454] p 191 N90-28827
- FORSBERG, ROGER C.**
Adjustable depth gage
[NASA-CASE-LEW-14880-1] p 187 N90-10415
- FOSS, J. F.**
The effects of forcing on a single stream shear layer and its parent boundary layer
p 169 A90-35219
- FOSS, JOHN F.**
The effects of forcing on a single stream shear layer and its parent boundary layer
[NASA-CR-186529] p 180 N90-21301
- FOSSUM, A. F.**
Probabilistic analysis of a materially nonlinear structure
[AIAA PAPER 90-1099] p 211 A90-29329
- FOX, D. S.**
Influence of alloying elements on the oxidation behavior of NbAl₃
p 113 A90-24861
- FOX, DENNIS S.**
Burner rig hot corrosion of silicon carbide and silicon nitride
p 121 A90-25267
- FRALICK, G. C.**
Frequency response of a thermocouple wire: Effects of axial conduction
[NASA-CR-180454] p 191 N90-28827
- FRALICK, GUSTAVE C.**
Results of an attempt to measure increased rates of the reaction D-2 + D-2 yields He-3 + n in a nonelectrochemical cold fusion experiment
[NASA-TM-102430] p 250 N90-17424
- FRANCIS, ROBERT W.**
Issues and opportunities in space photovoltaics
p 54 A90-14852
- FRANCISCUS, LEO C.**
RAMSCRAM: A flexible ramjet/scramjet engine simulation program
[NASA-TM-102451] p 27 N90-14235
- FRANCISCUS, LEO C.**
Supersonic through-flow fan engine and aircraft mission performance
[NASA-TM-102304] p 29 N90-21038
- FRANK, L. A.**
Spacelab 2 Plasma Diagnostics Package
p 39 A90-23263
- FRASCA, A. J.**
Neutron and gamma irradiation effects on power semiconductor switches
[NASA-TM-103200] p 155 N90-25278
- FREED, A. D.**
Viscoplasticity: A thermodynamic formulation
[NASA-TM-102388] p 216 N90-14640
- FREED, A. D.**
Steady-state and transient Zener parameters in viscoplasticity: Drag strength versus yield strength
[NASA-TM-102487] p 218 N90-18064
- FREED, A. D.**
A viscoplastic model with application to LiF-22 percent CaF₂ hypereutectic salt
[NASA-TM-103181] p 221 N90-23770
- FREED, A. D.**
Stress versus temperature dependent activation energies in creep
[NASA-TM-103192] p 221 N90-23773
- FREED, ALAN D.**
Model development in viscoplastic ratchetting
[NASA-TM-102509] p 219 N90-20431
- FREEDMAN, MARC R.**
Slurry-pressing consolidation of silicon nitride
p 121 A90-27691
- FREEDMAN, MARC R.**
Reliability analysis of a structural ceramic combustion chamber
[NASA-TM-103264] p 223 N90-28112
- FRENKLACH, MICHAEL**
On the driving force of PAH production
p 84 A90-32833
- FRENKLACH, MICHAEL**
Kinetics and mechanism of soot formation in hydrocarbon combustion
[NASA-CR-186162] p 106 N90-14305
- FRIEDBERG, R. A.**
Electro-impulse de-icing testing analysis and design
[NASA-CR-4175] p 18 N90-10031
- FRIEDMAN, ROBERT**
Fire safety applications for spacecraft
p 16 N90-17595
- FRIEMAN, JOSHUA A.**
Is the sub-millisecond pulsar strange?
p 264 A90-12669

- FRITSCH, KLAUS**
Modulated-splitting-ratio fiber-optic temperature sensor
p 185 A90-11706
- FRITSCH, KLAUS**
Silicon-etalon fiber-optic temperature sensor
[NASA-TM-102389] p 18 N90-13381
- FUJIKAWA, G.**
ATDRS payload technology research and development
[NASA-TM-103256] p 52 N90-28596
- FUJIKAWA, GENE**
Characterization of two MMIC GaAs switch matrices at microwave frequencies
[AIAA PAPER 90-0866] p 147 A90-25686
- FUJIKAWA, GENE**
Effects of amplitude distortions and IF equalization on satellite communication system bit-error rate performance
[AIAA PAPER 90-0878] p 140 A90-25697
- FUJIKAWA, GENE**
Characterization of two MMIC GaAs switch matrices at microwave frequencies
[NASA-TM-102449] p 50 N90-14273
- FUJIKAWA, GENE**
Performance measurements for a laboratory-simulated 30/20 GHz communication satellite transponder
[NASA-TM-102424] p 143 N90-17977
- FUJIKAWA, GENE**
Effects of amplitude distortions and IF equalization on satellite communication system bit-error rate performance
[NASA-TM-102415] p 144 N90-19454
- FUSARO, ROBERT L.**
Self-lubricating polymer composites and polymer transfer film lubrication for space applications
[NASA-TM-102492] p 128 N90-21862

G

- GABB, T. P.**
The high temperature deformation in cyclic loading of a single crystal nickel-base superalloy
p 108 A90-11534
- GABB, T. P.**
The role of interfacial dislocation networks in high temperature creep of superalloys
p 114 A90-33329
- GABB, T. P.**
Isothermal and nonisothermal fatigue behavior of a metal matrix composite
p 91 A90-36746
- GABB, TIMOTHY P.**
Heat treatment study of the SiC/Ti-15-3 composite system
[NASA-TP-2970] p 97 N90-19302
- GABB, TIMOTHY P.**
Characterization of failure processes in tungsten copper composites under fatigue loading conditions
[NASA-TM-102371] p 98 N90-21123
- GABB, TIMOTHY P.**
High temperature fatigue behavior of tungsten copper composites
[NASA-TM-102404] p 99 N90-21138
- GAGE, M. L.**
Corrosion prevention in copper combustion chamber liners of liquid oxygen/methane booster engines
[AIAA PAPER 90-2119] p 85 A90-42028
- GAGE, MARK L.**
Hydrocarbon-fuel/combustion-chamber-liner materials compatibility
[NASA-CR-185203] p 118 N90-21165
- GAIER, J. R.**
Properties of Pb(1-x)Bi(x)/Ba₂YCu₃O(x) composites - Reaction of Ba₂YCu₃O(x) with Pb and Bi
p 255 A90-33224
- GAIER, J. R.**
Synthesis and structural chemistry of Au(III)-substituted Ba₂YCu₃O(7-delta)
[NASA-TM-103292] p 108 N90-28696
- GAIER, JAMES R.**
Effect of heat-treatment temperature of vapor-grown graphite fibers. I - Properties of their bromine intercalation compounds
p 120 A90-16279
- GAIER, JAMES R.**
The effect of length and diameter on the resistivity of bromine intercalated graphite fibers
p 122 A90-33332
- GAIER, JAMES R.**
Density of intercalated graphite fibers
p 124 A90-49061
- GAIER, JAMES R.**
Density of intercalated graphite fibers
[NASA-TM-102411] p 126 N90-14362
- GAIER, JAMES R.**
Aeolian removal of dust from photovoltaic surfaces on Mars
[NASA-TM-102507] p 76 N90-19299
- GAIER, JAMES R.**
Feasibility of intercalated graphite railgun armatures
[NASA-TM-102546] p 128 N90-21181
- GAIER, JAMES R.**
Resistivity of pristine and intercalated graphite fiber epoxy composites
[NASA-TM-102576] p 128 N90-21192
- GAIER, JAMES R.**
Aeolian removal of dust from radiator surfaces on Mars
[NASA-TM-103205] p 81 N90-26068
- GAIER, JAMES R.**
The chemical effects of the Martian environment on power system component materials: A theoretical approach
[NASA-TM-103203] p 87 N90-26074

- GAJJAR, J. S. B.**
Amplitude-dependent neutral modes in compressible boundary layer flows
[NASA-TM-102524] p 178 N90-20326
- GALINAITIS, W. S.**
Health Monitoring System for the SSME-fault detection algorithms
[AIAA PAPER 90-1988] p 63 A90-40584
- GALINAITIS, WILLIAM S.**
Framework for a space shuttle main engine health monitoring system
[NASA-CR-185224] p 78 N90-21809
- GALLAGHER, RICHARD H.**
Compatibility conditions of structural mechanics for finite element analysis
[NASA-TM-102413] p 217 N90-17180
- GALLAGHER, RICHARD H.**
Integrated force method versus displacement method for finite element analysis
[NASA-TP-2937] p 218 N90-18081
- GALOFARO, JOEL T.**
Comparison of currents predicted by NASCAP/LEO model simulations with elementary Langmuir-type bare probe models for an insulated cable containing a single pinhole
[NASA-TM-102486] p 51 N90-26054
- GAMMON, ROBERT W.**
Critical speeding up in pure fluids
p 167 A90-26369
- GAMMON, ROBERT W.**
Critical fluid light scattering
p 251 N90-17087
- GANESAN, S.**
Solute redistribution in dendritic solidification with diffusion in the solid
p 253 A90-17399
- GANTOSE, DAVE**
Development of Ada language control software for the NASA power management and distribution test bed
p 236 A90-38082
- GANZ, MATTHEW W.**
Convergence of the SMI and the diagonally loaded SMI algorithms with weak interference
[AD-A22639] p 141 A90-36717
- GAO, Q.**
The equivalence between dislocation pile-ups and cracks
p 210 A90-29215
- GAO, Q.**
Characterization of the tip field of a discrete dislocation pileup for the development of physically based micromechanics
p 213 A90-43883
- GARDNER, WILLIAM B.**
Energy efficient engine program technology benefit/cost study. Volume 1: Executive summary
[NASA-CR-174766-VOL-1] p 34 N90-28564
- GARDNER, WILLIAM B.**
Energy efficient engine program technology benefit/cost study, volume 2
[NASA-CR-174766-VOL-2] p 35 N90-28565
- GARG, SANJAY**
Cooperative synthesis of control and display augmentation in approach and landing
p 36 A90-33061
- GARG, SANJAY**
Analysis of airframe/engine interactions - An integrated control perspective
[AIAA PAPER 90-1918] p 36 A90-40557
- GARG, SANJAY**
H-infinity based integrated flight/propulsion control design for a STOVL aircraft in transition flight
[AIAA PAPER 90-3335] p 36 A90-47595
- GARG, SANJAY**
H-infinity based integrated flight/propulsion control design for a STOVL aircraft in transition flight
[NASA-TM-103198] p 37 N90-26011
- GAUG, R. L.**
Convection phenomena in low-gravity processing - The GTE GaAs space experiment
[AIAA PAPER 90-0409] p 133 A90-25032
- GAYDA, J.**
Analysis of gamma prime shape changes in a single crystal Ni-base superalloy
p 109 A90-15206
- GAYDA, J.**
Isothermal and nonisothermal fatigue behavior of a metal matrix composite
p 91 A90-36746
- GAYDOSH, D. J.**
Microstructure and tensile properties of Fe-40 at. pct Al alloys with C, Zr, Hf, and B additions
p 108 A90-11651
- GAYDOSH, D. J.**
Influence of testing environment on the room temperature ductility of FeAl alloys
p 115 A90-39658
- GAYDOSH, D. J.**
1300 K compressive properties of several dispersion strengthened NiAl materials
p 116 A90-47091
- GAYDOSH, D. J.**
Compatibility of Fe-40Al with various fibers
p 94 A90-50496
- GAYDOSH, DARRELL J.**
Oxidation behavior of FeAl + Hf, Zr, B
p 113 A90-24858
- GAYLE, E. ROSE**
Effect of reduced aft diameter and increased blade number of high-speed counterrotation propeller performance
[AIAA PAPER 89-0438] p 4 A90-23650
- GEDDES, J.**
The 30-GHz monolithic receive module
[NASA-CR-180849] p 146 N90-24528

- GEDWILL, MICHAEL A.**
Cyclic oxidation of aluminide coatings on Ti3Al+ Nb
p 115 A90-39660
- GEMEINER, RUSSEL P.**
Characterization testing of a 40 ampere hour bipolar nickel-hydrogen battery p 56 A90-33940
Characterization testing of a 40 AHR bipolar nickel-hydrogen battery p 230 N90-20463
- GENERAZIO, E. R.**
Subtle porosity variation in the YBa2Cu3O(7-x) high-temperature superconductor revealed by ultrasonic imaging
[NASA-TM-102130] p 206 N90-17167
- GENERAZIO, EDWARD R.**
Ultrasonic and radiographic evaluation of advanced aerospace materials: Ceramic composites
[NASA-TM-102540] p 207 N90-21401
Recent advances in nondestructive evaluation made possible by novel uses of video systems
[NASA-TM-102491] p 207 N90-22801
Theory and experimental technique for nondestructive evaluation of ceramic composites
[NASA-TM-102561] p 207 N90-23754
Improved transverse crack detection in composites
[NASA-TM-103261] p 102 N90-27875
- GENG, STEVEN M.**
Results from baseline tests of the SPRE I and comparison with code model predictions
p 62 A90-38249
- GEOFFROY, L. M.**
High efficiency GaAs/Ge monolithic tandem solar cells p 224 A90-14858
- GEORGE, JEFFREY A.**
Multi-reactor configurations for multi-megawatt spacecraft power supplies
[AIAA PAPER 90-2111] p 66 A90-47207
- GERVER, M. J.**
Theory of plasma contactors in ground-based experiments and low earth orbit p 150 A90-47108
- GESSERT, T. A.**
An empirical investigation of the InP shallow-homojunction solar cell p 225 A90-14869
Hybrid solar cells based on dc magnetron sputtered films of n-ITO on APMOVPE grown p-InP p 225 A90-14893
Investigation of buried homojunctions in p-InP formed during sputter deposition of both indium tin oxide and indium oxide p 256 A90-36799
- GESSNER, F. B.**
Experimental investigation of turbulent flow through a circular-to-rectangular transition duct
[AIAA PAPER 90-1505] p 171 A90-38654
Experimental investigation of flow about a strut-endwall configuration
[AIAA PAPER 90-1541] p 171 A90-38685
- GOLDSTON, E.**
Space Station Freedom power management and distribution design status p 59 A90-38080
- GHORASHI, B.**
A circular combustor configuration with multiple injection ports for mixing enhancement p 158 A90-15389
A planar reacting shear layer system for the study of fluid dynamics-combustion interaction
[NASA-TM-102422] p 27 N90-13393
- GHOSH, LOUIS**
Fatigue crack growth in a unidirectional SCS-6/Ti-15-3 composite
[NASA-TM-103095] p 119 N90-22646
- GHOSH, LOUIS J.**
The unusual near-threshold FCG behavior of a single crystal superalloy and the resolved shear stress as the crack driving force p 111 A90-21009
Fatigue crack growth in unidirectional metal matrix composite
[NASA-TM-103102] p 220 N90-22117
- GIBALA, R.**
The effects of surface films on mechanical behavior of B2 ordered intermetallic alloys p 115 A90-44338
- GILCHRIST, B. E.**
The sheath structure around a negatively charged rocket payload p 48 A90-34780
- GILLAND, J. H.**
Multimegawatt electric propulsion system design considerations
[AIAA PAPER 90-2552] p 68 A90-52566
- GINLEY, D. S.**
Rapid thermal processing of high temperature superconducting fiber
[NASA-CR-186803] p 259 N90-24964
- GINSBERG, D. M.**
Experimental evidence of a dimensional crossover in Y1Ba2Cu3O(7-delta) p 255 A90-29739
- GINTY, C. A.**
Fundamental aspects and failure modes in high-temperature composites p 93 A90-50095
- GINTY, CAROL A.**
Fundamental aspects of and failure modes in high-temperature composites
[NASA-TM-102558] p 98 N90-20151
- GIRIJAN, J.**
Reflector surface distortion analysis techniques (thermal distortion analysis of antennas in space)
p 144 N90-19267
- GIVI, PEYMAN**
Model-free simulations of turbulent reactive flows
p 158 A90-15729
- GJERDE, HELEN B.**
Photovoltaic array environmental protection program
p 59 A90-38088
- GLADDEN, HERBERT J.**
Thermal/structural analyses of several hydrogen-cooled leading-edge concepts for hypersonic flight vehicles
[AIAA PAPER 90-0053] p 164 A90-23702
Thermal/structural analyses of several hydrogen-cooled leading-edge concepts for hypersonic flight vehicles
[NASA-TM-102391] p 177 N90-14511
- GLASSMAN, ARTHUR J.**
Advanced core technology - Key to subsonic propulsion benefits
[ASME PAPER 89-GT-241] p 19 A90-23890
- GLATT, L.**
Generalized Advanced Propeller Analysis System (GAPAS). Volume 2: Computer program user manual
[NASA-CR-185277] p 36 N90-29394
- GLICKSMAN, M. E.**
Effects of crystal-melt interfacial energy anisotropy on dendritic morphology and growth kinetics
p 253 A90-19284
Free dendritic growth in viscous melts - Cyclohexanol p 253 A90-19285
Evaluation of transport conditions during physical vapor transport growth of opto-electronic crystals
p 132 A90-20525
Flight software development for the isothermal dendritic growth experiment
[AIAA PAPER 90-0744] p 235 A90-22257
- GLICKSMAN, MARTIN E.**
Flight software development for the isothermal dendritic growth experiment
[NASA-TM-102412] p 238 N90-13988
- GLIEBE, P. R.**
An investigation of counterrotating tip vortex interaction
[NASA-CR-185135] p 247 N90-11549
High speed turboprop aeroacoustic study (counterrotation). Volume 1: Model development
[NASA-CR-185241] p 249 N90-26633
- GLIKSMAN, M. E.**
Determination of the mean solid-liquid interface energy of pivalic acid p 84 A90-22646
- GLOVER, DANIEL**
Design considerations for space flight hardware
[NASA-TM-102300] p 52 N90-14275
- GOLAN, ODED**
Minimum fuel trajectory for the aerospace-plane
[AAS PAPER 89-352] p 40 A90-46785
- GOLAN, ODED M.**
Minimum fuel trajectories for a low-thrust power-limited mission to the moon and to Lagrange points L4 and L5
[AAS PAPER 89-351] p 40 A90-46784
Minimum fuel lunar trajectories for a low-thrust power-limited spacecraft
[AIAA PAPER 90-2975] p 41 A90-53054
- GOLDSTEIN, M. E.**
Nonlinear evolution of oblique waves on compressible shear layers p 158 A90-15942
Nonlinear evolution of interacting oblique waves on two-dimensional shear layers p 158 A90-15943
On the instabilities of supersonic mixing layers - A high-Mach-number asymptotic theory p 8 A90-42644
Spatial evolution of nonlinear acoustic mode instabilities on hypersonic boundary layers
[NASA-TM-102431] p 177 N90-14517
- GOLDSTEIN, S. A.**
Experiments on a repetitively pulsed electrothermal thruster p 56 A90-27960
- GOMBOS, F. J.**
Development and refinement of test bed simulations
p 59 A90-38081
- GONZALEZ-SANABRIA, OLGA D.**
Energy storage considerations for a robotic Mars surface sampler
[AAS PAPER 87-245] p 42 A90-16544
- GOODEN, CLARENCE E.**
Feasibility of intercalated graphite railgun armatures
[NASA-TM-102546] p 128 N90-21181
- GOODRICH, JOHN W.**
Time-dependent viscous incompressible Navier-Stokes equations - The finite difference Galerkin formulation and streamfunction algorithms
p 156 A90-11598
- Hopf bifurcation in the driven cavity p 174 A90-48548
- Hopf bifurcation in the driven cavity
[NASA-TM-102334] p 175 N90-11969
- An unsteady time asymptotic flow in the square driven cavity
[NASA-TM-103141] p 181 N90-22016
- GORADIA, CHANDRA**
Predicted performance of near-optimally designed indium phosphide space solar cells at high intensities and temperatures p 225 A90-14898
- GORADIA, MANJU GHALLA**
Predicted performance of near-optimally designed indium phosphide space solar cells at high intensities and temperatures p 225 A90-14898
- GORDON, ELIOTT B.**
The entrainment rate for a row of turbulent jets
[NASA-CR-185278] p 15 N90-28504
- GORDON, W. L.**
Complex permittivity of lanthanum aluminate in the 20 to 300 K temperature range from 26.5 to 40.0 GHz
p 148 A90-37864
Millimeter-wave surface resistance of laser-ablated YBa2Cu3O(7-delta) superconducting films
p 257 A90-48694
Millimeter wave surface resistance of RbBa2Cu3O(7-delta) superconductors (R = Y, Eu, Dy, Sm, Er)
[NASA-TM-102571] p 259 N90-20886
Microwave conductivity of laser ablated YBaCuO superconducting films and its relation to microstrip transmission line p 155 N90-27844
- GOUKER, MARK A.**
Millimeter-wave/infrared rectenna development at Georgia Tech p 69 N90-10147
- GOULD, RICHARD D.**
Investigation of turbulent transport in an axisymmetric sudden expansion p 163 A90-23112
- GRADY, J. E.**
Evaluation of thermal and mechanical loading effects on the structural behavior of a SiC/titanium composite
[AIAA PAPER 90-1026] p 90 A90-29228
- GRADY, JOSEPH E.**
Evaluation of thermal and mechanical loading effects on the structural behavior of a SiC/titanium composite
[NASA-TM-102536] p 98 N90-20139
Low velocity impact analysis with NASTRAN p 221 N90-24647
Collision forces for compliant projectiles
[NASA-TM-4203] p 223 N90-28111
- GRAHAM, ROBERT W.**
Recent progress in research pertaining to estimates of gas-side heat transfer in an aircraft gas turbine
[NASA-TM-102460] p 27 N90-13394
Middle management of research
[NASA-TM-102417] p 262 N90-20901
Extraterrestrial life in the universe
[NASA-TM-102363] p 264 N90-22464
- GRAHAM, RON**
Detection of potential space station control/structure interaction with CO-ST-IN p 50 N90-21074
- GRATZ, ROY F.**
The 3F condensation polyimides: Review and update
[NASA-TM-102353] p 126 N90-14363
New Condensation polyimides containing 1,1,1-triaryl-2,2,2-trifluoroethane structures
[NASA-CASE-LEW-14346-1] p 86 N90-19300
Substituted 1,1,1-triaryl-2,2,2-trifluoroethanes and processes for their synthesis
[NASA-CASE-LEW-14345-2] p 107 N90-23497
- GRAY, D. E.**
Energy efficient engine program technology benefit/cost study. Volume 1: Executive summary
[NASA-CR-174766-VOL-1] p 34 N90-28564
Energy efficient engine program technology benefit/cost study, volume 2
[NASA-CR-174766-VOL-2] p 35 N90-28565
- GREBER, ISAAC**
The entrainment rate for a row of turbulent jets
[NASA-CR-185278] p 15 N90-28504
- GREEN, JAMES M.**
Catalytic ignition of hydrogen/oxygen p 107 N90-28627
- GREEN, MICHAEL J.**
CFD propels NASP propulsion progress p 172 A90-41163
- GREEN, ROBERT E., JR.**
Acousto-ultrasonic nondestructive evaluation of materials using laser beam generation and detection
[NASA-CR-186694] p 154 N90-23664
- GREENBERG, PAUL S.**
Non-contact temperature measurements in support of microgravity combustion experiments p 135 N90-17900

- New findings and instrumentation from the NASA Lewis microgravity facilities [NASA-TM-103189] p 136 N90-26163
- GRIEST, KIM**
Unity limits on the mass and radius of dark-matter particles p 264 A90-24671
- GRISAFFE, SALVATORE J.**
The Materials Division: A case study [NASA-TM-102380] p 86 N90-13597
- GROBSTEIN, TONI**
Oxidation of high-temperature intermetallics; Proceedings of the Workshop, Cleveland, OH, Sept. 22, 23, 1988 p 112 A90-24852
- GROBSTEIN, TONI L.**
Advanced refractory metals and composites for extraterrestrial power systems p 40 A90-48819
- GRODSINSKY, C. M.**
Low frequency vibration isolation technology for microgravity space experiments p 136 A90-46246
The vibro-acoustic mapping of low gravity trajectories on a Learjet aircraft [NASA-TM-103103] p 1 N90-21723
- GRODSINSKY, CARLOS M.**
Nonintrusive inertial vibration isolation technology for microgravity space experiments [AIAA PAPER 90-0741] p 132 A90-19999
Nonintrusive inertial vibration isolation technology for microgravity space experiments p 137 N90-11901 [NASA-TM-102386]
A new approach to active vibration isolation for microgravity space experiments [NASA-TM-102470] p 137 N90-17929
Development and approach to low-frequency microgravity isolation systems [NASA-TP-2984] p 138 N90-28754
- GROENEWEG, J. F.**
Unsteady Euler analysis of the flowfield of a propfan at an angle of attack p 5 A90-25028 [AIAA PAPER 90-0339]
Unsteady blade surface pressures on a large-scale advanced propeller - Prediction and data [AIAA PAPER 90-2402] p 9 A90-47220
Prediction of unsteady blade surface pressures on an advanced propeller at an angle of attack [NASA-TM-102374] p 11 N90-12560
Unsteady Euler analysis of the flow field of a propfan at an angle of attack [NASA-TM-102426] p 248 N90-18229
- GROENEWEG, JOHN F.**
Aeroacoustics of advanced propellers p 249 N90-26635 [NASA-TM-103137]
- GROENEWEG, MARK A.**
Ceramic port shields cast in an iron engine head p 196 A90-27095
- GROESBECK, DONALD E.**
Effects of fiber motion on the acoustic behavior of an anisotropic, flexible fibrous material p 247 A90-33313
- GROESBECK, W.**
Centaur upper stage p 44 A90-18017
- GROTH, MARY**
Attachment of lead wires to thin film thermocouples mounted on high temperature materials using the parallel gap welding process [NASA-TM-102442] p 189 N90-21361
- GROTH, MARY F.**
Mars in situ propellants - Carbon monoxide and oxygen ignition experiments [AIAA PAPER 90-1894] p 130 A90-50642
Mars in situ propellants: Carbon monoxide and oxygen ignition experiments [NASA-TM-103202] p 81 N90-26065
- GRUBER, R. P.**
Xenon ion propulsion for orbit transfer [AIAA PAPER 90-2527] p 67 A90-52562
- GRUSKA, C. J.**
Large scale prop-fan structural design study. Volume 1: Initial concepts [NASA-CR-174992] p 23 N90-10043
Large scale prop-fan structural design study. Volume 2: Preliminary design of SR-7 [NASA-CR-174993] p 23 N90-10044
- GRZEDZINSKI, J.**
Unsteady disturbances of streaming motions around bodies p 162 A90-21424
- GUHA, SUMIT**
Improving the low temperature ductility of NiAl p 110 A90-16940
- GULINO, DANIEL A.**
Ellipsometric studies of the diffusion of atomic oxygen through silicon dioxide thin films p 104 A90-36268
- GUO, Q.**
Measurement of the intrinsic bond strength of brittle thin films on flexible substrates p 256 A90-44022
- GUPTA, I. J.**
An experimental SMI adaptive antenna array for weak interfering signals [NASA-CR-185976] p 142 N90-11211
- GUPTA, INDER J.**
Effects of desired signal on the performance of a sidelobe canceller p 139 A90-13936
Adaptive antenna arrays for satellite communication [NASA-CR-185989] p 143 N90-12784
- GUPTA, MURI M.**
High accuracy solutions of incompressible Navier-Stokes equations [NASA-TM-102539] p 244 N90-21567
- GUSTAFSON, G.**
A high-speed GaAs MESFET optical controller p 186 A90-22483
- GUSTAFSON, KARL**
Hopf bifurcation in the driven cavity p 174 A90-48548
Hopf bifurcation in the driven cavity [NASA-TM-102334] p 175 N90-11969
- GUTE, DOUG**
Multi-level Hierarchical Poly Tree computer architectures p 236 A90-26082
- GYEKENYESI, J. Z.**
Nicalon/siliconoxycarbide ceramic composites p 94 A90-51924
- GYEKENYESI, JOHN P.**
Designing ceramic components with the CARES computer program p 235 A90-19147
A review of failure models for ceramic matrix composite laminates under monotonic loads p 89 A90-23842 [ASME PAPER 89-GT-153]
Calculation of Weibull strength parameters and Baldford flow-density constants for volume- and surface-flaw-induced fracture in ceramics p 212 A90-35462
Design of ceramic components with the NASA/CARES computer program [NASA-TM-102369] p 222 N90-26359
Ceramics Analysis and Reliability Evaluation of Structures (CARES). Users and programmers manual [NASA-TP-2916] p 223 N90-28099
Reliability analysis of a structural ceramic combustion chamber [NASA-TM-103264] p 223 N90-28112
- GYEKENYESI, JOHN Z.**
Polymer derived Nicalon/Si-C-O composites - Processing and mechanical behavior p 89 A90-27065
Nicalon/siliconoxycarbide ceramic composites [NASA-TM-102563] p 99 N90-21133

H

- HA, TRI T.**
A performance analysis of DS-CDMA and SCPC VSAT networks p 141 A90-39056
- HAAG, T. W.**
End-hall thrusters [AIAA PAPER 90-2595] p 64 A90-42570
- HAAG, THOMAS W.**
Design of a thrust stand for high power electric propulsion devices [NASA-TM-102372] p 73 N90-15992
Test facility and preliminary performance of a 100 kW class MPD thruster p 75 N90-18476
Arcjet cathode phenomena p 75 N90-18477
Arcjet nozzle design impacts p 76 N90-18478
- HAGGARD, J. B.**
Droplet combustion experiment drop tower tests using models of the space flight apparatus [NASA-TM-101472] p 133 N90-11196
- HAGGARD, JOHN B.**
N-decane-air droplet combustion experiments in the NASA-Lewis 5 Second Zero-Gravity Facility [AIAA PAPER 90-0649] p 104 A90-25038
- HAGGERTY, J. S.**
Nitriding kinetics of Si-SiC powder mixtures as simulations of reaction bonded Si₃N₄-SiC composites p 90 A90-27076
Properties of RBSN and RBSN-SiC composites p 94 A90-51920
- HAGSTROM, THOMAS**
Conditions at the downstream boundary for simulations of viscous incompressible flow [NASA-TM-102510] p 243 N90-18198
Asymptotic boundary conditions for dissipative waves: General theory [NASA-TM-102497] p 243 N90-18927
Asymptotic analysis of dissipative waves with applications to their numerical simulation [NASA-TM-103231] p 244 N90-26615
Consistency and convergence for numerical radiation conditions [NASA-TM-103262] p 244 N90-29124
- HAINLEY, DONALD C.**
Two-tiered design analysis of a radiator for a solar dynamic powered Stirling engine p 60 A90-38158
An improved algorithm for the modeling of vapor flow in heat pipes p 176 N90-13748 [NASA-CR-185179]
SP-100 power system conceptual design for lunar base applications [NASA-TM-102090] p 267 N90-15030
- HAISSIG, CHRISTINE M.**
Comparison of solution approaches for minimum-fuel, low-thrust, power-limited orbital transfers [AIAA PAPER 90-2960] p 41 A90-53035
- HAJELA, P.**
Neurobiological computational models in structural analysis and design [AIAA PAPER 90-1133] p 210 A90-29260
- HAKIM, NABIL S.**
Ceramic port shields cast in an iron engine head p 196 A90-27095
- HALASI, KADOSA**
Hopf bifurcation in the driven cavity p 174 A90-48548
Hopf bifurcation in the driven cavity [NASA-TM-102334] p 175 N90-11969
- HALEVI, Y.**
Performance analysis of Integrated Communication and Control System networks p 239 A90-51267
- HALFORD, G. R.**
Isothermal life prediction of composite lamina using a damage mechanics approach p 92 A90-48115
- HALFORD, GARY R.**
Thermal fatigue durability for advanced propulsion materials p 216 N90-14641
A nonlinear high temperature fracture mechanics basis for strainrate partitioning p 216 N90-14642 [NASA-TM-4133]
Finite element elastic-plastic-creep and cyclic life analysis of a cowl lip p 220 N90-22808 [NASA-TM-102342]
High temperature fatigue behavior of Haynes 188 p 119 N90-28642
- HALL, ARNOLD**
Bipolar nickel-hydrogen battery development - A program review p 62 A90-38288
- HALL, EDWARD J.**
3D Euler analysis of ducted propfan flowfields [AIAA PAPER 90-3034] p 8 A90-45873
Investigation of advanced counterrotation blade configuration concepts for high speed turboprop systems, task 1: Ducted propfan analysis [NASA-CR-185217] p 30 N90-22567
- HALL, KENNETH C.**
Calculation of unsteady Euler flows in turbomachinery using the linearized Euler equations p 2 A90-11778
Gust response analysis for cascades operating in nonuniform mean flows p 28 N90-18415
Development of a linearized unsteady aerodynamic analysis for cascade gust response predictions [NASA-CR-4308] p 14 N90-27655
- HALL, STEPHEN W.**
Effect of KOH concentration on LEO cycle life of IPV nickel-hydrogen flight battery cells [NASA-TM-103127] p 77 N90-21116
Effect of LEO cycling on 125 Ah advanced design IPV nickel-hydrogen battery cells p 78 N90-21808 [NASA-TM-103128]
- HALLINAN, GEORGE J.**
Design of the Space Station Freedom power system p 57 A90-38070
- HALLORAN, J. W.**
Rapid thermal processing of high temperature superconducting fiber [NASA-CR-186803] p 259 N90-24964
- HAMBOURGER, P. D.**
Properties of Pb(1-x)Bi(x)/Ba₂YCu₃O(x) composites - Reaction of Ba₂YCu₃O(x) with Pb and Bi p 255 A90-33224
Synthesis and structural chemistry of Au(III)-substituted Ba₂YCu₃O(7-delta) [NASA-TM-103292] p 108 N90-28696
- HAMBOURGER, PAUL D.**
Effect of heat-treatment temperature of vapor-grown graphite fibers. I - Properties of their bromine intercalation compounds p 120 A90-16279
Resistivity of pristine and intercalated graphite fiber epoxy composites [NASA-TM-102576] p 128 N90-21192
- HAMED, AWATEF**
The simulation of fluid dynamic uncertainties in the SSME turbopump [AIAA PAPER 90-2294] p 65 A90-42770
Three dimensional LDV flow measurements and theoretical investigation in a radial inflow turbine scroll p 9 A90-46860

- Probabilistic modeling for simulation of aerodynamic uncertainties in propulsion systems
[NASA-TM-102472] p 29 N90-21036
- HAMLEY, JOHN A.**
Arcjet load characteristics
[AIAA PAPER 90-2579] p 67 A90-47226
Arcjet load characteristics
[NASA-TM-103190] p 79 N90-25181
- HAMMOND, A. N.**
Electrical characterization of a Mapham inverter using pulse testing techniques
[NASA-TM-103254] p 82 N90-27784
- HAMMOUD, AHMAD M.**
A brief survey of radiation effects on polymer dielectrics p 123 A90-43119
- HAN, J. C.**
Augmented heat transfer in rectangular channels of narrow aspect ratios with rib turbulators p 157 A90-13091
Pressure drop and mass transfer in two-pass ribbed channels p 185 A90-24837
- HANCOCK, J. P.**
Analysis of results from wind tunnel tests of inlets for an advanced turbo-prop nacelle installation
[NASA-CR-174937] p 10 N90-10011
- HANDSCHUH, R. F.**
Efficiency testing of a helicopter transmission planetary reduction stage p 193 A90-21113
Topology of modified helical gears p 195 A90-21132
- HANDSCHUH, ROBERT F.**
Efficiency study comparing two helicopter planetary reduction stages p 199 A90-50644
Computerized inspection of gear tooth surfaces
[NASA-TM-102395] p 203 N90-22054
- HANNUM, NED P.**
The Pathfinder chemical transfer propulsion program p 74 N90-18471
- HANSEN, IRVING G.**
The effects of nonlinear loading upon the Space Station Freedom 20 kHz power system p 60 A90-38118
Variable speed induction motor operation from a 20-kHz power bus p 148 A90-38119
Induction motor control
[NASA-TM-102533] p 28 N90-19234
Aerospace induction motor actuators driven from a 20-kHz power link
[NASA-TM-102482] p 28 N90-20085
- HANSMAN, R. JOHN, JR.**
Heat transfer on accreting ice surfaces
[AIAA PAPER 90-0200] p 162 A90-22181
Modeling of surface roughness effects on glaze ice accretion p 16 N90-20925
Ultrasonic techniques for aircraft ice accretion measurement p 16 N90-20926
Investigation of surface water behavior during glaze ice accretion p 16 N90-20927
The influence of ice accretion physics on the forecasting of aircraft icing conditions p 17 N90-20928
- HANSON, D. B.**
Investigation of the near wake of a propfan p 7 A90-40686
- HARABURDA, FRANCIS M.**
Space Station Freedom electrical power system hardware commonality with the United States Polar Platform p 58 A90-38073
- HARABURDA, SCOTT S.**
Diagnostic evaluations of microwave generated helium and nitrogen plasma mixtures
[AIAA PAPER 90-2634] p 252 A90-42602
- HARDING, J. T.**
Iridium-coated rhenium thrusters by CVD p 114 A90-30480
- HARDY, T. L.**
Background, current status, and prognosis of the ongoing slush hydrogen technology development program for the NASP
[NASA-TM-103220] p 51 N90-26055
- HARDY, TERRY L.**
Slush Hydrogen (SLH2) technology development for application to the National Aerospace Plane (NASP)
[NASA-TM-102315] p 50 N90-14268
FLUSH: A tool for the design of slush hydrogen flow systems
[NASA-TM-102467] p 130 N90-17890
Prediction of the ullage gas thermal stratification in a NASP vehicle propellant tank experimental simulation using FLOW-3D
[NASA-TM-103217] p 131 N90-26160
- HARF, F. H.**
Filter clogging by the extracted gamma prime and its measurement p 116 A90-45620
- HARLOFF, G. J.**
Viscous three-dimensional analyses for nozzles for hypersonic propulsion
[NASA-CR-185197] p 27 N90-17635
- HARLOFF, GARY J.**
Hypersonic aerospace sizing analysis for the preliminary design of aerospace vehicles p 17 A90-23276
Three-dimensional compressible jet-in-crossflow calculations using improved viscosity models and adapted grid
[AIAA PAPER 90-2100] p 174 A90-47206
- HARROLD, JOSEPH L.**
On-board switching and processing p 150 A90-51168
- HART, HAROLD**
Linear acene derivatives - New routes to pentacene and naphthacene and the first synthesis of a triptycene with two anthracene moieties p 85 A90-49071
Bismatellation with a benzo(1,2-c:4,5-c'-prime) difuran equivalent - A new route to linear acene derivatives p 85 A90-49072
Iptycene synthesis: A new method for attaching a 2,3-anthracene moiety to the 9,10-positions of another anthracene moiety - Exceptional conditions for a Lewis acid catalyzed Diels-Alder reaction p 85 A90-49073
- HART, R. E., JR.**
High efficiency GaAs/Ge monolithic tandem solar cells p 224 A90-14858
Radiation resistance and comparative performance of ITO/InP and n/p InP homojunction solar cells p 226 A90-14933
Indium phosphide solar cell research in the United States: Comparison with non-photovoltaic sources p 229 N90-17758
- HART, RUSSELL E., JR.**
High altitude current-voltage measurement of GaAs/Ge solar cells p 226 A90-14910
InP homojunction solar cell performance on the LIPS III flight experiment p 226 A90-14921
Performance of GaAs concentrator cells under electron irradiations from 0.4 to 2.3 MeV p 227 A90-14956
- HARTLEY, J. G.**
Feasibility analysis of reciprocating magnetic heat pumps
[NASA-CR-186205] p 177 N90-15363
- HARTLEY, TOM T.**
The determination of third order linear models from a seventh order nonlinear jet engine model p 239 A90-52881
- HARTMAN, W. F.**
A forward error correction technique using a high-speed, high-rate single chip codec p 141 A90-48440
- HARTZ, WILLIAM G.**
Data compression techniques applied to high resolution high frame rate video technology
[NASA-CR-4263] p 143 N90-14452
- HASAN, MOHAMMAD H.**
Numerical investigation of the thermal stratification in cryogenic tanks subjected to wall heat flux
[NASA-TM-103194] p 184 N90-27984
- HASAN, MOHAMMAD M.**
Buoyancy effects on the vapor condensation rate on a horizontal liquid surface
[AIAA PAPER 90-0353] p 162 A90-22201
Vapor condensation on liquid surface due to laminar jet-induced mixing - The effects of system parameters
[AIAA PAPER 90-0354] p 163 A90-22202
Buoyancy effects on the vapor condensation rate on a horizontal liquid surface
[NASA-TM-102437] p 130 N90-13675
Vapor condensation on liquid surface due to laminar jet-induced mixing: The effects of system parameters
[NASA-TM-102433] p 176 N90-13751
- HASAN, MOHAMMED M.**
Numerical investigation of the thermal stratification in cryogenic tanks subjected to wall heat flux
[AIAA PAPER 90-2375] p 175 A90-52500
- HASSELMAN, D. P. H.**
Role of the interfacial thermal barrier in the effective thermal diffusivity/conductivity of SiC-fiber-reinforced reaction-bonded silicon nitride p 89 A90-25268
- HASTINGS, D. E.**
Theory of plasma contactors in ground-based experiments and low earth orbit p 150 A90-47108
- HASTINGS, DANIEL E.**
Ion drag for a negatively biased solar array in low earth orbit p 48 A90-36191
- HATHAWAY, MICHAEL D.**
Laser anemometer measurements in a transonic axial-flow fan rotor
[NASA-TP-2879] p 175 N90-11245
- HAVEN, V. E.**
High efficiency GaAs/Ge monolithic tandem solar cells p 224 A90-14858
- HAW, R. C.**
The effects of forcing on a single stream shear layer and its parent boundary layer p 169 A90-35219
- HAW, RICHARD C.**
The effects of forcing on a single stream shear layer and its parent boundary layer
[NASA-CR-186529] p 180 N90-21301
- HAWLEY, MARTIN C.**
Review of research and development on the microwave electrothermal thruster p 55 A90-16369
Diagnostic evaluations of microwave generated helium and nitrogen plasma mixtures
[AIAA PAPER 90-2634] p 252 A90-42602
- HAWMAN, MICHAEL W.**
Health monitoring system for the SSME - Program overview
[AIAA PAPER 90-1987] p 63 A90-40583
Framework for a space shuttle main engine health monitoring system
[NASA-CR-185224] p 78 N90-21809
- HAWMAN, MIKE W.**
Health monitoring system for the SSME - Hardware architecture study
[AIAA PAPER 90-1989] p 65 A90-42713
- HAYES, DAVID P.**
A performance analysis of DS-SSMA and SSMA VSAT networks p 141 A90-39056
- HEAD, V. L.**
Mixer-ejector nozzle for jet noise suppression
[AIAA PAPER 90-1909] p 247 A90-47202
- HEBSUR, M. G.**
Influence of alloying elements on the oxidation behavior of NbAl3 p 113 A90-24861
- HEDAYATPOUR, ALI**
Influence of bulk turbulence and entrance boundary layer thickness on the curved duct flow field
[AIAA PAPER 90-1502] p 171 A90-38651
- HEDSTROM, J.**
Regenerative fuel cell systems for project pathfinder p 74 N90-17708
- HEIDENREICH, G. R.**
Brayton advanced heat receiver development program p 61 A90-38170
- HEIDMANN, JAMES D.**
An analysis of the viscous flow through a compact radial turbine by the average passage approach
[NASA-TM-102471] p 12 N90-14206
- HEIGHWAY, J.**
Reflector surface distortion analysis techniques (thermal distortion analysis of antennas in space) p 144 N90-19267
- HEINBOCKEL, JOHN H.**
Mathematical optimization of photovoltaic converters for diode lasers p 228 A90-38110
- HEINEN, V. O.**
Complex permittivity of lanthanum aluminate in the 20 to 300 K temperature range from 26.5 to 40.0 GHz p 148 A90-37864
Performance and modeling of superconducting ring resonators at millimeter-wave frequencies
[NASA-TM-102526] p 151 N90-18634
Microwave conductivity of laser ablated YBaCuO superconducting films and its relation to microstrip transmission line p 155 N90-27844
High temperature superconducting thin film microwave circuits: Fabrication, characterization, and applications
[NASA-TM-103235] p 156 N90-28786
- HEINRICH, J. C.**
Finite element simulations of thermosolutal convection in vertical solidification of binary alloys p 132 A90-18292
The role of gravity on macrosegregation in alloys
[NASA-CR-186530] p 136 N90-25238
- HELLER, JACK A.**
The SP-100 space reactor as a power source for Mars exploration missions
[AAS PAPER 87-224] p 55 A90-16689
A feasibility assessment of installation, operation and disposal options for nuclear reactor power system concepts for a NASA growth space station
[NASA-TM-89923] p 70 N90-10174
- HELMICK, LARRY S.**
Determination of the thermal stability of perfluoroalkylethers
[NASA-TM-102493] p 127 N90-17875
- HEMANN, JOHN H.**
A review of failure models for ceramic matrix composite laminates under monotonic loads
[ASME PAPER 89-GT-153] p 89 A90-23842
- HENDRICKS, R. C.**
A laser based computer aided non-intrusive technique for full field flow characterization in macroscopic curved channels p 168 A90-32293
Numerical modeling of flows in simulated brush seal configurations
[AIAA PAPER 90-2141] p 198 A90-47209

PERSONAL AUTHOR INDEX

- Flow visualization and motion analysis for a series of four sequential brush seals
[AIAA PAPER 90-2482] p 199 A90-47222
- HENN, V.**
A geometric analysis of semicircular canals and induced activity in their peripheral afferents in the rhesus monkey p 234 A90-28084
- HENRY, D. P., JR.**
Advanced applications of BEM to inelastic analysis of solids p 213 A90-45770
- HEPP, A. F.**
Properties of $Pb(1-x)Bi(x)/Ba_2YCu_3O(x)$ composites - Reaction of $Ba_2YCu_3O(x)$ with Pb and Bi p 255 A90-33224
Subtle porosity variation in the $YBa_2Cu_3O(7-x)$ high-temperature superconductor revealed by ultrasonic imaging [NASA-TM-102130] p 206 N90-17167
Synthesis and structural chemistry of $Au(III)$ -substituted $Ba_2YCu_3O(7-\delta)$ [NASA-TM-103292] p 108 N90-28696
- HEPP, ALOYSIUS F.**
Thin-film sensors for reusable space propulsion systems [NASA-TM-102383] p 71 N90-13595
XANES and EXAFS study of Au-substituted $YBa_2Cu_3O(7-\delta)$ [NASA-TM-103291] p 260 N90-29219
- HERBELL, THOMAS P.**
Ceramic matrix composites in simulated SSME environments p 102 N90-28655
- HERCZFELD, P. R.**
High-speed analog fiber optic links for satellite communication p 46 A90-11822
- HERCZFELD, PETER R.**
Design for steering accuracy in antenna arrays using shared optical phase shifters p 138 A90-13935
- HERING, GARY T.**
Status of structural analysis of 30 cm diameter ion optics [AIAA PAPER 90-2649] p 215 A90-52571
- HEYWARD, ANN O.**
Application of heuristic satellite plan synthesis algorithms to requirements of the WARC-88 allotment plan [AIAA PAPER 90-0815] p 245 A90-25638
Application of a hybrid generation/utility assessment heuristic to a class of scheduling problems [NASA-TM-102367] p 245 N90-10674
Application of heuristic satellite plan synthesis algorithms to requirements of the WARC-88 allotment plan [NASA-TM-102479] p 245 N90-14856
Numerical Arc Segmentation Algorithm for a Radio Conference-NASARC (version 4.0) technical manual [NASA-TM-101453] p 144 N90-20264
Numerical Arc Segmentation Algorithm for a Radio Conference (NASARC), version 4.0: User's manual [NASA-TM-101454] p 145 N90-21250
- HICKMAN, J. M.**
Comparison of solar photovoltaic and nuclear reactor power systems for a human-tended lunar observatory p 42 A90-38030
- HICKOK, J. KYLE**
Vapor grown carbon fiber for space thermal management systems p 94 A90-50128
- HILL, JEFF T.**
Constitutive modeling for isotropic materials (HOST) [NASA-CR-179522] p 26 N90-13390
- HILL, S. M.**
High frequency GaAlAs modulator and photodetector for phased array antenna applications p 146 A90-11774
- HILMAS, GREGORY E.**
Microstructural changes in beta-silicon nitride grains upon crystallizing the grain-boundary glass p 120 A90-13230
- HINDS, C.**
Automotive Stirling engine development program [NASA-CR-180839] p 263 N90-11654
- HINGST, W. R.**
An LDA investigation of the normal shock wave boundary layer interaction p 10 A90-52618
- HIRSCHKRON, R.**
Convertible engine system for high speed rotorcraft [AIAA PAPER 90-2512] p 20 A90-40643
- HO, P. Y.**
Energy Efficient Engine acoustic supporting technology report [NASA-CR-174834] p 33 N90-28557
- HOBERECHT, MARK A.**
Space Station Freedom photovoltaic power module design status p 58 A90-38075
Launch packaging options for the PV power module cargo element p 45 A90-38078
- HOBSON, G. V.**
Fully elliptic incompressible flow calculations on regular grid by a new pressure substitution method [AIAA PAPER 90-0239] p 160 A90-19749
Computation of turbine flowfields with a Navier-Stokes code [AIAA PAPER 90-2122] p 8 A90-42731
- HOCHSTEIN, JOHN I.**
Prediction of self-pressurization rate of cryogenic propellant tankage p 55 A90-21219
- HOEKSTRA, CRAIG**
Review of research and development on the microwave electrothermal thruster p 55 A90-16369
- HOFF, G. E.**
Experimental performance and acoustic investigation of modern, counterrotating blade concepts [NASA-CR-185158] p 18 N90-23393
- HOFFMAN, D.**
Space Station Freedom power - A reliability, availability, and maintainability assessment of the proposed Space Station Freedom electric power system p 58 A90-38074
- HOLANDA, RAYMOND**
Attachment of lead wires to thin film thermocouples mounted on high temperature materials using the parallel gap welding process [NASA-TM-102442] p 189 N90-21361
- HOLDEN, JAMES D.**
Three-dimensional turbulent flow code calculations of hot gas ingestion p 21 A90-44726
- HOLLAND, F. A., JR.**
Investigation of Weibull statistics in fracture analysis of cast aluminum p 115 A90-45304
- HOLMAN, RICHARD**
Gravitational couplings of the inflator in extended inflation p 265 A90-40088
- HONEY, F. S.**
Characterization of interfacial failure in SiC reinforced Si3N4 matrix composite material by both fiber push-out testing and Auger electron spectroscopy p 91 A90-36802
- HOPKINS, D. A.**
Probabilistic structural analysis methods of hot engine structures [ASME PAPER 89-GT-122] p 56 A90-23821
Metal matrix composite micromechanics - In situ behavior influence on composite properties p 92 A90-45271
Probabilistic structural analysis methods development for SSME p 83 N90-28616
- HOPKINS, DALE A.**
Local and global accuracy estimates for boundary element analysis [AIAA PAPER 90-0930] p 211 A90-29324
- NOTES, DEBORAH**
Aeolian removal of dust from radiator surfaces on Mars [NASA-TM-103205] p 81 N90-26068
- NOTES, DEBORAH L.**
The effects of atomic oxygen on the thermal emittance of high temperature radiator surfaces [NASA-TM-103224] p 102 N90-28670
- HOUSER, D. R.**
Dynamic analysis of geared rotors by finite elements p 194 A90-21123
- HOUSER, DONALD R.**
Dynamic analysis of geared rotors by finite elements [NASA-TM-102349] p 201 N90-16286
Non-linear dynamic analysis of geared systems, part 2 [NASA-CR-180495] p 204 N90-23732
- HOUSHMAND, B.**
A comparison of reflector antenna designs for wide-angle scanning p 144 N90-19264
- HOVENAC, EDWARD A.**
Droplet sizing instrumentation used for icing research: Operation, calibration, and accuracy [NASA-CR-182293] p 187 N90-11999
Laser diffraction particle sizing: Instrument probe volume relocation and elongation [NASA-TM-102512] p 188 N90-18025
- HOWARD, BRIAN T.**
Laser-velocimeter-measured flow field around an advanced, swept, eight-blade propeller at Mach 0.8 [NASA-TP-2462] p 1 N90-20942
- HOWARTH, R.**
Automotive Stirling engine development program [NASA-CR-180839] p 263 N90-11654
- HOWE, DAVID C.**
Energy Efficient Engine program advanced turbofan nacelle definition study [NASA-CR-174942] p 34 N90-28560
Energy Efficient Engine integrated core/low spool test hardware design report [NASA-CR-168137] p 35 N90-28566
- Energy Efficient Engine: Control system preliminary definition report [NASA-CR-179578] p 35 N90-28569
Energy Efficient Engine: High-pressure compressor test hardware detailed design report [NASA-CR-180850] p 36 N90-28570
- HOWELL, M.**
Selection of phase-change and containment materials for thermal energy storage [NASA-CR-186228] p 229 N90-15506
- HOYNIK, DANIEL**
Aeroelastic detuning for stability enhancement of unstalled supersonic flutter p 19 A90-17462
- HRMA, PAVEL**
Instantaneously generated foam and its applicability to reduced gravity [NASA-CR-185208] p 135 N90-20237
- HSIEH, K.-C.**
Comparative study of computational efficiency of two LU schemes for non-equilibrium reacting flows [AIAA PAPER 90-0396] p 167 A90-26940
- HSU, ANDREW T.**
Three-dimensional compressible jet-in-crossflow calculations using improved viscosity models and adapted grid [AIAA PAPER 90-2100] p 174 A90-47206
A simple algebraic grid adaptation scheme with applications to two- and three-dimensional flow problems [NASA-TM-102446] p 178 N90-18667
- HSU, Y.**
Three-dimensional analysis of surface crack-Hertzian stress field interaction [NASA-CR-4254] p 215 N90-11332
- HU, ROGER**
Thin films of the $Bi_2Sr_2Ca_2Cu_3O(x)$ superconductor p 254 A90-24448
- HUANG, H. T.**
Application of HOST technology to the SSME HPFTP blade [ASME PAPER 89-GT-130] p 209 A90-23828
- HUANG, P. G.**
Time-accurate simulations of a shear layer forced at a single frequency p 163 A90-23111
Time-dependent calculation of a forced mixing layer using a k-epsilon turbulence model p 169 A90-35222
- HUBER, ROBERT D.**
Acousto-ultrasonic nondestructive evaluation of materials using laser beam generation and detection [NASA-CR-186694] p 154 N90-23664
- HUCKELBRIDGE, A. A.**
Boundary flexibility method of component mode synthesis using static Ritz vectors p 212 A90-35429
Characterization of structural connections using free and forced response test data p 213 A90-46172
- HUCKELBRIDGE, ARTHUR A.**
Characterization of damped structural connections for multi-component systems p 208 A90-16959
A global approach for the identification of structural connection properties [NASA-TM-102502] p 218 N90-18745
- HUFF, D. L.**
Application of an efficient hybrid scheme for aeroelastic analysis of advanced propellers [AIAA PAPER 90-0028] p 4 A90-22153
Application of an efficient hybrid scheme for aeroelastic analysis of advanced propellers [NASA-TM-102428] p 11 N90-13355
- HUFF, DENNIS L.**
Evaluation of three turbulence models in static air loads and dynamic stall predictions p 7 A90-31291
Numerical simulations of supersonic flow through oscillating cascade sections [NASA-TM-103100] p 13 N90-20051
- HUFF, J. R.**
Regenerative fuel cell systems for project pathfinder p 74 N90-17708
- HUGHES, W. F.**
A simplified model for two phase face seal design p 197 A90-40713
- HULL, D. R.**
The role of interfacial dislocation networks in high temperature creep of superalloys p 114 A90-33329
Microstructure of a SiC/Ti-15-3 composite p 91 A90-37663
- HULL, JOHN R.**
High-temperature superconductors for space power transmission lines [NASA-TM-103459] p 259 N90-24952
- HULL, P. R.**
Convertible engine system for high speed rotorcraft [AIAA PAPER 90-2512] p 20 A90-40643
- HUMPHREY, DONALD L.**
Reactions of SiC with $H_2/H_2O/Ar$ mixtures at 1300 C p 123 A90-45830

- Hydrogen-silicon carbide interactions
[NASA-TM-102382] p 125 N90-11144
- HUMPHREY, J. A. C.**
Investigation of turbulent flow in highly curved ducts with application to turbomachinery components
[NASA-CR-186060] p 175 N90-12882
- HUNG, CHING-CHEN**
Fluorinated graphite fibers as a new engineering material: Promises and challenges
[NASA-TM-102511] p 86 N90-19301
- HUNG, CHING-CHEN**
Brominated graphitized carbon fibers
[NASA-CASE-LEW-14698-2] p 126 N90-15262
- HURWITZ, F. I.**
Nicalon/siliconoxycarbide ceramic composites
p 94 A90-51924
- HURWITZ, FRANCES I.**
Polymer derived Nicalon/Si-C-O composites - Processing and mechanical behavior p 89 A90-27065
Nicalon/siliconoxycarbide ceramic composites
[NASA-TM-102563] p 99 N90-21133
- HUSAIN, HYDER S.**
Elliptic jets. I - Characteristics of unexcited and excited jets
p 159 A90-18071
- HUSSAIN, FAZLE**
Elliptic jets. I - Characteristics of unexcited and excited jets
p 159 A90-18071
- HUSSEY, S.**
20 kHz main inverter unit p 148 A90-38124
20 kHz, 25 kVA node power transformer p 149 A90-38275
- HUSTON, R. L.**
Comparison of boundary element and finite element methods in spur gear root stress analysis
p 193 A90-21107
Computer aided design of spur gear teeth p 195 A90-21131
Computer aided design of bevel gear tooth surfaces p 195 A90-21136
- HUSTON, RONALD L.**
Improvement of finite element meshes - Heat transfer in an infinite cylinder p 209 A90-19109
Finite element mesh refinement criteria for stress analysis p 209 A90-23013
Mesh refinement in finite element analysis by minimization of the stiffness matrix trace
[NASA-CR-185170] p 201 N90-15434
Computer simulation of gear tooth manufacturing processes
[NASA-CR-185200] p 138 N90-26171
- HUYNH, HUNG T.**
A nonoscillatory, characteristically convected, finite volume scheme for multidimensional convection problems
[AIAA PAPER 90-0015] p 159 A90-19633
A nonoscillatory, characteristically convected, finite volume scheme for multidimensional convection problems
[NASA-TM-102354] p 242 N90-11497
- HUYNH, T.**
Experimental study of the cross-polarization characteristics of rectangular microstrip antennas
p 141 A90-37312
- HYATT, M. J.**
Crystallization of a barium-aluminosilicate glass
p 121 A90-27107
- HYATT, MARK J.**
Crystallization kinetics of BaO-Al₂O₃-SiO₂ glasses
p 121 A90-21175
Phase transformations in xerogels of mullite composition p 123 A90-47093
- HYLTON, L. D.**
An experimental study of turbine vane heat transfer with leading edge and downstream film cooling
[ASME PAPER 89-GT-69] p 165 A90-23792
- IBRAHIM, AZMAN SYED**
Vibration dampers for cryogenic turbomachinery
[AIAA PAPER 90-2740] p 199 A90-47228
- IBRAHIM, M.**
Simulating transitional flow and heat transfer over the flat plate and circular cylinder using a K-epsilon turbulence model
p 168 A90-32171
- IBRAHIM, MOUNIR**
Two-dimensional numerical simulation of a Stirling engine heat exchanger
p 170 A90-38290
- IBRAHIM, MOUNIR B.**
Analysis of thermal energy storage material with change-of-phase volumetric effects
[NASA-TM-102457] p 181 N90-21974
Two-dimensional model of a Space Station Freedom thermal energy storage canister
[NASA-TM-103124] p 183 N90-26279
- IDE, R. F.**
Comparison of two droplet sizing systems in an icing wind tunnel
[NASA-TM-102456] p 200 N90-14617
- IDE, ROBERT F.**
Liquid water content and droplet size calibration of the NASA Lewis Icing Research Tunnel
[AIAA PAPER 90-0669] p 37 A90-22242
Comparison of two droplet sizing systems in an icing wind tunnel
[AIAA PAPER 90-0668] p 164 A90-23711
Liquid water content and droplet size calibration of the NASA Lewis Icing Research Tunnel
[NASA-TM-102447] p 200 N90-13797
Comparison of drop size distributions from two droplet sizing systems
[NASA-TM-102520] p 202 N90-17147
- ILHAN, ALI**
Instantaneously generated foam and its applicability to reduced gravity
[NASA-CR-185208] p 135 N90-20237
- INGEBO, ROBERT D.**
Gas-phase flowrate effect on disintegrating cryogenic liquid-jets
p 173 A90-46895
Gas-phase flowrate effect on disintegrating cryogenic liquid-jets
[NASA-TM-102357] p 187 N90-11277
Scattered-light scanner measurements of cryogenic liquid-jet breakup
[NASA-TM-102432] p 189 N90-22021
Optical characterization of clouds of fine liquid-nitrogen particles
[NASA-TM-103208] p 191 N90-26299
- ISENBERG, LON**
The SP-100 space reactor as a power source for Mars exploration missions
[AAS PAPER 87-224] p 55 A90-16689
- ISIKAWA, Y.**
Effects of lubrication on the performance of high speed spur gears
p 194 A90-21119
- ITOH, T.**
Performance and modeling of superconducting ring resonators at millimeter-wave frequencies
[NASA-TM-102526] p 151 N90-18634
Analysis of microstrip lines with alternative implementation of conductors and superconductors
[NASA-TM-103182] p 155 N90-27966
- IVANCIC, WILLIAM D.**
Satellite-matrix-switched, time-division-multiple-access network simulator
[AIAA PAPER 90-0848] p 147 A90-25671
Satellite-matrix-switched, time-division-multiple-access network simulator
[NASA-TP-2944] p 142 N90-11915
- J**
- JABLONSKI, DAVID A.**
High-temperature tensile properties of fiber reinforced reaction bonded silicon nitride
p 95 A90-52783
- JACOBSON, N. S.**
Mass spectrometric observations of metal oxychlorides produced by oxidation-chlorination reactions
p 103 A90-21215
- JACOBSON, NATHAN**
Corrosion of cordierite ceramics by sodium sulphate at 1000 C
p 121 A90-21214
- JACOBSON, NATHAN S.**
Reactions of SiC with H₂/H₂O/Ar mixtures at 1300 C
p 123 A90-45830
- JACOMIN, D. A.**
Materials for engine applications above 3000 deg F: An overview
[NASA-TM-100169] p 95 N90-10188
Hydrogen-silicon carbide interactions
[NASA-TM-102382] p 125 N90-11144
Thermodynamic properties of some metal oxide-zirconia systems
[NASA-TM-102351] p 126 N90-13666
- JACOBSON, T. P.**
Hardware development for the surface tension driven convection experiment
p 52 A90-36195
- JACOMIN, D. A.**
Convection phenomena in low-gravity processing - The GTE GaAs space experiment
[AIAA PAPER 90-0409] p 133 A90-25032
- JACOMIN, DAVID**
Parallel flows with Soret effect in tilted cylinders
p 167 A90-25594
- JAIN, LALIT K.**
Extension of a noninteractive reliability model for ceramic matrix composites
[NASA-CR-185267] p 129 N90-26142
- JAIN, R. K.**
Estimation of minority carrier diffusion lengths in InP/GaAs solar cells
[NASA-TM-103213] p 81 N90-26069
- JAMALI, M. M.**
A parallel pipelined architecture for a digital multicarrier demodulator
[AIAA PAPER 90-0812] p 46 A90-25635
- JANETZKE, DAVID C.**
Concurrent processing adaptation of aeroelastic analysis of propfans
[AIAA PAPER 90-1036] p 211 A90-29380
Concurrent processing adaptation of aeroplastic analysis of propfans
[NASA-TM-102455] p 217 N90-14656
- JANG, J. H.**
Mathematical modeling and analysis of heat pipe start-up from the frozen state
p 174 A90-48404
- JANG, JONG HOON**
Transient characteristics of a grooved water heat pipe with variable heat load
[NASA-CR-185280] p 183 N90-26272
- JANKOWSKI, D. F.**
Energy stability of thermocapillary convection in a model of the float-zone crystal-growth process
p 133 A90-48720
- JANUS, J. MARK**
Counterrotating prop-fan simulations which feature a relative-motion multiblock grid decomposition enabling arbitrary time-steps
[AIAA PAPER 90-0687] p 3 A90-19978
- JARRAH, YOUSEF MOHD**
Nonlinear interactions in mixing layers and compressible heated round jets
[NASA-CR-186303] p 182 N90-23674
- JASSOWSKI, D. M.**
Combustion interaction with radiation-cooled chambers
[AIAA PAPER 90-2121] p 64 A90-42030
- JAVIDI, S.**
Space Station Freedom power management and distribution design status
p 59 A90-38080
- JAWORSKE, DONALD A.**
Measurements of print-through in graphite fiber epoxy composites
p 91 A90-31555
Hot filament technique for measuring the thermal conductivity of molten lithium fluoride
[NASA-TM-102506] p 127 N90-19373
- JAYARAMAN, N.**
Torsional and biaxial (tension-torsion) fatigue damage mechanisms in Waspaloy at room temperature
p 109 A90-11925
Microstructure: Property correlation
[NASA-CR-180406] p 224 N90-28880
- JEFFERIES, KENT S.**
Concentration of off-axis radiation by solar concentrators for space power
p 60 A90-38163
- JENG, DUEN-REN**
Numerical simulation of rarefied gas flow through a slit
[AIAA PAPER 90-1694] p 170 A90-38397
- JENKINS, K. A.**
Millimeter wave surface resistance of RBa₂Cu₃O₇(δ -x) superconductors
[NASA-TM-102571] p 259 N90-20886
Laser ablated high T(sub c) superconducting thin YBa₂Cu₃O₇(δ -x) films on substrates suitable for microwave applications
p 260 N90-27808
- JENKINS, KIMBERLY A.**
Study of deposition of YBa₂Cu₃O₇-x on cubic zirconia
[NASA-TM-102350] p 257 N90-10737
- JENKINS, M. G.**
Determination of the stress distributions in a ceramic: Tensile specimen using numerical techniques
[NASA-TM-101914] p 129 N90-26132
- JENKINS, MICHAEL G.**
Empirical and analytical determination of the fracture resistance of a TiB₂ particle/SiC matrix composite
[NASA-TM-101940] p 96 N90-15143
- JENNINGS, M. J.**
A rotating hot-wire technique for spatial sampling of disturbed and manipulated duct flows
p 186 A90-41120
- JENSEN, KENNETH A.**
Secondary electron emission characteristics of molybdenum-masked, ion-textured OFHC copper
[NASA-TP-2967] p 117 N90-15211
- JENSEN, R. J.**
LOX/hydrocarbon combustion instability investigation
[NASA-CR-182249] p 71 N90-13589
Oxygen/methane combustion stability investigation
p 107 N90-28628

- JERACKI, ROBERT J.**
Effect of reduced aft diameter and increased blade number of high-speed counterrotation propeller performance
[AIAA PAPER 89-0438] p 4 A90-23650
Effect of reduced aft diameter and increased blade number on high-speed counterrotation propeller performance
[NASA-TM-102077] p 11 N90-13352
- JETT, T. A.**
Evaluation of power control concepts using the PMAD systems test bed p 42 A90-38083
- JEUNETTE, TIMOTHY T.**
Measurements of print-through in graphite fiber epoxy composites p 91 A90-31555
- JHA, S.**
Antiferromagnetism in Co-57-doped La₂CuO₄(-y) studied by Moessbauer spectroscopy p 255 A90-34011
Hyperfine magnetic field on Cd-111 in Heusler alloys Co₂MnZ (Z = Si, Ga, Ge, Sn) p 255 A90-34012
Fe-57 and Sn-119 Moessbauer study of La₂CuO₄(-y), YBa₂Cu₃O₇(-y) and SmBa₂Cu₃O₇(-y) p 256 A90-34020
- JI, HYUN-CHUL**
Prediction of self-pressurization rate of cryogenic propellant tankage p 55 A90-21219
- JIANG, BO-NAN**
Least-squares finite element method for fluid dynamics p 159 A90-18246
Least-squares finite element methods for compressible Euler equations p 9 A90-51013
A least-squares finite element method for incompressible Navier-Stokes problems
[NASA-TM-102385] p 242 N90-12231
- JIANG, HONG**
Absorbing boundary conditions for second-order hyperbolic equations p 242 A90-34549
- JIMENEZ, AMADOR P.**
Space Station Freedom photovoltaic power module design status p 58 A90-38075
- JIRBERG, RUSSELL**
LBR-2 earth stations for the ACTS program
[AIAA PAPER 90-0838] p 42 A90-25662
- JOHNS, ALBERT L.**
Engine inlet distortion in a 9.2 percent scaled vectored thrust STOVL model in ground effect
[AIAA PAPER 89-2910] p 5 A90-25043
Engine inlet distortion in a 9.2 percent scale vectored thrust STOVL model in ground effect
[NASA-TM-102358] p 12 N90-17561
Hot gas ingestion characteristics and flow visualization of a vectored thrust STOVL concept
[NASA-TM-103212] p 32 N90-26009
- JOHNSON, JEROME A.**
Investigation of methods to produce a uniform cloud of fuel particles in a flame tube
[NASA-TM-102376] p 178 N90-18665
- JOHNSON, PETER N.**
Advanced modulation technology development for earth station demodulator applications. Coded modulation system development
[NASA-CR-185149] p 145 N90-20270
- JOHNSON, S. D.**
A Brayton cycle solar dynamic heat receiver for space p 61 A90-38165
- JONES, C. W.**
Mixer-ejector nozzle for jet noise suppression
[AIAA PAPER 90-1909] p 247 A90-47202
- JONES, LEE W.**
Engine selection for the Space Exploration Initiative
[AIAA PAPER 90-1880] p 65 A90-47201
- JONES, ROBERT E.**
A forward error correction technique using a high-speed, high-rate single chip codec p 141 A90-48440
- JONES, WILLIAM R., JR.**
Determination of the thermal stability of perfluoroalkylethers
[NASA-TM-102493] p 127 N90-17875
- JONGEWARD, G. A.**
EPSAT - A workbench for designing high-power systems for the space environment
[AIAA PAPER 90-0637] p 245 A90-26975
- JONGEWARD, GARY A.**
The Environment-Power System Analysis Tool development program p 236 A90-38089
- JORASCH, RONALD E.**
Role of communications satellites in the fiber era
[AIAA PAPER 90-0792] p 139 A90-25617
Data distribution satellite system architecture concept
[AIAA PAPER 90-0885] p 46 A90-25704
- JORDAN, E. M.**
Biaxial constitutive modelling and testing of a single crystal superalloy at elevated temperatures p 110 A90-16741
- JORDAN, ERIC H.**
X-ray beam method for displacement measurement in hostile environments p 187 A90-44485
- JOU, W.-H.**
Progress in direct numerical simulations of turbulent reacting flows p 157 A90-12836
- JOULIN, G.**
The structure and stability of nonadiabatic flame balls p 105 A90-43674
- JUHAS, JOHN J.**
Improved process for HIP canning of composites
[NASA-CASE-LEW-14990-1-CU] p 97 N90-15147
One step HIP canning of powder metallurgy composites
[NASA-CASE-LEW-14719-1] p 101 N90-23493
- JULIAN, GLENN M.**
Antiferromagnetism in Co-57-doped La₂CuO₄(-y) studied by Moessbauer spectroscopy p 255 A90-34011
Hyperfine magnetic field on Cd-111 in Heusler alloys Co₂MnZ (Z = Si, Ga, Ge, Sn) p 255 A90-34012
Fe-57 and Sn-119 Moessbauer study of La₂CuO₄(-y), YBa₂Cu₃O₇(-y) and SmBa₂Cu₃O₇(-y) p 256 A90-34020
- JULIANTO, AGUS**
Ellipsometric studies of the diffusion of atomic oxygen through silicon dioxide thin films p 104 A90-36268

K

- KACKLEY, N.**
Oxygen electrodes for rechargeable alkaline fuel cells. II p 228 A90-33946
Oxygen electrodes for rechargeable alkaline fuel cells-II p 231 N90-20469
- KADIRAMANGALAM, MURALI N.**
Figure of merit studies of beam power concepts for advanced space exploration
[NASA-CR-186720] p 146 N90-26234
- KAFALAS, J. A.**
Interface demarcation in GaAs by current pulsing
[AIAA PAPER 90-0319] p 254 A90-19793
- KAHRAMAN, A.**
Dynamic analysis of geared rotors by finite elements p 194 A90-21123
- KAHRAMAN, AHMET**
Dynamic analysis of geared rotors by finite elements
[NASA-TM-102349] p 201 N90-16286
Non-linear dynamic analysis of geared systems, part 2
[NASA-CR-180495] p 204 N90-23732
- KALLURI, SREERAMESH**
High temperature fatigue behavior of Haynes 188 p 119 N90-28642
- KAM, MOSHE**
Design for steering accuracy in antenna arrays using shared optical phase shifters p 138 A90-13935
- KAMENETZ, JEFFREY**
Framework for a space shuttle main engine health monitoring system
[NASA-CR-185224] p 78 N90-21809
- KAMENETZ, JEFFRY K.**
Health monitoring system for the SSME - Hardware architecture study
[AIAA PAPER 90-1989] p 65 A90-42713
- KAMIONKOWSKI, MARC**
Unitarity limits on the mass and radius of dark-matter particles p 264 A90-24671
- KANG, P.**
A circular combustor configuration with multiple injection ports for mixing enhancement p 158 A90-15389
- KANKAM, M. DAVID**
An analysis of space power system masses
[NASA-TM-103199] p 80 N90-25184
- KANTZOS, PETER**
Fatigue crack growth in unidirectional metal matrix composite
[NASA-TM-103102] p 220 N90-22117
Fatigue crack growth in a unidirectional SCS-6/Ti-15-3 composite
[NASA-TM-103095] p 119 N90-22646
- KAO, CHIKUAN K.**
A new approach to active vibration isolation for microgravity space experiments
[NASA-TM-102470] p 137 N90-17929
- KAO, Y. C.**
Doped-channel heterojunction structures for millimeter-wave discrete devices and MMICs p 150 A90-48492
- KAPOOR, VIK J.**
Electron beam induced damage in PECVD Si₃N₄ and SiO₂ films on InP
[NASA-TM-102544] p 203 N90-20393
- KAPPES, J. MARK**
Advanced modulation technology development for earth station demodulator applications. Coded modulation system development
[NASA-CR-185149] p 145 N90-20270
- KARKI, K. C.**
Calculation of turbulent three-dimensional jet-induced flow in a rectangular enclosure
[AIAA PAPER 90-0684] p 161 A90-19976
Three-dimensional fluid flow calculations using a flux-spline method p 167 A90-27983
- KASCAK, A. F.**
Test and theory for piezoelectric actuator-active vibration control of rotating machinery p 198 A90-46226
- KASCAK, ALBERT F.**
Vibration dampers for cryogenic turbomachinery
[AIAA PAPER 90-2740] p 199 A90-47228
- KASSEMI, M.**
Two-dimensional convection and radiation with scattering from a Poiseuille flow p 161 A90-20519
- KASSEMI, MOHAMMAD**
Effect of gas and surface radiation on crystal growth from the vapor phase p 133 A90-49060
- KATEHI, P. B.**
Coplanar waveguide discontinuities for P-I-N diode switches and filter applications
[NASA-TM-102534] p 153 N90-21278
- KATZ, I.**
High-voltage plasma interactions calculations using NASCAP/LEO
[AIAA PAPER 90-0725] p 251 A90-22254
Plasma contactor modeling with NASCAP/LEO - Extending laboratory results to space systems
[AIAA PAPER 90-0726] p 251 A90-22255
Computer modeling of current collection by the CHARGE-2 mother payload p 252 A90-24933
Plasma sources for spacecraft neutralization
[AIAA PAPER 90-1556] p 49 A90-38697
- KATZ, IRA**
A Van der Waals-like theory of plasma double layers p 251 A90-10725
- KAUFMAN, A.**
Finite element implementation of Robinson's unified viscoplastic model and its application to some uniaxial and multiaxial problems p 208 A90-15704
- KAUFMAN, H. R.**
End-hall thrusters
[AIAA PAPER 90-2595] p 64 A90-42570
- KAUFMANN, K. J.**
A Brayton cycle solar dynamic heat receiver for space p 61 A90-38165
- KAZAROFF, J. M.**
Indium-coated rhenium thrusters by CVD p 114 A90-30480
- KAZAROFF, JOHN M.**
Advanced tube-bundle rocket thrust chamber
[AIAA PAPER 90-2726] p 67 A90-47227
Advanced tube-bundle rocket thrust chamber
[NASA-TM-103139] p 80 N90-25185
- KEEFER, DENNIS**
Numerical modeling of an arcjet thruster
[AIAA PAPER 90-2614] p 64 A90-42587
- KEER, L. M.**
Measurement of the intrinsic bond strength of brittle thin films on flexible substrates p 256 A90-44022
- KEITH, T. G.**
An LDA investigation of the normal shock wave boundary layer interaction p 10 A90-52618
- KEITH, THEO G. JR.**
A numerical simulation of the flow in the diffuser of the NASA Lewis Icing Research Tunnel
[AIAA PAPER 90-0488] p 166 A90-25034
Time domain flutter analysis of cascades using a full-potential solver
[AIAA PAPER 90-0984] p 6 A90-29374
Numerical simulation of rarefied gas flow through a slit
[AIAA PAPER 90-1694] p 170 A90-38397
Analysis and design of optimized truncated scarfed nozzles subject to external flow effects
[AIAA PAPER 90-2222] p 9 A90-47213
A numerical simulation of the flow in the diffuser of the NASA Lewis icing research tunnel
[NASA-TM-102480] p 38 N90-15965
Analysis and design of optimized truncated scarfed nozzles subject to external flow effects
[NASA-TM-103175] p 13 N90-25106
- KELLACKEY, C. J.**
Impact ice stresses in rotating airfoils
[AIAA PAPER 90-0198] p 15 A90-19735
- KENNEDY, E. M.**
EPSAT - A workbench for designing high-power systems for the space environment
[AIAA PAPER 90-0637] p 245 A90-26975
- KENNEDY, ERIC M.**
The Environment-Power System Analysis Tool development program p 236 A90-38089

- KENNY, BARBARA H.**
An analysis of space power system masses
[NASA-TM-103199] p 80 N90-25184
- KER, H. L.**
Properties of RBSN and RBSN-SiC composites
p 94 A90-51920
- KERCZEWSKI, ROBERT J.**
Performance measurements for a laboratory-simulated 30/20 GHz communication satellite transponder
[AIAA PAPER 90-0808] p 140 A90-25634
Effects of amplitude distortions and IF equalization on satellite communication system bit-error rate performance
[AIAA PAPER 90-0878] p 140 A90-25697
Performance measurements for a laboratory-simulated 30/20 GHz communication satellite transponder
[NASA-TM-102424] p 143 N90-17977
Effects of amplitude distortions and IF equalization on satellite communication system bit-error rate performance
[NASA-TM-102415] p 144 N90-19454
- KERSLAKE, THOMAS W.**
Analysis of thermal energy storage material with change-of-phase volumetric effects
[NASA-TM-102457] p 181 N90-21974
Two-dimensional model of a Space Station Freedom thermal energy storage canister
[NASA-TM-103124] p 183 N90-26279
- KERSLAKE, WILLIAM R.**
Effect of eleven years in earth orbit on a mirror surface
p 44 A90-36188
- KESSELI, JAMES B.**
The cavity heat pipe Stirling receiver for space solar dynamics
p 61 A90-38169
- KESSLER, WILLIAM J.**
H₂/O₂ three-body rates at high temperatures
[AIAA PAPER 90-1696] p 105 A90-38399
- KETELSEN, DEAN A.**
A new fabrication method for precision antenna reflectors for space flight and ground test
[AIAA PAPER 90-0803] p 139 A90-25627
- KHADER, N.**
Shaft flexibility effects on the forced response of a bladed-disk assembly
p 21 A90-43218
- KHADER, NAIM**
Shaft flexibility effects on aeroelastic stability of a rotating bladed disk
p 208 A90-16371
Blade mistuning coupled with shaft flexibility effects in rotor aeroelasticity
[ASME PAPER 89-GT-330] p 19 A90-23896
- KHATIBZADEH, A. M.**
Doped-channel heterojunction structures for millimeter-wave discrete devices and MMICs
p 150 A90-48492
- KHOO, BOO CHEONG**
Rate correlation for condensation of pure vapor on turbulent, subcooled liquid
p 174 A90-50511
- KHOSLA, P. K.**
A flux-split solution procedure for unsteady inlet flows
[AIAA PAPER 90-0585] p 6 A90-26967
Transient behavior of supersonic flow through inlets
[AIAA PAPER 90-2130] p 8 A90-42734
- KIEFFER, JONATHAN**
Computerized inspection of gear tooth surfaces
[NASA-TM-102395] p 203 N90-22054
- KIERNAN, M. T.**
Impact damage development in damaged composite materials
p 193 A90-18355
- KIM, CHEOL J.**
Superconducting glass-ceramics in the Bi-Sr-Ca-Cu-O system
p 256 A90-35153
- KIM, DONG-SANG**
Instantaneously generated foam and its applicability to reduced gravity
[NASA-CR-185208] p 135 N90-20237
- KIM, J. H.**
Transport properties of InAs(x)Sb(1-x) (x = 0-0.55) on InP grown by molecular-beam epitaxy
p 256 A90-36232
- KIM, J. T.**
The effects of surface films on mechanical behavior of B2 ordered intermetallic alloys
p 115 A90-44338
- KIM, JINHAN**
Application of the computational aeroacoustics method to an advanced counterrotating propfan configuration
[AIAA PAPER 90-0183] p 246 A90-19725
- KIM, K. S.**
Simulation of crack growth and crack closure under large cyclic plasticity
p 214 A90-50562
Elevated temperature crack growth
[NASA-CR-182247] p 222 N90-26355
- KIM, KWANG-SOO**
Skin friction measurements by laser interferometry in swept shock/boundary-layer interactions
p 3 A90-18153
- KIM, S. C.**
A new mixing length model for supersonic shear layers
[AIAA PAPER 90-0018] p 166 A90-25026
Calculations of gaseous H₂/O₂ thruster
[AIAA PAPER 90-2490] p 67 A90-47224
- KIM, S.-W.**
Calculation of reattaching shear layers in divergent channel with a multiple-time-scale turbulence model
[AIAA PAPER 90-0047] p 160 A90-19649
Near-wall turbulence model and its application to fully developed turbulent channel and pipe flows
p 169 A90-37328
Numerical investigation of separated transonic turbulent flows with a multiple-time-scale turbulence model
[NASA-TM-102499] p 180 N90-21962
- KIM, WALTER S.**
Thin-film sensors for reusable space propulsion systems
[NASA-TM-102383] p 71 N90-13595
Attachment of lead wires to thin film thermocouples mounted on high temperature materials using the parallel gap welding process
[NASA-TM-102442] p 189 N90-21361
- KIM, YONG-SUK**
Characterization of failure processes in tungsten copper composites under fatigue loading conditions
[NASA-TM-102371] p 98 N90-21123
High temperature fatigue behavior of tungsten copper composites
[NASA-TM-102404] p 99 N90-21138
- KIMNACH, G. L.**
Evaluation of power control concepts using the PMAD systems test bed
p 42 A90-38083
- KING, GALEN B.**
Saturated fluorescence measurements of the hydroxyl radical in laminar high-pressure flames
[NASA-CR-185218] p 190 N90-22022
- KING, ROGER J.**
Electrical performance characteristics of high power converters for space power applications
[NASA-CR-185947] p 72 N90-14279
A comparative study of electric power distribution systems for spacecraft
[NASA-CR-186531] p 77 N90-21113
- KINGTON, H.**
Development of impact design methods for ceramic gas turbine components
[AIAA PAPER 90-2413] p 197 A90-42165
- KIRBY, MARK S.**
Ultrasonic techniques for aircraft ice accretion measurement
p 16 N90-20926
- KIRCH, LUKE A.**
Space Station Freedom electric power system photovoltaic power module integrated launch package
[AIAA PAPER 90-1053] p 48 A90-29281
Protoflight photovoltaic power module system-level tests in the Space Power Facility
p 62 A90-38266
- KIRTLEY, K. R.**
Numerical analysis of secondary flow in a two-stage turbine
[AIAA PAPER 90-2356] p 66 A90-47216
- KISER, JAMES D.**
Slurry-pressing consolidation of silicon nitride
p 121 A90-27691
Matrix density effects on the mechanical properties of SiC/RBSN composites
[NASA-TM-103098] p 100 N90-21826
- KISER, LAMES D.**
Matrix density effects on the mechanical properties of SiC fiber-reinforced silicon nitride matrix properties
p 94 A90-51927
- KISH, JAMES A.**
Space Station power system autonomy demonstration
p 245 A90-10373
Automated electric power management and control for Space Station Freedom
[NASA-TM-103151] p 240 N90-23125
- KITAMURA, TAKAYUKI**
A nonlinear high temperature fracture mechanics basis for strainrange partitioning
[NASA-TM-4133] p 216 N90-14642
- KITTUR, MADAN G.**
Improvement of finite element meshes - Heat transfer in an infinite cylinder
p 209 A90-19109
Finite element mesh refinement criteria for stress analysis
p 209 A90-23013
Mesh refinement in finite element analysis by minimization of the stiffness matrix trace
[NASA-CR-185170] p 201 N90-15434
- KLEIN, WILLIAM E.**
Model OA wind turbine generator FMEA
[NASA-TM-102378] p 206 N90-12034
- KLEM, MARK D.**
Combustor design and analysis using the ROCKET Combustor Interactive Design (ROCCID) Methodology
[AIAA PAPER 90-2240] p 65 A90-45694
A comparison of analytical results for 20 K LOX/hydrogen instabilities
[AIAA PAPER 90-2241] p 130 A90-47214
Combustor design and analysis using the Rocket Combustor Interactive Design (ROCCID) methodology
[NASA-TM-103165] p 79 N90-24349
A comparison of analytical results for 20 K LOX/hydrogen instabilities
[NASA-TM-103166] p 80 N90-25186
- KLINEBERG, JOHN M.**
Advances in computational design and analysis of airbreathing propulsion systems
p 19 A90-12502
- KLINGSHIRN, EUGENE A.**
Analytical and experimental study of high phase order induction motors
[NASA-CR-186580] p 153 N90-21952
- KLOSKO, S. M.**
The GEM-T2 gravitational model
[NASA-TM-100746] p 234 N90-12984
- KNASEL, DON**
Solar Concentrator Advanced Development Program
[NASA-CR-185173] p 232 N90-22834
- KNIP, GERALD, JR.**
Advanced core technology - Key to subsonic propulsion benefits
[ASME PAPER 89-GT-241] p 19 A90-23890
- KNOLL, R. L.**
Tank Pressure Control Experiment - A low-g mixing investigation
[AIAA PAPER 90-2376] p 66 A90-47217
- KNOWLES, S. C.**
Qualification and life testing of a flight design hydrazine arcjet system
[AIAA PAPER 90-2576] p 64 A90-42559
- KOBAYASHI, ALBERT S.**
Empirical and analytical determination of the fracture resistance of a TiB₂ particle/SiC matrix composite
[NASA-TM-101940] p 96 N90-15143
- KOHOUT, LISA L.**
Cryogenic reactant storage for lunar base regenerative fuel cells
[IAF PAPER ICOSP89-3-8] p 227 A90-27709
A solar power system for an early Mars expedition
[NASA-TM-103219] p 246 N90-28393
- KOLB, EDWARD W.**
Gravitational couplings of the inflator in extended inflation
p 265 A90-40088
- KOLLMANN, W.**
The pdf approach to turbulent flow
p 168 A90-32225
- KONG, H. S.**
Deep-level dominated electrical characteristics of Au contacts on beta-SiC
p 147 A90-33726
- KONG, K. S.**
Performance and modeling of superconducting ring resonators at millimeter-wave frequencies
[NASA-TM-102526] p 151 N90-18634
- KONG, K.-S.**
Analysis of microstrip lines with alternative implementation of conductors and superconductors
[NASA-TM-103182] p 155 N90-27966
- KONKEL, C. R.**
User needs, benefits, and integration of robotic systems in a space station laboratory
[NASA-CR-185150] p 200 N90-13794
- KORKAN, K. D.**
Performance and acoustic prediction of counterrotating propeller configurations
[SAE PAPER 891035] p 246 A90-14342
A study of ice shape prediction methodologies and comparison with experimental data
[AIAA PAPER 90-0753] p 15 A90-26986
- KORSMEYER, DAVID**
A superconducting quenchgun for delivering lunar derived oxygen to lunar orbit
[AIAA PAPER 90-2369] p 43 A90-40627
- KORSMEYER, DAVID J.**
A trajectory generation and system characterization model for cislunar low-thrust spacecraft. Volume 2: Technical manual
[NASA-CR-185172] p 77 N90-21807
- KOSMAHL, HENRY G.**
Miniature traveling wave tube and method of making
[NASA-CASE-LEW-14520-1] p 153 N90-22724
- KOSMATKA, J. B.**
Generalized Advanced Propeller Analysis System (GAPAS). Volume 2: Computer program user manual
[NASA-CR-185277] p 36 N90-29394
- KOSS, D. A.**
Deformation behavior of NiAl-based alloys containing iron, cobalt, and hafnium
p 110 A90-16930

PERSONAL AUTHOR INDEX

- Microstructure and mechanical properties of multiphase NiAl-based alloys p 115 A90-35071
- KRAINER, A.**
Progress towards the development of an inviscid-viscous interaction method for unsteady flows in turbomachinery cascades p 2 A90-11806
- KRANTZ, TIMOTHY L.**
Efficiency study comparing two helicopter planetary reduction stages [AIAA PAPER 90-2156] p 199 A90-50644
- KRAWCZONEK, WALTER**
High power, high frequency component test facility [NASA-TM-102500] p 151 N90-19484
- KRAWCZONEK, WALTER M.**
Autonomous power expert system p 240 N90-22306
Autonomous power expert fault diagnostic system for Space Station Freedom electrical power system testbed p 80 N90-25521
- KREINER, D. M.**
ATTAP/AGT101 ceramics technology update [ASME PAPER 89-GT-105] p 195 A90-23814
- KREJSA, E. A.**
Mixer-ejector nozzle for jet noise suppression [AIAA PAPER 90-1909] p 247 A90-47202
- KREJSA, EUGENE A.**
Predicted and measured boundary layer refraction for advanced turboprop propeller noise [NASA-TM-102365] p 248 N90-17413
- KROPP, J. L.**
Droplet combustion experiment drop tower tests using models of the space flight apparatus [NASA-TM-101472] p 133 N90-11196
- KRUPP, JOSEPH C.**
Electric power scheduling: A distributed problem-solving approach [NASA-TM-103149] p 240 N90-22323
- KU, CHIEH C.**
Three dimensional full potential method for the aeroelastic modeling of propfans [AIAA PAPER 90-1120] p 7 A90-29392
- KUCUK, SENOL**
An adaptive human response mechanism controlling the V/STOL aircraft. Appendix 3: The adaptive control model of a pilot in V/STOL aircraft control loops [NASA-CR-186599] p 38 N90-21777
- KUCZMARSKI, M. A.**
Modeling of the SiC chemical vapor deposition process and comparison with experimental results p 105 A90-36810
- KUHARSKI, R. A.**
EPSAT - A workbench for designing high-power systems for the space environment [AIAA PAPER 90-0637] p 245 A90-26975
- KUHARSKI, ROBERT A.**
The Environment-Power System Analysis Tool development program p 236 A90-38089
- KUKICH, GEORGE**
An expert system for simulating electric loads aboard Space Station Freedom [NASA-TM-103150] p 240 N90-22325
- KUKULKA, J. R.**
Optimization of silicon 8 cm x 8 cm wrapthrough Space Station cells for 'on orbit' operation p 54 A90-14941
- KUMAR, K. S.**
1200 to 1400 K slow strain rate compressive properties of NiAl/Ni₂AlTi-base materials p 88 A90-16938
1100 to 1300 K slow plastic compression properties of Ni-38.5Al composites p 111 A90-19154
1300 K compressive properties of several dispersion strengthened NiAl materials p 116 A90-47091
High-temperature slow-strain-rate compression studies on CoAl-TiB₂ composites p 93 A90-48636
Compression behavior of the forged Li₂ compounds Al₆₇Ti₂₅Cr₈ and Al₆₆Ti₂₅Mn₉ p 116 A90-51298
- KUMAR, S.**
Slow plastic deformation of extruded NiAl-10TiB₂ particulate composites at 1200 and 1300 K p 92 A90-46133
- KUNATH, R. R.**
High-speed analog fiber optic links for satellite communication p 46 A90-11822
High-speed digital fiber optic links for satellite traffic p 250 A90-41247
Bit-error-rate testing of fiber optic data links for MMIC-based phased array antennas [NASA-TM-102523] p 145 N90-21261
ATDRS payload technology research and development [NASA-TM-103256] p 52 N90-28596
- KUNATH, RICHARD**
High-speed fiber-optic links for distribution of satellite traffic p 47 A90-41687

- KUNATH, RICHARD R.**
Design of an optically controlled Ka-band GaAs MMIC phased-array antenna [NASA-TM-103147] p 155 N90-26250
- KUNIN, B.**
A probabilistic approach to crack instability p 212 A90-41278
- KUNTZ, H. L.**
Interior noise in the untreated Gulfstream II Propfan Test Assessment aircraft p 17 A90-44736
- KURKI-SUONIO, HANNU**
Big bang nucleosynthesis and the quark-hadron transition p 265 A90-31407
- KURTH, W. S.**
Spacelab 2 Plasma Diagnostics Package p 39 A90-23263
- KUSSMAUL, MICHAEL**
Total hemispherical emittance measured at high temperatures by the calorimetric method [NASA-TM-102322] p 136 N90-10309
- KWAK, J. F.**
Rapid thermal processing of high temperature superconducting fiber [NASA-CR-186803] p 259 N90-24964
- KWATRA, S. C.**
Encoding Y,I,Q component estimates of an NTSC composite signal p 139 A90-23261
A parallel pipelined architecture for a digital multicarrier demodulator [AIAA PAPER 90-0812] p 46 A90-25635
- KWON, OH J.**
Numerical study of the effects of icing on finite wing aerodynamics [AIAA PAPER 90-0757] p 3 A90-20010
- KWOR, R.**
High frequency capacitance-voltage characteristics of thermally grown SiO₂ films on beta-SiC p 254 A90-21348
- KYR, DOUG**
Detection of potential space station control/structure interaction with CO-ST-IN p 50 N90-21074

L

- LABUS, THOMAS L.**
Solar dynamic power module design p 59 A90-38079
- LACEY, DOVIE E.**
Brayton advanced heat receiver development program p 61 A90-38170
- LACKNEY, JOSEPH J.**
Demonstration of capabilities of high temperature composites analyzer code HITCAN [NASA-TM-102560] p 219 N90-19629
- LACY, DOVIE E.**
The cavity heat pipe Stirling receiver for space solar dynamics p 61 A90-38169
Technology development program for an advanced microsheet glass concentrator [NASA-TM-102406] p 229 N90-14678
- LACY, R.**
Automotive Stirling engine development program [NASA-CR-180839] p 263 N90-11654
- LADDEN, R. M.**
Large scale prop-fan structural design study. Volume 1: Initial concepts [NASA-CR-174992] p 23 N90-10043
Large scale prop-fan structural design study. Volume 2: Preliminary design of SR-7 [NASA-CR-174993] p 23 N90-10044
- LAFLEN, J. H.**
A constitutive model for the inelastic multiaxial response of Rene 80 at 871 C and 982 C p 114 A90-32266
Simulation of crack growth and crack closure under large cyclic plasticity p 214 A90-50562
Elevated temperature crack growth [NASA-CR-182247] p 222 N90-26355
- LAGHARI, JAVAD R.**
A brief survey of radiation effects on polymer dielectrics p 123 A90-43119
- LAGIN, A.**
Reflector surface distortion analysis techniques (thermal distortion analysis of antennas in space) p 144 N90-19267
- LAHAMER, AMER**
Antiferromagnetism in Co-57-doped La₂CuO₄(-y) studied by Moessbauer spectroscopy p 255 A90-34011
Hyperfine magnetic field on Cd-111 in Heusler alloys Co₂MnZ (Z = Si, Ga, Ge, Sn) p 255 A90-34012
Fe-57 and Sn-119 Moessbauer study of La₂CuO₄(-y), YBa₂Cu₃O₇(-y) and SmBa₂Cu₃O₇(-y) p 256 A90-34020
- LAI, H. T.**
Viscous three-dimensional analyses for nozzles for hypersonic propulsion [NASA-CR-185197] p 27 N90-17635
- LAKE, MAX L.**
Vapor grown carbon fiber for space thermal management systems p 94 A90-50128
- LAKSHMINARAYANA, B.**
Computation of three dimensional turbulent boundary layers in internal flows, including turbomachinery rotor blades p 3 A90-12555
Fully elliptic incompressible flow calculations on regular grid by a new pressure substitution method [AIAA PAPER 90-0239] p 160 A90-19749
Computation of turbine flowfields with a Navier-Stokes code [AIAA PAPER 90-2122] p 8 A90-42731
- LALLI, VINCENT R.**
Model OA wind turbine generator FMEA [NASA-TM-102378] p 206 N90-12034
- LALONDE, RICK J.**
The determination of third order linear models from a seventh order nonlinear jet engine model p 239 A90-52881
- LAMANCUSA, J. S.**
Optimum structural design of robotic manipulators with fiber reinforced composite materials p 197 A90-46074
- LAMBERT, KEVIN M.**
Aperture taper determination for the half-scale accurate antenna reflector [NASA-CR-185215] p 153 N90-21282
- LANDAHL, M. T.**
On sublayer streaks p 168 A90-28143
- LANDIS, G. A.**
A V-grooved GaAs solar cell p 225 A90-14887
GaAs solar cells with V-grooved emitters p 229 N90-17754
Peelable film GaAs solar cells for space power [NASA-TM-103125] p 153 N90-21287
- LANDIS, GEOFFREY**
Degradation of the lunar vacuum by a moon base p 266 A90-35441
- LANDIS, GEOFFREY A.**
Photovoltaic power for a lunar base [IAF PAPER 89-254] p 42 A90-13409
Optics and materials considerations for a laser-propelled lightsail [IAF PAPER 89-664] p 54 A90-13668
Thin, light-trapping silicon solar cells for space p 226 A90-14900
Lunar production of space photovoltaic arrays p 226 A90-14930
Effect of crystal orientation on anisotropic etching and MOCVD growth of grooves on GaAs p 253 A90-15136
Lunar production of solar cells - A near-term product for a lunar industrial facility p 42 A90-24791
Solar power for the lunar night p 266 A90-24814
Wide-bandgap epitaxial heterojunction windows for silicon solar cells p 227 A90-28359
- LANGSTON, L. S.**
Asymmetrical boundary layer separation at the base of a two cylinder geometry p 159 A90-18505
- LANKFORD, JAMES**
Sliding seal materials for low heat rejection engines [NASA-CR-182262] p 125 N90-11882
- LANT, CHRISTIAN T.**
Feasibility study for the advanced one-dimensional high temperature optical strain measurement system, phase 3 [NASA-CR-185254] p 191 N90-25324
Progress in high temperature speckle-shift strain measurement system [NASA-TM-103255] p 191 N90-28031
- LARKIN, D. J.**
Growth of improved quality 3C-SiC films on 6H-SiC substrates p 255 A90-29596
Growth of high quality 6H-SiC epitaxial films on vicinal (0001) 6H-SiC wafers p 255 A90-29952
- LARKIN, M. J.**
Energy Efficient Engine exhaust mixer model technology report addendum; phase 3 test program [NASA-CR-174799] p 33 N90-28556
- LARSON, A. V.**
Feasibility analysis of reciprocating magnetic heat pumps [NASA-CR-186205] p 177 N90-15363
- LARSON, CATHERINE A.**
Optimal orbital rendezvous using high and low thrust [AAS PAPER 89-354] p 41 A90-46786
- LAU, S. Y.**
A simplified model for two phase face seal design p 197 A90-40713
- LAUBENTHAL, JAMES R.**
Design and test of a compact optics system for the pool boiling experiment [NASA-TM-102530] p 135 N90-20253

- LAUGHNER, JAMES W.**
Measurement of interfacial shear strength in SiC-fiber/Si₃N₄ composites p 87 A90-13237
- LAURENDEAU, NORMAND M.**
Saturated fluorescence measurements of the hydroxyl radical in laminar high-pressure flames [NASA-CR-185218] p 190 N90-22022
- LAVALLE, JAMES J.**
Aeropropulsion facilities configuration control: Procedures manual [NASA-TM-102541] p 207 N90-21399
- LAVERY, J. E.**
Solution of steady-state one-dimensional conservation laws by mathematical programming p 241 A90-21918
- LAVERY, JOHN E.**
Calculation of shocked one-dimensional flows on abruptly changing grids by mathematical programming p 162 A90-21937
Numerical simulation of thermocapillary bubble migration under microgravity for large Reynolds and Marangoni numbers p 164 A90-23213
- LAVIN, S. P.**
Energy Efficient Engine acoustic supporting technology report [NASA-CR-174834] p 33 N90-28557
- LAWRENCE, C.**
Characterization of structural connections using free and forced response test data p 213 A90-46172
- LAWRENCE, CHARLES**
Characterization of damped structural connections for multi-component systems p 208 A90-16959
A global approach for the identification of structural connection properties [NASA-TM-102502] p 218 N90-18745
Reaction-compensation technology for microgravity laboratory robots [NASA-TM-103271] p 205 N90-28062
- LAXMANAN, V.**
Efficient estimation of diffusion during dendritic solidification p 111 A90-20612
- LAYER, DAVID H.**
Advanced modulation technology development for earth station demodulator applications. Coded modulation system development [NASA-CR-185149] p 145 N90-20270
- LEE, C. M.**
High speed commercial transport fuels considerations and research needs [NASA-TM-102535] p 131 N90-21869
- LEE, C. T.**
Zirconia toughened SiC whisker reinforced alumina composites small business innovation research [NASA-CR-179629] p 125 N90-10294
- LEE, CHINWAI**
Influence of linear profile modification and loading conditions on the dynamic tooth load and stress of high contact ratio gears [NASA-TM-103136] p 204 N90-22796
Computer-aided design of high-contact-ratio gears for minimum dynamic load and stress [NASA-TM-103275] p 205 N90-28065
- LEE, D. S.**
Processing and microstructure of melt spun NiAl alloys p 110 A90-16941
- LEE, DAVID**
Side branch morphology and coarsening in directionally solidified Pb-8.4 at. pct Au p 109 A90-11658
- LEE, FRED C. Y.**
High-frequency ac power distribution in Space Station p 63 A90-39111
- LEE, H. Y.**
Performance and modeling of superconducting ring resonators at millimeter-wave frequencies [NASA-TM-102526] p 151 N90-18634
- LEE, H.-J.**
METCAN verification status [NASA-TM-103119] p 100 N90-21824
- LEE, H.-Y.**
Analysis of microstrip lines with alternative implementation of conductors and superconductors [NASA-TM-103182] p 155 N90-27966
- LEE, HONG-TAO**
Generation and tooth contact analysis of spiral bevel gears with predesigned parabolic functions of transmission errors [NASA-CR-4259] p 199 N90-12033
- LEE, K. F.**
Experimental study of the cross-polarization characteristics of rectangular microstrip antennas p 141 A90-37312
Microstrip subarray with coplanar and stacked parasitic elements p 141 A90-41586
- LEE, R. Q.**
Experimental study of the cross-polarization characteristics of rectangular microstrip antennas p 141 A90-37312
- Microstrip subarray with coplanar and stacked parasitic elements p 141 A90-41586
Coplanar waveguide fed phased array antenna [NASA-TM-102522] p 152 N90-21273
- LEE, S. W.**
On physical optics for calculating scattering from coated bodies p 250 A90-20151
A comparison of reflector antenna designs for wide-angle scanning p 144 N90-19264
- LEE, SHUNG WU**
Reflector spillover loss of an open-ended rectangular and circular waveguide feed p 141 A90-45398
- LEE, W. E.**
Crystallization of a barium-aluminosilicate glass p 121 A90-27107
- LEE, WILLIAM E.**
Microstructural changes in beta-silicon nitride grains upon crystallizing the grain-boundary glass p 120 A90-13230
- LEE, Y. Y.**
Mass spectrometric observations of metal oxychlorides produced by oxidation-chlorination reactions p 103 A90-21215
- LEI, C. K.**
Augmented heat transfer in rectangular channels of narrow aspect ratios with rib turbulators p 157 A90-13091
- LEI, JIH-FEN**
Development and characterization of PdCr temperature-compensated wire resistance strain gage [NASA-CR-185153] p 188 N90-13761
A resistance strain gage with repeatable and cancellable apparent strain for use to 800 C [NASA-CR-185256] p 53 N90-26063
- LEIB, S. J.**
Nonlinear evolution of oblique waves on compressible shear layers p 158 A90-15942
- LEIBECKI, HAROLD F.**
Modeling and optimization of a regenerative fuel cell system using the ASPEN process simulator [NASA-TM-103210] p 233 N90-26396
- LEISHMAN, D. K.**
Large scale prop-fan structural design study. Volume 1: Initial concepts [NASA-CR-174992] p 23 N90-10043
Large scale prop-fan structural design study. Volume 2: Preliminary design of SR-7 [NASA-CR-174993] p 23 N90-10044
- LEMKEY, F. D.**
Identification of a cast iron alloy containing nonstrategic elements [NASA-CR-185174] p 118 N90-18559
- LENHART, STEPHEN**
Bipolar nickel-hydrogen battery development - A program review p 62 A90-38288
- LEONARD, B. P.**
A cost-effective strategy for nonoscillatory convection without clipping [NASA-TM-102536] p 179 N90-21291
ULTRA-SHARP nonoscillatory convection schemes for high-speed steady multidimensional flow [NASA-TM-102568] p 244 N90-21570
- LEONHARDT, T. A.**
Microstructure of a SiC/Ti-15-3 composite p 91 A90-37663
- LEONHARDT, TODD A.**
Metallographic techniques for evaluation of thermal barrier coatings p 85 A90-44869
- LEONIDA, A.**
Hydrogen-oxygen proton-exchange membrane fuel cells and electrolyzers p 56 A90-33944
Hydrogen-oxygen proton-exchange membrane fuel cells and electrolyzers p 230 N90-20467
- LEPICOVSKY, J.**
Total temperature effects on centerline Mach number characteristics of freejets p 6 A90-25290
- LERCH, B. A.**
Evaluation of thermal and mechanical loading effects on the structural behavior of a SiC/titanium composite [AIAA PAPER 90-1026] p 90 A90-29228
Microstructure of a SiC/Ti-15-3 composite p 91 A90-37663
Fatigue crack propagation behavior of a single crystalline superalloy p 116 A90-48635
- LERCH, BRAD**
Cyclic deformation, fatigue and fatigue crack propagation in Ni-base alloys p 115 A90-34162
- LERCH, BRADLEY A.**
Heat treatment study of the SiC/Ti-15-3 composite system [NASA-TP-2970] p 97 N90-19302
Evaluation of thermal and mechanical loading effects on the structural behavior of a SiC/titanium composite [NASA-TM-102536] p 98 N90-20139
- LERCH, F. J.**
The GEM-T2 gravitational model [NASA-TM-100746] p 234 N90-12984
- LESKOVICH, R. THOMAS**
The effects of nonlinear loading upon the Space Station Freedom 20 kHz power system p 60 A90-38118
- LEVINE, STANLEY R.**
Materials for engine applications above 3000 deg F: An overview [NASA-TM-100169] p 95 N90-10188
- LEVINSON, LAURIE H.**
Flight software development for the isothermal dendritic growth experiment [AIAA PAPER 90-0744] p 235 A90-22257
Flight software development for the isothermal dendritic growth experiment [NASA-TM-102412] p 238 N90-13988
- LEVY, RALPH**
User's manual for PEPSIG NASA tip vortex version [NASA-CR-182178] p 10 N90-10835
Computation of the tip vortex flowfield for advanced aircraft propellers [NASA-CR-182179] p 10 N90-10836
- LEWICKI, D. G.**
Tooth contact shift in loaded spiral bevel gears p 193 A90-21112
Effect of advanced component technology on helicopter transmissions p 193 A90-21115
Transmission research activities at NASA Lewis Research Center [NASA-TM-103132] p 203 N90-21394
- LEZBERG, ERWIN A.**
Fuel-rich catalytic combustion - A fuel processor for high-speed propulsion [AIAA PAPER 90-2319] p 105 A90-42774
Fuel-rich catalytic combustion: A fuel processor for high-speed propulsion [NASA-TM-103177] p 107 N90-23518
- LI, G. Y.**
Robustness, generality and efficiency of optimization algorithms in practical applications [AIAA PAPER 90-1177] p 236 A90-29268
- LI, X.**
Hybrid solar cells based on dc magnetron sputtered films of n-ITO on APMOPE grown p-InP p 225 A90-14893
Investigation of buried homojunctions in p-InP formed during sputter deposition of both indium tin oxide and indium oxide p 256 A90-36799
Study of indium tin oxide films exposed to atomic oxygen p 257 A90-45193
- LIAO, M.**
Reflector surface distortion analysis techniques (thermal distortion analysis of antennas in space) p 144 N90-19267
- LIAO, MEI-HWA**
A transient plasticity study and low cycle fatigue analysis of the Space Station Freedom photovoltaic solar array blanket [NASA-TM-102516] p 218 N90-19617
- LICHTENFELTS, FRED**
Ultrasonic techniques for aircraft ice accretion measurement p 16 N90-20926
- LIEBERT, CURT H.**
Heat flux measurements [ASME PAPER 89-GT-107] p 165 A90-23815
- LIFF, DALE R.**
Development of a quadrupole-based Secondary-Ion Mass Spectrometry (SIMS) system at Lewis Research Center [NASA-TM-102531] p 87 N90-23476
- LIGHTFOOT, A.**
Nitriding kinetics of Si-SiC powder mixtures as simulations of reaction bonded Si₃N₄-SiC composites p 90 A90-27076
Properties of RBSN and RBSN-SiC composites p 94 A90-51920
- LILLEY, J. R., JR.**
Computer modeling of current collection by the CHARGE-2 mother payload p 252 A90-24933
- LILLINGTON, D. R.**
High efficiency GaAs/Ge monolithic tandem solar cells p 224 A90-14858
Optimization of silicon 8 cm x 8 cm wrapthrough Space Station cells for 'on orbit' operation p 54 A90-14941
- LIM, H. S.**
Electrochemical behavior of heavily cycled nickel electrodes in Ni/H₂ cells containing electrolytes of various KOH concentrations p 103 A90-24535
KOH concentration effect on the cycle life of nickel-hydrogen cells. IV - Results of failure analysis p 228 A90-33952
- LIM, SANG G.**
On the numerical solution of the dynamically loaded hydrodynamic lubrication of the point contact problem [NASA-TM-102427] p 178 N90-17076

PERSONAL AUTHOR INDEX

- LIM, TEIK C.**
Modal analysis of gear housing and mounts
p 192 A90-17018
- LIM, TEIK CHIN**
Vibration transmission through rolling element bearings in geared rotor system, part 1
[NASA-CR-186093] p 199 N90-12936
A review of gear housing dynamics and acoustics literature
[NASA-CR-185148] p 203 N90-21387
- LIN, AVI**
On the mathematical modeling of the Reynolds stress's equations
[AIAA PAPER 90-0498] p 161 A90-19878
Parallel algorithms for boundary value problems
[NASA-TM-102498] p 243 N90-19783
Parallel/distributed direct method for solving linear systems
[NASA-TM-103229] p 244 N90-26614
- LIN, CHIN-SHUN**
Buoyancy effects on the vapor condensation rate on a horizontal liquid surface
[AIAA PAPER 90-0353] p 162 A90-22201
Vapor condensation on liquid surface due to laminar jet-induced mixing - The effects of system parameters
[AIAA PAPER 90-0354] p 163 A90-22202
Numerical investigation of the thermal stratification in cryogenic tanks subjected to wall heat flux
[AIAA PAPER 90-2375] p 175 A90-52500
Buoyancy effects on the vapor condensation rate on a horizontal liquid surface
[NASA-TM-102437] p 130 N90-13675
Vapor condensation on liquid surface due to laminar jet-induced mixing: The effects of system parameters
[NASA-TM-102433] p 176 N90-13751
Numerical investigation of the thermal stratification in cryogenic tanks subjected to wall heat flux
[NASA-TM-103194] p 184 N90-27984
- LIN, H. H.**
Dynamic loading of spur gears with linear or parabolic tooth profile modifications
p 195 A90-21126
Profile modification to minimize spur gear dynamic loading
p 195 A90-21128
- LIN, HSIANG HSI**
Influence of linear profile modification and loading conditions on the dynamic tooth load and stress of high contact ratio gears
[NASA-TM-103136] p 204 N90-22796
Computer-aided design of high-contact-ratio gears for minimum dynamic load and stress
[NASA-TM-103275] p 205 N90-28065
- LIN, R. R.**
Test and theory for piezoelectric actuator-active vibration control of rotating machinery
p 198 A90-46226
- LIN, T. C.**
Robustness, generality and efficiency of optimization algorithms in practical applications
[AIAA PAPER 90-1177] p 236 A90-29268
- LIN, Y. C.**
Studies on the use of supercritical ammonia for ceramic nitride synthesis and fabrication
[NASA-TM-102570] p 106 N90-21843
- LINDHOLM, U. S.**
High temperature inelastic deformation under uniaxial loading - Theory and experiment
p 109 A90-13838
High temperature inelastic deformation of the B1900 + Hf alloy under multiaxial loading - Theory and experiment
p 112 A90-22656
Inelastic deformation under nonisothermal loading
p 112 A90-22657
- LINDHOLM, ULRIC S.**
Constitutive modeling for isotropic materials (HOST)
[NASA-CR-179522] p 26 N90-13390
Constitutive modeling for isotropic materials (HOST)
[NASA-CR-174718] p 26 N90-13391
- LING, H.**
On physical optics for calculating scattering from coated bodies
p 250 A90-20151
- LING, JERRI S.**
Design and test of a compact optics system for the pool boiling experiment
[NASA-TM-102530] p 135 N90-20253
- LINNE, DIANE L.**
Mars in situ propellants - Carbon monoxide and oxygen ignition experiments
[AIAA PAPER 90-1894] p 130 A90-50642
Mars in situ propellants: Carbon monoxide and oxygen ignition experiments
[NASA-TM-103202] p 81 N90-26065
- LIU, LUEN-WOEI**
Integrated Communication and Control Systems. III - Nonidentical sensor and controller sampling
p 239 A90-51266
- LIU, M.-S.**
Implicit solution of three-dimensional internal turbulent flows
[NASA-TM-103099] p 184 N90-27982
- LIU, MENG-SING**
The Osher scheme for real gases
[AIAA PAPER 90-0397] p 166 A90-25030
Splitting of inviscid fluxes for real gases
p 167 A90-25451
Inviscid flux-splitting algorithms for real gases with non-equilibrium chemistry
p 174 A90-52275
- LIPO, T. A.**
Performance testing of a high frequency link converter for Space Station power distribution system
p 148 A90-38128
- LITT, JONATHAN S.**
An expert system to perform on-line controller tuning
[NASA-TM-103101] p 240 N90-23991
An expert system to perform on-line controller restructuring for abrupt model changes
[NASA-TM-103609] p 241 N90-29121
- LITTLE, B. H.**
Propan Test Assessment (PTA): Flight test report
[NASA-CR-182278] p 24 A90-11738
Propan Test Assessment (PTA)
[NASA-CR-185138] p 25 A90-11739
- LITVIN, F. L.**
Tooth contact shift in loaded spiral bevel gears
p 193 A90-21112
Topology of modified helical gears
p 195 A90-21132
- LITVIN, FAYDOR L.**
Generation and tooth contact analysis of spiral bevel gears with predesigned parabolic functions of transmission errors
[NASA-CR-4259] p 199 N90-12033
Theory of gearing
[NASA-PP-1212] p 202 N90-19593
Computerized inspection of gear tooth surfaces
[NASA-TM-102395] p 203 N90-22054
- LIU, H. W.**
The equivalence between dislocation pile-ups and cracks
p 210 A90-29215
Characterization of the tip field of a discrete dislocation pileup for the development of physically based micromechanics
p 213 A90-43883
- LIU, J. T. C.**
Contributions to the understanding of large-scale coherent structures in developing free turbulent shear flows
p 158 A90-13907
- LIU, J. Z.**
Experimental evidence of a dimensional crossover in $\text{YBa}_2\text{Cu}_3\text{O}_{7-\delta}$
p 255 A90-29739
- LIU, N.-S.**
Reciprocal interactions of hairpin-shaped vortices and a boundary layer
[AIAA PAPER 90-0017] p 159 A90-19635
- LIZANICH, PAUL J.**
Effects of amplitude distortions and IF equalization on satellite communication system bit-error rate performance
[AIAA PAPER 90-0878] p 140 A90-25697
Effects of amplitude distortions and IF equalization on satellite communication system bit-error rate performance
[NASA-TM-102415] p 144 N90-19454
- LOCCI, I. E.**
Processing and microstructure of melt spun NiAl alloys
p 110 A90-16941
- LOCK, JAMES A.**
Laser diffraction particle sizing: Instrument probe volume relocation and elongation
[NASA-TM-102512] p 188 N90-18025
- LOEWY, R. G.**
Shaft flexibility effects on the forced response of a bladed-disk assembly
p 21 A90-43218
- LOEWY, ROBERT**
Shaft flexibility effects on aeroelastic stability of a rotating bladed disk
p 208 A90-16371
- LOEWY, ROBERT G.**
Blade mistuning coupled with shaft flexibility effects in rotor aeroelasticity
[ASME PAPER 89-GT-330] p 19 A90-23896
- LOFERSKI, JOSEPH J.**
Wide-bandgap epitaxial heterojunction windows for silicon solar cells
p 227 A90-28359
- LOFTIN, TIMOTHY A.**
Applications of high thermal conductivity composites to electronics and spacecraft thermal design
[AIAA PAPER 90-0783] p 89 A90-25609
- LOHMANN, R. P.**
Energy efficient engine pin fin and ceramic composite segmented liner combustor sector rig test report
[NASA-CR-179534] p 35 N90-28567
- LONG, KENWYN J.**
Analysis of a Mars-stationary orbiting microwave power transmission system
[NASA-TM-101344] p 138 N90-26172
- LONG, MARTIN**
Fluorinated graphite fibers as a new engineering material: Promises and challenges
[NASA-TM-102511] p 86 N90-19301
- LORD, W. K.**
Mixer-ejector nozzle for jet noise suppression
[AIAA PAPER 90-1909] p 247 A90-47202
- LOUTFY, R. O.**
Zirconia toughened SiC whisker reinforced alumina composites small business innovation research
[NASA-CR-179629] p 125 N90-10294
- LOVELY, R.**
Photovoltaic module on-orbit assembly for Space Station Freedom
p 45 A90-38071
- LOVELY, RONALD G.**
Solar dynamic power module design
p 59 A90-38079
- LOWELL, CARL E.**
The Materials Division: A case study
[NASA-TM-102380] p 86 N90-13597
The oxidation and corrosion of ODS alloys
[NASA-TM-102555] p 119 N90-25211
- LOYSELLE, PATRICIA**
Structural comparison of nickel electrodes and precursor phases
p 231 N90-20472
- LOYSELLE, PATRICIA L.**
Structural comparison of nickel electrodes and precursor phases
p 228 A90-33949
- LU, CHENG Y.**
Estimated performance and future potential of solar dynamic and photovoltaic power systems for selected LEO and HEO missions
p 62 A90-38307
- LUCHT, R.**
Combustion interaction with radiation-cooled chambers
[AIAA PAPER 90-2121] p 64 A90-42030
- LUCK, ROGELIO**
An observer-based compensator for distributed delays
p 239 A90-49899
- LUO, H. A.**
Green's functions for dislocations in bonded strips and related crack problems
[NASA-CR-185291] p 224 N90-28878
- LUO, H. L.**
Thin films of the $\text{Bi}_2\text{Sr}_2\text{Ca}_2\text{Cu}_3\text{O}(x)$ superconductor
p 254 A90-24448
- LUO, JIHMEI**
Linear acene derivatives - New routes to pentacene and naphthalene and the first synthesis of a triptycene with two anthracene moieties
p 85 A90-49071
Bisannulation with a benzo(1,2-c:4,5-c'-prime) difuran equivalent - A new route to linear acene derivatives
p 85 A90-49072
- LUTON, MICHAEL J.**
Preliminary investigation of a NiAl composite prepared by cryomilling
p 113 A90-25098
- LYMAN, FREDERIC A.**
Mass transfer from a sphere in an oscillating flow with zero mean velocity
[NASA-TM-102566] p 179 N90-20338
- LYMAN, V.**
Analysis of results from wind tunnel tests of inlets for an advanced turboprop nacelle installation
[NASA-CR-174937] p 10 N90-10011
- LYTLE, JOHN K.**
Three-dimensional compressible jet-in-crossflow calculations using improved viscosity models and adapted grid
[AIAA PAPER 90-2100] p 174 A90-47206
A simple algebraic grid adaptation scheme with applications to two- and three-dimensional flow problems
[NASA-TM-102446] p 178 N90-18667

M

- MA, T.-Z.**
A two-dimensional model of plasma expansion in the ionosphere
p 233 A90-43609
- MACIEJEWSKI, PAUL K.**
Effects of very high turbulence on heat transfer
p 169 A90-35247
- MACINNES, J. M.**
Time-accurate simulations of a shear layer forced at a single frequency
p 163 A90-23111
Time-dependent calculation of a forced mixing layer using a k-epsilon turbulence model
p 169 A90-35222
- MACKAY, R. A.**
Analysis of gamma prime shape changes in a single crystal Ni-base superalloy
p 109 A90-15206

- Influence of molybdenum on the creep properties of nickel-base superalloy single crystals p 113 A90-25233
- The role of interfacial dislocation networks in high temperature creep of superalloys p 114 A90-33329
- Isothermal and nonisothermal fatigue behavior of a metal matrix composite p 91 A90-36746
- Coarsening in high volume fraction nickel-base alloys p 115 A90-37719
- MACKAY, REBECCA A.**
Effect of fiber spacing on interfacial damage in a metal matrix composite p 88 A90-23188
- Heat treatment study of the SiC/Ti-15-3 composite system [NASA-TP-2970] p 97 N90-19302
- MACKIN, MICHAEL**
Development of Ada language control software for the NASA power management and distribution test bed p 236 A90-38082
- MACRAE, GREGORY S.**
Requirements for long-life operation of inert gas hollow cathodes - Preliminary results [AIAA PAPER 90-2586] p 69 A90-52570
- Status of structural analysis of 30 cm diameter ion optics [AIAA PAPER 90-2649] p 215 A90-52571
- Requirements for long-life operation of inert gas hollow cathodes: Preliminary report [NASA-TM-103242] p 82 N90-27783
- MADZBAR, G.**
Fabry-Perot interferometer development for rocket engine plume spectroscopy [AIAA PAPER 90-2234] p 187 A90-47212
- MADZBAR, GEORGE C.**
Digital filtering of plume emission spectra [AIAA PAPER 90-1994] p 67 A90-50643
- A fiber optic sensor for noncontact measurement of shaft speed, torque, and power [NASA-TM-102481] p 189 N90-21360
- Digital filtering of plume emission spectra [NASA-TM-103135] p 81 N90-26070
- MAEDA, KEI-ICHI**
Soft inflation p 265 A90-40093
- MAGLIOZZI, BERNARD**
Acoustic test and analysis of a counterrotating prop-fan model [NASA-CR-179590] p 247 N90-10683
- MAHEFFEY, E. T.**
Mathematical modeling and analysis of heat pipe start-up from the frozen state p 174 A90-48404
- MAHLE, CHRISTOPH E.**
The role of technology in influencing future civil communications satellites p 142 A90-51167
- MATLAND, DUNCAN J., IV**
Fiber optic sensing systems using high frequency resonant sensing heads with intensity sensors p 185 A90-10472
- MAJJIGI, R. K.**
An investigation of counterrotating tip vortex interaction [NASA-CR-185135] p 247 N90-11549
- MALACHOWSKI, M. J.**
Beam rider for an Articulated Robot Manipulator (ARM) accurate positioning of long flexible manipulators [NASA-CR-185151] p 241 N90-26581
- MALAK, MALAK FOUAD**
Three dimensional LDV flow measurements and theoretical investigation in a radial inflow turbine scroll p 9 A90-46860
- MALARIK, D. C.**
Autoclavable addition polyimides for 371 C composite applications [NASA-TM-103233] p 102 N90-27874
- MALDONADO, JAIME J.**
Supersonic through-flow fan engine and aircraft mission performance [NASA-TM-102304] p 29 N90-21038
- MALIK, S. N.**
Elevated temperature crack growth [NASA-CR-182247] p 222 N90-26355
- MALONEY, THOMAS M.**
Modeling and optimization of a regenerative fuel cell system using the ASPEN process simulator [NASA-TM-103210] p 233 N90-26396
- MANDEL, GEORGE**
Criss-cross directory of NASA N numbers and DOD AD numbers. Volume 2, part 1: AD to N, 1979-1986. N to AD, 1962-1986 [NASA-TM-101814] p 262 N90-12388
- Criss-cross directory of NASA N numbers and DOD AD numbers. Volume 2, part 2: AD to N, 1979-1986. N to AD, 1962-1986 [NASA-TM-101815] p 262 N90-12389
- MANDELL, M. J.**
High-voltage plasma interactions calculations using NASCAP/LEO [AIAA PAPER 90-0725] p 251 A90-22254
- Plasma contactor modeling with NASCAP/LEO - Extending laboratory results to space systems [AIAA PAPER 90-0726] p 251 A90-22255
- Computer modeling of current collection by the CHARGE-2 mother payload p 252 A90-24933
- The sheath structure around a negatively charged rocket payload p 48 A90-34780
- Plasma sources for spacecraft neutralization [AIAA PAPER 90-1556] p 49 A90-38697
- MANDERSCHIED, JANE M.**
Designing ceramic components with the CARES computer program p 235 A90-19147
- Analysis of whisker-toughened ceramic components - A design engineer's viewpoint p 88 A90-19149
- Noninteractive macroscopic reliability model for ceramic matrix composites with orthotropic material symmetry [ASME PAPER 89-GT-129] p 209 A90-23827
- Analysis of whisker-toughened ceramic components: A design engineer's viewpoint [NASA-TM-102333] p 97 N90-18504
- Design of ceramic components with the NASA/CARES computer program [NASA-TM-102369] p 222 N90-26359
- Ceramics Analysis and Reliability Evaluation of Structures (CARES). Users and programmers manual [NASA-TP-2916] p 223 N90-28099
- Reliability analysis of a structural ceramic combustion chamber [NASA-TM-103264] p 223 N90-28112
- MANI, R.**
High speed turboprop aeroacoustic study (counterrotation). Volume 1: Model development [NASA-CR-185241] p 249 N90-26633
- MANI, RAMANI**
The radiation of sound from a propeller at angle of attack [NASA-CR-4264] p 249 N90-21602
- MANKBADI, R. R.**
Evolution and interaction of two- and three-dimensional instability waves p 173 A90-46885
- MANKBADI, REDA R.**
Multiwave nonlinear interactions in the axisymmetric mode [AIAA PAPER 90-0365] p 166 A90-25029
- Phase development and its role on subharmonic control [AIAA PAPER 90-0503] p 166 A90-25035
- MANNAN, S. K.**
1200 to 1400 K slow strain rate compressive properties of NiAl/Ni₂AlTi-base materials p 88 A90-16938
- 1100 to 1300 K slow plastic compression properties of Ni-38.5Al composites p 111 A90-19154
- Elevated temperature slow plastic deformation of NiAl-TiB₂ particulate composites at 1200 and 1300 K p 92 A90-45621
- Slow plastic deformation of extruded NiAl-10TiB₂ particulate composites at 1200 and 1300 K p 92 A90-46133
- High-temperature slow-strain-rate compression studies on CoAl-TiB₂ composites p 93 A90-48636
- MANNING, ROBERT M.**
Radiative transfer theory for inhomogeneous media with random extinction and scattering coefficients p 260 A90-21904
- A unified statistical rain-attenuation model for communication link fade predictions and optimal stochastic fade control design using a location-dependent rain-statistic database p 141 A90-34914
- MANSOUR, N. N.**
Modeling of near-wall turbulence [NASA-TM-103222] p 184 N90-28009
- MANTENIEKS, M.**
Geometric effects in applied-field MPD thrusters [AIAA PAPER 90-2669] p 69 A90-52572
- Geometric effects in applied-field MPD thrusters [NASA-TM-103259] p 82 N90-27782
- MANTENIEKS, M. A.**
Test facility and preliminary performance of a 100 kW class MPD thruster p 75 N90-18476
- MANZELLA, DAVID H.**
Preliminary plume characteristics of an arcjet thruster [AIAA PAPER 90-2645] p 64 A90-42609
- Performance characterization of a segmented anode arcjet thruster [AIAA PAPER 90-2582] p 68 A90-52569
- The effect of electrode configuration on arcjet performance [NASA-TM-102346] p 70 N90-11081
- Preliminary plume characteristics of an arcjet thruster [NASA-TM-103241] p 81 N90-26071
- MANZO, MICHELLE**
Bipolar nickel-hydrogen battery development - A program review p 62 A90-38288
- MANZO, MICHELLE A.**
Characterization testing of a 40 ampere hour bipolar nickel-hydrogen battery p 56 A90-33940
- Nickel-hydrogen capacity loss on storage p 57 A90-33955
- NASA aerospace battery systems program update p 228 A90-38217
- Characterization testing of a 40 AHR bipolar nickel-hydrogen battery p 230 N90-20463
- Nickel-hydrogen capacity loss on storage p 231 N90-20478
- NASA aerospace flight battery systems program [NASA-TM-103237] p 233 N90-26397
- MARABITO, MARK**
Aeolian removal of dust from photovoltaic surfaces on Mars [NASA-TM-102507] p 76 N90-19299
- MARCHANT, R. D.**
Energy Efficient Engine: High-pressure compressor test hardware detailed design report [NASA-CR-180850] p 36 N90-28570
- MAREK, C. J.**
A planar reacting shear layer system for the study of fluid dynamics-combustion interaction [NASA-TM-102422] p 27 N90-13393
- MARINELLI, WILLIAM J.**
H₂/O₂ three-body rates at high temperatures [AIAA PAPER 90-1696] p 105 A90-38399
- MARK, HERMAN**
Effect of eleven years in earth orbit on a mirror surface p 44 A90-36188
- MARK, J. L.**
Research on a two-dimensional inlet for a supersonic V/STOL propulsion system. Appendix A [NASA-CR-174945] p 12 N90-18364
- MARSH, J. G.**
The GEM-T2 gravitational model [NASA-TM-100746] p 234 N90-12984
- MARSHALL, A. C.**
Scaling study for SP-100 reactor technology [NASA-TM-897140] p 249 N90-16496
- MARSHALL, DAVID T.**
A radiological assessment of nuclear power and propulsion operations near Space Station Freedom [NASA-CR-185185] p 76 N90-21108
- MARSHALL, MATTHEW FISK**
Evolutionary growth for Space Station Freedom electrical power system p 58 A90-38072
- MARTIN, DONALD F.**
Space Station Freedom solar array panels plasma interaction test facility [NASA-TM-102475] p 266 N90-22488
- MARTIN, RONALD E.**
Integrated regenerative fuel cell experimental evaluation [NASA-CR-185183] p 230 N90-18808
- MARTINEZ, J. C.**
Ka-band propagation characteristics of microstrip lines on GaAs substrates at cryogenic temperatures p 147 A90-33644
- MARTINI, WILLIAM R.**
Development of free-piston Stirling engine performance and optimization codes based on Martini simulation technique [NASA-CR-182210] p 263 N90-18326
- MARTZAKLIS, KONSTANTINOS S.**
Experimental investigations on channelized coplanar waveguide [NASA-TM-102494] p 151 N90-20286
- MASER, J. G.**
Parametric studies of advanced turboprops p 19 A90-21225
- MASON, A. V.**
Optimization of silicon 8 cm x 8 cm wrapthrough Space Station cells for 'on orbit' operation p 54 A90-14941
- MASON, LEE S.**
SP-100 power system conceptual design for lunar base applications [NASA-TM-102090] p 267 N90-15030
- MASTERS, R.**
Effect of Ga and P dopants on the thermoelectric properties of n-type SiGe p 256 A90-38140
- MATA, FERNANDO**
Application of heuristic satellite plan synthesis algorithms to requirements of the WARC-88 allotment plan [AIAA PAPER 90-0815] p 245 A90-25638
- A heuristic approach to worst-case carrier-to-interference ratio maximization in satellite system synthesis [AIAA PAPER 90-0816] p 46 A90-25639

- Application of heuristic satellite plan synthesis algorithms to requirements of the WARC-88 allotment plan [NASA-TM-102479] p 245 N90-14856
- MATTOSSIAN, J. N.**
Xenon ion sources for space applications p 56 A90-22874
Status of xenon ion propulsion technology p 56 A90-27961
High-power xenon ion thrusters [AIAA PAPER 90-2540] p 64 A90-42536
- MATTEDI, ANITA K.**
Framework for a space shuttle main engine health monitoring system [NASA-CR-185224] p 78 N90-21809
- MATTERN, DUANE L.**
H-infinity based integrated flight/propulsion control design for a STOVL aircraft in transition flight [AIAA PAPER 90-3335] p 36 A90-47595
H-infinity based integrated flight-propulsion control design for a STOVL aircraft in transition flight [NASA-TM-103198] p 37 N90-26011
- MATTHIEN, D. H.**
Interface demarcation in GaAs by current pulsing [AIAA PAPER 90-0319] p 254 A90-19793
Free float acceleration measurements aboard NASA's KC-135 Microgravity Research Aircraft [AIAA PAPER 90-0742] p 132 A90-20000
- MATUS, L. G.**
High frequency capacitance-voltage characteristics of thermally grown SiO₂ films on beta-SiC p 254 A90-21348
Growth of improved quality 3C-SiC films on 6H-SiC substrates p 255 A90-29596
Growth of high quality 6H-SiC epitaxial films on vicinal (0001) 6H-SiC wafers p 255 A90-29952
Deep-level dominated electrical characteristics of Au contacts on beta-SiC p 147 A90-33726
- MATZNER, RICHARD A.**
Big bang nucleosynthesis and the quark-hadron transition p 265 A90-31407
- MAUL, WILLIAM A., III**
Multi-sensor analysis techniques for SSME safety monitoring [AIAA PAPER 90-1990] p 45 A90-52499
Multi-sensor analysis techniques for SSME safety monitoring [NASA-CR-185260] p 45 N90-27732
- MAVRIPLIS, D.**
Comparison of boundary element and finite element methods in spur gear root stress analysis p 193 A90-21107
Computer aided design of spur gear teeth p 195 A90-21131
- MAVRIPLIS, DIMITRI**
Computer simulation of gear tooth manufacturing processes [NASA-CR-185200] p 138 N90-26171
- MAZELSKY, R.**
Evaluation of transport conditions during physical vapor transport growth of opto-electronic crystals p 132 A90-20525
- MCCARDLE, JACK G.**
Performance characteristics of a one-third-scale, vectorable ventral nozzle for SSTOVL aircraft [AIAA PAPER 90-2271] p 20 A90-37562
Analysis of internal flow in a ventral nozzle for STOVL aircraft [AIAA PAPER 90-1899] p 21 A90-42688
Performance characteristics of a one-third-scale, vectorable ventral nozzle for SSTOVL aircraft [NASA-TM-103120] p 2 N90-21725
Analysis of internal flow in a ventral nozzle for STOVL aircraft [NASA-TM-103123] p 31 N90-23404
Experimental and analytical study of close-coupled ventral nozzles for ASTOVL aircraft [NASA-TM-103170] p 31 N90-24273
- MCCARTHY, G. J.**
Constitutive and life modeling of single crystal blade alloys for root attachment analysis p 119 N90-28643
- MCCARTNEY, TIMOTHY P.**
A test matrix sequencer for research test facility automation [AIAA PAPER 90-2386] p 37 A90-42791
A test matrix sequencer for research test facility automation [NASA-TM-103108] p 39 N90-23416
- MCCARTY, K.**
Combustion interaction with radiation-cooled chambers [AIAA PAPER 90-2121] p 64 A90-42030
- MCCULLUNG, R. C.**
Application of the probabilistic approximate analysis method to a turbopump blade analysis [AIAA PAPER 90-1098] p 56 A90-29328
- MCCORMICK, DUANE C.**
Laser velocimeter and total pressure measurements in circular-to-rectangular transition ducts [NASA-CR-182286] p 177 N90-14494
- MCDANAL, A. J.**
The mini-dome lens space concentrator array - Recent component test results and current array development status p 60 A90-38155
Conceptual design study of a 5 kilowatt solar dynamic Brayton power system using a dome Fresnel lens solar concentrator [NASA-CR-185134] p 72 N90-14281
- MCDONALD, H.**
Reciprocal interactions of hairpin-shaped vortices and a boundary layer [AIAA PAPER 90-0017] p 159 A90-19635
- MCDONELL, V. G.**
Influence of the continuous and dispersed phases on the symmetry of a gas turbine air-blast atomizer [ASME PAPER 89-GT-303] p 163 A90-22651
Application of two-component phase Doppler interferometry to the measurement of particle size, mass flux, and velocities in two-phase flows p 186 A90-32853
An experimental and numerical study of particle-laden coaxial jet flows p 171 A90-38799
- MCDONNELL, V. G.**
Symmetry assessment of an air-blast atomizer spray p 172 A90-40930
- MCELROY, J.**
Hydrogen-oxygen proton-exchange membrane fuel cells and electrolyzers p 56 A90-33944
Hydrogen-oxygen proton-exchange membrane fuel cells and electrolyzers p 230 N90-20467
- MCGARRY, M. A.**
Research on a two-dimensional inlet for a supersonic V/STOL propulsion system. Appendix A [NASA-CR-174945] p 12 N90-18364
- MCGAW, MICHAEL A.**
The fatigue damage behavior of a single crystal superalloy p 120 N90-28644
- MCKISSOCK, B.**
Scaling study for SP-100 reactor technology [NASA-TM-897140] p 249 N90-16496
- MCKISSOCK, BARBARA I.**
Space nuclear reactor shields for manned and unmanned applications p 57 A90-37859
A solar power system for an early Mars expedition [NASA-TM-103219] p 246 N90-28393
- MCKNIGHT, R. L.**
Application of HOST technology to the SSME HPFTP blade [ASME PAPER 89-GT-130] p 209 A90-23828
- MCLALLIN, KERRY**
Evolutionary growth for Space Station Freedom electrical power system p 58 A90-38072
- MCNALLAN, M. J.**
Mass spectrometric observations of metal oxychlorides produced by oxidation-chlorination reactions p 103 A90-21215
- MCNELIS, MARK E.**
A modified VAPEPS method for predicting vibroacoustic response of unreinforced mass loaded honeycomb panels p 206 A90-43731
- MCVAY, J. W.**
The effects of surface films on mechanical behavior of B2 ordered intermetallic alloys p 115 A90-44338
- MEADOR, MARY ANN B.**
Processable, high temperature polymers from 1,4,5,8-tetrahydro-1,4,5,8-diepoxyanthracene and bis-dienes p 84 A90-21930
Photochemical approaches to ordered polymers p 84 A90-33222
- MEADOR, MICHAEL A.**
Photochemical approaches to ordered polymers p 84 A90-33222
- MEASE, KENNETH D.**
Comparison of solution approaches for minimum-fuel, low-thrust, power-limited orbital transfers [AIAA PAPER 90-2960] p 41 A90-53035
- MEEKS, CRAWFORD**
Development of a compact, light weight magnetic bearing [AIAA PAPER 90-2483] p 199 A90-47223
- MEI, YU**
Thin films of the Bi₂Sr₂Ca₂Cu₃O(x) superconductor p 254 A90-24448
- MEITNER, PETER L.**
Computer code for predicting coolant flow and heat transfer in turbomachinery [NASA-TP-2985] p 32 N90-27722
- MELCONIAN, JERRY O.**
Introducing the VRT gas turbine combustor [AIAA PAPER 90-2452] p 21 A90-42808
Introducing the VRT gas turbine combustor [NASA-TM-103176] p 137 N90-23591
- MELIS, MATTHEW E.**
Thermal/structural analyses of several hydrogen-cooled leading-edge concepts for hypersonic flight vehicles [AIAA PAPER 90-0053] p 164 A90-23702
Thermal/structural analyses of several hydrogen-cooled leading-edge concepts for hypersonic flight vehicles [NASA-TM-102391] p 177 N90-14511
COMGEN: A computer program for generating finite element models of composite materials at the micro level [NASA-TM-102556] p 219 N90-20438
Finite element elastic-plastic-creep and cyclic life analysis of a cowl lip [NASA-TM-102342] p 220 N90-22808
- MELLOR, PAMELA A.**
Electric power scheduling: A distributed problem-solving approach [NASA-TM-103149] p 240 N90-22323
Automated electric power management and control for Space Station Freedom [NASA-TM-103151] p 240 N90-23125
- MELLOTT, KENNETH D.**
Space Station Freedom solar array panels plasma interaction test facility [NASA-TM-102475] p 266 N90-22488
- MEMARZADEH, KAZEM**
Ellipsometric studies of the diffusion of atomic oxygen through silicon dioxide thin films p 104 A90-36268
- MENNERTIER, CHRISTOPHE**
Coupled effects of conduction in the crystal and thermo-solutal convection in a rectangular inclined enclosure [AIAA PAPER 90-0408] p 133 A90-25031
- MEOLA, J. E.**
Laser ablated high T_(sub c) superconducting thin YBa₂Cu₃O_{7-x} films on substrates suitable for microwave applications p 260 N90-27808
- MEOLA, JOSEPH E.**
Study of deposition of YBa₂Cu₃O_{7-x} on cubic zirconia [NASA-TM-102350] p 257 N90-10737
- MERCER, CAROLYN R.**
Active phase compensation system for fiber optic holography p 250 A90-11310
Fiber-optic projected-fringe digital interferometry [NASA-TM-103252] p 191 N90-28033
- MERRILL, W.**
A real time neural net estimator of fatigue life [NASA-TM-103117] p 239 N90-21564
- MERRILL, WALTER**
A failure diagnosis system based on a neural network classifier for the space shuttle main engine [NASA-TM-103607] p 83 N90-28659
- MERRILL, WALTER C.**
A real time microcomputer implementation of sensor failure detection for turbofan engines p 21 A90-45414
Advanced detection, isolation, and accommodation of sensor failures in turbofan engines: Real-time microcomputer implementation [NASA-TP-2925] p 37 N90-15112
Neuromorphic learning of continuous-valued mappings from noise-corrupted data. Application to real-time adaptive control [NASA-TM-4176] p 241 N90-25607
- MESEROLE, J. S.**
Tank Pressure Control Experiment - A low-g mixing investigation [AIAA PAPER 90-2376] p 66 A90-47217
- METZ, ROGER N.**
LEO high voltage solar array arcing response model, continuation 5 [NASA-CR-186505] p 232 N90-25418
- MEYER, CLAUDIA M.**
Rocket engine failure detection using system identification techniques [AIAA PAPER 90-1983] p 65 A90-47205
Rocket engine failure detection using system identification techniques [NASA-CR-185259] p 45 N90-25159
- MEYER, T. G.**
Constitutive modeling for isotropic materials (HOST) [NASA-CR-179522] p 26 N90-13390
Constitutive and life modeling of single crystal blade alloys for root attachment analysis p 119 N90-28643
- MEYER, WILLIAM V.**
NASA Laser Light Scattering Advanced Technology Development Workshop, 1988 [NASA-CP-10033] p 188 N90-17085
- MEYERS, GRANT G.**
Ellipsometric studies of the diffusion of atomic oxygen through silicon dioxide thin films p 104 A90-36268
- MICHAL, GARY M.**
Production and processing of Cu-Cr-Nb alloys p 114 A90-33340
Production and processing of Cu-Cr-Nb alloys [NASA-TM-102495] p 117 N90-16053

- MICHELASSI, V.**
Implicit solution of three-dimensional internal turbulent flows
[NASA-TM-103099] p 184 N90-27982
- MICKLOW, GERALD J.**
Effect of vane twist on the performance of dome swirlers for gas turbine airblast atomizers
[AIAA PAPER 90-1955] p 173 A90-47203
Effect of vane twist on the performance of dome swirlers for gas turbine airblast atomizers
[NASA-TM-103195] p 182 N90-25289
- MICU, C. J.**
Ceramic valve development for heavy-duty low heat rejection diesel engines p 196 A90-27091
- MIHALOE, JAMES R.**
STOVL aircraft simulation for integrated flight and propulsion control research
[NASA-TM-102419] p 26 N90-13389
- MILDICE, J. W.**
Bidirectional power converter control electronics
[NASA-CR-175070] p 70 N90-10175
- MILITELLO, C.**
Variational formulation of high-performance finite elements - Parametrized variational principles p 213 A90-46068
Developments in variational methods for high performance plate and shell elements p 214 A90-46288
- MILITELLO, CARMELO**
A variational justification of the assumed natural strain formulation of finite elements. I - Variational principles. II - The C(0) four-node plate element p 210 A90-24384
- MILLER, CHRISTOPHER J.**
Euler analysis comparison with LDV data for an advanced counter-rotation propfan at cruise
[AIAA PAPER 90-3033] p 9 A90-50637
Euler analysis comparison with LDV data for an advanced counter-rotation propfan at cruise
[NASA-TM-103249] p 14 N90-25946
- MILLER, D. R.**
Development and refinement of test bed simulations p 59 A90-38081
- MILLER, ERIC L.**
On the dynamic response of pressure transmission lines in the research of helium-charged free piston Stirling engines p 196 A90-38248
- MILLER, GABRIEL**
Figure of merit studies of beam power concepts for advanced space exploration
[NASA-CR-186720] p 146 N90-26234
- MILLER, JEFFREY H.**
Reaction-compensation technology for microgravity laboratory robots
[NASA-TM-103271] p 205 N90-28062
- MILLER, N. M.**
Free-vibration analysis of three-dimensional solids by BEM p 215 A90-52007
- MILLER, ROBERT A.**
TBCs for better engine efficiency p 83 A90-17294
Thermal barrier coatings for gas turbine and diesel engines
[NASA-TM-102408] p 117 N90-13636
Assessment of fundamental materials needs for Thick Thermal Barrier Coatings (TTBC's) for truck diesel engines
[NASA-TM-103130] p 119 N90-23536
- MILLER, SUSAN P.**
Advanced modulation technology development for earth station demodulator applications. Coded modulation system development
[NASA-CR-185149] p 145 N90-20270
- MILLER, THOMAS L.**
Icing Research Tunnel test of a model helicopter rotor p 15 A90-28179
- MILLIGAN, WALTER W.**
The correlation between the temperature dependence of the CRSS and the formation of superlattice-intrinsic stacking faults in the nickel-base superalloy PWA 1480 p 109 A90-11657
On the mechanism of cross slip in Ni3Al p 111 A90-20611
Micromechanics of cyclic deformation in SSME turbopump blade materials p 224 N90-28641
- MILLIS, MARC G.**
A candidate architecture for monitoring and control in chemical transfer propulsion systems
[AIAA PAPER 90-1882] p 52 A90-41980
Integrated controls and health monitoring for chemical transfer propulsion
[AIAA PAPER 90-2751] p 52 A90-47229
A candidate architecture for monitoring and control in chemical transfer propulsion systems
[NASA-TM-103161] p 52 N90-22595
Integrated controls and health monitoring for chemical transfer propulsion
[NASA-TM-103185] p 52 N90-25178
- MILLWATER, H. R.**
Application of the probabilistic approximate analysis method to a turbopump blade analysis
[AIAA PAPER 90-1098] p 56 A90-29328
Probabilistic analysis of a materially nonlinear structure
[AIAA PAPER 90-1099] p 211 A90-29329
Advanced probabilistic structural analysis method for implicit performance functions p 214 A90-49792
- MINCK, ROBERT**
Sodium-sulfur battery flight experiment definition study p 57 A90-33956
Sodium-sulfur battery flight experiment definition study p 231 A90-20479
- MINER, R. V.**
High temperature creep behavior of single crystal gamma prime and gamma alloys p 110 A90-16901
- MINNETYAN, LEVON**
Progression of damage and fracture in composites under dynamic loading
[AIAA PAPER 90-0916] p 210 A90-29318
Progression of damage and fracture in composites under dynamic loading
[NASA-TM-103118] p 100 N90-21825
Structural behavior of composites with progressive fracture
[NASA-TM-102370] p 100 N90-23477
- MINTER, JANET**
The role of NDE in ceramic turbine engine component development p 206 A90-35508
- MIRANDA, F. A.**
Complex permittivity of lanthanum aluminate in the 20 to 300 K temperature range from 26.5 to 40.0 GHz p 148 A90-37864
Millimeter-wave surface resistance of laser-ablated YBa2Cu3O(7-delta) superconducting films p 257 A90-48694
Millimeter wave surface resistance of RbBa2Cu3O(7-delta) superconductors (R=Y, Eu, Dy, Sm, Er) p 259 N90-20886
Microwave conductivity of laser ablated YBaCuO superconducting films and its relation to microstrip transmission line p 155 N90-27844
- MIRFAKHRAIE, KOOROSH**
Optimal cooperative time-fixed impulsive rendezvous
[AIAA PAPER 90-2962] p 41 A90-53037
- MIRTICH, MICHAEL J.**
Diamondlike carbon protective coatings for optical windows p 122 A90-34569
Effect of eleven years in earth orbit on a mirror surface p 44 A90-36188
Total hemispherical emittance measured at high temperatures by the calorimetric method
[NASA-TM-102322] p 136 N90-10309
- MISRA, A. K.**
Compatibility of Fe-40Al with various fibers p 94 A90-50496
- MISRA, AJAY K.**
Identification of thermodynamically stable ceramic reinforcement materials for iron aluminide matrices p 89 A90-25238
Thermodynamic analysis of chemical compatibility of ceramic reinforcement materials with niobium aluminides p 92 A90-44001
Reactions of SiC with H2/H2O/Ar mixtures at 1300 C p 123 A90-45830
Hydrogen-silicon carbide interactions
[NASA-TM-102382] p 125 N90-11144
Thermodynamic analysis of chemical stability of ceramic materials in hydrogen-containing atmospheres at high temperatures
[NASA-CR-4271] p 126 N90-16072
- MITAL, SUBODH K.**
Fiber pushout test: A three-dimensional finite element computational simulation
[NASA-TM-102565] p 99 N90-21131
Metal matrix composites microfracture: Computational simulation
[NASA-TM-103153] p 101 N90-24383
- MITCHELL, M. A.**
Rapid thermal processing of high temperature superconducting fiber
[NASA-CR-186803] p 259 N90-24964
- MITCHELL, T. E.**
Rapid thermal processing of high temperature superconducting fiber
[NASA-CR-186803] p 259 N90-24964
- MITI-KAVUMA, M.**
Creep and creep rupture of strongly reinforced metallic composites
[NASA-CR-185286] p 223 N90-28110
- MITROS, C.**
Antiferromagnetism in Co-57-doped La2CuO(4-y) studied by Moessbauer spectroscopy p 255 A90-34011
- Hyperfine magnetic field on Cd-111 in Heusler alloys Co2MnZ (Z = Si, Ga, Ge, Sn) p 255 A90-34012
Fe-57 and Sn-119 Moessbauer study of La2CuO(4-y), YBa2Cu3O(7-y) and SmBa2Cu3O(7-y) p 256 A90-34020
- MITTELHANN, H. D.**
Energy stability of thermocapillary convection in a model of the float-zone crystal-growth process p 133 A90-48720
- MIYOSHI, K.**
Plasma-deposited amorphous hydrogenated carbon films and their tribological properties p 123 A90-44864
Fundamental tribological properties of ion-beam-deposited boron nitride films p 124 A90-49054
- MIYOSHI, KAZUHISA**
Plasma-deposited amorphous hydrogenated carbon films and their tribological properties
[NASA-TM-102379] p 125 N90-11880
Fundamental tribological properties of ion-beam-deposited boron nitride films
[NASA-TM-102088] p 125 N90-11881
Studies of mechano-chemical interactions in the tribological behavior of materials
[NASA-TM-102545] p 128 N90-21182
- MIZUTANI, H.**
Effects of lubrication on the performance of high speed spur gears p 194 A90-21119
- MOCKLER, THEODORE T.**
Thermal/structural analyses of several hydrogen-cooled leading-edge concepts for hypersonic flight vehicles
[AIAA PAPER 90-0053] p 164 A90-23702
Thermal/structural analyses of several hydrogen-cooled leading-edge concepts for hypersonic flight vehicles
[NASA-TM-102391] p 177 N90-14511
- MOFFAT, ROBERT J.**
Effects of very high turbulence on heat transfer p 169 A90-35247
- MOHLER, WILLIAM**
Simple evaporation controller for thin-film deposition from a resistively heated boat p 149 A90-39761
- MOKHTARI, SIMIN**
ULTRA-SHARP nonoscillatory convection schemes for high-speed steady multidimensional flow
[NASA-TM-102568] p 244 N90-21570
- MOLDOVER, M. R.**
Critical exponent for the viscosity of carbon dioxide and xenon p 261 A90-43941
- MOLLS, FRANK B.**
Effect of spatial resolution on apparent sensitivity to initial conditions of a decaying flow as it becomes turbulent
[NASA-TM-102377] p 176 N90-13719
- MONGIA, H. C.**
Calculation of turbulent three-dimensional jet-induced flow in a rectangular enclosure p 161 A90-19976
Three-dimensional fluid flow calculations using a flux-spline method p 167 A90-27983
An experimental and numerical study of particle-laden coaxial jet flows p 171 A90-38799
- MONGIA, HUKAM C.**
Composite matrix cooling scheme for small gas turbine combustors
[AIAA PAPER 90-2158] p 22 A90-47210
- MONTAGUE, J.**
Test and theory for piezoelectric actuator-active vibration control of rotating machinery p 198 A90-46226
- MOORE, T. J.**
Preliminary study on pressure brazing and diffusion welding of Nb-12r to Inconel 718 p 196 A90-26899
- MORALES, WILFREDO**
Tribological reactions of perfluoroalkyl polyether oils with stainless steel under ultrahigh vacuum conditions at room temperature p 120 A90-16278
Decomposition of perfluoroalkylpolyethers (PFPE) in ultra-high vacuum under sliding conditions p 122 A90-40714
X-ray photoelectron spectroscopy peak assignment for perfluoropolyether oils p 124 A90-48550
- MORAN, MATTHEW E.**
Initial experimentation on the nonvented fill of a 0.14 cu m (5 cu ft) dewar with nitrogen and hydrogen
[AIAA PAPER 90-1681] p 136 A90-50641
Liquid Transfer Cryogenic Test Facility: Initial hydrogen and nitrogen no-vent fill data
[NASA-TM-102572] p 179 N90-21295
Initial experimentation on the nonvented fill of a 0.14m3 (5 ft. 3) dewar with nitrogen and hydrogen
[NASA-TM-103155] p 183 N90-26278
- MOREL, M.**
Optimal fabrication processes for unidirectional metal-matrix composites - A computational simulation p 93 A90-50096

PERSONAL AUTHOR INDEX

- Optimal fabrication processes for unidirectional metal-matrix composites: A computational simulation [NASA-TM-102559] p 100 N90-21143
- MOREL, M. R.**
Parallel eigenanalysis of finite element models in a completely connected architecture [NASA-CR-185166] p 217 N90-14652
- MOREL, MICHAEL R.**
Eigensolution of finite element problems in a completely connected parallel architecture [NASA-TM-102450] p 217 N90-17173
- MORGAN, WALTER L.**
Role of communications satellites in the fiber era [AIAA PAPER 90-0792] p 139 A90-25617
- MORI, SHIGEYUKI**
Tribological reactions of perfluoroalkyl polyether oils with stainless steel under ultrahigh vacuum conditions at room temperature p 120 A90-16278
Decomposition of perfluoroalkylpolyethers (PFPE) in ultra-high vacuum under sliding conditions p 122 A90-40714
X-ray photoelectron spectroscopy peak assignment for perfluoropolyether oils p 124 A90-48550
- MORIARTY, M. P.**
SP-100 advanced radiator designs for thermoelectric and Stirling applications p 62 A90-38202
- MOROSIN, B.**
Rapid thermal processing of high temperature superconducting fiber [NASA-CR-186803] p 259 N90-24964
- MORREN, W. EARL**
Performance and endurance tests of a laboratory model multipropellant resistorjet p 55 A90-21220
- MORRIS, MARTIN J.**
Experimental investigation of terminal shock sensors in mixed-compression inlets [AIAA PAPER 90-1931] p 186 A90-40560
- MORRIS, P. M.**
Energy efficient engine pin fin and ceramic composite segmented liner combustor sector rig test report [NASA-CR-179534] p 35 N90-28567
- MORRIS, RONALD W.**
A transient plasticity study and low cycle fatigue analysis of the Space Station Freedom photovoltaic solar array blanket [NASA-TM-102516] p 218 N90-19617
- MOSER, J. A.**
Processing and microstructure of melt spun NiAl alloys p 110 A90-16941
- MOSES, RANDOLPH L.**
Convergence of the SMI and the diagonally loaded SMI algorithms with weak interference [AD-A22639] p 141 A90-36717
Effects of additional interfering signals on adaptive array performance [NASA-CR-186508] p 145 N90-20271
- MOSTAFA, A. A.**
An experimental and numerical study of particle-laden coaxial jet flows p 171 A90-38799
- MOSTAFA, ABDU A.**
Introducing the VRT gas turbine combustor [AIAA PAPER 90-2452] p 21 A90-42808
Introducing the VRT gas turbine combustor [NASA-TM-103176] p 137 N90-23591
- MOUNT-CAMPBELL, CLARK A.**
A heuristic approach to worst-case carrier-to-interference ratio maximization in satellite system synthesis [AIAA PAPER 90-0816] p 46 A90-25639
- MROZ, THADDEUS S.**
The NASA Advanced Solar Dynamics Technology Program p 62 A90-38280
- MUEGGENBURG, H. H.**
A highly durable injector faceplate design concept for O₂/H₂ propellants [AIAA PAPER 90-2181] p 66 A90-47211
- MUELLER, D. C.**
Ignition and combustion characteristics of metallized propellants [NASA-CR-186870] p 107 N90-26911
- MULAC, M. W.**
Performance comparisons of nuclear thermal rocket and chemical propulsion systems for piloted missions to Phobos/Mars [IAF PAPER 89-027] p 53 A90-13262
- MULLEN, R. A.**
The numerical simulation of multistage turbomachinery flows p 29 N90-21025
- MULARZ, E. J.**
A planar reacting shear layer system for the study of fluid dynamics-combustion interaction [NASA-TM-102422] p 27 N90-13393
- MULLEN, R. L.**
Numerical modeling of flows in simulated brush seal configurations [AIAA PAPER 90-2141] p 198 A90-47209
- MULLEN, ROBERT L.**
Assumed strain distributions for a finite strip plate bending element using Mindlin-Reissner plate theory p 208 A90-16723
- MULLICAN, A.**
WINCOF-I code for prediction of fan compressor unit with water ingestion [NASA-CR-185157] p 1 N90-21724
- MUNDY, J.**
Automotive Stirling engine development program [NASA-CR-180840] p 264 N90-29260
- MUNROE, PAUL R.**
Improving the low temperature ductility of NiAl p 110 A90-16940
- MURRAY, K. A.**
The Gevaltig: An inertial fusion powered manned spacecraft design for outer solar system missions [NASA-CR-185163] p 50 N90-15985
- MURTHY, DURBHA V.**
Concurrent processing adaptation of aeroelastic analysis of propfans [AIAA PAPER 90-1036] p 211 A90-29380
Concurrent processing adaptation of aeroplastic analysis of propfans [NASA-TM-102455] p 217 N90-14656
- MURTHY, P. L. N.**
Metal matrix composite micromechanics - In situ behavior influence on composite properties p 92 A90-45271
Optimal fabrication processes for unidirectional metal-matrix composites - A computational simulation p 93 A90-50096
Optimal fabrication processes for unidirectional metal-matrix composites: A computational simulation [NASA-TM-102559] p 100 N90-21143
Computational simulation of structural fracture in fiber composites [NASA-TM-102505] p 100 N90-21821
METCAN verification status [NASA-TM-103119] p 100 N90-21824
Simplified design procedures for fiber composite structural components/joints [NASA-TM-103113] p 101 N90-24384
- MURTHY, PAPPU L. N.**
Progression of damage and fracture in composites under dynamic loading [AIAA PAPER 90-0916] p 210 A90-29318
Demonstration of capabilities of high temperature composites analyzer code HITCAN [NASA-TM-102560] p 219 N90-19629
Progression of damage and fracture in composites under dynamic loading [NASA-TM-103118] p 100 N90-21825
Structural behavior of composites with progressive fracture [NASA-TM-102370] p 100 N90-23477
- MURTHY, S. N. B.**
Application of large eddy interaction model to a mixing layer [NASA-CR-185123] p 11 N90-13328
WINCOF-I code for prediction of fan compressor unit with water ingestion [NASA-CR-185157] p 1 N90-21724
- MYERS, I. T.**
Electrical characterization of a Mapham inverter using pulse testing techniques [NASA-TM-103254] p 82 N90-27784
- MYERS, IRA T.**
Central electrical utility power for a satellite ring city in low earth orbit space p 150 N90-10166
High-temperature superconductors for space power transmission lines [NASA-TM-103459] p 259 N90-24952
- MYERS, NEIL B.**
Computer modeling of current collection by the CHARGE-2 mother payload p 252 A90-24933
- MYERS, R. M.**
Multimegawatt electric propulsion system design considerations [AIAA PAPER 90-2552] p 68 A90-52566
Geometric effects in applied-field MPD thrusters [AIAA PAPER 90-2669] p 69 A90-52572
Geometric effects in applied-field MPD thrusters [NASA-TM-103259] p 82 N90-27782
- MYERS, ROGER M.**
Preliminary plume characteristics of an arcjet thruster [AIAA PAPER 90-2645] p 64 A90-42609
Preliminary plume characteristics of an arcjet thruster [NASA-TM-103241] p 81 N90-26071
- NAGAMATSU, H. T.**
Nature of convection-stabilized dc arcs in dual-flow nozzle geometry. I - The cold flow field and dc arc characteristics. II - Optical diagnostics and theory p 252 A90-26665
- NAGIB, H. M.**
A rotating hot-wire technique for spatial sampling of disturbed and manipulated duct flows p 186 A90-41120
- NAGPAL, V. K.**
Probabilistic analysis of bladed turbine disks and the effect of mistuning [AIAA PAPER 90-1097] p 196 A90-29327
Probabilistic analysis of bladed turbine disks and the effect of mistuning [NASA-TM-102564] p 136 N90-21871
- NAGPAL, VINOD K.**
Probabilistic structural analysis of aerospace components using NESSUS [NASA-TM-102324] p 221 N90-22823
- NAGY, A.**
High temperature inelastic deformation of the B1900 + Hf alloy under multiaxial loading - Theory and experiment p 112 A90-22656
- NAGY, LAWRENCE A.**
Satellite range delay simulator for a matrix-switched time division multiple-access network simulation system [AIAA PAPER 90-0795] p 139 A90-25620
Satellite-matrix-switched, time-division-multiple-access network simulator [AIAA PAPER 90-0848] p 147 A90-25671
Satellite-matrix-switched, time-division-multiple-access network simulator [NASA-TP-2944] p 142 N90-11915
Satellite range delay simulator for a matrix-switched time division multiple-access network simulator [NASA-TM-102407] p 143 N90-12813
Rain-fade simulation and power augmentation for satellite communication systems [NASA-TM-103134] p 146 N90-28768
- NAHRA, HENRY K.**
Assessment of the effects of space debris and meteoroids environment on the Space Station solar array assembly p 54 A90-14929
The Space Station photovoltaic panels plasma interaction test program - Test plan and results [AIAA PAPER 90-0722] p 47 A90-22252
Review of the environmental effects on the Space Station Freedom photovoltaic power module p 59 A90-38087
The Space Station Photovoltaic Panels Plasma Interaction Test Program: Test plan and results [NASA-TM-102474] p 49 N90-13581
- NAKAZAWA, SHOHEI**
The MHOST finite element program: 3-D inelastic analysis methods for hot section components. Volume 2: User's manual [NASA-CR-182235-VOL-2] p 215 N90-10450
The MHOST finite element program: 3-D inelastic analysis methods for hot section components. Volume 3: Systems' manual [NASA-CR-182236] p 215 N90-10451
- NALETTE, T.**
Hydrogen-oxygen proton-exchange membrane fuel cells and electrolyzers p 56 A90-33944
Hydrogen-oxygen proton-exchange membrane fuel cells and electrolyzers p 230 N90-20467
- NALLASAMY, M.**
Unsteady Euler analysis of the flowfield of a propfan at an angle of attack [AIAA PAPER 90-0339] p 5 A90-25028
Unsteady blade surface pressures on a large-scale advanced propeller - Prediction and data [AIAA PAPER 90-2402] p 9 A90-47220
Prediction of unsteady blade surface pressures on an advanced propeller at an angle of attack [NASA-TM-102374] p 11 N90-12560
Unsteady Euler analysis of the flow field of a propfan at an angle of attack [NASA-TM-102426] p 248 N90-18229
Large-scale advanced propeller blade pressure distributions: Prediction and data [NASA-TM-102316] p 30 N90-22564
- NAMKOONG, D.**
Thermal energy storage flight experiments p 53 A90-11992
- NAMKOONG, DAVID**
Flight experiment of thermal energy storage p 61 A90-38172
- NARAGHI, M. H. N.**
Radiative configuration factors from cylinders to coaxial axisymmetric bodies p 167 A90-26334
- NATHAL, M.**
Processing and microstructure of melt spun NiAl alloys p 110 A90-16941

- NATHAL, M. V.**
Microstructure and tensile properties of Fe-40 at. pct Al alloys with Cr, Zr, Hf, and B additions p 108 A90-11651
High temperature creep behavior of single crystal gamma prime and gamma alloys p 110 A90-16901
Deformation behavior of NiAl-based alloys containing iron, cobalt, and hafnium p 110 A90-16930
Compressive strength of a B2 matrix NiAl-Nb intermetallic at 1200 and 1300 K p 111 A90-19157
Influence of molybdenum on the creep properties of nickel-base superalloy single crystals p 113 A90-25233
The role of interfacial dislocation networks in high temperature creep of superalloys p 114 A90-33329
Microstructure and mechanical properties of multiphase NiAl-based alloys p 115 A90-35071
Coarsening in high volume fraction nickel-base alloys p 115 A90-37719
Influence of testing environment on the room temperature ductility of FeAl alloys p 115 A90-39658
Compatibility of Fe-40Al with various fibers p 94 A90-50496
- NATHANSON, THEODORE H.**
Space Station Freedom electric power system photovoltaic power module integrated launch package [AIAA PAPER 90-1053] p 48 A90-29281
- NAUD, STEVEN**
Feasibility of intercalated graphite railgun armatures [NASA-TM-102546] p 128 A90-21181
- NAUJOKAS, GERALD J.**
A program for advancing the technology of space concentrators p 60 A90-38159
- NEAL, M. J.**
Rapid thermal processing of high temperature superconducting fiber [NASA-CR-186803] p 258 A90-24964
- NEIDZWECKI, R.**
A circular combustor configuration with multiple injection ports for mixing enhancement p 158 A90-15389
- NEINER, GEORGE**
Engine inlet distortion in a 9.2 percent scaled vectored thrust STOVL model in ground effect [AIAA PAPER 89-2910] p 5 A90-25043
Engine inlet distortion in a 9.2 percent scale vectored thrust STOVL model in ground effect [NASA-TM-102358] p 12 A90-17561
- NEINER, GEORGE H.**
Hot gas ingestion characteristics and flow visualization of a vectored thrust STOVL concept [NASA-TM-103212] p 32 A90-26009
- NEITZEL, G. P.**
Energy stability of thermocapillary convection in a model of the float-zone crystal-growth process p 133 A90-48720
- NELSON, A. J.**
Investigation of buried homojunctions in p-InP formed during sputter deposition of both indium tin oxide and indium oxide p 256 A90-36799
- NELSON, C. C.**
An annular gas seal analysis using empirical entrance and exit region friction factors [ASME PAPER 89-TR1B-46] p 196 A90-33555
- NELSON, H. D.**
An active optimal control strategy of rotor vibrations using external forces p 198 A90-46224
- NELSON, PAUL**
A radiological assessment of nuclear power and propulsion operations near Space Station Freedom [NASA-CR-185185] p 76 A90-21108
- NEMETH, EDWARD**
Health management system for rocket engines [NASA-CR-185223] p 131 A90-23574
- NEMETH, NOEL N.**
Designing ceramic components with the CARES computer program p 235 A90-19147
Design of ceramic components with the NASA/CARES computer program [NASA-TM-102369] p 222 A90-26359
Ceramics Analysis and Reliability Evaluation of Structures (CARES). Users and programmers manual [NASA-TP-2916] p 223 A90-28099
- NESARIKAR, V. V.**
Side branch morphology and coarsening in directionally solidified Pb-8.4 at. pct Au p 109 A90-11658
- NESBITT, J. A.**
Diffusional aspects of the high-temperature oxidation of protective coatings p 113 A90-28075
- NESBITT, JAMES A.**
Materials for engine applications above 3000 deg F: An overview [NASA-TM-100169] p 95 A90-10188
Heat transfer to throat tubes in a square-chambered rocket engine at the NASA Lewis Research Center [NASA-TM-102336] p 70 A90-11082
- Thermal modelling of various thermal barrier coatings in a high heat flux rocket engine [NASA-TM-102418] p 117 A90-16911
Durability of thermal barrier coatings in a high heat flux environment p 129 A90-28651
Thermal analysis of thermal barrier coatings in a high heat flux environment p 129 A90-28652
- NEUBERT, T.**
Computer modeling of current collection by the CHARGE-2 mother payload p 252 A90-24933
The sheath structure around a negatively charged rocket payload p 48 A90-34780
- NEUMAN, HARVEY E.**
Laser-velocimeter-measured flow field around an advanced, swept, eight-blade propeller at Mach 0.8 [NASA-TP-2462] p 1 A90-20942
- NEUSTADTER, MARC S.**
Data compression techniques applied to high resolution high frame rate video technology [NASA-CR-4263] p 143 A90-14452
- NG, DANIEL L. P.**
Multiwavelength pyrometry to correct for reflected radiation [NASA-TM-102578] p 190 A90-23714
- NG, LIAN LAI**
Instabilities and subharmonic resonances of subsonic heated round jets, volume 2 [NASA-CR-186058] p 181 A90-22017
- NGUYEN, H. L.**
Critical evaluation of Jet-A spray combustion using propane chemical kinetics in gas turbine combustion simulated by KIVA-II [AIAA PAPER 90-2439] p 105 A90-50645
GRID2D/3D: A computer program for generating grid systems in complex-shaped two- and three-dimensional spatial domains. Part 2: User's manual and program listing [NASA-TM-102454] p 237 A90-20708
GRID2D/3D: A computer program for generating grid systems in complex-shaped two- and three-dimensional spatial domains. Part 1: Theory and method [NASA-TM-102453] p 238 A90-22262
Critical evaluation of Jet-A spray combustion using propane chemical kinetics in gas turbine combustion simulated by KIVA-2 [NASA-TM-103173] p 138 A90-26170
- NGUYEN, H. LEE**
Effect of vane twist on the performance of dome swirlers for gas turbine airblast atomizers [AIAA PAPER 90-1955] p 173 A90-47203
Two-dimensional analysis of two-phase reacting flow in a firing direct-injection diesel engine [NASA-TM-102069] p 27 A90-13392
Effect of vane twist on the performance of dome swirlers for gas turbine airblast atomizers [NASA-TM-103195] p 182 A90-25289
Evaluation of a hybrid kinetics/mixing-controlled combustion model for turbulent premixed and diffusion combustion using KIVA-2 [NASA-TM-103196] p 185 A90-28792
- NGUYEN, HUNG LEE**
Reduced chemical kinetics for propane combustion [AIAA PAPER 90-0546] p 103 A90-19904
Introducing the VRT gas turbine combustor [AIAA PAPER 90-2452] p 21 A90-42808
Introducing the VRT gas turbine combustor [NASA-TM-103176] p 137 A90-23591
- NIEDRA, J. M.**
High frequency, high temperature specific core loss and dynamic B-H hysteresis loop characteristics of soft magnetic alloys [NASA-TM-103164] p 154 A90-23663
- NIEDZWECKI, R. W.**
High speed commercial transport fuels considerations and research needs [NASA-TM-102535] p 131 A90-21869
- NIEZGODA, THOMAS F.**
Investigation of methods to produce a uniform cloud of fuel particles in a flame tube [NASA-TM-102376] p 178 A90-18665
- NIKJOO, M.**
Calculation of turbulent three-dimensional jet-induced flow in a rectangular enclosure [AIAA PAPER 90-0684] p 161 A90-19976
- NIKNAPS, H. S.**
A cost-effective strategy for nonoscillatory convection without clipping [NASA-TM-102538] p 179 A90-21291
- NIRMALAN, V.**
An experimental study of turbine vane heat transfer with leading edge and downstream film cooling [ASME PAPER 89-GT-69] p 165 A90-23792
- NOEBE, R. D.**
Processing and microstructure of melt spun NiAl alloys p 110 A90-16941
- Observations on the brittle to ductile transition temperatures of B2 nickel aluminides with and without zirconium p 111 A90-19153
The effects of surface films on mechanical behavior of B2 ordered intermetallic alloys p 115 A90-44338
- NOEBE, RONALD**
Up-and-coming IMCs p 88 A90-17295
- NONAMI, K.**
Active vibration control for flexible rotor by optimal direct-output feedback control p 197 A90-46222
- NORDWALL, H. L.**
A Brayton cycle solar dynamic heat receiver for space p 61 A90-38165
- NORMAN, J. P.**
The application of cast SiC/Al to rotary engine components [NASA-CR-179610] p 25 A90-13385
- NOTTKE, NATHAN**
A superconducting quenchgun for delivering lunar derived oxygen to lunar orbit [AIAA PAPER 90-2369] p 43 A90-40627
A superconducting quenchgun for delivering lunar derived oxygen to lunar orbit [NASA-CR-185161] p 77 A90-21806
- NOWOTNY, H.**
Identification of a cast iron alloy containing nonstrategic elements [NASA-CR-185174] p 118 A90-18559
- NYLAND, TED W.**
Initial experimentation on the nonvented fill of a 0.14 cu m (5 cu ft) dewar with nitrogen and hydrogen [AIAA PAPER 90-1681] p 136 A90-50641
Liquid Transfer Cryogenic Test Facility: Initial hydrogen and nitrogen no-vent fill data [NASA-TM-102572] p 179 A90-21295
Acquisition and correlation of cryogenic nitrogen mass flow data through a multiple orifice Joule-Thomson device [NASA-TM-103121] p 182 A90-22761
Initial experimentation on the nonvented fill of a 0.14m3 (5 ft. 3) dewar with nitrogen and hydrogen [NASA-TM-103155] p 183 A90-26278
- O**
- O'BRIEN, J. E.**
Two-component phase-averaged turbulence statistics downstream of a rotating spoke-wheel wake generator p 156 A90-11559
Some characteristics of bypass transition in a heated boundary layer p 169 A90-35183
- O'BRIEN, JAMES E.**
A technique for measurement of instantaneous heat transfer in steady-flow ambient-temperature facilities p 172 A90-39625
- O'DONNELL, PATRICIA M.**
Energy storage considerations for a robotic Mars surface sampler [AAS PAPER 87-245] p 42 A90-16544
Space Electrochemical Research and Technology Conference, 2nd, Cleveland, OH, Apr. 11-13, 1989, Proceedings p 227 A90-33932
- O'NEILL, M. J.**
The mini-dome lens space concentrator array - Recent component test results and current array development status p 60 A90-38155
- O'NEILL, MARK J.**
An advanced space photovoltaic concentrator array using Fresnel lenses, gallium arsenide cells, and prismatic cell covers p 54 A90-14954
- O'REILLY, MICHAEL**
LBR-2 earth stations for the ACTS program [AIAA PAPER 90-0838] p 42 A90-25662
- OBBERHARDT, M. R.**
Theory of plasma contactors in ground-based experiments and low earth orbit p 150 A90-47108
- OBERLE, LAWRENCE G.**
TiCl4 as a source of TiO2 particles for laser anemometry measurements in hot gas [NASA-TM-102581] p 189 A90-20358
- OCANNOR, BRENDAN M.**
A trajectory generation and system characterization model for cislunar low-thrust spacecraft. Volume 2: Technical manual [NASA-CR-185172] p 77 A90-21807
- ODONNELL, PATRICIA M.**
NASA aerospace flight battery systems program [NASA-TM-103237] p 233 A90-26397
- OH, J. E.**
Molecular beam epitaxial growth of high-quality InSb on InP and GaAs substrates p 253 A90-12808
- OHAYON, R.**
Mixed variational formulation of finite element analysis of acoustoelastic/slosh fluid-structure interaction p 212 A90-34851

- OHAYON, ROGER**
Treatment of coupled fluid-structure interaction problems by a mixed variational principle p 159 A90-18288
- OLAN, EMMANUEL**
Vibration dampers for cryogenic turbomachinery [AIAA PAPER 90-2740] p 199 A90-47228
- OLDENBURG, J. R.**
Comparison of two droplet sizing systems in an icing wind tunnel [NASA-TM-102456] p 200 N90-14617
- OLDENBURG, JOHN R.**
Comparison of two droplet sizing systems in an icing wind tunnel [AIAA PAPER 90-0668] p 164 A90-23711
Spray nozzle investigation for the Improved Helicopter Icing Spray System (IHSS) [AIAA PAPER 90-0666] p 37 A90-25040
Comparison of drop size distributions from two droplet sizing systems [NASA-TM-102520] p 202 N90-17147
- OLEN, CARL**
Application of heuristic satellite plan synthesis algorithms to requirements of the WARC-88 allotment plan [AIAA PAPER 90-0815] p 245 A90-25638
Application of heuristic satellite plan synthesis algorithms to requirements of the WARC-88 allotment plan [NASA-TM-102479] p 245 N90-14856
- OLEN, CARL A.**
A heuristic approach to worst-case carrier-to-interference ratio maximization in satellite system synthesis [AIAA PAPER 90-0816] p 46 A90-25639
- OLINTO, ANGELA V.**
Is the sub-millisecond pulsar strange? p 264 A90-12669
- OLIVE, KEITH A.**
Neutron stars and white dwarfs in galactic halos? p 265 A90-30909
Big bang nucleosynthesis and the quark-hadron transition p 265 A90-31407
- OLMSTEAD, DEAN A.**
Advanced Communications Technology Satellite (ACTS) [AIAA PAPER 90-0839] p 140 A90-25663
- OLSON, S. L.**
Properties of $Pb(1-x)Bi(x)/Ba_2YCu_3O(x)$ composites - Reaction of $Ba_2YCu_3O(x)$ with Pb and Bi p 255 A90-33224
- OLSON, SANDRA I.**
Fire safety applications for spacecraft p 16 N90-17595
- OLSON, SANDRA L.**
Ignition and behavior of laminar gas-jet diffusion flames in microgravity p 103 A90-23107
Near-limit flame spread over a thin solid fuel in microgravity p 104 A90-32835
- ONEILL, MARK J.**
Conceptual design study of a 5 kilowatt solar dynamic Brayton power system using a dome Fresnel lens solar concentrator [NASA-CR-185134] p 72 N90-14281
- ORANGE, T. W.**
Simulation of crack growth and crack closure under large cyclic plasticity p 214 A90-50562
- ORANGE, THOMAS W.**
Method and models for R-curve instability calculations p 214 A90-50566
- ORTH, NORMAN W.**
Production and processing of Cu-Cr-Nb alloys p 114 A90-33340
Production and processing of Cu-Cr-Nb alloys [NASA-TM-102495] p 117 N90-16053
- ORTIZ, MILTON**
Thermal barrier coating life prediction model development, phase 1 [NASA-CR-182230] p 26 N90-13388
- OSAKI, H.**
Measurement of the intrinsic bond strength of brittle thin films on flexible substrates p 256 A90-44022
- OSWALD, F. B.**
Comparison of boundary element and finite element methods in spur gear root stress analysis p 193 A90-21107
Dynamic loading of spur gears with linear or parabolic tooth profile modifications p 195 A90-21126
Profile modification to minimize spur gear dynamic loading p 195 A90-21128
Computer aided design of spur gear teeth p 195 A90-21131
- OSWALD, FRED B.**
Experimental and analytical evaluation of dynamic load vibration of a 2240-kW (3000-hp) rotorcraft transmission p 192 A90-13750
- Improvement of finite element meshes - Heat transfer in an infinite cylinder p 209 A90-19109
Gear noise, vibration, and diagnostic studies at NASA Lewis Research Center [NASA-TM-102435] p 202 N90-18041
Influence of linear profile modification and loading conditions on the dynamic tooth load and stress of high contact ratio gears [NASA-TM-103136] p 204 N90-22796
Computer-aided design of high-contact-ratio gears for minimum dynamic load and stress [NASA-TM-103275] p 205 N90-28065
- OU, S.**
Augmented heat transfer in rectangular channels of narrow aspect ratios with rib turbulators p 157 A90-13091
- OUZTS, PETER**
H-infinity based integrated flight/propulsion control design for a STOVL aircraft in transition flight [AIAA PAPER 90-3335] p 36 A90-47595
- OUZTS, PETER J.**
Real-time simulation of an F110/STOVL turbofan engine [NASA-TM-102409] p 25 N90-12618
H-infinity based integrated flight/propulsion control design for a STOVL aircraft in transition flight [NASA-TM-103198] p 37 N90-26011
- OZGUVEN, H. N.**
Dynamic analysis of geared rotors by finite elements p 194 A90-21123
- OZGUVEN, H. NEVZAT**
Dynamic analysis of geared rotors by finite elements [NASA-TM-102349] p 201 N90-16286
- P**
- PADOVAN, JOE**
Multi-level Hierarchical Poly Tree computer architectures p 236 A90-26082
- PALASZEWSKI, BRYAN**
Lunar missions using advanced chemical propulsion - System design issues [AIAA PAPER 90-2431] p 67 A90-47221
- PALASZEWSKI, BRYAN A.**
Atomic hydrogen as a launch vehicle propellant [AIAA PAPER 90-0715] p 44 A90-23712
Atomic hydrogen as a launch vehicle propellant [NASA-TM-102459] p 73 N90-14284
Advanced launch vehicle propulsion at the NASA Lewis Research Center [NASA-TM-103096] p 45 N90-20110
- PALAZZOLO, A. B.**
Test and theory for piezoelectric actuator-active vibration control of rotating machinery p 198 A90-46226
- PALAZZOLO, ALAN B.**
Vibration dampers for cryogenic turbomachinery [AIAA PAPER 90-2740] p 199 A90-47228
- PALKO, JOSEPH L.**
Analysis of whisker-toughened ceramic components - A design engineer's viewpoint p 88 A90-19149
Analysis of whisker-toughened ceramic components: A design engineer's viewpoint [NASA-TM-102333] p 97 N90-18504
- PALUMBO, DANIEL L.**
Three approaches to reliability analysis p 206 A90-30706
- PAMULAPATI, J.**
Dielectric function of InGaAs in the visible [NASA-TM-103246] p 260 N90-26683
- PANK, D. R.**
Deformation behavior of NiAl-based alloys containing iron, cobalt, and hafnium p 110 A90-16930
Microstructure and mechanical properties of multiphase NiAl-based alloys p 115 A90-35071
- PANTIC, DRAGAN M.**
Electron-beam induced damage in thin insulating films on compound semiconductors p 151 N90-17987
[NASA-CR-185177]
Electron beam induced damage in PECVD Si₃N₄ and SiO₂ films on InP [NASA-TM-102544] p 203 N90-20393
- PAO, YOH-HAN**
Automating security monitoring and analysis for Space Station Freedom's electric power system [NASA-TM-103148] p 240 N90-22324
- PAPADOPOULOS, D. S.**
Autoclavable addition polyimides for 371 C composite applications [NASA-TM-103233] p 102 N90-27874
- PAPADOPOULOS, DEMETRIOS S.**
Use of unbalanced laminates as a screening method for microcracking p 94 A90-50217
Use of unbalanced laminates as a screening method for microcracking [NASA-TM-102517] p 98 N90-21124
- PAPELL, S. STEPHEN**
Liquid Transfer Cryogenic Test Facility: Initial hydrogen and nitrogen no-vent fill data [NASA-TM-102572] p 179 N90-21295
Acquisition and correlation of cryogenic nitrogen mass flow data through a multiple orifice Joule-Thomson device [NASA-TM-103121] p 182 N90-22761
- PARK, A.**
Constitutive parameter measurements of lossy materials [NASA-CR-183398] p 257 N90-11603
- PARK, J. S.**
Augmented heat transfer in rectangular channels of narrow aspect ratios with rib turbulators p 157 A90-13091
- PARKES, J. E.**
Test facility and preliminary performance of a 100 kW class MPD thruster p 75 N90-18476
- PARZYCH, DAVID**
Acoustic test and analysis of a counterrotating prop-fan model [NASA-CR-179590] p 247 N90-10683
- PASKIN, MARC D.**
Composite matrix cooling scheme for small gas turbine combustors [AIAA PAPER 90-2158] p 22 A90-47210
- PATANKAR, S. V.**
Three-dimensional fluid flow calculations using a flux-spine method p 167 A90-27983
- PATEL, G. B.**
The GEM-T2 gravitational model [NASA-TM-100746] p 234 N90-12984
- PATHAK, P. H.**
High-frequency asymptotic methods for analyzing the EM scattering by open-ended waveguide cavities [NASA-CR-186244] p 143 N90-16103
- PATNAIK, SURYA N.**
Compatibility conditions of structural mechanics for finite element analysis [NASA-TM-102413] p 217 N90-17180
Integrated force method versus displacement method for finite element analysis [NASA-TP-2937] p 218 N90-18081
- PATRICK, W. P.**
Investigation of the near wake of a propfan p 7 A90-40686
- PATRICK, WILLIAM P.**
Laser velocimeter and total pressure measurements in circular-to-rectangular transition ducts [NASA-CR-182286] p 177 N90-14494
- PATTERSON, A. G.**
Development and refinement of test bed simulations p 59 A90-38081
- PATTERSON, ALEXANDER G.**
Distortion and regulation characterization of a Mapham inverter p 148 A90-38125
- PATTERSON, M. J.**
Xenon ion propulsion for orbit transfer [AIAA PAPER 90-2527] p 67 A90-52562
Multimegawatt electric propulsion system design considerations [AIAA PAPER 90-2552] p 68 A90-52566
Electric propulsion options for 10 kW class earth-space missions p 75 N90-18474
- PATTERSON, MICHAEL J.**
5kW xenon ion thruster lifetest [AIAA PAPER 90-2543] p 68 A90-52564
- PATTERSON, RICHARD L.**
A fiber-optic current sensor for aerospace applications [NASA-TM-103152] p 190 N90-22773
- PATTON, A. D.**
Central electrical utility power for a satellite ring city in low earth orbit space p 150 N90-10166
- PAULSEN, PHILLIP E.**
Evaluation of atomic oxygen resistant protective coatings for fiberglass-epoxy composites in LEO p 84 A90-31581
The effects of atomic oxygen on the thermal emittance of high temperature radiator surfaces [NASA-TM-103224] p 102 N90-28670
- PAVLI, ALBERT J.**
Advanced tube-bundle rocket thrust chamber [AIAA PAPER 90-2726] p 67 A90-47227
Advanced tube-bundle rocket thrust chamber [NASA-TM-103139] p 80 N90-25185
- PAYSON, J. SCOTT**
Radiation resistance studies of amorphous silicon films p 227 A90-14952
- PEARSON, D. D.**
Influence of molybdenum on the creep properties of nickel-base superalloy single crystals p 113 A90-25233
- PEASE, D. M.**
X-ray beam method for displacement measurement in hostile environments p 187 A90-44485

- PEDDICORD, K. LEE**
A radiological assessment of nuclear power and propulsion operations near Space Station Freedom [NASA-CR-185185] p 76 N90-21108
- PEDERSEN, J.**
NASA/GE Energy Efficient Engine low pressure turbine scaled test vehicle performance report [NASA-CR-168290] p 34 N90-28563
- PENCIL, ERIC**
Attachment of lead wires to thin film thermocouples mounted on high temperature materials using the parallel gap welding process [NASA-TM-102442] p 189 N90-21361
- PENCIL, ERIC J.**
Performance characterization of a segmented anode arcjet thruster [AIAA PAPER 90-2582] p 68 A90-52569
- PENKO, PAUL F.**
Efficient Monte Carlo simulation of rarefied flow in a small nozzle [AIAA PAPER 90-1693] p 170 A90-38396
- PENNOCK, A. P.**
Analysis of results from wind tunnel tests of inlets for an advanced turboprop nacelle installation [NASA-CR-174937] p 10 N90-10011
- PEPPER, STEPHEN V.**
Fundamentals of tribology at the atomic level p 192 A90-14020
- PEREIRA, J. MICHAEL**
Improved transverse crack detection in composites [NASA-TM-103261] p 102 N90-27875
- PEREZ-DAVIS, MARLA E.**
Mars manned transportation vehicle [AAS PAPER 87-271] p 42 A90-16569
Aeolian removal of dust from photovoltaic surfaces on Mars [NASA-TM-102507] p 76 N90-19299
Energy storage for a lunar base by the reversible chemical reaction: $\text{CaO} + \text{H}_2\text{O}$ reversible reaction $\text{Ca}(\text{OH})_2$ [NASA-TM-103145] p 233 N90-25419
Aeolian removal of dust from radiator surfaces on Mars [NASA-TM-103205] p 81 N90-26068
The chemical effects of the Martian environment on power system component materials: A theoretical approach [NASA-TM-103203] p 87 N90-26074
- PERINO, MARIA ANTONIETTA**
Lunar production of solar cells - A near-term product for a lunar industrial facility p 42 A90-24791
- PERRY, J. L.**
The mini-dome lens space concentrator array - Recent component test results and current array development status p 60 A90-38155
- PERRY, JOHN G.**
Reusable rocket engine turbopump health monitoring system, part 3 [NASA-CR-182294] p 204 N90-26320
- PERRY, WILLIAM D.**
Hot filament technique for measuring the thermal conductivity of molten lithium fluoride [NASA-TM-102506] p 127 N90-19373
- PETERSON, ANDREW A.**
Spray nozzle investigation for the Improved Helicopter Icing Spray System (IHSS) [AIAA PAPER 90-0666] p 37 A90-25040
- PETERSON, TODD T.**
Update of the Solar Concentrator Advanced Development Project p 48 A90-38267
- PETIT, J. B.**
Deep-level dominated electrical characteristics of Au contacts on beta-SiC p 147 A90-33726
- PETRARCA, D. A.**
Hardware development for the surface tension driven convection experiment p 52 A90-36195
- PETRASEK, D. W.**
Refractory metal alloys and composites for space power systems p 116 A90-46677
- PETRASEK, DONALD W.**
Fiber reinforced superalloys p 91 A90-34169
- PETRIK, EDWARD J.**
Autonomous power expert system p 240 N90-22306
- PFEIFFER, S.**
Conceptual design of a Liquid Droplet Radiator space flight experiment [SAE PAPER 891565] p 48 A90-27527
- PFEIFFER, SHLOMO L.**
Conceptual design of liquid droplet radiator shuttle-attached experiment [NASA-CR-185164] p 71 N90-11805
Conceptual design of liquid droplet radiator shuttle-attached experiment technical requirements document [NASA-CR-185165] p 71 N90-11806
- PHAM, M.**
Hydrogen-oxygen proton-exchange membrane fuel cells and electrolyzers p 56 A90-33944
Hydrogen-oxygen proton-exchange membrane fuel cells and electrolyzers p 230 N90-20467
- PHARR, G. M.**
On the stability of the creep substructure in NaCl single crystals p 254 A90-21920
Creep substructure formation in sodium chloride single crystals in the power law and exponential creep regimes p 255 A90-33330
- PHILIPP, WARREN H.**
Studies on the use of supercritical ammonia for ceramic nitride synthesis and fabrication [NASA-TM-102570] p 106 N90-21843
Polysiloxanes derived from the controlled hydrolysis of tetraethoxysilane as precursors to silica for use in ceramic processing [NASA-TM-102489] p 128 N90-21858
- PHILLIPS, R. E.**
Thermal effects on the mechanical properties of SiC fibre reinforced reaction-bonded silicon nitride matrix composites p 92 A90-46999
- PHILLIPS, RONALD E.**
Laminate behavior for SiC fiber-reinforced reaction-bonded silicon nitride matrix composites p 90 A90-29927
- PIDGEON, DAVID J.**
Advanced propulsion for LEO and GEO platforms [AIAA PAPER 90-2551] p 68 A90-52565
Advanced propulsion for LEO and GEO platforms [NASA-TM-103228] p 82 N90-27785
- PIEPER, JERRY L.**
Combustor design and analysis using the ROCKET Combustor Interactive Design (ROCCID) Methodology [AIAA PAPER 90-2240] p 65 A90-45694
Combustor design and analysis using the Rocket Combustor Interactive Design (ROCCID) methodology [NASA-TM-103165] p 79 N90-24349
- PIERCE, F. J.**
The growth and development of a turbulent junction vortex system p 173 A90-46902
- PINON, ELFEGO, III**
A trajectory generation and system characterization model for cislunar low-thrust spacecraft. Volume 2: Technical manual [NASA-CR-185172] p 77 N90-21807
- PIPER, LAWRENCE G.**
H₂/O₂ three-body rates at high temperatures [AIAA PAPER 90-1696] p 105 A90-38399
- PISZCZOR, M. F.**
The mini-dome lens space concentrator array - Recent component test results and current array development status p 60 A90-38155
- PISZCZOR, MICHAEL F.**
An advanced space photovoltaic concentrator array using Fresnel lenses, gallium arsenide cells, and prismatic cell covers p 54 A90-14954
- PISZCZOR, MICHAEL, JR.**
NASA advanced space photovoltaic technology: Status, potential and future mission applications p 74 N90-17775
- PLA, FREDERIC**
Microgravity acoustic mixing for particle cloud combustors [NASA-CR-185159] p 248 N90-21600
- PLA, FREDERIC G.**
Investigation of methods to produce a uniform cloud of fuel particles in a flame tube [NASA-TM-102376] p 178 N90-18665
- PLASTINO, A.**
Phase transitions in fermionic systems with many-body interaction p 249 A90-19303
- PLATZER, M. F.**
Progress towards the development of an inviscid-viscous interaction method for unsteady flows in turbomachinery cascades p 2 A90-11806
- PLATZER, MAX F.**
Unsteady heat transfer on turbine blades p 161 A90-20511
- PLINE, A. D.**
Hardware development for the surface tension driven convection experiment p 52 A90-36195
- PLINE, ALEXANDER D.**
Development of an infrared imaging system for the surface tension driven convection experiment p 188 N90-17922
Spacelab qualified infrared imager for microgravity science experiments [NASA-TM-102503] p 189 N90-20352
- PODBOY, GARY G.**
Euler analysis comparison with LDV data for an advanced counter-rotation propfan at cruise [AIAA PAPER 90-3033] p 9 A90-50637
- Euler analysis comparison with LDV data for an advanced counter-rotation propfan at cruise [NASA-TM-103249] p 14 N90-25946
- PODDAR, K.**
A study of the unsteadiness of crossing shock wave turbulent boundary layer interactions [AIAA PAPER 90-1456] p 170 A90-38614
- POINSAATTE, PHILIP E.**
Convective heat transfer measurements from a NACA 0012 airfoil in flight and in the NASA Lewis Icing Research Tunnel [AIAA PAPER 90-0199] p 162 A90-22180
Convective heat transfer measurements from a NACA 0012 airfoil in flight and in the NASA Lewis Icing Research Tunnel [NASA-TM-102448] p 176 N90-13750
Heat transfer measurements from a NACA 0012 airfoil in flight and in the NASA Lewis icing research tunnel [NASA-CR-4278] p 13 N90-19203
- POIRIER, D. R.**
Solute redistribution in dendritic solidification with diffusion in the solid p 253 A90-17399
Efficient estimation of diffusion during dendritic solidification p 111 A90-20612
The role of gravity on macrosegregation in alloys [NASA-CR-186530] p 136 N90-25238
- POLAND, D. T.**
Propfan Test Assessment (PTA) [NASA-CR-185138] p 25 N90-11739
- PONCHAK, DENISE S.**
Numerical Arc Segmentation Algorithm for a Radio Conference-NASARC (version 4.0) technical manual [NASA-TM-101453] p 144 N90-20264
Numerical Arc Segmentation Algorithm for a Radio Conference (NASARC), version 4.0: User's manual [NASA-TM-101454] p 145 N90-21250
A technology assessment of alternative communications systems for the space exploration initiative [NASA-TM-103243] p 47 N90-27736
- PONCHAK, G. E.**
Coax-to-channelised coplanar waveguide in-phase N-way, radial power divider p 149 A90-41605
Channelized coplanar waveguide pin-diode switches [NASA-TM-102289] p 150 N90-11943
- PONCHAK, GEORGE E.**
Experimental investigations on channelized coplanar waveguide [NASA-TM-102494] p 151 N90-20286
A new rectangular waveguide to coplanar waveguide transition [NASA-TM-102477] p 145 N90-21263
Coplanar waveguide fed phased array antenna [NASA-TM-102522] p 152 N90-21273
Coplanar waveguide discontinuities for P-I-N diode switches and filter applications [NASA-TM-102534] p 153 N90-21278
- PONTANO, B. A.**
A users perspective of the ACTS hopping beam TDMA system [AIAA PAPER 90-0833] p 140 A90-25658
- PORDAL, H. S.**
A flux-split solution procedure for unsteady inlet flows [AIAA PAPER 90-0585] p 6 A90-26967
Transient behavior of supersonic flow through inlets [AIAA PAPER 90-2130] p 8 A90-42734
- POTAPCZUK, M. G.**
Swept wing ice accretion modeling [AIAA PAPER 90-0756] p 5 A90-25042
The low frequency oscillation in the flow over a NACA0012 airfoil with an 'iced' leading edge p 8 A90-46377
Experimental investigation of multielement airfoil ice accretion and resulting performance degradation p 9 A90-48954
- POTAPCZUK, MARK**
Modeling of surface roughness effects on glaze ice accretion p 16 N90-20925
- POTAPCZUK, MARK G.**
Predictions of airfoil aerodynamic performance degradation due to icing p 3 A90-16753
Swept wing ice accretion modeling [NASA-TM-103114] p 13 N90-21727
- POUCH, J. J.**
Plasma-deposited amorphous hydrogenated carbon films and their tribological properties p 123 A90-44864
Synthesis and structural chemistry of Au(III)-substituted Ba₂YCu₃O₇(δ) [NASA-TM-103292] p 108 N90-28696
- POUCH, JOHN J.**
Optical dispersion relations for diamondlike carbon films [NASA-TM-102356] p 257 N90-10738
Plasma-deposited amorphous hydrogenated carbon films and their tribological properties [NASA-TM-102379] p 125 N90-11880

PERSONAL AUTHOR INDEX

- POVINELLI, L. A.**
Implicit solution of three-dimensional internal turbulent flows
[NASA-TM-103099] p 184 N90-27982
- POVINELLI, LOUIS A.**
Advanced computational techniques for hypersonic propulsion p 156 A90-12606
Least-squares finite element method for fluid dynamics p 159 A90-18246
CFD propels NASP propulsion progress p 172 A90-41163
Computational modeling and validation for hypersonic inlets p 181 N90-22011 [NASA-TM-103111]
- POWELL, J. A.**
Growth of improved quality 3C-SiC films on 6H-SiC substrates p 255 A90-29596
Growth of high quality 6H-SiC epitaxial films on vicinal (0001) 6H-SiC wafers p 255 A90-29952
Modeling of the SiC chemical vapor deposition process and comparison with experimental results p 105 A90-36810
- POWERS, ALBERT G.**
COLD-SAT - An orbital cryogenic hydrogen technology experiment [IAF PAPER 89-057] p 53 A90-13282
- PRAHL, JOSEPH M.**
On the numerical solution of the dynamically loaded hydrodynamic lubrication of the point contact problem [NASA-TM-102427] p 178 N90-17076
- PRAKASH, C.**
The modelling of heat, mass and solute transport in solidification systems p 157 A90-13092
- PRAKASH, JAI**
Electrocatalysis for oxygen electrodes in fuel cells and water electrolyzers for space applications p 57 A90-33945
Electrocatalysis for oxygen electrodes in fuel cells and water electrolyzers for space applications p 230 N90-20468
- PRICE, KENT M.**
Role of communications satellites in the fiber era [AIAA PAPER 90-0792] p 139 A90-25617
Servicing communication satellites in geostationary orbit [AIAA PAPER 90-0830] p 39 A90-25655
Data distribution satellite system architecture concept [AIAA PAPER 90-0885] p 46 A90-25704
- PRIEM, RICHARD J.**
Combustion instability coupling with feed system acoustics p 108 N90-28629
- PROBST, HUBERT B.**
Effects of crucible wetting during solidification of immiscible Pb-Zn alloys p 132 A90-17825
Materials for engine applications above 3000 deg F: An overview [NASA-TM-100169] p 95 N90-10188
- PROKOPIUS, P.**
Regenerative fuel cell systems for project pathfinder p 74 N90-17708
- PROKOPIUS, PAUL R.**
The fuel cell in space - Yesterday, today and tomorrow p 56 A90-26837
The fuel cell in space: Yesterday, today and tomorrow [NASA-TM-102366] p 70 N90-11804
- PRUSSING, J. E.**
Optimal impulsive time-fixed orbital rendezvous and interception with path constraints [AIAA PAPER 90-2972] p 41 A90-53051
- PRUSSING, JOHN E.**
Optimal orbital rendezvous using high and low thrust [AAS PAPER 89-354] p 41 A90-46786
- PRYDZ, R. A.**
Interior noise in the untreated Gulfstream II Proplan Test Assessment aircraft p 17 A90-44736
- PUTNAM, R. M.**
EPSAT - A workbench for designing high-power systems for the space environment [AIAA PAPER 90-0637] p 245 A90-26975
- PUTNAM, RAND M.**
The Environment-Power System Analysis Tool development program p 236 A90-38089
- PUTNEY, B. H.**
The GEM-T2 gravitational model [NASA-TM-100746] p 234 N90-12984
- Q**
- QUEALY, ANGELA**
Hypercluster parallel processing library user's manual [NASA-CR-185231] p 237 N90-21552
- QUENTMEYER, R. J.**
Rocket combustion chamber life-enhancing design concepts [AIAA PAPER 90-2116] p 66 A90-47208
- QUENTMEYER, RICHARD J.**
Rocket combustion chamber life-enhancing design concepts [NASA-CR-185257] p 79 N90-25183
- QUINN, TODD**
Autonomous power expert system p 240 N90-22306
- QUINN, TODD M.**
Autonomous power expert system [NASA-CR-185263] p 80 N90-25187
Autonomous power expert fault diagnostic system for Space Station Freedom electrical power system testbed p 80 N90-25521
- QUINN, WILLIAM F.**
The effect of leveling coatings on the atomic oxygen durability of solar concentrator surfaces [NASA-TM-102557] p 76 N90-21110
- R**
- RAAD, PETER E.**
A 'transient' automated mapping procedure for complex geometries p 242 A90-26499
- RAAG, V.**
Effect of Ga and P dopants on the thermoelectric properties of n-type SiGe p 256 A90-38140
- RAHMATSAHIL, Y.**
A comparison of reflector antenna designs for wide-angle scanning p 144 N90-19264
- RAITANO, P.**
Test facility and preliminary performance of a 100 kW class MPD thruster p 75 N90-18476
- RAJ, R.**
Near wall flow parameters in the blade end-wall corner region p 156 A90-12636
- RAJ, S. V.**
Apparent activation volume for creep of copper and alpha brass at intermediate temperatures p 108 A90-10028
Observations on the brittle to ductile transition temperatures of B2 nickel aluminides with and without zirconium p 111 A90-19153
On the stability of the creep substructure in NaCl single crystals p 254 A90-21920
Creep substructure formation in sodium chloride single crystals in the power law and exponential creep regimes p 255 A90-33330
The mechanical properties of fluoride salts at elevated temperatures p 123 A90-44376
Deformation of as-cast LiF-22 mol pct CaF2 hypereutectic salt between 500 and 1015 K p 124 A90-49086
Stress versus temperature dependent activation energies in creep [NASA-TM-103192] p 221 N90-23773
- RAJ, SUBRAMANIAM V.**
Intergranular fracture of lithium fluoride-22 percent calcium fluoride hypereutectic salt at 800 K p 121 A90-25273
- RAJU, M. S.**
Analysis of rotary engine combustion processes based on unsteady, three-dimensional computations [AIAA PAPER 90-0643] p 163 A90-22237
Analysis of rotary engine combustion processes based on unsteady, three-dimensional computations [NASA-TM-102469] p 176 N90-13749
Computational experience with a three-dimensional rotary engine combustion model [NASA-TM-103104] p 183 N90-26275
- RAMAN, GANESH**
Phase development and its role on subharmonic control [AIAA PAPER 90-0503] p 166 A90-25035
- RAMASWAMY, V. G.**
A constitutive model for the inelastic multiaxial response of Rene 80 at 871 C and 982 C p 114 A90-32266
- RAMINS, PETER**
Spent-beam refocusing analysis and multistage depressed collector design for a 75-W, 59- to 64-GHz coupled-cavity traveling-wave tube [NASA-TP-3039] p 155 N90-27965
- RAMAUO, RICHARD J.**
Initial results from the joint NASA-Lewis/U.S. Army icing flight research tests p 16 A90-28180
NASA's program on icing research and technology p 16 N90-15062
- RAPP, DOUGLAS C.**
High energy-density liquid rocket fuel performance [AIAA PAPER 90-1968] p 130 A90-47204
High energy-density liquid rocket fuel performance [NASA-CR-185279] p 131 N90-28742
- RAQUET, JOHN F.**
Arcjet cathode phenomena p 75 N90-18477
- RASHIDNIA, N.**
Ground-based experiments on thermal and thermosolutal convection in inclined low-aspect-ratio enclosures [AIAA PAPER 90-0413] p 166 A90-25033
Numerical studies of convective heat transfer in an inclined semi-annular enclosure p 173 A90-45317
Thermocapillary migration of liquid droplets in a temperature gradient in a density matched system [NASA-CR-185178] p 177 N90-14512
- RAWLIN, V. K.**
Xenon ion propulsion for orbit transfer [AIAA PAPER 90-2527] p 67 A90-52562
- RAWLIN, VINCENT K.**
Performance of large area xenon ion thrusters for orbit transfer missions p 75 N90-18475
- RAWLINS, W. TERRY**
H2/O2 three-body rates at high temperatures [AIAA PAPER 90-1696] p 105 A90-38399
- RAY, A.**
Integrated Communication and Control Systems. III - Nonidentical sensor and controller sampling p 239 A90-51266
Performance analysis of Integrated Communication and Control System networks p 239 A90-51267
- RAY, ASOK**
An observer-based compensator for distributed delays p 239 A90-49899
- REAGAN, P. V.**
Research on a two-dimensional inlet for a supersonic V/STOL propulsion system. Appendix A [NASA-CR-174945] p 12 N90-18364
- REDDY, D. R.**
Comparison of 3-D viscous flow computations of Mach 5 inlet with experimental data p 6 A90-26970
Viscous three-dimensional analyses for nozzles for hypersonic propulsion [NASA-CR-185197] p 27 N90-17635
Comparison of 3-D viscous flow computations of Mach 5 inlet with experimental data [NASA-TM-102518] p 28 N90-20090
- REDDY, N. N.**
Proplan Test Assessment (PTA): Flight test report [NASA-CR-182278] p 24 N90-11738
- REDDY, T. S. R.**
Application of an efficient hybrid scheme for aeroelastic analysis of advanced propellers [AIAA PAPER 90-0028] p 4 A90-22153
Time domain flutter analysis of cascades using a full-potential solver [AIAA PAPER 90-0984] p 6 A90-29374
Application of an efficient hybrid scheme for aeroelastic analysis of advanced propellers [NASA-TM-102428] p 11 N90-13355
Numerical simulations of supersonic flow through oscillating cascade sections [NASA-TM-103100] p 13 N90-20051
- REED, BRIAN D.**
Advanced APS impacts on vehicle payloads p 75 N90-18472
- REEDER, M. F.**
Pressure-based real-time measurements in compressible free shear layers [AIAA PAPER 90-1980] p 8 A90-42709
- REID, MARGARET A.**
Impedance studies of nickel/cadmium and nickel/hydrogen cells using the cell case as a reference electrode p 228 A90-33950
Changes in impedance of Ni electrodes upon standing and cycling [NASA-TM-102438] p 229 N90-18097
Impedance studies of Ni/Cd and Ni/H2 cells using the cell case as a reference electrode p 231 N90-20473
- REILLY, CHARLES H.**
Application of heuristic satellite plan synthesis algorithms to requirements of the WARC-88 allotment plan [AIAA PAPER 90-0815] p 245 A90-25638
A heuristic approach to worst-case carrier-to-interference ratio maximization in satellite system synthesis [AIAA PAPER 90-0816] p 46 A90-25639
Application of heuristic satellite plan synthesis algorithms to requirements of the WARC-88 allotment plan [NASA-TM-102479] p 245 N90-14856
- REINMANN, JOHN J.**
NASA's program on icing research and technology p 16 N90-15062
- REISINE, H.**
A geometric analysis of semicircular canals and induced activity in their peripheral afferents in the rhesus monkey p 234 A90-28084

- RENCIS, JOSEPH J.**
Local and global accuracy estimates for boundary element analysis
[AIAA PAPER 90-0930] p 211 A90-29324
- RENNEISEN, JOHN D.**
Input-output characterization of fiber reinforced composites by P waves
[NASA-CR-185287] p 208 N90-28097
- RENO, CHARLES**
Interactive grid generation for turbomachinery flow field simulations p 6 A90-26553
- REPAS, G. A.**
A highly durable injector faceplate design concept for O₂/H₂ propellants
[AIAA PAPER 90-2181] p 66 A90-47211
- RESHOTKO, E.**
Some characteristics of bypass transition in a heated boundary layer p 169 A90-35183
- RESHOTKO, ELI**
The vibrating ribbon problem revisited p 168 A90-33516
Interactive calculation procedures for mixed compression inlets
[NASA-CR-186581] p 14 N90-25934
- RHATIGAN, JENNIFER L.**
Numerical model of solar dynamic radiator for parametric analysis p 61 A90-38168
On protection of Freedom's solar dynamic radiator from the orbital debris environment. Part 1: Preliminary analyses and testing
[NASA-TM-102458] p 73 N90-14285
- RHODES, ROBERT P.**
Numerical modeling of an arcjet thruster
[AIAA PAPER 90-2614] p 64 A90-42587
- RICE, EDWARD J.**
Phase development and its role on subharmonic control
[AIAA PAPER 90-0503] p 166 A90-25035
Effects of fiber motion on the acoustic behavior of an anisotropic, flexible fibrous material p 247 A90-33313
Control of flow separation and mixing by aerodynamic excitation
[NASA-TM-103131] p 13 N90-21733
- RICE, J. P.**
Experimental evidence of a dimensional crossover in Y₁Ba₂Cu₃O(7- δ) p 255 A90-29739
- RICHARD, M.**
A high-speed GaAs MESFET optical controller p 186 A90-22483
- RICHARD, M. A.**
Control of a GaAs monolithic Ka-band phase shifter using a high-speed optical interconnect p 150 A90-41700
Optical control of an 8-element Ka-band phased array using a high-speed optoelectronic interconnect
[NASA-TM-102550] p 152 N90-21275
- RICHARD, MARK A.**
Design of an optically controlled Ka-band GaAs MMIC phased-array antenna
[NASA-TM-103147] p 155 N90-26250
- RICHEY, A.**
Automotive Stirling engine development program
[NASA-CR-180840] p 264 N90-29260
- RICHTER, G. P.**
Background, current status, and prognosis of the ongoing slush hydrogen technology development program for the NASP
[NASA-TM-103220] p 51 N90-26055
- RICHTER, G. PAUL**
Slush Hydrogen (SLH₂) technology development for application to the National Aerospace Plane (NASP)
[NASA-TM-102315] p 50 N90-14268
- RICHTER, SCOTT W.**
Technology development program for an advanced microsheet glass concentrator
[NASA-TM-102406] p 229 N90-14678
- RIEKER, LORRA L.**
Space Station Freedom electrical power system hardware commonality with the United States Polar Platform p 58 A90-38073
- RILEY, B. R.**
Kinetic theory model for the flow of a simple gas from a two-dimensional nozzle p 169 A90-37124
- RILEY, JAMES J.**
Progress in direct numerical simulations of turbulent reacting flows p 157 A90-12836
- RINGER, MARK J.**
Autonomous power expert system
[NASA-CR-185263] p 80 N90-25187
- RITTER, J. E.**
Properties of RBSN and RBSN-SiC composites p 94 A90-51920
- RIVERA, A. L.**
Nicalon/siliconoxycarbide ceramic composites p 94 A90-51924
- RIVERA, ANN L.**
Nicalon/siliconoxycarbide ceramic composites
[NASA-TM-102563] p 99 N90-21133
- RIVERA, JUAN C.**
Protoflight photovoltaic power module system-level tests in the Space Power Facility p 62 A90-38266
- RIZK, M. H.**
Aerodynamic optimization by simultaneously updating flow variables and design parameters p 18 N90-20991
- ROBBINS, J. W.**
The GEM-T2 gravitational model
[NASA-TM-100746] p 234 N90-12984
- ROBINSON, D. N.**
Effects of state recovery on creep buckling under variable loading p 212 A90-41223
A creep model for metallic composites based on matrix testing: Application to Kanthal composites
[NASA-TM-103172] p 101 N90-25193
Creep and creep rupture of strongly reinforced metallic composites
[NASA-CR-185286] p 223 N90-28110
- ROBINSON, R. S.**
End-hall thrusters
[AIAA PAPER 90-2595] p 64 A90-42570
- ROBSON, R. R.**
Status of xenon ion propulsion technology p 56 A90-27961
- ROCHE, J. C.**
EPSAT - A workbench for designing high-power systems for the space environment
[AIAA PAPER 90-0637] p 245 A90-26975
- ROCHE, JAMES C.**
The Environment-Power System Analysis Tool development program p 236 A90-38089
- ROELKE, R. J.**
GRID2D/3D: A computer program for generating grid systems in complex-shaped two- and three-dimensional spatial domains. Part 2: User's manual and program listing
[NASA-TM-102454] p 237 N90-20708
GRID2D/3D: A computer program for generating grid systems in complex-shaped two- and three-dimensional spatial domains. Part 1: Theory and method
[NASA-TM-102453] p 238 N90-22262
- ROELKE, RICHARD J.**
Design of an air-cooled metallic high-temperature radial turbine p 20 A90-32960
- ROGERS, J. R.**
Modeling of collision and coalescence of droplets during microgravity processing of Zn-Bi immiscible alloys p 132 A90-22878
- ROGERS, JAN R.**
The effects of van der Waals attractions on cloud droplet growth by coalescence p 234 A90-38363
- ROHN, D. A.**
Efficiency testing of a helicopter transmission planetary reduction stage p 193 A90-21113
- ROHN, DOUGLAS A.**
Reaction-compensation technology for microgravity laboratory robots
[NASA-TM-103271] p 205 N90-28062
- ROHRER, NORMAN J.**
Sequentially evaporated thin film YBa₂Cu₃O(7-x) superconducting microwave ring resonator
[NASA-TM-103180] p 154 N90-25273
- ROLLBUHLER, R. JAMES**
Fuel-rich catalytic combustion - A fuel processor for high-speed propulsion
[AIAA PAPER 90-2319] p 105 A90-42774
Fuel-rich catalytic combustion: A fuel processor for high-speed propulsion
[NASA-TM-103177] p 107 N90-23518
- ROMAN, ROBERT F.**
Secondary electron emission characteristics of molybdenum-masked, ion-textured OFHC copper
[NASA-TP-2967] p 117 N90-15211
- ROMANOVSKY, R. R.**
Ka-band propagation characteristics of microstrip lines on GaAs substrates at cryogenic temperatures p 147 A90-33644
Performance and modeling of superconducting ring resonators at millimeter-wave frequencies
[NASA-TM-102526] p 151 N90-18634
Microwave conductivity of laser ablated YBaCuO superconducting films and its relation to microstrip transmission line p 155 N90-27844
High temperature superconducting thin film microwave circuits: Fabrication, characterization, and applications
[NASA-TM-103235] p 156 N90-28786
- ROMANOVSKY, ROBERT R.**
Universal nondestructive MM-wave integrated circuit test fixture
[NASA-CASE-LEW-14746-1] p 151 N90-17009
- Experimental investigations on channelized coplanar waveguide
[NASA-TM-102494] p 151 N90-20286
- ROMANOVSKY, R. R.**
Control of a GaAs monolithic Ka-band phase shifter using a high-speed optical interconnect p 150 A90-41700
- RONCACE, JAMES**
Mars in situ propellants - Carbon monoxide and oxygen ignition experiments
[AIAA PAPER 90-1894] p 130 A90-50642
Mars in situ propellants: Carbon monoxide and oxygen ignition experiments
[NASA-TM-103202] p 81 N90-26065
- RONNEY, P.**
The structure and stability of nonadiabatic flame balls p 105 A90-43674
- ROSE, A. H.**
A fiber-optic current sensor for aerospace applications
[NASA-TM-103152] p 190 N90-22773
- ROSE, GAYLE E.**
Effect of reduced aft diameter and increased blade number on high-speed counterrotation propeller performance
[NASA-TM-102077] p 11 N90-13352
- ROSENBAUM, D.**
Global pressure relaxation for laminar two-dimensional internal flow p 174 A90-51019
- ROSENBERG, S. D.**
Corrosion prevention in copper combustion chamber liners of liquid oxygen/methane booster engines
[AIAA PAPER 90-2119] p 85 A90-42028
Combustion interaction with radiation-cooled chambers
[AIAA PAPER 90-2121] p 64 A90-42030
- ROSKILLY, RONALD R.**
National space test centers, Lewis research center facilities
[NASA-TM-103187] p 44 N90-26030
- ROSNER, DANIEL E.**
Side-wall gas 'creep' and 'thermal stress convection' in microgravity experiments on film growth by vapor transport p 158 A90-14086
- ROSS, H. D.**
Surface reorientation and settling in cylinders upon step reduction in gravity p 172 A90-44541
- ROSS, HOWARD D.**
An investigation of flame spread over shallow liquid pools in microgravity and nonair environments
[NASA-TM-102425] p 134 N90-13680
New findings and instrumentation from the NASA Lewis microgravity facilities
[NASA-TM-103189] p 136 N90-26163
- ROSS, PHILLIP T.**
Composite matrix cooling scheme for small gas turbine combustors
[AIAA PAPER 90-2158] p 22 A90-47210
- ROSTAFINSKI, WOJCIECH**
Analysis of fully stalled compressor p 6 A90-27966
- ROTH, D. J.**
Subtle porosity variation in the YBa₂Cu₃O(7-x) high-temperature superconductor revealed by ultrasonic imaging
[NASA-TM-102130] p 206 N90-17167
Review and statistical analysis of the ultrasonic velocity method for estimating the porosity fraction in polycrystalline materials
[NASA-TM-102501-REV] p 207 N90-21402
- ROTH, DON J.**
Recent advances in nondestructive evaluation made possible by novel uses of video systems
[NASA-TM-102491] p 207 N90-22801
- ROTH, MARY ELLEN**
Preliminary evaluation of space station transmission line in a ring configuration
[NASA-TM-102461] p 74 N90-17677
High power, high frequency component test facility
[NASA-TM-102500] p 151 N90-19484
Electromechanical actuation for thrust vector control applications
[NASA-TM-102548] p 152 N90-21272
Autonomous power expert system p 240 N90-22306
Field oriented control of induction motors
[NASA-TM-103154] p 154 N90-22731
Autonomous power expert fault diagnostic system for Space Station Freedom electrical power system testbed p 80 N90-25521
- RUBIN, S. G.**
A flux-split solution procedure for unsteady inlet flows
[AIAA PAPER 90-0585] p 6 A90-26967
Transient behavior of supersonic flow through inlets
[AIAA PAPER 90-2130] p 8 A90-42734
Global pressure relaxation for laminar two-dimensional internal flow p 174 A90-51019

RUBINSTEIN, ASHER A.

- Crack-path effect on material toughness
[ASME PAPER 89-WA/APM-43] p 210 A90-28755
Mechanics of the crack path formation
[NASA-CR-185143] p 215 N90-10455
Micromechanical model of crack growth in fiber reinforced ceramics
[NASA-TM-4321] p 224 N90-28113

RUBINSTEIN, ROBERT

- Nonlinear Reynolds stress models and the renormalization group p 172 A90-44011
Investigation of methods to produce a uniform cloud of fuel particles in a flame tube
[NASA-TM-102376] p 178 N90-18665

RUBINSTEIN, ROBERT I.

- Structural tailoring of select fiber composite structures
[NASA-TM-102484] p 99 N90-21137
Microgravity acoustic mixing for particle cloud combustors
[NASA-CR-185159] p 248 N90-21600

RUCKMAN, MARK W.

- XANES and EXAFS study of Au-substituted YBa₂Cu₃O_{7-δ}
[NASA-TM-103291] p 260 N90-29219

RUDOFF, R.

- Advanced instrumentation for aircraft icing research
[NASA-CR-185225] p 18 N90-21006

RUDOFF, R. C.

- Development of a phase Doppler based probe for icing cloud droplet characterization
[AIAA PAPER 90-0667] p 186 A90-26978

RUFF, GARY A.

- Users manual for the NASA Lewis Ice Accretion Prediction Code (LEWICE)
[NASA-CR-185129] p 1 N90-20943

RUPPE, WALTER R.

- Modulated-splitting-ratio fiber-optic temperature sensor p 185 A90-11706

RUSSELL, L.

- A laser based computer aided non-intrusive technique for full field flow characterization in macroscopic curved channels p 168 A90-32293

RUSSELL, LOUIS M.

- Experimental determination of stator endwall heat transfer
[ASME PAPER 89-GT-219] p 165 A90-23880

RUSSELL, PAUL K.

- Servicing communication satellites in geostationary orbit
[AIAA PAPER 90-0830] p 39 A90-25655

RUSSO, MATHEW J.

- Shear stabilization of the capillary breakup of a cylindrical interface
[AD-A219268] p 159 A90-17578

RUTLEDGE, SHARON K.

- Evaluation of atomic oxygen resistant protective coatings for fiberglass-epoxy composites in LEO p 84 A90-31581

RUTLEDGE, SHARON K.

- Aeolian removal of dust from radiator surfaces on Mars
[NASA-TM-103205] p 81 N90-26068

RUTLEDGE, SHARON K.

- The effects of atomic oxygen on the thermal emittance of high temperature radiator surfaces
[NASA-TM-103224] p 102 N90-28670

RYS, JOHN R.

- Modulated-splitting-ratio fiber-optic temperature sensor p 185 A90-11706

RYU, DONGSU

- Neutron stars and white dwarfs in galactic halos? p 265 A90-30909
A model for the distribution of the intergalactic medium p 265 A90-34505

RYU, DONGSU

- A model for the distribution of dark matter, galaxies, and the intergalactic medium in a cold dark matter-dominated universe p 266 A90-45560

S**SAAD, EHAB**

- CryoTran user's manual, version 1.0
[NASA-TM-102468] p 237 N90-15622

SABLA, P. E.

- Energy Efficient Engine combustor test hardware detailed design report p 33 N90-28554
[NASA-CR-168301]

SABLA, P. E.

- Energy Efficient Engine (E3) combustion system component technology performance report p 33 N90-28555
[NASA-CR-168274]

SACKSTEDER, KURT

- A comparison of European and American microgravity combustion experimental techniques p 134 N90-16966

SACKSTEDER, KURT R.

- Facilities for microgravity combustion research
[NASA-TM-102014] p 134 N90-13679

SAEDI, R.

- High-speed digital fiber optic links for satellite traffic p 250 A90-41247

SAEDI, REZA

- High-speed fiber-optic links for distribution of satellite traffic p 47 A90-41687

SAIYED, NASEEM H.

- Acquisition and correlation of cryogenic nitrogen mass flow data through a multiple orifice Joule-Thomson device
[NASA-TM-103121] p 182 N90-22761

SAJBEN, MIKLOS

- Experimental investigation of terminal shock sensors in mixed-compression inlets
[AIAA PAPER 90-1931] p 186 A90-40560

SALAMA, E. E.

- Advanced gearbox technology
[NASA-CR-179625] p 32 N90-24274

SALEM, J. A.

- Determination of the stress distributions in a ceramic: Tensile specimen using numerical techniques
[NASA-TM-101914] p 129 N90-26132

SALEM, JONATHAN A.

- Strength and toughness of monolithic and composite silicon nitrides
[NASA-TM-102423] p 126 N90-14368

SALEM, JONATHAN A.

- Empirical and analytical determination of the fracture resistance of a TiB₂ particle/SiC matrix composite
[NASA-TM-101940] p 96 N90-15143

SALEM, JONATHAN A.

- Reliability analysis of a structural ceramic combustion chamber
[NASA-TM-103264] p 223 N90-28112

SALTIEL, C.

- Radiative configuration factors from cylinders to coaxial axisymmetric bodies p 167 A90-26334

SALTSMAN, JAMES F.

- High temperature fatigue behavior of Haynes 188 p 119 N90-28642

SALVINO, R. E.

- Equilibrium statistical thermodynamics of a many-particle system coupled to an external scalar field p 261 A90-31670

SAMIMY, M.

- Compressibility effects in free shear layers
[AIAA PAPER 90-0705] p 161 A90-19984

SAMIMY, M.

- Effects of compressibility on the characteristics of free shear layers p 6 A90-25285
Structure of a reattaching supersonic shear layer p 7 A90-36252

SAMIMY, M.

- Pressure-based real-time measurements in compressible free shear layers
[AIAA PAPER 90-1980] p 8 A90-42709

SAMUELSEN, G. S.

- Influence of the continuous and dispersed phases on the symmetry of a gas turbine air-blast atomizer
[ASME PAPER 89-GT-303] p 163 A90-22651

SAMUELSEN, G. S.

- Application of two-component phase Doppler interferometry to the measurement of particle size, mass flux, and velocities in two-phase flows p 186 A90-32853

SAMUELSEN, G. S.

- An experimental and numerical study of particle-laden coaxial jet flows p 171 A90-38799
Symmetry assessment of an air-blast atomizer spray p 172 A90-40930

SANCHEZ, B. V.

- The GEM-T2 gravitational model
[NASA-TM-100746] p 234 N90-12984

SANCHEZ, J.

- Optimization of silicon 8 cm x 8 cm wrapthrough Space Station cells for 'on orbit' operation p 54 A90-14941

SANDERS, WILLIAM A.

- Slurry-pressing consolidation of silicon nitride p 121 A90-27691
Materials for engine applications above 3000 deg F: An overview p 95 N90-10188

SANFACON, M. M.

- High efficiency GaAs/Ge monolithic tandem solar cells p 224 A90-14858

SANKAR, L. N.

- Evaluation of three turbulence models in static air loads and dynamic stall predictions p 7 A90-31291
Numerical simulation of unsteady rotational flow over propfan configurations p 10 N90-12500

SANKAR, LAKSHMI N.

- Numerical study of the effects of icing on finite wing aerodynamics
[AIAA PAPER 90-0757] p 3 A90-20010

SANKAR, N. L.

- Application of an efficient hybrid scheme for aeroelastic analysis of advanced propellers
[AIAA PAPER 90-0028] p 4 A90-22153

SANTORO, G.

- Application of an efficient hybrid scheme for aeroelastic analysis of advanced propellers
[NASA-TM-102428] p 11 N90-13355

SANTORO, G.

- Microgravity noncontact temperature requirements at NASA Lewis Research Center p 134 N90-17897

SARAVANOS, D. A.

- Multi-objective shape and material optimization of composite structures including damping
[AIAA PAPER 90-1135] p 210 A90-29262

SARAVANOS, D. A.

- Tailoring of composite links for optimal damped elasto-dynamic performance p 211 A90-30250
Optimum structural design of robotic manipulators with fiber reinforced composite materials p 197 A90-46074

SARAVANOS, D. A.

- Optimal fabrication processes for unidirectional metal-matrix composites - A computational simulation p 93 A90-50096

SARAVANOS, D. A.

- Mechanics of damping for fiber composite laminates including hygro-thermal effects
[NASA-TM-102329] p 95 N90-10185

SARAVANOS, D. A.

- An integrated methodology for optimizing structural composite damping
[NASA-TM-102343] p 96 N90-11808

SARAVANOS, D. A.

- Computational simulation of damping in composite structures
[NASA-TM-102567] p 219 N90-20432

SARAVANOS, D. A.

- Multi-objective shape and material optimization of composite structures including damping
[NASA-TM-102579] p 99 N90-21132

SARAVANOS, D. A.

- Optimal fabrication processes for unidirectional metal-matrix composites: A computational simulation
[NASA-TM-102559] p 100 N90-21143

SARAVANOS, DIMITRIS A.

- Unified micromechanics of damping for unidirectional and off-axis fiber composites p 90 A90-29929

SARMIENTO, CHARLES J.

- Low power arcjet performance
[AIAA PAPER 90-2578] p 68 A90-52568

SARMIENTO, CHARLES J.

- Low power arcjet performance
[NASA-TM-103280] p 83 N90-28657

SASAKI, S.

- The sheath structure around a negatively charged rocket payload p 48 A90-34780

SATER, B. L.

- Optimization of silicon 8 cm x 8 cm wrapthrough Space Station cells for 'on orbit' operation p 54 A90-14941

SATER, BERNARD L.

- The Space Station photovoltaic panels plasma interaction test program - Test plan and results
[AIAA PAPER 90-0722] p 47 A90-22252

SATER, BERNARD L.

- Photovoltaic array environmental protection program p 59 A90-38088
The Space Station Photovoltaic Panels Plasma Interaction Test Program: Test plan and results
[NASA-TM-102474] p 49 N90-13581

SAUNIER, P.

- Doped-channel heterojunction structures for millimeter-wave discrete devices and MMICs p 150 A90-48492

SAUNIER, PAUL

- AlGaAs/InGaAs heterostructures with doped channels for discrete devices and monolithic amplifiers p 146 A90-20861

SAUNIER, PAUL

- Minimum fuel trajectory for the aerospace-plane
[AAS PAPER 89-352] p 40 A90-46785

SAUNIER, PAUL

- Tooth contact shift in loaded spiral bevel gears p 193 A90-21112
Vibration signature analysis of multistage gear transmission p 194 A90-21124

SAVINO, JOSEPH M.

- A program for advancing the technology of space concentrators p 60 A90-38159

SAYOOD, KHALID

- Data compression for the microgravity experiments p 188 N90-16212

SCAVUZZO, R. J.

- An experimental evaluation of the tensile strength of impact ice p 83 A90-15049
Impact ice stresses in rotating airfoils
[AIAA PAPER 90-0198] p 15 A90-19735

SCHACHAM, S. E.

- Reflecting boundary conditions for graded p-n junctions p 150 A90-42400
Interface properties of various passivations of HgCdTe p 251 A90-45947

SCHERTLER, RONALD J.

- Contribution of the graded region of a HgCdTe diode to its saturation current p 257 A90-45948
Kinetic theory model for the flow of a simple gas from a two-dimensional nozzle p 169 A90-37124
Advanced Communications Technology Satellite (ACTS)
[AIAA PAPER 90-0839] p 140 A90-25663

- SCHIERMAN, JOHN D.**
Analysis of airframe/engine interactions - An integrated control perspective
[AIAA PAPER 90-1918] p 36 A90-40557
Extended implicit model following as applied to integrated flight and propulsion control
[AIAA PAPER 90-3444] p 239 A90-47697
- SCHLOSSER, HERBERT**
Liquid alkali metals - Equation of state and reduced-pressure, bulk-modulus, sound-velocity, and specific-heat functions p 102 A90-16280
Pressure dependence of the melting temperature of metals p 103 A90-16281
An accurate analytic approximation to the non-linear change in volume of solids with applied pressure p 261 A90-27612
- SCHLUMBERGER, JULIE A.**
Cooling of rocket thrust chambers with liquid oxygen [AIAA PAPER 90-2120] p 63 A90-42029
Cooling of rocket thrust chambers with liquid oxygen [NASA-TM-103146] p 78 N90-22605
- SCHMIDT, DAVID K.**
Cooperative synthesis of control and display augmentation in approach and landing p 36 A90-33061
Analysis of airframe/engine interactions - An integrated control perspective [AIAA PAPER 90-1918] p 36 A90-40557
Extended implicit model following as applied to integrated flight and propulsion control [AIAA PAPER 90-3444] p 239 A90-47697
- SCHMITZ, GREGORY V.**
Power transmission cable development for the Space Station Freedom electrical power system p 149 A90-38134
- SCHMITZ, PAUL C.**
A solar power system for an early Mars expedition [NASA-TM-103219] p 246 N90-28393
- SCHNEIDER, STEVEN J.**
Low thrust rocket test facility [AIAA PAPER 90-2503] p 43 A90-47225
Extended temperature range rocket injector [NASA-CASE-LEW-14846-1] p 73 N90-15130
Advanced APS impacts on vehicle payloads p 75 N90-18472
Zero-G phase detector and separator [NASA-CASE-LEW-14844-1] p 190 N90-22024
Low thrust rocket test facility [NASA-TM-103206] p 43 N90-25158
- SCHRAIG, R. L.**
Electro-impulse de-icing testing analysis and design [NASA-CR-4175] p 18 N90-10031
- SCHRAMM, DAVID N.**
The shocking development of lithium (and boron) in supernovae p 264 A90-17643
Big bang nucleosynthesis and the quark-hadron transition p 265 A90-31407
- SCHREIBER, JEFFREY G.**
Comparison of conceptual designs for 25 kW advanced Stirling conversion systems for dish electric applications p 229 A90-38254
Initial characterization of a modular heat exchanger with an integral heat pipe p 62 A90-38301
Preliminary designs for 25 kW advanced Stirling conversion systems for dish electric applications [NASA-TM-103188] p 263 N90-26729
- SCHULER, JAMES**
Electromagnetic finite elements based on a four-potential variational principle p 214 A90-49869
- SCHULTZ, DONALD F.**
Steam cooled rich-burn combustor liner [NASA-CASE-LEW-13609-1] p 106 N90-11824
- SCHULZE, NORMAN R.**
NASA aerospace battery systems program update p 228 A90-38217
- SCHUNK, R. W.**
A two-dimensional model of plasma expansion in the ionosphere p 233 A90-43609
- SCHUSTER, J. R.**
COLD-SAT - An orbital cryogenic hydrogen technology experiment [IAF PAPER 89-057] p 53 A90-13282
- SCHWAB, JOHN R.**
PROTEUS two-dimensional Navier-Stokes computer code, version 1.0. Volume 1: Analysis description [NASA-TM-102551] p 180 N90-21303
PROTEUS two-dimensional Navier-Stokes computer code, version 1.0. Volume 2: User's guide [NASA-TM-102552] p 180 N90-21306
PROTEUS two-dimensional Navier-Stokes computer code, version 1.0. Volume 3: Programmer's reference [NASA-TM-102553] p 180 N90-21307
- SCHWARZE, G. E.**
High frequency, high temperature specific core loss and dynamic B-H hysteresis loop characteristics of soft magnetic alloys [NASA-TM-103164] p 154 N90-23663
Neutron and gamma irradiation effects on power semiconductor switches [NASA-TM-103200] p 155 N90-25278
- SCHWEIGER, F. A.**
Revolutionary opportunities for materials and structures study [NASA-CR-179642] p 95 N90-10184
- SCOFIELD, JOHN H.**
Simple evaporation controller for thin-film deposition from a resistively heated boat p 149 A90-39761
- SCOTT, J. R.**
Analysis of nonuniform subsonic flows about a row of moving blades p 2 A90-11779
- SCOTT, JAMES R.**
Numerical solutions of the linearized Euler equations for unsteady vortical flows around lifting airfoils [AIAA PAPER 90-0694] p 5 A90-25041
Numerical solutions of the linearized Euler equations for unsteady vortical flows around lifting airfoils p 7 A90-30264
Numerical solutions of the linearized Euler equations for unsteady vortical flows around lifting airfoils [NASA-TM-102466] p 12 N90-17562
- SCOTT, M. J.**
Ignition and combustion characteristics of metallized propellants [NASA-CR-186870] p 107 N90-26911
- SEASHOLTZ, RICHARD G.**
TiCl₄ as a source of TiO₂ particles for laser anemometry measurements in hot gas [NASA-TM-102581] p 189 N90-20358
- SECUNDE, RICHARD R.**
Solar dynamic power module design p 59 A90-38079
- SEDGWICK, L. M.**
A Brayton cycle solar dynamic heat receiver for space p 61 A90-38165
- SEINER, J. M.**
Viscous effects on the instability of an axisymmetric jet [NASA-TM-102396] p 12 N90-16719
- SEKULA-MOISE, P. A.**
Dielectric function of InGaAs in the visible [NASA-TM-103246] p 260 N90-26683
- SEKULA-MOISE, PATRICIA A.**
Wide-bandgap epitaxial heterojunction windows for silicon solar cells p 227 A90-28359
- SENG, HAN-SONG**
Ultrasonic verification of five wave fronts in unidirectional graphite epoxy composite [NASA-CR-185288] p 208 N90-28858
- SERAFINI, JOHN A.**
Laser-velocimeter-measured flow field around an advanced, swept, eight-blade propeller at Mach 0.8 [NASA-TP-2462] p 1 N90-20942
- SERBETCI, ILTER**
Nature of convection-stabilized dc arcs in dual-flow nozzle geometry. I - The cold flow field and dc arc characteristics. II - Optical diagnostics and theory p 252 A90-26665
- SETO, S. P.**
Energy Efficient Engine combustor test hardware detailed design report [NASA-CR-168301] p 33 N90-28554
Energy Efficient Engine (E3) combustion system component technology performance report [NASA-CR-168274] p 33 N90-28555
- SETTLES, GARY S.**
Skin friction measurements by laser interferometry in swept shock/boundary-layer interactions p 3 A90-18153
- SHAH, A. R.**
Probabilistic analysis of bladed turbine disks and the effect of mistuning [NASA-TM-102564] p 136 N90-21871
- SHAH, ASHWIN**
Probabilistic analysis of bladed turbine disks and the effect of mistuning [AIAA PAPER 90-1097] p 196 A90-29327
- SHAKER, FRANCIS J.**
Dynamic analysis of space-related linear and non-linear structures [NASA-TM-103490] p 51 N90-25174
- SHALKHAUSER, K.**
High-speed digital fiber optic links for satellite traffic p 250 A90-41247
- SHALKHAUSER, K. A.**
Bit-error-rate testing of fiber optic data links for MMIC-based phased array antennas [NASA-TM-102523] p 145 N90-21261
- SHALKHAUSER, KURT**
High-speed fiber-optic links for distribution of satellite traffic p 47 A90-41687
- SHALKHAUSER, KURT A.**
Universal nondestructive MM-wave integrated circuit test fixture [NASA-CASE-LEW-14746-1] p 151 N90-17009
Rain-fade simulation and power augmentation for satellite communication systems [NASA-TM-103134] p 146 N90-28768
- SHALKHAUSER, MARY JO**
Satellite-matrix-switched, time-division-multiple-access network simulator [AIAA PAPER 90-0848] p 147 A90-25671
Digital codec for real-time processing of broadcast quality video signals at 1.8 bits/pixel p 142 A90-51306
Satellite-matrix-switched, time-division-multiple-access network simulator [NASA-TP-2944] p 142 N90-11915
Data compression for the microgravity experiments p 188 N90-16212
- SHALTENS, RICHARD K.**
Comparison of conceptual designs for 25 kW advanced Stirling conversion systems for dish electric applications p 229 A90-38254
Preliminary designs for 25 kW advanced Stirling conversion systems for dish electric applications [NASA-TM-103188] p 263 N90-26729
- SHAMROTH, S. J.**
Reciprocal interactions of hairpin-shaped vortices and a boundary layer [AIAA PAPER 90-0017] p 159 A90-19635
- SHAN, XIAOYIN**
Structural comparison of nickel electrodes and precursor phases p 228 A90-33949
Structural comparison of nickel electrodes and precursor phases p 231 N90-20472
- SHANTARAM, S. PAI**
Calculation of Weibull strength parameters and Batdorf flow-density constants for volume- and surface-flaw-induced fracture in ceramics p 212 A90-35462
- SHAPIRO, WILBUR**
Analysis and design of helium-buffered face seals for the SSME high-pressure oxygen turbopump [AIAA PAPER 90-2049] p 197 A90-42000
- SHARP, G. R.**
ATDRS payload technology research and development [NASA-TM-103256] p 52 N90-28596
- SHARP, G. RICHARD**
Applications of high thermal conductivity composites to electronics and spacecraft thermal design [AIAA PAPER 90-0783] p 89 A90-25609
A new fabrication method for precision antenna reflectors for space flight and ground test [AIAA PAPER 90-0803] p 139 A90-25627
- SHARP, R.**
Reflector surface distortion analysis techniques (thermal distortion analysis of antennas in space) p 144 N90-19267
- SHAUMEYER, J. N.**
Critical speeding up in pure fluids p 167 A90-26369
- SHAW, B. D.**
Theory of influence of a low-volatility, soluble impurity on spherically-symmetric combustion of fuel droplets p 104 A90-28771
- SHAW, NANCY J.**
Densification and coarsening during solid state sintering of ceramics: A review of the models. II - Grain growth p 120 A90-15375
Materials for engine applications above 3000 deg F: An overview [NASA-TM-100169] p 95 N90-10188
- SHAW, ROBERT J.**
Predictions of airfoil aerodynamic performance degradation due to icing p 3 A90-16753
NASA's program on icing research and technology p 16 N90-15062
- SHEFFLER, K. D.**
MATE (Materials for Advanced Turbine Engines) Program, Project 3. Volume 2: Design, fabrication and evaluation of an oxide dispersion strengthened sheet alloy combustor liner [NASA-CR-180892] p 117 N90-17868
- SHEFFLER, KEITH D.**
Mechanisms of degradation and failure in a plasma deposited thermal barrier coating [ASME PAPER 89-GT-132] p 84 A90-23830
- SHEH, M. Y.**
A crystallographic model for the tensile and fatigue response for Rene N4 at 982 C p 114 A90-28754

PERSONAL AUTHOR INDEX

- SHELDON, B. W.**
Nitriding kinetics of Si-SiC powder mixtures as simulations of reaction bonded Si₃N₄-SiC composites p 90 A90-27076
- SHELTON, SAM V.**
Feasibility analysis of reciprocating magnetic heat pumps [NASA-CR-186205] p 177 N90-15363
- SHEN, Y.**
Energy stability of thermocapillary convection in a model of the float-zone crystal-growth process p 133 A90-48720
- SHETLER, RUSSELL E.**
A 2.5 kW cascaded Schwarz converter for 20 kHz power distribution p 147 A90-36913
- SHETTY, DINESH K.**
Equivalence of physically based statistical fracture theories for reliability analysis of ceramics in multiaxial loading p 123 A90-43580
- SHIAO, MICHAEL C.**
A methodology for evaluating the reliability and risk of structures under complex service environments [AIAA PAPER 90-1102] p 211 A90-29332
Probability of failure and risk assessment of propulsion structural components p 218 N90-18470
Probabilistic structural analysis of aerospace components using NESSUS [NASA-TM-102324] p 221 N90-22823
- SHIH, T. H.**
An improved k-epsilon model for near-wall turbulence and comparison with direct numerical simulation [NASA-TM-103221] p 184 N90-27983
Modeling of near-wall turbulence [NASA-TM-103222] p 184 N90-28009
- SHIH, T. I.-P.**
GRID2D/3D: A computer program for generating grid systems in complex-shaped two- and three-dimensional spatial domains. Part 2: User's manual and program listing [NASA-TM-102454] p 237 N90-20708
GRID2D/3D: A computer program for generating grid systems in complex-shaped two- and three-dimensional spatial domains. Part 1: Theory and method [NASA-TM-102453] p 238 N90-22262
- SHIN, J.**
The growth and development of a turbulent junction vortex system p 173 A90-46902
- SHINGLER, M.**
Catalysts for ultrahigh current density oxygen cathodes for space fuel cell applications [NASA-CR-180650] p 232 N90-22835
- SHOEMAKER, NEIL S.**
Optical dispersion relations for diamondlike carbon films [NASA-TM-102356] p 257 N90-10738
- SHOHADAE, AHMAD A.**
Influence of bulk turbulence and entrance boundary layer thickness on the curved duct flow field [AIAA PAPER 90-1502] p 171 A90-38651
- SHUEN, JIAN SHUN**
Numerical study of chemically reacting flows using a lower-upper symmetric successive overrelaxation scheme p 3 A90-17989
- SHUEN, JIAN-SHUN**
Splitting of inviscid fluxes for real gases p 167 A90-25451
Inviscid flux-splitting algorithms for real gases with non-equilibrium chemistry p 174 A90-52275
- SHYNE, RICKEY J.**
Analysis and design of optimized truncated scarfed nozzles subject to external flow effects [AIAA PAPER 90-2222] p 9 A90-47213
Analysis and design of optimized truncated scarfed nozzles subject to external flow effects [NASA-TM-103175] p 13 N90-25106
- SIDI, AVRAM**
Convergence acceleration for vector sequences and applications to computational fluid dynamics [AIAA PAPER 90-0338] p 160 A90-19804
Quotient-difference type generalizations of the power method and their analysis [NASA-TM-102361] p 242 N90-10635
Efficient implementation of minimal polynomial and reduced rank extrapolation methods [NASA-TM-103240] p 244 N90-26616
- SIEG, R. E.**
Ellipsometric study of YBa₂Cu₃O_{7-x} laser ablated and co-evaporated films [NASA-TM-103223] p 259 N90-26682
Dielectric function of InGaAs in the visible [NASA-TM-103246] p 260 N90-26683
- SIEG, ROBERT M.**
Optical dispersion relations for diamondlike carbon films [NASA-TM-102356] p 257 N90-10738
- SIEGEL, ROBERT**
Some aspects of transient cooling of a radiating rectangular medium p 157 A90-13095
Emittance bounds for transient radiative cooling of a scattering rectangular region p 161 A90-20520
Solidification by radiative cooling of a cylindrical region filled with drops p 166 A90-24840
- SIEGERT, CLIFFORD E.**
Investigation of methods to produce a uniform cloud of fuel particles in a flame tube [NASA-TM-102376] p 178 N90-18665
- SIGNORELLI, ROBERT A.**
Fiber reinforced superalloys p 91 A90-34169
- SILK, JOSEPH**
Neutron stars and white dwarfs in galactic halos? p 265 A90-30909
- SIMITSES, GEORGE J.**
Analysis of shell-type structures subjected to time-dependent mechanical and thermal loading [NASA-CR-185077] p 222 N90-24653
- SIMONCIC, ROBERT**
AIRNET: A real-time communications network for aircraft [NASA-CR-186140] p 145 N90-24514
- SIMONEAU, R. J.**
Progress towards the development of an inviscid-viscous interaction method for unsteady flows in turbomachinery cascades p 2 A90-11806
- SIMONEAU, ROBERT J.**
Unsteady heat transfer on turbine blades p 161 A90-20511
- SIMONS, R. N.**
Coax-to-channelised coplanar waveguide in-phase N-way, radial power divider p 149 A90-41605
Channelized coplanar waveguide pin-diode switches [NASA-TM-102289] p 150 N90-11943
- SIMONS, RAINEE N.**
Synthesis and characterization of high-T(c) screen-printed Y-Ba-Cu-O films on alumina p 254 A90-21926
Experimental investigations on channelized coplanar waveguide [NASA-TM-102494] p 151 N90-20286
A new rectangular waveguide to coplanar waveguide transition [NASA-TM-102477] p 145 N90-21263
Coplanar waveguide fed phased array antenna [NASA-TM-102522] p 152 N90-21273
Coplanar waveguide discontinuities for P-I-N diode switches and filter applications [NASA-TM-102534] p 153 N90-21278
- SIMONS, STEPHEN N.**
Energy storage and thermal control system design status p 59 A90-38077
- SIMPSON, J. I.**
A geometric analysis of semicircular canals and induced activity in their peripheral afferents in the rhesus monkey p 234 A90-28084
- SINGER, JOSEPH**
Corrosion testing of candidates for the alkaline fuel cell cathode p 228 A90-33948
Corrosion testing of candidates for the alkaline fuel cell cathode p 231 N90-20471
O₂ reduction at the IFC orbiter fuel cell O₂ electrode [NASA-TM-102580] p 231 N90-21469
- SINGER, S.**
Magnification of starting torques of dc motors by maximum power point trackers in photovoltaic systems p 149 A90-38144
- SINGH, N. B.**
Effects of crystal-melt interfacial energy anisotropy on dendritic morphology and growth kinetics p 253 A90-19284
Free dendritic growth in viscous melts - Cyclohexanol p 253 A90-19285
Evaluation of transport conditions during physical vapor transport growth of opto-electronic crystals p 132 A90-20525
Determination of the mean solid-liquid interface energy of pivalic acid p 84 A90-22646
- SINGH, RAJENDRA**
Modal analysis of gear housing and mounts p 192 A90-17018
Vibration transmission through rolling element bearings in geared rotor system, part 1 [NASA-CR-186093] p 199 N90-12936
A review of gear housing dynamics and acoustics literature [NASA-CR-185148] p 203 N90-21387
Non-linear dynamic analysis of geared systems, part 2 [NASA-CR-180495] p 204 N90-23732
- SINGHAL, SURENDRA N.**
Demonstration of capabilities of high temperature composites analyzer code HITCAN [NASA-TM-102560] p 219 N90-19629
- SINHA, ALOK**
A new approach to active vibration isolation for microgravity space experiments [NASA-TM-102470] p 137 N90-17929
- SIRIGNANO, W. A.**
Effects of g-jitter on a thermal, buoyant flow [AIAA PAPER 90-0653] p 163 A90-22239
- SIROCKY, PAUL J.**
High temperature, flexible, thermal barrier seal [NASA-CASE-LEW-14672-1] p 201 N90-15444
- SIROCKY, PAUL J.**
High temperature flexible seal [NASA-CASE-LEW-14695-1] p 204 N90-23751
- SKUPINSKI, ROBERT C.**
Results from baseline tests of the SPRE I and comparison with code model predictions p 62 A90-38249
- SLABE, MELISSA E.**
Effect of heat-treatment temperature of vapor-grown graphite fibers. I - Properties of their bromine intercalation compounds p 120 A90-16279
Density of intercalated graphite fibers p 124 A90-49061
Density of intercalated graphite fibers [NASA-TM-102411] p 126 N90-14362
Resistivity of pristine and intercalated graphite fiber epoxy composites [NASA-TM-102576] p 128 N90-21192
- SLATE, E.**
Automotive Stirling engine development program [NASA-CR-180839] p 263 N90-11654
- SLINEY, HAROLD E.**
Some composite bearing and seal materials for gas turbine applications - A review [ASME PAPER 89-GT-144] p 195 A90-23838
Friction and wear of oxide-ceramic sliding against IN-718 nickel base alloy at 25 to 800 C in atmospheric air [NASA-TM-102291] p 124 N90-10262
Tribological properties of PM212: A high-temperature, self-lubricating, powder metallurgy composite [NASA-TM-102355] p 86 N90-12659
A new test machine for measuring friction and wear in controlled atmospheres to 1200 C [NASA-TM-102405] p 96 N90-12670
- SMALLEY, A. J.**
Spray automated balancing of rotors - How process parameters influence performance p 198 A90-46228
- SMEGGIL, J. G.**
Identification of a cast iron alloy containing nonstrategic elements [NASA-CR-185174] p 118 N90-18559
- SMIALEK, J. L.**
The oxidation of Ni-rich Ni-Al intermetallics p 112 A90-24855
Influence of alloying elements on the oxidation behavior of NbAl₃ p 113 A90-24861
- SMIALEK, JAMES L.**
Oxidation behavior of FeAl + Hf, Zr, B p 113 A90-24858
Burner rig hot corrosion of silicon carbide and silicon nitride p 121 A90-25267
Cyclic oxidation of aluminide coatings on Ti3Al + Nb p 115 A90-39660
Method of forming low cost, formable High T(subc) superconducting wire [NASA-CASE-LEW-14676-2] p 258 N90-17454
- SMITH, BRIAN S.**
InP homojunction solar cell performance on the LIPS III flight experiment p 226 A90-14921
- SMITH, C. FREDERIC**
Analysis of internal flow in a ventral nozzle for STOVL aircraft [AIAA PAPER 90-1899] p 21 A90-42688
Analysis of internal flow in a ventral nozzle for STOVL aircraft [NASA-TM-103123] p 31 N90-23404
Experimental and analytical study of close-coupled ventral nozzles for ASTOVL aircraft [NASA-TM-103170] p 31 N90-24273
- SMITH, J.**
Advanced instrumentation for aircraft icing research [NASA-CR-185225] p 18 N90-21006
- SMITH, J. N.**
Development of a phase Doppler based probe for icing cloud droplet characterization [AIAA PAPER 90-0667] p 186 A90-26978
- SMITH, JOHN R.**
Universal aspects of brittle fracture, adhesion, and atomic force microscopy p 83 A90-14021
- SMITH, M. M.**
Feasibility analysis of reciprocating magnetic heat pumps [NASA-CR-186205] p 177 N90-15363
- SMITH, S. D.**
Reaction zone microstructure in a Ti3Al + Nb/SiC composite p 91 A90-39627

- SMITH, SAMUEL O.**
Thin film eddy current impulse deicer
[AIAA PAPER 90-0761] p 17 A90-20012
- SMITH, TODD E.**
Aeroelastic stability analysis of a high-energy turbine blade
[AIAA PAPER 90-2351] p 66 A90-47215
- SMITHRICK, JOHN J.**
Effect of KOH concentration on LEO cycle life of IPV nickel-hydrogen flight battery cells
[NASA-TM-103127] p 77 N90-21116
Effect of LEO cycling on 125 Ah advanced design IPV nickel-hydrogen battery cells
[NASA-TM-103128] p 78 N90-21808
- SMOLINSKI, P.**
Parallel multi-time step integration on a transputer system
p 235 A90-20188
- SMOLINSKI, PATRICK J.**
Transient finite element computations on the transputer system
[NASA-CR-185199] p 218 N90-18071
- SNOW, D. B.**
Identification of a cast iron alloy containing nonstrategic elements
[NASA-CR-185174] p 118 N90-18559
- SNYDER, CHRISTOPHER A.**
Advanced core technology - Key to subsonic propulsion benefits
[ASME PAPER 89-GT-241] p 19 A90-23890
- SNYDER, DAVID B.**
Plasma interactions and effects for large systems
p 252 N90-25545
- SNYDER, P. G.**
Dielectric function of InGaAs in the visible
[NASA-TM-103246] p 260 N90-26683
- SNYDER, PAUL G.**
Study of indium tin oxide films exposed to atomic oxygen
p 257 A90-45193
- SNYDER, PHILIP H.**
Design of an air-cooled metallic high-temperature radial turbine
p 20 A90-32960
- SOBAJIC, DEJAN J.**
Automating security monitoring and analysis for Space Station Freedom's electric power system
[NASA-TM-103148] p 240 N90-22324
- SOEDER, RONALD H.**
NASA Lewis icing research tunnel user manual
[NASA-TM-102319] p 31 N90-23407
- SOH, W. Y.**
Time-dependent viscous incompressible Navier-Stokes equations - The finite difference Galerkin formulation and streamfunction algorithms
p 156 A90-11598
Computational analysis of the flowfield of a two-dimensional ejector nozzle
[AIAA PAPER 90-1901] p 21 A90-42690
Computational analysis of the flowfield of a two-dimensional ejector nozzle
[NASA-CR-185255] p 31 N90-23406
- SOH, WOO-YUNG**
Application of a lower-upper implicit scheme and an interactive grid generation for turbomachinery flow field simulations
[ASME PAPER 89-GT-20] p 4 A90-23762
- SOHN, K. H.**
Some characteristics of bypass transition in a heated boundary layer
p 169 A90-35183
- SOHN, PHILIP Y.**
Advanced Communications Technology Satellite (ACTS) and potential system applications
p 142 A90-51165
A technology assessment of alternative communications systems for the space exploration initiative
[NASA-TM-103243] p 47 N90-27736
- SOKOLOV, V.**
The 30-GHz monolithic receive module
[NASA-CR-180849] p 146 N90-24528
- SOMERVILLE, W. A.**
Issues and opportunities in space photovoltaics
p 54 A90-14852
- SONG, J.**
Development of impact design methods for ceramic gas turbine components
[AIAA PAPER 90-2413] p 197 A90-42165
- SONIN, AIN A.**
Rate correlation for condensation of pure vapor on turbulent, subcooled liquid
p 174 A90-50511
- SOTOS, RAYMOND G.**
An investigation of flame spread over shallow liquid pools in microgravity and nonair environments
[NASA-TM-102425] p 134 N90-13680
- SOULAS, G.**
Diagnostics and performance of a 1/4-scale MPD thruster
[AIAA PAPER 90-2665] p 65 A90-42625
- SOURS, T.**
Photovoltaic module on-orbit assembly for Space Station Freedom
p 45 A90-38071
- SOVEY, J.**
Geometric effects in applied-field MPD thrusters
[AIAA PAPER 90-2669] p 69 A90-52572
- SOVEY, J. S.**
Test facility and preliminary performance of a 100 kW class MPD thruster
p 75 N90-18476
- SOVEY, JAMES S.**
Performance and endurance tests of a laboratory model multipropellant resistojet
p 55 A90-21220
Advanced propulsion for LEO and GEO platforms
[AIAA PAPER 90-2551] p 68 A90-52565
Geometric effects in applied-field MPD thrusters
[NASA-TM-103259] p 82 N90-27782
Advanced propulsion for LEO and GEO platforms
[NASA-TM-103228] p 82 N90-27785
- SOVIE, AMY J.**
Arcjet nozzle design impacts
p 76 N90-18478
- SOVIE, R. J.**
Nuclear power systems for lunar and Mars exploration
[NASA-TM-103168] p 82 N90-26873
- SOVIE, RONALD J.**
Nuclear technology and the space exploration missions
[NASA-TM-103156] p 232 N90-22847
- SPALVINS, TALIVALDIS**
Advances and directions of ion nitriding/carburizing
[NASA-TM-102398] p 137 N90-11902
Influence of the deposition conditions on radiofrequency magnetron sputtered MoS₂ films
[NASA-TP-2994] p 137 N90-21210
- SPATZ, RAYMOND R.**
Space Station Freedom electric power system photovoltaic power module integrated launch package
[AIAA PAPER 90-1053] p 48 A90-29281
- SPEARS, DON H.**
Conceptual design study of a 5 kilowatt solar dynamic Brayton power system using a dome Fresnel lens solar concentrator
[NASA-CR-185134] p 72 N90-14281
- SPENCE, RODNEY L.**
Numerical Arc Segmentation Algorithm for a Radio Conference-NASARC (version 4.0) technical manual
[NASA-TM-101453] p 144 N90-20264
Numerical Arc Segmentation Algorithm for a Radio Conference (NASARC), version 4.0: User's manual
[NASA-TM-101454] p 145 N90-21250
A technology assessment of alternative communications systems for the space exploration initiative
[NASA-TM-103243] p 47 N90-27736
- SPISZ, ERNIE**
LBR-2 earth stations for the ACTS program
[AIAA PAPER 90-0838] p 42 A90-25662
- SPRISSLER, B.**
Elevated temperature slow plastic deformation of NiAl-TiB₂ particulate composites at 1200 and 1300 K
p 92 A90-45621
- SPURLOCK, O. F.**
Performance comparisons of nuclear thermal rocket and chemical propulsion systems for piloted missions to Phobos/Mars
[IAF PAPER 89-027] p 53 A90-13262
- SRIVASTAVA, R.**
Application of an efficient hybrid scheme for aeroelastic analysis of advanced propellers
[AIAA PAPER 90-0028] p 4 A90-22153
Numerical simulation of unsteady rotational flow over propfan configurations
[NASA-CR-186037] p 10 N90-12500
Application of an efficient hybrid scheme for aeroelastic analysis of advanced propellers
[NASA-TM-102428] p 11 N90-13355
- SRIVATSAN, T. S.**
An experimental evaluation of the tensile strength of impact ice
p 83 A90-15049
- STAN, M. A.**
Ellipsometric study of YBa₂Cu₃O_{7-x} laser ablated and co-evaporated films
[NASA-TM-103223] p 259 N90-26682
- STANDLEY, HILDA M.**
A general model for memory interference in a multiprocessor system with memory hierarchy
p 238 A90-37482
Multiprocessor architecture: Synthesis and evaluation
[NASA-CR-186618] p 235 N90-25579
Modeling and synthesis of multicomputer interconnection networks
[NASA-CR-186619] p 238 N90-25604
Computer architecture evaluation for structural dynamics computations: Project summary
[NASA-CR-186137] p 235 N90-26512
- STANG, D. B.**
Subtle porosity variation in the YBa₂Cu₃O_{7-x} high-temperature superconductor revealed by ultrasonic imaging
[NASA-TM-102130] p 206 N90-17167
- Review and statistical analysis of the ultrasonic velocity method for estimating the porosity fraction in polycrystalline materials
[NASA-TM-102501-REV] p 207 N90-21402
- STASKUS, JOHN V.**
The Space Station photovoltaic panels plasma interaction test program - Test plan and results
[AIAA PAPER 90-0722] p 47 A90-22252
The Space Station Photovoltaic Panels Plasma Interaction Test Program: Test plan and results
[NASA-TM-102474] p 49 N90-13581
- STEARNS, CARL A.**
Materials for engine applications above 3000 deg F: An overview
[NASA-TM-100169] p 95 N90-10188
- STEARNS, E. MARSHALL**
Energy Efficient Engine: Flight propulsion system final design and analysis
[NASA-CR-168219] p 34 N90-28558
Energy Efficient Engine core design and performance report
[NASA-CR-168069] p 34 N90-28559
Energy Efficient Engine integrated core/low spool design and performance report
[NASA-CR-168211] p 34 N90-28561
- STECURA, STEPHAN**
Two-layer thermal barrier coating. I - Effects of composition and temperature on oxidation behavior and failure
p 122 A90-33317
- STEEN, PAUL H.**
Shear stabilization of the capillary breakup of a cylindrical interface
[AD-A219268] p 159 A90-17578
- STEIGMAN, GARY**
The shocking development of lithium (and boron) in supernovae
p 264 A90-17643
- STEINBACH, R.**
Reflector surface distortion analysis techniques (thermal distortion analysis of antennas in space)
p 144 N90-19267
- STEINETZ, BRUCE M.**
Tribological properties of ceramic/Ti3Al-Nb sliding couples for use as candidate seal materials to 700 deg C
[NASA-TM-102401] p 86 N90-12658
High temperature, flexible, thermal barrier seal
[NASA-CASE-LEW-14672-1] p 201 N90-15444
High temperature flexible seal
[NASA-CASE-LEW-14695-1] p 204 N90-23751
- STEINKE, RONALD J.**
Application of a two-dimensional unsteady viscous analysis code to a supersonic throughflow fan stage
[NASA-TM-4141] p 25 N90-13387
- STEINMANN, PIERRE A.**
Influence of the deposition conditions on radiofrequency magnetron sputtered MoS₂ films
[NASA-TP-2994] p 137 N90-21210
- STELLA, PAUL M.**
Photovoltaic options for solar electric propulsion
[AIAA PAPER 90-2529] p 68 A90-52563
NASA advanced space photovoltaic technology: Status, potential and future mission applications
p 74 N90-17775
- STEPHENS, CRAIG A.**
An investigation into the numerical prediction of boundary layer transition using the K.Y. Chien turbulence model
[NASA-CR-185252] p 182 N90-26269
- STEPHENS, J. R.**
Influence of alloying elements on the oxidation behavior of NbAl₃
p 113 A90-24861
- STEPHENS, JOSEPH R.**
Composites boost 21st-century aircraft engines
p 90 A90-29704
Resources - Supply and availability
p 114 A90-34152
Materials Park, OH
NASA's HITEMP program for UHBR engines
[AIAA PAPER 90-2395] p 85 A90-39975
p 140 A90-47218
- STEPHENS, R.**
Refractory metal alloys and composites for space power systems
p 116 A90-46677
- STERN, A. M.**
Mixer-ejector nozzle for jet noise suppression
[AIAA PAPER 90-1909] p 247 A90-47202
- STERN, ALAN L.**
Spacecraft designs for VSAT networks
[AIAA PAPER 90-0895] p 140 A90-25681
- STEVENS, GRADY H.**
On-board switching and processing
p 150 A90-51168
- STEVENS, N. J.**
EPSAT - A workbench for designing high-power systems for the space environment
[AIAA PAPER 90-0637] p 245 A90-26975

PERSONAL AUTHOR INDEX

- STEVENS, N. JOHN**
The Environment-Power System Analysis Tool development program p 236 A90-38089
Conceptual definition of a high voltage power supply test facility [NASA-CR-185216] p 50 N90-25172
- STEVENSON, STEVEN M.**
An evolutionary communications scenario for Mars exploration [AAS PAPER 87-268] p 139 A90-16566
- STEVENSON, WARREN H.**
Investigation of turbulent transport in an axisymmetric sudden expansion p 163 A90-23112
- STIDHAM, CURTIS**
Total hemispherical emittance measured at high temperatures by the calorimetric method [NASA-TM-102322] p 136 N90-10309
- STINESPRING, C. D.**
Modeling of the SiC chemical vapor deposition process and comparison with experimental results p 105 A90-36810
- STITT, LEONARD E.**
Exhaust nozzles for propulsion systems with emphasis on supersonic cruise aircraft [NASA-RP-1235] p 29 N90-21037
- STOCK, T. A.**
Probabilistic simulation of uncertainties in composite uniaxial strengths [NASA-TM-102483] p 97 N90-16008
- STOCKER, DENNIS P.**
Ignition and behavior of laminar gas-jet diffusion flames in microgravity p 103 A90-23107
Effects of pressure on microgravity hydrocarbon diffusion flames [AIAA PAPER 90-0651] p 104 A90-25039
- STOLLER, H. M.**
The application of cast SiC/Al to rotary engine components [NASA-CR-179610] p 25 N90-13385
- STOTLER, C. L.**
PMR graphite engine duct development [NASA-CR-182228] p 23 N90-10037
- STOTTS, R.**
Automotive Stirling engine development program [NASA-CR-180839] p 263 N90-11654
- STOUFFER, D. C.**
A crystallographic model for the tensile and fatigue response for Rene N4 at 982 C p 114 A90-28754
A constitutive model for the inelastic multiaxial response of Rene 80 at 871 C and 982 C p 114 A90-32266
- STRAZISAR, A. J.**
An LDA investigation of the normal shock wave boundary layer interaction p 10 A90-52618
- STRAZISAR, ANTHONY J.**
Laser anemometer measurements in a transonic axial-flow fan rotor [NASA-TP-2879] p 175 N90-11245
- STROCK, T. W.**
Engine inlet distortion in a 9.2 percent scaled vectored thrust STOVL model in ground effect [AIAA PAPER 89-2910] p 5 A90-25043
Engine inlet distortion in a 9.2 percent scale vectored thrust STOVL model in ground effect [NASA-TM-102358] p 12 N90-17561
- STROCK, THOMAS W.**
Hot gas ingestion characteristics and flow visualization of a vectored thrust STOVL concept [NASA-TM-103212] p 32 N90-26009
- STROH, P.**
Space Station Freedom power management and distribution design status p 59 A90-38080
- STROUD, D.**
Surface entropy of liquids via a direct Monte Carlo approach - Application to liquid Si p 261 A90-31675
- STUART, THOMAS A.**
A 2.5 kW cascaded Schwarz converter for 20 kHz power distribution p 147 A90-36913
Electrical performance characteristics of high power converters for space power applications [NASA-CR-185947] p 72 N90-14279
A comparative study of electric power distribution systems for spacecraft [NASA-CR-186531] p 77 N90-21113
- STUFFLE, K. L.**
Zirconia toughened SiC whisker reinforced alumina composites small business innovation research [NASA-CR-179629] p 125 N90-10294
- SUDER, KENNETH L.**
Laser anemometer measurements in a transonic axial-flow fan rotor [NASA-TP-2879] p 175 N90-11245
- SUL, S. K.**
Performance testing of a high frequency link converter for Space Station power distribution system p 148 A90-38128
- SULLIVAN, T. J.**
Simulating transitional flow and heat transfer over the flat plate and circular cylinder using a K- ϵ swirl turbulence model p 168 A90-32171
- SUMMERS, ANNE M.**
Data compression for the microgravity experiments p 188 N90-16212
- SUN, D. C.**
A high-speed photography study of cavitation in a dynamically loaded journal bearing [NASA-TM-103178] p 204 N90-26338
- SUN, H.**
Comparison of boundary element and finite element methods in spur gear root stress analysis p 193 A90-21107
- SUNDBERG, GALE R.**
Advanced Launch System (ALS) actuation and power systems impact operability and cost p 69 A90-52955
Advanced Launch System (ALS): Electrical actuation and power systems improve operability and cost picture [NASA-TM-102547] p 152 N90-21271
Civil air transport: A fresh look at power-by-wire and fly-by-light [NASA-TM-102574] p 153 N90-21283
- SUNDBERG, RICHARD C.**
Frequency domain model for analysis of paralleled, series-output-connected Mapham inverters p 148 A90-38084
Distortion and regulation characterization of a Mapham inverter p 148 A90-38125
Development and testing of a 20 kHz component test bed p 43 A90-38126
- SURESH, AMBADI**
The Osher scheme for real gases [AIAA PAPER 90-0397] p 166 A90-25030
PROTEUS two-dimensional Navier-Stokes computer code, version 1.0. Volume 1: Analysis description [NASA-TM-102551] p 180 N90-21303
PROTEUS two-dimensional Navier-Stokes computer code, version 1.0. Volume 2: User's guide [NASA-TM-102552] p 180 N90-21306
PROTEUS two-dimensional Navier-Stokes computer code, version 1.0. Volume 3: Programmer's reference [NASA-TM-102553] p 180 N90-21307
- SUTLIFF, T. J.**
The vibro-acoustic mapping of low gravity trajectories on a Learjet aircraft [NASA-TM-103103] p 1 N90-21723
- SUTTER, JAMES K.**
Polymer solution phase separation: Microgravity simulation p 127 N90-17101
- SVOBODA, JAMES S.**
Effects of amplitude distortions and IF equalization on satellite communication system bit-error rate performance [AIAA PAPER 90-0878] p 140 A90-25697
Effects of amplitude distortions and IF equalization on satellite communication system bit-error rate performance [NASA-TM-102415] p 144 N90-19454
Rain-fade simulation and power augmentation for satellite communication systems [NASA-TM-103134] p 146 N90-28768
- SWANSON, S. R.**
Analysis of impact response in composite plates p 214 A90-47567
- SWARTZ, C. K.**
Radiation resistance and comparative performance of ITO/InP and n/p InP homojunction solar cells p 226 A90-14933
The mini-dome lens space concentrator array - Recent component test results and current array development status p 60 A90-38155
Indium phosphide solar cell research in the United States: Comparison with non-photovoltaic sources p 229 N90-17758
New directions in InP solar cell research [NASA-TM-103160] p 154 N90-23662
- SWARTZ, CLIFFORD K.**
Predicted performance of near-optimally designed indium phosphide space solar cells at high intensities and temperatures p 225 A90-14898
- SWEC, DIANE M.**
Diamondlike carbon protective coatings for optical windows p 122 A90-34569
- SWETTE, L.**
Oxygen electrodes for rechargeable alkaline fuel cells. II Oxygen electrodes for rechargeable alkaline fuel cells-II p 231 N90-20469
- SWICKARD, S. M.**
Review and statistical analysis of the ultrasonic velocity method for estimating the porosity fraction in polycrystalline materials [NASA-TM-102501-REV] p 207 N90-21402
- SWIFT, G.**
Propan Test Assessment (PTA): Flight test report [NASA-CR-182278] p 24 N90-11738
- SWIGART, R. J.**
Generalized Advanced Propeller Analysis System (GAPAS). Volume 2: Computer program user manual [NASA-CR-185277] p 36 N90-29394

T

- T'EN, JAMES S.**
Near-limit flame spread over a thin solid fuel in microgravity p 104 A90-32835
The possibility of a reversal of material flammability ranking from normal gravity to microgravity p 105 A90-42298
- TABAKOFF, WIDEN**
Three dimensional LDV flow measurements and theoretical investigation in a radial inflow turbine scroll p 9 A90-46860
- TACINA, ROBERT R.**
Space Station Freedom resistojet system study p 54 A90-16368
Low NO(x) potential of gas turbine engines [AIAA PAPER 90-0550] p 20 A90-25036
Combustor technology for future aircraft [AIAA PAPER 90-2400] p 22 A90-47219
Low NO(x) potential of gas turbine engines [NASA-TM-102452] p 27 N90-17636
- TADJFAR, M.**
A numerical study of the interaction between unsteady free-stream disturbances and localized variations in surface geometry p 161 A90-21422
- TAFTI, D. K.**
Hot gas environment around STOVL aircraft in ground proximity. II - Numerical study [AIAA PAPER 90-2270] p 21 A90-42766
- TAGHAVI, K.**
Inverse heat transfer analysis of Bridgman crystal growth p 157 A90-13093
- TAGHAVI, R.**
Modern developments in shear flow control with swirl [NASA-CR-186586] p 181 N90-22000
- TAGLIALAVORE, ANTONI P.**
Development of Si3N4 for gas turbine applications p 122 A90-35509
- TAHA, BADIE A.**
A general model for memory interference in a multiprocessor system with memory hierarchy p 238 A90-37482
- TALTY, T.**
Microstrip subarray with coplanar and stacked parasitic elements p 141 A90-41586
- TAM, CHRISTOPHER K. W.**
Theoretical model of discrete tone generation by impinging jets p 247 A90-35903
- TAM, KWA-SUR**
Modeling of power electronic systems with EMTF [NASA-TM-102375] p 245 N90-14060
- TAMASHIRO, R. N.**
K-band TWT using new diamond rod technology [AIAA PAPER 90-0870] p 147 A90-25691
- TAN, C. S.**
A multi-domain spectral computation of three-dimensional laminar horseshoe vortex flow using incompressible Navier-Stokes equations p 3 A90-17592
- TAN, C.-H.**
Comparison between pressure gradient method and MAC method on high Re calculation p 172 A90-44462
- TAN, H. Q.**
Computer simulation of the mathematical modeling involved in constitutive equation development: Via symbolic computations [NASA-TM-102532] p 219 N90-20428
Application of symbolic computations to the constitutive modeling of structural materials [NASA-TM-103225] p 222 N90-26364
- TANG, D.**
A fiber-optic current sensor for aerospace applications [NASA-TM-103152] p 190 N90-22773
- TANG, S. M.**
High frequency capacitance-voltage characteristics of thermally grown SiO2 films on beta-SiC p 254 A90-21348
- TANRIKUT, S.**
Energy efficient engine pin fin and ceramic composite segmented liner combustor sector rig test report [NASA-CR-179534] p 35 N90-28567
- TAUR, D.-R.**
Optimal impulsive time-fixed orbital rendezvous and interception with path constraints [AIAA PAPER 90-2972] p 41 A90-53051

- TAYA, MINORU**
Empirical and analytical determination of the fracture resistance of a TiB₂ particle/SiC matrix composite [NASA-TM-101940] p 96 N90-15143
- TAYLOR, J. R.**
Energy Efficient Engine combustor test hardware detailed design report [NASA-CR-168301] p 33 N90-28554
Energy Efficient Engine (E3) combustion system component technology performance report [NASA-CR-168274] p 33 N90-28555
- TELESMA, JACK**
The unusual near-threshold FCG behavior of a single crystal superalloy and the resolved shear stress as the crack driving force p 111 A90-21009
Fatigue crack growth in unidirectional metal matrix composite [NASA-TM-103102] p 220 N90-22117
Fatigue crack growth in a unidirectional SCS-6/Ti-15-3 composite [NASA-TM-103095] p 119 N90-22646
- TENG, N. G.**
Progress towards the development of an inviscid-viscous interaction method for unsteady flows in turbomachinery cascades p 2 A90-11806
- TENNER, V. J.**
Determination of the stress distributions in a ceramic: Tensile specimen using numerical techniques [NASA-TM-101914] p 129 N90-26132
- TEREN, FRED**
Space Station Freedom power management and distribution system design [IAF PAPER 89-078] p 54 A90-13295
- TEREPKA, F. M.**
Calibration approach to electron probe microanalysis: A study with PWA-1480, a nickel base superalloy [NASA-TM-102393] p 117 N90-14335
- TEVAARWERK, J. L.**
The measurement, modeling, and prediction of traction for rocket propellant 1 [NASA-CR-185186] p 131 N90-19386
- TEW, ROY C.**
Two-dimensional numerical simulation of a Stirling engine heat exchanger p 170 A90-38290
Recent Stirling engine loss-understanding results [NASA-TM-103122] p 77 N90-21114
- TEWARI, S. N.**
Side branch morphology and coarsening in directionally solidified Pb-8.4 at. pct Au p 109 A90-11658
Primary arm spacing in directionally solidified Pb-10 wt pct Sn alloys [AIAA PAPER 90-0740] p 132 A90-23713
Calibration approach to electron probe microanalysis: A study with PWA-1480, a nickel base superalloy [NASA-TM-102393] p 117 N90-14335
Primary arm spacing in directionally solidified Pb-10 wt percent Sn alloys [NASA-CR-185190] p 134 N90-14398
- THACKER, B. H.**
Application of the probabilistic approximate analysis method to a turbopump blade analysis [AIAA PAPER 90-1098] p 56 A90-29328
- THANEDAR, P. B.**
Robustness, generality and efficiency of optimization algorithms in practical applications [AIAA PAPER 90-1177] p 236 A90-29268
Composite laminate tailoring with probabilistic constraints and loads [NASA-TM-102515] p 98 N90-20138
- THESLING, WILLIAM**
Predicted performance of near-optimally designed indium phosphide space solar cells at high intensities and temperatures p 225 A90-14898
- THIEME, LANNY G.**
Recent Stirling engine loss-understanding results [NASA-TM-103122] p 77 N90-21114
- THOMAS, DAVID J.**
Reliability analysis of continuous fiber composite laminates [NASA-CR-185265] p 223 N90-26372
- THOMAS, J. KELLY**
A radiological assessment of nuclear power and propulsion operations near Space Station Freedom [NASA-CR-185185] p 76 N90-21108
- THOMAS, R. D.**
A V-grooved GaAs solar cell p 225 A90-14887
GaAs solar cells with V-grooved emitters p 229 N90-17754
Peeled film GaAs solar cells for space power [NASA-TM-103125] p 153 N90-21287
- THOMAS, RONALD L.**
Design of the Space Station Freedom power system p 57 A90-38070
The US space station and its electric power system [NASA-TM-101974] p 71 N90-13596
- THOMPSON, H. DOYLE**
Investigation of turbulent transport in an axisymmetric sudden expansion p 163 A90-23112
- THOMPSON, R. L.**
Structural response of SSME turbine blade airfoils p 224 N90-28649
- TIDMAN, D. A.**
Experiments on a repetitively pulsed electrothermal thruster p 56 A90-27960
- TIEN, JOHN K.**
Fiber reinforced superalloys p 91 A90-34169
- TIMKO, L. P.**
Energy Efficient Engine high pressure turbine component test performance report [NASA-CR-168289] p 33 N90-28553
- TITRAN, R. H.**
Refractory metal alloys and composites for space power systems p 116 A90-46677
Advanced refractory metals and composites for extraterrestrial power systems p 40 A90-48819
- TITRAN, ROBERT H.**
Creep strength of niobium alloys, Nb-1%Zr and PWC-11 [NASA-TM-102390] p 116 N90-11854
- TO, HING Y.**
Sequentially evaporated thin film YBa₂Cu₃O_{7-x} superconducting microwave ring resonator [NASA-TM-103180] p 154 N90-25273
- TO, W. M.**
The numerical simulation of multistage turbomachinery flows p 29 N90-21025
- TOBIN, S. P.**
High efficiency GaAs/Ge monolithic tandem solar cells p 224 A90-14858
- TODD, J. A.**
The high temperature creep deformation of Si₃N₄-6Y₂O₃-2Al₂O₃ p 121 A90-18879
- TOMSIK, T. M.**
Background, current status, and prognosis of the ongoing slush hydrogen technology development program for the NASP [NASA-TM-103220] p 51 N90-26055
- TOMSIK, THOMAS M.**
Prediction of the ullage gas thermal stratification in a NASP vehicle propellant tank experimental simulation using FLOW-3D [NASA-TM-103217] p 131 N90-26160
- TONG, MIKE**
Thermal/structural analyses of several hydrogen-cooled leading-edge concepts for hypersonic flight vehicles [AIAA PAPER 90-0053] p 164 A90-23702
Thermal/structural analyses of several hydrogen-cooled leading-edge concepts for hypersonic flight vehicles [NASA-TM-102391] p 177 N90-14511
- TOWER, LEONARD K.**
An improved algorithm for the modeling of vapor flow in heat pipes [NASA-CR-185179] p 176 N90-13748
- TOWNE, CHARLES E.**
PROTEUS two-dimensional Navier-Stokes computer code, version 1.0. Volume 1: Analysis description [NASA-TM-102551] p 180 N90-21303
PROTEUS two-dimensional Navier-Stokes computer code, version 1.0. Volume 2: User's guide [NASA-TM-102552] p 180 N90-21306
PROTEUS two-dimensional Navier-Stokes computer code, version 1.0. Volume 3: Programmer's reference [NASA-TM-102553] p 180 N90-21307
- TOWNSEND, D. P.**
Effect of advanced component technology on helicopter transmissions p 193 A90-21115
The role of thermal and lubricant boundary layers in the transient thermal analysis of spur gears p 194 A90-21118
Effects of lubrication on the performance of high speed spur gears p 194 A90-21119
Wear consideration in gear design for space applications p 194 A90-21121
Lubricant jet flow phenomena in spur and helical gears with modified addendums - For radially directed individual jets p 194 A90-21122
Vibration signature analysis of multistage gear transmission p 194 A90-21124
Dynamic loading of spur gears with linear or parabolic tooth profile modifications p 195 A90-21126
Profile modification to minimize spur gear dynamic loading p 195 A90-21128
- TOWNSEND, DENNIS P.**
Experimental and analytical evaluation of dynamic load vibration of a 2240-kW (3000-hp) rotorcraft transmission p 192 A90-13750
Surface pitting fatigue life of noninvolute, low-contact-ratio gears [AIAA PAPER 90-2153] p 197 A90-42049
- Gear noise, vibration, and diagnostic studies at NASA Lewis Research Center [NASA-TM-102435] p 202 N90-18041
Surface pitting fatigue life of noninvolute, low-contact-ratio gears [NASA-TM-103116] p 203 N90-22790
Influence of linear profile modification and loading conditions on the dynamic tooth load and stress of high contact ratio gears [NASA-TM-103136] p 204 N90-22796
Dynamics of multistage gear transmission with effects of gearbox vibrations [NASA-TM-103109] p 205 N90-28060
Computer-aided design of high-contact-ratio gears for minimum dynamic load and stress [NASA-TM-103275] p 205 N90-28065
- TRASH, L. M.**
Evaluation of power control concepts using the PMAD systems test bed p 42 A90-38083
- TREFNY, CHARLES J.**
On the use of external burning to reduce aerospace vehicle transonic drag [AIAA PAPER 90-1935] p 20 A90-40562
On the use of external burning to reduce aerospace vehicle transonic drag [NASA-TM-103107] p 30 N90-21762
- TRIPP, DAVID E.**
A review of failure models for ceramic matrix composite laminates under monotonic loads [ASME PAPER 89-GT-153] p 89 A90-23842
- TROUDET, T.**
A real time neural net estimator of fatigue life [NASA-TM-103117] p 239 N90-21564
- TROUDET, TERRY**
Neuromorphic learning of continuous-valued mappings from noise-corrupted data. Application to real-time adaptive control [NASA-TM-4176] p 241 N90-25607
- TROWBRIDGE, DANIEL A.**
Low velocity impact analysis with NASTRAN p 221 N90-24647
- TRUEBLOOD, B.**
Oxygen/methane combustion stability investigation p 107 N90-28628
- TRUONG, LONG V.**
Autonomous power expert fault diagnostic system for Space Station Freedom electrical power system testbed p 80 N90-25521
- TRUONG, LONG VAN**
Autonomous power expert system p 240 N90-22306
- TRURAN, JAMES**
The shocking development of lithium (and boron) in supernovae p 264 A90-17643
- TRYK, D.**
Catalysts for ultrahigh current density oxygen cathodes for space fuel cell applications [NASA-CR-180650] p 232 N90-22835
- TRYK, DONALD**
Electrocatalysis for oxygen electrodes in fuel cells and water electrolyzers for space applications p 57 A90-33945
Electrocatalysis for oxygen electrodes in fuel cells and water electrolyzers for space applications p 230 N90-20468
- TSAI, FU-SHENG**
High-frequency ac power distribution in Space Station p 63 A90-39111
- TSAI, TOMMY M.**
User's manual for PEPSIG NASA tip vortex version [NASA-CR-182178] p 10 N90-10835
Computation of the tip vortex flowfield for advanced aircraft propellers [NASA-CR-182179] p 10 N90-10836
- TSAI, Y.-L. PETER**
Comparative study of computational efficiency of two LU schemes for non-equilibrium reacting flows [AIAA PAPER 90-0396] p 167 A90-26940
- TSAU, F.**
Effects of g-jitter on a thermal, buoyant flow [AIAA PAPER 90-0653] p 163 A90-22239
- TSERNG, H. Q.**
Doped-channel heterojunction structures for millimeter-wave discrete devices and MMICs p 150 A90-48492
- TSERNG, HUA QUEN**
AlGaAs/InGaAs heterostructures with doped channels for discrete devices and monolithic amplifiers p 146 A90-20861
- TSUKAMOTO, S.**
Molecular beam epitaxial growth of high-quality InSb on InP and GaAs substrates p 253 A90-12808
Transport properties of InAs(x)Sb(1-x) (x = 0-0.55) on InP grown by molecular-beam epitaxy p 256 A90-36232

PERSONAL AUTHOR INDEX

- TU, Y. K.**
Vibration signature analysis of multistage gear transmission p 194 A90-21124
Dynamics of multistage gear transmission with effects of gearbox vibrations [NASA-TM-103109] p 205 N90-28060
- TULPUL, S.**
Health Monitoring System for the SSME-fault detection algorithms [AIAA PAPER 90-1988] p 63 A90-40584
- TULPUL, SHARAYU**
Health monitoring system for the SSME - Hardware architecture study [AIAA PAPER 90-1989] p 65 A90-42713
Framework for a space shuttle main engine health monitoring system [NASA-CR-185224] p 78 N90-21809
- TURNBERG, J. E.**
Large scale prop-fan structural design study. Volume 1: Initial concepts [NASA-CR-174992] p 23 N90-10043
Large scale prop-fan structural design study. Volume 2: Preliminary design of SR-7 [NASA-CR-174993] p 23 N90-10044
- TURNBERG, JAY E.**
Large-scale Advanced Prop-fan (LAP) static rotor test report [NASA-CR-180848] p 25 N90-12617
- TURNER, MICHAEL S.**
Dark matter candidates p 266 A90-44095
- TURNOK, STEPHEN R.**
Investigation of surface water behavior during glaze ice accretion p 16 N90-20927
- TURNQUIST, S. R.**
Space Station Freedom power - A reliability, availability, and maintainability assessment of the proposed Space Station Freedom electric power system p 58 A90-38074
- TURNQUIST, SCOTT R.**
Space Station Freedom electric power system availability study [NASA-CR-185181] p 50 N90-20120
- URNS, S. R.**
Ignition and combustion characteristics of metallized propellants [NASA-CR-186870] p 107 N90-26911
- TUROK, NEIL**
Phase transitions as the origin of large scale structure in the universe p 265 A90-35291
- TWOMBLY, M.**
Space Station Freedom power - A reliability, availability, and maintainability assessment of the proposed Space Station Freedom electric power system p 58 A90-38074
- TYLIM, A.**
Space Station Solar Dynamic Module modelling and simulation p 53 A90-11993
- TYLIM, ADRIAN**
Structural configuration options for the Space Station Freedom solar dynamic radiator [IAF PAPER ICOSP89-4-5] p 48 A90-27710
- U**
- UENISHI, K.**
An investigation of counterrotating tip vortex interaction [NASA-CR-185135] p 247 N90-11549
- ULBRICH, H.**
Actuator design for rotor control p 198 A90-46232
- ULBRICH, HEINZ**
Elements of active vibration control for rotating machinery [NASA-TM-102368] p 137 N90-22703
- V**
- VALCO, G. J.**
Photoresponse of YBa₂Cu₃O₇(δ) granular and epitaxial superconducting thin films [NASA-TM-103144] p 154 N90-22732
- VALCO, GEORGE J.**
Sequentially evaporated thin film YBa₂Cu₃O₇(δ) superconducting microwave ring resonator [NASA-TM-103180] p 154 N90-25273
- VALGORA, MARTIN E.**
Power considerations for an early manned Mars mission utilizing the Space Station [AAS PAPER 87-223] p 55 A90-16688
- VAN DALEN, ANTHONY**
Cosmic-string-induced hot dark matter perturbations p 264 A90-25889

- VAN FOSSEN, G. JAMES**
Convective heat transfer measurements from a NACA 0012 airfoil in flight and in the NASA Lewis Icing Research Tunnel [AIAA PAPER 90-0199] p 162 A90-22180
- VAN LEER, BRAM**
Splitting of inviscid fluxes for real gases p 167 A90-25451
Inviscid flux-splitting algorithms for real gases with non-equilibrium chemistry p 174 A90-52275
- VAN OMMEERING, GERT**
Energy storage and thermal control system design status p 59 A90-38077
- VAN STONE, R. H.**
A constitutive model for the inelastic multiaxial response of Rene 80 at 871 C and 982 C p 114 A90-32266
Simulation of crack growth and crack closure under large cyclic plasticity p 214 A90-50562
- VANDERBORGH, N. E.**
Regenerative fuel cell systems for project pathfinder p 74 N90-17708
- VANDERSANDE, J. W.**
Effect of Ga and P dopants on the thermoelectric properties of n-type SiGe p 256 A90-38140
- VANFOSSEN, G. JAMES**
Convective heat transfer measurements from a NACA 0012 airfoil in flight and in the NASA Lewis Icing Research Tunnel [NASA-TM-102448] p 176 N90-13750
- VANKA, S. P.**
Multigrad calculations of a jet in crossflow [AIAA PAPER 90-0444] p 167 A90-26952
Hot gas environment around STOVLC aircraft in ground proximity. II - Numerical study [AIAA PAPER 90-2270] p 21 A90-42766
- VANNUCCI, R. D.**
Autoclavable addition polyimides for 371 C composite applications [NASA-TM-103233] p 102 N90-27874
- VANOVERBEKE, T. J.**
Calculations of gaseous H₂/O₂ thruster [AIAA PAPER 90-2490] p 67 A90-47224
- VANOVERBEKE, THOMAS J.**
Three-dimensional turbulent flow code calculations of hot gas ingestion p 21 A90-44726
- VANSTONE, R. H.**
Elevated temperature crack growth [NASA-CR-182247] p 222 N90-26355
- VARALJAY, N.**
Photoresponse of YBa₂Cu₃O₇(δ) granular and epitaxial superconducting thin films [NASA-TM-103144] p 154 N90-22732
- VARALJAY, N. C.**
Growth and patterning of laser ablated superconducting YBa₂Cu₃O₇ films on LaAlO₃ substrates [NASA-TM-102436] p 259 N90-22421
- VARGAS-ABURTO, CARLOS**
Development of a quadrupole-based Secondary-Ion Mass Spectrometry (SIMS) system at Lewis Research Center [NASA-TM-102531] p 87 N90-23476
- VEDHA-NAYAGAM, M.**
Advanced spacecraft fire safety: Proposed projects and program plan [NASA-CR-185147] p 49 N90-12645
- VENTURINI, E. L.**
Rapid thermal processing of high temperature superconducting fiber [NASA-CR-186803] p 259 N90-24964
- VERDON, JOSEPH M.**
Gust response analysis for cascades operating in nonuniform mean flows p 28 N90-18415
Development of a linearized unsteady aerodynamic analysis for cascade gust response predictions [NASA-CR-4308] p 14 N90-27655
- VERHEY, TIMOTHY R.**
5kW xenon ion thruster lifetest [AIAA PAPER 90-2543] p 68 A90-52564
Requirements for long-life operation of inert gas hollow cathodes - Preliminary results [AIAA PAPER 90-2586] p 69 A90-52570
Requirements for long-life operation of inert gas hollow cathodes: Preliminary report [NASA-TM-103242] p 82 N90-27783
- VERHOFF, VINCENT G.**
An applicational process for dynamic balancing of turbomachinery shafting [NASA-TM-102537] p 202 N90-20392
- VERNON, S. M.**
High efficiency GaAs/Ge monolithic tandem solar cells p 224 A90-14858
- VERNON, STANLEY M.**
Wide-bandgap epitaxial heterojunction windows for silicon solar cells p 227 A90-28359

WAINAUSKI, HARRY S.

- VERRILLI, M. J.**
Isothermal life prediction of composite lamina using a damage mechanics approach p 92 A90-48115
- VERRILLI, MICHAEL J.**
Characterization of failure processes in tungsten copper composites under fatigue loading conditions [NASA-TM-102371] p 98 N90-21123
High temperature fatigue behavior of tungsten copper composites [NASA-TM-102404] p 99 N90-21138
- VERZWYVELT, S. A.**
Electrochemical behavior of heavily cycled nickel electrodes in Ni/H₂ cells containing electrolytes of various KOH concentrations p 103 A90-24535
KOH concentration effect on the cycle life of nickel-hydrogen cells. IV - Results of failure analysis p 228 A90-33952
- VESELY, E. J., JR.**
Mechanical properties of pure nickel alloys after long term exposures to LiOH and vacuum at 775 K [NASA-TM-102403] p 118 N90-20181
- VIERGUTZ, B. J.**
Ka-band propagation characteristics of microstrip lines on GaAs substrates at cryogenic temperatures p 147 A90-33644
- VIJAYAKUMAR, M.**
Calibration approach to electron probe microanalysis: A study with PWA-1480, a nickel base superalloy [NASA-TM-102393] p 117 N90-14335
- VINCENT, JAMES H.**
Flight control design considerations for STOVLC powered-lift flight [AIAA PAPER 90-3225] p 37 A90-49110
- VINER, ANDREW S.**
The impedance of a tubular electrode - A model for a porous electrode p 104 A90-33723
- VINET, PASCAL**
Pressure dependence of the melting temperature of metals p 103 A90-16281
- VINH, NGUYEN X.**
Comparison of solution approaches for minimum-fuel, low-thrust, power-limited orbital transfers [AIAA PAPER 90-2960] p 41 A90-53035
- VINYARD, SHANNON**
Sliding seal materials for low heat rejection engines [NASA-CR-182262] p 125 N90-11882
- VIRNIG, JOHN C.**
The implementation of STOVLC task-tailored control modes in a fighter cockpit [AIAA PAPER 90-3229] p 17 A90-49114
- VISHNIAC, ETHAN T.**
A model for the distribution of the intergalactic medium p 265 A90-34505
A model for the distribution of dark matter, galaxies, and the intergalactic medium in a cold dark matter-dominated universe p 266 A90-45560
- VISWANADHAM, R. K.**
1200 to 1400 K slow strain rate compressive properties of NiAl/Ni₂AlTi-base materials p 88 A90-16938
Elevated temperature slow plastic deformation of NiAl-TiB₂ particulate composites at 1200 and 1300 K p 92 A90-45621
Slow plastic deformation of extruded NiAl-10TiB₂ particulate composites at 1200 and 1300 K p 92 A90-46133
- VITTA, S.**
Ellipsometric study of YBa₂Cu₃O₇(δ) laser ablated and co-evaporated films [NASA-TM-103223] p 259 N90-26682
- VOGT, SCOTT T.**
Launch packaging options for the PV power module cargo element p 45 A90-38078
- VOLLER, V. R.**
The modelling of heat, mass and solute transport in solidification systems p 157 A90-13092
- W**
- WACHTER, JOSEPH P.**
COLD-SAT - An orbital cryogenic hydrogen technology experiment [IAF PAPER 89-057] p 53 A90-13282
- WAGNER, D. A.**
Advanced gearbox technology [NASA-CR-179625] p 32 N90-24274
- WAINAUSKI, HAROLD S.**
Large-scale Advanced Prop-fan (LAP) high speed wind tunnel test report [NASA-CR-182125] p 24 N90-10045
- WAINAUSKI, HARRY S.**
Large-scale Advanced Prop-fan (LAP) static rotor test report [NASA-CR-180848] p 25 N90-12617

WALKER, GILBERT H.

PERSONAL AUTHOR INDEX

- WALKER, GILBERT H.**
Mathematical optimization of photovoltaic converters for diode lasers p 228 A90-38110
- WALKER, J. D. A.**
Computation of three-dimensional turbulent boundary layers with heat transfer in a plane of symmetry using embedded wall-layer functions [AIAA PAPER 90-0307] p 180 A90-19788
Wall-layer eruptions in turbulent flows [NASA-TM-102362] p 175 N90-11250
- WALKER, K. P.**
High temperature inelastic deformation under uniaxial loading - Theory and experiment p 109 A90-13838
Biaxial constitutive modelling and testing of a single crystal superalloy at elevated temperatures p 110 A90-18741
Constitutive modeling for isotropic materials (HOST) [NASA-CR-174718] p 26 N90-13391
A new uniformly valid asymptotic integration algorithm for elasto-plastic-creep and unified viscoplastic theories including continuum damage [NASA-TM-102344] p 217 N90-14655
Steady-state and transient Zener parameters in viscoplasticity: Drag strength versus yield strength [NASA-TM-102487] p 218 N90-18064
A viscoplastic model with application to LiF-22 percent CaF2 hypereutectic salt [NASA-TM-103181] p 221 N90-23770
Stress versus temperature dependent activation energies in creep [NASA-TM-103192] p 221 N90-23773
- WALKER, KEVIN P.**
Model development in viscoplastic ratchetting [NASA-TM-102509] p 219 N90-20431
- WALKER, RICHARD E.**
Combustor design and analysis using the ROCKET Combustor Interactive Design (ROCCID) Methodology [AIAA PAPER 90-2240] p 65 A90-45694
Combustor design and analysis using the Rocket Combustor Interactive Design (ROCCID) methodology [NASA-TM-103165] p 79 N90-24349
- WALSTON, WILLIAM S.**
The effect of hydrogen and microstructure on the deformation and fracture behavior of a single crystal nickel-base superalloy [NASA-CR-185219] p 118 N90-21849
- WALTERS, JERRY L.**
Autonomous power expert system p 240 N90-22306
Autonomous power expert fault diagnostic system for Space Station Freedom electrical power system testbed p 80 N90-25521
- WALTON, E.**
Electromagnetic properties of material coated surfaces [NASA-CR-186466] p 144 N90-19466
- WALTON, ERIC K.**
Application of heuristic satellite plan synthesis algorithms to requirements of the WARC-88 allotment plan [AIAA PAPER 90-0815] p 245 A90-25638
A heuristic approach to worst-case carrier-to-interference ratio maximization in satellite system synthesis [AIAA PAPER 90-0816] p 46 A90-25639
Application of heuristic satellite plan synthesis algorithms to requirements of the WARC-88 allotment plan [NASA-TM-102479] p 245 N90-14856
- WANG, C.**
Catalysts for ultrahigh current density oxygen cathodes for space fuel cell applications [NASA-CR-180650] p 232 N90-22835
- WANG, EDWARD Y.**
The photovoltaic properties of an Al In As/InP heterojunctions grown by LPE method [NASA-CR-185996] p 229 N90-13886
- WANG, H. C.**
Advanced development of BEM for elastic and inelastic dynamic analysis of solids p 213 A90-45771
- WANG, L. W.**
Ground-based experiments on thermal and thermosolutal convection in inclined low-aspect-ratio enclosures [AIAA PAPER 90-0413] p 166 A90-25033
- WANG, L.-W.**
Numerical studies of convective heat transfer in an inclined semi-annular enclosure p 173 A90-45317
- WANG, N.**
Electromagnetic properties of material coated surfaces [NASA-CR-186466] p 144 N90-19466
- WANG, YUN**
Gravitational couplings of the inflaton in extended inflation p 265 A90-40088
- WANG, Z. Q.**
Surface entropy of liquids via a direct Monte Carlo approach - Application to liquid Si p 261 A90-31675
- WANHAINEIN, J. S.**
Hardware development for the surface tension driven convection experiment p 52 A90-36195
- WANHAINEIN, JOYCE S.**
A new fabrication method for precision antenna reflectors for space flight and ground test [AIAA PAPER 90-0803] p 139 A90-25627
- WANLASS, M. W.**
An empirical investigation of the InP shallow-homojunction solar cell p 225 A90-14869
Hybrid solar cells based on dc magnetron sputtered films of n-ITO on APMOPE grown p-InP p 225 A90-14893
Modeling and simulation of InP homojunction solar cells p 226 A90-14899
Investigation of buried homojunctions in p-InP formed during sputter deposition of both indium tin oxide and indium oxide p 256 A90-36799
- WARD, JAMES**
Effects of desired signal on the performance of a sidelobe canceller p 139 A90-13936
- WARK, C. E.**
A rotating hot-wire technique for spatial sampling of disturbed and manipulated duct flows p 186 A90-41120
- WARNER, J. D.**
Millimeter-wave surface resistance of laser-ablated YBa2Cu3O(7-delta) superconducting films p 257 A90-48694
Performance and modeling of superconducting ring resonators at millimeter-wave frequencies [NASA-TM-102526] p 151 N90-18634
Millimeter wave surface resistance of RBa2Cu3O(7-delta) (R=Y, Eu, Dy, Sm, Er) superconductors [NASA-TM-102571] p 259 N90-20886
Growth and patterning of laser ablated superconducting YBa2Cu3O7 films on LaAlO3 substrates [NASA-TM-102436] p 259 N90-22421
Photoreponse of YBa2Cu3O(7-delta) granular and epitaxial superconducting thin films [NASA-TM-103144] p 154 N90-22732
Ellipsometric study of YBa2Cu3O(7-x) laser ablated and co-evaporated films [NASA-TM-103223] p 259 N90-26682
Laser ablated high T(sub c) superconducting thin YBa2Cu3O(7-x) films on substrates suitable for microwave applications p 260 N90-27808
Microwave conductivity of laser ablated YBaCuO superconducting films and its relation to microstrip transmission line p 155 N90-27844
High temperature superconducting thin film microwave circuits: Fabrication, characterization, and applications [NASA-TM-103235] p 156 N90-28786
- WARNER, JOSEPH D.**
Study of deposition of YBa2Cu3O7-x on cubic zirconia [NASA-TM-102350] p 257 N90-10737
Sequentially evaporated thin film YBa2Cu3O(7-x) superconducting microwave ring resonator [NASA-TM-103180] p 154 N90-25273
- WARSHAWSKY, ISIDORE**
Foundations of measurement and instrumentation [NASA-RP-1222] p 189 N90-21351
- WARSHAY, MARVIN**
The fuel cell in space - Yesterday, today and tomorrow p 56 A90-26837
The NASA Advanced Solar Dynamics Technology Program p 62 A90-38280
The fuel cell in space: Yesterday, today and tomorrow [NASA-TM-102366] p 70 N90-11804
- WARS, S.**
Large-scale advanced propeller blade pressure distributions: Prediction and data [NASA-TM-102316] p 30 N90-22564
- WARS, SAIF A.**
User's guide to PMESH: A grid-generation program for single-rotation and counterrotation advanced turboprops [NASA-CR-185156] p 235 N90-14783
- WATERS, J. F.**
Autoclavable addition polyimides for 371 C composite applications [NASA-TM-103233] p 102 N90-27874
- WEAVER, ALFRED C.**
AIRNET: A real-time communications network for aircraft [NASA-CR-186140] p 145 N90-24514
- WEBER, K. E.**
Ceramic valve development for heavy-duty low heat rejection diesel engines p 196 A90-27091
- WEBER, R. M.**
Constitutive modeling for isotropic materials (HOST) [NASA-CR-179522] p 26 N90-13390
Constitutive modeling for isotropic materials (HOST) [NASA-CR-174718] p 26 N90-13391
- WEDHA-NAYAGAM, M.**
Opposed-flow flame spread and extinction in mixed-convection boundary layers p 168 A90-32841
- WEEKS, DAVID J.**
Space Station power system autonomy demonstration p 245 A90-10373
- WEIKLE, DONALD H.**
Heat flux measurements [ASME PAPER 89-GT-107] p 165 A90-23815
TiCl4 as a source of TiO2 particles for laser anemometry measurements in hot gas [NASA-TM-102581] p 189 N90-20358
- WEINBERG, I.**
Radiation resistance and comparative performance of ITO/InP and n/p InP homojunction solar cells p 226 A90-14933
Indium phosphide solar cell research in the United States: Comparison with non-photovoltaic sources p 229 N90-17758
New directions in InP solar cell research [NASA-TM-103160] p 154 N90-23662
- WEINBERG, IRVING**
Predicted performance of near-optimally designed indium phosphide space solar cells at high intensities and temperatures p 225 A90-14898
InP homojunction solar cell performance on the LIPS III flight experiment p 226 A90-14921
Indium phosphide solar cells - Recent developments and estimated performance in space p 57 A90-37854
- WEIR, L. J.**
Comparison of 3-D viscous flow computations of Mach 5 inlet with experimental data [AIAA PAPER 90-0600] p 6 A90-26970
Comparison of 3-D viscous flow computations of Mach 5 inlet with experimental data [NASA-TM-102518] p 28 N90-20090
- WEISLOGEL, MARK M.**
Surface reorientation and settling in cylinders upon step reduction in gravity p 172 A90-44541
- WEIZER, VICTOR G.**
Contact formation in gallium arsenide solar cells p 225 A90-14888
The kinetics of the Au-InP interaction p 254 A90-25084
Humidity-induced room-temperature decomposition of Au contacted indium phosphide p 105 A90-44689
Contact spreading and the Au3In-to-Au9In4 transition in the Au-InP system p 257 A90-48661
Lateral spreading of Au contacts on InP [NASA-TM-103133] p 232 N90-22843
An analysis of the contact sintering process in III-V solar cells [NASA-TM-103179] p 233 N90-25420
- WELCH, W. J. C.**
A numerical study of the interaction between unsteady free-stream disturbances and localized variations in surface geometry p 161 A90-21422
- WELSCH, G.**
The high temperature deformation in cyclic loading of a single crystal nickel-base superalloy p 108 A90-11534
- WENZLER, CARL J.**
Design of a CO2 laser power control system for a Spacelab microgravity experiment [NASA-TM-103112] p 192 N90-28833
- WERNET, MARK P.**
New space domain processing technique for pulsed laser velocimetry p 187 A90-48750
- WESTFALL, L. J.**
Compressive strength of a B2 matrix NiAl-Nb intermetallic at 1200 and 1300 K p 111 A90-19157
- WETHERHOLD, ROBERT C.**
Extension of a noninteractive reliability model for ceramic matrix composites [NASA-CR-185267] p 129 N90-26142
Reliability analysis of continuous fiber composite laminates [NASA-CR-185265] p 223 N90-26372
- WEY, C.**
A planar reacting shear layer system for the study of fluid dynamics-combustion interaction [NASA-TM-102422] p 27 N90-13393
- WEY, C. C.**
A planar reacting shear layer system for the study of fluid dynamics-combustion interaction [NASA-TM-102422] p 27 N90-13393
- WEY, MING-JYH**
Evaluation of a hybrid kinetics/mixing-controlled combustion model for turbulent premixed and diffusion combustion using KIVA-2 [NASA-TM-103196] p 185 N90-28792
- WHALEN, M. V.**
Background, current status, and prognosis of the ongoing slush hydrogen technology development program for the NASP [NASA-TM-103220] p 51 N90-26055

- WHALEN, MARGARET V.**
Performance and endurance tests of a laboratory model multipropellant resistojet p 55 A90-21220
Slush Hydrogen (SLH2) technology development for application to the National Aerospace Plane (NASP) [NASA-TM-102315] p 50 N90-14268
- WHALEN, THOMAS J.**
Improved silicon carbide for advanced heat engines [NASA-CR-180831] p 124 N90-10293
Improved silicon carbide for advanced heat engines [NASA-CR-182186] p 129 N90-28735
- WHATLEY, DAVID W.**
The implementation of STOVl task-tailored control modes in a fighter cockpit [AIAA PAPER 90-3229] p 17 A90-49114
- WHEELER, D. R.**
Measurement of the intrinsic bond strength of brittle thin films on flexible substrates p 256 A90-44022
- WHIPPLE, DANIEL Y.**
Laser-velocimeter-measured flow field around an advanced, swept, eight-blade propeller at Mach 0.8 [NASA-TP-2462] p 1 N90-20942
- WHITE, A.**
Conceptual design of a Liquid Droplet Radiator space flight experiment [SAE PAPER 891565] p 48 A90-27527
- WHITE, JAMES W.**
A "transient" automated mapping procedure for complex geometries p 242 A90-26499
- WHITEHAIR, STANLEY**
Review of research and development on the microwave electrothermal thruster p 55 A90-16369
- WHITFIELD, C. E.**
High speed turboprop aeroacoustic study (counterrotation). Volume 1: Model development [NASA-CR-185241] p 249 N90-26633
- WHITFIELD, DAVID L.**
Counterrotating prop-fan simulations which feature a relative-motion multiblock grid decomposition enabling arbitrary time-steps [AIAA PAPER 90-0687] p 3 A90-19978
- WHITTENBERGER, J. D.**
On the stability of the creep substructure in NaCl single crystals p 254 A90-21920
The mechanical properties of fluoride salts at elevated temperatures p 123 A90-44376
Slow plastic deformation of extruded NiAl-10TiB2 particulate composites at 1200 and 1300 K p 92 A90-46133
High-temperature slow-strain-rate compression studies on CoAl-TiB2 composites p 93 A90-48636
Deformation of as-cast LiF-22 mol pct CaF2 hypereutectic salt between 500 and 1015 K p 124 A90-49086
Compression behavior of the forged Li2 compounds Al67Ti25Cr8 and Al68Ti25Mn9 p 116 A90-51298
- WHITTENBERGER, J. DANIEL**
Properties of oxide dispersion strengthened alloys p 109 A90-14687
1200 to 1400 K slow strain rate compressive properties of NiAl/Ni2AlTi-base materials p 88 A90-16938
1100 to 1300 K slow plastic compression properties of Ni-38.5Al composites p 111 A90-19154
Compressive strength of a B2 matrix NiAl-Nb intermetallic at 1200 and 1300 K p 111 A90-19157
Preliminary investigation of a NiAl composite prepared by cryomilling p 113 A90-25098
Intergranular fracture of lithium fluoride-22 percent calcium fluoride hypereutectic salt at 800 K p 121 A90-25273
Solid state processing for high temperature alloys and composites p 196 A90-33225
Elevated temperature slow plastic deformation of NiAl-TiB2 particulate composites at 1200 and 1300 K p 92 A90-45621
1300 K compressive properties of several dispersion strengthened NiAl materials p 118 A90-47091
Mechanical properties of pure nickel alloys after long term exposures to LiOH and vacuum at 775 K [NASA-TM-102403] p 118 N90-20181
- WHYTE, WAYNE A., JR.**
Digital codec for real-time processing of broadcast quality video signals at 1.8 bits/pixel p 142 A90-51306
Data compression for the microgravity experiments p 188 N90-16212
Numerical Arc Segmentation Algorithm for a Radio Conference-NASARC (version 4.0) technical manual [NASA-TM-101453] p 144 N90-20264
Numerical Arc Segmentation Algorithm for a Radio Conference (NASARC), version 4.0: User's manual [NASA-TM-101454] p 145 N90-21250
A technology assessment of alternative communications systems for the space exploration initiative [NASA-TM-103243] p 47 N90-27736
- WICKSTROM, S. N.**
Measurements of dynamic Young's modulus in short specimens with the PUCOT p 112 A90-21174
- WIESERMAN, W. R.**
High frequency, high temperature specific core loss and dynamic B-H hysteresis loop characteristics of soft magnetic alloys [NASA-TM-103164] p 154 N90-23663
- WILCOX, JEFFREY**
Design for steering accuracy in antenna arrays using shared optical phase shifters p 138 A90-13935
- WILCOX, K. G.**
EPSAT - A workbench for designing high-power systems for the space environment [AIAA PAPER 90-0637] p 245 A90-26975
- WILCOX, KATHERINE G.**
The Environment-Power System Analysis Tool development program p 236 A90-38089
- WILLHOITE, BRYAN C.**
Energy storage and thermal control system design status p 59 A90-38077
- WILLIAMS, BEN R.**
Hot gas ingestion characteristics and flow visualization of a vectored thrust STOVl concept [NASA-TM-103212] p 32 N90-26009
- WILLIAMS, F. A.**
Theory of influence of a low-volatility, soluble impurity on spherically-symmetric combustion of fuel droplets p 104 A90-28771
- WILLIAMS, FORMAN A.**
N-decane-air droplet combustion experiments in the NASA-Lewis 5 Second Zero-Gravity Facility [AIAA PAPER 90-0649] p 104 A90-25038
- WILLIAMS, JAMES H., JR.**
Input-output characterization of fiber reinforced composites by P waves [NASA-CR-185287] p 208 N90-28097
Ultrasonic verification of five wave fronts in unidirectional graphite epoxy composite [NASA-CR-185288] p 208 N90-28858
- WILLIAMS, JOHN D.**
Plasma contactor research, 1989 [NASA-CR-185212] p 252 N90-22389
- WILLIAMS, KENNETH A.**
SPRITE - A computer code for the optimization of space based heat pipe radiator systems p 170 A90-38036
- WILLIAMS, MARC H.**
Propeller-wing interaction using a frequency domain panel method p 6 A90-26128
Three dimensional full potential method for the aeroelastic modeling of propfans [AIAA PAPER 90-1120] p 7 A90-29392
Counter-rotating propellant analysis using a frequency domain panel method p 7 A90-40937
An unsteady lifting surface method for single rotation propellers [NASA-CR-4302] p 14 N90-25940
- WILLIAMS, R.**
A constitutive model for the inelastic multiaxial response of Rene 80 at 871 C and 982 C p 114 A90-32266
- WILLIAMS, WALLACE D.**
Electron beam induced damage in PECVD Si3N4 and SiO2 films on InP [NASA-TM-102544] p 203 N90-20393
- WILLIAMSON, R. G.**
The GEM-T2 gravitational model [NASA-TM-100746] p 234 N90-12984
- WILLIS, E. A.**
Analysis of rotary engine combustion processes based on unsteady, three-dimensional computations [AIAA PAPER 90-0643] p 163 A90-22237
Analysis of rotary engine combustion processes based on unsteady, three-dimensional computations [NASA-TM-102469] p 176 N90-13749
Computational experience with a three-dimensional rotary engine combustion model [NASA-TM-103104] p 183 N90-26275
- WILLIS, EDWARD A.**
Performance of a supercharged direct-injection stratified-charge rotary combustion engine [NASA-TM-103105] p 32 N90-25982
- WILSON, D. F.**
Selection of phase-change and containment materials for thermal energy storage [NASA-CR-186228] p 229 N90-15506
- WILSON, JEFFREY D.**
Spent-beam refocusing analysis and multistage depressed collector design for a 75-W, 59- to 64-GHz coupled-cavity traveling-wave tube [NASA-TP-3039] p 155 N90-27965
- WILSON, R. B.**
Free-vibration analysis of three-dimensional solids by BEM p 215 A90-52007
- WILSON, SANFORD L.**
Convergence of the SMI and the diagonally loaded SMI algorithms with weak interference [AD-A222839] p 141 A90-36717
- WILT, D. M.**
A V-grooved GaAs solar cell p 225 A90-14887
GaAs solar cells with V-grooved emitters p 229 N90-17754
Peeled film GaAs solar cells for space power [NASA-TM-103125] p 153 N90-21287
- WILT, DAVID M.**
Effect of crystal orientation on anisotropic etching and MOCVD growth of grooves on GaAs p 253 A90-15136
- WINSA, EDWARD A.**
Flight software development for the isothermal dendritic growth experiment [AIAA PAPER 90-0744] p 235 A90-22257
Flight software development for the isothermal dendritic growth experiment [NASA-TM-102412] p 238 N90-13988
- WINSLOW, CINDY**
Space Station Freedom solar array design development p 58 A90-38076
- WINTER, JERRY M.**
CSTI high capacity power p 61 A90-38196
- WITHERS, C. C.**
Propan Test Assessment (PTA): Flight test report [NASA-CR-182278] p 24 N90-11738
Propan Test Assessment (PTA) [NASA-CR-185138] p 25 N90-11739
- WITHERS, J. C.**
Zirconia toughened SiC whisker reinforced alumina composites small business innovation research [NASA-CR-179629] p 125 N90-10294
- WOIKE, MARK R.**
An electronic pressure profile display system for aeronautic test facilities [NASA-TM-102478] p 38 N90-15964
- WOLFENDEN, A.**
Measurements of dynamic Young's modulus in short specimens with the PUCOT p 112 A90-21174
- WONG, E. W.**
Generalized Advanced Propeller Analysis System (GAPAS). Volume 2: Computer program user manual [NASA-CR-185277] p 36 N90-29394
- WONG, YAU SHU**
Absorbing boundary conditions for second-order hyperbolic equations p 242 A90-34549
- WOOD, C.**
Effect of Ga and P dopants on the thermoelectric properties of n-type SiGe p 256 A90-38140
- WOOD, JERRY R.**
Laser anemometer measurements in a transonic axial-flow fan rotor [NASA-TP-2879] p 175 N90-11245
- WOODS, CLAUDIA M.**
Modification of the SHABERTH bearing code to incorporate RP-1 and a discussion of the traction model [NASA-TP-3017] p 205 N90-28066
- WOODWARD, RICHARD P.**
Noise of a simulated installed model counterrotation propeller at angle-of-attack and takeoff/approach conditions [AIAA PAPER 90-0283] p 247 A90-32505
Comparison between design and installed acoustic characteristics of NASA Lewis 9- by 15-foot low-speed wind tunnel acoustic treatment [NASA-TP-2896] p 38 N90-19242
Noise of a simulated installed model counterrotation propeller at angle-of-attack and takeoff/approach conditions [NASA-TM-102440] p 248 N90-20794
- WOODYARD, JAMES R.**
Radiation resistance studies of amorphous silicon films p 227 A90-14952
- WOOLLAM, J. A.**
Dielectric function of InGaAs in the visible [NASA-TM-103246] p 260 N90-26683
- WOOLLAM, JOHN**
Ellipsometric studies of the diffusion of atomic oxygen through silicon dioxide thin films p 104 A90-36268
- WOOLLAM, JOHN A.**
Ellipsometric study of Al2O3/Ag/Si and SiO2/Ag/quartz ashed in an oxygen plasma p 120 A90-18217
Study of indium tin oxide films exposed to atomic oxygen p 257 A90-45193
- WRIGHT, DAVID L.**
Spacecraft designs for VSAT networks [AIAA PAPER 90-0895] p 140 A90-25681
Advanced Communications Technology Satellite (ACTS) and potential system applications p 142 A90-51165
- WRIGHT, TED**
Development of Ada language control software for the NASA power management and distribution test bed p 236 A90-38082

WU, CHI

WU, CHI

Fiber optic detector probes for laser light scattering
p 192 A90-11593

WU, JIUNN-CHI

Evaluation of three turbulence models in static air loads and dynamic stall predictions
p 7 A90-31291

WU, SHAOFU

Energy analysis of crack-damage interaction
p 213 A90-41372
Effect of crack-microcracks interaction on energy release rates
p 214 A90-49269

WU, Y.-T.

Probabilistic analysis of a materially nonlinear structure
[AIAA PAPER 90-1099]
p 211 A90-29329
Computational methods for probability of instability calculations
[AIAA PAPER 90-1139]
p 236 A90-29333
Advanced probabilistic structural analysis method for implicit performance functions
p 214 A90-49792

WUNDROW, D. W.

Spatial evolution of nonlinear acoustic mode instabilities on hypersonic boundary layers
[NASA-TM-102431]
p 177 N90-14517

WYNOSKY, T. A.

Energy Efficient Engine program advanced turbofan nacelle definition study
[NASA-CR-174942]
p 34 N90-28560

X

XIAN, X.

An experimental evaluation of the tensile strength of impact ice
p 83 A90-15049

XU, KANG

Micromechanical model of crack growth in fiber reinforced ceramics
[NASA-CR-4321]
p 224 N90-28113

XU, ZHI-YUE

The high temperature creep deformation of Si3N4-6Y2O3-2Al2O3
p 121 A90-18879

Y

YAHIA, A. H.

Modeling and simulation of InP homojunction solar cells
p 226 A90-14899

YAMAGUCHI, KEIKO

Heat transfer on accreting ice surfaces
[AIAA PAPER 90-0200]
p 162 A90-22181
Modeling of surface roughness effects on glaze ice accretion
p 16 N90-20925

YAMAMOTO, O.

Large-scale advanced propeller blade pressure distributions: Prediction and data
[NASA-TM-102316]
p 30 N90-22564

YANG, WEN-JEI

Numerical analysis of natural convection in liquid droplets by phase change
p 164 A90-23212

YANO, S. E.

Qualification and life testing of a flight design hydrazine arcjet system
[AIAA PAPER 90-2576]
p 64 A90-42559

YAO, H. D.

Dielectric function of InGaAs in the visible
[NASA-TM-103246]
p 260 N90-26683

YASHAN, DOREEN

Feasibility of intercalated graphite railgun armatures
[NASA-TM-102546]
p 128 N90-21181

YEAGER, E.

Catalysts for ultrahigh current density oxygen cathodes for space fuel cell applications
[NASA-CR-180650]
p 232 N90-22835

YEAGER, ERNEST

Electrocatalysis for oxygen electrodes in fuel cells and water electrolyzers for space applications
p 57 A90-33945
Electrocatalysis for oxygen electrodes in fuel cells and water electrolyzers for space applications
p 230 N90-20468

YEHIA, S.

Fe-57 and Sn-119 Moessbauer study of La2CuO4(y), YBa2Cu3O(7-y) and SmBa2Cu3O(7-y)
p 256 A90-34020

YEHIA, SHERIF

Antiferromagnetism in Co-57-doped La2CuO4(y) studied by Moessbauer spectroscopy
p 255 A90-34011
Hyperfine magnetic field on Cd-111 in Heusler alloys Co2MnZ (Z = Si, Ga, Ge, Sn)
p 255 A90-34012

YEUM, K. S.

Efficient estimation of diffusion during dendritic solidification
p 111 A90-20612

YI, ZHANG

Computerized inspection of gear tooth surfaces
[NASA-TM-102395]
p 203 N90-22054

YING, S.-J.

Critical evaluation of Jet-A spray combustion using propane chemical kinetics in gas turbine combustion simulated by KIVA-II
[AIAA PAPER 90-2439]
p 105 A90-50645
Critical evaluation of Jet-A spray combustion using propane chemical kinetics in gas turbine combustion simulated by KIVA-2
[NASA-TM-103173]
p 138 N90-26170

YING, SHUH-JING

Reduced chemical kinetics for propane combustion
[AIAA PAPER 90-0546]
p 103 A90-19904

YOKEL, S. A.

PMR graphite engine duct development
[NASA-CR-182228]
p 23 N90-10037

YOKOTA, JEFFREY W.

A nonoscillatory, characteristically convected, finite volume scheme for multidimensional convection problems
[AIAA PAPER 90-0015]
p 159 A90-19633
Diagonal inversion of lower-upper implicit schemes
p 242 A90-23110
Numerical analysis of three-dimensional viscous internal flows
p 168 A90-32456
Multigrid calculations of 3-D turbulent viscous flows
p 172 A90-42426

Diagonally inverted lower-upper factored implicit multigrid scheme for the three-dimensional Navier-Stokes equations
p 174 A90-49789

A nonoscillatory, characteristically convected, finite volume scheme for multidimensional convection problems
[NASA-TM-102354]
p 242 N90-11497
Multigrid calculations of 3-D turbulent viscous flows
[NASA-CR-185154]
p 1 N90-13323

YOKOYAMA, JUNICHI

Soft inflation
p 265 A90-40093

YOON, SEOKKWAN

Numerical study of chemically reacting flows using a lower-upper symmetric successive overrelaxation scheme
p 3 A90-17989
Application of a lower-upper implicit scheme and an interactive grid generation for turbomachinery flow field simulations
[ASME PAPER 89-GT-20]
p 4 A90-23762

YORK, T. M.

Diagnostics and performance of a 1/4-scale MPD thruster
[AIAA PAPER 90-2665]
p 65 A90-42625

YORK, THOMAS M.

The effects of magnetic nozzle configurations on plasma thrusters
[NASA-CR-186465]
p 76 N90-21109

YOUNG, PAUL G.

Electron beam induced damage in PECVD Si3N4 and SiO2 films on InP
[NASA-TM-102544]
p 203 N90-20393

YOUNGBLOOD, WALLACE W.

Advanced spacecraft fire safety: Proposed projects and program plan
[NASA-CR-185147]
p 49 N90-12645

YUHAS, J. S.

Spray automated balancing of rotors - How process parameters influence performance
p 198 A90-46228

YUNG, C.-N.

Numerical studies of convective heat transfer in an inclined semi-annular enclosure
p 173 A90-45317

Z

ZAKRAJSEK, J.

Dynamic analysis of geared rotors by finite elements
p 194 A90-21123

ZAKRAJSEK, J. J.

Dynamics of multistage gear transmission with effects of gearbox vibrations
[NASA-TM-103109]
p 205 N90-28060

ZAKRAJSEK, JAMES J.

Modal analysis of gear housing and mounts
p 192 A90-17018
An investigation of gear mesh failure prediction techniques
[NASA-TM-102340]
p 200 N90-13785
Dynamic analysis of geared rotors by finite elements
[NASA-TM-102349]
p 201 N90-16286
Gear noise, vibration, and diagnostic studies at NASA Lewis Research Center
[NASA-TM-102435]
p 202 N90-18041

ZAKRAJSEK, JUNE F.

Rocket engine failure detection using system identification techniques
[AIAA PAPER 90-1993]
p 65 A90-47205

Rocket engine failure detection using system identification techniques
[NASA-CR-185259]
p 45 N90-25159

ZAKRZWSKI, C.

Diagnostics and performance of a 1/4-scale MPD thruster
[AIAA PAPER 90-2665]
p 65 A90-42625

ZAMAN, K. B. M. Q.

Some observations on transitory stall in conical diffusers
[AIAA PAPER 90-0048]
p 4 A90-22158
The low frequency oscillation in the flow over a NACA0012 airfoil with an 'iced' leading edge
p 8 A90-46377
Some observations on transitory stall in conical diffusers
[NASA-TM-102387]
p 11 N90-12561
Viscous effects on the instability of an axisymmetric jet
[NASA-TM-102396]
p 12 N90-16719

ZAPLATYNSKY, ISIDOR

Plasma gun with coaxial powder feed and adjustable cathode
[NASA-CASE-LEW-14901-1]
p 252 N90-10718

ZARETSKY, E. V.

Investigation of Weibull statistics in fracture analysis of cast aluminum
p 115 A90-45304

ZARETSKY, ERWIN V.

Bearing and gear steels for aerospace applications
[NASA-TM-102529]
p 202 N90-20391
Bearing elastohydrodynamic lubrication: A complex calculation made simple
[NASA-TM-102575]
p 203 N90-22041
Liquid lubrication in space
[NASA-RP-1240]
p 205 N90-28063

ZELLER, M. V.

High frequency capacitance-voltage characteristics of thermally grown SiO2 films on beta-SiC
p 254 A90-21348

ZERNIC, MIKE

Evolutionary growth for Space Station Freedom electrical power system
p 58 A90-38072

ZHANG, J.

Computation of three dimensional turbulent boundary layers in internal flows, including turbomachinery rotor blades
p 3 A90-12555
Topology of modified helical gears
p 195 A90-21132

ZHU, W.

An active optimal control strategy of rotor vibrations using external forces
p 198 A90-46224

ZIERKE, W. C.

The measurement of boundary layers on a compressor blade in cascade. IV - Flow fields for incidence angles of -1.5 and -8.5 degrees
[ASME PAPER 89-GT-72]
p 165 A90-23793

ZIERKE, WILLIAM C.

The measurement of boundary layers on a compressor blade in cascade. Volume 1: Experimental technique, analysis and results
[NASA-CR-185118-VOL-1]
p 23 N90-10038
The measurement of boundary layers on a compressor blade in cascade. Volume 2: Data tables
[NASA-CR-185118-VOL-2]
p 23 N90-10039

ZIEVE, PETER B.

Thin film eddy current impulse deicer
[AIAA PAPER 90-0761]
p 17 A90-20012

ZIMMERMAN, M.

A comparison of reflector antenna designs for wide-angle scanning
p 144 N90-19264

ZIMMERMAN, MARTIN L.

Reflector spillover loss of an open-ended rectangular and circular waveguide feed
p 141 A90-45398

ZINGER, DON S.

Field oriented control of induction motors
[NASA-TM-103154]
p 154 N90-22731

ZIPP, MARK E.

The insertion of human dynamics models in the flight control loops of V/STOL research aircraft. Appendix 2: The optimal control model of a pilot in V/STOL aircraft control loops
[NASA-CR-186598]
p 38 N90-21776

ZUBE, DIETER M.

Preliminary plume characteristics of an arcjet thruster
[AIAA PAPER 90-2645]
p 64 A90-42609
Preliminary plume characteristics of an arcjet thruster
[NASA-TM-103241]
p 81 N90-26071

ZUMWALT, G. W.

Electro-impulse de-icing testing analysis and design
[NASA-CR-4175]
p 18 N90-10031

ZURAWSKI, ROBERT L.

The Pathfinder chemical transfer propulsion program
p 74 N90-18471
Catalytic ignition of hydrogen/oxygen
p 107 N90-28627

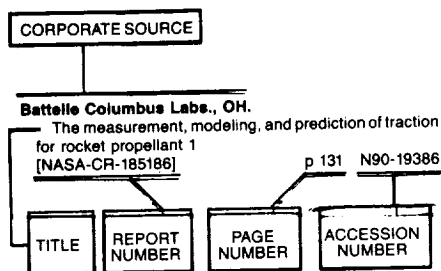
PERSONAL AUTHOR INDEX

ZUZEK, JOHN E.

Numerical Arc Segmentation Algorithm for a Radio
Conference-NASARC (version 4.0) technical manual
[NASA-TM-101453] p 144 N90-20264
Numerical Arc Segmentation Algorithm for a Radio
Conference (NASARC), version 4.0: User's manual
[NASA-TM-101454] p 145 N90-21250
A technology assessment of alternative communications
systems for the space exploration initiative
[NASA-TM-103243] p 47 N90-27736

CORPORATE SOURCE INDEX

Typical Corporate Source Index Listing



Listings in this index are arranged alphabetically by corporate source. The title of the document provides the user with a brief description of the subject matter. The report number helps to indicate the type of document cited (e.g., NASA report, translation, NASA contractor report). The accession number denotes the number by which the citation is identified. The titles are arranged under each corporate source in ascending accession number order.

A

Advanced Control Technology, Inc., Northridge, CA.
Development of a compact, light weight magnetic bearing
[AIAA PAPER 90-2483] p 199 A90-47223

Aeritalia S.p.A., Turin (Italy).
Lunar production of solar cells - A near-term product for a lunar industrial facility p 42 A90-24791

Aerodyne Research, Inc., Billerica, MA.
Modeling of the SiC chemical vapor deposition process and comparison with experimental results p 105 A90-36810

Aerojet Electrosystems Co., Azusa, CA.
Wear consideration in gear design for space applications p 194 A90-21121

Aerojet Technical Systems Co., Sacramento, CA.
Corrosion prevention in copper combustion chamber liners of liquid oxygen/methane booster engines
[AIAA PAPER 90-2119] p 85 A90-42028

Combustion interaction with radiation-cooled chambers p 64 A90-42030
[AIAA PAPER 90-2121]
Hydrocarbon-fuel/combustion-chamber-liner materials compatibility
[NASA-CR-185203] p 118 N90-21165

Aerojet TechSystems Co., Sacramento, CA.
Combustor design and analysis using the ROCKET Combustor Interactive Design (ROCCID) Methodology
[AIAA PAPER 90-2240] p 65 A90-45694

A highly durable injector faceplate design concept for O₂/H₂ propellants p 66 A90-47211
[AIAA PAPER 90-2181]
Fabry-Perot interferometer development for rocket engine plume spectroscopy
[AIAA PAPER 90-2234] p 187 A90-47212

Aerometrics, Inc., Sunnyvale, CA.
Development of a phase Doppler based probe for icing cloud droplet characterization
[AIAA PAPER 90-0667] p 186 A90-26978

Advanced instrumentation for aircraft icing research
[NASA-CR-185225] p 18 N90-21006

Aerospace Corp., El Segundo, CA.
Issues and opportunities in space photovoltaics p 54 A90-14852

Experimental investigation of flow about a strut-endwall configuration
[AIAA PAPER 90-1541] p 171 A90-38685

Aerostructures, Inc., Arlington, VA.
Finite element mesh refinement criteria for stress analysis p 209 A90-23013

Air Force Systems Command, Cleveland, OH.
An expert system to perform on-line controller tuning
[NASA-TM-103101] p 240 N90-23991

Akron Univ., OH.
Experimental and analytical evaluation of dynamic load vibration of a 2240-kW (3000-hp) rotorcraft transmission p 192 A90-13750

An experimental evaluation of the tensile strength of impact ice p 83 A90-15049

Impact ice stresses in rotating airfoils
[AIAA PAPER 90-0198] p 15 A90-19735

Two-dimensional convection and radiation with scattering from a Poiseuille flow p 161 A90-20519

Tooth contact shift in loaded spiral bevel gears p 193 A90-21112

The role of thermal and lubricant boundary layers in the transient thermal analysis of spur gears p 194 A90-21118

Vibration signature analysis of multistage gear transmission p 194 A90-21124

Parametric studies of advanced turboprops p 19 A90-21225

Multi-level Hierarchical Poly Tree computer architectures p 236 A90-26082

A laser based computer aided non-intrusive technique for full field flow characterization in macroscopic curved channels p 168 A90-32293

Experimental study of the cross-polarization characteristics of rectangular microstrip antennas p 141 A90-37312

Effects of state recovery on creep buckling under variable loading p 212 A90-41223

Numerical modeling of flows in simulated brush seal configurations
[AIAA PAPER 90-2141] p 198 A90-47209

Flow visualization and motion analysis for a series of four sequential brush seals p 199 A90-47222

The determination of third order linear models from a seventh order nonlinear jet engine model p 239 A90-52881

Temperature and melt solid interface control during crystal growth
[NASA-CR-186731] p 259 N90-26664

Creep and creep rupture of strongly reinforced metallic composites
[NASA-CR-185286] p 223 N90-28110

Alberta Univ., Edmonton.
Absorbing boundary conditions for second-order hyperbolic equations p 242 A90-34549

Alfred Univ., NY.
Measurement of interfacial shear strength in SiC-fiber/Si₃N₄ composites p 87 A90-13237

Allied-Signal Aerospace Co., Phoenix, AZ.
ATTAP/AGT101 ceramics technology update
[ASME PAPER 89-GT-105] p 195 A90-23814

The role of NDE in ceramic turbine engine component development p 206 A90-35508

Development of impact design methods for ceramic gas turbine components p 197 A90-42165

[AIAA PAPER 90-2413] p 197 A90-42165

Three dimensional LDV flow measurements and theoretical investigation in a radial inflow turbine scroll p 9 A90-46860

Advanced Turbine Technology Applications Project (ATTAP)
[NASA-CR-185109] p 263 N90-14153

Aluminum Co. of America, Alcoa Center, PA.
Reaction zone microstructure in a Ti₃Al + Nb/SiC composite p 91 A90-39627

Analex Corp., Cleveland, OH.

Buoyancy effects on the vapor condensation rate on a horizontal liquid surface p 162 A90-22201

[AIAA PAPER 90-0353] p 162 A90-22201

Vapor condensation on liquid surface due to laminar jet-induced mixing - The effects of system parameters
[AIAA PAPER 90-0354] p 163 A90-22202

Effects of amplitude distortions and IF equalization on satellite communication system bit-error rate performance
[AIAA PAPER 90-0878] p 140 A90-25697

Comparative thermal analysis of the Space Station Freedom photovoltaic deployable boom structure using TRASYS, NEVADA, and SINDA programs p 47 A90-27525

[SAE PAPER 891563] p 47 A90-27525

Distortion and regulation characterization of a Mapham inverter p 148 A90-38125

Data compression techniques applied to high resolution high frame rate video technology p 143 N90-14452

[NASA-CR-4263] p 143 N90-14452

Space Station Freedom electric power system availability study p 50 N90-20120

[NASA-CR-185181] p 50 N90-20120

Aperture taper determination for the half-scale accurate antenna reflector p 153 N90-21282

[NASA-CR-185215] p 153 N90-21282

Analex Corp., Fairview Park, OH.
Development and refinement of test bed simulations p 59 A90-38081

Numerical investigation of the thermal stratification in cryogenic tanks subjected to wall heat flux p 175 A90-52500

[AIAA PAPER 90-2375] p 175 A90-52500

Analytic Sciences Corp., Reston, VA.
A performance analysis of DS-CDMA and SCPC VSAT networks p 141 A90-39056

Applied Sciences Corp., Yellow Springs, OH.
Vapor grown carbon fiber for space thermal management systems p 94 A90-50128

Argonne National Lab., IL.
Experimental evidence of a dimensional crossover in Y₁Ba₂Cu₃O₇(δ) p 255 A90-29739

Arinc Research Corp., Annapolis, MD.
Space Station Freedom power - A reliability, availability, and maintainability assessment of the proposed Space Station Freedom electric power system p 58 A90-38074

Space Station Freedom electric power system availability study p 50 N90-20120

[NASA-CR-185181] p 50 N90-20120

Arizona State Univ., Tempe.
Analysis of airframe/engine interactions - An integrated control perspective p 36 A90-40557

[AIAA PAPER 90-1918] p 36 A90-40557

An active optimal control strategy of rotor vibrations using external forces p 198 A90-46224

Extended implicit model following as applied to integrated flight and propulsion control
[AIAA PAPER 90-3444] p 239 A90-47697

Energy stability of thermocapillary convection in a model of the float-zone crystal-growth process p 133 A90-48720

The photovoltaic properties of an Al In As/InP heterojunctions grown by LPE method p 229 N90-13886

[NASA-CR-185996] p 229 N90-13886

Arizona Univ., Tucson.
Experimental investigation of convective stability in a superposed fluid and porous layer when heated from below p 158 A90-15947

Solute redistribution in dendritic solidification with diffusion in the solid p 253 A90-17399

Finite element simulations of thermosolutal convection in vertical solidification of binary alloys p 132 A90-18292

Salt-finger convection under reduced gravity
[AIAA PAPER 90-0122] p 160 A90-19693

Efficient estimation of diffusion during dendritic solidification p 111 A90-20612

A new fabrication method for precision antenna reflectors for space flight and ground test p 139 A90-25627

[AIAA PAPER 90-0803] p 139 A90-25627

On the instabilities of supersonic mixing layers - A high-Mach-number asymptotic theory p 8 A90-42644

- Instabilities and subharmonic resonances of subsonic heated round jets, volume 2
[NASA-CR-186058] p 181 N90-22017
- Nonlinear interactions in mixing layers and compressible heated round jets
[NASA-CR-186303] p 182 N90-23674
- The role of gravity on macrosegregation in alloys
[NASA-CR-186530] p 136 N90-25238
- Army Air Mobility Research and Development Lab., Cleveland, OH.**
- Test and theory for piezoelectric actuator-active vibration control of rotating machinery p 198 A90-46226
- Army Aviation Engineering Flight Activity, Edwards AFB, CA.**
- Initial results from the joint NASA-Lewis/U.S. Army icing flight research tests p 16 A90-28180
- Army Aviation Research and Development Command, Cleveland, OH.**
- A planar reacting shear layer system for the study of fluid dynamics-combustion interaction
[NASA-TM-102422] p 27 N90-13393
- Liquid water content and droplet size calibration of the NASA Lewis Icing Research Tunnel
[NASA-TM-102447] p 200 N90-13797
- On the numerical solution of the dynamically loaded hydrodynamic lubrication of the point contact problem
[NASA-TM-102427] p 178 N90-17076
- Comparison of drop size distributions from two droplet sizing systems
[NASA-TM-102520] p 202 N90-17147
- Army Aviation Systems Command, Cleveland, OH.**
- Tooth contact shift in loaded spiral bevel gears p 193 A90-21112
- Efficiency testing of a helicopter transmission planetary reduction stage p 193 A90-21113
- Effect of advanced component technology on helicopter transmissions p 193 A90-21115
- Topology of modified helical gears p 195 A90-21132
- Liquid water content and droplet size calibration of the NASA Lewis Icing Research Tunnel
[AIAA PAPER 90-0669] p 37 A90-22242
- Comparison of two droplet sizing systems in an icing wind tunnel
[AIAA PAPER 90-0668] p 164 A90-23711
- Composite matrix cooling scheme for small gas turbine combustors
[AIAA PAPER 90-2158] p 22 A90-47210
- Efficiency study comparing two helicopter planetary reduction stages
[AIAA PAPER 90-2156] p 199 A90-50644
- Matrix density effects on the mechanical properties of SiC fiber-reinforced silicon nitride matrix properties p 94 A90-51927
- An investigation of gear mesh failure prediction techniques
[NASA-TM-102340] p 200 N90-13785
- The 3F condensation polyimides: Review and update
[NASA-TM-102353] p 126 N90-14363
- Mesh refinement in finite element analysis by minimization of the stiffness matrix trace
[NASA-CR-185170] p 201 N90-15434
- Assessment of worm gearing for helicopter transmissions
[NASA-TM-102441] p 27 N90-15923
- Dynamic analysis of geared rotors by finite elements
[NASA-TM-102349] p 201 N90-16286
- Theory of gearing
[NASA-RP-1212] p 202 N90-19593
- Transmission research activities at NASA Lewis Research Center
[NASA-TM-103132] p 203 N90-21394
- Surface pitting fatigue life of noninvolute, low-contact-ratio gears
[NASA-TM-103116] p 203 N90-22790
- Influence of linear profile modification and loading conditions on the dynamic tooth load and stress of high contact ratio gears
[NASA-TM-103136] p 204 N90-22796
- Computer code for predicting coolant flow and heat transfer in turbomachinery
[NASA-TP-2985] p 32 N90-27722
- Computer-aided design of high-contact-ratio gears for minimum dynamic load and stress
[NASA-TM-103275] p 205 N90-28065
- An expert system to perform on-line controller restructuring for abrupt model changes
[NASA-TM-103609] p 241 N90-29121
- Army Propulsion Lab., Cleveland, OH.**
- Laminate behavior for SiC fiber-reinforced reaction-bonded silicon nitride matrix composites p 90 A90-29927
- Spray automated balancing of rotors - How process parameters influence performance p 198 A90-46228

- Thermal effects on the mechanical properties of SiC fiber reinforced reaction-bonded silicon nitride matrix composites p 92 A90-46999
- High-temperature tensile properties of fiber reinforced reaction bonded silicon nitride p 95 A90-52783
- Oxidation effects on the mechanical properties of SiC fiber-reinforced reaction-bonded silicon nitride matrix composites
[NASA-TM-102360] p 96 N90-14287

B

- Battelle Columbus Labs., OH.**
- The measurement, modeling, and prediction of traction for rocket propellant 1
[NASA-CR-185186] p 131 N90-19386
- Boeing Aerospace Co., Seattle, WA.**
- A Brayton cycle solar dynamic heat receiver for space p 61 A90-38165
- Tank Pressure Control Experiment - A low-g mixing investigation
[AIAA PAPER 90-2376] p 66 A90-47217
- Boeing Helicopter Co., Philadelphia, PA.**
- Spray nozzle investigation for the Improved Helicopter Icing Spray System (IHIS) p 37 A90-25040
- Boycie Engineering International, Inc., Houston, TX.**
- Near wall flow parameters in the blade end-wall corner region p 156 A90-12636
- BP America, Warrensville, OH.**
- Laminate behavior for SiC fiber-reinforced reaction-bonded silicon nitride matrix composites p 90 A90-29927
- Brown Univ., Providence, RI.**
- Contributions to the understanding of large-scale coherent structures in developing free turbulent shear flows p 158 A90-13907
- Wide-bandgap epitaxial heterojunction windows for silicon solar cells p 227 A90-28359

C

- California State Univ., Long Beach.**
- Progress towards the development of an inviscid-viscous interaction method for unsteady flows in turbomachinery cascades p 2 A90-11806
- Fortified LEWICE with viscous effects
[AIAA PAPER 90-0754] p 15 A90-20009
- Unsteady heat transfer on turbine blades p 161 A90-20511
- The role of thermal and lubricant boundary layers in the transient thermal analysis of spur gears p 194 A90-21118
- Lubricant jet flow phenomena in spur and helical gears with modified addendums - For radially directed individual jets p 194 A90-21122
- California Univ., Berkeley.**
- Smoldering combustion under low gravity conditions
[AIAA PAPER 90-0648] p 103 A90-22238
- Unitarity limits on the mass and radius of dark-matter particles p 264 A90-24671
- Neutron stars and white dwarfs in galactic halos? p 265 A90-30909
- Investigation of turbulent flow in highly curved ducts with application to turbomachinery components
[NASA-CR-186060] p 175 N90-12882
- California Univ., Davis.**
- The pdf approach to turbulent flow p 168 A90-32225
- California Univ., Irvine.**
- Effects of g-jitter on a thermal, buoyant flow
[AIAA PAPER 90-0653] p 163 A90-22239
- Influence of the continuous and dispersed phases on the symmetry of a gas turbine air-blast atomizer
[ASME PAPER 89-GT-303] p 163 A90-22651
- Application of two-component phase Doppler interferometry to the measurement of particle size, mass flux, and velocities in two-phase flows p 186 A90-32853
- An experimental and numerical study of particle-laden coaxial jet flows p 171 A90-38799
- Symmetry assessment of an air-blast atomizer spray p 172 A90-40930
- California Univ., La Jolla.**
- Thin films of the Bi₂Sr₂Ca₂Cu₃O(x) superconductor p 254 A90-24448
- N-decane-air droplet combustion experiments in the NASA-Lewis 5 Second Zero-Gravity Facility
[AIAA PAPER 90-0649] p 104 A90-25038
- Theory of influence of a low-volatility, soluble impurity on spherically-symmetric combustion of fuel droplets p 104 A90-28771
- California Univ., Los Angeles.**
- Aeroelastic problems in turbomachines
[AIAA PAPER 90-1157] p 7 A90-29393
- Celapan-Buffalo Univ. Research Center, NY.**
- Phase and time-resolved measurements of unsteady heat transfer and pressure in a full-stage rotating turbine
[ASME PAPER 89-GT-135] p 165 A90-23832
- Development of an integrated BEM approach for hot fluid structure interaction
[NASA-CR-186214] p 177 N90-15364
- Heat transfer and pressure measurements for the SSME fuel-side turbopump
[NASA-CR-184928] p 31 N90-23405
- Carnegie-Mellon Univ., Pittsburgh, PA.**
- Gravitational couplings of the inflator in extended inflation p 265 A90-40088
- A simplified model for two phase face seal design p 197 A90-40713
- Base reaction optimization of redundant manipulators for space applications
[NASA-CR-186274] p 201 N90-15447
- The effect of hydrogen and microstructure on the deformation and fracture behavior of a single crystal nickel-base superalloy
[NASA-CR-185219] p 118 N90-21849
- A global approach for using kinematic redundancy to minimize base reactions of manipulators
[NASA-CR-186825] p 234 N90-25499
- Case Inst. of Tech., Cleveland, OH.**
- Interactive calculation procedures for mixed compression inlets
[NASA-CR-186581] p 14 N90-25934
- Case Western Reserve Univ., Cleveland, OH.**
- The high temperature deformation in cyclic loading of a single crystal nickel-base superalloy p 108 A90-11534
- Modulated-splitting-ratio fiber-optic temperature sensor p 185 A90-11706
- High frequency GaAlAs modulator and photodetector for phased array antenna applications p 146 A90-11774
- Assumed strain distributions for a finite strip plate bending element using Mindlin-Reissner plate theory p 208 A90-16723
- Processing and microstructure of melt spun NiAl alloys p 110 A90-16941
- Characterization of damped structural connections for multi-component systems p 208 A90-16959
- Synthesis and characterization of high-Tc superconductors in the Ti-Ca-Ba-Cu-O system p 253 A90-19300
- Phase transitions in fermionic systems with many-body interaction p 249 A90-19303
- Synthesis and characterization of high-T(c) screen-printed Y-Ba-Cu-O films on alumina p 254 A90-21926
- A high-speed GaAs MESFET optical controller p 186 A90-22483
- Local-global analysis of crack growth in continuously reinforced ceramic matrix composites
[ASME PAPER 89-GT-138] p 88 A90-23835
- Near-limit flame spread over a thin solid fuel in microgravity p 104 A90-32835
- Production and processing of Cu-Cr-Nb alloys p 114 A90-33340
- The vibrating ribbon problem revisited p 168 A90-33516
- Electrocatalysis for oxygen electrodes in fuel cells and water electrolyzers for space applications p 57 A90-33945
- Superconducting glass-ceramics in the Bi-Sr-Ca-Cu-O system p 256 A90-35153
- Some characteristics of bypass transition in a heated boundary layer p 169 A90-35183
- Boundary flexibility method of component mode synthesis using static Ritz vectors p 212 A90-35429
- Microwave response of a HEMT photoconductive detector p 147 A90-37301
- Complex permittivity of lanthanum aluminate in the 20 to 300 K temperature range from 26.5 to 40.0 GHz p 148 A90-37864
- Control of a GaAs monolithic Ka-band phase shifter using a high-speed optical interconnect p 150 A90-41700
- The possibility of a reversal of material flammability ranking from normal gravity to microgravity p 105 A90-42298
- Characterization of structural connections using free and forced response test data p 213 A90-46172
- Numerical modeling of flows in simulated brush seal configurations
[AIAA PAPER 90-2141] p 198 A90-47209
- Millimeter-wave surface resistance of laser-etched YBa₂Cu₃O(7-delta) superconducting films p 257 A90-48694

- New space domain processing technique for pulsed laser velocimetry p 187 A90-48750
Use of unbalanced laminates as a screening method for microcracking p 94 A90-50217
Nicalon/siliconoxycarbide ceramic composites p 94 A90-51924
- Three-dimensional analysis of surface crack-Hertzian stress field interaction p 215 N90-11332
[NASA-CR-4254]
Superconducting ceramics in the Bi_{1.5}SrCaCu₂O₇ sub x system by melt quenching technique p 258 N90-11606
[NASA-CR-185139]
Preparation of 110K (Bi, Pb)-Sr-Ca-Cu-O superconductor from glass precursor p 258 N90-14108
[NASA-CR-185162]
Superconducting Bi_{1.5}Pb_{0.5}Sr₂Ca₂Cu₃O_{7-x} ceramics by rapid melt quenching and glass crystallization p 258 N90-17465
[NASA-CR-185184]
Instantaneously generated foam and its applicability to reduced gravity p 135 N90-20237
[NASA-CR-185208]
Electrocatalysis for oxygen electrodes in fuel cells and water electrolyzers for space applications p 230 N90-20468
- Dynamic substructuring by the boundary flexibility vector method of component mode synthesis p 220 N90-22813
[NASA-CR-182445]
Catalysts for ultrahigh current density oxygen cathodes for space fuel cell applications p 232 N90-22835
[NASA-CR-180650]
The entrainment rate for a row of turbulent jets p 15 N90-28504
[NASA-CR-185278]
Green's functions for dislocations in bonded strips and related crack problems p 224 N90-28878
[NASA-CR-185291]
- Cellulose Conversion Enterprises, Berkeley, CA.**
Beam rider for an Articulated Robot Manipulator (ARM) accurate positioning of long flexible manipulators p 241 N90-26581
[NASA-CR-185151]
- Centre National de la Recherche Scientifique, Poitiers (France).**
The structure and stability of nonadiabatic flame balls p 105 A90-43674
- Chicago Univ., IL.**
The shocking development of lithium (and beryllium) in supernovae p 264 A90-17643
Unitarity limits on the mass and radius of dark-matter particles p 264 A90-24671
Cosmic-string-induced hot dark matter perturbations p 264 A90-25889
Big bang nucleosynthesis and the quark-hadron transition p 265 A90-31407
Gravitational couplings of the inflation in extended inflation p 265 A90-40088
Dark matter candidates p 266 A90-44095
- Chung Shan Inst. of Science and Technology, Lung Tan (China).**
Optimal impulsive time-fixed orbital rendezvous and interception with path constraints p 41 A90-53051
[AIAA PAPER 90-2972]
- Cincinnati Univ., OH.**
Torsional and biaxial (tension-torsion) fatigue damage mechanisms in Waspaloy at room temperature p 109 A90-11925
Improvement of finite element meshes - Heat transfer in an infinite cylinder p 209 A90-19109
Comparison of boundary element and finite element methods in spur gear root stress analysis p 193 A90-21107
Computer aided design of spur gear teeth p 195 A90-21131
Computer aided design of bevel gear tooth surfaces p 195 A90-21136
Finite element mesh refinement criteria for stress analysis p 209 A90-23013
A flux-split solution procedure for unsteady inlet flows [AIAA PAPER 90-0585] p 6 A90-26967
A crystallographic model for the tensile and fatigue response for Rene N4 at 982 C p 114 A90-28754
A constitutive model for the inelastic multiaxial response of Rene 80 at 871 C and 982 C p 114 A90-32266
Antiferromagnetism in Co-57-doped La₂CuO₄(-y) studied by Moessbauer spectroscopy p 255 A90-34011
Hyperfine magnetic field on Cd-111 in Heusler alloys Co₂MnZ (Z = Si, Ga, Ge, Sn) p 255 A90-34012
Fe-57 and Sn-119 Moessbauer study of La₂CuO₄(-y), YBa₂Cu₃O_{7-y} and SmBa₂Cu₃O_{7-y} p 256 A90-34020
Space vehicle propulsion systems - Environmental space hazards p 63 A90-40545
[AIAA PAPER 90-1881]
Transient behavior of supersonic flow through inlets [AIAA PAPER 90-2130] p 8 A90-42734
- The simulation of fluid dynamic uncertainties in the SSME turbopump p 65 A90-42770
[AIAA PAPER 90-2294]
Three dimensional LDV flow measurements and theoretical investigation in a radial inflow turbine scroll p 9 A90-46860
Global pressure relaxation for laminar two-dimensional internal flow p 174 A90-51019
Mesh refinement in finite element analysis by minimization of the stiffness matrix trace p 201 N90-15434
[NASA-CR-185170]
Electron-beam induced damage in thin insulating films on compound semiconductors p 151 N90-17987
[NASA-CR-185177]
Computer simulation of gear tooth manufacturing processes p 138 N90-26171
[NASA-CR-185200]
Microstructure: Property correlation p 224 N90-28880
[NASA-CR-180406]
- City Coll. of the City Univ. of New York, NY.**
Near wall flow parameters in the blade end-wall corner region p 156 A90-12636
- Clarkson Univ., Potsdam, NY.**
Progression of damage and fracture in composites under dynamic loading p 210 A90-29318
[AIAA PAPER 90-0916]
- Cleveland State Univ., OH.**
Fiber optic sensing systems using high frequency resonant sensing heads with intensity sensors p 185 A90-10472
Side branch morphology and coarsening in directionally solidified Pb-8 at. pct Au p 109 A90-11658
Modulated-splitting-ratio fiber-optic temperature sensor p 185 A90-11706
Predicted performance of near-optimally designed indium phosphide space solar cells at high intensities and temperatures p 225 A90-14898
Effect of heat-treatment temperature of vapor-grown graphite fibers. I - Properties of their bromine intercalation compounds p 120 A90-16279
Liquid alkali metals - Equation of state and reduced-pressure, bulk-modulus, sound-velocity, and specific-heat functions p 102 A90-16280
Pressure dependence of the melting temperature of metals p 103 A90-16281
Least-squares finite element method for fluid dynamics p 159 A90-18246
Analysis of whisker-toughened ceramic components - A design engineer's viewpoint p 88 A90-19149
Primary arm spacing in directionally solidified Pb-10 wt pct Sn alloys p 132 A90-23713
[AIAA PAPER 90-0740]
Noninteractive macroscopic reliability model for ceramic matrix composites with orthotropic material symmetry [ASME PAPER 89-GT-129] p 209 A90-23827
A review of failure models for ceramic matrix composite laminates under monotonic loads p 89 A90-23842
[ASME PAPER 89-GT-153]
Noninteractive macroscopic reliability model for whisker-reinforced ceramic composites p 89 A90-26561
Polymer derived Nicalon/Si-C-O composites - Processing and mechanical behavior p 89 A90-27065
An accurate analytic approximation to the non-linear change in volume of solids with applied pressure p 261 A90-27612
Measurements of print-through in graphite fiber epoxy composites p 91 A90-31555
Evaluation of atomic oxygen resistant protective coatings for fiberglass-epoxy composites in LEO p 84 A90-31581
Simulating transitional flow and heat transfer over the flat plate and circular cylinder using a K-epsilon turbulence model p 168 A90-32171
Properties of Pb(1-x)Bi(x)/Ba₂YCu₃O_{7-x} composites - Reaction of Ba₂YCu₃O_{7-x} with Pb and Bi p 255 A90-33224
Two-dimensional numerical simulation of a Stirling engine heat exchanger p 170 A90-38290
Developing a self-diagnostic system for piezoelectric sensors p 187 A90-42755
[AIAA PAPER 90-2230]
Density of intercalated graphite fibers p 124 A90-49061
Nicalon/siliconoxycarbide ceramic composites p 94 A90-51924
Primary arm spacing in directionally solidified Pb-10 wt percent Sn alloys p 134 N90-14398
[NASA-CR-185190]
Analytical and experimental study of high phase order induction motors p 153 N90-21952
[NASA-CR-186580]
Extension of a noninteractive reliability model for ceramic matrix composites p 129 N90-26142
[NASA-CR-185267]
- Colby Coll., Waterville, ME.**
LEO high voltage solar array arcing response model, continuation 5 p 232 N90-25418
[NASA-CR-186505]
- Colorado State Univ., Fort Collins.**
End-hall thrusters p 64 A90-42570
[AIAA PAPER 90-2595]
Plasma contactor research, 1989 p 252 N90-22389
[NASA-CR-185212]
- Colorado Univ., Boulder.**
Treatment of coupled fluid-structure interaction problems by a mixed variational principle p 159 A90-18288
Modeling of collision and coalescence of droplets during microgravity processing of Zn-Bi immiscible alloys p 132 A90-22878
A variational justification of the assumed natural strain formulation of finite elements. I - Variational principles. II - The C(0) four-node plate element p 210 A90-24384
Mixed variational formulation of finite element analysis of acoustoelastic/slosh fluid-structure interaction p 212 A90-34851
The effects of van der Waals attractions on cloud droplet growth by coalescence p 234 A90-38363
Variational formulation of high-performance finite elements - Parametrized variational principles p 213 A90-46068
Developments in variational methods for high performance plate and shell elements p 214 A90-46288
Hopf bifurcation in the driven cavity p 174 A90-48548
Electromagnetic finite elements based on a four-potential variational principle p 214 A90-49869
- Colorado Univ., Colorado Springs.**
High frequency capacitance-voltage characteristics of thermally grown SiO₂ films on beta-SiC p 254 A90-21348
Magnification of starting torques of dc motors by maximum power point trackers in photovoltaic systems p 149 A90-38144
- Columbia Univ., New York, NY.**
Interactive grid generation for turbomachinery flow field simulations p 6 A90-26553
Fiber reinforced superalloys p 91 A90-34169
Grid generation for the solution of partial differential equations p 237 A90-47188
- Commonwealth Scientific Corp., Alexandria, VA.**
End-hall thrusters p 64 A90-42570
[AIAA PAPER 90-2595]
- Communications Center, Clarksburg, MD.**
Role of communications satellites in the fiber era p 139 A90-25617
[AIAA PAPER 90-0792]
- Communications Satellite Corp., Clarksburg, MD.**
A users perspective of the ACTS hopping beam TDMA system p 140 A90-25658
[AIAA PAPER 90-0833]
The role of technology in influencing future civil communications satellites p 142 A90-51167
Advanced modulation technology development for earth station demodulator applications. Coded modulation system development p 145 N90-20270
[NASA-CR-185149]
- Connecticut Univ., Storrs.**
Biaxial constitutive modelling and testing of a single crystal superalloy at elevated temperatures p 110 A90-16741
Asymmetrical boundary layer separation at the base of a two cylinder geometry p 159 A90-18505
X-ray beam method for displacement measurement in hostile environments p 187 A90-44485
- Cornell Univ., Ithaca, NY.**
Shear stabilization of the capillary breakup of a cylindrical interface p 159 A90-17578
[AD-A219268]
Diagonal inversion of lower-upper implicit schemes p 242 A90-23110
The coupling of Marangoni and capillary instabilities in an annular thread of liquid p 171 A90-38978
- D**
- Dartmouth Coll., Hanover, NH.**
Improving the low temperature ductility of NiAl p 110 A90-16940
- Department of Energy, Washington, DC.**
Sliding seal materials for low heat rejection engines [NASA-CR-182262] p 125 N90-11882
Preliminary designs for 25 kW advanced Stirling conversion systems for dish electric applications [NASA-TM-103188] p 263 N90-26729
- Detroit Diesel Allison, MI.**
Ceramic valve development for heavy-duty low heat rejection diesel engines p 196 A90-27091

Detroit Diesel Allison

Ceramic port shields cast in an iron engine head
p 196 A90-27095

Detroit Diesel Allison, Indianapolis, IN.

Advanced Turbine Technology Applications Project (ATTAP)
[NASA-CR-185133] p 22 N90-10036

Digital Automation Associates, Bowling Green, OH.

Encoding Y,I,Q component estimates of an NTSC composite signal
p 139 A90-23261

Drexel Univ., Philadelphia, PA.

High-speed analog fiber optic links for satellite communication
p 46 A90-11822

Design for steering accuracy in antenna arrays using shared optical phase shifters
p 138 A90-13935

Big bang nucleosynthesis and the quark-hadron transition
p 265 A90-31407

High-speed digital fiber optic links for satellite traffic
p 250 A90-41247

High-speed fiber-optic links for distribution of satellite traffic
p 47 A90-41687

DWA Composite Specialties, Inc., Chatsworth, CA.

Applications of high thermal conductivity composites to electronics and spacecraft thermal design
[AIAA PAPER 90-0783] p 89 A90-25609

E

Electroimpact, Inc., Seattle, WA.

Thin film eddy current impulse deicer
[AIAA PAPER 90-0761] p 17 A90-20012

Elort Corp., Palo Alto, CA.

Efficient Monte Carlo simulation of rarefied flow in a small nozzle
[AIAA PAPER 90-1693] p 170 A90-38396

Elrod (Harold G.), Old Saybrook, CT.

Efficient numerical method for computation of thermohydrodynamics of laminar lubricating films
[NASA-CR-185136] p 175 N90-11256

Engineering Science Software, Inc., Smithfield, RI.

High temperature inelastic deformation under uniaxial loading - Theory and experiment
p 109 A90-13838

Biaxial constitutive modelling and testing of a single crystal superalloy at elevated temperatures
p 110 A90-16741

ENTECH Corp., Dallas-Fort Worth Airport, TX.

An advanced space photovoltaic concentrator array using Fresnel lenses, gallium arsenide cells, and prismatic cell covers
p 54 A90-14954

The mini-dome lens space concentrator array - Recent component test results and current array development status
p 60 A90-38155

Conceptual design study of a 5 kilowatt solar dynamic Brayton power system using a dome Fresnel lens solar concentrator
[NASA-CR-185134] p 72 N90-14281

Evansville Univ., IN.

Kinetic theory model for the flow of a simple gas from a two-dimensional nozzle
p 169 A90-37124

Exeter Univ. (England).

Amplitude-dependent neutral modes in compressible boundary layer flows
[NASA-TM-102524] p 178 N90-20326

Exxon Research and Engineering Co., Annandale, NJ.

Preliminary investigation of a NiAl composite prepared by cryomilling
p 113 A90-25098

F

Fermi National Accelerator Lab., Batavia, IL.

Is the sub-millisecond pulsar strange?
p 264 A90-12669

Unitarity limits on the mass and radius of dark-matter particles
p 264 A90-24671

Cosmic-string-induced hot dark matter perturbations
p 264 A90-25889

Neutron stars and white dwarfs in galactic halos?
p 265 A90-30909

Big bang nucleosynthesis and the quark-hadron transition
p 265 A90-31407

A model for the distribution of the intergalactic medium
p 265 A90-34505

Phase transitions as the origin of large scale structure in the universe
p 265 A90-35291

Gravitational couplings of the inflaton in extended inflation
p 265 A90-40088

Soft inflation
p 265 A90-40093

Dark matter candidates
p 266 A90-44095

A model for the distribution of dark matter, galaxies, and the intergalactic medium in a cold dark matter-dominated universe
p 266 A90-45560

Florida State Univ., Gainesville.

Theoretical model of discrete tone generation by impinging jets
p 247 A90-35903

Florida Univ., Gainesville.

Neurobiological computational models in structural analysis and design
[AIAA PAPER 90-1133] p 210 A90-29260

Effect of vane twist on the performance of dome swirlers for gas turbine airblast atomizers
[AIAA PAPER 90-1955] p 173 A90-47203

Flow Research, Inc., Kent, WA.

Progress in direct numerical simulations of turbulent reacting flows
p 157 A90-12836

Ford Aerospace and Communications Corp., Palo Alto, CA.

COLD-SAT - An orbital cryogenic hydrogen technology experiment
[IAF PAPER 89-057] p 53 A90-13282

Role of communications satellites in the fiber era
[AIAA PAPER 90-0792] p 139 A90-25617

Servicing communication satellites in geostationary orbit
[AIAA PAPER 90-0830] p 39 A90-25655

Data distribution satellite system architecture concept
[AIAA PAPER 90-0885] p 46 A90-25704

Sodium-sulfur battery flight experiment definition study
p 57 A90-33956

Energy storage and thermal control system design status
p 59 A90-38077

Sodium-sulfur battery flight experiment definition study
p 231 N90-20479

Ford Aerospace Corp., Newport Beach, CA.

Sodium-sulfur battery flight experiment definition study
p 57 A90-33956

Ford Aerospace Corp., Palo Alto, CA.

Bipolar nickel-hydrogen battery development - A program review
p 62 A90-38288

End-hall thrusters

[AIAA PAPER 90-2595] p 64 A90-42570

Ford Motor Co., Dearborn, MI.

Improved silicon carbide for advanced heat engines
[NASA-CR-180831] p 124 N90-10293

Improved silicon carbide for advanced heat engines
[NASA-CR-182186] p 129 N90-28735

Front Range Research, Fort Collins, CO.

End-hall thrusters
[AIAA PAPER 90-2595] p 64 A90-42570

G

Garrett Turbine Engine Co., Phoenix, AZ.

Advanced Turbine Technology Applications Project (ATTAP)
[NASA-CR-185240] p 263 N90-26728

General Dynamics/Astronautics, San Diego, CA.

COLD-SAT - An orbital cryogenic hydrogen technology experiment
[IAF PAPER 89-057] p 53 A90-13282

General Dynamics Corp., San Diego, CA.

Frequency domain model for analysis of paralleled, series-output-connected Mapham inverters
p 148 A90-38084

Distortion and regulation characterization of a Mapham inverter
p 148 A90-38125

Development and testing of a 20 kHz component test bed
p 43 A90-38126

Bidirectional power converter control electronics
[NASA-CR-175070] p 70 N90-10175

Evolutionary space station fluids management strategies
[NASA-CR-185137] p 49 N90-10983

General Dynamics/Fort Worth, TX.

The implementation of STOVL task-tailored control modes in a fighter cockpit
[AIAA PAPER 90-3229] p 17 A90-49114

General Electric Co., Cincinnati, OH.

Application of HOST technology to the SSME HPFTP blade
[ASME PAPER 89-GT-130] p 209 A90-23828

Simulation of crack growth and crack closure under large cyclic plasticity
p 214 A90-50562

PMR graphite engine duct development
[NASA-CR-182228] p 23 N90-10037

Full scale technology demonstration of a modern counterrotating unducted fan engine concept: Component test
[NASA-CR-180868] p 24 N90-10047

Full scale technology demonstration of a modern counterrotating unducted fan engine concept: Design report
[NASA-CR-180867] p 24 N90-10048

Full scale technology demonstration of a modern counterrotating unducted fan engine concept: Engine test
[NASA-CR-180869] p 24 N90-10049

Revolutionary opportunities for materials and structures study
[NASA-CR-179642] p 95 N90-10184

An investigation of counterrotating tip vortex interaction
[NASA-CR-185135] p 247 N90-11549

Altitude testing of the 2D V-STOL ADEN demonstrator on an F404 engine
[NASA-CR-174824] p 28 N90-17638

Experimental performance and acoustic investigation of modern, counterrotating blade concepts
[NASA-CR-185158] p 18 N90-23393

Elevated temperature crack growth
[NASA-CR-182247] p 222 N90-26355

High speed turboprop aeroacoustic study (counterrotation). Volume 1: Model development
[NASA-CR-185241] p 249 N90-26633

Energy Efficient Engine high pressure turbine component test performance report
[NASA-CR-186289] p 33 N90-28553

Energy Efficient Engine combustor test hardware detailed design report
[NASA-CR-186301] p 33 N90-28554

Energy Efficient Engine (E3) combustion system component technology performance report
[NASA-CR-186274] p 33 N90-28555

Energy Efficient Engine acoustic supporting technology report
[NASA-CR-174834] p 33 N90-28557

Energy Efficient Engine core design and performance report
[NASA-CR-168069] p 34 N90-28559

NASA/GE Energy Efficient Engine low pressure turbine scaled test vehicle performance report
[NASA-CR-168290] p 34 N90-28563

General Electric Co., Erie, PA.

A 2.5 kW cascaded Schwarz converter for 20 kHz power distribution
p 147 A90-36813

General Electric Co., Evendale, OH.

A constitutive model for the inelastic multiaxial response of Rene 80 at 871 C and 982 C
p 114 A90-32266

Energy Efficient Engine: Flight propulsion system final design and analysis
[NASA-CR-168219] p 34 N90-28558

Energy Efficient Engine integrated core/low spool design and performance report
[NASA-CR-168211] p 34 N90-28561

Energy Efficient Engine: Control system component performance report
[NASA-CR-174651] p 34 N90-28562

General Electric Co., Lynn, MA.

Convertible engine system for high speed rotorcraft
[AIAA PAPER 90-2512] p 20 A90-40643

General Electric Co., Princeton, NJ.

Spacecraft designs for VSAT networks
[AIAA PAPER 90-0895] p 140 A90-25681

General Electric Co., Schenectady, NY.

The modelling of heat, mass and solute transport in solidification systems
p 157 A90-13092

The radiation of sound from a propeller at angle of attack
[NASA-CR-4264] p 249 N90-21602

General Electric Co., Syracuse, NY.

High-speed fiber-optic links for distribution of satellite traffic
p 47 A90-41687

General Motors Corp., Indianapolis, IN.

Calculation of turbulent three-dimensional jet-induced flow in a rectangular enclosure
[AIAA PAPER 90-0684] p 161 A90-19876

An experimental study of turbine vane heat transfer with leading edge and downstream film cooling
[ASME PAPER 89-GT-89] p 165 A90-23792

Three-dimensional fluid flow calculations using a flux-spline method
p 167 A90-27983

Design of an air-cooled metallic high-temperature radial turbine
p 20 A90-32960

An experimental and numerical study of particle-laden coaxial jet flows
p 171 A90-38799

3D Euler analysis of ducted propfan flowfields
[AIAA PAPER 90-3034] p 8 A90-45873

Composite matrix cooling scheme for small gas turbine combustors
[AIAA PAPER 90-2158] p 22 A90-47210

Investigation of advanced counterrotation blade configuration concepts for high speed turboprop systems, task 1: Ducted propfan analysis
[NASA-CR-185217] p 30 N90-22567

Advanced gearbox technology
[NASA-CR-179625] p 32 N90-24274

General Motors Research Labs., Warren, MI.

Universal aspects of brittle fracture, adhesion, and atomic force microscopy
p 83 A90-14021

Efficient estimation of diffusion during dendritic solidification
p 111 A90-20612

George Washington Univ., Hampton, VA.

Advanced propulsion for LEO and GEO platforms
[AIAA PAPER 90-2551] p 68 A90-52565

CORPORATE SOURCE

- George Washington Univ., Washington, DC.**
Rotating primary flow induction using jet-flapped blades p 19 A90-12585
- Georgia Inst. of Tech., Atlanta.**
The correlation between the temperature dependence of the CRSS and the formation of superlattice-intrinsic stacking faults in the nickel-base superalloy PWA 1480 p 109 A90-11657
Numerical study of the effects of icing on finite wing aerodynamics p 3 A90-20010
On the mechanism of cross slip in Ni3Al p 111 A90-20611
Application of an efficient hybrid scheme for aeroelastic analysis of advanced propellers p 4 A90-22153
[AIAA PAPER 90-0028]
Evaluation of three turbulence models in static air loads and dynamic stall predictions p 7 A90-31291
Cyclic deformation, fatigue and fatigue crack propagation in Ni-base alloys p 115 A90-34162
Fatigue crack propagation behavior of a single crystalline superalloy p 116 A90-48635
Millimeter-wave/infrared rectenna development at Georgia Tech p 69 N90-10147
Numerical simulation of unsteady rotational flow over propfan configurations p 10 N90-12500
[NASA-CR-186037]
Feasibility analysis of reciprocating magnetic heat pumps p 177 N90-15363
[NASA-CR-186205]
Analysis of shell-type structures subjected to time-dependent mechanical and thermal loading p 222 N90-24653
[NASA-CR-185077]
Micromechanics of cyclic deformation in SSME turbopump blade materials p 224 N90-28641
- Giner, Inc., Waltham, MA.**
Oxygen electrodes for rechargeable alkaline fuel cells. II p 228 A90-33946
Oxygen electrodes for rechargeable alkaline fuel cells-II p 231 N90-20469
- Grumman Aerospace Corp., Bethpage, NY.**
Conceptual design of a Liquid Droplet Radiator space flight experiment p 48 A90-27527
[SAE PAPER 891565]
Conceptual design of liquid droplet radiator shuttle-attached experiment p 71 N90-11805
[NASA-CR-185164]
Conceptual design of liquid droplet radiator shuttle-attached experiment technical requirements document p 71 N90-11806
[NASA-CR-185165]
- GT-Devices, Alexandria, VA.**
Experiments on a repetitively pulsed electrothermal thruster p 56 A90-27960
- GTE Labs., Inc., Waltham, MA.**
Interface demarcation in GaAs by current pulsing p 254 A90-19793
[AIAA PAPER 90-0319]
Free float acceleration measurements aboard NASA's KC-135 Microgravity Research Aircraft p 132 A90-20000
[AIAA PAPER 90-0742]
- ## H
- Hamilton Standard, Windsor Locks, CT.**
Hydrogen-oxygen proton-exchange membrane fuel cells and electrolyzers p 56 A90-33944
Large scale prop-fan structural design study. Volume 1: Initial concepts p 23 N90-10043
[NASA-CR-174992]
Large scale prop-fan structural design study. Volume 2: Preliminary design of SR-7 p 23 N90-10044
[NASA-CR-174993]
Large-scale Advanced Prop-fan (LAP) high speed wind tunnel test report p 24 N90-10045
[NASA-CR-182125]
Large-scale Advanced Prop-fan (LAP) technology assessment report p 24 N90-10046
[NASA-CR-182142]
Two stage gear tooth dynamics program p 199 N90-10437
[NASA-CR-185110]
Acoustic test and analysis of a counterrotating prop-fan model p 247 N90-10683
[NASA-CR-179590]
Measurement of the steady surface pressure distribution on a single rotation large scale advanced prop-fan blade at Mach numbers from 0.03 to 0.78 p 32 N90-28552
[NASA-CR-182124]
- Hamilton Standard Div., United Aircraft Corp., Windsor Locks, CT.**
Large-scale Advanced Prop-fan (LAP) static rotor test report p 25 N90-12617
[NASA-CR-180848]
- Harris Corp., Melbourne, FL.**
LBR-2 earth stations for the ACTS program p 42 A90-25662
[AIAA PAPER 90-0838]

- Update of the Solar Concentrator Advanced Development Project p 48 A90-38267
A forward error correction technique using a high-speed, high-rate single chip codec p 141 A90-48440
Solar Concentrator Advanced Development Program [NASA-CR-185173] p 232 N90-22834
- Honeywell, Inc., Bloomington, MN.**
A high-speed GaAs MESFET optical controller p 186 A90-22483
Control of a GaAs monolithic Ka-band phase shifter using a high-speed optical interconnect p 150 A90-41700
The 30-GHz monolithic receive module p 146 N90-24528
[NASA-CR-180849]
- Houston Univ., TX.**
Elliptic jets. I - Characteristics of unexcited and excited jets p 159 A90-18071
- Hughes Aircraft Co., El Segundo, CA.**
Antenna beamforming using optical processing p 142 N90-11210
[NASA-CR-180844]
- Hughes Aircraft Co., Los Angeles, CA.**
Electrochemical behavior of heavily cycled nickel electrodes in Ni/H₂ cells containing electrolytes of various KOH concentrations p 103 A90-24535
- Hughes Aircraft Co., Torrance, CA.**
K-band TWT using new diamond rod technology p 147 A90-25691
[AIAA PAPER 90-0670]
KOH concentration effect on the cycle life of nickel-hydrogen cells. IV - Results of failure analysis p 228 A90-33952
- Hughes Research Labs., Malibu, CA.**
Xenon ion sources for space applications p 56 A90-22874
Status of xenon ion propulsion technology p 56 A90-27961
High-power xenon ion thrusters p 64 A90-42536
[AIAA PAPER 90-2540]
- ## I
- IBM Watson Research Center, Yorktown Heights, NY.**
Computer aided design of bevel gear tooth surfaces p 195 A90-21136
- Illinois Inst. of Tech., Chicago.**
A rotating hot-wire technique for spatial sampling of disturbed and manipulated duct flows p 186 A90-41120
- Illinois Univ., Chicago.**
Tooth contact shift in loaded spiral bevel gears p 193 A90-21112
Topology of modified helical gears p 195 A90-21132
Mass spectrometric observations of metal oxychlorides produced by oxidation-chlorination reactions p 103 A90-21215
A probabilistic approach to crack instability p 212 A90-41278
Energy analysis of crack-damage interaction p 213 A90-41372
Effect of crack-microcracks interaction on energy release rates p 214 A90-49269
Generation and tooth contact analysis of spiral bevel gears with predesigned parabolic functions of transmission errors p 199 N90-12033
[NASA-CR-4259]
Theory of gearing p 202 N90-19593
[NASA-RP-1212]
- Illinois Univ., Urbana.**
The shocking development of lithium (and boron) in supernovae p 264 A90-17643
On physical optics for calculating scattering from coated bodies p 250 A90-20151
Multigrid calculations of a jet in crossflow p 167 A90-26952
[AIAA PAPER 90-0444]
Experimental evidence of a dimensional crossover in Y1Ba2Cu3O(7-delta) p 255 A90-29739
Hot gas environment around STOVL aircraft in ground proximity. II - Numerical study p 21 A90-42766
[AIAA PAPER 90-2270]
The structure and stability of nonadiabatic flame balls p 105 A90-43674
Reflector spillover loss of an open-ended rectangular and circular waveguide feed p 141 A90-45398
Optimal finite-thrust spacecraft trajectories using collocation and nonlinear programming p 40 A90-46783
[AAS PAPER 89-350]
Optimal orbital rendezvous using high and low thrust p 41 A90-46786
[AAS PAPER 89-354]
Optimal cooperative time-fixed impulsive rendezvous p 41 A90-53037
[AIAA PAPER 90-2962]
Discrete approximations to optimal trajectories using direct transcription and nonlinear programming p 41 A90-53038
[AIAA PAPER 90-2963]

- Optimal impulsive time-fixed orbital rendezvous and interception with path constraints p 41 A90-53051
[AIAA PAPER 90-2972]
- Instron Corp., Canton, MA.**
High-temperature tensile properties of fiber reinforced reaction bonded silicon nitride p 95 A90-52783
- International Fuel Cells Corp., South Windsor, CT.**
Integrated regenerative fuel cell experimental evaluation p 230 N90-18808
[NASA-CR-185183]
- Iowa Univ., Iowa City.**
Spacelab 2 Plasma Diagnostics Package p 39 A90-23263
Robustness, generality and efficiency of optimization algorithms in practical applications p 236 A90-29268
[AIAA PAPER 90-1177]
- ## J
- Jet Propulsion Lab., California Inst. of Tech., Pasadena.**
The SP-100 space reactor as a power source for Mars exploration missions p 55 A90-16689
[AAS PAPER 87-224]
Iridium-coated rhenium thrusters by CVD p 114 A90-30480
Effect of Ga and P dopants on the thermoelectric properties of n-type SiGe p 256 A90-38140
Photovoltaic options for solar electric propulsion p 68 A90-52563
[AIAA PAPER 90-2529]
NASA advanced space photovoltaic technology: Status, potential and future mission applications p 74 N90-17775
- John Carroll Univ., Cleveland, OH.**
Modulated-splitting-ratio fiber-optic temperature sensor p 185 A90-11706
- Johns Hopkins Univ., Baltimore, MD.**
Acousto-ultrasonic nondestructive evaluation of materials using laser beam generation and detection p 154 N90-23664
[NASA-CR-186694]
- Jordan Univ. of Science and Technology, Irbid.**
Shaft flexibility effects on aeroelastic stability of a rotating bladed disk p 208 A90-16371
Blade mistuning coupled with shaft flexibility effects in rotor aeroelasticity p 19 A90-23896
[ASME PAPER 89-GT-330]
Shaft flexibility effects on the forced response of a bladed-disk assembly p 21 A90-43218

K

- Kansas State Univ., Manhattan.**
Hopf bifurcation in the driven cavity p 174 A90-48548
- Kansas Univ. Center for Research, Inc., Lawrence.**
Modern developments in shear flow control with swirl p 181 N90-22000
[NASA-CR-186586]
- Kentucky Univ., Lexington.**
Inverse heat transfer analysis of Bridgman crystal growth p 157 A90-13093
Opposed-flow flame spread and extinction in mixed-convection boundary layers p 168 A90-32841

L

- L'Air Liquide, Sassenage (France).**
Pressure dependence of the melting temperature of metals p 103 A90-16281
- La Plata Univ. (Argentina).**
Phase transitions in fermionic systems with many-body interaction p 249 A90-19303
- Lagos Univ. (Nigeria).**
Application of multi-grid methods for solving the Navier-Stokes equations p 243 N90-14002
[NASA-TM-102359]
- Large Scale Programs Inst., Austin, TX.**
A superconducting quenchgun for delivering lunar derived oxygen to lunar orbit p 43 A90-40627
[AIAA PAPER 90-2369]
A superconducting quenchgun for delivering lunar derived oxygen to lunar orbit p 77 N90-21806
[NASA-CR-185161]
A trajectory generation and system characterization model for cislunar low-thrust spacecraft. Volume 2: Technical manual p 77 N90-21807
[NASA-CR-185172]
- Lawrence Livermore National Lab., CA.**
The shocking development of lithium (and boron) in supernovae p 264 A90-17643
- Lehigh Univ., Bethlehem, PA.**
Computation of three-dimensional turbulent boundary layers with heat transfer in a plane of symmetry using embedded wall-layer functions p 160 A90-19788
[AIAA PAPER 90-0307]

Little (Arthur D.), Inc., Cambridge, MA.

- Conceptual design of a moving belt radiator shuttle-attached experiments: Technical requirement Document [NASA-CR-185168] p 73 N90-15996
- Conceptual design of a Moving Belt Radiator (MBR) shuttle-attached experiment [NASA-CR-185169] p 79 N90-23474

Lockheed Aeronautical Systems Co., Burbank, CA.

- Interior noise in the untreated Gulfstream II Propan Test Assessment aircraft p 17 A90-44736

Lockheed Aeronautical Systems Co., Marietta, GA.

- Total temperature effects on centerline Mach number characteristics of freejets p 6 A90-25290
- Theoretical model of discrete tone generation by impinging jets p 247 A90-35903
- Propan Test Assessment (PTA): Flight test report [NASA-CR-182278] p 24 N90-11738
- Propan Test Assessment (PTA) [NASA-CR-185138] p 25 N90-11739

Lockheed-Georgia Co., Marietta.

- Analysis of results from wind tunnel tests of inlets for an advanced turboprop nacelle installation [NASA-CR-174937] p 10 N90-10011

Lockheed Missiles and Space Co., Sunnyvale, CA.

- Space Station Freedom solar array design development p 58 A90-38076
- Photovoltaic array environmental protection program p 59 A90-38088

M

Maine Univ., Orono.

- Asymmetrical boundary layer separation at the base of a two cylinder geometry p 159 A90-18505

Manchester Univ. (England).

- A numerical study of the interaction between unsteady free-stream disturbances and localized variations in surface geometry p 161 A90-21422

Manhattan Coll., New York.

- Radiative configuration factors from cylinders to coaxial axisymmetric bodies p 167 A90-26334

MARC Analysis Research Corp., Palo Alto, CA.

- The MHOST finite element program: 3-D inelastic analysis methods for hot section components. Volume 2: User's manual [NASA-CR-182235-VOL-2] p 215 N90-10450
- The MHOST finite element program: 3-D inelastic analysis methods for hot section components. Volume 3: Systems' manual [NASA-CR-182236] p 215 N90-10451

Martin Marietta Corp., Baltimore, MD.

- 1200 to 1400 K slow strain rate compressive properties of NiAl/Ni₂AlTi-base materials p 88 A90-16938
- High-temperature slow-strain-rate compression studies on CoAl-TiB₂ composites p 93 A90-48636

Martin Marietta Labs., Baltimore, MD.

- 1100 to 1300 K slow plastic compression properties of Ni-38.5Al composites p 111 A90-19154
- Elevated temperature slow plastic deformation of NiAl-TiB₂ particulate composites at 1200 and 1300 K p 92 A90-45621
- Slow plastic deformation of extruded NiAl-10TiB₂ particulate composites at 1200 and 1300 K p 92 A90-46133

- 1300 K compressive properties of several dispersion strengthened NiAl materials p 116 A90-47091
- Compression behavior of the forged L2 compounds Al67Ti25Cr8 and Al66Ti25Mn9 p 116 A90-51298

Martin Marietta Space Systems, Inc., Denver, CO.

- On-orbit low gravity cryogenic scientific investigations using the COLD-SAT Satellite [AIAA PAPER 90-0718] p 39 A90-19988

Martini Engineering, Richland, WA.

- Development of free-piston Stirling engine performance and optimization codes based on Martini simulation technique [NASA-CR-182210] p 263 N90-18326

Maryland Univ., College Park.

- Critical speeding up in pure fluids p 167 A90-26369
- Comparison between pressure gradient method and MAC method on high Re calculation p 172 A90-44462

The GEM-T2 gravitational model

- [NASA-TM-100746] p 234 N90-12984

Massachusetts Inst. of Tech., Cambridge.

- Calculation of unsteady Euler flows in turbomachinery using the linearized Euler equations p 2 A90-11778
- A multi-domain spectral computation of three-dimensional laminar horseshoe vortex flow using incompressible Navier-Stokes equations p 3 A90-17592
- Heat transfer on accreting ice surfaces [AIAA PAPER 90-0200] p 162 A90-22181

Nitriding kinetics of Si-SiC powder mixtures as simulations of reaction bonded Si₃N₄-SiC composites

- p 90 A90-27076
- On sublayer streaks p 168 A90-28143
- Ion drag for a negatively biased solar array in low earth orbit p 48 A90-36191

Theory of plasma contactors in ground-based experiments and low earth orbit

- p 150 A90-47108

Rate correlation for condensation of pure vapor on turbulent, subcooled liquid

- p 174 A90-50511

Properties of RBSN and RBSN-SiC composites

- p 94 A90-51920

Ultrasonic techniques for aircraft ice accretion measurement

- p 16 N90-20926

Investigation of surface water behavior during glaze ice accretion

- p 16 N90-20927

The influence of ice accretion physics on the forecasting of aircraft icing conditions

- p 17 N90-20928

Input-output characterization of fiber reinforced composites by P waves

- [NASA-CR-185287] p 208 N90-28097

Ultrasonic verification of five wave fronts in unidirectional graphite epoxy composite

- [NASA-CR-185288] p 208 N90-28858

Massachusetts Inst. of Tech., Lexington.

- Convergence of the SMI and the diagonally loaded SMI algorithms with weak interference [AD-A22639] p 141 A90-36717

Massachusetts Univ., Amherst.

- Properties of RBSN and RBSN-SiC composites p 94 A90-51920

Materials and Electrochemical Research Corp., Tucson, AZ.

- Zirconia toughened SiC whisker reinforced alumina composites small business innovation research [NASA-CR-179629] p 125 N90-10294

Max-Planck-Inst. fuer Metallforschung, Stuttgart (Germany, F.R.).

- Preliminary investigation of a NiAl composite prepared by cryomilling p 113 A90-25098

Maxwell Labs., Inc., La Jolla, CA.

- EPSAT - A workbench for designing high-power systems for the space environment [AIAA PAPER 90-0637] p 245 A90-26975
- The sheath structure around a negatively charged rocket payload p 48 A90-34780

The Environment-Power System Analysis Tool development program

- p 236 A90-38089

Maxwell Labs., Inc., San Diego, CA.

- Computer modeling of current collection by the CHARGE-2 mother payload p 252 A90-24933

MCAT Inst., Moffett Field, CA.

- Application of a lower-order implicit scheme and an interactive grid generation for turbomachinery flow field simulations [ASME PAPER 89-GT-20] p 4 A90-23762

McDonnell Aircraft Co., Houston, TX.

- Research on a two-dimensional inlet for a supersonic V/STOL propulsion system. Appendix A [NASA-CR-174945] p 12 N90-18364

McDonnell Aircraft Co., Saint Louis, MO.

- Engine inlet distortion in a 9.2 percent scaled vectored thrust STOVL model in ground effect [AIAA PAPER 89-2910] p 5 A90-25043

McDonnell-Douglas Research Labs., Saint Louis, MO.

- Experimental investigation of terminal shock sensors in mixed-compression inlets [AIAA PAPER 90-1931] p 186 A90-40560

Mechanical Engineering Lab., Tsukuba (Japan).

- Effects of lubrication on the performance of high speed spur gears p 194 A90-21119

Mechanical Technology, Inc., Latham, NY.

- Analysis and design of helium-buffered face seals for the SSME high-pressure oxygen turbopump [AIAA PAPER 90-2049] p 197 A90-42000

Automotive Stirling engine development program

- [NASA-CR-180839] p 263 N90-11654

Medical Technology, Inc., Syracuse, NY.

- Automotive Stirling engine development program [NASA-CR-180840] p 264 N90-29260

Memphis State Univ., TN.

- Dynamic loading of spur gears with linear or parabolic tooth profile modifications p 195 A90-21126

- Profile modification to minimize spur gear dynamic loading p 195 A90-21128

Miami Univ., Oxford, OH.

- Antiferromagnetism in Co-57-doped La₂CuO₄(-y) studied by Moessbauer spectroscopy p 255 A90-34011

- Hyperfine magnetic field on Cd-111 in Heusler alloys Co₂MnZ (Z = Si, Ga, Ge, Sn) p 255 A90-34012

- Fe-57 and Sn-119 Moessbauer study of La₂CuO₄(-y), YBa₂Cu₃O(7-y) and SmBa₂Cu₃O(7-y) p 256 A90-34020

Michigan State Univ., East Lansing.

- Review of research and development on the microwave electrothermal thruster p 55 A90-16369

- The effects of forcing on a single stream shear layer and its parent boundary layer p 169 A90-35219

- Diagnostic evaluations of microwave generated helium and nitrogen plasma mixtures [AIAA PAPER 90-2634] p 252 A90-42602

- Linear acene derivatives - New routes to pentacene and naphthalene and the first synthesis of a triptycene with two anthracene moieties p 85 A90-49071

- Bisannulation with a benzo(1,2-c:4,5-c'-prime) difuran equivalent - A new route to linear acene derivatives p 85 A90-49072

- Triptycene synthesis: A new method for attaching a 2,3-anthracene moiety to the 9,10-positions of another anthracene moiety - Exceptional conditions for a Lewis acid catalyzed Diels-Alder reaction p 85 A90-49073

- The effects of forcing on a single stream shear layer and its parent boundary layer [NASA-CR-186529] p 180 N90-21301

Michigan Technological Univ., Houghton.

- The correlation between the temperature dependence of the CRSS and the formation of superlattice-intrinsic stacking faults in the nickel-base superalloy PWA 1480 p 109 A90-11657

- On the mechanism of cross slip in Ni₃Al p 111 A90-20611

- Time-accurate simulations of a shear layer forced at a single frequency p 163 A90-23111

- Structural comparison of nickel electrodes and precursor phases p 228 A90-33949

- Structural comparison of nickel electrodes and precursor phases p 231 N90-20472

Michigan Univ., Ann Arbor.

- Molecular beam epitaxial growth of high-quality InSb on InP and GaAs substrates p 253 A90-12808

- Numerical analysis of natural convection in liquid droplets by phase change p 164 A90-23212

- Splitting of inviscid fluxes for real gases p 167 A90-25451

- Transport properties of InAs(x)Sb(1-x) (x = 0-0.55) on InP grown by molecular-beam epitaxy p 256 A90-36232

- The effects of surface films on mechanical behavior of B2 ordered intermetallic alloys p 115 A90-44338

- Inviscid flux-splitting algorithms for real gases with non-equilibrium chemistry p 174 A90-52275

- Comparison of solution approaches for minimum-fuel, low-thrust, power-limited orbital transfers [AIAA PAPER 90-2960] p 41 A90-53035

Midwest Research Inst., Golden, CO.

- An empirical investigation of the InP shallow-homojunction solar cell p 225 A90-14869

- Hybrid solar cells based on dc magnetron sputtered films of n-ITO on APMOVPE grown p-InP p 225 A90-14893

- Modeling and simulation of InP homojunction solar cells p 226 A90-14899

- High altitude current-voltage measurement of GaAs/Ge solar cells p 226 A90-14910

- Radiation resistance and comparative performance of ITO/InP and n/p InP homojunction solar cells p 226 A90-14933

- Investigation of buried homojunctions in p-InP formed during sputter deposition of both indium tin oxide and indium oxide p 256 A90-36799

- Study of indium tin oxide films exposed to atomic oxygen p 257 A90-45193

Military Academy, West Point, NY.

- Diagnostic evaluations of microwave generated helium and nitrogen plasma mixtures [AIAA PAPER 90-2634] p 252 A90-42602

Minnesota Univ., Minneapolis.

- The modelling of heat, mass and solute transport in solidification systems p 157 A90-13092

- Three-dimensional fluid flow calculations using a flux-spline method p 167 A90-27983

- Neutron stars and white dwarfs in galactic halos? p 265 A90-30909

- Big bang nucleosynthesis and the quark-hadron transition p 265 A90-31407

Mississippi State Univ., Mississippi State.

- Counterrotating prop-fan simulations which feature a relative-motion multiblock grid decomposition enabling arbitrary time-steps [AIAA PAPER 90-0687] p 3 A90-19978

- An observer-based compensator for distributed delays p 239 A90-49899

Monash Univ., Clayton (Australia).

- Instrumented adhesion tests on plasma sprayed thermal barrier coatings p 111 A90-20255

- Tensile adhesion testing methodology for thermally sprayed coatings p 85 A90-43902

Mount Sinai School of Medicine, New York, NY.

A geometric analysis of semicircular canals and induced activity in their peripheral afferents in the rhesus monkey
p 234 A90-28084

Multi-Metals, Louisville, KY.

1200 to 1400 K slow strain rate compressive properties of NiAl/Ni₂AlTi-base materials p 88 A90-16938

N**National Aeronautics and Space Administration, Washington, DC.**

Advanced Communications Technology Satellite (ACTS) p 140 A90-25663
NASA aerospace battery systems program update p 228 A90-38217
NASA advanced space photovoltaic technology: Status, potential and future mission applications p 74 N90-17775

National Aeronautics and Space Administration, Ames Research Center, Moffett Field, CA.

Numerical study of chemically reacting flows using a lower-upper symmetric successive overrelaxation scheme p 3 A90-17989
Smoldering combustion under low gravity conditions [AIAA PAPER 90-0648] p 103 A90-22238
Application of a lower-upper implicit scheme and an interactive grid generation for turbomachinery flow field simulations p 4 A90-23762
[ASME PAPER 89-GT-20] p 4 A90-23762
Efficient Monte Carlo simulation of rarefied flow in a small nozzle p 170 A90-38396
[AIAA PAPER 90-1693] p 170 A90-38396
CFD propels NASP propulsion progress p 172 A90-41163

National Aeronautics and Space Administration, Lyndon B. Johnson Space Center, Houston, TX.

Hydrogen-oxygen proton-exchange membrane fuel cells and electrolyzers p 56 A90-33944

National Aeronautics and Space Administration, Langley Research Center, Hampton, VA.

CFD propels NASP propulsion progress p 172 A90-41163
Grid generation for the solution of partial differential equations p 237 A90-47188
Advanced propulsion for LEO and GEO platforms [AIAA PAPER 90-2551] p 68 A90-52565

National Aeronautics and Space Administration, Marshall Space Flight Center, Huntsville, AL.

Space Station power system autonomy demonstration p 245 A90-10373
Characterization testing of a 40 ampere hour bipolar nickel-hydrogen battery p 56 A90-33940
Engine selection for the Space Exploration Initiative [AIAA PAPER 90-1880] p 65 A90-47201

National Central Univ., Chung-Li (Taiwan).

Evaluation of three turbulence models in static air loads and dynamic stall predictions p 7 A90-31291

National Inst. of Standards and Technology, Gaithersburg, MD.

Critical exponent for the viscosity of carbon dioxide and xenon p 261 A90-43941

Naval Postgraduate School, Monterey, CA.

Progress towards the development of an inviscid-viscous interaction method for unsteady flows in turbomachinery cascades p 2 A90-11806

Unsteady heat transfer on turbine blades p 161 A90-20511

A performance analysis of DS-CDMA and SCPC VSAT networks p 141 A90-39056

Nebraska Univ., Lincoln.

Ellipsometric study of Al₂O₃/Ag/Si and SiO₂/Ag/quartz ashed in an oxygen plasma p 120 A90-18217
Ellipsometric studies of the diffusion of atomic oxygen through silicon dioxide thin films p 104 A90-36268
Study of indium tin oxide films exposed to atomic oxygen p 257 A90-45193

New York Univ., New York.

Figure of merit studies of beam power concepts for advanced space exploration [NASA-CR-186720] p 146 N90-26234

New York Univ. Medical Center.

A geometric analysis of semicircular canals and induced activity in their peripheral afferents in the rhesus monkey p 234 A90-28084

Nielsen Engineering and Research, Inc., Mountain View, CA.

Development of an unstructured mesh/Navier-Stokes method for aerodynamics of aircraft with ice accretions [AIAA PAPER 90-0758] p 4 A90-20011
Chemically reacting supersonic flow calculation using an assumed PDF model p 4 A90-22256 [AIAA PAPER 90-0731]

North Carolina State Univ., Raleigh.

Investigation of turbulent transport in an axisymmetric sudden expansion p 163 A90-23112
The impedance of a tubular electrode - A model for a porous electrode p 104 A90-33723
Deep-level dominated electrical characteristics of Au contacts on beta-SiC p 147 A90-33726
Characterization of reaction kinetics in a porous electrode [NASA-CR-186504] p 106 N90-19340

Silicon carbide semiconductor device fabrication and characterization [NASA-CR-186354] p 258 N90-19873

Northwestern Univ., Evanston, IL.

Measurement of the intrinsic bond strength of brittle thin films on flexible substrates p 256 A90-44022
Electrical properties of materials for high temperature strain gage applications [NASA-CR-186192] p 188 N90-14534

Norton Co., Northboro, MA.

Development of Si₃N₄ for gas turbine applications p 122 A90-35509

Notre Dame Univ., IN.

Analysis of nonuniform subsonic flows about a row of moving blades p 2 A90-11779
High frequency capacitance-voltage characteristics of thermally grown SiO₂ films on beta-SiC p 254 A90-21348
Unsteady disturbances of streaming motions around bodies p 162 A90-21424
Numerical solutions of the linearized Euler equations for unsteady vortical flows around lifting airfoils [AIAA PAPER 90-0694] p 5 A90-25041
Numerical solutions of the linearized Euler equations for unsteady vortical flows around lifting airfoils p 7 A90-30264

O**Oak Ridge National Lab., TN.**

Selection of phase-change and containment materials for thermal energy storage [NASA-CR-186228] p 229 N90-15506

Oberlin Coll., OH.

Simple evaporation controller for thin-film deposition from a resistively heated boat p 149 A90-39761

Office National d'Etudes et de Recherches Aeronautiques, Paris (France).

Treatment of coupled fluid-structure interaction problems by a mixed variational principle p 159 A90-18288

Office National d'Etudes et de Recherches Aeronautiques, Paris (France).

Mixed variational formulation of finite element analysis of acoustoelastic/slosh fluid-structure interaction p 212 A90-34851

Office of Naval Research, Arlington, VA.

Solution of steady-state one-dimensional conservation laws by mathematical programming p 241 A90-21918

Ohio State Univ., Columbus.

Microstructural changes in beta-silicon nitride grains upon crystallizing the grain-boundary glass p 120 A90-13230

Effects of desired signal on the performance of a sidelobe canceller p 139 A90-13936

Modal analysis of gear housing and mounts p 192 A90-17018

The shocking development of lithium (and boron) in supernovae p 264 A90-17643

Compressibility effects in free shear layers [AIAA PAPER 90-0705] p 161 A90-19984

On physical optics for calculating scattering from coated bodies p 250 A90-20151

Dynamic analysis of geared rotors by finite elements p 194 A90-21123

A numerical study of the interaction between unsteady free-stream disturbances and localized variations in surface geometry p 161 A90-21422

Effects of compressibility on the characteristics of free shear layers p 6 A90-25285

Application of heuristic satellite plan synthesis algorithms to requirements of the WARC-88 allotment plan [AIAA PAPER 90-0815] p 245 A90-25638

A heuristic approach to worst-case carrier-to-interference ratio maximization in satellite system synthesis [AIAA PAPER 90-0816] p 46 A90-25639

Crystallization of a barium-aluminosilicate glass p 121 A90-27107

Surface entropy of liquids via a direct Monte Carlo approach - Application to liquid Si p 261 A90-31675

Structure of a reattaching supersonic shear layer p 7 A90-36252

Convergence of the SMI and the diagonally loaded SMI algorithms with weak interference [AD-A222639] p 141 A90-36717

Diagnostics and performance of a 1/4-scale MPD thruster [AIAA PAPER 90-2665] p 65 A90-42625

Pressure-based real-time measurements in compressible free shear layers [AIAA PAPER 90-1980] p 8 A90-42709

Crystallization behavior and properties of BaO-Al₂O₃-2SiO₂ glass matrices p 95 A90-51933

An experimental SMI adaptive antenna array for weak interfering signals [NASA-CR-185976] p 142 N90-11211

Constitutive parameter measurements of lossy materials [NASA-CR-183398] p 257 N90-11603

Adaptive antenna arrays for satellite communication [NASA-CR-185989] p 143 N90-12784

Vibration transmission through rolling element bearings in geared rotor system, part 1 [NASA-CR-186093] p 199 N90-12936

High-frequency asymptotic methods for analyzing the EM scattering by open-ended waveguide cavities [NASA-CR-186244] p 143 N90-16103

Crystallization behavior and properties of BaO-Al₂O₃-2SiO₂ glass matrices [NASA-CR-185209] p 127 N90-19374

Electromagnetic properties of material coated surfaces [NASA-CR-186466] p 144 N90-19466

Effects of additional interfering signals on adaptive array performance [NASA-CR-186508] p 145 N90-20271

The effects of magnetic nozzle configurations on plasma thrusters [NASA-CR-186465] p 76 N90-21109

A review of gear housing dynamics and acoustics literature [NASA-CR-185148] p 203 N90-21387

Non-linear dynamic analysis of geared systems, part 2 [NASA-CR-180495] p 204 N90-23732

Ohio Univ., Athens. Parallel eigenanalysis of finite element models in a completely connected architecture [NASA-CR-185166] p 217 N90-14652

Old Dominion Univ., Norfolk, VA. Mathematical optimization of photovoltaic converters for diode lasers p 228 A90-38110

Optical Coating Lab., Inc., Santa Rosa, CA. Optimization of silicon 8 cm x 8 cm wrapthrough Space Station cells for 'on orbit' operation p 54 A90-14941

P**PDA Engineering, Santa Ana, CA.**

The application of cast SiC/Al to rotary engine components [NASA-CR-179610] p 25 N90-13385

Pennsylvania State Univ., New Kensington. The effects of nonlinear loading upon the Space Station Freedom 20 kHz power system p 60 A90-38118

Pennsylvania State Univ., State College. The measurement of boundary layers on a compressor blade in cascade. Volume 1: Experimental technique, analysis and results [NASA-CR-185118-VOL-1] p 23 N90-10038

The measurement of boundary layers on a compressor blade in cascade. Volume 2: Data tables [NASA-CR-185118-VOL-2] p 23 N90-10039

Pennsylvania State Univ., University Park. Computation of three dimensional turbulent boundary layers in internal flows, including turbomachinery rotor blades p 3 A90-12555

Deformation behavior of NiAl-based alloys containing iron, cobalt, and hafnium p 110 A90-16930

Skin friction measurements by laser interferometry in swept shock/boundary-layer interactions p 3 A90-18153

Fully elliptic incompressible flow calculations on regular grid by a new pressure substitution method [AIAA PAPER 90-0239] p 160 A90-19749

The measurement of boundary layers on a compressor blade in cascade. IV - Flow fields for incidence angles of -1.5 and -8.5 degrees [ASME PAPER 89-GT-72] p 165 A90-23793

On the driving force of PAH production p 84 A90-32833

Microstructure and mechanical properties of multiphase NiAl-based alloys p 115 A90-35071

Computation of turbine flowfields with a Navier-Stokes code [AIAA PAPER 90-2122] p 8 A90-42731

Optimum structural design of robotic manipulators with fiber reinforced composite materials p 197 A90-46074

Physical Sciences, Inc.

- An observer-based compensator for distributed delays p 239 A90-49899
- Integrated Communication and Control Systems. III - Nonidentical sensor and controller sampling p 239 A90-51266
- Performance analysis of Integrated Communication and Control System networks p 239 A90-51267
- Kinetics and mechanism of soot formation in hydrocarbon combustion [NASA-CR-186162] p 106 N90-14305
- Ignition and combustion characteristics of metallized propellants [NASA-CR-186870] p 107 N90-26911
- Physical Sciences, Inc., Andover, MA.**
- H₂/O₂ three-body rates at high temperatures [AIAA PAPER 90-1696] p 105 A90-38399
- Pittsburgh Univ., Johnstown, PA.**
- Two-component phase-averaged turbulence statistics downstream of a rotating spoked-wheel wake generator p 156 A90-11559
- Pittsburgh Univ., PA.**
- Parallel multi-time step integration on a transputer system p 235 A90-20188
- Growth of improved quality 3C-SiC films on 6H-SiC substrates p 255 A90-29596
- Growth of high quality 6H-SiC epitaxial films on vicinal (0001) 6H-SiC wafers p 255 A90-29952
- Transient finite element computations on the transputer system [NASA-CR-185199] p 218 N90-18071
- The insertion of human dynamics models in the flight control loops of V/STOL research aircraft. Appendix 2: The optimal control model of a pilot in V/STOL aircraft control loops [NASA-CR-186598] p 38 N90-21776
- An adaptive human response mechanism controlling the V/STOL aircraft. Appendix 3: The adaptive control model of a pilot in V/STOL aircraft control loops [NASA-CR-186599] p 38 N90-21777
- Pratt and Whitney Aircraft, East Hartford, CT.**
- Thermal barrier coating life prediction model development, phase 1 [NASA-CR-182230] p 26 N90-13388
- MATE (Materials for Advanced Turbine Engines) Program, Project 3. Volume 2: Design, fabrication and evaluation of an oxide dispersion strengthened sheet alloy combustor liner [NASA-CR-180892] p 117 N90-17868
- Energy Efficient Engine exhaust mixer model technology report addendum; phase 3 test program [NASA-CR-174799] p 33 N90-28556
- Energy Efficient Engine program advanced turbofan nacelle definition study [NASA-CR-174942] p 34 N90-28560
- Energy efficient engine program technology benefit/cost study. Volume 1: Executive summary [NASA-CR-174766-VOL-1] p 34 N90-28564
- Energy efficient engine program technology benefit/cost study, volume 2 [NASA-CR-174766-VOL-2] p 35 N90-28565
- Energy Efficient Engine integrated core/low spool test hardware design report [NASA-CR-188137] p 35 N90-28566
- Energy efficient engine pin fin and ceramic composite segmented liner combustor sector ng test report [NASA-CR-179534] p 35 N90-28567
- Energy Efficient Engine: Combustor component performance program [NASA-CR-179533] p 35 N90-28568
- Energy Efficient Engine: Control system preliminary definition report [NASA-CR-179578] p 35 N90-28569
- Energy Efficient Engine: High-pressure compressor test hardware detailed design report [NASA-CR-180850] p 36 N90-28570
- Constitutive and life modeling of single crystal blade alloys for root attachment analysis p 119 N90-28643
- Pratt and Whitney Aircraft, West Palm Beach, FL.**
- Assessment of High Temperature Superconducting (HTS) electric motors for rotorcraft propulsion [NASA-CR-185222] p 29 N90-21761
- Pratt and Whitney Aircraft Group, East Hartford, CT.**
- Mixer-ejector nozzle for jet noise suppression [AIAA PAPER 90-1909] p 247 A90-47202
- Princeton Univ., NJ.**
- Time-accurate simulations of a shear layer forced at a single frequency p 163 A90-23111
- N-decane-air droplet combustion experiments in the NASA-Lewis 5 Second Zero-Gravity Facility [AIAA PAPER 90-0649] p 104 A90-25038
- Time-dependent calculation of a forced mixing layer using a k-epsilon turbulence model p 169 A90-35222
- A study of the unsteadiness of crossing shock wave turbulent boundary layer interactions [AIAA PAPER 90-1456] p 170 A90-38614

- The structure and stability of nonadiabatic flame balls p 105 A90-43674
- Comparison of solution approaches for minimum-fuel, low-thrust, power-limited orbital transfers [AIAA PAPER 90-2960] p 41 A90-53035
- Program Development Corp., White Plains, NY.**
- The fundamentals of adaptive grid movement p 185 N90-29610
- Purdue Univ., Indianapolis, IN.**
- A block-based algorithm for the solution of compressible flows in rotor-stator combinations p 9 A90-46905
- Purdue Univ., West Lafayette, IN.**
- The unsteady aerodynamics of an oscillating cascade in a compressible flow field p 2 A90-11789
- Aeroelastic detuning for stability enhancement of unstalled supersonic flutter p 19 A90-17462
- Investigation of turbulent transport in an axisymmetric sudden expansion p 163 A90-23112
- Propeller-wing interaction using a frequency domain panel method p 6 A90-26128
- Three dimensional full potential method for the aerocoustic modeling of propfans [AIAA PAPER 90-1120] p 7 A90-29392
- Cooperative synthesis of control and display augmentation in approach and landing p 36 A90-33061
- Counter-rotating propellant analysis using a frequency domain panel method p 7 A90-40937
- Application of large eddy interaction model to a mixing layer [NASA-CR-185123] p 11 N90-13328
- WINCOF-I code for prediction of fan compressor unit with water ingestion [NASA-CR-185157] p 1 N90-21724
- Saturated fluorescence measurements of the hydroxyl radical in laminar high-pressure flames [NASA-CR-185218] p 190 N90-22022
- An unsteady lifting surface method for single rotation propellers [NASA-CR-4302] p 14 N90-25940

R

- Rensselaer Polytechnic Inst., Troy, NY.**
- Shaft flexibility effects on aeroelastic stability of a rotating bladed disk p 208 A90-16371
- Effects of crystal-melt interfacial energy anisotropy on dendritic morphology and growth kinetics p 253 A90-19284
- Free dendritic growth in viscous melts - Cyclohexanol p 253 A90-19285
- Evaluation of transport conditions during physical vapor transport growth of opto-electronic crystals p 132 A90-20525
- Flight software development for the isothermal dendritic growth experiment [AIAA PAPER 90-0744] p 235 A90-22257
- Blade mistuning coupled with shaft flexibility effects in rotor aeroelasticity [ASME PAPER 89-GT-330] p 19 A90-23896
- Nature of convection-stabilized dc arcs in dual-flow nozzle geometry. I - The cold flow field and dc arc characteristics. II - Optical diagnostics and theory p 252 A90-26665
- Shaft flexibility effects on the forced response of a bladed-disk assembly p 21 A90-43218
- Rensselaer Polytechnic Inst. of Connecticut, Inc., East Windsor Hill.**
- Determination of the mean solid-liquid interface energy of pivalic acid p 84 A90-22646
- Research Inst. of Industrial Science and Technology, Pohang (Republic of Korea).**
- Mass spectrometric observations of metal oxychlorides produced by oxidation-chlorination reactions p 103 A90-21215
- Research Triangle Inst., Research Triangle Park, NC.**
- The impedance of a tubular electrode - A model for a porous electrode p 104 A90-33723
- Ricardo-ITI, Westmont, IL.**
- A rotating hot-wire technique for spatial sampling of disturbed and manipulated duct flows p 186 A90-41120
- Rice Univ., Houston, TX.**
- On the stability of the creep substructure in NaCl single crystals p 254 A90-21920
- Creep substructure formation in sodium chloride single crystals in the power law and exponential creep regimes p 255 A90-33330
- Rocket Research Corp., Redmond, WA.**
- Qualification and life testing of a flight design hydrazine arcjet system [AIAA PAPER 90-2576] p 64 A90-42559
- Arcjet thruster research and technology. Phase 1: Executive summary [NASA-CR-182106] p 72 N90-14278

Rockwell International Corp., Canoga Park, CA.

- Space Station Solar Dynamic Module modelling and simulation p 53 A90-11993
- Effects of pressure on microgravity hydrocarbon diffusion flames [AIAA PAPER 90-0651] p 104 A90-25039
- Structural configuration options for the Space Station Freedom solar dynamic radiator [IAF PAPER ICOSP89-4-5] p 48 A90-27710
- Space Station Freedom electric power system photovoltaic power module integrated launch package [AIAA PAPER 90-1053] p 48 A90-29281
- Design of the Space Station Freedom power system p 57 A90-38070
- Photovoltaic module on-orbit assembly for Space Station Freedom p 45 A90-38071
- Evolutionary growth for Space Station Freedom electrical power system p 58 A90-38072
- Space Station Freedom photovoltaic power module design status p 58 A90-38075
- Energy storage and thermal control system design status p 59 A90-38077
- Launch packaging options for the PV power module cargo element p 45 A90-38078
- Solar dynamic power module design p 59 A90-38079
- Space Station Freedom power management and distribution design status p 59 A90-38080
- Development and refinement of test bed simulations p 59 A90-38081
- SP-100 advanced radiator designs for thermoelectric and Stirling applications p 62 A90-38202
- Enhanced heat transfer rocket combustor technology component hot-fire test results [AIAA PAPER 90-2182] p 64 A90-42063
- Determination of the durability of the fiberoptics in rocket engine environments [AIAA PAPER 90-2229] p 250 A90-42754
- LOX/hydrocarbon combustion instability investigation [NASA-CR-182249] p 71 N90-13589
- The Gevaltig: An inertial fusion powered manned spacecraft design for outer solar system missions [NASA-CR-185163] p 50 N90-15985
- Health management system for rocket engines [NASA-CR-185223] p 131 N90-23574
- Reusable rocket engine turbopump health monitoring system, part 3 [NASA-CR-182294] p 204 N90-26320
- Oxygen/methane combustion stability investigation p 107 N90-28628
- Integrated controls and health monitoring fiberoptic shaft monitor [NASA-CR-185210] p 191 N90-29622

S

- Sanders Associates, Inc., Nashua, NH.**
- The cavity heat pipe Stirling receiver for space solar dynamics p 61 A90-38169
- Sandia National Labs., Albuquerque, NM.**
- Rapid thermal processing of high temperature superconducting fiber [NASA-CR-186803] p 259 N90-24964
- Sandia National Labs., Livermore, CA.**
- Combustion interaction with radiation-cooled chambers [AIAA PAPER 90-2121] p 64 A90-42030
- Santa Clara Univ., CA.**
- A 'transient' automated mapping procedure for complex geometries p 242 A90-26499
- Science Applications International Corp., Albuquerque, NM.**
- SPRITE - A computer code for the optimization of space based heat pipe radiator systems p 170 A90-38036
- Science Applications International Corp., Torrance, CA.**
- Ignition and behavior of laminar gas-jet diffusion flames in microgravity p 103 A90-23107
- Effects of pressure on microgravity hydrocarbon diffusion flames [AIAA PAPER 90-0651] p 104 A90-25039
- Scientific Research Associates, Inc., Glastonbury, CT.**
- Reciprocal interactions of hairpin-shaped vortices and a boundary layer [AIAA PAPER 90-0017] p 159 A90-19635
- User's manual for PEP SIG NASA tip vortex version [NASA-CR-182178] p 10 N90-10835
- Computation of the tip vortex flowfield for advanced aircraft propellers [NASA-CR-182179] p 10 N90-10836
- SDRC, Inc., San Diego, CA.**
- Modal selection in structural dynamics p 209 A90-17001
- Selection of component modes [AIAA PAPER 90-1201] p 210 A90-26787

Sealco, Inc., Providence, RI.

- A simplified model for two phase face seal design
p 197 A90-40713

SOL-3 Resources, Inc., Reading, MA.

- Introducing the VRT gas turbine combustor
[AIAA PAPER 90-2452] p 21 A90-42808

Sony Magnetic Products, Inc., Miyagi (Japan).

- Measurement of the intrinsic bond strength of brittle thin films on flexible substrates p 256 A90-44022

Southern Methodist Univ., Dallas, TX.

- A 'transient' automated mapping procedure for complex geometries p 242 A90-26499

Southwest Research Inst., San Antonio, TX.

- High temperature inelastic deformation under uniaxial loading - Theory and experiment p 109 A90-13838
High temperature inelastic deformation of the B1900 + Hf alloy under multiaxial loading - Theory and experiment p 112 A90-22656
Inelastic deformation under nonisothermal loading p 112 A90-22657

- Application of the probabilistic approximate analysis method to a turbopump blade analysis
[AIAA PAPER 90-1098] p 56 A90-29328

- Probabilistic analysis of a materially nonlinear structure
[AIAA PAPER 90-1099] p 211 A90-29329

- Computational methods for probability of instability calculations
[AIAA PAPER 90-1139] p 236 A90-29333

- Spray automated balancing of rotors - How process parameters influence performance p 198 A90-46228
Advanced probabilistic structural analysis method for implicit performance functions p 214 A90-49792

- Sliding seal materials for low heat rejection engines
[NASA-CR-182262] p 125 N90-11882

- Constitutive modeling for isotropic materials (HOST)
[NASA-CR-179522] p 26 N90-13390

- Constitutive modeling for isotropic materials (HOST)
[NASA-CR-174718] p 26 N90-13391

Space Power, Inc., San Jose, CA.

- Advanced radiator concepts p 170 A90-38042

Special Libraries Association, Chicago, IL.

- Cross-cross directory of NASA N numbers and DOD AD numbers. Volume 2, part 1: AD to N, 1979-1986. N to AD, 1962-1986 p 262 N90-12388

- Cross-cross directory of NASA N numbers and DOD AD numbers. Volume 2, part 2: AD to N, 1979-1986. N to AD, 1962-1986 p 262 N90-12389

Spectrolab, Inc., Sylmar, CA.

- High efficiency GaAs/Ge monolithic tandem solar cells p 224 A90-14858

- InP homojunction solar cell performance on the LIPS III flight experiment p 226 A90-14921

- Optimization of silicon 8 cm x 8 cm wrapthrough Space Station cells for 'on orbit' operation p 54 A90-14941

Spire Corp., Bedford, MA.

- High efficiency GaAs/Ge monolithic tandem solar cells p 224 A90-14858

- Wide-bandgap epitaxial heterojunction windows for silicon solar cells p 227 A90-28359

Stanford Univ., CA.

- Computer modeling of current collection by the CHARGE-2 mother payload p 252 A90-24933

- The sheath structure around a negatively charged rocket payload p 48 A90-34780

- Time-dependent calculation of a forced mixing layer using a k-epsilon turbulence model p 169 A90-35222

- Effects of very high turbulence on heat transfer p 169 A90-35247

- Minimum fuel trajectories for a low-thrust power-limited mission to the moon and to Lagrange points L4 and L5
[AAS PAPER 89-351] p 40 A90-46784

- Minimum fuel trajectory for the aerospace-plane
[AAS PAPER 89-352] p 40 A90-46785

- Minimum fuel lunar trajectories for a low-thrust power-limited spacecraft
[AIAA PAPER 90-2975] p 41 A90-53054

- State Univ. of New York, Buffalo.

- Development of an integrated BEM for hot fluid-structure interaction
[ASME PAPER 89-GT-128] p 212 A90-32264

- A brief survey of radiation effects on polymer dielectrics p 123 A90-43119

- Advanced applications of BEM to inelastic analysis of solids p 213 A90-45770

- Advanced development of BEM for elastic and inelastic dynamic analysis of solids p 213 A90-45771

- Inelastic transient dynamic analysis of three-dimensional problems by BEM p 215 A90-51480

- Free-vibration analysis of three-dimensional solids by BEM p 215 A90-52007

- Reliability analysis of continuous fiber composite laminates p 223 N90-26372

- [NASA-CR-185265]

State Univ. of New York, Stony Brook.

- Fiber optic detector probes for laser light scattering p 192 A90-11593

- Consistency and convergence for numerical radiation conditions
[NASA-TM-103262] p 244 A90-29124

State Univ. of New York at Buffalo, Amherst.

- Model-free simulations of turbulent reactive flows p 158 A90-15729

Stuttgart Univ. (Germany, F.R.).

- Preliminary plume characteristics of an arcjet thruster
[AIAA PAPER 90-2645] p 64 A90-42609

Sundstrand Corp., Rockford, IL.

- Brayton advanced heat receiver development program p 61 A90-38170

Sverdrup Technology, Inc., Brook Park, OH.

- Probabilistic analysis of bladed turbine disks and the effect of mistuning
[AIAA PAPER 90-1097] p 196 A90-29327

- Preliminary design of a long-endurance Mars aircraft
[AIAA PAPER 90-2000] p 43 A90-40587

- A candidate architecture for monitoring and control in chemical transfer propulsion systems
[AIAA PAPER 90-1882] p 52 A90-41980

- Preliminary plume characteristics of an arcjet thruster
[AIAA PAPER 90-2645] p 64 A90-42609

- Analysis of internal flow in a ventral nozzle for STOVL aircraft
[AIAA PAPER 90-1899] p 21 A90-42688

- Computational analysis of the flowfield of a two-dimensional ejector nozzle
[AIAA PAPER 90-1901] p 21 A90-42690

- Fuel-rich catalytic combustion - A fuel processor for high-speed propulsion
[AIAA PAPER 90-2319] p 105 A90-42774

- Humidity-induced room-temperature decomposition of Au contacted indium phosphide p 105 A90-44689

- Rocket engine failure detection using system identification techniques
[AIAA PAPER 90-1993] p 65 A90-47205

- Three-dimensional compressible jet-in-crossflow calculations using improved viscosity models and adapted grid
[AIAA PAPER 90-2100] p 174 A90-47206

- Rocket combustion chamber life-enhancing design concepts
[AIAA PAPER 90-2116] p 66 A90-47208

- Aeroelastic stability analysis of a high-energy turbine blade
[AIAA PAPER 90-2351] p 66 A90-47215

- Unsteady blade surface pressures on a large-scale advanced propeller - Prediction and data
[AIAA PAPER 90-2402] p 9 A90-47220

- Low thrust rocket test facility
[AIAA PAPER 90-2503] p 43 A90-47225

- Advanced tube-bundle rocket thrust chamber
[AIAA PAPER 90-2726] p 67 A90-47227

- Integrated controls and health monitoring for chemical transfer propulsion
[AIAA PAPER 90-2751] p 52 A90-47229

- Experimental investigation of multi-element airfoil ice accretion and resulting performance degradation
p 9 A90-48954

- Mars in situ propellants - Carbon monoxide and oxygen ignition experiments
[AIAA PAPER 90-1894] p 130 A90-50642

- Multi-sensor analysis techniques for SSME safety monitoring
[AIAA PAPER 90-1990] p 45 A90-52499

- Multimegawatt electric propulsion system design considerations
[AIAA PAPER 90-2552] p 68 A90-52566

- Requirements for long-life operation of inert gas hollow cathodes - Preliminary results
[AIAA PAPER 90-2586] p 69 A90-52570

- Geometric effects in applied-field MPD thrusters
[AIAA PAPER 90-2669] p 69 A90-52572

- Preliminary design of a long-endurance Mars aircraft
[NASA-CR-185243] p 30 N90-21763

- Computational analysis of the flowfield of a two-dimensional ejector nozzle
[NASA-CR-185255] p 31 N90-23406

- Rocket engine failure detection using system identification techniques
[NASA-CR-185259] p 45 N90-25159

- Rocket combustion chamber life-enhancing design concepts
[NASA-CR-185257] p 79 N90-25183

- Feasibility study for the advanced one-dimensional high temperature optical strain measurement system, phase 3
[NASA-CR-185254] p 191 N90-25324

- A resistance strain gage with repeatable and cancellable apparent strain for use to 800 C
[NASA-CR-185256] p 53 N90-26063

- Transient characteristics of a grooved water heat pipe with variable heat load
[NASA-CR-185280] p 183 N90-26272

- Multi-sensor analysis techniques for SSME safety monitoring
[NASA-CR-185260] p 45 N90-27732

- High energy-density liquid rocket fuel performance
[NASA-CR-185279] p 131 N90-28742

Sverdrup Technology, Inc., Eglin AFB, FL.

- Aerodynamic optimization by simultaneously updating flow variables and design parameters p 18 N90-20991

Sverdrup Technology, Inc., Cleveland, OH.

- Time-dependent viscous incompressible Navier-Stokes equations - The finite difference Galerkin formulation and streamfunction algorithms p 156 A90-11598

- Numerical modeling of enclosure convection
[IAF PAPER 89-403] p 157 A90-13511

- Nonlinear evolution of oblique waves on compressible shear layers p 158 A90-15942

- A nonoscillatory, characteristically convected, finite volume scheme for multidimensional convection problems
[AIAA PAPER 90-0015] p 159 A90-19633

- Convergence acceleration for vector sequences and applications to computational fluid dynamics
[AIAA PAPER 90-0338] p 160 A90-19804

- An interactive grid generation procedure for axial and radial flow turbomachinery
[AIAA PAPER 90-0344] p 162 A90-22200

- Analysis of rotary engine combustion processes based on unsteady, three-dimensional computations
[AIAA PAPER 90-0643] p 163 A90-22237

- Diagonal inversion of lower-upper implicit schemes p 242 A90-23110

- Numerical analysis of natural convection in liquid droplets by phase change p 164 A90-23212

- Hypersonic aerospace sizing analysis for the preliminary design of aerospace vehicles p 17 A90-23276

- Application of a lower-upper implicit scheme and an interactive grid generation for turbomachinery flow field simulations
[ASME PAPER 89-GT-20] p 4 A90-23762

- Simulation of three-dimensional viscous flow within a multistage turbine
[ASME PAPER 89-GT-152] p 5 A90-23841

- Oxidation of high-temperature intermetallics; Proceedings of the Workshop, Cleveland, OH, Sept. 22, 23, 1988 p 112 A90-24852

- Influence of alloying elements on the oxidation behavior of NbAl3 p 113 A90-24861

- A new mixing length model for supersonic shear layers
[AIAA PAPER 90-0018] p 166 A90-25026

- Unsteady Euler analysis of the flowfield of a propan at an angle of attack
[AIAA PAPER 90-0339] p 5 A90-25028

- The Osher scheme for real gases
[AIAA PAPER 90-0397] p 166 A90-25030

- The kinetics of the Au-InP interaction p 254 A90-25084

- Identification of thermodynamically stable ceramic reinforcement materials for iron aluminate matrices p 89 A90-25238

- Splitting of inviscid fluxes for real gases p 167 A90-25451

- Effects of amplitude distortions and IF equalization on satellite communication system bit-error rate performance
[AIAA PAPER 90-0878] p 140 A90-25697

- Comparative study of computational efficiency of two LU schemes for non-equilibrium reacting flows
[AIAA PAPER 90-0396] p 167 A90-26940

- Comparison of 3-D viscous flow computations of Mach 5 inlet with experimental data
[AIAA PAPER 90-0600] p 6 A90-26970

- A methodology for evaluating the reliability and risk of structures under complex service environments
[AIAA PAPER 90-1102] p 211 A90-29332

- Equilibrium statistical thermodynamics of a many-particle system coupled to an external scalar field p 261 A90-31670

- Numerical analysis of three-dimensional viscous internal flows p 168 A90-32456

- Cooperative synthesis of control and display augmentation in approach and landing p 36 A90-33061

- Analysis of airframe/engine interactions - An integrated control perspective
[AIAA PAPER 90-1918] p 36 A90-40557

- Multigrid calculations of 3-D turbulent viscous flows p 172 A90-42426

- A brief survey of radiation effects on polymer dielectrics p 123 A90-43119

- Thermodynamic analysis of chemical compatibility of ceramic reinforcement materials with niobium aluminides p 92 A90-44001
- Nonlinear Reynolds stress models and the renormalization group p 172 A90-44011
- Metallographic techniques for evaluation of thermal barrier coatings p 85 A90-44869
- Thermal effects on the mechanical properties of SiC fibre reinforced reaction-bonded silicon nitride matrix composites p 92 A90-46999
- High energy-density liquid rocket fuel performance [AIAA PAPER 90-1968] p 130 A90-47204
- Numerical analysis of secondary flow in a two-stage turbine [AIAA PAPER 90-2356] p 66 A90-47216
- Calculations of gaseous H₂/O₂ thruster [AIAA PAPER 90-2490] p 67 A90-47224
- H-infinity based integrated flight/propulsion control design for a STOL aircraft in transition flight [AIAA PAPER 90-3335] p 36 A90-47595
- Contact spreading and the Au₃In-to-Au₉In₄ transition in the Au-In-P system p 257 A90-48661
- Diagonally inverted lower-upper factored implicit multigrid scheme for the three-dimensional Navier-Stokes equations p 174 A90-49789
- Parametric studies to determine the effect of compliant layers on metal matrix composite systems p 93 A90-50093
- Compatibility of Fe-40Al with various fibers p 94 A90-50496
- Inviscid flux-splitting algorithms for real gases with non-equilibrium chemistry p 174 A90-52275
- 5kW xenon ion thruster lifetest [AIAA PAPER 90-2543] p 68 A90-52564
- Performance characterization of a segmented anode arcjet thruster [AIAA PAPER 90-2582] p 68 A90-52569
- A supersonic through-flow fan engine airframe integration study [NASA-CR-185140] p 10 N90-10004
- Hydrogen-silicon carbide interactions [NASA-TM-102382] p 125 N90-11144
- A nonoscillatory, characteristically convected, finite volume scheme for multidimensional convection problems [NASA-TM-102354] p 242 N90-11497
- Droplet sizing instrumentation used for icing research: Operation, calibration, and accuracy [NASA-CR-182293] p 187 N90-11999
- Multigrid calculations of 3-D turbulent viscous flows [NASA-CR-185154] p 1 N90-13323
- An improved algorithm for the modeling of vapor flow in heat pipes [NASA-CR-185179] p 176 N90-13748
- Development and characterization of PdCr temperature-compensated wire resistance strain gage [NASA-CR-185153] p 188 N90-13761
- An interactive grid generation procedure for axial and radial flow turbomachinery [NASA-CR-185167] p 237 N90-13968
- Thermocapillary migration of liquid droplets in a temperature gradient in a density matched system [NASA-CR-185178] p 177 N90-14512
- User's guide to PMESH: A grid-generation program for single-rotation and counterrotation advanced turboprops [NASA-CR-185156] p 235 N90-14783
- Thermodynamic analysis of chemical stability of ceramic materials in hydrogen-containing atmospheres at high temperatures [NASA-CR-4271] p 126 N90-16072
- Viscous three-dimensional analyses for nozzles for hypersonic propulsion [NASA-CR-185197] p 27 N90-17635
- Users manual for the NASA Lewis Ice Accretion Prediction Code (LEWICE) [NASA-CR-185129] p 1 N90-20943
- Exhaust nozzles for propulsion systems with emphasis on supersonic cruise aircraft [NASA-RP-1235] p 29 N90-21037
- Thermomechanical deformation testing and modeling in the presence of metallurgical instabilities [NASA-CR-185188] p 219 N90-21420
- Hypercluster parallel processing library user's manual [NASA-CR-185231] p 237 N90-21552
- Microgravity acoustic mixing for particle cloud combustors [NASA-CR-185159] p 248 N90-21600
- Autonomous power expert system [NASA-CR-185263] p 80 N90-25187
- Sverdrup Technology, Inc., Mayfield, OH.**
- Microstructure of a SiC/Ti-15-3 composite p 91 A90-37663
- Complex permittivity of lanthanum aluminate in the 20 to 300 K temperature range from 26.5 to 40.0 GHz p 148 A90-37864
- Distortion and regulation characterization of a Mapham inverter p 148 A90-38125
- Two-tiered design analysis of a radiator for a solar dynamic powered Stirling engine p 60 A90-38158
- A program for advancing the technology of space concentrators p 60 A90-38159
- Results from baseline tests of the SPRE I and comparison with code model predictions p 62 A90-38249
- Sverdrup Technology, Inc., Middleburg Heights, OH.**
- Contact formation in gallium arsenide solar cells p 225 A90-14888
- Investigation of interfacial shear strength in a SiC fibre/Ti-24Al-11Nb composite by a fibre push-out technique p 88 A90-18973
- The oxidation of Ni-rich Ni-Al intermetallics p 112 A90-24855
- Three-dimensional adaptive grid generation for body-fitted coordinate system p 187 A90-26506
- Evaluation of atomic oxygen resistant protective coatings for fiberglass-epoxy composites in LEO p 84 A90-31581
- Characterization of interfacial failure in SiC reinforced Si₃N₄ matrix composite material by both fiber push-out testing and Auger electron spectroscopy p 91 A90-36802
- Development of Ada language control software for the NASA power management and distribution test bed p 236 A90-38082
- Frequency domain model for analysis of paralleled, series-output-connected Mapham inverters p 148 A90-38084
- Development and testing of a 20 kHz component test bed p 43 A90-38126
- On the dynamic response of pressure transmission lines in the research of helium-charged free piston Stirling engines p 196 A90-38248
- Test and theory for piezoelectric actuator-active vibration control of rotating machinery p 198 A90-46226
- Syracuse Univ., NY.**
- The equivalence between dislocation pile-ups and cracks p 210 A90-29215
- System Planning Corp., Arlington, VA.**
- Design for steering accuracy in antenna arrays using shared optical phase shifters p 138 A90-13935
- Systems Control Technology, Inc., Palo Alto, CA.**
- Flight control design considerations for STOL powered-lift flight [AIAA PAPER 90-3225] p 37 A90-49110
- Systems Science and Software, La Jolla, CA.**
- A Van der Waals-like theory of plasma double layers p 251 A90-10725
- High-voltage plasma interactions calculations using NASCAP/LEO [AIAA PAPER 90-0725] p 251 A90-22254
- Plasma contactor modeling with NASCAP/LEO - Extending laboratory results to space systems [AIAA PAPER 90-0726] p 251 A90-22255
- Plasma sources for spacecraft neutralization [AIAA PAPER 90-1556] p 49 A90-38697
- T**
- Tankley (W. L.) and Associates, Inc., Cleveland, OH.**
- Designing ceramic components with the CARES computer program p 235 A90-19147
- Calculation of Weibull strength parameters and Batdorf flow-density constants for volume- and surface-flaw-induced fracture in ceramics p 212 A90-35462
- Technion - Israel Inst. of Tech., Haifa.**
- High temperature inelastic deformation under uniaxial loading - Theory and experiment p 109 A90-13838
- High temperature inelastic deformation of the B1900 + Hf alloy under multiaxial loading - Theory and experiment p 112 A90-22656
- Interface properties of various passivations of HgCdTe p 251 A90-45947
- Contribution of the graded region of a HgCdTe diode to its saturation current p 257 A90-45948
- Performance analysis of Integrated Communication and Control System networks p 239 A90-51267
- Quotient-difference type generalizations of the power method and their analysis [NASA-TM-102361] p 242 N90-10635
- Technische Univ., Munich (Germany, F.R.).**
- Actuator design for rotor control p 198 A90-46232
- Teledyne Brown Engineering, Huntsville, AL.**
- User needs, benefits, and integration of robotic systems in a space station laboratory [NASA-CR-185150] p 200 N90-13794
- Temple Univ., Philadelphia, PA.**
- On the mathematical modeling of the Reynolds stress's equations [AIAA PAPER 90-0498] p 161 A90-19878
- Tennessee Univ., Tullahoma.**
- Influence of bulk turbulence and entrance boundary layer thickness on the curved duct flow field [AIAA PAPER 90-1502] p 171 A90-38651
- Tennessee Univ. Space Inst., Tullahoma.**
- Numerical modeling of an arcjet thruster [AIAA PAPER 90-2614] p 64 A90-42587
- Texas A&M Univ., College Station.**
- Augmented heat transfer in rectangular channels of narrow aspect ratios with rib turbulators p 157 A90-13091
- Performance and acoustic prediction of counterrotating propeller configurations [SAE PAPER 891035] p 246 A90-14342
- Application of the computational aeroacoustics method to an advanced counterrotating propeller configuration [AIAA PAPER 90-0183] p 246 A90-19725
- Measurements of dynamic Young's modulus in short specimens with the PUCOT p 112 A90-21174
- Pressure drop and mass transfer in two-pass ribbed channels p 165 A90-24837
- A study of ice shape prediction methodologies and comparison with experimental data [AIAA PAPER 90-0753] p 15 A90-26986
- An annular gas seal analysis using empirical entrance and exit region friction factors [ASME PAPER 89-TRIB-46] p 196 A90-33555
- Test and theory for piezoelectric actuator-active vibration control of rotating machinery p 198 A90-46226
- Vibration dampers for cryogenic turbomachinery [AIAA PAPER 90-2740] p 199 A90-47228
- An approximate model for the performance and acoustic predictions of counterrotating propeller configurations [NASA-CR-180667] p 248 N90-18228
- A radiological assessment of nuclear power and propulsion operations near Space Station Freedom [NASA-CR-185185] p 76 N90-21108
- Texas Instruments, Inc., Dallas.**
- AlGaAs/InGaAs heterostructures with doped channels for discrete devices and monolithic amplifiers p 146 A90-20861
- Doped-channel heterojunction structures for millimeter-wave discrete devices and MMICs p 150 A90-48492
- Texas Univ., Austin.**
- On physical optics for calculating scattering from coated bodies p 250 A90-20151
- Big bang nucleosynthesis and the quark-hadron transition p 265 A90-31407
- A model for the distribution of the intergalactic medium p 265 A90-34505
- A model for the distribution of dark matter, galaxies, and the intergalactic medium in a cold dark matter-dominated universe p 266 A90-45560
- Least-squares finite element methods for compressible Euler equations p 9 A90-51013
- An investigation into the numerical prediction of boundary layer transition using the K.Y. Chien turbulence model [NASA-CR-185252] p 182 N90-26269
- Textron Lycoming, Stratford, CT.**
- Introducing the VRT gas turbine combustor [AIAA PAPER 90-2452] p 21 A90-42808
- Thermo Electron Corp., Waltham, MA.**
- Effect of Ga and P dopants on the thermoelectric properties of n-type SiGe p 256 A90-38140
- Tokyo Univ. (Japan).**
- The sheath structure around a negatively charged rocket payload p 48 A90-34780
- Soft inflation p 265 A90-40093
- Toledo Univ., OH.**
- Application of an efficient hybrid scheme for aeroelastic analysis of advanced propellers [AIAA PAPER 90-0028] p 4 A90-22153
- Convective heat transfer measurements from a NACA 0012 airfoil in flight and in the NASA Lewis Icing Research Tunnel [AIAA PAPER 90-0199] p 162 A90-22180
- Encoding Y,I,Q component estimates of an NTSC composite signal p 139 A90-23261
- A numerical simulation of the flow in the diffuser of the NASA Lewis Icing Research Tunnel [AIAA PAPER 90-0488] p 166 A90-25034
- A parallel pipelined architecture for a digital multicarrier demodulator [AIAA PAPER 90-0812] p 46 A90-25635
- Time domain flutter analysis of cascades using a full-potential solver [AIAA PAPER 90-0984] p 6 A90-29374
- Concurrent processing adaptation of aeroelastic analysis of propfans [AIAA PAPER 90-1036] p 211 A90-29380
- A 2.5 kW cascaded Schwarz converter for 20 kHz power distribution p 147 A90-36913

CORPORATE SOURCE

Experimental study of the cross-polarization characteristics of rectangular microstrip antennas p 141 A90-37312

A general model for memory interference in a multiprocessor system with memory hierarchy p 238 A90-37482

Numerical simulation of rarefied gas flow through a slit [AIAA PAPER 90-1694] p 170 A90-38397

Microstrip subarray with coplanar and stacked parasitic elements p 141 A90-41586

Numerical studies of convective heat transfer in an inclined semi-annular enclosure p 173 A90-45317

Analysis and design of optimized truncated scarf nozzles subject to external flow effects [AIAA PAPER 90-2222] p 9 A90-47213

An LDA investigation of the normal shock wave boundary layer interaction p 10 A90-52618

Electrical performance characteristics of high power converters for space power applications p 72 N90-14279

Heat transfer measurements from a NACA 0012 airfoil in flight and in the NASA Lewis icing research tunnel [NASA-CR-4278] p 13 N90-19203

A comparative study of electric power distribution systems for spacecraft [NASA-CR-186531] p 77 N90-21113

Application of finite-element-based solution technologies for viscoplastic structural analyses [NASA-CR-185196] p 221 N90-23757

Finite element analysis of structural components using viscoplastic models with application to a cowl lip problem [NASA-CR-185189] p 221 N90-23769

Multiprocessor architecture: Synthesis and evaluation [NASA-CR-186618] p 235 N90-25579

Modeling and synthesis of multicomputer interconnection networks [NASA-CR-186619] p 238 N90-25604

Computer architecture evaluation for structural dynamics computations: Project summary [NASA-CR-186137] p 235 N90-26512

TRW, Inc., Redondo Beach, CA.
Solar dynamic power for the Space Station p 55 A90-16374

EPSAT - A workbench for designing high-power systems for the space environment [AIAA PAPER 90-0637] p 245 A90-26975

The Environment-Power System Analysis Tool development program p 236 A90-38089

Power transmission cable development for the Space Station Freedom electrical power system p 149 A90-38134

TRW Defense and Space Systems Group, Redondo Beach, CA.
Generalized Advanced Propeller Analysis System (GAPAS). Volume 2: Computer program user manual [NASA-CR-185277] p 36 N90-29394

TRW Space Technology Labs., Redondo Beach, CA.
Conceptual definition of a high voltage power supply test facility [NASA-CR-185216] p 50 N90-25172

Tulane Univ., New Orleans, LA.
Crack-path effect on material toughness [ASME PAPER 89-WA/APM-43] p 210 A90-28755

Mechanics of the crack path formation [NASA-CR-185143] p 215 N90-10455

Micromechanical model of crack growth in fiber reinforced ceramics p 224 N90-28113

U

Ultramet, Pacolma, CA.
Iridium-coated rhenium thrusters by CVD p 114 A90-30480

United Technologies Corp., East Hartford, CT.
Mechanisms of degradation and failure in a plasma deposited thermal barrier coating [ASME PAPER 89-GT-132] p 84 A90-23830

Free-vibration analysis of three-dimensional solids by BEM p 215 A90-52007

United Technologies Corp., Windsor Locks, CT.
Investigation of the near wake of a propfan p 7 A90-40686

Health monitoring system for the SSME - Hardware architecture study [AIAA PAPER 90-1989] p 65 A90-42713

United Technologies Research Center, East Hartford, CT.
Calculation of unsteady Euler flows in turbomachinery using the linearized Euler equations p 2 A90-11778

Simulation of three-dimensional viscous flow within a multistage turbine [ASME PAPER 89-GT-152] p 5 A90-23841

Influence of molybdenum on the creep properties of nickel-base superalloy single crystals p 113 A90-25233

Health monitoring system for the SSME - Program overview [AIAA PAPER 90-1987] p 63 A90-40583

Health Monitoring System for the SSME-fault detection algorithms [AIAA PAPER 90-1988] p 63 A90-40584

Investigation of the near wake of a propfan p 7 A90-40686

Health monitoring system for the SSME - Hardware architecture study [AIAA PAPER 90-1989] p 65 A90-42713

Laser velocimeter and total pressure measurements in circular-to-rectangular transition ducts [NASA-CR-182286] p 177 N90-14494

Gust response analysis for cascades operating in nonuniform mean flows p 28 N90-18415

Identification of a cast iron alloy containing nonstrategic elements [NASA-CR-185174] p 118 N90-18559

Framework for a space shuttle main engine health monitoring system [NASA-CR-185224] p 78 N90-21809

Development of a linearized unsteady aerodynamic analysis for cascade gust response predictions [NASA-CR-4308] p 14 N90-27655

University of South Florida, Tampa.
Reduced chemical kinetics for propane combustion [AIAA PAPER 90-0546] p 103 A90-19904

Critical evaluation of Jet-A spray combustion using propane chemical kinetics in gas turbine combustion simulated by KIVA-II [AIAA PAPER 90-2439] p 105 A90-50645

University of Southern California, Los Angeles.
The high temperature creep deformation of Si3N4-6Y2O3-2Al2O3 p 121 A90-18879

University of Southwest Jiaotong, Sichuan (China).
The equivalence between dislocation pile-ups and cracks p 210 A90-29215

Characterization of the tip field of a discrete dislocation pileup for the development of physically based micromechanics p 213 A90-43883

Utah State Univ., Logan.
Computer modeling of current collection by the CHARGE-2 mother payload p 252 A90-24933

A two-dimensional model of plasma expansion in the ionosphere p 233 A90-43609

Utah State Univ., Salt Lake City.
Equivalence of physically based statistical fracture theories for reliability analysis of ceramics in multiaxial loading p 123 A90-43580

Analysis of impact response in composite plates p 214 A90-47567

V

Valpey-Fisher Corp., Hopkinton, MA.
Measurements of dynamic Young's modulus in short specimens with the PUCOT p 112 A90-21174

Vermont Univ., Burlington.
A simplified model for two phase face seal design p 197 A90-40713

Virginia Polytechnic Inst. and State Univ., Blacksburg.
Impact damage development in damaged composite materials p 193 A90-18355

Role of the interfacial thermal barrier in the effective thermal diffusivity/conductivity of SiC-fiber-reinforced reaction-bonded silicon nitride p 89 A90-25268

An annular gas seal analysis using empirical entrance and exit region friction factors [ASME PAPER 89-TRIB-46] p 196 A90-33555

High-frequency ac power distribution in Space Station p 63 A90-39111

The growth and development of a turbulent junction vortex system p 173 A90-46902

Virginia Univ., Charlottesville.
AIRNET: A real-time communications network for aircraft [NASA-CR-186140] p 145 N90-24514

W

Waseda Univ., Tokyo (Japan).
Soft inflation p 265 A90-40093

Washington Univ., Saint Louis, MO.
Prediction of self-pressurization rate of cryogenic propellant tankage p 55 A90-21219

Washington Univ., Seattle.
Progress in direct numerical simulations of turbulent reacting flows p 157 A90-12836

Experimental investigation of turbulent flow through a circular-to-rectangular transition duct [AIAA PAPER 90-1505] p 171 A90-38654

Experimental investigation of flow about a strut-endwall configuration [AIAA PAPER 90-1541] p 171 A90-38685

Wayne State Univ., Detroit, MI.
Radiation resistance studies of amorphous silicon films p 227 A90-14952

Westinghouse Research and Development Center, Pittsburgh, PA.
Effects of crystal-melt interfacial energy anisotropy on dendritic morphology and growth kinetics p 253 A90-19284

Free dendritic growth in viscous melts - Cyclohexanol p 253 A90-19285

Evaluation of transport conditions during physical vapor transport growth of opto-electronic crystals p 132 A90-20525

Whittaker-Yardney Power Systems, Pawcatuck, CT.
Bipolar nickel-hydrogen battery development - A program review p 62 A90-38288

Wichita State Univ., KS.
Electro-impulse de-icing testing analysis and design [NASA-CR-4175] p 18 N90-10031

Wisconsin Univ., Madison.
Performance testing of a high frequency link converter for Space Station power distribution system p 148 A90-38128

High power density dc/dc converter: Selection of converter topology [NASA-CR-186129] p 151 N90-14467

Worcester Polytechnic Inst., MA.
Local and global accuracy estimates for boundary element analysis [AIAA PAPER 90-0930] p 211 A90-29324

Wright Research Development Center, Wright-Patterson AFB, OH.
Mathematical modeling and analysis of heat pipe start-up from the frozen state p 174 A90-48404

Wright State Univ., Dayton, OH.
Mathematical modeling and analysis of heat pipe start-up from the frozen state p 174 A90-48404

Wyle Labs., Inc., Huntsville, AL.
Advanced spacecraft fire safety: Proposed projects and program plan [NASA-CR-185147] p 49 N90-12645

Y

Yale Univ., New Haven, CT.
Side-wall gas 'creep' and 'thermal stress convection' in microgravity experiments on film growth by vapor transport p 158 A90-14086

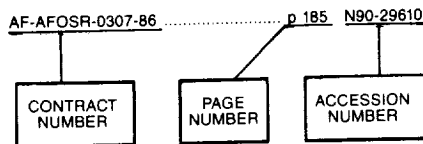
Yuan-Tze Memorial Coll. of Engineering (China).
Ground-based experiments on thermal and thermosolutal convection in inclined low-aspect-ratio enclosures [AIAA PAPER 90-0413] p 166 A90-25033

Z

Zurich Univ. (Switzerland).
A geometric analysis of semicircular canals and induced activity in their peripheral afferents in the rhesus monkey p 234 A90-28084

CONTRACT NUMBER INDEX

Typical Contract Number Index Listing



Listings in this index are arranged alphanumerically by contract number. Under each contract number the accession numbers denoting documents that have been produced as a result of research done under that contract are arranged in ascending order. The accession number denotes the number by which the citation is identified.

AF-AFOSR-0307-86 p 185 N90-29610
 AF-AFOSR-84-0315 p 133 A90-48720
 AF-AFOSR-86-0082 p 3 A90-18153
 AF-AFOSR-86-0307 p 237 A90-47188
 AF-AFOSR-87-0340 p 48 A90-36191
 AF-AFOSR-88-003 p 213 A90-41372
 AF-AFOSR-88-003 p 214 A90-49269
 AF-AFOSR-89-0033 p 170 A90-38614
 DA PROJ. 1L1-2211-A-47-A p 203 N90-21394
 DA PROJ. 1L1-61102-AH-45 p 175 N90-11256
 DA PROJ. 1L1-61102-AH-45 p 27 N90-13393
 DA PROJ. 1L1-61102-AH-45 p 200 N90-13786
 DA PROJ. 1L1-61102-AH-45 p 27 N90-15923
 DA PROJ. 1L1-61102-AH-45 p 178 N90-17076
 DA PROJ. 1L1-61102-AH-45 p 129 N90-23543
 DA PROJ. 1L1-61102-AH-45 p 204 N90-26338
 DA PROJ. 1L1-61102-AH-45 p 32 N90-27722
 DA PROJ. 1L1-61102-AH-45 p 241 N90-29121
 DA PROJ. 1L1-62209-A-47-A p 199 N90-12033
 DA PROJ. 1L1-62209-A-47-A p 201 N90-15434
 DA PROJ. 1L1-62209-A-47-A p 138 N90-26171
 DA PROJ. 1L1-62209-A-47-A p 205 N90-28060
 DA PROJ. 1L1-62209-AH-47-A p 203 N90-22054
 DA PROJ. 1L1-62209-AH-47-A p 202 N90-17147
 DA PROJ. 1L1-62209-AH-47-A p 202 N90-19593
 DA PROJ. 1L1-62209-AH-76 p 200 N90-13785
 DA PROJ. 1L1-62209-A4-7A p 200 N90-14617
 DA PROJ. 1L1-62209-A4-7A p 201 N90-16286
 DA PROJ. 1L1-62209-A4-7A p 202 N90-18041
 DA PROJ. 1L1-62209-A4-7A p 203 N90-22790
 DA PROJ. 1L1-62209-A47-A p 200 N90-13797
 DA PROJ. 1L1-62209-A47-A p 203 N90-21387
 DA PROJ. 1L1-62211-A-47-A p 205 N90-28065
 DA PROJ. 1L1-62211-A4-7A p 240 N90-23991
 DAAJ02-77-C-0031 p 94 A90-51920
 DDAJ02-77-C-0031 p 20 A90-32960
 DE-AB29-79ET-20370 p 206 N90-12034
 DE-AC02-76ER-03066 p 265 A90-40088
 DE-AC02-76ER-03066 p 266 A90-44095
 DE-AC02-80ER-10587 p 225 A90-14869
 DE-AC02-83CH-10093 p 225 A90-14893
 DE-AC02-83CH-10093 p 226 A90-14899
 DE-AC02-83CH-10093 p 256 A90-36799
 DE-AC02-83ER-40105 p 265 A90-30909
 DE-AC02-83ER-40105 p 265 A90-31407
 DE-AC02-84ER-80186 p 227 A90-28359
 DE-AC04-76DP-00789 p 249 N90-16496
 DE-AC04-76DP-00789 p 259 N90-24964
 DE-AC05-76OR-00033 p 121 A90-18879
 DE-AC05-84OR-21400 p 96 N90-15143
 DE-AC05-84OR-21400 p 229 N90-15506

DE-AI01-77CS-51040 p 129 N90-26132
 DE-AI01-85CE-50111 p 118 N90-18559
 DE-AI01-85CE-50112 p 22 N90-10036
 DE-AI01-85CE-50112 p 263 N90-11654
 DE-AI01-85CE-50112 p 264 N90-29260
 DE-AI01-85CE-50162 p 127 N90-16944
 DE-AI01-86CE-50162 p 125 N90-11882
 DE-AI01-86CE-50162 p 116 N90-11854
 DE-AI03-86SF-16310 p 126 N90-14368
 DE-AI05-87OR-21749 p 119 N90-23536
 DE-AT04-85AL-33408 p 263 N90-26729
 DE-FG02-85ER-45178 p 103 A90-21215
 DE-FG05-88ER-13839 p 159 A90-18071
 DEN3-282 p 118 N90-18559
 DEN3-329 p 196 A90-27091
 DEN3-329 p 263 N90-11654
 DEN3-329 p 264 N90-29260
 DEN3-329 p 195 A90-23814
 DEN3-329 p 206 A90-35508
 DEN3-329 p 122 A90-35509
 DEN3-329 p 197 A90-42165
 DEN3-329 p 263 N90-14153
 DEN3-329 p 263 N90-26728
 DEN3-336 p 22 N90-10036
 DEN3-352 p 125 N90-11882
 DLA900-83-C-1744 p 131 N90-19386
 DOT-MA91-85-C-50114 p 19 A90-12585
 DTFA03-83-A-00328 p 1 N90-21724
 FY1455-89-N-0655 p 82 N90-27784
 F08635-86-C-0039 p 186 A90-32853
 F08635-86-C-0039 p 172 A90-40930
 F19628-85-C-0002 p 141 A90-36717
 F19628-86-C-0056 p 252 A90-24933
 F33615-86-C-3615 p 36 A90-33061
 F33615-87-C-2790 p 158 A90-15729
 F33615-88-C-2820 p 174 A90-48404
 F49620-85-C-0027 p 6 A90-26967
 F49620-85-C-0027 p 8 A90-42734
 F49620-85-C-0067 p 157 A90-12836
 F49620-86-C-0028 p 158 A90-15729
 F49620-86-C-0109 p 159 A90-19635
 F49620-88-C-0022 p 233 A90-43609
 F49620-88-C-0022 p 162 A90-21424
 INTEL-SAT-INTEL-375 p 56 A90-27961
 MIPR-FY1455-89-N0655 p 151 N90-20301
 NAGW-1321 p 264 A90-17643
 NAGW-1340 p 264 A90-24671
 NAGW-1340 p 265 A90-30909
 NAGW-1340 p 265 A90-40088
 NAGW-1566 p 265 A90-40093
 NAGW-77 p 48 A90-34780
 NAGW-951 p 233 A90-43609
 NAGW-951 p 132 A90-22878
 NAGW-951 p 234 A90-38363
 NAG1-379 p 158 A90-13907
 NAG3-1000 p 257 N90-11603
 NAG3-1002 p 161 A90-19878
 NAG3-1004 p 187 A90-44485
 NAG3-1008 p 51 N90-25174
 NAG3-1011 p 158 A90-15729
 NAG3-1015 p 254 A90-24448
 NAG3-1026 p 21 A90-42766
 NAG3-1044 p 107 N90-26911
 NAG3-1046 p 105 A90-42298
 NAG3-1048 p 146 N90-26234
 NAG3-1086 p 210 A90-29260
 NAG3-108 p 153 N90-21952
 NAG3-1105 p 208 N90-28097
 NAG3-1105 p 208 N90-28858
 NAG3-1112 p 105 A90-50645
 NAG3-1138 p 41 A90-53037
 NAG3-1151 p 41 A90-53038
 NAG3-1159 p 187 A90-42755
 NAG3-122 p 64 A90-42587
 NAG3-140 p 156 A90-12636
 NAG3-159 p 14 N90-25934
 NAG3-159 p 245 A90-25638
 NAG3-159 p 46 A90-25639
 NAG3-159 p 245 N90-14856
 NAG3-166 p 197 A90-40713
 NAG3-172 p 193 A90-18355

NAG3-181 p 196 A90-33555
 NAG3-18 p 242 A90-26499
 NAG3-202 p 69 N90-10147
 NAG3-251 p 15 N90-28504
 NAG3-26 p 9 A90-46860
 NAG3-284 p 18 N90-10031
 NAG3-286 p 40 A90-46784
 NAG3-308 p 41 A90-53054
 NAG3-311 p 7 A90-29393
 NAG3-333 p 157 A90-13091
 NAG3-336 p 253 A90-19285
 NAG3-351 p 234 A90-28084
 NAG3-354 p 190 N90-22022
 NAG3-376 p 246 A90-14342
 NAG3-379 p 246 A90-19725
 NAG3-379 p 248 N90-18228
 NAG3-379 p 171 A90-38654
 NAG3-379 p 171 A90-38685
 NAG3-379 p 121 A90-41223
 NAG3-379 p 101 N90-25193
 NAG3-379 p 223 N90-28110
 NAG3-379 p 208 A90-18371
 NAG3-379 p 19 A90-23896
 NAG3-379 p 21 A90-43218
 NAG3-383 p 229 N90-13886
 NAG3-396 p 215 N90-11332
 NAG3-397 p 174 A90-51019
 NAG3-417 p 111 A90-20612
 NAG3-419 p 141 A90-45398
 NAG3-428 p 254 A90-21348
 NAG3-42 p 139 A90-23261
 NAG3-443 p 103 A90-22238
 NAG3-449 p 39 A90-23263
 NAG3-463 p 118 N90-21849
 NAG3-475 p 250 A90-20151
 NAG3-476 p 143 N90-16103
 NAG3-479 p 83 A90-15049
 NAG3-481 p 15 A90-19735
 NAG3-485 p 1 N90-21724
 NAG3-485 p 181 N90-22017
 NAG3-485 p 182 N90-23674
 NAG3-499 p 6 A90-26128
 NAG3-499 p 7 A90-29392
 NAG3-499 p 7 A90-40937
 NAG3-501 p 14 N90-25940
 NAG3-502 p 188 N90-14534
 NAG3-503 p 163 A90-23112
 NAG3-503 p 109 A90-11657
 NAG3-503 p 111 A90-20611
 NAG3-506 p 224 N90-28641
 NAG3-511 p 224 N90-28880
 NAG3-512 p 114 A90-28754
 NAG3-519 p 110 A90-16741
 NAG3-522 p 228 A90-33949
 NAG3-527 p 231 N90-20472
 NAG3-534 p 169 A90-35247
 NAG3-536 p 3 A90-18153
 NAG3-536 p 222 N90-24653
 NAG3-536 p 139 A90-13936
 NAG3-551 p 141 A90-36717
 NAG3-555 p 142 N90-11211
 NAG3-565 p 143 N90-12784
 NAG3-568 p 145 N90-20271
 NAG3-576 p 63 A90-39111
 NAG3-577 p 193 A90-21112
 NAG3-578 p 186 A90-41120
 NAG3-580 p 133 A90-48720
 NAG3-581 p 232 N90-25418
 NAG3-592 p 170 A90-38397
 NAG3-600 p 55 A90-21219
 NAG3-617 p 198 A90-46224
 NAG3-624 p 165 A90-23832
 NAG3-627 p 31 N90-23405
 NAG3-630 p 11 N90-13328
 NAG3-639 p 177 N90-15363
 NAG3-649 p 171 A90-38651
 NAG3-655 p 175 N90-12882
 NAG3-655 p 163 A90-22239
 NAG3-655 p 145 N90-24514
 NAG3-655 p 159 A90-18071
 NAG3-655 p 104 A90-33723
 NAG3-655 p 106 N90-19340
 NAG3-655 p 202 N90-19593

CONTRACT

CONTRACT NUMBER INDEX

D-2

CONTRACT NUMBER INDEX

NAS3-23940	p 214	A90-50562	NAS3-25209	p 62	A90-38202	NAS3-25653	p 186	A90-26978
	p 222	N90-26355	NAS3-25210	p 170	A90-38036	NAS3-25787	p 116	A90-51298
NAS3-23944	p 84	A90-23830	NAS3-25266	p 162	A90-22200	NAS3-25799	p 152	N90-21272
	p 26	N90-13388		p 166	A90-25026	NAS3-25836	p 17	A90-20012
NAS3-24080	p 247	N90-11549		p 166	A90-25030	NAS3-25867	p 260	N90-26683
	p 18	N90-23393		p 254	A90-25084	NAS3-25876	p 259	N90-24964
NAS3-24105	p 17	A90-23276		p 140	A90-25697	NAS3-25917	p 241	N90-26581
	p 167	A90-26506		p 6	A90-26970	NAS3-26266	p 163	A90-22237
	p 235	N90-14783		p 261	A90-31670	NAS8-32807	p 39	A90-23263
	p 27	N90-17635		p 148	A90-38084	NAS8-35350	p 48	A90-34780
NAS3-24210	p 183	N90-26272		p 43	A90-38126	NATO-343/85	p 158	A90-13907
	p 24	N90-10047		p 43	A90-40587	NCC2-582	p 170	A90-38396
	p 24	N90-10048		p 21	A90-42688	NCC3-105	p 154	N90-22732
	p 24	N90-10049		p 21	A90-42690		p 154	N90-25273
NAS3-24222	p 247	N90-10683		p 172	A90-44011	NCC3-109	p 259	N90-26664
NAS3-24227	p 157	A90-13091		p 105	A90-44689	NCC3-120	p 221	N90-23757
	p 165	A90-24837		p 130	A90-47204		p 221	N90-23769
NAS3-24229	p 157	A90-12836		p 65	A90-47205	NCC3-133	p 258	N90-11606
NAS3-24230	p 20	A90-32960		p 174	A90-47206		p 258	N90-14108
NAS3-24239	p 146	A90-20861		p 66	A90-47215		p 258	N90-17465
	p 150	A90-48492		p 67	A90-47224		p 127	N90-19374
NAS3-24252	p 147	A90-25686		p 257	A90-48661	NCC3-135	p 191	N90-28827
NAS3-24253	p 39	A90-25655		p 45	A90-52499	NCC3-140	p 177	N90-14512
NAS3-24339	p 17	A90-44736		p 10	N90-10004	NCC3-177	p 168	A90-28143
	p 24	N90-11738		p 187	N90-11999	NCC3-19	p 120	A90-16279
	p 25	N90-11739		p 11	N90-12560		p 255	A90-33224
NAS3-24341	p 32	N90-24274		p 1	N90-13323		p 128	N90-21192
NAS3-24350	p 161	A90-19976		p 176	N90-13748	NCC3-27	p 111	A90-20255
	p 163	A90-22651		p 188	N90-13761		p 85	A90-43902
	p 167	A90-27983		p 237	N90-13968	NCC3-56	p 181	N90-22000
	p 171	A90-38799		p 177	N90-14512	NCC3-58	p 185	A90-10472
NAS3-24384	p 172	A90-40930		p 177	N90-14517	NCC3-626	p 15	A90-26986
	p 124	N90-10293		p 126	N90-16072	NCC3-71	p 249	A90-19303
	p 129	N90-28735		p 27	N90-17635	NCC3-72	p 121	A90-25273
NAS3-24389	p 56	A90-29328		p 178	N90-18667		p 255	A90-33330
	p 211	A90-29329		p 144	N90-19454		p 124	A90-49086
	p 236	A90-29333		p 1	N90-20943	NCC3-75	p 151	N90-17987
	p 214	A90-49792		p 29	N90-21037	NCC3-81	p 209	A90-23827
NAS3-24564	p 140	A90-25697		p 219	N90-21420		p 89	A90-23842
	p 143	N90-14452		p 237	N90-21552		p 89	A90-26561
	p 144	N90-19454		p 248	N90-21600	NCC3-89	p 129	N90-26142
	p 50	N90-20120		p 30	N90-21763	NCC3-93	p 168	A90-32293
	p 153	N90-21282		p 232	N90-22843	NCC3-95	p 109	A90-11658
NAS3-24565	p 153	N90-22724		p 31	N90-23404		p 132	A90-23713
NAS3-24612	p 71	N90-13589		p 31	N90-23406		p 134	N90-14398
	p 107	N90-28628		p 45	N90-25159	NCC3-99	p 146	A90-11774
NAS3-24616	p 177	N90-14494		p 79	N90-25183	NGL-22-009-640	p 162	A90-22181
NAS3-24619	p 165	A90-23792		p 80	N90-25187		p 16	N90-20925
NAS3-24622	p 95	N90-10184		p 191	N90-25324		p 16	N90-20926
NAS3-24631	p 64	A90-42559		p 233	N90-25420		p 16	N90-20927
	p 72	N90-14278		p 53	N90-26063		p 17	N90-20928
NAS3-24635	p 228	A90-33946		p 183	N90-26272	NGT-50085	p 177	N90-14517
	p 231	N90-20469		p 183	N90-26275	NGT-50087	p 114	A90-33340
NAS3-24636	p 56	A90-27960		p 45	N90-27732	NGT-50088	p 104	A90-32835
NAS3-24640	p 104	A90-28771		p 131	N90-28742	NGT-50367	p 132	A90-22878
NAS3-24641	p 227	A90-28359		p 146	N90-28768	NIH-NS-13742	p 234	A90-28084
NAS3-24644	p 254	A90-19793	NAS3-25270	p 8	A90-45873	NRA-88-ARC-1(BJY)	p 126	N90-16072
	p 132	A90-20000		p 30	N90-22567	NSF AST-84-51736	p 265	A90-34505
NAS3-24645	p 197	A90-42000		p 132	A90-20525	NSF AST-85-15447	p 264	A90-17643
NAS3-24653	p 148	A90-38124	NAS3-25274	p 200	N90-13794		p 264	A90-25889
NAS3-24655	p 55	A90-16374	NAS3-25278	p 204	N90-26320	NSF AST-88-09616	p 264	A90-24671
NAS3-24667	p 149	A90-38275	NAS3-25279	p 199	N90-10437	NSF CBT-86-57228	p 105	A90-43674
NAS3-24670	p 48	A90-38267	NAS3-25281	p 18	N90-21006	NSF CHE-83-19578	p 85	A90-49071
	p 232	N90-22834	NAS3-25317	p 157	A90-13092	NSF CHE-87-12118	p 85	A90-49072
NAS3-24672	p 54	A90-14941	NAS3-25331	p 250	A90-42754		p 85	A90-49073
NAS3-24680	p 145	N90-20270	NAS3-25346	p 236	A90-38089	NSF CPE-80-14661	p 158	A90-15729
NAS3-24683	p 139	A90-25617	NAS3-25347	p 49	N90-10983	NSF DMC-87-07648	p 239	A90-51266
	p 46	A90-25704	NAS3-25354	p 57	A90-33956		p 239	A90-51267
NAS3-24847	p 25	N90-13385	NAS3-25355	p 231	N90-20479	NSF DMR-85-06705	p 115	A90-44338
NAS3-24855	p 18	N90-20991		p 73	N90-15996	NSF DMR-86-17820	p 192	A90-11593
NAS3-24861	p 209	A90-23828	NAS3-25356	p 79	N90-23474	NSF DMR-87-14555	p 255	A90-29739
NAS3-24872	p 125	N90-10294		p 71	N90-11805	NSF DMR-89-05314	p 243	N90-18927
NAS3-24877	p 72	N90-14281	NAS3-25357	p 71	N90-11806		p 244	N90-26615
NAS3-24881	p 10	N90-10835		p 49	N90-12645		p 244	N90-29124
	p 10	N90-10836	NAS3-25367	p 253	A90-19284	NSF ECS-86-57951	p 153	N90-21278
NAS3-24887	p 141	A90-39056	NAS3-25368	p 84	A90-22646	NSF ECS-88-00659	p 253	A90-12808
NAS3-24889	p 142	N90-11210		p 167	A90-26369		p 256	A90-36232
NAS3-24895	p 147	A90-25686	NAS3-25370	p 28	N90-18415	NSF INT-85-14196	p 158	A90-13907
NAS3-24897	p 147	A90-25691	NAS3-25425	p 14	N90-27655	NSF INT-87-02083	p 3	A90-12555
NAS3-25062	p 53	A90-13282		p 186	A90-40560	NSF IRI-88-10168	p 138	A90-13935
NAS3-25063	p 39	A90-19988	NAS3-25446	p 20	A90-40643	NSF MSM-83-20307	p 158	A90-13907
NAS3-25070	p 85	A90-42028	NAS3-25460	p 94	A90-50128	NSF MSM-83-51490	p 133	A90-48720
	p 118	N90-21165	NAS3-25470	p 56	A90-22874	NSF MSM-87-02732	p 158	A90-15947
NAS3-25079	p 59	A90-38088	NAS3-25553	p 64	A90-42536		p 160	A90-19693
NAS3-25082	p 53	A90-11993		p 17	A90-20012	NSF PHY-88-06567	p 265	A90-31407
	p 48	A90-27710	NAS3-25555	p 105	A90-38399	NSF 85-52702	p 16	N90-20925
	p 58	A90-38076	NAS3-25566	p 199	A90-47223		p 16	N90-20927
NAS3-25084	p 140	A90-25658	NAS3-25572	p 7	A90-29393	NSG-3079	p 2	A90-11778
NAS3-25087	p 141	A90-48440	NAS3-25574	p 4	A90-20011	NSG-3114	p 168	A90-32841
NAS3-25089	p 50	N90-25172	NAS3-25601	p 131	N90-23574	NSG-3139	p 6	A90-29374
NAS3-25117	p 29	N90-21761	NAS3-25625	p 63	A90-40583		p 209	A90-19109
NAS3-25193	p 37	A90-49110	NAS3-25626	p 63	A90-40584	NSG-3188	p 193	A90-21107
	p 17	A90-49114		p 65	A90-42713		p 195	A90-21131
NAS3-25199	p 228	A90-33948		p 78	N90-21809		p 195	A90-21136
	p 231	N90-20471	NAS3-25633	p 4	A90-22256		p 209	A90-23013
NAS3-25208	p 170	A90-38042	NAS3-25646	p 64	A90-42030		p 201	N90-15434

NSG-3220

CONTRACT NUMBER INDEX

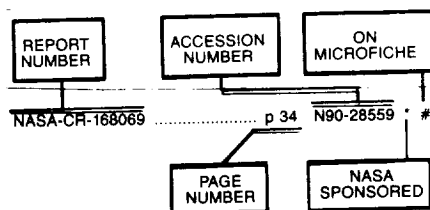
NSG-3220	p 138	N90-26171	p 23	N90-10039	p 178	N90-17076	
NSG-3238	p 186	A90-41120	p 242	N90-10635	p 258	N90-17465	
NSG-3264	p 159	A90-18505	p 175	N90-11250	p 86	N90-17811	
	p 185	A90-23793	p 187	N90-11277	p 87	N90-20130	
	p 23	N90-10038	p 242	N90-11497	p 119	N90-23536	
NSG-3266	p 23	N90-10039	p 175	N90-11969	p 119	N90-25211	
	p 3	A90-12555	p 216	N90-12041	p 129	N90-28735	
	p 160	A90-19749	p 242	N90-12231	p 130	N90-28740	
	p 8	A90-42731	p 11	N90-12561			
NSG-3299	p 55	A90-16369	p 11	N90-13323	505-63-1B	p 95	N90-10181
	p 252	A90-42602	p 11	N90-13328		p 215	N90-11332
NSG-3506	p 109	A90-11925	p 25	N90-13387		p 11	N90-13355
N00014-84-C-0359	p 157	A90-12836	p 27	N90-13393		p 96	N90-14294
N00014-85-C-0639	p 92	A90-45621	p 176	N90-13750		p 216	N90-14640
	p 93	A90-48636	p 237	N90-13968		p 217	N90-14652
N00014-85-K-0182-P005	p 147	A90-33726	p 243	N90-14002		p 217	N90-14656
N00014-85-K-0182	p 258	N90-19873	p 177	N90-14517		p 217	N90-17180
N00014-87-K-0168	p 7	A90-36252	p 243	N90-14844		p 218	N90-18064
N00014-87-K-0169	p 161	A90-19984	p 12	N90-16719		p 218	N90-18071
	p 6	A90-25285	p 217	N90-17173		p 218	N90-18081
N00014-87-K-0174	p 157	A90-12836	p 12	N90-17562		p 218	N90-18745
N00014-88-C-0512	p 259	N90-24964	p 178	N90-18005		p 98	N90-20138
N00014-90-J-1730	p 8	A90-42709	p 243	N90-18198		p 202	N90-20391
N00024-85-C-6041	p 197	A90-46074	p 178	N90-18667		p 219	N90-20431
SERC-GR/E/25702	p 161	A90-21422	p 243	N90-18927		p 219	N90-20432
SNSF-3,718,80	p 234	A90-28084	p 38	N90-19242		p 99	N90-21132
SWRI PROJ. 06-7576	p 26	N90-13390	p 243	N90-19783		p 219	N90-21420
	p 26	N90-13391	p 28	N90-20090		p 203	N90-22041
W-31-109-ENG-38	p 255	A90-29739	p 178	N90-20326		p 137	N90-22703
	p 259	N90-24952	p 179	N90-20337		p 129	N90-23543
W-7405-ENG-36	p 259	N90-24964	p 243	N90-20769		p 221	N90-23773
307-51-00	p 257	N90-10737	p 29	N90-21036		p 101	N90-24384
	p 258	N90-11606	p 179	N90-21291		p 222	N90-25367
	p 151	N90-18634	p 179	N90-21300		p 129	N90-26142
	p 259	N90-22421	p 180	N90-21303		p 223	N90-26373
316-30-19	p 47	N90-27736	p 180	N90-21306		p 102	N90-27875
316-60-13	p 52	N90-28596	p 180	N90-21307		p 205	N90-28063
323-53-62	p 49	N90-12645	p 237	N90-21552		p 223	N90-28099
324-01-00	p 125	N90-10294	p 244	N90-21567		p 223	N90-28111
326-31-31	p 267	N90-15030	p 244	N90-21570	505-63-1M	p 224	N90-28113
414-70-75-25	p 234	N90-12984	p 1	N90-21724		p 126	N90-14368
474-10-52	p 73	N90-14285	p 13	N90-21733	505-63-11	p 223	N90-28112
	p 181	N90-21974	p 106	N90-21842		p 95	N90-10185
	p 183	N90-26279	p 180	N90-21962		p 96	N90-11808
474-11-10	p 71	N90-13596	p 181	N90-22011		p 86	N90-13597
474-12-10	p 49	N90-13581	p 181	N90-22016		p 97	N90-16008
	p 50	N90-20120	p 189	N90-22021		p 97	N90-17817
474-42-10	p 245	N90-14060	p 14	N90-25948		p 98	N90-20139
474-46-10	p 218	N90-19617	p 182	N90-26269		p 99	N90-21137
	p 266	N90-22488	p 183	N90-26276	505-63-31	p 100	N90-21825
474-46-20	p 118	N90-20181	p 184	N90-26282		p 100	N90-23477
474-52-10	p 221	N90-23770	p 191	N90-26299		p 215	N90-10455
480-52-02	p 50	N90-25172	p 244	N90-26614	505-63-5A	p 219	N90-20438
488-10-12	p 77	N90-21806	p 244	N90-26615		p 199	N90-10437
488-51-03	p 240	N90-22323	p 244	N90-26616		p 202	N90-18041
	p 240	N90-22324	p 184	N90-27982		p 203	N90-21387
	p 240	N90-22325	p 184	N90-27983	505-63-51	p 205	N90-28060
	p 240	N90-23125	p 184	N90-28009		p 199	N90-12033
501-14-11	p 267	N90-23339	p 15	N90-28504		p 200	N90-13785
505-03-01	p 10	N90-10835	p 244	N90-29124		p 201	N90-15434
	p 10	N90-10836	p 38	N90-15964		p 201	N90-16286
505-05-01	p 12	N90-14206	p 202	N90-20392		p 203	N90-21394
505-31-3B	p 10	N90-10011	p 31	N90-23407		p 203	N90-22054
505-42-31	p 70	N90-11081	p 39	N90-25151		p 203	N90-22790
505-42-94	p 202	N90-19593	p 107	N90-23518		p 204	N90-22796
505-43-02	p 222	N90-26355	p 13	N90-25106		p 138	N90-26171
505-43-22	p 28	N90-17638	p 39	N90-23416	505-63-64	p 205	N90-28065
505-44-2C	p 259	N90-26682	p 13	N90-20051		p 204	N90-26338
505-45-58	p 1	N90-20942	p 30	N90-22567	505-68-1A	p 187	N90-11999
505-45-72	p 70	N90-10175	p 14	N90-25940	505-68-11	p 18	N90-10031
505-474-46	p 78	N90-21812	p 176	N90-13749		p 200	N90-13797
505-53-1A	p 127	N90-17875	p 175	N90-11245		p 200	N90-14617
505-60-01	p 189	N90-20358	p 27	N90-13392		p 38	N90-15965
505-62-OK	p 27	N90-15923	p 11	N90-14203		p 202	N90-17147
505-62-OK	p 199	N90-10437	p 27	N90-17636		p 1	N90-20943
	p 175	N90-11256	p 25	N90-11740		p 18	N90-21006
	p 202	N90-18041	p 25	N90-12618	505-69-31	p 13	N90-21727
	p 203	N90-21387	p 26	N90-13389	505-69-61	p 27	N90-14235
	p 240	N90-23991	p 12	N90-17561		p 10	N90-10004
	p 32	N90-27722	p 179	N90-20338		p 29	N90-21037
	p 205	N90-28060	p 2	N90-21725		p 29	N90-21038
	p 241	N90-29121	p 30	N90-22566	505-80-31	p 29	N90-21761
505-62-00	p 179	N90-21296	p 31	N90-23404		p 177	N90-14511
505-62-01	p 18	N90-13381	p 31	N90-24273	505-90-01	p 176	N90-13719
	p 188	N90-13761	p 32	N90-26009		p 184	N90-27985
	p 37	N90-15112	p 177	N90-14494		p 208	N90-28097
	p 250	N90-17424	p 70	N90-11082	506-41-11	p 208	N90-28858
	p 188	N90-18025	p 86	N90-12658		p 152	N90-21274
	p 153	N90-21277	p 86	N90-12659		p 153	N90-21287
	p 189	N90-21351	p 96	N90-12670		p 232	N90-22843
	p 190	N90-25323	p 117	N90-13636		p 87	N90-23476
	p 37	N90-26011	p 200	N90-13786		p 154	N90-23662
	p 53	N90-26063	p 258	N90-14108		p 233	N90-25420
505-62-11	p 32	N90-25982	p 117	N90-14335		p 81	N90-26069
	p 183	N90-26275	p 117	N90-16911	506-41-21	p 108	N90-28696
505-62-21	p 23	N90-10038	p 127	N90-16944		p 106	N90-12696
						p 229	N90-18097

CONTRACT NUMBER INDEX

	p 230	N90-20454		p 100	N90-21821		p 79	N90-22606
	p 77	N90-21116		p 100	N90-21824		p 232	N90-22847
	p 231	N90-21469		p 100	N90-21826	590-13-21	p 183	N90-26272
	p 78	N90-21808		p 106	N90-21843	590-13-31	p 154	N90-23663
	p 107	N90-21844		p 220	N90-22822		p 155	N90-25278
	p 233	N90-26397		p 190	N90-23714	590-13-41	p 190	N90-22773
506-41-3F	p 151	N90-20301		p 207	N90-23754	590-21-11	p 79	N90-25183
506-41-3G	p 70	N90-10174		p 101	N90-24382		p 191	N90-28033
506-41-3K	p 51	N90-26054		p 101	N90-24383		p 205	N90-28066
	p 82	N90-26873		p 222	N90-26359	590-21-21	p 79	N90-24349
506-41-31	p 72	N90-14281		p 102	N90-27874	590-21-31	p 14	N90-27655
	p 72	N90-14283	510-01-01	p 126	N90-13666	590-21-41	p 189	N90-21360
	p 229	N90-14678		p 97	N90-19302		p 81	N90-26070
	p 127	N90-19373		p 220	N90-22117	591-11-31	p 30	N90-21763
	p 76	N90-21110		p 119	N90-22646	591-14-11	p 87	N90-26074
506-41-41	p 126	N90-14362		p 221	N90-23757		p 267	N90-26789
	p 74	N90-17677		p 221	N90-23769		p 246	N90-28393
	p 86	N90-19301		p 101	N90-25193	591-14-3A	p 70	N90-11804
	p 151	N90-19484		p 223	N90-28110	591-14-41	p 76	N90-19299
	p 28	N90-20085	510-01-1A	p 207	N90-21401		p 81	N90-26068
	p 128	N90-21181		p 207	N90-22801		p 233	N90-26396
	p 128	N90-21192		p 222	N90-26364	591-21-00	p 182	N90-22761
	p 153	N90-21283	510-11-01	p 223	N90-26372	591-23-00	p 130	N90-13675
	p 51	N90-25173	533-04-1A	p 26	N90-13390		p 176	N90-13751
	p 80	N90-25184		p 26	N90-13391		p 237	N90-15622
	p 233	N90-25419	533-04-11	p 215	N90-10450		p 179	N90-21295
	p 82	N90-27784		p 215	N90-10451		p 184	N90-27984
506-42-00	p 73	N90-14284	535-03-01	p 24	N90-10045	591-23-21	p 183	N90-26278
	p 45	N90-20110		p 24	N90-10046	591-41-21	p 80	N90-25185
506-42-11	p 69	N90-10172		p 24	N90-10047	643-10-01	p 245	N90-10674
	p 78	N90-22604		p 24	N90-10048		p 245	N90-14856
506-42-21	p 52	N90-22595		p 24	N90-10049		p 144	N90-20264
	p 52	N90-25178		p 247	N90-11549		p 145	N90-21250
	p 191	N90-29622		p 25	N90-11739		p 138	N90-26172
506-42-31	p 73	N90-15992		p 11	N90-12560	650-20-26	p 145	N90-20270
	p 79	N90-25181		p 11	N90-13352	650-60-20	p 145	N90-21261
	p 81	N90-26071		p 248	N90-17413		p 153	N90-21282
	p 82	N90-27782		p 248	N90-18229		p 155	N90-26250
	p 82	N90-27783		p 248	N90-20794	650-60-23	p 142	N90-11915
	p 82	N90-27785		p 249	N90-21602		p 143	N90-12813
	p 82	N90-27786		p 30	N90-22564		p 50	N90-14273
	p 83	N90-28657		p 18	N90-23393		p 47	N90-15983
506-42-51	p 190	N90-22022		p 14	N90-25946		p 143	N90-17977
	p 43	N90-25158		p 249	N90-26635		p 144	N90-19454
	p 131	N90-28742		p 32	N90-28552		p 146	N90-28768
506-42-61	p 81	N90-26065	535-03-22	p 32	N90-24274	674-22-05	p 134	N90-13679
506-43-1C	p 137	N90-11902	535-05-01	p 95	N90-10188		p 134	N90-13680
506-43-11	p 124	N90-10262		p 235	N90-14783	674-24-05	p 136	N90-26163
	p 125	N90-11880		p 237	N90-20708		p 177	N90-14512
	p 125	N90-11881		p 128	N90-21858		p 183	N90-26273
	p 258	N90-12348		p 131	N90-21869	674-25-05	p 134	N90-14398
	p 206	N90-17167		p 238	N90-22262	674-26-05	p 135	N90-20237
	p 189	N90-20353		p 249	N90-26633	694-03-03	p 137	N90-11901
	p 128	N90-21182		p 15	N90-27657		p 200	N90-13794
	p 137	N90-21210	535-07-01	p 217	N90-14655		p 143	N90-14452
	p 207	N90-21402	535-505-01	p 24	N90-10891		p 134	N90-16087
	p 128	N90-21862	537-01-11	p 137	N90-23591		p 188	N90-17085
506-44-2B	p 155	N90-27965		p 182	N90-25289		p 137	N90-17929
506-44-2C	p 150	N90-11943		p 138	N90-26170		p 135	N90-20253
	p 151	N90-20286	537-02-11	p 185	N90-28792		p 189	N90-20352
	p 145	N90-21263	537-02-41	p 31	N90-23406		p 1	N90-21723
	p 152	N90-21273	549-03-1A	p 152	N90-21271		p 205	N90-28062
	p 153	N90-21278		p 152	N90-21272		p 138	N90-28754
	p 156	N90-28786	553-13-00	p 216	N90-14641	694-22-00	p 133	N90-11196
506-44-20	p 259	N90-20886		p 216	N90-14642	694-23-03	p 238	N90-13988
	p 152	N90-21275		p 117	N90-16053	694-24-00	p 178	N90-18665
	p 155	N90-27966		p 98	N90-21123		p 248	N90-21600
506-44-21	p 257	N90-10738		p 78	N90-21809	763-01-21	p 50	N90-14268
	p 117	N90-15211		p 118	N90-21849		p 27	N90-17635
	p 151	N90-17987		p 136	N90-21871		p 130	N90-17890
	p 203	N90-20393		p 220	N90-22808		p 30	N90-21762
	p 260	N90-26683		p 221	N90-22823		p 51	N90-26055
506-44-26	p 260	N90-29219		p 131	N90-23574		p 131	N90-26160
506-48-21	p 44	N90-10912		p 45	N90-25159	763-01-4B	p 219	N90-19629
	p 71	N90-13590		p 45	N90-27732	763-01-46	p 126	N90-16072
	p 52	N90-14275		p 125	N90-11144	776-81-63	p 263	N90-26729
506-48-4A	p 71	N90-11806	582-01-11	p 71	N90-13595	778-32-11	p 97	N90-18504
	p 73	N90-15996		p 216	N90-13819	946-02-20	p 28	N90-19234
	p 79	N90-23474		p 131	N90-19386		p 154	N90-22731
506-63-31	p 224	N90-28878		p 239	N90-21564			
506-64-12	p 77	N90-21807		p 192	N90-22784			
506-68-11	p 13	N90-19203		p 191	N90-25324			
510-01-0A	p 23	N90-10037		p 241	N90-25607			
	p 216	N90-12950		p 191	N90-28031			
	p 96	N90-14287		p 83	N90-28659			
	p 126	N90-14363	582-01-21	p 80	N90-25186			
	p 98	N90-19310	582-01-31	p 71	N90-13589			
	p 127	N90-19374		p 30	N90-23403			
	p 98	N90-20151	586-01-11	p 136	N90-10309			
	p 219	N90-20428		p 116	N90-11854			
	p 98	N90-21124		p 263	N90-18326			
	p 99	N90-21131		p 102	N90-28670			
	p 99	N90-21133	586-01-21	p 176	N90-13748			
	p 99	N90-21138	590-01-21	p 78	N90-22605			
	p 100	N90-21143	590-12-31	p 80	N90-25187			
	p 189	N90-21361	590-13-11	p 77	N90-21114			

REPORT/ACCESSION NUMBER INDEX

Typical Report Number Index Listing



Listings in this index are arranged alphanumerically by report number. The accession number denotes the number by which the citation is identified. An asterisk (*) indicates that the item is a NASA report. A pound sign (#) indicates that the item is available on microfiche.

AARL-P-90-1	p 76	N90-21109 *	#
AAS PAPER 87-210	p 55	A90-16676 *	
AAS PAPER 87-223	p 55	A90-16688 *	
AAS PAPER 87-224	p 55	A90-16689 *	
AAS PAPER 87-245	p 42	A90-16544 *	
AAS PAPER 87-268	p 139	A90-16566 *	
AAS PAPER 87-271	p 42	A90-16569 *	
AAS PAPER 89-350	p 40	A90-46783 *	
AAS PAPER 89-351	p 40	A90-46784 *	
AAS PAPER 89-352	p 40	A90-46785 *	
AAS PAPER 89-354	p 41	A90-46786 *	
AD-A216002	p 199	N90-10437 *	#
AD-A217844	p 200	N90-13785 *	#
AD-A217846	p 200	N90-13786 *	#
AD-A217851	p 126	N90-14363 *	#
AD-A217852	p 96	N90-14287 *	#
AD-A217853	p 199	N90-12033 *	#
AD-A219268	p 159	A90-17578 *	
AD-A219299	p 178	N90-17076 *	#
AD-A219303	p 201	N90-15434 *	#
AD-A221523	p 202	N90-17147 *	#
AD-A222639	p 141	A90-36717 *	
AD-A224492	p 204	N90-22796 *	#
AD-A224494	p 100	N90-21826 *	#
AD-A224967	p 203	N90-21394 *	#
AD-A224968	p 101	N90-24382 *	#
AD-A224969	p 240	N90-23991 *	#
AD-A225679	p 204	N90-26338 *	#
AD-A227148	p 138	N90-26171 *	#
AD-A227149	p 205	N90-28065 *	#
AD-A227150	p 129	N90-23543 *	#
AD-A227151	p 205	N90-28060 *	#
AD-A227392	p 118	N90-21165 *	#
AIAA PAPER 89-0438	p 4	A90-23650 *	#
AIAA PAPER 89-2910	p 5	A90-25043 *	#
AIAA PAPER 90-0015	p 159	A90-19633 *	#
AIAA PAPER 90-0017	p 159	A90-19635 *	#
AIAA PAPER 90-0018	p 166	A90-25026 *	#
AIAA PAPER 90-0028	p 4	A90-22153 *	#
AIAA PAPER 90-0047	p 160	A90-19649 *	#
AIAA PAPER 90-0048	p 4	A90-22158 *	#
AIAA PAPER 90-0053	p 164	A90-23702 *	#
AIAA PAPER 90-0122	p 160	A90-19693 *	#
AIAA PAPER 90-0183	p 246	A90-19725 *	#
AIAA PAPER 90-0198	p 15	A90-19735 *	#
AIAA PAPER 90-0199	p 162	A90-22180 *	#
AIAA PAPER 90-0200	p 162	A90-22181 *	#
AIAA PAPER 90-0239	p 160	A90-19749 *	#
AIAA PAPER 90-0245	p 160	A90-19752 *	#
AIAA PAPER 90-0283	p 247	A90-32505 *	#
AIAA PAPER 90-0307	p 160	A90-19788 *	#
AIAA PAPER 90-0319	p 254	A90-19793 *	#

AIAA PAPER 90-0338	p 160	A90-19804 *	#
AIAA PAPER 90-0339	p 5	A90-25028 *	#
AIAA PAPER 90-0344	p 162	A90-22200 *	#
AIAA PAPER 90-0353	p 162	A90-22201 *	#
AIAA PAPER 90-0354	p 163	A90-22202 *	#
AIAA PAPER 90-0365	p 166	A90-25029 *	#
AIAA PAPER 90-0391	p 164	A90-23706 *	#
AIAA PAPER 90-0396	p 167	A90-26940 *	#
AIAA PAPER 90-0397	p 166	A90-25030 *	#
AIAA PAPER 90-0408	p 133	A90-25031 *	#
AIAA PAPER 90-0409	p 133	A90-25032 *	#
AIAA PAPER 90-0413	p 166	A90-25033 *	#
AIAA PAPER 90-0444	p 167	A90-26952 *	#
AIAA PAPER 90-0488	p 166	A90-25034 *	#
AIAA PAPER 90-0498	p 161	A90-19878 *	#
AIAA PAPER 90-0503	p 166	A90-25035 *	#
AIAA PAPER 90-0546	p 103	A90-19904 *	#
AIAA PAPER 90-0550	p 20	A90-25036 *	#
AIAA PAPER 90-0585	p 6	A90-26967 *	#
AIAA PAPER 90-0600	p 6	A90-26970 *	#
AIAA PAPER 90-0637	p 245	A90-26975 *	#
AIAA PAPER 90-0643	p 163	A90-22237 *	#
AIAA PAPER 90-0648	p 103	A90-22238 *	#
AIAA PAPER 90-0649	p 104	A90-25038 *	#
AIAA PAPER 90-0651	p 104	A90-25039 *	#
AIAA PAPER 90-0653	p 163	A90-22239 *	#
AIAA PAPER 90-0666	p 37	A90-25040 *	#
AIAA PAPER 90-0667	p 186	A90-26978 *	#
AIAA PAPER 90-0668	p 164	A90-23711 *	#
AIAA PAPER 90-0669	p 37	A90-22242 *	#
AIAA PAPER 90-0684	p 161	A90-19976 *	#
AIAA PAPER 90-0687	p 3	A90-19978 *	#
AIAA PAPER 90-0694	p 5	A90-25041 *	#
AIAA PAPER 90-0705	p 161	A90-19984 *	#
AIAA PAPER 90-0715	p 44	A90-23712 *	#
AIAA PAPER 90-0718	p 39	A90-19988 *	#
AIAA PAPER 90-0719	p 44	A90-19989 *	#
AIAA PAPER 90-0722	p 47	A90-22252 *	#
AIAA PAPER 90-0725	p 251	A90-22254 *	#
AIAA PAPER 90-0726	p 251	A90-22255 *	#
AIAA PAPER 90-0731	p 4	A90-22256 *	#
AIAA PAPER 90-0740	p 132	A90-23713 *	#
AIAA PAPER 90-0741	p 132	A90-19999 *	#
AIAA PAPER 90-0742	p 132	A90-20000 *	#
AIAA PAPER 90-0744	p 235	A90-22257 *	#
AIAA PAPER 90-0753	p 15	A90-26986 *	#
AIAA PAPER 90-0754	p 15	A90-20009 *	#
AIAA PAPER 90-0756	p 5	A90-25042 *	#
AIAA PAPER 90-0757	p 3	A90-20010 *	#
AIAA PAPER 90-0758	p 4	A90-20011 *	#
AIAA PAPER 90-0761	p 17	A90-20012 *	#
AIAA PAPER 90-0783	p 89	A90-25609 *	#
AIAA PAPER 90-0792	p 139	A90-25617 *	#
AIAA PAPER 90-0795	p 139	A90-25620 *	#
AIAA PAPER 90-0803	p 139	A90-25627 *	#
AIAA PAPER 90-0808	p 140	A90-25634 *	#
AIAA PAPER 90-0812	p 46	A90-25635 *	#
AIAA PAPER 90-0815	p 245	A90-25638 *	#
AIAA PAPER 90-0816	p 46	A90-25639 *	#
AIAA PAPER 90-0830	p 39	A90-25655 *	#
AIAA PAPER 90-0833	p 140	A90-25658 *	#
AIAA PAPER 90-0836	p 42	A90-25662 *	#
AIAA PAPER 90-0839	p 140	A90-25663 *	#
AIAA PAPER 90-0848	p 147	A90-25671 *	#
AIAA PAPER 90-0850	p 46	A90-25673 *	#
AIAA PAPER 90-0866	p 147	A90-25686 *	#
AIAA PAPER 90-0870	p 147	A90-25691 *	#
AIAA PAPER 90-0878	p 140	A90-25697 *	#
AIAA PAPER 90-0885	p 46	A90-25704 *	#
AIAA PAPER 90-0895	p 140	A90-25681 *	#
AIAA PAPER 90-0916	p 210	A90-29318 *	#
AIAA PAPER 90-0930	p 211	A90-29324 *	#
AIAA PAPER 90-0984	p 6	A90-29374 *	#
AIAA PAPER 90-1026	p 90	A90-29228 *	#
AIAA PAPER 90-1036	p 211	A90-29380 *	#
AIAA PAPER 90-1053	p 48	A90-29281 *	#
AIAA PAPER 90-1097	p 196	A90-29327 *	#
AIAA PAPER 90-1098	p 56	A90-29328 *	#
AIAA PAPER 90-1099	p 211	A90-29329 *	#
AIAA PAPER 90-1102	p 211	A90-29332 *	#
AIAA PAPER 90-1120	p 7	A90-29392 *	#
AIAA PAPER 90-1133	p 210	A90-29260 *	#
AIAA PAPER 90-1135	p 210	A90-29262 *	#
AIAA PAPER 90-1139	p 236	A90-29333 *	#
AIAA PAPER 90-1157	p 7	A90-29393 *	#
AIAA PAPER 90-1177	p 236	A90-29268 *	#
AIAA PAPER 90-1201	p 210	A90-26787 *	#
AIAA PAPER 90-1456	p 170	A90-38614 *	#
AIAA PAPER 90-1502	p 171	A90-38651 *	#
AIAA PAPER 90-1505	p 171	A90-38654 *	#
AIAA PAPER 90-1541	p 171	A90-38685 *	#
AIAA PAPER 90-1556	p 49	A90-38697 *	#
AIAA PAPER 90-1672	p 49	A90-41566 *	#
AIAA PAPER 90-1681	p 136	A90-50641 *	#
AIAA PAPER 90-1693	p 170	A90-38396 *	#
AIAA PAPER 90-1694	p 170	A90-38397 *	#
AIAA PAPER 90-1696	p 105	A90-38399 *	#
AIAA PAPER 90-1880	p 65	A90-47201 *	#
AIAA PAPER 90-1881	p 63	A90-40545 *	#
AIAA PAPER 90-1882	p 52	A90-41980 *	#
AIAA PAPER 90-1894	p 130	A90-50642 *	#
AIAA PAPER 90-1899	p 21	A90-42688 *	#
AIAA PAPER 90-1901	p 21	A90-42690 *	#
AIAA PAPER 90-1909	p 247	A90-47202 *	#
AIAA PAPER 90-1918	p 36	A90-40557 *	#
AIAA PAPER 90-1931	p 186	A90-40560 *	#
AIAA PAPER 90-1935	p 20	A90-40562 *	#
AIAA PAPER 90-1955	p 173	A90-47203 *	#
AIAA PAPER 90-1968	p 130	A90-47204 *	#
AIAA PAPER 90-1980	p 8	A90-40587 *	#
AIAA PAPER 90-1987	p 63	A90-40583 *	#
AIAA PAPER 90-1988	p 63	A90-40584 *	#
AIAA PAPER 90-1989	p 65	A90-42713 *	#
AIAA PAPER 90-1990	p 45	A90-52499 *	#
AIAA PAPER 90-1993	p 65	A90-47205 *	#
AIAA PAPER 90-1994	p 67	A90-50643 *	#
AIAA PAPER 90-2000	p 43	A90-40587 *	#
AIAA PAPER 90-2049	p 197	A90-42000 *	#
AIAA PAPER 90-2100	p 174	A90-47206 *	#
AIAA PAPER 90-2111	p 66	A90-47207 *	#
AIAA PAPER 90-2116	p 66	A90-47208 *	#
AIAA PAPER 90-2119	p 85	A90-42028 *	#
AIAA PAPER 90-2120	p 63	A90-42029 *	#
AIAA PAPER 90-2121	p 64	A90-42030 *	#
AIAA PAPER 90-2122	p 8	A90-42731 *	#
AIAA PAPER 90-2130	p 8	A90-42734 *	#
AIAA PAPER 90-2141	p 198	A90-47209 *	#
AIAA PAPER 90-2153	p 197	A90-42049 *	#
AIAA PAPER 90-2156	p 199	A90-50644 *	#
AIAA PAPER 90-2158	p 22	A90-47210 *	#
AIAA PAPER 90-2181	p 66	A90-47211 *	#
AIAA PAPER 90-2182	p 64	A90-42063 *	#
AIAA PAPER 90-2222	p 9	A90-47213 *	#
AIAA PAPER 90-2229	p 250	A90-42754 *	#
AIAA PAPER 90-2230	p 187	A90-42755 *	#
AIAA PAPER 90-2234	p 187	A90-47212 *	#
AIAA PAPER 90-2240	p 65	A90-45694 *	#
AIAA PAPER 90-2241	p 130	A90-47214 *	#
AIAA PAPER 90-2270	p 21	A90-42766 *	#
AIAA PAPER 90-2271	p 20	A90-37562 *	#
AIAA PAPER 90-2294	p 65	A90-42770 *	#
AIAA PAPER 90-2319	p 105	A90-42774 *	#
AIAA PAPER 90-2351	p 66	A90-47215 *	#
AIAA PAPER 90-2356	p 66	A90-47216 *	#
AIAA PAPER 90-2369	p 43	A90-40627 *	#
AIAA PAPER 90-2375	p 175	A90-52500 *	#
AIAA PAPER 90-2376	p 66	A90-47217 *	#
AIAA PAPER 90-2386	p 37	A90-42791 *	#
AIAA PAPER 90-2389	p 261	A90-42152 *	#
AIAA PAPER 90-2400	p 22	A90-47218 *	#
AIAA PAPER 90-2402	p 9	A90-47220 *	#
AIAA PAPER 90-2413	p 197	A90-42165 *	#
AIAA PAPER 90-2417	p 20	A90-42168 *	#
AIAA PAPER 90-2431	p 67	A90-47221 *	#
AIAA PAPER 90-2439	p 105	A90-50645 *	#
AIAA PAPER 90-2452	p 21	A90-42808 *	#
AIAA PAPER 90-2482	p 199	A90-47222 *	#
AIAA PAPER 90-2483	p 199	A90-47223 *	#
AIAA PAPER 90-2490	p 67	A90-47224 *	#
AIAA PAPER 90-2503	p 43	A90-47225 *	#
AIAA PAPER 90-2512	p 20	A90-40643 *	#
AIAA PAPER 90-2527	p 67	A90-52562 *	#
AIAA PAPER 90-2529	p 68	A90-52563 *	#
AIAA PAPER 90-2540	p 64	A90-42536 *	#
AIAA PAPER 90-2543	p 68	A90-52564 *	#

AIAA PAPER 90-2551

REPORT NUMBER INDEX

AIAA PAPER 90-2551	p 68	A90-52565 *	AIAA-90-2645	p 81	N90-26071 *	DOT/FAA/CD-89/13	p 187	N90-11999 *
AIAA PAPER 90-2552	p 68	A90-52566 *	AIAA-90-2669	p 82	N90-27782 *			
AIAA PAPER 90-2576	p 64	A90-42559 *	AIAA-90-2726	p 80	N90-25185 *	DOT/FAA/CT-TN89/63	p 1	N90-21724 *
AIAA PAPER 90-2578	p 68	A90-52568 *	AIAA-90-2751	p 52	N90-25178 *			
AIAA PAPER 90-2579	p 67	A90-47226 *	AIAA-90-3593	p 44	N90-26030 *			
AIAA PAPER 90-2582	p 68	A90-52569 *	AIAA-90-3681	p 47	N90-27736 *			
AIAA PAPER 90-2586	p 69	A90-52570 *				E-2429	p 1	N90-20942 *
AIAA PAPER 90-2595	p 64	A90-42570 *	ARINC-4247-01-01-5032	p 50	N90-20120 *	E-2641	p 202	N90-19593 *
AIAA PAPER 90-2614	p 64	A90-42587 *				E-3622	p 70	N90-10174 *
AIAA PAPER 90-2634	p 252	A90-42602 *	ASME PAPER 89-GT-105	p 195	A90-23814 *	E-3734	p 95	N90-10188 *
AIAA PAPER 90-2645	p 64	A90-42609 *	ASME PAPER 89-GT-107	p 165	A90-23815 *	E-3786	p 189	N90-21351 *
AIAA PAPER 90-2649	p 215	A90-52571 *	ASME PAPER 89-GT-122	p 56	A90-23821 *	E-4030	p 119	N90-25211 *
AIAA PAPER 90-2665	p 65	A90-42625 *	ASME PAPER 89-GT-128	p 212	A90-32264 *	E-4137	p 32	N90-28552 *
AIAA PAPER 90-2669	p 69	A90-52572 *	ASME PAPER 89-GT-129	p 209	A90-23827 *	E-4152-1	p 12	N90-16719 *
AIAA PAPER 90-2726	p 67	A90-47227 *	ASME PAPER 89-GT-130	p 209	A90-23828 *	E-4161	p 77	N90-21795 *
AIAA PAPER 90-2740	p 199	A90-47228 *	ASME PAPER 89-GT-132	p 84	A90-23830 *	E-4224	p 200	N90-13786 *
AIAA PAPER 90-2751	p 52	A90-47229 *	ASME PAPER 89-GT-135	p 165	A90-23832 *	E-4279	p 18	N90-10031 *
AIAA PAPER 90-2960	p 41	A90-53035 *	ASME PAPER 89-GT-138	p 88	A90-23835 *	E-4307	p 216	N90-13819 *
AIAA PAPER 90-2962	p 41	A90-53037 *	ASME PAPER 89-GT-144	p 195	A90-23838 *	E-4367	p 138	N90-26172 *
AIAA PAPER 90-2963	p 41	A90-53038 *	ASME PAPER 89-GT-152	p 5	A90-23841 *	E-4391	p 37	N90-15112 *
AIAA PAPER 90-2972	p 41	A90-53051 *	ASME PAPER 89-GT-153	p 89	A90-23842 *	E-4441	p 106	N90-21843 *
AIAA PAPER 90-2975	p 41	A90-53054 *	ASME PAPER 89-GT-20	p 4	A90-23762 *	E-4480	p 175	N90-11245 *
AIAA PAPER 90-3033	p 9	A90-50637 *	ASME PAPER 89-GT-219	p 165	A90-23880 *	E-4527	p 128	N90-21858 *
AIAA PAPER 90-3034	p 8	A90-45873 *	ASME PAPER 89-GT-241	p 19	A90-23890 *	E-4538	p 187	N90-11999 *
AIAA PAPER 90-3225	p 37	A90-49110 *	ASME PAPER 89-GT-303	p 163	A90-22651 *	E-4586	p 133	N90-11196 *
AIAA PAPER 90-3229	p 17	A90-49114 *	ASME PAPER 89-GT-330	p 19	A90-23896 *	E-4601	p 246	N90-12282 *
AIAA PAPER 90-3335	p 36	A90-47595 *	ASME PAPER 89-GT-69	p 165	A90-23792 *	E-4604	p 218	N90-18081 *
AIAA PAPER 90-3444	p 239	A90-47697 *	ASME PAPER 89-GT-72	p 165	A90-23793 *	E-4655	p 243	N90-14002 *
			ASME PAPER 89-TRIB-46	p 196	A90-33555 *	E-4674	p 71	N90-13596 *
			ASME PAPER 89-WA/APM-43	p 210	A90-28755 *	E-4704	p 136	N90-10309 *
						E-4708	p 230	N90-20454 *
AIAA-89-0438	p 11	N90-13352 *	AVSCOM-TM-89-C-003	p 199	N90-10437 *	E-4722-1	p 223	N90-28099 *
AIAA-89-0501	p 133	N90-11196 *	AVSCOM-TM-89-C-005	p 200	N90-13785 *	E-4726	p 134	N90-13679 *
AIAA-89-1060	p 11	N90-12560 *	AVSCOM-TM-89-C-006	p 201	N90-16286 *	E-4733	p 216	N90-14642 *
AIAA-89-1395	p 217	N90-17173 *	AVSCOM-TM-89-C-009	p 203	N90-21387 *	E-4736	p 144	N90-20264 *
AIAA-89-2139	p 29	N90-21038 *	AVSCOM-TM-89-C-010	p 27	N90-15923 *	E-4768	p 202	N90-20392 *
AIAA-89-2140	p 10	N90-10004 *	AVSCOM-TM-89-C-012	p 200	N90-13786 *	E-4769	p 257	N90-10738 *
AIAA-89-2696	p 30	N90-22564 *	AVSCOM-TM-89-C-014	p 200	N90-13797 *	E-4780	p 262	N90-15846 *
AIAA-89-2829	p 73	N90-15992 *	AVSCOM-TM-89-C-015	p 200	N90-14617 *	E-4786	p 134	N90-16087 *
AIAA-89-2910	p 12	N90-17561 *	AVSCOM-TM-90-C-001	p 202	N90-17147 *	E-4788	p 177	N90-14511 *
AIAA-90-0028	p 11	N90-13355 *	AVSCOM-TM-90-C-003	p 138	N90-26171 *	E-4789	p 29	N90-21037 *
AIAA-90-0048	p 11	N90-12561 *	AVSCOM-TM-90-C-004	p 204	N90-22796 *	E-4813	p 142	N90-11915 *
AIAA-90-0053	p 177	N90-14511 *	AVSCOM-TM-90-C-006	p 203	N90-21394 *	E-4826	p 27	N90-13392 *
AIAA-90-0283	p 248	N90-20794 *	AVSCOM-TM-90-C-008	p 203	N90-22790 *	E-4837	p 11	N90-13352 *
AIAA-90-0339	p 248	N90-18229 *				E-4848	p 25	N90-13387 *
AIAA-90-0344	p 237	N90-13968 *				E-4850	p 125	N90-11881 *
AIAA-90-0353	p 130	N90-13675 *	AVSCOM-TR-88-C-035	p 202	N90-19593 *	E-4867	p 258	N90-12348 *
AIAA-90-0354	p 176	N90-13751 *	AVSCOM-TR-89-C-008	p 32	N90-27722 *	E-4911	p 202	N90-18740 *
AIAA-90-0391	p 11	N90-14203 *	AVSCOM-TR-89-C-011	p 203	N90-22054 *	E-4914	p 30	N90-22564 *
AIAA-90-0438	p 14	N90-25946 *	AVSCOM-TR-89-C-013	p 27	N90-13393 *	E-4915	p 188	N90-17085 *
AIAA-90-0488	p 38	N90-15965 *	AVSCOM-TR-89-C-014	p 199	N90-12033 *	E-4917	p 206	N90-17187 *
AIAA-90-0550	p 27	N90-17636 *	AVSCOM-TR-89-C-015	p 175	N90-11256 *	E-4920	p 221	N90-23789 *
AIAA-90-0643	p 176	N90-13749 *	AVSCOM-TR-89-C-017	p 126	N90-14363 *	E-4954	p 126	N90-16072 *
AIAA-90-0668	p 200	N90-14617 *	AVSCOM-TR-89-C-018	p 96	N90-14287 *	E-4956	p 178	N90-18005 *
AIAA-90-0669	p 12	N90-17562 *	AVSCOM-TR-89-C-020	p 202	N90-18041 *	E-4957-1	p 175	N90-11968 *
AIAA-90-0694	p 73	N90-14284 *	AVSCOM-TR-89-C-021	p 178	N90-17076 *	E-4959	p 150	N90-11943 *
AIAA-90-0715	p 44	N90-10912 *	AVSCOM-TR-90-C-003	p 101	N90-24382 *	E-4960	p 216	N90-12041 *
AIAA-90-0719	p 49	N90-13581 *	AVSCOM-TR-90-C-007	p 240	N90-23991 *	E-4963	p 124	N90-10262 *
AIAA-90-0722	p 134	N90-14398 *	AVSCOM-TR-90-C-008	p 100	N90-21826 *	E-4966	p 217	N90-17180 *
AIAA-90-0741	p 137	N90-11901 *	AVSCOM-TR-90-C-009	p 129	N90-23543 *	E-4967	p 241	N90-25607 *
AIAA-90-0744	p 238	N90-13988 *	AVSCOM-TR-90-C-013	p 204	N90-26338 *	E-4977	p 199	N90-12033 *
AIAA-90-0756	p 13	N90-21727 *	AVSCOM-TR-90-C-016	p 205	N90-28065 *	E-4979	p 52	N90-14275 *
AIAA-90-0808	p 143	N90-17977 *	AVSCOM-TR-90-C-018	p 241	N90-29121 *	E-4981	p 38	N90-19242 *
AIAA-90-0815	p 245	N90-14856 *	AVSCOM-TR-90-C-022	p 205	N90-28060 *	E-4985	p 97	N90-19302 *
AIAA-90-0850	p 47	N90-15983 *				E-4986	p 95	N90-10181 *
AIAA-90-0878	p 144	N90-19454 *	CMU-RI-TR-88-17	p 201	N90-15447 *	E-4987	p 145	N90-21250 *
AIAA-90-1681	p 183	N90-26278 *	CMU-RI-TR-89-9	p 234	N90-25499 *	E-4991	p 29	N90-21038 *
AIAA-90-1882	p 52	N90-22595 *				E-5001	p 50	N90-14268 *
AIAA-90-1894	p 81	N90-26065 *	CONF-891116-1	p 96	N90-15143 *	E-5007	p 71	N90-13590 *
AIAA-90-1899	p 31	N90-23404 *	CONF-891208-32	p 259	N90-24952 *	E-5009	p 117	N90-15211 *
AIAA-90-1901	p 31	N90-23406 *	CONF-891208-6	p 229	N90-15506 *	E-5012	p 30	N90-23403 *
AIAA-90-1935	p 30	N90-21762 *	CONF-900109-4	p 249	N90-16496 *	E-5013	p 215	N90-11332 *
AIAA-90-1955	p 182	N90-25289 *	CONF-900466-44	p 259	N90-24964 *	E-5015	p 31	N90-23407 *
AIAA-90-1968	p 131	N90-28742 *	CONF-900837-2	p 129	N90-26132 *	E-5016	p 216	N90-12950 *
AIAA-90-1990	p 45	N90-27732 *				E-5020	p 221	N90-22823 *
AIAA-90-1993	p 45	N90-25159 *	CTD-90/022	p 145	N90-20270 *	E-5034	p 95	N90-10185 *
AIAA-90-1994	p 81	N90-26070 *				E-5036	p 137	N90-22703 *
AIAA-90-2000	p 30	N90-21763 *	DE89-012331	p 96	N90-15143 *	E-5038	p 222	N90-26359 *
AIAA-90-2116	p 79	N90-25183 *	DE89-014778	p 229	N90-15506 *	E-5039	p 24	N90-10891 *
AIAA-90-2120	p 78	N90-22605 *	DE89-014967	p 249	N90-16496 *	E-5042	p 97	N90-18504 *
AIAA-90-2153	p 203	N90-22790 *	DE90-009725	p 259	N90-24952 *	E-5045	p 70	N90-11082 *
AIAA-90-2222	p 13	N90-25106 *	DE90-010499	p 129	N90-26132 *	E-5048	p 86	N90-12658 *
AIAA-90-2240	p 79	N90-24349 *	DE90-011236	p 259	N90-24964 *	E-5049	p 200	N90-13785 *
AIAA-90-2241	p 80	N90-25186 *				E-5050	p 220	N90-22808 *
AIAA-90-2271	p 2	N90-21725 *	DOE/NASA/0032-30	p 263	N90-11654 *	E-5051	p 96	N90-11806 *
AIAA-90-2319	p 107	N90-23518 *	DOE/NASA/0032-31	p 264	N90-29260 *	E-5052	p 217	N90-14655 *
AIAA-90-2375	p 184	N90-27984 *	DOE/NASA/0282-1	p 118	N90-18559 *	E-5054	p 70	N90-11081 *
AIAA-90-2386	p 39	N90-23416 *	DOE/NASA/0335-1	p 263	N90-14153 *	E-5057	p 216	N90-14641 *
AIAA-90-2389	p 78	N90-22604 *	DOE/NASA/0335-2	p 263	N90-26728 *	E-5058	p 201	N90-16286 *
AIAA-90-2417	p 30	N90-22566 *	DOE/NASA/0336-1	p 22	N90-10036 *	E-5059	p 257	N90-10737 *
AIAA-90-2450	p 185	N90-28792 *	DOE/NASA/0352-3	p 125	N90-11882 *	E-5060	p 126	N90-13666 *
AIAA-90-2452	p 137	N90-23591 *	DOE/NASA/16310-13	p 116	N90-11854 *	E-5062	p 126	N90-14363 *
AIAA-90-2503	p 43	N90-25158 *	DOE/NASA/20370-23	p 206	N90-12034 *	E-5063	p 27	N90-13393 *
AIAA-90-2551	p 82	N90-27785 *	DOE/NASA/21749-1	p 119	N90-23536 *	E-5064	p 258	N90-11606 *
AIAA-90-2578	p 83	N90-28657 *	DOE/NASA/33408-4	p 263	N90-26729 *	E-5066	p 86	N90-12659 *
AIAA-90-2579	p 79	N90-25161 *	DOE/NASA/50162-3	p 127	N90-16944 *	E-5068	p 10	N90-10004 *
AIAA-90-2586	p 82	N90-27783 *				E-5069	p 242	N90-11497 *
						E-5070	p 215	N90-10455 *

REPORT NUMBER INDEX

E-5071	p 187	N90-11277 * #	E-5224	p 106	N90-21842 * #	E-5359	p 152	N90-21272 * #
E-5072	p 12	N90-17561 * #	E-5228	p 13	N90-19203 * #	E-5360	p 203	N90-22041 * #
E-5074	p 96	N90-14287 * #	E-5229	p 178	N90-18667 * #	E-5361	p 87	N90-20130 * #
E-5075-1	p 177	N90-14517 * #	E-5231	p 200	N90-13797 * #	E-5365	p 153	N90-21275 * #
E-5077	p 242	N90-10635 * #	E-5232	p 176	N90-13750 * #	E-5366	p 180	N90-21303 * #
E-5078	p 175	N90-11250 * #	E-5234	p 50	N90-14273 * #	E-5367	p 180	N90-21306 * #
E-5080	p 264	N90-22464 * #	E-5235	p 217	N90-17173 * #	E-5368	p 180	N90-21307 * #
E-5081	p 248	N90-17413 * #	E-5236	p 27	N90-14235 * #	E-5372	p 219	N90-20438 * #
E-5083	p 267	N90-15030 * #	E-5237	p 27	N90-17636 * #	E-5373	p 153	N90-21282 * #
E-5084	p 70	N90-11804 * #	E-5238	p 13	N90-21727 * #	E-5375	p 76	N90-21110 * #
E-5086	p 245	N90-10674 * #	E-5240	p 200	N90-14617 * #	E-5376	p 153	N90-21277 * #
E-5089	p 100	N90-23477 * #	E-5241	p 238	N90-22262 * #	E-5378	p 98	N90-20151 * #
E-5090	p 98	N90-21123 * #	E-5242	p 237	N90-20708 * #	E-5379	p 100	N90-21143 * #
E-5093	p 96	N90-12670 * #	E-5243	p 219	N90-21420 * #	E-5380	p 219	N90-19629 * #
E-5094	p 205	N90-28063 * #	E-5244	p 181	N90-21974 * #	E-5381	p 207	N90-23754 * #
E-5095	p 51	N90-26054 * #	E-5245	p 73	N90-14285 * #	E-5383	p 99	N90-21133 * #
E-5102	p 116	N90-11854 * #	E-5246	p 73	N90-14284 * #	E-5384	p 204	N90-22796 * #
E-5104	p 73	N90-15992 * #	E-5247	p 27	N90-13394 * #	E-5388	p 136	N90-21871 * #
E-5105	p 217	N90-14856 * #	E-5248	p 74	N90-17677 * #	E-5389	p 99	N90-21131 * #
E-5107	p 69	N90-10172 * #	E-5249	p 176	N90-13749 * #	E-5391	p 78	N90-21812 * #
E-5108	p 11	N90-12580 * #	E-5249	p 183	N90-26275 * #	E-5392	p 101	N90-24384 * #
E-5109	p 245	N90-14060 * #	E-5250	p 101	N90-24382 * #	E-5395	p 259	N90-20886 * #
E-5110	p 178	N90-18665 * #	E-5251	p 152	N90-21274 * #	E-5396	p 179	N90-21295 * #
E-5112	p 188	N90-13761 * #	E-5252	p 96	N90-14294 * #	E-5402	p 153	N90-21283 * #
E-5113	p 203	N90-22054 * #	E-5253	p 72	N90-14283 * #	E-5403	p 207	N90-21401 * #
E-5115	p 176	N90-13719 * #	E-5255	p 130	N90-17890 * #	E-5406	p 128	N90-21192 * #
E-5116	p 1	N90-13323 * #	E-5256	p 237	N90-15622 * #	E-5407	p 205	N90-28066 * #
E-5117	p 206	N90-12034 * #	E-5257	p 137	N90-17929 * #	E-5408	p 151	N90-20301 * #
E-5118	p 125	N90-11880 * #	E-5258	p 12	N90-14206 * #	E-5409	p 190	N90-23714 * #
E-5119	p 86	N90-13597 * #	E-5259	p 29	N90-21036 * #	E-5410	p 99	N90-21132 * #
E-5120	p 125	N90-11144 * #	E-5260	p 49	N90-13581 * #	E-5411	p 231	N90-21469 * #
E-5122	p 71	N90-13595 * #	E-5261	p 266	N90-22488 * #	E-5412	p 189	N90-20358 * #
E-5123	p 243	N90-14844 * #	E-5262	p 127	N90-16944 * #	E-5413	p 119	N90-22646 * #
E-5124	p 242	N90-12231 * #	E-5263	p 145	N90-21263 * #	E-5416	p 267	N90-23339 * #
E-5126	p 143	N90-14452 * #	E-5264	p 38	N90-15964 * #	E-5417	p 45	N90-20110 * #
E-5127	p 137	N90-11901 * #	E-5265	p 245	N90-14856 * #	E-5420	p 184	N90-27982 * #
E-5128	p 11	N90-12561 * #	E-5266	p 27	N90-17635 * #	E-5421	p 13	N90-20051 * #
E-5129	p 216	N90-14640 * #	E-5267	p 97	N90-16008 * #	E-5422	p 240	N90-23991 * #
E-5130	p 18	N90-13381 * #	E-5269	p 38	N90-15965 * #	E-5426	p 220	N90-22117 * #
E-5131	p 258	N90-14108 * #	E-5270	p 189	N90-21360 * #	E-5427	p 1	N90-21723 * #
E-5137	p 12	N90-17562 * #	E-5271	p 28	N90-20085 * #	E-5428	p 14	N90-25940 * #
E-5138	p 117	N90-14335 * #	E-5272	p 99	N90-21137 * #	E-5430	p 32	N90-25982 * #
E-5139	p 249	N90-21602 * #	E-5273	p 219	N90-20428 * #	E-5431	p 30	N90-21762 * #
E-5141	p 134	N90-14398 * #	E-5276	p 218	N90-18064 * #	E-5432	p 39	N90-23416 * #
E-5142	p 118	N90-20181 * #	E-5278	p 223	N90-26373 * #	E-5433	p 205	N90-28060 * #
E-5143	p 219	N90-20432 * #	E-5279	p 97	N90-17817 * #	E-5435	p 181	N90-22011 * #
E-5144	p 44	N90-10912 * #	E-5280	p 135	N90-20237 * #	E-5436	p 192	N90-28833 * #
E-5147	p 25	N90-11740 * #	E-5282	p 207	N90-22801 * #	E-5438	p 203	N90-22790 * #
E-5148	p 137	N90-11902 * #	E-5283	p 128	N90-21862 * #	E-5440	p 100	N90-21825 * #
E-5151	p 237	N90-13968 * #	E-5284	p 151	N90-20286 * #	E-5442	p 100	N90-21824 * #
E-5152	p 235	N90-14783 * #	E-5285	p 117	N90-16053 * #	E-5443	p 249	N90-26635 * #
E-5153	p 106	N90-12696 * #	E-5286	p 138	N90-28754 * #	E-5446	p 2	N90-21725 * #
E-5155	p 14	N90-25948 * #	E-5287	p 243	N90-18927 * #	E-5448	p 182	N90-22761 * #
E-5156	p 99	N90-21138 * #	E-5291	p 243	N90-19783 * #	E-5449	p 77	N90-21114 * #
E-5158	p 229	N90-14678 * #	E-5292	p 180	N90-21962 * #	E-5450	p 31	N90-23404 * #
E-5159	p 143	N90-12813 * #	E-5295	p 151	N90-19484 * #	E-5451	p 153	N90-21287 * #
E-5160	p 117	N90-13636 * #	E-5297	p 207	N90-21402 * #	E-5453	p 129	N90-23543 * #
E-5162	p 25	N90-12618 * #	E-5298	p 202	N90-20391 * #	E-5454	p 155	N90-27965 * #
E-5167	p 126	N90-14362 * #	E-5300	p 128	N90-21182 * #	E-5455	p 77	N90-21116 * #
E-5170	p 238	N90-13988 * #	E-5301	p 218	N90-18745 * #	E-5457	p 78	N90-21808 * #
E-5177	p 47	N90-15983 * #	E-5303	p 189	N90-20352 * #	E-5458	p 119	N90-23536 * #
E-5180	p 144	N90-19454 * #	E-5304	p 100	N90-21826 * #	E-5460	p 13	N90-21733 * #
E-5181	p 137	N90-21210 * #	E-5306	p 100	N90-21821 * #	E-5462	p 203	N90-21394 * #
E-5182	p 98	N90-20138 * #	E-5307	p 127	N90-19373 * #	E-5469	p 232	N90-22843 * #
E-5183	p 262	N90-20901 * #	E-5308	p 76	N90-19299 * #	E-5472	p 183	N90-26279 * #
E-5184	p 117	N90-16911 * #	E-5309	p 86	N90-17811 * #	E-5474	p 30	N90-21763 * #
E-5185	p 26	N90-13389 * #	E-5310	p 219	N90-20431 * #	E-5475	p 146	N90-28768 * #
E-5186	p 32	N90-27722 * #	E-5311	p 243	N90-18198 * #	E-5476	p 81	N90-26070 * #
E-5187	p 221	N90-23757 * #	E-5312	p 86	N90-19301 * #	E-5478	p 80	N90-25185 * #
E-5188	p 126	N90-14368 * #	E-5313	p 127	N90-19374 * #	E-5491	p 107	N90-21844 * #
E-5189	p 143	N90-17977 * #	E-5314	p 188	N90-18025 * #	E-5492	p 181	N90-22016 * #
E-5190	p 134	N90-13680 * #	E-5315	p 189	N90-20353 * #	E-5493	p 79	N90-22606 * #
E-5191	p 248	N90-18229 * #	E-5317	p 244	N90-21570 * #	E-5494	p 39	N90-25151 * #
E-5192	p 177	N90-14512 * #	E-5320	p 218	N90-19617 * #	E-5495	p 154	N90-22732 * #
E-5193	p 178	N90-17076 * #	E-5321	p 28	N90-20090 * #	E-5496	p 233	N90-25419 * #
E-5195	p 176	N90-13748 * #	E-5322	p 243	N90-20769 * #	E-5497	p 78	N90-22605 * #
E-5196	p 11	N90-13355 * #	E-5323	p 202	N90-17147 * #	E-5498	p 31	N90-24273 * #
E-5197	p 11	N90-14203 * #	E-5324	p 152	N90-21273 * #	E-5499	p 155	N90-26250 * #
E-5198	p 250	N90-17424 * #	E-5327	p 145	N90-21261 * #	E-5500	p 240	N90-22324 * #
E-5200	p 189	N90-22021 * #	E-5330	p 178	N90-20326 * #	E-5502	p 240	N90-22323 * #
E-5201	p 176	N90-13751 * #	E-5331	p 128	N90-21181 * #	E-5503	p 240	N90-22325 * #
E-5202	p 179	N90-20338 * #	E-5332	p 179	N90-20337 * #	E-5504	p 240	N90-23125 * #
E-5204	p 202	N90-18041 * #	E-5333	p 151	N90-18634 * #	E-5505	p 190	N90-22773 * #
E-5205	p 259	N90-22421 * #	E-5334	p 179	N90-21296 * #	E-5513	p 101	N90-24383 * #
E-5206	p 130	N90-13675 * #	E-5335	p 179	N90-21291 * #	E-5514	p 156	N90-28786 * #
E-5207	p 229	N90-18097 * #	E-5336	p 135	N90-20253 * #	E-5515	p 154	N90-22731 * #
E-5208	p 98	N90-19310 * #	E-5339	p 87	N90-23476 * #	E-5516	p 183	N90-26278 * #
E-5210	p 248	N90-20794 * #	E-5341	p 28	N90-19234 * #	E-5517	p 232	N90-22847 * #
E-5211	p 127	N90-17875 * #	E-5342	p 153	N90-21278 * #	E-5518	p 220	N90-22822 * #
E-5212	p 27	N90-15923 * #	E-5343	p 131	N90-21869 * #	E-5524	p 184	N90-26282 * #
E-5214	p 98	N90-21124 * #	E-5345	p 248	N90-21600 * #	E-5527	p 154	N90-23662 * #
E-5215	p 223	N90-28111 * #	E-5347	p 98	N90-20139 * #	E-5528	p 52	N90-22595 * #
E-5216	p 258	N90-17465 * #	E-5349	p 244	N90-21567 * #	E-5529	p 192	N90-22784 * #
E-5217	p 239	N90-21564 * #	E-5350	p 207	N90-21399 * #	E-5530	p 78	N90-22604 * #
E-5218	p 189	N90-21361 * #	E-5351	p 203	N90-20393 * #	E-5531	p 14	N90-27655 * #
E-5219	p 179	N90-21300 * #	E-5356	p 152	N90-21271 * #	E-5533	p 154	N90-23663 * #
			E-5358			E-5536		

E-5537

REPORT NUMBER INDEX

E-5537	p 79	N90-24349 *	ESL-TR-716111-7	p 142	N90-11211 *	M/NA/TURB-1	p 11	N90-13328 *
E-5538	p 80	N90-25186 *	ESL-TR-719630-3	p 143	N90-16103 *			
E-5539	p 30	N90-22566 *				M/NAFA/89-1	p 1	N90-21724 *
E-5540	p 82	N90-26873 *	ESL-721837-1	p 257	N90-11603 *			
E-5543	p 222	N90-25367 *	ETEC-89-7	p 50	N90-15985 *	MSU-ENGR-90-006	p 180	N90-21301 *
E-5545	p 184	N90-27984 *						
E-5546	p 191	N90-25324 *	E19-666-1	p 191	N90-28827 *	MTI-87ASE555SA11	p 263	N90-11654 *
E-5547	p 81	N90-26068 *				MTI-87ASE575SA12	p 264	N90-29260 *
E-5547	p 204	N90-26338 *	FCR-10555A	p 230	N90-18808 *	NAS 1.15:100169	p 95	N90-10188 *
E-5548	p 31	N90-23406 *				NAS 1.15:100746	p 234	N90-12984 *
E-5550	p 101	N90-25193 *	FEF/PD/1101/89-VOL-2	p 215	N90-10450 *	NAS 1.15:101311	p 216	N90-13819 *
E-5551	p 138	N90-26170 *	FEF/PD/1102/89-VOL-3	p 215	N90-10451 *	NAS 1.15:101344	p 138	N90-26172 *
E-5552	p 82	N90-27786 *				NAS 1.15:101344	p 144	N90-20264 *
E-5553	p 13	N90-25106 *	GARRETT-31-8071(1)	p 263	N90-14153 *	NAS 1.15:101453	p 145	N90-21250 *
E-5554	p 137	N90-23591 *	GARRETT-31-8071(2)	p 263	N90-26728 *	NAS 1.15:101454	p 133	N90-11196 *
E-5555	p 107	N90-23518 *				NAS 1.15:101472	p 262	N90-12388 *
E-5556	p 233	N90-25420 *	GDSS-CRAD-89-002	p 49	N90-10983 *	NAS 1.15:101814	p 262	N90-12389 *
E-5557	p 154	N90-25273 *				NAS 1.15:101815	p 129	N90-26132 *
E-5559	p 221	N90-23770 *	G8558-8701	p 131	N90-19386 *	NAS 1.15:101914	p 96	N90-15143 *
E-5562	p 155	N90-27966 *				NAS 1.15:101940	p 95	N90-10181 *
E-5564	p 79	N90-25183 *	HSE-11518-VOL-1	p 23	N90-10043 *	NAS 1.15:101958	p 71	N90-13596 *
E-5568	p 184	N90-27985 *	HSE-11518-VOL-2	p 23	N90-10044 *	NAS 1.15:101974	p 134	N90-13679 *
E-5570	p 44	N90-26030 *	HSE-116227	p 25	N90-12617 *	NAS 1.15:102014	p 262	N90-15846 *
E-5571	p 43	N90-25158 *	HSE-11804	p 24	N90-10046 *	NAS 1.15:102034	p 134	N90-16087 *
E-5573	p 263	N90-26729 *	HSE-11894	p 24	N90-10045 *	NAS 1.15:102037	p 27	N90-13392 *
E-5575	p 136	N90-26163 *	HSE-12648	p 199	N90-10437 *	NAS 1.15:102069	p 11	N90-13352 *
E-5577	p 53	N90-26063 *				NAS 1.15:102077	p 125	N90-11881 *
E-5578	p 79	N90-25181 *	IAF PAPER ICOSP89-3-8	p 227	A90-27709 *	NAS 1.15:102088	p 267	N90-15030 *
E-5580	p 221	N90-23773 *	IAF PAPER ICOSP89-4-5	p 48	A90-27710 *	NAS 1.15:102090	p 206	N90-17167 *
E-5585	p 45	N90-25159 *				NAS 1.15:102130	p 178	N90-18005 *
E-5589	p 182	N90-25289 *	IAF PAPER 89-027	p 53	A90-13262 *	NAS 1.15:102288	p 150	N90-11943 *
E-5590	p 185	N90-28792 *	IAF PAPER 89-057	p 53	A90-13282 *	NAS 1.15:102289	p 216	N90-12041 *
E-5591	p 45	N90-27732 *	IAF PAPER 89-078	p 54	A90-13295 *	NAS 1.15:102290	p 124	N90-10262 *
E-5593	p 130	N90-28740 *	IAF PAPER 89-254	p 42	A90-13409 *	NAS 1.15:102291	p 267	N90-24220 *
E-5594	p 37	N90-26011 *	IAF PAPER 89-403	p 157	A90-13511 *	NAS 1.15:102296	p 52	N90-14275 *
E-5597	p 80	N90-25184 *	IAF PAPER 89-664	p 54	A90-13668 *	NAS 1.15:102300	p 29	N90-21038 *
E-5598	p 155	N90-25278 *				NAS 1.15:102303	p 71	N90-13590 *
E-5599	p 190	N90-25323 *	IAF-88-355	p 134	N90-13679 *	NAS 1.15:102313	p 50	N90-14268 *
E-5607	p 81	N90-26065 *	IAF-90-200	p 82	N90-26873 *	NAS 1.15:102316	p 30	N90-22564 *
E-5608	p 87	N90-26074 *				NAS 1.15:102319	p 31	N90-23407 *
E-5609	p 80	N90-25187 *	ICOMP-89-17	p 216	N90-12041 *	NAS 1.15:102320	p 216	N90-12950 *
E-5613	p 102	N90-27874 *	ICOMP-89-21	p 175	N90-11969 *	NAS 1.15:102322	p 136	N90-10309 *
E-5615	p 267	N90-26789 *	ICOMP-89-22	p 217	N90-14655 *	NAS 1.15:102324	p 221	N90-22823 *
E-5616	p 191	N90-26299 *	ICOMP-89-24	p 243	N90-14002 *	NAS 1.15:102329	p 95	N90-10185 *
E-5617	p 183	N90-26276 *	ICOMP-89-25	p 242	N90-10635 *	NAS 1.15:102333	p 97	N90-18504 *
E-5618	p 233	N90-26396 *	ICOMP-89-26	p 175	N90-11250 *	NAS 1.15:102334	p 175	N90-11969 *
E-5620	p 51	N90-25173 *	ICOMP-89-27	p 243	N90-14844 *	NAS 1.15:102336	p 70	N90-11082 *
E-5621	p 129	N90-26142 *	ICOMP-89-28	p 242	N90-12231 *	NAS 1.15:102340	p 200	N90-13785 *
E-5623	p 32	N90-26009 *	ICOMP-89-29	p 14	N90-25948 *	NAS 1.15:102341	p 24	N90-10891 *
E-5624	p 81	N90-26069 *	ICOMP-89-30	p 177	N90-14517 *	NAS 1.15:102342	p 220	N90-22808 *
E-5626	p 183	N90-26273 *	ICOMP-89-31	p 217	N90-17173 *	NAS 1.15:102343	p 96	N90-11808 *
E-5629	p 131	N90-26160 *	ICOMP-89-32	p 29	N90-21036 *	NAS 1.15:102344	p 217	N90-14655 *
E-5632	p 246	N90-28393 *	ICOMP-90-0017	p 184	N90-28009 *	NAS 1.15:102346	p 70	N90-11081 *
E-5634	p 51	N90-26055 *	ICOMP-90-01	p 243	N90-20769 *	NAS 1.15:102348	p 216	N90-14641 *
E-5635	p 184	N90-27983 *	ICOMP-90-02	p 243	N90-18927 *	NAS 1.15:102349	p 201	N90-16286 *
E-5636	p 184	N90-28009 *	ICOMP-90-03	p 243	N90-19783 *	NAS 1.15:102350	p 257	N90-10737 *
E-5637	p 259	N90-26682 *	ICOMP-90-04	p 180	N90-21962 *	NAS 1.15:102351	p 126	N90-13866 *
E-5640	p 102	N90-28670 *	ICOMP-90-05	p 243	N90-18198 *	NAS 1.15:102353	p 126	N90-14363 *
E-5641	p 222	N90-26364 *	ICOMP-90-06	p 178	N90-20326 *	NAS 1.15:102354	p 242	N90-11497 *
E-5644	p 82	N90-27785 *	ICOMP-90-07	p 179	N90-20337 *	NAS 1.15:102355	p 86	N90-12659 *
E-5645	p 244	N90-26614 *	ICOMP-90-09	p 179	N90-21291 *	NAS 1.15:102356	p 257	N90-10738 *
E-5647	p 244	N90-26615 *	ICOMP-90-10	p 244	N90-21567 *	NAS 1.15:102357	p 187	N90-11277 *
E-5650	p 102	N90-27875 *	ICOMP-90-11	p 99	N90-21131 *	NAS 1.15:102358	p 12	N90-17561 *
E-5656	p 233	N90-26397 *	ICOMP-90-12	p 244	N90-21570 *	NAS 1.15:102359	p 243	N90-14002 *
E-5658	p 244	N90-26616 *	ICOMP-90-13	p 184	N90-27982 *	NAS 1.15:102360	p 96	N90-14287 *
E-5659	p 81	N90-26071 *	ICOMP-90-14	p 101	N90-24383 *	NAS 1.15:102361	p 242	N90-10635 *
E-5662	p 82	N90-27783 *	ICOMP-90-15	p 184	N90-26282 *	NAS 1.15:102362	p 175	N90-11250 *
E-5665	p 47	N90-27736 *	ICOMP-90-16	p 184	N90-27983 *	NAS 1.15:102363	p 264	N90-22464 *
E-5667	p 131	N90-28742 *	ICOMP-90-18	p 244	N90-26614 *	NAS 1.15:102365	p 248	N90-17413 *
E-5668	p 183	N90-26272 *	ICOMP-90-19	p 244	N90-26615 *	NAS 1.15:102366	p 70	N90-11804 *
E-5670	p 224	N90-28113 *	ICOMP-90-20	p 244	N90-26616 *	NAS 1.15:102367	p 245	N90-10674 *
E-5672	p 260	N90-26683 *	ICOMP-90-21	p 244	N90-29124 *	NAS 1.15:102368	p 137	N90-22703 *
E-5676	p 14	N90-25946 *				NAS 1.15:102369	p 222	N90-26359 *
E-5677	p 15	N90-27657 *	INT-PATENT-CLASS-B64D-33/04	p 204	N90-23751 *	NAS 1.15:102370	p 100	N90-23477 *
E-5681	p 191	N90-28033 *				NAS 1.15:102371	p 98	N90-21123 *
E-5683	p 82	N90-27784 *	INT-PATENT-CLASS-F16J-15/46	p 204	N90-23751 *	NAS 1.15:102372	p 73	N90-15992 *
E-5684	p 191	N90-28031 *				NAS 1.15:102373	p 69	N90-10172 *
E-5686	p 205	N90-28065 *	INT-PATENT-CLASS-G01N-3/32	p 190	N90-23712 *	NAS 1.15:102374	p 11	N90-12560 *
E-5687	p 52	N90-28596 *				NAS 1.15:102375	p 245	N90-14060 *
E-5692	p 82	N90-27782 *	INT-PATENT-CLASS-H01J-25/34	p 153	N90-22724 *	NAS 1.15:102376	p 178	N90-18665 *
E-5695	p 244	N90-29124 *				NAS 1.15:102377	p 176	N90-13719 *
E-5699	p 223	N90-28112 *	KBO-FR-1	p 118	N90-21165 *	NAS 1.15:102378	p 206	N90-12034 *
E-5713	p 205	N90-28062 *				NAS 1.15:102379	p 125	N90-11880 *
E-5734	p 83	N90-28657 *	KU-FRL-724-4	p 181	N90-22000 *	NAS 1.15:102380	p 86	N90-13597 *
E-5751	p 260	N90-29219 *				NAS 1.15:102382	p 125	N90-11144 *
E-5752	p 108	N90-28696 *	L-89-600204	p 202	N90-19593 *	NAS 1.15:102383	p 71	N90-13595 *
E-5756	p 83	N90-28659 *				NAS 1.15:102384	p 243	N90-14844 *
E-5761	p 241	N90-29121 *	LC-86-23	p 35	N90-28567 *	NAS 1.15:102385	p 242	N90-12231 *
E-6657	p 52	N90-25178 *				NAS 1.15:102386	p 137	N90-11901 *
EDR-12909	p 32	N90-24274 *	LG85ER0105	p 10	N90-10011 *	NAS 1.15:102387	p 11	N90-12561 *
EDR-14232	p 22	N90-10036 *	LG89ER0026	p 24	N90-11738 *	NAS 1.15:102388	p 216	N90-14640 *
EDR-14622	p 30	N90-22567 *	LG89ER0064	p 25	N90-11739 *	NAS 1.15:102389	p 18	N90-13381 *
ESD-TR-90-048	p 141	A90-36717 *	LSPI-901	p 77	N90-21806 *	NAS 1.15:102390	p 116	N90-11854 *
			LSPI-903	p 77	N90-21807 *	NAS 1.15:102391	p 177	N90-14511 *
						NAS 1.15:102392	p 200	N90-13786 *

REPORT NUMBER INDEX

NAS 1.15:102393	p 117	N90-14335 *	#	NAS 1.15:102499	p 180	N90-21962 *	#	NAS 1.15:103119	p 100	N90-21824 *	#
NAS 1.15:102394	p 44	N90-10912 *	#	NAS 1.15:102500	p 151	N90-19484 *	#	NAS 1.15:103120	p 2	N90-21725 *	#
NAS 1.15:102395	p 203	N90-22054 *	#	NAS 1.15:102501-REV	p 207	N90-21402 *	#	NAS 1.15:103121	p 182	N90-22761 *	#
NAS 1.15:102396	p 12	N90-16719 *	#	NAS 1.15:102502	p 218	N90-18745 *	#	NAS 1.15:103122	p 77	N90-21114 *	#
NAS 1.15:102397	p 25	N90-11740 *	#	NAS 1.15:102503	p 189	N90-20352 *	#	NAS 1.15:103123	p 31	N90-23404 *	#
NAS 1.15:102398	p 137	N90-11902 *	#	NAS 1.15:102504	p 100	N90-21821 *	#	NAS 1.15:103124	p 183	N90-26279 *	#
NAS 1.15:102399	p 106	N90-12696 *	#	NAS 1.15:102505	p 127	N90-19373 *	#	NAS 1.15:103125	p 153	N90-21287 *	#
NAS 1.15:102401	p 86	N90-12658 *	#	NAS 1.15:102506	p 76	N90-19299 *	#	NAS 1.15:103126	p 129	N90-23543 *	#
NAS 1.15:102402	p 14	N90-25948 *	#	NAS 1.15:102507	p 86	N90-17811 *	#	NAS 1.15:103127	p 77	N90-21116 *	#
NAS 1.15:102403	p 118	N90-20181 *	#	NAS 1.15:102508	p 219	N90-20431 *	#	NAS 1.15:103128	p 78	N90-21808 *	#
NAS 1.15:102404	p 99	N90-21138 *	#	NAS 1.15:102509	p 243	N90-18198 *	#	NAS 1.15:103129	p 119	N90-23536 *	#
NAS 1.15:102405	p 96	N90-12670 *	#	NAS 1.15:102510	p 86	N90-19301 *	#	NAS 1.15:103130	p 13	N90-21733 *	#
NAS 1.15:102406	p 229	N90-14678 *	#	NAS 1.15:102511	p 188	N90-18025 *	#	NAS 1.15:103131	p 203	N90-21394 *	#
NAS 1.15:102407	p 143	N90-12813 *	#	NAS 1.15:102512	p 98	N90-20138 *	#	NAS 1.15:103132	p 232	N90-22843 *	#
NAS 1.15:102408	p 117	N90-13636 *	#	NAS 1.15:102513	p 189	N90-20353 *	#	NAS 1.15:103133	p 146	N90-28768 *	#
NAS 1.15:102409	p 25	N90-12618 *	#	NAS 1.15:102514	p 98	N90-20138 *	#	NAS 1.15:103134	p 81	N90-26070 *	#
NAS 1.15:102410	p 126	N90-14362 *	#	NAS 1.15:102515	p 218	N90-19617 *	#	NAS 1.15:103135	p 204	N90-22796 *	#
NAS 1.15:102411	p 238	N90-13988 *	#	NAS 1.15:102516	p 98	N90-21124 *	#	NAS 1.15:103136	p 249	N90-26635 *	#
NAS 1.15:102412	p 217	N90-17180 *	#	NAS 1.15:102517	p 28	N90-20090 *	#	NAS 1.15:103137	p 80	N90-25185 *	#
NAS 1.15:102413	p 47	N90-15983 *	#	NAS 1.15:102518	p 243	N90-20769 *	#	NAS 1.15:103138	p 107	N90-21844 *	#
NAS 1.15:102414	p 144	N90-19454 *	#	NAS 1.15:102519	p 202	N90-17147 *	#	NAS 1.15:103139	p 181	N90-22016 *	#
NAS 1.15:102415	p 262	N90-20901 *	#	NAS 1.15:102520	p 152	N90-21273 *	#	NAS 1.15:103140	p 79	N90-22606 *	#
NAS 1.15:102416	p 117	N90-16911 *	#	NAS 1.15:102521	p 145	N90-21261 *	#	NAS 1.15:103141	p 39	N90-25151 *	#
NAS 1.15:102417	p 26	N90-13389 *	#	NAS 1.15:102522	p 178	N90-20326 *	#	NAS 1.15:103142	p 154	N90-22732 *	#
NAS 1.15:102418	p 27	N90-13393 *	#	NAS 1.15:102523	p 179	N90-20337 *	#	NAS 1.15:103143	p 233	N90-25419 *	#
NAS 1.15:102419	p 126	N90-14368 *	#	NAS 1.15:102524	p 151	N90-18634 *	#	NAS 1.15:103144	p 78	N90-22605 *	#
NAS 1.15:102420	p 143	N90-17977 *	#	NAS 1.15:102525	p 179	N90-21296 *	#	NAS 1.15:103145	p 155	N90-26250 *	#
NAS 1.15:102421	p 134	N90-13680 *	#	NAS 1.15:102526	p 202	N90-20391 *	#	NAS 1.15:103146	p 240	N90-22324 *	#
NAS 1.15:102422	p 248	N90-18229 *	#	NAS 1.15:102527	p 135	N90-20253 *	#	NAS 1.15:103147	p 240	N90-22323 *	#
NAS 1.15:102423	p 178	N90-17076 *	#	NAS 1.15:102528	p 87	N90-23476 *	#	NAS 1.15:103148	p 240	N90-22325 *	#
NAS 1.15:102424	p 11	N90-13355 *	#	NAS 1.15:102529	p 219	N90-20428 *	#	NAS 1.15:103149	p 240	N90-23125 *	#
NAS 1.15:102425	p 11	N90-14203 *	#	NAS 1.15:102530	p 28	N90-19234 *	#	NAS 1.15:103150	p 190	N90-22773 *	#
NAS 1.15:102426	p 250	N90-17424 *	#	NAS 1.15:102531	p 153	N90-21278 *	#	NAS 1.15:103151	p 101	N90-24383 *	#
NAS 1.15:102427	p 177	N90-14517 *	#	NAS 1.15:102532	p 131	N90-21869 *	#	NAS 1.15:103152	p 154	N90-22731 *	#
NAS 1.15:102428	p 189	N90-22021 *	#	NAS 1.15:102533	p 98	N90-20139 *	#	NAS 1.15:103153	p 183	N90-26278 *	#
NAS 1.15:102429	p 176	N90-13751 *	#	NAS 1.15:102534	p 202	N90-20392 *	#	NAS 1.15:103154	p 232	N90-22847 *	#
NAS 1.15:102430	p 202	N90-18041 *	#	NAS 1.15:102535	p 179	N90-21291 *	#	NAS 1.15:103155	p 220	N90-22822 *	#
NAS 1.15:102431	p 259	N90-22421 *	#	NAS 1.15:102536	p 244	N90-21567 *	#	NAS 1.15:103156	p 184	N90-26282 *	#
NAS 1.15:102432	p 130	N90-13675 *	#	NAS 1.15:102537	p 207	N90-21401 *	#	NAS 1.15:103157	p 154	N90-23662 *	#
NAS 1.15:102433	p 229	N90-18097 *	#	NAS 1.15:102538	p 203	N90-21399 *	#	NAS 1.15:103158	p 52	N90-22595 *	#
NAS 1.15:102434	p 98	N90-19310 *	#	NAS 1.15:102539	p 128	N90-20393 *	#	NAS 1.15:103159	p 192	N90-22784 *	#
NAS 1.15:102435	p 248	N90-20794 *	#	NAS 1.15:102540	p 128	N90-21182 *	#	NAS 1.15:103160	p 78	N90-22604 *	#
NAS 1.15:102436	p 27	N90-15923 *	#	NAS 1.15:102541	p 152	N90-21181 *	#	NAS 1.15:103161	p 154	N90-23663 *	#
NAS 1.15:102437	p 189	N90-21361 *	#	NAS 1.15:102542	p 152	N90-21272 *	#	NAS 1.15:103162	p 79	N90-24349 *	#
NAS 1.15:102438	p 106	N90-21842 *	#	NAS 1.15:102543	p 87	N90-20130 *	#	NAS 1.15:103163	p 80	N90-25186 *	#
NAS 1.15:102439	p 178	N90-18667 *	#	NAS 1.15:102544	p 152	N90-21275 *	#	NAS 1.15:103164	p 30	N90-22566 *	#
NAS 1.15:102440	p 200	N90-13797 *	#	NAS 1.15:102545	p 180	N90-21303 *	#	NAS 1.15:103165	p 82	N90-26873 *	#
NAS 1.15:102441	p 176	N90-13750 *	#	NAS 1.15:102546	p 180	N90-21306 *	#	NAS 1.15:103166	p 31	N90-24273 *	#
NAS 1.15:102442	p 50	N90-14273 *	#	NAS 1.15:102547	p 180	N90-21307 *	#	NAS 1.15:103167	p 222	N90-25367 *	#
NAS 1.15:102443	p 217	N90-17173 *	#	NAS 1.15:102548	p 119	N90-25211 *	#	NAS 1.15:103168	p 101	N90-25193 *	#
NAS 1.15:102444	p 27	N90-14235 *	#	NAS 1.15:102549	p 219	N90-20438 *	#	NAS 1.15:103169	p 138	N90-26170 *	#
NAS 1.15:102445	p 27	N90-17636 *	#	NAS 1.15:102550	p 76	N90-21110 *	#	NAS 1.15:103170	p 82	N90-27786 *	#
NAS 1.15:102446	p 238	N90-22262 *	#	NAS 1.15:102551	p 98	N90-20151 *	#	NAS 1.15:103171	p 13	N90-25106 *	#
NAS 1.15:102447	p 237	N90-20708 *	#	NAS 1.15:102552	p 100	N90-21143 *	#	NAS 1.15:103172	p 137	N90-23591 *	#
NAS 1.15:102448	p 217	N90-14656 *	#	NAS 1.15:102553	p 219	N90-19629 *	#	NAS 1.15:103173	p 107	N90-23518 *	#
NAS 1.15:102449	p 200	N90-14617 *	#	NAS 1.15:102554	p 207	N90-23754 *	#	NAS 1.15:103174	p 204	N90-26338 *	#
NAS 1.15:102450	p 181	N90-21974 *	#	NAS 1.15:102555	p 153	N90-21277 *	#	NAS 1.15:103175	p 233	N90-25420 *	#
NAS 1.15:102451	p 73	N90-14285 *	#	NAS 1.15:102556	p 99	N90-21277 *	#	NAS 1.15:103176	p 154	N90-25273 *	#
NAS 1.15:102452	p 73	N90-14284 *	#	NAS 1.15:102557	p 136	N90-21133 *	#	NAS 1.15:103177	p 221	N90-23770 *	#
NAS 1.15:102453	p 27	N90-13394 *	#	NAS 1.15:102558	p 99	N90-21871 *	#	NAS 1.15:103178	p 155	N90-27966 *	#
NAS 1.15:102454	p 74	N90-17677 *	#	NAS 1.15:102559	p 179	N90-21131 *	#	NAS 1.15:103179	p 52	N90-25178 *	#
NAS 1.15:102455	p 101	N90-24382 *	#	NAS 1.15:102560	p 219	N90-20338 *	#	NAS 1.15:103180	p 184	N90-27985 *	#
NAS 1.15:102456	p 96	N90-14294 *	#	NAS 1.15:102561	p 244	N90-20432 *	#	NAS 1.15:103181	p 44	N90-26030 *	#
NAS 1.15:102457	p 12	N90-17562 *	#	NAS 1.15:102562	p 78	N90-21570 *	#	NAS 1.15:103182	p 263	N90-26729 *	#
NAS 1.15:102458	p 130	N90-17890 *	#	NAS 1.15:102563	p 106	N90-21812 *	#	NAS 1.15:103183	p 136	N90-26163 *	#
NAS 1.15:102459	p 237	N90-15622 *	#	NAS 1.15:102564	p 259	N90-21843 *	#	NAS 1.15:103184	p 79	N90-25181 *	#
NAS 1.15:102460	p 176	N90-13749 *	#	NAS 1.15:102565	p 179	N90-20886 *	#	NAS 1.15:103185	p 221	N90-23773 *	#
NAS 1.15:102461	p 137	N90-17929 *	#	NAS 1.15:102566	p 153	N90-21295 *	#	NAS 1.15:103186	p 184	N90-27984 *	#
NAS 1.15:102462	p 12	N90-14206 *	#	NAS 1.15:102567	p 203	N90-21283 *	#	NAS 1.15:103187	p 185	N90-27982 *	#
NAS 1.15:102463	p 29	N90-21036 *	#	NAS 1.15:102568	p 128	N90-22041 *	#	NAS 1.15:103188	p 37	N90-26011 *	#
NAS 1.15:102464	p 72	N90-14283 *	#	NAS 1.15:102569	p 151	N90-21192 *	#	NAS 1.15:103189	p 80	N90-25184 *	#
NAS 1.15:102465	p 49	N90-13581 *	#	NAS 1.15:102570	p 190	N90-20301 *	#	NAS 1.15:103190	p 155	N90-25278 *	#
NAS 1.15:102466	p 266	N90-22488 *	#	NAS 1.15:102571	p 99	N90-23714 *	#	NAS 1.15:103191	p 190	N90-25323 *	#
NAS 1.15:102467	p 127	N90-16944 *	#	NAS 1.15:102572	p 231	N90-21132 *	#	NAS 1.15:103192	p 81	N90-26065 *	#
NAS 1.15:102468	p 145	N90-21263 *	#	NAS 1.15:102573	p 189	N90-20358 *	#	NAS 1.15:103193	p 87	N90-26068 *	#
NAS 1.15:102469	p 38	N90-15964 *	#	NAS 1.15:102574	p 267	N90-23339 *	#	NAS 1.15:103194	p 81	N90-25158 *	#
NAS 1.15:102470	p 245	N90-14856 *	#	NAS 1.15:102575	p 119	N90-22646 *	#	NAS 1.15:103195	p 43	N90-26789 *	#
NAS 1.15:102471	p 38	N90-15965 *	#	NAS 1.15:102576	p 45	N90-20110 *	#	NAS 1.15:103196	p 267	N90-26299 *	#
NAS 1.15:102472	p 189	N90-21360 *	#	NAS 1.15:102577	p 100	N90-21826 *	#	NAS 1.15:103197	p 191	N90-26276 *	#
NAS 1.15:102473	p 28	N90-20085 *	#	NAS 1.15:102578	p 184	N90-27982 *	#	NAS 1.15:103198	p 183	N90-26396 *	#
NAS 1.15:102474	p 97	N90-16008 *	#	NAS 1.15:102579	p 13	N90-20051 *	#	NAS 1.15:103199	p 233	N90-25173 *	#
NAS 1.15:102475	p 99	N90-21137 *	#	NAS 1.15:102580	p 240	N90-23991 *	#	NAS 1.15:103200	p 51	N90-26009 *	#
NAS 1.15:102476	p 152	N90-21274 *	#	NAS 1.15:102581	p 220	N90-22117 *	#	NAS 1.15:103201	p 32	N90-26069 *	#
NAS 1.15:102477	p 51	N90-26054 *	#	NAS 1.15:102582	p 1	N90-21723 *	#	NAS 1.15:103202	p 81	N90-26273 *	#
NAS 1.15:102478	p 218	N90-18064 *	#	NAS 1.15:102583	p 183	N90-26275 *	#	NAS 1.15:103203	p 183	N90-26160 *	#
NAS 1.15:102479	p 223	N90-26373 *	#	NAS 1.15:102584	p 32	N90-25982 *	#	NAS 1.15:103204	p 246	N90-28393 *	#
NAS 1.15:102480	p 128	N90-21858 *	#	NAS 1.15:102585	p 30	N90-21762 *	#	NAS 1.15:103205	p 51	N90-26055 *	#
NAS 1.15:102481	p 97	N90-17817 *	#	NAS 1.15:102586	p 39	N90-23416 *	#	NAS 1.15:103			

NAS 1.15:103231

REPORT NUMBER INDEX

NAS 1.15:103231	p 244	N90-26615 *	NAS 1.26:182262	p 125	N90-11882 *	NAS 1.26:185287	p 208	N90-28097 *
NAS 1.15:103233	p 102	N90-27874 *	NAS 1.26:182278	p 24	N90-11738 *	NAS 1.26:185288	p 208	N90-28858 *
NAS 1.15:103235	p 156	N90-28786 *	NAS 1.26:182286	p 177	N90-14494 *	NAS 1.26:185291	p 224	N90-28878 *
NAS 1.15:103237	p 233	N90-26397 *	NAS 1.26:182293	p 187	N90-11999 *	NAS 1.26:185947	p 72	N90-14279 *
NAS 1.15:103239	p 130	N90-28740 *	NAS 1.26:182294	p 204	N90-26320 *	NAS 1.26:185976	p 142	N90-11211 *
NAS 1.15:103240	p 244	N90-26616 *	NAS 1.26:182445	p 220	N90-22813 *	NAS 1.26:185989	p 143	N90-12784 *
NAS 1.15:103241	p 81	N90-26071 *	NAS 1.26:183398	p 257	N90-11603 *	NAS 1.26:185996	p 229	N90-13886 *
NAS 1.15:103242	p 82	N90-27783 *	NAS 1.26:184928	p 31	N90-23405 *	NAS 1.26:186037	p 10	N90-12500 *
NAS 1.15:103243	p 47	N90-27736 *	NAS 1.26:185077	p 222	N90-24653 *	NAS 1.26:186058	p 181	N90-22017 *
NAS 1.15:103246	p 260	N90-26683 *	NAS 1.26:185109	p 263	N90-14153 *	NAS 1.26:186060	p 175	N90-12882 *
NAS 1.15:103249	p 14	N90-25946 *	NAS 1.26:185110	p 199	N90-10437 *	NAS 1.26:186093	p 199	N90-12936 *
NAS 1.15:103250	p 15	N90-27657 *	NAS 1.26:185118-VOL-1	p 23	N90-10038 *	NAS 1.26:186129	p 151	N90-14467 *
NAS 1.15:103252	p 191	N90-28033 *	NAS 1.26:185118-VOL-2	p 23	N90-10039 *	NAS 1.26:186137	p 235	N90-28512 *
NAS 1.15:103254	p 82	N90-27784 *	NAS 1.26:185123	p 11	N90-13328 *	NAS 1.26:186140	p 145	N90-24514 *
NAS 1.15:103255	p 191	N90-28031 *	NAS 1.26:185129	p 1	N90-20943 *	NAS 1.26:186162	p 106	N90-14305 *
NAS 1.15:103256	p 52	N90-28596 *	NAS 1.26:185133	p 22	N90-10036 *	NAS 1.26:186192	p 188	N90-14534 *
NAS 1.15:103259	p 82	N90-27782 *	NAS 1.26:185134	p 72	N90-14281 *	NAS 1.26:186205	p 177	N90-15363 *
NAS 1.15:103261	p 102	N90-27875 *	NAS 1.26:185135	p 247	N90-11549 *	NAS 1.26:186214	p 177	N90-15364 *
NAS 1.15:103262	p 244	N90-29124 *	NAS 1.26:185136	p 175	N90-11256 *	NAS 1.26:186228	p 229	N90-15506 *
NAS 1.15:103264	p 223	N90-28112 *	NAS 1.26:185137	p 49	N90-10983 *	NAS 1.26:186244	p 143	N90-16103 *
NAS 1.15:103271	p 205	N90-28062 *	NAS 1.26:185138	p 25	N90-11739 *	NAS 1.26:186274	p 201	N90-15447 *
NAS 1.15:103275	p 205	N90-28065 *	NAS 1.26:185139	p 258	N90-11606 *	NAS 1.26:186303	p 182	N90-23674 *
NAS 1.15:103280	p 83	N90-28657 *	NAS 1.26:185140	p 10	N90-10004 *	NAS 1.26:186354	p 258	N90-19873 *
NAS 1.15:103291	p 260	N90-29219 *	NAS 1.26:185143	p 215	N90-10455 *	NAS 1.26:186465	p 76	N90-21109 *
NAS 1.15:103292	p 108	N90-28696 *	NAS 1.26:185147	p 49	N90-12645 *	NAS 1.26:186466	p 144	N90-19466 *
NAS 1.15:103459	p 259	N90-24952 *	NAS 1.26:185148	p 203	N90-21387 *	NAS 1.26:186504	p 106	N90-19340 *
NAS 1.15:103490	p 51	N90-25174 *	NAS 1.26:185149	p 145	N90-20270 *	NAS 1.26:186505	p 232	N90-25418 *
NAS 1.15:103607	p 83	N90-28659 *	NAS 1.26:185150	p 200	N90-13794 *	NAS 1.26:186508	p 145	N90-20271 *
NAS 1.15:103609	p 241	N90-29121 *	NAS 1.26:185151	p 241	N90-26581 *	NAS 1.26:186529	p 180	N90-21301 *
NAS 1.15:14133	p 216	N90-14642 *	NAS 1.26:185153	p 188	N90-13761 *	NAS 1.26:186530	p 136	N90-25238 *
NAS 1.15:14141	p 25	N90-13387 *	NAS 1.26:185154	p 1	N90-13323 *	NAS 1.26:186531	p 77	N90-21113 *
NAS 1.15:14176	p 241	N90-25607 *	NAS 1.26:185156	p 235	N90-14783 *	NAS 1.26:186580	p 153	N90-21952 *
NAS 1.15:14203	p 223	N90-28111 *	NAS 1.26:185157	p 1	N90-21724 *	NAS 1.26:186581	p 14	N90-25934 *
NAS 1.15:897140	p 249	N90-16496 *	NAS 1.26:185158	p 18	N90-23393 *	NAS 1.26:186586	p 181	N90-22000 *
NAS 1.15:89715	p 261	N90-26693 *	NAS 1.26:185159	p 248	N90-21600 *	NAS 1.26:186598	p 38	N90-21776 *
NAS 1.15:89923	p 70	N90-10174 *	NAS 1.26:185161	p 77	N90-21806 *	NAS 1.26:186599	p 38	N90-21777 *
NAS 1.26:168069	p 34	N90-28559 *	NAS 1.26:185162	p 258	N90-14108 *	NAS 1.26:186618	p 235	N90-25579 *
NAS 1.26:168137	p 35	N90-28566 *	NAS 1.26:185163	p 50	N90-15985 *	NAS 1.26:186619	p 238	N90-25604 *
NAS 1.26:168211	p 34	N90-28561 *	NAS 1.26:185164	p 71	N90-11805 *	NAS 1.26:186694	p 154	N90-23664 *
NAS 1.26:168219	p 34	N90-28558 *	NAS 1.26:185165	p 217	N90-14652 *	NAS 1.26:186720	p 146	N90-26234 *
NAS 1.26:168274	p 33	N90-28555 *	NAS 1.26:185166	p 71	N90-11806 *	NAS 1.26:186731	p 259	N90-26664 *
NAS 1.26:168289	p 33	N90-28553 *	NAS 1.26:185167	p 237	N90-13968 *	NAS 1.26:186803	p 259	N90-24964 *
NAS 1.26:168290	p 34	N90-28563 *	NAS 1.26:185168	p 73	N90-15996 *	NAS 1.26:186825	p 234	N90-25499 *
NAS 1.26:168301	p 33	N90-28554 *	NAS 1.26:185169	p 79	N90-23474 *	NAS 1.26:186870	p 107	N90-26911 *
NAS 1.26:174651	p 34	N90-28562 *	NAS 1.26:185170	p 201	N90-15434 *	NAS 1.26:4175	p 18	N90-10031 *
NAS 1.26:174718	p 26	N90-13391 *	NAS 1.26:185172	p 77	N90-21807 *	NAS 1.26:4254	p 215	N90-11332 *
NAS 1.26:174766-VOL-1	p 34	N90-28564 *	NAS 1.26:185173	p 232	N90-22834 *	NAS 1.26:4259	p 199	N90-12033 *
NAS 1.26:174766-VOL-2	p 35	N90-28565 *	NAS 1.26:185174	p 118	N90-18559 *	NAS 1.26:4263	p 143	N90-14452 *
NAS 1.26:174799	p 33	N90-28556 *	NAS 1.26:185177	p 151	N90-17987 *	NAS 1.26:4264	p 249	N90-21602 *
NAS 1.26:174824	p 28	N90-17638 *	NAS 1.26:185178	p 177	N90-14512 *	NAS 1.26:4271	p 126	N90-16072 *
NAS 1.26:174834	p 33	N90-28557 *	NAS 1.26:185179	p 176	N90-13748 *	NAS 1.26:4278	p 13	N90-19203 *
NAS 1.26:174937	p 10	N90-10011 *	NAS 1.26:185181	p 50	N90-20120 *	NAS 1.26:4302	p 14	N90-25940 *
NAS 1.26:174942	p 34	N90-28560 *	NAS 1.26:185183	p 230	N90-18808 *	NAS 1.26:4308	p 14	N90-27655 *
NAS 1.26:174945	p 12	N90-18364 *	NAS 1.26:185184	p 258	N90-17465 *	NAS 1.26:4321	p 224	N90-28113 *
NAS 1.26:174992	p 23	N90-10043 *	NAS 1.26:185185	p 76	N90-21108 *	NAS 1.55:10016	p 77	N90-21795 *
NAS 1.26:174993	p 23	N90-10044 *	NAS 1.26:185186	p 131	N90-19386 *	NAS 1.55:10033	p 188	N90-17085 *
NAS 1.26:175070	p 70	N90-10175 *	NAS 1.26:185188	p 219	N90-21420 *	NAS 1.55:3056	p 230	N90-20454 *
NAS 1.26:179522	p 26	N90-13390 *	NAS 1.26:185189	p 221	N90-23769 *	NAS 1.60:2462	p 1	N90-20942 *
NAS 1.26:179533	p 35	N90-28568 *	NAS 1.26:185190	p 134	N90-14398 *	NAS 1.60:2879	p 175	N90-11245 *
NAS 1.26:179534	p 35	N90-28567 *	NAS 1.26:185196	p 221	N90-23757 *	NAS 1.60:2916	p 223	N90-28099 *
NAS 1.26:179578	p 35	N90-28569 *	NAS 1.26:185197	p 27	N90-17635 *	NAS 1.60:2925	p 37	N90-15112 *
NAS 1.26:179590	p 247	N90-10683 *	NAS 1.26:185199	p 218	N90-18071 *	NAS 1.60:2937	p 218	N90-18081 *
NAS 1.26:179610	p 25	N90-13385 *	NAS 1.26:185200	p 138	N90-26171 *	NAS 1.60:2944	p 142	N90-11915 *
NAS 1.26:179625	p 32	N90-24274 *	NAS 1.26:185203	p 118	N90-21165 *	NAS 1.60:2949	p 246	N90-12282 *
NAS 1.26:179629	p 125	N90-10294 *	NAS 1.26:185208	p 135	N90-20237 *	NAS 1.60:2957	p 258	N90-12348 *
NAS 1.26:179642	p 95	N90-10184 *	NAS 1.26:185209	p 127	N90-19374 *	NAS 1.60:2967	p 117	N90-15211 *
NAS 1.26:180406	p 224	N90-28880 *	NAS 1.26:185210	p 191	N90-29622 *	NAS 1.60:2970	p 97	N90-19302 *
NAS 1.26:180454	p 191	N90-28827 *	NAS 1.26:185212	p 252	N90-22389 *	NAS 1.60:2984	p 138	N90-28754 *
NAS 1.26:180495	p 204	N90-23732 *	NAS 1.26:185215	p 153	N90-21282 *	NAS 1.60:2985	p 32	N90-27722 *
NAS 1.26:180650	p 232	N90-22835 *	NAS 1.26:185216	p 50	N90-25172 *	NAS 1.60:2994	p 137	N90-21210 *
NAS 1.26:180667	p 248	N90-18228 *	NAS 1.26:185217	p 30	N90-22567 *	NAS 1.60:2996	p 38	N90-19242 *
NAS 1.26:180831	p 124	N90-10293 *	NAS 1.26:185218	p 190	N90-22022 *	NAS 1.60:3005	p 30	N90-23403 *
NAS 1.26:180839	p 263	N90-11654 *	NAS 1.26:185219	p 118	N90-21849 *	NAS 1.60:3017	p 205	N90-28066 *
NAS 1.26:180840	p 264	N90-29260 *	NAS 1.26:185222	p 29	N90-21761 *	NAS 1.60:3039	p 155	N90-27965 *
NAS 1.26:180844	p 142	N90-11210 *	NAS 1.26:185223	p 131	N90-23574 *	NAS 1.61:1212	p 202	N90-19593 *
NAS 1.26:180848	p 25	N90-12617 *	NAS 1.26:185224	p 78	N90-21809 *	NAS 1.61:1222	p 189	N90-21351 *
NAS 1.26:180849	p 146	N90-24528 *	NAS 1.26:185225	p 18	N90-21006 *	NAS 1.61:1228	p 202	N90-18740 *
NAS 1.26:180850	p 36	N90-28570 *	NAS 1.26:185226	p 237	N90-21552 *	NAS 1.61:1235	p 29	N90-21037 *
NAS 1.26:180867	p 24	N90-10048 *	NAS 1.26:185240	p 263	N90-26728 *	NAS 1.61:1240	p 205	N90-28063 *
NAS 1.26:180868	p 24	N90-10047 *	NAS 1.26:185241	p 249	N90-26633 *	NAS 1.71:LEW-14672-1	p 201	N90-15444 *
NAS 1.26:180869	p 24	N90-10049 *	NAS 1.26:185243	p 30	N90-21763 *	NAS 1.71:LEW-14676-2	p 258	N90-17454 *
NAS 1.26:180892	p 117	N90-17868 *	NAS 1.26:185252	p 182	N90-26269 *	NAS 1.71:LEW-14698-2	p 126	N90-15262 *
NAS 1.26:182106	p 72	N90-14278 *	NAS 1.26:185254	p 191	N90-25324 *	NAS 1.71:LEW-14746-1	p 151	N90-17009 *
NAS 1.26:182124	p 32	N90-28552 *	NAS 1.26:185255	p 31	N90-23406 *	NAS 1.71:LEW-14776-1	p 201	N90-15445 *
NAS 1.26:182125	p 24	N90-10045 *	NAS 1.26:185256	p 53	N90-26063 *	NAS 1.71:LEW-14795-1	p 251	N90-15733 *
NAS 1.26:182142	p 24	N90-10046 *	NAS 1.26:185257	p 79	N90-25183 *	NAS 1.71:LEW-14846-1	p 73	N90-15130 *
NAS 1.26:182178	p 10	N90-10835 *	NAS 1.26:185259	p 45	N90-25159 *	NAS 1.71:LEW-14880-1	p 187	N90-10415 *
NAS 1.26:182179	p 10	N90-10836 *	NAS 1.26:185260	p 45	N90-27732 *	NAS 1.71:LEW-14901-1	p 252	N90-10718 *
NAS 1.26:182186	p 129	N90-28735 *	NAS 1.26:185263	p 80	N90-25187 *	NAS 1.71:LEW-14990-1-CU	p 97	N90-15147 *
NAS 1.26:182210	p 263	N90-18326 *	NAS 1.26:185265	p 223	N90-26372 *			
NAS 1.26:182228	p 23	N90-10037 *	NAS 1.26:185267	p 129	N90-26142 *			
NAS 1.26:182230	p 26	N90-13388 *	NAS 1.26:185277	p 36	N90-29394 *			
NAS 1.26:182235-VOL-2	p 215	N90-10450 *	NAS 1.26:185278	p 15	N90-28504 *			
NAS 1.26:182236	p 215	N90-10451 *	NAS 1.26:185279	p 131	N90-28742 *			
NAS 1.26:182247	p 222	N90-26355 *	NAS 1.26:185280	p 183	N90-26272 *			
NAS 1.26:182249	p 71	N90-13589 *	NAS 1.26:185286	p 223	N90-28110 *			
						NASA-CASE-LEW-13609-1	p 106	N90-11824 *
						NASA-CASE-LEW-14124-1	p 190	N90-23712 *
						NASA-CASE-LEW-14345-2	p 107	N90-23497 *
						NASA-CASE-LEW-14346-1	p 86	N90-19300 *
						NASA-CASE-LEW-14520-1	p 153	N90-22724 *
						NASA-CASE-LEW-14672-1	p 201	N90-15444 *

REPORT NUMBER INDEX

NASA-CASE-LEW-14676-2	p 258	N90-17454 *	NASA-CR-185137	p 49	N90-10983 *	NASA-CR-186244	p 143	N90-16103 *
NASA-CASE-LEW-14695-1	p 204	N90-23751 *	NASA-CR-185138	p 25	N90-11739 *	NASA-CR-186274	p 201	N90-15447 *
NASA-CASE-LEW-14698-2	p 126	N90-15262 *	NASA-CR-185139	p 258	N90-11606 *	NASA-CR-186303	p 182	N90-23674 *
NASA-CASE-LEW-14719-1	p 101	N90-23493 *	NASA-CR-185140	p 10	N90-10004 *	NASA-CR-186354	p 258	N90-19873 *
NASA-CASE-LEW-14746-1	p 151	N90-17009 *	NASA-CR-185143	p 215	N90-10455 *	NASA-CR-186465	p 76	N90-21109 *
NASA-CASE-LEW-14776-1	p 201	N90-15445 *	NASA-CR-185147	p 49	N90-12645 *	NASA-CR-186466	p 144	N90-19486 *
NASA-CASE-LEW-14795-1	p 251	N90-15733 *	NASA-CR-185148	p 203	N90-21387 *	NASA-CR-186504	p 106	N90-19340 *
NASA-CASE-LEW-14844-1	p 190	N90-22024 *	NASA-CR-185149	p 145	N90-20270 *	NASA-CR-186505	p 232	N90-25418 *
NASA-CASE-LEW-14846-1	p 73	N90-15130 *	NASA-CR-185150	p 200	N90-13794 *	NASA-CR-186508	p 145	N90-20271 *
NASA-CASE-LEW-14880-1	p 187	N90-10415 *	NASA-CR-185151	p 241	N90-26581 *	NASA-CR-186529	p 180	N90-21301 *
NASA-CASE-LEW-14901-1	p 252	N90-10718 *	NASA-CR-185153	p 188	N90-13761 *	NASA-CR-186531	p 136	N90-25238 *
NASA-CASE-LEW-14990-1-CU	p 97	N90-15147 *	NASA-CR-185154	p 1	N90-13323 *	NASA-CR-186531	p 77	N90-21113 *
			NASA-CR-185156	p 235	N90-14783 *	NASA-CR-186580	p 153	N90-21952 *
NASA-CP-10016	p 77	N90-21795 *	NASA-CR-185157	p 1	N90-21724 *	NASA-CR-186581	p 14	N90-25934 *
NASA-CP-10033	p 188	N90-17085 *	NASA-CR-185158	p 18	N90-23393 *	NASA-CR-186586	p 181	N90-22000 *
NASA-CP-3056	p 230	N90-20454 *	NASA-CR-185159	p 248	N90-21600 *	NASA-CR-186598	p 38	N90-21776 *
			NASA-CR-185161	p 77	N90-21806 *	NASA-CR-186599	p 38	N90-21777 *
NASA-CR-168069	p 34	N90-28559 *	NASA-CR-185162	p 258	N90-14108 *	NASA-CR-186618	p 235	N90-25579 *
NASA-CR-168137	p 35	N90-28566 *	NASA-CR-185163	p 50	N90-15985 *	NASA-CR-186619	p 238	N90-25604 *
NASA-CR-168211	p 34	N90-28561 *	NASA-CR-185164	p 71	N90-11805 *	NASA-CR-186694	p 154	N90-23664 *
NASA-CR-168219	p 34	N90-28558 *	NASA-CR-185165	p 71	N90-11806 *	NASA-CR-186720	p 146	N90-26234 *
NASA-CR-168274	p 33	N90-28555 *	NASA-CR-185166	p 217	N90-14652 *	NASA-CR-186731	p 259	N90-26664 *
NASA-CR-168289	p 33	N90-28553 *	NASA-CR-185167	p 237	N90-13968 *	NASA-CR-186803	p 259	N90-24964 *
NASA-CR-168290	p 34	N90-28563 *	NASA-CR-185168	p 73	N90-15996 *	NASA-CR-186825	p 234	N90-25499 *
NASA-CR-168301	p 33	N90-28554 *	NASA-CR-185169	p 79	N90-23474 *	NASA-CR-186870	p 107	N90-26911 *
NASA-CR-174651	p 34	N90-28562 *	NASA-CR-185170	p 201	N90-15434 *	NASA-CR-4175	p 18	N90-10031 *
NASA-CR-174718	p 26	N90-13391 *	NASA-CR-185171	p 77	N90-21807 *	NASA-CR-4254	p 215	N90-11332 *
NASA-CR-174766-VOL-1	p 34	N90-28564 *	NASA-CR-185173	p 232	N90-22834 *	NASA-CR-4259	p 199	N90-12033 *
NASA-CR-174766-VOL-2	p 35	N90-28565 *	NASA-CR-185174	p 118	N90-18559 *	NASA-CR-4263	p 143	N90-14452 *
NASA-CR-174799	p 33	N90-28556 *	NASA-CR-185177	p 151	N90-17987 *	NASA-CR-4264	p 249	N90-21602 *
NASA-CR-174824	p 28	N90-17638 *	NASA-CR-185178	p 177	N90-14512 *	NASA-CR-4271	p 126	N90-16072 *
NASA-CR-174834	p 33	N90-28557 *	NASA-CR-185179	p 176	N90-13748 *	NASA-CR-4278	p 13	N90-19203 *
NASA-CR-174937	p 10	N90-10011 *	NASA-CR-185181	p 50	N90-20120 *	NASA-CR-4302	p 14	N90-25940 *
NASA-CR-174942	p 34	N90-28560 *	NASA-CR-185183	p 230	N90-18808 *	NASA-CR-4308	p 14	N90-27655 *
NASA-CR-174945	p 12	N90-18364 *	NASA-CR-185184	p 258	N90-17465 *	NASA-CR-4321	p 224	N90-28113 *
NASA-CR-174992	p 23	N90-10043 *	NASA-CR-185185	p 76	N90-21108 *			
NASA-CR-174993	p 23	N90-10044 *	NASA-CR-185186	p 131	N90-19386 *	NASA-RP-1212	p 202	N90-19593 *
NASA-CR-175070	p 70	N90-10175 *	NASA-CR-185188	p 219	N90-21420 *	NASA-RP-1222	p 189	N90-21351 *
NASA-CR-179522	p 26	N90-13390 *	NASA-CR-185189	p 221	N90-23769 *	NASA-RP-1228	p 202	N90-18740 *
NASA-CR-179533	p 35	N90-28568 *	NASA-CR-185190	p 134	N90-14398 *	NASA-RP-1235	p 29	N90-21037 *
NASA-CR-179534	p 35	N90-28567 *	NASA-CR-185191	p 221	N90-23757 *	NASA-RP-1240	p 205	N90-28063 *
NASA-CR-179578	p 35	N90-28569 *	NASA-CR-185197	p 27	N90-17635 *			
NASA-CR-179590	p 247	N90-10683 *	NASA-CR-185199	p 218	N90-18071 *	NASA-TM-100169	p 95	N90-10188 *
NASA-CR-179610	p 25	N90-13385 *	NASA-CR-185200	p 138	N90-26171 *	NASA-TM-100746	p 234	N90-12984 *
NASA-CR-179625	p 32	N90-24274 *	NASA-CR-185203	p 118	N90-21165 *	NASA-TM-101311	p 216	N90-13819 *
NASA-CR-179629	p 125	N90-10294 *	NASA-CR-185208	p 135	N90-20237 *	NASA-TM-101344	p 138	N90-26172 *
NASA-CR-179642	p 95	N90-10184 *	NASA-CR-185209	p 127	N90-19374 *	NASA-TM-101453	p 144	N90-20264 *
NASA-CR-180406	p 224	N90-28880 *	NASA-CR-185210	p 191	N90-29622 *	NASA-TM-101454	p 145	N90-21250 *
NASA-CR-180454	p 191	N90-28827 *	NASA-CR-185212	p 252	N90-22389 *	NASA-TM-101472	p 133	N90-11196 *
NASA-CR-180455	p 204	N90-23732 *	NASA-CR-185215	p 153	N90-21282 *	NASA-TM-101814	p 262	N90-12388 *
NASA-CR-180495	p 232	N90-22835 *	NASA-CR-185216	p 50	N90-25172 *	NASA-TM-101815	p 262	N90-12389 *
NASA-CR-180650	p 248	N90-18228 *	NASA-CR-185217	p 30	N90-22567 *	NASA-TM-101914	p 129	N90-26132 *
NASA-CR-180667	p 124	N90-10293 *	NASA-CR-185218	p 190	N90-22022 *	NASA-TM-101940	p 96	N90-15143 *
NASA-CR-180831	p 263	N90-11654 *	NASA-CR-185219	p 118	N90-21849 *	NASA-TM-101958	p 95	N90-10181 *
NASA-CR-180839	p 264	N90-29260 *	NASA-CR-185222	p 29	N90-21761 *	NASA-TM-101974	p 71	N90-13596 *
NASA-CR-180840	p 142	N90-11210 *	NASA-CR-185223	p 131	N90-23574 *	NASA-TM-102014	p 134	N90-13679 *
NASA-CR-180844	p 25	N90-12617 *	NASA-CR-185224	p 78	N90-21809 *	NASA-TM-102034	p 262	N90-15846 *
NASA-CR-180849	p 146	N90-24528 *	NASA-CR-185225	p 18	N90-21006 *	NASA-TM-102037	p 134	N90-16087 *
NASA-CR-180850	p 36	N90-28570 *	NASA-CR-185231	p 237	N90-21552 *	NASA-TM-102069	p 27	N90-13392 *
NASA-CR-180867	p 24	N90-10048 *	NASA-CR-185240	p 263	N90-26728 *	NASA-TM-102077	p 11	N90-13352 *
NASA-CR-180868	p 24	N90-10047 *	NASA-CR-185241	p 249	N90-26633 *	NASA-TM-102088	p 125	N90-11881 *
NASA-CR-180869	p 24	N90-10049 *	NASA-CR-185243	p 30	N90-21763 *	NASA-TM-102090	p 267	N90-15030 *
NASA-CR-180892	p 117	N90-17868 *	NASA-CR-185252	p 182	N90-26269 *	NASA-TM-102130	p 206	N90-17167 *
NASA-CR-182106	p 72	N90-14278 *	NASA-CR-185254	p 191	N90-26324 *	NASA-TM-102288	p 178	N90-18005 *
NASA-CR-182124	p 32	N90-28552 *	NASA-CR-185255	p 31	N90-23406 *	NASA-TM-102289	p 150	N90-11943 *
NASA-CR-182125	p 24	N90-10045 *	NASA-CR-185256	p 53	N90-26063 *	NASA-TM-102290	p 216	N90-12041 *
NASA-CR-182142	p 24	N90-10046 *	NASA-CR-185257	p 79	N90-25183 *	NASA-TM-102291	p 124	N90-10262 *
NASA-CR-182178	p 10	N90-10835 *	NASA-CR-185259	p 45	N90-25159 *	NASA-TM-102296	p 267	N90-24220 *
NASA-CR-182179	p 10	N90-10836 *	NASA-CR-185260	p 45	N90-27732 *	NASA-TM-102300	p 52	N90-14275 *
NASA-CR-182186	p 129	N90-28735 *	NASA-CR-185263	p 80	N90-25187 *	NASA-TM-102303	p 29	N90-21038 *
NASA-CR-182210	p 263	N90-18326 *	NASA-CR-185265	p 223	N90-26372 *	NASA-TM-102304	p 71	N90-13590 *
NASA-CR-182228	p 23	N90-10037 *	NASA-CR-185267	p 129	N90-26142 *	NASA-TM-102313	p 50	N90-14268 *
NASA-CR-182230	p 26	N90-13388 *	NASA-CR-185277	p 36	N90-29394 *	NASA-TM-102316	p 30	N90-22564 *
NASA-CR-182235-VOL-2	p 215	N90-10450 *	NASA-CR-185278	p 15	N90-28504 *	NASA-TM-102319	p 31	N90-23407 *
NASA-CR-182236	p 215	N90-10451 *	NASA-CR-185279	p 131	N90-28742 *	NASA-TM-102320	p 216	N90-12950 *
NASA-CR-182247	p 222	N90-26355 *	NASA-CR-185280	p 183	N90-26272 *	NASA-TM-102322	p 136	N90-10309 *
NASA-CR-182249	p 71	N90-13589 *	NASA-CR-185286	p 223	N90-28110 *	NASA-TM-102324	p 221	N90-22823 *
NASA-CR-182262	p 125	N90-11882 *	NASA-CR-185287	p 208	N90-28097 *	NASA-TM-102329	p 95	N90-10185 *
NASA-CR-182278	p 24	N90-11738 *	NASA-CR-185288	p 208	N90-28858 *	NASA-TM-102333	p 97	N90-18504 *
NASA-CR-182286	p 177	N90-14494 *	NASA-CR-185291	p 224	N90-28878 *	NASA-TM-102334	p 175	N90-11969 *
NASA-CR-182293	p 187	N90-11999 *	NASA-CR-185947	p 72	N90-14279 *	NASA-TM-102336	p 70	N90-11082 *
NASA-CR-182294	p 204	N90-26320 *	NASA-CR-185976	p 142	N90-11211 *	NASA-TM-102340	p 200	N90-13785 *
NASA-CR-182445	p 220	N90-22813 *	NASA-CR-185989	p 143	N90-12784 *	NASA-TM-102341	p 24	N90-10891 *
NASA-CR-183398	p 257	N90-11603 *	NASA-CR-185996	p 229	N90-13888 *	NASA-TM-102342	p 220	N90-22808 *
NASA-CR-184928	p 31	N90-23405 *	NASA-CR-186037	p 10	N90-12500 *	NASA-TM-102343	p 96	N90-11808 *
NASA-CR-185077	p 222	N90-24853 *	NASA-CR-186058	p 181	N90-22017 *	NASA-TM-102344	p 217	N90-14655 *
NASA-CR-185109	p 263	N90-14153 *	NASA-CR-186060	p 175	N90-12882 *	NASA-TM-102346	p 70	N90-11081 *
NASA-CR-185110	p 199	N90-10437 *	NASA-CR-186093	p 199	N90-12936 *	NASA-TM-102348	p 216	N90-14641 *
NASA-CR-185118-VOL-1	p 23	N90-10038 *	NASA-CR-186129	p 151	N90-14467 *	NASA-TM-102349	p 201	N90-16286 *
NASA-CR-185118-VOL-2	p 23	N90-10039 *	NASA-CR-186137	p 235	N90-26512 *	NASA-TM-102350	p 257	N90-10737 *
NASA-CR-185123	p 11	N90-13328 *	NASA-CR-186140	p 145	N90-24514 *	NASA-TM-102351	p 126	N90-13666 *
NASA-CR-185129	p 1	N90-20943 *	NASA-CR-186162	p 106	N90-14305 *	NASA-TM-102353	p 126	N90-14363 *
NASA-CR-185133	p 22	N90-10036 *	NASA-CR-186192	p 188	N90-14534 *	NASA-TM-102354	p 242	N90-11497 *
NASA-CR-185134	p 72	N90-14281 *	NASA-CR-186205	p 177	N90-15363 *	NASA-TM-102355	p 86	N90-12659 *
NASA-CR-185135	p 247	N90-11549 *	NASA-CR-186214	p 177	N90-15364 *	NASA-TM-102356	p 257	N90-10738 *
NASA-CR-185136	p 175	N90-11256 *	NASA-CR-186228	p 229	N90-15506 *	NASA-TM-102357	p 187	N90-11277 *

NASA-TM-102358	p 12	N90-17561 *	NASA-TM-102466	p 12	N90-17562 *	NASA-TM-102569	p 78	N90-21812 *
NASA-TM-102359	p 243	N90-14002 *	NASA-TM-102467	p 130	N90-17890 *	NASA-TM-102570	p 106	N90-21843 *
NASA-TM-102360	p 96	N90-14287 *	NASA-TM-102468	p 237	N90-15622 *	NASA-TM-102571	p 259	N90-20886 *
NASA-TM-102361	p 242	N90-10635 *	NASA-TM-102469	p 176	N90-13749 *	NASA-TM-102572	p 179	N90-21295 *
NASA-TM-102362	p 175	N90-11250 *	NASA-TM-102470	p 137	N90-17929 *	NASA-TM-102573	p 153	N90-21283 *
NASA-TM-102363	p 264	N90-22464 *	NASA-TM-102471	p 12	N90-14206 *	NASA-TM-102574	p 203	N90-22041 *
NASA-TM-102365	p 248	N90-17413 *	NASA-TM-102472	p 29	N90-21036 *	NASA-TM-102575	p 128	N90-21192 *
NASA-TM-102366	p 70	N90-11804 *	NASA-TM-102473	p 72	N90-14283 *	NASA-TM-102576	p 151	N90-20301 *
NASA-TM-102367	p 245	N90-10674 *	NASA-TM-102474	p 49	N90-13581 *	NASA-TM-102577	p 190	N90-23714 *
NASA-TM-102368	p 137	N90-22703 *	NASA-TM-102475	p 266	N90-22488 *	NASA-TM-102578	p 99	N90-21132 *
NASA-TM-102369	p 222	N90-26358 *	NASA-TM-102476	p 127	N90-18944 *	NASA-TM-102579	p 231	N90-21469 *
NASA-TM-102370	p 100	N90-23477 *	NASA-TM-102477	p 145	N90-21263 *	NASA-TM-102580	p 189	N90-20358 *
NASA-TM-102371	p 98	N90-21123 *	NASA-TM-102478	p 38	N90-15864 *	NASA-TM-102581	p 267	N90-23339 *
NASA-TM-102372	p 73	N90-15992 *	NASA-TM-102479	p 245	N90-14856 *	NASA-TM-103094	p 119	N90-22646 *
NASA-TM-102373	p 69	N90-10172 *	NASA-TM-102480	p 38	N90-15865 *	NASA-TM-103095	p 45	N90-20110 *
NASA-TM-102374	p 11	N90-12560 *	NASA-TM-102481	p 189	N90-21360 *	NASA-TM-103096	p 100	N90-21826 *
NASA-TM-102375	p 245	N90-14060 *	NASA-TM-102482	p 28	N90-20085 *	NASA-TM-103097	p 184	N90-27982 *
NASA-TM-102376	p 178	N90-18665 *	NASA-TM-102483	p 97	N90-16008 *	NASA-TM-103098	p 13	N90-20051 *
NASA-TM-102377	p 176	N90-13719 *	NASA-TM-102484	p 99	N90-21137 *	NASA-TM-103099	p 240	N90-23991 *
NASA-TM-102378	p 206	N90-12034 *	NASA-TM-102485	p 152	N90-21274 *	NASA-TM-103100	p 220	N90-22117 *
NASA-TM-102379	p 125	N90-11880 *	NASA-TM-102486	p 51	N90-26054 *	NASA-TM-103101	p 1	N90-21723 *
NASA-TM-102380	p 86	N90-13597 *	NASA-TM-102487	p 218	N90-18064 *	NASA-TM-103102	p 183	N90-26275 *
NASA-TM-102382	p 125	N90-11144 *	NASA-TM-102488	p 223	N90-26373 *	NASA-TM-103103	p 32	N90-25882 *
NASA-TM-102383	p 71	N90-13595 *	NASA-TM-102489	p 128	N90-21858 *	NASA-TM-103104	p 30	N90-21762 *
NASA-TM-102384	p 243	N90-14844 *	NASA-TM-102490	p 97	N90-17817 *	NASA-TM-103105	p 39	N90-23416 *
NASA-TM-102385	p 242	N90-12231 *	NASA-TM-102491	p 207	N90-22801 *	NASA-TM-103106	p 205	N90-28060 *
NASA-TM-102386	p 137	N90-11901 *	NASA-TM-102492	p 128	N90-21862 *	NASA-TM-103107	p 181	N90-22011 *
NASA-TM-102387	p 11	N90-12561 *	NASA-TM-102493	p 127	N90-17875 *	NASA-TM-103108	p 192	N90-28833 *
NASA-TM-102388	p 216	N90-14640 *	NASA-TM-102494	p 151	N90-20286 *	NASA-TM-103109	p 101	N90-24384 *
NASA-TM-102389	p 18	N90-13381 *	NASA-TM-102495	p 117	N90-16053 *	NASA-TM-103110	p 13	N90-21727 *
NASA-TM-102390	p 116	N90-11854 *	NASA-TM-102496	p 179	N90-21300 *	NASA-TM-103111	p 203	N90-22790 *
NASA-TM-102391	p 177	N90-14511 *	NASA-TM-102497	p 243	N90-18927 *	NASA-TM-103112	p 239	N90-21564 *
NASA-TM-102392	p 200	N90-13786 *	NASA-TM-102498	p 243	N90-19783 *	NASA-TM-103113	p 100	N90-21825 *
NASA-TM-102393	p 117	N90-14335 *	NASA-TM-102499	p 180	N90-21962 *	NASA-TM-103114	p 100	N90-21824 *
NASA-TM-102394	p 44	N90-10912 *	NASA-TM-102500	p 151	N90-19484 *	NASA-TM-103115	p 2	N90-21725 *
NASA-TM-102395	p 203	N90-22054 *	NASA-TM-102501-REV	p 207	N90-21402 *	NASA-TM-103116	p 182	N90-22761 *
NASA-TM-102396	p 12	N90-16719 *	NASA-TM-102502	p 218	N90-18745 *	NASA-TM-103117	p 77	N90-21114 *
NASA-TM-102397	p 25	N90-11740 *	NASA-TM-102503	p 189	N90-20352 *	NASA-TM-103118	p 31	N90-23404 *
NASA-TM-102398	p 137	N90-11902 *	NASA-TM-102504	p 100	N90-21821 *	NASA-TM-103119	p 183	N90-26279 *
NASA-TM-102399	p 106	N90-12696 *	NASA-TM-102505	p 127	N90-18373 *	NASA-TM-103120	p 153	N90-21287 *
NASA-TM-102401	p 86	N90-12658 *	NASA-TM-102506	p 76	N90-19299 *	NASA-TM-103121	p 129	N90-23543 *
NASA-TM-102402	p 14	N90-25948 *	NASA-TM-102507	p 86	N90-17811 *	NASA-TM-103122	p 77	N90-21116 *
NASA-TM-102403	p 118	N90-20181 *	NASA-TM-102508	p 219	N90-20431 *	NASA-TM-103123	p 78	N90-21808 *
NASA-TM-102404	p 99	N90-21138 *	NASA-TM-102509	p 243	N90-18198 *	NASA-TM-103124	p 119	N90-23536 *
NASA-TM-102405	p 96	N90-12670 *	NASA-TM-102510	p 86	N90-19301 *	NASA-TM-103125	p 13	N90-21733 *
NASA-TM-102406	p 229	N90-14678 *	NASA-TM-102511	p 188	N90-18025 *	NASA-TM-103126	p 203	N90-21394 *
NASA-TM-102407	p 143	N90-12813 *	NASA-TM-102512	p 189	N90-20353 *	NASA-TM-103127	p 232	N90-22843 *
NASA-TM-102408	p 117	N90-13636 *	NASA-TM-102513	p 98	N90-20138 *	NASA-TM-103128	p 146	N90-28768 *
NASA-TM-102409	p 25	N90-12618 *	NASA-TM-102514	p 218	N90-19617 *	NASA-TM-103129	p 81	N90-26070 *
NASA-TM-102410	p 126	N90-14362 *	NASA-TM-102515	p 98	N90-21124 *	NASA-TM-103130	p 204	N90-22796 *
NASA-TM-102411	p 238	N90-13988 *	NASA-TM-102516	p 28	N90-20090 *	NASA-TM-103131	p 249	N90-26635 *
NASA-TM-102412	p 217	N90-17180 *	NASA-TM-102517	p 243	N90-20769 *	NASA-TM-103132	p 80	N90-25185 *
NASA-TM-102413	p 47	N90-15983 *	NASA-TM-102518	p 202	N90-17147 *	NASA-TM-103133	p 107	N90-21844 *
NASA-TM-102414	p 144	N90-19454 *	NASA-TM-102519	p 152	N90-21273 *	NASA-TM-103134	p 181	N90-22016 *
NASA-TM-102415	p 262	N90-20901 *	NASA-TM-102520	p 145	N90-21261 *	NASA-TM-103135	p 79	N90-22606 *
NASA-TM-102416	p 117	N90-16911 *	NASA-TM-102521	p 178	N90-20326 *	NASA-TM-103136	p 39	N90-25151 *
NASA-TM-102417	p 26	N90-13389 *	NASA-TM-102522	p 179	N90-20337 *	NASA-TM-103137	p 154	N90-22732 *
NASA-TM-102418	p 27	N90-13393 *	NASA-TM-102523	p 151	N90-18634 *	NASA-TM-103138	p 233	N90-25419 *
NASA-TM-102419	p 126	N90-14368 *	NASA-TM-102524	p 179	N90-21296 *	NASA-TM-103139	p 78	N90-22605 *
NASA-TM-102420	p 143	N90-17977 *	NASA-TM-102525	p 202	N90-20391 *	NASA-TM-103140	p 155	N90-26250 *
NASA-TM-102421	p 134	N90-13680 *	NASA-TM-102526	p 135	N90-20253 *	NASA-TM-103141	p 240	N90-22324 *
NASA-TM-102422	p 248	N90-18229 *	NASA-TM-102527	p 87	N90-23476 *	NASA-TM-103142	p 240	N90-22323 *
NASA-TM-102423	p 178	N90-17076 *	NASA-TM-102528	p 219	N90-20428 *	NASA-TM-103143	p 240	N90-22325 *
NASA-TM-102424	p 11	N90-13355 *	NASA-TM-102529	p 28	N90-19234 *	NASA-TM-103144	p 240	N90-23125 *
NASA-TM-102425	p 11	N90-14203 *	NASA-TM-102530	p 153	N90-21278 *	NASA-TM-103145	p 190	N90-22773 *
NASA-TM-102426	p 250	N90-17424 *	NASA-TM-102531	p 131	N90-21869 *	NASA-TM-103146	p 101	N90-24383 *
NASA-TM-102427	p 177	N90-14517 *	NASA-TM-102532	p 98	N90-20139 *	NASA-TM-103147	p 154	N90-22731 *
NASA-TM-102428	p 189	N90-22021 *	NASA-TM-102533	p 202	N90-20392 *	NASA-TM-103148	p 183	N90-26278 *
NASA-TM-102429	p 176	N90-13751 *	NASA-TM-102534	p 179	N90-21291 *	NASA-TM-103149	p 232	N90-22847 *
NASA-TM-102430	p 202	N90-18041 *	NASA-TM-102535	p 244	N90-21567 *	NASA-TM-103150	p 220	N90-22822 *
NASA-TM-102431	p 259	N90-22421 *	NASA-TM-102536	p 207	N90-21401 *	NASA-TM-103151	p 184	N90-26282 *
NASA-TM-102432	p 130	N90-13675 *	NASA-TM-102537	p 207	N90-21399 *	NASA-TM-103152	p 154	N90-23662 *
NASA-TM-102433	p 229	N90-18097 *	NASA-TM-102538	p 203	N90-20393 *	NASA-TM-103153	p 52	N90-22595 *
NASA-TM-102434	p 98	N90-19310 *	NASA-TM-102539	p 128	N90-21182 *	NASA-TM-103154	p 192	N90-22784 *
NASA-TM-102435	p 248	N90-20794 *	NASA-TM-102540	p 128	N90-21181 *	NASA-TM-103155	p 78	N90-22804 *
NASA-TM-102436	p 27	N90-15923 *	NASA-TM-102541	p 152	N90-21271 *	NASA-TM-103156	p 154	N90-23663 *
NASA-TM-102437	p 189	N90-21361 *	NASA-TM-102542	p 152	N90-21272 *	NASA-TM-103157	p 79	N90-24349 *
NASA-TM-102438	p 106	N90-21842 *	NASA-TM-102543	p 87	N90-20130 *	NASA-TM-103158	p 80	N90-25186 *
NASA-TM-102439	p 178	N90-18667 *	NASA-TM-102544	p 152	N90-21275 *	NASA-TM-103159	p 30	N90-22566 *
NASA-TM-102440	p 200	N90-13797 *	NASA-TM-102545	p 180	N90-21303 *	NASA-TM-103160	p 82	N90-26873 *
NASA-TM-102441	p 176	N90-13750 *	NASA-TM-102546	p 180	N90-21306 *	NASA-TM-103161	p 31	N90-24273 *
NASA-TM-102442	p 50	N90-14273 *	NASA-TM-102547	p 180	N90-21307 *	NASA-TM-103162	p 222	N90-25367 *
NASA-TM-102443	p 217	N90-17173 *	NASA-TM-102548	p 119	N90-25211 *	NASA-TM-103163	p 101	N90-25193 *
NASA-TM-102444	p 27	N90-14235 *	NASA-TM-102549	p 219	N90-20438 *	NASA-TM-103164	p 138	N90-26170 *
NASA-TM-102445	p 27	N90-17636 *	NASA-TM-102550	p 76	N90-21110 *	NASA-TM-103165	p 82	N90-27786 *
NASA-TM-102446	p 238	N90-22262 *	NASA-TM-102551	p 98	N90-20151 *	NASA-TM-103166	p 13	N90-25106 *
NASA-TM-102447	p 237	N90-20708 *	NASA-TM-102552	p 100	N90-21143 *	NASA-TM-103167	p 137	N90-23591 *
NASA-TM-102448	p 217	N90-14658 *	NASA-TM-102553	p 219	N90-19629 *	NASA-TM-103168	p 107	N90-23518 *
NASA-TM-102449	p 200	N90-14617 *	NASA-TM-102554	p 207	N90-23754 *	NASA-TM-103169	p 204	N90-26338 *
NASA-TM-102450	p 181	N90-21974 *	NASA-TM-102555	p 153	N90-21277 *	NASA-TM-103170	p 233	N90-25420 *
NASA-TM-102451	p 73	N90-14285 *	NASA-TM-102556	p 99	N90-21133 *	NASA-TM-103171	p 154	N90-25273 *
NASA-TM-102452	p 73	N90-14284 *	NASA-TM-102557	p 136	N90-21871 *	NASA-TM-103172	p 221	N90-23770 *
NASA-TM-102453	p 27	N90-13394 *	NASA-TM-102558	p 99	N90-21131 *	NASA-TM-103173	p 155	N90-27966 *
NASA-TM-102454	p 74	N90-17677 *	NASA-TM-102559	p 179	N90-20338 *	NASA-TM-103174	p 52	N90-25178 *
NASA-TM-102455	p 101	N90-24382 *	NASA-TM-102560	p 219	N90-20432 *	NASA-TM-103175	p 184	N90-27985 *
NASA-TM-102456	p 96	N90-14294 *	NASA-TM-102561	p 244	N90-21570 *	NASA-TM-103176	p 44	N90-26030 *
NASA-TM-102457			NASA-TM-102562			NASA-TM-103177		
NASA-TM-102458			NASA-TM-102563			NASA-TM-103178		
NASA-TM-102459			NASA-TM-102564			NASA-TM-103179		
NASA-TM-102460			NASA-TM-102565			NASA-TM-103180		
NASA-TM-102461			NASA-TM-102566			NASA-TM-103181		
NASA-TM-102462			NASA-TM-102567			NASA-TM-103182		
NASA-TM-102463			NASA-TM-102568			NASA-TM-103183		
NASA-TM-102464			NASA-TM-102569			NASA-TM-103184		
NASA-TM-102465			NASA-TM-102570			NASA-TM-103185		

REPORT NUMBER INDEX

NASA-TM-103188	p 263	N90-26729 * #	PWA-5574-223-VOL-2	p 117	N90-17868 * #	US-PATENT-CLASS-428-551	p 101	N90-23493 *
NASA-TM-103189	p 136	N90-26163 * #	PWA-5594-231	p 35	N90-28566 * #	US-PATENT-CLASS-428-552	p 101	N90-23493 *
NASA-TM-103190	p 79	N90-25181 * #	PWA-5594-251-VOL-2	p 35	N90-28565 * #	US-PATENT-CLASS-431-352	p 106	N90-11824 *
NASA-TM-103192	p 221	N90-23773 * #	PWA-5594-258-VOL-1	p 34	N90-28564 * #	US-PATENT-CLASS-528-188	p 86	N90-19300 *
NASA-TM-103194	p 184	N90-27984 * #	PWA-5594-271-ADD	p 33	N90-28556 * #	US-PATENT-CLASS-528-229	p 86	N90-19300 *
NASA-TM-103195	p 182	N90-25289 * #	PWA-5594-287	p 36	N90-28570 * #	US-PATENT-CLASS-528-352	p 86	N90-19300 *
NASA-TM-103196	p 185	N90-28792 * #	PWA-5594-329	p 35	N90-28568 * #	US-PATENT-CLASS-528-353	p 86	N90-19300 *
NASA-TM-103198	p 37	N90-26011 * #	PWA-5594-331	p 35	N90-28569 * #	US-PATENT-CLASS-549-241	p 107	N90-23497 *
NASA-TM-103199	p 80	N90-25184 * #	PWA-5594-333	p 35	N90-28567 * #	US-PATENT-CLASS-55-160	p 190	N90-22024 *
NASA-TM-103200	p 155	N90-25278 * #	PWA-5970-40	p 26	N90-13388 * #	US-PATENT-CLASS-55-203	p 190	N90-22024 *
NASA-TM-103201	p 190	N90-25323 * #				US-PATENT-CLASS-55-204	p 190	N90-22024 *
NASA-TM-103202	p 81	N90-26065 * #	REPT-716111-09	p 143	N90-12784 * #	US-PATENT-CLASS-562-413	p 107	N90-23497 *
NASA-TM-103203	p 87	N90-26074 * #	REPT-89-3	p 182	N90-26269 * #	US-PATENT-CLASS-562-415	p 107	N90-23497 *
NASA-TM-103205	p 81	N90-26068 * #	REPT-89B00244	p 234	N90-12984 * #	US-PATENT-CLASS-562-417	p 107	N90-23497 *
NASA-TM-103206	p 43	N90-25158 * #				US-PATENT-CLASS-60-730	p 106	N90-11824 *
NASA-TM-103207	p 267	N90-26789 * #	RI/RD-89-179	p 71	N90-13589 * #	US-PATENT-CLASS-60-732	p 106	N90-11824 *
NASA-TM-103208	p 191	N90-26299 * #	RI/RD-90-177	p 191	N90-29629 * #	US-PATENT-CLASS-73-799	p 190	N90-23712 *
NASA-TM-103209	p 183	N90-26276 * #				US-PATENT-CLASS-73-845	p 190	N90-23712 *
NASA-TM-103210	p 233	N90-26396 * #	RI/RD89-171-PT-3	p 204	N90-26320 * #	US-PATENT-CLASS-75-228	p 101	N90-23493 *
NASA-TM-103211	p 51	N90-25173 * #						
NASA-TM-103212	p 32	N90-26009 * #	RPT/D0406-54	p 118	N90-21165 * #	US-PATENT-4,819,438	p 106	N90-11824 *
NASA-TM-103213	p 81	N90-26069 * #				US-PATENT-4,845,167	p 86	N90-19300 *
NASA-TM-103215	p 183	N90-26273 * #	R82AEB401	p 33	N90-28555 * #	US-PATENT-4,885,116	p 107	N90-23497 *
NASA-TM-103217	p 131	N90-26180 * #	R82AEB406	p 33	N90-28553 * #	US-PATENT-4,904,538	p 101	N90-23493 *
NASA-TM-103219	p 246	N90-28393 * #	R82AEB470	p 34	N90-28559 * #	US-PATENT-4,911,738	p 190	N90-22024 *
NASA-TM-103220	p 51	N90-26055 * #	R82AEB472	p 33	N90-28554 * #	US-PATENT-4,916,954	p 190	N90-23712 *
NASA-TM-103221	p 184	N90-27983 * #	R83AEB143	p 34	N90-28563 * #	US-PATENT-4,917,302	p 204	N90-23751 *
NASA-TM-103222	p 184	N90-28009 * #	R83AEB143	p 34	N90-28558 * #			
NASA-TM-103223	p 259	N90-26682 * #	R83AEB488	p 34	N90-28558 * #			
NASA-TM-103224	p 102	N90-28670 * #	R83AEB503	p 34	N90-28561 * #			
NASA-TM-103225	p 222	N90-26364 * #	R83AEB623	p 34	N90-28562 * #			
NASA-TM-103228	p 82	N90-27785 * #	R84AEB246	p 33	N90-28557 * #			
NASA-TM-103229	p 244	N90-26614 * #	R88-900064-F	p 10	N90-10835 * #			
NASA-TM-103231	p 244	N90-26615 * #	R88-900064-F	p 10	N90-10836 * #			
NASA-TM-103233	p 102	N90-27874 * #	R89-917447-32	p 118	N90-18559 * #			
NASA-TM-103235	p 156	N90-28786 * #	R89AEB-325	p 222	N90-26355 * #			
NASA-TM-103237	p 233	N90-26397 * #	R90-957907-2	p 14	N90-27655 * #			
NASA-TM-103239	p 130	N90-28740 * #						
NASA-TM-103240	p 244	N90-26616 * #	SAE PAPER 891035	p 246	A90-14342 *			
NASA-TM-103241	p 81	N90-26071 * #	SAE PAPER 891563	p 47	A90-27525 *			
NASA-TM-103242	p 82	N90-27783 * #	SAE PAPER 891565	p 48	A90-27527 *			
NASA-TM-103243	p 47	N90-27736 * #	SAE PAPER 892213	p 20	A90-28571 *			
NASA-TM-103246	p 260	N90-26683 * #						
NASA-TM-103249	p 14	N90-25946 * #	SAE SP-800	p 20	A90-28571 *			
NASA-TM-103250	p 15	N90-27657 * #						
NASA-TM-103252	p 191	N90-28033 * #	SAND-89-1635C	p 249	N90-16496 * #			
NASA-TM-103254	p 82	N90-27784 * #	SAND-90-1229C	p 259	N90-24964 * #			
NASA-TM-103255	p 191	N90-28031 * #						
NASA-TM-103256	p 52	N90-28596 * #	SWRI-06-7576/13	p 26	N90-13391 * #			
NASA-TM-103259	p 82	N90-27782 * #	SWRI-06-7963	p 125	N90-11882 * #			
NASA-TM-103261	p 102	N90-27875 * #	SWRI-7576/45	p 26	N90-13390 * #			
NASA-TM-103262	p 244	N90-29124 * #						
NASA-TM-103264	p 223	N90-28112 * #	TBE-SSD-P601-89-191	p 200	N90-13794 * #			
NASA-TM-103271	p 205	N90-28062 * #						
NASA-TM-103275	p 205	N90-28065 * #	TSF1-R-014	p 180	N90-21301 * #			
NASA-TM-103280	p 83	N90-28657 * #						
NASA-TM-103291	p 260	N90-29219 * #	UPI307-51-00	p 154	N90-25273 * #			
NASA-TM-103292	p 108	N90-28696 * #						
NASA-TM-103459	p 259	N90-24952 * #	US-Patent-4,890,036	p 153	N90-22724 *			
NASA-TM-103490	p 51	N90-25174 * #						
NASA-TM-103607	p 83	N90-28659 * #	US-PATENT-APPL-SN-130058	p 153	N90-22724 *			
NASA-TM-103609	p 241	N90-29121 * #	US-PATENT-APPL-SN-159071	p 107	N90-23497 *			
NASA-TM-4133	p 216	N90-14842 * #	US-PATENT-APPL-SN-292146	p 204	N90-23751 *			
NASA-TM-4141	p 25	N90-13387 * #	US-PATENT-APPL-SN-326757	p 101	N90-23493 *			
NASA-TM-4176	p 241	N90-25607 * #	US-PATENT-APPL-SN-326786	p 190	N90-22024 *			
NASA-TM-4203	p 223	N90-28111 * #	US-PATENT-APPL-SN-376488	p 252	N90-10718 * #			
NASA-TM-897140	p 249	N90-16496 * #	US-PATENT-APPL-SN-376738	p 187	N90-10415 * #			
NASA-TM-89715	p 261	N90-26693 * #	US-PATENT-APPL-SN-392239	p 151	N90-17009 * #			
NASA-TM-89923	p 70	N90-10174 * #	US-PATENT-APPL-SN-396263	p 190	N90-23712 *			
			US-PATENT-APPL-SN-404291	p 251	N90-15733 * #			
			US-PATENT-APPL-SN-433863	p 97	N90-15147 * #			
			US-PATENT-APPL-SN-441672	p 201	N90-15444 * #			
			US-PATENT-APPL-SN-443289	p 126	N90-15262 * #			
			US-PATENT-APPL-SN-443523	p 73	N90-15130 * #			
			US-PATENT-APPL-SN-452465	p 106	N90-11824 *			
			US-PATENT-APPL-SN-458274	p 201	N90-15445 * #			
			US-PATENT-APPL-SN-458467	p 258	N90-17454 * #			
			US-PATENT-APPL-SN-924470	p 86	N90-19300 *			
			US-PATENT-APPL-SN-924474	p 107	N90-23497 *			
			US-PATENT-CLASS-165-156	p 106	N90-11824 *			
			US-PATENT-CLASS-165-81	p 106	N90-11824 *			
			US-PATENT-CLASS-165-83	p 106	N90-11824 *			
			US-PATENT-CLASS-210-512.1	p 190	N90-22024 *			
			US-PATENT-CLASS-210-97	p 190	N90-22024 *			
			US-PATENT-CLASS-239-265.11	p 204	N90-23751 *			
			US-PATENT-CLASS-260-386	p 107	N90-23497 *			
			US-PATENT-CLASS-260-395	p 107	N90-23497 *			
			US-PATENT-CLASS-277-158	p 204	N90-23751 *			
			US-PATENT-CLASS-277-34	p 204	N90-23751 *			
			US-PATENT-CLASS-315-3.5	p 153	N90-22724 *			
			US-PATENT-CLASS-315-3	p 153	N90-22724 *			
			US-PATENT-CLASS-331-82	p 153	N90-22724 *			
			US-PATENT-CLASS-419-24	p 101	N90-23493 *			
			US-PATENT-CLASS-419-36	p 101	N90-23493 *			
			US-PATENT-CLASS-419-37	p 101	N90-23493 *			
			US-PATENT-CLASS-419-8	p 101	N90-23493 *			
OSU-TR-716111-8	p 145	N90-20271 * #						
OSU-TR-720964-5	p 144	N90-19466 * #						
PDA-86-FR-5333-00-06	p 25	N90-13385 * #						
PW-FR-20668	p 29	N90-21761 * #						
PWA-5394-315	p 34	N90-28560 * #						

Report Documentation Page

1. Report No. NASA TM-103753		2. Government Accession No.		3. Recipient's Catalog No.	
4. Title and Subtitle Bibliography of Lewis Research Center Technical Publications Announced in 1990				5. Report Date August 1991	
				6. Performing Organization Code	
7. Author(s)				8. Performing Organization Report No. E-6007	
				10. Work Unit No. None	
9. Performing Organization Name and Address National Aeronautics and Space Administration Lewis Research Center Cleveland, Ohio 44135-3191				11. Contract or Grant No.	
				13. Type of Report and Period Covered Technical Memorandum	
12. Sponsoring Agency Name and Address National Aeronautics and Space Administration Washington, D.C. 20546-0001				14. Sponsoring Agency Code	
15. Supplementary Notes Compiled by Technical Information Services Division, Lewis Research Center.					
16. Abstract This compilation of abstracts describes and indexes the technical reporting that resulted from the scientific and engineering work performed and managed by the Lewis Research Center in 1990. All the publications were announced in the 1990 issues of STAR (Scientific and Technical Aerospace Reports) and/or IAA (International Aerospace Abstracts). Included are research reports, journal articles, conference presentations, patents and patent applications, and theses.					
17. Key Words (Suggested by Author(s)) Bibliographies Abstracts Documentation Indexes (Documentation)			18. Distribution Statement Unclassified - Unlimited Subject Category 82		
19. Security Classif. (of this report) Unclassified		20. Security Classif. (of this page) Unclassified		21. No. of pages 435	
				22. Price* A19	

National Aeronautics and
Space Administration

Lewis Research Center
Cleveland, Ohio 44135

Official Business
Penalty for Private Use \$300

FOURTH CLASS MAIL

ADDRESS CORRECTION REQUESTED



Postage and Fees Paid
National Aeronautics and
Space Administration
NASA 451

NASA
